TRANSACTIONS

OF THE

AMERICAN SOCIETY

OF

CIVIL ENGINEERS

(INSTITUTED 1852)

VOLUME 119

1954

Edited by the Secretary, under the direction of the Committee on Publications.

Reprints from this publication, which is copyrighted, may be made on condition that the full title of paper, name of author, and page reference (or paper number) are given.

NEW YORK
PUBLISHED BY THE SOCIETY

1954

Transp.
TA
1
.A526
v.119

Copyright 1954, by the American Society of Civil Engineers.

Note.—The Society is not responsible for any statement made or opinion expressed in its publications.

Transportation
Library

Gift

FEB 3 '58

CONTENTS

PAPERS AND DISCUSSIONS

(Alphabetical Indexes Begin on Page 1371)

No. PAGE

2656 ICE PRESSURE AGAINST DAMS: A SYMPOSIUM 1
STUDIES OF THE EFFECTS OF TEMPERATURE VARIATIONS
By **Bertil Löfquist** 6
Discussion:
By G. E. Monfore 17
Edwin Rose 18
Bertil Löfquist 20

SOME INVESTIGATIONS IN CANADA
By **A. D. Hogg** 22

EXPERIMENTAL INVESTIGATIONS BY THE BUREAU OF RECLAMATION
By **G. E. Monfore** 26
Discussion:
By Edwin Rose 39
G. E. Monfore 41

2657 STIFFNESS CHARTS FOR GUSSETED MEMBERS UNDER AXIAL LOAD
By **John E. Goldberg** 43
Discussion:
By Leonard K. Stevens 58
John E. Goldberg 59

2658 ELECTRONIC DEVICES IN AIR TRANSPORT
By **F. B. Lee** 60
Discussion:
By P. C. Sandretto 70
F. B. Lee 72

2659 DAM MODIFICATIONS CHECKED BY HYDRAULIC MODELS
By **E. S. Harrison and Carl E. Kindsvater** 73
Discussion:
By G. H. Hickox 90
E. S. Harrison and Carl E. Kindsvater 92

2660 RAPID COMPUTATION OF FLEXURAL CONSTANTS
By **Thomas G. Morrison** 93
Discussion:
By Henry Malter 103
Paul Rogers 106
Thomas G. Morrison 107

No. PAGE

2661 SPECIAL DESIGN FEATURES OF THE YORKTOWN BRIDGE
By **Maurice N. Quade** 109

2662 UNIFIED MASS-TRANSPORTATION SYSTEM FOR NEW YORK
By **William Reid** 127

Discussion:
By JOHN F. KRAUS 132

2663 SLACKWATER IMPROVEMENT OF THE COLUMBIA RIVER
By **O. E. Walsh** 135

2664 AERONAUTICAL CHARTING AND MAPPING
By **Charles A. Schanck** 151

Discussion:
By E. S. FABIAN 158
PHIL M. MILES 161
CHARLES A. SCHANCK 162

2665 CITY PLANNING TECHNIQUES
By **Russell H. Riley** 163

2666 EARTHQUAKE STRESSES IN SHEAR BUILDINGS
By **M. G. Salvadori** 171

Discussion:
By JOHN A. BLUME 194
E. F. MASUR 201
EDWARD COHEN, EDWARD LAING, AND LEON S. LEVY 203
M. G. SALVADORI 205

2667 VELOCITY MEASUREMENT OF AIR-WATER MIXTURES
By **Lorenz G. Straub, John M. Killen, and Owen P. Lamb** 207

2668 RADIAL IMPACT ON AN ELASTICALLY SUPPORTED RING
By **Edward Wenk, Jr.** 221

Discussion:
By JOHN C. BURGESS 246
EDWARD WENK, JR. 247

2669 RAINFALL STUDIES USING RAIN-GAGE NETWORKS AND RADAR
By **H. E. Hudson, Jr., G. E. Stout, and F. A. Huff** 248

Discussion:
By VEN TE CHOW 274
H. E. HUDSON, JR., G. E. STOUT, AND F. A. HUFF 275

2670 ZONING MAPS FOR AIRPORTS
By **Benjamin Everett Beavin, Sr.** 277

Discussion:
By HAROLD M. LEWIS 286
BENJAMIN EVERETT BEAVIN, SR. 290

2671 THE EQUIVALENT RECTANGLE IN PRESTRESSED CONCRETE DESIGN
By **John J. Peebles** 292

Discussion:
By FRED E. KOEBEL 303
JOHN J. PEEBLES 306

No. Page

2672 **NONELASTIC BEHAVIOR OF BRIDGES UNDER IMPULSIVE LOADS**
By **S. J. Fraenkel and L. E. Grinter** 309

Discussion:
By Robert J. Hansen and John S. Archer 329
S. J. Fraenkel and L. E. Grinter 330

2673 **FRICTION FACTORS FOR TURBULENT FLOW IN PIPES**
By **Edward F. Wilsey** 331

Discussion:
By George A. Whetstone 337

2674 **GROUP LOADINGS APPLIED TO THE ANALYSIS OF FRAMES**
By **I. F. Morrison** 338

Discussion:
By Bernard L. Weiner 353
I. F. Morrison 354

2675 **DESIGN OF SIDE WALLS IN CHUTES AND SPILLWAYS**
By **D. B. Gumensky** 355

Discussion:
By Leland S. Rhodes 362
G. S. Sarkaria 363
J. H. Douma 364
Edgar E. Foster 368
Thomas J. Rhone 368
D. B. Gumensky 371

2676 **THE DESIGN OF FLEXIBLE BULKHEADS**
By **James R. Ayers and R. C. Stokes** 373

Discussion:
By W. F. Heavey 384
Morgan S. Campbell 385
Walter C. Boyer 386
P. W. Rowe 388
Gregory P. Tschebotarioff 390
J. Owen Lake 392
Nai C. Yang 394
David Hopkins 396

2677 **RATING CURVES FOR FLOW OVER DRUM GATES**
By **Joseph N. Bradley** 403

Discussion:
By Guido Wyss 421
Sam Shulits 421
Bob Buehler 421
F. B. Campbell and A. A. McCool 428
Joseph N. Bradley 431

2678 **SEWAGE DISPOSAL IN TIDAL ESTUARIES**
By **Alexander N. Diachishin, Seth G. Hess, and William T. Ingram** 434

Discussion:
By Isadore Nusbaum 448
Alexander N. Diachishin, Seth G. Hess, and William T. Ingram 451

No. PAGE

2679 A DIRECT STEP METHOD FOR COMPUTING WATER-SURFACE PROFILES
By **Arthur A. Ezra** 453

Discussion:
By I. H. Steinberg 463
C. A. M. Gray 469
Bob Buehler 470
Monir M. Kansoh 475
Arthur A. Ezra 477

2680 OFFSHORE PETROLEUM INSTALLATIONS
By **Jack S. Toler** 480

2681 RECENT AIRPORT DESIGN AND DEVELOPMENT
By **Philip A. Hahn** 489

Discussion:
By Louis A. Nees 497
Philip A. Hahn 498

2682 DEFLECTION OF MEMBERS OF VARIABLE MOMENT OF INERTIA
By **Anthony Hoadley** 499

2683 THE GRANBY PUMPING PLANT: A SYMPOSIUM 509

FOUNDATIONS AND DESIGN
By **W. R. Judd and W. H. Wolf** 510

CONSTRUCTION
By **R. J. Willson** 525

2684 SPECIAL PROCEDURES FOR PAVEMENT DESIGN
By **L. A. Palmer** 542

Discussion:
By R. Horonjeff 561
L. A. Palmer 563

2685 NUMERICAL ANALYSIS OF CONTINUOUS FRAMES IN SPACE
By **James Michalos** 565

2686 REVENUE BOND FINANCING FOR AIRPORT IMPROVEMENTS
By **James C. Buckley** 583

2687 SNOW HYDROLOGY FOR MULTIPLE-PURPOSE RESERVOIRS
By **Herbert S. Riesbol** 595

Discussion:
By Ray K. Linsley 614
R. W. Gerdel 615
Harold D. Hafterson 619
David M. Rockwood 621
Herbert S. Riesbol 624

2688 WAVE-WASH CONTROL ON MISSISSIPPI RIVER LEVEES
By **Rudolf Hertzberg** 628

2689 DESIGN CURVES FOR ANCHORED STEEL SHEET PILING
By **Walter C. Boyer and Henry M. Lummis, III** 639

Discussion:
By Gregory P. Tschebotarioff 651
Walter C. Boyer and Henry M. Lummis, III 655

No. PAGE

2690 ALGAE RESPONSIBLE FOR ODOR AND TASTE IN WATER SUPPLIES
By George J. Turre 658

2691 ANALYSIS OF CORRECTIVE ACTIONS FOR HIGHWAY LANDSLIDES
By R. F. Baker 665
Discussion:
By D. P. Krynine and Richard J. Woodward 690
R. F. Baker 696

2692 POST-BUCKLING STRENGTH OF REDUNDANT TRUSSES
By E. F. Masur 699

2693 THE ENGINEER'S ROLE IN METROPOLITAN TRAFFIC PLANNING
By Lloyd Braff 713
Discussion:
By James L. Foley, Jr. 719

2694 DEFLECTION OF LAMINATED BEAMS
By L. G. Clark 721

2695 BRIDGES ON THE WEST VIRGINIA TURNPIKE
By Elmer K. Timby 737

2696 HIPPED PLATE ANALYSIS, CONSIDERING JOINT DISPLACEMENTS
By Ibrahim Gaafar 743
Discussion:
By Herman Craemer 771
James M. Paulson and L. C. Maugh 772
R. Gartner 776
Ibrahim Gaafar 779

2697 PUTTING A SEWAGE TREATMENT PLANT INTO OPERATION
By Benjamin Benas 785

2698 STRESSES IN THE CORNERS OF RIGID FRAMES
By Harvey C. Olander 797

2699 CONTINUOUS COMPOSITE STEEL AND CONCRETE BEAMS
By John Sherman 810

2700 LATERAL BUCKLING OF CHANNELS AND Z-BEAMS
By H. N. Hill 829

2701 RELIEF WELL SYSTEMS FOR DAMS AND LEVEES
By W. J. Turnbull and C. I. Mansur 842
Discussion:
By P. T. Bennett 862
John A. Focht, Jr. 870
W. H. Jervis 874
W. J. Turnbull and C. I. Mansur 875

2702 WIND LOADS ON TRUSS BRIDGES
By John M. Biggs 879
Discussion:
By F. B. Farquharson 893
John M. Biggs 896

No. PAGE

2703 MASS-CONCRETE OPERATIONS IN THE ROCKY MOUNTAINS
By George P. McIndoe 899

2704 AMPLIFICATION OF STRESS IN FLEXIBLE STEEL ARCHES
By Robert S. Rowe 910

Discussion:
By Milo S. Ketchum 926
Robert S. Rowe 926

2705 FREQUENCY OF EXCESSIVE RAINFALLS IN FLORIDA
By David B. Smith 927

2706 PLATES WITH BOUNDARY CONDITIONS OF ELASTIC SUPPORT
By S. J. Fuchs 935

Discussion:
By M. Z. v. Krzywoblocki 959
R. H. Wood 960
S. J. Fuchs 966

2707 AN INTERSTATE ROUTE AND ITS URBAN CONNECTIONS
By D. W. Ormsbee 969

2708 LIVE LOADING FOR LONG-SPAN HIGHWAY BRIDGES
Bv R. J. Ivy, T. Y. Lin, Stewart Mitchell, N. C. Raab, V. J. Richey, and C. F. Scheffey 981

Discussion:
By Louis Balog 995
Glenn B. Woodruff 999
William G. Byers 1001
Kuang-Han Chu 1002
R. J. Ivy, T. Y. Lin, Stewart Mitchell, N. C. Raab, V. J. Richey, and C. F. Scheffey 1003

2709 PEAK DISCHARGE FOR HIGHWAY DRAINAGE DESIGN
By Carl F. Izzard 1005

Discussion:
By Max A. Kohler 1016
Roy F. Warner 1017
N. E. Minshall 1018
Carl F. Izzard 1022

2710 DESIGN CHARTS FOR AIR CHAMBERS ON PUMP LINES
By W. E. Evans and C. C. Crawford 1025

Discussion:
By C. E. Withers 1037
Henry M. Paynter 1039
W. E. Evans and C. C. Crawford 1045

2711 ELECTRICAL ANALOGS OF STATICALLY LOADED STRUCTURES
By Frederick L. Ryder 1046

2712 RIVER-BED SCOUR DURING FLOODS
By E. W. Lane and W. M. Borland 1069

Discussion:
By E. E. Dittbrenner 1080
Emmett M. Laursen and Arthur Toch 1084
E. W. Lane and W. M. Borland 1087

No. Page

2713 HIGHWAY BRIDGES ON DEEP FOUNDATIONS
By **Louis Duclos** 1090

Discussion:
By Arthur V. Walker 1100

2714 MECHANICS OF MANIFOLD FLOW
By **John S. McNown** 1103

Discussion:
By Julio Escobar 1119
M. R. Carstens and John Roberson 1123
James J. Hartigan 1128
Sadiq M. Niaz 1132
James R. Barton 1134
Ralph W. Powell 1136
John K. Vennard and Darrel I. Dentoni 1136
John S. McNown 1140

2715 DESIGN OF FRAMES BY RELAXATION OF YIELD-HINGES
By **J. Morley English** 1143

Discussion:
By Noel W. Murray 1154
Herman Tachau 1155
J. Morley English 1156

2716 LAMINAR TO TURBULENT FLOW IN A WIDE OPEN CHANNEL
By **W. M. Owen** 1157

Discussion:
By Yuichi Iwagaki 1165
J. W. Delleur 1167
Ralph W. Powell and Chesley J. Posey 1170
Henry Maksoud 1172
W. M. Owen 1174

2717 ANALYSIS OF WATER HAMMER BY CHARACTERISTICS
By **C. A. M. Gray** 1176

Discussion:
By Pin-Nam Lin 1190
Henry M. Paynter 1191
C. A. M. Gray 1193

2718 JOINT TRANSLATION BY CANTILEVER MOMENT DISTRIBUTION
By **L. E. Grinter and C. H. Tsao** 1195

Discussion:
By T. C. Kavanagh 1204
Ralph W. Stewart 1205
W. Merchant 1206
Jack R. Benjamin 1206
Joseph G. Perri 1207
Richard H. Hadley 1207
Ming-Lung Pei 1208
L. E. Grinter and C. H. Tsao 1209

2719 TURBULENT BOUNDARY LAYER ON STEEP SLOPES
By **William J. Bauer** 1212

Discussion:
By G. Halbronn 1234
William J. Bauer 1240

No. PAGE

2720 ANCHORED BULKHEADS

By Karl Terzaghi 1243

Discussion:

By T. H. Wu 1281
W. D. Bigler 1284
J. Brinch Hansen 1285
Gregory P. Tschebotarioff 1287
Paul Baumann 1296
Rudolf Briske 1298
Norman D. Lea 1299
S. Packshaw 1301
J. Verdeyen and V. Roisin 1307
Karl Terzaghi 1311

2721 THE ENGINEER AND WORLD POPULATION: ADDRESS AT THE SUMMER CONVENTION, ATLANTIC CITY, N. J., JUNE 16, 1954

By Daniel V. Terrell, President 1325

MEMOIRS OF DECEASED MEMBERS: ABSTRACTS 1331

PAPERS PUBLISHED JULY, 1953-SEPTEMBER, 1954, INCLUSIVE, AS ASCE PROCEEDINGS-SEPARATES, ACCEPTED FOR FUTURE PUBLICATION IN TRANSACTIONS, BUT NOT INCLUDED IN VOL. 119

No.		*Proceedings-Separates*
200	**SAND COMPACTION BY VIBROFLOTATION** By Elio d'Appolonia, Callix E. Miller, Jr., and Thomas M. Ware	July, 1953
205	**BENDING OF A CONSTRAINED CIRCULAR BEAM RESTING ON AN ELASTIC FOUNDATION** By Enrico Volterra and Randall Chung	July, 1953
211	**PHOTOELASTIC ANALOGY FOR NON-HOMOGENEOUS FOUNDATIONS** By Allen J. Curtis and F. E. Richart, Jr.	July, 1953
214	**PLANNING AND OPERATING TURNPIKES** By Charles M. Noble	July, 1953
216	**THE JOHN E. MATHEWS BRIDGE** By Maurice N. Quade and Richard S. M. Lee	July, 1953
218	**WIND VELOCITIES DURING HURRICANES** By Robert C. Gentry	July, 1953
219	**INVESTIGATION OF THE DEAD LOAD STRESSES IN THE MISSISSIPPI RIVER VETERANS MEMORIAL BRIDGE AT EAST ST. LOUIS, ILLINOIS** By L. T. Wyly, R. W. Kluge, K. H. Lenzen, L. B. McCammon, M. B. Lagaard, and E. W. Larson, Jr.	July, 1953
223	**APPLICATIONS OF THE RELAXATION TECHNIQUE IN FLUID MECHANICS** By John S. McNown, En-Yun Hsu, and Chia-Shun Yih	July, 1953
226	**DEVELOPMENT OF THE CHEMICAL AND ALLIED INDUSTRY IN THE SOUTH** By C. O. Hoyer	July, 1953
227	**UNUSUAL FOUNDATION CONDITIONS ENCOUNTERED ON THE CENTRAL AND SOUTHERN FLORIDA PROJECT** By Paul H. Shea	July, 1953
228	**REDUCTION IN SOIL STRENGTH WITH INCREASE IN DENSITY** By Charles R. Foster	July, 1953
229	**SELECTION OF PUMPS AND DESIGN OF HIGH VOLUME-LOW HEAD PUMPING STATIONS** By George F. Snodgrass	July, 1953
230	**TOTAL SEDIMENT LOAD MEASURED IN TURBULENCE FLUME** By P. C. Benedict, M. L. Albertson, and D. Q. Matejka	August, 1953
233	**DETERMINATION OF RADII OF CURVATURE OF TAXIWAYS** By John Hugh Jones and Robert Horonjeff	August, 1953

No. | *Proceedings-Separates*

235 CALIFORNIA EXPERIENCE IN CORRECTION OF LANDSLIDES AND SLIPOUTS
By A. W. Root .... August, 1953

236 HIGHWAY ENGINEERING EDUCATIONAL PROGRAMS AND PROBLEMS
By Harner E. Davis and Ralph A. Moyer .... August, 1953

243 STRUCTURAL WELDMENT INSPECTION
By John L. Beaton and Paul G. Jonas .... August, 1953

255 AIRPORT TRAFFIC AND THE PUERTO RICO INTERNATIONAL AIRPORT
By Walther Prokosch .... August, 1953

271 A PROPOSED METHOD FOR THE TRANSIT LINING OF HIGH-SPEED TRACK
By Neil R. Berndt .... September, 1953

280 PROGRESS REPORT ON STUDIES ON THE DESIGN OF STABLE CHANNELS BY THE BUREAU OF RECLAMATION
By E. W. Lane .... September, 1953

283 FLOCCULATION AND FLOCCULATION BASINS
By Thomas R. Camp .... September, 1953

286 INELASTIC BEHAVIOR OF REINFORCED CONCRETE MEMBERS SUBJECTED TO SHORT-TIME STATIC LOADS
By L. H. N. Lee .... September, 1953

287 IMPULSIVE MOTION OF ELASTO-PLASTIC BEAMS
By H. H. Bleich and M. G. Salvadori .... September, 1953

291 LATERAL BUCKLING OF I BEAMS UNDER THRUST AND UNEQUAL END MOMENTS
By M. G. Salvadori .... October, 1953

292 STRENGTH OF COLUMNS ELASTICALLY RESTRAINED AND ECCENTRICALLY LOADED
By P. P. Bijlaard, G. P. Fisher, and George Winter .... October, 1953

294 RECENT ADDITIONS AND IMPROVEMENTS TO THE HALES BAR HYDROELECTRIC PLANT
By Adolph A. Meyer .... October, 1953

295 DISCHARGE CHARACTERISTICS OF TAINTER GATES
By Arthur Toch .... October, 1953

297 HIGH VELOCITY TESTS IN A PENSTOCK
By Maxwell F. Burke .... October, 1953

302 STABILIZATION OF MUNICIPAL REFUSE BY COMPOSTING
By P. H. McGauhey and Harold B. Gotaas .... October, 1953

304 CHESAPEAKE BAY BRIDGE
By E. F. Ball .... October, 1953

No.		*Proceedings-Separates*
310	**SEWAGE AERATION PRACTICE IN THE SANITARY DISTRICT OF CHICAGO** By Norval E. Anderson	October, 1953
311	**ESTIMATING THE TRUE CONSOLIDATION BEHAVIOR OF CLAY FROM LABORATORY TEST RESULTS** By John H. Schmertmann	October, 1953
318	**SOME ECONOMIC ASPECTS OF WATERWAY PROJECTS** By Haywood R. Faison	October, 1953
321	**ERECTION OF THE MAIN RIVER SPAN, PASSAIC RIVER CROSSING, NEW JERSEY TURNPIKE** By Jonathan Jones	November, 1953
343	**DESIGN AND RESEARCH FOR WELDED STRUCTURES** By La Motte Grover	November, 1953
344	**STEEL FOR WELDED BRIDGES AND BUILDINGS** By Simon A. Greenberg	November, 1953
345	**FABRICATION AND CONSTRUCTION OF STRUCTURAL STEEL FOR BUILDINGS** By C. L. Kreidler	November, 1953
346	**STATUTORY CONTROL OF GROUND WATER** By S. T. Harding	November, 1953
353	**THE IMPORTANCE OF SHORAN SURVEYING IN THE SOUTHERN HEMISPHERE** By Carl I. Aslakson	November, 1953
365	**EFFECT OF WELL SCREENS ON FLOW INTO WELLS** By Jack S. Petersen, Carl Rohwer, and M. L. Albertson	December, 1953
375	**DEFLECTIONS OF A CIRCULAR BEAM OUT OF ITS INITIAL PLANE** By Enrico Volterra	December, 1953
381	**OPEN CHANNELS WITH NONUNIFORM DISCHARGE** By Wen-Hsiung Li	January, 1954
382	**HYDRAULIC MODEL STUDIES OF MARTIN DAM DRAFT TUBES** By Carl E. Kindsvater and R. R. Randolph, Jr.	January, 1954
383	**BACKWATER FUNCTIONS BY NUMERICAL INTEGRATION** By Clint J. Keifer and Henry Hsien Chu	January, 1954
390	**A NEW CONCEPT OF FLOW IN ROUGH CONDUITS** By Henry N. Morris	January, 1954
434	**ANALYSIS AND TESTS OF A CYLINDRICAL SHELL ROOF MODEL** By Bruno Thurlimann and Bruce G. Johnston	April, 1954
440	**THE WORK OF THE RESEARCH COUNCIL ON RIVETED AND BOLTED JOINTS** By W. C. Stewart	May, 1954

No.		*Proceedings-Separates*
441	LABORATORY TESTS OF HIGH TENSILE BOLTED STRUCTURAL JOINTS By W. H. Munse, D. T. Wright, and N. M. Newmark	May, 1954
466	FLOW IN OPEN CHANNELS By Edward F. Wilsey	August, 1954
467	TRANQUIL FLOW THROUGH OPEN-CHANNEL CONSTRICTIONS By Carl E. Kindsvater and Rolland W. Carter	August, 1954
469	FATIGUE IN RIVETED AND BOLTED SINGLE LAP JOINTS By J. W. Carter, K. H. Lenzen, and L. T. Wyly	August, 1954
470	COMPARATIVE BEHAVIOR OF BOLTED AND RIVETED JOINTS By Frank Baron and Edward W. Larson, Jr.	August, 1954
484	SLIP OF JOINTS UNDER STATIC LOADS By R. A. Hechtman, D. R. Young, A. G. Chin, and E. R. Savikko	September, 1954
485	STRUCTURAL APPLICATION OF HIGH-STRENGTH BOLTS By T. R. Higgins and E. J. Ruble	September, 1954

ERRATA

Transactions, Vol. 117, 1952

Page 482, Fig. 26, the point at which the envelope intersects the left ordinate should be designated as point "F."

Transactions, Vol. 118, 1953

Page 557, line 7, change "meterology" to "meteorology."

Page 602, line 29, change "shop mooring" to "ship mooring."

Pages 838, 846, 1289, and 1356, the name, "Joseph Sorkin," should be changed to "Josef Sorkin."

Page 1020, Eq. 15, in the second term in the right-hand member, change "b_w" to "b^2_w."

Page 1021, Eq. 16, in the first and second terms in the right-hand member, change "b_w" to "b^2_w." Throughout the paragraph directly following Eq. 16, change "b_w" to "b^2_w." In the second paragraph following Eq. 16, in the two occurrences of the term, "$\frac{2\,Q}{b_w\,g\,H^3}\,\frac{\partial Q}{\partial x}$," change "$b_w$" to "$b^2_w$."

Page 1036, line 1, change "$(I = 0)$" to "$(I = O)$."

Transactions, Vol. CT, 1953

Page 319, line 19 from the bottom of the page, change "Greely" to "Greeley."

Page 542, in the caption of Fig. 3, "Washington" should read "Idaho."

Pages 665, 1274, 1287, 1304, and 1310, the name, "F. J. Cleary," should be changed to "E. J. Cleary."

Transactions, Vol. 119, 1954

Page 151, the name of the author should read "Charles A. Schanck, M. ASCE."

Page 1152, Fig. 8(*b*), the value "−7" should be changed to "−17."

AMERICAN SOCIETY OF CIVIL ENGINEERS
Founded November 5, 1852
TRANSACTIONS

Paper No. 2656

ICE PRESSURE AGAINST DAMS

A SYMPOSIUM

PAGE

Foreword
By the ASCE Joint Division Committee on Masonry Dams, through its Subcommittee on Ice Pressure Against Dams 2

Studies of the Effects of Temperature Variations
By Bertil Löfquist 6

Some Investigations in Canada
By A. D. Hogg 22

Experimental Investigations by the Bureau of Reclamation
By G. E. Monfore 26

FOREWORD

The magnitude of the pressure exerted by ice sheets against dams remains one of the major uncertainties in the design of retaining structures. Some allowance for this thrust must be made when it is known that the surface of the reservoir to be formed by a dam may freeze. Estimates of the force have ranged as high as 50,000 lb per ft, although values much lower than this are in common use. Since the ice pressure must be taken as acting at or near the maximum water level, the economic importance of the uncertainty is obvious. It has been the concern of this subcommittee to attempt to increase the understanding of this complex matter with a view to making design procedures more certain.

Background of the Problem.—In 1947, Edwin Rose[1] presented a review of data, derived from laboratory experiments and field observations, on the magnitude of the thrusts that may be expected upon dams as a result of the formation of ice sheets on the surfaces of the reservoirs. Using the conclusions reached as a result of laboratory experiments, and based on a number of reasonable simplifying assumptions, Mr. Rose showed theoretically that thrusts of the order of from 5 kips per lin ft to 20 kips per lin ft of dam were possible for North American climatic conditions.

Since the subject matter of the paper by Mr. Rose is highly specialized, it is not surprising that its discussion attracted only a few contributors. One of these contributors was Ernest Brown,[2] whose work during 1931–1932 (jointly with George C. Clarke, M. ASCE) provided Mr. Rose with much of his factual data. Mr. Brown was appointed a member of this subcommittee when it was instituted, but his death in 1949 deprived the members of the benefit of his experience and wise counsel.

In a discussion of Mr. Rose's paper, R. E. Kennedy, M. ASCE, presented a singularly interesting table of ice-sheet thicknesses as observed by the Bureau of Reclamation, United States Department of the Interior (USBR). From these observations he derived a simple equation by means of which an estimate of ice thickness may be obtained if latitude and elevation are known. Experimental confirmation of this formula was naturally suggested as desirable. Another contribution to the discussion of Mr. Rose's paper from the USBR was that of B. R. McGrath. Following a discussion of theoretical aspects of ice pressure, Mr. McGrath pointed to the vital need for further laboratory and field experiments and observations, stressing particularly three directions in which work must be pursued if the questions still associated with ice pressure are to be answered satisfactorily. These may be expressed briefly thus:

---

[1] "Thrust Exerted by Expanding Ice Sheet," by Edwin Rose, *Transactions*, ASCE, Vol. 112, 1947, p. 895.

[2] Discussion of "Ice Thrust in Connection with Hydro-Electric Plant Design," by Ernest Brown and George C. Clarke, *The Engineering Journal*, August, 1932, pp. 393–397.

a. Field measurements of actual ice pressures together with other relevant local factors such as ice thicknesses and temperature;

b. Analysis of climatic data in relation to ice sheet formation; and

c. Laboratory tests to determine the physical properties of ice.

These are major tasks, far more complex than would appear at first sight, calling for long-term research projects and field observations widely distributed geographically. The field observations should be of a long-term character because of the vagaries of the weather. Clearly, such programs cannot be the responsibility of any one organization acting alone. No easy or quick solution to the many associated problems will be found. Correlation of the results of many endeavors will be necessary. It appears to be the function of this subcommittee to stimulate research programs in the directions indicated and to assure that the results thus obtained will be correlated for the general benefit of the profession.

The subcommittee was formed in 1947. Inquiries have been pursued in a number of directions, with little result except as herein described. A general appeal for information was published in the October, 1948, issue of *The Journal of Glaciology* (official journal of the British Glaciological Society, the only body known to be concerned solely with problems of snow and ice). This inquiry revealed no information, which was a further indication of the dearth of factual data.

R. F. Legget, M. ASCE (member of the subcommittee), was able to discuss the matter with Scandinavian engineers in Norway and Sweden in 1948, and with Swiss scientists later in the same year. As a result of these personal contacts and the work of members of the subcommittee, the following brief notes are presented summarizing the situation in the countries noted.

Switzerland.—Although Switzerland possesses a research institution devoted solely to problems of snow and ice (at Davos), no record of any experimental work in connection with ice pressure against dams has been found. The subcommittee is reliably informed that the ice pressure problem in connection with dams in the high Alps is dealt with by the regular lowering of water levels in the reservoirs in the early winter. If this does not effectively break up the ice sheets on the reservoirs, the pressure from the ice is exerted at elevations well below the maximum water levels and therefore need not be considered in the structural design of the dams.

Norway.—At one time an allowable load as high as 30,000 lb per lin ft was used in Norway for the design of dams. Practically all Norwegian dams are subjected to ice pressure every winter. The design load has been reduced consistently, and a value of 3,350 lb per ft is in regular use in conjunction with dams that have sloping upstream faces. No experimental work appears to have been done in Norway, but the fact that no Norwegian dam has yet given any indication of failure is taken as evidence justifying the low design load now in use. Many Norwegian dams are relatively thin structures of reinforced concrete, so that field observations on dam performance have special value.

Sweden.—In Sweden, it is the practice to use 20,100 lb per lin ft as a maximum allowable ice pressure. The contrast of this design value with that used in the neighboring country of Norway is interesting. In discussing this value it developed that some experimental work had been done in Sweden by Bertil Löfquist. From the paper by Mr. Löfquist, it will be seen that careful study has been given the problem in Sweden. The subcommittee has been engaged in solving the same problem in North America.

Canada.—The problem of ice pressure is one of special concern in Canada. It seems to be general practice for normal dam construction in Canada to use 10,000 lb per lin ft, although higher allowable loads have been used. The Hydro-Electric Power Commission of Ontario is probably responsible for more dam construction than any other Canadian organization and has, consequently, a special interest in this problem. Within the past few years the commission has inaugurated research investigations of the problem.

The National Research Council of Canada has conducted a number of investigations into problems of snow and ice but these have not been correlated with the specific problem of ice pressure against dams. With the formation of a new Division of Building Research in 1947, the medium for this correlation has been provided. The division engages in experimental work, particularly in the physical properties of ice, and works with the Hydro-Electric Power Commission of Ontario in field studies.

United States of America.—The interest of engineers in the United States in the problem was clearly indicated in the paper by Mr. Rose and in its discussion. The USBR has continued the studies described in Mr. Rose's paper.

Reading References.—The following list of references on ice pressures have not been mentioned specifically elsewhere in this Symposium, but will prove of value to those studying this subject:

1. "The Problem of an Expanding Ice Sheet," by G. E. Monfore and Frank W. Taylor, *Proceedings*, Western Snow Conference, Colorado Agri. Experiment Station, Fort Collins, Colo., 1948, pp. 30–45.
2. "Ice Temperature Measurements at Eleven Mile Canon Dam, January 11 to April 14, 1947," by G. E. Monfore, *Laboratory Report No. SP-16*, Bureau of Reclamation, U. S. Dept. of the Interior, Denver, Colo., October 23, 1947.
3. "Thrust of Ice Against Dams," by G. Albenga, *Annali Lavori Pubblici*, Vol. 3, 1921, pp. 71–74.
4. "Ice Engineering," by H. T. Barnes, Renouf Pub. Co., Montreal, Que., Canada, 1928.
5. "Ice Formation," by H. T. Barnes, John Wiley & Sons, Inc., New York, N. Y., 1906.
6. "Results of Experiments on Strength of Ice," by G. C. Bell, *Proceedings*, Maine Soc. of Civ. Eng., Vol. 1, 1911, pp. 44–46.
7. "Tests on the Shearing Strength of Ice," by J. F. Finlayson, *Canadian Engineer*, Vol. 53, 1927, pp. 101–103.
8. "Safeguarding Hydro Plants Against the Ice Menace," by Paul E. Gisiger, *Civil Engineering*, ASCE, January, 1947, p. 24.
9. "Field Measurement of Ice Pressures at Hastings Lock and Dam," by H. M. Hill, *The Military Engineer*, March-April, 1935, pp. 119–122.
10. "Ice As Affecting Power Plants: Final Report of Committee of Power Division," *Transactions*, ASCE, Vol. 95, 1931, p. 1143.

11. "Observations and Experiments on Ice Expansion," by W. H. Sawyer, *Proceedings*, Maine Soc. of Civ. Eng., Vol. 1, 1911, pp. 27–40.

12. "Suitability of Ice for Aircraft Landings," by R. F. Sharp, *Transactions*, Am. Geophysical Union, Vol. 28, 1947, pp. 111–119.

13. "Bending and Shear Tests on Lake Ice," by J. T. Wilson and J. M. Horeth, *ibid.*, Vol. 29, December, 1948, pp. 909–912.

Additional references have been mentioned specifically in the papers of this Symposium and such references appear as footnotes where they apply.

SUMMARY

One may wonder why a problem which appears to be relatively straightforward on superficial examination should still be unsolved despite the attention that has been and is being devoted to it. Detailed study reveals that the complexities of the problem, whether attacked in the field or in the laboratory, make it a singularly difficult one. Field observations necessarily mean interference with an ice sheet by means of materials having physical properties different from those of the ice itself. This introduces complications that are further intensified by the restraining effect along the entire boundary of an ice sheet adjacent to a dam. New methods of attack are being studied, but reliable field observations are probably more difficult than laboratory research. In the laboratory, all experimental work is complicated by the critical control exercised by temperature variations. The fact that ice is a crystalline material with significant plastic properties renders experimental work unusually complex.

The investigations of the subcommittee have shown that the problem, difficult as it is, is being attacked generally along the lines suggested in the discussion of Mr. Rose's paper. It will be several years before enough information is obtained from field observations in particular, to make possible a further advance toward a complete solution of the problem. The subcommittee therefore recommends that the interested organizations be encouraged to develop their work in connection with ice pressure against dams, and be urged to maintain mutual liaison in this field.

Respectfully submitted,

R. L. Hearn, *Chairman*
R. F. Legget, *Vice-Chairman*
D. A. Buzzell
D. McHenry
L. S. McLennan
E. N. Peterson
G. R. Strandberg

STUDIES OF THE EFFECTS OF TEMPERATURE VARIATIONS

BY BERTIL LÖFQUIST[1]

WITH DISCUSSION BY MESSRS. G. E. MONFORE, EDWIN ROSE, AND BERTIL LÖFQUIST

SYNOPSIS

The problem relating to the magnitude of the horizontal ice pressure produced by a solid sheet of ice as a result of rapidly rising temperatures has not found a satisfactory solution. Investigations have yielded unreliable and somewhat contradictory results. This paper describes an investigation that was undertaken by the Swedish State Power Board. In the experiments, made with an arrangement installed in a freezing chamber, a pressure of 20 tons per m (13,400 lb per lin ft) was obtained with ice 60 cm (23.62 in.) thick. This result is somewhat unreliable, however, owing to the presence of certain additional effects during the experiment. From calculations made on the buckling of an ice sheet, a probable maximum ice pressure of from 30 tons per m to 40 tons per m (20,000 lb per lin ft to 27,000 lb per lin ft) is found. It would seem that an ice pressure of similar magnitude may also be set up under certain unfavorable local conditions in consequence of variations in the water level, with an ice sheet having a limited expanse of from 20 m to 40 m (65 ft to 130 ft). As a rule the ice pressure resulting from variations in the water level will be less, but it may occur in many places with appreciably greater frequency than ice pressure resulting from extreme temperature variations.

PRIOR INVESTIGATIONS

Numerous different opinions have been expressed concerning the magnitude of the horizontal pressure set up by a solid sheet of ice as a result of increased temperatures. Originally, it was believed that the ice pressure was limited by the compressive strength or elasticity of the ice, and in such cases—even under very favorable assumptions—very high working pressures were assumed. Despite the fact, however, that many dams that would be entirely incapable of withstanding pressures calculated in the foregoing manner were found to stand up well for long periods, it was recognized that this method of approach was not correct. It is now known that it is the plasticity of the ice that reduces the magnitude of the pressure considerably, and consequently lower values for the ice pressure were assumed subsequently. It has even been asserted that

---

NOTE.—Published, essentially as printed here, in December, 1952, as *Proceedings-Separate No. 160.* Positions and titles given are those in effect when the paper or discussion was received for publication.

[1] Chf., Structural Research Div., State Power Board, Stockholm, Sweden.

the plasticity of the ice is so great that the pressure at increased temperatures could be ignored.

In Sweden, when dimensioning dams and other structures in rivers and lakes, it is usual to assume a horizontal pressure from a solid ice sheet varying between 5 tons per m and 30 tons per m according to the geographical position and the judgment of the designer.

The first investigations of a more exhaustive nature relating to ice pressure from rapidly rising temperatures, in which allowance was made both for the course of the temperature and the actual deformation properties of the ice, were carried out in the year 1922 by Nils Royen.[2] As the result of these investigations a maximum ice pressure of 30 tons per m was found with an ice thickness of 1 m (40 in.).

The interesting and well-known experiments that were undertaken in 1932 by Ernest Brown and George C. Clarke,[3] M. ASCE, represented a valuable contribution to knowledge on the deformation properties of ice. The experiments did not lead to a solution of the problem concerning the maximum ice pressure, however, since the relation between change of temperature and the stresses was only ascertained for an ice temperature with a linear rise. The course of events is more complicated in an ice sheet as the temperature curves are bent, and as the bends vary with the time and with the depth below the surface of the ice. The application of the test results, therefore, is accompanied by difficulties.

An attempt to compute the ice pressure on the basis of the Brown-Clarke experimental data was made by Edwin Rose[4] and B. R. McGrath.[5] These writers based their work partly on the Brown-Clarke curve for the relation between the rates of temperature rise and increase in pressure, and partly on the course of the temperature in the ice sheet, determined by a numeral method.

In this manner, ice pressures were obtained by a summation process, these values in general appearing reasonable. However, the method is not quite correct. An integration of the component forces will be mathematically permissible only if a linear relation exists between the stress and strain (principle of superposition). In the present case, this is true only with a linear temperature rise, according to the experiments. From the physical point of view it is not permissible, as a rule, to add to a component of force set up in the ice at a given point of time, in consequence of restrained temperature expansion, another component of force set up at a later point of time. The first component has actually been reduced to some extent at the later point of time on account of the plasticity. The concept of the distribution of stresses in the ice sheet obtained by this method will therefore be improbable. Moreover, as demonstrated subsequently, the relation between the ice pressure and the thickness of the ice obtained by the method in question is also improbable, since it increases almost linearly with the ice thickness. Investigations described in this paper

---

[2] "Ice Pressure by Temperature Rise," by Nils Royen, *Homage Book in Honour of V. Hansen*, Swedish State Power Board, Stockholm, Sweden, 1922 (in Swedish).

[3] "Ice Thrust in Connection with Hydro-Electric Plant Design," by Ernest Brown and George C. Clarke, *The Engineering Journal*, January, 1932.

[4] "Thrust Exerted by Expanding Ice Sheet," by Edwin Rose, *Transactions*, ASCE, Vol. 112, 1947, p. 871.

[5] Discussion by B. R. McGrath of "Thrust Exerted by Expanding Ice Sheet," by Edwin Rose, *ibid.*, p. 887.

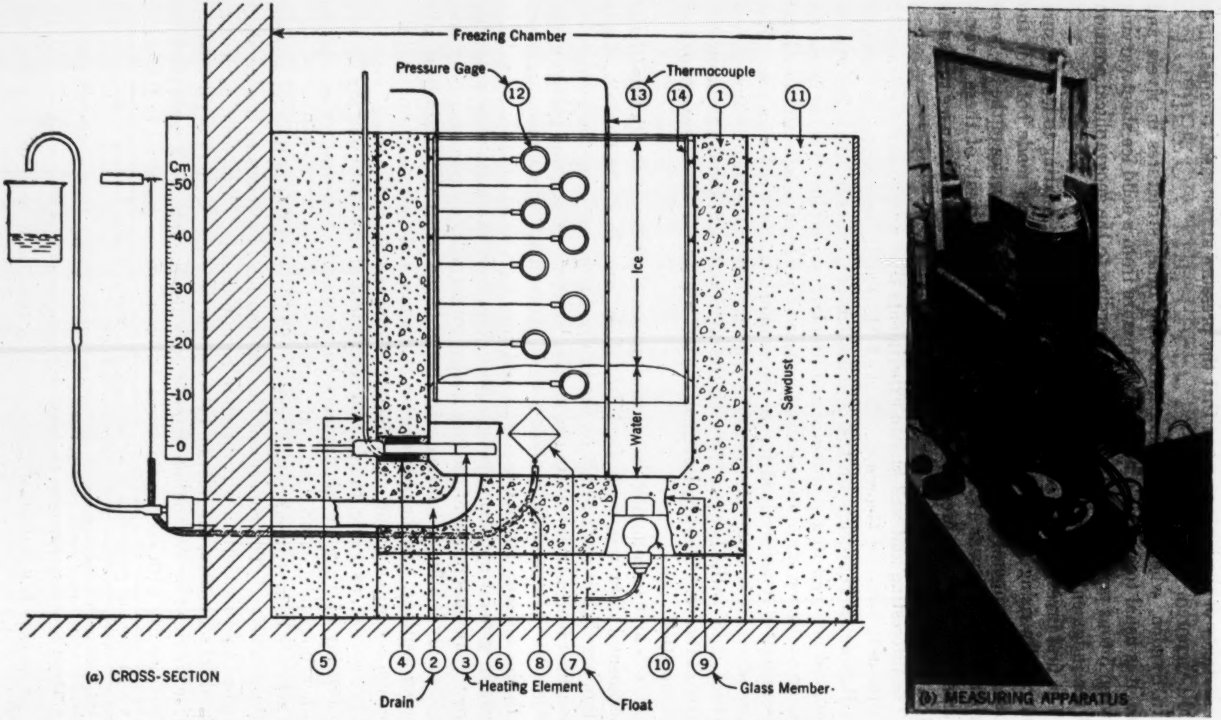
Freezing Chamber
Pressure Gage
Thermocouple
12
13
14
1
11
Cm
50
40
30
20
10
0
Ice
Water
Sawdust
5
4
2
3
6
8
7
10
9
Drain
Heating Element
Float
Glass Member

(a) CROSS-SECTION

(b) MEASURING APPARATUS

Fig. 1.—Laboratory Apparatus for Measuring Ice Pressure

tend rather to show that the ice pressure already reaches its maximum value with an ice thickness of about half a meter, after which the pressure falls slightly with increasing thickness; or, in any case, it increases only to a relatively insignificant extent.

Computations of the ice pressure based on elementary experiments, with small sample blocks of ice, yield unreliable results, since the effect on the plasticity of the sample's size and the distribution of the stresses are difficult to determine. When it is desired to obtain reliable figures for the ice pressure, the best method for doing so consists of measuring the forces in question directly on an ice sheet in the field. Admittedly, it is scarcely possible to measure the maximum pressure directly, because it occurs only under exceptional conditions, but it should nevertheless be possible, after taking a large number of measurements in the field, to obtain a good starting point for determining the probable maximum pressure. With a combination of systematic laboratory experiments and field measurements it should become possible to solve the old problem of ice pressure by temperature rise in an entirely satisfactory manner. The ice pressure measurements made on natural sheets of ice begun by the Bureau of Reclamation[6] (USBR), United States Department of the Interior, are therefore of great value in this respect.

ICE PRESSURE MEASUREMENTS UNDER LABORATORY CONDITIONS

In 1943 the writer attempted to solve the ice pressure problem with the help of an experimental arrangement in a freezing chamber. Although the experiment did not lead to an entirely satisfactory result, some observations were made during the course of the tests that are of interest. The underlying idea consisted of attempting to reproduce in a freezing chamber the conditions encountered in a sheet of ice in the field, and then measuring the course of the temperature and the stresses set up in the ice directly.

Experimental Arrangement.—The experimental arrangement is illustrated in Fig. 1 referring to the numbered points in Fig. 1(*a*): It consists essentially of a cylindrical concrete vessel (1) having an internal diameter of 50 cm (20 in.), filled with water, and thermally insulated with sawdust (11). The vessel is placed in a freezing chamber and, when the temperature is lowered, a sheet of ice is formed in the vessel in a manner similar to that occurring in nature. The heat transmission in the ice, when cooled and heated, takes place only in a vertical direction.

The stresses in the ice are measured by pressure gages (12) of a special type, and the temperature in the air, ice, water, and concrete is observed with the help of a number of thermo-elements (13).

The pressure gages (Fig. 2) consist in principle of two flat steel plates, electrically insulated from one another and from the outer, thicker pressure plates by thin sheets of mica. The electrical capacity of the device is sensitive to changes of pressure. Deformation in the direction of pressure is extremely small and may be neglected when taking measurements in ice. Since the pressure gage is constructed of steel (which has approximately the same coefficient of thermal expansion as the reinforced concrete in the experimental vessel), the relative expansion between the pressure gage and the ice, on changes of temperature, can be ignored.

---

[6] "Ice Pressure Measurements at Eleven Mile Canon Reservoir During January, 1949," by G. E. Monfore, *Report No. SP-21*, Structural Research Lab., Bureau of Reclamation, U. S. Dept. of the Interior, Denver, Colo., April 28, 1949.

The thickness of the ice is measured by a float (7). The float is held by a thin steel wire that runs in a tube (8) filled with mercury. Thus, the thickness of the ice can be read on a scale outside the freezing chamber.

In order to prevent freezing at the bottom and to regulate the thickness of the ice, an electric heating element (3) is placed at the bottom of the vessel. A protective plate (6) covering the heating element distributes the rising water that has been heated. To prevent leakage, which might cause short circuits and burned insulation, the bushing at point 4, Fig 1(*a*), was packed with cement and an inside filling of wood tar. This wood tar filling was placed under a higher pressure than the water at the same level by means of a rising tube (5), thus insuring complete safety. The vessel is provided with bottom illumination (10) through a glass member (9) so that the formation of cracks in the ice can be seen clearly. Finally, a bottom drain (2) is fitted to carry off the water displaced during freezing.

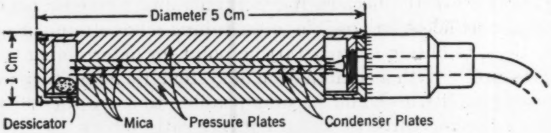

Note: Cm = 0.3937 In.

FIG. 2.—ICE PRESSURE GAGE

When the ice sheet increases in thickness and the temperature falls, tensile stresses are set up in the ice, giving rise to cracks. In the first two experiments, it was found that the cracks were formed when the temperature at the surface of the ice had fallen to about − 12 °C (10 °F). The fine cracks did not spread down to the underside of the ice and could not be filled with water and freeze again, as in the case of open cracks in a natural ice sheet of wide expanse. No great ice pressure could occur, therefore, during the subsequent temperature rise. In the two first tests the pressure amounted to approximately 5 tons per m with an ice thickness of 50 cm. This value thus corresponds to the ice pressure in ice sheets of small extent, such as those encountered in small reservoirs where continuous cracks of sufficient width do not occur.

In order to produce the same conditions for ice pressure as those existing in a large ice sheet, double cylindrical plates (14) were arranged in the concrete vessel and connected at the bottom and at the sides. In this manner an air-filled gap (a cylindrical contraction joint) was obtained so that the ice could be cooled to the desired temperature without cracking. Before raising the temperature, the gap was carefully filled with water that froze to ice. However, in this operation, it was not possible to eliminate crack formation in the ice sheet entirely, which probably exercised a reducing action on the ice pressure set up subsequently.

RESULTS OF THE EXPERIMENTS

Figs. 3 to 6 show the results of a typical test that gave a maximum pressure of 20 tons per m (13,400 lb per lin ft) when the temperature of the air was raised from − 30 °C to + 6 °C in 17 hr. Two further tests, under similar conditions, also gave a maximum pressure of about 20 tons per m. In consequence of the thermal expansion of the concrete vessel, the conditions did not correspond to perfect restraint. The pressure in the case of perfect restraint can be estimated to be about 25% higher.

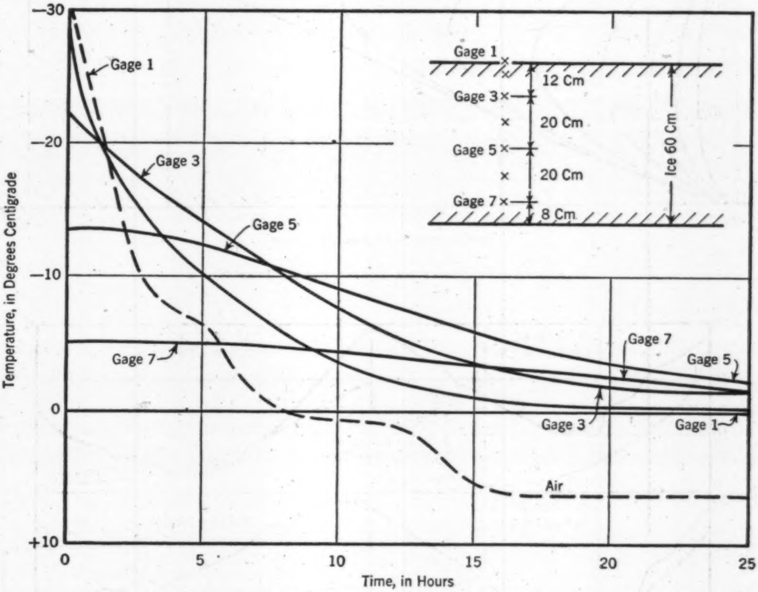

FIG. 3.—TIME RATE OF TEMPERATURE RISE, TEST NO. 4

Two effects made their appearance during the experiments, however, which exercised a disturbing action on the results in different directions. On the one hand, as stated, a number of cracks were formed in the ice when filling the air gap, and these cracks probably exercised a reducing effect on the ice pressure. The irregularities, visible in the curves for pressure in Fig. 5, may be ascribed mainly to the effect of these cracks. On the other hand, the expansion of the ice in a vertical direction at the walls of the vessel is prevented to a certain extent by adhesion. The additional vertical stresses thus set up produce compressive stresses in a horizontal direction in the central depth of the ice sheet and tensile stresses at the surface. The action of the compressive stresses nevertheless preponderates, so that the result will be a certain increase in the total ice pressure. Had it been possible to eliminate the effects in question, the "pear" shape appearance of the pressure distribution in Fig. 6 would probably have been less pronounced.

In principle, however, the curves should not present a changed appearance since, if the temperature at the surface of the ice is 0 °C, or close to it, when the total maximum pressure is reached, the compressive stresses in the surface layer itself must be relatively small. It was observed that the surface of the ice, which was smooth at the outset, had become buckled at the conclusion of the experiment as a result of the compressive stresses, and presented a rough appearance. This phenomenon is probably one of the reasons for the relatively small pressure in the surface layer.

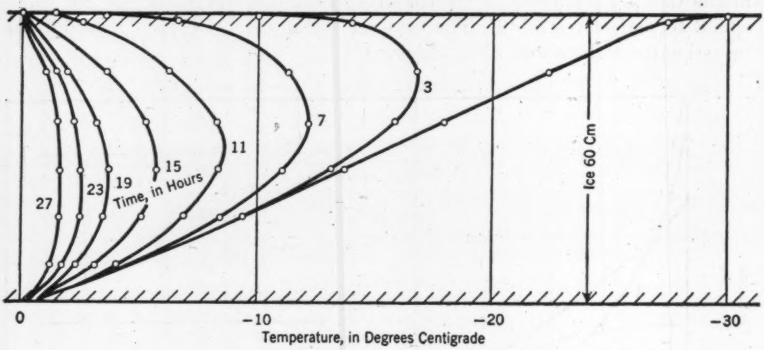

Fig. 4.—Temperature Distribution, Test No. 4

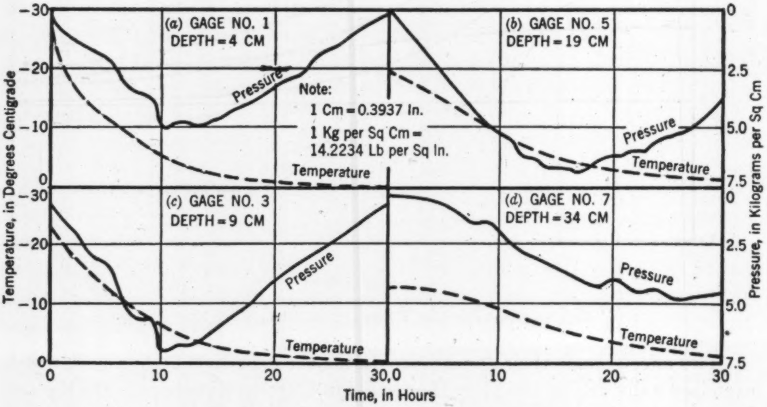

Fig. 5.—Time Variation of Pressure and Temperature for Same Gage, Test No. 4

In Fig. 7 the results of two of the most successful experiments have been drawn on a diagram of the type produced by Messrs. Brown and Clarke. The difference between the curves obtained by varying means is considerable, and illustrates fairly clearly the difficulty of obtaining a correct grasp of the ice pressure problem. The difference, of course, results in part from the fact that the upper curve is based on experiments in which the conditions of stress are mainly uni-dimensional whereas the lower curve is based on chiefly two-dimensional stresses. Moreover, an appreciable difference may exist between different kinds of ice—a circumstance concerning which current knowledge is still very imperfect. In the experiments described, tap water was used for producing the ice. The water was heated to the boiling point to reduce the air content. On applying pressure parallel to the surface of the ice, a compression strength at 0 °C of about 50 kg per sq cm was obtained with sawed out ice cubes.

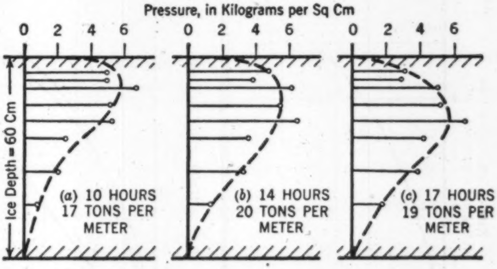

Note:
1 Cm = 0.3937 In.
1 Ton per Meter = 670 Lb per Lin Ft
1 Kg per Sq Cm = 14.2234 Lb per Sq In.

FIG. 6.—PRESSURE DISTRIBUTION IN A CROSS SECTION OF ICE

In ice investigations of this kind, the salt content of the water (ice) should always be stated exactly, as the plastic properties appear to vary considerably with the salt content, even when the latter is low.

Although the results of the experiments are unreliable as regards the absolute magnitude of the ice pressure, they nevertheless afford the possibility of throwing some light on another interesting question—namely, the relation between the ice pressure and ice thickness. The general opinion seems to be that ice pressure of the kind concerned increases appreciably with the thickness of the ice even in the case of thick ice. Closer investigation tends to show that the ice pressure reaches its maximum at a thickness of about half a meter, and thereafter it falls slightly, or in any case only increases to an insignificant extent. The reason for this behavior is that the rate of temperature rise in ice is rapidly reduced as the thickness of the ice increases. This effect compensates for the action of the increased thickness.

As will be seen from Fig. 7, the ice pressure increases with the rate of temperature rise in accordance with a curve that only appears to bend slightly within the actual range. If a certain course of the temperature in the air is assumed, such as a change from − 30 °C to 0 °C in 10 hr, after which it remains constant at 0 °C, it is possible to calculate the course of the ice's mean temperature mathematically. On the basis of the temperature variations in the ice, the diffusivity constant of the ice can be computed by means of difference equations at 0.0048 m per hr, which agrees fairly closely with the particulars given in the literature on the subject. Experiments showed that the maximum pressure was produced when the mean temperature reached about − 4 °C (see Figs. 3 to 6). On this assumption, and on the basis of the temperature's mean rate of rise, it is possible to calculate approximately the relative maximum pressure with different ice thicknesses. A maximum is found with an ice thickness of about 0.5 m (Fig. 8, curve A). It is nevertheless possible that the maximum pressure may occur at a somewhat lower temperature than − 4 °C, with a considerable thickness of ice, since the temperature will then follow a slower course. When this fact is taken into consideration, the maximum point will be displaced to a greater thickness of ice, but the increase for thicknesses exceeding 0.5 m will not be appreciable (Fig.8, curve B).

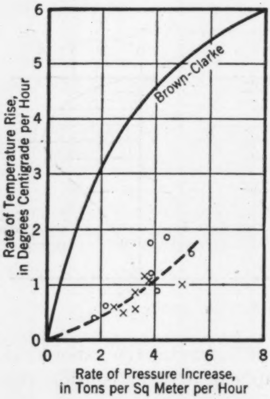

Fig. 7.—Relation Between Temperature Rise and Pressure Rise, Tests 3 and 4

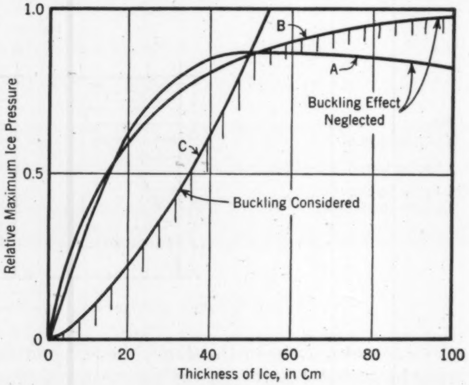

Fig. 8.—Probable Relation Between Maximum Ice Pressure and Ice Thickness

The foregoing reasoning is based solely on the properties of the ice itself. Under field conditions in most cases the heating of the ice begins in the morning after a cold night and proceeds during the entire day. With small thicknesses of ice the maximum pressure may then be obtained before the temperature falls again in the evening, whereas this is not the case with greater thicknesses of ice, which require a time of 20 hr or more to attain the maximum pressure. This fact also argues in favor of the probability of an ice pressure maximum in nature with an ice thickness of about 0.5 m.

Buckling of an Ice Sheet

When the horizontal pressure in a sheet of ice attains a certain magnitude, the ice will buckle. This phenomenon may frequently be observed with a thickness of ice as great as from 20 cm to 30 cm, whereas it appears to occur very rarely with a thickness of 50 cm. This fact indicates a method of estimating the ice pressure by calculation. The difficulty here, as in the case of other ice pressure problems, is to find a correct value for the modulus of elasticity of the ice with due regard to the plasticity. As will be seen, however, an erroneous assumption will not have the same far-reaching effect as when the ice pressure is determined directly from the thermal expansion.

The buckling of an ice sheet can be computed by the theories for beams or slabs resting on an elastic bed. In an ice sheet of wide extent the buckling load H will be

$$H = \sqrt{\frac{k\,d^3\,E\,m^2}{3\,(m^2 - 1)}} \quad \text{(1)}$$

in which k is the modulus of reaction (the uplift in water); d is the thickness of the ice; E is the modulus of elasticity; and m is the Poisson ratio.

To account for the plastic character of the ice, E is replaced by a "modulus of deformation," F, which includes both the elastic and the plastic deformation as well as the effect of lateral restraint. Eq. 1 can then be written:

$$H = \sqrt{\frac{k\,d^3\,F}{3}} \quad \text{(2)}$$

When investigating the lifting force of an ice sheet,[7] the following expression for the modulus of deformation was found to agree satisfactorily with measurements of the deflection of a natural sheet of ice:

$$\frac{1}{F} = \frac{1}{E} + \frac{C\,\sqrt[3]{h}}{t + 1} \quad \text{(3)}$$

in which C is a constant equal to 8×10^{-5} when calculating in tons, meters, degrees Centigrade, and hours; h is the time in hours; and t is the ice temperature in degrees Centigrade with reversed sign.

When using Eq. 3, it is necessary to know the ice temperature and the time for the buckling process. The value of $1/E$ can here be neglected in relation to $1/F$. The maximum pressure occurred when the mean temperature of the ice was about $-$ 4°C. On deflection, however, the upper and lower extreme "fibers" of the ice sheet will be most active, so in this case the effective mean temperature can be assumed at about $-$ 2.5 C. The time for the buckling process can be estimated on the basis of the curves in Fig. 5 at 2 hr to 4 hr at least, if visible buckling is to be produced. Thus, for an ice thickness of 0.5 m, $t = 2.5$ and $h = 3$, according to Eq. 3 it is found that $F = 30{,}000$ tons per sq m, and according to Eq. 2, $H = 35$ tons per m. In general, if the assumptions are varied within the limits of probability, buckling forces between 30 tons per m and 40 tons per m are obtained.

In Fig. 8, curve C, shows the manner in which the buckling load varies with the ice thickness in accordance with the foregoing assumption. Thus, it will be seen that the buckling load determines the magnitude of the ice pressure with lesser thicknesses than about 0.5 m and that the reduction in the ice pressure thus produced is appreciable. The relation between curve C and curves A and B in Fig. 8 is based on the assumption that an ice sheet thicker than 0.5 m will not buckle.

---

[7] "Lifting Force and Bearing Capacity of an Ice Sheet," by Bertil Löfquist, *Technical Translation, TT-164*, National Research Council of Canada, Ottawa, Ont., Canada, 1951 (From Teknisktidskrift, No. 25, Stockholm, Sweden, 1944).

These calculations are open to discussion in many respects, of course, but they should suffice to show that it is possible in this manner to determine the maximum ice pressure within fairly narrow limits.

ICE PRESSURE CAUSED BY VARIATIONS OF WATER LEVEL

Buckling results not only from temperature rises but is caused far more frequently by variations in the water level. When the water level falls, the ice sheet is subjected to tensile stresses if it is frozen to the shore. Thus, wide open cracks may be produced in the ice in a moment. The cracks may freeze again, and a horizontal pressure is set up in the ice sheet when the water level rises.

A similar effect may also occur because of the fact that, on changes of water level, the ice is repeatedly broken by bending forces produced at the shore or against a dam structure, and the cracks fill with water and freeze again. If open chanels are formed in the ice (as is frequently the case in rivers and waterways), the ice will have a tendency to move out from the shore and will thereby exercise a horizontal force on structures that obstruct its movement. Many cases of trouble caused by ice pressure of this kind have been observed.

The magnitude of the ice pressure with variation of water level is largely dependent on local conditions, and it is consequently difficult to obtain any general value. For ice sheets of wide extent in a plane, the pressure in question seemed to be comparatively moderate, but in smaller ice sheets it appears that the forces of pressure may be of the same order of magnitude as in the case of extreme temperature variations. In particular cases it is possible to make approximate calculations for the pressure with the help of Eq. 3 for the modulus of deformation and with the help of formulas for the buckling load, and assumptions concerning the form of the ice sheet. It would seem that the most unfavorable conditions prevail, as a rule, with a span across the ice sheet of from 20 m to 40 m, when the ice sheet may form a complete arch between supports.

Perhaps ice pressure of the kind in question will not be so great in many places as the maximum ice pressure resulting from temperature variations. It will probably occur far more frequently, however, since it does not require the coincidence of so many unfavorable conditions as in the case of ice pressure caused by temperature variations. In order to obtain wider knowledge on this subject, further measurements must be made in the field, mainly leveling ice sheets with different spans at varying water levels.

When the water level rises, the ice sheet can also exert lifting forces that are of special significance for smaller hydraulic constructions.[7]

ACKNOWLEDGMENT

The pressure gage in Fig. 2 was designed by C. H. Johannssen[8] and J. O. Linde at the Royal Institute of Technology in Stockholm, Sweden.

---

[8] "Neue Kondensatordruckkraftmesser," by C. H. Johannssen, *Annaler der physik*, Vol. 27, 1936, p. 742.

DISCUSSION

G. E. Monfore[9].—The experimental approach used by Mr. Löfquist in investigating ice pressure indicates thoughtful planning and careful measurements. This approach, which involved the use of what might be called a laboratory ice sheet 20 in. in diameter and 24 in. thick, is intermediate to the methods used by the Bureau of Reclamation (USBR), United States Department of the Interior. The investigations conducted by the USBR[10] consisted of field measurements of pressure and temperatures at several reservoirs and laboratory measurements on 4-in.-by-4-in. ice cylinders. The investigations by Mr. Löfquist and by the USBR are thus entirely independent and so provide a valuable check on each other.

Solar radiation, which is an important factor in the temperature changes in an ice sheet in the field, is difficult to simulate in a laboratory ice sheet. The flow of energy into the laboratory ice sheet must come mainly from the air that is in contact with the ice surface, whereas in the field ice sheet, energy comes not only from the air but by absorption of solar radiation. The limited USBR experiments indicated that about 35% of the solar energy is absorbed after passing through 1 in. of ice and 60% is absorbed after passing through 25 in. of ice.[6] Thus, much radiant energy is transformed to heat near the ice surface, and additional heat is generated lower in the ice sheet. It follows that a given rate of air temperature rise in the laboratory will produce a lower rate of increase in the ice temperature of the laboratory ice sheet than that produced in the field ice sheet exposed to solar radiation in addition to the same air temperature rise. Variation of ice temperature with depth in the laboratory ice sheet will probably differ from that in field ice sheets.

It was interesting to note that the author found a marked reduction in the maximum pressure when there were contraction cracks in the laboratory ice sheet. The USBR observed the same phenomenon in their field measurements. Apparently under some field conditions, the contraction cracks fill with water which then freezes, but under other conditions the cracks remain open. The open cracks prevent the development of high pressures. A better understanding of the factors that allow open cracks to persist in field ice sheets might aid in fixing an upper limit for ice thrust.

The pressure curves obtained by Mr. Löfquist from the laboratory ice sheet and the curves that the USBR obtained from field ice sheets and from small laboratory samples are all of a similar shape. As the ice temperature increased, the ice pressure increased to a maximum value and then decreased. The temperature at which the maximum pressure occurs may be considerably less than the melting point of ice. These pressure curves indicate that the maximum pressure that can be developed in an ice sheet is limited by plastic flow of the ice.

---

[9] Research Engr., Bureau of Reclamation, U. S. Dept. of the Interior, Denver, Colo.

[10] "Ice Pressure Against Dams: Experimental Investigations by the Bureau of Reclamation," by G. E. Monfore, *Transactions*, ASCE, Vol. 119, 1954, p. 26.

The data from Fig. 5 may be compared with the results of the USBR laboratory study as shown in curves published in a companion paper.[11] The data from Gage No. 5, Fig. 5(*b*), were used for comparison because the ice temperature in this case increased almost linearly until the maximum pressure was reached. Linear rates of ice temperature rise were used in the USBR laboratory study. According to Fig. 5(*b*), the initial ice temperature was −2° F, and the ice temperature increased from −2° F to 24° F in 17 hr, a rate of rise of 1.5° F per hr. The maximum pressure registered by Gage No. 5 was 95 lb per sq in.

The maximum pressure obtained in the USBR laboratory study for similar temperature conditions may be read from the previously mentioned USBR curves.[11] An ice temperature rise of 1.5° F per hr from an initial temperature of −2° F resulted in a maximum pressure of 125 lb per sq in. which occurred in from 5 hr to 6 hr.

In the USBR laboratory study, the ice samples were maintained at a constant length, whereas in the author's work the ice sheet could expand a small amount because of the thermal expansion of the concrete vessel and the deformation of the vessel under load. This limited expansion of the laboratory ice sheet would decrease the magnitude of the maximum pressure and increase the time required for the maximum pressure to develop. Mr. Löfquist estimates that if there were no thermal expansion of the vessel, the maximum pressure would have been about 25% greater. This corrected maximum pressure would be $95 + \frac{95}{4} = 120$ lb per sq in., which is in excellent agreement with the pressure of 125 lb per sq in. measured in the USBR laboratory study.

Edwin Rose.[12]—The results of the tests performed by Mr. Löfquist represent a definite contribution toward obtaining a better understanding of the ice-pressure problem. In a paper published in 1947,[4] the writer presented a basis for estimating ice pressures against hydraulic structures by the application of the ice temperature-pressure relationship established by Messrs. Brown and Clarke in 1932.[3] The writer stated that more data, both from the laboratory and from the field, were needed to verify this relationship and to make it possible to prepare more reliable design criteria. Additional data have been presented by Mr. Löfquist, some of which differ considerably from the data presented by Messrs. Brown and Clarke.

The measured temperatures shown in Fig. 4 can be checked by the method of computation presented in the writer's paper. Applying the relationships obtained by Messrs. Brown and Clarke to these temperature changes, and estimating the effect of restraint by the use of Poisson's ratio equal to 0.365, results in an estimated maximum pressure of approximately 4,000 lb per lin ft rather than the 13,400 lb per lin ft shown in Fig. 6. Results of the author's experiments show that considerably greater pressure is developed than is indicated by the basic data presented by Messrs. Brown and Clarke. Figs. 5 and 6 reveal a pear-shaped pressure distribution, with the maximum intensity reached in the upper parts of the ice sheet and varying to a lower value at the top surface, and to zero pressure at the bottom of the ice sheet. Fig. 6 shows intensities of pressure that build up to a maximum and then undergo a characteristic relief of pressure with the passage of time. This plastic-flow effect presents a more logical behavior for this material than the distribution of ice pressure obtained by Messrs. Brown and Clarke.[13]

---

[11] "Ice Pressure Against Dams: Experimental Investigations by the Bureau of Reclamation," by G. E. Monfore, *Transactions*, ASCE, Vol. 119, 1954, p. 36, Fig. 9.

[12] Structural Engr., Bureau of Reclamation, U. S. Dept. of the Interior, Denver, Colo.

It appears that the curve in Fig. 7 yields results that are different from the results obtained by the use of Figs. 3 to 6, inclusive. This seems to be caused by the fact that relief of pressure with time cannot be evaluated from the type of curve shown in Fig. 7.

For thicker ice sheets a lower rate of pressure increase occurs, but a maximum pressure (per linear foot) may not be reached when the ice sheet is 2-ft thick. Some pressure increase will probably develop in thicker ice sheets for the same air temperature and other conditions. A sample computation of curves A and B in Fig. 8 would aid in illustrating the method by which values on these curves were determined. It would also indicate whether the application of the mean-temperature concept might lead to pressure values of doubtful accuracy. The writer has stated that the high pressures shown for thick ice sheets were unlikely because these pressures were dependent on a sustained rate of air-temperature rise, and that pressure would be relieved by plastic flow with the passage of time.[14,15,16] These statements were made because a conservative approach was believed justified in the application of the data obtained by Messrs. Brown and Clarke. Mr. Löfquist's experiments, and those of Mr. Monfore,[10] indicate that the pressures determined by Messrs. Brown and Clarke were low, especially in the lower range of ice-temperature rises. Also, their curves did not show the relief of pressure with the elapse of time after the maximum value had been reached, although this characteristic is mentioned in the text of the paper, under the heading, "Prior Investigations."

It would be helpful to have information on the following:

a. Test data for more rapid rates of ice-temperature rise to extend the curve in Fig. 7.

b. The field use of pressure gages in a large ice sheet, especially if this ice were thick.

c. Ice pressures that might develop if the water in the bottom of the freezing chamber were prevented from escaping as the ice froze. This would explain the effect of (1) confinement and (2) size of well or pit in the development of forces caused by a volume expansion as a result of the freezing process. Under what conditions of size and restraint does this force become important?

---

[13] "Thrust Exerted by Expanding Ice Sheet," by Edwin Rose, *Transactions*, ASCE, Vol. 112, 1947, pp. 896–898.

[14] *Ibid.*, p. 883.

[15] *Ibid.*, p. 897.

[16] *Ibid.*, p. 898.

In reviewing the data shown in Figs. 3 and 5, differences are noted in the depths of the gages. It is assumed that the depths given in Fig. 5 are the correct ones.

The pressures obtained by Mr. Löfquist are higher than the pressures obtained by Messrs. Brown and Clarke. These higher pressures are caused partly by the two-dimensional stress conditions existing in Mr. Löfquist's tests, possible variations in test procedure, and ice crystal structure. However, some further explanation should be made of the differences. Ultimately a new and consistent set of basic data should be set up when such data are well founded.

Thus the problem does not appear entirely solved. Perhaps a precise solution is not possible, but some revision to the writer's curves or some new data should be prepared—coordinating the findings of Messrs. Löfquist and Monfore with the findings of A. D. Hogg[17]—when sound and consistent results are established. The data should be presented in a form to permit quick and easy use by designers of hydraulic structures to aid them in their judgment of the magnitude of ice pressures to be assumed in the design of such structures.

Bertil Löfquist.[18]—Mr. Monfore has shown by an example that the writer's values for the maximum ice pressure are in good agreement with the pressures measured in the USBR laboratory study. The time required to reach this maximum pressure varies, however. The difference may be caused by a variation in the crystalline structure of the ice, but it more probably results from differing strain conditions. In the USBR study, the ice cylinder was restrained in the axial direction; but in the writer's study, the ice cylinder was restrained in the radial directions. The ice pressure is expected to be greater under the latter conditions, but other factors in the tests may compensate for this difference—such as adhesion between the ice and the bearing blocks in the USBR study and cracks in the ice in the writer's study.

Solar radiation is generally insignificant during the winter in northern Sweden, but it is surely an important factor in the ice pressures in more southerly areas.

The ice pressures measured in the USBR field investigations are, at present, the most reliable. As the values are in good agreement with laboratory tests, they represent a definite source of information concerning ice pressure.

The relation between the ice pressure and ice thickness is a problem that needs further investigation. Mr. Rose does not agree that the ice pressure has a maximum at a thickness of approximately 2 ft, and thereafter decreases slightly, or in any case only increases to an insignificant extent (Fig. 8). This conception is a result of computations based on the writer's test and some simplified assumptions as given in the paper. Mathematical treatment of ice-pressure problems is apt to be misleading, however, and the writer will not stress these results. If solar radiation is considered, another relation must exist.

---

[17] "Ice Pressure Against Dams: Some Investigations in Canada," by A. D. Hogg, *Transactions*, ASCE, Vol. 119, 1954, p. 22.

[18] Chf. Inspector, Swedish State Power Board, Stockholm, Sweden.

The disagreement between the data in Figs. 3 and 5, to which Mr. Rose refers, is explainable. The "gages" in Fig. 3 are thermocouples, and the "gages" in Fig. 5 are pressure gages. The gage numbers in the two figures do not correspond.

SOME INVESTIGATIONS IN CANADA

BY A. D. HOGG[1]

SYNOPSIS

Experimental apparatus for determining ice pressure on dams has been developed in the course of research on the subject by the Hydro-Electric Power Commission of Ontario, Canada. This paper describes the methods of investigation adopted by the Commission, and details the field installations used in recording ice pressures.

INTRODUCTION

The interest of the Hydro-Electric Power Commission of Ontario in the subject of ice pressure on dams is a very natural one since it operates and is building a large number of dams located in practically all areas of the province except the most northern areas. The winter temperatures at many of these dams drop to −40°F, or even lower, resulting in thick ice and thus the possibility of high ice pressures. Future dams for which design data are required may be built in even more northerly areas.

The design basis for ice pressure being used for dams on the Ottawa River and in western Ontario, north of the Great Lakes, is 10,000 lb per lin ft of dam, assumed to be acting 1 ft below the regulated water level. In common with the practice of other designers, various values have been used in the past depending on the interpretation of the best information available at the time.

The ultimate objective of the Commission's investigation is to determine the maximum ice pressure that may act on dams in which the Commission is interested. This is recognized as ambitious because of the many variables affecting ice pressure. However, although an ideal solution may not be obtained, it is hoped that the investigation will add substantially to the knowledge of ice pressure, and so aid in the design of safe and economical dams.

INVESTIGATIONAL METHODS

In view of the number of factors affecting ice pressure, it was decided to concentrate on the direct measurement of the force of the ice acting on the dam, and to record together with this value as many of the influencing factors as possible. From these data, the local weather records and any additional measurements and observations that may prove desirable, it was hoped that a method would be derived for determining the probable maximum ice pressure for any particular situation.

NOTE.—Published, essentially as printed here, in December, 1952, as *Proceedings-Separate No. 161*. Positions and titles given are those in effect when the paper was received for publication.

[1] Research Engr., Research Div., The Hydro-Electric Power Commission of Ontario, Canada.

Fig. 1 shows, schematically, the system that has been evolved for measuring the force on the dam. This is essentially a platform scale with the platform in a vertical rather than a horizontal plane. The ice pressure acting over the width of the platform, or "panel," is transmitted to load-measuring cells. The electrical output of these cells (which is proportional to the load) is recorded on a suitable instrument. If the load acting on the panel is to be equal to the load on a corresponding length of the dam, the panel and associated equipment must exhibit the same degree of rigidity as the concrete replaced. This has not been found feasible, but an investigation, based on conservative assumptions, has shown that by the use of a massive reinforced concrete panel and deflection compensating load cells, the loss in accuracy from this source should be relatively minor.

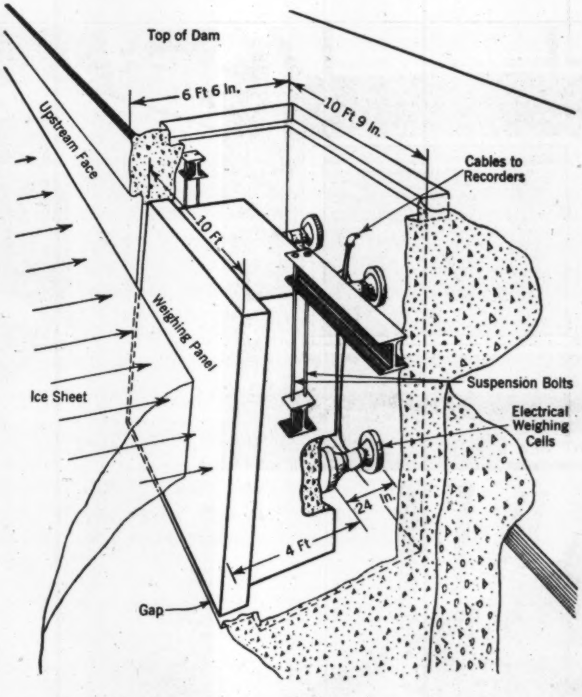
Top of Dam
6 Ft 6 In.
10 Ft 9 In.
Upstream Face
Cables to Recorders
10 Ft
Weighing Panel
Suspension Bolts
Ice Sheet
Electrical Weighing Cells
24 In.
4 Ft
Gap

Fig. 1.—Device for Measurement of Ice Pressure on Dams

In addition to the ice pressure, simultaneous records of air and ice temperatures, ice thickness, elevation of the forebay, wind direction and velocity, and incident radiation are made. In so far as possible, a record is also kept of the snow cover and the condition of the ice, for example, whether it is clear or cloudy. Information is also obtained about the nature of the shores of the forebay.

The panel system of ice pressure measurement has some shortcomings, chief among which is the fact that (*a*) it is rather costly and so can be used in only a limited number of locations and (*b*) it can be installed only at the time a dam is constructed. In view of these shortcomings, consideration was given to the means of measuring the ice pressure at any point in the ice sheet. Although there are a number of ways in which this might be done, the way that seems most promising is to freeze into the ice load sensitive cells known as "stress meters." This name has been applied to meters independent of strain. Some work has been done on the development of such meters by other investigators, but there appears to be none on the market suitable for ice pressure work. The design of a suitable meter was thus considered.

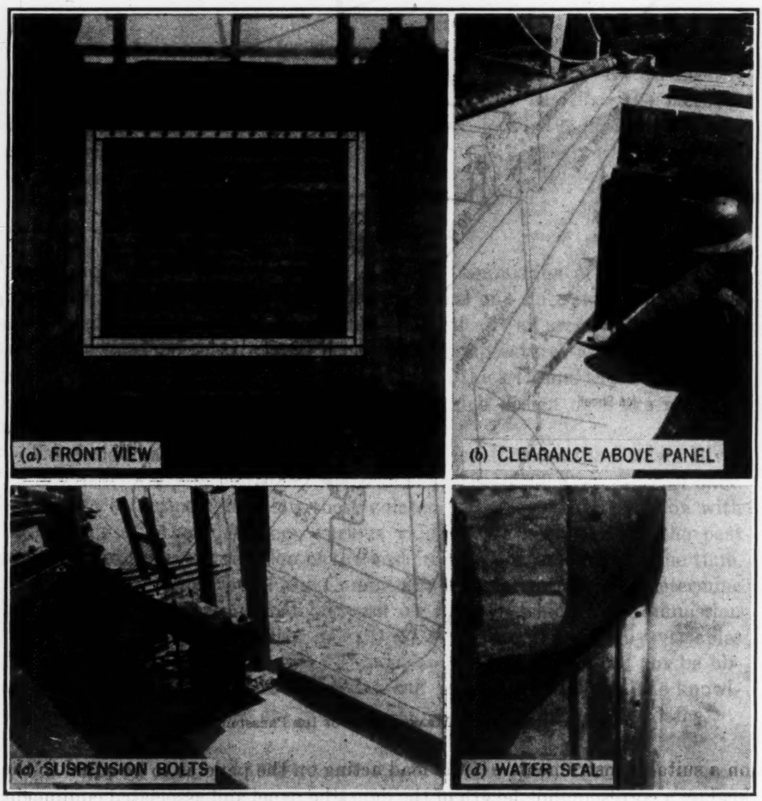

FIG. 2.—FIELD INSTALLATION FOR MEASUREMENT OF ICE PRESSURE

STATUS OF THE WORK

As of August, 1950, the reinforced concrete panels were suspended in position at the Des Joachims Dam (on the Ottawa River) and Pine Portage Dam (on the Nipigon River) and plans are being made for a similar installation at the LaCave Dam (on the Ottawa River near Ottawa, Ont., Canada). Fig. 2 shows various features of these installations, such as the method of suspension and of water sealing. As shown, two suspension bolts are used at each end of the panel. These are arranged to include between them the plane of the center of gravity. Since the location of this plane cannot be predicted exactly, the use of two bolts makes it possible to keep the panel hanging vertically.

The water seal consists of a flat rubber gasket held down by two sets of steel sealing plates, one of which is bolted to the panel and the other to the dam. In applying the seal, the recess formed for it was first prepared by grinding down or building up the concrete, as required, to produce a relatively smooth surface. This surface, together with the adjacent steel and the mating rubber surface, was then "doped" with adhesive, and the rubber gasket and hold-down plates were applied and bolted down. Normal water pressure on these seals has not developed any signs of leaks.

The load cells are in the design stage (1950). In mind is a liquid-type cell provided with a liquid-filled bottle connected to the cell by a tube. A heater in the bottle, controlled from sensing elements suitably disposed about the panel, will provide sufficient heat to expand the liquid as required to compensate for the deflection of the panel and supporting structure.

It is planned to use a commercial pyrheliometer for radiation measurement, resistance thermometers for temperatures and ice thickness, a resistance wire-type pressure gage for forebay elevations, and commercial wind direction and velocity instruments for atmospheric conditions. All these quantities, together with the load on the panel, are recorded on a high-speed recording potentiometer.

EXPERIMENTAL INVESTIGATIONS BY THE BUREAU OF RECLAMATION

BY G. E. MONFORE[1]

WITH DISCUSSION BY MESSRS. EDWIN ROSE, AND G. E. MONFORE

SYNOPSIS

The pressures produced by the thermal expansion of thick ice sheets are considered by the Bureau of Reclamation (USBR), United States Department of the Interior, in the designs of some dams and accessory structures. The USBR conducted experimental investigations of ice pressure from 1946 to 1951. These investigations included field studies at several reservoirs located in the mountains of Colorado and laboratory studies performed in the Engineering Laboratories of the USBR in Denver, Colo. The purpose of this paper is to summarize the more important findings of these field and laboratory investigations.

FIELD INVESTIGATIONS

The primary aim of the field investigation was to measure directly the pressures that develop in natural ice sheets. However, before pressures could be measured, it was necessary to design and perfect suitable gages. A gage diameter of 2.5 in. was chosen because it was small enough to allow the determination of a pressure gradient between the top and the bottom of an ice sheet. The pressure resulting from an increase in temperature of a restrained ice sheet would be expected to be greatest at the top surface where the temperature change is greatest, and zero on the bottom surface where the temperature remains constant at 32° F. Proper values for gage modulus and pressure range were known only after considerable experimentation in both the laboratory and field.

Electric Resistance Pressure Gage[2].—One type of pressure gage that proved successful is shown in Fig. 1. The gage consisted of two steel plates between which was a strain-sensitive element. As the gage was subjected to external

---

NOTE.—Published, essentially as printed here, in December, 1952, as *Proceedings-Separate No. 162.* Positions and titles given are those in effect when the paper or discussion was received for publication.

[1] Research Engr., Bureau of Reclamation, U. S. Dept. of the Interior, Denver, Colo.

[2] "Ice Pressure Measurements at Eleven Mile Canon Reservoir During January 1949," by G. E. Monfore, *Report No. SP-21*, Structural Research Lab., Bureau of Reclamation, U. S. Dept. of the Interior, Denver, Colo., April 28, 1949.

pressure, the separation between the plates decreased by a minute amount. This slight movement was measured by determining the change in electrical resistance of a grid of fine wire that was stretched as the gage deformed.

The strain-sensitive grid consisted of 0.001-in. Advance wire wound on two small glass rods that were contained in a recess between the gage plates. The longer glass rod was supported on the edge of the recess, but the shorter rod was held only by the wire. When the gage was deformed, the shorter glass rod was forced away from the longer rod and thus the wire was stretched. The resistance of the grid was adjusted to about 120 ohms in order that changes in resistance could be measured with commercial bridges.

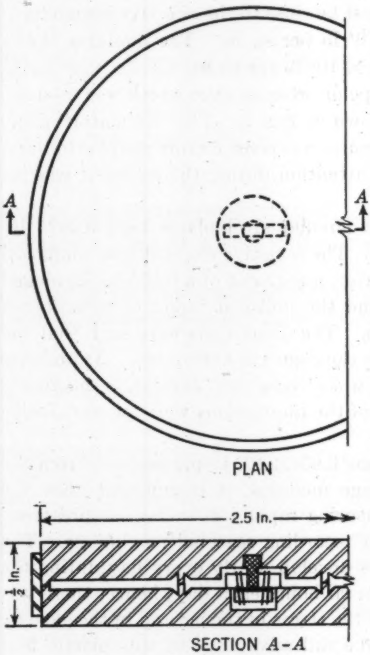

FIG. 1.—ELECTRIC PRESSURE GAGE

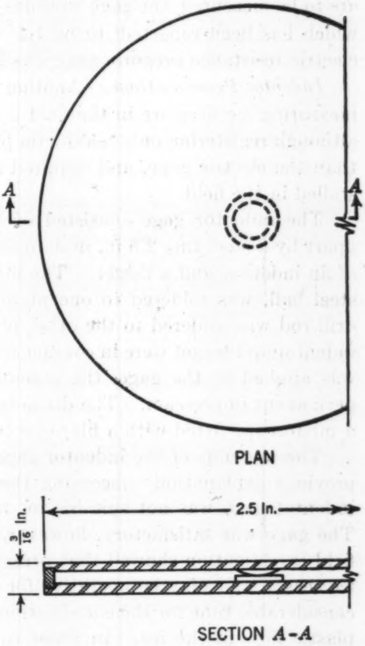

FIG. 2.—INDENTOR PRESSURE GAGE

The gage was compensated for temperature change by employing a "dummy" grid (not shown in Fig. 1) which was similar to the active grid except that it was not subjected to strain as a result of gage deformation. The grids were connected so as to form two adjacent arms of a Wheatstone bridge circuit. Resistance changes caused by temperature variation alone do not affect the balance of the bridge if the active and dummy grids are exactly matched.

It has been shown[3] that the modulus of a gage, which is defined as the pressure applied to the gage divided by the change in thickness per unit thickness at the center of the gage, should be equal to, or slightly higher than, the modulus of the material in which the gage is embedded. Although ice is plastic, and hence the theory of elasticity does not apply strictly, its behavior will approach that of an elastic solid for short time changes. If rapid changes in ice pressure are to be measured, the gage modulus must be close to the effective ice modulus which has been reported[4] to be 1.4×10^6 lb per sq in. The modulus of the electric resistance pressure gage was 2.0×10^6 lb per sq in.

Indentor Pressure Gage.—Another type of pressure gage which was used for measuring ice pressure in the field is shown in Fig. 2. This "indentor" gage, although registering only maximum pressure, was considerably simpler to build than the electric gage, and required no attention during the period it was installed in the field.

The indentor gage consisted of two circular steel plates held 0.0625 in. apart by a steel ring 2.5 in. in diameter. The sensitive element was composed of an indentor and a target. The indentor, a segment of a 0.375-in. hardened steel ball, was soldered to one plate, and the polished target of unhardened drill rod was soldered to the other plate. The dimensions were such that the indentor and target were in contact when the gage was assembled. As pressure was applied to the gage, the indentor was driven into the target making a permanent impression. The diameters of the impressions were measured with a microscope fitted with a filar eyepiece.

The modulus of the indentor gage was 0.03×10^6 lb per sq in. From the previous explanation concerning the gage modulus, it is apparent that the indentor gage was not suitable for measuring rapidly changing ice pressures. The gage was satisfactory, however, for recording seasonal maximums. The field investigation showed that pressures develop nearly every day during the ice season and may be operative for several hours each day; hence, there was considerable time for the equalization of the stress in the ice and in the gage by plastic flow in the ice. In order to take full advantage of this plastic flow there must be no tendency for the gage plates to return to a position of zero stress during periods of zero ice pressure. For this reason, the plates were adjusted so that, were the indentor and target removed, the space between the plates would be about 0.002 in. less than the combined thickness of the indentor and target. Thus there was an initial outward bending of the plates, which kept the indentor and target in contact at all times.

Pressure Measurements.—Before either the electric gages or the indentor gages were installed in the field, they were embedded in thin mortar panels as indicated in Fig. 3. The panel was installed with the three gages in a vertical line. The gages were spaced so as to be symmetric in an 18-in. ice sheet. The center of the top gage was placed 2.5 in. below the top ice surface, the center of the bottom gage was 2.5 in. above the lower ice surface, and the middle gage was at the center of the ice sheet. The mortar panels were installed at the reservoirs after the ice had reached sufficient thickness for safety. Holes were cut through the sheet and the panels were supported by wires at the proper height. The panels were not removed until the ice had melted in the spring.

---

[3] "An Analysis of the Stress Distributions in and near Stress Gages Embedded in Elastic Solids," by G. E. Monfore, *Report No. SP-26*, Structural Research Lab., Bureau of Reclamation, U. S. Dept. of the Interior, Denver, Colo., June 26, 1950.

[4] "Sonic Determination of the Elastic Properties of Ice," by T. D. Northwood, *Canadian Journal of Research*, Vol. 25, Section A, March, 1947, p. 88.

Ice pressures were measured with six of the electric gages at Eleven Mile Canon Reservoir[2] during a period of two weeks in January, 1949. This reservoir is part of Denver's municipal water system, and is located in central Colorado at El. 8600 ft, a latitude of 38° 54′ N, and a longitude of 105° 28′ W. The dam is a concrete arch, 445 ft long and 125 ft high. The shores of the reservoir in the vicinity of the dam are very steep and rocky. A typical gage location is shown in Fig. 4.

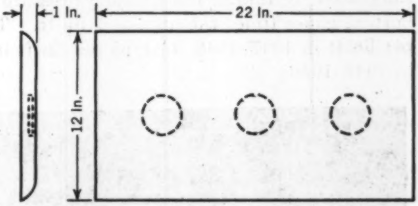

FIG. 3.—POSITIONS OF PRESSURE GAGES IN MORTAR PANEL

The gages were read four or five times during daylight hours every day for two weeks. In general, high pressures occurred during relatively warm weather following periods of cold weather. The highest pressure recorded was 150 lb per sq in. at 12:45 p.m. on January 22 by a top gage. At the same time, the middle gage showed 50 lb per sq in., and the bottom gage, 0 lb per sq in. By 3 p.m., the pressure on the top gage had decreased to 100 lb per sq in., the pressure on the middle gage had increased to its peak value of 80 lb per sq in., and the pressure on the bottom gage was 5 lb per sq in. The average pressure was highest at 12:45 p.m., when it was $(150 + 50 + 0)/3 = 67$ lb per sq in. Because the ice sheet was 18 in. thick at the time, the thrust was calculated as $67 \times 12 \times 18 = 14$ kips per lin ft. The highest average pressure, 74 lb per sq in., occurred on January 20. The thrust corresponding to this average pressure was 16 kips per lin ft.

On several occasions, pressures were measured when there was a strong wind, and at each of these times rapid variations in the readings were noted. Undoubtedly, these variations were caused by the wind, which was very gusty in Eleven Mile Canon. The magnitudes of the variations were estimated by observing the bridge for a period of several minutes and adjusting it for both the high and low points of fluctuation. The greatest variation from the mean pressure was 3 kips per lin ft for a wind that reached gusts of perhaps 30 miles per hr.

During one severe cold period, numerous cracks that did not close during the day were observed in the top of the ice sheet. Apparently the ice was cold enough to freeze the water that entered the contraction cracks from beneath the sheet before the cracks were filled. During this cold period the pressures were generally low, and the highest pressures were recorded, not by the top gage, but by the middle gage.

Several indentor gages were installed at Eleven Mile Canon Reservoir[5,6] during each of the winters of 1947–1948, 1948–1949, and 1949–1950. As with the electric gages, the indentor gages indicated that the highest pressures usually occurred at the top of the ice sheet and the lowest at the bottom. There was some uncertainty in translating the pressure readings of the indentor gages to values of thrust because the impressions of the top, middle, and bottom gages may have occurred at different times. Thrusts were usually calculated by taking the average pressure recorded by the top, middle, and bottom gages times the area of 1 lin ft. The seasonal maximum was 16 kips per lin ft in 1947–1948, 14 kips per lin ft in 1948–1949, and 20 kips per lin ft in 1949–1950.

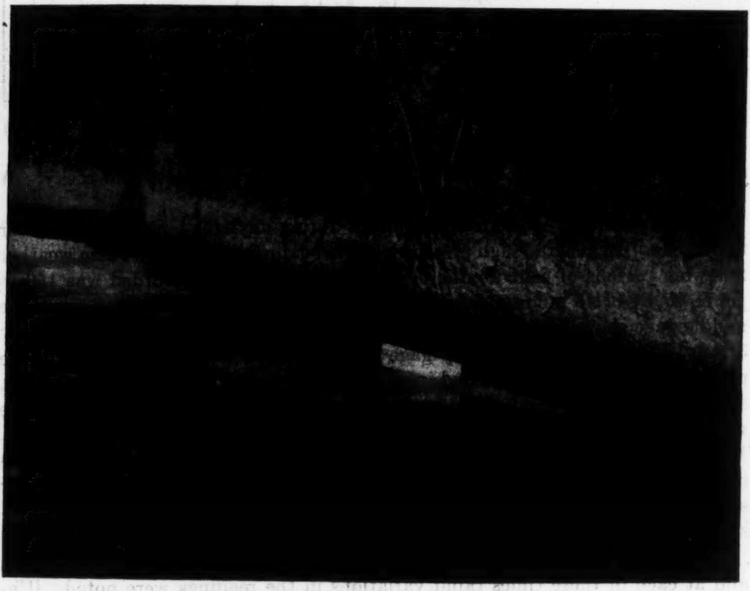

FIG. 4.—PRESSURE GAGE INSTALLATION AT ELEVEN MILE CANON RESERVOIR

It is reasonable to expect that the shores of a reservoir would influence the thrust developed in an ice sheet. If the shores yield under load, the thrust should be relieved accordingly. If the ice sheet can slide up a gently sloping shore, the thrust should also be relieved.

Tests made in the winter of 1950–1951 at several reservoirs[7] offering a considerable variety of shore conditions seemed to confirm this expectation.

---

[5] "Ice Pressure Measurements by Means of Indentor Gages at Eleven Mile Canon Reservoir, Winters of 1947–48 and 1948–49," by G. E. Monfore, *Report No. SP-22*, Structural Research Lab., Bureau of Reclamation, U. S. Dept. of the Interior, Denver, Colo., August 4, 1949.

[6] "Ice Pressure Measurements by Means of Indentor Gages at Eleven Mile Canon Reservoir for the Winter of 1949-50," by G. E. Monfore, *Report No. SP-28*, Structural Research Lab., Bureau of Reclamation, U. S. Dept. of the Interior, Denver, Colo., October 16, 1950.

[7] "Ice Pressure Measurements by Means of Indentor Gages for the Winter of 1950-51," by G. E. Monfore, *Report No. SP-33*, Structural Research Lab., Bureau of Reclamation, U. S. Dept. of the Interior, Denver, Colo., December 12, 1951.

Indentor gages were installed at Antero (El. 9000), Evergreen (El. 7050), Shadow Mountain (El. 8370), and Tarryall (El. 9000) reservoirs. All are in Colorado. The highest thrust at Antero Reservoir was 3.6 kips per lin ft and at Shadow Mountain, 5.8 kips per lin ft. Both reservoirs have flat shores. The greatest thrust at Evergreen Reservoir, which has moderately steep shores, was 9.4 kips per lin ft. The highest thrust for the winter, 17 kips per lin ft, was recorded at Tarryall Reservoir which has steep, rocky shores in the vicinity of the dam where the gages were located. These results indicate that the type of shore can have an important effect on the thrust developed.

In seeming contradiction to these results, however, were those obtained at Eleven Mile Canon Reservoir. The thrust recorded during the winter of 1949–1950 near a shallow sandy beach that was located a mile above the dam was nearly the same as that measured near vertical rock faces in the vicinity of the dam.[6] In this case, the gently sloping shore did not relieve ice pressure.

The explanation for these apparently contradictory results may be the strength of the bond between an ice sheet and a flat shore. The location of the shore and its orientation relative to surrounding surface features and to solar radiation could influence the bond strength and thereby the maximum thrust.

Other Measurements.—Ice temperatures were measured at Eleven Mile Canon Reservoir[2] during January, 1949, at depths in the ice sheet of 1 in., 2 in., 4 in., 8 in., and 16 in. One set of iron-constantan thermocouples was put in ice that was clear of snow, and another set was placed in ice that had a 5-in. snow cover. Four or five readings were made during daylight hours at each thermocouple. The temperature at the top of the sheet began increasing at about 9 a.m. and increased until about 3 p.m. At lower levels in the ice sheet the temperature began increasing at a later time and continued until later in the afternoon. The effect of snow in insulating the ice was remarkable. The temperature at the top of the clear ice increased an average of 13.5° F from the low to the high during a nine-day period, while the temperature at the top of the ice with a 5-in. snow cover increased an average of only 3.3° F. The lowest temperature recorded at the 1-in. depth in clear ice was − 7° F, and the greatest rate of rise in ice temperature was 7° F per hr. The effect of these ice temperature changes on pressure will be further discussed subsequently under the heading, "Calculation of Ice Thrust."

Air temperatures were recorded continuously at Eleven Mile Canon Reservoir during the winter of 1948–1949, and daily maximum and minimum temperatures were read for the other winters of test. The extremes for the two months of January and Februrary were as follows:

Year	Minimum temperature, in degrees Fahrenheit	Maximum temperature, in degrees Fahrenheit
1948	−45	52
1949	−29	51
1950	−16	54
1951	−30	60

The only air temperature records for the other reservoirs where pressure gages were installed in the winter of 1950–1951 were maximum and minimum readings. The extremes for the two months of January and Februrary were the following: At Antero Reservoir, a minimum of −50° F and a maximum of 66° F; at Evergreen Reservoir, a minimum of − 32° F and a maximum of 72° F; and at Shadow Mountain Reservoir, a minimum of − 41° F and a maximum of 51° F. No records were available for Tarryall Reservoir, but it is located only 20 miles from Eleven Mile Canon Reservoir and has approximately the same elevation.

The absorption of solar radiation by an ice sheet is an important factor influencing the temperature of the ice. The intensity of solar radiation was measured at Eleven Mile Canon Reservoir during the winter of 1946–1947, and some tests[2] were made in January, 1949, to determine the amount of energy absorbed in the ice. The absorption data were widely scattered but indicated that the absorption in ice is nearly the same as that in water.[8]

The thickness of the ice sheet at Eleven Mile Canon Reservoir was measured several times each winter. The maximum thickness was 24 in. in 1948, and 20 in. in 1949 and 1950. The ice reached a thickness of 19 in. at Evergreen Reservoir in 1951.

LABORATORY INVESTIGATION[9]

The purpose of the laboratory investigation was to supplement the field program in determining the magnitude of thrust and to provide basic information on the action of ice under changing temperature and pressure. Ice cylinders were subjected to rising temperature, and the pressures necessary to prevent axial expansion were determined. This is basically the procedure used by Ernest Brown and George C. Clarke,[10] M. ASCE, in their laboratory investigation of ice pressure. However, the apparatus used in the present investigation was entirely different, and the results were significantly different in magnitude.

Samples.—Cylinders 4 in. in diameter were cut from cakes of field ice in such a manner that the axes of the cylinders corresponded to the horizontal direction in the original ice sheet. Loads applied to the ends of the cylinders were thus in the same direction relative to the crystal structure as thrusts that develop in the field. The cylinders were cut to a length of 4 in., and bearing blocks consisting of brass plates ½ in. thick and plaster of Paris cylinders 4 in. by 4 in. were frozen to each end. This particular construction of the bearing blocks was found to provide a uniform temperature distribution within the ice sample.

Apparatus.—The insulated chamber in which the pressure tests were conducted was 9 in. in diameter by 12 in. high. The ice sample with its bearing block assembly was placed between masonite plugs, 6 in. in diameter by 4 in. long, located at the top and bottom of the test chamber. These masonite plugs served not only as insulators for the ends of the test chamber, but also as part of the loading system. The construction of the test chamber and the position of the ice sample are shown in Fig. 5. Loads were applied to the sample by a small hydraulic ram connected to a hand pump that was equipped with a pressure gage.

---

[8] "Properties of Ordinary Water-Substance," by N. E. Dorsey, Reinhold Publishing Corp., New York, N. Y., 1940, p. 333.

[9] "Laboratory Investigation of Ice Pressure," by G. E. Monfore, *Report No. SP-31*, Structural Research Lab., Bureau of Reclamation, U. S. Dept. of the Interior, Denver, Colo., October 8, 1951.

[10] "Ice Thrust in Connection with Hydro-Electric Plant Design," by Ernest Brown and George C. Clarke, *The Engineering Journal*, January, 1932, pp. 18–25.

The temperature of the ice sample was controlled by circulating air of the desired temperature through the test chamber. The air was furnished by an air temperature controller consisting principally of a centrifugal fan, an open mesh wire basket containing dry ice, and an electric heating element controlled by a variable transformer. The various components were housed in a large insulated box to which the test chamber was attached. A damper in the controller made it possible to circulate all the air through the dry ice basket, to by-pass the dry ice and circulate the air over the heating element, or to circulate a portion of the air through the dry ice and the remainder over the heating element.

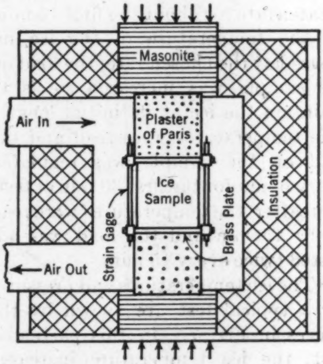

FIG. 5.—TEST CHAMBER

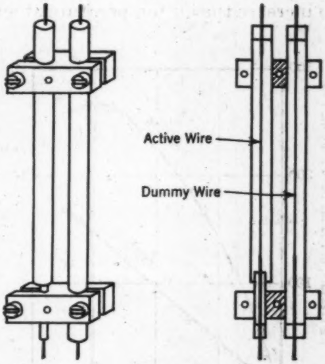

FIG. 6.—STRAIN GAGE

The temperature of the air stream through the test chamber was measured with 36-gage copper-constantan thermocouples, and ice temperatures were measured with similar thermocouples embedded in the ice. The values of thermal electromotive force were measured with a manual potentiometer that was sensitive to a change of 0.001 mv. This corresponds to approximately 0.05° F for copper-constantan thermocouples.

The requirements for a gage needed to insure a constant length for an ice sample during a temperature rise may be estimated by assuming the sample to be elastic. If the modulus of ice is taken to be 1.4×10^6 lb per sq in., an error in length of the sample corresponding to a strain of one part in a million would result in an error of 1.4 lb per sq in. in the stress in the ice. Because a finite time was required to adjust the load on the ice, and because ice is a plastic solid, the actual error would be less than that calculated on the assumption of an elastic sample.

A gage that was sensitive to a strain of one part in a million was devised and perfected in the laboratories of the USBR. A drawing of this unbonded elastic wire gage is shown in Fig. 6. The gage consisted of an active wire that was sensitive to length changes in the specimen, and a dummy wire that was included in the bridge circuit for temperature compensation. The dummy tube also served as a holder for the gage when it was not in use. The gage was fastened to the brass plates at each end of the ice sample. The clamping screw that held the dummy tube to the upper gage block was loosened and the dummy tube was lowered until it was free from the upper block. The active wire was then stretched to about one half of its elastic limit and clamped. Any change in length of the ice made the same change in length of the active wire. It was thus possible to keep the length of the ice sample constant to within one part in a million.

Test Procedure.—With the strain gages attached and the sample in place in the test chamber, the air temperature was brought to the desired initial temperature and held constant until equilibrium was established. In order to obtain a given linear rate of increase in the ice temperature, it was necessary to increase the air temperature at a much greater rate for about the first 15 min. As the temperature of the ice increased at the chosen rate, the load on the sample was increased so as to maintain the ice at its initial length. The temperatures were read and the load on the sample was regulated every 5 min for the first 30 min of test; thereafter, the temperatures were read every 15 min and the load was adjusted twice every 15 min.

The ice temperatures and pressures for a typical test are shown by the curves in Fig. 7. In this particular test, the ice temperature increased from an initial temperature of −10.5° F at a uniform rate of 5° F per hr. The pressure increase was fairly linear for the first part of the test, then curved to a maximum, and decreased. Many tests were performed under various temperature conditions, and invariably the pressure increased to a maximum and then decreased.

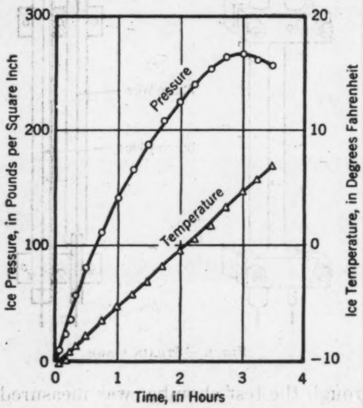

FIG. 7.—TYPICAL ICE PRESSURE TEST

Results.—Check tests were run on several samples to determine the reproducibility of the apparatus and technique. The average deviation in the maximum pressures for duplicate tests on a given sample was 6%. This was considered satisfactory precision.

Much larger variations, an average of 25%, were found in the maximum pressures reached by different ice samples tested under the same conditions. Similarly large variations in the physical properties of ice have been reported by other investigators.

A possible explanation for such large variations in otherwise apparently identcal samples might lie in the arrangement of the crystals. Therefore, it was decided to examine the crystal structure of some of the samples that had been included in the pressure tests. The whole samples were placed between crossed polaroids, and the crystal arrangements were studied. This was later done with sections ½ in. thick, also. Photographs were made of those orientations which seemed to be important. Fig. 8 shows cross sections of the crystals in two samples. Sample A showed poorly defined crystals and no sharp division lines. The maximum pressure obtained with this sample was 326 lb per sq in. when tested from an initial temperature of −10° F with a temperature rise in the ice of 5° F per hr. Sample B, although having poorly defined crystals, did show a sharp division line extending at roughly 45° to the load axis. This sample reached a maximum pressure of only 145 lb per sq in. under the same test conditions as those used for sample A. The indications would seem to be that slippage along the sharp division surface caused the lower pressure in sample B. A study of the other samples revealed similar situations; that is, the samples that exerted low maximum pressures contained crystal surfaces or other sharp divisions along which slippage might occur.

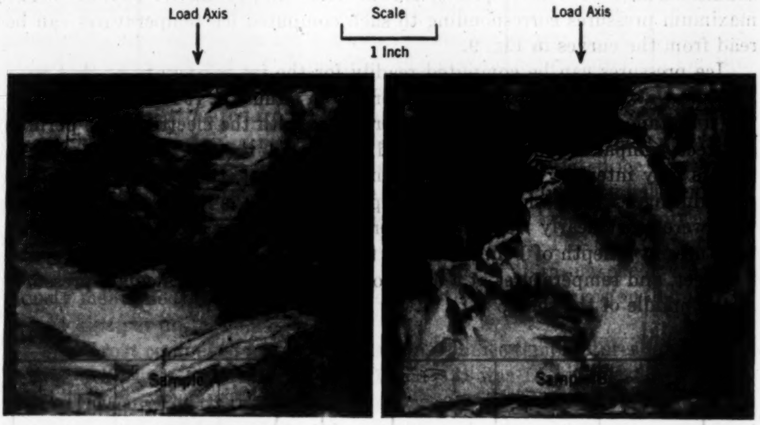

Fig. 8.—Crystal Structure of a Strong Sample and a Weak Sample

Pressure tests were made with initial temperatures of −30° F, −10° F, and +10° F, and with rates of temperature rise in the ice of 2° F per hr, 5° F per hr, 10° F per hr, and 15° F per hr. Curves similar to those in Fig. 7 were obtained for each test. For a given rate of temperature rise, the maximum pressure that the sample reached increased as the initial temperature decreased; and, for a given initial temperature, the maximum pressure increased as the rate of temperature rise increased. The times required for the maximum pressures to develop, and the relationships between maximum pressure and rate of temperature rise for several initial temperatures are shown by the series of curves in Fig. 9. These curves represent the averages obtained from more than 100 tests performed on 24 ice samples.

Computation of Ice Thrust

The laboratory data can be used to calculate ice thrusts that may develop in the field, if information on ice sheet temperatures is available. Analytical methods for computing temperatures in ice sheets for various assumed weather conditions have been developed by Edwin Rose[11] and Frank W. Taylor.[12] The maximum pressures corresponding to such computed ice temperatures can be read from the curves in Fig. 9.

Ice pressures can be computed readily for the ice temperatures that were measured at Eleven Mile Canon Reservoir in January, 1949. Furthermore, the simultaneous measurement of ice pressures with the electric gages permits a direct comparison of measured and calculated thrusts. Because several factors may interfere with the development of thrust, there are probably few days during a winter when the highest possible thrust is reached. Three days that were most nearly free of interference were selected for study. Ice temperatures at a depth of 1 in. were used to calculate pressures at the top of the ice sheet, and temperatures at a depth of 8 in. were used to calculate pressures in the middle of the sheet.

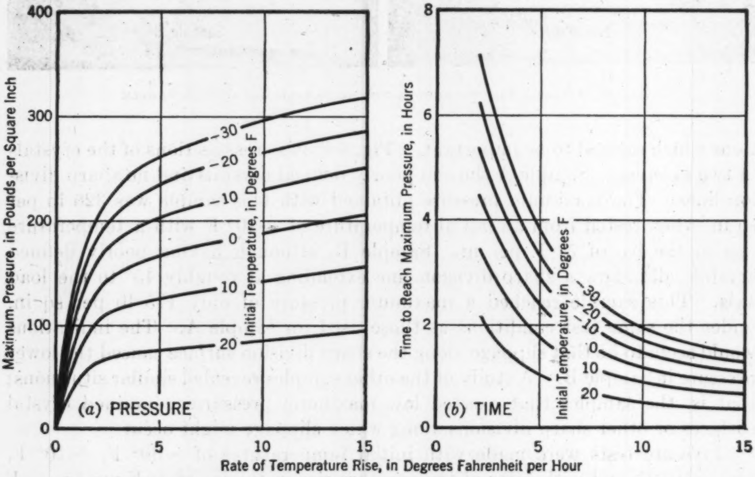

Fig. 9.—Maximum Ice Pressure and Time of Temperature Rise Related to Rate of Ice Temperature Rise

The steps in computing thrusts from ice temperatures can best be illustrated by considering one case in detail. The ice at the top of the sheet reached a minimum temperature of 14° F on the morning of January 22, 1949. The ice temperature began increasing at about 9 a.m. and continued increasing for about 6 hr. The greater part of the rise occurred, however, in 4 hr. The rate of rise that would be applicable for computing thrust was estimated as 3.6° F per hr. The maximum pressure resulting from a temperature rise of 3.6° F per hr from an initial temperature of 14° F is found to be 100 lb per sq in. from the curves of Fig. 9(*a*), and the time required to reach this maximum pressure is 2 hr from Fig. 9(*b*). The minimum temperature measured in the ice sheet at a depth of 8 in. on the morning of January 22 was 19° F, and the rate of rise for this point was 1.3° F per hr. The maximum pressure from Fig. 9(*a*) for an initial temperature of 19° F and a rise of 1.3° F per hr is seen to be 55 lb per sq in. It is estimated from Fig. 9(*b*) that approximately 3 hr were required to develop the maximum pressure under these conditions. The temperature records showed that over 6 hr were available. The calculated ice pressure at the bottom of the sheet is zero because the ice temperature remained constant at 32° F. The average pressure through the sheet was taken as simply 100 + 55 + 0 divided by three which equals 52 lb per sq in. The maximum thrust was then $52 \times 12 \times 18 = 11$ kips per lin ft for the 18-in. ice sheet. As previously mentioned, the thrust measured with the electric gages on January 22 was 14 kips per lin ft.

---

[11] "Thrust Exerted by Expanding Ice Sheet," by Edwin Rose, *Transactions*, ASCE, Vol. 112, 1947, p. 895.

[12] "Temperature Changes in an Ice Sheet, with the Lower Surface in Contact with Water at Freezing Temperature, for Various Conditions of Exposure on Upper Surface," by Frank W. Taylor, Memorandum of November 29, 1945, Bureau of Reclamation, U. S. Dept. of the Interior, Denver, Colo.

The thrust computed in a similar fashion from ice temperatures for January 14 was 6 kips per lin ft and that for January 21 was 13 kips per lin ft. The thrusts measured with the pressure gages were 6 kips per lin ft and 12 kips per lin ft, respectively.

Because the reservoir in the vicinity of the pressure gages was nearly free of snow, the thrusts computed here were correctly based on temperatures measured in clear ice. Temperatures were also measured in ice that had a 5-in. snow cover. The thrusts that might develop in a reservoir completely covered by 5 in. of snow may be calculated from these temperature readings. The thrust thus computed for January 14 was 1 kip per lin ft, that for January 21 was 3 kips per lin ft, and that for January 22 was 3 kips per lin ft. These thrusts are to be compared to thrusts of 6 kips per lin ft, 13 kips per lin ft, and 11 kips per lin ft, which were calculated for ice free of snow.

The most rapid ice temperature rises recorded at Eleven Mile Canon Reservoir were 7° F per hr at a depth of 1 in. and 1.8° F per hr at a depth of 8 in. The lowest recorded ice temperatures, which were not recorded on the same day as the most rapid rises, were −7° F at a depth of 1 in. and 9° F at a depth of 8 in. It was then assumed that the most rapid rises could occur from the lowest ice temperatures. The maximum thrust calculated for these severe conditions was 22 kips per lin ft.

CONCLUSIONS

The highest seasonal thrusts measured with indentor gages at Eleven Mile Canon Reservoir for three winters ranged from 14 kips per lin ft to 20 kips per lin ft. Because the shores of the reservoir where the measurements were made offer as severe restraint to an ice sheet as any to be found, these ice thrusts probably represent maximum values for the ice thickness and weather conditions prevailing during the tests. The results obtained with the indentor gages were subject to some uncertainty, but they were in good agreement with the highest thrust of 16 kips per lin ft which was measured with the electric gages during January, 1949.

These values of thrust were further substantiated by the laboratory investigation. This investigation indicated that the pressure that can develop in a restrained ice sample as the result of a temperature rise is limited by plastic flow. The maximum pressure depends on the initial temperature of the ice and on the rate at which the temperature is increased. The laboratory data were used to calculate the thrusts corresponding to ice temperatures measured at Eleven Mile Canon Reservoir. The thrusts thus calculated were in good agreement with the thrusts measured directly by the electric pressure gages.

The maximum thrusts that might develop in other locations could be calculated from the laboratory data, provided information on ice temperatures becomes available. Temperature measurements in ice sheets at reservoirs of various latitudes and elevations, and during periods extending over several years, would be necessary.

ACKNOWLEDGMENT

Valuable assistance was received from Douglas McHenry, M. ASCE (former head of the Structural Research Laboratory of the USBR), who supervised the investigations.

Field and laboratory investigations mentioned in this paper have been described in reports of the engineering laboratories of the USBR.

DISCUSSION

Edwin Rose.[13]—The results of extensive field and laboratory investigations are a worthwhile addition to the information regarding the development of ice pressure caused by the expansion of an ice sheet resulting from temperature changes.

Mr. Monfore has obtained a favorable comparison between ice pressures obtained from direct field measurement and those computed by application of the temperature-pressure relationships established in the laboratory to the corresponding ice temperatures measured in the field.

Although they are not in a form that permits direct comparisons, the ice-pressure values shown in Figs. 7 to 9 appear to differ from the results of similar tests conducted in 1932 by Messrs. Brown and Clarke.[10] Figs. 7 and 9 show that for a given rate of ice-temperature rise, the rate of ice-pressure rise is very rapid for 1 hr to 3 hr. A maximum pressure is reached in from 1 hr to 6 hr depending on the initial ice temperatures and the rate of ice-temperature rise. After the maximum value is reached, the pressure decreases. During the early period, the rate of pressure increase is greater than that shown by the tests performed by Messrs. Brown and Clarke. In a paper published in 1947[14] the writer computed curves in a form convenient for design purposes based on the ice temperature-pressure relationship established by Messrs. Brown and Clarke. Use of the author's test data, in a similar manner, indicates that greater pressures would result in the case of a low rate of ice-temperature rise and in ice sheets 2 ft or less in thickness. Cases of more rapid temperature rises and for thicker ice sheets indicate that maximum pressures are more nearly comparable.

Under the heading, "Computation of Ice Thrust," Mr. Monfore used the maximum values at the top surface and the 8-in. depth to obtain the total pressure through the ice. Since these pressures did not occur at the same time, this procedure yields too large a maximum value of total pressure. By observation of the curves in Figs. 7 and 9, the author shows that the pressure at a given point increases to a maximum in from 1 hr to 6 hr and then decreases. This general pattern is also shown by the field data on pressures measured with the electric gages. This characteristic property should be used in the computation procedure.

To permit computation of pressures at various depths of the ice sheet at different increments of time, it would be helpful if the curve in Fig. 7 could be extended to show the pressure decrease past the maximum as the ice-temperature continues to rise at a uniform rate. Such pressure values could then be integrated to obtain the total pressure in the ice sheet at a given time, and from this the maximum pressure value could be determined. Bertil Löfquist[15] described experiments involving pressures measured at various depths in an ice sheet. He found that the surface pressure reached a maximum a few hours after the start of the temperature rise, whereas the total pressure was not a maximum at that time because of the lag in the increase of temperature in the interior of the ice. Mr. Löfquist found that maximum total pressure occurs at a later time when the surface pressure is past its peak but the interior pressure is at a maximum. This results in a "pear-shaped" pressure curve.

---

[13] Structural Engr., Bureau of Reclamation, U. S. Dept. of the Interior, Denver, Colo.

[14] "Thrust Exerted by Expanding Ice Sheet," by Edwin Rose, *Transactions*, ASCE, Vol. 112, 1947, pp. 871–900.

[15] "Ice Pressure Against Dams: Studies of the Effects of Temperature Variations," by Bertil Löfquist, *Transactions*, ASCE, Vol. 119, 1954, p. 6.

An attempt was made by the writer to estimate the effect on a 2-ft-thick ice sheet with a minimum surface temperature of −30° F and to compare these results with those obtained by Mr. Monfore and Messrs. Brown and Clarke. For an air-temperature rise of 5° F, 10° F, and 15° F, respectively, the pressures obtained (using the relationships determined by Messrs. Brown and Clarke) would be 4,500 lb per lin ft, 5,000 lb per lin ft, and 7,000 lb per lin ft. Using the data derived by Mr. Monfore the pressures would be 20,000 lb per lin ft, 22,000 lb per lin ft, and 23,000 lb per lin ft.

These values are estimates, but wide differences are noted. These differences are caused partly by the variation in the structure and the variation in the arrangement of the ice crystals. In the field, ice structure and strength are bound to differ at various locations. It is likely that test procedure and test methods also are a factor.

It would be helpful if the air-temperature curve were plotted in Fig. 7 to show graphically the rapid increase in the air temperature required during the first fifteen minutes of the test. This would permit study of the lag in the ice-temperature rise relative to the air-temperature rise in these early stages and the influence on ice pressures.

The field observations made by Mr. Monfore regarding ice-pressure variations caused by the effect of restraint at the reservoir shores, the amount of snow cover, solar radiation, and wind conform to the expectations set forth in the writer's paper and elsewhere.

The wide variation of the basic data on the temperature-pressure relation as established by Mr. Monfore and Messrs. Brown and Clarke indicates the necessity for an explanation of these differences. Recognizing that the tests performed by the author were extensive, precise, and supported by field measurements, it is believed that verification is needed from independent sources—such as the test results from Sweden and Canada.[15,16] When a reasonably consistent relationship has been established, then a revised set of design curves or tables should be prepared. Such design data should be in an easily adaptable form and should be in terms of variables that can be readily determined or accurately estimated. Generally, it would not be convenient to measure ice temperatures over a period of several years, as suggested by the author, but records of changes of air temperature and ice thicknesses usually would be available or could be estimated.

Until general agreement is reached on the basic properties affecting the development of ice pressure and these properties are supported by field measurements, the writer believes that the data presented in his 1947 paper, when

---

[16] "Ice Pressure Against Dams: Some Investigations in Canada," by A. D. Hogg, *Transactions*, ASCE, Vol. 119, 1954, p. 22.

used with judgment, can serve as a reasonable basis for estimating ice thrust. Before selection of a final value, some allowance should be made for the larger pressures indicated by Mr. Monfore.

Further field information is especially desirable, and since suitable gages have been developed, it is possible that they can be used under a wide variety of conditions. Measurement of pressures in smaller areas of ice sheets, such as in pumping-plant pits or in narrow channels where confinement is closer than in a large reservoir, would provide valuable data for use in the design of such structures.

G. E. MONFORE.[17]—In presenting the results of the USBR's experimental investigations of ice pressure it was recognized that much work remained to be done. When the program was discontinued in 1951, it was decided to make generally available the data which had been gathered up to that time. The results of the laboratory investigation were in agreement with the results obtained by Mr. Löfquist,[15] A detailed comparison is contained in a discussion of Mr. Löfquist's paper.[18]

The pressure near the top of an ice sheet reaches a maximum before that of points lower in the sheet. Thrusts which were calculated from the pressures measured with electric pressure gages were based on the actual pressure gradient existing at a given time. These results are presented under the heading, "Field Investigations: Pressure Measurements." The method of using maximum pressures in computing thrusts on the basis of the laboratory tests and field ice temperatures was chosen because of its simplicity, and also because the results thus obtained were only slightly greater than the true values based on instantaneous gradients. For example, the greatest thrust measured at Eleven Mile Canon Reservoir on January 22, 1949, was 14 kips per lin ft. The thrust computed on the basis of maximum pressures without regard to time was 17 kips per lin ft. Similarly, the greatest measured thrust for January 20, 1949, was 16 kips per lin ft, and that computed on the basis of maximum pressures without regard to time was 17 kips per lin ft.

Although some of the earlier laboratory tests were continued considerably beyond the time required for the maximum pressure to develop, the pressure-time curve for ice can be given with certainty only to times which are approximately 25% greater than the time required for the maximum pressure to develop. It was found that the pressure-time curves, expressed in a dimensionless form, were nearly identical for the various initial temperatures and rates of temperature rise. The curve shown in Fig. 10 represents an average of many tests.

Temperatures were measured at several points in a laboratory ice sample for various air-temperature conditions in preliminary tests that have been described.[9] The air temperature and corresponding ice temperature for one typical test are shown in Fig. 11. This is the same test which is shown in

---

[17] Research Engr., Bureau of Reclamation, U. S. Dept. of the Interior, Denver, Colo.

[18] Discussion by G. E. Monfore of "Ice Pressure Against Dams: Studies of the Effects of Temperature Variations," by Bertil Löfquist, *Transactions*, ASCE, Vol. 119, 1954, p. 17.

Fig. 7. The rapid increase in air temperature for the first fifteen minutes was necessary to obtain a linear increase in ice temperature.

It is true that air temperatures are easier to measure in the field than are ice-sheet temperatures, but it is also true that the computation of ice temperatures from air temperatures is difficult. Surface conditions provide elements of uncertainty in such computations. The measurement of ice-sheet temperatures, compared to the measurement of ice pressures, is relatively simple; such data from various locations would be valuable, not only for direct estimation of thrust but also as a check on the methods of computing ice temperatures.

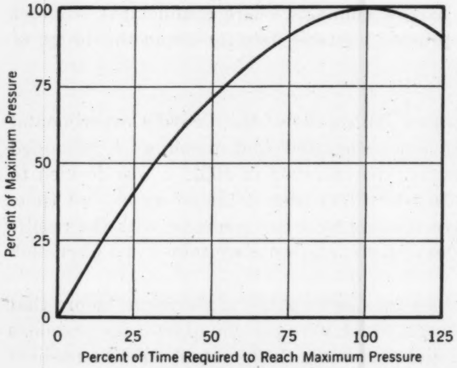

Fig. 10.—Average Pressure-Time Curve

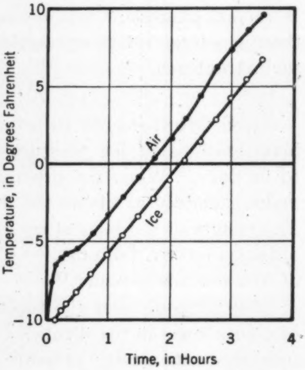

Fig. 11.—Air and Ice Temperatures for Typical Laboratory Test

The presentation of data in an easily used form is desirable, but it must be remembered that no matter how convenient a table or set of curves may be, the accuracy of the presentation cannot be any greater than the accuracy of the original experimental data.

AMERICAN SOCIETY OF CIVIL ENGINEERS
Founded November 5, 1852
TRANSACTIONS

Paper No. 2657

STIFFNESS CHARTS FOR GUSSETED MEMBERS UNDER AXIAL LOAD

BY JOHN E. GOLDBERG,[1] M. ASCE

WITH DISCUSSION BY MESSRS. LEONARD K. STEVENS, AND JOHN E. GOLDBERG

SYNOPSIS

Charts are presented that show the slope-deflection flexural coefficients, under axial compression or axial tension conditions, for members consisting of a uniform middle part and infinitely rigid end regions of equal or unequal lengths up to 25% of the total length of the member. Assuming that the actual gussets at the ends of a member may be replaced by shorter gussets of infinite rigidity, the charts may be used in the analysis of secondary stresses in gusset-connected trusses and in the stability analysis of such trusses by either the moment-distribution method or the slope-deflection method. Because the fundamental theories of secondary stresses and of stability analysis have been discussed elsewhere (see subsequent footnotes), these theories are not covered in this paper.

There exist two major problems in the design and analysis of gusset-connected trusses in which it is essential that reasonably accurate values for the flexural rigidity of the various members be used. These problems are as follows: (1) The calculation, in certain cases, of so-called secondary stresses resulting from the angular distortion of the panels as a consequence of axial strains; and (2) the calculation of the critical loading that causes a general instability of the truss. Both problems may be approached by the slope-deflection method or by the moment-distribution method both of which depend for their correct application on the use of reasonably accurate values of the true flexural stiffnesses of the various members.

H. Manderla, in 1880, published[2] an exact solution for secondary stresses in trusses, which included correct expressions for the end moments of a uniform

---

NOTE.—Published, essentially as printed here, in March, 1953, as *Proceedings-Separate No. 179.* Positions and titles given are those in effect when the paper was received for publication.

[1] Associate Prof. of Structural Eng., Purdue Univ., Lafayette, Ind.

[2] "Die Berechnung der Sekundärspannungen, welche in einfachen Fachwerke infolge starrer Knotenverbindungen entstehen," by H. Manderla, *Allgemeine Bauzeitung*, 1880, p. 34.

member as functions of the end rotations and the axial load. Applications of this solution and of simplified slope-deflection and moment-distribution methods that neglect the effect of axial load upon flexural rigidity are treated in a number of references.[3,4,5,6,7,8,9] Benjamin Wyly James[10] extended the moment-distribution method to include the effect of axial load upon flexural rigidity and presented curves that facilitate solution of such problems. The effect of finite length of joints and gussets on secondary stresses and on stress analysis of rigid frames was discussed by L. T. Wyly,[11,12,13] M. ASCE.

Eugene E. Lundquist,[14] M. ASCE, has developed a moment-distribution method for determining the stability of a structural frame and has prepared stiffness tables[15,16] that reduce the labor in stability analyses. The stability analysis of trusses and frames has been further discussed and refined by George Winter, M. ASCE, and associates[17]; Harold E. Wessman and Thomas C. Kavanagh,[18] Members, ASCE; P. P. Bijlaard,[19] M. ASCE; and N. J. Hoff, M. ASCE, and associates.[20] Numerical examples are given in these references. The methods used are usually of the moment-distribution type or the slope-deflection type. Messrs. Hoff[20] and Bijlaard[19] have included the effect of gussets of equal length on the buckling of trusses, and have presented graphs from which modified factors may be read directly. Using a limited amount of test data, Mr. Bijlaard[19] and Jacob Karol,[21] M. ASCE, have developed empirical relations

---

[3] "Secondary Stresses in Bridge Trusses," by C. R. Grimm, John Wiley & Sons, Inc., New York, N. Y., 1908.

[4] "The Theory and Practice of Modern Framed Structures," by J. B. Johnson, C. W. Bryan, and F. E. Turneaure, John Wiley & Sons, Inc., New York, N. Y., 10th Ed., 1929, Pt. II, Chapter VII, pp. 469–476.

[5] "Technische Mechanik," by O. Mohr, Wilhelm Ernst and Son, Berlin, Germany, 1906, pp. 420–430.

[6] "Simplified Methods for the Analysis of Multiple Joint Rigid Frames," by John E. Goldberg and George A. Maney, *Bulletin*, Northwestern Univ., Evanston, Ill., 1932.

[7] "Wind Stresses by Slope Deflection and Converging Approximations," by John E. Goldberg, *Transactions*, ASCE, Vol. 99, 1934, pp. 962–975.

[8] "Statically Indeterminate Stresses," by John Ira Parcel and George Alfred Maney, John Wiley & Sons, Inc., New York, N. Y., 2d Ed., 1936, pp. 266–281.

[9] "Analysis of Continuous Frames by Distributing Fixed-End Moments," by Hardy Cross, *Transactions* ASCE, Vol. 96, 1932, pp. 1–156.

[10] "Principal Effects of Axial Load on Moment Distribution Analysis of Rigid Structures," by Benjamin Wyly James, *Technical Note No. 534*, National Advisory Committee for Aeronautics, Washington, D. C., July, 1935.

[11] Discussion by L. T. Wyly of "Analysis of Multiple Span Rigid Frame Bridges by the Slope Deflection Method," by George A. Maney, *Journal*, A. C. I., September–October, 1936, pp. 767–770.

[12] "Two Problems in Bridge Design," by L. T. Wyly, *Bulletin No. 454*, A.R.E.A., September–October, 1945, pp. 27–53.

[13] "The Equivalent Joint Method of Rigid Frame Analysis—Modification of Slope Deflection by Successive Approximations," by L. T. Wyly, *Bulletin No. 502*, A.R.E.A., June–July, 1952, pp. 3–44.

[14] "Stability of Structural Members Under Axial Load," by Eugene E. Lundquist, *Technical Note No.* 617, National Advisory Committee for Aeronautics, Washington, D. C., October, 1937.

[15] "Tables of Stiffness and Carry-Over Factors for Structural Members under Axial Load," by E. E. Lundquist and W. D. Kroll, *Technical Note No. 652*, National Advisory Committee for Aeronautics, Washington, D. C., June, 1938.

[16] "Extended Tables of Stiffness and Carry-Over Factors for Structural Members under Axial Load," by E. E. Lundquist and W. D. Kroll, *Wartime Report L-255* (*ARR4B 24*), National Advisory Committee for Aeronautics, Washington, D. C., February, 1944.

[17] "Buckling of Trusses and Rigid Frames," by George Winter, P. T. Hsu, Benjamin Koo, and M. H. Loh, *Bulletin No. 36*, Cornell Univ. Eng. Experiment Station, Ithaca, N. Y., April, 1948.

[18] "End Restraints on Truss Members," by Harold E. Wessman and Thomas C. Kavanagh, *Transactions* ASCE, Vol. 115, 1950, pp. 1135–1153.

[19] "Investigation on Buckling of Rigid Joint Structures—First Progress Report," by P. P. Bijlaard, School of Civ. Eng., Cornell Univ., Ithaca, N. Y., November 1, 1949 (mimeographed).

[20] "Buckling of Rigid-Jointed Plane Trusses," by N. J. Hoff, Bruno A. Boley, S. V. Nardo, and Sara Kaufman, *Transactions*, ASCE, Vol. 116, 1951, p. 958.

[21] Discussion by Jacob Karol of "Buckling of Rigid-Jointed Plane Trusses," by N. J. Hoff, Bruno A. Boley, S. V. Nardo, and Sara Kaufman, *ibid.*, p. 987.

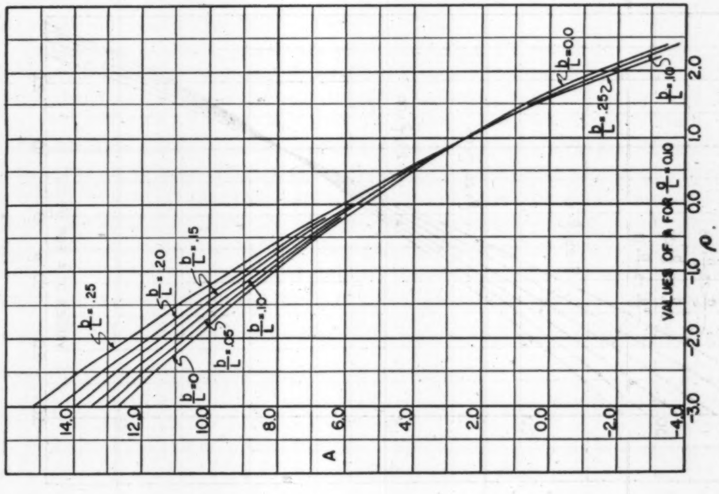
A
14.0
12.0
10.0
8.0
6.0
4.0
2.0
0.0
-2.0
-4.0
-3.0
-2.0
-1.0
0.0
1.0
2.0
$\frac{b}{L} = .25$
$\frac{b}{L} = .20$
$\frac{b}{L} = .15$
$\frac{b}{L} = 0$
$\frac{b}{L} = .05$
$\frac{b}{L} = .10$
$\frac{b}{L} = 0.0$
$\frac{b}{L} = .25$
$\frac{b}{L} = .10$
VALUES OF A FOR $\frac{a}{L} = 0.10$
ρ

FIG. 2

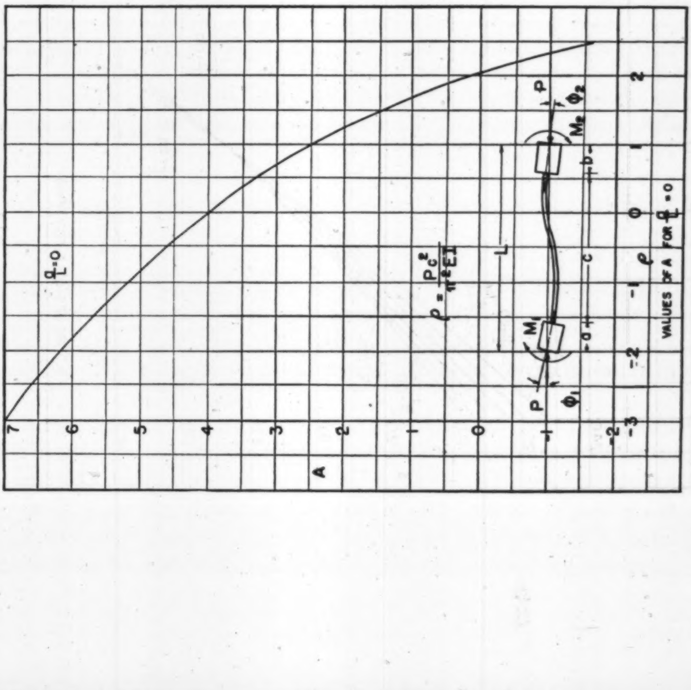
A
7
6
5
4
3
2
1
0
-1
-2
-3
-3
-2
-1
0
1
2
$\frac{a}{L} = 0$
$\rho = \frac{Pc^2}{\pi^2 EI}$
L
P
P
M_1
M_2
ϕ_1
ϕ_2
a
c
b
VALUES OF A FOR $\frac{a}{L} = 0$
ρ

FIG. 1

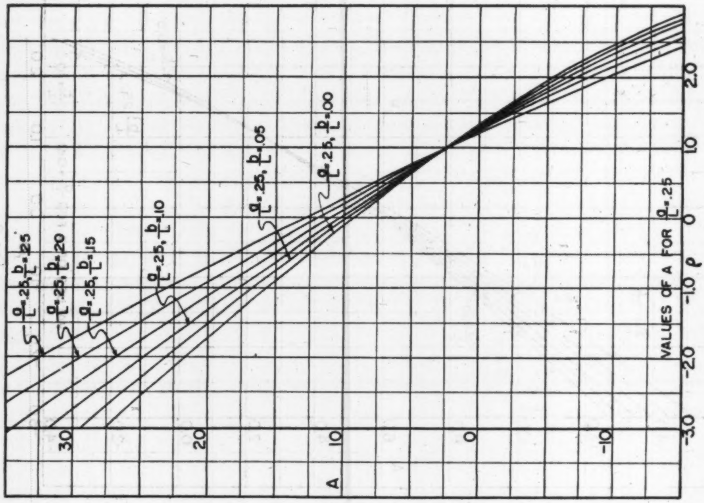
A
30
20
10
0
-10
-3.0
-2.0
-1.0
0
1.0
2.0
VALUES OF A FOR a/L=.25 ρ
a/L=.25, b/L=.25
a/L=.25, b/L=.20
a/L=.25, b/L=.15
a/L=.25, b/L=.10
a/L=.25, b/L=.05
a/L=.25, b/L=.00

FIG. 4

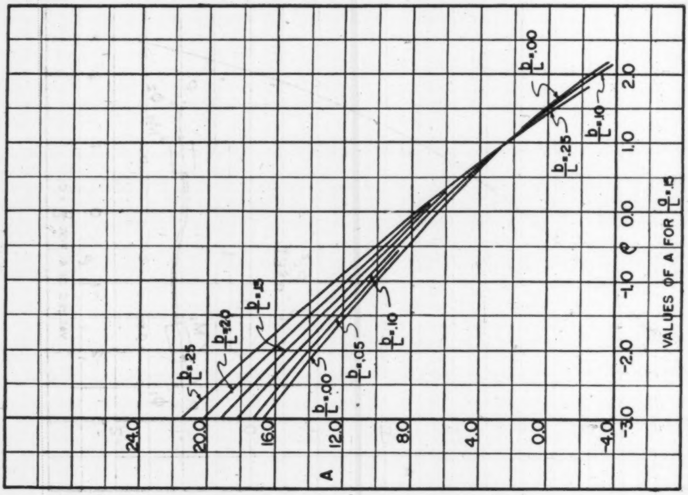
A
24.0
20.0
16.0
12.0
8.0
4.0
0.0
-4.0
-3.0
-2.0
-1.0
0.0
1.0
2.0
VALUES OF A FOR a/L=.15 ρ
b/L=.25
b/L=.20
b/L=.15
b/L=.00
b/L=.05
b/L=.10
b/L=.25
b/L=.00
b/L=.10

FIG. 3

between the actual length of a gusset and the reduced length of an equivalent but infinitely rigid gusset.

In the present paper, charts are presented (Figs. 1 through 12) which show the coefficients to be used in a generalized slope-deflection formula (Eq. 3) for an idealized truss member consisting of a uniform middle portion and infinitely rigid end portions of equal or unequal lengths up to 25% of the total length of the member. In these charts, the coefficients are presented as functions of the magnitude and sign of the axial load. Derivations for the equations on which these charts are based are to be found in Appendix I and Appendix II. These charts may be used, under appropriate circumstances, to facilitate the slope-deflection analysis or the moment-distribution analysis of secondary stresses and the determination of stability limits of gusset-connected trusses by the methods described in the references that have been cited. Charts for the values $\frac{a}{L} = 0.05$ and $\frac{a}{L} = 0.20$ (Figs. 9 through 12) appear subsequently in this paper in relation to a specific numerical example.

In the case of initially straight members, the flexural stiffness is determined by (*a*) the parameter $E\,I$ of the basic member, in which E is the modulus of elasticity and I is the moment of inertia; (*b*) the sublengths of the member and its reinforced portions, such as gusset regions; (*c*) the flexural stiffness and type of attachment of the gussets or other reinforcement; and (*d*) the magnitude (and sign) of the axial load acting on the member.

Under certain obvious conditions an actual member (including two gussets of finite rigidity) may, with sufficient accuracy, be replaced by an idealized member that includes two gussets of infinite rigidity but of reduced length. One may assume, for example, that appropriate conditions prevail if the gussets are integrally and continuously attached to the main member and have flexural rigidities several times as great as that of the main member. Thus, the replacement procedure and the charts of the stiffness coefficients may be used with confidence in the analysis of a welded truss if the relative flexural rigidities of the gussets are sufficiently great. The stiffness charts also may be used in the analysis of a riveted truss if the rivet loads are so small that rivet slip is precluded. Recent research has indicated that the clamping action obtained by the use of high-strength bolts may be great enough to eliminate slip. If this is true, it may be possible to use the stiffness charts with confidence for well-designed bolted trusses, at least for moderately heavy and light joint loads. In the case of trusses that are subject to the possibility of rivet slip, the direct use of the charts, that is, the neglect of rivet slip, usually should lead to a conservative analysis of the secondary stresses, but to an unconservative estimate of the stability limit of the truss.

Assuming that the gussets are several times as stiff as the basic member and that they are attached integrally to the basic member, one may, for purposes of analysis, replace the large but finite rigidity of the gusset in the end region by an infinitely rigid gusset of somewhat shorter length. Of course, the difference between the real length of the finite gusset and the effective length of the infinitely stiff gusset is to be added to the clear length of the member.

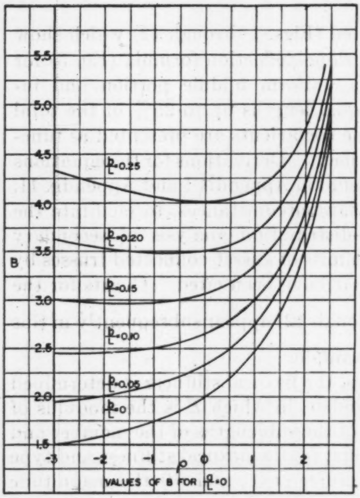

FIG. 5

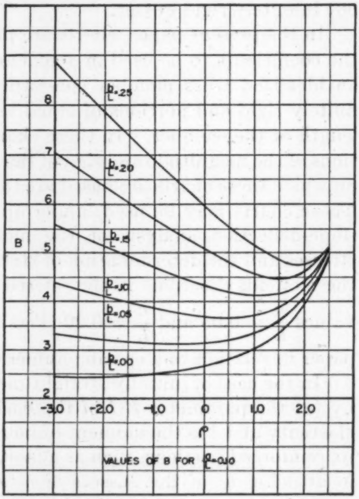

FIG. 6

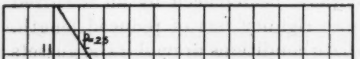

FIG. 7

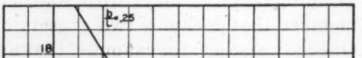

FIG. 8

Several methods are extant by which the actual member may be reduced to a simplified member with infinitely rigid end regions. The most simple method may suffice if the gusset is several times as stiff as the member. Let it be specified, for example, that the flexural rigidity of a gusset of length a' (measured from the center of the joint outward along the member to the outermost point of attachment) is $(E\,I)_g$, that the flexural rigidity of the basic member is $(E\,I)_m$, and that its clear length is c'. The true stiffness in the gusset region usually will be $(E\,I)_g$ plus $(E\,I)_m$ because the gusset is essentially added to the sides of the basic member. For a constant bending moment M, the angular change in the gusset region will be $\frac{M}{(E\,I)_g + (E\,I)_m}\,a'$. A length a'' of the basic member will have the same angular change if

$$a'' = \frac{(E\,I)_m}{(E\,I)_g + (E\,I)_m}\,a' \qquad \text{(1a)}$$

In the case of a trapezoidal gusset, in which $(E\,I)_g$ varies appreciably, it may be desirable to use

$$a'' = (E\,I)_m \int_0^{a'} \frac{1}{(E\,I)_g + (E\,I)_m}\,da' \qquad \text{(1b)}$$

Hence, for this approximate method, it is necessary merely to add the dimension a'' to the clear length of the member and subtract a'' from the actual length of the gusset. A similar procedure is applied at the other end to reduce the gusset of length b'. One thus arrives at an approximately equivalent simplified member consisting of a uniform clear length, c, equal to $c' + a'' + b''$ with a rigidity $(E\,I)_m$ having at each end infinitely rigid gussets of lengths a and b, respectively, such that

$$a = a' - a'' \qquad \text{(2a)}$$

$$b = b' - b'' \qquad \text{(2b)}$$

$$c = L - a - b \qquad \text{(2c)}$$

in which L is the over-all length of the member and gussets, and b'' is computed in a manner similar to that used for computing a''.

This method of replacement is admittedly approximate. However, other methods may be developed along the same lines. The significant fact is that, for practical purposes, a gusset, or a reinforcement of finite rigidity usually may be replaced in the analysis by an infinitely stiff gusset or reinforcement of reduced length. It is emphasized that the reinforcement is assumed to be attached ideally to the member and that such dislocations as rivet slip are neglected or must be otherwise included.

The problem of determining the flexural rigidity of a member that is reinforced by gussets is thus reduced to a problem for which graphical aids may be obtained. With this idea in mind, graphs have been prepared showing the flexural stiffness coefficients of idealized members having infinitely rigid end portions that are subjected simultaneously to axial load. These graphs give the coefficients A and B which appear in a generalized form of the slope-deflection equation:

$$M_1 = \frac{E\,I}{c}\,(A\,\phi_1 + B\,\phi_2) \ldots\ldots\ldots\ldots\ldots\ldots\ldots (3)$$

in which ϕ is the slope of the infinitely rigid end portion and the subscript members denote opposite ends of a member and in which M_1 is the moment at one end of the member (see Fig. 13). The coefficients A and B are presented as functions of the three parameters, $\frac{a}{L}$, $\frac{b}{L}$, and $\frac{P\,c^2}{\pi^2\,E\,I}$, in which P is the applied axial load.

A transverse displacement having the value Δ (in inches), which rotates the chord of the member in a clockwise direction, is equivalent to counter-clockwise end rotation of $-\frac{\Delta}{L}$ applied at each end. Therefore, the basic equation may be generalized as follows:

$$M_1 = \frac{E\,I}{c}\left[\,A\,\phi_1 + B\,\phi_2 - (A + B)\,\frac{\Delta}{L}\right] \ldots\ldots\ldots\ldots (4)$$

A corresponding formula may be written for M_2 if the parameters $\frac{a}{L}$ and $\frac{b}{L}$ are interchanged.

The charts may be used to obtain factors for use in moment-distribution analysis. The quantity $A\left(\frac{E\,I}{c}\right)$ is the true stiffness of the member, and, therefore, any set of quantities proportional to $A\left(\frac{E\,I}{c}\right)$ for the various members will serve as distribution factors.

The carry-over factor from M_1 to M_2 may be determined as follows: For specified values of $\frac{a}{L}$, $\frac{b}{L}$, and ρ (see Eq. 16, Appendix II), the coefficient A may be determined. For the same value of ρ but with the original $\frac{a}{L}$ and $\frac{b}{L}$ interchanged, one may determine the coefficient B. The carry-over factor from M_1 to M_2 is $\frac{B}{A}$. The carry-over factors from each end usually will be different. As an example, consider a member for which $\frac{a}{L} = 0.05$, $\frac{b}{L} = 0.20$, and $\rho = +0.5$. The coefficient A is given by the stiffness charts as 3.72 (see Figs. 9 and 10). For values of $\frac{a}{L} = 0.20$, $\frac{b}{L} = 0.05$, and $\rho = +0.5$, the value of the coefficient B is given as 4.13 (see Figs. 11 and 12). Therefore the carry-over factor from M_1 to M_2 is $\frac{4.13}{3.72}$, or 1.11. The carry-over factor from M_2 to M_1 is determined in a similar manner and is found to be $\frac{4.13}{5.34}$, or 0.77. One item in the stress

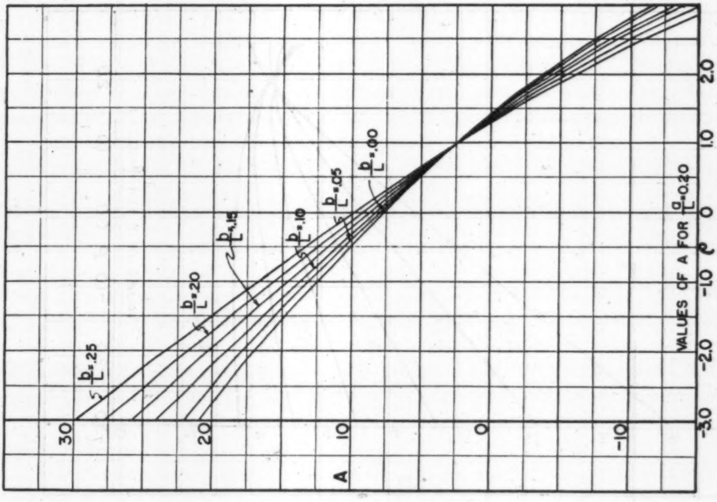
30
20
10
0
-10
A
-3.0
-2.0
-1.0
0
1.0
2.0
VALUES OF A FOR $\frac{a}{L}$=0.20
ρ
$\frac{b}{L}$=.25
$\frac{b}{L}$=.20
$\frac{b}{L}$=.15
$\frac{b}{L}$=.10
$\frac{b}{L}$=.05
$\frac{b}{L}$=.00

Fig. 10

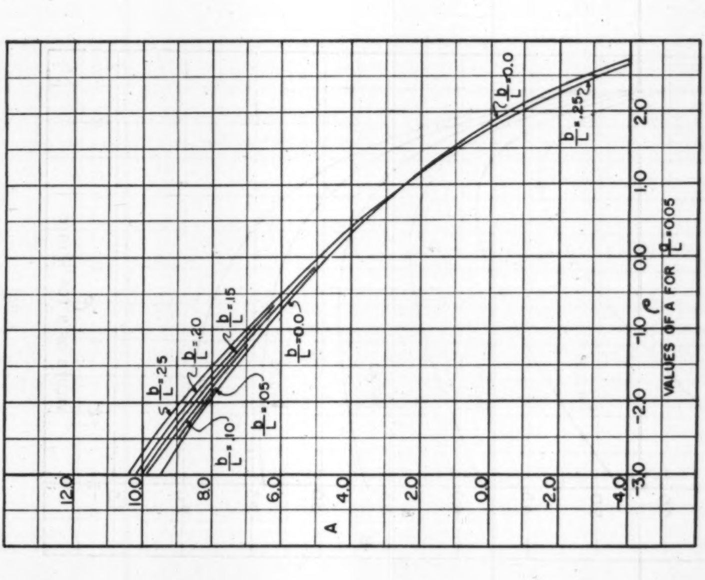
12.0
10.0
8.0
6.0
4.0
2.0
0.0
-2.0
-4.0
A
-3.0
-2.0
-1.0
0.0
1.0
2.0
VALUES OF A FOR $\frac{a}{L}$=0.05
ρ
$\frac{b}{L}$=.25
$\frac{b}{L}$=.20
$\frac{b}{L}$=.15
$\frac{b}{L}$=.10
$\frac{b}{L}$=.05
$\frac{b}{L}$=0.0
$\frac{b}{L}$=0.0
$\frac{b}{L}$=.25

Fig. 9

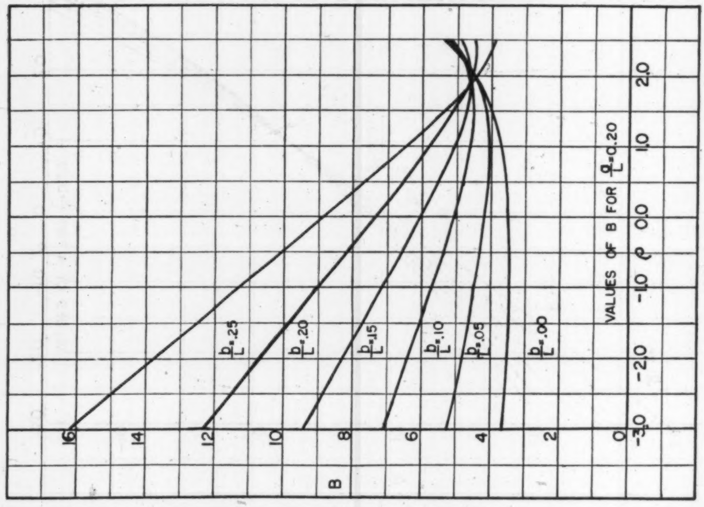
B
0
2
4
6
8
10
12
14
16
-3.0
-2.0
-1.0
0.0
1.0
2.0
$\frac{b}{L}$=.25
$\frac{b}{L}$=.20
$\frac{b}{L}$=.15
$\frac{b}{L}$=.10
$\frac{b}{L}$=.05
$\frac{b}{L}$=.00
ρ
VALUES OF B FOR $\frac{a}{L}$=0.20

FIG. 12

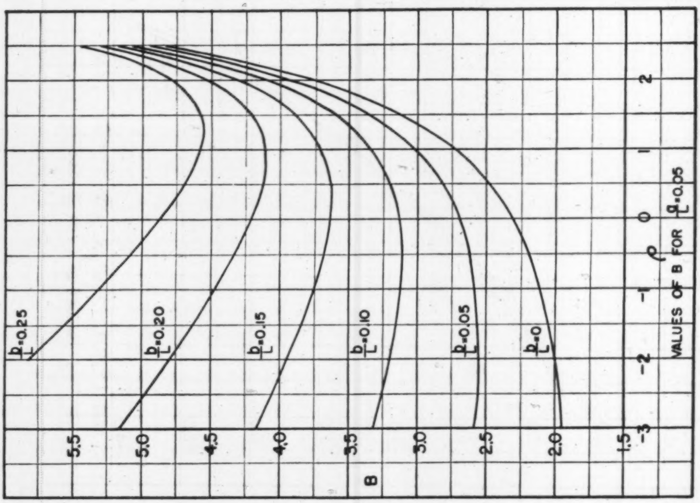
B
1.5
2.0
2.5
3.0
3.5
4.0
4.5
5.0
5.5
-3
-2
-1
0
1
2
$\frac{b}{L}$=0.25
$\frac{b}{L}$=0.20
$\frac{b}{L}$=0.15
$\frac{b}{L}$=0.10
$\frac{b}{L}$=0.05
$\frac{b}{L}$=0
ρ
VALUES OF B FOR $\frac{a}{L}$=0.05

FIG. 11

analysis of riveted trusses frequently is overlooked. When the secondary end moments become large, the rivet pattern which attaches the member to the gussets is subjected not only to an "axial" force in the longitudinal direction of the member but also to a significant shearing force acting in a direction perpendicular to the member and, further, to a moment about the effective centroid of the rivet pattern. The last two of these load components may have an appreciable effect on the resultant stress in the critical rivets.

CONCLUSIONS

Charts have been presented which give the slope-deflection constants for idealized members, consisting of a uniform middle part, plus two infinitely rigid end regions, under the action of axial load. These charts may be used in the secondary stress and stability analysis of gusset-connected trusses, if the actual members which include gussets of finite rigidity may be replaced, by some rational method, with idealized members. One simple rational method of replacement has been suggested. It is assumed that the truss is welded or, if riveted or bolted, the effects of slip can be neglected. This assumption may, in turn, require careful computation of the resultant rivet or bolt loads and friction forces.

The circumstances under which it is advisable or necessary to analyze for secondary stresses have been discussed elsewhere.[22] It is generally held that plastic flow, particularly under near-static load conditions, may be relied on to redistribute the critical stresses; and therefore it may be assumed that the secondary stresses do not reduce the strength of the structure. Discussion of this theory is beyond the scope of the present paper. Under repeated load and other fatigue conditions, however, the amplitude of the secondary stresses may be such as to cause local failure after a sufficient number of load repetitions. Also, although secondary stresses may become important in heavy bridge trusses composed of stiff members, the stiffness of these members usually will be such as to minimize the effect of the axial load on the flexural stiffness.

APPENDIX I. STIFFNESS FACTORS FOR A UNIFORM BAR

The bending moment at a distance x measured logitudinally from the end of a compressed bar that is subjected simultaneously to end couples M_1 and M_2 (see Fig. 13(a)) is

$$M = M_1 + P\,y - \frac{M_1 + M_2}{L}\,x.$$

Use of the well-known relation between the bending moment and the second derivative of the deflection leads to the following differential equation:

$$E\,I\,\frac{d^2y}{dx^2} + P\,y = -\,M_1 + \frac{M_1 + M_2}{L}\,x \quad\ldots\ldots\ldots\ldots\ldots(5)$$

---

[22] "Effect of Secondary Stresses Upon Ultimate Strength," by John I. Parcel and Eldred B. Murer, *Transactions*, ASCE, Vol. 101, 1936, pp. 289–343.

The particular solution of this equation that satisfies the conditions of zero displacement at the ends of the member is

$$y = \frac{M_1}{P}\cos p\,x - \frac{M_1 \cos p\,L + M_2}{P \sin p\,L}\sin p\,x - \frac{M_1}{P} + \frac{M_1 + M_2}{P\,L}\,x \quad\ldots(6)$$

in which

$$p = \sqrt{\frac{P}{E\,I}} \quad\ldots\ldots\ldots\ldots(7)$$

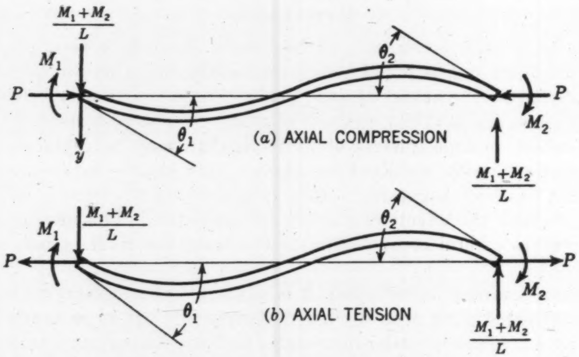
$\frac{M_1+M_2}{L}$
M_1
P
θ_2
P
M_2
θ_1
y
(a) AXIAL COMPRESSION
$\frac{M_1+M_2}{L}$
M_1
$\frac{M_1+M_2}{L}$
θ_2
P
P
M_2
θ_1
(b) AXIAL TENSION
$\frac{M_1+M_2}{L}$

FIG. 13.—BENDING OF A UNIFORM BAR RESISTING AXIAL LOAD AND END COUPLES

The general expression for the slope of the bar is

$$\frac{dy}{dx} = \frac{-M_1}{P}\,p \sin p\,x - \frac{M_1 \cos p\,L - M_2}{P \sin p\,L}\,p \sin p\,x + \frac{M_1 + M_2}{P\,L} \quad\ldots(8)$$

Evaluating Eq. 8, at $x = 0$ and at $x = L$, and denoting the respective values of the end slopes by θ_1 and θ_2,

$$\left.\begin{aligned} \theta_1 &= M_1 \frac{1}{L}\left(\frac{1}{P} - p \cot p\,L\right) + M_2\,\frac{1}{P}\left(\frac{1}{L} - p \csc p\,L\right) \\ \theta_2 &= M_1 \frac{1}{P}\left(\frac{1}{L} - p \csc p\,L\right) + M_2 \frac{1}{P}\left(\frac{1}{L} - p \cot p\,L\right) \end{aligned}\right\}\ldots\ldots(9)$$

The simultaneous solution of Eqs. 9 yields

$$M_1 = \frac{E\,I}{L}\left[\frac{\sin p\,L - p\,L \cos p\,L}{\frac{2}{p\,L}(1 - \cos p\,L) - \sin p\,L}\,\theta_1 - \frac{\sin p\,L - p\,L}{\frac{2}{p\,L}(1 - \cos p\,L) - \sin p\,L}\,\theta_2\right] \quad\ldots(10)$$

Eq. 10 may be written in the form:

$$M_1 = \frac{E\,I}{L}\left(A_0\,\theta_1 + B_0\,\theta_2\right) \quad\ldots\ldots\ldots(11)$$

in which A_0 and B_0 are the respective coefficients of θ_1 and θ_2 within the brackets of Eq. 10.

In a entirely analogous manner, a bar (see Fig. 13(*b*)) that is subjected simultaneously to end couples and to axial tension (that is, a negative axial load) satisfies the differential equation:

$$E\,I\,\frac{d^2y}{dx^2} - P\,y = -\,M_1 + \frac{M_1 + M_2}{L}\,x \qquad (12)$$

The particular solution of Eq. 12 that yields a value of $y = 0$ at $x = 0$ and at $x = L$ is

$$y = \frac{-\,M_1}{P}\cosh p\,x + \frac{M_1\cosh p\,L + M_2}{P\sinh p\,L}\sinh p\,x + \frac{M_1}{P} - \frac{M_1 + M_2}{P\,L}\,x \qquad (13)$$

Evaluating the slopes at the two ends of the bar, and solving the resulting simultaneous equations, yields

$$M_1 = \frac{E\,I}{L}\left[\frac{p\,L\cosh p\,L - \sinh p\,L}{\frac{2}{p\,L}(1 - \cosh p\,L) + \sinh p\,L}\,\theta_1 - \frac{p\,L - \sinh p\,L}{\frac{2}{p\,L}(1 - \cosh p\,L) + \sinh p\,L}\,\theta_2\right] \qquad (14)$$

which also may be written in the form of Eq. 11.

The coefficients A_0 and B_0 are clearly functions only of the parameter $p\,L$. However, by Eq. 7, $p\,L = L\sqrt{\frac{P}{E\,I}} = \pi\sqrt{\frac{P}{P_{cr}}}$ in which, P_{cr} is Euler's load, $\frac{\pi^2 E\,I}{L^2}$, for the equivalent pin-ended member. Thus, the coefficients A_0 and B_0 are functions of the single parameter $\rho = \frac{P}{P_{cr}}$.

APPENDIX II. MODIFICATION OF STIFFNESS FACTORS BY RIGID END PORTIONS

It is now assumed that the gusset regions are replaced by equivalent perfectly rigid end portions having lengths, *a* and *b*, respectively (see Fig. 14). The remaining part, *c*, of the total length of the member then may be assumed to be of uniform section.

For small deflections, the cosine of the local slope may be taken as unity. Consequently, the bending moments at the interior ends of the gussets, or at the ends of the clear length *c*, are

$$\left.\begin{aligned} M_a &= \frac{E\,I}{c}(A_0\,\theta_1 + B_0\,\theta_2) \\ M_b &= \frac{E\,I}{c}(B_0\,\theta_1 + A_0\,\theta_2) \end{aligned}\right\} \qquad (15)$$

in which A_0 and B_0 are the coefficients for the uniform member of length c and are therefore functions of the single parameter,

$$\rho = \frac{P\,c^2}{\pi^2\,E\,I} \qquad (16)$$

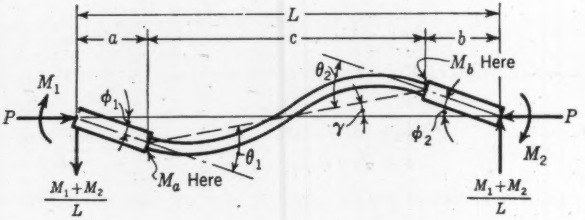

FIG. 14.—DISTORTION OF A MEMBER HAVING INFINITELY RIGID END PORTIONS

If M_1 and M_2 are the moments at the extreme ends of the member—that is, at the centers of rotation—then the moments M_a and M_b may be expressed in terms of the end moments and the axial load:

$$\left.\begin{aligned} M_a &= M_1 + P\,a\,\phi_1 - \frac{M_1 + M_2}{L}\,a \\ M_b &= M_2 + P\,b\,\phi_2 - \frac{M_1 + M_2}{L}\,b \end{aligned}\right\} \qquad (17)$$

The rotation, γ, of the uniform middle part of the beam is $\gamma = \frac{a\,\phi_1 + b\,\phi_2}{c}$. Therefore,

$$\left.\begin{aligned} \theta_1 &= \phi_1 + \gamma = \phi_1\left(1 + \frac{a}{c}\right) + \phi_2\,\frac{b}{c} \\ \theta_2 &= \phi_2 + \gamma = \phi_2\left(1 + \frac{b}{c}\right) + \phi_1\,\frac{a}{c} \end{aligned}\right\} \qquad (18)$$

Substituting Eqs. 17 and 18 into Eq. 15 yields two simultaneous equations in M_1 and M_2. The solution of these is

$$M_1 = \frac{E\,I}{c}\left(\frac{L}{c}\right)$$

$$\times\left[\begin{aligned} &\left\{\left[A_0\left(1+\frac{a}{c}\right)+B_0\frac{a}{c}-\frac{P\,c^2}{E\,I}\frac{a}{c}\right]\left(1-\frac{b}{L}\right)+\left[A_0\frac{a}{c}+B_0\left(1+\frac{a}{c}\right)\right]\left(\frac{a}{L}\right)\right\}\phi_1 \\ &+\left\{\left[A_0\frac{b}{c}+B_0\left(1+\frac{b}{c}\right)\right]\left(1-\frac{b}{L}\right)+\left[A_0\left(1+\frac{b}{c}\right)+B_0\frac{b}{c}-\frac{P\,c^2}{E\,I}\frac{b}{c}\right]\left(\frac{a}{L}\right)\right\}\phi_2 \end{aligned}\right]. \qquad (19)$$

and a similar expression for M_2.

It is seen that Eq. 19 may be written

$$M_1 = \frac{E\,I}{c}\,(A\,\phi_1 + B\,\phi_2)\ldots\ldots\ldots\ldots\ldots\ldots\ldots(20)$$

in which A and B are defined by Eq. 19 and are functions of (*a*) the coefficients A_0 and B_0 for the sublength c of the bar, (*b*) the geometric ratios $\frac{a}{L}$ and $\frac{b}{L}$, and (*c*) the parameter ρ, as defined by Eq. 16.

Values of A and B have been computed by Eqs. 15 through 20 and are presented in charts for a wide range of the parameters.

DISCUSSION

Leonard K. Stevens.[23]—The stiffness charts presented by the author are very useful in the elastic analysis of the behavior of rigid-jointed trusses.

Mr. Lundquist's method of stability analysis assumes that the members of a rigid-jointed truss remain straight and are centrally loaded up to the point of failure, at which point they suddenly buckle. In actuality, the end moments introduced by the joint translations resulting from the axial deformations of the members produce curvatures, and the strut is not straight at failure. However, the ultimate load capacity of an eccentrically loaded, elastic strut is not significantly less than when loaded centrally, although large lateral deflections may occur before the maximum load is reached. For this reason, it is considered that Mr. Lundquist's method of analysis gives reasonably accurate results. Experimental work has shown good agreement in the elastic range.

It is possible that the secondary stresses produced by the end moments may lead to combined stresses approaching the yield point of the material, even though the average axial stress is still within the elastic range. If the yield point is reached in a slender strut, the load capacity decreases rapidly. The determination of the secondary stresses in a stability analysis of a truss with struts having medium slenderness ratios is therefore very important—especially when the analysis indicates that the average axial stress for limiting stability is 70% or more of the yield-point stress.

Most structures have members in the medium-to-low slenderness-ratio range. The yield point of the material is the major factor in determining the ultimate loads. As Mr. Goldberg states, plastic flow can sometimes be relied on to redistribute the critical stresses. The action when yielding has commenced in a rigid-jointed truss has not been fully investigated. For a strut having a low slenderness ratio, the appearance of initial yielding does not necessarily indicate imminent collapse; in fact, the ultimate useful load capacity can be considerably higher. An exact secondary-stress analysis can determine the load at which initial yielding begins. This load will be the lower limit of the ultimate load capacity. The upper limit is fixed by the load producing an average stress equal to the yield stress. These limits enable the collapse load to be closely bracketed. It is in this respect that the charts presented offer a valuable aid to the analysis.

It is interesting to note the effect of rigid-gusset plates and axial load on the moments found in a secondary-stress analysis. Rigid-jointed trusses with gusset plates having a ratio of a/L equal to 0.125 and strut slenderness ratios of from 55 to 110 have been analyzed by the writer. Near the load at which yielding began, the joint moments were as much as 53% greater than the moments computed by the classical methods which ignored gusset lengths and axial load.

---

[23] Research Assistant, Civ. Eng. Dept., Univ. of Melbourne, Melbourne, Victoria, Australia.

John E. Goldberg,[24] **M. ASCE.**—Mr. Stevens' manifest interest in the stiffness charts which have been presented by the writer, and his informative and constructive comments are appreciated. His statements in support of the contention regarding the effect of gusset lengths and axial loads on the magnitude of the secondary stresses are gratifying. It is interesting and significant that Mr. Stevens, by using the stiffness charts, has found that the effect of gusset length and axial load can increase the secondary bending moments by as much as 53%, even in the case of trusses composed of members in the intermediate-slenderness range.

Mr. Stevens is entirely correct in his statement that

> "For a strut [in a rigid-jointed truss] having a low slenderness ratio, the appearance of initial yielding does not necessarily indicate imminent collapse, * * *. An exact secondary-stress analysis can determine the load at which initial yielding begins."

A rigidly connected truss is a highly redundant structure, and it appears to the writer that one can apply the limit-design concepts and can also invoke the general rule that a strut must develop three complete plastic zones before it will collapse.

---

[24] Associate Prof. of Structural Eng., Purdue Univ., Lafayette, Ind.

AMERICAN SOCIETY OF CIVIL ENGINEERS
Founded November 5, 1852
TRANSACTIONS

Paper No. 2658

ELECTRONIC DEVICES IN AIR TRANSPORT

By F. B. Lee[1]

With Discussion by Messrs. P. C. Sandretto, and F. B. Lee

Synopsis

Some of the aspects and implications of electronic devices used in air transport today, and those to be used in the immediate future, are treated in this paper. It is imperative for the groups interested in electronic navigation devices to exchange views with the groups interested in surveying, mapping, and charting, since navigation and charting are inseparably bound together. The development of the transportation and communications industries was made possible by the surveys, maps, and charts that preceded them. Conversely, those industries are placing increasing requirements on the mapping and charting industries to obtain more reliable charts and charts of extremely specialized natures.

An old map of the United States entitled "Standard Air Trail Maps" (presumably published in the late 1920's or the early 1930's) was essentially a record of the railroads, with major cities and towns served by them. Very meager terrain information was shown, and no radio information of any nature was indicated. The only navigation information, except for the old "iron compass" of the railroads, was the lines of magnetic variation. The reverse side of the chart contained matter explaining the use of the chart and information relating to air navigation. One statement on this old chart contained a lasting truth:

> "One of the important navigational instruments is an accurate air map; in fact, some of the other instruments of navigation are of value only as related to the map."

Concepts of navigation have changed greatly since the time of air trails maps which gave predominance to the railroads as a navigation device. Basic air navigation has progressed from the art of observing and recognizing objects on the ground with the unaided human eye to the art of observing position by

---

Note.—Published, essentially as printed here, in February, 1953, as *Proceedings-Separate No. 173.* Positions and titles given are those in effect when the paper or discussion was received for publication.

[1] Deputy Administrator for Operations, Civ. Aeronautics Administration, Washington, D. C.

reference to instruments in the cockpit. This change of emphasis has been caused by the development of electronic devices for air navigation. This development has only begun, and future developments cannot be foreseen. Therefore, the writer will discuss only those devices which are either available and in service or which are planned to be placed into service in the very near future.

The electronic devices used in the operation of aircraft, both in the cockpit and on the ground, by the government—by scheduled and other civil aircraft operators—are of such great quantity and variety that mere designation and description would consume considerable time. The devices used in air navigation are relatively few but are of tremendous importance to the welfare and security of the United States. The U. S. Armed Forces depend heavily on air transportation for the prompt and efficient movement of men and material. Schedule reliability is important to both the military and the civilian activities. In case of war, the ability to move bombers, fighters, and military transport aircraft in large numbers, regardless of weather, would be critical to the national defense. An air navigation system which will bring with it a higher degree of scheduled air carrier dependability and reliability would be extremely beneficial to the economy of the United States and could be measured in substantially increased passenger and cargo business. Manufacturers of private aircraft will reap benefits from any air navigation devices that will increase the use of small aircraft for business and pleasure.

The Civil Aeronautics Administration (CAA) is engaged in providing the ground facilities to be used in an air navigation system that has the attributes of the system just described. It was developed by the aviation industry itself including civil and military govermental, commercial, and private aviation interests. The name "common system" was chosen because there must be one system of air navigation and traffic control to be used in common by all aviation—civil and military—in the United States.

The "common system" was formally conceived in 1947 when the Radio Technical Commission for Aeronautics established Special Committee No. 31 to undertake a study for the purpose of developing recommendations for the control of expanding air traffic. That committee was composed of government agencies, aviation trade associations, radio manufacturers, airline pilot organizations, and others interested in, and connected with, aviation.

The committee reviewed and recognized the individual problems peculiar to specialized aviation operations, such as those of the scheduled airlines, military air transport, and other nontactical services, as well as the problem of commercial and private aircraft operators. The needs and requirements of all groups were studied, and a report was produced, accepted by government and industry, and adopted as a guide in the implementation and further development of the "common system" for the common good. Shortly thereafter, the Air Navigation Development Board (composed of representatives of the departments of Commerce and Defense who are specifically represented by the CAA, the Air Force, and the Army and Navy, with a chairman from industry) was created to guide and supervise the development of the electronic devices needed to implement the report of Special Committee No. 31 (RTCA-SC-31). In addition, the Air Coordinating Committee established an Air Navigation and

Traffic Control Panel (ANTCP) and charged it with the responsibility for developing the operational requirements for aids to air navigation and traffic control. This panel consists of government agencies (military and civil), representatives of the aviation industry, and private citizens responsible for the implementation of the "common system" or concerned with the use of the federal airways. Thus, the users of the air space have an active voice in molding the future character of the airways system.

The operational requirements developed by the ANTCP are forwarded to the Air Navigation Development Board which, guided by the requirements, formulates a unified program for research on, and development of, aids for the "common system." After an aid has been developed by the board, the specifications for the aid are presented to the implementing agencies. Under this system, the CAA has the responsibility to plan, install, and operate the ground aids required for the "common system" and to advise the users of the air space regarding airborne equipment.

In January, 1950, the ANTCP established an operational policy group to review the RTCA-SC-31 report and all other papers dealing with the "common system." This group was authorized to review and evaluate all information and materials pertaining to present and anticipated operational policies and procedures; it formulates programs for equipment development and makes reports and recommendations accordingly; and it was charged with taking into account the needs of the national defense and special problems of the users of the air space. The group was composed of representatives of the government, air transport and airline pilot organizations, airport operators, and others. Its report[2] deals with the immediate future and contains the latest industry-wide thinking with respect to the "common system." The major electronic devices specified in the report which are related to air navigation and charting are especially timely.

The special working group report deals primarily with the "transition program," or a program that will raise aviation from its World War II status to the "common system" plane. Basically, the transition program (1) converts the navigation system to a new system which provides the pilot with continuous information as to his position in space; (2) utilizes radar as a traffic-control facility in congested terminal areas; (3) provides direct communications between the pilot and the air route traffic controllers; and (4) utilizes electronic and electro-mechanical techniques for the display and relaying of information.

The basic facility in the transition air navigation system is the very-high-frequency omni-directional radio range which will replace the low and medium frequency four-course radio ranges that have been in use since the 1930's.

The omni-range, as its name implies, provides an infinite number of tracks radiating from the transmitting site. For convenience, each omni-range is considered to have 360 tracks (of 1° width) which are designated as "radials" in magnetic degrees from the station. The omni-range operates in a very-high-frequency spectrum between 112 and 118 megacycles. The radio characteristics of that frequency band are such that the omni-range is virtually static free but, at the same time, its propagation is limited to radio line-of-sight which is only slightly greater than optical line-of-sight. In general, the omni-range may be received at a distance of 30 miles at 500 ft above the ground station, 45 miles at 1,000 ft, with this reception distance increasing to 200 miles at 20,000 ft.

---

[2] "Air Traffic Control and the National Security;" Report of the Operational Policy Group of the Air Traffic Control and Navigation Panel, December, 1950, U. S. Govt. Printing Office, Washington, D. C.

Inasmuch as the normal minimum altitude of aircraft operating on instruments is 1,000 ft above the terrain in nonmountainous areas and 2,000 ft above the terrain in mountainous areas, an area coverage of 45-mile radius is normally expected at minimum instrument altitudes.

The omni-range imposes some requirements on the airborne receiving system that were not present under the old low-frequency system in that the function of interpretation is transferred from the pilot to the electronic equipment in the new "common system." Under the old system, the airborne receiver picked up the ground signal, and the pilot detected courses and quadrants through discrimination of the relative signal strength of the Morse code characters *A* and *N*. The omni-directional receiver itself detects and interprets the course signals produced by the ground equipment and displays them visually to the pilot. The pilot is thus relieved of the monotonous task of listening continually to air navigation signal information and now merely needs to glance at an indicator to learn whether he is flying to or from the range station and whether his magnetic bearing is to or from the station.

Distance-measuring equipment (DME) has been developed to furnish additional safety and convenience, inasmuch as this equipment continuously informs the pilot of distance from the ground station. The distance-measuring equipment utilizes radar pulse techniques to measure the time interval for radar pulse travel from the aircraft to the ground equipment and return to the aircraft. Since the radar pulses travel at the uniform velocity of light, or 186,000 miles per sec, it is a relatively simple matter for the distance-measuring equipment to convert the time intervals into distances and display those distances in the cockpit on a meter graduated in miles. Thus, a pilot with equipment will know, continually and accurately, his distance and direction from the ground equipments located at fixed geographical points and, therefore, can determine his position in space accurately.

The development of an additional piece of electronic gear, the course line computer, has been coordinated with the development of the omni-range and distances-measuring equipment. This computer—an airborne electronic device—makes it unnecessary to fly directly to or from an omni-range because, with it, a pilot can fly a straight course between any two selected points covered by omni-range and DME signals. The computer using intelligence received from the omni-range and DME continuously solves the specific trigonometric problems involved in presenting information with respect to preselected courses and relieves the pilot of the burden of piloting and solving these navigational problems.

A further refinement of an electronic device to use information transmitted by omni-range and DME is the pictorial computer. Various pictorial computers are being developed, but essentially all of them receive azimuth information from an omni-range and distance information from DME, and portray this intelligence on a chart as a moving marker which corresponds accurately to the position of the aircraft over the surface of the earth. These computers vary in size and complexity from a small lap model, in which the pilot manually inserts paper charts and information desired and observes his progress by watching a simple "crab" crawling over the chart, to more complex devices which may be mounted in instrument panels and which will project the proper chart and position of his aircraft thereon merely by turning in the appropriate ground station. Research studies conducted by the CAA indicate the possibility of navigating, with an ease and simplicity never before thought possible, by using pictorial display.

The omni-range and DME, with their various airborne receiving and interpreting devices, are basically provided for en route or point-to-point navigation and are generally not considered to be suitable as precision approach aids. However, recent experiments and tests by the CAA have indicated that, although the omni-range may not be regarded as a precision approach aid, it offers more accuracy, reliability under atmospheric static conditions, ease of operation, and orientation than any low-frequency or medium-frequency aid currently used for making instrument approaches. Thus, the omni-range can serve two functions—(*a*) it is a means of providing en route guidance and (*b*) it is an adequate instrument approach device at those locations where density of traffic does not justify a precision approach aid.

The "common system" has within it two electronic devices for making precision instrument approaches during adverse weather conditions—the instrument landing system and precision approach radar. The two may be used separately, but the best results are obtained when both are considered and used as complementary facilities.

The instrument landing system (ILS) uses ground transmitters located at the airport to project two radial beams into space. One beam, called the "localizer," is directed down the runway into the approach zone. It provides lateral guidance to aircraft approaching the airport, keeping them on an electronic track over the runway center line, extended. The second beam, called the "glide path," controls the plane's rate of descent and angle of approach in the vertical plane. The pilot making an ILS approach watches a cross-pointer indicator in the cockpit and controls his course of flight by reference to these indicators. The use of the instrument landing system requires that the aircraft be equipped with a specialized receiver which will intercept and interpret the localizer and glide path signals and display them in convenient visual form to the pilot.

The precision approach radar is simpler to operate in so far as the pilot is concerned because no specialized receiver is required and the pilot merely follows the instructions issued to him from the ground controller in making an approach to the runway. The ground controller watches the aircraft on two radar scopes, one of which gives him the distance and the azimuth of the aircraft with respect to the touchdown point on the runway, and the other provides him with information on height or angle of elevation. Thus the controller follows the movement of the aircraft in the approach zone and directs the pilot down to the runway by transmitting instructions over the radio telephone. Precision approach radar provides a means whereby a partly equipped aircraft may make an approach to an airport in a congested terminal area.

The CAA supplies both an instrument landing system and precision approach radar at the dense traffic airports which constitute the safest and surest landing method known. In general, aircraft equipped with ILS facilities employ those facilities in making the approach, and the CAA personnel monitor guides the aircraft on its approach with precision approach radar. Thus, two functionally different and independent electronic instrument landing devices are used as a double check to provide the highest possible safety for the users of federal airways.

The CAA is providing additional radar facilities to act as the eyes of the airport traffic controllers during periods of restricted visibility. These facilities are designated as airport surveillance radar (or ASR), and they show the controller, on a plan-position indicator, the location of all aircraft within 30 miles of the terminal. The ASR serves several general purposes in addition to the obvious one of reducing collision hazards. It is used to guide aircraft to positions where the precision approach radar can pick them up and pilot them down to safe landings, or to "vector" departing aircraft direct to their en route airway, thus greatly reducing departure delays. The ASR is also used to "vector" or "monitor" aircraft proceeding through the terminal area when necessary because of congestion. This facility introduces another strong element of certainty by ground monitoring, by revealing the direction of aircraft operating in reduced visibility, and by providing flexibility of routes in the terminal area.

The identification of aircraft by radar is somewhat laborious and time consuming, unless additional aids are used. One of the ground aids available for, and suitable to, this purpose is (very-high-frequency) automatic direction finding equipment used in association with airport surveillance radar. This equipment provides the controller with a visual means of identifying aircraft in voice contact with the controller. When the pilot presses his microphone button, a radial line appears on the radar scope bisecting the "pip" on the radar representing his aircraft. An airborne radar safety beacon provides an immediate means of identifying a radar target and greatly increases the range and the usefulness of the radar. In addition to the transition program of the "common system" used by the pilots, the ground personnel require a large number of electronic devices to be used behind the scenes to handle a large volume of high-speed aircraft. Some of these devices include automatic air-traffic-control plotting displays, remote radar displays for long-range radar, mechanical interlock units to expedite the exchange of information relating to the status of air traffic at specific locations, automatic relay and display of aircraft movement messages, high-speed communication networks interconnecting the air traffic centers, and other similar devices. Some of these devices are now in partial or experimental use and others are only in the developmental stage. Added together, they promise safety, efficiency, and reliability in the air transport field which will insure the dominance of the United States in the aviation field and will further integrate air transportation as a part of the economy and daily life in this country. The effect of this program is being reflected in the steadily increasing volume of instrument flying in the United States, the increasing efficiency of the air-traffic-control system, the increasing reliability of scheduled air carriers, and the sureness with which the military can perform their missions.

Some of the foregoing equipment is expensive and complicated, and it requires relatively large ground forces to operate and maintain. The CAA must weigh the needs of air traffic against the cost of providing facilities that will offer complete reliability, essentially, under all weather conditions at all airports. Literally, billions of dollars would be involved if the federal government undertook an ambitious program of providing all-weather operations at all airports. Hundreds of millions of dollars would be involved if the CAA contemplated a program of installing at each airport served by a scheduled air carrier the aids that would permit the degree of all-weather operation that is now technically feasible. Realizing that programs of such magnitude are economically impractical, the CAA has carefully analyzed the needs and requirements of air traffic, and it has developed a program that will benefit the most people—one that can be implemented within the bounds of economic justification.

Traditionally, the CAA has established air navigation facilities to meet the operational needs indicated by the total volume of air traffic existing at the time the facility was established. Other factors, such as prevailing weather conditions, the mixed operation of various classes of aircraft, the proximity of other airports, and the pecularities of the geographical location have been taken into account.

As air traffic continues to increase, the problem of planning for adequate air traffic control, communications, airports, and air navigation aids becomes increasingly complex. Implementation can no longer be planned to meet all operational requirements without giving increased emphasis to the economic questions involved. Implementation plans must meet those operational needs that reflect an optimum return in terms of service rendered within the bounds of the national economic structure. This is not a compromise between safety and economics, but a realistic endeavor to provide maximum safety and reliability within available means. Since safety must not, and cannot, be compromised, aeronautical activity in areas not having complete facilities must be limited to meet required safety standards.

The search for an answer to the question of the extent to which the CAA may reasonably and profitably provide the modern electronic devices called for under the "common system" has led to intensive studies of air commerce and civil aviation in general. The studies are providing a firm and solid foundation for building an electronic system that is economically sound, in addition to being technically superior to any other system in common use in the world today.

The findings of these studies are neither startling nor new. In their simplest form, they merely reveal that the distribution and concentration of population within the continental United States establish the pattern and control the apportionment of air transportation in, and between, the communities. It is said that a community's population, size, and its economic character fix its volume of terminal air commerce. Furthermore, the flow of air transportation between pairs of communities varies directly with the size of their population product, and inversely with the distance between them when allowance is made for such secondary factors as differences in the air-surface-distance ratio, the minimum effective distance for present day aircraft, the economic character of each community in a pair, and the density of communities within a geographic area.

The population of a community is obviously a fundamental factor in determining its volume of air traffic, since air transportation is the movement of people and things from one place to another. However, the population is not the sole factor, inasmuch as places in the same size group do not generate equivalent volumes of air traffic. Variations in the air traffic of communities within the same size group are associated with differences in their economic character, or the manner in which the economic livelihood of the community is achieved.

The volume of air passengers or aircraft operations in a community is not due to chance but is fixed by the community's population and economic character in the same way as are retail sales, automobile registrations, and trade outlets. Studies of air commerce from 1940 through 1950 show a high degree of correlation through the years, and thus provide a basis for making reasonable forecasts of a community's air transportation volume and, hence, its requirements for aviation facilities.

The 1950 census reveals that there are 4,720 urban places in the United States with a population of 2,500 or more. Of these 4,720 urban places, only 320 of them had a population of 25,000 or more. These 320 places account for 93% of the urban population and 59.3% of the total population of the United States; they are the focal points for the nation's entire economic system.

The civil aviation pattern follows the concentration of population. Some of the significant findings in this area reveal that 93% of all passengers, 95% of the air mail, and 96% of the air cargo originated at the top 126 of the approximately 500 communities served by the scheduled air carriers. The 139 communities of less than 10,000 population generated less than 2% of the passengers, less than 1% of the mail, and less than 0.5% of the cargo; but, they required more than 7% of the air carriers take-off and landing operations to glean this small revenue. The conclusions are that air commerce is concentrated in the large metropolitan areas and that the small cities played relatively unimportant roles in the field of air transportation.

A study of the airline passenger pattern reveals that the volume of traffic between a pair of communities is controlled by factors affecting both the communities rather than by factors affecting only one of the communities. The definition of air transportation establishes the population of communities in a pair as one of the primary factors affecting passenger flow. The combined effect of the population could be stated as either the sum or the product of the population of the two communities. The population product has been selected as the correct measurement of the combined effect of the population of the two communities in a pair because it takes into account the relative size of both places. Substantial airline passenger traffic occurs only between series of communities having large population products.

The location of the large standard metropolitan areas, particularly the ones with a population of one million or more, determines the basic airline passenger pattern in the United States. The pattern can be likened to a series of wheels, the hubs of which are communities like New York, N. Y., Chicago, Ill., Los Angeles, Calif., Washington, D. C., and San Francisco, Calif., which are connected by "wheel spokes" to lesser "hubs" and "rim" points. High-density traffic moves between hubs, and there is a significant volume that occurs between a hub and a rim point. The volume of passengers for pairs in small cities is relatively unimportant.

In general, civil aviation follows essentially the same pattern of concentration in the large communities as do scheduled air carrier operations. One of the best indicators of general aviation activity is the civil aircraft population in a community. A study of the civil aircraft population indicates that the average number of civil aircraft registered in the large metropolitan areas is three hundred and this average dwindles to forty for the independent cities. Of the 3,000 locations with one or more civil aircraft as of January 1, 1950, nearly one half of them had less than ten aircraft and only fifty eight had more than two hundred.

The number of civil itinerant operations was measured and it was found that the large metropolitan districts averaged 22,500 operations annually, as compared with 7,500 operations with the independent cities.

A study of instrument approaches executed in 1950 indicated that the large metropolitan districts averaged 1,850 approaches annually, 1,500 of which were air carrier, 150 civil, and 200 military, whereas the smaller independent cities averaged 420 approaches, 350 of which were air carrier.

This knowledge about the economic demand for air transportation by the community has been related to the requirements for the "common system" electronic aids. The CAA has examined the benefits to be produced by each of these aids and has established criteria that specify whether or not a given community has sufficient civil aviation activities to qualify for the particular aids.

A specific example is the criteria for the establishment of a CAA airport traffic control tower. The more important ones included:

(1) The number of domestic enplaned passengers,
(2) The tons of domestic air mail dispatched,
(3) The tons of domestic enplaned air cargo,
(4) The number of domestic air carrier departures,
(5) The number of civil aircraft,
(6) The number of civil and military operations, and
(7) The number of itinerant operations.

Any one could have been selected as they have substantially the same community pattern. Air carrier operations were selected because they are most directly related to the primary function of a CAA airport traffic control tower—that is, the traffic control of interstate aircraft operations.

It would be desirable to have a tower at every airport if cost were not a factor. In order to provide maximum benefits with minimum costs, it was determined that airport traffic control service would be justified at airports having 7,000 or more annual scheduled operations, or at airports generating 4,000 scheduled operations annually if other classes of traffic are high enough in volume to qualify on the basis of a traffic count formula. Other exceptions may be made where peculiar or exceptional circumstances warrant.

Criteria for all other aids have been developed on a similar basis. The number of aircraft operations, or traffic density, governs the degree and type of service the CAA will provide at each location. Criteria, programs, and civil aviation requirements are reviewed continuously in order to provide the flying public with maximum benefits of the new electronic miracles at a price that can be afforded by the national economy.

DISCUSSION

P. C. Sandretto.[3]—World War II ended in 1945, and in 1946 the population of the United States began to think seriously of peaceful living. The airlines had been operating with every aircraft filled to capacity with passengers and cargo. A large percentage of airline passengers were military personnel until 1946, when the public began to fly the airlines and found that the airlines continued to have not only accidents but also long periods of waiting as the aircraft circled the major air terminals. Immediately, there were protests from all persons concerned. Three magazines carried articles concerning navigational facilities.[4,5,6] The House of Representatives, United States Congress, held hearings to investigate what was wrong with air-transportation aids and air-navigation aids, and the report of that investigation committee was published in July, 1947.[7]

Many of the articles and investigations criticized the proposed CAA navigation program. The CAA had begun, in 1936, the development of very-high-frequency navigation facilities and instrument low-approach systems. On its small budget it had worked diligently through the years to produce better aids to replace those which had been designed in 1927. The CAA was prepared to install new aids when World War II began. There had been approximately six fixed-beam approach systems installed in various major terminals in the United States, and a line of very-high-frequency radio ranges was operating between Salt Lake City, Utah, and Los Angeles. During World War II the CAA did not have access to the classified systems used by the military. The CAA did, however, continue to improve the very-high-frequency range and the fixed-beam approach systems. When the end of the war came the CAA program had been formulated. Many of the accusations made at that time were that the CAA's program was not "modern" because it did not include radar devices. The CAA engineers may not have been well acquainted with the radar developments, but, similarly, many radar designers were equally unfamiliar with civil aviation, its high standards of safety, and low cost, which are necessary in civil air operations.

The confused reports reaching the federal government impeded progress on the implementation of an air-navigational aid program in 1946 and 1947. Credit should go to Delos W. Rentzel for convincing the federal government that the RTCA-SC-31 should be given the opportunity to resolve these differences of opinion. The RTCA-SC-31 did its work in two phases—the first phase (completed in twelve meetings and under the chairmanship of Col. J. B. Duckworth, United States Air Force) determined the operational requirements.

---

[3] Brig. Gen., USAFR, Asst. Technical Director, Federal Telecommunication Labs., Inc. Nutley, N. J.

[4] "What's Wrong With the Airlines?", *Fortune*, August, 1946.

[5] "Is the Air Full?" *Harper's*, July, 1946.

[6] "For Landings Sake," *Collier's*, January 3, 1948.

[7] "Safety in Air Navigation," by John H. Frederick, Committee on Interstate and Foreign Commerce, House of Representatives, U. S. Cong., Washington, D. C., July 24, 1947, p. 21.

The second phase (under the chairmanship of Capt. A. S. Born, United States Navy, meeting almost continuously from October, 1947, to February, 1948) took the operational requirements of phase one and established the programs referred to as the "common system."

The RTCA-SC-31 began work by examining the aids that had been developed by the CAA. The committee did not find that the developments made by the CAA should be discarded but, on the contrary, concluded that these equipments formed the backbone of the only system which was ready to be installed. Through the many newly-proposed systems presented before the committee, it was evident that the CAA devices did not constitute the optimum design which could be produced by utilizing the best of the war-developed techniques. However, it was equally evident that they constituted completely workable, usable, and practical equipments which would go a long way toward improving air operations in the United States. The committee next investigated what improvement to the system would result by adding some of the devices developed during World War II. These devices were GCA (ground control approach)-radar low-approach system, surveillance radar, very-high-frequency direction finders, responder beacons, and distance measuring equipment. Distance measurement, by the use of pulse techniques had become common during the war, but the equipment the RTCA-SC-31 specified was to be a new development. After outlining a system based on the equipment described by Mr. Lee (eventually known as the "interim program"), it was found to have a factor of merit of 67%. This rating is recorded in the final report.

In spite of many weeks of debate, unanimous agreement on the installation of the interim system was impossible, so the committee spent a number of months developing the ultimate system. The ultimate system offered a coordinated program and, among other features, specified air-borne navigational equipment[8] which would weigh 20 lb, have an azimuth accuracy of $\frac{1}{2}°$, have a distance accuracy of 0.2 mile, and provide for instrument landings and other services. With promises that the ultimate system could be realized within fifteen years, the recalcitrant members of the RTCA-SC-31 agreed to the interim program and the final report was issued.

Since this RTCA-SC-31 meeting, the CAA has pursued the interim program. This group is to be commended for the manner in which it has attempted to carry out the recommendations of the RTCA-SC-31 which have, in fact, no official standing. The RTCA-SC-31 report stopped all criticism and brought together the various persons interested in aeronautical navigational aids. However, it is necessary to examine the "ultimate" program.

It is felt that Americans do things rapidly, but the history of air navigation does not bear this out. Aircraft are still flying the four-course radio range that was first applied to the airways in 1927. The instrument landing system[9] devised by H. Diamond and S. W. Dunmore (1928) was first used in Europe in modified form. World War II interrupted the work, and in the United States commercial carriers did not make operational-instrument very-low approaches until 1947—twenty years after their original development. Navigational programs cannot be executed on the spur of the moment, but require years of solid effort.

---

[8] "Air Traffic Control," Special Committee 31, Radio Technical Commission for Aeronautics, Washington, D. C., May 12, 1948, pp. 55–58.

[9] "A Radio Beacon and Receiving System for Blind Landing of Aircraft," *Proceedings*, Inst. of Radio Engrs., Vol. 19, April, 1931.

Mr. Lee outlined the economic questions involved in the installation of further radio aids, therein suggesting that the interim system must be used beyond the fifteen-year period which the RTCA-SC-31 envisioned. The interim program is satisfactory for today's (1953) needs, but will confusion once again force remedial action? The RTCA-SC-31 attempted to exercise foresight by planning a program fifteen years in advance, known as the ultimate system which "sold" the common system to the operating air agencies of the United States. If there is delay in effecting the program for the ultimate system, it can be envisioned that the "air that is full" again places limitations on air operations and national security.

F. B. Lee[10].—The excellent discussion by General Sandretto shows a keen insight into the major problems facing the federal government in providing air navigation and traffic control facilities and services. There must be continuous research, development, and planning to enable the air navigation and traffic control services to keep ahead of the requirements of the aviation industry. General Sandretto summarized the problem succinctly when he asserted that "* * * navigational programs cannot be executed on the spur of the moment, but require years of solid effort."

It is the intent of the CAA, and all those working with navigational systems, to meet the ultimate requirements of the users of the common system of air navigation and to maintain the high standards of safety and low cost essential to the development of aviation.

---

[10] Administrator of Civ. Aeronautics, Civ. Aeronautics Administration, Washington, D. C.

AMERICAN SOCIETY OF CIVIL ENGINEERS
Founded November 5, 1852
TRANSACTIONS

Paper No. 2659

DAM MODIFICATIONS CHECKED BY HYDRAULIC MODELS

BY E. S. HARRISON[1] AND CARL E. KINDSVATER,[2]
MEMBERS, ASCE

WITH DISCUSSION BY MESSRS. G. H. HICKOX; AND E. S. HARRISON AND CARL E. KINDSVATER

SYNOPSIS

Reconsideration of the maximum design flood, and a review of the stability analyses for the 25-year-old Bartlett's Ferry Dam, on the Chattahoochee River near Columbus, Ga., showed that the dam was deficient in freeboard and stability. Furthermore, a review of assumptions made for the original design indicated that, with the reservoir at normal pool level or above, the concrete spillway section was probably subject to tensile stresses. Field measurements also showed that high uplift pressures existed within the dam. Measures undertaken to remedy these conditions are described herein. Structural modifications, which were completed in 1950, included the installation of drains, the raising and strengthening of the non-overflow sections of the dam, and the addition of prestressed, reinforced concrete buttresses to the spillway section. Questions regarding the effect of the latter modification on the hydraulics of spillway operation called for extensive hydraulic model studies. Models were used also to obtain information pertinent to the structural design of the buttresses and certain appurtenances. Results of the uplift measurements, a description of the structural modifications to the dam, and a discussion of the model tests are given in this paper.

DESIGN FLOOD AND STABILITY INVESTIGATIONS

The investigation reported in this paper was started in 1946, when a power company in Georgia initiated studies to determine the adequacy of spillway capacity and the structural stability of eight of its major dams. These dams

---

NOTE.—Published, essentially as printed here, in April, 1953, as *Proceedings-Separate No. 184*. Positions and titles given are those in effect when the paper or discussion was received for publication.

[1] Hydr. Engr., Georgia Power Co., Atlanta, Ga.

[2] Prof. of Civ. Eng., Georgia Inst. of Technology, Atlanta, Ga.

were designed and built between 1900 and 1926, at which time rainfall and flood-flow data were meager. Longer hydrologic records show, for most sections of the United States, rainfall and flood flows much larger than those shown by records available at the time the dams were built. Later methods of analysis applied to the long-term records resulted in greater design floods than those used in the original designs. Thus, in reviewing the hydrology of these projects, the power company sought to determine the adequacy of the dams in the light of the greater storms that have occurred since their construction. Only those storms experienced east of the Mississippi River were considered.

Of the eight dams, only Bartlett's Ferry Dam, near Columbus, Ga., was shown to require remedial measures. Here, a revised design flood resulted in a calculated reservoir level which would reach the top of the earth non-overflow sections. Stability computations based on modern practice also indicated that the spillway section should be strengthened to provide adequate safety. Furthermore, observations in the field indicated that excessive uplift pressures existed in this section of the dam. It was apparent that immediate remedial measures were needed.

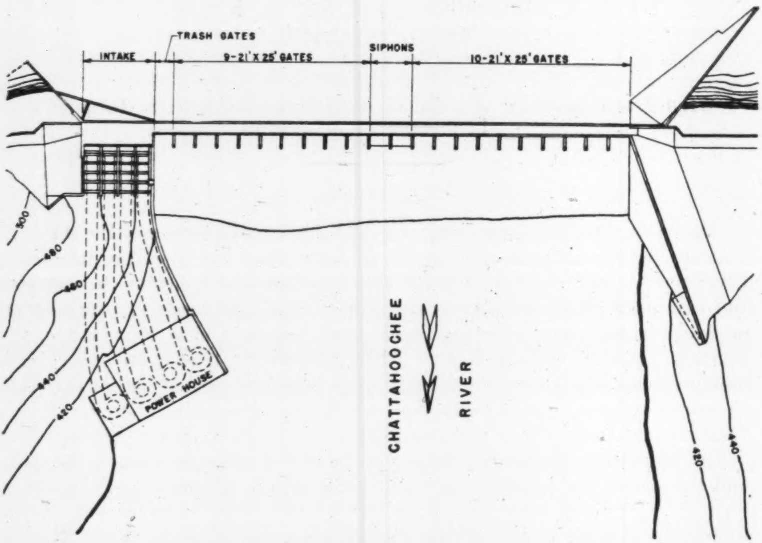

Fig. 1.—General Plan of the Original Structure, Bartlett's Ferry Dam Near Columbus, Ga.

Description of Bartlett's Ferry Dam

Bartlett's Ferry Dam was built in 1925, and was purchased by a power company in 1929. It consists of a concrete gravity spillway section, a concrete intake section, and two earthfill abutments. The maximum height of the spillway section, measured from the river bed to the normal pool level, is approximately 140 ft. A plan of the development is shown in Fig. 1. This dam is described in greater detail elsewhere.[3,4,5,6]

Fig. 2 shows a cross section of the spillway of the dam as originally built. This figure also illustrates the uplift assumption used in the original design. It was assumed that the uplift would vary from two thirds of full headwater at the upstream face of the dam to no uplift at the longitudinal drain, which was 15 ft downstream from the reservoir. No allowance was made for the uplift within the body of the dam. Below El. 400, as illustrated in Fig. 2, base widths used in the design were increased by including a part of the spillway bucket. These increased widths were based on an assumed change in slope beginning at El. 400. Because of the latter assumption in the original design, and because no allowance was made for uplift above the foundation line, review computations which included uplift indicated that the critical plane from the standpoint of stability was at El. 400. Here, assuming a 50% uplift, the calculated stress at the upstream face was approximately 27 lb per sq in. tension. This stress value is based on the assumption that the reservoir would be at normal level, El. 521, which corresponds to the elevation of the top of the spillway gates.

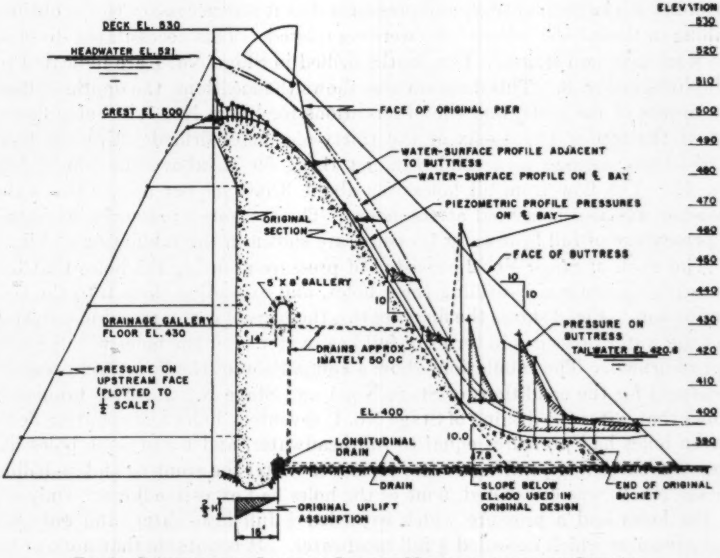
ELEVATION
530
520
510
500
490
480
470
460
450
440
430
420
410
400
390
DECK EL. 530
HEADWATER EL. 521
CREST EL. 500
FACE OF ORIGINAL PIER
WATER-SURFACE PROFILE ADJACENT TO BUTTRESS
WATER-SURFACE PROFILE ON ℄ BAY
PIEZOMETRIC PROFILE PRESSURES ON ℄ BAY
ORIGINAL SECTION
FACE OF BUTTRESS
10
10
5'X 8' GALLERY
10
6
DRAINAGE GALLERY FLOOR EL. 430
14'
4'
DRAINS APPROXIMATELY 50' OC
PRESSURE ON BUTTRESS
TAILWATER EL. 420.6
PRESSURE ON UPSTREAM FACE (PLOTTED TO ½ SCALE)
EL. 400
10.0
7.8
LONGITUDINAL DRAIN
DRAIN
SLOPE BELOW EL. 400 USED IN ORIGINAL DESIGN
END OF ORIGINAL BUCKET
⅔H
ORIGINAL UPLIFT ASSUMPTION
15'

FIG. 2.—SECTION OF THE SPILLWAY, SHOWING MODIFICATIONS TO THE ORIGINAL STRUCTURE AND PIEZOMETRIC PROFILES FOR THE MODIFIED SECTION

---

[3] "Water Power Engineering," by H. K. Barrows, McGraw-Hill Book Co., Inc., New York, N. Y., 1943, p. 524

[4] *Ibid.*, p. 536

[5] *Ibid.*, pp. 744–748.

[6] "The Bartlett's Ferry Hydroelectric Development," by H. A. Hageman and T. B. Parker, *Journal*, Boston Soc. of Civ. Engrs., March, 1926, pp. 93–125.

Because there was every reason to believe that uplift water pressures existed in the concrete dam above the rock line, immediate steps were taken to relieve this pressure as much as possible. Diamond drill holes of 3-in. diameter were drilled from the drainage gallery, at El. 430, into the rock foundation. The purpose of these drill holes was to relieve the existing internal water pressure, and, also, to determine, if possible, what the existing water pressures were. The internal water pressure conditions revealed by these holes were unusual.

UPLIFT PRESSURES IN THE SPILLWAY SECTION

Thirty-one 3-in. drain holes were drilled vertically downward from the gallery in the spillway section of the dam. In fifteen of the holes, the drill struck water in such large quantities and pressures that it was necessary to discontinue drilling in these holes before they were completed. This necessitated dividing the work into two stages. The depths drilled in Stage No. 1 are indicated by solid lines in Fig. 3. This diagram also shows the locations, the depths drilled, the results of the tests, and the observations for Stage No. 1. Water flowed out of the top of twenty-six of the thirty-one holes drilled. Upward flows varied from seepage to a solid 3-in. jet rising 59 in. above the top of hole No. 52. The flow from all holes was about 3,400 gal per min. The water pressure was also measured at the holes. The measured pressures, expressed in percentage of full headwater pressure, are shown in the tabulation of Fig. 3.

The work of Stage No. 2 consisted of pressure-grouting the holes that had excessive discharges, re-drilling these holes, and extending them into the rock foundation. Fig. 3 shows the final depths, the bags of cement used in grouting, and the water pressures in terms of full headwater after the holes were grouted and re-drilled. The tabulations show a comparison of the flows and pressures measured for the conditions of Stage No. 1 and Stage No. 2. This tabulation shows that, after the drilling of Stage No. 1, seventeen holes had spouting flows, eleven holes had pressures equal to full headwater, and twenty-one holes had pressures exceeding $\frac{1}{2}$ full headwater pressure. After the grouting and re-drilling (Stage No. 2) was completed, none of the holes had excessive flows. Only one of the holes had a pressure which exceeded $\frac{1}{2}$ full headwater, and only five had pressures which exceeded $\frac{1}{3}$ full headwater. It is notable that none of the holes drilled during either stage indicated excessive leakage at the rock line.

Fig. 3 shows nine holes designated by numbers and by the letter A. These were diamond drill holes 1.5 in. in diameter, drilled midway between those 3-in. holes which were grouted. The purpose of these holes was to test the effectiveness of the grouting. In every case, only small flows were encountered in the test holes. In one, a grout core approximately $\frac{3}{16}$ in. thick was recovered.

Holes of 3-in. diameter were also drilled from the crest of the dam to the drainage gallery. None of these holes indicated excessive leakage.

STRENGTHENING OF THE DAM

The modified dam is designed to withstand a reservoir level 8 ft higher than that used in the original design. At this higher pool level the estimated maximum spillway discharge is 337,000 cu ft per sec, which is 68% larger

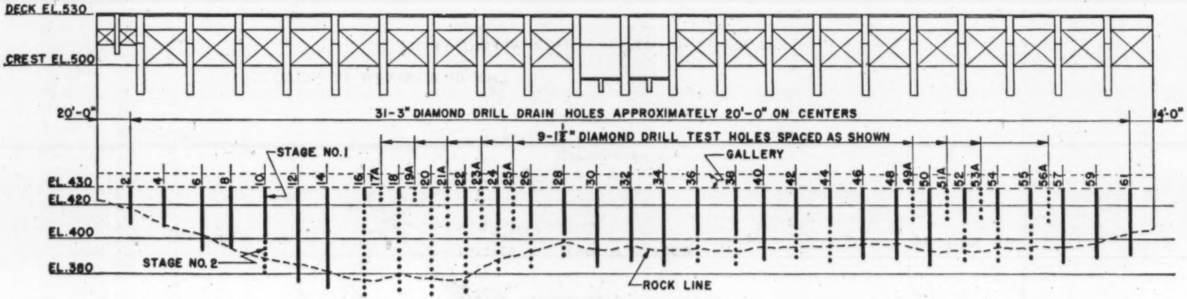
DECK EL.530
CREST EL.500
20'-0"
31-3" DIAMOND DRILL DRAIN HOLES APPROXIMATELY 20'-0" ON CENTERS
14'-0"
9-1½" DIAMOND DRILL TEST HOLES SPACED AS SHOWN
STAGE NO.1
GALLERY
EL.430
EL.420
EL.400
EL.380
STAGE NO.2
ROCK LINE
2
4
6
8
10
12
14
16
17A
18
19A
20
21A
22
23A
24
25A
26
28
30
32
34
36
38
40
42
44
46
48
49A
50
51A
52
53A
54
55
56A
57
59
61

LONGITUDINAL SECTION

HOLE NUMBER	STAGE NO. 1				STAGE NO. 2				
	DEPTH DRILLED	HEIGHT JET (1)	DEPTH TO WATER (2)	MEASURED PRESSURE (3)	BAGS OF CEMENT	DEPTH DRILLED	HEIGHT JET (1)	DEPTH TO WATER (2)	MEASURED PRESSURE (3)
2	21'-8"	S(4)	...	69	...	...	S	...	35
4	21'-8"	S	...	0	...	...	S	...	0
6	37'-0"	S	...	59	...	...	S	...	2
8	35'-4"	...	27'-5"	...	...	...	...	27'-0"	...
10	29'-0"	11"	...	100	28	49'-6"	S	...	9
12	54'-6"	1/2"	...	61	...	...	S	...	0
14	59'-0"	...	27'-5"	...	...	...	...	27'-1"	...
16	7'-0"	11"	...	100	50	64'-0"	...	18'-6"	...
17A	...	...	...	...	...	8'-0"	S	...	...
18	6'-8"	25"	...	100	75	60'-6"	...	27'-1"	...
19A	...	...	...	...	...	8'-0"	1/4"	...	...
20	6'-8"	17"	...	100	20	63'-0"	S	...	0
21A	...	...	...	...	17	22'-0"	1/4"	...	...
22	21'-8"	8"	...	80	55	61'-5"	S	...	49
23A	...	...	...	...	...	23'-0"	2 1/2"	...	...
24	21'-8"	57"	...	100	67	49'-0"	S	...	14
25A	...	...	...	...	...	23'-0"	S	...	...
26	21'-8"	7"	...	100	30	46'-5"	S	...	2
28	26'-8"	2 1/2"	...	100	15	40'-0"	...	27'-0"	...
30	46'-2"	...	24'-2"	...	...	...	...	19'-8"	...
32	43'-0"	...	8'-7"	...	...	...	...	2'-0"(6)	...
34	46'-0"	...	8'-7"	...	...	...	...	6'-0"	...
36	26'-8"	4 1/2"	...	77	15	43'-0"	S	...	0(7)
38	26'-8"	9"	...	91	25	45'-3"	1/4"	...	49(8)
40	43'-0"	1 3/4"	...	93	...	...	S	...	9(9)
42	21'-4"	3"	...	53	7	41'-4"	...	27'-0"	...
44	21'-8"	2"	...	100	20	42'-6"	S	...	0(5)
46	41'-0"	4"	...	91	...	...	S	...	46
48	41'-0"	1"	...	29	...	...	...	27'-6"	...
49A	...	...	...	...	...	19'-0"	S	...	0
50	45'-4"	3 1/2"	...	91	...	...	S	...	69
51A	...	...	...	...	...	18'-6"	S	...	0
52	17'-7"	59"	...	100	50	42'-8"	S	...	0
53A	...	...	...	...	...	18'-6"	...	3"	...
54	17'-0"	47"	...	100	35	43'-3"	S	...	0
55	17'-0"	42"	...	100	50	40'-6"	S	...	0
56A	...	...	...	...	...	18'-6"	...	12'-9"	...
57	42'-0"	S	...	0	...	...	S	...	0
59	39'-10"	S	...	0	...	...	S	...	0
61	36'-8"	S	...	0	...	...	S	...	0

NOTES: (1) ABOVE TOP OF HOLE. (2) BELOW GALLERY FLOOR. (3) PERCENT OF FULL HEAD. (4) S-SEEP. (5) PRESSURE 29% WITH 46 CLOSED. (6) SMALL FLOW WITH 34, 36, 38 & 40 CLOSED (PRESSURE 0%) (7) 32% WITH 38 & 40 CLOSED. (8) 60% WITH 36 & 40 CLOSED. (9) 35% WITH 34, 36 & 38 CLOSED.

Fig. 3.—Plan and Log of Drilling Operations

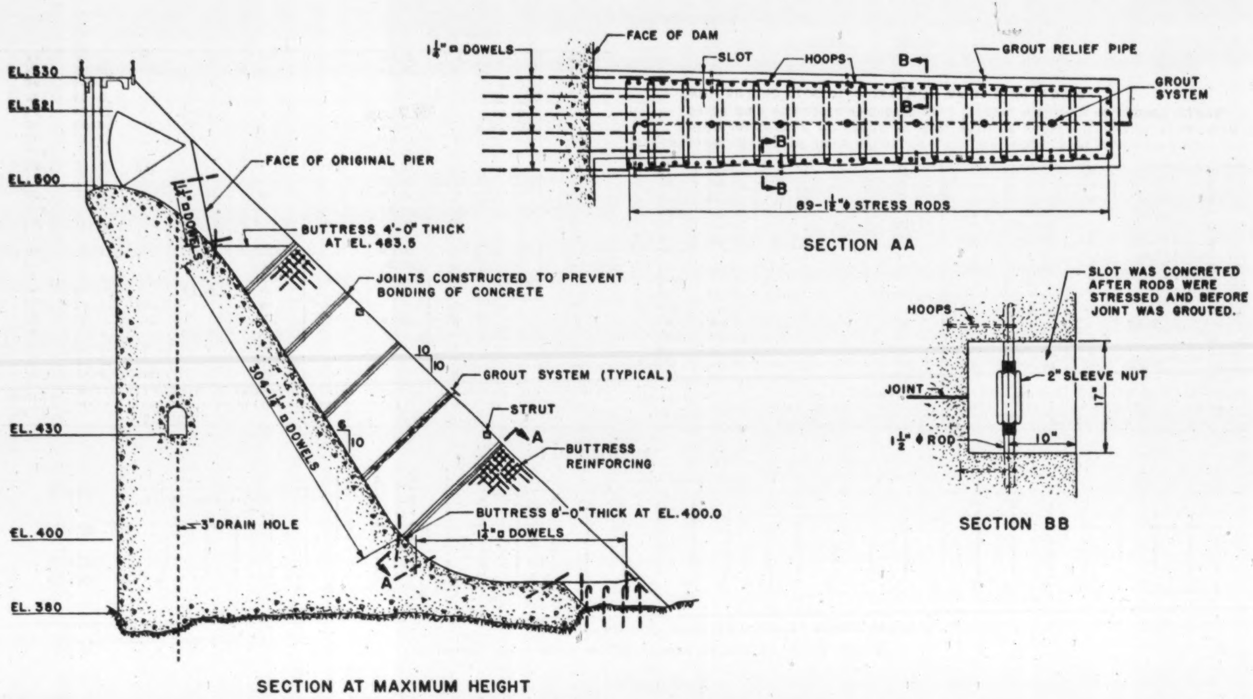
EL. 530
EL. 521
EL. 500
EL. 430
EL. 400
EL. 380
FACE OF ORIGINAL PIER
1½" ◻ DOWELS
BUTTRESS 4'-0" THICK AT EL. 463.5
JOINTS CONSTRUCTED TO PREVENT BONDING OF CONCRETE
10
10
6
10
304-1½" ◻ DOWELS
GROUT SYSTEM (TYPICAL)
STRUT
A
BUTTRESS REINFORCING
BUTTRESS 8'-0" THICK AT EL. 400.0
1½" ◻ DOWELS
3" DRAIN HOLE
SECTION AT MAXIMUM HEIGHT
1½" ◻ DOWELS
FACE OF DAM
SLOT
HOOPS
B
GROUT RELIEF PIPE
GROUT SYSTEM
89-1½" ϕ STRESS RODS
SECTION AA
SLOT WAS CONCRETED AFTER RODS WERE STRESSED AND BEFORE JOINT WAS GROUTED.
HOOPS
JOINT
2" SLEEVE NUT
17"
1½" ϕ ROD
10"
SECTION BB

FIG. 4.—DETAILS OF SPILLWAY BUTTRESS CONSTRUCTION

then the original design discharge. To meet these new requirements, the earth abutments were raised 5 ft and were strengthened by adding rock fills. Wave walls 4 ft high were added to the tops of the earth sections.

Strengthening of the spillway section of the dam was required because of the possible large tensile stresses revealed by the uplift measurements and the stability analyses. The structural modification adopted to accomplish this purpose consisted of adding prestressed, reinforced concrete buttresses to the downstream side of the spillway, one at each of the existing crest-gate piers. Fig. 4 shows certain details of the buttresses, and Fig. 5 shows the spillway after modification.

The design of the modified spillway section was based on the following considerations: (1) The buttresses would be added to the dam while it was in a stressed condition; (2) after completion, the buttresses would be made to carry a predetermined part of the load by means of adjustable stress rods embedded in the buttresses; (3) the total shear stress between the existing dam and the buttresses would be carried by steel dowels; and (4) the uplift pressure, at any horizontal plane, would be assumed to vary from 50% of full headwater to zero pressure, or tailwater, and would be assumed to be applied to 100% of the base area.

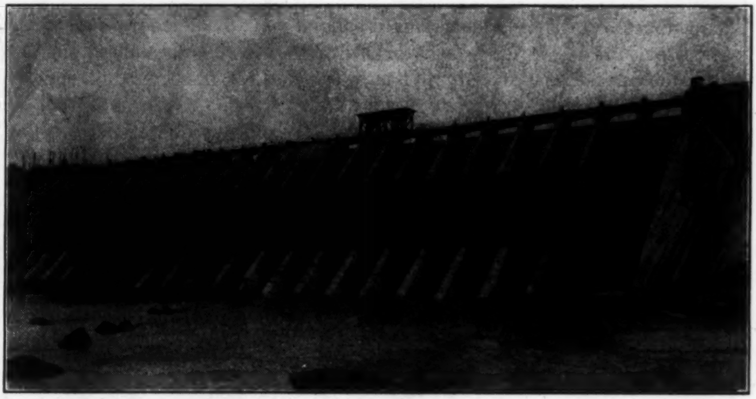

FIG. 5.—THE MODIFIED STRUCTURE BEFORE REMOVAL OF THE ACCESS STAIRWAYS

The design requirement that the buttresses be prestressed was imposed by the apparent large tensile stresses in the existing dam when subjected to normal reservoir levels, and by the fact that the reservoir could not be lowered enough to reduce these existing stresses to values permitting the construction of unstressed buttresses that would eliminate tensile stresses with maximum headwater conditions.

The principal steps used in the stability analysis of the modified structure involved the determination of (1) stresses in the existing structure with lowered headwater, (2) stresses induced by the addition of the buttresses, (3) stresses induced in the modified structure by loading of the buttresses, (4) stresses induced in the modified structure by raising the headwater to maximum level, and (5) the combination of all conditions to determine the maximum stresses.

The conventional elastic theory was used in the design. Allowable unit stresses used for the design of the buttresses were purposely kept low (one half the usual values) to provide large factors of safety.

Fig. 4 shows the general details of the buttresses. The buttresses were added in separate blocks, as indicated. The top of each block was formed to provide a smooth surface and was oiled to prevent bonding to the next lift. Steel stress rods, with sleeve nuts at each lift joint, were installed for the purpose of prestressing the buttresses after they were completed. The buttresses were anchored to the existing dam by grouting 1.25-in. steel dowels 8 ft and 10 ft into the old gravity dam. These dowels were designed to carry the total shear at the contact line between the old dam and the buttresses, no allowance being made for the development of shear between the old and the new concrete. The old concrete was chipped down an average of 6 in. under areas of new construction. The temporary stairways shown on the sides of the buttresses in Fig. 5 were provided to give access to the stress nuts. Fig. 6 shows workmen on one of these stairways during the stressing operations.

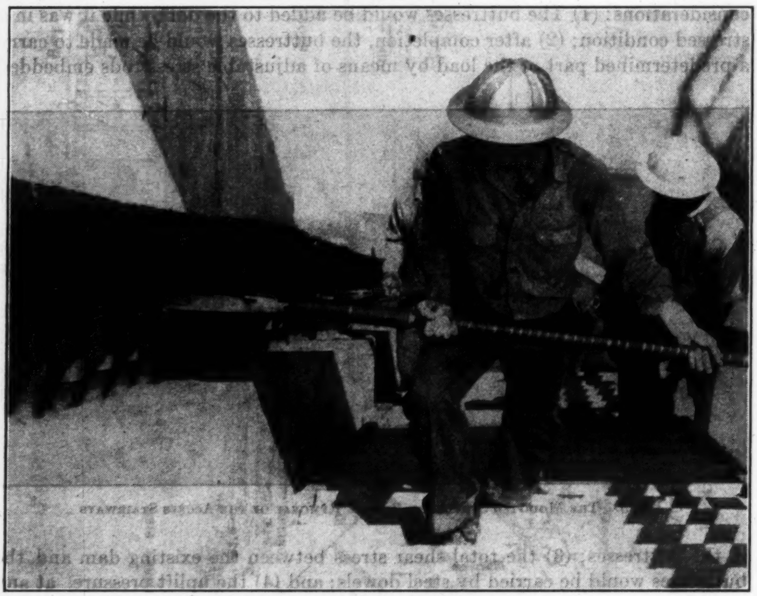

FIG. 6.—WORKMEN SHOWN TIGHTENING STRESS NUTS IN ONE OF THE BUTTRESSES DURING PRESTRESSING OPERATIONS

PRESTRESSING THE SPILLWAY BUTTRESSES

During the period when the buttresses were under construction, the reservoir was drawn 11 ft below normal pool level. After their completion, the reservoir was lowered an additional 10 ft, and the buttresses were then loaded to predetermined values. Because it was not feasible to lower the reservoir further, the existing dam remained in a stressed condition, and, for this reason, it was necessary to prestress the buttresses so that they might assume their assigned part of the total load.

Stress was applied to the buttresses by means of the stress (sleeve) nuts. This operation involved a systematic tightening of the nuts with torque wrenches previously calibrated by a testing laboratory. Ten sets of rods and sleeve nuts, duplicates of those in the buttresses, were used in laboratory calibration in order to determine the uniformity of thread friction. The tests showed a very consistent relationship between the rod load and the wrench-dial readings. To insure an even distribution of stress in the rods in all the buttresses, the torque-wrench loads were applied in increments. An initial loading of 50% of the predetermined final stress was applied to all rods. In successive steps, loads equivalent to 75%, 85%, 90%, and progressively higher percentages of the full load were applied. A final check was made at each sleeve nut before the access slots were filled with concrete. The last operation consisted of pressure-grouting the buttress lift joints, and the joints between the buttresses and the face of the original structure. An embedded grout-pipe system, shown in Fig. 4, had been provided for this purpose. A considerable amount of grout was injected into all the lift joints. Very little grout was taken by the face joints.

NECESSITY FOR MODEL TESTS

When the planning studies for the modification of the spillway section of the dam indicated that the buttress plan might be the most economical, some uncertainty arose concerning the effects of the buttresses on flow conditions in the area below the spillway. Although a negligible amount of erosion had occurred during the life of the original structure, it was suggested that the "nozzling" effect of the buttresses might cause excessive scour below the dam. It is to be noted that the effective flow width at the bottom of the spillway was reduced approximately 28% by the addition of the buttresses. Continued studies raised other questions, including the magnitude of the hydraulic forces on the buttresses, the design of the spillway bucket extensions required to accommodate the buttresses, the height and location of construction cofferdams, and the coefficient of discharge for the modified spillway. The need for model studies was clearly indicated, and arrangements were made to conduct these studies in the hydraulics laboratory at the Georgia Institute of Technology, at Atlanta.

BACKGROUND FOR MODEL STUDIES—PROTOTYPE EXPERIENCES

A complete understanding of the model test program and results is not possible without a brief review of certain unusual prototype operating conditions and experiences. As Bartlett's Ferry Dam had been in operation for more than 20 years, it was possible to interpret the model observations in the light of those recorded experiences, and the resulting conclusions were especially significant.

As constructed, the original structure did not include the customary elaborate provisions for the development of a stilling basin below the spillway, despite the abnormally low tailwater depths which occur at the site. Thus, for almost all conditions of operation, the tailwater was swept off the spillway bucket, exposing foundation rock near the toe of the dam to high-velocity flows. It is remarkable, however, that during the 25 years of the dam's existence, no significant movement of the foundation rock had taken place, and erosion had never been a serious problem.

During the time that the project had been in operation, several large floods were experienced. These included the flood of March, 1929, for which the peak spillway discharge was estimated to be approximately 135,000 cu ft per sec. Of greater significance, perhaps, is the fact that several gates had been opened during a considerable part of each year in order to pass normal flows. Early observations during high flows at the dam indicated that excessive spray and wave action made it undesirable to open spillway gates in the vicinity of the powerhouse. Following the flood of 1929, the powerhouse training wall was raised 5 ft to prevent overtopping during high flows.

The normal power-pool level for the Bartlett's Ferry Project is at El. 521, which corresponds to the top of the spillway crest gates. The revised maximum flood-pool level is at El. 530. Maximum spillway discharge capacities are computed on the basis of 19 full spillway bays, 2 trash gates, and 4 siphons, all in operation. The combined capacity of the trash gates and siphons is very small. The siphons, which occupy a width equal to 2 spillway bays, are normally closed, but can be opened for flood discharge. In recent years, the last gate on the east end of the spillway has been opened infrequently, in order to avoid concentrations of the flow along the foot of the retaining wall.

THE 1/80-SCALE MODEL

Two models were constructed, the first of which was a 1/80-scale comprehensive model of the spillway and powerhouse sections of the dam, plus a length of the river extending approximately 700 ft (prototype) downstream from the dam. For purposes of the model tests, the spillway crest gates were numbered from 1 to 19, beginning at the powerhouse end of the dam, as shown in Fig. 9, appearing subsequently. One bay, adjacent to the powerhouse, which is occupied by trash gates, was reproduced as an additional spillway bay, designated by the letter T. Two bays representing the siphons were designated S_1 and S_2, reading from west to east. The models of the proposed buttresses, each of which required special fitting to conform to the irregular spillway bucket, were assembled as a single unit to facilitate installation. River bed topography was reproduced in concrete except for scour tests, during which a short section of the bed immediately below the spillway was composed of pea gravel. Fig. 7, illustrating the original and modified structure, shows the completed 1/80-scale model.

The objectives of tests on this model were (1) to contrast flow conditions below the original spillway structure with conditions which might occur if the buttresses were added; (2) to develop a satisfactory design for the spillway bucket extension; (3) to determine a satisfactory gate-opening sequence for passing floodwaters over the spillway; (4) to explore the necessity for raising the original powerhouse training wall, and to develop a satisfactory design for this modification, if required; and (5) to determine the best location and height of cofferdam for the two-stage construction of the buttresses.

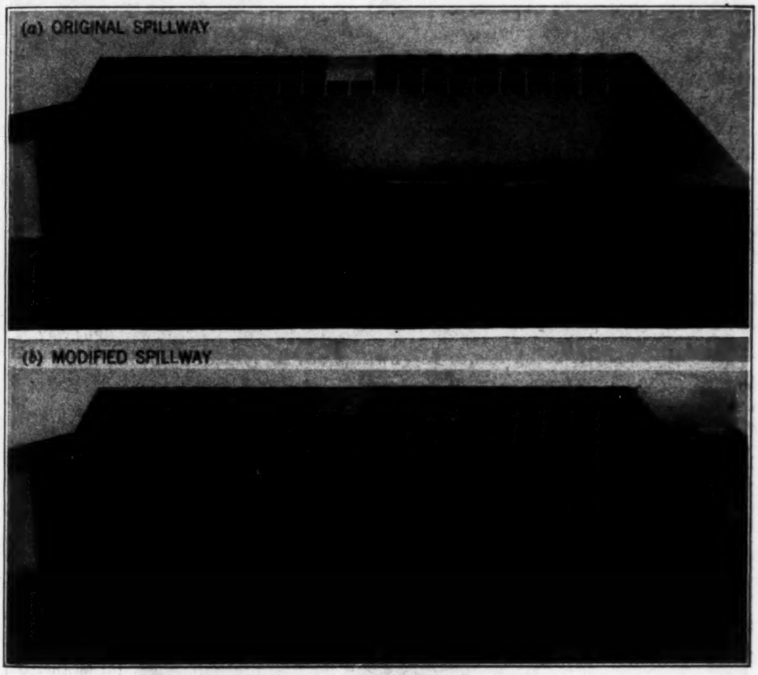

Fig. 7.—Model Built to Scale of 1/80

In this limited space, only the more important test results, with little of the supporting data, can be examined.

Effect of the Buttresses on the Stilling Basin.—Tests on both the movable-bed model and the fixed-bed model indicated that, in general, erosive tendencies would be lessened by the addition of buttresses to the original spillway. The fairly obvious explanation of this conclusion lies in the observed effect of the buttresses in dividing the nappe into separate jets, which discharge freely off the spillway bucket, falling on the tailwater blanket a considerable distance downstream from the end of the dam. In contrast, tests on the original bucket indicated that the lack of free air below the continuous sheet of water passing across the bucket resulted in negative pressures under the nappe, unstable flow, and a lowered trajectory. When the results of the model tests were compared with the recorded performance of the original structure, it could be concluded that conditions in the stilling basin would not be unfavorably affected by the proposed construction. Fig. 8 illustrates the characteristic differences in behavior of the original and the modified spillways. Typical results of comparative scour tests are shown in Figs. 9 and 10. In all the tests illustrated by Figs. 8, 9, and 10, the model was operating at normal reservoir level, at El. 521, with all gates opened wide, corresponding to a prototype flow of 172, 000 cu ft per sec.

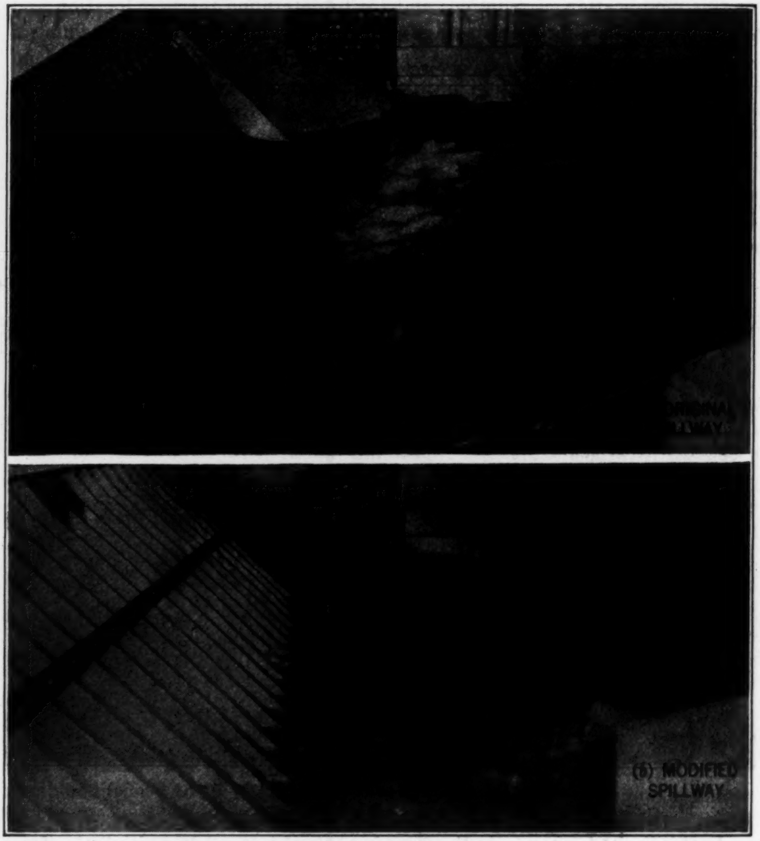

Fig. 8.—A Discharge Corresponding to 172,000 Cu Ft per Sec

Design of Spillway Bucket Extension.—As shown in Fig. 2, the spillway bucket on the original structure was of a minimum length and did not include any type of end sill or baffle blocks. As shown in Fig. 4, the bucket had to be lengthened from 13 ft to 23 ft (variable because of different apron elevations across the length of the spillway) to accommodate the added buttresses. Thus, an important objective of the model tests was to develop a satisfactory design for the apron extension. The only type of sill considered for comparison with a horizontal extension was a simple "flip" sill with plane faces sloping up in the downstream direction. The design that was adopted finally called for the construction of a sill 1 ft high and 6 ft in base width in every gate bay except Nos. T, 1, 2, and 3 at the powerhouse end of the spillway. This design appeared to give optimum performance, considering scour, wave action, and spray. The sills were omitted in the 4 bays nearest the powerhouse in order not to increase the objectionable spray which normally occurs as a result of the unfortunate orientation of the powerhouse with respect to the spillway. Sills in the bays nearer the opposite end of the spillway, where the bucket is much higher, caused considerable spray in the model, but greatly reduced scour around the retaining wall. As these sills are far removed from the powerhouse, spray was not believed to be a serious consideration. Fig. 10 shows the results of a typical scour test on Design C, which differs from the final design only in the inclusion of sills in bays T to 3, inclusive.

Gate-Opening Sequence.—The problem of determining a most satisfactory gate-opening sequence for floodwater release was, of course, limited to flows less than the full capacity of the spillway at top-of-gates level, El. 521. The criteria for evaluating various gate-opening arrangements included surface currents, waves, spray, and stilling-basin scour. The schedule of operation as finally developed necessitated opening the gates in the following sequence (see Fig. 9): Nos. 10, 12, 14, 16, 18, 9, 8, 7, 6, 5, 11, 13, 15, 17, 19, 4, 3, 2, 1, T. It was indicated that the siphons could be opened at any time. The adopted sequence obviously develops quite logically, but it was made clear during the tests that undesirable flow conditions frequently result from gate arrangements which, without the benefit of the model studies, would appear to be just as logical. In the model, as in the prototype, it was demonstrated that gates adjacent to the powerhouse should be opened last.

Other Objectives.—A secondary objective of tests on the 1/80-scale model, which developed as the tests proceeded, involved the raising of the powerhouse training wall to resist and to deflect spray and overriding flow from spillway bays near the powerhouse that normally would be opened only during extreme floods. The final design for this modification necessitated raising the wall 4 ft and adding a 4-ft overhanging extension at the top to serve as a wave deflector. It is important to note that the necessity for this modification was due primarily to powerhouse orientation and not to the addition of buttresses on the spillway.

The height and location of cofferdams required for two-stage construction of the spillway buttresses was also determined in brief tests on the 1/80-scale model. A unique result of this study was the enlargement of the cofferdam to permit flooding of, and discharge into, the cofferdam areas in the event of

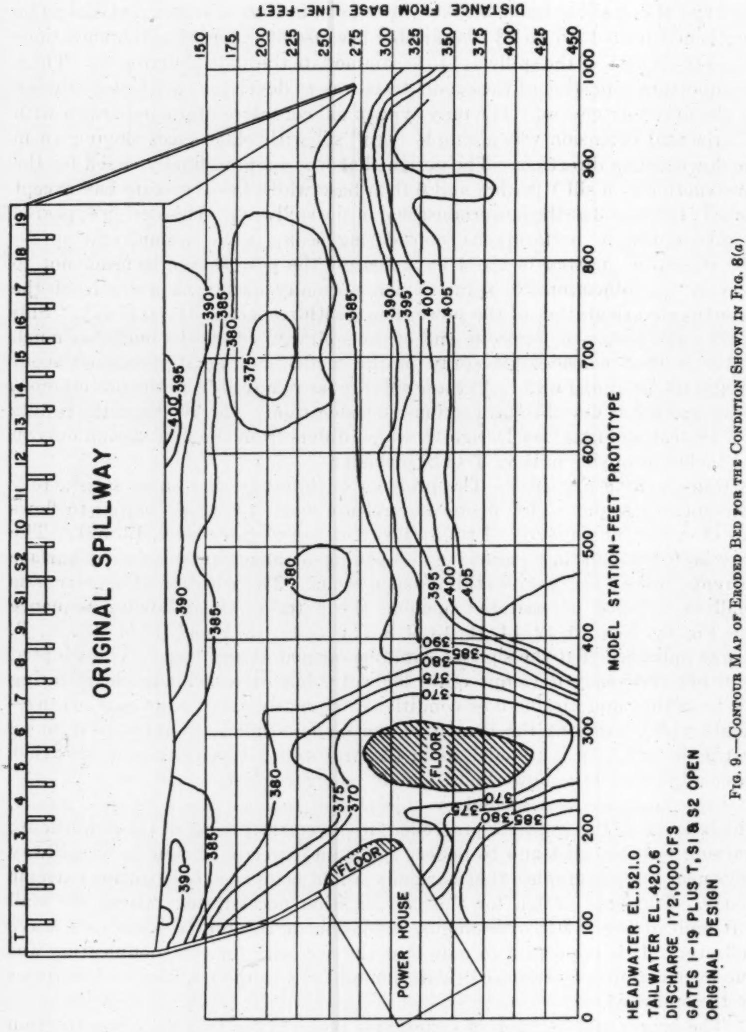
ORIGINAL SPILLWAY
T
1
2
3
4
5
6
7
8
9
S1
S2
10
11
12
13
14
15
16
17
18
19
POWER HOUSE
FLOOR
FLOOR
DISTANCE FROM BASE LINE-FEET
150
175
200
225
250
275
300
325
350
375
400
425
450
MODEL STATION-FEET PROTOTYPE
0
100
200
300
400
500
600
700
800
900
1000
390
385
380
375
370
375
380
385
370
375
380
385
390
395
400
405
390
385
380
375
380
390
385
400
395
390
385
380
385
390
395
400
405

HEADWATER EL. 521.0
TAILWATER EL. 420.6
DISCHARGE 172,000 CFS
GATES 1-19 PLUS T, S1 & S2 OPEN
ORIGINAL DESIGN

FIG. 9.—CONTOUR MAP OF ERODED BED FOR THE CONDITION SHOWN IN FIG. 8(a)

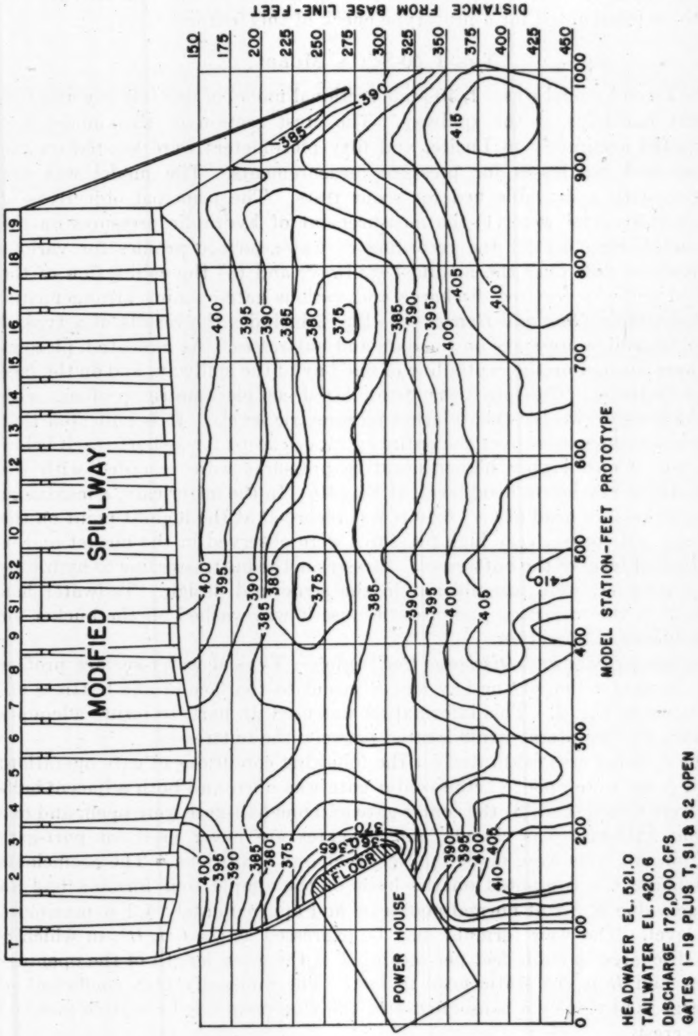
DISTANCE FROM BASE LINE-FEET
150
175
200
225
250
275
300
325
350
375
400
425
450
MODEL STATION-FEET PROTOTYPE
0
100
200
300
400
500
600
700
800
900
1000
MODIFIED SPILLWAY
T
1
2
3
4
5
6
7
8
9
S1
S2
10
11
12
13
14
15
16
17
18
19
POWER HOUSE
FLOOR
365
370
375
380
385
390
395
400
405
410
415

HEADWATER EL. 521.0
TAILWATER EL. 420.6
DISCHARGE 172,000 CFS
GATES 1–19 PLUS T, S1 & S2 OPEN
DESIGN C WITH 1'X 6' END SILLS

FIG. 10.—Contour Map of Eroded Bed for the Condition Shown in Fig. 8(b)

the occurrence of a flood larger than could be passed through the unenclosed spillway bays. Fortunately, construction operations at the dam site did not have to be interrupted for a prototype check of this feature.

THE 1/40-SCALE MODEL

The second model was a 1/40-scale sectional model of one full bay and two adjacent half-bays of the spillway. The crest section of this model was constructed accurately in Lucite, and fifty piezometers were located on the spillway and buttresses for pressure measurements. The model was not equipped with a movable bed for scour tests. The principal objectives of tests on this model were (1) the measurement of hydraulic pressures on the dam and buttresses; (2) the recording of water-surface profiles for various conditions of flow over the modified spillway; and (3) the calibration of the modified spillway for free discharge and various gate-opening arrangements.

Pressures on Dam and Buttresses.—Fig. 2 includes the results of a typical test to determine pressures on the dam and buttresses. As indicated, piezometers were located on the center line of one bay of the spillway, and on the face of one buttress. Pressure data are plotted as piezometric profiles, with straight lines drawn between plotted piezometric levels. It is indicated that positive pressures exist over the entire spillway except for a short reach below the crest. Considerably higher negative pressures were recorded with the headwater at maximum flood level, at El. 530. In the latter case, a maximum negative pressure head of (−) 6.40 ft was recorded at the highest point on the spillway. Of course, very high pressures were observed in the bucket and in the adjacent faces of the buttresses. Stresses in the buttresses due to hydraulic forces, however, were insignificant in the structural design. Tailwater had no effect on the measured pressures because it was washed off the bucket for all conditions of operation.

Surface Profiles and Discharge Calibration.—Typical water-surface profiles along the center line of one bay and adjacent to the face of one buttress are also shown in Fig. 2. This information was used, in part, to insure adequate clearance for the lateral struts located between the buttresses.

The spillway was calibrated for the following conditions of gate operation: (1) All gates were open; (2) the center gate was open and both adjacent half-gates were closed; and (3) the center gate and one half-gate were open, and one adjacent half-gate was closed. As the gates are never used for part-gate operation, all tests were made for free-discharge conditions. The coefficients of discharge (C) computed on the basis of the simple weir formula had an average value of 3.7 at normal pool level and approximately 4.2 at maximum flood level. The weir formula may be expressed as $Q=C\ L\ H^{3/2}$, in which Q is the discharge in cubic feet per second, L is the gross length of the openings in feet, and H is the static head in feet. The unusually high coefficient of discharge is obviously a consequence of the aforementioned negative pressure on the crest.

ACKNOWLEDGMENTS

The owner of Bartlett's Ferry Dam at the time of these investigations was the Georgia Power Company in Atlanta. The investigations were under

the direct supervision of E. S. Harrison, M. ASCE, and under the general direction of W. P. Hammond, vice-president of the Georgia Power Company. Consulting engineers were S. H. Woodard, O. G. Thurlow, and N. F. Williams, Members, ASCE. R. R. Randolph, of Southern Services, Incorporated, assisted by engineering personnel of the Georgia Power Company, conducted the model tests under the direction of one of the writers. The laboratory studies were made in the hydraulic laboratory of the Georgia Institute of Technology by arrangement with the Georgia Tech Research Institute.

DISCUSSION

G. H. Hickox,[7] **M. ASCE.**—A praiseworthy description of an unusually complete set of model tests has been presented by the authors. This paper presents an excellent example of the type of model testing that is necessary for the design of a new dam or the reconstruction of an old dam. The authors have arrived at completely satisfactory conclusions. Only a few comments, accordingly, on the general subject of model tests for dams shall be added.

It has been assumed that considerable erosion would occur in the river bed below a dam, even in rock, if special provisions were not made to prevent it. There is considerable evidence to support this assumption. Wilson Dam on the Tennessee River, near Florence, Ala., is founded on limestone but it was not provided with an apron. Considerable erosion occurred at the toe when the dam was first placed in operation. Extension of the apron served merely to transfer the erosion to a point further downstream. It seems probable that properly conducted model tests might have abolished this problem. Messrs. Harrison and Kindsvater describe a dam that is 25 years old, which, although lacking an apron, has sustained considerable flow without any significant erosion of the river bed. The experiments were conducted on models having erodible beds in which considerable movement occurred. The results of the model tests were used for comparative purposes only, however, and no attempt was made to claim that erosion in the prototype would agree quantitatively with erosion in the model. The fundamental difficulty appears to be a lack of knowledge about the erodibility of various rocks under the flow conditions to which they are subjected. Without such knowledge, the designer must be cautious.

The authors made tests on models at two different scales for various purposes. These objectives were to study the following: (1) Effect of the buttresses on erosive tendencies; (2) effect of sills at the end of the apron on erosion; (3) most suitable schedule of gate operation; (4) location of struts between buttresses; (5) elevation of the powerhouse training wall; (6) elevation and location of construction cofferdams; (7) pressures on the face of the spillway; (8) water surface profiles; and (9) spillway discharge calibration.

A large model of a section of the spillway was built at a 1/40-scale to determine the last three objectives. A smaller, 1/80-scale model of the entire dam, powerhouse, and a part of the river channel was built for the first six objectives. The paper indicates clearly that it is not sufficient to build a large-scale model for one or two bays of a spillway to study the erosion at the toe of a dam. There is usually a problem of erosion at the end of the spillway adjacent to the non-overflow section of the dam or adjacent to the powerhouse. Whenever the overflow section of the spillway is away from either bank, an eddy current is set up in the region of relatively quiet water between the end of the spillway and the adjacent river bank. At the base of the dam, or in the powerhouse tailrace, the eddy current moves toward the spillway section where the water surface is depressed. At the junction of the high-velocity stream from the spillway and the lateral current from the eddy, local eddy currents of considerable intensity and erosive power are formed. These local eddies cause scouring at the end of the spillway or at the training wall (if a training wall exists at that point). Extension of the training wall in a downstream direction does not eliminate the difficulty except at a prohibitive cost. The solution to the problem usually requires a training wall with a proper combination of height, length, and location, and river bed paving. The proper combination can be determined only by a study of a complete model of the entire spillway and river and cannot be determined by tests made on a sectional model.

---

[7] Associate Director, Eng. Experiment Station, Univ. of Tennessee, Knoxville, Tenn.

The Bartlett's Ferry Dam is unusual with respect to the relative locations of the powerhouse and the spillway. At this dam the powerhouse tailrace is directly below a part of the spillway. The training wall dividing the spillway from the tailrace is subjected to an increase in both water surface and water pressure on the spillway side, rather than reduction in elevation, as is usually the case when the dam is straight.

The results reported as having occurred with the use of a sloping sill at the end of the apron are in agreement with the experience of the Tennessee Valley Authority (TVA). Aprons of most TVA dams are terminated with a sloping sill which reduces the erosive tendencies at the end of the apron. TVA experience also agrees with that reported by Messrs. Harrison and Kindsvater that the slope of the upstream face is usually a compromise between the depth of erosion and the height of the waves produced in the river channel below the dam. The steeper sills produce the least erosion and the highest waves. The flat sills increase erosive tendencies but reduce the wave height. The slope adopted is generally chosen with regard to the importance of erosion at the toe of the sill and the effect of waves on navigation and erosion of the bank.

It is encouraging to note that the authors considered conditions during construction. Model tests of high dams are frequently made without regard to conditions existing during diversion. A stilling basin that may be entirely satisfactory for the maximum flood discharge of a stream after the completion of the dam may be wholly inadequate when it is required to handle a much smaller flood under entirely different conditions. During the construction period, flow may be diverted through a narrowed river channel or, occasionally, through tunnels by-passing a cofferdam. In either case, the flow is concentrated, and considerable damage may result. This is especially true when diversion occurs through spillway blocks which have not reached their final height. This circumstance causes concentration and direction of flow that are quite different from those of the completed structure, and the erosive effects may be quite unexpected. The concentration of flow over a fraction of a long apron may result in eddies that move debris and gravel onto the apron and, by continual movement of this material, cause serious scour. Such conditions can be predicted only by simulating construction conditions and expected floods with models.

It is gratifying to note that observations on the model have been made for rather small prototype discharges. One of the reasons why satisfactory comparisons of model and prototype operations are uncommon is that many models are tested only for the worst design condition, which is usually at or near maximum discharge. Extreme discharges occur very rarely in the prototype. Comparisons of model and prototype are therefore available only when the experimenter has had sufficient foresight to conduct tests in the normal operating range. The meager accumulation of knowledge about the reliability of models will increase if careful test data are obtained in the range of normal, or relatively frequent, prototype operating conditions.

Another somewhat neglected phase of model testing is the effect of gate operations on erosive tendencies. As indicated by the authors, concentration of flow is usually undesirable and nearly uniform distribution is greatly preferred. Tests on a model with an erodible bed are an extremely valuable method of determining the erosive effect caused by various methods of gate operations. Similar tests with a fixed-bed model are also valuable in determining the effect of concentrated discharges on surface currents which may hinder or improve navigation. It would seem preferable to learn these combinations by model testing rather than by interfering with navigation.

The importance of having model tests designed, carried out, and interpreted by a competent, well-trained staff should be emphasized. It is known that in any argument the conclusions reached are always a function of the initial premises. If the model experimenter assumes that only a single sectional model will be sufficient for the problem at hand, the answers obtained will be a function of the particular model. For example, such a model would be adequate for determining the effect of the height of the sill on erosion. If, however, it is assumed that there may be lateral flow problems, a complete model should be built to explore the situation. In such a case, the results discovered may be other than those predicted by use of the sectional model. Similar considerations apply to the use of fixed and movable beds. Model tests should therefore be made and interpreted by the most competent investigators available. The requirements should include both field experience with operating structures and training in fundamental hydraulics and fluid mechanics.

E. S. HARRISON,[8] AND CARL E. KINDSVATER,[9] MEMBERS, ASCE.—The writers are indebted to Mr. Hickox for his comprehensive discussion of the model testing aspects of the paper. His general comments and admonitions are an invaluable complement to the paper. The writers also wish to acknowledge their use of the uplift measurements made at Bartlett's Ferry Dam.[10]

---

[8] Asst. Chf. Engr., Georgia Power Co., Atlanta, Ga.

[9] Prof. of Civ. Eng., Georgia Inst. of Technology, Atlanta, Ga.

[10] "Uplift in Masonry Dams": Final Report of the Subcommittee on Uplift in Masonry Dams of the Committee on Masonry Dams of the Power Division, 1951, *Transactions*, ASCE, Vol. 117, 1952, p. 1243.

AMERICAN SOCIETY OF CIVIL ENGINEERS
Founded November 5, 1852
TRANSACTIONS

Paper No. 2660

RAPID COMPUTATION OF FLEXURAL CONSTANTS

By Thomas G. Morrison,[1] A. M. ASCE

With Discussion by Messrs. Henry Malter, Paul Rogers, and Thomas G. Morrison

Synopsis

Short algebraic formulas for computing stiffness, fixed-end moments, and carry-over factors in terms of three functions and their components are given. This paper has attempted to systematize and thereby simplify the evaluation of these factors by the introduction of the flexural functions. A numerical method for rapidly computing the values of the functions for nonprismatic beams is presented.

Notation

The letter symbols adopted for use in this paper are defined where they first appear, in the illustrations or in the text, and are arranged alphabetically for reference in the Appendix.

Introduction

Computation of the flexural constants for nonprismatic beams by the usual methods involves considerable hidden repetition in the numerical work. This repetition indicates the existence of simpler functions, of which the flexural constants are composed. Investigation discloses that the flexural constants can be computed by combining a system of three functions that cannot be simplified further.

In this paper, all quantities are taken as positive and evident physical relationships are relied upon to keep the signs of moments correct.

Definitions

The three flexural functions are defined as

$$\left.\begin{aligned}\Phi_0 &= \int_0^1 \frac{I_a}{I_x}\,dx\\ \Phi_1 &= \int_0^1 \frac{I_a}{I_x}\,x\,dx\\ \Phi_2 &= \int_0^1 \frac{I_a}{I_x}\,x^2\,dx\end{aligned}\right\}\ldots\ldots\ldots\ldots\ldots\ldots\ldots\ldots(1)$$

Note.—Published, essentially as printed here, in February, 1953, as *Proceedings-Separate No. 170.* Positions and titles given are those in effect when the paper or discussion was received for publication.

[1] Cons. Engr., Chicago, Ill.

in which I_a is the moment of inertia evaluated at the small end of the beam, and I_x is the moment of inertia at any section. The distance $x\,L$ is indicated in Fig. 1.

For computing the fixed-end moment coefficients, additional components of Φ_0, Φ_1, and Φ_2 will be required, corresponding to each load position $r\,L$:

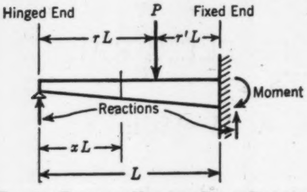

Fig. 1.—Beam of Varying Cross Section

$$\left.\begin{aligned}\Phi_{0,r} &= \int_r^1 \frac{I_a}{I_x}\,dx\\ \Phi_{1,r} &= \int_r^1 \frac{I_a}{I_x}\,x\,dx\\ \Phi_{2,r} &= \int_r^1 \frac{I_a}{I_x}\,x^2\,dx\end{aligned}\right\}\ldots\ldots\ldots\ldots\ldots\ldots(2)$$

If the computations are carried out by numerical integration, no significant additional work is required to obtain the functions of Eqs. 2.

For use in computing $\Phi_{0,r}$, $\Phi_{1,r}$, and $\Phi_{2,r}$ by numerical integration, the following factors are defined:

$$\left.\begin{aligned}\Phi'_{0,r} &= \int_r^{r+\frac{1}{n}} dx\\ \Phi'_{1,r} &= \int_r^{r+\frac{1}{n}} x\,dx\\ \Phi'_{2,r} &= \int_r^{r+\frac{1}{n}} x^2\,dx\end{aligned}\right\}\ldots\ldots\ldots\ldots\ldots\ldots(3)$$

In Eqs. 3, n is the number of intervals into which the beam is divided for numerical integration. By Eq. 3, $\Phi'_{0,r}$ is the reciprocal of n.

A fourth function can be defined as

$$\Phi_3 = \int_0^1 \frac{I_a}{I_x}\,x^3\,dx\ldots\ldots\ldots\ldots\ldots\ldots(4a)$$

The function in Eq. 4a is convenient for computing the fixed-end moment factors for a beam carrying a uniformly distributed load. The factors $\Phi'_{3,r}$ are defined as follows:

$$\Phi'_{3,r} = \int_r^{r+\frac{1}{n}} x^3\,dx\ldots\ldots\ldots\ldots\ldots\ldots(4b)$$

These factors can be tabulated for various n-values and are convenient for computing Φ_3 by numerical integration.

An infinite set of functions—

$$\Phi_m = \int_0^1 \frac{I_a}{I_x}\,x^m\,dx\ldots\ldots\ldots\ldots\ldots\ldots(5)$$

—can be defined. In Eq. 5, m is any integer. The functions up to and including Φ_m could be used to compute the fixed-end moment factors for a distributed load varying as x^{m-3}. Actually, for such loading it is easier to sum the fixed-end moment factors for concentrated loading, each weighted by the proper factor.

WORKING FORMULAS

Having computed the flexural functions, the coefficients for the flexural constants can be computed from the following formulas, which can be easily derived by the moment-area method or by a similar method. The carry-over factor at the small end is

$$C_{ab} = \frac{(\Phi_1 - \Phi_2)}{\Phi_2}$$

—and at the large end

$$C_{ba} = \frac{(\Phi_1 - \Phi_2)}{(\Phi_0 - \Phi_1) - (\Phi_1 - \Phi_2)} \qquad \ldots\ldots (6)$$

The stiffness factors are

$$\left.\begin{aligned} k_a &= (\Phi_0 - \Phi_1) - C_{ab}\,\Phi_1 \\ k_b &= \Phi_1 - C_{ba}\,(\Phi_0 - \Phi_1) \end{aligned}\right\} \ldots\ldots (7)$$

If N is a quantity defined as follows—

$$N = \frac{\Phi_{2,r} - r\,\Phi_{1,r}}{\Phi_2} \ldots\ldots (8)$$

then the angle-of-rotation factor at the small end is

$$\theta_{a,r} = N\,\Phi_1 - \Phi_{1,r} + r\,\Phi_{0,r} \ldots\ldots (9a)$$

The fixed-end moment factor for the beam of Fig. 1 is

$$F'_{b,r} = r' - N \ldots\ldots (9b)$$

and for a beam having both ends fixed, the fixed-end moment factors are

$$\left.\begin{aligned} F_{a,r} &= \frac{1}{k_a}\,\theta_{a,r} \\ F_{b,r} &= F'_{b,r} - C_{ab}F_{a,r} \end{aligned}\right\} \ldots\ldots (9c)$$

For uniform loading,

$$\theta_{a,u} = \tfrac{1}{2}\left[\frac{\Phi_3\,\Phi_1}{\Phi_2} - \Phi_2\right] \ldots\ldots (10a)$$

$$F'_{b,u} = \tfrac{1}{2}\left[1 - \frac{\Phi_3}{\Phi_2}\right] \ldots\ldots (10b)$$

$$\left.\begin{aligned} F_{a,u} &= \frac{1}{k_a}\,\theta_{a,u} \\ F_{b,u} &= F'_{b,u} - C_{ab}\,\frac{1}{k_a}\,\theta_{a,u} \end{aligned}\right\} \ldots\ldots (10c)$$

If the fixed-end moments for concentrated loads are required, the function Φ_3 need not be computed. Instead, $F_{a,u}$ and $F_{b,u}$ can be calculated from the expressions:

$$\left.\begin{aligned} F_{a,u} &= \frac{1}{n-1}\sum_{r} F_{a,r} \\ F_{b,u} &= \frac{1}{n-1}\sum_{r} F_{b,r} \end{aligned}\right\} \dots\dots\dots\dots\dots\dots\dots (11)$$

in which n is the number of intervals into which the member is divided for the computation of $F_{a,r}$ and $F_{b,r}$.

Fixed–End Moment Factors

Usually, $F_{a,r}$ and $F_{b,r}$ are computed directly, and are used for computing $F'_{a,r}$ and $F'_{b,r}$ by algebraic reduction. This procedure is cumbersome, time-consuming, and inaccurate because, to obtain $F_{a,r}$ and $F_{b,r}$ directly, simultaneous equations usually must be solved. The evident reason for the relative difficulty of direct computation of $F_{a,r}$ and $F_{b,r}$ is that of all the flexural constants they alone are defined for doubly indeterminate beams. However, $F'_{a,r}$ and $F'_{b,r}$ are defined for singly indeterminate beams. When flexural functions are employed, the numerical work is the least if $F'_{b,r}$ and $\theta_{a,r}$ are computed directly, and $F_{a,r}$ and $F_{b,r}$ then obtained from these. No steps are wasted by using this procedure.

Numerical Integration

Although the flexural functions theoretically can be computed by integration, it is well known to engineers that, even for so simple a beam as a slab having a parabolic soffit, evaluation of the resulting integrals becomes quite formidable. Furthermore, for a beam whose soffit is a compound curve, the work is greatly increased. Because of these practical problems, it usually will be found simpler to evaluate the flexural functions by numerical integration. This method has the additional advantage that the components of the functions required for obtaining the fixed-end moment factors can be obtained without significant additional work.

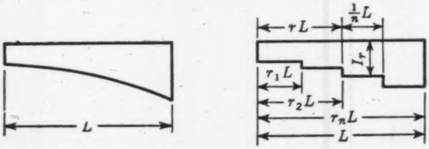

Fig. 2.—Stepped Equivalent Beam for Numerical Integration (Beams Are Approximately Equal)

For purposes of numerical integration, the actual beam is replaced by an approximately equivalent beam consisting of n segments (taken of equal length for convenience only), each segment being of constant moment of inertia. This condition is illustrated in Fig. 2. Then,

$$\int_0^1 \frac{I_a}{I_x} x^m \, dx = \sum_{q=r_0}^{q=r_{n-1}} \frac{I_a}{I_q} \int_q^{q+\frac{1}{n}} x^m \, dx \dots\dots\dots\dots (12a)$$

or, in terms of flexural functions,

$$\Phi_m = \sum_{q=r_0}^{q=r_{n-1}} \frac{I_a}{I_q} \Phi'_{m,\,q} \quad \text{(12}b\text{)}$$

Similarly,

$$\Phi_{m,\,r} = \sum_{q=r}^{q=r_{n-1}} \frac{I_a}{I_q} \Phi'_{m,\,q} \quad \text{(12}c\text{)}$$

In Eqs. 12, q is the segment designation. Because the factors $\Phi'_{m,r}$ are independent of the beam shape, they can be tabulated for various values of n. Tables of $\Phi'_{0,r}$, $\Phi'_{1,r}$, and $\Phi'_{2,r}$ are given for $n = 4$, 6, 8, 10, and 12.

Errors in Numerical Integration.—It should be observed that Eqs. 12 are theoretically accurate. The only approximation in the process is the substitution of the stepped beam for the continuously varying beam as illustrated in Fig. 2. The margin of error is indicated in Table 1, in which the values of Φ_0, Φ_1, and Φ_2 have been computed for the beam of continuously varying depth shown and for three stepped, approximately equivalent beams. For the worst case ($n = 4$), Φ_0 is only 2% in error and for $n = 12$, the error is reduced to 0.25%. These values are approximate because they were all computed with a slide rule, but they are therefore indicative of the accuracy to be expected in an actual problem. The percentage of error in the final stiffness, carry-over factor, and fixed-end moment would be three or four times that of the individual functions because of the magnification of the errors by subtraction.

TABLE 1.—COMPARISON BETWEEN VALUES OF Φ COMPUTED BY EXACT AND APPROXIMATE METHODS

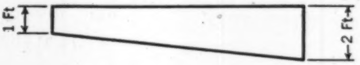

Flexural functions for beam	Theoretical value (exact)	$n = 4$		$n = 8$		$n = 12$	
		Value by numerical method	% error	Value by numerical method	% error	Value by numerical method	% error
Φ_0	0.37500	0.3675	2.00	0.37300	0.53	0.374	0.27
Φ_1	0.12500	0.1260	0.80	0.12564	0.51	0.12536	0.29
Φ_2	0.06815	0.06905	1.32	0.06837	0.32	0.06838	0.34

For concrete beams, accuracy greater than 5% is of academic importance only. For steel beams having uniform depth and stepped cover plates, the numerical method involves no intrinsic inaccuracy.

EXAMPLES

Two examples are presented to illustrate the method. For the first, a simple problem is selected that occurs frequently in practice. This is the problem of a prismatic beam having infinitely rigid ends.

The flexural constants for the top beam of the nonsymmetrical bent shown in Fig. 3 are required. For this problem, symbolic integration is easier than numerical integration, and therefore the problem offers a good illustration of the basic theory without the secondary complications of numerical integration.

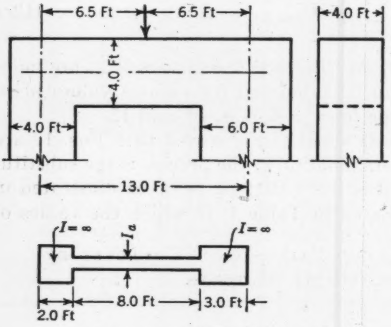

FIG. 3.—NONSYMMETRICAL BENT

As is conventional with most moment-distribution formulas for beams of variable section, the constant value of moment of inertia, "I_a," given in the formulas is that at the small or left-hand end. It should be observed that this choice is quite arbitrary and conventional and that any particular value of I_a might just as well have been selected with only the provision that the same value be used throughout any given set of computations. In the present problem, because the moments of inertia at the ends of the beam are infinite and therefore indeterminate, I_a is taken as the moment of inertia of the central portion.

The limits of integration are 2/13 = 0.154 and 10/13 = 0.769. Thus, the flexural functions are as follows:

$$\Phi_0 = \int_0^1 \frac{I_a}{I_x}\,dx = \int_0^{0.154} \frac{I_a}{\infty}\,dx + \int_{0.154}^{0.769} \frac{I_a}{I_a}\,dx + \int_{0.769}^{1} \frac{I_a}{\infty}\,dx$$

$$= 0 + 0.769 - 0.154 + 0 = 0.615 \ldots (13a)$$

Similary,

$$\Phi_1 = \int_{0.154}^{0.769} \frac{I_a}{I_a}\,x\,dx = 0.284 \ldots\ldots\ldots\ldots (13b)$$

and

$$\Phi_2 = \frac{x^3}{3}\Bigg|_{0.154}^{0.769} = 0.150 \ldots\ldots\ldots\ldots (13c)$$

For the fixed-end moments produced by a concentrated load at the center of the beam,

$$\left.\begin{aligned} \Phi_{0,\,0.5} &= \int_{0.5}^{0.769} \frac{I_a}{I_a}\,dx = 0.269 \\ \Phi_{1,\,0.5} &= 0.171 \\ \Phi_{2,\,0.5} &= 0.110 \end{aligned}\right\} \ldots\ldots\ldots\ldots (14)$$

Similarly,

and

Then, from Eqs. 6,

$$C_{ab} = \frac{\Phi_1 - \Phi_2}{\Phi_2} = \frac{0.284 - 0.150}{0.150} = 0.894$$

$$C_{ba} = \frac{\Phi_1 - \Phi_2}{(\Phi_0 - \Phi_1) - (\Phi_1 - \Phi_2)} = 0.680,$$

and, from Eqs. 7, $k_a = 0.077$ and $k_b = 0.059$. As a check, the known property $\frac{C_{ab}\,k_b}{C_{ba}\,k_a} = 1$ is used. Thus, $\frac{0.894 \times 0.059}{0.680 \times 0.077} = 0.992$, indicating an error of less than 1%.

TABLE 2.—COMPUTATION OF DIMENSIONLESS FACTORS FOR STIFFNESS, FIXED-END MOMENTS, AND CARRY-OVER FACTORS FOR A NONPRISMATIC BEAM

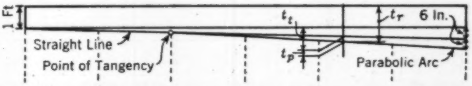

Line No.	Term or factor						
1	t_t	0.50	1.50	2.50	3.50	4.50	5.50
2	t_p	0.00	0.00	0.09	0.84	2.34	4.60
3	t_r	12.50	13.50	14.59	16.34	18.84	22.10
4	$I_a/I_r = (t_a/t_r)^3$	1.000	0.795	0.630	0.448	0.292	0.181
5	$\Phi'_{0,r}\,I_a/I_r$	0.1667	0.1323	0.1050	0.0746	0.0487	0.0302
6	$\Phi_{0,r}$		0.3908	0.2585	0.1535	0.0789	0.0302
7	Φ_0	0.5575					
8	$\Phi'_{1,r}\,I_a/I_r$	0.0139	0.0331	0.0437	0.0435	0.0365	0.0276
9	$\Phi_{1,r}$		0.1844	0.1513	0.1076	0.0641	0.0276
10	Φ_1	0.1983					
11	$\Phi'_{2,r}\,I_a/I_r$	0.0015	0.0086	0.0185	0.0256	0.0275	0.0254
12	$\Phi_{2,r}$		0.1056	0.0970	0.0785	0.0529	0.0254
13	Φ_2	0.1071					
14	$\Phi_0 - \Phi_1$	0.3592					
15	$\Phi_1 - \Phi_2$	0.0912					
16	$(\Phi_0 - \Phi_1) - (\Phi_1 - \Phi_2)$	0.2680					
17	By Eqs. 6 and 7: $C_{ab} = 0.851$, $C_{ba} = 0.341$, $k_a = 0.190$, $k_b = 0.076$. Check: $\frac{C_{ab}\,k_b}{C_{ba}\,k_a} = 0.999$						
18	$r\,\Phi_{1,r}$		0.0307	0.0504	0.0538	0.0427	0.0230
19	$\Phi_{2,r} - r\,\Phi_{1,r}$		0.0749	0.0466	0.0247	0.0102	0.0024
20	N		0.7000	0.435	0.231	0.094	0.022
21	$N\,\Phi_1$		0.1388	0.0863	0.0458	0.0186	0.0044
22	$r\,\Phi_{0,r}$		0.0651	0.0862	0.0768	0.0526	0.0252
23	$N\,\Phi_1 + r\,\Phi_{0,r}$		0.2039	0.1725	0.1226	0.0712	0.0296
24	$\Theta_{a,r}$		0.0195	0.0212	0.0150	0.0071	0.0020
25	r'		0.8333	0.6667	0.5000	0.3333	0.1667
26	$F'_{b,r}$		0.1333	0.2317	0.269	0.2393	0.1447
27	$F_{a,r}$		0.1028	0.1118	0.0790	0.0347	0.0105
28	$C_{ab}\,F_{a,r}$		0.0174	0.0189	0.0133	0.0063	0.0018
29	$F_{b,r}$		0.1159	0.2128	0.2557	0.2330	0.1429
30	$\Sigma F_{a,r}$	0.3415					
31	$F_{a,u}$	0.0683					
32	$\Sigma F_{b,r}$	0.9603					
33	$F_{b,u}$	0.1921					

The actual stiffness factors are (using a value of 1 for *E*)

$$K_a = \frac{1 \times 4 \times 4.5^3}{12 \times 0.077 \times 13} = 30.4 \text{ kip-ft}$$

$$K_b = \frac{1 \times 4 \times 4.5^3}{12 \times 0.059 \times 13} = 39.6 \text{ kip-ft.}$$

For the fixed-end moment for a concentrated load at the center of the beam,

$$N = \frac{\Phi_{2,\,0.5} - r\,\Phi_{1,\,0.5}}{\Phi_2} = \frac{0.110 - (0.5 \times 0.171)}{0.150} = 0.167$$

and

$$\Phi_{0,\,0.5} = N\,\Phi_1 - \Phi_{1,\,0.5} + r\,\Phi_{0,\,0.5} = 0.167 \times 0.284 - 0.171 + (0.5 \times 0.269) = 0.0110.$$

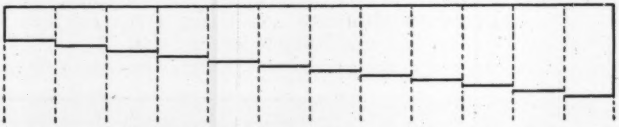

n	Factor												
$n = 12$	$\Phi'_{0,r}$	0833											
	$\Phi'_{1,r}$	0035	0104	0174	0243	0313	0382	0451	0521	0590	0660	0729	0799
	$\Phi'_{2,r}$	0002	0014	0037	0071	0118	0176	0245	0326	0418	0523	0639	0766
$n = 10$	$\Phi'_{0,r}$	1000											
	$\Phi'_{1,r}$	0050	0150	0250	0350	0450	0550	0650	0750	0850	0950		
	$\Phi'_{2,r}$	0003	0023	0063	0123	0203	0303	0423	0563	0723	0903		
$n = 8$	$\Phi'_{0,r}$	1250											
	$\Phi'_{1,r}$	0078	0234	0391	0547	0703	0859	1016	1172				
	$\Phi'_{2,r}$	0007	0046	0124	0241	0397	0592	0827	1100				
$n = 6$	$\Phi'_{0,r}$	1667											
	$\Phi'_{1,r}$	0139	0417	0694	0972	1250	1528						
	$\Phi'_{2,r}$	0015	0108	0293	0571	0941	1404						
$n = 4$	$\Phi'_{0,r}$	2500											
	$\Phi'_{1,r}$	0313	0938	1563	2188								
	$\Phi'_{2,r}$	0052	0365	0990	1927								

FIG. 4.—CHART OF FACTORS $\Phi'_{0,r}$, $\Phi'_{1,r}$, AND $\Phi'_{2,r}$ FOR USE IN COMPUTING FLEXURAL FUNCTIONS—MULTIPLY ALL VALUES BY 10^{-4}

By substitution into Eqs. 9,

$$F'_{b,\,0.5} = 0.500 - 0.167 = 0.333$$

and

$$F_{a,\,0.5} = \frac{0.011}{0.077} = 0.143.$$

These values may be substituted into Eq. 9*c* to yield $F_{b,\,0.5} = 0.205$.

For the second example, a beam having a compound soffit curve composed of a straight line and a tangent parabolic arc is chosen. Table 2 shows a sketch of the beam, and the complete computations for carry-over factors, stiffness factors, and fixed-end moment factors for uniform load. The computations are arranged in systematic order.

The flexural functions are evaluated by numerical integration, the beam being divided into six equal parts for the purpose. The ordinates t_t and t_p as well as the total ordinate t_r are computed at the center of each increment. Then, since the width of the beam is assumed uniform, the value of I_a/I_r is the value of $(t_a/t_r)^3$ for each increment. The thickness t_a is taken as 12.5 in., the first ordinate.

The values in lines 5, 8, and 11 of Table 2 are obtained by multiplying the values in line 4 by the factors in Fig. 4 for a value of $n = 6$ (six increments). It should be observed that the numbers in lines 6, 9, and 12 are each the sum of the numbers immediately above and to the right. The rest of the values in Table 2 are the numerical evaluation of the formulas given, and need no explanation.

To make the solution complete, it may be assumed that the slab shown in cross section is 1 ft wide and 35 ft long. Then, assuming E to be 1 kip per sq in.,

$$K_a = \frac{E\,I_a}{k_a\,L} = 24.4 \text{ kip-in. per ft}$$

$$K_b = \frac{E\,I_a}{k_b\,L} = 61.0 \text{ kip-in. per ft.}$$

To obtain the flexural functions for any given beam, divide the beam into n equal segments, n being a convenient arbitrary number. Then compute the value of I_a/I for each segment; I_a is a constant value of the moment of inertia—usually taken for the left-end segment. Multiply each value of I_a/I by the factors $\Phi'_{0,r}$, $\Phi'_{1,r}$, and $\Phi'_{2,r}$ for the corresponding segment and the same value of n. The values of these factors may be obtained from Fig. 4. The factors $\Phi_{0,r}$, $\Phi_{1,r}$, and $\Phi_{2,r}$ are obtained by summing these products from right to left (see lines 4 through 13 of Table 2, in which $n = 6$).

APPENDIX. NOTATION

The following symbols, adopted for use in the paper and for the guidance of discussers, comform essentially with American Standard Letter Symbols for Structural Analysis (ASA Z10.8-1949), prepared by a Committee of the American Standards Association, with Society representation and approved by the Association in 1942:

C_{ab} = the carry-over factor at the small ($x = 0$)-end;
C_{ba} = the carry-over factor at the large ($x = 1$)-end;
E = the modulus of elasticity;
$\left.\begin{matrix}F_{a,r}\\F_{b,r}\end{matrix}\right\}$ = the fixed-end moment factors at the small and large ends, respectively, for a beam having both ends fixed and a concentrated load, P, at distance $r\,L$ from the small end, for use in the formula: (fixed-end moment) = $F\,P\,L$;

$\left.\begin{array}{r}F'_{a,r}\\ F'_{b,r}\end{array}\right\}$ = the fixed-end moment factors for a beam having one end hinged and the other end fixed and a concentrated load at distance $r\,L$ from the hinged end;

$\left.\begin{array}{r}F_{a,u}\\ F_{b,u}\\ F'_{a,u}\\ F'_{b,u}\end{array}\right\}$ = the fixed-end moment factors as the foregoing for a unit uniformly distributed load;

I_x = the moment of inertia at $x\,L$;

$\left.\begin{array}{r}k_a\\ k_b\end{array}\right\}$ = the dimensionless stiffness factors at the small and large ends, respectively, for use in the formula: Stiffness equals $K = \dfrac{E\,I_a}{k\,L}$;

L = the length of a member;

m = an integer signifying the degree of the flexural function;

N = a factor defined by Eq. 8;

n = the number of differential segments;

P = a concentrated load;

q = the segment designation;

$r\,L$ = the position coordinate for the concentrated load—constant during integration;

t_r = total depth of beam at a section;

$\left.\begin{array}{r}t_p\\ t_t\end{array}\right\}$ = depths of parts of a beam, as shown in Table 2;

$x\,L$ = the variable of integration;

Φ = a flexural function;

Φ' = a factor for computing Φ;

$\theta_{a,r}$ = the angle-of-rotation factor at the small end of the beam, corresponding to a unit load at a distance $r\,L$ from the small end, for use in the formula: $\theta = \theta_{a,r}\,\dfrac{P\,L^2}{E\,I_a}$, in which θ is the angle at rotation at the small end of the beam; and

$\theta_{a,u}$ = the angle-of-rotation factor at the small end corresponding to a unit uniform load.

(The subscript "a" refers to the small end of the beam shown in Fig. 1, at which end x equals zero, except that I_a is a "reference" value, taken at any stipulated section. The subscript "b" refers to the large end of the beam, at which x equals unity. The first subscript on the flexural functions Φ are the m-values that apply. The second subscript r on Φ, F, F', and θ corresponds to the position of the concentrated load and takes values 1 through n in sequence. A second subscript u on any symbol corresponds to a unit uniform load. The values of x and r are dimensionless.)

DISCUSSION

Henry Malter,[2] A. M. ASCE.—A method of numerical integration that differs from the author's method for computing stiffnesses, carry-over factors, and fixed-end-moment factors has been developed by N. M. Newmark,[3] M. ASCE. Mr. Newmark's method involves no new theoretical concepts; however, by a systematization of computations an answer can be obtained quickly. As in any numerical procedure, exact solutions are not found, but the degree of accuracy obtained is sufficient on consideration of all the variables involved in the problem that is ordinarily encountered. The accuracy of any solution can be improved by increasing the number of subdivisions of the beam. After becoming familiar with the technique of solution, the matter of subdivisions is one of individual discretion. The time spent must be balanced against the accuracy desired, with a constant realization of the limitations on accuracy imposed by the conditions of the problem.

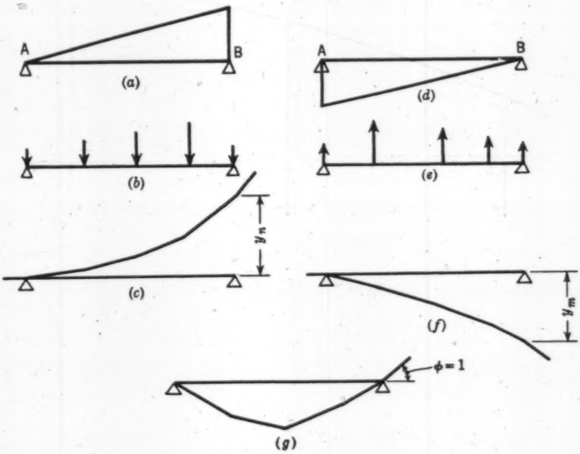

Fig. 5.—Basic Concepts of the Newmark Method

General Solution.—Using the method developed by Mr. Newmark, a moment is introduced into beam AB at end B in Fig. 5(*a*). The moment diagram is changed into a series of concentrated angle changes α that are considered to be loads in Fig. 5(*b*). With zero slope at A, and progressively adding each concentrated angle change α, the final deflection at B and the shape of the elastic curve are obtained as shown in Fig. 5(*c*). To correct for the deflection y_n at B, a moment is introduced at A in the correction diagram of Fig. 5(*d*). This results in the series of load concentrations shown in Fig. 5(*e*). With zero slope at A, the concentrated angle changes are added, thus obtaining the deflection y_m at B (Fig. 5(*f*)). If this deflection of B is of opposite sign to that obtained in Fig. 5(*c*), y_n/y_m times the correction diagram (Fig. 5(*f*)) is added to the deflection diagram (Fig. 5(*c*)) to form a deflection diagram having zero slope at A and zero deflection at B (Fig. 5(*g*)). The slope at B is reduced to unity and the moments and the deflections are reduced accordingly. This produces a unit rotation at B, and the moment accompanying this rotation is the beam stiffness. The deflected line is an influence line for the moment at B, using the Müller-Breslau principle, and the carry-over factor is the ratio of the final corrected moment at A to the moment at B.

---

[2] Head, Dept. of Civ. Eng., Robert College, Istanbul, Turkey.

[3] "Numerical Procedure for Computing Deflections, Moments, and Buckling Loads," by N. M. Newmark, *Transactions*, ASCE, Vol. 108, 1943, pp. 1161–1234.

Sign Convention.—A numerical procedure requires a sign convention for rapid computations, and the convention adopted by Mr. Newmark will be retained. Any method of obtaining panel concentrations from distributed loads is approximate. A suggested procedure is illustrated in Fig. 6.

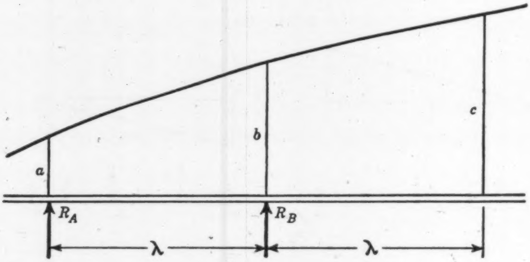

FIG. 6.—LOADING CURVE

The formulas derived by Mr. Newmark,

$$R_A = \frac{\lambda}{12}\,\frac{1}{2}\,(7\,a + 6\,b - c)\ldots\ldots\ldots\ldots\ldots\ldots(15a)$$

and

$$R_B = \frac{\lambda}{12}\,(a + 10\,b + c)\ldots\ldots\ldots\ldots\ldots\ldots\ldots(15b)$$

assume that the loading curves are parabolic and continuous. For problems involving discontinuities, two R_A-values are combined.

Numerical Integration.—The steps to be used are illustrated in Table 3 and are as follows (the lines refer to the lines in Table 3):

a. A moment M_b (some multiple of the number of subdivisions) is applied to the beam AB at point B (line 6).

b. The moment values at the subdivisions are changed to α-values $\left(\text{equal to } \frac{M}{E\,I}\right)$ at the particular point (line 7).

c. The distributed α-values are changed to $\bar{\alpha}$-concentrations by using the appropriate relationship. The factor $h/12$ is included in the right-hand column (line 8).

d. Assuming zero slope at point A, the slope in each subdivision is computed by adding each $\bar{\alpha}$-concentration successively (line 9).

e. Assuming zero deflection at point A, the deflection at each point is determined by successively adding the various slopes (line 10). The factor h is included as a common multiplier in changing the factor to $b^2/12$.

This satisfies the condition of the problem that the slope at point A be zero. However, the second condition—that the deflection at point B be zero—is not satisfied. To make the necessary correction, a correction-configuration diagram must be added by applying a moment at point A.

f. A moment M_a is applied at end A (line 1).

g. The moment values are changed to α-values (line 2).

h. The $\bar{\alpha}$-concentrations are computed (line 3).

i. Assuming zero slope at point A, the slope in each subdivision is computed (line 4).

j. Assuming zero deflection at point A, the deflection at each point is successively determined (line 5).

k. To make the deflection at point B zero, it is necessary to add a proportion of the deflection found in line 5 to that found in line 10. The correction ratio is the deflection y_m at point B (line 10) divided by the deflection y_n at point B (line 5) with the appropriate sign to produce a total deflection at point B equal to zero. This correction ratio is then multiplied by each of the values in line 5 to obtain y_c (line 11).

l. Lines 10 and 11 are then added to determine the final deflections (line 12).

m. The slope ϕ at point B is computed. This consists of three steps: The first step is the determination of the slope to the left of point B, the second step is the computation of $\bar{\alpha}$ at point B, and the third step is to determine the corrected value of $\bar{\alpha}$ from the correction configuration.

TABLE 3.—SOLUTION OF ILLUSTRATIVE PROBLEM

Line	Term or factor	DISTANCE FROM LEFT SUPPORT, IN FEET				
		0.00	3.25	6.50	9.75	13.00
1	Applied moment, M_a	0	+6	+12	+18	+24
2	α-values	Determined semi-graphically				
3	$\bar{\alpha}$-concentrations	−1.28	−17.97	−39.00	−30.39	−0.17
4	Slope, ϕ	+87.53	+69.56	+30.56	+0.17	
5	Deflection, y_n	−187.82	−100.29	−30.73	−0.17	0
6	Applied moment, M_b	+24	+18	+12	+6	0
7	α-values	Determined semi-graphically				
8	$\bar{\alpha}$-concentrations	−4.64	−45.10	−39.00	−14.38	−0.05
9	Slope, ϕ	+98.53	+53.43	+14.43	+0.05	
10	Deflection, y_m	−166.44	−67.91	−14.48	−0.05	0
11	Deflection, y_c	+166.44	+88.71	+27.30	+0.15	0
12	Deflection, y	0	+20.80	+12.82	+0.10	0

These steps allow for the determination of the stiffness, the carry-over factor, and the fixed-end-moment factor for both distributed and concentrated loads for point B.

To illustrate the application of Mr. Newmark's method, the author's first problem is analyzed in Table 3. Inasmuch as the stiffness is infinite at both ends for varying distances, resulting in zero $\left(\frac{M}{E\,I}\right)$-area, a semigraphical method was used to obtain the α-values at the evenly-spaced points.

For this problem, the slope ϕ at point B was

$$\phi = +\,20.80 + 4.64 - 1.13 = 24.31 \text{.............} (16a)$$

the stiffness was

$$K_a = \frac{24 \times 4 \times 3.25}{24.31}\frac{E\,I}{L} = 30.0 \text{ kip-ft............} (16b)$$

the carry-over factor was

$$C_{ab} = \frac{166.44}{187.82} = 0.887 \text{....................} (16c)$$

and the fixed-end-moment factor was

$$F_{a,\,0.5} = \frac{12.82\,P\,h}{24.31} = 0.132 \text{..................} (16d)$$

In a similar manner, the stiffness, the carry-over factor, and the fixed-end-moment factor for the right-hand side of the bent were computed. To compare the results obtained by the use of Mr. Newmark's method with those obtained by the author, Table 4 has been prepared. This table is presented to demonstrate the technique involved, and not to question the physical meaning of the constants derived. Although beam dimensions may take on sudden changes, distributed angle changes (moment areas) are stress-strain relationships, and all changes must be gradual.

TABLE 4.—COMPARISON OF RESULTS

Method	TERM OR FACTOR					
	K_a, in kip-feet	C_{ab}	$F_{a,\,0.5}$	K_b, in kip-feet	C_{ba}	$F_{b,\,0.5}$
Morrison.........	30.4	0.894	0.143	39.6	0.680	0.205
Newmark.........	30.0	0.887	0.132	38.6	0.680	0.216

PAUL ROGERS,[4] M. ASCE.—Although numerical methods such as moment distribution and relaxation system have become so widely accepted that the classical analyses for most computations are practically obviated. Their use is usually limited to prismatic members. There are tabulated constants for straight and parabolic haunches available, but these consider only a few of the most commonly applied loadings.

The fundamental theory of moment distribution supplies the tools with which the stiffness factors, distribution factors, carry-over factors, and the proper fixed-end moments can be computed for almost all possible loadings and shapes of the supporting members. In actual practice, however—unless the structure is of utmost importance, or is repeated to such an extent that even minute savings can amount to considerable economies—designing engineers cannot afford the time necessary to make refined computations.

---

[4] Cons. Engr., Rogers and Snitoff, Inc., Cons. Engrs.. Chicago, Ill.

Mr. Morrison recognized that the tedious computations for the required constants are made laborious by needless repetitions of numerical computations. By proper grouping, registering, and tabulating the obtained values, the author's method allows for their use in further computations, at once saving time and eliminating some sources for numerical errors.

The only systems to be considered in practical design (apart from academic studies or research), are those which afford speedy and accurate results. It has been found that even for prismatic members there is a need for tabulated values for fixed-end moments because loadings on structures are complex and usually unsymmetrical. The writer has tabulated fixed-end moment constants.[5] Because of the unlimited variety of possible shapes for the supporting members, the constants are limited to prismatic members.

Mr. Morrison's basic formulas may be varied to such an extent that his numerical computations might be combined with tabulated constants. Such combination would give the moment-distribution method widespread practical application.

Thomas G. Morrison,[6] A.M. ASCE.—Mr. Malter has reviewed Mr. Newmark's approximate method for obtaining deflection curves and has applied the method to the first illustrative problem. It is of interest to note that, for the triangular loading used by Mr. Malter, the slopes ϕ (given in lines 4 and 9 of Table 3) are, respectively, $\phi_{1,r} \frac{I_0}{I} M\,L$ and $(\phi_{0,r} - \phi_{1,r}) \frac{I_0}{I} M\,L$ in which $M\,L$ is the product of the applied moment (24 ft kips) and the beam length (13 ft). These values can be obtained more quickly and accurately by use of the flexural functions in lieu of the semigraphical integration used by Mr. Malter. For a less simple problem—for example, the second illustrative problem—the flexural functions would certainly give the slopes more accurately and quickly. Similarly, for the loadings used, the exact values for the deflections y_n are proportional to $(r\,\phi_{1,r} + \phi_{2,r})$ and the deflections y_m are proportional to $(r'\,\phi_{1,r} - \phi_{2,r})$.

Several other well-known methods have been used for obtaining the flexural constants—the column analogy and the conjugate beam are two of the more popular. Most of these methods are simple in physical theory but entail more numerical work than is necessary when used for computing flexural constants. Because the flexural functions are the "building blocks" of which the beam constants are built, all of these methods can be expressed in terms of the flexural functions when arranged for the computation of the flexural constants.

Mr. Rogers refers to the many excellent tables that are available for obtaining fixed-end moments. In these tables are cited many of the conditions encountered in building construction. However, the data published for continuous bridge design are incomplete, and (for the reason given by Mr. Rogers) must so remain. Lack of a suitable, quick, accurate method for obtaining the flexural constants has influenced bridge designers to adopt soffit curves solely because tabulated flexural constants were available for the curves used—to the economic and artistic detriment of the design. The ungainly, half-horizontal, half-parabolic soffit curve used for the end spans of so many otherwise beautifully-proportioned concrete bridges is a case in point. Introduction of the flexural functions and the tabulated values for $\phi'_{0,r}$, $\phi'_{1,r}$, and $\phi'_{2,r}$ has freed the bridge engineer and architect from the few tabulated forms for soffit curves. Bridges can be proportioned for economy and grace without the necessity for an analytic expression and without increasing the difficulty of design.

---

[5] "Tables and Formulas for Fixed End Moments of Members of Constant Moment of Inertia," by Paul Rogers, Frederick Ungar Pub. Co., New York, N. Y., 1953.

[6] Cons. Engr., Chicago, Ill.

AMERICAN SOCIETY OF CIVIL ENGINEERS
Founded November 5, 1852
TRANSACTIONS

Paper No. 2661

SPECIAL DESIGN FEATURES OF THE YORKTOWN BRIDGE

By Maurice N. Quade,[1] M.ASCE

Synopsis

Many unique problems were encountered in the design of the George P. Coleman Memorial Bridge at Yorktown, Va. The ultimate solutions to these problems and a brief description of the construction of the central span are included in this paper.

The design features of this structure include the use of two swing spans in tandem, hollow, concrete supporting piers, and steel caissons specially designed for the construction of the piers. Details of the substructure and superstructure are given, as well as information on the operating features of the bridge.

Design Features

The three special features of the York River Bridge at Yorktown, Va., are: (1) The lightweight, hollow pier bases that made possible the design of tall piers with unusually low bearing pressures at the bottom, as required by soil conditions; (2) the design of the steel caissons used in constructing the piers; and (3) the use of two swing spans placed in tandem, each span longer than any previous swing span built.

Description of Bridge

The structure, known as the George P. Coleman Memorial Bridge, was opened to traffic in May, 1952. It connects Yorktown on the south bank of the York River with Gloucester Point on the north bank. At Gloucester Point the river is 2,600 ft wide—only one quarter of the 2-mile width above and below the bridge site. The river crossing is achieved by seven deck truss spans completely symmetrical about the center channel span, as shown in Fig. 1. Approaches on either side consist of deck, plate-girder, spans terminating

---

Note.—Published, essentially as printed here, in January, 1953, as *Proceedings-Separate No. 168.* Positions and titles given are those in effect when the paper was received for publication.

[1] Partner, Parsons, Brinckerhoff, Hall & Macdonald, Engrs., New York, N. Y.

in abutments located at the top of a natural slope on the south bank and on a 40-ft-high artificial embankment on the north side. The total length of the bridge is 3,750 ft.

At the center of the channel span, the roadway attains a height of 115 ft above the water by means of 4.5% grades on either side and a vertical curve 1,000 ft long between them to provide ample sight distance for highway safety.

Normally, each end of a swing span rests on a pier or an abutment, but in the case of the Yorktown Bridge the forward arms of the two swing spans provide the required 450-ft clear width of channel for navigation, and obviously the center of that channel is not the place to locate a pier. Piers could have been placed at the shore ends of each swing span, but this would have resulted in a span length on either side of the channel of only 250 ft (which is too short for economy because of the great depth of the river and the resulting high cost of the piers). Moreover, the architects and the structural engineers agreed that it would have created a most unpleasant appearance.

To increase the length of the spans adjacent to the channel and to permit a curved bottom chord in these spans, the fixed trusses in the adjoining spans are cantilevered four panels (140 ft) beyond the pier and, in the closed position, the shore end of each swing span rests on the end of a cantilever arm. The length of each flanking span is thus increased from 250 ft to 390 ft.

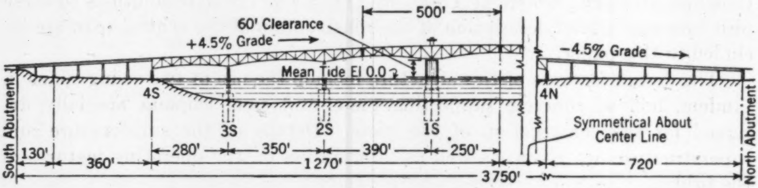

FIG. 1.—ELEVATION OF YORK RIVER BRIDGE, YORKTOWN, VA.

On each side of the channel, the next span toward the shore is an anchor span 350 ft long, and beyond these is a second cantilever arm 70 ft long that supports one end of a 210-ft suspended span. Since the shore end of the suspended span rests on a pier located near the edge of the river, the end truss spans are 280 ft long.

The two-lane roadway is 26.0 ft wide between curbs 10 in. high. Each curb has a width of 2.5 ft, which is sufficient to serve as an emergency sidewalk.

FOUNDATION CONDITIONS AND DESIGN CRITERIA

Subsurface Conditions.—Water depths at the sites of the six river piers vary from 50 ft to 80 ft, the average depth being 70 ft (see Table 1). One or more borings taken at each site showed that the river bed is of rather soft mud, sometimes containing small quantities of loose sand. The depth of mud varies from 10 ft to 40 ft, the bottom of the stratum being 85 ft to 110 ft below the water surface. The mud is generally underlain by sand or silt strata, some of which contain clay and broken shells. The sand is predominantly fine to very fine. Although most of the piers are actually founded on these strata, the borings—some of which were driven to a depth of 200 ft below the water surface—show that the principal material supporting the piers is a medium to stiff clay. Fig. 2 illustrates a typical boring log.

Pier Design Criteria.—Both the resistances to driving the sample spoon, and the laboratory tests of undisturbed samples obtained from borings, led to the conclusion that the net unit bearing from vertical loads must be limited to 2.0 tons per sq ft in excess of that resulting from the weight of the existing overburden at the depth of the bottom of the pier base. Since permanent vertical loads exert more influence on pier settlement than horizontal forces (which are generally at a maximum for only a short duration), a maximum edge pressure of 3.5 tons per sq ft was considered permissible for vertical loads in combination with horizontal forces tending to overturn the piers.

Obviously with such criteria, the depth of penetration of the pier base into the bed of the river becomes a variable in the design, since in most cases the depths at which the piers are founded exceed the minimum depths required for lateral stability against horizontal movement. As designed, bearing pressures (after deducting for the buoyancy of the submerged parts of the pier) do not exceed 4.0 tons per sq ft for the total direct vertical load. The weight of the overburden above the bottom of the pier base is 2.0 tons per sq ft; hence, the net differential direct pressure is 2.0 tons per sq ft for all vertical loads. Horizontal forces (such as those from wind on the parts of the bridge above water and river currents below water) increase the edge pressure by an additional 1.8 tons per sq ft (maximum). From the total bearing pressure, it has been considered reasonable to deduct 0.3 ton per sq ft as an allowance for permanent skin friction on the embedded depth of the caisson base. This is equal to an average unit friction of 200 lb per sq ft.

TABLE 1.—SUMMARY OF PIER DEPTHS AND BORING DATA

Pier (Fig. 1)	DEPTHS, IN FEET			BOTTOM OF BASE	
	Water	Mud	Silt, sand, and shells	Elevation	Material
3S	75	10	50	−135	Very fine sand and shells
2S	80	30	35	−150	Stiff green clay and shells
1S	80	20	49	−150	Gray clay with shells
1N	72	18	50	−141	Fine gray sand with shells
2N	60	40	41	−141	Silt and shells
3N	50	30	45	−135	Green sand with shells

To reach a stratum capable of supporting the net bearing load previously described, piers 1S and 2S were sunk to a depth of 150 ft below mean tide level (Fig. 1). Piers 1N and 2N have been founded at El. −141 and the two piers nearest the shores, 3S and 3N, at a depth of 135 ft. Laboratory analyses indicate that even the low pressures produced at these depths may cause slight settlements during the first fifty years of the life of the bridge. If they occur at all, they will be small in magnitude, uniform in character, and will create no serious structural or maintenance problems. If settlements should become a nuisance to the next generation, they will find that their predecessors have

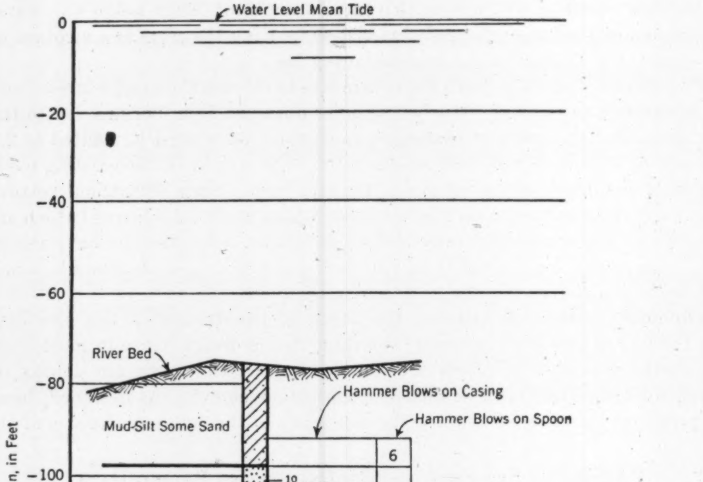
Water Level Mean Tide
0
-20
-40
-60
-80
-100
-120
-140
-160
-180
-200
Elevation, in Feet
River Bed
Hammer Blows on Casing
Hammer Blows on Spoon
Mud-Silt Some Sand
Coarse Gray Sand
Very Fine Gray Sand
Very Fine Gray Sand Many Shells
Very Fine Gray Sand Few Shells
Fine Gray Sand
Gray Clay, Little Very Fine Gray Sand Some Shells
Gray Clay
Gray Clay Few Shells
10 18 26
29 26 22
28 25 14
15 18 20
23 30 29
35 36 40
41 31 27
29 28 32
32 36 75
59 42 40
35 35 41
45 60 62
80 74 149
92 84 82
90 90 87
90 94 105
114 130 160
6
5
5
5
11
7
6
9
8
10
9
Size of Casing 2.5 In.
Size of Spoon 2-In. Round
Weight of Hammer 290 Lb
Drop 24 In.
For Both Casing and Spoon

FIG. 2.—TYPICAL BORING LOG

made it comparatively easy to correct for settlement by jacking up the steel superstructure.

PIERS

A rough idea of the problem of limiting the gross bearing pressure to 4 tons per sq ft may be obtained from considering that the tallest pier is 210 ft high (about the height of an eighteen-story building) and that a column of concrete 1 ft square and 210 ft high has a bearing pressure of more than 15 tons per sq ft. Obviously, solid piers of normal stepped and tapered design would not leave much of a margin for supporting the superstructure, which after all, is the only function of a bridge pier.

Therefore, the pier bases were designed as hollow, reinforced concrete boxes, having exterior walls 4 ft thick.[2] One transverse and two longitudinal interior walls—each 3 ft thick—divide each base into six cells and mutually brace one another and the exterior walls.

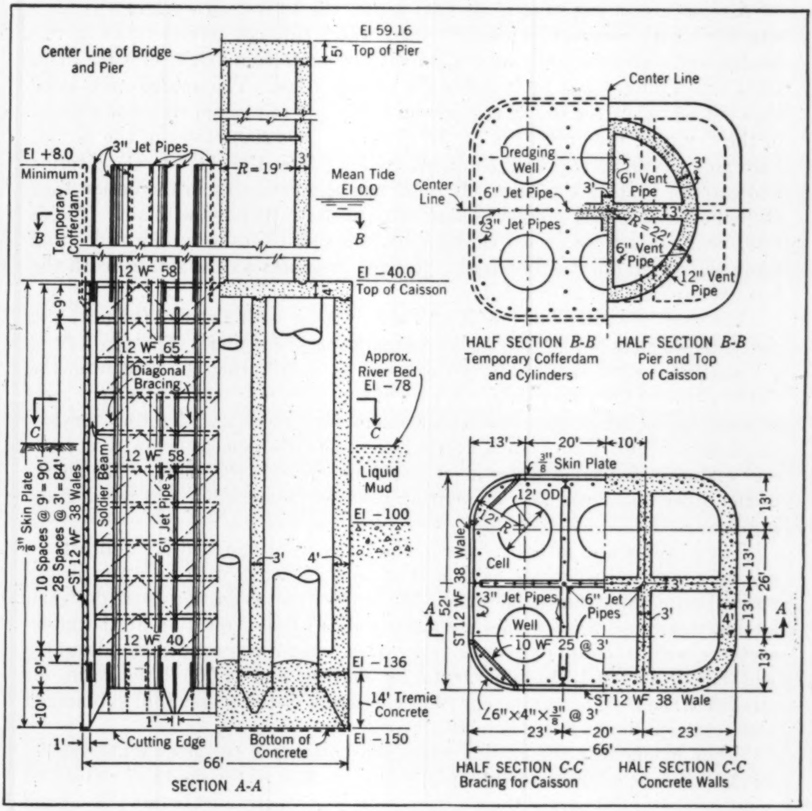
Center Line of Bridge and Pier
El 59.16
5'
Top of Pier
El +8.0
Minimum
3" Jet Pipes
R = 19'
3'
Mean Tide
El 0.0
B
B
Temporary Cofferdam
12 WF 58
El −40.0
Top of Caisson
4'
9'
12 WF 65
Diagonal Bracing
Approx. River Bed
El −78
C
C
12 WF 58
Liquid Mud
Soldier Beam
6" Jet Pipe
El −100
3/8" Skin Plate
10 Spaces @ 9' = 90'
28 Spaces @ 3' = 84'
ST 12 WF 38 Wales
3'
4'
12 WF 40
9'
El −136
14' Tremie Concrete
10'
1'
Cutting Edge
Bottom of Concrete
El −150
1'
66'
SECTION A-A
Center Line
Dredging Well
Center Line
6" Jet Pipe
3" Jet Pipes
3'
6" Vent Pipe
3'
3'
R = 22'
6" Vent Pipe
12" Vent Pipe
HALF SECTION B-B
Temporary Cofferdam and Cylinders
HALF SECTION B-B
Pier and Top of Caisson
13'
20'
10'
3/8" Skin Plate
12' OD
12' R
Wale
Cell
52'
ST 12 WF 38
3" Jet Pipes
6" Jet Pipes
Well
10 WF 25 @ 3'
3'
3'
4'
A
A
13'
13'
26'
13'
13'
ST 12 WF 38 Wale
∠6"×4"×3/8" @ 3'
23'
20'
23'
66'
HALF SECTION C-C
Bracing for Caisson
HALF SECTION C-C
Concrete Walls

Fig. 3.—Typical Dimensions, Pivot Pier 1S

The bases for the two pivot piers supporting the swing spans (Fig. 3) are 66 ft by 52 ft in plan, the corners being rounded on a 12-ft radius. The other four bases are similar in plan to the pivot pier bases but are slightly smaller (66 ft by 42 ft).

---

[2] "Deep Lightweight Piers for Bridge at Yorktown, Va., Built by Caisson Method," by Maurice N. Quade and George Vaccaro, *Civil Engineering*, Vol. 21, 1951, p. 79.

The pier bases were designed for construction by the open dredge caisson method. Since the tops of the bases of all river piers have a plan elevation of −40, the highest caisson base was 110 ft tall and the shortest, 95 ft. Follower cofferdams 48 ft high, designed by the contractor, were used in the construction of the underwater parts of the pier shafts.

After a caisson was sunk to its final depth, the 10-ft-deep working chamber was filled with concrete deposited under water through tremie tubes in the dredge wells, and the wells were filled with concrete to a height of 4 ft. The total depth of seal was 14 ft above the cutting edge. The dredge wells were then cut off below the top of the caisson and a 4-ft reinforced slab was poured in the dry over the entire top of the caisson. This slab closes in the hollow base and serves, as required, to distribute load from the shaft to the interior and exterior walls of the base. It could not be anticipated in the design that the hollow spaces in the base would remain permanently filled with air. Therefore, vent pipes were placed through the top slab to insure uniform flooding when the cofferdam was removed. Bearing pressures on the soil beneath the base were computed accordingly.

The shaft of each pivot pier is a hollow cylinder with a shell 3 ft thick, and two interior cross walls, 3 ft thick, mutually perpendicular. The top 5 ft of the shaft is a solid slab reinforced to assist in distributing the load from the center pivot of the swing span. A part of the interior spaces above river level is used for housing electrical transformers for power and lighting service. Here again, vents insure equal flooding of the interior spaces below river level and maintain the same water level inside and outside the shaft. The shafts of the other four river piers supporting fixed spans are solid, and rectangular in plan.

The exterior and interior walls in the bases were designed for hydrostatic pressure incurred when the caisson is at its final depth with no water in the spaces surrounding the dredge wells. The curved corner sections were designed as unsymmetrical fixed arches assuming points of zero rotation at the intersections with the interior walls. For this temporary condition, allowable working stresses of 1,350 lb per sq in. for concrete and 22,000 lb per sq in. for steel were used. The permanent load, consisting of the pressure of submerged soil, results in much lower stresses.

Reinforcement in the cutting edges and bottoms of the cross walls was designed for edge support during sinking but, because of the depth of water and mud, a substantial part of the concrete walls was constructed before the caisson became nonbuoyant; hence, only a comparatively small percentage of steel is needed to resist bending caused by edge support. The depth-span ratio is large. Steel in the cutting edges and cross walls was checked for its capacity to resist the wedge action of the sloping sides of the tremie seal.

Design of Caissons

Some of the caissons were sunk through 80 ft of water and for design purposes were assumed to reach a depth of 115 ft before the soil became sufficiently firm to support them. The necessary buoyancy was provided by steel boxes, within which the reinforced concrete walls were constructed in stages.

Since a steel caisson is in reality a piece of construction equipment, it is usually designed by the contractor. Preliminary designs soon indicated, however, that the design and construction of each pier and the design of its caisson were inseparable problems; hence, detailed designs for the caissons were included in the contract plans. Basic design criteria for the completed pier were outlined in the specifications, and bidders were permitted to submit proposals based on an alternate design for the caissons conforming to those criteria. However, the lowest alternate bid received exceeded the lowest bid on the contract plan design by more than $1,600,000.

As designed, the caissons were welded throughout and were made of a $\frac{3}{8}$-in. continous skin plate, reinforced by horizontal steel wales 3 ft on centers, consisting of continuous 12-in. structural tees. The wales, in turn, were supported by six vertical soldier beams (18WF70) in the planes of the cross walls. The soldier beams were supported by 12-in. wide-flange struts of varying weights at 9-ft centers, braced by double-angle diagonals. Since the struts and diagonals are in the planes of the cross walls, they became embedded in concrete as the walls were poured in successive lifts. Each level of longitudinal and transverse struts is offset vertically by 6 in. to eliminate splicing.

At the points where the struts crossed, an extra heavy pipe, 6 in. in diameter, extended from top to bottom of the caisson through holes in the webs of the 12-in., wide-flange struts. The pipes were welded to the struts and served as structural posts. In addition, they were used for jetting during sinking and were extended for this purpose when the follower cofferdam was added.

Because of the interrelation between the design of the completed pier, the caisson used to build it, and the sequence of construction, stresses and buoyancy conditions were computed for twenty-six separate and consecutive stages of sinking and construction for pier 1S, for example. The results were included in the bidding documents to acquaint the bidders thoroughly with the scope of the work and the problems involved. The stages were subsequently studied and modified to some extent by the contractor.[3]

The development of the design followed a rather definite sequence, although there was much "cutting and trying" in the process. After the dimensions of the caisson and the concrete wall thicknesses were determined, some height-of-wall pour had to be assumed. This height was made such as to permit placement of a practicable volume of concrete per lift; yet, during the buoyant stages of construction (up to a 115-ft depth)—while the caisson was still afloat and its depth below the water surface could not be controlled by dredging—the weight added to the caisson in each lift was limited by the permissible increase in hydrostatic head acting on those parts of the steel caisson that were not effectively reinforced by seasoned concrete. Using a trial design, the draft, freeboard, and hydrostatic head were computed for each added increment of concrete.

The successive stages that were studied indicated that a head of 23 ft above the top of seasoned concrete of the exterior wall occurred frequently and that, after the first 20 ft of all the walls had been placed simultaneously, the 23-ft head would be considerably exceeded during certain stages, unless the exterior walls were advanced ahead of the interior walls by separate pours. As constructed, the interior walls were 20 ft lower than the exterior walls, at times, and the required differential was maintained until the caisson was firmly seated and did not float. Within the range of differential pours, the exterior walls were provided with keys and dowels to insure effective transfer of stress.

---

[3] "Floating Caissons for Yorktown, Va., Bridge Sunk to 150-Ft Depth in Swift-flowing Tidal Water," by John N. Newell, *Civil Engineering*, Vol. 21, 1951, p. 406.

Since the construction of the interior walls lagged behind, many of the caisson struts and soldier beams are relatively heavier because they are subjected to greater hydrostatic heads than the shell plate and wales. This is economical because most of the 3,700 tons of structural steel in the six caissons is in the skin plate and wales. A design based entirely on simultaneous pours for all walls would substantially increase the head on the skin plate and wales and, therefore, the quantity of steel required.

The skin plate is ⅜ in. thick. A check of the unit stress in the plate, when computed in accordance with usual structural practice, reveals that, for a ⅜-in. plate continuous over 3-ft supports and loaded by a hydrostatic head of 23 ft (nearly 1,500 lb per sq ft), the combined bending and tensile stresses in the plate is about 46,000 lb per sq in. However, it is generally agreed that the usual theoretical analysis for plates subjected to this type of action is exceptionally conservative, as proved by tests. The designers then adopted the method used in the design of steel ships for determining the required thickness of rectangular plates under fluid pressure.

Although any similarity of these caissons to warships is coincidental, the method used in design was that described for warships by William Hovgaard.[4] Other authorities are in substantial agreement. The method is largely empirical and is based primarily on tests. The simplified method,[5] applicable to this particular problem (Fig. 4), consists of the fact that, when the longer dimension of a rectangular plate supported on four sides is three or more times the shorter dimension (as is the case in these caissons), the coefficient in the design formula may be taken as unity with negligible error.

In Fig. 4, the ordinates are plotted as the ratio s/t in which s is the length of the short side of the rectangle and t is the thickness of the plate. The abscissas are plotted equal to the equivalent head, $K_A\ h$, in which K_A is a coefficient dependent upon the ratio r between the long and short sides of the rectangle, and h is the actual head of water. In this design r is greater than 3 and K_A is 1; hence, the head is read directly.

In Fig. 4, curve A corresponds to the case in which the plate reaches the yield point—that is, it has no permanent set if the head indicated is not exceeded. For the particular case under study, with ⅜-in. plate and a 3-ft span ($s/t = 96$), the head is 13 ft.

Curve B corresponds to the case in which the permanent set in the plate is about 20% of the total deflection under the given head, and when the head is exceeded, the permanent set begins to increase rapidly. In ship design this is the curve used for the shell plating of submarines and for ordinary watertight bulkheads.

---

[4] "The Structural Design of Warships," by William Hovgaard, The U. S. Naval Inst., Annapolis, Md., 1940.

[5] *Ibid.*, Plate IV, facing p. 124.

The designers were not quite willing to adopt curve B, entirely, and adopted a 23-ft head for the ⅜-in. skin plate supported on 3-ft centers, which is about one third the distance between curves A and B and corresponds to an 8% permanent set in the plate and a deflection of about ⅞ in.

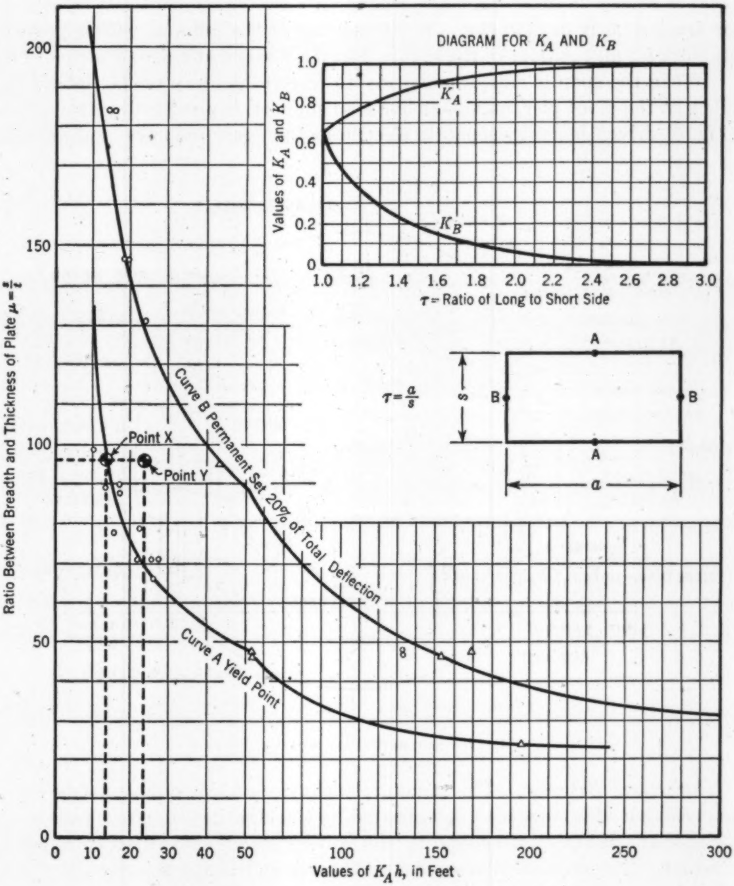

FIG. 4.—DIAGRAM FOR THE DESIGN OF A CAISSON SKIN PLATE

During the towing of one of the caissons to the site, rough weather was encountered and the caisson listed. The water line was observed at the time and was found to be 36 ft above the concrete. This is almost three times the head that produces yield point stresses, but there was no evidence of damage to the skin plate or any other part of the caisson.

Superstructure

Each of the 500-ft swing spans weighs about 1,200 tons. When the span is in motion or free to rotate, it is supported on a single center pivot. Lateral stability of the span when so supported is provided by four pairs of cast steel balance wheels 28 in. in diameter, rolling on a twelve-segment cast steel circular track 34.5 ft in diameter. A 90° spacing of the pairs of wheels provides stability for all positions of the span. Fig. 5 is a schematic plan of a pivot pier.

When the span is closed and ready to receive highway traffic, lateral stability at the pivot pier, as well as live load support, is provided by two wedges (Fig. 6) driven home by separate electric motors, gear reducers, and linkages.

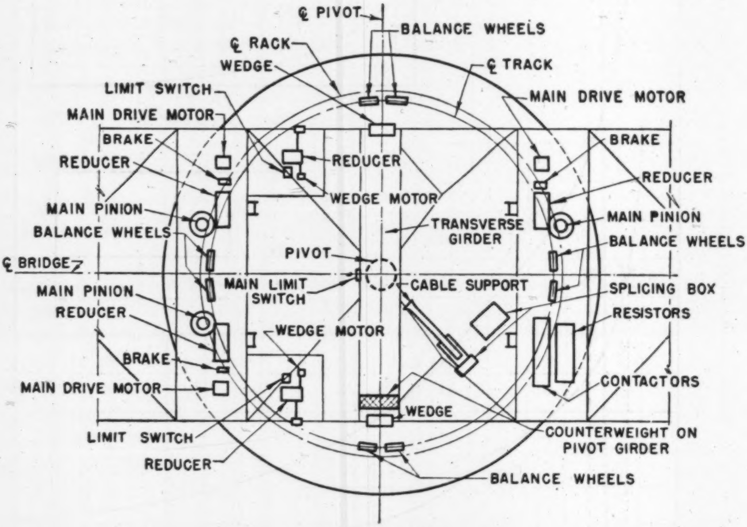
℄ PIVOT
BALANCE WHEELS
℄ RACK
WEDGE
℄ TRACK
LIMIT SWITCH
MAIN DRIVE MOTOR
MAIN DRIVE MOTOR
BRAKE
BRAKE
REDUCER
REDUCER
REDUCER
WEDGE MOTOR
MAIN PINION
TRANSVERSE GIRDER
MAIN PINION
BALANCE WHEELS
BALANCE WHEELS
PIVOT
℄ BRIDGE
MAIN LIMIT SWITCH
CABLE SUPPORT
MAIN PINION
SPLICING BOX
REDUCER
RESISTORS
WEDGE MOTOR
BRAKE
CONTACTORS
MAIN DRIVE MOTOR
WEDGE
LIMIT SWITCH
COUNTERWEIGHT ON PIVOT GIRDER
REDUCER
BALANCE WHEELS

Fig. 5.—Schematic Plan at Pivot Pier

Structural Behavior.—The structural behavior of this double swing bridge under live load is somewhat complicated by the fact that the shore ends of the swing spans rest on elastic supports (the cantilever ends of the fixed truss spans). Theoretically, a vehicle at any point on the five central spans (except at a point directly over a pier) will produce stress in every main truss member in all five spans. Similarly, a load applied to one of the end spans will stress the main truss members in all other spans except the end span on the opposite side of the river. Practically, this is of little significance from the standpoint of stresses or deflections. There will be slightly more vibration in the structure. A person standing on the bridge might be somewhat puzzled by a slight vibration caused by a vehicle that he can neither see nor hear. The motorist is happily unaware of the fact that his vehicle disturbs more than 2,000 ft of structure.

Span Connections.—The elastic end supports for the swing spans present problems other than those involving stresses. Ordinarily, swing bridges are equipped with wedge end lifts to insure a positive dead-load and live-load reaction at the ends of the span. In this double swing span, it is useless to provide end lifts because they would only result in rotating the spans about the center pivots throwing objectionable load on the balance wheels and causing the two forward arms at midchannel to drop. It has been necessary, therefore, to use bascule-type shear locks to provide live-load supports for the ends of the swing spans.

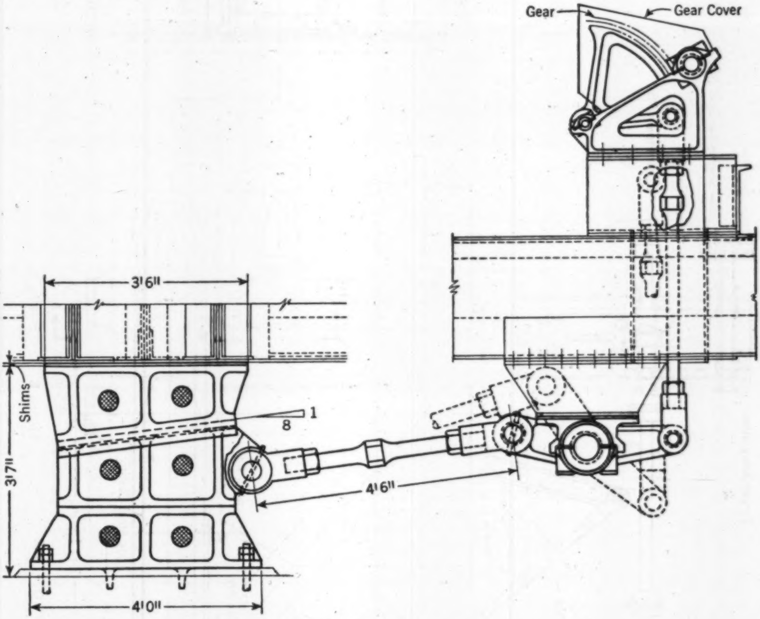

Fig. 6

In the closed position, two large motor-operated movable lock bars (Fig. 7) at the shore end of each swing span engage bearing slots on the cantilever end of the adjacent fixed truss span. A single motor operates both lock bars through a gear reducer which, in turn, applies power to a pinion gear engaging a rack on the lock bar.

A similar pair of locks connects the forward ends of the swing spans where they meet at the center of the channel. The movable spans are thus securely held in the closed position vertically and horizontally and are connected to each other and to the adjacent fixed spans. All three pairs of locks transfer live-load shear from one part of the bridge to another.

The requirements for the locking devices are unprecedented in movable bridge design. Normal operating clearances, together with inevitable wear

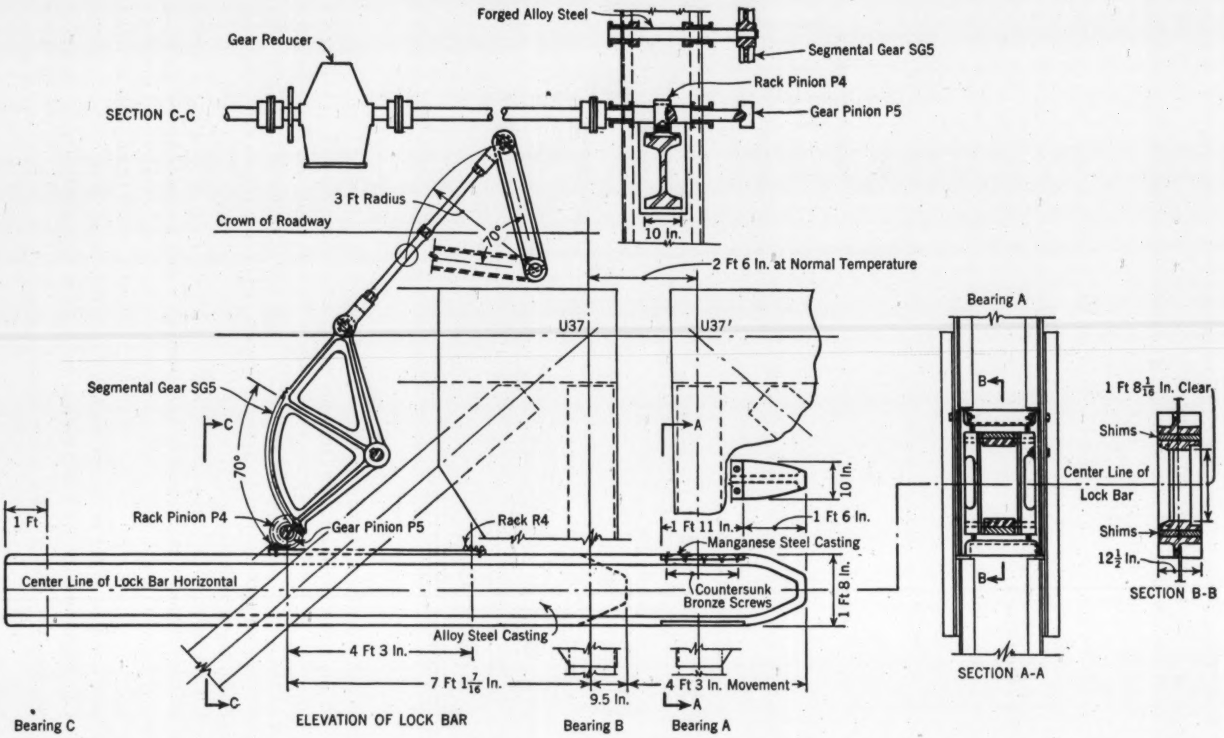
Forged Alloy Steel
Gear Reducer
Segmental Gear SG5
Rack Pinion P4
SECTION C-C
Gear Pinion P5
3 Ft Radius
Crown of Roadway
70°
10 In.
2 Ft 6 In. at Normal Temperature
Bearing A
U37
U37′
Segmental Gear SG5
C
70°
A
B
1 Ft 8$\frac{1}{16}$ In. Clear
Shims
Center Line of Lock Bar
10 In.
Rack Pinion P4
Gear Pinion P5
Rack R4
1 Ft 11 In.
1 Ft 6 In.
Shims
1 Ft
Manganese Steel Casting
12$\frac{1}{2}$ In.
Center Line of Lock Bar Horizontal
Countersunk Bronze Screws
1 Ft 8 In.
B
SECTION B-B
Alloy Steel Casting
4 Ft 3 In.
SECTION A-A
7 Ft 1$\frac{7}{16}$ In.
4 Ft 3 In. Movement
9.5 In.
C
A
Bearing C
ELEVATION OF LOCK BAR
Bearing B
Bearing A

FIG. 7.—SPAN LOCKS

throughout years of operation, will allow the spans to tip slightly on the pivot piers, thus causing some misalinement of the lock bar and the socket that it engages. Temperature and wind pressure will cause further misalinement by producing horizontal and vertical warping of the span itself and of adjacent fixed spans; yet, the locks must be designed not only to engage under all these conditions but also to move and distort the swing span as required to lock it securely in its fully closed position. Some appreciation of the magnitude of the problem may be gained from the fact that each lock bar is a heavy I-shaped alloy steel casting, 18 in. deep, 10 in. wide, and more than 18 ft long. It travels 4.25 ft in locking the span. The surfaces of the lock bars that are subject to wear consist of detachable manganese steel plates. These plates are

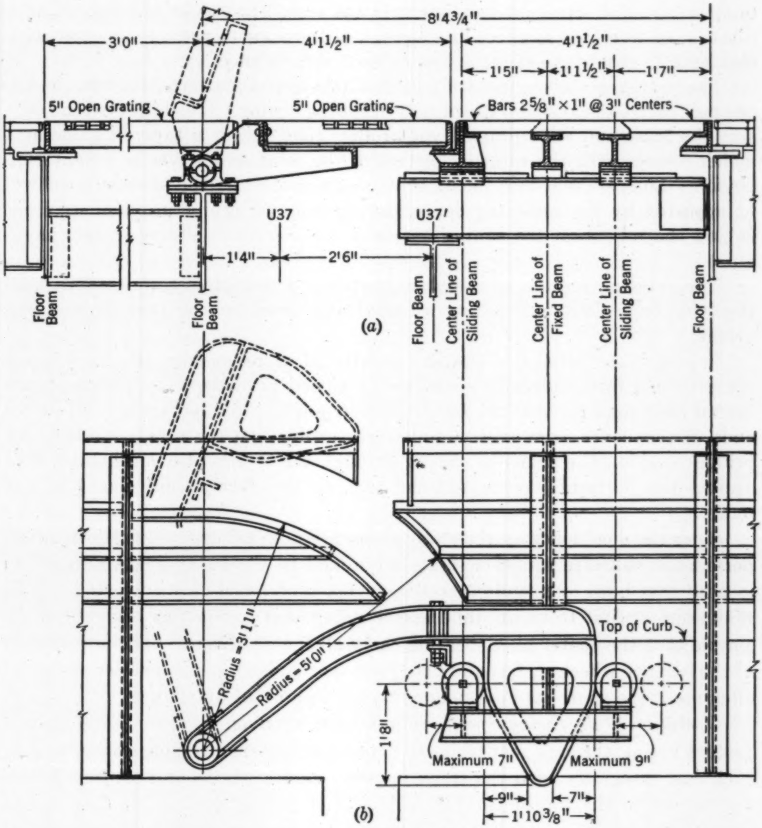
8'4¾"
3'0"
4'1½"
4'1½"
1'5"
1'1½"
1'7"
5" Open Grating
5" Open Grating
Bars 2⅝" × 1" @ 3" Centers
U37
U37'
1'4"
2'6"
Floor Beam
Floor Beam
Floor Beam
Center Line of Sliding Beam
Center Line of Fixed Beam
Center Line of Sliding Beam
Floor Beam
(a)
Radius = 3'11"
Radius = 5'0"
Top of Curb
1'8"
Maximum 7"
Maximum 9"
9"
7"
1'10⅜"
(b)

FIG. 8.—FLOOR JOINTS

hard and confine most of the wear to the softer carbon steel bearing plates in the sockets. The carbon bearing plates can be easily adjusted and can be easily and inexpensively replaced when necessary.

Floor Joints.—The floor joints at the three points where the spans separate also involved special problems not ordinarily encountered (Fig. 8). The solution was found in providing at each joint both a sliding section of floor that allows temperature and live-load movement in the closed and locked position, and a rotating section that in effect lifts enough of the floor to provide the necessary clearance to rotate the swing spans without interference.

The sliding section consists of longitudinal steel bars alternately attached to one pair of fixed beams and to one pair of sliding beams. The latter extend outside the truss and are equipped with rollers that engage a tapered guide arm which rotates with the rotating section of the joint and serves as a centering device. Longitudinal movement that may occur while the span is open will be adjusted by the centering device during the closing operation since in engaging the rollers on the sliding beams it will move the sliding section as required.

The rotating section is operated by the lock machinery and moves with the lock bars, thus eliminating an additional step in the operation of the bridge.

Superstructure Details.—Positive rotational stops against the fixed spans are provided for alining the spans in the closed position, thus insuring exact lateral alinement for the lock bars and floor joints. Air buffers located at the ends of cantilever arms and mounted vertically (like those on a vertical lift bridge) cushion the spans in closing through the action of a mechanism that applies the horizontal energy of the span to the vertical movement of the buffer.

Since the dead loads on the swing spans are not entirely symmetrical, small, permanent concrete counterweights are added to the swing spans and are so located that both longitudinal and transverse unbalances are corrected. This may seem at first to be an unnecessary refinement but in this bridge it is desirable that the center pivot-bearing carry all the dead load. The adjustment of the balance wheels, locks, and floor joint mechanisms is much easier and more effective if the span has no tendency to tip because of unbalance.

Operation of the Swing Spans.—Each span is driven by three 20-hp electric motors acting through gear trains to main pinion gears engaging a circular gear rack cast integrally with the track for the balance wheels and securely bolted and keyed to the top of the pier. If necessary, any two of the motors can operate the bridge under all conditions at an overload that is permissible for short temporary periods. Electrically-operated brakes are provided in sufficient number and size to stop the span or hold it in any open position.

Normally, each span will be operated by electric power furnished through a submarine cable to transformers located in the south pivot pier. From this point, the power is distributed as required throughout the bridge. An emergency power source is maintained in the form of a gasoline engine-generator set located in an enclosed machinery room below the bridge deck at the south pivot pier. This standby source will supply sufficient emergency power for the complete operation of both spans.

To prevent highway traffic from entering the open draw, a traffic light, warning gong, and warning gate are placed 280 ft from the shore end of each swing span. A barrier gate of heavier construction is located 140 ft on either side of the open draw. All gates are operated by electric motors.

Normally, the bridge is controlled by only one operator. In order that he may have an unobstructed and clear view of both the bridge roadway and the river, the operator's house has been placed at a clear height of 18 ft above the roadway at the south pivot pier. This house consists of a single room with adequate windows for vision in all directions. It contains the switchboards and a control desk from which every motor, brake, light, or signal for the operation of the bridge may be controlled.

The movable spans are fully equipped with all safety devices, including a complete interlocking sequence of the various steps in opening and closing the spans. Perhaps the only unusual feature of the control is the built-in device for operating the spans singly and in proper sequence for the first 8° of rotation in opening, and the last 8° of rotation in closing, the spans. In all other positions, the spans move simultaneously.

There is no attendant on the north swing span and, unlike most movable spans, it is inaccessible except by water in the open position. If a contactor should stick, or if some other trouble should develop in that span, the operator who is located on the south span has ready, for his use when needed, a non-sinkable aluminum rowboat swung from davits mounted on a platform near river level at the south pivot pier.

CONCLUSION

The final layout of this bridge is not the most economical nor the most desirable from several points of view. Circumstances compelled consideration of other factors in addition to economy and engineering. The design of the hollow, lightweight piers and their caissons would have been a part of the engineering for any crossing involving piers in the river. Those design problems that had to be solved in connection with the 500-ft swing spans are unique to this layout.

AMERICAN SOCIETY OF CIVIL ENGINEERS
Founded November 5, 1852
TRANSACTIONS

Paper No. 2662

UNIFIED MASS-TRANSPORTATION SYSTEM FOR NEW YORK

BY WILLIAM REID[1]

WITH DISCUSSION BY MR. JOHN F. KRAUS

SYNOPSIS

An adjustment in transportation philosophy, as applied to commuters in a metropolitan area, is proposed in this paper. Using the metropolitan area of Greater New York City as a "laboratory specimen," the author maintains that rail lines should most logically be used for mass transportation to the heart of the area, with feeder bus lines and private cars serving the rail-loading points.

INTRODUCTION

Despite the large population growth in the metropolitan suburban areas of New York, N. Y., and despite the appalling highway congestion, no public official nor public body has taken effective action to bring into being a modern, unified mass-transportation system for people residing within that great metropolitan area. As a consequence, more and more people are resorting to the use of automobiles and buses, and they probably will continue to do so in increasing numbers until proper and convenient mass-transportation facilities are provided.

The New York metropolitan region contains industry and business of every kind and description. It is made up of about 14,000,000 people, 7,900,000 of whom live within the city and the remainder in the surrounding cities or suburban areas.

Years ago, New York City recognized that a basic problem was one of moving people—all the people, not alone the ones who then rode in horse and buggies and, later, in automobiles and buses—and so constructed a great transit system which, however, was limited to the areas within the city.

NOTE.—Published, essentially as printed here, in February, 1953, as *Proceedings-Separate No. 171*. Positions and titles given are those in effect when the paper or discussion was received for publication.

[1] President, Hudson & Manhattan Railroad Co., New York, N. Y.

A METROPOLITAN AREA-WIDE PUBLIC AUTHORITY IS A PARAMOUNT NECESSITY

State and city boundaries must be ignored when considering the transportation needs of the population in this area. The real need is the creation of a comprehensive, modern system for the entire region. No local governmental body alone can cope with the over-all need for such a system. Only a combination of the several states, working in unison, can bring about a solution. A metropolitan area-wide public body is a "must." It should do what needs to be done to consolidate and modernize existing services; and it should coordinate all private and public transportation facilities, thereby benefitting by the efficiency of such unified operation.

TRANSPORTATION ON RUBBER REACHING SATURATION POINT

The writer agrees wholeheartedly with a statement[2] made in 1951 that

> "* * * the problem involves more than one railroad, one city or one state. What is needed is a broad, regional approach toward giving fast and comfortable transportation to all the millions in the metropolitan area."

The entire area has now come to the crossroads so far as transportation on rubber is concerned. In 1950, 6,000,000 cars were sold in the United States, and as many more were sold in 1951. It seems far too often as if these 12,000,000 cars were all sold for use in and around New York!

Any one, for example, who attends the World Series baseball games has discovered that the subway is the quickest way to reach the ball parks, and almost everywhere else in New York City for that matter. All the highways that money can build will not provide adequate mass-transportation facilities. There are "through" traffic highways and parkways, one-way streets, a parking ban on some streets—although not nearly enough—and many traffic controls and regulations have been introduced. Nevertheless, traffic congestion continues to increase because more and more cars are pouring into the city, over highway facilities, faster than such facilities can be built.

There is parking on hundreds of miles of city streets 24 hr each day, much of it double parking. Under these conditions, business deliveries choke the streets, and buses and taxis are continually being delayed. Thus, the person who operates an automobile but refuses to—or cannot afford to—use a parking lot, is favored over the vast majority who must depend upon public vehicles for commuting. Thousands of these parked cars come from sections outside the city via the various subsidized facilities.

It is known that the streets were not built as substitutes for parking lots and garages, and it is generally admitted that some way must be found to dislodge all-day parkers from the city streets. The solution to the traffic problem is to remove parked automobiles from the streets, not to build more facilities for more cars and hence increase the congestion. In the writer's opinion, the most effective method is to construct the type of modern mass-transportation system that would induce people to ride to work by rail instead of by automobile.

---

[2] "Railroads and Rubber," *The New York Herald-Tribune*, New York, N. Y., October 10, 1951 (an editorial).

NEED FOR A UNIFIED SYSTEM LONG RECOGNIZED

Long ago, the Regional Plan Association recognized the need for a unified system but, for one reason or another, only transportation on rubber has been considered and has been furnished with the latest facilities—at the taxpayer's expense. The value of these facilities will soon be greatly reduced because of sticky, molasses-like progress on highways due to the rapid increase in vehicular traffic.

In 1920, by amendment of the original 1887 Act to Regulate Commerce, Congress directed the Interstate Commerce Commission to prepare and adopt, as soon as practicable, a plan for the consolidation of the railway properties of the continental United States into a limited number of systems. No authority, however, was given the commission to compel the railroad consolidation recommended by it in 1921, 1929, and 1932, and the railroads themselves have continued to resist any program for unification of properties which would have reduced their individual operating expenses. However, if only the proper public officials will take hold of the problem, the writer believes that the necessary legislation could be obtained to make possible the consolidation of essential existing facilities, so that this desperately needed unified mass-transportation system for all the people in the New York metropolitan area may become a reality.

COORDINATION OF RAIL AND BUS SERVICE

Although it is recognized that both rail and bus services have certain obvious advantages over each other, the public interest would best be served by preserving the inherent advantages of both types of service. This objective, of course, is a stated policy of the Transportation Act.

As a result of the pressure of population growth, there has been an intensive suburban development in recent years which has had the effect of locating commuters away from the immediate vicinity of railroad terminals and stations. Slowly, but inevitably, the efficient and economical rail commutation facilities have been disappearing under the burden of increasing costs and motor vehicle diversion. Any further development of the pattern of commuter traffic which does not encourage the coordination of feeder bus lines with railroad commutation service will continue to affect the railroads' financial condition adversely, with a resultant deterioration of service.

Because of this trend, the Hudson & Manhattan Railroad Company petitioned the Interstate Commerce Commission in 1951 to initiate, on its own motion, an investigation of commutation services in the New York metropolitan area for the purpose of determining the respective places of rail, rail-bus, and all-bus service in the future improvement and development of such commutation services, and to invite the public authorities of the states of New York and New Jersey, and the officials of the municipalities affected, to participate in such investigation and determination. The commission also has had requests from other areas with similar commuter problems, but has not yet ordered such investigation. A study could well result in the establishment of principles that would be applicable to conditions in other sections of the United States as well.

GREATER USE OF RAILS A SOLUTION TO TRAFFIC CONGESTION PROBLEM

In the suburban areas, the emphasis in the past has been placed on attempts to solve the traffic problem without proper regard for the main objective of transporting people in mass. Expressways, tunnels, and bridges will not solve the traffic congestion problem. They have made it worse in many sections. The answer lies in the provision of a modern, unified mass-rapid-transit system of large passenger-carrying capacity, operating wherever required in order to bring people into and out of the city quickly and at a fare they can afford to pay.

Because of the high-density morning and evening peak-period use of rolling stock, and competition from automobiles and buses operating on public-financed freeways, bridges, and tunnels, rapid-transit commuter services are rarely self-sustaining; and, because of constantly increasing costs, the financial condition of the forgotten and forsaken commuter railroads becomes worse and worse, resulting in progressively poorer equipment and service.

In 1951, a statement[3] appeared that

> "It is not hard to see that ever-increasing fares for public transit and railroad travel will encourage greater use of the automobile (and many drivers do not reckon the dollar cost of this use), and that this will increase traffic congestion, and multiply our street and parking problems, at public expense."

This should prove—if it need be—that rail-commuter services are practically indispensable if large communities are to be kept from choking to death from automotive traffic congestion.

Strange as it may seem, the annual trans-Hudson river passenger traffic into and out of New York City has not increased since 1932 but has shifted from rail to rubber as the number of cars has increased and as new highway facilities have been built. In 1925, there were 1,635,337 vehicles registered in New York State, and 579,978 in New Jersey. In 1950, New York had 3,856,270 and New Jersey 1,599,003. All this evidence leads to the inevitable conclusion that commuter railroads must be acknowledged to be a public problem, and that steps must be taken by the proper public officials to introduce corrective measures by the integration of railroads and rapid-transit facilities in the New York metropolitan area.

INTEGRATION OF RAILROADS AND RAPID-TRANSIT FACILITIES

In a substantial degree, the present railroad setup in the New York metropolitan area is a large economic waste because of the duplication of routes, noncapacity usage, and dormant and abandoned railroads—particularly in the New Jersey sector. Seven major factors must be analyzed and activated to bring into being this comprehensive metropolitan rapid-transit service: (1) Eliminating duplication of services, (2) the acquisition of rights of way, (3) the allocation of freight service, (4) the allocation, and determination of the construction costs of tunnels for railroad and vehicular traffic, (5) the function of bus facilities, (6) the coordinated operation setup, and (7) the financial structure.

---

[3] "Public Transit," *The New York Times*, New York, N. Y., October 15, 1951 (an editorial).

1. Eliminating Duplication of Services.—There are all kinds of needless duplication of competition between railroads as well as between railroads and buses. For instance, the Pennsylvania Railroad and the Hudson & Manhattan Railroad use the same tracks from Newark, N. J., to a point east of Journal Square Station, Jersey City, N. J. Pennsylvania Railroad passengers destined for downtown New York transfer to Hudson Tubes trains at Exchange Place Station, Jersey City. There is no reason why these Pennsylvania passengers could not change to Hudson & Manhattan trains at Newark and thus make it unnecessary for the Pennsylvania Railroad to maintain its Jersey City station, because some time ago it abandoned its ferry service between Jersey City and New York.

Passenger service to Asbury Park, N. J., and other New Jersey shore points, is furnished jointly from a point near Perth Amboy, N. J., by both the Pennsylvania and the Jersey Central railroads. The Pennsylvania Railroad carries passengers via Newark whereas the Jersey Central Railroad takes them to its Jersey City terminal where they board ferries running to Liberty Street, New York City.

There seems to be useless duplication in the Lackawanna Railroad and Erie Railroad, together with bus lines, providing service to the same suburban communities, thereby "cutting each other's throat" in the process.

The railroads that continue to run ferries do so at a substantial loss. At a hearing before the New Jersey Board of Public Utility Commissioners, in 1951, testimony was presented to show that the Lackawanna, Erie, and West Shore railroads lose approximately $2,500,000 each year on ferry operations.

A number of bus lines run from the northern New Jersey suburbs to the New York City bus terminal of the Port of New York Authority, through the Lincoln and Holland tunnels, and several bus companies carry passengers from Newark, as well as from Jersey City, into other parts of New York City through the same facilities, all competing with the railroads.

There are hundreds of buses daily feeding thousands of passengers into the subway lines at Jamaica, Flushing, and elsewhere on Long Island, which service in many instances parallels the Long Island Railroad, while the latter in substantial part is far from being used to capacity. It would not be an expensive or a difficult engineering feat to make connections at or near Jamaica, between the subway lines and the Long Island Railroad lines, thereby eliminating many long bus rides.

It is a known fact that having so many buses on the roads in direct competition with the railroads helps neither the congested highway condition nor the railroads' financial plight.

2. The Acquisition of Rights of Way.—A study should determine the railroad rights of way that should be eliminated in commuter service and the ones that should be retained. The retained rights of way should be part of a joint system and, in most cases, would have to be leased from the railroads owning such rights of way, as the railroads' bond indenture provisions generally make it impossible to do anything else but lease them.

3. Allocation of Freight Service.—The Long Island Railroad obtains about 28% of its revenues from freight and 67% from passenger service. Studies have been made in the past suggesting that these services be separated and the freight handled by one organization and passengers by another. The reason given for this proposed separation, at the time, was that the Long Island freight traffic was then tied in with the Pennsylvania Railroad. Whether such a division in an over-all metropolitan rapid-transit plan would be advisable so far as the Long Island Railroad was concerned could be determined only after a tentative plan was set up and studied.

In New Jersey, on the other hand, although it would undoubtedly be wise to carry freight and commuters by a joint system (because this would reduce the cost of freight handling) it would probably be impossible to persuade the railroads to agree to such an arrangement. They seem willing to abandon their commuter services but wish to retain their respective freight business.

4. The Allocation of Tunnels for Railroad and Vehicular Traffic.—A tunnel under the Hudson River reaching New York somewhere between Fiftieth Street and Sixtieth Street has been advocated by some who have studied the needs of the large number of New Jersey people who work in uptown New York. The New York City Board of Transportation has proposed that a tunnel be constructed under the East River reaching New York somewhere between Seventieth and Eightieth Street where it would tie in with the proposed Second Avenue Subway, so as to provide better service for people coming in from Long Island.

The cost of tunnels for railroad cars would be substantially greater than for subway cars. Before a decision is reached with respect to the size of a tunnel, however, a determination should be made as to whether passengers alone are to be carried or whether freight also would be carried. It would also be decided whether in New Jersey a transfer center should be established for unloading freight and, no doubt, passengers, before the correct size tunnel could be determined. A tunnel 23 ft in diameter would be required for the ordinary railroad car as compared with a diameter of 18.5 ft for subway cars. The cost of the larger tunnel would be approximately 50% greater than that of the smaller one for subway cars.

5. The Role of Buses in a Unified System.—One of the problems to be considered is the sound and practicable integration of buses into a metropolitan transit system so that their value and desirability would be increased to the best advantage of both the public and the bus-operating companies.

Some people argue that mass-transportation needs can be met by building more and bigger highways and tunnels to accommodate the ever-increasing number of buses and automobiles. Also, it is natural that the bus companies should want to take whatever advantage they can of the new and greater facilities provided by public authorities at no investment outlay by the bus companies. This is shown by the steadily growing number of bus applications to bring more local bus lines into the center of New York City. Some of these applications are for extensions from purely local, neighborhood service to interstate service operating for miles to and from the Port Authority bus terminal. This expansion of commuter bus service poses several major problems so far as the public is concerned: It reduces transportation efficiency; it reduces the efficient use of existing facilities which are fundamentally better able to transport large numbers of passengers quickly; and it brings about greater and greater demands on the public purse for more and more facilities, thereby increasing traffic congestion rather than reducing it.

Those who state that buses alone can handle mass transportation make sense only when they refer to small cities, but in great metropolitan centers the bus is inadequate. It simply is not possible to transport so many persons as far, as quickly, and as efficiently by bus as it is by train. A 10-car subway train, during rush hours, carries 1,600 passengers and is operated by 3 men. It would require twenty-five buses, each carrying 64 passengers, to transport 1,600 people, and each bus would require 1 operator. So far as speed is concerned, the result is just another bus in the general congestion of vehicles.

Rail rapid transit in major metropolitan communities is indispensable. However, a well-integrated system of transportation should have buses operating as feeder lines serving the rapid-transit stations.

6. The Organization of a Unified System.—Railroads in the New York metropolitan area are supervised by the Interstate Commerce Commission if they operate in both New York and New Jersey; by the Public Service Commission with respect to New York operations; and by the Board of Public Utility Commissioners for New Jersey operations. A study should be made relative to this distribution of authority, and the necessary legislation should be enacted to eliminate supervision by these multiple commissions if found advisable and in the public interest.

The Port Authority was given the right to purchase, construct, lease, and operate any terminal or transportation facility within its boundaries, which now comprise a radius of about 25 miles from City Hall, New York. These boundaries may be changed if necessary by joint action of the New York and New Jersey legislatures to enlarge the present boundary lines. The Port Authority is now practically tax exempt. It has the power to fix rates or charges for the services it provides. It is free from supervision by any state or federal governmental agency. Thus, there would be no problem, rate-wise or tax-wise, if it were to take over the operation of a metropolitan mass-transportation system or, if some other authority were given similar powers. Thus, the supervision by a multiplicity of governmental agencies would not exist.

The drafters of the law giving the Port Authority full power and use of all modes of transportation for the carriage of persons or property intended that transportation facilities within its boundaries be provided for all the people, not for a favored group. However, for many years the Port Authority has been confining its efforts to providing facilities for those who travel by bus and automobile and has avoided the responsibility of providing modern railroad facilities for the vast majority of people in this area.

7. The Financial Structure.—It would greatly simplify the problem if the Port Authority brought into being and operated a metropolitan mass-transportation system because of its backlog of credit. The low interest on its tax-exempt bonds, together with exemption from real estate and income taxes, makes low operating costs possible. This simplifies the fare problem compared with the present railroad tariffs. Because the states of New York and New Jersey, and the commuters who live therein, would be the beneficiaries of such a system, any operating deficits should be financed by them. However, if such a complete over-all system were established, any deficiency would be unlikely, if the experience of existing subsidized facilities now provided for automobiles and buses is any criterion.

SUMMARY

The foregoing is a succinct statement of an acute problem. It offers a broad definition of the problem and a practical outline for a possible solution.

DISCUSSION

John F. Kraus.[4]—A clear, concise, and factual presentation of the mass-transportation problem and its solution has been given by the author. The writer's comments have been made in the hope that various issues may be clarified for those who are not thoroughly acquainted with this problem in the New York metropolitan region.

In the Introduction, Mr. Reid stated that

> "* * * no public official nor public body has taken effective action to bring into being a modern, unified mass-transportation system for people residing within that great metropolitan area."

However, in the spring of 1952 (subsequent to the preparation of Mr. Reid's paper), the states of New Jersey and New York enacted legislation, creating commissions to develop jointly plans and specifications for the improvement and coordination of the rapid transit facilities of the New York metropolitan region, and to recommend all necessary measures. Commission appointments were made by the Hon. Alfred E. Driscoll, Governor of New Jersey, on July 31, 1952, and by the Hon. Thomas E. Dewey, Governor of New York, on November 13, 1952, but the commissions have not met jointly and no work has been done to date (1953). It was intended that the commissions ultimately would become the agency to build and operate the proposed project.

Because rubber-tired transportation has reached its practical limits, the need is not for more vehicular facilities, but for relief. This relief, as Mr. Reid states, is mass transportation by rail. The existing (1953) trend from rail to rubber is not a solution, because the railroads still form the life-blood arteries between communities. The trend from rail to rubber has been caused by the lack of comparable investments in railroad facilities as in vehicular facilities, the latter partly by subsidies. This trend has not only unbalanced the transportation system, but has presented the following problems, the cost of which is borne by both the user and the nonuser of transportation facilities:

1. The traffic problem is growing daily. The New York Regional Plan Association stated[5] that if the use of railroads for commuting is permitted to decline in favor of motor-vehicle commuting, traffic congestion in the region's central business areas and costs of relieving such congestion will increase out of all proportion to the number of persons transported.
2. Increased parking facilities are required. It is interesting to note that one trainload of commuters is estimated to require four acres of parking space if carried by private automobiles.
3. The adverse effect on business of traffic congestion and lack of parking facilities has resulted (in some cases) in decentralization.
4. Highway construction and maintenance costs are mounting. They are estimated to be more than $5,000,000,000 a year for the period from 1953 to 1963.

---

[4] Chairman, Inter-Municipal Group for Better Rail Service, North Plainfield, N. J.

[5] "New York's Commuters," *Report of July 1951*, Regional Plan Assn., Inc., New York, N. Y.

5. Losses of tax ratables, as a result of the building of vehicular facilities, are mounting.

6. The cost of automobile insurance is rising.

7. (*a*) The number of accidents is rapidly mounting. Up to 1951, the total number of persons killed in automobile accidents was over one million, and in 1952 the number exceeded the total number of all Americans killed in all wars since the Revolution.

(*b*) The Institute of Life Insurance reports payments of $69,000,000 under some 39,000 policies for automobile accident death claims during 1952. This figure is four times the amount of life insurance death claims arising from the first 2 years of the Korean War.

The need for a unified transportation system has long been recognized. Municipalities have contended before regulatory bodies and governmental agencies that one of the keys to the long-range solution of the mass-transportation problem lies in the consolidation of competing railroads with wasteful and expensive duplicating facilities. This contention is borne out by a report (December 1, 1949) of the Secretary of Commerce to the President of the United States, which stated that the problem of railroad consolidation is particularly urgent because the continued existence of an adequate railroad system is necessary for peacetime commerce and for wartime emergency. This report emphasizes the fact that, following considerable study of unnecessary duplication of facilities and other waste and unnecessary expenses in railroad operations, savings of approximately $800,000,000 annually could have been made in 1932 and 1933. The report also states that 10 years later, the Board of Investigation and Research reported that increased efficiency could save the railroads approximately $1,400,000,000 on an annual basis. This report recommended that action toward the obtaining of the most efficient railroad plant should be initiated immediately. The report also stated that, although the carriers could do much in this direction on their own initiative, it was clear that they needed active support and direction from the federal government, involving a mixture of incentives and compulsory action.

An integrated transportation system is a necessity. Within such a system, buses play an active part in furnishing feeder service to the railroads. The basic problem, however, has been the Interstate Commerce Commission's interpretation of national policy with respect to transportation. This policy was confirmed by the report of the Secretary of Commerce, in which it was stated that there has been a "* * * shift in emphasis and possible modification of the Transportation Act of 1940." Further confirmation was contained in a report of the United States Senate Committee on Interstate and Foreign Commerce. This report (October, 1952) held that the "* * * poor financial condition of certain railroads is due in large part to unsound regulatory and promotional policies of the Federal Government."

In the New York metropolitan region, the Port Authority of New York has not acted on the legislated master plan under the Compact under which it was set up by the states of New Jersey and New York. This plan was abandoned in the early 1930's when the Port Authority's activities were shifted from finding a solution for the railroad-steamship port problems to the construction and operation of vehicular tunnels, bridges, and airports. These facilities, instead of promoting the plan, have had the opposite effect.

In a Senate report it is stated that any further decline in railroad traffic would lead to insolvency for most of the industry and that, if there is any practical solution to commuter service, it will have to be devised through the joint efforts of the railroads and the local governments. Alexander H. Elder states[6] that the intent of the two states in setting up the Port of New York Authority was to realize the benefits of the "Comprehensive Physical Plan," the theory of which was the unification of railroad terminal operations. As railroads are privately owned and operated, they are required to compete in the terminal area where activity is greatest, and where there is an inherent conflict between terminal competition and terminal unification. The railroads could hardly have been expected to initiate such a unification if, indeed, they could legally do so. It is the responsibility of the state commissions to solve this problem. Failure can result only in the eventual breakdown of the transportation system.

It has been frequently stated that civilization is measured in terms of transportation or man's ability to surmount the limitations of nature with respect to time, space, and natural laws for his economic well-being. It is therefore appropriate to note the interest in this important problem of mass transportation.

---

[6] "New Jersey-New York Port Problem," by Alexander H. Elder, New Jersey Dept. of Conservation and Economic Development, December, 1952.

AMERICAN SOCIETY OF CIVIL ENGINEERS
Founded November 5, 1852
TRANSACTIONS

Paper No. 2663

SLACKWATER IMPROVEMENT OF THE COLUMBIA RIVER

By O. E. Walsh[1]

Synopsis

Navigation on the Columbia River and its tributaries is vital to the economy of the Columbia River basin. This paper presents a description and history of the basin and describes the effects of the many slackwater improvement projects in this area.

It is concluded that great economic benefits are yielded by navigational improvements in this basin, and that coordination with other water uses and with other forms of transportation is feasible.

Introduction

Rivers were the highways for the pioneers and, as such, they played an important part in the early settlement of many regions. However, other forms of transportation developed, along with the development of the tributary area, and many rivers lost their statures as important arteries of commerce and were forced to adopt new roles in the economy of their regions. No great river ever remained an unimportant resource for long, but in many instances it has taken centuries for the full worth of a river to be realized and for its full potential to be developed. The Columbia River, long recognized as one of the great rivers of the west, has only in recent years begun its climb into a place of national importance as one of the great rivers of the world. Attention is focused (1953) on the Columbia River because of its tremendous hydroelectric power potential because in the Columbia River and its tributaries are concentrated approximately one third the potential water power of the United States. In a period of industrial expansion—in which there is an ever growing need for greater supplies of economical electrical energy—the vast resources of the Columbia River can be tapped for the benefit of the nation and, thus, the

---

Note.—Published, essentially as printed here, in April, 1953, as *Proceedings-Separate No. 181*. Positions and titles given are those in effect when the paper was received for publication.

[1] Brig.-Gen., Corps of Engrs., U. S. Dept. of the Army, North Pacific Div., Portland, Ore.

world. Although much has been said about Columbia River power, and much more can and will be said about this great resource, this paper is devoted to another phase of the Columbia River development which has guided, and will continue to guide, the economic growth of the region. Navigation has been an important function of the Columbia River since the day Capt. Robert Gray sailed his ship, *The Columbia*, into its mouth in 1792. It truly served as a highway for the pioneer settlers, even though it was a rough one in many spots. Although the commerce of the lower river has continued to grow for more than 150 years, those "rough spots" in the upper river highway have retarded the growth of river commerce above tidewater since the hardy days of iron men and wooden ships. It has been only through the use of equipment of better design and as a result of continued improvements around and through these spots of turbulent white water that river commerce has remained in active competition with the paralleling railroads and highways and has grown remarkably. For the swift and rugged Columbia River and for the principal tributary, the Snake River, adequate navigation can be provided only by slackwater improvement similar to that of the great tonnage carrier, the Ohio River.

Description of Basin

To understand the problems and potentialities of Columbia River navigation better, the geography and economic development of the region should first be examined and also its navigation history. The Columbia River, with its tributaries, drains an area of 259,000 sq miles on the Pacific slope of the North American continent, mostly between the Rocky Mountains and the Cascade Range. In the part that is of maximum length the basin extends north of the international boundary 270 miles into Canada and south into the United States approximately 550 miles. The widest part of the basin is from the mouth of the Columbia River at Astoria, Ore., to the headwaters of the Snake River in Yellowstone Park in western Wyoming, a distance of 730 miles. Fig. 1 shows that the 219,500 sq miles of the basin in the United States includes most of Idaho, the greater parts of Washington and Oregon, all of Montana west of the continental divide, and small areas of Wyoming, Nevada, and Utah. The basin boundaries are mostly mountain ranges, which comprise a large percentage of the basin area.

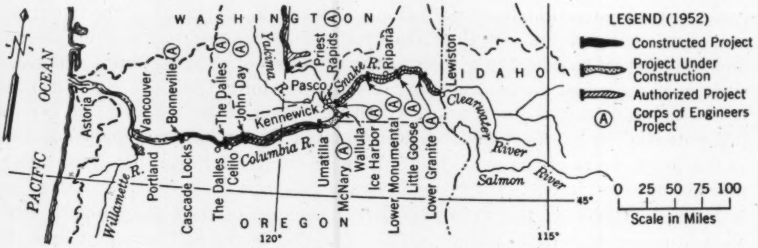
WASHINGTON
PACIFIC OCEAN
Astoria
Vancouver
Bonneville Ⓐ
The Dalles Ⓐ
John Day Ⓐ
Yakima R.
Priest Rapids Ⓐ
Pasco
Snake R.
Riparia
Lewiston
IDAHO
Kennewick
Columbia R.
Clearwater River
Salmon River
Willamette R.
Portland
Cascade Locks
The Dalles
Celilo
Umatilla
McNary Ⓐ
Wallula
Ice Harbor Ⓐ
Lower Monumental Ⓐ
Little Goose Ⓐ
Lower Granite Ⓐ
OREGON
120°
115°
45°
LEGEND (1952)
Constructed Project
Project Under Construction
Authorized Project
Ⓐ Corps of Engineers Project
0 25 50 75 100
Scale in Miles

Fig. 1.—Part of Columbia River Basin

The Columbia River has its source in Columbia Lake in the Rocky Mountains of Canada, and flows a distance of 462 miles through British Columbia before crossing the international boundary at the northeast corner of the State of Washington. In the United States, it flows generally south through the central part of Washington to a junction with the Snake River and then turns westerly to the Pacific Ocean, a total distance of 1,207 miles from its source in Columbia Lake. The total fall of the river from its source to the ocean is 2,652 ft. The Snake River contributes slightly more than one fifth of the 180,000,000 acre-ft of mean annual runoff of the Columbia basin and drains 109,000 sq miles. The Snake River falls a distance of 9,000 ft in the 1,070 miles from its headwaters to a junction with the Columbia River near Pasco, Wash.

The climate of the Columbia basin varies between the mild coastal conditions at the mouth of the river, to the dry semidesert climate of the inland valleys and plains, and between the extremes of temperature and precipitation found in the mountain altitudes. Annual precipitation ranges from 7 in. per yr to 150 in. per yr. Seasonal high water, usually a maximum in May or June, is caused by a rapid melting of the accumulated snow pack from the previous winter, and is often accelerated by the melting action of late spring rains. Winter runoff is frequently extremely low because of freezing weather which occasionally extends to the lower reaches of the river west of the Cascade Mountain Range. The discharge of the Columbia River varies from the mean annual of about 200,000 cu ft per sec, to an upper limit of 1,240,000 cu ft per sec attained at The Dalles, Wash., during the maximum flood of record in 1894, and downward to a lower limit of only 36,000 cu ft per sec at the same point during the freeze-up of January, 1937. The mean annual runoff is approximately 13 in. over the watershed area at the mouth, and a little more than 11 in. at The Dalles.

The population of the Columbia River basin was approximately 3,000,000 in 1950. Half the population is rural, about equally divided between farmers and nonfarmers. Its distribution is characteristically that of an immature, rapidly growing region. Concentrations are small, occurring in conjunction with the conversion of near-by natural resources. The only two large cities within the basin are Portland, Ore., with a population of 371,011 in 1950 or 24.6% of the population of the State of Oregon, and Spokane, Wash., with a population of 160,484. The population of the Columbia basin increased 28.3% between 1940 and 1950 or at twice the rate of the nation; and the population forecasts indicate a substantially greater growth in the future than for the United States as a whole.

The most important natural resources of the Columbia River basin are its agricultural land, forests, mineral deposits, fish, and, of course, its water resources. In direct relation to these resources, the most important industries are agriculture, lumbering, and mining. Since 1940 the availability of hydroelectric power, the development of new processing techniques, and the impetus of war-expanded markets have greatly accelerated the growth of manufacturing in the basin. Although timber products continue to lead in importance—more than 300,000,000,000 board ft, log scale, of timber exist in the United States section of the basin, yielding more than one third the nation's total lumber production, and there is a sound policy of harvesting on a perpetual yield basis—electrochemical and electrometallurgical plants have been continuously attracted to the region because of the economical power rate and have threatened to change the manufacturing picture. Aluminum reduction plants lead the light metals activity, and a titanium industry now (1953) is directing its attention to the region's great power potential. Although the basin produced 41% of the primary aluminum supply of the nation in 1945, growth since that time has been small, and further large expansion of all such industries must await an increased power supply. The exportation of raw material and partly processed commodities, and the importation of manufactured goods, characterize the trade of the region. The trend and aim of the region are to carry on the processing of local materials to the end product, thus greatly extending its industrial foundation and expanding its economy. The principal exports are lumber, wheat, orchard fruits, flour, refined and unrefined metals and mineral products, manufactured wood products and wood pulp, and canned salmon and tuna. The chief imports are petroleum and related products, steel, iron, and manufactured consumer goods.

Great distances and topographic barriers, not only between centers of population outside the basin but also between points within the basin, have made transportation facilities of vital importance to the development of the region. Many areas remain isolated and undeveloped because of the lack of adequate transportation facilities. This is particularly true of the area above Lewiston, Idaho, in the Snake River Canyon. Although the basin is served by six transcontinental railways, by numerous federal and state highways, and by many secondary roads, the water highway of the Columbia River still remains an important artery of commerce and, as it is canalized, becomes of increasing importance to more and larger areas of the basin.

In the pioneer settlement days, the Columbia River and its tributaries provided the principal means of transportation, and many streams were extensively traveled by water and by portage. With the coming of roads, railroads and, later, improved highways, navigation lost some of its importance on most of the Columbia River tributaries. Navigation by ocean-going vessels having as much as a 35-ft draft is possible between the mouth of the Columbia River and Vancouver, Wash.—a distance of 105 miles. The lower 12 miles of the Willamette River, from its confluence with the Columbia to Portland, also is navigable by ships of this size. This provides a total distance of 112 miles from the ocean to the head of deep-water navigation. Portland, Vancouver, and the lower Columbia River ports have grown tremendously because they are ports and handle water-borne commerce, and continued growth in this water commerce is indicated for the future. Shallow-draft navigation is important on the Willamette River above Portland and on the Columbia River to Pasco and Kennewick, Wash., at the mouth of the Snake River, 328 miles by river from the mouth. Navigation on the Snake River to Lewiston, an additional 140 miles inland, now constitutes a potential more than a recognized commerce because of the swift water, the inadequate depths, and the attendant hazards of the unimproved Snake River. However, small, high-powered launches operate 92 miles upstream from Lewiston to serve the few isolated inhabitants of the Snake River Canyon and, for many of them, provide the only means of ready access to the outside world. Little river traffic has ever developed on the Columbia River above Kennewick, although the river is navigable for an additional 65 miles to the foot of the Priest Rapids.

HISTORY OF COLUMBIA RIVER NAVIGATION

The history of navigation in the tidal reaches of the lower Columbia and Willamette rivers has paralleled the history of the region. Under John McLaughlin, the Hudson Bay Company's fur-trading post at Vancouver was the economic and social center of the vast Oregon country until about 1845, and nearly all transportation was by water. Canoes, flatboats, and other small craft traveled the tributary streams and sailing ships came into Vancouver with supplies to exchange for furs. The furs were carried to China and converted to goods for the European trade. The first steamship on the Pacific was *The Beaver*, constructed in England and sent to Vancouver for the fur trade. By the 1830's, settlements in the Oregon country were producing exportable surpluses of the same commodities that still make up a large part of the present exports—namely, grain and lumber; and clipper ships rounded Cape Horn to carry these products to world markets. By 1870, following the dredging of a bar on the lower Willamette River—the first federal navigation project in the region—Portland became the commercial center of the area. Improvement of the entrance to the Columbia River was authorized in 1877 and progressively deeper river channels were authorized in 1902, 1912, and 1930. The present project, adopted in 1930, provides for a river channel 500 ft wide and 35 ft deep, extending from the mouth to Portland and Vancouver. A depth of 40 ft over the bar has been maintained since 1918, and the feasibility of deepening the entrance channel to 48 ft is now under study at the request of shipping interests. Commerce, conducted by deep-draft vessels, on the lower Columbia River has grown from modest fur shipments in the early settlement days and from 430,586 tons in 1909, the start of reliable commercial statistics, to more than 9,500,000 tons in 1949. Commerce, conducted by shallow-draft vessels, on the river amounted to nearly 9,000,000 tons in 1949, composed primarily of log rafts and barge tows. In 1945, Portland reached eleventh place in tonnage among the ports of the United States, and second among the seaports of the Pacific Coast for ocean and local commerce combined. In this tidal reach of the river, navigation is both practical and economical, and its continued growth can be expected with the growth of the region and the development of the contributary upper Columbia River area.

The upper Columbia River and its logical navigation extension up Snake River has a different and more troubled history. The first record of travel on these streams comes from the report of the Lewis and Clark expedition of 1804–1805. Coming over the continental divide between the Missouri River basin and the Salmon River, the Lewis and Clark expedition proceeded north into the Bitterroot Valley. While crossing this valley to the Clearwater River, they built boats and followed the Clearwater, Snake, and Columbia rivers to the Pacific Ocean. The Snake River once was called the "Lewis

Fork" of the Columbia River and, as the third largest Columbia tributary, is still called the "Clark Fork." Subsequent to the adventures of Lewis and Clark, trappers and pioneer settlers blazed a transportation route known as the Oregon Trail. This famous route, used by the early emigrants to the great Oregon country, essentially followed the Snake and Columbia rivers, except in the lower Snake River Canyon below Fort Boise and at the Cascade Gorge of the Columbia River, just above its principal terminus at Fort Vancouver. River commerce by light-draft vessel and portage developed and prospered until 1882, when completion of a railroad paralleling the south bank of the Columbia River from Wallula, Wash., near the mouth of the Snake River, to Portland interposed serious competition. Shortly afterward regular river service was abandoned. Various attempts were made later to revive navigation in the upper river, but the difficulties of navigating the swift and treacherous river could not be overcome with profit to the operations in the face of the rate-cutting competition of railroads.

In almost 50 years of upper river navigation during the pioneer period, before the coming of railroads, many tons of freight and thousands of passengers were hauled through the white water of the Columbia and Snake rivers or portaged over its worst falls at the Cascade Rapids and Celilo, Wash. In the upper section of the Columbia River from the mouth of the Snake River to Celilo, the river flows in a series of pools and rapids. Within this 124-mile distance, there is a fall of 185 ft, 86 ft of which is concentrated in sixteen rapids having an aggregate length of 19 miles. The river slope at low water in these rapids, or natural dams, is from 3 ft per mile to 8 ft per mile, and, in the slackwater reaches between the rapids, the slope averages less than 1 ft per mile. In the stretch between the upper and middle sections of the river, a distance of 12 miles, there is a fall of 81 ft at low water, primarily concentrated at Celilo Falls. There was a drop at low water of only 4 ft in the 43-mile middle stretch past The Dalles to the head of Cascade Rapids. Before the days of Bonneville Dam, the river had a fall of 37 ft in a distance of 7 miles between its middle and lower sections, in a reach that terminated at the head of tide at Warrendale, Ore., a short distance below the site of Bonneville Dam. Of this 37-ft drop, 25 ft were concentrated in a distance of 3,000 ft through the Cascade Rapids proper. The Columbia River, in this narrow gorge section, cuts directly across the heavily timbered Cascade Mountain Range. The narrow gorge, with precipitous slopes and cliffs that rise in many places to more than 3,000 ft above the river channel, turned most of the early pioneers southward to a safer passage for their wagons and possessions over the mountains—a much longer passage that was filled with the difficulties and hazards of high mountain passes.

In pioneer days, boats traveled in these three main sections of the Columbia River but seldom passed the separating Cascade Rapids or Celilo Falls sections. The first portages around Cascade Rapids, between the tidal section and The Dalles pool, were made by wagons. In 1859 a tramway was built and later steam portage railways were built on both sides of the river. Construction of the Cascade Lock and Cascade Canal was begun in 1878, but these structures were not opened to traffic until November, 1896. Because of the obstructions to navigation between the foot of Three Mile Rapids (about 1½ miles above the town of The Dalles) and Celilo, the head of navigation was at The Dalles, and freight and passengers were transferred by means of wagons over a wagon road between The Dalles and Celilo. A portage railroad was completed in about 1862, following the Oregon bank of the river to the town of Celilo, about 1 mile above Celilo Falls, where freight was transferred to boats. In 1882, this portage railroad became a part of the main line of the railroad between Portland and Wallula (later the Union Pacific Railroad). Because of gold discoveries on the Salmon River in Idaho in 1862, the following few years witnessed the greatest era of steamboat activity on the river above Celilo. In 1864 steamers carried 36,000 passengers to and from the Idaho mining regions on the Salmon and Clearwater rivers. The boats ran regularly as far as Lewiston and frequently trips were made up the Clearwater River and up the Snake River above Lewiston. Navigation rapidly declined between 1866 and 1870, and during high-water periods most of the boats were taken to lower river points. In 1882 navigation above Celilo Falls almost ceased.

Between 1891 and 1894 and again from 1905 to 1910, active efforts were made to revive upper river navigation. The Dalles-Celilo Canal was opened to traffic in May, 1915, and another attempt was made to revive navigation on the river above Celilo. However, it was unsuccessful because of lack of patronage, and boat operations were discontinued in 1917. The failure of upper river navigation in these periods can be charged primarily to lack of control over railroad rates. The absence of the stipulation of fixed rates by state and interstate commissions made it possible for the railroads to reduce rates at will for a time sufficient to force boats from the river whenever a steamboat company attempted to establish service. During the period from 1926 to 1930, no freight traffic passed through The Dalles-Celilo Canal. Although there were some experimental shipments in 1931, regular traffic was not revived until 1932, when a total movement of 408 tons passed through the canal, and tonnage has increased rapidly since that time. This increase is indicated by Fig. 2, which also shows a projected straight-line curve for commerce after 1950. The horizontal line designated "50-year average" is the estimated average tonnage for a 50-year period immediately following completion of the through waterway and is set at 4,828,000 tons. With the authorization of the Bonneville Lock and Dam in 1933, a slackwater development program was initiated on the upper Columbia River. This program revived navigation on the upper river to a full-scale commercial operation.

SLACKWATER IMPROVEMENT

In the year before the Bonneville Dam Lock was opened, the traffic through The Dalles-Celilo Canal totaled 5,626 tons, representing primarily a new navigation venture in the upstream barge movement of petroleum products. In 1938, the year Bonneville Lock was opened, the tonnage quickly multiplied nearly eight times to a total of 44,349 tons. In 1939 it tripled, and it nearly tripled again in 1940 with a tonnage of 325,900 before it leveled out for a more gradual increase. In 1949, traffic through The Dalles-Celilo Canal totaled 900,246 tons, probably more tons of commerce than had passed over the upper river in its entire history prior to and including 1940. There are many reasons for this increase in navigation on the upper river, one of which is the Bonneville Lock and the slackwater now available to the entrance of The Dalles-Celilo Canal, which completely eliminated the navigation hazards of past years in the Columbia Gorge stretch of the lower river. The Cascade Lock walls extending above the normal Bonneville pool of El. 72 ft still remain as visible mementos of early days.

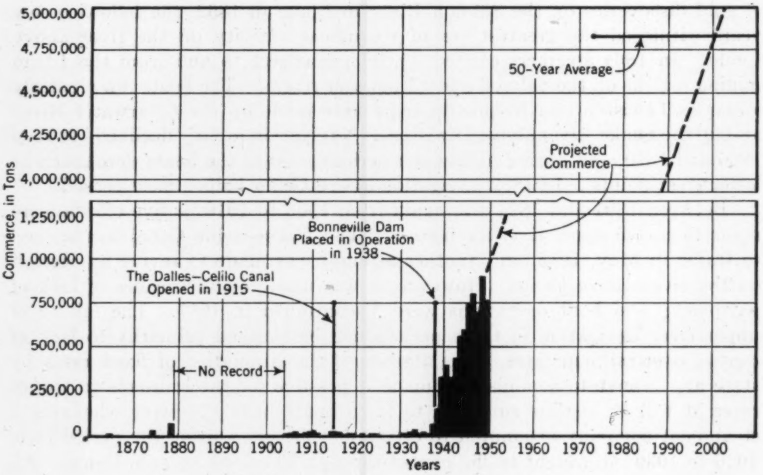

FIG. 2.—COMMERCE THROUGH THE DALLES-CELILO CANAL SECTION OF THE COLUMBIA RIVER

Bonneville Dam, located at the head of tidewater, 145 miles upstream from the ocean and 42 miles east of Portland, is the project farthest downstream from a series of locks and dams planned for construction on the Columbia and Snake rivers (Fig. 3). A site in the Bonneville Dam vicinity was proposed by the Corps of Engineers, United States Army, in its Columbia River "308" Report[2] of 1932, as a part of a long range plan to develop fully the power potential of the Columbia River. Construction was begun in 1933 as a Federal Emergency Administration project, was authorized by Congress in 1935 as a federal navigation project, and was placed in operation with two power units in 1938. Although the original 86,400 kw of installed capacity were considered far beyond the immediate needs of the region, additional units were found to be in demand immediately and, between 1938 and 1943, eight additional 54,000-kw generating units were added to complete the project. The phenomenal growth of the power load was no greater a surprise than the phenomenal navigation growth. The navigation lock at Bonneville was constructed to lift coastal steamers the 59 ft to the normal pool level of 72 ft above mean sea level. The pool, which extends upstream about 48 miles to the foot of The Dalles-Celilo Canal, affords a navigable channel with depths of 30 ft or more from the dam to The Dalles. To complete the ship channel connection between The Dalles and the ocean, a channel 27 ft deep and 300 ft wide was authorized from Vancouver to The Dalles and, although excavation was started on the open channel work involved, work was stopped by World War II. The part of the channel between Vancouver and Bonneville was completed in 1949 and the remainder has been held in abeyance, awaiting a greater need for such a channel. Above Celilo, a channel 7 ft deep and 150 ft wide was authorized, to extend as far as Wallula, and a channel of no specific depth and width thence upstream to Kennewick. This improvement, to be obtained by the removal of rock pinnacles and shoals, has been essentially completed simultaneously with the ever growing river traffic. Similar open river improvements were also made on the Snake River from its mouth to above Lewiston, but a minimum controlling depth of less than 1 ft to Lewiston limited navigation to favorable river stages and prevented the Columbia River growth from extending up the Snake River.

---

[2] "Columbia River and Minor Tributaries," *House Document 103*, 73rd Cong., 1st Session (2 volumes), U. S. Govt. Printing Office, Washington, D. C., June 30, 1932.

Commercial navigation on the Columbia River above Vancouver is conducted principally with powerful shallow-draft tugs and barges. The towboats (which actually push, closely coupled to the barge) range from 200-hp shuttle boats to twin-screw, tunnel bottom diesel boats of more than 5,000 hp, but draw less than 7 ft of water. Even with the more powerful towboats, the use of four-barge tows is practicable only approximately 30% of the time because of the swift water and narrow channels. Specially constructed steel barges, usually about 40 ft by from 165 ft to 175 ft, are utilized on the upper river. Many of these barges are designed to carry petroleum products upstream as large tankers and to carry wheat downstream as a deck load. These two-way pay loads consist of 290,000 gal of liquid petroleum products or 1,000 tons of wheat. Fig. 4 shows a load of petroleum being transported.

Navigation problems that remained to be solved were the following: The swift currents, in excess of 10 miles per hr through the rapids at medium stages; the insufficient depth and width of the channel during a large part of the year; the narrow, rock-bound channels lined with points on the sides and pinnacles on the bottom; the excessive time required for shuttle passage of barge tows through The Dalles-Celilo Canal; and the shallow water between the main channel and those installations at which the exchange of cargo between land and river takes place. Complete removal of the narrow sections through the many rapids would serve only to lower the intervening pools and would cause additional problems. Restricting the swift water to deeper channels would serve to increase the velocities, which already caused the downstream barge tows to travel at unusually high speed in order to maintain steerage way. Although river improvement would be possible at great expense, the solution of Columbia River and Snake River navigation problems was seen at an early date to rest with locks, dams, and slackwater. The fear, expressed by irrigationists, that open channel navigation would require more water also indicated a slackwater project.

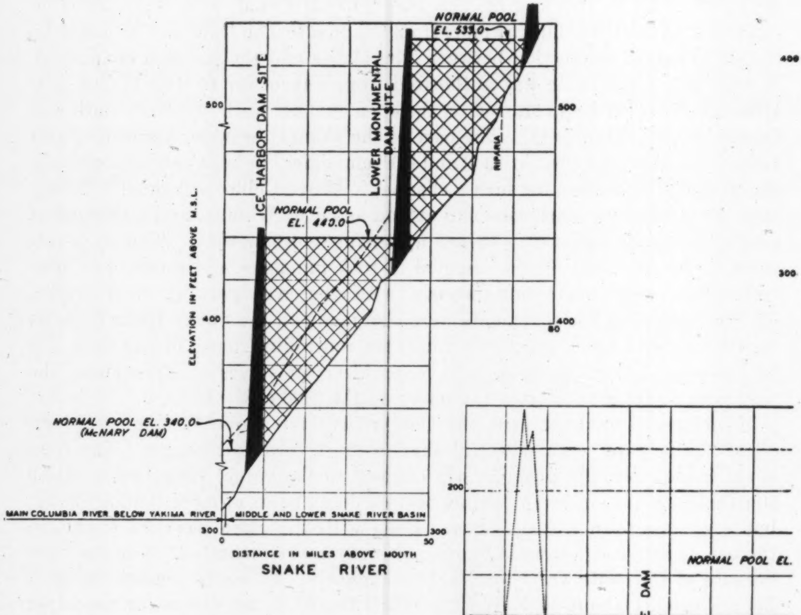

FIG. 3.—PROFILE OF THE COLUMBIA RIVER BELOW THE YAKIMA RIVER

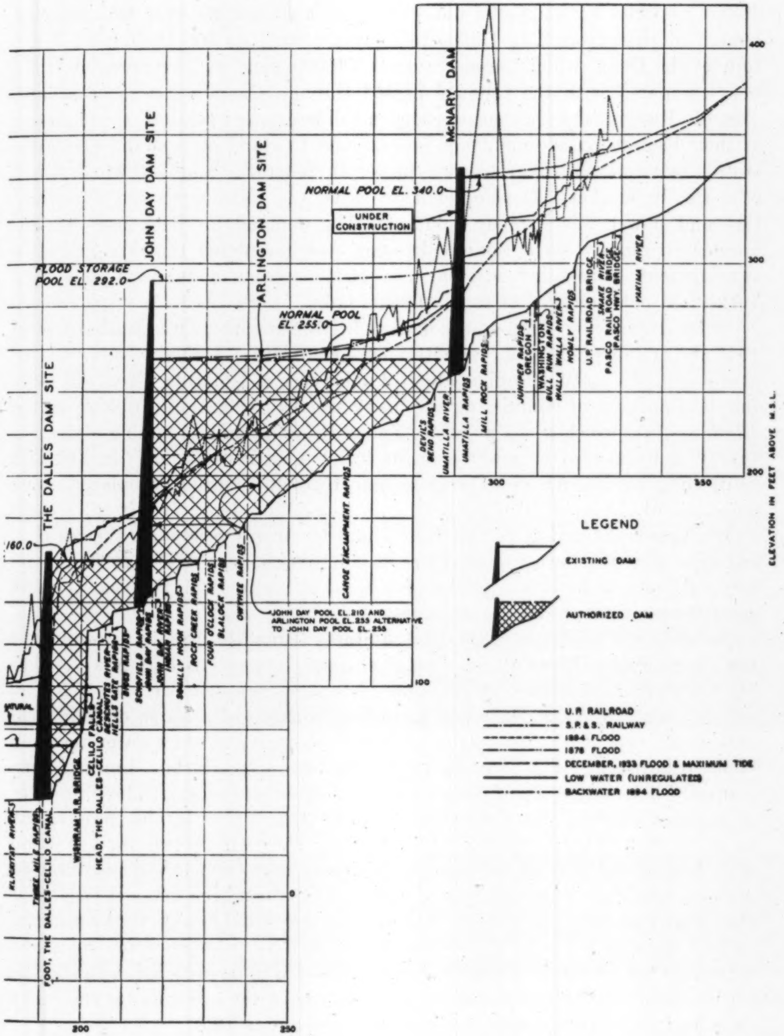

AND OF THE LOWER SNAKE RIVER, SHOWING MAJOR DAM PROJECTS

The commerce that could hardly support the expense of open river improvement could never be expected to justify the many hundreds of millions of dollars required for locks and dams to provide slackwater over this 275-mile stretch of river from The Dalles to Lewiston with its 650 ft of fall. Even Bonneville Dam, which passed over 1,500,000 tons of commerce in 1952—as compared with the tonnage passed through Cascade Locks or around Cascade Rapids, which never exceeded much over one twentieth that amount in their biggest years—could not be expected to stand on a sound enonomic footing without the hydroelectric power it generates and for which there is a steady market. Development to serve the joint purposes of navigation and power was a ready solution. The demand for both uses has increased so rapidly since Bonneville Dam was completed that the complete development, considered visionary in 1931, became a justified and fully authorized potentiality less than 20 years later.

After Bonneville Dam was completed, McNary Dam was authorized in 1945 and is now (1953) approximately 70% complete. McNary Dam, located at the foot of Umatilla Rapids, about 2 miles east of Umatilla, Ore., will serve the dual purpose of eliminating the many serious navigation problems in the 45 miles of river below the mouth of Snake River as well as adding a sizeable supply of hydroelectric power from its 980,000-kw installation. In lieu of a controlling depth of 6 ft in a narrow channel through Umatilla Rapids (in which velocities would reach 10 miles per hr), a controlling depth of 9 ft will extend above Kennewick and up Snake River about 10 miles, overlapping the Ice Harbor Dam site, the lowest dam of the Snake River series. The McNary Dam pool will be raised to its normal elevation of 340 ft in 1953, the year the first generators will be placed in operation.

In 1945, the Congress of the United States also authorized improvement of the lower Snake River to provide slackwater navigation and power. The most economical plan to develop this 140-mile reach of river with 375 ft of fall, between McNary Dam and Lewiston, consists of a series of four locks and dams, each with from 90 ft to 100 ft of drop and slackwater reservoir pools in between. The projects have been named Ice Harbor, Lower Monumental, Little Goose, and Lower Granite, in upstream order. These projects, in addition to providing slackwater navigation, will also develop power; but, as in the case of the Columbia River projects, they will be run-of-river plants with limited drawdowns for pondage purposes only, which will not interfere with navigation. The initiation of these projects has been delayed because of the alleged possible interference and damage they would cause to the valuable salmon runs that utilize the Snake River and its tributaries for spawning. Funds for the initiation of Ice Harbor are expected to be included in the budget for the fiscal year 1954, and the national defense power schedule for the region calls for its completion with first power on the line in 1957.

The 100 miles of open river between the town of The Dalles and Umatilla Rapids was left, temporarily, without authorized slackwater improvement, although the plans included either two or three dams to close the gap. The most hazardous navigable rapids of the Columbia River will be eliminated by McNary Dam, but others will remain. The most serious bottleneck, the narrow, outmoded The Dalles-Celilo Canal, still remains temporarily at least. In the Corps of Engineers' Columbia River "308" Report,[2] dated October, 1948, there was recommended an extensive, coordinated plan of development for the entire basin, including dams at The Dalles and John Day sites for navigation and power to close this gap.[3] These were included in a total of seven additional multiple-purpose dams that were proposed as part of the Main Control Plan to meet the present and immediate future needs of the Columbia River basin for navigation, flood control, power, and other water uses. Combined with open river improvements to Lime Point, Idaho, on Snake River, 30 miles above Lewiston, and with the previously authorized projects, the Main Control Plan will provide a fully developed channel for inland navigation on the Columbia and Snake rivers from Portland to Lime Point, a distance of 405 miles. In addition, the Main Control Plan will provide positive control of floods equal to the greatest of record on the lower Columbia River, 4,400,000 kw of additional prime power, irrigation for new lands, and many other local, regional, and national benefits. Most of these projects, including The Dalles and John Day dams, were authorized by Congress in the Omnibus River and Harbor and Flood Control Act of 1950 substantially as recommended.

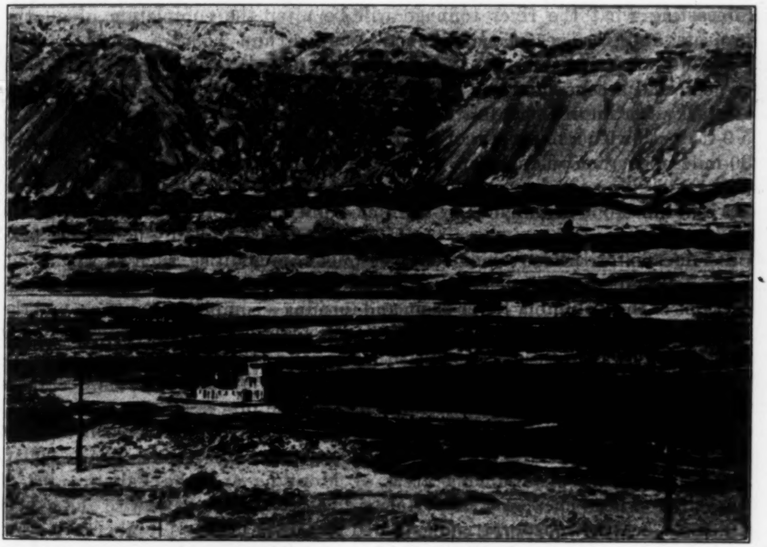

FIG. 4.—BARGE TOW, MIDDLE JOHN DAY RAPIDS, COLUMBIA RIVER

The Dalles Dam, started in December, 1951, at the downstream end of The Dalles-Celilo Canal and just above the town of The Dalles, will raise the water about 88 ft to a normal pool of El. 160. This pool will drown out The Dalles-Celilo Canal, Celilo Falls, and 25 miles of open river to the foot of the John

---

[3] "Columbia River and Tributaries, Northwestern United States," *House Document 531*, 81st Cong., 2nd Session (8 volumes), U. S. Govt. Printing Office, Washington, D. C., Oct. 1, 1948.

Day Dam. The John Day Dam in turn would cause another 92-ft lift to a normal pool of El. 252 which would extend to McNary Dam, 75 miles upstream. The Dalles Dam was started early in 1951 as a defense measure with funds for 7% completion of the project appropriated to December, 1952. The construction program provides for first power and a full pool for navigation in 1957. Plans have been initiated toward construction of other dams in the basin. Construction is scheduled to begin on Monumental Dam in 1957, on Little Goose Dam in 1958, and on Granite Point and John Day dams in 1959.

What effect the completion of these individual projects will have on navigation is a matter of conjecture. Even more interesting is the problem of forecasting what the river tonnage will be after the completion of all the projects and the necessary terminal facilities and harbors on the pools. Certainly an increase in tonnage can be expected with the completion of each project, and a continued and rapid increase in tonnage can be expected after all slackwater improvements are completed and a safe channel is maintained at a 9-ft depth with a minimum of 250 ft of width to Lewiston. In addition, the 30-mile open river channel on the Snake River between Lewiston and Lime Point will give an open river channel of 6 ft by 150 ft to tap large deposits of ore and limestone in the vicinity of Lime Point, now isolated from transportation. The advantage of water transportation is the basically lower cost over other means for the movement of large bulk commodities, such as wheat, oil, logs, or lumber. The generally mountainous terrain dividing the various sections of the Columbia River basin and forming a complete closure around the basin, except as cut by the rivers, causes the higher cost of transportation by rail and highway. Because of this situation, and the fact that a large percentage of the production of raw materials and crops are shipped long distances from the basin to market, and a large part of the processed commodities and finished products are shipped long distances into and within the basin, the cost of transportation is a vital problem in the Columbia River basin. In particular, the extensive wheat-producing areas of Montana and the Palouse area of Washington need cheaper transportation to tidewater for coastwise and export trade. Cheaper transportation is needed to deliver logs and lumber to market and cheaper transportation is needed between tidewater and the central parts of the Columbia River basin for a large tonnage of petroleum products. Economical transportation of any kind is needed in moving the ores and other minerals of the lower Snake basin to tidewater and to market. For all of these, the low cost of bulk shipment on a slackwater river is attractive. In estimating the tonnage that would be available for water shipment, careful studies were made of the production and consumption potentialities of the areas contributory to the navigation system. These totals have been discounted to allow for local consumption, and for movement in other directions, or by other transportation means.

For example, 65% of the wheat production was considered to be potential tonnage for barge movement. Generally, 20% of the inland lumber production was estimated to be available for river movement. Limestone and ore, previously inaccessible in the Snake River Canyon, will be moved by water in quantities determined by the probable future demands indicated by the trend of economic development, and will be influenced also by the depletions of the resources in other sections of the nation which are now in heavy use. Petroleum products, the largest single item to be carried upstream, can be estimated on the basis of per capita consumption (currently determined by authoritative sources to be approximately 1 ton per capita annually) and by means of estimates of future population. It is estimated that 80% of the petroleum products now moving into this interior region moves by river barge. It is difficult to evaluate what net effect the oil pipe line from eastern sources (completed in 1950) will have on this commerce. Although it has diverted tonnage that otherwise would have moved by river, there has not been any reduction to date (1953) because of it. Doubtless the large future demands and possible future increases in per capita consumption will bring about further increase in movement of petroleum products.

The results of these studies yield an estimated future average annual commerce for the Columbia River and Snake River slackwater system of nearly 5,000,000 tons, more than three times the 1952 commerce. The transportation savings expected to be realized in this commerce have been estimated at nearly $7,500,000 annually. Because the transportation system that makes these savings possible assumes a through and uninterrupted artery of commerce, all navigation improvements in the system must be provided to accomplish the system's savings and must share equitably in the total benefits. Accordingly, these benefits can be prorated to the improvements composing the river system by first assigning benefits equal to the annual cost of the single-use navigation improvements and distributing the balance of the benefits among the projects on the basis of ton-miles of commerce transported over the length of river improved by each project. Although the use of the cost of single-purpose navigation facilities only, in this computation, neglects the possible total charges upon final allocation of the total project costs among the uses served, application of this procedure indicated a balance of benefits to distribute in the Columbia River system—actually a benefit-to-cost ratio for system navigation of 2 to 1.

The addition of each individual slackwater pool prior to completion of the system eliminates another stretch of rough, dangerous water. Within this stretch, new water tonnage will originate and terminate, and through tonnage will move faster, more economically and, as a result, in larger amounts.

With the elimination of the Cascade Locks and Cascade Canal, as a result of the completion of Bonneville Dam, a new impetus was given to up-river traffic. The reservoir behind McNary Dam will eliminate several miles of rapids, including two of the most dangerous. Slackwater port facilities will be available at Pasco and Kennewick. Although no appreciable volume of through tonnage up the Snake River can be expected to result until the lower Snake River is slackwatered, the tonnage originating or terminating in the pool may be expected to exceed 500,000 tons annually within a reasonable number of years with no further system additions. This would be approximately half the system potential of the Snake River (the estimated average annual comparable commerce after the system is completed), but it would represent a substantial increase over previous commerce. A larger addition can be expected with the completion of The Dalles Dam after the elimination of the bottleneck of The Dalles-Celilo Canal. In this case, the principal beneficiary will be through traffic. On the other hand, addition of the Ice Harbor Dam will add some tonnage directly tributary to its own pool and some from seasonal open river operations upstream as far as 100 miles to Lewiston. However, completion of the improvement to Lime Point is necessary to tap heavy tonnage. Each project will make a contribution which will grow and be added to, as another "link in the chain" is completed. By 1970, the Columbia-Snake slackwater system probably will be complete; and before that time, consideration will be given to extending the system up the Columbia River or up the Snake River for the development of additional territory. By that time the Main Control Plan will be effective not only in supporting considerable commerce in slackwater navigation, but also in providing large amounts of electrical energy, and controlling floods on the lower river.

SUMMARY

The slackwater improvement of the Columbia River has been established as definitely the most feasible method of providing safe, efficient, and successful navigation on the Columbia and lower Snake rivers. A comprehensive plan to this end, originally proposed in the early 1930's as a possibility for the distant future, became an authorized reality less than 20 years later. In fact, it is well on the way toward achievement with the completion of Bonneville Dam, with McNary Dam and The Dalles Dam under construction, and with the Ice Harbor project under serious consideration for early initiation. Completion of the first step in this improvement, the opening of the Bonneville Lock in 1938, marked a sharp and even phenomenal increase in navigation tonnage which continued at a high rate for several years before it leveled off. With each additional new increment in the system, added tonnage may be expected. The average annual tonnage of the completed system over the 50 years following completion of the last project by 1970, is estimated at nearly 5,000,000 tons as shown in Fig. 2—five times the tonnage carried into the upper river in 1949 and possibly one-thousand times the average tonnage for the 50 years preceding the completion of Bonneville Dam. Water transportation has been a major factor in the economic and social life of the Columbia River basin. The growth and full development of the region will be as dependent on the adequacy of transportation in the future as it has been in the past, and the part that the Columbia River played in the early economic history of its basin will be followed by a sequel in the future. Railroads and highways also have played an important part in this development and will continue to do so in the future. The problems of early competition between these land forms of transportation and water transportation have been greatly reconciled, and further reconciliation will be achieved in the Columbia basin, as has been done in other more highly-developed areas in the east. In many areas, it has been shown that the growth of navigation has resulted in a comparable growth in the railroads and highways that either parallel or feed the waterways. Water commerce will continue to play an increasingly important part in the development of the United States and will continue in the Columbia River for many years after completion of the slackwater improvement.

AMERICAN SOCIETY OF CIVIL ENGINEERS
Founded November 5, 1852
TRANSACTIONS

Paper No. 2664

AERONAUTICAL CHARTING AND MAPPING

By Charles A. Schanck[1]

With Discussion by Messrs. E. S. Fabian, Phil M. Miles, and Charles A. Schanck

Synopsis

Charting and mapping standards of the United States Coast and Geodetic Survey are outlined in this paper. Special charts needed by the aviator and by those who lay out air transport lanes and terminal facilities are classified. Among the specialty maps described are the "Sectional Aeronautical Charts of the United States," world aeronautical charts, small landing charts, and the related problems of assembling data for such purposes.

Introduction

The aeronautical charting program of the Coast and Geodetic Survey, United States Department of Commerce (USCGS), was initiated in about 1930 to provide necessary charts for aviation. Progressive cartographic developments in the nautical charting work of the USCGS, covering a period of more than one hundred years, have resulted in improved charting techniques that have given the nautical chart its present high standard in precision, and its scientific status. Because of the basic similarity between nautical and aeronautical charts, the production of the latter was also delegated to the USCGS as a result of the Air Commerce Act of 1926 and subsequent legislative action.

The need for special maps or charts for air navigation was realized as early as 1888 when steps were taken in Europe to produce maps for the navigation of lighter-than-air craft. With the limited air speeds of the early days of aviation, it was possible for the aviator to use standard topographic maps for identifying prominent landmarks in navigating his plane. The British incorporated special features into an "aero" map produced in 1912 to emphasize details pertinent to the aviator. This early aeronautical map emphasized roads, railways, and lakes by hand coloring on a photoprint of an ordnance survey map at a scale of 1 in. = 1 mile.

The practice of using existing topographic maps, with the addition of special information by hand, continued during the early days of World War I, but

---

Note.—Published, essentially as printed here, in February, 1953, as *Proceedings-Separate No. 172*. Positions and titles given are those in effect when the paper or discussion was received for publication.

[1] Comdr., Coast and Geodetic Survey, U. S. Dept. of Commerce, Washington, D. C., formerly Asst. Chf., Div. of Charts.

the growth of aviation during that war emphasized the need for special air maps. By the end of the war, the British had produced special air charts for use over the coastal areas of the British Isles and a special aviation map of France. These maps are thought to be the first ever produced in quantity for use in the air. They conformed generally to existing topographic maps except in the simplification of certain detail and the showing of aeronautical data, such as aerodromes, landing areas, and dangers to navigation. Air speeds were slow, with flying largely confined to good weather, and navigation was mainly by contact flying or piloting.

An important development in the period immediately following World War I was the International Convention of Air Navigation held in 1920 for the purpose of standardizing cartographic practice to simplify the problems of the aviator when flying outside his own country. General aeronautical charts at the scale of 1:1,000,000, with larger scales for selected areas, were proposed and standard symbols for showing aeronautical data were agreed upon. Existing topographic series, such as the "International Map of the World," were adapted for use in the air by means of an aeronautical overprint. These overprints showed aerodromes, landing areas, dangers, obstructions, prohibited areas, lines of magnetic declination, and radio data. The overprint was reproduced in a conspicuous color, such as red or purple, but was printed so as not to obliterate existing detail on the map.

Charting in the United States

In the United States, the Army Air Corps first considered the needs for aeronautical charts in the early 1920's. When F. L. Martin and his crew made their round-the-world flight in 1924, they accomplished their mission without the aid of aeronautical charts. The flight was made with road maps, topographic maps, nautical charts, and other types—all that were then available. This undertaking and other activities emphasized the need for special charts for use in aviation, and in 1924, the Air Corps inaugurated a project which included 35 strip maps for military use covering limited areas of operation, primarily between major Air Corps fields. The USCGS cooperated with the Air Corps in this undertaking by organizing its first unit for the preparation of aeronautical charts. This unit produced a number of strip maps covering areas 80 miles wide along principal airways to meet immediate demands. In 1927, the printing order for strip maps was increased to 500 copies, which represented a full year's supply.

In 1929, the Federal Board of Surveys and Maps recognized the problem, appointing a committee on aerial navigation maps to make recommendations for a charting program. Work was started in 1930 by the USCGS on the first of the Department of Commerce charts. The first series was laid out on an area basis to cover the United States in 87 charts known as the "Sectional Aeronautical Charts of the United States." The Chicago (Ill.) chart, published in December, 1930, was the first to be issued of the new series. By 1935, all 87 charts were completed and the Air Corps in the meantime discontinued the use of strip maps in favor of the new sectional charts.

The present-day aeronautical charting activities of the USCGS include the compilation and printing of aeronautical charts of the United States, its territories and possessions, as required for civil aviation and for military use where these requirements are parallel. In addition, such aeronautical charts covering international airways as are required primarily by United States civil aviation are compiled and printed by the USCGS.

Aeronautical charts on issue in 1952 totaled 1,191, including 276 standard and auxiliary charts, 761 instrument approach and landing charts, and 154 radio facility charts. Approximately 9,000,000 copies of the standard aeronautical charts are distributed annually. In addition, more than 29,000,000 of the page-size airport and radio facility charts are issued each year. These charts are issued in several different types and scales, depending on their use. Charts in use for the United States in 1952 included the sectional series at the scale of 1:500,000; 43 world aeronautical charts at the scale of 1:1,000,000; route charts at the scale of 1:2,000,000; and planning, direction-finding, local, instrument-approach and landing, radio-facility, and aircraft-position charts at varying scales.

The sectional charts are considered as the basic all-purpose series designed by the USCGS for contact flying, or flying by reference to visible landmarks. For this reason, they include all prominent topographic features that can be seen from the air, all air navigation aids, and many outstanding landmarks and other items of value to pilots which do not appear on conventional topographic maps.

The world aeronautical charts, at the scale of 1:1,000,000, were designed primarily for radio navigation and, being at a smaller scale, do not show the completeness of detail appearing on the sectional charts. The route charts were designed especially for long-range navigation to meet the requirements of air carriers operating at high altitudes with high-speed aircraft. Aeronautical charts for radio direction finding at the scale of 1:2,000,000 have been constructed for simple and quick plotting of radio bearings. Planning charts of the United States and Alaska at the scale of 1:5,000,000 are published for planning routes between distant points.

The small approach and landing (AL) charts serve the needs of the pilot when approaching an airport on instruments under conditions of low visibility. They also serve as contact charts, after a break-through on instruments, and as airport vicinity charts. Charts of the series are published for use with instrument-landing systems and automatic direction-finding equipment. Each type of chart has its primary purpose and has been developed after careful study has been made of the problems involved.

AERONAUTICAL CHART PRODUCTION

Aeronautical charts constitute a new development in cartography with the primary objective of providing for the needs of the aviator in as simple and characteristic a form as possible. Primary requirements are the ready solution of certain problems of direction and distance and a comprehensive indication of intervening terrain which may be gained at a glance. The features to be stressed are those relevant to air navigation in a rapidly moving plane. The airway route should be clearly defined, and prominent landmarks either natural or otherwise conspicuous—such as the general trend of railways and highways, their intersections, and the positions of industrial landmarks—are clearly shown or emphasized. Sinuosities of streams should be generalized, and minor roads and details that may confuse the aviator are omitted. Simplicity is desired so that the aviator may grasp at a glance the relative location of the places in which he is interested and which will serve him in maintaining his course.

From the beginning of a compilation until the final product is placed in the hands of the pilot, it is constantly borne in mind that aeronautical charts are not ordinary maps, but highly specialized charts intended for one purpose—to provide the aviator with the simplest and most accurate instrument for proceeding safely to any chosen destination and for identifying terrain features en route. In keeping with these requirements, many details appearing on ordinary maps are omitted because they would only obscure details of greater navigational importance.

As aeronautical charts require special consideration of geographic fundamentals, the merits of a suitable system of projection and proper control become significant in respect to the facility of laying out courses, fixing features, and measuring distances. Therefore, the first step in aeronautical chart production is the determination of the best framework on which to delineate as true a representation of the earth's surface as is practicable for this purpose. Two properties, both of which are vital in air navigation, are the speed and accuracy with which navigational problems may be solved.

In selecting a projection, these factors must be considered:

(*a*) Correct representation of topographic features visible to the airman by preserving true shapes of physical features, including correct angular relationships and the representation of areas in their correct relative proportions;
(*b*) True scale values for measuring distances; and
(*c*) Representation of great circles as straight lines.

Other factors to be considered are the following:

(*d*) Solution of problems of celestial navigation;
(*e*) Determination of position in the air by dead reckoning from accurate courses and distances;
(*f*) Use of radio bearings for position fixing; and
(*g*) Junctions of all adjacent sheets on the same scale.

CHART PROJECTION

After thorough investigation, the USCGS selected the Lambert conformal conic projection for the aeronautical charts of the United States. This projection permits a perfect junction between any number of charts in any direction. It is unexcelled for scaling distances in all directions for a large geographical area, such as the United States. Azimuths obtained from this projection conform closely to directions on the earth. The Lambert projection affords a simple and satisfactory solution for all problems of dead reckoning, not excepting the rhumb line; it affords a simple means of practical great-circle navigation; it is well suited for celestial navigation and all problems requiring the plotting of positions; and it is unsurpassed for all types of radio navigation.

The meridians and parallels of the earth are projected upon a cone that intersects the surface of the earth along two standard parallels. The standard parallels on the earth and on the cone coincide, and along them the scale is therefore exact. Between the standard parallels, the earth is projected inward upon the cone, and the scale of the cone is somewhat smaller than the scale of the larger earth. Outside the standard parallels, the earth's surface is projected outward, and the scale of the cone is slightly larger than that of the earth. The standard parallels of true scale adopted for aeronautical charts of the United States are latitudes 33° and 45°. The tables have been extended by the USCGS with additional bands for world-wide charting; and the aeronautical charts published of world areas by the U. S. Air Force contain this system of projection.

Marginal scales in statute miles are printed in the borders of the charts, and the meridians are graduated for use of the nautical mile. The border scales in statute miles on charts of a scale of 1:1,000,000 series, and larger, are based on the scale of the central parallel of the chart. Consequently, the distances measured by these scales along the central parallel are exact, and the distances between points on opposite sides of the central parallel and equidistant from it are exact also, regardless of the direction between them. Distances can be measured on these projections with surprising accuracy.

The use of a transverse or oblique Mercator projection in the production of aeronautical charts has received considerable attention in the past few years due to the development of great-circle navigation. Projection tables for each five degrees of azimuth have been computed and published, thereby making world-wide coverage, based on this projection, possible. The oblique Mercator projection has excellent properties for air navigation. By selecting the projection table that is nearest in azimuth to that of an air-route scale, distortion is kept to a minimum, and for all practical purposes no correction is necessary for radio bearings since all straight lines closely approximate great circles.

The Base of the Aeronautical Chart

When the projection to be used in the aeronautical chart has been selected, the next step is the selection of the source material for the various chart features. One source may be best for roads, another for railroads, another for relief and drainage, and still another for city shapes.

Only a small percentage of the base information that goes into its aeronautical charts originates with the USCGS. This information covers areas adjacent to shore lines where field surveys have been conducted by the USCGS in connection with its natural charting program. Control surveys by the USCGS in the interior serve to verify and augment information from other sources. For most of the base material that goes into the aeronautical charts, the USCGS must rely on the mapping activities of other agencies. The quadrangles established by the Geological Survey, United States Department of the Interior (USGS), are the greatest single source of topographic information. Accurate, up-to-date, topographic maps, regardless of their source, provide the ideal information for the compilation of the aeronautical chart base. Unfortunately, vast areas of the United States have not been mapped adequately. In these areas, the USCGS relies on information from a wide variety of sources, including county road maps and property maps, railroad plans and profiles, drainage maps, aerial photographs, planimetric maps, trigonometric leveling data, and cadastral survey and others.

THE AERONAUTICAL OVERPRINT

Complete aeronautical data are furnished by the Civil Aeronautics Administration, United States Department of Commerce (CAA). These data convert the topographic map into an aeronautical chart. They include accurate locations of airports and auxiliary landing fields, types and facilities of airports, navigational lights, radio ranges, civil airways, high-frequency and low-frequency radio facilities, and other aids, as well as power lines and other obstructions to air navigation.

THE FINISHED CHART

As an expression of natural conditions, the finished chart delineates geographic features and aeronautical information partly in the form of a reduced outline and partly in the form of symbols of various kinds. In addition to the proper use of conventional signs and symbols, attention is given to details such as lettering, balance of chart, and the number and selection of charted details. A critical study is made of the area to be charted in order to secure a selection of details that is simple, representative, and practical. By maintaining a sense of proportion and propriety, the cartographer supplies the artistic element indicative of good charting without sacrificing any essential detail.

To afford maximum legibility and ready identification in the air, aeronautical charts are lithographed in colors. Projection lines, names, roads, and railroads are black; city outlines are yellow; drainage is dark blue; and contours are brown. Gradient tints of one or two shades of green and up to five shades of brown are used. Aeronautical information is in magenta and offset blue.

AIRPORT OBSTRUCTION PLANS

In 1945, the CAA requested the USCGS to prepare a new series for a different purpose. Regulations of the CAA prescribed maximum weight limitations for aircraft of transport category. The weight limitations vary with the type of aircraft, and with wind and temperature conditions, as well as with the length, elevation, and gradient of the runway being used, and the locations and elevations of obstructions in the vicinity. It was for the study of these latter factors governing weight limitations that the series of "Airport Obstruction Plans" was designed. The plans are also useful tools for city zoning in the airport vicinity, and for the airport engineer in planning new construction.

Each plan shows the airport runway pattern and the location and elevation of objects in the vicinity of the airport that may be potential hazards to air traffic. These objects are those that extend above several imaginary surfaces, varying in extent, shape, and elevation. A general note on each plan defines those surfaces.

The official airport elevation and a generalized profile of each runway are also shown on each obstruction plan. The profiles extend outward from the end of each runway to a point just beyond the last potential hazards or to a maximum of 10,200 ft for noninstrument runways and 50,000 ft for instrument runways.

Airport obstruction plans are compiled from accurate field surveys and recent aerial photographs, usually taken with the nine-lens camera. The field survey parties identify on the photographs the features to be shown on the plan. The elevations of these features and of the airport runways, the lengths and azimuths of the runways, and the horizontal control necessary for the compilation of the plan are also determined during the field surveys. The plans are compiled in the Washington, D. C., office of the USCGS from the aerial photographs and the ground survey data, at a scale of 1 in. = 1,000 ft.

Each field survey presents its interesting problems. It should be remembered that obstructions in the approach areas and the conical section are defined by sloping surfaces. The reconnaissance for the identification of an obstruction in these areas requires methods peculiar to airport obstruction surveys. In the parts of the approach areas that are visible from the runway ends, obstructions can be readily identified by setting the glide angle on the vertical circle of the instrument and scanning the horizon. Trial elevations must be taken to identify observations in other parts of the area surveyed. A stereoscopic study of the aerial photographs will reveal areas where obstructions are likely.

Once the obstructions are identified, their elevations are determined by any of a number of suitable methods. No great accuracy is required on such surveys. Permissible elevation tolerances are 15 ft in the conical section, 10 ft in the horizontal area, 1.5 ft in the runway area, and 1.5 ft per 5,000 ft from runway ends in the approach areas.

FUTURE CHARTING

Requirements for aeronautical charts will be changing continually for years to come. The flying farmers, the pleasure flyers, the crop dusters, and the operators of small chartered planes can be expected to continue the use of the sectional aeronautical charts. These charts will be improved as new types of topographic mapping become available. Meanwhile, the operator of the jet-propelled aircraft operating over long distances at high altitudes and at speeds of many hundred miles per hour becomes less and less interested in topographic detail on this chart, except at the take-off and the landing. New types of charts for use for instrument landing systems are already in use. The cartographer must constantly strive to improve his techniques and devise better methods of presenting these facilities so that the aeronautical charts will keep abreast of the rapid developments in the aviation industry.

DISCUSSION

E. S. Fabian,[2] A.M. ASCE.—An excellent presentation of the development of aeronautical charting and mapping has been offered by Commander Schanck. The author has stated clearly the many problems involved in preparing the several kinds of aeronautical charts and maps which will best satisfy specific aeronautical needs.

The most obvious need for the aeronautical chart is in connection with aerial navigation. Aerial navigation is a complex operation requiring specialized training, specialized navigational instrumentation and aids, and the high degree of skill that is developed with experience. In general, the problem of aerial navigation consists of three parts: First, the preparation of the flight plan or "laying out" the course of flight from the point of departure to the point of destination; second, the establishment of a sequence of check points along the course of flight by which the navigator can check the aircraft's progress while in the air; and third, the actual execution of the flight plan with the full and correct knowledge at any time of the exact position of the aircraft along the flight course.

The importance of an accurate aeronautical chart in the solution of the first two parts of navigational problems is quite obvious. The chart must correctly represent the geographic relations of both distance and direction of the landing fields and it must show the geographic location of the most prominent topographic features which will serve as recognizable "check points." These points must be shown for the entire area represented by the map. Either through errors of navigation or the action of the elements, aircraft frequently stray from the planned line of flight and become "lost." The navigator must then be able to establish the aircraft's position by reference to recognizable features on the ground which are represented on the chart, so that the aircraft can be promptly returned to the planned route or to an alternate route.

If the flight is to be executed on instruments, the topographic features shown on the map will be of little navigational value. The features will be obscured by the weather or darkness or they will be unrecognizable at a high altitude. Instrument flight must be guided by radio navigational aids such as radio ranges, radio beacons, and the various types of markers. If the aeronautical chart is to serve as a guide for instrument navigation, it must show the correct geographic location of these aids and unmistakably identify each.

When only the first two parts of the problem of aerial navigation are considered, namely, the preparation of a flight plan and of the flight control, the cartographer's problem appears to be relatively simple—not much more difficult than that of producing a good geographic map. It is only when the third part of the problem of aerial navigation is considered—the execution of the flight plan by use of the aeronautical chart—that "the psychology of space orientation" occurs. The aerial navigator must be oriented at all times; he must know the exact position of his craft within some familiar framework. Complete orientation without any maps or charts is possible over only a very limited territory with which the navigator is completely familiar. In any other case the framework of orientation is the aeronautical chart on which the aircraft is represented as a point to be correctly located at any moment, with reference to the symbols shown on the chart. The orientation consists in establishing correctly the correspondence between the signals received from the earth below, whether the signals be photographic images or radio signals. To establish this correspondence the aeronautical chart must be an exact image of only those features on the surface of the earth which can be unmistakably translated (by the navigator) from a signal to a symbol.

---

[2] Prof. of Civ. Eng., Univ. of Tennessee, Knoxville, Tenn.

Selection of the most recognizable land features and adoption of chart symbols that will permit the easiest and most reliable translation from signal to symbol are the cartographer's most difficult problems. Enough features of the visible landscape must be shown to permit a complete coverage of the area shown on the chart. If too many features are shown, they will confuse the navigator; if too few are shown, the navigator lacks possible means of orientation. The powers of observation and comprehension vary among navigators. A good chart will not show all geographic and topographic details, but only those features which trained observation will grasp quickly and trained comprehension will identify unmistakably. The selection of the features to be shown on the chart must be made from the navigator's point of view and with reference to the mental process involved in space orientation. The teacher of navigation, the navigator, and the cartographer must cooperate to produce a good aeronautical map.

The selection of symbols by which the recognizable features are to be represented on the chart in their proper relations is a difficult problem. Some features, such as roads and their intersections, railroads, and rivers are best symbolized by their likenesses. Others, such as swamps, lakes, and large bodies of water are best represented by outline, shading, and color, and still other features, such as cities, towns, bridges, industrial areas, and navigational aids, by suggestive symbols or brief descriptions. The adopted symbols must permit the easiest identification from the signal received so that the correspondence of the ground below can be quickly and correctly established to the part of the chart which it represents.

Cartographers have ably solved these problems in producing navigational maps and charts. The charts are accurate, and their general composition permits quick training in observation for comprehension and the development of the power of space orientation. The present methods of aerial navigation, whether in accordance with contact flight rules or instrument flight rules, are well served by existing navigational charts.

These charts can be improved, if they are regarded as representing only a stage in the long process of cartographic evolution. The fact remains that aircraft get lost, sometimes with disastrous results. How many and what proportion of navigational errors are chargeable to human frailty and the failure of navigational instrumentation and how many and what proportion to the shortcomings of the charts must be determined by careful studies. Aviation psychologists might be able to indicate the direction of chart improvements as has been done in the fields of pilot training and selection, in instrumentation, and in other fields. Improvements in technical factors of aeronautical charting can also be expected, because, as Commander Schanck indicates, cartography is not a static science.

The charts are adequate for the usual methods of aerial navigation. However, there are increased navigational requirements for both the improved aircraft and navigational aids. Universal adoption of the omnidirectional range as a navigation aid will render the existing charts inadequate. A successful development of ground and airborne radar as instruments for navigation and air traffic control might render these navigational charts obsolete. The basic problem, however, will remain the same for the science of cartography; it must still provide a framework for orientation in space on which the correspondence between the signal and the symbol must be established by the aerial navigator. Experience indicates that the production of charts and maps as adequate as those which are used for the existing methods of aerial navigation may be expected of the science of cartography. It is probable that these charts will be superior, in view of the expected improvements in the art of map making.

The reliability of the aeronautical charts—their accurate and full representation of all features necessary for the solution of navigational problems—deserves special comment. There are continuous changes in the condition of the airports. New landing fields are being built, and new landing facilities are being added. Airways are frequently relocated, and new ground navigational aids are commissioned. There are also frequent changes in the landscape resulting from the building of new highways and the relocation of the old ones. The contours of lakes and rivers are frequently changed by the building of dams. New industrial areas are constantly being developed. All these changes on the surface of the earth render navigational charts inaccurate from one issue to the next. Just what are the criteria for determining the obsolescence of the charts and what are the factors which determine the necessity of a new issue? The normal procedure of supplementing the navigational charts and maps and indicating the pertinent changes is by use of a bi-weekly volume issued by the Office of Aviation Development of the CAA. In addition to the changes in flight rules, this volume contains corrections, changes, and additions to the aeronautical maps and charts. This information is compiled from reports of the CAA district airport offices, from airway communication centers, and from CAA regional offices. Thus the navigational information is made accurate every two weeks. More urgent information is transmitted to the flight control centers by use of teletype, and immediately urgent information is broadcast directly to the aircraft by use of radio communication. Much of this information is only of temporary importance, but some of it represents permanent departure from the information shown on the charts in use, and necessitates their revision.

The large distribution of aeronautical charts indicates that the charts must be used by others besides aircraft personnel; federal, state, and private aviation planning agencies make use of the various types of charts in planning regional aviation development. While directing aviation development in Tennessee, the writer has used sectional charts as base maps for planning a development of secondary airways, in locating intermediate and secondary airports, and in preparing an air marking plan. The various charts were also used in making aviation facility inventories and in planning the development of additional facilities. Cooperation with the CAA in carrying out the National Airport Plan required continuous reference to aeronautical charts of various types.

Airport managers, planners, and engineers make excellent use of airport, radio facility, and airport obstruction plans. Commander Schanck mentions specifically the use of airport obstruction plans in connection with zoning studies and in the planning of new airport construction. When used in connection with topographic and aerial survey maps, the aeronautical charts permit preliminary location and engineering studies for airports. The charts also minimize the number of field surveys necessary for preparing construction plans.

Aeronautical charts and maps are necessary aids and references in traffic control, in planning and controlling aircraft operations in airline offices, in aircraft accident investigations, and in the many other activities of the CAA and the Civil Aeronautics Board. The very characteristics of these charts which make them useful for air navigation are responsible for their usefulness on the ground. The charts are probably used in greater volume in connection with ground aeronautical activities than for aerial navigation.

The usefulness of the charts as teaching aids and instruments for classroom practice must not be overlooked. Flight schools, aeronautical ground schools, traffic control training centers, airline training schools, and engineering schools find the charts not only useful but necessary in the training of students. It is this widespread usefulness and excellence of aeronautical charts and maps which account for their annual multi-million distribution. The volume of distribution may well be an index to the growth of aviation.

PHIL M. MILES.[3]—The history of the development of aeronautical charts and their use in the United States has been presented by Commander Schanck. An examination of the production and use of these charts, both in the United States and other countries, leads to the conclusion that their quality is unsurpassed.

It is vital to the development of aviation that a complete series of aeronautical charts, from relatively large-scale instrument-approach and landing charts to small-scale charts required for navigation of high-speed aircraft, be produced and maintained. The cost of production and development of a complete series of charts is an infinitesimal part of the cost of conducting the aviation industry.

The USCGS and other agencies and groups are constantly endeavoring to develop more useful cartographic designs for aeronautical charts. These charts will enable all pilots, and especially the inexperienced pilot, to make better use of such material. A more complete and easily interpretable presentation of relief and prominent landmark objects is the objective of cartographic development. For example, current (1953) aeronautical charts show relief by a color-gradient tint that represents intervals of 1,000 ft or 2,000 ft and contours at 500-ft intervals. This leaves much to be desired in illustrating the roughness of the terrain, and this is most important in selecting flight routes for light aircraft. In the event of power failure or adverse weather conditions, the availability of suitable emergency-landing areas is of utmost importance to the light-aircraft operator.

---

[3] Chf., Maps and Minerals Div., Agri. and Industrial Development Board, Frankfort, Ky.

Notable development work is being conducted (1953) at Ohio State University, at Columbus, under the direction of George Harding, A.M. ASCE. This cartographic unit is experimenting effectively with various methods of relief presentation on maps and charts. Some of these methods show promise. Noteworthy also are the accomplishments of the USCGS in supplying excellent aeronautical charts, despite inadequate topographic coverage in the United States.

The expansion of large-scale topographic operations following World War II, especially in the eastern and middle-western areas of the United States, will enable the USCGS to correct many errors that were beyond its control in earlier charts. Unfortunately, few users of aeronautical charts appreciate either the efforts of the USCGS cartographers to show accurately the information required, or the efforts continually made to improve the charts.

CHARLES A. SCHANCK,[4] M. ASCE.—The comments of Messrs. Fabian and Miles are valuable contributions to the subject of aeronautical charting and mapping. Exception can be taken to Mr. Fabian's statement that aeronautical charts are probably used more frequently in connection with ground activities than for aerial navigation. It is unlikely that accurate figures are available on the number of aeronautical charts used in various fields of the aviation industry. Certainly, however, many charts are used which are never carried in an airplane.

It is regrettable that everyone is not as aware as Mr. Fabian is of the usefulness of these charts as training aids. As he writes, "aircraft get lost." Perhaps fewer of them would get lost if pilots were thoroughly instructed in map reading during their pre-flight training.

Mr. Miles' statement that much is still to be desired in illustrating the roughness of terrain cannot be refuted. Every governmental agency engaged in charting or mapping constantly strives to find a remedy for this unsatisfactory condition. These efforts are well coordinated. The agencies also follow closely the developmental work being conducted at Ohio State University and other research centers. It is this compilation, by all interested groups, of cartographic knowledge that will produce better aeronautical charts.

---

[4] Comdr., Coast and Geodetic Survey, U. S. Dept. of Commerce, Washington, D. C.; formerly **Asst.** Chf., Div. of Charts.

AMERICAN SOCIETY OF CIVIL ENGINEERS
Founded November 5, 1852
TRANSACTIONS

Paper No. 2665

CITY PLANNING TECHNIQUES

By Russell H. Riley,[1] M. ASCE

Synopsis

The growth and development of cities, if properly planned, involve long and careful study by laymen and engineers working with city officials. This paper describes and evaluates some of the procedures followed in preparing a city plan, and provides a general description of the most desirable method. Particular stress is placed on the roles of the engineer and of the private citizen.

Introduction

A complete study of city planning techniques is difficult because more than a thousand American cities have prepared city plans or are engaged in city planning activities. It is impossible, therefore, to be completely familiar with all the different practices and procedures. However, the writer has had the privilege of assisting in the preparation of many city plans and of studying many others—experiences affording a fair cross section of information on current planning practices. Some of the following comments may seem critical of certain procedures; however, they are presented in an effort to show both advantages and defects.

City Planning Compared with Other Phases of Engineering

Before discussing the different practices or techniques of city planning, it is desirable to recognize a major difference that exists between usual engineering practice and city planning. This difference is people—the relationship of the program to the public. In designing and supervising a sewerage system or water system, a power plant, dams, or similar projects, the engineer is normally responsible to a small committee or to a few officials, and the public has little interest in the plan or its details unless there are long delays during construction, or unless defects develop soon after completion. The situation is different in city planning. Each phase of the plan affects some or all of the property within the city. Property owners protest vigorously when it is proposed that

---

Note.—Published, essentially as printed here, in June, 1953, as *Proceedings-Separate No. 194*. Positions and titles given are those in effect when the paper was received for publication.

[1] Partner, Harland Bartholomew and Associates, St. Louis, Mo.

a major street traverse a residential district, or when a grade-separation structure hinders access to a commercial building. Even a recommendation to change a bus route may bring forth much opposition. However, public reaction is particularly widespread in regard to zoning. The state enabling acts facilitate the opportunity to protest—and properly so—since they require duly advertised public hearings before zoning and other phases of the plan can be adopted or amended. Planning techniques and practices should be such that they will keep public opposition to a minimum.

MAJOR TYPES OF PLANNING TECHNIQUES

With so many cities engaged in planning, there are countless combinations of practices used in preparing a comprehensive city plan. The dominant techniques, however, can be grouped into three major classifications, which are summarized as follows:

Planning by Citizens and Inexperienced Technicians.—Although many suburban communities and smaller towns—of 50,000 population and less—have engaged experienced technicians to prepare their city plans and zoning ordinances, many others have attempted to have the work done by citizens' committees assisted by local city officials or by a young graduate from a technical school. The failure of the legislative body to appropriate adequate funds for planning purposes is a major reason for this practice.

The work is usually initiated with considerable enthusiasm, the first step being the acquisition of a number of plans and ordinances from other cities of similar size. These are studied to determine which parts would be applicable to the local community. Efforts are made to combine selected parts of several plans into a plan for the local city and, as might be expected, large gaps or missing sections frequently result. A few field inspections are usually made, but, for the most part, the citizens rely on their memory of existing conditions.

After many hours of meetings, enthusiasm begins to wane, and a long period usually elapses before any plan is presented for public consideration and comment. Even the public comment may be very critical since it is layman's opinion against layman's opinion.

Any defects in this practice or technique are certainly not the fault of the citizen planners. They give far more time and effort than should be required in any civic endeavor. It is unreasonable to expect citizens engaged in their own personal business to spend so much time on unfamiliar technical details. Citizens play an important part in any planning program, but it should be primarily in judging the proposals rather than in making them.

Furthermore, the local officials are usually too busy with their normal duties to devote much time to handling the routine details of preparing a plan. As a result, sufficient time is not given to considering existing conditions and probable future requirements. The basic defect, however, is the lack of technical experience and background.

Compilation of Data Followed by Incomplete Planning.—A second type of planning technique sometimes followed, even in large cities having relatively large staffs, involves the devoting of almost all efforts to the compilation of data regarding existing conditions and trends. Such information is necessary as the basis for a plan, but it has only limited value unless the plan is actually prepared.

Routine administrative duties admittedly absorb much of the time of the average planning staff. This is particularly true of the time required for enforcement of subdivision regulations and for making zoning changes and revisions (almost all the larger cities have zoning ordinances, even though they may be the only existing part of a city plan). Almost all state enabling legislation providing for city planning, however, clearly states that the major duty of a plan commission is to prepare and adopt a comprehensive plan. Such legislation further provides for changes and amendments in the plan. Thus, there should be a comprehensive plan and it should be continuously adjusted to unexpected changes in conditions and trends. This responsibility for preparing a plan should be delegated to a group or committee of any local staff. The staff should not devote its entire efforts to routine administration or compilation of mere facts—interesting as the latter may be. If the staff cannot be augmented, outside technical assistance should be secured to prepare the plan and participate in its revisions.

A variation of the foregoing technique is the preparation of one or two phases of a comprehensive plan, usually a major street plan or possibly a plan for a grouping of public buildings. In numerous instances, the study or plan may be only for an individual project that is contemplated for early construction, rather than for a system of such facilities serving the entire urban area. This partial planning should produce certain beneficial results, but its potentialities are limited in comparison with those of a comprehensive plan. In some cities, these "piecemeal" plans receive little or no publicity, and few persons other than the plan commission and some officials are familiar with the proposals. This procedure may prevent public objection or criticism, but it hinders attempts by individuals or corporations to adjust their improvements to a long-range plan.

One large midwestern city had been engaged in a planning program for more than ten years. Vast amounts of data had been compiled—some of which was becoming obsolete—but a complete plan, or even a major section thereof, had never been prepared and submitted to the public. As a result, the commission was beginning to receive so much criticism from both citizens and officials that its standing and prestige were impaired. This commission finally engaged a planning firm to prepare such parts of a comprehensive plan as could be developed from its existing data. The partial plan was prepared within a few months, and received considerable newspaper publicity. A much more favorable attitude developed toward the commission and its work; in fact, the legislative bodies have since provided additional funds to complete the comprehensive plan.

A Complete Plan Based on Engineering Principles.—The third major type of planning technique is the one most commonly used in modern programs. The procedures involved are generally the same as those observed in studying and designing other engineering projects. New Orleans, La., has completed a comprehensive revision of its original city plan, which was prepared in the late 1920's. The program required approximately 3 years, during which the local staff compiled the data and did the drafting, and the consultants furnished two experienced planners. In addition, frequent visits were made by members of the firm to direct the work, to decide on recommendations, and to discuss the findings and proposals with the commission, officials, and citizens.

Before starting preliminary studies and plans for the average engineering project, it is necessary to spend considerable time in determining the dominant requirements and major physical and economic characteristics of the proposed project. Similar investigations, probably of a more intensive nature, are necessary in the initial phases of a city planning program. Topographical, climatological, and geological characteristics frequently exert a major influence on the type of city and on its physical requirements. For example, the low, level topography has been a major factor in influencing the character of development found in New Orleans. The difficulties of storm-water disposal, caused by the topography and periods of heavy rainfall, and the high costs of foundations and footings (required because of local soil conditions) have resulted in such high land-improvement costs that land use is much more intensive than in many other cities of comparable size. For example, there were only 4.63 acres of developed land per 100 persons in New Orleans (1950), as opposed to 6.11 acres for the same number of persons in eleven other cities of comparable size. In New Orleans, the residential lots are narrow, and two-family houses and multiple-dwelling structures are much more dominant than in similar cities—particularly those in the midwest and in the south. The high land cost and the intensive use of land, together with the comparable lack of vacant property (except in the extreme outlying sections), have also resulted in small school grounds and in few neighborhood parks. Many other cities have particular characteristics which affect the recommendations and proposals comprising a satisfactory plan.

Another major study that should be made in determining the background and future requirements of city planning is an analysis of employment opportunities and conditions that have influenced the growth of the particular city. In New Orleans, the harbor and water transportation facilities exerted the major influence on its early growth. Not only did they facilitate the establishment and development of commerce and industry, but they were, and have continued to be, a major source of employment. This fact clearly reveals that the plan for this city must provide amply for the expanison of ports and other modern forms of transportation. During World War II, the city experienced a tremendous increase in industrial development, a trend which continued after the war's end. Accordingly, there has been a need for providing large tracts of land that can be made available for industrial expansion. Of particular importance is the fact that the industrial growth has provided a wider and more balanced economic diversification. This indicates excellent possibilities for employment and continued growth.

The second step in the study of the average engineering project is the determination of its size and future requirements. The same is true of a city planning program. The major objective of the city plan is to provide more efficient and adequate physical facilities for present and future citizens. Careful studies of population growth and development are essential, therefore, in order that data be available as to how many citizens will reside within the area during the next 25 or 30 years.

The first phase of the population study is an analysis of past trends and factors influencing growth, and the preparation of estimates as to the size of the probable future population. Some unexpected conditions may affect the population estimates, but for the most part, there can be reasonable approximations. The second phase requires a careful study as to where this future population should, and probably will, be located. Without these data, it is impracticable to decide the location and size of the future physical facilities—such as major streets, schools, parks, sewers, and drainage facilities—for most effective service to the future citizens.

Several different factors, including existing land uses, trends in building development, and topography affect distribution of population. For example, in the New Orleans area, some sections of the vacant and undeveloped property were found to be 6 ft or more below sea level. Other large unimproved sections of the city had elevations only slightly above sea level. Improvement of the low areas, with particular regard to facilities for disposing of the storm water, would be expensive. Therefore, the population should be encouraged to settle in the areas that can be most economically developed.

One further factor that should be mentioned in connection with population studies is that much of the future distribution probably will occur beyond present corporate limits; the area that should be considered in a planning program is an urban area that may be much larger than the city's incorporated area.

Just as an engineer or architect, after having determined the size of a building, must next decide upon the arrangement of its various portions or rooms, so the next step in normal city planning practice is to determine the general location and extent of the major land-use areas. These areas include those for single-family and two-family residences, multiple dwellings, commercial structures, and the various types of industries. Past experience has indicated that each use functions much more efficiently when it is near other similar uses and not when widespread intermingling occurs. Arrangement and control of land uses in city planning are known as zoning, and all too frequently have been considered as the dominant or sole phase of planning.

Preparation of a land-use plan and zoning ordinance involves most careful study and consideration of existing conditions and probable future needs. A field survey to determine the location and extent of existing land uses is imperative. Of particular interest to engineers is the fact that studies have revealed a close relationship between land-use areas and units of population. This relationship is usually expressed in acres of land use per 100 persons. For example, in New Orleans, the land-use survey (1950) revealed an average of 0.14 acre of commercial development per 100 persons and an average of 0.31 acre of industrial development per 100 persons. A study of a large number of land-use surveys reveals a marked similarity of ratio between land use and population in different communities of similar size. Some such surveys have also been made at intervals of 20 or 25 years in the same cities, and very minor changes in the ratio were noted during the intervening periods.

The land-use ratios provide a sound basis, therefore, for determining the areas that will be required for the various uses, especially since these ratios can be related to the estimates of future population. A zoning ordinance can thus provide for adequate land uses on a sound engineering basis, rather than on individual opinions or guesses. Admittedly, the average zoning ordinance provides a greater area for industry, commerce, and (usually) for multiple dwellings than the land-use computations indicate as being needed. The major reason for this apparent lack of balance is that the existing development is usually so scattered that the districts must be larger than would normally be necessary. Zoning can and should, however, be based on sound engineering standards and principles—just as is the design of a sewer or water system.

After the determination of the extent of population, and the location and extent of the land-use areas necessary for this population, the next step in New Orleans was to determine the location, character, and extent of the public physical improvements required to serve these areas in accordance with modern standards. The physical facilities normally considered in the modern city plan are the following: Major streets; street and off-street parking facilities; public schools; public parks and recreation facilities; transportation facilities, including rail, water, air, and truck transportation; transit facilities (streetcars, trolley coaches, and buses); public buildings; and housing. It will be noted that, with the possible exception of housing and some of the transit and transportation facilities, all the foregoing are the responsibility of public agencies or are under some type of public control and regulation. Even private housing is affected by public controls and has a definite relation to the public welfare.

In the average city, and certainly in a city as large as New Orleans, a special study and report is made on each of these major physical facilities comprising the comprehensive plan. Furthermore, in making this study and in determining the recommendations regarding their future location, extent, and character, the most careful consideration is given to existing facilities, modern standards, and probable future requirements. In the major street study, it is possible to estimate the volume of traffic which will originate in major sections of the city, how much will originate in or be destined for areas beyond the city, and where the major objectives will be within the urban area. The future capacities of the entire street system can be determined, and the proposed individual improvements related thereto. Similarly, careful estimates can be made for future school enrollments and, when adjusted to modern standards, the school and park system can be planned in close relationship to future requirements.

In city planning, just as in many other engineering projects, it is frequently impossible to meet recognized and desirable standards completely. Fixed conditions are usually the major obstacles. The application of sound technical judgment can, nonetheless, result in a workable and satisfactory solution. For example, the computations and standards might indicate the need for a major street accommodating three lanes of moving traffic in each direction during the peak period of traffic movement. Existing streets in the area to be served have a right of way of only 70 ft, and the frontage is so completely occupied with expensive structures that any widening of this right of way would be financially prohibitive. A logical and practicable solution might be to widen the pavement to only 58 ft, prohibiting parking on the side of the street that carries the dominant traffic movement during the peak hours. Another possibility may be two one-way streets. There are undoubtedly many opportunities to expedite traffic flow through traffic control and public education, rather than through expensive improvement projects.

The practice and procedures as well as the standards to be followed in planning have been mentioned in regard to only a few of the several physical improvements. The same general policies should be followed in planning for the other facilities, and several instances will probably be encountered in which some readjustments will be necessary in the preliminary recommendations as additional phases are considered. One of the fundamental advantages of planning is providing for the proper relationship between the several parts of the city design. Such coordination should begin as the plan is being prepared.

Preparation and even the adoption of the best city plan can insure satisfactory results only if the plan is followed consistently. One of the most effective means of securing adherence to the plan is the preparation of a 5-year or 10-year public works program after all other phases of the planning program have been completed. This work program involves a selection of those physical improvements which the studies revealed as being most seriously needed, and which would result in maximum benefits to the population. Preliminary estimates also should be made of the cost of these improvements, followed by an analysis of the financial status and potentialities of the several public agencies to be responsible for the projects. The number and type of projects selected for construction each year can thus be closely adjusted to available funds; no serious tax burden should result at any one time.

Relationship of the Planning Program to Citizens

Throughout this paper, emphasis has been placed upon the close relationship that exists—or should exist—between the city plan and the citizens. The fact that city planning is an engineering science has also been stressed. It may seem inconsistent that laymen can force changes in a city plan that is based upon sound facts and proved engineering principles. Ability to do so remains a proved fact. Furthermore, this condition will continue under the present (and desirable) form of government in the United States. What steps can be taken to improve the situation?

Two measures seem to offer major potentialities. One is to encourage the use of citizen committees to advise with the planning commission concerning the preliminary reports or any changes or adjustments in any part of the plan after it is officially adopted. The fact that the total membership of such citizens' committees will represent only a small percentage of the total population can be partly offset if the membership comprises prominent leaders representing all the varied community interests. Citizens' committees not only acquaint more persons with the need and advantages of the plan, but also give other citizens a feeling that their interests are being protected.

The second measure is to follow procedures used by business organizations, and to engage experienced public relations personnel as a part of the planning staff. It has always been the writer's belief that members of the technical profession have limited ability in public relations—primarily because their training and experience are of such a specialized nature. Many people now agree that the weakest part of planning is not the preparation of a good plan, but the means of making the general public familiar with the plan and with its advantages. It is only logical that a part of the planning program be handled by a personnel staff able to secure widespread public understanding and support, since these can be so beneficial. The cost would be small in comparison with the potential advantages.

Summary

City planning has made marked progress in its scope and practice since the early 1920's. Although many more subjects have been included in later studies than were in those made earlier, the basic fact remains that city planning is primarily concerned with the physical facilities of urban areas. Even though a sound plan includes consideration of economic and social characteristics as well as of financial problems in carrying out the plan, studies of the physical facilities comprise the major work of the modern planning program.

Members of the civil engineering profession are from their experience and training eminently qualified to deal with these physical facilities and some have helped to develop many sound practices and techniques. This paper has emphasized the fact that, although several different practices and techniques are used in preparing a plan, the best results can be obtained only when the same sound procedures are followed as are required in any other phase of civil engineering. There is no reason why the engineer cannot play a most important part in improving city planning techniques and practices in the future, and in formulating even sounder and more complete plans than have been prepared in the past.

AMERICAN SOCIETY OF CIVIL ENGINEERS
Founded November 5, 1852
TRANSACTIONS

Paper No. 2666

EARTHQUAKE STRESSES IN SHEAR BUILDINGS

BY M. G. SALVADORI,[1] A. M. ASCE

WITH DISCUSSION BY MESSRS. JOHN A. BLUME; E. F. MASUR; EDWARD COHEN, EDWARD LAING, AND LEON S. LEVY; AND M. G. SALVADORI

SYNOPSIS

The elastic stresses in a multistory building due to earthquake displacements of its foundation are determined by means of the normal modes of vibration of the building and numerical integration. The building is assumed to move due to the deflection of its columns, and the mass of the structure is concentrated at the floors, which are infinitely rigid. The rocking of the building on an elastic soil and the influence of internal damping are taken into account. The stresses in the multistory building are compared with those obtained by assuming the building to act as a cantilever shear beam. A numerical example illustrates the application of the method and permits an evaluation of its accuracy and efficiency by comparison with a rigorous solution of the same problem.

1. INTRODUCTION

The dynamic behavior of an elastic framed building acted upon by impressed displacements (earthquakes) or time-varying forces (blasts) is of great practical importance. Unfortunately, the mathematical difficulties involved in the solution of dynamic problems have prevented a rational design of such structures; hence, any step in the simplification of their solution is to be welcomed.

The dynamical analysis of framed structures is considerably simplified whenever the structure has a height-to-width ratio of 5 or less[2] and whenever its columns are relatively flexible, in which case the structure will be called a "shear building." In a shear building it is possible to neglect the influence of direct stresses in the columns and to assume that: (1) The motion of the building is due to the bending deflection of the columns only; and (2) the mass of the building is lumped at the floor levels. Within the limits of elastic behavior,

---

NOTE.—Published, essentially as printed here, in March, 1953, as *Proceedings-Separate No. 177.* Positions and titles given are those in effect when the paper or discussion was received for publication.

[1] Associate Prof. of Civ. Eng., Columbia Univ., New York, N. Y., and Cons. Engr., Ammann & Whitney, New York, N. Y.

[2] "Wind Bracing," by H. V. Spurr, McGraw-Hill Book Co., Inc., New York, N. Y., 1930.

the building acts as an elastic system with as many degrees of freedom as there are floors, and the determination of the stresses is reduced to the integration of a set of simultaneous ordinary differential equations.

In what follows, a method for the solution of this problem is presented for the case of earthquake stresses. The same procedures could be applied, practically without change, to the blast problem.

Notation.—Letter symbols in this paper are defined where they first appear, in the text or by diagram. Throughout, the symbol i, used as a subscript, refers the main symbol to its appropriate floor; and the symbol j, used as a subscript, denotes one of the N vibrational modes of the structure. Single or double-dots over any symbol denote differentiation with respect to time.

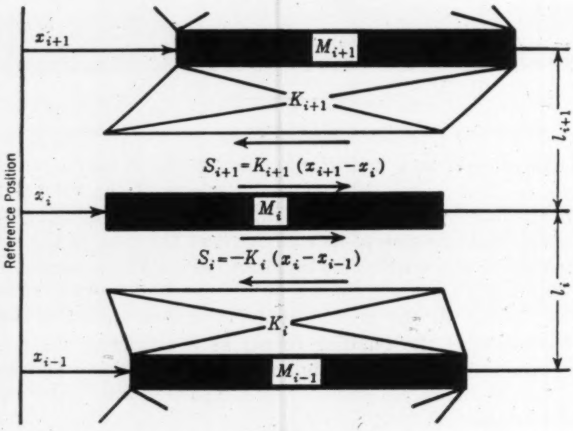

FIG. 1

2. THE FREE VIBRATIONS OF A SHEAR BUILDING

Consider a slice of a framed building, one unit wide, with N floors. In Fig. 1, let:

M_i = the mass concentrated at the ith floor ($i = 0, 1, 2, \ldots, N$);

S_i = the total horizontal shear force at the ith floor;

l_i = the story height between the $(i - 1)$th and the ith floors;

K_i = the spring constant under the ith floor—that is, the shear at the ith floor necessary to displace that floor horizontally by one unit relative to the $(i - 1)$th floor;

$X(i)$ = the modal displacement at the ith floor;

$x_i(t)$ = the absolute horizontal displacement of the ith floor at a time t; and

$x_0(t)$ = the impressed horizontal motion of the foundation of the building, considered identical with the earthquake displacement component in the plane of the frame.

The equation of motion of the ith floor is obtained from Newton's second law ($F = m\,a$) in the form:

$$M_i\,\ddot{x}_i = K_{i+1}\,(x_{i+1} - x_i) - K_i\,(x_i - x_{i-1}) \quad (i = 1, 2, \ldots, N) \ldots\ldots (1)$$

in which the dots connote differentiation with respect to time.

The free vibrations of the structure are characterized by the fact that each floor moves in simple harmonic motion. The structure can vibrate freely in N different modes defined by the equation[3]

$$x_i(t) = X(i) \sin \omega\, t \ldots\ldots\ldots\ldots\ldots\ldots\ldots\ldots (2)$$

in which $X(i)$ is the displacement at the ith floor in the mode of frequency ω. Substituting Eqs. 2 in Eqs. 1, the ordinates $X(i)$ are found to satisfy the system of N homogeneous linear equations—

$$-\,k'_i\,X(i-1) + (k_i - \omega^2)\,X(i) - k''_i\,X(i+1) = 0 \quad (i = 1, 2, \ldots, N) \ldots (3)$$

in which

$$k''_i = \frac{K_{i+1}}{M_i} \ldots\ldots\ldots\ldots\ldots\ldots\ldots\ldots (4a)$$

$$k_i = \frac{K_{i+1} + K_i}{M_i} \ldots\ldots\ldots\ldots\ldots\ldots\ldots\ldots (4b)$$

and

$$k'_i = \frac{K_i}{M_i} \ldots\ldots\ldots\ldots\ldots\ldots\ldots\ldots (4c)$$

Eqs. 3 have roots $X(i)$ different from zero only if their determinant vanishes, thus:

$$\begin{vmatrix} (k_1 - \omega^2) & -\,k''_1 & 0 & \ldots\ 0 & 0 & 0 \\ -\,k'_2 & (k_2 - \omega^2) & -\,k''_2 & \ldots\ 0 & 0 & 0 \\ \cdots & \cdots & \cdots & \cdots & \cdots & \cdots \\ \cdots & \cdots & \cdots & \cdots & \cdots & \cdots \\ 0 & 0 & 0 & -\,k'_{N-1} & (k_{N-1} - \omega^2) & -\,k''_{N-1} \\ 0 & 0 & 0 & 0 & -\,k'_N & (k_N - \omega^2) \end{vmatrix} = 0 \ldots (5)$$

The N roots ω^2_j of Eq. 5 ($j = 1, 2, \ldots, N$) are the squares of the frequencies of the N modes. Once the values ω_j have been found, Eqs. 3 determine the "co-ordinates" $X_j(i)$ of the jth mode within a multiplying constant c. This constant may be chosen so as to make

$$\sum_{i=1}^{N} [c^2\,X^2_j(i)\,M_i] \equiv \sum_{i=1}^{N} [\phi^2_j(i)\,M_i] = 1 \quad (j = 1, 2, \ldots, N) \ldots\ldots (6a)$$

in which case the modes

$$\phi_j(i) \equiv c\,X_j(i) = \frac{X_j(i)}{\sqrt{\sum_{i=1}^{N} X^2_j(i)\,M_i}} \quad (j = 1, 2, \ldots, N) \ldots\ldots (6b)$$

---

[3] "Mathematical Methods in Engineering," by Th. von Kármán and M. A. Biot, McGraw-Hill Book Co., Inc., New York, N. Y., 1940, Chapter V.

—are said to be normalized. It can be proved[3] that the modes ϕ_j (or X_j) are orthogonal; that is, that

$$\sum_{i=1}^{N} \phi_j(i)\, \phi_k(i)\, M_i = 0 \quad (j \neq k) \qquad (7)$$

3. The Forced Vibrations of a Shear Building

The displacements $x_i(t)$ of the structure due to any impressed displacement, or applied force, can be expressed[3] as a series of products of the modes $\phi_j(i)$ and of unknown functions $q_j(t)$, called the "generalized co-ordinates" of the structure. In the study of earthquake displacements it is convenient to expand, in terms of generalized co-ordinates, the displacements of the ith floor relative to the foundation—that is, to set—

$$x_i(t) = x_0(t) + \sum_{j=1}^{N} [\phi_j(i)\, q_j(t)] \qquad (8)$$

By substitution of Eqs. 8 in the expressions for the kinetic energy: $T = \frac{1}{2} \sum_{i=1}^{N} (M_i\, \dot{x}^2_i)$, and the potential energy: $U = \frac{1}{2} \sum_{i=1}^{N} [K_i\, (x_i - x_{i-1})^2]$—of the structure, and by Eqs. 6 and 7, it may be seen that

$$T = \frac{1}{2} M\, \dot{x}^2_0 + \dot{x}_0 \sum_{j=1}^{N} (\alpha_j\, \dot{q}_j) + \frac{1}{2} \sum_{j=1}^{N} \dot{q}^2_j \qquad (9)$$

and

$$U = \frac{1}{2} \sum_{j=1}^{N} \omega^2_j\, q^2_j \qquad (10)$$

in which M is the total mass of the building and

$$\alpha_j = \sum_{i=1}^{N} [\phi_j(i)\, M_i] \qquad (11)$$

The equations of motion of the structure in terms of its generalized co-ordinates q_j are Lagrange's equations,[3]

$$\frac{d}{dt}\left(\frac{\partial T}{\partial \dot{q}_k}\right) + \frac{\partial U}{\partial q_k} = Q_k \quad (k = 1, 2, \ldots, N) \qquad (12a)$$

and

$$\frac{d}{dt}\left(\frac{\partial T}{\partial \dot{x}_0}\right) + \frac{\partial U}{\partial x_0} = Q_0 \qquad (12b)$$

where the "generalized force" Q_k is given, in terms of the force P_i applied to the ith floor, by

$$Q_k = \sum_{i=0}^{N} P_i \frac{\partial x_i}{\partial q_k} \quad (k = 1, 2, \ldots, N) \qquad (13a)$$

$$Q_0 = \sum_{i=0}^{N} P_i \frac{\partial x_i}{\partial x_0} \qquad (13b)$$

Eq. 13*b* could be used to determine the force exerted by the ground on the foundation, but will not be considered in this paper. In the present case the only external force is applied at the foundation and $Q_k = P_0 \frac{\partial x_0}{\partial q_k}$; but x_0 is not a function of the q_k and hence all the Q_k are zero. By means of Eqs. 9 and 10, the Lagrangian equations become

$$\ddot{q}_j + \omega^2{}_j \, q_j = - \alpha_j \, \ddot{x}_0 \ldots\ldots\ldots\ldots\ldots\ldots (14)$$

The acceleration graphs supplied by strong-motion records[4] are so jagged that it is often inconvenient to integrate Eqs. 14. Then it becomes practical to introduce new generalized co-ordinates $p_j(t)$ defined by the equation:

$$q_j = \alpha_j \, (p_j - x_0) \ldots\ldots\ldots\ldots\ldots\ldots (15)$$

in terms of which the equations of motion become

$$\ddot{p}_j + \omega^2{}_j \, p_j = \omega^2{}_j \, x_0 \ldots\ldots\ldots\ldots\ldots\ldots (16)$$

and contain the displacement x_0, as a forcing function, rather than the acceleration $\ddot{x}_0$. Eqs. 14 and 16 demonstrate the advantage gained by the use of generalized co-ordinates and normal modes. The burdensome integration of the original system of N simultaneous equations (Eqs. 1) has been reduced to the much simpler task of integrating the N separate Eqs. 14 or 16. Moreover, it will often be found sufficient from an engineering point of view to take into account only the first few (two or three) modes of the structure. The problem becomes thus substantially simpler and hence more economical.

Since the motion of the building starts from rest at a time that can be selected as origin ($t = 0$), the initial conditions require that

$$x_i(0) = x_0(0) + \sum_{j=1}^{N} [\phi_j(i) \, q_j(0)] = 0 \ldots\ldots\ldots\ldots (17a)$$

and

$$\dot{x}_i(0) = \dot{x}_0(0) + \sum_{j=1}^{N} [\phi_j(i) \, \dot{q}_j(0)] = 0 \ldots\ldots\ldots\ldots (17b)$$

Multiplying each of Eqs. 17 by $M_i \, \phi_k(i)$, summing with respect to i, and remembering Eqs. 6 and 7,

$$\alpha_k \, x_0(0) + q_k(0) \equiv \alpha_k \, p_k(0) = 0 \ldots\ldots\ldots\ldots (18a)$$

and

$$\alpha_k \, \dot{x}_0(0) + \dot{q}_k(0) \equiv \alpha_k \, \dot{p}_k(0) = 0 \ldots\ldots\ldots\ldots (18b)$$

Hence, whatever the values of $x_0(0)$ and $\dot{x}_0(0)$, the initial conditions for p_j are

$$p_j(0) = 0 \ldots\ldots\ldots\ldots\ldots\ldots (19a)$$

$$\dot{p}_j(0) = 0 \ldots\ldots\ldots\ldots\ldots\ldots (19b)$$

---

[4] "Earthquake Investigations in California 1934-1935," *Special Publication No. 201*, Coast and Geodetic Survey, U. S. Dept. of Commerce, Washington, D. C.

Substituting the value $\dot{q}_k(0) = -\alpha_k \dot{x}_0$ from Eq. 18*b* in Eq. 17*b*, the velocity $\dot{x}_i(0)$ takes the form:

$$\dot{x}_i(0) = \dot{x}_0(0)\left[1 - \sum_{j=1}^{N} \alpha_j \phi_j(i)\right] = 0$$

Whenever $\dot{x}_0(0) \neq 0$ and an approximate solution of the earthquake problem is obtained by means of the first $N' < N$ modes, the ratios—

$$r_{N'}(i) = \frac{\dot{x}_i(0)}{\dot{x}_0(0)} = 1 - \sum_{j=1}^{N'} [\alpha_j \phi_j(i)] \quad \text{(20)}$$

—give a quantitative idea of the accuracy with which the initial conditions have been satisfied. (Although $\dot{x}_0(0)$ must vanish for physical reasons, it is sometimes convenient to approximate $x_0(t)$ by means of curves whose first derivative does not vanish at the origin.)

Whenever $x_0(t)$ is an elementary analytic function, the solutions of Eqs. 16 satisfying the initial conditions of Eqs. 19 are given by

$$p_j(t) = \omega_j \int_0^t x_0(\tau) \sin \omega_j (t - \tau)\, d\tau \quad \text{(21)}$$

For example, if

$$x_0(t) = X_0 \sin \omega_0 t \quad \text{(22)}$$

Eq. 21 gives

$$p_j(t) = \frac{X_0 \omega_j}{\omega^2{}_j - \omega^2{}_0}(\omega_j \sin \omega_0 t - \omega_0 \sin \omega_j t); \quad (\omega_0 \neq \omega_j) \quad \text{(23a)}$$

and

$$p_k(t) = \tfrac{1}{2} X_0 (\sin \omega_0 t - \omega_0 t \cos \omega_0 t); \quad (\omega_0 = \omega_k) \quad \text{(23b)}$$

and the corresponding displacements become, by Eqs. 8:

$$x_i(t) = X_0\left[1 + \omega^2{}_0 \sum_{j=1}^{N} \frac{\alpha_j \phi_j(i)}{\omega^2{}_j - \omega^2{}_0}\right] \sin \omega_0 t - X_0 \omega_0 \sum_{j=1}^{N} \frac{\alpha_j \omega_j \phi_j(i)}{\omega^2{}_j - \omega^2{}_0} \sin \omega_j t; \quad (\omega_j \neq \omega_0) \quad \text{(24a)}$$

and

$$x_i(t) = X_0\left[1 + \omega^2{}_0 \sum_{\substack{j=1\\ j\neq k}}^{N} \frac{\alpha_j \phi_j(i)}{\omega^2{}_j - \omega^2{}_0}\right] \sin \omega_0 t - X_0 \omega_0 \sum_{\substack{j=1\\ j\neq k}}^{N} \frac{\alpha_j \omega_j \phi_j(i)}{\omega^2{}_j - \omega^2{}_0} \sin \omega_j t - \tfrac{1}{2} X_0 \alpha_k \phi_k(i) [\sin \omega_0 t + \omega_0 t \cos \omega_0 t]; \quad (\omega_0 = \omega_k) \quad \text{(24b)}$$

By superposition, the displacements due to a half-sine pulse ground displacement—

$$x_0(t) = \begin{cases} X_0 \sin \omega_0 t; & 0 < t \leq \dfrac{\pi}{\omega_0} \\ 0 & ; \quad \dfrac{\pi}{\omega_0} \leq t \end{cases} \quad \text{(25)}$$

—are given by

$$x_{i,p}(t) = \begin{cases} x_i(t) & ; \quad 0 < t \leq \dfrac{\pi}{\omega_0} \\ x_i(t) + x_i\left(t - \dfrac{\pi}{\omega_0}\right); & \dfrac{\pi}{\omega_0} \leq t \end{cases} \qquad (26)$$

The solutions of Eqs. 24 may be used in connection with each sine component of the expansion of $x_0(t)$ into a Fourier series and are of practical importance in connection with the graph of maximum amplitude as functions of the frequency given by Frank Neumann,[5] for each grade of the modified Mercalli earthquake scale.

When $x_0(t)$ is not an elementary function, and particularly when $x_0(t)$ is known experimentally, the integration of Eqs. 16 is conveniently performed by numerical methods, as shown in Sect. 8, or by analog machines.

4. THE INFLUENCE OF INTERNAL DAMPING

Although little is known about the type of internal damping developed in actual structures, experimental evidence shows[6] that damping in steel occurs as if the coefficient of viscous damping in any given mode were proportional to the frequency of that mode. Since viscous damping is easily handled mathematically, this result is assumed to apply to a complete structure, and a viscous term is added to Eqs. 16:

$$\ddot{p}_j + 2 f_j \dot{p}_j + \omega^2{}_j p_j = \omega^2{}_j x_0 \qquad (27)$$

The value of the logarithmic decrement in the jth mode—

$$r_j = e^{-2\pi f_j/\omega_j} \qquad (28)$$

—has an upper value (seldom attained) of 0.9; and, hence, an upper value for the coefficient of viscous damping is

$$f_j \leq - \frac{\log_e 0.9}{2\pi} \omega_j = 0.017\, \omega_j \qquad (29)$$

The solution of Eqs. 27 when $x_0(t)$ is a sine function is

$$x_i(t) = X_0 \{\sin \omega_0 t + e^{-f_j t} [A_j \cos \sqrt{\omega^2{}_j - f^2{}_j}\, t + B_j \sin \sqrt{\omega^2{}_j - f^2{}_j}\, t] + C_j \cos \omega_0 t + D_j \sin \omega_0 t\} \qquad (30)$$

in which

$$A_j = - C_j = \frac{\alpha_j \omega^2{}_0 + 2 f_j \omega_0}{(\omega^2{}_j - \omega^2{}_0)^2 + (2 f_j \omega_0)^2} \qquad (31a)$$

$$B_j = - \frac{\alpha_j \omega_0}{\sqrt{\omega^2{}_j - f^2{}_j}} \frac{\omega^2{}_j (\omega^2{}_j - \omega^2{}_0) + 2 f^2{}_j \omega^2{}_j}{(\omega^2{}_j - \omega^2{}_0)^2 + (2 f_j \omega_0)^2} \qquad (31b)$$

---

[5] "Ground Amplitudes and Periods Associated With Earthquake Intensity: A Preliminary Statement," by Frank Neumann, Supplement, *Quarterly Engineering Seismology Bulletin*, MST-75, October, November, December, 1950.

[6] "Response of Damped Elastic Systems to Transient Disturbances," by R. D. Mindlin, F. W. Stubner, and H. L. Cooper, *Bell Telephone System Tech. Publications*, Monograph B 1561 (or *Proceedings*, Soc. for Experimental Stress Analysis, Vol. 5, No. 2, 1948.)

and

$$D_j = \frac{\alpha_j \, \omega^2{}_0 \, (\omega^2{}_j - \omega^2{}_0)}{(\omega^2{}_j - \omega^2{}_0)^2 + (2 \, f_j \, \omega_0)^2} \ldots\ldots\ldots\ldots\ldots\ldots (31c)$$

Inasmuch as the largest stresses due to earthquakes occur, in general, a short time after the beginning of the earthquake, and since the logarithmic decrement r_j is nearly 1, the influence of damping on elastic earthquake stresses is often negligible. Its essential feature is to damp out, rapidly, the higher modes of vibration.

5. Rocking of Building on an Elastic Soil

It was assumed in the preceding sections that the motion of the foundation was purely horizontal. When a building rests on an elastic soil, instead, the earthquake displacements will produce, not only horizontal displacements of the floors, but also rotation of the foundation about an axis through its centroid perpendicular to the plane of motion. (It is assumed that no relative horizontal displacement takes place between foundation and soil.) This additional motion is usually called the "rocking" of the building.

Calling θ the rotation of the foundation in radians, indicate by B (elastic stiffness coefficient for rocking motion) the reactive elastic moment of the soil per unit depth of the building when $\theta = 1$. The value of B was computed by M. A. Biot[7] in terms of the elastic constants E(Young's modulus) and ν (Poisson's ratio) of the soil:

$$B = \frac{\pi}{4} \frac{E}{1 - \nu^2} \left(\frac{b}{2} \right)^2 \ldots\ldots\ldots\ldots\ldots\ldots (32)$$

in which b is the width of the foundation.

The modes of the elastic structure rocking on its foundation are conveniently determined by means of the concept of "complementary systems" evolved by Hans H. Bleich, M. ASCE.[8] As "complementary system A," consider the building in which the "shear springs" are frozen: System A is a rigid beam elastically restrained against rotation at one end. As "complementary system B," consider the building in which the "shear springs" are free to act, but in which rocking is prevented. The modes ϕ_j of system B are, therefore, the modes, previously determined, of the building on a rigid soil.

The differential equation of free vibration of the rigid building (system A) is

$$\ddot{\theta} + \omega^2{}_A \, \theta = 0 \ldots\ldots\ldots\ldots\ldots\ldots (33)$$

in which the frequency ω_A is given by

$$\omega_A = \sqrt{\frac{B}{I}} \ldots\ldots\ldots\ldots\ldots\ldots (34)$$

and

$$I = \sum_{i=0}^{N} M_i \left[L^2{}_i + \frac{b^2}{12} \right] \ldots\ldots\ldots\ldots\ldots\ldots (35)$$

---

[7] "Analytical and Experimental Methods in Engineering Seismology," by M. A. Biot, *Transactions*, ASCE, Vol. 108, 1943, p. 365.

[8] "Frequency Analysis of Beam and Girder Floors," by Hans H. Bleich, *ibid.*, Vol. 115, 1950, p. 1023.

is the moment of inertia of the structure about the axis of rotation, L_i indicating the height of the ith floor above the foundation (Fig. 2). The corresponding mode $\phi_A(i)$ is a straight line

$$\phi_A(i) = \frac{L_i}{\sqrt{\sum_{i=1}^{N} M_i L^2_i}} \qquad (36)$$

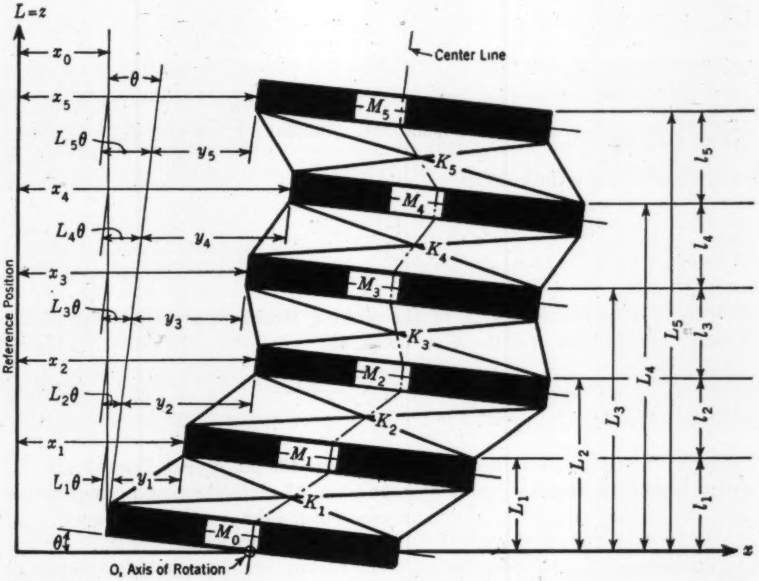
L = z
Center Line
x_0
θ
x_5
$L_5\theta$
y_5
M_5
K_5
x_4
$L_4\theta$
y_4
M_4
K_4
x_3
$L_3\theta$
y_3
M_3
K_3
x_2
$L_2\theta$
y_2
M_2
K_2
x_1
$L_1\theta$
y_1
M_1
K_1
M_0
θ
O, Axis of Rotation
Reference Position
L_1
L_2
L_3
L_4
L_5
l_1
l_2
l_3
l_4
l_5
x

FIG. 2

Mr. Bleich[8] has shown that the modes $\psi_k(i)$ of the rocking structure can be represented by a linear combination of $\phi_A(i)$ and $\phi_j(i)$, thus:

$$\psi_k(i) = c_k\, \phi_A(i) + \sum_{j=1}^{N} c_{kj}\, \phi_j(i); \quad (k = 1, 2, \ldots, N) \qquad (37)$$

The coefficients of this linear combination are given by

$$\frac{\omega^2_A}{\Omega^2_k} c_k = \sum_{i=1}^{N} [\phi_A(i)\, \psi_k(i)\, M_i] \qquad (38)$$

and

$$\frac{\omega^2_j}{\Omega^2_k} c_{kj} = \sum_{i=1}^{N} [\phi_j(i)\, \psi_k(i)\, M_i] \qquad (39)$$

in which Ω_k is the frequency of the mode ψ_k. Substituting in Eqs. 38 and 39 the value of ψ_k defined by Eq. 37 and letting

$$b_j = \sum_{i=1}^{N} M_i \, \phi_A(i) \, \phi_j(i) \tag{40}$$

it follows that

$$c_k \left(\frac{\omega^2_A}{\Omega^2_k} - 1 \right) = \sum_{j=1}^{N} b_j \, c_{kj} \tag{41a}$$

and

$$c_{kj} = \frac{b_j}{\dfrac{\omega^2_j}{\Omega^2_k} - 1} \, c_k \tag{41b}$$

Substitution of Eq. 37 in the normalizing condition $\sum_{i=1}^{N} [\psi^2_k \, (i) M_i] = 1$ shows that c must satisfy the condition,

$$\omega^2_A \, c^2_k + \sum_{j=1}^{N} \omega^2_j \, c^2_{kj} = \Omega^2_k \tag{42}$$

if the ψ_k are to be normal modes.

The $N + 1$ frequencies Ω_k of the rocking structure are the roots of the determinantal equation of the $N + 1$ Eqs. 41:

$$\frac{\omega^2_A}{\Omega^2_k} - 1 = \sum_{j=1}^{N} \frac{b^2_j}{\dfrac{\omega^2_j}{\Omega^2_k} - 1} \tag{43}$$

Once the Ω_k values have been found from Eq. 43, the $N + 1$ Eqs. 41*b* and 42 define c_k and c_{kj} for each value of k, and Eq. 37 gives the new normal modes ψ_k of the rocking structure. (An analysis of Eq. 43 shows that Ω_1 is lower than both ω_A and ω_1, and that any other Ω_k is bound by two successive ω_j.)

The generalized co-ordinates p_k of the rocking structure satisfy the first or second of the equations

$$\ddot{p}_k + \Omega^2_k \, p_k = \Omega^2_k \, x_0 \tag{44a}$$

and

$$\ddot{p}_k + 2 \, f_k \, p_k + \Omega^2_k \, p_k = \Omega^2_k \, x_0 \tag{44b}$$

depending upon whether friction is neglected or taken into account; and the initial conditions are

$$p_k(0) = 0; \quad \text{and} \quad \dot{p}_k(0) = 0 \tag{45}$$

The absolute displacements of the rocking structure are given, as usual, by

$$x_i(t) = x_0(t) + \sum_{k=1}^{N} \psi_k(i) \, q_k(t) \tag{46}$$

in which, as in Eq. 15, $q_k = \alpha_k(p_k - x_0)$.

It is now interesting to notice that the stresses in the rocking building are due exclusively to the shear components of the displacements x_i. These are obtained by subtracting from the total modes ψ_k the rotational components

$c_k\,\phi_A$ to obtain the "shear modes,"

$$\psi_{k,s}(i) = \sum_{j=1}^{N} [c_{kj}\,\phi_j(i)] \tag{47}$$

The shear displacements are then simply given by

$$x_{i,s}(t) = \sum_{k=1}^{N} \psi_{k,s}(i)\,q_k(t) \tag{48}$$

6. The Numerical Evaluation of the Modes

When the number of stories N of the building is greater than 4 or 5, the writing and the solution of the determinantal equation for the frequencies (Eq. 5) becomes a lengthy task requiring particular care. It is simpler in such cases to obtain the frequencies and the modes by the classical procedure of successive approximations developed by L. Vianello and A. Stodola, which makes use of the fact that the modes are the deflections of the elastic structure loaded by its own inertia forces.

To determine the first mode $X_1(i)$ by the Vianello-Stodola method:

(1) Assume a deflection $X_1^{(0)}(i)$, which possibly is not too different from $X_1(i)$;

(2) Apply to the structure the horizontal loads $P_i = \omega^2_1\,M_i\,X_1^{(0)}(i)$;

(3) Determine the shear S_k at the kth floor: $S_k = \sum_{i=N}^{k} P_i$

(4) Determine the displacement of the kth floor, relative to the $(k-1)$th floor: $\Delta X_k = S_k/K_k$ (in which K_k is the spring constant under the kth floor)

(5) Determine the new displacement $X_1^{(1)}(i)$ of the ith floor by summing the ΔX_k from the foundation up: $X_1^{(1)}(i) = \sum_{k=1}^{i} \Delta X_k$.

The displacement $X_1^{(1)}$ is a better approximation of X_1 which can now be used as the initial deflection to obtain a nearer approximation $X_1^{(2)}$, and the process is continued until the difference between two successive approximations becomes negligible.

In practice, since ω^2_1 is unknown, the structure is loaded with loads $P_i = M_i\,X_1^{(0)}(i)$ and the deflections $X_1^{(1)}(i)$ are ω^2_1 times smaller than they should be. Hence the ratio of any $X_1^{(r)}(i)$ to the corresponding $X_1^{(r+1)}(i)$ gives an approximate value of ω^2_1.

The best possible value of ω^2_1 is obtained by taking the ratio of the weighted averages of $X_1^{(r)}$ and $X_1^{(r+1)}$,

$$\omega^4_1 = \frac{\sum_{i=1}^{N} [X_1^{(r)}(i)]^2\,M_i}{\sum_{i=1}^{N} [X_1^{(r+1)}(i)]^2\,M_i} \tag{49}$$

The normalized mode $\phi_1(i)$ is given, in terms of the last approximation $X_1^{(n)}(i)$ by Eq. 6*b*.

The second mode ϕ_2 may be obtained by the same procedure, provided the initial approximation $X_2^{(0)}$ is chosen orthogonal to ϕ_1 and the successive approximations $X_2^{(r)}$ are made orthogonal to ϕ_1. It is easy to see that, given any function $\overline{X}(i)$, the function—

$$X(i) = \overline{X}(i) - \phi_1(i) \sum_{i=1}^{N} [\overline{X}(i)\ \phi_1(i)\ M_i] \qquad (50)$$

—is orthogonal to ϕ_1. Hence, X may be chosen as $X_2^{(0)}$, and Eq. 50 may be used to obtain functions $X_2^{(r)}$ orthogonal to ϕ_1, by means of the rth approximation $\overline{X}_2^{(r)}$, which, in general, will not be orthogonal to ϕ_1.

The determination of the third mode may similarly be started by means of any function $\overline{X}$ and of the formula,

$$X(i) = \overline{X}(i) - \phi_1(i) \sum_{i=1}^{N} [\overline{X}(i)\ \phi_1(i)\ M_i] - \phi_2(i) \sum_{i=1}^{N} [\overline{X}(i)\ \phi_2(i)\ M_i] \qquad (51)$$

which makes X orthogonal to both ϕ_1 and ϕ_2.

In order to be able to follow the convergence of the method it is practical to normalize the approximations $X_j^{(r)}$ at each step. Since the results converge more rapidly when the initial approximations are near the true modes, it pays to obtain good initial guesses. These may be obtained, for example, from the modes of a "shear beam."

7. THE MODES AND FREQUENCIES OF THE SHEAR BEAM

Refer the building on a rigid soil to a vertical z-axis with the origin at the foundation (Fig. 2), and let:

$z_i = L_i$, the height of the ith floor above the foundation;

$l_i = z_i - z_{i-1}$, the height of the ith story;

$m = \dfrac{M_i}{l_i}$, the average mass per unit length (assumed to be constant);

$k = K_i\, l_i$, the average spring constant per unit length (assumed to be constant);

$L = \sum_{i=1}^{N} l_i$, the height of the building;

$M = \sum_{i=1}^{N} M_i$, the total mass of the building; and

$\overline{K} =$ the common value of K_i, when K_i does not vary from story to story.

Letting

$$x_i(t) = x(z, t); \quad x_{i+1} - x_i = \Delta x; \quad z_i - z_{i-1} = \Delta z \qquad (52)$$

—Eqs. 1 take the form:

$$m\,\Delta z\,\ddot{x} = \Delta\left(\frac{k}{\Delta z}\Delta x\right) = \frac{k}{\Delta z}\Delta^2 x$$

and, dividing by Δz and taking the limit as Δz approaches zero, the partial differential equation of a so-called "shear beam" becomes

$$\frac{\partial^2 x}{\partial t^2} = \frac{k}{m}\frac{\partial^2 x}{\partial z^2} \qquad \text{(53)}$$

In this equation k and m (and hence their ratio k/m) are assumed to be independent of z. (The solution of the corresponding equation for a linear variation of k/m has been obtained by the writer in connection with further studies on the dynamics of shear buildings.[9]) When k/m is constant, it is easy to prove[10] that the normal modes of the shear beam are given by

$$\phi_n(z) = \sqrt{\frac{2}{m\,L}}\sin\,(2\,n-1)\frac{\pi\,z}{2\,L};\quad (n = 1, 2, 3, \ldots) \qquad \text{(54)}$$

and that the corresponding frequencies are given by

$$\omega_n = (2\,n-1)\frac{\pi}{2\,L}\sqrt{\frac{k}{m}};\quad (n = 1, 2, 3, \ldots) \qquad \text{(55)}$$

Merit P. White,[11] M. ASCE, has proved, moreover, that as soon as the number of floors N is larger than 3, the first few frequencies—hence, the first few modes—of the lumped building, for all practical purposes, are sufficiently well approximated by those of the uniform shear beam.

Hence, when the ratios $\frac{k}{m} = \frac{K_i\,l^2_i}{M_i}$ are approximately constant, one may obtain good approximations to the lower frequencies and modes of the building by using for k, in Eq. 55, its average value—

$$k \doteq \frac{1}{N}\sum_{i=1}^{N} K_i\,l_i \qquad \text{(56)}$$

—and for m in Eqs. 54 and 55 its average value

$$m \doteq \frac{M}{L} \qquad \text{(57)}$$

obtaining

$$\phi_j(i) \doteq \sqrt{\frac{2}{M}}\sin\,(2\,j-1)\frac{\pi}{2}\frac{L_i}{L} \qquad \text{(58)}$$

and

$$\omega_j \doteq (2\,j-1)\frac{\pi}{2}\sqrt{\frac{\sum_{i=1}^{N}(K_i\,l_i)}{N\,M\,L}} \qquad \text{(59)}$$

---

[9] "Approximate Determination of Dynamic Stresses in Buildings," by M. G. Salvadori, *Proceedings*, Eighth International Cong. on Theoretical and Applied Mechanics, Istanbul, Turkey, 1952.

[10] "Natural Periods of Uniform Cantilever Beams," by L. S. Jacobsen, *Transactions*, ASCE, Vol. 104 1939, p. 402.

[11] *Ibid.* p. 433.

Moreover, if M_i, K_i and l_i are independently constant (uniform building of constant story height), Eqs. 58 and 59 reduce to

$$\phi_j(i) \doteq \sqrt{\frac{2}{M}} \sin\,(2\,j - 1)\,\frac{i}{N}\,\frac{\pi}{2} \tag{60a}$$

and

$$\omega_j \doteq (2\,j - 1)\,\frac{\pi}{2}\sqrt{\frac{\overline{K}}{N\,M}} \tag{60b}$$

As shown by the illustrative example in Sect. 9, these formulas give fairly good approximations to the lower modes and frequencies of a building even if $\frac{K_i}{M_i}\,l^2_i$ is not rigorously constant.

8. The Numerical Integration of the Equations of Motion

As pointed out in Sect. 3, the equations of motion (Eqs. 16 or 27) must be integrated numerically whenever $x_0(t)$ is not a simple analytical function. Numerous methods of step-by-step integration are available for second-order equations, but few are as simple and as powerful as those advanced by Noumerov, and by L. Fox and R. T. Goodwin,[12] and applicable to Eqs. 16 and 27.

To integrate Eq. 16

$$\ddot{p} + \omega^2 p = \omega^2 x_0 \tag{61}$$

Eq. 61 is multiplied through by the square of the time spacing $h = \Delta t$, the second derivative is approximated by the first two terms $\left(\delta^2 - \frac{\delta^4}{12}\right) p$ of its central difference expansion[13,14] and both sides of the equation are then operated upon by $\left(1 + \frac{\delta^2}{12}\right)$. Letting

$$p(rh) = p_r \tag{62a}$$

$$\omega^2{}_0\, x_0(rh) = f_r \tag{62b}$$

$$\delta^2 p_r = p_{r+1} - 2\,p_r + p_{r-1} \tag{62c}$$

$$c = \frac{2 - \frac{5}{6}\,h^2\,\omega^2}{1 + \frac{1}{12}h^2\,\omega^2} \tag{62d}$$

and

$$F_r = \frac{h^2}{12}\,\frac{f_{r+1} + 10\,f_r + f_{r-1}}{1 + \frac{1}{12}\,h^2\,\omega^2} \tag{62e}$$

—Eq. 61 reduces to the simple recurrence equation

$$p_{r+1} = -\,p_{r-1} + c\,p_r + F_r + e_{r+1} \tag{63}$$

---

[12] "Some New Methods for the Numerical Integration of Ordinary Differential Equations," by L. Fox and R. T. Goodwin, *Proceedings*, Cambridge Physical Soc., Vol. 45, Pt. 3, 1949, p. 373.

[13] "Central Difference Formulae," by W. F. Sheppard, *Proceedings*, London Mathematical Soc., Vol. 31, 1899.

[14] "Numerical Computation of Buckling Loads by Finite Differences," by M. G. Salvadori, *Transactions*, ASCE, Vol. 116, 1951, p. 590.

in which the truncation error e_{r+1} takes the form:

$$e_{r+1} = \frac{-1}{1 + \frac{1}{12} h^2 \omega^2} \left(\frac{\delta^6}{240} - \frac{13\,\delta^8}{13{,}120} + \dots \right) p_r \dots\dots\dots (64)$$

The truncation error is of the order of h^6 and the convergence of the process is very rapid.

In order to be able to apply Eq. 63, p must be known at $r = 0$ and $r = 1$. Although p_1 could be evaluated by means of a Taylor expansion around $t = 0$, due to the uncertainties in the value of x_0 and its derivatives at $t = 0$, it is more convenient and accurate to evaluate p_1 by means of the initial conditions expressed in terms of averaged central differences. Neglecting differences of order higher than the fourth, as was done in obtaining Eq. 63, Eqs. 19 yield

$$p(0) = p_0 = 0 \dots\dots\dots (65a)$$

and

$$\begin{aligned} \dot{p}(0) &\doteq \mu \left(\delta - \frac{\delta^3}{6} \right) p_0 \\ &= \frac{1}{2\,h} \left[p_1 - p_{-1} - \tfrac{1}{6} \left(p_2 - 2\,p_1 + 2\,p_{-1} - p_{-2} \right) \right] = 0 \,..\, (65b) \end{aligned}$$

whereas, by applying Eq. 63 at $r = -1, 0, 1$, and noticing that $F_{-1} = 0$,

$$c\,p_{-1} - p_{-2} = 0 \dots\dots\dots (66a)$$

$$p_1 + p_{-1} = F_0 \dots\dots\dots (66b)$$

and

$$p_2 - c\,p_1 = F_1 \dots\dots\dots (66c)$$

Solving Eqs. 66 and Eq. 65a for p_1 and p_2,

$$p_1 = \tfrac{1}{2} \left(F_0 + \frac{F_1}{8 - c} \right) \dots\dots\dots (67a)$$

and

$$p_2 = \tfrac{1}{2} \left(c\,F_0 + \frac{16 - c}{8 - c}\,F_1 \right) \dots\dots\dots (67b)$$

and the application of Eq. 63 is begun at $r = 2$, neglecting the error e_{r+1}. Once p_r is evaluated at the required points, e_{r+1} may be obtained by differencing the values p_r for $r = 3, 4, 5, \dots$ and by extrapolation at sight for $r = 1, 2, 3$. These values are introduced in Eq. 63, at each step, to obtain improved values of p_r. It is seldom that this correction need be used in practical cases.

Substituting for the derivatives the first term of their central difference expansions,[13,14] the following recurrence formula for the integration of Eqs. 27 is similarly obtained:

$$p_{r+1} = -\,c_1\,p_{r-1} + c_2\,p_r + F_r + e'_{r+1} \dots\dots\dots (68)$$

in which

$$c_1 = \frac{1 - hf}{1 + hf} \qquad (69a)$$

$$c_2 = \frac{2 - h^2 \omega^2}{1 + hf} \qquad (69b)$$

$$F_r = \frac{\omega^2 x_0(rh)}{1 + hf} \qquad (69c)$$

and

$$e'_{r+1} = \frac{1}{1 + hf}\left[\left(\frac{\delta^4}{12} - \frac{\delta^6}{90} + \dots\right) p_r + 2 f h \mu \left(\frac{\delta^3}{6} - \frac{\delta^5}{30} + \dots\right) p_r\right] \qquad (69d)$$

In Eq. 69*d*, f is the coefficient of viscous friction. The initial values p_0 and p_1 are both equal to zero in this case, and the truncation error is proportional to h^4.

9. ILLUSTRATIVE EXAMPLE

a. Modes and Frequencies of Building on Rigid Soil.—The methods presented in the previous section will be illustrated by means of the simple example of a five-story building, whose geometric and elastic characteristics are given in Table 1.

TABLE 1.—GEOMETRIC AND ELASTIC CHARACTERISTICS OF A FIVE-STORY BUILDING ON RIGID SOIL

Floor i (1)	Height l_i $\times 10^{-2}$ in. (2)	Height L_i $\times 10^{-2}$ in. (3)	$M_i \times \left(\frac{\text{lb-sec}^2}{\text{in.}}\right)$ (4)	$K_i \times 10^{-3} \frac{\text{lb}}{\text{in.}}$ (5)	$-k''_i$ (6)	k_i (7)	$-k'_i$ (8)	$\frac{K_i l^2_i}{M_i} \times 10^{-6}$ (9)
5	1.44	7.44	11.65	6.84	—	587	−587	12.17
4	1.44	6.00	15.53	7.98	−440	954	−514	10.66
3	1.44	4.56	15.53	9.12	−514	1,101	−587	12.18
2	1.44	3.12	15.53	10.26	−587	1,248	−661	13.70
1	1.68	1.68	15.53	11.40	−661	1,395	—	20.72
0	—	—	62.08	—	—	—	—	—

$L = \sum_{i=1}^{5} l_i = 744$ in.; and $M = \sum_{i=1}^{5} M_i = 73.77$ lb-sec² per in.

The roots of the corresponding determinantal equation, Eq. 5, are given in Table 2; they were evaluated by Newton's method and synthetic division in about one hour. Solving Eqs. 3 successively with these values of ω_j by taking $X_j(5) = 1$, the $X_j(i)$ are obtained; and, by Eq. 6*b*, the modes $\phi_j(i)$ are found and entered in Table 3(*a*).

TABLE 2.—ROOTS OF EQ. 5, FIVE-STORY BUILDING

j	ω^2_j	ω_j	ω_j of Shear Beam	e%
1	57.11	7.557	7.84	3.7
2	424.89	20.61	23.53	14.1
3	1,009.73	31.78	39.21	23.3
4	1,596.19	39.95	54.90	37.4
5	2,197.09	46.87	70.58	50.5

TABLE 3.—COMPARISON OF MODES COMPUTED BY EQS. 6*b* AND 58, FOR SEVERAL VALUES OF *j*

Floor i	(*a*) MODES $\phi_j(i)$, BY EQ. 6*b*					(*b*) APPROXIMATE MODES ϕ_j BY SHEAR BEAM (Eq. 58)				
	Values of j equal to:									
	1	2	3	4	5	1	2	3	4	5
5	0.165	−0.166	0.149	−0.093	0.020	0.165	−0.165	0.165	−0.165	0.165
4	0.149	−0.046	−0.107	0.160	−0.055	0.157	−0.101	0.009	0.087	−0.151
3	0.118	0.095	−0.116	−0.120	0.116	0.135	0.041	−0.164	0.072	0.114
2	0.080	0.149	0.076	−0.039	−0.168	0.101	0.151	−0.025	−0.164	−0.057
1	0.040	0.102	0.130	0.127	0.139	0.057	0.144	0.161	0.101	−0.008

The uniformly distributed mass and spring constant of the five-story building are, by Eqs. 57 and 56, respectively, $m = 0.0992$ lb-sec^2 per sq in., and $k = 1.37 \times 10^6$ lb. The frequencies of the first five modes of the corresponding shear beam, computed from Eq. 59, appear in Table 2 together with their percentage errors. They show that, although the ratios $K_i\, l^2_i/M_i$ (Table 1) are not constant, the first frequency is fairly well approximated by the fundamental frequency of the shear beam. The modes of the shear beam, computed by Eq. 58, appear for comparison in Table 3(*b*).

Table 4, which is self-explanatory, shows the evaluation of the first mode by the Stodola-Vianello method, according to Sect. 6, starting from an assumed deflection $X_1^{(0)}$. The second approximation, $\phi_1^{(2)}(i)$, has errors of not more than 1 unit in the third significant figure, when compared with the true mode ϕ_1 of Table 3(*a*). The corresponding frequency, evaluated by Eq. 49, is $\omega^4{}_1 \doteq \dfrac{0.9217}{0.0002823} = 3{,}265$; and $\omega_1 \doteq 7.559$—and has an error of less than 0.03%.

The evaluation of the second mode by the Stodola-Vianello method appears in Table 5: The assumed deflection $\overline{X}_2$ is normalized by means of Eq. 6 to obtain $\overline{\phi}_2{}^{(0)}$; and $\overline{\phi}_2{}^{(0)}$ is made orthogonal to ϕ_1 by means of Eq. 50 to obtain the initial approximation $\phi_2{}^{(0)}$. The first approximation $X_2{}^{(1)}$ is then obtained by the same operations used in Table 4 to derive $X_1{}^{(1)}$ from $X_1{}^{(0)}$. The displacement $X_2{}^{(1)}$ is normalized, $\overline{\phi}_2{}^{(1)}$, and made orthogonal to ϕ_1, $\phi_2{}^{(1)}$. In this example $\overline{\phi}_2{}^{(1)}$ is already orthogonal to ϕ_1 and hence $\overline{\phi}_2{}^{(1)} = \phi_2{}^{(1)}$. (This indicates that, when the approximate deflection is near the true mode, one need not orthogonalize the solution at each step.) Repeating the process, $\phi_2{}^{(2)}$ is found to differ from the true ϕ_2 of Table 3(*a*) by no more than three units in the third significant figure—that is, by less than 3%. The corresponding value of the frequency after the second approximation is $\omega^4{}_2 \doteq \dfrac{\sum_{i=1}^{N} [\phi_2{}^{(1)}(i)]^2 M_i}{\sum_{i=1}^{N} [X_2{}^{(2)}(i)]^2 M_i}$ $= \dfrac{1}{5.426 \times 10^{-6}}$; and, $\omega_2 \doteq 20.72$—with an error of 0.53%; and, after the third approximation, $\omega_2 = 20.63$, with an error of 0.05%.

TABLE 4.—EVALUATION OF THE FIRST

i	M_i	$X_1^{(0)}$	$10^{-3} M_i X_1^{(0)}$	$10^{-3} S_i^{(0)}$	$10^{-3} K_i$	$\Delta X_1^{(1)}(i) = \dfrac{S_i^{(0)}}{K_i}$	$X_1^{(1)}$	$M_i X_1^{(1)}$
(1)	(2)	(3)	(4)	(5)	(6)	(7)	(8)	(9)
5	11.65	9	0.105	0.105	6.84	0.0153	0.158	1.836
4	15.53	8	0.124	0.229	7.98	0.0287	0.142	2.210
3	15.53	6.5	0.101	0.330	9.12	0.0362	0.114	1.765
2	15.53	4.5	0.070	0.400	10.26	0.0390	0.078	1.203
1	15.53	2.5	0.039	0.439	11.40	0.0385	0.039	0.598

TABLE 5.—EVALUATION OF THE SECOND

i	$\bar{X}_i$	$\bar{\phi}_2^{(0)}$	$\phi_2^{(0)}$	$M_i \phi_2^{(0)}$	$S_i^{(0)}$	$10^3 \Delta X_2^{(1)}$	$10^3 X_2^{(1)}$	$\bar{\phi}_2^{(1)}$	$\phi_2^{(1)}$	$M_i \phi_2^{(1)}$	$S_i^{(1)}$	$10^3 \Delta X_2^{(2)}$
(1)	(2)	(3)	(4)	(5)	(6)	(7)	(8)	(9)	(10)	(11)	(12)	(13)
5	−10	−0.153	−0.152	−1.767	−1.767	−0.258	−0.338	−0.159	−0.159	−1.852	−1.852	−0.271
4	0	0	0.001	0.018	−1.749	−0.219	−0.080	−0.038	−0.038	−0.582	−2.435	−0.305
3	0	0	0.001	0.014	−1.734	−0.190	0.139	0.066	0.066	1.019	−1.416	−0.155
2	10	0.153	0.154	2.386	0.652	0.064	0.330	0.155	0.155	2.409	0.993	0.097
1	10	0.153	0.153	2.381	3.033	0.266	0.266	0.125	0.125	1.944	2.937	0.258

The third mode was not computed since it did not contribute substantially to the solution, as shown in Sect. 9*c*.

b. Modes and Frequencies of Rocking Building.—A soft elastic soil with $E = 10{,}000$ lb per sq in., and Poisson's ratio $\nu = \frac{1}{3}$, has an elastic stiffness coefficient for the rocking motion of a unit strip of a building 60 ft wide, given by Eq. 32; thus: $B = 1.145 \times 10^9$ in.-lb. The moment of inertia of the building, about an axis through the centroid of its foundation, by Eq. 35, with M_i and L_i as in Table 1 and $b = 60$ ft, is $I = 2.308 \times 10^7$ lb-in.-sec². Hence, the frequency of the rigid building, by Eq. 34, is $\omega_A = 7.043$ ($\omega^2_A = 49.60$). The corresponding mode ϕ_A, computed by Eq. 36, appears in Table 6 together with the first two modes ϕ_1 and ϕ_2 of the shear building on a rigid soil, taken from Table 3(*a*).

The modes of the rocking structure have been computed approximately by means of these three modes only. From Eq. 40 and Table 6, $b_1 = 0.998$; and $b_2 = -0.049$; and with $\omega^2_1 = 57.11$, $\omega^2_2 = 424.9$ (from Table 2) the frequency

TABLE 6.—MODES OF ROCKING STRUCTURE

i	$\phi_A(i)$	$\phi_1(i)$	$\phi_2(i)$	$\psi_1(i)$	$\psi_{1,e}(i)$	$\psi_2(i)$	$\psi_{2,e}(i)$
5	0.179	0.165	−0.166	0.173	0.077	0.162	0.129
4	0.145	0.149	−0.046	0.147	0.069	0.040	0.014
3	0.110	0.118	0.095	0.114	0.055	−0.099	−0.119
2	0.075	0.080	0.149	0.077	0.037	−0.151	−0.165
1	0.041	0.040	0.102	0.040	0.018	−0.102	−0.109

Mode by the Stodola–Vianello Method

$M_i[X_1^{(1)}(i)]^2$ (10)	$S_i^{(1)}$ (11)	$10^3\,\Delta X_1^{(2)}$ (12)	$10^3\,X_1^{(2)}(i)$ (13)	$10^6[X_1^{(2)}]^2$ (14)	$10^6 M_i[X_1^{(2)}]^2$ (15)	$\phi^{(2)}_1(i) = \frac{X^{(2)}_1(i)}{\sqrt{\Sigma_2}}$ (16)	i (1)
0.290	1.836	0.268	2.764	7.640	89.0	0.164	5
0.315	4.046	0.507	2.495	6.225	96.7	0.148	4
0.201	5.811	0.637	1.988	3.952	61.4	0.118	3
0.093	7.013	0.684	1.351	1.825	28.3	0.080	2
0.023	7.611	0.668	0.668	0.446	6.9	0.040	1
$\Sigma_1 = 0.922$					$\Sigma_2 = 282.3$		

Mode by the Stodola–Vianello Method

$10^3\,X_2^{(2)}$ (14)	$M_i[X_2^{(2)}]^2$ (15)	$\bar{\phi}_2^{(2)}$ (16)	$\phi_2^{(2)}$ (17)	$M_i\,\phi_2^{(2)}$ (18)	$S_i^{(2)}$ (19)	$10^3\,\Delta X_2^{(3)}$ (20)	$10^3\,X_2^{(3)}$ (21)	$M_i[X_2^{(3)}]^2$ (22)	$\bar{\phi}_2^{(3)}$ (23)	$\phi_2^{(3)}$ (24)	i (1)
−0.377	1.655	−0.162	−0.162	−1.885	−1.885	−0.276	−0.385	1.730	−0.164	−0.164	5
−0.106	0.175	−0.046	−0.046	−0.707	−2.592	−0.325	−0.110	0.187	−0.047	−0.047	4
0.199	0.615	0.085	0.085	1.326	−1.265	−0.139	0.215	0.719	0.092	0.092	3
0.354	1.950	0.152	0.152	2.362	1.097	0.107	0.354	1.944	0.151	0.151	2
0.258	1.031	0.111	0.111	1.718	2.814	0.247	0.247	0.947	0.105	0.105	1
	$\Sigma_2 = 5.426$							$\Sigma_3 = 5.527$			

equation, Eq. 43, becomes

$$\frac{49.60}{\Omega^2_k} - 1 = \frac{0.996}{57.11/\Omega^2_k - 1} + \frac{0.0024}{424.9/\Omega^2_k - 1}.$$

The first two roots of this equation are

$$\Omega^2_1 = 26.57; \quad \Omega_1 = 5.155$$
$$\Omega^2_2 = 421.1; \quad \Omega_2 = 20.52$$

Hence, by Eq. 41*b*, for $k = 1$:

$$c_{11} = \frac{0.998}{57.11/26.57 - 1}\,c_1 = 0.868\,c_1$$

and

$$c_{12} = \frac{-\,0.049}{424.9/26.57 - 1}\,c_1 = -\,0.003\,c_1$$

—and, by Eq. 42: $49.60\,c^2_1 + 57.11(0.868\,c_1)^2 + 424.9(-\,0.003\,c_1)^2 = 26.57$, from which $c_1 = 0.536$; $c_{11} = 0.465$; and $c_{12} = -\,0.002$. Repeating the computations for Ω_2: $c_2 = 0.184$; $c_{21} = -\,0.212$; and $c_{22} = -\,0.990$. Hence, the first two modes of the rocking structure are given by

$$\psi_1(i) \doteq 0.536\,\phi_A(i) + 0.465\,\phi_1(i) - 0.002\,\phi_2(i)$$

and

$$\psi_2(i) \doteq 0.184\,\phi_A(i) - 0.212\,\phi_1(i) - 0.990\,\phi_2(i)$$

The shear modes $\psi_{k,s}$ of the rocking structure are evaluated by setting $\phi_A = 0$ in these equations. Table 6 contains the modes ψ_k and $\psi_{k,s}$ for $k = 1$ and $k = 2$.

c. Motion of Building on Rigid Soil for a Sinusoidal Foundation Displacement.—In order to evaluate the influence of the various modes on the motion of the building and to gage the convergence of the Noumerov-Fox step-by-step integration method, the building of Table 1 was subjected to a sinusoidal ground displacement of unit amplitude and period $T_0 = 1.2$ sec (the period of an important Fourier component of an actual earthquake record). With $\omega_0 = \dfrac{2\pi}{T_0} = 5.236$, and $\omega^2_0 = 27.42$, with ω_1 and ω_2 selected from Table 2, and ϕ_1 and ϕ_2 from Table 3(*a*), Eq. 24 gives the displacements:

$$x_i(t) = [1 + 7.318\ \phi_1(i) + 0.188\ \phi_2(i)] \sin \omega_0 t \\ - 10.563\ \phi_1(i) \sin \omega_1 t - 0.741\ \phi_2(i) \sin \omega_2 t \quad (70)$$

TABLE 7.—MOTION OF A BUILDING ON RIGID SOIL FOR A SINUSOIDAL FOUNDATION DISPLACEMENT

i	(*a*) SINE COEFFICIENTS OF $x_i(t)$ IN THE SOLUTION BY MODES					(*b*) SATISFACTION OF REST CONDITIONS				
	$\sin \omega_0 t$ (Mode 1) (1)	$\sin \omega_0 t$ (Modes 1 and 2) (2)	$\sin \omega_0 t$ (all modes) (3)	$\sin \omega_1 t$ (4)	$\sin \omega_2 t$ (5)	r_1 (6)	r_2 (7)	r_3 (8)	r_4 (9)	r_5 (10)
5	2.204	2.173	2.178	−1.738	0.123	−0.304	0.149	−0.070	−0.015	0.000
4	2.087	2.078	2.076	−1.569	0.034	−0.177	−0.052	0.106	−0.040	0.000
3	1.866	1.884	1.878	−1.250	−0.070	0.062	−0.196	−0.026	0.084	0.000
2	1.588	1.616	1.617	−0.849	−0.111	0.303	−0.045	−0.155	−0.120	0.001
1	1.290	1.310	1.318	−0.419	−0.075	0.685	0.407	0.216	−0.100	0.000

Cols. 1, 2, and 3 of Table 7(*a*) contain, respectively, the coefficients of the forced term $\sin \omega_0 t$, when 1, 2, and 5 modes are taken into account in Eq. 24. (These last coefficients have been obtained independently from a rigorous solution of the same problem by the Laplace transform method.) These results indicate that in the present problem the contribution of the higher modes to the forced vibrations is negligible and that it is permissible to take into account only two modes. Cols. 4 and 5 of Table 7(*a*) contain the coefficients of $\sin \omega_1 t$ and $\sin \omega_2 t$, the contributions of the first two modes of free vibration.

It was noticed in Sect. 3 that the initial conditions of rest for the co-ordinates p_j cannot be rigorously satisfied unless all the modes are taken into account. Table 7(*b*) gives the values of the ratios $r_{N'}(i)$, from Eq. 20, for $N' = 1$, 2, 3, 4, 5, and shows that the rest conditions are very poorly satisfied at the lower floors unless one takes into account all the modes. This is to be expected, since the jump between $\dot{x}_0(0) \neq 0$ and $\dot{x}_i(0) = 0$ cannot be well approximated by a Fourier series. The values r_5, which should be identically zero, have been computed as a numerical check. It is noteworthy (and also lucky) that the solution of this problem is not too sensitive to the initial conditions.

d. The Step-by-step Integration of the Lagrangian Equations.—The displacements of the structure due to a sinusoidal motion of the ground were evaluated in Sect. 9*c* by means of the solution of Eqs. 16 given by Eqs. 23. The values of $p_1(t)$ and $p_2(t)$, for $X_0 = 1$ and $\omega_0 = 5.236$, in steps of 0.1 for p_1 and of 0.025 for p_2, appear in Table 8, for values of t between 0 and $t = 1.5\ T_0 = 1.8$ sec.

TABLE 8.—STEP-BY-STEP INTEGRATION OF THE LAGRANGIAN EQUATIONS FOR $p(t)$

r (1)	Approximate p_r (2)	True p_r (3)	r (1)	Approximate p_r (2)	True p_r (3)	r (1)	Approximate p_r (2)	True p_r (3)	r (1)	Approximate p_r (2)	True p_r (3)
(*a*) INTEGRATION OF p_1											
0	0	0	5	1.770	1.755	10	−2.963	−2.940	15	3.197	3.179
1	0.032	0.048	6	1.335	1.311	11	−2.173	−2.156	16	2.275	2.276
2	0.312	0.335	7	0.172	0.155	12	−0.465	−0.466	17	0.574	0.593
3	0.884	0.901	8	−1.351	−1.352	13	1.497	1.480	18	−1.173	−1.147
4	1.507	1.508	9	−2.599	−2.583	14	2.909	2.885	—	—	—
(*b*) INTEGRATION OF p_2											
1	0.004	0.006	19	0.752	0.748	37	−1.123	−1.118	55	0.870	0.866
2	0.041	0.044	20	0.749	0.744	38	−1.220	−1.214	56	1.081	1.075
3	0.135	0.138	21	0.682	0.676	39	−1.252	−1.245	57	1.236	1.229
4	0.293	0.295	22	0.537	0.533	40	−1.199	−1.192	58	1.311	1.304
5	0.505	0.505	23	0.320	0.318	41	−1.059	−1.055	59	1.296	1.291
6	0.744	0.742	24	0.054	0.054	42	−0.851	−0.849	60	1.202	1.199
7	0.974	0.970	25	−0.227	−0.224	43	−0.606	−0.606	61	1.056	1.056
8	1.157	1.151	26	−0.482	−0.477	44	−0.361	−0.364	62	0.894	0.895
9	1.265	1.258	27	−0.680	−0.674	45	−0.153	−0.157	63	0.750	0.753
10	1.284	1.278	28	−0.800	−0.795	46	−0.004	−0.008	64	0.652	0.654
11	1.221	1.217	29	−0.843	−0.839	47	0.078	0.076	65	0.610	0.610
12	1.099	1.096	30	−0.823	−0.823	48	0.106	0.106	66	0.615	0.614
13	0.951	0.950	31	−0.777	−0.777	49	0.107	0.109	67	0.645	0.641
14	0.813	0.815	32	−0.733	−0.735	50	0.113	0.117	68	0.666	0.660
15	0.716	0.718	33	−0.724	−0.726	51	0.158	0.162	69	0.643	0.637
16	0.673	0.675	34	−0.767	−0.769	52	0.261	0.264	70	0.553	0.548
17	0.680	0.680	35	−0.862	−0.862	53	0.426	0.427	71	0.387	0.383
18	0.717	0.715	36	−0.991	−0.989	54	0.639	0.638	72	0.154	0.154

The values of these functions at the same points have also been evaluated by the Noumerov-Fox step-by-step procedure. For $j = 1$, with $\omega^2{}_1 = 57.11$ and $h = 0.10$, Eqs. 62 give: $c_1 = 1.455$; and $F_{r,1} = 0.0454\ [\sin 0.524\ (r + 1) + 10 \sin 0.524\ r + \sin 0.524\ (r - 1)]$; and Eqs. 67 give: $p_{1,1} = 0.317$; and $p_{2,1} = 0.312$. With these constants and starting values, Eq. 63 gives the values of $p_{r,1}$ in Table 8(*a*). A comparison with the true values indicates satisfactory agreement although h is about one eighth of the period $T_1 = \dfrac{2\pi}{7.557} = 0.831$. For $j = 2$, similarly: $c_2 = 1.740$; $F_{r,2} = 0.02165\ [\sin 0.131\ (r + 1) + 10 \sin 0.131\ r + \sin 0.131\ (r - 1)]$; $p_{1,2} = 0.0041$; and $p_{2,2} = 0.0410$. By Eq. 63, the results are as shown in Table 8(*b*). These results agree satisfactorily with the true values after seventy-two steps, although the spacing h is of the order of $\frac{1}{12}$ the period $T_2 = 0.305$ sec.

The seventy-two steps in the integration of p_2 took approximately 20 min., once the sine functions had been tabulated. The error e_{r+1} was evaluated but not used, since it did not influence the results within the accuracy of the computations.

e. Influence of Damping.—It was stated in Sect. 4 that the influence of damping on the earthquake displacements consists, essentially, in reducing the importance of the higher modes. This is revealed by the case of the structure under study, if a logarithmic decrement equal to 0.9 is assumed, leading to a value of the damping coefficients (Eq. 29): $f_1 = 0.017 \times 7.557 = 0.127$; and $f_2 = 0.017 \times 20.61 = 0.350$. Solving Eqs. 27 with these values of the damping coefficient f_j for a sinusoidal ground motion of unit amplitude and period $T = 1.2$ sec.—and using the modes $\phi_1(i)$ and $\phi_2(i)$ of the undamped structure of Table 3(*a*)—the floor displacements become

$$\begin{aligned} x_i(t) = {} & \sin \omega_0 t + 7.311\, \phi_1(i) \sin (\omega_0 t - 2°31') \\ & + 0.190\, \phi_2(i) \sin (\omega_0 t - 8°8') - 10.568\, e^{-0.127t}\, \phi_1(i) \sin (\omega_1 t + 1°45') \\ & - 0.740\, e^{-0.350t}\, \phi_2(i) \sin (\omega_2 t - 2°5'). \end{aligned}$$

A comparison of this equation with Eq. 70 of Sect. 9*c* shows that the coefficients of the forced vibration are practically unchanged. The amplitude of the higher modes, instead, is rapidly damped out, and the frequencies are practically unchanged by friction.

10. CONCLUSIONS

The methods outlined in this paper permit the solution of dynamic problems of shear buildings whatever the applied forces or displacements may be. They must be compared with other methods on the basis of efficiency and flexibility.

A direct measure of their efficiency has been gained by the writer in solving the problem of the structure without rocking in three different ways:

(1) By direct integration of the equations of motion, using the Laplace transform;

(2) By numerical integration of the same equations, using an extension of the Noumerov-Fox method[15]; and

(3) By modes and numerical integration, using the methods of this paper.

The time involved in the three solutions was roughly in the ratio of 3:3:1; but this ratio of times does not indicate the main advantages of the use of modes—(a) the possibility of simplifying the solution by using a limited number of modes, and (b) the small amount of additional work necessary to analyze the structure under various types of external loads or displacements.

The solution of the rocking building by direct numerical integration is complicated[15] and requires 30 min for each step, whereas the use of complementary systems permits the evaluation of the rocking modes in a remarkably easy manner. The direct analytical integration of the same problem, whenever possible, is very cumbersome.

The introduction of internal damping does not present difficulties by the present methods, but complicates the other two types of solution considerably. It seems possible to state, therefore, that the methods presented herein may be more efficient and flexible than others used to date. The availability of such procedures should encourage the designer to abandon the simplified and unrealistic methods of analysis suggested by codes (such as the $0.1g$ method) with obvious gains in economy and safety.

---

[15] "A Comprehensive Numerical Method for the Analysis of Earthquake Resisting Structures," by C. S. Whitney, B. G. Anderson, and M. G. Salvadori, *Journal*, A.C.I., Vol. 23, No. 1, September, 1951.

Finally, analogous methods are applicable to tall buildings, in which direct stresses are prevalent, and they may be extended to include the elasto-plastic behavior of structures under dynamic loads.

11. Acknowledgments

The writer is highly indebted to his colleague, Mr. Bleich, associate professor of civil engineering, Columbia University, New York, N. Y., for suggesting the application of his method of complementary systems to the present problem and for invaluable advice in the writing of this paper.

E. Cohen, J. M. ASCE, assistant engineer, Ammann & Whitney, in New York, N. Y., read the paper and gave valuable advice based on numerical experience gained in solving the illustrative problem by other methods. All the numerical work in the paper has been checked by M. L. Baron and F. DiMaggio, Junior Members, ASCE, both research associates at Columbia University.

DISCUSSION

JOHN A. BLUME,[16] M. ASCE.—There has been considerable technical literature concerning the analysis of buildings subjected to earthquakes. A great deal of this revived interest in building dynamics has undoubtedly been induced by the possible application of earthquake-resistant design methods to blast design. Such renewed interest is heartily welcomed. A word of caution is required, however, regarding the general acceptance of mathematical or numerical methods based on idealized structures as constituting complete earthquake-resistant design. Caution is especially necessary when the buildings are conveniently subjected, for the purpose of analysis, to sinusoidal motion of specific characteristics, or even to a few cycles of sinusoidal motion of different characteristics.

The author's contribution can be considered another method of investigating building dynamics, but neither this paper, that by C. S. Whitney, M. ASCE, B. G. Anderson, and the author,[15] nor any other idealized mathematical treatment should be thought to constitute a panacea. In this regard, reference is made to the statement in Mr. Salvadori's conclusions:

> "The availability of such procedures should encourage the designer to abandon the simplified and unrealistic methods of analysis suggested by codes (such as the 0.1g method) with obvious gains in economy and safety."

The mere assumption of static lateral forces, whether based on 0.1g or any other percentage of *g*, is an unrealistic approach to a dynamic problem. Building codes, including the San Francisco (Calif.) code and the 1952 Uniform Building Code,[17] vary the seismic factor with the height or number of stories. A suggested code[18] approaches the problem from a more realistic viewpoint—permitting decreases in lateral design forces with flexibility and considering actual damage and earthquake records. It is untrue that the use of assumed static lateral forces in design is entirely or even largely caused by the lack of numerical procedures for dynamic analysis. There are actually many methods and techniques—mathematical, experimental, and empirical. Two mathematical methods which can be used to obtain building periods in much less time than the method suggested by Mr. Salvadori will be presented.

Some of the factors involved in the design of buildings to resist earthquakes greatly complicate and make questionable the implied accuracy and security of any rigorous analysis as a sole criterion. These factors are:

1. The motion of the earth in the general area of the greatest energy release is not a simple sinusoidal movement or even a superimposition of only a few such waves of variable period, amplitude, and acceleration. The motion is violent, chaotic, and in three directions. It may last from 30 sec to 40 sec or more. The motion is exceedingly complex and variable.

---

[16] Cons. Civ. and Structural Engr., San Francisco, Calif.

[17] "Uniform Building Code," Pacific Coast Building Officials Conference, Los Angeles, Calif., Vol. I, 1952, p. 280.

[18] "Lateral Forces of Earthquake and Wind," *Transactions*, ASCE, Vol. 117, 1952, Appendix I.—Lateral Force Code, p. 746.

2. The epicenter is not known in advance, although active faults usually are.
3. There are many active faults that may affect structures in some localities. The assumption, therefore, that distant shocks may transmit smoother waves of lesser intensity (but more subject to analysis) can be dangerous as the only basis for design.
4. The natural periods of the building, which are greatly affected by the walls, fireproofing, ground conditions, and adjacent structures, are subject to change during an earthquake. With increased amplitude the periods shorten as more partitions, walls, and other items come into structural action, and the periods lengthen as cracks and failure occur.
5. The damping is not only conveniently viscous but is frictional and varies not only with materials and types of construction but with amplitude and damage.
6. The concept of using dominant ground periods or important Fourier components of actual records as disturbing forces or motions is subject to more exploration before being a reliable basis for design. Moreover, such characteristics may be not only local, but local for a specific origin of energy release, which point may not be the same in future shocks.

There are several other factors complicating rigorous aseismic design. This approach should be joined with (a) the study of actual damage (and lack of damage) in exposed structures; (b) field research; (c) dynamic laboratory research (shaking table and similar equipment); (d) mathematical research; (e) obtaining and analyzing reliable earthquake records, particularly for the response of various systems of one and more masses to such motion, with various damping coefficients, and spectrum studies; (f) practical design considerations; (g) practical considerations of function, economy, and risk; (h) complete drawings showing details; (i) adequate construction supervision; (j) code requirements; and (k) committee work and discussion.

The writer has been engaged in all of these phases of the problem and wishes to defend (at the present state of knowledge) modern (1953) methods using assumed lateral forces for codes. It is suggested that such codes be constantly improved as experience and knowledge indicate. The static lateral forces can be, and to some extent have been, based on dynamics and mathematics as well as on many other considerations. Special structures are often designed dynamically. Earthquake-resistant design is essentially an art which uses either assumed static forces or dynamic forces (or both) as a means to an end. No code, mathematical method, or assumed force can remove the basic requirement for sound, practical judgment and experience. Above all, continued research is needed.

Research was performed at Stanford University at Stanford, Calif., in 1933 with Lydik S. Jacobsen as faculty sponsor.[19] This work disclosed many interesting factors concerning the dynamic characteristics of a building and the methods of computing these characteristics. The results of this research were not widely distributed because they were considered interesting but academic in view of the many other factors in the design problem. Many of the writer's comments on the author's paper are based on that research.

---

[19] "The Reconciliation of the Computed and Observed Periods of Vibration of a Fifteen-Story Building," by John August Blume and Harry Leonard Hesselmeyer, thesis presented to Stanford University, at Stanford, Calif., in 1934, in partial fulfilment of the requirements for the degree of Engineer.

Shear versus Flexure.—The natural vibration frequencies of a hypothetical five-story structure have been developed by Mr. Salvadori from generalized equations based on certain assumptions. There is little error involved in the assumption that the mass of each story is concentrated at the corresponding floor level when four or more stories are involved. This assumption was the construction basis of dynamic building models at Stanford University by Mr. Jacobsen. However, in the introduction the author states that a structure with an height-to-width ratio of 5 or less can be termed a "shear building," and the influence of direct stresses (flexure of the building as a whole) can be neglected. The listed reference[2] does not reconcile the difference between wind and earthquake design. Normal wind design for framed buildings considers frame resistance to all wind forces, whereas earthquake design usually considers not only the frame, but fireproofing, walls, and other structural elements—in proportion to their relative rigidities. Of course, there are some exceptions in both cases. If the walls and fireproofing are neglected, the shear distortion between level floors is much greater than the deflection caused by direct stress in the columns, and the 5-to-1 ratio applies. In earthquake design, however, the walls, floors, fireproofing, permanent partitions, and shear walls provide not only mass but rigidity and strength. Many practicing engineers are convinced of the value of a good frame as a secondary defense,[18] but they do not neglect the walls or other structural elements which can provide both strength and rigidity and which may constitute a hazard to personnel.

An actual fifteen-story building was analyzed in detail at Stanford University.[19] The height-to-width ratio in one direction was 3.27. The fundamental period computed for this same direction with shear alone (neglecting flexure and ground movement) was 0.605 sec as compared to 1.026 sec if shear and flexure were both considered. The error of the former is 70%. When ground flexibility is introduced the period becomes 1.32 sec. In the other direction, the height-to-width ratio was 2.85 and the fundamental period with shear alone was 0.764 sec as compared to 1.04 sec with shear and flexure; the error was therefore 36%. With ground movement in this direction, T_1 was 1.23 sec. An error in T_2 for the same building caused by neglecting flexure would be from 15% to 20%. The walls of this building contained a considerable number of windows—about 47% of the wall length in the first direction and 60% in the other direction.

For buildings with an height-to-width ratio of 5, and with other slenderness ratios, flexure as a whole should be considered in the determination of the first, second, and possibly the third modes.

The First Mode.—The first mode of an hypothetical building is evaluated in Table 4 by the Stodola-Vianello method. Other methods give results with less expenditure of work and time and with greater ease of introducing factors such as flexure, ground rotation, and ground translation. One simple solution for the first mode for any number of different masses and for different spring constants can be made directly without trial and with only elementary mathematics; the Lord Rayleigh potential energy method is applied to d'Alembert's principle and the basic equations of motion. Although mathematically approximate, the solution can be considered sufficiently accurate for engineering purposes, which involve many factors for which the value of the second significant figure is doubtful.

This method will be demonstrated by using the same geometric and elastic properties as set forth in Table 1. It is assumed that the dynamic deflection curve for this mode is the same as the static deflection curve of the system loaded laterally by its own weight. Table 9 illustrates the entire process and has an extra column, M_i, which would ordinarily be eliminated since W would be entered directly in pounds or kips. The equation,

TABLE 9.—DIRECT COMPUTATION OF APPROXIMATE FIRST–MODE FREQUENCY

i	M_i	$W = M_i\,g$	$\Sigma\,W$	$K_i \times 10^{-3}$	$d\Delta_s = \frac{\Sigma W}{K_i}$	Δ_s	Δ^2_s	$W\,\Delta_s$	$W\,\Delta^2_s$
(1)	(2)	(3)	(4)	(5)	(6)	(7)	(8)	(9)	(10)
5	11.65	4,502	4,502	6.84	0.658	8.478	71.88	38,168	323,604
4	15.53	6,001	10,503	7.98	1.316	7.820	61.15	46,928	366,961
3	15.53	6,001	16,504	9.12	1.810	6.504	42.30	39,031	253,842
2	15.53	6,001	22,505	10.26	2.193	4.694	22.03	28,169	132,202
1	15.53	6,001	28,506	11.40	2.501	2.501	6.26	15,009	37,506
								$\Sigma\,W\,\Delta_s =$ 167,305	$\Sigma\,W\,\Delta^2_s =$ 1,114,115

$$\omega^2_1 = g\,\frac{\Sigma\,W_i\,\Delta_i}{\Sigma\,W_i\,\Delta^2_i}\qquad(71)$$

can easily be proved valid by equating the maximum potential energy in the fully deflected position to the maximum kinetic energy when vibrating through the static equilibrium position. It is simple to add the flexural deflection, Δ_f, and ground rotation values, Δ_g, to the shear deflections before computing $W\,\Delta$ and $W\,\Delta^2$.

From Table 9 and Eq. 71,

$$\omega^2_1 = 386.4 \times \frac{167{,}305}{1{,}114{,}115} = 58.025\qquad(72a)$$

from which

$$\omega_1 = 7.617\qquad(72b)$$

The value of ω_1 computed in one step is 0.79% in error from the value (7.557) determined from Eq. 5. This error from the classical solution is much less than the knowledge of the actual modulus of elasticity of concrete or steel.

It should be noted that ω_1 ("frequency" in the author's nomenclature) is actually the angular velocity in radians per second. The frequency is $\frac{\omega_1}{2\,\pi}$. The first period, T_1, is $\frac{2\,\pi}{\omega_1}$, which is 0.824 sec according to results of Table 9.

Fig. 3 is a qualitative plot of the first-mode curve, wherein the values obtained from Table 9 are reduced in proportion to the maxima obtained by the two methods.

A more accurate method of computing ω_1 and all natural frequencies involves a trial type of solution, but less labor than Mr. Salvadori's procedure. This procedure[19] will be demonstrated subsequently. It was adapted to building dynamics (apparently for the first time) from a device first given by H. Holzer[20] and applied to the torsional vibration problem of a shaft by S. Timoshenko.[21]

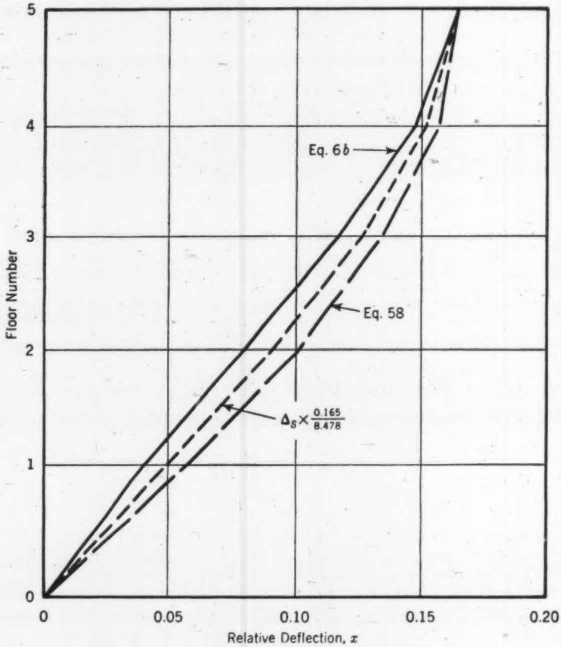

FIG. 3

General Method for Shear Vibration.—For convenience and flexibility in introducing variable ground characteristics in the research at Stanford University,[19] the top story (in lieu of the lowest story) was called 1 in the i series and the nth story the lowest. In order to avoid confusion with the author's notation, the notation z is used instead of i (see Fig. 4).

From d'Alembert's principle,

$$M_z \ddot{x}_z + K_z (x_z - x_{z+1}) - K_{z-1} (x_{z-1} - x_z) = 0 \dots\dots\dots (73)$$

---

[20] "Die Berechnung der Drehschwingungen," by H. Holzer, J. Springer Verlag, Berlin, 1921.

[21] "Vibration Problems in Engineering," by S. Timoshenko, D. Van Nostrand Co., Inc., New York, N. Y., 2d Ed. 1937, p. 263.

and by the addition of the n equations of motion.

$$\sum_{1}^{n} M_z \ddot{x}_z + K_n (x_n) = 0 \qquad (74)$$

Assuming simple harmonic motion (for the natural system, not the forcing distrubance),

$$x_z = X_z \sin \omega t \qquad (75)$$

and

$$\ddot{x}_z = - X_z \omega^2 \sin \omega t \qquad (76)$$

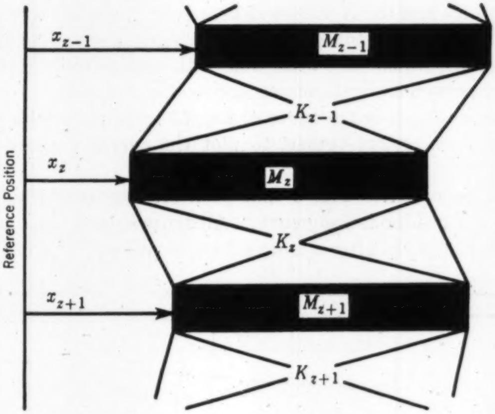

FIG. 4

Substituting and letting $\sin \omega t$ equal unity, for maximum motion,

$$- \sum_{1}^{n} M_z \omega^2 X_z + K_n X_n = 0 \qquad (77)$$

Also, for the zth mass it can be shown that

$$X_z = X_{z-1} - \frac{1}{K_{z-1}} \sum_{1}^{z-1} M \omega^2 X \qquad (78)$$

The process can best be undertaken in tabular form as in Table 10, which uses the same geometric and elastic values established by the author.

The first step in this process is to assume an ω-value and then to assume that X is equal to unity. Since frequencies of such a system are independent of amplitude, the X-values can later be proportionally adjusted, if desired. At a solution for an harmonic period, Eq. 77 must be satisfied.

$$6992.1 + 11{,}400\,(-0.6138) = -5 \approx 0$$

TABLE 10.—EXAMPLE OF FREQUENCY CALCULATION WITH ω ASSUMED EQUAL TO 20.61

i (1)	M (2)	$M\omega^2$ (3)	X (4)	$M\omega^2 X$ (5)	$\Sigma M\omega^2 X$ (6)	$\frac{1}{K} \times 10^3$ (7)	$\frac{1}{K}\Sigma M\omega^2 X$ (8)
5	11.65	4948.6	1.000	4948.6	4948.6	0.1462	0.7235
4	15.53	6596.7	0.2765	1824.0	6772.6	0.1253	0.8486
3	15.53	6596.7	−0.5721	−3774.0	2998.6	0.1096	0.3286
2	15.53	6596.7	−0.9007	−5941.6	−2943.0	0.0975	−0.2869
1	15.53	6596.7	−0.6138	−4049.1	−6992.1	0.0877	

In this case (in Table 10) the solution is for the second mode since the criterion is essentially met and the X-values indicate two nodes, or second-mode movement. The procedure is to select various values of ω and to plot the results. With a few trials, which take little time with a calculating machine, solutions for frequency as well as mode shapes are readily obtained.

The curve in Fig. 5 is the curve of Eq. 77 for the author's building. It is ordinarily unnecessary, of course, to plot the curve except near the desired frequency.

It should be noted in Fig. 5 that each crossing of the vertical zero axis represents a natural-mode frequency. All those shown agree with those computed by Mr. Salvadori after a more laborious process. In Fig. 3 the shape of the fundamental mode coincides exactly with the curve obtained from Eq. 6*b*. The X-values of Table 10, when proportioned to the author's top-story value, agree with his second-mode values of Table 3(*a*).

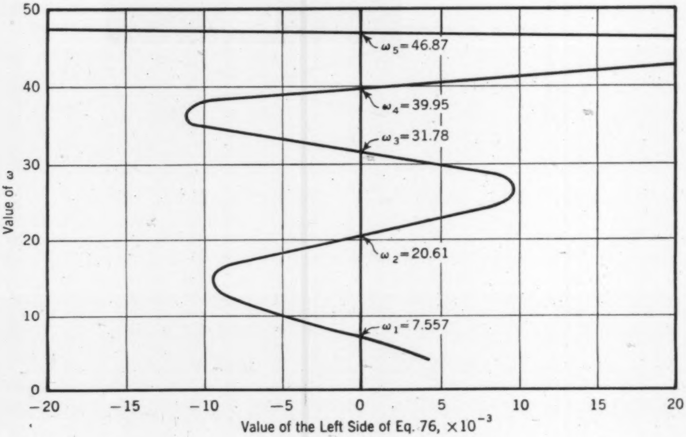

FIG. 5

The mathematical research undertaken at Stanford University did not limit the computation of the first or second modes to shear only, but included flexure of the building as a whole, ground rotation, ground translation, the effectiveness of brick filler walls in conjunction with the steel frame, and other considerations. Actually the computation methods were means to the end of learning how multistory buildings vibrate. It has been most interesting to substitute Mr. Salvadori's hypothetical building values in the equations and in the methods developed in 1933, and to obtain the same results as did the author.

E. F. MASUR.[22]—It is gratifying to note that Mr. Salvadori's paper marks a return to the "classical" procedure of determining the dynamic response of an elastic system to a set of applied forces by expanding that response in terms of the natural modes of vibration of the system. This approach has the further advantage (in addition to the ease of computation mentioned by the author) of permitting the study of various loading conditions with a minimum of additional effort.

It is felt that the concept of a shear building needs further elucidation. Other than the two conditions stated in the Introduction, the author also assumes that the floors are infinitely rigid. This simplification leads to the almost diagonal form of the frequency determinant in Eq. 5. There is some doubt, however, whether the error thus introduced is negligible in the case of actual structural-design practice. In fact, the existence of joint rotations lessens the resistance of a structure against sidesway to such an extent that it is reasonable to expect appreciably smaller natural frequencies of vibration than those based on the idealization of complete floor rigidity. This weakening effect is well recognized in conventional wind-bracing analysis, in which the stiffness of the floor girders is as much a factor as that of the columns.

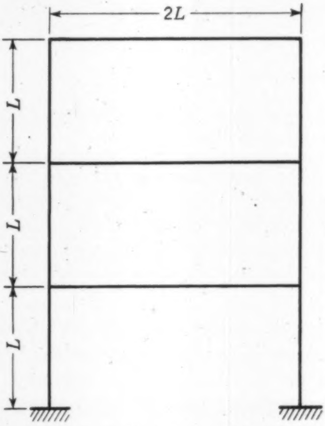

FIG. 6

---

[22] Associate Prof. of Civ. Eng., Illinois Inst. of Technology, Chicago, Ill.

To illustrate this point numerically the simple one-bay, three-story frame shown in Fig. 6 should be considered. The mass, modulus of elasticity, and moment of inertia are, respectively, M, E, and I for the columns, and 8 M, E, and 4 I for the girders. When the distributed spandrel masses are combined with the respective floor masses, the frequency equation, on the assumption of rigid girders, takes the form:

$$\begin{vmatrix} (48\,D - 10\,\omega^2) & -24\,D & 0 \\ -24\,D & 48\,D - 10\,\omega^2 & -24\,D \\ 0 & -24\,D & 24\,D - 9\,\omega^2 \end{vmatrix} = 0 \quad \text{(79a)}$$

in which

$$D = \frac{E\,I}{M\,L^3} \quad \text{(79b)}$$

The roots of Eq. 79*a*—that is, the natural frequencies of the idealized structure, are

$$\omega^2{}_1 = 0.50\,D \quad \text{(80a)}$$

$$\omega^2{}_2 = 3.84\,D \quad \text{(80b)}$$

and

$$\omega^2{}_3 = 7.92\,D \quad \text{(80c)}$$

These results differ from the exact values (that is, "exact" within the other two assumptions regarding shear buildings) of

$$\omega^2{}_1 = 0.31\,D \quad \text{(81a)}$$

$$\omega^2{}_2 = 2.81\,D \quad \text{(81b)}$$

and

$$\omega^2{}_3 = 7.17\,D \quad \text{(81c)}$$

It can be seen that the nonrigidity of the floors affects the magnitude of the natural frequencies of vibration to a significant extent. Furthermore, it can be shown that the effect on the modes is as great, or greater, than the effect on the natural frequencies of vibration.

It is possible, however, to make some allowance for the joint rotations without sacrificing the simplicity of the form of the author's equations of motion. This can be done by assuming that all columns and girders display a point of contraflexure at their midpoints. In that case, the conventional analysis shows that the spring constant K_i, as used by Mr. Salvadori, must be multiplied by a factor,

$$c = \frac{\sum_G S}{\sum_M S} \quad \text{(82)}$$

in which $\sum_G$ extends over all the girders and $\sum_M$ extends over all the members (that is, girders and columns) meeting at a joint. In Eq. 82, S is used to denote the stiffness of a member.

If this procedure is applied to the example under consideration, the frequency equation is modified to

$$\begin{vmatrix} (30\,D - 10\,\omega^2) & -\,12\,D & 0 \\ -\,12\,D & (26\,D - 10\,\omega^2) & -\,14\,D \\ 0 & -\,14\,D & 14\,D - 9\,\omega^2 \end{vmatrix} = 0 \quad (83)$$

The roots of Eq. 83 are

$$\omega^2{}_1 = 0.31\,D \quad (84a)$$

$$\omega^2{}_2 = 2.47\,D \quad (84b)$$

and

$$\omega^2{}_3 = 4.37\,D \quad (84c)$$

It is apparent that the proposed method yields a good approximation of the fundamental frequency (and, to a lesser extent, of the fundamental mode) of vibration. Conversely, the accuracy of the method at the high frequencies is less than the accuracy obtained by the author. This lessening of the accuracy appears reasonable if it is considered that the higher modes involve nodes which reduce the magnitude of the joint rotations.

Edward Cohen[23] and Edward Laing,[24] Junior Members, ASCE, and Leon S. Levy.[25]—A valuable contribution to the solution of dynamic problems involving shear buildings has been made by the author. The writers have utilized the material presented by Mr. Salvadori for the dynamic analysis of structures subjected to impulsive loads. In the course of this work it was noted that the rotational mode, as defined by Eq. 36, is valid only for buildings with large height-to-width ratios where the distribution of mass across the width can be neglected. However, under these conditions, the number of actual modes and frequencies in a building subject to shear and rocking will not exceed the number of stories. As described by Mr. Bleich,[26] the

> "*** total number [of frequencies] can include a trivial root $\omega = \infty$, however [and a mode equal to zero], which happens in the special case in which the complete system contains only masses which already form part of system B."

For structures in which the distribution of mass across the width cannot be neglected, the actual rotational modes can be derived as follows (in the same manner as the shear modes):

The derivation of the modes from Eq. 33,

$$I\,\ddot{\theta} + B\,\theta = 0 \quad (85)$$

will be valid only when the proper dimensionality has been introduced.[27]

---

[23] Asst. Engr., Ammann & Whitney, New York, N. Y.

[24] Structural Designer, Ammann & Whitney, New York, N. Y.

[25] Professional Assistant (Mathematics), Ammann & Whitney, New York, N. Y.

[26] "Frequency Analysis of Beam and Girder Floors," by Hans H. Bleich, *Transactions*, ASCE, Vol. 115, 1950, p. 1035.

[27] "Mathematical Methods in Engineering," by Th. von Kármán and M. A. Biot, McGraw-Hill Book Co., Inc., New York, N. Y., 1940, p. 177.

Thus, setting x_i equal to $L_i \theta$ and dividing Eq. 85 by L_i, there results

$$\frac{L}{L^2_i} \ddot{x}_i + \frac{B}{L^2_i} x_i = 0 \cdots (i = 1,2,\cdots, N) \ldots\ldots\ldots\ldots (86)$$

Eq. 86 on application of the normalizing condition for the rotational mode, leads to

$$\sum_{i=1}^{N} c^2 x^2(i) \frac{I}{L^2_i} = \sum_{i=1}^{N} \phi^2_A(i) \frac{I}{L^2_i} = 1 \ldots\ldots\ldots\ldots (87a)$$

from which

$$\phi_A(i) = \frac{x(i)}{\sqrt{\sum_{i=1}^{N} x^2(i) \frac{I}{L^2_i}}} \ldots\ldots\ldots\ldots (87b)$$

Remembering that the physical condition necessitates that $x(i) = c\, L_i$,

$$\phi_A(i) = \frac{L_i}{\sqrt{I}} = \frac{L_i}{\sqrt{\sum_{i=1}^{N} M_i \left(L^2_i + \frac{b^2}{12} \right)}} \ldots\ldots\ldots\ldots (88)$$

Thus, the rotational modes include a factor of the width of the building, and, as anticipated, the use of this factor reduces the rotational mode and the rotation. In the illustrative example, where the building has a height-to-width ratio of 1, an error of approximately 15% is introduced by the use of Eq. 36.

It should be noted that modification of the normalizing condition (following Eq. 41*b*) and of the orthogonality condition also becomes necessary.

The writers question the validity of Mr. Salvadori's statement that

> "Inasmuch as the largest stresses due to earthquakes occur, in general, a short time after the beginning of the earthquake, and since the logarithmic decrement r_j is nearly 1, the influence of damping on elastic earthquake stresses is often negligible."

For any given earthquake the maximum structural distortions occur as the result of either the severe discontinuous shocks relatively close to the epicenter or the sustained oscillations of lower acceleration and longer period which occur farther away from the epicenter.

In the case of the sustained oscillations, it is apparent that damping, even of small magnitude, must play an important part in reducing the effects of resonance for structures whose natural period approximates the period of the ground motions. However, even in the former case, damping cannot be neglected. It was found[28] that, in the case of the earthquake of May 18, 1940, at El Centro, Calif., the response of an idealized structure could be reduced by more than 50% by the addition of 2% of critical damping. Damping in ordinary buildings has been found to range from 7.5% to 14% of critical damping for concrete structures and 1.5% to 5% for steel structures.

---

[28] Discussion by R. R. Martel, G. W. Housner, and J. L. Alford, of "Lateral Forces of Earthquake and Wind," *Transactions*, ASCE, Vol. 117, 1952, p. 769, Fig. 17.

M. G. **Salvadori**,[29] A.M. ASCE.—Mr. Blume justifiably warns the engineer about the complexities of earthquake-resistant design, and the writer wholeheartedly agrees with him. Mr. Blume has performed a valuable service to the profession by listing (in factors 1 to 6 and (*a*) to (*k*)) some of the essential points governing the dynamics of earthquake motion in buildings. However, one must realize that the research engineer must confine his studies to the influence of some of these factors lest he be hampered by the complexity of the phenomenon. It is not a matter of controversy that the improvements in procedures stipulated in some building codes depend essentially on the results achieved by mathematical and experimental methods. The faster these results are incorporated into the codes, provided this is done intelligently, the better practical earthquake design will become.

The writer's procedures combine the classical approach with the numerical approach to obtain an increase in efficiency. The methods of Lord Rayleigh and H. Holzer are well known, but it is often a matter of familiarity that decides the designer's preference. It was gratifying to learn that Mr. Blume was able to reproduce, by other methods, the writer's numerical results.

The influence of bending on the frequencies and modes of a building, which acts primarily as a shear building, can obviously be substantial, as shown by Mr. Blume. This influence can be accounted for in the procedures suggested by the writer.

The writer is aware of the existence of other numerical and mathematical procedures which are well adapted to the solution of the earthquake problem and did not mean to imply that empirical methods should be discarded entirely. His intention was to compare the efficiency of three methods of solving a simplified earthquake problem, in the hope of adding some knowledge to a complex field of investigation.

Mr. Masur's suggestion to account approximately for the influence of joint rotation seems to be applicable only in connection with the first mode. Since this mode can easily be obtained by Rayleigh's method, the writer does not feel that, in general, its use would be justified.

Messrs. Cohen, Laing, and Levy take issue with the writer's statement concerning the influence of damping on earthquake motion. The influence of damping on the over-all response of a building depends essentially on (1) whether there is resonance between the Fourier components of the earthquake and the natural modes of the building, and (2) the amount of energy dissipated through friction. Although it is quite possible to encounter cases in which these two factors are of fundamental importance, it is not possible to state beforehand that this should always be the case. It would be of interest to study the influence of friction on earthquake motion from a mathematical viewpoint.

Even though the influence of the width of the building is not among the most important factors in dynamic design, it can be easily taken into account by substituting for Eqs. 6*a*, 7, 36, 37, and 38, respectively, the following, in which θ_k is the rotational component of the *k*th mode:

---

[29] Prof. of Civ. Eng., Columbia Univ., New York, N. Y., and Cons. Engr., Ammann & Whitney, New York, N. Y.

$$\sum_{i=1}^{N} \psi^2{}_k\,(i)\,M_i + \theta^2{}_k \sum_{i=1}^{N} M_i\,\frac{b^2}{12} = 1 \quad \text{(89)}$$

$$\sum_{i=1}^{N} \psi_k\,(i)\,\psi_j\,(i)\,M_i + \theta_k\,\theta_j \sum_{i=1}^{N} M_i\,\frac{b^2}{12} = 0 \quad \text{(90)}$$

$$\phi_A\,(i) = \frac{L_i}{\sqrt{I}} \quad \text{(91a)}$$

$$\theta_A = \frac{1}{\sqrt{I}} \quad \text{(91b)}$$

$$\psi_k\,(i) = c_k\,\phi_A\,(i) + \sum_{j=1}^{N} c_{kj}\,\phi_{kj}\,(i) \quad \text{(92a)}$$

$$\theta_k = c_k\,\theta_A \quad \text{(92b)}$$

and

$$\frac{\omega^2{}_A}{\Omega^2{}_k}\,c_k = \sum_{i=1}^{N} [\phi_A\,(i)\,\psi_k\,(i)\,M_i] + \theta_k\,\theta_A \sum_{i=1}^{N} M_i\,\frac{b^2}{12} \quad \text{(93)}$$

AMERICAN SOCIETY OF CIVIL ENGINEERS
Founded November 5, 1852
TRANSACTIONS

Paper No. 2667

VELOCITY MEASUREMENT OF AIR-WATER MIXTURES

BY LORENZ G. STRAUB,[1] M. ASCE, JOHN M. KILLEN,[2] AND OWEN P. LAMB[3]

SYNOPSIS

The search for an adequate explanation of the physical phenomena of natural occurrences is invariably held in abeyance by the lack of suitable measuring instruments and standards of measurement. Once accurate and detailed measurements can be made, the analytical treatment of a wide range of conditions is usually possible on the completion of basic experimentation. The insufflation of air into high-velocity streams of water in open channels is one of the many fluid mechanics phenomena still retarded in its complete analytical explanation by the inadequacy of instrumentation required for experimental observations. This paper traces the development and use of a velocity-measuring instrument at the St. Anthony Falls Hydraulic Laboratory, University of Minnesota, at Minneapolis. This instrument, referred to as the St. Anthony Falls (SAF) velocity meter, is particularly useful in the undertaking of velocity traverses in air-water mixtures.

INTRODUCTION

The capacity of high-velocity streams of water to entrap and contain large quantities of air is apparent in flows over spillways or down steep chutes. The "white water" produced by this air insufflation by open-channel flows is a heterogeneous mixture, varying in bulk density throughout the depth of flow and exhibiting pulsating density variations at all depths. The behavior of air-entrained flow as regards bulking, velocity, depth, and slope relationships, is important to the designing engineer. However, there is a meager supply

---

NOTE.—Published, essentially as printed here, in May, 1953, as *Proceedings-Separate No. 193.* Positions and titles given are those in effect when the paper was received for publication.

[1] Director, St. Anthony Falls Hydr. Lab., Univ. of Minnesota, Minneapolis, Minn.

[2] Asst. Scientist, St. Anthony Falls Hydr. Lab., Minneapolis, Minn.

[3] Research Fellow, St. Anthony Falls Hydr. Lab., Minneapolis, Minn.

of conclusive data on which to base quantitative estimates of these factors when design for freeboard and energy dissipation in steep-gradient structures is being considered. Typical patterns of air-water mixtures in high-velocity flows in open channels are shown in Figs. 1 and 2. Fig. 1 shows the water surface for flow in an inclined channel, and Fig. 2 shows the profile (through a transparent wall) of an air-entrained stream at a steep gradient. Both photographs were taken at speeds of 1/50,000 sec.

LABORATORY EQUIPMENT

The St. Anthony Falls Hydraulic Laboratory at the University of Minnesota, at Minneapolis, is uniquely suited for making high-velocity studies under favorable conditions. Large quantities of water are available at the natural head of 50 ft for the falls. Channels can readily be built to use the head and discharge under easily controllable conditions.

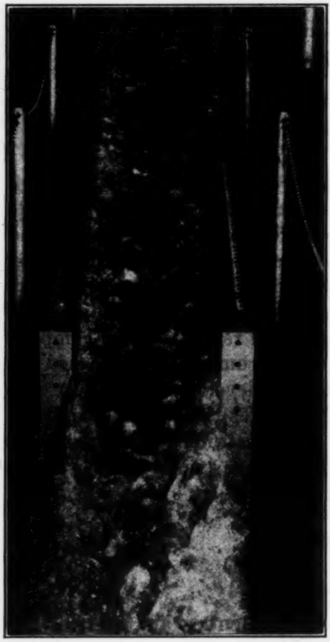

FIG. 1.—AERATED FLOW IN HIGH-VELOCITY CHANNEL

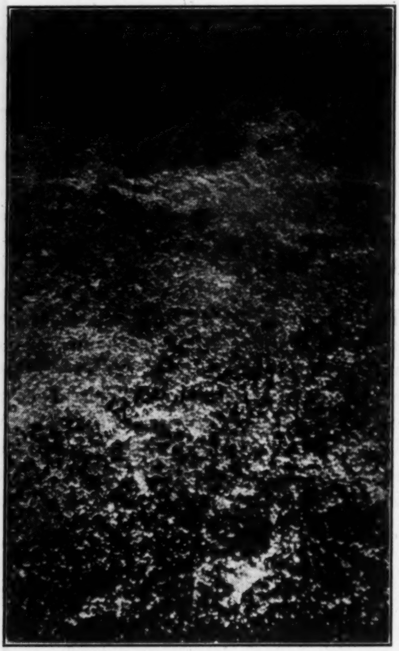

FIG. 2.—PROFILE OF AERATED FLOW

The first of these channels was constructed in 1940, in the turbine pit, at the St. Anthony Falls Hydraulic Laboratory, which is a large vertical shaft inside the laboratory walls extending from above the normal headwater pool elevation of the falls to the tailwater pool elevation. Both headwater and tailwater pools extend as canals into the laboratory. This air-entrainment test channel could be set at any slope from horizontal to 45° with the horizontal. The research program using this flume did not include detailed velocity measurements, but air-concentration traverses and photographic studies on this experimental setup proved to be invaluable in gaining an understanding of the air-entrainment problem and in developing specialized instruments for a subsequent, more comprehensive program.

A larger and more versatile air-entrainment test channel has replaced the earlier setup at the same location in the laboratory. The new flume is 18 in. wide, 12 in. deep, and 50 ft long, and can be set at any slope from the horizontal to the vertical. The design features of this channel will not be covered in this paper. However, the headbox design provides a region of uniform velocity at the inlet end of the flume which has proved useful for testing the velocity meters through a wide range of velocities.

Instrumentation has been incidental to the entire experimental program of aerated flow so that the sequence of steps leading to the St. Anthony Falls (SAF) velocity meter was supplementary to the studies using both the old and the new test channels. Intermediate models of the instrument were used extensively in the course of the experimental program before the later improvements were made.

A separate report has been issued by the St. Anthony Falls Hydraulic Laboratory in which the development of a separate instrument is described for use in measuring air concentration in flowing air-water mixtures.[4] The SAF velocity meter described in this paper is used in conjunction with the air-concentration measuring device to obtain detailed information regarding aerated flows. The functions of the two instruments are complementary, in so far as they are both needed in observations to define air-entrained flows completely. The two devices are completely self-sufficient; however, the accuracies and limitations of either instrument are independent of those of the other.

STUDIES AND INSTRUMENTATION

A summary and bibliography of the literature relative to air entrainment,[5] assembled as an initial phase of the present investigations, reveals that the main experimental effort has been directed toward the determination of air content of flows. When velocity measurements were considered, they were usually used as a means for obtaining a better estimate of the bulk ratio of air to water in various flows under laboratory or field conditions. There are no precise data on velocity distribution in air-entrained flows that might be used in detailed analyses of shear distribution, energy loss, or other internal flow characteristics.

R. Ehrenberger, in pioneering studies of air-entrainment phenomena, assumed that the velocity distributions in the aerated test channel flows were linear between surface velocities obtained with floats and velocities measured near the flume bottom, where there was little entrained air.[6] With this estimate of the velocity distribution, Mr. Ehrenberger use a pitot tube to obtain air-concentration distribution in vertical traverses, the assumption being that any differences between the stagnation pressure to be expected at the assumed velocity and the stagnation pressure actually obtained were caused by the presence of air in the flow at the point of measurement.

---

[4] "An Electrical Method for Measuring Air Concentration in Flowing Air-Water Mixtures," by Owen P. Lamb and John M. Killen, *Technical Paper No. 2, Series B*, St. Anthony Falls Hydraulic Lab., Univ. of Minnesota, Minneapolis, Minn., 1950.

[5] "Air-Entrainment in Flowing Water, A Summary and Bibliography of Literature," by Owen P. Lamb, *Project Report No. 19*, St. Anthony Falls Hydraulic Lab., Univ. of Minnesota, Minneapolis, Minn., 1949.

With methods of measuring the air-concentration distribution directly by independent means, the question arises as to the feasibility of using the pitot tube to obtain applicable velocity measurements in conjunction with the data on air content. If the mixture of air and water were considered to be replaced at every point by a homogeneous fluid with a density equal to the bulk density of the mixture, the pitot tube could be used to measure the velocity. However, the mechanical function of the pitot tube involves the concept of a point or region of stagnation in the flow. It is necessary, therefore, to evaluate the possible difference in behavior between homogeneous and mixed flows in the vicinity of this stagnation point to weigh the applicability of the pitot tube in measuring the velocity of mixtures. In the case of points of flow where the volume of air entrained is small, the curvature of the streamlines at the end of the tube will cause separation of the air and water, as compared to the normal mixture. At higher levels of air concentration there occurs a succession of impingements against the end of the pitot tube in contrast to a stagnation point, and the validity of the measured values is doubtful. In addition to these and other inherently questionable features of the pitot tube, the accuracy of the velocity measurements would be limited to, rather than independent of, the accuracy of the air-concentration measurements.

The basic concept of velocity (distance divided by time) provides the most direct method for determining velocities in open channels. The oldest hydraulic techniques are based on this concept. Various float methods are used in river and canal velocity observations, in the form of surface floats, subsurface floats, rod floats, and other similar devices. A somewhat later development was the use of dye cloudlets over extended river stretches to determine mean velocities.

Salt-Velocity Method.—The salt-velocity method, introduced by C. M. Allen, for determining mean velocities and flow quantities by observations over long stretches of channels or conduits, marked an advance in measurements of this character.[7] Salt was substituted for coloring material in the injection techniques and then was detected by the passage of the salt cloud at some downstream station. This passage was recorded with an ammeter by an increase in conductivity between two electrodes placed in the flow at the downstream station. Various refinements and revised versions of this method were introduced by other investigators. Probably the most practical applications of this salt-velocity method were made in closed penstocks, pipe lines, and flow through hydraulic machinery for the purpose of establishing efficiencies of the hydroelectric plants. The Bureau of Reclamation, United

---

[6] "Wasserbewegung in steilen Rinnen (Schusstennen) mit besonder Berücksichtigung der Selbstbelüftung," by R. Ehrenberger, *Osterreichischer Ingenieur-und Architektverein*, Nos. 15/16 and 17/18, 1926.

[7] "The Salt-Velocity Method of Water Measurement," by C. M. Allen and E. A. Taylor, *Transactions*, ASME, Vol. 45, 1923, p. 285.

States Department of the Interior (USBR), in a study of air-entrained flows, used the salt-velocity methods to obtain mean velocities in extensive reaches of high-velocity open-channel streams in flumes of constant cross section.[8] The velocity measurements were used to estimate the amount of air entrained in the stream.

SELECTION OF A VELOCITY-MEASURING METHOD

The mean velocity of flow through a cross section is readily computed in homogeneous fluid streams where the discharge and cross section can be determined directly. Even this basic information becomes inconclusive when air insufflation occurs because the air discharge and the cross-sectional area are uncertain. In fact, the data available to various investigators are so inconclusive that contradictory statements have been published as to whether the presence of entrained air results in an increase or a decrease of the mean velocity of flow.

In the design of a velocity meter, the range of conditions that might confront the instrument is important. Insufflation might be encountered in streams having a mean velocity as low as 4 ft per sec, but usually the velocities are much greater. Thus, the instrument refinements necessary for accuracy at low velocities are unimportant. At higher velocities, where air entrainment is common, the instrument must be rugged, positive in action, and sufficiently versatile to give a reasonable accuracy of velocity measurement throughout a wide aeration-density range.

The customary concept of fluid density, applicable to homogeneous fluids, is not directly applicable to heterogeneous fluid mixtures of macroscopic proportions. In considering the flow pattern of such a mixture, the filament is made up of random air-and-water regions. The concept of mean bulk density of the filament might be introduced for convenience, but not without discernment as to the limitations of this concept.

Extensive vertical traverses of air concentration conducted during studies at the St. Anthony Falls Hydraulic Laboratory indicate that the distribution of air concentration can be approximated by an equation of the logarithmic type when progressing from the flume bottom to the flow surface. Situations might arise in which the flow near the bottom of the stream is virtually devoid of entrained air, whereas near the surface the filament is almost 100% air. At lower levels of air concentration, where the volume of water exceeds the volume of air, the air might be expected to take the form of bubbles in the flowing stream of water. At levels where the mean air concentration is very high, it is to be expected that water droplets will be entrained in a moving stream of air. The transition between these two extremes from bottom to top provides a less clearly defined air-water mixture. Observations by means of high speed photography show other large-scale pulsating phenomena in the air-water flows. At some combinations of slopes and discharges, definite train-wave phenomena are superimposed upon the general air-entrainment pattern. Macroscopic air pockets may develop at some flow conditions, with the pockets extending far down into the flow. Some of these conditions are evident in Figs. 1 and 2.

---

[8] "Progress Report on Studies of the Flow of Water in Open Channels with High Gradients," by C. W. Thomas, *Hydraulic Laboratory Report No. 35*, Bureau of Reclamation, U. S. Dept. of the Interior, Denver, Colo., July 27, 1938.

This description of the general character of air-water mixtures produced by insufflation in open-channel flow of high velocity immediately directs attention toward the limitations of many customary methods of measuring velocity.

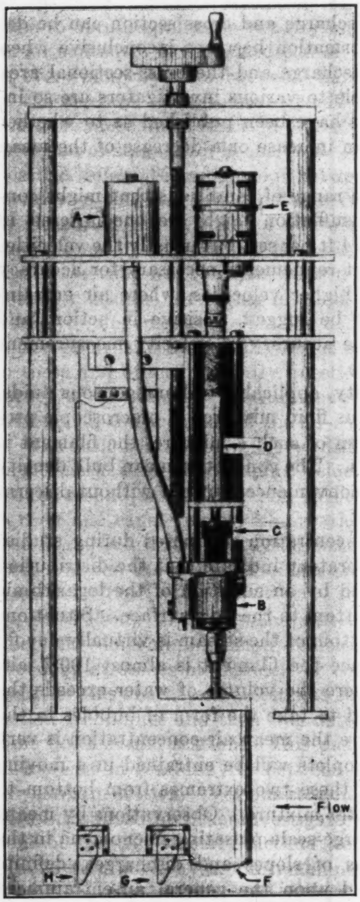
A
E
D
C
B
Flow
H
G
F

Fig. 3.—Probe and Injection System of SAF Velocity Meter

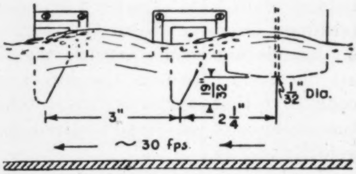
$\frac{19}{32}$"
$\frac{1}{32}$" Dia.
3"
2 $\frac{1}{4}$"
~30 fps

(a) Preliminary Nozzle

(b) Undesirable Cloudlet

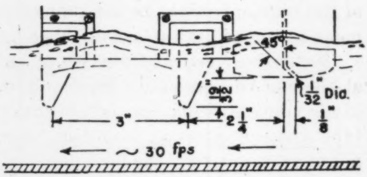
45°
$\frac{1}{32}$" Dia.
3"
2 $\frac{1}{4}$"
$\frac{1}{8}$"
~30 fps

(c) Final Nozzle

(d) Desirable Cloudlet

Fig. 4.—Design of Injection System and Nozzle

OPERATING PRINCIPLES OF THE SAF VELOCITY METER

The SAF velocity meter makes use of electronic methods for measuring very short time intervals that were developed extensively during World War II for radar, sonar, and other similar applications. The meter also makes use of the salt-velocity principle (which was initially applied to the measure of mean velocities over long reaches of channel) so as to minimize errors in the observation of time intervals. By measuring time intervals by electronics, the distance necessary to observe a velocity accurately can be shortened to such an extent that point velocities can be obtained and, accordingly, velocity traverses over a cross section can be made. Even turbulent pulsations can be observed by using very short distance intervals of measurement. The application of an instrument of such basic design for the determination of velocities in fluid mixtures can be checked against conventional instruments in homogeneous flows.

The operating principle of the SAF velocity meter consists basically of marking a small element of a flowing mixture, and then recording the time interval required for this marked element to traverse a fixed distance. The marking is accomplished by making a diminutive portion of flowing water more highly conductive to electrical current by injecting a very small amount of salt solution or similar electric conductor into the stream. The passage of this ionized cloudlet is then detected by electrodes at fixed stations in the flow path. The injection must be rapid enough to identify a very small portion of flowing fluid. The momentum of the injection must be low enough to avoid introducing a significant change in the velocity of flow.

Based on the foregoing principles, the SAF velocity meter combines a mechanical injection system with an electric timing and indicating system for the purpose of measuring velocities in air-water mixtures. The meter can complete the entire velocity measurement from the injection to the recording within a distance of 6 in. along the flow filament. The marking is done by injecting a miniature slug of 6% saline solution into the flowing stream within a time interval of less than 1/600 sec. The volume of each injection is approximately 0.03 cu cm, a quantity small enough to cause no significant momentum effects upon the flowing stream, although the velocity of injection is high.

The salt solution immediately ionizes the water particles that it contacts. An ionized cloudlet is formed which enters a filament of flow. The velocity of this filament is measured when the cloudlet is swept past the two electrode stations which are arranged in tandem along the flow path. Indications are transmitted to the electrical circuit when the front of this ionized cloudlet arrives at each electrode station. By making adjustments to the electrical circuit, the time lapse between the instant that the peak indication near the front of the cloudlet arrives at the first electrode station and the instant it arrives at the second station can be accurately measured. In the SAF meter, the distance between the electrode stations has been fixed at 3 in. Only the very tips of the electrodes are left uninsulated and exposed to flow.

In the development of the instrument, much experimental work was done in determining optimum conditions for the injection of the salt solution. The front of the cloudlet is of special importance because it must be both sharply defined and vertical, so as to assure sharp and accurate readings. This is accomplished by an abrupt and rapid injection using an injector pump from a diesel engine as the main component of the system. The injector pump is driven repetitively by a trip hammer, which is powered by a small electric drill motor. The salt solution to be injected is stored in a small reservoir and is gravity-fed into the injector pump. Metering of the quantity injected at each stroke of the plunger is possible because the pump plunger is slotted for variable delivery. For the open-channel aerated flows at the St. Anthony Falls Hydraulic Laboratory, it has been found that a rate of 15 injections per sec is most advantageous. At each stroke of the injector-pump plunger, the pressure is built up to a point at which it abruptly opens a spring-loaded valve in the outlet port of the injector. This valve closes immediately after the peak of the pressure pulse has passed. The fluid charge then passes through a small injection tube leading from the outward port of the injection pump to the point of injection into the flow stream. At the point of injection, the diminutive slug of salt solution in the end of the needle is abruptly forced out into the flow to form the ionized cloudlet, of which the passage is recorded at the electrode stations.

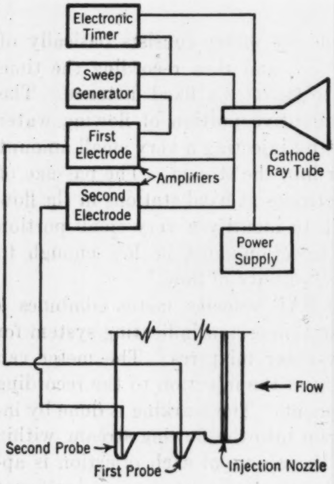

Fig. 5.—Schematic Diagram of Electrical Circuit for SAF Velocity Meter

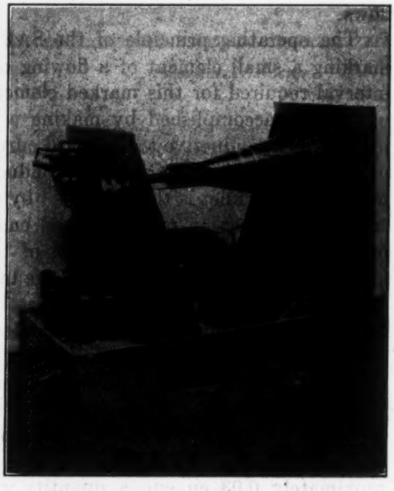

Fig. 6.—Indicating and Time Circuits in Unit Chassis

Fig. 3 shows the injection system. The salt solution from reservoir A flows down through the tube to the inlet port in the diesel injector pump B. The pinion C, which is attached to the pump plunger, can be rotated to set the proper delivery volume. The pump plunger is actuated by the trip hammer D, which in turn is driven by the electric motor E. The injection pulse from the pump is transmitted through the injection tube to the point of injection F.

If the injected slug encounters any water, its downward movement will be dissipated, and the small mass will almost immediately attain stream velocity. The ionized cloudlet in the water will then pass by the tips of the electrodes G and H, which are spaced 3 in. apart, and a velocity reading will be obtained. If the injected spray does not encounter any water, but is fired directly into an air pocket, the momentum of the injection will carry the salt solution down past the level of the electrode tips and there will be no indication. The spacings between the two electrode stations, the distance between the point of injection and the first electrode station, and the difference in level between the point of injection and the electrode tips were all selected so that the salt cloudlets that have attained stream velocity would be the only ones carried past both electrodes, thus forming indications for the meter.

The threaded shaft in Fig. 3 is used to position the electrode tips in a vertical direction. The lower plate is the only part of the instrument actually inserted in the flow. This plate is ⅛ in. wide and is sharpened at all edges so that it can be inserted into the high velocity flows without excessive splashing.

Design of the injection system and the nozzle at the end of the injection tube proved critical in obtaining true velocity readings with the instrument. During the study motion picture films of injection sequences were made. Fluorescein dye was substituted for the salt solution, so that the shape of the cloudlet would be visible. The injection produced by the arrangement shown in Fig. 4(*a*) was undesirable because the front of the salt cloudlet was inclined with the vertical, and it had a slight break near the level of the electrode tips, as shown in Fig. 4(*b*). Since the front of the cloudlet is the point at which the beginning of the indication is relayed to the electrical circuit, this injection would tend to promote erroneous readings. Fig. 4(*c*) illustrates a desirable injection system, in which the salt cloudlet was compact and the leading edge was vertical, as shown in Fig. 4(*d*).

The electrical circuit is shown schematically in Fig. 5. The leads from each of the electrode stations in the probe are connected to the cathode-ray tube through their respective electrical amplifiers. The power supply and sweep generator circuits are necessary for the operation of the cathode-ray tube. The circuits are all enclosed in the chassis shown in Fig. 6. The electronic timing circuit is similar to a type developed for radar timing during World War II. The function of the electronic timing is to place marks on the cathode-ray tube screen at the beginning and at the end of each timing interval. Separate knobs on the electrical control panel allow the operator to position the limits of the timing interval at the peaks of the indications from the electrode stations. When the time-interval markers are positioned accurately on the indications from the electrodes, the reading on the phantastron dial on the panel can be directly converted into stream velocity. The phantastron dial can be set with extreme sensitivity as it has one thousand separate divisions on its 10-turn range. The timing circuit accuracy is on the order of ±0.025 millisec.

Typical indications which appear on the face of the cathode-ray tube are shown in Fig. 7(*a*). The marks showing the extremities of the timing interval are positioned at the peaks of the indications from the respective electrodes. Repetitive injections result in a succession of such indications on the cathode-ray tube screen. All the indications fall close to one another, but there are small differences because each indication represents an instantaneous sample of the longitudinal velocity at a point in the flow, and the flows in which the measurements are being taken are highly turbulent. At the rate of 15 injections per sec, the visual averaging of the small differences of the indication peak positions and proper positioning of the timing marks by the operator have given satisfactory results.

Fig. 7(*b*) is a motion picture strip of indications appearing on the cathode-ray tube from successive injections. The timing marks were not positioned on the peaks of the indications when these pictures were taken so that the independence of their spacing could be illustrated.

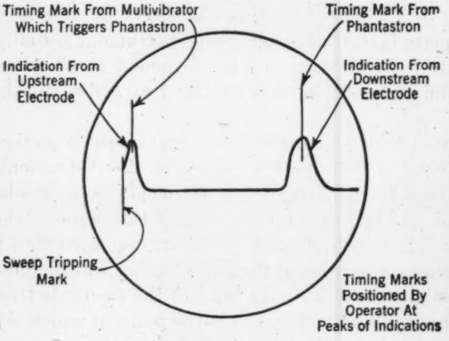
Timing Mark From Multivibrator Which Triggers Phantastron
Timing Mark From Phantastron
Indication From Upstream Electrode
Indication From Downstream Electrode
Sweep Tripping Mark
Timing Marks Positioned By Operator At Peaks of Indications

(*a*) GENERAL SKETCH

(*b*) PICTURE RECORD

FIG. 7.—CATHODE-RAY TUBE INDICATIONS

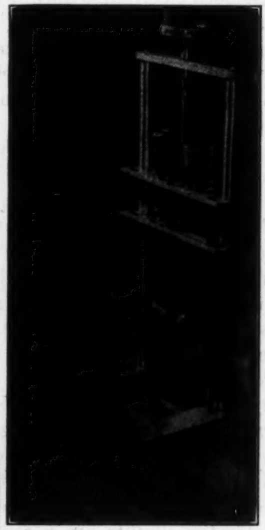

FIG. 8.—SAF VELOCITY METER MOUNTED FOR OPEN-CHANNEL MEASUREMENTS

Fig. 8 shows the SAF velocity meter with the probe elevated above the high-velocity flow. In operation each reading with the instrument requires about 2 min. This includes the time necessary for the operator to position the instrument in the flow, start the injection motor, observe the indications on the cathode-ray tube, position the timing marks, and read the velocity on the phantastron dial. The actual procedure can be readily learned, as the only adjustments necessary for determining the indicated velocity are the two timing marks.

The instrument is limited with regard to making accurate measurements close to the wall. The mounting permits it to be used as close as ⅜ in.

from the side walls; it is doubtful whether accurate readings could be obtained closer than this distance from the wall because of electrode interference set up by the steel-wall boundaries. When the point of measurement is closer than ⅜ in. to the bottom of the channel, there will probably be excessive interference with the injection cloudlets. Such interference would promote erroneous measurements.

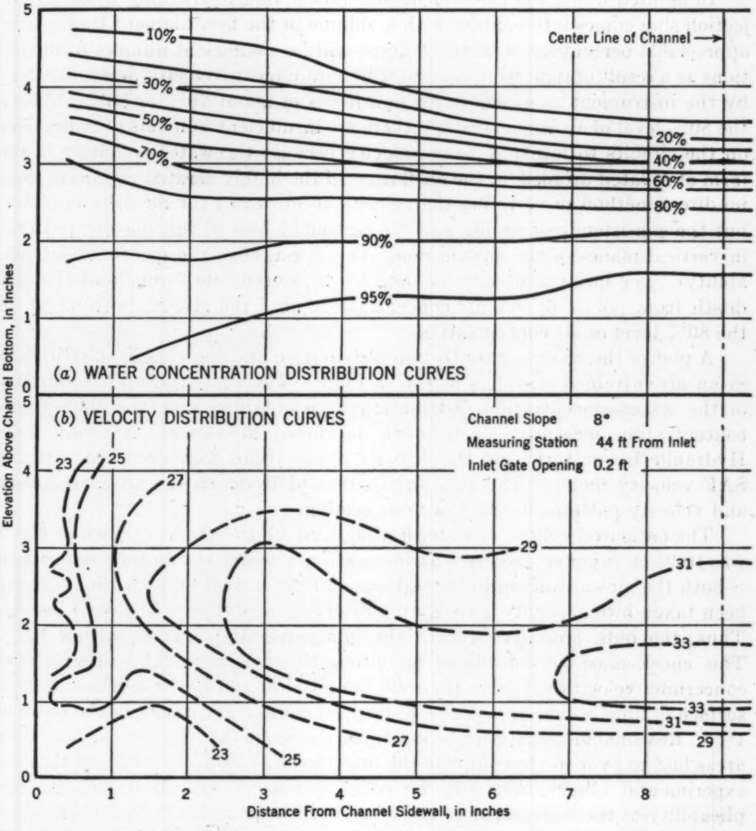

FIG. 9.—VELOCITY AND WATER CONCENTRATION TRAVERSES OF AERATED FLOW WITH SAF INSTRUMENTS

TEST VERIFICATIONS

Various experiments have been made to test the practicality of operation, the effectiveness, and the accuracy of the SAF velocity meter. The most direct check possible is a comparison with a pitot tube in a nonaerated stream. The velocities indicated by the SAF meter were found to be slightly lower than those obtained by the pitot tube at the same point and flow condition.

That is, nearly all points fall slightly below a line of perfect correlation. The apparent tendency of the SAF meter is to indicate velocities 1% or 2% lower than the velocities obtained by the pitot tube. This might be attributable to the velocity deficiency caused by the drag of the first electrode since the tips of the electrodes are the only obstructions in the flow at the level of the filament being measured.

In aerated flows, the instrument indicates a velocity reading when the injection slug comes into contact with a volume in the flow filament that has an appreciable percentage of water. There will be a sufficient number of indications as a result of repetitive injections to obtain mean-velocity determinations by the instrument at air-concentration levels of about 70% or 80%. Above the 80% level of air concentration, there are insufficient numbers of indications on the circuits to measure mean velocity because the water is mainly in the form of isolated droplets in the air flow. In the highly aerated regions of flow, no direct method of verifying the velocity recording of the meter is available, but the consistency of results and the reasonableness of the velocity patterns in vertical planes of the stream cross section establish the measurement reliability. The instrument may be used for measurements throughout the flow depth from points of low air concentration, near the stream bottom, up to the 80% level of air concentration.

A plot of the water-concentration distribution and the velocity distribution in an air-entrained stream is shown in Fig.9. The experimental observations of the water-concentration distribution were obtained with the electric air-concentration measuring instrument developed at the St. Anthony Falls Hydraulic Laboratory, and the velocity observations were obtained with the SAF velocity meter. The two distribution plots define the air-entrainment and velocity patterns in the flow cross section.

The measured volume of water flowing through the channel shown in Fig. 9 was 10.95 cu ft per sec, whereas an integration of water flow in the cross section —both the air-entrainment observations and the velocity observations having been taken into account—gave a bulk discharge of water of 10.8 cu ft per sec. Thus, the bulk flow agreed with the integrated discharge to within 1.5%. This check must be considered fortuitous because the several uncertainties concerning velocities close to the solid boundaries, and near the indefinite free surface of flow, would appear not to warrant normal accuracies of the order of 1%. Reasonable assumptions concerning the water discharge in the boundary areas had to be made to complete the integration. However, the fact that the experimental observations can be correlated so closely illustrates the applicability of the instrument to the types of flow for which it was designed.

STATUS OF THE SAF VELOCITY METER IN 1951

The SAF meter has been mounted in a manner that will facilitate velocity traverses in the aerated open-channel flows being studied at the St. Anthony Falls Hydraulic Laboratory. The new mounting is shown in Fig. 10, in which the letters denote items which are the same as in Fig. 3.

The electrical circuits have been developed further, so that the placing of the limits of the timing sequence on the paths of the velocity indications is done automatically. The averaging of these indicated times is also accomplished by the electrical circuit, eliminating operator-judgment in placing the timing marks. Furthermore, the circuit dispenses with the need for the cathode-ray tube which was essential to the developmental phases of the instrument. This allows for more convenient packaging of the entire electrical circuit. The mean velocity is read directly on the meter, making the instrument entirely objective and simple to use in an experimental study.

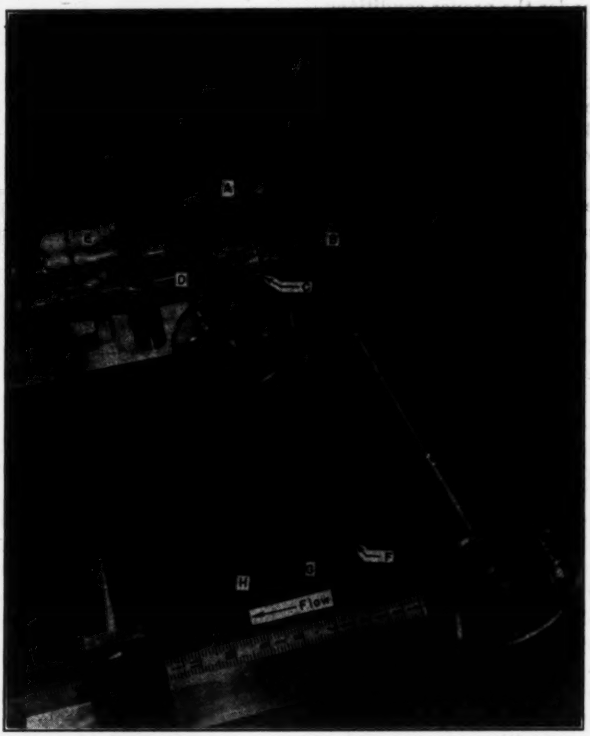

FIG. 10.—SAF VELOCITY METER MOUNTED FOR TRAVERSING LABORATORY OPEN-CHANNEL FLOWS

CONCLUSION

Incorporation of the injection tube and the electrode stations into a single plate proved a most satisfactory arrangement for a device that must be inserted into high-velocity streams. There should be little difficulty in constructing a similar probe on a larger scale for investigating aerated flows in large-scale field structures. The compact portable electrical system by which the velocities can be read directly on an electrical meter is particularly adaptable to field conditions.

The SAF velocity meter used with the cathode-ray tube is quite satisfactory for laboratory observations, and it delivers an individual reading accurately on the order of 2% of the actual velocity. It is quite sensitive to velocity changes and permits detailed study of aerated flows. Exploratory studies indicate that the instrument might be used for turbulence measurements in water. Its use for measuring velocities in other fluid mixtures is also possible under the proper conditions.

ACKNOWLEDGMENTS

The development of the SAF velocity meter is one phase of a comprehensive experimental and analytical investigation of air insufflation and air-entrained flows first undertaken at the St. Anthony Falls Hydraulic Laboratory, prior to 1943. This investigation was initially sponsored by the Engineering Foundation (United Engineering Trustees, Incorporated) and the committee on Research, Hydraulics Division, ASCE. More recently, the studies have been sponsored by the Office of Naval Research, United States Department of the Navy.

AMERICAN SOCIETY OF CIVIL ENGINEERS
Founded November 5, 1852
TRANSACTIONS

Paper No. 2668

RADIAL IMPACT ON AN ELASTICALLY SUPPORTED RING

By Edward Wenk, Jr.,[1] J. M. ASCE

With Discussion by Messrs. John C. Burgess, and Edward Wenk, Jr.

Synopsis

The study of free vibrations of a circular ring, as developed by A. E. H. Love and S. Timoshenko, has been extended for the case of a circular ring that has radial and tangential elastic support and that is subjected to a radial impulse in the plane of the ring. Equations are developed for the frequencies of rigid-body motion and flexural vibration, and infinite series solutions are obtained for displacements and bending moments produced by an impulsive load analytically defined as a half-sine wave. In the development of the theory, the vibrations are assumed to be inextensional, and damping effects, rotatory inertia, and shear are neglected.

The theory was investigated experimentally by tests of a 24-in.-diameter ring radially supported by a large number of coil springs. Impulses of half-sine characteristic were delivered by a pendulum, and the force of impact was accurately measured with a dynamometer especially developed for this study. The parameters of elastic support and of the duration and intensity of load were varied during the test; and the strains, radial displacements, and external loads were recorded.

The observed frequencies of vibration agreed with those computed by the theory very closely up to the seventh mode of flexural motion. Also, the observed strains and displacements were found to correlate with the computed values both for the time interval during the pulse and for the subsequent free vibrations.

It is concluded that the theory is valid within the bounds of the assumptions, provided that the depth of cross section of the ring is small compared with the diameter.

Note.—Published, essentially as printed here, in November, 1952, as *Proceedings-Separate No. 157*. Positions and titles given are those in effect when the paper or discussion was received for publication.

[1] Head, Structures Div., Structural Mech. Lab., David Taylor Model Basin, Washington, D. C.

NOTATION

The letter symbols are defined where they first appear, in the illustrations or in the text, and are arranged alphabetically for reference in Appendix I.

INTRODUCTION

Fundamental to this investigation is the differential equation for the static bending of a thin curved element, that was established by J. Boussinesq,[2]

$$M = E\,I\left(\frac{1}{r + \Delta r} - \frac{1}{r}\right) = \frac{E\,I}{r^2}\left(\frac{\partial^2 u}{\partial \theta^2} + u\right) \qquad (1)$$

in which M is a flexural couple acting about the x-axis on a cross section of the ring—positive if it increases the curvature of the ring; E is the modulus of elasticity; I is the moment of inertia about the x-axis of a cross section of the ring; r is the mean radius of the ring; u is the radial displacement, measured positive toward the center of the ring; and θ is the central angle of the ring, measured positive counterclockwise. The same differential equation was apparently derived independently by H. Lamb.[3] These solutions have been applied to the bending analysis of a thin circular ring statically loaded in its plane.[4,5] The analysis of circular rings with radial elastic support has been studied by A. J. S. Pippard and W. E. Francis,[6] who also obtained experimental verification by static tests of wire wheels. Their instrumentation was confined to Marten optical extensometers for measuring strains in the radial spokes, from which measurements the bending moments and radial displacements of the ring were inferred. Similar theoretical analyses have been developed by L. H. Donnell and others,[7] and by M. I. Hetényi.[8]

The vibrations of a circular ring were first investigated by R. Hoppe,[9] who derived the frequency equation,

$$p^2_i = \frac{i^2(i^2 - 1)^2}{1 + i^2}\,\frac{g\,E\,I}{A\,\gamma\,r^4} \qquad (2)$$

in which p_i is the circular frequency of a vibrating ring at a mode designated by an integer i; g is the acceleration due to gravity; A is the area of a cross section of the ring; and γ is the density of the material. A. E. H. Love[10] later studied the fundamental equations of motion for both a complete ring and an incomplete ring with a cross section that was also circular. For these solutions, the important assumption was made that the center line of the ring is free of any extension.

---

[2] "Résistance d'un anneau à la flexion, quand sa surface extérieure supporte une pression normal, contante par unité de longuer de sa fibre moyenne," by J. Boussinesq, *Comptes Rendus*, Paris, France, Vol. 97, 1883, p. 843.

[3] "On the Flexure and Vibrations of a Curved Bar," by H. Lamb, *Proceedings*, London Math. Soc., Vol. 19, 1888, p. 365.

[4] "Strength of Materials," by S. Timoshenko, D. Van Nostrand, Inc., New York, N. Y., Vol. 2, 2d Ed., 1940, p. 101.

[5] *Ibid.*, p. 218.

[6] "On a Theoretical and Experimental Investigation of the Stresses in a Radially Spoked Wire Wheel under Loads Applied at the Rim," by A. J. S. Pippard and W. E. Francis, *Philosophical Magazine*, Series 7, Vol. 11, No. 69, 1931, pp. 233–285.

[7] "Analysis of Spoked Rings," by L. H. Donnell, H. B. Gibbons, and E. L. Shaw, *Journal of Applied Mechanics*, Vol. 8, No. 2, 1941, pp. 67–73.

[8] "Beams on Elastic Foundations," by M. I. Hetényi, Univ. of Michigan Press, Ann Arbor, Mich., 1946.

[9] "Vibrationen eines Ringes in seiner Ebene," by R. Hoppe, *Journal für die Reine und Angewandt Mathematik*, Vol. 73, 1871, pp. 158–170.

[10] "A Treatise on the Mathematical Theory of Elasticity," by A. E. H. Love, Dover Publications, 4th Ed., 1944, pp. 451–453.

The flexural vibration of a circular ring, when the possible extension of the center line is considered, is discussed by F. W. Waltking,[11] and by K. Federhofer.[12] Vibrations of ring-shaped frames out of the plane of the frame are discussed by J. H. Michell,[13] by Mr. Love,[10] and by F. H. Brown,[14] and torsional vibrations are also treated by Mr. Love.[10]

More recently, G. F. Carrier[15] has given a mathematical analysis of vibrations of a circular ring that is rotating at high speed so as to develop important centrifugal effects and that is either rigidly or elastically supported by radial spokes.

As a further development of the mechanics of circular rings, there is investigated in this paper the dynamical behavior of a ring with both radial and tangential elastic support, subjected to a concentrated radial force that has the time characteristic of a half-sine wave. A frequency equation for flexural and rigid-body motion is derived and, by application of procedures used by S. Timoshenko[16] and W. H. Hoppmann, II,[17] for the impact loading of straight beams, normal mode solutions are obtained for bending displacements in the plane of the ring. These solutions developed in 1948 may be considered only as first-order approximations; a second-order approximation that leads to the buckling load for an elastically supported ring has also been developed and is contained in a Taylor Model Basin (TMB) report.

The validity of the theoretical analysis was investigated experimentally by tests of a circular ring with a diameter of 24 in., radially supported by thirty-eight coil springs intended to simulate pure radial elastic support. The ring was subjected to a radial impulse of controlled duration and intensity during which time the impulse and the resulting strains and displacements were measured with electrical instruments. The ring was also subjected to a harmonically varying force over a continuous frequency spectrum to determine the frequencies of flexural vibration by observation of resonance.

Several new experimental instruments and techniques were developed for these tests, including a method for applying, controlling, and precisely measuring a transient impulse. These are described in detail.

The paper concludes with a comparison of theoretical and experimental results for the various cases of loading.

---

[11] "Schwingungszahlen und Schwingungsformen von Kreisbogentragern," by F. W. Waltking, *Ingenieur-Archive*, Vol. 5, 1934, pp. 429–449.

[12] "Über die Eigenschwingungen des senkrecht zu einer Ebene schwingenden Kreisbogens," by K. Federhofer, Akadamie der Wissenschaften, Berlin, Germany, ab IIa, Vol. 145, 1936, pp. 29–50.

[13] "The Small Deformations of Curves and Surfaces with Application to the Vibration of a Helix and Circular Rings," by J. H. Michell, *Messenger of Mathematics*, Vol. 19, 1890, pp. 68–82.

[14] "Lateral Vibrations of Ring-Shaped Frames," by F. H. Brown, *Journal*, Franklin Inst., Vol. 218, No. 1, 1934, pp. 41–48.

[15] "On the Vibrations of the Rotating Ring," by G. F. Carrier, *Quarterly of Applied Mathematics*, Vol. 3, No. 3, 1945, pp. 235–245.

[16] "Vibration Problems in Engineering," by S. Timoshenko, D. Van Nostrand, Inc., New York, N. Y., 2d Ed., 1937, pp. 405–410.

[17] "Impact of a Mass on a Damped Elastically Supported Beam," by W. H. Hoppmann, II, *Journal of Applied Mechanics*, Vol. 15, No. 2, June 1948, pp. 125–136.

THEORETICAL ANALYSIS

The subject of this investigation is a plane circular ring of constant and symmetrical cross section whose dimensions are small compared with the radius of the center line; one of the principal axes of the cross section is assumed to be situated in the plane of the ring. Furthermore, the ring is considered to have uniform radial and tangential supports that are completely elastic and that exercise constraints at the centroid of the cross section of the ring. Damping and body forces are neglected in the analysis, and external forces are restricted to radial orientation in the plane of the ring.

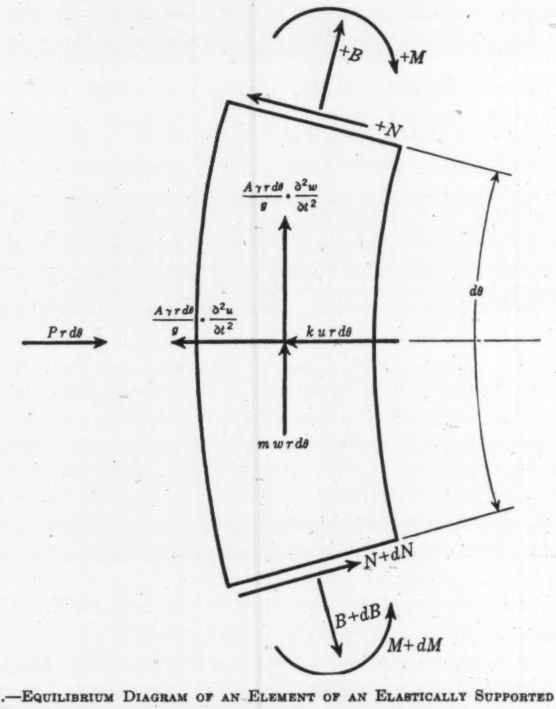

+B
+M
+N
$\frac{A\gamma r\,d\theta}{g}\cdot\frac{\partial^2 w}{\partial t^2}$
$d\theta$
$\frac{A\gamma r\,d\theta}{g}\cdot\frac{\partial^2 u}{\partial t^2}$
$P r\,d\theta$
$k u r\,d\theta$
$m w r\,d\theta$
N+dN
B+dB
M+dM

FIG. 1.—EQUILIBRIUM DIAGRAM OF AN ELEMENT OF AN ELASTICALLY SUPPORTED RING

The Differential Equation of Motion.—Consider first an element of the ring as shown in Fig. 1. Equations of equilibrium are derived, taking into account the internal shear force denoted by N; the normal force denoted by B; the flexural moments, M (all imposed by contiguous ring elements); the radial and tangential components of particle accelerations; the external loads, P; and the radial and tangential elastic supports.

In the radial direction, the forces are as follows:

$$\frac{\partial N}{\partial \theta} + B = \frac{A\,\gamma\,r}{g}\frac{\partial^2 u}{\partial t^2} + k\,u\,r - P\,r \ldots\ldots\ldots\ldots\ldots (3a)$$

in which k is the modulus of elastic support expressed in units of pounds per inch of circumference per inch of radial displacement, u designates radial displacement taken positive toward the center, and t is the time variable.

In the tangential direction, the forces are

$$\frac{\partial B}{\partial \theta} - N = \frac{A\,\gamma\,r}{g}\,\frac{\partial^2 w}{\partial t^2} + m\,w\,r \ldots\ldots\ldots\ldots\ldots\ldots (3b)$$

in which m is the modulus of tangential support and w is the tangential displacement taken positive in the counterclockwise direction.

If rotatory inertia is neglected, the equation of equilibrium involving moments is

$$\frac{\partial M}{\partial \theta} + N\,r = 0 \ldots\ldots\ldots\ldots\ldots\ldots\ldots\ldots (3c)$$

Terms corresponding to effects of shearing distortion have also been neglected, but the possible error thus introduced has been found by Mr. Timoshenko[18] to be unimportant for bars with vibrational wave lengths of at least ten times the depth of the cross section.

The tangential displacements, w, are now assumed to occur in such a form that the extension of the center line is zero. This condition of inextensional vibration was expressed by Mr. Love as

$$u = \frac{\partial w}{\partial \theta} \ldots\ldots\ldots\ldots\ldots\ldots\ldots\ldots\ldots (4)$$

If the change in curvature in terms of bending displacements is represented by the equation given by Mr. Boussinesq[2] for bending of a curved beam—

$$M = E\,I\left(\frac{1}{r + \Delta r} - \frac{1}{r}\right) = \frac{E\,I}{r^2} = \left(\frac{\partial^2 u}{\partial \theta^2} + u\right) \ldots\ldots\ldots (5)$$

—then, by use of Eqs. 4 and 5, the equations of equilibrium (Eqs. 3*a*, 3*b*, and 3*c*) may be reduced to eliminate the terms involving M, N, and B. This gives the partial differential equation of motion in terms of tangential displacements:

$$\frac{E\,I}{r^4}\left(\frac{\partial^6 w}{\partial \theta^6} + 2\,\frac{\partial^4 w}{\partial \theta^4}\,\frac{\partial^2 w}{\partial \theta^2}\right) + k\,\frac{\partial^2 w}{\partial \theta^2} - m\,w - \frac{\partial P}{\partial \theta} = \frac{A\,\gamma}{g}\,\frac{\partial^2}{\partial t^2}\left(w - \frac{\partial^2 w}{\partial \theta^2}\right) \ldots (6a)$$

By differentiating Eq. 6*a* with respect to θ and applying Eq. 4, a relationship may be obtained for the radial displacements:

$$\frac{E\,I}{r^4}\left(\frac{\partial^6 u}{\partial \theta^6} + 2\,\frac{\partial^4 u}{\partial \theta^4} + \frac{\partial^2 u}{\partial \theta^2}\right) + k\,\frac{\partial^2 u}{\partial \theta^2} - m\,u - \frac{\partial^2 P}{\partial \theta^2} = \frac{A\,\gamma}{g}\,\frac{\partial^2}{\partial t^2}\left(u - \frac{\partial^2 u}{\partial \theta^2}\right) \ldots (6b)$$

In the usual fashion for the homogeneous case, it is assumed that the radial displacement expressed by u is the product of a characteristic function, $U(\theta)$, and a time function, $\Gamma(t)$; thus,

$$u = U\,\Gamma \ldots\ldots\ldots\ldots\ldots\ldots\ldots\ldots\ldots (7)$$

---

[18] "Vibration Problems in Engineering," by S. Timoshenko, D. Van Nostrand, Inc., New York, N. Y., 2d Ed., 1937, p. 337.

With the variables thus separated, the time function represented by Γ is found (by substitution of Eq. 7 in Eq. 6*b*) to be in the simple harmonic form, of circular frequency p, as follows:

$$\Gamma = C \cos p\,t + D \sin p\,t = \cos (p\,t + \delta) \dots\dots\dots\dots (8)$$

in which C, D, and δ are constants. This condition yields the following ordinary differential equation for U, the characteristic function of radial displacement:

$$\frac{d^6U}{d\theta^6} + 2\frac{d^4U}{d\theta^4} + \left[1 + \frac{\left(k - \frac{A\,\gamma}{g}p^2\right)}{E\,I} r^4\right]\frac{d^2U}{d\theta^2} + \frac{r^4}{E\,I}\left(\frac{A\,\gamma\,p^2}{g} - m\right)U = \frac{1}{\Gamma}\left(\frac{r^4}{E\,I}\right)\frac{d^2P}{d\theta^2} \dots (9a)$$

The homogeneous equation describing the motion of the freely vibrating ring, when $P = 0$, is of the form:

$$\frac{d^6U}{d\theta^6} + 2\frac{d^4U}{d\theta^4} + \nu\frac{d^2U}{d\theta^2} + \mu\,U = 0 \dots\dots\dots\dots (9b)$$

in which the coefficients appearing in Eq. 9*a* have been replaced by the symbols ν and μ. The solution of this equation is given by Mr. Love[10] to be

$$U = \sum_{n=1}^{n=3} (C_n \cos i_n\,\theta + D_n \sin i_n\,\theta) \dots\dots\dots\dots (10)$$

in which n is an integer and i_1, i_2, and i_3 are roots of the equation,

$$i^6{}_n - 2\,i^4{}_n + \nu\,i^2{}_n - \mu = 0 \dots\dots\dots\dots (11)$$

Eq. 11 follows from the substitution of Eq. 10 in the differential equation (Eq. 9*b*).

Frequency Equation for Free Vibration.—In the usual dynamical analysis of bars, physical boundary conditions would be available from which the constants of integration of the differential equation could be determined. In the problem of a complete ring, however, no boundary conditions exist for bending displacements or their functions. However, the requirement exists that the solution be univalued in θ. Thus, for a complete ring, there is the recurrence condition that

$$u_\theta = u_{\theta+2\pi} = u_{\theta+4\pi} = u_{\theta+2n\pi} \dots\dots\dots\dots (12)$$

in which $n = 0, 1, 2, 3, 4, 5, \dots \infty$. This requires that the i_n-terms appearing in Eq. 10 must be integers, which condition establishes the frequency equation. By employing the explicit coefficients of Eq. 9*a* ,Eq. 11 may be solved for the frequency p_i as

$$p^2{}_i = \frac{g}{A\,\gamma}\frac{1}{1 + i^2}\left[\frac{E\,I}{r^4}(1 - i^2)^2\,i^2 + k\,i^2 + m\right] \dots\dots\dots (13)$$

Here, the integer values of i_n are represented simply by i, a quantity greater than unity which defines the number of wave lengths of flexural vibration that may develop in the circumference. The cases wherein i equals zero and unity are the cases of rigid-body rotation and translation of the ring, respectively.

Radial Displacements and Bending Moments Produced by an Harmonically Varying Radial Force.—From Eqs. 8 and 10, the radial displacements may be expressed as an infinite series, as noted previously; thus:

$$u = \sum_{n=1}^{n=\infty} (C_n \cos i_n \theta + D_n \sin i_n \theta) \cos (p\, t + \delta) \ldots\ldots\ldots (14)$$

A single concentrated external force applied at $\theta = 0$ produces symmetrical vibrations, and consequently the odd functions $\sin i_n \theta$ must not appear in the displacement function. This is accomplished by making the coefficients D_n equal to zero. Then,

$$u = \sum_{i=1}^{\infty} a_i \cos i\, \theta \ldots\ldots\ldots\ldots\ldots\ldots\ldots\ldots (15a)$$

and

$$w = \sum_{i=1}^{\infty} \frac{a_i}{i} \sin i\, \theta \ldots\ldots\ldots\ldots\ldots\ldots\ldots\ldots (15b)$$

in both of which a_i-values are functions of time and are taken as the generalized coordinates.

The Lagrange equation of motion may be restated as

$$\frac{d}{dt}\left(\frac{\partial T}{\partial \dot{a}_i}\right) + \frac{\partial V}{\partial a_i} = Q_i \ldots\ldots\ldots\ldots\ldots\ldots\ldots\ldots (16)$$

in which Q_i is the external generalized force, measured positive toward the center; the dotted quantities in this and subsequent equations are derivatives taken with respect to time t. The potential energy, V, of the system is expressed by

$$V = \frac{1}{2}\int \frac{M^2}{E\, I}\, ds + \frac{k}{2}\int u^2\, ds + \frac{m}{2}\int w^2\, ds$$

$$= \frac{E\, I}{2\, r^4}\int_0^{2\pi} \left(\frac{\partial^2 u}{\partial \theta^2} + u\right)^2 r\, d\theta + \frac{k}{2}\int_0^{2\pi} u^2\, r\, d\theta + \frac{m}{2}\int_0^{2\pi} w^2\, r\, d\theta \ldots (17a)$$

in which ds is an increment of the circumference.

Similarly, the kinetic energy, T, of the vibrating ring is

$$T = \frac{A\, \gamma}{2\, g}\int_0^{2\pi} (\dot{u}^2 + \dot{w}^2)\, r\, d\theta \ldots\ldots\ldots\ldots\ldots\ldots (17b)$$

By substitution of the series solutions (Eq. 15a), the Lagrange equation (Eq. 16) then yields:

$$\frac{\pi\, r\, A\, \gamma}{g}\left(1 + \frac{1}{i^2}\right)\ddot{a}_i + \left[(1 - i^2)^2\, \frac{\pi\, E\, I}{r^3} + \pi\, k\, r + \frac{\pi\, m\, r}{i^2}\right] a_i = Q_i \ldots (18a)$$

This equation reduces to—

$$\ddot{a}_i + p^2_i\, a_i = \frac{g}{\pi\, r\, A\, \gamma}\left(\frac{i^2}{1 + i^2}\right) Q_i \ldots\ldots\ldots\ldots\ldots (18b)$$

—the solution of which is

$$a_i = H_i \cos p_i\, t + F_i \sin p_i\, t + \frac{1}{p_i}\,\frac{g}{\pi\, r\, A\, \gamma}\,\frac{i^2}{1 + i^2}\int_0^{t_1} Q_i \sin p_i\,(t_1 - t)\, dt \ldots (19)$$

in which t_1 is a particular time at which the behavior is described. The constants of integration, H_i and F_i, depend on initial conditions of displacement and velocity of the ring and are taken here to be zero.

To study the case of steady-state forced vibration, a radial force P, concentrated at $\theta = 0$, is applied with simple harmonic oscillation of frequency ω and maximum intensity P_o so that $P = P_o \sin \omega\, t$. On a generalized coordinate:

$$\text{Increment of work} = P\,\Delta u = P\,\Delta a_i \cos i\,\theta = Q_i\,\Delta a_i \ldots\ldots (20)$$

The generalized force thus becomes

$$Q_i = P \cos i\,\theta = P_o \sin \omega\, t \cos i\,\theta\,\big|_{\theta=0} = P_o \sin \omega\, t \ldots\ldots (21)$$

Denoting the coefficients by $\alpha = \dfrac{g}{\pi\, r\, A\, \gamma}$, $\beta = \dfrac{g\, E\, I}{\pi\, r^3\, A\, \gamma}$, $i_a = \dfrac{i^2}{1 + i^2}$, and $i_b = \dfrac{i^2\,(1 - i^2)}{1 + i^2}$, and integrating the particular integral of Eq. 19 corresponding to the transient response, the generalized coordinates or amplitude functions corresponding to the steady-state forced vibration are given by

$$a_i = \frac{P_o\, \alpha\, i_a}{P_i\,(\omega^2 - p^2_i)}\,(\omega \sin p_i\, t_1 - p_i \sin \omega\, t_1) \ldots\ldots\ldots\ldots (22)$$

If η_i is equal to the ratio $\dfrac{\omega}{p_i}$ of forcing frequency to the frequency corresponding to any mode of response, then (by Eq. 15a) the radial displacements are given by

$$u_1 = P_o\, \alpha \sum_{i=1}^{\infty} \frac{i_a}{p^2_i\,(\eta^2_i - 1)}\,(\eta_i \sin p_i\, t - \sin \omega\, t) \cos i\,\theta \ldots\ldots (23a)$$

Similarly, the equation for bending moment is found from Eq. 5 to be

$$M_1 = P_o\, \beta \sum_{i=1}^{\infty} \frac{i_b}{p^2_i\,(\eta^2_i - 1)}\,(\eta_i \sin P_i\, t - \sin \omega\, t) \cos i\,\theta \ldots\ldots (23b)$$

The time variable, t_1, has been changed to t for convenience in notation. The significance of the subscript numeral for u and M is discussed subsequently.

Thus Eqs. 23 define the response of the elastically supported ring to a steady-state forced vibration. The frequencies of free vibration are given by Eq. 13.

Radial Displacements and Bending Moments Produced by Transient Loading.—Consider the response of the system to a radial impulse defined as a half-sine wave of duration τ and a maximum intensity P_o (Fig. 2). Following the procedure adopted by Mr. Hoppmann[17] for the case of an infinite bar, a harmonic force, P', of identical amplitude and frequency is superposed on P, as shown in Fig. 2. The P' force is initiated 180° out of phase with P, that is, at a time t equal to τ which is equal to π/ω.

The time variable for the force P' is denoted by t' and the following relationships obtain between the time coordinates t and t':

$$t' = t - \tau \dots\dots\dots\dots\dots\dots (24a)$$

and

$$t'_1 = t_1 - \tau \dots\dots\dots\dots\dots\dots (24b)$$

in which t_1 is the instant at which response is to be determined.

The response of the system to the force P' may be treated by transforming the time variable, so that an expression is obtained for the generalized coordinate a'_i similar to that for a_i given by Eq. 22.

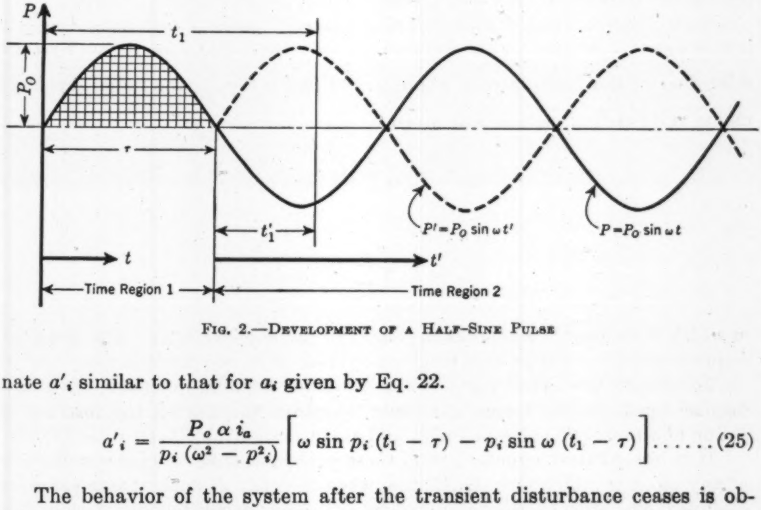

FIG. 2.—DEVELOPMENT OF A HALF-SINE PULSE

$$a'_i = \frac{P_o \, \alpha \, i_a}{p_i \, (\omega^2 - p^2_i)} \left[\omega \sin p_i \, (t_1 - \tau) - p_i \sin \omega \, (t_1 - \tau) \right] \dots\dots (25)$$

The behavior of the system after the transient disturbance ceases is obtained by superposing the steady-state forced vibration produced by P' upon that produced by P so that

$$a''_i = a_i + a'_i \dots\dots\dots\dots\dots\dots (26)$$

in which a''_i represents the new set of generalized coordinates corresponding to the transient force $P - P'$. By making use of Eqs. 22 and 25 and noting that $\cos \omega \tau = -1$ and $\sin \omega \tau = 0$, Eq. 27 results—

$$a''_i = \frac{P_o \, \alpha \, i_a \, \omega}{P_i \, (\omega^2 - p^2_i)} \left[(1 + \cos p_i \, \tau) \sin p_i \, t_1 - \sin p_i \, \tau \cos p_i \, t_1 \right] \dots (27)$$

The expressions corresponding to a''_i for radial displacement and bending moment, after convenient trigonometric simplification, reduce to

$$u_2 = P_o\,\alpha \sum_{i=1}^{\infty} \frac{2\,\eta_i \cos \frac{p_i\,\eta}{2}}{p^2{}_i\,(\eta^2{}_i - 1)}\, i_a \cos i\,\theta \sin p_i \left(t - \frac{\tau}{2}\right) \ldots\ldots\ldots (28a)$$

and

$$M_2 = P_o\,\beta \sum_{i=1}^{\infty} \frac{2\,\eta_i \cos \frac{p_i\,\tau}{2}}{p^2{}_i\,(\eta^2{}_i - 1)}\, i_b \cos i\,\theta \sin p_i \left(t - \frac{\tau}{2}\right) \ldots\ldots\ldots (28b)$$

Again, the time variable has been changed from t_1 to t for convenience in notation.

The response of the ring to a transient pulse is computed for $t < \tau$ by Eqs. 23 and for $t > \tau$ by Eqs. 28. The symbols for displacements (u) and bending moments (M) for the two time regions corresponding to $t < \tau$ and $t > \tau$ have been given the subscripts 1 and 2, respectively.

Static Loading Treated As a Limiting Case of Transient Loading.—Implicit in this dynamic analysis is the solution for the case of static loading. By consideration of the limiting case where $\omega \rightarrow 0$ and $\omega\,t \rightarrow \frac{\pi}{2}$, the radial displacements and bending moments as given by Eqs. 23 reduce to

$$u_s = P_o\,\alpha \sum_{i=1}^{\infty} \frac{i_a}{p^2{}_i} \cos i\,\theta \ldots\ldots\ldots\ldots\ldots\ldots (29a)$$

and

$$M_s = P_o\,\beta \sum_{i=1}^{\infty} \frac{i_b}{p^2{}_i} \cos i\,\theta \ldots\ldots\ldots\ldots\ldots\ldots (29b)$$

in which the subscript s denotes the behavior under static load. The transient response after the disturbance as given by Eqs. 28 is, of course, zero.

The Solution in Series Form.—Eqs. 23 define bending moments and radial displacements during forced harmonic vibration and during the interval of action of a transient half-sine pulse, and are in recognizable normal mode form.

It is immediately apparent from these equations that resonance will occur at any mode in which $\eta_i = 1$—that is, when $\omega = p_i$. If such unique cases are excluded, convergence can be proved by examining separately the various factors that appear in each series term, and by application of the ratio test of succeeding terms. Convergence is proved for the bending moments defined by Eq. 23*b*, except that the presence of the $(1 - i^2)$-term in the numerator of each series term retards convergence.

A similar test of Eqs. 28 (for free vibration after termination of a transient) also discloses convergence, even when $\eta_i = 1$.

Comparison of the Series Solution with a Closed-Form Solution for the Case of Static Load.—The differential equation of the elastically supported ring will very easily yield a closed-form solution with a static load concentrated at

$\theta = 0$, thus providing an opportunity to check both the accuracy of the derivation and the rate of convergence of the functions. With available closed-form solutions,[8] and the series of solutions of Eqs. 29, computations were made of the bending moments and radial displacements in a ring statically loaded at $\theta = 0$; the dimensions corresponded to the ring employed in later tests. The series solution was extended through ten terms; the numerical results of both calculations are given in Table 1. The locations of the stations are shown subsequently in Fig. 5.

EXPERIMENTAL ANALYSIS OF A RADIALLY SUPPORTED RING

Because of the simplifying assumptions necessary to render feasible a mathematical solution, a collateral experiment was performed to confirm the analysis. For this purpose, measurements were required of (1) the frequencies of various modes of flexural vibration, and (2) the response of the ring to a transient pulse of half-sine characteristic.

TABLE 1.—COMPARISON OF SERIES SOLUTION WITH CLOSED–FORM SOLUTION FOR STATIC BEHAVIOR OF RADIALLY SUPPORTED RING

ORIENTATION		RADIAL DISPLACEMENT, u, IN MILS		BENDING MOMENT, M, IN INCH–POUNDS	
Station	Degrees θ	Series solution	Closed-form solution	Series solution	Closed-form solution
1	0	8.911	8.98	−1.340	−1.70
A	4.7	8.745	...	−1.237	−1.24
B	23.7	5.687	...	0.060	0.002
D	61.6	−0.962	...	0.457	0.413
E	80.5	−2.316	...	0.218	0.290
11	94.7	−2.655	−2.43	...	...
J	175.3	−1.847	...	−0.120	−0.110
21	189.4	−1.863	−1.84	...	...

Ring parameters: $k = 6.8$, $m = 0$, $E = 29.2$, $\gamma = 0.292$, $P = 1$ at $\theta = 0$, $r = 12$ in., cross section = 1 in. by ⅛ in.

For a ring of given dimensions, the transient reponse is a function of duration and intensity of the pulse as well as of the elastic support of the ring, and therefore it was necessary to provide means for developing a half-sine impulse and for varying its duration and intensity.

The pulse generator used to deliver to the ring a transient pulse of controllable intensity and duration, and the instrument for measuring the applied load are briefly described in this section; the design and operation of all test apparatus have been discussed in considerable detail elsewhere.[19]

Description of the Ring and Elastic Support.—The ring selected for the test had a diameter of 24 in. and a rectangular cross section of 1 in. by 0.125 in; it was manufactured from flat bar stock by rolling a hoop and welding the two ends together. The material was cold-rolled steel with a modulus of elasticity of 29.2 × 10^6 lb per sq in.

---

[19] "A Theoretical and Experimental Investigation of a Dynamically Loaded Ring with Radial Elastic Support," by E. Wenk, Jr., *TMB Report No. 704*, David Taylor Model Basin, Washington, D. C., July, 1950.

For test purposes, only radial support was desired. Two different stiffnesses of elastic support for the ring were selected—one to increase the frequency of the first flexural mode of vibration of the unconstrained ring by a multiple of two, and the other to increase it by a multiple of four. The corresponding required values of k were computed to be 6.33 lb per in. per in. and 31.6 lb per in. per in., respectively. After a study of various systems to furnish elastic sup-

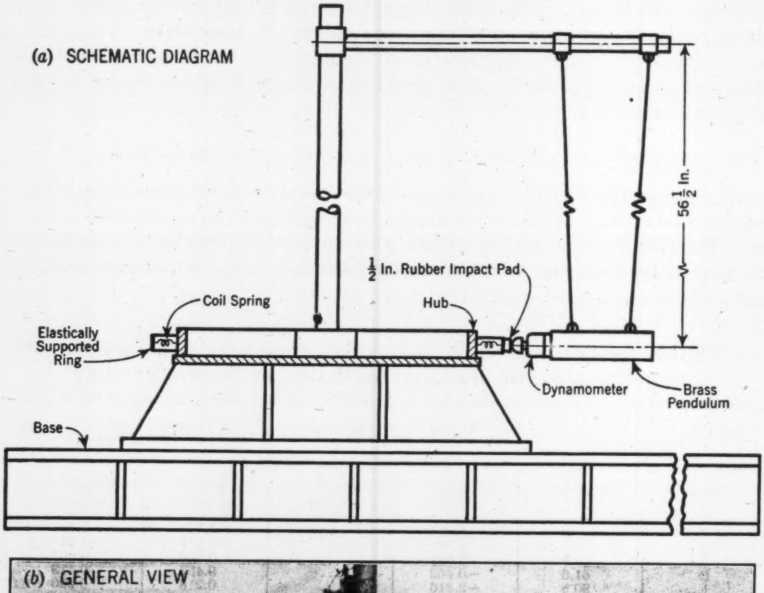
(a) SCHEMATIC DIAGRAM
$56\frac{1}{2}$ In.
$\frac{1}{2}$ In. Rubber Impact Pad
Coil Spring
Hub
Elastically Supported Ring
Dynamometer
Brass Pendulum
Base
(b) GENERAL VIEW

Fig. 3.—Apparatus for Direct Loading of the Ring by a Pendulum

port, coil springs were selected, oriented radially, and spaced at 2-in. intervals around the periphery. As shown in Fig. 3, the ring was positioned horizontally, and its weight was supported by the lateral stiffness of the springs. To provide elastic support with radial displacements in both directions, the springs were installed with uniform initial tension.

All coil springs were individually calibrated to check stiffness prior to installation, and the values of k actually obtained were 6.80 lb per in. per in. and 31.6 lb per in. per in. plus or minus 5%; these values have been employed in all calculations.

Excitation of Steady-State Forced Vibrations.—For the purpose of determining natural frequencies of flexural vibration before impact tests, a heavy-duty loud speaker element, driven by an audio-oscillator, was attached to the ring for excitation over a continuous frequency spectrum. Resonance was very easily detected by sounds emanating from the vibrating ring, as well as by visual observation of strain-gage signals; driving power was sufficient to excite the eighth flexural mode without difficulty.

Pulse Generator for Applying Transient Loads.—To deliver a radial impulse with a pure half-sine characteristic, frequent use has been made of a small sphere dropped onto the test specimen from a controlled height. Computations of the duration, intensity, and shape of the applied load were made by the application of the contract theory of H. Hertz.[20] This indirect estimate of the impact characteristic may introduce undesirable errors. Furthermore, a limit to the validity of the contact theory occurs when the specimen being struck has diminutive mass or stiffness compared with that of the striking sphere. Also implicit in the Hertz theory are short durations of contact compared with the fundamental period of ring vibration. Because longer durations of contact and greater accuracy were desired for this investigation, it was necessary to explore other methods of dynamically loading the ring.

From preliminary experiments, it was found that the desired half-sine pulse could be developed readily by striking the ring with a small body moving at constant velocity. Furthermore, the critical parameters—intensity and duration of impact—could be independently controlled as a function of the mass and the velocity of the moving impact body, and of the mass and the stiffness of the elastically supported ring. Approximate relationships defining the mechanics of impact were derived for use in the design of the apparatus and for control during the test.

These were as follows:

$$\tau = \pi \sqrt{\frac{u_s/P_o\,(W_r + W_p)}{g}} \qquad \text{(30}a\text{)}$$

$$P_o = \frac{u_s(\max)}{u_s/P_o} = \frac{2\,W_p\,\sqrt{W_p + W_r}}{(2\,W_p + W_r)\,\sqrt{Y\,g}}\,v \qquad \text{(30}b\text{)}$$

and

$$v = \sqrt{\frac{g}{L}}\,d \qquad \text{(30}c\text{)}$$

---

[20] "Über die Berechnung Fester Elastichen Köper," by H. Hertz, *Journal für die Reine und Angewandt Mathematik*, Vol. 92, 1881, pp. 155–170.

in which P_o is the maximum intensity of the pulse; W_r is the combined weight of the ring and coil spring system; W_p is the weight of the impact body; v is the terminal velocity of the impact body, at the time of impact; u_s is the static deflection of the ring at the point of application; L is the length of the pendulum; and d is the stroke of the pendulum.

TABLE 2.—COMPARISON BETWEEN OBSERVED AND COMPUTED CHARACTERISTICS OF TRANSIENT LOADING

Modulus of elastic foundation, k (lb per in. per in.) (1)	Computed unit static deflection, $\frac{u_s}{P_o}$ (in. per lb) (2)	Weight of pendulum W_p (lb) (3)	Impact pad during test (4)	Stroke of pendulum, d (in.) (5)	DURATION τ (SEC) Computed (6)	DURATION τ (SEC) Observed (7)	LOADING, P_o (LB) Computed (8)	LOADING, P_o (LB) Observed (9)
6.8	0.0090	5.2	yes	. . .	0.043	0.047	. . .	. . .
6.8	0.0090	2.2	yes	6	0.034	0.032	6.5	7.3
31.6	0.0021	2.2	no	. . .	0.016	0.016	. . .	. . .
31.6	0.0021	2.2	yes	18	0.016	0.023	41.3	39.7
31.6	0.0021	1.2[a]	no	. . .	0.014	0.012	. . .	. . .

[a] In this test a ball 2 in. in diameter was substituted for the brass impact body to confirm the loading relationships and to verify inapplicability of the Hertz contact theory in this experiment.

A comparison between observed characteristics and those computed by Eqs. 30, given in Table 2, shows agreement within 10% for the duration values and for the intensity values.

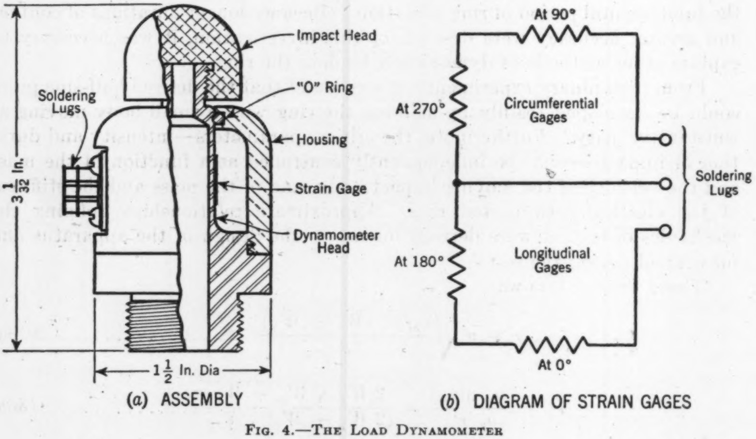

(a) ASSEMBLY (b) DIAGRAM OF STRAIN GAGES

FIG. 4.—THE LOAD DYNAMOMETER

For the tests of the ring, the impact body was designed as a pendulum composed of a cylindrical brass bar having a 2-in. diameter and a length sufficient to provide the mass required for a specified loading characteristic. The bar was suspended on phosphor-bronze wires as shown in Fig. 3.

The Load Dynamometer.—To measure the impact load, a special dynamometer was developed that permitted remote electrical recording of the load simultaneously with measurements of ring response. This dynamometer was designed as a short, cylindrical steel tube, $\frac{1}{2}$ in. in diameter, fitted with electrical strain gages oriented for maximum response to an axially applied load and minimum response to bending and torsion, as shown in Fig. 4. Steel for the dynamometer was SAE 4340, and the housing was of aluminum. Lucite, aluminum, and steel were all satisfactory materials for impact heads. Complete details are available in a TMB report.[19] The dynamometer was calibrated statically, and its response was linear and completely free of temperature instability. Its sensitivity, which depended on wall thickness was 2.37 micro-in. per in. per lb of load, permitting the measurement of forces as small as 5 lb. Its natural frequency which depended on the length was high enough to insure accurate detection of forces having durations as short as 0.01 milli-sec. Type A-B wire resistance strain gages were used in the dynomometer.

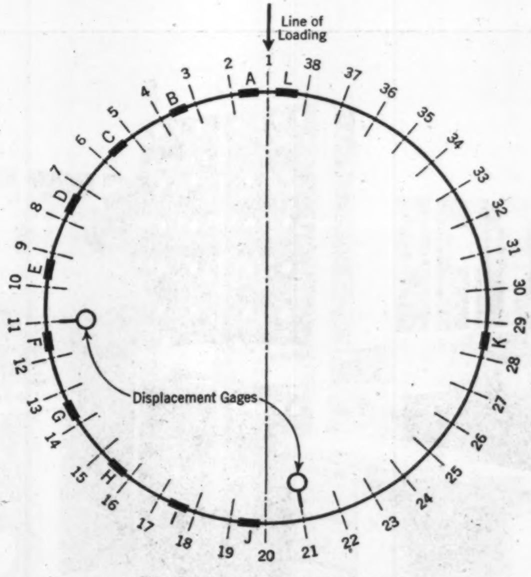

FIG. 5.—ARRANGEMENT OF GAGES

For these tests, a TMB type 1A strain indicator[21] was used with the dynamometer because of its great sensitivity. It operates on a carrier frequency of 2,200 cycles per sec and has a linear response from 0 cycles per sec to 200 cycles per sec, which was ample for these tests, in which the duration of load always exceeds 15 milli-sec.

---

[21] "A Carrier-Type Strain Indicator," by G. W. Cook, *TMB Report No. 565*, David Taylor Model Basin, Washington, D. C., November, 1946.

Instrumentation to Measure Strains and Displacements.—The response of the ring was considered definable in terms of bending moments and radial displacements, and instrumentation was provided for their measurement.

The bending moments were computed from strains measured by wire-resistance gages, mounted in pairs on both faces of the ring at each station so as to double the electrical output and insure temperature compensation. Gage locations are shown in Fig. 5, in which the numbers indicate spring locations and the letters indicate strain gages. Signals from the gages were carried through TMB type 1A amplifier equipment which included a calibration system.

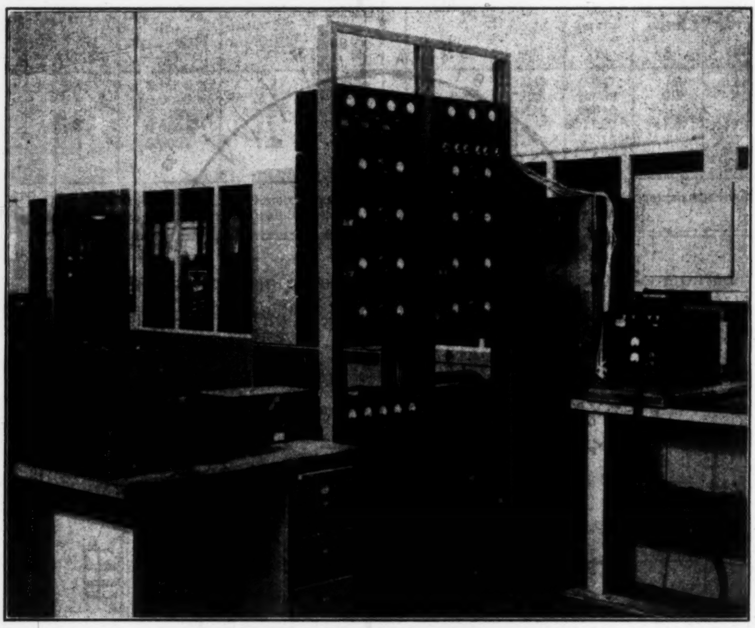

FIG. 6.—AUXILIARY ELECTRONIC AND RECORDING EQUIPMENT

Radial displacements were measured with linear variable differential transformer gages.[22] These gages were used with an auxiliary driving unit[23] that furnished 1,000-cycle alternating current to the gage and included sense discriminating and rectifier circuits that give a direct-current output (with a sense of direction) proportional to the measured displacement. The gages were calibrated after they were in place by means of a mechanical device with a dial indicator.

---

[22] "The Linear Variable Differential Transformer," by H. Schaevitz, *Proceedings*, Soc. for Experimental Stress Analysis, Vol. 4, No. 2, 1947, pp. 79–88.

[23] "Differential Transformer Unit Driver and Demodulator Type 10L," *TMB Electronic Instrument Instruction Manual*, David Taylor Model Basin, Washington, D. C., March, 1949.

A string oscillograph was used for recording amplified electrical signals from the various pickups. A 60-cycle-per-sec signal was also recorded as a timing trace. Fig. 6 shows (left to right) a cathode-ray oscilloscope with external sweep generator, relay racks containing one five-channel differential transformer driving unit (middle of left rack) and eight strain indicators with power supplies, and the string oscillograph (at far right). This constituted all the auxiliary equipment. Errors in measurement were estimated as shown in Table 3. The consistency of results indicated that some errors were compensating so as collectively to be on the order of 5%.

TABLE 3.—EXPERIMENTAL ERRORS, IN PERCENTAGES

Measurement	SYSTEMATIC			ACCIDENTAL	
	Gage factor or calibration device	Nonlinearity		Scaled Amplitude	
		Gage	Galvanometer	Response	Calibration
Strain	2	...	1	2	2
Displacement	0.5	6	1	3	3
Load	0.5	...	1	2	2

EXPERIMENTAL RESULTS AND COMPARISON WITH THEORY

Free Vibration.—Vibration tests were conducted using springs of two different stiffnesses. The frequencies of vibration corresponding to the states of resonance are given in Table 4, which also lists the frequencies as computed from Eq. 13 (Appendix II).

For all the flexural modes up to the seventh (that is, for $i > 1$) the agreement between the observed and computed values is excellent. Such a correlation with the use of two different values of elastic support was interpreted as reassuring evidence o the validity of the theory and also of the satisfactory mechanical arrangement of the supported ring. This was one of the most important results of the experiment.

TABLE 4.—FREQUENCIES OF FREE VIBRATION ON AN ELASTICALLY SUPPORTED RING, IN CYCLES PER SECOND

Mode, i	MODULUS OF ELASTIC SUPPORT, k (LB PER IN. PER IN.)			
	6.8		31.6	
	Computed[a]	Observed	Computed[a]	Observed
1 (Eq. 13)	28.74	37.5	62.0	73.8
1(a) (Eq. 32)	33.50	37.5	72.1	73.8
2	41.49	42.6	80.9	84.8
3	68.50	66.0	100.6	98.9
4	115.5	111.3	138.0	134.7
5	180.0	176.9	195.2	191.9
6	260.7	254.0	271.8	276.5
7	356.8	358.0	365.5	362.0
8	468.2	...	475.0	474.0

[a] Computations, except for $i = 1(a)$, were based on Eq. 13, with $m = 0$, $\gamma = 0.322$ lb per in.^{3}, and $E = 29.2 \times 10^6$ lb per in^2.

Rigid-Body Translation and the Presence of Tangential Constraint.—One obvious discrepancy in frequencies is noted in the case of rigid-body translation where $i = 1$ (Table 4). An alternate calculation of rigid-body translation of a radially supported ring was made by the following elementary procedure, with the assumption that all springs were combined as one of the constant K:

$$K = \sum k_n \cos \theta_n = 4\, k_n\, r \int_0^{\frac{\pi}{2}} \cos \theta \, d\theta = 4\, k_n\, r \text{..........} \quad (31)$$

and

$$p'_1 = \sqrt{\frac{K\, g}{2\, \pi\, r\, A\, \gamma}} = \sqrt{\frac{2}{\pi}} \sqrt{\frac{k_n\, g}{A\, \gamma}} \text{...............} \quad (32)$$

in which p'_1 is the circular frequency of rigid-body motion, and k_n is the stiffness constant associated with each individual spring that furnishes radial support.

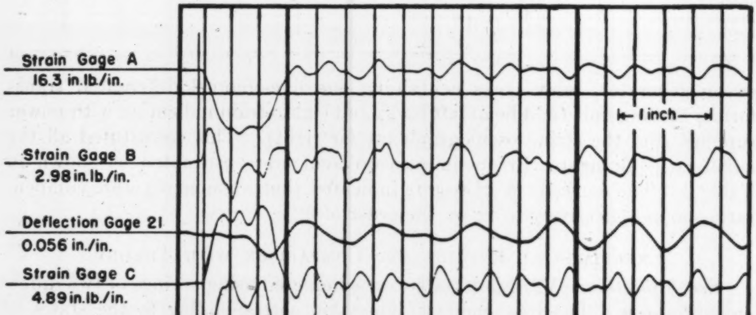

FIG. 7.—OSCILLOGRAM OF RING RESPONSE

This derivation of rigid-body motion takes into account the capacity of a radial spring to exert tangential constraint. As shown in Table 4, the frequency of vibration p'_1 as obtained with this computation is in better agreement with the observed frequency than with the value computed using Eq. 13. In this application of the theoretical analysis it was assumed that only radial elastic support could occur with radial displacement, but it is believed that during the test the coil springs, intended only for radial support, inadvertently offered tangential support. Thus the condition that $m = 0$ was not experimentally achieved, and the difference between computed and observed frequencies for the case of rigid-body motion is explained.

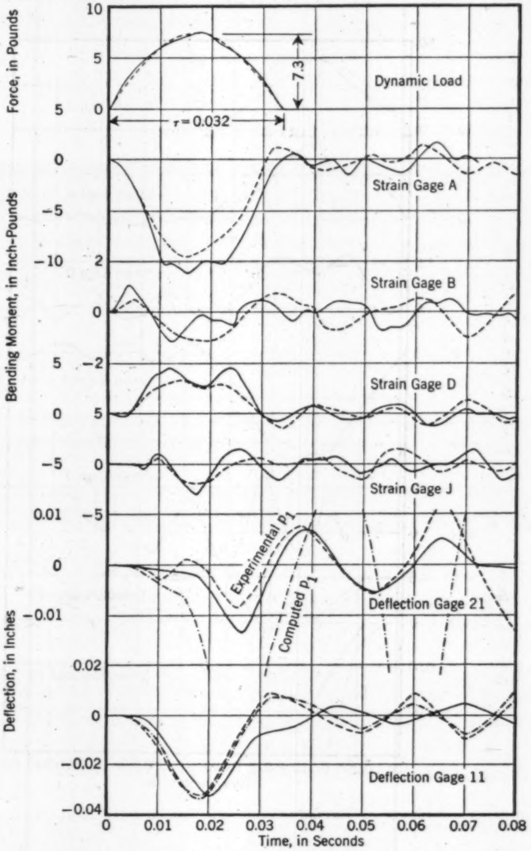

FIG. 8.—COMPARISON OF EXPERIMENTAL AND THEORETICAL RESULTS, $k = 6.8$

The frequency corresponding to rigid-body motion was of some significance in computing radial displacements but not in computing the bending moments because the term $i = 1$ does not appear in the moment equation.

Results of Tests with Transient Loading.—Transient loading of the ring was produced by dropping the pendulum of selected mass through a predetermined stroke. Simultaneously recorded were the indications of the load, strain at seven stations, deflections at two stations, and a 60-cycle-per-sec timing pulse. Scales were established for these various quantities by using the height of calibration steps recorded prior to each dynamic test. A typical oscillogram is shown in Fig. 7, corresponding to a test in which k was equal to 6.8 lb per in. per in. and the force was applied directly, using a 2.21-lb pendulum having a 6-in. stroke. Along the left margin, calibration scales are given for each gage. The variety in character of response at different stations is immediately apparent. At stations near the point of application of load (stations A and L), the bending moments during loading are similar in pattern to the loading pulse, whereas irregular undulations appear elsewhere. The delay in incidence of response at stations remote from the point of impact is also apparent.

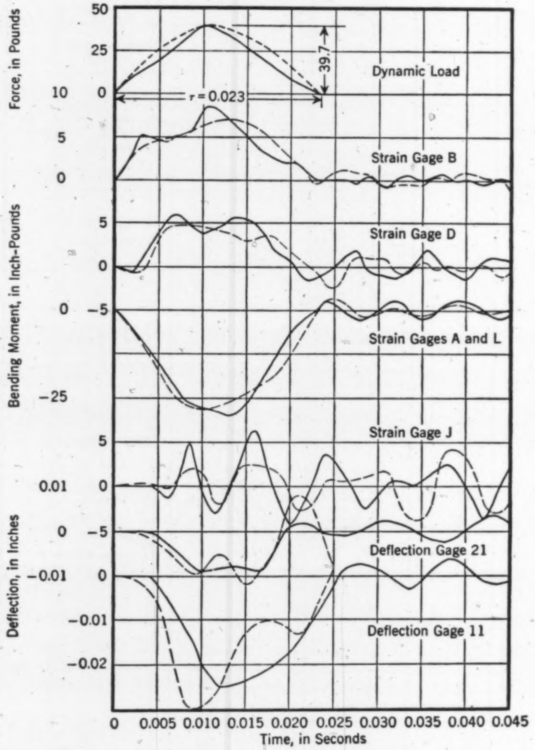

FIG. 9.—COMPARISON OF EXPERIMENTAL AND THEORETICAL RESULTS, $k = 31.6$

Displacements Produced by Transient Loading.—The computed theoretical responses were plotted separately in Figs. 10 and 11. (For computations and plotted curves, see Appendix II.) Aggregate values of the responses corresponding to $k = 6.8$ were plotted as broken lines in Fig. 8. Experimental results in the form of oscillogram records were plotted as solid lines for comparison. This was also done for the value of $k = 31.6$, as shown in Fig. 9.

It is apparent that agreement between the computed and observed behavior is found both during and after the transient disturbance. Not only are the intensities of response comparable, but similar patterns are found in both the experimental and computed curves. The extent of agreement both confirms the theory and demonstrates that experimental techniques were satisfactory.

Summary and Conclusions

Restatement of Important Equations of Response.—Equations have been derived for radial displacements and bending moments in a circular ring having elastic radial and tangential support and subjected to either steady-state forced vibration or transient loading. These equations are in the form of infinite series given by Eqs. 23 for steady-state forced vibration and for the period of action of a half-sine pulse, and by Eqs. 28 for free vibration subsequent to a transient pulse. Solutions for the limiting case of static loading are given by Eqs. 29.

The frequency of free vibration, including the effects of radial and tangential elastic support, is given by Eq. 13. It was found that the addition of moderate elastic tangential support influences primarily the radial displacements and the frequency of rigid-body translation.

Experimental Investigation.—An experiment has been performed with a ring of 24-in. diameter having a cross section 1 in. by 0.125 in. supported radially with thirty-eight coil springs and subjected to a radial impulse having as its time history a half-sine pulse. The intensity and duration of the pulse and the stiffness of the springs were varied, and the response was observed.

A special pulse generator and a dynamometer were developed for the purpose of applying an analytically described transient load to the ring, and for measuring this load.

Measurements were made of the frequencies of free vibration and of the bending moments and radial displacements produced by transient loading. The experimental errors present in the test were carefully investigated, and (on the basis of consistency of results) were of the order of 5%.

Agreement Between Theory and Experiment.—It was observed that, with steady-state forced vibrations, the frequencies of the various modes agreed with values computed by the theory within a small percentage, even up to the seventh flexural mode. Furthermore, the computed curves of displacement and bending moment as functions of time agreed reasonably well with experimental data.

Conclusions.—It is therefore concluded that (1) the experimental procedures in this test were satisfactory, (2) the simplifying assumptions of the analysis do not vitiate its accuracy, and (3) the mathematical analysis for an elastically supported ring is applicable to a ring in which the thickness is small in comparison to the diameter.

ACKNOWLEDGMENTS

The writer wishes to acknowledge the support and encouragement given this investigation by Capt. R. A. Hinners, USN, William R. Osgood, M.ASCE, formerly of the David W. Taylor Model Basin (Washington, D. C.), and Comdr. T. H. Frost, USNR, of the Bureau of Ships.

The writer also wishes to acknowledge the assistance of Margaret E. Duke, R. L. Hughes, and V. L. Mildenberg in making computations and in conducting the experiment.

Parts of this paper were abstracted from a dissertation submitted in partial fulfilment of the requirements for the degree of Doctor of Engineering at The Johns Hopkins University, Baltimore, Md. The thesis work was conducted under the guidance of Mr. Hoppmann and J. Trueman Thompson, M. ASCE.

APPENDIX I. NOMENCLATURE

The following letter symbols, adopted for use in the paper and its discussions, conform essentially to American Standard Letter Symbols for Structural Analysis (ASAZ10.8–1942) and to American Standard Letter Symbols for Mechanics of Solid Bodies (ASAZ10.3–1948) prepared by committees of the American Standards Association with Society representation, and approved by the Association in 1942 and 1948, respectively.

A = area of a cross section of the ring;
a_i = generalized coordinates;
B = normal force on a cross section of the ring;
C, D = constants;
d = stroke of the pendulum;
E = modulus of elasticity;
F_i, H_i = constants;
g = acceleration of gravity;
I = moment of inertia about the x-axis of a cross section of the ring;
i = integer designating the mode of vibration;
K = constant for combined springs of constant k_n which simulate the elastic foundation;
k = modulus of radial elastic foundation;
k_n = stiffness constant for individual springs that simulate elastic foundation;
L = length of the pendulum;
M = flexural couple acting about the x-axis on a cross section of the ring —positive if it increases the curvature of the ring;
m = modulus of tangential elastic foundation;
N = shear in a radial direction on a cross section of a ring;
P = external load (force per inch of circumference)—positive toward the center of the ring;
P_o = maximum value of P;
p = circular frequency of a vibrating ring;
p_i = circular frequency of a vibrating ring at mode i;
Q_i = generalized external force, measured positive toward the center;
r = radius of the ring;

s = circumference of the ring;
T = kinetic energy;
t = time variable;
t_1 = particular time at which behavior is stated;
U = characteristic radial displacement function;
u = radial displacement, measured positive toward the center of the ring;
V = potential energy;
v = terminal velocity of the body at the time of impact with the ring;
W = tangential displacement function;
W_p = weight of body striking ring;
W_r = combined weight of the ring and spring system;
w = tangential displacement of the ring, measured positive if counterclockwise;
α, β = constants;
Γ = time function;
γ = density;
δ = constant.
$\eta_i = \omega/p_i$;
θ = central angle of the ring, measured positive counterclockwise;
ν, μ = constants defined by Eqs. 9*a* and 9*b*;
τ = duration of the half-sine pulse;
ω = circular frequency of the external periodic exciting force $\omega = \pi/\tau$; and

---

APPENDIX II. NUMERICAL EXAMPLE OF SERIES SOLUTION WITH DYNAMIC LOADING

To evaluate the analysis, computations have been made of an example of the behavior of a radially supported ring with impact loading.

For these calculations, the parameters were assigned the values of those of the test ring: $P = 1$ lb, $r = 12$ in., $A = 0.125$ in.^{2}, $I = 162.8 \times 10^{-6}$ in.^{4}, $E = 29.2 \times 10^6$ lb per in.^{2}, $\gamma = 0.322$ lb per in.^{3}, $k = 6.8$ and 31.2 lb per in. per in., $m = 0$, and $\tau = 0.032$ sec and 0.23 sec.

It will be noted that the value chosen for density γ includes a correction for effective mass of the springs, a part of each of which may be expected to vibrate with the ring. This correction was applied as follows: The density of the cold-rolled steel was 0.292 lb per in.^{3} and the weight of the ring was 2.73 lb. The springs weighed 0.45 lb, of which 0.33 lb was assumed active. Thus, the effective density was increased by 11% to $\gamma = 0.322$. The frequencies p_i for both rigid-body motion and flexural vibration were computed from Eq. 13 and were listed in Table 4. A graphical demonstration of the first six modes of vibration is presented in Fig. 10, in which the arrows indicate the point and direction of application of the pulsating load.

By employing the values of τ (the duration of the half-sine pulse) actually observed during experiments, the response of the ring has been computed for the time intervals during and after the pulse. With the elastic support of modulus $k = 6.8$, τ was 0.032 sec, and with $k = 31.6$, τ was 0.023 sec.

The bending moments were computed at positions on the ring corresponding to four stations A, B, D, and J, and displacements were computed at stations 11

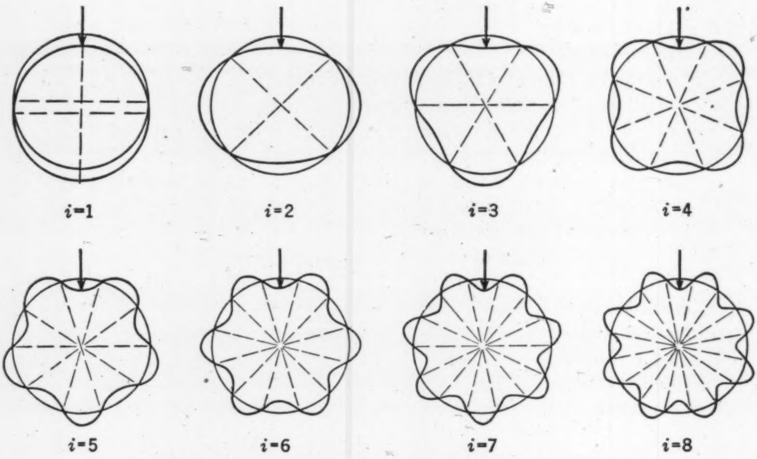
i=1
i=2
i=3
i=4
i=5
i=6
i=7
i=8

FIG. 10.—RING DEFORMATIONS FOR DIFFERENT MODES

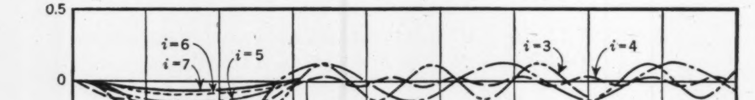

FIG. 11.—RESPONSE CURVES, $k = 6.8$ LB PER IN. PER IN.

and 21; also, experimental observations were made at all the stations whose locations were shown in Fig. 5. The computed response corresponding to contributions of each of the different modes up to $i = 7$ are plotted for two values of θ in Figs. 11 and 12; none were shown where the amplitude was less than 2% of the maximum value. Because the observed frequency of rigid-body vibra-

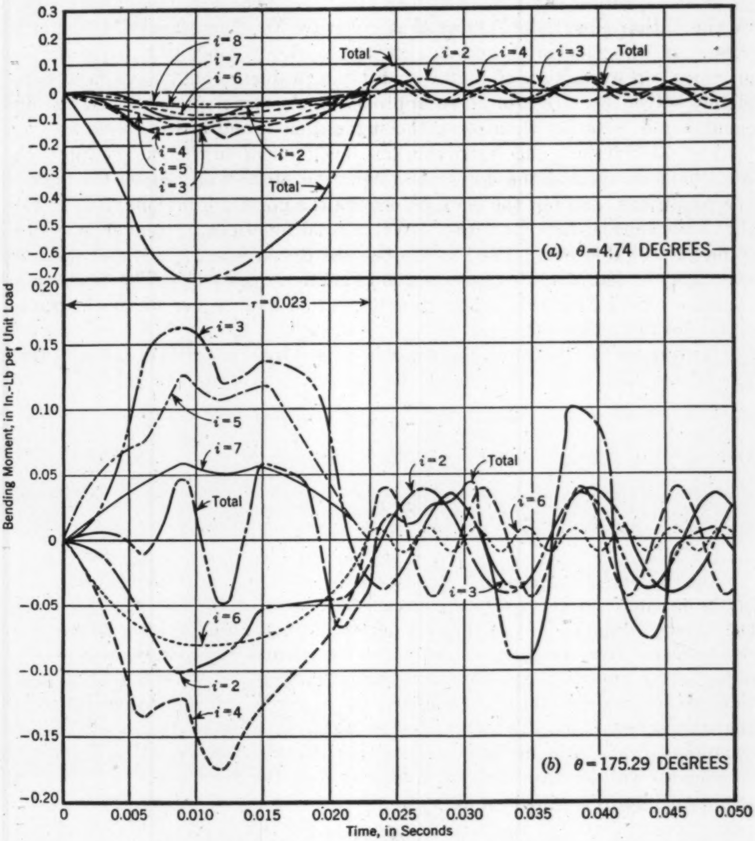

FIG. 12.—RESPONSE CURVES, $k = 31.6$ LB PER IN. PER IN.

tion was found to differ from the computed frequency as shown in Table 4, numerical calculations of response were made for $i = 1$, using observed values of p_1 as well as computed values.

The total response at any instant is the algebraic sum of the contributions from all modes, and plots of the aggregate responses are given in Figs. 8 and 9, where experimental and theoretical results are compared.

DISCUSSION

John C. Burgess,[24] J.M. ASCE.—The theoretical development presented by the author essentially follows that given by Mr. Timoshenko,[25] in that it uses both the elemental and energy approaches. Since the paper is not primarily an exposition of method, and the problem could have been completely solved by either of these approaches, the development seems unduly encumbered. Rather than using the suggestions found in the literature[26] for his normal functions and restricting his development to the energy approach, Mr. Wenk integrated the differential equation of motion. Since the boundary conditions, and not the load, determine the normal functions, Eq. 14 (for the homogeneous case) gives the correct normal functions. To avoid a change in method at this point, Eq. 15*a* can be substituted into Eq. 6*b*, and the load expanded in terms of the same normal function ($\cos i\,\theta$). The result is a combination of Eqs. 18*b* and 21 directly, rather than a use of the Lagrange equations of motion.

With regard to notation, confusion is caused by the choice of index in Eqs. 12 and 14. These equations might be more clear if written as follows:

$$u_\theta = \cdots = u_{\theta+2k\pi},\ k = 0, 1, 2, \cdots \qquad (33)$$

and

$$u = \sum_{i=1}^{\infty} (C_i \cos i\,\theta + D_i \sin i\,\theta) \cos (p_i\,t + \delta) \qquad (34)$$

Eqs. 22 and 23 represent "steady-state" solutions only for specific ratios of the forcing and natural frequencies. The solution that usually represents the steady state is one having no terms corresponding to free vibrations. Solutions for vibration problems in which the natural damping is small may be obtained by omitting explicit recognition of damping in the differential equation, and taking account of it implicitly by adjusting the complete solution for the undamped case. The reasoning is that, because of the small natural damping always present in a physical system, the free-vibration terms (or transients) will decrease with time, leaving only the forcing terms.[27] Eq. 22 might therefore be rewritten as

$$a_i = -\frac{P_0\,\alpha\,i_a}{\omega^2 - p^2_i} \sin \omega\,t_1 \qquad (35)$$

with Eqs. 23 changed accordingly.

---

[24] Research Asst., Stanford Univ., Stanford, Calif.

[25] "Vibration Problems in Engineering," by S. Timoshenko, D. Van Nostrand, Inc., New York, N. Y., 2d Ed., 1937, Chapter VI.

[26] *Ibid.*, pp. 408-409.

[27] *Ibid.*, p. 350.

Edward Wenk, Jr.,[28] J. M. ASCE.—The careful study undertaken and the suggestions offered by Mr. Burgess are most welcome. Either the elemental or the energy approaches to the problem under consideration would, of course, have been valid. In this type of problem, the choice is usually a matter of personal preference. Any detailed discussion of the merits of various approaches is not within the scope of the paper.

The primary considerations in using both methods were (1) to arrive at the frequency equation (Eq. 13) with as few arbitrary assumptions as possible, and (2) to develop solutions for response to impact in terms of the normal modes of vibration so as to facilitate the interpretation of any numerical results. The avoidance of the change in method proposed by Mr. Burgess could have been accomplished only by expansion of the load in terms of normal functions. For the concentrated load selected for analysis, this procedure introduces a form of the solution that is too cumbersome for numerical computation.

In suggesting that the free vibration terms of Eqs. 22 and 23 be omitted, Mr. Burgess follows the assumption, made by many theorists, that these vibrations are so rapidly "damped out" as to be unimportant. However, the effects of damping, at least with respect to the lower modes, are not likely to be this severe for the interval during which the impact load is acting on the structure. The importance of these free vibration terms is demonstrated in Figs. 11and 12 as deviations from the simple sine form, for $t<\tau$. Other more detailed illustrations of this effect are given elsewhere.[29] By neglecting these terms, as proposed by Mr. Burgess, agreement between the theoretical analysis and the experimental results would not have been as good. The loss in accuracy thus introduced could be avoided by using the complete form of the solution, as given in the paper, which in itself is not difficult to solve. Perhaps the importance of retaining these terms in impact problems, contrary to the usual practice,[27] should be emphasized.

---

[28] Head, Structures Div., Structural Mech. Lab., David Taylor Model Basin, Washington, D. C.

[29] "A Theoretical and Experimental Investigation of a Dynamically Loaded Ring with Radial Elastic Support," by E. Wenk, Jr., *TMB Report No. 704*, David Taylor Model Basin, Washington, D. C., July, 1950. pp. 18-21, Figs. 5 and 6.

AMERICAN SOCIETY OF CIVIL ENGINEERS
Founded November 5, 1852
TRANSACTIONS

Paper No. 2669

RAINFALL STUDIES USING RAIN-GAGE NETWORKS AND RADAR

BY H. E. HUDSON, JR.,[1] M. ASCE, G. E. STOUT,[2] AND F. A. HUFF[3]

WITH DISCUSSION BY VEN TE CHOW; AND H. E. HUDSON, JR., G. E. STOUT, AND F. A. HUFF

SYNOPSIS

The results of three years' work on concentrated rain-gage networks and on measurements of rainfall extent and intensity by means of radar are described. Thunderstorm rainfall is shown to be multicellular, so that the application of area-depth data is more complex than is usually assumed.

The orientation, duration, and path of storm cells are shown to have marked effects on area-depth curves for a given basin. Data on area-depth relationships are presented for networks having areas of 5.2 sq miles, 95 sq miles, and 280 sq miles.

The effects of gage density on mean rainfall errors are investigated. The heaviest storms were found to be associated with cold fronts.

The theory and development of radar for rainfall measurement are reviewed. Available methods of measuring rainfall by radar are discussed. Data collected in the study on radar signal strength and rainfall intensity are presented and analyzed using a new analytical approach. It is concluded that radar is able to depict rainfall extent better than rain gaging, and that radar can measure rainfall intensities as ably as do the rain-gage networks generally used.

INTRODUCTION

The standard rain gage that has provided engineers with limited rainfall data may be replaced in the age of electronics. Radar, a high-frequency radio device, that became a reality during World War II, has since been used

---

NOTE.—Published, essentially as printed here, in March, 1953, as *Proceedings-Separate No. 178*. Positions and titles given are those in effect when the paper or discussion was received for publication.

[1] Head, Eng. Subdivision, Illinois State Water Survey, Urbana, Ill.

[2] Meteorologist, Eng. Subdivision, Illinois State Water Survey, Urbana, Ill.

[3] Meteorologist, Eng. Subdivision, Illinois State Water Survey, Urbana, Ill.

by the Illinois Water Survey to detect, track, and measure quantitatively rainfall over the northern half of Illinois. The detection and tracking of rainfall were recognized by the military users of radar, but were not deeply explored by them for their application in the field of hydrometeorology.

Prior to the use of radar, rain-gaging techniques have not provided the accuracy desired by engineers and meteorologists. On the smaller watersheds under study in Illinois prior to 1948, gage densities of 15 sq miles per gage were used, but large differences of rainfall were encountered, especially when the precipitation occurred in the form of local showers or thunderstorms. In Illinois, the bulk of the year's precipitation comes from such storms.

When rainmaking was introduced in 1947, the Illinois Water Survey began to gather data on it. A corn company in El Paso, Ill., in cooperation with the Illinois Water Survey, organized a program to evaluate the possibilities of induced precipitation. A war surplus radar set was purchased by the cooperating group to be used for the tracking of both aircraft and rainfall during any rainmaking attempts. Gradually, although rainmaking did not seem to prove necessary in Illinois, the utility of the radar unit at El Paso for portraying the areal extent of the rainfall became evident. It was thought that, with this equipment, the quantity of rainfall could be determined, as well as the areal extent. Practically, it appeared that a radar scanning a radius of 70 miles or 15,000 sq miles could also determine the quantity of rainfall de-

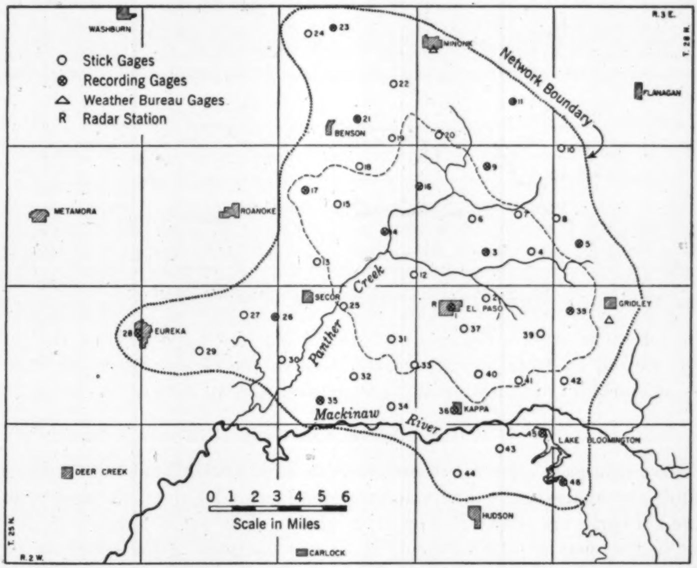
○ Stick Gages
⊗ Recording Gages
△ Weather Bureau Gages
R Radar Station
WASHBURN
MINONK
FLANAGAN
BENSON
METAMORA
ROANOKE
SECOR
EUREKA
EL PASO
GRIDLEY
KAPPA
LAKE BLOOMINGTON
DEER CREEK
HUDSON
CARLOCK
Network Boundary
Panther Creek
Mackinaw River
0 1 2 3 4 5 6
Scale in Miles
R.3E.
T.28N.
T.25N.
R.2W.
R
1
2
3
4
5
6
7
8
9
10
11
12
13
14
15
16
17
18
19
20
21
22
23
24
25
26
27
28
29
30
31
32
33
34
35
36
37
38
39
40
41
42
43
44
45
46

Fig. 1.—Panther Creek Rain-Gage Network (1948–1949)

posited in that area and thus supplement or even eliminate the standard rain gage.

As a check on the possibilities of the cloud-seeding work planned, a rain-gage network was installed in the vicinity of El Paso in the spring of 1948. This network, continued in revised form in 1949 and 1950, proved of little value for radar studies because of "ground clutter" appearing on the radar scope, caused by trees and structures close to the radar. However, the El Paso network did produce much thunderstorm rainfall data.

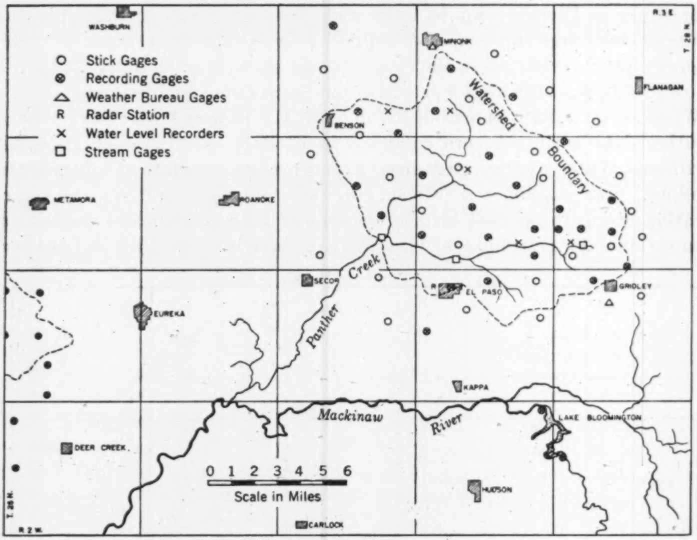
WASHBURN
○ Stick Gages
⊗ Recording Gages
△ Weather Bureau Gages
R Radar Station
× Water Level Recorders
□ Stream Gages
MINONK
FLANAGAN
R 3 E
T 28 N
BENSON
Watershed
Boundary
METAMORA
ROANOKE
Creek
Panther
SECOR
EL PASO
GRIDLEY
EUREKA
KAPPA
Mackinaw
River
LAKE BLOOMINGTON
DEER CREEK
0 1 2 3 4 5 6
Scale in Miles
HUDSON
CARLOCK
T. 25 N.
R 2 W.

FIG. 2.—PANTHER CREEK RAIN-GAGE NETWORK (1950)

GAGE NETWORKS USED

Three rain-gage networks were available from 1948 through 1950 to make possible the analysis of the character of the storms involved in these studies. These networks are shown in Figs. 1, 2, and 3. The network covering 280 sq miles in the vicinity of El Paso (Fig. 1) was initiated in the spring of 1948. It was reorganized at the close of the 1949 thunderstorm season. Beginning in the spring of 1950, the Panther Creek network, as shown in Fig. 2, having an area of 95 sq miles, has been operated in conjunction with a detailed hydrologic study on that watershed located north of El Paso. The edge of the Farm Creek (a tributary of the Illinois River) network appears on the extreme left of Fig. 2. To obtain more rainfall data for this type of watershed, a different area of the same size and shape was chosen from the 280-sq-mile network in the area of maximum gage density. No distinct topographic or climatic features exist in the region. The superimposed area is shown by the dashed outline in Fig. 1. The network of 5.2 sq miles, located on Boneyard Creek, at Champaign-Urbana, Ill., is shown in Fig. 3. This network has been operated since the fall of 1948 in cooperation with the Civil Engineering Department of the University of Illinois, at Urbana.

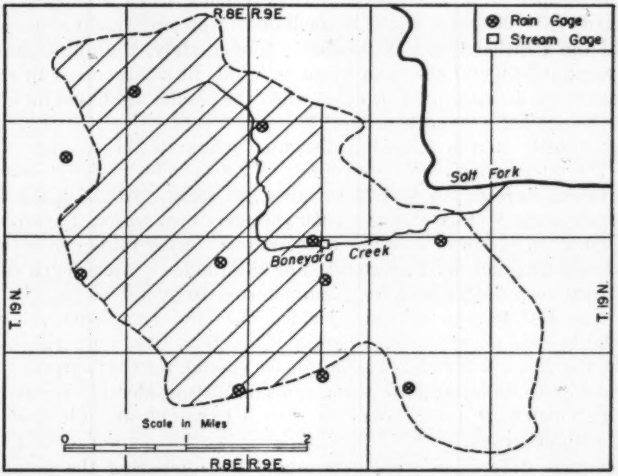

Fig. 3.—Boneyard Creek Rain-Gage Network, Urbana-Champaign, Ill.

The area of 280 sq miles, gaged in 1948–1949, contained a total of 29 stick gages and 17 recording gages, or an average of 1 gage per 6.1 sq miles. Within this area was the watershed of 95 sq miles that had 14 stick gages and 6 recording gages during the 1948 and 1949 seasons, corresponding to an average of 1 gage per 4.75 sq miles. During the 1950 thunderstorm season, 30 stick gages and 26 recording gages were located on, or in, the vicinity of the watershed of 95 sq miles. The Boneyard watershed included 7 recording gages, or an average of 1 gage per 0.7 sq mile.

AREA-DEPTH RELATIONSHIPS

For many engineering design purposes, a detailed knowledge of duration-area-depth relationships for small areas is essential. Few published data are available for areal units of less than 100 sq miles. Rain-gage networks of sufficient density to permit area-depth extrapolations (with reasonable accuracy) to such small areas seldom have existed. Rainfall data, collected on three networks of 5.2 sq miles, 95 sq miles, and 280 sq miles in central Illinois, have been analyzed in an attempt to furnish some concrete information on the characteristics of the area-depth curve for small watersheds in thunderstorm rainfall. The present analysis is concerned chiefly with the basin having an area of 95 sq miles, for which three years' data are available.

More limited data for the areas of 280 sq miles and 5.2 sq miles have been used to supplement this study. Only data for the thunderstorm season, between May and September, have been used in the analysis.

Effect of Gage Density on Area-Depth Curve.—During the summer of 1950, 40 gages were located on, or within, the boundaries of the 95-sq-mile Panther Creek watershed. For the 1948 and 1949 seasons, when a much larger area was gaged, only 20 gages could be included in an area having the size and shape of the Panther Creek watershed. Immediately, the question arose as to the comparability of the data—that is, what differences exist in the area-depth curve for an area of 95 sq miles when the results are based on a 40-gage network as against a 20-gage network?

Gage density in the following discourse refers to the average area per gage. The 40-gage network corresponds to 2.4 sq miles per gage and the 20-gage network corresponds to 4.75 sq miles per gage. To check the effect of gage density, the 8 storms of the 1950 thunderstorm season, having an areal mean rainfall in excess of 0.50 in., were analyzed using rain-gage networks of 40 gages and 20 gages on the watershed of 95 sq miles. Area-depth curves for each storm were determined by planimetering isohyetal maps. It was assumed that the 40-gage network yielded the true area-depth relationship. Interpolation was not extended to areas of less than 10 sq miles because it was felt that the 20-gage network was not dense enough for this purpose. (There is a tendency to underestimate the mean rainfall considerably for small units of area in which gage densities are insufficient to sample small intense cores of rainfall with accuracy.)

Percentage differences were determined by comparing the points representing areas of 10 sq miles, 25 sq miles, 50 sq miles, 75 sq miles, and 95 sq miles on area-depth curves for 20-gage networks and 40-gage networks. Although the 20-gage network did not provide isohyetal patterns of such fine detail, the variation in the constructed area-depth curves was less than 7% in each of the 8 storms studied. The mean variation was 1.2%. It was felt, therefore, that the 1948–1949 network of 20 gages per 95 sq miles (4.75 sq miles per gage) could be used for analysis with confidence in the results.

Because the 20-gage network seemed to give area-depth curves very close to the true curve, it was decided to investigate further the effect of gage density on the area-depth curve obtained. To do this, area-depth curves obtained from gage densities of 4.75 sq miles per gage, 9.5 sq miles per gage, and 19.5 sq miles per gage (20 gages, 10 gages, and 5 gages) for the 15 heaviest storms during the 1948–1950 period were compared. The results for densities of 9.5 sq miles per gage and 19.5 sq miles per gage were expressed as percentage differences from those obtained with the density of 4.75 sq miles per gage. The mean errors for the density of 9.5 sq miles per gage ranged from 3% to 6%; for the density of 19.5 sq miles per gage, they were from 4% to 7%. The results indicated, as would be expected, an increasing error with decreasing gage density, the error being greatest at the smaller units of area. Departures from the true mean were predominantly negative, demonstrating the tendency of the sparser networks to miss or underestimate the heavier cores of rainfall.

The 5-gage network was not extrapolated to areas of less than 25 sq miles because it correponds to only 1 gage per 19.5 sq miles.

Thunderstorm Rainfall.—H. R. Byers and R. R. Braham, Jr.,[4] have shown that, as a result of radar-thunderstorm studies in Ohio and Florida, the thunderstorm is normally of a multicellular nature. Usually a thunderstorm consists of three or more adjacent cells, each manifesting itself in the surface rainfall pattern. They found that single, isolated thunderstorm cells were comparatively rare and usually weak. The duration of moderate or heavy rain from a single cell of a storm was found to vary from a few minutes to almost an hour, depending upon the life of the cell.

The thunderstorm squalls preceding cold fronts, probably the most frequent source of heavy rainfall in the Panther Creek region and in much of the midwest, were found, in the writers' study, to be composed most frequently of several squall lines comprising a squall zone rather than a single line of thunderstorms. This discovery leads to the conclusion that the surface rainfall pattern is dependent on several factors—including the number, size, and longevity of the individual cells affecting the area, and their distribution of showers within the area of interest.

In the thunderstorm studies, described by Messrs. Byers and Braham,[4] it was found that these cells may vary from 1 mile to more than 30 miles in diameter. Consequently, these factors will be reflected in the area-depth curve. The complexity of the rainfall pattern will tend to increase with area and decrease with time; that is, the number of cores or centers of heavy rainfall associated with the individual cells will tend to increase with the area, especially with squall line conditions. The increasing number of cells crossing an area with progressing time will usually tend to make the total storm pattern more uniform because of the overlapping effect. For relatively large basins and short storm durations, the area-depth curve will often reflect a composite effect of several rainfall cores or centers within the area, rather than a pattern of high rainfall at one place decreasing progressively outward from the single center.

Some Factors Affecting Area-Depth Relationships on Individual Basins

The area-depth curve will be influenced by the size and shape of the basin, the orientation of the storm with respect to the basin, the topography, the duration of the storm, and the type of storm. The Panther Creek studies have been concentrated chiefly on the summer thunderstorm type of rainfall over this watershed, which is comprised of relatively flat terrain with no distinct topographic features. Therefore, for this investigation, three variables—the size and the shape of the basin, the general type of the storm, and the topography—are fixed. Efforts have been made to study the effects of storm duration and storm location with respect to the basin.

With respect to storm location, it may be stated that a given storm, consisting of a single rainfall core or storm center traveling along the minor axis of a rectangular basin, will produce an area-depth curve of greater slope than the same storm having its center coinciding with the major axis of the basin; that is, the range of rainfall values from the lower end to the upper end of the curve will be greater. Similarly, when the storm axis passes near, or outside, the basin boundary, the slope will be greater than when the storm center passes through, or near, the basin center.

---

[4] "The Thunderstorm," Report of the Thunderstorm Project (A joint project of the U.S.A.F., U. S. Navy, National Advisory Committee for Aeronautics, U. S. Weather Bureau), Superintendent of Documents, Washington, D. C., June, 1949.

Area-Depth Analysis, Watershed of 95 Sq Miles, 1948–1950.—During the 1948–1950 period, 28 storms having mean rainfalls in excess of 0.50 in. for the watershed of 95 sq miles were used in the study. Of these, 14 had the axis of the rainfall core passing near the center of the basin; the remaining 14 passed near the boundary of the basin. As would be expected, the heaviest areal rainfall occurred with those storms having their area of heaviest rainfall near the basin center. Because these are the storm types producing the heaviest rainfall for a given area, they have been analyzed separately. The results should be quite typical of area-depth relationships in heavy rainstorms.

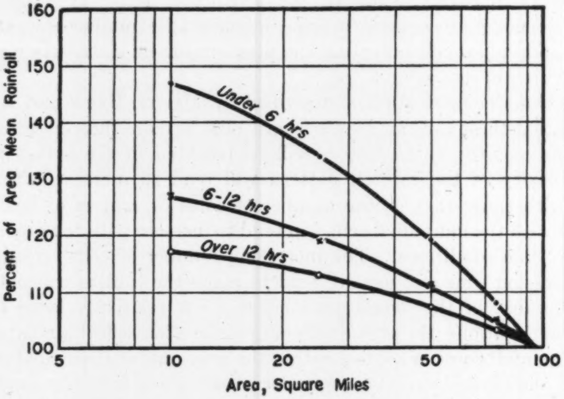

Fig. 4.—Percentage-Area-Depth Curves for 3 Storm Durations (1948–1950) Data

Percentage area-depth relationships for these 14 storms were listed in three classes, corresponding to rainfall durations of more than 12 hr (3 storms), 6 hr to 12 hr (5 storms), and less than 6 hr (6 storms). Fig. 4 shows mean-percentage area-depth curves for each of the duration classifications. Partial storm periods for several of the heavier storms have been used in the analysis because they comprised unit storms within the over-all storm period representing the passage of squall lines or zones. A further breakdown, involving the orientation of storm cores with respect to the basin axis, was not possible with the limited data. However, in these cases, it should be a minor factor because the basin is not of an elongated nature, being roughly equivalent to a rectangle of 9 units by 11 units.

Fig. 4 indicates that the slope of the area-depth curve tends to decrease considerably as the rainfall duration increases. This tendency is most pronounced when proceeding from the relatively short duration (from 1 hr to 5 hr) to moderate durations (from 6 hr to 12 hr). Variations between the percentage area-depth curves for individual storms became smaller as the rainfall duration increased. For a specific duration, the variations between individual storms were less for large areas than for small areas. Considering the nature of thunderstorm rainfall, these indicated tendencies are quite logical. As mentioned previously, the thunderstorm is multicellular in nature, so that as storm duration increases and as the number of individual cells crossing a given area increases, there will be a greater tendency toward uniform areal rainfall.

Fig. 5 shows a comparison between 14 storms with storm axes located near the boundary of the 95-sq-mile watershed, with 6 storms having their core of heaviest rainfall near the central part of the basin. A comparison could be made only for storms having durations of less than 6 hr because all 14 boundary storms fell into this classification. As would be expected, the slope of the boundary storm curve is greater, as a rule. With respect to a basin, the rainfall gradient decreases mostly in one direction in the boundary storms. As a result, the mean rainfall for the total area decreases considerably compared to that of the same storm passing near the basin center. However, the maximum rainfall remains as great, or nearly so, as when the storm core is well within the watershed boundaries. This condition, of course, results in a greater slope for the area-depth curve in the case of boundary storms.

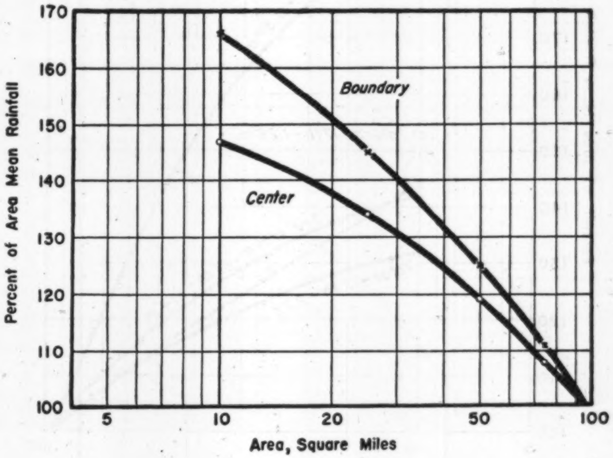

FIG. 5.—STORM CENTER LOCATION AND AREA-DEPTH DISTRIBUTION

The limited data did not permit a thorough analysis of the possible effects of the magnitude of storm rainfall on the slope of the area-depth curve. The Weather Bureau (United States Department of Commerce) study[5] of 38 6-hr partial storm periods found no evidence of any significant change in slope with increased mean rainfall in these 6-hr periods. The 14 storms examined in the writers' study give similar indications. In comparing the 3 storms of greater than 12-hr duration, no significant differences in percentage values are evident, although mean rainfall varies from 2.57 in. to 5.22 in. Similarly, for the 5 storms of a duration of from 6 hr to 12 hr, there seems to be no significant correlation with mean rainfall, although amounts range from 1.14 in. to 2.77 in. A similar conclusion may be drawn from an examination of the storms of less than a duration of 6 hr. Rainfall duration appears to be more important than total thunderstorm rainfall in determining the slope of the area-depth curve.

---

[5] "Thunderstorm Rainfall," *Hydrometeorological Report No. 5*, U. S. Dept. of Commerce, Weather Bureau, and U. S. War Department, Corps of Engrs., Waterways Experiment Station, Vicksburg, Miss., 1947.

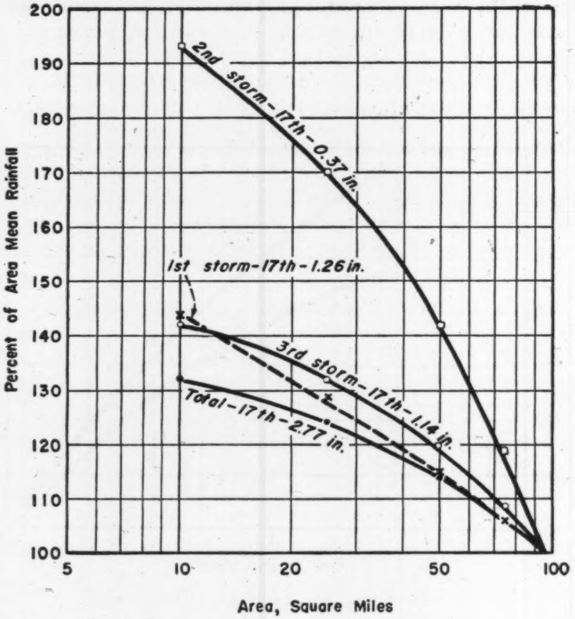

FIG. 6.—PERCENTAGE AREA-DEPTH COMPARISONS FOR PARTIAL STORM PERIODS AND FOR THE TOTAL STORM, JULY 17, 1950

The tendency for the area-depth curve to decrease in slope, with increasing duration of rainfall, is further illustrated in Fig. 6, in which percentage area-depth relationships for 3-hr intervals in the storm of July 17, 1950, are compared with the same values for the total 9-hr storm period. This storm consisted of two 3-hr periods of relatively heavy rainfall separated by a 3-hr period of relatively light precipitation. In connection with Fig. 6, it is interesting to note that the 3-hr period of light rainfall having the greatest slope showed the heaviest rainfall amounts near the edge of the watershed, but the axis of the rainfall core in the 2 heavy storms passed well within the watershed boundaries.

Comparison of Watersheds of 5.2 Sq Miles, 95 Sq Miles, and 280 Sq Miles.—A comparison of the area-depth data for the 95-sq-mile watershed was made with those collected from the Boneyard watershed of 5.2 sq miles and the 280-sq-mile Panther Creek area. A comparison of the three areas was possible only for storms of a duration of less than 6 hr because insufficient data for the Boneyard watershed were available for longer durations. Fig. 7 shows this comparison for storms whose heaviest rainfall was located near the central part of the watersheds.

From Fig. 7, the tendency for storm rainfall variability to increase with increasing basin area is apparent. In referring to Fig. 7, it should be remembered that the average relationships for the watershed of 5.2 sq miles are not strictly representative of the maximum relationships for areas of 5 sq miles in the larger watersheds. With the increasing basin area, the number of thunderstorm cells, and, consequently, the number of intense cores of rainfall, tend to increase. This condition results in a trend toward lesser variability in the area-depth curve within the very small areas of heaviest rainfall in the larger watersheds.

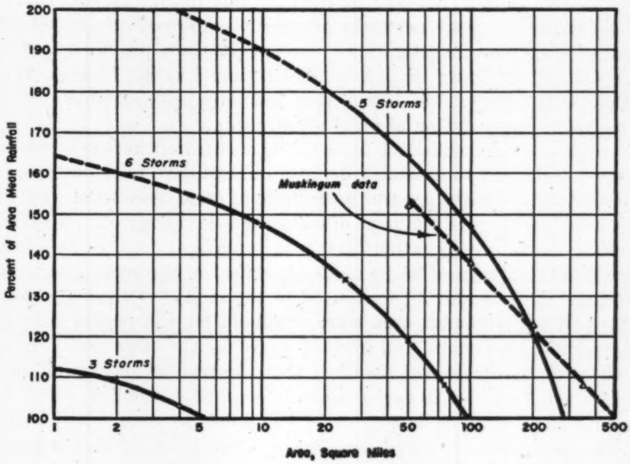

Fig. 7.—Percentage Area-Depth Curves for 3 Networks in Illinois

The dashed parts of the curves in Fig. 7 represent estimated relationships. Because the three curves for the individual watersheds are strikingly similar in shape, the curves for the basins of 5.2 sq miles and of 95 sq miles were used as guides in extrapolating the curve for the basin of 280 sq miles. This extrapolation was done by plotting the necessary parts of the two lower curves at the upper end of the curve for the area of 280 sq miles. Similarly, the curve for the area of 5.2 sq miles was used as a guide in extrapolating the 95-sq-mile curve. The results are presented as an approximation of the actual relationships, in the absence of more concrete data. As stated before, the direct application of the actual percentage values for a small watershed to the upper end of a curve for a larger watershed would tend to produce erroneously high values. As an example, the ratio of the rainfall on 1 sq mile to the areal mean rainfall determined for the 95-sq-mile basin would be 1.71 by this method, but that obtained by the extrapolation method was 1.64.

The Muskingum data in Fig. 7 represent average values obtained from an analysis of 38 storms on the Muskingum Basin, in Ohio, by the Hydrometeorological Section of the Weather Bureau.[6]

Relations Between Gage Density and Mean Rainfall

It is important to know the reliability of mean rainfall values obtained from rain-gage networks of varying density which may be used for the determination of basin rainfall-runoff relationships. This fact is especially true for small watersheds with thunderstorm rainfall where only limited information is available because the rain-gage networks ordinarily employed do not provide sufficient data for such an investigation. Except for those provided by P. Light,[5] A.M. ASCE, W. B. Langbein,[6] A.M. ASCE, and Ray K. Linsley, M. ASCE, and Max. A. Kohler,[7] A.M. ASCE, very few data are available on the errors involved in the computation of areal mean rainfall.

Although the data collected from the concentrated networks used in this study are too limited to establish definite quantitative relationships, it is believed that they show the general magnitude of error associated with different gage densities for the size and type of watersheds investigated. The investigation is being continued to gather further information.

Data from the basin of 95 sq miles, described in the section on area-depth relationships (Figs. 1 and 2), were used in the study. Observations from 20 gages on this experimental area were available for the period between May and September, 1948–1949, and from 40 gages for the same period in 1950.

Analysis of Data.—It was assumed that the true mean rainfall was determined by the network of 20 gages on the 95-sq-mile watershed. This network corresponds to an average density of 4.75 sq miles per gage. Although, necessarily, the assumption involved some error, it was believed that it would be of small magnitude. As a partial check on the assumption, a comparison of results from 40-gage networks and 20-gage networks on the 95-sq-mile watershed for 1950 was made. This comparison revealed that maximum differences obtained from the two networks were less than 0.06 in.

Mean Error as Related to Gage Density.—The reliability of mean rainfall, as determined from networks of 10 gages, 5 gages, 3 gages, and 1 gage on the 95-sq-mile watershed, was investigated next. These networks correspond to average densitites of 9.5 sq miles per gage, 19.5 sq miles per gage, 32 sq miles per gage, and 95 sq miles per gage. Stations were chosen to give as uniform a network as possible in each case. In places where only one gage was used, it was the one most centrally located. Mean rainfall was classified into four intervals of from 0.01 in. to 0.20 in., from 0.21 in. to 0.50 in., from 0.51 in. to 1.00 in., and from 1.01 in. to 3.00 in., to determine the effect of storm magnitude on the error involved with each rain-gage network. The error in each case was determined from the difference between the 20-gage mean rainfall and that obtained from the network in question.

---

[6] "Error in Computation of Mean Areal Precipitation," by W. B. Langbein, U. S. Geological Survey, Superintendent of Documents, Washington, D. C., August, 1946.

[7] "Variations in Storm Rainfall over Small Areas," by Ray K. Linsley and Max A. Kohler, *Transactions*, Am. Geophysical Union, Vol. 32, No. 2, April, 1951, pp. 245–250.

The results are shown in Fig. 8. It can be seen that, although the absolute magnitude of the error (in inches) increases with increased mean rainfall, it is proportionally smaller with the heavier storms. Based on an average for a number of storms, the mean error is relatively small, except for the heavier storms with the single gage. For general climatic purposes, therefore, it appears that concentrated networks, such as those employed in the 3-yr period studied, are not justifiable.

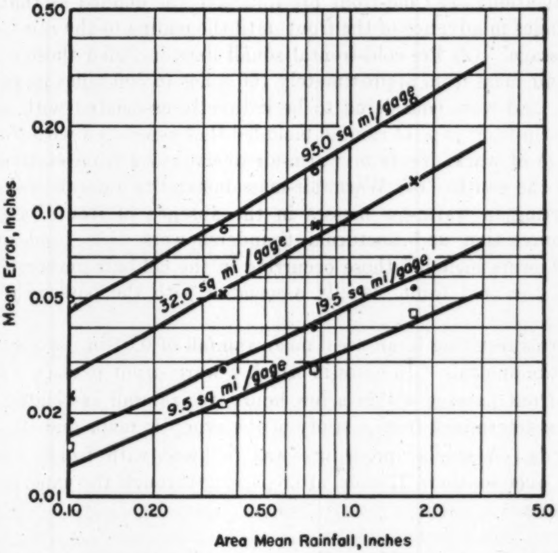

FIG. 8.—EFFECT OF GAGE DENSITY AND MEAN STORM RAINFALL ON MEAN ERROR, AREA OF 95 SQ MILES, 1948–1950

Error as Related to Gage Density, on a Monthly and Seasonal Basis.—Analysis was made of the errors for different gage densities by storms, on a monthly and seasonal basis. The data indicate that, for monthly rainfall, a network having 1 gage per 95 sq miles gave a mean error of less than 10% during two thirds of the months, especially during the months having the heavier areal rainfalls. Because the greatest errors would ordinarily occur during the thunderstorm season, it seems that a network of 1 gage per 100 sq miles should be sufficient for the determination of monthly or seasonal mean rainfall for most purposes. Monthly and seasonal accuracy improve only slightly with increasing gage density. The errors were predominantly negative, illustrating the tendency of the less dense networks to miss, or underestimate, areas of most intense rainfall. This fact, of course, is also true for storm rainfall.

Storm Type and Resultant Rainfall

Areal Mean Rainfall as Related to Storm Type.—The frequency distribution of areal mean rainfall by storm types over the 95-sq-mile basin for the thunderstorm seasons 1948–1950 was investigated. Storm precipitation was divided into five classes for this study. These classes included rainfall occurring with cold fronts, with pre-cold-frontal squall lines, with warm fronts or warm-air overrunning, with instability of warm-air masses, and with instability of cold-air masses.

The storm type associated with each rainfall occurrence was determined from the daily synoptic maps of the Weather Bureau. For the purpose of this investigation: (1) Cold-front precipitation was defined as that occurring from 100 miles in advance of the front until the ending of the rainfall with the frontal passage. (2) Pre-cold-frontal squall lines included those occurring in the warm-air mass from approximately 100 miles to 300 miles in advance of a cold front, and were considered to be indirectly associated with cold fronts. (3) The warm-front type of rainfall included that associated with the approach and passage of warm fronts or warm-air overrunning from stationary fronts located to the south. (4) Warm-air-mass instability rainfall was defined as that occurring in warm-air masses in the absence of fronts, and included thermal convection and nocturnal thundershowers. (5) Cold-air-mass instability showers included those occurring in the cold-air mass well after the passage of the cold front, usually associated with the passage of a trough aloft.

All storms resulting in an areal mean rainfall of 0.01 in., or more, were included in the analysis. In cases in which a warm-front passage was followed by a cold-front passage within a few hours, the rainfall associated with each system was determined from a study of the synoptic maps and the recording-gage records. A similar procedure was followed with fronts that became stationary over southern Illinois, after passing through the experimental area as cold fronts.

TABLE 1.—Areal Mean Rainfall as Related to Storm Type

Storm type	No. of storms	Percentage of total storms	Rainfall amount, in inches	% of total areal rainfall	Maximum individual storm, in inches
Cold front	49	38	18.66	40	2.02
Pre-cold-frontal squall line	16	12	12.42	26	2.77
Warm front	30	23	10.74	23	2.56
Instability of:					
Warm-air masses	30	23	5.28	11	0.76
Cold-air masses	5	4	0.12	0.3	0.05
Cold front plus squall line	65	50	21.08	66	

In Table 1, a comparison between storm type and areal mean rainfall has been summarized. As should be expected in the region in which the experimental area lies, precipitation was most frequently associated with cold fronts during the thunderstorm season. Similarly, the largest proportion of the areal mean rainfall was either directly, or indirectly, associated with cold fronts. During the 3-yr period, cold fronts and pre-cold-frontal squall lines accounted for 50% of the total storms and 66% of the total rainfall.

Perhaps more significant to the hydrologist and meteorologist is the frequency distribution of the heavier areal mean rainfalls by storm type. Table 2 shows a comparison between storm type and areal mean rainfalls of 0.50 in. or more. It can be seen that cold-frontal squall lines and pre-cold-frontal squall lines were again dominant, accounting for 80% of the storm rainfalls of 1.00 in. or more and 71% of those equaling or exceeding 0.50 in. No warm-air-mass type (which includes heat-convection thunderstorms) gave an areal mean rainfall of 1.00 in. or more. Although the heat-convection thunderstorms may produce heavy rainfall intensities, they consist, normally, of scattered or isolated storm cells of small areal extent and short duration. Opportunities for heavy areal rainfall on a watershed of 95 sq miles are considerably greater with the multicellular-thunderstorm lines, or zones, associated with the approach and passage of cold fronts, in which rainfall may continue for several hours.

TABLE 2.—AREAL MEAN RAINFALL AS RELATED TO STORM TYPE

Storm type	Minimum Depth of Rainfall, in Inches			
	0.50		1.00	
	No. of storms	Percentage of total storms	No. of storms	Percentage of total storms
Cold front	13	42	5	50
Pre-cold-frontal squall line	9	29	3	30
Warm front	5	16	2	20
Instability of:				
Warm-air masses	4	13	0	0
Cold-air masses	0	0	0	0
Cold front plus squall line	22	71	8	80

Rainfall Intensity as Related to Storm Type.—A study was made of the excessive rainfall rates recorded on the watershed of 95 sq miles between May and September, 1948–1950. Only data from recording gages could be used for this purpose. During the 1948 and 1949 seasons, 8 recording gages were included in the 20-gage basin network. The number of recording gages was increased to 24 during 1950.

Excessive rainfall rates were determined from the following Weather Bureau formula for short-period, high-intensity storms: $H = 0.01\ (t + 20)$, in which H is the rainfall, in inches, and t is the time, in minutes. Excessive rates were determined for 30-min, 1-hr, and 2-hr storm periods. Because weekly recording charts were used on the gages, the analysis of excessive rates for smaller units of time was not practical. Excessive rates for 30 min, 1 hr, and 2 hr correspond to 0.50 in., 0.80 in., and 1.40 in., respectively.

During the three thunderstorm seasons, there was a total of 25 storms in which excessive 30-min rates were recorded by one or more of the recording gages. Similarly, there were 19 storms in which excessive 1-hr rates occurred, and 9 storms with excessive 2-hr rates.

Storms associated either directly, or indirectly, with cold fronts were the chief sources of heavy intensities. Cold fronts and pre-cold-frontal squall lines accounted for 75% of the storms with excessive 30-min rates, 84% of those with excessive 1-hr rates, and 89% of the storms with excessive 2-hr rates. The maximum intensities recorded by an individual station occurred with a pre-cold-frontal squall line on July 16, 1950. A 30-min total of 1.46 in. was recorded by one station, whereas another recorded 1-hr and 2-hr totals of 2.25 in. and 2.72 in., respectively. This storm was also the source of the most widespread occurrence of excessive rates. For 30-min amounts exceeding 1.00 in., the cold-front systems were dominant, accounting for 7 out of 8 storms, with one or more stations recording over 1.00 in. in 30 min. Thus, storms associated either directly, or indirectly, with cold fronts were the most frequent source of rainfall, the source of the heaviest mean storm rainfalls, and the source of the heaviest rates of rainfall in the 95-sq-mile experimental area.

Radar Studies

The very close correspondence between the storm pattern shown by the radar and the rainfall pattern occurring on the ground has been established, but the possible application of this relationship in engineering meteorology has not been explored. Studies have been made by the Massachusetts Institute of Technology (MIT) Weather Radar Research Project, at Cambridge, whose report of December, 1946,[8] summarized the results previous to that date.

The United States Signal Corps has played a leading role in sponsoring the MIT work, and in carrying on a number of separate studies.[9,10,11] The British, through J. W. Ryde,[12] J. S. Marshall, and others of the Canadian Army Operational Research Group,[13] have contributed much to the theoretical knowledge of the relation of radar echo to rainfall and other meteorological parameters.

In the application of radar for storm detection, the Army-Navy-National Advisory Committee on Aeronautics-Weather Bureau Thunderstorm Project explored the structure and dynamics of the thunderstorm in great detail. In a preliminary study the possible use of radar in estimating the amount of rainfall over a small area[14] was established by Mr. Byers and others. The All-Weather Flying Division of the United States Air Force (USAF) recognized the possible uses of radar in aviation meteorology, and D. Atlas combined the theoretical and empirical weather radar equations to form the basis for a simplified radar-rain intensity computer.[15]

---

[8] "M.I.T. Weather Radar Research, 1946," First Technical Report under Signal Corps Project, Dept. of Meteorology, Massachusetts Inst. of Technology, Cambridge, Mass., December 31, 1946.

[9] "Preliminary Report on Optimum Wave-length for Storm Detection," by D. Swingel and R. Wexler, *Technical Memorandum No. 183-R*, Evans Signal Labs., Belmar, N. J., November 7, 1945.

[10] "Rainfall Intensities and Attenuation of Centimeter Electromagnetic Waves," by J. Weinstein and R. Wexler, Evans Signal Labs., Belmar, N. J., 1947.

[11] "Ground Weather Test of AN/APQ-13A," by H. B. Brooks, *Technical Memorandum No. 193-R*, Evans Signal Labs., Belmar, N. J., April 17, 1946.

[12] "The Attenuation and Radar Echoes Produced at Centimeter Wave-lengths by Various Meteorological Phenomena," by J. W. Ryde, The Physical Soc. and the Royal Meterological Soc., Report of a conference held on April 8, 1946, pp. 169–189.

[13] "Measurement of Rainfall by Radar," by J. S. Marshall, R. C. Langille, W. McK. Palmer, *Journal of Meterology*, December, 1947, pp. 186–192.

[14] "The Use of Radar in Determining the Amount of Rain Falling Over a Small Area," by H. R. Byers, et al., *Transactions*, Am. Geophysical Union, Vol. 29, No. 2 April, 1948, pp. 187–196.

However, none of the foregoing projects has provided sufficient data and conclusions to establish radar as a dependable quantitative instrument.

PRINCIPLE OF RADAR

The radar set emits a short, intense pulse of energy which may be focused into a narrow beam, and which travels at the speed of light. If the beam strikes an object, such as an airplane or a rainstorm, a small portion of the energy is reflected and returns as an "echo" to the point of transmission. It is then amplified and presented on a cathode-ray tube. The range and bearing of the object are determined readily. The beam usually travels along a "line-of-sight," hence, the radar cannot detect distant subjects that are near the earth's surface.

Theory.—Studies in this field indicate that the radar echoes from precipitation are the result of the scattering of radio energy by water drops falling through the atmosphere or suspended by strong vertical currents. The theoretical expression that has been developed[16] indicates that the energy (power) received from precipitation (reflected back to the radar antenna) is

$$P_r = C\,h\,P_t\,\frac{N\,a^6}{R^2} \qquad (1)$$

in which P_r is the received power; C is a constant for the equipment used; h is the radar pulse width (duration, expressed as a distance); P_t represents the peak pulse transmitted power; N is the number of raindrops per unit volume; a^6 denotes the mean sixth power of the radii of the raindrops; and R equals the distance to the object. Eq. 1 may be expressed as $P_r = K_1 \frac{N\,a^6}{R^2}$, in which K_1 includes several of the constants.

From data collected by J. O. Laws and D. A. Parsons,[17] which indicate a relationship between raindrop size and intensity of rainfall, R. Wexler[18] has concluded that

$$\log N\,a^6 = 1.441 \log I - 17.302 \qquad (2)$$

in which I represents the rainfall intensity expressed in millimeters per hour; hence,

$$P_r = K_2\,\frac{I^{1.441}}{R^2} \qquad (3)$$

Therefore, the problem in using radar for rainfall-intensity measurement seems to center around determining the power received (P_r) because that is a function of the intensity of the rainfall.

---

[15] "Preliminary Report on New Techniques in Quantitative Radar Analysis," by D. Atlas, *Memorandum Report AWNW 7-4*, Pt. I, All-Weather Flying Div., AMC, U.S.A.F., October 22, 1947.

[16] "The Effect of Rain and Fog on the Propagation of Very Short Radio Waves," by J. A. Stratton, *Proceedings*, Inst. of Radio Engrs., June, 1930, pp. 1064–1074.

[17] "The Relation of Raindrop-Size to Intensity," by J. O. Laws and D. A. Parsons, *Transactions*, Am. Geophysical Union, Vol. 24, Pt. II, 1943, pp. 452–459.

[18] "Radar Detection of a Frontal Storm, June 18, 1946," by R. Wexler, *Journal of Meteorology*, February, 1947, pp. 38–44.

Radar Storm Presentation.—Fig. 9(*a*) represents a hypothetical storm 5 miles deep, of which the nearest edge is 15 miles east of the radar. The contours represent lines of equal rain intensity, the core of heavy rain being the innermost area. Numbers on the contour lines denote the rain intensity in inches per hour. When the radar antenna is directed along axis AB, Fig. 9(*b*) represents the hypothetical received-power curve, corrected for range and attenuation. The "A-scope," a cathode-ray tube presentation used in many radar sets, portrays the observed data in a similar form. However, the receiver sensitivity is normally maintained at a high level so that light rain may be observed. As a result, the amplitude of the received-power curve exceeds the capacity of the receiver circuits, distorting the signal so that moderate rain intensities and cores of heavy rain cannot be distinguished.

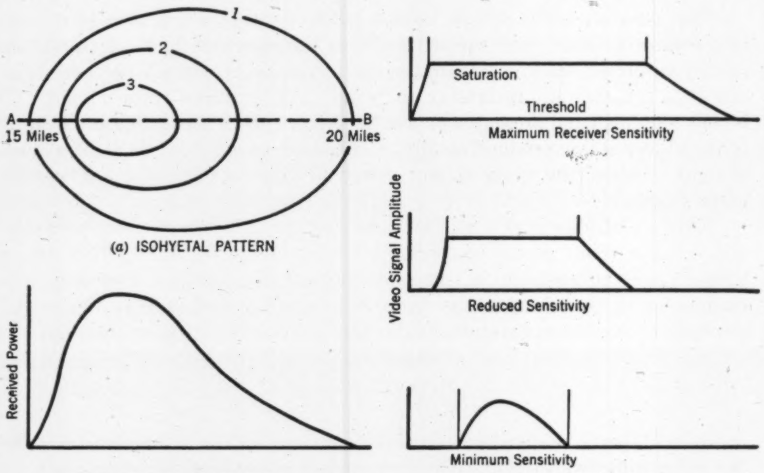

(*a*) ISOHYETAL PATTERN

(*b*) RECEIVED-POWER CURVE

(*c*) A-SCOPE PROFILES

FIG. 9.—RECEIVED-POWER PROFILES (NO ATTENUATION)

The portion of the received-power curve observed by the radar operator on the A-scope is shown in Fig. 9(*c*). At maximum receiver sensitivity, only the base of the received-power wave form is presented. This base represents the area of light rain, but the heavier rainfall drives the circuits to saturation, thus flattening the top of the received-power curve. When the receiver sensitivity is reduced, greater received power is necessary to reach the threshold of visibility. It is necessary for the rain intensity to be greater for it to produce a detectable signal. Thus, the area of medium rainfall is presented. The receiver sensitivity may be reduced until only the received power from the core of heaviest rain is perceptible. The received power that will cause a barely-perceptible image on the scope is readily measurable.

A different type of presentation is obtained with the plan position indicator (PPI) scope. As the rotating antenna scans the entire area around the radar set, the PPI presents an image of the storm as if it were laid out on polar coordinates. The area of rain glows, whereas the rest of the face of the scope is dark. Thus, the location and the areal extent of the storm are readily observed. Fig. 10(*a*) presents such a view, showing the scope and data of August 28, 1950, at 3:01 p.m., Central Daylight Time. Fig. 10(*a*) shows a heavy rain near Galesburg, Ill., 80 miles from the radar. For observing summer thunderstorm rainfall, the equipment used seemed to have an effective range of approximately 75 miles. To the right of the scope in Fig. 10(*a*) may be seen the date card, the 24-hr watch used to record the time of observation, the antenna-tilt indicator, and the light signals of the step-position indicator.

The outline of the image at different receiver-sensitivity levels should correspond to a rainfall-intensity contour. If the image on the PPI is recorded at several receiver-sensitivity levels, superimposing the areas enables construction of radar-rain-intensity contours that should coincide with actual rain-intensity contours.

Methods Available.—Two methods of varying the receiver sensitivity were used by the All-Weather Flying Division of the USAF.[18,19]

In one method, the receiver-sensitivity control was calibrated in terms of the echo power necessary for the threshold of visibility of the PPI. The operator changed the sensitivity manually, photographed the PPI image in each setting, and recorded the receiver-sensitivity setting for each picture. A picture taken at maximum sensitivity showed the outline of the entire storm and, at minimum sensitivity, the picture showed the locations of the cores of heavy rain (Figs. 10(*b*), 10(*c*), 10(*d*), 10(*e*), and 10(*f*)).

The second method used by the USAF all-weather group was the video-inversion method, which presents the storm structure as alternate bands of bright and dark areas. The light rain around the outside of the storm (the area between contours 1 and 2 in Fig. 9(*a*)) would appear bright, heavier rain (contours 2 to 3) would show as a dark area, and the core of the heaviest rain (inside contour 3) would appear as a bright area for the center of the storm. This method necessitates considerable additional circuitry.

Neither method seemed to fill all the immediate requirements. The video-inversion method requires a large number of additional tubes and associated circuits. Manual recording of sensitivity settings seemed laborious when several pictures were taken every minute. Because an automatic system of film recording was already in use, an automatic system of receiver-sensitivity control (synchronized with the camera) was developed.

METHOD

An AN/APS-15 3-cm radar set was used for the study. The radar set was located in El Paso. It was calibrated in nautical miles, and its peak power output averaged 25 kw. For this study, receiver sensitivity was varied by predetermined steps, and the storm pattern on the PPI scope was recorded on

---

[19] "Some Experimental Results of Quantitative Radar Analysis of Rain Storms," by D. Atlas, *Memorandum AWNW 7-4*, Pt. II, All-Weather Flying Div., AMC, USAF, May 1, 1948.

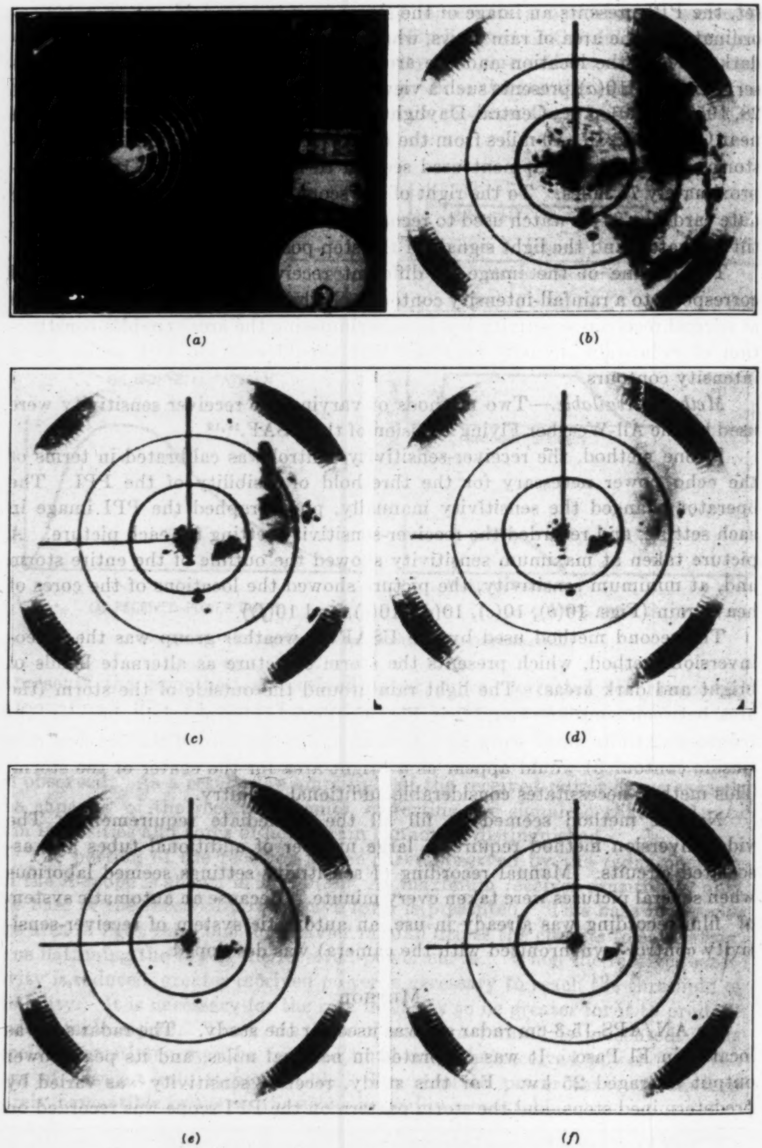
(a) (b) (c) (d) (e) (f)

FIG. 10.—RAIN-INTENSITY CONTOURS

a 16-mm moving-picture film. An automatic photographic-recording and sensitivity-stepping circuit was devised. Known values of receiver power were put into the equipment to calibrate the circuit. A series of negatives exposed on August 30, 1950 (Fig. 10), shows the effect of step-wise receiver-sensitivity changes on the image on the PPI scope. The entire series was taken in a period of 1 min, with 10-sec intervals.

The first picture is on step 1 (Fig. 10(*b*)). The range-marking circles are at intervals of 10 nautical miles. Ground clutter, caused by reflections from buildings, extends out to almost 8 miles. The main area of the rain is the black portion to the northeast. A small area extends from 5 to 10 miles due east, and 4 showers are clustered about 10 miles to the south. In the second picture (Fig. 10(*c*)), the sensitivity is reduced to step 2. The areas of the rainfall images are reduced. The areas of light rain become imperceptible. Each successive step reduces the area of rain that is visible. On step 4, the core of only 1 of the 4 showers to the south is visible. On step 5, the core of heavy rain in the shower 8 miles east is the only rain visible.

All rainfall detected on the radar scope from June, 1950, through September, 1950, was recorded on film. The equipment was kept in readiness for operation 24 hr a day, and round-the-clock operators were present whenever synoptic conditions indicated the possibility of precipitation.

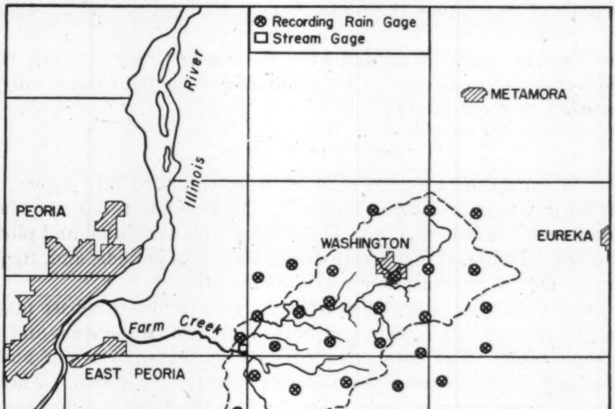

FIG. 11.—FARM CREEK RAIN-GAGE NETWORK, 1950

Rainfall Measurements.—To gather reliable rainfall data outside the zone of ground clutter, a network of weighing-bucket rain gages was placed in service in July, 1950, in the vicinity of Washington, Ill. The network of 31 gages, 15 miles west of the radar station in El Paso, covers the watershed area of Farm Creek and some adjacent areas above East Peoria, Ill. The gages are generally spaced about 1½ miles apart (see Fig. 11). Collectors of 12.648-in. diameter were used instead of the standard units of 8-in. diameter. This use of larger diameter collectors expanded the sensitivity of the gages 2.5 times. The standard drum clock was geared for one drum revolution in a 6-hr period. Thus, 5-min rainfall amounts were easily determined, and 1-min rates-of-fall were computed with fair accuracy. A laboratory check is being conducted on the lag in the operation of the gages.

Rain fell during 18 days of the 74-day period of operation of the Farm Creek network. On 10 of these days, the average amount for the network was less than 0.10 in. On the remaining 8 days of rain, the daily totals were as follows: 0.12 in., 0.25 in., 0.31 in., 0.61 in., 0.75 in., 1.33 in., 1.47 in., and 2.54 in. Widespread shower activity, that produced rainfall between the network and the radar set, occurred on several days. This condition introduced an attenuation effect so that only 2 of the rainstorms could be used in the analysis described in this paper. On several occasions the radar set was not functioning properly, and data collected at those times were eliminated. The data from rainfalls of September 19, September 20, and September 21, 1950, were usable.

There were no cases of rainfall over the Farm Creek network that the radar did not detect and record. On a number of the light rains, only a part of the network received rainfall.

ANALYSIS OF DATA

The data from the rain-gage network were compiled into a form readily available for any type of analysis required. Mean 5-min totals, the maximum rate during each 5-min period, and 1-min rates were tabulated and plotted for selected cases. Isohyetal maps were drawn for 5-min periods, and, frequently, for 1-min periods of precipitation over the network.

The radar data were transcribed from the 16-mm film to a base map 11 in. by 17 in., by projecting the photograph through a mirror system and a glass-topped copy table. The total area covered during each 1-min and 5-min period for each different receiver-sensitivity setting was drawn. These maps were termed "radar echo contour maps." Fig. 12 shows a 1-min radar echo contour map and the corresponding precipitation map. Discrepancies between the two patterns can be attributed to: (1) Failure of the radar to detect the entire depth of the storm because of attenuation; (2) time lag caused by the time of fall from the elevation at which the radar detects the raindrops to the earth; (3) lateral drift of the raindrops in falling; and (4) evaporation of the raindrops while falling. The areal extent of the precipitation, as observed by radar, correlates very well with the measured-rainfall pattern.

Mr. Atlas[19] found that there was a significant correlation between the intense rainfall cores, as observed in the lower 5,000 ft of the atmosphere, and those measured on the ground below. His best correlation resulted when the surface rainfall was measured at the core of the corresponding precipitation pattern as the average rate over a 5-min interval immediately after the radar observation.

To compensate for the fall time and the drift of raindrops from the average height of between 2,000 ft and 3,000 ft, observed by the radar, successive 1-min maps of radar contours and of surface rainfall were used. The 1-min rainfall rates were determined from the slope of the curve on the rain-gage chart. Using the sensitive rain gages, it was not difficult to observe rainfall depths as small as 0.005 in., with a time resolution of 1 min. Every change of slope, either large or small, was considered valid and used in the evaluation. In most cases, very minor irregularities did not have to be considered because fairly consistent rates persisted for at least 2 min or 3 min.

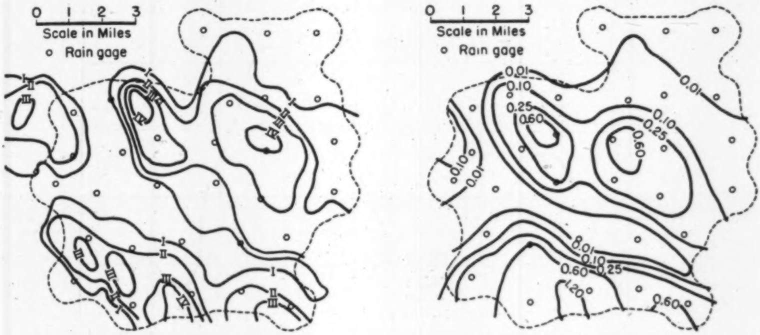

(a) Radar lines of equal received power

(b) Rain gage isohyetal pattern

FIG. 12.—STORM PATTERNS DURING A 1-MIN PERIOD—BY RADAR AND BY RAIN-GAGE NETWORKS

The direction and the amount of drift were determined from the movement of the radar cores for several consecutive minutes. The fall time of the raindrops was approximated by comparing a chosen 1-min radar profile along an appropriate radial from the radar station with consecutive 1-min surface rainfall profiles along the same radial line, after applying a drift correction to the surface rainfall pattern.

The successive 1-min rainfall profiles were compared with the radar profile until a matching of peaks for location was obtained (Fig. 13). The radar profile in Fig. 13 is along radial No. 5, between the hours of 0844.5 and 0845.5 on September 19, 1950. Only those cases in which the indicated time lag was less than 5 min, with the drift not greater than 1.5 miles, were used in the analysis. Cases involving intervening rain and core centers moving off the network were excluded. If the operators' log showed the possibility of instrumental error, or other observational inconsistencies, the data were discarded. Examples of very light shower activity were not considered. When more than one core of rainfall existed, it was often found that the time lag or the drift (or both) varied for each cell. Because the development stage of adjacent cells may vary considerably, this variation should be expected.

Fig. 14 summarizes the available data. For comparison with published measurements, a function of the received power was used for correlation. Values of $\frac{P_r R^2}{P_t}$ were plotted against the surface rainfall intensities, I_s, in inches per hour. A curve was fitted to the median values of the groups of values.

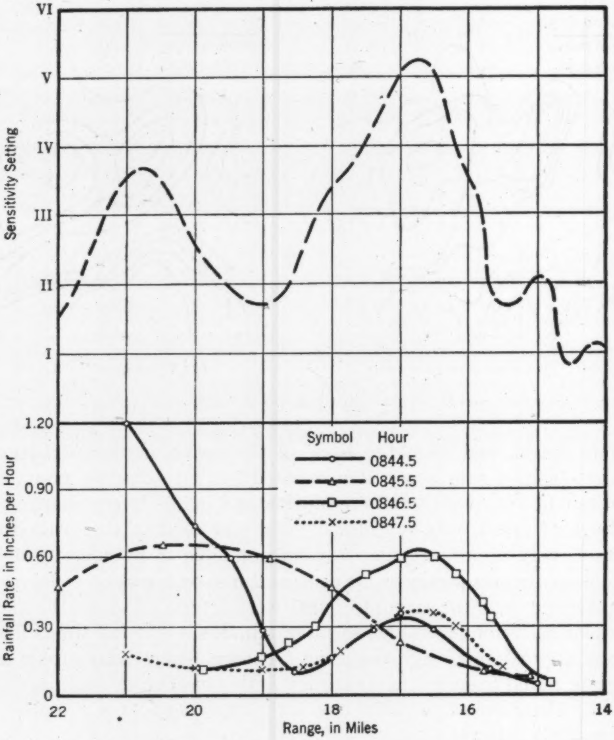

Fig. 13.—Profiles of Radar-Received Power and Rainfall Intensities

Conclusions

At rainfall rates below 0.7 in. per hr, there is reasonably good agreement between the observations gathered in this study and those made by Mr. Atlas. For higher rainfall rates, there are significant differences in returned-signal strength. The Illinois data failed to indicate the expected exponential relation between rainfall intensities and received power.

Previous studies have indicated that the received power from rainstorms should follow closely the Rayleigh scattering effect. The best available information on drop size[20] indicates that received power should be exponentially

---

[20] "Drop Size, Intensity, and Radar Echo of Rain," by A. F. Spilhaus, *Journal of Meterology*, August, 1948, pp. 161–164.

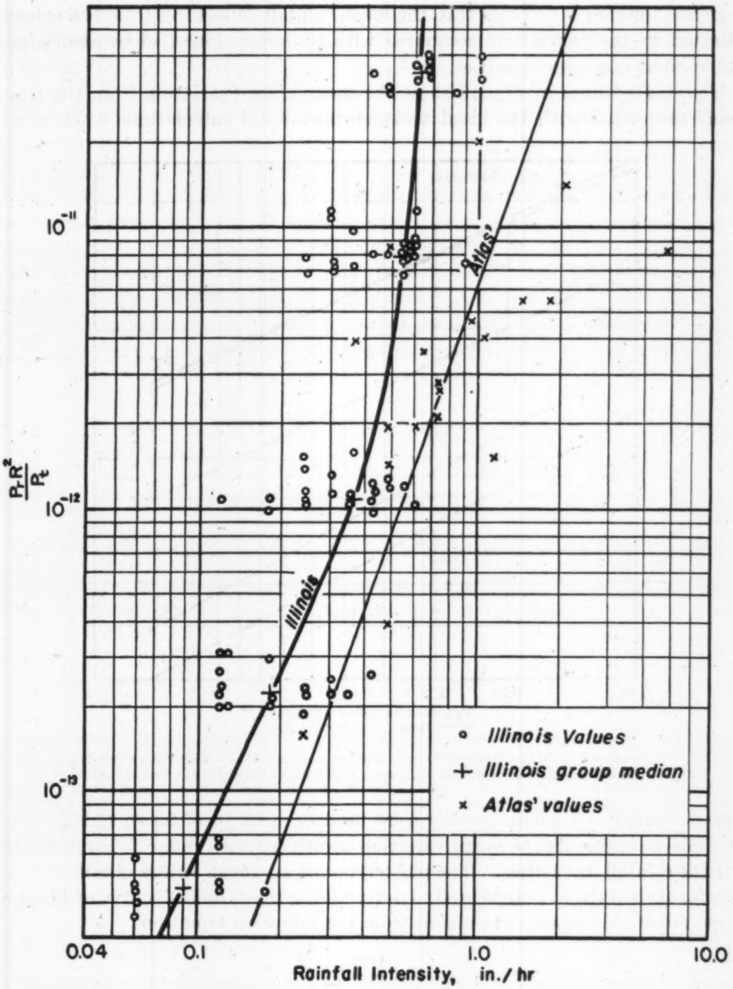

FIG. 14.—RECEIVED-POWER AND RAINFALL INTENSITY

related to rainfall intensity. These drop-size measurements were made at the ground surface, however, and the high received-power values at higher rainfall rates may indicate that large drops are present in higher concentrations at the elevations observed by the radar.

The scatter of actual measured-rainfall rates (by rain gages) shown in Fig. 14 was analyzed further to see whether the departures from the curve were such as to indicate any significant lack of correlation with signal strength and range measurements. To do this, the mean rainfall departures from the values indicated by the curve were compared with the errors found to be associated with various rain-gage densities.

The dashed lines in Fig. 15 show the mean error (variation from the true mean) associated with the areal mean-storm-rainfall calculations when rain-gage networks of various density were used on a basin of 95 sq miles. The solid curve represents the mean variation associated with radar determinations of point rainfall intensities. The plotted points are mean values obtained from data for each of the five steps used in determining the "Illinois" curve of Fig. 14. These mean values were calculated from the following equation:

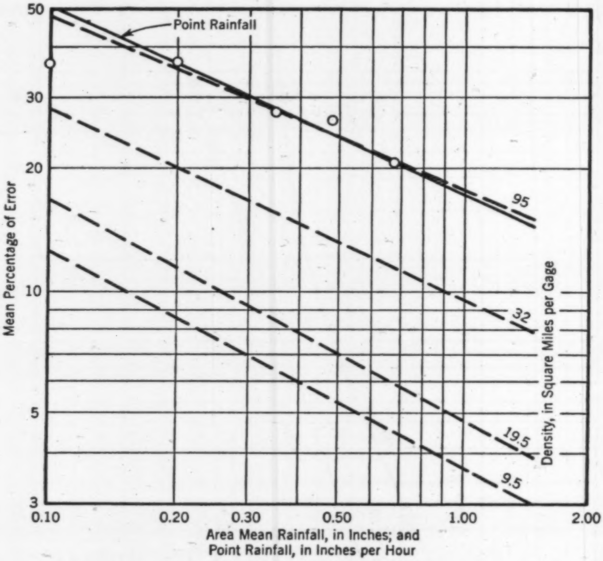

FIG. 15.—COMPARISON OF MEAN OBSERVATIONAL ERRORS—AREAL MEAN RAINFALL FROM RAIN-GAGE NETWORKS COMPARED WITH POINT RAINFALL INTENSITIES FROM RADAR OBSERVATIONS

$$V = \frac{100}{N} \sum \frac{D}{I_g} \qquad \text{(4)}$$

in which V equals the mean variations; D equals the deviation of rain-gage rainfall intensity from the experimental curve value; I_g equals the rain-gage rainfall intensity in inches per hour; and N equals the number of observations.

Despite the limitations of the equipment used, the radar set appeared capable of determining point rainfall intensities as accurately as a rain gage network of 1 gage per 100 sq miles measured the mean areal rainfall.

Experience gained in this study indicated that the radar was equivalent to gage networks having approximately 1 gage per 3 sq miles for determining the areal extent of rainfall. As further work is done, it is expected that increasingly close correlations between radar observations and rainfall intensities will be obtained.

Utility of Radar.—During the summer of 1950, regular rainfall reports, based on radar observations, were provided industry, agriculture, and the public through a local radio station. The Weather Bureau put the radar observations on its teletype to augment its information. In highway construction in central Illinois, it was found that the precise rainfall-location data often allowed the extension of operation beyond the usual periods of pouring concrete. Special short-range rainfall forecasts were made for the operations of a hybrid corn company, for the commencement exercises of a large university, and for the 1949 and 1950 Illinois state fairs.

Radar can depict precipitation patterns associated with flash floods, large floods, tornadoes, hurricanes, frontal weather, and freezing rain in winter. It should prove useful in irrigation works, and in controlling water-supply reservoirs and hydroelectric plants.

During succeeding years, radar will provide the answers to the area-depth questions asked by engineers.

Acknowledgments

These studies owe much to the interest, encouragement, and material assistance of Lester Pfister, president of the Pfister Hybrid Corn Company, at El Paso. This company helped to organize the project. The radar set used in this work was located in the Pfister Building, at El Paso.

Many staff members of the Illinois State Water Survey have contributed to this study. The radar work was begun under the initiative of A. M. Buswell, chief, and the entire study has been carried forward with his strong encouragement. W. J. Roberts, A.M. ASCE, associate engineer, procured the radar set and directed its assembly. Douglas Jones, meteorologist, stationed at El Paso, directed the 1950 field operations. G. W. Farnsworth, assistant engineer, had the responsibility for the design and the construction of modifications to the radar, for the maintenance of the equipment, and for some of the analysis of the data collected. Much of the processing of the data was done by Homer Hiser, a graduate assistant. Mr. Byers, meteorological consultant, contributed many valuable suggestions.

DISCUSSION

Ven Te Chow,[21] A.M. ASCE.—The writer has discussed the problem of area-depth relationships for thunderstorm rainfall.[22,23] It was assumed that any observed storm pile can be converted into one which has circular horizontal sections, symmetrical with respect to the vertical axis of the pile. The storm pile is simply a three-dimensional representation of the rainfall isohyetals. By a mathematical treatment, a theoretical general equation for rainfall area-depth distribution for all types of storms was developed. This equation is in the form of an infinite series,

$$H = a + b\,A^{\frac{1}{2}} + c\,A + d\,A^{\frac{3}{2}} + e\,A^2 + \ldots\ldots\ldots\ldots\ldots \quad (5)$$

in which H is the average depth of rainfall on an area A, and a, b, c, d, and e are coefficients.

A further mathematical manipulation shows that Eq. 5 can be expressed as

$$H = \frac{1}{\alpha + \beta\,\sqrt{A}} = (\alpha + \beta\,\sqrt{A})^{-1} \ldots\ldots\ldots\ldots\ldots \quad (6)$$

in which α and β are coefficients. By expanding Eq. 6 there results

$$H = \alpha^{-1} + (-\,1)\,\alpha^{-2}\,\beta\,A^{\frac{1}{2}} + \frac{(-\,1)\,(-\,2)}{1 \times 2}\,\alpha^{-3}\,\beta^2\,A + \frac{(-\,1)\,(-\,2)\,(-\,3)}{1 \times 2 \times 3}\,\alpha^{-4}\,\beta^3\,A^{\frac{3}{2}} + \ldots\ldots\ldots\ldots\ldots \quad (7)$$

which is mathematically exactly in the same form as the Eq. 5. The simplified equation can be written as

$$H^{-1} = \alpha + \beta\,\sqrt{A} \ldots\ldots\ldots\ldots\ldots\ldots \quad (8)$$

which indicates that the reciprocal of H plotted against the square root of area will result in a straight-line relationship for all types of rainfall storms.

If H_0 is the maximum point-rainfall depth measured at the gage site, the ratio of the average rainfall to the point rainfall can be expressed as

$$\frac{H}{H_0} = \frac{1}{1 + \frac{\beta}{\alpha}\,\sqrt{A}} \ldots\ldots\ldots\ldots\ldots\ldots \quad (9)$$

which is a reduction coefficient to account for a decrease of rainfall depth with increase in drainage area. The value of the ratio β/α is variable and depends mainly on the locality. A study of the data[24] results in an average value of β/α equal to 0.005 (with A expressed in square miles) for the central sections of the United States.

---

[21] Asst. Prof. of Civ. Eng., Univ. of Illinois, Urbana, Ill.

[22] Discussion of "Area-Depth Studies for Thunderstorm Rainfall in Illinois," by F. A. Huff and G. E. Stout, by Ven Te Chow, *Transactions*, Am. Geophysical Union, August, 1953.

[23] "Hydrologic Studies of Urban Watersheds, Rainfall and Runoff of Boneyard Creek Watershed, Champaign-Urbana, Illinois," by Ven Te Chow, *Hydraulic Eng. Series No. 2*, Civ. Eng. Studies, Dept. of Civ. Eng., Univ. of Illinois, Urbana, Ill., November 1, 1952.

H. E. Hudson, Jr.[25] M. ASCE, G. E. Stout,[26] and F. A. Huff.[27]—The writers are indebted to Mr. Chow for his contributions to the development of the area-depth relationships. They are also indebted to him for a discussion[22] of an earlier paper[28] which is directly related to the present subject. In the earlier paper it was shown that, when area-depth data for thunderstorms were presented as a plotting of average depth of rainfall (H) against the square root of the area (A) within which the rainfall occurs, a linear relation between the two parameters results which can be expressed by Eq. 5, eliminating the higher coefficients c, d, e....

In discussing Eq. 5, Mr. Chow treated the storm pile as a surface of revolution. The analysis revealed that point rainfall is also linearly related to the distance from the center of the storm:

$$y = C + D\,r \qquad (10)$$

in which y is the point rainfall, r is the distance from the center of the storm, and—for a given thunderstorm—C and D are constants. Accordingly, it was concluded that the storm pile was equivalent to a cone of similar dimensions. From this analysis, the writers have determined that $a = C$ and $b = -\,0.376\,D$, so that

$$H = C - 0.376\,D\,\sqrt{A} \qquad (11)$$

It should be remembered that thunderstorm patterns usually resemble elongated ellipses rather than circles. However, the area-depth data appear to be well correlated when treated as though they were yielded from circular patterns.

It is significant that C is the hypothetical, maximum point rainfall at the center of a storm. The measured maximum point value will probably be smaller than C because of sampling errors and the differences between actual occurrences and analyses. The constant D is, of course, the rainfall gradient, and it is interesting to note that it usually appears to be uniform in nearly all the thunderstorms studied.

Eq. 10 can be used to construct hypothetical area-depth curves for design purposes on small basins when the maximum point rainfall at the storm center can be obtained from frequency data, such as those obtained by D. L. Yarnell,[29] provided that the rainfall gradient or mean rainfall on the basin can be estimated from a local rain-gage network. The State Water Survey Division of Illinois is at present (1953) investigating the magnitude of thunderstorm rainfall gradients from data collected on small Illinois watersheds in the hope that more concrete information can be obtained on this subject.

---

[24] "Storm Rainfall of Eastern United States," by the Engineering Staff of the District, *Technical Reports*, Miami Conservancy District, Part V, Dayton, Ohio, 1917.

[25] Head, Eng. Subdivision, Illinois State Water Survey, Urbana, Ill.

[26] Meteorologist, Eng. Subdivision, Illinois State Water Survey, Urbana, Ill.

[27] Meteorologist, Eng. Subdivision, Illinois State Water Survey, Urbana, Ill.

[28] "Area-Depth Studies for Thunderstorm Rainfall in Illinois," by F. A. Huff and G. E. Stout, *Transactions*, Am. Geophysical Union, August, 1952.

[29] "Rainfall Intensity-Frequency Data," by D. L. Yarnell, *Miscellaneous Publication No. 204*, U.S.D.A., Washington, D. C., August, 1935.

Mr. Chow's discussion of relationships in large storms expands the subject. The writers have not had the opportunity to test Eqs. 5 to 9 with data from large storms.

AMERICAN SOCIETY OF CIVIL ENGINEERS
Founded November 5. 1852
TRANSACTIONS

Paper No. 2670

ZONING MAPS FOR AIRPORTS

BY BENJAMIN EVERETT BEAVIN,[1] SR., M. ASCE

WITH DISCUSSION BY MESSRS. HAROLD M. LEWIS, AND BENJAMIN EVERETT BEAVIN, SR.

SYNOPSIS

Airport zoning may be defined simply as the protection of approaches. In practice, the term encompasses the defining of sloping approaches to standards evolved through long experience, and effectually protecting them from encroachment of man-made or naturally grown flight hazards by purchasing adjoining land, securing avigation (aerial navigation) easements, or by enacting and enforcing zoning ordinances.

The purpose of this paper is to call attention to the desirability of early and effective zoning and to suggest methods of further simplifying and standardizing zoning surveys and maps.

An engineer engaged in the design and supervision of construction theoretically occupies a semijudicial position with definite responsibilities, not only to his client but also to the contractor whose work he oversees. Likewise, in zoning for airports, he has responsibilities to his client (usually somebody representing a segment of the general public) and also to those persons whose safety and properties are affected by whatever zoning measures are adopted.

Ideally, airport zoning should begin during the reconnaissance stage, before the site has been selected finally. The effect of the airport operations on neighboring properties should be weighed carefully. The noise factor should not be overlooked. Quite often a small rotation of all or part of a runway layout will result in greater approach clearances and therefore less property damage. It should be borne in mind constantly that a zoning ordinance, no matter how well drawn, cannot contravene the constitutional provision that properties may not be taken for public use without adequate compensation. Surely the act of restricting the heights of the structures that may be built in residential areas to something less than that of a two-story house, or fixing less than a reasonable height for a stack, water tank, or other necessary struc-

---

NOTE.—Published, essentially as printed here, in February, 1953, as *Proceedings-Separate No. 174*. Positions and titles given are those in effect when the paper or discussion was received for publication.

[1] Cons. Engr., Baltimore, Md.

tures in industrial areas, may only be construed as a taking away of a considerable part of the value of properties so restricted.

It is not meant to suggest that airport zoning is bad, but rather to urge that public safety and property damage be considered along with all other factors in selecting the location for airports.

As soon as the site has been selected and the position and elevations of runway ends determined, four steps—(1) zoning of the airport, (2) purchasing of land in approach zones, (3) the securing of avigation easements (a comparatively recent development), or (4) a combination of all three—should be undertaken.

The importance of early and effective protection for airport approaches cannot be overstressed. The safety of passengers, neighbors, and aircraft and, indeed, the value of the entire project, may be jeopardized by the encroachment of flight hazards.

The preparation of zoning ordinances is a complex legal problem and should be undertaken in cooperation with competent legal counsel. Much useful legal information is readily available through the Civil Aeronautics Administration, United States Department of Commerce (CAA). The art of drawing legal descriptions of the zones, and the preparation of necessary zoning maps, calls for the highest order of engineering to insure that the resulting ordinance may be simple, clear, and easy to administer. Not so long ago approach and turning zones were defined by distances from irregular airport boundaries and by heights above runways of varying elevations. Zones so defined were scalloped in plan view, wavy in surface, and difficult to define mathematically.

Recent practice tends toward simplification of the geometrics of approaches, making the understanding, and successful administration, of a zoning ordinance much easier.

The best source of information concerning the avigation requirements naturally is the Civil Aeronautics Administration. Most of the zoning ordinances for civil airports have been guided by the administration's published material, the latest of which is *Technical Standard Order No. N 18*, issued on April 16, 1950. This order outlines the procedure for determining obstructions, defines imaginary governing surfaces, and limits the heights above ground of objects in various areas at or near airports. Obviously, then, any suggestion as to further simplification of civil zoning practice must largely be a discussion of this technical order. In the text, the words or phrases in quotation marks are taken from the order.

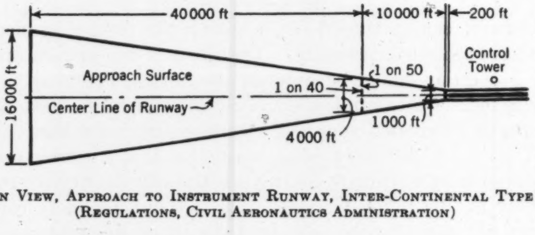

FIG. 1.—PLAN VIEW, APPROACH TO INSTRUMENT RUNWAY, INTER-CONTINENTAL TYPE OF AIRPORT (REGULATIONS, CIVIL AERONAUTICS ADMINISTRATION)

The inclined paths followed by aircraft approaching or leaving runways are protected by the prohibition of the construction or maintenance of obstacles protruding through an imaginary inclined surface known as an "approach surface." That part of the earth directly below an approach surface is known as an "approach area" (Fig. 1).

In plan view the "approach surfaces" begin 200 ft outward from the end of the runway and, for instrument approaches, they are 1,000 ft wide, flare out to 4,000 ft wide at a distance of 10,200 ft from the end of the runway, and continue to flare out to a total width of 16,000 ft at a distance of 50,200 ft from the end of the runway. Non-instrument runway approaches vary in width according to the service classification of the airport. For instrument runways the approach slope ratio is specified by the CAA as 1 on 50 for the 10,000-ft section and as 1 on 40 for the outer 40,000-ft section (Fig. 2).

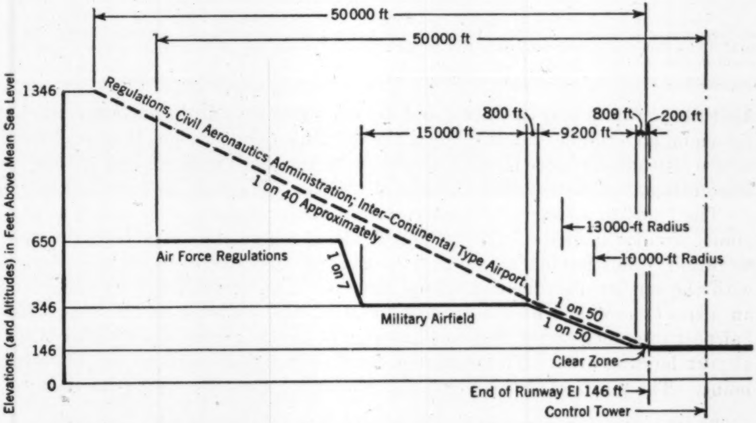
50000 ft
50000 ft
Elevations (and Altitudes) in Feet Above Mean Sea Level
1346
650
346
146
0
Regulations, Civil Aeronautics Administration; Inter-Continental Type Airport
1 on 40 Approximately
800 ft
800 ft
200 ft
15000 ft
9200 ft
13000-ft Radius
10000-ft Radius
Air Force Regulations
1 on 7
Military Airfield
1 on 50
1 on 50
Clear Zone
End of Runway El 146 ft
Control Tower

FIG. 2.—PROFILES OF APPROACH SURFACES, BASED ON AN ESTABLISHED AIRPORT ELEVATION OF 150 FT

The technical order can be simplified further by tabulating the widths and giving altitudes rather than slopes. For one reason, curvature of the earth amounts to approximately 60 ft in the 50,000 ft involved. Also, it is desirable that the altitudes of imaginary surfaces, above mean sea level, be easily comparable with surface contours referred to the same datum. An improvement over present practice would be to tabulate the geometrics of approach surfaces as shown in Table 1.

The state coordinates should be given to fix the position of all runway ends horizontally. The ultimate ends should be protected, rather than intermediate stages of construction.

At first glance the values in Table 1 may seem to be the same as the current CAA regulations. However, a moment's reflection indicates that the current regulations are based on slope ratios referred to a plane tangent to the earth's surface at the runway end, whereas the tabulated values are obtained by adding increments of altitude. By the slope-ratio method the altitude at the end of 50,200 ft would be approximately 1,260 ft instead of the 1,200 ft shown in Table 1. The error (due to using 2,000-ft intervals in part of the table) seems negligible; but intervals of 1,000 ft or less may be tabulated if so desired.

TABLE 1.—DIMENSIONS OF APPROACH SURFACES, INSTRUMENT RUNWAY, IN FEET

Distance[a] (1)	Width (2)	Height[b] (3)	Altitude[b] (4)	Distance[a] (1)	Width (2)	Height[b] (3)	Altitude[b] (4)	Distance[a] (1)	Width (2)	Height[b] (3)	Altitude[b] (4)
200	1,000	0		5,200	2,500	100		10,200	4,000	200	
1,200	1,300	20		6,200	2,800	120		12,200	4,600	250	
2,200	1,600	40		7,200	3,100	140		14,200	5,200	300	
3,200	1,900	60		8,200	3,400	160		16,200	5,800	350	
4,200	2,200	80		9,200	3,700	180		52,200	16,000	1,200	

[a] Distance in feet from the zero end of the runway. At the zero end, the width (Col. 2) is 1,000 ft and the height (Col. 3) is zero. [b] Height in feet above the zero end of the runway. To convert values in Col. 3 to altitudes (feet above mean sea level), add the elevation of the zero end, at a given airport, and enter the result in Cols. 4.

Altitude contours may be drawn and are comparable with the surface contours shown on government maps. From the airmen's point of view, it seems better to use altitudes because aircraft are flown by reference to them rather than to slope ratios.

The "horizontal surface," under current CAA regulations, is described as a plane, circular in shape, with its height 150 ft above the "established airport elevation," and having a radius from the "airport reference point" varying with the service classification of the airport. The "established elevation" of an airport is defined as the highest point of the usable landing area. The "airport reference point" is defined as a point at the approximate center of the airport landing area. The control tower is frequently used as the reference point. The position of this point also should be fixed by giving its state coordinates. The "horizontal surface" is referred to a plane different from that of each runway end (Fig. 3).

TABLE 2.—ELEVATIONS FOR TURNING-BOWL SURFACES (CONTINENTAL TYPE AIRPORTS), IN FEET

Line	Elevations[a]	Radius from Airport Reference Point (Thousands of Feet):					
		0 to 10	10 to 11	11 to 12	12 to 13	13 to 14	14 to 15
1	Height above established airport elevations	150	200	250	300	350	400
2	Altitude above mean sea level						

[a] To correct values in line 1 to altitudes, add established elevations at the given airport, and enter the result, rounded to the next highest 10 ft, in line 2.

Extending outward and upward, from the periphery of the "horizontal surface" is a "conical surface" with a slope ratio of 1 on 20, its horizontal dimensions varying with the service classification of the airport.

To simplify the description of these surfaces further, the writer proposes that they be combined in one tabulation and known by a simple name, such as the "turning-bowl surface" (Table 2).

"Transitional surfaces" (Fig. 4) are defined as inclined planes with a slope of 1 on 7 measured outward and upward at right angles to the runway center line. These surfaces are designed to merge, gradually, the approach surfaces with the "horizontal and conical surfaces" (or the bowl surface if the writer's suggestion is followed). The adoption of tabulated altitudes for the "approach surface" should cause little or no difficulty in defining the "transitional surfaces" by the usual slope-ratio method. Transitional surfaces usually are limited in extent and the effect of curvature of the earth is not important. It should be noted that under current regulations the transition surface just outside the turning bowl begins with a vertical face nearly 500 ft high which does not permit tying the altitude contours of this transition surface into those of the turning bowl.

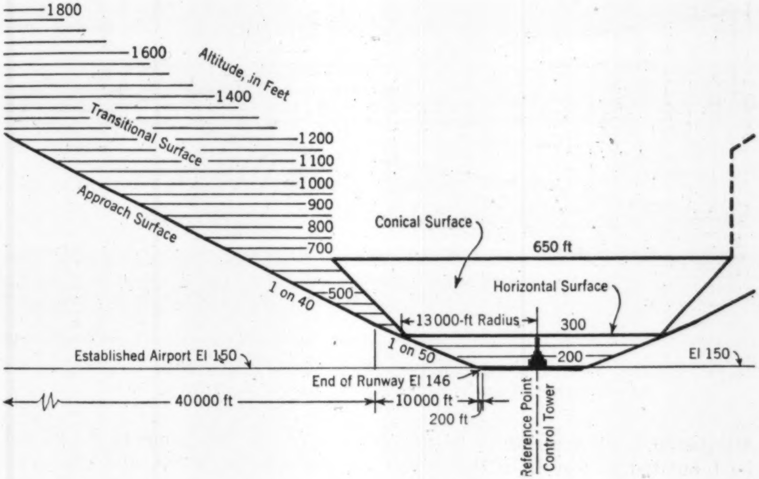
1800
1600
Altitude, in Feet
1400
Transitional Surface
1200
1100
1000
900
800
700
Approach Surface
Conical Surface
650 ft
Horizontal Surface
1 on 40
500
13000-ft Radius
300
1 on 50
200
Established Airport El 150
El 150
End of Runway El 146
40000 ft
10000 ft
200 ft
Reference Point
Control Tower

FIG. 3.—HORIZONTAL AND CONICAL SURFACES, INTER-CONTINENTAL TYPE AIRPORT (REGULATIONS, CIVIL AERONAUTICS ADMINISTRATION)

In addition to the requirements previously stated, *Technical Standard Order No. N 18* lists (under Section B) limiting heights of objects that may be considered obstructions to air navigation "unless special aeronautical study indicates otherwise." The method of defining the height of these objects above runways is the same as that proposed by the writer for the imaginary surfaces—namely, by listing heights which, when added to the elevation of the runway end or other reference points, give altitudes. Here the resemblance ceases. Alternate limitations are given in heights above ground and the tabulated distances are given in statute miles rather than in feet. Also, the tabulated distances in the case of instrument approaches are given in statute miles from runway ends and in all other parts of the airport are given in statute miles from the airport reference point. One attempt to present these regulations graphically or mathematically for inclusion in a zoning ordinance is enough to discourage the most ardent zoning advocate. Assuming, however, that they are justified, there seems to be no reason why the requirements should not be tabulated in feet from the airport reference point and in altitudes comparable to other requirements discussed in this paper.

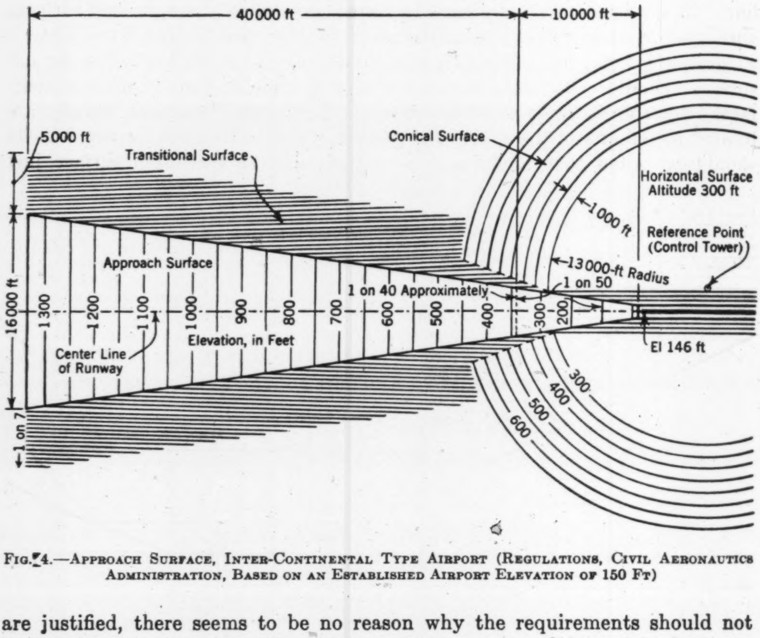
40000 ft
10000 ft
5000 ft
Transitional Surface
Conical Surface
Horizontal Surface Altitude 300 ft
1000 ft
Reference Point (Control Tower)
13000-ft Radius
Approach Surface
1 on 40 Approximately
1 on 50
16000 ft
1300
1200
1100
1000
900
800
700
600
500
400
300
200
Center Line of Runway
Elevation, in Feet
El 146 ft
300
400
500
600
1 on 7

Fig. 4.—Approach Surface, Inter-Continental Type Airport (Regulations, Civil Aeronautics Administration, Based on an Established Airport Elevation of 150 Ft)

There are further limitations of objects "whose elevation would increase the final approach minimum flight altitude within a civil airway" and "within certain established Military Coastal Corridors." The administration of the requirements of Section B presupposes that there are zoning officials capable of performing "special aeronautical study," with zoning powers extending far beyond the limits of the airport. The average zoning commission does not have such powers or such a staff. The writer does not know of a single case in which the requirements of Section B have been written into a zoning ordinance.

A further commentary on *Technical Standard Order No. N 18* is that many of the existing airports cannot come close to meeting the requirements, and the available sites for new airports meeting the requirements are difficult to find. There seems to be no real reason why the engineer should not prepare his zoning map and descriptions in the simplified manner advocated in this paper. Officials of the CAA could have no valid objections because the adding of increments of altitude for "approach surfaces" results in a slightly flatter approach slope than does the slope-ratio method.

The requirements for military airfields have led to the establishment of different criteria for their approaches (Fig 5). Air Force Regulation 86-3 sets forth dimensional criteria for United States Air Force airfields. Air Force requirements are stated in somewhat simpler terms than those for civil airfields, but the dimensions are entirely different. A "clear zone" at the end of each runway is defined as

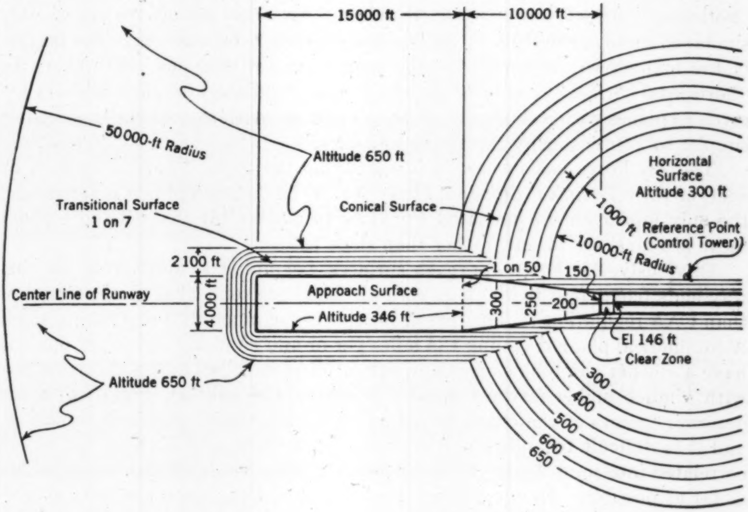
15000 ft
10000 ft
50000-ft Radius
Altitude 650 ft
Horizontal Surface Altitude 300 ft
Transitional Surface 1 on 7
Conical Surface
1000 ft
Reference Point (Control Tower)
10000-ft Radius
2100 ft
1 on 50
150
Center Line of Runway
Approach Surface
4000 ft
300
250
200
Altitude 346 ft
El 146 ft
Clear Zone
300
400
500
600
650
Altitude 650 ft

FIG. 5.—INSTRUMENT RUNWAY, MILITARY AIRFIELD, BASED ON AN ESTABLISHED AIRPORT ELEVATION OF 150 FT (REGULATIONS, U. S. AIR FORCE)

> " * * * the area immediately adjacent to the end of a runway which has been cleared of all above-ground obstructions and graded to prevent damage to aircraft undershooting or overrunning the runway. The standard clear zone dimensions are 1,000 ft long (measured along the extended runway center line) and 1,500 ft wide (750 ft on each side of the extended runway center line).

Beyond the clear zone is an "approach zone" which is an area beyond each clear zone, extending on the ground for a distance of 25,000 ft along and symmetrical about the extended center line of the runway. The width of the approach zone at the end of the clear zone is 1,500 ft; it flares to 4,000 ft at 10,000 ft from the end of the clear zone; and it remains 4,000 ft wide for the additional 15,000 ft.

The "approach surface" is an imaginary plane covering the "approach zone," beginning at the end of the "clear zone" at the elevation of the end of the runway and rising over the "approach zone" on a slope of 1 on 50 (known as the glide angle) for an horizontal distance of 10,000 ft (200 ft above the elevation of the end of the runway). From this point the controlling elevation of the approach surface remains at 200 ft until the end of the approach zone (25,000 ft from the end of the clear zone).

In the case of an "airfield reference point," "established airfield elevation," "horizontal surface," and "conical surface," Air Force definitions are roughly similar to those of the CAA. Air Force regulations tabulate widths and heights in the manner recommended by the writer for civil airfields. However, the "horizontal surface" is referred to as a "plane" and the approach surfaces are given as planes with a slope of 1 on 50. These regulations could be made much simpler to administer by specifying altitudes.

The Air Force has succeeded in specifying the type of hazard covered by Section B of *Technical Standard Order No. N 18*, in a simplified manner, and the only improvement indicated would be to make clear that altitudes above mean sea level are meant, rather than slope ratios.

Obviously, Air Force approach surfaces, beginning 1,000 ft from the runway ends (compared to 200 ft in civil airfields) are somewhat more restrictive than CAA regulations. The reason for this is the much flatter climbing slope. A commerical plane traveling 125 miles per hr and climbing 500 ft per min will have a steeper climbing slope than, say, a jet plane climbing at the same rate with a much higher forward speed. However, the military aircraft of today determine many of the characteristics of the commercial planes of tomorrow, and it is difficult to understand why the requirements of both should not be correlated into joint Army-Navy-Air Force-Civil zoning regulations, simplified as far as possible. In one project, the airfield is zoned approximately according to CAA regulations. An important Air Force base was contemplated which required Air Force zoning regulations. As a further problem, the obstruction map prepared by the Coast and Geodetic Survey, United States Department of Commerce (USCGS), shows an airport reference point that is several hundred feet away from the point used by the other two. To complicate matters further, the so-called "horizontal surface" is actually zoned at this airport with a radius of 4 miles; CAA regulations call for a radius of 13,000 ft; and Air Force Regulations require that a radius of 10,000 ft be shown on approach drawings.

Avigation easements offer a means of controlling airport approaches and of reimbursing property owners for the damages suffered, without resorting to the outright purchase and subsequent eviction of families from homes to which they may be deeply attached, or from farms or business locations providing their livelihood. Avigation easements usually should be attempted only when zoning imposes real hardship or when they may be obtained at less cost than outright purchase would entail. Avigation easements also may be the only solution where political boundaries or lack of enabling legislation make zoning impracticable. Simplified maps and descriptions should be used in the taking of avigation easements in the same manner as in zoning practice.

SUMMARY

Summing up briefly, the desirable features of airport zoning maps are as follows:

1. Airport reference point and runway ends fixed by state coordinates;
2. Horizontal limits of imaginary surfaces fixed by radial distances, in feet, from the airport reference point, wherever possible;
3. The elevation of all runway ends referred to mean sea level;
4. The number of imaginary surfaces reduced to a minimum with altitudes referred to mean sea level; and
5. Ground contours and landmarks shown in dashed lines.

A zoning map meeting these requirements can be plotted on other maps without recourse to field work and may easily be used by engineers and zoning ordinance administrators.

Even with the best of airport approach protection, vigilance and administrative effort will always be required to prevent the encroachment of growing trees and man-made hazards. It is doubted that any existing airports live up to their ordinances completely. By doing so, however, safety features of the airport and its neighborhood are enhanced, the capital investment is protected, the capacity of the port is maintained, and early obsolescence may be averted.

DISCUSSION

Harold M. Lewis,[2] M. ASCE.—The CAA requirements for clearances on airport approaches have been clearly presented by the author. There is an obvious need for protecting these approaches through the use of zoning ordinances. The Zoning Commission of New Castle County, Delaware, has attempted to do this in a zoning code[3] prepared under the direction of the writer. The code supplies an interesting example of the way in which Mr. Beavin's objectives have been adapted to a specific case.

Airport zoning by use of the usual municipal ordinances is handicapped by the fact that the runway approaches (which should be protected) generally extend far beyond the limits of the municipality. This was not the case in New Castle County, where there is now (1953) only one major airport—the New Castle County Airport—situated about 5½ miles southwest of the center of the city of Wilmington, Del. The airport is located near the western approach of the Delaware Memorial Bridge and it is within an area that experienced very rapid development in the period following World War II. Designated as Class 1 by the CAA, the airport is used as a training center for jet airplanes by the Air Force. The airport management, the pilots, the county officials, the local population, and the real estate interests all recognize the need for some control for the sake of safety and orderly development.

The proposed zoning code for New Castle County will apply to all the unincorporated areas of the county. These areas represent 95% of the total county area of 433 sq miles, with a population in 1950 of 80,413 (approximately 37% of the total county population). The municipality nearest the airport is New Castle, the center of which is 1½ miles from the eastern edge of the airport. Newark, Del., an important industrial community, lies 5½ miles to the west of the airport.

Because the county is large and most of its population is concentrated in its northern section, the zoning maps are in ten sections. Such a procedure was authorized in the enabling legislation. Each section corresponds, with one minor exception, to one of the various "Hundreds" into which the county is divided. These "Hundreds" are representative and census-enumeration districts but have no local government; their boundaries, in general, follow watercourses, thus making them natural subdivisions for zoning purposes.

Hearings on the proposed zoning code were started in November, 1952, and nine hearings had been held prior to July, 1953, the last four of these hearings being devoted both to the code and to three of the sectional maps (including the New Castle County Airport and its principal approaches) which had been completed. At each of these hearings there was also presented a map entitled "Height Regulations on Approaches to New Castle County Airport." The essential features of this map are shown in Fig. 6. This map supplements, but does not legally form a part of, Article XVI of the code

---

[2] Cons. Engr. and City Planner, New York, N. Y.

[3] "Proposed Zoning Code of New Castle County, Delaware, Revision of March 3, 1953," prepared for the New Castle County Zoning Comm. by Harold M. Lewis, New York, N. Y. (mimeographed).

("Special Regulations Around Airports"). It contains the following desirable features for airport zoning maps:

1. The airport reference point is given by latitude and longitude, rather than by state coordinates as recommended by Mr. Beavin.

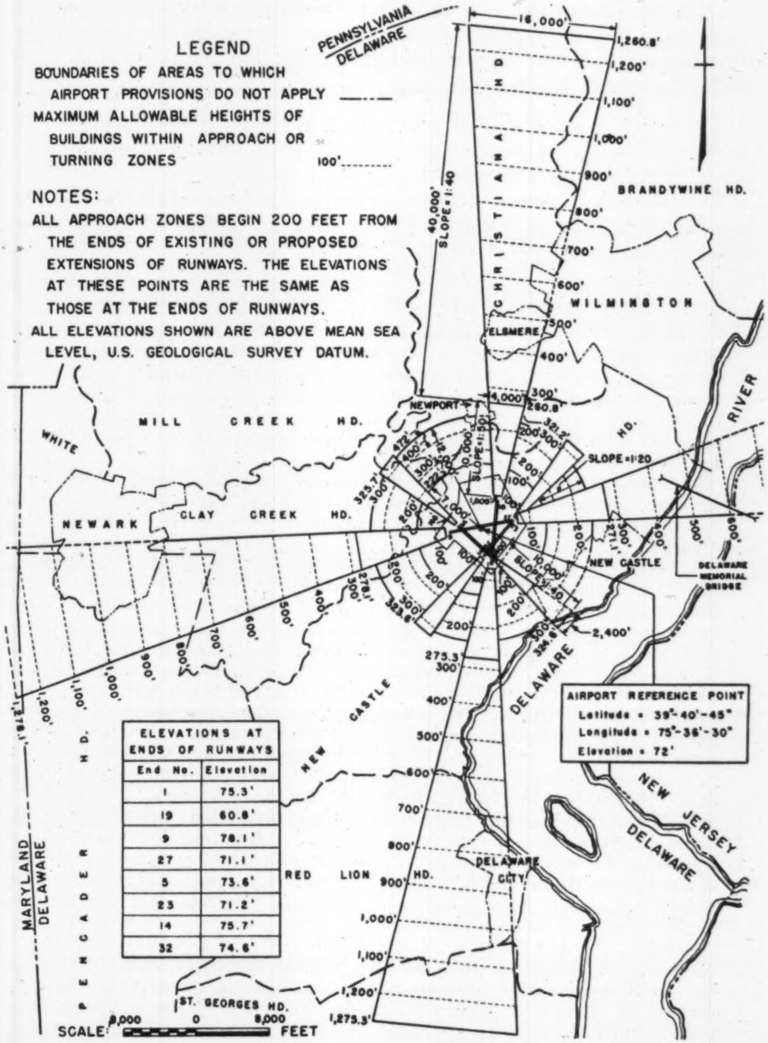

LEGEND

BOUNDARIES OF AREAS TO WHICH AIRPORT PROVISIONS DO NOT APPLY —.—.—

MAXIMUM ALLOWABLE HEIGHTS OF BUILDINGS WITHIN APPROACH OR TURNING ZONES 100'--------

NOTES:

ALL APPROACH ZONES BEGIN 200 FEET FROM THE ENDS OF EXISTING OR PROPOSED EXTENSIONS OF RUNWAYS. THE ELEVATIONS AT THESE POINTS ARE THE SAME AS THOSE AT THE ENDS OF RUNWAYS.

ALL ELEVATIONS SHOWN ARE ABOVE MEAN SEA LEVEL, U.S. GEOLOGICAL SURVEY DATUM.

ELEVATIONS AT ENDS OF RUNWAYS

End No.	Elevation
1	75.3'
19	60.8'
9	78.1'
27	71.1'
5	73.6'
23	71.2'
14	75.7'
32	74.6'

AIRPORT REFERENCE POINT
Latitude = 39°-40'-45"
Longitude = 75°-36'-30"
Elevation = 72'

PENNSYLVANIA
DELAWARE
16,000'
1,260.8'
1,200'
1,100'
1,000'
900'
800'
700'
600'
500'
400'
300'
260.8'
40,000' SLOPE = 1:40
CHRISTIANA HD.
BRANDYWINE HD.
WILMINGTON
ELSMERE
NEWPORT
4,000'
MILL CREEK HD.
WHITE
NEWARK
CLAY CREEK HD.
SLOPE = 1:20
SLOPE = 1:30
10,000'
NEW CASTLE
DELAWARE MEMORIAL BRIDGE
RIVER
DELAWARE
2,400'
275.3'
NEW CASTLE HD.
NEW JERSEY
DELAWARE
DELAWARE CITY
RED LION HD.
PENCADER HD.
ST. GEORGES HD.
MARYLAND
DELAWARE
1,278.1'
1,273.3'
SCALE 8,000 0 8,000 FEET

FIG. 6.—HEIGHT REGULATIONS ON THE APPROACHES TO THE NEW CASTLE COUNTY AIRPORT, NEW CASTLE COUNTY, DELAWARE

2. Horizontal limits of areas within which controls are established are fixed by radial distances from the airport reference point and by wedge-shaped areas extending beyond each runway end.

3. The elevation of the airport reference point and of runway ends is referred to mean sea level.

4. The elevations above mean sea level of all points within the approach areas subject to height control, with the permitted elevations of new structures, are shown by 100-ft contours and 20-ft ground contours and the existing street system throughout the area of the map.

The writer believes that the combination of this map and the sections of the code relating to it provides a practical example of the application of zoning to the control of airport approaches.

The following airport zoning restrictions in the New Castle County code have met with such general endorsement that no changes have been made since the initial hearing.[3]

ARTICLE XVI—SPECIAL REGULATIONS AROUND AIRPORTS

Section 1. Purpose.—In order to provide free air space for the safe descent, landing, and ascent of aircraft and to prevent undue hazard to the life or property of the occupants of buildings within airport approach or turning zones, the following special regulations in this Article shall apply to any land airport, other than a helicopter landing facility, owned and operated by a public agency or an instrumentality thereof and designated by Resolution of the Levy Court as a "major airport."

Section 2. Limitation of Height Within Approach Zones.—Within the air space above the approach zone to each end of each airport runway no building structure shall be erected or altered to project above the following planes:

(1) In the case of runway used or designed to be used for instrument landings, a plane with a slope of 1 (vertical) to 50 (horizontal) projected from a point two hundred (200) feet beyond the end of the existing runway or proposed extension thereof for a distance of ten thousand (10,000) feet, said plane to be in the shape of a symmetrical trapezoid one thousand (1,000) feet in width at its lowest point and four thousand (4,000) feet in width at its highest point; combined with a second plane with a slope of 1 (vertical) to 40 (horizontal) extending from the upper edge of the first plane for an additional distance from the airport runway of forty thousand (40,000) feet, said plane to be in the shape of a symmetrical trapezoid four thousand (4,000) feet in width at its lowest point and sixteen thousand (16,000) feet in width at its highest point.

(2) In the case of any other runways, a plane with a slope of 1 (vertical) to 40 (horizontal) projected from a point two hundred (200) feet beyond the end of the existing runway or proposed extension thereof for a distance of ten thousand (10,000) feet, said plane to be a symmetrical trapezoid four hundred (400) feet wide at its lowest point and two thousand four hundred (2,400) feet wide at its highest point.

Section 3. Limitation of Height Within Turning Zone.—Within twelve thousand (12,000) feet from the airport reference point as established by the Civil Aeronautics Administration, no building or structure shall be erected or altered to project within the air space of the airport turning zone defined as the space above the following surfaces:

(1) A horizontal surface one hundred and fifty (150) feet above the established airport elevation as determined by the Civil Aeronautics

Administration and extending seven thousand (7,000) feet radially from the airport reference point as determined by the Civil Aeronautics Administration.

(2) A conical surface beginning at the outer edge of the horizontal surface as described in the above paragraph and extending outward with each element thereof rising on a slope of 1 (vertical) to 20 (horizontal) to a distance of twelve thousand (12,000) feet from the airport reference point as determined by the Civil Aeronautics Administration.

Section 4. Map showing Application of Provisions.—A map showing the approximate maximum heights to which any building or structure may be built within the area subject to the controls set forth above shall be on file in the office of the Building Inspector of New Castle County.

Section 5. Existing Obstructions.—Any present existing obstructions of record on the date of adoption of this Code shall be exempt therefrom, but nothing herein contained shall be interpreted to prevent negotiations, or the exercise of right of eminent domain by a public agency, for the removal of such present obstructions.

Section 6. Exception to Above Provisions.—In no case shall the provisions of this Code prevent the erection of a building or structure distant one hundred (100) feet or more from the boundary of an airport to a maximum height of twenty (20) feet above natural ground level.

The Zoning Commission of New Castle County plans to submit its final report on the entire code, together with maps for the five northern sections to the Levy Court (the county's legislative body) in the fall of 1953.

Two of the runways on New Castle County Airport are designed to be used for instrument landings and their approaches follow the pattern shown in Fig. 1. It is indicated in Fig. 1 that the controlled areas for their approaches extend to a distance of 50,000 ft from a point 200 ft beyond the ends of the runways, with a slope of 1 on 50 for the first 10,000 ft and a slope of 1 on 40 beyond. For the other two runways, controls extend to a distance of 10,000 ft from a point 200 ft beyond the end of the runways with a slope of 1 on 40. The approaches to the east-west instrument runway extend over a portion of New Jersey on the east and just over the Maryland-Delaware boundary line on the west. These areas outside New Castle County and the incorporated municipalities in the county are not subject to the zoning provisions, but it will be noted that the approach areas avoid all but a negligible corner of New Castle and all of Wilmington except some small residential sections on the extreme western edge. The town of Elsmere, Del., lies directly in the northern approach to an instrument runway, but at this location the approach surface is approximately 300 ft above the ground. Although the southern part of Newark is also within an instrument runway approach, the permissible height of a structure at that distance would be 800 ft above ground level, making the control nonrestrictive.

The edge of the conical-shaped section of the turning zone area, extending 12,000 ft from the airport reference point, extends over a part of New Castle and just reaches Newport, Del.

The only points at which the proposed controls would hit developed areas are at the southern end of the north-south instrument runway and near the eastern corner of the airport where an instrument and a noninstrument runway intersect.

Section 1 of that part of the code previously quoted aroused discussion at the public hearings, since the county also contains airports (owned by industrial companies) which are used primarily for experimental purposes. It should be noted that the code applies only to a

> "* * * land airport, other than a helicopter land facility, owned and operated by a public agency or an instrumentality thereof and designated by the Resolution of the Levy Court as a 'major airport'."

It is expected that only the New Castle County Airport will be designated as a "major airport," but the code provisions would apply to any additional airport of similar character that might be constructed and so designated.

Section 5 (previously quoted) implies that, in some cases, additional control might be exercised through eminent domain. Mr. Beavin has stated that "* * * restricting the heights of the structures that may be built in residential areas to something less than that of a two-story house * * * may only be construed as a taking away of a considerable part of the value of the properties so restricted." In conformance with this theory, Section 6 provides that the code would not prevent the erection of a building to a height of 20 ft if located 100 ft or more from the boundary of the airport.

No attempt was made to incorporate in the code any control over the "transitional surfaces" shown in Figs. 4 and 5 and covered in the *Technical Standard Order No. N 18* of the CAA. No objection to this omission was made at the public hearings.

The writer feels that the descriptive presentation supplemented by a map (as developed for New Castle County) has advantages over such a tabular presentation as Mr. Beavin proposes. It is also easier for the layman to comprehend. The map shows at a glance all the areas where height controls will apply, and permits an owner or prospective builder to determine (from a simple scaling of the map and computations of differences between ground elevation and permissible structure elevation) the approximate height to which a structure can be erected at any specific location.

BENJAMIN EVERETT BEAVIN, SR.,[4] M. ASCE.—The technique followed by Mr. Lewis in preparing a zoning code for New Castle County is commendable and should provide an instrument whereby the zoning commission can protect both the approaches to the airport and the interests of its neighbors.

Although in Fig. 6 it was not possible to show in extensive detail, the positions of the runway ends (with relation to the airport reference point), and the azimuths of the approach zones were undoubtedly fixed in the zoning ordinance.

Because of the facility with which engineers and surveyors can settle possible conflicts between proposed construction and zoning restrictions, state plane coordinates are preferable to the geographic coordinates used by Mr. Lewis at New Castle County Airport. Given the geographic coordinates, however, the state coordinates can be computed readily. If the astronomic bearings of the approaches are given in the ordinance, a correction must be applied before computing the state coordinates of the runway ends and other points. It would seem better to fix all positions by plane coordinates in the ordinance, rather than to cause the same computations to be made several times during the life of the ordinance. It also may be desirable to have the geographic coordinates of the airport reference point given in zoning ordinances, in addition to the state plane coordinates.

---

[4] Partner, Porter, Urquhart & Beavin, Newark, N. J., and Baltimore, Md.

The writer hopes that the paper and the discussion by Mr. Lewis will be of service to other members of the profession. It is also hoped that further efforts by the profession may lead to the correlation of zoning regulations among governmental agencies of the United States.

AMERICAN SOCIETY OF CIVIL ENGINEERS
Founded November 5, 1852
TRANSACTIONS

Paper No. 2671

THE EQUIVALENT RECTANGLE IN PRESTRESSED CONCRETE DESIGN

By John J. Peebles,[1] J. M. ASCE

With Discussion by Messrs. Fred E. Koebel, and John J. Peebles

Synopsis

A simple procedure is presented for selecting cross-sectional shapes and dimensions for prestressed concrete beams in a manner similar to that used for selecting structural steel shapes. The required section modulus is computed from the bending moments and from the allowable working stress in concrete. From an equation utilizing an equivalent rectangular cross section, or by use of a chart, the dimensions of the selected shape can be determined rapidly.

Notation

The letter symbols adopted for use in this paper are defined where they first appear, in the illustrations or in the text, and are arranged alphabetically for reference in the Appendix.

Introduction

Prestressed concrete members differ from conventional reinforced concrete members in that compression is introduced into the member to counteract tensile stresses caused by the applied loads. Prestressed structures utilize more efficiently the compressive strength of concrete and the tensile strength of steel in the form of high-strength, cold-drawn wires or cables. As a result, much greater spans and load capacities are possible with prestressed concrete than would be feasible with conventional reinforced concrete. Thus, prestressing tends to place concrete in a much better competitive position relative to other structural materials.

One type of member that affords outstanding possibilites for economy of materials is the prestressed concrete beam. The most efficient cross section for this type of beam is usually an I, a T, or a hollow rectangle. These shapes

---

Note.—Published in April, 1953, as *Proceedings-Separate No. 187*. Positions and titles given are those in effect when the paper or discussion was received for publication.

[1] Engr., Bureau of Reclamation, U. S. Dept. of the Interior, Columbia Falls, Mont.

do not lend themselves to rapid determination of cross-sectional properties such as areas and moments of inertia. Consequently, the design computations often become extremely tedious when the final dimensions for a given set of conditions must be obtained by assuming a series of trial sections.

DEVELOPMENT OF BASIC EQUATIONS

Rectangular cross sections lend themselves to a fairly direct method of design. For any given irregular-shaped section such as an I, a T, or a hollow rectangle, a solid rectangular section exists that is equivalent in area and moment of inertia about a given axis. This equivalent rectangle usually will have a height different from that of the actual section.

The basic design equation for prestressed concrete is of the form: $s = \frac{P}{A} \pm \frac{M\,y}{I}$, in which s is the unit fiber stress, P is the effective prestressing force, A represents the area of the gross concrete section, M denotes bending moment, y is the distance from the center of gravity of the gross concrete section (CGG) to the fiber to be investigated, and I is the moment of inertia of the gross section about its center of gravity.

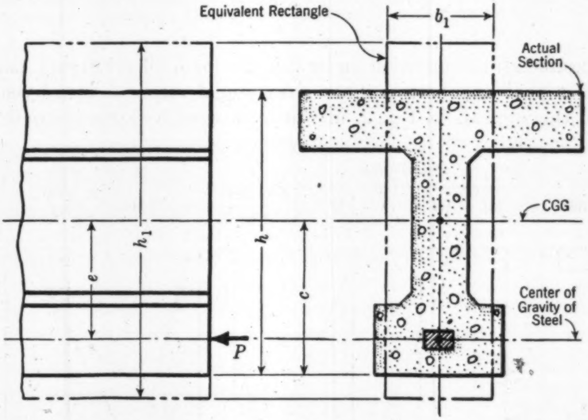

FIG. 1.—RELATIONSHIP BETWEEN THE EQUIVALENT RECTANGLE AND THE ACTUAL CROSS SECTION

In the direct stress expression,

$$s = \frac{P}{A} \quad\quad (1a)$$

the stress depends on the force and the area only and is independent of the shape of the section. In the flexural stress expression,

$$s = \frac{M\,y}{I} \quad\quad (1b)$$

in which a straight-line variation is assumed, the stress is dependent on the shape of the section inasmuch as the moment of inertia and the fiber distance are dependent on this property. Therefore, the equivalent rectangle can be used as a basis for determining the required area and moment of inertia of the cross section if coefficients are applied to the fiber distances to compensate for the differences in height.

Fig. 1 shows superimposed on a T-section a rectangular section of height h_1 and width b_1, having a moment of inertia about the horizontal axis identical to that of the T-section and having the same CGG as has the T-section. The height of the actual section is h. The ratio of the bottom fiber distance to the height of the actual section may be expressed as

$$i = \frac{c}{h} \qquad (2)$$

(For cross sections having horizontal axes of symmetry, $i = 0.500$.) Similarly,

$$i_1 = \frac{c}{h_1} \qquad (3a)$$

and

$$i_2 = \frac{e}{h_1} \qquad (3b)$$

The desired stress condition under full live load, all prestress losses having occurred, is that the bottom fiber stress equal zero. A step-by-step illustration of this appears in Fig. 2, in which compressive stresses are designated positive, and tensile stresses are designated negative. The desired bottom fiber stress is expressed as follows:

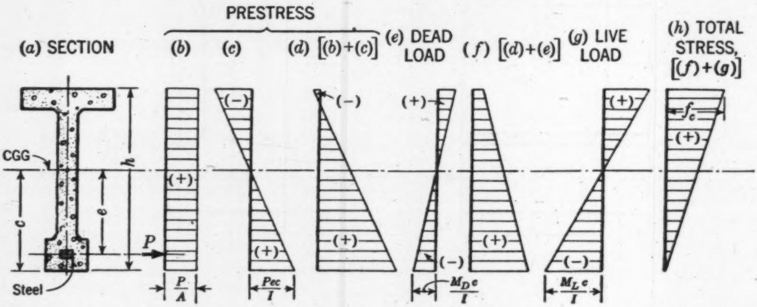

FIG. 2.—LONGITUDINAL STRESS DISTRIBUTION IN A PRESTRESSED CONCRETE T-SECTION

$$s = \frac{P}{A} + \frac{P\,e\,c}{I} - \frac{M_D\,c}{I} - \frac{M_L\,c}{I} = 0 \qquad (4)$$

in which the subscripts D and L correspond to dead load and live load. Fig. 2 also shows that the direct stress portion of the prestress at the CGG is

$$\frac{P}{A} = \frac{c}{h} f_c = i\,f_c \qquad (5a)$$

in which f_c is the working stress in concrete. Therefore, the equation for the prestress force is

$$P = i\, f_c\, A \tag{5b}$$

The area of the equivalent rectangle is expressed as

$$A = b_1\, h_1 \tag{6a}$$

and, consequently,

$$P = i\, f_c\, b_1\, h_1 \tag{6b}$$

The moment of inertia of the equivalent rectangle is

$$I = b_1 \frac{h^3_1}{12} \tag{7}$$

Substituting Eqs. 3, 6, and 7 into Eq. 4 and, reducing,

$$s = i\, f_c + 12\, i\, f_c\, i_1\, i_2 - \frac{12\, M_D\, i_1}{b_1\, h^2_1} - \frac{12\, M_L\, i_1}{b_1\, h^2_1} = 0 \tag{8}$$

It is emphasized that Eq. 8 shows the dimensions of the cross section to be independent of the properties of the steel prestressing wires and—for any given cross-sectional shape—to depend only on the bending moments and the allowable concrete working stress. Thus, the concrete sectional dimensions can be selected first, and the details of the prestressing steel can be determined later by using Eq. 5*b*.

The following equalities may be specified:

$$b_1 = z\, h_1 \tag{9a}$$

$$M_D + M_L = M_T \tag{9b}$$

and

$$i\,(1 + 12\, i_1\, i_2) = K \tag{9c}$$

Substituting into Eq. 8 the symbols defined by Eqs. 9, and collecting terms,

$$K\, f_c - \frac{12\, M_T\, i_1}{z\, h^3_1} = 0 \tag{10a}$$

or

$$\frac{M_T}{K\, f_c} = \frac{z\, h^3_1}{12\, i_1} \tag{10b}$$

Eq. 10*b* indicates the section modulus of the equivalent rectangular section. The required section modulus based on the total moment is Z_T, expressed as the quotient,

$$\frac{M_T}{K\, f_c} = Z_T \tag{11a}$$

and $h_1 = \dfrac{c}{i_1} = \dfrac{i\, h}{i_1}$. Therefore,

$$\left.\begin{aligned} Z_T &= \left(\frac{i^3\, z}{12\, i^4_1}\right) h^3 \\ &\text{or} \\ h &= \sqrt[3]{\left(\frac{12\, i^4_1}{i^3\, z}\right) Z_T} \end{aligned}\right\} \tag{11b}$$

Fig. 2 indicates that, if the ratio of live load to dead load is large, the live-load fiber stress may control the design. This fiber stress must not exceed the allowable working stress, f_c, because if it does, the bottom fiber stress will exceed f_c when the live load is not acting on the beam. In this case, the last element of Eq. 8—the expression $\frac{12\,M_L\,i_1}{b_1\,h^2_1}$—is equal to f_c. By the same procedure followed in arriving at Eqs. 11*b*, therefore,

$$\left.\begin{aligned} Z_L &= \left(\frac{i^3\,z}{12\,i^4_1}\right) h^3 \\ &\text{or} \\ h &= \sqrt[3]{\left(\frac{12\,i^4_1}{i^3\,z}\right) Z_L} \end{aligned}\right\} \qquad (12a)$$

in which

$$Z_L = \frac{M_L}{f_c} \qquad (12b)$$

In Eqs. 12*a*, Z_L is computed using the live-load moment and the working stress,

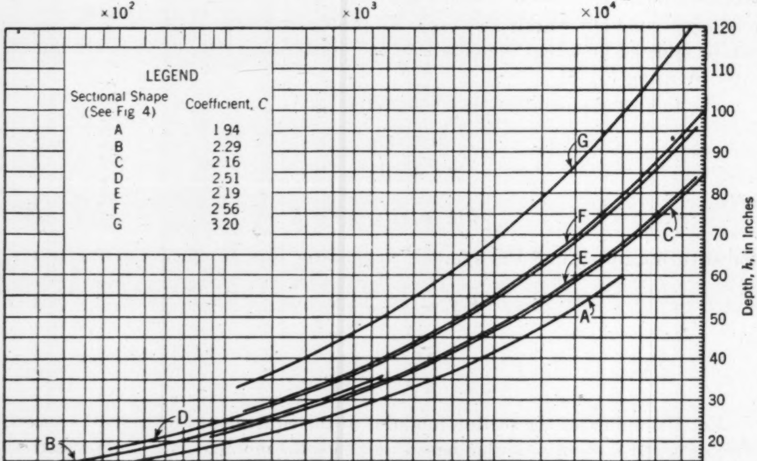

FIG. 3.—CHART FOR DETERMINING THE DEPTH OF THE CROSS SECTION

whereas Z_T in Eqs. 11*b* is computed using the sum of the dead-load moments and live-load moments and the working stress modified by the prestressing factor, *K*.

Fig. 3 is a chart based on Eqs. 11 and 12 for the various cross-sectional shapes shown in Fig. 4. The cubic equations for these shapes would be represented by parallel straight lines on logarithmic graph paper, but semilogarithmic paper was used so that the vertical scale would be uniform. Each curve is identified by its value of the coefficient $C = \sqrt[3]{\frac{12\,i_1^4}{i^3\,z}}$, as it appears in the equation, $h = C\,\sqrt[3]{Z}$, in which Z is either Z_L or Z_T as they are expressed in Eqs. 11 and 12.

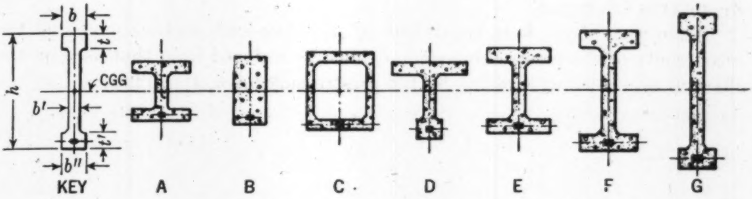

FIG. 4.—SECTIONAL SHAPES

TABLE 1.—SECTIONAL PROPERTIES[a] CORRESPONDING TO FIG. 4[b]

Geometric ratios	SECTION DESIGNATION IN FIG. 4						
	A	B	C	D	E	F	G
$\frac{b}{h}$	1.000	0.500	0.875	1.000	0.750	0.500	0.250
$\frac{b'}{h}$	0.200		0.100	0.167	0.143	0.111	0.091
$\frac{b''}{h}$	1.000		0.100	0.333	0.750	0.500	0.250
$\frac{t}{h}$	0.200		0.125	0.167	0.167	0.143	0.125
$\frac{t'}{h}$	0.200		0.125	0.250	0.167	0.143	0.125
i	0.500	0.500	0.500	0.622	0.500	0.500	0.500
i_1	0.396	0.500	0.395	0.534	0.390	0.394	0.422
i_2	0.317	0.400	0.346	0.426	0.325	0.338	0.369
K	1.253	1.700	1.320	1.864	1.261	1.300	1.435
z	0.326	0.500	0.230	0.256	0.210	0.138	0.093
$\frac{A}{h^2}$	0.520	0.500	0.368	0.347	0.345	0.222	0.131
$\frac{w_D}{h^2}$	0.542	0.521	0.384	0.362	0.360	0.231	0.136
$\frac{I}{h^4}$	0.0690	0.0417	0.0492	0.0392	0.0475	0.0298	0.0153

[a] Properties of the equivalent rectangle also appear, and are defined by Fig. 1 and Eqs. 3, 6*a*, 7, 9*a*, and 9*c*.

[b] The center of gravity of the steel (Fig. 4, Key) is at the center of gravity of the bottom flange.

The best procedure for determining the required cross-sectional dimensions is to obtain the value of h from Fig. 3, based on the live-load section modulus,

Z_L. Using this h-value for computing the first trial dead-load moment, h is again determined from Fig. 3, based on the total load section modulus, Z_T. Usually one or two adjustments of the dead-load moment will result in the correct section for the latter case, which is the same procedure used in the selection of structural steel shapes. The larger h-value based on either Z_L or Z_T governs the design.

When the depth h is controlled by the live-load section modulus, the eccentricity of the prestressing steel, e, must be reduced from that used on the chart to prevent overstressing by the prestressing force, P. Thus,

$$K f_c - \frac{M_T}{Z_L} = 0 \qquad (13)$$

The required K-value is given by $K = \frac{M_T}{f_c Z_L}$; so that, using Eq. 9c,

$$i_2 = \frac{K - i}{12\, i\, i_1} \qquad (14)$$

Using the relationships, $e = i_2 h_1$ and $h_1 = \frac{i\,h}{i_1}$, which were indicated previously, it is found that

$$e = \left(\frac{K - i}{12\, i^2{}_1}\right) h \qquad (15)$$

The eccentricity of the prestressing wires can be adjusted at any section along the beam to compensate for the difference in moment by multiplying e by the ratio, $\frac{M_x}{M_T}$, in which M_x and M_T are the sum of the dead-load moments and live-load moments at a distance x along the beam and at the point of maximum moment, respectively. Thus, the eccentricity over the supports is zero.

Based on the four elements of Eq. 4, fiber stresses can be checked for conformance with design specifications in the intermediate stages. The fiber stress is expressed as follows:

$$s = i f_c \mp \frac{(i f_c A)\, e}{Z} \pm \frac{M_D}{Z} \pm \frac{M_L}{Z} \qquad (16)$$

in which Z is the section modulus for the top or bottom fiber, depending on which fiber is to be investigated.

Theoretically, the fiber stresses should be checked on the basis of the area of the net concrete section, A_c, and the moment of inertia of the net concrete section, I_c. These properties and those of the transformed section can be computed at the designer's option after the sectional shape and dimensions have been determined. However, the usual design assumptions and the inherent inconsistency of concrete render questionable the justification for such refinements.

Referring to Fig. 4, theory and practice support the indication that a decrease in the depth of the section is accompanied by an increase in the required area. Conversely, the deeper the section, the smaller the required area. Thus, a sectional shape may be chosen from a purely economical standpoint. For example, in a multistory building, although shallow beams will be more costly in themselves than will deep beams, the possibility for savings in the total height of the building may be a consideration.

In the case of bridges, overpasses, and similar structures, headroom may be an important consideration, and the most shallow practicable beam may be desirable. However, in many situations headroom is not a governing factor, and the most economical beam can be utilized. Also, cases occur in which these two extremes must be balanced against each other and some average section may be desired in which each condition is partly satisfied.

Although economy apparently favors deeper beams, considerations of practicability tend to limit the depth. Tensile stresses in the top fibers of the beam over the supports (where the bending moments become zero) increase with increased depth of the beam. Provisions must be made to resist these stresses regardless of the shape of the beam, but the cost of such provisions increases with increased depth-span ratio of the beam. Also, deep, thin sections exhibit an increased tendency toward buckling, and more web stiffeners therefore are required. The seven shapes shown in Fig. 4 probably will cover most design conditions, but the variety of shapes that could be used is unlimited.

Eqs. 11 and 12 can be developed for other shapes, and curves can be drawn in the same manner as those in Fig. 3. In determining the various properties for the shapes shown in Fig. 4 (as listed in Table 1), the first step was to assume the flange and web proportions as some fraction of the height, h. These appear as the first five lines in Table 1. To avoid complicated algebraic expressions, actual dimensions of typical sections were used to determine the center of gravity of the section and to compute values of the area and of the moment of inertia about the horizontal axis through the CGG. Next, the dimensions of the equivalent rectangle were determined from Eqs. 2, 3*a*, 6*a*, and 7.

The center of gravity of the prestressing steel was assumed to be at the center of gravity of the bottom flange, and thus i_2 was some fraction of i_1. (The value of i_2 is different if the live load controls the design, but this fact does not affect the preparation of the curves.)

Eqs. 9*a* and 9*c* were used in evaluating K and z. Values for A and w_D in terms of h^2, and of I in terms of h^4, also were determined in order to facilitate rapid computation of these properties when h is known.

EXAMPLES

To illustrate the use of the equivalent rectangle in designing prestressed concrete beams, two examples are presented. Table 2 shows the initial steps in the computations. For the 100-ft span, a value of Z_L is found by dividing values in Col. 2 by those in Col. 3. Entering Fig. 3 with a value for Z_L yields and h-value of 41.1 in., which is used to compute the first trial value for Col. 8. The value of Z_T is obtained from Eq. 11*a*. Re-entering Fig. 3 with the value from Col. 9, an h-value of 47.4 in. is obtained, which does not agree with the value in Col. 6. A second trial value of h equal to 52 in. yields the values:

$M_D = 11{,}700$ kip-in. and $M_T = 19{,}200$ kip-in. The new value for Z_T is 8,200 in^3. Using this value, a depth of $h = 51.6$ in. is obtained from Fig. 3. This is satisfactory.

Eq. 16 is used to check fiber stresses, yielding a top fiber stress of 1,800 lb per sq in. and a bottom fiber stress of 0 lb per sq in. Eq. 5*b* yields a prestressing force P equal to 532 kips.

TABLE 2.—COMPUTATIONS FOR PRESTRESSED BEAMS (FIRST TRIAL)

Span, in feet (1)	$M_L \times 10^{-3}$, in kip-inches (2)	f_c, in lb per sq in. (3)	Shape (Fig. 4) (4)	Z_L, in inches cubed (5)	Depth, h, in inches[a] (6)	Trial $M_D \times 10^{-3}$, in kip-inches[b] (7)	$M_T \times 10^{-3}$, in kip-inches (8)	Z_T, in inches cubed (9)
100	7.500	1,800	F	4,160	41.1	7.330	14.830	6,350
40	4.800	2,250	D	2,135	32.3	1.131	5.931	1,413

[a] From Fig. 3. [b] The trial dead-load moment equals $w_D L^2/8$, plus 25% for the deck, stiffeners, and other components.

The required area of steel depends on the tensile strength of the wires or cables to be used. Fiber stresses in the concrete also can be checked using the initial prestressing force required to compensate for the subsequent prestress losses of approximately 15%.

For the 40-ft span, the Z_T-value in Col. 9, Table 2, is less than the value of Z_L in Col. 5, indicating the h-value of 32.3 in. (Col. 6) to be satisfactory. Thus, the live load controls the design and a new value of e must be obtained. Introducing values from Table 2 into Eq. 13 gives a K-value to be substituted into Eq. 15. The eccentricity is 5.79 in., the top fiber stresses are found to be 2,250 lb per sq in., and the bottom fiber stresses vanish. The required prestressing force is $P = 507$ kips.

CONCLUSIONS

A method has been presented whereby the shape and dimensions of regular and irregular cross sections of prestressed concrete beams can be determined rapidly in the same manner as that used for selecting structural steel shapes. The method has the following advantages:

a. The time-consuming method of selecting trial sections and then checking the stresses is eliminated.

b. The method is not limited to any particular sectional shapes.

c. No complicated equations are involved.

d. The method is particularly helpful to those who have had little or no previous experience in the design of prestressed concrete beams and thus have no basis for selecting trial sections.

e. When making economic comparisons of beams of various materials, the quantities for the prestressed concrete beam can be determined quickly with the assurance that the stress conditions in the beam will be satisfactory under the given loading.

The method has the following disadvantages:

I. If sections other than those shown in Fig. 4 are used, the designer must formulate Eqs. 11 and 12 in order to determine the dimensions.

II. The required height of the section, *h*, may not be controlled by the sum of the dead-load moments and live-load moments, but may be controlled by the live-load moment alone—a situation which entails two computations for *h*.

APPENDIX. NOTATION

The following symbols, adopted for use in the paper and for the guidance of discussers, conform essentially with "American Standard Letter Symbols for Structural Analysis" (ASA–Z10.8–1949), prepared by a committee of the American Standards Association with Society participation, and approved by the Association in 1949:

A = the area of the gross concrete section;

A_c = the net area of concrete;

b = the top flange width:

b' = the web thickness;

b'' = the bottom flange width;

b_1 = the width of the equivalent rectangle;

C = the coefficient in the equation, $h = C\,Z^{\frac{1}{3}}$;

c = the distance from the CGG to the bottom fiber;

e = the eccentricity of the steel area with respect to the CGG;

f_c = the allowable working stress in concrete;

h = the height of the actual section;

h_1 = the height of the equivalent rectangle;

I = the moment of inertia of the gross concrete section referred to the CGG;

I_c = the moment of inertia of the net concrete section about its centroidal axis;

i = the ratio of the bottom fiber distance to the height of the actual section:

i_1 = the ratio of the bottom fiber distance of the actual section to the height of the equivalent rectangle;

i_2 = the ratio of the steel eccentricity to the height of the equivalent rectangle;

K = a prestressing factor;

L = the span;

M = the bending moment:

M_D = the dead-load moment;
M_L = the live-load moment;
M_T = the total moment;

P = the effective prestressing force;
s = the unit stress;
t = the top flange thickness;
t' = the bottom flange thickness;
w_D = a uniform dead load;
x = the horizontal distance along a beam:
y = the vertical distance from the CGG;
Z = the section modulus:

Z_L = the section modulus based on the live-load moment;
Z_T = the section modulus based on the total moment; and

z = the ratio of the width of the equivalent rectangle to its height.

DISCUSSION

Fred E. Koebel,[2] J. M. ASCE.—Much valuable information has been contributed by the author to those engineers who are interested in the design of structural members made from prestressed concrete. Tabular and graphical solutions for sections have been sought by design engineers since the introduction of prestressing (on a large scale) into the United States (1946). The establishment of certain ratios (such as flange width to height, flange thickness to height, and web thickness to height) in Table 1, and the assumption of a ratio of width to depth for the equivalent rectangle (Fig. 1), limit the designer to a given section for any condition. In some instances, a design may require a specific headroom clearance; in other extreme instances, as much height is available as is desired by the engineer. This variation in requirements for the depth of the beam hinders the application of the assumed ratios. Unless tables and figures are available for all practical height variations, the design is likely to be uneconomical. Obviously tables and figures can be prepared for many variations. However, it is questionable if the preparation of such material is feasible. The practical use of the author's system would also be difficult in cases where composite action can be obtained—as in highway-girder design. Composite action is important and often leads to economical designs for highway-bridge spans.

In general, the live load or superimposed moment controls the required section modulus for post-tensioned girders, if provision is made for the loss of prestressing force required for the dead-load stresses and for the live-load stresses. This is true, because (generally) as the prestressing forces are applied, the beam rises from the soffit and the dead load stresses act simultaneously with those stresses caused by prestressing. Thus, the required section modulus can be approximated by use of

$$\frac{I}{c_b} = \frac{M_L}{K_1 f^b_c} \qquad \text{(17)}$$

in which f^b_c is the allowable initial compression on the bottom fibers and K_1 is a factor based on the section properties and the percentage loss in stress from the initial prestressing force.

The designer can then obtain the required section modulus and can choose a cross-sectional shape. With the knowledge of the design limitations which are present, an approximation of the section can be made, and if the ratio of I/c obtained is of the same value as that shown or required, the stress conditions are confirmed. The design can then be refined and made practical for construction.

From Cols. 4 and 6, Table 2, it can be seen that for the beam having a 40-ft span, the section designation is D, and the depth h is 32.2 in. Therefore, from Table 1,

$$I = h^4 \, (0.0392) = 42{,}500 \text{ in.}^4 \qquad \text{(18a)}$$

$$A = h^2 \, (0.347) = 360 \text{ in.}^2 \qquad \text{(18b)}$$

$$c = h \, (0.622) = 20.1 \text{ in.} \qquad \text{(18c)}$$

---

[2] Vice-Pres. and Chf. Engr., Prestressing, Inc., San Antonio, Tex.

and

$$r^2 = \frac{I}{A} = 118 \text{ in.}^2 \quad \text{(18d)}$$

From Table 2,

$$M_L = 4.8 \times 10^6 \text{ in-lb} \quad \text{(19a)}$$

$$M_D = 1.131 \times 10^6 \text{ in-lb} \quad \text{(19b)}$$

and from Table 1,

$$W_D = h^2 (0.362) = 378 \text{ lb per ft} \quad \text{(19c)}$$

Therefore, the fiber stresses are as follows:

In the top fiber, under dead load,

$$f^t{}_D = 1.131 \times 10^6 \times \frac{12.2}{42{,}500} = + 325 \text{ lb per sq in.} \quad \text{(20a)}$$

In the bottom fiber, under dead load,

$$f^b{}_D = 1.131 \times 10^6 \times \frac{20.1}{42{,}500} = - 536 \text{ lb per sq in.} \quad \text{(20b)}$$

In the top fiber, under live load,

$$f^t{}_L = 4.8 \times 10^6 \times \frac{12.2}{42{,}500} = + 1{,}380 \text{ lb per sq in.} \quad \text{(20c)}$$

In the bottom fiber, under live load,

$$f^b{}_L = 4.8 \times 10^6 \times \frac{20.1}{42{,}500} = - 2{,}270 \text{ lb per sq in.} \quad \text{(20d)}$$

From the stresses given in Eqs. 20, it can be seen that, even if no tensile stresses are allowed in the top fibers at initial prestressing, a greater eccentricity can be used than is shown by the author (5.79 in.). That is, the eccentricity can remain within the kern and a greater value can be obtained. The depth of the kern can be determined from

$$d_k = \frac{r^2}{y_t} = \frac{118}{12.2} = 9.7 \text{ in.} \quad \text{(21)}$$

in which d_k is the depth of the kern and y_t is the distance from the CGG to the top fiber. If e is assumed to be 9.7 in., then the prestressing force required is

$$P = \frac{2{,}806 \times 360}{0.85 \left(1 + \frac{9.7 \times 20.1}{118}\right)} = 450 \text{ kips} \quad \text{(22)}$$

Thus the stresses caused by only the prestressing are

$$f^t{}_p = \frac{450{,}000}{360} \left[1 - \frac{9.7\ (12.2)}{118}\right] = 0 \quad \text{(23a)}$$

and

$$f^b{}_p = \frac{450{,}000}{360}\left[1 + \frac{9.7\,(20.1)}{118}\right] = +\,3{,}320 \text{ lb per sq in.} \tag{23b}$$

After losses the value of $f^b{}_p$ will decrease to 2,820 lb per sq in. Combining the stresses from the prestressing and the dead load results in

$$f^t{}_{Dp} = +\,325 - 0 = +\,325 \text{ lb per sq in.} \tag{24a}$$

and

$$f^b{}_{Dp} = -\,526 + 3{,}320 = +\,2{,}794 \text{ lb per sq in.} \tag{24b}$$

Combining the total-load stresses and the prestressing stresses after losses have occurred results in

$$f^t{}_{Tp} = +\,1{,}705 - 0 = +\,1{,}705 \text{ lb per sq in.} \tag{25a}$$

and

$$f^b{}_{Tp} = -\,2{,}806 + 2{,}820 = +\,14 \text{ lb per sq in.} \tag{25b}$$

However, even with an eccentricity of 9.7 in., the maximum possible eccentricity is not being used because the dead load comes on to the beam as the prestressing force is applied. Also, it is acceptable to allow some small amount of initial tension on the top fibers caused by the initial prestressing. Thus the eccentricity can be increased to 15 in. in which case the value of P would be 334 kips (including losses), $f^t{}_p = -\,510$ lb per sq in. (after losses $f^t{}_p = -\,434$ lb per sq in.), and $f^b{}_p = +\,3{,}320$ lb per sq in. (after losses $f^b{}_p = +\,2{,}820$ lb per sq in.). Combining stresses leads (before losses) to $f^t{}_{Dp} = -\,185$ lb per sq in. and $f^b{}_{Dp} = +\,2{,}784$ lb per sq in. After losses the stress $f^t{}_{Tp} = +\,1{,}289$ lb per sq in. and $f^b{}_{Dp} = +\,14$ lb per sq in.

Thus, by taking full advantage of the available section, the magnitude of the prestressing force is 34% less than that given by Mr. Peebles. This reduction will result in a large saving in the final cost of the member. The cables are, of course, laid in a catenary so that the stresses are within the allowable limit along the entire length of the beam. Even with pretensioning, the results from the investigation in which $e = 9.7$ in. indicate that a much larger value of e could be used. It would appear, therefore, that the use of the equivalent rectangle is not valid when applied to unsymmetrical sections. This invalidity is caused by the fact that the center of gravity of the rectangle is not the same as the center of gravity of the unsymmetrical section. Since these centers are not the same, the resulting stress conditions cannot be the same and the equations developed fail to give satisfactory results.

It should be realized that prestressed concrete is a very adaptable material; it should not be restricted to parameters for any given conditions. The skilful designer can make use of many practical shapes, the end result being a structurally sound and economical design. This takes no special skills, charts, or tables, but it does require a firm knowledge of the basic fundamentals of structural analysis.

JOHN J. PEEBLES,[3] J.M. ASCE.—Mr. Koebel has increased the value of the writer's paper by indicating that, although the design procedure proposed for the case in which the live load controls the design satisfies the stress limitations, a greater eccentricity and a smaller prestressing force could satisfy these limitations with a saving in steel and prestressing costs. However, the results that Mr. Koebel obtained are not entirely satisfactory, and the statements concerning these results are not correct (in some particulars) for the following reasons:

1. The results obtained by the proposed method are the final stress conditions, all prestress losses having taken place.
2. The stresses must be within the allowable limits, not only when the live load is on or off the member after prestress losses have occurred, but also when the member is subject only to the dead load—before prestress losses have taken place. Thus, by increasing the eccentricity to 15 in. (in the second example), the top fiber is stressed to −185 lb per sq in. and the bottom fiber is overstressed by 24% in compression under dead load before prestress losses take place; and the top fiber is stressed to −90 lb per sq in. under dead load even after prestress losses have taken place. Although Mr. Koebel states that it is acceptable to allow some tension in the top fibers of the member, it is doubtful whether this tension would be permitted by the average building code or design specification; tension is not permitted in the design of conventional reinforced-concrete structures.
3. The statement that the center of gravity of the equivalent rectangle is not the same as the center of gravity of the unsymmetrical section is in error. It is a geometrical fact that the centers of gravity coincide, as shown by Eqs. 6*a* and 7. From these equations the dimensions of the equivalent rectangle are obtained by making its area and moment of inertia equal to the area and moment of inertia of the given symmetrical or unsymmetrical section, both moments of inertia being about their respective centers of gravity. A reduction in the prestressing force was shown by Mr. Koebel, not because of a disparity between the centers of gravity of the sections, but as a result of increasing the eccentricity in the given section and reducing the prestressing force to obtain certain predetermined stress conditions. Also, the fact that the particular shape was unsymmetrical was of no consequence.

In presenting his material, the writer endeavored to illustrate the general application of the theory of the equivalent rectangle. Refinements in design—such as minor adjustments in cross sections and accounting for prestress losses—were purposely omitted (although important) to simplify the presentation. Rarely does any design method produce the final desired results without the need for some refinements and adjustments to comply with special conditions. It is agreed that no design method or short cut should take the place of sound engineering judgment.

Mr. Koebel suggests proportioning the cross section by trial and error to obtain the required section modulus. This may be a relatively simple operation for rectangular sections, but for **I**, **T**, hollow-rectangular, and similar irregular shapes, considerable time and energy may be expended before a satisfactory shape is obtained. One of the main advantages of the proposed method of design is virtually to eliminate such tedium.

---

[3] Engr., Bechtel Corp., San Francisco, Calif.

It is not claimed that any one of the limited number of cross sections shown in Fig. 4 is the most economical—a term which is relative, anyway, and depends on the specific application. Probably "efficiency" would be a better term to characterize the cross sections in Fig. 4. In general, the cross sections increase in efficiency from A to G. There is no limit to the number of variations in shapes that could be devised. Contrary to Mr. Koebel's statement that sectional ratios limit the designer to a given section for any condition, there actually would be less limitation with a reasonably wide selection of shapes than there is with structural-steel shapes.

The **T**-shape (D in Fig. 4) can be used for floor systems and bridge decks so that advantage can be taken of composite action. In themselves, unsymmetrical sections of this type generally are less efficient than symmetrical sections. However, by incorporating the top flange in the slab or deck, efficiency usually can be attained.

When the live-load section modulus (computed from Eq. 12*b*) is greater than the total-load section modulus (computed by Eq. 11*a*, in which K reflects a reduction in section modulus as a result of the prestressing force), the required height of the section is controlled by the live-load fiber stress. This case will not be encountered often because it indicates that the ratio of live load to dead load is large, a condition usually associated with short spans. Although prestressed concrete members certainly are not limited to long spans, the greatest economy is generally demonstrated by using the members in this way.

In the usual case, in which the live load does not control the design, no adjustment in the cross section will be required to compensate for prestress losses resulting from both the plastic flow in the concrete and the creep in the steel; and the eccentricity, of course, already has its greatest attainable value at the point of maximum moment. Thus (in the first example), if it is desired to check the fiber stresses at the time of the initial prestressing, the required force P should be 626,000 lb. This force will result in top and bottom fiber stresses (when the beam is under the influence of both the prestress and dead load) of +790 lb per sq in. and +1,330 lb per sq in., respectively—each stress being less than the allowable stress of +1,800 lb per sq in.

To refine the design in the less common case in which the live load controls the design, it is usually necessary to reduce the allowable stress by from 15% to 20% in computing the live-load section modulus; otherwise the bottom fiber will be overstressed during initial prestressing, as was indicated in Mr. Koebel's computations. Thus, in the second example, by reducing the allowable concrete stress by 400 lb per sq in., the life-load section modulus would be 2,600 in^3. In a manner similar to that used in the second example, a slightly greater value of h equal to 34.5 in. is obtained. In order to establish the optimum value of e so that the top fiber stress will be zero and the bottom fiber stress will be f_c (under the influence of dead load, before prestress losses have occurred), the expression for the required K-value should be

$$K = \left(\frac{i}{1 - i}\right)\left(\frac{M_D}{f_c\,Z_b} + 1\right) \qquad (26)$$

in which Z_b is the section modulus for the bottom fiber. It should be noted that the only reason that the value of K must be changed from the value shown in Table 1 is that the value of i_2, which is a measure of e, has changed (Eq. 9*c*). All other factors remain the same as indicated in Table 1. The value of e from Eq. 15 is therefore 14.00 in. The required initial prestressing force is

$$P = (1 - i)\,f_c\,A = 350{,}000 \text{ lb} \qquad (27)$$

To compute stresses for this special case, Eq. 4 should be used instead of Eq. 16. Checking by use of Eq. 4, the stress in the top fiber is zero and the stress in the bottom fiber is +2,250 lb per sq in. under dead load and before prestress losses have occurred.

The prestressing force will reduce to 300,000 lb after losses of about 15%. From Eq. 4, the top fiber stress is +35 lb per sq in., and the bottom fiber stress is +1,850 lb per sq in. (under the influence of prestress and dead load). Under full load the top fiber stress is +1,170 lb per sq in., and the bottom fiber stress is zero.

Thus, the prestressing force has been reduced considerably, as advocated by Mr. Koebel, and also the limiting stresses of zero and +2,250 lb per sq in. have not been breeched under the influence of dead load before losses or under the influence of dead load or total load after losses.

Although there are those engineers who are apparently reluctant to utilize new design methods, charts, and tables to increase the efficiency of their operations, it is believed that the material presented by the writer can be used to simplify greatly the design of prestressed concrete members. As with most design methods, the results obtained may require minor adjustments to fit specific conditions. However, the bulk of the work required in the usual trial-and-error method of proportioning the cross section is eliminated by this design procedure, and the resulting stresses are within the allowable limits.

AMERICAN SOCIETY OF CIVIL ENGINEERS
Founded November 5, 1852
TRANSACTIONS

Paper No. 2672

NONELASTIC BEHAVIOR OF BRIDGES UNDER IMPULSIVE LOADS

BY S. J. FRAENKEL[1] AND L. E. GRINTER,[2] M. ASCE

WITH DISCUSSION BY MESSRS. ROBERT J. HANSEN AND JOHN S. ARCHER; AND S. J. FRAENKEL AND L. E. GRINTER

SYNOPSIS

A method for predicting the effects of loads that vary with time on bridges and other structures when deformations extend into the plastic range is presented in this paper. Although such analyses are necessarily more complex than the use of statics, the method presented requires only numerical techniques. Hence, the computations are of a routine nature fitted to the procedures of a design office. The bridge studies reported in this paper aid in determining which bridges, under atomic attack, are most susceptible to damage, and the bridge characteristics that are desirable for resisting blast.

Because the immediate questions would be whether the span should be long or short, whether mass is to be added or avoided, whether girders or trusses are to be preferred, and what effect is to be expected from change of elevation above the water, the answers to these questions were sought. In order to reduce the number of variables, a group of simple railway spans ranging from 50 ft to 519 ft were studied to determine the permanent deflections produced by the explosion of a nominal atomic bomb 2,000 ft vertically above the center of the span. The numerical answers obtained are not as significant, of course, as the relative damage sustained as a function of span, mass, elevation, and type of structure.

PRELIMINARY CONSIDERATIONS

The determination of dynamic effects on bridges is not new since much has been written about impact loadings on bridge spans and related phenomena. However, the problem of blast damage differs in two important aspects from previous work in this field. Former studies have been concerned with dynamic

---

NOTE.—Published in April, 1953, as *Proceedings-Separate No. 185.* Positions and titles given are those in effect when the paper or discussion was received for publication.

[1] Asst. Chairman, Structural Research Dept., Armour Research Foundation of Illinois Inst. of Tech., Chicago, Ill.

[2] Dean of Graduate School, and Director of Research, Univ. of Florida, Gainesville, Fla.

forces originating from wheel unbalance that produces a periodic forcing function traveling along the span, whereas the concern in this study is a nonperiodic uniformly distributed loading, which is a function of time. The methods proposed do not limit the variation of the load with time as long as this variation can be expressed mathematically or graphically.

The second departure from conventional engineering considerations lies in the emphasis which is placed on the nonelastic behavior of the bridge. In determining the amount of damage that a given bridge may suffer as a result of an explosion, only the plastic range of behavior is of interest. Moreover, the changing configuration of the bridge, after the forces have deformed it beyond the elastic limit, must be established.

The principal simplification available for the study of configuration follows from the common assumption of plasticity that yielding of a single member of a statically determinate truss transforms the structure into a mechanism. Irrespective of the questions that may be raised as to the influence of gussets, rivet holes, welds, continuity of chords, and other structural details, present design practice assumes that any properly designed truss or girder span must deflect well into the plastic range before fracture occurs because brittle fracture is not contemplated in standard specifications. Hence, analysis based on the mechanism concept is believed to be a satisfactory method of evaluating the relative influence of a parameter, such as length of span, on the resistance to deflection from atomic blast for bridges that are essentially similar. Once this concept of transformation of the structure into a mechanism consisting of two rigid bodies joined by a plastic member is accepted, the motion of each body may be studied by the equations of dynamic equilibrium. Such equations can be solved by numerical stage-by-stage analysis using an appropriate interval of time between successive stages.

The structures selected as examples for study are simple-span trusses and girders of a single-track railway type. The uniform impulsive loading chosen is that produced by an atomic explosion of a 20-kiloton bomb (equivalent to 20,000 tons of trinitrotoluene (TNT) at 2,000 ft directly above the span. The method of analysis developed could be adjusted, with only moderate complication, to handle nonuniform loading and statically indeterminate spans such as suspension bridges, continuous girders, and rigid frame bridges. An impulsive load of any type may be handled as long as the pressure-time variation is completely known. The character of the differential equations that describe the motion of the bridge does not encourage the hope that a closed solution may be obtained, and it seems likely that numerical methods will continue to be required for the solution of the equations. The amount of labor involved in carrying through a stage-by-stage analysis of the type suggested is well within reason, however.

Definition of Damage.—Reference has already been made to relative damage as a measure of the resistance of a bridge to atomic blast. For quantitative comparisons it is necessary to define structural damage in numerical terms despite the realization that the degree of damage assigned to any structure after a blast will be dependent on such factors as the difference between wartime and peace, the importance of the structure to a given operation, the possibility of control over traffic, the visibility of the damage, and other similar factors. In this paper, the ratio of the maximum nonrecoverable deflection to the span length is taken as a quantitative index of structural damage. This index is related to such physical factors as the slope of the floor, the change in the critical internal angle of the truss triangle, and the external angle that develops between the two rigid bodies joined by the plastic member.

The ratio of deflection to span is readily determined, and it seems to be a reasonable criterion of structural damage, considering the symmetrical uniform loading and the expressed intention to study large nonelastic movements. It might properly be suggested that a better index of damage would be, for example, the percentage of actual change of length to the permissible change of length of the plastic member. However, until more is known about the action of built-up tension and compression members in the plastic range so that limits may be assigned to total axial deformations for members of different lengths, cross sections, and end conditions, a simpler index of damage such as the one described seems preferable. Hence, all procedures of analysis presented herein furnish values of the maximum deflection as the final result.

DEVELOPMENT OF A PROCEDURE OF ANALYSIS

The analytical processes comprise the determination of the loading acting on the bridge; the movement within the elastic range, resulting in the maximum elastic deflection; and the movement within the plastic range which produces nonrecoverable deflection.

Determination of Loads.—The first step in computing the loads acting on the bridge requires consideration of some of the basic phenomena surrounding the explosion of an atomic bomb. Such an explosion creates pressures in the atmosphere—varying with both time and distance from the point of explosion—which can be described roughly as shock waves expanding spherically around the source. The pressure difference existing between the undisturbed air in front of the shock wave and the air behind it is called the "over-pressure," which decreases gradually to zero. The variation (with time) of free air pressure at a point is given by the expression:[3]

$$p_s = (P_s)_{\max} \left(1 - \frac{t}{t_0}\right) e^{-t/t_0} \qquad \text{(1)}$$

in which p_s equals the over-pressure in shock wave at the time t; $(P_s)_{\max}$ is equal to the peak over-pressure (often termed "side-on" pressure); t represents time, measured from the beginning of the positive phase; and t_0 denotes the duration of the positive phase of the blast wave.

It also can be determined that, at a distance of 2,000 ft from an exploding nominal bomb, the peak over-pressure is 24 lb per sq in., which decreases to zero in a period of 0.45 sec, according to the upper curve[4] in Fig. 1. Thus, it is possible to determine the over-pressure existing at any time during the positive phase for the particular case of interest.

---

[3] "The Effects of Atomic Weapons," U. S. Govt. Printing Office, Washington, D. C., 1950, p. 124.

[4] *Ibid.*, p. 135.

For bridge locations displaced laterally from beneath the point of explosion of the bomb, the "Mach stem" will produce an essentially horizontal side-on shock to the bridge.[5,6] The intensification of the pressure in the Mach stem and the small lateral resistance in some bridges may cause greater vulnerability to such loadings than to the vertical loadings considered herein. This vulnerability can be determined only by a study of the methods to be discussed.

However, knowledge of the variation of over-pressure with time at the location of the bridge is not sufficient for determining vertical loads. The loading on the bridge depends largely on the geometry of the bridge itself because the pressures and their variation with time during the action of the shock wave on the bridge are functions of the size and shape of the structure. When the shock front first arrives at the bridge floor, it increases immediately to the "reflected pressure" which is two or more times the original over-pressure. This excess pressure then flows around the edges of the object struck in order to equalize itself with the surrounding over-pressures; this process is referred to as "diffraction" and is dependent on the size and shape of the object struck by the shock front. Considering the simple rectangular shape of a bridge structure viewed from above, and the predominant contribution made by the solid deck of the bridge to the total area struck by the wave, the structure will be idealized to that of a flat plate (corresponding to the deck) that is struck by a shock wave. It is important to recall that it is the expressed objective to determine relative nonelastic deflections for several bridges and that approximations having a comparable effect on all structures may be accepted. With this simplification, results from shock tube experiments may be used to determine the pressure distribution as a function of time during the diffraction process. A shock tube is a pipe in which pressure can be built up and then suddenly released, causing a shock wave to travel down the tube. The data used actually were obtained for a thin plate fixed at the bottom of the shock tube and struck normally by a passing shock wave of intensity comparable to an over-pressure of 24 lb per sq in. The results are derived from interfero-

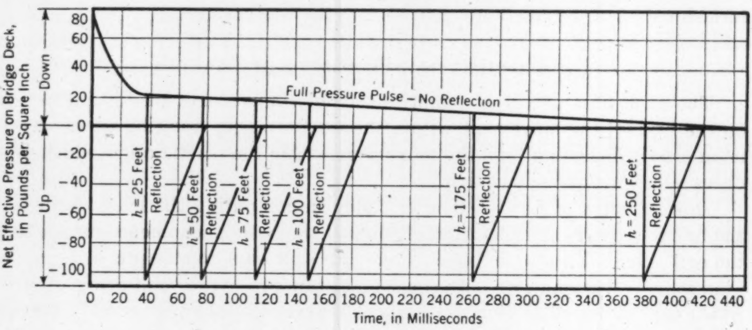

FIG. 1.—PRESSURE-TIME CURVE FOR 519-FT BRIDGE

---

[5] "The Effects of Atomic Weapons," U. S. Govt. Printing Office, Washington, D. C., 1950, p. 67.
[6] *Ibid.*, p. 76.

metric measurements and are in terms of dimensionless pressure ratios expressed as functions of time.[7] For reasons of symmetry the thin plate used in shock tube studies is considered to represent the half-width of the bridge deck. It is suggested that, in studies of this kind, the flat plate that simulates the bridge deck in the shock tube be considered to represent the width of the bridge between the outboard edges of the chords, rather than that of the deck proper, in order to compensate, as far as is practicable, for the neglect of the resistance to the vertical shock of the individual truss members.

The diffraction period is followed by a relatively long period of drag that is caused by the flow of air away from the explosion during the positive phase. Shock tube data are limited, for practical reasons, to the initial diffraction period, but it can be shown that conventional drag formulas give values of pressures that agree well with the end values of the shock tube information. It seems permissible, therefore, to extend the pressure-time curve based on shock tube results with a straight line passing through zero pressure at the end of the positive phase. A typical curve of this kind is shown in Fig. 1, in which it is designated as "Full Pressure Pulse—No Reflection."

The loading phenomena previously described are those which would be expected to occur if the bridge were located by itself in an infinite atmosphere, or were so far removed from other obstructions to the shock wave that it would not be affected by their presence. Actually, this is not likely to be the case except where the elevation of the span above the ground or water surface is unusually great. It becomes necessary, therefore, to consider the effects of elevation of the span above the surface of the earth, and it will be shown that the reflection of the shock wave from the ground or water beneath the bridge will alter the loading considerably.

It is helpful to draw first a qualitative picture of the successive phenomena in the reflection process. First, the original shock wave impinges on the top side of the bridge floor and is diffracted around it. The shock wave is reformed underneath the bridge and impinges on the ground or water surface below, whereupon it is reflected with intensified strength and travels upward into a "once-shocked" region. The mass flow behind the returning shock wave is zero—that is, the air is at rest. The reflected shock wave impinges on the bottom surface of the bridge floor, exerting upward pressure on it. The reflected shock wave is then diffracted around the deck and travels farther upward, after reforming above the deck. Following this, no further air forces act on the bridge.

A quantitative treatment of this procedure will not be given in this paper because it would require far too much space. However in the performance of other investigations of this kind it should be kept in mind that both water and earth, being of high acoustic impedance relative to air, reflect shock without appreciable loss of energy and that, until further experimental data become available, the upward diffraction process must be approximated from the same shock tube data as the initial downward diffraction. Also, because of the presence of a turbulent region immediately beneath the deck, the strength of the returning shock wave, reflected from the earth's surface below, should be reduced by one third when the reflected pressure on the underside of the deck is computed. Attention must be paid to the fact that the returning shock wave enters a region in which the over-pressure is continuously decreasing. Assuming the latter to remain constant is probably permissible for elevations up to about 100 ft with a shock of 24 lb per sq in., but this assumption will introduce serious error for greater heights or stronger shocks.

---

[7] "The Diffraction of Shock Waves around Obstacles and the Resultant Transient Loading of Structures," by D. R. White, D. K. Weimer, and W. Bleakney, *Technical Report II-6*, Princeton Univ., Princeton, N. J., August 1, 1950.

The pressure-time relations that are obtained for various elevations of a 510-ft span are shown in Fig. 1, in which the bridge deck elevation is expressed as *h*. It is apparent that the case of no reflection differs radically in its pressure-time relationship from the case of reflection from any commonly encountered height. The time required for the reflected shock to make itself felt increases with increasing elevation of the bridge, and the upward impulse furnished by the reflection becomes a progressively smaller percentage of the downward impulse as the elevation increases. The large upward forces exerted by the reflected shock waves may account for the phenomenon observed in Hiroshima and Nagasaki, in Japan, where even those bridges close to "ground zero" suffered little structural damage. Unfortunately, evidence on this point is very meager.[8]

Present knowledge of the actual loading is surrounded by many uncertainties. An analytical treatment of this problem seems virtually impossible, and only fragmentary experimental data applicable to diffraction around complex structures have been published. Therefore, the numerical results obtained from such data are open to question as to their accuracy, although it should be kept in mind that in this study accuracy of loading is secondary to the establishment of general relations between bridge characteristics and damage. The validity of such comparisons is not influenced by the accuracy of the loading information to as great an extent as are individual numerical answers.

Motion in the Elastic Range.—The initial motion of the bridge under the applied load is in the elastic range. The theoretical response to a suddenly applied load is the excitation of the various elastic modes of the bridge. Because consideration is restricted herein to uniform loading on a symmetrical bridge, there is no need for the inclusion of even harmonics that correspond to unsymmetrical deflection profiles. The treatment may be simplified further by assuming the elastic response configuration to be the static deflection profile or, essentially, by using the first mode of vibration. Since experimental evidence justifies this assumption for the case of a concentrated central dynamic load, it seems certain that a uniformly distributed load would follow the static deflection profile even more closely.[9]

It is desirable, as a matter of convenience, to reduce the problem of determining the center deflection as a function of time to that of determining the motion-time history of a lumped single-degree-of-freedom system. The motion of such a system may be treated with Duhamel's integral, although other methods are also possible. Considering the nonmathematical character of the forcing function—that is, the pressure variation with time—it is desirable to express the integral in incremental form for tabular integration,[10,11] as follows:

---

[8] "The Effects of Atomic Weapons," U. S. Govt. Printing Office, Washington, D. C., 1950, p. 152.

[9] "Investigation of Bridge Impacts with a Mechanical Oscillator," *Bulletin*, AREA, 1948, p. 61.

$$y_1 = y_0 \cos \omega \Delta + \frac{\dot{y}_0}{\omega} \sin \omega \Delta + \frac{F}{m\, \omega^2} (1 - \cos \omega \Delta) \ldots\ldots\ldots (2a)$$

and

$$\frac{\dot{y}_1}{\omega} = - y_0 \sin \omega \Delta + \frac{\dot{y}_0}{\omega} \cos \omega \Delta + \frac{F}{m\, \omega^2} \sin \omega \Delta \ldots\ldots\ldots\ldots (2b)$$

in which y is equal to the center deflection, in feet; $\dot{y}$ equals the center velocity, in feet per second (the dot notation for time derivatives is used here and throughout this paper); F represents the total applied load, in pounds; m equals the mass of the entire bridge, in pound-feet per second per second; ω is equal to the natural frequency of the bridge in the fundamental mode, in cycles per second; Δ denotes the time interval, in seconds; and the subscripts 0 and 1 correspond to deflections at any two consecutive instants.

The equivalent linear oscillator should not only possess the same natural frequency as the bridge, but it also should undergo the same static deflections. If the entire mass of the bridge is used as the mass m of the oscillator, and if the natural frequencies of the bridge and the oscillator are equal, then the oscillator will have an excessive stiffness k. Consequently, a fictitious driving force must be used for equal static deflections of the bridge and the oscillator model, which is obtained by multiplying the actual forcing function by the ratio of the stiffness of the oscillator to that of the bridge. The adjustment can also be made by using a suitably reduced mass and retaining the actual forcing function.

The integration of Eqs. 2a and 2b requires that the natural frequency of the bridge and its limiting elastic deflection be computed. The following relations are available for the determination of these frequencies:

For truss railway bridges, in which δ_{st} is the dead load deflection in inches,

$$\frac{\omega}{2\,\pi} = f = \frac{12}{\sqrt{\delta_{st}}} \ldots\ldots\ldots\ldots\ldots\ldots\ldots\ldots (3)$$

in which f is the natural frequency, in cycles per second; and for girder railway bridges,

$$f = \frac{12.4}{\sqrt{\delta_{st}}} \ldots\ldots\ldots\ldots\ldots\ldots\ldots\ldots (4)$$

Variations of the moment of inertia along the span need not be considered and the center value may be used in the determination[12] of δ_{st}.

The determination of the limiting elastic deflection is necessary in order to terminate the stage-by-stage integration of Eqs. 2a and 2b when the deflection passes from the elastic into the plastic region. Eqs. 2a and 2b do not apply beyond this point, of course. The computation of the limiting elastic deflection is simple in principle, although rather laborious, and is illustrated through the description of the various steps involved for a truss bridge, as follows:

---

[10] "Advanced Dynamics," by S. Timoshenko and D. H. Young, McGraw-Hill Book Co., Inc., New York, N. Y., 1948, p. 54.

[11] *Ibid.*, p. 311.

[12] "A Mathematical Treatise on Vibrations in Railway Bridges," by Sir Charles E. Inglis, Cambridge University Press, Cambridge, England, 1934, p. 11.

1. The dead load stresses in each member are determined.
2. The capacity of each member, which may be taken as the yield stress times the effective cross-sectional area, is determined, with allowance for buckling in compression members.[13]
3. The remaining capacity of each member is computed by subtracting the dead load stress from the computed capacity.
4. The live load stress in each member is determined for a uniformly distributed live load.
5. The deflection produced at the center by the live load is computed from step 4.
6. By proportion, the uniformly distributed live load that will exhaust the remaining capacity (as obtained in step 3) is computed for the most highly stressed member.
7. The deflection caused by the live load obtained in step 6 is computed. This deflection is the limiting elastic deflection.

The integration of Eqs. 2*a* and 2*b* for the elastic range can be illustrated readily by the numerical example in the Appendix.

Motion in the Plastic Range.—The terminal values for the elastic range, obtained as explained in the Appendix, furnish the limiting elastic deflection, the time at which this deflection is reached, and the downward velocity of the bridge at that time. These terminal values of the elastic case constitute the initial conditions for the plastic range.

The basic treatment of the plastic case is based on the consideration that yielding in a single member in a statically determinate structure (or of the last redundant member plus one in an indeterminate system) converts the structure into a mechanism. The equations of motion for constrained rigid bodies may be used to follow the ensuing motion in the plastic range. Hence, for the statically determinate truss, it is assumed that only one plastic member exists and that the members that remain elastic form essentially rigid links in a kinematic chain. Actually, these links are elastic and will be vibrating elastically. Their individual elastic displacements, however, are so small in relation to the sum of the elastic and plastic displacements of the entire span that they will be neglected. Also, when dealing with bridges with solid deck floors, it appears satisfactory for purposes of comparison to assume the trusses to be equivalent to bars in the plane of the floor. Where greater numerical accuracy is desired, the actual mass distribution of the truss can be taken into account readily in the computations.

It seems reasonable to make the assumption that a condition of "perfect plasticity" exists—that is, no account will be taken of possible strain hardening. This assumption is justified for strains less than from ten to twenty times the elastic strains in structural steels, as is confirmed by the stress-strain diagram and the tests of actual laboratory structures. Beyond the range of deformation the structure develops added resistance by virtue of strain hardening that will be neglected in the computations. Other simplifying assumptions include the neglect of strain-rate and multi-axial effects, the omission of secondary stress, the convention of frictionless joints in trusses, and the convenient use of a total plastic cross section when the yield point is reached in the extreme fiber of girder sections. It is believed that none of these approximations affect the validity of the results significantly, at least as far as comparative computed damage for generally similar structures is concerned.

---

[13] "Design of Modern Steel Structures," by L. E. Grinter, The Macmillan Co., New York, N. Y., 1941, p. 185, Fig. 97.

The equations of motion in the plastic range are derived for a girder bridge, a truss bridge with flow occurring in the top chord, and a truss bridge with flow occurring in the bottom chord. The equations have been derived in the general form and then have been simplified successively in each case for small angles of rotation and also for a symmetrical deflection configuration. In the case of girder bridges symmetry exists. However, even a symmetrical bridge no longer can be considered as such when inertia forces are involved because one end of the span is pinned whereas the other is free to slide, so that the bridge becomes, in effect, a slider-crank type of mechanism. The complete derivation of the equations would require too much space to be included herein; instead, the derivation of a simple case will be given in outline form and the equations for all other cases will be written in final form.

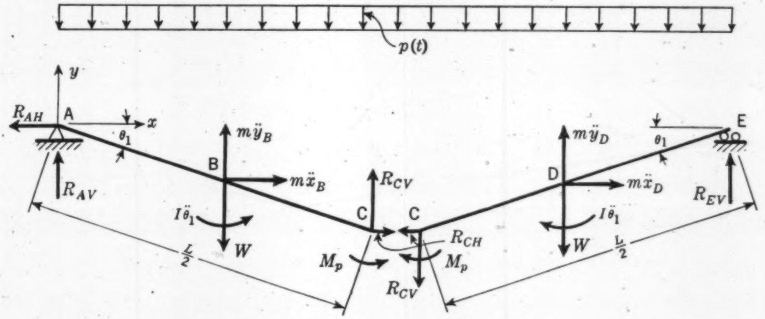

FIG. 2.—GEOMETRY OF GIRDER IN PLASTIC RANGE

Equations of Motion for a Girder Bridge.—The equation of motion for any rigid link, such as is shown in the left-hand part of Fig. 2, may be written by an equation of dynamic equilibrium which makes use of the inertia forces $m\,\ddot{y}_B$, $m\,\ddot{x}_B$, and $I_B\,\ddot{\theta}_1$; the loads, p, W; and the reactions at both ends of the link. The symbol x indicates horizontal displacement, the symbol I denotes the mass moment of inertia about the point indicated by the subscript, and W is the dead load over one half of the span. A convenient expression is obtained from the equation $\Sigma\, M_A = 0$ for the forces of Fig. 2, in which M is a moment about the point indicated by the subscript. It will be recalled that the moment of the three inertia terms about A is equivalent to $I_A\,\ddot{\theta}_1$ in which the subscript 1 refers to the left half of the bridge. Hence,

$$\Sigma\, M_A = 0 = \tfrac{1}{8}\,p\,L^2\cos^2\theta_1 + \tfrac{1}{4}\,W\,L\cos\theta_1 - M_p - R_{CH}\left(\frac{L}{2}\sin\theta\right) - R_{CV}\left(\frac{L}{2}\cos\theta\right) - I_A\,\ddot{\theta}_1.$$

Transferring the inertia moment to the opposite side of the equation and expressing R_{CV} and R_{CH} from their values obtained from the equations, $\Sigma F_x = 0$ and $\Sigma F_y = 0$, applied to Fig. 2,

$$I_A \ddot{\theta}_1 = \tfrac{1}{8} p L^2 \cos^2 \theta_1 - M_p + \tfrac{1}{4} m L^2 \sin \theta_1 (\cos \theta_1 \dot{\theta}^2{}_1 + \sin \theta_1 \ddot{\theta}_1) + \tfrac{1}{4} W L \cos \theta_1 \quad (5)$$

The equation for small angles of rotation, θ, is

$$I_A \ddot{\theta}_1 - 3 I_A \theta_1 \dot{\theta}^2{}_1 = \tfrac{1}{8} p L^2 - M_p + \tfrac{1}{4} W L \quad (6)$$

in which I_A denotes the mass moment of inertia of the left half of the bridge about point A; θ_1, $\dot{\theta}_1$, and $\ddot{\theta}_1$ equal angular displacement, velocity, and acceleration about point A, respectively; M_p represents the maximum plastic moment of the girder section; and W denotes the weight of one half of the girder. All other symbols are illustrated in Fig. 2.

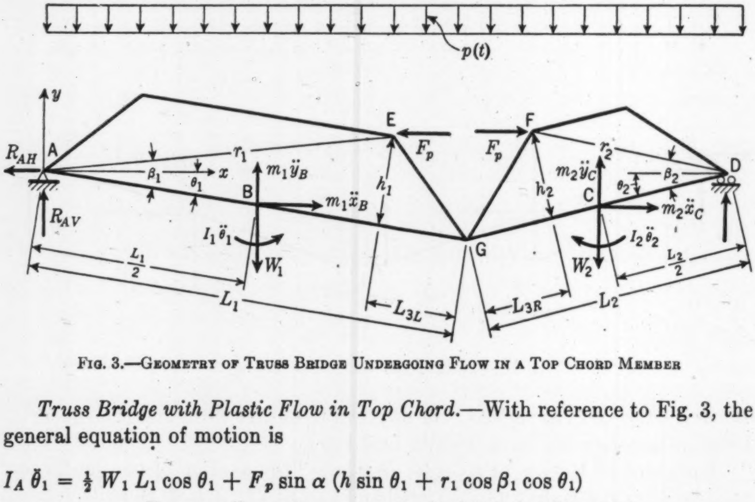

FIG. 3.—GEOMETRY OF TRUSS BRIDGE UNDERGOING FLOW IN A TOP CHORD MEMBER

Truss Bridge with Plastic Flow in Top Chord.—With reference to Fig. 3, the general equation of motion is

$$I_A \ddot{\theta}_1 = \tfrac{1}{2} W_1 L_1 \cos \theta_1 + F_p \sin \alpha (h \sin \theta_1 + r_1 \cos \beta_1 \cos \theta_1) - F_p \cos \alpha (h \cos \theta_1 - r_1 \cos \beta_1 \sin \theta_1) + \tfrac{1}{2} p L^2{}_1 \cos^2 \theta_1 + R_{GV} L_1 \cos \theta_1 - R_{GH} L_1 \sin \theta_1 \quad (7)$$

in which I_A equals the mass moment of inertia of the left part of the bridge about point A; W_1 is equal to the weight of the left part of bridge; F_p represents the force in the plastic member; $\alpha = \tan^{-1} \frac{(y_F - y_E)}{(x_F - x_E)}$;

$$R_{GC} = -\tfrac{1}{2} p (L_1 \cos \theta_1 - L_2 \cos \theta_2) - (W_1 - m_1 \ddot{y}_B) \frac{\tfrac{1}{2} L_1 \cos \theta_1}{L_1 \cos \theta_1 + L_2 \cos \theta_2} - F_p \sin \alpha + \frac{I_1 \ddot{\theta}_1 - I_2 \ddot{\theta}_2}{L_1 \cos \theta_1 + L_2 \cos \theta_2} + \frac{1}{L_1 \cos \theta_1 + L_2 \cos \theta_2} \times [(m_1 \ddot{x}_B + m_2 \ddot{x}_C) \tfrac{1}{2} L_1 \sin \theta_1 - (m_2 \ddot{y}_C - W_2) \tfrac{1}{2} L_2 \cos \theta_2];$$

and

$$R_{GH} = m_2\,\ddot{x}_C + F_p \cos \alpha.$$

The equation for small angles of rotation, θ, is

$$\left[\tfrac{1}{3}\, m_1\, L^2{}_1 \left(1 - \frac{L_1}{L_1 + L_2}\right) + \tfrac{1}{3}\, \frac{L_1}{L_1 + L_2}\, m_2\, L_1\, L_2\right] \ddot{\theta}_1$$
$$- \left[m_2\, \frac{L_1}{L_1 + L_2}\, (L^2{}_1 + L_1\, L_2)\right] \theta_1\, \dot{\theta}^2{}_1 = \tfrac{1}{2}\, W_1\, L_1 \left(1 - \frac{L_1}{L_1 + L_2}\right)$$
$$+ \tfrac{1}{2}\, W_2\, L_2\, \frac{L_1}{L_1 + L_2} - F_p\, (h + L_{3L}\, \theta_1) - F_p\, \alpha\, L_{3L} + \tfrac{1}{2}\, p\, L_1\, L_2 \ldots (8)$$

The equation for small angles of rotation, θ, and for the symmetrical mode of yielding is

$$\tfrac{1}{3}\, m_1\, L^2{}_1\, \ddot{\theta}_1 - m_1\, L^2{}_1\, \theta_1\, \dot{\theta}^2{}_1 = \tfrac{1}{2}\, W_1\, L_1 - F_p\, (L_{3L}\, \theta_1 + h) + \tfrac{1}{2}\, p\, L^2{}_1 \ldots (9)$$

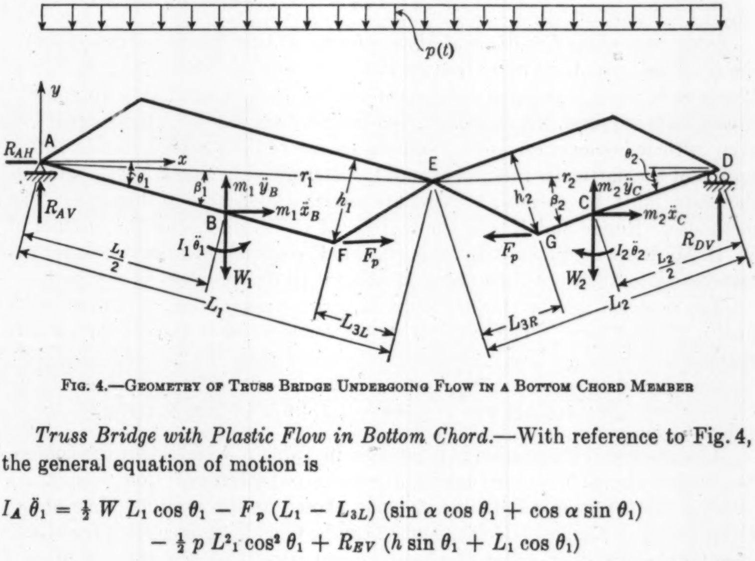

FIG. 4.—GEOMETRY OF TRUSS BRIDGE UNDERGOING FLOW IN A BOTTOM CHORD MEMBER

Truss Bridge with Plastic Flow in Bottom Chord.—With reference to Fig. 4, the general equation of motion is

$$I_A\, \ddot{\theta}_1 = \tfrac{1}{2}\, W\, L_1 \cos \theta_1 - F_p\, (L_1 - L_{3L})\, (\sin \alpha \cos \theta_1 + \cos \alpha \sin \theta_1)$$
$$- \tfrac{1}{2}\, p\, L^2{}_1 \cos^2 \theta_1 + R_{EV}\, (h \sin \theta_1 + L_1 \cos \theta_1)$$
$$+ R_{EH}\, (h \cos \theta_1 - L_1 \sin \theta_1) \ldots (10)$$

in which $\alpha = \tan^{-1} \dfrac{(y_G - y_F)}{(x_G - x_F)}$;

$$R_{EV} = -\tfrac{1}{2}\, p\, (L_1 \cos \theta_1 - L_2 \cos \theta_2) - (W_1 - m_1\, \ddot{y}_B)\, \frac{\tfrac{1}{2}\, L_1 \cos \theta_1}{L_1 \cos \theta_1 + L_2 \cos \theta_2}$$
$$+ F_p \sin \alpha + \frac{I_1\, \ddot{\theta}_1 - I_2\, \ddot{\theta}_2}{L_1 \cos \theta_1 + L_2 \cos \theta_2} + \frac{1}{L_1 \cos \theta_1 + L_2 \cos \theta_2}$$
$$\times \left[(m_1\, \ddot{x}_B + m_2\, \ddot{x}_C)\, \tfrac{1}{2}\, L_1 \sin \theta_1 - (m_2\, \ddot{y}_C - W_2)\, \tfrac{1}{2}\, L_2 \cos \theta_2)\right];$$

and

$$R_{EH} = m_2\,\ddot{x}_C - F_p \cos \alpha.$$

The equation for small angles of rotation, θ, is

$$\left[\tfrac{1}{3}\, m_1\, L^2{}_1 + \frac{L_1}{L_1 + L_2}\left(\tfrac{1}{6}\, m_1\, L^2{}_1 - \tfrac{1}{6}\, m_2\, L_1\, L_2\right) + m_2\, \frac{2\, L_1\, L_2 + L^2{}_1}{2\, L_2}\, h\, \theta_1\right] \ddot{\theta}_1$$
$$+ \left[m_2\, \theta_1 \left(\frac{L^3{}_1 + L^4{}_1/L_2}{2\,(L_1 + L_2)} - L^2{}_1 - \frac{L^3{}_1}{2\, L_2}\right) + m_2\, h \left(L_1 + \frac{L^2{}_1}{2\, L_2}\right)\right] \dot{\theta}^2{}_1$$
$$= \tfrac{1}{2}\, W_1\, L_1 \left(1 - \frac{L_1}{L_1 + L_2}\right) + \tfrac{1}{2}\, W_2\, L_2\, \frac{L_1}{L_1 + L_2}$$
$$- \tfrac{1}{2}\, p\, [(L_1 - L_2)\, h\, \theta_1 - L_1\, L_2] - F_p\, (h - L_{3L}\, \theta_1) + F_p\, \alpha\, L_{3L} \quad \text{..(11)}$$

The equation for small angles of rotation, θ, and for the symmetrical mode of yielding is

$$\left(\tfrac{1}{3}\, m_1\, L^2{}_1 + \tfrac{3}{2}\, m_1\, L_1\, h\, \theta_1\right) \ddot{\theta}_1 - m_1\, L_1\, \left(L_1\, \theta_1 - \tfrac{3}{2}\, h\right) \dot{\theta}^2{}_1$$
$$= \tfrac{1}{2}\, W_1\, L_1 + F_p\, (L_{3L}\, \theta_1 - h) + \tfrac{1}{2}\, p\, L^2{}_1 \quad \text{..(12)}$$

Integration of the Equations of Motion for the Plastic Region.—Inspection of the simplified equations of motion for the plastic range—that is, Eqs. 6, 9, and 12—reveals that the integration of second-order nonlinear ordinary differential equations is required. A closed solution has not been found for these equations even in their homogeneous form, and the nature of the forcing function $p(t)$ is such that the particular integral cannot be determined. Numerical integration therefore must be used and there are several applicable techinques. The methods of Runge and Kutta, the method of C. Störmer, and the method of W. E. Milne, as modified by L. R. Ford, could be employed. In this paper the last-named method has been used, adapting it to this problem as required.

The problem will be clarified by considering an equation of motion in its final numerical form. The example chosen corresponds to the case of a 519-ft span:

$$\ddot{\theta}_1 = \frac{3{,}405\, \theta_1 - 1{,}471}{764 + 1{,}471\, \theta_1}\, \dot{\theta}^2 - \frac{279}{764 + 1{,}471\, \theta_1} + p\, \frac{258 + 17.5\, \theta_1}{764 + 1{,}471\, \theta_1} \quad \text{....(13)}$$

The process of integration is illustrated in Table 1, which gives the column headings of the table actually used in the numerical solution. Cols. 1 and 2 are self-explanatory, the initial time, t, being chosen as the terminal time of the elastic range. Similarly, Cols. 3 and 12 can be filled in at once from the elastic case for the initial time, but at all subsequent times Col. 3 is obtained from a Taylor expansion, as follows:

$$\theta\Big|_{t_1 = t_0 + \Delta} = \theta\Big|_{t = t_0} + \frac{\Delta}{2}\, \dot{\theta}\Big|_{t = t_0} + \frac{1}{2}\left(\frac{\Delta}{2}\right)^2 \ddot{\theta}\Big|_{t = t_0} \quad \text{..........(14)}$$

in which Δ is the time interval selected. Col. 12 requires a similar prediction of $\dot{\theta}$; hence,

$$\dot{\theta}\Big|_{t_1 = t_0 + \Delta} = \dot{\theta}\Big|_{t = t_0} + \frac{\Delta}{2}\, \ddot{\theta}\Big|_{t = t_0} \quad \text{..................(15)}$$

Values for θ_0 and $\dot{\theta}_0$ thus having been established for Cols. 3 and 12, respectively, it is possible to complete all columns up to and including Col. 14. According to the equation itself, the algebraic addition of Cols. 10, 11, and 14 gives a value for $\ddot{\theta}_0$, shown in Col. 15. It becomes necessary to obtain an improved value of θ_0 and of $\dot{\theta}_0$ (designated θ_1 and $\dot{\theta}_1$, respectively) for the next iteration cycle. The particular formulas used are[14]

TABLE 1.—TABULAR SOLUTION OF EQ. 13

Time, t (sec) (1)	Pressure, p (lb per sq in.) (2)	Angular displacement, θ_0 (radians) (3)	$1,471\,\theta_0$ (4)	$17.5\,\theta_0$ (5)	$3,405\,\theta_0$ (6)	$764 + 1,471\,\theta_0$ (7)

$258 + 17.5\,\theta_0$ (8)	$1,470 - 3,405\,\theta_0$ (9)	$p\,\frac{258 + 17.5\,\theta_0}{764 + 1,471\,\theta_0}$ (10)	$\frac{279}{764 + 1,471\,\theta_0}$ (11)	Angular velocity, $\dot{\theta}_0$ (radians per sec) (12)

$\dot{\theta}^2_0$ (13)	$\frac{1,470 - 3,405\,\theta_0}{764 + 1,471\,\theta_0}\,\dot{\theta}^2_0$ (14)	Angular acceleration, $\ddot{\theta}_0$ (radians per sec per sec) (15)	$\dot{\theta}_1$ (radians per sec) (16)	θ_1 (radians) (17)	$\ddot{\theta}_1$ (radians per sec per sec) (18)	$\dot{\theta}_2$ (radians per sec) (19)	θ_2 (radians) (20)

$$\left.\begin{aligned} \dot{\theta}\Big|_{t=t+2\Delta} &= \dot{\theta}_t + \frac{\Delta}{3}\left[\ddot{\theta}_t + 4\,\ddot{\theta}\Big|_{t+\Delta} + \ddot{\theta}\Big|_{t+2\Delta}\right] \\ \theta\Big|_{t=t+2\Delta} &= \theta_t + \frac{\Delta}{3}\left[\dot{\theta}_t + 4\,\dot{\theta}\Big|_{t+\Delta} + \dot{\theta}\Big|_{t+2\Delta}\right] \end{aligned}\right\}\ldots\ldots\ldots\ldots(16)$$

A slight variation of these formulas is desirable for the initial interval Δ in order to obtain greater accuracy in the beginning. By using Eqs. 16 it is possible to complete Cols. 16 and 17. At this point a new cycle of iteration begins and the procedure repeats itself since the values of $\dot{\theta}_1$ and θ_1 in Cols. 16 and 17 are analogous to $\dot{\theta}_0$ and θ_0 given in Cols. 12 and 3. The results of the next cycle are given in Cols. 18, 19, and 20. Column headings for the second iteration cycle are not shown in Table 1 because Cols. 4 to 14 would simply repeat themselves, with all subscripts changed from 0 to 1, and from 1 to 2.

---

[14] "Differential Equations," by L. R. Ford, McGraw-Hill Book Co., Inc., New York, N. Y., 1933, p. 159.

Actual numerical solutions are not presented because of the voluminous character of the computations. It was found that agreement between θ_2 in Col. 20 and θ_1 in Col. 17 was close enough to permit the iteration procedure to be terminated after the second cycle.

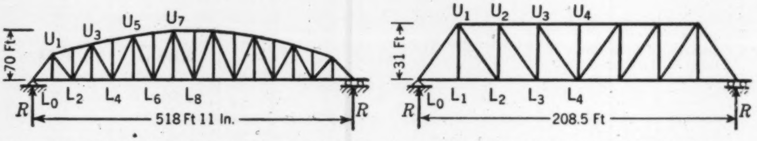

U1
U3
U5
U7
70 Ft
L0
L2
L4
L6
L8
R
R
518 Ft 11 In.
U1
U2
U3
U4
31 Ft
L0
L1
L2
L3
L4
R
R
208.5 Ft

(a) SYMMETRIC THROUGH TRUSS, 27 FT WIDE (d) THROUGH TRUSS, 20.5 FT WIDE

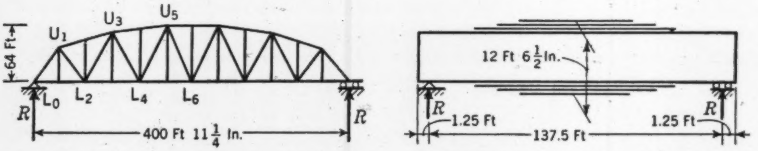

U1
U3
U5
64 Ft
L0
L2
L4
L6
R
R
400 Ft 11¼ In.
12 Ft 6½ In.
R
R
1.25 Ft
137.5 Ft
1.25 Ft

(b) SYMMETRIC THROUGH TRUSS, 24 FT WIDE (e) THROUGH PLATE GIRDER, 20.5 FT WIDE

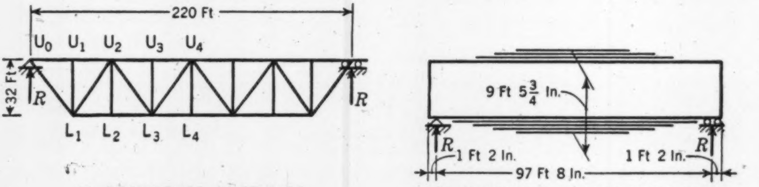

220 Ft
U0
U1
U2
U3
U4
32 Ft
R
R
L1
L2
L3
L4
9 Ft 5¾ In.
R
R
1 Ft 2 In.
1 Ft 2 In.
97 Ft 8 In.

(c) DECK TRUSS, 21 FT WIDE (f) DECK PLATE GIRDER, 11.7 FT WIDE

FIG.—5. SINGLE-TRACK BRIDGES

APPLICATIONS OF ANALYTICAL PROCEDURE

The methods developed in the foregoing sections have been applied to seven single-track steel railway bridges, designed for Cooper's E-65 or E-72 loading, and supported by pins at one end and by rollers at the other. All, except the 140-ft girder span, have solid deck floors of standard weight, and all are statically determinate. The specific structures investigated are those shown in Figs. 5 and a 50-ft rolled-beam bridge, which is not shown. The particular variables investigated were the effect of span length on resistance to impulsive loading resulting from an atomic explosion 2,000 ft above the bridge, the difference between deck and through construction with respect to such resistance, and the effect of elevations between 50 ft and 175 ft above ground or water surface (for the 519-ft bridge) on the damage from such an explosion.

PRESENTATION OF RESULTS

The immediate result obtained from a "plastodynamic" analysis is the value of the center or maximum deflection of the bridge as a function of time. The time at which the plastic deformation terminates may be inherent in the loading and the resistance of the structure or plastic flow may continue virtually indefinitely. However, deformation that is greater than a certain limiting range of values is of little interest. For example, if it is assumed that a ratio of maximum deflection to a span length of 5% corresponds to total uselessness or collapse of the bridge, it is unimportant to determine how much larger the deflection could grow. This assumption makes possible the use of the equations for small angles of rotation which represent a vast simplification of the general case. It must be further understood that the equations presented apply only while the angular velocity $\dot{\theta}$ remains positive because the reverse motion implies

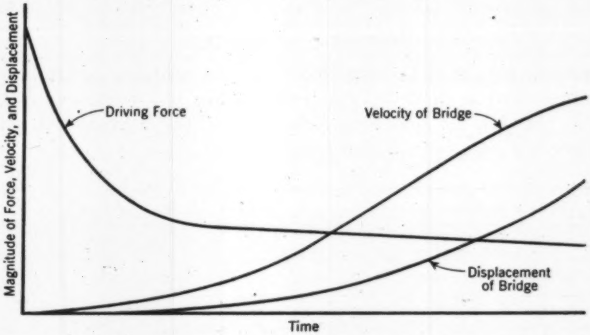

FIG. 6.—DRIVING FORCE AND BRIDGE RESPONSE VARIATION WITH TIME

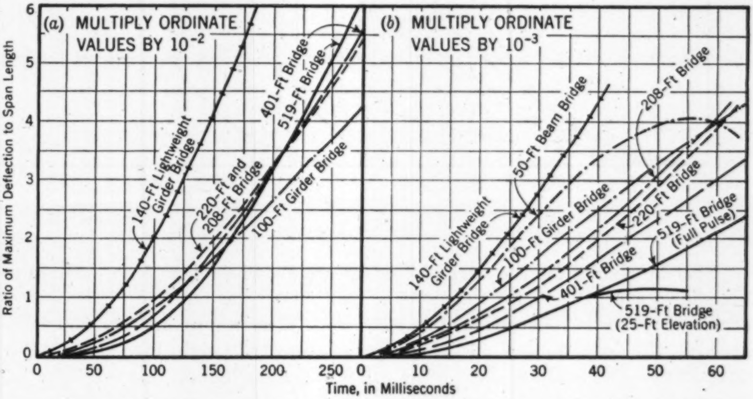

FIG. 7.—VARIATION WITH TIME OF THE RATIO OF MAXIMUM DEFLECTION TO SPAN LENGTH

elastic behavior of the structure rather than constant resistance to deformation. In any event, the procedure may be terminated when the physically significant limit of the deflection of the deflection-span ratio, or of any other selected criterion of damage, is judged to have been reached. This limit depends on the particular structure. For example, it seems reasonable to assume that the limiting value for highway bridges would be significantly higher than that for railway bridges.

Discussion of Results

The general nature of the displacement-time relations determined by the foregoing procedure is shown qualitatively in Fig. 6. These curves illustrate the time lag between the increasing deflection and the decreasing driving force, and they are typical of all the spans investigated.

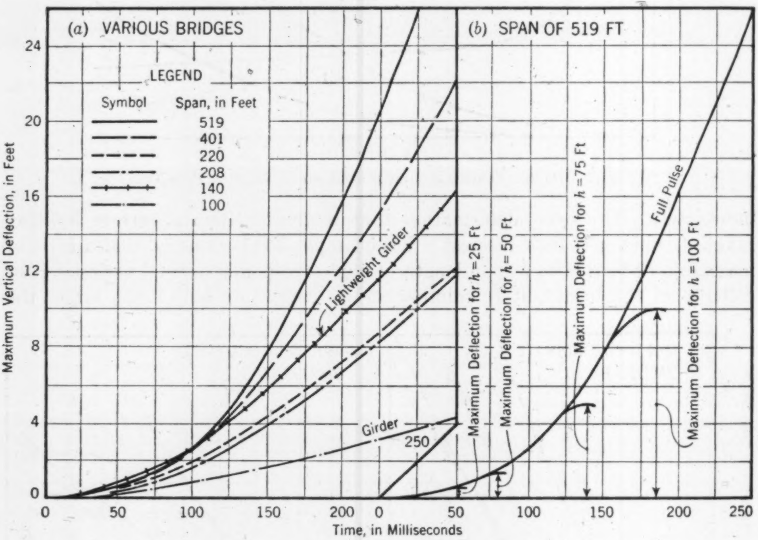

Fig. 8.—Relation Between Time and Maximum Vertical Deflection

Specific results for the various bridges are shown in Fig. 7(*a*). All spans are shown except the 50-ft rolled-beam span which was omitted for reasons of scale. From this illustration it is seen that, after approximately 250 milliseconds, the deflections of all the bridges of standard weight increase with the span length, and that the given pulse will produce the highest ratio of deflection to span length for the longest bridge. The situation is reversed in the early stages, as is shown more clearly in Fig. 7(*b*), because the greater inertia of the longer spans delays the development of speed and displacement. Thus, it can be seen that ultimate damage should increase with increasing span. The 140-ft girder span forms a rather remarkable exception to this pattern, and its behavior has been attributed to its lightweight construction and unusually large deck area. The curve for the 140-ft span indicates that a reduction of mass may lead to very undesirable consequences in bridges acted upon by pressure pulses of this type. It is not possible to isolate completely the effect of mass variation by means of the results shown, however, because no two bridges studied differed in mass only.

It may be noted also that the difference in behavior between the 220-ft deck bridge and the 208-ft through bridge is negligible. Therefore, it may be accepted that deck and through bridges have approximately the same resistance to blast and that no reason exists (on the basis of the present evidence) to favor one over the other.

The variation with time of the deflection-span ratio is shown to an expanded time scale in Fig. 7(*b*), so that the initial phases of the motion become distinguishable. It is clearly seen that, in the early stages of motion, the deflection-span ratio increases with decreasing span length. The motion of the 50-ft span is illustrated, and it is noticed that its motion remains elastic throughout. This result agrees with the earlier conclusion that damage increases with increasing span length. The lower curve in Fig. 7(*b*) illustrates the effect of reflection from an elevation of 25 ft on the 519-ft span and shows graphically that this bridge, which is the most vulnerable of all the spans, would not even enter the plastic range if it were located within 25 ft of the ground or of the water surface.

The relations represented in Fig. 8(*a*) are essentially similar to those shown in Fig. 7 but give the actual deflection in feet as a function of time. Again, the maximum deflection increases with span length, except for the lightweight, unballasted 140-ft span which shows deflections that might be expected of a 300-ft span of standard ballasted construction.

The remarkable effects of elevation above the surface are illustrated for the 519-ft bridge in Fig. 8(*b*). The short segments of curves correspond to the motions for the heights shown, whereas the full curve coincides with that shown in Fig. 8(*a*) for this span. It is apparent that, for elevations substantially exceeding 100 ft, the downward deflection of the bridge is so great by the time the upward pulse arrives that the latter has no significantly helpful effect, and the bridge must be presumed to have been rendered useless. It is obvious, on the other hand, that, for elevations of less than 75 ft, the effects of reflection are drastic and that this effect may save such a span from destruction. This conclusion agrees with the observations made after the Hiroshima and Nagasaki bombings.

By studying Fig. 7 some interesting conclusions may be drawn regarding the maximum height above ground for which an important inhibiting effect is exerted on the damage to spans of various lengths. The curves in Fig. 7 show that, after about 220 milliseconds, a given ratio of maximum deflection to span length is reached at a later time for shorter spans. Considering a certain ratio of permanent deflection to span, or a specified extent of damage, more time can be allowed for the return of the shock wave for short spans because the length of time required to produce this extent of damage is greater for short spans. Therefore, the benefit derived from the returning shock wave may be obtained during a longer period of time while the bridge is being deformed. This longer time corresponds to the reflection period for an increased elevation above the ground or water surface. Thus, it can be concluded that the maximum elevation, for which reflection has an important inhibiting effect on damage, increases with decreasing span length.

One further observation should be made which does not refer directly to the aforementioned illustrations. A comparison of the differential equations of motion for girder and truss bridges, Eqs. 6 and 12, show that the "resistance" term is $-M_p$ for the girder and $-F_p(h - L_{3L}\theta_1)$ for the truss. Assuming that a girder and a truss bridge of equal span weigh the same, when designed for the same loading, the inertia and weight terms need be of no concern in this comparison. If the deck area is also the same for the two bridges, the same driving force will be exerted, and the resulting nonelastic deflection will depend inversely and approximately on the resistance terms. However, it will be noted that the magnitude of the resistance term for the girder is constant, M_p, but that of the truss bridge decreases with increasing rotation θ_1. Thus, it may be presumed that a truss bridge will suffer greater permanent deflection and damage than a girder bridge, provided both are of the same weight and span and are designed according to the same specifications. Unfortunately, it is not possible to include such a pair of comparable examples herein, and the results obtained do not permit isolation of the effect of span length from that of truss or girder construction. On the other hand, the extreme reduction of deflection from the 208-ft truss bridge to the 100-ft girder bridge, shown in Fig. 8(*a*), does not appear wholly attributable to a reduction in the span alone. Therefore, it may be concluded that the numerical results are not inconsistent with the presumption that there is a significant difference between the inelastic behavior of truss and girder bridges.

Summary and Conclusions

This paper has proposed a method for the determination of deflections produced by impulsive vertical loadings on simple-span bridges of truss and girder types. These procedures cover both elastic and large nonelastic deflections, and their use involves only moderate expenditures of time and technical effort. The method can be extended to treat statically indeterminate structures.

The development of the procedures involves the use of several physical assumptions, which are discussed in the body of the paper. The two most important assumptions are the equivalence of a plastically deformed bridge to a mechanism involving rigid and plastic parts, and the feasibility of extrapolating transient shock loading data obtained from small shock tube models to full-size structures. The numerical solution of the differential equations of motion is essentially exact from the engineering viewpoint for both the elastic and the plastic ranges.

The procedures suggested have been applied to the case of an impulsive loading produced by the explosion of a nominal atomic bomb at 2,000 ft above the bridge. Simple-span truss and girder bridges of steel ranging from 50 ft to 519 ft in length were investigated. Since incomplete information on the validity of the underlying assumptions should not vitiate conclusions based on comparisons between the computed response of different bridges of the same general type, the results obtained are believed to justify the following specific conclusions:

1. Damage from nonelastic vertical deflection produced by an atomic blast, measured either directly or as a percentage of span length, increases with increasing span.
2. Damage increases with increasing width of bridge—all other things remaining equal.
3. Damage to two bridges of the same span and differing only in weight should be greater for the bridge having the smaller weight.
4. Height of a bridge above ground or water influences markedly the damage sustained. A bridge that may be destroyed in the absence of shock wave reflection from the ground may suffer no damage at all if it is sufficiently close to the ground or water surface.
5. In the case of the 519-ft bridge, computations show that the maximum elevation above ground for which a significant benefit is derived from reflection is about 100 ft. At greater heights, the returning shock wave arrives too late to prevent the bridge from being rendered useless.
6. It has been found that the maximum elevation above ground for which the reflected shock wave will have an important inhibiting effect on damage will increase with decreasing length of the bridge.
7. The elastic and nonelastic behaviors of deck bridges and through truss bridges are essentially alike under an overhead atomic blast, and there appears to be no reason to prefer one or the other from this aspect.
8. If a truss bridge and a girder bridge have the same weight and span, and if they are designed under the same specifications, it may be reasoned from mathematical considerations that blast damage of the girder bridge should be less than that of the truss bridge.

APPENDIX. NUMERICAL EXAMPLE

The equations of motion for the elastic range (Eqs. 2) take the following form for the 519-ft through truss bridge:

$$y_1 = 0.9992\, y_0 + 0.0389\, \frac{\dot{y}_0}{9.73} + 0.001334\, p \ldots\ldots\ldots\ldots (17a)$$

and

$$\frac{\dot{y}_1}{9.73} = -\,0.0389\, y_0 + 0.9992\, \frac{\dot{y}_0}{9.73} + 0.00685\, p \ldots\ldots\ldots (17b)$$

(Subscripts 0 and 1 refer to consecutive values of y and $\dot{y}$ with respect to time.) The tabular solution then proceeds as shown in Table 2, in which the first three fines of the integration process are given. Col. 1 gives the time, at intervals of four milliseconds. The corresponding values of the pressure are then read from the pressure-time curve in Fig. 1. Cols. 3 and 4 then follow, and values of zero may be entered for Cols. 5 and 8 in the first line because the bridge is presumed to be initially at rest. The deflection y after $t = 0.004$ sec, in the second line, may be obtained from Eq. 17*a*, as follows:

$$y\Big|_{t=0.004} = 0.9992\, y\Big|_{t=0} + 0.0389\, \frac{\dot{y}|_{t=0}}{9.73} + 0.0001334\, p\Big|_{t=0.004}$$
$$= 0 + 0 + 0.00846 = 0.00846.$$

TABLE 2.—Solution of Eqs. 17

Time, t (sec) (1)	Pressure, p (lb per sq in.) (2)	$0.00685\, p$ (lb per sq in.) (3)	$0.0001334\, p$ (lb per sq in.) (4)	Deflection, y (ft) (5)	$0.9992\, y$ (ft) (6)	$0.0389\, y$ (ft) (7)	$\frac{\dot{y}}{9.73}$ (ft per sec) (8)	$0.9992\, \frac{\dot{y}}{9.73}$ (ft) (9)	$0.0389\, \frac{\dot{y}}{9.73}$ (ft) (10)
0	75	0.514	0.01001	0			0		
0.004	63.5	0.435	0.00846	0.00846	0.00845	0.00033	0.435	0.435	0.015
0.008	54	0.369	0.00720	0.03065	0.03065	0.00119	0.804	0.804	0.0313

Cols. 6 and 7 then follow by direct multiplication. The second equation is used to obtain $\dot{y}$:

$$\frac{\dot{y}|_{t=0.004}}{9.73} = -\,0.0389\, y\Big|_{t=0} + 0.9992\, \frac{\dot{y}|_{t=0}}{9.73} + 0.00685\, p\Big|_{t=0.004}$$
$$= 0 + 0 + 0.435 = 0.435,$$

which is shown in Col. 8. Cols. 9 and 10 follow directly. For the next line, in which $t = 0.008$—

$$y\Big|_{t=0.008} = 0.9992\, y\Big|_{t=0.004} + 0.0389\, \frac{\dot{y}}{9.73}\Big|_{t=0.004} + 0.0001334\, p\Big|_{t=0.008}$$

or, the values in Col. 5, line 3, are obtained by adding together the values in Col. 6, line 2; Col. 10, line 2; and Col. 4, line 3. Thus, $y\Big|_{t=0.008} = 0.03065$. Similarly, $\frac{\dot{y}}{9.73}\Big|_{t=0.008} = 0.804$, obtained by adding algebraically the following values: Col. 7, line 2; Col. 9, line 2; and Col. 3, line 3. This procedure continues in this manner until y reaches the limiting elastic deflection beyond which it is no longer applicable.

DISCUSSION

Robert J. Hansen,[15] A. M. ASCE, and John S. Archer,[16] J. M. ASCE.—The authors' paper is of considerable value to engineers concerned with the vulnerability of bridges to attack from atomic weapons. The analysis as presented is limited to the case of attack from directly above the bridge and only mentions the possibility of attack from weapons that are detonated to either side or end of the bridge. For a thorough assessment of vulnerability, a complete consideration should be made of attack situations in which the blast wave approaches the bridge from the side. In many cases this situation would be most likely to cause failure of the bridge. The procedures of analysis presented by the authors, however, can be utilized for the latter conditions.

Several factors not mentioned by Messrs. Fraenkel and Grinter deserve consideration. First—as regards the side loading condition—the possibility of sliding a bridge off its piers through failure of the anchor bolts is a mechanism of failure which deserves investigation. Second, truss members in compression that are subject to lateral loading from the air blast are particularly vulnerable if the axis of the member is normal to the direction of the air blast. The lateral-blast loading enhances the possibility of buckling of the member under its axial load.

It should be apparent that the blast-load impulse is dependent on the percentage of openings in the bridge deck as well as on the width of the deck. The load impulse transmitted to an open-deck (steel-grid) highway bridge or an open-deck railroad bridge may be so small as to leave the bridge undamaged from a nominal atomic bomb burst 2,000 ft in the air over the bridge, without regard to the height of the bridge above the ground.

The engineer should have a thorough background[17,18,19,20,21] on the subject of air-blast loading and dynamic analysis before attempting to analyze bridges for the type of behavior mentioned by the authors.

---

[15] Associate Prof. of Structural Eng., Dept. of Civ. and San. Eng., Massachusetts Inst. of Technology, Cambridge, Mass.

[16] Asst. Prof. of Structural Eng., Dept. of Civ. and San. Eng., Massachusetts Inst. of Technology, Cambridge, Mass.

[17] "Shock Loading of Rectangular Structures," by Walter Bleakney, *Technical Report II-11*, Princeton University Press, Princeton, N. J., January, 1952.

[18] "A Simple Method for Evaluating Blast Effects on Buildings," Armour Research Foundation of Illinois Inst. of Technology, Technology Center, Chicago, Ill., July, 1952.

[19] "Wind Loads on Truss Bridges," by J. M. Biggs, *Transactions*, ASCE, Vol. 119, 1954.

[20] "Proceedings of the Conference on Building in the Atomic Age," Dept. of Civ. and San. Eng., Massachusetts Inst. of Technology, Cambridge, Mass., June, 1952.

[21] "Proceedings of the Symposium of Earthquake and Blast Effects on Structures," Earthquake Eng. Research Inst. and Univ. of California, Los Angeles, Calif., June, 1952.

S. J. Fraenkel[22] and L. E. Grinter,[23] M. ASCE.—The interest of Messrs. Hansen and Archer in bridges subjected to impulsive loads is greatly appreciated. The writers are in agreement with the points cited by the discussers. It is entirely possible that atomic explosions resulting primarily in the lateral loading of bridges may have greater military effect than explosions which occur directly over a bridge. Lateral loading would be much more likely, for example, to produce alternate types of damage to the bridge—such as rigid-body tumbling or the sliding of the bridge off the supporting pier. As it was not the writers' intent to establish a military doctrine for attack on bridges, consideration of these other possible causes of damage to bridge structures was purposely ignored.

It is evident that openings in the bridge deck will have an effect on the damage sustained. Quantitative extrapolation to open-deck bridges cannot be made from the material presented. However, there is reason to believe that the general relations derived (in terms of bridge length, width, and height above ground) will also apply to open-deck bridges.

Two items are worthy of additional emphasis. The first is the effect of longitudinal inertia—which is included in the equations characterizing bridge behavior, and which is the principal feature distinguishing this paper from the usual single-degree-of-freedom treatment of structural vulnerability. The importance of the longitudinal inertia is approximately the same as that of the rotary inertia, and it does not seem generally permissible to omit the longitudinal-inertia term from consideration. The second item relates to the failure criterion (the ratio of deflection to span length). The criterion is admittedly simple, but it does have the great advantage of lending itself to computation and of having significance (to a greater or lesser degree) for all types of bridges. It is possible that for given bridge types, and for given functional purposes, more pertinent and more specific criteria could be given. If this were done, the establishment of general rules of behavior would be rendered most difficult (if not impossible), and not even an approximate generalized treatment could be given to this subject.

It should be realized that it was the writers' purpose to develop and illustrate a convenient method of handling the bridge-vulnerability problem and to derive certain general relations applicable to all bridges. It was not their intent to provide quantitative information on the vulnerability of any specific bridge. As a result of the continually changing state of knowledge concerning blast loading, quantitative answers for specific bridges should always be obtained with reference to the most recent information.

---

[22] Mgr., Propulsion and Structural Research Dept., Armour Research Foundation of Illinois Inst. of Tech., Chicago, Ill.

[23] Dean of Graduate School, and Director of Research, Univ. of Florida, Gainesville, Fla.

AMERICAN SOCIETY OF CIVIL ENGINEERS
Founded November 5, 1852
TRANSACTIONS

Paper No. 2673

FRICTION FACTORS FOR TURBULENT FLOW IN PIPES

BY EDWARD F. WILSEY[1]

WITH DISCUSSION BY MR. GEORGE A. WHETSTONE

SYNOPSIS

It was the author's opinion that curves for determining values of the friction factor f could be fitted to the hyperbolic cotangent of x, some function of **R**, the Reynolds number. This is because coth x has an infinite value when x is equal to zero. As x increases, but remains of small magnitude, coth x decreases rapidly. As x increases further in value, the rate of decrease of coth x lessens until, for all practical purposes, coth x reaches unity when x is equal to, or exceeds, 3.5. On this basis two formulas are presented that permit the computation of the friction factor throughout the entire range of Reynolds numbers for turbulent flow in pipes.

DEVELOPMENT OF THE FORMULAS

Rough Pipes.—The basic formula relating the friction factor f to x some function of the Reynolds number can be written as

$$f = f_{min} \left[\coth \left(\log_{10} x\right)\right]^n \qquad (1)$$

in which n is an undetermined exponent.

J. Nikuradse[2] has shown that the value of the minimum friction factor is

$$f_{min} = \frac{0.25}{\left(\log_{10} 3.7 \frac{D}{k}\right)^2} \qquad (2)$$

in which k/D is the relative roughness of the pipe. Relative roughness is defined as the ratio of the average height k of the protuberances on the pipe

---

NOTE.—Published, essentially as printed here, in June, 1953, as *Proceedings-Separate No. 197*. Positions and titles given are those in effect when the paper or discussion was received for publication.

[1] Former Prof. of Civ. Eng., Ohio Univ., Athens, Ohio. (Mr. Wilsey died on June 30, 1952.)

[2] "Laws of Flow in Rough Pipe," by J. Nikuradse, *Technical Memorandum No. 1292*, National Advisory Committee for Aeronautics, November, 1950, p. 11.

surface to the diameter D of the pipe. The logarithmic function was introduced to change Reynolds numbers ranging from 4,000 to 10,000,000 to numbers varying from 3.5 to 7.

The first step in determining the final form of Eq. 1 was to find a value for x whose logarithm is approximately 3.5 when the friction factor would be a minimum. The function adopted was

$$x = \mathsf{R}\,\frac{k}{D} = V\,\frac{k}{\nu} \quad \text{(3)}$$

in which R is the Reynolds number, V is the velocity of the fluid, and ν is the kinematic viscosity.

TABLE 1.—FRICTION FACTORS COMPUTED FROM EQ. 5 AND FRICTION

Reynolds Number $\mathsf{R} \times 10^{-5}$	*D/k*, INVERSE VALUE OF THE											
	40		70		100		200		400		1,000	
	$f_5^{(a)}$	$f_4^{(b)}$	f_5	f_4	f_5	f_4	f_5	f_4	f_5	f_4	f_5	f_4
0.04	5.95	5.9	5.13	5.2	4.82	4.9	4.72	4.7	5.62	4.3	12.1	4.3
0.06	5.78	5.8	4.88	5.0	4.50	4.6	4.18	4.2	4.44	3.9	7.10	3.7
0.08	5.62	5.7	4.76	4.8	4.31	4.4	3.88	3.9	3.86	3.6	5.30	3.4
0.1	5.60	5.7	4.62	4.7	4.22	4.3	3.70	3.7	3.57	3.5	4.45	3.3
0.2	5.47	5.5	4.50	4.5	4.04	4.1	3.38	3.4	3.02	3.1	3.06	2.8
0.4	....	....	....	....	3.93	3.9	3.24	3.3	2.76	2.8	2.51	2.5
0.6	5.35	5.4	4.37	4.3	3.85	3.9	3.18	3.2	2.70	2.7	2.33	2.3
0.8	5.34[c]	5.3	4.35	4.3	3.82	3.8	3.15	3.2	2.65	2.7	2.24	2.2
1.0			4.34	4.3	3.81	3.8	3.13	3.1	2.62	2.6	2.18	2.1
1.4			4.32[c]	4.3	....	....	....	....	....	....	....	....
2.0					3.80[c]	3.8	3.08	3.1	2.56	2.5	2.11	2.1
4.0							3.05[c]	3.0	2.52	2.5	2.04	2.0
6.0									2.50	2.5	2.01	2.0
8.0									2.49[c]	2.5	1.99	2.0
10											1.99	2.0
20											1.97[c]	2.0
40												
60												
80												
100												
200												
400												
600												
800												
$f_{\min}^{(d)}$	5.30		4.29		3.78		3.03		2.48		1.96	

[b] The term f_5 is herein used to signify the value of the friction factor, multiplied by 100, obtained from curves of the Colebrook formula, Eq. 4. [c] At this point $\mathsf{R}\,k/D$ is equal to 2,000. [d] Values of $f_{\min}$ have been

The final step was to fit the equation to the accepted values of the friction factor by determining a suitable value for n. In order to avoid computation, values of f from the formula of C. F. Colebrook[3]:

$$\frac{1}{\sqrt{f}} = -2 \log_{10}\left(\frac{k}{3.7D} + \frac{2.51}{\mathsf{R}\,\sqrt{f}}\right) \quad \text{(4)}$$

were taken from curves plotted from this formula.[4] From these values it was found that $n = 3$, so that

---

[3] "Turbulent Flow in Pipes, with Special Reference to the Transition Region between Smooth and Rough Pipe Laws," by C. F. Colebrook, *Journal*, Inst. of C. E., London, England, Vol. 11, 1938–1939, p. 133.

[4] "Hydraulics," by H. W. King, C. O. Wisler, and J. G. Woodburn, John Wiley & Sons, Inc., New York, N. Y., 5th Ed., 1948, p. 192.

$$f = f_{min}\left[\coth\left(\log_{10} \mathsf{R}\,\frac{k}{D}\right)\right]^3 \tag{5}$$

Table 1 illustrates the fact that values for the friction factor obtained from Eq. 5 approximate the values obtained from Eq. 4 for all values of $\mathsf{R}\,\frac{k}{D}$ equal to, or greater than, 25. It also illustrates the fact that the friction factor is a minimum when $\mathsf{R}\,\frac{k}{D}$ is equal to, or exceeds, 2,000. When the value of $\mathsf{R}\,\frac{k}{D}$ is less than 25, the computed friction factor rises abruptly, indicating a change in the type of flow. When $\mathsf{R}\,\frac{k}{D}$ is approximately equal to 25, smooth-pipe flow is similar to rough-pipe flow.

FACTORS READ FROM CURVES OF THE COLEBROOK FORMULA

RELATIVE ROUGHNESS OF PIPE										Reynolds Number $\mathsf{R} \times 10^{-5}$
2,000		4,000		10,000		20,000		40,000		
f_5	f_4	f_5	f_4	f_5	f_4	f_5	f_4	f_5	f_4	
										0.04
										0.06
										0.08
7.45	3.15									0.1
3.80	2.7	6.41	....							0.2
2.61	2.5	3.27	2.5	7.38	....					0.4
2.30	2.3	2.58	2.2	4.29	2.13					0.6
2.14	2.2	2.24	2.0	3.21	1.94					0.8
2.04	2.0	2.08	1.9	2.70	1.87	4.68	....	17.4	....	1.0
....	....	....	....	....	....	....	....	....	....	1.4
1.86	1.9	1.76	1.8	1.85	1.65	2.38	1.6	4.16	....	2.0
1.79	1.8	1.60	1.6	1.52	1.5	1.64	1.4	2.12	....	4.0
1.75	1.8	1.57	1.6	1.41	1.4	1.45	1.4	1.67	1.35	6.0
1.74	1.7	1.54	1.5	1.36	1.4	1.34	1.3	1.45	1.3	8.0
1.72	1.7	1.52	1.5	1.33	1.3	1.26	1.2	1.34	1.2	10
1.70	1.7	1.49	1.5	1.27	1.3	1.17	1.2	1.14	1.1	20
1.68[c]	1.7	1.46	1.5	1.24	1.2	1.12	1.1	1.04	1.0	40
		1.45	1.5	1.22	1.2	1.10	1.1	1.02	1.0	60
		1.45[c]	1.5	1.21	1.2	1.09	1.1	1.00	1.0	80
				1.20	1.2	1.07	1.1	0.98	0.99	100
				1.20[c]	1.2	1.06	1.1	0.96	0.97	200
						1.06[c]	1.1	0.95	0.96	400
								0.94	0.95	600
								0.94[c]	0.94	800
1.67		1.44		1.19		1.05		0.933		f_{min}(d)

Eq. 5. [b] The term f_4 is herein used to signify the value of the friction factor, multiplied by 100, obtained from
computed from Eq. 2.

Smooth Pipes.—For smooth pipes k/D is equal to zero, and Eq. 5 must be modified. If the position of $\log_{10} x$ on the hyperbolic cotangent curve were moved, the exponent in the formula for the friction factor would change. Further investigation resulted in

$$f = 0.001\left[\coth\left(\frac{\log_{10} \mathsf{R}}{12.8}\right)\right]^3 \tag{6}$$

The coefficient 12.8 was chosen in order that the smooth-pipe equation and the rough-pipe equation would be equal when $\mathsf{R}\,\frac{k}{D}$ is equal to 25. Eq. 6 illustrates that the minimum friction factor for a smooth pipe is 0.001.

The values for the friction factor in smooth pipes agree favorably with the values computed from the formula developed by L. Prandtl, T. von Kármán, Hon. M. ASCE, and Mr. Nikuradse,[5,6]

$$\frac{1}{\sqrt{f}} = 2 \log_{10} \frac{\mathsf{R}\sqrt{f}}{2.51} \qquad (7)$$

Other formulas for the friction factor of smooth pipes have been developed. Mr. Nikuradse has suggested the expression[7]:

$$f = 0.0032 + 0.221\, \mathsf{R}^{-0.237} \qquad (8)$$

and T. B. Drew, E. C. Koo, and W. H. McAdams proposed the following[8]:

$$f = 0.0056 + 0.500\, \mathsf{R}^{-0.32} \qquad (9)$$

TABLE 2.—COMPARISON OF SMOOTH PIPE FRICTION FACTORS

Reynolds number $\mathsf{R} \times 10^{-5}$	Wilsey (Eq. 6)	Prandtl, von Kármán, and Nikuradse (Eq. 7)	Nikuradse (Eq. 8)	Drew, Koo, and McAdams (Eq. 9)
0.04	0.0482	0.040	0.034	0.041
0.06	0.0421	0.035	0.031	0.036
0.08	0.0386	0.033	0.029	0.034
0.10	0.0328	0.031	0.028	0.032
0.20	0.0292	0.026	0.024	0.027
0.40	0.0244	0.022	0.021	0.022
0.60	0.0217	0.020	0.020	0.020
0.80	0.0203	0.019	0.018	0.019
1.00	0.0194	0.018	0.018	0.019
2.00	0.0166	0.015	0.015	0.016
4.00	0.0142	0.014	0.014	0.013
6.00	0.0131	0.013	0.013	0.013
8.00	0.0125	0.012	0.012	0.012
10.00	0.0120	0.012	0.012	0.011
20.00	0.010	0.010	0.010	0.010
40.00	0.0093	0.0093	0.0092	0.0095
60.00	0.0087	0.0087	0.0087	0.0090
80.00	0.0084	0.0083	0.0083	0.0087
100.00	0.0081	0.0080	0.0081	0.0085

Table 2 shows a comparison of values for the friction factors obtained from Eqs. 6, 7, 8, and 9 for Reynolds numbers ranging in value from 4,000 to 10,000,000. The friction factors from Eq. 7 were read from curves plotted by R. C. Binder.[9] There is a fair agreement for values of the friction factors obtained with Reynolds numbers greater than 100,000. For values of R less than 100,000, they diverge because in this region coth x changes quite rapidly, and laboratory measurements are subject to error. Any other divergency can

---

[5] "Turbulence and Skin Friction," by T. von Kármán, *Journal of the Aeronautical Sciences*, January, 1934, p. 1.

[6] "Mechanische Ahnlichkeit und Turbulenz," by T. von Kármán, *Proceedings*, Third Congress for Applied Mech., Stockholm, Sweden, Vol. 1, 1930, p. 85.

[7] "Gesetzmässigkeit der turbulenten Strömung in glatten Röhren," by J. Nikuradse, *Verein Deutscher Ingenieur, Forschungsscheft No. 356*, 1932.

[8] "The Friction Factor for Clean Round Pipes," by T. B. Drew, E. C. Koo, and W. H. McAdams, *Transactions*, Am. Inst. of Chemical Engrs., Vol. 28, 1932, p. 56.

[9] "Fluid Mechanics," by R. C. Binder, Prentice-Hall, New York, N. Y., 2d Ed., 1949, p. 85.

be explained by the realization that Eqs. 7, 8, and 9 were fitted to data, whereas Eq. 6 was designed to meet Eq. 5 at the point where $\mathbf{R}\,\frac{k}{D}$ is equal to 25.

In order to investigate further the validity of Eq. 6, a comparison was made with the data of measured friction factors for smooth brass pipe, reported by Victor L. Streeter,[10] M. ASCE. Table 3 shows these data arranged in the order of increasing Reynolds numbers. The measured friction factors are compared with values from Eq. 6 and values obtained from a curve of Mr. von Kármán's equation.[9] There is a scattering of the measured friction factors for the lower Reynolds numbers. For these low values of Reynolds numbers there appears to be no way of determining the true value of *f*. As the Reynolds number increases, Eq. 5 conforms more closely with the experimental results.

TABLE 3.—COMPARISON OF FRICTION FACTORS FOR SMOOTH BRASS PIPES

Reynolds number $\mathbf{R} \times 10^{-5}$	Streeter	Wilsey	Prandtl, von Kármán, and Nikuradse	Reynolds number $\mathbf{R} \times 10^{-5}$	Streeter	Wilsey	Prandtl, von Kármán, and Nikuradse
0.179	0.0310	0.0300	0.026	5.35	0.0129	0.0135	0.0129
0.238	0.0201	0.0259	0.0248	5.42	0.0136	0.0135	0.0129
0.400	0.0198	0.0244	0.0219	5.47	0.0134	0.0135	0.0128
0.407	0.0194	0.0241	0.0218	5.50	0.0131	0.0134	0.0128
0.482	0.0206	0.0229	0.0208	5.61	0.0130	0.0134	0.0128
0.575	0.0216	0.0224	0.0200	5.92	0.0133	0.0135	0.0127
0.643	0.0188	0.0215	0.0195	5.96	0.0129	0.0133	0.0127
0.736	0.0198	0.0208	0.0190	6.08	0.0126	0.0131	0.0127
0.752	0.0191	0.0206	0.0190	6.19	0.0129	0.0131	0.0126
0.817	0.0196	0.0203	0.0185	6.27	0.0126	0.0130	0.0125
0.860	0.0182	0.0201	0.0180	6.34	0.0130	0.0130	0.0125
0.933	0.0182	0.0197	0.0180	6.49	0.0124	0.0129	0.0125
1.034	0.0177	0.0192	0.0176	6.61	0.0130	0.0129	0.0123
1.147	0.0174	0.0186	0.0175	6.76	0.0129	0.0128	0.0123
1.33	0.0168	0.0182	0.0170	6.82	0.0126	0.0128	0.0123
1.51	0.0168	0.0176	0.0165	6.85	0.0126	0.0127	0.0122
1.63	0.0164	0.0174	0.0160	6.86	0.0126	0.0127	0.0122
1.68	0.0165	0.0172	0.0160	7.21	0.0124	0.0126	0.0121
1.88	0.0160	0.0170	0.0157	7.28	0.0127	0.0126	0.0121
2.10	0.0158	0.0166	0.0153	7.67	0.0126	0.0126	0.0120
2.21	0.0125	0.0164	0.0153	7.76	0.0123	0.0125	0.0120
2.25	0.0160	0.0160	0.0150	7.80	0.0122	0.0125	0.0120
2.44	0.0141	0.0158	0.0148	8.05	0.0124	0.0124	0.0120
2.61	0.0143	0.0154	0.0148	8.15	0.0125	0.0123	0.0120
2.73	0.0149	0.0153	0.0147	8.36	0.0120	0.0123	0.0119
2.73	0.0156	0.0153	0.0147	8.40	0.0120	0.0122	0.0119
2.75	0.0151	0.0153	0.0147	8.71	0.0119	0.0122	0.0119
2.84	0.0147	0.0153	0.0145	8.73	0.0120	0.0122	0.0119
3.16	0.0144	0.0151	0.0141	9.42	0.0121	0.0121	0.0118
3.16	0.0143	0.0151	0.0141	9.46	0.0121	0.0120	0.0118
3.33	0.0158	0.0149	0.0140	9.46	0.0118	0.0120	0.0118
3.40	0.0143	0.0149	0.0140	9.48	0.0119	0.0119	0.0118
3.50	0.0141	0.0147	0.0140	10.19	0.0117	0.0118	0.0117
3.52	0.0141	0.0147	0.0139	10.62	0.0115	0.0118	0.0117
3.73	0.0137	0.0145	0.0138	10.85	0.0113	0.0117	0.0116
3.73	0.0142	0.0145	0.0138	11.02	0.0114	0.0117	0.0116
3.93	0.0129	0.0144	0.0138	11.08	0.0114	0.0117	0.0116
3.96	0.0140	0.0143	0.0138	11.22	0.0114	0.0116	0.0115
4.09	0.0132	0.0142	0.0135	11.53	0.0108	0.0116	0.0115
4.26	0.0139	0.0141	0.0135	12.02	0.0111	0.0116	0.0114
4.48	0.0139	0.0140	0.0133	12.30	0.0107	0.0115	0.0113
4.66	0.0140	0.0139	0.0132	12.39	0.0111	0.0115	0.0113
4.67	0.0140	0.0139	0.0131	13.30	0.0110	0.0114	0.0112
4.78	0.0132	0.0138	0.0131	13.93	0.0107	0.0112	0.0112
4.90	0.0136	0.0138	0.0131	14.42	0.0108	0.0112	0.0110
5.06	0.0137	0.0137	0.0130	15.00	0.0104	0.0111	0.0109
5.17	0.0127	0.0137	0.0130	15.62	0.0106	0.0109	0.0108
5.22	0.0127	0.0136	0.0130	15.96	0.0108	0.0106	0.0107

---

[10] "Frictional Resistance in Artificially Roughened Pipes," by Victor L. Streeter, *Transactions*, ASCE, Vol. 101, 1936, p. 687.

CONCLUSIONS

To facilitate the use of the equations which have been developed for determining a suitable value of the friction factor, the following procedure outline is presented:

1. If $\mathsf{R}\,\frac{k}{D}$ is greater than 25 and less than 2,000, use Eq. 5.
2. When $\mathsf{R}\,\frac{k}{D}$ is greater than 2,000, use Eq. 2.
3. Eq. 6 should be used when $\mathsf{R}\,\frac{k}{D}$ is less than 25.

When R is less than 2,000—that is, when the flow is laminar—the familiar equation, $f = 64/\mathsf{R}$, should be used.

Eqs. 5 and 2 give results that agree closely with accepted values for the friction factor. The results from Eq. 6 diverge somewhat from the results obtained with other formulas when the Reynolds number has a low value. This divergency indicates a need for further investigation of flow having low values of the Reynolds number.

It may be felt that the new formulas are complicated. This is not so, since all that is needed for the computations is a set of mathematical tables. In defense of simple formulas, the following has been stated[11]:

> "Daniel Bernoulli often said to me to eschew all complicated formulas; he believing that the organization of Nature is too simple to lead to them; and should one find such, the explanation is that one's computations were based upon false hypotheses."

However, the writer feels that the findings in scientific research are truly a revelation, and the way to reveal "Nature's" plan is to work hard, pray to God for guidance, and be sceptical of authoritarianism.

---

[11] "Biographies Relating to the History of Civilization in Switzerland," by R. Wolf, Vol. III, 1860, p. 176.

DISCUSSION

GEORGE A. WHETSTONE,[12] A.M. ASCE.—The formulas proposed by Mr. Wilsey would seem to have the advantage of easy logarithmic computation as contrasted with the complex arithmetic operations implicit in formulas such as Eqs. 4 and 7. The proposed formulas do fulfill one of the criteria of a good engineering formula—the criterion of simplicity. This criterion, however, can also be complied with by use of a table or chart. Thus, an algebraic expression such as the Ganguillet-Kutter formula for open channels,

$$C = \frac{41.65 + \frac{0.00281}{S} + \frac{1.811}{n}}{1 + \left(41.65 + \frac{0.00281}{S}\right)\frac{n}{\sqrt{R}}} \qquad (10)$$

is, from the standpoint of the user who has a table, just as simple as the author's formula which requires a table of coth ($\log_{10} x$).

A much more important engineering criterion is that of accuracy. Accepting Eq. 4 as perhaps the best expression for f in the transition range, it must be agreed that the results obtained by use of Eq. 5 agree closely with the results obtained from Eq. 4 for values of $\mathsf{R}\,\frac{k}{D}$ that are between 25 and 2,000. Mr. Colebrook, however, imposed no such limits on the validity of Eq. 5 but made the equation asymptotic to the smooth and rough pipe laws. The author's statement (under the heading, "Development of the Formulas: Rough Pipes")—"When the value of $\mathsf{R}\,\frac{k}{D}$ is less than 25, the computed friction factor rises abruptly, indicating a change in the type of flow"—seems unwarranted. Nothing of physical significance is involved—the two different types of expression merely diverge for these values.

The statement (under the heading, "Development of the Formulas: Smooth Pipes"), "Eq. 6 illustrates that the minimum friction factor for a smooth pipe is 0.001," is as misleading as would be the equally justifiable statements that Eq. 8 illustrates this limit to be 0.0032 and that Eq. 9 illustrates the limit to be 0.0056.

Table 2 indicates good agreement for values of $\mathsf{R} \times 10^{-5}$ between 6 and 100. For values of R that are less than this range, Eq. 6 gives larger values than do other formulas, except for R equal to 60,000. A recomputation of this value indicates that it should be 0.0220 rather than 0.0217.

Thus the formulas proposed by Mr. Wilsey have no claim to accuracy above that obtained from Eqs. 4, 7, 8, and 9 which they were intended to fit. Actually the author's formulas have a range of validity that is much more restricted.

Perhaps the greatest failing of the formulas is their apparent lack of rationality. In the writer's opinion any significant advance in the practical treatment of pipe friction should follow the broad outlines given by Charles W. Harris,[13] M. ASCE.

---

[12] Associate Prof. of Civ. Eng., Texas Technological College, Lubbock, Tex.

[13] "An Engineering Concept of Flow in Pipes," by Charles W. Harris, *Transactions*, ASCE, Vol. 115, 1950, pp. 909–958.

AMERICAN SOCIETY OF CIVIL ENGINEERS
Founded November 5, 1852
TRANSACTIONS

Paper No. 2674

GROUP LOADINGS APPLIED TO THE ANALYSIS OF FRAMES

By I. F. Morrison[1]

With Discussion by Messrs. Bernard L. Weiner, and I. F. Morrison

Synopsis

In the analysis of highly indeterminate frame structures, the task of setting up and solving the elastic equations becomes time-consuming. Several methods have been developed by which the work may be shortened considerably. Of these, among the classical methods, perhaps that of group loading is the best and most comprehensive method.

The paper sets forth, in detail, the theory of this method in analytical form. Examples in algebraic form, followed by illustrative numerical computations, are used to make clear the engineering application of the theory.

A still further reduction in the number of elastic equations is effected by the choice of a statically indeterminate primary structure. A numerical application of this is also included.

Introduction

The primary purpose of the theory of group loadings is a reduction in the effort required to solve the simultaneous linear equations that arise in the analysis of statically indeterminate structures.

The customary procedure for such analysis is to select a statically determinate primary structure by the choice of such redundant forces and couples as are necessary to obtain the complete solution. This is done by making cuts through the members, inserting hinges, and removing reaction components and other forces in the original structure. The number of these is always *n*, for an *n*-fold indeterminate case. By any one of several well-known procedures, a set of simultaneous equations results:

$$\sum \delta_{ij} X_j = \delta_{io} \quad \text{(1)}$$

Note.—Published, essentially as printed here, in April, 1953, as *Proceedings-Separate No. 183*. Positions and titles given are those in effect when the paper or discussion was received for publication.

[1] Prof. of Applied Mech., Dept. of Civ. and Municipal Eng., Univ. of Alberta, Edmonton, Alta., Canada.

in which the terms X_j are the redundants. The subscripts j and i are integers from 1 to n. The terms δ_{ij} are coefficients depending only on the size and shape of the original structure and the terms δ_{io} are the loading terms that depend both on geometry and on the load and its arrangement. The required stresses are then obtained by the principle of superposition. By the general term "stresses" in this paper is meant reactions, moments, direct stresses in truss members, and other forces of this kind. The superposition of stresses yields

$$Z = Z_0 - z_1 X_1 - z_2 X_2 - z_3 X_3 \ldots - z_n X_n \ldots\ldots\ldots\ldots (2)$$

in which the terms z_i are the stresses produced by the loading $X_i = -1$ and the terms Z_0 are the stresses produced by the actual loading on the statically determinate primary structure.

In the procedure to be followed in this paper, the elements in the square matrix, δ_{ij}, are found from the self-stressed conditions obtained by placing in turn each X_j-term equal to -1, whereas all the other redundants are assumed to be zero. Each of these conditions is called "Condition $X_j = -1$." For frames or girders, sketches are made of each of the bending moment diagrams for the statically determinate primary structure with the single loadings $X_j = -1$ and from them are obtained the elements of the structure matrix by means of the Maxwell-Mohr work equation:

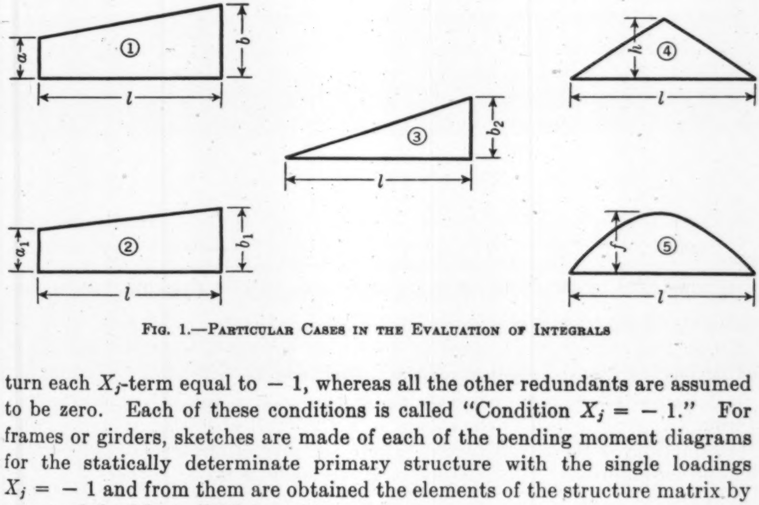

FIG. 1.—PARTICULAR CASES IN THE EVALUATION OF INTEGRALS

$$\delta_{ij} = \sum \int_0^l \frac{N_i\, N_j\, ds}{E\, A} + \sum \int_0^l \frac{m_i\, m_j\, ds}{E\, I} + \cdots \ldots\ldots\ldots\ldots (3)$$

in which E denotes the modulus of elasticity, A is the cross-sectional area of a member, N is the direct stress in a member, m is the moment produced by a unit load, s represents distance, and I is the moment of inertia. Eq. 3 is not the complete work equation. The terms relate to frames. The first term is usually small relative to the second and, therefore, only the last term will be retained as is customary. Other terms dependent on temperature changes, shrinkage, and displacement of supports have not been included. Neglecting the first term, $\delta_{ij} = \sum \int_0^l \frac{m_i\, m_j\, ds}{E\, I}$ represents the displacements, in an assigned direction at the point of application i of the redundant X_i, produced by the loading $X_j = -1$—that is, the work done by $X_i = -1$ as a result of the deformation produced by $X_j = -1$.

The summation incorporates all the members of the frame. The modulus of elasticity will be assumed to be constant for the frame and I will be assumed to be constant for each member.

The definite integrals, which are in all cases quite simple, can best be evaluated by means of the Müller-Breslau tables,[2] a part of which follows, with the notation defined in Fig. 1. All the cases required in this paper are listed here, and case numbers are encircled in Fig. 1:

Case	$\int m_i\, m_j\, ds$
1–1	$\frac{l}{3}(a^2 + a\,b + b^2)$
1–2	$\frac{l}{6}[a_1(2\,a + b) + b_1(a + 2\,b)]$
1–3	$l\,\frac{b_2}{6}(2\,a + b)$
3–4	$\frac{h\,b_2\,l}{4}$
3–5	$\frac{f\,b_2\,l}{3}$

Because of the Maxwell theorem, the outlined procedure always leads to a symmetrical matrix and, therefore, it is necessary to determine $\frac{n\,(n+1)}{2}$ elements of the matrix, if n is the number of redundants. This task, in itself, may be long, but it can always be done, and the set of simultaneous linear equations then must be solved for the redundants X_j.

If any, or all, of the coefficients δ_{ij}, in which $i \neq j$, can be reduced to zero through a proper choice of the redundants, the effort of setting up and solving the equations is thereby reduced. There are several methods by which this can be accomplished. The method of group loadings is one of them.

GROUP LOADINGS

Group loadings are used to reduce the set of equations (Eq. 1) to one-term simultaneous equations of the form, $\delta_{ii}\, X_i = \delta_{io}$, the simple solution of which is $X_i = \frac{\delta_{io}}{\delta_{ii}}$, by making $\delta_{ij} \neq 0$ when $i = j$ and $\delta_{ij} = 0$ when $i \neq j$. Such a process is called "orthogonalization" of the equations.

A necessary and sufficient choice of the redundants for this purpose is, however, not apparent except in very simple cases; and it is usually desired to discover the conditions that will lead to such orthogonalization. To accomplish this, a linear relationship is established between the chosen X_i and a group of secondary redundants Y_k by means of the linear transformation:

---

[2] "Die Graphische Statik der Baukonstruktionen," Vol. II, Pt. 2, Alfred Kröner Verlag, Leipzig, Germany, p. 56.

$$X_j = \sum \alpha_{jk} \, Y_k \ldots\ldots\ldots\ldots\ldots\ldots\ldots\ldots \quad (4)$$

in which k is an integer from 1 to n. This relationship is shown in detail in Table 1, which the writer will call the α-pattern.

The number of Y-terms and X-terms will always be n. Thus, the α-pattern will form a square matrix of the order n.

If Y_k equals -1, all other Y-values being equal to zero, a group of values, $X_j = -\alpha_{jk}$, results so that, instead of a set of self-stressed conditions caused by a single redundant loading $X_j = -1$, one has a set of self-stressed conditions caused by a group of redundant loadings expressed as $X_j = -\alpha_{jk}$, which is called condition $Y_k = -1$. Considering the terms Y_k to be the redundants provides a work equation that is similar to Eq. 1. This equation

TABLE 1.—THE α-PATTERN

X_j	Y_k				
	Y_a	Y_b	Y_c	...	Y_n
X_a	α_{aa}	α_{ab}	α_{ac}	...	α_{an}
X_b	α_{ba}	α_{bb}	α_{bc}	...	α_{bn}
X_c	α_{ca}	α_{cb}	α_{cc}	...	α_{cn}
.	.	.	.	...	.
.	.	.	.	...	.
.	.	.	.	...	.
X_n	α_{na}	α_{nb}	α_{nc}	...	α_{nn}

is $\sum \gamma_{ik} \, Y_k = \gamma_{io}$, in which the coefficients γ_{io} are the loading terms obtained from the group loading Y_i and the displacements of the structure produced by the actual loads. It is the γ_{ik}-terms that are to be orthogonalized. This process is expressed by the condition equations: $\gamma_{ik} \neq 0$ when $i = k$; and $\gamma_{ik} = 0$ when $i \neq k$. When this has been accomplished, Y_i becomes equal to $\frac{\gamma_{io}}{\gamma_{ii}}$, and the redundants X_j are obtained by substitution in Eqs. 4, with k equal to i. Thus, the α-pattern is to be so formed that the following condition prevails:

$$\sum \int \frac{m_k \, m_i \, ds}{E \, I} = 0 \ldots\ldots\ldots\ldots\ldots\ldots\ldots \quad (5)$$

in which k is not equal to i. The moments m_k and m_i are produced by the group loadings, $Y_k = -1$ and $Y_i = -1$. Eq. 5 makes the equilibrium condition, $Y_k = -1$, orthogonal to the displacement condition of $Y_i = -1$.

It is useful to let $\bar{m}_i$ be the moment produced by the loads $X_i = -1$, and to let m_i be the moment produced by the loads $Y_i = -1$. For abbreviation, the following will be used:

$$\delta_{ik} = \sum \int \frac{\bar{m}_i \, \bar{m}_k \, ds}{E \, I} \ldots\ldots\ldots\ldots\ldots\ldots\ldots \quad (6a)$$

which is the work done by the redundant, $X_k = -1$, with the displacement produced by the load, $X_i = -1$. Obviously, $\delta_{ik} = \delta_{ki}$. Similarly,

$$\beta_{ik} = \sum \int \frac{\bar{m}_i \, m_k \, ds}{E\,I} \tag{6b}$$

is the work done by the load condition, $Y_k = -1$, with the displacement produced by the load, $X_i = -1$ and $\beta_{ik} \neq \beta_{ki}$. The work accomplished by the group loading, $Y_k = -1$, with the displacement produced by the load, $X_i = -1$, is not equal to the work done by $Y_i = -1$ with the displacement $X_k = -1$. Finally,

$$\gamma_{ik} = \sum \int \frac{m_i \, m_k \, ds}{E\,I} \tag{6c}$$

is the work done by the load condition, $Y_k = -1$, with the displacements, $Y_i = -1$, and $\gamma_{ik} = \gamma_{ki}$.

Setting $m_j = \sum \alpha_{ij} \, \bar{m}_i$, and omitting the summation signs that incorporate the members, the second member of Eq. 6*c* can be written as

$$\int \frac{m_j \, m_k \, ds}{E\,I} = \sum \int \alpha_{ij} \frac{\bar{m}_i \, m_k \, ds}{E\,I} = \sum \alpha_{ij} \int \frac{\bar{m}_i \, m_k \, ds}{E\,I} \tag{7}$$

in which the summation is to be taken for the load group. Thus,

$$\gamma_{jk} = \sum \alpha_{ij} \, \beta_{ik} \tag{8}$$

In order to obtain a system of orthogonal functions, α_{ij}, γ_{jk} must be placed equal to zero, with j not equal to k, yielding—

$$\sum \alpha_{ij} \, \beta_{ik} = 0, \qquad j \neq k$$

from which it is desired to determine the coefficient α_{ij}. One way to do this will be described herein. For the group Y_a, it is suggested that the designer choose arbitrarily the single value, $\alpha_{aa} = +1$, and make all other values of α_{ia}, in the vertical column under Y_a in Table 1, zero. Thus, $X_a = Y_a$ and, therefore, condition $Y_a = -1$ becomes equivalent to condition $X_a = -1$.

For the group Y_b,

$$\gamma_{ba} = \alpha_{ab} \, \beta_{aa} + \alpha_{bb} \, \beta_{ba} + \alpha_{cb} \, \beta_{ca} + \ldots = 0 \tag{9a}$$

from which it is desired to determine α_{ab}. To do this, it is assumed that $\alpha_{bb} = +1$, and all other values of α_{ib} equal zero excepting α_{ab}. Then,

$$\alpha_{ab} = -\frac{\beta_{ba}}{\beta_{aa}} \tag{9b}$$

and

$$\gamma_{ab} = \alpha_{aa} \, \beta_{ab} + \alpha_{ba} \, \beta_{bb} + \alpha_{ca} \, \beta_{cb} + \ldots = 0 \tag{9c}$$

Then, because all α_{ia}-values have been assumed to be zero except α_{aa},

$$\beta_{ab} = 0 \tag{9d}$$

For the group Y_c, there are two equations:

$$\left.\begin{aligned}\gamma_{cb} &= \alpha_{ac}\,\beta_{ab} + \alpha_{bc}\,\beta_{bb} + \alpha_{cc}\,\beta_{cb} + \ldots = 0\\ \gamma_{ca} &= \alpha_{ac}\,\beta_{aa} + \alpha_{bc}\,\beta_{ba} + \alpha_{cc}\,\beta_{ca} + \ldots = 0\end{aligned}\right\}\ldots\ldots\ldots\ldots(10)$$

If α_{cc} is set equal to $+ 1$, Eqs. 10 yield

$$\alpha_{bc} = - \frac{\beta_{cb}}{\beta_{bb}}\ldots\ldots\ldots\ldots\ldots\ldots\ldots\ldots(11a)$$

and

$$\alpha_{ac} = - \frac{\alpha_{bc}\,\beta_{ba}}{\beta_{aa}} - \frac{1\,\beta_{ca}}{\beta_{aa}}\ldots\ldots\ldots\ldots\ldots\ldots(11b)$$

Also, the conditions:

$$\gamma_{ac} = 0 \text{ and } \gamma_{bc} = 0$$

yield

$$\beta_{ac} = 0 \text{ and } \beta_{bc} = 0.$$

This process can be continued until all the required α_{ij}-values have been determined. The α-pattern of Table 1 becomes the new arrangement shown in Table 2.

TABLE 2.—THE α-PATTERN CONFORMING TO EQ. 5

X_j	Y_k					
	Y_a	Y_b	Y_c	Y_d	...	Y_n
X_a	+1	α_{ab}	α_{ac}	α_{ad}	...	α_{an}
X_b	0	+1	α_{bc}	α_{bd}	...	α_{bn}
X_c	0	0	+1	α_{cd}	...	α_{cn}
X_d	0	0	0	+1	...	α_{dn}
.	.	.	.	.	...	.
.	.	.	.	.	...	.
X_n	0	0	0	0	...	+1

This is not the only arrangement of the arbitrarily chosen values of α. Others are possible and sometimes more desirable. For example, when the structure is symmetrical, it is expedient to take advantage of that fact in choosing the α-values. However, the number of the α_{ij}-values that can be chosen arbitrarily is always $\dfrac{n\,(n + 1)}{2}$.

The β-values may be computed systematically. The term δ_{ia} is the displacement corresponding to the redundant $X_i = - 1$ produced by $X_a = - 1$ but, because X_a is equal to Y_a,

$$\beta_{ia} = \delta_{ia}\ldots\ldots\ldots\ldots\ldots\ldots\ldots\ldots(12a)$$

All values of β_{ib} are the displacements corresponding to the redundants $X_i = - 1$ of the primary structure produced by the loads $Y_b = - 1$; that is, by the group loadings, $X_b = - 1$ and $X_a = - \alpha_{ab}$.

Thus, putting $m_b = \bar{m}_b + \alpha_{ab}\,\bar{m}_a$ into Eq. 6b, with k equal to b, yields

$$\beta_{ib} = \delta_{ib} + \alpha_{ab}\,\delta_{ia}\ldots\ldots\ldots\ldots\ldots\ldots\ldots(12b)$$

and, because $\alpha_{ab} = -\frac{\beta_{bc}}{\beta_{aa}} = -\frac{\delta_{ba}}{\delta_{aa}}$ from Eq. 9*b*,

$$\beta_{ib} = \delta_{ib} - \frac{\delta_{ba}\,\delta_{ia}}{\delta_{aa}} \tag{12c}$$

for all values of i. In the same way,

$$\beta_{ic} = \delta_{ic} - \frac{\delta_{ca}\,\delta_{ia}}{\delta_{aa}} - \frac{\beta_{cb}\,\beta_{ib}}{\beta_{bb}} \tag{12d}$$

EXAMPLES

A careful study of the following examples will make the process clearer. After an α-pattern has been established for a certain type of structure, it can be retained and the numerical values filled in.

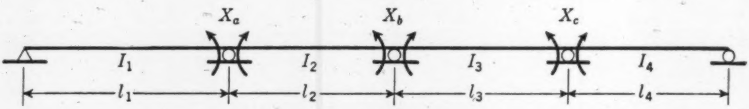

(*a*) CONTINUOUS GIRDER

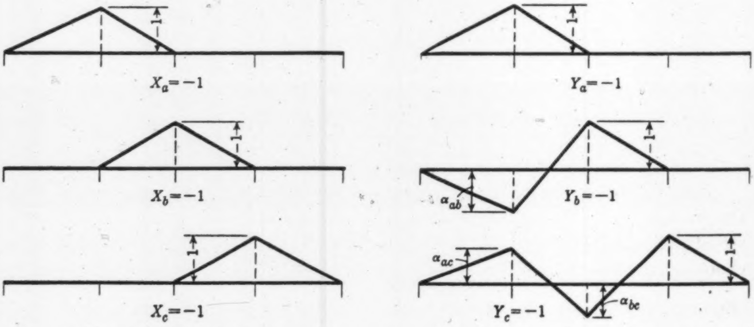

(*b*) MOMENT DIAGRAMS

(*c*) MOMENT DIAGRAMS (GROUP)

FIG. 2.—GIRDER MOMENTS

Continuous Girder.—Fig. 2(*a*) shows a girder on five supports. The length of the span is l, and the value $l' = \frac{l}{I}$—called the modified span—will be used for abbreviation. The redundants have been taken as X_a, X_b, and X_c, which are the moments at the inner supports. Fig. 2(*b*) shows the moment diagrams for the conditions $X_a = -1$, $X_b = -1$, and $X_c = -1$, respectively. By means of the Müller-Breslau tables, or by direct integration, the following can be written:

$$\delta_{aa} = \frac{l'_1 + l'_2}{3}, \qquad \delta_{ab} = \frac{l'_2}{6}, \qquad \delta_{ac} = 0$$

$$\delta_{ba} = \frac{l'_2}{6}, \qquad \delta_{bb} = \frac{l'_2 + l'_3}{3}, \qquad \delta_{bc} = \frac{l'_3}{6}$$

$$\delta_{ca} = 0, \qquad \delta_{cb} = \frac{l'_3}{6}, \qquad \delta_{cc} = \frac{l'_3 + l'_4}{3}$$

By Eqs. 9*b* and 12*a*,

$$\alpha_{ab} = -\frac{\delta_{ba}}{\delta_{aa}} = -\frac{l'_2}{2\,(l'_1 + l'_2)} \quad \text{(13a)}$$

Eqs. 11 and 12 lead to

$$\alpha_{bc} = -\frac{2\,l'_3\,(l'_1 + l'_2)}{4\,(l'_2 + l'_3)\,(l'_1 + l'_2) - (l'_2)^2} \quad \text{(13b)}$$

and

$$\alpha_{ac} = +\frac{l'_3\,l'_2}{4\,(l'_2 + l'_3)\,(l'_1 + l'_2) - (l'_2)^2} \quad \text{(13c)}$$

Fig. 1(*c*) shows the moment diagrams for the group loadings $Y_a = -1$, $Y_b = -1$, and $Y_c = -1$, respectively. The coefficients γ_{ab}, γ_{bc}, and γ_{ca} are all equal to zero, and the following expressions can be solved:

$$\left.\begin{aligned} Y_a &= +\frac{\gamma_{ao}}{\gamma_{aa}} \\ Y_b &= +\frac{\gamma_{bo}}{\gamma_{bb}} \\ Y_c &= +\frac{\gamma_{co}}{\gamma_{cc}} \end{aligned}\right\} \quad \text{(14)}$$

From Eq. 4 values are obtained for X_a, X_b, and X_c. The moment diagram resulting from the actual loads on the primary structure has not been shown here. It can always be drawn for any loads that may be placed on the simple spans. From it and each of the moment diagrams of Fig. 1(*c*), the γ_{io}-values can be determined immediately.

Unsymmetrical Bent.—As a second example, an α-pattern is established for the frame shown in Fig. 3(*a*) which is indeterminate to the third degree. The statically determinate primary structure has been selected by the insertion of three hinges at points a, b, and c, respectively, and the redundants have been taken as the moments at those points. The location of the hinge at point a has been left indeterminate for convenience. The procedure involves making the substitution, $\frac{l_c}{l_b} = \nu$, and finding $h_0 = \frac{2}{3}\,\frac{(h_1\,\nu + h_2)}{(1 + \nu)}$. Instead of following the previous procedure, an adequate α-pattern is adopted through the choice of six of the α-values as shown in Fig. 3(*b*).

Fig. 4(*a*) shows the bending moment diagrams for the following conditions: $X_a = -1$, $X_b = -1$, and $X_c = -1$. The symbol *m* in Fig. 4 designates moments at the corner joints and rigid column bases. These moments are

$$m_1 = \frac{h_1\,(\nu + 1)}{(h_1\,\nu + h_2)}, \qquad m_3 = \frac{h_2}{(h_1\,\nu + h_2)}, \qquad m_5 = \frac{h_1}{(h_1\,\nu + h_2)}$$

$$m_2 = \frac{h_2\,(\nu + 1)}{(h_1\,\nu + h_2)}, \qquad m_4 = \frac{h_2\,\nu}{(h_1\,\nu + h_2)}, \qquad m_6 = \frac{h_1\,\nu}{(h_1\,\nu + h_2)}$$

Therefore, $\nu\, m_3 = m_4$, and $\nu\, m_5 = m_6$. Because $Y_a = -1$ is the same as $X_a = -1$, Eq. 6c yields the following by means of the Müller-Breslau tables:

$$\gamma_{aa} = \frac{4}{9\,h^2_0}\left[\frac{h'_1\,h^2_1}{4} + \frac{h'_2\,h^2_2}{4} + \frac{l'}{3}\,(h^2_1 + h_1\,h_2 + h^2_2)\right] \ldots\ldots (15)$$

in which h' is equal to $\frac{h}{I}$. Because β_{aa} is not equal to zero, if it is desired to make α_{ab} equal to zero, it is necessary that (from Eq. 9a) $\alpha_{bb}\,\beta_{ba} + 1\,\beta_{ca} = 0$

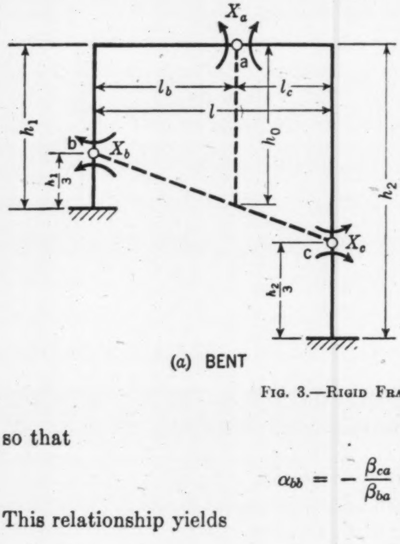

(a) BENT

X_j	Y_k		
	Y_a	Y_b	Y_c
X_a	+1	0	α_{ac}
X_b	0	α_{bb}	$-\alpha_{bc}$
X_c	0	+1	+1

(b) THE α-PATTERN

FIG. 3.—RIGID FRAME ANALYSIS

so that

$$\alpha_{bb} = -\frac{\beta_{ca}}{\beta_{ba}} = -\frac{\delta_{ca}}{\delta_{ba}} \ldots\ldots (16a)$$

This relationship yields

$$\alpha_{bb} = +\frac{h_1}{h_2} \ldots\ldots (16b)$$

The condition $\alpha_{bb} = +1$ could have been chosen, but it would have been necessary to compute α_{ab} which would, in general, not be zero.

The column under Y_b in Fig. 3(b) has been established, and Fig. 4(b) shows the condition, $Y_b = -1$. From Fig. 4(b), and by means of the Müller-Breslau tables,

$$\gamma_{bb} = \frac{3}{4}\left[\frac{h'_1\,h^2_1 + h'_2\,h^2_2}{h^2_2}\right] \ldots\ldots (17)$$

The next step is to obtain expressions for α_{ac} and α_{bc}. From Eq. 11*a*, the following is true:

$$-\alpha_{bc} = -\frac{\beta_{cb}}{\beta_{bb}} \qquad (18a)$$

From the conditions: $X_c = -1$, $Y_b = -1$, and $X_b = -1$, $Y_b = -1$, it is found that, according to Eq. 6*b*, $\beta_{cb} = +\frac{3}{4}h'_2$, $\beta_{bb} = +\frac{3}{4}\frac{h'_1 h_2}{h_2}$, so that

$$\alpha_{bc} = +\frac{h'_2 h_2}{h'_1 h_1} \qquad (18b)$$

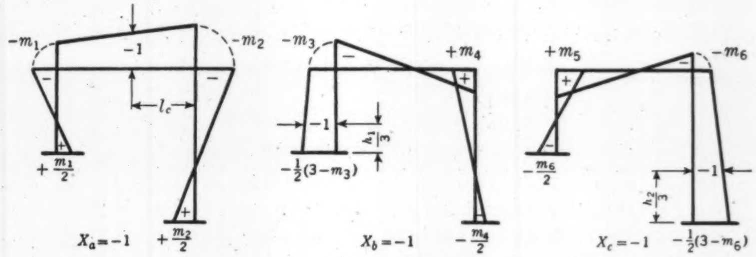
$-m_1$
-1
$-m_2$
$-m_3$
$+m_4$
$+m_5$
$-m_6$
l_c
$+\frac{m_1}{2}$
-1
$\frac{h_1}{3}$
$-\frac{1}{2}(3-m_3)$
$-\frac{m_6}{2}$
-1
$\frac{h_2}{3}$
$X_a=-1$
$+\frac{m_2}{2}$
$X_b=-1$
$-\frac{m_4}{2}$
$X_c=-1$
$-\frac{1}{2}(3-m_6)$

(*a*) MOMENT DIAGRAMS

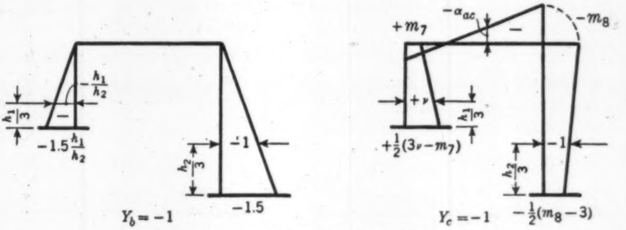
$-\frac{h_1}{h_2}$
$\frac{h_1}{3}$
$-1.5\frac{h_1}{h_2}$
$\frac{h_2}{3}$
-1
-1.5
$Y_b=-1$
$-\alpha_{ac}$
$+m_7$
$-m_8$
$+\nu$
$\frac{h_1}{3}$
$+\frac{1}{2}(3\nu-m_7)$
-1
$\frac{h_2}{3}$
$Y_c=-1$
$-\frac{1}{2}(m_8-3)$

(*b*) MOMENT DIAGRAMS (GROUP)

FIG. 4.—MOMENTS IN THE FRAME OF FIG. 3

If ν is so chosen that it equals $\frac{h'_1 h_1}{h'_2 h_2}$, it follows that $\alpha_{bc} = \frac{1}{\nu}$. To compute α_{ac}, substitution into Eq. 11*b* yields

$$\alpha_{ac} = \frac{1}{\nu}\frac{\beta_{ba}}{\beta_{aa}} - \frac{1}{\nu}\frac{\beta_{ca}}{\beta_{aa}} \qquad (19a)$$

Because $\delta_{ca} = -\frac{h_1}{h_2}\delta_{ba}$, it may be written that $\alpha_{ac} = +\frac{\delta_{ba}}{\delta_{aa}}\frac{(h_2 + \nu\, h_1)}{\nu\, h_2}$, which is equivalent to

$$\alpha_{ac} = \frac{3}{2}\, l'\, h_0 \frac{\left[\frac{1}{\nu}(2\,h_1 + h_2) - (2\,h_2 + h_1)\right]}{\frac{3}{2}(h'_1\, h^2_1 + h'_2\, h^2_2) + 2\, l'\,(h^2_1 + h_1\, h_2 + h^2_2)} \qquad (19b)$$

Fig. 4(*b*) shows the moment diagram for the condition, $Y_c = -1$, from which the coefficient γ_{cc} may be determined.

Because the purpose of this analysis is to demonstrate the method rather than to obtain algebraic formulas for any particular frame, the algebra will not be carried further. In practice, one works directly with the numerical values. Moreover, in this particular example, the elastic center method may perhaps be shorter but it has the same purpose—namely, to reduce the elastic equations to one-term equations.

If the frame is symmetrical, the α-pattern becomes quite simple, because $\nu = 1$ and $\frac{h_1}{h_2} = 1$. Also, $\alpha_{ac} = 0$ and $\alpha_{bc} = +1$. Therefore, the α-pattern is as shown in Table 3.

TABLE 3.—THE α-PATTERN (SYMMETRIC FRAME)

Y_k / X_i	Y_a	Y_b	Y_c
X_a	+1	0	0
X_b	0	+1	−1
X_c	0	+1	+1

INDETERMINATE PRIMARY STRUCTURES

In the preceding analysis, the primary structure in each case has been chosen as a statically determinate structure. The only reason for this is that the bending moment diagrams always can be readily sketched.

However, if there are at hand indeterminate cases that have previously been solved, the primary structure may be chosen as being made up of statically indeterminate parts. In a previous paper, the writer has directed attention to the "Rahmenformeln" of A. Kleinlogel, which serves the purpose admirably.[3]

Rigid Frame.—A simple numerical example is presented to show the application of the theory of group loadings, assisted by the use of an n'-fold statically indeterminate primary structure.

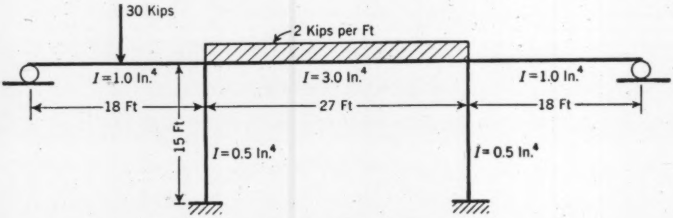

FIG. 5.—LOADED STRUCTURE

Fig. 5 shows the original structure. It is symmetrical, and it is 5-fold statically indeterminate. The primary structure can be selected in several ways, one of which appears in Fig. 6(*a*). It is 3′-fold statically indeterminate, and the number of redundants is two.

Because the original structure is symmetrical, the two redundants X_a and X_b have been symmetrically arranged. Therefore, the α-pattern for a symmetrical 2-fold statically indeterminate structure may be chosen as shown in Fig. 6(*b*).

---

[3] "On the Extended Use of Kleinlogel's Rahmenformeln," by I. F. Morrison, *Canadian Journal of Research*, F, 26, December, 1948, pp. 552–564.

Fig. 7 shows the two cases, $Y_a = -1$, $Y_b = -1$, and also "Condition 0," defining the stresses Z_0 (see Eq. 2) produced by the loads on the primary structure.

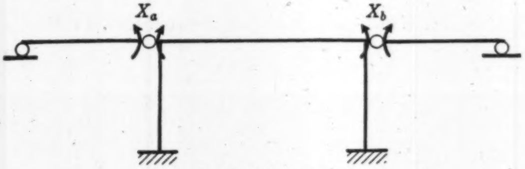

(*a*) REDUNDANTS

X_j \ Y_k	Y_a	Y_b
X_a	+1	-1
X_b	+1	+1

(*b*) THE α-PATTERN

FIG. 6.—PRIMARY STRUCTURE

The γ-values can be computed directly from the moment diagrams of Fig. 7 with the aid of the Müller-Breslau tables:

$$\gamma_{aa} = +16.57, \qquad \gamma_{ao} = -1{,}290.9$$
$$\gamma_{cc} = +14.86, \qquad \gamma_{bo} = +\ \ 607.5.$$

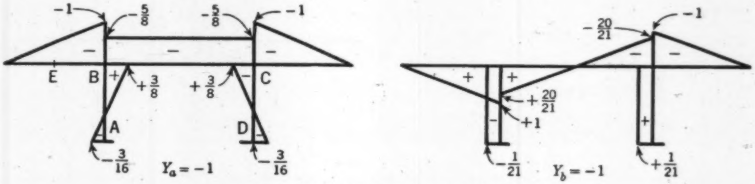
-1
$-\frac{5}{8}$
$-\frac{5}{8}$
-1
$-$
$-$
$-$
E
B
C
$+$
$+\frac{3}{8}$
$+\frac{3}{8}$
$-$
A
D
$-\frac{3}{16}$
$Y_a = -1$
$-\frac{3}{16}$
$-\frac{20}{21}$
-1
$-$
$-$
$+$
$+$
$+\frac{20}{21}$
$+1$
$-$
$+$
$-\frac{1}{21}$
$Y_b = -1$
$+\frac{1}{21}$

(*a*) MOMENT DIAGRAMS (GROUP)

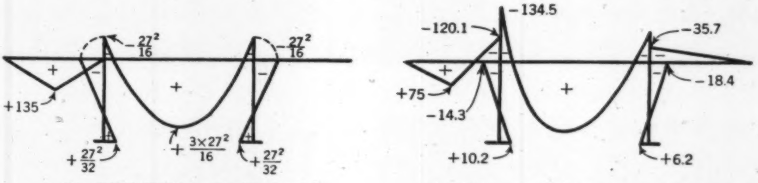
$-\frac{27^2}{16}$
$-\frac{27^2}{16}$
$+$
$-$
$+$
$-$
$+135$
$+\frac{27^2}{32}$
$+\frac{3\times 27^2}{16}$
$+\frac{27^2}{32}$
-134.5
-120.1
-35.7
$+$
$-$
$+$
$-$
$+75$
-14.3
-18.4
$+10.2$
$+6.2$

(*b*) CONDITION 0, IN KIP-FEET (*c*) COMPLETE MOMENTS, IN KIP-FEET

FIG. 7.—MOMENTS IN THE FRAME OF FIG. 5

The group loadings may be computed as $Y_a = -\dfrac{1{,}290.9}{16.57} = -77.9$; and $Y_b = +\dfrac{607.5}{14.86} = +42.2$. The redundants are $X_a = -77.9 - 42.2 = -120.1$; and $X_b = -77.9 + 42.2 = -35.7$.

Table 4, based on Eq. 2, shows the moments at several points. From these values the complete bending moment diagram can be drawn as shown in Fig. 7(*c*).

Three-Bay Frame.—As a second numerical example, the frame shown in Fig. 8(*a*) is considered. This structure is 9-fold statically indeterminate.

TABLE 4.—MOMENT VALUES, IN KIP-FEET, FOR THE STRUCTURE IN FIG. 5

Condition	Term	POINT (FIG. 7 (*a*))								
		A	B	B (BC)	B (BA)	C (CD)	C (CB)	C	D	E
0	Z_0	+22.78	0	− 45.56	−45.56	−45.56	−45.56	0	+22.78	+135.0
$Y_a = -1$	$-Y_a z_1$	−14.61	− 77.9	− 48.70	+29.22	+29.22	−48.70	−77.9	−14.61	− 38.95
$Y_b = -1$	$-Y_b z_2$	+ 2.01	− 42.2	− 40.19	+ 2.01	− 2.01	+40.19	+42.2	− 2.01	− 21.10
Final	Z	+10.18	−120.1	−134.45	−14.33	−18.35	−54.07	−35.7	+ 6.16	+ 74.95

The 6′-fold statically indeterminate primary structure is shown in Fig. 8(*b*), leaving three redundant quantities; and the α-pattern is shown subsequently in Fig. 9(*d*). In this α-pattern, $V_0 = X_a$, $H_0 = X_b$, and $M_0 = X_c$.

Fig. 9(*a*) shows the conditions, $X_a = -1$, $X_b = -1$, and $X_c = -1$. Because of the antisymmetry of the condition, $X_a = -1$, the following equations result: $\delta_{ca} = 0$ and $\delta_{ba} = 0$. Therefore, if $\alpha_{ab} = 0$, it follows that $\alpha_{bb} = \frac{0}{0} = 1$.

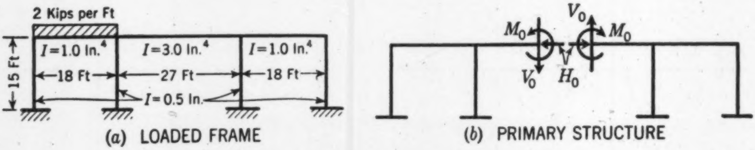

(*a*) LOADED FRAME (*b*) PRIMARY STRUCTURE

FIG. 8.—THREE-BAY FRAME

From Eqs. 11*b* and 12*a*, $\alpha_{ac} = \frac{\alpha_{bc}\,\delta_{ba} - \delta_{ca}}{\delta_{aa}}$, and because $\delta_{ca} = \delta_{ba} = 0$, it is true that $\alpha_{ac} = 0$. Also, from Eq. 11*a*, $\alpha_{bc} = \frac{\beta_{cb}}{\beta_{bb}}$. However,

$$\beta_{cb} = \delta_{cb} - \frac{\delta_{ba}\,\delta_{ca}}{\delta_{aa}} = \delta_{cb}$$

and

$$\beta_{bb} = \delta_{bb} - \frac{\delta_{ba}\,\delta_{ba}}{\delta_{aa}} = \delta_{bb}$$

and, therefore, $\alpha_{bc} = \frac{\delta_{cb}}{\delta_{bb}}$.

From Fig. 9(*a*), $\frac{1}{2}\,\delta_{cb} = \frac{1{,}247.5}{121}$, $\frac{1}{2}\,\delta_{bb} = \frac{43{,}312.5}{121}$, and $\alpha_{bc} = +\,0.02882$.

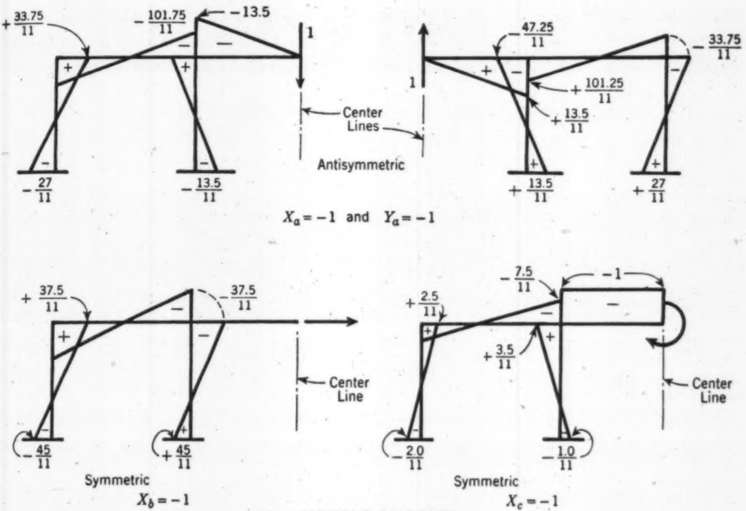
+ $\frac{33.75}{11}$
− $\frac{101.75}{11}$
−13.5
1
− $\frac{27}{11}$
− $\frac{13.5}{11}$
Center Lines
Antisymmetric
− $\frac{47.25}{11}$
− $\frac{33.75}{11}$
1
+ $\frac{101.25}{11}$
+ $\frac{13.5}{11}$
+ $\frac{13.5}{11}$
+ $\frac{27}{11}$
$X_a = -1$ and $Y_a = -1$
+ $\frac{37.5}{11}$
− $\frac{37.5}{11}$
Center Line
− $\frac{45}{11}$
+ $\frac{45}{11}$
Symmetric
$X_b = -1$
− $\frac{7.5}{11}$
−1
+ $\frac{2.5}{11}$
+ $\frac{3.5}{11}$
Center Line
− $\frac{2.0}{11}$
− $\frac{1.0}{11}$
Symmetric
$X_c = -1$

(*a*) MOMENT DIAGRAMS

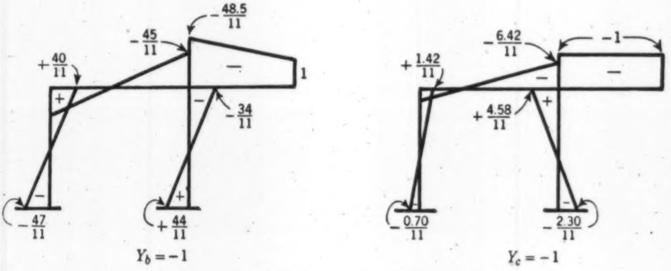
− $\frac{48.5}{11}$
− $\frac{45}{11}$
+ $\frac{40}{11}$
1
− $\frac{34}{11}$
− $\frac{47}{11}$
+ $\frac{44}{11}$
$Y_b = -1$
− $\frac{6.42}{11}$
−1
+ $\frac{1.42}{11}$
+ $\frac{4.58}{11}$
− $\frac{0.70}{11}$
− $\frac{2.30}{11}$
$Y_c = -1$

(*b*) MOMENT DIAGRAMS (GROUP)

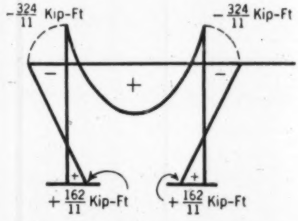
− $\frac{324}{11}$ Kip-Ft
− $\frac{324}{11}$ Kip-Ft
+ $\frac{162}{11}$ Kip-Ft
+ $\frac{162}{11}$ Kip-Ft

(*c*) CONDITION 0

X_j	Y_a	Y_b	Y_c
X_a	+1	0	α_{ac}
X_b	0	α_{bb}	$-\alpha_{bc}$
X_c	0	+1	+1

(*d*) THE α-PATTERN

FIG. 9.—MOMENTS IN THE FRAME OF FIG. 8

The α-pattern in Fig. 9(*d*) is thus complete. Fig. 9(*b*) shows the conditions, $Y_b = -1$ and $Y_c = -1$, and Fig. 9(*c*) shows Condition 0 readily obtained from the Kleinlogel "Rahmenformeln." The γ-values are as follows:

$$\gamma_{aa} = \frac{216{,}512.7}{121}, \qquad \gamma_{ao} = -\frac{360{,}855}{121}$$
$$\gamma_{bb} = \frac{162{,}602.5}{121}, \qquad \gamma_{bo} = -\frac{26{,}730}{121}$$
$$\gamma_{cc} = \frac{1{,}843.2}{121}, \qquad \gamma_{co} = -\frac{26{,}730}{121}.$$

The group loadings are: $Y_a = -\frac{360{,}855}{216{,}513} = -1.67$ kips; $Y_b = -\frac{26{,}730}{162{,}602} = -0.164$ kips; and $Y_c = -\frac{26{,}730}{1{,}843.2} = -14.5$ kip-ft. The values of the redundants are

$$V_0 = -1.67 \text{ kips}$$
$$H_0 = +0.254 \text{ kips}$$
$$M_0 = -14.66 \text{ kip-ft.}$$

It seems unnecessary to carry the numerical computation further because the procedure has been shown in the preceding numerical example.

DISCUSSION

Bernard L. Weiner,[4] M. ASCE.—An excellent method of solving simultaneous linear equations occurring in the analysis of statically indeterminate structures has been presented by the author. Although equations of this type are not as important as they were before the development of the moment-distribution method, the need for a simple and direct method of solution will always exist. The analysis of structures having a large number of degrees of freedom of joint translation (sidesway) is a case in point.

Mr. Morrison's method, therefore, should be considered not as competing with moment distribution and similar methods, but as supplementing them. It is doubtful whether any method can compete with moment distribution in cases where the latter gives the complete solution.

It is unfortunate that Mr. Morrison did not use matrix algebra in his presentation. Although matrix algebra does not generally reduce the amount of numerical work required for a solution, it is an invaluable tool for study and research and often reveals useful properties which would otherwise remain hidden. This case is no exception in this respect and since the method lends itself readily to the use of matrices, the procedure would be clarified thereby.

Mr. Morrison states that the number of α_{ij}-values which can be chosen arbitrarily is $\frac{n(n+1)}{2}$. This is not completely accurate as can be seen by referring to Eq. 4 and expanding one typical equation to yield

$$X_a = \alpha_{aa} Y_a + \alpha_{ab} Y_b + \alpha_{ac} Y_c + \cdots \qquad (20)$$

Letting

$$Y_k = \frac{Z k}{\alpha_{aa}} \qquad (21a)$$

and substituting it into Eq. 20 results in

$$X_a = Z_a + \frac{\alpha_{ab}}{\alpha_{aa}} Z_b + \frac{\alpha_{ac}}{\alpha_{aa}} Z_c + \cdots \qquad (21b)$$

The value X_a will be fully determined if the α-ratios and Z_k are determined. Any other coefficient could obviously have been used instead of α_{aa} in Eq. 21*a*.

Actually, if one α-value in each equation is left undetermined, it will cancel out of the solution. Since any one α-value in each equation may be considered to be a factor, it can be given any value except zero, and the simplest value to assign to it is usually unity. There are therefore only $(n - 1)$-values of α in each equation to be determined and since there are n equations, it follows that there are a total of $n(n - 1)$ undetermined values of α_{ij}. Half of this number may be chosen arbitrarily, and the remaining half is determined from the conditions that γ_{ij} equals zero when i does not equal j, and that γ_{ij} does not equal zero when i equals j.

---

[4] Cons. Engr., New York, N. Y.

Matrix-algebra analysis reveals that, although the total number of α_{ij}-values which may usefully be chosen arbitrarily is $\frac{n(n-1)}{2}$, some choices are not permissible. A restriction on the choice of values is imposed because, in the solution, the α-coefficients separate into independent groups with n-elements in each group. Since one element must be made unity (or given some other convenient value) or left undetermined but cannot be set equal to zero, $(n-1)$-elements remain to be determined in each group. It is obviously not permissible to use more than $(n-1)$-conditions in one group and to compensate by using fewer conditions in another independent group. If this were done, contradictory results would be obtained in the former group, and all the α-values could not then be determined in the latter group.

Mr. Morrison is to be congratulated for presenting a basic concept which should lead to even more valuable results upon further study.

I. F. MORRISON.[5]—Mr. Weiner's interest in the writer's work is appreciated. The method presented by the writer is not as "attractive" as it might be because the advantage of the method is not apparent when expressed in algebraic form. The use of matrix algebra was considered but was rejected as it was thought that there would be relatively few structural engineers who would be sufficiently familiar with this branch of mathematics. Moreover, the method of moment distribution is also not "attractive" when expressed in algebraic form.

In reference to the number of α-values which can be chosen arbitrarily, the writer fails to see how this number can be both $\frac{n\,(n+1)}{2}$ and $\frac{n\,(n-1)}{2}$. Obviously the number of values in the α-matrix is n^2, and it is also clear that none of the values on the main diagonal can be equal to zero. Examination of Table 2 reveals that all the values below the diagonal can be taken to be zero, and therefore the values above the diagonal must be computed. The number of these values is $\frac{n\,(n-1)}{2}$, and there are $\frac{n\,(n-1)}{2}$ equations from which they are obtained. Thus, the number of arbitrary values is

$$n + \frac{n\,(n-1)}{2} = \frac{n\,(n+1)}{2} \qquad (22)$$

It has been suggested that other arrangements of the α-pattern may be more desirable because it is sometimes possible to obtain a more simple moment diagram which reduces the numerical work. An example of this kind of moment diagram is that for $Y_b = -1$ in Fig. 4(b). It is difficult to appreciate the process until one has worked directly with numerical values. When one is sufficiently familiar with the process, the α-values can be written by inspection from moment diagrams such as those given in Fig. 4.

---

[5] Prof. of Applied Mech., Dept. of Civ. and Muncipal Eng., Univ. of Alberta, Edmonton, Alta, Canada.

AMERICAN SOCIETY OF CIVIL ENGINEERS
Founded November 5, 1852
TRANSACTIONS

Paper No. 2675

DESIGN OF SIDE WALLS IN CHUTES AND SPILLWAYS

By D. B. GUMENSKY,[1] M. ASCE

With Discussion by Messrs. Leland S. Rhodes, G. S. Sarkaria, J. H. Douma, Edgar E. Foster, Thomas J. Rhone, and D. B. Gumensky

Synopsis

Water confined between vertical walls and flowing down an inclined plane exerts a lateral pressure of diminishing intensity on the walls as the steepness of the fall increases. The limit in such a case is a vertical fall when the lateral pressure equals zero.

When the flow of water is deflected by a vertical curve as at the bottom of a chute or in a "flip bucket" of a spillway, the centrifugal force increases the pressure on the bottom and on the walls of the confining channel. The effect of this increase in pressure is as though the water were much denser than it really is—in some actual cases as much as twelve times the density of water.

Introduction

When designing chutes, wasteways, and spillways, the hydraulic design is the first and the most important phase. The structural design follows the completion of the hydraulic design. In the structural design, the principal features are the thickness and the reinforcement of the side walls and (in spillways where they are used) of the intermediate training walls. It has been the writer's experience that much time is spent in discussing and in determining the proper criteria for the design of these walls. Because little treatment of this subject has been found in engineering literature, this presentation is submitted in the hope that it may help the practicing engineer both to save time in getting the job done and to save his client a considerable amount of money. The usual engineering practice, because of a lack of understanding, is to overdesign such walls by about twice the necessary requirement. On the other hand, the effect of the centrifugal force in deflected streams is seldom evaluated and the walls often remain standing in a condition near failure.

Note.—Published, essentially as printed here, in February, 1953, as *Proceedings-Separate No. 175*. Positions and titles given are those in effect when the paper or discussion was received for publication.

[1] Cons. Engr., Water Dept., Ministry of Agriculture, Tel-Aviv, Israel.

PRESSURE IN STILL WATER

The intensity of pressure in still or slowly moving water varies directly with the depth and equals the depth times the specific weight (see Fig. 1). This pressure is expressed as

$$p = \gamma\, h = 62.5\, h \ldots\ldots\ldots\ldots\ldots\ldots\ldots (1a)$$

in which p equals the intensity of pressure, in pounds per square foot; γ equals the weight of water, in pounds per cubic foot; and h equals the depth of water from the surface, in feet.

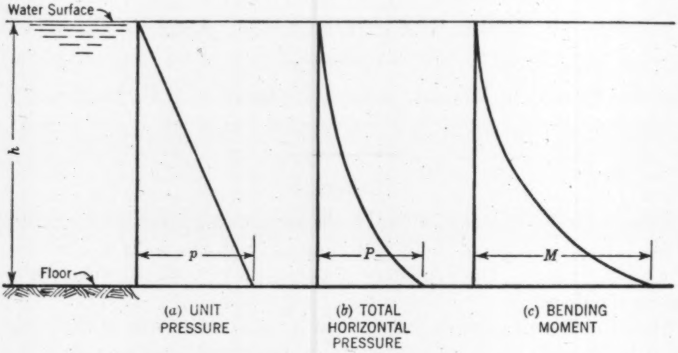

FIG. 1.—PRESSURE AND MOMENT ON A VERTICAL WALL IN STILL WATER

In this case, the total horizontal pressure on a unit length of a vertical wall will be

$$P = \tfrac{1}{2}\, \gamma\, h^2 = 31.2\, h^2 \ldots\ldots\ldots\ldots\ldots\ldots\ldots (1b)$$

in which P equals the total pressure, in pounds per unit length of wall. The moment about the base of the wall caused by this pressure will be

$$M = \tfrac{1}{6}\, \gamma\, h^3 = 10.4\, h^3 \ldots\ldots\ldots\ldots\ldots\ldots\ldots (1c)$$

PRESSURE IN A STEEPLY INCLINED STREAM

In a stream flowing down a steeply inclined slope, the pressure pattern is modified from the static condition. The water, which is supported on a slope, has a negligible shearing value. Therefore, the floor supports only the normal component of the weight of the water.

The component of the weight parallel to the floor is used either to accelerate the water down the slope or to overcome friction, or both. This condition is illustrated in Fig. 2. The shaded unit volume of water weighs γ pounds. This weight is resolved into components that are normal and parallel to the floor. The component of the weight parallel to the floor produces no pressure and is expended in producing acceleration down the slope and in overcoming friction. The component of the weight normal to the floor produces the pressure on the floor (and on the walls) and equals in value the weight multiplied by the cosine of the angle which the floor makes with the horizontal. Measuring the depth of water in the direction normal to the floor, and using the subscript α to designate the inclined floor and stream, the pressure intensity at the floor becomes

$$p_\alpha = \gamma\, h \cos \alpha \qquad (2a)$$

The value of h is modified by the cosine of the angle only in the evaluation of the intensity of the pressure. In computing the total horizontal pressure on an element of a wall, the pressure intensity acts over the full value of h so that the overturning force becomes

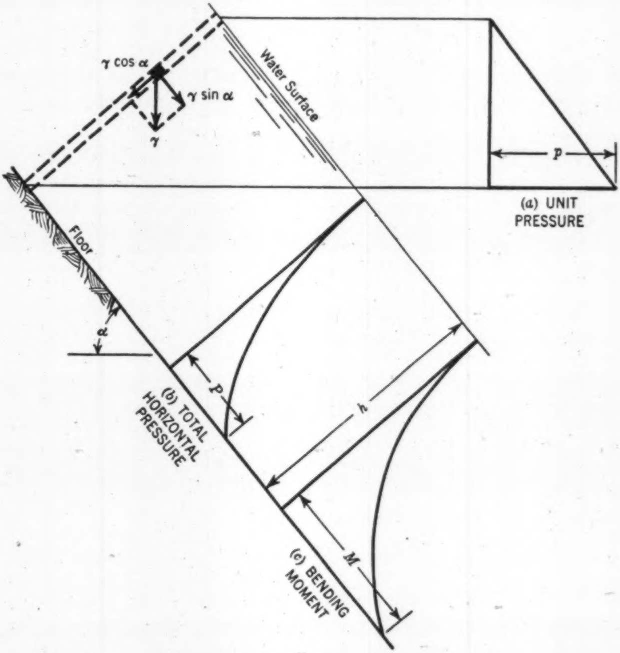

FIG. 2.—PRESSURE IN WATER FLOWING ON AN INCLINE

$$P_\alpha = \tfrac{1}{2}\, \gamma\, h^2 \cos \alpha \qquad (2b)$$

and the overturning moment is expressed as

$$M_\alpha = \tfrac{1}{6}\, \gamma\, h^3 \cos \alpha \qquad (2c)$$

The fallacy of using the vertical depth for determining pressures of flowing water on steep slopes, as is done by some engineers, becomes apparent at the limiting condition of the slope. If the floor were vertical, the water would fall down within the confinement of the floor and the walls. Any pressure developed on these confining surfaces would be merely nominal.

PRESSURE IN A DEFLECTED STREAM

If a flowing stream is deflected by a curving vane, such as a vertical curve in a chute or a flip bucket at the bottom of a spillway, the pressure of the water is increased by centrifugal force. This increase in pressure may be easily evaluated. If a bucket of water is rotated in a vertical plane as shown in Fig. 3, and, if F_c represents the centrifugal force, ρ is the mass per unit volume of water, ω denotes the angular velocity in radians per second, and r equals the radius of curvature, in feet, then

$$F_c = \rho\,\omega^2\,r \quad \ldots\ldots (3)$$

Considering an element of the water in the bucket of Fig. 3, having a cross-sectional area (dA), of one square foot and a depth h, the mass of water in the bucket is expressed as

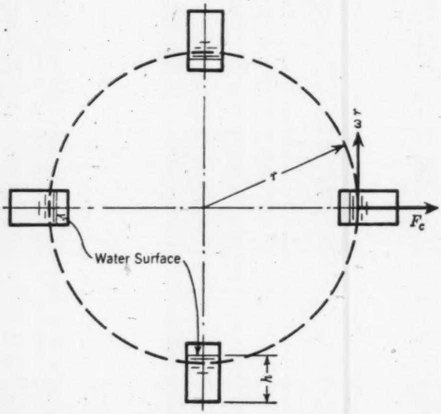

FIG. 3.—CENTRIFUGAL FORCE ON WATER IN ROTATING BUCKETS

$$\rho = \frac{\gamma\,h\,dA}{g} = 1.94\,h \quad \ldots\ldots (4)$$

Substituting this value of ρ into Eq. 3 yields

$$F_c = 1.94\,\omega^2\,r\,h \quad \ldots\ldots (5)$$

From Eq. 5 it is apparent that the centrifugal force will not only vary directly as ω^2 and as r, but will also vary directly as h. This also can be deduced logically from Eq. 3 because the mass of the water in the container varies directly with the depth h and, therefore, the centrifugal force varies directly with h. Further examination of Eq. 5 shows that the expression $1.94\,\omega^2\,r$, on the right-hand side of the equation, is equivalent to the unit weight of a liquid in the expression for hydrostatic pressure at depth h.

For the specific case of a flip bucket at the bottom of the spillway of Pine Flat Dam, on Kings River, in California, which the writer helped to design, the velocity of water was 139 ft per sec and the radius of the flip bucket was 50 ft. Substituting these values in Eq. 5, $F_c = 1.94\left(\frac{139}{50}\right)^2 50\,h = 749\,h$.

Comparing the value 749 lb per ft with 62.5 lb per ft makes obvious the fact that the centrifugal pressure of the water in the flip bucket is equal to the static pressure created by a liquid having a specific gravity about twelve times that of water. Considering the static pressure, which is not included in the formula for centrifugal pressure, the wall of the flip bucket should be designed for a loading equal to thirteen times the loading on an equivalent wall holding static water to the same depth as the flow depth in the bucket.

The unit liquid pressure for which the side walls should be designed in concave vertical curves of chutes or flip buckets (Fig. 4) is expressed by the equation

$$p_{vc} = (1.94\,\omega^2 r + 62.5)\,h \qquad \text{(6a)}$$

The total horizontal pressure on the unit length of the wall then becomes

$$P_{vc} = \tfrac{1}{2}\,p_{vc}\,h^2 \qquad \text{(6b)}$$

and the bending moment at the base of wall—

$$M_{vc} = \tfrac{1}{6}\,p_{vc}\,h^3 \qquad \text{(6c)}$$

Convex curvatures exist at the tops of spillways and in some chutes. In such cases, the forces acting on the element of the water are the weight of the water, the kinetic force of the stream, the restraining effect of walls, and the support of the bottom.

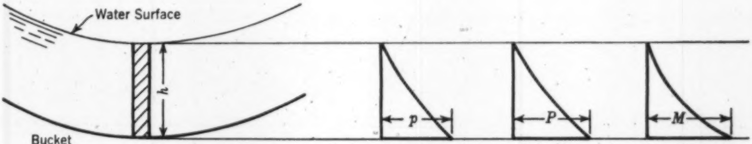

(a) UNIT PRESSURE

(b) TOTAL HORIZONTAL PRESSURE

(c) BENDING MOMENT

FIG. 4.—PRESSURE IN WATER FLOWING IN A CIRCULAR VERTICAL CURVE

Sometimes the convex curvature of the bottom is so sharp that the acceleration of the force of gravity is insufficient to make it follow the bottom. The stream then tends to separate from the bottom and negative pressures result. The water pressures on side walls in such cases are reduced to nominal resistance to confinement, and the stream temporarily acts as a jet. All cases of convex curvature can be investigated graphically very easily and quickly.

EFFECT OF AIR ENTRAINMENT

At velocities of about 20 ft per sec and faster, air becomes entrained in the water, swelling its volume and increasing its depth. Numerous measurements were made on fast flowing water in chutes and spillways, and some correlation between velocity and air entrainment was established.[2] However, there are no experimental data on the distribution of pressure in such "white water." Some idea of it can be gleaned from logical reasoning based on physical facts.

---

[2] "Air Entrained in Fast Water Affects Design of Training Walls and Stilling Basins," by D. B. Gumensky, *Civil Engineering*, December, 1949, p. 35.

In Fig. 5, the probable pressure distribution in a stream with entrained air is illustrated. Because the weight of the water supported by the floor is the same whether or not there is entrained air, the intensity of the pressure on the bottom of the channel will be $\gamma\, h$ for both cases. The intensity of the pressure at any position above the floor is equal to the weight of the water above a horizontal unit area at that level. For a uniform mixture of air and water (extreme hypothesis), the intensity at any depth will be represented by the straight line 2–4. Since the volume of the entrained air is a maximum near the surface and gradually diminishes toward the bottom, the actual pressure will be represented by some curve 2–5–4 between lines 2–4 and 2–1. However, because of the varying ratio between distances 1–4 and 1–3, depending on the velocity and the depth of the flow, the writer was unable to find any general curve equation which would be suitable for all conditions. For design purposes, it seems best to use the extreme hypothetical assumption of the uniform air distribution as represented by line 2–4, which errs on the side of safety. Because the flow with air entrainment occurs on steep slopes, the correction for the vertical angle is introduced. Substituting lighter unit weight, $\gamma_a = \gamma \frac{h}{h_a}$ for the water-air mixture, and using the subscript *a* for the flow of water with entrained air, the design equations become

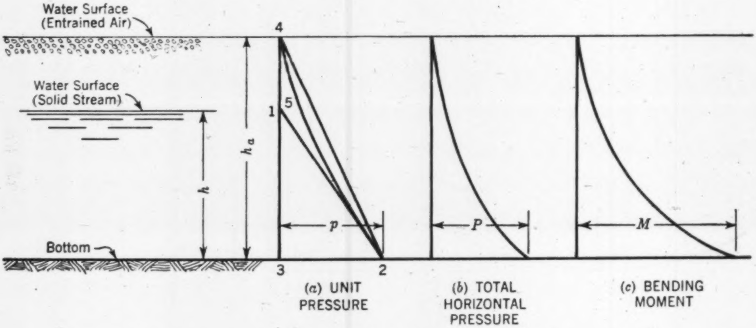
Water Surface (Entrained Air)
Water Surface (Solid Stream)
Bottom
h
h_a
4
5
1
3
2
p
P
M
(a) UNIT PRESSURE
(b) TOTAL HORIZONTAL PRESSURE
(c) BENDING MOMENT

FIG. 5.—PRESSURE IN WATER WITH ENTRAINED AIR

$$p_a = \gamma\, h \cos \alpha \quad \text{(7a)}$$

$$P_a = \tfrac{1}{2}\, \gamma\, h\, h_a \cos \alpha \quad \text{(7b)}$$

and

$$M_a = \tfrac{1}{6}\, \gamma\, h\, h^2_a \cos \alpha \quad \text{(7c)}$$

Although specific data are not available, it appears that, when a stream with entrained air is deflected by a vertical curve, the centrifugal force tends both to drive the air out of the stream and to force it into solution. Therefore, until data are available showing the effect of vertical curves on air entrainment, the design of walls in vertical curves should be based on Eqs. 7. Fig. 6 illustrates the flow of water with entrained air down the face of a spillway and through a flip bucket at the bottom of the spillway. (This photograph was kindly supplied by the Denver (Colo.) office of the Bureau of Reclamation.) It shows the swelling of the stream caused by air entrainment, with subsequent vertical contraction in the flip bucket in which the air is partly driven out by centrifugal force.

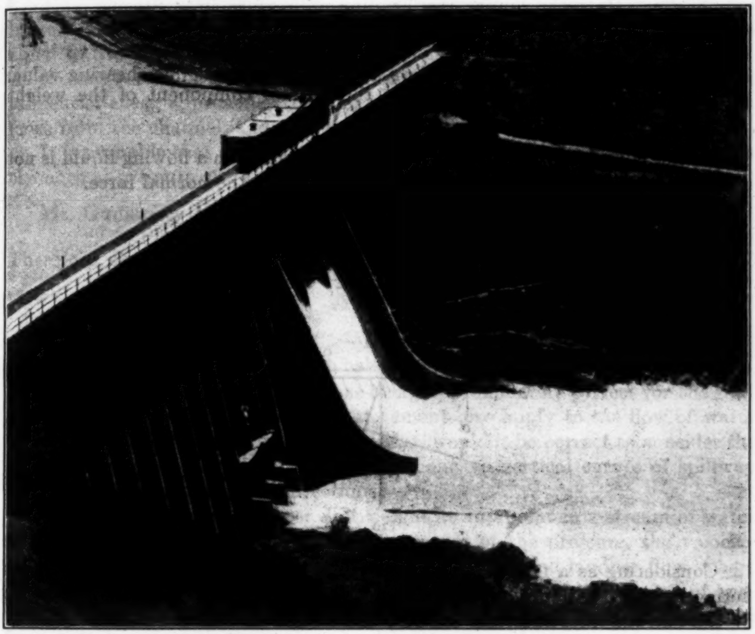

FIG. 6.—STONY GORGE DAM, ORLAND PROJECT (UNITED STATES BUREAU OF RECLAMATION), CALIFORNIA

DISCUSSION

LELAND S. RHODES.[3]—Some excellent points have been brought out by Mr. Gumensky. However, under the heading, "Pressure in a Steeply Inclined Stream," there appears the statement that

> "The water, which is supported on a slope, has a negligible shearing value. Therefore, the floor supports only the normal component of the weight of the water."

This is not completely true, because the shearing force in a flowing liquid is not a negligible quantity, but may be even greater than the normal force.

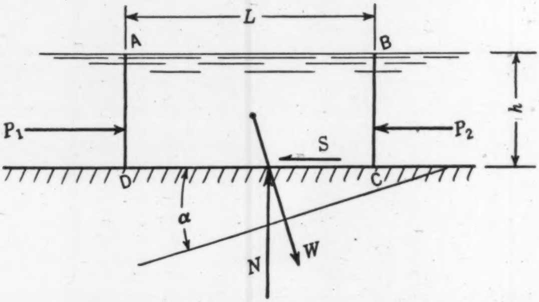

FIG. 7

Considering as a free-body the water in Fig. 7, labeled ABCD, the forces acting on the free-body are the two forces P_1 and P_2, which are the pressures of the surrounding water on ABCD, the weight of the water $W = \gamma\, b\, h\, L$, in which b is the width of the channel, N the normal pressure force of the channel bottom against the water, and S the shearing force between the channel surfaces and the water.

When the water begins to flow down the channel, the weight component $W \sin \alpha$ is larger than the shearing force S and therefore the water accelerates. Higher velocities produce higher values of S until, in a rather short length of channel, the velocity has reached a value at which $S = W \sin \alpha$, and there is equilibrium of forces and no further acceleration, since $P_1 = P_2$.

Since

$$N = W \cos \alpha = \gamma\, b\, h\, L \cos \alpha \qquad (8)$$

the pressure intensity on the floor is

$$p = \frac{N}{A} = \frac{\gamma\, b\, h\, L \cos \alpha}{b\, L} = \gamma\, h \cos \alpha \qquad (9)$$

---

[3] Prof. of Civ. Eng., Pennsylvania State College, State College, Pa.

as shown in Eq. 2*a*. The shearing force is

$$S = W \sin \alpha = \gamma\, b\, h\, L \sin \alpha \qquad (10)$$

and the unit shearing stress is equal to Eq. 10 divided by the area $(b + 2\,h)L$. If b is very large in comparison to $2\,h$ (a wide, shallow channel), $s = \gamma\, h \sin \alpha$. This means that in addition to the normal water pressure on the bottom and sides, there is a tangential shearing force which at $\alpha = 45°$ is equal to the normal force, and at steeper angles will exceed the normal force. As the angle α approaches 90° the normal pressure approaches zero, and the tangential shear approaches the weight of water. At 90° the flow can break loose from the channel, and the shear will drop to zero.

It is probable that a correct structural design should take into account both the normal pressure and the friction drag or shear on the bottom and sides.

Mr. Gumensky has defined ρ as the mass per unit volume; that is $\rho = \frac{\gamma}{g}$. Therefore, should not Eq. 4 show the total mass M equal to $\frac{\gamma\, h\, d\, A}{g}$, and Eq. 3 read $F_c = M\, \omega^2\, r$?

G. S. Sarkaria,[4] J.M. ASCE.—In static water the water pressure intensity is uniform at the same depth below the surface and is the same in all directions. This can also be considered as being approximately correct for the slow laminar flow of water. Would this statement also apply to the flow of water down steep chutes or dam spillways? Also, would it be correct to consider the hydrodynamic pressure at a point on the concave vertical curves of spillway buckets as being equal in all directions?

The total head or energy per unit weight at any point in a stream of water flowing down an inclined slope will be the sum of the pressure, the velocity heads, and the elevation. In the case of gradually varied laminar flow, where the accelerative forces are negligible, the pressure head would be constant over any transverse section of the chute. This means that the pressure head would be equal at the side walls and center of the channel. This pressure head is determined from Eq. 2*a*. If the angle α is small, the pressure will be approximately equal to the product of γ and the vertical depth of water. This pressure, synonymous with hydrostatic pressure at a point, is equal in all directions and should be used for the design of the side walls. The velocity head is active on planes normal to the direction of flow and may be neglected when design pressure on the side walls is being considered.

The problem of flow along a concave vertical curve and the determination of the resultant pressures on the side walls differs from the problem of flow along a steep incline. This difference is caused by the fact that centrifugal force must be taken into consideration in the former problem. As shown in Fig. 3, the centrifugal force acts in a direction normal to the direction of the flow of water and increases the pressure on the bucket floor. Mr. Gumensky assumes that the pressure on the side walls will be increased by the amount of the centrifugal force. In other words, the author assumes that the velocity of the water along the walls is the same as at the center of the chute and that the increase in hydrodynamic pressure, as a result of centrifugal force, will be the same in all directions.

---

[4] Asst. Design Engr., Punjab Irrig. Branch, Simla, India.

The velocity of water flowing in a channel is not uniform across the cross section. It is a maximum near the center of the section; and at the sides of the section it is less than the average velocity of the section. This is also true for water flowing down vertically-concave steep chutes at velocities greater than the critical velocity. In such cases there will be secondary movements along the side walls, resulting in local eddies and a reduction in the velocity of water flowing along the walls. Thus, the centrifugal force of the water flowing along the walls will be smaller than that in the center of the channel.

The small centrifugal force along the walls will act in a radial direction on the bucket floor. There will be no hydrodynamic forces acting on the side walls unless there are acceleration components acting in the plane of the cross section or at right angles to the general direction of flow. This would be possible to some extent, if the cross section of the spillway chute or bucket were curved or concave instead of rectangular or trapezoidal. Any flow at right angles to the general direction of flow will exert additional hydrodynamic pressure on the side walls of such a chute in the form of centrifugal force.

By investigating Mr. Gumensky's approach to the inclusion of centrifugal forces in the design pressures on side walls of spillway buckets, the writer wants to illustrate the complex nature of the problem. Mr. Gumensky states that walls built along the sides of the curved bottom of a spillway chute, where the centrifugal force had not been included in the design, are near the point of failure. No walls are known to have failed because of the omission of the effect of centrifugal force. This shows that the inclusion of such a force in the design would result in a over-designed structure. Experimental observations of pressure on the walls of laboratory models would remove most of the doubts concerning the effects of centrifugal force. Such experimental results would be more reliable then deductions based on a theoretical approach to the problem.

J. H. Douma,[5] A.M. ASCE.—Basic design considerations of side walls for high-velocity chutes and spillways containing vertical curves are investigated by the author. Previous to this paper, incorrect design methods have been used; in some cases, the effect of centrifugal action has been completely neglected.

Although not specifically stated by Mr. Gumensky, centrifugal pressures occurring on the surface of the spillway bucket are equal to pressures occurring at the base of the spillway side walls. Bucket pressure must be considered in the stability analysis of the dam, and in the case of a buttress dam with a downstream spillway deck, the deck slab must be designed to withstand centrifugal pressures.

Because hydraulic loads resulting from centrifugal pressures are inversely proportional to the bucket radius, those loads can be held to reasonable limits by selecting the proper radius. For buttress dams it is desirable, in some cases, to select a longer radius than is needed to satisfy the hydraulic requirements, so that the spillway side walls and the downstream face deck will not be excessively thick.

---

[5] Hydr. Engr., Office of the Chf. of Engrs., Corps of Engrs., U. S. Dept. of the Army, Washington, D. C.

Centrifugal pressures in a spillway bucket are computed by the expression,

$$p_c = \frac{\gamma q}{v} \frac{2 h_1}{g} \ldots\ldots\ldots\ldots\ldots\ldots (11a)$$

which is obtained by substituting $d = \frac{q}{V}$ and $V = \sqrt{2 g h_1}$ in the generalized equation for centrifugal pressure,

$$p_c = \frac{\gamma d v^2}{g r} \ldots\ldots\ldots\ldots\ldots\ldots (11b)$$

In Eqs. 11, p_c is the centrifugal pressure, in pounds per square foot; q denotes the discharge per foot of spillway, in cubic feet per second; h_1 is the head from the maximum reservoir level to a point on the bucket, in feet (Fig. 8(*a*)); and g represents the acceleration of gravity, in feet per second per second.

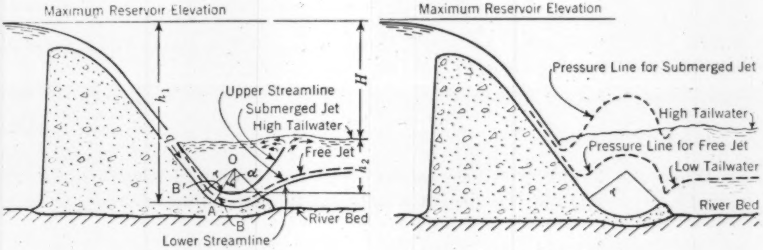
Maximum Reservoir Elevation
h_1
H
Upper Streamline
Submerged Jet
High Tailwater
Free Jet
h_2
d
O
r
α
B′
A
B
River Bed
Lower Streamline
Maximum Reservoir Elevation
Pressure Line for Submerged Jet
High Tailwater
Pressure Line for Free Jet
Low Tailwater
r
River Bed

(*a*) FLOW (*b*) PRESSURE

FIG. 8.—SPILLWAY BUCKETS

The advantage of using Eq. 11*a* instead of Eq. 5 is that values of h_1 can be determined more readily than the velocity. Although h_1 should be taken as the distance from the energy gradient to the bucket surface, the small head losses as a result of flow down the face of a dam may be neglected without appreciably affecting the thickness of the deck slabs or the side walls.

Eq. 11*a* yields variable centrifugal pressures because of variations in the value of h_1 throughout the bucket. The minimum and maximum centrifugal pressures in a bucket occur at the highest and lowest points of the bucket, respectively. The variation in centrifugal pressures is greater in a bucket of a low dam than in a bucket of a high dam because the relative variation in heads is greater for low dams.

Eq. 11*a* is applicable to roller-bucket stilling basins when h_1 is replaced by h_2, the head in feet, from the reservoir elevation to the tailwater elevation as in Fig. 8(*a*). The computed pressures will be approximate because the water-surface elevation of the bucket roller is seldom the same as the tailwater elevation. The approximate bucket pressure and the maximum side-wall pressures are obtained by adding the computed centrifugal pressures to the hydrostatic pressures corresponding to the tailwater depth.

Eqs. 11 are based on the assumption that streamlines instantly assume the paths dictated by the bucket radius at the beginning of curvature. The flow net theory indicates, however, that streamlines are influenced somewhat upstream of this point and continue to be influenced for some distance downstream of the point. A similar transition zone occurs at the downstream point of tangency. Therefore, actual pressure distributions in a bucket are realistically represented in Fig. 8(*b*), which is based on data obtained from model studies of Grand Coulee Dam, in Washington, Pine Flat Dam, in California, and Popolopen Dam at West Point, N. Y.

For a dam flow net, streamlines near the bucket boundary are circular; hence, the velocity is tangential at all points. These streamlines are determined by the function:

$$\psi = c \log r = \text{constant} \qquad (12)$$

and equipotential lines are determined by

$$\phi = C\,\theta = \text{constant} \qquad (13)$$

The slope of the potential surface in the direction of flow equals the tangential velocity, and thus the absolute velocity is expressed by

$$V = \frac{d\phi}{dr} = -\frac{c}{r} \qquad (14)$$

When the flow occurs between two circular boundaries whose radii are r_1 and r_2 $(r_2 > r_1)$, and the discharge between the two boundaries is q, then

$$q = \int_{r_1}^{r_2} V\,dr = \int_{r_1}^{r_2} \frac{c}{r}\,dr = -c\,(\log r_2 - \log r_1) \qquad (15a)$$

from which

$$c = -\frac{q}{\log (r_2/r_1)} \qquad (15b)$$

Substituting Eq. 15*b* into Eq. 13,

$$V = \frac{q}{r \log (r_2/r_1)} \qquad (16)$$

Referring to Fig. 8(*a*), if r_2 is the bucket radius and r_1 = OB, the velocity at point A for free-jet flow is

$$V_A = \frac{q}{r_2 \log (r_2/r_1)} \qquad (17)$$

At point B on the upper streamline the velocity is

$$V_B = \frac{q}{r_1 \log (r_2/r_1)} \qquad (18)$$

From Bernoulli's theorem, the pressure head at point A is

$$\frac{p}{\gamma} = h_1 - \frac{1}{2\,g}\left[\frac{q}{r_2 \log (r_2/r_1)}\right]^2 \ldots\ldots\ldots\ldots\ldots\ldots (19)$$

Since the pressure head at point B is zero, Bernoulli's equation becomes

$$h_1 - (r_2 - r_1) \cos \alpha - \frac{1}{2\,g}\left[\frac{q}{r_1 \log (r_2/r_1)}\right]^2 = 0 \ldots\ldots\ldots (20)$$

If values of h_1, α, q, and r_2 are known for any point, the corresponding values of r_1 may be determined by solution of Eq. 20. Then the pressure at the corresponding point on the bucket is determined from Eq. 19.

When the tailwater submerges the high-velocity jet, as in Fig. 8(*a*), the pressure on the upper streamline at point B is not zero but approximates the back-pressure caused by the tailwater. Then Eq. 20 becomes

$$h_1 - (r_2 - r_1) \cos \alpha - \frac{1}{2\,g}\left[\frac{q}{r_1 \log (r_2/r_1)}\right]^2 = h_2 \ldots\ldots\ldots (21)$$

and

$$H = h_1 - h_2 - (r_2 - r_1) \cos \alpha \ldots\ldots\ldots\ldots\ldots\ldots (22)$$

Solving Eqs. 21 and 22 simultaneously,

$$r_1 \log \left(\frac{r_2}{r_1}\right) = \frac{q}{\sqrt{2\,g\,H}} \ldots\ldots\ldots\ldots\ldots\ldots\ldots\ldots (23)$$

From Eq. 23, values of r_1 may be computed if values of q, H, and r_2 are known. Corresponding bucket pressures are computed by use of Eq. 19.

A graphical solution for the pressure distribution in a spillway bucket, based on construction of the flow net, has been presented by Hunter Rouse,[6] M. ASCE. This solution is based on assumed flow conditions approaching the bucket curve. It is to be noted that the effect of the bucket curve on pressure extends beyond the two points of tangency.

The methods presented by the author and the writer for determining pressures in spillway buckets and on side walls furnish conservative design loads when maximum computed pressures are used. The present (1953) state of knowledge is inadequate for safe reduction of design loads in the vicinity of the two points of tangency unless pressures in those areas are verified by model tests.

Generalized model tests are required to evaluate the following factors for flow in spillway buckets: (1) The approach flow conditions, (2) the upper water-surface profiles for free and submerged jets, and (3) the relationship between the tailwater depth and the hydrostatic bucket pressures for the submerged-jet condition. When these factors are determined in terms of head and discharge, Eqs. 18, 19, and 22 and the graphical solution can be modified to permit a precise determination of the pressures on side walls and upstream and downstream from, and within, spillway buckets.

---

[6] "Engineering Hydraulics," by Hunter Rouse, *Proceedings*, Fourth Hydraulics Conference, Iowa Inst. of Hydr. Research, John Wiley & Sons, Inc., New York, N. Y., 1950.

Edgar E. Foster,[7] M. ASCE.—Certain factors in the design of walls for spillways, chutes, and similar structures have been clarified by the author. As he states, the functional design should be the first consideration; that is, the various dimensions and general layout should be fixed by the required hydraulic capacity. After that step the structural dimension can be fixed by the loads imposed.

The loads imposed by the flowing water, however, are not the only loads to be considered, except in the case of walls such as those shown for the spillway in Fig. 6. In many cases spillway and chute walls are backed by an earth fill which imposes loads that control the design because the walls are constructed to safe heights above the maximum water surface. Earth-imposed loads would have the greatest effect during periods of low water.

In general, it appears that small slopes would have little effect on altering either the water loads or earth-imposed loads. For steep slopes, such as those shown in Fig. 6, the effect would be great. It also seems logical to assume that steep slopes parallel to the wall would tend to diminish the earth-imposed loads in a manner similar to the decrease shown for water loads. It would be most helpful if this assumption were investigated.

Thomas J. Rhone,[8] A. M. ASCE.—The author's analysis of the problem and his working equations are most commendable. It is apparent that an allowance should be made for the effects of centrifugal force, and the use of Mr. Gumensky's equations provides for such allowances.

When hydraulic model studies are made for an over-all evaluation of design, the side-wall pressures can be easily evaluated. Two examples of pressures in spillway side walls have been prepared from data obtained during model studies conducted in the hydraulic laboratory of the Bureau of Reclamation in Denver, Colo. The examples were taken from two different types of structures and indicate the conditions under which side-wall pressures may be investigated.

Example No. 1.—The data used in this example were obtained from hydraulic model studies made in 1936 on the stilling basin (a submerged roller bucket) for Grand Coulee Dam, on the Columbia River. The wall on which the pressure studies were made separates the stilling basin from the powerhouse tailrace and is completely submerged by the tailwater at the larger of the two discharges used in this example.

The pressure curves shown in Fig. 9 were derived by two methods: Curves A and C were computed from Eq. 6*a*, whereas curves B and D are pressures obtained from piezometers placed in the dividing wall. Curves A and B illustrate the conditions at a flow of 1,000,000 cu ft per sec and curves C and D show the conditions for a flow of 500,000 cu ft per sec. At a flow of 1,000,000 cu ft per sec, the water surface at the piezometers is at El. 997.5; and at 500,000 cu ft per sec, the water surface is at El. 975.2.

The measured pressures were taken from six piezometers placed normal to the face of the wall. The wall has a slight batter, but the pressure readings have been plotted in Fig. 9 on a horizontal line at the elevation of the piezometer. The pressures shown at the base of the wall were determined from a piezometer placed in the invert of the bucket rather than in the wall. The pressures computed from Eq. 6*a* also made use of model data; the velocity was determined from pitot tube measurements; the valve used for *r* for pressure values near the wall base was equal to the radius of the bucket, but for other pressure values was equal to the approximate radius of the flow lines at the point under investigation.

---

[7] Chf., Eng. & Cons. Div., Technical Cooperation for Iran, Teheran, Iran.

[8] Hydr. Engr., Bureau of Reclamation, U. S. Dept. of the Interior, Denver, Colo.

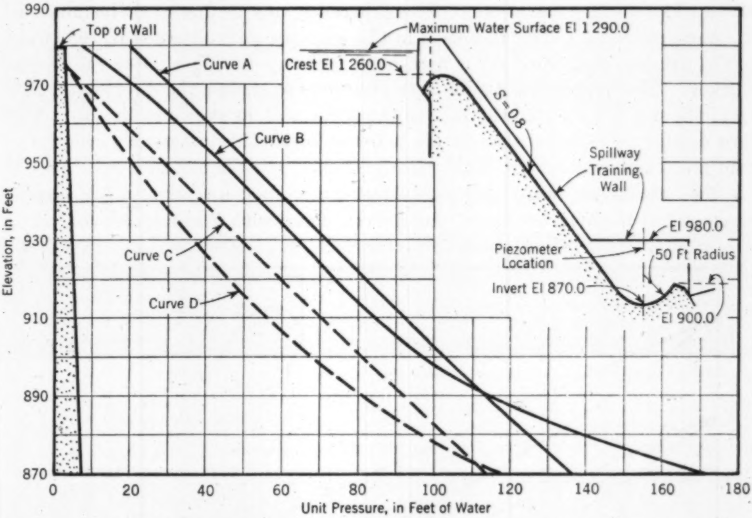

FIG. 9.—SIDE-WALL PRESSURES AT GRAND COULEE DAM STILLING BASIN

The reverse flow near the water surface in the bucket was considered as having no velocity; therefore, there is no pressure caused by centrifugal force in the upper part of curves A and C.

The velocities in the submerged roller bucket (in a vertical plane directly over the invert of the bucket) were comparatively small—only 50 ft per sec at El. 870—and decreasing to 22 ft per sec at El. 910. With these velocities, the maximum pressure caused by centrifugal force was only 1.5 ft of water. Therefore, for all practical purposes, curves A and C represent the hydrostatic pressure.

In comparing the computed pressures with the measured pressures, the computed pressures for both discharges are greater than the measured pressures except near the base of the wall. For a discharge of 500,000 cu ft per sec, the computed and measured pressures are almost the same at the base of the wall. For a discharge of 1,000,000 cu ft per sec, the measured pressure is approximately 30% greater than the computed pressure. This difference may have been caused by the reflection of some impact head from the flow by the floor piezometer. However, the lowest of the wall piezometers (El. 885) also shows a pressure greater than the computed pressure (Fig. 9). Example No. 1 seems to indicate that the pressure resulting from the centrifugal force need not be considered when the flow becomes submerged with a resulting severe reduction in velocity.

Of further interest in this example is the fact that the measured pressures (over most of the range) are less than the hydrostatic pressures based on the given water-surface elevations. This difference may be due to air insufflation.

Example No. 2.—The data used in this example were obtained in 1953 from model studies performed on a high-head spillway having a 60-ft radius flip bucket. The bucket is not submerged but acts to change the direction of flow from the slope of the spillway face to the horizontal, as shown in Fig. 10. The flow discharges into the atmosphere between vertical training walls which contain piezometers.

Two discharges were also used in this example, and the wall pressures measured at the invert of the bucket are compared with the pressures computed from Eq. 6*a*. Curves E and G in Fig. 10 are the computed pressures, and curves F and H are the measured pressures. Curves E and F show the conditions at a flow of 56,100 cu ft per sec, and curves G and H illustrate the conditions for a flow of 35,600 cu ft per sec. At a flow of 56,100 cu ft per sec, the water surface at the piezometers is at El. 8.52; and at 35,600 cu ft per sec, the water surface is at El. 5.80. The velocity used in the computations is the average velocity obtained from

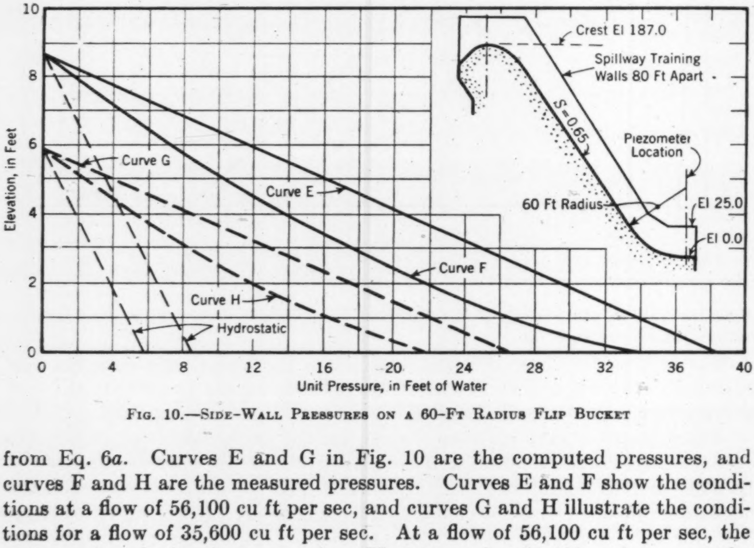

FIG. 10.—SIDE-WALL PRESSURES ON A 60-FT RADIUS FLIP BUCKET

$$V = \frac{Q}{A} \quad \text{.......................} \quad (24)$$

in which A is the product of the spillway width and the flow depth measured at the bucket invert. The value used for r in Eq. 6*a* is the radius of the flip bucket.

Fig. 10 shows that for both discharges the computed pressures are higher than the measured pressures for the full depth. A comparison of the pressures near the base of the wall shows that, at a flow of 56,100 cu ft per sec, the piezometer pressures and the computed pressures are, respectively, 4.0 and 4.5 times as great as the hydrostatic pressure. For a discharge of 35,600 cu ft per sec the piezometer pressures and the computed pressures are, respectively, 3.6 and 4.6 times as great as the hydrostatic pressure.

Example No. 2 shows that, although the computed pressures are higher than the measured pressures, they are not excessive. However, if the centrifugal force had not been included in the pressure value, the computed value would be only 25% of the actual force.

D. B. Gumensky,[9] M. ASCE.—Many thanks are due the engineers who have shared with the profession some of their time, knowledge, and energy by contributing their discussions of the writer's paper. The discussions further elucidate the problem introduced in the paper. Theoretical deductions are supported by experimental measurements, new formulas for the computations of pressures in spillway buckets are offered, and some clarifying and critical observation are presented.

Mr. Rhodes, in Fig. 7 and in Eqs. 8 to 10, develops a value for the shearing stress of a sliding block ABCD. Eq. 10 is entirely applicable in a case of a solid block sliding down the surface. However, in the case of flowing water, most of the weight component parallel to the bottom of the channel is expended either in giving the water an acceleration or in imparting to the water a turbulence which consumes the energy as internal friction. The remarks of Mr. Rhodes regarding Eqs. 3 and 4 appear appropriate and are noted with gratitude. The slight confusion in these equations was caused by the use of the symbol F_c for both the unit centrifugal force in Eq. 3 and for the total centrifugal force for depth h in Eq. 5.

Mr. Foster acknowledges the necessary steps in the functional and structural design outlined by the writer and appropriately points out the need for the inclusion of loads imposed by earth fills. Such loads, especially in connection with earth dams, frequently control the structural design of the walls of water channels. The evaluation of lateral pressures caused by earth loads placed on sloping ground is somewhat complicated by the shearing strength of the earth which will vary between relatively simple cases of granular soils having internal friction but no cohesion, and difficult cases of highly cohesive clays which, in addition, may have expanding properties depending on their mineral composition.

Mr. Sarkaria discusses various phenomena connected with the flow of water on a slope and along concave surfaces in a bucket of a spillway. He indicates the complex nature of the problem by noting the uneven distribution of velocities in a flowing stream, and he questions the need for including in the design of bucket walls the increase in pressure caused by the centrifugal force. Mr. Sarkaria asks for experimental results rather than theoretical deductions. It appears that the experimental data given by Messrs. Douma and Rhone should satisfy Mr. Sarkaria's request.

---

[9] Civ. and Structural Engr., Berkeley, Calif.

Mr. Douma calls attention to the necessity of considering centrifugal-force pressures in stability analyses and in the structural design of concrete gravity and buttress dams. This is a welcome reminder which could be extended into several particulars.

The use of Eq. 8*a* for the computation of centrifugal pressures in the bucket should be excellent in cases of low and moderate height dams. However, in cases of dams exceeding 150 ft in height the friction and turbulence losses probably would justify a more accurate, although a more tedious, analysis. The writer was impressed by the mathematical exposition of the relationship between pressures, velocities, heads, and radii in various parts of a discharge bucket as shown by Mr. Douma.

Figs. 8 are most valuable because they show the physical actuality of the behavior of a deflected water stream in a free jet and in a submerged jet. Much valuable information can be derived from the study of these figures.

The experimental data furnished by Mr. Rhone are a valuable contribution to the study of pressures in a spillway bucket. Mr. Rhone's discussion of these data is illuminating and furnishes a reliable tie between theoretical deductions and experimental measurements. In a case of a free jet the theory appears to be well supported by experiment.

AMERICAN SOCIETY OF CIVIL ENGINEERS
Founded November 5, 1852
TRANSACTIONS

Paper No. 2676

THE DESIGN OF FLEXIBLE BULKHEADS

BY JAMES R. AYERS,[1] M. ASCE, AND R. C. STOKES[2]

WITH DISCUSSION BY MESSRS. W. F. HEAVEY, MORGAN S. CAMPBELL, WALTER C. BOYER, P. W. ROWE, GREGORY P. TSCHEBOTARIOFF, J. OWEN LAKE, NAI C. YANG, AND DAVID HOPKINS

SYNOPSIS

In the design of flexible bulkheads, the engineer is limited by a lack of knowledge concerning the actual behavior of varying soil masses.

Bulkhead design literature contains many theories and mathematical studies on the action and effect of earth pressure. The very number of these analyses supports the fact that no single method has universal application, and that a wide range of error in the assessing of pressures can be expected.

The purpose here is not to advance a new procedure that will remove all uncertainties from bulkhead design. Instead, this paper presents a description of the design and construction procedures followed by the Bureau of Yards and Docks, United States Department of the Navy, for varying site and soil conditions, together with methods for reducing pressures, proper construction sequences, and practical rules which are axiomatic for bulkhead design.

ENGINEERING DATA REQUIRED

The procurement of site and soil data is of paramount importance. A site survey that includes the history and general geology of the area is essential.

Unless soil conditions are known with certainty, borings should be taken at representative locations throughout the site. Undisturbed samples of cohesive type soils and disturbed samples of cohesionless materials should be tested for their physical properties. Active and passive earth pressures should be determined from these data.

SOIL PRESSURE THEORIES

The loads for which bulkheads are designed depend on the pressure exerted by natural earth deposits and earth fills. The wide variation in physical properties among different types of soil is responsible for the range in magnitude of lateral pressure exerted against various types of restraining structures. The classical theories relating to the physical properties of granular materials

---

NOTE.—Published, essentially as printed here, in January, 1953, as *Proceedings-Separate No. 166*. Positions and titles given are those in effect when the paper or discussion was received for publication.

[1] Head, Waterfront Structures Section, Bureau of Yards and Docks, U. S. Dept. of the Navy, Washington, D. C.

[2] Asst. Head, Waterfront Structures Section, Bureau of Yards and Docks, U. S. Dept. of the Navy, Washington, D. C.

have been quite universally accepted. These are based on the assumption that the earth is composed of granular particles without cohesion. Active pressures computed on this basis are frequently larger than those found in nature, and computed passive pressures are smaller than those observed.

There are so many variables affecting the magnitude of earth pressure that some practical procedure is necessary to arrive at values that are usable for the design of safe structures at reasonable cost.

The Bureau of Yards and Docks has built bulkheads of many types designed to meet a large variety of site and soil conditions. It has been Navy practice to compute earth pressures in the following manner:

(*a*) The active pressures and passive pressures for granular material are both computed by the Rankine-Coulomb formulas, neglecting the effect of wall friction.

(*b*) For fine-grained and cohesive materials, the earth pressures are based on both frictional and cohesive resistance, with allowance for pore pressure in unconsolidated material.

(*c*) Uniform surcharges are converted to equivalent heights of the backfill material.

The design is predicated on providing an actual safety factor of from 1.5 to 2.0 for the passive resistance. By use of the pressures computed as outlined above, the minimum depth of penetration required for stability of the sheet piles is determined. This minimum depth is considered sufficient to give the required factor of safety for sheet piling driven into natural undisturbed soils.

Pressure and Loading Diagrams

Pressure and loading diagrams for several general types of bulkheads are shown. Fig. 1 shows idealized pressure diagrams for a cantilever bulkhead. The diagram in Fig. 1(*a*) indicates minimum penetration of the sheeting as required for stability. This bulkhead is subject to progressively increasing deflection as the soil at the surface of the ground yields under pressure and with time. The deflection can be reduced by increasing the penetration of the sheet piles as shown in Fig. 1(*b*). For bulkheads where alinement and safety are important, increased penetration above the minimum required for stability is essential. Cantilever bulkheads should be of limited height and should be restricted to use in consolidated or compacted soils. Fig. 2 is an example of a bulkhead with single anchorage. Two loading diagrams having

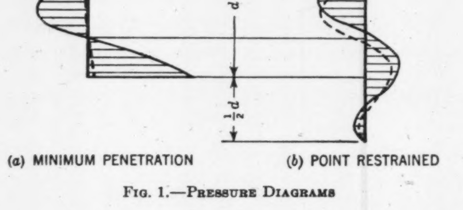

(*a*) MINIMUM PENETRATION (*b*) POINT RESTRAINED

Fig. 1.—Pressure Diagrams

equal areas of active pressure are shown. Fig. 2(*a*) is for sheet piling driven to the minimum penetration required for stability. Fig. 2(*b*) shows longer piling with the point restrained by passive pressure mobilized on both sides, thus reducing the bending moment and tie-rod pull. It is evident that the additional penetration will provide for higher active pressures or lower passive pressures than assumed, and for possible overdredging or scouring.

Fig. 3 illustrates a bulkhead with support for the sheet piles at two different levels. The angle of repose of the material is designated by ϕ. The additional support may be required because of lower values for the physical properties of the backfill material, increased bulkhead heights above low water level, greater water depths, and unbalanced water heads. The unbalanced water head usually is caused by a wide range of tide levels and is assumed to be about one half of the tide range. By proper choice of granular material for the backfill against the piling, it should be possible to restrict the elevation differential of the water lag. This bulkhead is considerably more difficult to construct because of the underwater work required to place the lower waling and tie rods. However, if a suitable anchorage can be provided economically, the wall should cost less than one with a relieving platform.

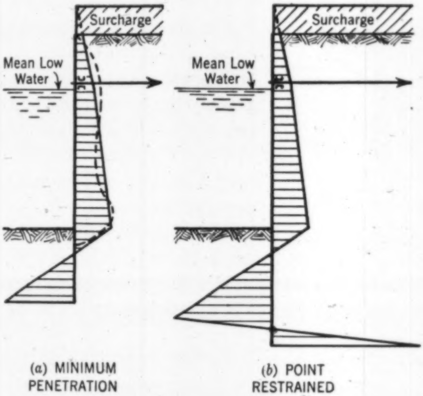

(*a*) MINIMUM PENETRATION

(*b*) POINT RESTRAINED

FIG. 2—LOADING DIAGRAMS—BULKHEAD WITH SINGLE ANCHORAGE

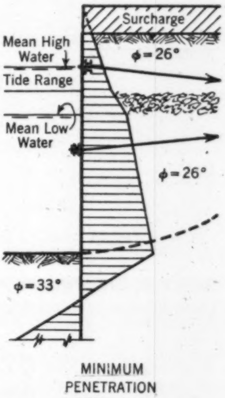

MINIMUM PENETRATION

FIG. 3.—LOADING DIAGRAM—BULKHEAD WITH DOUBLE ANCHORAGE

Bulkheads backfilled by the hydraulic method frequently are subjected to active pressures during filling that are greater than those occurring after completion. Fig. 4 shows a comparison between typical loading diagrams for these two conditions. The combined earth pressure and water pressure above mean low water during hydraulic filling produce larger loads than those resulting from the surcharge after completion. However, larger stresses in the sheet piles are permissible for the temporarily increased construction loads, provided the tie rods and anchorages are adequate. For this loading condition, a check on the adequacy of the anchorage and of the penetration of the sheet piles should be made.

METHODS OF REDUCING PRESSURES

Lateral loads at deep-water sites, or those resulting from soft materials, may become too large for bulkheads of the conventional type. Several methods are used by the Navy for reducing lateral pressures.

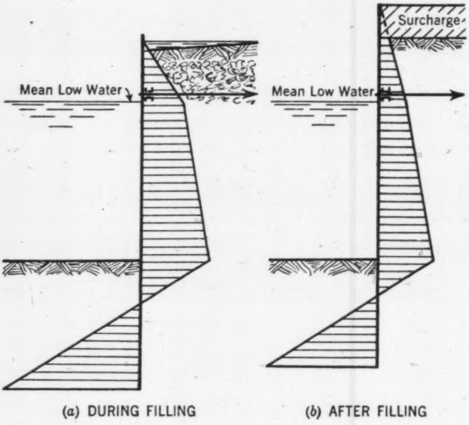

Surcharge
Mean Low Water
Mean Low Water

(a) DURING FILLING (b) AFTER FILLING

FIG. 4.—LOADING DIAGRAMS—BULKHEAD WITH HYDRAULIC FILL

Frequently, the site for a bulkhead is overlain by a considerable depth of soft material. Two possible solutions to this problem are shown in Fig. 5. In Fig. 5(*a*), the sheet piles are driven to obtain advantage of a constraining moment at the bottom. In the loading diagram, the effect of the soft material is shown clearly by the greatly increased area just below the elevation of the original bottom. In Fig. 5(*b*), the site is predredged and the mud removed. A sand blanket is deposited from the top of the firm strata to the level of final dredged bottom before the driving of sheet piling. The effect of a sand blanket in reducing the pressures is quite evident by comparison of the loading diagrams. The use of a sand blanket is the most economical method for constructing bulkheads at sites with poor bottom conditions for those cases in which the heaviest piling is inadequate.

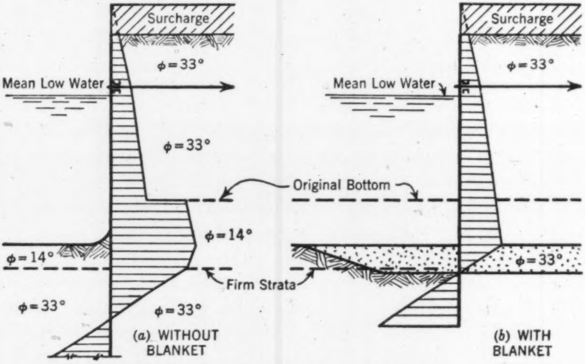

Surcharge
φ=33°
Mean Low Water
φ=33°
Original Bottom
φ=14°
φ=14°
Firm Strata
φ=33°
φ=33°
Surcharge
φ=33°
Mean Low Water
φ=33°

(a) WITHOUT BLANKET (b) WITH BLANKET

FIG. 5.—LOADING DIAGRAMS—BULKHEAD WITH SAND BLANKET

The effect of a sand dike in reducing the lateral pressure from poor quality backfill material is shown in Fig. 6. In this case, the existing material is assumed to be of good quality at the level of the dredged bottom, overlain by a few feet of somewhat poorer material. A hydraulic fill is deposited to tie-rod level above which a blanket of good quality granular material is dumped. The hydraulic fill is assumed to be fine grained, partly consolidated material which develops a pore pressure. The effect of this pore pressure is clearly indicated in Fig. 6(*a*). In Fig. 6(*b*), a dike of granular material is deposited immediately adjacent to the sheet piles. Behind this dike, the same poor quality hydraulic fill is assumed as in Fig. 6(*a*). Laboratory tests have indicated that the load on the sheet piles from a hydraulic fill with pore pressure can be reduced to approximately that from a full granular fill by depositing a dike of granular material against the bulkhead to its full height. Thus, the pressure diagram for Fig. 6(*b*) has ordinates of the same magnitude as those that would apply for a granular fill throughout the entire bulkhead height. Therefore, it is not necessary that the backfill consist entirely of a granular material for an indefinite distance behind the sheet piling. In a bulkhead of this type, settlement of the surface is to be anticipated because of the slow consolidation of the hydraulic fill. Certain advantages are gained by depositing the upper blanket of bank run material instead of carrying the hydraulic fill to the surface of the completed work. These advantages include accelerated consolidation of the hydraulic fill, better distribution of surcharges, and elimination of pressures from water level differentials during hydraulic filling.

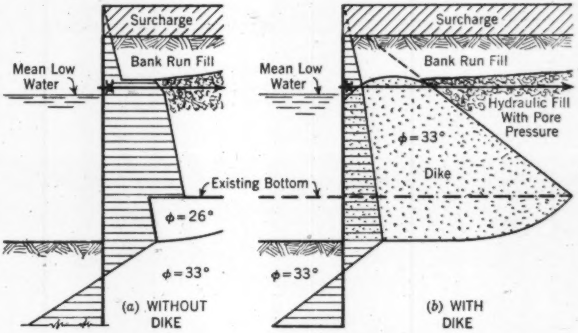

Fig. 6.—Loading Diagrams—Bulkhead with Dike

For water depths in excess of approximately 30 ft, or at locations where removal of soft material is impractical, it is necessary to provide other means for limiting the lateral pressure. One of the most common methods for accomplishing this is the relieving platform shown in Fig. 7. The deck of the platform is constructed within 1 ft or 2 ft of mean low water level. The supporting piles under the platform are designed to carry the entire weight of material and surcharge above the platform, thus relieving the earth immediately below the platform of any vertical load. The batter piles at the rear of the platform furnish the necessary sheet pile anchorage. In Fig. 7, the material existing between the original bottom and the dredged bottom has been left in place beneath the platform. The differences in the physical properties of the soil account for the changes in the loading diagram at the level of the original bottom. By using backfill material of minimum density and high shearing resistance, a relieving platform has been constructed in 48 ft of water by depositing a dike of oyster shells adjacent to the sheet piles.

In contrast to the bulkhead with relieving platform, Fig. 8 shows sheet piling located inboard of the platform. The active pressure against the bulkhead at any level is that produced by the full height of fill behind the platform, but the unsupported length of the sheet piles is reduced greatly. This construction possesses a distinct advantage over any other type, in that it may be adapted to any water depth by providing the requisite width of platform to allow for a stable slope in front of the sheet piles. An open type of wharf structure may be built instead of the platform in locations where favorable loading conditions prevail.

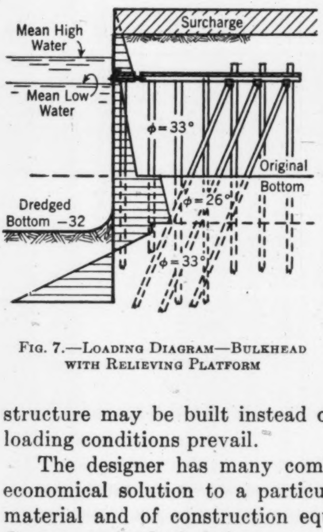

Fig. 7.—Loading Diagram—Bulkhead with Relieving Platform

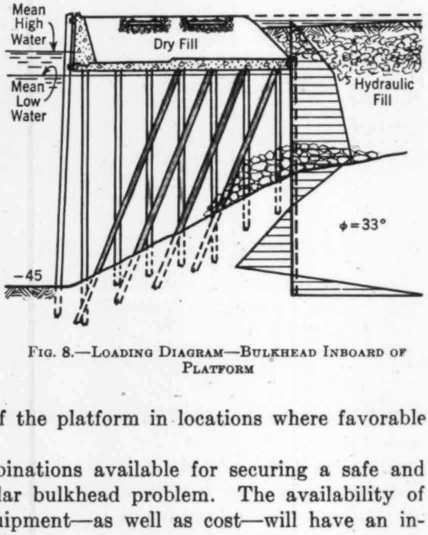

Fig. 8.—Loading Diagram—Bulkhead Inboard of Platform

The designer has many combinations available for securing a safe and economical solution to a particular bulkhead problem. The availability of material and of construction equipment—as well as cost—will have an influence on the final choice.

Types of Anchorage

Either one or both of two methods may be used for transferring tie-rod loads to the earth. One method derives its resistance from the passive pressures developed in front of a buried deadman, the other from a structural arrangement of brace piles. Several forms of typical anchorages are shown in Fig. 9. The simple deadman, Fig. 9(*a*), is suitable for use at a site where the existing ground level is at or above the bottom of the anchor. A concrete deadman can be either precast or cast in place, depending on economy of construction and the type of equipment available. Preferably, the concrete is cast in a trench in undisturbed firm material. Otherwise, the material in front of the deadman should be of select quality and throughly compacted to minimize lateral movement and resulting misalinement of the bulkhead. This type of anchorage is subject to tipping caused by unequal passive resistances in the earth and should not be used on important structures unless very favorable soil conditions exist. A **T**-shaped or **L**-shaped deadman will give improved stability against tipping.

In Fig. 9(*b*), sheet piles are used as an anchorage. The piling may be placed as a continuous wall, or in separate groups centered at each tie rod. The longer sheet piles are driven into the ground at each tie rod to provide vertical support for the assembly during erection and backfilling. This anchorage is suitable for sites having firm soils with varying ground elevations.

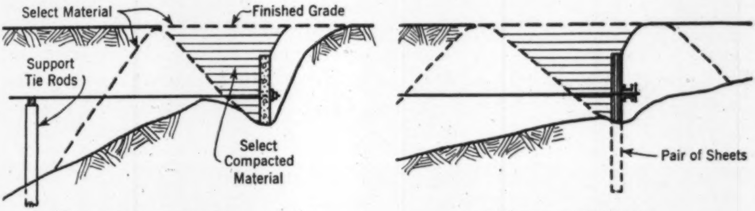

(*a*) SIMPLE DEADMAN (*b*) SHEET PILE DEADMAN

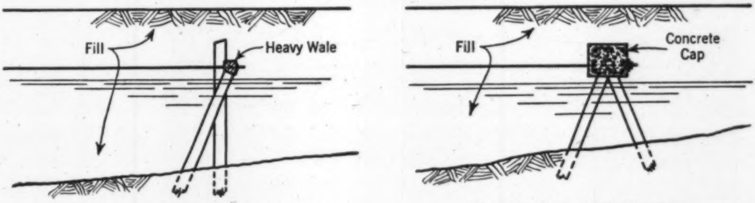

(*c*) BATTERED PILE ANCHORAGE (*d*) A-FRAME PILE ANCHORAGE

FIG. 9.—TYPES OF ANCHORAGE

In locations where the existing grade is low, anchorages of the type shown in Figs. 9(*c*) and 9(*d*) are effective. Because the resistance of this anchorage is not dependent primarily on passive pressure, it is well adapted to the hydraulic placing of fill. The principal resistance is derived from the batter piles, although in the case shown by Fig. 9(*d*) a large passive resistance eventually may be mobilized. Steel or concrete piles may be substituted for wood piles for increased capacity.

The location of an anchorage is of primary importance. If an anchorage depends entirely on passive earth pressure, it should be located far enough back from the bulkhead so that a region sufficient to develop this pressure exists behind the region producing active pressure. Anchorages of this type should not be closer to the bulkhead than from two to three times the distance from mean tide level to the dredged bottom. Anchorages depending on batter piles should be placed behind the region contributing active pressure to the bulkhead. Live load surcharges and settlements accompanying natural compaction of the backfill produce high tensile stresses in the tie rods and overloads on the anchorages. Therefore adequate vertical supports for the tie rods are essential in order to prevent sag of the rods both before and after placing of the backfill.

MOVEMENT OF BULKHEADS

A nominal amount of bulkhead movement should be anticipated to allow for bending of sheet piles, removal of sag and elastic lengthening in tie rods, and shift of anchorages to mobilize resistance. Movements of much larger magnitude often occur in well-designed and well-constructed bulkheads. Sites having predominantly clay soils must be examined for stability against the development of a general outward slide. Two other potential causes are illustrated in Fig. 10. A heavy surcharge placed immediately behind the anchorage may cause the anchorage to shift because of the bulb of pressure created by this loading condition. Unless the heavy surcharge can be located quite far behind the anchorage, vertical pile supports are required. If an underlying stratum of soft material is unconfined outboard of the bulkhead (such as the material indicated by a value of ϕ equal to 18° in Fig. 10), the loads from the bulkhead fill, and surcharges may cause a slow lateral flow of the soft material toward the channel, resulting in a translation of the bulkhead area as a whole. Such a translation is difficult to prevent. Driving of the sheet piles through the unconsolidated layer and provision of steel **A**-frame anchorages driven to bearing below the soft stratum is indicated. Another possible solution is a relieving platform supported on piles with points bearing below the soft stratum.

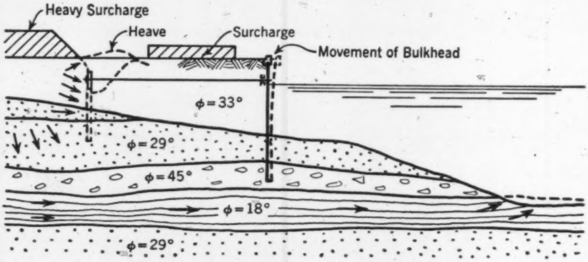

FIG. 10.—MOVEMENT OF BULKHEADS

IMPORTANCE OF CONSTRUCTION SEQUENCES

There is no single factor having more influence upon the success or failure of a given bulkhead than the sequence of construction. Overloading, lateral displacement, and actual failure result from improper construction methods as often as from poor design. Proper inspection is necessary to insure that requirements of the design are met.

The time and method of performing the dredging is often critical. Removal of soft material, when contemplated in the design, should precede the driving of sheet piles. If the existing material behind the sheeting is to be left in place, it will be advantageous to dredge in front of the bulkhead after completion of the structure. Because the lateral loads during backfilling are usually larger than those occurring at any other time, it is well to take advantage of the lateral resistance from material existing above the level of the final dredged bottom. In such a case, dredging after completion of the bulkhead allows a certain time for settlement with a consequent reduction in the active pressure. Dredging adjacent to the sheet piling after completion should preferably be done in two or three vertical stages to avoid rapid changes in load differential. The site should be predredged for open-type platform structures. Certain construction sequences are necessary with respect to the anchor system. Care should be taken to pretension the tie rods as uniformly as possible in order to avoid uneven alinement in the finished bulkhead wall under the load of the entire backfill. If the anchorage depends on passive resistance, there should be no filling against the sheet piles until the backfill has been properly deposited in front of, and to finished grade above, the anchorage.

The process of backfilling must be rigidly controlled. Backfill should be deposited by working away from the sheet piling rather than toward it. The trapping of soft material adjacent to the sheet piles must be avoided. In the filling of a relieving platform type of structure, the area under the back portion of the platform should be filled to deck level, the deck over the batter piles placed, and filling continued to grade. The area adjacent to the sheets may then be filled and the structure completed. In hydraulic filling operations, it is well to locate the discharge line on, or in front of, the anchorage. Openings in the sheet piles should be provided at intervals of about 100 ft to allow the escape of discharge water and thus prevent the formation of pools and the development of excessive hydraulic heads.

MATERIALS OF CONSTRUCTION

Several factors influence the selection of materials used in the construction of bulkheads. Among these are the depth of the water, the soil conditions, the presence of destructive marine organisms, the availability of construction equipment, and the permanency of the structure. Timber should not be used where destructive marine organisms are known to be active. All untreated timber should be located below the permanent wet line to avoid decay. Only treated timber should extend to a higher elevation. Tie rods should be painted and wrapped, or encased, for a distance of about 6 ft adjacent to the bulkhead and should be fully protected in acid soils or in certain cinder fills. Wire rope should not be used in the anchor system because of the rapid deterioration of the small wires. Steel wales and sheet piling corrode rapidly in the tide zone. The wales should, preferably, be located on the inner face of the piling. For increased life, all steel should be protected with bituminous coatings or concrete jackets above a level of 3 ft below mean low water. Concrete sheet piles with adequate cover give good service, but alinement is difficult to maintain when driving through large depths of relatively firm material. If there will be deep dredging in fine sand after completion of the structure, steel sheet piles usually are preferable because of their tight joints. Fill material should be predominantly granular. The percentage of fine-grained soil should be kept at a sufficiently low level to preclude the development of pore pressure.

Design Stresses

Assignment of uniform working stresses for wales, tie rods, and sheet piles—applicable to all conditions—is not realistic. The region of maximum corrosion is usually critical for the wales and tie rods. The maximum bending stress in the sheet piles usually occurs well below the water line where there is a minimum of corrosion. Limited data from prototype measurements of tie-rod tension indicate that the pulls resulting from pressures of backfill may be reduced by as much as 25% in one year's time. However, there are indications that the beneficial effect of this reduction may be overcome by the residual stresses developed by surcharges of long duration lying over extensive areas. Surcharges of short duration lying on small areas have little effect, but the increased tension from surcharges of long duration is released slowly after removal of the surcharge. Therefore, frequent repetition of extensive surcharges may cause tie-rod stresses considerably larger than those computed by theoretical methods. The tie rods may also develop increased stress resulting from earth settlement. Because of the uncertainty relating to soil pressures, unbalanced water heads, and the effects of corrosion, conventional working stresses are used for designing the wales and tie rods. Because records of failure for sheet piles are almost unknown, an increase of from 10% to 15% in excess of conventional working stresses may be used safely for ordinary conditions of loading. In order to care for loads during hydraulic filling, the Navy frequently permits increases of from 25% to 50% in excess of conventional working stresses for the sheet piles and increases of from 10% to 15% for wales and tie rods.

Axioms for Bulkhead Construction

The more important lessons learned from experience may be summarized as follows: (*a*) Study the general geology and history of the bulkhead site; (*b*) determine the properties of the underlying soil and of the backfill material; (*c*) remove soft unconsolidated material that overlays the site to depths exceeding 5 ft and replace it with predominantly granular material if required; (*d*) prepare a separate loading diagram and stability analysis for bulkheads to be backfilled hydraulically; (*e*) provide ample sheet pile penetration to care for accidental overdredging; (*f*) provide ample anchorage and locate it in a stable soil zone; (*g*) provide vertical supports for tie rods; (*h*) protect the tie rods and wales adjacent to the bulkhead against corrosion; (*i*) deposit the backfill by working away from or along the line of sheet piles; (*j*) never permit a mud wave to develop behind the structure; (*k*) when a choice must be made between backfill materials, consider the maintenance cost caused by the consolidation of fine-grained soils; (*l*) guard against the development of high water heads behind the structure; and (*m*) load relieving platforms before filling behind them.

CONCLUSION

Several branches of science have contributed to the fund of knowledge of bulkhead design. Beginning with Coulomb in 1773, extensive effort has been expended on theoretical and analytical methods. The relatively new science of soil mechanics is responsible for greatly improved means for evaluating earth pressures, based on the sampling and testing of materials. The most promising avenue to further progress seems to be in the field of prototype measurements for testing the validity of existing design methods.

DISCUSSION

W. F. Heavey,[3] M. ASCE.—There is no question that there is still a wide range of error in the assessment of the pressures of different soil masses behind bulkheads, despite many theoretical and approximate methods of computing these pressures. The paper by Messrs. Ayers and Stokes does much to illustrate this fact.

In this connection it is of interest to review the foundation problems encountered in the design and construction of Wharf 16 on the Houston Ship Channel (1951) at Houston, Tex. Borings disclosed that under a layer of very soft organic muck there were several layers of very fine silty sand before silty clay was encountered from El. −40 to El. −60. Below El. −63 a stiff to hard sandy clay-marly with shale was found. Two wharves have slipped out into the channel in the years prior to the construction of Wharf 16 because of these foundation difficulties.

A straight sheet-steel piling bulkhead with two levels of tie-rod supports attached to a sheet-pile anchor wall appeared to be the solution to the problem. The rear sheet-steel piling anchor wall was to extend from El. −26 to El. +9. Construction of this type of anchor wall would not have been so simple as the design indicated because of the inherent difficulty with the two levels of the tie rods and the anchor wall. The problems of bracing and of dewatering the particular site indicated that the cost of this solution would be high. Further study indicated that to assure the effectiveness of the two levels of tie rods, the site would have to be dewatered so that the important lower level of the tie rods could be placed in the dry.

Recourse was taken to changing the design to a series of joined circular sheet-steel piling cells. With this type of piling it was necessary only to remove the layer of organic muck prior to driving the interlocking sheet-steel piling. The 56-ft-wide cells were filled to the top with densified and compacted sands, as was the area between the rear of the cells and the bank to El. +5. Above that elevation the earth was rolled. Care was taken to fill the cells progressively so that the fill inside each cell was always higher than the fill outside it and never more than 5 ft higher than the fill in the adjacent cells.

The sheet piling was driven to El. −53. Each cell acted as a stable unit in resisting both the lateral and vertical loads. As designed, the factor of safety against overturning was 4.0. The factor of safety against sliding along the base of the cell was 5.0, caused by the cohesion of the soil on the shear plane plus the passive resistance of the soil at the toe of the cells on the channel side.

To the valuable axioms listed under the heading, "Axioms for Bulkhead Construction," might be added—where foundation conditions make it economical, the use of circular sheet-steel piling cells, filled with well-consolidated materials, may prove advantageous.

---

[3] Formerly Director, Port of Houston, Houston, Tex.; Project Engr., Frederic R. Harris, Inc., New York, N. Y.

Morgan S. Campbell,[4] M. ASCE.—The manner in which the authors have presented the design problem is to be commended. By carefully avoiding the involved theories of soil pressures acting on flexible bulkheads, they have been able to present an uncomplicated picture of the general problem.

The section entitled "Methods of Reducing Pressures" is interesting and informative, as it describes methods applicable to bulkheads having greater heights and more severe loading conditions than those usually encountered. The "Axioms for Bulkhead Construction" give valuable criteria to be followed in design and construction. To axiom (*e*) might be added an item concerning the possible removal of material from the toe of a bulkhead by scouring action from flowing streams and by propeller wash in boat anchorages and turning basins.

Both concrete and steel sheet-piling bulkheads have been designed and built by the Galveston (Tex.) District of the Corps of Engineers, United States Department of the Army. These walls have ranged in height from 10 ft to 35 ft, and a majority of them have been constructed on navigable waterways. Experience in the design and construction of these walls confirms the design considerations covered by Messrs. Ayers and Stokes.

In the construction of the higher bulkheads in the Galveston District, dikes of oyster shell, similar to the dike shown in Fig. 6(*b*), have been used as the fill behind the bulkhead to obtain reduced lateral pressures. Various types of anchorages, all generally similar to those shown in Fig. 9, have been used with success by the Galveston District. The selection of the type of anchorage has been decided on the bases of economy, availability of materials, and site conditions.

The behavior of bulkheads of steel-sheet piling, when subjected to unusual conditions, and the repair of damage to such structures may be important considerations for some installations. Several of the walls constructed in the Galveston District are located on the Gulf-Intracoastal Waterway, and have been struck at various times by barge traffic. The walls have shown unexpected strength under such collisions. The sheet piling has been bent and flattened but not badly torn or ruptured at the interlocks, and there has been very little loss of fill material. The part of the piling usually damaged has been between the top of the wall and a point a few feet below the water surface. Repair procedure has consisted of removing the fill immediately behind the damaged section, cutting out and removing the damaged piling, installing new sections of sheet piling above the undamaged portions of the old piling, and splicing the new sections to the old ones. In some instances the old piling has been pulled up several feet to raise the joint above the water before making a welded splice. After the splice has been made, the piling is redriven to grade, wale and tie-rod connections are made, and the backfill is replaced. This method of repair has been found to be economical and it does not cause undue obstruction of the waterway.

---

[4] Chf. of Design, Corps of Engrs., U. S. Dept. of the Army, Galveston, Tex.

Walter C. Boyer,[5] A. M. ASCE.—The authors are to be commended for presenting a valuable addition to the literature concerning flexible-bulkhead design. The determination of the pressure distribution under various conditions of backfill is admittedly complex; hence the classical theories provide a rational solution. The applications of these theories, however, are subject to many variations among designers. Consequently, the statement of the practice of the Bureau of Yards and Docks, which is based on extensive research and experience, will serve as a valuable guide.

It would be helpful if the authors would show the manner in which cohesive resistance and allowance for pore pressure in unconsolidated materials are accounted for in their design procedure. In examples of bulkhead design generally found in the literature, this has been neglected. The work of Gregory P. Tschebotarioff,[6] M. ASCE, gives promise of yielding important concepts in this matter. There are two methods of accounting for cohesive resistance often employed. One method utilizes a rational weighted value for the angle of friction which is depicted as ϕ_w in Fig. 11. The determination of the maximum normal stresses that are developed in the backfill is essential to this method. It is noted that the normal stresses increase with the height of the wall, with a consequent reduction in the value of ϕ_w. This is, in effect, a rational refinement of the method of selecting a ϕ-value from a table of soil types—a method found in some specifications. Another method involves the development of pressure diagrams using the value of ϕ in the Rankine formula, and subsequently, reducing this pressure by the cohesive resistance P_c defined by the relationship:

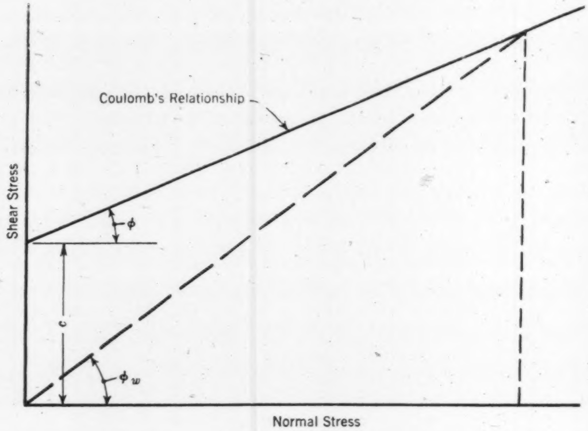

Fig. 11.—Relation Between Shear Stress and Normal Stress for a Soil.

$$P_c = \frac{2\,c}{\sqrt{K_p}} \qquad (1)$$

---

[5] Asst. Prof., The Johns Hopkins Univ., Baltimore, Md.

[6] "Final Report—Large Scale Earth Pressure Tests with Model Flexible Bulkheads," by Gregory P. Tschebotarioff, Princeton Univ., Princeton, N. J., January 31, 1949.

in which c is the cohesion and K_p denotes Rankine's passive coefficient. This may be recognized as the normal modification of the Rankine formula that inincludes cohesive resistance and is utilized occasionally in the design of retaining walls. The pore pressure presumably can be accounted for by adjusting the conditions of the shear test on which the data for pressure coefficients are based.

The designs of the Bureau of Yards and Docks (as stated by the authors under the heading, "Soil Pressure Theories") are "* * * predicated on providing an actual safety factor of from 1.5 to 2.0 for the passive resistance." Does this constitute an actual reduction in passive pressure in the computations? When driving in sand, is the Rankine passive coefficient increased by a factor of 2.0, as recommended by H. Blum based on the tests[7] of O. Franzius? Do the authors consider that the Rankine coefficient, with its neglect of friction between the fill and the wall, actually constitutes a factor of safety?

The methods described for reducing pressures are well conceived and present practical solutions to a number of intricate situations. Although these cover the majority of cases encountered, another situation is worthy of emphasis. The problem of extending harbor facilities by cutting out soil existing at or above water level is occasionally encountered. If the area is excavated, followed by the placing of the wall and the subsequent backfilling, it will fall into the class described by the authors. Another construction procedure for this situation may involve driving the wall and then excavating in front of it. This method is advantageous as it causes little disturbance to the natural soil. If the in-place soil is of a cohesive nature, an economic advantage may be derived by such a construction sequence. In this respect, however, the advice of the authors regarding the development of balanced pressures must be strictly adhered to in the dredging operation.

A bulkhead and relieving platform with the sheet pile located inboard of the platform is shown in Fig. 8. Such a system can cause difficulties if the relieving platform is not surcharged prior to the placing of the hydraulic fill behind the sheet pile. The placing of a surcharge on the relieving platform initially permits interaction of the batter piles and the plumb piles in carrying both the vertical loads and the transverse thrusts. Failure to follow such a sequence of loading may cause poor alinement of the pier face or actual failure of the relieving platform. Examination of Fig. 8 illustrates that the sequence described is the procedure followed by the Bureau of Yards and Docks and is worthy of emphasis.

C. Martin Duke,[8] A.M. ASCE, has described a field study of a sheet-pile bulkhead. An important result of this study is the considerable redistribution of both wall pressure and tie-rod tension when settlement of the backfill occurred. It can be concluded that the support system for the tie rods assumes considerable importance under such conditions. Measures for reducing or eliminating the resulting increases in tie-rod pressures (by placing the rods in conduits) represent additional expense in sheet-pile construction. A description of the measures used by the Bureau of Yards and Docks for this condition would be informative.

---

[7] "Versuche mit passiven Druck," by O. Franzius, *Der Bauingenieur*, 1924.

[8] "Field Study of A Sheet-Pile Bulkhead," by C. Martin Duke, *Transactions*, ASCE, Vol. 118, 1953, p. 1131.

The writer is particularly interested in the section entitled "Materials of Construction." Concrete jackets should be used to resist corrosion; however, this is not economically feasible on many installations, with the result that the less expensive bituminous coatings are specified. Experience seems to indicate, however, that even with reasonable care on the part of the contractor such coatings are far from successful. One of the most pressing needs in flexible-bulkhead construction is the development of an inexpensive coating for sheet piles—a coating which can resist the normal handling necessary on the project and the abrasion to which the wall is subjected during its life.

P. W. Rowe.[9]—A useful record of the practical considerations required for sheet-pile wall construction has been presented by the authors. However, there have been further developments in the knowledge of fundamental factors influencing the stability in cohesionless soil of this type of wall.

During the period from 1947 to 1951 a large number of tests[10] were made in Scotland on model sheet-pile walls of varying heights, stiffnesses, and materials. Other variables investigated were the effects of surcharge, dredge level, tie-rod locations, and sand conditions. The results of these tests, which agreed with all other published records of experiments concerned with sheet piling, proved that the bending moment and the tie-rod loads of a sheet-pile wall depend principally on the flexibility of the wall and the density of the subsoil.

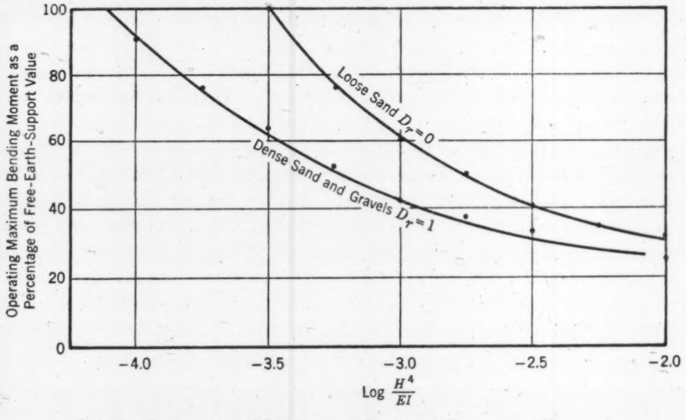

Fig. 12.—Reduction of Moment with Change in Flexibility Number

Briefly, a stiff wall will be subject to free-earth-support conditions of pressure. If the wall is made more flexible, the pressure distribution will approach that assumed by the fixed-earth-support pressure diagram, and at very high flexibilities the pressure distribution will approach that corresponding to complete fixity. The change is a continuous process, independent of all variables in the design other than the relative density of the subsoil. The results of the investigations conducted in Scotland are shown in the two empirical moment-reduction curves. In Fig. 12 H is the total height of the sheet piling in feet; E denotes the modulus of elasticity of the sheet-pile material in pounds per square inch; I is the moment of inertia of the sheet-pile cross section in inches^4 per foot of sheet-pile wall; D_r represents the relative density of the subsoil; α is the ratio of the free height of the piling to the total length of the piling; and $\frac{H^4}{EI}$ signifies the flexibility number of the sheet piling. The curves of Fig 12 are valid for all values of α between 0.6 and 0.8. Theoretical investigations have proven these curves to be correct.

---

[9] Lecturer in Civ. Eng., Univ. of Manchester, Manchester, England.

[10] "Anchored Sheet-Pile Walls," by P. W. Rowe, *Proceedings*, Inst. of C. E., London, England, Vol. 1, Pt. 1, 1952, p. 27.

The results of the Scotland investigations signify that the flexibility, and therefore the nature of the material of the piling, must be considered in the design. Specific moment-flexibility curves for different materials of wall are shown in Fig. 13(b) which allow the choice of the most economical type of wall and size of section. In Fig. 13(b) M is the maximum bending moment on the sheet-pile wall in pound inches per foot of wall length. Curve A was plotted from the maximum free-earth support moment and by interpolating values from Fig. 12 for D_r = 0.5. Curves B show the approximate relationship between the unit moment which the particular wall can withstand, and the wall's flexibility number. In the computations for Curves B, the allowable wood fiber stress was 2,000 lb per sq in.; the allowable steel stress was 18,000 lb per sq in.; and the reinforced concrete allowable stresses f_c were 750 lb per sq in. and 1,250 lb per sq. in. In this example the correct design sections are obtained from the intersection of Curve A with appropriate Curve B.

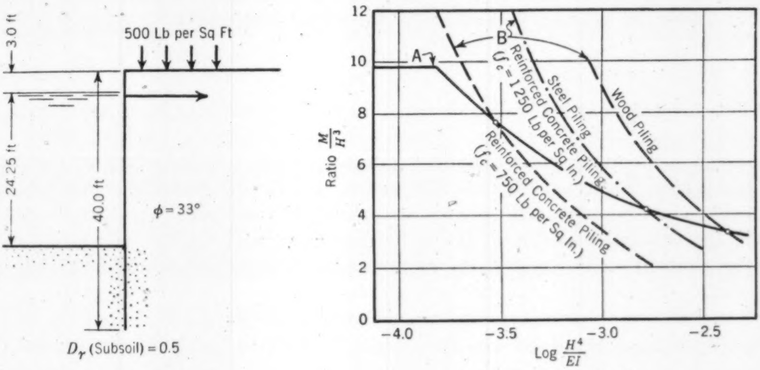

(a) SITE CONDITIONS (b) DESIGN CURVES

FIG. 13.—THE EFFECT OF MATERIAL OF CONSTRUCTION ON THE DESIGN OF A WALL

Having determined the required size of the section, the designer generally has to choose the nearest commercially available size. Normally a stiffer section would be chosen. However, it can be seen that the choice of the next lighter section does not lead to the large stress increase as is supposed, since the increase in flexibility of the sheeting causes a further reduction in moment from that corresponding to the design flexibility.

It has been generally assumed (an assumption also endorsed by the authors) that the deeper the piling is driven, the greater the reduction of the bending moment on the sheeting as a result of increased fixity. A slight increase in fixity does occur, but it is a very expensive way of reducing the moment on the sheeting by a few percent. If the wall is stiff and the subsoil loose, the wall would have to be embedded by a length at least as great as its free height before any appreciable fixity commenced. If the wall is flexible and the soil dense, full fixity remains until sudden failure occurs at a penetration of approximately one tenth of the free height. In either case, the earth-pressure distribution is the free-earth-support diagram at failure. For these reasons the free-earth-support method should be used for the computation of the depth of embedment and the maximum moment acting on a stiff wall. The curves of moment reduction with flexibility for the particular density of subsoil can then be applied to this value.

Under the heading, "Conclusion," the authors state that

> "The most promising avenue to further progress seems to be in the field of prototype measurements for testing the validity of existing design methods."

This suggests that if a wall is designed by a certain method, built, and tested, and it is found to have approximately the design moment, it follows that the design was correct and economical. In fact, if the free-earth-support theory is assumed, the design leads to a stiff section which would cause the prototype to behave in accordance with the free-earth-support computation and thus result in the computed moment. If the fixed-earth-support theory were assumed, the moment would be less, the section more flexible, and some fixity would result. Probably this theory would also be shown to be valid on the prototype. Thus, no prototype or field measurements on pile walls are likely to be useful until the influence of soil density and pile flexibility is thoroughly understood.

GREGORY P. TSCHEBOTARIOFF,[11] M. ASCE.—A valuable survey of the various practical considerations which must be evaluated by the designer of flexible anchored bulkheads has been presented by the authors. They are to be complimented for summarizing, in so comprehensive a manner, their extensive experience in this field.

The writer would like to comment on the remarks made by Messrs. Ayers and Stokes concerning the need for preventing high tensile stresses in the tie rods as a result of the consolidation of the backfill. The provision of "adequate vertical supports for the tie rods" (under the heading," Types of Anchorage"), presumably of the type shown in Fig. 9(*a*), may not be sufficient in some cases. Negative friction, caused by the consolidation of the backfill along the skin of such pile supports, can force the piles into the ground and thus overload the anchors which the piles are supposed to support. For this reason, it has been found necessary, in some localities, to encase the tie rods in a hollow box or in a cylindrical conduit so that the fill can settle without loading the tie rods.[12]

---

[11] Prof. of Civ. Eng., Princeton Univ., Princeton, N. J.

[12] "Soil Mechanics, Foundations and Earth Structures," by Gregory P. Tschebotarioff, McGraw-Hill Book Co., Inc., New York, N. Y., 1951, pp. 511–516.

The authors' recognition of the contributions made by soils engineers to the knowledge of bulkhead design is gratifying. On the basis of the theory of soil mechanics, however, there are several factors that require clarification. For example, no explanation is given as to why the authors state (under the heading, "Soil Pressure Theories") that the "* * * minimum depth of penetration required for stability of the sheet piles * * *"—if computed in the manner described—is considered sufficient to give a factor of safety of from 1.5 to 2.0. This condition is apparently attributed to some unspecified properties of "natural undisturbed soils." Other investigators have also used this method of approach—which can lead to overdesign in some cases and underdesign in others.[13] The reasons for this variation are given subsequently.

Model tests have clearly indicated that in the case of sand soils wall friction is fully mobilized below the dredge line in front of the bulkhead. It is this factor which accounts for the very high measured passive resistances.[14] These resistances were, in some cases, three to four times greater than the maximum values theoretically possible if the effect of wall friction is neglected. By thus neglecting the effect of wall friction in computing the passive pressures for granular material, the authors can obtain the desired factor of safety—or even a higher one. For cohesive soils, however, the effect of shearing stresses along the wall on the increase of passive resistance will be much smaller than in the case of granular materials. Therefore, by neglecting the effect of wall friction (or adhesion), and by using the minimum depth of penetration required for stability of the sheet piles, a factor of safety may be obtained for clay soils that is less than the minimum value of 1.5.

Another matter of both theoretical and practical importance which was not entirely clarified concerns the criteria that should be used to decide whether and when the depth of penetration should be increased beyond the depth necessary for stability, so that the pile point can be considered to be restrained and the fixed earth support method of design can be used instead of the free earth support method.

Both of these factors—questioned because they lead to ultra-conservative designs in some cases of granular soils—have been discussed by the writer.[15]

The writer agrees with Messrs. Ayers and Stokes that much information may be gained from prototype measurements, testing the validity of design methods. The importance of such measurements has long been recognized; however, at this time (1953) the results of only one such complete set of measurements on anchored bulkheads have been published.[8] Opportunities for field observations have been by-passed because of (1) a deficiency of funds for such observations, (2) the lack of specially trained personnel to conduct such observations and to be responsible for them, and (3) the wide-spread feeling among engineers responsible for waterfront construction that allocation of funds from a specific project is not justified unless the observations can be relied on to produce results of value to that particular project.

---

[13] "Design Curves for Anchored Steel Sheet Piling," by Walter C. Boyer and Henry M. Lummis, *Transactions*, ASCE, Vol. 119, 1954, p. 639.

[14] "Soil Mechanics, Foundations and Earth Structures," by Gregory P. Tschebotarioff, McGraw-Hill Book Co., Inc., New York, N. Y., 1951, p. 300.

[15] Discussion by Gregory P. Tschebotarioff of "Design Curves for Anchored Steel Sheet Piling," by Walter C. Boyer and Henry M. Lummis, *Transactions*, ASCE, Vol. 119, 1954, p. 651.

This latter feeling is responsible for the fact that years go by with nothing being done to check the unsatisfactory methods of design in use. It is therefore essential that funds be appropriated for such observations and that these observations be placed in the hands of specialized research personnel.

It should be remembered that no matter how well full-scale field observations are organized, such observations alone cannot form the basis for a rapid advance of knowledge of the actual performance of earth-retaining structures. The number of conditions affecting the performance of such structures is so great that (in accordance with the theory of probability) there is little chance that these factors would vary from one observed structure to another in a manner that would permit the numerical evaluation of the separate influence of each factor. In order to accomplish this evaluation under controlled conditions, model testing is essential.

The authors present an example of the important results achieved by model testing. The laboratory experiments that they state as having justified the use of sand dikes to reduce the pressures of fluid hydraulic fill were model tests performed under the sponsorship of the Bureau of Yards and Docks.[16] The writer, in this discussion, presents another example of the importance of model test results in their effect on the estimation of the factors of safety for a known depth of sheet-pile penetration.[14, 16]

Further progress can therefore be best achieved by a continuous effort to correlate the results of full-scale observations, model tests, and theoretical analyses.[17]

J. OWEN LAKE,[18] A.M. ASCE.—A useful summary of the various factors to be considered in the design of bulkheads has been presented by the authors. Unfortunately, however, the description of earth-pressure computation (under the heading, "Soil Pressure Theories") is not sufficiently explicit to allow detailed discussion. It would be enlightening if the authors' method of determining the active and passive earth pressures for silts and clays could be explained.

Messrs. Ayers and Stokes state that earth pressures for fine-grained and cohesive materials are based on both frictional and cohesive properties. However, soils are shown in Figs. 3, 5, and 10 with ϕ-values of 14°, 18°, and 26° with no mention of cohesion and no indication on the loading diagrams to show that cohesion is allowed for. Because soils having values of ϕ that are less than approximately 30° inevitably possess cohesion, neglect of this property will nullify the validity of any pressure computation. Also, an analysis of the initial stability of bulkheads sustaining pressure caused by fully saturated clays should be based on the clay possessing a ϕ-value equal to zero, as this is the result obtained in undrained triaxial tests, which generally represent immediate post-construction conditions before any water content change has occurred.

---

[16] "Soil Mechanics, Foundations and Earth Structures," by Gregory P. Tschebotarioff, McGraw-Hill Book Co., Inc., New York, N. Y., 1951, pp. 293–297.

[17] "Some Unsolved Problems of Importance for the Design of Earth Retaining Structures," by Gregory P. Tschebotarioff, *Bulletin No. 33*, Permanent International Assn. of Nav. Congs., 1950.

[18] Cons. Engr., Toronto, Ont., Canada.

The authors compute the active and passive pressures of granular materials acting on bulkheads by the Rankine-Coulomb formulas, neglecting the effect of wall friction, and then apparently design the bulkhead for simple support. Such a procedure will generally overestimate the required strength of the sheet piling by approximately 25% to 50%, in comparison to a design that uses the fixed earth support method[19] based on angles of wall friction equal to zero for active pressure, and equal to $\frac{2}{3}\,\phi$ for passive pressure. This latter procedure has been the basis of design adopted by the writer for considerable bulkhead construction in the United Kingdom and in many other parts of the world, and at least some confirmation of the general validity of this design procedure lies in the fact that there has been no indication that stress in these bulkheads has exceeded the anticipated design value of one half the yield stress.

The generally satisfactory results obtained from the fixed earth support method when applied to bulkheads founded in cohesionless soils are made apparent in the results of model tests described by Mr. Rowe,[10] who has presented, for the first time, quantitative information concerning the influence of bulkhead flexibility on the maximum bending moment which bulkheads sustain. In a discussion of Mr. Rowe's tests, S. Packshaw and the writer have shown comparisons between typical designs based on the conventional fixed earth support method with no allowance for flexibility, and designs based on the results of Mr. Rowe's research.[20] It was demonstrated that generally even the fixed earth support method considerably overestimates the bending moment. The comparisons did disclose that sheet-pile bulkheads of normal flexibility having a yield stress of about 36,000 lb per sq in., penetrating into loose cohesionless soil and exceeding approximately 40 ft in height, did not achieve the degree of fixity assumed in the fixed earth support method. However, the existence of uniform deposits of entirely cohesionless sand in a minimum state of compaction, although not unknown, is not often encountered in bulkhead construction. Furthermore, the use of high-tensile steel sheet piling would generally develop the necessary flexibility at one half the yield stress to achieve fixity even in loose sand.

Thus, the use of high-tensile steel having a yield stress of from 50,000 lb per sq in. to 55,000 lb per sq in. can, under appropriate conditions, result in economy amounting to about 35% saving in weight and 25% saving in cost when compared with the use of steel having a yield stress of approximately 36,000 lb per sq in.

Although the authors consider that the greatest water depth for conventional anchored bulkheads set in granular material is about 30 ft, it is of interest to note that the writer has been concerned with a design involving 42 ft of water, and a conventional bulkhead with a single anchorage system located at water level was adopted with success. In this design the steel sheet piling was a standard section having a section modulus of 55.1 cu in. per ft of wall, but strengthened in the region of maximum bending moment to result in a section modulus of 82.2 cu in. per ft of wall. Similar designs have been proposed and adopted in Canada, with resulting economy.

---

[19] "The Application of Steel Sheet Piling to Engineering Construction," by S. Packshaw, *Civil Engineering*, London, England, December, 1932—January, 1933.

[20] Correspondence of S. Packshaw and J. Owen Lake on "Anchored Sheet-Pile Walls," by P. W. Rowe, *Proceedings*, Inst. of C. E., London, England, Vol. 1, Pt. 1, 1952, p. 621.

NAI C. YANG,[21] A. M. ASCE.—The writer takes issue with the authors' statement (under the heading, "Soil Pressure Theories") that

> "By use of the pressures computed as outlined above [Rankine-Coulomb formulas], the minimum depth of penetration required for stability of the sheet piles is determined. This minimum depth is considered sufficient to give the required factor of safety for sheet piling driven into natural undisturbed soils."

It is known that the magnitude of earth pressure is related to the amount of wall movement. This movement indicates the mobilization of the shearing strength in the soil. The conventional earth pressure theory assumes that the shearing strength of the soil is fully mobilized to create the active or passive stress. In so far as the state of stress is concerned, the active pressure computed by the Rankine-Coulomb formulas is the minimum thrust on the wall, and the passive pressure is the maximum resistance that the soil can afford.

In known cases of bulkhead failure, the wall moves outward near the dredge line a distance more than the movement at the anchorage. This type of wall movement prevents the soil from fulfilling the basic assumption of the Rankine-Coulomb theory. For active earth pressure, the pressure shifts toward the anchor point at which the anchorage confines the wall movement. According to reported field measurements,[22] the observed active pressure does not differ greatly in the total thrust from the pressure as computed by the Coulomb formula. It can be assumed that the ordinary wall movement might create an active pressure state in the backfill. Coulomb's formula should be used in designing the bulkhead only to estimate the magnitude of the total active thrust, not its distribution on the wall.

To create the maximum passive resistance, the wall must move more than the distance that is required to develop the active thrust. Although the backfill reaches a state of active pressure, the same wall movement is not sufficient to mobilize fully the passive resistance of the front soil. The actual passive resistance is thus appreciably smaller than the theoretical resistance. The dredge line is sometimes assumed to extend horizontally from the bulkhead. If this were the case, there would be an unrealistic increase in computing the passive resistance. With the dredge line set at a slope equal to the angle of repose of the soil, there will theoretically be no passive resistance at all.

If the limitations of earth pressure theory are ignored, the bulkhead design by the Rankine-Coulomb formulas eventually will be found to be unstable. In most cases, bulkhead failures have resulted when the bulkhead collapsed massively along a potential sliding surface somewhere under the sheeting. The second major cause of failure was the inadequacy of the anchorage. This inadequacy tended to make the wall tilt. There have been few cases in which the sheet pile broke near the dredge line where, according to the conventional earth pressure theory, the bending moment should be a maximum.

---

[21] Foundation Engr., Madigan-Hyland, Cons. Engr., Long Island City, New York, N. Y.

[22] "Earth Pressure Measurements in Open Cuts," by R. B. Peck, *Transactions*, ASCE, Vol. 108, 1943, pp. 1008–1036.

In designing bulkheads, it should be noted that:

1. The stability of the entire bank is the most important aspect to be investigated. The penetration of the sheet pile should meet the requirement for slope stability.

2. A study of the possible movement of the anchorage should be more important than that of its potential resistance.

3. The earth pressure on the sheeting is of relatively minor importance. The bending moment of the sheeting can be estimated, however, by use of the conventional earth pressure theory. Any such computation is of only academic interest unless the primary assumptions of the theory are fulfilled.

Hydraulic Backfill.—On the basis of experience the most desirable site for the use of hydraulically-placed backfill is in shallow water. The soil condition of the foreshore usually consists of a fine-grained deposit that has never been subjected to a pressure greater than its prevailing overburden. Such a deposit is usually referred to as being normally loaded, and it is always soft to a considerable depth below the surface. The hydraulic fill generally affords an economical way for the disposal of the dredged materials. It is not uncommon for the hydraulic fill to be silted upon soft virgin ground. For sheet-pile bulkheads with hydraulic backfill, experience indicates that: (1) Failure occurs more frequently than for bulkheads with dry backfill; (2) sheet piles are usually broken near the anchor point; and (3) many filling enclosures fail to stand at the outboard corners.

Excessive water pressure in the fill is usually thought to be the immediate cause of bulkhead failure. The authors (under the heading, "Methods of Reducing Pressures") have presented their experiences concerning "The effect of a sand blanket in reducing the lateral pressure * * *." The application is limited to the condition that "* * * the existing material is assumed to be of good quality at the level of the dredged bottom, overlain by a few feet of somewhat poorer material." However, they realize that "Frequently, the site for a bulkhead is overlain by a considerable depth of soft material." It is unlikely that the concept of a sand dike can be used extensively in hydraulic-filling operations.

Because of the weight of the fill, the subsoil tends to consolidate. According to the elastic theory of settlement, the edges of a large-area filling basin should subside about one half the amount that the fill subsides, and the corners should subside approximately one quarter of the amount. The differential settlement at the edge is about one half the total settlement of the fill, and the differential settlement at the corners is three quarters of the total settlement. It is important that excessive settlement is always anticipated in a normally loaded deposit. In the case of sheet-pile bulkhead with hydraulic backfill, the anchorage should settle more than the sheeting. Because of the differential settlement, the anchorage tends to pull the sheeting against the fill. This type of wall movement contradicts the fundamental assumption (in conventional bulkhead design) that the sheeting tends to pull the anchorage. The backfill consequently by-passes the active state of earth pressure and reaches the passive one. The tie-rod tension and the bending moment in the sheeting increase considerably—as the passive earth pressures do with increasing wall movement. The more differential settlement that occurs, the more possibility there will be for bulkhead failure.

If the fill is assumed to be cohesionless, sandy soil with $\phi = 30°$ and a saturated weight of 115 lb per cu ft, according to the Coulomb formulas the active pressure for dry fill is 38 lb per sq ft, the active pressure for hydraulic fill equals 80 lb per sq ft, and the passive pressure for hydraulic fill is 220 lb per sq ft.

The active pressure in the hydraulic fill is approximately twice that in a dry fill. By changing the state of stress, however, the earth pressure may increase as much as six times. In usual design practice, the working stress of a structural material is taken to be one third of its stress at failure; it is therefore unlikely that a stress that is twice the working stress will cause an immediate failure. These numerical quantities are purely illustrative. They show that, unless there is a change of state of stress (from active to passive), the excessive water pressure is not principally responsible for the failure of a bulkhead with hydraulic backfill.

The sand dike does reduce the excessive water pressure on the sheeting. Nevertheless, a preconsolidation of the area along the fill edges will result from the placement of the sand dike. As the hydraulic fill is placed, the differential settlement between the sheeting and the anchorage will increase. Thus, the advantage of using a sand dike is not offset by its potential harm.

David Hopkins,[23] A.M. ASCE.—A clear and concise summary of basic principles has been presented by the authors. The paper will undoubtedly be of assistance to engineers responsible for bulkhead design. It is regrettable that references to earth-pressure analyses and research performed by Mr. Terzaghi and several others[10,20,24,25,26,27,28,29] have not been included.

The conclusions reached by model investigators and research workers should lead to considerable modification of the design criteria used by the Bureau of Yards and Docks. Present knowledge (1953) indicates that certain design criteria in use by the Navy are ultra-conservative and wasteful.

Design Principles.—Publications describing model tests have been confusing because their writers have advocated conflicting design methods for solving bulkhead design problems. J. P. R. N. Stroyer, for example, attributed an observed reduction in bending moment to soil arching, and he derived an empirical formula to evaluate this reduction.[28,29] Research by Mr. Rowe illustrated the fact that the bending moment reduction is only partly a result of soil arching; the major causes are flexure of the piling and fixity of the toe.[10]

---

[23] Civ. Engr., Parsons, Brinckerhoff, Hall & Macdonald, New York, N. Y.

[24] Correspondence of G. P. Tschebotarioff on "Anchored Sheet-Pile Walls," by P. W. Rowe, *Proceedings*, Inst. of C. E., London, England, Vol. 1, Pt. 1, 1952, p. 616.

[25] Correspondence by Karl Terzaghi on "Anchored Sheet-Pile Walls," by P. W. Rowe, *ibid.*, p. 619.

[26] "Large-Scale Model Earth Pressure Tests on Flexible Bulkheads," by G. P. Tschebotarioff, *Transactions*, ASCE, Vol. 114, 1949, p. 415.

[27] "Theoretical Soil Mechanics," by Karl Terzaghi, John Wiley & Sons, Inc., New York, N. Y., 1943, p. 216.

[28] "Earth-Pressure on Flexible Walls," by J. P. R. N. Stroyer, *Journal*, Inst. of C. E., London, England, Vol. 1, 1935–1936, p. 94.

[29] Correspondence of "Earth-Pressure on Flexible Walls," by J. P. R. N. Stroyer, *ibid.*, p. 550.

Despite such disagreement as to the best method of bulkhead design, the results obtained from the various model tests are substantially in agreement. A number of basic principles are well established, which can be briefly summarized as follows:

The active and passive pressures of a granular soil on a flexible bulkhead generally follow the Coulomb theory with full wall friction. The magnitude and distribution of the earth pressures, however, and the bending moment in the sheet piling, will depend on (1) the amount of yield of the tie rod under load, (2) the flexure of the sheet piling, and (3) the density of the soil which provides the toe embedment for the sheet piling.

1. Tie-Rod Yield.—The amount of tie-rod yield and anchorage yield under load has considerable influence on the magnitude and distribution of active pressure. In the hypothetical case of a rigidly-supported rigid bulkhead, the active earth pressure would be equal to or greater than the earth pressure at rest. Since cases of zero yield cannot occur in practice, however, earth pressure at rest need not be considered.

When the tie rod yields, the active earth pressure decreases until it becomes approximately equal to the Coulomb value—but with a soil-arching effect which results in a pressure redistribution, as illustrated in Fig. 2(*a*). If the tie-rod yield increases, the soil-arching effect disappears, and the active pressure follows a straight line distribution equal to, or slightly less than, the Coulomb value with full wall friction.

Thus, for the range of yield normally encountered in tie rods and anchorages, the active pressure may be assumed—without serious error—to be equal to the Coulomb value with full wall friction. However, if the tie-rod yield is restricted, as in the case of a stiff batter pile anchorage with a very short tie rod, there will be a concentration of pressure at the tie-rod level, and a resulting increase in tie-rod pull. As a general rule, however, yield of the tie rod has the effect of slightly relieving the active pressure on the bulkhead.

2. Flexure of the Piling.—Flexibility of the sheet piling is the most important factor contributing to the active-pressure reductions and bending-moment reductions observed by investigators. The causes of the reduction are complex, but they are generally related (*a*) to the amount of end fixity provided by the embedment of the toe of the pile, and (*b*) to the reduction in effective span which occurs if the pile is flexible. In the case of a sheet pile of average stiffness, where the toe has a good penetration in a dense soil, the negative bending moment at the toe will approximately agree with classical fixed-earth-support computations, and there will be a corresponding reduction in the positive moment at midspan.

If the sheet-pile section is very stiff, however, and the toe is embedded in a loose soil, the toe of the pile may not be fixed, even though the pile has been driven to a penetration that should theoretically provide end fixity. In this case, the positive bending moment may be equal to the moment in a simply-supported beam spanning from tie-rod level to the centroid of the passive pressure. The bending moment in this extreme case may be double or more than double the bending moment for the preceding case.

3. Soil Density and Passive-Pressure Distribution.—The effects of pile flexure and the soil density are closely related in the determination of the toe fixity. The distribution of passive pressure is similarly affected by both pile flexure and the soil density. However, the full Coulomb passive pressure is not usually mobilized. Only in the case of a sheet pile driven to a minimum penetration to resist sliding is the magnitude and the distribution of the passive pressure exactly equal to the Coulomb value.

The possible variations in the passive pressure are illustrated in Fig. 14, which shows three typical cases. The active pressure on the sheet piling is assumed to be the same in each case. In Fig. 14 the effective span is denoted by L_e.

Fig. 14(*a*) shows a pile driven to a minimum penetration, with the passive pressure P_1 equal to the Coulomb passive pressure. The minimum penetration varies from one-fifth to one-third of the pile length in an average bulkhead design, depending on the ϕ-value and other design factors.

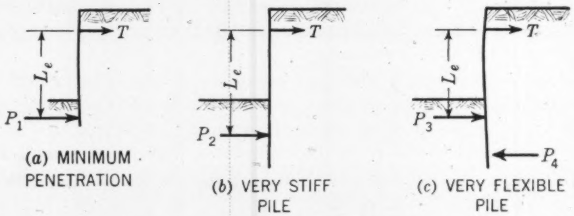

FIG. 14.—PASSIVE-PRESSURE DISTRIBUTION

Fig. 14(*b*) shows a very stiff pile driven to a greater penetration in a loose soil, where the full passive pressure is not mobilized. The passive pressure P_2 is slightly greater than P_1, and the bending moment is larger because of the increase in effective span.

Fig. 14(*c*) shows an extremely flexible pile driven into a dense soil. The full passive pressure is mobilized, but it does not follow a straight line distribution because of the pile contraflexure. In this case, P_3 is approximately equal to P_1 plus P_4. The bending moment in the pile is reduced by the amount of the end-fixing moment.

Design Analyses.—The most comprehensive series of model tests of flexible bulkheads is the investigation undertaken by Mr. Rowe in 1952.[10] The results of his measurements are shown in an abbreviated and simplified form in Figs. 15 and 16, which illustrate the effect of pile flexure and soil density on the bending moment of the pile. It can be seen how critical these factors are, and how wide a range of bending moments can occur under varying conditions.

A survey of Mr. Rowe's results shows that for a pile of average stiffness in a soil of average density (Fig. 15(*b*)) the bending moment is of the same order of magnitude as the bending moment computed by the conventional fixed earth support method. If a very stiff pile has a toe embedment in a loose soil (Fig. 15(*a*)), the bending moment may be considerably larger. For a very flexible pile in a dense soil (Fig. 16(*c*)) the bending moment may be smaller than that computed by the fixed earth support method.

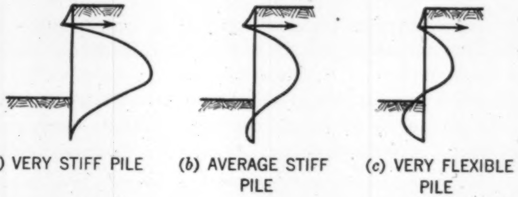

FIG. 15.—BENDING-MOMENT DIAGRAMS FOR BULKHEADS IN VERY LOOSE SOIL

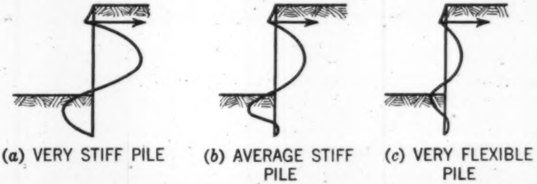

FIG. 16.—BENDING-MOMENT DIAGRAMS FOR BULKHEADS IN DENSE SOIL

It should be noted that in the following arbitrary pile classification (according to varying degrees of stiffness), it is assumed that (1) piles of average stiffness include steel sheet piles in the lengths normally used for anchored sheet-pile bulkheads; (2) very stiff piles include reinforced concrete sheet piles and short lengths of the heavier sections of steel sheet pile; and (3) very flexible piles include timber sheeting and longer-than-average lengths of steel sheet piles.

As an example of relative stiffness, a pile 50 ft to 55 ft long with an MZ 38 section would be typical of piling having an average stiffness, whereas a similar section 30 ft to 35 ft long would be very stiff.

It should also be noted that the higher the working stress is, the greater the pile flexure will be. Hence, overstressing a pile in bending will automatically relieve the pressure on it, and consequently reduce the bending moment.

It is unfortunate that Mr. Rowe's method for design analysis is unwieldy and presupposes more exact information about soil properties than is usually available to the designer. It is clear, however, that an allowance for bending moment variations must be included in practical design computations, and the most convenient method of making the necessary adjustments to design moments appears to be an empirical adaptation of the fixed earth support analysis.

The following graphical procedure (which is approximate, but practical) has been found to be in reasonable agreement with more rigorous analytical methods:

(*a*) The active and passive pressures are computed using full wall friction equal to $\frac{2}{3}\phi$. To avoid arithmetical work in the computations, the Rankine values of active pressure can be used—neglecting wall friction—and the error will be small. In computing passive pressures, wall friction must be included, and the passive pressure can be twice the Rankine value or more. Values of K_p can be obtained from tables or graphs to include wall friction. It is also important that account be taken of the effects of hydrostatic or pore pressures as a result of tidal fluctuations or ground water on the pressure diagram.

(*b*) The force polygon is drawn from the vector diagram. There is no need to locate the closing line precisely by the elastic line method, however, since its position depends on the degree of fixity of the toe, and is extremely variable.

In Fig. 17(*a*), the force polygon has been drawn, and the closing line, which will constitute the base line of the bending moment diagram, will pass through point O (point O lies on the line of action of the tie rod). The base line will actually lie somewhere in between line OT (which is tangential to the force polygon), and line OA (which is drawn so that $M_n = M_p$). If there is no fixity at the toe, the maximum will be M_O; if the toe is completely fixed, the maximum value will be M_p (which is equal to M_n).

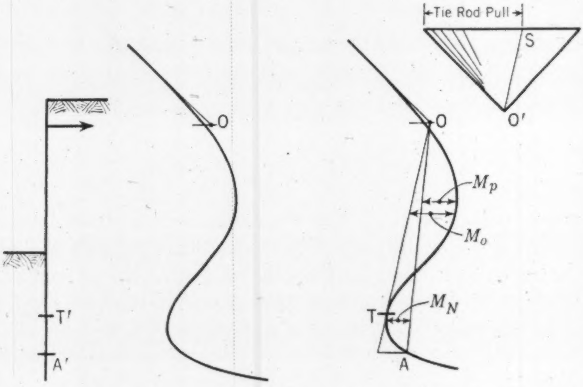

(*a*) FORCE POLYGON (*b*) MOMENT DIAGRAM

FIG. 17.—GRAPHICAL ANALYSIS

(*c*) The tie-rod pull is obtained from the vector diagram by drawing a vector O'S parallel to line OT, and measuring the resultant force. The value of the tie-rod pull obtained by this procedure (assuming that there is no toe fixity) is a maximum. In most cases where toe fixity occurs, the tie-rod pull is less, but by using the maximum figure an adequate safety factor is automatically introduced into the design. No safety factor is required other than the use of a normal working stress for the tie rod—20,000 lb per sq in. if structural steel is used.

(*d*) The required penetration of the toe of the pile is determined after the amount of toe fixity has been estimated. The toe penetration depends on (1) the density of the soil and (2) the section modulus of the sheet piling. Sand and gravel can generally be considered to be dense, unless it is from a recently deposited bed or in a loose, cohesionless state.

If it is proposed for economic or other reasons to use a sheet pile with a section modulus adequate for the maximum bending moment, the toe can be cut off at the elevation of the point T′. Alternatively, if the soil is dense enough to develop full toe fixity, a lighter section of sheet pile can be used; the toe penetration is then extended to the elevation of point A. In order to provide a reasonable margin of safety against toe failure, the actual length of pile must be increased so that the penetration is least 20% more than the minimum penetration found by this method. (For an average bulkhead design this requires a pile length approximately 5% greater than the theoretical length.)

(*e*) For piles of average stiffness, the positive moment M_p can be used to obtain the required section modulus (assuming that M_n equals M_p, as shown in Fig. 17(*b*)).

For very flexible sheet piling, the actual bending moments will be smaller than M_n or M_p, but it is not advisable to make any further reduction in the section modulus of the sheet pile without a very thorough investigation of soil properties and a rigorous analysis of earth pressures and moments for the particular pile section that it is proposed to use.

For very stiff piles or for piles embedded in a loose soil, the bending moment can be taken as the full positive value without end fixity (M_O in Fig. 17(*b*)). In the case in which the density of the soil is doubtful, a value of M_n equal to $\frac{1}{2}\ M_p$ can be used.

In all cases a working stress of 24,000 lb per sq in. or greater can be used for regular sheet-pile sections, and the factor of safety will be adequate if the soil properties have been reasonably estimated. If severe corrosion is anticipated, it is necessary either to increase the thickness of the steel section or to resort to cathodic protection.

Conclusions.—In conclusion, the following suggestions are advanced:

1. Consolidation and correlation of existing knowledge are more important than further model research. In particular, a convenient method for evaluating pile flexibility and soil density and their influence on pile bending moments is urgently required.
2. A full-scale experimental verification of pile flexibility effects is required to support model test data.

3. Free earth support analyses which compensate for toe fixity by including a bending moment reduction factor are liable to be misleading; fixed earth support methods should always be used.

4. Design analyses should be suitable for practical design use. In view of the approximations involved in "idealizing" geologic sections and assessing soil properties, design computations should not depend on arithmetical accuracy to several decimal places.

AMERICAN SOCIETY OF CIVIL ENGINEERS
Founded November 5, 1852
TRANSACTIONS

Paper No. 2677

RATING CURVES FOR FLOW OVER DRUM GATES

BY JOSEPH N. BRADLEY,[1] A. M. ASCE

WITH DISCUSSION BY MESSRS. GUIDO WYSS; SAM SHULITS; BOB BUEHLER; F. B. CAMPBELL AND A. A. McCOOL; AND JOSEPH N. BRADLEY

SYNOPSIS

With water becoming more valuable in the western states each year, there is an increasing demand for better methods of measurement and additional rating structures. This condition applies not only to the requirements for main canals and laterals of irrigation works but also to the regulation and measurement of flow at dams. In fact, the need has reached the point at which operators are desirous of metering the flow at nearly all control devices in irrigation systems, and in other water supply or control systems.

The primary purpose of this paper is to point out that there are numerous control structures in existence that will serve a dual purpose—that of a metering station as well as that of a regulating device. Examples of such structures include spillways, with or without gates; outlet works for dams using gates or valves; and canal regulating structures using gates. With the accumulation of information from hydraulic model studies made by the Bureau of Reclamation (USBR), United States Department of the Interior, it is now possible to prepare reasonably accurate rating curves for many such structures without the construction of models and without access to the prototypes. The method is especially useful for the rating of existing structures. This paper describes the method as it applies to the rating of drum gates and the paper is concluded with an engineering example. The method is also applicable to the rating of the Volet gate used in France, the bascule gate manufactured in the United States, and others in which the sector of a circle is hinged at or near the crest of a spillway.

NOTE.—Published, essentially as printed here, in February, 1953, as *Proceedings-Separate No. 169.* Positions and titles given are those in effect when the paper or discussion was received for publication.

[1] Hydr. Engr., Bureau of Reclamation, U. S. Dept. of the Interior, Denver, Colo.

INTRODUCTION

The drum gate is a type of gate that floats in a chamber and is buoyed into position by regulating the water level in that chamber. A medium-sized gate of this type is shown in Fig. 1. To use drum gates as metering devices, it is essential that each gate be equipped with an accurate position indicator. This indicator may consist of an arm or pointer connected directly to one of the gate pins, and is usually located inside an adjacent pier. The scale, which commonly indicates "position of high point of gate," may be a cast-metal arc mounted on the wall under the pointer, or a scale painted on the wall.

This paper presents a method of computing rating curves for all positions of the gate with an accuracy comparable to that which can be obtained from an average current-meter traverse of the river. The information required for rating a drum gate consists of the over-all dimensions of the gate and overflow crest, the information contained in this paper, and the coefficient of discharge for any appreciable head on the spillway with the gate in the completely lowered position. Should the coefficient data be lacking, the coefficient of discharge for the designed head can be estimated for nearly any overflow section by a method previously published.[2]

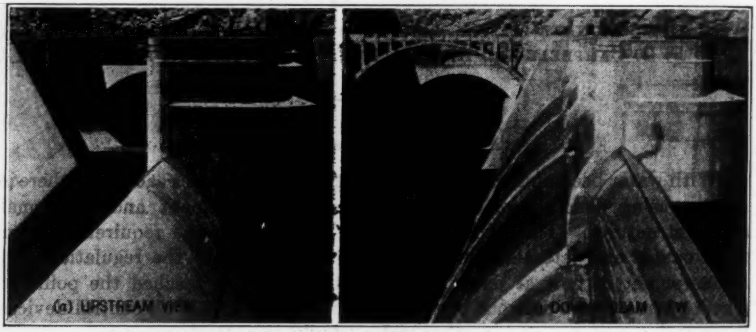

FIG. 1.—DRUM GATE, 100 FT BY 16 FT, AT HOOVER DAM (ARIZONA-NEVADA)

The method of rating described here is not intended to replace the measurements taken at river gaging stations. However, it has the following advantages: (1) The gates can be set in a few minutes to pass a desired discharge and (2) in time of flood, the gaging station may be out of order but the gate calibration is as accurate as usual. The flood that passed over Grand Coulee Dam (Washington) in 1948 is an example. The river gage, in the pier of a bridge downstream, was in error because of a drawdown in the water surface, adjacent to the pier, at the higher flows. Current-meter measurements were also attempted during the flood, but the swiftness of the current and other difficulties rendered these only partially successful. As a result, the discharge at the peak of the flood, which was finally estimated as 638,000 sec-ft, is questionable. Measurement of the flow over the drum gates, which is now possible, would have afforded a continuous record and one that would be as accurate for floods as for normal flows.

---

[2] "Discharge Coefficients for Irregular Overfall Spillway Sections," by J. N. Bradley, *Engineering Monograph No 9*, Bureau of Reclamation, U. S. Dept. of the Interior, Denver, Colo., March, 1952.

CHARACTERISTICS OF THE DRUM GATE

As a measuring device, the drum gate resembles a sharp-crested weir with a curved upstream face over the greater part of its travel. With an adequate positioning indicator, the drum gate can serve as a very satisfactory metering device.

When the drum gate simulates a sharp-crested weir—that is, when a line drawn tangent to the downstream lip of the gate makes a positive angle with the horizontal, as in Fig. 2(*a*), four principal factors are involved. These factors are H, the total head above the high point of the gate; θ, the angle made by a line drawn tangent to the downstream lip of the gate and the horizontal; r, the radius of the gate or an equivalent radius, should the curvature of the gate involve a parabola; and C_q, the coefficient of discharge in $Q = C_q\, L\, H^{3/2}$, in which Q is the discharge in second-feet, and L is the length of the gate.

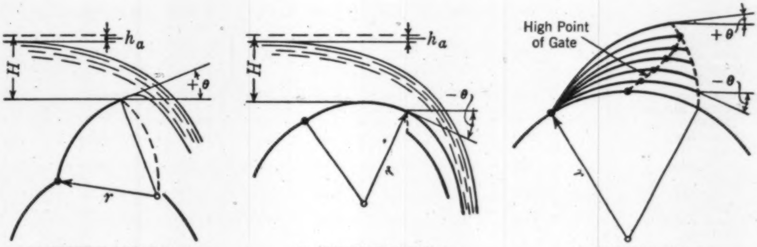

(*a*) POSITIVE ANGLE, θ (*b*) NEGATIVE ANGLE, θ (*c*) CONTROL POINT

FIG. 2.—DRUM-GATE POSITIONS

The depth of approach was not included as a variable because drum-gate installations studied were for medium and high dams at which approach effects were negligible. When the approach depth, measured below the high point of the gate, is equal to or greater than twice the head on the gate, it has been shown[3] that a further increase in approach depth produces very little increase in the coefficient of discharge. Most drum-gate installations satisfy this condition, especially when the gate is in a raised position. Therefore, with adequate approach depth the four variables H, θ, r, and C_q completely define the flow over this type of gate for positive angles of θ, Fig. 2(*a*).

For negative values of θ, Fig. 2(*b*), the downstream lip of the gate no longer controls the flow. Rather, the control point shifts upstream to the vicinity of the high point of the gate for each setting as illustrated in Fig. 2(*c*), and flow conditions gradually approach those of the free crest (as the gate is lowered). Although other factors enter the problem, the similitude also holds for this case down to an angle of approximately −15°.

---

[3] "Studies of Crests for Overfall Dams," *Bulletin No. 3*, Pt. VI, Boulder Canyon Final Reports, Bureau of Reclamation, U. S. Dept. of the Interior, Denver, Colo., 1948.

SOURCES OF INFORMATION

The data for this drum-gate study were obtained from hydraulic models of various sizes and scales. The experiments were performed over a period of about eighteen years. The spillway drum gates tested, the principal dimensions of each, the model scale, the laboratory where the tests were conducted, and other information are given in Table 1. Gates for the first three dams listed in the table—Grand Coulee Dam (Washington), Bhakra Dam (India), and Shasta Dam (California)—are identical except for the length and number. The models of each were tested at different times by different personnel. The results of the tests are nearly identical, which fact indicates the consistency possible in this type of test. Although identical gates are of value in indicating the consistency of results, test results on dissimilar gates are desirable because they can give assurance that all factors involved in the establishment of similitude have been considered. The study includes only eleven gates (Table 1), but the dimensions of these vary over a fairly wide range, and the consistency indicated in compiling the results was quite satisfactory.

TABLE 1.—PRINCIPAL DIMENSIONS OF DRUM GATES TESTED

Dam	No. of gates	Length of gate, in ft	Height of gate, in ft	Radius of gate, in ft	Approach depth, in ft	Maximum head on crest,[a] in ft	Model scale	Hydraulic laboratory
Grand Coulee (Washington)	11	135	28	66.25	360	31.65	1:30	Fort Collins (Colo.)
Bhakra (India)	2	135	28	66.25	410	28	1:80	Customhouse (Denver, Colo.)
Shasta (California)	3	110	28	66.25	460	28	1:68	Customhouse
Hamilton (Texas)	1	300	28	74.17	50	32	1:30	Fort Collins
Hoover, Shape 4-M3[b] (Ariz.-Nev.)	4	100	16	26.8	50	26.6	1:20	Montrose, Colo.
Hoover, Shape 8-M5[b] (Ariz.-Nev.)	4	100	16	36.0	50	26.6	1:20	Montrose
Hoover, Shape 7-C4[b] (Ariz.-Nev.)	4	100	16	26.0	50	26.6	1:60	Fort Collins
Friant (California)	3	100	18	47.0	140	19.0	1:25	Fort Collins
Norris (Tennessee)	3	100	14	34.0	200	27.0	1:72	Fort Collins
Madden (Canal Zone)	4	100	18	30.0	120	30.0	1:72	Fort Collins
Capilano (British Columbia)	1	70	23	71.0	200	23.0	1:60	Denver Federal Center

[a] Gate down. [b] Refers to the shape of the spillway cross section.

Cross sections of representative examples of the spillway overflow sections and drum gates listed in Table 1 are shown in Fig. 3. For Hoover Dam, Shape 4-M3 is shown. The data relating the coefficient, C_q, to the head for the model drum gates tested are tabulated in Table 2.

RESULTS OF BAZIN ON STRAIGHT INCLINED WEIRS

The straight inclined weir is comparable to a drum gate, having infinite radius, thus the results of Bazin serve as an introduction to this study.

Bazin, in his classical experiments, studied inclined sharp-crested weirs.[4] The angle of the weir was varied in increments from 14° to 90° with the horizontal, and each weir was 3.7 ft high (vertical dimension). The head on the crest of the weirs ranged from 0.32 ft to 1.48 ft. The results, presented in Fig. 4, show θ plotted against the Bazin coefficient, C_b (in the formula, $Q = C_b\, L\, h \sqrt{2\, g\, h}$), in which h does not include the velocity head of approach (h_a). The angle θ is also plotted with respect to C_q (in the expression, $Q = C_q\, L\, H^{\frac{3}{2}}$) in which H is the total head. This latter expression will be used throughout the paper.

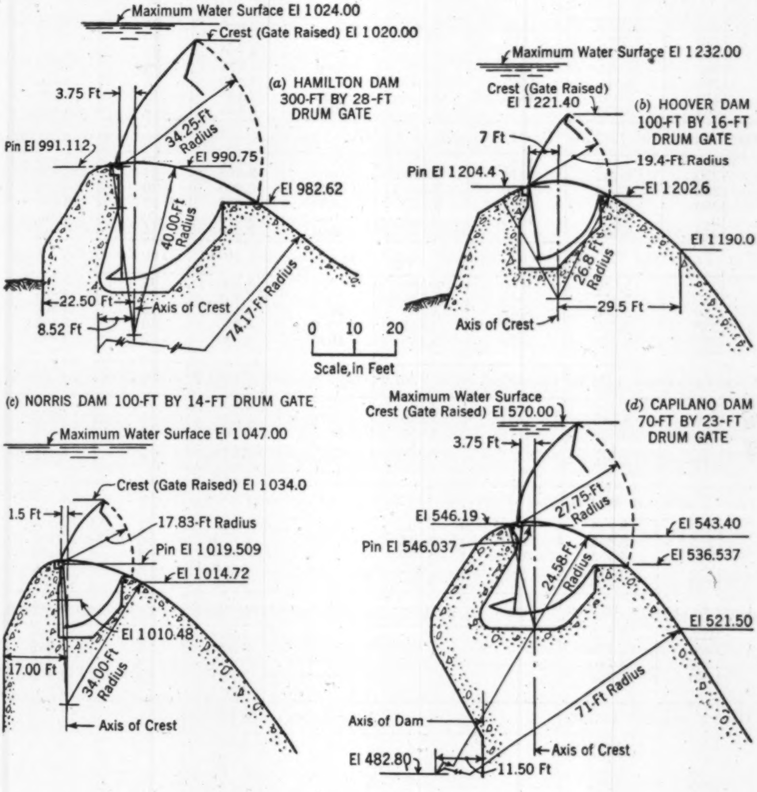
Maximum Water Surface El 1 024.00
Crest (Gate Raised) El 1 020.00
(a) HAMILTON DAM
300-FT BY 28-FT
DRUM GATE
3.75 Ft
34.25-Ft Radius
Pin El 991.112
El 990.75
El 982.62
40.00-Ft Radius
74.17-Ft Radius
22.50 Ft
Axis of Crest
8.52 Ft
0 10 20
Scale, in Feet
Maximum Water Surface El 1 232.00
Crest (Gate Raised)
El 1 221.40
(b) HOOVER DAM
100-FT BY 16-FT
DRUM GATE
7 Ft
19.4-Ft Radius
Pin El 1 204.4
El 1 202.6
El 1 190.0
26.8 Ft Radius
29.5 Ft
Axis of Crest
(c) NORRIS DAM 100-FT BY 14-FT DRUM GATE
Maximum Water Surface El 1 047.00
Crest (Gate Raised) El 1 034.0
1.5 Ft
17.83-Ft Radius
Pin El 1 019.509
El 1 014.72
El 1 010.48
17.00 Ft
34.00-Ft Radius
Axis of Crest
Maximum Water Surface
Crest (Gate Raised) El 570.00
(d) CAPILANO DAM
70-FT BY 23-FT
DRUM GATE
3.75 Ft
27.75-Ft Radius
El 546.19
El 543.40
Pin El 546.037
24.58-Ft Radius
El 536.537
El 521.50
71-Ft Radius
Axis of Dam
Axis of Crest
El 482.80
11.50 Ft

FIG. 3.—EXAMPLES OF DRUM-GATE CROSS SECTIONS

By reference to Fig. 4 it can be observed (1) that the coefficient, C_q, varies only slightly with the observed head on the weir, (2) that there is a rather

---

[4] "Recent Experiments on the Flow of Water over Weirs," by H. Bazin, *Annales des Ponts et Chaussées*, October, 1888. (Translation by Arthur Marichal and John C. Trautwine, Jr., *Proceedings*, Engineers' Club of Philadelphia, Pa., Vol. IX, No. 4, 1892, p. 316.)

TABLE 2.—DRUM-GATE COEFFICIENTS[a]

GRAND COULEE DAM (Washington)		BHAKRA DAM (India)		SHASTA DAM (California)		HAMILTON DAM (Texas)	
Reservoir elevation, in feet	Coefficient, C_q	Reservoir elevation, in feet	Coefficient, C_q	Reservoir elevation, in feet	Coefficient, C_q	Total head on gate, in feet	Coefficient, C_q
GATE ELEVATION[b] 1260.0		GATE ELEVATION[b] 1552.0		GATE ELEVATION[b] 1037.0		GATE ELEVATION[b] 992.0	
1295	3.920	1580	3.680	1075	3.895	35	3.710
1290	3.842	1575	3.645	1070	3.835	30	3.645
1285	3.745	1570	3.550	1065	3.760	25	3.580
1280	3.635	1565	3.420	1060	3.675	20	3.500
1275	3.510	1560	3.275	1055	3.575	15	3.400
1270	3.352	1555	3.120	1050	3.465	10	3.290
1265	3.220			1045	3.335	5	3.160
GATE ELEVATION 1263.51		GATE ELEVATION 1557.0		GATE ELEVATION 1039.0		GATE ELEVATION 995.52	
1295	3.530	1580	3.430	1075	3.637	30	3.400
1290	3.442	1575	3.380	1070	3.565	25	3.310
1285	3.360	1570	3.295	1065	3.490	20	3.223
1280	3.280	1565	3.170	1060	3.417	15	3.150
1275	3.220	1560	3.040	1055	3.340	10	3.085
1270	3.182			1050	3.250	5	3.040
GATE ELEVATION 1267.02		GATE ELEVATION 1562.0		GATE ELEVATION 1041.0		GATE ELEVATION 999.0	
1295	3.530	1580	3.550	1075	3.550	25	3.450
1290	3.457	1576	3.355	1070	3.494	20	3.390
1285	3.380	1572	3.290	1065	3.432	15	3.300
1280	3.300	1568	3.345	1060	3.365	10	3.195
1275	3.213	1564	3.465	1055	3.290	5	3.080
1270	3.120						
GATE ELEVATION 1270.48		GATE ELEVATION 1567.0		GATE ELEVATION 1045.0		GATE ELEVATION 1006.0	
1295	3.600	1580	3.665	1075	3.637	18	3.640
1290	3.530	1577	3.650	1070	3.565	15	3.635
1285	3.462	1573	3.600	1065	3.490	12	3.605
1280	3.410	1570	3.535	1060	3.415	9	3.560
1275	3.375			1055	3.330	6	3.505
				1050	3.220		
GATE ELEVATION 1274.01		GATE ELEVATION 1572.0		GATE ELEVATION 1050.0		GATE ELEVATION 1013.0	
1300	3.725	1580	3.780	1075	3.717	12	3.718
1295	3.695	1579	3.755	1070	3.670	10	3.690
1290	3.662	1578	3.690	1065	3.615	8	3.645
1285	3.630	1577	3.500	1060	3.560	6	3.595
1280	3.600	1576	3.150	1055	3.495	4	3.530
GATE ELEVATION 1277.50				GATE ELEVATION 1055.0		GATE ELEVATION 1020.0	
1295	3.750			1075	3.854	6	3.630
1290	3.738			1070	3.827	5	3.610
1285	3.740			1065	3.800	4	3.540
1280	3.765			1060	3.780	3.5	3.400
				1055	3.763		
GATE ELEVATION 1281.02				GATE ELEVATION 1060.0			
1295	3.730			1075	3.645		
1292	3.708			1072	3.683		
1288	3.705			1069	3.740		
1285	3.725			1066	3.815		
				1063	3.920		
GATE ELEVATION 1284.50				GATE ELEVATION 1065.0			
1300	3.840			1076	3.810		
1296	3.830			1074	3.865		
1292	3.875			1072	3.910		
1288	3.950			1070	3.950		
GATE ELEVATION 1288.0							
1296	3.750						
1294	3.720						
1292	3.670						
1290	3.580						

[a] Coordinates of curves prepared by plotting original data. [b] Gate down.

TABLE 2.[a]—(*Continued*)

FRIANT DAM (California)		NORRIS DAM (Tennessee)		MADDEN DAM (Canal Zone)		CAPILANO DAM (British Columbia)	
Reservoir elevation, in feet	Coefficient, C_q	Reservoir elevation, in feet	Coefficient, C_q	Total head on gate, in feet	Coefficient, C_q	Reservoir elevation, in feet	Coefficient, C_q
GATE ELEVATION[b] 560.0		GATE ELEVATION[b] 1020.0		GATE ELEVATION[b] 232.0		GATE ELEVATION[b] 547.0	
580	3.650	1055	3.915	35	3.900	580	3.775
577	3.625	1050	3.845	30	3.770	575	3.705
574	3.550	1045	3.765	25	3.660	570	3.625
571	3.460	1040	3.670	20	3.560	565	3.530
568	3.340	1035	3.550	15	3.460	560	3.415
565	3.175	1030	3.390	10	3.365	555	3.250
562	2.965	1025	3.125	5	3.280		
GATE ELEVATION 561.5		GATE ELEVATION 1022.0		GATE ELEVATION 236.0		GATE ELEVATION 555.4	
580	3.340	1055	3.785	30	3.810	580	3.615
577	3.300	1050	3.725	25	3.750	577	3.580
574	3.250	1045	3.655	20	3.675	574	3.540
571	3.200	1040	3.570	15	3.590	571	3.485
568	3.125	1035	3.460	10	3.500	568	3.420
564	2.950	1030	3.300	5	3.410	565	3.320
		1025	3.000				
GATE ELEVATION 563.0		GATE ELEVATION 1024.0		GATE ELEVATION 240.0		GATE ELEVATION 561.1	
580	3.320	1055	3.760	30	3.960	583	3.560
577	3.280	1050	3.720	25	3.890	580	3.530
574	3.240	1045	3.670	20	3.835	577	3.490
571	3.175	1040	3.605	15	3.800	574	3.435
568	3.080	1035	3.520	10	3.775	571	3.355
565	2.960	1030	3.380	5	3.740	568	3.130
		1025	3.000				
GATE ELEVATION 566.0		GATE ELEVATION 1026.0		GATE ELEVATION 245.0		GATE ELEVATION 568.5	
580	3.450	1055	3.835	25	3.900	583	3.785
577	3.410	1050	3.810	20	3.900	580	3.850
574	3.340	1045	3.780	15	3.890	577	3.890
571	3.240	1040	3.740	10	3.910	574	3.925
568	3.085	1035	3.685	5	3.935		
		1030	3.580				
GATE ELEVATION 569.0		GATE ELEVATION 1028.0		GATE ELEVATION 250.0			
580	3.625	1055	3.890	20	3.750		
578	3.605	1050	3.880	15	3.780		
576	3.575	1045	3.865	10	3.860		
574	3.550	1040	3.845	5	3.980		
572	3.500	1035	3.815				
570	3.400	1030	3.745				
GATE ELEVATION 572.0		GATE ELEVATION 1030.0					
580	3.725	1055	3.890				
578	3.720	1050	3.890				
576	3.680	1045	3.885				
574	3.620	1040	3.880				
		1035	3.875				
GATE ELEVATION 573.0		GATE ELEVATION 1032.0					
580	3.760	1055	3.870				
578	3.760	1050	3.875				
576	3.765	1045	3.880				
575	3.780	1040	3.895				
574	3.900	1035	3.920				
GATE ELEVATION 575.0		GATE ELEVATION 1034.0					
580	3.780	1055	3.815				
578	3.790	1050	3.835				
577	3.840	1045	3.855				
576	3.950	1040	3.885				
		1036	3.945				

[a] Coordinates of curves prepared by plotting original data. [b] Gate down.

TABLE 2.[a]—(*Continued*)

HOOVER DAM (Arizona-Nevada) SHAPE 4-M3		HOOVER DAM (Arizona-Nevada) SHAPE 8-M5		HOOVER DAM (Arizona-Nevada) SHAPE 7-C4	
Total head on gate, in feet	Coefficient, C_q	Total head on gate, in feet	Coefficient, C_q	Total head on gate, in feet	Coefficient, C_q
GATE ELEVATION[b] 1205.4		GATE ELEVATION[b] 1205.4		GATE ELEVATION[b] 1205.4	
26	3.670	28	3.735	26	3.665
22	3.605	25	3.705	22	3.615
18	3.540	20	3.650	18	3.540
14	3.472	15	3.565	14	3.450
10	3.405	10	3.460	10	3.360
6	3.338	5	3.335	6	3.200
GATE ELEVATION 1209.4		GATE ELEVATION 1209.4		GATE ELEVATION 1209.0	
20	3.675	24	3.590	23	3.725
17	3.645	20	3.540	19	3.650
14	3.615	16	3.492	15	3.580
11	3.585	12	3.428	11	3.508
8	3.555	8	3.330	7	3.415
GATE ELEVATION 1213.4		GATE ELEVATION 1213.4		GATE ELEVATION 1213.0	
20	3.880	20	3.765	19	3.800
17	3.875	16	3.765	16	3.845
14	3.875	12	3.725	13	3.825
11	3.870	8	3.668	10	3.750
8	3.870	4	3.600	7	3.640
GATE ELEVATION 1217.4		GATE ELEVATION 1217.4		GATE ELEVATION 1217.0	
14	3.960	15	3.900	15	3.960
12	3.980	12	3.890	13	3.930
10	4.010	9	3.900	11	3.935
8	4.075	6	3.930	9	3.970
				7	4.020
GATE ELEVATION 1221.4		GATE ELEVATION 1221.4		GATE ELEVATION 1221.4	
10	3.890	11	3.830	14	3.815
8	3.930	9	3.840	12	3.820
6	4.020	7	3.875	10	3.823
5	4.100	5	3.935	8	3.825

[a] Coordinates of curves prepared by plotting original data. [b] Gate down.

sharp reversal in the curve when the angle θ approaches 28°, and (3) that the coefficient of discharge is a maximum at this angle. As the angle θ is increased from 28° to 90°, contraction of the jet gradually reduces the coefficient to approximately 3.33, which occurs when the weir is vertical. As θ is decreased from 28° to 0° the coefficient is gradually reduced—either by approach conditions, friction, or both—to that for a broad-crested weir, which may be some value between 2.8 and 3.1. As the principal difference between the drum gate and the straight inclined weir lies in the curvature of the gate, the trends for the two should be similar.

An inconsistency exists in Fig. 4—namely, the coefficient of discharge for a vertical sharp-crested weir should approximate 3.33, but Fig. 4 shows that Bazin obtained 3.45. This conclusion is supported by the fact that the USBR, Ernest W. Schoder, M.ASCE, and Kenneth B. Turner,[5] and others have not

---

[5] "Precise Weir Measurements," by Ernest W. Schoder and Kenneth B. Turner, *Transactions*, ASCE, Vol. 93, 1929, p. 999.

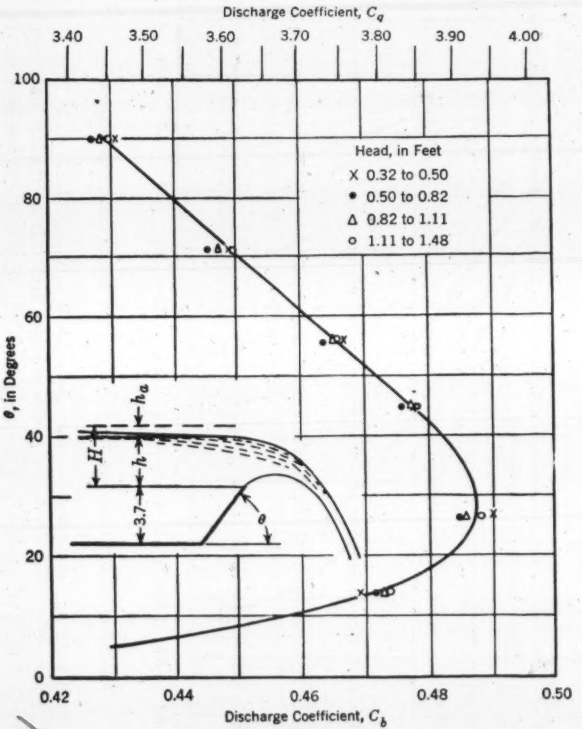

FIG. 4.—RESULTS OF BAZIN'S EXPERIMENTS ON SLOPING WEIRS

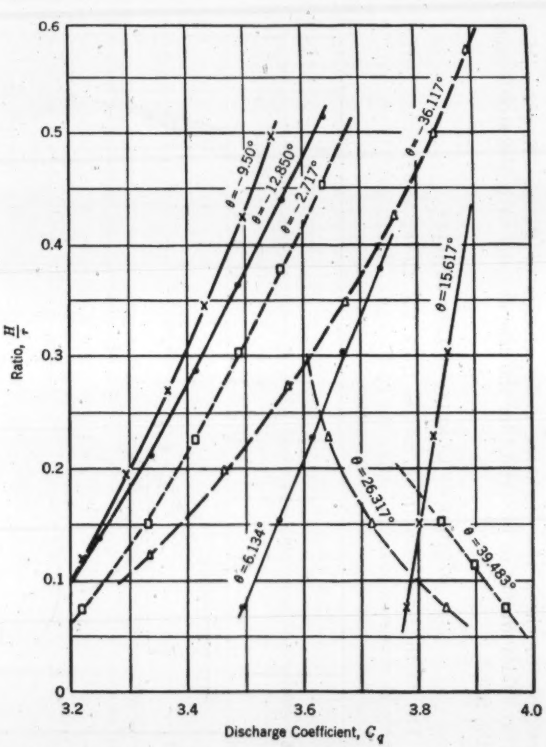

FIG. 5.—DIMENSIONLESS PLOTTING OF DATA FROM MODEL OF SHASTA DAM DRUM GATE

been able to check the discharge measurements of Bazin. However, the actual values are not so important for the case at hand as is the significance of the trend.

METHOD OF COMBINING TEST RESULTS

The method for combining results from the eleven drum gates tested (Table 2) consisted of first plotting the coefficient of discharge data separately for each gate as illustrated by the sheet for the Shasta Dam gate (Fig. 5). With the coefficient of discharge as the abscissa and H/r as the ordinate, each curve in Fig. 5 represents a different gate angle θ, which the tangent to the downstream lip of the gate makes with the horizontal. In all cases, H is the

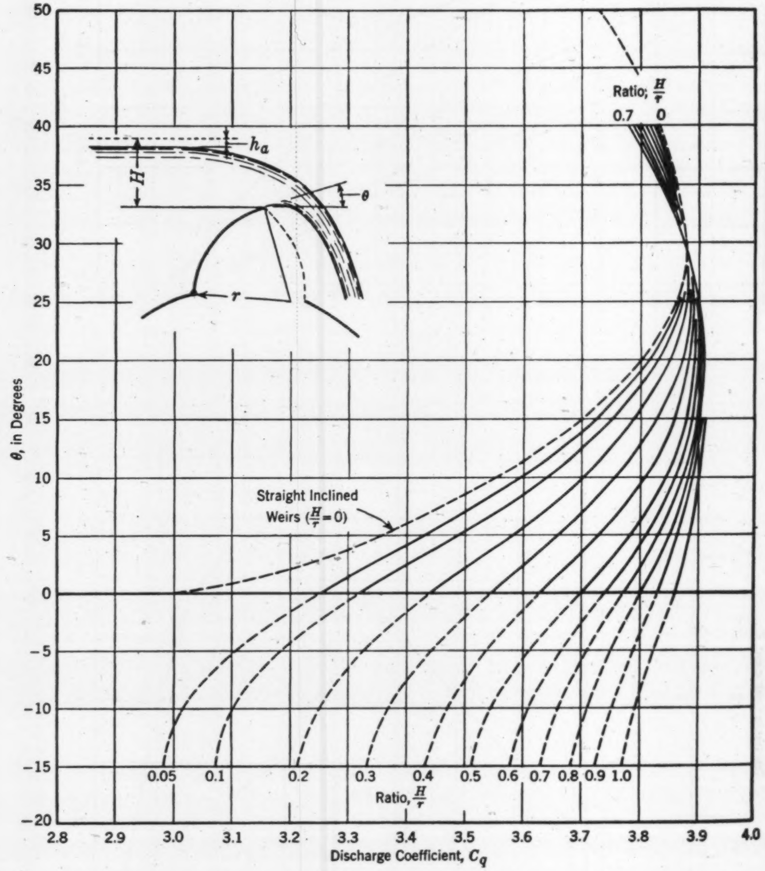

FIG. 6.—GENERAL CURVES FOR THE DETERMINATION OF DISCHARGE COEFFICIENTS

total head, including the velocity head of approach, measured above the high point of the gate, and r is the radius of the gate. In Fig. 5, C_q is based on the relationship, $Q = C_q L H^{3/2}$. For positive values of θ, the head was measured above the lip of the gate, whereas for negative angles it was observed above the high point, or crest, of the gate proper. The method of measuring the head is illustrated in Fig. 2.

Upon completion of a similar set of curves for each gate tested, the eleven sets of curves were replotted and combined into the chart exhibited as Fig. 6. The results from the various gates showed good general agreement; and the curves in Fig. 6 constitute the general experimental information needed for determining the discharge coefficients for gates in raised or partly raised positions. The supporting points are not shown in Fig. 6, but the individual information for each gate is listed in Table 2.

ANALYSIS OF TEST RESULTS

The curves in Fig. 6 show a tendency toward reversal, similar to that exhibited by the Bazin curve in Fig. 4, but the points of inflection vary from $\theta = 20°$ to $\theta = 30°$, depending on the value of H/r. Fig. 4 showed the coefficients to vary only slightly with the head, but in this case the coefficients definitely vary with the head.

A matter of significance is the reversal of the (H/r)-order which occurs at 29° (Fig. 6). The coefficient of discharge has but one value, 3.88, when θ approximates 29°; thus, it is insensitive to both the radius and the head on the gate for this angle. The curve for $H/r = 0$ approximates a drum gate of infinite radius and was obtained from the data of Bazin (Fig. 4) by applying a uniform adjustment.

As stated previously, similitude is valid for small negative angles of θ, as well as for positive angles up to 90°; thus, the curves in Fig. 6 are shown and recommended for use down to $\theta = -15°$. As the gate is lowered beyond this angle, the curves double back and converge, finally terminating in the free flow coefficient.

The discharge coefficients in the region between $\theta = -15°$ and the gate completely down are determined by graphical interpolation. Interpolation is accomplished by plotting head-discharge curves for several gate angles between $-15°$ and the maximum positive angle. Also the head-discharge curve is plotted for the free crest. This information is then cross-plotted to obtain values in the transition zone. The method will be explained in the example that follows. It will be discovered that negative angles greater than $-15°$ (with the exception of the free crest) are not particularly important from an operator's standpoint, as a change in gate position has little effect on the discharge in this range.

It must be assumed that the coefficient of discharge is known for at least one value of the head on the free crest (gate completely down) for the particular spillway under consideration. With the coefficient known for one or more heads, the complete coefficient curve for the free crest can be plotted by consulting Fig. 7, in which H_e and C_e are the designed head and the coefficient for the designed head, respectively. This chart was reproduced from a previous publication[2] and represents a curve well supported by tests of some fifty overfall spillway crests having wide variation in shape and operating conditions.

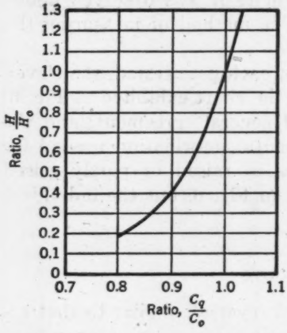

FIG. 7.—COEFFICIENTS OF DISCHARGE FOR OTHER THAN THE DESIGNED HEAD

APPLICATION OF RESULTS

From the plan and section of the Black Canyon Diversion Dam (Idaho), shown in Figs. 8 and 9, assume that it becomes necessary to compute and construct a rating curve for one drum gate for each 0.5 ft of gate elevation. The scale on the gate position indicator is calibrated to show the elevation of the high point of the gate, and the gate has a constant radius of 21.0 ft. The gate is 64 ft long. The coefficient of discharge for the free crest is $C_o = 3.48$ for the designed head (H_o) of 14.5 ft.

With the coefficient of discharge known for free flow at the designed head, the entire free-flow coefficient curve can be established by consulting Fig. 7. The free-flow coefficient curve for Black Canyon Dam spillway (for which $H_o = 14.5$ ft

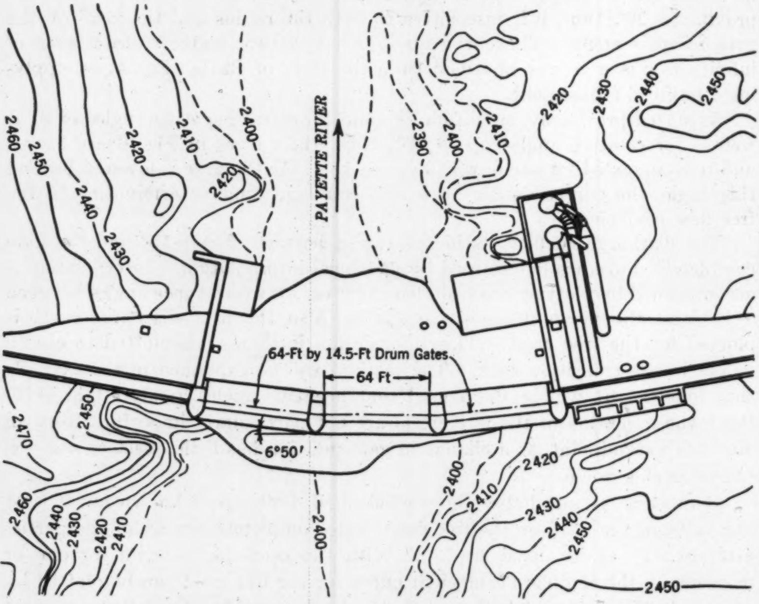
2460
2450
2440
2430
2420
2410
2420
2400
PAYETTE RIVER
2390
2400
2410
2420
2430
2440
2450
64-Ft by 14.5-Ft Drum Gates
64 Ft
6°50′
2450
2470
2460
2440
2430
2420
2410
2400
2400
2410
2420
2430
2440
2450
2450

FIG. 8.—PLAN OF BLACK CANYON DIVERSION DAM IN IDAHO

and $C_e = 3.48$) is constructed by arbitrarily assuming several values of H/H_e and reading the corresponding values of C/C_o from Fig. 7. The method is illustrated in Table 3, and the head-coefficient curve for free flow (gate down), obtained in this manner, is shown in Fig. 10.

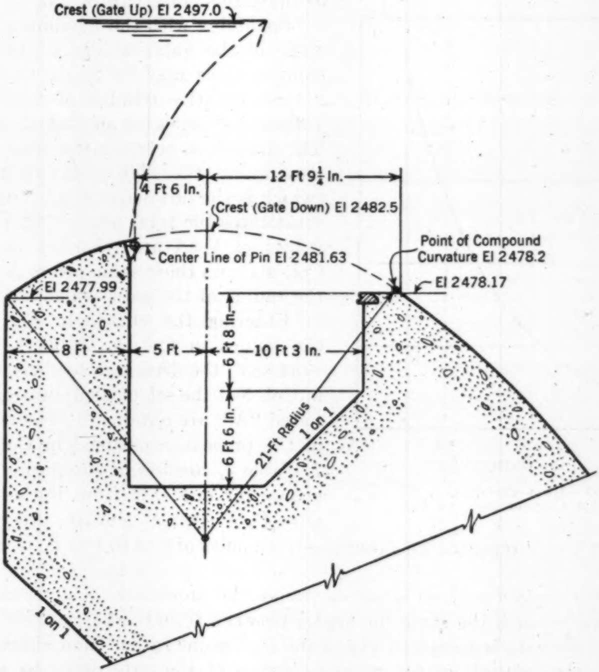
Crest (Gate Up) El 2497.0
4 Ft 6 In.
12 Ft 9¼ In.
Crest (Gate Down) El 2482.5
Center Line of Pin El 2481.63
Point of Compound Curvature El 2478.2
El 2478.17
El 2477.99
8 Ft
5 Ft
10 Ft 3 In.
6 Ft 8 In.
6 Ft 6 In.
21-Ft Radius
1 on 1
1 on 1

FIG. 9.—SPILLWAY CREST DETAIL, BLACK CANYON DAM IN IDAHO

TABLE 3.—HEAD AND DISCHARGE COMPUTATIONS FOR A FREE CREST (BLACK CANYON DAM IN IDAHO)

Total head, H, in ft (1)	Reservoir elevation, in ft (2)	Ratio,[a] H/H_e (3)	Ratio,[b] C_e/C_o (4)	Coefficient, C_e (5)	Q, in cu ft per sec[c] (6)
17	2499.5	1.172	1.020	3.55	15,950
16	2498.5	1.104	1.012	3.52	14,420
14.5	2497.0	1.0	1.0	3.48	12,296
12	2494.5	0.827	0.980	3.41	9,072
10	2492.5	0.690	0.960	3.34	6,759
8	2490.5	0.552	0.940	3.27	4,736
6	2488.5	0.414	0.905	3.135	2,949
4	2486.5	0.276	0.850	2.957	1,514
3	2485.5	0.207	0.815	2.835	943
2	2484.5	0.138	0.760	2.642	478

[a] $H_e = 14.5$ ft. [b] $C_o = 3.48$. [c] The discharge for one gate: $Q = C_e L H^{3/2}$, in which $L = 64.0$ ft.

Before considering the rating of the spillway with gates in raised positions, it is necessary to construct a diagram such as that shown in Fig. 11 to relate gate elevation to the angle θ for the Black Canyon Dam gate. The tabulation in Fig. 11 shows the angle θ for corresponding elevations of the downstream lip of the gate at intervals of 2 ft.

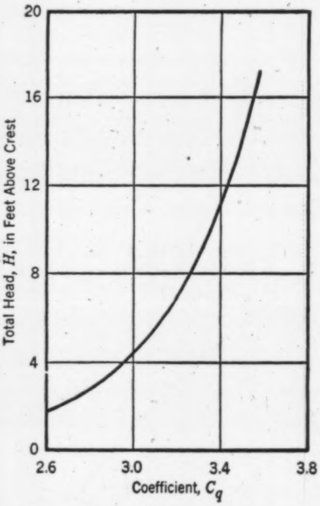

Fig. 10.—Head-Coefficient Curve, Black Canyon Dam, in Idaho

Beginning with the maximum positive angle of the gate, which is 34.883°, the computations may be begun by choosing a representative number of reservoir elevations as indicated in Col. 2, Table 4. The difference between the reservoir elevation and the high point of the gate (which is the downstream lip in this case) constitutes the total head on the gate, and values of head are recorded in Col. 3. Col. 4 shows these same heads divided by the radius of the gate, which is 21.0 ft.

Entering the curves in Fig. 6 with the values in Col. 4, Table 4, for $\theta = +34.883°$, the discharge coefficients, listed in Col. 5 of the set of computations designated "A," are obtained. The remainder of the procedure outlined in Cols. 6 and 7, Table 4, consists of computing the discharge for one gate from the expression, $Q = C_q\, L\, H^{3/2}$. A similar procedure of computation is repeated for other positive angles of θ as in sets B, C, and D of Table 4.

As the angle θ is given negative values, the procedure for determining the discharge remains the same for angles between 0 and −15°, except that the head on the gate is measured above the high point rather than above the lip. Discharge computations for negative angles of the gate down to −15.017° are tabulated in E, F, and G of Table 4.

Plotting values of discharge, reservoir elevation, and gate elevation from Table 4 results in the seven curves in Fig. 12 for which the points are denoted by circles. The extreme lower curve, on which the points are identified by x-marks, represents the discharge of the free crest with the gate completely down. The latter values were obtained from Table 3.

The discharge values shown in Fig. 12 are for one gate only. When more than one gate is in operation, the discharges from the separate gates may be totaled providing the gates are each raised the same amount. The experimental models contained from one to four gates (with the exception of that of Grand Coulee Dam, which contained eleven) so a reasonable allowance for pier effect on the discharge is already present in the results.

The intervals between the eight curves identified by points (Fig. 12) are too great for rating purposes, especially the gap between gate elevations, 2485.75 ft and 2482.5 ft. This is remedied by cross-plotting the eight curves for various constant values of the discharge as shown in Fig. 13. Fortunately, the result is a straight-line variation for any constant value of discharge. The lines in Fig. 13 are not quite parallel and there is no assurance that they will be straight for every drum gate. Nevertheless, this will not detract appreciably from the accuracy obtained. Interpolated information from Fig. 13 is then utilized to construct the additional curves in Fig. 12. If all curves are considered, Fig. 12 shows the completed rating for the Black Canyon Dam spillway for 0.5-ft gate intervals. For intermediate values, straight-line interpolation is permissible.

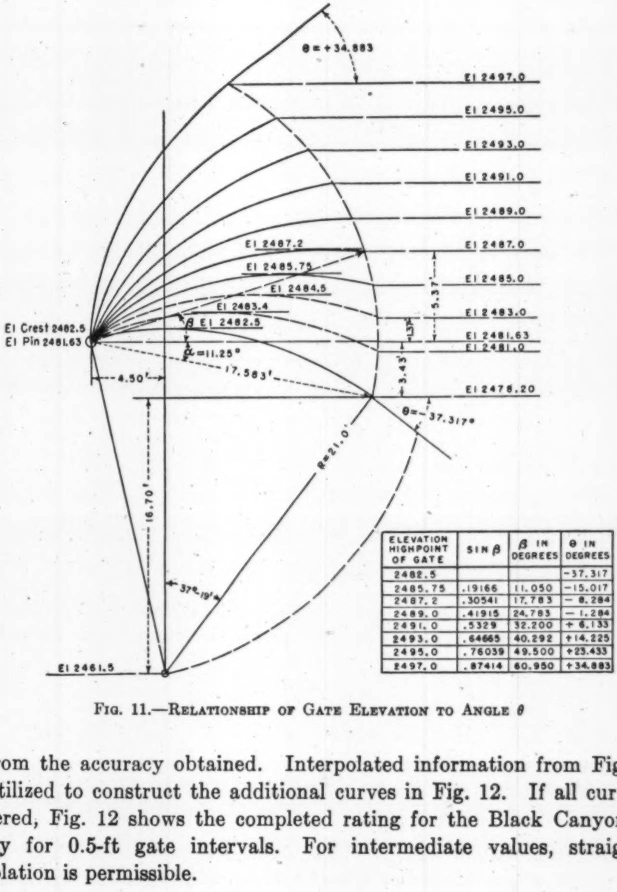
θ = +34.883
El 2497.0
El 2495.0
El 2493.0
El 2491.0
El 2489.0
El 2487.2
El 2487.0
El 2485.75
El 2485.0
El 2484.5
El 2483.4
El 2483.0
β El 2482.5
El Crest 2482.5
El Pin 2481.63
El 2481.63
El 2481.0
5.37'
1.37'
α = 11.25°
17.583'
4.50'
3.43'
El 2478.20
θ = -37.317°
R = 21.0'
16.70'
37°-19'
El 2461.5

ELEVATION HIGHPOINT OF GATE	SIN β	β IN DEGREES	θ IN DEGREES
2482.5			-37.317
2485.75	.19166	11.050	-15.017
2487.2	.30541	17.783	− 8.284
2489.0	.41915	24.783	− 1.284
2491.0	.5329	32.200	+ 6.133
2493.0	.64665	40.292	+14.225
2495.0	.76039	49.500	+23.433
2497.0	.87414	60.950	+34.883

FIG. 11.—RELATIONSHIP OF GATE ELEVATION TO ANGLE θ

CONCLUSIONS

This paper has demonstrated how an existing control structure, such as the Black Canyon Dam spillway, can also serve as a rating station. The accuracy of rating curves obtained by the method is estimated to approach that of an average current-meter traverse of the river providing that (1) the gate position indicators are made as large as possible and are accurately calibrated, (2) the reservoir gage can be read to within 0.05 ft, (3) nearly atmospheric pressure exists under the sheet of water after it springs from the gate, and (4) all gates are set at approximately the same elevation.

TABLE 4.—HEAD AND DISCHARGE COMPUTATIONS FOR DRUM GATES IN RAISED POSITIONS

Set (1)	Reservoir elevation, in ft (2)	H, in ft[a] (3)	Ratio, $\frac{H}{r}$ (4)	Coefficients, C_q (5)	$H^{3/2}$, in ft (6)	Q, in cu ft per sec[b] (7)
GATE ELEVATION 2497.0; $\theta = +34.88°$						
A	2498.0	1	0.048	3.86	1	247
	2499.0	2	0.095	3.86	2.828	699
	2500.0	3	0.143	3.86	5.196	1.283
GATE ELEVATION 2495.0; $\theta = +23.43°$						
B	2496.0	1	0.048	3.85	1	246
	2497.0	2	0.095	3.86	2.828	698
	2498.0	3	0.143	3.87	5.196	1,284
	2499.0	4	0.190	3.87	8.00	1,979
	2500.0	5	0.238	3.88	11.18	2,770
GATE ELEVATION 2493.0; $\theta = +14.22°$						
C	2494.0	1	0.048	3.69	1	236
	2495.0	2	0.095	3.73	2.828	675
	2496.0	3	0.143	3.75	5.196	1,247
	2498.0	5	0.238	3.80	11.18	2,719
	2500.0	7	0.333	3.84	18.52	4,552
GATE ELEVATION 2491.0; $\theta = +6.13°$						
D	2492.0	1	0.048	3.47	1	222
	2493.0	2	0.095	3.51	2.828	635
	2494.0	3	0.143	3.57	5.196	1,187
	2496.0	5	0.235	3.63	11.18	2,597
	2498.0	7	0.333	3.70	18.52	4,386
	2500.0	9	0.429	3.77	27.00	6,515
GATE ELEVATION 2489.0; $\theta = -1.28°$						
E	2490.0	1	0.048	3.21	1	205
	2491.0	2	0.095	3.28	2.828	594
	2492.0	3	0.143	3.34	5.196	1,111
	2494.0	5	0.238	3.45	11.18	2,469
	2496.0	7	0.333	3.545	18.52	4,202
	2498.0	9	0.429	3.63	27.00	6,273
	2500.0	11	0.524	3.695	36.48	8,627
GATE ELEVATION 2487.2; $\theta = -8.28°$						
F	2488.0	0.8	0.038	3.02	0.716	138
	2489.0	1.8	0.086	3.10	2.415	479
	2490.0	2.8	0.133	3.17	4.685	950
	2492.0	4.8	0.229	3.31	10.52	2,229
	2494.0	6.8	0.324	3.43	17.73	3,892
	2496.0	8.8	0.419	3.51	26.10	5,863
	2498.0	10.8	0.515	3.58	35.49	8,131
	2500.0	12.8	0.610	3.635	45.79	10,653
GATE ELEVATION 2485.75; $\theta = -15.02°$						
G	2487.0	1.25	0.060	3.00	1.398	268
	2488.0	2.25	0.107	3.07	3.375	663
	2489.0	3.25	0.155	3.15	5.859	1,181
	2491.0	5.25	0.250	3.275	12.03	2,522
	2493.0	7.25	0.345	3.375	19.52	4,216
	2495.0	9.25	0.440	3.465	28.13	6,238
	2497.0	11.25	0.536	3.54	37.73	8,548
	2499.0	13.25	0.631	3.595	48.23	11,097

[a] H is the total head on the gate. [b] The discharge for one gate: $Q = C_q L H^{3/2}$.

In connection with provision (3), the blunt piers on the Black Canyon Dam spillway, Figs. 8 and 9, provide effective aeration under the overfalling sheet of water for all but very small heads with gate completely raised. In the case of provision (4), uniform operation of the gates is also most desirable from the standpoint of stilling basin operation for minimum erosion downstream.

Discharge measurements on the prototype are desirable whenever possible as a check on the accuracy of the foregoing method. Sufficient observations should be taken, however, to establish the fact that the prototype information is consistent and reliable.

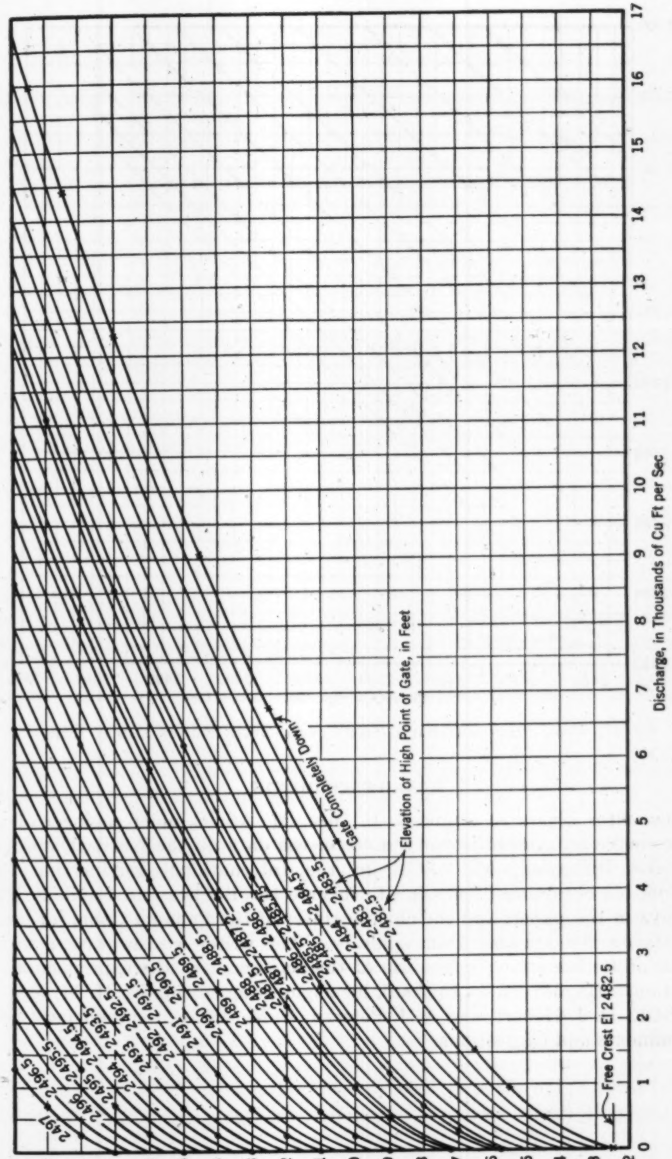

FIG. 12.—RATING CURVES FOR BLACK CANYON DAM DRUM-GATE SPILLWAY IN IDAHO

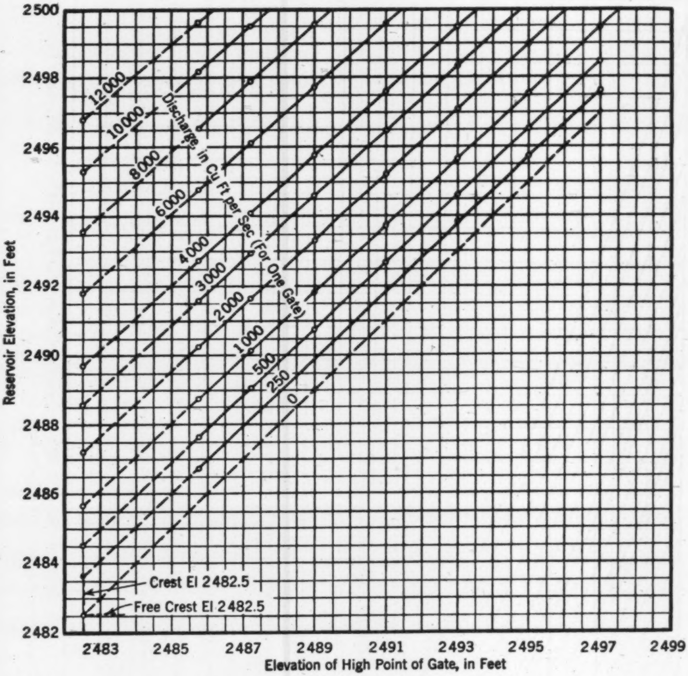

FIG. 13.—CROSS-PLOTTED INITIAL RATING CURVES, BLACK CANYON DAM IN IDAHO

ACKNOWLEDGMENTS

The writer wishes to thank C. E. Blee, M. ASCE, chief engineer of the Tennessee Valley Authority for the use of the data on the Norris Dam Spillway; Hal Birkeland, M. ASCE, of the International Engineering Corporation, for obtaining permission to include the Bhakra and Capilano Dam spillways in the paper; and the chief engineer of the Panama Canal for use of the data on the Madden Dam spillway. The writer is also grateful to the Bureau of Reclamation for the use of the remainder of the experimental information. He also wishes to thank his engineering associates, H. M. Martin, M. ASCE, D. J. Hebert, and A. J. Peterka, A. M. ASCE, for their most helpful comments and suggestions.

DISCUSSION

Guido Wyss[6].—The information presented by Mr. Bradley is of utmost value for determining the quantities of discharge over drum gates under various heads for any gate position. This information will permit operators in the field to adjust the gate position from corresponding chart values in such a manner as to obtain the desired flow. The use of drum gates as an actual metering device for spillway quantity discharges is unique and the results obtained are more practicable and reliable than those obtained by stream gaging, especially when this gaging is conducted during periods of high floods.

It would have been interesting if the author had presented an investigation of the flow, profiles of the upper and lower nappe surfaces, as well as the actual water pressures on the upstream plate of the drum gate by use of charts. This would afford an opportunity to obtain the true loading conditions on the gate during the cycle of operation from fully-raised gate to fully-lowered gate. This information would be important in the determination of the buoyancy and loading criteria of the gate structure.

Sam Shulits,[7] M. ASCE.—An outstanding contribution to the design and operation of drum gates has been presented in this report of the author's work at the USBR. The paper and its complement[2] fill a great need.

Since 1928, when the Freeman Scholarships were established, there has been a tremendous development of hydraulic model research in the laboratories of the United States. Although these laboratories are unexcelled in size and quality, many hydraulic engineers have pondered the procession of models (spillways, stilling pools, and river reaches) in the period from 1928 to 1953 with few, if any, summaries or proposals for design to reduce the dependence on models. In Mr. Bradley's work there is strong evidence that the laboratories will produce correlations and syntheses—not more models.

When it is realized that many of the most famous and productive laboratories in the United States did not exist prior to 1928, the lack of correlation and synthesis for general use is understandable. The hope is that other works of similar quality will be added to engineering literature.

Bob Buehler,[8] A. M. ASCE.—An interesting and clever use of data has resulted in a method by which records of gate settings at dams can be made a substitute for missing stream-flow records and can be used to augment existing records. The construction of a dam and reservoir often floods an established stream gage. Unless the gage is replaced below the dam or upstream from the reservoir, subsequent stream flow usually is not accurately known. Sometimes a series of dams (each causing the water to back up to the dam above) prevents continuing established gages at the strategic points where they had been located. The less accurate—and more costly—slope stations are not completely satisfactory alternatives to the single-line rating stations.

---

[6] Mech. Engr., Bureau of Reclamation, U. S. Dept. of the Interior, Denver, Colo.

[7] Associate Prof., Director, Hydr. Lab., Civ. Eng. Dept., Pennsylvania State College, State College, Pa.

[8] Hydr. Engr., TVA, Knoxville, Tenn.

If the spillway of a dam can be rated with an accuracy comparable to the accuracy obtainable with a gage (as demonstrated by Mr. Bradley for certain spillway types), and if allowance is made for flow through other water outlets such as turbines, locks, and sluices, the structure is then superior in some respects to the gage. For example, the rating of the dam should be permanent, whereas the rating of a gage usually requires frequent checking.

Mr. Bradley's method for rating drum gates not only allows records for ordinary stream flow to be supplemented, but also probably gives a more accurate determination of extreme flood rates than do most gages. He has made an important contribution to the planning and design of drum-gated structures.

The author has presented a method for rating a spillway at all heads provided the coefficient for one appreciable head is known. He also states that a coefficient for the designed head can be estimated for most spillways by a method previously published.[2] The writer, on the other hand, offers a method by which an ogee spillway can be rated, provided its profile shape is known. The method is based on an equation derived by R. N. Brudenell, A. M. ASCE, incidental to studies made on radial gates.[9] Mr. Brudenell's equation is

$$Q = \frac{3.97\,L\,H^{1.62}}{H^{0.12}{}_{D}} \qquad \text{(1)}$$

in which Q is the spillway discharge, in cubic feet per second; L denotes the length of the spillway, in feet; H is the total head on the spillway crest, in feet;

TABLE 5.—FREE DISCHARGES FOR BLACK CANYON DAM IN IDAHO

Total head, in feet (1)	Discharge, in cubic feet per second[a] (2)	USING EQ. 1		USING FIG. 14	
		Discharge, in cubic feet per second (3)	Difference, in percent (4)	Discharge, in cubic feet per second (5)	Difference, in percent (6)
17	15,950	15,847	−0.65	15,910	−0.25
16	14,420	1,4363	−0.39	14,421	−0.01
14.5[b]	12,296	12,247[c]	−0.40	12,296	0
12	9,072	9,013	−0.65	9,049	−0.25
10	6,759	6,708	−0.75	6,735	−0.36
8	4,736	4,673	−1.33	4,692	−0.93
6	2,949	2,932	−0.58	2,944	−0.20
4	1,514	1,521	+0.46	1,527	+0.86
3	943	954	+1.17	958	+1.59
2	478	494	+3.35	496	+3.76

[a] From Col. 6, Table 3. [b] Head at which $C_q = 3.48$. [c] C_q would be 3.466 for this discharge.

and H_D represents the design head in feet. The design head is that head which produces a standard lower nappe that agrees closely with the spillway profile.

---

[9] "Flow over Rounded Crests," by R. N. Brudenell, *Engineering News-Record*, July 18, 1935, p. 95.

Eq. 1 was intended to be used with heads greater than $H_D/4$, although the equation has been found to agree closely with model data for somewhat lower heads. Without knowing any coefficients, Eq. 1 gives discharges that agree closely with those obtained by Mr. Bradley for Black Canyon Dam. In the case of Black Canyon Dam, Mr. Bradley used one known coefficient and the curve of Fig. 7. Free-flow discharges computed by the two methods are shown in Cols. 2 and 3, Table 5. The procedure by which Eq. 1 was applied will be described subsequently.

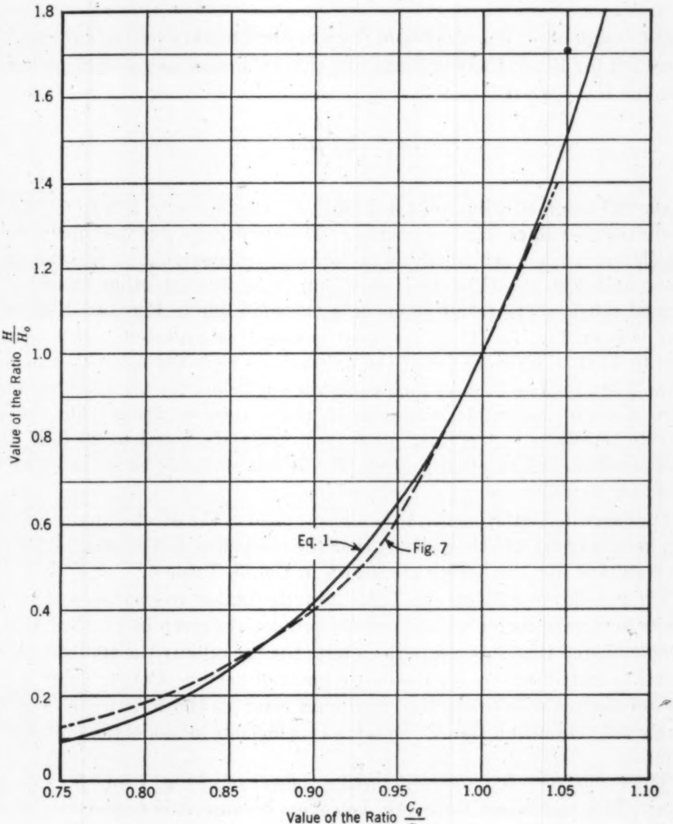

FIG. 14.—COMPARISON OF VALUES OBTAINED FROM FIG. 7 AND EQ. 1

It is assumed that in choosing Black Canyon Dam for his example, the author knew that his method would yield discharges close to known values. The good agreement for all except the low heads shows that, in this example, Eq. 1 (using only the shape of the spillway) also produces suitable results.

This good agreement suggests, too, that there must be a close relationship between the curve in Fig. 7 and a similar curve that can be derived from Eq. 1. To examine the relationship, theoretical discharge coefficients were computed by using

$$Q = C_q \, L \, H^{3/2} \qquad (2)$$

and Eq. 1, from which

$$C_q = \frac{3.97 \; H^{1.62}}{H^{0.12}{}_D \; H^{3/2}} \qquad (3)$$

The design head, H_D, was found (by a method to be described subsequently) to be 45 ft for Black Canyon Dam, and this value was used in making the test. Thus, for $H_D = 45$ ft,

$$C_q = \frac{2.5143 \; H^{1.62}}{H^{3/2}} \qquad (4)$$

For several assumed values of total head, H, varying from 2 ft to 58.5 ft, corresponding C_q-values were computed. The resulting C_q of 3.97 for a head of 45 ft (H_o) was taken arbitrarily as the known coefficient, C_o. Then the (H/H_o)-ratios and the (C_q/C_o)-ratios were computed for all other heads in the assumed range. The resulting curve is the solid line in Fig. 14. The dashed curve is from Fig. 7. The agreement is close—as expected. Still using H_D equal to 45 ft, the remainder of the process was repeated using the coefficient for the 25-ft head as C_o, and then using the coefficient for the 12-ft head as C_o. There was no discernible difference in the curves resulting from the three separate selections. A similar procedure, using H_D equal to 20 ft in Eq. 1, also showed no differences from Fig. 14. It can probably be proved that there should be no difference.

The curve derived from Eq. 1 then was applied to the Black Canyon Dam spillway, assuming (as did the author) that the coefficient is 3.48 at a 14.5-ft head. The resultant free discharges are shown in Col. 5, Table 5.

The free-flow coefficients in Table 2 invite further comparisons with Eq. 1 for the four projects for which spillway profiles are given in Fig. 3. It should be remembered that this comparison tests the use of only the spillway shape as a guide to free discharge for the entire range of heads. Col. 4, Table 6, shows that for appreciable heads the maximum error in the four cases is approximately 2% (Hamilton Dam). Observed coefficients in model tests often scatter as much.

The same coefficients permit testing the curve in Fig. 7 for all eleven spillways. This test is not as severe, however, because it is necessary to assume one known coefficient at which head agreement becomes perfect. At near-by higher and lower heads, large divergences would not be expected. Col. 6, Table 6, shows that for appreciable heads the maximum error is slightly greater than 2% (Hoover Dam, shape 8-M5). The base coefficient selected to obtain C_q from the (C_q/C_o)-ratios is designated by a footnote for each project. These arbitrary selections were made for medium high heads.

The solid-line curve in Fig. 14 also was tested in this manner. The same coefficient at each project was assumed to be known as when the curve in Fig. 7 was tested. Col. 8, Table 6, shows that for appreciable heads the maximum error is slightly more than 2% (Madden Dam).

These comparisons show that the direct application of Eq. 1, Fig. 7 (or Fig. 14) (derived from Eq. 1), all give highly accurate free-flow spillway dis-

TABLE 6.—COMPARISON OF FREE-FLOW SPILLWAY COEFFICIENTS

Total head, in feet	Coefficient obtained from model test	USING EQ. 1		USING FIG. 7		USING FIG. 14	
		C_q	Difference, in percent	C_q	Difference, in percent	C_q	Difference, in percent
(1)	(2)	(3)	(4)	(5)	(6)	(7)	(8)
			GRAND COULEE DAM (WASHINGTON)				
35	3.920			3.914	− 0.15	3.902	−0.46
30	3.842			3.831	− 0.29	3.827	−0.39
25	3.745			3.745[a]	0	3.745[a]	0
20	3.635			3.655	+ 0.55	3.651	+0.44
15	3.510			3.550	+ 1.14	3.524	+0.40
10	3.352			3.370	+ 0.54	3.356	+0.12
5	3.220			3.138	− 2.54	3.168	−1.62
			BHAKRA DAM (INDIA)				
28	3.680			3.736	+ 1.52	3.732	+1.41
23	3.645			3.645[a]	0	3.645[a]	0
18	3.550			3.547	− 0.08	3.543	−0.20
13	3.420			3.434	+ 0.41	3.404	−0.47
8	3.275			3.215	− 1.83	3.208	−2.04
3	3.120			2.748	−11.92	2.854	−8.53
			SHASTA DAM (CALIFORNIA)				
38	3.895			3.910	+ 0.39	3.899	+0.10
33	3.835			3.839	+ 0.10	3.831	−0.10
28	3.760			3.760[a]	0	3.760[a]	0
23	3.675			3.677	+ 0.05	3.674	−0.03
18	3.575			3.591	+ 0.45	3.568	−0.20
13	3.465			3.455	− 0.29	3.429	−1.04
8	3.335			3.215	− 3.60	3.230	−3.15
			HAMILTON DAM (TEXAS) H_D = 52 FT				
35	3.710	3.785	+2.02	3.741	+ 0.84	3.730	+0.54
30	3.645	3.716	+1.95	3.662	+ 0.47	3.659	+0.38
25	3.580	3.635	+1.54	3.580[a]	0	3.580[a]	0
20	3.500	3.539	+1.11	3.494	− 0.17	3.490	−0.29
15	3.400	3.420	+0.59	3.394	− 0.18	3.369	−0.91
10	3.290	3.258	−0.97	3.222	− 2.07	3.208	−2.50
5	3.160	2.997	−5.16	3.000	− 5.06	3.029	−4.14
			FRIANT DAM (CALIFORNIA)				
20	3.650			3.717	+ 1.84	3.706	+1.53
17	3.625			3.639	+ 0.39	3.632	+0.19
14	3.550			3.550[a]	0	3.550[a]	0
11	3.460			3.458	− 0.06	3.452	−0.23
8	3.340			3.348	+ 0.24	3.319	−0.63
5	3.175			3.142	− 1.04	3.131	−1.38
2	2.965			2.723	− 8.15	2.812	−5.16

[a] Coefficient assumed to be known.

TABLE 6.—(*Continued*)

Total head, in feet	Coefficient obtained from model test	Using Eq. 1		Using Fig. 7		Using Fig. 14	
		C_q	Difference, in percent	C_q	Difference, in percent	C_q	Difference, in percent
(1)	(2)	(3)	(4)	(5)	(6)	(7)	(8)
Norris Dam (Tennessee) H_D = 35 Ft							
35	3.915	3.969	+1.38	3.934	+ 0.49	3.923	+0.20
30	3.845	3.897	+1.35	3.852	+ 0.18	3.848	+0.08
25	3.765	3.812	+1.25	3.765^a	0	3.765^a	0
20	3.670	3.711	+1.12	3.675	+ 0.14	3.671	+0.03
15	3.550	3.586	+1.01	3.569	+ 0.53	3.543	−0.20
10	3.390	3.416	+0.77	3.388	− 0.06	3.373	−0.50
5	3.125	3.143	+0.58	3.155	+ 0.96	3.185	+1.92
Madden Dam (Canal Zone)							
35	3.900			3.825	− 1.92	3.814	−2.20
30	3.770			3.744	− 0.69	3.740	−0.80
25	3.660			3.660^a	0	3.660^a	0
20	3.560			3.572	+ 0.34	3.568	+0.22
15	3.460			3.470	+ 0.29	3.444	−0.46
10	3.365			3.294	− 2.11	3.279	−2.55
5	3.280			3.067	− 6.49	3.096	−5.61
Capilano Dam (British Columbia) H_D = 48 Ft							
33	3.775	3.797	+0.58	3.783	+ 0.21	3.775	0
28	3.705	3.720	+0.40	3.705^a	0	3.705^a	0
23	3.625	3.634	+0.25	3.623	− 0.05	3.620	−0.14
18	3.530	3.529	−0.03	3.538	+ 0.23	3.516	−0.40
13	3.415	3.394	−0.62	3.405	− 0.29	3.379	−1.05
8	3.250	3.201	−1.51	3.168	− 2.52	3.183	−2.06
Hoover Dam (Arizona-Nevada) Shape 4-M3, H_D = 50 Ft							
26	3.670	3.670	0	3.681	+ 0.30	3.677	+0.19
22	3.605	3.597	−0.22	3.605^a	0	3.605^a	0
18	3.540	3.512	−0.79	3.526	− 0.40	3.522	−0.51
14	3.472	3.408	−1.84	3.439	− 0.95	3.414	−1.67
10	3.405	3.273	−3.88	3.306	− 2.91	3.280	−3.67
6	3.338	3.077	−7.82	3.064	− 8.21	3.082	−7.67
Hoover Dam Shape 8-M5							
28	3.735			3.814	+ 2.12	3.800	+1.74
25	3.705			3.752	+ 1.27	3.749	+1.19
20	3.650			3.650^a	0	3.650^a	0
15	3.565			3.537	− 0.78	3.530	−0.98
10	3.460			3.387	− 2.11	3.358	−2.94
5	3.335			3.059	− 8.28	3.088	−7.41
Hoover Dam Shape 7-C4							
26	3.665			3.691	+ 0.71	3.687	+0.60
22	3.615			3.615^a	0	3.615^a	0
18	3.540			3.535	− 0.14	3.532	−0.23
14	3.450			3.449	− 0.03	3.423	−0.78
10	3.360			3.315	− 1.34	3.290	−2.08
6	3.200			3.073	− 3.97	3.091	−3.41

charges for ogee dams at all but low heads. Eq. 1, applied directly to the spillway shape, has the advantage that no coefficients need be known or estimated in advance.

The comparisons in Table 6 show a tendency toward errors of some importance at low heads when Eq. 1 or its companion curve in Fig. 14 is used, as well as when Fig. 7 is used. In most cases the errors are negative. These errors are of little concern in planning the safety of a structure against extreme floods, or in considering most other operations such as emptying the reservoir. The errors nonetheless affect the analytical rating of drum gates in the lowered or slightly raised positions. The free-flow coefficients help to determine the direction of the general curves at the large negative angles shown in Fig. 6. Free discharges form the base curve of the rating curves in Fig. 12 and help define the curvature of the low ends of the cross-plot curves in Fig. 13. Low to ordinary heads, corresponding to normal stream flow, can exist for a large part of the time at dams whose reservoir capacities are small. Further study of data for low heads might lead to valuable refinements.

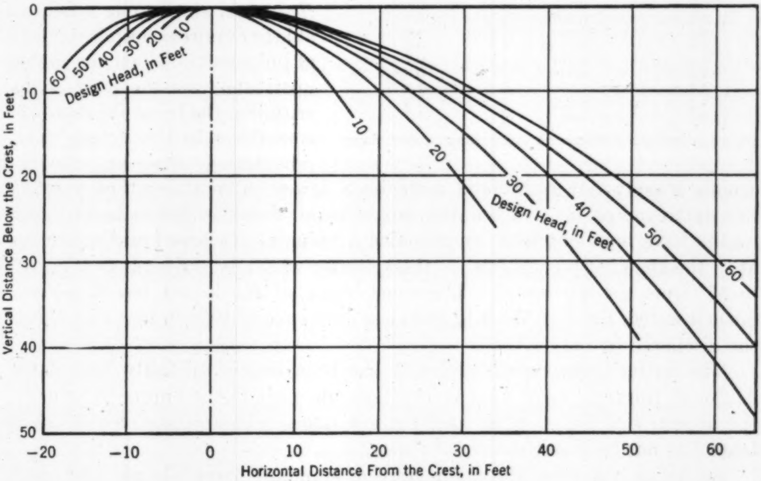

FIG. 15.—STANDARD SPILLWAY SHAPES

Application of Eq. 1.—Since the factor H_D in Eq. 1 represents the head at which a standard lower nappe shape is a reasonable approximation of the spillway shape (as designed or built), it is only necessary to find this head to apply the formula. Spillway coordinates for a standard crest having a vertical upstream face have been used to find this head.[10] These coordinates are shown in Table 7. The last column in Table 7 refers the horizontal (x) coordinates to the spillway crest because this form is the simplest to apply. In Table 7, y is the distance below the crest elevation.

Using these dimensionless coordinates, standard spillway shapes were plotted (Fig. 15) for values of H_D from 10 ft to 60 ft. In Fig. 15 negative horizontal distances indicate the distance upstream from the crest. The spillway shape as designed or built is then drawn on transparent paper. This paper is laid over Fig. 15, and the value of H_D which gives the best fit is selected. In deciding the best fit it may be found that the profile upstream from the crest indicates one value and the downstream profile indicates a different value. The higher of the two indicated values of H_D should be used. For example, the shape of Black Canyon Dam spillway upstream from the crest indicated a value of approximately 45 ft for H_D. The downstream shape indicated a value of approximately 25 ft. The larger value was used.

---

[10] "Hydroelectric Handbook," by William P. Creager and Joel D. Justin, John Wiley & Sons, Inc., New York, N. Y., 2d Ed., 1950, p. 362.

The determination of the H_D-value which gives a reasonable fit requires a certain amount of judgment. When the profile upstream from the crest is the criterion, the lip of the dam will sometimes be the determinant. Sometimes, however, the lip droops sharply downward and indicates a lower value than other parts of the upstream profile. When the downstream shape is the criterion, good results have been obtained by assigning a value of H_D based on the average fit in the zone between points on the spillway where tangents range from 20° to 35° from the horizontal. The exact value of H_D is not too important. Since it enters Eq. 1 in the 0.12 power, a difference of 10% in its value affects the discharge by only 1.15%.

TABLE 7.—COORDINATES OF A STANDARD SPILLWAY CREST

Value of $\frac{x}{H_D}$	Value of $\frac{y}{H_D}$	Value of $\frac{x}{H_D}$ referred to crest
0	0.126	−0.3
0.1	0.036	−0.2
0.2	0.007	−0.1
0.3	0	0
0.4	0.007	0.1
0.6	0.063	0.3
0.8	0.153	0.5
1.0	0.267	0.7
1.2	0.410	0.9
1.4	0.590	1.1
1.7	0.920	1.4
2.0	1.31	1.7

The writer's application of Eq. 1 has been limited to fairly high dams. Although the total head used in Eq. 1 should include the approach velocity, the accuracy of Eq. 1 when used for low dams, where approach velocity is large, has not been tested.

So far as is known, the application of standard nappe shapes (for which discharge coefficients are known) to actual spillways on a basis of reasonable best fit was first suggested by W. M. Borlund.[11] Mr. Borlund used a curve of observed C_q-value plotted against H/H_o. In 1942, C. E. Kindsvater, M. ASCE, suggested a similar procedure in which the curve of C_q versus H/H_o was derived from Eq. 1. Mr. Kindsvater's work (not published) should give results comparable to those obtained herein.

The material presented is regarded as an excellent check on that part of Mr. Bradley's work which relates to free discharge over an ogee spillway.

F. B. CAMPBELL,[12] M. ASCE, AND A. A. McCOOL,[13] J. M. ASCE.—The experimental data on discharge coefficients for flow over drum gates are a welcome addition to the published information on flow over spillways, or the observation and recording of the flow of streams. A paper by Robert E. Horton has been a guide for the estimation of flows over spillways since its publication.[14] The basic information for the discharge over curved crests which fit the under side of a nappe from a sharp-crested weir can be deduced from investigations made by Bazin,[15,16] although the published record of these experiments has not been generally available to engineers in the United States. The investigations conducted by the USBR (proposed by E. W. Lane, M. ASCE) embraced and extended the scope of Bazin's work which is often used as the basis for overflow spillway shapes.[3] Although good estimates for discharge over free-overflow crests can be accomplished rather simply, the problem becomes complicated when flow through partly opened crest gates is involved.

---

[11] "Flow over Rounded Crest Weirs," by W. M. Borlund, thesis presented to the University of Colorado, at Boulder, Colo., in 1938, in partial fulfilment of the requirement for the degree of Master of Science.

[12] Chf. Hydr. Engr., Analysis Branch, Corps of Engrs., U. S. Waterways Experiment Station, Vicksburg, Miss.

[13] Hydr. Engr., U. S. Waterways Experiment Station, Vicksburg, Miss.

The commonly used types of crest gates are vertical lift gates, tainter or radial gates, and drum gates. The coefficient for a partly opened vertical lift gate depends on the location of the plane of the skin plate or lip with respect to the axis of the curved crest. The discharge coefficient for tainter gates is affected by the radius of the skin plate, the elevation of the trunnion with respect to the crest, and the location of the gate seat with respect to the axis as well as the crest curvature. To complicate any investigations further, observers define the gate opening variously as (1) the length of the arc from the gate seat to the gate lip, (2) the vertical distance from the lip to the face, and (3) the distance from the lip to the face measured normal to the face. The last method is believed to give the proper dimension, whereas the foregoing considerations are geometrical. The effective head for a partly opened vertical lift or tainter gate depends on the pressures on the face of the concrete and the pressures within the issuing jet. The author has given a good outline of the geometrical variables and the head-measurement method for analyzing partly raised drum gates.

The drum gate has the very attractive feature of requiring no mechanical hoisting equipment for operation. Many of the dams constructed by the USBR have spillways controlled by drum gates. For example the Arrowrock Dam in Idaho (constructed in 1915) and the Tieton Dam in Washington (constructed in 1925) are both equipped with drum gates. B. F. Thomas and D. A. Watt credit H. M. Crittenden with the design of what is apparently the first drum gate.[17] The gates were installed in Dam No. 1 on the Osage River in Missouri in 1911. However, the refinements of the modern drum gate have been developed principally by the USBR.

The discharge coefficients presented by the author are based on model studies. There should be opportunity to check the coefficients for relatively low heads with partly raised gates in the prototype by current-meter measurements. Only on rare occasions with large floods is it possible to verify the coefficients for high prototype heads over the drum gates in the lowered position. The author's mention of the failure to obtain discharge measurements during the 1948 flood over the Grand Coulee Dam spillway emphasizes the importance of this condition. The writers have studied the basic data for high heads over the drum gate in the lowered position.

---

[14] "Weir Experiments, Coefficients and Formulas," by Robert E. Horton, *Water Supply and Irrigation Paper No. 200*, Coast and Geodetic Survey, U. S. Dept. of Commerce, Washington, D. C., 1907 (revision of Paper No. 150).

[15] "Recent Experiments on the Flow of Water over Weirs," by H. Bazin, *Annales des Ponts et Chaussées*, October, 1888. (Translation by Arthur Marichal and John C. Trautwine, Jr., *Proceedings*, Engineers' Club of Philadelphia, Pa., Vol. VII, No. 5, 1890, p. 259.)

[16] *Ibid.*, Vol. IX, No. 3, 1892, p. 231.

[17] "The Improvement of Rivers," by B. F. Thomas and D. A. Watt, John Wiley & Sons, Inc., New York, N. Y., 2d Ed., 1913.

It becomes evident from a study of Table 2 that the ratio of gate radius to maximum head has a wide range. The writers use the ratio r/H_D, in which H_D is the design head for the spillway. This is the inverse of the ratio used by Mr. Bradley, used so that circular arcs can be traced on dimensionless profiles of x/H_D and y/H_D.

A comparison has been made of the coefficients for various (r/H_D)-values with the gate down. Only the high-overflow sections with negligible velocity of approach were selected from Table 2 for a study of discharge coefficients. Table 8 shows the value of the discharge coefficients for the condition when the drum gate is down. The percentage difference of the coefficient from that of the Madden Dam coefficient is also shown. It is expected that the accuracy of the discharge measurements and thus the coefficient of discharge is less than 1%.

TABLE 8.—COMPARISON OF DISCHARGE COEFFICIENT WITH THE GATE DOWN

Dam	Radius of gate, in feet[a]	Maximum head on crest, in feet[a]	Ratio, $\frac{r}{H_D}$	Coefficient,[b] C_q	Difference, in percent, from Madden Dam
Madden (Canal Zone)	30.0	30.0	1.00	3.77	0.0
Norris (Tennessee)	34.0	27.0	1.26	3.80	0.8
Grand Coulee (Washington)	66.2	31.6	2.09	3.87	2.6
Shasta (California)	66.2	28.0	2.37	3.76	−0.3
Friant (California)	47.0	19.0	2.47	3.64	−3.5
Capilano (British Columbia)	71.0	23.0	3.08	3.62	−4.0

[a] From Table 1. [b] From Table 2.

The dams for which the data are listed in Table 8 are in the approximate chronological order of the time of their design conception.

Because of the increase in the ratio of r/H_D (Table 8), it is of interest to plot the profile for the lower surface of the nappe from a sharp-crested weir with an approach slope of 2 on 3 in terms of x/H_D and y/H_D and to superimpose on it the arcs of circles with radii of r/H_D equal to 1, 2, and 3, as is done in Fig. 16. The center of the radius is located on the axis of the crest. It can be seen that the arc represented by r/H_D equal to 1 is a fair approximation of the true nappe shape. The arcs of r/H_D equal to 2 and 3 indicate a very flat curvature in comparison to the shape of the nappe.

One is tempted to assume, for a crest with a ratio $r/H_D = 3$, that the coefficient would be that for one third the design head of a crest with $4/H_D = 1$.

Model studies for Madden Dam reported by Richard R. Randolph, Jr.,[18] indicate that the coefficient for such a condition is approximately 3.40. Such a coefficient is not in agreement with that for Capilano Dam with r/H_D equal to 3.62 at full head. The lack of agreement does not necessarily vitiate the initial assumption. The difference in the coefficient may be caused by the difference in shape of the two crests upstream from the circular arc. Furthermore, the scale ratio of the Madden Dam model was only 1:78, and a 10-ft prototype head would be 0.128 ft on the model, which is near the lower limit of reliability for conformity of the discharge coefficient.

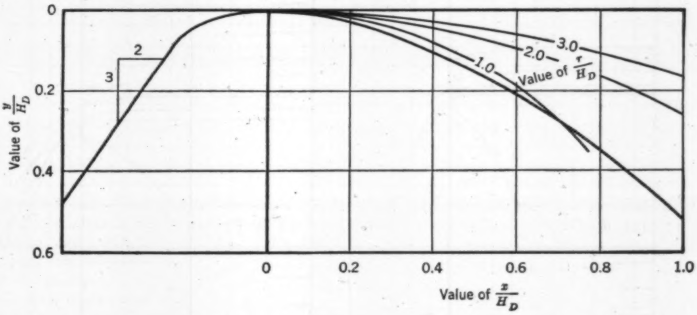

FIG. 16.—LOWER SURFACE OF NAPPE FROM SLOPING WEIR COMPARED WITH CIRCULAR ARCS

JOSEPH N. BRADLEY,[19] A.M. ASCE.—Mr. Shulits' statements regarding the lack of correlation in laboratory studies are well founded, and the writer is in complete agreement with his views.

Mr. Buehler's analysis for the determination of the designed head, H_D, for overflow sections formed by a single radius, or for a shape that conforms closely to a single radius, gives satisfactory results. The comparison of discharge coefficients for free flow over various dams, using Eq. 3 with the method offered in the paper, is gratifying. Mr. Buehler's method certainly has merit because following the determination of H_D, coefficients of discharge can be computed directly for all heads.

Messrs. Campbell and McCool undertook to show that a definite relationship exists between the coefficient of discharge at the designed head and the ratio r/H_D for overflow shapes. This relationship is valid if the overflow shape can be approximated by an arc of a single radius and if the approach conditions are favorable—that is, if the approach depth below the crest is at least twice H_D. This method results in a coefficient of discharge for the designed head only. When overflow sections are encountered where a single radius does not approximate the overflow shape, or when the approach conditions are unusual, an engineering monograph[2] may prove helpful.

---

[18] "Hydraulic Tests on the Spillway of the Madden Dam," by Richard R. Randolph, Jr., *Transactions*, ASCE, Vol. 103, 1938, p. 1091.

[19] Hydr. Engr., Bureau of Reclamation, U. S. Dept. of the Interior, Denver, Colo.

Mr. Wyss suggested that pressures and water surfaces for drum gates at various positions and reservoir levels would be useful to designers in computing gate loadings. A limited amount of information is available, and this will be presented.

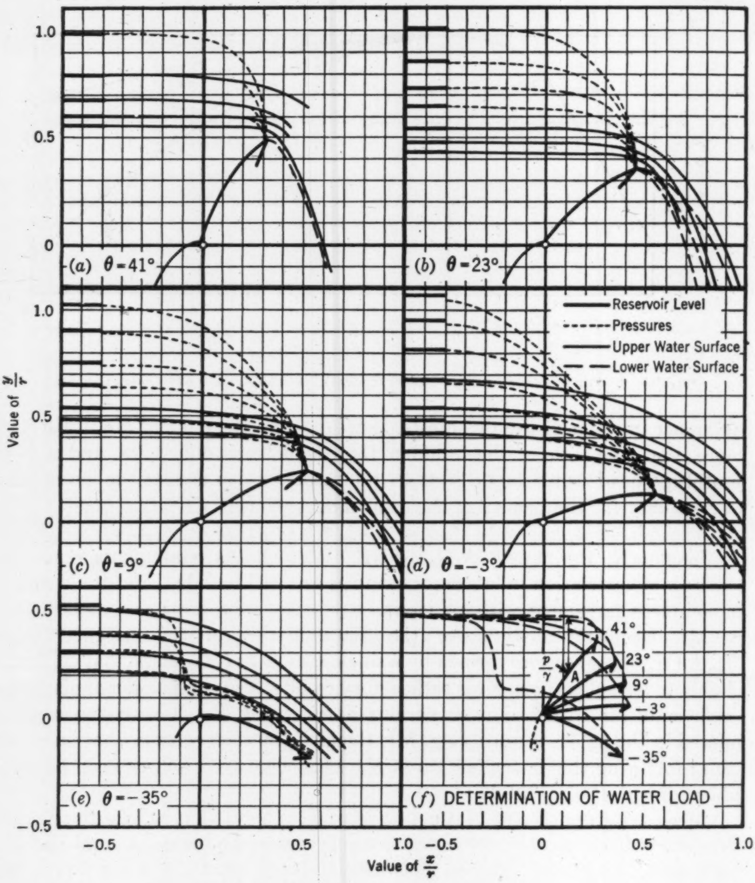

FIG. 17.—PRESSURE AND WATER-SURFACE PROFILES

Because there was good correlation among the discharge coefficients, it was reasoned that the pressures and related flow patterns would also be well correlated through the same variables.

Pressures and water-surface profiles are plotted in dimensionless coordinates (in terms of the radius of the gate) in Fig. 17. Five positions of the gate are shown for various reservoir levels producing flow over the gate. Pressures and water surfaces are shown for some levels whereas only pressures are available for others. The broken lines represent pressure, measured vertically, for the reservoir levels indicated at the left of the charts. Upper water-surface profiles are shown by solid lines, and lower water-surface profiles are identified by dash lines. The charts represent a composite, in graphical form, of information from model tests performed on the Grand Coulee, Hamilton, Norris, Friant, and Hoover dams.

To determine graphically the most adverse water load on a particular gate, it is necessary to investigate the pressures for several gate positions. Assuming that the first position is $\theta = 41°$, the gate is drawn in this position on a piece of transparent paper to the same scale as that used in Fig. 17. The maximum expected reservoir is indicated for this gate position on the left side of the transparent sheet.

The transparent sheet is then placed over Fig. 17 (*a*), disregarding the origin of coordinates, and matching only the downstream tips of the two gates. The downstream part of all drum gates, regardless of size or radius, will coincide for any given value of θ. The height of the gate, or length of arc, can be expected to vary; this will have a negligible effect on pressures or water-surface profiles in the majority of cases. Should the gate under investigation differ from the height shown in Fig. 17 (*a*), a small increase or decrease in the approach-depth results.

Beginning with the chosen reservoir level, the pressure curve is traced from Fig. 17 (*a*) onto the transparent paper. It may be necessary to interpolate between two of the pressure curves. The result will be similar to that shown in Fig. 17 (*f*).

A similar procedure is then followed for gate positions of 23°, 9°, −3°, and −35°, utilizing Figs. 17 (*b*), 17 (*c*), 17 (*d*), and 17 (*e*), respectively. The result is a composite plot similar to that shown in Fig. 17 (*f*). It should be noted that the pressures shown for negative angles of the gate are not as reliable as those for positive angles. Fortunately, the greater water loads occur for positive angles.

Water loads can be determined by scaling the pressures vertically over the gate as indicated by point A in Fig. 17 (*f*). If a gate angle other than those shown is desired, interpolation can be made directly on the sheet corresponding to Fig. 17 (*f*). Following the establishment of the maximum-pressure curve, values of x/r and y/r are scaled from the sheet corresponding to Fig. 17 (*f*) and are transferred to dimensional values by multiplying by r. Should water-surface profiles be desired, the same method of tracing and scaling can be used.

AMERICAN SOCIETY OF CIVIL ENGINEERS
Founded November 5, 1852
TRANSACTIONS

Paper No. 2678

SEWAGE DISPOSAL IN TIDAL ESTUARIES

By Alexander N. Diachishin,[1] J. M. ASCE, Seth G. Hess,[2] M. ASCE, and William T. Ingram,[3] A. M. ASCE

With Discussion by Messrs. Isadore Nusbaum; and Alexander N. Diachishin, Seth G. Hess, and William T. Ingram

Synopsis

The determination of water volumes available for the dilution of sewage in tidal estuaries and the detention time of this sewage is often necessary in the formulation of pollution abatement projects. This paper presents information on the nature of tidal actions with emphasis on those aspects of interest to the sanitary engineer. Techniques used in determining dilution volumes and detention periods are discussed with the purpose of determining how these methods are in accord with accepted concepts of tidal flow.

The type of subsidiary tide induced in tidal estuaries may be either the "progressive wave," "stationary wave," or hydraulic flow type. Salinity, currents, winds, and changes in atmospheric pressure can influence each of these tide types.

The quantity of water available for the dilution of contaminants introduced into tidal waters has been estimated as being equal to the water volume of a tidal prism calculated for an entire water body. However, in many instances, the basic assumptions inherent in an estimation by a tidal prism are not in accord with fact. A modification, which theoretically confines mixing in any tidal cycle to segments of the tidal waters rather than the waters as a whole, is a closer approximation of actual tidal actions. Salinity determinations are a valuable check on the validity of any assumed tidal action, since the salinity of sea water serves as a "tracer."

The influence of the tide on sewage discharged into tidal waters varies widely for individual areas. Hence, it is difficult to estimate dilution volumes and detention periods in a given estuary without an individual study of tidal action in the estuary.

Note.—Published, essentially as printed here, in January, 1953, as *Proceedings-Separate No. 167*. Positions and titles given are those in effect when the paper or discussion was received for publication.

[1] Prin. Engr., Interstate Sanitation Comm., New York, N. Y.

[2] Director and Chf. Engr., Interstate Sanitation Comm., New York, N. Y.

[3] Associate Prof. of Public Health Eng., New York Univ., New York, N. Y.

INTRODUCTION

New York Harbor (New York, N. Y.) has a tidal range, on an average, of only 4.5 ft, as compared to the average range of 39.4 ft at Folly Point in the Bay of Fundy (eastern Canada). Tidal action in New York Harbor has an influence on the distribution and detention of the sewage contributed to the harbor. However, opinions as to the magnitude of this influence have diverged widely. One school of thought has held that tidal action produces a fresh surge of water in each cycle that flushes the harbor of its wastes. The other school is of the opinion that the tidal waters do little more than oscillate back and forth ceaselessly, and merely circulate the contained impurities.

To arrive at a true understanding of tidal actions in bays and estuaries it is desirable to examine the intrinsic nature of tides and tidal currents.

GENERAL TIDE THEORY

Tides, the periodic vertical movements of bodies of water, and the associated tidal currents, or horizontal movements, are caused by the gravitational attraction between the waters of the earth and the sun, moon, and planets. The tidal forces produced by these bodies are directly proportional to the mass of the body and inversely proportional to the cube of the distance. By computing the relative importance of these bodies, it is found that the moon is 2.25 times more effective than the sun in producing tides and greater than 10,000 times more effective than any of the planets. For all practical purposes, only the tidal forces produced by the moon and the sun need to be considered.

If the relative motions of the earth, moon, and sun were such that the moon and sun appeared only on the celestial equator, and these bodies remained the same distance from the earth, the tidal forces could be resolved into two semidiurnal components. The lunar period would be one of 12 hr 25 min, and the solar period 12 hr 0 min. These forces can be resolved into semidiurnal, rather than diurnal, components, since the tide producing force is such that the same force is produced both when the moon or sun is on the meridian and when these bodies are 180° removed from the meridian. The tide producing forces can be assumed to be created by two moons—one, the real moon, and the other, the anti-moon—and by two suns. The magnitude of the semidiurnal forces would vary with the latitude but they would be the sole tide producing forces. Hence, it would be relatively simple to extrapolate local tide records of a few days indefinitely into the future, if the effects of wind and weather could be evaluated.

The moon and sun do not always remain on the celestial equator. In consequence of the inclination of the lunar and solar orbits, the tide producing forces repeat themselves diurnally rather than semidiurnally. This is compensated for by adding to the semidiurnal component, a diurnal component whose magnitude varies with the orbital inclination of the respective bodies. To allow for the varying distances of the moon and sun from the earth, other components must also be introduced. The characteristics of five principal components are as follows: (1) Semidiurnal lunar component, (2) semidiurnal solar component, (3) component for variation in distance of the moon from the earth and (4) and (5) components for a change in the moon's declination. The characteristics of a tide may be evaluated. Although these components are the principal ones, as many as twenty or thirty may be evaluated. Generally a period of 19 yr is taken as constituting a full tidal cycle. Therefore, it may appear possible, although laborious, to estimate a full tidal cycle of 19 yr, given its location. Such is not the case, however. It is true that, by use of a 19-yr tidal record of a gaging station, the general characteristics of the tide at this station can be predicted, but the results of this analysis cannot be applied to other localities. A striking example of this fact may be found at the Panama Canal. At Colon, on the Atlantic side, the tides have an average rise and fall of less than a foot, with but one high water and low water in a day, whereas, on the Pacific side at Balboa, two high waters and two low waters occur each day, and the tide has an average range of more than 12 ft. The present state of knowledge is such that, with the aid of past records, engineers are reasonably able to forecast tides at a given locality, but they are unable to provide universal forecasts for all localities.

Several theories have been proposed to explain the relation of the tides over the entire face of the earth. G. B. Airy,[4] in the nineteenth century, conceived of the oceanic tide as a progressive wave. A progressive wave (Fig. 1) is similar to that produced by vertical agitation of the entire depth of water at one end of a tank. The wave produced will travel from one end of the tank to the other, the outline of the wave resembling a cosine curve. This wave is not to be confused with that produced by a pebble dropped into a pool. The latter is primarily a surface wave whereas the extent of the progressive wave is felt throughout the depth of the water. The rate of advance of the progressive wave is equal to

$$V = \sqrt{gH} \qquad \text{.........................(1)}$$

in which V is the rate of advance, g is the acceleration of gravity, and H is the depth of the water. It is important to differentiate between the movement of the wave itself and of the water particles. Although the wave form moves in accordance with Eq. 1, there is no comparable movement of the water particles. For any given point, a plot of the vertical displacement of the water level (or tide) versus the time will give a cosine curve, as will a plot of the horizontal velocities (or tidal currents) versus the time. The change in direction of the tidal current occurs at the original level of the water, and the maximum tidal current occurs at high-water level or low-water level.

Whewell[4] has presented an elaboration of Airy's progressive wave theory, the "Southern Ocean" theory. Supposedly, a tidal wave originates in the relatively unobstructed ocean expanses of the Southern Hemisphere and progresses northward, its speed being determined by the changing depths of ocean. The types of tides encountered at different locations are explained by the local topographical peculiarities and the difference in the times of arrival of various subsidiary waves.

---

[4] "Evaluation of Present State of Knowledge of Factors Affecting Tidal Hydraulics and Related Phenomena," *Report No. 1*, Committee on Tidal Hydraulics, Corps of Engrs., U. S. Dept. of the Army, Washington, D. C., 1950.

Rollin A. Harris has proposed an opposing theory,[5] that of the stationary wave. A stationary wave (Fig. 1(*b*)) can be produced by elevating one end of a water-filled tank suddenly and then returning it to a level position. The water at the ends of the tank will lower and rise periodically, in opposition to each other while the water in the center of the tank will remain at the original level. The vertical movement of the water level at any part of the tank (the tide), when plotted against time, will form a cosine curve. Since the horizontal movement of the water particles (tidal current) must stop at the same time as the vertical movement, the minimum tidal current occurs at the time of high water and low water, whereas the maximum current occurs between high water and low water. This relation of current to tide is the reverse of the relations in the progressive wave.

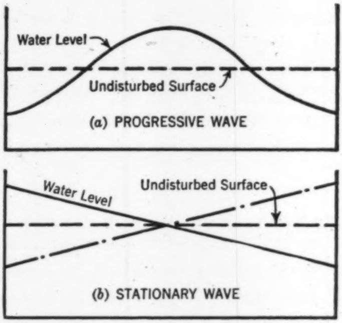

FIG. 1

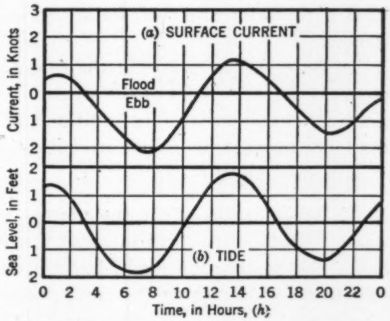

FIG. 2.—OBSERVATIONS, NEW YORK HARBOR, AUGUST, 1922

According to Mr. Harris, oscillatory waves are set up in the various oceans and seas. The position and alinement of these waves is such that their natural period of oscillation is equal to the periodicity of the major semidiurnal tide producing forces.

The sparcity of factual data is the major reason for the lack of a generally accepted explanation of world-wide tidal phenomena. Many tide and current readings are available for coastal locations, but as yet no practical method has been developed to measure the rise and fall of the waters in oceans and open seas.

DERIVED TIDES AND TIDAL CURRENTS

Progressive Wave.—Regardless of their world-wide occurrence, oceanic tides induce subsidiary tides in the adjacent bays, sounds, and estuaries.

The type of tide normally induced is generally agreed to be similar to the progressive wave. Fig. 2 is a plot of the tide and tidal current at the mouth of the Hudson River in New York Harbor. The marked resemblance between the current and tide curves, typical of the progressive wave, may be noted. The maximum flood current occurs at about the time of high tide, and the maximum ebb at time of low tide. The observed speed of the tidal wave as it progresses up the Hudson River checks closely with the theoretical velocity, 30 miles per hr as against 27 miles per hr. As the wave progresses upstream, there is a changing tendency in the relation of tide to tidal current. Farther upstream the relationship is more nearly hydraulic, the flow is controlled mainly by the surface water slope, and the highest velocity occurs when the slope of the water is steepest.

---

[5] "Manual of Tides," by Rollin A. Harris, Coast and Geodetic Survey, U. S. Dept. of Commerce, Washington, D. C., 1897.

Fifty miles above the mouth of the Hudson River at West Point, N. Y., the strength of the current occurs 45 min before high tide and low tide; at Poughkeepsie, N. Y., 75 miles above the mouth, the strength of the current occurs 1.5 hr before local high water and low water; and at Albany, N. Y., 145 miles above the mouth, the strength of the current occurs about 3 hr before local high water and low water, or approximately when the water slope is steepest.

In general, the nature of the tide and tidal currents is determined by the physical characteristics of the stream. Among the factors that will determine the tidal characteristics, in addition to the tide at the mouth of the river, are the following: (1) Shore line irregularities and obstructions, (2) cross-sectional stream area, and (3) depth.

1. Irregularities affect the normal and uniform propagation of the tidal wave. Obstructions will increase the velocity and range of the tide at and below the obstruction itself, but will decrease the tidal range above the obstruction by decreasing the tidal prism. If the waterway is terminated abruptly, as by a dam, the tides and associated currents will be modified considerably by the waves reflected downstream.

2. Since frictional losses tend to decrease the amplitude of the tide, in order to maintain the tidal current, it is necessary that the cross-sectional area decrease. Theoretically, a funnel-shaped stream with constantly decreasing cross section will maintain a constancy of tidal amplitude and current.

3. The average depth determines the speed of tidal propagation and affects the rate at which the tidal amplitude is reduced in its upstream travel due to friction. Theoretically, since the speed of wave travel varies with depth, the difference in depth at high water and low water should cause a shortening of the time of tidal rise and a lengthening of the time of fall. However, this theory has not been borne out too well by observed results.

Stationary Wave.—In some bays and sounds connected with the ocean, a type of tide prevails that cannot be readily explained by a progressive wave. Long Island Sound, connected at its western extremity to New York Harbor by a strait known as the East River, is a good example of this type of tidal action.

At the eastern end of Long Island Sound, opening to the sea, the tidal range is about 2.5 ft, and at its western end, at Willets Point, the tidal range is nearly 7.5 ft. At its midpoint (the place of greatest width) the range is about 6 ft.

This increase in tidal range landward is opposite to that expected from a progressive wave.

A progressive wave would traverse the 92-mile length of the sound, with its average depth of 65 ft, in about 5 hr. Instead, high water occurs at the western end of the sound barely 30 min later than at the eastern end. Furthermore, the current changes occur almost simultaneously throughout the sound, and these changes occur at about the times of high tide and low tide. Clearly, this type of tidal movement is characterized by a stationary, rather than a progressive wave. It is similar to the type of movement that has been described previously, as exemplified by the half of a stationary wave in a tank of water.

The natural period of oscillation (T) of such a wave is equal to

$$T = \frac{4\,L}{\sqrt{g\,H}} \qquad \text{(2)}$$

which, for Long Island Sound, is equal to 11.8 hr. In Eq. 2, L is the length of travel, or "fetch," which is equal to one half the length of the stationary wave in Fig. 1(*b*). This natural period is approximately equal to the periodicity of the semidiurnal tide producing forces. When these periods are about equal for a given body of water, a composite wave is to be expected, one component due to an induced progressive wave derived from the ocean, and the other an oscillatory stationary wave of its own. The tide in the Bay of Fundy (the largest tidal range in the world) has been explained on the basis of a stationary wave.

Hydraulic Flow.—Other than the progressive and stationary wave types, a brief previous mention has been made of a third kind of tidal flow—the hydraulic type that occurs at Albany. This flow is also characteristic of the East River, into which the water flows from the body of water having temporarily the higher level. The velocity of this current of water increases as the difference in level increases, the maximum velocity occurring at the time of the greatest difference in level.

Fig. 3 is a plot of the various heights of water at both ends of the East River.[6] The numbers on the ends of the various connecting lines denote the time as referred to the moon's meridian passage over Fort Hamilton, Brooklyn. At any time the slope line in the East River is given by the lines connecting the heights of the water levels at both ends of the stream. This simple hydraulic flow explains the seemingly complicated tidal phenomena that occur in the East River. From Fig. 3 it is clear that the range in tidal amplitude decreases upstream from the Battery, at the south end of Manhattan Island, for about one fourth of the distance to Willets Point, and then increases the remainder of the way. The times of high water and low water are also seen to vary in a manner that is not readily explicable by other than hydraulic flow.

---

[6] "Tides and Currents in New York Harbor," by H. A. Marmer, *Special Publication No. 111*, Coast and Geodetic Survey, U. S. Dept. of Commerce, Washington, D. C., 1935 (revised edition).

The time of high tide and low tide varies for different stretches of the stream, whereas the time of current change is practically simultaneous for its entire length, occurring when the slope is zero, at about 3 h and 9 h.

An interesting aspect of the tides in the East River is revealed by the shape of the low-water line. The line joining the low-water points at the Battery and Willets Point is not straight, but is curved upward. A practical application of this curve shape would result in a considerable saving in channel dredging since it is not necessary to dredge to a uniform depth below mean sea level.

Salinity Currents.—The flow in the East River is such that there is no great vertical stratification of velocity. The flow is in accordance with hydraulic theory, for open channels, and the changes in current occur for all depths at practically the same time. However, when fresh-water streams are considered, such is not the case; the factor of salinity differences introduces complications.

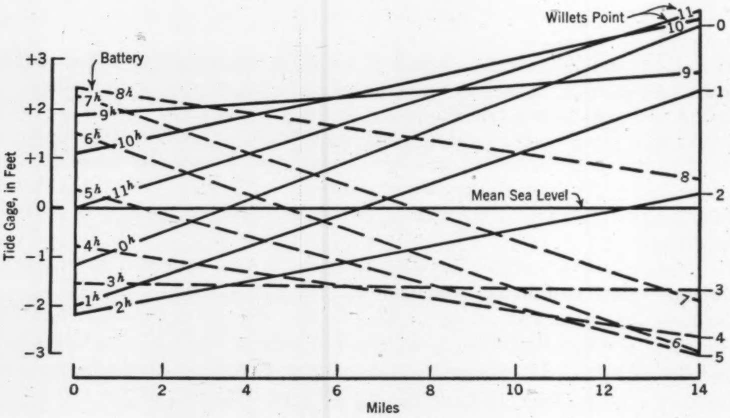

Fig. 3.—Hourly Slope Lines, East River, New York

It is apparent that fresh-water river flow will tend to increase the duration and strength of the flood current, thereby altering the relationship of tide to tidal current. In addition, the fresh river water, due to its lesser density as compared to sea water, will tend to flow on the surface, and thereby induce a circulatory pattern. An understanding of the underlying causes governing this circulation may be obtained by reference to Fig. 4, which presents a hypothetical situation in which the bottom pressures at sections 1 and 2 are equal. The average density at section 1 is 1.02, approximately the density in the Lower Bay of New York Harbor. The density at section 2 is that of some point farther upstream. At both sections the sea water is overrun by the same depth of fresh water. On the average, the density of section 1 is greater than that at section 2. In order to maintain equal bottom pressures, therefore, a greater depth must prevail at section 2. If the horizontal pressure differences between the two sections are computed and plotted, a distribution such as that in Fig. 4(*b*) will be obtained. In general this pressure distribution will induce a flow proportional to the pressure differences, and will tend to increase the depth at section 1. With this increase in depth, a pressure pattern similar to that in Fig. 4(*c*) will be established, which in turn, will initiate a circulatory flow. The seaward bound fresh water will flow at the surface, above a seaward flow of somewhat saline water, both overriding a return upstream flow of salt sea water.

From a purely empirical standpoint, one can assume that a return flow is necessary to maintain the more or less constant average salinities that have been observed in tidal rivers. The net flow toward the sea is somewhat saline; to balance this net loss of salt, a return flow is necessary. This return flow, because of its greater density, is restricted to the lower layers.

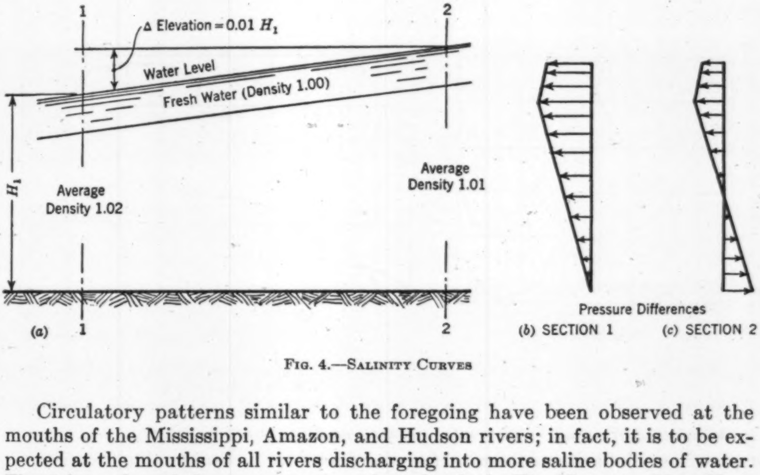

FIG. 4.—SALINITY CURVES

Circulatory patterns similar to the foregoing have been observed at the mouths of the Mississippi, Amazon, and Hudson rivers; in fact, it is to be expected at the mouths of all rivers discharging into more saline bodies of water. Fig. 5 is a plot of the currents at various depths in The Narrows, New York Harbor.[7] The ebb flow at the 17-ft depth is seen to be greater than the flood by a rough comparison of the areas above and below the line of zero velocity. At the 44-ft depth the ebb and flow volumes seem to be about equal, but at the 77-ft depth it is apparent that the net flood flow exceeds the net ebb flow.

In general, with respect to salinity currents, five conclusions can be stated, as follows:

1. The tidal wave, its dimensions, form rate of propagation, and velocity are materially affected by the salinity and its distribution.
2. The ocean water entering a tidal stream does so in the form of a wedge—its entering point along the bottom of the stream. A salt-water interfall

---

[7] "The Tide," by H. A. Marmer, D. Appleton and Co., New York, N. Y., 1926.

(interface), generally not well defined, lies between the top fresh water and the salt-water wedge. Its thickness increases downstream, as does its density from top to bottom. The interface obtains its salt content by erosion from the salt-water wedge.

3. The salt-water wedge enters and begins advancing upstream while the fresh water at the top is still being discharged to the ocean. In Fig. 5 it is to be noticed that at 10 *h*, the 17-ft depth has a southerly ebb velocity of about 1.5 knots while the current at the 70-ft depth has a northerly flood velocity of 0.5 knot.

4. The distance that the wedge advances is governed by the range of the tide, the resistance to flow offered by channel irregularities, and the rate of stream discharge.

5. As the fresh-water flow increases, the amount of salt water eroded from the wedge increases, thus tending to decrease the salinity at a given point.

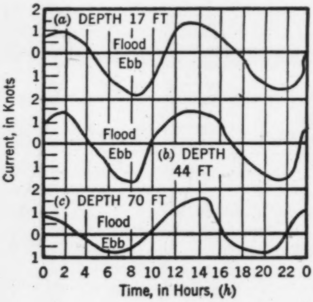

FIG. 5.—CURRENT CURVES, NEW YORK HARBOR, AUGUST, 1922

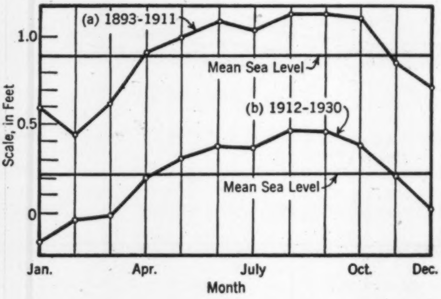

FIG. 6.—MONTHLY VARIATION IN SEA LEVEL, THE NARROWS, NEW YORK HARBOR

Wind and Weather.—The wind, as well as differences in salinity, will induce a circulatory velocity pattern. If a wind blows for a considerable time in one direction on a body of water, the surface particles are carried from their orignal position by the impingement of the air upon them. The wind will then tend to raise the level of water in the direction of the wind and to diminish the level on the opposite shore. In shallow bodies of water this rise may be considerable, whereas in deep bodies of water with steep and abrupt shores the effect is negligible because the forces due to the wind do not act alike upon the particles at all depths, as do the tidal forces; the wind acts primarily on the surface. The increase of depth engendered by the wind creates a flow at the lower depths in a direction approximately reversed to the direction of the wind. Since this lower current has a greater cross-sectional area than does the surface current, its velocity will not be so great. Rather than taking a direction exactly in the direction of the wind, the surface current is deflected to the right of the wind in the Northern Hemisphere, due to the rotation of the earth. Hence a wind of 30 miles per hr will induce a surface current, not in the direction of the wind, but about 20° to the right of the wind.

The barometric pressure, or rather the pressure gradient, may also affect the height of mean sea level. For instance, if the barometric pressure in New York Harbor were to drop suddenly while the atmospheric pressure over the ocean remained constant, a rise in water level can be expected in the harbor, represented by a differential pressure of 1 in. of mercury, causing a difference in water level of about 1 ft. This effect may explain the observed seasonable variation in sea at New York Harbor, shown in Fig. 6, which represents the monthly heights as determined from 19-yr averages; and an obvious trend toward higher mean sea levels in the summer and fall is indicated. A correlation of the pressure differences between New York Harbor and some points in the Atlantic Ocean would establish whether this seasonal variation is, in fact, due to atmospheric pressure differences. It has been established, from a meteorological viewpoint, that higher pressures exist over land areas as opposed to water areas during the winter months, due to the more rapid cooling of the land areas. This cooling of the air over land areas results in denser air masses. Conversely, in the summer months, higher air pressures are expected over water areas.

TIDES AND SEWAGE DISPOSAL

For tidal bays and estuaries and straits, this paper has described the various types of tidal action that may occur (either progressive wave, stationary wave, or hydraulic flow) and how these are influenced by density currents, wind, and weather. It is in the application of this information, however, that the primary interest lies. How have these facts been used in determining the criteria for sewage disposal? How have detention periods and dilutions been estimated?

Classical Theory of the Tidal Prism.—The classical tidal prism theory constituted the first attempt to evaluate the role of the tidal action in sewage disposal. Supposedly, the entire volume of water between mean high water and mean low water—the tidal prism—is available for sewage dilution in each tidal cycle. In each cycle, the prism is renewed with a supply of fresh sea water that mixes completely with the water below the mean low-water line.

For instance, in Upper New York Bay, where the tidal prism is approximately 2,000 cu ft and the volume below mean low water is about 12,000 cu ft, one may expect a renewal of $\frac{2.10^9}{12.10^9} \times 100 = 16.7\%$ of the water in the bay in every tidal cycle. Since the water in the bay is assumed to be completely mixed, 83.3% of the sewage introduced during a tidal cycle can be expected to remain. Of the sewage introduced during the previous cycle, there would be 83.3%, or 69.4%, remaining. The total volume of sewage remaining after n cycles would be

$$\sum (x + x^2 + x^3 + \cdots + x^n) = \frac{x\,(1 - x^n)}{1 - x} \qquad \text{(3)}$$

which for large values of n will be approximated by

$$Q = \frac{x}{1 - x} \qquad (4)$$

In Eqs. 3 and 4, x is the decimal amount remaining after one cycle, and Q is the total sewage in the harbor, expressed as a multiple of the sewage discharged in one tidal cycle. For $x = 0.833$ there will be present in the bay $\frac{0.833}{0.167} = 4.98$ times the pollutional load introduced in one tidal cycle, or approximately 2.5 times the daily pollutional load. The time required for the pollutional load introduced during a cycle to be reduced by one half is approximately equal to four tidal cycles, or roughly two days.

From a consideration of the tide and tidal currents discussed in a previous section of this paper, it can be shown that the classical tidal prism theory usually overevaluates the cleansing action of the tide. The theory does not take tidal rivers into account. If the derived tide forms a progressive wave (which generally occurs in tidal estuaries), the entire tidal prism is not filled with fresh sea water in a tidal cycle. The wave form undulates, and high and low tides do not occur at the same time in all parts of the harbor or bay, as is implied by the classical concept of the tidal prism. Moreover, by consideration of the tidal currents, it is obvious that, in order to fill the tidal prism with new sea water, the horizontal water velocities must be such as to transport the water throughout the entire tidal area. For example, if the maximum surface tidal current observed in a harbor is 2 miles per hr, then, since the current curve approximates a cosine curve, the ratio of the mean current to the maximum current is 2:1.55. Application of this ratio gives a mean current of about 1.3 miles per hr. For an ebb or flow current lasting 6.2 hr, a particle of water is expected to be carried about 8 miles. For the Hudson River the theoretical transport distance, derived in this manner, has checked closely with results obtained by means of floats.

Applying the classical tidal prism theory to a harbor that is 20 miles long, and if there is only a total transport on any tide amounting to 5 miles, the calculated dilution will be much larger than the actual dilution. In this case, it is physically impossible for the sea water to renew itself in each tidal cycle in accordance with the classical theory. In many instances, the basic assumptions of the theory—(1) a renewal of fresh sea water equal to the tidal prism occurs in each tidal cycle and (2) there is a complete mixing of all the waters affected by the tide—are not in accord with fact.

Modified Theory of the Tidal Prism.—A modified tidal prism theory, more in keeping with the physical nature of tidal action, has been proposed by B. H. Ketchum.[8] To remove the objection that the strength of the tidal currents may not be able to transport tidal water for the entire extent of the estuary, Mr. Ketchum has separated the estuary into segments. Each of these segments has a length that can be determined by the average movement of a

---

[8] "The Flushing of Tidal Estuaries," by B. H. Ketchum, *Sewage and Industrial Wastes*, Vol. 23, 1951, p. 198.

particle on the flood tide. Rather than use the actual tidal currents to determine the average movement, however, Mr. Ketchum conceives of the tide as entering a given segment and pushing the low-tide water upstream, the distance of its displacement being equal to the length of the segment. Thus the low-tide volume is equal to the volume of the adjacent landward segment. The segmentation starts at the inner end of the estuary, defined as the section above which the volume of the tidal prism is contributed entirely by the river flow. From this section the length of the successive seaward segments is determined by the aforementioned relationship. These segments are defined only for a given river flow. With a change in river flow the upper end of the estuary will change and thus define a different segmentation.

For a constant river flow it is assumed that the net seaward transport of water, per tidal cycle in each segment, is equal to the fresh-water flow for the same period of time. During periods of constant flow it is also assumed that there is no net salt exchange in any given segment.

As in the classical tidal prism theory, the percentage of water removed, r, by each ebb flow in each segment is equal to

$$r = \frac{P}{P + B} \qquad (5)$$

in which P is the intertidal volume and B is the low-tide volume. Since (by hypothesis) the volume of water that proceeds seaward in each cycle is equal to the river flow for the cycle, and since there is complete mixing in each segment, it also follows that

$$r = \frac{R}{Q_r} \qquad (6)$$

in which R is the volume of river flow during the tidal cycle, and Q_r is the tidal volume of river water in the segment.

The mean age of sewage in any segment is defined as the average length of time required for the fresh river water to pass through the segment. The mean age for sewage introduced at the inner end of an estuary is the total of the mean ages in all the component segments.

As in the classical prism theory, the quantity of water available for dilution is equal to the intertidal volume except that the dilution is on the basis of segmental prisms rather than the entire estuarial prism. A partial check on the volume of water available for dilution can be made by means of salinity data. The water available for dilution, as determined by the intertidal volume, should be equal to the total river flow during the tidal cycle divided by the ratio of fresh water to sea water.

The use of salinities in the determination of x, the proportion of sewage remaining after one tidal cycle, has been discussed by Richard G. Tyler,[9] M. ASCE. This question perhaps is best understood by an examination of a survey made in Gray's Harbor, Washington. The salinity of the harbor water under consideration was 14,790 ppm, the corresponding chloride content in the sea water being 17,500 ppm. To obtain the average harbor salinity then requires a mixing of 5.46 cu ft of sea water with 1 cu ft of fresh water. Since the fresh-water flow is known, this relationship can be used to determine the total volume of sea water that must enter and leave in each tidal cycle to maintain the observed harbor salinity. The ratio of this sea water added to the total quantity of water in the harbor will then give the percentage renewed in each cycle—in this case, 1.2%. Therefore, the fraction retained in each cycle, x, equals $1.00 - 0.012 = 0.988$.

---

[9] "Disposal of Sewage into Tidal Waters," by Richard G. Tyler, *Sewage and Industrial Wastes*, Vol. 22, 1950, pp. 685–698.

To estimate the total quantity of sewage in the harbor, Eq. 4 yields $Q = \frac{x}{1 - x} = 82.3$. Hence, the total volume of sewage in the harbor equals 82.3 times the sewage discharged in one tidal cycle or—since the tidal cycle for Gray's Harbor is 12.42 hr—42.7 times the daily pollutional load. This will give an estimate of the dilution that occurs in the harbor.

The average detention time can be estimated by the total fresh water in the harbor, divided by the river discharge per tidal cycle. For Gray's Harbor, with a flow of 709 cu ft per sec, this amounts to 42 days.

SUMMARY

In some instances the assumptions inherent in the methods outlined in this paper approximate the truth; the factors that have not been considered are of minor importance, and more accurate results will be obtained than in those instances where factors cannot be ignored. Hence, the usefulness of one method will vary from place to place—perhaps even from time to time. It is the intent of this paper to demonstrate the type of situation in which any one or the other of the methods is applicable, and to determine how closely any of the situations for which these methods are ideally suited is encountered under actual conditions.

The classical tidal prism theory assumes a complete vertical and horizontal mixing throughout the tidal estuary. In Mr. Ketchum's modification, mixing is confined to segments of the estuary. The use of segments takes into account the strength of the tidal current, as has been shown previously, thus reducing the horizontal extent of mixing; but complete vertical mixing is assumed within any segment.

In all tidal estuaries there is some vertical stratification; hence, to an extent all the methods are in error. In some locations, such as Commencement Bay, Puget Sound (Washington), there is extreme stratification, and most of the river water is confined to the upper few feet of the water. In a case such as this, a study of the surface flow may give a sufficiently accurate estimate of the fate of the sewage load. Even in Commencement Bay, however, if a sizable portion of the solids in the sewage settled into the underlying salt-water wedge, and if the dissolved and colloidal matter remained in the upper layers, a study of the bay throughout its depth would be required.

The problem of evaluating the effect of factors such as the wind and the long-range tidal components presents a major difficulty. If the effect of such factors on the tide is to be evaluated, it would be necessary to take long-range observations. Such observations would be costly, and even if made the relationship of other factors which are not necessarily periodic (such as the river flow and the volume of sewage) will be difficult to evaluate.

The development of a salinity-temperature-depth (STD) instrument offers hope that, in the future, necessary data may be gathered much more quickly, efficiently, and economically. This instrument makes possible instantaneous determinations of salinity, temperature, and density, and its use provided data for the analysis of Commencement Bay in a period of four days.

Even with the use of the STD indicator, tidal bodies of water do not lend themselves to the testing of tidal hypotheses, especially when the disposal of sewage is the primary concern. There are a host of variables which are difficult to evaluate, and the control of many of these variables is impossible.

Model studies are useful in the study of tidal phenomena and the testing of hypotheses. The Corps of Engineers,[4] working with models, has demonstrated a marked ability to reproduce these phenomena. The range of the tide, the effect of density current, changes in river flow, and ocean level can be readily examined.

With the use of models and with the further gathering of field data to correlate model and prototype phenomena, one can arrive at a truer understanding of the rate of tidal actions in general, and the impact of these actions on sewage disposal.

DISCUSSION

Isadore Nusbaum,[10] A.M. ASCE.—Technical literature is replete with investigations into the disposal of wastes in tidal waters, but no part of the field of sanitary engineering applied to liquid-waste disposal has less applicable knowledge. During the first half of the twentieth century there were extensive investigations in New York Harbor to determine the capacity of the harbor to receive municipal and industrial wastes, yet at the present time (1953) there is little more published material on the subject despite the years and money expended on this project.

Since the centers of population on both the east and west coasts of the United States are located on tidal waters, these communities must dispose of sewage and industrial wastes into the tidal waters. The saline parts of the surface waters influenced by tidal movement have little or no use as a source of water supply for domestic and agricultural purposes. However, many economical, beneficial uses of great significance have been adversely affected by indiscriminate discharge into an apparently unlimited reservoir for disposal.

Before any adequate attack on the problem of tidal flushing of estuaries can be made, the estuaries must be classified in terms of the important factors that influence mixing and movement of water masses. D. W. Pritchard has presented an excellent review of several classifications.[11] One such classification is in terms of fresh-water inflow and evaporation. A "positive" estuary is one in which there is a measurable dilution of sea water by land drainage. An "inverse" estuary has a mixture of high-salinity estuarine waters and sea water. In a third classification, neither fresh-water inflow nor evaporation dominates; this is known as a "neutral" estuary.

A classification scheme presented by Henry Stommel[12] is based on the predominant physical causes of movement and mixing of water in the estuary. Tide, wind, or river flow are indicated as the principal causes. In many cases no single cause of movement and mixing predominates. For example, in some estuaries the tidal motion will dominate near the channel connecting the estuary with the ocean, whereas well within the bay both wind and tide may contribute to the motion and the mixing. The classification of estuaries according to the type of tide which appears to influence the water movement leads to considerable misinterpretation of the forces effective in the little understood phenomena of flushing.

Studies by Mr. Pritchard,[13] J. P. Tully,[14] and Mr. Ketchum[15] have demonstrated that in the estuaries on the coastal plain of the Atlantic coast of the

---

[10] Water Pollution Control Engr., State Water Pollution Control Board, San Diego, Calif.

[11] "A Review of Our Present Knowledge of the Dynamics and Flushing of Estuaries," by D. W. Pritchard, *Technical Report No. IV*, Chesapeake Bay Inst., Johns Hopkins Univ., Baltimore, Md., March, 1952.

[12] "Recent Developments in the Study of Tidal Estuaries," by Henry Stommel, *Technical Report, Ref. No. 51-33*, Oceanographic Inst., Woods Hole, Mass.

[13] "The Physical Structure, Circulation, and Mixing in a Coastal Plain Estuary," by D. W. Pritchard, *Technical Report No. III*, Chesapeake Bay Inst., Johns Hopkins Univ., Baltimore, Md., May, 1952.

[14] "Oceanography and Prediction of Pulp Mill Pollution," by John P. Tully, *Bulletin No. LXXXIII*, Fisheries Research Board of Canada, Ottawa, Ont., Canada, 1949.

[15] "The Exchange of Fresh and Salt Waters in Tidal Estuaries," by Bostwick H. Ketchum, *Journal of Marine Research*, Vol. X, No. 1, Sears Foundation, June 30, 1951, pp. 18-38.

United States and the fiords on the western coast of Canada the predominant physical cause of mixing appears to be the tide. The principal reason for the movement of suspended and dissolved material out of the estuary is the inflow of fresh water. In the case of an inverse estuary, attempts have been made to obtain flushing parameters by the determination of a negative inflow of fresh water, or through the loss of fresh water by evaporation. The flushing problems of San Diego Bay (California) (essentially a neutral estuary) have not been successfully solved. In this bay, salinity determinations have been of little value since there is no significant difference between the saline content of the greatest part of the bay water and the surrounding ocean. In the extreme south end of the bay, which is very shallow, some increase in salinity is found during the summer months. There are no significant vertical salinity gradients in the bay. Under these and other circumstances, temperature gradients can have an important effect on the dynamic characteristics of the estuary. It has also been stated by Mr. Pritchard that in large estuaries the deflecting force of the earth's rotation may have an important effect on the distribution of salinity.

The effects on the progressive wave caused by the reflection and resonance of waves have not been stressed by the authors. These factors are important, as are those changes which influence the progress of the tidal wave up an estuarial river. At several places along the Hudson River, between the mouth and Albany, N. Y., the tide and current tables for the Atlantic coast indicate tidal changes that are not merely frictional.

Standing waves such as those occurring in Long Island Sound (New York) can be considered as composed of two progressive waves—the incoming wave and the reflected wave—traveling in opposite directions. When the period of the reflected wave coincides with the period of the incoming wave, a standing wave is formed.

The designation of a third type of tidal wave form as the hydraulic type leads to some peculiar conclusions. The characterization of the flow in the Hudson River at Albany as being of the same type as that in the East River is not demonstrated by the data presented. Actually, H. A. Marmer described the tidal and current phenomena in the East River as caused by the "* * * interference of tide waves * * *" between that water entering the East River from Long Island Sound and that water entering the East River from the Upper Bay of New York Harbor.[7] This description made a nonmathematical discussion of the phenomena almost impossible, and Mr. Marmer presented the following explanation based on the fact that high water and low water at each end of the East River occur at different times:

> "* * * The movement of the water in East River is brought about by the fact that part of the time the level of the water in Upper Bay is higher than in Long Island Sound and part of the time it is lower. East River thus acts merely as a channel through which the water flows from the body having, temporarily, the higher level to the one having the lower level. In other words, the movement of the water in East River is primarily hydraulic in character.* * *"

Movement of water through the East River is thus "hydraulic" in both directions—and not at all similar to the flow occurring in the Hudson River.

Under the heading, "Derived Tides and Tidal Currents: Salinity Currents," it is stated that the fresh-water flow will tend to increase the duration and strength of the flood current. This is contrary to both theory and experience since the duration and strength of the ebb current are increased by the fresh-water flow because the accumulation of fresh water and tidal water at "flood" must find its way out on the ebb.

The attempt to explain (by the use of pressure diagrams) the fact that the net movement of the less saline water in the upper strata of the estuarine waters is seaward whereas the net movement of the deeper waters is upstream is not entirely adequate. Excellent discussions of this water movement have been given by Messrs. Pritchard,[13] Tully,[14] and Ketchum.[16] It has been observed that as the upper layer of the less saline water moves seaward it gets progressively more saline as additional sea water is transferred through the boundary. To provide this sea water there must be a flow in a landward direction. The purely empirical reasons for the reverse flow are more satisfactory than the description of pressure differentials. It should be possible to prove such a theory by a series of measurements of depth and the determination of the vertical and horizontal salinity gradients at and between carefully selected points.

Circulatory patterns such as described by the authors and the writer have been found in the coastal plain estuaries of the Atlantic coast and in some fiords. It is doubtful, however, whether the salt-wedge formations at the mouths of the Mississippi and Amazon rivers are strictly comparable to New York Harbor conditions. These rivers, with their tremendous outflow of fresh water, are cases in which the position of the salt wedge is entirely dependent on the river flow. It is doubtful whether any such well-defined salt wedge exists in New York Harbor. In the Hudson River, the position of the wedge would be influenced by, and probably dependent on, the tide.

It has been stated by the authors that a wind of 30 miles per hr will induce a surface current—not in the direction of the wind—but about 20° to the right of the wind. Actually, V. W. Ekman found that surface currents caused by the wind were in a direction 45° to the right of the wind in the Northern Hemisphere and 45° to the left in the Southern Hemisphere.[17] This is true, however, only for an ocean of infinite depth, and Mr. Ekman found that near shore, the wind-driven current was much modified by the direction of the coast line. Depending on the angle between the coast line and the direction of the wind, the deviation of the current could vary from 0° to 53°. In shallow water, the current flows in the direction of the stress at all depths. In all cases, the current is the resultant of several forces including the tidal current, the wind-driven current, and currents caused by river discharge and other nontidal drifts.

Abrupt changes in the barometric gradient in the vicinity of any estuary lead to surface oscillations having the characteristics of standing waves.

---

[16] "The Oceanography of the New York Bight," by B. H. Ketchum, A. C. Redfield, and John C. Ayers, *Physical Oceanography and Meteorology*, Massachusetts Inst. of Technology, Cambridge, Mass., and the Oceanographic Inst., Woods Hole, Mass., Vol. XII, No. 1, 1951, p. 28.

[17] "The Oceans," by H. V. Sverdrup, M. H. Johnson, and R. H. Flemming, Prentice-Hall, Inc., New York, N. Y., 1942.

These waves are long-period waves known as "seiches." The seiche superimposes another wave form upon that of the tide wave and gives the tide wave a "sawtooth" appearance. The seiche does not increase the mean range of the tide. Variations in sea level have been ascribed to variations in the average density of water columns as well as to other causes.[17]

Under the heading, "Tides and Sewage Disposal: Modified Theory of the Tidal Prism," the statement should be made: "Thus the low-tide volume of a given segment is equal to the high-tide volume of the adjacent landward segment." It should be noted that Mr. Ketchum postulates a net positive flow of fresh water seaward. In the case of a neutral estuary, Mr. Ketchum's theory would indicate no flushing. Where an inverse estuary exists, the flushing might be determined by assuming a negative inflow of fresh water. The deficiencies of the modified tidal-prism theory have been noted where stratification exists. Mr. Pritchard[11] has indicated that where the tidal wave has the features of a progressive wave, the successive estuary segments may have to be defined by means other than the average excursion of a particle of water on the flooding tide.

The waste-disposal capacities of many estuaries are limited by the extent of the chemical and biological changes acting within the estuary and the immediate, available dilution. When wastes are discharged at the head of the estuary, the tide has little influence on the actual effects produced by the waste or the natural processes of purification. Near the mouth of an estuary, where tidal effects are at a maximum, waste disposal can be considered as if the disposal were into the open ocean. Under some circumstances the sanitary engineer should ignore tidal "flushing" in computing the waste-receiving capacity of an estuary.

ALEXANDER N. DIACHISHIN,[18] J.M. ASCE, SETH G. HESS,[19] M. ASCE, AND WILLIAM T. INGRAM,[20] A.M. ASCE.—The writers are substantially in accord with Mr. Nusbaum's introductory statement that

> "* * * no part of the field of sanitary engineering applied to liquid-waste disposal has less applicable knowledge"

than the disposal of wastes in tidal waters. However, it is the very lack of this applicability and the widespread use of tidal waters as a receiver of liquid-borne waste materials that make the problem of tidal-waste disposal both challenging and valuable to sanitary engineers.

Mr. Nusbaum is to be commended for amplifying some aspects of the pertinent tidal phenomena. The matter of classifying estuaries in terms of the important factors that influence the mixing and movement of the water masses serves to emphasize the individual nature of estuaries. Because (under almost all conditions) no single cause of movement and mixing predominates, it is doubtful that any system of classification, as such, can be of other than academic interest. In addition to the variation of tidal "flushing" characteristics and other estuarial phenomena between individual estuaries, emphasis should also be placed on the variation within a given harbor. This intra-estuarial variation applies not only to geographical variation, as discussed by Mr. Nusbaum, where

---

[18] Prin. Engr., Interstate Sanitation Comm., New York, N. Y.

[19] Director and Chf. Engr., Interstate Sanitation Comm., New York, N. Y.

[20] Associate Prof. of Public Health Eng., New York Univ., New York, N. Y.

> "For example, in some estuaries the tidal motion will dominate near the channel connecting the estuary with the ocean, whereas well within the bay both wind and tide may contribute to the motion and the mixing"

but also to variations with time.

Certainly, at the same location in a harbor, radically different regimes have been observed between different seasons and even between successive weeks of the same season. At present (1953) the writers are engaged in a long-range study of pollution distributions in Upper New York Bay. For the same location, at a depth of 20 ft, there has been recorded—within the same year—a variation of (1) from less than 1.8 to 700 Most Probable Number of coliforms per milliliter; (2) from 7,630 ppm to 15,320 ppm of chlorides; and (3) from 28% to 88% of dissolved oxygen saturation. The site under discussion is half a mile from the shore and at least one mile from any major source of pollution.

Although intra-estuarial variation is implied in most studies which specify "flushing" times and other parameters (characterizing the distribution and detention of the water-borne wastes as a function of river flow and other factors), more emphasis should be placed on the effect of intra-estuarial variations. The over-all variation of estuarial characteristics both within and between estuaries is perhaps best summarized by paraphrasing the old adage to the effect that each harbor and even the components of a harbor are laws unto themselves. However, it was the original intent of the writers to outline those factors which can have an important influence on the movements of estuarial tidal-water masses and not to specify a quantitative description applicable to all estuaries. Both the original presentation and Mr. Nusbaum's discussion have realized this original intent and, by so doing, have indicated a more realistic approach to the appraisal of waste-disposal practices in estuarial waters.

AMERICAN SOCIETY OF CIVIL ENGINEERS
Founded November 5, 1852
TRANSACTIONS

Paper No. 2679

A DIRECT STEP METHOD FOR COMPUTING WATER-SURFACE PROFILES

By Arthur A. Ezra,[1] J. M. ASCE

With Discussion by Messrs. I. H. Steinberg, C. A. M. Gray, Bob Buehler, Monir M. Kansoh, and Arthur A. Ezra

Synopsis

The direct step method is proposed to replace the computations by trial and error used in the standard step method for tracing water-surface profiles in natural channels. It is a semigraphical method applying Bernoulli's theorem and includes the effect of velocity-head changes. The effect of eddy losses, bridge-pier losses, and overbank flow can also be included when necessary. The proposed method, which is conveniently applicable in general, has been found by the author to be especially advantageous when several water-surface profiles must be determined in the same channel.

Notation

The letter symbols adopted for use in this paper are defined where they first appear, in the illustrations or in the text, and are arranged alphabetically for reference in the Appendix.

Introduction

The proposed method seeks to eliminate the trial-and-error computations necessary in the standard step method for determining water-surface profiles in natural channels. This is accomplished by indicating the hydraulic properties of each section in a length of river channel by means of graphs in such a fashion that, knowing the water-surface level at any section, the water-surface level at the next section (upstream or downstream) can be obtained by direct computation.

Theory

Fig. 1 represents the water-surface profile for varied flow between two sections in an open channel.

Because the total energy at section (1) is equal to the total energy at section (2) plus losses,

$$Z_1 + \frac{V^2_1}{2\,g} = Z_2 + \frac{V^2_2}{2\,g} + \text{losses} \qquad (1)$$

Note.—Published, essentially as printed here, in March, 1953, as *Proceedings-Separate No. 180.* Positions and titles given are those in effect when the paper or discussion was received for publication.

[1] Structural Engr., Corps of Engrs., San Francisco, Calif.

The losses in the reach (1)–(2) that are usually taken into account in profile computations consist of the loss of head caused by friction, the eddy losses caused by enlargement or contraction of the channel, and bend losses.

The friction loss in the reach will be computed by Manning's formula.

The eddy losses (the part of the velocity head that is not recovered) are usually taken into account in determinations of water-surface profiles as follows:

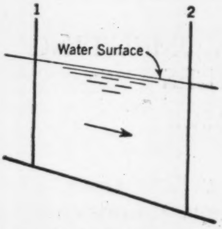

FIG. 1.—SURFACE PROFILE—VARIED FLOW IN AN OPEN CHANNEL

(*a*) They are included in the value of the roughness coefficient n in the Manning formula, and S is determined. This can be done when the value of n has been determined from observations of water-surface profiles in the same or similar reaches. The value of S in this case will represent the total rate of loss of energy head including both eddy and friction losses.

(*b*) The eddy losses are considered as a certain percentage of the change in velocity head between two sections. The total loss of head between two consecutive sections then will be the sum of the loss of head caused by friction the reach plus the eddy losses.

Let the friction losses between sections (1) and (2) in Fig. 1 be denoted by $S_{\text{aver}}\,L$, in which S_{aver} is the average of the rates of loss of head due to friction at sections (1) and (2), and L is the length of the reach measured along the center line between sections (1) and (2).

Limiting consideration of losses to friction and eddy losses, the loss of energy head between sections (1) and (2) in Fig. 1 is

$$S_{\text{aver}}\,L + K\left(\frac{V^2_1}{2\,g} - \frac{V^2_2}{2\,g}\right) = \tfrac{1}{2}\,(S_1 + S_2)\,L + K\left(\frac{V^2_1}{2\,g} - \frac{V^2_2}{2\,g}\right)$$

in which the quantity in parentheses is the numerical difference between the arger and smaller velocity heads, irrespective of which is the larger, and S_1 and S_2 are the rates of loss of head due to friction if eddy losses are computed separately as $K\left(\frac{V^2_1}{2\,g} - \frac{V^2_2}{2\,g}\right)$. For abrupt expansions and contractions $K = 0.5$ approximately. For a gradually diverging reach K may be taken as 0.2 and for a gradually converging reach, K may be taken from 0 to 0.1, approximately.[3]

When the effect of eddy losses is included in the roughness coefficient n in Manning's formula, S_1 and S_2 (as determined from Manning's formula) represent rates of loss of energy head at sections (1) and (2).

Substituting the foregoing expression for losses in Eq. 1 yields

$$Z_1 + \frac{V^2_1}{2\,g} = Z_2 + \frac{V^2_2}{2\,g} + \tfrac{1}{2}\,(S_1 + S_2)\,L + K\left(\frac{V^2_1}{2\,g} - \frac{V^2_2}{2\,g}\right)$$

---

[3] U. S. Corps of Engineers Engineering Manual for Civil Works, Part CXIV, May, 1952, Chapter 9, "Computation of Backwater Curves in River Channels," Paragraph 9-06.

or

$$Z_1 + \frac{V^2{}_1}{2\,g} - \tfrac{1}{2}\,S_1\,L = Z_2 + \frac{V^2{}_2}{2\,g} + \tfrac{1}{2}\,S_2\,L + K\left(\frac{V^2{}_1}{2\,g} - \frac{V^2{}_2}{2\,g}\right)\ldots\ldots(2)$$

For a given discharge Q and a given roughness coefficient n, Manning's formula yields

$$Z_1 + \frac{V^2{}_1}{2\,g} - \left(\frac{L}{2}\right)\frac{n^2 V^2{}_1}{2.2\,R^{4/3}{}_1} = Z_2 + \frac{V^2{}_2}{2\,g} + \left(\frac{L}{2}\right)\frac{n^2 V^2{}_2}{2.2\,R^{4/3}{}_2} + K\left(\frac{V^2{}_1}{2\,g} - \frac{V^2{}_2}{2\,g}\right).$$

Because $V_1 = Q/A_1$ and $V_2 = Q/A_2$ it is found that

$$\begin{aligned} Z_1 + \frac{Q^2}{2\,g\,A^2{}_1} - \left(\frac{L}{2}\right)\frac{Q^2\,n^2}{2.2\,A^2{}_1\,R^{4/3}{}_1} \\ = Z_2 + \frac{Q^2}{2\,g\,A^2{}_2} + \left(\frac{L}{2}\right)\frac{Q^2\,n^2}{2.2\,A^2{}_2\,R^{4/3}{}_2} + K\left(\frac{V^2{}_1}{2\,g} - \frac{V^2{}_2}{2\,g}\right)\ldots(3) \end{aligned}$$

in which the term $K\left(\frac{V^2{}_1}{2\,g} - \frac{V^2{}_2}{2\,g}\right)$ is always taken as positive as the quantity in parentheses is merely the numerical difference as explained previously. Thus, for a constant discharge Q, a given roughness coefficient n, and a given distance L between sections, the expressions: $\frac{Q^2}{2\,g\,A^2{}_1} - \left(\frac{L}{2}\right)\frac{Q^2\,n^2}{2.2\,A^2{}_1\,R^{4/3}{}_1}$ and $\frac{Q^2}{2\,g\,A^2{}_2} + \left(\frac{L}{2}\right)\frac{Q^2\,n^2}{2.2\,A^2{}_2\,R^{4/3}{}_2}$—are functions of the water-surface elevation on which the values of A and R depend. The expressions of the form: $\frac{Q^2}{2\,g\,A^2} - \left(\frac{L}{2}\right)\frac{Q^2\,n^2}{2.2\,A^2\,R^{4/3}}$—may be denoted by $f(Z)$ and the expression of the form: $\frac{Q^2}{2\,g\,A^2} + \left(\frac{L}{2}\right)\frac{Q^2\,n^2}{2.2\,A^2\,R^{4/3}}$—may be denoted by $\phi(Z)$.

Eq. 3 therefore can be rewritten as

$$Z_1 + f(Z_1) = Z_2 + \phi(Z_2) + K\left(\frac{V^2{}_1}{2\,g} - \frac{V^2{}_2}{2\,g}\right)\ldots\ldots\ldots\ldots(4)$$

when Q is constant.

DESCRIPTION OF PROCEDURE

The direct step solution consists of the graphical application of Eq. 4. For each chosen section in the natural channel under consideration, the values of A and R for a range of water-surface elevations are determined and tabulated. This procedure is common to both the standard step solution and the proposed direct step solution. At least three water-surface elevations for each section are chosen, in the range in which the water-surface profile is expected to lie, and are used for computing the hydraulic properties.

For given values of Q and n, values of $\frac{V^2}{2\,g}$ and S are determined at each section for each of these elevations, and the corresponding values of $f(Z)$ and

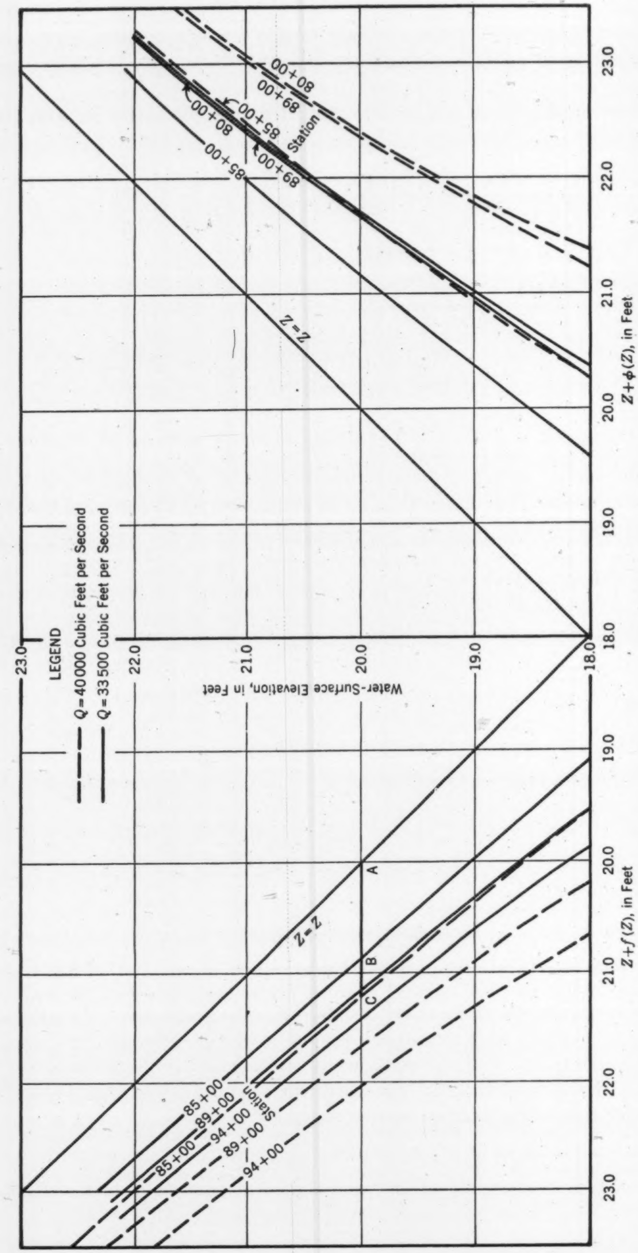

FIG. 2.—CURVES FOR THE DETERMINATION OF WATER-SURFACE PROFILES

$\phi(Z)$ are obtained. Curves of $Z + f(Z)$, $Z + \phi(Z)$, and $K \frac{V^2}{2g}$ are plotted against Z for each section, as shown in Fig. 2. For flows above critical depth, the water-surface profile is determined in upstream order. Starting with a given water-surface elevation at a section, the value of $Z + \phi(Z)$ is obtained from the appropriate curve.

Neglecting the term $K\left(\frac{V^2_1}{2g} - \frac{V^2_2}{2g}\right)$ in Eq. 4 when the effect of eddy losses is included in the value of the roughness coefficient n, it can be seen that the resulting value of $Z + \phi(Z)$ is equal to $Z + f(Z)$ for the next upstream section. Entering the curve for $Z + f(Z)$ for the next upstream section with this value, the corresponding water-surface elevation is determined directly. This procedure is repeated from section to section, tracing the desired water-surface profile. For flows below critical depth, the water-surface profile is traced downstream and the procedure is similar. Starting with the value of $Z + f(Z)$ at a section and taking this value to the $Z + \phi(Z)$ curve for the next downstream section, the corresponding water-surface elevation is determined.

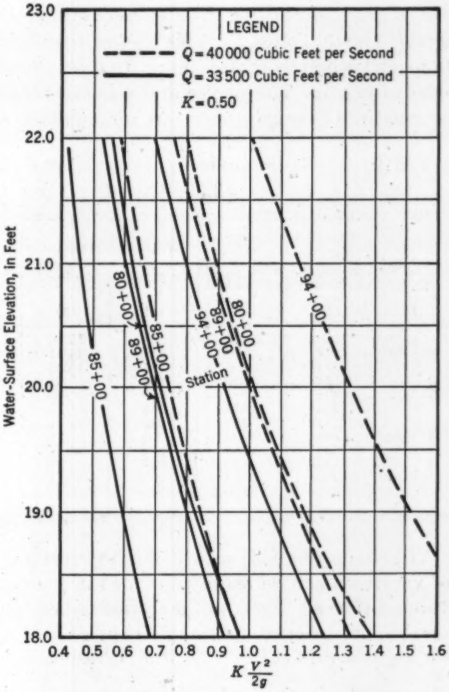

FIG. 3.—CORRECTION TO BE APPLIED TO $Z + \phi(Z)$

If it is desired to consider the eddy losses separately as a percentage of the velocity-head change between the upstream and downstream end sections of a reach, the procedure is modified. After finding the water-surface elevations for two consecutive sections when proceeding upstream (as described previously) by neglecting the term $K\left(\frac{V^2_1}{2g} - \frac{V^2_2}{2g}\right)$ in Eq. 4, the values of $K \frac{V^2}{2g}$ are found for these water-surface elevations from previously plotted curves, as shown in Fig. 3. The difference is then added to the value of $Z + \phi(Z)$ for the lower of the two sections. This corrected value is taken to the $Z + f(Z)$ curve for the higher of the two sections, and the corresponding corrected water-surface elevation is determined.

For flows below critical depth, the procedure is similar, Eq. 4 being applicable. However, the water-surface profile should be traced downstream and the correction for eddy losses $\left(\frac{K\,V^2_1}{2\,g} - \frac{K\,V^2_2}{2\,g}\right)$ should be deducted from the value of $Z + f(Z)$ for a section before this value is transferred to the $Z + \phi(Z)$ curve.

Corrections for bend losses or bridge-pier losses[3] in a reach may be made in a manner similar to that described for eddy losses.

In computing the values of $f(Z)$ used to plot the $Z + f(Z)$ curve, the value of L downstream from that section should be used. Similarly, in computing $\phi(Z)$-values for plotting the $Z + \phi(Z)$ curve, the value of L upstream from that section should be used. This insures that values of L will be common to sections at both ends of any reach, that is, the same value of L is used on both sides of Eq. 4. This choice of the L-value is important because sections taken on a natural channel usually are not equidistant from each other.

TABLE 1.—HYDRAULIC PROPERTIES OF CROSS SECTIONS, FOR VALUES OF Q = 33,500 CU FT PER SEC AND n = 0.030

Station (1)	Water-surface elevation, Z, in feet (2)	Cross-sectional area, A, in square feet (3)	Wetted perimeter, P, in feet (4)	Hydraulic radius, R, in feet (5)	Mean velocity, V, in feet per second (6)	$\frac{V^2}{2\,g}$, in feet (7)	Gradient, S (8)	$0.5\,\frac{V^2}{2\,g}$, in feet (9)
80+00	18.0	3000	238	12.60	11.17	1.94	0.00173	0.97
	20.0	3500	248	14.11	9.57	1.42	0.00110	0.71
	22.0	3970	258	15.39	8.44	1.11	0.00076	0.56
85+00	18.0	3580	265	13.51	9.36	1.36	0.00111	0.68
	20.0	4100	273	15.02	8.17	1.04	0.00073	0.52
	22.0	4630	282	16.42	7.24	0.82	0.00051	0.41
89+00	18.0	3080	248	12.42	10.88	1.84	0.00167	0.92
	20.0	3550	258	13.76	9.44	1.39	0.00111	0.70
	22.0	4050	268	15.11	8.27	1.06	0.00075	0.53
94+00	18.0	2650	225	11.78	12.64	2.48	0.00243	1.24
	20.0	3100	235	13.19	10.81	1.81	0.00153	0.91
	22.0	3550	245	14.49	9.44	1.39	0.00102	0.70

In computing $f(Z)$ or $\phi(Z)$ for any section, the effect of overbank flow and of varying n can be readily included in the computations by using a weighted value of the velocity V for the sections when tabulating the hydraulic properties for the purpose of computing $f(Z)$ and $\phi(Z)$. Also, after $f(Z)$ has been obtained for a given value of $Q = Q_1$, the corresponding values of $f(Z)$ and $\phi(Z)$ for any other discharge Q_2 can be obtained by multiplying by the factor $\left(\frac{Q_2}{Q_1}\right)^2$.

The examples comprising the remainder of this paper may help to illustrate the use of the proposed direct step method.

EXAMPLE NO. 1

If a discharge of 33,500 cu ft per sec is measured in the San Lorenzo River at Santa Cruz, Calif., let it be required to determine the water-surface profile from station 80 + 00 to station 94 + 00. The water-surface elevation at station 80 + 00 is 18.5 ft above mean sea level for a discharge of 33,500 cu ft per sec. Assume that the value of Manning's n is 0.030, and that it includes the effect of eddy losses.

---

[3] "Handbook of Hydraulics," by H. W. King. McGraw-Hill Book Co., Inc., New York, N. Y., 1939, p. 416.

Eq. 4 is applied graphically as explained previously, neglecting the term $K\left(\frac{V^2_1}{2\,g} - \frac{V^2_2}{2\,g}\right)$. The plotted cross sections from station 80 + 00 to station 94 + 00 have been omitted from this presentation, but the hydraulic properties for each section are tabulated in Table 1 for the range in which the water-surface profile is expected to lie.

TABLE 2.—COMPUTATION OF $Z + f(Z)$ AND $Z + \phi(Z)$ FOR VALUES OF $Q = 33{,}500$ CU FT PER SEC AND $n = 0.030$

Station (1)	Z, in feet (2)	$\frac{1}{2}\,S\,L_d$, in feet (3)	$\frac{1}{2}\,S\,L_u$, in feet (4)	$f(Z)$, in feet (5)	$\phi(Z)$, in feet (6)	$Z + f(Z)$, in feet (7)	$Z + \phi(Z)$, in feet (8)
80 + 00	18.0		0.43		2.37		20.37
	20.0		0.28		1.70		21.70
	22.0		0.19		1.30		23.30
85 + 00	18.0	0.28	0.22	1.08	1.58	19.08	19.58
	20.0	0.18	0.15	0.86	1.19	20.86	21.19
	22.0	0.13	0.10	0.69	0.92	22.69	22.92
89 + 00	18.0	0.33	0.42	1.51	2.26	19.51	20.26
	20.0	0.22	0.28	1.17	1.67	21.17	21.67
	22.0	0.15	0.19	0.91	1.25	22.91	23.25
94 + 00	18.0	0.61		1.87		19.87	
	20.0	0.38		1.43		21.43	
	22.0	0.26		1.13		23.13	

The computations for $f(Z)$ and $\phi(Z)$ for three elevations are shown in Table 2. Curves of $Z + f(Z)$ and $Z + \phi(Z)$ were plotted against Z for each cross section, as shown in Fig. 2.

From Manning's formula, $S = \frac{n^2\,V^2}{2.2\,R^{4/3}}$; L_d was taken as the length of a reach downstream from a particular cross section; and L_u was taken as the length of a reach upstream from a particular cross section.

At station 80 + 00, for a water-surface elevation of 18.5 ft, the value of $Z + \phi(Z)$ is found from the appropriate curve in Fig. 2 to be 20.70. Taking this value to the $Z + f(Z)$ curve for the next upstream section at station 85 + 00, the corresponding water-surface elevation is found to be 19.83 ft. This procedure is repeated until station 94 + 00 is reached. The results of the profile computations have been tabulated in Table 3. This method is very advantageous in the determination of water-surface profiles in a natural channel if several profiles, each for a different elevation at the initial section, are required.

TABLE 3.—WATER-SURFACE PROFILE, FOR A VALUE OF $Q = 33{,}500$ CU FT PER SEC

Station (1)	$Z + f(Z)$, in feet (2)	$Z + \phi(Z)$, in feet (3)	Water-surface elevation, Z, in feet (4)
80 + 00		20.70	18.50
85 + 00	20.70	21.03	19.83
89 + 00	21.03	21.55	19.85
94 + 00	21.55		20.15

Examples of this type of problem are the tracing of water-surface profiles in a tributary stream, for different stages in the main river; in a river with a tidal estuary, for different tidal elevations; or in a channel connecting two reservoirs whose elevations vary.

EXAMPLE No. 2

Assume that it is required to trace the water-surface profile from station 80 + 00 to station 94 + 00 in the previous problem for a value of $Q = 40{,}000$ cu ft per sec. The roughness coefficient n in Manning's formula is equal to 0.030, and the effect of eddy losses is included in the value of n. The water-surface elevation at station 80 + 00 is 19.0 ft above mean sea level for a value of $Q = 40{,}000$ cu ft per sec.

TABLE 4.—VALUES OF $Z + f(Z)$ AND $Z + \phi(Z)$ FOR VALUES OF $Q = 40{,}000$ CU FT PER SEC AND $n = 0.030$

Station (1)	Z, in feet (2)	$f(Z)$, in feet (3)	$\phi(Z)$, in feet (4)	$Z + f(Z)$, in feet (5)	$Z + \phi(Z)$, in feet (6)
80+00	18.0		3.39		21.39
	20.0		2.43		22.43
	22.0		1.86		23.86
85+00	18.0	1.54	2.26	19.54	20.26
	20.0	1.23	1.70	21.23	21.70
	22.0	0.99	1.32	22.99	23.32
89+00	18.0	2.16	3.24	20.16	21.24
	20.0	1.67	2.39	21.67	22.39
	22.0	1.30	1.79	23.30	23.79
94+00	18.0	2.67		20.67	
	20.0	2.03		22.03	
	22.0	1.62		23.62	

The values of $f(Z)$ and $\phi(Z)$ may be obtained for a value of $Q = 40{,}000$ cu ft per sec from the corresponding values in the previous problem, in which $Q = 33{,}500$ cu ft per sec, by multiplying them by $\left(\frac{40{,}000}{33{,}500}\right)^2 = 1.43$. The values of $f(Z)$ and $\phi(Z)$ obtained in this manner have been tabulated in Table 4, and the corresponding values of $Z + f(Z)$ and $Z + \phi(Z)$ have been plotted in Fig. 2.

TABLE 5.—WATER-SURFACE PROFILE DETERMINATION FOR A VALUE OF $Q = 40{,}000$ CU FT PER SEC

Section (1)	$Z + f(Z)$, in feet (2)	$Z + \phi(Z)$, in feet (3)	Water-surface elevation, Z, in feet (4)
80+00		21.85	19.0
85+00	21.85	22.25	20.70
89+00	22.25	22.85	20.72
94+00	22.85		21.04

This also can be accomplished by a simple graphical method. In Fig. 2 straight line $Z = Z$ may be drawn along with the $Z + f(Z)$ curve and the $Z + \phi(Z)$ curve. For example, for station 85 + 00 the intercept AB between the line $Z = Z$ and the curve for $Z + f(Z)$ is equal to $Z + f(Z) - Z = f(Z)$ for $Q = 33{,}500$ cu ft per sec and a water-surface elevation of 20.00 ft. If a pair of proportional dividers is set at the ratio 1.43:1, the intercept AB may be set off at the small end of the dividers, and the intercept AC is laid off with the large end as shown—at the same water-surface elevation. The intercept AC therefore will be the intercept between the line $Z = Z$ and the curve for $Z + f(Z)$ for the value of $Q = 40{,}000$ cu ft per sec. Hence, C is a point on the curve of $Z + f(Z)$ for $Q = 40{,}000$ cu ft per sec. Other points on the same curve can be obtained similarly, and curves of $Z + f(Z)$ and $Z + \phi(Z)$ can be obtained for each section for $Q = 40{,}000$ cu ft per sec from the curves for $Q = 33{,}500$ cu ft per sec. The water-surface profile then may be determined from this new set of curves. The computations are tabulated in Table 5.

Example No. 3

For a discharge of 33,500 cu ft per sec in the San Lorenzo River at Santa Cruz, it is required to determine the water-surface profile from station 80 + 00 to station 94 + 00. For this discharge, the water-surface elevation at station 80 + 00 is 18.5 ft above mean sea level. The value of Manning's $n = 0.030$. Eddy losses are to be computed as 50% of the change in velocity head when the velocity head is decreasing downstream. Eddy losses may be neglected when the velocity head increases downstream.

TABLE 6.—Water-Surface Profile Determination,[a] Treating Eddy Losses Separately, for Values of $Q = 33{,}500$ Cu Ft per Sec and $K = 0.5$

Station (1)	$Z + f(Z)$ (2)	Corrected $Z + f(Z)$ (3)	$Z + \phi(Z)$ (4)	$K \frac{V^2}{2g}$ (5)	Eddy losses (6)	$Z + \phi(Z)$ + eddy losses (7)	Trial Z-value (8)	Corrected Z-value (9)
80 + 00			20.70	0.91			18.50	18.50
85 + 00	20.70		21.03	0.53		21.21	19.83	19.83
89 + 00	21.03	21.21	21.70	0.71	0.18	21.86	19.85	20.05
94 + 00	21.70	21.86		0.87	0.16		20.35	20.53

[a] All values are in feet.

The water-surface profile may be determined by application of Eq. 4, taking into account eddy losses. The value of K will be 0.5, and the corresponding terms are tabulated in Table 1. In Fig. 3 the curves of $K \frac{V^2}{2g}$ for $K = 0.5$ have been plotted and should be used to correct for eddy losses as explained previously. The computations for the determination of the water-surface profile are tabulated in Table 6. Beginning at station 80 + 00 with a water-surface elevation of 18.50 ft (Col. 9, Table 6), the value of $Z + \phi(Z)$ may be found from the appropriate curve in Fig. 2 to be 20.70 ft (see Col. 4, Table 6). The corresponding value of $K \frac{V^2}{2g}$ is 0.91 (see Col. 5, Table 6). Taking the value of 20.70 ft to the $Z + f(Z)$ curve for the next upstream section at station 85 + 00 (Col. 2, Table 6), the corresponding water-surface elevation (shown in Col. 8, Table 6) is 19.83 ft, and the value of $K \frac{V^2}{2g}$ is 0.53 (Col. 5, Table 6). Therefore, the velocity is increasing downstream and eddy losses are neglected so that the corrected water-surface elevation is still 19.83

ft, as shown in Col. 9, Table 6. The value of $Z + \phi(Z)$ at station 85 + 00 for a water-surface elevation of 19.83 ft is found to be 21.03 ft. Going with this value to the $Z + f(Z)$ curve for the next upstream section at station 89 + 00, the water-surface elevation is found to be 19.85 ft and the corresponding value of $K \frac{V^2}{2\,g}$ is 0.71. Therefore, the velocity head has decreased downstream from station 89 + 00 to station 85 + 00, and the eddy losses are 0.71 ft − 0.53 ft = 0.18 ft. In order to include the effect of these eddy losses, add 0.18 ft to 21.03 ft which was previously found to be the value of $Z + \phi(Z)$ at station 85 + 00, yielding the value 21.21 ft. Going to the $Z + f(Z)$ curve for station 89 + 00 with this value, the water-surface elevation is found to be 20.05 ft.

This procedure is repeated, accounting for eddy losses when necessary, until the water-surface profile has been computed over the required distance.

APPENDIX. NOTATION

The following symbols, adopted for use in the paper and for the guidance of discussers, conform essentially with "Letter Symbols for Hydraulics" (ASA Z10.2—1942):

A = area of the cross section, in square feet;
q = acceleration due to gravity, in feet per second per second;
K = ratio of eddy losses to velocity-head change between any two consecutive sections;
L = length of a reach, in feet;
n = roughness coefficient in the Manning formula;
P = wetted perimeter, in feet;
Q = discharge, in cubic feet per second;
R = hydraulic radius in feet;
S = rate of loss of head caused by friction at any section, as determined by the Manning formula;
V = mean velocity of flow at any section, in feet per second; and
Z = water-surface elevation at any section, in feet.

DISCUSSION

I. H. Steinberg.[4]—The advantages of any graphical or semigraphical solution over the trial-and-error methods of flow line computations lie in the frequent use of the derived curves. Where only a relatively few profiles of given discharges and conditions are required, it has been found practicable to draw the elevation-area curves and elevation-($A\,R^{2/3}$) curves to a convenient scale and use the trial-and-error method for tracing the water-surface profile. There have been many occasions, however, when it was necessary for the writer to compute numerous water-surface profiles over the same stretch of river. It would have been an insurmountable task were it not for the fact that it was possible to use graphical solutions. In most of the graphical methods corrections for velocity head were not considered.

The author has presented a relatively simple graphical method of computing directly the water-surface profiles in natural and artificial watercourses. Where profiles for discharges of different magnitudes are required, it would be desirable to present the pairs of curves for the discharges on separate axes for each reach. Thus, only the curves of $Z + \phi(Z)$ for station 80 + 00 and the curves of $Z + f(Z)$ for station 85 + 00 for the discharges of 33,500 cu ft per sec and 40,000 cu ft per sec would be shown in Fig. 2. The curves for the other reaches could be shown in a similar manner.

Mr. Ezra uses a weighted value for the velocity of flow when both channel flow and overbank flow are involved. A suggested method is to weight the velocities in accordance with the respective channel and overbank discharges. A weighted-area curve which can be applied directly to the discharges to obtain the weighted velocities can then be derived. Therefore,

$$\bar{V} = \frac{Q_c\,V_c + Q_o\,V_o}{Q} \quad \text{.......................} (5)$$

in which $\bar{V}$ is the weighted velocity in feet per second, Q_c is the channel flow in cubic feet per second, V_c denotes the velocity of flow in the channel, Q_o represents the overbank flow in cubic feet per second, V_o is the velocity of overbank flow, and Q is the total discharge in cubic feet per second.

Because

$$V = \frac{Q}{A} \quad \text{.........................} (6a)$$

then

$$\frac{Q^2}{A_w} = \frac{Q^2{}_c}{A_c} + \frac{Q^2{}_o}{A_o} \quad \text{.......................} (6b)$$

in which A_w is the weighted cross-sectional area, and A_c and A_o are the cross-sectional areas of the channel flow and the overbank flow, respectively.

From the Manning formula,

$$Q_c = C_c\,h^{1/2}{}_f \quad \text{.......................} (7a)$$

$$Q_o = C_o\,h^{1/2}{}_f \quad \text{.......................} (7b)$$

---

[4] Superv. Hydr. Engr., Corps of Engrs., U. S. Dept. of the Army, San Francisco, Calif.

and

$$Q = (C_e + C_o)\, h^{\frac{1}{2}}{}_f = C\, h^{\frac{1}{2}}{}_f \quad \text{(7c)}$$

in which

$$C = \frac{1.486}{n} \frac{A\, R^{\frac{2}{3}}}{L^{\frac{1}{2}}} \quad \text{(8)}$$

and h_f is the friction loss in feet in the distance L. From Eq. 6*b*,

$$\frac{C^2\, h^2{}_f}{A_w} = \frac{C^2{}_c\, h_f}{A_c} + \frac{C^2{}_o\, h_f}{A_o} \quad \text{(9a)}$$

or

$$\frac{1}{A_w} = \frac{1}{A_c}\left(\frac{C_c}{C}\right)^2 + \frac{1}{A_o}\left(\frac{C_o}{C}\right)^2 \quad \text{(9b)}$$

from which

$$A_w = A_c \left[\frac{\left(\frac{C}{C_c}\right)^2}{1 + \left(\frac{A_c}{A_o}\right)\left(\frac{C_o}{C_c}\right)^2}\right] \quad \text{(9c)}$$

Either Eq. 9*b* or Eq. 9*c* can be used to compute the weighted-area curve. Where the channel and overbank lengths are equal, the term L will cancel and therefore can be omitted from Eq. 8. Where the reach lengths are different for channel and overbank, the average lengths for adjacent reaches upstream and downstream from the section should be used in Eq. 7.

If the velocity head rather than the velocity is weighted, the expression for the weighted-area curve will be

$$A_w = A_c \left\{\frac{1}{\left[\left(\frac{C_c}{C}\right)^3 + \left(\frac{C_o}{C}\right)^3\left(\frac{A_c}{A_o}\right)^2\right]^{\frac{1}{2}}}\right\} \quad \text{(10)}$$

A number of graphical and semigraphical charts and graphs have been developed for eliminating the trial-and-error computations in tracing the water-surface profile. The writer devised a method which required a nomograph for the solution.[5] In most methods the velocity-head corrections have not been taken into account. However, Francis F. Escoffier has presented a solution which is similar to the direct step method developed by Mr. Ezra in the respect that pairs of curves are plotted for each reach. A sloping straight line drawn from the known point on one curve to the intersection of the second curve gives the required water-surface elevation. The slope of the line is a function of the discharge. Thus, only one set of basic curves is required for a wide range of discharges.

The writer has also developed a graphical solution utilizing "slope curves" in which velocity head corrections are provided for. In this method the water-surface elevations at the lower end of the reach and the discharges are plotted as ordinates and abscissas, respectively, whereas the falls, or differences in water-surface elevation between the upstream and downstream end of the reach, are plotted as the parameter. The curves can also be plotted with the elevation at the upper end of the reach as the parameter. Eq. 1 can be written as

---

[5] "The Nomograph As an Aid in Computing Backwater Curves," by I. H. Steinberg, *Civil Engineering*, Vol. 9, 1939, p. 365.

$$Z_1 + \frac{V^2_1}{2\,g} = Z_2 + \frac{V^2_2}{2\,g} + h_f + h_o \quad \text{.............. (11a)}$$

in which

$$h_o = K\left(\frac{V^2_1}{2\,g} - \frac{V^2_2}{2\,g}\right) \quad \text{.................. (11b)}$$

Using the Manning formula for computing the friction loss,

$$h_f = Q^2\left(\frac{n}{1.486\,A_m\,R^{\frac{2}{3}}_m}\right)^2 L = \left(\frac{Q}{C_m}\right)^2 \quad \text{........... (12a)}$$

in which

$$C_m = \frac{1.486}{n}\,\frac{A_m\,R^{\frac{2}{3}}_m}{L^{\frac{1}{2}}} \quad \text{.................. (12b)}$$

The subscript *m* is used to denote the mean value for the reach, and attention is directed to the different method of applying the hydraulic elements to obtain the average slope in the reach from that used in Mr. Ezra's derivation. The mean value for the reach can be based on the average of the end value or on the value as defined by the midpoint elevation of the reach. The writer uses the latter system because of the greater simplicity in computing the basic slope curves.

Eq. 1 can also be written as

$$Z_1 - Z_2 = F = \left(\frac{Q_m}{C_m}\right)^2 - \left(\frac{V^2_1}{2\,g} - \frac{V^2_2}{2\,g}\right) + K\left(\frac{V^2_1}{2\,g} - \frac{V^2_2}{2\,g}\right) \quad \text{... (13a)}$$

and

$$F = \left(\frac{Q}{C_m}\right)^2 - \left(\frac{V^2_1}{2\,g} - \frac{V^2_2}{2\,g}\right)(1 - K) \quad \text{............ (13b)}$$

However,

$$V = \frac{Q}{A} \quad \text{......................... (14a)}$$

Therefore,

$$F = \left(\frac{Q}{C_m}\right)^2 - \left[\left(\frac{Q}{8.03\,A_1}\right)^2 - \left(\frac{Q}{8.03\,A_2}\right)^2\right](1 - K) \quad \text{...... (14b)}$$

and

$$F = \left(\frac{Q}{C_m}\right)^2\left\{1 - \left[\left(\frac{C_m}{8.03\,A_1}\right)^2 - \left(\frac{C_m}{8.03\,A_2}\right)^2\right](1 - K)\right\} = \left(\frac{Q\,M}{C_m}\right)^2 \text{. (14c)}$$

in which

$$M^2 = 1 - \left[\left(\frac{C_m}{8.03\,A_1}\right)^2 - \left(\frac{C_m}{8.03\,A_2}\right)^2\right](1 - K) \ldots\ldots\ldots (15a)$$

and

$$Q = \frac{C_m}{M}(F)^{\frac{1}{2}} \ldots\ldots\ldots\ldots\ldots\ldots\ldots\ldots (15b)$$

Any given values of midpoint elevation and of fall, F, in a reach will define corresponding values of C_m, A_1, and A_2. The value of M can be computed from Eq. 15a and the value of Q then determined from Eq. 15b. For development of the "slope curves," Eqs. 15a and 15b are solved for a range of values of midpoint elevation and fall. The resulting points are plotted as curves on appropriate graphs.

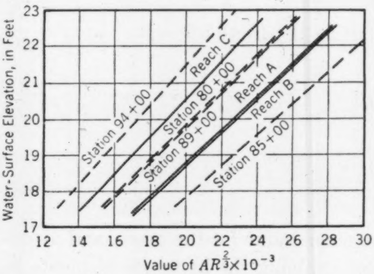

FIG. 4.—ELEVATION—($A\,R^{\frac{2}{3}}$) CURVES

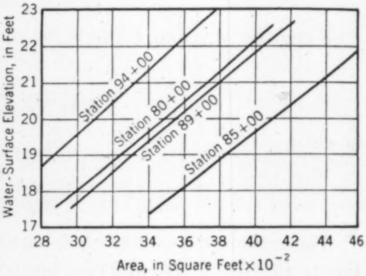

FIG. 5.—ELEVATION—AREA CURVES

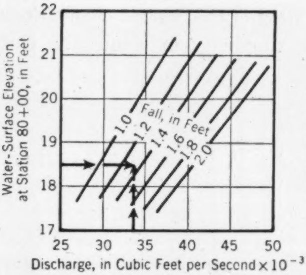

FIG. 6.—SLOPE CURVES FOR REACH A

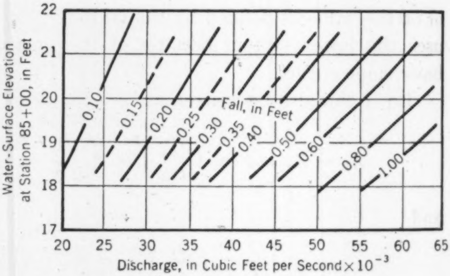

FIG. 7.—SLOPE CURVES FOR REACH B

To illustrate the application of the "slope curve" graphical method in which a velocity-head correction is included, Example No. 1 will be used. Values of K equal to 0.5 for decelerating flow and K equal to $-$ 0.1 for accelerating flow have been adopted. The negative value of K for accelerating flow has been used to conform with Eq. 15a.

Table 7 contains the same basic data as given in Table 1, except that the values of $A\,R^{\frac{2}{3}}$ have been computed. Elevation-($A\,R^{\frac{2}{3}}$) curves and elevation-area curves, based on Table 7, are shown in Figs. 4 and 5. Table 8 illustrates the computations for reach A (station 80 + 00 to station 85 + 00). The values of $A R^{\frac{2}{3}}$ (Col. 5) and areas (Cols. 6 and 7) were obtained from the curves in Figs. 4 and 5. The resulting slope curves are shown in Fig. 6. The curves for reaches B (station 85 + 00 to station 89 + 00) and C (station 89 + 00 to station 94 + 00) are shown in Figs. 7 and 8.

TABLE 7.—HYDRAULIC PROPERTIES OF CROSS SECTIONS

Station (1)	Water-surface elevation, Z, in feet (2)	Cross-sectional area, A, in square feet (3)	Wetted perimeter P, in feet (4)	$A R^{\frac{2}{3}}$ (5)
80 + 00	18.0	3,000	238	16,210
	20.0	3,500	248	20,400
	22.0	3,970	258	24,580
85 + 00	18.0	3,580	265	20,400
	20.0	4,100	273	25,000
	22.0	4,630	282	29,800
89 + 00	18.0	3,080	248	16,400
	20.0	3,550	258	20,500
	22.0	4,050	268	24,750
94 + 00	18.0	2,650	225	13,710
	20.0	3,100	235	17,350
	22.0	3,550	245	21,000

TABLE 8.—COMPUTATIONS FOR DEVELOPING THE SLOPE CURVES FOR REACH A

Midpoint elevation, in feet	Fall, F, in feet	WATER-SURFACE ELEVATION, IN FEET		$A R^{\frac{2}{3}}$	C_m	CROSS-SECTIONAL AREA, IN SQUARE FEET		M^2	Discharge, Q, in cubic feet per second
		Z_2, Station 80 + 00	Z_1, Station 85 + 00			A_2, Station 80 + 00	A_1, Station 85 + 00		
(1)	(2)	(3)	(4)	(5)[a]	(6)[b]	(7)[c]	(8)[c]	(9)[d]	(10)[e]
18.5	1.0	18.0	19.0	19,450	43,100	3,000	3,840	2.39	27,800
	1.2	17.9	19.1			2,970	3,865	2.47	30,000
	1.4	17.8	19.2			2,950	3,895	2.55	31,800
	1.6	17.7	19.3			2,920	3,920	2.63	33,600
	1.8	17.6	19.4			2,900	3,950	2.71	35,050
	2.0	17.5	19.5			2,880	3,975	2.80	36.400
19.5	1.0	19.0	20.0	21,600	47,800	3,255	4,100	2.37	31,050
	1.2	18.9	20.1			3,230	4,130	2.45	33,500
	1.4	18.8	20.2			3,205	4,155	2.54	35,600
	1.6	18.7	20.3			3,180	4,185	2.62	37,400
	1.8	18.6	20.4			3,155	4,210	2.71	38,900
	2.0	18.5	20.5			3,130	4,235	2.79	40,500
20.5	1.0	20.0	21.0	23,800	52,600	3,500	4,370	2.40	33,900
	1.2	19.9	21.1			3,475	4,395	2.48	36,600
	1.4	19.8	21.2			3,450	4,420	2.56	38,900
	1.6	19.7	21.3			3,425	4,445	2.65	40,900
	1.8	19.6	21.4			3,400	4,470	2.74	42,900
	2.0	19.5	21.5			3,380	4,500	2.82	44,400
21.5	1.0	21.0	22.0	26,000	57,500	3,740	4,630	2.41	37,050
	1.2	20.9	22.1			3.715	4,655	2.49	39,950
	1.4	20.8	22.2			3,690	4,685	2.58	42,400
	1.6	20.7	22.3			3,665	4,710	2.67	44,500
	1.8	20.6	22.4			3,640	4,735	2.75	46,600
	2.0	20.5	22.5			3,620	4,760	2.83	48,200

[a] Values of $A R^{\frac{2}{3}}$ obtained from Fig. 4. [b] Values of C_m determined from Eq. 12*b* with $n = 0.030$ and $L = 500$ ft. [c] Values of A obtained from Fig. 5. [d] Values of M^2 computed from Eq. 15*a* with $K = 0.5$ when $A_1 < A_2$ and $K = -0.1$ when $A_1 > A_2$. [e] Values of Q determined from Eq. 15*b*.

To compute the water-surface profile, it is necessary only (1) to enter the slope curves with the given elevation at the lower end of the reach and the given discharge, (2) to read the corresponding fall, and (3) to add to the given elevation to obtain the elevation at the upper end of the reach, which then becomes the given elevation at the lower end of the next upstream reach. This procedure is illustrated in Table 9. The computed water-surface profile shown in Table 9 agrees closely with that shown in Table 6.

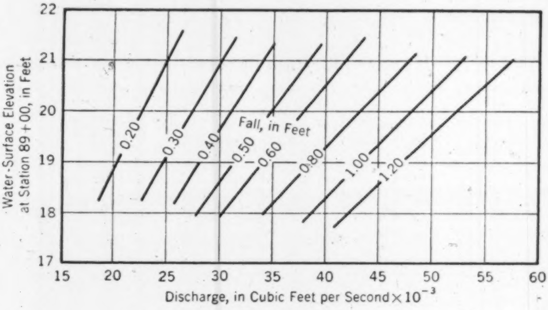

FIG. 8.—SLOPE CURVES FOR REACH C

TABLE 9.—COMPUTATION OF WATER-SURFACE PROFILE FOR A VALUE OF Q = 33,500 CU FT PER SEC

Station (1)	Reach (2)	Water-surface elevation, Z, in feet (3)	Fall, F, in feet (4)
80 + 00		18.50	
	A		1.33
85 + 00		19.83	
	B		0.21
89 + 00		20.04	
	C		0.48
94 + 00		20.52	

TABLE 10.—DOWNSTREAM COMPUTATION OF WATER-SURFACE PROFILE FOR A VALUE OF Q = 33,500 CU FT PER SEC

Station (1)	Reach (2)	Water-surface elevation, Z, in feet (3)	Trial water-surface elevation at lower end of reach (4)	Fall, F, in feet (5)	Computed water-surface elevation at upper end of reach (6)
94 + 00		21.00			
	A		20.60 20.57	0.42 0.43	21.02 21.00
89 + 00		20.57			
	B		20.35 20.38	0.19 0.19	20.54 20.57
85 + 00		20.38			
	C		19.25 19.20	1.18 1.18	20.43 20.38
80 + 00		19.20			

It should be noted that the slope curves have been drawn for computing upstream. The same curves can be readily adapted, however, for computing downstream by trial and error. In this case—(*a*) the elevation at the lower end of the reach is assumed and (*b*) the fall is obtained from the slope and added to the assumed elevation. This elevation is checked against the given elevation at the upper end of the reach. Usually two, or perhaps three, trial computations are required to obtain the correct fall. An illustration of the procedure is given in Table 10.

C. A. M. GRAY,[6] A. M. ASCE.—An ingenious variant of the standard step method has been presented by the author. As the solution is direct and the labor involved is considerable, the question of how long the steps are to be made is most important. It seems worthwhile, therefore, to investigate the measure of the error introduced by the selection of an arbitrary length of step.

Eq. 2, neglecting the eddy-loss term, is obtained from the "exact" integral relationship,

$$Z_2 + \frac{V^2_2}{2\,g} = Z_1 + \frac{V^2_1}{2\,g} - \int_1^2 S\,dx \ldots\ldots\ldots\ldots\ldots (16)$$

when the integral is evaluated by the trapezoidal rule. An alternative value would be $S_M\,L$ in which S_M is the value of S at the midpoint of the interval L. If the integral is denoted by I, it can be shown that

$$\frac{S_1 + S_2}{2}\,L > I > S_M\,L \ldots\ldots\ldots\ldots\ldots\ldots (17a)$$

or

$$S_M\,L > I > \frac{S_1 + S_2}{2}\,L \ldots\ldots\ldots\ldots\ldots\ldots (17b)$$

depending on whether the curve of S versus x is concave upward or concave downward. In the former case, Mr. Ezra's solution would give too small a value for Z, and in the latter case it would result in too great a value. Using the mean value of S will give an opposite result. An estimate of S_M can be obtained by use of the data required for Fig. 2. If

$$\left(Z + \frac{V^2}{2\,g}\right)_{x=L/2} = Z_1 + \frac{V^2_1}{2\,g} - j \ldots\ldots\ldots\ldots\ldots (18a)$$

and

$$\lambda < S < \mu \ldots\ldots\ldots\ldots\ldots\ldots\ldots\ldots (18b)$$

in the range $0 < x < L$, then

$$\frac{\lambda\,L}{2} < j < \frac{\mu\,L}{2} \ldots\ldots\ldots\ldots\ldots\ldots\ldots\ldots (18c)$$

Hence,

$$Z_1 + \frac{V^2_1}{2\,g} - \frac{\mu\,L}{2} < E_M < Z_1 + \frac{V^2_1}{2\,g} - \frac{\lambda\,L}{2} \ldots\ldots\ldots\ldots (19a)$$

---

[6] Senior Lecturer in Civ. Eng., Univ. of Sydney, Sydney Australia

in which

$$E_M = \left(\frac{V^2}{2g} + Z\right)_{x=L/2} \quad \text{(19b)}$$

From the properties of the section at $x = L/2$, limits can be set for S_M. Unfortunately, the data are not available. For purposes of investigation it can be assumed, however, that the cross section is constant between stations.

From Tables 1 and 3 it can be seen that, in the interval from station 80 + 00 to station 85 + 00,

$$0.00076 < S < 0.00162 \quad \text{(20a)}$$

and the value of E at station 80 + 00 is 20.31. Hence, from Eq. 19*a*,

$$0.40 + 20.31 = 20.71 > E_M > 0.19 + 20.31 = 20.50 \quad \text{(20b)}$$

From Table 1

$$0.00149 > S_M > 0.00139 \quad \text{(20c)}$$

which is greater than the mean value $\frac{S_1 + S_2}{2}$, indicating that the curve of S versus x is concave downward.

Hence, at station 85 + 00,

$$E < 20.31 + 0.75 = 21.06 \quad \text{(21a)}$$

and from Table 1

$$Z < 20.02 \quad \text{(21b)}$$

Under these conditions, at station 85 + 00,

$$19.83 < Z < 20.02 \quad \text{(22a)}$$

and

$$20.90 < E < 21.06 \quad \text{(22b)}$$

Upper and lower bounds to Z at station 85 + 00 have thus been established, and the separation of these values gives a measure of the accuracy achieved with the assumed length of step.

Bob Buehler,[7] A. M. ASCE.—A method has been presented by Mr. Ezra which should be welcomed by those engaged in computing water-surface profiles in natural streams or reservoirs. If profiles for several flows and downstream starting elevations are to be determined, use of this method, as opposed to the standard trial-and-error procedure, will save time and avoid drudgery. The method has been tried successfully on a typical stream, and it is believed to be superior to most others.

This discussion (1) seeks confirmation or simplification of a method presented by the writer for the consideration of overbank flow; (2) offers alternate plotting procedures; and (3) seeks further confirmation of (*a*) the application of channel-roughness coefficients which vary from reach to reach, (*b*) the determination of these coefficients from observed flood profiles, and (*c*) the determination of channel coefficients under conditions in which there is a substantial amount of overbank flow.

---

[7] Hydr. Engr., TVA, Knoxville, Tenn.

Inclusion of Overbank Flow.—Table 11, showing hydraulic properties, is a variation of Table 1 in that flow in an assumed overbank has been added. For brevity, only the reach from station 80 + 00 to station 85 + 00 has been used. Table 11 shows, for each elevation, two values for the area and two values for the hydraulic radius. The upper figure is the channel value used in Table 1, and the lower figure is the overbank value that has been assumed for illustration. The value of *n* for the overbank has been taken as 0.05. If discharge is represented by

TABLE 11.—HYDRAULIC PROPERTIES OF CROSS SECTIONS FOR Q = 33,500 CU FT PER SEC, n for CHANNEL = 0.03, AND n FOR OVERBANK = 0.05

Station (1)	Water-surface elevation Z, in feet (2)	Cross-sectional area A, in square feet (3)	Hydraulic radius R, in feet (4)	$Q\,S^{-\frac{1}{2}}$ (5)	Flow Q, in cubic feet per second (6)	$S^{\frac{1}{2}}$ (7)	Friction gradient (8)	Velocity V, in feet per second (9)	$V^2 Q$ (10)	Weighted V^2 (11)	Weighted $\frac{V^2}{2g}$ (12)
80+00	18.0	3,000	12.60	805,000							
		0	0.00	0	0						
					33,500	0.0416	0.00173	11.17			1.94
	20.0	3,500	14.11	1,012,000	32,508			9.29	2,800,000		
		500	3.00	30,900	992			1.98	3,890		
				1,042,900	33,500	0.0321	0.00103		2,803,890	83.7	1.30
	22.0	3,970	15.39	1,217,000	31,000			7.81	1,891,000		
		1,000	6.00	98,100	2,500			2.50	15,620		
				1,315,100	33,500	0.0255	0.000650		1,906,620	56.9	0.88
85+00	18.0	3,580	13.51	1,005,000							
		0	0.00	0	0						
					33,500	0.0333	0.00111	9.36			1.36
	20.0	4,100	15.02	1,237,000	33,161			8.09	2,170,000		
		300	1.70	12,660	339			1.13	433		
				1,249,660	33,500	0.0268	0.000718		2,170,433	64.8	1.01
	22.0	4,630	16.42	1,482,000	31,823			6.87	1,502,000		
		900	5.00	78,100	1,677			1.86	5,800		
				1,560,100	33,500	0.0215	0.000462		1,507,800	45.0	0.70

$$Q = \frac{1.486\,A\,R^{\frac{2}{3}}\,S^{\frac{1}{2}}}{n} \qquad (23a)$$

then

$$\frac{Q}{S^{\frac{1}{2}}} = \frac{1.486\,A\,R^{\frac{2}{3}}}{n} \qquad (23b)$$

In Col. 5, Table 11, $Q\,S^{-\frac{1}{2}}$ can be computed first for the channel section, and next for the overbank; then the two values are added. For El. 20.0 at station 80 + 00, $Q\,S^{-\frac{1}{2}}$ is 1,012,000 in the channel, 30,900 in the overbank, thus totalling 1,042,900. The true total discharge is known to be 33,500 cu ft per sec. Therefore, Cols. 7 and 8 (Table 11) can be determined. With $S^{\frac{1}{2}}$ known, the parts of the total flow carried respectively by the channel and overbank can be computed and entered in Col. 6, Table 11. The velocities and weighted velocity head for the total section can be found and entered in Cols. 9 through 12, Table 11.

Table 12 shows, for this same reach, the computation for $\phi(Z)$ and $f(Z)$ for the base flow of 33,500 cu ft per sec using the slopes and weighted velocity heads found in Table 11. Other entries in Table 12 will be explained subsequently.

TABLE 12.—COMPUTATION FOR $Z + f(Z)$ AND $Z + \phi(Z)$ FOR REACH FROM STATION 80 + 00 TO STATION 85 + 00 WITH n FOR CHANNEL = 0.03, n FOR OVERBANK = 0.05, AND $L/2$ = 250 FT

Station	Water-surface elevation Z, in ft	VALUES FOR Q = 33,500 CU FT PER SEC				VALUES OF $\phi(Z)$ OR $f(Z)$ FOR FLOW Q, IN CU FT PER SEC				VALUES OF $Z + \phi(Z)$ OR $Z + f(Z)$ FOR FLOW Q, IN CU FT PER SEC			
		$S\frac{L}{2}$	Weighted $\frac{V^2}{2g}$	$\phi(Z)$	$f(Z)$	10,000	20,000	30,000	40,000	10,000	20,000	30,000	40,000
80 + 00	18.0	0.43	1.94	2.37		0.21	0.84	1.90	3.37	18.21	18.84	19.90	21.37
	20.0	0.26	1.30	1.56		0.14	0.56	1.25	2.22	20.14	20.56	21.25	22.22
	22.0	0.16	0.88	1.04		0.09	0.37	0.83	1.48	22.09	22.37	22.83	23.48
85 + 00	18.0	0.28	1.36		1.08	0.10	0.38	0.87	1.54	18.10	18.38	18.87	19.54
	20.0	0.18	1.01		0.83	0.07	0.30	0.66	1.18	20.07	20.30	20.66	21.18
	22.0	0.12	0.70		0.58	0.05	0.21	0.46	0.83	22.05	22.21	22.46	22.83

Alternate Plotting Procedures.—Adaptation to specific needs as well as to individual preference determines the most convenient method of plotting. For example, if curves were to be prepared which would be suited to a wide variety of flows, the form used by the author would become unwieldy. It would seem logical, therefore, to use one plotting sheet for each reach, showing on each a family of discharge curves. An example for the reach from station 80 + 00 to station 85 + 00 is shown in Fig. 9 which was prepared from Table 12. Values of $\phi(Z)$ and $f(Z)$ in Table 12 for the various flows were computed from the base value for 33,500 cu ft per sec, using the ratio of the discharges squared, as suggested by Mr. Ezra. The solid lines in Fig. 9 were drawn from computed values of $Z + \phi(Z)$ and $Z + f(Z)$. The dashed intermediate lines were interpolated by use of construction lines based on the computed curves. The form of this plot differs from that presented by the author. In this form, if eddy losses are ignored, the upper curves can be entered with the known elevation at the downstream section and flow—for example, El. 20.32 at station 80 + 00 and 37,000 cu ft per sec. This intersection is carried vertically downward to the lower curves until the proper discharge is reached. This lower intersection gives a resulting elevation of 21.28 at station 85 + 00. The values of $Z + \phi(Z)$

and $Z + f(Z)$ need not be tabulated since they only represent guide lines connecting the upper curves for station 80 + 00 to the lower curves for station 85 + 00.

The basic form of the curve in which Z is plotted against $Z + \phi(Z)$ and $Z + f(Z)$ has serious limitations if the water-surface elevations at a given section will vary over a wide range. A scale on a convenient size of graph paper can be read with sufficient accuracy if the graph covers an elevation range of perhaps 10 ft, but not if it covers a range of 50 ft or more. For any given reach, however, there usually is a reasonable limit in the elevation differences at the two ends. The functions $\phi(Z)$ and $f(Z)$ are closely related to the rise in a reach, suggesting a rearrangement of Eq. 4. Neglecting eddy losses, Eq. 4 can be written as

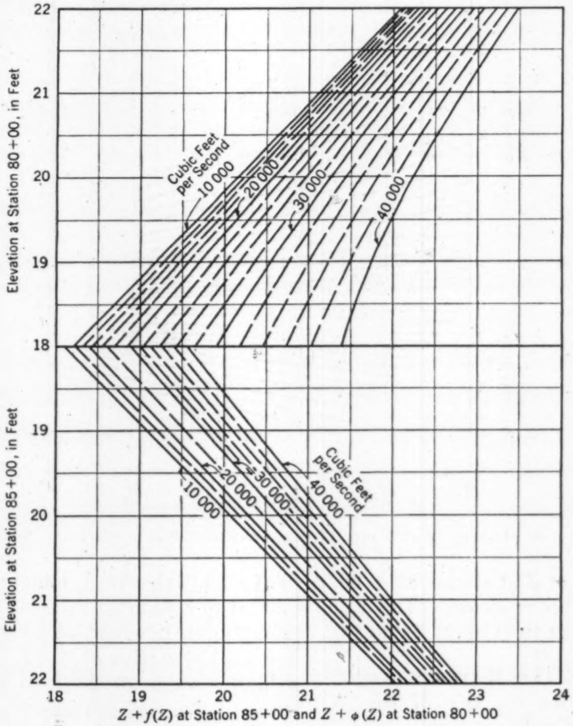

FIG. 9.—CURVES FOR COMPUTING WATER-SURFACE PROFILE

$$Z_1 = Z_2 + \phi(Z_2) - f(Z_1) \qquad (24)$$

For any reach, a curve can be drawn for the downstream section showing $\phi(Z)$ versus Z. Another curve can also be drawn for the upstream section showing $f(Z)$ against $Z + f(Z)$. Fig. 10 is an example of this in which the reach from station 80 + 00 to 85 + 00 has been used. Fig. 10 was plotted from the data in Table 12. Table 13 shows the water-surface profile for a flow of 37,000 cu ft per sec and illustrates the use of the curves. Starting with

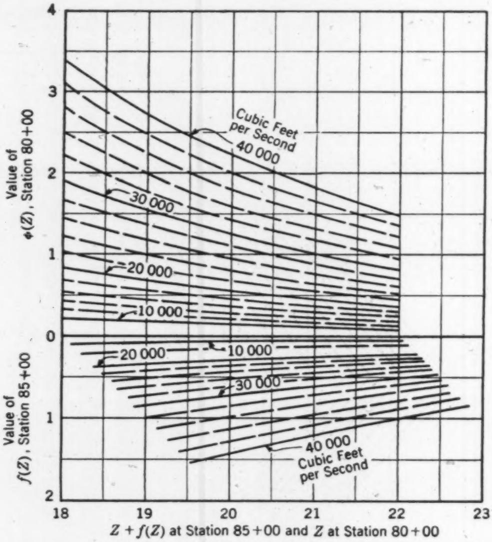

FIG. 10.—CURVES OF $\phi(Z)$ AND $f(Z)$ FOR COMPUTING WATER-SURFACE PROFILES

El. 20.32 or Z at station 85 + 00, $\phi(Z)$ (Col. 3, Table 12) is found to be 1.78 from the upper curves. This value is added to Z to get a value of $Z + \phi(Z)$ equal to 22.10 (Col. 4, Table 13). From Eq. 4, however, this value equals $Z + f(Z)$ at station 85 + 00. Entering with this value of 22.10 in the lower curves, $f(Z_1)$ (Col. 5, Table 13), is found to be 0.82. The value of Z at station 85 + 00 (El. 21.28) is Col. 5, Table 13, subtracted from Col. 4, Table 13. In this procedure, elevations are not read from the curves. Instead, factors comprising the difference in elevations are read. The operation requires more tabulating than when Fig. 9 is used; but with the same size graph paper, it is far more accurate whenever wide elevation ranges must be accommodated. Of course, it is presumed that reaches will be short enough so that values of $\phi(Z)$ and $f(Z)$ will be sufficiently small to plot with reasonable accuracy.

TABLE 13.—WATER-SURFACE PROFILE FOR $Q = 37{,}000$ CU FT PER SEC

Station (1)	Water-surface elevation Z, in feet (2)	Value of $\phi(Z)$ (3)	Value of $Z+\phi(Z)$ (4)	Value of $f(Z)$ (5)
80 + 00	20.32	1.78	22.10	
85 + 00	21.28			0.82

Roughness Coefficients and their Determination.—Whenever possible, it has been the writer's practice to use roughness coefficients that were computed from observed flood profiles for known flows. If a choice of floods for this purpose is available, the preferred flood is one which just fills the channel part of the cross section without extending into the overbank. The resulting computed channel coefficients are then tested on one or more higher floods to aid in assigning a suitable roughness coefficient to the overbank. Channel-roughness values usually vary enough, and are critical enough, so that different values are required in each reach. Overbank values (*a*) are more difficult to compute with assurance, (*b*) are usually less critical than channel values, and (*c*) are often assumed to be constant for long stretches of a stream. Channel-roughness factors are computed, and applied, with the friction slope based on the average of the areas and the hydraulic radii at the two sections bounding each reach.

Mr. Ezra uses a different procedure in the application of area and of hydraulic radius. The rate of friction slope is found for each section using its area and hydraulic radius. The total friction slope in a reach is, then, the average of the rates at its two end points times the length. If roughness factors vary in each reach, the rate of friction loss at each section must be computed twice—once for use in an upstream direction, and once for use in a downstream direction. This would require two columns for S in Table 1, one headed S_u and one S_d. It would be similar to the need for both Cols. 3 and 4, in Table 2, in which $\frac{1}{2} L$ may differ in the upstream and downstream directions. Also, Col. 3, Table 2, would then be entitled $\frac{1}{2} S_d L_d$ and Col. 4, Table 2, would be entitled $\frac{1}{2} S_u L_u$.

When overbank flow is not involved, roughness factors can presumably be computed from a marked flood profile of known flow using Eq. 3. All quantities in this equation are known except the value of n. When n must be computed from a flood involving appreciable overbank flow, however, the determination of the channel values, even with the value of n in the overbanks assumed, becomes a cumbersome operation. Were it not necessary to weight the channel and overbank velocity heads, the overbank flow could be computed first and deducted from the known total flow, thereby leaving the necessary known quantities with which the channel roughness can be computed. This would be a reasonable expedient if the overbank flows were not large. When overflow is large, however, and when it appears necessary to use a weighted velocity head (even with an assumed overbank n), it seems necessary to make successive estimates of the value of n for the channel until a value is found that will satisfy Eq. 3 (modified to include overbank flow). An application of this principle to a typical stream required the use of a 20-column table to reach a satisfactory solution.

Monir M. Kansoh.[8]—The method proposed by the author is a valuable contribution to the problem of plotting water-surface profiles. It facilitates plotting and saves time, especially once the necessary tables and graphs are computed and prepared.

---

[8] Asst. Prof., Faculty of Eng., Univ. of Alexandria, Alexandria, Egypt.

Mr. Ezra describes his method as being a general one. Actually, however, the method is limited to cases involving gradually varying flow in which departure from hydrostatic conditions is so negligible that the potential energy can be expressed by the terms Z_1 or Z_2 in Eq. 1. The method is based on the assumption that the velocity is uniformly distributed over the area of any cross section.

The term "S" varies with the rugosity factor which can be supposed to be constant between two consecutive stations, as well as with the velocity of flow and with the proportions of the section of the channel. The average rate of friction loss of head can then be taken to be equal to

$$S_{\text{aver}} = \left(\frac{n}{1.486}\,\frac{V_{\text{aver}}}{R_{\text{aver}}^{2/3}}\right)^2 \dots\dots\dots\dots (25)$$

Assuming, in a uniform canal, that

$$V_{\text{aver}} = \frac{V_1 + V_2}{2} \dots\dots\dots\dots (26a)$$

and

$$R_{\text{aver}} = \frac{R_1 + R_2}{2} \dots\dots\dots\dots (26b)$$

then

$$S_{\text{aver}} = \left(\frac{n}{1.486}\right)^2 \left(\frac{V_1 + V_2}{2}\right)^2 \left(\frac{2}{R_1 + R_2}\right)^{4/3}$$

$$= \left(\tfrac{1}{2}\right)^{2/3} \frac{n^2}{2.2}\,\frac{(V_1 + V_2)^2}{(R_1 + R_2)^{4/3}} \dots\dots\dots\dots (27)$$

Eq. 27 shows that S_{aver}, as derived, does not equal $\frac{1}{2}\,(S_1 + S_2)$, nor $\frac{1}{2}\,\frac{n^2}{2.2}\left(\frac{V^2{}_1}{R^{4/3}{}_1} + \frac{V^2{}_2}{R^{4/3}{}_2}\right)$ as proposed by the author.

It should be realized that the area, the perimeter, the hydraulic mean depth or radius, and consequently $\frac{Q^2}{g\,A^2}$ and $\frac{Q^2\,n^2}{2.2\,A^2\,R^{4/3}}$ are functions of the depth of flow and not of the elevation of the water surface above a chosen datum. It is not correct, then, to denote that (in general)

$$\frac{Q^2}{2\,g\,A^2} \pm \frac{L}{2}\,\frac{Q^2\,n^2}{2.2\,A^2\,R^{4/3}} = \phi\,(Z) \text{ and } f\,(Z).$$

This is true only in particular cases for particular cross sections selected beforehand.

It would be helpful if a plot were presented of the same surface profiles computed by Mr. Ezra's method and according to the methods developed by Bresse, Bakhmeteff, and Tolkmitt (as well as some of the simplified analytical and graphical methods) to show the discrepancy.

ARTHUR A. EZRA,[9] J. M. ASCE.—Mr. Kansoh is correct in stating that the proposed method is limited to conditions in which the potential energy can be expressed by the terms Z_1 or Z_2 in Eq. 1. This limitation corresponds to the boundary conditions (found in the theory of varied flow in open channels) on which are based the generally used methods of determining water-surface profiles. The velocities used are usually the mean or weighted velocities at a section. The area, the perimeter, the hydraulic radius, and consequently the terms $\frac{A^2}{g\,A^2}$ and $\frac{A^2\,n^2}{2.2\,A^2\,R^{4/3}}$ are functions of the depth of flow and the elevation of the water surface above a chosen datum. The reason for this interrelationship is that the depth of flow is a function of the difference between the water-surface elevation and the elevation of the channel bottom. The elevation of the channel bottom is expressed implicitly in the values of A and R that correspond to a given water-surface elevation at a section.

Mr. Kansoh's question regarding the value of S_{aver} appears to be a matter of definition. The writer defined S_{aver} as that value of S which is the arithmetic mean of the values S_1 and S_2. These values of S are determined individually from Manning's formula using V_1, R_1, and V_2, R_2, respectively. Mr. Kansoh defines S_{aver} as that value of S which is obtained by substituting in Manning's formula the arithmetic mean of V_1 and V_2 together with the arithmetic mean of R_1 and R_2. Naturally, the value of S_{aver} as defined by Mr. Kansoh will not equal $\frac{1}{2}(S_1 + S_2)$. The writer's usage of $\frac{1}{2}(S_1 + S_2)$ as the average rate of loss of head corresponds to that used by George E. Russell.[10] The writer's method gives plots of surface profiles corresponding to those obtained by the standard step method which is based on trial and error. Mr. Kansoh's suggestion of plotting the same surface profiles for comparison by Bresse's, Bakhmeteff's, and Tolkmitt's methods is profitable.

The writer is indebted to Mr. Gray for his analysis of the relative accuracy of the approximation used to establish the friction-head loss in a reach in comparison to the results obtained by using $\int S\,dx$ and $S_M\,L$. From Table 3 the difference in water-surface elevations between station 85 + 00 and station 80 + 00 is 1.33 ft. Using Mr. Gray's method of analysis, the difference in water-surface elevations computed by using $\int_1^2 S\,dx$ is between 1.33 ft and 1.52 ft. On the basis of this analysis, the writer's approximation yields a result for a 500-ft-long interval that is within 12% of the result that would be obtained by using $\int S\,dx$. This inaccuracy is small in comparison to the inaccuracies involved in the choice of a value of the roughness coefficient n, especially since S varies as n^2.

Mr. Buehler has made a valuable contribution to the method of computing water-surface profiles. His suggestions for alternate plotting procedures are very appropriate. It is agreed that one plotting sheet should be used for each reach, as shown in Fig. 9. The form used in Fig. 2 was presented for the purpose of illustrating the application of the proposed method. The method of plotting shown in Fig. 10 is an ingenious solution to the practical difficulty involved in plotting a graph to cover a range of 50 ft in elevation at a section. It has been found that the method of inclusion of overbank flow, proposed in Eqs. 23 and Table 11, is a commonly used expedient. Basically, this method corresponds to the use of the function,[11]

---

[9] Senior Harbor Engr., Port of San Francisco, Calif.

[10] "Hydraulics," by George E. Russell, Henry Holt and Co., New York, N. Y., 5th Ed., 1947, p. 292.

$$K\,d = \frac{1.486}{n}\,A\,R^{\frac{2}{3}} \qquad (28)$$

Although some engineers may object to this procedure on the grounds that the value of $A\,R^{\frac{2}{3}}$ for a cross section taken as a whole is not equal to the sum of the $(A\,R^{\frac{2}{3}})$-values of its component parts, it should be realized that the difference is not great for moderate amounts of overbank flow. If the value of n is determined from observed flood profiles (using the sum of the $(A\,R^{\frac{2}{3}})$-values for channel and overbank), the computation of surface profiles should also use this n-value.

Mr. Buehler is correct in his interpretation of the procedure to be followed in applying the proposed method to channels where it is necessary to use a different roughness coefficient for each reach. The computations in Table 11 and Eq. 23 show how it is possible to use different roughness coefficients at the same cross section for different parts of the cross section. The writer agrees with Mr. Buehler that it is a cumbersome operation to determine the value of the roughness factor from flood observations when there is appreciable overbank flow.

Mr. Steinberg makes a welcome suggestion regarding the use of a weighted-area curve that can be applied directly to the discharges to obtain weighted velocities when overbank flow is involved. It has been observed, however, that the use of Eq. 5 involves less work and is simpler than the use of Eq. 9*c* or Eq. 10 to prepare a weighted-area curve.

Mr. Steinberg's discussion makes it obvious that it was not made sufficiently clear that the proposed method is a rigorous, although semigraphical, solution of the basic equation of varied flow given by Eq. 1. With this solution, it is not necessary to ignore the velocity-head terms or to make trial-and-error computations. The method, although perfectly applicable to channels of uniform cross section and roughness, is especially suited to natural channels in which (1) the velocity varies from reach to reach, (2) consecutive lengths of reach are not equal, (3) each reach has a different roughness coefficient, (4) conditions of overbank flow prevail, (5) the same cross section has different roughness coefficients for different water-surface elevations, and (6) the effect of eddy losses and bridge-pier losses can readily be included when necessary. Mr. Steinberg is correct in showing that, in most graphical and semigraphical methods which seek to eliminate trial-and-error computations, the velocity head corrections have not been taken into account. That is, these methods solve Eq. 1 by omitting consideration of the terms $\frac{V^2_1}{2\,g}$ and $\frac{V^2_2}{2\,g}$, and furthermore by assuming that the difference in elevations Z_1 and Z_2 at the two ends of a reach are equal to the friction-head loss only. Although these simplifying assumptions are useful and not inaccurate when the velocity heads at each end of a reach are equal (in which case there is no varied flow), or when the difference between velocity heads is small compared to the friction-head loss in the reach (which is not the case when short lengths of reach are used under conditions of varied flow), they cannot be termed a rigorous attempt to solve the equation of varied flow.

---

[11] "Handbook of Hydraulics," by H. W. King, McGraw-Hill Book Co., Inc., New York, N. Y., 1939, pp. 530–531.

Mr. Steinberg presents a method of using a graphical solution for the equation of varied flow. Since the computation of M from Eq. 15*a* requires the determination of the properties of a midsection, as well as of the ends of a reach, the additional work involved is not worth while since no greater precision is obtained as Table 9 shows in comparison with Table 6.

AMERICAN SOCIETY OF CIVIL ENGINEERS
Founded November 5, 1852
TRANSACTIONS

Paper No. 2680

OFFSHORE PETROLEUM INSTALLATIONS

BY JACK S. TOLER[1]

SYNOPSIS

The development of the petroleum resources lying offshore from the coasts of Louisiana and Texas has presented many problems to the engineering profession. The large and prolific reservoirs of oil and gas located and developed inshore along the Gulf of Mexico indicate that many areas equally or more productive are to be found offshore. Financial and operational risks involved in locating and recovering these resources are such that large-scale exploratory and development work did not appear to be justified prior to 1942. Following World War II, however, demands for petroleum and petroleum products made it necessary for the petroleum industry to develop engineering and operating techniques for drilling below the Gulf of Mexico.

INTRODUCTION

Drilling operations conducted prior to 1942 in the comparatively shallow depths off the coasts of Louisiana and Texas brought attention to the many operational problems in open-water drilling. These operations led to greater recognition of the need for careful study of both structural design and foundation design and also of the need for the development of special construction techniques and seagoing construction equipment. It is necessary only to view the destructive results of a hurricane along the "Gulf Coast" of the United States to understand the limitations of conventional design and operation procedures, particularly in the more exposed areas offshore from the 30-ft depth contour.

Before the petroleum industry ventured to move its operations into the deeper waters of the Gulf of Mexico, its engineering staffs, private engineering firms, and consultants spent several years developing reliable criteria concerning wave action, analyzing the soft silt-clay strata underlying the Gulf of Mexico, and studying various foundation and structural designs. The first operations were conducted in 1948, from 6 to 8 miles offshore, in depths greater than 30 ft of water. These operations followed research and study without benefit of precedence and actual experience. The concern for the safety of the fifty-man

---

NOTE.—Published, essentially as printed here, in September, 1953, as *Proceedings-Separate No. 289*. Positions and titles given are those in effect when the paper was received for publication.

[1] Asst. Div. Civ. Engr., Louisiana Div., Humble Oil and Refining Co., New Orelans, La.

drilling and technical crews and the huge investments in platforms and rig equipment made many operators apprehensive lest some unknown critical design factor had not been considered. Most companies considered costs second to safety in the design and operations of the initial phases, feeling that with the knowledge and information gained through experience, techniques would subsequently be developed to reduce costs to compare favorably with marsh and inshore water drilling.

During the period from 1947 to 1952, many advancements were made which more clearly defined the engineering problems in drilling and production operations. The principal considerations are as follows:

1. Oil and gas must be located, produced, and delivered to inland terminals at a cost that will assure the operator a profitable return on his investment.
2. Operating plans should accommodate the conditions imposed by the particular location, depth of water, and proposed development (whether exploratory or field development).
3. Drilling equipment and rig arrangements should be designed to afford maximum utility on a minimum of deck area, and to distribute loadings for the safest and most economical design of both the foundation and the structure.
4. Criteria for design should be further developed and standardized, particularly with reference to the intensity and the nature of the loadings imposed by wave forces on exposed foundation and structural members.
5. Greater understanding of the characteristics of the soils underlying the bottom of the Gulf of Mexico is required for more economical design of the deep-penetration, high-bearing pile supports.
6. Structural design and construction techniques should afford a maximum of economy in materials, fabrication, and construction operations.
7. Construction equipment should be seaworthy and able to operate continuously during ordinary rough seas. The equipment should be maneuverable and able to withstand storms of hurricane intensity.
8. Adequate protection should be provided against the corrosive effects of salt water and atmosphere.

Considerable progress was made from 1947 to 1952 in the development of design criteria, structural design, and design and layout of drilling equipment. Safety and efficiency in drilling operations were also greatly increased. More must be done in the field of engineering research, however, to assure the development of the most adequate and economical installations for deep-water operations, and to make possible operations in water depths greater than present (70 ft) operating depths.

Prior to 1953, the petroleum industry had invested more than $261,000,000 for leasing, exploration, and development offshore along the Gulf Coast. During the years of the "tidelands" controversy, the United States Congress was unable to pass legislation to fix ownership or to establish necessary procedures for interim operations. The importance of the tidelands in the development of the petroleum resources of the United States is apparent in the fact that, from 1947 through 1951, a total of 242 wells were drilled with approximately 130 completed as oil, gas, or gas-condensate producers. More than twenty producing areas were discovered in the waters of the Gulf of Mexico during this same period.

To continue these operations, approximately seventy separate drilling platforms have been erected (as of January 1, 1953) in water depths to 70 ft. A number of the larger platforms cost more than $1,250,000. Several costly oil and gas pipelines were built to carry the products to shore terminals. One of the larger fields was electrified by the construction of high-voltage transmission lines across many miles of marshland and into the Gulf of Mexico.

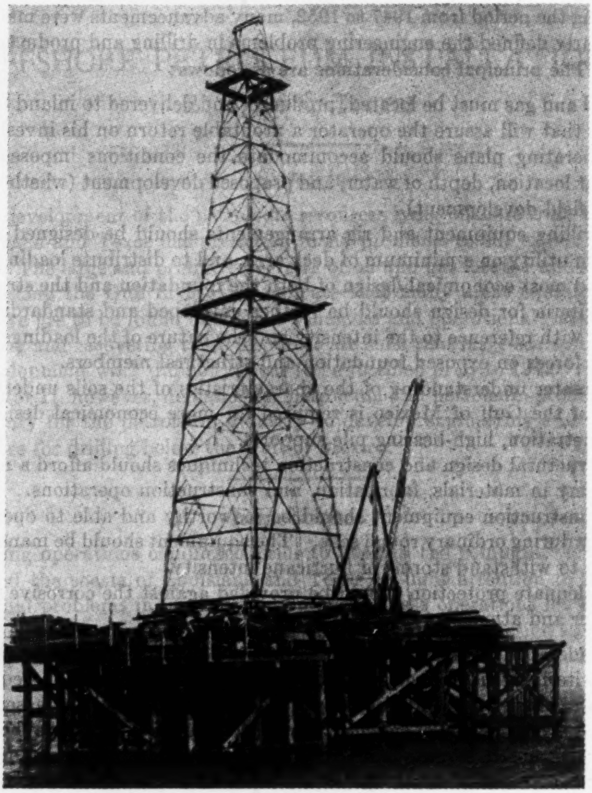

FIG. 1.—DRILLING PLATFORM LOCATED OFFSHORE FROM HIGH ISLAND, TEX.

Actual drilling operations in the tideland area of Louisiana and Texas have been conducted by seventeen oil companies. A number of other companies hold leases or have performed geophysical exploration in the area. The operating problems have, in general, been the same. However, the development of engineering and operating techniques by the operators has varied considerably. This paper treats primarily with the design considerations, methods of construction, and operating facilities in use by one of the major companies engaged in offshore petroleum operations.

EARLY OPERATIONS IN THE GULF OF MEXICO

One of the first drilling operations in the Gulf of Mexico was conducted in 1938 off McFadden Beach near High Island, Tex. Five wells were drilled in this area, the one farthest offshore being 7,600 ft from land in 18 ft of water. The five wells were drilled from conventional-type, timber-pile foundations and structures similar to those used for inland-bay drilling and marsh drilling. In 1938 there was very little reliable oceanographic or soils data available for guidance in design. As can be seen in Fig. 1, the unobstructed spacing between pile supports and the structural members above mean sea level was limited by the low-strength timber construction used. A total of 100 piles, 65 ft long, was used to support the 70-ft by 122-ft drilling deck set 15 ft above mean Gulf of Mexico water level (MGL). In comparison, a structure erected in the Gulf of Mexico, approximately 6 miles offshore from Grand Isle, La., is located in 55 ft of water and has a 60-ft-by-80-ft deck 44 ft above MGL. The structure was supported by a templet-type foundation with sixteen 10-in. by 57-lb steel piles, 275 ft long. The piles are driven with a penetration of 180 ft and have a cutoff at El. 40 MGL.

Although these conventional, inland platforms provided foundations for successful drilling operations, they were inadequate for conditions imposed by the frequent storms and gales; operations were handicapped by damage and loss of drilling time incurred during rough seas. A number of intense storms and hurricanes have been experienced which would have, in all probability, destroyed the original installations at McFadden Beach.

There were a number of other early operations in water depths of 20 ft along the Gulf Coast, notably those in the Creole Field off the coast from Cameron, La. Approximately twenty-five wells were drilled from conventional pile foundations in shallow waters off the Gulf Coast from 1937 to 1942.

DESIGN CONSIDERATIONS

Wind and Waves.—Design criteria in general use prior to the fall of 1949 were based on a probable maximum wave height of 32 ft, with a 5-ft storm tide in water depths of 40 ft, giving a maximum crest height of 29 ft above MGL. It was considered possible that a storm of long duration, with wind velocities above 125 miles per hr, would develop tide and wave heights considerably greater than those previously listed. Based on a study of hurricanes along the Gulf Coast, it was considered unlikely, however, that storms generating wave-crest heights in excess of 29 ft above MGL would occur on a frequency of more than once in 40 to 50 years.

In October, 1949, a small but intense hurricane formed in the Gulf of Mexico off the coast of Merida, Mexico, and moved in a northerly direction to the coast of the United States in the vicinity of Freeport, Tex. Data obtained at a drilling site located in the path of the storm revealed wave-crest heights which closely approximated the maximum heights previously considered probable. As a result of the 1949 hurricane, a number of designers changed their criteria and increased their wave-force computations to provide for a probable maximum 40-ft wave with a 10-ft storm tide in water depths of 65 ft above

MGL. This would produce a breaking wave with a crest height of 40 ft above MGL.

Although most engineers agreed on the safe limits of probable maximum wind-and-sea conditions to be expected, they differ widely in their interpretations of available theoretical data concerning the action of waves, and in their understanding of the severity and exact nature of the loadings imposed upon structures during storm periods. A curve[2,3] for the design of a permanent drilling platform is shown in Fig. 2. This chart shows the wave profile and pressure diagram for a wave 40 ft high, 380 ft long, with a period of 9 sec in 65 ft of water with a 10-ft storm tide. The pressures shown are maximum, and they occur at the crest of the breaking wave on a tubular pile 1 ft in diameter. For cylindrical sections of other sizes, the forces shown should be multiplied by the diameter in feet. The pressure resultant is 9,008 lb acting on the pile 12.36 ft above MGL. A factor of 5.9 is used in computing the forces on flat surfaces. This criteria curve is by no means accepted as final, nor is it universally used; some designers use forces of less magnitude, whereas the criteria used by others give considerably greater forces—especially with respect to the unit pressures between zero and 35 ft above MGL.

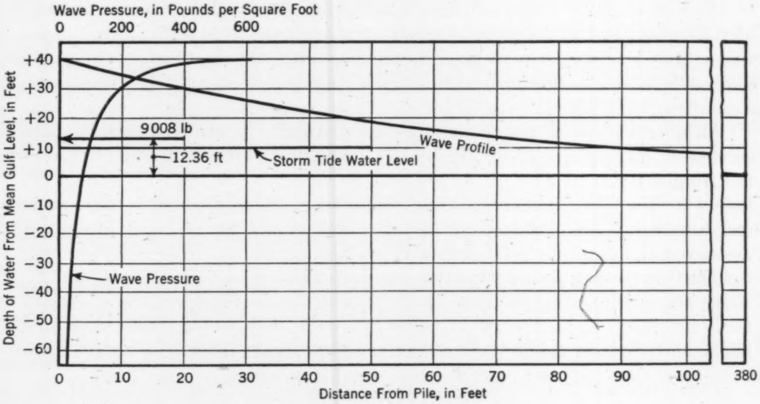

Fig. 2.—Design Curve for a Permanent Drilling Platform

Three storms of near-hurricane or above-hurricane intensity were experienced between 1947 and 1952 in areas where drilling platforms were located. There was evidence of wave heights from 22 ft to 29 ft above MGL. From observations of the wave effect on the structures lying within the storm paths, one fact appears to be significant: Extensive damage and destruction were sustained by those installations with flat deck and structural surfaces exposed to the forces of the waves, whereas those with deck and superstructure set

---

[2] "The Solitary Wave Theory and Its Application to Surf Problems," by Walter H. Munk, *Annals*, New York Academy of Sciences, Vol. 51, May, 1949, pp. 376–424.

[3] "Wave Action on Structures," by Walter H. Munk, *Petroleum Development and Technology*, Am. Inst. Mining and Metallurgical Engrs., 1949, p. 11.

above wave height were relatively undamaged. The effects of these storms enabled engineers to review certain basic design factors in the light of actual conditions. The difficulty in obtaining measured (or observed) data at the height of storm periods, or under laboratory conditions, however, has limited the accumulation or verification of other facts necessary for agreement of the criteria to be used by designers. Further development of the factors involved in the design for wave forces is essential for more complete and uniform understanding among those engaged in design.

Foundation.—Prior to 1946, little reliable data were available concerning the characteristics of the soil below the Gulf of Mexico. Several different procedures had been followed by various operators in conducting soils investigation. These investigations depended on the operator's scope of operations and the proximity of the operator's locations to the delta formations of the large silt-carrying streams, where erratic strata of sand, silt, and clay can be expected.

In order to obtain data for foundation design, Raymond F. Dawson,[4] M. ASCE (in 1946 and 1947), aided in the investigation of the soils below the Gulf of Mexico, in an area extending from the west side of the Mississippi River delta west to Timbalier Bay, in Louisiana. Seven core-test holes were drilled at various points on land between Tiger Pass in Louisiana and Timbalier Island. Another core test was drilled from a platform constructed on a 24-in. test pile driven approximately 6 miles offshore from Grand Isle. To supplement the core-test information, 24-in. tubular test piles were driven in the Gulf of Mexico at ten prospective platform locations. The core tests were drilled to depths of approximately 400 ft, and the test piles were driven with penetrations of 165 ft.

Unconfined compression tests of the samples collected by Mr. Dawson were used to measure shear strengths of the soils, and consolidation tests were made to aid in determining the probable maximum settlement to be expected. It was found that, except for surface variations, the soil formations throughout the area investigated consisted of a soft, silty clay having a comparatively low shear strength and extending 200 ft or more below the Gulf of Mexico. Although the soil profiles were not uniform, there was sufficient similarity in all borings to furnish reliable average values of cohesion. The average value of cohesion from various depths of penetration to the floor of the Gulf of Mexico was determined by use of the average of all borings taken. This average value of cohesion was used as a guide in determining the depth of penetration required for individual piling loads at various platform locations. Borings taken over the area investigated indicated the absence of a thick stratum of dense sand to furnish end bearing for piles—therefore, all piles are considered to act as friction piles.

Driving data recorded on piles show that the driving characteristics of individual 10-in. by 57-lb steel H-piles are very irregular for the first 125 ft to 135 ft of penetration, with appreciably low resistance to driving. Resistance gradually increases and driving characteristics become more uniform as penetrations of approximately 185 ft are approached. This trend indicates that, when sufficient penetration is reached, the average soil conditions in the area are such that uniform results are obtained, even though the formations may be of an irregular nature. It would appear, however, that these average conditions should not be relied on where foundations are to be built near the outlets of large, silt-carrying streams such as the Mississippi and Atchafalaya rivers, because of the extremely erratic soil formations to be encountered. Near such outlets borings should be taken at the location either prior to, or at, the time when the platform is to be erected. The pile penetrations should be determined from an analysis of the borings.

---

[4] "Report on Soil Tests from Timbalier and Tiger Pass," by Raymond F. Dawson, Humble Oil and Refining Co., New Orleans, La., November, 1947.

Soils studies were continued by Mr. Dawson in 1949, in order to determine more exactly the characteristics of the shallow formations in the floor of the Gulf of Mexico. Offshore borings were made at several locations to depths of approximately 50 ft below the bottom. The results of the borings indicated a predominance of soft, silt clay, with cohesive strengths varying from 40 lb per sq ft to 400 lb per sq ft.

Based on this study, and as an additional factor of safety, modifications were made in later templet-type foundations to reduce the possibility of excessive bending stresses under maximum storm loading conditions. These modifications included increasing the length of the templet legs to provide a penetration of 27 ft, and increasing the area and strength of the templet legs below the mud line. On existing installations the soft soils were strengthened and consolidated by placing an 18-in. layer of shell and a 3-ft layer of 6-in. crushed rock on the floor under and around the foundations.

OPERATIONAL FACILITIES

Drilling and producing operations offshore involve engineering study and advance planning, with consideration given to location, depth of water, drilling depths, and the operator's plan for development—whether exploratory or field development drilling. In addition to constructing a drilling platform, it may be necessary to provide moorings for drilling tenders and barges, oil storage batteries, marine pipelines, and land terminal facilities from which operations can be conducted. Experience has proved that these accessory facilities are costly and that as much attention must be given to their design and installation as is given to the drilling platform itself.

Drilling Platforms.—Drilling operations have followed two plans: (1) The use of a large self-contained platform with crew quarters, mess facilities, drilling equipment, pipe and mud storage—all contained on the platform; and (2) the use of a small platform to contain the minimum of rig equipment with the pumping equipment, pipe and mud storage, living quarters, and other required service facilities placed on a moored drilling tender. Although some operators have preferred one type of platform over the other for economy or convenience in operation, each type has a place in the over-all development of a productive area.

One of the first, deep, wildcat, offshore operations was conducted from a large, double-deck, self-contained platform erected 7 miles south of Grand Isle in a water depth of 48 ft. Although four producing wells were drilled from this platform, and several additional wells were proposed, the large investment involved in such an installation is considered prohibitive to wildcat drilling where the first well drilled, if dry, might result in the abandonment of the prospect. The operations conducted prior to 1952 were primarily exploratory; subsequent drilling was performed with a smaller type of platform and World War II surplus landing ships were used as drilling tenders.

The first drilling-tender platforms were 50 ft by 150 ft. They provided drilling positions for three wells spaced 10 ft on centers in the longitudinal direction of the platform. A 50-ft by 50-ft area at the forward end of the platform was used for pipe storage, with rig equipment arranged in the 50-ft by 100-ft space at the rear. At a number of drilling locations the pipe-storage space was eliminated and the pipe was moved directly from the tender to the derrick floor. Later developments resulted in a much more satisfactory arrangement; the rig and the equipment were placed on a 90-ft by 120-ft deck, with well centers alined with the transverse axis of the structure. This arrangement provided five drilling locations, and increased the deck space by 45%. The platform cost was slightly less than that of the 50-ft by 150-ft, three-well platform. A number of smaller single-well platforms were erected for drilling wells to shallow depths where no directional drilling was anticipated.

Also built were eighteen, single-deck, drilling-tender platforms for exploratory work in the Louisiana area. Many changes made in the rig arrangements and the equipment layouts led to greater economy in operations and lower "per-well-platform cost." A 60-ft by 80-ft platform was constructed without pipe racks. This platform was designed to support a heavy rig for drilling wildcat tests to 14,000-ft depths. This layout and design permit the drilling of two wells with a reduction of approximately 50% in the cost of the well platform. Initial construction plans were designed to make possible platform extension to 90 ft by 120 ft with pipe racks and drilling locations for five wells, in the event that extensions be desired later, to provide a 120-ft by 120-ft self-contained platform for drilling a total of ten wells. Significant features of this plan were: (*a*) A minimum platform investment was made in drilling the first well, and, in the event that the prospect was dry and abandoned, all materials with the exception of the piling below the mud line could be salvaged for use elsewhere; and (*b*) in the event that drilling the initial well yielded production, and additional directional wells were desired, the platform could be expanded to a 90-ft by 120-ft, five-well structure without loss of drilling time, while the second well was being drilled from the initial platform.

A two-well platform similar to that described was used for drilling at Grand Isle Block 16, State Lease 799 F-1. Its deck, set at El. 44 MGL is supported by sixteen 10-in. by 57-lb steel H-piles driven through the legs of four 10-ft-square by 80-ft-long pipe templets.

Drilling tenders used in conjunction with the smaller platforms were former landing vessels converted to accommodate drilling operations. The barge is moored with its bow approximately 25 ft from the end of the platform, and is connected to the platform by a movable, ramp-carrying walkway and pipe chute. A 35-ton-capacity gantry crane is installed near the bow of the vessel and is used to load cargo and supplies and to transfer material to and from the platform. The design of the drilling-tender moorings is critical, as these moorings must be strong enough to hold the vessel in a safe position under extreme wind-and-sea conditions. Arrangements must be made to swing the stern of the barge through a considerable angle so that its axis can be held as nearly parallel as possible to the sea-current direction. Fixed moorings with high-test anchor chains connected to heavily-reinforced spud piles driven into firm soil well below the floor of the Gulf of Mexico have provided satisfactory moorings for the drilling tenders.

Offshore drilling operations have been conducted from multiple-well platforms rather than from single-well platforms, with the first well being drilled vertically into the geological formations. Additional wells can then be drilled by directional methods to other drilling objectives. Although the cost of drilling directional wells is usually greater than straight-hole drilling, analysis of costs indicates that it is more economical if more than one well is to be drilled in a given area.

Experience has shown that drilling from self-contained platforms is more efficient than from drilling-tender platforms. However, the cost of this type of installation is such that the tender-type platform is more economical for the drilling of a limited number of wells. In an area where extensive field drilling is contemplated and drilling depths are such that a number of wells can be drilled directionally, cost analysis may indicate that directional drilling would be more economical from a self-contained platform than from any other type.

Conclusion

Offshore petroleum operations have presented many unusual problems in the fields of civil, petroleum, and marine engineering as well as in the associated field of oceanography. At the outset of deep-water operations, there was little experience to guide operators in planning their operations and in designing their installations to withstand the forces encountered in the open waters of the Gulf of Mexico. Experience gained through actual construction and drilling operations has greatly increased the knowledge of essential design factors and has furthered the development of operating techniques. These techniques will permit profitable development of the offshore petroleum reserves in the Gulf of Mexico. Further study and investigation of design factors involved are requisite, however, to a common understanding among the engineers engaged in offshore operations. This need will be intensified in the case of installation development beyond the water-depth limit for pile foundations.

AMERICAN SOCIETY OF CIVIL ENGINEERS
Founded November 5, 1852
TRANSACTIONS

Paper No. 2681

RECENT AIRPORT DESIGN AND DEVELOPMENT

BY PHILIP A. HAHN[1]

WITH DISCUSSION BY MESSRS. LOUIS A. NEES, AND PHILIP A. HAHN

SYNOPSIS

The recent developments and trends in airport design and construction are common knowledge to the engineer. This paper presents the reasons for these trends and developments. These advances have been based on a desire to follow engineering principles which are basically sound and economically wise in planning, surveying, and structural endeavors. There is still another important factor which controls airport engineering and that is the need for providing the necessary aeronautical requirements to insure the safe operation of aircraft in the vicinity of the airport, in turning zones or areas, in the approaches, and on the airport.

AIRPORT SIZE AND TYPE

Since the adoption of the Federal Airport Act of 1946,[2] several changes have been made by the Civil Aeronautics Administration, United States Department of Commerce (CAA), in airport nomenclature and design criteria. One of the first major changes was to dispense with the categorization of airports as Class 1, 2, 3, and so on. This classification was based on the length of the longest runway at each airport. The situation was further confused because the CAA Class 1 was the smallest airport, whereas Class 1 was the largest airport in the classification system used by the military air groups. The revised classification system categorizes the various airports by the type of air activity or service that occurs at the airport. Therefore, airports are identified as follows:

Personal.—For light aircraft usage at small communities and urban areas.

Secondary.—For larger aircraft usage, up to a gross weight of 15,000 lb, engaged in nonscheduled flying activities.

NOTE.—Published, essentially as printed here, in June, 1953, as *Proceedings-Separate No. 196*. Positions and titles given are those in effect when the paper or discussion was received for publication.

[1] Chf., Airport Eng. Div., Office of Airports, Civ. Aeronautics Administration, U. S. Dept. of Commerce, Washington, D. C.

[2] *Public Law 377*, 79th Cong., 2d Session, Washington, D. C.

Feeder.—To serve all planes up to certificated feeder airlines.

Trunk.—For the servicing of intermediate communities on airline trunk routes.

Express.—To serve relatively large cities or junction points on trunk routes.

Continental.—For the servicing of aircraft making long nonstop domestic flights.

Intercontinental.—Airports that are terminal points for long international flights.

Intercontinental Express.—Airports that serve the highest type of transoceanic flights.

Coupled with these categories is the CAA Technical Standard Order (TSO) N-6a, which indicates the maximum extent of runways, taxiways, and landing strips for which the government will afford federal aid. Also listed in TSO N-6a are the correction formulas as to runway length which must be made for airport elevations, temperature, and runway gradient. In many cases shorter lengths will be satisfactory for the type of service encountered. The issuance of TSO N-6a was necessary in eliminating confusion as to the dimensional sizing of runways to be applied to airport developments at various locations and areas. It was only after extensive coordination with the entire aviation industry had been achieved that TSO N-6a was issued.

AIRPORT CONFIGURATION

Airport configuration—as related to the number and orientation of runways, taxiways, lead-off taxiways, warm-up aprons, parking aprons, and terminal areas—is a very vital item to be considered in the development of airports and, more particularly, in the development of master plan layouts. Too much emphasis cannot be placed on the need for careful, detailed, and prolonged studies for the master plan. A review of airport configurations indicates that, whereas certain airports are sound and very usable by the standards of engineering and aeronautics, many of them do not have maximum efficiency. To emphasize the need for good airport configuration, the CAA issued a policy governing the number of runways to be established at airport projects receiving federal aid. The basic aim of this policy is to construct, at existing and proposed airports, traffic-bearing runways which will provide a maximum degree of utilization. This policy is commonly known as the "one-runway" policy. Actually, this is a misnomer because the policy does not curtail an airport to one bi-directional runway, but does emphasize that not more than one runway should be constructed at a site unless traffic warrants the development of two or more runways. The traffic capacity of a single runway has been established as 40 operations per peak-hour per runway, whether the operations are landings, take-offs, or a combination of landings and take-offs. If it is determined that there is a need for multiple runways at an airport, the most efficient orientation pattern would be a parallel arrangement with a separation of at least 3,000 ft and preferably 4,000 ft. The reason for such a separation is to provide maximum efficiency in the operation of aircraft under all weather conditions, during both landings and take-offs. In adverse weather, landings and take-offs can be conducted with the aid of radar facilities and other electronic devices which are essential to speeded-up instrument operations. Any deviation from the ideal configuration will decrease the efficiency or capacity of the runways.

Modified configurations consisting of nonintersecting divergent runways separated by at least 700 ft in the apex area and diverging at an angle of at least 15° can approach the ideal under some operational conditions. However, intersecting runway patterns afford poor efficiency because they provide only a slight increase in capacity over a single runway and, therefore, should be avoided.

In certain instances the land area will restrict developments and can reduce operational efficiency, but the goal should be to adapt that system which provides maximum efficiency under the existing conditions. Once the runway layout is established, careful consideration must be given the configuration and location of taxiways (especially lead-off taxiways) and the size and location of run-up aprons at runway ends to provide for a rapid clearance of aircraft from the runways. A preliminary study of lead-off taxiway and run-up apron configurations was conducted from 1949 to 1951.

To make this study, certain airports throughout the United States were selected on the basis of the existing configuration and traffic density, which provided the desired variations in local conditions and traffic. Various aspects were explored to determine the effect of factors on the landings with respect to touchdown, turnoff, and time on the runway. These studies revealed that—

1. Data on night or day landings were essentially the same.
2. Data for instrument or visual landings showed no notable difference.
3. Landing roll, in many instances, was influenced by the intended destination at the airport.
4. The available length of runway had no apparent effect on the point of touchdown or landing-roll distance.
5. The length of the landing roll was approximately inversely proportional to the touchdown distance.
6. Angular lead-off taxiways reduce the operating time of aircraft on the runway as opposed to the use of right-angle turnoffs. Angularity between 30° and 60° does not reflect any difference in time on the runway.

Less than 1% of the aircraft made the touchdown within 100 ft of the threshold, but 93% of the aircraft "touched down" within a distance of 1,500 ft. Table 1 shows the average turnoff distances from the threshold for various aircraft. It was found that relatively few aircraft turn off the runway in less than 2,000 ft from the threshold and that practically all aircraft complete the landing roll before reaching a point 5,000 ft from the threshold, except in cases of excessive overshooting. The optimum locations of lead-off taxiways have been determined as 2,500 ft, 3,500 ft, and 4,500 ft from the threshold. These locations are somewhat flexible and should be adjusted to fit the runway length, with the realization that exits located less than 2,000 ft, or more than 5,000 ft, from the threshold are of little value.

A review of run-up apron data revealed that, during off-peak periods of traffic, the average run-up time was generally in proportion to the size of the aircraft. The data also show that the average run-up time increased as the traffic increased and that, in periods of peak traffic, run-up time was about equal for all types of aircraft. The size of the run-up apron required at each location will depend principally on the rate of peak traffic on a particular runway. For peak traffic on a runway serving both landings and take-offs, an average run-up time of 10 min, as compared with 6 min for runways serving take-offs only, should be used as a basis for determining the run-up apron size.

Table 2 is a guide for the design of apron lengths. The apron should not be designed to accommodate less than two large airplanes nor more than five large airplanes. It is desirable to locate the run-up aprons in a position as close as possible to the intersection of the runway and the taxiway and still fulfil safe clearance requirements.

Another vital factor to consider in the over-all configuration of the airport is whether the proposed arrangement lends itself readily to the fulfilment of the criteria for determining obstructions to air navigation with particular reference to turning zones and approach areas as they affect instrument and visual operations. The latter criteria are all contained in CAA TSO N-18. The drawing contained in this order, frequently referred to as Drawing No. 814, depicts the various phases of imaginary surfaces and limiting heights above ground for all types of airports. The intricacy of the arrangement of the drawing has precipitated adverse comments as to the difficulty with which it can be applied and interpreted. The fact that all airports of all categories are described in the one drawing may give rise to such comments. However, when the requirements of the drawing are applied to an individual airport, it will be found that many of the apparent mathematical and developmental intricacies resolve themselves into relatively easy problems. A simple visual concept of TSO N-18 is that of an ordinary kitchen pie plate. It is not anticipated that each requirement may be met in every instance. However, careful thought should be given its application in order to minimize intricate landing procedures with particular reference to those necessary for instrument operations.

TABLE 1.—DISTANCE FROM THRESHOLD TO TURNOFF

Airplane type	DISTANCE, IN FEET	
	Minimum	Average
Single engine	1,000	2,750
DC-3	1,500	2,950
Convair 240	1,650	3,300
Martin 202	2,200	3,500
DC-4	2,200	3,400
DC-6	2,175	3,400
Constellation	2,225	3,800
Boeing 377	2,275	3,700
All aircraft	1,000	3,200

TABLE 2.—THE EFFECT OF OPERATING CONDITIONS ON APRON LENGTHS

Runway system	Rate of take-off per hour	Apron length, in feet
Take-offs and landings	15	200
	20	300
	30	500
Take-offs only	15	200
	20	200
	30	300
	40	400

When developing master plan layouts, it is important to provide areas for the location of all electronic aids necessary for the navigation of aircraft, whether these aids occur within or without the confines of the airport boundaries.

Much interest has been expressed and a great deal of curiosity aroused as to the effects of the operation of jet aircraft on runway, taxiway, and apron layouts of an airport. All statements regarding special requirements as a result of jet transport operations are necessarily vague since the operation of jet transports has been extremely limited; but it may be assumed that any changes from existing requirements will be of a minor nature. Until definite information on the effect of jet aircraft on runways becomes available, the CAA does not plan to introduce any changes in airport-design standards. In this connection, however, studies leading to the improvement of standards will be made and are being given special consideration.

PAVEMENT DESIGN

In the early days of airport development it was felt that highway pavement design methods would suffice for aircraft loadings. This was a reasonable assumption for the type of aircraft in use at the time. However, as airport experience broadened, standards were revised to allow for the specialized requirements of airport pavements. Standards were also revised to provide for the greater strength needed to support the ever-increasing loads superimposed on the pavements by new developments in aircraft design. These revisions have been made from studies of experimental investigations, accelerated traffic tests, and pavement performance under service conditions.

Design based on performance is generally rule-of-thumb. The users of the methods mentioned do not claim them to be the final answer, but the fact remains that they are the most reliable available at the present time. Satisfactory methods for determining pavement-thickness requirements, on the basis of stress analysis within the pavement and in the supporting subgrade, have not been developed. Even the Westergaard method, which has been widely accepted in the field of rigid-pavement design, must be modified in accordance with the behavior of pavements in service.

Studies of pavement performance have yielded information regarding the relative importance of static, dynamic, and impact loads. The studies have also furnished information on the pavement areas that are most critical from the standpoint of aircraft use, as well as data on the relationship between the stability of the soil, the magnitude of the applied loads, and the pavement thickness.

Each governmental agency charged with the development of design standards has prepared procedures to be followed by the engineers in that particular group. Although these methods differ in details, they are basically similar in so far as soils are classified or indexed according to certain physical properties determined by specified laboratory or field tests. From observed behavior and a knowledge of climatic variables at the site, pavement-thickness requirements are estimated. In general, the determination is made from a series of curves which gives the relationship between pavement thickness, wheel loading, and subgrade soil. The validity of these design curves are being checked continuously against pavement performance, and adjustments are made if the curves are found to be in error. The reliability of the design depends on the proper interpretation of test results and good judgment in predicting the behavior of the soils under the moisture and climatic conditions encountered.

There are obvious drawbacks to a design procedure which depends almost entirely on a few soil tests and a great deal of experience. It would be more logical if it were possible to determine accurately the bearing power of subgrade soil and then to analyze the pavement requirements on the basis of a distribution of stresses in the pavement and in the soil. However, because of the changes in stability of a given subgrade soil produced by variations in moisture, climate, and the arrangement of the soil layers, a method of determining a definite or absolute value of bearing strength remains to be decided. This lack of a reliable value for the bearing strength is the most serious obstacle to the development of the analytical methods of design. Until the bearing strength of the subgrade soil can be determined and controlled, it will be necessary to continue using the existing methods of estimating this strength on the basis of observed pavement behavior correlated with subgrade conditions. As of 1952 these methods are a satisfactory guide to pavement design, as has been proved by the performance of pavements constructed in accordance with these design criteria.

The development of acceptable analytical methods is progressing as a result of extensive investigations conducted by the CAA; the Bureau of Public Roads, United States Department of Commerce; the Corps of Engineers, United States Department of the Army; and the Bureau of Yards and Docks, United States Department of the Navy. These investigations are producing accurate information on the distribution of stresses in subgrade soils under loads applied at the surface and on the ways and means of controlling the moisture and volume changes that occur in soils, so as to provide support of a more permanent and uniform nature.

Operation of jet aircraft has raised many questions concerning the performance of airport pavements subjected to fuel spillage and high exhaust temperatures. It is believed that spillage is not a serious problem. However, the effect of the jet blast is significant. Observations made on fields where jet aircraft operations are of a sufficient magnitude so as to furnish performance data disclose that the areas seriously affected are small in extent and are confined to locations where sustained run-up periods occur, thus subjecting the pavement to sustained blasts. No damage has been observed so long as the jet aircraft is in motion.

The effect of the blast on the pavement will depend on the design of the aircraft with respect to the velocity of the blast and the angle of the exhaust. As the direction of blast approaches the horizontal, the less important the blast becomes, so far as pavements are concerned. Because of this, observations of transport types of jet aircraft indicate that there is no detrimental effect on the airport pavement.

TERMINAL BUILDINGS AND AREA

In the development of terminal areas and buildings, the goal is to determine facility sizing and layout criteria and to develop basic site planning and layout considerations for the entire building area. To be successful and acceptable, such criteria should not force architectural design by formula, nor should the criteria lean toward "standard" or "stereotyped" plans. There is no attempt to encroach on the designers' prerogatives relating to freedom of architectural design and treatment.

Analyses of passenger and visitor activities at a large number of airports of varying passenger volume revealed a fairly consistent pattern of relationships between total annual passengers and the number of passengers that would have to be accommodated during a typical peak hour. In addition to the passenger activity patterns, significant data were found on the number of visitors and patrons of the concessions. Therefore, the peak-hour passenger is the common denominator in determining the area requirements for airline, public, and concessionaire space needs. Along with this information, passenger-volume forecasting methods allow extrapolation of data in order that terminal buildings may be sized to accommodate passenger volumes ten years in advance of the construction of the facility. This extrapolation results in initial oversizing of the building, but it allows for increase in passenger volume without requiring additions to the structure for an extended period. Consistent functional relationships exist between the various spaces and activities in a terminal building for the processing of passengers and the accommodation of the visitors. These relationships have been so distorted that confusion and delays befell the "using" public, operational inefficiencies developed for the airlines, and financial losses were incurred by the concessionaires and airport owners. The new approach to this situation is the development of schematic space-relationship diagrams and flow diagrams which show graphically the accepted relationships between the functions and spaces of a terminal building. These diagrams do not restrict the freedom of the designer in the development of an individualized scheme. However, the schemes have done much toward making industry agree on the basic principles of terminal-building operation, and great strides have been taken toward this goal.

The matter of site planning and development has been treated in much the same manner as have been the space relationships—through the development of area-use diagrams which schematically depict accepted relationships of the various operational areas of an airport. Here again, predesign has been purposely avoided, and the functional disposition of the required activities and their relationships to surrounding areas and associated activities have been indicated.

There has been an attempt to bring out the "whats" and leave the "hows" to the designer. Economic practicability, amortization potentialities, and functional efficiency should be the prime considerations in allocating space. However, expansibility and flexibility are the prime considerations in the design and construction of airport terminal buildings.

AIRPORT LIGHTING

Great strides have been made in improving airport lighting facilities since 1946. The most important improvement has been the elevated runway and taxiway lights and their subsequent use as replacements for the semiflush-type lights.

The semiflush lights presented many problems which are relatively unsolvable. For example, it is almost impossible to keep the system operative because most of the unit is below ground. This condition made it extremely difficult to keep the system dry, and, consequently, many "shorting outs" occurred. Another difficulty of the system is that bare current-carrying parts of the unit are below ground, making electrical maintenance a never-ending job. The optical system was of such a character that the light beams were literally "bent around a corner" to allow for pilot observation. Also, because of the low height of the unit, the light beams were readily obscured by dirt, snow, or even a 4-in. growth of grass.

With the elevated type of light, from 13 in. to 30 in. above ground, any current-carrying parts of the unit below ground are sealed into watertight housings. This sealing eliminates all the shorting out encountered with semiflush lights. With the same wattage lamp, the efficiency of the optical system is five times greater.

There appear to be two solutions which offer good possibilities for the protection of underground cable from lightning strikes. The first is to install a counterpoise system, consisting of a bare copper conductor installed in the same trench with the underground cables and about 4 in. above the cables. This bare copper circuit is then connected to a ground rod at several points around the airport so that any lighting surges in the vicinity of the airport will be carried away from the underground lighting cables and off to a good established ground. The second solution is quite similar to the first, except that the underground cables are manufactured with a shielding metallic tape. This metallic tape completely encircles the underground cable and protects it in the same manner as the counterpoise system. Those airports that have installed cable with a metallic shielding tape have had some encouraging results.

One of the greatest sources of trouble in an airport lighting system has been the inability to obtain good splices during construction. To overcome this situation, rubber-covered insulating transformers have been developed with leads that have special rubber-covered connectors for underground circuits. However, because the rubber covering is molded directly to the transformer windings, the potential for moisture entering the equipment is eliminated.

Because efficient lighting equipment is so important as a visual aid to pilots in the approaches as well as on the ground, there is a constant search for improvement of the over-all picture.

CONCLUSION

It is apparent that aviation is an important and expanding industry. Consequently, engineers cannot remain stagnant with outdated criteria for the development of aircraft facilities, but must seek improved standards and designs. Engineers who are, or will be, concerned with airport development, therefore, must keep abreast of the advances in design suggestions and standards.

DISCUSSION

Louis A. Nees,[3] **A.M. ASCE.**—The writer concurs in the author's opinion concerning intersecting runway patterns. The development of heavier aircraft with more stability against beam winds, and the development of crosswind landing gears, tend to eliminate the necessity for intersecting runways that provide for all possible wind variations.

Table 2 would be increased in value if it were expanded to indicate the type of aircraft for which the size determinations are listed. It does not seem probable that Table 2 could be applied to a wide range of aircraft types.

The writer would question the author's statements regarding the drawbacks in the present (1953) design methods for aircraft pavements. It is true that design guides are generally empirical. However, to a great extent, the criteria (especially those adopted by the Corps of Engineers) are the result of extensive and continuing correlation with tests and analyses of existing pavements. It is extremely possible that a theoretical analysis can never determine subgrade strengths and pavement thicknesses. Judgment and experience must always play a major part in this particular type of design. However, the progress made (by various governmental agencies) in improving design procedures has resulted in logical and reliable methods of pavement design.

Mr. Hahn states that the spillage of jet fuels is not a serious problem, but he considers that the effect of the jet blast is significant. On the basis of the writer's limited experience with pavements subjected to both of these factors, it is believed that the reverse is true. The jet-blast effects appear to be significant only while the airplane is stationary; deterioration of the pavement is appreciable only on asphaltic types of construction and on seeded shoulders. In military operations, these problems have been solved by the use of portable blast deflectors and by the provision of appropriate stabilization in areas where warm-ups would otherwise cause erosion of the shoulders. Moreover, the use of Portland-cement concrete in such areas eliminates a great many of the problems connected with jet blast. Spillage, however (as a result of the relatively low volatility of the fuels), can be a significant factor—especially on aprons and work areas where the pavements are constructed of asphaltic concrete. In the writer's opinion, there has not yet (as of 1953) been produced an asphaltic pavement which provides any reliable resistance to damage from spillage of jet fuels. It is in this field that continuing study and development are especially needed if bituminous pavements are to compete satisfactorily with Portland-cement concrete.

It is noted that the author makes no mention of the problem of noise suppression and control. With the advent of increased traffic and higher-powered, jet-engine-propelled aircraft this factor becomes an important one, not only in the effect on surrounding areas but also in the effect on workers engaged in the maintenance and overhaul facilities. Considerable strides in the study of this problem have been made both by aircraft manufacturers and by the

---

[3] Chf., Eng. Branch, Installations Div., Headquarters Air Materiel Command, Wright-Patterson Air Force Base, Dayton, Ohio.

United States Air Force (USAF). From the USAF's continuing study, engine-test cells have evolved which are capable of accommodating all present (1953) types and contemplated future types of jet engines without exceeding the permissible noise levels in work areas around the cells. A number of aircraft manufacturers have interested themselves in this problem to the extent of devising and constructing "noise barriers" and portable devices to suppress aircraft noises during run-up periods. There still exists a need for a great deal of study and effort, but the problem is being vigorously attacked by both the USAF and private industry, and practical solutions appear to be within the grasp of the profession.

It is interesting to note that Mr. Hahn's statements regarding the use of counterpoise systems for lighting installations are in conformance with USAF policy in these matters. Such devices are required on all new airfield lighting installations built by the USAF.

PHILIP A. HAHN.[4]—With respect to Mr. Nees' suggestion that Table 2 would be of more value if it were expanded to indicate the type of aircraft for which the size dimensions are listed, it should be noted that the values are for the current (1953) types of four-engine aircraft used in civil operations.

In connection with his discussion on pavement design, Mr. Nees has misinterpreted the statements covering certain drawbacks in design methods. Actually, these design methods are satisfactory, and the proof of their suitability is found in the performance of pavements designed on the basis of these criteria. Mr. Nees is correct in regarding experience and judgment as major bases for pavement design.

The intent of the writer in noting the drawbacks was to supply engineers with a brief review of the present (1953) status of pavement-design criteria as well as to indicate the studies necessary for improving the design procedures. When and if analytical methods or rational methods of design are developed from investigations, the basic information must still be obtained from the correlation of pavement performance with the characteristics of the subgrade soil, the paving materials, and the wheel loadings.

---

[4] Chf., Airport Eng. Div., Civ. Aeronautics Administration, U. S. Dept. of Commerce, Washington, D. C.

AMERICAN SOCIETY OF CIVIL ENGINEERS
Founded November 5, 1852
TRANSACTIONS

Paper No. 2682

DEFLECTION OF MEMBERS OF VARIABLE MOMENT OF INERTIA

By Anthony Hoadley,[1] M. ASCE

Synopsis

A method is herein developed with which the deflections of all points on a curved beam having a variable moment of inertia can be found from the bending-moment curve for the applied loading. The method is analogous to the Williot-Mohr construction method for finding the deflection of trusses. In a truss, the relative joint deflections are found as a result of a change in the length of the truss members. In this paper the relative motions of points along the neutral axis are determined from the bending stress in each segment of the beam.

The resulting deflection diagram gives the x-component and y-component for all points along the structural member. The construction of the deflection diagram can be extended to include the effect of direct stress if that stress is large enough to be of importance.

Development of Geometrical Relationships

The determination of the deflections in a structure or machine is important. From knowledge of the deflections one can (1) determine the camber needed to overcome dead-load and live-load deflections in structures, and (2) check the clearances in machinery. Indirectly, deflection diagrams are useful in the construction of influence lines, and this may be their most important use.

The method which will be described makes it possible to construct the deflected position of a curved or irregularly shaped structural member of varying moment of inertia provided that the moment diagram can be obtained for the applied loading. The method is a semigraphical one that, in a single diagram, gives the absolute deflection for each point on the structure. It is assumed that the deflections are not large enough to change significantly the geometry of the structure. Basically, the method consists of (*a*) finding the relative deflections of points at the ends of each segment of a curved beam, (*b*) graphically deter-

---

Note.—Published, essentially as printed here, in August, 1953, as *Proceedings-Separate No. 256*. Positions and titles given are those in effect when the paper was received for publication.

[1] Prof. of Civ. Eng., Union College, Schenectady, N. Y.

mining the deflections of these points from an assumed tangent, and (*c*) rotating the deflected beam until the points of support reach their known relative positions.

The geometrical relationships involved in finding the motion of segments of a curved beam relative to the fixed end of the beam at point o are shown in Fig. 1. The light line represents segments 1 and 2 of the unloaded beam. The heavy line represents the final position of these segments resulting from the deflection of the beam. If segment 2 were perfectly rigid, its position as a result of the deflection of segment 1 would be as shown by the dashed lines.

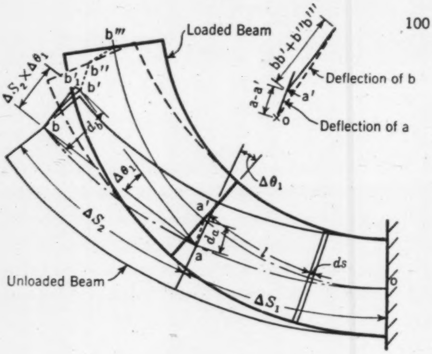
b'''
Loaded Beam
$\Delta S_2 \times \Delta\theta_1$
b'
b''
b
d_b
$bb' + b''b'''$
$a\text{-}a'$
a'
o
Deflection of b
Deflection of a
$\Delta\theta_1$
$\Delta\theta_1$
ΔS_2
a'
a
d_a
l
ds
Unloaded Beam
ΔS_1
o

FIG. 1.—GEOMETRICAL RELATIONSHIPS

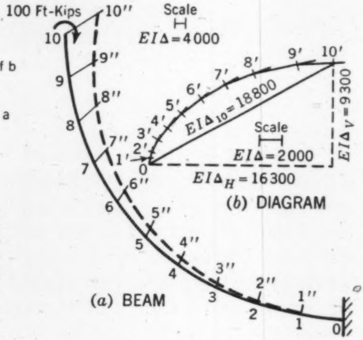
100 Ft-Kips
10''
Scale
$EI\Delta = 4000$
10
9''
9
8''
8
7''
7
6''
6
5''
5
4''
4
3''
3
2''
2
1''
1
0
1'
2'
3'
4'
5'
6'
7'
8'
9'
10'
$EI\Delta_{10} = 18800$
Scale
$EI\Delta = 2000$
$EI\Delta_H = 16300$
$EI\Delta_V = 9300$

(*a*) BEAM (*b*) DIAGRAM

FIG. 2.—CIRCULAR RIB WITH CONSTANT MOMENT OF INERTIA

Because of the applied loads, the left face of segment 1 undergoes a deflection d_a and has an angular displacement of $\Delta\theta_1$. Point b in the left face of segment 2, which is considered to be rigid, is moved to point b′ as a result of the rotation of segment 1. Because of the deflection d_a of point a, point b′ is moved an equal distance in the direction of d_a. Then, because of the bending of segment 2, point b″ is deflected to its final position b‴.

It is assumed that the deflections are small enough so that line b″-b‴ is perpendicular to chord a-b. The deflection of point b relative to point a is thus equal to the length of segment 2 times the angular rotation at point a plus the deflection of point b from the tangent at point a.

As a result of the relative magnitude of the angular changes and of the displacements in comparison to the length of the segment, it is assumed that the deflection of a segment takes place in a direction perpendicular to the chord of that segment. The close agreement between the analytical and graphical solutions would seem to substantiate the validity of this assumption.

It can be seen that the displacements of the ends of the various segments can be found graphically by plotting successively—to scale—(1) the deflection d_a at right angles to chord o-a of segment 1, (2) the sum of displacements d_b and b″-b‴ (d_a) at right angles to chord a-b of segment 2, and continuing in a similar fashion for the subsequent segments.

The change in slope in a differential length of the segment ds is $\int \frac{m\,ds}{E\,I}$ in which m is the bending moment at any point, E denotes the modulus of elasticity, and I is the moment of inertia. The total angular change $\Delta\theta_1$ in length ΔS_1 will be

$$\Delta\theta_1 = \int \frac{m\,ds}{E\,I} = \frac{M\,\Delta S_1}{E\,I} \quad \text{(1)}$$

in which M is the average bending moment. The length ΔS_1 should be chosen so that Eq. 1 is applicable to within the desired accuracy. Special care must be exercised near a sharp peak in the moment curve such as that found at the supports of a continuous beam. The displacement d_a in Fig. 1 will be

$$d_a = \int \frac{l\,M\,ds}{E\,I} = \frac{\Delta S_1}{2}\,\frac{M\,\Delta S_1}{E\,I} \quad \text{(2)}$$

and will be approximately perpendicular to the chord o-a of segment 1. The displacement d_b will be

$$d_b = \Delta S_2\,\Delta\theta_1 = \Delta S_2\,\frac{M\,\Delta S_1}{E\,I} \quad \text{(3)}$$

and will be perpendicular to chord a-b of segment 2.

In general terms, the deflection of point n with respect to point n-1 is given by

$$\frac{\Delta S_n}{2}\,\frac{M_n\,\Delta S_n}{E\,I} + \Delta S_n \sum_0^{n-1} \frac{M\,\Delta S}{E\,I} \quad \text{(4a)}$$

or

$$\frac{\Delta S_n}{2}\,\Delta\theta_n + S_n \sum_0^{n-1} \Delta\theta \quad \text{(4b)}$$

in which ΔS is the length of the segment n measured along the neutral surface.

Circular Rib with Constant Moment of Inertia.—The deflected position of the circular rib shown in Fig. 2(*a*) illustrates the application of the graphical method. The rib has a constant radius of curvature R of 12.75 ft and a constant moment of inertia. It is fixed at point 0 and carries a moment of 100 ft-kips at point 10. The general procedure would be the same for (*a*) a beam of variable moment of inertia, (*b*) a beam of variable radius of curvature, and (*c*) a beam subjected to any type of loading. The conditions shown in Fig. 2 simplify the analytical solutions used to check the graphical results.

The relative deflections of the arch rib segments are computed in Table 1. As both the moment of inertia and the bending moment are constant, the angular change $\Delta\theta$ for each segment is $\frac{100 \times 2}{E\,I}$. The total deflection of segment n (Col. 6, Table 1) with respect to segment n-1 is equal to the deflection caused by the bending of segment n (Col. 3, Table 1) plus the deflection caused by the rotation of segment n (Col. 5, Table 1). The value of Δs has been taken as 2 ft for each segment.

TABLE 1.—RELATIVE DEFLECTIONS FOR THE CURVED BEAM IN FIG. 2

Segment (1)	Bending moment M, in foot-kips (2)	$E\,I\,\frac{\Delta\theta\,\Delta s}{2}$ (3)	$E\,I\sum_{0}^{n-1}\Delta\theta$ (4)	$E\,I\,\Delta s\sum_{0}^{n-1}\Delta\theta$ (5)	$E\,I$ × relative deflection (6)
1	100	200	0		200
2	100	200	200	400	600
3	100	200	400	800	1,000
4	100	200	600	1,200	1,400
5	100	200	800	1,600	1,800
6	100	200	1,000	2,000	2,200
7	100	200	1,200	2,400	2,600
8	100	200	1,400	2,800	3,000
9	100	200	1,600	3,200	3,400
10	100	200	1,800	3,600	3,800

From point 0′ a distance of 200 is drawn in the direction of the radius to the center of segment 1, thus establishing point 1′ of Fig. 2(*b*). From point 1′ the line 1′-2′ is drawn 600 units long and parallel to the radius to the center of segment 2. All points are located similarly. The line 0′-1′ represents the motion of point 1′ with respect to the fixed point 0. The line 1′-2′ represents the motion of point 2 relative to point 1 so that the line 0′-2′ represents the absolute motion of point 2. The absolute motion of any point on the beam is given by a line drawn from 0′ to the corresponding point in Fig. 2(*b*).

The deflected position of the loaded circular beam is found by drawing, to scale, lines 1–1″, 2–2″, . . . , 10–10″ in Fig. 2(*a*) parallel to rays 0′–1′, 0′–2′, . . . , 10–10′ in Fig. 2(*b*). The curve connecting points 0, 1″, 2″, . . . , 10″ was found to be circular as would be expected in the case of a beam loaded only with a bending moment. The horizontal and vertical components of the deflection of point 10 agree with those found by an analytical solution with an error of less than 1%.

REINFORCED CONCRETE ARCH

The deflected position of a fixed-ended reinforced concrete arch with a span of 123 ft which carries a 10-kip load near the quarter-point has been found and is shown in Fig. 3. The related computations are given in Table 2.

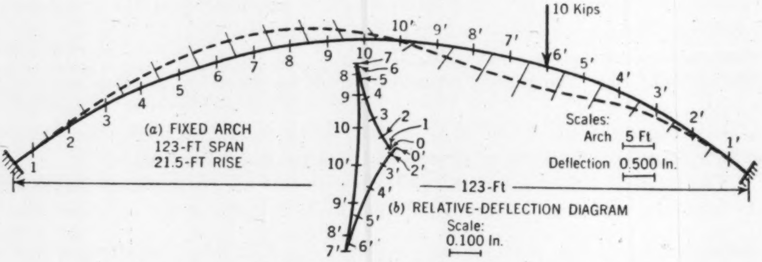

FIG. 3.—DEFLECTION OF FIXED ARCH

The heading for Col. 4, Table 2, is $\frac{M}{540}\frac{\Delta s}{I}$. The values in Col. 4 are $10^6 \times \Delta\theta$ for each segment. The modulus of elasticity for the arch is 3×10^6 lb

TABLE 2.—RELATIVE DEFLECTIONS FOR THE ARCH IN FIG. 3

Segment (1)	$\frac{\Delta s}{I}$ (2)	Bending moment M, in kip-feet (3)	$\frac{M}{540}\frac{\Delta s}{I}$ (4)	Adjustment $\times 10^3$ (5)	Adjusted $\Delta\theta$, in radians $\times 10^3$ (6)	Δs, in inches (7)	$\frac{\Delta s}{2}\Delta\theta$, in inches $\times 10^3$ (8)	$\sum_0^{n-1}\Delta\theta$, in inches $\times 10^3$ (9)	$\Delta s \times \sum_0^{n-1}\Delta\theta$, in inches $\times 10^3$ (10)	Relative deflection, in inches $\times 10^3$ (11)
1	2.47	+70.41	+0.322	1	+0.321	93.0	+14.93			+ 14.9
2	4.36	+41.88	+0.337	1	+0.336	87.8	+14.75	+0.321	+ 28.2	+ 43.0
3	6.89	+19.40	+0.247	1	+0.246	83.8	+10.32	+0.657	+ 55.1	+ 65.4
4	9.35	+ 2.01	+0.035	1	+0.034	80.5	+ 1.44	+0.903	+ 72.7	+ 74.1
5	10.71	−10.01	−0.1985	1	−0.200	78.2	− 7.82	+0.937	+ 73.2	+ 65.4
6	11.53	−17.81	−0.380	1	−0.381	76.6	−14.60	+0.737	+ 56.5	+ 41.9
7	12.27	−22.14	−0.503	1	−0.502	75.2	−18.85	+0.356	+ 26.8	+ 8.0
8	12.98	−23.03	−0.553	2	−0.555	74.5	−20.70	−0.146	− 10.87	− 31.6
9	13.35	−20.89	−0.516	1	−0.517	74.0	−19.13	−0.701	− 52.0	− 71.1
10	13.54	−15.72	−0.394	1	−0.395	73.8	−14.56	−1.218	− 89.9	−104.5
10′	13.54	− 7.10	−0.1781	1	−0.179	73.8	− 6.60	−1.613	−119.0	−125.6
9′	13.35	+ 4.98	+0.1233	0	+0.123	74.0	+ 4.55	−1.792	−132.6	−128.0
8′	12.98	+20.08	+0.482	1	+0.481	74.5	+17.90	−1.629	−121.3	−103.4
7′	12.27	+38.21	+0.868	2	+0.866	75.2	+32.50	−1.148	− 86.4	− 53.9
6′	11.53	+59.79	+1.278	3	+1.275	76.6	+48.80	−0.282	− 21.6	+ 27.2
5′	10.71	+23.33	+0.462	1	+0.461	78.2	+18.02	+0.953	+ 74.5	+ 92.5
4′	9.35	− 8.81	−0.1525	0	−0.152	80.5	− 6.14	+1.414	+113.6	+107.5
3′	6.89	−35.77	−0.457	1	−0.458	83.8	−19.20	+1.262	+105.7	+ 86.5
2′	4.36	−57.55	−0.465	1	−0.466	87.8	−20.45	+0.804	+ 70.6	+ 50.1
1′	2.47	−73.27	−0.335	1	−0.336	93.0	−15.61	+0.338	+ 31.45	+ 15.8
0′		−78.20								

per sq in. or 432 × 10^6 lb per sq ft. The moment of inertia of the transformed section I_T is 1.25 I. From Eq. 1,

$$\Delta\theta = \frac{M\,\Delta s}{E\,I_T} = \frac{M\,\Delta s}{(432 \times 10^6)(1.25\,I)} = \frac{M\,\Delta s}{540 \times 10^6 \times I} \quad \text{(5)}$$

The sum of the angular changes computed in Col. 4, Table 2, is not zero as it should be. The error was distributed proportionately to the size of the angle change in each segment, and the adjusted angle was entered in Col. 6, Table 2. Data on the arch axis were prepared by Clarence W. Dunham,[2] M. ASCE. Under the applied loading, Fig. 3 shows that the middle half of the arch has an appreciable shift to the left. The vertical component of the deflection at the left quarter-point was found to be 0.230 in. as compared with the 0.236 in. given by Mr. Dunham's analytical solution. The deflection curve is also the influence line for the deflection at panel point 6.

Effect of Direct Stress.—The effect of direct stress on the deflection of the arch rib can be found in the following manner: A line is drawn from point 1 of the relative-deflection diagram (Fig. 3(*b*)) so that it is parallel to the thrust acting on segment 1 of the arch. The length of this line should equal the shortening of segment 1 as a result of direct stress and will extend downward to the left from point 1 of the relative-deflection diagram. This new point gives the deflection of the right end of segment 1 caused by both direct stress and bending. The effect of direct stress in the other segments is found in a similar manner. The effect of direct stress in the arch was negligible for a 10-kip load placed at panel point 6′.

---

[2] "Theory and Practice of Reinforced Concrete," by Clarence W. Dunham, McGraw-Hill Book Co., Inc., New York, N. Y., 1944.

Deflection of Curved Beams with Hinged Ends

In the case of structures which do not have a fixed point or a point at which the slope of the tangent to the neutral axis is known, it becomes necessary to find the deflections of the panel points with respect to an assumed tangent and then to rotate the structure until the points of support have the correct relative elevation.

Dead-Load Deflections of a Rigid-Frame Bridge.—The dead-load deflection curve for an unsymmetrical rigid-frame bridge with hinged ends is an apt illustration of the solution of a problem of this type. Data on the bridge shown in Fig. 4 and its dead-load moments were obtained by Arthur G. Hayden and Maurice Barron,[3] Members, ASCE. The deflections relative to point 11.5 of the panel points were computed from the dead-load moments and from the elastic properties of the bridge on a tabular form similar to that shown in Table 2. The relative-deflection diagram was then drawn as shown by the light lines and primed points in Fig. 4(*b*). The light solid line in Fig. 4(*a*) shows the position of the bridge relative to a tangent to the neutral axis at panel point

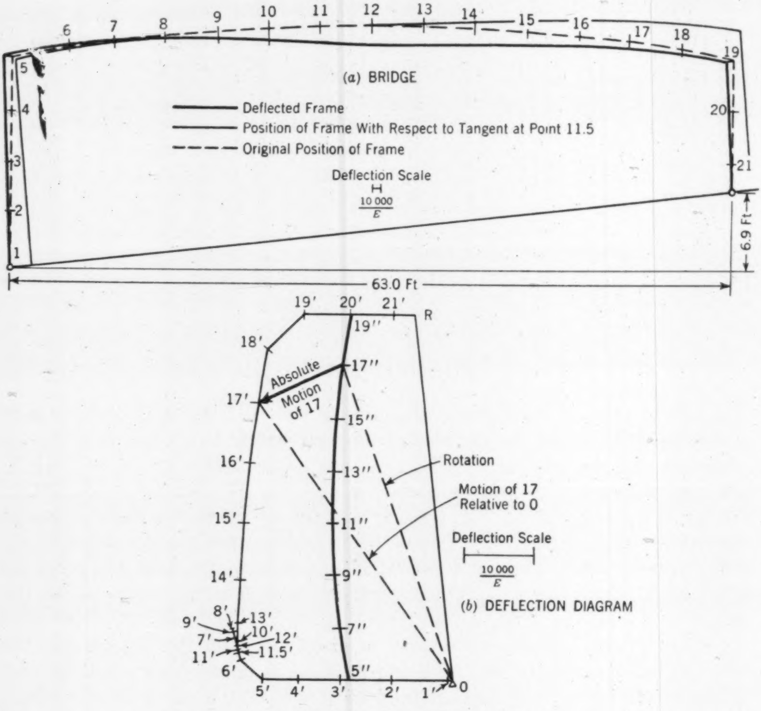
(a) BRIDGE
Deflected Frame
Position of Frame With Respect to Tangent at Point 11.5
Original Position of Frame
Deflection Scale
10 000/E
1
2
3
4
5
6
7
8
9
10
11
12
13
14
15
16
17
18
19
20
21
63.0 Ft
6.9 Ft
19′
20′
21′
R
18′
19″
17″
Absolute Motion of 17
17′
15″
16′
13″
Rotation
Motion of 17 Relative to 0
15′
11″
Deflection Scale
10 000/E
14′
9″
(b) DEFLECTION DIAGRAM
8′
9′
13′
10′
7′
12′
11′
11.5′
7″
6′
5″
5′
4′
3′
2′
1′
0

Fig. 4.—Rigid-Frame Bridge

---

[3] "The Rigid-Frame Bridge," by Arthur G. Hayden and Maurice Barron, John Wiley & Sons, Inc., New York, N. Y., 1950.

11.5. This shows that, with point 11.5 fixed, the left end of the bridge has moved to the right and slightly below its original position. At the same time, the right end of the bridge has moved to the right and a considerable distance above its original position. It is necessary to rotate the bridge about its left end until the right end is the original distance (6.9 ft) above the left end. The motion of any panel point caused by this rotation will be proportional to its distance from the left hinge and will be perpendicular to the line connecting these two points. In Fig. 4(*b*) the vertical distance between points 0 and R represents, to scale, the distance that the right end of the bridge must be dropped to bring the ends of the bridge to their correct elevations. From point 0 a rigid frame, whose span in 0-R, is drawn so that it is rotated 90° with respect to the real bridge. The distance from a panel point to point 0 on this correction diagram will then represent the motion of the corresponding point of the rigid frame when the rotation occurs. For panel point 17 this is shown as line 17″-0. The motion of point 17 relative to point 0 is shown as line 0–17′. The absolute motion of point 17 is the resultant of these motions, or the distance 17″–17′ in Fig. 4(*b*). The deflections in Fig. 4(*a*) are shown to half the scale used in drawing the deflections in Fig. 4(*b*). The deflections shown are the values for the face of each segment which is farthest from point 11.5.

Deflection Curve for Continuous Beam.—The construction of the deflection curve for a beam 20 ft long which is supported at its left end and midpoint, and which carries a 1-lb load acting vertically upward at its right end, is shown in Table 3 and Fig. 5. The beam has a constant moment of inertia and Δs is taken as 2 ft. Substituting these values into Eq. 4*a* and multiplying by $E\,I$ results in

TABLE 3.—DEFLECTION AND INFLUENCE VALUES FOR TWO-SPAN CONTINUOUS BEAM

Segment (1)	$2\,M$ (2)	$\sum_0^{n-1} 4\,M$ (3)	Relative deflection (4)	Scaled vertical deflection (5)	Influence ordinate (6)
a	18		18	85	0.128
b	14	36	50	200	0.302
c	10	64	74	342	0.516
d	6	84	90	498	0.752
e	2	96	98	663	1.000
a′			18	−49	0.074
b′			50	−65	0.098
c′			74	−56	0.084
d′			90	−33	0.045
e′			98	0	

$$E\,I \times \delta_{n,n-1} = 2\,M_n + \sum_0^{n-1} 4\,M \qquad (6)$$

in which $\delta_{n,n-1}$ is the relative deflection of segments n and n-1 and M is the moment at the center of a segment caused by the 1-lb load. The relative deflections shown in Col. 4, Table 3 (which are $E\,I$ times the actual relative deflection), are plotted from point 10′ of Fig. 5(*b*) in a direction perpendicular to the tangent to the beam at the center of each segment. This results in the straight line 10′–20′. The deflections are then plotted at the appropriate points on the beam giving the dotted deflection curve shown in Fig. 5(*c*) which is relative to a tangent at point 10. Fig. 5(*b*) shows point 0′ to be the distance 10′–0′ above point 0. Actually, the left end of the beam must rest on the point of support 0. This condition will be attained when the dotted deflection curve is rotated until 0′ drops to 0. This can be done by drawing a Mohr correction diagram as shown in Fig. 5(*b*). The diagram has been drawn at right angles to the original beam, with the length of one span equal to the distance that 0′ must drop (or the line 0′–10′ on the relative deflection diagram). The distance from a point on the Mohr diagram to the corresponding point on the relative-deflection diagram will give the absolute deflection of that point on the beam.

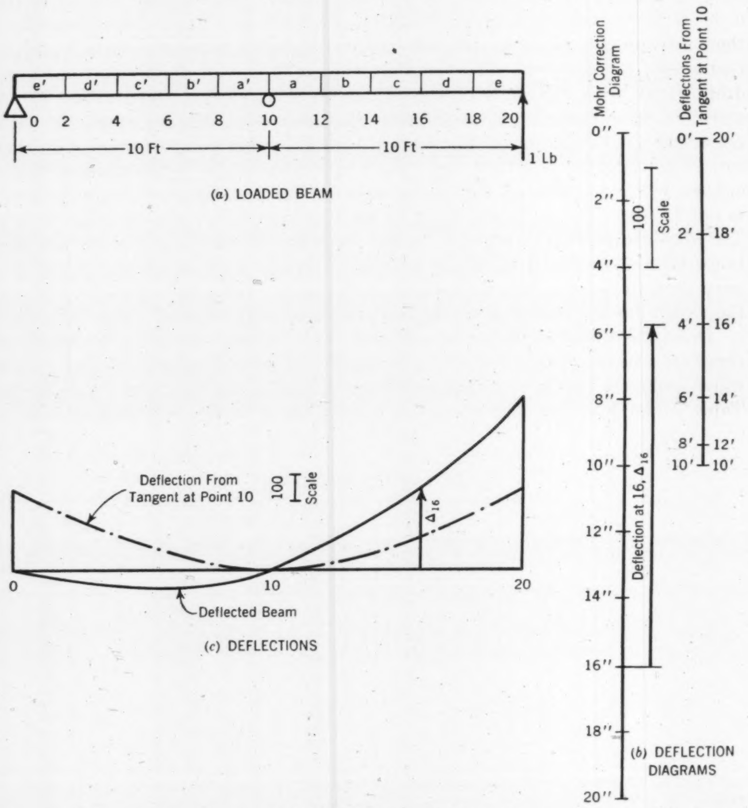
e′
d′
c′
b′
a′
a
b
c
d
e
0 2 4 6 8 10 12 14 16 18 20
10 Ft
10 Ft
1 Lb
Deflection From Tangent at Point 10
100
Scale
Δ16
0
10
20
Deflected Beam
Mohr Correction Diagram
Deflections From Tangent at Point 10
0″ 2″ 4″ 6″ 8″ 10″ 12″ 14″ 16″ 18″ 20″
0′ 20′
2′ 18′
4′ 16′
6′ 14′
8′ 12′
10′ 10′
100
Scale
Deflection at 16, Δ16

(*a*) LOADED BEAM

(*c*) DEFLECTIONS

(*b*) DEFLECTION DIAGRAMS

FIG. 5.—CONTINUOUS BEAM

These scaled distances were recorded in Col. 5, Table 3, and were used to plot the final deflection curve shown in Fig. 5(*c*). The actual deflections would be the value from Col. 5, Table 3, divided by $E I$. This method of finding deflection curves for beams can be applied to haunched or reinforced beams by using the average I for each segment in performing the summation in Eq. 4*a*.

Influence Line for Continuous Beam.—H. Müller-Breslau,[4] D. B. Steinman,[5] M. ASCE, and others have shown that the deflection curve caused by a load acting in place of the reaction of an indeterminate beam is proportional to the influence line for the redundant reaction. The influence ordinates for a vertical reaction at point 20 were obtained by dividing the scaled deflections of Col. 5, Table 3, by 663.

APPENDIX

Chord versus Arc.—For computing the rotational effect, the correct distance to use is the chord a-b in Fig. 1. For the bending of the segment, ΔS as measured along the arc should be used. When ΔS for a curved beam is so chosen that the angle subtended by the segment is 20°, the arc will be ½% longer than the segment. For a subtended angle of 28° the differences in length will be 1%. Segment lengths can be chosen so that the difference in length of chord and arc is less than the accuracy in the drawing.

Direction of Rotational Deflection.—Even in an extreme case of elastic deflection, the tangent b-b′ in Fig. 1 is a satisfactory approximation for arc b-b′. If the depth of a curved beam (fixed at one end) is $L/20$, the length is L, and the moment of inertia I and the moment at any point M are constant, then the change in slope at the free end of the beam will be

$$\Delta\theta = \frac{M L}{E I} \qquad (7a)$$

or

$$\Delta\theta = \frac{f L}{E c} \qquad (7b)$$

in which

$$M = \frac{f I}{c} \qquad (7c)$$

f is the allowable fiber stress, and c is the distance from the neutral axis to the extreme fiber. The rotational deflection (b-b′) of the end segment is $\frac{\Delta S f L}{E c}$. The difference in direction between arc b-b′ and tangent b-b′$_1$ is the angle b′-b-b′$_1$ in Fig. 1. This angle is $\Delta\theta/2$.

---

[4] "Graphische Statik der Baukonstructionen," by H. Müller-Breslau, Alfred Kröner, Vol. 2. Pt. 1, Leipzig, 5th ed., 1912.

[5] *Engineering Record*, November 25, 1916, p. 648.

For steel with $f = 20{,}000$ lb per sq in. and $c = L/40$,

$$|\text{b-b}'| = \frac{\Delta S\, f\, L}{E\, c} \quad \text{(8a)}$$

$$|\text{b-b}'| = \frac{20{,}000 \times 40}{30 \times 10^6}\, \Delta S = 0.0267\, \Delta S \quad \text{(8b)}$$

$$\frac{\Delta\theta}{2} = \frac{f\, L}{2\, E\, c} \quad \text{(8c)}$$

and

$$\frac{\Delta\theta}{2} = \frac{20{,}000 \times 40}{2 \times 30 \times 10^6} = 0.0133 \text{ radian} = 46 \text{ min.} \quad \text{(8d)}$$

The average angular error in a beam for which the bending moment is between zero and a maximum, or from maximum negative to maximum positive, would be much smaller.

Stiff Beams.—When the ratio d/R (in which d is the depth of the beam) is comparatively large, a modified moment of inertia must be used. It has been shown[6] that

$$\Delta\theta = \frac{M\, \Delta S}{E\, I \left[1 + \frac{4}{15}\left(\frac{d}{2\, R}\right)^2\right]} \quad \text{(9)}$$

for curved beams having a rectangular cross section. Values of the moment-of-inertia factor $\left[1 + \frac{4}{15}\left(\frac{d}{2\, R}\right)^2\right]$ for ratios of d/R equal to $\frac{1}{2}$, $\frac{1}{5}$, and $\frac{1}{10}$ are 1.0167, 1.0027, and 1.0007, respectively.

---

[6] "Theory of Structures," by S. Timoshenko and D. H. Young, McGraw-Hill Book Co., Inc., New York, N. Y., 1945, p. 423.

AMERICAN SOCIETY OF CIVIL ENGINEERS
Founded November 5, 1852
TRANSACTIONS

Paper No. 2683

THE GRANBY PUMPING PLANT

A SYMPOSIUM

Foundations and Design
By W. R. Judd, A.M. ASCE, and W. H. Wolf................ 510

Construction
By R. J. Willson.. 525

FOUNDATIONS AND DESIGN

By W. R. Judd,[1] A. M. ASCE, and W. H. Wolf[2]

Synopsis

At Granby Reservoir, in Colorado, the peculiarities of the foundation material and an unusual margin of forebay fluctuation dictated the special features of the pumping plant built to divert water across the Continental Divide. The foundation conditions at the Granby Pumping Plant, their relation to the design, and the unusual design analyses of this structure are described herein.

Alternate designs were studied. Open-cut construction was used, and a rectangular structure having semicircular ends was built. It was strengthened by heavy transverse frames, the design of which was particularly complex.

Introduction

The Granby Pumping Plant (in Colorado) is a major feature of the Colorado-Big Thompson Project (Fig. 1). The project is a transmountain diversion development which takes waters from Grand Lake, in Colorado,

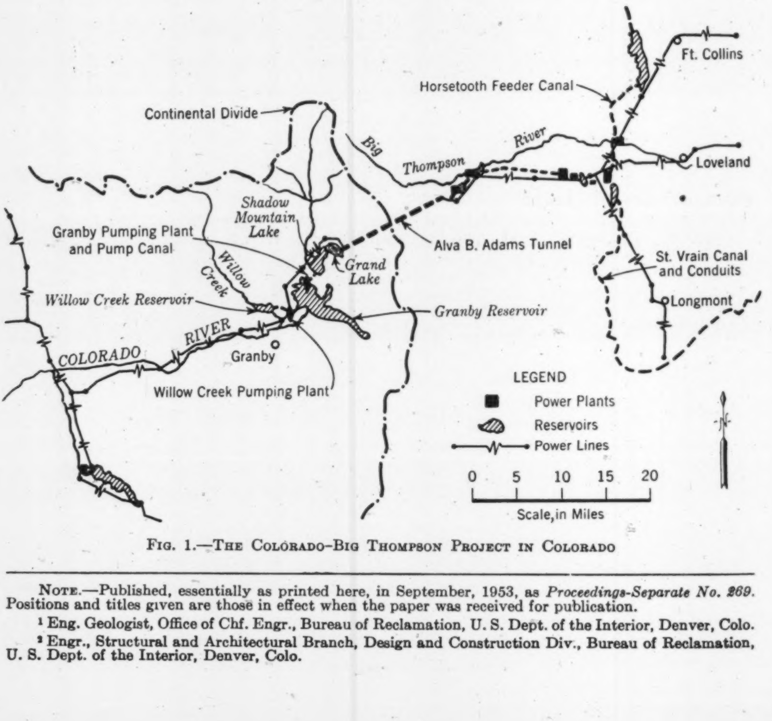
Ft. Collins
Horsetooth Feeder Canal
Continental Divide
Big
Thompson
River
Loveland
Shadow Mountain Lake
Granby Pumping Plant and Pump Canal
Alva B. Adams Tunnel
Willow Creek
Grand Lake
St. Vrain Canal and Conduits
Willow Creek Reservoir
Granby Reservoir
Longmont
RIVER
COLORADO
Granby
Willow Creek Pumping Plant
LEGEND
■ Power Plants
▨ Reservoirs
—∿— Power Lines
0 5 10 15 20
Scale, in Miles
N

Fig. 1.—The Colorado-Big Thompson Project in Colorado

Note.—Published, essentially as printed here, in September, 1953, as *Proceedings-Separate No. 269.* Positions and titles given are those in effect when the paper was received for publication.

[1] Eng. Geologist, Office of Chf. Engr., Bureau of Reclamation, U. S. Dept. of the Interior, Denver, Colo.

[2] Engr., Structural and Architectural Branch, Design and Construction Div., Bureau of Reclamation, U. S. Dept. of the Interior, Denver, Colo.

(the headwaters of the Colorado River), situated on the western slope of the Colorado section of the Rocky Mountains. By means of the Alva B. Adams Tunnel through the Continental Divide, this water is diverted to the Big Thompson River on the eastern slope. To supplement the water supply available from the drainage area above Grand Lake, water from tributaries below the lake is collected on the western slope by Granby Reservoir and Willow Creek Reservoir, and is pumped to Shadow Mountain Reservoir (all in Colorado). From this point, gravity causes the water to flow through Grand Lake and the Adams Tunnel to the eastern slope—where it is stored for later release as a supplemental supply for the irrigation of 708,000 acres of fertile farm land in the Platte Valley of eastern Colorado. On the eastern slope, the natural drop of the water (2,800 ft between the outlet of the tunnel and the foothills storage reservoirs) is utilized in generating power. The Granby Pumping Plant is on the north shore of Granby Reservoir. It lifts the water from the reservoir to the head of a canal which conveys the water to Shadow Mountain Reservoir at a maximum rate of 1,100 cu ft per sec.

The elevation of the reservoirs on the western slope can be regulated by remote control from the pumping plant. Diversion through the Adams Tunnel can be regulated, and telemetering equipment housed in the plant informs the operators concerning the elevation and discharges of the various reservoirs. As shown in Fig. 2, the pumping plant is an unusual structure, being the equivalent of a fifteen-story reinforced concrete building 187 ft high, except that 133 ft of it is underground.

Foundation Conditions

Granby Reservoir lies in a natural valley created by glaciers moving westward from the front range of the Rocky Mountains. The glaciers, in their downward sweep from the mountains, carved new valleys in the soft beds of siltstone and sandstone that had been deposited in the Tertiary period. They left in their wake a mass of glacial debris composed of a heterogeneous mixture of sand, gravel, boulders, and silt. After the glaciers had retreated, the present drainage patterns of the country were formed. The path of a tributary glacier became the present valley of the Colorado River in the vicinity of Granby Reservoir.

In the area of the reservoir, recent alluvial materials overlying glacial debris have been found. These alluvial materials, in turn, overlie siltstones and soft sandstones near the top of the Tertiary North Park formation. This formation also has been injected with lava flows; but lava was not encountered at the structure site. The reservoir lies in a broad U-shaped valley with steep walls. These walls have numerous exposures of the basement rock, which is granite and granite gneiss.

The broad U-shaped valley provided an excellent reservoir site into which sufficient water could be impounded by constructing Granby Dam and four small dikes. The next problem was to move water from Granby Reservoir up to Shadow Mountain Reservoir and Grand Lake, which were between 85 ft higher (at maximum high water in Granby Dam) and 180 ft higher (at low water) (Fig. 3). Numerous sites for the necessary pumping plant were investi-

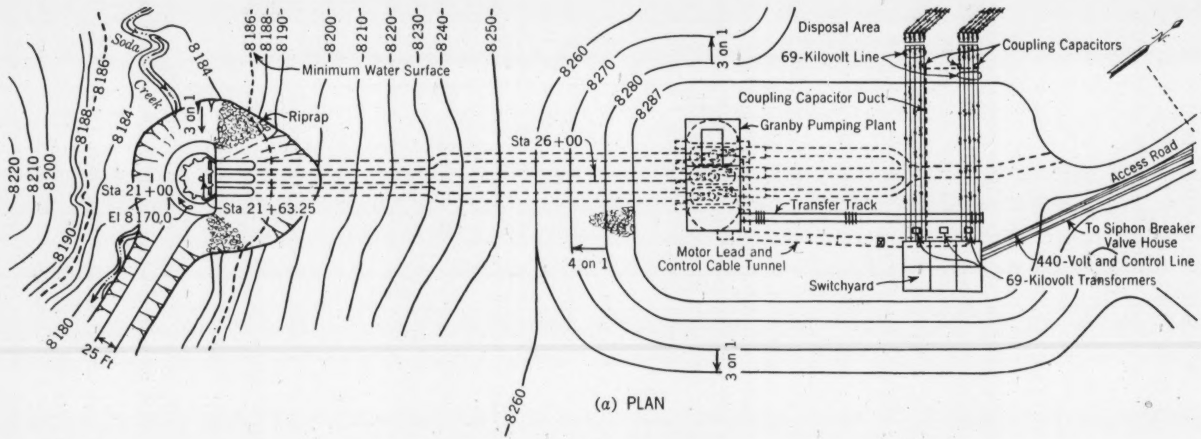
Soda Creek
8220
8210
8200
8190
8188
8186
8184
8180
25 Ft
3 on 1
Sta 21+00
El 8170.0
Sta 21+63.25
Riprap
8186
8188
8190
Minimum Water Surface
8200
8210
8220
8230
8240
8250
8260
8270
8280
8287
Sta 26+00
4 on 1
3 on 1
3 on 1
Disposal Area
69-Kilovolt Line
Coupling Capacitors
Coupling Capacitor Duct
Granby Pumping Plant
Transfer Track
Motor Lead and Control Cable Tunnel
Switchyard
69-Kilovolt Transformers
440-Volt and Control Line
To Siphon Breaker Valve House
Access Road

(a) PLAN

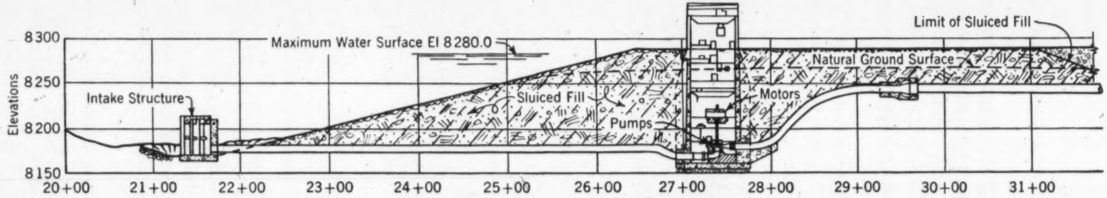
Elevations
8300
8250
8200
8150
20+00
21+00
22+00
23+00
24+00
25+00
26+00
27+00
28+00
29+00
30+00
31+00
Intake Structure
Maximum Water Surface El 8280.0
Sluiced Fill
Pumps
Motors
Natural Ground Surface
Limit of Sluiced Fill

(b) PROFILE ALONG CENTER LINE

FIG. 2.—GRANBY PUMPING PLANT IN COLORADO

gated. After brief studies, many sites were eliminated because of obvious construction difficulties or exceedingly high costs. (In Fig. 3, areas without symbols indicate that the bedrock is completely covered with glacial till or topsoil.) Intensive studies were made on what appeared to be four comparable preliminary schemes called A-1, A-2, B, and C. The A-1 and A-2 schemes involved building 3,000 ft of discharge conduit and 2 miles of canal at the northwest end of Granby Lake; open excavation and backfilling were necessary. The A-1 scheme required three surge suppressors and three reinforced concrete discharge conduits of 7.25-ft diameter. The embankment to fill this cut would have been raised 7 ft above the maximum high-water surface. The A-2 design also involved the construction of a valve house containing three slide valves, and of a larger plant to house the discharge valves. With this scheme, one surge tank was utilized, with one 11-ft-diameter discharge conduit.

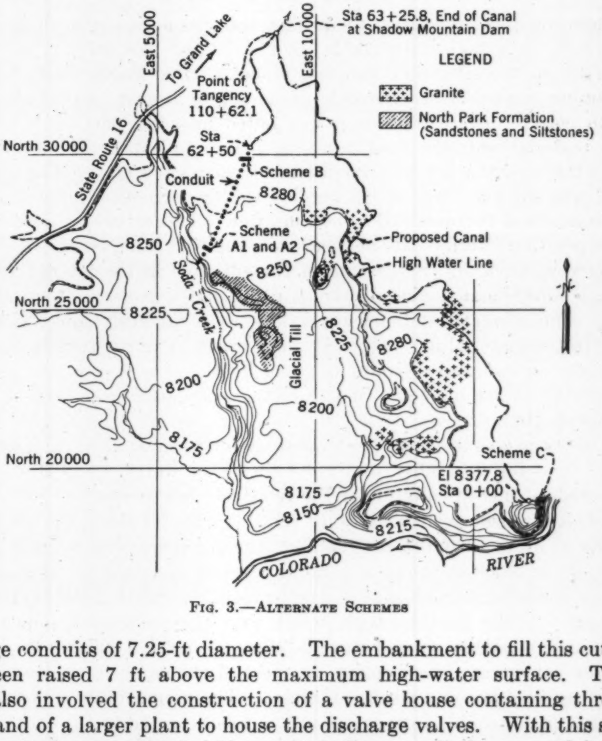
Sta 63+25.8, End of Canal at Shadow Mountain Dam
LEGEND
Granite
North Park Formation (Sandstones and Siltstones)
East 5000
East 10000
To Grand Lake
Point of Tangency 110+62.1
State Route 16
North 30000
Sta 62+50
Scheme B
Conduit
8280
8250
Scheme A1 and A2
Proposed Canal
High Water Line
Soda Creek
8250
North 25000
8225
Glacial Till
8225
8280
8200
8200
8175
North 20000
Scheme C
El 8377.8 Sta 0+00
8175
8150
8215
COLORADO
RIVER

Fig. 3.—Alternate Schemes

Scheme B necessitated an intake tunnel 11 ft in diameter, a vertical stope to the surface of the plant site, and a circular building (73 ft in diameter), using the face of the excavation for the exterior form.

Under scheme C the pumping plant was situated some distance down the reservoir rim, and the plant would have been placed in granite. A tunnel intake and discharge would have been required, as well as a side-hill canal from 6 miles to 7 miles long. At this elevation and in this climate considerable difficulty with freezing and side-hill drainage would have been encountered.

The costs, operation, and construction of these preliminary designs were analyzed. Scheme A-1 with modifications (such as the elimination of the surge tank) was selected because: (1) It would be possible to take any one of the three units out of service; (2) it involved only open-cut construction, which would permit simultaneous operations; (3) both the construction and operating hazards were minimized; and (4) the rectangular plant with semicircular ends was relatively more conventional, and thus offered better operation facilities.

FOUNDATION EXPLORATION

Exploration of the fundation by drilling, test pitting, and trenching revealed the presence of a high-water table, and indicated the primary foundation material to be the siltstones and sandstones of the North Park formation. The siltstone was friable, moderately cemented, light gray to reddish buff and brown in color. Severe fracturing was noted near the surface of the beds; but the material near the final pumping plant grade became more massive, although there were a few thin laminae and partings of clay. The cementing material was silt and clay, which implied that construction difficulties would be encountered if the excavation became wet. The siltstones were found to occupy a position intermediate between soils and rock, and, therefore, exhibited characteristics of both. Saturation of the siltstone in the laboratory caused dilation, a subsequent increase in voids ratio, and a decrease in strength and density. The strength and density values were probably lower than those inherent in the material in its original state, where saturation occurred because of the consolidation and restraint imposed by the overlying beds. However, the laboratory tests indicated that swelling and spalling during excavation could be expected.

The siltstone was tested in the laboratory for permeability, compressibility, elasticity, and for durability under conditions of wetting and drying. The samples yielded inelastically under the relatively low stresses of 100 lb per sq in. The compression tests were quite variable, the wet strength ranging from 200 lb per sq in. to 1,240 lb per sq in., and the dry strength varying from 1,320 lb per sq in. to 5,000 lb per sq in. Sonic tests for the modulus of elasticity of the wet samples yielded values of E ranging from 167,000 lb per sq in. to 454,000 lb per sq in. Static modulus tests, which were also conducted, indicated that the moduli of elasticity ranged from 0 lb per sq in. to 2,600,000 lb per sq in. The latter value was the exception, as most of the samples were so soft that accurate test results could not be obtained. The permeability was sufficiently low so that little trouble from water inflow was expected in the excavation.

Triaxial shear tests on a recompacted sample of soft, reddish-brown siltstone having an average dry density of 109 lb per cu ft and a moisture content of 19% gave values of tan ϕ of 0.62 and cohesion of 9.3 lb per sq in. A sample of very hard, bluish-gray siltstone, with an average density of 129 lb per cu ft and a moisture content of 5% (after recompaction) gave values of tan ϕ of 0.86 and cohesion of 26.0 lb per sq in. The specific gravity of both samples was 2.65. The samples were recompacted as the undisturbed siltstone was too hard to be prepared with standard procedures. The relationship between the laboratory shear values of the remolded samples and those values that existed in the field was somewhat speculative, but it was assumed that, whereas the laboratory cohesion values might be considerably different from the in-place values, the laboratory friction values would be acceptable. As a result of these studies, 6.25 tons per sq ft was permitted as a design load for the siltstone.

Geologic study disclosed minor slumping in the natural valley slopes of between 3 on 1 and 4 on 1. These slumps occurred in areas of oversteepening and at ground-water seeps. It was thought that the valley sides might heave and flow during reservoir inundation and thus close the inlet channel, and that protection should be provided to prevent leveling of the natural slopes and erosion caused by wave action. Because of the instability of the slopes, it was decided to grade a hill adjacent to the inlet to a stable slope, placing riprap wherever the bare siltstone would be exposed to wave action. It was further decided that the excavation slopes should be 1 on 1 during construction, that the embankment on the intake side of the plant would have slopes of 4 on 1 to match the adjacent topography, and that they would be riprapped to prevent erosion.

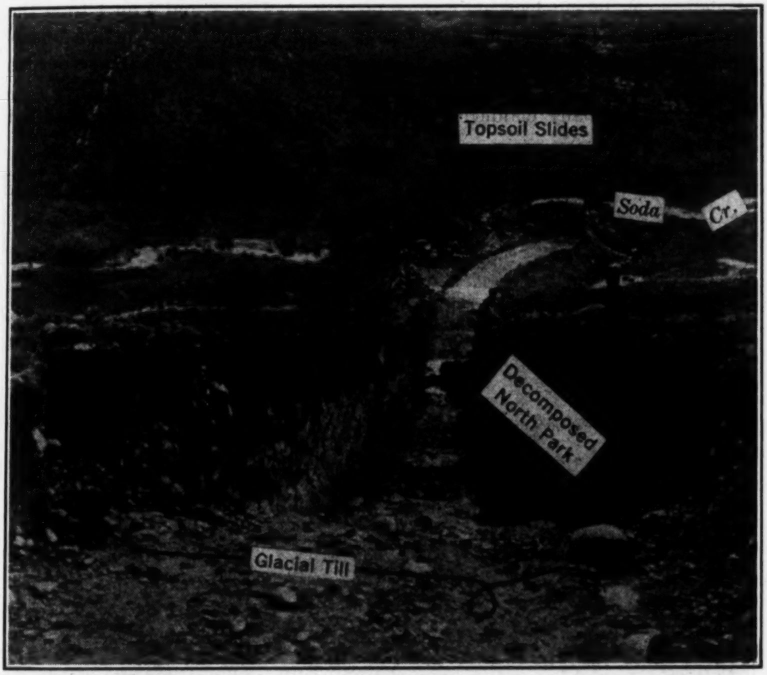

FIG. 4.—EXPLORATORY TRENCH

Fig. 4 shows an exploratory trench which was excavated along the pumping plant site. The siltstone seemed quite hard and durable, indicating that blasting might be required for excavation. However, during an inspection of the trench, a heavy rain occurred and the siltstone in the bottom of the trench was softened and became clayey underfoot.

Construction Difficulties Due to Geologic Conditions

From the outset, concern was expressed because the slopes planned for the excavation would have to be very flat for stability. Laboratory tests indicated, however, that the slope of 1 on 1 should be stable. It was recommended that a 10-ft berm be excavated on top of the siltstone, and that the overlying glacial gravels be cut back on a slope of between 1 on 1 and ½ on 1 from the berm. This berm was omitted, however, during initial construction operations until it was found that continual raveling of the glacial overburden material endangered the workmen in the cut below; the berm was then constructed as originally planned and further troubles from this cause were not experienced (Fig. 5).

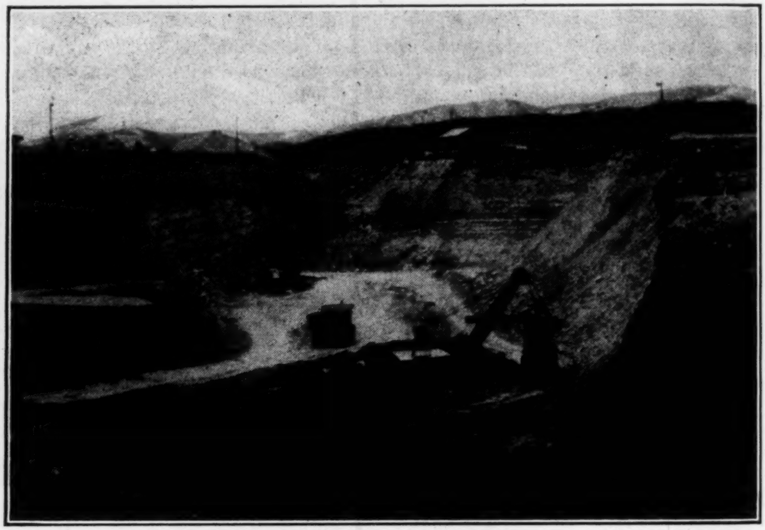

Fig. 5.—Initial Excavation

During excavation, faults were exposed in the walls. There was a severe fault on both the left and right excavation walls. It was concluded that these faults could cause slides and result in overexcavation, but major damage was not expected. This was later verified when three slides occurred on the left-hand side. One of the slides is shown in Fig. 6. No damage resulted from the slides, but overexcavation was required. All three slides were caused by the existence of fault zones and lubrication from ground water.

The siltstone was also found to be quite susceptible to deterioration by moisture because of the silt-clay cementing material (Fig. 7). If water was allowed to collect on the floor of the excavation, and if, subsequently, trucks

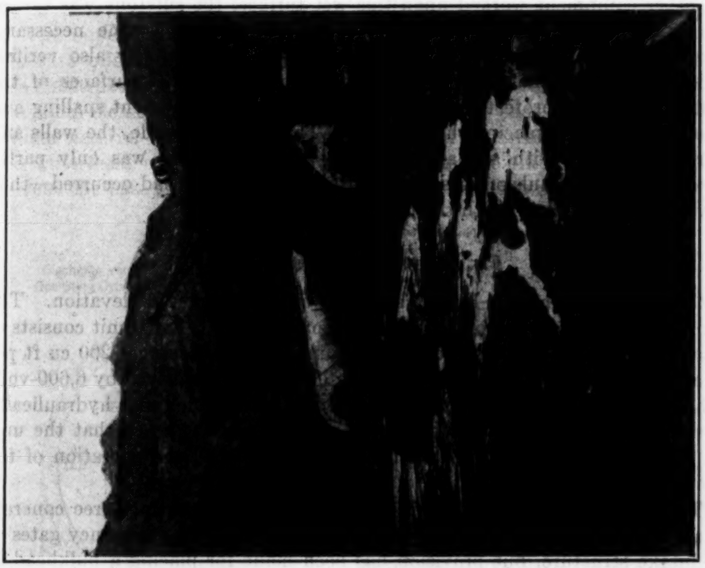

FIG. 7.—DETERIORATION OF SILTSTONE

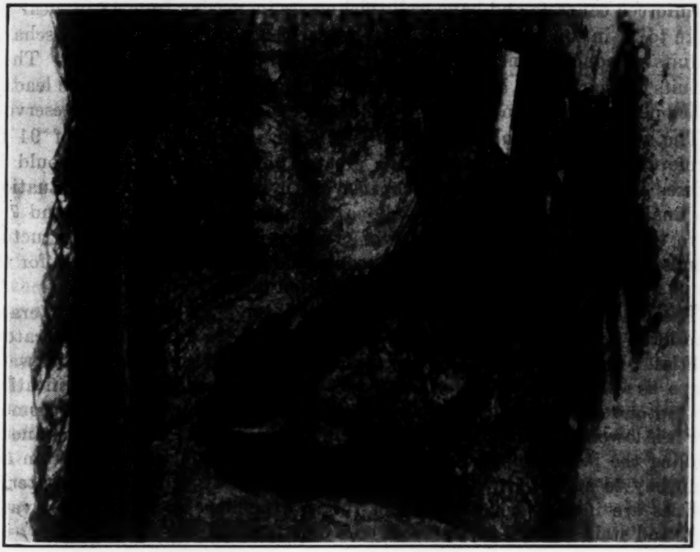

FIG. 6.—A SLIDE CAUSED BY A FAULT

and other equipment worked upon this wet surface, the siltstone was turned into a mud slurry which soon became impassable. It became necessary, therefore, to keep the excavation well drained. This difficulty also verified earlier conclusions that, at final grade, the newly exposed surfaces of the siltstone should be protected with some type of lining to prevent spalling and deterioration before placing the concrete. Thus, at final grade, the walls and floor were coated with asphalt emulsion. This treatment was only partly successful, as the emulsion was placed after some spalling had occurred—thus preventing a good bond with the rock.

Final Design of the Plant

General Arrangement.—Fig. 2 shows the over-all plan and elevation. The pumping plant structure contains three pumping units. Each unit consists of a single-stage, vertical-shaft, centrifugal pump which discharges 200 cu ft per sec at a rated head of 186 ft at 327 rpm. The pumps are driven by 6,600-volt, 3-phase, 60-cycle, 6,000-hp motors, and each unit is provided with hydraulically operated butterfly valves on the intake and discharge sides so that the unit can be inspected and repaired without interfering with the operation of the others.

The intake structure is semicircular in plan with room for three concrete conduits having inside diameters of 7.25 ft. There are no emergency gates at the intake structure, but provision has been made for placing a bulkhead to close the entrance to each of the three intake pipes. The intake conduits are of reinforced concrete and have wall thicknesses increasing from 18 in. near the intake to 27 in. under the maximum fill near the plant. The three discharge conduits are concrete-encased, steel pipes having 87-in. inside diameters. These conduits discharge into an 11-ft pressure conduit of reinforced concrete leading to the open canal section that carries the water to Shadow Mountain Reservoir.

The surface of Granby Reservoir has a maximum fluctuation of 94 ft; therefore, the pumping plant has a greater vertical height than would be required in a plant of the same capacity with a normal forebay fluctuation. The final yard elevation is 22 ft above the natural ground surface and 7 ft above the maximum water surface of Granby Reservoir. The substructure extends 133 ft below the yard so as to provide adequate submergence for the pumps at the minimum water-surface elevation in the reservoir.

The superstructure contains a machine shop having a 50-ton bridge crane, in addition to a control room, battery and switchgear rooms, and operator's facilities. On the first floor below yard level are the air compressors and water pumps, as well as equipment for cable spreading and oil storage and purification. The motor room is provided with a 25-ton crane for handling all equipment after it is lowered to that level by the machine-shop crane. A 12.5-ton crane for handling the pump impeller and intermediate shaft may be moved from one pump bay to another by the motor-room crane. The sump and unwatering facilities are in one end of the substructure; and the cable shaft, elevator shaft, and stair well are at the other end.

STRUCTURAL ARRANGEMENT

The superstructure presented no unusual design difficulties. The substructure offered the major design problems because of its unusual depth. The substructure, shown in Fig. 8, is cellular in construction and consists of four main elements: The base slab, the semicircular ends or arches, the longitudinal exterior walls, and the cross walls and buttresses. The cross walls and buttresses combine to serve as diaphragms or transverse plates which prevent the base slab and longitudinal walls from deflecting inward.

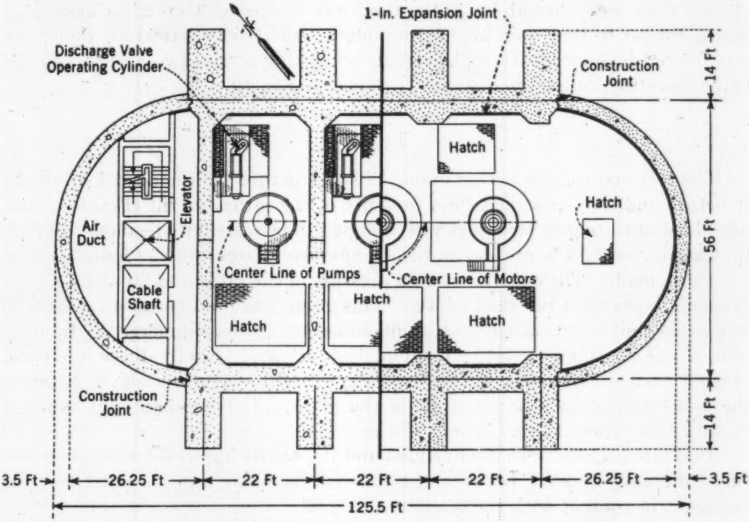
1-In. Expansion Joint
Discharge Valve Operating Cylinder
Construction Joint
14 Ft
Hatch
Elevator
Air Duct
Hatch
56 Ft
Center Line of Pumps
Center Line of Motors
Cable Shaft
Hatch
Hatch
Hatch
Construction Joint
14 Ft
3.5 Ft
26.25 Ft
22 Ft
22 Ft
22 Ft
26.25 Ft
3.5 Ft
125.5 Ft

(*a*) HALF PLAN, PUMP FLOOR
(EL 8186.25)

(*b*) HALF PLAN, MOTOR FLOOR
(EL 8211.25)

FIG. 8.—PLAN OF SUBSTRUCTURE

Early studies indicated that the semicircular ends were naturally adapted to the over-all design. The hydrostatic loading places them in direct compression and thereby makes them more watertight. Furthermore, since the loads are carried in a horizontal direction, major concentrations of moment and thrust are not introduced into the base slab, as would have been the case if buttresses had been used on the end walls. These semicircular ends were increased in thickness for a short distance above the base slab to resist the local bending stresses at the junction of the base and the arches. As shown in Fig. 9, all the floor slabs up to and including the one at El. 8252.50 were separated from the longitudinal exterior walls and from the semicircular ends by a 1-in. expansion joint. This separation insured that the exterior walls spanned in a horizontal direction. The thickness of the longitudinal exterior

walls was increased with depth to resist the horizontal loading acting normal to them.

The transverse plates are the major structural elements in the substructure and are 133 ft high and 84 ft wide. Each plate has an opening 50 ft wide and 33 ft high at the motor room, and a second opening 28 ft wide and 11 ft high near the top.

The expense of installing an exterior, four-ply waterproofing membrane was eliminated by taking two major precautions to minimize shrinkage cracks: (1) After the base slab and the concrete walls up to the motor floor were placed, they were cooled by water that was circulated through a system of piping similar to that used in concrete dams. (2) Each vertical lift thereafter was poured in four separate placements consisting of the two arches and the two connecting longitudinal walls, as shown in Fig. 10.

LOADS

The two major loads acting upon the substructure are the dead load of the structure and the equivalent fluid pressure of the saturated fill (Fig. 9). The dead load of the entire structure was assumed to be distributed—down through the exterior walls, the arches, and the transverse plates—to the foundation as a uniform load. The equivalent fluid pressure of the saturated fill was assumed to be 85 lb per sq ft per ft of depth. This value was used because the backfill was to be sluiced into place and would subsequently be submerged. In addition, it was felt that a relatively rapid fluctuation of Granby Reservoir could cause a 10-ft difference in the hydraulic gradient, or saturation level, between the two longitudinal exterior walls of the plant. This gradient was assumed to vary as a straight line between the two walls.

Two minor loads were the live load and the thrust imposed by the temperature difference of 25°F between the exterior members and the interior cross walls not in contact with the saturated backfill.

STRUCTURAL DESIGN

The design plan of the substructure of the pumping plant may be divided into three parts: (1) The base slab, (2) the exterior walls, and (3) the transverse frame. The base slab was designed to (*a*) provide a continuous beam spanning the cross walls and the semicircular ends and (*b*) resist the vertical cantilever action of the exterior longitudinal walls and of the semicircular ends. Because of the cantilever action of the exterior walls, moments and thrusts caused by the horizontal loads were applied at the edges of the base slab; and the principal stresses in the base slab were computed.

The horizontal reinforcement in the longitudinal walls, cross walls, and semicircular ends was determined by analyzing horizontal frames cut from the structure at various heights. These frames (Fig. 8) were analyzed by moment distribution, the moments being distributed to the cross walls, the semicircular ends, and the longitudinal walls. The lowest horizontal frame was selected at an elevation above the base slab where the vertical cantilever action

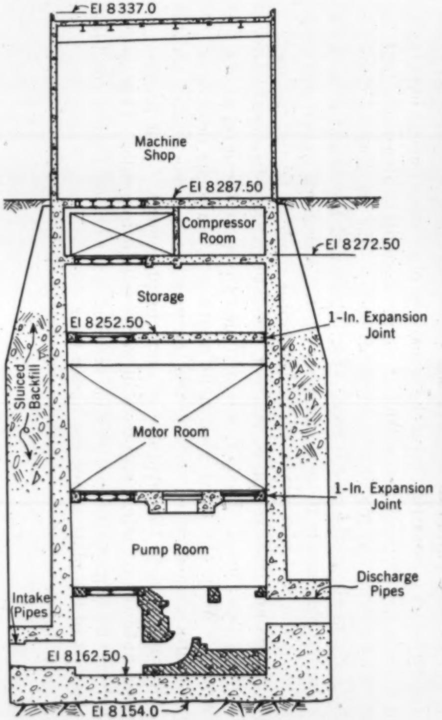
El 8337.0
Machine Shop
El 8287.50
Compressor Room
El 8272.50
Storage
El 8252.50
1-In. Expansion Joint
Sluiced Backfill
Motor Room
1-In. Expansion Joint
Pump Room
Discharge Pipes
Intake Pipes
El 8162.50
El 8154.0

FIG. 9.—TRANSVERSE SECTION

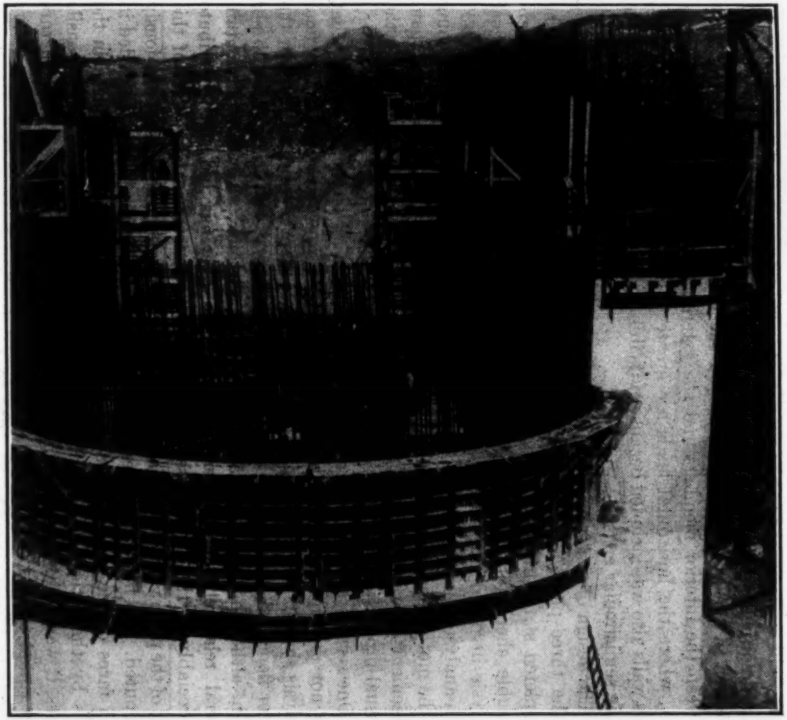

FIG. 10.—POURING OF WALLS AND ARCHES

in the walls was assumed to be nonexistent. Each frame was designed to carry the full equivalent fluid pressure at that level, including the effect of the 10-ft variation in the hydraulic gradient and the temperature differential of 25°F between the interior members and the exterior members. Below the motor floor, where the horizontal loads are greatest, the rib shortening in the end cross walls also was included because of its influence on the moments and thrusts in the semicircular ends.

The design of the transverse frame (Fig. 9) proved to be the most complex of the three parts. In the preliminary design, a trial-load analysis of the completed structure was made for the ultimate loading. It proved to be a valuable check for the detailed design of the transverse frame. The final analysis involved the use of moment distribution and the column analogy. Both analyses showed that the inflection points in the buttresses at the opening for the motor room were actually inside the supports and not in the clear span. Agreement between the two methods was exceptionally close, considering the unusual proportions of the frame.

One serious problem was encountered in the design of the cross walls that was not anticipated when the trial-load analysis was requested. The final analysis showed that, because of dead and live loads, the cross walls below the motor floor had unexpected diagonal tensile stresses of the order of 250 lb per sq in. although the wall is 57 ft high and 3 ft thick. These walls contain several relatively small openings, but these openings did not contribute appreciably to the high stress. Photoelastic and stress-coat analyses of this part of the plate verified the magnitude of the diagonal tensile stresses previously computed. To help resist these stresses, diagonal reinforcement was added in both faces of the walls. Because the compressive stresses introduced in the walls by the saturated backfill would tend to relieve these diagonal tensile forces, it was desirable that some backfill be placed before the entire structure was completed. Consequently, backfilling operations were begun before concrete had been placed to El. 8272.50.

The sequence of construction of the transverse plate was of prime importance from a design standpoint, as is true of many monolithic structures that are subjected to large horizontal and vertical loads. The framing of the intermediate floors above the motor room (Fig. 9) limited the height of many of the concrete placements to approximately 10 ft. A separate design was made, considering the first placement above the motor room to be the top member of the frame and the weight of the wet concrete in the placement above it acting as a dead load. Backfill was assumed to be at the level of the first placement. When the third placement above was added as dead load, the first two lifts were assumed to form the top member of a new frame, and the backfill was raised to the level of the previous placement. This process was repeated until the structure and backfill were brought to grade. This method of analysis and sequence of construction resulted in the critical loading condition for the part of the plate above the motor floor.

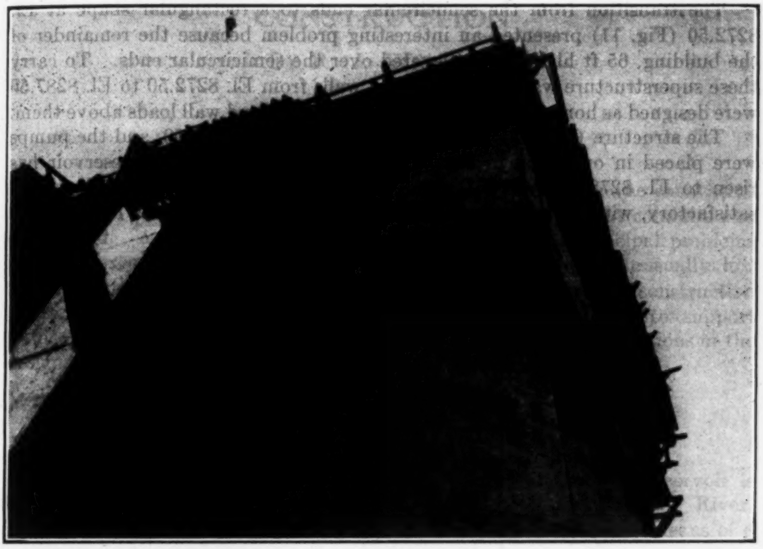

FIG. 11.—CANTILEVERING AT THE ENDS

FIG. 12.—COMPLETED STRUCTURE

The transition from the semicircular ends to a rectangular shape at El. 8272.50 (Fig. 11) presented an interesting problem because the remainder of the building, 65 ft high, is cantilevered over the semicircular ends. To carry these superstructure walls, the basement walls from El. 8272.50 to El. 8287.50 were designed as horizontal girders to carry the floor and wall loads above them.

The structure (Fig. 12) was completed in September, 1950, and the pumps were placed in operation in January, 1951. The water in the reservoir has risen to El. 8278 (July, 1953), and the performance of the plant has been satisfactory, with no leakage evident.

CONSTRUCTION

By R. J. Willson[1]

Synopsis

Approximately four construction seasons were required for the excavation and erection of the Granby Pumping Plant and its appurtenant conduits and switchyard. A joint-venture group built the plant. The principal problems included excavation in wet siltstone, curing of concrete at unusually low temperatures, and special precautions to avoid seepage through construction joints. A somewhat novel use of native logs—for scaffolding to support forms—is described. The paper also describes a few special adaptations of the designs that were necessary under unexpected conditions.

Plant Construction

The Granby Pumping Plant on the north shore of Granby Reservoir is situated adjacent to Soda Creek, a small tributary of the Colorado River. This location provides access to high ground north of the plant by means of a minimum length of closed conduit and access to the reservoir floor by means of a 115-ft-deep excavation on the left bank of the creek and three intake conduits 518 ft long.

Construction of the plant was begun on March 31, 1947, and was completed in the late fall of 1950. Actually, the major concrete work on the building proper was completed in the fall of 1949. The principal work which had to be completed in 1950 was the construction of the plant parapet, the embedment of pumps, and other second-stage concrete work (such as the placement of the bonded floor topping). Also to be constructed were a cable tunnel from the plant to the switchyard and the switchyard structure foundations. The final dressing of the area also remained.

Construction by Contract.—The Granby Constructors, a joint-venture group organized purposely to construct Granby Dam in 1946, were successful in obtaining the contract for the pumping plant and its appurtenant works. The group was comprised of seven contracting firms.

Included in the contract were the plant building; the intake structure and 3 reinforced concrete intake conduits with internal diameters of 7¼ ft; the reinforced concrete discharge conduit with an internal diameter of 11 ft; and the silt-retention and diversion facilities, consisting of an earth dike located upstream from the intake structure on Soda Creek and a diversion channel ½-mile long, extending from Soda Creek to adjacent Stillwater Creek. The contract did not provide for the installation of the pumps, motors, operating equipment, nor for such facilities as the heating, ventilating, and electrical

---

Note.—Published, essentially as printed here, in September, 1953, as *Proceedings-Separate No. 270.* Positions and titles given are those in effect when the paper was received for publication.

[1] Engr., Design and Construction Div., Bureau of Reclamation, U. S. Dept. of the Interior, Denver, Colo.

control apparatus. These were installed under separate contract on completion of the major concrete construction in 1949. A large steel surge tank which was to have been constructed under the general contract was eliminated by a change in the design of the discharge conduits.

Progress.—During the first year, the excavation proceeded rapidly, but steel shortages and consequent late delivery of embedded materials considerably delayed the concrete work. The supply of steel reinforcement was particularly short and was obtainable only after many weeks of advanced planning and scheduling with steel mills. Equipment manufacturers, because of the steel shortage, were reluctant to set definite delivery dates, and the designs necessarily suffered. In some instances, the designs had to be changed to facilitate utilization of obtainable equipment or suitable alternatives. These factors contributed to the requirement of an additional year for construction.

The weather was an important consideration in construction progress. Winters are severe in the subartic, or alpine, region of the western Rocky Mountains above El. 8000 and limit the working season. Frost penetrates to depths of from 6 ft to 7 ft; temperatures of from −10° to −40° are often encountered; and a snow depth of from 3 ft to 4 ft is not uncommon. During only 4 months or $4\frac{1}{2}$ months of the year can concrete be placed without elaborate and expensive protection. Excavation and earthwork are impossible between November 10 and May 10 of most years. The years 1947 and 1948 followed the usual weather pattern, but an open fall in 1949 contributed materially to the progress made.

Construction Facilities

While the contractor was proceeding with the excavation in 1947, several plant and office buildings were constructed. A Quonset hut was assembled for use as office space. A fully automatic batching and mixing plant was erected. A carpenter shop (consisting of steel framework covered by canvas) was fashioned from a surplus airplane hanger, and a small utility building was built for housing compressors, small parts, and pipe and electrical shops. A frame warehouse for the storage of government-furnished materials completed the number of construction-plant buildings erected during the first year.

In 1948 a gantry-type crane, used during World War II in the west coast shipbuilding program, was purchased and was shipped to Granby, Colo. Upon arrival, it was converted into a whirley-type crane and was installed at the pumping plant, after a steel substructure had been built. As shown in Fig. 1, the crane transferred concrete buckets from the truck to the forms in all parts of the plant building. In 1949, on the completion of Granby Dam, a small truck-repair shop was established at the plant to service and maintain the equipment used for excavation and hauling. Previously, all repair and maintenance work had been done in the contractor's well-equipped shops at the dam.

Excavation equipment consisted of numerous draglines, power shovels, carryalls, and scrapers. Hauling equipment, in addition to the carryalls, consisted of end-dump trucks and bottom-dump trucks having capacities of 10 cu yd and 13 cu yd, respectively. Both the excavation and hauling equipment were utilized on both Granby Dam and the pumping plant as the need arose and were shifted frequently.

Labor.—Securing and maintaining an adequate force of skilled and unskilled labor was a problem to most contractors in the area. During the summer months college men were available to supplement the normal labor supply. At the advent of cool weather, the students and other workers left to return to school or to the fall harvests. In an attempt to secure a sufficient labor supply, the contractor maintained contact with employment offices in all sections of

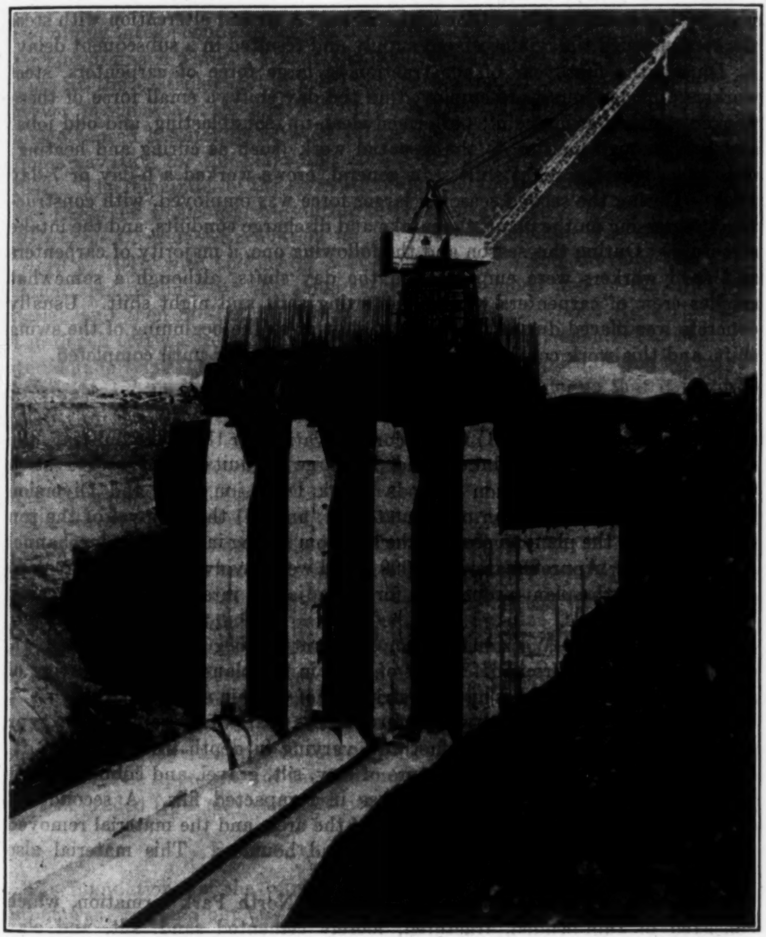

Fig. 1.—The Whirley Crane, Placing Concrete

Colorado, in the adjoining states of Kansas, Wyoming, Nebraska, Utah, and as far south as Texas. Strikes did not hamper the progress of work on the western slope as much as on the eastern slope of the Colorado section of the Rocky Mountains; however, in the spring of 1948, a strike of steel workers (which broke out on the former slope) delayed the erection of a crane so that work was materially affected for that season. A second altercation with steel workers impeded the reinforcement supply and resulted in a subsequent delay.

During the first year of construction, a large force of carpenters, steel workers, and laborers were employed on the day shift; a small force of these workers on the "swing" shift performed clean-up, sandblasting, and odd jobs; and only enough men to do the essential work (such as curing and heating) were placed on the night shift. In general, crews worked a 6-day or 7-day week. During the second season a larger force was employed, with construction progressing on the plant, the intake and discharge conduits, and the intake structure. During this season and the following one, a majority of carpenters and steel workers were employed on the day shifts, although a somewhat smaller crew of carpenters worked the swing shift and night shift. Usually concrete was placed during the late day shift or at the beginning of the swing shift, and this work continued on into the night shift or until completed.

EXCAVATION

The contract included (1) the major excavation for the plant building, the intake structure, and the intake and discharge conduits; (2) the excavation necessary for the foundation of Soda Creek Diversion Dike and Diversion Channel; (3) the excavation of fill materials; and (4) the removal of the top of a hill east of the plant to prevent the hill from sliding into the intake channel and structure. Approximately 275,000 cu yd were involved in the 115-ft-deep excavation for the plant proper and for the adjacent intake and steel-encased discharge conduits.

Pumping Plant.—Work on the pumping plant was begun on March 31, 1947, with the removal of from 1 ft to 2 ft of snow in the plant area, the clearing of sage brush and a few trees, and the stripping of organic material.

The manner of excavating was determined as nearly as possible by the type of material encountered. The first cut, varying in depth from 1 ft to 8 ft, provided for the removal of a mixture of clay, silt, gravel, and cobbles. This material was stock-piled for future use in compacted fills. A second cut extended the excavation to the bedrock of the area, and the material removed consisted of silty-sandy gravel, cobbles, and boulders. This material also was stock-piled for later use as sluiced backfill.

The balance of the excavation was in the North Park formation, which consisted of thin-bedded, fractured, loosely cemented sand, silt, and clay stone that was of variable hardness and was referred to as siltstone. For this excavation, the draglines were converted to shovels. Light blasting of the siltstone was attempted but was abandoned because of the unsatisfactory results caused by the fractured condition and the variable hardness of the formation. However, the shovels were able to dig the siltstone effectively, and minimum difficulty was encountered in the excavation in so far as the hardness of the siltstone was concerned. The plant excavation was staked on a slope of one on one in both the siltstone and overburden. Minor faults were intersected, producing slides that required approximately 960 cu yd of additional excavation (including the excavation of the overhanging "drummy" and loosely consolidated siltstone).

The only other problem encountered in the excavation for the plant and the adjoining intake conduits was caused primarily by the seepage of irrigation water and drainage water. Within the plant area, this water was collected in a sump at the east end of the plant excavation and caused little difficulty. However, in the area of the intake conduits, infiltrating water as well as surface drainage caused a softening of some of the siltstone and bogging equipment. Major excavation for the plant and intake conduits was completed on June 3, 1947. The remainder of the excavation required for the intake conduits and intake trashrack was completed during the following year.

Discharge Conduit.—Excavation for the discharge conduit was also begun on April 3, 1947, with the use of a 2½-cu yd dragline and shovel. The excavation area outlined by the slope stakes was stripped first of all organic material, and then of the clay overburden. The latter varied from 1 ft to 6 ft in depth and was removed and stock-piled along the trench. The coarse material underlying the clay was then excavated and stock-piled behind the clay for future use. The material was segregated in this manner so that it might be used for backfill. With the exception of the excavation for the three concrete-encased steel discharge pipes, the steel-encased Y branch, and the first few sections of the discharge conduit, all excavation for the discharge works was above the siltstone.

Soda Creek Diversion Channel and Dike.—On April 19, 1947, a 2½-cu yd dragline started excavation for the Soda Creek Diversion Channel at Stillwater Creek. Tractor-drawn carryalls having capacities of 12 cu yd stripped the organic material from the surface. The clay overburden was next removed and stock-piled for building the zoned dike. The dragline then excavated the remaining material (which was a mixture of clay, silt, sand, gravel, and cobbles) and segregated it for possible use in the dike. Some siltstone was found in the bottom of the diversion channel, but it was removed without special blasting. The foundation for the dike consisted generally of gray clay, with some thin gravel layers dispersed throughout, and with siltstone near the south abutment. The upper part of the abutments was primarily alluvium, reasonably well-graded from clay-size particles to boulders.

Preparation of Foundations

The foundation for the pumping plant proper and the adjacent intake conduit was "roughed out" by a power shovel. Next, the outline of the substructure for the plant was staked, and the siltstone was trimmed to neat lines with power spades and hand tools, as shown in Fig. 2. To avoid any possible disturbance to the outline material, blasting of siltstone was discontinued when excavation approached neat foundation lines for the substructure. All loose fragments and "drummy" siltstone were removed by hand. The mud was removed by scraping with hand shovels and by the use of air-water jets. At first, asphalt emulsion was applied to the exposed siltstone foundation to reduce air and water slaking, but the results were not entirely satisfactory, especially where the siltstone had become moist from seepage. In these damp areas, the emulsion bonded poorly with the siltstone. Approximately one half of the foundation was covered with the emulsion (as called for in the specifications), and the area was dusted with cement to prevent the wet siltstone from sticking to the workmen's feet. Even with care, the asphalt emulsion had peeled off by the time forms were ready for the placement of concrete. Use of the emulsion was therefore abandoned, and instead the foundation was kept dampened at all times in an effort to reduce the slaking. Immediately prior to the placement of concrete, the foundation was cleaned by the use of air and water jets.

Fig. 2.—Foundation Trimming

The siltstone foundation for the intake conduits was prepared in the same manner as was the foundation for the pumping plant proper, except in overexcavated areas where seepage was a problem. In these areas, gravel drains were provided on top of the siltstone prior to the placement of concrete. In preparation for the placement of concrete for the discharge conduit, all rock exceeding 3 in. in diameter was removed from the surface, which was thoroughly dampened prior to compaction with a one-drum, sheepsfoot-type roller. Where overexcavation occurred, an 8-in. layer of clay was placed and rolled. If necessary, additional 8-in. layers of clay were consolidated until the foundation had reached desired grade. Sufficiency of compaction of the clay was determined by field density tests.

The blue clay or siltstone foundation material for the Soda Creek Dike was prepared by dewatering and removing loose material. Cofferdams were placed upstream and downstream from the dike-foundation area, and the water within the area was pumped out.

Forming

The forms used in building the pumping plant and its appurtenant works varied as to type. Wooden forms, fabricated in a manner so as to produce board marks running either horizontally or vertically between major breaks within the plant (such as between the floor at one elevation and the ceiling above), were used throughout the plant building. Shop-fabricated panels were used extensively. For the substructure, studs, 2 in. by 6 in., and 2 in. by 8 in., were sheeted in a horizontal direction with 6-in. shiplap; the forms were braced externally, as seen in Fig. 3. Panels constructed with the shiplap sheeting running in a vertical direction formed the exterior walls and buttresses on the intermediate structure of the plant. Most of the interior walls were formed with shop-fabricated panels in which the sheeting ran horizontally.

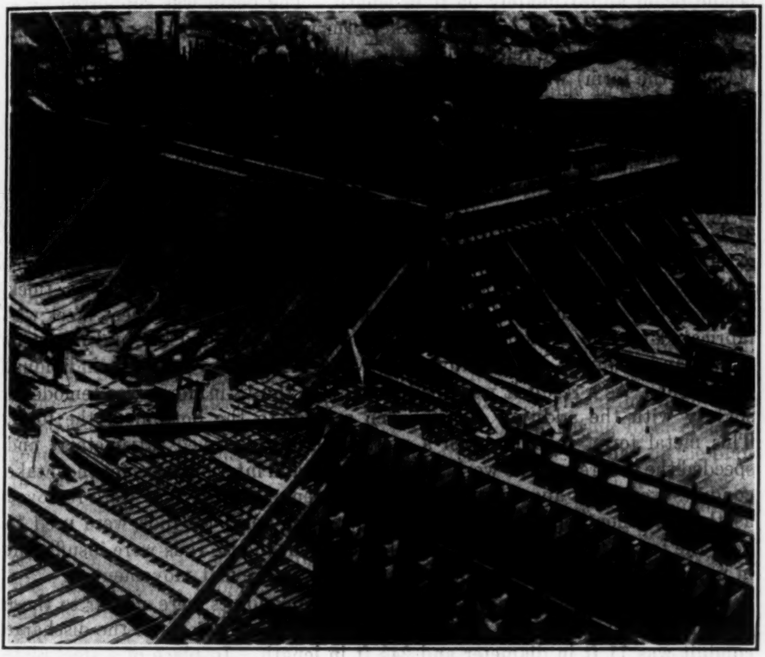

FIG. 3.—SHOP-FABRICATED SUBSTRUCTURE FORMS

Form ties of various types were used in the early part of the work, but most of them were discarded in favor of the conventional "she-bolt" ties. After the first few concrete placements, little difficulty was encountered in holding the forms in place. Changing the location of tie rods helped materially in this respect.

The usual bracing, scaffolding, and supports were provided for the floors and beams. An innovation was the use of native logs for the bridging and staging in support of the floor at El. 8252.50 (approximately 41 ft above the next lower floor). To support this floor and its beams, the native timbers were fabricated into bents, cross-braced securely, and properly capped. At first, there was some concern regarding the amount of settlement that might occur in the use of the green timbers because of drying shrinkage, but careful checking disclosed nothing unusual.

Except as noted, steel forms were utilized in constructing the discharge and intake conduits and were of the conventional type. The interior forms were collapsible, with the invert section omitted. The interior form for the intake conduits was 7.25 in. in diameter and 25 ft in length, supported by a needle beam approximately 55 ft in length. The beam was supported by a screw jack at each end, and, when the form was moved to the next adjacent section, the jacks were released and the needle beam (attached to and held in place by the form) was rolled ahead and reset. The form was then collapsed and moved forward. The forms were used as designed except the bolting of two plates adjacent to the lower end, which reduced the invert opening of 13 in. in order to prevent fresh concrete from "boiling" up into the invert during placement operations.

Where backfill load was greatest, the concrete of the intake conduits was 27 in. thick; the remainder was 18 in. thick. The contractor secured sufficient exterior steel forms for the 18-in.-thick intake conduits, but because of the steel shortage it was impossible to secure steel exterior forms for the 27-in.-thick parts of the conduits. At first, a wooden form lined with sheet steel was fabricated for the thicker conduit sections. This form racked, did not strip easily, and required construction of a wooden bulkhead for each individual placement. As a result it was abandoned, and the 18-in. form was remodeled slightly with the addition of a wooden section to the bottom of the form. This metal form, together with a metal bulkhead, proved satisfactory, and speeded the progress of the work. The exterior and interior forms for the intake conduits were held apart by temporary wooden spreaders that were removed as the placement of concrete progressed. "She-bolt" tie rods were used to hold the forms together. As originally designed, the tie rods were insufficient in number, and exterior bracing was necessary to prevent movement.

Forms for the construction of the discharge conduits were similar to those used in construction of the intake conduits. The inside form of the discharge conduit was 11 ft in diameter and 24½ ft in length. In place of a steel plate to reduce the entry of fresh concrete in the invert, "boil strips" consisting of a piece of lumber 2 in. by 6 in. were bolted to the lower edge of the form and extended downward into the fresh concrete. Tie rods and spreaders similar to those for the intake-conduit forms were used. To eliminate external bracing an additional row of tie rods was placed along the bottom of the outside form. "Floating" of the forms caused little trouble.

Most of the horizontal and vertical bends were formed with wooden shop-fabricated interior forms and built-in-place exterior forms. The wood forms for all the work were well-designed and fabricated. Their use both simplified and expedited construction.

All forms were treated with appropriate types of oil. Steel forms stripped easily and, unless the form was left in place for a long time, there was only minor damage to the formed surfaces. As an experiment, some of the interior plant forms were coated with plastic. This was tried in an effort to reduce the work necessary in the cleaning and preparation of the forms for re-use, and to prolong the usefulness of the forms. The extra expense of applying the plastic and the care of the forms thus coated was not considered justifiable, and coating of plastic was therefore discontinued.

PLACEMENT OF STEEL AND EMBEDDED MATERIALS

Reinforcement.—In accordance with the specifications, the contractor furnished all reinforcement bars. They were already cut and bent when purchased. Because of the steel shortage and the time spent in cutting and bending, shipping, and subsequent on-sight fabrication, the contractor scheduled the rolling of reinforcements with the steel mills at least 2 months in advance of each concrete placement.

The fabrication and placement of reinforcing was subcontracted to a construction company from Virginia. Upon receiving the cut and bent steel, the subcontractor fabricated the cages necessary for the intake and discharge conduits, and (wherever possible) mats for various parts of the plant and its appurtenances. This work was done in a steel yard adjacent to the plant building. The fabricated cages and mats were then transported on a low-boy truck and were set into place in the conduits by a dragline, and in the plant by a crane.

The design required that the splicing of reinforcement bars be limited. Most of the steel reinforcing within the plant was placed and tied by hand. Minimizing the vertical splices often resulted in steel extending from 20 ft to 30 ft above the previous placement—thereby complicating form erection, concrete placement, and the movement of materials from one bay of the plant to another.

Embedded Materials.—Similar to all structures of its kind, numerous materials were embedded in the concrete of the plant, including metal sealing strips, metal water stops, asphalt seals, pump-intake pipes, cast-iron drain tile, pipe sleeves, copper tubing, grout tubing and fittings, metal inserts, anchor bolts, both metal and transite electrical conduit and ground wires. The work of placing the embedded materials was time-consuming and was complicated by the heavily reinforced walls, floors, and beams; but little additional difficulty was encountered.

Watertightness was a prime requisite in constructing the plant, the lower 133 ft of which is below the maximum high-water surface of Granby Reservoir. Construction joints were held to a minimum number, commensurate with the type of design used, and all horizontal joints were provided with metal water stops. The only vertical joints in the exterior walls below water level were those between the rectangular section of the plant and the semicircular arch rings at each end, and (of course) those between the intake and discharge conduits and the plant building. All other vertical construction joints were placed in the interior cross walls.

In addition to monel-metal and stainless-steel water seals, asphalt seals were provided in the vertical and horizontal construction joints of the 8-sectional base slab. The asphalt seal was built in each construction joint of the substructure by forming an opening 5½ in. square. The block-out was formed for the first half of the opening, and in the other half (in the adjacent block) sheet steel embedded in the concrete formed the opening. A system of ½-in. pipe was also embedded in this block-out so that, when necessary, steam could be circulated in the opening to warm both the concrete slabs and the asphalt that was placed in the block-out. Results accomplished were extremely satisfactory.

At first, difficulty was encountered in the welding of the monel-metal and stainless-steel sealing strips for the substructure blocks. The strips were bent, as specified in drawings, and the joints of half of the strip to be embedded in the first placement were welded. The half to be embedded in the second block was bent 90° and loosely tacked to the forms with the joints unwelded. Upon stripping the forms and rebending the strips to their normal position, an attempt was made to weld the remaining half of the joints. Numerous pin holes and cracks developed in these latter welds. Welders experienced in the use of monel metal and stainless steel were asked to demonstrate the proper flux, flame, and procedure, and there was some improvement. Finally, however, it was concluded that the heat of the welding expanded the exposed metal, whereas the metal embedded in the previous block was held rigid. The differential expansion caused the cracking. Since the work was being delayed, the contractor decided to try welding all joints except the corner joints before embedding the first half of the strip. This resulted in only minor difficulties and delays.

The welds in metal water-sealing strips were tested by smearing the weld with soap suds and blowing compressed air against the other side. Any holes in the welds were indicated by a soap bubble.

The concrete was cooled using horizontal coils of thin-walled tubing having a 1-in. outside diameter. Two series of coils were enclosed in each block of the substructure, one in the center and the other near the bottom. Coils of tubing were also embedded in the buttresses at horizontal intervals of 3 ft. Before the placement of concrete, all tubing was tested for leaks under 100 lb of air pressure.

Concrete Production

Under earlier contracts, aggregate had been obtained from river deposits a mile below Grand Lake on the Colorado River prior to its inundation by Shadow Mountain Reservoir. The aggregate had been transported to the pumping-plant area and stock-piled in five sizes. The sizes were: (1) Sand, less than 3/16 in.; (2) gravel, between 3/16 in. and ½ in.; (3) gravel, between ½ in. and 1 in.; (4) gravel, between 1 in. and 2 in.; and (5) gravel, between ½ in. and 1½ in. The fully automatic batching and mixing plant erected adjacent to the aggregate storage area (Fig. 4) included a 2-cu yd weighing hopper and a 2-cu yd tilting-type mixer. The batching and mixing facilities normally maintained a sufficient quantity of fresh concrete.

Cement for the work was transported in bulk by rail and by bottom-dump hopper cars to Granby, fifteen miles from the Granby Pumping Plant. A bucket elevator and a 1,600-bbl storage silo at Granby provided for unloading and storage of the delivered cement. Specially covered dump trucks having a capacity of approximately 60 bbl transported the cement from the railhead to the pumping plant. Upon arrival, the trucks dumped the cement into a road-level hopper, and the cement was lifted by bucket elevator to the 500-bbl silo in the top story of the batching and mixing plant. Two trucks were sufficient to supply cement during placing operations.

Cement was furnished by the contractor, under the terms of the specifications. An automatic recorder in the batching plant produced a graphic record of the individual weights of all materials that entered the concrete, except mixing water. Payments to the contractor for cement used were based on the record thus produced. Mixing water was measured by means of a water meter. Periodic checks of the batching equipment and recorder were made to assure their accuracy.

FIG. 4.—AUTOMATIC BATCHING AND MIXING PLANT

Darex, in commercial solution, was used as an air-entraining agent, enough being used to produce between 3% and 5% entrained air in the concrete. The agent was dispensed, by means of a standard Darex dispenser, directly into the mixer water charging line.

Mixing water was pumped from near-by Soda Creek into a storage tank adjacent to the mixing and batching plant. During cold weather, the water was heated at first by an oil water heater; and later a stationary boiler was installed that was also utilized in supplying hot water for curing and heating within the pumping plant proper. In general, water-cement ratios for the concrete on all features averaged 0.50, the maximum being 0.53.

CONCRETE HANDLING

Fresh concrete was transported from the batching and mixing plant to the forms in bottom-dump buckets of between 1-cu yd and 2-cu yd capacity, carried on flat-bed trucks. During the first year of construction, the buckets were handled at the forms entirely by draglines. After the whirley crane was erected in the spring of 1948, it was used for placing concrete within the plant and in the intake and discharge conduits within its reach. Having a 125-ft boom, the crane was able to reach all parts of the plant (Fig. 1).

Clean-up Prior to Concrete Placement

The clean-up of construction joints to receive fresh concrete consisted at first of wet sandblasting and flushing with air-water jets to remove any laitance or construction debris that may have collected on the previously placed concrete surfaces. Later, air and water jets only were used, accomplishing an early cutting of the fresh surface at the first stage of final set. The desired results were not always obtained by the air-water jetting, and in these instances sandblasting was used. If placement of a subsequent lift was to be delayed, such as that occasioned by a winter shut-down of operations, the joints were sandblasted to a sandy finish, followed by copious flushing with air-water jets. In all instances, horizontal or vertical joints were conditioned by water 72 hr in advance of the placement of fresh concrete.

Placement of Concrete

The first placement of concrete in the pumping plant began on June 30, 1947, in the massive substructure.

The fluid pressure which the forms would withstand and the rate of delivery of fresh concrete controlled the method of placement in the substructure slabs having thicknesses of 8 ft or 9 ft, involving approximately 3,100 cu yd each. As a result, the fresh concrete was consolidated in stepped lifts of between 1 ft and 2 ft to avoid the development of a cold joint. A concrete mix containing aggregate of 2-in. maximum diameter was used in the substructure and in all subsequent placement within the pumping area and conduits, until the supply of this maximum sized aggregate had been depleted. Concrete-containing aggregate of a maximum size of 1½ in. was used to complete the work. A mix having a water-cement ratio of 0.53 and a 3-in. slump was best suited for the work and was sufficiently cohesive to avoid segregation. Concrete was consolidated with both electric and pneumatic vibrators, the latter being preferred.

The specifications for the work required that the alternate blocks of the substructure be placed first, and after being properly cooled, the intervening blocks were to be placed. This procedure reduced subsequent shrinkage as much as possible. Late delivery of anchor bolts for butterfly valves necessitated some slight change in the sequence of block placement shown on the plans, but the general scheme of placing alternate blocks was followed. The first placement of concrete above the substructure was in the cross wall adjacent to the spring line of the east arch (the right arch in Fig. 1) and work continued on the walls, buttresses, arch rings, and intake block-outs without interruption until November 3, 1947, when operations were stopped for the winter. Completed work at this stage of construction is pictured in Fig. 5, which shows the plant and intake conduits.

The placement of concrete in the plant was resumed the following season, May 25, 1948, on completing the erection of the whirley crane. Cold weather caused a winter stoppage of work on December 10, 1948. Resuming construction for the third season on April 28, 1949, the constructors completed all major exterior concrete work on the building, conduits, and intake structure before cold weather again halted work. After the walls and roof of the plant building were completed, interior work continued throughout the winter by temporary installation of the electric heaters later to be incorporated in the plant heating system.

At first, concrete in the walls and buttresses was placed directly from the buckets whenever possible, but, where the vertical reinforcement (having 4-in. spacing vertically, horizontally, and diagonally) extended far above the placement and in the narrow walls, direct pouring was impractical. Consequently, a side chute was used to guide the concrete into the form. Baffles prevented segregation, and thorough vibration was required in order to consolidate the concrete properly and to overcome segregation produced when the concrete was "screened" by the vertical steel mats. In the latter part of the first season, concrete buggies were used more extensively to distribute the concrete to the narrow walls, and this method produced better results.

FIG. 5.—COMPLETED EXCAVATION, AND PROGRESS ON STRUCTURES

The location of the vertical construction joints in the pumping plant dictated the sequence of placing operations. The only vertical construction joints within the plant proper were between the rectangular part of the plant and the arch walls. Horizontal construction joints were usually spaced at 5 ft to 8 ft. Considerable care had to be taken, therefore, to avoid "cold joints" within a pour. The slow rate of delivery of fresh concrete required that the contractor's foreman and government inspectors be constantly alert in order to prevent a cold joint, and, therefore, placement of fresh concrete in lifts of between 1 ft and 2 ft was the general procedure.

For placing concrete in conduits, a somewhat similar procedure was followed. Concrete was dumped by bucket onto chutes inserted in two series of trapdoors in the outside form, one below the spring line and one above it. When the invert and the sides of the forms were filled to the sills, the lower doors were closed and the concrete was placed through the upper ones until its top surface was a foot or more above the spring line. The upper doors were then closed and the remaining concrete placed and vibrated from the top of the form. Sufficient space for a vibrator operator remained between the mats of steel within the conduit forms, except where the intake conduit was only 18 in. thick. Best placement of concrete resulted if a small amount was deposited in one place at a time. There were relatively few rock pockets. After the form had been filled, the top was screeded and wood-floated. The concrete (having between a 3-in. and 3½-in. slump value) for the conduits was placed and worked well at this value. Concrete having wetter slumps than 3½ in. caused difficulty in that it boiled up within the open invert of the interior form. The placement of the steel plates on the intake-conduit interior forms and the added strip on the discharge-conduit forms (described previously) reduced this boiling tendency but did not eliminate it. In general, forms within the plant were stripped not earlier than from 36 hr to 48 hr after the concrete was poured, and those of the discharge and intake conduits were stripped between 12 hr and 14 hr after placement. In colder weather, either the forms were left in place for a longer period of time, or calcium chloride was added (maximum addition, 1½%) to make possible earlier stripping.

CURING, COOLING, AND PROTECTION OF CONCRETE

Specifications provided for the water curing of the interior concrete of the pumping plant and all other exposed surfaces. On the unexposed surfaces of the plant, on the intake and discharge conduits, and on similar surfaces, white-pigmented curing compound was applied.

To provide for the cooling of the interior of the massive substructure and buttresses, water was circulated through systems of coils installed for the purpose prior to placement of concrete. Water was circulated for a period of 10 days after placement for the substructure blocks and 7 days for the buttresses. Each day, the direction of flow within the coils was reversed. Water supplied from Soda Creek was used for the purpose. The temperature of the cooling water tended to become uniform after the fourth day. It was also required that the blocks of the substructure be cooled at least 7 days before the adjacent blocks could be placed. After the cooling was completed, the cooling coils were grouted under pressure of 100 lb per sq in. until completely filled.

The specifications required that the temperature of the concrete exposed to freezing should be maintained at 50°F or higher for not less than 72 hr after placement, or until it had hardened thoroughly. It was also specified that concrete be protected from freezing for at least 2 weeks immediately after being placed. The protection of concrete to meet these requirements was a burdensome and expensive job (as is indicated by yearly temperature records for the area). On an average, there was only 1 month of each year during which temperatures remained above freezing. Minor protection of fresh concrete in the area may be necessary at any time through June and again after the middle of September. Thereafter, through the following April, elaborate protection is essential.

Complex measures were taken to secure the minimum protection required to prevent the concrete from freezing. These precautions included the use of conventional orchard-type "salamanders" (some of which were equipped with electrically powered blowers); airplane-type motor warmers; electric heaters with blowers; steam; and—during the fall and winter of 1948—two coal furnaces that were placed in the plant building. Even with these measures, and with the plant and other placement locations fully housed in canvas, a minimum of protection was all that could be made available. Orchard-type salamanders, on a platform hung from the bottom of the exterior wall forms, were surrounded by the canvas spread over the plant wall forms, as shown in Fig. 6. These heaters were probably the most efficient for the exterior work, and the electric heaters with blowers proved best for the interior work. Fortunately, the large quantity of heating equipment produced few accidental conflagrations, although soot, smoke, and fumes were a usual occurrence.

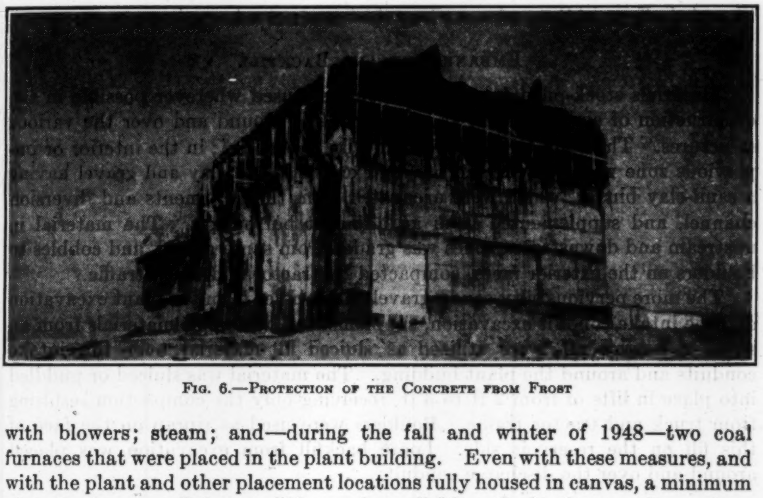

FIG. 6.—PROTECTION OF THE CONCRETE FROM FROST

FINISHING

The forming and finishing procedures that were made standard specifications for all work of the Bureau of Reclamation, United States Department of the Interior (USBR), after 1947 were not in effect in time for inclusion in the specifications for the pumping plant; however, the contractor accepted these new procedures as a guide to the type of finishing desired throughout the construction work. With little exception, all floors within the pumping plant were left from 1 in. to 2 in. below grade to allow for a bonded floor topping.

This topping was one of the last jobs completed, after all major construction work within the plant proper had been finished in 1949.

The accumulation of soot and smoke from the heaters, rust stains from curing water, form oil stains, and laitance from a spillage of concrete or from seepage of cement-laden waters from forms above, made necessary the cleaning of all exposed surfaces of the plant and of other structures permanently exposed to view. As little cleaning as possible was required in storerooms and in locations not generally observable, but the main rooms of the plant building and its exterior above ground level were cleaned by the use of wire brushes, and by wet and dry sandblasting. Wet sandblasting was applied to interior walls where sand in the air was objectionable. Dry sandblasting was more effective and less costly, and this treatment was used in all places that could be sealed off, or in those places where dust was not a hazard.

EMBANKMENT AND BACKFILL

Materials stock-piled from excavation were used wherever possible in the construction of embankments and in backfilling around and over the various structures. The Soda Creek Diversion Dike was zoned; in the interior or impervious zone were placed sand having excess silt and clay and gravel having a sand-clay binder, which were excavated from the abutments and diversion channel, and supplemented from an adjacent borrow pit. The material in upstream and downstream zones was graded from sand, gravel, and cobbles to boulders on the exterior faces, compacted by tractor and truck traffic.

The more pervious silty-sandy gravel and cobbles from the plant excavation and the intake conduit excavation, supplemented by similar materials from an adjacent borrow pit, were utilized as sluiced fill material over the intake conduits and around the plant building. The material was sluiced or puddled into place in lifts of from 2 ft to 3 ft, receiving only the compaction resulting from truck and tractor traffic. Boulders were used as riprap on the face of this fill on the reservoir side. Loose backfill from excavation was placed around and over the discharge conduit.

CONSTRUCTION CONTROL

The excavations for the pumping plant, the conduits, and the intake structure were slope-staked from their respective center lines and were properly referenced. The horizontal control for the pumping plant was established for each reference line by monuments on each side of the structure. All bench marks about the pumping plant were set from a circuit between two USBR precise-datum bench marks, each construction point was set by the intersection of two reference lines, and the proper elevation was determined from near-by bench marks. A crew of four men established this control and set all points for the construction work.

The inspection of the actual construction work, the placement and handling of the concrete for the pumping plant and conduits, and the construction of the diversion dike and channel were provided by USBR personnel at the pumping plant. The handling of the aggregate for the concrete and the inspection within the batching and mixing plant were under the supervision of the USBR technicians and inspectors of the area laboratory, who also performed the necessary testing of concrete and made routine aggregate moisture tests and grading tests.

ACKNOWLEDGMENTS

The design and construction of the Colorado-Big Thompson Project, of which the Granby Pumping Plant is a part, were under the direction of L. N. McClellan, M. ASCE, chief engineer (USBR). Construction within the area was under the direction of George R. Highley, construction engineer (USBR) until Februrary, 1950, at which time he was succeeded by U. V. Engstrom. E. H. Honnen was project manager for the Granby Constructors.

AMERICAN SOCIETY OF CIVIL ENGINEERS
Founded November 5, 1852
TRANSACTIONS

Paper No. 2684

SPECIAL PROCEDURES FOR PAVEMENT DESIGN

BY L. A. PALMER[1]

WITH DISCUSSION BY MESSRS. R. HORONJEFF, AND L. A. PALMER

SYNOPSIS

In building airfield pavements to resist the heavy loads and thermal shock produced by improved types of aircraft, the Bureau of Yards and Docks, United States Department of the Navy, has established the testing procedures and design criteria described herein.

Material must fulfil special requirements to be used on runway ends, and the structural properties of the base course and subbase for the entire runway must conform to high standards. This paper describes the requirements of such material, the types of tests used, and the principles on which the pavement construction methods are based.

INTRODUCTION

As a consequence of the development of new and heavier types of naval aircraft, the Bureau of Yards and Docks of the United States Department of the Navy has established tentative testing procedures and general design criteria for the construction of new pavements and the reinforcement of existing ones.

Simultaneously with the pursuance of its huge pavement construction program, the Navy has planned and has conducted research in its laboratories in an effort to find new materials and procedures for constructing pavements having high resistance to the repeated thermal shock produced by the hot exhaust gases from jet aircraft. Such materials, if found, should have the following properties: They must be economical; they must have low thermal conductivity so that they may be used as a cover to protect existing pavements; they must possess structural stability; and they must have low thermal expansivity. Also, they must resist the solvent action of petroleum distillates that are used as fuels. These properties are required particularly in the end zones of runways, at junctures of taxiways and runways, in warm-up aprons where

---

NOTE.—Published in June, 1953, as *Proceedings-Separate No. 195*. Positions and titles given are those in effect when the paper or discussion was received for publication.

[1] Eng. Consultant, Soil Mechanics and Paving, Bureau of Yards and Docks, U. S. Dept. of the Navy, Washington, D. C.

jet planes check power before taking off, and to a somewhat lesser extent in taxiways where the jet aircraft must stop and start frequently. In the intermediate stretches of runways between the end zones, no special materials are needed; but the design of bituminous mixes for surfacing, and of the base course and subbase for flexible pavements, must be adequate for single tire loads of 20,000 lb with a tire inflation pressure of 250 lb per sq in. and for single tire loads as great as 50,000 lb with a tire pressure of 150 lb per sq in.

The complete stress analysis for multi-layered systems of infinite lateral extent and of variable (yet finite) thicknesses of the separate-layered components remains to be accomplished. Donald M. Burmister,[2] M. ASCE, has presented a precise solution limited for the most part to two-layered systems. His published solution applies only to the settlement or deflection of points on the axis of symmetry when a load is distributed uniformly over a circular area (either by means of a rigid plate or by other means). Expressions for shearing stresses and normal stresses within and below the separate-layered components apparently await further studies.

For the case of a load that is uniformly distributed over a circular area on a single homogeneous layer of great depth, both S. D. Carrothers[3] and A. E. H. Love[4] have shown that a basin-shaped surface extends from the perimeter to a depth that depends on the assumed value for the Poisson ratio, at all points of which surface the shearing stress is a maximum and equal to w/π, w being the unit load. For a Poisson ratio of 0.5, the depth of maximum shear is about 0.7 r, in which r is the radius of the uniformly loaded area. In the case of multi-layered systems, such as flexible pavements, the depth to which the occurrence of maximum shearing stresses extends is not known. Because all the layered components of a flexible pavement tend to spread the load more than does the subgrade, certainly the region of maximum shear does not extend to depths greater than 0.7 r in flexible pavements, and an assumption on the side of safety is that shearing stresses equal to w/π extend to this depth. For a tire load having an inflation pressure of 250 lb per sq in., the actual contact pressure between the tire and the pavement is 250 lb per sq in. plus 10% of this amount, or 275 lb per sq in. Thus, the maximum shearing stress (assuming the tire footprint to be circular) is 87.6 lb per sq in. For the greater tire load of 50 kips, with tire pressure equal to 150 lb per sq in., the depth within which the shearing stress is a maximum is approximately 7 in.

Thus, approximately 7 in. of the flexible-type pavement must have shearing resistance equal to not less than $165/\pi = 52.5$ lb per sq in. This stress condition demands an especially tough surfacing and a base course, the top few inches of which must have high shearing resistance. For the tire load of 20 kips at a tire pressure of 250 lb per sq. in., the shearing resistance must be not less than 87.6 lb per sq in. in the upper 5 in. of pavement. This stress condition demands a surfacing of unusual toughness.

---

[2] "The Theory of Stresses and Displacements in Layered Systems and Application to the Design of Airport Runways," by Donald M. Burmister, *Proceedings*, Highway Research Board, National Research Council, Washington, D. C., Vol. 23, 1943, pp. 126–148.

[3] "Elastic Equivalence of Statically Equipollent Loads," by S. D. Carrothers, *Proceedings*, International Mathematical Cong., Toronto University Press, Toronto, Ont., Canada, Vol. 2, 1924, p. 527.

[4] "The Stress Produced in a Semi-Infinite Solid by Pressure on Part of the Boundary," by A. E. H. Love, *Philosphical Transactions*, Royal Soc. of London, Series A., Vol. 228, 1929.

Experience has evidenced that the required total or over-all flexible pavement thickness is that which will assure a settlement not exceeding 0.2 in. under the severest conditions of loading—which must take into account both tire load and tire pressure. Thus, it may be shown that for the two conditions—a 20-kip tire load with tire pressure equal to 250 lb per sq in., and a 50-kip tire load with tire pressure equal to 150 lb per sq in.—the latter condition is the determining factor in estimating the required total thickness of flexible pavement.

Therefore, the high tire pressures that characterize new models of naval aircraft require an especially tough, asphaltic concrete surfacing and a base course of which at least the top few inches must have a correspondingly high shearing resistance. Experience has demonstrated the economic feasibility of designing and constructing asphalt-surfaced pavements that meet these requirements. The total pavement thickness required for the 50-kip tire load at a tire pressure or 150 lb per sq in. is determined by loadings on trial pavement sections having a base course of fixed thickness and a subbase of variable thickness. A circular steel plate, 20 in. in diameter, is used for this purpose. The required pavement thickness is obtained by first loading the compacted subgrade and computing the modulus of compression E_2 of the subgrade, then obtaining E_1 for the pavement by loading the base course after this course has been compacted on the subgrade and thereafter using Mr. Burmister's influence curves.

For the design of concrete pavement, loading tests are made either on the compacted subgrade or on a prepared subbase of variable thickness to determine the modulus, *k*, for use in the Westergaard analysis.

Essential Features of Pavement Design

For the flexible-type pavement, quality (especially toughness) of the pavement is a consideration equal in importance to pavement thickness. The required pavement quality is determined by the tire pressure, and the required over-all pavement thickness depends on the magnitude of the greatest anticipated wheel load, with proper consideration being given to tire pressure and the essential differences in requirements for loads on single tires, dual tires, and dual-tandem tires. On the basis of experience, field tests, and observations, quality indexes have been tentatively adopted by the Bureau of Yards and Docks for the following paving components and procedures: Asphaltic concrete surfacing, base courses for flexible pavements, subbases, subgrade preparation, the use of trial pavement sections, and proving of the design by studying pavement performance.

Asphaltic Concrete Surfacing.—The design of the bituminous mix for both the binder course and the wearing course is based on the Marshall test. Traffic tests made for the Bureau of Yards and Docks by the Corps of Engineers, United States Department of the Army, at the Waterways Experiment Station, at Vicksburg, Miss.,[6] in addition to the Marshall stability tests made with cored specimens of asphaltic concrete taken from pavements in use at naval air stations, have led to the adoption of the following standard requirements for the binder course:

---

[6] "Effect of Traffic with Small High-Pressure Tires on Asphalt Pavements," *Technical Memorandum No. 3-314*, Corps of Engrs., U. S. Dept. of the Army, Vicksburg, Miss., June, 1950.

Test property	Values
Marshall stability (pounds)	$> 1,500$
Flow (hundredths of an inch)	< 16
Voids (%)	$4 < n < 6$
Voids filled with asphalt (%)	$70 < X < 82$

The standard requirements for the wearing course are the same with the following exceptions: Voids (%) $3 < n < 5$; and voids filled with asphalt (%) $75 < X < 85$. Asphalt paving mixtures are designed for a tire pressure of 250 lb per sq in., based on tests of cylindrical specimens compacted in a mold by applying seventy-five blows on each flat surface with the commonly used Marshall equipment. The optimum asphalt content is the average of the different asphalt contents at the following points on curves (test property as related to asphalt content):

Test property	Point for selection of asphalt content
Stability	Peak of curve
Unit weight, total mix	Peak of curve
Unit weight, aggregate only	Peak of curve
Voids (%)	5
Voids filled with asphalt (%)	78

Specifications for the placing and rolling of binder and wearing courses require that compaction produce a density that is 98% of the density (corresponding to the optimum asphalt content) obtained in the laboratory compaction of the specimen, which requires seventy-five blows per flat surface.

A characteristic of mixes designed in this manner is the tendency toward leanness in asphalt—that is, "dryness." One of the greatest sources of danger when using high-pressure tires is the extraction of asphalt from the surfacing material as the result of kneading action of the tires, best described as "working" of the asphalt out of the surfacing material. A certain residual void space to contain asphalt "worked out" by progressive compaction under unlimited traffic and a low asphalt content to permit desirable aggregate interlocking and maximum internal frictional resistance are absolutely necessary. Dense gradation of hard and durable aggregates and a careful determination of optimum asphalt and mineral filler content are sufficient for meeting all requirements. The asphalt penetration usually ranges from 70 to 100.

New asphalt surfacing construction is proof-tested by repeated coverages (cycles of operation) over tracks of two-tire widths with vehicles of the type shown in Fig. 1. A thousand coverages are sufficient for a test. The tire inflation pressure for these tests is 250 lb per sq in., and the load on a single tire is 9,000 lb. The Marshall stability and flow, the percentage of voids, the percentage of voids filled with asphalt, and the bulk density are determined both before and subsequent to the traffic tests from cored specimens, 4 in. in diameter.

The compacted asphalt surfacing (binder course plus wearing courses) is 3 in. thick for the types of tire loads described, and the seal coat usually is omitted at the time of construction.

Base Courses for Flexible Pavements.—The following types of base courses are being constructed: Mechanically stabilized aggregate, dry-bound macadam, water-bound macadam, limerock, bituminous concrete (black base), and penetration macadam. For overlays on existing flexible pavements and existing concrete pavements the black base type and the asphalt penetration macadam type usually are preferred. After tack coating these adhere well to the old pavement. For runway extensions and other new pavement construction, mechanically stabilized aggregate tends to be the most economical generally. Dry-bound macadam and water-bound macadam permit slightly thinner pavements than does stabilized aggregate, and they are often preferred where there are long hauls of aggregates or other transportation difficulties. The use of stabilized aggregate and limerock effects a substantial saving in the time required for construction of the base.

A minimum soaked (4 days of soaking) California Bearing Ratio (CBR) of 80 is recommended as a quality index for the mechanically stabilized or select aggregate base course. This index is made necessary by the high shearing stresses caused by high-pressure tires. In nearly all instances, this minimum has been exceeded without difficulty. Of course, it is not practicable to utilize the CBR test in the design of the other types of bases. For the black base, a minimum Marshall stability of 1,000 lb and a flow value not exceeding 16 is the usual requirement.

The only quantitative index to the relative bearing values of in-place base courses, such as the dry-bound and water-bound macadams, the black base, and the penetration macadam, is the plate loading test. This index is expressed in terms of a "modulus," E_1, obtained after first loading the prepared subgrade with a steel plate 20 in. or 30 in. in diameter, and thereafter loading with the same plate a layer of known thickness of the base course constructed on the same prepared subgrade of measured modulus, E_2. The procedure for computing both E_1 and E_2 with the aid of influence curves has been completely described by Mr. Burmister.[2] The measured moduli of base courses tend to vary over a wide range, those for stabilized aggregate base course being generally between 25,000 lb per sq in. and 100,000 lb per sq in. The moduli for well-constructed penetration macadam, black base, and water-bound macadam usually tend to exceed 100,000 lb per sq in., and, in some instances, are as high as 200,000 lb per sq in. There has been little work done toward a careful and thorough analysis of the large number of load-test data obtained (1953), but it is apparent that such an analysis will definitely serve to classify base courses from the standpoint of their load-distributing characteristics. This classification is particularly desirable in the case of bituminous-treated aggregates and other processed aggregates for which the soaked CBR test has no application. The importance of quality of the flexible-type pavement has been minimized by the overemphasis attached to pavement thickness alone. The attainment of high quality of pavement with respect to high shearing resistance and load-distributing properties is a matter of both good design and good construction. Neither one without the other can produce an adequate pavement.

Fig. 2 shows the general relation or lack of relation between soaked CBR-values and the moduli, E_2 for subgrades and E_1 for base courses. The moduli were obtained without presoaking any of the materials. This difference should be of relatively little importance in the case of base courses consisting of densely graded select aggregates of the 2-in. size and smaller. A lack of relationship would be expected in the case of silt and clay subgrades. In this case, the soaked CBR-values and not the in-place CBR-values were measured, whereas the plate loading tests were made either on the subgrades under existing pavements or on compacted subgrades that were at or near their optimum moisture contents during the course of construction of trial pavement sections. Nevertheless, a correlation between CBR-values and E_2-values of subgrades is indicated in Fig. 2.

FIG. 1.—LOADING VEHICLE FOR NEW ASPHALT SURFACING

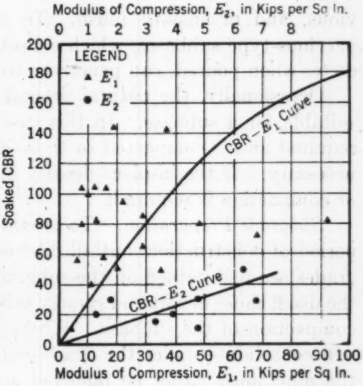

FIG. 2.—RELATION BETWEEN MODULI OF COMPRESSION AND SOAKED CBR-VALUES

Subbases.—The general policy for the design of subbases is to construct progressively tougher pavement components from the subgrade up to and including the surfacing for flexible pavements, with the base course designed to function as the principal structural component. Contingent on relative costs and availability of materials, the general policy is to maintain also a fixed thickness of base course in constructing trial pavement sections and to vary the pavement thickness in these sections by varying that of the compacted subbase. The fixed thickness of the base course is intended to insure against failure by shear within the pavement caused by excessive tire pressures. The thickness of the subbase is then estimated from the plate loading test as being that thickness required to avoid the subgrade yielding beyond an extent such that the maximum anticipated tire load causes a plate settlement exceeding 0.2 in. In a few instances, the cost of subbase materials that were not near the site has been equal to or greater than the cost of good base course material that was locally available. In all such cases the subbase is omitted, and the thickness of the base course is varied in the trial sections.

For flexible pavements, suitable subbase materials commonly used are chert, caliche, pit-run uncrushed gravel and sand, decomposed or partly decomposed granite, sand-clay, and mixtures of sand-clay with shell or crusher-run stone.

The essential, recommended requirements for subbase material for flexible pavements are as follows: A 4-day soaked CBR of not less than 45; a liquid limit of material passing the No. 40 sieve of not more than 25%; and a plasticity index less than 8%. The fraction passing the No. 200 sieve shall not exceed one half the fraction passing the No. 40 sieve. For concrete pavements, the recommended minimum soaked CBR is 30 and all other requirements are the same as those for subbase in flexible-type pavements. Base courses, comparable to those in flexible pavements, are not used to support concrete pavements. The subbase for concrete pavements must be dense, relatively impervious, and of smooth finish. To be avoided are open-type subbases and pervious-type subbases, which collect and hold water and into which the concrete, when poured, can penetrate and bond.

Occasionally, the natural ground or material available for fills is in itself suitable for a subbase. In this case, the material is loosened or removed as required and is compacted to those depths indicated by loading tests as being necessary. If the in-place density in cuts is sufficient, no removal, scarifying, or compaction is required.

Subgrade Preparation.—To provide adequate drainage of the site during the period of construction, outfall ditches are dug in the subgrade, and transverse grades are maintained on the subgrade to permit runoff. Failure to do this is the usual cause of soft and spongy subgrades that render impossible the effective compaction of the subbase. Where there is to be fill over a mud layer that will consolidate under the dead load produced by the fill plus the pavement, the mud must either be removed and replaced with more granular or stable material or be stabilized. Stabilization is achieved by constructing interconnecting vertical sand drains and overloading the mud by adding extra surcharge which is cut away and removed after a few weeks when the mud becomes so well consolidated that no slow settlement will be realized with final grades established. Because the time-consolidation relation for very peaty soil differs radically from that of normal silt and clay soils, no attempt is made to stabilize peat by the use of sand drains. Peat soils must be removed and replaced.

Trial Pavement Sections.—Much could be written about trial pavement sections. The proper selection of sites for trial sections within the area to be paved requires elaborate description and nothing can be substituted for experience. The trial section is a full-size model test. A loading test on a trial section is a test of the finished product—the pavement—and it reflects the combined influence of a multiplicity of factors, each unpredictable from "piecemeal" studies in the laboratory. Among other things, the construction of trial sections tends often to disclose unexpected difficulties in compacting the pavement components. It is well to discover such difficulties prior to preparing the final plans and specifications. As an example—it was found in one instance to be inadvisable to construct a penetration macadam base course on a sand-clay subbase. In the trial section the sand-clay, compacted to more than 95% of maximum density (by the laboratory compaction procedure given by the modified (Corps of Engineers) form of Test T99-49 of the American Association of State Highway Officials[6]), was readily penetrated when the coarse aggregate was rolled on it. Changing the base course to a select, graded, and mechanically stabilized type was more feasible than changing the subbase and, when this alteration was made, all went well and issuance of a change order after award of the contract was avoided.

By loading first the compacted subgrade and then a subbase and base course of arbitrary thicknesses to find the separate moduli of these materials, an estimate of the required pavement thickness may be made by using the Burmister procedure and influence curves. A trial section comprised of three adjoining plots not less than 20 ft by 20 ft is then constructed so that the combined thickness of the base course and the subbase is equal to the estimated value in one plot, one half to two thirds of the estimated thickness in a second plot, and 1.5 times the estimated required thickness in a third plot (see Fig. 3). Load tests then are made on each plot with a circular steel plate of area equal to the tire footprint of the greatest anticipated tire loading that the pavement is to accommodate. Corrections of the observed plate deflections under the full

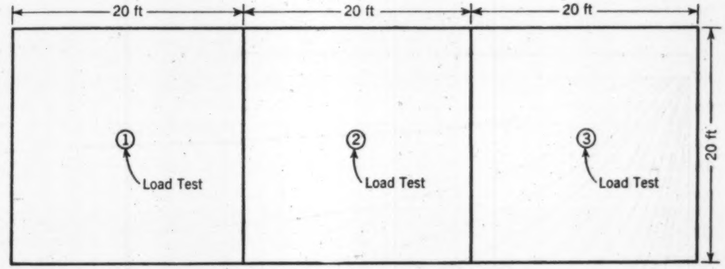

(*a*) PLAN OF TRIAL PAVEMENT PANELS

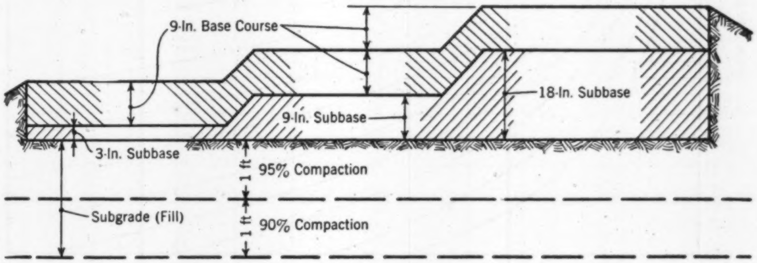

(*b*) CROSS SECTION

FIG. 3.—TYPICAL SECTION OF A TRIAL PAVEMENT

load in each case may be made for any assumed future increase in moisture content of the subgrade that may seem reasonable. If the subgrade modulus, E_2, is known for various subgrade moisture contents, it is preferable to make the correction by using theory. The design basis for flexible pavement thickness is an upper limit of settlement of 0.2 in. For a rigid plate of radius, r,

---

[6] "Standard Specifications for Highway Materials and Methods of Sampling and Testing, Part II." A.A.S.H.O., Washington, D. C., 1950.

$$E_2 = \frac{3\,\pi\,w\,r}{8\,\Delta} \qquad (1)$$

in which w is the average pressure of the plate on the soil and Δ is the settlement. Succeeding paragraphs demonstrate the design procedure.

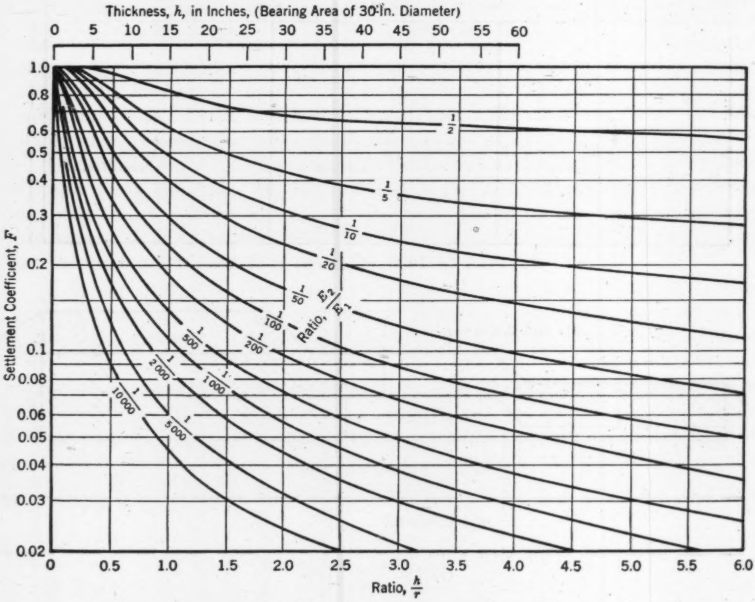

FIG. 4.—INFLUENCE CURVES FOR THE SETTLEMENT COEFFICIENT, F, FOR THE TWO-LAYER SYSTEM

By loading on a subgrade compacted to 96% of maximum density at optimum moisture, with a 30-in.-diameter loading plate, the observed value for w at $\Delta = 0.2$ in. was 40 lb per sq in. Then $E_2 = 3{,}535$ lb per sq in. by Eq. 1. When the same subgrade was loaded four years later, using the same plate, the subgrade moisture at the same location was found to have increased to 4% above optimum and the observed w-value for this condition was 32 lb per sq in. The corrected value of E_2 became 2,830 lb per sq in.

The Burmister settlement factor is

$$F = \frac{E_2\,\Delta}{1.18\,w\,r} \qquad (2)$$

By loading on 12 in. of base course for the first condition, the observed w-value was 130 lb per sq in. at a Δ-value of 0.2. This yields an F-value equal to 0.307. If the thickness of the reinforcing or pavement layer is h, and is equal to 12 in. (the equivalent of 0.8 r), a set of influence curves developed by Mr. Burmister (Fig. 4) yields a value of $\frac{1}{80}$ for the ratio, $\frac{E_2}{E_1}$ corresponding to the F-value for this case. Therefore, $E_1 = 282{,}900$ lb per sq in. Similarly, for the second (wetter subgrade) condition, and with E_1 already evaluated, $\frac{E_2}{E_1}$ is approximately $\frac{1}{100}$.

A circle of 20-in. diameter has approximately the area of the print of a tire carrying a load of 50 kips at a tire pressure of 150 lb per sq in. (165 lb per sq in. of tire contact). If the thickness, h, of base course is required for this tire load for each of the two subgrade conditions, a uniform load on a circular area has a settlement factor expressed as

$$F = \frac{E_2 \, \Delta}{1.5 \, w \, r} \qquad (3)$$

TABLE 1.—COMPARISON OF IN-PLACE SUBGRADE CONDITIONS BEFORE THE INACTIVATION OF THREE AIR STATIONS AND AFTER A FIVE-YEAR INACTIVE PERIOD AT THESE STATIONS

Air station	Value	In-Place Dry Density, in Lb per Cu Ft		In-Place Moisture Content in Percentage of Dry Weight		In-Place Voids Ratio		In-Place Saturation, in Percentages	
		1944	1951	1944	1951	1944	1951	1944	1951
Kingsville, Tex. North Field	Minimum	94.0	91.0	7.0	7.1	0.501	0.460	44.3	33.0
	Maximum	112.0	115.0	18.0	28.0	0.865	0.844	80.9	100.0
	Average	101.4	105.0	12.1	16.5	0.714	0.598	61.6	73.0
Kingsville, Tex. South Field	Minimum	80.6	89.0	9.4	11.0	0.554	0.435	36.5	61.0
	Maximum	108.0	117.0	24.1	32.0	0.907	0.886	84.0	100.0
	Average	94.6	100.4	17.3	21.1	0.774	0.672	60.7	84.5
Edenton, N. C.	Minimum	92.0	97.8	6.0	4.9	0.391	0.354	26.5	19.6
	Maximum	127.0	123.5	21.3	20.0	0.817	0.710	99.1	100.0
	Average	110.4	105.5	14.6	10.6	0.514	0.585	76.1	48.6

For the subgrade at optimum moisture, $F = 0.286$. Interpolation in Fig. 4, using the proportion, $\frac{E_2}{E_1} = \frac{1}{80}$, yields $\frac{h}{r} = \frac{h}{10} = 0.87$, or $h = 8.7$ in.

For the wet subgrade condition, $F = 0.229$ and $\frac{E_2}{E_1} = \frac{1}{100}$, as found. Interpolating again from Fig. 4, $h = 10.6$ in. Thus, the 12 in. of base course (exclusive of 2.5 in. of tough asphaltic concrete surfacing) was more than ample for the design load, even for the wettest condition of subgrade found anywhere under the pavement in an evaluation study of the field.

As an aid in the substitution of facts for prevalent suppositions concerning the probable wetting of subgrades under airport pavements, the data of Table 1 are shown. Subgrade conditions prior to and following a long period of inactivity of three airfields are listed. During the period of inactivity (about five years in each case) there was neither plane traffic nor pavement maintenance. The subgrades of the two airfields at Kingsville, Tex., are clays of the CL and CH plasticity types, and the subgrade at the field at Edenton, N. C., varies from SF to ML. The surfacings at all three fields were badly cracked, and every condition favored the wetting of the subgrade. Normally, subgrades under airport pavements in use do not show these extreme conditions.

The average optimum moisture contents of the subgrades at the three air stations were found to be the following:

Air station	Moisture (%)
North Field, Kingsville	12.5
South Field, Kingsville	16.1
Edenton	12.8

In 1951, following the long period of inactivity, the average percentage increases above optimum (Table 1) were 4.0 and 5.0 for the first two of the aforementioned fields, respectively, whereas in the case of the Edenton field, the subgrade moisture dropped to 2.2% below optimum. Significantly, however, the in-place subgrade density also increased simultaneously with the increase of subgrade moisture at the Kingsville airfields.

The average maximum subgrade densities were found to be 117.6 lb per cu ft, 112.2 lb per cu ft, and 119.2 lb per cu ft for North Field and South Field at Kingsville and at Edenton, respectively. For 1951 conditions, the corresponding in-place dry densities were 89.3%, 89.5% and 88.5% of the maximum densities, respectively, representing a small increase in percentage of maximum density for the Kingsville stations and a small decrease for the Edenton station.

The data of Table 1 may be summarized further as follows:

Kingsville, North Field.—In the period from 1944 to 1951, during five years of which (1946 to 1951) the field was inactive, the average in-place subgrade density increased 3.6 lb per cu ft, the average in-place moisture increased 4.4%, the average voids ratio diminished by 0.116, and a corresponding higher percentage of the voids space became filled with water; that is, the subgrade was consolidated slightly during this period.

Kingsville, South Field.—The average in-place subgrade density increased by 5.8 lb per cu ft and the average in-place moisture increased 3.8%. Again, the average voids ratio decreased (that is, the subgrade consolidated slightly) with a consequent increase in percentage saturation.

Edenton.—In this case, the average in-place density decreased by 4.9 lb per cu ft, but the average in-place moisture content also decreased by 4.0%. The average voids ratio increased with a consequent decrease in the average percentage saturation. In other words, the subgrade rebounded or recovered in a manner similar to that observed when there is a release of the load on a loaded soil mass.

The asphalt surfacing at the three airfields had no seal coat application during the period of inactivation and tended to become brittle, to oxidize, and to deteriorate during the five years they were without traffic. Even with these unusually favorable conditions for wetting subgrade, there seems to be no reason for extreme conservatism in applying a correction factor to the design thickness of a flexible pavement as indicated from loading tests on trial sections. At a total of seventy-two Navy and Marine Corps air stations, including principal stations in the United States, and islands of the Caribbean Sea and the Pacific Ocean, the in-place subgrade moisture has been found to exceed only occasionally the optimum by as much as 3% for fields that have been in use for from four years to nine years.[7] Many of these field studies were made during wet seasons and at the time of spring thaw.

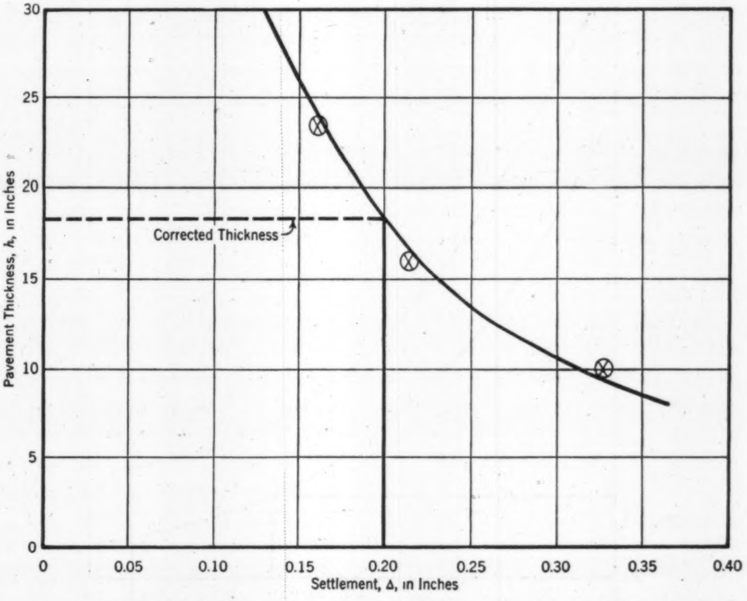

FIG. 5.—PLOTTING OF DATA OBTAINED BY LOADING THE TRIAL SECTIONS

The plotting of data obtained by loading on trial sections is shown in Fig. 5. In each of the three panels of the trial pavement section (Fig. 3) the pavement thickness is corrected as may be indicated for possible future increase of subgrade moisture in the manner already described. The corrected thicknesses are then plotted against the observed settlements and the best possible curve is drawn through the points. The thickness corresponding to 0.2 in. of plate settlement is taken as the over-all design pavement thickness. In constructing the trial sections, the asphaltic surfacing is omitted—an equivalent thickness of base course being substituted for it.

---

[7] "Pavement Evaluation by Loading Tests at Naval and Marine Corps Air Stations," by L. A. Palmer and James B. Thompson, *Proceedings*, Second International Conference on Soil Mechanics, Vol. 2, 1948, p. 227, Table 1.

Pavement design and evaluation on the basis of plate loading tests have been found to be generally reliable and economical procedures in Navy experience. It is hoped that the field tests may be simplified and reduced by finding correlations between laboratory test data obtainable from soil tests such as unconfined compression tests or in-place CBR tests (or both) and the E_2-moduli as determined by plate loading.

Trial sections for concrete pavement involve only the construction of compacted subbase panels 20 ft square in cut-and-fill areas of runways, taxiways, aprons, and runway ends, and at transitions between cut-and-fill areas. In the use of the well-known Westergaard analysis, the design requirement is that, when loading on the compacted subbase, the foundation modulus, *k*, must not be less than 200 lb per cu in. after a reasonable correction (based largely on experience) has been made for probable future increase in moisture of the compacted subgrade and subbase. The policy requires the use of a factor of safety of about 1.4 based on values of the moduli of rupture obtained by testing

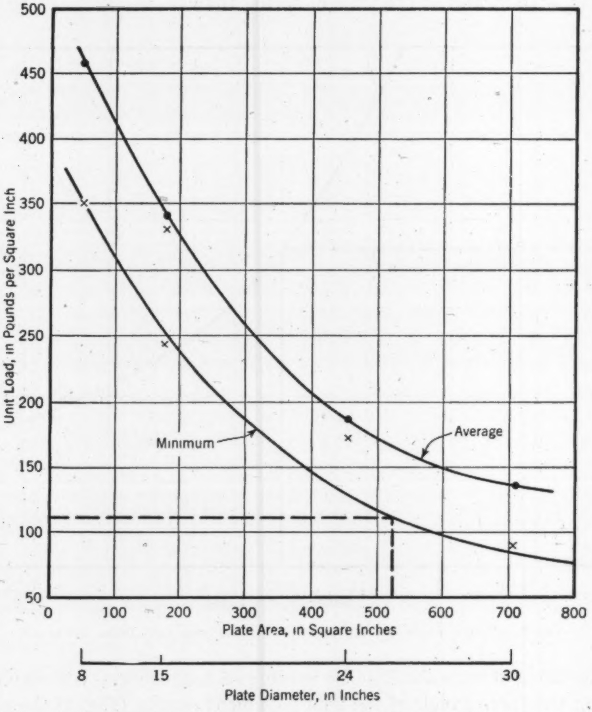

FIG. 6.—EXAMPLE OF THE GRAPHICAL METHOD OF DETERMINING THE SAFE WHEEL LOADS FOR FLEXIBLE PAVEMENTS

beams after 28 days of wet-curing. Extensive pavement evaluation studies have shown that such a factor of safety at 28 days may reasonably be expected to increase to about 1.6 at the end of a year in the actual pavement, and the elapse of a year may be expected between the time of construction and the time when the pavement begins to carry a considerable volume of traffic of the heaviest type planes. Subbase thicknesses have varied from 6 in. to 18 in. as determined by loading on trial sections with a plate 30 in. in diameter in all cases. The primary consideration is to obtain a permanency and uniformity of k-modulus throughout the paved area during its period of use. Experience has proved that, with initially low k-values of from 50 to 100, "mushroom" subgrade support of the slab almost always results after a year or more. Pumping at joints and all attendant evils resulting from low k-values render the cost of a well-designed and well-constructed subbase small in comparison with the greater cost of the extra maintenance made necessary when the earth support is given little or no consideration.

Design Proved by Pavement Performance.—The basis for flexible pavement design as described herein is a maximum allowable plate settlement of 0.2 in. This corresponds to a greater settlement realized when the same load on the same area is applied uniformly. A 0.2-in. settlement of a rigid plate is equivalent to $\frac{1.5}{1.18} \times 0.2$ in., or 0.254 in., of settlement under a tire load of the same magnitude, the loaded areas being the same for both the plate and the tire.

The evaluation of pavements already constructed utilizes the criterion of a 0.2-in. allowable settlement. More than 3,000 plate loading tests have been made since 1944 in the evaluation of pavements at seventy-two Navy and Marine Corps air stations. The safe maximum tire loads corresponding to different tire pressures were established for the pavements of each runway, taxiway, parking area, and similar areas at each airfield.

The simple graphical method of establishing these loads is illustrated in Fig. 6, in which two curves are shown, designated as the "average" and "minimum" curves. The ordinates are the unit loads producing a 0.2-in. settlement. Points on the average curve are obtained by averaging the unit loads that produced a 0.2-in. settlement when loading on steel plates having diameters of 8 in., 15 in., 24 in., and 30 in. Having drawn the curve for averages, the minimum curve is drawn as nearly parallel as possible to the average curve and through the points of minimum values obtained by loading the flexible runway pavement at different carefully selected sites. The minimum curve is used for evaluating the pavement in terms of tire-load capacity. The tire contact pressure on the pavement is taken as the tire pressure increased by 10%. Thus, for a tire pressure of 100 lb per sq in. (Fig. 6) the contact pressure is 110 lb per sq in., and this ordinate value on the minimum curve corresponds to a plate area (also a tire contact area) of 525 sq in. and a safe maximum tire load at this tire pressure of 525 × 110 = 57,750 lb, or 58.0 kips to the nearest half-kip. Additional results thus obtained are tabulated as follows:

Tire pressure, in pounds per square inch	Contact pressure, in pounds per square inch	Safe wheel load, in kips
80	88	58
100	110	56.5
140	154	55
180	198	53
220	242	46
260	286	37
300	330	23

Many of the pavements evaluated by this procedure were originally designed by the method of trial pavement sections. Because of the progressive compaction of base and subgrade materials by traffic, the general tendency was toward an increase in load capacity, subsequent to construction, beyond that for which the pavement was originally designed. This tendency was especially marked in the case of sandy subgrades. Most of the pavements were designed and constructed during World War II and were intended to accommodate only light training planes. In these cases the pavement thicknesses were determined by judgment and not by trial sections or any other test method of pavement design. After two or more years of use, most of these pavements withstood the traffic of planes having single tire loads of 30 kips or more without damage beyond abrasion of the thin asphalt surfacing. This was quickly remedied by resurfacing. A description of the pavements of twenty of the airfields was published in 1946.[8]

With the exception of one runway (Naval Air Station, Los Alamitos, Calif.), the writer knows no instance of pavement failure caused by tire loads that did not exceed the rated capacities. The error at Los Alamitos resulted from too few loading tests. This was subsequently corrected. At a considerable number of the airfields the tire loads exceeded the rated capacities by from 20% to 50% without noticeable damage. At the Naval Air Station, at North Kingsville, Tex., tire loads of from 30 kips to 37 kips, at tire pressures of approximately 90 lb per sq in., caused complete failure in certain sections of pavement rated at 12.5 kips and 15 kips at 90 lb per sq in. In other sections of the same two runways, no damage was noticeable. Failure was mostly at the runway ends where there was dynamic loading on take-offs. At the Naval Air Station, Johnsville, Pa., there was repeated failure under tire loads exceeding the rated load capacity by 50%.

The basic principle utilized in the evaluation of the load capacity of a pavement is the same as that which is applied in the method of loading trial pavement sections when designing new pavements. The 0.2-in. allowable plate settlement has proved to be a reliable index for both new design and evaluation purposes. The Burmister theory (which is thoroughly sound from every angle) is not the yardstick of design. It is a means of obtaining a first estimate of the required pavement thickness for the construction of trial sections of different thicknesses. There must be no misinterpretation of the procedure from this standpoint. The procedure used by the Bureau of Yards and Docks is a mixture of the rational and empirical methods.

---

[8] "The Evaluation of Wheel Load Bearing Capacities of Flexible Types of Pavement," by L. A. Palmer, *Proceedings*, Highway Research Board, National Research Council, Washington, D. C., Vol. 26, 1946, pp. 72–97.

The pavement evaluation data were used in estimating the required extent of "beefing up" of the old pavements for aircraft considerably heavier than the rated tire-load capacities.

THE REINFORCEMENT OF OLD PAVEMENTS

Flexible-Type Pavement.—Values obtained from the plate loading tests made on the subgrade and on the surface of the existing pavement during the course of extended field studies, when the pavements at the air stations were evaluated, made it possible to estimate (by means of theory) the additional overlay in the form of flexible pavement reinforcement that was required to sustain safely tire loads that would exceed the rated capacity of the existing pavement. In this connection, there is no more reason to distrust theory as related to flexible pavement than to distrust the theory that has been applied for years in the design of concrete pavement—or to distrust the use of handbooks, all based on various theories, that engineers use generally.

Typical Example.—A runway at the Naval Air Station at Memphis, Tenn., is to be reinforced to carry a 50-kip load on a single tire at a tire pressure of 150 lb per sq in. The measured over-all pavement thickness is 8 in., of which 6 in. are base course and 2 in. are asphalt surfacing. At this field 1 in. of the surfacing is equivalent to 2 in. of base in load-bearing capacity. Thus, in computations, the pavement is considered as a single layer—as base course having a thickness of 10 in. By loading on the subgrade with the plate of 30-in. diameter, a value of 25 lb per sq in. is conservative for producing a settlement of 0.2 in. By loading with the same plate on the surface of the pavement, consideration of all the data shows that a conservative value of 58 lb per sq in. corresponds to 0.2 in. of plate deflection. The subgrade moisture was at about 2% above optimum in this runway after it was used six years. It is not assumed that it will become wetter after reinforcement of the old pavement.

Then, from Eq. 1, E_2 is 2,213 lb per sq in. and from Eq. 2 (with $w = 58$), F is 0.41. By interpolating in Fig. 4 for $F = 0.41$ and $h = 10$ in. $= 0.67\ r$, the ratio $\frac{E_2}{E_1}$ is $\frac{1}{50}$. Then $E_1 = 110{,}650$ lb per sq in. Use Eq. 3, setting $r = 10$ in. and $w = 165$ lb per sq in., corresponding to a uniformly distributed load of 165 lb per sq in. on a circular area having a radius of 10 in. (a total load of 51,810 lb, which is close enough to 50,000 lb for estimating). From Eq. 3, the new F-value is 0.18. Interpolating again in Fig. 4 to find a value of $\frac{h}{r}$ corresponding to $\frac{E_2}{E_1} = \frac{1}{50}$ and $F = 0.18$, it is seen that $\frac{h}{r} = 1.7$, so that $h = 1.7 \times 10 = 17$ in., which is the total pavement thickness required. Therefore, the required additional overlay must be equivalent to 7 in. of material having an E_1 of 110,650 lb per sq in.; that is, the reinforcement must produce a spreading of the load equivalent to 7 in. of the existing, well-compacted base course. This requirement must be checked by plate loading tests.

Judicious use of loading tests as a yardstick in pavement design must necessarily be based on long study and experience. Usually, such experience is not amenable to analysis and cannot be passed on to others in written form. Various contradictions may arise when the loading tests are not preceded by thorough analyses of soils, pavement materials, and topographic and drainage studies of the site. The in-place densities and moisture contents of all materials must be the same if direct comparisons of the relation of different pavement thicknesses to the plate settlement are to be made. Failure to eliminate all variables other than pavement thickness invariably leads to erratic and unreliable results.

In the foregoing example, it must be considered that the additional 7 in. of pavement reinforcement must be firmly bonded to the old pavement. Cleaning and tack coating of the old pavement before applying reinforcement are essential. Overlays that slide on the old surface must be avoided. Base courses of the bituminous types, such as black base and penetration macadam, have distinct advantages in this connection. Flexible-type pavements are adaptable to stage construction, but the additional reinforcement must become an integral part of the entire built-up pavement.

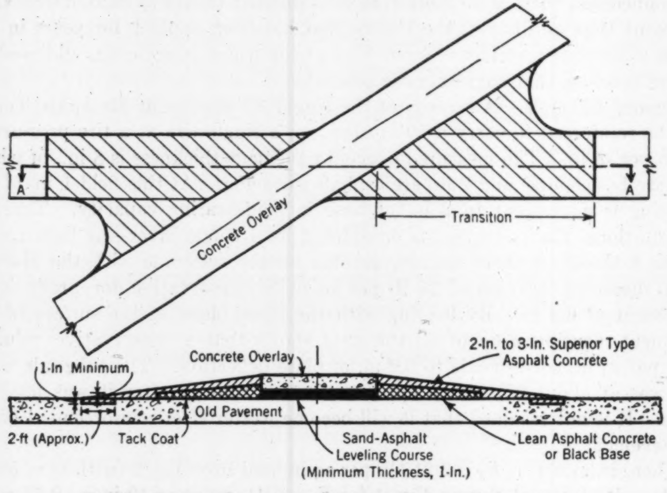
Concrete Overlay
A
A
Transition
1-In Minimum
Concrete Overlay
2-In. to 3-In. Superior Type Asphalt Concrete
Old Pavement
2-ft (Approx.)
Tack Coat
Sand-Asphalt Leveling Course (Minimum Thickness, 1-In.)
Lean Asphalt Concrete or Black Base

FIG. 7.—GENERAL SCHEME FOR RAMPS AT RUNWAY INTERSECTIONS

In very few instances in the 1950–1953 rebuilding program of the Bureau of Yards and Docks have old pavements been dug out, spoiled, and replaced with new materials, although some engineers have recommended this extravagant procedure. The old pavement is an investment and should be utilized. Evaluation studies have proved conclusively that (at least at naval air stations) old pavements usually have been pounded down by traffic to higher densities and bearing values than they had when newly constructed. Furthermore, from the standpoint of effective surface drainage, it is invariably advantageous to keep the pavement high in relation to the surrounding terrain. In one instance out of forty it was found advisable to scarify an old, poorly designed, and poorly constructed pavement and recompact it to produce a higher in-place CBR and a greater density before adding the reinforcement overlay.

If the reinforced runway pavement intersects a taxiway or runway that is not to be reinforced, the problem of transitions is encountered. In the present practice (1953) of the Bureau of Yards and Docks, the built-up runway pavement is "ramped" down on the adjacent paved areas with asphaltic concrete of quality equal to that used in surfacing landing strips for jet airplanes. Fig. 7 shows the usual scheme that is followed. At the outer end of each transition, grooves are sawed in the concrete and a keyway is chipped out. The length of the transition is determined by the difference in elevation between the old pavement and the overlay; the transition is ramped at a rate of change of grade not to exceed 0.3% per 100 ft. The longitudinal slope is not allowed to exceed 1%.

At those runway ends which are of flexible pavement and which are not to be extended, the overlay reinforcement of the ends is of reinforced concrete for a distance of 500 ft from the end.

Overlays on Concrete Pavements.—Old concrete runway pavements that will be overstressed by anticipated heavy tire loads are being reinforced with flexible-type pavement overlays, except at ends that are not to be extended, where the overlay in the last 500 ft is concrete. Old concrete taxiways and parking areas are reinforced with concrete overlays with few exceptions.

The preferred flexible-type overlays on existing concrete are asphaltic penetration macadam, with a maximum size of 2.5 in. for the coarse aggregate, and black base made with densely graded aggregate ranging from 1.5 in. down to fines and asphalt cement having penetration grades of from 85 to 100, with a 3-in. asphaltic surfacing in each case. The asphalt penetration grade for the penetration macadam to cover concrete is kept low—from 40 to 60. All old concrete pavements are thoroughly cleaned and primed with not more than 0.1 gal per sq yd of rapid-cure cutbacks, emulsion, or road tar (RT-2 or RT-3) prior to applying flexible-type overlays. Leveling, to fill minor depressions, is usually done with a sand-asphalt mix. In this case it is expedient, economical, and generally adequate to rake out dirt-filled and poorly-bonded seals in the old concrete joints and thereafter fill them with the sand-asphalt mix prior to constructing the flexible over-lay. Sometimes the only overlay required is the asphaltic concrete surfacing.

In estimating the thickness of required flexible overlay on concrete pavement, the Burmister analysis for the three-layer system is followed. In this procedure, the modulus E_3 for the subgrade is computed from the k-modulus determined from previous evaluation studies, and E_2 for the concrete is assumed to be 4,000,000 lb per sq in. It is safe to assume E_1 for the bituminous overlay. A value of 100,000 lb per sq in. is conservative for penetration macadam or black base that is always covered with 3 in. of a superior type of asphaltic concrete surfacing. In terms of k, obtained by loading the earth under the concrete,

$$E_3 = 1.18\, r\, k\, F \ldots\ldots\ldots\ldots\ldots\ldots\ldots\ldots (4)$$

The allowable settlement, Δ(under the tire load in this case), is taken as 0.1 in. Greater deflections would involve cracking of the concrete. However, the allowable settlement in this case should be determined with reference to the actual deflection of the concrete slab, exclusive of the "plastico-viscous" yielding within the bituminous overlay.

When the subgrade support under concrete is firm to the extent that overloading of a "cracked out" piece of the slab does not push the piece downward into the earth, thus forming a local depression, it is observed that the asphalt surfacing covering an old concrete pavement tends to remain intact without either noticeable cracks or unevenness. This favorable condition may even continue when there is progressive cracking of the concrete through repeated overloading. The cost of maintaining joints in old concrete is eliminated by a well-designed and well-constructed bituminous overlay, although other maintenance costs, such as periodic seal coating, are made necessary.

DISCUSSION

R. HORONJEFF,[9] A. M. ASCE.—A concise presentation of the method used by the Navy for designing airfield pavements has been offered by the author. There is little that can added except some general comments.

Mr. Palmer asserts that the determination of the thicknesses of the individual components of a pavement is as important as the determination of the total pavement thickness. Most design procedures evaluate the total thickness of pavement required. The total load on a single or dual wheel is used as the criterion for design. It is important to note that, normally, the gross load on a wheel is more important than the contact pressure for determining the total thickness of pavement. However, contact pressure becomes increasingly important for the design of the layers near the surface of the pavement because of the high shearing stresses induced in the material. The stresses induced by aircraft operating during World War II did not normally exceed the shearing resistance of a well-compacted base and bituminous surfacing. Therefore, most pavement failures were attributed to the failure of the subgrade material because of the inadequate total thickness required to distribute the load to the subgrade. As tire pressures increase, more attention will have to be given to the design of those components near the surface. The Navy criterion of 50,000-lb load at a pressure of 150 lb per sq in. usually governs for the determination of the total pavement thickness, but the pressure of 250 lb per sq in. associated with a wheel load of 20,000 lb is probably the governing factor in the design of the bituminous wearing surface. In this connection, Mr. Palmer states that attention is being given to the design of asphalt mixes in order that the pavements may withstand the exceedingly high pressures imposed by some jet aircraft.

The author has emphasized that the Navy method of design is not dependent on formulas but on the results of trial pavement sections. The formulas are used only to estimate the required pavement thickness for the construction of trial sections. In order to use the formulas, however, it is necessary to determine the modulus E_2 of the subgrade by plate-bearing tests; this type of test is cumbersome. In many instances, an estimate of the thickness for the construction of trial pavements might be made by utilizing design methods which do not require plate loading. Approximate correlation between CBR-values and E-values have been presented by the author and could be used for this purpose.

The Navy procedure emphasizes wheel load and corresponding contact pressure as the governing criteria for determining pavement thickness. In many areas of the United States extreme frost conditions are encountered. In these areas a blanket of non-frost-susceptible materials—to insulate the subgrade completely or partly—is required. The thickness of such a blanket might be greater than the thickness of the pavement computed only on the basis of wheel load and tire pressure. In such cases the greater of the two thicknesses is adopted for design.

---

[9] Lecturer and Research Engr., Inst. of Transportation and Traffic Eng., Univ. of California, Berkeley, Calif.

Mr. Palmer asserts that one of the advantages of the procedure used by the Navy is that it permits an evaluation of the load-distributing characteristics of various types of base courses. It is further stated that the moduli of base courses vary from 25,000 lb per sq in. to 200,000 lb per sq in. The writer has attempted to illustrate the effect of variable strength base courses on the required thickness of pavement in Fig. 8. Fig. 8 shows, for example, that, for a subgrade whose E_2-modulus is 1,000 lb per sq in., an increase in the modulus of the base course (E_1) from 50 kips to 100 kips permits a decrease in pavement thickness of 16 in. for a single-wheel load of 50,000 lb at a contact pressure of 150 lb per sq in.

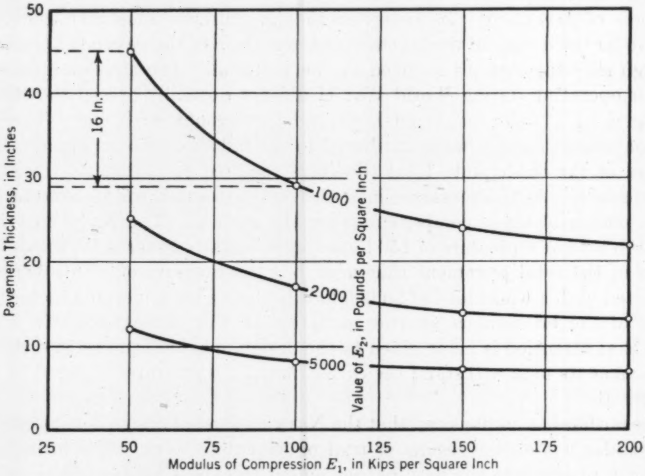

FIG. 8.—THE EFFECT OF LOAD-DISTRIBUTING CHARACTERISTICS OF BASE COURSES

From this relationship several observations can be made. As the moduli of the base course increase, large differences in moduli do not produce large changes in thickness. If the E_1-moduli are increased from 100 kips to 150 kips, the thickness is reduced by approximately 6 in. compared to the 16-in. reduction when the moduli are increased from 50 kips to 100 kips.

From Fig. 8 it can be seen that the distributing characteristic of asphaltic concrete surfacing laid on bases whose E_1-moduli are between 25 kips and 100 kips might be quite important, and the substitution of base course for asphaltic concrete in the trial sections may be questionable in these instances. It would be of interest to know the range of moduli of various asphaltic mixes, if such values were available.

L. A. Palmer.[10]—Mr. Horonjeff's discussion helps to clarify certain items. It is believed that Fig. 8 may tend to be somewhat misleading because the range of subgrade moduli (from 1 kip per sq in. to 5 kips per sq in.) does not represent the most unfavorable subgrade condition. Fig. 9 shows similar relationships for a very wide range of subgrade and pavement conditions. From Fig. 9 it can be seen that the total over-all pavement thickness, with E_1 equal to 200 kips per sq in., varies from 11 in. to 40 in. as E_2/E_1 varies from 1/100 to 1/500. This range of ratios represents a subgrade modulus range of from 400 lb per sq in. to 2,000 lb per sq in.—a rather normal range when fine-grained soils and high water tables are encountered.

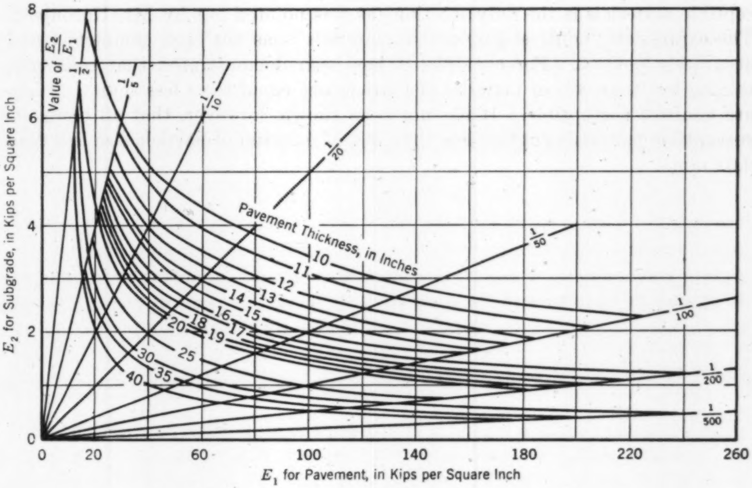

Fig. 9.—Thickness of Flexible Pavement for Tire Load of 50,000 Lb and Tire Pressure of 150 Lb per Sq In.

Fig. 9 shows that maximum information is obtained when the ratio E_2/E_1 (rather than the individual values) is considered. The curves in Fig. 8 show pavement thicknesses for a constant E_2 and a variable E_1. Fig. 9 shows variations in pavement thickness for a constant E_2 and a variable (E_2/E_1)-ratio. These variations are quite pronounced for E_1 exceeding 200 kips per sq. in. These theoretical relationships have been verified by actual plate loadings. There are great differences among load-spreading characteristics of different soils, subbases, and base courses. The mass of in-situ material that is affected in CBR tests is too small and too poorly representative to indicate these wide differences.

It is true that plate loading requires much time and effort, and it would be desirable, if possible, to use quicker and simpler test procedures. However, the economy realized by the use of procedures outlined by the writer has been substantial; it does not seem advisable to risk the loss of these savings until a very reliable correlation between these procedures and more simple ones has been established.

---

[10] Eng. Consultant, Soil Mechanics and Paving, Bureau of Yards and Docks, U. S. Dept. of the Navy, Wshington, D. C.

It is fortunate that granular subgrades exist at most air stations in the North Atlantic coastal areas. However, frost-heave problems have been encountered, to some extent, in these areas, and a blanket of nonfrost-susceptible materials is the only solution (as was pointed out by Mr. Horonjeff). The expression "nonfrost-susceptible materials" has not been completely and accurately defined. For example, it has been demonstrated that soils containing less than 3% of material of particle size equal to or less than 0.02 mm are nonfrost susceptible. It has not been shown, however, that all nonfrost-susceptible materials contain less than 3% of material of particle size less than 0.02 mm.

AMERICAN SOCIETY OF CIVIL ENGINEERS

Founded November 5, 1852

TRANSACTIONS

Paper No. 2685

NUMERICAL ANALYSIS OF CONTINUOUS FRAMES IN SPACE

By James Michalos,[1] M. ASCE

Synopsis

A numerical procedure, involving successive corrections, is presented for determining moments in continuous girders and frames whose members join at arbitrary angles in space. The component parts of these structures may be of constant or variable cross section.

Introduction

An analytical investigation of the structural behavior of a continuous building frame is usually made by neglecting the torsional resistance of girders at right angles to the particular bent under study. Usually, this simplification has not caused great concern among designers. The effect of these girders and the effect on these girders can be appraised, providing one knows—or can approximate—the relationship between angle of twist and torque for such members. An analysis that includes the torsional resistance of members at right angles to a frame can be made by application of the ordinary method of moment distribution[2] to all members framing into each joint. This has been explained elsewhere.[3,4,5]

Structures may be built whose members frame into each other at various angles in space rather than at right angles. It seems probable that requirements of clearance, space, and architecture will accelerate the use of structures having nonorthogonal framing, not only in building construction but also in connection with urban expressway construction. Simplifications are neither so obvious nor so acceptable as in those cases in which only relatively small moments are introduced into the joint by members at right angles to a bent.

NOTE.—Published, essentially as printed here, in September, 1953, as *Proceedings-Separate No. 261.* Positions and titles given are those in effect when the paper was received for publication.

[1] Prof. of Civ. Eng., Iowa State College, Ames, Iowa.

[2] "Analysis of Continuous Frames by Distributing Fixed-End Moments," by Hardy Cross, *Transactions*, ASCE, Vol. 97, 1932, p. 1.

[3] "Design of Reinforced Concrete in Torsion," by Paul Andersen, *ibid.*, Vol. 103, 1938, p. 1503.

[4] "Reinforced Concrete Structures," by Dean Peabody, Jr., John Wiley & Sons, Inc., New York, N. Y., 2d Ed., 1946, p. 419.

[5] "Analysis of Three-Dimensional Beam and Girder Framing," by Phil M. Ferguson, *Journal*, A.C.I., September, 1950, p. 61.

In this paper a numerical procedure is presented for analyzing girders and frames that are continuous in space. It is limited herein to straight members, but these may be of constant or variable section. Furthermore, the members may be oriented in space in any arbitrary fashion, both with respect to their longitudinal axes and to the principal axes of their cross sections. In general, the paper deals with structures in which there is no joint translation, or in which such movement is negligible, but the handling of cases in which translation occurs is outlined and illustrated by means of a numerical example.

The method involves successive corrections and can be carried to any desired precision. It is an extension into space of the philosophy of moment distribution, and it is based on a concept wherein all defined properties and moments are referred to a system of rectangular axes.

Expressions for the physical constants used in the numerical procedure are derived for the general case of a member in space subjected to moments about each of three rectangular axes, none of which is parallel to the longitudinal axis of the member or to the principal axes of the cross section. Simplified expressions are obtained for several special, or more usual, cases. The numerical procedure is then outlined, and examples are presented.

STIFFNESS AND CARRY-OVER FACTORS

When the method of moment distribution is used in the analysis of a frame lying in a plane, the unbalanced moment at each joint is distributed to all members framing into that joint. The portion of the unbalanced moment taken by each member is in proportion to its "stiffness," which is defined as the moment necessary to rotate one end of a member through a unit angle when the other end is fixed and there is no relative displacement of the ends of the member. But a distributed moment, resulting from rotation at one end of a member, induces moment at the other (fixed) end. This moment is determined by multiplying the distributed moment by a "carry-over factor," which is defined as the ratio of the moment induced at a fixed end to the moment producing rotation at the other end.

In the method presented in this paper, all moments are referred to a system of three rectangular axes, and a joint is considered free to rotate about one axis at a time. Consider a member that is not parallel to any of the three orthogonal planes associated with an arbitrarily chosen system of rectangular axes. If moment is applied about one of the reference axes at one end—and if rotation is prevented about the other two axes at that end and all three reference axes at the other end—carry-over moments will be induced at each end about the axes of no rotation. Stiffness factors will be required for rotation about each of the three reference axes. Five carry-over factors will be required for each of the three axes; two for the end at which rotation has occurred, and three for the opposite end. The adopted sign convention is shown in Fig. 1, wherein positive end moments and rotations are represented vectorially. The reader should use the right-hand rule for the sense of moments and rotations. Thus, if the thumb of the right hand is pointed in the direction of the arrow, the curved fingers indicate the direction of the moment or rotation.

Several views of a member supported at both ends are shown in Fig. 2. In addition to an arbitrarily chosen set of rectangular axes, x, y, and z, an auxiliary pair of axes, x_1 and z_1, is introduced, but only as an aid in the derivation of expressions for stiffness and carry-over. They have no role in the procedure itself. The z_1-axis is parallel to the xz-plane, and the x_1-axis forms a right angle with the longitudinal axis of the member, its projection in the xz-plane coinciding with the projection of the longitudinal axis of the member in the same plane. The axis 1–1 and the axis 2–2 are the principal axes of the cross section. The angles ψ and ζ are true angles, and α is the projection of an angle upon the xz-plane. The positive sense of these angles is indicated by arrows.

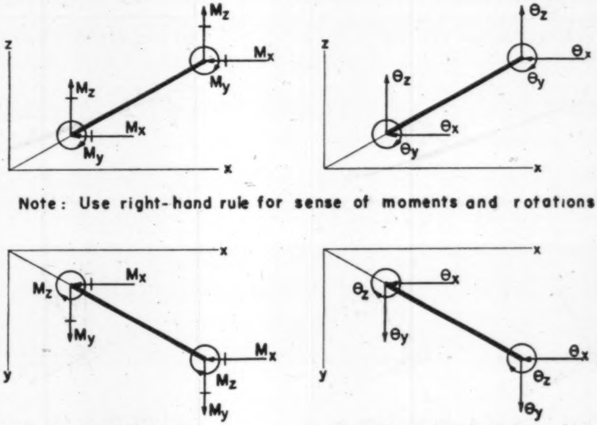

Note: Use right-hand rule for sense of moments and rotations

(a) MOMENTS (b) ROTATIONS

FIG. 1.—POSITIVE MOMENTS AND ROTATIONS AT THE ENDS OF A MEMBER

If a moment K_z applied about the z-axis at end A of the member in Fig. 2(a) produces a unit rotation about the same axis, while no rotation is allowed to take place about the x-axis and the y-axis at end A or about any of the axes at end B, the moments necessary to prevent rotation about these axes can be written as shown in Fig. 2(a). The moment K_z is the defined stiffness about the z-axis at end A, and C_{xz} and C_{yz} are carry-over factors to the x-axis and the y-axis, respectively, at the same end, whereas C'_{zz}, C'_{xz}, and C'_{yz} are carry-over factors to the far end, B. The contributions of the moments K_z, C_{xz}, K_z, and $C_{yz} K_z$ to torsional moment and to bending moments about principal axes at end A, as shown in Figs. 2(b) and 2(c), can be obtained as follows:

$$\left.\begin{aligned} M_t &= K_z \sin\alpha \sin\zeta - C_{xz} K_z \cos\alpha \sin\zeta + C_{yz} K_z \cos\zeta \\ M_{n1} &= K_z \cos\alpha \cos\psi - K_z \sin\alpha \cos\zeta \sin\psi + C_{xz} K_z \sin\alpha \cos\psi \\ &\quad + C_{xz} K_z \cos\alpha \cos\zeta \sin\psi + C_{yz} K_z \sin\zeta \sin\psi \\ M_{n2} &= K_z \cos\alpha \sin\psi + K_z \sin\alpha \cos\zeta \cos\psi + C_{xz} K_z \sin\alpha \sin\psi \\ &\quad - C_{xz} K_z \cos\alpha \cos\zeta \cos\psi - C_{yz} K_z \sin\zeta \cos\psi \end{aligned}\right\} \quad \ldots (1)$$

The bending moments induced about the principal axes at B are $C^{1-1}_{AB}\,M_{n1}$ and $C^{2-2}_{AB}\,M_{n2}$, as shown in Fig. 2(*d*). The terms C^{1-1}_{AB} and C^{2-2}_{AB} are carry-over factors from A to B, with respect to axis 1–1 and axis 2–2, respectively. The value of these carry-over factors is 0.5 for prismatic members. Values for nonprismatic members can be obtained from available charts or tables.[6]

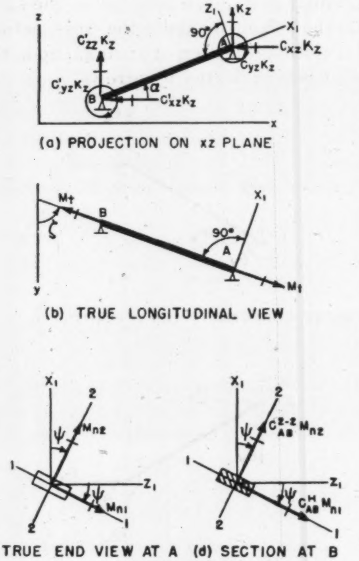
z
Z₁
K_z
90°
X₁
C′_zz K_z
C_xz K_z
C_yz K_z
C′_yz K_z
α
B
A
C′_xz K_z
x
Mt
B
X₁
90°
A
ζ
y
Mt
X₁
2
ψ
Mn2
1
Z₁
ψ
Mn1
2
1
X₁
2
C^{2-2}_{AB} Mn2
ψ
1
Z₁
ψ
C^{1-1}_{AB} Mn1
2
1

(a) PROJECTION ON xz PLANE

(b) TRUE LONGITUDINAL VIEW

(c) TRUE END VIEW AT A (d) SECTION AT B

FIG. 2.—MOMENT RELATIONSHIPS

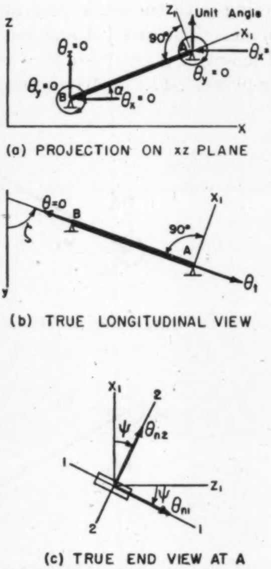
Z
Z₁
Unit Angle
90°
X₁
θ_z = 0
θ_x = 0
θ_y = 0
θ_y = 0
B
A
α
θ_x = 0
X
θ=0
B
X₁
90°
A
ζ
y
θ₁
X₁
2
ψ
θn2
1
Z₁
ψ
θn1
2
1

(a) PROJECTION ON xz PLANE

(b) TRUE LONGITUDINAL VIEW

(c) TRUE END VIEW AT A

FIG. 3.—ROTATION RELATIONSHIPS

In Fig. 3(*a*) the end A of the member has been rotated through a unit angle about the *z*-axis only. The contributions of the unit angle to twist and to rotation about principal axes at end A, as shown in Figs. 3(*b*) and 3(*c*), can be obtained as follows:

$$\left.\begin{aligned}\theta_t &= \sin\alpha\sin\zeta\\ \theta_{n1} &= \cos\alpha\cos\psi - \sin\alpha\cos\zeta\sin\psi\\ \theta_{n2} &= \cos\alpha\sin\psi + \sin\alpha\cos\zeta\cos\psi\end{aligned}\right\}\ldots\ldots\ldots\ldots\ldots(2)$$

This angle of twist and these rotation angles can be related to the moments of Eq. 1 by means of stiffnesses k_{n1}, k_{n2}, and k_t. The terms k_{n1} and k_{n2} represent the bending stiffnesses associated with moment distribution. Their values, for prismatic members, are $\frac{4\,E\,I_1}{L}$ and $\frac{4\,E\,I_2}{L}$, respectively. In these expressions, E is the modulus of elasticity in tension and compression, L is the length of the member, and I_1 and I_2 are the moments of inertia about axis 1–1 and axis 2–2, respectively. For nonprismatic members, values of k_{n1} and k_{n2} are available elsewhere.[6] The term k_t represents the moment necessary to twist one end of a member through a unit angle when the other end is fixed. Its value for prismatic members is $\frac{G\,J}{L}$, G being the modulus of elasticity in shear and J being a torsion factor, such that $G\,J$ represents the torque necessary to twist a member through a unit angle per unit length. The value of k_t for nonprismatic members can be determined through the use of the shear and torsion analogy.[7]

---

[6] "Handbook of Frame Constants," Portland Cement Assn., Chicago, Ill., 1947.

Three equations, relating end moments and end rotations about the longitudinal axis and the principal axes, can be written as follows:

$$\frac{1}{k_t}\left(\sin\alpha\sin\zeta\,K_z - \cos\alpha\sin\zeta\,C_{xz}\,K_z + \cos\zeta\,C_{yz}\,K_z\right) = \sin\alpha\sin\zeta \;..\;(3a)$$

$$\begin{aligned}&\frac{1}{k_{n1}}\left[(\cos\alpha\cos\psi - \sin\alpha\cos\zeta\sin\psi)\,K_z + (\sin\alpha\cos\psi + \cos\alpha\cos\zeta\right.\\&\left.\times\sin\psi)\,C_{xz}\,K_z + (\sin\zeta\sin\psi)\,C_{yz}\,K_z\right] = \cos\alpha\cos\psi - \sin\alpha\cos\zeta\sin\psi \;..\;(3b)\end{aligned}$$

$$\begin{aligned}&\frac{1}{k_{n2}}\left[(\cos\alpha\sin\psi + \sin\alpha\cos\zeta\cos\psi)\,K_z + (\sin\alpha\sin\psi\right.\\&\qquad\left. - \cos\alpha\cos\zeta\cos\psi)\,C_{xz}\,K_z - (\sin\zeta\cos\psi)\,C_{yz}\,K_z\right]\\&\qquad\qquad = \cos\alpha\sin\psi + \sin\alpha\cos\zeta\cos\psi \;..\;(3c)\end{aligned}$$

In an identical manner, similar groups of equations are obtained as the result of applying a moment K_x about the x-axis and a moment K_y about the y-axis in Fig. 2(*a*).

From the application of K_x—

$$\frac{1}{k_t}\left(\cos\alpha\sin\zeta\,K_x - \sin\alpha\sin\zeta\,C_{zx}\,K_x - \cos\zeta\,C_{yx}\,K_x\right) = \cos\alpha\sin\zeta \;..\;(4a)$$

$$\begin{aligned}&\frac{1}{k_{n1}}\left[(\sin\alpha\cos\psi + \cos\alpha\sin\psi\cos\zeta)\,K_x + (\cos\alpha\cos\psi\right.\\&\qquad\left. - \sin\alpha\sin\psi\cos\zeta)\,C_{zx}\,K_x + \sin\psi\sin\zeta\,C_{yx}\,K_x\right]\\&\qquad\qquad = \sin\alpha\cos\psi + \cos\alpha\sin\psi\cos\zeta \;..\;(4b)\end{aligned}$$

and

$$\begin{aligned}&\frac{1}{k_{n2}}\left[(\sin\alpha\sin\psi - \cos\alpha\cos\psi\cos\zeta)\,K_x + (\cos\alpha\sin\psi\right.\\&\qquad\left. + \sin\alpha\cos\psi\cos\zeta)\,C_{zx}\,K_x - \cos\psi\sin\zeta\,C_{yx}\,K_x\right]\\&\qquad\qquad = \sin\alpha\sin\psi - \cos\alpha\cos\psi\cos\zeta \;..\;(4c)\end{aligned}$$

From the application of K_y—

$$\frac{1}{k_t}\left(\cos\zeta\,K_y + \sin\alpha\sin\zeta\,C_{zy}\,K_y - \cos\alpha\sin\zeta\,C_{xy}\,K_y\right) = \cos\zeta \;....\;(5a)$$

$$\begin{aligned}&\frac{1}{k_{n1}}\left[\sin\psi\sin\zeta\,K_y + (\cos\alpha\cos\psi - \sin\alpha\sin\psi\cos\zeta)\,C_{zy}\,K_y\right.\\&\qquad\left. + (\sin\alpha\cos\psi + \cos\alpha\sin\psi\cos\zeta)\,C_{xy}\,K_y\right] = \sin\psi\sin\zeta \;..\;(5b)\end{aligned}$$

---

[7] "Laterally Loaded Plane Structures and Structures Curved in Space," by Frank Baron and James P. Michalos, *Transactions*, ASCE, Vol. 117, 1952, p. 279.

and

$$\frac{1}{k_{n2}}[-\cos\psi\sin\zeta\, K_y + (\cos\alpha\sin\psi + \sin\alpha\cos\psi\cos\zeta)\, C_{xy}\, K_y + (\sin\alpha\sin\psi - \cos\alpha\cos\psi\cos\zeta)\, C_{zy}\, K_y] = -\cos\psi\sin\zeta \quad\text{(5c)}$$

From the solution of the three groups of simultaneous equations (Eqs. 3, 4, and 5) expressions for the three stiffnesses (K_z, K_y, and K_x) and the six near-end carry-over factors (C_{xz}, C_{yz}, C_{yx}, C_{zx}, C_{zy}, and C_{xy}) were obtained and are shown at the top of Fig. 4. The coefficients, N, have been introduced for convenience, and they are defined in Fig. 5. These coefficients are functions of the angles only, and some of the expressions are greatly simplified—as shown in the bottom half of Fig. 5—in the usual case in which the angle ψ is equal to zero.

$$K_z = k_t N_4 - k_{n1}(N_6 - N_7) + k_{n2}(N_5 + N_8) \qquad C_{xz} = \frac{-k_t N_1 + k_{n1}(N_2 + N_{22}) - k_{n2}(N_2 - N_3)}{K_z} \qquad C_{zx} = C_{xz}\frac{K_z}{K_x}$$

$$K_x = k_t N_{12} + k_{n1}(N_5 + N_{14}) - k_{n2}(N_6 - N_{13}) \qquad C_{yz} = \frac{k_t N_9 + k_{n1}(N_9 - N_{11}) - k_{n2}(N_9 + N_{10})}{K_z} \qquad C_{zy} = C_{yz}\frac{K_z}{K_y}$$

$$K_y = k_t N_{19} + k_{n1} N_{21} + k_{n2} N_{20} \qquad C_{yx} = \frac{-k_t N_{15} + k_{n1}(N_{17} + N_{16}) + k_{n2}(N_{16} - N_{17})}{K_x} \qquad C_{xy} = C_{yx}\frac{K_x}{K_y}$$

$$C'_{xz} = N_1 - C_{xz}N_{12} + C_{yz}N_{15} + (C^{1-1}_{AB} - C^{2-2}_{AB})(N_2 + C_{xz}N_5 + C_{yz}N_{17}) + C^{1-1}_{AB}(N_{22} + C_{xz}N_{14} + C_{yz}N_{18}) + C^{2-2}_{AB}(N_3 + C_{xz}N_{13} + C_{yz}N_{16})$$

$$C'_{zz} = -N_4 + C_{xz}N_1 - C_{yz}N_8 + (C^{1-1}_{AB} - C^{2-2}_{AB})(-N_5 + C_{xz}N_2 + C_{yz}N_9) + C^{1-1}_{AB}(N_7 + C_{xz}N_{22} - C_{yz}N_{11}) + C^{2-2}_{AB}(N_8 + C_{xz}N_3 + C_{yz}N_{10})$$

$$C'_{yz} = -N_9 + C_{xz}N_{15} - C_{yz}N_{19} + (C^{1-1}_{AB} - C^{2-2}_{AB})(N_9 + C_{xz}N_{17}) + C^{1-1}_{AB}(-N_{11} + C_{xz}N_{18} + C_{yz}N_{21}) + C^{2-2}_{AB}(-N_{10} + C_{xz}N_{16} + C_{yz}N_{20})$$

$$C'_{xx} = -N_{12} + C_{zx}N_1 + C_{yx}N_{15} + (C^{1-1}_{AB} - C^{2-2}_{AB})(N_5 + C_{zx}N_2 + C_{yx}N_{17}) + C^{1-1}_{AB}(N_{14} + C_{zx}N_{22} - C_{yx}N_{18}) + C^{2-2}_{AB}(N_{13} + C_{zx}N_3 + C_{yx}N_{16})$$

$$C'_{zx} = N_1 - C_{zx}N_4 - C_{yx}N_8 + (C^{1-1}_{AB} - C^{2-2}_{AB})(N_2 - C_{zx}N_5 + C_{yx}N_9) + C^{1-1}_{AB}(N_{22} + C_{zx}N_7 - C_{yx}N_{11}) + C^{2-2}_{AB}(N_3 + C_{zx}N_8 - C_{yx}N_{10})$$

$$C'_{yx} = N_{15} - C_{zx}N_8 - C_{yx}N_{19} + (C^{1-1}_{AB} - C^{2-2}_{AB})(N_{17} + C_{zx}N_9) + C^{1-1}_{AB}(N_{18} - C_{zx}N_{11} + C_{yx}N_{21}) + C^{2-2}_{AB}(N_{16} - C_{zx}N_{10} + C_{yx}N_{20})$$

$$C'_{xy} = N_{15} - C_{xy}N_{12} + C_{zy}N_1 + (C^{1-1}_{AB} - C^{2-2}_{AB})(N_{17} + C_{xy}N_5 + C_{zy}N_2) + C^{1-1}_{AB}(N_{18} + C_{xy}N_{14} + C_{zy}N_{22}) + C^{2-2}_{AB}(N_{16} + C_{xy}N_{13} + C_{zy}N_3)$$

$$C'_{zy} = -N_8 + C_{xy}N_1 - C_{zy}N_4 + (C^{1-1}_{AB} - C^{2-2}_{AB})(N_9 + C_{xy}N_2 - C_{zy}N_5) + C^{1-1}_{AB}(-N_{11} + C_{xy}N_{22} + C_{zy}N_7) + C^{2-2}_{AB}(-N_{10} + C_{xy}N_3 + C_{zy}N_8)$$

$$C'_{yy} = -N_{19} + C_{xy}N_{15} - C_{zy}N_9 + (C^{1-1}_{AB} - C^{2-2}_{AB})(C_{xy}N_{17} + C_{zy}N_9) + C^{1-1}_{AB}(N_{21} + C_{xy}N_{18} - C_{zy}N_{11}) + C^{2-2}_{AB}(N_{20} + C_{xy}N_{16} - C_{zy}N_{10})$$

FIG. 4.—GENERAL EXPRESSIONS FOR STIFFNESS AND CARRY-OVER FACTORS

The carry-over moments at end B of Fig. 2(*a*) can be written in terms of the torsional and bending moments at the same end as follows:

$$\left.\begin{aligned}
C'_{xz}M_z &= -M_t\sin\alpha\sin\zeta + C^{1-1}{}_{AB}M_{n1}(\cos\psi\cos\alpha - \sin\psi\cos\zeta \\
&\quad \times \sin\alpha) + C^{2-2}{}_{AB}M_{n2}(\sin\psi\cos\alpha + \cos\psi\cos\zeta\sin\alpha) \\
C'_{yz}M_z &= -M_t\cos\zeta + C^{1-1}{}_{AB}M_{n1}\sin\psi\sin\zeta - C^{2-2}{}_{AB}M_{n2}\cos\psi\sin\zeta \\
C'_{zz}M_z &= M_t\sin\zeta\cos\alpha + C^{1-1}{}_{AB}M_{n1}(\cos\psi\sin\alpha + \sin\psi\cos\zeta \\
&\quad \times \cos\alpha + C^{2-2}{}_{AB}M_{n2}(\sin\psi\sin\alpha - \cos\psi\cos\zeta\cos\alpha)
\end{aligned}\right\}\quad\text{(6)}$$

If the right-hand sides of Eqs. 1 are substituted for M_t, M_{n1}, and M_{n2} in Eqs. 6, expressions for the far-end carry-over factors can be obtained in terms of the two carry-over factors at A and the two carry-over factors that are re-

For the general case of a member in space:

$N_1 = \sin\alpha\cos\alpha\sin^2\zeta$

$N_2 = (\cos^2\alpha - \sin^2\alpha)\sin\psi\cos\psi\cos\zeta$

$N_3 = \sin\alpha\cos\alpha(\sin^2\psi - \cos^2\psi\cos^2\zeta)$

$N_4 = \sin^2\alpha\sin^2\zeta$

$N_5 = 2\sin\alpha\cos\alpha\sin\psi\cos\psi\cos\zeta$

$N_6 = \sin^2\alpha\cos^2\psi\cos^2\zeta + \cos^2\alpha\sin^2\psi$

$N_7 = \sin^2\alpha\sin^2\psi\cos^2\zeta + \cos^2\alpha\cos^2\psi$

$N_8 = \sin\alpha\sin\zeta\cos\zeta$

$N_9 = \cos\alpha\sin\psi\cos\psi\sin\zeta$

$N_{10} = \sin\alpha\cos^2\psi\sin\zeta\cos\zeta$

$N_{11} = \sin\alpha\sin^2\psi\sin\zeta\cos\zeta$

$N_{12} = \cos^2\alpha\sin^2\zeta$

$N_{13} = \cos^2\alpha\cos^2\psi\cos^2\zeta + \sin^2\alpha\sin^2\psi$

$N_{14} = \cos^2\alpha\sin^2\psi\cos^2\zeta + \sin^2\alpha\cos^2\psi$

$N_{15} = \cos\alpha\sin\zeta\cos\zeta$

$N_{16} = \cos\alpha\cos^2\psi\sin\zeta\cos\zeta$

$N_{17} = \sin\alpha\sin\psi\cos\psi\sin\zeta$

$N_{18} = \cos\alpha\sin^2\psi\sin\zeta\cos\zeta$

$N_{19} = \cos^2\zeta$

$N_{20} = \cos^2\psi\sin^2\zeta$

$N_{21} = \sin^2\psi\sin^2\zeta$

$N_{22} = \sin\alpha\cos\alpha(\cos^2\psi - \sin^2\psi\cos^2\zeta)$

When $\psi =$.

$N_2 = 0$

$N_3 = -\sin\alpha\cos\alpha\cos^2\zeta$

$N_5 = 0$

$N_6 = \sin^2\alpha\cos^2\zeta$

$N_7 = \cos^2\alpha$

$N_9 = 0$

$N_{10} = \sin\alpha\sin\zeta\cos\zeta$

$N_{11} = 0$

$N_{13} = \cos^2\alpha\cos^2\zeta$

$N_{14} = \sin^2\alpha$

$N_{16} = \cos\alpha\sin\zeta\cos\zeta$

$N_{17} = 0$

$N_{18} = 0$

$N_{20} = \sin^2\zeta$

$N_{21} = 0$

$N_{22} = \sin\alpha\cos\alpha$

FIG. 5.—COEFFICIENTS FOR USE IN THE EXPRESSIONS OF FIG. 4

When: $\zeta = 90°$ and
$\psi = 0$:-

$K_z = k_t\sin^2\alpha + k_{n1}\cos^2\alpha$

$K_x = k_t\cos^2\alpha + k_{n1}\sin^2\alpha$

$K_y = k_{n2}$

$$C_{xz} = \frac{(k_{n1} - k_t)\sin\alpha\cos\alpha}{K_z}$$

$$C_{zx} = \frac{(k_{n1} - k_t)\sin\alpha\cos\alpha}{K_x}$$

$C_{yz} = 0$; $C_{yx} = 0$

$C_{zy} = 0$; $C_{xy} = 0$

$$\begin{aligned} C'_{xz} = {} & (C^{1-1}_{AB} + 1)\sin\alpha\cos\alpha \\ & + C_{xz}(C^{1-1}_{AB}\sin^2\alpha - \cos^2\alpha) \end{aligned}$$

$$\begin{aligned} C'_{zz} = {} & C^{1-1}_{AB}\cos^2\alpha - \sin^2\alpha \\ & + C_{xz}\sin\alpha\cos\alpha(C^{1-1}_{AB} + 1) \end{aligned}$$

$$\begin{aligned} C'_{xx} = {} & C^{1-1}_{AB}\sin^2\alpha - \cos^2\alpha \\ & + C_{zx}\sin\alpha\cos\alpha(C^{1-1}_{AB} + 1) \end{aligned}$$

$$\begin{aligned} C'_{zx} = {} & (C^{1-1}_{AB} + 1)\sin\alpha\cos\alpha \\ & + C_{zx}(C^{1-1}_{AB}\cos^2\alpha - \sin^2\alpha) \end{aligned}$$

$C'_{yz} = 0$; $C'_{yx} = 0$

$C'_{zy} = 0$; $C'_{xy} = 0$

$C'_{yy} = C^{2-2}_{AB}$

When: $\zeta = 0$ $(\therefore \psi = 0)$:-

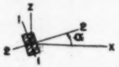

$K_z = k_{n2}\sin^2\alpha + k_{n1}\cos^2\alpha$

$K_x = k_{n2}\cos^2\alpha + k_{n1}\sin^2\alpha$

$K_y = k_t$

$$C_{xz} = \frac{(k_{n1} - k_{n2})\sin\alpha\cos\alpha}{K_z}$$

$$C_{zx} = \frac{(k_{n1} - k_{n2})\sin\alpha\cos\alpha}{K_x}$$

$C_{yz} = 0$; $C_{yx} = 0$

$C_{zy} = 0$; $C_{xy} = 0$

$$\begin{aligned} C'_{xz} = {} & (C^{1-1}_{AB} - C^{2-2}_{AB})\sin\alpha\cos\alpha \\ & + C_{xz}(C^{1-1}_{AB}\sin^2\alpha + C^{2-2}_{AB}\cos^2\alpha) \end{aligned}$$

$$\begin{aligned} C'_{zz} = {} & (C^{1-1}_{AB} - C^{2-2}_{AB})C_{xz}\sin\alpha\cos\alpha \\ & + C^{1-1}_{AB}\cos^2\alpha + C^{2-2}_{AB}\sin^2\alpha \end{aligned}$$

$$\begin{aligned} C'_{xx} = {} & (C^{1-1}_{AB} - C^{2-2}_{AB})C_{zx}\sin\alpha\cos\alpha \\ & + C^{1-1}_{AB}\sin^2\alpha + C^{2-2}_{AB}\cos^2\alpha \end{aligned}$$

$$\begin{aligned} C'_{zx} = {} & (C^{1-1}_{AB} - C^{2-2}_{AB})\sin\alpha\cos\alpha \\ & + C_{zx}(C^{1-1}_{AB}\cos^2\alpha + C^{2-2}_{AB}\sin^2\alpha) \end{aligned}$$

$C'_{yz} = 0$; $C'_{yx} = 0$

$C'_{zy} = 0$; $C'_{xy} = 0$

$C'_{yy} = -1$

Note: For prismatic members, $C^{1-1} = C^{2-2} = 0.5$

FIG. 6.—SIMPLIFIED EXPRESSIONS FOR USE IN COMMON CASES

lated to the principal axes. The resulting expressions for C'_{xz}, C'_{zz}, and C'_{yz} are given in Fig. 4, in terms of coefficients, N, which are defined in Fig. 5.

Similarly, the application of a moment K_x, instead of K_z, at A in Fig. 2(*a*) would lead to expressions for the three far-end carry-over factors C'_{xx}, C'_{zx}, and C'_{yx}, and the application of a moment K_y at A would lead to expressions for C'_{xy}, C'_{zy}, and C'_{yy}. The expressions for these carry-over factors are included in Fig. 5. In each case, the first subscript indicates the axis to which moment is carried, and the second subscript indicates the axis about which moment is applied.

The expressions for stiffness and for carry-over factors, as shown in Fig. 4, are for the general case. However, for the majority of cases which may be encountered in practice, the expressions are much simplified, as shown in the bottom half of Fig. 5 and in Fig. 6.

THE NUMERICAL PROCEDURE

Before the numerical procedure can be applied, it is necessary to compute the stiffnesses and the carry-over factors. In the great majority of cases, ψ is equal to zero, and the expressions are greatly simplified. If, in addition, ζ is equal to 90° or to zero, the expressions in Fig. 6 are directly applicable.

Only relative values of k_{n1}, k_{n2}, and k_t are necessary, and for prismatic members both $C^{1-1}{}_{AB}$ and $C^{2-2}{}_{AB}$ are equal to 0.5, thus further simplifying the expressions for carry-over factors. In dealing with prismatic members, or with symmetrically haunched members, the required stiffness values are the same for each end, but otherwise two sets of stiffness values must be determined for each member, one set for each end.

The application of the numerical procedure can be outlined in the following steps:

1. The fixed-end moments, about the principal axes, are computed for each end of all loaded members.
2. These moments are resolved to fixed-end moments about the rectangular axes of the selected reference system. In general, this will result in unbalanced moments about the reference axes at each joint.
3. At each joint, the unbalanced moment about each axis is distributed, in turn, to all members framing into the joint in proportion to their relative stiffnesses about each of the axes. The distribution at each joint is algebraic, and signs are determined automatically.
4. Each distributed moment is multiplied (with due regard to signs) by the appropriate carry-over factors in turn, and the resulting moments are carried over to the proper axes at both the near and far ends.
5. Steps 3 and 4 are repeated until a desired convergence is reached.
6. All values following Step 2 are totalled algebraically to obtain the end moments about the reference axes.
7. The values obtained in Step 6 are resolved into bending moments about the principal axes and into torsional moments.

The girder shown in Fig. 7 is fixed at ends A and C and is continuous over support B. Members AB and BC, both of which lie in the xz-plane, are identical in length and cross section, with relative bending stiffness about axis 1–1 equal to ten, and relative torsional stiffness equal to one. Because the load is applied normal to the xz-plane and the angle ψ is equal to zero, there will be no moments about the y-axis. As a result of this, it is not necessary to determine stiffnesses or carry-over factors associated with that axis. The required constants are readily determined from the simplified expressions ($\psi = 0; \zeta = 90°$) in Fig. 6. Ends A and C are fixed, and there will be no carry-over from A to B or from C to B.

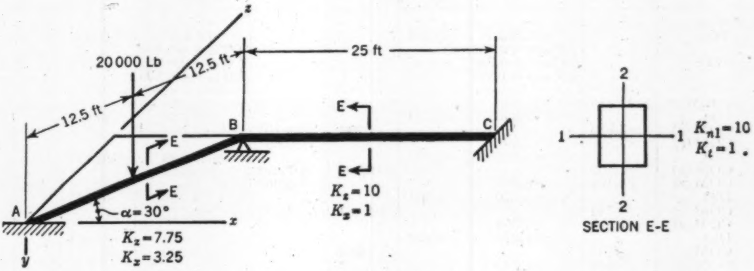

FIG. 7.—CONTINUOUS BEAM

It can be seen by inspection that, for member BC, K_z is equal to k_{n1}, and K_x is equal to k_t. Likewise, the carry-over factors from B to C are C_{xz} (equal to -1.0) and C'_{xz} (equal to $+0.5$). For convenience in distributing unbalanced moments, the ratio of the stiffness of each member to the sums of the stiffnesses of the members at each joint, for a particular axis, is entered in Table 1 as a distribution factor. For example, the distribution factors for moments about the x-axis at joint B are $\dfrac{3.25}{3.25 + 1} = 0.765$ for member BA, and $\dfrac{1}{3.25 + 1}$ $= 0.235$ for member BC.

As previously mentioned, a prime symbol used in connection with a carry-over factor indicates carry-over to the far end, whereas the absence of such a mark indicates carry-over to an axis at the end about which the distribution was made. That is, a moment distributed to an x-axis is multiplied by C_{xz} to obtain the moment induced about the z-axis at the same end of the member, but the distributed moment is multiplied by C'_{xz} to obtain the induced moment about the z-axis at the opposite end of the member.

To determine the fixed-end moments about the x-axis and the z-axis, at both joint A and joint B, one must first obtain the fixed-end moments about axis 1–1. These values are equal to $(\frac{1}{8})$ (20,000) 25, or 62,500 lb-ft, at each end. The fixed-end moments about the reference axes are 62,500 sin 30° = 31,250 lb-ft about the x-axis, and 62,500 cos 30° = 54,125 lb-ft about the z-axis. These values, with appropriate signs, are entered in Table 1.

The tabulated fixed-end moments create a statical unbalance at joint B, and the unbalance about each axis is distributed to the two members at B in

TABLE 1.—ANALYSIS OF THE CONTINUOUS BEAM OF FIG. 7.

DESCRIPTION[a]	MOMENTS ABOUT THE x-AXIS, IN POUND-FEET				MOMENTS ABOUT THE z-AXIS, IN POUND-FEET			
	Joint A	Joint B		Joint C	Joint A	Joint B		Joint C
	Member AB	Member BA	Member BC	Member CB	Member AB	Member BA	Member BC	Member CB
Factor:								
Dist.		+0.765	+0.235			+0.437	+0.563	
C.O.		$C'_{xx} = +0.154$ $C'_{zx} = +0.799$ $C_{zx} = +1.199$	$C'_{xx} = -1.0$			$C'_{zz} = +0.452$ $C'_{xz} = +0.335$ $C_{xz} = +0.503$	$C'_{zz} = +0.5$	
F.E.M.	−31,250	+31,250			−54,125	+54,125		
Dist.		−23,906	−7,344			−23,653	−30,472	
COM (x)	−3,682			+7,344	−19,101	−28,663		
COM (z)	−7,924	−11,897			−10,691			−15,236
Dist.		+9,101	+2,796			+12,526	+16,137	
COM (x)	+1,402			−2,796	+7,272	+10,912		
COM (z)	+4,196	+6,301			+5,662			+8,068
Dist.		−4,820	−1,481			−4,769	−6,143	
COM (x)	−742			+1,481	−3,851	−5,779		
COM (z)	−1,598	−2,399			−2,156			−3,072
Dist.		+1,835	+564			+2,525	+3,254	
COM (x)	+283			−564	+1,466	+2,200		
COM (z)	+846	+1,270			+1,141			+1,627
Dist.		−972	−298			−961	−1,239	
COM (x)	−150			+298	−777	−1,165		
COM (z)	−322	−483			−434			−620
Dist.		+369	+114			+509	+656	
COM (x)	+57			−114	+295	+442		
COM (z)	+171	+256			+230			+328
Dist.		−196	−60			−193	−249	
COM (x)	−30			+60	−157	−235		
COM (z)	−64	−97			−87			−124
Dist.		+74	+23			+103	+132	
COM (x)	+11			−23	+59	+89		
COM (z)	+34	+52			+46			+66
Dist.		−40	−12			−39	−50	
COM (x)	−6			+12	−32	−48		
COM (z)	−13	−20			−18			−25
Dist.		+15	+5			+21	+27	
Total	−38,781	+5,693	−5,693	+5,698	−75,258	+17,947	−17,947	−8,988

[a] Abbreviations: Dist. = Distribution; C.O. = Carry-Over; F.E.M. = Fixed-End Moment; COM (x) = Carry-Over Moment from the x-Axis; COM (z) = Carry-Over Moment from the z-Axis.

proportion to their relative stiffnesses about the corresponding axes. For example, the unbalanced moment of +31,250 lb-ft at joint B is distributed so that 23,906 lb-ft are resisted by member BA and 7,344 lb-ft are resisted by member BC. The distributed moments are entered in Table 1 with signs opposite to that of the unbalanced moment, and the sum of +31,250 lb-ft and −23,906 lb-ft is in balance with −7,344 lb-ft. Since joint A is fixed, there can be no unbalance at that joint; therefore, no moment is distributed to member AB at that end.

The carry-over moments (COM) are obtained by multiplying the distributed moments by the appropriate carry-over factors. Carry-over moments induced by a moment distributed to the x-axis are placed opposite the designation COM (x), and carry-over moments induced by a moment distributed to the z-axis are placed opposite the designation COM (z). To illustrate, the carry-over moments induced by the distributed moment of −23,906 lb-ft are the following: At the far end, joint A, the carry-over moments are COM(x) = − 23,906 (+0.154) = − 3,682 lb-ft about the x-axis, and COM (x) = − 23,906 (+0.799)

$= -19{,}101$ lb-ft about the z-axis; at the near end, joint B, COM (x) $= -23{,}906$ $(+1.199) = -28{,}663$ lb-ft about the z-axis. The distributed moment of $-7{,}344$ lb-ft induces a moment at the far end, C, whose value is COM (x) $= -7{,}344\ (-1.0) = +7{,}344$ lb-ft about the x-axis.

The carry-over moments resulting from the moments distributed to the z-axis at joint B are obtained in a similar manner, and are recorded opposite the designation COM (z).

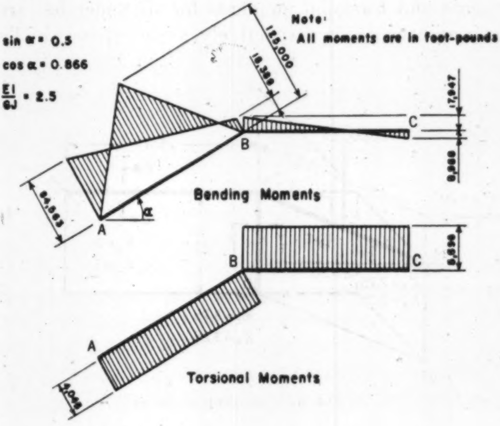

(a) Moment Diagrams Plotted Along the Structure

ΣF_x

+(125,000)(25)(0.5)(0.5) = +781,250
-(84,563)(25)(0.5)(0.5) = -528,519
-(18,388)(25)(0.5)(0.5) = -114,925
+(4,045)(25)(2.5)(0.866) = +218,936
-(5,698)(25)(2.5) = -356,125
+617

ΣF_z

-(125,000)(25)(0.5)(0.866) = -1,353,125
+(84,563)(25)(0.5)(0.866) = 915,394
+(18,388)(25)(0.5)(0.866) = 199,090
+(4,045)(25)(2.5)(0.5) = 126,406
+(17,947)(25)(0.5) = 224,337
-(8,988)(25)(0.5) = -112,350
-248

ΣM_y (about c)

-(8,988)(25)(0.5)(8.33) = -935,875
+(17,947)(25)(0.5)(16.67) = 3,739,706
+(18,388)(25)(0.5)(29.98) = 6,890,903
-(125,000)(25)(0.5)(34.15) = -53,359,375
+(84,563)(25)(0.5)(38.32) = 40,505,677
+(4,045)(25)(2.5)(12.5) = 3,160,156
1,192

(b) Numerical Check

FIG. 8.—MOMENTS AND NUMERICAL CHECK FOR THE CONTINUOUS BEAM OF FIG. 7

At each joint, the new unbalance resulting from moments carried over is distributed in proportion to the relative stiffnesses, and the resulting values are entered in the tabulation opposite the designation "Dist." No distribution is made at the fixed ends. The procedure of successively carrying over and distributing is continued to a desired degree of convergence, and the totals are obtained. In this example the process has been terminated after a distribution. It is a matter of academic interest that the moments balance at joint B, but the moments about the x-axis at the ends of member BC are not exactly equal

(5,693 lb-ft as against 5,698 lb-ft) as torsional moments should be. If the last distribution is omitted, the latter moments will balance exactly, but the moments at joint B will not.

Diagrams of bending moments and torsional moments are shown in Fig. 8(*a*). The bending moment diagram for AB was drawn by superimposing moments resulting from continuity on the moment diagram for beam AB considered as simply supported. Since member BC is parallel to the x-axis, the bending moments and torsional moments for that member are the moments about the z-axis and the x-axis, respectively, as determined in Table 1. To ob-

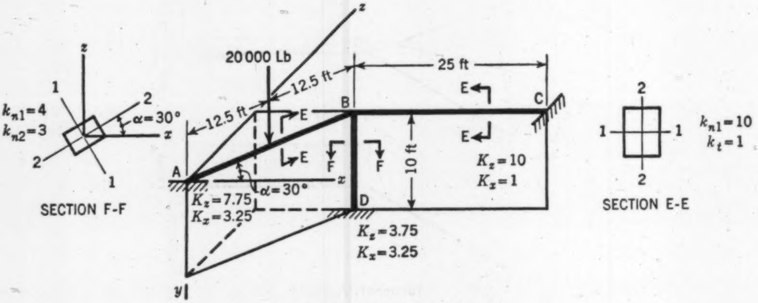
z
1
2
$k_{n1}=4$
$k_{n2}=3$
$\alpha=30°$
x
2
1
SECTION F-F
20000 Lb
12.5 ft
12.5 ft
25 ft
B
C
E
E
E
E
F
F
10 ft
A
x
$\alpha=30°$
$K_z=7.75$
$K_x=3.25$
D
$K_z=10$
$K_x=1$
$K_z=3.75$
$K_x=3.25$
y
2
1
1
2
SECTION E-E
$k_{n1}=10$
$k_t=1$

FIG. 9.—CONTINUOUS FRAME

TABLE 2.—ANALYSIS OF THE

Line No.	DESCRIPTION	MOMENTS ABOUT THE x-AXIS, IN POUND-FEET					
		Joint A	Joint B			Joint C	Joint D
		Member AB	Member BA	Member BC	Member BD	Member CB	Member DB
	Factors:						
1	Dist.		0.433	0.134	0.433		
2	C.O.		$C'_{xx}=+0.154$ $C'_{zx}=+0.799$ $C_{zx}=+1.199$	$C'_{xx}=-1.0$	$C'_{xx}=+0.500$ $C'_{zx}=+0.067$ $C_{zx}=+0.133$		
3	F.E.M.	−31,250	+31,250				
4	Dist.		−13,531	−4,188	−13,531		
5	COM (x)	−2,084				+4,188	−6,766
6	COM (z)	−6,527	−9,801		−1,089		−549
7	Dist.		+4,715	+1,460	+4,715		
8	COM(x)	+726				−1,460	+2,358
9	COM (z)	+2,174	+3,264		+363		+183
10	Dist.		−1,570	−487	−1,570		
11	COM (x)	−241				+487	−785
12	COM (z)	−757	−1,137		−126		−64
13	Dist.		+547	+169	+547		
14	COM (x)	+84				−169	+274
15	COM (z)	+252	+379		+42		+21
16	Dist.		−182	−57	−182		
17	COM (x)	−28				+57	−91
18	COM (z)	−88	−132		−15		−7
19	Dist.		+64	+19	+64		
20	COM (x)	+10				−19	+32
21	COM (z)	+29	+44		+5		+2
22	Dist.		−21	−7	−21		
23	Totals	−37,700	+13,889	−3,091	−10,798	+3,084	−5,392

tain the bending moments and torsional moments for member AB, the moments obtained in Table 1 were resolved into components about the bending axis and the axis of twist.

A solution of a statically indeterminate structure is correct, providing the requirements of continuity are satisfied. To satisfy these requirements, the angle changes—as determined by means of the moments and the defined properties of the material—must "balance" around a closed circuit. By "balance" it is meant that the distribution of angle changes must be such that the sum of the angle changes about any axis equals zero, and the sum of the products of angle changes times distances about any axis at a support—that is, the displacement at a support—equals zero. Stated algebraically,

$$\left.\begin{array}{ll} \Sigma d\theta_x = 0, & \delta_x = \Sigma z d\theta_y + \Sigma y d\theta_z = 0 \\ \Sigma d\theta_y = 0, & \delta_y = \Sigma x d\theta_z + \Sigma z d\theta_x = 0 \\ \Sigma d\theta_z = 0, & \delta_z = \Sigma x d\theta_y + \Sigma y d\theta_x = 0 \end{array}\right\} \quad \ldots\ldots\ldots (7)$$

In Eqs. 7, $d\theta_x$, $d\theta_y$, and $d\theta_z$ are angle changes about the x-axis, the y-axis, and the z-axis, respectively; and δ_x, δ_y, and δ_z are displacements of one end of a circuit relative to the other end along the x-axis, the y-axis, and the z-axis, respectively.

If angle changes are treated as forces along their axes of rotation, a displacement can be computed as a moment of these "forces" about the axis of displacement. The requirements of geometry stated in Eqs. 5 can be written as

CONTINUOUS FRAME OF FIG. 9

Line No.	Moments About the z-Axis, in Pound-Feet					
	Joint A	Joint B			Joint C	Joint D
	Member AB	Member BA	Member BC	Member BD	Member CB	Member DB
1		0.360	0.465	0.175		
2		$C'_{zz} = +0.452$ $C'_{zz} = +0.335$ $C_{zz} = +0.503$	$C'_{zz} = +0.5$	$C'_{zz} = +0.500$ $C'_{zz} = +0.058$ $C_{zz} = +0.115$		
3	−54,125	+54,125				
4		−19,485	−25,168	−9,472		
5	−10,811	−16,224		−1,800		−907
6	−8,807				−12,584	−4,736
7		+6,489	+8,381	+3,154		
8	+3,767	+5,653		+627		+316
9	+2,933				+4,190	+1,577
10		−2,261	−2,920	−1,099		
11	−1,254	−1,882		−209		−105
12	−1,022				−1,460	−550
13		+753	+972	+366		
14	+437	+656		+73		+37
15	+340				+486	+183
16		−262	−339	−128		
17	−145	−218		−24		−12
18	−118				−170	−64
19		+87	+113	+42		
20	+51	+72		+9		+4
21	+40				+56	+21
22		−29	−38	−14		
23	−68,714	+27,474	−18,999	−8,475	−9,482	−4,237

analogous requirements of statics, as follows:

$$\begin{array}{ll} \textbf{For rotations:} & \textbf{For displacements:} \\ \Sigma F_x = 0, & \Sigma M_x = 0 \\ \Sigma F_y = 0, & \Sigma M_y = 0 \\ \Sigma F_z = 0, & \Sigma M_z = 0 \end{array} \Bigg\} \ldots\ldots\ldots\ldots\ldots (8)$$

In Fig. 8(*b*) a check is made of the solution through application of the appropriate relationships from Eqs. 8. Angle changes were first obtained about the principal axis of bending and the axis of twist using the moments in Fig. 8(*a*) and the appropriate values of bending and torsional stiffness per unit length of a member. Such angle changes are obtained by dividing bending moments by $E\,I$ and torsional moments by $G\,J$. It is only necessary to use relative values of $E\,I$ and $G\,J$. The angle changes about the x-axis and the z-axis ("forces" in the x and z directions, respectively) were obtained by use of the appropriate functions of angle α. In Fig. 8(*b*), all values of angles are based on relative values of $E\,I$ and $G\,J$ equal to 2.5 lb-sq ft and 1.0 lb-sq ft, respectively. The results of the check in 8(*b*) show that the requirements of geometry are satisfied.

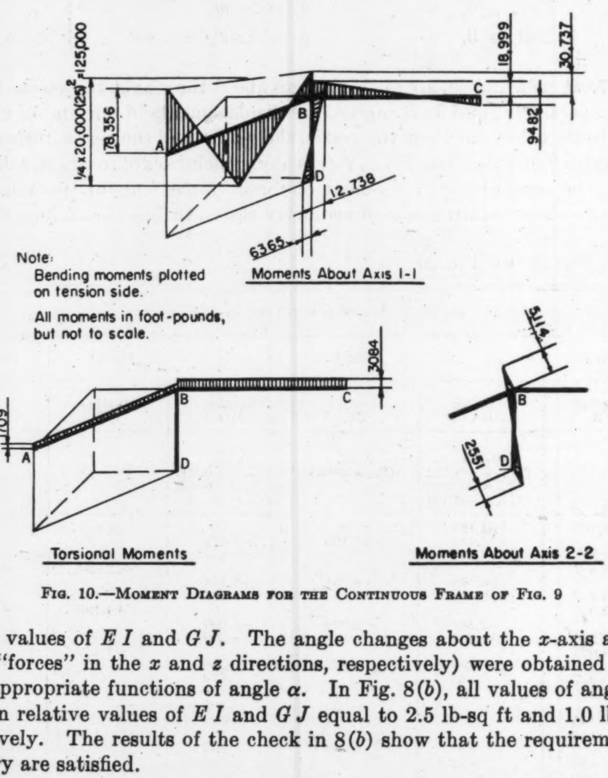
1/4 x 20,000(25)² = 125,000
78,356
A
B
C
D
18,999
30,737
9482
12,738
6365
Moments About Axis 1-1
Note:
Bending moments plotted on tension side.
All moments in foot-pounds, but not to scale.
3084
1709
A
B
C
D
Torsional Moments
5114
2551
B
D
Moments About Axis 2-2

Fig. 10.—Moment Diagrams for the Continuous Frame of Fig. 9

Except for the addition of column BD, the structure shown in Fig. 9 and analyzed in Table 2 is identical to that in Fig. 7. The column is so oriented that the principal axis 2–2 of the section is parallel with the longitudinal axis of

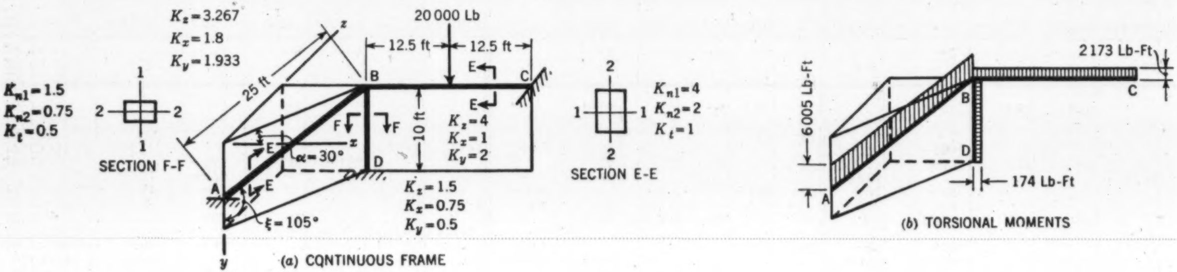
$K_{n1}=1.5$
$K_{n2}=0.75$
$K_t=0.5$
1
2
2
1
SECTION F-F
$K_z=3.267$
$K_x=1.8$
$K_y=1.933$
z
25 ft
20 000 Lb
12.5 ft
12.5 ft
B
C
E
E
F
F
10 ft
$K_z=4$
$K_x=1$
$K_y=2$
z
E
$\alpha=30°$
D
A
E
$\xi=105°$
y
$K_z=1.5$
$K_x=0.75$
$K_y=0.5$
2
1
1
2
SECTION E-E
$K_{n1}=4$
$K_{n2}=2$
$K_t=1$
6005 Lb-Ft
B
D
A
174 Lb-Ft
2 173 Lb-Ft
C

(a) CONTINUOUS FRAME

(b) TORSIONAL MOMENTS

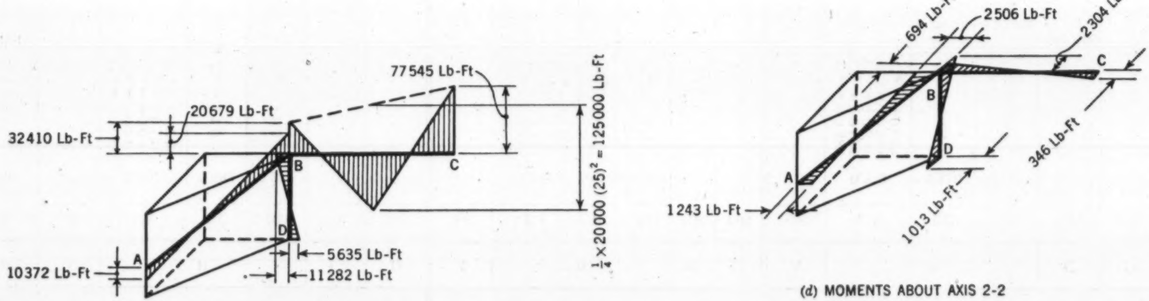
32410 Lb-Ft
20679 Lb-Ft
77545 Lb-Ft
$\frac{1}{4}\times 20000\ (25)^2 = 125000$ Lb-Ft
B
C
A
D
10372 Lb-Ft
5635 Lb-Ft
11 282 Lb-Ft
694 Lb-Ft
2 506 Lb-Ft
2 304 Lb-Ft
C
B
D
A
346 Lb-Ft
1 243 Lb-Ft
1013 Lb-Ft

(c) MOMENTS ABOUT AXIS 1-1

(d) MOMENTS ABOUT AXIS 2-2

FIG. 11.—CONTINUOUS FRAME AND MOMENT DIAGRAMS (BENDING MOMENTS PLOTTED ON THE TENSION SIDE)

TABLE 3.—ANALYSIS OF THE CONTINUOUS FRAME OF FIG. 11

Line	MOMENT	MOMENT ABOUT THE x-AXIS, IN POUND-FEET						MOMENT ABOUT THE y-AXIS, IN POUND-FEET						MOMENT ABOUT THE z-AXIS, IN POUND-FEET						Line
	JOINT	A	B			C	D	A	B			C	D	A	B			C	D	
	MEMBER	AB	BA	BC	BD	CB	DB	AB	BA	BC	BD	CB	DB	AB	BA	BC	BD	CB	DB	
1	Factors: Dist.		0.507	0.282	0.211				0.431	0.455	0.114				0.373	0.456	0.171			1
2	C.O.		$C'_{xx} = -0.083$ $C'_{yx} = -0.241$ $C'_{zx} = +0.690$ $C_{yx} = -0.121$ $C_{zx} = +0.706$	$C'_{xx} = -1.0$	$C'_{xx} = +0.5$				$C'_{xy} = -0.225$ $C'_{yy} = +0.448$ $C'_{zy} = +0.129$ $C_{xy} = -0.112$ $C_{zy} = +0.064$	$C'_{yy} = +0.5$	$C'_{yy} = -1.0$				$C'_{xz} = +0.380$ $C'_{yz} = +0.076$ $C'_{zz} = +0.394$ $C_{xz} = +0.389$ $C_{yz} = +0.038$	$C'_{zz} = +0.5$	$C'_{zz} = +0.5$			2
3	F.E.M.															−62,500		+62,500		3
4	Dist.														+23,313	+28,500	+10,688			4
5	COM (x)																			5
6	COM (y)																			6
7	COM (z)	+8,859	+9,069					+1,772	+886					+9,185				+14,250	+5,344	7
8	Dist.		−4,598	−2,557	−1,914				−382	−403	−101									8
9	COM (x)	+382				+2,557	−957	+1,108	+556					−3,173	−3,246					9
10	COM (y)	+86	+43					−171				−202	+101	−49	−24					10
11	COM (z)																			11
12	Dist.		−22	−12	−9				−240	−253	−63				+1,220	+1,491	+559			12
13	COM (x)	+18				+12	−4	+5	+3					−15	−16					13
14	COM (y)	+54	+27					−108				−126	+63	−31	−15					14
15	COM (z)	+464	+475					+93	+46					+481				+746	+274	15
16	Dist.		−255	−142	−105				−21	−22	−6				+12	+14	+5			16
17	COM (x)	+21				+142	−52	+61	+31					−176	−180					17
18	COM (y)	+5	+2					−9				−11	+6	−2	−1					18
19	COM (z)	+5	+5					+1						+5				+7	+2	19
20	Dist.		−4	−2	−1				−13	−14	−4				+68	+83	+30			20
21	COM (x)					+2		+1						−3	−3					21
22	COM (y)	+3	+1					−6				−7	+4	−2	−1					22
23	COM (z)	+26	+26					+5	+3					+27				+42	+15	23
24	Dist.		−14	−8	−5				−1	−2					+2	+2				24
25	Totals	+9,923	+4,755	−2,721	−2,034	+2,713	−1,013	+2,752	+868	−694	−174	−346	+174	+6,247	+21,129	−32,410	+11,282	+77,545	+5,635	25

member AB. From the expressions in Fig. 6 ($\zeta = 0$), the stiffnesses and carry-over factors for BD were determined. The numerical procedure follows in a manner similar to that in Table 1. Moment diagrams are shown in Fig. 10. A check of the angle changes along the circuit ABC and along the circuit DBC showed an almost perfect balance.

In the frame in Fig. 11 (*a*), member AB does not lie in any of the three orthogonal planes. The projected angle α of this member is equal to 30°, the angle ζ is equal to 105°, and the angle ψ is equal to zero. Column BD is so oriented that the principal axes of its cross section are parallel to the chosen reference

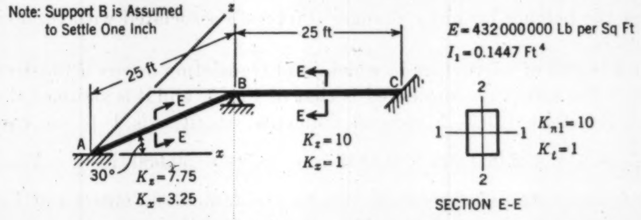

FIG. 12.—EFFECTS OF TRANSLATION

TABLE 4.—ANALYSIS OF THE EFFECTS OF TRANSLATION OF THE CONTINUOUS BEAM OF FIG. 12

DESCRIPTION	MOMENTS ABOUT THE x-AXIS, IN POUND-FEET				MOMENTS ABOUT THE z-AXIS, IN POUND-FEET			
	Joint A	Joint B		Joint C	Joint A	Joint B		Joint C
	Member AB	Member BA	Member BC	Member CB	Member AB	Member BA	Member BC	Member CB
Factor: Dist.		0.765	0.235			0.437	0.563	
C.O.		$C'_{xx} = +0.154$ $C'_{zx} = +0.799$ $C_{zx} = +1.199$	$C'_{xx} =$ −1.0			$C'_{zz} = +0.452$ $C'_{xz} = +0.335$ $C_{xz} = +0.503$	$C'_{zz} =$ +0.5	
F.E.M.	−25,000	−25,000			−43,300	−43,300	+50,000	+50,000
Dist.		+19,125	+5,875			−2,928	−3,772	
COM (x)	+2,945			−5,875	+15,281	+22,931		
COM (z)	−981	−1,473			−1,323			−1,886
Dist.		+1,127	+346			−10,021	−12,910	
COM (x)	+174			−346	+900	+1,351		
COM (z)	−3,357	−5,041			−4,529			−6,455
Dist.		+3,856	+1,185			−590	−761	
COM (x)	+594			−1,185	+3,081	+4,693		
COM (z)	−198	−297			−267			−380
Dist.		+227	+70			−2,051	−2,642	
COM (x)	+35			−70	+181	+272		
COM (z)	−687	−1,032			−927			−1,321
Dist.		+789	+243			−119	−153	
COM (x)	+122			−243	+630	+946		
COM (z)	−40	−60			−54			−76
Dist.		+46	+14			−413	−533	
COM (x)	+7			−14	+37	+55		
COM (z)	−138	−208			−187			−266
Dist.		+159	+49			−24	−31	
COM (x)	+24			−49	+127	+191		
COM (z)	−8	−12			−11			−16
Dist.		+9	+3			−86	−108	
Totals	−26,508	−7,785	+7,785	−7,782	−30,361	−29,093	+29,090	+39,600

axes, thus making angle α for this member equal to zero. Girders AB and BC are identical in cross section. Values of stiffnesses and carry-over factors for member AB were determined through use of the general expressions in Fig. 4. Because the principal axes of the cross sections of members BC and BD are parallel to the reference axes, their stiffnesses about the latter axes are identical to those about the corresponding principal axes. The structure is analyzed in Table 3.

Diagrams of bending moments and torsional moments for the structure are shown in Fig. 11. Again a check of the angle changes along the circuits ABC and DBC showed a very good balance. Of course, in this case it was necessary to check the balance for angle changes ("forces") associated with the x, z, and y directions.

The analysis of a structure in which joint translation occurs is illustrated in Fig. 12. The structure considered is that of Fig. 7, and it is assumed that the support B settles 1 in. Fixed-end moments, about axis 1–1, are equal to $6\,E\,I\,\frac{\Delta}{L^2} = 6 \times 432{,}000{,}000 \times 0.1447 \times \frac{1/12}{-\,(25)^2} = 50{,}000$ lb-ft. Fixed-end moments about the reference axes were next obtained and entered in Table 4, and the procedure was applied as before.

SUMMARY

A procedure has been presented for the structural analysis of girders and frames that are continuous in space. As herein presented, it is applicable to structures composed of straight members; the members may be of either constant or variable cross section. The method involves successive corrections of an assumed solution, and consequently lends itself to approximate or precise analyses.

ACKNOWLEDGMENT

The writer wishes to express his thanks to F. E. Hogan, A.M. ASCE, of Louisiana Polytechnic Institute, at Ruston, who made all the numerical computations.

AMERICAN SOCIETY OF CIVIL ENGINEERS
Founded November 5, 1852
TRANSACTIONS

Paper No. 2686

REVENUE BOND FINANCING FOR AIRPORT IMPROVEMENTS

By JAMES C. BUCKLEY[1]

SYNOPSIS

The reluctance to provide adequate airport facilities with public funds frequently may be overcome through the use of airport revenue bonds. However, if such a method of financing is to be used, it must be thoroughly understood by the engineer so that he will design the facilities on the basis of the economic requirements imposed. Special factors to be considered in such a design are described in general.

INTRODUCTION

Before the end of World War II, the subject of this paper would have had little more than academic interest even for builders of airports. In 1953, however, there is no subject (with the possible exception of future federal appropriations for airport aid) which bears so directly on the volume and type of municipal airport improvements to be expected in the immediate future.

The explanation is simple. Municipalities have a pressing need for airport improvements that will cost hundreds of millions of dollars. Most of them, however, have an even more pressing need for streets, schools, sewers, libraries, hospitals, and other essential municipal facilities; and there is not enough margin within the limits of their general obligation debt to cover all the needs. Many of the needed airport improvements will not be made unless they can be financed outside the debt limit with some type of revenue obligation.

This situation is in large measure a result of World War II. Compressed into the five war years was a four-fold increase in air passenger traffic and increases in the size and weight of transport aircraft which otherwise might well have taken a decade—or even longer. However, there were almost no improvements at civil airports during the war years, except at those airports used wholly or in part by the military.

NOTE.—Published, essentially as printed here, in September, 1953, as *Proceedings-Separate No. 260*. Positions and titles given are those in effect when the paper was received for publication.

[1] Pres., James C. Buckley, Inc., New York, N. Y.

At the beginning of World War II, the civil airport system was generally geared to the modest requirements of the DC-3 aircraft. This meant a required runway length at sea level of only 3,300 ft; a pavement strength adequate for aircraft with a gross weight of only 25,000 lbs; loading positions with a diameter of only 125 ft; and terminals geared only to the peak-hour loads of a 21-passenger aircraft serving an annual air travel market of only 3,500,000 people. Such relatively small and inexpensive facilities could usually be provided with proceeds from the scale of general obligation bonds without conflicting seriously with other municipal requirements.

At the close of World War II, however, essentially the same civil airport system was faced with the problem of meeting the greatly increased physical requirements imposed by a four-fold increase in air traffic and the introduction of the DC-4, the DC-6, and the Constellation aircraft. This meant a required runway length at sea level of 5,000 ft; a pavement strength adequate for aircraft with a gross weight of as much as 100,000 lb; loading positions with a diameter of as much as 160 ft; and terminals geared to the peak-hour loads of aircraft carrying as many as 58 passengers, these terminals serving an annual air-travel market of more than 12,000,000 people. It is not surprising, therefore, that terminal facilities at major air centers were overcrowded; that makeshift expansions were accomplished at many terminals; and that many certificated airline stops were without service entirely, or served only on a restricted basis, because of inadequacies in landing-area facilities.

Airport planning naturally became a common topic of conversation in many communities—planning not just for the needs of the immediate post-war period, but for the needs of Stratocruisers, the DC-6B's, and the Super-Constellations of the early 1950's, and for the needs of the even larger and heavier aircraft of the more distant future. With this planning came the first real appreciation of the astronomical increase in municipal investment which would be required to provide an adequate system of civil airports.

The City of New York (N. Y.) discovered that the development of the International Airport at Idlewild might require an ultimate investment of $200,000,000—approximately ten times its investment in the much smaller La Guardia Airport—and it soon realized that the capital budget could not cover this large airport debt. This same problem faced the City of Newark (N. J.) when it was discovered that it would cost $55,000,000 to redevelop Newark Airport—more than five times the original investment in the facility.

The City of Detroit (Mich.) learned that it would cost $20,000,000 or more to replace the obsolete Detroit Municipal Airport with a new airport. Unable to provide such a facility, Detroit still uses Willow Run Airport, 32 miles away, for scheduled air service.

The City of Philadelphia (Pa.) initiated a development program for its Southwest Airport which ultimately will require the investment of $50,000,000, much of which still remains to be appropriated.

The City of Cleveland (Ohio) submitted to the voters a proposition for issuing airport terminal bonds three times before securing approval, and this development was then threatened by the specter of insufficient funds as a result of sharp increases in construction costs.

In large and small communities throughout the United States the situation has been the same. The problem has been alleviated to some extent by grants-in-aid from the United States government under the Federal Airport Act.[2] However, the dwindling appropriations under this act, and the increasing requirements of civil aviation, leave a growing balance of needed local investment in civil airports. Much of this will be financed, if at all, only on the security of the basic earning power of airport facilities. Here lies an opportunity as well as a challenging responsibility for the engineer.

The financing of airport improvements with revenue bonds presents an opportunity for the engineer to perform a real public service by helping a community to secure the needed airport improvements that otherwise might be long delayed or never built, and also to provide those improvements without burden to the taxpayers. Therefore, the revenue-bond financing of airport improvements presents an opportunity deserving earnest attention.

To grasp this opportunity, however, places a challenging responsibility on both the engineer and the architect because the ultimate success of revenue-bond projects at airports mainly depends on the engineer's understanding of the fundamental problems involved, and on his technical ability to develop solutions to those problems. It would be presumptuous for the writer to discuss the technical aspects of the engineering and architectural approach to problems involved in revenue-bond projects at airports. The writer can, however, suggest the fundamental points on which he feels the engineer must be informed in order to utilize his technical skills effectively.

THE AIRPORT

Understanding of the Nature and Functions of an Airport.—An airport should not be considered merely a transportation terminal designed to accommodate aircraft and to process their passengers and cargo. With such a concept, consideration of airport revenue bonds would be pointless. The available revenues would fall far short of meeting the costs of providing, operating, and maintaining the necessary facilities, and there would be no margin to attract and protect revenue-bond purchasers.

Fortunately, the airport has many other functions which, with proper design and under proper development, can be more productive of revenues than can the strictly aeronautical activities. For example:

1. The airport is as important a terminal for ground transportation as it is for air transportation, since all the people and goods which move by air must also move to and from an airport by some mode of ground transportation. Adequate provision must therefore be made for access to highways, loading platforms for passengers, loading docks for cargo, space for taxicab holding lines, storage space for "for-hire" automobiles, and automobile parking areas.

That this ground transportation problem is no small task is indicated by the fact that, at La Guardia Airport in 1951, approximately 400,000 taxicabs left the airport with passengers; more than 1,200,000 passengers rode in airport limousines; and more than $300,000 was received from public automobile parking.

---

[2] Federal Airport Act, *Public Law 377*, 79th Cong., 2d Session, Chapter 251, approved May 13, 1946.

2. Of course, the airport is also a service station for aircraft. This involves facilities for (*a*) the repair and servicing of aircraft, (*b*) the overhaul of aircraft components and accessories, and (*c*) the inside and outside storage of aircraft. Cleveland, for example, has completed arrangements for the construction of a $3,500,000 hangar at Cleveland Hopkins Airport, to be 1,375 ft long and to have 5 acres of concrete ramp.

3. The airport is also a service center for all passengers and visitors. The air passenger, the friends who meet him on arrival or accompany him at departure, and the casual visitors whom the aeronautical activities attract to the airport—all have a variety of consumption requirements that must be met. These requirements range from shoeshines to deluxe meals, but all are part of the airport complex which must be understood if the needs of its customers are to be met. This again is no small business as evidenced by the fact that the volume of restaurant and bar business at Stapleton Airfield in Denver, Colo., is now (1953) averaging more than $1,250,000 per year.

4. The airport is also a recreational and entertainment center for the community. The restaurants, shops, and services necessarily provided at an airport as a service to air passengers and their friends, combined with the drawing power of the aeronautical activity at the airport, inevitably make modern airports a center of attraction for the entire community. This is strongly evidenced by the fact that an average of more than 1,000,000 people per year visited the observation gallery at La Guardia Airport between 1946 and 1952.

5. Also, the airport is a center for governmental activities concerned with aviation. Most airports of large or medium size have control towers operated by the Civil Aeronautics Administration (CAA), and a federally-operated weather station. In New York City, these two agencies have made their regional headquarters at Idlewild Airport, where they occupy a specially constructed $4,000,000 building. Many state aviation commissions also make their headquarters at airports.

6. In addition, the airport is important as an industrial site. More and more industries are finding that the increasing importance of air transportation, both for people and goods, makes the land adjacent to the airport highly desirable for industrial use. At Friendship International Airport in Baltimore, Md., for example, an electronics corporation is completing (1952) a $9,000,000 plant which is expected to employ 3,500 workers.

7. This complex of activities makes the airport also a major employment center in the community—actually an industry in its own right. At Love Field in Dallas, Tex., a check in 1951 revealed that 2,850 persons were employed at the airport and an additional 800 persons with flying jobs were based at the airport. The total annual payroll for these two groups together, representing community income flowing from airport employment, was $14,500,000.

8. Finally, these many activities of which the complex economic mechanism of a modern airport is composed, all depend on and support each other. The automobile parking lots are patronized by airline passengers, visitors, and employees. The use of the landing area depends as much on the availability of hangar and base facilities for various classes of aircraft and on the avail-

ability of good terminal facilities as it does on the availability of good runways and taxiways. Industrial development at the airport means much to terminal-area revenues from employee patronage of terminal concessions.

This means that the design of facilities at airports must recognize and provide for the requirements of all types of airport activity if a sound basis is to be established for financing with revenue bonds.

AIRPORT REVENUE BOND

Understanding of the Meaning of the Airport Revenue Bond.—Municipalities in the United States have from two to six billion dollars invested in airport facilities. The portion of this total resulting from the issuance of revenue bonds is infinitesimal.

The Port of New York Authority, through December 31, 1951, issued airport revenue bonds in the total face amount of $72,400,000—but these bonds enjoyed the support of a reserve composed of revenues from bridges, tunnels, and other facilities, and were not marketed solely on the security of the revenues to be derived from the facilities to be established.

The Dade County Port Authority, at Miami, Fla., has issued airport revenue bonds to improve and extend the Miami International Airport, but these bonds were secured by a pledge of the revenues of the entire airport rather than by the revenues from the facilities constructed with the proceeds of the issue.

The only major airport revenue bond issue secured solely by the revenues of the facilities to be constructed with the proceeds of the bond issue was marketed in 1951 by the City and County of Denver to secure funds for the terminal development program at Stapleton Airfield. This issue totaled $1,750,000 and was sold at an average effective interest rate of 3.3% to a syndicate headed by two firms from New York City.

A few small bond issues have been marketed under the name "revenue bonds," but these have required not only the pledge of the revenues from facilities other than those to be constructed with the proceeds of the bond issue (or even of the revenues of the entire airport), but also, in some cases, the mortgaging of the entire airport as additional security. Although this procedure has made possible the raising of capital without burden to the taxpayer, the pledging of airport revenues as a whole to support only one facility, or the mortgaging of the airport, creates a threat to flexibility in the future airport program (and even a threat to the continued existence of the airport as such) which most municipalities wish to avoid.

Therefore, the writer believes that in planning, the engineer should think of an airport revenue bond as an instrument which is usually to be secured only by the revenues of the facilities to be created with its proceeds. Sometimes, of course, it may be necessary to pledge additional revenues—up to the revenues of the entire airport—and even to mortgage the airport in order to accomplish essential airport financing. However, one should recognize that the revenue unit, which is the basis of the revenue bond financing, is completely flexible—it can be the airport as a whole, but it can also be an individual facility, a group of facilities, or even a part of one facility, as long as the revenues and related expenses can be properly segregated and designated.

Ability to Issue Airport Revenue Bonds.—Many airport officials have only a rudimentary appreciation of the difference between a revenue bond and a general obligation bond. Many seem to feel that, when the debt limit is reached and the municipality can no longer issue general obligation bonds for airport purposes, it is a matter of simple financial technique to issue, forthwith, revenue bonds for needed airport improvements.

A consideration frequently forgotten, but one which must always be understood, is that the revenue bond depends for its market on the assurance that net revenues from the facilities whose revenues are pledged will be sufficient to pay interest and amortization on the bonds as those payments become due. If such assurance is not reasonably evident from the data available on the facilities, it will be impossible to issue revenue bonds because no market will exist.

In this respect, the airport is no different from a private corporation offering its unsecured bonds in the market. Such bonds can be sold if there is reasonable assurance that the corporation has (*a*) a market for its product; (*b*) a plant that is neither too large nor too costly for its operations (one that will be economical to maintain and economical in production); and (*c*) a management and staff that will operate its plant and produce its product efficiently and economically.

If the airport has a good market, an economical plant, and an efficient management, it can reasonably expect net revenues which will permit it to issue revenue bonds. It is the job of engineers to make certain that the airport has the kind of plant that will give it a sound basis for revenue bond financing.

Necessity of Evidence of Continuing Demand.—Bond investment is long-term investment. The buyer of revenue bonds must depend on net revenues to meet his claims for interest and bond repayment over long periods of time. He is not nearly so interested in whether the pledged facility will earn its debt service three times in a certain year as he is in receiving reasonable assurance that it will earn it perhaps one and one half times on an average over the entire life of his bond.

At an airport, such assurance depends on the continued demand for facilities—that is, the continued traffic potential at the airport. The term "traffic potential" is used because, although there are some exceptions, the bulk of the activity at an airport depends on the continued flow of air traffic through the airport. This is the life blood that keeps the fees and rentals flowing into the airport treasury.

There is nothing so comforting to the buyer of revenue bonds as to have the revenue bond facilities rented to tenants with prime credit ratings for the entire period of the bonds at rentals that will assure the payment of interest and bond amortization when due. This does not happen very often in the airport business, and a sound evaluation of traffic expectancy must be available both as an assurance to the buyer of revenue bonds and as a basis for the design and engineering of airport facilities.

PLANNING

Engineering for Low-Capital Cost.—No compromise is suggested in the quality of the efficient functional layout of facilities financed through revenue bonds. However, the engineer should be aware of what is needed, build within these restrictions, and avoid expensive features and ornamentation not required for the efficient functioning of the facility. The importance of this subject will be appreciated if it is remembered that, if one is trying to finance with twenty-five year, 4%-income bonds, for example, and have an indicated debt service coverage of 1.5, a 10% decrease in the construction cost will increase the debt service coverage to 1.66. This decrease will provide a more attractive bond in the market and may result in a lower effective interest cost.

To find out what construction is required, one must study traffic forecasts as well as activity forecasts, which show the types of activity that may reasonably be anticipated at the airport. Together, these will provide a basis for predicting plane movements, the type of traffic, and the airport population.

These are the raw materials on which one can base a study of requirements as to space and design, which will show the physical facilities required to accommodate reasonably the aeronautical and other activities in prospect. This is the design basis for a new airport or for a new facility on an existing airport. Of major importance in all airport construction—particularly in cases of facilities financed through revenue bonds—is designing and building slightly beyond near-term demand but avoiding the creation of civic monuments that have plagued airport development programs at cities throughout the United States.

The nature of an airport is such that the landing-area facilities will require much the same construction whether the demand will be for 100% of the capacity, or only 35%. A runway and related taxiways are needed regardless of how many plane movements are anticipated. However, little extra capacity is gained from three runways as compared with two runways—or even one runway—if the airport is primarily an airline airport used by large aircraft that can land considerably off the prevailing wind. In landing-area design, therefore, it may be possible to effect large savings in capital cost with little or no effect on capacity or revenue potential by reducing the number of runways to two—or even one—instead of the conventional three.

In terminal building work, economy in construction rests on a sound study of the requirements of space and design, and on a recognition of the functions of the various parts of a terminal building. Basically, the terminal is a working headquarters for the servicing of aircraft, the processing of air passengers and air cargo, and the vending of food, merchandise and services to the public. The areas meriting costly treatment should be a relatively small percentage of the total area, and the income-producing areas must be a relatively high percentage of the total if the facility is to lend itself to revenue bond financing.

Designing for Economical Expansion.—Not only does the revenue bond buyer properly require assurance of a continued demand for the services of the airport facilities he finances—but also assurance that the facility he finances will not lose its market because it cannot be expanded economically to keep pace with growing demand. These facts are especially true of airports because this industry has barely tapped its full potential market. Naturally, this market rises and falls, which is why initial over-building is not advisable. It is equally true that the long-term trend is definitely upward, and airports and airport facilities must be designed for economical expansion. This trend indicates the inadvisability of placing airports where expansion is limited by railroad tracks, major highways, mountains, waterways, or other obstacles that cannot be overcome if more area is needed.

With respect to the runway layout, considerations as to future expansion require planning ahead for the possibility of longer runways and so placing them that such extensions will be possible without unreasonable cost for land acquisition or obstruction removal. It also means planning the bearing capacity of runways to accommodate larger and heavier aircraft later. In an airport that may reasonably require the capacity of parallel runways it is equally important to place the terminal area between the ultimate parallel runways, instead of having both runways on one side of the terminal. With parallel runways on either side of the terminal building, more than twice the capacity of a single runway will be realized when the parallel stage is reached. With both parallel runways on one side of the terminal building, less than twice the capacity of a single runway is obtained because of the necessity of moving aircraft to and from the far runway across the near runway, with consequent decrease in the capacity of the near runway to accept aircraft.

In planning the terminal building, the land reserved for terminal purposes must permit economical extension of the building and of the aircraft loading positions that serve it, as well as economical extension of ancillary facilities such as automobile parking areas, taxicab lines, circulation area for commercial vehicles, and similar features. This is equally true of hangar areas in which space should be reserved to meet the increasing needs of the aeronautical users of the airport.

Within the terminal building itself, the same type of problem exists. As airline business grows, the companies need more area for ticket counters, operational offices and passenger service, baggage and freight handling, and related activities. To build initially far in advance of demand is not feasible; but one can plan a facility so that the inevitable expansion of specific functions within the building can be made with a minimum of added expense. This is equally true of concession areas and public space in the terminal building, since they are all a function of the terminal population which increases with air traffic.

In summarizing the problem of expansion from the standpoint of the engineer and the architect, sound design and engineering for airport facilities typically require more professional work in relation to initial costs than do most construction projects because of the necessity of planning for almost inevitable expansion. This is a feature sometimes difficult for airport operators to appreciate, but it is essential that it be understood and that it be authorized in the case of revenue bond facilities.

Planning to Produce Maximum Revenues.—The initial factor contributing to the realization of adequate net revenues to support revenue bonds is a maximum development of gross revenues; and the production of maximum gross revenues can be realized only when that objective is kept constantly in mind—first, in the location of the airport itself, and then in the location and design of its facilities.

Much of the revenue of modern airports is received from the visitors from adjacent communities. That location having the greatest consumer market readily available will produce the greatest revenue.

Also important are convenient access facilities (preferably on or adjacent to main highways) having direct service by public transportation vehicles. The airport should be within a reasonable cab fare of the city center.

The revenue potential of an airport also depends on space—to permit necessary expansion of the landing area in order to accommodate larger aircraft, to accommodate all the various types of activity that reasonably can be expected at the airport, and for expansion of individual facilities such as the terminal building and the hangers. Land at airports is seldom expensive in relation to the revenue that can be realized from its full development. Only by encouraging the provision of an adequate area initially can the planner be sure of having room to accommodate the balanced development essential to the production of maximum revenues.

The terminal area is the major revenue source at most modern airports. As a result, it stands to lose or gain most by the attention paid to revenue production at the design stage. Unless the terminal is designed to exploit fully the revenue potentially available, the chances of a feasible revenue bond program are almost nil.

The basic problem of designing air terminals for revenue production has vast ramifications. A few examples are presented.

At active terminals, an observation gallery is an important source of revenue—if there is no convenient free area from which to see the same activities. An observation gallery certainly should be provided—but free competition must not be permitted. The observation gallery will produce more revenue if it has convenient plumbing and electric connections to permit the installation of refreshment stands and vending machines.

Concessions provide considerable airport revenue—if they are exposed to all the people who use the terminal. Customers will not hunt for a place to spend their money. All the concession space reasonably required for the anticipated terminal population should be provided, but the flow of people should be centralized so that the people will be exposed to all the concessions in a concentrated area.

Automobile parking fees are sources of revenue at larger airports, provided parking spaces are adjacent to the terminal building and protected from equally desirable free competition. These ideas should be remembered when planning the areas adjacent to the terminal building. This fact applies also to taxicabs and car-rental agencies. They will produce revenue for the airport if allotted convenient storage area and service points so that they can develop business.

The submetering of electricity can be an important source of revenue at large airports—if it is possible under the rate schedules of the public utility and if the electrical distribution system is designed for it.

This simply means that revenue production at an airport is not a specialized activity which may be begun after the airport is built; to achieve the full potential at an airport, this phase must be provided for in the design stage.

Design for Economical Operation.—Another factor contributing to the realization of net revenues adequate to support revenue bonds is a minimum operating cost, which also depends largely on design, engineering, and construction materials. A few of the many operating factors that deserve attention will be described.

Snow removal with heavy equipment is relatively economical compared to snow removal with small equipment or by hand. Operating expense should be reduced at the design stage by eliminating or keeping to a minimum the sharp angles and constricted areas on the loading ramp where snow removal will require small equipment or hand work.

Every point at the airport that must be manned around the clock seven days a week will cost the airport the wages of four or five men. This includes guard stations, public-address control, pneumatic-tube control, telephone switchboards, and similar functions. By placing two or more of these activities at common or adjacent points, significant savings in the annual operating budget will be effected.

Public toilets are expensive to keep clean and are costly from the standpoint of the wages of attendants. The expense can be substantially reduced, and in large terminals eliminated, by transferring responsibility to a concessionaire—if the necessary facilities are concentrated in a few large installations rather than scattered throughout the public areas of a terminal.

Cleaning services comprise a large percentage of terminal operating costs, and vary widely depending on the materials used for walls and floors. Some materials are much better suited to the use of mechanical cleaning equipment than are others. A review of proposed construction materials with the airport custodial service or with a sanitation maintenance contractor can result in important savings.

It is necessary to meter utilities provided by the airport to its tenants. Usually of minor importance is the electricity supplied for illumination to miscellaneous tenants, and meters usually need not be provided. However, of great concern are the steam and hot water supplied to the restaurant concessionaire, and the electricity (for power and illumination) supplied to CAA, the United States Weather Bureau, the airlines, and the restaurant concessionaire. To the airport, these represent important costs which, when estimated, usually will be compromised on a basis favorable to the tenants and unfavorable to the airport. These utilities should be metered to protect the airport from loss.

Although these examples are not too significant individually, they indicate the responsibility of the engineer and the architect to contribute to the economical operation of the completed facility at the design stage.

Economical Use by Tenants.—Still another factor contributing to the realization of net revenues adequate to support revenue bonds is the provision of a facility that may be used economically by tenants. The more economical the tenants' operation, the more willing and more able they are to pay a proper rent or fee for the use of the facility.

The easiest way to discover which features and layout will be most economical for the tenants is to consult them—the concessionaires, ground transportation firms, government agencies, oil companies, airlines, and other major users of the airport. It may not be possible to supply all their requirements, but it will certainly be possible to offer them most of the features for which they are willing to pay.

Significant savings can be realized in tenants' operating costs by considering their problems at the design stage; for example—the distance, time, and cost of taxiing can be kept to a minimum if the terminal and hangar areas are located as close as possible to the runway ends. Also, the taxiing distance can be reduced and time and expenses saved by constructing frequent turnoffs from the runways to the taxiways. Of even greater benefit to airline tenants is the provision of adequate runway length and strength to permit tenants to use the field with their usual aircraft without restriction on payload.

Within the terminal area, both the airlines and the concessionaires have special operating problems which need recognition at the design stage if operating costs are to be kept to a minimum. The restaurant concessionaire, for example, will profit if food is prepared in a kitchen which has been designed to suit his particular type of operating needs. All concessionaires will benefit if convenient and accessible storage space is provided. Each airline will save if its operations space is convenient to the loading gates which it uses, and if the total space is concentrated into groupings which will avoid needless duplication of personnel.

In the hangar areas there are equally significant opportunities to achieve operating savings through proper design. A lighting installation with short-lived lamps can easily cost more in maintenance expenses plus capital costs, than a more expensive system requiring attention less frequently. The selection of a heating system should not only be based on its capital cost in relation to the area to be heated, but it should reflect other factors such as fuel savings (possible with added insulation) and possible savings from radiant heating in very high hangars.

Emphasizing the inclusion of the ideas of the tenants and users in the design of the airport facilities reflects the writer's conviction that the experience record of engineers is too limited to expect any large development of the market for airport revenue bonds without the cooperation of airport tenants and users, and also that their cooperation is increased if the facilities are made economical for them to use.

Independent Evaluation of the Engineer's Work.—This concept is important in the engineer's approach to financing airports through revenue bonds because the reaction of engineers to the "bankers' report" or "feasibility report" varies so widely. Perhaps this condition results partly from the fact that such reports vary rather widely also, with respect both to their scope and to the extent of the detailed investigation.

In the development of airport revenue bonds, the type of security is so new and the scope of airport activities so complex that one can confidently expect to have the work evaluated independently as part of a feasibility report on any issue of consequence. Such an evaluation is necessary not only to assure the investor as to the soundness of the design, the engineering, and the cost estimates, but also to relate the engineer's work to other factors outside the scope of his responsibility.

It may aid understanding of the feasibility report and of the problems of the individual who must prepare it if it is called, instead, an "audit of future prospects"—which it is indeed. As such, it must review not only the design, specifications, cost estimates, and construction schedules prepared by the engineers and architects, but also the following:

a. The traffic, activity, and population forecasts on which that work is based;

b. The reliability of the techniques used to convert those forecasts into requirements as to space and facilities;

c. The validity of the proposed budget for operation and maintenance expenses;

d. The reasonableness of the proposed structure and level of rates, and the resulting revenue forecasts;

e. The reasonableness of the effective interest rate anticipated for the proposed bond issue; and

f. The efficiency of existing management and the future prospects for efficient and economical administration of the airport.

In addition, the feasibility report must consider many contingent threats to the security of the proposed bond issue, including factors such as—

1. The threat of recapture by the federal government under existing agreements;
2. The obligation to provide free space and runway use to the federal government under existing agreements;
3. The effect of existing long-term leases with airlines and other tenants;
4. The danger of an assessment of real property taxes against airport property;
5. The possible reduction in airport capacity as the result of air space congestion;
6. The extent to which the aerial approaches to the airport may be endangered by uncontrolled construction that would impinge on flight paths; and
7. The danger of disastrous floods that might destroy the entire earning power of the facility.

Only when the work of the engineer and the architect has been evaluated and related to all these other factors does the bond buyer have an integrated picture of the future prospects of the facility he is being asked to finance solely on the security of those prospects. Therefore, he can hardly be blamed for feeling that "two heads are better than one" in protecting his interests.

CONCLUSION

A great quantity of needed airport construction will not be accomplished unless it is financed with revenue bonds. This fact provides an opportunity for engineers and architects to help their communities and to stimulate business if they can develop such projects as will pass the scrutiny of the buyer of revenue bonds. To do so, the engineer must recognize and understand some fundamental factors affecting the offering of airport revenue bonds such as have been described herein, and he must apply them in his work on such issues.

AMERICAN SOCIETY OF CIVIL ENGINEERS
Founded November 5, 1852
TRANSACTIONS

Paper No. 2687

SNOW HYDROLOGY FOR MULTIPLE-PURPOSE RESERVOIRS

By Herbert S. Riesbol,[1] M. ASCE

With Discussion by Messrs. Ray K. Linsley, R. W. Gerdel, Harold D. Hafterson, David M. Rockwood, and Herbert S. Riesbol

Synopsis

Snow is a form of precipitation possessing certain characteristics which can be evaluated and applied to advantage, both from an hydrologic and an economic viewpoint, in the planning and design of multiple-purpose storage reservoirs. This paper describes briefly the processes of snow melting and runoff, and presents criteria and examples of procedures followed in applying the knowledge of these processes to determine reservoir space allocations and spillway capacities. The writer calls attention to the gap existing between detailed physical knowledge of evaporation and melting processes and application of this knowledge to practical design problems.

Introduction

Hydraulic engineers responsible for planning and designing multiple-purpose storage reservoirs recognize snow as a form of precipitation possessing certain characteristics which can be evaluated and applied to advantage, from both an hydrologic and an economic viewpoint. In northern latitudes and at high elevations, snow falls and accumulates on the earth's surface in frozen crystalline form and usually remains until a proper sequence of meteorologic events provides the thermodynamic conditions essential for either evaporation or melting. Periodic snow surveys provide a reliable index of the relative snow accumulation. With knowledge of the processes of storage, evaporation, and melting, the engineer can predict, with reasonable accuracy (for normal climatic conditions and for a known snow pack), the characteristics and the stream flow to be expected. These predictions are then applied in determining multiple-purpose reservoir capacities and in designing spillways. In contrast, forecasts of amounts of rainfall can at best be made only a few

---

Note.—Published, essentially as printed here, in May, 1953, as *Proceedings-Separate No. 189*. Positions and titles are those in effect when the paper or discussion was received for publication.

[1] Asst. Chf., Hydrology Branch, Project Planning Div., Bureau of Reclamation, U. S. Dept. of the Interior, Denver, Colo.

hours before the actual storm, and runoff occurs almost immediately after the rain has fallen.

In the United States, the greatest total snowfall and accumulation occur in the high mountain areas and extreme northern latititudes. In the western states, the economy of the arid and semi-arid lands lying between the mountain ranges is increasingly dependent on the development of multiple-purpose storage reservoirs to utilize the stream flow originating in the high mountain snow packs. Engineers of the western states accept as a blessing the fact that the predictable characteristics of this stream flow enable economies in planning and designing multiple-purpose reservoirs by the joint use of space allocated to the various functions and by the reduction of spillway capacities. They continually seek fuller understanding of the processes of snow evaporation, melting, and runoff, and of their application to determining reservoir and spillway capacities as expressed in the following sections of this paper.

Snow Evaporation, Melting, and Runoff

Snow has the desirable characteristic of being stored on the earth's surface for a considerable period of time before it evaporates, or melts and infiltrates into the soil, or runs off into stream channels (usually at a moderate rate). The snow cover, because of its structure, will store and hold considerable quantites of the rain which falls on it and will facilitate the infiltration of temporarily stored water into the underlying soil mantle. Thus, it tends to retard and regulate the runoff from excessively rapid precipitation. Runoff from snow melt is seasonal in occurrence, of long duration, of relatively large volume, and of moderate rate, and can be forecast in terms of total volume on the basis of snow surveys, precipitation, and temperature.

The melting and evaporation of a snow cover are fundamentally a matter of thermodynamics. Walter T. Wilson,[2] A.M. ASCE, has presented an admirable outline of the thermodynamic relationships. The sun is the ultimate source of energy. This heat energy can reach the snow through several indirect paths in the atmosphere and by direct radiation. For practical application, however, the temperature of the air seems to be the most significant single index of melting conditions. Snow-melt rates frequently are expressed as functions of air temperatures measured in degree-days above freezing. Such expression incorrectly implies that other effects are either negligible or constant, or that they are simple functions of temperature. The significant paths by which solar energy actually reaches the snow may be divided into two categories. The first category consists of three major paths: Radiation, convection or turbulent exchange, and condensation or latent heat. The second category is composed of three minor paths: Conduction from air, conduction from underlying soil, and warm rain. As melt occurs, the melt water accumulates in and moves through the snow pack in accordance with certain physical laws. Robert W. Gerdel,[3] M. ASCE, has studied, and reported on, these relationships in some detail.

---

[2] "An Outline of the Thermodynamics of Snowmelt," by Walter T. Wilson, *Transactions*, Am. Geophysical Union, 1941, Pt. I, pp. 182-195.

[3] "The Dynamics of Liquid Water in Deep Snow Packs," by R. W. Gerdel, *ibid.*, Vol. 26, Pt. I, August, 1945, pp. 83-90.

Much has been accomplished in identifying the physical factors contributing to the processes of snow melting and evaporation, and in determining the intricate relationships existing among these factors. Regardless of these accomplishments, the engineer who must apply them in the planning and design stage finds that usually it is not practicable, with the hydrologic and meteorologic data available (1952), to apply all these factors and their relationships on a watershed basis. He is compelled, therefore, to utilize his knowledge of the physics of snow evaporation and snow melt largely as a guide to judgment, and to turn to empirical relationships which make use of available data when he is performing his computations. As a backlog of data covering the various pertinent hydrologic and meteorologic factors becomes available, it will be possible to apply the results of research and to obtain a more precise and economic design.

The problem of predicting the shape of the snow-melt hydrograph is usually approached from the premise that, with a full snow cover, an excess of 1° of temperature above a given base (usually 32° F) would produce a constant volume of runoff.

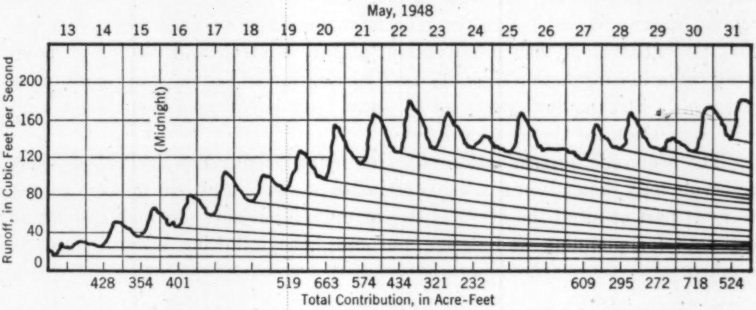

FIG. 1.—SNOW-MELT RUNOFF, ST. LOUIS CREEK NEAR FRASER, COLO. (AREA 32.8 SQ MILES)

It has been demonstrated by W. U. Garstka,[4] M. ASCE, and others, working with relatively complete data from an experimental watershed in the Fraser Experimental Forest in the Rocky Mountains of Colorado, that the melt from one day of temperature excess will reach a peak within a certain lag time, after which the remainder of the runoff will follow a recession curve having a fairly constant slope factor, as shown in Fig. 1, in which the total contribution to runoff made by the day's snow melt has been computed from a recession-curve analysis of the hydrograph. In this connection, it is recognized that the runoff is divided into three components: (1) Overland flow directly into stream channels; (2) subsurface flow through the mantle of decayed vegetation and soil; and (3) ground-water flow from ground-water tables in the underlying rock. Overland flow usually is reflected in the immediate daily peak of the hydrograph, and subsurface and ground-water flow are reflected in the recession curve—the change in dominance from one to the other appearing as a change in slope. Application of this knowledge permits an analysis somewhat similar to the approach based on the unit hydrograph and recession curve, as commonly used in the development of stream-flow hydrographs from rainfall.

---

[4] "Report No. 1, the 1948 Snowmelt Season, Progress in Snow Investigations at the Fraser Experimental Forest," Cooperative Snow Investigations, prepared and published jointly by the Bureau of Reclamation, U. S. Dept. of the Interior, and Forest Service, U. S. D. A., November, 1949.

CAPACITIES OF MULTIPLE-PURPOSE RESERVOIRS

In multiple-purpose reservoirs, storage capacities allocated to such functions as irrigation, hydroelectric power generation, flood control, and navigation are determined by operation studies in which historical stream flows are regulated to satisfy the multiple requirements. The historical stream flows are derived either from recorded discharge measurements, or, if necessary, by correlation with recorded stream flows or other data in the same climatic and physiographic area. Water-storage requirements are determined by studying demands of the various multiple uses after unregulated sources have been utilized. A release for one purpose may serve several other purposes; for example, water released for power generation may also be used for navigation, pollution abatement, fish preservation, salinity control, and similar purposes prior to, or in conjunction with, its use for irrigation and other water-consuming purposes. Stream flow produced by snow melt is compatible in many ways with regulation for these purposes.

The economic determination of space requirements in a multiple-purpose reservoir may depend on a reliable estimate of space that can be used jointly to meet part or all of the needs of two or more functions. In making such an estimate for planning and design purposes, the following criteria must be applied:

a. Irrigation storage capacity (both single-purpose and joint-use) must be filled during the runoff season. Favorable allowance is made for probable overestimate of the forecasted seasonal runoff.

b. Flood-control storage capacity (both inviolate and joint-use), as required for the control of the predicted flood at any time during a given season, must be definitely available on the specified date. Necessary allowance is made for a probable underestimate of the forecasted flood runoff.

c. Water for power, as required—in addition to usable irrigation and other functional releases for generation of prime power to meet contract schedules throughout the year—must be stored entirely during the runoff season.

d. If storage requirements are also established for other functions, such as pollution and salinity control, criteria must be applied.

The key feature of reservoir operating plans involving joint use of storage for irrigation and flood control, or variable allocations to flood control, is the set of operating curves commonly called operation "parameters." In Fig. 2 an example of these operating parameters is shown for the Palisades Reservoir on the Snake River, in southeastern Idaho. They show anticipated runoff from any given date until July 31. A typical method for deriving and applying these parameters will be outlined briefly, omitting details. Similar procedures, suited to the stream-flow characteristics of other basins, are "tailor-made" to meet the particular situation.

Runoff Forecasting Curves.—These curves are the first essential feature of a reservoir operating plan based on variable allocations to flood control. The curves can be derived only when the basic data are adequate for reliable corre-

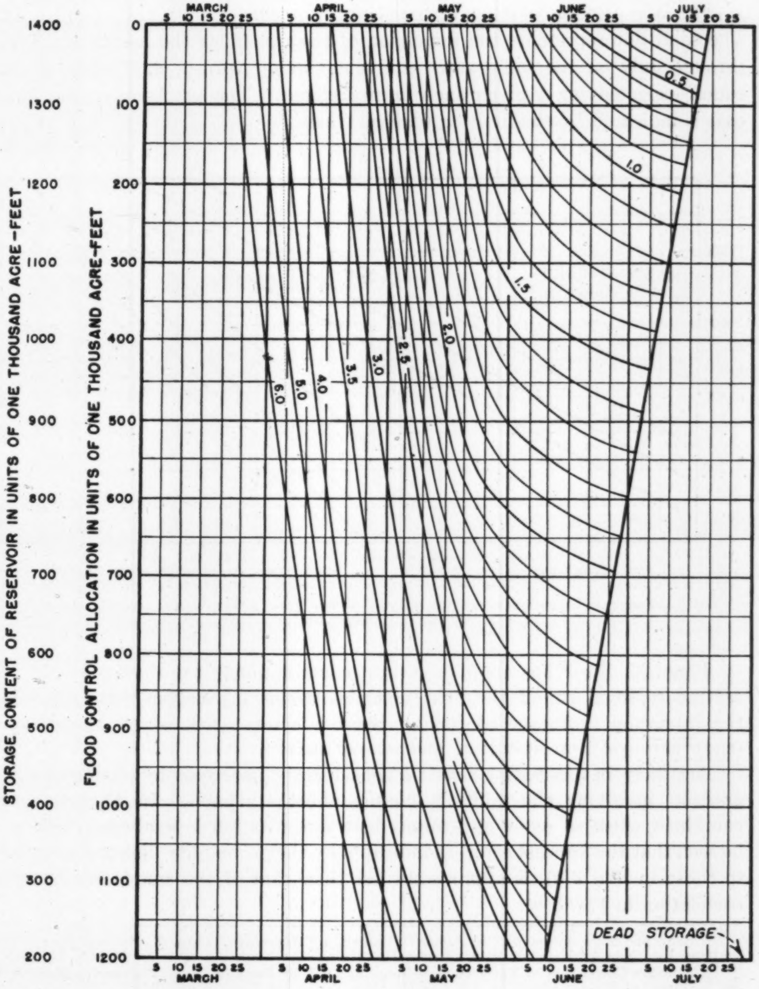

FIG. 2.—ALLOCATION OF FLOOD-CONTROL SPACE ON THE BASIS OF ANTICIPATED FLOOD-SEASON RUNOFF (PARAMETERS ARE IN MILLIONS OF ACRE-FEET)

lations between snow indices and natural runoff at the potential reservoir site. Reliable, seasonal runoff forecasts are limited at the present time to streams deriving most of their flood-producing runoff from snow melt during the spring and early summer months. James E. Church,[5] a leader and early pioneer in the field of snow surveying and runoff forecasting, has done much excellent writing on the subject.

Fig. 3(*a*) is a forecast curve based on snow survey data and runoff data. The solid line represents the regression of the runoff for the months of April through July on the snow-water equivalent as of April 1, and indicates the runoff expected for a given snow measurement. The precision of the forecast is indicated by the limiting (dashed) lines.

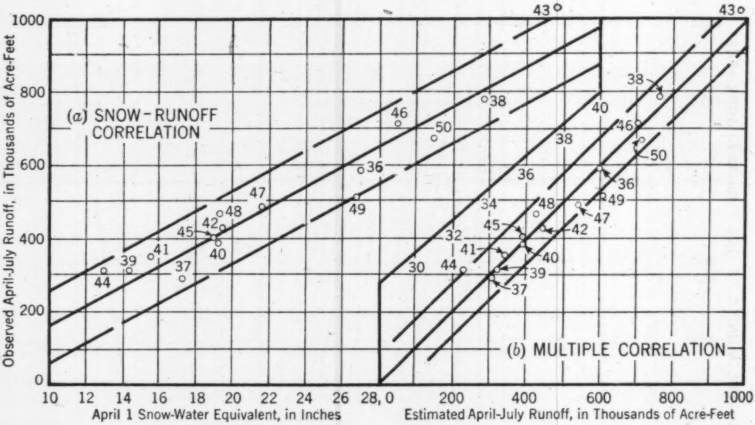

FIG. 3.—FORECAST CURVES FOR THE SOUTH FORK OF THE BOISE RIVER AT ANDERSON RANCH DAM NEAR BOISE, IDAHO

Perry M. Ford[6] has made important contributions to the methods of forecasting seasonal runoff through multiple-correlation analysis for evaluating the integrated influence of such measured factors as snow on the ground (snow surveys[7]), precipitation, and temperature.

Accuracy in forecasting may be considerably improved by means of a regression involving the multiple factors affecting runoff. In Fig. 3(*b*) the combined effect of snow and antecedent precipitation is evaluated. It will be seen that the forecast error, as indicated by the probability limits comparable to those in Fig. 3(*a*), is appreciably less than that of the simple snow-runoff correlation in Fig. 3(*a*).

---

[5] "Snow and Snow Surveying," by James E. Church, in "Hydrology," Oscar E. Meinzer, Dover Publications, Inc., New York, N. Y., 1949, Chapter IV.

[6] "Multiple Correlation in Forecasting Seasonal Runoff," by Perry M. Ford, ***Engineering Monograph No. 2***, Bureau of Reclamation, U. S. Dept. of the Interior, Denver, Colo., April, 1949.

[7] "Snow Surveying," by James C. Marr, ***Miscellaneous Publication No. 380***, U. S. D. A., Washington, D. C., June, 1940.

In Fig. 3 the encircled points are identified by the last two digits in the applicable year. The values of the snow-water equivalent represent averages as of April 1 covering the period of record for five snow courses in Idaho. The forecast derived from Fig. 3(*b*) is based on conditions of April 1, 1950. The equation for the solid-line curve in Fig. 3(*a*) is

$$y = 26.89\,x - 95.53 \qquad (1)$$

in which x represents abscissa values and y represents ordinates. The solid-line curve in Fig. 3(*b*) may be expressed as

$$y = 17.0\,x_2 + 21.4\,x_3 - 126.0 \qquad (2)$$

in which, for the forecast of April 1, 1950, x_2 is the precipitation observed from October, 1949, through January, 1950, and x_3 is the snow-water equivalent of April 1, 1950. In Fig. 3(*a*) the dashed-line limits have departures from the mean line equal to ± 98,200 acre-ft; and in Fig. 3(*b*), departures equal to ± 79,450 acre-ft.

TABLE 1.—ANALYSIS OF AN HISTORICAL FLOOD

Period (1)		Volume[a] (2)	Summation[a] (3)	Volume[a,b] (4)	Summation[a,b] (5)
Feb.	1-15	94.4	4,382.6		
	16-28	87.0	4,288.2		
March	1-15	93.5	4,201.2		
	16-31	126.8	4,107.7		
April	1-15	122.9	3,980.9	−477.1	0
	16-30	239.1	3,858.0	−360.9	200.2
May	1-9	296.2	3,618.9	−63.8	561.1
	10-15	297.4	3,322.7	57.4	624.9
	16-31	1,135.7	3,025.3	495.7	567.4
June	1-7	351.8	1,889.6	71.8	71.8
	8-15	278.6	1,537.8		
	16-30	514.4	1,259.2		
July	1-15	454.7	744.8		
	16-31	290.1	290.1		

[a] In thousands of acre-feet. [b] For runoff greater than 20,000 cu ft per sec.

Analysis of Historical Floods.—In developing parameters, each historical flood at the reservoir site is analyzed to determine the storage space required, and to control that flood to a specified maximum release (usually the nondamaging downstream channel capacity), at the same time, having the reservoir at the maximum safe level at the end of the flood season. In that regard it is necessary to have the following basic information: The maximum release through outlets at the dam (normally equal to the safe channel capacity at critical downstream points); the active storage capacity of the reservoir; the daily discharges for significant floods of record (care having been taken to include relatively small floods occurring either early or late in the snow-melt season, as these floods may prove valuable as control points); and the date when snow-melt inflow generally becomes negligible.

Each flood also is analyzed to determine the storage space required at various time intervals to limit the flood to the specified maximum release. In

Table 1 the procedure is illustrated by a hypothetical example in which the maximum release is 20,000 cu ft per sec; the end of the snow-melt period is July 31; the routing time interval, 15 days; the active storage capacity 1,200,000 acre-ft; and daily discharge data are available. After the flood-storage requirements are computed for each flood, the storage requirement volumes are plotted against time.

Daily discharges were analyzed for selected periods shown in Col. 1, Table 1. All intermediate periods were chosen as 15-day or 16-day periods excepting the period from May 1 to May 9, which was selected from daily records because the snow-melt runoff began to exceed the channel capacity on May 10, and the period from June 1 to June 7, which was selected from daily records to be the end of the flood season.

The summations of daily discharges exceeding 20,000 cu ft per sec during each period are converted in Col. 4, Table 1, to thousands of acre-feet. Negative volumes indicate periods when drawdown could be made and show how much can be released within the safe channel capacity. When daily flows begin to exceed the safe channel capacity, water must be stored. Minor rises above channel capacity, followed by periods of flow below channel capacity, are disregarded.

For example in Table 1, drawdown was required beginning on April 9, storage was required beginning on May 10, and the flood storage was completed on June 7, after which the daily discharge remained below 20,000 cu ft per sec. The summation of Col. 4, Table 1, from June 7 backward through April 9, as listed in Col. 5, shows the storage space necessary at the beginning of each period to control the flood of Col. 2 to a release of 20,000 cu ft per sec. The April 9 date was determined by an analysis of daily records showing that the total of daily flows under 20,000 cu ft per sec was 200,200 acre-ft between April 15 and April 9.

After the flood-storage requirements have been computed for each flood, the storage requirement volumes (Col. 5, Table 1) are plotted against time. For the example presented in Table 1, the plotting would consist of the following data, in thousands of acre-feet:

Date	Flood-control reservations	Remaining flood volume
April 9	0	3,900
April 16	200.2	3,900
May 1	561.1	3,600
May 10	624.9	3,300
May 16	567.5	3,000
June 1	71.8	1,900

The dates would be plotted as the abscissa values, and the ordinates would be the flood-control reservations. The remaining flood volumes are indicated by a third set of variables (see the family of curves in Fig. 2).

The next step is to draw curves that envelope critical points. These curves, drawn for selected parameter intervals and smoothed for continuity and spacing without changing their enveloping characteristics, are the operating parameters of the example shown in Fig. 2. The remaining flood volumes of the foregoing tabulation are the variables indicated by these curves.

Ordinarily the first drawing of the enveloping parameter curves will require some adjustment to assure ideal multiple-purpose operation. It is desirable to test the parameters by operating the reservoir through critical flood and drought periods, using the runoff forecasting curves and the parameter curves under simulated operating conditions. Frequently, daily operation is necessary during critical periods. This testing and adjustment of the parameters is particularly beneficial to irrigation interests. In many cases, permissible adjustments can be made in the lower (right-hand) part of the parameters, permitting greater storage contents at the end of the snow-melt season.

The operating plan for reservoirs for which variable flood-control allocation are to be made should be, essentially, a set of general regulations covering application of the operating parameters. Technical detail should be kept to a minimum, and matters of basic operating policy should be paramount. The actual forecast curves and operation parameters are subject to continual revision on the basis of new data and experience.

APPLICATION TO SPILLWAY DESIGN

The spillway and surcharge storage capacity for any dam and reservoir project are determined by the inflow design flood. This flood may be from snow melt, or rainfall, or both, depending on the source area. The inflow design flood usually is equal to the maximum probable flood. The maximum probable flood is defined as the largest flood that can be reasonably expected on a given stream at a selected point, and is distinguished from the maximum possible flood by rational consideration of the chance of simultaneous occurrence of the maximum (or minimum) of the several elements or conditions contributing to the flood.

The practical determination of a maximum probable snow flood is at present (1952) generally dependent on empirical relationships derived from studies of observed runoff, precipitation, temperatures, and wind velocities, reapplied under the assumption of reasonable concurrence of maximum conditions. Empirical relationships and procedures to be applied vary with geographical location—with the size, elevation, and topography of the basin—and with the type and quantity of available hydrologic data.

The maximum probable snow flood may be generated by snow melt alone, or by a combination of snow melt and rainfall. The "combination" flood falls into one or the other of two categories—namely, the "rain-on-snow" flood and the "snow-melt-followed-by-rain" flood. The first of these results from rain falling directly on the surface of the snow pack. The rain water is then transmitted either directly and rapidly through the snow pack to the underlying soil or rock surface, or it is absorbed within the snow pack. The absorbed water or prolonged storage with some concurrent melting of the snow continues until the combined rain water and melt water is released either as infiltration into the underlying soil and rock, or runs off into stream channels. Floods of the second category result from rain falling on the wetted soil left when the snow pack has melted. Runoff occurs according to normal rainfall-runoff relationships. In this case, the rain flood usually "rides" downstream on the recession of the antecedent snow flood to form a secondary peak which may exceed the snow-flood peak in magnitude.

Flood from Snow Melt Alone.—Several recognized procedures exist for developing hydrographs for the maximum probable flood from snow melt alone, the selection of procedure depending on the location, the size, and the elevation of the watershed, and on the available hydrologic and meteorologic data. One procedure now (1952) being applied by the Bureau of Reclamation, United States Department of Interior (USBR), for developing the maximum probable snow flood for small areas where the occurrence of rain on snow during the winter season is not probable, is demonstrated as follows:

TABLE 2.—DETERMINATION OF THE RELATION BETWEEN TEMPERATURE AND SNOW-MELT RUNOFF

Year	MAXIMUM 15-DAY RUNOFF[a]		TEMPERATURE STATION A		Melting rate of runoff, in inches per degree-day[e]	TOTAL SNOWMELT RUNOFF	
	(Cu ft per sec)-day	Inches	Accumulated[b] temperature[c] above 32° F	Degree-days adjusted to basin[d]		(Cu ft per sec)-day	Inches
(1)	(2)	(3)	(4)	(5)	(6)	(7)	(8)
1944	39,610	4.91	294	234	0.0210	77,200	9.57
1942	26,460	3.28	266	206	0.0159	67,040	8.31
1941	25,250	3.13	376	316	0.0099	42,350	5.25
1938	22,760	2.82	269	209	0.0135	67,280	8.34
1937	32,670	4.05	360	300	0.0135	76,960	9.54
1936	28,880	3.58	259	199	0.0180	72,360	8.97
1935	56,950	7.06	305	245	0.0288	98,740	12.24
1933	53,160	6.59	374	314	0.0210	84,700	10.50
1932	40,170	4.98	392	332	0.0150	66,070	8.19
1931	30,010	3.72	294	234	0.0159	53,480	6.63
1930	26,780	3.32	230	170	0.0195	79,860	9.90
1929	27,750	3.44	251	191	0.0180	62,680	7.77
1928	45,980	5.70	289	229	0.0249	138,910	17.22
1926	46,870	5.81	329	269	0.0216	95,840	11.88
1925	37,430	4.64	420	360	0.0129	60,020	7.44
1924	53,320	6.61	264	204	0.0324	119,800	14.85
1923	51,060	6.33	292	232	0.0273	134,070	16.62
1922	47,520	5.89	353	293	0.0201	106,970	13.26
1921	77,120	9.56	337	277	0.0345	132,140	16.38

[a] The contributing area is 300 sq miles. [b] Over a 15-day period. [c] Daily mean, in degrees Fahrenheit. [d] The lapse rate is 4° per 1,000 ft. [e] Values in Col. 6 are found by dividing the runoff of Col. 3 by the degree-days of Col. 5.

1. The maximum experienced snow-melt runoff rates for the basin are computed either in inches, or in (cubic feet per second)-days, per degree-day of temperature, for the years in which little or no precipitation occurred during the period of high snow-melt runoff. Normally, during any one season, the period of high snow-melt runoff is confined to a period of from 10 days to 20 days. In the example shown in Table 2, a 15-day runoff period is used.

2. The part of the basin that will contribute to the snow-melt flood runoff is estimated from the approximate elevation of the snow line as observed during the maximum runoff period of record. The judgment of the engineer making the study is all-important. The aspect, exposure, and latitude of the watershed all have bearing on the selected elevation. It is assumed in this example

that 300 sq miles, of a total of 460 sq miles, above the proposed dam site, would contribute.

3. From a temperature station near to, and representative of, the basin, the accumulated degree-days of temperature above 32° F corresponding to each of the maximum 15-day runoff periods are computed and adjusted according to the mean change in temperature per 1000 ft of elevation (lapse rate) to the mean elevation of that part of the basin which contributes to the snow-melt runoff (see Table 2, Col. 4). If the stream-gaging station is a considerable distance from the snow-melt area, it is necessary to determine time lag between snow-melting temperatures and runoff.

4. The maximum 15-day runoff expressed in inches is divided by the accumulated and adjusted degree-days for the period to determine the melting rate of runoff.

5. For each year tabulated, the total runoff that occurred during the entire snow-melt season until the daily mean flow receded to the ground-water recession curve (see Table 2, Col. 8) is computed in inches. This is the "index" runoff.

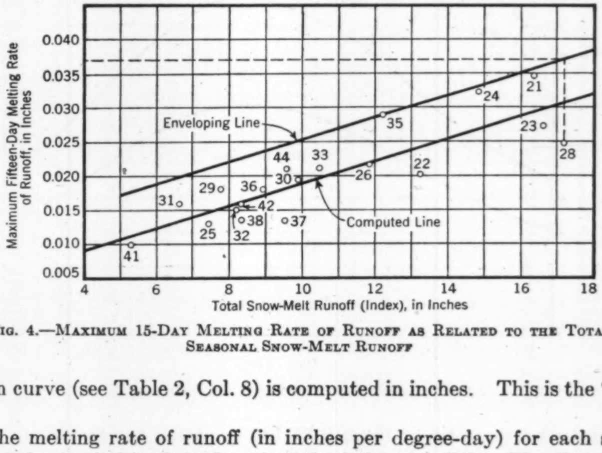

FIG. 4.—MAXIMUM 15-DAY MELTING RATE OF RUNOFF AS RELATED TO THE TOTAL SEASONAL SNOW-MELT RUNOFF

6. The melting rate of runoff (in inches per degree-day) for each selected annual 15-day period is plotted against the index runoff (see Fig. 4). A mean line through these points is computed using the method of least squares, and an enveloping line is drawn through the maximum point, parallel to the computed line. The slope of the computed line in Fig. 4 is 0.00165 in. per in., and the vertical intercept is 0.00257 in.

7. In the example shown in Fig. 4, the year of greatest runoff from snow melt is 1928, with an index runoff of 17.22 in. Entering the graph of Fig. 4 with this value (17.22 in.) indicates a melting rate of runoff of 0.0369 in. per degree-day on the enveloping line (as shown by the dashed line). This computed melting rate of runoff is selected as the maximum probable melting rate of runoff for computation of the maximum probable snow-melt flood.

8. The maximum probable snow-melt flood volume is computed by multiplying the melting rate of runoff (in this example 0.0369 in. per degree-day) by

the recorded maximum accumulative 15 days of mean temperatures above 32° F, as observed during periods of snow melt, adjusted to the basin. It is important that the maximum 15-day temperature accumulation be selected from a long period of record, preferably of at least twenty years. Lack of such a record within the basin usually necessitates transposing to the basin the most comparable long-term record available from a near-by point outside the basin. In the example cited, a maximum 15-day total of 377 degree-days, adjusted to the basin, was obtained. This accumulation of temperature would give 13.91 in. of snow-melt runoff, or 112,210 (cu ft per sec)-days.

Distribution of the design volume can be accomplished realistically by augmentation of the maximum, or near-maximum, 15-day recorded hydrograph by the ratio of the respective volumes. In this example, the 1921 runoff having the maximum 15-day volume of 77,120 (cu ft per sec)-days was augumented by the ratio of 112,210/77,120 to obtain the maximum probable snow-melt flood hydrograph shown in Fig. 5. Theoretical distribution of the design volume can also be accomplished by assuming that the maximum accumulative 15 days of mean temperature will follow a thermogram taken from the most severe temperature distribution of record. The runoff for each day, as computed from the daily temperature excesses of the thermogram and the melting rate of runoff, is distributed by a unit hydrograph derived from data such as those discussed previously. The total hydrograph is the sum of these daily flows.

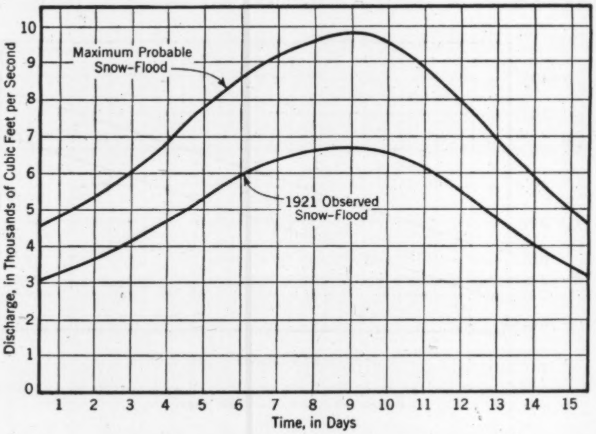

Fig. 5.—Design Snow-Flood Hydrograph

Flood Produced by Rain on Snow.—In the high Sierra Nevada range of California, meterological conditions are such that the greatest precipitation and the most severe floods usually occur during the months of November through March. Precipitation during these months can occur as rainfall at elevations up to 10,000 ft or 1,000 ft, and it is not unusual for a rain storm to occur immediately after previous storms have deposited a cover of snow over the watersheds. The runoff resulting from the rainstorm then depends on a delicate balance between the depth and the density of snow cover and the depth, intensity, and duration of the rainstorm. If a deep and "dry" snow cover exists, it may absorb and detain most of the rainfall, so that little runoff will result. On the other hand, with moderate snow cover and considerable intense rain, the snow cover temporarily "holds" rain until the snow melts, whereupon the "held" rain, plus the water content of the snow cover, is released rapidly, causing runoff exceeding that which would result from the rainstorm alone. The Sacramento River Basin floods of late November, 1950, are examples of this situation. In developing hydrographs for inflow design floods for dam sites in this terrain, the critical consideration is the potential flood from an early winter rainstorm falling on a watershed having optimum snow cover. The snow-melt contribution may not be the dominant factor, but it is very significant in developing the inflow design flood. The melting rate of snow, the effect of the snow cover on the rain-fed runoff, and the losses into the soil are some of the problems to be resolved. An attempt was made early in 1951 to bring these factors together in a manner satisfactory for engineering applications in order to derive an inflow design flood for Sly Park Dam site, in the Central Valley Basin of California.

By applying the formula[8] of Phillip Light, A.M. ASCE, the Hydrometeorological section of the Weather Bureau (United States Department of Commerce) and the Corps of Engineers[9] (United States Department of the Army) had computed melting rates for watersheds within the Sacramento River Basin on the basis of turbulent transfer of heat and moisture between the air and the snow surface. As applied, relating the rate of melt over a drainage area to observation of wind velocity, temperature, and humidity at standard levels above the surface, the formula is

$$D = 0.00184\,K\,U\,[(t - 32)\,10^{-0.0000156Z} + 0.00578\,(p - 6.11)] \quad \ldots\ldots(3)$$

in which D is melt, in inches of water per 6-hr period; U is the wind velocity in miles per hour at the 50-ft level; t is the temperature, in degrees Fahrenheit at the 10-ft level; p is the vapor pressure, in millibars at the 10-ft level; Z is the elevation, in feet above mean sea level; and K is a regional or basin constant.

The merit of Mr. Light's formula has been demonstrated further by its application to snow-melt computations in connection with research conducted by the USBR in cooperation with the Forest Service (United States Department of Agriculture), at the Fraser Experimental Forest, at Fraser, Colo.[10]

Joseph B. Paulson, Jr., also had devised a method[11] of utilizing the Sacramento River Basin melting rates in such a manner as to provide increments of

---

[8] "Analysis of High Rates of Snow-Melting," by Phillip Light, *Transactions*, Am. Geophysical Union, Pt. I, 1941, pp. 195–205.

[9] "Maximum Possible Precipitation, Sacramento River Basin," *Hydrometeorological Report No. 3*, Weather Bureau, U. S. Dept. of Commerce, and Corps of Engs., U. S. Dept. of the Army, 1943.

[10] "Report No. 2, the 1949 Snowmelt Season, Progress in Snowmelt Investigations at the Fraser Experimental Forest, Colorado," Cooperative Snow Investigations, prepared and published jointly by the Bureau of Reclamation, U. S. Dept. of the Interior and Forest Service, U. S. D. A., June, 1951.

[11] "A Method for Calculating the Effect of Snow on Runoff During a Rainstorm," by Joseph B. Paulson, Jr., *Transactions*, Am. Geophysical Union, Pt. 1, 1944, pp. 15–21.

"equivalent rainfall" that were mean values for the basin and that could be applied to some method of computing a rain-runoff hydrograph. The Sacramento District office of the Corps of Engineers, in computing the inflow design flood for Pine Flat Dam on Kings River,[12] had made use of Mr. Paulson's method as modified to provide for the effect of a varying infiltration rate.

In the study of Sly Park damsite on Sly Park Creek, a northern tributary of the Mokelumne River, California, made by the USBR, the basic assumptions of the foregoing methods were re-examined in view of observations reported in November, 1950, at the Central Sierra Snow Laboratory, near Soda Springs, Calif., by D. H. Miller, J. M. ASCE, of the Corps of Engineers. The drainage area of 16 sq miles above Sly Park ranges in elevation from about 3,300 ft to nearly 5,800 ft. Three elevation zones were considered: One beween 3,000 ft and 4,000 ft containing 57.5% of the area; one between 4,000 ft and 5,000 ft, containing 34.9% of the area; and one between 5,000 ft and 6,000 ft, representing 7.6% of the area. The watershed was assumed to be covered by snow from a storm which shortly preceded the design rainstorm. Hydrometeorological studies[9] indicated 12 hr as the minimum interval possible between the end of a snowstorm and the beginning of a maximum probable rainstorm. Table 3 lists the water content in inches of assumed antecedent snow cover from *Hydrometeorological Report No. 3*,[9] the assumed density (explained subsequently), and the depth of snow in inches by elevation zones at the time rainfall would begin.

TABLE 3.—DESCRIPTION OF SNOW COVER

Elevation band, in feet	Water content, in inches	Density, (%)	Snow depth, in inches
3,000–4,000	6.00	17	35.30
4,000–5,000	5.10	16	31.86
5,000–6,000	3.60	15	24.00

The snow on the ground preceding the rain was "new-fallen." Density of new-fallen snow varies, but only on rare occasions does it reach 20%. According to Mr. Miller, the snowfall density on November 16, 1950, with a temperature of 30° F, at the Central Sierra Snow Laboratory (elevation approximately 7,000 ft), was over 13%. For the Sly Park study, it was assumed that, under maximum probable conditions, density of the new snow would vary uniformly from 20% at El. 1000 to 10% at El. 10000.

An accumulation of 1.5 in. of melt water was assumed to have been retained on the watershed before the beginning of the inflow design flood computations. Additional retention during the rain and melt period was taken from a curve plotted in such a manner that 6-hr increments of retention were indicated from total accumulative retention. Only the application of values from this curve is pertinent to the present discussion.

The data of Table 3 were then utilized as follows: During the 6-hr period preceding the design rain a small amount of melting begins as the result of rising temperatures. As the design rain starts, melting of the snow cover is accelerated by warmer temperatures and turbulence from accompanying winds. The water initially released by melting and from rain is stored in the snow pack.[13] The density of the snow pack increases and its actual depth decreases as the process continues. When the density reaches the retention-capacity limit of the snow pack, the excess water will be released either to infiltration or runoff. The snow pack will attain a "saturated" density and will continue to decrease in depth during infiltration and runoff until the storm ends and temperatures fall below 32° F. If snow remains at the end of the storm, it will have a density equal to that at which it ceased to store water.

---

[12] *Corps of Engineers Definite Project Report*, Pine Flat Dam and Reservoir, Kings River, Calif., April, 1947, Corps of Engrs., U. S. Dept. of the Army.

TABLE 4.—ANALYSIS OF RAINFALL ON SNOW HAVING AN ASSUMED INITIAL DENSITY OF 17%; FOR THE ELEVATION ZONE BETWEEN 3,000 FT AND 4,000 FT IN THE SLY PARK STUDY

Procedure:

Col. 3 is taken directly from storm data.
Col. 4 represents potential snow melt, and is computed from Eq. 3 using observed data.
Col. 5 is obtained from Col. 4 by dividing those values by the values in Col. 7 for the preceding period.
Col. 6 begins with the value of the depth of the antecedent snow cover (the given water content divided by 17%). Each subsequent value is obtained from the preceding value by adding the depth of any new snowfall (not applicable to this example) and subtracting the value in Col. 5.
Col 7 is computed by dividing the values in Col. 9 by those in Col. 6.
Col. 9 begins with the value of the water content of the antecedent snow cover. Subsequent values are obtained from the preceding value in Col. 14 by adding the value in Col. 3 (plus snowfall, if applicable).
Col. 10 shows the excess of values in Col. 9 over those in Col. 8, or the values from the retention curve, whichever are smaller.
Col. 11 shows the accumulation of values in Col. 10.
Col. 12 is obtained by subtracting the values in Col. 10 from those in Col. 9.
Col. 13 is the excess of each value in Col. 12 over the corresponding value in Col. 8.
Col. 14 is obtained by subtracting the values in Col. 13 from those in Col. 12, and cannot exceed corresponding values in Col. 8.
Col. 15 is equal to Col. 13 multiplied by the ratio of the band area to the total basin area (0.575 for this band).

6-HR TIME INCREMENT		Increment of rain, in inches	INCREMENT OF SNOW MELT, IN INCHES		Depth of snow on the ground,[a,b] in inches	Density of the snow,[c] in %	Water-holding capacity at 40% density,[d] in inches	Accumulated unreduced water content,[e] in inches	Increment of retention, in inches	Accumulated retention,[f] in inches	Accumulated reduced water content,[g] in inches	Increment of water excess, in inches	Residual water content,[h,b] in inches	Contribution to the basin mean water excess, in inches
Start	End		Water content	Depth										
(1)	(2)	(3)	(4)	(5)	(6)	(7)	(8)	(9)	(10)	(11)	(12)	(13)	(14)	(15)
					35.30	17	14.12	6.00	0	1.50[i]	6.00	0	6.00	0
−6	0		0.4[j]	2.35	32.95	18.2	13.18	6.00	0	1.50	6.00	0	6.00	0
0	6	1.4	1.00	5.49	27.46	27	10.98	7.40	0	1.50	7.40	0	7.40	0
6	12	2.4	1.00	3.70	23.76	40	9.50	9.80	0.3	1.80	9.50	0	9.50	0
12	18	3.7	1.20	3.00	20.76	40	8.30	13.20	1.77	3.57	11.43	3.13	8.30	1.80
18	24	1.0	0.70	1.75	19.01	40	7.60	9.30	1.50	5.07	7.80	0.20	7.60	0.12
24	30	0.3	0.70	1.75	17.26	40	6.90	7.90	1.00	6.07	6.90	0	6.90	0
30	36	4.8	1.60	4.00	13.26	40	5.30	11.70	1.20	7.27	10.50	5.20	5.30	2.99
36	42	7.2	2.00	5.00	8.26	40	3.30	12.50	1.03	8.30	11.47	8.17	3.30	4.70
42	48	5.4	1.60	4.00	4.26	40	1.70	8.70	0.90	9.20	7.80	6.10	1.70	3.51
48	54	3.4	1.20	3.00	1.26	40	0.50	5.10	0.77	9.97	4.33	3.83	0.50	2.20

[a] Cannot be less than zero. [b] The depth of snow left at the end of the storm (last line) equals 1.26 in., with a water content of 0.50 in.; if melted in the following 6-hr period, this quantity would be absorbed by retention. [c] Holding capacity of the snow mass, not to exceed 40%. [d] Maximum capacity of the snow mass to prevent significant retention. [e] The accumulated water content unreduced for retention or surface runoff during the period. [f] Used as a parameter for retention capacity. [g] The accumulated water content after reduction for retention during the period. [h] Total water content carried forward into next period. [i] Assumed initial accumulated retention. [j] Melting preceding design rain.

---

[13] "A New Technique for the Determination of Heat Necessary to Melt Snow," by Merrill Bernard and Walter T. Wilson, *Transactions*, Am. Geophysical Union, 1941, Pt. I, pp. 178–181.

According to Mr. Miller, during the flood of November, 1950, the snow remaining on the ground after approximately 16 in. of rain had fallen upon it had a density of from 40% to 45%.

In the Sly Park study, it was assumed that no release of water from the snow pack would occur until the snow attained a density of 40%, and that all water in the snow pack above a density of 40% would be available to infiltration and runoff. Table 4 shows the computation for the zone between 3,000 ft and 4,000 ft. If snow had fallen during the storm, it would have been necessary to add a column between Cols. 2 and 3, entitled "Increment of Precipitation," and two columns to the left of Col. 4, under the general heading, "Increment of Snowfall." The first column under this general heading would have shown the water content and the second the depth of the snow, the second set of values having been obtained by dividing all the water-content values by 17%, the assumed initial density. These values affect those in Col. 6. If snow had fallen at the end of the storm, runoff would have stopped.

Addition of the values of the contributions to the mean water excess for the basin (Col. 15, Table 4), computed from each elevation band, provided incremental runoff values that were applied to a unit hydrograph for the watershed in order to determine the hydrograph for the inflow design flood.

Inflow Design Flood Based on Seasonal Snow Melt.—Safe utilization of joint-use storage space for the control of the inflow design flood in areas where the snow flood is dominant can be assured by the development of an inflow design flood portraying maximum probable snow-melt runoff from the beginning of the melting season to its cessation and including runoff from a rainstorm that reasonably could be expected to occur concurrently with, or immediately following, the high discharges from melting snow.

Numerous methods exist by which such a seasonal hydrograph can be developed. Fundamentally, they are all based on the concept of a winter of high snowfall and continuing low temperature, followed by a period of unusually high temperature, and accompanying rainfall which produces maximum rates and volumes of runoff from the melting of the accumulated snow pack. The 1948 flood of the Columbia River[14] was an actual example of this type of event.

In January, 1951, Bertram S. Barnes, M. ASCE, working with data from the South Fork Flathead River in Montana (an upper tributary of the Columbia River) developed a procedure utilizing observed temperature sequences to compute favorable reproductions of observed seasonal runoff. This procedure of the USBR is being expanded for application in deriving the maximum probable flood. Mr. Barnes' procedure involves the following major steps and assumptions:

1. A "base" temperature can be derived, which, when subtracted from the maximum daily temperatures at a near-by observation station during an observed snow flood, will give the best index of melting temperatures over a watershed.

2. The direct runoff occurring during the snow flood will reflect the index of melting temperatures. Direct runoff is observed runoff from which groundwater flow has been subtracted by standard methods.

---

[14] "Floods of May–June 1948 in Columbia River Basin," *Water-Supply Paper No. 1080*, Geological Survey, U. S. Dept. of the Interior, Washington, D. C., 1949.

3. Before index melting temperatures will be properly reflected in a reproduction of the computed direct runoff, the proper base temperature must be determined by trial and error. This is done by using a device referred to as the "hydrothemogram."

4. The hydrothermogram is a hypothetical discharge hydrograph computed on the assumption that each effective degree of temperature above the base temperature will generate the same amount of runoff volume. Of this runoff volume, the maximum daily runoff occurs on the first day, thereafter decreasing at a normal rate such as illustrated in Fig. 1. The runoff on the first day is assumed to be one unit per degree of temperature. The second day's runoff from that same generation is the depletion factor (0.816 for the South Fork Flathead River) times the runoff for the first day; the third day is the depletion factor times the runoff for the second day; and the values for succeeding days are computed in the same way. For a given sequence of daily effective temperatures above a given base, the process is similar to that approach which involves unit hydrographs for successive unit periods of excess rainfall. The sample computations in Table 5 are from one of the work sheets, starting at the beginning of the snow-melt season.

TABLE 5.—COMPUTATIONS FOR A HYDROTHERMOGRAM

Date, in April (1)	Maximum temperature (in degrees) above 54° (2)	Residual,[a] in (cubic feet per second)-days (3)	Total daily runoff, in (cubic feet per second)-days (4)
14	2	....	2.0
15	8	1.6	9.6
16	15	7.8	22.8
17	3	18.6	21.6

[a] The previous total from Col. 4 multiplied by the depletion factor, 0.816.

In reproducing an observed seasonal hydrograph with a recorded temperature sequence, the procedure is applied with successive base temperatures until the best fit is obtained between the hydrothermogram and the hydrograph of direct runoff. The melting rate of runoff necessary to convert the thermogram to the observed runoff becomes apparent at this stage of the analysis. Fig. 6(*a*) shows the hydrograph of direct runoff for the South Fork Flathead River during April and May, 1948, and the derivation of the daily depletion factor. Fig. 6(*b*) demonstrates the comparison of hydrothermograms for differing base temperatures with this hydrograph of direct runoff. The base temperatures are noted on the curves. A base temperature of 57° F provided the best fit.

Application of the base temperature, the maximum melting rate of runoff, and the hydrothermogram—in order to determine the maximum probable snow flood hydrograph—requires prediction of the design snow-flood volume and of the melting period. The design volume can be computed by several procedures from an estimate of the maximum probable snow pack which would accumulate during a cold winter of heavy snowfall. The total design volume may then be divided into two parts: The direct runoff which follows the

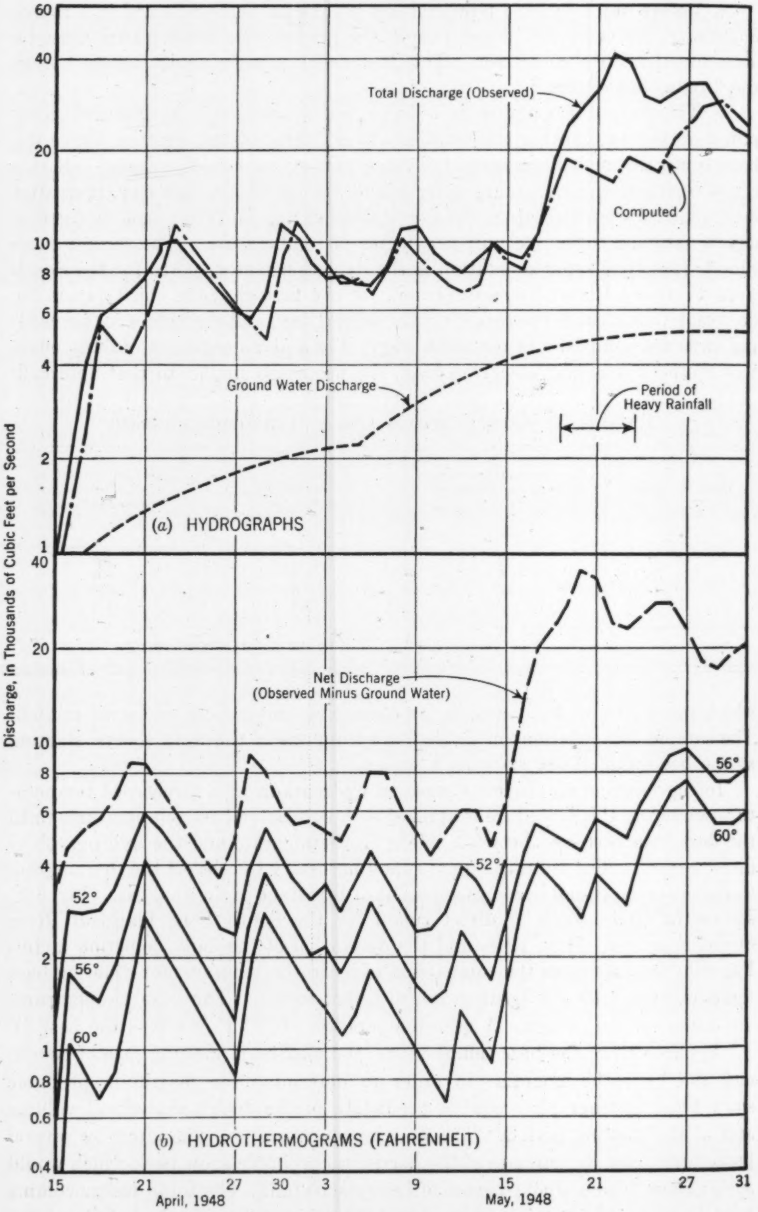

FIG. 6 —RUNOFF, SOUTH FORK FLATHEAD RIVER

thermogram pattern and the direct runoff in the hydrograph recession. The design volume is proportioned into these two parts by analyzing several observed hydrographs. The volume falling into each of the two parts may then be expressed as a percentage of the total direct runoff. The hydrothermogram of the maximum probable temperature sequence and the maximum melting rate of runoff are then applied until the first part of the design volume is satisfied.

CONCLUSIONS

The water resources of the western states can be developed economically only by taking advantage of every opportunity for full utilization of the limited stream flows. The construction of multiple-purpose reservoirs on surface streams is one of the most common methods for attaining this objective. In the determination of space allocation for each of the multiple uses and spillway capacities of multiple-purpose reservoirs, economy can be obtained by considering stream-flow and snow-melt characteristics. This paper has presented a summary of the principles involved and a few typical examples. No attempt has been made to cover the subject historically or in full detail. Those interested will find such detail available in the published reports of the agencies engaged in such planning and design. Great refinement in procedure, with corresponding economy in both design and operation, will result from continued research in the field of snow hydrology and from the extension of networks for the collection of data so that they include pertinent elements on a watershed basis.

ACKNOWLEDGMENTS

The specific examples given herein have been taken from the files of the Hydrology Branch, Project Planning Division of the USBR. Many of the procedures have been developed from data-gathering and research activities in collaboration with the Corps of Engineers, the U. S. Weather Bureau, the Soil Conservation Service (United States Department of Agriculture), and the Forest Service.

DISCUSSION

Ray K. Linsley,[15] A.M. ASCE.—The accumulation of snow in the mountains of the western United States is economically important. Without this snow the development of this area would have taken a far different and probably less favorable course. To the engineer, however, this snow constitutes a troublesome design factor. Many approximations and assumptions are necessary in any computation of the runoff rates to be expected from melting snow. Mr. Riesbol has performed a service in presenting a fine summary of snow-hydrology practices.

The hydrothermogram procedure outlined by the author (under the heading, "Application to Spillway Design: Inflow Design Flood Based on Seasonal Snow Melt") is an interesting commentary on the present (1953) status of snow hydrology. The method is an application of the "degree-day" approach in which temperature above some base value is taken as an index of the melting rate. It is similar in many respects to the procedure suggested by the writer[16] and basically the same as that proposed by G. D. Clyde,[17] M. ASCE.

A great deal of fundamental research in the field of snow physics has been conducted. Many features of the subject are imperfectly understood, but a skeleton theory exists which should permit one to go beyond the degree-day approach to include in the melting index such parameters as solar radiation, humidity, and wind.

Mr. Barnes did not use these parameters (under the heading, "Application to Spillway Design: Inflow Design Flood Based on Seasonal Snow Melt") because the necessary data for their use on an engineering scale were not available to him. A region of heavy snow accumulation is a region of scanty meteorological and hydrologic data. The variability of meteorological and hydrologic elements in rugged terrain and the economic importance of the region suggest that a station density greater than the national average might be in order. Continued research will fill out the skeleton of knowledge regarding snow physics. With this knowledge the basic data required to utilize it should also be available.

The amount of snow melted from a given basin in any period of time depends on the area of the snow pack exposed to melting conditions. This area is bounded by the lower edge of the snow cover and by the upper limit of the melting temperatures. Neither of these boundaries is strictly an elevation contour. Meteorological data may suffice to define the level to which melting temperatures extend, but the lower limit of the snow cover can be determined only by field location. Aerial photography offers one of the best means of obtaining these data, although terrestrial photography and reconnaisance mapping methods contribute to local determinations. It seems axiomatic that a rational computation of snow melt cannot be performed without some knowledge of the controlling area of the melting zone, just as the runoff from rainfall on a basin cannot be estimated without first knowing the drainage area.

---

[15] Associate Prof. of Hydr. Eng., Stanford Univ., Stanford, Calif.

[16] "A Simple Procedure for the Day-to-Day Forecasting of Runoff from Snowmelt," by R. K. Linsley, *Transactions*, Am. Geophysical Union, Pt. 3, 1943, pp. 62–67.

[17] "Snow-Melting Characteristics," by G. D. Clyde, ***Bulletin No. 231***, Utah Agri. Experiment Station, Logan, Utah, 1931.

It is necessary in some cases to vary both the base temperature for the hydrothermogram and the degree-day factor, or melting rate of runoff, as the season progresses. The variation in the base temperature results from the fact that the melting zone moves progressively higher above the temperature station as the melting proceeds. Similarly, the variation in the melting rate of runoff must result from the change in area of the melting zone. Other factors such as the seasonal variation in solar radiation are undoubtedly important, but there is clearly a need for data defining the critical melting zone.

In Fig. 1 is shown an analysis which has been applied to the computation of the snow-melt hydrograph of a small area. When this analysis is applied to the hydrographs of snow-melt runoff from large areas, it is often found that the recessions of the daily increments of snow melt intersect the falling limb of the total hydrograph. A more rational approach seems to visualize the total hydrograph as the sum of a hydrograph of direct runoff and a ground-water (or subsurface flow) hydrograph (Fig. 6(*a*)). This approach makes apparent the many problems which hamper the application of experience gained in the study of small basins to the engineering problems of large basins. It is quite probable that the development of techniques must wait for available data on large basins.

Under the heading, "Capacities of Multiple-Purpose Reservoirs: Runoff Forecasting Curves," Mr. Riesbol mentions only the use of snow surveys, whereas successful forecasts of seasonal runoff have been made using precipitation data recorded at regular stations of the Weather Bureau.[18] Existing records of rainfall make possible forecasts of runoff for areas where snow surveys are not available. These records offer a better source of data for statistical analysis than do the snow-survey records. Since the data on precipitation are regularly available, the cost of the forecasts is less than the cost of forecasts made from snow surveys. It appears that the accuracy of the forecasts based on precipitation data is as good as those based on snow surveys, although the superiority of either method depends on the local area and the data available. Precipitation data for forecasts of this type certainly deserve consideration for use in snow hydrology.

R. W. Gerdel,[19] M. ASCE.—An improved approach to the development of operational procedures for multiple-purpose reservoirs in areas where precipitation in the form of snow is the dominant hydrologic element has been presented by Mr. Riesbol. The author has emphasized the fact that the hydrologic engineer is compelled to use empirical relationships to develop suitable design and operation criteria despite the considerable amount of research that has been conducted on snow-melt and runoff problems. The gaps in the scientific literature concerning snow may be sufficiently large to justify the use of empirical relationships, but the use of hypotheses not compatible with experimental evidence or the known physical properties of snow is not justified.

---

[18] "Recent Developments in Water Supply Forecasting from Precipitation," by M. A. Kohler and R. K. Linsley, *Transactions*, Am. Geophysical Union, 1949, pp. 427–436.

[19] Chf., Field Operations and Analysis Branch, Snow, Ice and Permafrost Research Establishment, U. S. Dept. of the Army, Wilmette, Ill.

The literature on snow hydrology, mechanics, and physics contains sufficient references to the liquid-water holding capacity of snow and to the metamorphic processes which occur in snow to refute any assumption that a snow pack must achieve a density of 40% before discharge of rain or snow-melt water will take place. Also, there is no basis for assuming that a snow pack will not continue to increase to a density of more than 40% without storage of liquid, or that it will not retain that increase in the form of the solid phase.

In 1948 the writer examined the existing pertinent literature in a search for information about the physical properties of a ripe, discharging snow pack, for a report to the International Commission on Snow and Glaciers.[20] It was found that densities between 25% and 56.5% for a ripe, melting, actively discharging snow pack were reported by several investigators. A snow pack usually consists of a number of readily identifiable layers which are the products of separate storms. The variation in density between these layers may be large at the time of deposition and will be maintained even in the ripe pack. R. A. Work found that homogeneous density was never obtained in a ripe pack and that the density of different layers in a late-April, ripe snow pack varied between 45% and 58%.[21] In the Central Sierra Snow Laboratory observers found variations of more than 10% between the densities of ripe, discharging, spring snow packs at different sample points in the 4-sq-mile basin.

The results of investigations of the discharge of water from a melting snow pack made by the Weather Bureau at the Soda Springs Cooperative Research Project, in California, showed that a pack of 52.8% density, rapidly melting under an air temperature of 65°F, had a total liquid and solid water-equivalent content of 14.8 in. at 3:30 p.m.[22] This content consisted of 13.4 in. of water-equivalent snow crystals and 1.4 in. of liquid water. At 8:30 the following morning, when temperatures had been low enough during the night to prevent or retard melting, the pack density was still 53%, whereas the total water equivalent was only 13.8 in., consisting of 13.4 in. of water-equivalent snow crystals and 0.4 in. of liquid water. The studies showed that no liquid water was frozen in the snow during the night and that the 1-in. loss in water equivalent of the pack during the night could be accounted for by the drainage of the 1 in. of liquid water from the pack during the same period. The maintenance of almost constant density was due to shrinkage and reduction in voids.

The 1944–1945 report from this project presented the results of investigations of a heavy rain on new and old snow.[23] A new snow, five inches deep and of 10% density, had been deposited on top of an old pack of 38.3% density. In places, the new snow was deposited on clean black top and concrete roadways.

---

[20] "Physical Changes in Snow-Cover Leading to Runoff, Especially to Floods," by R. W. Gerdel, Union géodesique et géophysique internationale, Association d'Hydrologie Scientifique, Assemblée générale d'Oslo, Vol. II, Oslo, Norway, 1948, pp. 42–54.

[21] "Snow Layer Density Changes," by R. A. Work, *Transactions*, Am. Geophysical Union, Vol. 29, 1948, pp. 525–546.

[22] "Snow Studies at the Cooperative Snow Research Project, Soda Springs, California," *Annual Report*, Weather Bureau, U. S. Dept. of Commerce, Washington, D. C., 1943–1944, pp. 11–14.

[23] "Snow Studies at the Cooperative Snow Research Project, Soda Springs, California," *Annual Report*, Weather Bureau, U. S. Dept. of Commerce, Washington, D. C., 1944–1945, pp. 10–13.

During one day, 1.44 in. of rain fell upon the new snow. At the height of the storm the new snow, overlying the old snow, contained only 13% of liquid water. On the paved roadway, where water was impounded in depressions, the slush that developed had a free-water content of 30%. Under no circumstances could such a high free-water content be attributed to the water-holding capacity of the snow. It was definitely the result of snow floating on, or being submerged in, water impounded in a depression with an impervious bottom. It is of interest to note that when efforts were made to measure the density of the slush by the usual tube sampling and weighing procedure, the water drained out of the sample so rapidly that the maximum measured density was only 16.5%—much less than the 40% density assumed to be required before melt or rain water could be discharged from the pack.

During the period between 1943 and 1950, when the writer was actively engaged in snow-hydrology research in the western United States for the Weather Bureau and the Corps of Engineers, a number of experiments were performed to determine the effect of large amounts of water on the shrinkage and increase in density of monolithic cylindrical samples of snow. A cylindrical container equipped with a cutter was used to obtain snow core samples (8 in. in diameter and 24 in. long) from sensibly homogeneous horizons in the pack. A screen bottom was applied to the container, the sample was weighed, and was then saturated with water at 32°F. The core was returned to the pack to establish natural capillary tension through the screen bottom. At the end of approximately 4 hr, the core was removed from the container, carefully calipered and weighed, and the free-water content was measured by the calorimetric method. These studies showed that an 18%-density dry snow at a temperature of 32°F underwent a reduction in volume and thus increased its density to 26% with an unfrozen water content of 1.5%. During the shrinkage process more than 2 in. of the previously applied water drained out of the sample, but there was no loss of solids. A 24%-density snow was increased to a density of 31% by this process. Repeated addition of liquid water, equal to three times the water equivalent of the original solid snow crystals in the core sample, changed the density from 22% to 34% by reducing the volume while allowing more than 15 in. of liquid water to pass through the initial 24-in.-long core of snow. The water equivalent of the sample at the beginning and end of the experiment was 5.28 in. and 5.48 in., respectively. The positive increase of 0.2 in. in water equivalent probably represents the amount of liquid retained in the core.

The results of these studies have not been published heretofore because the investigations were limited to high mountain snow covers where steeply sloping land provided rapid drainage and because there was lacking the time and equipment to collect sufficient data with which to demonstrate the extent of application of the results. They are presented in this discussion in hope that the 40%-hypothesis may be subject to a revision based on experimental evidence rather than on empirical judgment.

In another paper[24] the writer has discussed some experiments performed on the water transmission and retention capacity of snow as measured with an electronic capacitance meter developed for this type of investigation. It was found that for snow of 35% to 46% density, water applied to the surface of the snow (in quantities of 0.5 in. to 2.0 in.) was transmitted through 0.9 in. to 24 in. of snow per min. This velocity appears to indicate a limited temporary detention capacity. The permanent retention capacity, when free drainage was available, was approximately 0.1 in. of water per ft of 50%-density snow. It was shown that the movement of water through the snow pack follows definite channels which develop perpendicularly and horizontally within the pack. These channels have been recognized by glaciologists who term them "firn pipes" or "glands." The channels develop into drains filled with coarse-grained crystals in the melting seasonal layer of snow and are similar to the rock-filled drains used in agricultural and other soil-engineering practices. When the ground is exposed as a melting snow pack recedes in the mountains, the flow channels which have developed at the contact between the snow pack and the ground are evident on some soils, as a dendritic pattern of erosion marks. When these channels develop over rock or less erodible soils, they appear as arched piping in the bottom snow layer.

---

[24] "The Transmission of Water Through Snow," by R. W. Gerdel, Minnesota International Hydraulics Convention, Univ. of Minnesota, Minneapolis, Minn., August 31–September 4, 1953.

There is little experimental evidence to indicate that a deep and dry snow cover will retain appreciable amounts of rainfall, as stated by the author. The presence of free water induces a rapid metamorphic process which reduces the surface area of the individual snow crystals to the minimum area compatible with the mass and stable form of the crystal. That is, the feather-like, or dendritic, snow flakes are converted to small crystals of hexagonal form which resemble a mass of table salt or rock salt. The surface detention capacity of the snow flake is rapidly reduced by the metamorphic process, and the water which may have been retained on the larger surface area is discharged. This metamorphic process is not uniform throughout the pack. The process appears to proceed more rapidly at one place than at another, a phenomenon which accounts for the development of the flow zones within the pack and at the ground surface.

The size of the metamorphosed grains in a spring snow pack is the same as the size of a mixture of fine and coarse sands, about 0.02 mm to 2.0 mm in diameter. A reference to the literature on soil moisture shows that a sand with such a size distribution and free drainage will hold from 1% to 3% of liquid water, the same quantity as has been measured and reported for a spring snow pack.

The temporary detention of liquid water in snow is a function of the time required for the development of internal flow channels; hydrologically, these channels are effective temporary supplemental tributaries to the normal drainage pattern of the basin. There is no evidence that snow must achieve a 40% density before this supplemental tributary system becomes operative nor that, having achieved this density, the supplemental tributary drainage can be considered as having a discharge capacity which is a function of the density in excess of 40%.

In presenting this discussion the writer does not wish to detract from the value of Mr. Riesbol's paper. This discussion is submitted so that hydrologists may give more recognition to the known physical and thermodynamic properties of snow and the associated hydraulic phenomena in developing snow-melt runoff formulas and design and operational criteria for multiple-purpose reservoirs.

As a source of information, attention is called to a bibliography of six thousand items on snow, ice, and frozen ground available in the Engineering Societies' Library, New York, N. Y.[25]

HAROLD D. HAFTERSON,[26] A.M. ASCE.—One of the most important aspects of the multiple-purpose use of major reservoirs in the western and northern sections of the United States has been investigated by Mr. Riesbol. This subject was previously examined in a symposium—one of the papers of which was written by Albert L. Cochran,[27] M. ASCE.

The ability to forecast the volume and shape of the flood-runoff hydrograph is a valuable asset in operating multiple-purpose reservoirs and in realizing the purposes which these reservoirs have been designed to meet. The author rightly states (under the heading, "Conclusions") that

> "Great refinement in procedure, with corresponding economy in both design and operation, will result from * * * the extension of networks for the collection of data so that they include pertinent elements on a watershed basis."

Continual study of forecasting procedures and operating criteria—to utilize available information on snow depths, areal coverage, and melting processes—is being made (1953) by all reservoir-operating agencies in areas where snow-melt runoff provides a large part of the storable flow. Snow surveys are constantly being conducted to cover ever-widening areas. New methods of measuring depths and water content of the snow pack are being devised. Experiments are being continued to determine the relationship of snow melt to some of the more easily measured meteorological factors such as temperature, air movement, and relative humidity.

It is worthwhile to note that the development of forecasting procedures, and the application of resulting forecasts to the operation of multiple-purpose reservoirs, have provided methods whereby relatively full use of certain storage facilities can be made for functions which are ordinarily in opposition to each other. For example, in certain areas it is possible to use the full capacity of certain reservoirs both for flood control and irrigation, or for other conservation purposes, despite the fact that flood control requires reservation of reservoir space whereas irrigation demands the assured accumulation of storage for subsequent use.

Mr. Riesbol's use of the term "operation 'parameters' " might readily have been clarified by a definition of exactly what these parameters denote. The mathematical definition of a parameter is any constant or element whose values characterize one or more of the variables entering into a system of expressions or functions. Thus, the operating curves (which the author referred to under the heading, "Capacities of Multiple-Purpose Reservoirs") show the relationship between the storage space required to control the forecasted flood within specified limits of outflow and the volume of runoff which is anticipated between any given dates and the normal end of the flood season. The curves shown in Fig. 2, empirically derived from floods of record, are curves that envelop the storage requirements for various volumes of total forecast runoff from any given date to July 31. An additional safety factor has been added to Fig. 2 to assure adequate reservation of space at the beginning of the flood period. This factor was added to account for the possible forecasting errors shown in the computations in Fig. 3.

---

[25] "Annotated Bibliography on Snow, Ice and Permafrost," *SIPRE Report 12*, Vol. III, Snow, Ice and Permafrost Research Establishment, Corps of Engrs., U. S. Dept. of the Army. Prepared by the Library of Congress, Washington, D. C., January, 1953.

[26] Chf., Hydrology Branch, Project Planning Div., Bureau of Reclamation, U. S. Dept. of the Interior, Region 1, Boise, Idaho.

[27] "Their Use for Flood Control," by Albert L. Cochran, from "Multiple-Purpose Reservoirs: A Symposium," *Transactions*, ASCE, Vol. 115, 1950, p. 818.

To be more complete, Table 1 might have included a split period beginning on April 9 and continuing through April 16 so that the negative values could be shown to balance the positive values of required storage space. By means of this inclusion, the summations shown in Col. 5, Table 1, would be correctly referenced as to date.

The author's presentation of three methods for applying snow hydrology to spillway design includes the best of the available (1953) methods for deriving spillway-design floods of snow melt or combination rain and snow-melt types. It is gratifying to note that Mr. Riesbol suggests either the use of the unitgraph method or the augmentation of an actual snow-melt event to distribute the design snow-melt volume. Both procedures are practical and are superior to the widely used scheme of proportioning runoff directly to a design thermogram, ignoring the runoff characteristics of the basin.

It is felt that the detailed approach described in the second method (under the heading, "Application to Spillway Design: Flood Produced by Rain on Snow") is an admirable attempt to account for causative snow-melt factors other than air temperature. However, the number of assumptions necessary and the type of data required in the method prevent its practical use in most localities. Almost none of the numerous watersheds in the northwestern parts of the United States (for which spillway floods have been derived or will be derived by the USBR) has a temperature record within the watershed. The determination of values for K, U, and p in Eq. 3 and the determination of the required infiltration rates for such watersheds are highly speculative.

It is advantageous to use the hydrothermogram method for the derivation of spillway floods for large watersheds where seasonal snow-melt floods of several months' duration are prevalent. An examination of the method or methods for converting an actual and a design thermogram into corresponding runoff (through the hydrothermogram approach) would have been helpful to the potential user of this approach.

In determining the relationship between temperature and snow-melt runoff (Table 2), a correction should be made for the area contributing to snow melt during a given recorded event. In some cases, snow-course data can be used to correct continuously the contributing area during the given snow-melt flood. The author states (under the heading, "Application to Spillway Design: Flood from Snow Melt Alone"):

"If the stream-gaging station is a considerable distance from the snow-melt area, it is necessary to determine time lag between snow-melting temperatures and runoff."

The location of the stream gage is only one of the factors which can cause a lag between temperature and runoff. The location of the temperature station with respect to the snow-melt area is another factor. A third factor is the time which is required for the heat in the air to convert the snow into water. The first two factors cause variance in the apparent time lag observed in different snow-melt floods because of differences in the direction and speed of the respective causative warm-air mass. The third factor varies, depending on the depth and quality of the snow.

Should not the vertical axis of Fig. 4 be labeled, "Maximum fifteen-day melting rate of runoff, in inches per degree day" rather than "Maximum * * * of runoff, in inches?"

In the application of the detailed and somewhat theoretical method for deriving a design flood produced by rain on snow (Table 4), it appears that consideration should be given to the melting of the snow by the heat of the rain water. This amount of melting can be computed from

$$M = \frac{P\,(T_w - 32)}{144} \qquad (4)$$

in which M is the snow melt in inches, P denotes the precipitation in inches, and T_w is the wet-bulb temperature (assumed to be the temperature of the rain). Although generally regarded as insignificant, the heat in 7.2 in. of precipitation of the maximum 6-hr period at an assumed 50° F could cause 0.90 in. of additional snow melt in the example cited in Table 4—thus increasing the contribution to the mean-water excess of the basin from 4.70 in. to 5.60 in. for that single 6-hr period.

The relationship of snow melt to runoff has not been given as much consideration in the design and operation of multiple-purpose projects as its importance warrants. The qualitative use of available knowledge on this subject, applied through the judgment of the engineer, should be bolstered by continuous improvement of procedures to apply this increasing knowledge quantitatively.

David M. Rockwood,[28] A. M. ASCE.—The problems of snow hydrology as related to the design and operation of water-control projects have been described by the author. Mr. Riesbol has also summarized methods for determining rates of snow melt, reservoir capacities, seasonal forecasts, design floods, and storage of liquid water in the snow pack.

The purpose of reservoir storage in the regulation of streams is twofold. This storage can be used for supplementing deficiencies in the natural flow for specified purposes, or it can be used for reducing overbank flows to specified channel capacities. In rivers where the occurrences of low and high flows invariably follow a seasonal pattern, the reservoir-storage space can be used to meet both purposes compatibly, provided proper operational procedures are established. In rivers where the stream flow is primarily the result of snow melt, and when there is normally a delay between the accumulation and melt periods, optimum use of storage space can be made because the volume of runoff during the melt period can be forecast two or three months in advance. The Columbia River in the Pacific Northwest is a notable example of a stream with these characteristics and is particularly susceptible to the development of multiple-purpose reservoir storage.

---

[28] Technical Director, Snow Investigations, Corps of Engrs., U. S. Dept. of the Army, North Pacific Div., Portland, Ore.

Efficiency of design and operation of multiple-purpose reservoir projects on snow-fed streams is dependent on the accuracy with which the stream flows can be forecast. In the matter of project design, the application of snow hydrology involves determination of reservoir-storage requirements and the derivation of design floods to meet the criteria for spillways and appurtenances for the structure. For the operation of the project, knowledge of snow hydrology is a requirement for forecasting rates of flow for day-to-day operation, and also for volumetric-runoff forecasts in order to establish long-term operating criteria on a seasonal basis.

Engineers of the Corps of Engineers have long recognized the importance of snow hydrology for efficient design and operation of their projects, particularly those projects in the western United States. In 1945 the Corps of Engineers entered into a cooperative snow-investigation program with the Weather Bureau—with limited cooperation from other governmental agencies—for the purpose of determining criteria to be used in snow-hydrology problems. That program included (1) operation of three basin snow laboratories in the mountains of the western United States for periods of from 4 yr to 7 yr ,(2) processing and publishing the hydrometeorological data from the laboratories, (3) maintaining an analytical unit for performing basic research in snow hydrology, and (4) disseminating information to participating offices. The cooperative phase of the program ended in 1952; however, the Snow Investigations Unit was continued by the Corps of Engineers with offices (1953) in the North Pacific Division office. The activities of the unit were directed, almost entirely, toward specific analytical problems which were divided into two categories. The first was the analysis of physical processes affecting snow deposition and snow melt. The second was the practical application of procedures to basin snow-hydrology problems, which dealt with forecasting rates of stream flow and estimating seasonal volume of runoff.

The use of degree-day factors provides a quick method of approximating daily increments of snow melt from readily available meteorological data because air temperature is an index of heat transfer by several processes. The complexity and variability of these processes require that temperature-index methods be used with considerable judgment. This judgment can be obtained only by study and evaluation of the components of heat transfer for various meteorological and basin conditions. For example, on clear days the processes of heat transfer in a forest-covered area are quite different from those processes for open areas, whereas the total daily energy exchange may be approximately equal. An air-temperature index in the forest area for this condition is much more reliable than for an open area because the air temperature is a less reliable index for solar radiation than for convective heat transfer and long-wave radiation from the forest canopy. Differences in meteorological factors, such as vertical and horizontal distribution of moisture and temperature of the air (together with the associated cloud layers, air drainage, and stability), are related to the general atmospheric circulation, which in turn produces changes in these properties with respect to time. All these properties affect the rate of heat exchange in a manner which cannot be defined by air temperature at only a few surface index stations. The problem of accuracy becomes a matter of economic necessity. The project design or operation must warrant the expenditure of time and effort to obtain the required basic data and to analyze the meteorological and basin effects for each day's melt. When the requirements are such that empirical day-degree relationships are adequate, application and limitations of the method should be understood.

The examination by Mr. Riesbol of spillway-design floods resulting from snow melt alone is based on an analysis of historical stream-flow and temperature records for a particular stream. Empirical melt rates were determined, and interpolation to design conditions was made on the basis of a maximum observed runoff and a maximum enveloping melt rate corresponding to that runoff. These values do not necessarily represent the maximum flood potential of the basin, when one considers such important factors as the maximum possible snow accumulation, the minimum basin losses, the optimum flood-producing temperature sequence, the meteorological events leading to the greatest rate of heat transfer at the time of the flood peak, and the maximum snow cover that can reasonably be expected at the time of the peak. The simultaneous occurrence of these important flood-producing factors would probably lead to a much greater flood flow than that derived from the analysis of a relatively few years of stream-flow records—during which time it is quite unlikely that maximum flood-producing conditions have occurred.

Floods produced by rain on snow are more complex and less certain of analysis than those caused by snow melt alone. Eq. 3 is used to evaluate heat transfer by convection and condensation but does not account for heat transfer by solar or long-wave radiation. The application of Eq. 3 to basin analysis depends on an evaluation of the basin constant, K. In the example shown for the Sly Park Dam site, it was not explained how K was determined for this particular drainage basin. The use of Eq. 3 for this example is valid, inasmuch as short-wave radiation is negligible under these conditions, and net long-wave exchange is primarily a function of air temperature. However, it should be realized that, for the evaluation of total heat exchange, radiation ordinarily causes a large part of the total melt.

The retention of liquid water in the snow pack has been the subject of much speculation. Qualitatively, the pack has been considered a "sponge" capable of retaining large amounts of liquid water entering as a result of rainfall or surface melt, thereby reducing the rates of flow that would have resulted from the same excess water being deposited on saturated ground. Observations (1953) on the impervious snow lysimeter at the snow laboratory in the Central Sierras near Soda Springs indicate that the permanent retention of liquid water in a 100-in.-thick snow pack of 31% initial density during a

5-in. rainstorm was approximately 1 in., which included 0.3 in. as a result of the increase in temperature of the pack (isothermally) to 0°C. There was, in addition, transitory storage of liquid water in the pack, in the amount varying from 1 in. to 2 in., but this water drained out completely within 10 hr after cessation of rainfall and snow melt. In deriving the water-holding capacity of the snow, Mr. Riesbol assumed for Table 4 that the snow pack must reach a density of 40% before any water excess is available at the ground for contribution to the stream flow. From the observations at the Central Sierra Laboratory, runoff from the snow pack commenced after the pack density increased to 32.5%; the maximum density was 34%. In Table 4, it is not clear how the increments of snow melt shown in Col. 4 could total 11.0 in. when the initial water equivalent of the snow pack was 6.0 in. Also (considering the total storm period) there were 29.6 in. of rainfall and 6.0 in. of snow-water equivalent, of which 0.5 in. remained in storage in the pack at the end of the period and 1.5 in. were retained initially in the ground. Thus, a total of 33.6 in. was available at the ground surface during the storm period. The total water excess, which is the sum of the increments listed in Col. 13, is 26.63 in. The loss then is 7.0 in. during the 54-hr period, which is equivalent to an average loss rate of 0.13 in. per hr. For design-flood conditions, the value appears to be rather high for this area. In general, the retention and detention of liquid water in the relatively shallow snow pack shown by this example appears to be too great.

Herbert S. Riesbol,[29] M. ASCE.—The writer is indebted to Messrs. Gerdel, Hafterson, Linsley, and Rockwood for their constructive discussion and criticism of the paper. The purpose of the paper was to demonstrate the engineering application of scientific knowledge and data of snow hydrology to the planning, design, and operation of multiple-purpose reservoirs. Mr. Gerdel has urged that this application not include the use of hypotheses incompatible with "* * * experimental evidence or the known physical properties of snow * * *." Mr. Hafterson emphasizes the fact that the application must be based on the judgment of the engineer, and that procedures must be continuously developed to bridge the gap between physical knowledge and engineering application. Each of the discussers had emphasized the need for new and improved methods of measurement and for more basic data. The writer agrees with these recommendations.

Mr. Gerdel has shown that, under a variety of conditions, the density of a ripe, melting, actively discharging snow pack can vary over a wide range. Undoubtedly, this is correct. However, the writer has made the conservative engineering assumption (under the heading, "Application to Spillway Design: Flood Produced by Rain on Snow") that "* * * no release of water from the snow pack would occur until the snow attained a density of 40% * * *." This assumption was based on an examination of considerable data which has been corroborated by Walter T. Wilson, A.M. ASCE. Mr. Wilson has stated[30]:

---

[29] Asst. Chf., Hydrology Branch, Project Planning Div., Bureau of Reclamation, U. S. Dept. of the Interior, Denver, Colo.

[30] "Storage and Movement of Liquid Water in a Snowpack," by Walter T. Wilson, Weather Bureau, U. S. Dept. of Commerce, Washington, D. C., October 12, 1953.

> "The appended table gives average density as a function of number of days since establishment of the snow cover. The values given are based on a large mass of data including shallow and deep snow, short seasons and long seasons, high and low elevations and a wide range of other conditions. Of course, particular instances frequently vary considerably from the average values, but experience has shown the average values to be reliable * * *."

Mr. Wilson's table of the average-density trend contains the following information:

Time since beginning of snow cover, in days	Average density (percentage)
0	8
1	12
2	14
5	16
10	20
20	25
50	30
100	40
200	50

Most of the snow floods which are dealt with in the design and operation of multiple-purpose reservoirs occur within 100 days to 200 days after the beginning of the snow cover.

Mr. Gerdel has stated that the temporary detention of liquid water in snow is a function of the time required for the development of internal flow channels, and Mr. Hafterson states that the detention varies with the depth and quality of the snow. In this connection Mr. Wilson[30] presents the following information and practical formula for water movement through a deep snow pack:

> "If a dense snowpack is deep enough to warrent routing, instead of merely lagging the rain or melt * * *, after its waterholding capacity has been satisfied the rates of rainfall or snowmelt may be expressed as a hydrograph of inflow to the pack at its upper surface. The outflow hydrograph at the snow-ground interface may be approximated by lagging the inflow and routing it by reservoir analogy. If the snow depth is d feet, the lag is $0.3d$, and the routing coefficient is $0.5d$, both in hours. Using the Muskingum notation, K in hours equals half the snow depth in feet, X is zero, and the hydrograph is translated a number of hours equal to three-tenths of the snow depth in feet."

Mr. Hafterson has shown that, in the derivation of a design flood produced by rain or snow, consideration should be given to the melting of snow by the heat of the rain water. As Mr. Hafterson states, this source of melting is usually regarded as being of minor significance; however, in the Sly Park study, it appears that the melt from this source might contribute considerably to the flood runoff. Usually, the rain forms at a higher elevation and lower temperature than is indicated by the surface dew point. Thus the rain would be subject to some evaporative cooling during its descent, and, as a result, when the rain reaches the surface, it might be at a temperature several degrees lower than the surface dew point. This lower temperature would reduce the melt potential.

Mr. Linsley notes the similarity between the hydrothermogram and his (1943) procedure and states that the method is basically the same as that offered by Mr. Clyde (1931). It is believed that any valid procedure for constructing the hydrograph of discharge from snow melt would necessarily resemble Mr. Linsley's procedure. However, the only similarity between the writer's procedure and Mr. Clyde's procedure for net yield is in the assumption of a constant volume of melt per degree day. Actually, a more general and more flexible procedure is now (1953) in use in which both the basic temperature and the discharge factor are considered to be variable functions of the accumulated percentage of the seasonal runoff volume. Methods have been developed by engineers of the USBR for constructing and adjusting the relationships among these functions, using only temperature and runoff data, so that a knowledge of the elevations, the area of the melting zone, and the lapse rate is not essential. Such data, if readily available, could perhaps be used to refine the procedure. Data concerning the wind velocity, humidity, and solar radiation could also be used to refine the procedure; however, these data are seldom available for design-flood studies.

The hydrothermogram procedure developed by Mr. Barnes differs from the methods cited by Mr. Linsley as follows:

1. Ground-water flow and direct runoff are computed independently and concurrently from separate hydrothermograms. Different lag times, depletion factors, base temperatures, and discharge factors are used for the two elements of flow.
2. The base temperature and discharge factor are considered to be variables and are determined from the accumulated percentage of the seasonal runoff.
3. The runoff volume generated each day is expressed directly as the maximum daily discharge in cubic feet per second.
4. The subsequent distribution of the runoff is accomplished by combining all the flows (of direct runoff or of ground water) that are in the channel and by applying the appropriate constant depletion factor to the total.

Mr. Rockwood is correct in stating that the methods presented by the writer for the derivation of the spillway design flood resulting from snow melt will not yield the maximum possible flood potential from that source. These methods are used as a rational procedure to obtain a maximum probable flood event which would have a magnitude somewhat less than the maximum possible event. This maximum probable flood is of sufficient magnitude to justify its selection for prudent design purposes. Snow floods developed by these procedures are considerably in excess of maximum experienced floods for the area of derivation.

Mr. Rockwood inquires how the increments of snow melt in Col. 4, Table 4, could total 11.0 in. when the initial water equivalent of the snow pack was 6.0 in. The values in Col. 4, Table 4, are melt potential computed from Eq. 3 and are used only as a method of distributing the depth of snow on the ground at the beginning and end of each 6-hr time increment (Col. 5 and Col 6, Table 4) after accounting for the increase in density (Col. 7, Table 4) up to the 40% limit. Following the attainment of a pack density of 40%, the values shown in Col. 4, Table 4, reduce the waterholding capacity of the pack (Col. 8, Table 4) by equivalent amounts. Mr. Rockwood states that "* * * a total of 33.6 in. was available at the ground surface during the storm period." Actually, this amount should be 35.1 in. as the 1.5 in. shown at the head of Col. 12, Table 4, is the retention which was assumed to have occurred during a previous event. This assumption provides a reasonable starting point on the retention-time curve. The average loss rate over a period of 54 hr of approximately 0.16 in. per hr falls within the range of retention rates derived by the writer for the area from hydrograph analysis.

The cooperative snow-investigation program, referred to by Mr. Rockwood, has contributed greatly to the physical theory underlying snow hydrology and to the practical applications of that theory. The USBR has maintained a close contact with that program, including the contribution of approximately four man-years of technical assistance. As the results of the program are fully analyzed and presented, they will become even more valuable to all engineers engaged in the planning, design, and operation of multiple-purpose reservoirs that receive their inflow from snow-fed streams.

AMERICAN SOCIETY OF CIVIL ENGINEERS
Founded November 5, 1852
TRANSACTIONS

Paper No. 2688

WAVE-WASH CONTROL ON MISSISSIPPI RIVER LEVEES

By Rudolf Hertzberg,[1] M. ASCE

Synopsis

Unprotected levees along the lower Mississippi River are subject to serious wave-wash damage where the foreshore is narrow and without protective vegetation. The need for protection works is almost continuous below New Orleans, La., and intermittent as far upstream as Baton Rouge, La. Above New Orleans the situation is less severe because ship traffic is lighter and the river banks are generally high enough to contain the river at ordinary stages, limiting wave-wash attack on the levees to periods of high water. Many types of protection have been suggested, and most of them have been tried, but no single type has met reasonable criteria for economy and effectiveness. Present practice (1953) is to use either of two major types of protection for the levee, and under special conditions, a supplemental structure to keep the wave-wash protection work from being undermined.

Conditions

Destructive waves in the river are caused by wind and passing ships. Storm damage is potentially most dangerous when river stages are high and wave-wash damage could weaken the levee sufficiently to cause a crevasse. Damage from ship wash is intermittent but cumulative, and in many places below New Orleans, can occur throughout the year. The levees in the lower river generally are built of clays that are rather resistant to erosion, and normal waves would seldom cause serious damage on sodded slopes of such materials if it were not for the effect of drift. Logs batter the face of the levee with considerable force, starting damage that ordinary wave action can then extend. A heavy log can seriously damage the less substantial forms of wave-wash protection, particularly when it becomes partly anchored and pounds repeatedly on the same spot. A secondary form of wave-wash damage occurs in several areas below New Orleans where the foreshore is low enough to be

---

Note.—Published, essentially as printed here, in September, 1953, as *Proceedings-Separate No. 275.* Positions and titles given are those in effect when the paper was received for publication.

[1] Chf., Levee Section, New Orleans Dist., Corps of Engrs., U. S. Dept. of the Army, New Orleans, La.

submerged during much of the year and where the surface stratum consists of light, easily eroded soils. Protective vegetation will not grow in such locations and waves can break in the shallow water near the levee without restraint. Under such circumstances, the light surface soils are washed away, and the wave-wash-protection structure is undermined.

PROTECTION WORKS

Heavy protection works, as used on large earth dams, would be adequate for all levee purposes, but since levees aggregating more than 120 miles in the New Orleans district require such protection, and since the life expectancy of levees is limited by the meandering tendencies of the Mississippi River, it is apparent that a less expensive form of protection is necessary. The various formulas available for computing wave impact values are not useful in designing such works because the destructive potential of drift cannot be evaluated. It has been necessary, therefore, to examine earlier work and to experiment, adapting and improving the earlier designs, and discarding unsuccessful and unduly expensive features. By compensating for—or eliminating—weaknesses, designs have been developed which assure useful life commensurate with cost.

Emergency wave-wash protection works, used during floods to prevent development and extension of damage already incurred, include fences of wood and sheet piling, of light-gage steel, sacked earth, and riprap. These have value only for a limited range of river stages and are temporary since they must be removed when the levee is repaired. Another class of temporary protection includes old levees left standing between the new levee and the river, and debris from clearing and stripping operations piled riverward of the new levee borrow pit. These are destroyed by caving banks in a few years, but it is customary to get as much use as is practicable from these free protection works before permanent works are placed.

Permanent wave-wash protection works include wooden bulkheads or fences, generally called "wooden revetments," and various types of pavement applied to the river-side slope of the levee.

Wooden revetments, in a variety of types, have been used since the days of the first levees, and still protect more than fifty miles of levee in the New Orleans district. The type in current use has evolved over the years into a well-balanced structure capable of long and dependable service. It is subject, however, to hazards that cannot be eliminated in planning. Sound timber is always useful, and revetments frequently lose framing and planking by theft in the more isolated places. The braces interfere with proper mowing and maintenance of the river-side slope of the levee, and during the dry season, grass and trash fires sometimes are responsible for severe damage. Wooden revetments withstand attack well and are damaged only by heavy drift. Drift damage normally reduces but does not destroy the effectiveness of the revetment, and repairs can be made quickly, even during flood and storm conditions, without use of heavy mechanical equipment.

Three general types of pavement have been tried on a scale large enough to provide an adequate basis for preliminary evaluation. Various modifications of these basic types have shown no significant advantages in economy or performance.

Compacted asphaltic pavement, which is a densely-graded sheet asphalt 2.5 in. thick, containing approximately 10% asphalt cement, was used for some years as a by-product of the asphalt subaqueous and bank revetment operations. Natural deposits in bars provided aggregate; and loess deposits along the river provided filler. Construction was largely mechanized by use of modified road building equipment, although considerable hand work was necessary in the preliminary operations. The last levee pavement constructed by this method was placed in 1941, after which the equipment was diverted to military construction. The high density of the pavement made it quite effective in reducing the volume of seepage through the levee, but the thin pavement is extremely vulnerable to damage by drift, and maintenance has been expensive. Weathering and vegetation have caused further damage, and much of the pavement has deteriorated so far that further maintenance is impracticable.

Uncompacted asphaltic pavement was developed during World War II, when labor and equipment were scarce. It is poorly graded sand asphalt, 4.5 in. thick, containing 6% asphalt cement. The material is applied hot, then spread, and roughly finished with rakes and shovels. No compaction is used. The pavement lacks the strength to withstand battering by drift, and because of the porosity resulting from coarse grading, low asphalt content, and lack of compaction, it has little value in reducing seepage and is particularly susceptible to damage by vegetation, which grows within and through the pavement. Although the weakness of the pavement has created a maintenance problem in exposed places, repair of local damage is simple and relatively inexpensive, and the pavement has performed adequately in light service.

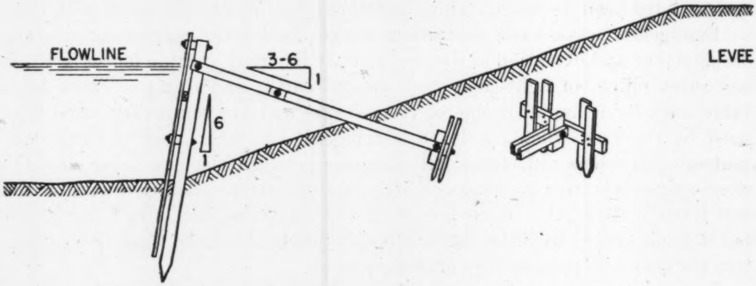

Fig. 1.—Standard Wooden Revetment

Concrete pavement has been used successfully for many years, and several such pavements placed in the early years of the century are still (1953) in good condition. No record exists of such cast-in-place concrete pavement having failed under attack by waves and drift, although there have been failures caused by undermining. The principal objection to concrete has been its relatively high first cost. Probably, unnecessary refinement of detail has contributed to high construction costs, and present (1953) construction is simply planned, using large panels of low-strength concrete with butt joints and screeded finish.

Undermining has become a major problem along shores below New Orleans with the gradual increase in ship traffic. In several areas where ship waves had caused severe washing of the foreshore, and undermining of the wave-wash protection works had occurred or was imminent, low brush dikes have been constructed between the levee and the river to break up waves before they reach the levee. When stages are appreciably higher than the top of the dike, the depth of water over the foreshore is sufficient to cushion the impact of the waves. Cross dikes act as retards and induce deposit of river-borne sediment near the levee during high water periods.

The wooden revetment shown in Fig. 1 is constructed of No. 2 common rough pine lumber that is given a 10-lb open-cell creosote treatment after being cut to size. Planking is 2 in. thick, and from 8 in. to 12 in. wide. The posts are capped with sheet metal or bituminous material. Anchors are buried deeply in the levee and are designed to resist tension in the braces as well as normal forces, since anchors of earlier design have failed when large waves rolled over and pushed out the revetment from behind. Major connections are made with bolts with cast iron ogee washers.

FIG. 2.—WOODEN REVETMENT, THREE YEARS OLD

The top of the planking is 2 ft above the maximum flow line; the bottom is generally 3 ft below ground surface, with increased penetration where undermining is possible. Penetration of the posts is approximately 1.5 ft more than that of the planking. The batter of the face of the revetment is 6 vertical on 1 horizontal; slope of bracing is not steeper than 1 vertical on 3 horizontal. An intermediate rail is provided when the top and bottom rails are more than 7 ft apart.

Fig. 2 shows a wooden revetment in excellent condition about three years after construction. The heavy growth of Johnson grass on the levee slope is typical of such installations because the braces interfere with the use of powered mowing equipment.

Fig. 3 shows a section of concrete pavement of current (1953) design. The slab has an average thickness of 4 in.; the minimum acceptable thickness is 3.5 in. A cut-off wall is provided at the top to prevent infiltration of rain water from the slope and crown above. The toe of the slab is placed at least 3 ft below natural ground surface, and the toe trench is backfilled with earth. A longitudinal expansion joint is provided near the ground surface to allow for some settlement in the levee embankment without damage to the pavement. This and other necessary extension joints are made with premolded mastic or cypress boards with suitable seal. The maximum permissible panel size on old, well-compacted earth surfaces is 40 ft by 40 ft. Smaller panels must be used on fresh fills. The average compressive strength of the concrete is 2,000 lb per sq in.

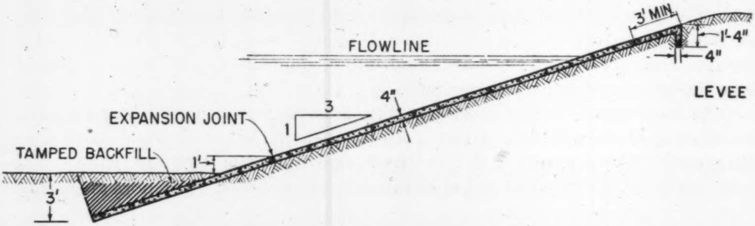

FIG. 3.—CROSS SECTION, CONCRETE SLOPE PAVEMENT

Fig. 4 shows concrete pavement seven years old. This pavement was constructed with small panels separated by thin expansion joints made with asphalted felt. The joints are not tight, and grass and weeds grow through

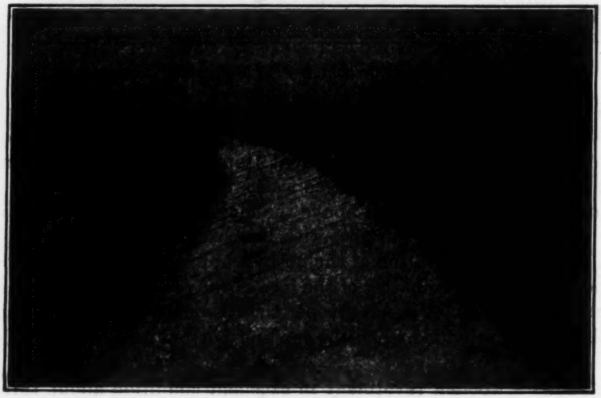

FIG. 4.—CONCRETE SLOPE PAVEMENT

them. No damage from vegetation has appeared in this particular pavement, but spalling has resulted from similar growth in some locations. This pavement is on an open reach of river and has been subjected to battering by the heaviest drift without visible damage.

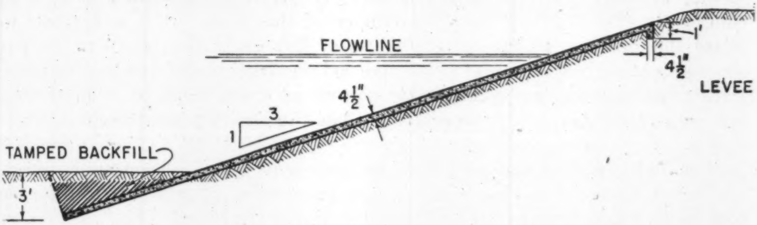

FIG. 5.—CROSS SECTION, UNCOMPACTED ASPHALT SLOPE PAVEMENT

A section of uncompacted asphaltic pavement is shown in Fig. 5. The design is similar to that of concrete pavement in regard to cut-off wall and toe penetration. The slab thickness averages 4.5 in., the minimum acceptable thickness being 4 in. The material is composed of sand aggregate that may contain as much as 30% gravel, with 6% by weight of asphalt cement having between 85 and 100 penetration. The graded earth surface receives a weed-killing treatment of sodium chlorate or salt before the pavement is placed.

Fig. 6 shows an uncompacted asphaltic pavement. In the foreground is a typical growth of Johnson grass, part of which has been recently mowed. In the middle distance is an area completely bare of vegetation; and brush and small willow trees have claimed the lower third of the levee slope. The entire

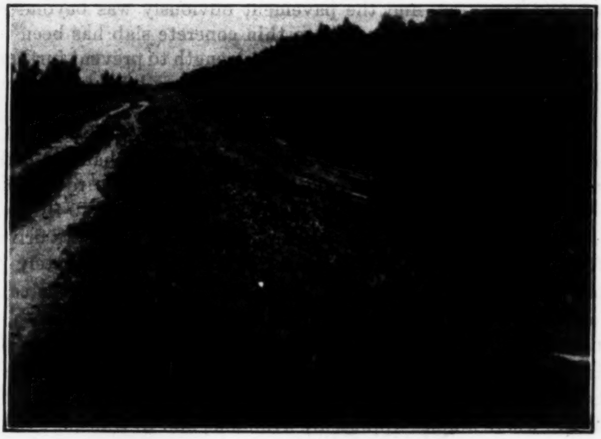

FIG. 6.—UNCOMPACTED ASPHALT SLOPE PAVEMENT

area received the same treatment with sodium chlorate or salt. At this stage the pavement has not been seriously weakened by vegetation, but since every stalk, in pushing its way through the pavement, pulverizes and destroys the material in its path and breaks out a sizable chip at the surface, the pavement becomes progressively more porous and correspondingly more vulnerable to further growth. Perhaps only prohibitively expensive treatment would be completely effective in preventing damage of this kind. It is interesting to relate this problem to the successful use of thin asphaltic pavement for encouraging rapid production of protective sod on airfields and in ditch bottoms. Pavements containing a considerable volume of gravel seem to be somewhat less subject to damage by vegetation than the straight sand-asphalt pavements.

Fig. 7 shows a toe-wall used to repair pavement that has been undermined. Creosoted lumber sheathing is driven to a penetration of from 3 ft to 6 ft; the broken pavement is removed and placed as riprap riverward of the wall. Lost embankment is restored with a tamped earth backfill, and a new concrete slab is placed to join the toe-wall to the undisturbed slope pavement. An attempt has been made to control the conditions that make such work necessary by construction of brush dikes, as shown subsequently in Figs. 9 and 10.

Fig. 8 shows what happens to a weak pavement in an exposed location. Some of the drift that aggravates the situation can be seen on the levee slope; this is relatively small drift since the larger logs continue down the river to do damage elsewhere. The original pavement was compacted asphalt, which was seriously damaged by vegetation, waves, and drift. Extensive repairs were made with uncompacted asphalt, but further damage soon appeared in both the original pavement and in the patches. The foreshore was washed away intermittently by wave action at low river stages, and the pavement was undermined. The toe-wall treatment was applied where necessary; holes on the levee slope were patched with concrete. When the photograph was taken, new holes had appeared, and the pavement obviously was beyond repair on any reasonable basis. Subsequently, a thin concrete slab has been placed on top of the old pavement to provide sufficient strength to prevent further damage by drift. It is probable (1953) that more toe-wall or brush dike construction will be necessary to prevent further undermining.

The form and positioning of brush dikes are illustrated by Fig. 9. Brush dikes vary in height from 3 ft to 6 ft, but are rarely more than 4 ft high for any considerable distance. The base width is 5 ft. A double row of light, untreated piling is driven with 5-ft transverse spacing and 10-ft longitudinal spacing. In the first stage of construction, piles in one row are driven to the full 15-ft penetration; those in the other row are left approximately 2 ft high. After the brush filling has been placed between the rows and the cables have been drawn up tight, the high piles are driven to full penetration to compress the filling and to produce the maximum practicable tension in the cables. In early plans for such dikes, it was contemplated that drift would be used for filling, but it has been found both better and cheaper to cut willow brush and poles on bars where ample supplies are available, and to transport the material to the work site by barge. It is common practice to obtain brush and poles

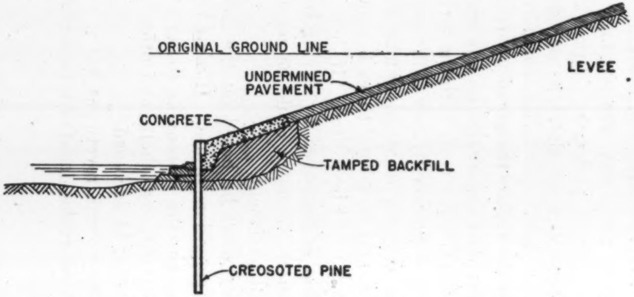
ORIGINAL GROUND LINE
LEVEE
UNDERMINED PAVEMENT
CONCRETE
TAMPED BACKFILL
CREOSOTED PINE

Fig. 7.—Slope Pavement Repair Using a Timber Toe-Wall

Fig. 8.—Damaged Asphalt Pavement

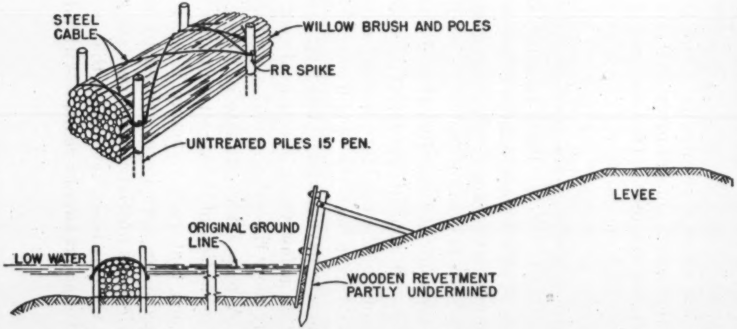
STEEL CABLE
WILLOW BRUSH AND POLES
RR SPIKE
UNTREATED PILES 15' PEN.
LEVEE
ORIGINAL GROUND LINE
LOW WATER
WOODEN REVETMENT PARTLY UNDERMINED

Fig. 9.—Brush Dike

Fig. 10.—A Brush Dike on the Mississippi River

as far as fifty miles from the work site; in one extreme case the contractor chose to get his material near Plaquemine, La., two hundred miles by river from the work. The lacing cable is ⅜-in. seven-wire galvanized strand. Transverse ties, which are under somewhat greater stress during the redriving operation, are ½-in. nineteen-wire galvanized strand. Railroad spikes are driven into the piles to hold the cables. The only major item of plant needed for brush dike construction is a small dragline on a barge. Brush and poles are easily handled with slings and tongs. Piles are driven with a light hammer suspended from the boom. Much hand work is necessary, however—all of it wet and much of it difficult and aggravating.

Fig. 10 was taken in September, 1951, and shows a brush dike that was completed in January, 1951—just prior to the flood season, which was of long duration but not severe. Before construction of the dike the foreshore had been nearly denuded by low-water wave action; all vegetation had been washed away except for a few dying willow trees with exposed roots, and the wooden revetment was in imminent danger of being undermined. During the flood season following completion of the dike, substantial deposits were made adjacent to the wooden revetment—ending any immediate threat of undermining. Some new growth is evident on the deposits, indicating that the foreshore is high enough to support vegetation.

ECONOMICS

For average conditions, where the total effective height of necessary protection works, including penetration, is 15 ft, comparative construction costs (adjusted to reflect 1953 contract prices plus engineering and overhead) are about $15 per lin ft for uncompacted asphalt pavement; $20 per lin ft for wooden revetment; and $25 per lin ft for concrete pavement. Brush dike, which belongs in a somewhat different category, costs about $8 per lin ft. First costs for the three principal classes are only superficially comparable, since circumstances and conditions may properly require the use of a particular one without regard to cost. Annual costs cannot be compared on any reasonable basis because of the wide variation in maintenance costs with the severity of exposure and the difficulty of establishing acceptable figures of life expectancy. If asphalt pavement is used in an exposed location, annual costs, because of the need for constant maintenance, may be several times as much as would have been the case if concrete pavement had been used. If, however, concrete pavement is placed on a levee that is destroyed by caving banks within a few years, the annual cost of concrete pavement could be considerably more than the annual cost of an asphalt pavement.

A reasonable estimate of life expectancy must be based on the rate of deterioration of the structure under normal conditions of use. It must be assumed that each structure is used only within the reasonable limits of its capabilities, and losses caused by river meander, fire, theft, and other considerations unrelated to wave-wash attack, must be excluded.

On this basis, it appears that a creosoted wooden revetment has a useful life of about twenty years. Within that period, replacement of broken, stolen, and deteriorated members is feasible and economical. After about twenty years complete replacement would normally be sound economy.

The first installation of uncompacted asphaltic pavement was made in 1944, and this type of pavement has not been in use long enough for failure to develop through deterioration alone. When used in locations where heavy drift cannot destroy it, it appears that the major factor affecting its useful life is the damage done by vegetation. On the basis of the damage now evident (1953) in the average 9-yr-old pavement in place, and assuming that the pavement will become progressively more susceptible to damage by vegetation, it seems that disintegration will be so far advanced in ten years more that further maintenance will be impracticable. The useful life, therefore, appears to be not more than twenty years.

The useful life of concrete pavement appears to be determined by design and conditions of use rather than by the material. No significant deterioration of material is evident in pavements nearly fifty years old. It is probable, however, that in any reasonably economical design, infiltration of rain water and river water at the joints, over a long period of time, will produce cavities in the slopes large enough to cause the slabs to tilt and the joints to open. This is the only basis for estimating the useful life to be as short as forty years.

CONCLUSIONS

Uncompacted asphaltic pavement is the least expensive form of wave-wash protection in so far as first costs are concerned, and is adequate in areas where attack by waves and drift is not too severe. No extenisve new levee protection work has been done with this material since 1946, but uncompacted asphalt has been widely used in repair work and for river bank pavement that is deeply submerged at stages when drift is heavy. There may be economic justification for use of uncompacted asphalt pavement in semi-protected areas on levees whose life expectancy is less than twenty years.

Wooden revetments will continue in use. This is the only form of protection that can be constructed during high or rising river stages, and for that reason is used to advantage on embankments completed late in the working season, when construction of pavement might be interrupted by flood stages. Wooden revetments can be used on new embankment where the amount of shrinkage and subsidence expected would militate against early construction of pavement, and small isolated units can be economically constructed with hand tools where moblization of the plant needed for pavement construction would be prohibitively expensive.

Concrete pavement is the only type of protection in use that is able to withstand the heaviest attack. It is the only type that remains useful over a long period of time without regular maintenance. Where wave attack aggravated by drift would destroy a weaker structure, the use of concrete pavement is obviously essential, and its long life and low maintenance requirements seem to justify the relatively high first cost on any levee having an anticipated life in excess of twenty years.

Brush dikes are still in the experimental stage. In 1953 there is ample evidence that they have successfully accomplished their purpose in preventing undermining of wave-wash protection works and inducing deposit of river-borne material on submerged foreshore areas. The success is gratifying, but the rapid deterioration of the structures has resulted in heavy maintenance costs, and it is apparent that a more durable structure is needed. The major factor in deterioration is the loss of brush filling. This loss is caused in part by failure to obtain adequate tensioning of cables and compression of the brush during construction, and in part by wave-wash, which causes sufficient scour under the dike to permit expansion of the brush filling and slackening of the cables. Permanent improvement of the low foreshore areas can be obtained only if the dikes remain effective until the induced fill becomes consolidated and growth of vegetation produces natural protection against wave action. It is hoped, therefore, that improved methods of design and construction will produce more long-lived structures.

AMERICAN SOCIETY OF CIVIL ENGINEERS
Founded November 5, 1852
TRANSACTIONS

Paper No. 2689

DESIGN CURVES FOR ANCHORED STEEL SHEET PILING

By Walter C. Boyer,[1] J. M. ASCE, and
Henry M. Lummis, III,[2] J. M. ASCE

With Discussion by Messrs. Gregory P. Tschebotarioff; and
Walter C. Boyer and Henry M. Lummis, III

Synopsis

The design of anchored steel sheet piling bulkheads is a procedure normally encountered in many pier development projects. Although no design method has met with universal acceptance, it is felt that the "free-earth-support method" will yield a sufficiently rational approach for preliminary design considerations. A set of curves introduced with this paper will simplify preliminary design computations.

Introduction

Anchored sheet piling depends for its stability on the embedment of the lower part of the sheeting assisted by an anchorage system as near to the top as is consistent with the durability of the anchor rods. Such reactions, therefore, are yielding supports under the effects of the backfill and surcharge forces. The sheeting must be of sufficient strength to sustain the lateral pressures involved. Since walls of this type experience considerable yield, it is rational to assume that the soil attains Rankine's active state.[3] This assumption forms the basis for the normal methods of design as demonstrated by Raymond P. Pennoyer[4] and others.

A set of curves provides an excellent basis for the preliminary design of sheet-pile bulkheads. Consistent with certain assumptions, it is possible to develop such curves quite readily for the major factors involved in sheet-pile design, provided the relationships involved are developed in efficient form for calculation.

Note.—Published, essentially as printed here, in January, 1953, as *Proceedings-Separate No. 165.* Positions and titles given are those in effect when the paper or discussion was received for publication.

[1] Asst. Prof. of Civ. Eng., The Johns Hopkins University, Baltimore, Md.

[2] Engr., Sverdrup & Parcel, Cons. Engrs., St. Louis, Mo.

[3] "Fundamentals of Soil Mechanics," by Donald W. Taylor, John Wiley & Sons, Inc., New York, N. Y., 1948, p. 487.

[4] "Design of Steel Sheet-Piling Bulkheads," by Raymond P. Pennover, *Civil Engineering*, Vol. 3, 1933, pp. 615–619.

Selection of Design Procedure

The three primary factors of interest in anchored sheet-pile design are the depth of embedment, the bending moment in the sheeting, and the anchor pull. There is varied thought as to the procedure to be followed in the determination of these factors. The "free-earth-support method" produces minimum penetration depth resulting in increased bending moment. The "fixed-earth-support method" produces increased penetration depth, resulting in constraining action of the earth with resultant reduction in bending moment. The material-utilization factor is essentially the same in either case, but the latter method is purported to give a greater factor of safety against toe "push out," and reduced cost of the anchorage system.

In the development of passive resistance it has become quite popular to increase the Rankine passive coefficient by a factor of two as recommended by H. Blum based on the tests of O. Franzius.[5] This practice has been questioned by Gregory P. Tschebotarioff,[6] M. ASCE, who terms it "a dangerous oversimplification." The writers concur completely in this statement.

On the basis of the foregoing considerations, the method of design utilized in this paper is the "free-earth-support method" in which the penetration is obtained by taking moments about the anchor point but without doubling the increment of passive pressure. Under this condition, the driving costs are reduced while the depth of penetration is still adequate. Moreover, experience indicates that the additional cost of anchorage is money well spent. In several sheet-pile installations that exhibited signs of distress, it was observed that the anchorage system had proved to be inadequate for the surcharge forces involved.

Basic Assumptions

Fig. 1 indicates the cross section of a typical sheet-pile wall and its anchorage system. The variables involved in the design are as follows: H_s is the height of surcharge; H is the height of sheet pile above water; H_w is the depth of water; ϕ is the angle of internal friction of dry soil; ϕ' is the angle of internal friction of wet soil; W is the weight of dry soil; W' is the buoyed-up weight of soil; H_p is the depth of penetration; T is the tension in tie-rod pounds per foot of wall; and M is the maximum bending moment per foot of wall.

The symbols H_s, H, and H_w, as well as the factors defining the soil properties, denote situation variables obtained prior to actual design. The first problem is to solve for the depth of penetration, H_p, necessary to hold the wall in equilibrium; secondly, the tension, T, in the tie rod must be determined; and, finally, the maximum bending moment, M, must be found. Other design considerations such as the anchorage system, wales, and incidental details are not a part of this paper.

In the development of the formulas that follow, the following assumptions are made to simplify the problem:

---

[5] "Versuche mit Passiven Druck," by O. Franzius, *Der Bauingenieur*, 1924.

[6] "Final Report—Large Scale Earth Pressure Tests with Model Flexible Bulkheads," by Gregory P. Tschebotarioff, Princeton, Univ. Princeton, N. J., January 31, 1949, p. 61.

1. The specific gravity of the soil particles is assumed to be equal to 2.65—a commonly accepted constant.

2. The placement of the tie is assumed at the mean water level. The tie rod is normally placed at or near the mean water level in the zone of saturation to reduce corrosion effects. It is undesirable to place the tie deeper than 2 ft below water level since workers must be paid divers' wages when working below this depth.[7]

3. The Rankine coefficients are assumed to be applicable. Since sheet pile installations have yielding supports, it is rational to assume that they deflect sufficiently to develop the active and passive Rankine coefficients.

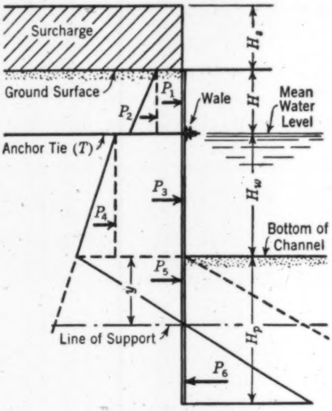

Surcharge
Ground Surface
Anchor Tie (T)
P_1
P_2
Wale
Mean Water Level
H_s
H
H_w
P_3
P_4
Bottom of Channel
P_5
y
Line of Support
H_p
P_6

FIG. 1

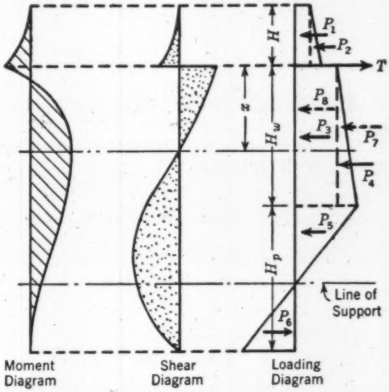

P_1
P_2
T
H
x
H_w
P_8
P_3
P_7
P_4
P_5
H_p
Line of Support
P_6
Moment Diagram
Shear Diagram
Loading Diagram

FIG. 2

4. The soil is considered to have a reduced friction angle for the submerged condition, an assumption which is consistent with usual design procedure. Paul Andersen,[8] M. ASCE, states:

> "This design conventionality may be justified by the fact that the upper portion of the backfill is usually made up of selected material, while the lower portion is the natural soil considerably disturbed by the construction."

5. The soil is assumed to be homogeneous. This assumption is necessary in the development of the curves and is fundamental to most design procedures. However, if boring data indicate definite soil stratification, the curves developed are not applicable.

DEVELOPMENT OF RELATIONSHIPS

With due regard to these five assumptions, the development of the relationships upon which the curves are based is as follows: The y-distance to the line of support (Fig. 1) is readily obtained by setting the active pressure equal to the passive pressure; thus,

---

[7] *U. S. Steel Sheet Piling*, Carnegie-Illinois Steel Corp., p. 9.

[8] "Substructure Analysis and Design," by Paul Andersen, Irwin-Farnham Pub. Co., Chicago, Ill. 1948, p. 49.

$$y\,W'\,K_3 = H_s\,W\,K_2 + H\,W\,K_2 + H_w\,W'\,K_2 + Y\,W'\,K_2 \ldots\ldots (1)$$

Solving Eq. 1 results in

$$y = \frac{K_2\,(H_s\,W + H\,W + H_w\,W')}{W'\,(K_3 - K_2)} \ldots\ldots (2)$$

in which

$$\left.\begin{aligned} K_1 &= \frac{1 - \sin\phi}{1 + \sin\phi} \\ K_2 &= \frac{1 - \sin\phi'}{1 + \sin\phi'} \\ K_3 &= \frac{1 + \sin\phi'}{1 - \sin\phi'} \end{aligned}\right\} \ldots\ldots (3)$$

The various forces exerted on the wall are evaluated in the following manner:

$$\left.\begin{aligned} P_1 &= W\,H\,H_s\,K_1 \\ P_2 &= \frac{W\,H^2\,K_1}{2} \\ P_3 &= W\,H_w\,K_2\,(H_s + H) \\ P_4 &= \frac{W'\,H^2_w\,K_2}{2} \\ P_5 &= \frac{K^2_2\,(H_s\,W + H\,W + H_w\,W')^2}{2\,W'\,(K_3 - K_2)} \\ P_6 &= [W'\,H_p\,(K_3 - K_2) - K_2\,(H_s\,W + H\,W + H_w\,W')]\left[\frac{H_p}{2} - \frac{y}{2}\right] \end{aligned}\right\} (4)$$

The solution for H_p is obtained by taking moments about the tie; thus,

$$\sum M\text{ (tie)} = P_1\frac{H}{2} + P_2\frac{H}{3} - P_3\frac{H_w}{2} - P_4\frac{2\,H_w}{3} - P_5\left(H_w - \frac{y}{3}\right)$$
$$+ P_6\left(H_w + H_p - \frac{H_p}{3} + \frac{y}{3}\right) = 0 \ldots\ldots (5)$$

Substituting for the *P*-forces the expressions in Eqs. 4, and simplifying, Eq. 5 becomes

$$H^3_p\,\frac{W'\,(K_3 - K_2)}{3} + H^2_p\,\frac{H_w\,W'\,(K_3 - K_2)}{2} - \frac{H^2_p\,K_2\,(H_s\,W)}{2}$$
$$- \frac{H^2_p\,K_2\,(H\,W + H_w\,W')}{2} - H_p\,H_w\,K_2\,(H_s\,W + H\,W + H_w\,W')$$
$$+ \frac{W\,H^2\,H_s\,K_1}{2} + \frac{W\,H^3\,K_1}{6} - \frac{H^2_w\,K_2\,(3\,H_s\,W + 3\,H\,W + 2\,H_w\,W')}{6} = 0 \ldots (6)$$

Eq. 6 can be expressed in the general form:

$$f(H_p, H, H_s, H_w, \phi, \phi', W, W') = 0 \ldots\ldots\ldots\ldots\ldots (7)$$

By applying the principles of dimensional analysis, Eq. 7 can be reduced to an equation of dimensionless variables, thereby reducing the number of variables by the number of primary quantities involved.[9] Since there are two primary quantities in Eq. 6—force and length—an equation can be obtained, involving six dimensionless variables, as follows:

$$f'\left(\frac{H_p}{H_w}, \frac{H}{H_w}, \frac{H_s}{H_w}, \phi, N, \frac{W}{W'}\right) = 0 \ldots\ldots\ldots\ldots\ldots (8)$$

in which $N = \phi'/\phi$. However, observing that W is the product of a constant and the specific gravity of the soil particles (G), and that W' is the product of the same constant and the quantity $G - 1$,

$$\frac{W}{W'} = \frac{G}{G - 1} \ldots\ldots\ldots\ldots\ldots (9)$$

Since the specific gravity has been assumed constant, this ratio is also constant. Therefore, if both ϕ and N are considered constant, the general formula, Eq. 9, reduces to

$$f''\left(\frac{H_p}{H_w}, \frac{H}{H_w}, \frac{H_s}{H_w}\right) = 0 \ldots\ldots\ldots\ldots\ldots (10)$$

Calling $\frac{H_p}{H_w} = C_p$; $\frac{H}{H_w} = C$; $\frac{H_s}{H_w} = C_s$; $A = (K_3 - K_2)$; $B = \frac{K_2\, W}{2\, W'}$; and $D = \frac{K_1\, W}{2\, W'}$, and dividing Eq. 6 by $W'\, H^3{}_w$, the following expression is obtained:

$$C^3{}_p \frac{A}{3} + C^2{}_p \frac{A}{2} - C^2{}_p \left(C_s B + C\, B + \frac{K_2}{2}\right) - C_p\, (2\, C_s B + 2\, C\, B + K_2)$$
$$+ C^2\, C_s D + C^3 \frac{D}{3} - C_s B - C\, B - \frac{K_2}{3} = 0 \ldots\ldots\ldots\ldots (11)$$

Simplifying Eq. 11 and arranging it in the most convenient form:

$$C_s = \frac{\left[C^3{}_p \frac{A}{3} + C^2{}_p \left(\frac{A - K_2}{2}\right) - C_p\, K_2 - \frac{K_2}{3}\right]}{B\, (C^2{}_p + 2\, C_p + 1) - C^2\, D}$$
$$- \frac{C\, [B\, (C^2{}_p + 2\, C_p + 1)] + C^3 \frac{D}{3}}{B\, (C^2{}_p + 2\, C_p + 1) - C^2\, D} \ldots\ldots\ldots\ldots (12)$$

The next unknown to be determined is the tension in the tie. If an equation of equilibrium is written for horizontal forces (Fig. 1),

$$T = P_1 + P_2 + P_3 + P_4 + P_5 - P_6 \ldots\ldots\ldots\ldots (13)$$

---

[9] "Fluid Mechanics for Hydraulic Engineers," by Hunter Rouse, McGraw-Hill Book Co., Inc., New York, N. Y., 1938, pp. 14–24.

Substituting the values for the *P*-forces (Eq. 4), and simplifying,

$$T = W\,H\,H_s\,K_1 + \frac{W\,H^2\,K_1}{2} + W\,H_w\,H_s\,K_2 + W\,H_w\,H\,K_2 + W'\,\frac{H^2_w\,K_2}{2} - \frac{W'\,H^2_p\,(K_3 - K_2)}{2} + K_2\,H_p\,(H_s\,W + H\,W + H_w\,W') \ldots\ldots (14)$$

or, in general form:

$$f(T, H_s, H, H_w, H_p, \phi, N, W, W') = 0 \ldots\ldots\ldots\ldots\ldots (15)$$

Taking advantage of the principles of dimensional analysis once again, and considering ϕ and N constant,

$$f'\left(\frac{T}{W\,H^2_w}, \frac{H}{H_w}, \frac{H_s}{H_w}, \frac{H_p}{H_w}\right) = 0 \ldots\ldots\ldots\ldots\ldots (16)$$

Therefore, Eq. 14 is divided by $W\,H^2_w$, calling

$$C_t = \frac{T}{W\,H^2_w} \ldots\ldots\ldots\ldots\ldots (17a)$$

$$E = \frac{W'\,(K_3 - K_2)}{2\,W} \ldots\ldots\ldots\ldots\ldots (17b)$$

and

$$F = \frac{K_2\,W'}{2\,W} \ldots\ldots\ldots\ldots\ldots (17c)$$

Thus,

$$C_t = 2\,F\,C_p + F - C^2_p\,E + K_2\,(C_p + 1)(C_s + C) + C\,K_1\left(C_s + \frac{C}{2}\right) \ldots (18)$$

The final value that must be computed is the maximum bending moment in the pile. Formulas must be developed for the bending moment at three different points—at the tie, between the tie and the bottom of the channel, and between the bottom of the channel and the bottom of the pile. Fig. 2 shows the loading on the piling and the resulting shear and moment diagram.

Assuming that the maximum moment occurs at a point, distance x below the tie (in which x is less than H_w), the first step is to locate this point by determining the section where the summation of shear forces is equal to zero. That is,

$$P_1 + P_2 + P_7 + P_8 - T = 0 \ldots\ldots\ldots\ldots\ldots (19)$$

in which

$$P_7 = \frac{W\,x^2\,K_2}{2}$$

and

$$P_8 = W\,x\,K_2\,(H_s + H) \quad \Bigg\} \ldots\ldots\ldots\ldots\ldots (20)$$

Substituting the values of the *P*-forces in Eq. 20, Eq. 19 becomes

$$W\,H\,H_s\,K_1 + \frac{W\,H^2\,K_1}{2} + \frac{W'\,x^2\,K_2}{2} + W\,x\,K_2\,(H_s + H) - T = 0 \ldots (21)$$

Taking advantage of the fact again that W/W' is constant, and considering ϕ and N constant, Eq. 21 is divided by $W\,H^2{}_w$ which reduces the number of variables by two; thus,

$$C^2{}_x\,F + C_x\,[K_2\,(C_s + C)] + \left[C\,C_s\,K_1 + C^2\,\frac{K_1}{2} - C_t\right] = 0 \ldots\ldots (22)$$

in which $C_x = \dfrac{x}{H_w}$.

Solving for C_x,

$$C_x = \frac{-\,K_2\,(C_s + C) \pm \sqrt{[K_2\,(C_s + C)]^2 - 4\,F\left(C\,C_s\,K_1 + C^2\,\dfrac{K_1}{2} - C_t\right)}}{2\,F} \ldots (23)$$

Taking moments about the point thus obtained,

$$\begin{aligned} M &= P_1\left(\frac{H}{2} + x\right) + P_2\left(\frac{H}{3} + x\right) - T\,x + P_8\,\frac{x}{2} + P_7\,\frac{x}{3} \\ &= \frac{W\,H^2\,H_s\,K_1}{2} + W\,H\,H_s\,x\,K_1 + \frac{W\,H^3\,K_1}{6} + \frac{W\,H^2\,x\,K_1}{2} - T\,x \\ &\quad + \frac{W\,x^2\,K_2\,H_s}{2} + \frac{W\,x^2\,K_2\,H}{2} + \frac{W'\,x^3\,K_2}{6} \ldots\ldots\ldots\ldots (24) \end{aligned}$$

Once again dimensional analysis is employed, and since ϕ and N are considered constant, Eq. 24 is divided by $W\,H^3{}_w$ and arranged in the most convenient form:

$$\begin{aligned} C_m = C^2\,C_s\,\frac{K_1}{2} + C^3\,\frac{K_1}{6} - C^3{}_x\,\frac{2}{3}\,F \\ - C^2{}_x\left[\frac{K_2}{2}\,(C_s + C)\right] \ldots (25) \end{aligned}$$

in which $C_m = \dfrac{M}{W\,H^3{}_w}$.

By taking moments about the tie and reducing to dimensionless form, the equation for moment at the tie is

$$C_m = C^2\,C_s\,\frac{K_1}{2} + C^3\,\frac{K_1}{6} \ldots\ldots\ldots\ldots (26)$$

Eq. 26 is the same as the first two terms of Eq. 25.

If the point of zero shear falls below the bottom of the channel, Eq. 25 is not valid and another equation must be derived. Fig. 3 shows that part of the piling below the channel with the loads acting on it. Since P_9 must equal P_6,

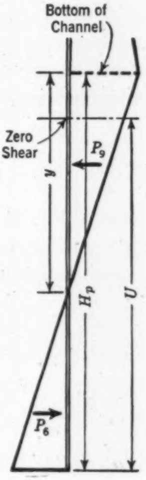

FIG. 3

$$U = 2\,(H_p - y) = 2\,H_p - \frac{2\,K_2}{W'\,(K_3 - K_2)}\,(H_s\,W + H\,W + H_w\,W') \ldots (27)$$

Applying dimensional analysis to Eq. 27, divide through by H_w and simplify.

Let $U/H_w = C_u$ and

$$C_u = 2\,C_p - \frac{K_2}{E}(C_s + C) - \frac{2\,K_2}{A} \quad \text{.............. (28)}$$

Taking moments about the point of zero shear,

$$M = \frac{5\,P_6}{3}(H_p - y) - \frac{P_9}{3}(H_p - y) \quad \text{.............. (29)}$$

and

$$M = \frac{U^2}{24}\left[5\,W'\,H_p\,(K_3 - K_2) - 5\,K_2\,(W\,H_s + W\,H + W'\,H_w) - W'\,(K_3 - K_2)\,\frac{U}{2}\right] \quad \text{.................. (30)}$$

Consider ϕ and N constant and divide Eq. 30 by $W\,H^3_w$ to convert Eq. 30 into dimensionless terms:

$$C_m = \frac{C^2_u}{4.8}\left[2\,E\,C_p - K_2\,(C_s + C) - 2\,F - \frac{E\,C_u}{5}\right] \quad \text{....... (31)}$$

Simplifying,

$$C_m = \frac{E}{6}\,C^3_u \quad \text{........................ (32)}$$

In reviewing the relationships developed, it is well to note that the dependent variables are all functions of the same independent variables when ϕ and ϕ' are considered constant. Note that in Eq. 12

$$C_p = f\,(C, C_s) \quad \text{...................... (33a)}$$

in Eq. 18,

$$C_t = f\,(C, C_s, C_p) = f'\,(C, C_s) \quad \text{.............. (33b)}$$

and, in Eq. 25,

$$C_m = f\,(C_x, C, C_s) \quad \text{...................... (33c)}$$

—but, since (in Eq. 23),

$$C_x = f\,(C, C_s, C_t) = f'\,(C, C_s) \quad \text{.............. (34)}$$

then

$$C_m = f\,(C, C_s) \quad \text{...................... (35)}$$

Likewise, in Eq. 26,

$$C_m = f\,(C, C_s) \quad \text{...................... (36a)}$$

and, in Eq. 32,

$$C_m = f\,(C_u) \quad \text{...................... (36b)}$$

—but, since

$$C_u = f\,(C_p, C, C_s) = f'\,(C, C_s) \quad \text{.............. (37)}$$

then

$$C_m = f\,(C, C_s) \quad \text{...................... (38)}$$

As it has been demonstrated that C_p, C_t, and C_m are functions of C and C_s alone, when ϕ and ϕ' are considered constant, lines of constant C_p, C_t, and C_m can be plotted with C the ordinate and C_s the abscissa. This procedure lends itself to an efficient construction of diagrams.

METHOD OF DEVELOPING DATA FOR CHARTS

The curves were plotted with values of C_s as the abscissas and values of C as the ordinates, each set for a particular value of ϕ and N ($N = \phi'/\phi$). Each set provides the constants, C_p, C_t, and C_m, over a practical range of values, by which the depth of penetration, the tension force in the tie rod per foot, and the maximum bending moment per foot may be determined for a particular problem.

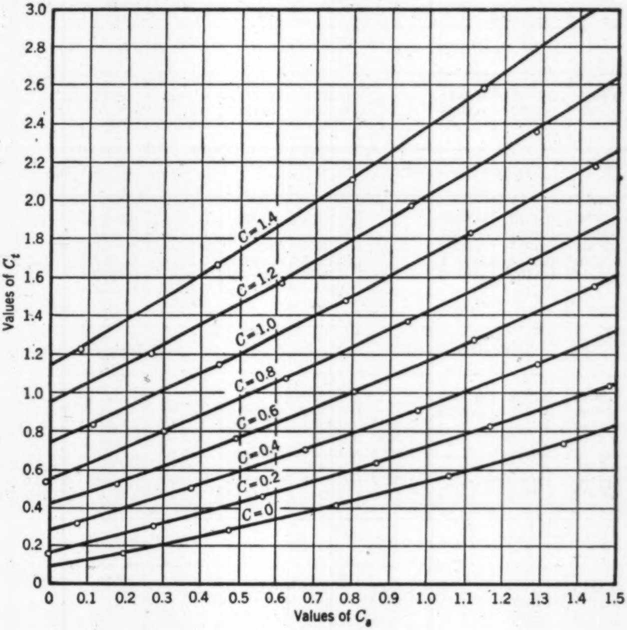

FIG. 4.—SAMPLE INTERPOLATION CURVE FOR C_t (ϕ = 30° AND $N = \frac{1}{2}$)

The first series of solutions was made for C_p utilizing Eq. 12. Actually, by assuming constant values for C_p and varying C, values for C_s were determined. By considering C_s as the dependent variable, the necessity of solving a cubic equation was avoided.

The next parameter considered was C_t. Using the values of C, C_s, and C_p previously determined, Eq. 18 yielded odd values of C_t. Therefore, a series of interpolation curves was drawn with values of C_t as the ordinates and values of C_s as the abscissas (Fig. 4). Thus, for any desired value of C_t, C_s was determined from the interpolation curves with C as the parameter.

A series of solutions for C_m was found by using Eqs. 25, 26, or 32, after having determined the location of the maximum moment by Eqs. 23 and 28. A set of interpolation curves was drawn for C_m similar to those for C_t in Fig. 4.

A complete log of the data for the condition of $\phi = 30°$ and $N = \frac{3}{4}$ is presented in Table 1. Similar data were determined for three values of ϕ (20°, 30°, and 40°) each associated with three values of N ($\frac{1}{2}$, $\frac{3}{4}$, and 1). The corresponding graphs for $\phi = 30°$ and $\phi = 40°$ are presented in Fig. 5. Supplementing information in Fig. 5, the design constants for $\phi = 20°$, 30°, and 40° are given in Table 2 for the special case $C = 0$ and $C_s = 0$.

TABLE 1.—ANCHORED STEEL SHEET PILING DATA FOR CONSTRUCTION DESIGN CURVES ($\phi = 30°$ AND $N = \frac{3}{4}$)

$C =_w$ H/H	$C_s = H_s/H_w$ (1)	C_t (Eq. 17*a*) (2)	$C_x = x/H_w$ (3)	$C_u = U/H_w$ (4)	C_m (Eq. 32) (5)	$C_s = H_s/H_w$ (1)	C_t (Eq. 17*a*) (2)	$C_x = x/H_w$ (3)	$C_u = U/H_w$ (4)	C_m (Eq. 32) (5)
	(*a*) $C_p = H_p/H_w = 0.8$					(*b*) $C_p = H_p/H_w = 1.0$				
0	0.195	0.1636	0.8151	....	0.0793	0.4710	0.2802	0.8518	....	0.1338
0.2	−0.005	0.1670	0.8058	....	0.0765	0.2735	0.3074	0.8536	....	0.1327
0.4	....	....	....	....	....	0.0771	0.3220	0.8575	....	0.1314
	(*c*) $C_p = H_p/H_w = 1.2$					(*d*) $C_p = H_p/H_w = 1.4$				
0	0.7580	0.4143	0.8941	....	0.2018	1.0580	0.5693	0.9426	....	0.2878
0.2	0.5624	0.4631	0.8981	....	0.2005	0.8650	0.6424	0.9483	....	0.2870
0.4	0.3705	0.5035	0.9092	....	0.1986	0.6770	0.7093	0.9627	....	0.2843
0.6	0.1790	0.5324	0.9174	....	0.1954	0.4922	0.7613	0.9677	....	0.2711
0.8	−0.0174	0.5407	0.9185	....	0.1892	0.3038	0.8056	0.9810	....	0.2642
1.0	....	....	....	....	....	0.1186	0.8403	0.9935	....	0.2564
1.2	....	....	....	....	....	−0.0804	0.8431	....	1.4060	0.2500
	(*e*) $C_p = H_p/H_w = 1.6$					(*f*) $C_p = H_p/H_w = 1.8$				
0	1.3640	0.7398	0.9899	....	0.3887	....	....	....	....	....
0.2	1.1680	0.8285	0.9928	....	0.3840	1.4810	1.0380	....	1.7569	0.5049
0.4	0.9780	0.9134	....	1.5993	0.3808	1.2970	1.1540	....	1.7441	0.4940
0.6	0.8040	1.0090	....	1.5785	0.3662	1.1220	1.2750	....	1.7241	0.4771
0.8	0.6270	1.0829	....	1.5601	0.3535	0.9490	1.3780	....	1.7025	0.4594
1.0	0.4500	1.1550	....	1.5417	0.3411	0.7810	1.4830	....	1.6769	0.4390
1.2	0.2700	1.2100	....	1.5257	0.3305	0.6130	1.5770	....	1.6513	0.4192
1.4	0.0824	1.2390	....	1.5158	0.3242	0.4440	1.6700	....	1.6265	0.4006
	(*g*) $C_p = H_p/H_w = 2.0$					(*h*) $C_p = H_p/H_w = 2.2$				
0.6	1.4440	1.5533	....	1.8665	0.6054	....	....	....	....	....
0.8	1.2730	1.6860	....	1.8433	0.5831	....	....	....	....	....
1.0	1.1130	1.8325	....	1.8113	0.5534	1.4410	2.1790	....	1.9489	0.6892
1.2	0.9550	1.9755	....	1.7777	0.5230	1.2890	2.3560	....	1.9105	0.6492
1.4	0.7999	2.1120	....	1.7425	0.4926	1.1420	2.5850	....	1.8681	0.6069

Design Example.—To demonstrate the use of a design chart such as Fig. 5, assume $H_s = 4$ ft, $H = 8$ ft, $H_w = 22$ ft, $W = 100$ lb per cu ft, $\phi = 30°$, and $\phi' = 30°$. With these data, it is possible to compute $C = H/H_w = 8/22 = 0.364$; $C_s = H_s/H_w = 4/22 = 0.182$; and $N = \phi'/\phi = 30/30 = 1$. With

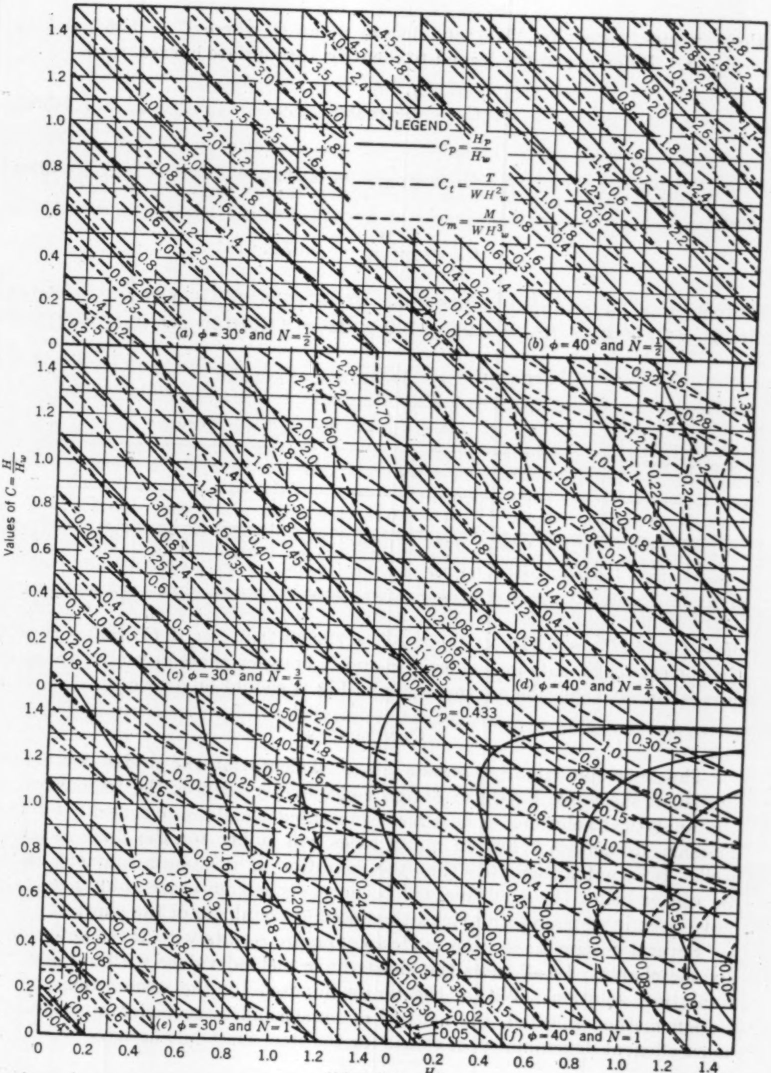

Fig. 5.—Design Curves for Anchored Steel Sheet Piling

these values, enter Fig. 5(*e*) and locate point O where $C = 0.364$ and $C_s = 0.182$. Referring to the legend to identify appropriate curves, read

$$C_p = \frac{H_p}{H_w} = 0.63 \ldots\ldots\ldots\ldots \quad (39a)$$

$$C_t = \frac{T}{W\,H^2_w} = 0.24 \ldots\ldots\ldots\ldots \quad (39b)$$

and

$$C_m = \frac{M}{W\,H^3_w} = 0.075 \ldots\ldots\ldots\ldots \quad (39c)$$

Solving Eqs. 39 for appropriate values—$H_p = C_p \times H_w = 0.63 \times 22 = 13.86$ ft; $T = C_t \times W \times H^2_w = 0.24 \times 100 \times \overline{22}^2 = 11{,}616$ lb per ft of wall; and $M = C_m \times H^3_w = 0.075 \times 100 \times \overline{22}^3 = 79{,}860$ ft-lb per ft of wall. To find the correct coefficients for values of ϕ and N between those given in the design curves, an interpolation curve similar to Fig. 4 should be drawn.

TABLE 2.—DESIGN CONSTANTS

Constant	Equation	ANGLE OF FRICTION, ϕ (FOR $C = C_s = 0$)								
		20°			30°			40°		
N	8	0.5	0.75	1	0.5	0.75	1	0.5	0.75	1
C_p	12	1.850	1.125	0.770	1.130	0.660	0.410	0.762	0.408	0.225
C_t	17*a*	0.290	0.160	0.110	0.158	0.080	0.050	0.108	0.057	0.030
C_m	32	0.160	0.100	0.057	0.110	0.045	0.026	0.057	0.026	0.013

CONCLUSION

The development of dimensionless coefficients for the design factors required in sheet-pile bulkhead design considerably reduces the tediousness of the analytical solution. The curves presented should prove useful for preliminary design work and in many cases will suffice for the final design as well. It is not anticipated that the condition of maximum moment at the tie rod or below the mud line will be normally encountered—but these cases have been investigated to extend the possible usefulness of the charts.

Several designs have been made to compare results with those determined by the charts. In all cases the charts have yielded values within 2% of the analytical solution. Within the limits imposed by the assumptions of the design method selected, the method of dimensionless coefficients permits the most efficient development of charts for the steel sheet-pile design.

DISCUSSION

Gregory P. Tschebotarioff,[10] **M. ASCE.**—The method of design described by the authors under the heading, "Selection of Design Procedure," is identified as

> "* * * the 'free-earth-support method' in which the penetration is obtained by taking moments about the anchor point but without doubling the increment of passive pressure. Under this condition, the driving costs are reduced while the depth of penetration is still adequate."

Messrs. Boyer and Lummis also state that the writer has questioned the practice of doubling the Rankine passive coefficient and termed it "a dangerous oversimplification."

The writer regrets that these words have been removed from their context. The writer's practical conclusions are diametrically opposed to those attributed to him by the authors. The relevant passage is as follows:[6]

> "In recent years there has been a tendency to assume that the passive earth pressure can always be taken as double its conventional value * * * irrespective of the values and of the direction of the angle of wall friction. This tendency appears to have been based on the results of tests performed in 1924 by Professor Franzius at Hannover * * * it is on these tests that Blum based his recommendations to double the passive earth pressure * * * Blum's recommendation that the passive earth pressure be doubled is said to have been made: 'to allow for the additional resistance due to the undisturbed and naturally compact soil into which the sheet piling is driven.' This is a dangerous oversimplification, especially where sands are concerned."

Only the justification for doubling the conventional Rankine passive coefficient was questioned here, since reliance on unspecified properties of undisturbed soil meant that the doubling of the coefficient might be considered justified under almost all field conditions. To show that this was not permissible the writer has stated[6] that "if the wall is pulled out in respect to the soil * * * the value of K' * * * will decrease to less than one third of its original value." Such a condition can arise in the case of a sheet-pile wall driven on the land side of a light relieving platform.[11] For an anchored sheet-pile bulkhead of the type investigated by the authors, however, the writer indicated that the passive earth pressure coefficient K_P (recorded during most of the tests with model flexible bulkheads) was equal to or greater than the value[6] of 12. During several tests,[12] K_P-values varied from 9 to 15. That is, since ϕ was equal to 36°, values of K_P were from 2.3 to 3.9 times higher than the values expected on the basis of the Rankine passive earth pressure coefficient (K' equal to 3.85), which neglected the effect of wall friction. Tests performed in 1953 confirmed the fact that, for the conditions of anchored bulkheads described by the authors, the doubling of the Rankine coefficient K' is entirely justified.[13] This conclusion is contrary to that reached by the authors.

---

[10] Prof. of Civ. Eng., Princeton Univ., Princeton, N. J.

[11] "The Effects of Restraining Boundaries on the Passive Resistance of Sand," by Gregory P. Tschebotarioff and Edmund G. Johnson, Princeton University Report, Princeton, N. J., June 1, 1953, Fig. III.

[12] "Final Report—Large Scale Earth Pressure Tests with Model Flexible Bulkheads," by Gregory P. Tschebotarioff, Princeton Univ., Princeton, N. J., January 31, 1949, Figs. 65, 67, 69, 71, 73, 77, 79, 81, 86, and 88.

Messrs. Boyer and Lummis do not explain why the minimum depth of penetration obtained without doubling the increment of passive pressure is considered to be adequate. A similar opinion has been reached by James R. Ayers, M. ASCE, and R. C. Stokes, in a paper discussed by the writer.[14] It was shown that for sand soils this approach can lead to very high (although uneconomical) factors of safety, whereas in the case of clay soils it can lead to dangerously low factors of safety.

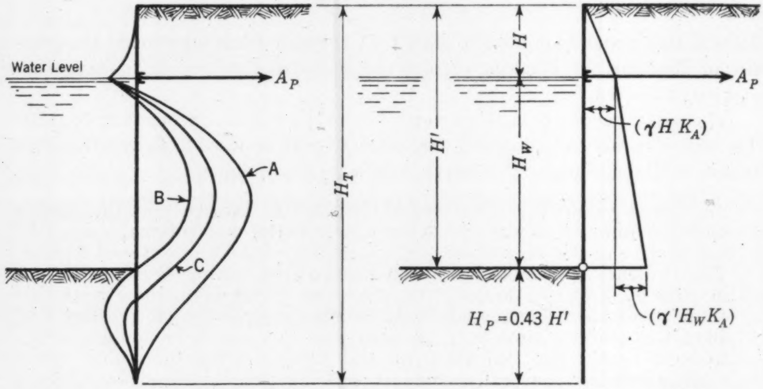

(*a*) BENDING-MOMENT CURVES

(*b*) FIXED EARTH SUPPORT METHOD

FIG. 6.—COMPARISON OF METHODS OF SHEET-PILE BULKHEAD DESIGN

The design curves developed by the authors are useful for the practical design of very rigid walls in loose sands. For flexible anchored sheet-pile bulkheads in medium to dense sands, however, the design will be uneconomical.

The free-earth-support method, illustrated in Figs. 1 and 2, results in a bending moment diagram similar to curve A in Fig. 6(*a*). Two independent series of model tests performed by the writer[15] and P. W. Rowe[16] have indicated that, for flexible bulkheads in clean medium to dense sands, definite restraint at the point of the piling is present—even at depths of penetration barely sufficient to provide a factor of safety of unity if the effect of wall friction on the passive resistance of the sand is neglected. For the same depth of penetration, the amount of restraint increases with the flexibility of the bulkhead and with the stiffness of the soil.

---

[13] "The Effects of Restraining Boundaries on the Passive Resistance of Sand," by Gregory P. Tschebotarioff and Edmund G. Johnson, Princeton University Report, Princeton, N. J., June 1, 1953, p. VIII.

[14] Discussion by Gregory P. Tschebotarioff of "The Design of Flexible Bulkheads," by James R. Ayers and R. C. Stokes, *Transactions*, ASCE, Vol. 119, 1954, p. 390.

[15] "Final Report—Large Scale Earth Pressure Tests with Model Flexible Bulkheads," by Gregory P. Tschebotarioff, Princeton Univ., Princeton, N. J., January 31, 1949.

[16] "Anchored Sheet-Pile Walls," by P. W. Rowe, *Proceedings*, Inst. of C. E., London, England, Vol. 1, Pt. 1, 1952, p. 27.

Tests have shown that for H_P equal to 0.43 H' the point of contraflexure very closely coincides with the dredge line (curve B, Fig. 6(*a*)).[15] On the basis of these test results, the writer proposed the modified fixed-earth-support method illustrated by Fig. 6(*b*).[17] A hinge is assumed at the dredge line, and bending moments above the dredge are computed for a beam on two supports with an overhanging end. The active earth pressure coefficient K_A was determined from

$$K_A = \left(1 - \frac{H}{f' H'}\right) 0.33 f''' \ldots\ldots\ldots\ldots\ldots\ldots (40)$$

The coefficients f' and f''' were assumed to equal 3.5 and 0.9, respectively.

This design procedure was based on the analysis of the summary of the test results given in Fig. 7, which covers the twelve tests performed with clean sands.[18] The same model bulkhead (steel plate, $\frac{1}{4}$ in. thick) was used throughout all the tests. The bulkhead's flexibility, however, was varied by changing (to the same scale) the distance H' from the top of the backfill to the dredge line and the distance H from the top of the backfill to the anchor level. The depth of embedment H_P was also varied. The total bulkhead length H_T was varied from a maximum of 98 in. to a minimum of 57 in.

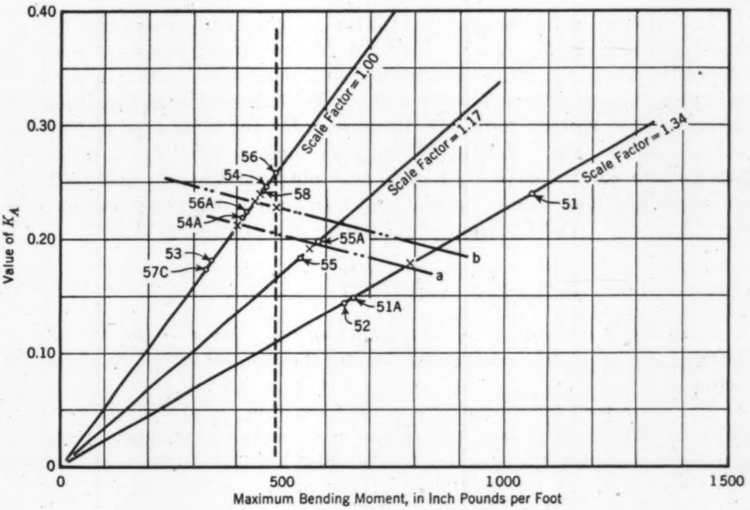

FIG. 7.—BULKHEADS FOUNDED IN CLEAN SANDS

The three lines radiating from the origin in Fig. 7 show the theoretical relationship between various values of the active lateral earth-pressure coefficient K_A, based on intergranular pressures, and the maximum bending moment values, computed according to Fig. 6(*b*), for the three scale factors used in a series of tests.[15] By plotting the measured bending-moment values on these lines, the corresponding K_A-values are obtained. It will be noted from Fig. 7 that the values of K_A obtained in this manner decrease with an increasing flexibility as given by the scale factor. The line a–a in Fig. 7 connects the average values of the tests with the same depth of embedment (H_P) equal to 0.63 H' at each of the three scale factors. Points 54 and 54A show that the procedure suggested by Fig. 6(*b*) is valid for a depth of embedment of H_P equal to or greater than 0.43 H'. It should be noted that model similarity was based on the similarity of both dimensions and stresses and was shown to exist for bending moments not exceeding the value of 490 in. lb per ft.[19] This value is indicated by a vertical dashed line in Fig. 7. Eq. 40 is based on a value of K_A equal to 0.23 that was the intersection of the dashed line with the line b–b.[20]

---

[17] "Soil Mechanics, Foundations and Earth Structures," by Gregory P. Tschebotarioff, McGraw-Hill Book Co., Inc., New York, N. Y., 1951, p. 506.

[18] "Final Report—Large Scale Earth Pressure Tests with Model Flexible Bulkheads," by Gregory P. Tschebotarioff, Princeton Univ., Princeton, N. J., January 31, 1949, Fig. 42.

The writer's conclusions (based on the foregoing tests) have been amplified by model tests performed by Mr. Rowe.[16] Mr. Rowe's tests constituted a greater range of bulkhead flexibilities at a somewhat smaller model scale (H_T equal to 42 in.) than those performed by the writer. For bulkhead flexibilities identical to those of the writer's tests, Mr. Rowe recorded the same type of bending-moment curve. For bulkheads stiffer than those tested by the writer, an intermediate curve (curve C, Fig. 6) was obtained whereas, for very stiff bulkheads and loose sands, curve A and a free earth support condition were found to apply. The flexibility of the bulkhead was expressed by

$$\rho = \frac{H^4_T}{E\,I} \qquad \text{(41)}$$

in which H_T is equal to the entire length of the pile; E is the modulus of elasticity of the pile material; and I denotes the moment of inertia of the pile section.

Mr. Rowe used the coefficient ρ in the form of log ρ, whereby H was measured in feet, E in pounds per square inch, and I in inches^4. Complete agreement between the writer's test results and Mr. Rowe's test results was then obtained[21] for flexibilities of the bulkhead used by the writer—which were greater than log $\rho = -2.97$. This value corresponds to ρ equal to 22.5 sq in. per lb. (It should be noted that ρ has dimensions that are equal to the reciprocal of stress; Mr. Rowe's procedure of determining model similarity is thus fundamentally similar to the writer's method.)[22]

In contrast to the procedure illustrated in Fig. 6(*b*), based on the fixed-earth-support method and a hinge at the dredge line, Mr. Rowe began from the opposite possible limit condition and based his design on the assumption of free earth support. The maximum moment of curve A (Fig. 6(*a*)) was then reduced by an empirical coefficient.[21]

---

[19] "Final Report—Large Scale Earth Pressure Tests with Model Flexible Bulkheads," by Gregory P. Tschebotarioff, Princeton Univ., Princeton, N. J., January 31, 1949, p. 40.

[20] *Ibid.*, p. 70.

[21] "Anchored Sheet-Pile Walls," by P. W. Rowe, *Proceedings*, Inst. of C. E., London, England, Vol. 1, Pt. 1, 1952, p. 45, Fig. 14.

[22] Correspondence by G. P. Tschebotarioff on "Anchored Sheet-Pile Walls," by P. W. Rowe, *Proceedings*, Inst. of C. E., London, England, Vol. 1, Pt. 1, 1952, p. 616.

A detailed comparison of the two methods of design will not be undertaken at this time; both have advantages and limitations. It should be noted that it would be erroneous to consider Mr. Rowe's method a free-earth-support method in the same sense that this term applies to the design curves presented by the authors. The bending moments computed according to all free-earth-support methods, including the one developed by the authors, increase with an increase in the depth of penetration. This increase in moment is contrary to experience with medium to dense sands. In Mr. Rowe's procedure, the free-earth-support method is followed by a reduction of bending moments to account for the effect of fixation at the toe on the change of bending moments. This reduction is shown by the change of curve A to the bending-moment curves illustrated by curves B and C of Fig. 6(*a*). The writer's method (Fig. 6(*b*) and Eq. 40) can also be adapted, by varying the coefficient f''' so that the maximum bending moments shown by curve B will reflect conditions of the type corresponding to curve C in Fig. 6(*a*). This latter procedure is more flexible and can more readily reflect many imponderables which lead to the inevitable scattering of results which occurs in the field. This scattering of results was observed during the tests performed by the writer (Fig. 7).

For flexible bulkheads, appreciable reductions of the bending moments proposed by the authors are indicated. Under the heading, "Method of Developing Data for Charts: Design Example," a sample design is presented in which H_P/H' is equal to 0.53. This value exceeds that needed for full fixation in the case of medium to dense sand (H_P/H' equal to 0.43). Computations based on Fig. 6(*b*) result in a maximum positive bending moment of + 34,400 ft lb in the sheet piling. This moment is 43% of the bending moment of 79,860 ft lb computed by the authors' free-earth-support method. Mr. Rowe's data[23] shows that steel piling stressed to 18,000 lb per sq in., as well as reinforced concrete piling stressed to $f_c = 1,250$ lb per sq in. (permissible in concrete with a 28-day strength of $f'_c = 2,760$ lb per sq in.), will also be subjected to approximately 45% of the bending-moment values obtained by use of the free-earth-support method. This proves that the writer's design procedure (Fig. 6(*b*)) automatically gives the strength required by the corresponding flexibility of steel sheet piling and of piling made of medium quality concrete. For timber piling and for higher quality concrete, designs according to Fig. 6(*b*) will give conservative values; such designs will be on the unsafe side only for low-grade concrete ($f_c = 750$ lb per sq in., $f'_c = 1,670$ lb per sq in.).[23] Such poor concrete should never be used in waterfront structures.

WALTER C. BOYER,[24] A. M. ASCE, AND HENRY M. LUMMIS, III,[25] J. M. ASCE.—Mr. Tschebotarioff has contributed a stimulating discussion, and has pointedly indicated the area of usefulness of the design charts. His interpretation, however, is subject to careful scrutiny and is a matter of opinion.

The function of the paper was to present a useful tool to the practicing engineer. In no sense can it be construed to be a paper reporting the research on flexible-pile bulkheads. The writers were faced with the problem of adopting generalized criteria which could be considered applicable to a complete range of pile flexibilities and soil conditions. Mr. Tschebotarioff has termed the resultant work "conservative." Since the charts were intended primarily for preliminary design, this is felt to be necessary and desirable. No claim has been made to originality in the fundamental assumptions, but these have been set forth clearly to permit appraisal of the resultant charts. Accordingly, it is difficult to conceive that a designer would utilize the charts without realizing their inherent limitations.

---

[23] Discussion by P. W. Rowe of "The Design of Flexible Bulkheads," by James R. Ayers and R. C. Stokes, *Transactions*, ASCE, Vol. 119, 1954, p. 389, Fig. 13(*b*).

[24] Asst. Prof. of Civ. Eng., The Johns Hopkins Univ., Baltimore, Md.

[25] Engr., Sverdrup & Parcel, Cons. Engrs., St. Louis, Mo.

Mr. Tschebotarioff has questioned the interpretation placed on his writings concerning the increase of Rankine's passive coefficient by a factor of 2, as recommended by Mr. Blum. In further writings, however, he has stated:[26]

> "It should be noted in this connection that the doubling of the K_p value, as compared with the value obtained from Equation (10–7), was undertaken by Blum not because he considered the beneficial effect of wall friction (Art. 1–5), but because of the results of previous tests by Franzius (Ref. 136, 1927) at Hannover. During these tests, Franzius obtained very high values of passive resistance and recommended doubling the values of passive resistance obtained by the use of the heretofore customary equation (10–14a). The direction of the wall friction (Art. 10–5) was not given any consideration by this recommendation, which should therefore not be used indiscriminately. The test box used by Franzius was 3.3 feet wide and 4.9 feet high. Therefore, side-wall friction may have had a very great influence on the increase of the passive resistance of the soil in the box when the front wall was pushed in. It is questionable whether his test data can be applied to a normally long wall under field conditions."

Other writers[27] have indicated similar concern with this procedure; accordingly, the use of Rankine's passive coefficient, K_p, without increase was adopted in this paper. Mr. Tschebotarioff's findings[11,13] were not available at the time this paper was prepared. However, one can question the advisability of interpreting ultimate toe-pressure development as an increased value of Rankine's passive coefficient. Presumably the toe pressure is a function of pile flexibility, wall friction, toe shear, and the vertical component of active soil as proposed by Mr. Rowe.[28] One should not conclude that doubling the value of Rankine's passive coefficient will result in substantial reductions in the design characteristics of sheet-pile walls, as can be seen from Table 3. It can be noted from Table 3 that doubling the value of Rankine's passive coefficient primarily influences the depth of penetration in the free-earth-support method of design but does not similarly influence the anchor tension or maximum bending moment. Using a value of K_p equal to unity results

---

[26] "Soil Mechanics, Foundations, and Earth Structures," by Gregory P. Tschebotarioff, McGraw-Hill Book Co., Inc., New York, N. Y., 1951, p. 499.

[27] "Design of Steel Sheet-Piling Bulkheads," by Raymond P. Pennoyer, *Civil Engineering*, Vol. 3, 1933, p. 615.

[28] "Anchored Sheet-Pile Walls," by P. W. Rowe, *Proceedings*, Inst. of C. E., London, England, Vol. 1, Pt. 1, 1952, p. 60.

TABLE 3.—THE EFFECT OF VARYING K_p

Design characteristic	Design charts	Analytical solution	
Coefficient of Passive Resistance	K_p	K_p	$2\,K_p$
Maximum bending moment, in foot-pounds per foot of wall	79,860	79,589	72,060
Anchor tension, in pounds per foot of wall	11,616	11,625	11,168
Depth of penetration, in feet	13.86	14.02	11.63

in a depth of penetration that is considered adequate without an additional increase as normally recommended in design procedures.

Mr. Tschebotarioff has placed a limitation on the value of the charts, relegating their usefulness to the practical design of very rigid walls in loose sands. This conclusion is based on a chart[21] similar to Fig. 8. In Fig. 8, M_D is the design moment reduced as a result of Mr. Rowe's tests, and M represents the bending moment as determined from the charts. Reference to Fig. 8 indicates that for very rigid walls ($\log \rho > 3.5$) and loose soil, no moment reduction is permissible. Fig. 8 also forms the basis for Mr. Tschebotarioff's statement that, for the design example, the reduction chart offered by Mr. Rowe causes a design moment which is 45% of the value, 79,860 ft lb per ft. This conclusion is concurred in, and it is strongly recommended that the design charts be used in conjunction with Mr. Rowe's reduction chart. Under this condition, the charts have a wide area of usefulness—ranging from relatively rigid concrete piling to flexible timber piling.

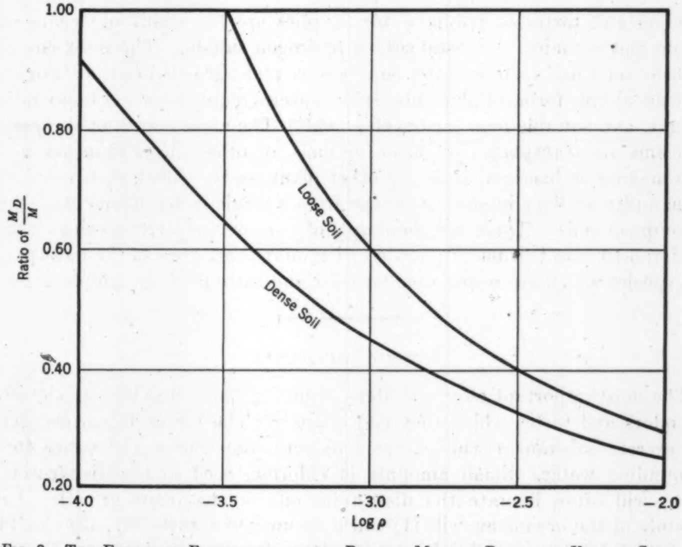

FIG. 8.—THE EFFECT OF FLEXIBILITY ON THE BENDING-MOMENT RATIO FOR VARIOUS SOILS

AMERICAN SOCIETY OF CIVIL ENGINEERS
Founded November 5, 1852
TRANSACTIONS

Paper No. 2690

ALGAE RESPONSIBLE FOR ODOR AND TASTE IN WATER SUPPLIES

BY GEORGE J. TURRE[1]

SYNOPSIS

Odors and tastes in public water supplies are the result of decomposed organic matter, mineral substances, or hydrogen sulfide. The most common origins of odor and taste in water supplies are plant growths of the algae type. Algae are simple forms of plant life—most species requiring warm temperature, sunlight, and suitable food for development. The algae spores of the various organisms are transported by wind, animals, or other physical means in the same manner as bacteria, yeast, or other plant seeds. Most algae are microscopic and may vary in size and shape from a single cell to filaments, chains, or groups of cells. There are thousands of variously colored species of algae. It is impossible to become acquainted with more than a few of the most prominent species which are responsible for odor and taste in water supplies.

EFFECTS OF ALGAE

The most important effects of algae in public water supplies are the offensive odors and tastes which they can cause.[2,3] The living organisms secrete and excrete substances which impart objectionable odors and tastes to the surrounding water. Small amounts of chlorine, used in the disinfection of water, will often liberate the distasteful oils of the plant growth. Large amounts of the organisms will (1) cause an unsightly turbidity, (2) clog filter beds, (3) inhibit proper floc formation, (4) reduce filtration rates, (5) reduce flow rates in pipe lines, and (6) stain plumbing fixtures.

From a health standpoint algae are not significant; they are not a cause of disease in man or the higher animals. An unusually large number of the common microscopic organisms found in drinking water can, however, produce

---

NOTE.—Published essentially as printed here, in September, 1953, as *Proceedings-Separate No. 267.* Positions and titles given are those in effect when the paper was received for publication.

[1] San. Engr., Board of Water Commissioners, Denver, Colo.

[2] "Microscopy of Drinking Water," by G. C. Whipple, John Wiley & Sons, Inc., New York, N. Y., 4th Ed., 1948.

[3] "The Use of Copper Sulfate in Control of Microscopic Organisms," by Frank E. Hale, Phelps Dodge Refining Corp., New York, N. Y., 1950.

digestive disturbances in the users of the water. Water of this kind would generally be too offensive to use without treatment.

Most algae grow in the presence of sunlight by the process of photosynthesis —that is, by acquiring their own food from the dissolved gases and mineral salts normally present in the water. Therefore, wherever practical, it is important to have all filtered-water storage reservoirs covered to exclude sunlight.

The distinctive odors produced by algae can be grouped in three general classifications—aromatic, grassy, and fishy.

FIG. 1.—ASTERIONELLA (400×)

Aromatic Odors.—Aromatic odors are caused principally by diatomaceae. The strongest odor is produced by the asterionella. The asterionella (the "little star") is shown in Fig. 1. This organism, when present in sufficient numbers (500 standard units or more), will impart an aromatic, geranium odor during the process of cell splitting, or reproduction. In larger numbers they may give the water a fishy odor. Asterionellae are brownish in color and are prevalent in the spring and fall months. The organisms are fragile; they may cause trouble by penetrating filter material; and they inhibit proper floc formation.

Grassy Odors.—Grassy odors are produced mainly by the cyanophyceae. The anabaena is the most common offender in this group of algae. There are two species which have slightly different odors. The circinalis species, which resembles a string of beads, is shown in Fig. 2(*a*). The prevalent color is brownish-green, or brown. Anabaenae are found free-floating; their vegetative cells are spherical, and the filaments are without sheaths. Anabaenae impart a grassy odor and taste. When present in large numbers, this species imparts a vile pig-pen odor, especially during the summer months. This organism is one of the most common offenders; it is easily destroyed with a dose of 1 lb of copper sulfate per million gallons of water.

In Fig. 2(*b*) there is shown the flos-aquae species of the anabaena. This species resembles a curled spring. The odor and taste produced may be characterized as moldy, grassy, nasturtium, or "pig pen." In the summer months this species is especially prevalent.

Fishy Odors.—Fishy odors are perhaps the most disagreeable of any detected in drinking water. Water, rich in uroglenae, often imparts a cod-liver odor. Volvox, eudorinae, and pandorinae also produce a fishy odor.

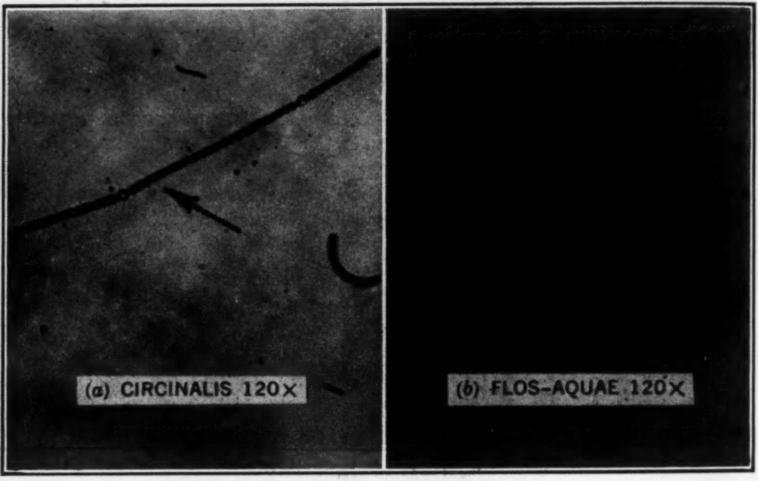

FIG. 2.—ANABAENA

Volvox, shown in Fig. 3, is one of the most beautiful forms to observe under a low-powered microscope. This species is characterized by a number of cells arranged in clusters located just within the periphery of a gelatinous sheath. The number of cells varies from two hundred to many thousands. The organism has a rolling motion, often visible to the naked eye. Volvox imparts a fishy odor and taste. This species is most prevalent in the summer months.

In Fig. 4 there is shown a photomicrograph of a pandorina. This organism contains an even number of cells, from 16 to 32. The cell colonies are mobile and resemble a hollow sphere. The colony is enclosed in a copious hyaline, gelatinous sheath. The organism is very resistant to chemical treatment, especially with copper sulfate. Pandorinae impart a faint fishy odor and taste, especially during the summer months.

ALGAE GROUPS

Diatomaceae.—In diatomaceae, the diatoms comprise a large number of organisms which are mainly one-celled plants, the wall material being inclosed in a marked cell wall of tough silicious substance. These markings appear as dots and ridges; some are so coarse that they can be resolved by a low-powered microscope, and some are so fine that they almost defy the resolving power of the highest aperature oil-immersion objectives. Diatoms, which existed ages ago and whose silicious parts settled in lake beds, formed the diatomaceous earth which is used commercially as an ingredient in silver polish, tooth paste, and insulation material. In addition to their green coloring matter (chlorophyll), diatoms also have a brownish coloring matter which is easily observed under a microscope.

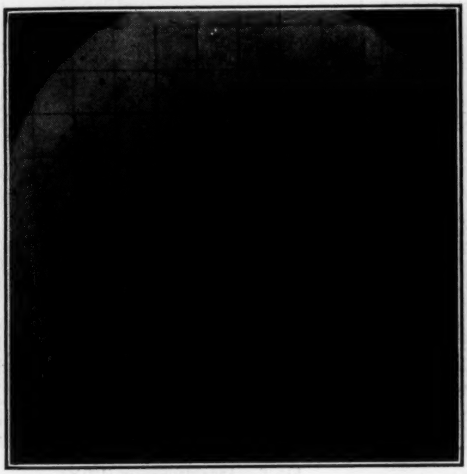

FIG. 3.—VOLVOX (25×)

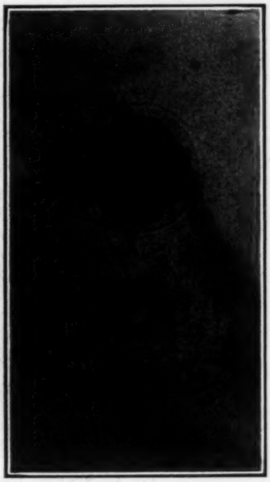

FIG. 4.—PANDORINA (120×)

A synedra organism is shown in Fig. 5. This organism resembles a fine-tooth comb, with straight, almost parallel, sides. The synedra contains a silicious substance; it is brown in color; and it often inhibits proper floc formation. This organism is prevalent in the spring and summer months.

The first diatoms were described in 1800, and since then (as of 1953) more than 15,000 forms have been described and classified. Diatoms live wherever there is sunlight and moisture. The perfection that exists in microscope lenses results from the use of fossil diatoms, as "test objects," by the early workers in that field.

It is interesting to consider the importance of the role played by the living diatoms in the food cycle of the higher forms of life, including man. The diatoms are the "grass of the sea." Like all green plants, these minute cells manufacture their food from inorganic materials and then are themselves eaten by a host of small animals, such as protozoa, hydra, worms, rotifers, and crustacea. These then serve as food for larger animals—invertebrates, fish-fry, and tadpoles—which in turn are then eaten by still larger aquatic forms such as bullfrogs, large fish, and whales. The cycle ends when man eats these aquatic forms.

Thus, diatoms constitute one of the largest and most fundamental groups, standing at the base of the food pyramid, synthesizing inorganic minerals into organic compounds for a large part of the earth's inhabitants.

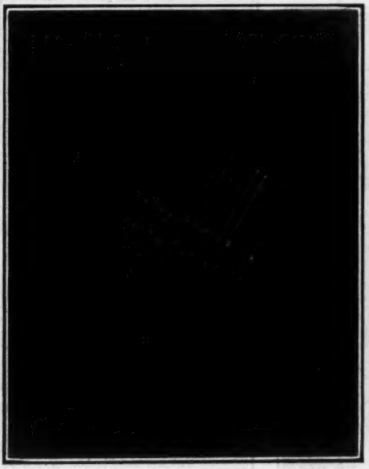

FIG. 5.—SYNEDRA (400 X)

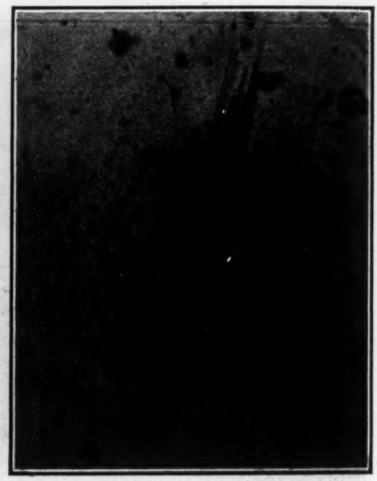

FIG. 6.—APHANIZOMENON (120 X)

Cyanophyceae.—Cyanophyceae often form a dark-green froth on the water surface, and are referred to as "water blooms." There are several species often found in the summer months, but cyanophyceae have also been found during the winter, growing under the ice. They may grow in polluted water, or in water containing considerable organic matter. Cyanophyceae are blue-green in color and are either free-floating or in gelatinous masses or strata. They appear as single cells, filaments, or chains. Some cyanophyceae are bead-like in structure and do not necessarily have a definite cell structure. Two common species are anabaena (Fig. 2) and aphanizomenon which produce a grassy odor and taste, or a vile pig-pen odor.

Aphanizomenon, shown in Fig. 6, usually appear in attached masses similar to a sheaf of wheat. They are found free-floating with long and oval spores. The filaments are tapered and will easily clump together. Aphanizomenon contain blue-green coloring matter and impart a moldly, grassy, vile and offensive odor. This organism is prevalent in the summer months.

Chlorophyceae.—A large number of species, green in color (caused by the presence of chlorophyll) are included in the chlorophyceae group. This group comprises a wide range of organisms, from single-cell to multicellular and flagellate forms, which reproduce asexually or sexually. This group includes thousands of forms, from the stringy filaments frequently found attached to walls and sides of tanks and open channels to single free-floating forms. Volvox (Fig. 3) is an example of this group. The spirogyra (Fig. 7) forms a stringy mass near the surface of the water and produces a vegetable odor.

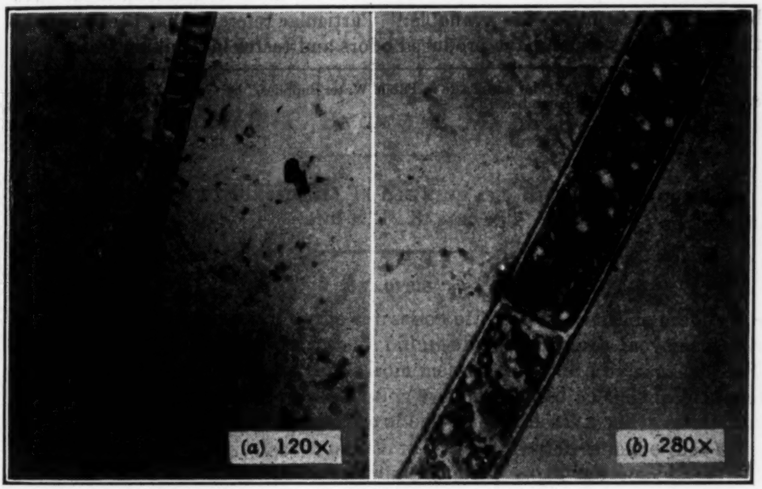

Fig. 7.—Spirogyra

The spirogyra is green alga containing chlorophyll in spiral bands. Conjugation is one of its methods of reproduction. The cells are generally cylindrical and attach themselves to form masses which are found free-floating near the surface of the water.

Protozoa.—Protozoa are the lowest form of animal life. Many forms exist on the borderline between plants and animals, possessing some of the characteristics of both. They are unicellular in structure although they may gather into colonies. The dinobryon, which often produces an aromatic or fishy odor and taste, and the synura, which imparts a cucumber, fishy, or bitter taste, are examples of protozoa.

Schizomycetes.—Schizomycetes are bacteria which are closely allied to the algae. Examples of this group are the beggiatoa ("sulfur bacteria"), which cause a decayed hydrogen-sulfide odor, and the crenothrix ("iron bacteria"), which also cause an offensive decayed odor.

Fungi.—Fungi are flowerless plants which lack chlorophyll and starch. They are seldom found in clean water. Fungi are common in sewage or in other organic wastes. They will grow in the absence of sunlight.

CONCLUSION

It is evident that knowledge, recognition, and the control of algae in public water supplies is of great importance to sanitary engineers and others in charge of public water supplies. It is not only their duty and responsibility to furnish safe water from the bacteriological standpoint, but they should also furnish water which is free from odor and taste.

A few actual photomicrographs of some of the most troublesome algae have been presented—others are available.[4] Particular reference has been made to those organisms which have produced odors and tastes in drinking water.

---

[4] "Algae Responsible for Odor and Taste in Public Water Supplies," by George J. Turre, *Proceedings-Separate No. 267*, ASCE, September, 1953.

AMERICAN SOCIETY OF CIVIL ENGINEERS
Founded November 5, 1852
TRANSACTIONS

Paper No. 2691

ANALYSIS OF CORRECTIVE ACTIONS FOR HIGHWAY LANDSLIDES

By R. F. Baker,[1] A. M. ASCE

With Discussion by Messrs. D. P. Krynine and Richard J. Woodward; and R. F. Baker

Synopsis

A semirational approach to the correction of highway landslide problems is presented in this paper. Only those failures involving earth movements are considered, and their analysis varies from methods described by some authorities in that (1) the landslide classification system is based on the mechanics of the movements; (2) a more general use of basic mechanics is made in estimating the effectiveness of a corrective measure; (3) a suggestion is made that there is more than one method for controlling a given earth movement; (4) the problem is primarily described as economic rather than academic; and (5) the statement is made that the determination of the mechanics of a landslide is more important than "the" cause. It is concluded that there is a need for a rational approach to the analysis of highway landslides and that that approach should have a scientific basis. It is also concluded that most corrective measures can be checked for stability by the use of a formula of the form used to determine the safety factor in soil mechanics. The proposed analysis is considered semirational, and for its general application, extensive development and observations are still necessary.

Introduction

Landslides are a critical problem throughout the world, but were never quite so prevalent as during the winter of 1950–1951 when there were almost daily reports of large-scale earth movements. West Virginia was greatly affected, and during the year 1950, approximately $125,000 was spent in extraordinary maintenance to resurface or remove debris from primary roads damaged by landslides. This sum does not include expenditures on secondary

---

Note.—Published, essentially as printed here, in May, 1953, as *Proceedings-Separate No. 190.* Positions and titles given are those in effect when the paper or discussion was received for publication.

[1] Engr. of Soil Mechanics, State Rd. Comm., Charleston, W. Va.

roads, on permanent corrections, nor on new construction projects. Although the winter and spring of 1950 and 1951 were particularly critical with regard to landslides, the State Road Commission of West Virginia has been bothered with similar problems for many years.

Numerous publications have carried detailed accounts of landslides. One of the most comprehensive reports was prepared by George E. Ladd for the American Railway Engineering Association.[2] Another publication in which the theories of earth and rock movement are thoroughly discussed is that by C. F. S. Sharpe.[3] Karl Terzaghi, Hon. M. ASCE, not only summarized the theories of soil mechanics but showed their application to earth movements in one of his works.[4] Paul H. Price, geologist for the State of West Virginia, prepared an unpublished report in 1940 about some of the landslides that had damaged West Virginia highways, and drew conclusions as to proper procedures in design, construction, and maintenance. Extensive bibliographies are included in the publications by Messrs. Sharpe and Ladd.

However, there is no known reference that presents a systematic approach to the use of the various methods of corrective action and the types of investigation necessary. Mr. Ladd refers briefly to nearly all the methods mentioned in this paper, but suggests that the basis for design is experience—which is not too helpful either to newcomers or to those who deal with slides sporadically.[2] Those who have become familiar with one method will use (or perhaps overuse) that same method because of their familiarity with the design and construction. Also, if more than one engineer or geologist is asked to make recommendations to counteract a slide, more than one answer is almost certain. Since there is a diversity of opinion as to proper corrective action, there is an obvious need for a method of analysis and evaluation that will clarify the factors involved.

The purpose of the following analysis is to suggest an approach to the design and use of corrective measures for earth movements that are threatening or affecting highway structures. The approach is basically one of highway engineering, although use is made of soil mechanics and geology. The study is not all-inclusive since there is no attempt to study failures that involve bedrock movement, subsidences, settlements of embankments over marsh or swamp areas, rock falls, rock weathering, or failures due to earthquakes. These are fundamentally different problems involved in mass movements and, therefore, are not included. The analysis presented is suggested for use in all other cases of earth masses in motion. The writer's experience has been in an area where earth movements represent at least 90% of the highway mass movements.

Undoubtedly, the technique suggested is an oversimplification, and, for general use, would require elaboration and attention to variables. However, for numerous small earth movements where an overdesign is not too costly, where the value of the structure to be protected is not great, and where there are no trained, experienced personnel to study the slide in detail, the suggested approach will permit better engineering than is possible with only experience as a guide. When it is realized that landslides in West Virginia number in the hundreds each year, the need for an immediate, usable, and rational method of approach is understandable.

---

[2] "Landslide, Subsidences and Rock-Falls," by George Edgar Ladd, *Bulletin*, A.R.E.A., Vol. 37, No. 377, July, 1935.

[3] "Landslides and Related Phenomena," by C. F. S. Sharpe, Columbia University Press, New York, N. Y., 1938.

[4] "Mechanism of Landslides," by Karl Terzaghi, *Berkey Volume*, The Geological Soc. of America, 1950.

DEFINITIONS

Landslides have been defined by Mr. Ladd[2] as

> "* * *superficial earth movements having essentially a horizontal component, usually involving slopes varying from very gentle to very steep, but rarely involving vertical cliffs at one extreme, and level but unsupported ground at the other."

Mr. Terzaghi[4] states of landslides:

> "The term landslide refers to a rapid displacement of a mass of rock, residual soil or sediments adjoining a slope, in which the center of gravity of the moving mass advances in a downward and outward direction."

These definitions and others are in general agreement. The main difference lies in the element of time. Mr. Terzaghi states that a landslide is a "rapid displacement" as differentiated from his definition of creep which he states is a "* * *similar movement proceeding at an imperceptible rate* * *." Messrs. Ladd,[2] Sharpe,[3] and others recognize the factor of time in landslides and in the phenomenon commonly termed creep. However, there is less accord as to the mechanics involved, particularly for creep. Mr. Terzaghi divides creep into continuous and seasonal types and defines the latter as a relatively shallow failure related to changes in moisture and temperature. He defines continuous creep as a relatively deep movement produced by the force of gravity, often caused by the presence of various strata with different elastic properties, and he asserts that, when the mass is stressed below the "average shearing strength" of the system, the weaker materials deform like a "very viscous liquid." Mr. Terzaghi also writes of the "fundamental strength" of elastic materials in contrast with the "compressive strength." The former term relates to the much smaller but continuous load under which the failure of the material begins. Perhaps the most important physical distinction that Mr. Terzaghi makes between landslides and creep is that landslides involve a body of material with "well-defined boundaries," but creep may involve areas in which "* * *no sharp boundaries exist between stationary and moving materials." This latter statement is important because of the potential clarity in identifying the type of displacement that has occurred.

Many methods have been proposed for classifying mass movements. Messrs. Ladd[2] and Sharpe[3] give excellent resumés of past efforts as well as proposed systems. Mr. Ladd presents a method of classification that excludes the term, creep, because of the inference that time is an element, whereas time is not a factor in his other classifications. Mr. Sharpe has recommended a classification that is quite complete and includes time as a most essential factor. A brief method of classifying mass movements was advanced by Mr. Price to cover the types of landslides encountered in West Virginia.

From the viewpoint of highway engineering, there is little value in classifying earth movements in too great detail. Mr. Sharpe states that mass movement may be classified as slides and flows. In the former, he includes all movements in which a slip-surface is involved, whereas the latter movement is a shifting of the mass and does not involve a surface of slippage. This distinction is shown in Fig. 1. From a corrective viewpoint, the difference need not be greatly amplified in order to serve adequately for classification purposes.

In this paper, four classifications of earth movements will be used, and the advantages of these classifications will become evident as the analysis progresses. Basically, the classification is a variation of a part of Mr. Sharpe's system.

Slides.—Earth movements that produce a slip-surface that is curved or partly curved in a direction parallel to movement are classified as slides. The slide area is surrounded by well-defined cracks except at the toe where "heaving" or "rolling" delineate the limits. Should the cracks be discontinuous, an earth movement could not be classified as either a slide or debris slide. Slides also produce "benches," or approximately horizontal surfaces near the top of the slide. These benches are typical of slides that have produced curved slip-surfaces. It is not unusual to find trees, poles, and houses in a relatively undisturbed vertical condition because the failure may be deep. The earth movement is sudden, in comparison to creep and flow, and is very likely to come to a temporary rest.

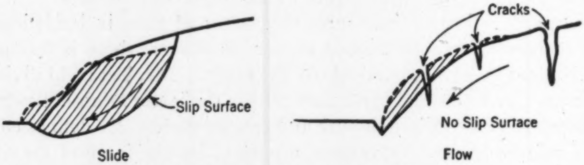

FIG. 1.—SLIDE AND FLOW IN EARTH MASSES

Debris Slides.—This movement differs from slides in that the plane of failure is straight in a direction parallel to the direction of movement. Upon a surface investigation, a debris slide will resemble some types of slides. However, the open crack at the top of the slide will not expose a slide plane because the material breaks away, rather than slides. Furthermore, the characteristic "heaving" or rotation at the toe of a slide will not be present for a debris slide.

Creep.—An earth movement which produces no slip-surface is termed creep. There is no clear line of cracks parallel to the movement to delineate the lateral extent of the slide area. The surface of the area contains some cracks perpendicular to the movement, but normally has a series of rolls or humps on the surface of the slide and no open cracks. Mr. Terzaghi suggests that it would be well to differentiate between seasonal and continuous creep. The distinction is based on the depth that is affected by variation in temperature and rainfall. Seasonal creep, as suggested by Mr. Terzaghi, could actually be classified as flow.

Movement is assumed to be caused by the successive failure of weaker strata or the forces being greater than the fundamental strength. With the exception of the cause, the movements are similar to those termed talus-creep and soil-creep by Mr. Sharpe.

Flows.—This movement is essentially the same as creep except that the primary cause of displacement is defined as the presence of an excessive quantity of water. This approximates the movement termed earth-flow by Mr. Sharpe, although the definition used in this paper states that, with the development of a sliding surface, a flow becomes a slide. Flows are not too common in the Appalachian province particularly within the Allegheny Plateau province of West Virginia, and occur in soil and soil-boulder materials having a high moisture content. The slope of the transported material is correspondingly flat in comparison to surrounding topography. The movement is more rapid than creep and may be differentiated from a slide primarily on the basis of the higher moisture content, flatter slopes, lack of continuity in the cracks, lack of a slip-surface, and open cracks that do not expose a slick, sliding surface.

Rock Slides.—A movement involving bedrock material is classified as a rock slide. Rock movements should be identified as such, although this analysis does not consider corrective action. Generally, displacements involving bedrock are obvious from a surface examination, but this type is most difficult to identify if it consists of a general subsidence due to the ejection of a weak layer, or due to cavities formed by nature or by man. Open cracks develop at the top of the slide, and subsurface exploration shows the presence of rock strata.

Omitted from consideration in this study are the following types as classified by Mr. Sharpe: Rock-creep, rock-glacier creep, solifluction, mudflow, debris-avalanche, debris-fall, rock-slide, rock-fall, and subsidences. Also eliminated is failure directly attributed to earthquakes.

The terms slip-plane, surface of failure, slip-surface, and other similar terms refer to the surface that divides the mass in motion from the stable material. A curved or straight slip-plane always refers to the shape of an assumed line, which lies on the surface of failure, parallel to the direction of movement, and is considered as being characteristic of the predominant shape of the slip-surface.

Mass movement is a term used by geologists and refers to all types of rock and soil displacements in which the material moves as a mass under the force of gravity. Earth movements and landslides refer to only those mass movements occurring in soil or soil-boulder materials, specifically excluding phenomena involving the movement of bedrock.

FUNDAMENTAL CONSIDERATIONS

Water is present as a contributing factor in almost all earth movements. The damaging action of the water is most often attributed to the weight added to the soil mass, the reduction of shear characteristics of the soil, and the lubricating action on the sliding plane. Hyde Forbes, M. ASCE, writes that, under certain conditions, seepage water could produce geochemical and physical changes in the soil and underlying bedrock.[5] Mr. Terzaghi[4] and others assert that water produces piezometric or hydrostatic pressures that, in effect, "float" the material away. All authorities agree that the removal of water represents a sound approach to a slide correction. The importance that is placed on drainage varies. In Mr. Forbes' paper, other corrective actions are mentioned, but details are given for drainage solutions only. Mr. Ladd states that drainage represents a very favorable type of correcting action, but gives considerable coverage to other corrective measures.[6] Mr. Price states that drainage as a corrective action has been overemphasized. He points out that to drain an area successfully, the soil must be permeable and nearly free of clay. This latter statement is undoubtedly true unless excess hydrostatic pressure is relieved prior to contact with the displaced mass.

---

[5] "Landslide Investigation and Correction," by Hyde Forbes, *Transactions*, ASCE, Vol. 112, 1947, p. 377.

A fundamental consideration in the use of corrective measures is the fact that all mass movements will continue until the topographic bottom of the area is reached. The time required for the mass to reach the bottom may be many hundreds of years. The importance of the role of landslides as "topographic-shapers" is emphasized by Mr. Ladd,[2] who states that "* * *'erosion' alone, should be given less credit for playing the major role." It may be assumed that most natural earth slopes, and particularly old slides, are near an equilibrium or balance point. The works of man accelerate or decelerate the ultimate rate of movement.

For landslides whose slip-surface is at the contact point between soil and underlying rock, the failure occurs in the soil. This is pointed out by Mr. Forbes,[5] and frequently observed in West Virginia. "Failure in the soil" means that soil fails in shear, and the shear characteristics of the soil at the slip-plane can be applied in a stability analysis. If the soil merely slips over the surface of the underlying rock, the mechanics for estimating the shearing resistance before failure require an entirely different approach based on the friction value between the earth mass and the rock.

There are several methods of correcting any given highway landslide problem, but it should be realized that the correction of all earth movements is not economically feasible. The corrective measure to be used depends primarily on economics, which means that the highway engineer has a totally different approach than others engaged in solving landslide problems. Many past studies have dealt with landslides of large areas or movements that were threatening particularly valuable structures. The writer believes that some of the methods that were suggested for these types of problems are not feasible for many highway situations. Mr. Forbes mentions spending seven months to study a landslide threatening a million-dollar structure. The methods applied to that situation should not be compared with the method used to save a thousand-dollar section of highway, even if the slide were of the same magnitude. It is entirely possible that an expedient method—one that is satisfactory for a period of from five to ten years—is the best answer to a highway landslide. This approach should not be used as an excuse for poor engineering, or for the elimination of an investigation.

---

[6] "Landslides and Their Relation to Highways," by George E. Ladd, *Public Roads*, Pt. 1, Vol. 8, 1927, p. 21, and Pt 2, Vol. 9, 1928, p. 153.

From a highway engineering viewpoint it is generally accepted that the solution to a landslide problem need not be a corrective action for the earth movement. The problem is not to eliminate the displacement but to correct a situation involving either costly maintenance or a threat to life, or to a structure, by the use of engineering principles.

The accurate determination of "the" cause of a landslide is not always essential to the solution of a highway landslide problem; equally important are the mechanics of the movement. For some earth movements and types of corrective measures, complete information as to the cause and the contributing factors is not needed except for academic reasons. The determination of "the" cause is often misleading since almost all landslides result from a combination of causes, with one factor being finally dominant. Of great importance is the fact that by eliminating or by modifying the effect of any one of the causes the stability will increase. The approach to landslide problems is still so uncertain that quite often engineers and geologists cannot agree on the final, decisive cause. Disagreement has arisen on the basic causes for many large-scale landslides, but increased expenditures and the increased likelihood of the loss of life in the event of failure require increased care and detail in the investigation and design.

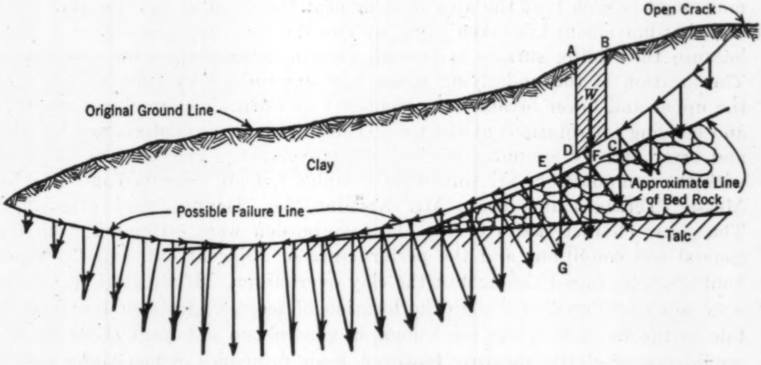

FIG. 2.—A SLIDE SHOWING THE SLIP-SURFACE

The slide surface is sometimes believed to lie along the dipping strata of underlying rock, even though there is ample evidence of horizontal bedding. In areas of horizontal bedding, the bedrock that underlies earth masses often presents a "sloping" face to the overlying earth mass. However, this slope has developed by differential weathering or erosion of the various strata at the time the bedrock was exposed to air and water, and is a series of small vertical or sloping steps, as seen subsequently in Fig. 3. The over-all slope is dependent upon the nature of the bedrock, the length of time the face was exposed to weathering or erosion, and the geochemical and physical changes caused by percolating ground water.[5]

The fact that the force of gravity is the one cause common to all mass movements is too often subjugated to other factors, particularly to the effect of water. Constant use is made of drainage as a corrective action, and, although drainage should be considered, the fundamental basis for an analysis of a landslide correction is the principle that gravity is tending to move the material to the topographic bottom. From a practical viewpoint, the correction of some slides by drainage alone would result in an expenditure greater than the cost of the removal of the entire mass.[7]

Basic mechanics should be applied to all landslides. Several engineers have recognized the importance of mechanics in the study of earth movement. Mr. Terzaghi and Ralph B. Peck[8] (M. ASCE), D. P. Krynine[9] (M. ASCE), R. G. Hennes[10] (M. ASCE), Donald W. Taylor[11] (A. M. ASCE), T. W. Lambe[12] (J. M. ASCE), and others have discussed the use of theoretical formulas for estimating the forces at work. All of them wisely qualify the application of the theories. One section of a slide area along the Ohio River on the Neptune-Belleville Project in West Virginia is shown diagrammatically in Fig. 2.

The condition of stability of the area at the time of, and shortly after, the movement is such that the area is at or near the point of equilibrium. The fact that movement has taken place justifies the foregoing assumption. Also, because the sliding surface is curved, certain other factors are important. The location of the underlying strata was determined by core-borings, and the upper and lower breaks were identified by open, deep cracks at the top, and heaving (or rotation) at the toe. The slip-plane was determined by trial and error and by assuming no bedrock movement. The theories involved with the computations are somewhat complex but are described in detail by Messrs. Terzaghi and Peck, Mr. Krynine, Mr. Hennes, and others.[8,9,10] The shear characteristics of the clay overburden were estimated from the general soil conditions and the performance of adjacent cut slopes. Many boulders were found throughout the clay overburden. Hydrostatic pressures were not considered, nor were the location of seepage strata or the layer of talc in the bedrock. The conditions, in general, do not meet those for the application of elastic theories; however, basic principles of mechanics justify the approximations that were made.

In Fig. 2, the narrow segment ABCD is selected for study. Assuming that the slip-plane is straight for the part of the slide under consideration introduces an error well within the limits of accuracy. The earth exerts a downward force equal to its weight. This vertical force (FG) at any point of failure along the slip-plane has a component perpendicular to the plane of failure and another component parallel to the plane of failure. This resolution of forces is indicated in Fig. 2. Those forces perpendicular to the plane are normal forces (EG), and those parallel to the plane are shear forces (EF). Further study of Fig. 2 shows that the shear forces are those that cause movement, and these forces are largest near the top of the slide. At the toe of the slope are the greatest part of the resisting normal forces as well as the shear forces that are acting to resist the slide due to the vertical or rotational effect.

---

[7] "Earth Slip Hazards and Control in Highway Maintenance," by William S. Downs, *Engineering News-Record*, May 15, 1930, p. 794.

[8] "Soil Mechanics in Engineering Practice," by Karl Terzaghi and Ralph B. Peck, John Wiley & Sons Inc., New York, N. Y., 1948.

[9] "Soil Mechanics," by D. P. Krynine, McGraw-Hill Book Co., Inc., New York, N. Y., 1941.

[10] "Analysis and Control of Landslides," by Robert Graham Hennes, *Bulletin No. 91*, Univ. of Washington Eng. Experiment Station, Seattle, Wash., June, 1936.

[11] "Fundamentals of Soil Mechanics," by Donald W. Taylor, John Wiley & Sons, Inc., New York, N. Y., 1948.

[12] Discussion by T. W. Lambe of "Landslide Investigation and Correction," by Hyde Forbes, *Transactions*, ASCE, Vol. 112, 1947, p. 407.

The stability of the slope can be estimated by computing (1) the normal and shear forces for successive increments and (2) the total normal and shear forces. The width of the increment is governed by the accuracy desired. Considering a segment 1 ft wide, perpendicular to movement, the following equation represents the stability of the slope:

$$N = \frac{\sum F_n \tan\phi + c\,L}{\sum F_t} \quad \text{.....................} (1)$$

in which N is equal to the safety factor (1.0 at equilibrium); F_n represents the normal force, in tons; ϕ is the angle of internal friction; c denotes the cohesion, in tons per square foot; L is the length of the slip-plane, in feet; and F_t represents the shear force, in tons. The numerator represents the shearing resistance and the denominator equals the shearing forces. For clay soils with an angle of internal friction equal to 0°, the shearing resistance is equal to $c\,L$.

The shearing resistance can be estimated by assuming a safety factor of 1.0 as suggested by E. M. Buckingham,[13] A. M. ASCE. Although there have been instances in which slopes have remained stable at values of 0.8 for the safety factor, an estimate of relative stability can be obtained by assuming a value of 1.0.

From an analysis of Eq. 1 and a study of Fig. 2, it can be seen that earth removed from the top of the slide, or a load applied at the toe of the slope, will increase the value of N for the slope. Since the earth mass represents the major part of the force, any change in the distribution of the earth will have an important effect on the stability of the slope.

The principles of landslides, as represented in Fig. 2, are fundamental and essential to a clear understanding of nearly all corrective actions that can be taken. The following semirational analysis is based on evaluating the stability through estimates of the safety factor, in which the theories of hydrostatic pressures, seepage forces, undisturbed samples for shear determinations, and other refinements may be applied. The analysis is based on the weight of the mass acting vertically, with a component perpendicular to the slip-plane and another component parallel to the slip-plane. Also, the position and shape of the failure plane are approximated. The landslide must be at rest at or near the balance point between movement and stability, resisted by essentially the same shearing resistance that existed just prior to failure. Any method of correction can be evaluated immediately as being essentially helpful or primarily harmful on the basis of the suggested approach. An estimate of the degree of improvement is dependent on an estimate of the shear forces as well as the shearing resistance. This estimate will depend on shear test data or on an estimate of the shear resistance based on the conditions immediately prior to movement, or both.

---

[13] Discussion by E. M. Buckingham of "Landslide Investigation and Correction," by Hyde Forbes, *Transactions*, ASCE, Vol. 112, 1947, p. 435.

The forces of gravity involved in debris-slides are as outlined in Fig. 3. For this type of movement, the ratio between the shear and normal forces will be equal to the tangent of the slope. The numerical value of the forces will be dependent on the amount of overburden, which will generally be largest at the toe of the slide. The movement cannot retain the classification of a debris-slide, as defined, unless the material that is sliding is cleared from the toe. If the material accumulates, the shape of the slip-surface will change from straight to curved, and a more stable situation will develop. Therefore, a debris-slide normally exists along a stream unless the toe is cleared by a highway maintenance crew. For debris-slides, a reduction of shear forces may be brought about by the removal of material from the sliding mass, but

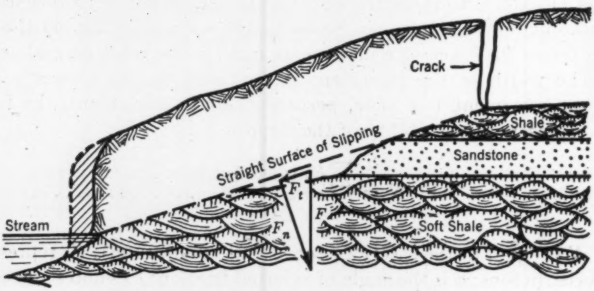
Crack
Shale
Sandstone
Straight Surface of Slipping
F_t
F
F_n
Stream
Soft Shale

FIG. 3.—THE MECHANICS OF A DEBRIS-SLIDE

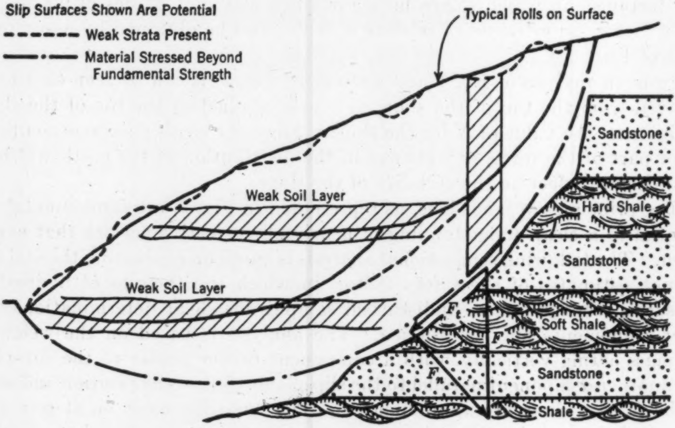
Slip Surfaces Shown Are Potential
------ Weak Strata Present
—·— Material Stressed Beyond Fundamental Strength
Typical Rolls on Surface
Sandstone
Weak Soil Layer
Hard Shale
Sandstone
Weak Soil Layer
F_t
Soft Shale
F
F_n
Sandstone
Shale

FIG. 4.—THE MECHANICS OF CREEP MOVEMENT

the location of the removal is less important than in the case of landslides with a curved slip-plane. The degree of stability brought about by the removal of material is dependent on the slope of the slip-plane since the normal and shear forces are reduced by a constant proportion for a given condition.

For earth movements classified as either creep or flow, the analysis is more involved. The over-all stability should be estimated because these types commonly develop into landslides.[3] The mechanics resemble those of slide analyses, the differences lying in the irregular potential slip-surface of the creep movement and the lower shear characteristics of the flow type. Figs. 4 and 5 illustrate creep and flow movements. The ratio between shear and normal forces will vary, the assumed slip-plane being curved; since this is a potential surface, it does not exist until an over-all failure occurs. For the control of the creep movement, corrective action should tend to reduce the load on any weak strata or on the entire earth mass. For flow movement, an effort should be made to reduce shearing forces and to increase shearing resistance. Also, because the cohesive strength of the soil involved in this type of movement is low, the removal of water would aid in the control of flow. Retaining devices should not be designed to eliminate displacement entirely if the landslide is extensive since a large part of the weight of the soil mass should not be concentrated against a rigid resistance. Creep and flow failures are rare types and, because of the complicated nature of the movements, these failures should be referred to an authority in that field.

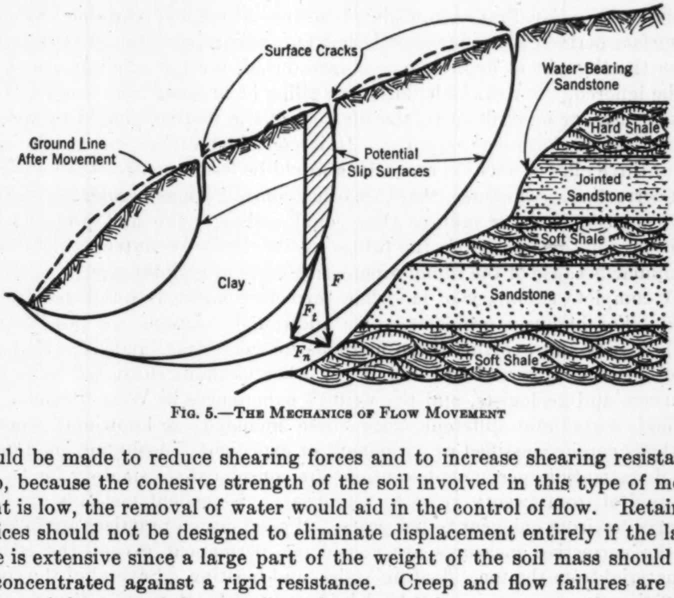

FIG. 5.—THE MECHANICS OF FLOW MOVEMENT

DISCUSSION OF METHODS OF CORRECTION

If the geomorphologists' land-forming hypothesis that landslides occur in a mass which is inevitably moving toward the topographic bottom of an area is accepted, it is important to realize that any method short of complete removal cannot be a permanent cure in terms of hundreds of years, and that the value and life expectancy of the structure are intimately associated with the solution of the problem. Therefore, design life must be a factor in arriving at a solution to any landslide condition, and of all the factors involved in the design or investigation, none is more complex or difficult to estimate. The determination of the factors contributing to a landslide usually is possible. The absence of these factors will delay the movement for some finite period. In several cases with which the writer is familiar, the time variable for the occurrence or nonoccurrence of a given landslide, as influenced by one factor, could well have ranged from a few seconds to nearly fifty years. The only estimate for this phase of the mass-movement problem is the degree of stability in such terms as "obviously weak," "questionable," or "obviously safe." If, for instance, the slope appears to be "very safe," the area should be considered stable for an extended period of time. Continuing observations are desirable for several years.

Another consideration related to permanency and design life is the maintenance of landslides. A. V. Bowhay[14] referred to this consideration in a discussion of a San Francisco, Calif., landslide which was contained by oiling the surface periodically to prevent the entrance of surface water into the ground. When the thought of maintenance is introduced, the full implications should not be ignored. For example, although piling or blasting may result in bent, broken piles, or in settlement, the life cost of the method should be weighed against the performance required. It is conceivable that, in certain cases, two or three piles or blasting operations would be less expensive than a permanent correction. Of course, there are other considerations besides life cost and performances, such as failures that could endanger life and property. In addition, solutions based on the future availability of maintenance funds are unpopular because of the rapidly increasing costs of maintenance.

A complete summary of landslide corrective methods was listed by Mr. Ladd. For highway problems, some additional solutions are possible, and Table 1 lists and explains those methods for correcting landslides that were mentioned by Messrs. Ladd and Price, other methods suggested by various engineers and geologists, and the writer's experiences in West Virginia. No method, essentially different from those included, is knowingly omitted. Methods can be classified as permanent or expedient. Assuming good design and investigation, permanent solutions are considered satisfactory for at least a period of from twenty years to fifty years. Expedient methods are likely to serve for from one year to ten years. If good design practices are followed, all the corrective measures are considered permanent except the removal of material from the toe, "floating" piles, and blasting. Several of the corrective measures are recommended solely for use with other corrective measures and are rarely solutions in themselves.

The theory that landslides result from unbalanced forces leads to solutions based on changing the balance between contributing and resisting forces at work in or on the earth mass. All landslide control methods rely upon the restoration of balance for their success. A general distinction does exist as to whether the method attempts to rebalance by draining, retaining, direct

---

[14] Discussion by A. V. Bowhay of "Landslide Investigation and Correction," by Hyde Forbes, *Transactions*, ASCE, Vol. 112, 1947, p. 428.

TABLE 1.—FACTORS IN THE DESIGN OF CORRECTIVE MEASURES

Corrective measure	Best application	Principles involved	Remarks
1. Relocation	All types.	Structure moved to location where mass movement is not present. Permanent solution.	Due to degree of permanency, a very desirable solution. Very often this is the most economical solution. Its use will depend on obtaining a satisfactory line and grade.
2. Excavate, drain, and backfill	Shallow soil or deep soil in combination with light weight backfill.	The sliding mass is removed and the area stabilized by the removal of water and by improving foundation conditions. Permanent solution.	All slide material should be excavated to solid rock, drains placed to intercept seepage, and the area backfilled. Unless highly organic, the same soil can be used for backfill. Good construction methods must be used. Where bedrock is not encountered, stability estimates based on shear values of reworked soil should be made, and a 2-ft-deep granular course should be placed at the bottom.
3. Drainage: Surface Subsurface Jacked-in-place pipe Tunnels	Subsurface is good method for shallow soil. Tunnel and jacking good for deep soil when water source is deep.	Removal of water results in: (1) A lower density of the soil; (2) a higher soil cohesion; (3) an elimination of lubrication of slip plane; (4) a removal of excess hydrostatic pressure; (5) a removal of seepage forces. Permanent solutions.	Surface drainage should be assured for all types of corrective measures. Generally, drainage should be designed to intercept water before it enters the slide. In an impervious soil, the water source must be reached to be effective in controlling movement. Subsurface drainage may not be feasible due to the undermining of slide material above the excavation.
4. Removal of material:			For shallow soil profiles, consideration should be given to a solution involving the entire removal of the slide. For deep soil profiles, the removal of material at the top of the slide will increase stability. For all removal corrections, undermining of areas should be considered. The removal of the material at the toe of a slide is rarely desirable, although at times necessary, in order to open a road for traffic. If the only corrective action applied is the removal from the toe, the slide will continue. Partial removal of material from the top has less influence on a debris slide.
Entirely	Shallow soil.	Entire slide mass is removed. Permanent solution.	
Partial at toe	Clear road for traffic.	Condition relieved temporarily. Expedient solution.	
Partial at top	Deep soil.	A large part of the main source of shearing force is removed. Permanent solution.	
5. Buttress at toe	Good foundation at toe in shallow or deep soil. Buttress should extend below the slip plane.	Large mass blocks the mass movement and any further movement involves displacement of the buttress. Permanent solution.	An excellent method of correction when the situation at the toe permits. Action is that of a retaining device. Much less expensive than cribbing or a retaining wall. The buttress should be founded below the slip surface, for, unless the sliding material has an angle of internal friction greater than 15°, the added normal force of a buttress has little influence on the safety factor.

TABLE 1.—(*Continued*)

Corrective measure	Best application	Principles involved	Remarks
6. Bridging	Steep hillside locations with a narrow failure parallel to road in deep soil.	The troublesome area is bridged and future movement passes under the structure. Permanent solution.	Very satisfactory solution. The foundations must be bedrock that is not subject to movement or erosion. Too costly for general application.
7. Cribbing—timber, concrete, or metal	Shallow soil with good foundations.	A retaining mass, with or without additional lateral restraint, placed in path of the mass movement. Further movement involves displacement of the retaining mass. Permanent solution.	Good method where applicable but relatively costly. Less stable foundation required than for retaining wall as shifting is permissible before cribbing fails. Resistance offered is the weight of the crib unless bedrock is excavated to give resistance to lateral thrust. Recommended for shallow soil profiles. Weight of the crib-wall can be compared with weight of material removed for an estimate of the relative degree of stability offered by the cribbing. In slide areas, the resistance required can be estimated by using the formula for the safety factor. Not recommended in creep and flow areas.
8. Retaining wall of stone or concrete	Shallow soil with good foundations.	A retaining mass with lateral restraint, placed in path of the mass movement. Further movement involves displacement of the retaining wall. Permanent solution.	The applications are similar to those of cribbing. The cost is a deterrent. Walls are advantageous in urban areas. A wall requires a foundation in bedrock or good soil below the slip surface. Standard practice is to include weep holes in designing the wall. The formula for the safety factor may be used to estimate resistance required to lateral thrust. Retaining walls in creep and flow movements may take full weight of soil.
9. Piling:			
Floating	Shallow soil to hold temporarily.	Piling offers a retaining influence. For soil masses the piling may tend to "pin" the moving and stable materials, and bring about a more lengthy slip-surface with a corresponding increase in shearing resistance. Floating piles are expedients. All others are permanent solutions.	Floating piles do not appreciably penetrate bedrock or the slip-surface. As an expedient, such methods have lasted for from 1 year to 10 years. With a slip-surface at bedrock, the fixed piling penetrating for a distance of from 3 ft to 5 ft into bedrock offers resistance equal to the force required to bend the piling. If the soil is wet and fine-grained, movement in the area is likely to be due to extrusion between the piles. For piling in deep soil, where the base of the pile penetrates 5 ft past the slip-surface, the recommendation of Krynine is to estimate the forces on a slip-surface curving under the piling.[a] Stability can be estimated by the formula for the safety factor. For piling with provisions for preventing extrusion (such as I-beam and cribbing combinations), the principles of a retaining wall apply.
Fixed—no provision for preventing extrusion	Shallow soil with numerous large rocks.		
Fixed—provision for preventing extrusion	Shallow soil.		
10. Sealing joint planes and open seams	Deep source of water.	The same benefits are sought as for a drainage solution. Permanent solution.	It is essential to locate the source of water and to block its entrance by grouting. Difficult to achieve and to estimate quantities. The effect of blocking the water should be studied for the area above and around the slide. This method of correction is still experimental.

---

[a] "Landslides and Pile Action," by D. P. Krynine, *Engineering News-Record*, Vol. 107, 1931, p. 860.

TABLE 1.—(*Continued*)

Corrective measure	Best application	Principles involved	Remarks
11. Cementation of loose material	Permeable material only, unless "column" principle is to be used.	An attempt to improve the shear characteristics of the soil. For "columns," the weight of the structure is carried to firm foundations. Some lateral restraint is offered. Permanent solution.	Stability is achieved by cementing the slide material. In order to produce deep soil stabilization, a permeable material is essential. By drilling holes and pressure grouting, columns of uncertain diameter will tend to stabilize the area even in clay soil. This method is experimental.
12. Chemical treatment—flocculation	Permeable material.	Same principles as 11, except chemicals are used. Permanent solution.	This is essentially the same as cementation, except chemicals are used. The value of "columns" for clay materials is of less importance than for cementation. This method is experimental.
13. Tie-rodding slopes	Shallow soil with large rock fragments.	The retaining device insufficient to withstand movement is anchored to bedrock. Permanent solution.	A retaining device, such as steel plates or piles with cribbing, is anchored by steel bars to solid rock and is generally a costly operation. This method has been described by T. H. Cutler[b] and others.[c] The resistance to movement can be checked by the formula for the safety factor.
14. Blasting	Shallow soil underlain by good rock.	An attempt is made to disrupt the sliding surface as well as to develop a drainage system. An expedient solution.	The soil should be shallow with a hard rock underneath. The blast should be heavy, particularly at the toe. Recommended spacing is 6-ft centers in a T form. Explosives experts should be consulted as to size of charge. If used under an impermeable clay-soil, the method will be ineffective unless the source of water is tapped. Continued settlement of the area is to be expected. According to Mr. Ladd, the slip-surface will not be permanently broken up nor will drainage be effective indefinitely.
15. Reshaping slide material	Face of slide has open fissures. Benches cause ponding of water.	See 3. Method generally used in combination with other actions.	Area improved by sealing surface so as to prevent the entrance of water. Also removed "ponds."
16. Slope treatment	Shallow soil in combination with other methods, or any erosion problem.	See 3. Method generally used in combination with other actions.	Area improved by sealing surface so as to prevent the entrance of water, and to minimize erosion. Use seeding or sodding, blanketing with cinders, "guniting," or oiling of surface.
17. Lightweight fill	In cases where loading is critical.	Reduction of the weight causing movement. Rarely a solution in itself.	The heavier soil is replaced with a lighter, permeable material. Often valuable when it is desirable to hold a given grade.

[b] "Slipping Road Fill Held Up by Steel Suspenders," by T. H. Cutler, *Engineering News-Record*, Vol. 109, 1932, p. 684. [c] "Device Prevents Slides on Road and Railway Fills," *ibid.*, Vol. 104, 1930, p. 787.

rebalancing of the forces, or some combination of these three. This difference in principle is indicated in Table 1.

ANALYZING A LANDSLIDE FOR CORRECTIVE MEASURES

There are four factors about which information is needed to analyze a landslide for corrective measures. One of the most important is involved with the geology and geologic structure of the area. In movements involving only the soil overburden, this information will consist primarily of a topographic description of the surface of the underlying bedrock. It is essential, also, to determine if there is a movement of the bedrock material. The type, nature, and extent of the bedrock are important if the corrective action requires a solid foundation.

Also important is the location of seepage strata which might contribute to the landslide. This location may not be essential to the solution of the problem, but the knowledge of the location of the underground water is certain to result in a better understanding of the mechanics of the earth movement.

The third type of information needed is a topographic survey of the ground surface in the landslide area. Normally, this will be for the purpose of estimating either the costs or the degree of stability. A hand-level survey will be sufficiently accurate unless subsequent movements of the slide are to be measured.

Finally, information is needed about the soil. The required detail will vary; however, data giving the unit weight, moisture content, gradation, and plasticity characteristics are almost always necessary. For this information the shear characteristics can often be estimated with sufficient accuracy. Until good approximations of shear data can be made, undisturbed soil samples may be required. The status of the corrective actions for landslides is not sufficiently developed to permit too high a degree of refinement. When the problem is obviously complex or the investment involved is large, the engineer must recognize the need for a specialist. Otherwise, the refinements need not be more than those recognized by highway engineers.

In analyzing a landslide relative to solving a highway problem, the first step is a preliminary field study. This is followed by a detailed field study, an office investigation, and, finally, a construction and supplemental investigation. In some cases, primarily those involving relocation projects or very small-scale movements, the second and third steps may be practically eliminated.

Preliminary Field Investigation.—In the preliminary field investigation, the area should be carefully inspected and the landslide classified. The depth of the soil mass, the boundaries of the moving area, and the relation of the structure to the movement are then estimated. From these, the type of corrective measures that seems feasible is determined and the information needed for the design of the corrective measures is indicated.

The slide should be classified as either a slide, a debris slide, a creep, a flow, or a rock movement. The depth of the soil mass is a critical factor in arriving at an adequate design. Normally this depth is determined by subsurface exploration. However, as an aid in estimating the probable corrective actions, the preliminary reconnaissance should state whether the soil mass is likely to be deeper than 15 ft. This depth is the approximate dividing line between the values of shallow and deep soil profiles discussed in Table 1. The best guides to approximate soil depth are excavations in the area and the steepness of the slope in the slide area. Generally, steeper slopes will have relatively shallow soil profiles. A familiarity with land forms will aid materially. However, experience is the best guide in estimating soil depths.

The outline of the displaced area is normally quite simple to identify. Active slides and debris-slides are accompanied by characteristic open cracks in the earth's surface as seen in Fig. 6. Creep may have (and flows will have) cracks near the top of the area. Normally, it is assumed that failure has not occurred in the area above the last open crack. Movement cracks are readily differentiated from shrinkage cracks since the former are perpendicular to the movement of the landslide. In some instances, smaller cracks may appear above the last pronounced crack due to a secondary failure caused by the primary movement. In such cases, the secondary failures should be included in the analysis. The toe of the slide is unmistakable even though the landslide occurred some time previously. It is characterized by either an unnatural, vertical hump that appears to have been lifted or rotated, as in Fig. 7, or a roll that has apparently been shoved laterally over a firm base. The toe is normally at the topographic bottom of the area, although exceptions to this are not uncommon. At times, the lateral extent of creep or flow is difficult to determine but it may be assumed that failure has not occurred beyond the limits of the cracks in the earth's surface.

FIG. 6.—DELINEATION OF A SLIDE AREA BY OPEN CRACKS

The best corrective action for the landslide will vary considerably with the location of the structure relative to the movement. Any location other than the top or the toe of the landslide is likely to have a stability problem both above and below the structure. The relative position of the structure can be determined after the boundaries have been established.

A fundamental assumption in the analysis is that there is more than one solution to an earth-movement problem, and certain types of corrective actions do not require complete investigations. Also, it is assumed that the mechanics, rather than the cause, of the landslide are the more important issue. Therefore, only the information needed for corrective action need be obtained. Arriving at an accurate preliminary estimate is the step most subject to the experience of the investigator. This estimate will vary not only with the investigator but with the area involved, and the type and value of the structure to be safeguarded. However, failure to estimate accurately the corrective action should result only in a higher investigational cost.

FIG. 7.—SLICK SURFACE OF THE SLIDE-PLANE

In considering which of the corrective methods will be feasible, many will be eliminated easily, because of obvious nonapplicability. For the remaining corrective measures, rough estimates will indicate an extremely expensive action, relative to the estimates for other measures. The expensive corrective actions should then be dropped from further consideration until the less expensive methods prove unfeasible.

For each method of correction, certain information is considered essential to produce design data. Table 2 is a summary of the data needed for the design computations for each of the methods. Details relative to the costs of the

TABLE 2.—INVESTIGATION NEEDED FOR VARIOUS CORRECTIVE MEASURES

Corrective measure	Topographic survey ground surface	Bedrock profile	Source of water	Undisturbed soil sample	General soil condition
1. Relcoation	For new location only.	Sometimes needed to check stability of new area.	No	No	No
2. Excavation, drain, and backfill	Area and depth for cost and stability estimates.	Depth for cost and stability estimates.	For cost, drainage, and stability estimates.	Not essential.	Moisture content for locating water and soil characteristics for estimating shear data.
3. Drainage: Surface Subsurface Jacked-in-place pipe Tunnels	For depths and lengths in cost estimates for all but surface drainage.	For depths, lengths, and cost estimates for all but surface drainage.	For locating position of drainage installation.	Essential for permeability only if drainage is to be installed to drain soil, rather than to intercept seepage strata.	Moisture content for locating water source.
4. Removal of material:					
Entirely	For cost estimate only.	For cost estimate only.	No	No	No
Partial at toe	For cost estimate (partial survey).	No	No	No	No
Partial at top	For cost and stability estimates.	Surface only, for cost and stability estimates.	Not essential.	To compute stability of slope.	Density and moisture variations for stability estimates.
5. Buttress at toe	For stability estimate.	Surface only, for stability estimate.	Not essential.	For stability estimate.	Density and moisture variations for stability estimates.
6. Bridging	At abutments only, for cost estimate.	At abutments only, to determine foundations.	Not essential.	At abutments if spread footers are used.	Not essential.
7. Cribbing—timber, concrete, metal	For computing forces against wall, and height determinations.	For depth to foundation, type of foundation, and stability estimate.	Not essential.	To compute forces against wall.	Density and moisture variations for stability estimate.

TABLE 2.—(*Continued*)

Corrective measure	Topographic survey ground surface	Bedrock profile	Source of water	Undisturbed soil sample	General soil condition
8. Retaining wall (stone or concrete)	For computing forces against wall and height determinations.	For depth to foundation, type of foundation, and stability estimate.	Not essential.	To compute forces against wall.	Density and moisture variations for stability estimate.
9. Piling:					
Floating	Partly for soil depths in cost estimate.	Partly for soil depths in cost estimate.	No	No	For moisture and gradation for determining flow possibilities.
Fixed, no provision for preventing intrusion	For soil depth in cost estimate.	For soil depth in cost estimate and type of foundation.	Not essential.	Not essential.	For moisture and gradation for determining flow possibilities.
Fixed, provision for preventing intrusion	For soil depth in cost estimate.	For soil depth in cost estimate and type of foundation.	Not essential.	To compute forces.	For density and moisture in determining stability.
10. Sealing joint planes and open seams	For depths in cost estimate.	For determining strata to be blocked.	For determining strata to be blocked.	No	No
11. Cementation of loose material	For depth and area in cost estimate.	Surface only for cost estimate.	Not essential.	For determining permeability to cementing material.	Density, moisture, gradation for determining feasibility of method.
12. Chemical treatments—flocculation	For depth and area in cost estimate.	Surface only for cost estimate.	Not essential.	For determining permeability to chemicals.	Density, moisture, texture for determining feasibility of method.
13. Tie-rodding slopes	Area and depth for stability and cost estimates.	For depth in cost and stability estimates. Also type of foundation.	Not essential.	For stability estimate.	For texture, moisture and density for stability estimate.
14. Blasting	For depths in cost estimates.	For depth in cost estimate and type of rock.	Not essential.	Not essential.	Density and moisture.
15. Reshaping slide material	For cost estimate.	No	Not essential.	No	No
16. Slope treatment	Area for cost estimate only	No	Not essential.	Not essential.	For agricultural purposes or for texture.
17. Lightweight fill	Depth and area for cost and stability estimates.	Surface only for depth in stability estimate.	Not essential.	For load reduction in stability estimate.	Density for stability estimate.

corrective actions are vital information in the design, and Table 3 shows the estimates of costs based on average prices in West Virginia in 1950.

Detailed Field Investigation.—An excellent summary of subsurface exploration methods has been prepared by M. Juul Hvorslev,[15] M. ASCE. The importance of geology in subsurface work is to be emphasized. The proper interpretation of land forms, exposed bedrock, and the general geologic conditions of the area will greatly expedite the subsurface investigation. One of the most troublesome deficiencies in a rational correction of landslide problems is the lack of an efficient, practicable, and direct method of obtaining subsurface information. The uses of the hand auger, the test pits, the power auger, the well-drill, the churn-drill, the core-drill, and the geophysical surveys are the most common methods for obtaining this information. There is, also, the method suggested by Mr. Forbes, which is that of obtaining information during the construction phase of the corrective measure.

TABLE 3.—1950 UNIT COSTS FOR USE IN ESTIMATING EXPENDITURES FOR CORRECTIVE MEASURES

Corrective measure	Item	Cost, in dollars	Unit
1. Relocation	Excavation	0.75	Cubic yard
	Pavement	3.00	Square yard[a]
	Right of way	Variable	
2. Excavate, drain, and backfill	Excavation	3.50	Cubic yard[b]
	Drainage pipe	1.00	Foot[c]
3. Drainage[d]	Drainage pipe	1.00	Foot[c]
	Excavation	3.00	Cubic yard
	Porous backfill	2.50	Cubic yard[e]
	Jacked-in-place pipe	2.00	Foot[f]
4. Removal of material[d]	Excavation	0.75	Cubic yard
	Right of way	Variable	
5. Buttress at toe	Excavation	1.00	Cubic yard
	Backfill	3.00	Cubic yard
	Drainage pipe	1.00	Foot
	Right of way	Variable	
6. Bridging	Roadway surface	15.00	Square foot
7. Cribbing[d]	Face of cribbing	4.00	Square foot[g]
8. Retaining wall[d]	Face of wall	7.00	Square foot[g]
9. Piling[d]	Length of pile	5.00	Foot[h]
10. Sealing joint planes and open seams	Equipment rental	75.00	Day
	Drilling	3.00	Foot
	Cement	4.00	Barrel[e,j]
11. Cementation of loose material	Equipment rental	75.00	Day
	Drilling	3.00	Foot
	Cement	4.00	Barrel[e,j]
12. Chemical treatments—flocculation	Equipment rental	75.00	Day
	Drilling	3.00	Foot[j]
	Admixture	Variable	
13. Tie-rodding slopes	Length of pile	5.00	Foot[h]
	Drilling	3.00	Foot
	Steel	0.20	Pound[e]
	Concrete	45.00	Cubic yard[e]
14. Blasting	Drilling	3.00	Foot
	Black powder	......	

[a] For flexible type pavement. [b] Earth moved twice. [c] Perforated pipe 6 in. in diameter. [d] Subheadings same as in Tables 1 and 2. [e] In place. [f] Pipe 6 in. in diameter, in place. [g] In place, 8 ft high, gravity-type concrete. [h] Steel, in place. [j] Quantities difficult to estimate.

The most generally used method is core-drilling in conjunction with steel casing driven through the overburden material. Unfortunately, the cost of core-drilling is relatively high, ranging in West Virginia (in 1950) from $2.75 per ft to $5.00 per ft. The area must be very thoroughly and systematically drilled if a complete picture of the subsurface condition is to be obtained. The "checker-board" layout, similar to that used for topographic surveying, is sometimes used.

---

[15] "Sub-surface Exploration and Sampling of Soils for Civil Engineering Purposes," by M. Juul Hvorslev, Report of a Research Project of the ASCE, The Engineering Foundation, Harvard Univ., Cambridge, Mass., 1950.

Of the two hand-methods, the auger is by far the cheaper and more generally applicable. A good two-man crew should average from 50 ft to 60 ft of investigation per day, for hole depths of from 10 ft to 14 ft. One advantage of this method is the reliable information that can be obtained about the variation of the soil and the moisture conditions. With additional equipment, relatively undisturbed samples can be removed. There are several limitations, however, the first being that rarely will a crew be able to bore deeper than 15 ft and the second being that the auger is stopped by rock boulders and most bedrock.

Test pits produce excellent information and often prove to be desirable, if subsurface drainage is a probable method of correction. However, the pits are uneconomical if numerous holes are needed in the design. The depth that can be reached is limited to from 10 ft to 15 ft unless problems of shoring and earth removal are solved.

If information at depths in excess of 15 ft is needed, power equipment is almost a necessity. Power augers are economical, the operating costs ranging from one third to one half that of core-drilling. Detailed soil information is sometimes difficult to obtain with power augers because many of the boring-rigs for deep work do not allow frequent withdrawals, nor do they cut through hard boulders or bedrock material. Even light rigs can drill to depths of from 60 ft to 75 ft.

Well-drills and churn-drills will penetrate bedrock and disclose the existence of seepage layers. The cost is approximately the same as for power augers. Since cores are not obtained, the type and character of the bedrock cannot be determined conclusively.

The subsurface methods holding the most promise are geophysical surveys, of either the electrical resistivity type or the seismic type. Since these methods are conducted from the surface, limited core-drilling for correlation purposes is usually desirable. Unfortunately, there have been very few efforts to apply these techniques to landslides. The initial efforts to use electrical resistivity surveys in West Virginia showed a surprisingly small difference of resistance between the soil and the bedrock shale and sandstone. The recent geophysical successes in highway engineering seem to justify the belief that eventually electrical resistivity and seismic methods will facilitate subsurface investigations of landslides. The cost of these studies may be as low as one tenth the cost of core-drilling.

In searching for underlying sources of water, it is well to realize that water generally follows a pattern in making its way through bedrock. The type of layer the water is traveling through may be observed in open cuts. Generally, water will travel through jointed sandstone or limestone and avoid the impervious shales. There are exceptions, of course. Water also is found seeping through the contact between soil and bedrock, or at the contact between embankment and foundation soil. In coal areas, water is likely to be located just above the coal seam.

The presence of tilted trees, posts, poles, or structures is valuable evidence in locating a sliding surface. This not only verifies the fact that movement of the area has taken place, but also indicates the possibility that the depth of movement does not exceed the depth reached by the roots or the foundations. It is not uncommon to see landslides upon which trees, poles, and houses have moved horizontally and downward with little or no disturbance of vertical alinement. Obviously, such cases involve a slide plane that is deeper than the depth penetrated by the tilted object. The location of the slip-plane may be obtained from the drill records.

Office Investigation.—The office investigation will consist of plotting data, computing the forces at work, designing the corrective action, estimating the cost for the corrective action, and preparing a final report.

The plotting of data concerning slides will be routine and should show cross sections of the existing ground surface, the underlying bedrock, the location of drill holes, the data from the drill holes, the seepage strata, the pavements or structures, and other information considered pertinent to the slide. The number of cross sections will vary, depending on the detail desired; for example, in a study involving a narrow area (100 ft), the distance between sections may be as short as 25 ft. Cross sections should be available on the solid areas immediately adjacent to each end of the slide. The sections should be continued above and below the slide so that a complete analysis of the effects of a corrective action can be anticipated. In some cases, sections perpendicular to the movement will be desirable.

A plan view is normally included showing the general limits of the slide area, the location of drill holes and corrective action, and other pertinent information. The best possible estimate of the location of the plane of failure should be made. The notes of the field work should be studied closely for evidences determined from visual examination and from the drill work.

The shearing resistance or the shearing forces should be estimated following the principles previously outlined, and more completely covered by Messrs. Terzaghi and Peck,[8] Mr. Krynine,[9] Mr. Hennes,[10] Mr. Buckingham,[13] and others.

On obtaining an estimate of the stability of the area before the failure, the safety factor should be computed to determine the advantage produced by the corrective action. The final corrective action should result in a more stable area than existed prior to the movement. The extent of improvement is dependent upon the economy of producing such stability. All else being equal, the method with the greatest safety factor is the most desirable.

Unless measurements and analyses are made to determine the influence of hydrostatic pressures and seepage forces, rarely will it be feasible to estimate, in terms of the safety factor, the benefit achieved by a drainage solution. Failure to take account of the many variables may produce a misleading safety factor; however, this refinement may be advisable under certain conditions. If the factor is neglected in both the "before failure" and "after correction" computations, the estimate will be on the safe side, except in cases where the corrective measure increases the excess hydrostatic pressure or seepage forces, or where the pressures existed during failure but not after movement ceased.

The investigation of debris-slides will be essentially the same as that for slides, differing in the fact that the surface of failure will be straight, and the reshaping or terracing of the area will not be more effective than a uniform reduction of the slope. The stability estimate will be a relatively simple application of the more complicated slide approach because the entire weight may be used instead of dividing the area into sections, as in Fig. 3. Corrective actions for this type are influenced greatly by the slope of the slip-plane, and the displacement is more likely to have been caused by excess hydrostatic pressures or seepage forces.

For creep investigations, cross sections and a plan view are desirable. There is presumed, by definition, to be no plane of failure. In the investigation, emphasis should be placed on the accurate location of the weaker strata as well as seepage phenomena. Data relative to the surface of the bedrock are also of value. If one accepts the theory of Mr. Terzaghi—that successive failures of weak layers or the existence of stresses greater than the fundamental strength cause creep—the design should tend to alleviate the overstressed conditions. The over-all stability should be estimated because the movement often develops into a slide. The weak layers undoubtedly will influence the slip-plane, as in Fig. 4. The conditions of hydrostatic pressures and seepage forces are more important in this type of failure than in the previously mentioned types, and a more specialized approach is necessary.

By definition, flow has no plane of failure, but has a more rapid movement than creep, and generally results from excessive moisture. Such failures may be caused by failure of the weaker strata. If this is the case, then the movement is classified as creep. Since excessive moisture is the principal contributor, a drainage solution should be found. The over-all slope stability is important because these movements tend to develop into slides, as seen in Fig. 5.

Construction and Supplemental Investigations.—If the preliminary and abbreviated field investigations indicate that one type of corrective action is the most feasible solution, it is often desirable to combine with the construction a more complete investigation. This is particularly true for deep drainage solutions. This technique has been used to some extent by Mr. Forbes. For any corrective measure, sight should not be lost of the fact that the existing methods of subsurface exploration are not infallible. The construction should be watched, and the corrective measure, bedrock layers, and seepage strata should be restudied. The drainage of all water-bearing strata or pockets should be worked into any corrective measure as an additional safety factor. If the construction exposes conditions not anticipated in the design, the corrective action must be re-evaluated.

For an indefinite period after completing the corrective action, observations should be continued. Any evidences of movement should be studied, and, if necessary, further corrective actions should be undertaken. Immediate action in such cases is very important, in order to make full use of the original corrective action.

CONCLUSION

The following facts and ideas have been presented in this study:

1. For landslides with slip-surfaces at or near the contact between soil and bedrock, a shear failure occurs in the soil.

2. All earth-movement problems can be corrected, but it is not always economically feasible to do so.

3. There are numerous instances in which the determination of "the" cause has only academic interest since the elimination of one or more "contributing factors" will bring about a higher degree of stability.

4. The presence of the force of gravity in every mass-movement problem should be a fundamental consideration. The earth mass represents not only the source of the trouble but also an economical source of resistance. The best method of applying these facts is through estimates based on the theories of soil mechanics. These theories involve the shear characteristics of the soil.

5. An inexpensive method of subsurface investigation is needed. Very few earth-movement problems can be satisfactorily considered without knowledge of subsurface conditions.

6. The method suggested herein for estimating the degree of stability for a corrective measure in a given situation is a step toward a rational analysis of earth movements. However, considerable development and extended observations are required before the method will progress to a fully rational procedure.

DISCUSSION

D. P. Krynine,[16] M. ASCE, and Richard J. Woodward,[17] A.M. ASCE.—The types of slides in a given region are influenced by the geology, topography, and climatic conditions of that region. To Mr. Baker's observations made in West Virginia the writers wish to add their observations made in California and in other localities where the aforementioned factors—and hence the slide types—differ, or may differ, from those mentioned by the author. In California—where a part of the year is rainless and the other part has much rain—the writers had a good opportunity to observe the contrasts in the stability of the same slope at different seasons and to understand clearly that excess moisture is a powerful contributing factor in producing slides. The writers have been enabled to study and correct slides affecting small properties, and they fully share Mr. Baker's opinion that, because corrective measures of landslides depend primarily on economics, expensive works in slide rehabilitation cannot be considered in these and similar cases.

Definition of a Slide.—A slide (or landslide) is a downward and outward movement of a portion of the soil (or soil-rock) mass with respect to that portion remaining in place. This movement is accompanied by a breaking of the bond connecting the separated and remaining portion of the mass. The separation is apparently preceded by more or less slow movements along the potential sliding surface followed by a more rapid movement of the separated portion.

Slides generally exhibit a characteristic topography. There is a typical area near the upper end of the slide from which the material has been carried away (excavation), and a part near the lower end in which the material has been deposited. The excavated part of the slide is usually bounded by a well defined continuous crack which is the exposed part of the sliding surface; this crack often has a parabolic shape both in the plan view and in the front elevation of the slide. The over-all shape of a slide is a closed curve which, however, is sometimes difficult to locate near the lower end of the slide. The closed curve bounding the slide generally has a confined "girt" as indicated in Fig. 8.

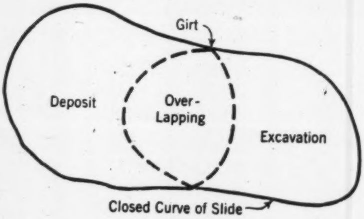

Fig. 8.—Plan of a Slide

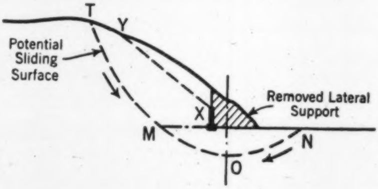

Fig. 9.—Removal of Lateral Support

---

[16] Cons. Engr., San Francisco, Calif.

[17] Partner, Woodward, Clyde & Associates, Soil and Foundation Engrs., Oakland, Calif.

This girt approximately corresponds to the boundary between the excavation and the deposit.

Types of Slides.—Two basic types of slides are considered, deep slides and shallow slides. The essential difference between these two types of slides consists in the shape of the surface which bounds the separated part of the earth material from that remaining in place. Deep slides are bounded by curved slip surfaces resembling, in section, an arc of a circle. Shallow slides are bounded by slip surfaces which resemble a plane surface, rather than a regular curved surface.

Deep slides are formed by rotation about some center (Fig. 1), and the separated part of the soil or soil-rock material is a well-defined three-dimensional body. All failures of this type can be classified as being "in the soil" according to Mr. Baker. However, the writers have observed sliding surfaces passing through both the soil and the underlying soft shale.

Shallow slides which have been observed are of two types: (1) A slab slide occurs when a slab of earth material, approximately 5 ft thick, is separated from the rest of the earth mass by slip surfaces roughly parallel to the ground surface. Such slides, in front elevation, are also bounded by closed curves. Although similar in appearance to debris slides, slab slides are not always produced by the removal of the material at the toe. The slab slides often start from a crack at the top followed by a heaving at the toe of the slide. (2) A shallow "break-through" slide may be produced by the pushing action of the rising ground water as explained subsequently under the heading, "Upper Subsurface Water."

Both deep and shallow slides are produced in two steps: Part of the earth mass becomes separated from the main formation, and the earth mass moves downward and outward under the influence of gravity. The separation may be caused by (1) the increase in horizontal forces acting on the separated portion and a consequent increase in tangential stresses along the potential sliding surface; (2) a partial relief of the normal pressure acting on the potential sliding surface; and (3) a combination of these two factors. A change in physical properties of the mass, because of climatic factors, may also contribute to the occurrence of slides.

Removal of Lateral Support.—A relief, or more accurately, a weakening of the normal pressure acting on the potential sliding surface can be produced by the removal of the lateral support of the mass, as shown schematically in Fig. 9. In Fig. 9 the removed lateral support is shown by crosshatching. This removal is reflected in the general weakening of the normal pressure against the potential sliding surface TN and especially a decrease in tangential stresses along the part ON of the sliding surface contributing to the stability of the slope. Another factor contributing to slope failures, in the case of the removal of lateral support, is the tensile stresses that develop on the unsupported surface of the slope above the cut. These tensile stresses tend to produce vertical cracks in the slope, a phenomenon which is especially pronounced if the slope is composed of expansive materials. A laterally supported slope can only expand and shrink vertically whereas, when the lateral support is removed, the slope is free to expand and shrink laterally. Shrinkage in expansive soils causes forces which result in wide cracks that are filled with water during the subsequent rainy season. This fact contributes to the decrease in shearing strength of the soil and subsequent slope failure.

Drainage as a corrective measure may or may not be helpful. It should be realized that the most efficient solution, in the case of the removal of lateral support, consists in constructing a retaining wall or flattening the slope. Both measures can be combined (dotted line XY in Fig. 9). In the general case, retaining walls are not too efficient in the rehabilitation of slides; however, the case of the removal of the lateral support is decidedly an exception. Addition of buttresses to the wall is helpful, but it is not always feasible because of lack of space.

Pore Pressure.—Another factor operative in the weakening of the normal pressure on the potential sliding surface is the pore pressure. Under the conditions shown in Fig. 10, the ground-water flow is constricted in the sandy aquifer below points A and B. If a boring is made to reach point A, water in the boring will rise to point A_1 in the dry season and to point A_2 in the rainy season. The loci of points A_1 and A_2 are piezometric surfaces in dry and rainy seasons, respectively. It can be concluded from Fig. 10 that during heavy rains the soil material at point A_2 is raised by a force equal to the distance from A to A_2 multiplied by the unit weight of water. Because of this force, the normal pressure on a potential sliding surface is decreased. Consequently, the shearing resistance of the soil material at point A_2 is decreased which may lead to a failure. If the impervious layer at point C is thin, the water in the underlying aquifer either will reach the ground surface by capillarity or will simply break through the impervious layer, thus causing a slide that should be classified as a shallow slide as mentioned under the heading, "Types of Slides." If an excessively deep excavation is made above point C, there is a probability that such an excavation will be periodically flooded. If a slide occurs above point

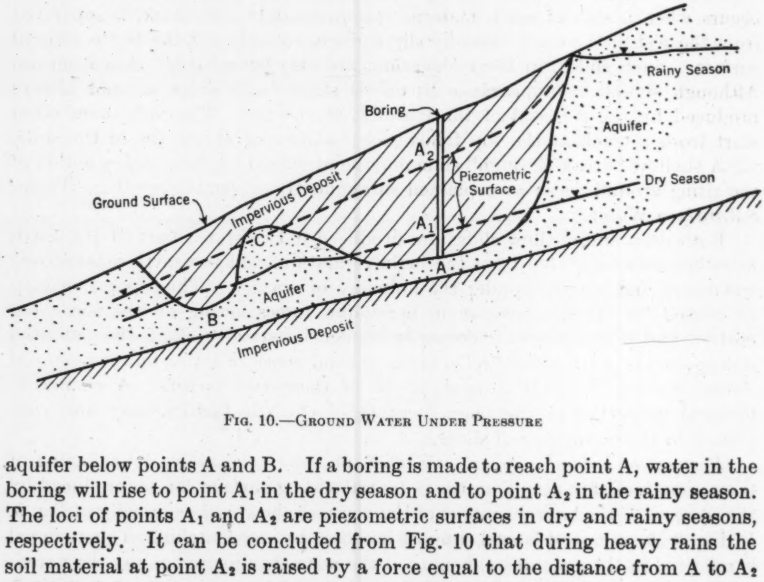

FIG. 10.—GROUND WATER UNDER PRESSURE

C because of the breaking through of the thin impervious layer, such a slide should be corrected with great care. If not adequately corrected, the slide will recur at the same place when the corresponding piezometric surface has again risen sufficiently. In fact, such a slide has the same action on the ground water as a safety valve has on a boiler.

Removal of Excess Ground Water.—Slides caused by an excessive rise of the ground-water level should be corrected by removing the detrimental part of the ground-water flow—thus holding the piezometric surface. A common method of removal is the use of "hydraugers," also termed "horizontal drains." The term, hydrauger (that is, hydraulic auger), is used on the west coast of the United States and does not describe correctly the device which contains no auger. The drains in question are also not horizontal, but sloping—5% being approximately the minimum value of the slope. In pervious soils, the hydrauger drains may consist of 2-in.-diameter or 4-in.-diameter pipes placed in the ground to increase the cross section of the draining area. The drains are provided with slots, about $\frac{1}{4}$ in. wide and from 2 in. to 3 in. long. Approximately 3 slots per lin ft are ordinarily used for a 2-in.-diameter pipe; the slots are made with an acetylene torch. In order to set the drains in place a slightly oversized hole is drilled by a machine which is a combination drill and wash borer. After the hole is drilled the drains are jacked into the hole, and the sections are welded together while the pipe is inserted. It is often convenient to place hydrauger drains in a fan-shaped arrangement with a common point of discharge.

In removing ground water from a stratified mass with impervious inclusions, it is often advisable, in conjunction with the hydraugers, to sink vertical holes (approximately 24 in. in diameter) to a convenient depth and to backfill the holes with crushed rock or gravel. In this arrangement one vertical well may be connected to each hydrauger. Rather than using hydraugers or trenches backfilled with rock or gravel, drainage is sometimes accomplished by sinking a row of vertical wells 30 in. in diameter, spaced approximately 7 ft on centers. Specially trained workers operating in the wells place drains by tunneling from hole to hole. Such an operation proves economical when substituted for short-drain trenches in remote places where the use of a trencher would be too expensive or where excessively long hydraugers would be required.

Increase in Tangential Stresses.—Placing a load (often a new embankment or fill) next to the top of a slope is another cause of deep slides. The failure in this case is the result of an over-all increase in tangential (shear) stresses along the potential sliding surface, although the normal pressure acting on that surface may not essentially change.

An effect similar to the placing of a load next to the top of a slope is caused by the removal of a load next to the toe of a slope (point N in Fig. 9). In New Haven, Conn., several buildings were erected on a slightly sloping street, close to each other. Demolition of one building in the row was causing continuous cracking of glass in the large windows of a building located several doors away. The cracking stopped when the demolished building was restored.

Correction of slides caused by the placement or removal of a load should be effected by removing or replacing the corresponding load.

Upper Subsurface Water.—Water in different stages (that is, hygroscopic, capillary, in the form of vapor, or locally condensed vapor retained between the particles) located above the water table, is termed "vadose" by the geologists. Perched water apparently is not included in this classification. When it rains continually during a long period, some of the rain water flows down the slope, and a part of the water is absorbed by the ground and moves downward. The upper soil layer, which has undergone a certain weathering process, is often rather pervious. This circumstance permits an easy downward movement of the rain water to the underlying impervious layer. As soon as the few upper inches of the latter are saturated, a "curtain" preventing further downward penetration of the rain water is formed. The still-falling rain water is then forced to flow down the slope on top of this curtain until it fills the soil mass to the top. If there is sudden flattening (break) at any point of the slope—not necessarily at the foot of the slope—the lower part of the slope has less discharge capacity than the upper part. As water continues to collect in the steeper part of the slope, the impossibility of further discharge through the vertical plane separating the upper and the lower parts of the break will be resolved either by pushing out a portion of the earth mass (crosshatched in Fig. 11) thus producing a slide, or forming a swamp condition at the break. The presence of the break is favorable, but it is not a compulsory condition for slides of this type.

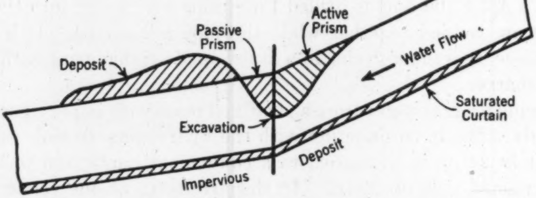

FIG. 11.—SLIDE AT THE BREAK OF A SLOPE

Slide scars on natural slopes may be observed in abundance in regions of young geology. The cause of these slides is apparently the intrinsic instability of the slopes that tend to reach stable equilibrium. In some places the slide scars are so abundant that they really should be considered as characteristic landforms of the region.

Efficient rehabilitation of the slides caused by the upper subsurface water is difficult. In hilly regions with extensive slopes, water should be prevented from reaching the places where it could be detrimental, so far as the formation of slides is concerned. It is advisable to stop water as close as possible to the source or at least as high as possible on the slope, although no general statement can be made for this case. Hydraugers may be used to stop the water, but they are not fully efficient following initial installation. In a given condition, a combination of hydraugers with rock-filled drains or other drainage features should be considered.

Slab Sliding.—Slides produced by the sliding of huge earth slabs on an almost frictionless surface often located at a depth of approximately 5 ft can be termed slab slides. These slides occur during continuous rainstorm periods and often are caused by agencies similar to those causing deep slides, such as the placing of a fill or the removal of the lateral support. A fill not placed next to the top of the slope, but somewhere at the middle of this slope, may cause a shallow slab slide of large magnitude. This fact suggests that additional loads on the area, such as a building with shallow footings, may increase the weight of the slab and push it down. It should be realized that the foregoing statement requires considerable verification. Slab sliding is generally corrected by proper drainage.

Slide Causes.—A slide is actually caused by a complex of causes in which the force of gravity and ground water are always present. Dry slides have been reported as rare exceptions. In a complex of causes one cause is predominant, all others being contributing factors. In addition to the predominant cause and the contributing factors in a complex of causes leading to a slide, the "immediate cause" should be considered, especially in legal cases. For example, if a portion of the mass is in a state close to limit equilibrium—that is, if its safety factor is close to unity—a slight increase in either the load or the intensity of the rainfall may cause a slide, thus being the immediate cause of the slide. The immediate cause should be sharply distinguished from the real cause of the slide.

Mr. Baker is quite correct in stating (under the heading, "Fundamental Considerations") that

> "Of great importance is the fact that by eliminating or by modifying the effect of any one of the causes the stability [of the slope] will increase."

The writers would suggest the substitution of the words "contributing factors" for "causes" in this statement. Since the detrimental action of ground water is always a contributing factor in the production of a slide, it is easy to understand that drainage represents "a sound approach to a slide correction." It is known, however, that looking for the cause of the slide is essential. In fact, if the slide has been caused by a load placed at the top of the slide, a drainage solution will not be sufficient. With regard to legal cases (and these are many), the engineering expert has to give to the court a clear answer as to the cause of the slide.

Creep.—The writers were most interested in the mechanics of creep movement as presented in Fig. 4. This type of earth movement has been insufficiently studied, and the explanation of creep by the presence of various potential slip surfaces within the creeping mass is perhaps an ingenious guess. It is believed that, since the creeping mass (as shown in Fig. 4) is reposing on a firm sloping base and slowly moves down, it should be in the state of unstable equilibrium alternated with microscopic translation. If this is so, the creep should be caused by very small oscillations of the center of gravity of the whole mass caused by readjustment of its constituents. It is probable that changes in moisture content are responsible for these readjustments.

In addition to the classical example of creep (Fig. 4), there are movements that lie somewhere between sliding and creeping. The following phenomenon is cited as an example. In a shallow valley (near Oakland, Calif.) with a clayey floor and a longitudinal slope along the thalweg of approximately 20%, a well-defined slide 500-ft long was produced with a regular crack and a "shelf" at the top. The following year, in bulldozing the locality, the toe of the slide was undermined. The slide moved bodily approximately 1 ft and continued moving slowly for a period of at least three months, during which there was no rainfall.

Mr. Baker's advice to refer the creep and flow cases to an authority in this field is good, provided such an authority exists.

Surveying a Slide.—Surveying existing slides and searching for potential ones is greatly facilitated by the use of aerial photographs. This source of information clearly discloses the features of the slide area—even those that have escaped the attention of the engineer during the survey. The cost of aerial photography is not as great as it is often believed.

Conclusion.—Mr. Baker's activities in the theoretical and practical study of landslides are well known to engineers active in this particular field. The paper constitutes additional valuable information in this field of endeavor.

R. F. BAKER,[18] M. ASCE.—The comments of Messrs. Krynine and Woodward are particularly helpful as their experience with landslide problems, particularly in the western part of the United States, have suggested factors that are also true in West Virginia. Many of the ideas contained in the paper might not apply throughout the United States, but the discussion indicates that many of the principles are the same.

Of particular interest is the differentiation offered by Messrs. Krynine and Woodward between "shallow" slides and "deep" slides. Their approach is a realistic one, particularly when applied to the investigation of corrective measures. In fact, it is probable that many of the suggested methods for treatments of landslides could be divided on the basis of their applicability to deep or shallow movements. In West Virginia the practice has been to estimate the depth of the overburden in the manner suggested, and the technique has been found to be helpful.

The writer was also interested in the comments concerning failures in underlying shale formations. Only one such failure has been observed in West Virginia, and this was a case in which extremely heavy blasting operations were involved. Other such failures in the Appalachian Plateau province have been reported in Pennsylvania. Failures in consolidated sediments are not considered to be average conditions, however, as a failure in the shale implies that the shearing resistance of the soil is greater than that of the shale, or that the two resistances are essentially equal.

In 1947 a theory was suggested[13] by Mr. Buckingham that a landslide analysis based on $\phi = 0°$ was a valid approach. Several of the ideas expressed by Messrs. Krynine and Woodward would indicate that such an assumption cannot be warranted as a generality. Specifically, the statement is made that the loss of lateral support near the toe of a slope results in a reduction of the shearing resistance. In addition, general acceptability of horizontal drainage is implied. Neither of these ideas could be valid for an analysis based on $\phi = 0°$. The writer does not know whether Messrs. Krynine and Woodward intended such an implication, but such an interpretation would verify observations of slides in West Virginia. The discussion concerning the use of horizontal drainage is particularly important as the western states have long used this technique. For the area within the Applachian Plateau very little use has been made of this method. The first application of the method in West Virginia was completed in the summer of 1953.

---

[18] Engr. of Soil Mechanics, State Rd. Comm., Charleston, W. Va.

The principle of horizontal drilling changes the entire concept of landslide correction as an effective installation can be accomplished at a minimum cost. It is felt that drainage as a corrective measure has been overemphasized; in West Virginia, drainage methods have not been economical for many of the slide conditions. However, use of horizontal drainage does permit a much wider application of drainage corrections.

It has been found that general statements concerning the application of specific types of corrective measures to certain types of landslide causes are not valid. Two such generalities were mentioned by Messrs. Krynine and Woodward. One (under the heading, "Increase in Tangential Stresses") is that "Correction of slides caused by the placement or removal of a load should be effected by removing or replacing the corresponding load." Although there is no question of the validity of the principle, the approach would not work often enough in West Virginia for such a generality to be made. The use of a retaining wall is not always valid where there has been a loss of lateral support unless very shallow slides or quantities are involved. The statement by Messrs. Krynine and Woodward may be based on conditions of extremely stable slopes prior to the loss of lateral support. Under such conditions, replacement of the loss with a mass of approximately the same resistance should lead to the same stability as existed prior to the excavations. However, for deep, ancient slides near the point of limiting equilibrium, retaining devices to replace the loss of lateral support have not been found to be successful in West Virginia.

Perhaps the most significant part of the discussion was concerned with the legal aspects of landslides. There is little in the literature concerning this important division of landslide work. Although the writer's experience does not correspond completely with that of Messrs. Krynine and Woodward, the intelligent appraisal of "cause" and "contributing factor" is most essential. The one cause and several contributing factors do not always constitute the "complex of causes." The writer does accept the words "contributing factor" for "cause" as a valuable change. Perhaps the disagreement is not that one cause predominates, but that it is practically impossible to ascertain which is the predominate cause, and what is the exact effect of the contributing factors.

One of the principal difficulties in relying on the designation of a "predominant cause" can be illustrated by the following: If it is assumed that an excavation has resulted due to a loss of lateral support, but that heavy seepage also exists beneath the surface of the ground, both factors should be recognized immediately as "contributing factors." If one states that the excavation is the "predominant cause," could not the slide have occurred without the presence of water? If, however, the water is the predominant cause, would the slide have occurred without the excavation? Certainly the removal of the lateral support must be partly at fault, regardless of other conditions. If some peculiar conditions such as a leaking water main or reservoir or extremely adverse climatic conditions had led to extreme seepage conditions, the situation would be changed. Many such conditions can arise, and the statement that either cause is the predominant one can lead to an impasse. Landslides have been rare about which a dogmatic statement can be made as to the predominant cause with the exclusion of other specific factors.

In the legal phases of landslide work, the writer has been in the position of either (1) defending an action specified as leading to damage, or (2) condemning an action as having damaged the client. For the first condition the most certain escape from a claim appears to be in proving that the action could not have been even a contributing factor. If the action has been a contributor to the movement, then the difficult task is to prove some other contributor has a greater influence and would undoubtedly have produced the failure even without the minor help of the action defended. The second type of claim is generally less difficult, for the major step is to prove that the action was a contributor. Quite often this is evident as being true or untrue, and the client can be so advised. Of course, if a major contributing factor exists, one must estimate whether the action in question could have accelerated the movement.

A helpful concept to the writer in dealing with the legal aspect of landslides is the geomorphology principle mentioned by Messrs. Krynine and Woodward. In the paper, the idea was expressed that the soil mass is inevitably headed for the topographic bottom of the area. If the action in question has assisted in accelerating or increasing the motion under consideration, some degree of contributancy appears to be involved. If an action has contributed to the movement, the action is most difficult to defend. In fact, if the action is a contributor to movement, a degree of liability will automatically exist in many cases. The extent of the liability then becomes debatable and may often be decided satisfactorily with a quantitative approach based on the principles of soil mechanics.

AMERICAN SOCIETY OF CIVIL ENGINEERS
Founded November 5, 1852
TRANSACTIONS

Paper No. 2692

POST-BUCKLING STRENGTH OF REDUNDANT TRUSSES

By E. F. Masur[1]

Synopsis

The load-carrying capacity of redundant rigid-jointed trusses after the trusses have buckled in their own plane is investigated. It is shown that (unlike similar statically determinate frameworks) such trusses buckle under increasing external forces, which generally approach limiting values as buckling progresses. The computation of the ultimate load is facilitated by the use of two theorems establishing upper and lower limits of the ultimate loads. Thus, the carrying capacity of the truss can be estimated by "surrounding" the unknown load between two easily calculable values. Of these limits, the lower bound can be computed to any desired accuracy.

Introduction

The problem of the resistance of rigid-jointed trusses to buckling in their own plane has been the subject of numerous investigations. Current (1953) codes for structural design still ignore the continuity of the truss members, although few structures are constructed without some degree of rigidity. For this reason, only rigid-jointed trusses are investigated herein. However, the principles developed (in a modified and simplified form) are also applicable to pin-jointed trusses. In fact, since a buckled bar behaves similarly to a perfectly plastic one, the analysis of a buckled pin-jointed truss closely follows the analysis of an equivalent "rigid-plastic" structure.[2]

It is apparent from simple analysis that statically determinate trusses become unsafe when subjected to critical loads—that is, when subjected to external forces corresponding to neutral equilibrium. Actually such structures are incapable of supporting loads in excess of the critical loads when the structures are in the buckled state. Assuming perfect elasticity throughout the structure, the external forces remain constant during the buckling process.

Note.—Published essentially as printed here in November, 1953, as *Proceedings-Separate No. 332*. Positions and titles given are those in effect when the paper was received for publication.

[1] Associate Prof. of Civ. Eng., Illinois Inst. of Technology, Chicago, Ill.

[2] "Limit Design of Beams and Frames," by H. J. Greenberg and W. Prager, *Transactions*, ASCE, Vol. 117, 1952, p. 447.

The constancy of the forces has been demonstrated in a series of comprehensive tests.[3]

It will be shown that trusses which are redundant with respect to their axial-force distribution buckle under loads that usually increase, and never decrease, as the joint rotations progress. At the same time, there occurs a redistribution of the internal forces in conjunction with the reduced chord lengths of the bent bars. In the general case, the state of stress in the truss approaches a limiting condition corresponding to the ultimate load. The ultimate load represents the final load-bearing capacity of the structure and is usually in excess of the loads under which the truss buckles initially.

THE EQUATIONS GOVERNING THE BUCKLED STATE

In the development of the equations for the buckled state, it is assumed that the structure is subjected to a set of external loads which are known, except for a common multiplying factor λ_0. Letting $\lambda_o X_i$ and $\lambda_o Y_i$ denote the Cartesian components of the external force acting on the *i*th joint, and having S_{ij} and M_{ij} equal, respectively, the axial force and moment with which the bar connecting joints i and j acts on joint i, at which all quantities are to be measured positive as shown in Fig. 1, the equations of equilibrium for joint i are

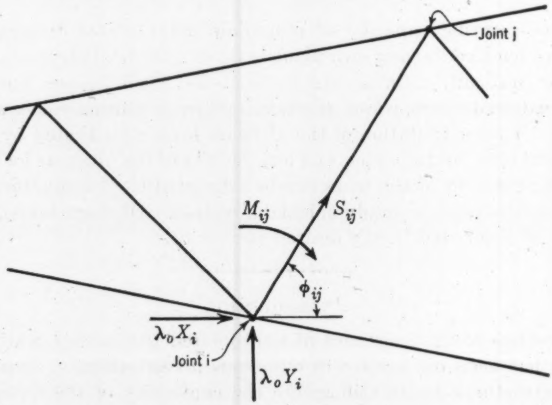

FIG. 1.—DIAGRAM OF A TYPICAL JOINT

$$\sum_j S_{ij} \cos \phi_{ij} + \lambda_o X_i = 0, \; (i = 1,2, \cdots n) \ldots\ldots\ldots\ldots (1a)$$

$$\sum_j S_{ij} \sin \phi_{ij} + \lambda_o Y_i = 0, \; (i = 1,2, \cdots n) \ldots\ldots\ldots\ldots (1b)$$

and

$$\sum_j M_{ij} = 0, \; (i = 1,2, \cdots n) \ldots\ldots\ldots\ldots\ldots\ldots\ldots\ldots (2)$$

in which ϕ_{ij} is the inclination of the bar ij in the undeflected state, and the summation extends over all the bars connected at joint i.

---

[3] "Buckling of Rigid-Jointed Plane Trusses," by N. J. Hoff, Bruno A. Boley, S. V. Nardo, and Sara Kaufman, *Transactions*, ASCE, Vol. 116, 1951, p. 958.

If the bar ij is elastic and initially straight, and if the effect of the linear joint displacement is ignored, the moments M_{ij} can be expressed in the form:[4]

$$M_{ij} = \frac{4\,E_{ij}\,I_{ij}}{L_{ij}} K_{ij}\,(\theta_i + C_{ij}\,\theta_j) \qquad (3)$$

in which E_{ij} is the modulus of elasticity of member ij, I_{ij} denotes the moment of inertia of bar ij, L_{ij} is the length of member ij, and θ_i and θ_j represent, respectively, the angular displacement of joints i and j and are measured positive in a counterclockwise direction,

$$K_{ij} = \frac{3\,\beta_{ij}}{4\,\beta^2_{ij} - \alpha^2_{ij}} \qquad (4a)$$

Furthermore,

$$C_{ij} = \frac{\alpha_{ij}}{2\,\beta_{ij}} \qquad (4b)$$

in which

$$\alpha_{ij} = 6\,\frac{1 - \epsilon_{ij}\,\mathrm{csch}\,\epsilon_{ij}}{\epsilon^2_{ij}} \qquad (5a)$$

$$\beta_{ij} = 3\,\frac{\epsilon_{ij}\coth\epsilon_{ij} - 1}{\epsilon^2_{ij}} \qquad (5b)$$

and

$$\epsilon_{ij} = \sqrt{\frac{S_{ij}\,L^2_{ij}}{E_{ij}\,I_{ij}}} \qquad (6)$$

It should be noted that for bars in compression ϵ becomes imaginary, in which case the hyperbolic terms in Eqs. 5 are replaced by similar expressions involving trigonometric functions.

To ignore the effect of linear joint displacement and to establish Eq. 1 with reference to the geometry of the undeflected structure is permissible for most types of trusses. Those for which the joint translations become important, however (such as latticed struts or trusses used as lateral bracing for the upper chords of through-type bridges), are excluded.

If Eq. 3 is substituted into Eq. 2, a set of n linear, homogeneous equations involving the n unknown joint rotations, θ_i, is obtained. In order that these equations can have a nontrivial solution, it is necessary and sufficient that the determinant of the coefficients a_{ij} of the joint rotations vanish, or

$$f(\lambda_0) \equiv |a_{ij}| = 0 \qquad (7)$$

in which

$$a_{ii} = \sum_{l} \frac{4\,E_{il}\,I_{il}}{L_{il}} K_{il} \qquad (8a)$$

and

$$a_{ij} = a_{ji} = \frac{4\,E_{ij}\,I_{ij}}{L_{ij}} C_{ij}\,K_{ij}\ (i \neq j) \qquad (8b)$$

in which the summation in Eq. 8a extends over all the bars joined at joint i.

---

[4] "Principal Effects of Axial Load on Moment-Distribution Analysis of Rigid Structures," by B. W. James, *Technical Note No. 534*, National Advisory Committee for Aeronautics, Washington, D. C., 1935.

Eq. 7 (the "instability equation") represents the familiar "determinant criterion."[5]

In a statically determinate truss, the bar forces S_{ij} are uniquely determined by Eqs. 1 for any given value of λ_o. Conversely, if the truss be of the mth degree of redundancy, the internal forces can be expressed in the form:

$$S_{ij} = \sum_{\alpha=0}^{m} \lambda_\alpha S^\alpha{}_{ij} \quad \text{(9)}$$

in which the $(m + 1)$-force systems $S^r{}_{ij}$ are subject to the restrictions,

$$\sum_{j} S^r{}_{ij} \cos \phi_{ij} + \delta_{or} X_i = 0, \; (i = 1,2,\cdots, n) \quad \text{(10a)}$$
$$(r = 0,1,2,\cdots, m)$$

and

$$\sum_{j} S^r{}_{ij} \sin \phi_{ij} + \delta_{or} Y_i = 0, \; (i = 1,2,\cdots n)$$
$$(r = 0,1,2,\cdots, m) \quad \text{(10b)}$$

in which δ_{pq} is the Kronecker delta ($\delta_{pp} = 1$ and $\delta_{pq} = 0$ if $p \neq q$).

It should be noted that the force systems $S^r{}_{ij}$ are not determined uniquely by Eqs. 10. It is convenient to select the forces $S^r{}_{ij}$ $(r = 1, 2,\cdots, m)$ in such a way that

$$\sum_{k} \frac{S^r{}_k S^s{}_k L_k}{A_k E_k} = \delta_{rs} \; (r,s = 1,2,\cdots, m) \quad \text{(11)}$$

in which S_k is the axial force in the kth bar and the summation extends over all the bars in the truss. The instability equation (Eq. 7) for the redundant truss takes the form:

$$f(\lambda_0, \lambda_1,\cdots, \lambda_m) = |a_{ij}| = 0 \quad \text{(12)}$$

The unknown parameters $(\lambda_0, \lambda_1,\cdots, \lambda_m)$ for the buckled truss are now determined by use of the geometric requirement that there exist a set of linear joint displacements (u_i, v_i) such that

$$\Delta L_k = (u_j - u_i) \cos \phi_{ij} + (v_j - v_i) \sin \phi_{ij} \quad \text{(13)}$$

in which ΔL_k represents the change in the chord length (of the kth bar connecting joints i and j) from the unloaded state. If both sides of Eq. 13 are multiplied by $S^r{}_k$ $(r = 1,2,\cdots, m)$ and summed over all the bars, and if Eqs. 10 and the fact that $\phi_{ij} = \phi_{ji} \pm \pi$ are considered, (after regrouping the sums on the right side) the following set of equations is obtained:

$$\sum_{k} S^r{}_k \Delta L_k = 0, \; (r = 1,2,\cdots, m) \quad \text{(14)}$$

If it is possible to have a system of initial stresses,

$$S^*{}_k = \sum_{\alpha=1}^{m} \lambda^*{}_\alpha S^\alpha{}_k \quad \text{(15)}$$

---

[5] "Numerical Methods for the Calculation of Elastic Instability," by B. A. Boley, *Journal of the Aeronautical Sciences*, June, 1947, p. 337.

then

$$\Delta L_k = \frac{(S_k - S^*_k)\, L_k}{A_k\, E_k} - \delta_k \dots\dots\dots\dots\dots\dots (16)$$

in which δ_k represents the shortening of the chord length corresponding to the bending of the kth bar.

It is also assumed, without loss of generality, that the state $S_{ij} = S^0{}_{ij}$ represents the force system in the unprestressed, unbuckled truss for λ_0 equal to unity. Since, in this case, S^*_k and δ_k both vanish for all bars, substitution of Eq. 16 into Eq. 14 leads to the set of "least-strain-energy" equations—

$$\sum_k \frac{S^0{}_k\, S^r{}_k\, L_k}{A_k\, E_k} = 0, \; (r = 1,2,\cdots, m) \dots\dots\dots\dots\dots (17)$$

In the general case, after substituting Eq. 16 into Eq. 14 and considering Eqs. 9, 11, 15, and 17, there results the system of "compatibility" equations,

$$\lambda_r = \lambda^*_r = \sum_k S^r{}_k\, \delta_k, \; (r = 1,2,\cdots, m) \dots\dots\dots\dots\dots (18)$$

In the Appendix it is shown that the right side of Eq. 18 can be represented by

$$\sum_k S^r{}_k\, \delta_k = \omega \frac{\partial f}{\partial \lambda_r}, \; (r = 0,1,2,\cdots, m) \dots\dots\dots\dots\dots (19)$$

in which ω is a measure of the magnitude of the angular displacements and is defined by

$$\omega = \frac{1}{2} \frac{\sum_i \theta^2{}_i}{\sum_i A_{ii}} \dots\dots\dots\dots\dots\dots\dots\dots\dots (20)$$

in which A_{ii} is the cofactor associated with a_{ii} in the instability determinant, and the summations extend over all the joints. If Eqs. 19 and 20 are substituted into Eq. 18,

$$\lambda_r - \lambda^*_r = \omega \frac{\partial f}{\partial \lambda_r}, \; (r = 1,2,\cdots, m) \dots\dots\dots\dots\dots\dots (21)$$

The term $\partial f / \partial \lambda_r$ has been investigated[6] and can be expressed most conveniently by the equation,

$$\frac{\partial f}{\partial \lambda_r} = \sum_{i=1}^{n} \sum_{j=1}^{n} b^r{}_{ij}\, A_{ij}, \; (r = 1,2,\cdots, m) \dots\dots\dots\dots (22a)$$

in which

$$b^r{}_{ii} = \frac{\partial a_{ii}}{\partial \lambda_r} = \sum_l \frac{E_{il}\, I_{il}}{L_{il}} K_{il} \frac{2\, S^r{}_{il}}{S_{il}} (1 - 4\, C^2{}_{il}\, K_{il}) \dots\dots\dots (22b)$$

$$b^r{}_{ij} = \frac{\partial a_{ij}}{\partial \lambda_r} = \frac{E_{ij}\, I_{ij}}{L_{ij}} K_{ij} \frac{2\, S^r{}_{ij}}{S_{ij}} (1 + 2\, C_{ij} - 4\, C_{ij}\, K_{ij}), \; (i \neq j) \dots (22c)$$

---

[6] "The Effect of Prestressing on the Buckling Loads of Statically Redundant Rigid-Jointed Trusses," by E. F. Masur, *Proceedings*, First U. S. National Cong., of Applied Mechanics, Edwards Brothers, Inc., Ann Arbor, Mich., 1952.

and A_{ij} is the cofactor of a_{ij} in Eq. 12. The constants K and C are defined by Eqs. 4 and have been tabulated individually and in a number of combinations that are frequently of practical interest.[7]

EXAMPLE AND GENERAL DISCUSSION

To trace the history of the structure throughout the buckling process, the engineer is faced with the task of solving the $(m + 1)$ transcendental equations (Eqs. 12 and 21) explicitly for the $(m + 1)$ unknowns $\lambda_0, \lambda_1, \cdots, \lambda_m$ as functions of the independent variable ω. Care must be taken to admit only the smallest positive real root λ_0 since it alone corresponds to neutral equilibrium and is of interest to the engineer.

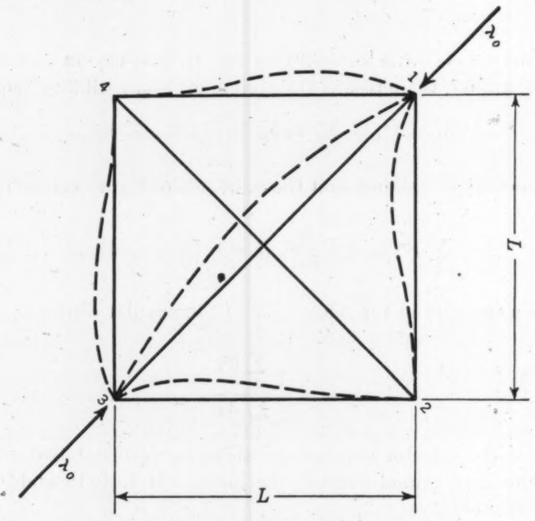

FIG. 2.—EXAMPLE OF A SINGLY REDUNDANT TRUSS

In evaluating the angular joint displacements, it should be remembered that the θ_i-values are proportional to the cofactors of an arbitrary row of the instability determinant. Thus, if

$$\theta_i = c_m\, A_{mi} \quad \text{(23)}$$

in which m is arbitrary, then (after finding all the factors and cofactors in the determinant for a given value of ω) c_m can be computed by substituting Eq. 23 into Eq. 20, which yields

$$c^2_m = 2\,\omega\,\frac{\sum\limits_i A_{ii}}{\sum\limits_i A^2_{mi}} \quad \text{(24a)}$$

---

[7] "Extended Tables of Stiffness and Carry-Over Factor for Structural Members under Axial Load," by E. E. Lundquist and W. D. Kroll, *Wartime Report L-255* (originally 4B24, 1944), National Advisory Committee for Aeronautics, Washington, D. C.

By considering Eq. 12 and the fact that $A_{ij} = A_{ji}$, Eq. 24a can be simplified to take the form:

$$c^2_m = \frac{2\,\omega}{A_{mm}} \qquad (24b)$$

The foregoing process was applied to the singly redundant truss shown in Fig. 2 in which all members are assumed to be made of the same material and to have the same moment of inertia. The diagonal members are solid circular bars having twice the cross-sectional area as the nondiagonal members. The dashed lines represent the buckling mode corresponding to neutral equilibrium. The results of this study, for which the numerical computational details are available,[3] are given in Fig. 3. The ordinate represents the percentage increase

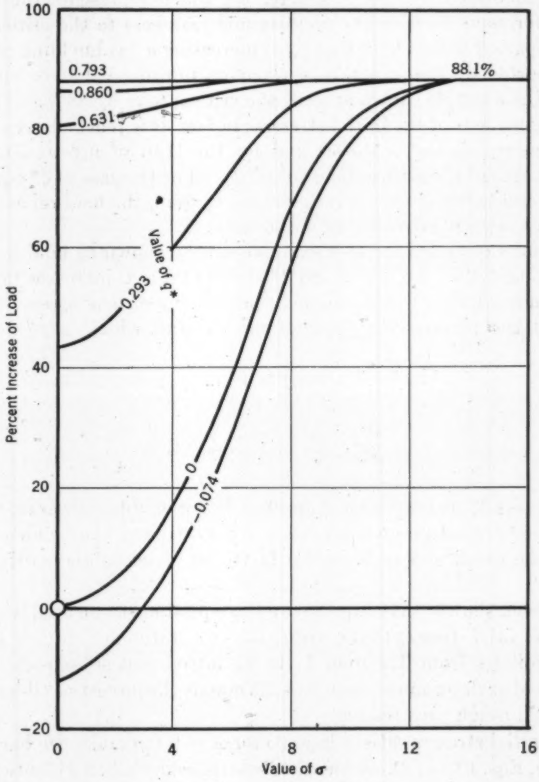

FIG. 3.—THE PERCENTAGE INCREASE OF THE EXTERNAL LOAD IN THE BUCKLED STATE

of the load sustained during buckling above that load under which the unprestressed truss is about to buckle—that is, the load which is considered to be critical in conventional design. If the axial compressive unit stress in member 1–3, which corresponds to that critical load, is termed the critical stress, the abscissa in Fig. 3 is the ratio σ of the variable maximum bending stress in bar 1–3 during buckling to the "critical stress." The selection of σ as the independent variable eliminates the influence of the diameter of bar 1–3 on the results. The history of the truss is traced for various prestressing conditions. These are identified by the parameter q^*, which represents the ratio of the initial compressive force in the nondiagonal members to the critical load.

---

[3] "The Stability of Statically Indeterminate, Rigid-Jointed Trusses," by E. F. Masur, thesis presented in 1951 to Illinois Inst. of Technology, at Chicago, Ill., in partial fulfilment of the requirements for the degree of Doctor of Philosophy in Mechanics.

It is apparent from Fig. 3 that with increasing σ (as buckling proceeds) the loads supported by the structure approach a limiting value, or ultimate load, which for the example shown exceeds the critical load by 88%. This ultimate load is independent of the initial stresses; in fact, it is reached even for the case of over-prestressing ($q^* > 0.793$) and for the kind of prestressing which reduces the value of the critical load ($q^* < 0$). For the case of q^* equal to 0.793, which represents the optimum initial stress system, the load remains constant; for all other cases it increases monotonically.

The results obtained for this example can be shown to hold in the general case. An inspection of Eqs. 12 and 21 shows that as ω increases (and provided that λ_r remains finite) the structure approaches a state of stress which is independent of the prestressing parameters, λ^*_r, and which is governed by the equations,

$$f = 0 \quad \text{(25a)}$$

and

$$\frac{\partial f}{\partial \lambda_r} = 0, \; (r = 1, 2, \cdots, m) \quad \text{(25b)}$$

The factors λ_r usually remain finite. It is possible, however, to construct trusses which exhibit no ultimate loads. Such trusses can be identified by the fact that the conditions of Theorem II (to be given subsequently) cannot be satisfied.

It has been shown[9] that Eqs. 25 are the equations to be used in determining a system of initial stresses that corresponds to a stationary value of the buckling load. It follows from Theorem I (to be introduced subsequently) that the ultimate load as determined from Eqs. 25 equals the largest of all buckling loads obtainable through prestressing.

If the initial stresses satisfy Eqs. 25 for $\omega = 0$ (to make the buckling load a maximum), Eqs. 12 and 21 are identically satisfied by λ_r being identically equal to λ^*_r—that is, constant for all values of ω. Thus, for this system of prestresses a truss buckles similarly to a statically determinate truss with constant internal and external forces, as exemplified by the case of q^* equal to 0.793 in Fig. 3. For all other prestressing systems, the state of stress in a truss approaches that governed by Eqs. 25, whereas the value of the external loads is a monotonically increasing[9] function of ω.

---

[9] "Lower and Upper Bounds to the Ultimate Loads of Buckled Redundant Trusses," by E. F. Masur, *Quarterly of Applied Mathematics*, No. 4, January, 1954, pp. 385–392.

UPPER AND LOWER BOUNDS TO THE ULTIMATE LOAD

The example shown in Fig. 2 was selected for its relative numerical simplicity. For more intricate trusses, the calculation of the ultimate load presents formidable computational difficulties. These obstacles can be overcome by the use of two theorems which establish readily calculable lower and upper bounds to the ultimate load. Through the use of these theorems, the designer can easily determine two load values of which one is known to be smaller, the other larger, than the exact value of the ultimate load. Furthermore, the designer can approach the ultimate load "from below" as closely as he deems desirable, although a similar approach "from above" is not feasible.

For the sake of clarity it is restated that, in all cases in which there is more than one applied load, the ratio between the loads is assumed to be held constant; in such cases the term "load" refers to the load parameter λ_0. In addition, a load $\lambda_o > 0$ is termed critical if there exists a set of parameters λ_r $(r = 1,2,\cdots, m)$ such that the truss is in neutral equilibrium with its internal forces identified by $(\lambda_0, \lambda_1, \lambda_2,\cdots, \lambda_m)$.

Theorem I.—The ultimate load of a redundant truss is its largest critical load. From this theorem a corollary can be deduced. If an arbitrary set of internal forces S_{ij} be in equilibrium with external loads identified by $\lambda_0 = \lambda'_0 > 0$, and if the truss be in stable equilibrium with its internal forces so defined,

$$\lambda^U{}_0 > \lambda'_0 \qquad (26)$$

in which $\lambda^U{}_0$ identifies the ultimate load.

The usefulness of this corollary in establishing lower bounds to the ultimate load is apparent since the question of the stability of a truss for an assumed internal force system can readily be settled by a number of criteria. Among these criteria, a common one is based on the convergence or divergence of a modified moment-distribution process and was established by E. E. Lundquist,[10] M. ASCE, and proved by N. J. Hoff.[11] For the truss shown in Fig. 2, various arbitrary forces in bar 1–2 were assumed. Notice was then taken of the convergence or divergence of the moment-distribution procedure for different values of the applied load. The largest safe external force (found in a few trials) was

$$\lambda'_0 = \frac{30\,E\,I}{L^2} \qquad (27)$$

It is apparent that the ultimate carrying capacity of the truss in question is at least equal to this value. The correct value of the ultimate load is

$$\lambda^U{}_0 = \frac{33.7\,E\,I}{L^2} \qquad (28)$$

which exceeds the critical load of $\frac{17.90\,E\,I}{L^2}$ in the unprestressed truss by 88%.

---

[10] "Stability of Structural Members under Axial Load," by E. E. Lundquist, *Techincal Note No. 617*, National Advisory Committee for Aeronautics, Washington, D. C., 1937.

[11] "Stable and Unstable Equilibrium of Plane Frameworks," by N. J. Hoff, *Journal of the Aeronautical Sciences*, March, 1941, p. 115.

Having thus obtained a set of lower bounds (to an arbitrary degree of accuracy) to the ultimate load, the designer can establish an upper bound by using a second theorem. This theorem is based on the kinematic consideration that a truss of m degrees of redundancy can be converted into a rigid-link mechanism of one degree of freedom by the removal of s members ($s \leq m + 1$) and by considering the remaining members to be pin-connected. If it is possible to select these S-members in such a way that the resulting mechanism has joint velocity vectors corresponding to a shortening of all the members to be removed, a second theorem can be established.

Theorem II.—If the s members be assigned compressive forces equal to $S_k = - 4 \pi^2 E_k I_k L^{-2}_k$ ($k = 1,2,\cdots, s$), and if the remaining bar forces be so selected as to be in equilibrium with the forces S_k and the external loads identified by $\lambda_0 = \lambda''_0 > 0$,

$$\lambda^U_0 \leq \lambda''_0 \qquad (29)$$

Although it is possible to establish an upper bound to the ultimate load, it should be recognized that for a well-designed truss the value so obtained is usually not close enough to the value of the ultimate load to be of much practical use because λ''_0 is computed on the basis of a collapse mode which involves no joint rotations and is therefore physically unrealistic. The usefulness of Theorem II is further restricted by the fact that the degree of approximation to the ultimate load from above is limited by the usually small number of bar selections which satisfy the stringent conditions of the theorem.

Theorem II is thus in marked contrast to the two theorems proposed by H. J. Greenberg and W. Prager,[2] M. ASCE, which established lower and upper bounds to the collapse loads of beams and bents by introducing plastic yield hinges. Fortunately, however, it is the lower bound that is of primary interest to the designer for reasons of safety. Furthermore, although the gap between the lower and upper bounds cannot be narrowed arbitrarily, the degree of accuracy obtained by following the procedure outlined in Theorem I can readily be estimated.

If the conditions of Theorem II are applied to the truss shown in Fig. 2, it is clear that an upper limit of the ultimate load can be determined by assuming a compressive force of magnitude $4 \pi^2 E_k I_k L^{-2}_k$ in bar 1–3 and in one of the nondiagonal members. This leads to

$$\lambda''_0 = 75.4 \frac{E I}{L^2} \qquad (30)$$

This value of λ''_0 is much larger than the ultimate load, as was to be expected from the foregoing discussion.

Conclusions

It has been shown that current (1953) design methods, as applied to the stability of statically indeterminate trusses, leave untapped a reservoir of strength which, if utilized, can lead to more rational designs with a subsequent saving of material. It is understood, however, that this investigation is merely an introduction into a field in which little work has been done.

Before any practical benefit can be derived from this type of analysis, a number of points must be studied and clarified. Aside from the lack of experimental data, the validity of the idealizations require verification. Conversely, the effect of initial curvatures, eccentric connections, and other modifying factors on the magnitude of the ultimate load requires intensive investigation.

The assumption of elastic buckling is valid only for slender truss members. For heavier trusses, the buckling curves shown in Fig. 3 should be drastically modified for plastic yielding as buckling proceeds beyond values that depend primarily on the slenderness ratios of the bars. However, it is for such structures that prestressing may prove to be most useful.

APPENDIX

If the kth member of a truss is subjected to a force system such as is shown in Fig. 4, the deflection y_k at any point x along the bar is governed by the differential equation,

$$\frac{d^2}{dx^2}\left(E_k I_k \frac{d^2 y_k}{dx^2}\right) - S_k \frac{d^2 y_k}{dx^2} = 0 \quad \text{.................} \quad (31)$$

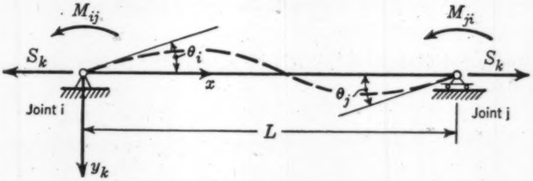

FIG. 4.—DIAGRAM OF A TYPICAL BAR

whereas the geometric boundary conditions are given by

$$y_k|_{x=0} = y_k|_{x=L} = 0 \quad \text{....................} \quad (32a)$$

$$\left.\frac{dy_k}{dx}\right|_{x=0} = -\theta_i \quad \text{.......................} \quad (32b)$$

and

$$\left.\frac{dy_k}{dx}\right|_{x=L} = -\theta_j \quad \text{.......................} \quad (32c)$$

The end moments can be expressed either by Eq. 3 or by

$$M_{ij} = E_k I_k \left.\frac{d^2 y_k}{dx^2}\right|_{x=0} \quad \text{.......................} \quad (33a)$$

and

$$M_{ji} = -E_k I_k \left.\frac{d^2 y_k}{dx^2}\right|_{x=L} \quad \text{..................} \quad (33b)$$

If there are two systems of bar forces S_{kp} and S_{kq}, to which there correspond two systems of deflection modes $y^p{}_k$ and $y^q{}_k$, then the term U_{pq} is defined by:

$$U_{pq} = \sum_k \int_0^L E_k I_k \frac{d^2 y^p{}_k}{dx^2} \frac{d^2 y^q{}_k}{dx^2}\, dx \ldots\ldots\ldots\ldots (34)$$

in which the summation extends over all the members. By partial integrations, the right side of Eq. 34 takes the form:

$$\sum_k E_k I_k \frac{d^2 y^p{}_k}{dx^2} \frac{dy^q{}_k}{dx} \bigg|_0^L - \sum_k \int_0^L \frac{d}{dx}\left(E_k I_k \frac{d^2 y^p{}_k}{dx^2}\right) \frac{dy^q{}_k}{dx}\, dx \ldots\ldots (35)$$

By considering the boundary conditions (Eqs. 32*b*, 32*c*, 33) and Eqs. 3, and through a rearrangement of the summation, the first sum in Eq. 35 can be represented by

$$\sum_i \left(\sum_j M^p{}_{ij}\right) \theta^q{}_i = \sum_i \sum_j a^p{}_{ij}\, \theta^q{}_i\, \theta^p{}_j \ldots\ldots\ldots\ldots (36)$$

in which the superscripts refer to the modes with which each term is associated. The second sum (after a partial integration and in consideration of Eq. 32*a*) is transformed into

$$\sum_k \int_0^L \frac{d^2}{dx^2}\left(E_k I_k \frac{d^2 y^p{}_k}{dx^2}\right) y^q{}_k\, dx \ldots\ldots\ldots\ldots (37)$$

If Eq. 37 (after substitution of Eq. 31) be integrated partly once more, Eq. 34 takes the form:

$$U_{pq} = \sum_i \sum_j a^p{}_{ij}\, \theta^q{}_i\, \theta^p{}_j - \sum_k S_{kp} \int_0^L \frac{dy^p{}_k}{dx} \frac{dy^q{}_k}{dx}\, dx \ldots\ldots\ldots (38)$$

Since $U_{pq} = U_{qp}$ by definition, and considering that $a_{ij} = a_{ji}$, the relationship,

$$\sum_k (S_{kp} - S_{kq}) \int_0^L \frac{dy^p{}_k}{dx} \frac{dy^q{}_k}{dx}\, dx = \sum_i \sum_j (a^p{}_{ij} - a^q{}_{ij})\, \theta^p{}_i\, \theta^q{}_j \ldots\ldots (39)$$

is obtained.

It is of interest to note that, if the force systems and deflection modes considered in Eq. 39 represent actual buckling modes, the right side of the equation vanishes. If, in addition, the two force systems correspond to the same redundant parameters, λ_r ($r = 1, 2, \cdots, m$)—only the load parameters, λ_0, being different—Eq. 39 reduces to the general orthogonality relationship:

$$\sum_k S^0{}_k \int_0^L \frac{dy^p{}_k}{dx} \frac{dy^q{}_k}{dx}\, dx = 0 \ldots\ldots\ldots\ldots (40)$$

if p does not equal q.

Eq. 39 can also be utilized to develop Eqs. 19. In fact, since the force systems considered are entirely arbitrary, it is permissible to select them in such a way that

$$S_{kp} - S_{kq} = (\lambda^p{}_r - \lambda^q{}_r)\, S^r{}_k \ldots\ldots\ldots\ldots (41)$$

in which r is an arbitrary, nonnegative integer not exceeding m. That is, the two force systems are chosen in accordance with Eq. 9, subject to the condition that all parameters except one (λ_r) be the same for both. In this case Eq. 39 (on consideration of Eq. 41) takes the form:

$$\sum_k S^r{}_k \int_0^L \frac{dy^p{}_k}{dx}\frac{dy^q{}_k}{dx}\,dx = \sum_i \sum_j \frac{a^p{}_{ij} - a^q{}_{ij}}{\lambda^p{}_r - \lambda^q{}_r}\,\theta^p{}_i\,\theta^q{}_j \ldots\ldots\ldots (42)$$

If the two force systems and deflection modes are permitted to approach one another, and as the limit of $(\lambda^p{}_r - \lambda^q{}_r)$ approaches zero, Eq. 42 is transformed into the relationship:

$$\frac{1}{2}\sum_k S^r{}_k \int_0^L \left(\frac{dy_k}{dx}\right)^2 dx = \frac{1}{2}\sum_i \sum_j \frac{\partial a_{ij}}{\partial \lambda_r}\,\theta_i\,\theta_j,\ (r = 0,1,2,\cdots,m)\ldots (43)$$

Eq. 43 can also be derived in a direct manner.[8]

It is apparent that the left side of Eq. 43 coincides with that of Eq. 19 since

$$\delta = \frac{1}{2}\int_0^L \left(\frac{dy}{dx}\right)^2 dx \ldots\ldots\ldots\ldots\ldots\ldots (44)$$

is the customary first approximation to the difference between the chord length and the arc length of a bent bar.

For the right side of Eq. 43, if the angles θ_i satisfy (nontrivially) the set of equations,

$$\sum_{j=1}^{n} a_{ij}\,\theta_j = \mu\,\theta_i\ (i = 1,2,\cdots,n)\ldots\ldots\ldots\ldots\ldots (45a)$$

then

$$\sum_{i=1}^{n}\sum_{j=1}^{n} a_{ij}\,\theta_i\,\theta_j = \mu \sum_{i=1}^{n} \theta^2{}_i \ldots\ldots\ldots\ldots\ldots\ldots (45b)$$

It is also assumed that all the terms appearing in Eqs. 45a are differentiable functions of the parameter λ.

If both sides of Eq. 45b are differentiated with respect to λ, and in consideration of Eqs. 45a and of $a_{ij} = a_{ji}$, the equation,

$$\sum_i \sum_j a'{}_{ij}\,\theta_i\,\theta_j = \mu' \sum_i \theta^2{}_i \ldots\ldots\ldots\ldots\ldots\ldots (46)$$

is obtained in which, for simplicity, primes have been used to denote derivatives with respect to λ. However, a necessary and sufficient condition for the nontriviality of the solution of Eq. 45a is given by

$$g(\lambda) = f[\mu(\lambda),\lambda] = |b_{ij}| \equiv |a_{ij} - \mu\,\delta_{ij}| = 0 \ldots\ldots\ldots (47)$$

Therefore, it follows that

$$g' = \frac{\partial f}{\partial \mu}\mu' + \frac{\partial f}{\partial \lambda} = -\mu' \sum_i B_{ii} + \frac{\partial f}{\partial \lambda} = 0 \ldots\ldots\ldots (48a)$$

or

$$\mu' = \frac{\dfrac{\partial f}{\partial \lambda}}{\sum_i B_{ii}} \qquad (48b)$$

in which B_{ii} is the cofactor of b_{ii} in Eq. 47.

If the angles θ_i correspond to a buckling mode (that is, to the case of $\mu = 0$) the determinant appearing in Eq. 47 is the same as that in the instability equation (Eq. 12) and $B_{ii} = A_{ii}$. Thus, by substituting Eqs. 44 and 46 into Eq. 43, and in consideration of Eq. 48*b*, the relationship,

$$\sum_k S^r{}_k \, \delta_k = \omega \frac{\partial f}{\partial \lambda_r}, \; (r = 0,1,2,\cdots, m) \qquad (19)$$

in which

$$\omega = \frac{1}{2} \frac{\sum_i \theta^2{}_i}{\sum_i A_{ii}} \qquad (20)$$

is determined.

Acknowledgment

The writer is greatly indebted to L. H. Donnell, research professor of mechanics, Illinois Institute of Technology, in Chicago, for his assistance in conducting the work on which this paper is based.

AMERICAN SOCIETY OF CIVIL ENGINEERS
Founded November 5, 1852
TRANSACTIONS

Paper No. 2693

THE ENGINEER'S ROLE IN METROPOLITAN TRAFFIC PLANNING

BY LLOYD BRAFF[1]

WITH DISCUSSION BY MR. JAMES L. FOLEY, JR.

SYNOPSIS

Departmental cooperation within the city government makes possible effective long-range traffic planning. The engineer is involved in this work in several specialized capacities. The organization and application of highway capacity studies and origin-destination surveys, the prediction of trends in the density of traffic, and the coordination of public utility planning under the over-all plan are all functions of the engineer. The problems found in this work are many and varied, and their solution is vital to community growth.

INTRODUCTION

Everyone who drives in almost any urban area is aware of traffic congestion, delay, accident hazards, inadequate streets, and lack of parking spaces. He recognizes that the increasing number of automobiles has expanded the area of cities and created demands for better streets and highways. In rapidly growing areas, motorists have seen many small rural roads suddenly exposed to traffic as a cotton field is converted into a subdivision full of homes.

In most urban areas, the engineer is assigned the prodigious task of solving the traffic problems. Throughout the evolution and revolution created by the automobile, the engineer has studied causes and effects. During this process he has created engineering specializations such as traffic engineering and traffic planning.

The attack on the traffic dilemma is divided into those activities that can be accomplished immediately, and those classified as long-range plans. The immediate activities are the less expensive methods of increasing the capacity of existing streets in the interim period before a long-range plan can be completed. This phase might be classified in three broad categories: Operations, planning, and construction. In smaller cities, all three usually are the re-

---

NOTE.—Published, essentially as printed here, in May, 1953, as *Proceedings-Separate No. 191*. Positions and titles given are those in effect when the paper or discussion was received for publication.

[1] City Traffic Engr., Dallas, Tex.

sponsibility of one engineer, but as the city grows, these become separated into departments for traffic, planning, and public works, and each is headed by a separate engineer.

The purpose of this paper is to describe the role of the engineer in attacking both the immediate and long-range traffic programs. Inasmuch as most cities are using similar methods to cope with the immediate problem, this phase will be minimized. Emphasis will be placed on those techniques developed by engineers which are applicable to the development of a long-range traffic plan.

IMMEDIATE PROGRAM

Operations.—Traffic engineers use many devices to obtain maximum efficiency and safety from the existing street system. Through national standardization of signs, signals, and markings, motorists may travel throughout the United States and expect to have uniform markings and warnings. By this means, the stranger may be guided with safety over any street system.

As traffic volumes increase on city streets, the traffic engineer may prohibit parking during rush hours (and at all times on narrow streets); he may protect major streets by erecting stop signs at minor streets; and he may signalize intersections of major streets. Also, he may create one-way streets, eliminate "jogs" along major streets, and channelize dangerous intersections.

In areas of heavy parking demand, the traffic engineer may establish parking time limits to cause a "turnover" of curb space, and he may lessen congestion by establishing orderly bus zones and truck spaces. At some intersections where traffic volumes exceed the capacity of the streets, he may eliminate the congestion by completely redesigning the roadways, or by adding storage lanes so that the capacity of the new intersection equals that of the streets leading to it. These are only a few of many devices by which the engineer may increase the efficiency of the existing street system.

Planning.—The planning engineer also has at his disposal methods by which he may assist in the immediate problem of getting the most out of existing facilities. Through zoning, the planning engineer can require off-street parking areas in connection with the construction of new buildings. Through this device, each vehicle taken off the street provides more area of street surface for moving traffic. Zoning control, such as the elimination of strip zoning, does much to relieve traffic arteries of the marginal conflict created by uncontrolled development. In subdivision regulations, the planning engineer may reserve rights of way adequate for major thoroughfares and secondary thoroughfares and for providing drainage easements. Through proper subdivision regulations, both the immediate problems and the long-range problems may be handled simultaneously.

Construction.—The public works engineer also is in a strategic position to gain maximum efficiency from the existing street system. By concentrating street improvements on the major thoroughfare system, maximum traffic volumes can be accommodated with minimum expenditures. He designs streets of adequate size to accommodate present traffic volumes and is guided by future traffic estimates to make provisions in his design so that the street may be altered for anticipated volumes. Every city has several intersections at which traffic volumes exceed the capacity of the existing pavement. Through relatively inexpensive construction, the roadways can be redesigned by adding lanes so that the resulting capacity of the intersection will equal the capacity of the roadways leading to it.

The functioning of the major thoroughfare plan depends on the street standards established by the public works engineer and the programming of street repaving and resurfacing at locations where traffic demands are greatest.

LONG-RANGE PLAN

Officials responsible for traffic have long recognized the need for techniques to determine the traffic requirements for metropolitan areas which will meet present needs and be adaptable to future traffic movements. They accept the fact that a comprehensive major thoroughfare plan is a necessity. However, because of the rapid increases in vehicle registration and vehicular use during the decade ending in 1952, traffic volumes have reached such proportions that it has been necessary to study the traffic capacities of streets and to determine all elements which affect capacity. Such a study[2] has been made and reported by O. K. Normann of the United States Bureau of Public Roads (USBPR). Through this research, engineers now have a tool to guide them in traffic planning.

Another tool recognized as a vital necessity is the comprehensive origin-destination survey also developed by the USBPR. In this type of survey, the origin and destination of all trips made within a metropolitan area are determined through a proved sampling procedure.

Traffic engineers and planning engineers who have access to the origin-destination survey can make a sound approach to the study of the traffic requirements of a city for both present and future conditions. Armed with these basic data, they can test the adequacy of the existing street system and the major thoroughfare plan, and revise the plan, if necessary. By proper procedures, they can make a logical approach to the establishment of priorities in their capital improvement programs.

Revision of the Dallas, Tex., Major-Thoroughfare Plan.—To illustrate the role of the engineer in planning for traffic, the City of Dallas is an example of one way in which a city is endeavoring to solve its traffic dilemma. During the past few years, the growth of Dallas has been phenomenal. Its population increased from 294,734, in 1940, to 432,927, in 1950. The city's population on January 1, 1953, was estimated to be 535,000. Similarly, Dallas County, in Texas, increased from 398,564 persons, in 1940, to 612,318, in 1950. Dallas County is the most densely populated county in Texas and exceeds by more than 50% the second most densely populated county, in persons per square mile. The area of the City of Dallas in 1945 was 45 sq miles, and at the end of 1952 was 172 sq miles. It is probable that the area will exceed 200 sq miles by 1954.

This rapid growth has far surpassed any predictions made as late as 1947. Population in 1952 exceeded that predicted for 1970. Similarly, vehicle registration has outgrown the most optimistic predictions. More than 250,000 vehicles were registered in Dallas County in 1952. In 1950, there were 2.95 persons per passenger vehicle in Dallas County. The use of the automobile in Dallas equals that of any part of the United States.

---

[2] "Principles of Highway Capacity Research," by O. K. Normann, *Transactions*, ASCE, Vol. 117, 1952, p. 913.

During this period of rapid expansion, the construction of major thoroughfares lagged. Dallas has extended beyond the area encompassed by its original major thoroughfare plan. Because of all these factors, it was found necessary to restudy the original major thoroughfare plan and to establish a realistic priority program for capital improvements. During 1952, the city began a comprehensive analysis of both present and future street needs so that it could revise its major thoroughfare plan.

Before starting such an undertaking, the city recognized the need for the best available basic data. At the request of the city in 1950, the Texas Highway Department, the USBPR, and the County of Dallas joined to conduct an origin-destination survey. This survey covered a metropolitan area of 230 sq miles. In addition, origin-destination information was obtained at all roads leading to six cities beyond the metropolitan area.

In selecting the sample for the origin-destination survey, a complete land-use map was prepared for the entire metropolitan area. For this purpose, the location of every dwelling was noted. This detail was considered vital in order to make the origin-destination survey adaptable to future expansion. After the survey, the City Planning Department completed the land-use map for the remainder of Dallas County.

The results of the survey were first made available for application in March, 1952. The first use of the survey data was to analyze three proposed routes for an east-west expressway. The survey made it possible to select the route that would best serve the city.

Traffic-volume counts are not helpful as a guide in planning the major thoroughfare system in Dallas. Many of the streets are narrow and, during rush hours, traffic "spills over" into adjacent parallel streets. In many instances, motorists make circuitous trips to avoid congested areas. For the purpose of conducting a thorough study, therefore, traffic volume data were not used. Origin-destination survey data were used exclusively. The major thoroughfare system was superimposed on a map of zones used for the origin-destination survey. Each major thoroughfare was coded. Traffic between all zones was allocated to major thoroughfares on the most logical route between the zones, on the assumption that all major thoroughfares were equally good. By this process, the 1950 traffic volumes were assigned to the entire network of thoroughfares, and the average daily allocated traffic was known for every section of that street. These data included both trucks and passenger vehicles. It is reiterated that this flow map is 1950 "allocated" traffic flow as distinguished from 1950 actual traffic flow.

Another of the studies being conducted concerns the available right of way and pavement width over the entire major-thoroughfare network. From these data, the theoretical capacity of every section of every major street will be computed. By comparing these capacities to the 1950 traffic allocated to the same network, the deficiencies in the existing network will be known. The next study will be the computation of traffic capacities based on the maximum pavement that could be constructed on the existing rights of way.

Both of these procedures will guide engineers in selecting priorities and geometric standards for improvements in the thoroughfare network. Neither of these steps, however, provides for probable future needs.

For future traffic requirements, predictions will be made of population increases for a twenty-year period. The increment of population increase during this period will be distributed to the zones used for the origin-destination survey. By utilizing the land-use maps, by zoning, and through knowledge of the limitations of future population distribution imposed by the Dallas drainage area, future population distribution can be predicted with reasonable accuracy. The 1950 origin-destination data will be expanded, by zones, on the basis of a composite of these factors: (1) The ratio of future population to 1950 population; (2) the trend of number of persons per vehicle; and (3) the trend of gasoline consumption in gallons per vehicle per year. The added trips by a larger population, the fact that more persons will operate automobiles, and the fact that vehicles will be driven more miles each year will all be taken into consideration. It is assumed that the type of trips will remain the same. In approximately ten areas where it is known that new industrial or retail areas will be established, a new origin-destination distribution will be made of those areas based on patterns established in similar areas in the 1950 survey. From these expanded origin-destination data, a new set of desire lines will be made for the purpose of determining the possibility of a shift in the directions and relative size of the major desire lines. This information will be used to determine where a network of expressways should be planned to serve future traffic movements.

When a network of expressways has been located, it will be superimposed over the major thoroughfare system on the map of zones. The expanded origin-destination data then will be allocated to the combined network of expressways and major thoroughfares. When this is completed, a comparison of the ultimate traffic demands and the 1950 demands will serve as a guide to discovering those places where additional rights of way are required, and the size of streets needed to accommodate future volumes.

It would be unwise to plan a comprehensive street system costing millions of dollars unless a comparison were made of present needs and of estimated future needs, because a network of expressways will change the travel pattern in many locations by a rotation of 90°. For example, traffic north of a city under an existing street system may be concentrated on north-south major streets. If a north-south expressway were built to supplement the street system, a majority of motorists would use the expressway and then confine their surface travel from the expressway to their homes on an east-west street. Unless an analysis of the future network of expressways and major streets were made, therefore, expenditures would have been made on the north-south streets (in this example); but in the outlying area the east-west streets would carry the majority of traffic and otherwise might have been neglected. This fact is frequently overlooked.

In Dallas, the city manager has established a Capital Improvements Review Board consisting of the finance officer, the director of public works, the superintendent of water and sanitary sewers, the city planning engineer, and the traffic engineer. It is the function of this board to coordinate all capital improvements in the city. Through this committee, no street improvement will be undertaken until any water, sewer, or other utility work is completed first. Priorities of all agencies must fit into the program. When a program is developed, it is presented to the city council as a guide for action. The technique of traffic planning described in this paper, even though incomplete, has guided the city council in one bond program for street improvements.

This technique will make it possible to estimate all the street deficiencies, estimate the cost of improvements, and prepare a construction program. It is anticipated that, once a community is cognizant of the deficiencies in its street system and the cost to modernize it, it will request that a comprehensive study of financing methods be made to accelerate the realization of the street program.

These have been the highlights of the numerous problems involved in planning for traffic in Dallas. Such planning in Dallas (or in any other metropolitan area) responds to engineering analysis and requires the coordination and cooperation of traffic engineers, planning engineers, and public works engineers, all of whom must concentrate on a common objective. In Dallas, that coordination and cooperation are to be found, and it is hoped that the plan will be adopted and put into practice.

DISCUSSION

James L. Foley, Jr.,[3] A. M. ASCE.—A lucid description of the role of the engineer in solving one of the most vexing of city planning problems has been presented by Mr. Braff.

Implied, but not emphasized, by the author are two important functions which are (or should be) the traffic engineer's responsibility. Public parking facilities and mass-transit service are such integral parts of the street transportation system that the engineer should exercise a considerable influence on their design and operation. This influence may be exercised directly if the engineer has full responsibility within his organization, or indirectly, through interdepartmental coordination.

The rapid growth in motor-vehicle registration during the period following World War II indicates the necessity of obtaining the greatest traffic efficiency possible within the existing rights of way. To achieve this end, it appears that rush-hour parking eventually will have to be prohibited on most major thoroughfares.

As stated by the author (under the heading, "Immediate Program: Operations") regulation of curb parking is one of the devices available to the engineer for improving the efficiency of a street system. In spite of the obvious advantages of the elimination of curb parking, the engineer often must "sell" good engineering practices to the laymen in a municipal government. In addition to the regulation of curb parking, the traffic engineer should approve the functional design of off-street parking facilities. It is imperative that the engineer review and approve the plans for all off-street facilities because operational defects (such as lack of adequate reservoir space or poor entrance design) can reduce the efficiency of a street as greatly as does curb parking.

It is obviously impossible for most cities to provide all the parking space likely to be required in the future. To meet this need for space, close cooperation is required between the various engineers charged with the responsibility of determining and planning for future traffic. If based on sound criteria, zoning regulations give some assurance that in the new growth and redevelopment areas of cities the streets will be available for the movement of traffic. Additional studies are necessary to provide data for determining sound criteria. J. T. Thompson, M. ASCE, and J. T. Stegmaier, J. M. ASCE, have suggested a method of obtaining these criteria from origin-destination studies.[4]

Before the Chicago (Ill.) zoning ordinance was revised to require adequate off-street parking facilities, studies were made of the parking needs of various land uses. The results of these studies were incorporated in the proposed revision to the zoning ordinance.[5] This ordinance is a good example of interdepartmental coordination in that the studies and recommendations were the result of the joint efforts of the Bureau of Street Traffic of the Chicago Plan Commission and other interested departments.

---

[3] Traffic Engr., J. E. Greiner Co., Cons. Engrs., Baltimore, Md.

[4] "The Effect of Building Space Usage on Traffic Generation and Parking Demand," by J. T. Thompson and J. T. Stegmaier, *Proceedings*, Highway Research Board, National Research Council, Washington, D. C., Vol. 28, 1948, p. 320.

[5] "Proposal for Amendment of Chicago Zoning Ordinance in Reference to Off-Street Parking Facilities," *Committee Pamphlet No. 15*, City Clerk, Chicago, Ill., July, 1953.

Transit.—Adequate off-street parking, improved traffic-control devices, grade separations at major intersections, and similar remedial measures do much to improve the flow of traffic. It appears, however, that mass-transit service must be provided (at least in the larger cities) if such cities are to continue to exist as at present (1953). A city's reliance on mass transit is a direct function of the city's size. Some major cities have struggled along without transit service for short periods of time. Detroit (Mich.) is one of the largest cities to have done so. However, certain cities (such as New York, N. Y., Chicago, and Boston, Mass.) would be practically paralyzed by the lack of mass-transit facilities. It is physically impossible to park the number of passenger cars that would be required to transport the people normally present in the central business districts of these cities.

It behooves the traffic engineer, in planning adequate highways, to do all that possibly can be done to encourage general use of mass transit and to assist the transit company in its efforts to provide convenient, expeditious service. The traffic engineer should promote the type of long-range planning which makes adequate provision for mass-transit service.

AMERICAN SOCIETY OF CIVIL ENGINEERS
Founded November 5, 1852
TRANSACTIONS

Paper No. 2694

DEFLECTION OF LAMINATED BEAMS

BY L. G. CLARK[1]

SYNOPSIS

A theory is developed to determine the deflection of a beam composed of two or more laminations and riveted or fixed at certain points along the beam. The laminations can be of different sizes and materials but must be long in comparison with the cross-sectional dimensions of the beam. Although the problem investigated is based on only two laminations, the same approach can be used to provide for any number of laminations. The final result is in a form such that particular problems can be solved in a manner similar to the area-moment method. It is shown that for two laminations joined at an infinite number of points the problem reduces to that of a simple beam. Two different cases of simply supported beams were tested and the satisfactory results are presented.

NOTATION

The letter symbols adopted for use in this paper are defined where they first appear, in the illustrations or in the text, and are arranged alphabetically for convenience of reference in the Appendix.

INTRODUCTION

It is known that a beam composed of laminations placed freely upon one another deflects more under a given load than does a solid beam of the same cross section under the same loading conditions. The difference in deflection is caused by the fact that in the solid beam all longitudinal planes can support shear, whereas a freely laminated beam cannot resist shearing load on the planes that separate the individual laminations. This inability to resist horizontal shear has led to the use of various devices such as riveting, welding, or bolting, to connect the laminations so that the laminated beam can be made to act similarly to a solid beam. The problem of building such a beam is not new to the engineer. Unfortunately, however, the general feeling seems to be that as

---

NOTE.—Published, essentially as printed here, in November, 1953, as *Proceedings-Separate No. 331*. Positions and titles given are those in effect when the paper was received for publication.

[1] Instructor, Dept. of Eng. Mechanics, Univ. of Michigan, Ann Arbor, Mich.

long as the method of joining the laminations will resist the longitudinal shear, as predicted by ideal beam theory, the problem is solved. That is, a built-up beam seems to be a result of guesswork in the matter of deflections.

TWO LAMINATIONS JOINED AT ARBITRARY POINTS

The analysis to be developed is easily extended to the case of a beam composed of more than two laminations. However, such an extension involves extensive algebraic computations which will do little to aid in the understanding of the problem. The analysis will determine the slope and deflection relationships between two points of the beam. These points will be chosen where the laminations are joined, and there will be no joining of the laminations between the chosen joints.

The following assumptions are made concerning the two laminations shown in Fig. 1(*a*):

1. The deflections are small.
2. Any separation of the laminations is small in comparison with the distances a_1 and a_2. The symbol a_1 denotes the distance from the neutral axis of the upper lamination to the contact plane between the laminations. The distance from the neutral axis of the lower lamination to the contact plane between the laminations is represented by a_2. The subscripts "1" and "2" will be used in this manner; the subscript "1" will refer to the upper of two laminations and the subscript "2" will refer to the lower lamination. It is important to note that separation is not neglected but merely assumed to be small.

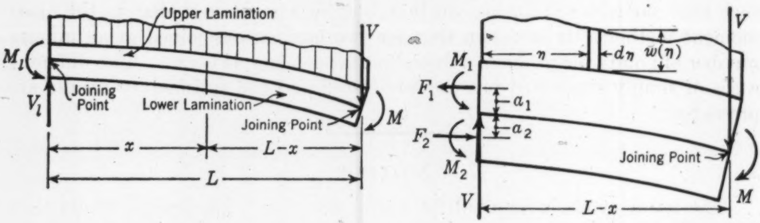

(*a*) BEAM (*b*) FREE-BODY DIAGRAM

FIG. 1.—DOUBLY LAMINATED BEAM

3. The total elongation of the contact plane is the same for both laminations. This does not imply that the strain is the same at corresponding points of the laminations, but only that the integrated effect is the same.
4. There is no friction between the contact surfaces. This, of course, is not true in a real problem, but the assumption is made because the friction cannot be analytically determined. More important is the fact that any forces caused by friction will serve to improve rather than harm the characteristics of the beam.

It can be seen from a consideration of the equilibrium of the free-body shown in Fig. 1(*b*) (the right half of the beam shown in Fig. 1(*a*)) that

$$F_1 = F_2 = F \qquad (1)$$

and the forces are constant over the length L. Letting

$$\bar{a} = a_1 + a_2 \qquad (2)$$

and taking moments with respect to the left end of the free-body,

$$M_1 + M_2 = V\,(L - x) - F\,\bar{a} + M + \int_0^{L-x} w\,(\eta)\,\eta\,d\eta \qquad (3)$$

in which the integral is the bending moment caused by the distributed load. The integral is a function of x and will be designated by

$$\int_0^{L-x} w\,(\eta)\,\eta\,d\eta = f(x) \qquad (4)$$

The following representations will also be used:

$$\int f(x)\,dx = g(x) \qquad (5a)$$

and

$$\int g(x)\,dx = h(x) \qquad (5b)$$

From Eqs. 4 and 5 it will be noted that

$$f(L) = g(L) = h(L) = 0 \qquad (6)$$

Eq. 3 can be expressed as

$$M_1 + M_2 = V\,(L - x) - F\,\bar{a} + M + f(x) \qquad (7)$$

Elongation of the Contact Plane.—From ordinary beam theory, the strain, γ, of a longitudinal fiber at the contact plane of the upper lamination is

$$\gamma_1 = -\frac{M_1\,a_1}{E_1\,I_1} + \frac{F}{A_1\,E_1} \qquad (8a)$$

and for the lower lamination

$$\gamma_2 = \frac{M_2\,a_2}{E_2\,I_2} - \frac{F}{A_2\,E_2} \qquad (8b)$$

in which E is the modulus of elasticity, I denotes the moment of inertia of the cross section, A is the cross-sectional area, and tensile forces are considered to be positive.

For the total elongation of the two laminations at the contact plane to be equal,

$$\int_0^L \left(\frac{F}{A_1 E_1} - \frac{M_1 a_1}{I_1 E_1} \right) dx = \int_0^L \left(\frac{M_2 a_2}{E_2 I_2} - \frac{F}{A_2 E_2} \right) dx \ldots\ldots (9)$$

from which

$$L F \left(\frac{1}{A_1 E_1} + \frac{1}{A_2 E_2} \right) = \int_0^L \frac{M_2 a_2}{E_2 I_2} dx + \int_0^L \frac{M_1 a_1}{E_1 I_1} dx \ldots\ldots (10)$$

Because

$$\frac{M_1}{I_1 E_1} = \frac{d^2 y_1}{dx^2} \ldots\ldots (11a)$$

and

$$\frac{M_2}{I_2 E_2} = \frac{d^2 y_2}{dx^2} \ldots\ldots (11b)$$

then

$$a_1 \int_0^L \frac{d^2 y_1}{dx^2} dx = a_1 \left[\left(\frac{dy_1}{dx} \right)_{x=L} - \left(\frac{dy_1}{dx} \right)_{x=0} \right] \ldots\ldots (11c)$$

and

$$a_2 \int_0^L \frac{d^2 y_2}{dx^2} dx = a_2 \left[\left(\frac{dy_2}{dx} \right)_{x=L} - \left(\frac{dy_2}{dx} \right)_{x=0} \right] \ldots\ldots (11d)$$

in which y is the deflection of the beam from an unloaded position.

From Fig. 2 it can be seen that

$$\left(\frac{dy_1}{dx} \right)_{x=0} = \left(\frac{dy_2}{dx} \right)_{x=0} = \theta_0 \ldots\ldots (12a)$$

and

$$\left(\frac{dy_1}{dx} \right)_{x=L} = \left(\frac{dy_2}{dx} \right)_{x=L} = \theta_L \ldots\ldots (12b)$$

Substitution of Eqs. 12 into Eqs. 11*c* and 11*d*, and subsequent substitution of Eqs. 11*c* and 11*d* into Eq. 10, results in

$$F L \left(\frac{1}{A_1 E_1} + \frac{1}{A_2 E_2} \right) = a_1 (\theta_L - \theta_0) + a_2 (\theta_L - \theta_0) \ldots\ldots (13a)$$

from which

$$F L \left(\frac{1}{A_1 E_1} + \frac{1}{A_2 E_2} \right) = (a_1 + a_2) (\theta_L - \theta_0) = \bar{a} (\theta_L - \theta_0) \ldots\ldots (13b)$$

From Fig. 2 it can also be seen that

$$\theta_L - \theta_0 = \phi \ldots\ldots (14a)$$

With

$$b = \frac{1}{A_1 E_1} + \frac{1}{A_2 E_2} \ldots\ldots (14b)$$

Eq. 13*b* becomes

$$F\,L\,b = \bar{a}\,\phi \qquad (15)$$

Eq. 7 can be expressed as

$$E_1\,I_1\,\frac{d^2y_1}{dx^2} + E_2\,I_2\,\frac{d^2y_2}{dx^2} = (V\,L - F\,\bar{a} + M) - V\,x + f(x) \qquad (16)$$

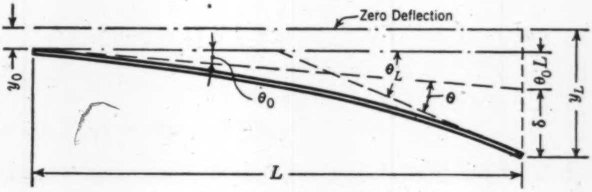

FIG. 2.—DEFLECTION DIAGRAM

Integration of Eq. 16 results in

$$E_1\,I_1\,\frac{dy_1}{dx} + E_2\,I_2\,\frac{dy_2}{dx} = (V\,L - F\,\bar{a} + M)\,x - \frac{V\,x^2}{2} + g(x) + K_a \qquad (17)$$

in which K_a is the constant of integration. At x equal to zero, Eq. 12*a* is applicable and

$$K_a = \theta_0\,(E_1\,I_1 + E_2\,I_2) - g(0) \qquad (18)$$

If

$$c = (E_1\,I_1 + E_2\,I_2) \qquad (19)$$

Eq. 17 becomes

$$E_1\,I_1\,\frac{dy_1}{dx} + E_2\,I_2\,\frac{dy_2}{dx} = (V\,L - F\,\bar{a} + M)\,x - \tfrac{1}{2}\,V\,x^2 + g(x) - g(0) + c\,\theta_0 \qquad (20)$$

Integrating Eq. 20 results in

$$E_1\,I_1\,y_1 + E_2\,I_2\,y_2 = \tfrac{1}{2}\,(V\,L - F\,\bar{a} + M)\,x^2 - \tfrac{1}{6}\,V\,x^3 + h(x) - g(0)\,x + c\,\theta_0\,x + K_b \qquad (21)$$

in which K_b is the integration constant. At x equal to zero,

$$y_1 = y_2 = y_0 \qquad (22)$$

Thus, from Eq. 21,

$$K_b = c\,y_0 - h(0) \qquad (23)$$

and Eq. 21 becomes

$$E_1\,I_1\,y_1 + E_2\,I_2\,y_2 = \tfrac{1}{2}\,(V\,L - F\,\bar{a} + M)\,x^2 - \tfrac{1}{6}\,V\,x^3 - g(0)\,x - h(0) + h(x) + c\,\theta_0\,x + c\,y_0 \qquad (24)$$

Although Eq. 24 is a deflection equation, it is of no practical use in this form.

At x equal to L, the boundary conditions are

$$\left(\frac{dy_1}{dx}\right)_{x=L} = \left(\frac{dy_2}{dx}\right)_{x=L} = \theta_L \tag{25a}$$

and

$$(y_1)_{x=L} = (y_2)_{x=L} = y_L \tag{25b}$$

Thus Eqs. 20 and 24 become

$$c\,\theta_L = (V\,L - F\,\bar{a} + M)\,L - \tfrac{1}{2}\,V\,L^2 - g(0) - c\,\theta_0 \tag{26a}$$

and

$$c\,y_L = \tfrac{1}{2}\,(V\,L - F\,\bar{a} + M)\,L^2 - \tfrac{1}{6}\,V\,L^3 - g(0)\,L - h(0) + c\,\theta_0\,L + c\,y_0 \tag{26b}$$

or

$$0 = (V\,L - F\,\bar{a} + M)\,L - \tfrac{1}{2}\,V\,L^2 - g(0) - c\,(\theta_L - \theta_0) \tag{27a}$$

$$0 = \tfrac{1}{2}\,(V\,L - F\,\bar{a} + M)\,L^2 - \tfrac{1}{6}\,V\,L^3 - g(0)\,L - h(0) - c\,(y_L - \theta_0\,L - y_0) \tag{27b}$$

and from Eq. 15,

$$F = \frac{\bar{a}}{L\,b}\,\phi \tag{28}$$

From Fig. 2 it can be seen that

$$\delta = y_L - y_0 - \theta_0\,L \tag{29}$$

Therefore, Eq. 27b reduces to

$$0 = (V\,L - F\,\bar{a} + M)\,L - \tfrac{1}{2}\,V\,L^2 - g(0) - c\,\phi \tag{30a}$$

and

$$0 = \tfrac{1}{2}\,(V\,L - F\,\bar{a} + M)\,L^2 - \tfrac{1}{6}\,V\,L^3 - g(0)\,L - h(0) - c\,\delta \tag{30b}$$

Thus, Eqs. 30 and 28 can be solved for ϕ and δ in terms of the known quantities. Using Eqs. 28 and 30a one obtains

$$\phi = \frac{b}{\bar{a}^2 + c\,b}\left[\tfrac{1}{2}\,V\,L^2 + M\,L - g(0)\right] \tag{31}$$

Eq. 31 is used to determine the angle between the tangents drawn at the ends of the section considered.

Using Eqs. 28 and 31 with Eq. 30b results in

$$\delta = \frac{V\,L^3}{c}\left[\frac{\bar{a}^2 + 4\,c\,b}{12\,(\bar{a}^2 + c\,b)}\right] + \frac{M\,L^2}{2}\left(\frac{b}{\bar{a}^2 + c\,b}\right) - \frac{g(0)}{c}\left[\frac{L\,(\bar{a}^2 + 2\,c\,b)}{2\,(\bar{a}^2 + c\,b)}\right] - \frac{h(0)}{c} \tag{32}$$

Eq. 32 is used to determine the distance between the right jointing point (Fig. 2) and the tangent at the left end. Thus, Eqs. 31 and 32 can be used to find the deflections of any doubly laminated beam. The values of δ and ϕ are then used in the same manner as in the area-moment method.

Unfortunately, the method presented herein will not give a solution for the deflection of the beam at points other than those that join the laminations. This is not a severe handicap as a close approximation can be made for the deflection at other points. The deflection y_1 is nearly equal to the deflection y_2, and by setting them equal, Eqs. 24, 31, and 32 will result in the solution for the deflection at any point.

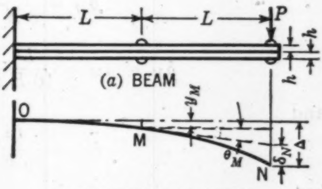

(a) BEAM

(b) DEFLECTION DIAGRAM

FIG. 3.—DOUBLY LAMINATED CANTILEVER BEAM SUBJCETED TO CONCENTRATED LOAD

Example No. 1.—To illustrate the simplicity of this procedure the problem of a cantilever beam composed of two laminations will be used. For ease of computation the laminations will be assumed to be of equal size and of the same material. These assumptions eliminate the need for subscripts to differentiate between the laminations. The beam is shown in Fig. 3. From basic considerations,

$$I = \frac{1}{12} A\, h^2 \quad \text{(33a)}$$

$$\bar{a} = h \quad \text{(33b)}$$

$$b = \frac{2}{A\, E} = \tfrac{1}{6}\,\frac{h^2}{E\, I} \quad \text{(33c)}$$

$$c = 2\, E\, I \quad \text{(33d)}$$

and

$$b\, c = \tfrac{1}{3}\, h^2 \quad \text{(33e)}$$

Because there are no distributed loads, Eqs. 4 and 5 equal zero and Eqs. 31 and 32 become

$$\phi = \frac{b}{\bar{a}^2 + b\, c}\left(\tfrac{1}{2}\, V\, L^2 + M\, L\right) \quad \text{(34a)}$$

and

$$\delta = \frac{V\, L^3}{c}\left[\frac{\bar{a}^2 + 4\, b\, c}{12\,(\bar{a}^2 + c\, b)}\right] + \frac{M\, L^2}{2\, c}\left(\frac{c\, b}{\bar{a}^2 + c\, b}\right) \quad \text{(34b)}$$

or (using Eqs. 33),

$$\phi = \frac{L}{8\, E\, I}\left(\tfrac{1}{2}\, V\, L + M\right) \quad \text{(35a)}$$

and

$$\delta = \frac{7\, V\, L^3}{96\, E\, I} + \frac{M\, L^2}{16\, E\, I} = \frac{L^2}{16\, E\, I}\left(\frac{7}{6}\, V\, L + M\right) \quad \text{(35b)}$$

From Fig. 3, it can be seen that

$$V_M = P \quad \text{(36a)}$$

$$M_M = P\, L \quad \text{(36b)}$$

$$V_N = P \quad \text{(36c)}$$

and

$$M_N = 0 \qquad (36d)$$

Thus,

$$\theta_M = \frac{L}{8\,E\,I}\left(\frac{3}{2}P\,L\right) = \frac{3\,P\,L^2}{16\,E\,I} \qquad (37a)$$

$$\delta_M = y_M = \frac{L^2}{16\,E\,I}\left(\frac{7\,P\,L}{6} + P\,L\right) = \frac{13\,P\,L^3}{96\,E\,I} \qquad (37b)$$

and

$$\delta_N = \frac{L^2}{16\,E\,I}\left(\frac{7}{6}P\,L\right) = \frac{7\,P\,L^3}{96\,E\,I} \qquad (37c)$$

but

$$\Delta = y_M + \theta_M\,L + \delta_N \qquad (38a)$$

Therefore,

$$\Delta = \frac{13\,P\,L^3}{96\,E\,I} + \frac{3\,P\,L^3}{16\,E\,I} + \frac{7\,P\,L^3}{96\,E\,I} \qquad (38b)$$

or

$$\Delta = \frac{19\,P\,L^3}{48\,E\,I} \qquad (38c)$$

The deflection of a solid beam of the same dimensions and under the same load has the value,

$$\Delta_s = \frac{P\,(2\,L)^3}{3\,E\,I_s} \qquad (39a)$$

in which the subscript "*s*" denotes the solid beam, I_s equals 8 I and is the moment of inertia of the entire cross section, and 2 L is the total length of the solid beam. Therefore,

$$\Delta_s = \frac{8\,P\,L^3}{24\,E\,I} \qquad (39b)$$

It is of interest to note that the relative deflection between the solid and laminated beams is

$$\frac{\Delta}{\Delta_s} = 1.189 \qquad (40)$$

which means that the deflection of the laminated beam is only 19% more than the deflection of the solid beam.

If the two laminations had been riveted only at the end,

$$\frac{\Delta}{\Delta_s} = 1.75 \qquad (41)$$

which indicates a substantial increase in stiffness as a result of the rivet at the center.

Example No. 2.—As an example, the case of the cantilever beam made of two laminations riveted only at the free end and supporting a uniformly distributed load will be investigated. This beam is shown in Fig. 4.

It can be seen that

$$g(0) = -\frac{w\,L^3}{6} \tag{42a}$$

and

$$h(0) = \frac{w\,L^4}{24} \tag{42b}$$

from which Eqs. 31 and 32 can be written as

$$\phi = \frac{b}{\bar{a}^2 + b\,c}\left(\tfrac{1}{2}\,V\,L^2 + M\,L + \frac{w\,L^3}{6}\right) \tag{43a}$$

and

$$\delta = \frac{V\,L^3}{c}\left[\frac{\bar{a}^2 + 4\,c\,b}{12\,(\bar{a}^2 + c\,b)}\right] + \frac{M\,L^2}{2\,c}\left(\frac{c\,b}{\bar{a}^2 + c\,b}\right) + \left[\frac{L\,(\bar{a}^2 + 2\,c\,b)}{2\,(\bar{a}^2 + c\,b)}\right]\left(\frac{w\,L^3}{6\,c}\right) - \frac{w\,L^4}{24\,c} \tag{43b}$$

Using the same notation as in Example No. 1 and realizing that

$$V = 0 \tag{44a}$$

and

$$M = 0 \tag{44b}$$

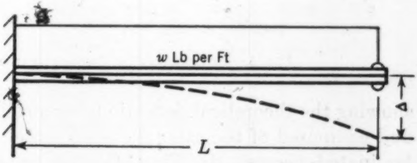

FIG. 4.—DOUBLY LAMINATED CANTILEVER BEAM SUBJECTED TO UNIFORM LOAD

at the free end of the beam, then

$$\Delta = \frac{w\,L^3}{12\,E\,I}\left(\frac{L \times \frac{5}{3}\,h^2}{2 \times \frac{4}{3}\,h^2}\right) - \frac{w\,L^4}{48\,E\,I} \tag{45a}$$

or

$$\Delta = \frac{3\,w\,L^4}{96\,E\,I} \tag{45b}$$

For a solid beam,

$$\Delta_s = \frac{w\,L^4}{64\,E\,I} \tag{46}$$

and

$$\frac{\Delta}{\Delta_s} = 2.00 \tag{47a}$$

For the case in which a rivet is used in the beam midway between the ends and at the end,

$$\frac{\Delta}{\Delta_s} = 1.25 \tag{47b}$$

EXPERIMENTAL RESULTS

As a verification of the theory, two cases of a simply supported beam with a centrally placed concentrated load were solved and compared with experimental results. The results of Case I are shown in Fig. 5(*a*). Case I had steel laminations (16 in. by 1$\frac{3}{4}$ in. by $\frac{5}{64}$ in.) joined by spot welds at the center of the span and at the two supports. The results of Case II are shown in Fig. 5(*b*). Case II had steel laminations (32 in. by 1$\frac{1}{4}$ in. by $\frac{1}{8}$ in.) joined by tapered pins at the quarter points of the beam. In Figs. 5(*a*) and 5(*b*) curves have been plotted showing the theoretical deflections for a solid beam having the same dimensions and composed of the same material (steel, $E = 30 \times 10^6$ lb per sq in.) as the laminated beams. In Fig. 5(*b*) the measured-deflection points have had a curve drawn through them to show the divergence from the theoretical deflections. In Fig. 5(*a*) the points of measured deflection agreed closely with the theoretical deflection curve.

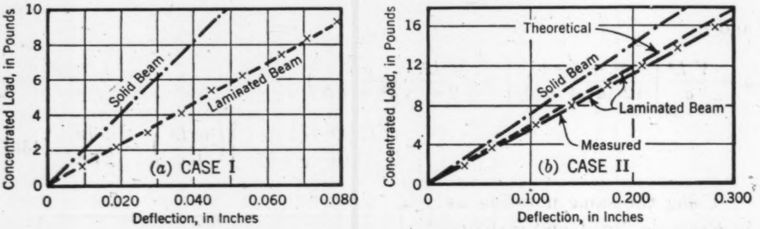

FIG. 5.—COMPARISON OF THEORETICAL AND EXPERIMENTAL DEFLECTIONS

It is believed that, if larger loads had been used in Case I, the theoretical and actual curves would have separated at the higher loads as in Case II. At the time of the testing for Case I it was not considered necessary to go beyond the loads indicated. Graphite was placed between the laminations of the beam in Case II which would tend to eliminate any friction effect. It is believed that the deflections were larger than predicted because of the straining of the pins. Also, in Case I the laminations were spot welded, which would eliminate any stress concentration which would occur with tapered pins.

LIMITING THE DEFLECTION

The question now arises as to the determination of the number of rivets (or joints) necessary to limit the deflection so that it will be within a certain percentage of the deflection of the solid beam of the same dimensions. This question will be investigated by the consideration of the cantilever beam shown in Fig. 6. The beam consists of two laminations joined at uniformly distributed points l units apart. If there are $(m + 1)$ spaces between joints in the beam, the joints are numbered from right to left, and the right end of the beam is the zero end.

Then,

$$\Delta = \sum_{n=1}^{m} (\delta_n + n\, l\, \phi_n) + \delta_0 \ldots\ldots\ldots\ldots\ldots\ldots (48)$$

in which ϕ_n is the angle between the tangents at joint n, and joint $(n + 1)$ and δ_n denote the vertical distance between joint n and the tangent at joint $(n + 1)$. There are also the relations:

$$\frac{L_c}{m + 1} = l \ldots\ldots\ldots\ldots\ldots\ldots (49a)$$

$$V_n = P \ldots\ldots\ldots\ldots\ldots\ldots (49b)$$

and

$$M_n = P_n\, l \ldots\ldots\ldots\ldots\ldots\ldots (49c)$$

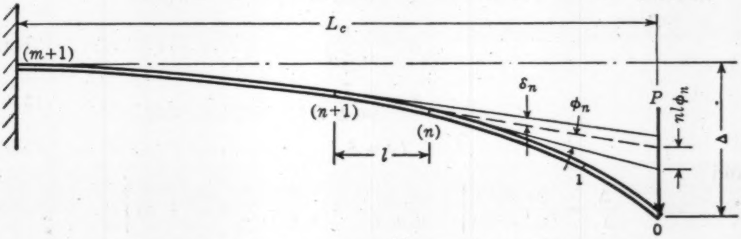

FIG. 6.—DOUBLY LAMINATED CANTILEVER BEAM JOINED AT MANY POINTS

in which the subscript n denotes the values at the nth joint of the beam. From Eqs. 31 and 32,

$$\phi_n = \alpha \left(\tfrac{1}{2} V_n\, l^2 + M_n\, l\right) \ldots\ldots\ldots\ldots\ldots\ldots (50a)$$

in which

$$\alpha = \frac{b}{\bar{a}^2 + b\, c} \ldots\ldots\ldots\ldots\ldots\ldots (50b)$$

and

$$\delta_n = \beta\, V_n\, l^3 \frac{\alpha}{2} M_n\, l^2 \ldots\ldots\ldots\ldots\ldots\ldots (50c)$$

in which

$$\beta = \frac{\bar{a}^2 + 4\, c\, b}{12\, c\, (\bar{a}^2 + c\, b)} \ldots\ldots\ldots\ldots\ldots\ldots (50d)$$

Therefore,

$$\Delta = \sum_{n=1}^{m} \left[\beta\, V_n\, l^3 + \tfrac{1}{2}\, \alpha\, M_n\, l^2 + n\, l\, \alpha \left(\tfrac{1}{2} V_n\, l^3 + M_n\, l\right)\right] + \beta\, V_0\, l^3 \ldots (51a)$$

or

$$\Delta = \sum_{n=1}^{m} \left[V_n\, l^3 \left(\beta + \tfrac{1}{2}\, \alpha\, n\right) + M_n\, l^2 \left(\tfrac{1}{2}\, \alpha + n\, \alpha\right)\right] + \beta\, V_0\, l^3 \quad (51b)$$

By use of Eqs. 49, Eq. 51b becomes

$$\Delta = P\, l^3 \sum_{n=1}^{m} \left[\beta + \tfrac{1}{2}\, \alpha\, n + \alpha\, n \left(\tfrac{1}{2} + n\right)\right] + \beta\, P\, l^3 \ldots\ldots (52a)$$

which is simplified to yield

$$\Delta = P\left(\frac{L_e}{m+1}\right)^3\left[\beta + \sum_{n=1}^{m}(\beta + \alpha\, n + \alpha\, n^2)\right] \tag{52b}$$

The ratio of deflections between the laminated beam and the solid beam, therefore, is

$$\frac{\Delta}{\Delta_s} = \frac{3\,E\,I_s}{(m+1)^3}\left[\beta\,(m+1) + \alpha\sum_{n=1}^{m} n\,(1+n)\right] \tag{53a}$$

in which

$$\Delta_s = \frac{P\,L_e^3}{3\,E\,I_s} \tag{53b}$$

Example No. 3.—For a beam composed of equal laminations,

$$\alpha = \frac{1}{8\,E\,I} \tag{54a}$$

$$\beta = \frac{7}{96\,E\,I} \tag{54b}$$

$$I_s = 8\,I \tag{54c}$$

and

$$\frac{\Delta}{\Delta_s} = \frac{24\,E\,I}{(m+1)^3}\left[\frac{7\,(m+1)}{96\,E\,I} + \frac{1}{8\,E\,I}\sum_{n=1}^{m} n\,(1+n)\right] \tag{54d}$$

or

$$\frac{\Delta}{\Delta_s} = \frac{3}{(m+1)^3}\left[\frac{7\,(m+1)}{12} + \sum_{n=1}^{m} n\,(1+n)\right] \tag{55}$$

By use of Eq. 55 the following values have been computed:

m	$\frac{\Delta}{\Delta_s}$
0	1.750
1	1.188
2	1.083
3	1.047
4	1.030
5	1.021

The number of joining points can thus be chosen depending on the deflection desired.

It can be seen from the previously listed values for Δ/Δ_s that the advantage gained by adding an extra joining point decreases very rapidly as the number of joining points increases. Although this particular case is quite simple, it indicates a direct method of solving for the optimum number of rivets in a laminated beam. That is, by this theory there is no longer any need for a trial-and-error solution to find the necessary number of rivets to limit the deflection to a given amount. It should also be noted that friction will serve to reduce the values as given in the preceding tabulation. Consequently, the theory presents the worst situation possible.

MORE THAN TWO LAMINATIONS

The case of the laminated beams composed of more than two laminations will not be treated in detail. As might be suspected, the mathematical manipulation increases rapidly with the increase in number of laminations; therefore, only an indication of the procedure will be given.

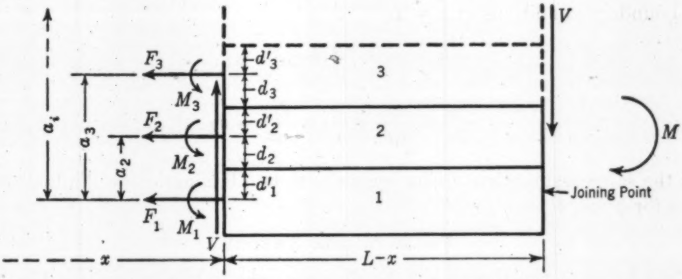

FIG. 7.—FREE-BODY DIAGRAM OF MULTIPLY LAMINATED BEAM

Assuming that a beam is composed of k laminations, the section between two adjacent joining points will be investigated (Fig. 7). Taking as a free-body the section of length $(L - x)$, the following equations may be written:

$$F_1 + F_2 + F_3 + \cdots + F_k = 0 \quad \text{(56a)}$$

and

$$M_1 + M_2 + \cdots + M_k = V\,(L - x) + M + f(x) - [F_2\,a_2 + F_3\,a_3 + \cdots + F_k\,a_k] \quad \text{(56b)}$$

—in which

$$a_2 = d'_1 + d_2 \quad \text{(57a)}$$

$$a_3 = a_2 + d'_2 + d_3 \quad \text{(57b)}$$

and

$$a_i = a_{i-1} + d'_{i-1} + d_i \quad \text{(57c)}$$

and d_i is the distance between the neutral axis of the ith lamination and the contact surface of the lamination immediately below it.

Assuming the integral of the strains for the contact surface of two laminations to be equal, one can write:

$$\int_0^L \left(\frac{M_1\,d'_1}{E_1\,I_1} + \frac{F_1}{A_1\,E_1}\right) dx = \int_0^L \left(-\frac{M_2\,d_2}{E_2\,I_2} + \frac{F_2}{A_2\,E_2}\right) dx \quad \text{(58a)}$$

$$\int_0^L \left(\frac{M_2\,d'_2}{E_2\,I_2} + \frac{F_2}{A_2\,E_2}\right) dx = \int_0^L \left(-\frac{M_3\,d_3}{E_3\,I_3} + \frac{F_3}{A_3\,E_3}\right) dx \quad \text{(58b)}$$

and

$$\int_0^L \left(\frac{M_i\,d'_i}{E_i\,I_i} + \frac{F_i}{A_i\,E_i}\right) dx = \int_0^L \left(-\frac{M_{i+1}\,d_{i+1}}{E_{i+1}\,I_{i+1}} + \frac{F_{i+1}}{A_{i+1}\,E_{i+1}}\right) dx \quad \text{(58c)}$$

Thus, Eqs. 56, 57, and 58, the boundary conditions at $x = 0$,

$$y_1 = y_2 = y_3 = \cdots = y_k = y_0 \qquad (59a)$$

and

$$\frac{dy_1}{dx} = \frac{dy_2}{dx} = \cdots = \frac{dy_k}{dx} = \theta_0 \qquad (59b)$$

the boundary conditions at $x = L$,

$$y_1 = y_2 = \cdots = y_k = y_L \qquad (60a)$$

and

$$\frac{dy_1}{dx} = \frac{dy_2}{dx} = \cdots = \frac{dy_k}{dx} = \theta_L \qquad (60b)$$

and the same assumptions as for beams with two laminations will allow one to solve for ϕ and δ.

PROOF OF THE THEORY

The proof of the theory will be rigorous only to the extent that the area-moment proposition is realized as the number of joined sections of a laminated beam approaches infinity. The proof will be offered for a doubly laminated beam—its extension to a more complicated system will be obvious.

If any two points on a doubly laminated beam with m joined points between them are considered, the case of a solid beam is approached by allowing m to increase indefinitely. Fig. 8 (b) is an enlarged view of the section between joints n and $(n + 1)$ of Fig. 8 (a) and Fig. 8 (c) in the bending-moment diagram of the section. As l becomes smaller the loading can be considered as concentrated at the joined points.

Using Eqs. 31 and 32,

$$\phi = \sum_{n=0}^{m} \phi_n = \alpha \sum_{n=0}^{m} \left(\tfrac{1}{2} V_n l^2 + M_n l\right) \qquad (61a)$$

and

$$\Delta = \sum_{n=0}^{m-1} (\delta_n + n\,\phi_n\, l) + \delta_0 \qquad (61b)$$

Examination of the right side of Eq. 61a reveals that the term in parentheses is the area of the bending-moment diagram in Fig. 8 (c). It is thus seen that ϕ is the sum of the bending-moment areas over the section, multiplied by α. This is the first area-moment proposition except that the term α allows for a varying modulus of elasticity over the cross section.

By taking a term from Eq. 61b which corresponds to the section between joints n and $(n + 1)$—and with suitable manipulation—it can be shown that

$$\delta_n + n\,\phi_n\, l = \left(\beta\, V_n\, l^3 + \tfrac{1}{2}\,\alpha\, M_n\, l^2\right) + \alpha\, Z_n\, A_n \qquad (62a)$$

in which

$$Z_n = n\ l \qquad (62b)$$

and A_n is the area of the bending-moment diagram for the section.

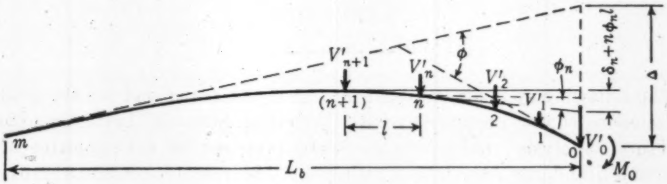
V'_{n+1}
V'_n
ϕ
V'_2
ϕ_n
$\delta_n+n\phi_n l$
Δ
V'_1
$(n+1)$
n
2
1
0
V'_0
M_0
m
l
L_b

(a) BEAM

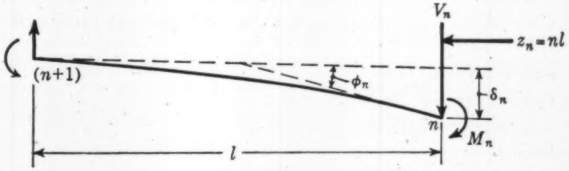
V_n
$z_n = nl$
$(n+1)$
ϕ_n
δ_n
n
M_n
l

(b) ENLARGED SECTION

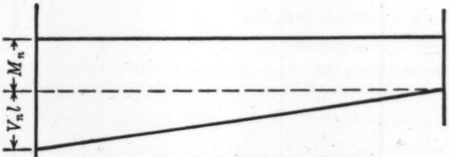

(c) BENDING-MOMENT DIAGRAM

FIG. 8.—DOUBLY LAMINATED BEAM

If l approaches zero, and the higher order terms are canceled, Eq. 61*b* becomes

$$\delta = \sum_{n=0}^{m \to \infty} \alpha \, Z_n \, A_n \dots\dots\dots\dots\dots\dots (63a)$$

or (noting that $A_n = M \, dz$)

$$\delta = \int_0^L \alpha \, M \, Z \, dZ \dots\dots\dots\dots\dots\dots (63b)$$

This is the second area-moment proposition except that α allows for a varying modulus of elasticity over the cross section, as before.

CONCLUSIONS

It should be noted that no attempt has been made to account for a shear deflection of the rivets or pins; this was not considered necessary for this analysis. Strains of this type could be brought into the problem by adding a term to Eqs. 9 and 58 which must express the shear strain in the rivets or pins that join the laminations.

APPENDIX

The following symbols, adopted for use in the paper and for the guidance of discussers, conform essentially with "American Standard Letter Symbols for Structural Analysis" (ASA Z10.8—1949), prepared by a Committee of the American Standards Association with Society representation, and approved by the Association in 1949:

A = cross-sectional area;
a = distance from neutral axis of the lamination to the contact plane;
$\bar{a}$ = the distance between neutral axes of adjacent laminations (defined by Eq. 2);
b = defined by Eq. 14b;
c = defined by Eq. 19;
E = modulus of elasticity;
F = axial load;
I = rectangular moment of inertia;
K_a = constant of integration in Eq. 17;
K_b = constant of integration in Eq. 20;
L = distance between joining points;
L_c = length of a cantilever beam;
l = uniform spacing of joints;
M = bending moment at a joint;
M_l = bending moment at the left end of Fig. 1(a);
P = concentrated load;
V = lateral shear at a joint;
V_l = lateral shear at the left end of Fig. 1(a);
w = uniform loading;
x = horizontal distance from arbitrary section;
y = deflection of the beam from the unloaded condition;
α = defined in Eq. 50b;
β = defined in Eq. 50d;
γ = strain of a longitudinal fiber;
Δ = total end deflection;
δ = vertical distance between tangent drawn through beam at $x = 0$ and beam at $x = L$;
η = distance coefficient for applied nonuniform loading;
θ = slope of tangent drawn to deflected beam; and
ϕ = defined by Eq. 14a.

The subscripts 1 and 2 are used to denote the upper and lower laminations, respectively. The subscripts 0 and L are used to signify the end of the beam at $x = 0$ and $x = L$, respectively. A solid beam of the same dimensions and material as the laminated beam is denoted by the subscript s.

AMERICAN SOCIETY OF CIVIL ENGINEERS
Founded November 5, 1852
TRANSACTIONS

Paper No. 2695

BRIDGES ON THE WEST VIRGINIA TURNPIKE

BY ELMER K. TIMBY,[1] M. ASCE

SYNOPSIS

· The difficult terrain and relatively light total traffic requirements made the designing of structures on the West Virginia Turnpike a somewhat unusual experience. Prior to bond issuance, it was necessary to secure government release of materials and to estimate costs and obtain contractors' commitments. This paper describes the first project of the West Virginia Turnpike system and is indicative of further extensions of a north-south turnpike route across the eastern states.

INTRODUCTION

Developments in the West Virginia Turnpike project—from the initial feasibility studies to the financing—influenced the design of bridges for the turnpike. Therefore, a paper on bridges for the West Virginia Turnpike would be incomplete without reference to these early developments.

The firm with which the writer is associated was engaged as general consultant to the West Virginia Turnpike Commission in May, 1950, shortly before the Korean War began. Governmental control of materials followed thereafter, with consequent fluctuations in the revenue-bond market. These economic factors, as well as the difficult terrain and the relatively light total traffic capacity requirements in West Virginia, affected significantly the chain of events leading to final bridge design.

PRELIMINARY STUDIES

The engineering investigations were divided into three phases, the first of which consisted of a study—using maps, traffic data, and field reconnaissance—of one quarter of the state's area. This study indicated a traffic need in West Virginia for a turnpike route, approximately 118 miles long, from Fairplain to a short distance east of Princeton. Adequate facilities for collection and dispersal of traffic were available at both ends of the route. The second phase

---

NOTE.—Published, essentially as printed here, in September, 1953, as *Proceedings-Separate No. 263*. Positions and titles given are those in effect when the paper was received for publication.

[1] Partner of Howard, Needles, Tammen and Bergendoff, New York, N. Y.

included a detailed study of all alternate routes, resulting in the selection of a more precisely defined location. The third and final phase prior to financing consisted of final cost, traffic, and revenue studies made in sufficient detail to justify the sale of bonds. During this phase of study, the investment bankers decided that the line must be shortened to 88 miles by eliminating the 30 miles north of Charleston. It was also stipulated that bonds could not be sold unless the West Virginia Turnpike Commission had definite commitments for the furnishing, fabrication, and erection of the steel bridge superstructures at the time when the bonds were offered to the public. This paper subsequently describes the means by which this unusual requirement was satisfied.

Origin-and-destination counts and interviews by the consulting traffic engineers with the majority of the operators of commercial trucks in the area revealed that the total anticipated traffic volumes did not require a four-lane divided highway. This, plus the compelling fact that such volumes of traffic would not support the cost of a four-lane divided highway in this rugged, mountainous terrain, led to the construction of a pavement 24 ft wide, flanked by paved shoulders each 9 ft wide, or a total improved width of 42 ft. Where grades exceeded momentum grades for commercial vehicles, the design cross section was altered to provide a 36-ft paved width with a paved shoulder 9 ft wide on the downhill side of the highway, and a paved shoulder 2 ft wide on the uphill side adjacent to the added 12-ft-wide lane, which was extended over the crest a distance sufficient to allow trucks to regain speed. This arrangement provided a total improved width of 47 ft. At those crests where the third lanes overlapped, the total improved width was 52 ft.

After these decisions were made, the construction cost estimate for the initial turnpike was completed in detail. A stadia survey was run along the selected line. Adjustments in the planned location to fit the actual ground conditions were made as the survey progressed. This stadia survey and the accompanying work provided a reasonably accurate ground profile. Also included in the survey were measurements of cross slopes for use in estimating earthwork, examination of the ground to provide an initial soil survey and to determine drainage requirements, and the obtaining of preliminary clearances and other data for all bridge structures. The remainder of this paper will deal with the work only as it related to bridges.

Preliminary Bridge Investigations.—The stadia survey was made during the winter when foliage was sparse; its average progress was between two and three miles per day when weather was clear and brush not heavy. Notes taken during a day were plotted that evening. This work was extended to include (1) the laying of a roadway profile grade, (2) the estimation of earthwork, and (3) the revision of the roadway profile in order to obtain economy in the use of earthwork and structures, and to obtain improved geometric characteristics where possible. A highway engineer and an experienced bridge designer and estimator participated in this work. The plan of the line was plotted carefully on the photostatic enlargements (1,000 ft equals 1 in.) of the Geological Survey (United States Department of the Interior) topographic sheets, and both the ground profile and the revised roadway profile were plotted.

After this work was done, the bridge designer went to each of the eighty-seven bridge sites with sketching board, notebook, and pocket transit and made a bridge-site survey. In addition to this information, plus roadway widths and design loadings as previously established, preliminary layouts and designs were prepared which included the determination of the sizes of principal members and estimates of structural steel tonnages, weights of castings and other special features, the weight of steel reinforcement, the volume of concrete, and the volume of excavation for structures. For the larger bridges, the data obtained by the designer in the field were forwarded to the home office for the development of preliminary designs and the preparation of estimates of quantities. Following completion of the preliminary design computations, the home office prepared preliminary drawings. These included typical cross sections, typical details for shoes, expansion joints, hand rails, scuppers, framing plans and arrangement of spans, and tabulated quantities. Each structure was identified with these details and data by its number.

Tentative specifications for fabrication and erection of steel superstructures were then prepared, together with a route map at a scale of 1 mile to the inch. This map identified the general location of each bridge by number, indicated whether it was a grade separation, a stream crossing, or a bridge for some other purpose, and whether it was an overpass or an underpass. Adjacent rail lines and access highways were also shown and identified in order to assist in studying erection.

Bond Issuance.—The foregoing preliminary drawings, tentative specifications and route map comprised the informational basis for the invited proposals submitted by contractors for the fabrication and erection of steel. The proposals were on a unit-price basis and contained nine different bid items. The breakdown was such that certain items could be assigned to one contractor and the remainder to another, with the result that each contractor would fabricate all, or a significant continuous length, of each bridge. By selecting the low price for each item, the result was that the contract for the steel to be fabricated was equally allocated between the Bethlehem Steel Company and the American Bridge Company (since 1952, the American Bridge Division of the U. S. Steel Corporation). The latter company submitted the only proposal for erection.

The proposals for furnishing, fabricating, and delivering were accepted by parts as indicated above, and the proposal for erection was accepted. Acceptance by the West Virginia Turnpike Commission was prior to the sale of bonds and was conditioned upon (1) receipt by the commission of proceeds from the sale of bonds, and (2) the subsequent preparation and execution of definitive contracts containing mutually agreeable provisions.

Also prior to the sale of bonds, the commission obtained a letter from the Bureau of Public Roads, United States Department of Commerce (USBPR), the claimant agency for the allocation of steel to be used in highway construction. The letter read in part as follows: "In our judgment it will be possible by the time construction can possibly be initiated, to carry forward without undue delay," and stated that, within certain reasonable stipulations, the construction schedule would be approved when submitted.

The acceptance of the proposals for furnishing, fabricating, delivering, and erecting steel (with the letter from the USBPR) formed the basis for this assertion in the prospectus offering the bonds to the public:

> "Designs for all steel structures throughout the length of the Turnpike have been made in sufficient detail to determine major steel requirements, and firm proposals from the American Bridge Company and the Bethlehem Steel Company for the furnishing, fabrication, delivery and erection of this steel are now in the possession of the Turnpike Commission. The agreements with the two steel companies contain their standard escalator provisions. These proposals, in the amount of $9,523,000, reduce to a minimum the item of contingency so far as these structures are concerned. The federal authorities have given assurances of the availability of critical materials and approval of the quarterly construction schedules when submitted."

Bonds were sold on April 10, 1952, and the definitive contract documents, containing more detailed specifications for furnishing, fabricating, delivering, and erecting all steel structures, were later executed. The preliminary expenses for the West Virginia Turnpike were jointly underwritten by Bear, Stearns and Company, and by Byrne and Phelps, Inc. The former managed the syndicate that marketed the $96,000,000 revenue-bond issue. Final plans for each structure have not (1953) been supplied to the fabricators.

Another preliminary step verified the adequacy of the previously described preliminary estimates prior to sale of bonds, although this step was not completed in time to enter into the steel negotiations. An early decision had been made to have topographic maps prepared from aerial surveys using a scale of 200 ft to the inch and a 5-ft contour interval. This decision was made early enough to permit photography during winter months. Its principal purpose was to shorten the construction schedule by several months by substituting extensive office studies for the necessarily slower and less thorough field surveys usually used to establish the final line after the sale of bonds. As these topographic maps became available, the previously selected tentative line was placed on them; ground and roadway profiles were plotted; cross sections were plotted; and quantities were re-estimated for all critical lengths, and for certain typical lengths. The earlier work was thus verified and the geometric characteristics were improved.

DESIGN AND CONSTRUCTION

Final Design.—These same aerial maps, with the tentative alinement added, and accompanied by such other quantity studies as had been made, formed the starting point for the final design of line, grade, grading and drainage, and paving by the section engineers. The turnpike was divided into three sections having lengths of 20 miles, 30 miles, and 38 miles, respectively, and the final design work on each section was done by a different firm. All final bridge design drawings were made by the general consultants, by whom the preliminary designs were made. The number of bridges was reduced to 76. A firm of tunnel specialists designed the tunnel, which is a half mile long.

A device (called "design data drawings") was used to convey all necessary information for any one bridge. In such a device, a plan view of the proposed bridge and all adjacent features are included. Borings are indicated and referenced. The skew angle and roadway width are dimensioned. Roads, railroads, streams, and buildings are identified. An elevation of the bridge is also shown on the design data drawing. Span lengths and vertical clearances are dimensioned—as are lateral clearances if these are not shown on the plan view. The plan view and the elevation view together give complete information with respect to line and grade for the turnpike center line. Profiles for the artery crossed (highway or railway) are shown at an enlarged scale on a separate view. Another view shows the cross section of the bridge deck, including sidewalks as required, and any special provisions for utilities. Each design data drawing also includes a vicinity map to assist officials of the West Virginia State Road Commission (and of any railroad concerned) in locating the bridge with regard to their respective systems. Finally, each drawing contains a space for designating the loading, for referring the location to the topographic maps, for identifying location by mileage, and for any other special information, such as references to pertinent correspondence or conferences. A space is provided for the approving signature of each party concerned.

The design data drawings for the turnpike bridges were prepared in the Charleston, (W. Va.) office of the general consultants. When completed and approved, copies were distributed to all persons whose approval was required, to the design office to govern the final design, and to the section engineer for use in designing adjacent grading and drainage. In this way, all work was correlated and everyone was informed completely and concisely.

Except for an appreciable number of modifications in detail requirements, Division III of the 1949 specifications of the American Association of State Highway Officials (AASHO)[2] governed the design of the bridges. There are none that carry railroads. The design load was H20–S16, except for a few bridges carrying secondary roads. Widths between curbs were 30 ft for a two-lane roadway, 36 ft for a three-lane roadway, 30 ft on two of the three major bridges, and 32 ft on the third. Safety walks on each side were 18 in. on all except the three major bridges and certain bridges over the turnpike adjacent to populated areas. Sidewalks 3 ft wide were provided on these bridges.

Three-span construction with small abutments is being used for all small bridges to provide better visibility. Few of these will be on piles. Either shale or sandstone is near the surface at most of the bridge sites and will form a large portion of the embankment material. In the vicinity of abutments, highly compacted embankments will be constructed for the spread footings. Rock is to be excluded from the embankments where piles are used under abutments.

Construction.—Supervision of construction for the three larger bridges and for the tunnel will be provided by the general consultants, who will also prepare the designs for—and supervise construction of—all common features such as toll collection equipment, lighting, guard rail, fencing, pavement markings, delineators, signs, and layouts of service and maintenance areas. All other construction will be supervised by two of the firms who prepared the final designs.

---

[2] "Standard Specifications for Highway Bridges," A.A.S.H.O., Washington, D. C., 1949.

Bids on the first grading, drainage, and substructure contract were taken on August 19, 1952. Ground was broken ten days later. The 88-mile turnpike, 22 miles shorter than the pre-existing highway route, will be opened to traffic on August 1, 1954.

CONCLUSION

This paper describes only the first project of the West Virginia Turnpike system. This first project will break the mountain barrier to traffic (there are no north-south railroads, and the existing highways are both steep and tortuous) by providing an expressway having a maximum grade of 5% and a sharpest curve of 5°30′. The present trust agreement provides for issuing additional bonds sufficient (1) to extend the first project southward to the Virginia state line and (2) to make the turnpike a four-lane highway as soon as traffic volume justifies such additions.

Other projects will follow this first unit of a north-south turnpike route, just as the east-west turnpike route has grown from the original section of the Pennsylvania Turnpike. The critical transportation needs of citizens, industry, and national defense thus will be served.

AMERICAN SOCIETY OF CIVIL ENGINEERS
Founded November 5, 1852
TRANSACTIONS

Paper No. 2696

HIPPED PLATE ANALYSIS, CONSIDERING JOINT DISPLACEMENTS

By Ibrahim Gaafar,[1] A. M. ASCE

With Discussion by Messrs. Herman Craemer; James M. Paulson and L. C. Maugh; R. Gartner; and Ibrahim Gaafar

Synopsis

Both theoretical and experimental investigations of the structural action of hipped plate structures are presented in this paper. The relative displacements of the joints of such structures under loading, neglected in the approximate theory of design described by G. Ehlers and H. Craemer, are shown to affect the results materially, and are taken into consideration by a more accurate, but still practical, method of analysis.

Tests on a $\frac{1}{40}$-scale aluminum model of a hipped plate roof have justified the assumptions and verified the analytical results. The results obtained by use of various theories are compared and checked against the experimental results.

The results of the approximate theory of Messrs. Ehlers and Craemer showed an average discrepancy of 200% in the values of the longitudinal stresses, and at some points gave opposite signs to the experimental results. The proposed treatment showed an average discrepancy of 40% for the same case. Referring to the transverse stresses, the approximate theory errs greatly (from + 60% to − 280%) on the unsafe side, and the proposed theory errs by 20% on the safe side.

The analytical values of the displacements of the joints yielded by the proposed theory agreed well with the experimental values. The difference between both results ranged from 2% for large displacements to 25% for small displacements.

Note.—Published, essentially as printed here, in April, 1953, as *Proceedings-Separate No. 182.* Positions and titles given are those in effect when the paper or discussion was received for publication.

[1] Assist. Prof. of Structural Eng., Ibrahim Univ., Cairo, Egypt.

NOTATION

The letter symbols in this paper are defined where they first appear, in the text or by diagram, and are assembled alphabetically in the Appendix.

INTRODUCTION

No particular sign convention was found necessary for the displacements, the forces, or the stresses. Any assumed displacements may be considered positive. A negative value in the result means an opposite sense of displacement to the one first assumed. Consistency in working out the solution, rather than a specified sign convention, is essential. For the sake of brevity as suggested by G. Winter, M. ASCE, and M. Pei,[2] J. M. ASCE, bending of a plate out of its plane will be designated as slab action and bending in its plane, plate action.

Previous Theory.—The principle of hipped plate construction was first developed by G. Ehlers in Germany in 1924. He wrote the first technical paper[3] on this subject in 1930. In his method of analysis he considered the various plate elements as beams supported at the cross and end diaphragms, shown in Fig. 1. Along the longitudinal edges, the plates were assumed to be connected by hinged joints that do not slide longitudinally and that are considered capable of transferring only edge shears, V, between the contiguous plate elements. Such connections neglected entirely the connecting moments transmitted between the plates due to the rigidity of the joints. The uniform loads on the plates were transformed to the line loads P acting at the joints. These loads P were resolved into two components, P_{cd} and P_{cb}, parallel to the two adjacent plates as shown in Fig. 1. The plates, acting as beams between the diaphragms, carried the loads P. At the same time, the shear stresses V were created to maintain equal longitudinal strains along the common edges. This strain condition at each joint was used to determine the magnitude and distribution of the edge shear stresses V.

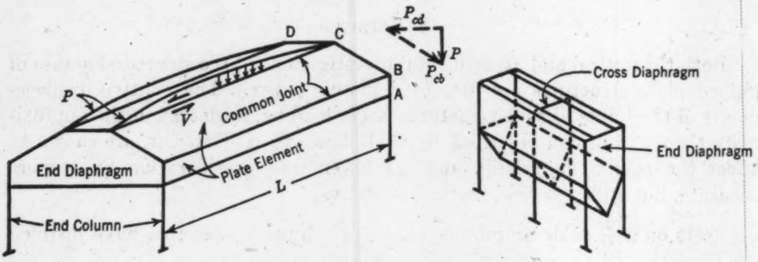

FIG. 1.—HIPPED PLATE STRUCTURES

In 1932, E. Gruber published a paper[4] in which he considered the effect of the rigidity of the joints, the connecting moments acting along the common edges of the plates, and the effect of the relative displacements between the joints. As a first approximation, the hipped roof was assumed to be hinged along the joints. By using this assumed hinged structure as a basic system, he developed his solution in the form of simultaneous differential equations of the fourth order, which could be solved by rapidly converging series. For a hipped roof of $r + 1$ plates, r being the number of joints, the total number of unknowns is $7\,r + 2$. For a roof of five plates, this will involve thirty unknowns. The solution is complicated even if trigonometric series are used. In his solution, Mr. Gruber showed that the maximum longitudinal stresses on a cross section and the maximum deflections for a roof with hinged plates were about twice as great as those for the rigidly connected plates. Consequently, he concluded that the influence of the rigid connections ought not to be neglected as it had been according to the usual practice.

---

[2] "Hipped Plate Construction," by G. Winter and M. Pei, *Journal*, A. C. I., January, 1947.

[3] "Ein neues Konstruktionprinzip, " by G. Ehlers, *Bauingenieur*, Vol. 9, 1930, p. 125.

[4] "Berechnung prismatischer Scheibenwerke," by E. Gruber, *Memoirs*, International Assn. of Bridge and Structural Eng., Vol. 1, 1932, p. 225

Later, the theory was further developed and expanded in many respects by H. Craemer,[5,6] Mr. Gruber,[7] and others. The European literature on the subject, mostly in German, is fairly extensive. All the treatments of the theory by German authors are developed from elasticity equations in the form of simultaneous algebraic and differential equations mathematically involved. With the exception of Mr. Gruber,[4] all writers have made the same simplifying assumption of neglecting the effect of the relative deflections of the joints—including Messrs. Craemer[5,6,8] and Ehlers[3] who first established the current simplified theory, taking into consideration the rigidity of the joints and the resulting transverse connecting moments.

In January, 1947, Messrs. Winter and Pei of Cornell University at Ithaca, N. Y., published a paper[2] on hipped plate construction in which they transformed the algebraic solution into a stress distribution method, which has the advantage of numerical simplicity over the other procedures. However, they also made the same simplifying assumption of neglecting the effect of the relative deflections of the joints.

In a dissertation[9] submitted to Cornell University in 1948, Mr. Pei presented a method of analysis considering joint displacements. The method requires the solution of $6\,n + 1$ simultaneous algebraic equations in which n is the number of plates. For a roof of five plates as shown in Fig. 1, the number of equations is thirty one.

None of the mathematical investigations previously mentioned gives any experimental evidence to substantiate the assumptions and verify the analytical procedures that were used. It seems that no previous experimental evidence from either actual structures or small-scale models has been obtained to support the theoretical analysis.

In the development of the analysis proposed in this paper, it was found necessary to depend on a study of the deformations and joint displacements in small-scale models to check and support the proposed theoretical analysis.

---

[5] "Der heutige Stand der Theorie der Scheibentraeger und Faltwerke, in Eisenbeton," by H. Craemer, *Beton und Eisen*, Vol. 36, 1937, p. 264.

[6] *Ibid.*, p. 297.

[7] "Die Berechnung pyramidenartiger Scheibenwerke und ihre Anwendung auf Kaminkeuhler," by E. Gruber, *Memoirs*, International Assn. of Bridge and Structural Eng., Vol. 2, 1933–1934, p. 206.

[8] "Theorie der Faltwerke," by H. Craemer, *Beton und Eisen*, Vol. 29, 1930, p. 276.

[9] "Hipped Plate Structures," by M. Pei, thesis presented to Cornell University, at Ithaca, N. Y., 1948, in partial fulfilment of the requirements for the degree of Doctor of Philosophy.

LIMITATIONS

The limitations governing Mr. Gruber's solution[4] will also be used in the theoretical investigation. They are as follows: (1) All plates are of rectangular shape. (2) The length of each plate is more than twice its width. This limitation makes it possible to treat the plates as one-way slabs, to assume linear distribution of bending stresses, and to neglect the effect of torsional rigidity. This treatment is justified by the experimental results obtained (see Fig. 28, appearing subsequently). (3) The structure is monolithically built. All joints are rigid. (4) Each plate is of uniform thickness. (5) The material is homogeneous and elastic. The theoretical and experimental investigations given herein are readily applicable to hipped plate structures built of steel or of any elastic material. As for application to reinforced concrete, this paper provides some light on the subject, and it is recommended that further experimental and analytical studies be made of reinforced concrete models. (6) In any plate, plane sections remain plane after deformation. The measured longitudinal strains shown in Figs. 23 and 24, appearing subsequently, are fairly linear across each plate and seem to justify this assumption. Plane cross sections of the entire structure do not necessarily remain plane after deformation.

RELATIVE TRANSVERSE DISPLACEMENTS BETWEEN JOINTS

In the method of analysis proposed in this paper, the relative transverse displacement Δ, between any two consecutive joints, is chosen as an unknown, and is treated as an additional load on the roof. These displacements will affect the slab moments, shears, and, consequently, the plate loads, P, and the plate deflections, δ. For a loading that is symmetrical about the middle section of the roof, the relative displacements are maximum at the middle of the span and are zero at the end diaphragms. If the maximum relative displacements between two joints are assigned a value Δ_0, three points will be given on the curve for the relative displacement. The general form of the curve is known but its exact equation is not known. The best approximation for such a curve may be the elastic line of a beam loaded in a way similar to that of the roof. That is, if the roof is uniformly loaded (which is usually the case), then the Δ-curve may be assumed to follow the elastic line of a uniformly loaded beam.

In the case of single-span roofs symmetrically loaded with respect to the middle of the span, the relaitve Δ-values can be represented by a half wave of a sine curve, instead of assuming them to vary as the elastic line of the corresponding loaded beam. This is shown by studying and comparing the curves represented by Eqs. 1, as follows:

The elastic line of a beam that carries a uniform load, having the maximum deflection Δ_0 at the middle, is expressed by

$$\Delta = \Delta_0 \left(\frac{16}{5} \frac{x^4}{L^4} - \frac{24}{5} \frac{x^2}{L^2} + 1 \right) \ldots\ldots\ldots\ldots\ldots\ldots (1a)$$

The equation for the elastic line of a beam loaded with a concentrated load at the middle, and also having the maximum deflection Δ_0 at the middle, is

$$\Delta = \Delta_0 \left(4 \frac{x^3}{L^3} - 6 \frac{x^2}{L^2} + 1 \right) \ldots\ldots\ldots\ldots\ldots\ldots (1b)$$

and that for a half sine wave is

$$\Delta = \Delta_0 \sin \frac{\pi x}{L} \qquad \text{(1c)}$$

In the foregoing expressions, x represents distance parallel to the joints, measured from the left end of the structure. These three curves, when plotted, are so nearly alike as to be almost indistinguishable. They have the same maximum ordinate Δ_0, and at the quarter points of the span these curves have their ordinates equal to $\frac{57}{80}\Delta_0$, $\frac{55}{80}\Delta_0$, and $\frac{56.6}{80}\Delta_0$, respectively.

When Eqs. 1 are treated as load curves on the plate elements of the roof, their correcting effects, δ_2, on the plate deflections, δ, at the middle of the span will be still more alike. If the relative deflections are assumed to vary according to Eqs. 1*b* and 1*c*, respectively, then the respective values for δ_2 will be 0.1010 multiplied by a constant (for Eq. 1*b*) and 0.1024 multiplied by the same constant (for Eq. 1*c*). These two values agree well, and, in the case of Eq. 1*a* and the sine curve (Eq. 1*c*), the agreement of results will be still closer.

This agreement suggests the adoption of Eq. 1*c*, the half sine wave, to represent the manner in which the Δ-values vary in single-span roofs. If this procedure is adopted, the loads on the roof may be either uniform or concentrated, provided that they are symmetrical about the middle of the span. Such use of the sine curve greatly simplifies the analytical treatment.

In the case of multispan roofs, or of roofs on which the loads are far from being symmetrical about the middle of the span, this sine wave treatment cannot be used with accuracy, and the elastic line of the corresponding loaded beam would have to be adopted—for the present. However, there may be a way of introducing a simplification, even in such a case.

PROPOSED METHOD OF ANALYSIS

The proposed method of analysis will be explained in terms of its application to the roof shown in Fig. 2. Of primary concern is the analytical determination of the relative transverse displacements (Δ) of the joints and their effect on the magnitude and distribution of the internal transverse and longitudinal stresses in the structure.

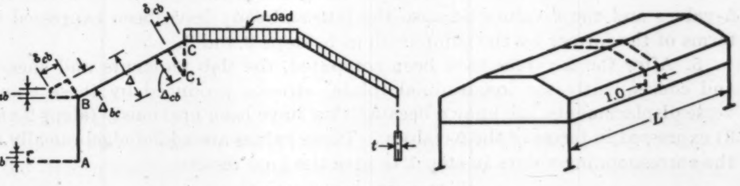

FIG. 2.—A HIPPED PLATE ROOF

1. The first step in the analysis is the computation of the forces and of the transverse and longitudinal stresses acting at the edges of each plate element, neglecting the effect of the relative displacement of the joints. The analytical

procedure used by Messrs. Winter and Pei[2,9] provides a convenient solution for this problem. In this procedure, the roof in the transverse direction is considered as a continuous one-way slab supported on rigid supports at the joints, and thus the shear forces Q are readily obtained. The Q-forces at each joint are then resolved into two component P-forces parallel to the contiguous plates. The plates, acting as beams between the diaphragms, carry the P-loads (plate action). At the same time, edge shear stresses (V) are created along the edges to maintain equal longitudinal strains along the common edges. The longitudinal (plate) stresses at a section of the roof, caused by the P-forces only, are corrected in a manner similar to the moment-distribution method, to include the effect of the edge shear stresses V.

2. The second step in the analysis is to provide for the effect that the relative transverse displacement of the joints has on the transverse and longitudinal stresses. This operation is most easily accomplished by choosing the relative transverse displacements (Δ) between each pair of consecutive joints as unknowns, determining the corresponding transverse (slab) fixed-end moments in terms of the Δ-values, and correcting for rotation at the ends of the slab strips by the moment-distribution method. After the end moments have been determined, the Q-forces and P-forces are computed in the same manner as in step 1. This operation must be repeated for each different Δ-value. For unsymmetrical loading, the number of unknown Δ-values for the structure in Fig. 2 is equal to three, but there is only one unknown for symmetrical loading.

3. After the Q-forces and P-forces have been expressed in terms of the Δ-values, the corresponding longitudinal (plate) stresses are computed in the same manner as in step 1.

4. From the values of the longitudinal stresses yielded in steps 1 and 3, the plate deflections δ_1 and δ_2 are computed. Therefore, the sum, δ, of these plate deflections is in terms of the applied load and the relative transverse deflection Δ. It will be found that there is only one set of Δ-values that will satisfy the algebraic relations between the Δ-values and the δ-values imposed by the geometrical requirements of the cross section and the equilibrium conditions. The values of Δ can be computed from the geometrical relations between the Δ-values and the δ-values because the latter already have been expressed in terms of the former by the computations in steps 2 and 3.

5. After the Δ-values have been computed, the slab moments and shears, and consequently the longitudinal (plate) stresses produced by these transverse displacements, are known because they have been previously (steps 2 and 3) expressed in terms of the Δ-values. These values are added algebraically to the corresponding values in step 1 to give the final results.

The application of the foregoing procedure to a $\frac{1}{40}$-scale aluminum model is illustrated in the following pages.

EXAMPLES

Example No. 1.—The dimensions of a $\frac{1}{40}$-scale aluminum model of a hipped plate roof, similar to that shown in Fig. 2, are given in Fig. 3. The model is loaded with a uniform load distributed entirely upon the top plate CC′, and it is required to determine the maximum transverse and longitudinal stresses, produced by this loading, in the model.

Step 1.—For the case of external loads and nonyielding supports, a transverse strip 1.0 in. wide at the middle of the span is considered, treating it as a continuous slab supported at the joints by nonyielding supports. The moment-distribution factors obtained from the stiffness coefficient, c, and the rigidity coefficient, $k = \frac{E\,I}{h}$, are evaluated for this example in Table 1.

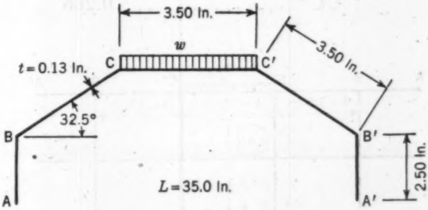

FIG. 3.—ROOF FOR EXAMPLE No. 1

The fixed-end moment at joint C is equal to $\frac{w\,h^2}{12}$. The bending moments and shears for this case are given in Fig. 4. The Q-forces, that is, the shear forces per unit length, acting on the joints, are given in Fig. 5.

TABLE 1.—MOMENT-DISTRIBUTION FACTORS AT JOINT C

Member (1)	Stiffness coefficient, c (2)	Rigidity coefficient, k, in inch-pounds (3)	$c\,k$ (4)	Moment-distribution factor (5)
CB	3	1	3	0.60
CC′	2	1	2	0.40
			5	1.00

For the determination of the P-forces acting on the plates, the positive sense for the P-forces may be assumed to be as indicated in Fig. 6. Then—

$$P_{ab} = +\,0.05\,w\,h\,\frac{1}{\cos\theta_b} = +\,0.05\,w\,h\,\frac{1}{0.8434} = +\,0.0593\,w\,h \ldots (2a)$$

$$P_{bc} = -\,0.05\,w\,h\,(\tan\theta_b + \cot\theta_b) - 0.5\,w\,h\,\frac{1}{\sin\theta_b} = -\,1.0424\,w\,h \,..\, (2b)$$

and, similarly, the P-force in plate CC′ is zero. In the foregoing computations, $h = 3.5$ in., and the subscripts indicate the joints between which the forces act.

To determine the "free edge" bending moments and the corresponding stresses at the middle section, each plate may be treated as a beam carrying the loads P and spanning between the end diaphragms, with no edge shear V along the joints. The moments, in inch-pounds, are

$$M_{ab} = P_{ab}\,\frac{L^2}{8} = (+\,0.0593\,w\,h)\,\frac{35.0^2}{8} = +\,31.80\,w \ldots\ldots\ldots (2c)$$

and

$$M_{bc} = P_{bc}\,\frac{L^2}{8} = (-\,1.0424\,w\,h)\,\frac{35.0^2}{8} = -\,560.0\,w \ldots\ldots\ldots (2d)$$

and for plate CC′, the moment is zero.

The corresponding fiber stresses are as follows:

Plate	Section modulus, Z, in cubic inches	Fiber stress, s, in pounds per square inch
AB	0.1354	$\pm 235.0\, w$
BC	0.266	$\pm 2105.0\, w$
CC′	0.266	0.0

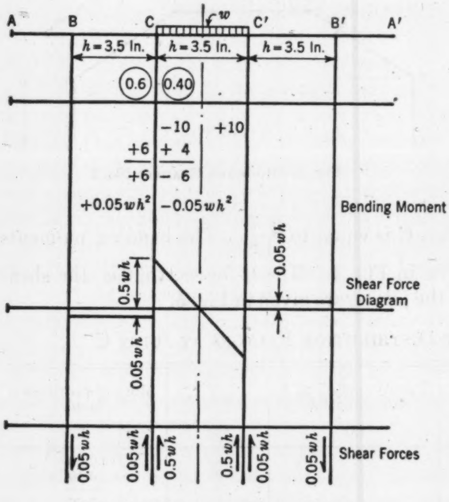
A
B
C
w
C′
B′
A′
h = 3.5 In.
h = 3.5 In.
h = 3.5 In.
0.6
0.40
−10
+10
+6
+ 4
+6
− 6
+0.05wh²
−0.05wh²
Bending Moment
0.05wh
0.5wh
Shear Force Diagram
0.05wh
0.05wh
0.05wh
0.5wh
0.5wh
0.05wh
0.05wh
Shear Forces

FIG. 4.—MOMENT AND SHEAR VALUES

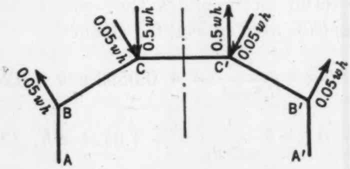
0.05wh
0.5wh
0.5wh
0.05wh
C
C′
0.05wh
B
B′
0.05wh
A
A′

FIG. 5.—LOCATIONS AND DIRECTIONS OF THE Q-FORCES

These free edge stresses are shown in Fig. 7. The signs for the stresses depend on the sense of the corresponding P-loads. The free edge stresses correspond to the case in which longitudinal sliding hypothetically takes place between the adjacent plates. However, this longitudinal sliding is eliminated by the presence of the longitudinal edge shears V between the adjacent edges. To correct the free edge stresses so that they include the effect of edge shear stresses, two equal and opposite forces are introduced, one at each joint. The process is similar to that used in the moment-distribution method.

The stresses in two rectangular sections AB and BC that are acted upon by two equal and opposite edge forces F are shown in Fig. 8. It can be concluded[2] that the stress-distribution coefficients at the joints are as follows:

At joint B,

$$K_{ba} = \frac{\dfrac{4\,F}{A_{ba}}}{\dfrac{4\,F}{A_{ba}} + \dfrac{4\,F}{A_{bc}}} = \frac{A_{bc}}{A_{bc} + A_{ba}} = \frac{3.50}{2.50 + 3.50} = 0.58 \ldots\ldots (3a)$$

Similarly,

$$K_{bc} = \frac{A_{ba}}{A_{ba} + A_{bc}} = 0.42 \ldots\ldots\ldots\ldots\ldots\ldots (3b)$$

and at joint C,

$$K_{cb} = - K_{cc'} = 0.50 \ldots\ldots\ldots\ldots\ldots\ldots\ldots\ldots (3c)$$

The carry-over factor equals $- \frac{1}{2}$.

The free edge stresses are corrected in Table 2. They are given in the second line of the table; the stresses, after distribution, are given in the last line, and are shown on a section of the model Fig. 9. Table 2 shows one half of the symmetrical structure. These stresses represent the longitudinal (plate) stresses at the middle section for the case of external loads, neglecting the effect of the relative displacements of the joints, which will be considered in the next step.

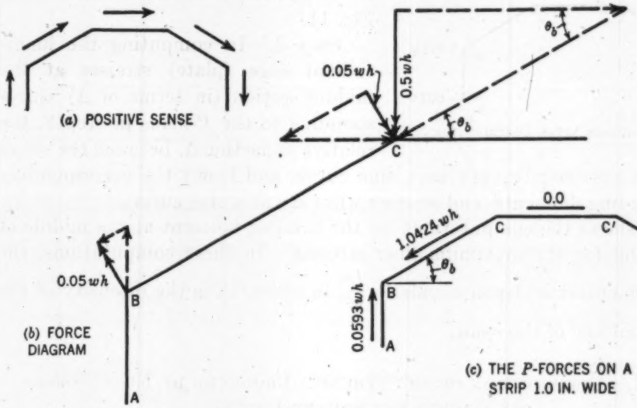
(a) POSITIVE SENSE
0.05wh
0.5wh
θ_b
θ_b
C
0.05wh
B
A
(b) FORCE DIAGRAM
0.0
1.0424wh
C
C'
θ_b
0.0593wh
B
B'
A
A'
(c) THE P-FORCES ON A STRIP 1.0 IN. WIDE

FIG. 6.—DETERMINATION OF THE *P*-FORCES

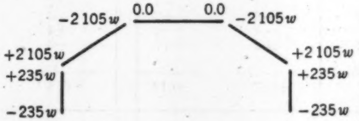
−2105w
0.0
0.0
−2105w
+2105w
+235w
−235w
+2105w
+235w
−235w

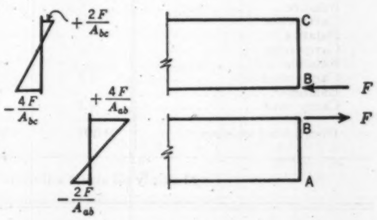
$+\frac{2F}{A_{bc}}$
$-\frac{4F}{A_{bc}}$
$+\frac{4F}{A_{ab}}$
$-\frac{2F}{A_{ab}}$
C
B
F
F
B
A

FIG. 7.—FREE EDGE STRESSES

FIG. 8.—STRESSES PRODUCED BY EDGE FORCES

Step 2.—In determining the effect of the relative displacements of the joints, a transverse strip at the middle of the model 1.0 in. wide is considered, and the relative displacement (see Fig. 2) between edges B and C at the middle of the strip is given by $\Delta = \Delta_{bc} + \Delta_{cb}$.

The fixed-end moment at edge C, with edge B free to rotate, equals $3 \frac{E\,I}{h}\left(\frac{\Delta}{h}\right) = 3\,\alpha$, in which I equals the moment of inertia of a strip 1.0 in.

wide. For the plate in this example, $I = 183 \times 10^{-6}$ in.^{4}. The symbol E is the modulus of elasticity of aluminum, which is equal to 10.5×10^6 lb per sq in., and $\alpha = \frac{E\,I}{h}\left(\frac{\Delta}{h}\right) = 156.5\,\Delta$.

The fixed-end moments are distributed, and the moments and the shear forces are shown in Fig. 10. The Q-forces and the P-loads are indicated in Fig. 11.

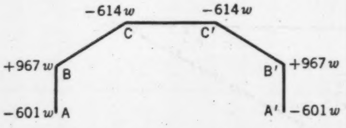

FIG. 9.—STRESSES AFTER DISTRIBUTION

Step 3.—In computing the longitudinal edge (plate) stresses at the middle section (in terms of Δ) corresponding to the P-loads in step 2, the relative deflection Δ, between the edges B and C, is assumed to vary as a sine curve, and hence the corresponding P-loads, bending moments, and stresses will vary as a sine curve.

Table 3 shows the computations for the bending moment at the middle of the span, and for the maximum fiber stresses. In these computations, the bending moment at midspan equals $P_0 \frac{L^2}{\pi^2}$, in which P_0 is the intensity of the load at the middle of the span.

TABLE 2.—DISTRIBUTION OF THE STRESSES PRODUCED BY EDGE FORCES, IN POUNDS PER SQUARE INCH[a]

Description	Edge A	Joint B		Joint C	
Distribution coefficients		0.58	0.42	0.5	0.5
Free edge stresses	−235	+235	+2105	−2105	0.0
Balance		+1085	−785	+1052	−1052
Carry over	−542		−526	+392	+526
Balance		−305	+221	+67	−67
Carry over	+152	.	−33	−110	+33
Balance		−19	+14	+72	−72
Carry over	+10		−36	−7	+36
Balance		−21	+15	+21.5	−21.5
Carry over	+10		−11	−7	+11
Balance		−6	+5	+9	−9
Carry over	+3		−4	−2	+4
Balance		−2	+2	+3	−3
Carry over	+1				
Distributed stresses	−601	+967	+967	−614	−614

[a] Multiply all stress values in this table by the unit load, w.

The free edge stresses shown in Fig. 12 are distributed by the stress distribution method to include the effect of the edge shears V. The same coefficients and method used in step 1 are used to solve for the stresses shown in Fig. 13.

Step 4.—In determining the displacements δ, parallel to the plate elements, the deflection at the middle of a beam loaded with a uniform load is given by

$$\delta_0 = \frac{s_0}{E\,h}\,\frac{5}{48}\,L^2 = \delta_1 \ldots\ldots\ldots\ldots\ldots\ldots\ldots\ldots (4)$$

to yield an approximate value of δ. The difference between the maximum fiber stresses at the middle of span L is expressed as s_0, and h is the depth of the beam.

The deflection[10] at the middle of a beam loaded with a distributed load varying as a half sine wave is expressed as

$$\delta_0 = \frac{s_0}{E\,h}\,\frac{L^2}{\pi^2} = \delta_2 \ldots\ldots\ldots\ldots\ldots\ldots\ldots\ldots (5)$$

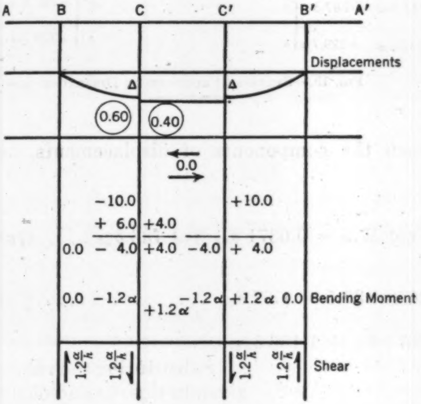
A
B
C
C′
B′
A′
Displacements
Δ
Δ
0.60
0.40
0.0
−10.0
+10.0
+ 6.0
+4.0
0.0
− 4.0
+4.0
−4.0
+ 4.0
0.0
−1.2α
+1.2α
−1.2α
+1.2α
0.0
Bending Moment
$1.2\frac{\alpha}{h}$
Shear

FIG. 10.—MOMENT AND SHEAR VALUES

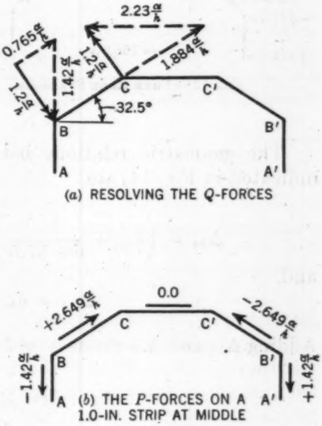
$2.23\frac{\alpha}{h}$
$0.765\frac{\alpha}{h}$
$1.42\frac{\alpha}{h}$
$1.2\frac{\alpha}{h}$
$1.884\frac{\alpha}{h}$
$1.2\frac{\alpha}{h}$
C
C′
32.5°
B
B′
A
A′
(a) RESOLVING THE Q-FORCES
0.0
$+2.649\frac{\alpha}{h}$
$-2.649\frac{\alpha}{h}$
C
C′
B
B′
$-1.42\frac{\alpha}{h}$
$+1.42\frac{\alpha}{h}$
A
A′
(b) THE P-FORCES ON A 1.0-IN. STRIP AT MIDDLE

FIG. 11.—OBTAINING THE P-FORCES

TABLE 3.—COMPUTATIONS OF FREE EDGE STRESSES

Plate (1)	Load intensity at midspan, P_0, in lb per in. (2)	Bending moment at midspan, M_0, in in.-lb (3)	Section modulus, Z, in in.^{3} (4)	Maximum fiber stress, s_0, in lb per sq in. (5)
AB	$-1.42\ \alpha/h$	$-50.40\ \alpha$	0.1354	$\pm 372.0\ \alpha$
BC	$+2.649\ \alpha/h$	$+94.10\ \alpha$	0.266	$\pm 353.0\ \alpha$
CC′	0.0	0.0	0.266	0.0

in which δ_2 is a correction to be applied to δ_1. Hence, the deflections δ of the plate elements produced by the two cases of loading discussed in steps 1 and 3 are as follows:

$$\delta_{ab} = \frac{(601 + 967)\,w}{E \times 2.50} \times \frac{5}{48} \times 35.0^2 - \frac{(329.7 + 287.3)\,\alpha}{E \times 2.50} \times \frac{35.0^2}{\pi^2}$$

---

[10] "The Analysis of Hipped Plate Structures Considering the Relative Displacements of the Joints," by Ibrahim Gaafar, thesis presented to the University of Michigan, at Ann Arbor, Mich., in 1949, in partial fulfilment of the requirements for the degree of Doctor of Science, Appendix II, pp. 107 to 111.

Setting α equal to 156.5 Δ yields

$$\delta_{ab} = 7.63 \times 10^{-3}\, w - 0.457\,\Delta \quad \text{(6a)}$$

Similarly,

$$\delta_{bc} = 5.50 \times 10^{-3}\, w - 0.2195\,\Delta \quad \text{(6b)}$$

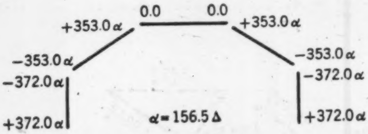
+353.0 α
0.0
0.0
+353.0 α
−353.0 α
−372.0 α
+372.0 α
α = 156.5 Δ
−353.0 α
−372.0 α
+372.0 α

FIG. 12.—FREE EDGE STRESSES

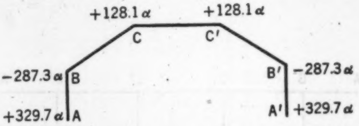
+128.1 α
+128.1 α
C
C′
−287.3 α
B
B′
−287.3 α
+329.7 α
A
A′
+329.7 α

FIG. 13.—STRESSES PRODUCED BY DISPLACEMENTS OF JOINTS

The geometric relations between the components of displacements, as indicated in Fig. 14, are

$$\Delta_{bc} = \left(\delta_{bc} + \frac{\delta_{ab}}{\cos 57.5}\right) \cot 57.5 = 0.6371\,\delta_{bc} + 1.186\,\delta_{ab} \quad \text{(7a)}$$

and

$$\Delta_{cb} = \delta_{bc} \times \cot 32.5 = 1.57\,\delta_{bc} \quad \text{(7b)}$$

Adding Δ_{bc} and Δ_{cb} yields $\Delta = 2,2071\,\delta_{bc} + 1.186\,\delta_{ab}$.

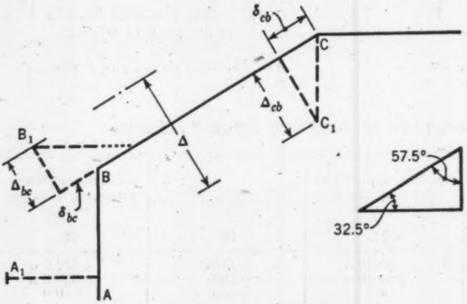
δ_{cb}
C
Δ_{cb}
C_1
B_1
Δ
B
Δ_{bc}
δ_{bc}
A_1
A
57.5°
32.5°

FIG. 14.—EDGE DISPLACEMENTS

Substituting the values given in Eqs. 6a and 6b for δ_{ab} and δ_{bc},

$$\Delta = 10.46 \times 10^{-3}\, w$$

in which Δ is expressed in inches.

Step 5.—Substitution of the value for Δ in the stress values obtained in step 3 yields stresses expressed in terms of the applied load w:

$$\alpha = 156.5\,\Delta = 1.638\, w.$$

The maximum longitudinal stresses at the middle section of the model, as computed by the approximate theory,[2] together with those resulting from the relative displacements of joints and those computed by the proposed theory, are given in Table 4. The necessary correction for the relative displacement of the joints ranges in magnitude between 34% and 90% of the result of the approximate theory.

In computing the bending moment in a transverse strip 1.0 in. wide, the approximate theory, in which external loads and nonyielding supports are considered, yields as the connecting moment $-M_e = 0.05\, w\, h^2 = 0.612\, w$. The maximum moment in span CC′ is $\frac{w\, h^2}{8} = 1.530\, w$. Both moments are in units of inch-pounds, and are illustrated by "Case 1" in Fig. 15. "Case 2" is the moment resulting from the relative deflection of joints, in inch-pounds:

TABLE 4.—THE MAXIMUM LONGITUDINAL STRESSES, IN POUNDS PER SQUARE INCH, PRODUCED BY A UNIFORM LOAD ON THE MODEL OF EXAMPLE No. 1[a]

Edge	Method of Computation		
	"Approximate" theory	Joint displacement	Proposed theory[b]
(1)	(2)	(3)	(4)
C	−614	+210	−404
B	+967	−470	+497
A	−601	+540	−61

[a] Multiply all stress values in this table by the unit load, w. [b] To obtain the values in Col. 4, add the values in Col. 2 to those in Col. 3.

$M_e = 1.2\, \alpha = 1.20 \times 1.638\, w = 1.96\, w$. In "Case 3," the proposed theory, the moments are added, as shown by the bending moment diagrams in Fig. 15.

A serious change in the transverse bending moment of "Case 1" is caused by the relative displacements of the joints, the increase in the value of the bending moment being $\frac{1.96}{0.918} \times 100 = 213\%$ at the middle of span CC′, and $\frac{-1.96}{0.612} \times 100 = -320\%$ at joints C and C′.

TABLE 5.—COMPUTATION OF PLATE LOADS, MOMENTS, AND STRESSES[a]

Plate (1)	Load, P, in pounds (2)	Free edge bending moment, M_0, in inch-pounds (3)	Maximum fiber stress, s_0, in pounds per square inch (4)
AB	0.0	0.0	0.0
BC	−0.466	−5.44	±20.45
CC′	0.0	0.0	0.0

[a] Multiply all values in this table by the total load, W.

Example No. 2.—The same aluminum model of Example No. 1 will be analyzed for the case of four concentrated vertical forces of 58.35 lb. each, acting on the model as shown in Fig. 16. The maximum longitudinal and the maximum transverse stresses at the middle of the model will be computed, and will subsequently be compared with the experimental results obtained for the same case.

Step 1.—For the case of external loads acting at the joints, the loads $W/4$ are resolved in the directions of the two adjacent plates (assuming nonyielding supports). The P-loads acting on the plates (Fig. 17) are yielded directly. These loads, and the resulting moments and stresses at the middle section, are listed in Table 5. The free edge stresses are shown in Fig. 18. Using the same stress distribution procedure and the same coefficients given in the preceding example, the stresses after distribution are as shown in Fig. 19.

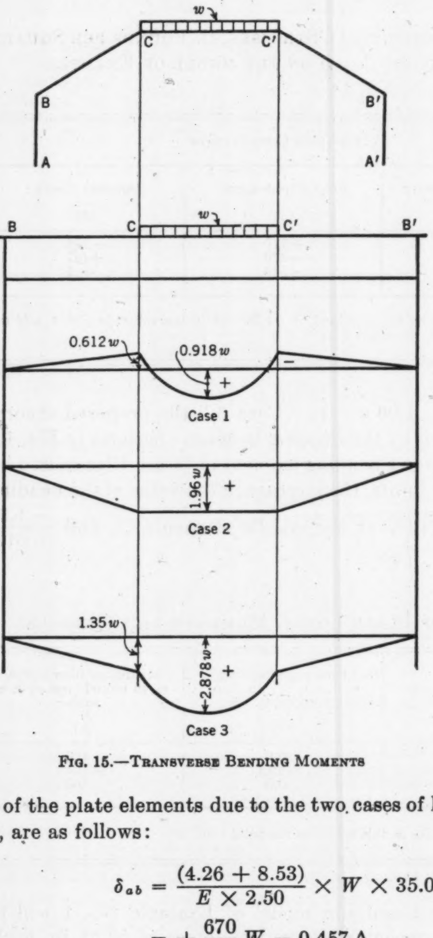

FIG. 15.—TRANSVERSE BENDING MOMENTS

Steps 2 and 3.—The procedure and the results for these steps are identical with those in Example No. 1.

Step 4.—The deflection[9] at the middle of a beam loaded with two concentrated loads at the $\frac{1}{3}$-points of the span is $\delta_0 = \frac{s_0 L^2}{E h} \times \frac{23}{216} = \delta_1$, in which s_0 is the difference between the maximum fiber stresses at the middle of span L.

The deflection[10] at the middle of a beam loaded with a distributed load varying as a half sine wave is expressed by $\delta_0 = \frac{s_0}{E h} \times \frac{L^2}{\pi^2} = \delta_2$. Hence, the deflections δ of the plate elements due to the two cases of loading, described in steps 1 and 3, are as follows:

$$\delta_{ab} = \frac{(4.26 + 8.53)}{E \times 2.50} \times W \times 35.0^2 \times \frac{23}{216} - 0.457\,\Delta$$

$$= +\frac{670}{E} W - 0.457\,\Delta$$

$$= 0.638 \times 10^{-4}\,W - 0.457\,\Delta.$$

Similarly,

$$\delta_{bc} = 0.510 \times 10^{-4}\,W - 0.2195\,\Delta.$$

The geometrical relations between the components of the edge displacements of the model hold true and are independent of the applied loads. The same geometrical relation of Example No. 1 will be used herein, namely: $\Delta = 2.2071\,\delta_{bc} + 1.186\,\delta_{ab}$. Substituting the values given for δ_{ab} and δ_{bc} into the geometrical relation yields $\Delta = 0.928 \times 10^{-4}\,W$ in. The positive sign of Δ indicates that Δ is assumed in the correct direction.

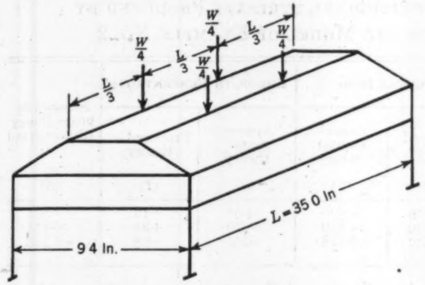

Fig. 16.—Application of Loads, Example No. 2

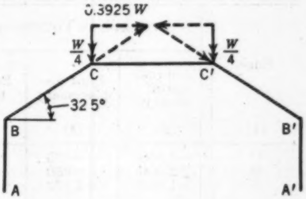

Fig. 17.—Determination of *P*-Loads

Step 5.—Substituting the value for Δ in the stresses obtained in step 3 gives these stresses expressed in terms of the applied load, W:

$$\alpha = E\,\Delta\,(14.90) \times 10^{-6} = 156.5\,\Delta$$
$$= 156.5 \times 0.928 \times 10^{-4}\,W = 0.0145\,W.$$

The applied load is $W = 4 \times 58.35 = 233.4$ lb.

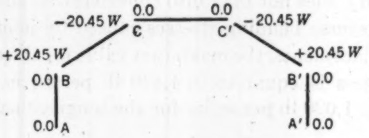

Fig. 18.—Free Edge Stresses

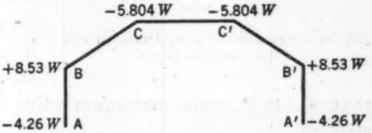

Fig. 19.—Stresses After Distribution

The maximum longitudinal stresses at the middle section of the model, obtained by means of the approximate theory,[2] the relative displacements of the joints and the proposed theory are listed in Table 6, together with the experimental results. The methods of analysis are found in the column headings of Table 6.

The necessary correction ranged between 32% and 112% of the approximate values, and resulted in changing the sign of the stress at edge A.

The bending-moment diagram on a transverse strip 1.0 in. wide, at the middle of the model, is shown in Fig. 20. No transverse bending moment is found by the approximate theory because the external loads are applied directly at the joints. Consideration of the relative displacements of the joints yields

$M_e = 1.2\,\alpha = 1.2 \times 0.0145\,W = 4.065$ in.-lb. Superposition of these two conditions yields the result by the proposed theory.

The maximum fiber stresses corresponding to this bending moment are

$$s = \pm \frac{M\,y}{I} = \pm \frac{4.065}{183 \times 10^{-6}} \times \frac{0.13}{2} = \pm\ 1{,}440 \text{ lb per sq in.}$$

TABLE 6.—MAXIMUM LONGITUDINAL STRESSES PRODUCED BY CONCENTRATED LOADS ON THE MODEL OF EXAMPLE NO. 2

Edge	STRESSES, IN POUNDS PER SQUARE INCH				ERROR, IN PERCENTAGES		Stresses by beam theory (lb per sq in.)
	"Approximate" theory	Joint displacement	Proposed theory*	Experimental values	"Approximate" theory	Proposed theory	
(1)	(2)	(3)	(4)	(5)	(6)	(7)	(8)
C	−1,360	+435	−925	−820	+66	+13	−537
B	+2,000	−980	+1,020	+740	+170	+38	+166
A	−1,000	+1,122	+122	+378	−365	−68	+1,102

* Values in Col. 4 are found by adding the values in Col. 2 to those in Col. 3.

The tensile force in plate CC′ found by relative displacements of the joints is $P_{cc'} = 2.23\,\frac{\alpha}{h} = 2.23 \times \frac{0.0145\,W}{3.5} = 0.00924\,W = 2.16$ lb per longitudinal in. The corresponding direct stress is + 16.6 lb per sq in., in tension.

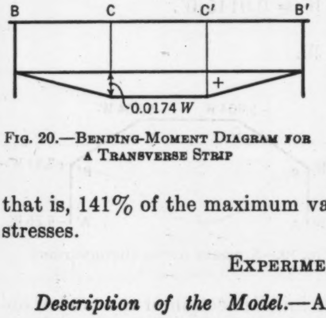

FIG. 20.—BENDING-MOMENT DIAGRAM FOR A TRANSVERSE STRIP

In the foregoing example, it should be noted that, although the approximate theory does not take into consideration any transverse bending stresses caused by joint displacements, the maximum value for these stresses is equal to ± 1,440 lb per sq in., that is, 141% of the maximum value of 1,020 lb per sq in. for the longitudinal stresses.

EXPERIMENTAL INVESTIGATION

Description of the Model.—An aluminum (24 S-T) model on a $\frac{1}{40}$-scale was used for the experimental investigation of the distribution of stresses and strains in a hipped plate structure. The general dimensions of the model are shown in Fig. 21. The supporting angles and base plates were of steel. The load was applied at four points on the model, as shown by the arrows on the diagrams in Fig. 21. To measure the longitudinal strains, SR-4 resistance gages (types A1 and A12) were placed at section C-C, D-D, and E-E. These longitudinal gages were placed on both sides of the plate and connected in series to yield the average strain. Transverse strains were measured at eight points by means of type A7 resistance gages. These gages are represented by

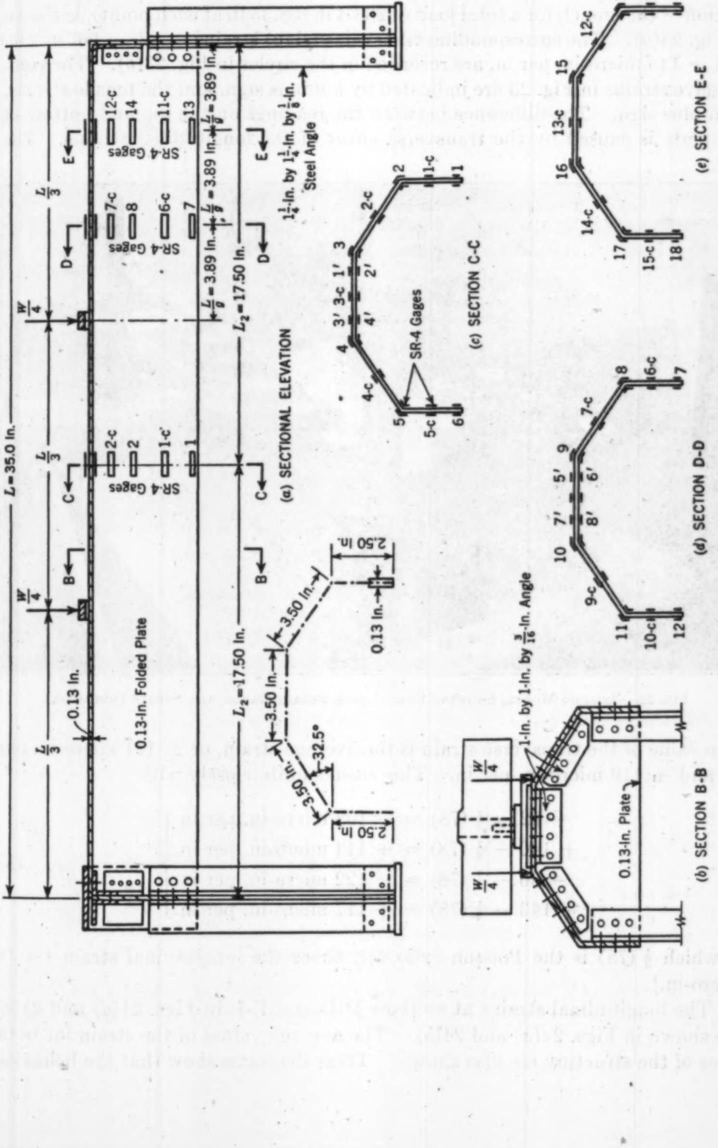
L = 35.0 In.
L/3
L/3
L/3
W/4
W/4
0.13 In.
0.13-In. Folded Plate
B
B
C
C
D
D
E
E
SR-4 Gages
SR-4 Gages
SR-4 Gages
2-c
2
1-c
1
7-c
8
6-c
7
12-c
14
11-c
13
L₂ = 17.50 In.
L₂ = 17.50 In.
L/9 = 3.89 In.
L/9 = 3.89 In.
L/9 = 3.89 In.
1½-In. by 1¼-In. by ⅛-In. Steel Angle
(a) SECTIONAL ELEVATION
3.50 In.
3.50 In.
3.50 In.
3.50 In.
32.5°
2.50 In.
2.50 In.
0.13 In.
1-In. by 1-In. by 3/16-In. Angle
W/4
W/4
0.13-In. Plate
(b) SECTION B-B
SR-4 Gages
5
4-c
4
3'
3-c
1'
3
2-c
2
4'
2'
5-c
6
11-c
1
(c) SECTION C-C
11
9-c
10
7'
5'
9
7-c
8
10-c
8'
6'
6-c
12
7
(d) SECTION D-D
17
14-c
16
13-c
15
12-c
14
15-c
11-c
18
13
(e) SECTION E-E

FIG. 21.—DETAILS OF THE HIPPED PLATE ROOF MODEL

1′, 2′, 3′, ⋯, 8′ as indicated in Figs. 21(*c*) and 21(*d*). These gages (on both sides of a plate element) were wired independently, thus giving the transverse strains at the outer and inner surfaces of the roof separately. A picture of the model appears as Fig. 22.

Results.—The distribution of the longitudinal (plate) strains at the middle section of the model, for a total load of 233.4 lb (58.35 lb at each point), is shown in Fig. 23(*a*). The corresponding transverse (slab) strains − 82, − 96, + 140, and + 143 micro-in. per in. are recorded in the circles in Fig. 23(*b*). The compressive strains in Fig. 23 are indicated by a minus sign, and the tensile strains, by a plus sign. The difference between the readings on the top and bottom of the plate is caused by the transverse effect of the longitudinal strains. The true value of the transverse strain is the average strain, or ± 111 micro-in. per in. and ± 119 micro-in. per in. This checks quite closely with

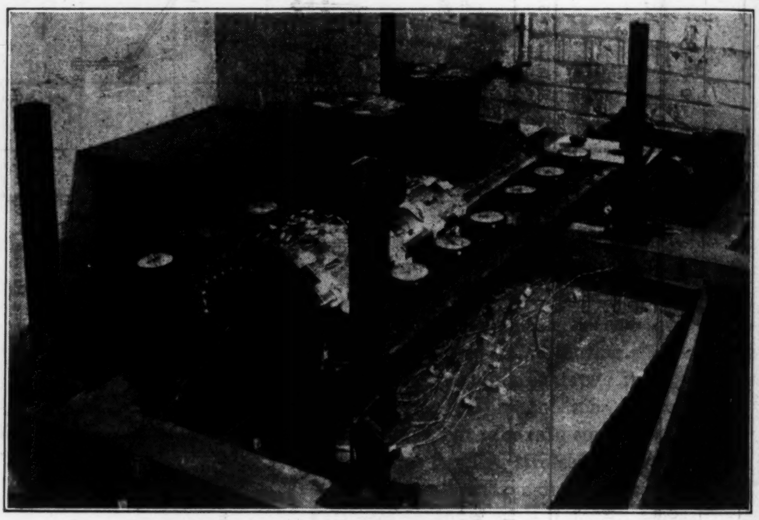

FIG. 22.—LOADED MODEL, SHOWING DIAL GAGES, STRAIN GAGES, AND STRAIN INDICATOR

$$\left.\begin{aligned} -82 - \tfrac{1}{3}(78) &= -108 \text{ micro-in. per in.}\\ +140 - \tfrac{1}{3}(78) &= +114 \text{ micro-in. per in.}\\ -96 - \tfrac{1}{3}(78) &= -122 \text{ micro-in. per in.}\\ +143 - \tfrac{1}{3}(78) &= +117 \text{ micro-in. per in.}\end{aligned}\right\}\quad\ldots\ldots\ldots\ldots(8)$$

in which $\frac{1}{3}(78)$ is the Poisson ratio ($\frac{1}{3}$), times the longitudinal strain (− 78 micro-in.).

The longitudinal strains at sections D-D and E-E in Figs. 21(*d*) and 21(*e*) are shown in Figs. 24(*a*) and 24(*b*). The average values of the strain for both sides of the structure are also shown. These diagrams show that the behavior

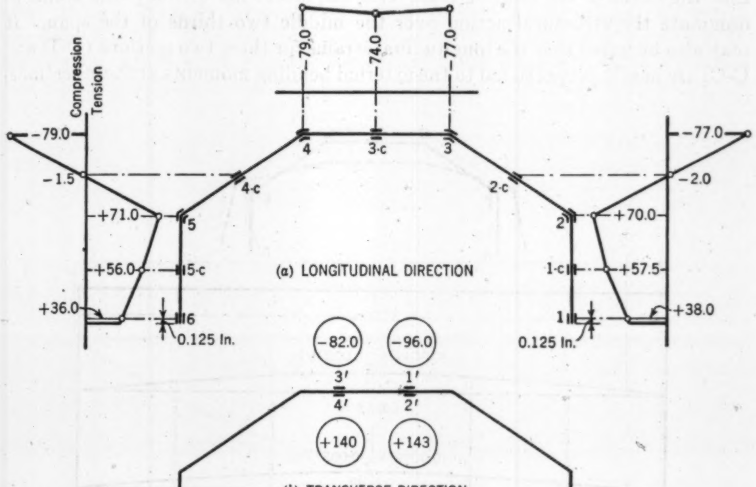
Compression
Tension
−79.0
−74.0
−77.0
−79.0
−1.5
+71.0
+56.0
+36.0
0.125 In.
4
3-c
3
4-c
5
5-c
6
−77.0
−2.0
2-c
2
+70.0
1-c
+57.5
1
+38.0
0.125 In.
−82.0
−96.0
3′
1′
4′
2′
+140
+143

(*a*) LONGITUDINAL DIRECTION

(*b*) TRANSVERSE DIRECTION

FIG. 23.—DISTRIBUTION OF UNIT STRAINS AT MIDDLE SECTION OF MODEL, IN MICRO-INCHES PER INCH

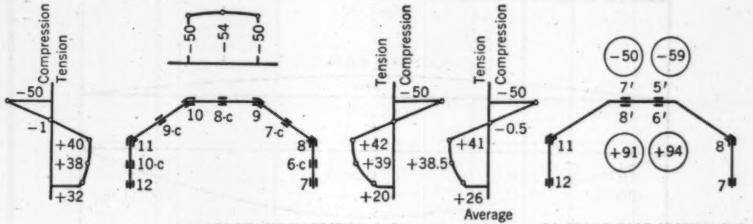
Compression
Tension
−50
−1
+40
+38
+32
−50
−54
−50
10
8-c
9
9-c
7-c
11
10-c
12
8
6-c
7
Tension
Compression
−50
+42
+39
+20
Tension
Compression
−50
−0.5
+41
+38.5
+26
Average
−50
−59
7′
5′
8′
6′
+91
+94
11
12
8
7

(*a*) LONGITUDINAL, SECTION D-D

(*c*) TRANSVERSE, SECTION D-D

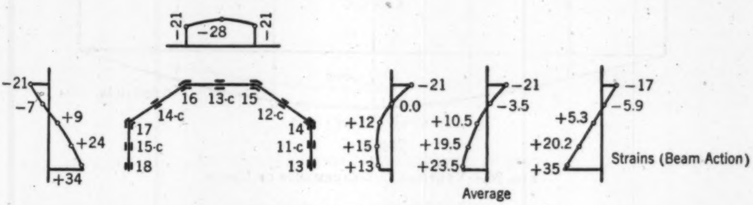
−21
−28
−21
−21
−7
+9
+24
+34
16
13-c
15
14-c
12-c
17
15-c
18
14
11-c
13
−21
0.0
+12
+15
+13
−21
−3.5
+10.5
+19.5
+23.5
Average
−17
−5.9
+5.3
+20.2
+35
Strains (Beam Action)

(*b*) LONGITUDINAL, SECTION E-E

FIG. 24.—STRAINS AT CERTAIN SECTIONS OF THE MODEL, IN MICRO-INCHES PER INCH

at section D-D is similar to that at the middle, section C-C. This fact indicates that the effect of the relative transverse displacements of the joints seems to dominate the structural action over the middle two thirds of the span. It may also be noted that the longitudinal strains for these two sections (D-D and C-C) are nearly proportional to the external bending moments at these sections, computed on the basis of simple end supports. However, at section E-E, where the translation of the edges is small, the distribution of the longitudinal strains more nearly approaches that for ordinary beam action, as shown, although some effect of the change of shape of the cross section is apparent. Transverse strains at section D-D are shown in Fig. 24(*c*).

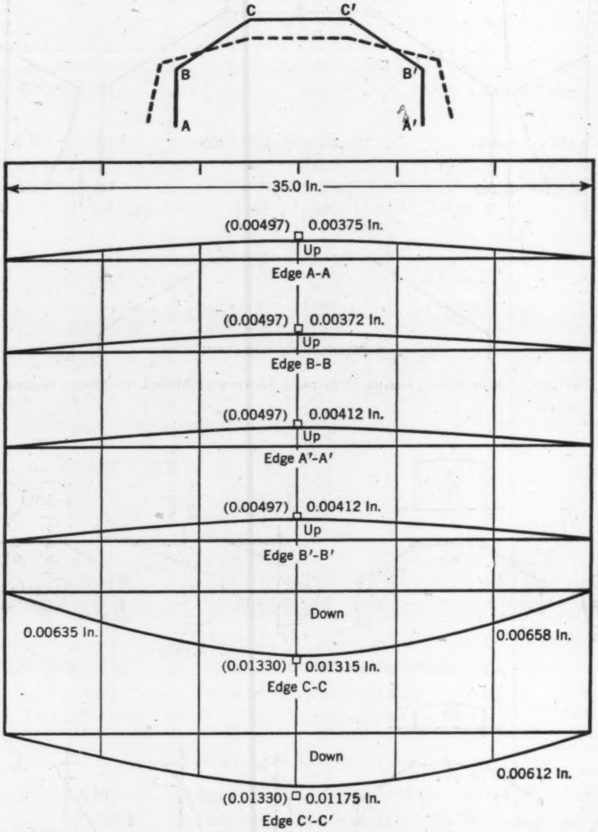

FIG. 25.—VERTICAL DISPLACEMENTS OF EDGES

The measured vertical and horizontal displacements of the edges are shown in Figs. 25 and 26, respectively. The theoretical displacements (in inches) computed according to the proposed theory are shown between parentheses in the same figures. The vertical displacements of the elements AB and A′B′ are upward, which agree with the theoretical value obtained. This motion is comparatively small, but very significant. The horizontal movements of edges B and B′ are of the same order of magnitude as the vertical movements of C and C′. A comparison of the theoretical and measured values of edge translations is given in Table 7. The computed values of the displacements agreed quite well with the measured values.

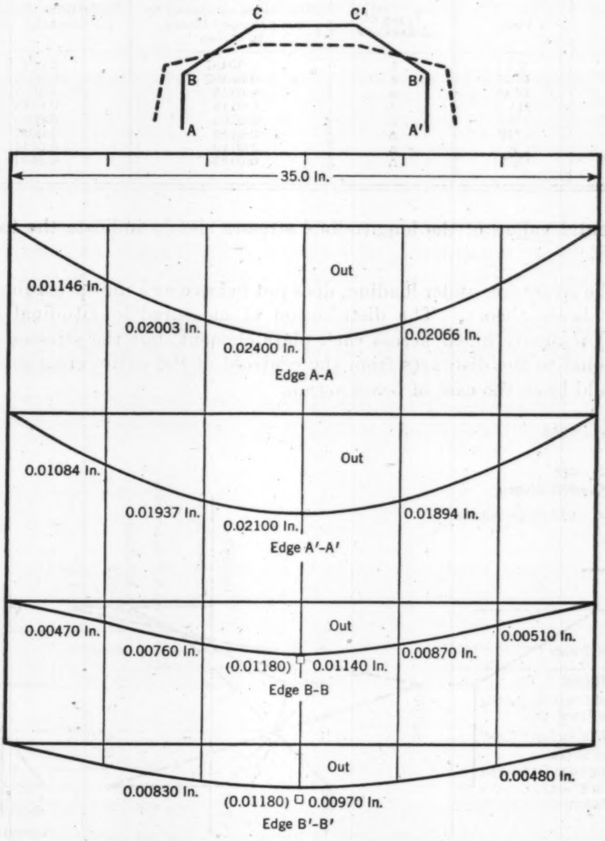

FIG. 26.—HORIZONTAL DISPLACEMENTS OF EDGES

The longitudinal stresses determined by the various theories and test results are listed in Table 6 and are presented graphically in Fig. 27. The correction diagram corresponding to edge translation is included in Fig. 27. The experimental values of the longitudinal stresses clearly indicate the following facts:

TABLE 7.—MODEL DEFLECTIONS AT THE MIDDLE SECTION (EXAMPLE NO. 2)

Edge	Plate	Types of deflections	Deflections computed by the proposed theory, in inches	Deflections evaluated experimentally, in inches
A′	A′B′	δ	0.00497	0.00412
B′	B′A′	δ	0.00497	0.00412
B′	B′A′	Δ	0.0118	0.0097
B	BA	Δ	0.0118	0.0114
B′	B′C′	Δ	0.0105	0.0092
C′	C′B′	Δ	0.0112	0.0099
C	CB	Δ	0.0112	0.0111
C	CC′	Δ	0.0133	0.0131

1. The structure, under loading, does not behave as a unit according to the ordinary beam theory. The distribution of measured longitudinal stresses (Fig. 27) is nearly linear across each plate element, but the stresses are not proportional to the distances from the centroid of the entire cross section, as they would be in the case of beam action.

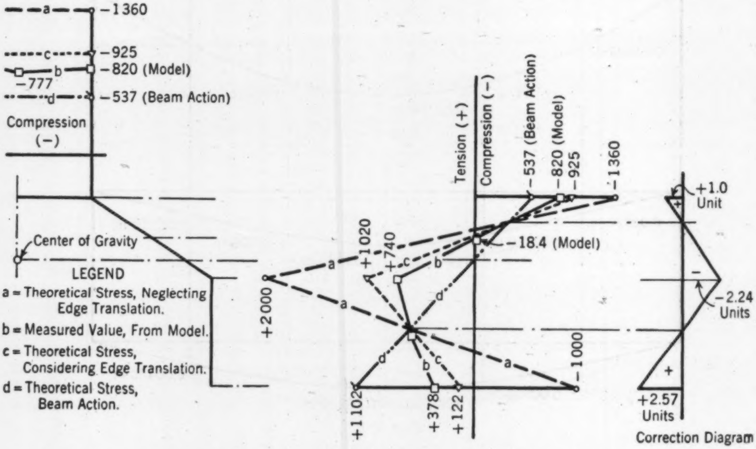

FIG. 27.—COMPARISON BETWEEN THE MEASURED AND THEORETICAL LONGITUDINAL STRESSES AT THE MIDDLE SECTION OF THE MODEL, IN POUNDS PER SQUARE INCH

2. When the relative transverse displacements of the joints are not taken into consideration, the stress values as computed by the approximate theory are much higher than the experimental values. The errors at the joints from top to bottom of the cross section (Fig. 27) are (joint C) + 66%, (joint B) + 170%, and (joint A) − 365%. These errors are given in Table 6.

3. The approximate theory may not even predict the right sense of the longitudinal stresses, as shown by the opposite signs obtained at edges A and A′ for experimental and current theoretical values.

4. On the other hand, when the relative displacements of the joints are considered, the values of the longitudinal stresses agree much better with the experimental results. The errors at the joints from top to bottom of the cross section are (joint C) 13%, (joint B) 38%, and (joint A) − 68%, respectively—that is, about one fifth of the corresponding errors produced by the approximate theory.

TABLE 8.—MAXIMUM TRANSVERSE STRESSES, IN POUNDS PER SQUARE INCH (EXAMPLE NO. 2)

Points (see Fig. 28) (1)	Values obtained experimentally (2)	Values yielded by the proposed theory (3)	Average percentage of error (4)
1′ and 2′	∓1,170	∓1,440	18.5
3′ and 4′	∓1,260	∓1,440	

The transverse stresses determined experimentally and by the proposed theory are listed in Table 8 and are presented graphically in Fig. 28, in which the measured values of stresses are indicated by small circles. These stresses correspond to the transverse strains shown in Figs. 23 and 24. Because the relative joint displacements are neglected in the approximate theory, the values of the transverse stresses yielded thereby are zero. From the results presented in Table 8 and in Fig. 28, together with the comments at the end of Example No. 1 and Example No. 2, it can be noted that:

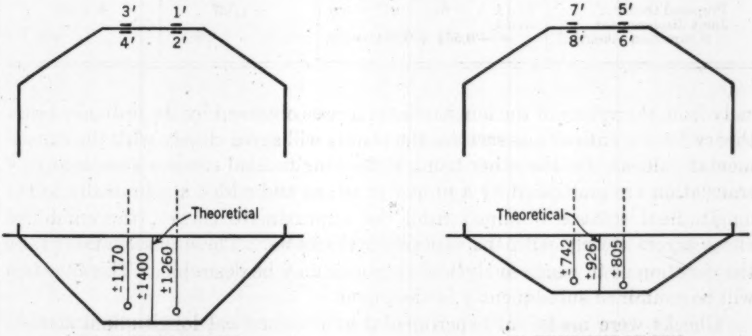

(*a*) TRANSVERSE BENDING STRESSES AT SECTION C-C

(*b*) TRANSVERSE BENDING STRESSES AT SECTION D-D

FIG. 28.—COMPARISON BETWEEN THEORETICAL AND EXPERIMENTAL TRANSVERSE STRESSES IN THE MODEL (ALL STRESSES IN POUNDS PER SQUARE INCH)

a. Although the transverse stresses are of the same order of magnitude as the longitudinal stresses (or even larger), the approximate theory misses them completely in the case of concentrated loads acting at the joints, or of tangential forces acting on the plates.

b. In the case of uniform loads acting on the roof (Example No. 1), the approximate theory still errs greatly on the unsafe side, the error varying from + 60%to − 280%. The error in the transverse bending moment (Fig. 15) that governs the slab design is quite serious.

c. The proposed theory presents a correct picture of the transverse stresses in the cases of concentrated, tangential, or uniform loads.

d. The error in the case of the proposed theory is on the safe side and is about 19%, as is indicated in Fig. 28.

The correction diagram representing the effect of joints displacements on the longitudinal stresses is shown separately in Fig. 27. An interesting fact brought out in Fig. 27 is that the different longitudinal stress diagrams pass through two common points which correspond to the two zero points of the correction diagram. This condition indicates that, if the ordinates of the correction diagram are multiplied by a proper constant and subtracted algebraically from the values of the longitudinal stresses obtained by the ordinary beam theory for the entire cross section, the results will agree closely with the experimental values. On the other hand, if the longitudinal stresses accompanying translation are multiplied by a proper constant and added algebraically to the longitudinal stresses obtained from the approximate theory, the combined effect agrees closely with the experimental results. These observations raise the question as to which analytical approach may be desirable. This question will be examined subsequently in the paper.

TABLE 9.—CHECK ON THE EXPERIMENTAL AND LONGITUDINAL STRESSES AT THE MIDDLE SECTION OF THE MODEL

Determination of stresses	Summation of stresses, in pounds per square inch	BENDING MOMENTS, IN INCH-POUNDS	
		Internal	External
Experimental	$E\,\Sigma\,\epsilon\,dA = E\,(-69.75 + 69.449) \approx 0.0$	+ 1,357	+ 1,350
Proposed theory	$\Sigma s\,dA = -842 + 837 \approx 0.0$	+ 1,357	+ 1,360
Joint displacement (Correction diagram)	$\Sigma s\,dA = -0.564 + 0.564 = 0.0$	0.0	0.0

Checks were made[11] of experimental and theoretical longitudinal stresses against basic equations of equilibrium, the conditions of equilibrium being fulfiled in every case. Table 9 summarizes these results. In the equations in Table 9, ϵ represents the unit linear strains, and A the cross-sectional area of the metal.

Hipped Plate Structures Compared with Ordinary Beams.—In hipped plate structures, the thickness t of each plate element is relatively small as compared to the other dimensions of the cross section of the structure. Consequently, the section of the structure changes its shape under loading, and the part of the load carried by each plate element varies with the position of the load on the cross section (Fig. 29), depending on the position of the load relative to the plate element under consideration. Also, there are forces and bending moments acting in the transverse direction (slab action). The condition of a plane section before deformation remaining plane after deformation does not hold for the cross section as a whole, except under very special cases of loading; but it holds fairly well for each individual plate element, especially for cross sections that are distant from the diaphragm.

---

[11] "The Analysis of Hipped Plate Structures Considering the Relative Displacements of the Joints," by Ibrahim Gaafar, thesis presented to the University of Michigan at Ann Arbor, Mich., in 1949, in partial fulfilment of the requirements for the degree of Doctor of Science, Appendix III, pp. 112–117.

If a member under load is to behave as an ordinary beam, certain requirements must be fulfiled. The thickness t should be large enough in comparison with the other dimensions of the cross section to prevent the section from changing its shape when the member is deflected longitudinally under loading—otherwise, internal diaphragms must be used to prevent distortion of the cross section. Under ordinary beam action, the cross section only moves parallel to itself, and the whole cross-sectional plane that existed before bending remains plane after bending. No transverse bending or deflection should exist under beam action, or the section will change its shape. Referring to Fig. 29, the longitudinal stress distribution over the cross section is not affected by changing the points of application of the loads, so long as the loads are symmetrical with respect to the vertical axis of symmetry of the cross section. Each plate element of the member carries a constant fraction of the total applied load, depending only on the dimensions of the cross section. Beam action can be a very special case in the behavior of a hipped plate structure under the following conditions: External forces must be either line loads or concentrated loads acting only at the edges and distributed in a very special manner so that each of the final resultant P-loads on each individual plate equals the P-load on the same plate if the structure were to behave as an ordinary beam. Any distributed load or concentrated load acting between the joints will result in transverse bending and, consequently, in a change in the shape of the cross section.

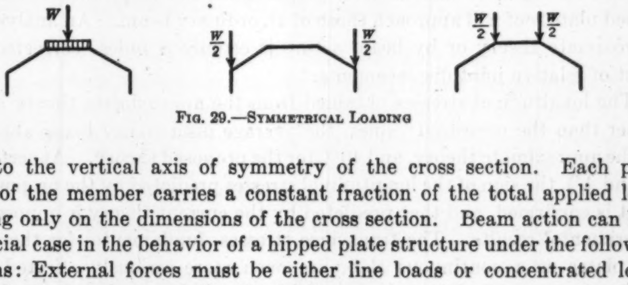

FIG. 29.—SYMMETRICAL LOADING

Therefore, it is evident that, if an effort is made to solve the hipped plate roof described previously by beginning from the preliminary assumption of a beam action and trying to correct it to obtain the longitudinal stresses of a hipped plate structure, two corrections for the longitudinal stresses obtained from beam action must be applied. These corrections are as follows:

(a) Longitudinal stresses resulting from the difference between the plate loads P included in the assumption of beam action, and the plate loads P obtained from the actual external loads, must be included. Under the preliminary assumption of beam action, a certain part of the total loads must be assumed to be carried by each plate element, which is not necessarily the case. However, beam action can be acquired by applying certain restraining line loads along the joints, and removing them by means of the first correction. The analytical work for carrying out this correction is very similar to that used in correcting for the relative displacements of the joints.

(*b*) Longitudinal stresses corresponding to the change in the *P*-loads resulting from the relative deflections of the joints must be determined because, in beam action, transverse deflections are not taken into consideration. The writer has described the procedure for this correction previously.

It can be seen from the foregoing discourse that more analytical work will be involved by trying to solve the problem from the beam action approach because correction for the relative displacements of the joints must be made.

Summary and Conclusions

A (24 S-T) aluminum model is both convenient and satisfactory for studying the structural action of hipped plate roofs. The effect of the relative displacements of the joints appears to dominate the structural action over the middle two thirds of the span. If the relative displacements of the joints are eliminated by introducing more intermediate diaphragms, the longitudinal stresses of a hipped plate roof will approach those of an ordinary beam. An analysis by the approximate theory or by beam action is erroneous unless corrected for the effect of relative joint displacements.

The longitudinal stresses obtained from the approximate theory are much higher than the measured values, the average discrepancy being about 200% for the approximate theory, and 40% for the proposed theory. At certain edges (A and A′), the sign of the longitudinal stresses predicted by the proposed treatment is confirmed, and that predicted by the current theory is opposed by the experimental results. The transverse stresses, fundamental for the design of the plates as a continuous slab, are even more seriously affected by joint displacements. The approximate theory errs greatly on the unsafe side. The necessary correction to be applied to the transverse stresses found by that theory may be as much as 320%, with a change of sign (see Example No. 1). In the case of concentrated loads at the joints (Example No. 2), the maximum transverse stresses were experimentally found to be 150% of the maximum longitudinal stresses. The proposed treatment gives a correct picture of the experimental stresses both in magnitude and in sign, the discrepancy being 20% on the safe side.

The proposed theory offers a solution for the problem in the form of simple linear algebraic equations in which the number of unknowns is $(r - 1)$ for unsymmetrical loading and $\left(\frac{r}{2} - 1\right)$ for symmetrical loading, in which r is the number of joints. For a roof of five plates (that is, four joints) the number of equations is three for unsymmetrical loading and one for symmetrical loading.

FURTHER INVESTIGATION

The effect of intermediate diaphragms and the effects of change of thickness t, width h, and span L of plate elements, on the behavior of the model, all merit investigation. The effect of the shape of the cross section on the behavior of the model is worthy of study, and the effect of continuous spans in both directions should be considered. Deep beam action is a subject affecting this type of structure. Studies of the behavior of models just before failure and of reinforced concrete models are also suggested.

ACKNOWLEDGMENTS

The writer wishes to express his appreciation to L. C. Maugh, M. ASCE, of the University of Michigan, at Ann Arbor, for his valuable advice and suggestions in regard to the conduct of this work, and for the time he has kindly given for consultation.

The writer wishes to thank the ASCE reviewers for criticism, the meeting of which added considerably to the clarity of the paper. Thanks are also due to the Egyptian Education Bureau at Washington, D. C., and to the Engineering Research Institute of the University of Michigan for partly financing the work.

APPENDIX. NOTATION

The following symbols, adopted for use in the paper, and for the guidance of discussers, conform essentially with American Standard Letter Symbols for Structural Analysis (ASA Z10.8—1942), prepared by a Committee of the American Standards Association, with Society representation, and approved by the Association in 1942:

A = the cross-sectional area of a plate, $h\,t$;

a, b, c = the subscripts used to denote edges and plate elements A, B, $\cdots$, etc.;

c = the stiffness coefficient of a member;

h_{ab} = the width of plate AB, or distance between edges A and B measured along the center line of the cross section of a plate;

k = the rigidity coefficient $\left(k = \frac{E\,I}{h}\right)$;

L = the span of the roof between end diaphragms;

M = the moments resisted by the plates;

P = the force components of the slab shears Q, parallel to the adjacent plates and resisted by plate action;

Q_{bc} = the slab shearing force per unit length, acting from joint B on plate BC in the direction perpendicular to BC;

t_{ab} = the thickness of plate AB;

V_b = the shear stresses per unit length parallel to edge B, acting from joint B along the edges of the adjacent plates;

w = the uniformly distributed load on the roof;

W = the total vertical force on the roof;

Z = the section modulus of a plate, considered to act as a beam $\left(Z = \frac{t h^2}{6}\right)$;

0 = the subscript used to denote the middle of a beam or a plate;

Δ_{bc} = the component of the displacement of edge B perpendicular to plate BC, corresponding to slab action;

Δ_{cb} = the component of the displacement of edge C perpendicular to plate BC (slab action);

δ_{bc} = the component of the displacement of edge B in the plane of plate BC (plate action);

$\delta_{cb} = \delta_{bc}$;

δ_0 = the deflection at the middle of a beam;

δ_1 = the plate deflection at its middle according to the approximate theory; and

δ_2 = the correction to the plate deflection produced at the middle section by the relative transverse displacements of the joints.

DISCUSSION

Herman Craemer.[12]—Following World War II hipped plate design was once again undertaken after it had been ignored for fifteen years preceding the war. Many investigations, valuable and otherwise have been conducted. Mr. Gaafar is to be congratulated for his valuable contribution to the field.

During the investigations conducted by Mr. Ehlers[3] and the writer,[5, 6, 8] the effect of the deflection of the edges was greatly underrated. Mr. Gaafar's statements (under the heading, "Introduction—Previous Theory") that "* * * the plates were assumed to be connected by hinged joints" and that the connecting moments of the slabs along the edges were "neglected entirely" were erroneous, however, because it was clearly stated (by Mr. Ehlers and the writer) that in the direction normal to the edges, the system behaves like a continuous slab rigidly supported at the edges. Thus, the oversimplification does not consist in neglecting the continuity but only in neglecting the translation of the edges. The comparison of the "approximate theory" with Mr. Gaafar's approach is therefore somewhat misleading.

The writer has conducted an investigation[13] which is based on the same assumptions listed under the heading "Limitations." It was found that the behavior of the system depends on the stiffness coefficient,

$$c = \frac{K\, t^3\, L^4}{h^6} \qquad \text{(9)}$$

in which K is a function of the shape of the cross section and the distribution of a load across the latter. If $c = 0$, the writer's elementary theory—but not the "approximate theory" in Mr. Gaafar's meaning—is correct. If c is infinite, the cross section as a whole behaves like an ordinary beam with a linear distribution of the longitudinal stresses. Thus, there is a gradual transition from "pure shell effect" ($c = 0$) to "pure beam effect" ($c = \infty$).

Although the writer's work[13] is probably easier to understand than the papers by Mr. Gruber,[4, 7] it is necessarily more complex than Mr. Gaafar's work because the writer's investigation takes into consideration the geometrical compatibility along the whole length of edges, thus leading to differential equations.

One of the author's principal simplifying statements is that the edge-translations are sinusoidal. However, since the transverse moments depend linearly on the latter, the transverse moments should also be sine waves. For a system approximating pure beam effect, however, this is not correct. This case is similar to the case of a narrow rectangular slab supported at the four edges and subjected to a uniform load, within which the moments in the direction of the short span are sensibly constant except near the short edges. This cannot be described by one sine wave. There is too much interaction in a prismatic shell between the various statical and geometrical effects occurring at a number of edges to allow for a simple approach covering the whole range of stiffness coefficients. Mr. Gaafar's work may nonetheless be useful for systems that approximate the pure shell effect.

---

[12] Civ. Engr., Germany.

[13] "Design of Prismatic Shells," by H. Craemer. *Journal*, A. C. I., No. 6, February, 1953.

For large values of c, a first approximation might be the assumption of pure beam effect; to this condition corrections to fulfill the geometrical conditions might be applied. There is a great need for theoretical research in hipped plate design and analysis.

James M. Paulson,[14] **J. M. ASCE, and L. C. Maugh,**[15] **M. ASCE.**—This paper provides much valuable information concerning the analysis of hipped plate or prismatic roof structures which consist of an assemblage of plate elements rigidly connected at their edges. Mr. Gaafar asserts (and it is substantiated by model tests) that both the transverse and longitudinal stresses are influenced considerably by the components of the edge displacements normal to the planes of the various plate elements. As the analysis is greatly complicated by this distortion of the cross section, it is of importance to determine whether such displacements need be considered when uniformly distributed forces only are acting. This problem had been investigated by Mr. Craemer,[13] although the arrangement of the material and procedure is quite different from that given by the author. Mr. Craemer was concerned more with the deviation from the linear distribution of the longitudinal stresses (as given by the ordinary beam formula) than with the discrepancies in the approximate hipped plate theory. Mr. Gaafar has noted that this theory does not consider the effect of edge displacements.

TABLE 10.—VALUE OF THE RATIO s_c/s_a AT THE EDGES OF THE EDGE BEAMS

Edge-beam depth, in feet	WIDTH-TO-LENGTH RATIO					
	0.288		0.407		0.576	
	Top edge	Bottom edge	Top edge	Bottom edge	Top edge	Bottom edge
7.5	+0.034	−0.028	+0.0092	−0.0076	+0.0023	−0.0019
3.75	+0.36	−0.19	+0.12	−0.062	+0.029	−0.015
1.875	+4.52	−0.56	+2.23	−0.29	+0.83	−0.098
0.9375	−3.43	−0.87	−2.80	−0.71	−1.60	−0.41

The writers have evaluated the error in the results obtained by the approximate method for structures of various proportions when subjected to a uniformly distributed vertical load. In Table 10 a comparison is shown of the correction s_c of the longitudinal stress caused by edge displacements to the stress s_a which is obtained by the approximate method in terms of the ratio s_c/s_a. The term s_c is the difference in the longitudinal stress between the

---

[14] Asst. Prof. in Civ. Eng., Wayne Univ., Detroit, Mich.

[15] Prof. of Civ. Eng., Univ. of Michigan, Ann Arbor, Mich.

approximate method and Mr. Gaafar's solution which considers edge displacements. The values given in Table 10 are for a structure similar to the hipped plate roof shown in Fig. 2. Such a structure is designated as a "three-segment roof." Table 10 shows the variation in s_c/s_a at the top and bottom edges for various depths of edge beams and for various width-to-span ratios. In the computations the width of the structure was kept constant (36 ft) whereas the length was varied. The effect of the edge displacements becomes more pronounced as the depth of the edge beam decreases, and as the width-to-length ratio decreases. In these computations the torsional resistance of the edge beam has been neglected as in Mr. Gaafar's analysis. For large edge beams this factor may be appreciable, particularly on the value of the transverse moments.

The variation of the ratio s_c/s_a for roofs with various numbers of plate elements with horizontal projections when acting with two stiff vertical edge beams of 7.5-ft depth is shown in Table 11. These values are for a constant width-to-length ratio of 0.288 and for a uniform vertical loading. In the range of cases investigated, the values indicate that the importance of edge displacements increased with the number of plate elements.

TABLE 11.—Value of the Ratio s_c/s_a for a Width-to-Span Ratio of 0.288 and an Edge-Beam Depth of 7.5 Ft

Number of roof plates with horizontal projection	Top	Bottom
2	+0.041	−0.021
3	+0.034	−0.028
4	−1.64	+0.43
5	−2.39	+1.04

TABLE 12.—The Effect of Edge-Beam Depth on the Stress and Transverse Moment Corrections

Edge-beam depth, in feet	(a) $\frac{s_c}{s_a}$ – Ratio[a]		(b) $\frac{M'_c}{M_{ap}}$ – Ratio[b]		
	Three-segment roof	Five-segment roof	Width-to-Length Ratio		
			0.288	0.407	0.576
7.5	+0.034	−2.40	0.26	0.07	0.02
3.75	+0.36	−2.40	1.58	0.52	0.12
1.875	+4.52	−2.74	4.11	2.11	0.72
0.9375	−3.42	−3.94	5.65	4.69	2.65

[a] At the top edge of an edge beam in a roof with a width-to-length ratio of 0.288. [b] At joint C in a three-segment roof.

The importance of the number of plate elements extending over the width of the roof and of the stiffness of the vertical edge beams is further indicated by the results given in Table 12(*a*).

For a roof with five plate elements and two vertical edge beams, the results in Table 12(*a*) show that the approximate method is greatly in error even with extremely stiff edge beams. Evidently, the effect of the edge displacements on the longitudinal stresses can be several times the stress obtained from the approximate method which neglects the edge movement.

In Table 12(*b*) the effect of edge displacements on the transverse moments is shown for a three-segment roof with vertical edge beams subjected to uniform vertical loading. The ratio of M'_c (the correction of the moment at edge C in the three-segment roof of Fig. 2) to M_{ap} (the same moment at edge C by the approximate method) is given for various depths of edge beams for various width-to-span ratios.

Table 13 gives results similar to those in Table 12(*b*) for a roof with five plate elements across the width and two vertical edge beams. Table 13 also illustrates the importance of the correction for edge displacement irrespective of the edge-beam depth or the width-to-span ratio.

TABLE 13.—VALUE OF THE RATIO $\frac{M'_c}{M_{ap}}$ FOR FIVE-SEGMENT ROOFS

Edge-beam depth, in feet	Width-to-Span Ratio					
	0.288		0.407		0.576	
	Joint C	Joint D	Joint C	Joint D	Joint C	Joint D
7.5	−1.42	+1.20	−1.44	+1.07	−1.33	+0.96
3.75	+0.31	+4.51	−0.70	+2.08	−1.01	+1.13
1.875	+3.16	+10.22	+1.32	+5.39	+0.08	+2.04
0.9375	+4.91	+14.40	+3.88	+10.40	+2.38	+4.75

A graphical illustration is shown in Fig. 30 of the effect of varying the stiffness of the edge beams and the width-to-span ratio on the value of the total transverse edge moment. The values, which are for a uniform vertical loading over the entire roof, have been determined by use of Mr. Gaafar's method of analysis.

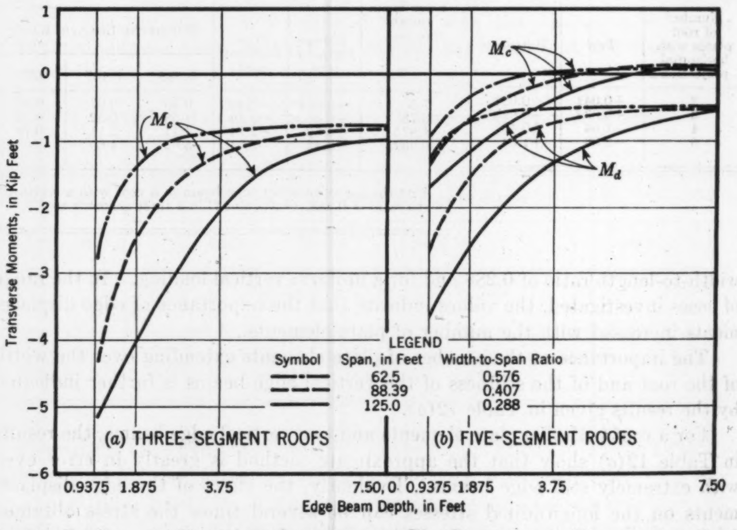

FIG. 30.—THE EFFECT OF VARYING THE STIFFNESS OF THE EDGE BEAMS AND THE WIDTH-TO-SPAN RATIO ON THE VALUE OF THE TOTAL TRANSVERSE MOMENT

A comparison is given in Fig. 31 of the actual longitudinal stress distribution at the midspan of a hipped plate structure of 36-ft width and spans of 62.5 ft, 88.39 ft, and 125 ft (as given by Mr. Gaafar's solution) to the corresponding values given by the ordinary beam formula assuming a linear distribution of stress. The ratio of the stress, s_g (that is given by the author's solution) to the corresponding value given by the ordinary beam formula,

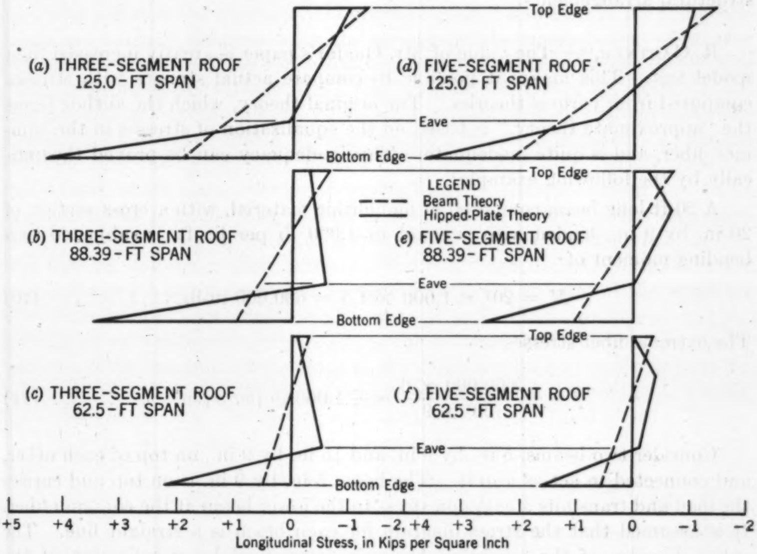

Fig. 31.—Distribution of the Longitudinal Stress at Midspan (1.875-Ft-Deep Edge Beam)

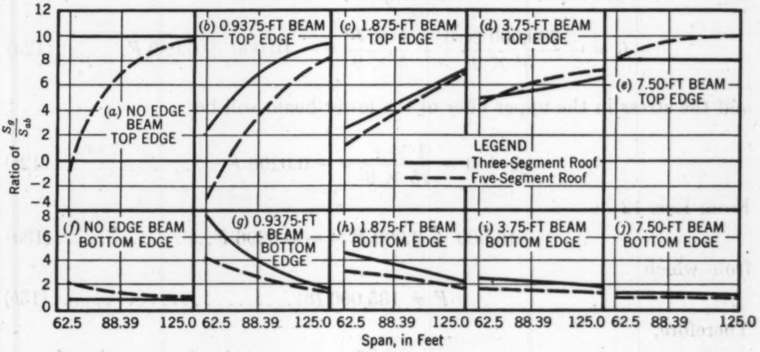

Fig. 32.—The Effect of Various Spans and Edge-Beam Depths in Three-Segment and Five-Segment Roofs on the Ratio s_g/s_{ab}

s_{ob}, is shown in Fig. 32 for the top and bottom edges for various width-to-span ratios and for various depths of edge beams. It is apparent that the assumption of a linear stress distribution is not sufficiently accurate for most structural arrangements.

R. GARTNER,[16].—The value of Mr. Gaafar's paper is greatly increased by a model test. This makes it possible to compare actual stresses with stresses computed from various theories. The original theory, which the author terms the "approximate theory," is based on the equalization of stresses in the common fiber, and is quite inadequate. This inadequacy can be proved theoretically by the following example:

A 20-ft-long beam composed of monolithic material, with a cross section of 20 in. by 9 in., loaded with w equal to 1,000 lb per lin ft, is subjected to a bending moment of

$$M = 20^2 \times 1{,}000 \times 1.5 = 600{,}000 \text{ in-lb} \qquad (10)$$

The extreme fiber stresses are

$$f = \pm \frac{600{,}000 \times 6}{20^2 \times 9} = \pm 1{,}000 \text{ lb per sq in.} \qquad (11)$$

Consider two beams, 5 in. by 9 in. and 15 in. by 9 in., on top of each other, and connected to act as a unit. The beam 5 in. by 9 in. is on top and carries the load and transmits a common stress to the lower beam at the common fiber. It is assumed that the stress diagram for each beam is a straight line. The stress diagram of the combined beam is determined by equalization of the stresses of the common fiber. There will be a shear stress, F, in this fiber. The stress in the lower fiber of the upper beam will be

$$f_b = -\frac{600{,}000 \times 6}{5^2 \times 9} + \frac{4 \times F}{5 \times 9} = -16{,}000 + 0.089\,F \qquad (12a)$$

and the stress in the upper fiber of the lower beam will be

$$f_b = 0 - \frac{4 \times F}{15 \times 9} = -0.0296\,F \qquad (12b)$$

From Eqs. 12

$$-16{,}000 + 0.089\,F = -0.0296\,F \qquad (13a)$$

from which

$$F = 135{,}000 \text{ lb} \qquad (13b)$$

Therefore,

$$f_a = +\frac{600{,}000 \times 6}{5^2 \times 9} - \frac{2 \times 135{,}000}{5 \times 9} = 10{,}000 \text{ in-lb} \qquad (14a)$$

$$f_b = -0.0296 \times 135{,}000 = -4{,}000 \text{ in-lb} \qquad (14b)$$

---

[16] Cons. Civ. Engr., Capetown, Union of South Africa.

and

$$f_c = 0 + \frac{2 \times F}{15 \times 9} = 2{,}000 \text{ in-lb} \ldots\ldots\ldots\ldots\ldots (14c)$$

The stresses in the common fiber are equal, but the stresses in the composite beam are entirely different from the stresses in the single beam. That the stresses determined for the composite beam are impossible is shown by the fact that, according to the stresses, the upper beam would be sagging, and the lower beam would be curved upward. Evidently, equalization of the common fiber stresses is inadequate, and a further condition must be imposed. It can be deduced that the upper beam presses down upon the lower, which therefore takes a part of the load, relieving the upper beam by the same amount, p. The distribution of p in the longitudinal direction is dependent on the deflection curve. As the beam deflects (as a result of a uniformly distributed load) p will also be uniformly distributed. Therefore, both deflection curves must have the same form, both should be sagging, and (on account of the equalization) the common fiber must have the same length. The two curves are then identical. As a second condition, either one point of the deflection line can be assumed to be common, or the slope of the deflection lines at any point can be assumed to be identical for the two beams. With the load carried by the lower beam designated as p, the upper beam carries a load of $(1{,}000 - p)$.

The angle of the deflected upper beam at the support is

$$E\,\gamma = \frac{1}{3} \times 20 \times 12 \, \frac{(1{,}000 - p) \times 20^2 \times 1.5 - F \times 2.5}{-\,5^3 \times 9} \times 12 \ldots (15a)$$

and for the lower beam the angle is

$$E'\,\gamma = \frac{1}{3} \times 20 \times 12 \, \frac{p \times 20^2 \times 1.5 - F \times 7.5}{15^3 \times 9} \times 12 \ldots\ldots (15b)$$

Because the angles are equal

$$280\,p + F = 270{,}000 \ldots\ldots\ldots\ldots\ldots\ldots (16a)$$

the equalization results in

$$14.222\,p + 0.11874\,F = 16{,}000 \ldots\ldots\ldots\ldots\ldots (16b)$$

from which

$$p = 844 \text{ lb} \ldots\ldots\ldots\ldots\ldots\ldots\ldots\ldots (17a)$$

$$1{,}000 - p = 156 \text{ lb} \ldots\ldots\ldots\ldots\ldots\ldots (17b)$$

and

$$F = 33{,}638 \text{ lb} \ldots\ldots\ldots\ldots\ldots\ldots\ldots (17c)$$

Computing the stresses from these values in the same manner as previously, they prove to be identical to those of the monolithic beam.

Considering the hipped beam shown in Fig. 3 to be subjected to vertical experimental loads of 58.4 lb at C and C′, it is of interest to compute, from the given average stresses, the forces which each plate carries in the longitudinal direction. The forces are, for plate AB,

$$p_1 = 17.1 \text{ lb} \qquad (18a)$$

and for plate BC,

$$W - p_2 = 108 - 38.5 = 69.5 \text{ lb} \qquad (18b)$$

The shear forces are, at point B,

$$F_1 = 180.5 \text{ lb} \qquad (19a)$$

and at point C,

$$F_2 = 163.3 \text{ lb} \qquad (19b)$$

In contrast to Mr. Gaafar's solution, the load W is (in this case) the load at each third point of span L.

With these loads, the free moments are, for plate AB,

$$M_0 = \frac{35}{3} \times 17.1 = 199 \text{ in-lb} \qquad (20a)$$

and for plate BC,

$$M_0 = \frac{35}{3} \times 69.5 = 810 \text{ in-lb} \qquad (20b)$$

The final stresses are, at point A in plate AB,

$$f_{A,AB} = \frac{199}{0.1354} - \frac{2 \times 180.5}{0.325} = 1{,}470 - 1{,}110 = +\,360 \text{ lb per sq in} \qquad (21a)$$

at point B, in plate AB,

$$f_{B,AB} = -\,1{,}470 + 2{,}220 = +\,750 \text{ lb per sq in} \qquad (21b)$$

at point B, in plate BC,

$$f_{B,BC} = +\,\frac{810}{0.266} - \frac{4 \times 180.5}{0.455} - \frac{2 \times 163.3}{0.455} = 3{,}050 - 1{,}590 - 718 = +\,742 \text{ lb per sq in} \qquad (21c)$$

at point C, in plate BC,

$$f_{C,BC} = -\,3{,}050 + 795 + 1{,}436 = -\,819 \text{ lb per sq in} \qquad (21d)$$

at point C, in plate CC′,

$$f_{C,CC'} = -\,\frac{2 \times 163.3}{0.455} = -\,718 \text{ lb per sq in} \qquad (21e)$$

The stresses computed in Eqs. 21 should be compared with those given in Col. 5, Table 6. The stress computed in Eq. 21*e* which should correspond to that of Eq. 21*d* has an error of 14%. If it is considered that the values of p_1, p_2, F_1, and F_2 vary slightly, this error is not too large—especially as the difference in stresses and deflections measured at the two sides of the model is, at some points, as great as 13%.

If the stresses computed by Mr. Gaafar are used rather than the stresses measured from the model, the following approximate values for the forces are obtained:

$$p_1 = 14.7 \text{ lb} \qquad (22a)$$

$$W - p_2 = 108 - 25.8 = 82.2 \text{ lb} \qquad (22b)$$

$$F_1 = 186 \text{ lb} \qquad (22c)$$

$$F_2 = 210 \text{ lb} \qquad (22d)$$

These values give very nearly the same stresses as those determined by Mr. Gaafar.

Conclusions.—It can be seen that mere equalization of stresses at the junction is not sufficient; another condition must be introduced in order to determine the actual stress conditions in a structure. The condition that Mr. Gaafar introduced seems to be adequate, but may be simplified if the exact equation can be used, together with the equation for equalization. Instead of using several steps, the solution could be obtained in one operation. More tests on larger models would be useful. In the model used by the author there seems to have been a slight twist, as the deflections on one side are all larger than the corresponding deflections on the opposite side. The method advanced by Mr. Gaafar is an important step forward in the solution of this problem.

IBRAHIM GAAFAR,[17] A. M. ASCE.—The interesting discussions contributed by Mr. Craemer, Messrs. Paulson and Maugh, and Mr. Gartner are gratifying to the writer.

The historical information to which Mr. Craemer has taken exception is true only of the work to which it referred—namely, Mr. Ehlers' work.[3] Mr. Craemer extended the statements about Mr. Ehlers' assumptions to his own works[5,6,8] which were referred to in another statement. That statement contained the facts restated by Mr. Craemer in his discussion—namely, that the current approximate theory, or "elementary theory," assumes the plates to be rigidly connected at the joints and takes into consideration the resulting transverse connecting moments but neglects the translation of the edges.

The sinusoidal treatment of edge translations has been questioned by Mr. Craemer on the basis that the transverse moments, claimed to be linearly related to them, would then be sinusoidal also, which is not true of systems in which the pure beam effect is approximated. However, the relation between transverse moments and edge displacements is not entirely linear. Transverse moments depend in part on the distribution of the external loads on the roof, and partly on the relative edge displacements (the word "relative" being particularly significant). They are therefore sinusoidal only in the latter part which has been thus computed, the former part having been computed through the approximate theory in the paper. Moreover, the more nearly a system approximates a beam, the smaller are the relative edge displacements; these relative displacements disappear entirely in the case of a pure beam system. Thus, in systems in which the pure beam effect is approximated, the sinusoidal part of the transverse moments nearly vanishes.

---

[17] Asst. Prof. of Structural Eng., Ibrahim Univ., Cairo, Egypt.

Can the proposed hipped plate theory be applied to a system having dimensions and load distribution such that the structure deforms like a beam? Will the proposed theory yield zero relative edge displacements and consequently indicate the longitudinal stresses computed by the pure beam theory or approximate theory? That this is so will be shown by applying the proposed theory to a pure beam system as follows:

Example No. 3.—The forces acting on a small element length dx of a beam loaded with a load w pounds per unit length, the beam cross section, and the shear stress diagram on that cross section are shown in Fig. 33. By equating to zero the moments about point u of all forces acting on prism 1 1 2 2, shown in Fig. 33(*b*), one may write

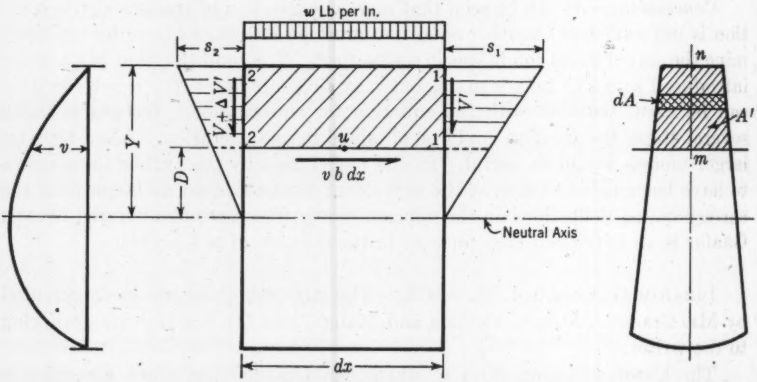

(*a*) SHEAR STRESSES (*b*) FORCES ON A BEAM ELEMENT (*c*) CROSS SECTION

FIG. 33.—STRESS DISTRIBUTION IN A BEAM

$$\int_m^n \frac{s_1 - s_2}{Y}\, y\, dA\, (y - D) - V'\, dx = 0 \ldots\ldots\ldots\ldots (23)$$

in which V' is the vertical shearing force acting on the shaded area, A', of the cross section and y is the centroidal distance. Therefore, if prime superscripts designate properties of the shaded area in Fig. 33,

$$\frac{V'}{V} = \frac{I' - A'\, y'\, D}{I} \ldots\ldots\ldots\ldots\ldots\ldots (24)$$

The dimensions of the cross section of the aluminum model are given in Fig. 34.

$$I = 3.637 \text{ in.}^4 \ldots\ldots\ldots\ldots\ldots\ldots\ldots\ldots (25a)$$

The moment of inertia of the sectional area of the plates AB and A′B′ about the neutral axis is

$$I' = 2.208 \text{ in.}^4 \ldots\ldots\ldots\ldots\ldots\ldots\ldots\ldots (25b)$$

Thus, by Eq. 24, the portion V' carried by side plates AB and A′B′ is 0.472 V lb. That is, under pure beam behavior, plates AB and A′B′ carry 0.472 of the total load on the model.

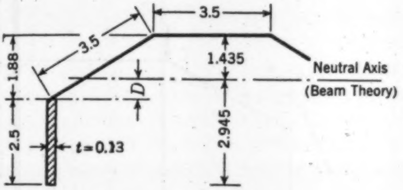

FIG. 34.—DIMENSIONS OF CROSS SECTION, IN INCHES

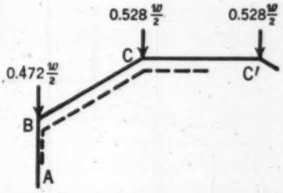

FIG. 35.—LOAD DISTRIBUTION, BEAM EFFECT

The aluminum model will be analyzed for a uniform vertical line load of w lb per lin in. of the model, distributed along the edges in such a way as to produce pure beam deformation. The line-load distribution is shown in Fig. 35.

If the structure deforms as a beam, the analytical stresses at the midspan are

$$s_a = + w \frac{35^2}{8} \times \frac{2.945}{3.637} = + 124\, w \ldots\ldots\ldots\ldots (26a)$$

$$s_b = + 18.7\, w \ldots\ldots\ldots\ldots\ldots\ldots\ldots\ldots (26b)$$

and

$$s_c = - 60.3\, w \ldots\ldots\ldots\ldots\ldots\ldots\ldots\ldots (26c)$$

Analysis by Proposed Theory.—The P-forces, the free edge bending moments at midspan, and the free edge stresses for the different plates are computed in the same manner as in Example No. 1.

The free edge stresses are corrected to include the effect of edge shear forces by the procedure of Table 2. The stresses after correction are: At edge A, + 125.8 w; at edge B, + 16.4 w; and at edge C, − 59.75 w. These are nearly the same values as those of Eqs. 26.

In determining the effect of the relative displacements of the joints on stresses, all computations and results given in steps 2 and 3 of Example No. 1 are applicable. Hence, as in Eq. 6 and Fig. 14, $\delta_{ab} = - 0.533 \times 10^{-3}\, w - 0.457\, \Delta$, and $\delta_{bc} = + 0.265 \times 10^{-3}\, w - 0.2195\, \Delta$.

The same geometrical relation of Example No. 1 applies herein—namely, $\Delta = 1.186\, \delta_{ab} + 2.2071\, \delta_{bc}$. Substituting the values for δ_{ab} and δ_{bc} in this geometrical relation yields $2.026\,\Delta = (+\,0.585 - 0.633)\,10^{-3}\,w$, or $\Delta \approx 0.0$, the required condition for pure beam behavior. The values between the parentheses should have yielded zero; the discrepancy corresponding to an average of 2.5% change in approximate-theory stresses is caused by the small original difference between approximate-theory stresses and beam-theory stresses, and by slide-rule inaccuracies.

Example No. 4.—The aluminum model loaded with uniform line load $w/2$ lb per lin in. of edges C and C′ (Fig. 36) has been analyzed by first assuming pure beam behavior as in Example No. 3 and then applying the two corrections explained in the paper (under the heading, "Hipped Plates Compared with Ordinary Beams") and designated therein as corrections (*a*) and (*b*). Loads for correction (*a*) are shown in Fig. 37 and resemble those for correction (*b*) due to Δ, shown in Figs. 10 and 11 (*a*). The stresses in terms of Δ due to the latter correction are the same as those due to Δ in any of the previous examples; and the stresses due to the former correction (*a*) are proportional to them. The procedure used in Example No. 1 in steps 4 and 5 serves to give the final results. The final stress values have been computed and appear in Table 14, Col. 5. The same problem has been analyzed by the proposed-theory procedure, and the results are given in Table 14, Col. 8.

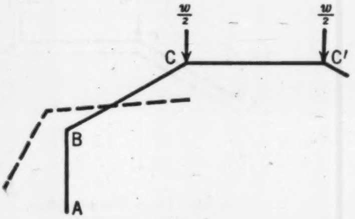

FIG. 36.—LOAD DISTRIBUTION FOR EXAMPLE NO. 4

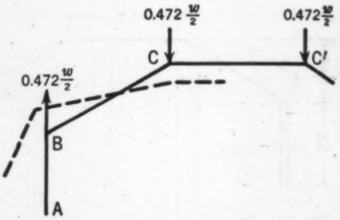

FIG. 37.—LOADS FOR CORRECTION (*a*)

TABLE 14.—MAXIMUM LONGITUDINAL STRESSES AT MIDSPAN

Edge	Example No. 4[a]							Example No. 2[e]		
	Beam-Theory Approach				Approximate-Theory Approach			Beam theory	Corr'ns. (*a*) + (*b*)	Final values
	Beam theory	Corrections		Final values						
		(*a*)	(*b*)		AT[b]	JD[c]	PT[d]			
(1)	(2)	(3)	(4)	(5)	(6)	(7)	(8)	(9)	(10)	(11)
C	− 60.3	− 92.2	+ 47.5	−105.0	−152.0	+ 47.5	−104.5	− 537	−383	− 920
B	+ 18.7	+205.3	−106.5	+117.5	+221.8	−106.5	+115.3	+ 166	+860	+1,026
A	+124.0	−236.0	+122.5	+ 10.5	−110.2	+122.5	+ 12.3	+1,102	−988	+ 114

[a] All values are to be multiplied by w, giving stresses, in pounds per square inch. [b] Values computed by the approximate theory. [c] Values resulting from relative displacements of joints. [d] Values computed by the proposed theory. [e] Stresses, in pounds per square inch.

Example No. 2 has been analyzed from the beam action approach, and the results are given in Table 14 for comparison with those of Table 6. Although both approaches (Table 14) lead to practically the same results, the proposed-theory approach, being the shorter, is the better.

Any single-span, symmetrically loaded hipped plate system can be solved by the technique of the proposed theory either by beginning from the pure shell effect (as in the writer's paper) or from the pure beam effect, and correcting for external load distribution and edge translations.

These examples answer Mr. Craemer's question as to the range of applicability of the analytical treatment developed in the paper. They show it to be generally applicable within the working conditions defined. Although application of the method is generally possible, it is not always advisable. To correct for relative edge displacements where they are too small will not be worth while, and the approximate theory will be accurate enough. Mr. Craemer's investigation[13] serves to indicate qualitatively where the proposed theory might profitably be applied, as is also indicated by Messrs. Paulson and Maugh in their valuable discussion. However, the writer does not consider Mr. Craemer's method a safe indicator for systems that approximate a beam since a beam system will become a hipped plate system through a slight change in the distribution of loads. In Example No. 3, for instance, if the loads on the joints are made 0.5 $w/2$ each, instead of 0.472 $w/2$ and 0.528 $w/2$, the plates will rotate slightly, and the system will become a hipped plate system although ω—the practical indicator—remains unchanged ($\omega = L/H \sqrt{t/h}$). The system of Example No. 3 has been changed to a hipped plate system in Example No. 4 by changing the distribution of loads. This shows clearly that a pure beam system is a special case of a hipped plate system, not a limiting case as indicated by Mr. Craemer.[18]

It is interesting to compare the conclusions Messrs. Paulson and Maugh deduced from examples they solved using the proposed theory with similar conclusions deducible from the paper by Mr. Craemer.[13] Studying Fig. 11 for open sections in Mr. Craemer's paper,[18] the deviation of the longitudinal stresses (when edge translations are considered) from those due to the approximate or pure shell theory ($\omega = 0$) is seen to increase as ω increases. This result agrees with the conclusions reached by Messrs. Paulson and Maugh using the proposed theory—namely, s_c/s_a increases as L increases, as the depth of the end beams decreases, and as the number of plates increases—that is, as h decreases. The writer is especially interested in the agreement between results obtained by the two entirely different methods of treatment of Mr. Craemer and the writer.

Mr. Gartner has used the average longitudinal stresses measured at the edges of the model (Fig. 27) to compute the forces resisted by each plate in the longitudinal direction and shows his results in Eqs. 18 and 19. These forces are used to compute the stresses in Eq. 21. However, in this computation, Mr. Gartner has overlooked the fact that the average measured longitudinal stresses as shown in Fig. 27 are not exactly linear across each plate.

---

[18] "Design of Prismatic Shells," by H. Craemer, *Journal*, A.C.I., No. 6, February, 1953, p. 558, Fig. 11.

The corresponding strains appear in Fig. 23(*a*). This oversight explains the discrepancies in the values of stresses obtained in Eq. 21. The slight curvature was considered in the check given in Table 9.

Mr. Gartner's observation that the deflections show a slight twist in the model is correct. The twist is so slight that its effect on the results is negligible. However, Mr. Gartner's suggestion concerning the use of the exact equation for simplification is not clear. His suggestion of eliminating the steps and reducing the method to one operation is, in the writer's opinion, out of the question.

AMERICAN SOCIETY OF CIVIL ENGINEERS
Founded November 5, 1852
TRANSACTIONS

Paper No. 2697

PUTTING A SEWAGE TREATMENT PLANT INTO OPERATION

By Benjamin Benas,[1] M. ASCE

Synopsis

The careful consideration of operating procedures when designing a sewage treatment plant, the proper selection and training of personnel, and the thorough checking of equipment are found to be of importance in placing a sewage treatment plant in operation. This paper describes experiences with new plants in San Francisco, Calif. An intimate knowledge of the layout and equipment of a plant should be obtained at the outset, and special measures for doing this are described. Adjustment of equipment to allow for deviations from original design values of flow, sewage strength, and other factors should be made as soon as possible. Such initial precautions are frequently justified by savings in cost.

Operating Procedures for Sewage Treatment Plant

The plan for placing a sewage treatment plant in operation starts with the original design and continues until the operating conditions are relatively normal or stabilized. This paper describes the procedures used in the North Point and Southeast Sewage Treatment Plants of the City of San Francisco, Calif., which commenced operation in December, 1951.

These plants are part of a master plan whose objective is the treatment of all sewage discharged into the surrounding bay or ocean. The master plan is based on a program recommended in a report to the Director of Public Works in 1935 by a board of consulting engineers. The recommendations of this board have been generally followed except that the degree of sewage treatment required has been changed to meet the more advanced standards of quality and conditions at outfalls prescribed by the California State Department of Public Health and the Water Pollution Control Boards in California. All the plants provide primary treatment; there is sufficient chlorination of the effluent to reduce the number of coliform organisms in the recreational shore areas to less than 10 per milliliter, 80% of the time.

Note.—Published, essentially as printed here, in August, 1953, as *Proceedings-Separate No. 257.* Positions and titles given are those in effect when the paper was received for publication.

[1] Senior Engr., Sewage and Waste Treatment Div., Bureau of Eng., San Francisco, Calif.

Sewage of San Francisco is treated (1953) in two plants—the Richmond-Sunset Plant and the North Point Plant. A third plant known as the Southeast Plant was placed in operation in November, 1952. Fig. 1 shows the plant locations and tributary areas. The shaded parts refer to those areas that were awaiting completion of collecting sewers when this map was prepared in 1952.

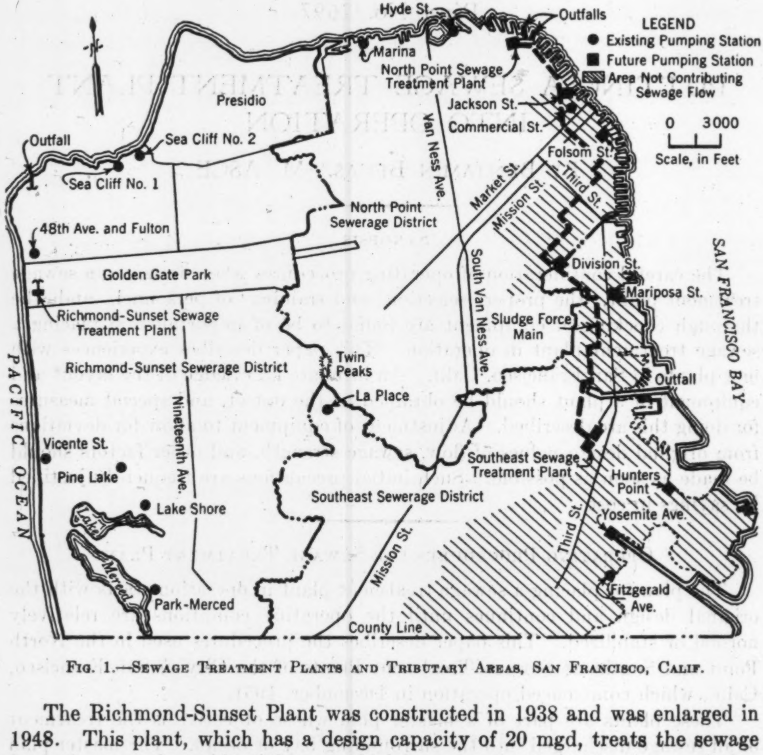
Hyde St.
Outfalls
LEGEND
● Existing Pumping Station
■ Future Pumping Station
▨ Area Not Contributing Sewage Flow
0 3000
Scale, in Feet
Marina
North Point Sewage Treatment Plant
Presidio
Jackson St.
Commercial St.
Van Ness Ave.
Outfall
Sea Cliff No. 2
Sea Cliff No. 1
Folsom St.
Market St.
Mission St.
Third St.
North Point Sewerage District
48th Ave. and Fulton
SAN FRANCISCO BAY
Division St.
Golden Gate Park
Mariposa St.
Richmond-Sunset Sewage Treatment Plant
Sludge Force Main
South Van Ness Ave.
PACIFIC OCEAN
Twin Peaks
Richmond-Sunset Sewerage District
Outfall
La Place
Nineteenth Ave.
Vicente St.
Southeast Sewage Treatment Plant
Pine Lake
Hunters Point
Southeast Sewerage District
Lake Shore
Yosemite Ave.
Lake Merced
Third St.
Mission St.
Park-Merced
Fitzgerald Ave.
County Line

Fig. 1.—Sewage Treatment Plants and Tributary Areas, San Francisco, Calif.

The Richmond-Sunset Plant was constructed in 1938 and was enlarged in 1948. This plant, which has a design capacity of 20 mgd, treats the sewage from the westerly residential area, which has an estimated ultimate population of 300,000. The plant provides pre-chlorination for odor control, screening by coarse and fine bar screens, removal of grit and grease from aerated Imhoff-type grit-grease tanks, pre-flocculation by mechanical means, sedimentation, and post-chlorination of the effuent before discharge into the ocean. Sludge removed from the sedimentation tanks, together with grease, is thickened, digested in two-stage digesters, elutriated, and filtered by vacuum units. The filter cake is being hauled (1953) to city parks for use as a soil conditioner, but in the future it will be hauled to the Southeast Plant to be dried. Screenings are incinerated, and grit and sand are hauled to a city dump.

Construction was started on the North Point Sewage Treatment Plant in 1949 and was completed in 1951 at a contract cost of $8,500,000. This plant provides only primary treatment, handling sewage and industrial wastes from combined sewers from the northeasterly section of the city. Since it has no sludge-treatment facilities, the sludge is pumped 6 miles to the Southeast Plant.

The North Point Plant has a design capacity of 65 mgd, received from an estimated ultimate population of 835,000; it has a maximum capacity of 150 mgd, including the runoff from light rains. Light rains are treated to prevent contamination of the recreational shore areas, particularly during the summer months. Provision is made for the discharge of excessive storm flows or of all flows directly to the bay when the plant is by-passed.

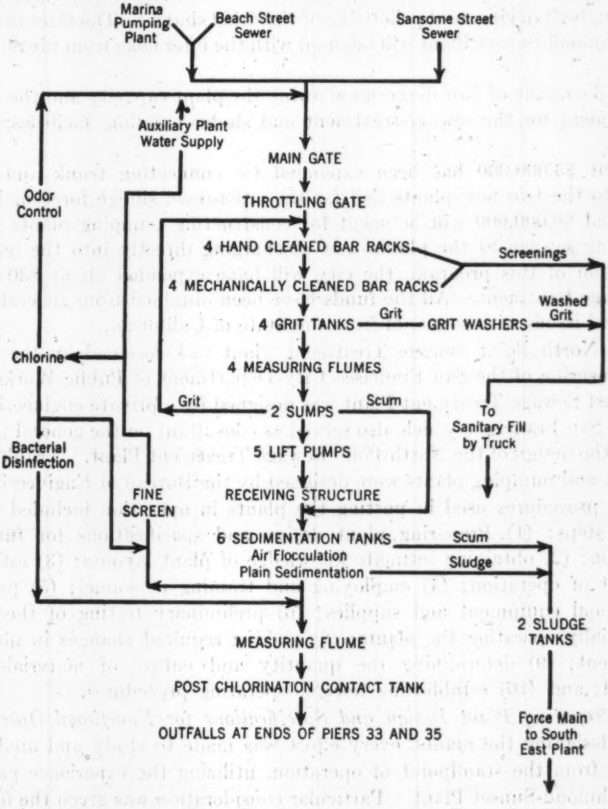
Marina Pumping Plant
Beach Street Sewer
Sansome Street Sewer
Auxiliary Plant Water Supply
MAIN GATE
Odor Control
THROTTLING GATE
4 HAND CLEANED BAR RACKS
Screenings
4 MECHANICALLY CLEANED BAR RACKS
Grit
Washed Grit
4 GRIT TANKS
GRIT WASHERS
Chlorine
4 MEASURING FLUMES
Grit
Scum
2 SUMPS
To Sanitary Fill by Truck
Bacterial Disinfection
5 LIFT PUMPS
FINE SCREEN
RECEIVING STRUCTURE
6 SEDIMENTATION TANKS
Scum
Air Flocculation
Plain Sedimentation
Sludge
2 SLUDGE TANKS
MEASURING FLUME
POST CHLORINATION CONTACT TANK
Force Main to South East Plant
OUTFALLS AT ENDS OF PIERS 33 AND 35

FIG 2.—FLOW DIAGRAM FOR THE NORTH POINT SEWAGE TREATMENT PLANT, SAN FRANCISCO, CALIF.

Fig. 2 is a flow diagram showing the plant capacity and the method of treatment.

Two contracts totaling $7,000,000 were let in 1949 and 1950 for the Southeast Sewage Treatment Plant. There are actually two separate plants on one site, one for sewage treatment and the other for sludge digestion, filtration, and drying. The sewage treatment part has a design capacity of 30 mgd and will treat sewage from combined sewers from an estimated population of 400,000. The type of treatment which this plant provides is similar to that at the North Point Sewage Treatment Plant.

The sludge-handling facilities include thickening of the raw sludge from the North Point Plant and Southeast Plant, primary and secondary digestion in digesters having floating covers, primary and secondary elutriation, vacuum filtration, heat drying, and pelletizing of the dried sludge. The filter cake from the Richmond-Sunset Plant will be dried with the filter cake from the Southeast Plant.

Fig. 3 consists of flow diagrams showing the plant capacity and the method of treatment for the sewage-treatment and sludge-handling facilities, respectively.

About $3,000,000 has been expanded for connecting trunk and outfall sewers to the two new plants and for the cross-town sludge force main. An additional $6,000,000 will be spent for constructing pumping plants and for conveying sewage to the plants now discharging directly into the bay. On completion of this program, the city will have expended about $30,000,000 for sewage treatment. All the funds have been obtained from general obligation bond issues with some aid from the State of California.

The North Point Sewage Treatment Plant was designed by the Bureau of Engineering of the San Francisco City Department of Public Works. The Southeast Sewage Treatment Plant was designed by a private engineering concern, in San Francisco, which also served as consultant on the general program and on the design of the North Point Sewage Treatment Plant. Trunk sewers, outfalls, and pumping plants were designed by the Bureau of Engineering.

The procedures used in putting the plants in operation included the following steps: (1) Preparing plant design and specifications for functional operation; (2) obtaining intimate knowledge of plant layouts; (3) estimating the cost of operation; (4) employing and training personnel; (5) procuring operational equipment and supplies; (6) preliminary testing of the plants; (7) initially operating the plants; (8) making required changes in plant and equipment; (9) determining the quantity and nature of materials to be handled; and (10) establishing normal operating procedures.

1. Preparing Plant Design and Specifications for Functional Operation.— While designing the plants, every effort was made to study and analyze the layouts from the standpoint of operation, utilizing the experience gained at the Richmond-Sunset Plant. Particular consideration was given the following factors: Maintenance requirements for plant and equipment; working space around units and space for removal of units; lifting facilities, such as hooks embedded in the concrete, hoists, and other machines; sampling of sewage; duplication of units; a comparison between automatic operation and manual operation; by-passes; power operation of large gates; water for cleaning and flushing, cleaning of channels, tanks, and similar equipment; protection around openings and walkways; adequate lighting and ventilation; safety facilities; tool boards at convenient locations; inter-plant communication, signal systems

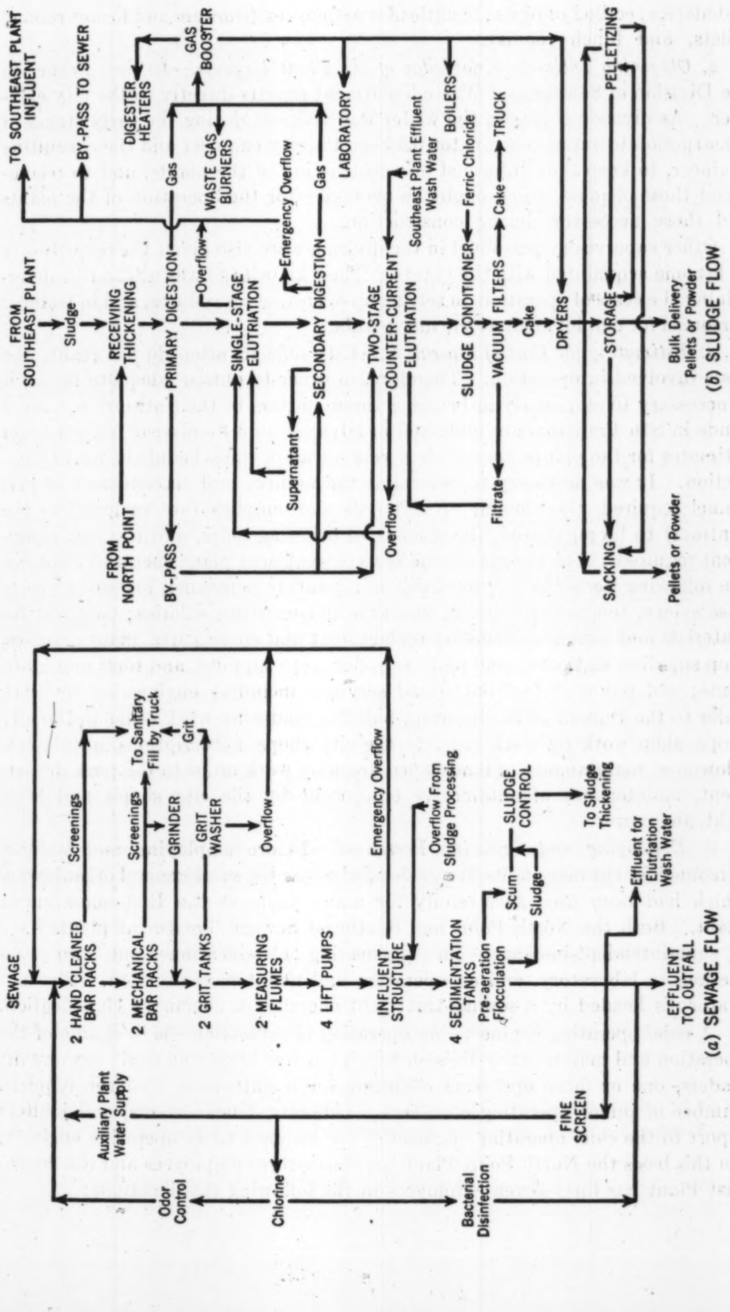
SEWAGE
2 HAND CLEANED BAR RACKS
Screenings
2 MECHANICAL BAR RACKS
Screenings
GRINDER
To Sanitary Fill by Truck
Grit
2 GRIT TANKS
GRIT WASHER
Overflow
2 MEASURING FLUMES
4 LIFT PUMPS
Emergency Overflow
INFLUENT STRUCTURE
Overflow From Sludge Processing
4 SEDIMENTATION TANKS
Pre-aeration Flocculation
Scum
Sludge
SLUDGE CONTROL
To Sludge Thickening
Effluent for Elutriation Wash Water
EFFLUENT TO OUTFALL
FINE SCREEN
Auxiliary Plant Water Supply
Odor Control
Chlorine
Bacterial Disinfection
(a) SEWAGE FLOW
FROM SOUTHEAST PLANT
Sludge
RECEIVING THICKENING
FROM NORTH POINT
BY-PASS
PRIMARY DIGESTION
Gas
TO SOUTHEAST PLANT INFLUENT
BY-PASS TO SEWER
DIGESTER HEATERS
GAS BOOSTER
Overflow
Emergency Overflow
WASTE GAS BURNERS
SINGLE-STAGE ELUTRIATION
SECONDARY DIGESTION
Gas
LABORATORY
Supernatant
Overflow
TWO-STAGE COUNTER-CURRENT ELUTRIATION
Southeast Plant Effluent Wash Water
BOILERS
SLUDGE CONDITIONER
Ferric Chloride
Filtrate
VACUUM FILTERS
Cake
TRUCK
Cake
DRYERS
PELLETIZING
STORAGE
SACKING
Pellets or Powder
Bulk Delivery Pellets or Powder
(b) SLUDGE FLOW

FIG. 3.—FLOW DIAGRAMS, SOUTHEAST SEWAGE TREATMENT PLANT, SAN FRANCISCO, CALIF.

and alarms; coding of pipes; facilities for employees (showers and locker rooms, toilets, and lunch rooms).

2. Obtaining Intimate Knowledge of the Plant Layouts.—In San Francisco the Division of Sewage and Waste Treatment reports directly to the city engineer. As division engineer, the writer was assigned during the early stages of construction to act as coordinator between the city engineer and the consulting engineer, to keep fully informed on construction of the plants, and to recommend those changes which might be necessary for the operation of the plants and those necessary during construction.

Other supervisory personnel in the division were also given the opportunity to become acquainted with the plants. Their knowledge was utilized in determining the costs of operation, in setting up operating procedures, and in training personnel for employment at the new plants.

3. Estimating the Cost of Operation.—City officials often do not realize the costs involved in operation. Therefore, in order to obtain adequate funds, it is necessary to start early in bringing these matters to their attention. Since funds in San Francisco are budgeted in advance on a fiscal-year basis, budget estimates for the plants were made a year ahead of the scheduled time of completion. It was necessary to determine the number and classification of personnel required, the amount of materials and supplies (not included in the contract) to be purchased, the services of other agencies, and the new equipment required. The budget for the sewage treatment plant operation contains the following items: Wages for daily and monthly personnel, including yearly base salary, temporary salaries, vacation and overtime salaries; payment for materials and supplies, including replacement and spare parts, plant supplies, shop supplies, stationery and office supplies, auto supplies, and fuels and lubricants; and payment for contractual services, including engineering by work order to the Bureau of Engineering, building trades by work order to the city shops, shop work by work order to the city shops, subscriptions, automobile allowance, maintanance of landscaped areas by work order to the park department, maintenance of automotive equipment by the city shops, and heat, light, and power.

4. Employing and Training Personnel.—Before employing and training personnel for the new plants, it was decided to use the same general organization which had been used successfully for many years at the Richmond-Sunset Plant. Both the North Point and Southeast Sewage Treatment plants have a superintendent-in-charge—an engineering classification—and two subsections, a laboratory, and an operation and maintenance section. The laboratory is headed by a sewage-treatment chemist—a chemistry classification.

A chief operating engineer—an operating classification—is in charge of the operation and maintenance division which has five operating engineers as shift leaders, one or more operating engineers for maintenance, and the required number of junior operating engineers. Laborers, truck drivers, and janitors report to the chief operating engineer or are assigned to an operating engineer. On this basis the North Point Plant has thirty-three employees and the Southeast Plant has forty-seven employees in the following classifications:

North Point Plant.—One sewage-treatment superintendent, one clerk-stenographer, one sewage-treatment chemist, two assistant chemists (1 for routine analyses, 1 for bacteriology), one chief operating engineer, six operating engineers, fifteen junior operating engineers, four laborers, one truck driver, and one janitor.

Southeast Plant.—One sewage-treatment superintendent, one clerk-stenographer, one sewage-treatment chemist, three assistant chemists (for routine analyses), one chief operating engineer, seven operating engineers, twenty-seven junior operating engineers, five laborers, and one janitor.

All employees are procured from San Francisco civil service lists and must be residents of the city. The position of superintendent is promotional from sewage-treatment chemist and from engineering lists of a lower pay rate; those of chief operating engineer and operating engineer are promotional from operating engineer and junior operating engineer, respectively. Lists for operating personnel are for general city service and not specifically for sewage treatment plants. The state Civil Service Commission was advised in sufficient time to conduct examinations so that the required number of employees would be available when needed. Funds were requested and included in the budget to provide a training period for certain classifications of personnel before the plants began operating. The purpose of this training was to acquaint the personnel with the operation of sewage treatment plants in general and with the details of their job assignments. Training schedules lasted three months for superintendents and chemists, six months for chief operating engineers, two months for operating engineers, and one month for junior operating engineers and assistant chemists. Actually, these training periods were extended because the plants were not completed on schedule.

All employees in the training program were first assigned to the Richmond-Sunset Plant where they received instruction from the superintendent, chemist, or chief operating engineer. This training period extended from one week to one month for the operation classifications and from one to three months for the chemistry classifications. The superintendents, who had previously been employed as chemists, trained the chemists, who then served as instructors for the assistant chemists. On completion of the training at the Richmond-Sunset Plant, the men were assigned to their respective plants for on-the-job instruction.

The chief operating engineer was the first employee assigned to the new plant so that he could become familar with details of the plant layout. He thus was able to instruct new operators in care and maintenance of equipment, to assist inspection forces, and to obtain information about equipment from manufacturers' representatives. Then, superintendents and chemists were assigned. They first familiarized themselves with the details of the plants, set up the training program for new personnel in cooperation with the chief operating engineer, and determined the operating procedures to be followed when the plant would open. As operating engineers were assigned to the plant, they received instructions from the chief operating engineer on the general plant layout and equipment and assisted in the marking and identification of the piping, checking of supplies, and conducting preliminary tests.

Junior operating engineers were assigned to the plant a month after the operating engineers began their work. Each operating engineer served as an instructor to a small group of junior operating engineers who were trained in their particular job assignments and then were fully informed about other details of the plant.

Frequent conferences were held, and sketches and drawings of the piping details were used as training aids. These conferences enabled supervisory personnel to become better acquainted with each operator's qualifications; thereby, suitable work was assigned to personnel. Every effort was made to answer all questions asked by operating personnel. Particular attention was given to directions on steps to be taken in the event of an emergency, such as power failure, overloading, breakage, or stoppage. After completion of the training program, all the plant personnel assisted in the preliminary tests.

5. Procuring Operational Equipment and Supplies.—Only a part of the supplies and equipment needed for operating the plant, shop laboratory, and office were included in construction contracts. The balance was obtained through the use of bond funds for fixed items of equipment and plant funds for other items. No attempt was made to stock supply items that normally are purchased on a yearly basis after actual requirements are known.

6. Preliminary Testing of the Plants.—The construction specifications provided for the testing and checking of all equipment by the contractors before initial operation, and for the submission of a statement by equipment manufacturers that their equipment was correctly installed and ready for operation.

It was decided that it would be to the advantage of the City of San Francisco and to the contractor to make this preliminary program a joint venture. Accordingly, a schedule was planned by the inspection forces of the Construction Division with the cooperation and approval of the individual contractor and the operation and design forces of the city. Whenever possible, fresh water was used to check pipe lines for leaks and obstructions, tanks for leaks, and pumps and other equipment for performance. This checking made it possible to correct any difficulties before the plant commenced operation. The inspectors made a test-check schedule for each building or group of buildings which constituted a stage in the process. Each schedule listed all specified test requirements for the equipment and detailed step-by-step test procedures. The following program was followed at the North Point Sewage Treatment Plant and for all units at the Southeast Sewage Treatment Plant except the sludge filtering and drying facilities: (*a*) All equipment was checked for a conformity to the approved drawings and specifications; (*b*) all electric circuits were tested; (*c*) tanks, as required, were calibrated to determine quantities for measurements; (*d*) water systems, air systems, lighting, and ventilation were examined; (*e*) all hydraulic gates were operated with water; (*f*) sedimentation tanks were filled with water which was circulated through the plant for checking the operation of pumps, motors, flights, and other equipment, and for ascertaining the tightness of pipe lines and water lines; and (*g*) a check was made of miscellaneous equipment.

At the Southeast Sewage Treatment Plant, digesters were filled with wate over the corbels, and the water was circulated through the units. Examination of the filtering and drying system was delayed until sludge was available.

As a result of the preliminary test, many changes and corrections were made which were the contractor's responsibility. This preliminary testing was greatly responsible for the success of the initial operating period.

7. *Initially Operating the Plants.*—The city authorities were required to place the plants in operation for a 30-day test period (after completion of the preliminary tests) and to furnish the operating staff, water, power, and chemicals.

The contractor was required to instruct and supervise the operating staff in the care and operation of the equipment, to change or replace any defective material, and to assume all responsibility for any damage to the plant or equipment during this period.

Past experience proved that it was advisable to operate one unit at a time and to place all units in operation gradually as conditions and experience warranted. In the beginning, as many units as possible were operated during the day period. Twenty-four-hour operation was started as soon as conditions were uniform and the necessary corrections were made. This method provided concentration of forces and more extensive training of employees and minimized confusion. During this initial operating period the quantity of the flow, the strength and characteristics of the sewage, and the quantity of materials removed were determined, and operating problems were evaluated. Duty assignments were changed when conditions necessitated a rotation of personnel.

Sample forms were prepared to record pertinent data before the initial operation period so that the quantity and characteristics of the sewage and sludge could be evaluated and the operation of the equipment and process could be controlled. Certain readings were taken at regular intervals to ascertain that operators were actually observing and checking the operations. No attempt was made to establish normal sampling procedures during this period; information was desired only to determine how the units were operating and whether the specification requirements were being met.

At the North Point Plant sewage was first run through one bar screen and grit tank. After it was shown that the influent control gates were operating properly, other grit tanks were gradually placed in service so that, at the end of one week, all the tanks had been operated singly or in combination with others.

Each of the two pump sumps was operated separately, and the sump scum skimmers and equipment for grit and sand removal were tested. The controls for automatically cutting the main lift pumps in and out were adjusted so that the pumping rate followed the flow rate of the influent as closely as possible.

Discharge from the pumps was run through one sedimentation tank at a time, the operation of the air flocculation system and the flights were observed, and necessary adjustments were made. As conditions permitted, the number of sedimentation tanks in service was gradually increased so that at the end of the 30-day period all the tanks were in service.

All flow-metering equipment was tested for correlation of the metering of influent and effluent with the meter control of chlorination. All auxiliary equipment, such as air deodorizing systems, effluent filters, and automatic samplers, was checked and adjusted during the 30-day period. The laboratory was prepared, studies and testing of the sewage and sludge were started, and sampling schedules were determined.

The chlorination system was not started until the 30-day testing period was nearly finished. Before chlorinating, the chlorine storage tanks were filled with dry air for one week, and air was then removed. Two 1-ton cylinders of chlorine were connected to the system, the lines were checked, and the units were adjusted. After these preliminaries were completed, a tank car of chlorine was transferred to permanent storage. Chlorination units were tested at low dosage, and the dosage was increased after final adjustments were made by the manufacturer.

During this initial operating period, the sludge removed from the sedimentation tanks was pumped directly to the bay with the effluent. Before sludge was pumped through the cross-town line to the Southeast Plant, the line was filled with fresh water to check for leaks, and a chain-covered rubber ball was forced through the line to test for obstructions. Sludge was not transferred through the line until a sufficient quantity of seeding material was available in the digestion system at the Southeast Plant, allowing digestion to proceed under the most favorable conditions without the possibility of foaming.

The operation of starting the digestion system at the Southeast Plant is of special interest. One primary digester was seeded with 1,000,000 gal of digested sludge hauled from the Richmond-Sunset Plant in 5,200-gal tank trucks during a 30-day period. Before adding the seeding material, the digester was heated to 95°F, using natural gas, and this temperature was maintained. Raw sludge was added when 500,000 gal of seeding material had accumulated in the digester in an amount equal to 10% of the solids loading in the digester; this ratio was maintained as the amount of solids in the digester increased. Thirty days after seeding operations began, 60,000 lb per day of raw sludge was being added to three digesters.

Gas production from the seeded digester was first noticed on the eighth day after the start of the seeding sludge transfer. A total of 3,600 cu ft of gas was recorded for the 24-hr period, 10 days after seeding operations began. Gas production was 125,000 cu ft per 24 hr, 6 days after raw sludge feeding began, and thereafter, the rate of gas production reflected the load of raw sludge added to the digesters. Digester gas was used for heating the digesters and dryers after February 15, 1952.

In March, 1952, supernatant and bottom sludge from primary digesters was transferred to the secondary digesters with intermediate single-stage elutriation; by the middle of April, there was sufficient storage of digested sludge to permit operation of one dryer at its rated capacity for 30 days. During this time, digester conditions were checked for volatile acids, alkalinity, volatile matter, pH, and composition of the gas.

During March, all auxiliary equipment for the filters was checked for operation. This was done by the plant organization in cooperation with representatives of the manufacturer of the filters. After this check, filter drums were soaked, being revolved continuously in a bath of water for 168 hr, after which the filter cloths were installed. Production of filter cake, using elutriated sludge, was started on April 7 (as scheduled) and was continued on an intermittent basis in order to check and adjust secondary elutriation, filtration, and conveying equipment under operating conditions; to insure a steady and adequate supply of filter cake for drying; and to determine the nature of the filter cake produced. After one week the filters were operating satisfactorily, and it was possible to start the dryer tests.

The representative of the manufacturer of the dryers reported to the plant two weeks prior to the scheduled date of dryer operation. During this time he tested the electric circuits, dryer controls, and motors with the cooperation of electrical and mechanical inspectors employed by the City of San Francisco, and with the cooperation of plant operating personnel. Plant operators were given different duties during this period so as to familiarize as many men as possible with this equipment.

Dryer operation was started on April 14, 1952, as scheduled. Each dryer was operated on a 8-hr basis for three weeks and then for one week continuously as a shakedown. During the six weeks of operation, frequent meetings of operating personnel with the representative of the manufacturer of the dryer were held to elicit comments, criticisms and questions. In addition to familiarizing the operators with the equipment, the preliminary operations had the following objectives: (1) Testing and adjustment of all components of the system; (2) development of proper operating procedure (especially in connection with starting and stopping of the dryers) and coordination between the operation of the filters and dryers; and (3) unofficial check of each dryer prior to official acceptance runs.

Dryers were stopped on May 26, 1952, for a two-week period to inspect the equipment and to allow the manufacturer to make some adjustments and changes before the official performance tests.

The official performance test determined the water evaporation capacity of each unit, the total horsepower required per ton of dried solids, and the number of British thermal units of fuel per ton of dried solids.

The dried-sludge conveying system, the storage hoppers, the removal equipment, and the pelletizing equipment were operated at the same time as were the dryers. During this time, the manufacturers made necessary changes and checked the operation of the equipment to insure conformity to specification requirements.

8. Making Required Changes in Plant and Equipment.—Regardless of the care taken in the original design, it is almost impossible to design a plant which can be placed in operation without several changes. It is the contractor's responsibility to construct the plant in accordance with approved drawings and specifications—not to correct any errors or omissions in design. It is always necessary, therefore, to provide funds for corrections or additions. In this case, funds were available partly from construction bond issues and partly from plant operating funds. The engineer must bring this matter to the attention of officials responsible for allocation of funds so that they may be prepared for these expenditures when the need arises.

9. Determining Quantity and Nature of Materials to Be Handled.—The basic design factors of flow, sewage strength, and quantities of sludge and other materials to be removed often differ from the actual quantities found during plant operation. These factors change the cost of operation by affecting the personnel required, the number of units operated, the power consumed, the chemicals required, the materials and quantities handled, and other related items of cost. Actual quantities and qualities should be determined as soon as possible, and operating personnel and procedures should be adjusted accordingly. If necessary, additional funds should be obtained.

10. Establishing Normal Operating Procedures.—The program for normal operation can be developed only after all basic factors are known and evaluated. Permanent duty assignments and schedules for operation, sampling, and testing then can be made. There should be a proper balance between sampling, testing, and operating requirements, but the sampling and testing program should be complete enough to give data for essential plant records as well as for control of plant operation. Preliminary forms should be reviewed and permanent forms, preferably of standard size, should be prepared.

CONCLUSIONS

The experience gained in starting these plants leads the writer to conclude the following:

(1) It is necessary to consider operation in design; (2) consideration should be given to obtaining plant personnel well in advance of the starting date; (3) an adequate personnel training program should be initiated; (4) adequate funds should be obtained in advance of plant operation; (5) an intimate knowledge of the plant and its processes should be acquired before starting operation; (6) the design, inspection, and operation forces should cooperate in checking the plant before and during initial operation; (7) if possible, it is best to place all units in operation gradually, rather than at full load at one time; (8) it is essential to develop employee interest by making each person feel he has an active and important part; and (9) if possible, plants should be placed in operation when flow and other characteristics are normal.

ACKNOWLEDGMENT

The two plants described are under the jurisdiction of the Division of Sewage and Waste Treatment of the Bureau of Engineering, San Francisco City Department of Public Works. Sherman P. Duckel, A.M. ASCE, is director of public works, and Ralph G. Wadsworth, M. ASCE, is city engineer. R. H. Owens, A.M. ASCE, is in charge of the Division of Design.

AMERICAN SOCIETY OF CIVIL ENGINEERS
Founded November 5, 1852
TRANSACTIONS

Paper No. 2698

STRESSES IN THE CORNERS OF RIGID FRAMES

BY HARVEY C. OLANDER,[1] M. ASCE

SYNOPSIS

By applying the wedge theory to the corners of rigid frames, a method is developed for analyzing the stresses which occur in these corners. Following the determination of the stresses, photoelastic tests were performed which yielded results that agreed closely with the analysis. The divergence of the experimental results from the computed results is analyzed, and it is shown that the accuracy of the analysis can be improved by the application of the basic principles of mechanics. However, this refinement is not a necessary one as the results of the basic method are well within the limit of accuracy deemed necessary for structural analysis.

NOTATION

The letter symbols adopted for use in this paper are defined where they first appear, in the illustrations or in the text, and are arranged alphabetically, for convenience of reference, in Appendix III.

INTRODUCTION

A simple method, based on the theory of a wedge, is developed for computing the stresses in the corners of rigid frames where the extreme fibers are not parallel. The general problem was presented in 1939 by William R. Osgood.[2] However, Mr. Osgood's solution was not widely adopted, as is evidenced by the frequent appearance of discussions of the problem. These discussions are based on the erroneous assumption that the ordinary beam theory is applicable to straight sections across members with nonparallel flanges. That these assumptions may be considerably in error, depending on the shape, was demonstrated by Mr. Osgood. It is probable that the application of the wedge theory to this problem would have come into more general use if the equations had been less difficult and if the analyses had been made

---

NOTE.—Published, essentially as printed here, in August, 1953, as *Proceedings-Separate No. 249.* Positions and titles given are those in effect when the paper was received for publication.

[1] Engr., Canals Branch, Design and Cons. Div., Bureau of Reclamation, U. S. Dept. of the Interior, Denver, Colo.

[2] "Theory of Flexure for Beams with Nonparallel Extreme Fibres," by W. R. Osgood, *Transactions*, ASME, Vol. 61, 1939.

to follow a procedure similar to that used for beams with parallel flanges. Therefore, a method is proposed which is based on an approximate solution for wedge-shaped beams (using the familiar beam formulas), and, in order to exhibit the accuracy of the method, the computed stresses are compared to the stresses measured during a series of photoelastic tests.

METHOD OF ANALYSIS

The method of analysis consists of (1) taking circular sections that cut the extreme fibers at right angles, such as section A–B shown in Fig. 1(*a*); (2) developing the section, as shown in Fig. 1(*b*); and (3) obtaining the area A and the moment of inertia I of the developed section. All forces to the right of section A–B are resolved into the components P_O, V_O, and M_O about point O, the center of the arc. The force P_O passes through the center of gravity of section A–B, the force V_O is normal to P_O, and the moment M_O is the moment of the forces about point O. From these forces, the stresses on section A–B can be computed, as for an ordinary beam, and the shear can be determined from M_O. The total shear V on section A–B is expressed as

$$V = \frac{M_O}{r} \ldots\ldots\ldots\ldots (1)$$

and the unit shear along section A–B is

$$\tau_{r\theta} = \frac{V\,Q}{I\,b} \ldots\ldots\ldots\ldots (2)$$

The stresses normal to the section are

$$\sigma_r = \frac{P_O}{A} \pm \frac{M\,c}{I} \ldots\ldots\ldots\ldots (3)$$

in which

$$M = M_O + V_O\,r \ldots\ldots\ldots\ldots (4)$$

The moment M is the moment of the forces to the right of the section about the center of gravity, point X; r is the radius of the sectional arc; and c is the distance from the neutral axis to the extreme fiber. It may seem unnecessary first to find V_O and M_O, and then to find their moments about point X, but, because it is essential to determine M_O in order to compute the shear and to determine P_O to find P_O/A, it is no extension of the problem to resolve all the forces about point O.

Following this procedure, circular sections are taken across the corner with the requirement that each section cut the extreme fibers at right angles. Thus, the sides of the wedges are tangent to the extreme fibers.

Limitations.—This method results in an approximate solution for wedge-shaped beams, and its accuracy varies according to the central angle β, being more accurate for the smaller values of β. In general, angles of β greater than 45° will not have to be considered, and for β equal to 45° the approximate solutions give results within 5% of the more rigorous solutions. Greater accuracy is obtainable for built-up members and for various combinations of loads. Mr. Osgood has developed[2] many formulas related to the stresses which occur in wedge-shaped beams.

The shear force V_O does not contribute to the shear on the circular sections. A consideration of the forces shown in Fig. 2(*b*) will clarify this situation. All the stresses σ_r intersect at the center O, and therefore the resultant of these stresses must pass through point O. Furthermore, the resultant is equal and opposite to V_O. Therefore, the stresses σ_r balance V_O, and no tangential forces, $\tau_{r\theta}$, can be present.

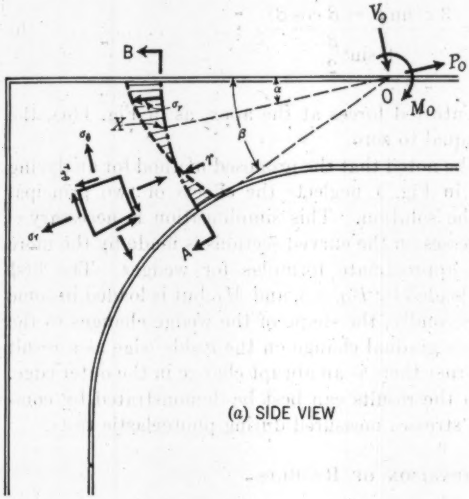
B
V_O
P_O
O
M_O
α
σ_r
X
σ_θ
β
τ
A

(*a*) SIDE VIEW

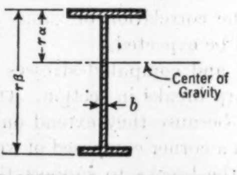
rα
rβ
Center of Gravity
b

(*b*) SECTION A–B (DEVELOPED)

FIG. 1

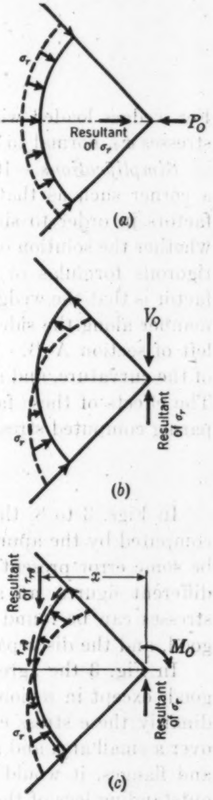
σ_r
Resultant of σ_r
P_O
(a)
V_O
σ_r
Resultant of σ_r
(b)
Resultant of $\tau_{r\theta}$
x
M_O
σ_r
Resultant of σ_r
(c)

FIG. 2

The stresses resulting from the moment M_O are both shear forces, $\tau_{r\theta}$, and normal stresses, σ_r (Fig. 2(*c*)). The resultant of $\tau_{r\theta}$ is a vertical force equal and opposite to the resultant of σ_r, but these resultants are applied at a distance, x, from each other—forming a couple which balances M_O. For example, for a section of uniform thickness,[2] the resultants S of σ_r and $\tau_{r\theta}$ can be expressed as

$$S = \frac{8\,M_O \sin^3 \frac{\beta}{2}}{3\,r(\sin\beta - \beta\cos\beta)} \qquad (5)$$

but they are of opposite signs, and

$$x = \frac{3\,r(\sin\beta - \beta\cos\beta)}{8\sin^3 \frac{\beta}{2}} \qquad (6)$$

For wedges loaded with concentrated forces at the apex, as in Fig. 1(*a*), the stresses σ_θ, normal to σ_r, are equal to zero.

Simplifications.—It should be noted that the proposed method for analyzing a corner such as that shown in Fig. 1 neglects the effects of two principal factors in order to simplify the solution. This simplification is necessary—whether the solution of the stresses on the curved sections is made by the more rigorous formulas or by the approximate formulas for wedges. The first factor is that the wedge is not loaded by P_O, V_O, and M_O but is loaded in some manner along the side OA. Secondly, the shape of the wedge changes to the left of section A–B. There is a gradual change on the inside edge as a result of the curvature, and at the corner there is an abrupt change in the outer edge. The effects of these factors on the results can best be demonstrated by comparing computed stresses with stresses measured during photoelastic tests.

Comparison of Results

In Figs. 3 to 8, the measured stresses are plotted as solid lines, and those computed by the approximate method are plotted as dotted lines. There will be some error present in the measured stress values, but, by comparing the different figures, an average discrepancy between measured and computed stresses can be found for the various sections. The correlation of values is good, and the discrepancies occur where they would be expected.

In Fig. 3 the agreement between the measured and computed stresses is good, except in regions near the vicinity of the sharp breaks in section. Ordinarily these stress concentrations are not critical because they extend only over a small area and are of a secondary nature. In a corner composed of web and flanges, it would be well to add stiffeners at the breaks to support the outstanding legs of the flanges.

In Figs. 4 to 7, the inside radius has been varied from 5 in. to 2 in. Fig. 8 is of the same shape as Fig. 7 except that the sharp outside corner has been rounded off. Agreement is good along the outside edges of all corners. The greatest discrepancies occur on the inside edges toward the center of the arc and are greatest where the internal angle of the wedge section is 45°. The average agreement is within 8% for internal angles of less than 30°. It should be noted, however, that the point at which the disagreement is greatest is beyond the region where maximum stresses occur so that the error at point A is usually of no importance. Furthermore, sections A–B in Figs. 4 to 7

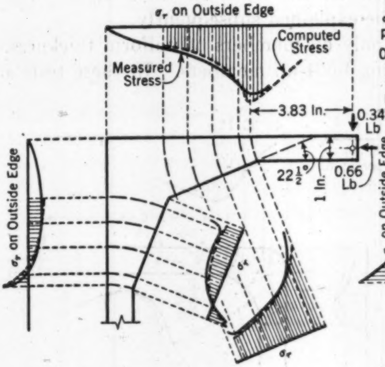
σ_r on Outside Edge
Computed Stress
Measured Stress
3.83 In.
0.34 Lb
$22\frac{1}{2}°$
1 In.
0.66 Lb
σ_r on Outside Edge
σ_t
σ_r

FIG. 3

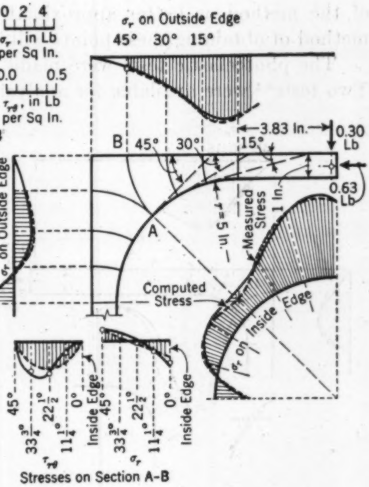
0 2 4
σ_r, in Lb per Sq In.
0.0 0.5
$\tau_{r\theta}$, in Lb per Sq In.
σ_r on Outside Edge
45° 30° 15°
3.83 In.
0.30 Lb
B
45°
30°
15°
0.63 Lb
1 In.
r = 5 In.
A
Measured Stress
Computed Stress
σ_r on Outside Edge
σ_r on Inside Edge
45°
$33\frac{3}{4}°$
$22\frac{1}{2}°$
$11\frac{1}{4}°$
0°
Inside Edge
$\tau_{r\theta}$
45°
$33\frac{3}{4}°$
$22\frac{1}{2}°$
$11\frac{1}{4}°$
0°
Inside Edge
σ_r
Stresses on Section A-B

FIG. 4

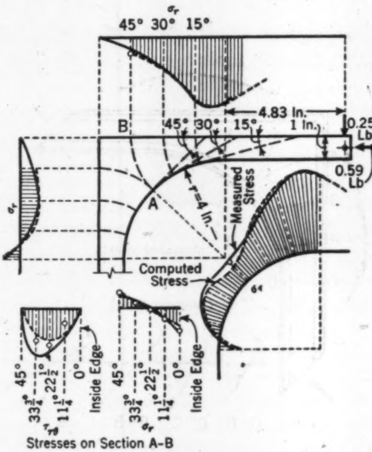
σ_r
45° 30° 15°
4.83 In.
1 In.
0.25 Lb
B
45°
30°
15°
0.59 Lb
r = 4 In.
A
Measured Stress
Computed Stress
σ_r
σ_t
45°
$33\frac{3}{4}°$
$22\frac{1}{2}°$
$11\frac{1}{4}°$
0°
Inside Edge
$\tau_{r\theta}$
45°
$33\frac{3}{4}°$
$22\frac{1}{2}°$
$11\frac{1}{4}°$
0°
Inside Edge
σ_r
Stresses on Section A-B

FIG. 5

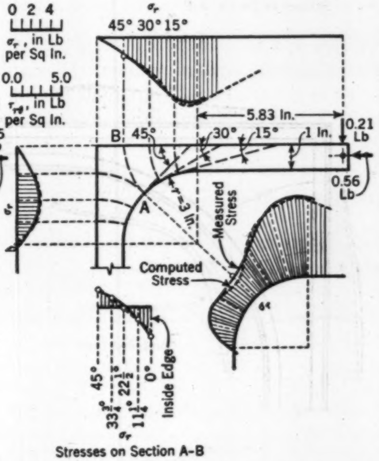
0 2 4
σ_r, in Lb per Sq In.
0.0 5.0
$\tau_{r\theta}$, in Lb per Sq In.
σ_r
45° 30° 15°
5.83 In.
0.21 Lb
B
45°
30°
15°
1 In.
0.56 Lb
r = 3 In.
A
Measured Stress
Computed Stress
σ_r
σ_t
45°
$33\frac{3}{4}°$
$22\frac{1}{2}°$
$11\frac{1}{4}°$
0°
Inside Edge
σ_r
Stresses on Section A-B

FIG. 6

indicate that the overstress occurs only near the extreme fiber and therefore does not extend over a large area.

Sections were taken as indicated. On the curved corners, they occur at intervals having internal angles equal to 15°, 30°, and 45°. The circled points indicated on sections A–B in Figs. 4 to 7 were obtained by further refinement of the method or better approximations of the loads on the wedges. The method of obtaining these points will be explained subsequently.

The photoelastic tests were made only on members of uniform thickness. Two tests[3,4] were available for analyzing built-up members. In these tests a comparison could be made between the measured stresses and those stresses obtained using the approximate method. The comparisons are shown in

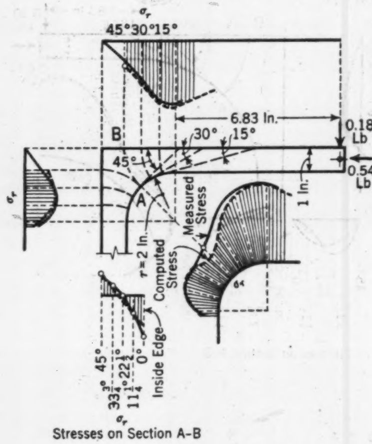
σr
45°30°15°
6.83 In.
0.18 Lb
B
30°
15°
45°
0.54 Lb
A
1 In.
Measured Stress
Computed Stress
r = 2 In.
σt
σr
45°
33¾°
22½°
11¼°
0°
Inside Edge
σr
Stresses on Section A-B

FIG. 7

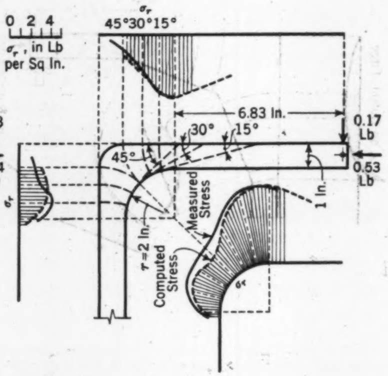
0 2 4
σr, in Lb per Sq In.
σr
45°30°15°
6.83 In.
0.17 Lb
30°
15°
45°
0.53 Lb
1 In.
Measured Stress
Computed Stress
r = 2 In.
σt
σr

FIG. 8

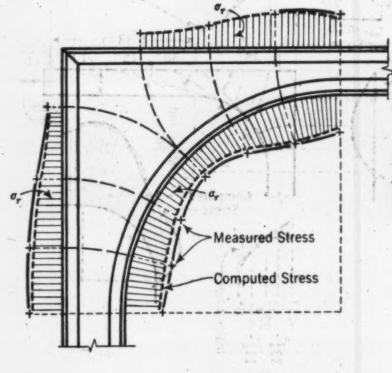
σr
σr
σt
Measured Stress
Computed Stress

FIG. 9

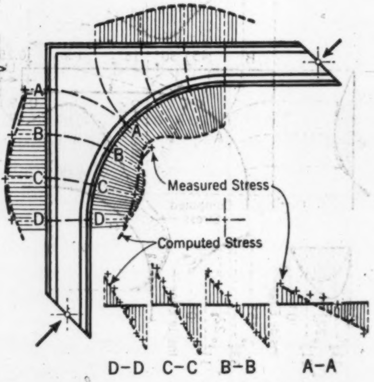
A
B
C
D
A
B
C
D
Measured Stress
Computed Stress
D-D
C-C
B-B
A-A

FIG. 10

---

[3] "An Investigation of Steel Rigid Frames," by Inge Lyse and W. E. Black, *Transactions*, ASCE, Vol. 107, 1942.

[4] "Strength of Riveted Steel Rigid Frame Having a Curved Inner Flange," by Ambrose H. Stang, Martin Greenspan, and William R. Osgood, *Research Paper RP 1161*, National Bureau of Standards, Washington, D. C., 1938.

Figs. 9 to 10. The results for these tests show the same general agreement between measured and computed stress around the corners, as in the photoelastic tests. The agreement is good and within the accuracy expected between design computations and actual tests.

Influence of Simplifications.—Of the two factors which were neglected in order to simplify the problem, the replacing of the loads along the wedge surface by the forces P_O, V_O, and M_O appears to influence the results more than the change of the shape of the wedge. By the use of St. Venant's principle, this simplification would have little influence on the stresses on the outside edge, such as those at point B on section A–B in Fig. 11, but would have the greatest effect at point A on the inside edge; it is significant that the greatest discrepancies occur along the inside edge. The change in cross section to the left of section A–B does not appear to influence greatly the results for extreme fiber stresses because, in regions where the local effects of the applied loads are small, there is good agreement between the measured and computed stresses. For example, the values agree everywhere along the outer edges, in all tests; in Fig. 3, where the inside edges are straight, agreement is good on both edges even near the sharp breaks in section.

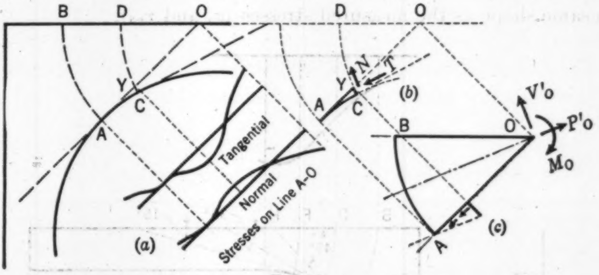

Fig. 11

To substantiate these observations further, an attempt was made to load the wedge AOB (Fig. 11) along the side OA in a manner that would show the local effect of these loads on the sections A–B. In doing so, the stresses indicated by the circled points on sections A–B in Figs. 4 to 7 were obtained. These stresses show good agreement and seem to account for the major part of the discrepancies between measured and computed stresses.

The wedge AOB (Fig. 11) is loaded along the face OA by the stresses that exist on section O–A. These stresses will be tangential, normal, somewhat of the nature shown in Fig. 11(*a*), and always equal to zero at point A. The local effect of the stresses along the line AO on section A–B diminishes as the distance from point A is increased, so that beyond point Y the manner in which the stresses are applied to the wedge is not important. Therefore, those forces from points Y to O can be replaced with concentrated forces at point O. That is, to obtain better results on section A–B only those stresses from point A to point Y in the manner that they exist along this distance need be applied. Having assumed that the stresses on section C–D have been previously determined, the total tangential and normal stresses from point A to point Y can be determined from a section, such as section C–D, by balancing the forces T and N on the element ACX in Fig. 11(*b*). The normal stresses from point A to point Y were small and were found to have little influence; therefore, only the tangential stresses from point A to point Y were applied as such. Furthermore, to simplify the work, these stresses were assumed to have a triangular distribution (Fig. 11(*c*)). Lastly, these stresses and the external forces were balanced about point O by adjusting P'_O and V'_O; then, with the system of forces shown in Fig. 11(*c*), the stresses were determined. These approximations yield results which are in better agreement with the measured stresses on sections A–B; the general shape of the stress-distribution curves on the sections has the same shape as the measured stresses (σ_r and $\tau_{r\theta}$).

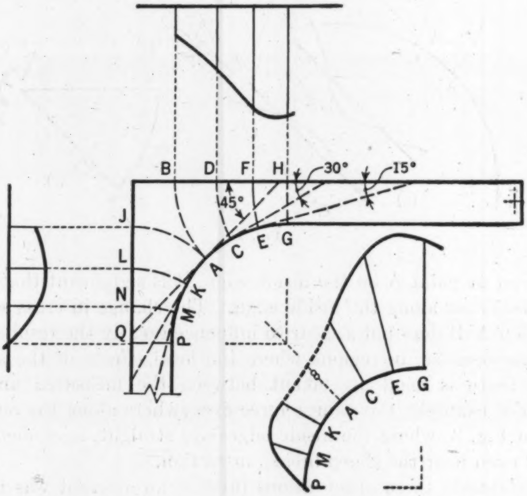

FIG. 12

It should be noted that this correction of the stresses on sections A–B in Figs. 4 to 7 was attempted as a matter of interest and is not recommended as a practical method. The method is still approximate and, in order to improve it, more elaborate methods must be developed to load the wedge with the stresses as they exist along the side OA. Even if this were possible, the work could hardly be justified because these stresses are not critical from a design standpoint. A reasonable approximation of the stress at point A can be made in a simple manner.

Sources of Errors.—The results obtained on the outer straight edges are satisfactory, and the results along the inner curved edge can be determined by this method with the use of an internal wedge angle of 30°, or less, with an expected error of less than 10%. At the center of the curved edge, where the internal angle is 45° (point A, Fig. 12), the greatest discrepancies occur. However, it has been shown that for ordinary structural members and for any combination of loads the stresses are not critical at this point—and therefore not important. In determining the stresses at point A, it is found that the stresses at point A from sections A–B and A–J do not always coincide. The divergence of values is dependent on the type of loading.

The deviation of values is indicated by the two circled points on the stress diagram for the inside edge at point A, in Fig. 12. However, after the stresses at points K and C have been determined and after the results of the photoelastic tests have been considered, it is a simple matter to estimate the stress at point A by considering the general shape of the curve to either side of point K and point C. The value of the stress at point A can be determined by interpolation. This interpolation is effected in Fig. 12 by the dotted line.

APPLICATION

This method can also be applied to the investigation of the bracket shown in Fig. 13.

Two centers are used for taking circular sections. These sections, shown by the dashed lines, have the center O_1, and other sections, such as section A–D, have the center O_2.

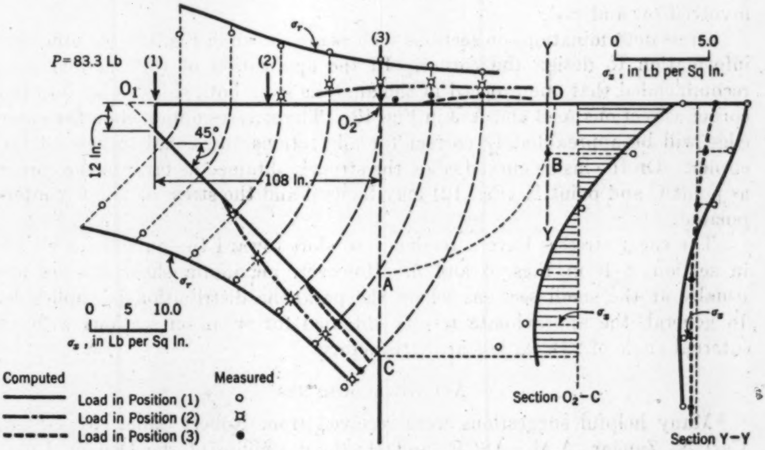
P=83.3 Lb
(1)
(2)
(3)
O_1
O_2
45°
12 In.
108 In.
σ_r
σ_r
D
B
Y
Y
A
C
0 5.0
σ_x, in Lb per Sq In.
0 5 10.0
σ_x, in Lb per Sq In.
σ_x
σ_x
Computed
Measured
Load in Position (1) ○
Load in Position (2) ¤
Load in Position (3) ●
Section O_2-C
Section Y−Y

FIG. 13

The σ_x-stresses on sections O_2–C are shown for the load in position 1. There are also shear stresses τ_{xy} and stresses σ_y on this section, but they are not shown. The stresses σ_x, τ_{xy}, and σ_y are determined at any point along section O_2–C from the stresses σ_r and $\tau_{r\theta}$ of a circular section through that point.

To determine the stress at point B on section A–D, the wedge O_2AD must be considered. This wedge is loaded along the side O_2A by stresses σ_x and τ_{xy}. Because point B is some distance from side O_2A, the wedge O_2AD can be considered to be loaded with concentrated forces P_O, V_O, and M_O at point O_2. These forces are obtained by resolving the stresses σ_x and τ_{xy} from point O_2 to point A about point O_2. The load P to the left of section O_2–C is not used, in this case, to determine the concentrated forces at point O_2, but when the wedge becomes large enough so that the side O_2–A is equal to or greater than O_2–C, P can be used because it will then be equal to the stresses σ_x and τ_{xy} from points O_2 to C, resolved about point O_2.

The σ_x-stresses on section Y–Y are shown in Fig. 13 for two positions of the load. These stresses were determined by taking several circular sections (such as section A–D) and finding the stresses at points such as point B along the line YY. Formulas and stress curves for straight sections such as YY, which simplify this part of the work, are presented in Appendix I.

It should be realized that in a problem of this type, a free surface near section Y–Y will have a considerable effect on the results.

CONCLUSION

The proposed method is not difficult to use, is easy to remember, and will give results within the accuracy usually obtained in structural design. This method determines the extreme fiber stresses directly and simplifies the problem, because by taking circular sections, only two types of stress are involved (σ_r and $\tau_{r\theta}$).

Stress determinations on sections such as are shown in Fig. 12 give sufficient information to design the corner. In the application of this method it is recommended that one proceed in the analysis from both sides as far into the corner as sections A–B and A–J in Fig. 12. The stresses obtained on the outer edge will be approximately correct for all sections and equal to zero at the corner. On the inside curved edge, the stresses obtained as far into the corner as point C and point K (Fig. 12) may be used and the stress at point A interpolated.

The shear stresses have a tendency to shift toward the outside, as shown in section A–B in Figs. 4 and 5. However, maximum shear stresses are usually at the small sections where the parabolic distribution is applicable. In general, the approximate results obtained for shear on sections with an internal angle of 22½° or less are satisfactory.

ACKNOWLEDGMENTS

Many helpful suggestions were received from Robert Sailer, M. ASCE, Carl N. Zangar, A.M., ASCE, and H. Boyd Phillips of the Denver, Colo., office of the Bureau of Reclamation, United States Department of the Interior, and C. K. Wang, A.M. ASCE, of the University of Colorado, at Boulder. The tests referred to were performed in the photoelastic laboratory of the Bureau of Reclamation in Denver.

APPENDIX I

The formulas presented in Fig. 14, for wedges loaded along one face, were developed from the basic equations presented by S. Timo-

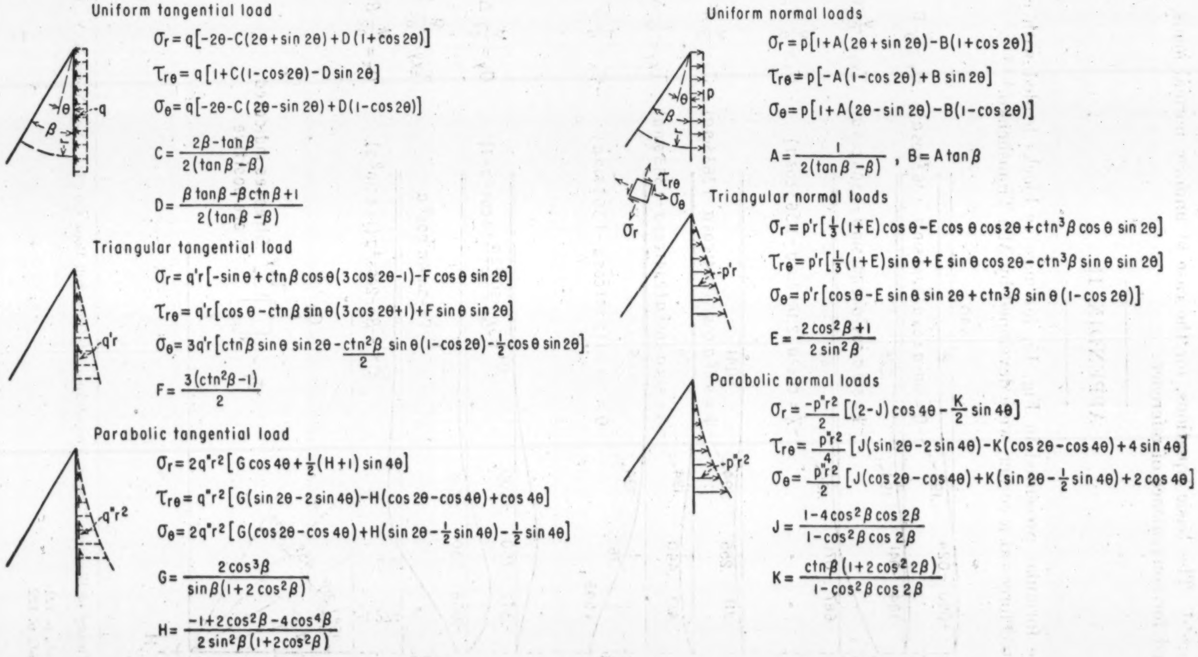

Uniform tangential load

$$\sigma_r = q[-2\theta - C(2\theta + \sin 2\theta) + D(1 + \cos 2\theta)]$$

$$\tau_{r\theta} = q[1 + C(1 - \cos 2\theta) - D \sin 2\theta]$$

$$\sigma_\theta = q[-2\theta - C(2\theta - \sin 2\theta) + D(1 - \cos 2\theta)]$$

$$C = \frac{2\beta - \tan\beta}{2(\tan\beta - \beta)}$$

$$D = \frac{\beta\tan\beta - \beta\,\mathrm{ctn}\,\beta + 1}{2(\tan\beta - \beta)}$$

Triangular tangential load

$$\sigma_r = q'r[-\sin\theta + \mathrm{ctn}\,\beta\cos\theta(3\cos 2\theta - 1) - F\cos\theta\sin 2\theta]$$

$$\tau_{r\theta} = q'r[\cos\theta - \mathrm{ctn}\,\beta\sin\theta(3\cos 2\theta + 1) + F\sin\theta\sin 2\theta]$$

$$\sigma_\theta = 3q'r[\mathrm{ctn}\,\beta\sin\theta\sin 2\theta - \frac{\mathrm{ctn}^2\beta}{2}\sin\theta(1 - \cos 2\theta) - \tfrac{1}{2}\cos\theta\sin 2\theta]$$

$$F = \frac{3(\mathrm{ctn}^2\beta - 1)}{2}$$

Parabolic tangential load

$$\sigma_r = 2q''r^2[G\cos 4\theta + \tfrac{1}{2}(H+1)\sin 4\theta]$$

$$\tau_{r\theta} = q''r^2[G(\sin 2\theta - 2\sin 4\theta) - H(\cos 2\theta - \cos 4\theta) + \cos 4\theta]$$

$$\sigma_\theta = 2q''r^2[G(\cos 2\theta - \cos 4\theta) + H(\sin 2\theta - \tfrac{1}{2}\sin 4\theta) - \tfrac{1}{2}\sin 4\theta]$$

$$G = \frac{2\cos^3\beta}{\sin\beta(1 + 2\cos^2\beta)}$$

$$H = \frac{-1 + 2\cos^2\beta - 4\cos^4\beta}{2\sin^2\beta(1 + 2\cos^2\beta)}$$

Uniform normal loads

$$\sigma_r = p[1 + A(2\theta + \sin 2\theta) - B(1 + \cos 2\theta)]$$

$$\tau_{r\theta} = p[-A(1 - \cos 2\theta) + B\sin 2\theta]$$

$$\sigma_\theta = p[1 + A(2\theta - \sin 2\theta) - B(1 - \cos 2\theta)]$$

$$A = \frac{1}{2(\tan\beta - \beta)}, \quad B = A\tan\beta$$

Triangular normal loads

$$\sigma_r = p'r[\tfrac{1}{3}(1+E)\cos\theta - E\cos\theta\cos 2\theta + \mathrm{ctn}^3\beta\cos\theta\sin 2\theta]$$

$$\tau_{r\theta} = p'r[\tfrac{1}{3}(1+E)\sin\theta + E\sin\theta\cos 2\theta - \mathrm{ctn}^3\beta\sin\theta\sin 2\theta]$$

$$\sigma_\theta = p'r[\cos\theta - E\sin\theta\sin 2\theta + \mathrm{ctn}^3\beta\sin\theta(1 - \cos 2\theta)]$$

$$E = \frac{2\cos^2\beta + 1}{2\sin^2\beta}$$

Parabolic normal loads

$$\sigma_r = \frac{-p''r^2}{2}[(2 - J)\cos 4\theta - \frac{K}{2}\sin 4\theta]$$

$$\tau_{r\theta} = \frac{p''r^2}{4}[J(\sin 2\theta - 2\sin 4\theta) - K(\cos 2\theta - \cos 4\theta) + 4\sin 4\theta]$$

$$\sigma_\theta = \frac{p''r^2}{2}[J(\cos 2\theta - \cos 4\theta) + K(\sin 2\theta - \tfrac{1}{2}\sin 4\theta) + 2\cos 4\theta]$$

$$J = \frac{1 - 4\cos^2\beta\cos 2\beta}{1 - \cos^2\beta\cos 2\beta}$$

$$K = \frac{\mathrm{ctn}\,\beta(1 + 2\cos^2 2\beta)}{1 - \cos^2\beta\cos 2\beta}$$

Fig. 14

shenko.[5,6,7] The basic equations, for the case of uniform normal loads, are included for convenience of reference.

APPENDIX II

The formulas presented in Fig. 15, for massive blocks loaded with concentrated forces at a corner, were developed by Mr. Timoshenko.[5,6,7]

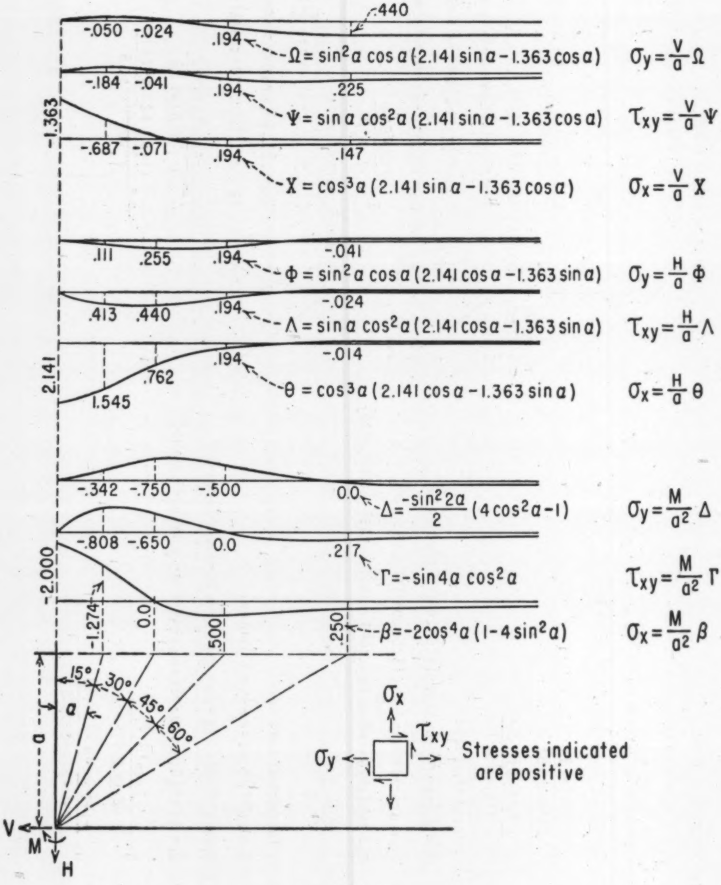
.440
-.050 -.024
.194
$\Omega = \sin^2\alpha \cos\alpha (2.141 \sin\alpha - 1.363 \cos\alpha)$
$\sigma_y = \frac{V}{a}\Omega$
-.184 -.041
.194
.225
$\Psi = \sin\alpha \cos^2\alpha (2.141 \sin\alpha - 1.363 \cos\alpha)$
$\tau_{xy} = \frac{V}{a}\Psi$
-1.363
-.687 -.071
.194
.147
$X = \cos^3\alpha (2.141 \sin\alpha - 1.363 \cos\alpha)$
$\sigma_x = \frac{V}{a}X$
.111 .255
.194
-.041
$\Phi = \sin^2\alpha \cos\alpha (2.141 \cos\alpha - 1.363 \sin\alpha)$
$\sigma_y = \frac{H}{a}\Phi$
.413 .440
.194
-.024
$\Lambda = \sin\alpha \cos^2\alpha (2.141 \cos\alpha - 1.363 \sin\alpha)$
$\tau_{xy} = \frac{H}{a}\Lambda$
2.141
.194
-.014
.762
1.545
$\theta = \cos^3\alpha (2.141 \cos\alpha - 1.363 \sin\alpha)$
$\sigma_x = \frac{H}{a}\theta$
-.342 -.750 -.500
0.0
$\Delta = \frac{-\sin^2 2\alpha}{2}(4\cos^2\alpha - 1)$
$\sigma_y = \frac{M}{a^2}\Delta$
-.808 -.650 0.0
.217
-2.000
$\Gamma = -\sin 4\alpha \cos^2\alpha$
$\tau_{xy} = \frac{M}{a^2}\Gamma$
-1.274 0.0 .500 .250
$\beta = -2\cos^4\alpha (1 - 4\sin^2\alpha)$
$\sigma_x = \frac{M}{a^2}\beta$
15° 30° 45° 60°
a
α
σ_x
τ_{xy}
σ_y
Stresses indicated are positive
V
M
H

FIG. 15

---

[5] "Theory of Elasticity," by S. Timoshenko, McGraw-Hill Book Co., Inc., New York, N. Y., 1932, p. 114.

[6] *Ibid.*, p. 121.

[7] *Ibid.*, p. 122.

APPENDIX III. NOTATION

The following symbols, adopted for use in the paper and for the guidance of discussers, conform essentially with "American Standard Symbols for Structural Analysis" (ASA Z10.8-1949) prepared by a committee of the American Standards Association with Society representation, and approved by the Association in 1949:

A = area of the developed section;
c = distance from the center of gravity to the extreme fiber;
I = moment of inertia of the developed section;
M = moment of the forces to the right of the section about the center of gravity of the developed section;
M_O = bending moment at point O;
N = normal force shown in Fig. 11;
O = center of the arch which is used to take the section;
P = concentrated load;
P_O = axial force at point O;
Q = static moment, about the center of gravity of the section, of the material to the outside of the point of the section in question;
r = radius of the sectional arc;
S = resultant of either σ_r or $\tau_{r\theta}$, defined in Eq. 5;
T = tangential force shown in Fig. 11;
V = total shear on the section;
V_O = normal shear at point O;
X = the point which locates the center of gravity of the developed section;
x = distance between the resultants of σ_r and $\tau_{r\theta}$, defined in Eq. 6;
Z = section modulus of the developed section;
β = central angle of the wedge-shaped section;
σ = unit stresses:
    σ_r = stress normal to the section;
    σ_x = stress shown in Fig. 13;
    σ_y = stress shown in Fig. 13;
    σ_θ = stress tangential to the section;
τ = unit shear:
    $\tau_{r\theta}$ = tangential shear along the section; and
    τ_{xy} = shear stress shown in Fig. 13.

AMERICAN SOCIETY OF CIVIL ENGINEERS
Founded November 5, 1852

TRANSACTIONS

Paper No. 2699

CONTINUOUS COMPOSITE STEEL AND CONCRETE BEAMS

BY JOHN SHERMAN,[1] M. ASCE

SYNOPSIS

The composite steel and concrete beam is used extensively in the construction of highway bridges. It is assumed in the analysis of such bridges that a part of the roadway slab between the adjacent stringers acts in conjunction with the steel beam in resisting the compressive stresses which the positive bending moment produces in the top flange of the beam. For a simply supported composite steel and concrete beam, the top flange is in compression throughout the length of the beam, and, if more concrete acts with the beam than was assumed, the only effect is added rigidity.

For the analysis of continuous composite steel and concrete beams, it is customary to assume that the steel beam takes all of the stresses caused by (1) the weight of the composite beam and the roadway slab, and (2) the negative bending moment produced by the dead and live load. The composite beam is presumed to take all of the stresses caused by the positive bending moment produced by the live load, live load impact, and the superimposed dead load. In a computation of the stresses resulting from the weight of the steel beam and the weight of the roadway slab, allowance is made for the variation in moment of inertia of the steel beam; and in computing the stresses produced by the loads taken by the composite beam, the moment of inertia of the composite beam is assumed to be uniform. This manner of analysis of continuous composite beams is termed the "approximate method."

This paper presents an analysis of continuous composite steel and concrete beams based on the assumption that, because the concrete does not take tension, the moment of inertia of the composite beam is effective only for those parts of the span where the bending moment is positive. The moment of inertia does not have the abrupt change which this assumption indicates, but changes gradually. The effect of this gradual change is somewhat counteracted by the fact that the moment of inertia of the composite beam has a slight variation[2]—being larger at the point of maximum moment than at the points of contraflexure.

NOTE.—Published, essentially as printed here, in August, 1953, as *Proceedings-Separate No. 251*. Positions and titles given are those in effect when the paper was received for publication.

[1] Engr. American Bridge Div., United States Steel Co., Roanoke, Va.

[2] "Strength of Materials," by S. Timoshenko, D. Van Nostrand Co., Inc., New York, N. Y., 2d Ed. 1941, Pt. II, p. 58, Fig. 42.

The analysis is restricted to symmetrical two-span and three-span continuous composite beams. The results of the analysis show that the continuous composite beam is not as stiff as is indicated by the approximate method, and that the assumptions used for the design of simply supported composite beams are not applicable to the design of continuous composite beams.

NOTATION

The letter symbols adopted for use in this paper are defined where they first appear, in the illustrations or in the text, and are arranged alphabetically for convenience of reference in the Appendix.

INTRODUCTION

The composite beam is composed of three essential parts: The steel beam, the concrete slab, and the shear connectors. The steel beam may be a rolled beam with or without cover plates, a plate girder, or a weldment composed of three plates.

The effective width b' (in inches) of the concrete part of a composite beam of length L (in inches) and thickness t (in inches) which is placed a distance (on centers) of s (in inches) from the adjacent beam is limited by the American Association of State Highway Officials[3] (AASHO) to less than $L/4$, s, or $12\,t$. The AASHO also requires that, for concrete having a strength of from 3,000 lb per sq in. to 3,900 lb per sq in., n (the ratio of the modulus of elasticity of steel, E_s, to the modulus of elasticity of concrete, E_c) is to be taken as 10 for strength determinations and 8 for computing the deflections. These values of n are for reinforced concrete beams, and although the specification does not give any value of n to be used for composite beams, it is usual to assume that these values also apply to composite beam construction. Having selected a value for n, the area of the concrete part of the composite beam (in terms of the steel) is $b'\,t/n$, and the properties of the composite beams are determined in a manner similar to that used for T-beams. Because the bond between the top flange of the steel beam and the concrete slab is not dependable, mechanical shear connectors are provided to develop the horizontal shear which occurs at the faying surface of the steel beam and the concrete slab. There are various types of shear connectors—bent or looped bars, beam or channel lugs, and serpentine or spiral rods—which are welded to the top flange of the steel beam.

MATHEMATICAL OPERATIONS

In the subsequent analysis it will be required to solve cubic and quartic equations. The roots of these equations will be M_n, the negative support moment in inch-pounds in some cases, and s_c, the distance from the point of contraflexure to the nearest support (in inches) in other cases; since these terms will be taken as factors of the product of the load and L, they will be numbers less than unity. The most direct method of solving such equations is termed "Horner's method." This method was developed by W. G. Horner and is supposed to have been known by the Chinese in the thirteenth century. The method consists of forming an equation for each figure of the root, the formation of the equations being done by synthetic division. This method was selected because it requires no more work to solve equations of the type that occurs in the solution of the problem under investigation than it does to reduce a cubic equation to the form required for a solution by radicals or to obtain the cubic resolvent of a quartic equation. Since the root to be determined is always a small positive number, it is not necessary to enter into the complexities of the general case of the method, the subsequent analysis being a sufficient description for the purposes of this investigation.

---

[3] "Standard Specifications for Highway Bridges," A.A.S.H.O., Washington, D. C., 5th Ed., 1949.

When the positive root of the equation,

$$x^3 + H\,x^2 + B\,x - U = 0 \ldots\ldots\ldots\ldots\ldots\ldots (1)$$

is a small decimal, the first figure of the root is equal to the absolute term divided by the penultimate coefficient. Denoting the first figure of the root by *l*, then

$$l = \frac{U}{B} \ldots\ldots\ldots\ldots\ldots\ldots\ldots\ldots (2)$$

If all of the roots of Eq. 1 are reduced by *l*, there results

$$x^3 + H'\,x^2 + B'\,x - U' = 0 \ldots\ldots\ldots\ldots\ldots\ldots (3)$$

from which the second figure of the root is equal to U'/B'. This process can be continued until the desired accuracy is obtained.

Eq. 3 is formed as follows:

1. Eq. 1 is divided by $(x - l)$ from which there results a quadratic equation which is denoted by X, and a remainder equal to U' in Eq. 3.
2. Eq. X is divided by $(x - l)$, resulting in an equation of the first degree which is denoted by Y and a remainder equal to B' in Eq. 3.
3. Eq. Y is divided by $(x - l)$ from which there results a remainder equal to H' in Eq. 3.

In this process, if *l* is made equal to $-H/3$, then H' will be zero and Eq. 3 will be in the form required for solution by radicals.

Example.—Given the equation,

$$x^3 + 4.89\,x^2 + 5.45\,x - 0.66 = 0 \ldots\ldots\ldots\ldots\ldots (4a)$$

then

$$l = \frac{0.66}{5.45} = 0.1 \ldots\ldots\ldots\ldots\ldots\ldots\ldots\ldots (4b)$$

First Operation.—

$$\begin{array}{r|rrrr|l}
\underline{x - 0.1} & x^3 & + 4.890\,x^2 & + 5.450\,x & - 0.6600 & \underline{x^2 + 4.99\,x + 5.949} \\
 & \underline{x^3} & \underline{- 0.100\,x^2} & & & \\
 & & + 4.990\,x^2 & + 5.450\,x & & \\
 & & \underline{+ 4.990\,x^2} & \underline{- 0.499\,x} & & \\
 & & & + 5.949\,x & - 0.6600 & \\
 & & & \underline{+ 5.949\,x} & \underline{- 0.5949} & \\
 & & & & - 0.0651 & = U' \ldots\ldots\ldots\ldots\ldots (5a)
\end{array}$$

Second Operation.—

$$\begin{array}{r|l}
\underline{x - 0.1} & x^2 + 4.99\,x + 5.949 \;\underline{|\; x + 5.09} \\
 & \underline{x^2 - 0.10\,x} \\
 & \qquad + 5.09\,x + 5.949 \\
 & \qquad \underline{+ 5.09\,x - 0.509} \\
 & \qquad\qquad\qquad + 6.458 = B' \ldots\ldots\ldots\ldots\ldots\ldots (5b)
\end{array}$$

Third Operation.—

$$\begin{array}{r|l}
\underline{x - 0.1} & x + 5.09 \\
 & \underline{x - 0.10} \\
 & \quad + 5.19 = H' \ldots\ldots\ldots\ldots\ldots\ldots\ldots (5c)
\end{array}$$

Therefore, the new equation is

$$x^3 + 5.19\,x^2 + 6.458\,x - 0.0651 = 0 \ldots\ldots\ldots\ldots\ldots (6)$$

The second figure of the root is $0.0651/6.458 = 0.01$ and the value of the root (to two decimal places) is 0.11.

This procedure is simplified and compacted by the use of synthetic division. Writing only the literal parts of the first equation, there results

$$\begin{array}{r|l}
\underline{1 - 0.1} & 1 + 4.89 + 5.45 \;\; - 0.66 \\
 & 1 + 4.99 + 5.949 - 0.0651
\end{array}$$

This corresponds to the first operation, the second line being formed as

$$\begin{aligned}
4.89 + 0.10 &= 4.99 \\
5.45 + 0.10 \times 4.99 &= 5.949
\end{aligned}$$

and

$$-0.66 + 0.10 \times 5.949 = -0.0651.$$

The second operation is written as

$$\begin{array}{r|l}
\underline{1 - 0.1} & 1 + 4.99 + 5.949 \\
 & 1 + 5.09 + 6.458
\end{array}$$

in which

$$4.99 + 0.10 = 5.09$$

and

$$5.949 + 0.10 \times 5.09 = 6.458.$$

The third operation is formed as

$$\begin{array}{r|l}
\underline{1 - 0.1} & 1 + 5.09 \\
 & 1 + 5.19
\end{array}$$

in which

$$5.09 + 0.10 = 5.19.$$

The three steps can be combined into the following compact form, and the formation of new equations continued as

$$\begin{array}{l|llll}
\underline{1 - 0.1} & 1 + 4.89 + 5.45 & - 0.66 & & \\
 & \underline{1 + 4.99 + 5.949} & \underline{- 0.0651} & & \\
 & \quad + 5.09 + 6.458 & \quad 0^* & & l' = \dfrac{0.0651}{6.458} = 010. \\
\underline{1 - 0.01} & \quad \underline{+ 5.19 + 6.510^*} & & & \\
 & \quad + 5.20^* & & & l'' = 0.
\end{array}$$

The literal terms of the third equation obtained by reducing the roots of the second equation by 0.01 are marked by an asterisk. The absolute term of this equation is zero; therefore 0.11 is an exact root of the first equation.

To obtain the other two roots, the roots of the first equation are reduced by 0.11;

$$\begin{array}{l|ll}
\underline{1 - 0.11} & 1 + 4.89 + 5.45 & - 0.66 \\
 & 1 + 5.00 + 6.00 & \quad 0\ ,
\end{array}$$

the other two roots being contained in the quadratic equation,

$$x^2 + 5x + 6 = 0 \qquad (7)$$

The remaining roots are -2 and -3.

Comparison of Results

When the results obtained by the method used herein are compared with the results obtained by the approximate method, the maximum unit stresses in the steel beam will be used as the basis of comparison. Because detailed considerations are beyond the scope of this investigation, a composite beam with the following characteristics will be used as an example:

1. The moment caused by the uniform live load is 85% larger than the moment resulting from the live concentrated load.
2. The impact factor is 30%.
3. The section modulus of the composite beam for the stress in the bottom flange of the steel beam is 50% larger than the section modulus of the steel beam.

Denoting the intensity of the dead and live uniform loading by w_d and w_l, respectively, the maximum positive moment resulting from the uniform dead load is a factor of $w_d L^2$ which is denoted by M_{pd}, and the maximum positive moment resulting from the uniform live load is a factor of $w_l L^2$ and is denoted by M_{pl}. Denoting by f_p the relative unit stress caused by the dead and live load positive moments when the uniform dead load is 50% larger than the uniform live load,

$$f_p = M_{pd} + M_{pl} \frac{1.85 \times 1.30}{1.5 \times 1.5} = M_{pd} + 1.07\, M_{pl} \qquad (8)$$

When the uniform dead load is three times the uniform live load,

$$f_p = M_{pd} + 0.535\, M_{pl} \qquad (9)$$

Designating the maximum negative moments as M_{nd} and M_{nl} to be factors of $w_d L^2$ and $w_l L^2$, respectively, with the relative unit stress resulting from the dead and live load negative moments indicated by f_n when the uniform dead load is 50% larger than the uniform live load,

$$f_n = M_{nd} + 1.61\, M_{nl} \ldots\ldots\ldots\ldots\ldots\ldots\ldots (10)$$

When the uniform dead load is three times the uniform live load,

$$f_n = M_{nd} + 0.815\, M_{nl} \ldots\ldots\ldots\ldots\ldots\ldots\ldots (11)$$

Eqs. 8, 9, 10, and 11 are used subsequently to compute the relative unit stresses used for comparison with the relative unit stresses obtained by the approximate method.

THE TWO-SPAN CONTINUOUS COMPOSITE BEAM

The two-span beam bridge is an infrequent type of construction as compared to the three-span beam bridge, but, because the equations for the two-span beam are used in forming the equations for loading in the exterior span of a three-span beam, a brief investigation will be made of the two-span beam.

In Fig. 1 there is shown the moment diagram of a continuous uniformly distributed load in the exterior span of a continuous beam. Taking as unity the length of the span, the intensity, w, of the uniform load, and the moment of inertia of the steel beam—the negative support moment M_n will be a factor of $w L^2$ and the moment of inertia of the composite beam will be i. That is,

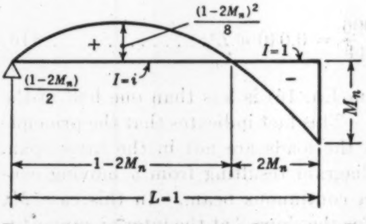

FIG. 1.—MOMENT DIAGRAM FOR A CONTINUOUS BEAM SUPPORTING A UNIFORMLY DISTRIBUTED LOAD

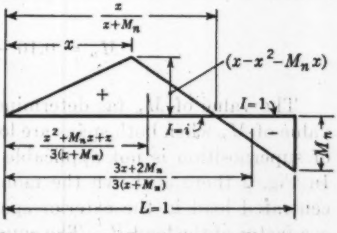

FIG. 2.—MOMENT DIAGRAM FOR A CONTINUOUS BEAM SUBJECTED TO A MOVING CONCENTRATED LOAD IN THE EXTERIOR SPAN

$$i = \frac{I_{co}}{I_s} \ldots\ldots\ldots\ldots\ldots\ldots\ldots (12)$$

in which I_{co} is the moment of inertia of the composite beam, and I_s is the moment of inertia of the steel beam. The equation for the slope, S, of the elastic curve at the interior support is

$$S = \frac{(1 - 2\,M_n)^4}{24\,i} - \frac{M^2_n}{3}(3 + 2\,M_n) + \frac{2\,M^3_n}{3}(1 - M_n) \ldots\ldots (13)$$

Expanding Eq. 13*a*, collecting the terms, and reversing the signs,

$$\begin{aligned} M^4_n (i - 1) - 2\,M^3_n (i - 1) + 1.5\,M^2_n (i - 1) \\ + 0.5\,M_n - 0.0625 + 1.5\,S\,i = 0 \end{aligned} \qquad (13b)$$

When S is equal to zero, Eq. 13*b* is the equation for the support moment of a symmetrical, two-span, continuous, composite beam with both spans loaded with a continuous uniformly distributed load. Substituting S equal to zero and i equal to 2 into Eq. 13*a*, there results

$$M^4_n - 2\,M^3_n + 1.5\,M^2_n + 0.5\,M_n - 0.0625 = 0 \qquad (14)$$

The factor of M_n when i is equal to unity is 0.125. Therefore, the roots of Eq. 14 are reduced by 0.1 as follows:

$$\begin{array}{r|lllll} 1 - 0.1 & 1 - 2 & + 1.5 & + 0.5 & - 0.0625 \\ & 1 - 1.90 & + 1.31 & + 0.631 & + 0.0006 \\ \hline & \quad - 1.80 & + 1.13 & + 0.744. & \end{array}$$

Then

$$M_n = 0.100 - \frac{0.0006}{0.744} = 0.099\,w\,L^2 \qquad (15)$$

which is 25% less than the value of M_n obtained by the approximate method.

When only one span is loaded S is equal to $M_n/3$, the penultimate coefficient in Eq. 14 is increased by unity, and

$$M_n = 0.10 - \frac{0.1006}{1.744} = 0.040\,w\,L^2 \qquad (16)$$

The value of M_n (as determined from Eq. 16) is less than one half of the value of M_n when both spans are loaded. This fact indicates that the principle of superposition is not applicable when the loads are not in the same span. In Fig. 2 there is shown the moment diagram resulting from a moving concentrated load in the exterior span of a continuous beam. In this case M_n is a factor of the load P. The equation for the slope S at the interior support is

$$S = x^2 \frac{1 - x - M_n}{6\,i\,(x + M_n)^2} (x^2 + M_n x + x) - \frac{M^2_n}{6} \frac{3\,x + 2\,M_n}{(x + M_n)^2} \qquad (17a)$$

Expanding Eq. 17*a*, collecting the terms, and reversing the signs, there results

$$\begin{aligned} 2\,M^3_n\,i + M^2_n (x^3 + 3\,i\,x + 6\,S\,i) + 2\,M_n (x^4 + 6\,S\,i\,x) \\ - x^3 + x^5 + 6\,S\,i\,x = 0 \end{aligned} \qquad (17b)$$

When S is equal to $M_n/3$ in Eq. 17*b*, the equation becomes the equation for the support moment of a symmetrical, two-span, continuous, composite beam with a moving load in one span. Therefore,

$$2\,M^3_n\,i + M^2_n (7\,i + x^2) + 2\,M_n\,x^2 (i + x^2) - x^3 + x^5 = 0 \qquad (18)$$

For the case of a single load in each span, symmetrically placed, with S equal to zero, Eq. 17*b* becomes

$$2\,M^3_n\,i + M^2_n\,x\,(3\,i + x^2) + 2\,M_n\,x^4 - x^3 + x^5 = 0 \quad \text{......} (19)$$

Taking x equal to 0.5 and i equal to 2 in Eq. 19, dividing this equation by 4, and reducing the roots by 0.15 as follows:

$$\begin{array}{r|l} \underline{1 - 0.15} & 1 + 0.783 + 0.0313 - 0.0243 \\ & \quad\;\; \underline{+\,0.933 + 0.1713 + 0.0014} \\ & \quad\;\; +\,1.083 + 0.3334 \end{array}$$

then

$$M_n = 0.150 - \frac{0.0014}{0.3334} = 0.146\,P\,L \quad \text{..............} (20a)$$

Solving Eq. 18 for M_n results in

$$M_n = 0.060\,P\,L \quad \text{.....................} (20b)$$

which is less than one half the value of M_n for the two loads.

TABLE 1.—EFFECT OF VARYING i IN FIG. 3

Value of i	(*a*) FACTORS OF M_n (MULTIPLY BY 10^{-3})									(*b*) Area under the influence line (Multiply by 10^{-3})	(*c*) MOMENTS CAUSED BY CONTINUOUS UNIFORMLY DISTRIBUTED LOAD (MULTIPLY BY 10^{-3})			
	Value of $\frac{x}{L}$													
	0.1	0.2	0.3	0.4	0.5	0.6	0.7	0.8	0.9		$M_{1,n}$	$M_{2,n}$	$M_{1,p}$	$M_{2,p}$
1.0	25	48	68	84	94	96	89	72	43	62.5	62.5	125.0	94.0	70.3
1.5	19	38	55	66	73	75	67	55	34	48.7	48.5	111.0	102.0	75.5
2.0	15	31	41	53	60	62	57	47	28	39.7	40.0	99.0	106.0	80.4
3.0	11	26	34	40	45	46	43	35	16	29.7	29.6	84.0	111.0	86.5

Table 1 contains values of M_n for a load applied at the tenth points of one span for values of i equal to 1, 1.5, 2, and 3. The moment diagram for Table 1 is shown in Fig. 3. Table 1 also contains the area under the influence lines for the moving load and the corresponding values of $M_{1,n}$ caused by a continuous uniformly distributed load in one span, as determined from Eq. 13*b*. The corresponding values of $M_{1,n}$ and the areas are in close agreement. From this close agreement it can be concluded that the principle of superposition is applicable when the loads are in the same span. Also included in

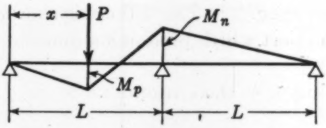

FIG. 3.—MOMENT DIAGRAMS FOR A TWO-SPAN BEAM SUPPORTING A MOVING CONCENTRATED LOAD

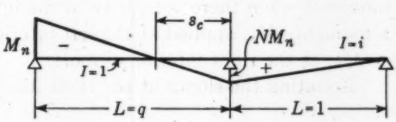

FIG. 4.—MOMENT DIAGRAM FOR A CONTINUOUS BEAM SUBJECTED TO A BENDING MOMENT ON ONE END

Table 1 are values of (1) the support moment $M_{2,n}$ resulting from a continuous uniformly distributed load in both spans, (2) the maximum positive moment $M_{1,p}$ caused by uniform loading in one span, and (3) the maximum positive moment $M_{2,p}$ resulting from a continuous uniformly distributed load in both spans.

Taking values of M_n and M_p from Table 1, computing the unit stresses f_n and f_p from Eqs. 8, 9, 10, and 11, and comparing these unit stresses with those obtained by the approximate method, the errors (given in Table 2) in the approximate method can be obtained.

TABLE 2.—PERCENTAGE ERROR IN APPLYING THE APPROXIMATE METHOD TO FIG. 3

Value of i	(a) ERROR IN DETERMINATION OF f_n		(b) ERROR IN DETERMINATION OF f_p	
	Value of $\frac{w_d}{w_l}$			
	1.5	3.0	1.5	3.0
1.5	+ 7.8	+ 5.3	− 4.7	−3.8
2.0	+12.5	+ 9.3	− 7.0	−5.6
3.0	+18.7	+14.2	−10.5	−7.8

It is evident that the unit stresses caused by the maximum negative and positive moments (as obtained by the approximate method) are larger and smaller, respectively, than those obtained by the proposed method. These errors (Table 2) will be increased by the superimposed dead load, particularly for the outside stringers; if more of the slab acts with the composite beam than was assumed, the errors will be further increased. It therefore appears that, when i is larger than 2, some limitation should be placed on the unit stresses if the design is based on the approximate method.

THE THREE-SPAN, CONTINUOUS, COMPOSITE BEAM

It is first necessary to determine the relationship between the support moments when there is no load in the interior span. In Fig. 4 there is shown a moment, M_n, applied at the left interior support which produces a moment, $N\,M_n$, at the right interior support.

Equating the slopes at the right interior support, there results

$$i\,(1 - s_c)^2\,q - N\,s_c\,(3\,q - s_c) = 2\,N \quad \text{............} (21)$$

Noting that

$$s_c = \frac{N}{1 + N} \quad \text{........................} (22)$$

Eq. 21 becomes

$$N^3\,(2\,q + 2) + N^2\,(3\,q + 4) + 2\,N - q\,i = 0 \quad \text{........} (23)$$

Having obtained the value of N from Eq. 23, the value of S with its sign reversed is

$$S = \frac{M_n}{6}(2 - N)\,q \ldots\ldots\ldots\ldots\ldots\ldots\ldots\ldots (24)$$

Taking q equal to unity and i equal to 1.5 in Eq. 23 results in

$$4\,N^3 + 7\,N^2 + 2\,N - 1.5 = 0 \ldots\ldots\ldots\ldots\ldots\ldots (25)$$

Dividing Eq. 25 by 4 and reducing its roots by 0.3,

$$\begin{array}{l|l} \underline{1 - 0.3} & 1 + 1.75 + 0.500 - 0.3750 \\ & \underline{1 + 2.05 + 1.115 - 0.0405} \\ & \quad + 2.35 + 1.820 \end{array}$$

Therefore

$$N = 0.300 + \frac{0.0405}{1.82} = 0.321 \ldots\ldots\ldots\ldots\ldots\ldots (26)$$

Fig. 5 shows the variation of N with respect to i for several values of q.

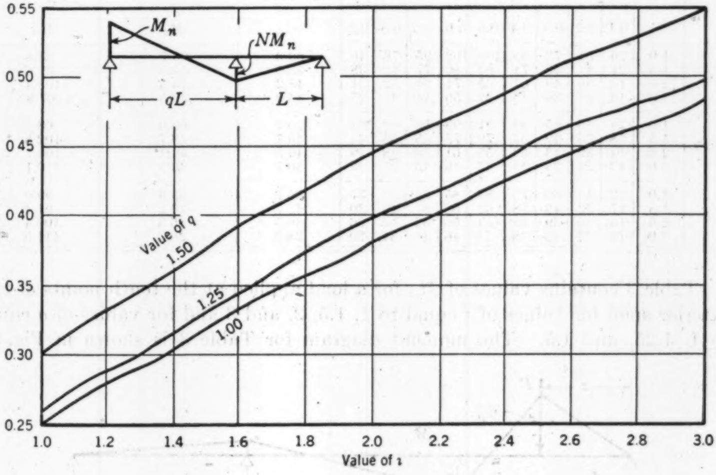

FIG. 5.—VARIATION OF N WITH RESPECT TO i FOR SEVERAL VALUES OF q

For the case of a uniform load in the exterior span of a symmetrical three-span continuous composite beam, Eq. 24 is substituted into Eq. 13b and thus yields

$$M^4_n(i - 1) - 2\,M^3_n(i - 1) + 1.5\,M^2_n(i - 1) \\ + 0.25\,M_n[2 + (2 - N)\,i\,q] - 0.0625 = 0 \ldots\ldots\ldots (27)$$

Taking q equal to unity and i equal to 1.5 in Eq. 27, dividing by 0.5, and reducing the roots by 0.05 leads to

$$\begin{array}{l|rrrrr} \underline{1 - 0.05} & 1 & -\,2.00 & +\,1.500 & +\,2.259 & -\,0.1250 \\ & & -\,1.95 & +\,1.598 & +\,2.338 & -\,0.0081 \\ \cline{3-6} & & -\,1.90 & +\,1.693 & +\,2.422. & \end{array}$$

Then

$$M_n = 0.0500 + \frac{0.0081}{2.422} = 0.0533\,w\,L^2 \ldots\ldots\ldots\ldots\ldots (28)$$

For the case of a moving load in the exterior span of a symmetrical, three-span, composite beam, Eq. 24 is substituted into Eq. 17*b* to result in

$$M^3_n\,i\,[2 + (2 - N)\,q] + M^2_n\,x\,[x^2 + 3\,i + 2\,i\,(2 - N)\,q] + M_n\,x^2\,[2\,x^2 + i\,(2 - N)_q] - x^3 + x^5 = 0 \ldots\ldots\ldots\ldots (29)$$

TABLE 3.—EFFECT OF VARYING q AND i IN FIG. 6

Value of q	Value of i	(a) FACTORS OF M_n (MULTIPLY BY 10^{-3}) — Value of $\frac{x}{L}$: 0.1	0.2	0.3	0.4	0.5	0.6	0.7	0.8	0.9	(b) Area under the influence line (Multiply by 10^{-3})	(c) MOMENTS CAUSED BY CONTINUOUS UNIFORMLY DISTRIBUTED LOAD IN THE EXTERIOR SPAN (MULTIPLY BY 10^{-3}): M_n	M_p
1.0	1.0	26	51	73	89	100	102	95	76	46	66.6	66.7	93.8
	1.5	21	41	58	71	80	82	77	61	38	53.5	53.3	99.6
	2.0	18	35	49	61	68	71	64	52	31	45.2	45.5	103.4
	3.0	14	27	36	46	52	56	50	41	25	34.9	35.5	107.8
1.25	1.0	24	46	65	83	91	93	86	69	41	60.0	60.0	68.0
	1.5	18	35	49	63	70	72	68	55	33	46.7	46.7	102.8
	2.0	14	32	43	53	59	61	58	48	29	40.3	40.4	106.7
	3.0	13	25	35	41	45	48	45	37	22	30.7	30.6	110.1
1.5	1.0	22	43	60	75	83	85	79	64	37	55.2	55.3	99.0
	1.5	17	32	46	58	62	68	62	49	30	42.7	43.2	91.4
	2.0	15	26	39	49	54	56	53	43	26	36.5	36.3	106.4
	3.0	12	21	30	38	43	46	41	34	20	28.7	28.3	111.3

Table 3 contains values of M_n for a load applied at the tenth points of the exterior span for values of i equal to 1, 1.5, 2, and 3 and for values of q equal to 1, 1.25, and 1.5. The moment diagram for Table 3 is shown in Fig. 6.

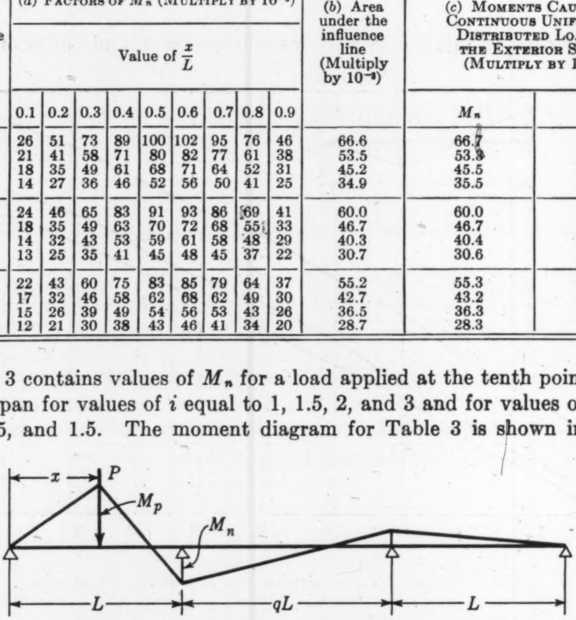

FIG. 6.—MOMENT DIAGRAM FOR A THREE-SPAN CONTINUOUS BEAM SUPPORTING A MOVING CONCENTRATED LOAD IN THE EXTERIOR SPAN

Table 3 also contains the area under the influence lines for the moving load and the corresponding values of M_n—both caused by a continuous uniformly distributed load in the exterior span, as determined from Eq. 27. The corresponding values of M_n and the areas are in close agreement. From this close agreement it can be concluded that the principle of superposition can be applied when the loads are in the same span. Table 3 also contains the values of the maximum positive moment M_p resulting from uniform loading in the exterior span. Fig. 7 shows the moment diagram resulting from a continuous uniformly distributed load in the interior span. The value of s_c is

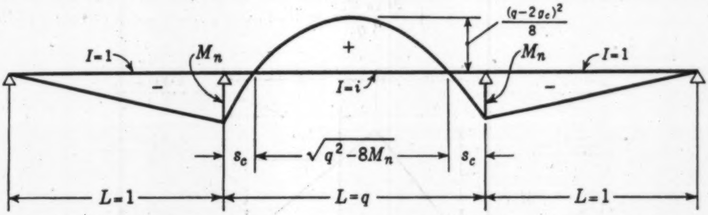

FIG. 7.—MOMENT DIAGRAM FOR A THREE-SPAN CONTINUOUS BEAM SUBJECTED TO A CONTINUOUS UNIFORM LOAD IN THE INTERIOR SPAN

$$s_c = q - \frac{(q^2 - 8\,M_n)^{\frac{1}{2}}}{2} \qquad \text{(30a)}$$

from which

$$M_n = s_c\,\frac{q - s_c}{2} \qquad \text{(30b)}$$

The equation for the condition when the slope of the elastic curve is the same for each interior support is

$$\frac{M_n}{3} + \frac{M_n\,s_c}{2} - \frac{s^3_c}{12} - \frac{(q - 2\,s_c)^3}{24\,i} = 0 \qquad \text{(31)}$$

Substituting Eq. 30*b* into Eq. 31 results in

$$8\,s^3_c\,(i - 1) - 2\,s^2_c\,[6\,q - i\,(3\,q - 2)] + 2\,s_c\,q\,(3\,q + 2\,i) - q^3 = 0 \qquad \text{(32)}$$

Solving Eq. 32 for s_c and substituting this result into Eq. 30*b*, M_n is obtained.

Fig. 8 shows the moment diagram resulting from a moving load in the interior span. The equations for s_{cl} and s_{cr} are

$$s_{cl} = \frac{M_{1n}\,q}{b - M_{1n} + M_{2n}} \qquad \text{(33a)}$$

and

$$s_{cr} = \frac{M_{2n}\,q}{a + M_{1n} - M_{2n}} \qquad \text{(33b)}$$

Equating the slopes at the interior supports, the following two equations are obtained:

$$\frac{M_{1n}}{3} + \frac{M_n\,s_{cl}}{6\,q}\,(3\,q - s_{cl}) - \frac{a - s_{cl}}{6\,q\,i}\,(b - s_{cr})(q + b - s_{cl} + s_{cr}) + \frac{M_{2n}\,s^2_{cr}}{6\,q} = 0 \qquad \text{(34a)}$$

and

$$\frac{M_{2n}}{3} + \frac{M_{2n}\, s_{cr}}{6\,q}(3\,q - s_{cr}) - \frac{(a - s_{cl})}{6\,q\,i}(b - s_{cr})(q + a + s_{cl} - s_{cr}) + \frac{M_{1n}\, s^2_{cl}}{6\,q} = 0 \ldots\ldots\ldots\ldots\ldots\ldots\ldots (34b)$$

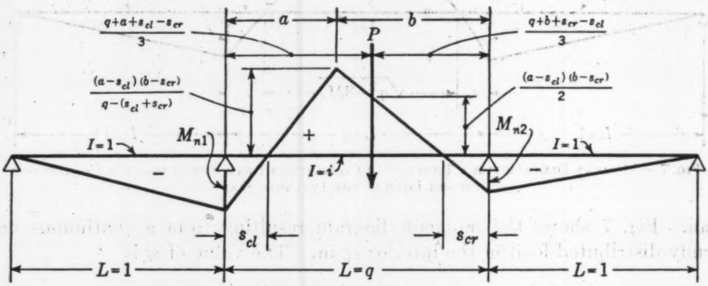
a
b
P
$\frac{q+a+s_{cl}-s_{cr}}{3}$
$\frac{q+b+s_{cr}-s_{cl}}{3}$
$\frac{(a-s_{cl})(b-s_{cr})}{q-(s_{cl}+s_{cr})}$
$\frac{(a-s_{cl})(b-s_{cr})}{2}$
M_{n1}
M_{n2}
+
I=1
I=i
I=1
−
−
s_{cl}
s_{cr}
L=1
L=q
L=1

FIG. 8.—MOMENT DIAGRAM OF A THREE-SPAN CONTINUOUS BEAM SUBJECTED TO A MOVING CONCENTRATED LOAD IN THE CENTER SPAN

The penultimate term in Eqs. 34 is small in comparison with the other terms; therefore these terms are discarded to yield

$$M_{1n}\, i\,[2\,q + s_{cl}\,(3\,q - s_{cl})] - (a - s_{cl})(b - s_{cr})(q + b - s_{cl} + s_{cr} = 0 \ldots (35a)$$

and

$$M_{2n}\, i\,[2\,q + s_{cr}\,(3\,q - s_{cr})] - (a - s_{cl})(b - s_{cr})(q + a + s_{cl} - s_{cr}) = 0 \ldots (35b)$$

Eqs. 35 must be solved by trial and error. The solution is made easy by the fact that M_n can be computed directly when the load is at midspan. In this case a is equal to b, s_{cl} is equal to s_{cr}, and M_{1n} is equal to M_{2n}. Eqs. 34 become

$$6\,M^2_n\,(i - 1) + M_n\,q\,(2\,q + 3\,i) - 0.375\,q^3 = 0 \ldots\ldots\ldots (36)$$

With M_n computed for x equal to $0.5\,q$ by Eq. 36 and with the influence line for i drawn equal to unity, the influence line is used to approximate M_{1n} and M_{2n} for any other value of x. Using these approximate values, s_{cl} and s_{cr} are determined from Eqs. 33. These values of s_c are used to obtain new values of M_{1n} and M_{2n} from Eqs. 35. From the new values of M_n the value of s_c is recomputed. This procedure is repeated until Eqs. 33 and 35 are in close agreement.

Table 4 contains values of M_n for a load applied at the tenth points of the interior span for i equal to 1, 1.5, 2, and 3 and q equal to 1, 1.25, and 1.5. The moment diagram for this case is shown in Fig. 9. Table 4 also contains the area under the influence line for the moving load and the corresponding values of M_n resulting from a continuous uniformly distributed load in the interior span as computed from Eqs. 30b and 32. The corresponding values

TABLE 4.—EFFECT OF VARYING q AND i IN FIG. 9

Value of q	Value of i	(a) FACTORS OF M_n (MULTIPLY BY 10^{-3}) Value of $\frac{x}{L}$									(b) Area under the influence line (Multiply by 10^{-3})	(c) MOMENTS CAUSED BY CONTINUOUS UNIFORMLY DISTRIBUTED LOAD IN THE EXTERIOR SPAN (MULTIPLY BY 10^{-3})	
		0.1	0.2	0.3	0.4	0.5	0.6	0.7	0.8	0.9		M_n	M_p
1.0	1.0	39	64	77	80	75	64	49	32	15	50.0	50.0	75.0
	1.5	31	52	62	64	60	52	41	27	16	40.8	40.8	84.0
	2.0	27	43	51	54	52	46	55	23	11	34.4	34.4	92.0
	3.0	21	34	40	42	38	35	27	20	9	26.7	26.9	98.0
1.25	1.0	54	88	106	109	102	86	65	42	19	84.8	84.8	111.0
	1.5	45	74	85	90	85	72	57	37	18	71.0	71.0	124.0
	2.0	37	67	73	76	71	58	48	35	15	62.3	62.3	133.0
	3.0	27	48	56	59	57	49	38	25	12	46.7	46.9	148.0
1.5	1.0	70	114	136	138	130	109	82	51	24	130.0	130.0	151.0
	1.5	59	94	113	116	108	91	70	42	20	102.7	107.6	174.0
	2.0	45	75	97	99	92	81	63	38	18	92.3	92.3	189.0
	3.0	59	63	78	80	74	64	51	31	17	75.3	75.3	206.0

of M_n and the areas are in close agreement. Therefore it can be concluded that the principle of superposition can be applied when the loads are in the same span. Also given in Table 4 is the value of M_p, the maximum positive moment caused by a uniform loading in the interior span.

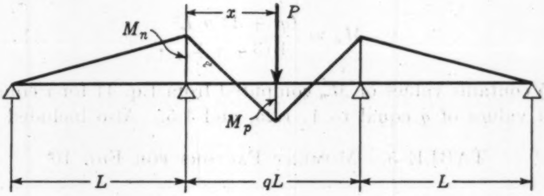

FIG. 9.—MOMENT DIAGRAM OF A THREE-SPAN CONTINUOUS BEAM SUPPORTING A MOVING CONCENTRATED LOAD IN THE INTERIOR SPAN

For the case of a continuous uniformly distributed load in all three spans, reference is made to Fig. 7. The slope at the left interior support is given by

$$S = -M_n\left[\frac{q-(q^2-8\,M_n)^{\frac{1}{2}}}{4}\right]+\frac{1}{96}\,[q-(q^2-8\,M_n)]^3 - \frac{(q^2-8\,M_n)^{\frac{1}{2}}}{24\,k} \qquad (37)$$

Eq. 37, when substituted into Eq. 13*b*, will result in a complex equation. To avoid this, Eq. 37 must be rationalized by use of the binomial expansion of the radicals so as to obtain an approximate solution. This solution has been found to be sufficiently precise for the purposes of this investigation.

Because the first term of Eq. 37 is small in comparison to the third term, the first two terms of the binomial expansion of the radical in the first term are rearranged to result in

$$(q^2 - 8\,M_n)^{\frac{1}{2}} = q - \frac{4\,M_n}{q} \qquad (38)$$

For the third term of Eq. 37 the first three terms of the binomial expansion of the radical are rearranged to yield

$$(q^2 - 8\,M_n)^{\frac{3}{2}} = q^3 - 12\,M_n\,q + 24\,\frac{M^2{}_n}{q} \qquad (39)$$

Substituting Eqs. 38 and 39 into Eq. 37 yields

$$S = -\,\frac{24\,M^2{}_n\,(i - 1) - 12\,M_n\,q^2 + q^4}{6\,i\,q} \qquad (40)$$

Substituting S (with its sign reversed) into Eq. 13*b* and discarding all powers of M_n above the second power (because the coefficient of $M^2{}_n$ is large) yields

$$24\,M^2{}_n\,(i - 1)\,(q + 1) + 4\,M_n\,q\,(3\,q + 2) - q\,(q^3 + 1) = 0 \qquad (41)$$

For the case of a uniform moment of inertia, Eq. 41 becomes

$$M_n = \frac{(q^3 + 1)\,w\,L^2}{4\,(3\,q + 2)} \qquad (42)$$

Table 5 contains values of M_n computed from Eq. 41 for i equal to 1, 1.5, and 2, and values of q equal to 1, 1.25, and 1.5. Also included in Table 5 are values of M_{pe} and M_{pi} (the maximum positive moments in the exterior and interior spans, respectively) caused by a continuous uniformly distributed load in all three spans. The moment diagram for Table 5 is shown in Fig. 10.

TABLE 5.—MOMENT FACTORS FOR FIG. 10

Value of q	(a) FACTORS OF M_n (MULTIPLY BY 10^{-3})				(b) FACTORS OF M_{pi} (MULTIPLY BY 10^{-3})				(c) FACTORS OF M_{pe} (MULTIPLY BY 10^{-3})			
	Value of i											
	1.0	1.5	2.0	3.0	1.0	1.5	2.0	3.0	1.0	1.5	2.0	3.0
1.00	100	90	84	73	25	35	41	52	80	84	87	91
1.25	126	118	108	98	69	77	87	102	70	73	77	81
1.50	168	151	131	115	113	130	150	166	55	61	68	73

Taking the moments from Tables 3, 4, and 5, computing the unit stresses f_n and f_p by Eqs. 8, 9, 10, and 11, and comparing these unit stresses with those obtained by the approximate method result in errors in this method which are given in Table 6.

It can be seen that (as was the case with the two-span, continuous, composite beam) the approximate method indicates that the stresses caused by the positive moment are too small, and that the stresses resulting from the negative moment are too large, when compared to the stresses determined from the moments computed by the proposed equations. The errors in the exterior span are small, but the errors in the interior span indicate that some limitation should be placed on the unit stresses used for design when *i* is larger than 1.5.

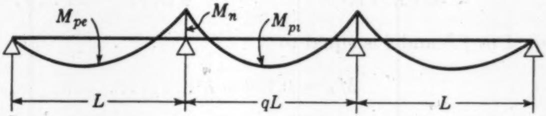

Fig. 10.—Moment Diagram of a Three-span Continuous Beam Supporting a Continuous Uniformly Distributed Load in All Three Spans

TABLE 6.—Percentage Error in Applying the Approximate Method to Fig. 10

Value of i	Value of $\frac{w_d}{w_L}$	Bending Moment								
		M_{pi}			M_{pe}			M_n		
		Value of q								
		1.00	1.25	1.50	1.00	1.25	1.50	1.00	1.25	1.50
		Unit Stresses								
		f_{pi}			f_{pe}			f_n		
1.5	1.5	− 9.5	− 7.4	− 8.7	−3.3	−4.0	−3.1	+11.4	+ 9.5	+10.7
	3.0	− 7.7	− 5.5	− 6.2	−3.1	−2.4	−2.8	+ 8.2	+ 7.3	+ 7.7
2.0	1.5	−17.2	−12.2	−14.5	−5.5	−6.4	−4.4	+20.6	+16.4	+17.8
	3.0	−13.9	− 9.4	−10.2	−3.8	−4.9	−3.7	+13.7	+11.3	+12.7
3.0	1.5	−23.8	−20.6	−21.1	−8.3	−8.0	−8.1	+20.0	+27.6	+26.0
	3.0	−18.5	−15.6	−15.0	−5.3	−5.8	−5.6	+20.4	+19.8	+18.7

In the three-span composite beam the maximum live-load deflection occurs at the center of the interior span when the uniform live load covers the interior span. The equation (by the approximate method) for *y*, the deflection, is

$$y = \frac{5\, w\, q^4\, L^4}{384\, E_s\, I_{co}} - \frac{M_n\, q^2\, L^2}{8\, E_s\, I_{co}} \ldots\ldots\ldots\ldots\ldots\ldots (43)$$

Referring to Fig. 7 and assuming that the moment of inertia of the composite beam is effective only in the positive sections of the moment diagram,

$$y = w\,L^4 \frac{(q - 2\,s_c)^3}{384\,E_s\,i\,I_s}\,(5\,q + 6\,s_c) - \frac{M\,s^2_c\,L^2}{6\,E_s\,I_s} + \frac{w\,s^4_c\,L^4}{24\,E_s\,I_s} \quad \ldots\ldots (44)$$

If q is equal to 1.5 and i is equal to 3,

$$M_n = 0.130\,w\,L^2 \quad \ldots\ldots (45)$$

for the condition of a uniform moment of inertia. Substituting these values into Eq. 43 results in

$$y = \frac{w\,L^4}{3\,E_s\,I_s}\,(0.01302 \times 1.5^2 - 0.125 \times 0.130) = \frac{0.0093\,w\,L^4}{E_s\,I_s} \quad \ldots (46)$$

In using Eq. 44, it is found that

$$M_n = 0.0753\,w\,L^2 \quad \ldots\ldots (47)$$

and s_c is equal to $0.11\,L$. Then

$$y = \frac{w\,L^4}{E_s\,I_s}\left(\frac{1.28^3 \times 8.16}{384 \times 3} - \frac{0.0753 \times 0.11^2}{6} + \frac{0.11^4}{24}\right) = \frac{0.0150\,w\,L^4}{E_s\,I_s} \quad .. (48)$$

which is 60% larger than the deflection obtained by the approximate method. When q is equal to unity and i is equal to 1.5, the deflection obtained from Eq. 44 is 35% larger than the deflection obtained by the approximate method.

For the case of a concentrated load placed at the center of the interior span, the deflection at the load by the approximate method is

$$y = \frac{P\,q^3\,L^3}{48\,E_s\,I_{co}} - \frac{M_n\,q^2\,L^2}{8\,E_s\,I_{co}} \quad \ldots\ldots (49)$$

Referring to Fig. 8 and taking $a = b = L/2$, and assuming that the moment of inertia of the composite beam is effective only in the positive parts of the moment diagram,

$$y = P\,L^3 \frac{(q - 2\,s_c)^2}{E_s\,i\,I_s}\,(q + s_c) - \frac{M_n\,s^2_c}{6\,E_s\,I_s} \quad \ldots\ldots (50)$$

When a beam has the same proportions as that used to obtain Eq. 50, the deflection (using Eq. 49) is

$$y = \frac{0.0117\,P\,L^3}{E_s\,I_s} \quad \ldots\ldots (51)$$

The deflection (using Eq. 50) is

$$y = \frac{0.0164\,P\,L^3}{E_s\,I_s} \quad \ldots\ldots (52)$$

which is 40% larger than the deflection obtained by the approximate method.

It can be seen from the foregoing examples that the composite beam is not so stiff as computations by the approximate method would indicate.

CONCLUSION

The AASHO does not specify a value of n to be used with composite beams. In the case of a simply supported composite beam, the use of the values of n given in the specification[3] results in a conservative design since it is customary to design shear connectors for the dead and live load shear to provide for the possibility of more concrete acting with the composite beam than was assumed. In the case of a continuous composite beam, it has been shown that there is a definite relationship between the moment distribution and the amount of concrete which acts with the composite beam. It can therefore be concluded that the assumptions used in the design of simply supported composite beams will not result in conservative designs when applied to the design of continuous composite beams.

To obtain a conservative design for a continuous composite beam when the moment distribution is determined by the proposed method, n should be taken larger for stress and deflection computations than for the value used to determine the moment distribution. When the approximate method is used to determine the moment distribution, the value of n used for stress and deflection computations should be taken larger than 10, and i should be limited to 3.

The modulus of elasticity for concrete is subject to variations; therefore, I_{co} and i are approximate quantities. Since in the case of a continuous composite beam the moment distribution is determined by i (which in turn depends on E_c), the analysis of continuous composite beams is not so precise as is the analysis of continuous beams made of steel. Therefore, some limitation should be placed on the design of continuous composite beams through specifications which will result in conservative designs.

APPENDIX

The following symbols, adopted for use in the paper and for the guidance of discussers, conform essentially with "American Standard Letter Symbols for Structural Analysis" (ASA Z10.8–1949), prepared by a committee of the American Standards Association with Society representation, and approved by the Association in 1949:

B = coefficient used in Eq. 1;

b' = effective width of the concrete;

E_c = modulus of elasticity of concrete;

E_s = modulus of elasticity of steel;

f_n = relative unit stress resulting from the dead and live load negative moments;

f_p = relative unit stress resulting from the dead and live load positive moments;

H = coefficient used in Eq. 1;
I_{co} = moment of inertia of the composite beam;
I_s = moment of inertia of the steel beam;
i = ratio of I_{co} to I_s;
L = length of the beam;
l = first figure of the root of Eq. 1;
M = bending moment:
M_n = negative support moment;
M_{nd} = negative moment caused by the uniform dead load;
M_{nl} = negative moment caused by the uniform live load;
M_{1n} = negative moment caused by the uniformly distributed load in one span;
M_{2n} = negative moment caused by the uniformly distributed load in two spans;
M_p = positive support moment;
M_{pd} = positive moment caused by the uniform dead load;
M_{pe} = maximum positive moment in the exterior span;
M_{pi} = maximum positive moment in the interior span;
M_{pl} = positive moment caused by the uniform live load;
M_{1p} = positive moment caused by the uniformly distributed load in one span;
M_{2p} = positive moment caused by the uniformly distributed load in two spans;
N = coefficient defined in Fig. 4;
n = ratio between E_s and E_c;
P = concentrated load;
q = ratio of the length of the interior span to the length of the exterior span;
S = slope of the elastic curve:
s = distance, center to center, of the beams;
s_c = distance from the point of contraflexure to the nearest support;
s_{cl} = distance from the point of contraflexure to the left support in Fig. 8;
s_{cr} = distance from the point of contraflexure to the right support in Fig. 8;
t = thickness of the beam;
U = coefficient used in Eq. 1;
w = intensity of the uniform load:
w_d = intensity of the uniform dead load;
w_l = intensity of the uniform live load;
x = unknown horizontal distance; and
y = deflection of the beam.

AMERICAN SOCIETY OF CIVIL ENGINEERS
Founded November 5, 1852
TRANSACTIONS

Paper No. 2700

LATERAL BUCKLING OF CHANNELS AND Z-BEAMS

BY H. N. HILL,[1] M. ASCE

SYNOPSIS

Beams having moments of inertia that differ when referred to the two principal axes may buckle in the direction of least stiffness when loaded in the direction of greater stiffness. The author presents the results of a series of investigations into the lateral buckling of channel sections and Z-sections that are loaded in the direction of greater stiffness. The investigations included tests on beams and an analytical consideration of the problem which were aimed at devising a rational procedure for the design of such beams. Because of the resistance to twist, arising from the restraint to warping of the cross sections of the beams, the torsion-bending factor is introduced. This factor is shown to be a property of the cross section as vital to proper design as the commonly used section modulus and moment of inertia.

NOTATION

The letter symbols introduced in this paper are defined where they first appear, in the text or illustration, and are assembled alphabetically in Appendix II for convenience of reference.

INTRODUCTION

A beam which has a greater moment of inertia about one principal axis than about the other principal axis is subject to failure, by buckling, in the direction of the least stiffness when loaded so as to produce bending in the direction of the greatest stiffness. Several experimental investigations have been conducted to study this lateral buckling as applied to deep rectangular beams[2] and I-beams.[3,4] The unsymmetrical nature of channel sections and Z-sections introduces considerations not encountered in rectangular beams and I-beams.

NOTE.—Published, essentially as printed here, in November, 1953, as *Proceedings-Separate No. 334*. Positions and titles given are those in effect when the paper was received for publication.

[1] Asst. Chf., Eng. Design Div., Aluminum Co. of America, New Kensington, Pa.

[2] "The Lateral Instability of Deep Rectangular Beams," by C. Dumont and H. N. Hill, *Technical Note No. 601*, National Advisory Committee for Aeronautics, Washington, D. C., May, 1937.

[3] "The Lateral Stability of Equal-Flanged Aluminum Alloy I-Beams Subjected to Pure Bending," by C. Dumont and H. N. Hill, *Technical Note No. 770*, National Advisory Committee for Aeronautics, Washington, D. C., August, 1940.

[4] "The Lateral Instability of Unsymmetrical I-Beams," by H. N. Hill, *Journal of the Aeronautical Sciences*, March, 1942.

The investigation described herein is concerned with the lateral buckling of equal-flanged channel and **Z**-beams when subjected to pure bending in a plane parallel to the web. The investigation included tests on beams and an analytical consideration of the problem which was directed toward devising a rational procedure for the design of such beams.

The Tests

The specimens tested were extruded aluminum alloy 17S-T6. Cross sections of the beams are shown in Fig. 1. The maximum variation of the individual measurements from the average values was less than 1%. The average measured dimensions were used in computing the section elements shown in Table 1.

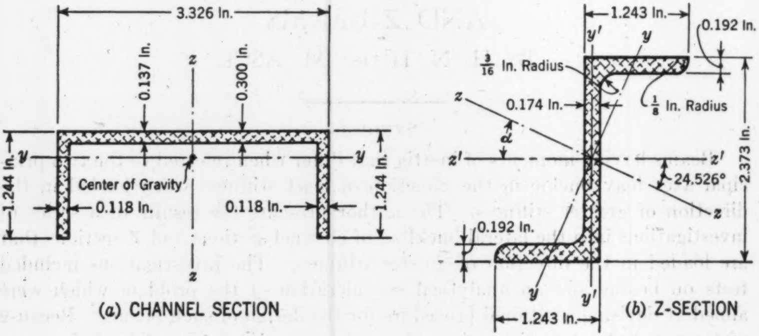

(*a*) CHANNEL SECTION

(*b*) Z-SECTION

Fig. 1.—Dimensions and Section Elements

TABLE 1.—Values of the Section Elements for the Test Beams

Section element	Channel section	Z-section
I_z, moment of inertia about the z-axis, in.^{4}	0.8090	1.0221
I'_z, moment of inertia about the z'-axis, in.^{4}	0.6822	
I_y, moment of inertia about the y-axis, in.^{4}	0.0728	0.0903
I'_y, moment of inertia about the y'-axis, in.^{4}	0.1996	
J, torsion factor, in.^{4}	0.00936	0.00392
Z, section modulus, in.^{3}	0.5750	0.6317
C_s, torsion-bending factor, in.^{6}	0.1401	0.1565

The tensile properties, as determined from flange specimens of the different lengths of material from which the beams were cut, are listed in Table 2. The modulus values are typical for this alloy and were used in the computations involved in the investigation. The modulus of elasticity E was 10,500,000 lb per sq in. and the modulus of rigidity G was 3,900,000 lb per sq in.

In order to provide a stable test setup, the beams were tested in pairs and loaded so as to subject the unsupported length to pure bending. Fig. 2 shows the general arrangement of the test. For both the channel sections and the **Z**-sections, four pairs of beams, having laterally unsupported lengths of 65 in., 45 in., 30 in., and 20 in., were tested.

TABLE 2.—MECHANICAL PROPERTIES OF TEST MATERIAL

Section	Unsupported beam length, in inches	Tensile strength, in pounds per square inch	Tensile yield strength,ᵃ in pounds per square inch	Elongation, percentage in 2 in.
Channel	65	62,770	44,900	17.0
Channel	45	56,070	39,900	24.5
Channel	30	62,770	44,900	17.0
Channel	20	57,110	39,700	25.0
Z	65	53,140	36,800	27.0
Z	45	53,010	36,300	25.0
Z	30	53,140	36,800	27.0
Z	20	53,190	36,400	24.0

ᵃ 0.2% offset.

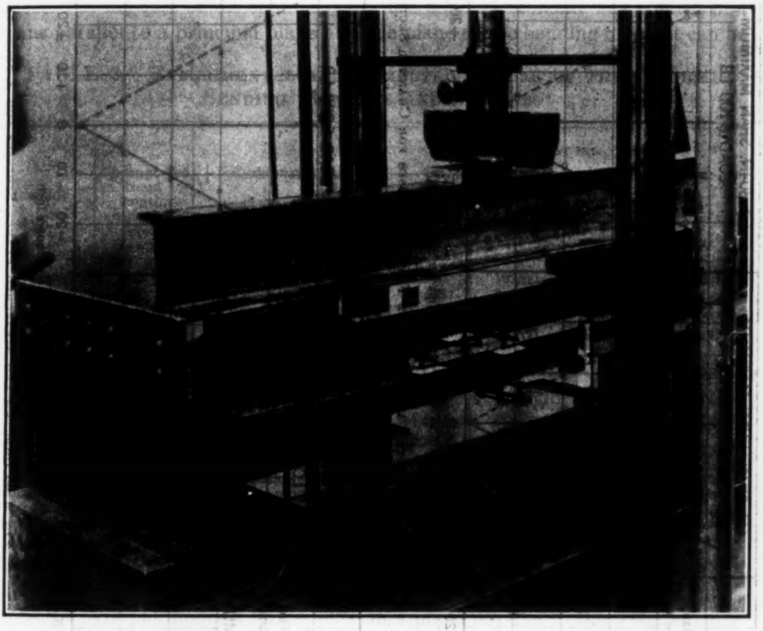

FIG. 2.—TEST ARRANGEMENT

The tests were made in a 40,000-lb-capacity testing machine. The load was applied in increments and continued to be applied until failure occurred. Strains were measured near midspan with tensometers of 1-in. gage length, mounted at the toe and heel of both flanges of one beam of each pair. The tensometers were removed before failure.

TEST RESULTS

Figs. 3 and 4 show that there was good agreement between the computed stress values and the stresses measured on both flanges of one beam of each

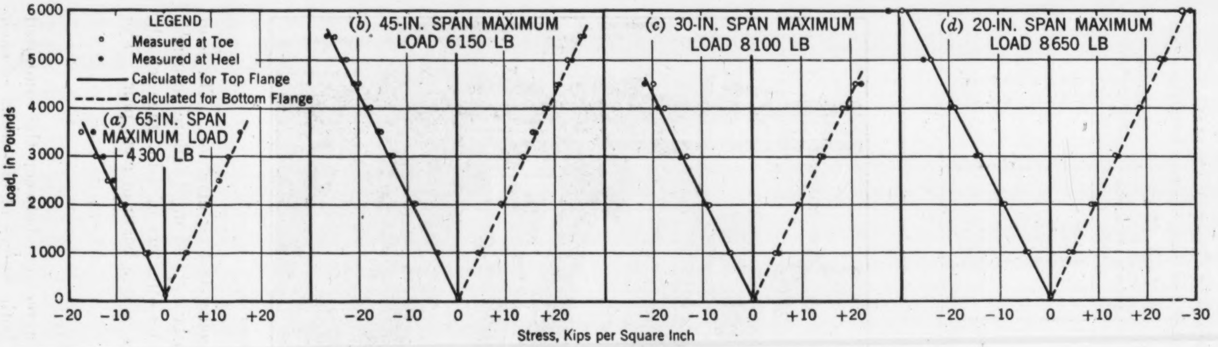

FIG. 3.—COMPUTED AND MEASURED FLANGE STRESSES FOR CHANNEL SECTIONS

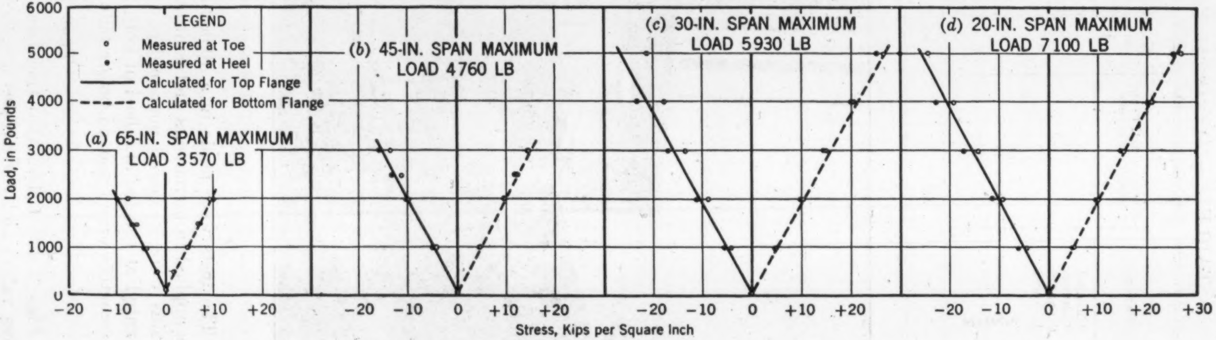

FIG. 4.—COMPUTED AND MEASURED FLANGE STRESSES FOR Z-SECTIONS

pair tested. This agreement indicates that both beams of the pair were equally loaded.

The difference in the stress measured at the toe and at the heel of the compressive (top) flanges is associated with the lateral deflection of these flanges resulting from a slight initial crookedness, and it does not indicate horizontal bending of the beams. This statement is supported by the fact that, in the tension (bottom) flange, no appreciable difference between the stress at the toe and at the heel was encountered.

Because of the manner in which the moments were applied to the beams, the unsymmetrical character of the channel sections and **Z**-sections did not affect the stress distribution. The resulting stresses were those that could be computed by the beam formula, $s = M/Z$, in which s is the normal unit stress and M denotes the bending moment. The stress distribution was not affected in the case of the channel, since the bending moment was applied in a plane parallel to a principal plane and the plane of the bending moment can be considered as containing the shear center of the section. Thus, no twisting of the channel section would be anticipated. In the case of the **Z**-beams, since the external moment was applied in a plane parallel to the web, which is not a principal plane, it can be expected that the applied moment would have components in both principal planes and that there would be horizontal as well as vertical bending, with a consequent unsymmetrical stress distribution. However, the bending moment was introduced at the end of the unsupported length in the form of uniform stresses in the flanges, and this stress condition must persist throughout the unsupported length. In order to attain this stress distribution, the bending moment in the plane of the web must be accompanied by a moment in a plane perpendicular to the web. These horizontal moments, acting on both beams, are self-balancing in the end frames.

TABLE 3.—EXPERIMENTAL AND COMPUTED VALUES OF THE CRITICAL BENDING MOMENTS AND STRESSES

Section	Unsupported beam length, in inches	EXPERIMENTAL		COMPUTED			
				$K = 1$[a]		$K = 0.5$[b]	
		M_c[c]	s[d]	M_c[c]	s[d]	M_c[c]	s[d]
Channel	65	12,900	20,400	6,500	10,300	16,500	26,100
Channel	45	18,450	29,200	10,400	16,500	29,600	46,900
Channel	30	24,300[e]	38,400	18,600	29,400	60,200	95,400
Channel	20	25,950[e]	41,000	36,100	57,100	138,500	219,000
Z	65	10,710	18,600	7,800	13,600	17,600	30,600
Z	45	14,280	24,800	11,900	20,700	29,000	50,500
Z	30	17,790	30,900	19,500	33,900	54,000	94,000
Z	20	21,300	37,000	34,400	59,800	109,000	190,000

[a] When the fixity coefficient $K = 1$, the ends of the unsupported lengths are simply supported against lateral bending. [b] When the fixity coefficient $K = 0.5$, the ends of the unsupported lengths are fixed against lateral bending. [c] The critical bending moment, in inch-pounds. [d] The stress, in pounds per square inch, computed from $s = M_c/Z$. [e] Failure originated as crumpling of the compression flange.

The maximum bending moments and the corresponding modulus of failure values for the beams of various unsupported lengths are shown in Table 3.

Failure occurred by a sudden buckling in all tests, accompanied by a "falling off" of the load. Only the beams with unsupported lengths of 65 in. failed in the elastic range. Failure of the beams of shorter length involved plastic action—probably only to a slight extent in the beams with 45-in. unsupported lengths. In the two shortest spans of the channel beams, failure occurred by crumpling of the compression flange followed by lateral buckling of the beams.

ANALYSIS OF TEST RESULTS

J. N. Goodier obtained an equation for computing the critical bending moments for beams having equal-flanged **I**-sections, channel sections, or **Z**-sections when subjected to pure bending in the principal planes.[5] This equation is of the form:

$$P_n\,M_z^2 + Q_n\,M_y^2 - P_n\,Q_n\,T_n\,r^2 = 0 \tag{1a}$$

in which M_z is the bending moment in the plane normal to the y-axis; M_y denotes the bending moment in the plane normal to the z-axis; r is the radius of gyration of the section about an axis through the shear center and normal to the x-axis and y-axis;

$$P_n = E\,I_y\left(\frac{\pi}{K\,L}\right)^2 \tag{1b}$$

$$Q_n = E\,I_z\left(\frac{\pi}{K\,L}\right)^2 \tag{1c}$$

and

$$r^2\,T_n = E\,C_s\left(\frac{\pi}{K\,L}\right)^2 + G\,J \tag{1d}$$

in which L is the unsupported length.

For the equal-flanged channel section, with bending applied in the plane of the web, $M_z = 0$; and the equation for the critical bending moment can be written as

$$M_c = \frac{\pi}{K\,L}\sqrt{\left[G\,J + \left(\frac{\pi}{K\,L}\right)^2 E\,C_s\right] E\,I_y} \tag{2}$$

In the tests on the **Z**-beams, bending moments were applied parallel to and normal to the web, rather than in the principal planes. The moment normal to the web had a definite relationship to the applied moment, M, in the plane of the web because the restraining frames prevented horizontal deflection of the beams (except as related to lateral buckling). The relative magnitude of the horizontal bending moment, and the values for bending moments in the principal planes of the **Z**-section corresponding to the applied moments, are investigated in Appendix I. The equations derived are

$$M_y = 1.079\,M \tag{3a}$$

and

$$M_z = 0.044\,M \tag{3b}$$

---

[5] "Flexural-Torsional Buckling of Bars of Open Sections," by J. N. Goodier, *Bulletin No. 28*, Cornell Univ. Eng. Experiment Station, Ithaca, N. Y., January, 1942.

Substitution of Eqs. 3 into Eq. 1*a* yields, for the critical bending moment of the Z-beams loaded as described previously,

$$M_c = 0.927 \frac{\pi}{K\,L}\sqrt{\left[G\,J + \left(\frac{\pi}{K\,L}\right)^2 E\,C_s\right] E\,I_y} \ldots\ldots\ldots (4)$$

The term C_s is introduced into Eqs. 2 and 4 because of the additional resistance to twist arising from the restraint to warping of the cross sections of the beam.[6,7,8,9] For channel sections, C_s can be expressed as follows:

$$C_s = \frac{I_f\,h^2}{2}\left(4 - \frac{18}{\dfrac{A_w}{A_f} + 6}\right) \ldots\ldots\ldots\ldots\ldots\ldots\ldots\ldots (5)$$

and for Z-sections, C_s can be expressed as

$$C_s = \frac{I_f\,h^2}{2}\,4 - 6\,\frac{A_f}{A} \ldots\ldots\ldots\ldots\ldots\ldots\ldots\ldots (6)$$

in which I_f is the moment of inertia of one flange about an axis through the centroid of the flange and parallel to the web, h denotes the height of the web, A_w is the area of the web, A_f is the area of one flange, and A is the total cross-sectional area.[10]

Substitution of the dimensions of the sections into Eqs. 5 and 6 yields the values for the torsion-bending factor listed in Table 1. In computing the values for the torsion factor J given in Table 1, it was assumed that the torsion factor for the section was equal to the sum of the torsion factors for the rectangles comprising the section. That part of the section common to the web and flange was considered in both the web and flange rectangles.

The derivation of Eqs. 2 and 4 is based on the assumption that the material is elastic. In Table 3 a comparison can be seen between the critical bending moments determined from the tests and corresponding values computed according to Eqs. 2 and 4. Computed stress values corresponding to the critical bending moment values are also listed. Only the values above the horizontal lines in Table 3 are within the region of elastic action. The experimental stress values and the computed bending moment and stress values below these lines, therefore, do not represent true values. The values listed as experimental stress values are modulus of failure values for the beams.

Only the beams with unsupported lengths of 65 in. failed within the elastic range (Table 3). The critical bending moment values determined from the tests on these beams are between the corresponding computed values for simply supported and fixed-end conditions. The degree of end fixity obtained in the

---

[6] "Torsion and Buckling of Open Sections," by H. Wagner, *Technical Memorandum No. 807*, National Advisory Committee for Aeronautics, Washington, D. C., 1936.

[7] "Torsion and Buckling of Open Sections," by H. Wagner and W. Pretschner, *Technical Memorandum No. 784*, National Advisory Committee for Aeronautics, Washington, D. C., 1936.

[8] "Twisting Failure of Centrally Loaded Open-Section Columns in the Elastic Range," by R. Kappus, *Technical Memorandum No. 851*, National Advisory Committee for Aeronautics, Washington, D. C., 1938.

[9] "Torsional and Flexural Buckling of Bars of Thin-Walled Open Section under Compressive and Bending Loads," by J. N. Goodier, *Journal of Applied Mechanics*, September, 1942.

[10] "Torsion of Flanged Members with Cross Sections Restrained Against Warping," by H. N. Hill, *Technical Note No. 888*, National Advisory Committee for Aeronautics, Washington, D. C., March, 1943.

tests can be evaluated by substituting the experimentally determined values of critical bending moment into Eqs. 2 and 4 and solving for the fixity factor K. Accordingly, the fixity factors for the tests on the beams with unsupported lengths of 65 in. are, for the channels, $K = 0.59$ and, for the **Z**-beams, $K = 0.76$. Complete fixity was not attained in either test. The ends of the unsupported lengths of the channel beams were not as completely fixed as were the **I**-beams in tests previously reported.[3] This was not unexpected, since in the **I**-beam tests both flanges were tightly fitted into slots machined into the top and bottom plates of the end frames; in the tests reported on herein, fixity depended on bolted connections. The K-value for the **Z**-beam is appreciably greater than 0.5, since the restraint is supplied for bending normal to the web. However, buckling occurs in the principal plane of least stiffness, which is at an angle of 24.526° to the plane of maximum restraint.

For design purposes, it is convenient to solve problems involving buckling beyond the region of elastic action by the equivalent slenderness-ratio method.[11] In this method the expression for the critical stress is equated to the expression for the critical stress for a column $\frac{\pi^2 E}{(K\,L/r)^2}$, and the equation is solved for $K\,L/r$. The desired value for the critical stress is then obtained for this equivalent slenderness ratio from a column curve or table of column strengths

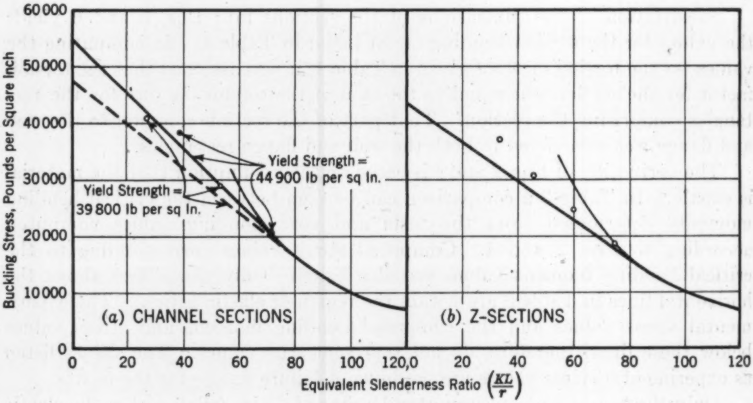

FIG. 5.—EQUIVALENT COLUMN CURVES

for the material. A satisfactory column curve for aluminum alloy 17S-T6 can be constructed on the basis of the yield strength of the material.[12] In bending both tensile and compressive yielding occur. Compression tests were not made on the material of the beams tested in this investigation. However, from other tests on a similar product, it was determined that the average of compressive and tensile yield strengths will not vary by more than 5% from the tensile yield strength. The tensile yield strength values have been used in constructing the equivalent column curves in Fig. 5.

---

[11] *Alcoa Structural Handbook*, Aluminum Co. of America, Pittsburgh, Pa., 1948.

[12] "Column Strength of Various Aluminum Alloys," by R. L. Templin, R. G. Sturm, E. C. Hartmann, and M. Holt, *Technical Paper No. 1*, Aluminum Research Labs., New Kensington, Pa., 1938.

In Fig. 5(*a*) two branches of the column curve are shown for the region above elastic action because, as shown in Table 2, there was considerable variation in the yield strength of the material of the different channel beams. The upper branch corresponds to a yield strength value of 44,900 lb per sq in., and the lower line represents a value of 39,800 lb per sq in. Arrows to the plotted points indicate the proper comparisons. The straight-line section of the equivalent column curve for the **Z**-beams (Fig. 5(*b*)) represents an average yield strength value of 36,600 lb per sq in.

The points in Fig. 5 represent the test results, expressed as modulus of failure values, M_c/Z, plotted against equivalent slenderness ratio values using for the fixity factor the values determined from the test results for the beams that buckled in the elastic range.

For both the channels (Fig. 5(*a*)) and the **Z**-beams (Fig. 5(*b*)), the beams that buckled in the plastic range failed at modulus of failure values higher than those indicated by the equivalent slenderness ratio method using straight-line column curves. This is consistent with results obtained from tests on I-beams.[3]

DESIGN CONSIDERATIONS

When channels or **Z**-beams are used to carry concentrated or distributed loads on their flanges, nonuniform stress distributions will be present in the flanges unless restraints against lateral bending and rotation are introduced at points of loading and support. The design of **Z**-beams is generally complicated by the occurrence of unsymmetrical bending, resulting from the fact that the plane of loading does not generally contain a principal axis, and each case requires special consideration. In the instances in which an unsupported length of the **Z**-beam is subjected to pure bending, the lateral buckling problem can be solved as indicated.

It is not uncommon to have unsupported lengths of channels under pure bending in the direction of greatest stiffness. The solution to the lateral buckling problem is contained in Eq. 2. The only term in this equation not common to design engineers is the torsion-bending factor C_s. It would seem that the inclusion of this factor in the table of section properties of standard structural sections would be most useful. This factor is as much a property of the cross section as the moments of inertia and the torsion factor. In addition to appearing in equations for the lateral buckling of beams, this torsion-bending factor is essential in an analysis of the torsional buckling of columns and also enters into the determination of the strength and stiffness of a structural member subjected to torsion in such a manner that one or more of the cross sections are restrained against warping.[10]

Since values of C_s are not included in tables of section properties, the designer interested in investigating the lateral buckling of a channel beam may do one of three things:

1. Compute the value of C_s in accordance with Eq. 5, making approximate allowances for such flange tapers and fillets as may exist.

2. Evaluate C_s according to the approximate relationship,

$$C_s = \frac{I_f\, h^2}{2} \qquad (7)$$

3. Use the approximate relationship,

$$C_s = \frac{I_y\, h^2}{4} \qquad (8)$$

For symmetrical I-sections, Eqs. 7 and 8 are essentially the same. For channels, Eq. 7 will yield values for C_s smaller than the correct value, and Eq. 8 will give values larger than the correct value. The use of Eq. 7 for evaluating C_s is equivalent to the treatment given in a handbook[11] for the lateral buckling of channels. The use of Eq. 8 is equivalent to the design method included in the proposed specifications for aluminum alloy 14S-T6.[12]

Computations for the torsion-bending factor in accordance with Eqs. 5, 7, and 8 have been made for the thirty-eight standard and fifteen special channels listed in a handbook.[11] Results of these computations indicate that C_s-values computed in accordance with Eq. 7 are low by from 25% to 58%, whereas with the use of Eq. 8 values for C_s result which are high by from 11% to 43%. Although these are serious errors in the evaluation of the torsion-bending factor, these errors have a greatly decreased effect in evaluating the lateral buckling strength. In Eq. 2, C_s enters only in the second term under the radical. This term becomes an important part of the total value under the radical when the ratio C_s/J is large, as in the case of channels with thin webs. The second term also increases in importance as the unsupported length $K\,L$ becomes small.

In order to evaluate the effect on the critical buckling stress of errors resulting from the use of approximate expressions for obtaining C_s, computations have been made for the channel sections listed in Table 4 in which the approximate methods for evaluating C_s are in error as indicated. The term in Eq. 2 containing C_s becomes of increasing importance as the unsupported length decreases. For small values of $K\,L$, buckling will involve stresses in the plastic ranges, and in the region of plastic buckling the critical moment becomes relatively insensitive to variations in C_s. The computations

TABLE 4.—THE PERCENTAGE EFFECT ON THE CRITICAL STRESS CAUSED BY AN ERROR IN THE TORSION-BENDING FACTOR

Channel elements	ERRORS IN C_s		ERRORS IN CRITICAL STRESS	
	Eq. 7	Eq. 8	Eq. 7	Eq. 8
3-in. by 0.170-in. web.........	−34	+21	− 3.4	+2.5
6-in. by 0.200-in. web.........	−41	+18	−12.5	+5.5
6-in. by 0.500-in. web.........	−49	+43	− 7	+5
12-in. by 0.300-in. web.........	−46	+15	−20	+6

---

[12] "Specifications for Heavy Duty Structure of High-Strength Aluminum Alloy: Progress Report of the Committee of the Structural Division on Design in Lightweight Structural Alloys," *Proceedings-Separate No. 22*, ASCE, June, 1950.

have been made for values of $K L$ which result in buckling stresses of approximately 50,000 lb per sq in. This is considered a reasonable upper limit for elastic action in the high-strength structural aluminum alloys. The errors in buckling stress resulting from the use of the approximate values for C_s are given in Table 4. It can be seen that Eq. 7 results in a conservative estimate of the critical buckling stress. The use of Eq. 8 results in critical stress values which are higher than the correct values but by not more than 6%.

It would appear, therefore, that the use of either Eq. 7 or Eq. 8 for approximating C_s could be permissible in designing channel beams for lateral buckling. The relative simplicity of Eq. 8 is evident, since it contains terms which can be taken directly from tables of section elements. This simplicity, coupled with the fact that the errors introduced are quite small, would seem to support a recommendation that until C_s-values are available for channel sections, Eq. 8 be used to approximate the value needed in computing the critical buckling stress for channel beams.

Substitution of Eq. 8 into Eq. 2 yields as an expression for the critical moment

$$M_e = \frac{\pi^2 E I_y}{(K L)^2}\frac{h}{2}\sqrt{1 + \frac{4}{\pi^2}\left(\frac{K L}{h}\right)^2 \frac{G J}{E I_y}} \quad \text{..............} \quad (9)$$

Eq. 9 is applicable to both channels and I-beams.

CONCLUSIONS

The following conclusions have been drawn from the results and discussions of tests involving lateral buckling of aluminum alloy **Z**-beams and channels subjected to pure bending:

1. Considering the lack of complete lateral fixity of the ends of the unsupported lengths, the results of the tests on specimens that failed by elastic buckling are not incompatible with the theoretical solution obtained by Mr. Goodier.

2. For cases in which buckling occurred at stresses beyond the elastic range of the material, the equivalent slenderness ratio method, used with a straight-line column curve, was found to estimate the critical stress conservatively.

3. Values for the torsion-bending factor C_s should be included in tables of section elements for standard structural sections.

4. The design of **Z**-beams requires special attention for each application. Cases involving lateral buckling under pure bending applied in the plane of the web can be handled by the methods described.

5. For lateral buckling of channels under pure bending, a handbook design method[11] is conservative, probably by as much as 20% in extreme cases.

6. Until values for C_s are readily available, Eq. 9 should be used as a basis for the design of both I-beams and channels subjected to lateral buckling under pure bending. When applied to channels this method gives results which are high by 6% in extreme cases.

APPENDIX I. BENDING MOMENTS IN PRINCIPAL PLANES OF A Z-SECTION

The condition of uniform stress in the flanges obtained in the tests on the Z-beams indicated that there was no lateral deflection of the beam (excepting that associated with lateral buckling). This means that, in addition to the vertical bending moment applied in the plane of the web, there must have been a horizontal bending moment arising from the restraint of the end frame. Components of the vertical and horizontal bending moments can be resolved into the principal planes.

If M'_y equals the bending moment applied in the plane of the web and M'_z denotes the bending moment normal to the plane of the web,

$$M_y = M'_y \cos\alpha + M'_z \sin\alpha \qquad (10)$$

and

$$M_z = M'_y \sin\alpha - M'_z \cos\alpha \qquad (11)$$

The deflection δ in the direction of the y-axis and the z-axis can be expressed as

$$\delta_y = \frac{B}{I_z}\left(M'_y \cos\alpha + M'_z \sin\alpha\right) \qquad (12)$$

and

$$\delta_z = \frac{B}{I_y}\left(M'_y \sin\alpha - M'_z \cos\alpha\right) \qquad (13)$$

in which B is a coefficient involving the length, the conditions of loading and restraint, and the modulus of elasticity of the material.

The significant condition is that there is no horizontal deflection—that is, $\delta'_z = 0$; hence,

$$\delta'_z = \delta_y \sin\alpha - \delta_z \cos\alpha \qquad (14)$$

By substituting Eqs. 12 and 13 into Eq. 14, and reducing,

$$M'_z\left(I_y \sin^2\alpha + I_z \cos^2\alpha\right) = M'_y\left(I_z - I_y\right)\sin\alpha\cos\alpha \qquad (15)$$

By substitution of Eq. 15 into Eqs. 10 and 11, and simplifying,

$$M_y = \frac{M}{\cos\alpha + \dfrac{I_y \sin^2\alpha}{I_z \cos\alpha}} \qquad (16a)$$

and

$$M_z = \frac{M}{\sin\alpha + \dfrac{I_z \cos^2\alpha}{I_y \sin\alpha}} \qquad (16b)$$

in which $M = M'_y$ is the bending moment applied in the plane of the web.

By substituting for α, I_z, and I_y, the values given in Fig. 1(*b*), and Table 1, Eqs. 16 reduce to

$$M_y = 1.079\ M \qquad (3a)$$

and

$$M_z = 0.044\ M \qquad (3b)$$

APPENDIX II. NOTATION

The following symbols, adopted for use in this paper and for the guidance of discussers, conform essentially with American Standard Letter Symbols for Structural Analysis (ASA Z10.8-1949), prepared by a Committee of the American Standards Association, with Society representation and approved by the Association in 1949.

A = total area of the cross-sectional area:
  A_f = area of one flange;
  A_w = area of the web;
B = a coefficient;
C_s = torsion-bending factor;
E = modulus of elasticity of the material;
G = modulus of rigidity of the material;
h = height of the web;
I_f = moment of inertia of one flange about an axis through the centroid of the flange and parallel to the web:
  I_y = moment of inertia about the y-axis;
  I'_y = moment of inertia about the y'-axis;
  I_z = moment of inertia about the z-axis;
  I'_z = moment of inertia about the z'-axis;
J = torsion factor;
K = fixity coefficient for ends of unsupported spans;
L = unsupported span length;
M = bending moment applied in the plane of the web:
  M_c = critical bending moment;
  M_y = bending moment in the plane normal to the z-axis;
  M'_y = bending moment applied in the plane of the web;
  M_z = bending moment in the plane normal to the y-axis;
  M'_z = bending moment applied normal to the plane of the web;
r = radius of gyration of the section about an axis through the shear center and normal to the x-axis and y-axis;
Z = section modulus of the cross section;
α = angle between the principal plane of least stiffness and the plane of maximum restraint;
δ = deflection of the beam:
  δ_y = deflection of the beam in the direction of the y-axis;
  δ_z = deflection of the beam in the direction of the z-axis; and
  δ'_z = horizontal deflection of the beam.

AMERICAN SOCIETY OF CIVIL ENGINEERS
Founded November 5, 1852
TRANSACTIONS

Paper No. 2701

RELIEF WELL SYSTEMS FOR DAMS AND LEVEES

BY W. J. TURNBULL,[1] M. ASCE, AND
C. I. MANSUR,[2] J. M. ASCE

WITH DISCUSSION BY MESSRS. P. T. BENNETT; JOHN A. FOCHT, JR.; W. H. JERVIS; AND W. J. TURNBULL AND C. I. MANSUR

SYNOPSIS

Excessive seepage and sand boils occur frequently during high water where dams or levees are underlain by strata of pervious sands and gravels. This paper presents the results of an investigation in which sand models were used to study: (1) The phenomena of underseepage; (2) the use of pressure relief wells as a means of controlling underseepage and sand boils along the lower Mississippi River levees; (3) the operation of relief wells; (4) well and seepage flows; and (5) landward substratum pressures with and without relief wells in operation, for various foundations, seepage entrances, and top strata. The conditions studied were those considered to represent qualitatively conditions commonly encountered in the lower Mississippi River valley.

Relief wells in the models, with proper spacing and penetration, effectively reduced excess hydrostatic pressure landward of levees or dams underlain by a pervious foundation for a wide range of seepage entrances, foundation conditions, and landward top strata. Seepage emerging landward of a levee without a well system was reduced materially with adequate well spacing and penetration, although the total underseepage flow was increased slightly. The model studies indicated the importance of insuring that the wells penetrate into the principal water-carrying strata in order to obtain efficient pressure relief. Borrow pits, excavated to sand, riverward of a levee, were found to increase underseepage and to have a pronounced effect on the design of a relief well system. Factors influencing the operation of the well systems in the models were: Well spacing, well penetration, seepage entrance conditions,

---

NOTE.—Published, essentially as printed here, in May, 1953, as *Proceedings-Separate No. 192*. Positions and titles given are those in effect when the paper or discussion was received for publication.

[1] Chf., Soils Div., Waterways Experiment Station, Corps of Engrs., U. S. Dept. of the Army, Vicksburg, Miss.

[2] Chf., Design and Analytical Section, Embankment and Foundation Branch, Soils Div., Waterways Experiment Station, Corps of Engrs., U. S. Dept. of the Army, Vicksburg, Miss.

stratification of the foundation, depth and permeability of the pervious stratum, and characteristics of the landside top stratum. The diameter of the wells is known to be another factor which influences the performance of a well system, although the effect of well diameter was not investigated in this series of tests.

In addition to these factors that influence the design of a well system, there are other practical considerations that must be taken into account. Some of these are design of the well, maintenance of the system, corrosion, disposal of seepage, and degree of pressure relief or seepage interception desired. These factors were not a part of the model studies reported in this paper.

INTRODUCTION

Excessive seepage and sand boils during high water are common occurrences behind some sections of the levee system in the lower Mississippi River valley. Seepage and sand boils most commonly occur where the levees are founded on a thin top stratum of relatively impervious soils underlain by deep strata of pervious sands and gravels. Fig. 1 presents a generalization of this condition.

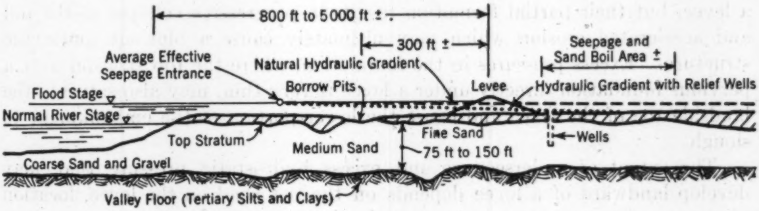

800 ft to 5000 ft ±
300 ft ±
Seepage and Sand Boil Area ±
Average Effective Seepage Entrance
Natural Hydraulic Gradient
Flood Stage
Borrow Pits
Levee
Hydraulic Gradient with Relief Wells
Normal River Stage
Top Stratum
Fine Sand
Wells
Medium Sand
75 ft to 150 ft
Coarse Sand and Gravel
Valley Floor (Tertiary Silts and Clays)

FIG. 1.—CROSS SECTION OF GEOLOGIC STRATA AND LEVEES

The use of relief wells for controlling underseepage beneath dams and levees has been investigated, and a number of installations have been made during the period from 1941 to 1951. However, most of the theoretical analyses and model analyses made in connection with the design of pressure-relief well systems have been made for the case of a homogeneous pervious foundation overlain by an impervious top stratum with a vertical seepage entrance at some given distance from the line of wells. This paper presents the results of a series of model tests conducted to study the operation of relief wells for various generalized foundation conditions, seepage entrances, and landside strata, some of which are not covered by any presently available methods of analysis. A brief discussion of the conditions which cause sand boils also is included as are some of the considerations pertinent to the design of well systems for the control of underseepage.

UNDERSEEPAGE AND SAND BOILS

Sand boils and piping, landward of levees or dams, are the result of excessive hydrostatic pressures and seepage into and through pervious substrata which provide for a communication of pressure and seepage from the river or reservoir to landside of the structure, as in Fig. 1. Under certain circumstances these conditions may produce subterranean pressures that become greater than the submerged weight of the top stratum at any locality landward of a levee or dam, and the excess pressure will cause heaving of the overlying soil. This may result in a concentration of seepage flow in the form of sand boils which may eventually cause failure by piping. Where the foundation and top strata are heterogeneous in character, as is usually the case, seepage tends to appear at localized spots instead of causing the entire top stratum to heave or become "quick." Such seepage may start a process of subsurface erosion or piping that may culminate in the formation of a passage, or pipe, beneath the structure without any heaving action. K. Terzaghi, Hon. M. ASCE, and R. B. Peck, M. ASCE, have stated that the mechanics of this latter type of piping defy a theoretical approach.[3]

Any tendency of the subterranean pressure to increase above the submerged weight of the top stratum only causes further expansion of the soil with increased percolation, thus creating a condition favorable for subsurface erosion. If such localized erosion is allowed to continue, piping may develop beneath the dam or levee. In general, continuous pipes rarely form through or under a levee, but their partial formation results in progressive collapse of the soil and accelerated erosion which may ultimately cause a blowout under the structure. Excess pressures in the foundation, where the top stratum over a pervious foundation directly under a levee is very thin, may also saturate the landside toe of the levee and cause the lower portion of the embankment to slough.

The extent of underseepage and excess hydrostatic pressure that may develop landward of a levee depends on the net head on the levee, location of seepage entrance, thickness and perviousness of the landside top stratum, and carrying capacity of the pervious substratum. If there were a completely impervious landside stratum overlying the pervious foundation and there were no flow of water landward, the hydrostatic pressure head beneath the landside blanket would equal the net head on the levee. This condition seldom exists, as there is usually some water flowing landward through the pervious foundation and upward through the surface stratum with a consequent landward decrease of pressure head, as shown in Fig. 1. This dissipation of head was observed in some of the models and partly explains why sand boils have not occurred in some areas where, without such head loss, subsurface pressures during high-water stages would have been sufficiently great to cause heaving or sand boils in the landside blanket.

CONTROL OF UNDERSEEPAGE WITH RELIEF WELLS

The prevention of sand boils and the control of underseepage require some measure that will reduce excess pressure beneath the landside top stratum to a safe value and will control erosional seepage. One method of accomplishing this is to tap the underlying pervious strata with a properly designed series of wells which will provide pressure relief and controlled seepage outlets that offer little resistance to flow and, at the same time, will prevent erosion of the foundation soils.

---

[3] "Soil Mechanics in Engineering Practice," by K. Terzaghi and R. B. Peck, John Wiley & Sons, Inc., New York, N. Y., 1948.

The primary requirements of a relief well system for the control of excess pressures due to underseepage are the following:

1. The wells should penetrate into the principal water-carrying strata and be spaced sufficiently close together so as to intercept the seepage and reduce the pressure which otherwise would act beyond the wells.
2. The wells must offer little resistance to water flowing into and out of them; they must prevent infiltration of sand into the well after initial pumping; and they must resist the deteriorative action of the water and soil.

Relief wells offer several advantages as compared to gravel toes, pervious blankets, or other surface drainage measures where the foundation consists of stratified deposits of pervious materials, in that they penetrate into the more pervious strata in which pressure relief is necessary.

THEORETICAL ANALYSIS OF RELIEF WELL SYSTEMS

A method of analysis frequently used in the design of relief well systems is one based on a mathematical solution by Morris Muskat.[4] Mr. Muskat assumed an infinite line of equispaced wells completely penetrating a uniform, semi-infinite, pervious stratum overlain by a uniform, absolutely impervious top stratum and underlain by a horizontal impervious stratum. The seepage entrance was assumed to be a vertical plane parallel to, and at a given distance from, the line of wells. An analysis for the case of wells partly penetrating the pervious stratum has been accomplished by using electrical analogy models.[5]

The formulas for the generalized conditions assumed by Mr. Muskat and in the paper by T. A. Middlebrooks, A. M. ASCE, and W. H. Jervis, M. ASCE, are not always applicable to field conditions. For example, the landside blanket is usually slightly pervious; in other cases the seepage may enter the pervious foundation through the top stratum or through open borrow pits riverward of a levee. In some cases the landward or downstream blanket may be of finite length as a result of landward borrow pits which extend through the top stratum, and in other cases there may be an impervious deposit which blocks the landward extent of the pervious foundation. Many combinations of conditions exist which cannot be covered completely by any single theory.

Approximate formulas for the design of well systems have been developed by Messrs. Middlebrooks and Jervis, R. A. Barron,[6] A. M. ASCE, and P. T. Bennett,[7, 8] M. ASCE, that permit taking into consideration some of the conditions described in the previous paragraph.

---

[4] "The Flow of Homogeneous Fluids Through Porous Media," by Morris Muskat, McGraw-Hill Book Co., Inc., New York, N. Y., 1937.

[5] "Relief Wells for Dams and Levees," by T. A. Middlebrooks and W. H. Jervis, *Transactions*, ASCE, Vol. 112, 1947, p. 1321.

[6] "The Effect of a Slightly Pervious Top Blanket on the Performance of Relief Wells," by R. A. Barron, *Proceedings*, Second International Conference on Soil Mechanics, Vol. IV, 1948.

[7] "The Effect of Blankets on Seepage Through Pervious Foundations," by P. T. Bennett, *Transactions*, ASCE, Vol. 111, 1946, p. 215.

[8] "Comments on the Design of Relief Wells," by P. T. Bennett, from "Conference on Control of Underseepage," Waterways Experiment Station, Vicksburg, Miss., 1945.

As indicated, the assumptions made in the previously described methods of analysis seldom are realized in the field. Therefore, the sand model tests to be described subsequently were performed, not only to study the general uses of wells for controlling underseepage, but also to obtain information for the design of well systems for various generalized foundation conditions not subject to the aforementioned formulas. The results of the model tests are not directly applicable to the design of any specific well system. However, the results obtained may be of use in a qualitative sense, and to some extent quantitatively, where theoretical formulas are not applicable, provided proper corrections are made for the conditions at hand and sound engineering judgment is exercised.

PURPOSE AND SCOPE OF INVESTIGATION

The general purpose of these investigations was to study the operation of relief wells with various well spacings and penetrations, and to observe well and seepage flows and landward pressures, with and without wells in operation, for different selected conditions. Specific purposes of the investigation were:

a. To obtain information on well flows and landward pressure for different well spacings and penetrations, and for various seepage entrances such as in a river bed or in riverside borrow pits excavated to sand;

b. To determine the capacity of a line of wells to intercept underseepage where the landside top stratum is not impervious and the initial landward pressures are low without relief wells;

c. To determine the increase of total flow caused by wells where there is a considerable amount of natural seepage without wells and the landside top stratum is not impervious;

d. To verify, where applicable, available design data obtained from theoretical and electrical model studies for homogeneous foundation conditions; and

e. To study the effect of stratification on the efficiency of a well system as regards well penetration.

DESCRIPTION OF MODELS

Four sand models, designated A, B, C, and D, with different generalized foundation conditions, were constructed and tested. Variables studied in these models were: Well spacing and penetration; river bank and borrow pit seepage entrances; impervious, relatively impervious, and no landside top strata; and stratification of the foundation. The foundation and seepage conditions studied were those considered to represent qualitatively conditions commonly encountered in the lower Mississippi River valley. However, the results of the tests are also considered qualitatively applicable to similar conditions.

The model studies were conducted in a steel flume approximately 28 ft long, 4 ft high, and 3.5 ft wide, as shown in Fig. 2. One side of the flume was tapped at numerous points so that piezometers could be attached for measuring pressures beneath the top stratum and within the foundation. The other side of the flume was composed of plate glass ½ in. thick that permitted the use of fluorescein dye lines for tracing flow patterns.

The primary requirements for similitude of sand models are that the flow be laminar, that the model be an undistorted geometrical reproduction of the prototype, and that the permeabilities of the various strata have the same ratio as the permeabilities in nature. The absolute permeabilities of the strata affect only the rate of seepage; they have no effect on the pressure distribution within the foundation.

Variable-elevation overflow funnels were used to control the elevation of the water riverside of the levee. Similarly, shallow pans or circular overflow weirs were used to maintain a constant tailwater elevation landside of the levee. The distribution of the hydrostatic pressure within the pervious substratum for the various test conditions was obtained from the piezometers previously referred to. The discharge from the wells and seepage through the landside top stratum were measured separately in model A.

FIG. 2.—STEEL FLUME FOR MODEL STUDIES

All dimensions, well diameters and spacings, seepage and well flows, and head measurements in the models have been adjusted to prototype units in this paper. Well and seepage flows are given in gallons per minute per foot of net head, and hydrostatic pressures are given as a percentage of the total net head. All flow measurements have also been adjusted to a temperature of 20° C.

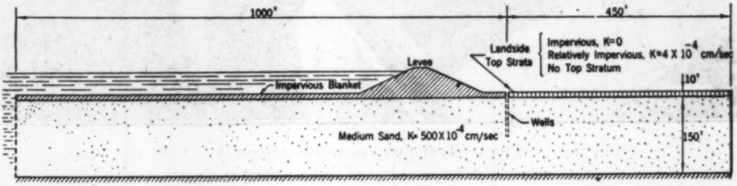

MODELS A-a-1, 2, 3

Seepage Entrance at River

FIG. 3.—HOMOGENEOUS FOUNDATION, MODEL A

The relief well systems were simulated in the models by a series of wells near and parallel to the levee toe, spaced so that different well spacings could be obtained by plugging various combinations of wells. The wells were so spaced that the sides of the flume always represented a plane midway between the wells, regardless of well spacing. The wells in the model consisted of copper tube riser pipe ½ in. in diameter and a monel or brass screen fully penetrating the pervious foundation. Various penetrations of well screens into the pervious foundation were obtained by plugging the lower section of the screens at the desired elevation.

Homogeneous Foundation—Model A.—The foundation, seepage entrance, and top stratum conditions tested in model A are shown in Fig. 3. Landside top strata simulated were an impervious top stratum (model A-a-1), a relatively impervious top stratum 10 ft thick with a coefficient of permeability approximately equal to 4 × 10⁻⁴ cm per sec (model A-a-2), and no top stratum (model A-a-3).

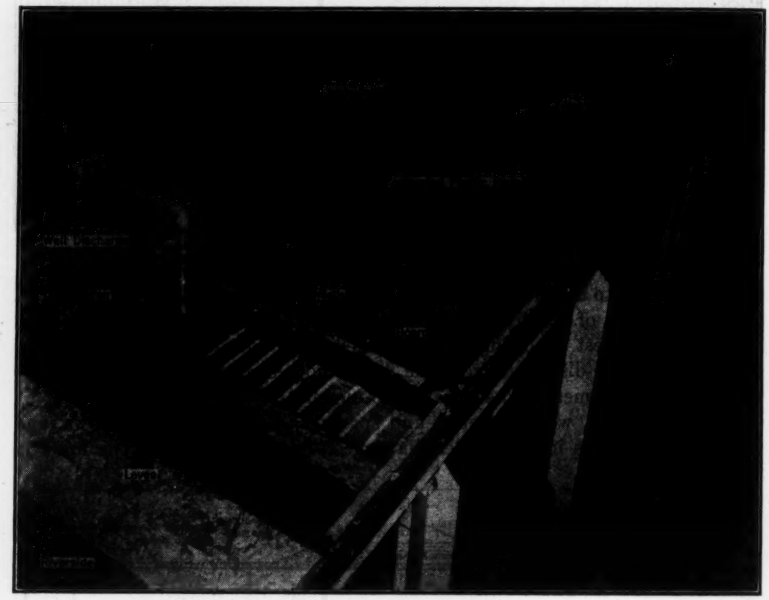

Fig. 4.—Test Conditions for Model A

The relatively impervious landside top stratum of model A-a-2 was simulated by means of a plastic plate ⅛ in. thick perforated with 0.025-in. holes spaced on 2½-in. by 2½-in. centers. This landside top stratum, with no wells in operation, resulted in hydrostatic heads at the line of wells of 36% of the net head when the seepage entrance was at the river 1,000 ft from the well line. The sand used for the pervious foundation was a uniform, round-grained sand.

The arrangement of wells, landside top stratum, and overflow weirs for model A are shown in Fig. 4. Well penetrations of 25%, 50%, and 100%, and spacings of 23.6 ft, 43.3 ft, 86.6 ft, 130 ft, and 260 ft were tested in this model. As seen in Fig. 4, flow from the wells was kept apart from the seepage through the landside top stratum by means of a board placed immediately landward of the well line. The tailwater at the wells and over the landside top stratum was maintained at the same elevation by the constant-level weirs shown in Fig. 4.

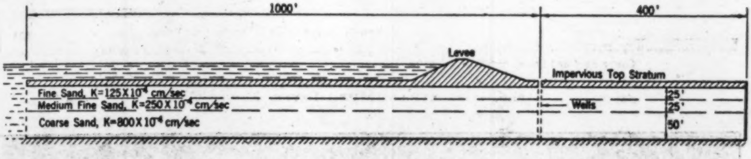
1000'
400'
Levee
Impervious Top Stratum
Fine Sand, K=125X10-4 cm/sec
Medium Fine Sand, K=250X10-4 cm/sec
Coarse Sand, K=800X10-4 cm/sec
Wells
25'
25'
50'

MODEL B-a

Seepage Entrance at River

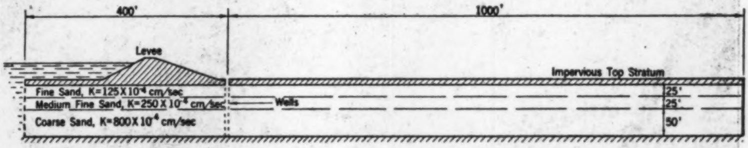
400'
1000'
Levee
Impervious Top Stratum
Fine Sand, K=125X10-4 cm/sec
Medium Fine Sand, K=250X10-4 cm/sec
Coarse Sand, K=800X10-4 cm/sec
Wells
25'
25'
50'

MODEL B-aa

Seepage Entrance at River

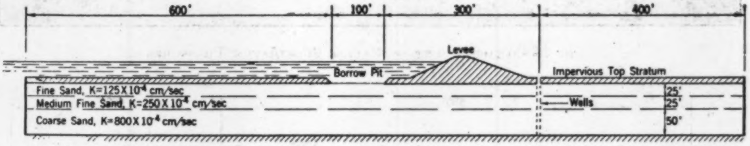
600'
100'
300'
400'
Levee
Borrow Pit
Impervious Top Stratum
Fine Sand, K=125X10-4 cm/sec
Medium Fine Sand, K=250X10-4 cm/sec
Coarse Sand, K=800X10-4 cm/sec
Wells
25'
25'
50'

MODEL B-b

Seepage Entrance in Borrow Pit Only

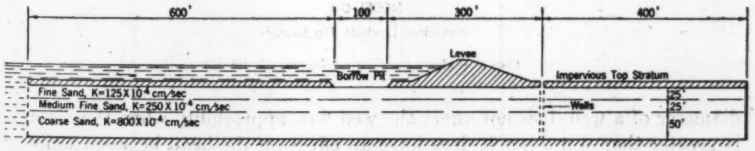
600'
100'
300'
400'
Levee
Borrow Pit
Impervious Top Stratum
Fine Sand, K=125X10-4 cm/sec
Medium Fine Sand, K=250X10-4 cm/sec
Coarse Sand, K=800X10-4 cm/sec
Wells
25'
25'
50'

MODEL B-c

Seepage Entrance at River and Borrow Pit

FIG. 5.—STRATIFIED FOUNDATION, MODEL B

The 1:75 scale of model A resulted in the diameter of the ½-in.-diameter well screens being equivalent to an actual diameter of 3 ft. This well diameter is somewhat larger than normally used in actual practice, which is from 3 in. to 24 in., depending on the type of well and the diameter of the filter. The diameter of a well does not affect the well flow appreciably when the diameter is greater than 6 in., but it does have an effect on the head between wells.

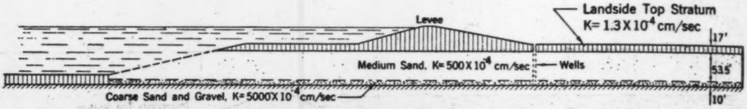
Landside Top Stratum
K= 1.3 X 10⁻⁴ cm/sec
Levee
17'
Medium Sand. K= 500 X 10⁻⁴ cm/sec
Wells
53.5'
Coarse Sand and Gravel, K= 5000 X 10⁻⁴ cm/sec
10'

FIG. 6.—GREENVILLE (MISS.) LEVEE, MODEL C

Wells (Plugged)
Sand Boil
Silt Top Stratum

FIG. 7.—MEASUREMENT OF EXCESS SUBSTRATUM PRESSURES

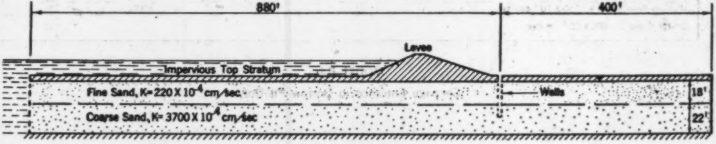
880'
400'
Levee
Impervious Top Stratum
Fine Sand, K= 220 X 10⁻⁴ cm/sec
Wells
18'
Coarse Sand, K= 3700 X 10⁻⁴ cm/sec
22'

MODEL D-a

Impervious Landside Top Stratum

FIG. 8.—Memphis (Tenn.) Levee, Model D

Stratified Foundation—Model B.—The foundation and seepage entrance conditions tested in models B-a, B-b, and B-c are shown in Fig. 5. This particular foundation was designed to simulate foundation conditions frequently encountered beneath Mississippi River levees. Model B had a scale

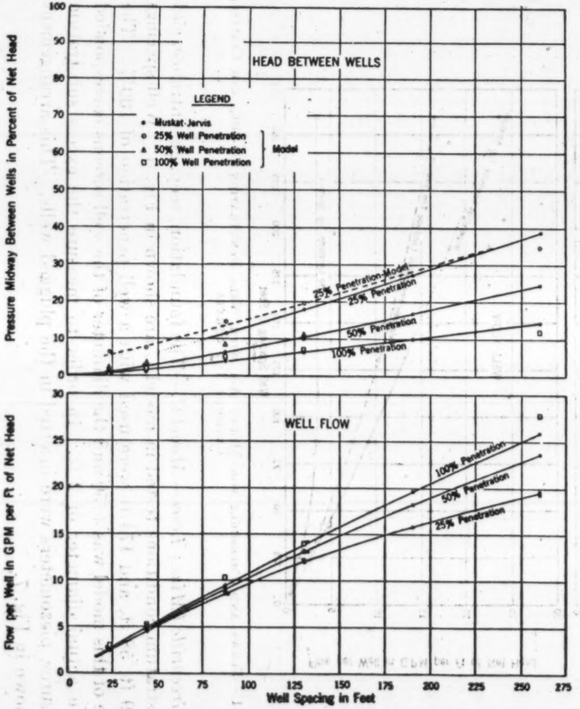

FIG. 9.—FLOWS AND PRESSURES FOR MODEL A-a-1

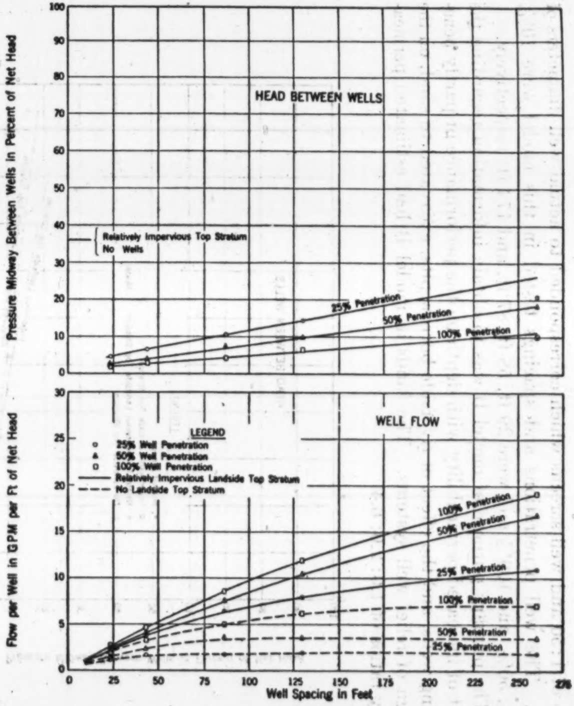

FIG. 10.—FLOWS AND PRESSURES FOR MODEL A-a-2 AND MODEL A-a-3

ratio of 1:50 and well screens which corresponded to actual well diameters of 2 ft. The well penetrations and spacings tested in this model were 10%, 25%, 50%, and 100% and were 29 ft, 58 ft, 87 ft, and 174 ft, respectively.

The primary purpose of model B was to obtain information regarding the effect of increased permeability with depth on the performance of partly penetrating wells, and the effect of riverside borrow pits, excavated to sand, on the design of relief well systems. The sands in model B had estimated permeability ratios of 1.0: 2.0: 6.4.

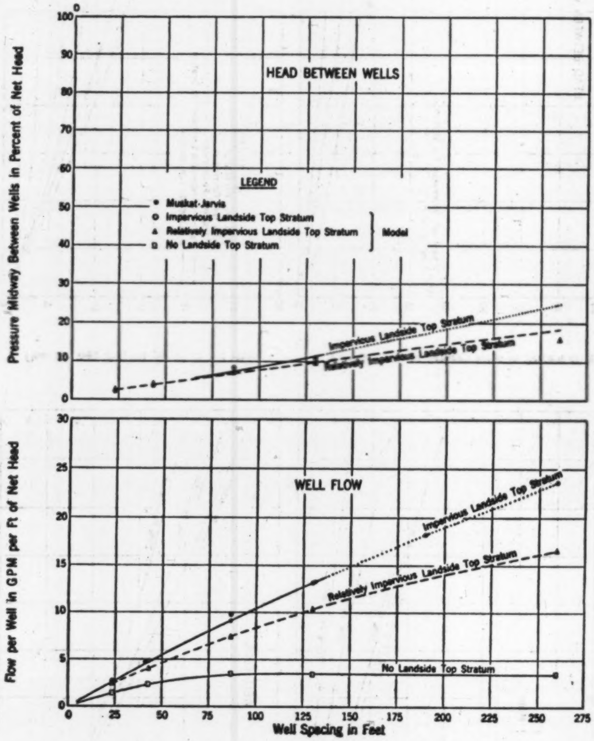

FIG. 11.—FLOWS AND PRESSURES FOR MODEL A-a WITH WELL PENETRATION OF 50% AND VARYING LANDSIDE TOP STRATA

Greenville (Miss.) Levee—Model C.—The foundation, seepage, entrance, and top stratum conditions tested in model C are shown in Fig. 6. Well spacings of 19 ft, 58 ft, and 174 ft were used with a well penetration of 100%. The scale of this model was 1:50 and the diameter of the well screens corresponded to an actual diameter of 2 ft. In order to measure the excess substratum pressures, piezometers were inserted in the plugged wells. This arrangement is shown in Fig. 7.

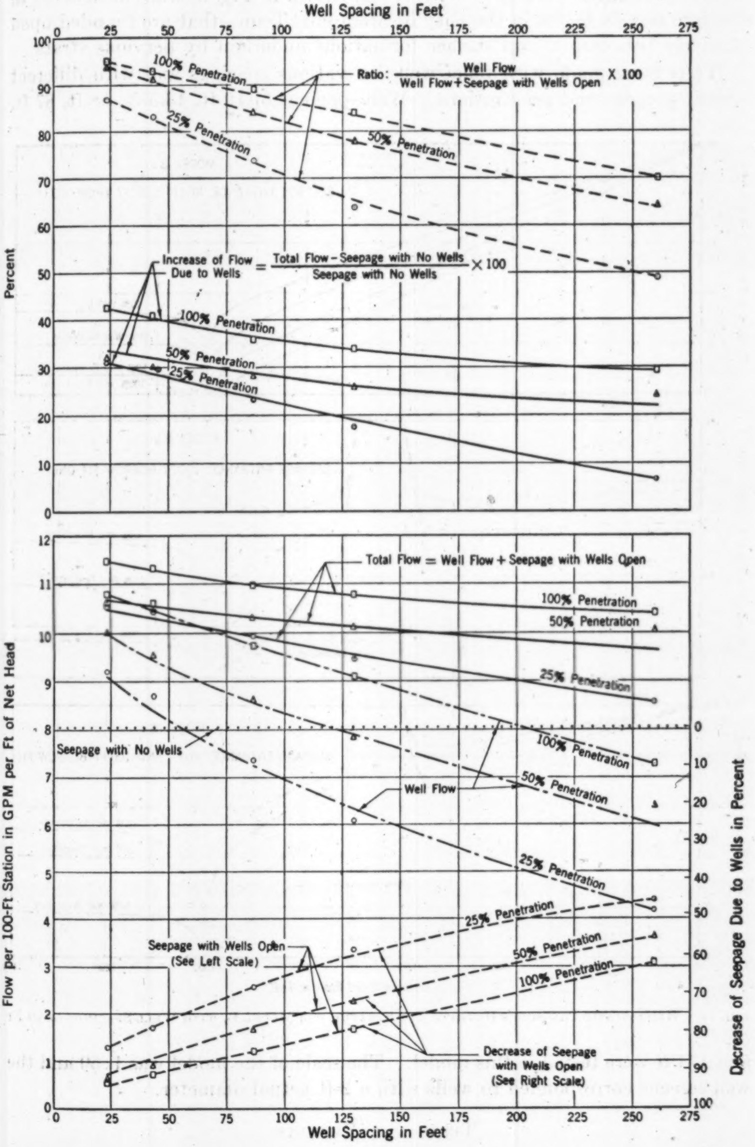

FIG. 12.—FLOW AND SEEPAGE FOR MODEL A-a-2

Memphis Levee—Model D.—Model D, shown in Fig. 8, was constructed to simulate certain levees in the City of Memphis, Tenn., that are founded upon relatively thin impervious surface formations underlain by pervious strata.

Tests were made with relief wells on various spacings and with different screen openings and penetrations. Well spacings of 19 ft, 43.5 ft, 58 ft, 87 ft, and 174 ft were tested in this model. The scale of the model was 1:50 and the well screens corresponded to wells with a 2-ft actual diameter.

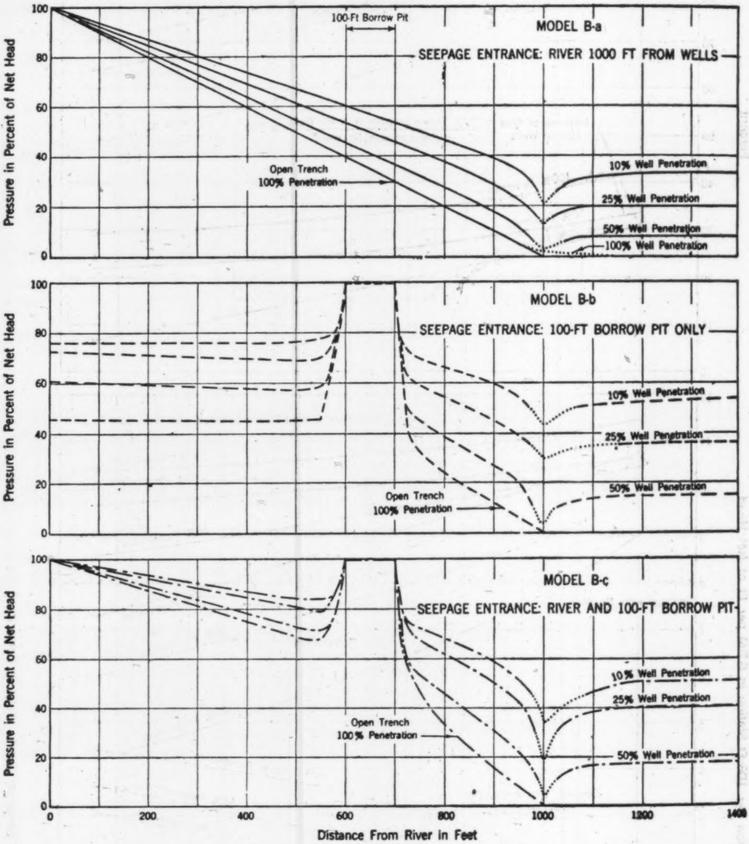

FIG. 13.—HYDROSTATIC PRESSURES BENEATH TOP STRATUM FOR MODEL B, WITH WELL SPACINGS OF 29 FT

TESTS AND RESULTS

The test results obtained in models A, B, C, and D are shown in Figs. 9 through 19. The results obtained in the various models, as shown in the

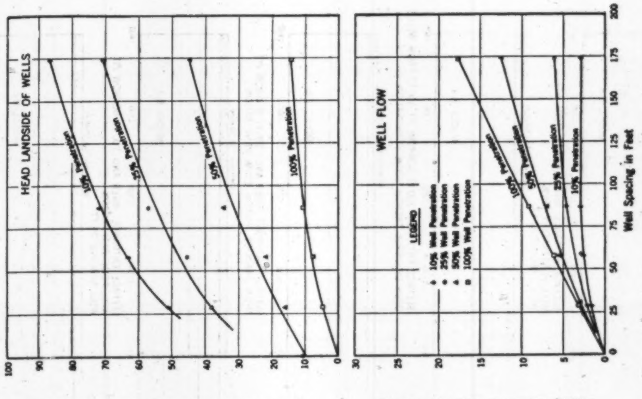

Fig. 16.—Flows and Pressures for Model B-c

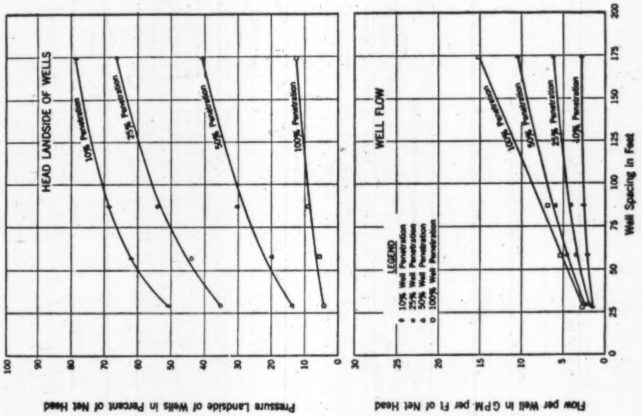

Fig. 15.—Flows and Pressures for Model B-b

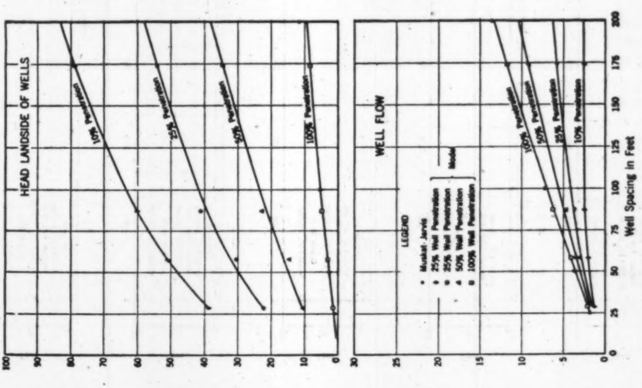

Fig. 14.—Flows and Pressures for Model B-a

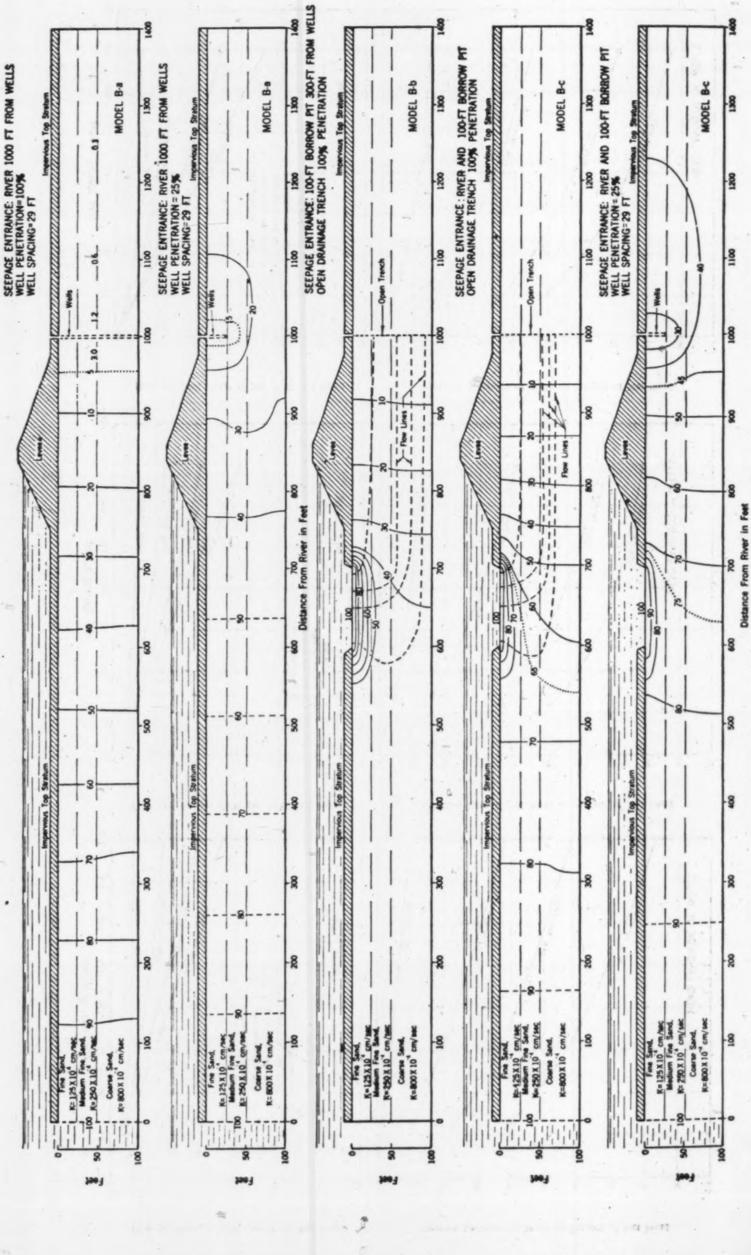
SEEPAGE ENTRANCE: RIVER 1000 FT FROM WELLS
WELL PENETRATION=100%
WELL SPACING=29 FT
MODEL B-a
SEEPAGE ENTRANCE: RIVER 1000 FT FROM WELLS
WELL PENETRATION=25%
WELL SPACING=29 FT
MODEL B-a
SEEPAGE ENTRANCE: 100-FT BORROW PIT 300-FT FROM WELLS
OPEN DRAINAGE TRENCH 100% PENETRATION
MODEL B-b
SEEPAGE ENTRANCE: RIVER AND 100-FT BORROW PIT
OPEN DRAINAGE TRENCH 100% PENETRATION
MODEL B-c
SEEPAGE ENTRANCE: RIVER AND 100-FT BORROW PIT
WELL PENETRATION=25%
WELL SPACING=29 FT
MODEL B-c
Impervious Top Stratum
Levee
Wells
Open Trench
Flow Lines
Fine Sand, K=125 X 10⁻⁴ cm/sec
Medium Fine Sand, K=250 X 10⁻⁴ cm/sec
Coarse Sand, K=800 X 10⁻⁴ cm/sec
Feet
0
50
100
Distance From River in Feet
0
100
200
300
400
500
600
700
800
900
1000
1100
1200
1300
1400

FIG. 17.—EQUIPOTENTIAL AND FLOW LINES FOR MODEL B

FIG. 17.—EQUIPOTENTIAL AND FLOW LINES FOR MODEL B

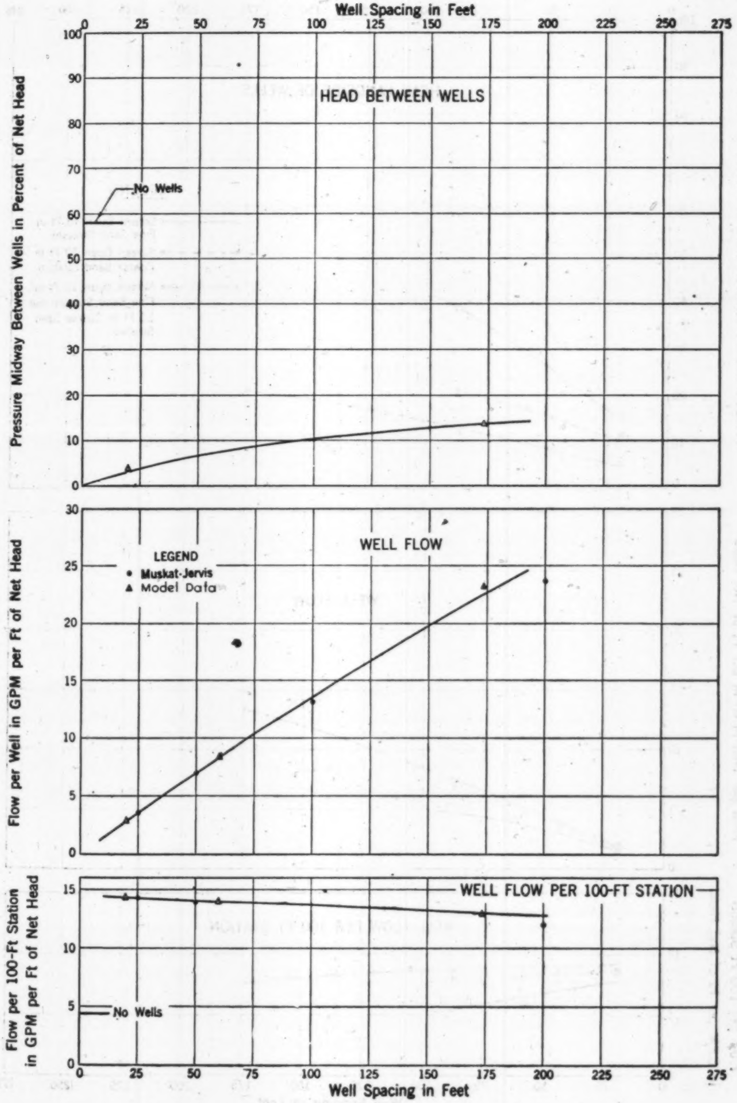

FIG. 18.—FLOWS, SEEPAGE, AND PRESSURES FOR MODEL C

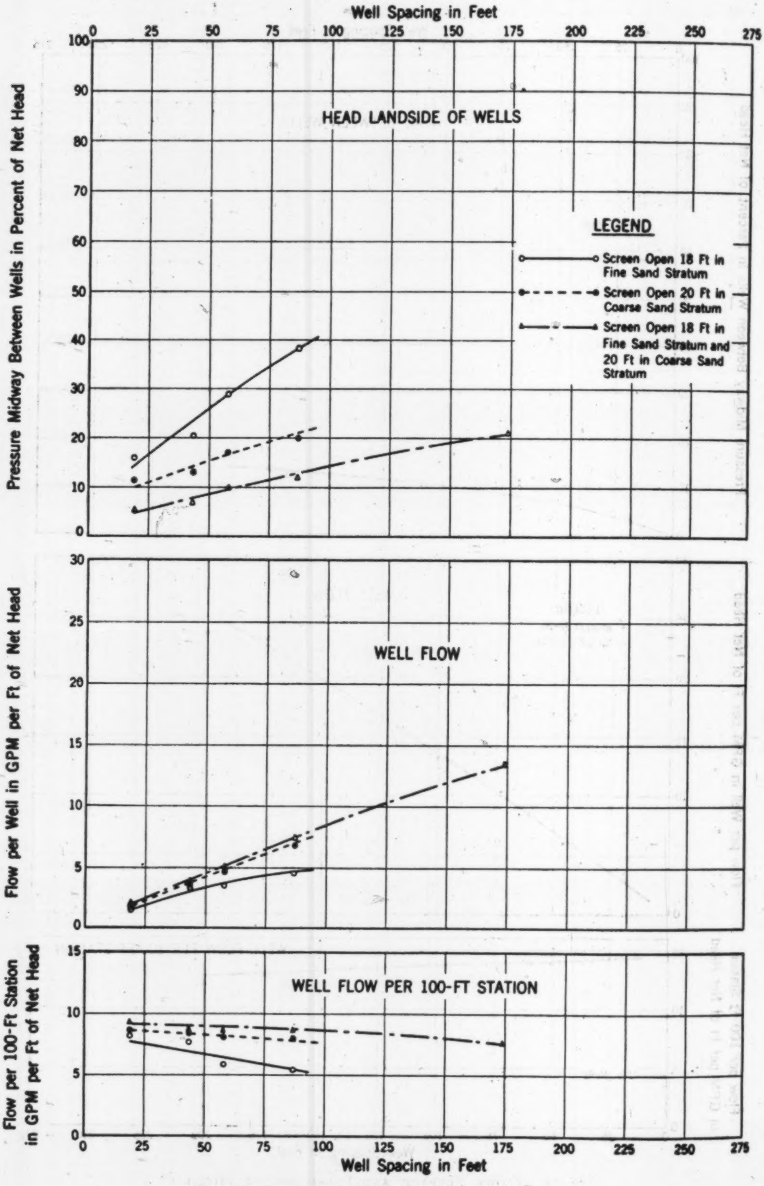

FIG. 19.—FLOWS AND PRESSURES FOR MODEL D

figures, are in terms of prototype head (percentage) and seepage flow. All data regarding seepage entrance, foundation conditions, landside top strata, well spacing, and penetration are presented in each figure showing results of the model tests. A summary of certain important test results obtained in each model is given in Table 1. The data shown pertain only to the particular model and wells being discussed. Application of the model results to any specific field problem would require that proper consideration be given to any

TABLE 1.—MODEL TEST RESULTS

Model	Seepage entrance	Landside top stratum	Test results
A-a-1	River bank 1,000 ft from wells	Impervious	The landside pressure was reduced 90% with either of the following combinations of well-spacing *a* and penetration *W* (Fig. 5): $W = 25\%$, $a = 60$ ft; $W = 50\%$, $a = 125$ ft; $W = 100\%$, $a = 190$ ft. Well spacings of less than 200 ft and penetrations greater than 25% had relatively little effect on well flow per 100-ft station, but did have a significant effect on the residual pressure between wells (Fig. 9).
A-a-2	River bank 1,000 ft from wells	Relatively impervious	An excess pressure of 36% *H* at the levee toe with no wells was reduced to 5% *H* with a well spacing of 50 ft and a penetration of 50% (Fig. 10). Natural seepage through the landside blanket with no wells was reduced approximately 80% by wells on 85-ft centers with a penetration of 50%. For this case, wells increased well flow plus seepage with wells only 28% above the natural seepage with no wells (Fig. 12).
A-a-3	River bank 1,000 ft from wells	None	Wells with a penetration of 50%, spaced on 50-ft centers, reduced natural seepage by approximately 50%. For this case, the wells increased the total seepage only 3% more than natural seepage with no wells.
A-a-1, -2, -3	River bank 1,000 ft from wells	..	See Fig. 11.
B-a	River bank 1,000 ft from wells	Impervious	Wells fully penetrating the coarse sand stratum on 100-ft centers gave a pressure reduction of 95% *H*, whereas wells on the same spacing, but only penetrating the top 25 ft of fine sand, reduced landward pressures by 58% *H* (Fig. 14).
B-b	100-ft borrow pit only, 300 ft from wells	Impervious	A 100-ft borrow pit, located riverside of the levee, with the river at an infinite distance, permitted approximately 15% more seepage to enter the foundation, for the same drainage facilities, than entered the foundation in model B-a with the river 1,000 ft from the wells (Figs. 14 and 15). To obtain the same landward pressure reduction required closer well spacing for model B-b than for model B-a.
B-c	River bank and 100-ft borrow pit	Impervious	Where seepage entered the foundation at both river and borrow pit, well flows were increased approximately 50% over those where seepage entered the foundation at the river only (Fig. 16).
B-a, B-b, B-c	....	Impervious	Where the foundation is stratified, drainage wells must penetrate the principal water-carrying strata to reduce pressures effectively (Figs. 14, 15, and 16). For a comparison of the hydrostatic pressures beneath the top stratum for various well spacings and seepage entrance conditions see Fig. 13. For the effect of open borrow pits on the seepage flow pattern for the foundation simulated by model B see Fig. 17.
C	River bank 600 ft from wells	Impervious	For the same well spacing and 100% penetration, drainage wells gave approximately the same pressure reduction for model C as for models A and B (Figs. 9, 14, and 18).
D	River bank 880 ft from wells	Impervious	As in model B, where the foundation is stratified, relief wells must penetrate the principal water-carrying strata to reduce pressure effectively (Fig. 19).

change in well diameter and penetration, foundation conditions, seepage entrance, or top strata, from that tested in the model. The term "seepage" as used in the figures for model A is limited to the seepage or water rising to the surface through the top stratum landward of the line of relief wells.

The well and seepage flows for distances from the line of wells to the seepage entrance at the river other than 1,000 ft may be computed for various well penetrations and spacings for model A-a from the following formula based on a straight-line variation of head beyond 300 ft riverward from the line of wells to the river.

$$Q = \frac{112{,}500\, H\, K\, q}{q(s - 1{,}000) + 11{,}250} \cdots\cdots\cdots\cdots \text{(1)}$$

in which Q is the well or seepage flow per 100 ft of the prototype levee in gallons per minute, H is equal to the net head in feet, K is the coefficient of permeability in feet per minute, q represents the well or seepage flow in gallons per minute per 100 ft of levee as determined from the model studies, and s denotes the distance from the line of wells to the river in feet, equal to or greater than 300 ft.

The hydrostatic head midway between the wells may also be computed for distances at which s does not equal 1,000 ft from the following formula:

$$P = \frac{150\, H\, (\%)}{0.0133\, q(s - 1{,}000) + 150} \cdots\cdots\cdots\cdots \text{(2)}$$

in which P is the head in feet midway between wells, when s is equal to or greater than 300 ft, and (%) is equal to the percentage of head between wells as obtained for s equal to 1,000 ft.

CONCLUSIONS

On the basis of the model studies that were undertaken, it can be concluded that relief wells with proper spacing and penetration will effectively reduce excess hydrostatic pressures landward of levees underlain by a pervious foundation for a wide range of seepage entrances, foundation stratification, and landward top strata. The pressures between wells and the well discharges are always slightly less for a relatively impervious landside blanket than for a completely impervious landside blanket, since the impervious blanket contributes to pressure relief. Therefore, well flows and residual landside pressures for relatively impervious landside blankets will be less than those computed for an impervious landside top stratum.

Another conclusion that can be made is that, with adequate well spacing and penetration, seepage normally emerging through a relatively impervious top stratum landward of a levee without wells may also be materially reduced, although the total of well flow plus seepage with open wells will be somewhat increased.

For the models tested and test conditions applicable, there was close agreement between the observed well flows, landside pressures, values computed from theoretical formulas, and electrical analogy studies.

Further study of the test results leads to the realization that it is important that the wells penetrate into the principal water-carrying strata, in order to obtain efficient pressure relief where the pervious foundation is stratified. The curves for partial penetration derived by Mr. Muskat and Messrs. Middlebrooks and Jervis are not applicable to this type of foundation. However, Mr. Muskat's formula for 100% penetration is applicable if the average horizontal permeability is used for computing the well flow.

Borrow pits excavated to sand on the riverside of a levee or dam increase underseepage and have a pronounced effect on the operation of relief well systems.

Finally, although the tests reported in this paper cover only certain specific foundation conditions, it is considered that the results obtained can, through the use of good judgment, be of use in designing well systems where conditions are generally similar.

DISCUSSION

P. T. Bennett,[9] M. ASCE.—The four sand models described by the authors corroborate their statement that many combinations of conditions exist which cannot be covered completely by any single theory for the design of relief wells.

In models representing specific local conditions, such as model C and model D, an attempt to draw generalized conclusions from the results is unnecessary because the conclusions can be applied only to the prototype. It is highly desirable whenever possible to obtain quantitative data from generalized models such as model A and model B.

Interpretation of model-study results and their application is vastly simplified by separating the effects of well spacing, well diameter, and depth of penetration from the effects of the relatively remote boundary conditions (such as the distance to the effective source of seepage, and the conditions of flow landward of the line of wells) of the seepage system. The possibilities of such a division of the whole system into component parts are illustrated in Figs. 13 to 17.

In model B no seepage was permitted to escape on the landside of the wells. The pressure gradient consequently approaches zero, and the "effective landside exit distance" is infinite for all three cases shown in Fig. 13. The "effective riverside distance" can be obtained graphically from Fig. 13 by drawing a tangent to the pressure-gradient curves at the points of inflection between the line of wells and the open borrow pit. This riverside tangent and the corresponding landside tangent intersect at the line of wells at a pressure defined as the average head in the line of wells. Extension of the riverside tangent gradient riverward to intersect the line representing the 100% head establishes the effective riverside distance. These tangents result in effective riverside distances of approximately 1,000 ft, 700 ft, and 560 ft for models B-a, B-b, and B-c, respectively.

These effective distances are defined by the pressure gradients at the top of the sand stratum. From Fig. 17 it can be seen that an entirely different set of gradients and effective distances would be obtained from piezometers placed at the bottom or midpoint depth in the sand. However, if it is assumed that the flow through the entire depth of the foundation is proportional to the gradient at the elevation indicated by Fig. 13, then

$$Q_w = C\,A\,(S_r - S_l) \quad \text{.....................} \quad (3)$$

in which Q_w denotes the flow from the well, C is an unknown constant, A denotes the well spacing, S_r is the riverside gradient, and S_l represents the landside gradient. For model B, S_l is zero in all three cases. If the mean head in the line of wells divided by the entire depth of the formation is designated as P_a, the total head by P_t, and the effective riverside distance by L_r—

$$S_r = \frac{P_t - P_a}{L_r} \quad \text{.......................} \quad (4)$$

---

[9] Chf., Geology, Soils and Materials Branch, Eng. Div., Missouri River Div., Corps. of Engrs., U. S. Dept. of the Army, Omaha, Nebr.

Combining Eqs. 3 and 4 results in

$$\frac{Q_w L_r}{A\,(P_t - P_a)} = C \ldots\ldots\ldots\ldots\ldots\ldots\ldots\ldots (5)$$

Eq. 5 is completely independent of any dimensions of the well system since Q_w/A is the seepage per linear foot and the well spacing A is introduced because the flow in Figs. 14 to 16 is in terms of Q_w. Consequently, if the experimental data fit Eq. 5 with reasonable accuracy, the flow per unit length from the line of wells is directly related to the exterior boundary conditions, and the relation is reasonably independent of the size, spacing, and penetration of the wells.

TABLE 2.—EVALUATIONS OF CONSTANTS C AND C_n FROM MODEL DATA

Test	C, in gal per min per lin ft	C_n, in gal per min per sq ft	Test	C, in gal per min per lin ft	C_n, in gal per min per sq ft
a-58-10	72	0.068	a-58-50	70	0.39
b-58-10	67	0.058	b-58-50	70	0.34
c-58-10	70	0.068	c-58-50	67	0.40
Mean		0.065	Mean		0.38
a-87-10	70	0.048	a-87-50	73	0.24
b-87-10	64	0.042	b-87-50	69	0.23
c-87-10	66	0.049	c-87-50	69	0.23
Mean		0.046	Mean		0.23
a-174-10	69	0.018	a-174-50	80	0.15
b-174-10	52	0.020	b-174-50	68	0.15
c-174-10	74	0.020	c-175-50	74	0.16
Mean		0.019	Mean		0.15
a-58-25	68	0.16	a-58-100	74	1.7
b-58-25	75	0.14	b-58-100	70	1.6
c-58-25	64	0.094	c-58-100	68	1.3
Mean		0.13	Mean		1.5
a-87-25	73	0.11	a-87-100	76	1.4
b-87-25	70	0.086	b-87-100	60	0.87
c-87-25	67	0.092	c-87-100	64	1.0
Mean		0.096	Mean		1.1
a-174-25	76	0.064	a-174-100	75	0.75
b-174-25	69	0.053	b-174-100	66	0.72
c-174-25	65	0.049	c-174-100	66	0.72
Mean		0.055	Mean		0.73

Table 2 seems to substantiate the previous assumptions. In Table 2, the designation "a-58-25" indicates that test data from model B-a with a well spacing of 58 ft and a penetration of 25%, has been taken from Figs. 14 to 16 to compute the assumed constant C from Eq. 5.

Considering the dimensions of the well system as opposed to the general relations between the system and the remote boundary conditions, it can be assumed that

$$\frac{Q_w}{A} = C_n\,P_a \ldots\ldots\ldots\ldots\ldots\ldots\ldots\ldots (6)$$

in which C_n is a coefficient presumed to be constant for a given well installation and is independent of the precise nature of the exterior or remote boundary conditions. The tabular values (Table 2) compiled from the data in Figs. 14 to 16 appear to substantiate Eq. 6.

The development of well-system formulas need not be complicated by introducing the possible exterior boundary conditions in the field. Also, the effect of any drainage system on a given set of field conditions can be studied without going into the details of the particular set of wells to be provided. (This statement must be qualified if the length of the drainage system is short, as in the case of a few wells.)

The electric analogy model studies described by Messrs. Middlebrooks and Jervis[5] also can be taken as illustrations of this principle. These studies were made with exterior boundary conditions similar to those in model A, but the results were reported in a form facilitating the entire elimination of exterior boundary conditions. In the writer's discussion of the paper by Messrs. Middlebrooks and Jervis, it was shown that the effective distances to the source and landside exit, and to the heads at source and exit, can be eliminated or generalized by substitution of the riverside and landside seepage gradients which determine the flow of the wells.[10] This elimination of specific exterior boundary conditions involved the substitution of the concept of a mean head in the line of wells for the "extra length" concept of Messrs. Middlebrooks and Jervis. There is no essential difference between these two concepts since the mean head P_a (referred to head at well) and the extra length L_x have the simple relation:

$$L_x\,(S_r - S_l) = P_a \quad \text{(7)}$$

The formula developed by Mr. Barron[6] for finite effective landside and riverside distances can also be transformed into an identity with the extra length or mean pressure formulas for fully penetrating wells. For partial penetration wells, no purely analytic formula is available, and the charts of Messrs. Middlebrooks and Jervis have been the only available guide. The use of these charts involves double interpolation (with respect to D/A and penetration), and for that reason they have not been used to full advantage. The term D is used to denote the depth of the pervious stratum.

The data of Messrs. Middlebrooks and Jervis were re-evaluated in the hope that some method could be developed to facilitate interpolation for any value of D/A and percentage of penetration. As the first step in the re-evaluation, the extra-length concept was replaced by the mean-head approach, so that the two sets of original curves[5] showing the "extra length" and the midpoint head might be replaced by a single set of curves involving midpoint head and mean heads only. Model data for these heads were replotted against the logarithm of A/R_w, as shown in Fig. 20. The term R_w denotes the radius of the well. For the penetrations shown in Fig. 20 the ratio D/A is equal to 3.

---

[10] Discussion by P. T. Bennett of "Relief Wells for Dams and Levees," by T. A. Middlebrooks and W. H. Jervis, *Transactions*, ASCE, Vol. 112, 1947, p. 1376.

In drawing lines through the experimentally determined data, a considerable degree of individual judgment is involved. It appeared that the semi-log plots defined nearly straight lines, and that the lines for midpoint and mean heads were nearly parallel for a given well installation. Analytic support for the interpretations of these lines as straight and parallel can be stated as follows:

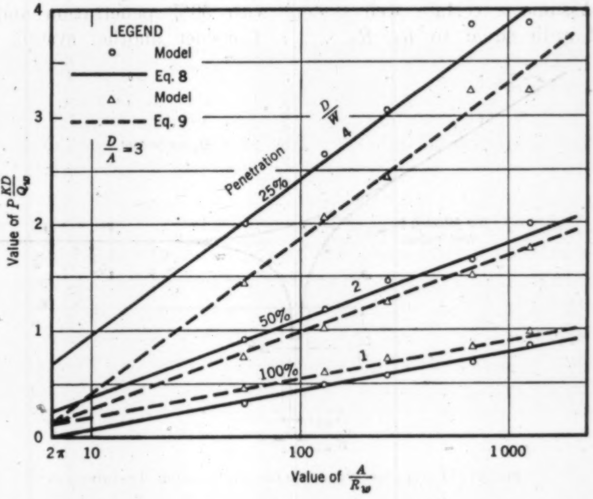

FIG. 20.—COMPARISON OF EMPIRICAL EQUATIONS WITH MODEL TEST DATA

1. In the region of the wells, the flow is composed of radial components toward the wells and a linear component normal to the line of wells. Only the radial components contribute to the flow and drawdown of the wells, and the other components can be neglected.

2. In the immediate vicinity of any one well, the radial components caused by other wells are quite small, and the flow to the well in question can be considered to be purely radial to it. For radial flow, the pressure is proportional to the logarithm of the radial distance.

3. For two or more well systems having all dimensions identical (except for the radius of the well) and having identical well flow, the pressure distribution will be identical except that, as the well radius becomes smaller, an increment of head loss proportional to an increment of $\log_e R_w$ will be added. This condition is illustrated in Figs. 21 and 22.

4. For successive systems which are identical or geometrically similar except for well radius, the difference between the mean and midpoint heads is constant, and the difference between the midpoint—or mean—head and the head at the well varies as $\log_e R_w$. The assumption of straight and parallel plots of pressure versus $\log_e (A/R_w)$ is therefore justified.

Another principle developed as a result of the re-evaluation was that, for systems similar except for the well penetration, the slope of the straight-line plots (Fig. 22) is inversely proportional to the percentage of penetration. The physical basis for this principle can be illustrated by reference to Fig. 22 and the following:

a. Assume a certain well system with 50% penetration and a series of well radii equal to R_1, R_2, ... Consider another system with the same series of radii, but with 25% penetration, and let the well discharge be identical for all cases.

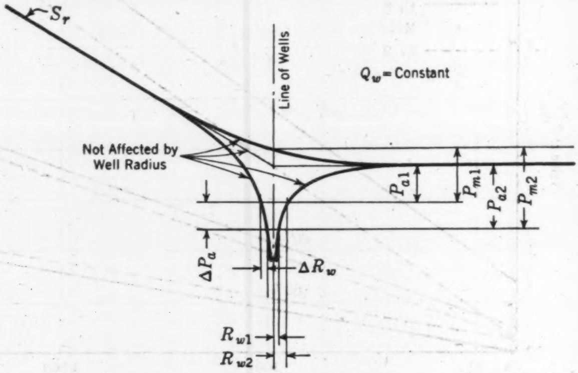
S_r
Line of Wells
Q_w = Constant
Not Affected by Well Radius
P_{a1}
P_{m1}
P_{a2}
P_{m2}
ΔP_a
ΔR_w
R_{w1}
R_{w2}

FIG. 21.—EFFECT OF WELL RADIUS ON PRESSURE DISTRIBUTION

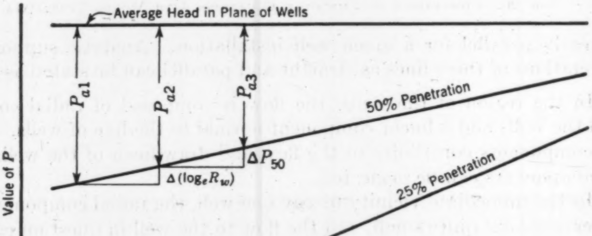

FIG. 22.—EFFECT OF WELL PENETRATION AND RADIUS ON PRESSURE DISTRIBUTION

b. Since the 25% penetration well has just half the length of the 50% penetration well, the intensity of flow will be doubled in the immediate vicinity of the well. The logarithmic pressure gradient will therefore be twice as steep. If the head increases by ΔP_{50} in changing from R_2 to R_3 in the 50% system, it will change by $2\Delta P_{50}$ in the same interval in the 25% system. The same principle holds for any amount of penetration provided the permeability does not change with depth.

It should be noted that these analytic principles do not define the absolute values of the midpoint and mean heads. However, with absolute values experimentally available, these principles assist materially in the process of smoothing out observational irregularities.

The slope of the semi-log plot for 100% penetration is known analytically from Mr. Muskat's formulas.[4] By use of the slope-penetration relationship, theoretical slopes were determined for the penetrations used in the original Vicksburg (Miss.) electric-analogy models. These slopes having been predetermined, straight lines were drawn through the plotted data. The intercepts of these lines were taken from the charts at an arbitrary value of A/R_w equal to 1,000, and they in turn were plotted against D/A and the reciprocal of percent penetration, designated by D/W. The term W is used to denote the depth of the well. These plots were linear with respect to both D/A and D/W, and it was therefore possible to interpolate algebraically the value of the midpoint and mean pressures for any combination of D/A and D/W with the arbitrarily chosen value of A/R_w equal to 1,000. In lieu of drawing a set of curves on charts similar to Fig. 20, the family of curves can be represented by the following:

$$P_a \frac{K\,D}{Q_w} = \frac{P_a}{A\,S} = \frac{D}{2\,\pi\,W} \log_e \frac{A}{2\,\pi\,R_w} + 0.11\left(\frac{D}{A} - 1\right)\left(\frac{D}{W} - 1\right) \ldots \quad (8)$$

and

$$P_m \frac{K\,D}{Q_w} = \frac{P_m}{A\,S} = \frac{D}{2\,\pi\,W} \log_e \frac{A}{2\,\pi\,R_w} + 0.11 \ldots\ldots\ldots\ldots \quad (9)$$

in which S equals the algebraic sum of the mean gradients normal to the line of wells, P_m is the head midway between wells at the top of the sand stratum, and $0.11 = \log_e 2/(2\,\pi)$. Eqs. 8 and 9 are empirical, even though certain analytic principles were used in their formulation. It should be noted that the equations are derived from the early basic work reported by Messrs. Middlebrooks and Jervis.[5] The only significant difference between the original work and the new form in which it is herein presented lies in the greater ease of accurate interpolation afforded by the equations.

The question arises as to whether the results from model B can be correlated with the generalized results from the early Vicksburg models, as stated in Eqs. 8 and 9. To investigate this question, it is first necessary to transform the nonhomogeneous sand strata of model B into an equivalent homogeneous system. Taking the total depth of the three strata as the unit of length, and the permeability of the top stratum as the unit of permeability, the horizontal transmissibility T_h of the system is

$$T_h = 0.25 \times 1 + 0.25 \times 2 + 0.50 \times 6.4 = 3.95 \ldots\ldots \quad (10a)$$

The vertical transmissibility (T_v) of the system is

$$T_v = \frac{1}{\frac{0.25}{1} + \frac{0.25}{2} + \frac{0.50}{6.4}} = 2.2 \qquad (10b)$$

The transformed homogeneous permeability both vertically and horizontally is

$$K_t = \sqrt{T_h T_v} = 2.96 \qquad (10c)$$

and the transformed depth is

$$D_t = D\sqrt{\frac{T_h}{T_v}} = 1.34\,D \qquad (10d)$$

The transformed depths of the individual strata become (1) for the top—

$$25 \times \frac{1}{2.96} = 8.5 \text{ ft} \qquad (11a)$$

(2) for the middle—

$$25 \times \frac{2}{2.96} = 17.0 \text{ ft} \qquad (11b)$$

and (3) for the bottom—

$$50 \times \frac{6.4}{2.96} = 108.0 \text{ ft} \qquad (11c)$$

resulting in a total transformed depth (*D'*) of 133.5 ft.

Corresponding to the authors' percentage penetration expressed in depth, the effective penetrations based on transmissibility are as follows:

Depth, in percentage	Transmissibility, in percentage
10	2.54
25	6.35
50	19.0
100	100

Transformed ratios of depth to well spacing were obtained by using a transformed total depth of 134 ft.

By using the transformed dimensions of model B, it is possible to compute theoretical values for $\frac{P_a}{A\,S}$ from Eq. 7, and also the observed values obtained from the model. A comparison of the observed and computed values is shown in Table 3. The underlined value is computed from the empirical formula.

The correlation between computed and observed data is quite satisfactory, considering that (1) basic data were taken visually from charts, (2) the foundation gradients are not uniform with depth, and (3) the transformation methods for obtaining effective penetrations and (*D*/*A*)-ratios are approximations. It would be interesting to compare computed midpoint heads with model results.

TABLE 3.—THEORETICAL AND OBSERVED VALUES OF $\frac{P_a}{A\,S}$

Well spacing A, in feet	Value of $\frac{D'}{A}$	Model	PERCENTAGE PENETRATION (DEPTH)			
			10	25	50	100
			PERCENTAGE PENETRATION (TRANSMISSIBILITY)			
			2.54	6.35	19.0	100
29	4.6		25.4	9.8	3.0	0.24
		B-a	21.1	9.7	4.0	0.7
		B-b	24.7	13.3	3.9	1.0
		B-c	19.7	11.8	3.7	0.9
58	2.3		19.8	7.8	2.5	0.35
		B-a	17.9	7.4	3.0	0.5
		B-b	19.7	9.5	3.0	0.7
		B-c	16.3	7.5	2.7	0.7
87	1.54		19.1	7.6	2.5	0.42
		B-a	17.3	8.0	3.3	0.6
		B-b	17.3	9.1	3.4	0.8
		B-c	16.5	8.5	3.4	0.7
174	0.77		20.2	8.1	2.7	0.53
		B-a	21.6	6.9	3.1	0.5
		B-b	14.5	7.8	2.7	0.5
		B-c	22.5	7.5	2.6	0.5

It is felt that the results of the authors' model tests strongly support the writer's contention that the characteristics of a well system can be determined independently of the over-all seepage system, and vice-versa. The results of the model studies performed by Messrs. Middlebrooks and Jervis, when expressed as Eqs. 7 and 8, appear to be applicable to nonuniform foundation conditions after transformation of the latter to an equivalent uniform condition. For that reason, in future model and analytic studies, attention might well be centered on those exterior features of the system which determine the effective distance to the "source" or "landside exit."

Model B illustrates the possibilities in the field. Fig. 13 shows the effective upstream resistance for model B-b to be 700 ft which can be considered as composed of the 350 ft from the line of wells to the center of the borrow pit, plus the equivalent of 350 ft involved in the vertical entrance through the borrow pit. In model B-c, this equivalent resistance through the borrow pit floor is in "parallel" with the 650 ft of resistance from the borrow pit to the open face at the river, and these two are in "series" with the 350 ft between the borrow pit and the wells. The total "resistance" of model B-c, computed from these partial resistances, is $\frac{1}{1/350 + 1/650} + 350 = 230 + 350 = 580$ ft, which closely approximates the effective riverside distance obtained experimentally. Following the experimental determination of the effective resistance of the borrow pit entrance, the total resistance of a system with such a pit at any location could be estimated by these methods.

Thus, it appears that generalized conclusions can be drawn from model studies of typical exterior systems—entirely independent of the particular drainage system used. Such general results, combined with those available for relief-well systems, should provide the method of attacking a variety of problems with a minimum of model studies.

Real progress in the field of relief-well design is also dependent on obtaining reasonably accurate basic information on the stratification of the foundation and top strata, with respect to permeability. Field permeability tests and observation of existing well systems are the best approach to this basic problem.

John A. Focht, Jr.,[11] J.M. ASCE.—A definite need has always existed for verification of theoretical methods of analysis of relief-well systems at locations where the landside top stratum is semipervious. Although reference was made by the authors to the approximate solutions which have been developed, no comparison was made between the model results and the theoretical analyses.

Mr. Barron developed approximate formulas which can be used to compute the pressure midway between fully penetrating wells and the well flows where there is a semipervious, landside top stratum.[6] The pressure beneath the top stratum midway between partially penetrating wells can be computed approximately by applying a correction factor to the pressure computed for fully penetrating wells. This correction factor is the ratio of the head midway between partially penetrating wells (computed from the curves developed by Messrs. Middlebrooks and Jervis[12]) to the head midway between fully penetrating wells for an impervious, landside top stratum. This correction factor is approximate but, as will be shown, yields results comparable to those indicated by the models.

Mr. Bennett also has developed an approximate solution for fully or partially penetrating wells in which the landside top stratum is semipervious. Mr. Bennett's method of analysis[13] will yield the average pressure in the plane of the wells and the well flows. The ratio of the maximum pressure midway between the wells to the average pressure in the plane of the wells for an impervious top stratum can be computed as a ratio between the curves determined by Messrs. Middlebrooks and Jervis.[12] Application of this ratio to the computed average pressure will indicate the maximum pressure midway between wells. This ratio can be computed and applied as a correction for either partially or fully penetrating wells.

It is of interest to compare the data obtained from Model A-a-2 (Fig. 10) with results obtained by theoretical analyses in order to prove or disprove the validity of the theoretical analyses. To make this comparison, the permeability and thickness of the prototype top stratum (Fig. 3) and the prototype well radius were used in the procedures outlined by Messrs. Barron and Bennett to obtain the maximum head midway between wells for various well spacings and penetrations. The computed maximum head midway between wells for 50% and 100% penetration wells is shown in Fig. 23 for different well spacings. Also shown are the observed model data taken from Fig. 10. In addition, a curve indicating the maximum pressure between wells, which would exist if the landside top stratum were impervious, has been plotted in Fig. 23. A similar group of curves for 25% penetration wells is given in Fig. 24.

---

[11] Associate Engr., Greer and McClelland, Cons. Foundation Engrs., Houston, Tex.

[12] "Relief Wells for Dams and Levees," by T. A. Middlebrooks and W. H. Jervis, *Transactions*, ASCE, Vol. 112, 1947, p. 1333, Figs. 8(*a*) and 8(*b*).

[13] Discussion by P. T. Bennett of "Relief Wells for Dams and Levees," by T. A. Middlebrooks and W. H. Jervis, *ibid.*, pp. 1378–1382.

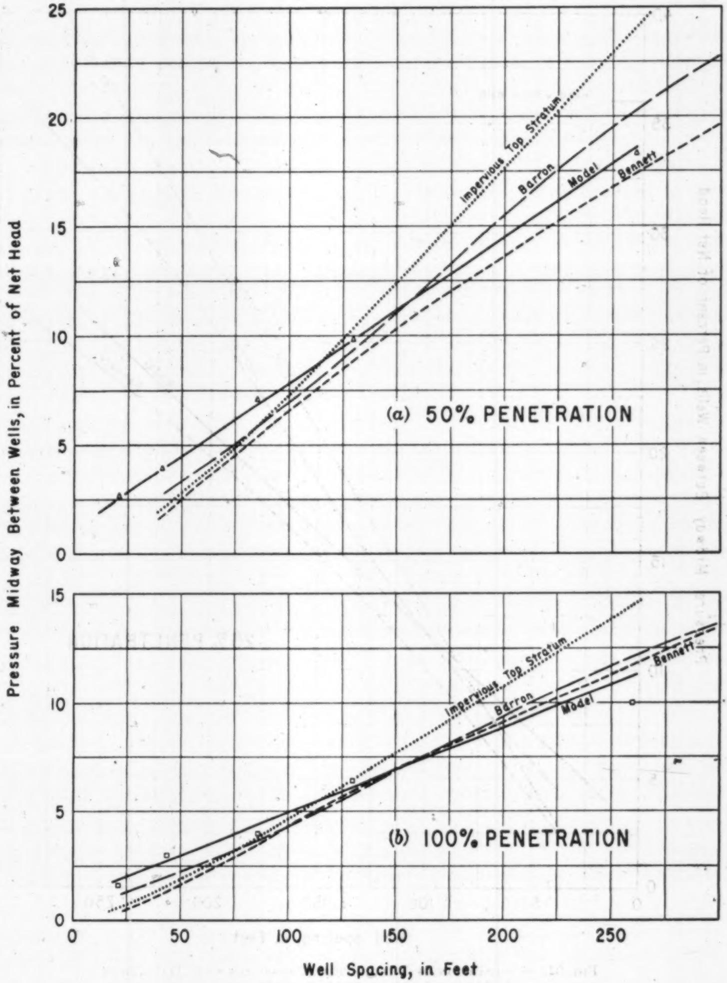

FIG. 23.—COMPARISON OF THEORETICAL PRESSURES WITH DATA FROM MODEL A-a-2 FOR VARIOUS WELL PENETRATIONS

Good agreement between both theoretical curves and the model data is indicated for fully penetrating wells. It should be noted that in Figs. 23 and 11, for small well spacings, both the model data and Mr. Barron's solution show a head between wells greater than that indicated for an impervious top stratum. This condition is one which cannot exist because the pressure at any location where the landside top stratum is semipervious must be less than that for an impervious top stratum.

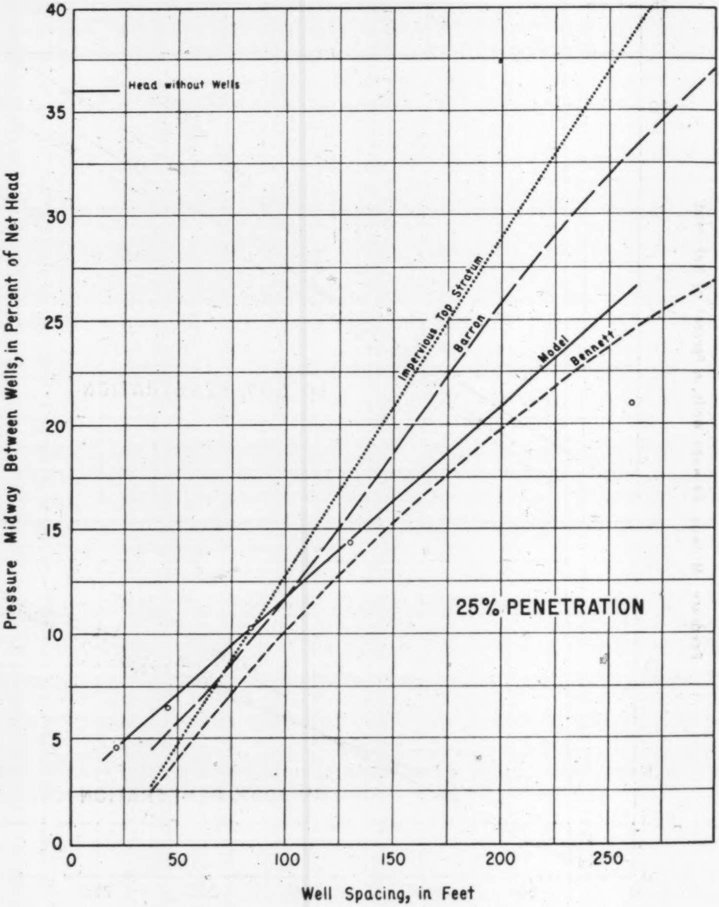

FIG. 24.—COMPARISON OF THEORETICAL PRESSURES WITH DATA FROM MODEL A-a-2 FOR 25% WELL PENETRATION

For 50% penetration wells, there is more divergence between the model data and the theoretical results. A considerable difference is indicated for the wells penetrating 25% into the pervious stratum. An inconsistency is evident in Fig. 24 as the pressures computed from Mr. Barron's solution for large well spacing are indicated to be greater than the pressure without any wells. The inherent error introduced into the correction factor for the small partial penetration results in a computed pressure greater than that which can actually occur. The average pressure in the line of wells for 25% penetration, as computed by Mr. Bennett's procedure (which is not shown in Fig. 24), is comparable to the model data for pressure midway between wells.

From a study of Figs. 23 and 24, it can be concluded that either Mr. Barron's procedure or Mr. Bennett's procedure will indicate satisfactory pressures midway between wells as compared to the model data for well penetrations between 50% and 100%. However, inasmuch as both the model data and results from Mr. Barron's analysis show (for small well spacings) pressures greater than those indicated for an impervious top stratum and, inasmuch as the pressures computed by Mr. Barron's analysis for large well spacings and small penetration may be greater than the pressure without any wells, the solution as outlined by Mr. Bennett—extended to obtain the maximum pressure between wells—appears preferable for numerical solutions. If a well system is to be designed on the basis of the average pressure in the line of wells, the method originally suggested by Mr. Bennett will be satisfactory. A comparison which would indicate results similar to those shown for the pressure midway between wells could also be made for the well flows.

Although Eqs. 1 and 2 make allowance for variation in the distance to the effective source of seepage, they do not permit a solution for a landside top stratum with a thickness or permeability different from the model prototype. Thus, the use of the approximate theoretical analyses seems preferable to the use of Eqs. 1 and 2. However, to utilize the theoretical analyses, an estimate of the distance from the proposed line of wells to the effective exit for seepage is required. The best information would be from piezometers installed previously at the proposed site; but an approximation[7] can be made if the average top stratum thickness and the permeability are known. At the present time (1953) a precise determination of the effective top stratum thickness and the ratio of top stratum permeability to pervious stratum permeability, as they exist in the field, is probably impossible.

At the present time (1953), an investigation of a number of underseepage sites along the lower Mississippi River levees is under way in which the writer has assisted. This investigation was directed partially toward an improvement in the procedure for estimating the effective top stratum thickness and the permeability ratio between the top stratum and the pervious stratum. It is hoped that, when this investigation is completed (1954), satisfactory methods for computing or estimating the necessary factors will have been derived.

One point on which preliminary results of the Mississippi River levee investigation were quite clear is that the minor local geologic features are extremely important. In fact, their significance is so great that, following the completion of the office design of a relief-well system, the final location of the wells along a levee should be made by the design engineer—modifying the spacing slightly to shift wells to more critical locations. This procedure was followed on large installations of relief wells along the Mississippi River between St. Louis, Mo., and Gale, Ill., in the St. Louis District, Corps of Engineers. In reality, this procedure illustrates that a completely precise solution is neither possible nor necessary since the landside conditions and the distribution of pressure and flow on the landside are too variable.

Summary.—The writer has endeavored to show that the authors' model tests verified approximate theoretical methods. These methods were developed for determining substratum pressures and well flows for pressure-relief well systems.

W. H. JERVIS,[14] M. ASCE.—An excellent presentation of a thorough hydraulic-model study has been made by the authors. The relief well is a useful tool for any engineer confronted with a deep-seepage problem. In fact, depending on the depth of the well, the saving in cost when compared to other methods of treatment is considerable.

The model studies illustrate one significant point. That point is related to the quantities of water which must be handled so as to obtain a reasonably complete pressure relief. For example, flow from wells on 100-ft centers and 100% penetration as observed in Models B, C, and D for a head of 20 ft would amount to the following:

Model	Well Flow in gallons per minute	in cubic feet per second
B–a	140	0.31
B–b	175	0.39
B–c	210	0.47
C	270	0.60
D	170	0.38

A head of 20 ft is possible on the main levees on the lower Mississippi River, and a well spacing of 100 ft and penetration of 100% might be required for adequate pressure relief. In the previously tabulated models for the given well spacing and penetration, pressure relief of from 85% to 95% was obtained. This relief is probably more than would be sought in the field. However, when the variations in the pervious layers underlying the levee are considered, it is doubtful whether it would be possible to design a system which would maintain a definite percentage relief. Such a system would require valves (controlled by piezometer installations) placed on the wells.

When it is realized that the levees along the lower Mississippi River protect flat areas where drainage is naturally poor, it can be seen that for a large-scale installation the problem of water removal could, in some cases, be material. For example, there are several hundred miles of levee surrounding the delta area of the Yazoo River (Mississippi) and the Mississippi River. At a rate of seepage of 0.4 cu ft per sec per 100-ft station, each mile of levee would yield 21 cu ft per sec of water which in some cases might have to be pumped back over the levee. This factor alone has led to some opposition to the installation of relief-well systems on the Mississippi River levees. Data from field installations of wells and piezometers are being gathered, and the progress of this work will be watched attentively by all interested persons.

---

[14] Resident Partner, Porter-Urquhart, Skidmore, Owings & Merrill, Associated, Casablanca, French Morocco.

The ultimate question is whether or not relief wells are necessary—that is, whether sand boils cause levee failures. The writer is convinced that they are a potential cause of levee failure and probably have been a cause in the past. However, determining the cause of a levee failure on a system as large as that on the Mississippi River is extremely difficult. It is not similar to watching seepage develop at a dam in a relatively confined space. If a failure occurs, it may occur suddenly, in a remote place, where there are no competent witnesses. The writer has questioned many people who have witnessed crevasses, and the causes as reported by them have varied from sand boils to "burrowing animals" to overtopping for the same crevasse. Obviously, such testimony is not convincing, and it is doubted whether any cause can be definitely assigned to any given crevasse. When a crevasse occurs, it is impossible to examine it afterward because there is nothing left but a big hole. The writer, nevertheless, is suspicious of underseepage as a leading cause of failures.

Meanwhile, the responsible engineers are confronted by a difficult problem. It is a problem with which the writer is familiar and with which he is sympathetic. The model studies described by Messrs. Turnbull and Mansur are a welcomed addition to this field of endeavor.

W. J. TURNBULL,[15] M. ASCE, and C. I. MANSUR,[16] J. M. ASCE.—The development by Mr. Bennett of generalized formulas for the design of relief-well systems from additional analyses of data from model B and electrical-analogy studies[5] of relief wells has added materially to this paper. The transformation of a stratified foundation to an equivalent homogeneous system and comparison of the computed values of $P_a/(A\ S)$ with those obtained in model B is also enlightening.

Mr. Bennett has stated that the value of C in Eq. 3 is an unknown constant. In actuality, when it is assumed that the flow through the entire depth of the foundation is proportional to the gradient at the top of the sand (as Mr. Bennett assumes), then the flow,

$$Q_w = k_h\, D\, A\, (S_r - S_l) = C\, A\, (S_r - S_l) \qquad (12)$$

thus,

$$C = k_h\, D \qquad (13)$$

in which k_h is the average horizontal permeability of the pervious foundation. In model B, $C = k_h\, D = 0.10 \times 100 = 10$ cu ft per min per ft or 75 gal per min per ft which corresponds closely with the average value for C of 69 gal per min per ft for all the C-values in Table 2.

It has been implied by Mr. Bennett that the flow per unit length of levee from a line of wells is reasonably independent of the well spacing and penetration. The model data show that well spacing and penetration do have an effect on well flow; however, this does not invalidate Eqs. 3 and 5, as changes in S_l and P_a with different well spacings and penetrations are compensated by a corresponding change in Q_w.

---

[15] Chf., Soils Div., Waterways Experiment Station, Corps of Engrs., U. S. Dept. of the Army, Vicksburg, Miss.

[16] Chf., Design and Analytical Section, Embankment and Foundation Branch, Soils Div., Waterways Experiment Station, Corps of Engrs., U. S. Dept. of the Army, Vicksburg, Miss.

In designing a well system for a given site by the use of the formulas (Eqs. 5, 8, and 9) offered by Mr. Bennett, it is necessary to determine first the permissible head beneath the top stratum which can exist at the landside toe of the levee without causing dangerous sand boils or piping. The well system is then designed so that the pressure, P_m, midway between wells does not exceed this allowable head. It is probably preferable to select first the desired well radius and the percentage penetration of the aquifer. With the distance to the effective source of seepage and the total design head, P_t, on the dam or levee known, a trial value for the well spacing can be assumed, and Eqs. 8, 9, and 5 (substituting $k\ D$ for C) can be solved simultaneously for Q_w, P_a, and P_m. This procedure can then be repeated for various values of well spacing until the well spacing having a head midway between the wells equal to the allowable head beneath the top stratum is obtained. In practical design problems, the hydraulic head losses in the well must also be considered, as these losses add to the head midway between wells. It is also necessary to allow for end effects when the well system consists of a comparatively short line of wells, rather than an infinite line of wells, because the head midway between the wells near the ends of the system is greater than that at the central part of the system. Equal heads midway between wells on the ends of a short line of wells can be obtained by either decreasing the well spacing or by increasing the penetration of the wells at the ends of the well line.

It should be noted that in Table 3 the theoretical values of $P_a/(A\ S)$ for 100% penetration have been compared to model values of $P_m/(A\ S)$. Therefore, in order to obtain a comparison of Mr. Bennett's formulas with the model data, it is necessary to compute the theoretical values of $P_m/(A\ S)$. The computed values of $P_m/(A\ S)$ for the cases shown can be obtained by adding 0.11 to the underlined values in the column for 100% well penetration. All the other values shown in Table 3, both theoretical and observed, are $P_a/(A\ S)$.

Mr. Focht's comparisons of the model data and the heads computed from theoretical formulas are most interesting. As Mr. Focht notes, there is some slight scattering in the model data which results in a minor deviation from the theoretical values. However, the deviation is not considered to be important because, in the design of relief-well systems, many of the factors affecting the design cannot be evaluated with precise accuracy. It is therefore believed that the deviations between the model data and the theoretical values are of a minor nature in comparison with the uncertainties which can exist in the evaluation of factors in the field that affect the design of well systems.

Mr. Jervis has stated that the installation of relief wells will greatly increase the amount of seepage or water landward of a levee during periods of high water. The primary purpose of relief wells is to reduce the hydrostatic pressure on the landside (or downstream side) of levees or dams. By so doing, the hydraulic gradient from the river or reservoir toward the landside is increased, which in turn increases the landward flow to some degree. It is believed that this increase does not assume the proportions suggested by Mr. Jervis for the following reasons:

First, along most levee systems—and certainly along those in the upper and lower Mississippi River valleys—only a relatively small proportion (20% to 40%) of the levees is critical with respect to dangerous substratum pressures. Thus, the need for pressure relief is not continuous throughout the entire length of the levee system.

Second, the flow (resulting from surface runoff and general seepage during flood time) that must be accommodated by any existing surface drainage system landward of the levees is appreciable without relief wells. The increase in this flow which would be caused by the installation of relief wells along certain reaches of the levee would be relatively small during high water when one considers the total length of the levee system.

Third, most areas landward of levees that are critical with respect to underseepage are usually subject to heavy seepage or sand boils during periods of high flood stages without pressure-relief measures. If relief wells are installed, they will intercept a large part of this natural seepage without excessively increasing the total flow passing beneath the levee, particularly at the higher river stages. This is illustrated by subsequent examples of model data, field observations, and hypothetical computations.

In Model A-a-2 with a net head of 25 ft (Figs. 3 and 12)—a model fairly representative of conditions along the Mississippi River levees—relief wells on 100-ft centers penetrating half the depth of the pervious foundation reduced the hydrostatic pressure landward of the levee to 2.0 ft or only 8% of the net head on the levee, decreased uncontrolled seepage by 77%, and increased the total flow passing beneath the levee by 28%.

This example is supported by actual field measurements of seepage and substratum pressures along a levee reach without any wells (at Trotters, Mississippi) during the high water in 1950 and by similar measurements made during a high water in 1951 of seepage and flow from relief wells subsequently installed at the same site. The total natural seepage in 1950 passing beneath the levee, determined from piezometer readings and known foundation characteristics, was 156 gal per min per 100 ft of levee. In 1951, with a line of drainage wells on 100-ft centers along the toe of the levee, with 50% penetration of the sand aquifer and a net head on the levee of 7.55 ft, the flow from the wells was 123 gal per min per 100-ft station. Adjusted to the same head on the levee that existed in 1950 when the natural seepage was measured without wells, the well flow would have been 218 gal per min per 100-ft station. That is, at this site, the relief wells increased the total flow passing beneath the levee by 40%. There was no measurable natural seepage landward of the wells in 1951, primarily because the wells discharged into a collector ditch and a natural landward drainage ditch which carried the well flow without overflowing.

Another illustration of the amount that relief wells increase flow passing beneath a levee during high flood stages is demonstrated by a subsequent computation for a soil condition that could be critical in flood time. The maximum hydrostatic pressure that can exist landward of a levee with a height of 25 ft, a top stratum thickness of 8 ft, an assumed critical gradient of

0.8, and a saturated foundation is 6.4 ft. (Any substratum pressure greater than this would either raise the landside blanket or be self-relieved through sand boils.) Therefore, the net hydrostatic head causing landward flow would be $\Delta H = 25 - 6.4 = 18.6$ ft. The flow resulting from this decrease in head will emerge somewhere landward of the levee as general seepage or as flow from sand boils. If a sufficient number of drainage wells were installed so as to lower the residual pressure on the landside to approximately 2.0 ft, the landward flow would be that corresponding to a head drop of 23 ft (25 ft − 2 ft). That is, the wells would increase the landward flow by 24%.

On the basis of the foregoing model data, field data, and theoretical computations, it can be seen that the additional flow for a continuous length of levee resulting from drainage wells at intervals would be relatively small (10% to 30%) in most instances when one considers the total flow that must normally be cared for by the surface drainage system. An additional amount of water of from 10% to 30% will probably not materially add to the difficulties which already exist. As a corollary, if pumping is necessary, it will be made necessary primarily by the natural seepage and rainfall which would exist with no relief wells.

During low floods which may not completely saturate the landward top stratum, the increase of total flow beneath a levee caused by relief wells may be somewhat more than that shown by the previous examples for relatively high (12 ft to 15 ft or greater) floods. The objection to well flow during low flood stages has been partly met in the design of an extensive system of relief wells for levees in the St. Louis District, Corps of Engineers, United States Department of the Army, by installing a standpipe (on top of each well) which would automatically overflow when the hydrostatic pressure at the well exceeds approximately one fourth the thickness of the top stratum. When the standpipes begin to overflow, they are to be removed so that the well system can function as designed.

Mr. Jervis expressed the hope that the model studies would be extended to field studies. Such studies of full-scale field installations of relief wells have been made. Information has been obtained on the functioning of a well system at Trotters during high river stages in 1951 and 1952. Also, extensive installations of relief wells have been and are presently (1954) being installed along Mississippi River levees in the St. Louis District. The writers have been—and are presently—closely associated with the field studies at Trotters and the design of the relief wells in the St. Louis District.

At the time the original model data were analyzed, it was considered desirable to assemble in a single volume certain relief-well-design formulas for various geological and stratigraphical soil conditions. Clarification of symbols, terminology, and various phases of well design could be accomplished in such a volume. This was done in an appendix to a publication.[17] Since the time of this publication, however, additional data have been developed and in one or two instances certain corrections to formulas have been made. Although further development and improvement in relief-well design will take place, another compilation bringing the 1949 publication[17] up to date would be extremely useful to engineers relatively unfamiliar with well-design problems.

---

[17] "Relief Well Systems for Dams and Levees on Pervious Foundations; Model Investigations," *Technical Memorandum No. 3-304*, Waterways Experiment Station, Vicksburg, Miss., November, 1949.

AMERICAN SOCIETY OF CIVIL ENGINEERS
Founded November 5, 1852
TRANSACTIONS

Paper No. 2702

WIND LOADS ON TRUSS BRIDGES

By John M. Biggs,[1] A. M. ASCE

With Discussion by Messrs. F. B. Farquharson, and John M. Biggs

Synopsis

Model tests indicate that the spacing of bridge trusses considerably affects wind resistance, and that the resistance produced by the floor bears little relation to its unshielded area. Other similarly useful information may be derived from small wood and brass bridge models such as those described in this paper. Component parts of the models were tested singly and in combinations in a wind tunnel to determine the effects of different components on the total resistance. The wind direction and velocity were also varied. The paper presents the results of these experiments.

Introduction

Design specifications for wind loadings on railroad and highway bridges remained essentially unchanged throughout the first half of the twentieth century, although facilities for the experimental determination of these loads were developed during that time.

Research has yielded data concerning the aerodynamic stability of suspension bridges, but wind loads determined in tests of suspension-bridge cross sections are limited in value by the differences between the proportions of these sections and those of other types of bridges.

This paper presents the results of wind-tunnel tests on two scale models of a typical double-track railroad bridge. Other data have been obtained for highway bridges and for various truss spacings through modification of one of the models. Test results presented herein should be found useful in the design of simple-span truss bridges.

Note.—Published, essentially as printed here, in July, 1953, as *Proceedings-Separate No. 201*. Positions and titles given are those in effect when the paper was received for publication.

[1] Asst. Prof. of Structural Eng., Massachusetts Inst. of Technology, Cambridge, Mass.

Models, Equipment, and Procedure

The prototype is a double-track, open-deck railroad bridge of the subdivided Warren type having a span of 350 ft and a depth of 49.2 ft. All truss members are fabricated of plates and angles to form box sections or I-sections. The floor system is of the conventional floor beam-and-stringer type.

One of the two models tested (shown in Fig. 1) was constructed of wood, to a scale of 1:120. As much detail was included as this material and scale would permit. In the model, U-sections and H-sections were simulated by

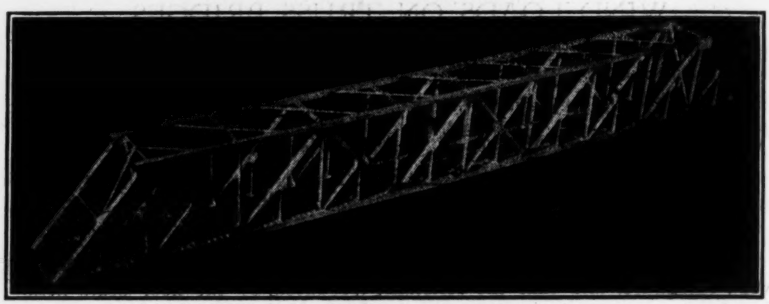

Fig. 1.—Wooden Model of Double-Track Railroad Bridge

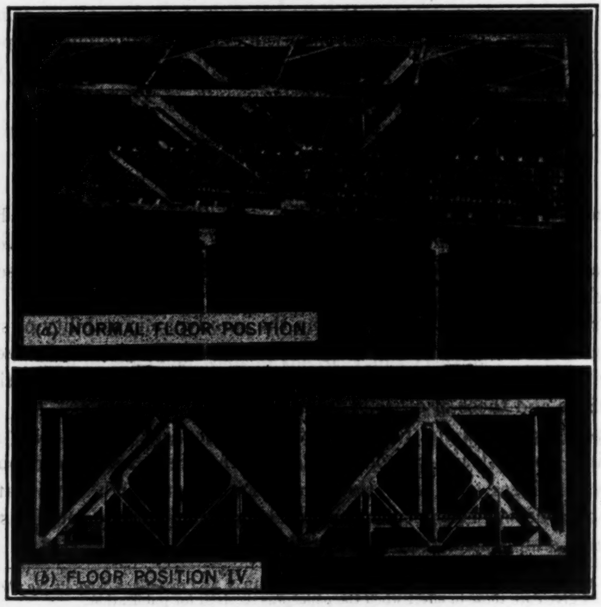

Fig. 2.—Brass Model, Two Floor Positions

routing one or two sides of solid rectangular cross sections. Members having lacing bars on one or two sides were represented by rectangular pieces in which circular holes had been drilled so that the ratio of net area to enclosed area equalled that of the prototype.

The other model (shown in Fig. 2) was constructed of brass, to a scale of 1:40. Unlike the first model, it included only eight interior panels, or two fifths of the span. The details of the prototype were carefully reproduced in an attempt to ensure the same aerodynamic properties. All gusset plates, lacing angles, batten plates, and projections on the individual members were reproduced to scale.

When the models were constructed it was thought that their drag coefficients might differ because (1) the brass model contained more detail, (2) the aspect ratio (length divided by width), which affects the drag coefficient of solid plates, differed widely between the models (being 7.1 for the wood model and 2.8 for the brass one), and (3) end effects might be present on the brass models. Despite these differences the data indicated close agreement between the wind pressures on the two models. In Fig. 3, the wind pressure on each model is plotted against the angle of attack, α—which is the angle between the wind direction and a horizontal plane. The side elevation area of the wooden truss, A_T, was 48.25 sq in., and that of the brass truss was 203.1 sq in. The wind velocity was 70 miles per hr.

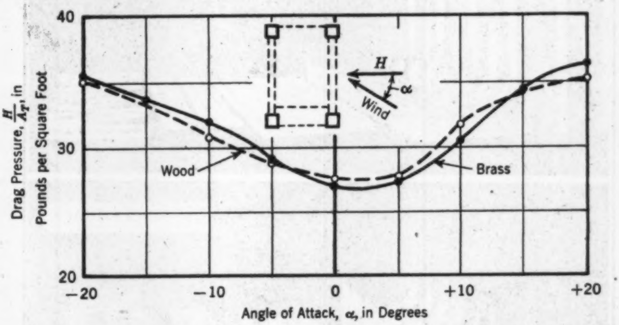

Fig. 3.—Comparison of Drag Pressures on Two Models of a Double-Track Railroad Bridge

Because it was desirable to obtain more basic data—for bridges other than the prototype—the brass model was constructed so that its main parts could be assembled and tested in any combination, as illustrated by Fig. 4. The contributions of the various parts to the total wind force could thus be determined, and a general method for computing wind loads could be devised.

The cross sections in Fig. 5 indicate the various arrangements of members. The following sequence of testing was adopted: (1) A single truss; (2) both trusses without the floor system or lateral bracing, spaced by small rods having little resistance to the air stream; (3) both trusses connected by the floor system and the bottom lateral bracing; and (4) the complete bridge. A second floor system having only two stringers and a width corresponding to a single-track railroad bridge was also constructed. This floor, together with narrow lateral bracing systems, was combined with the two trusses and tested in the same sequence to give results for a single-track bridge. Replacing tracks and ties with a solid plywood slab having curbs gave a reasonable facsimile of a highway bridge. It was expedient to use the same floor framing and lateral systems for the highway bridges as for the railroad bridges. Therefore, typical road widths were not possible. The roadways tested were 14.6 ft and 26.2 ft at full scale including curbs. The latter is approximately a two-lane width.

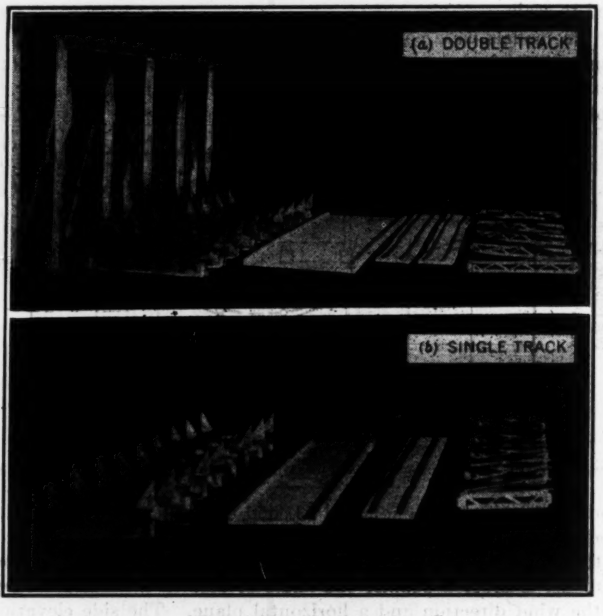

FIG. 4.—TEST COMPONENTS

The tests were conducted according to standard wind-tunnel procedures at wind velocities of 50 miles per hr, 60 miles per hr, and 70 miles per hr. The aerodynamic coefficients obtained at all three velocities were in agreement.

TEST RESULTS

The first test was run on a single truss completely removed from the remainder of the structure. The horizontal drag forces determined at three wind velocities for various angles of attack are plotted in Fig. 6. In the expression,

$$H_o = A_T C_D \rho \frac{v^2}{2} \qquad (1)$$

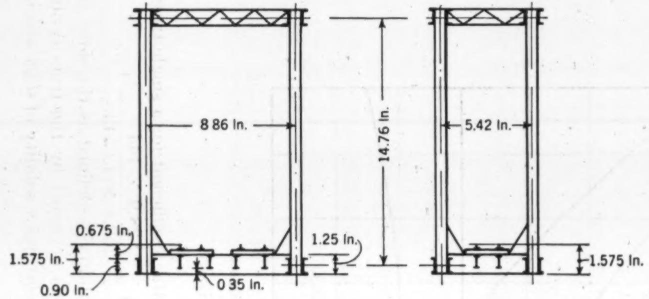
8 86 In.
14.76 In.
5.42 In.
0.675 In.
1.575 In.
0.90 In.
0 35 In.
1.25 In.
1.575 In.

(*a*) RAILROAD

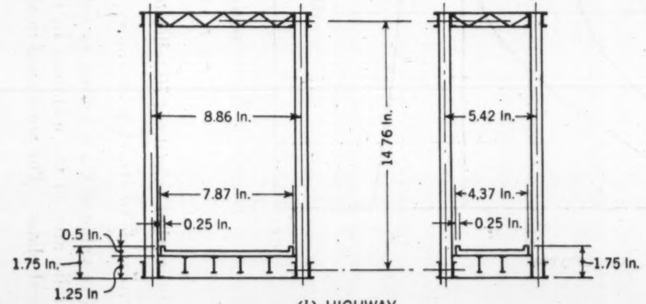
8.86 In.
14 76 In.
5.42 In.
7.87 In.
4.37 In.
0.25 In.
0.25 In.
0.5 In.
1.75 In.
1.25 In
1.75 In.

(*b*) HIGHWAY

FIG. 5.—CROSS SECTIONS, NORMAL FLOOR POSITION (SCALE = 1:40)

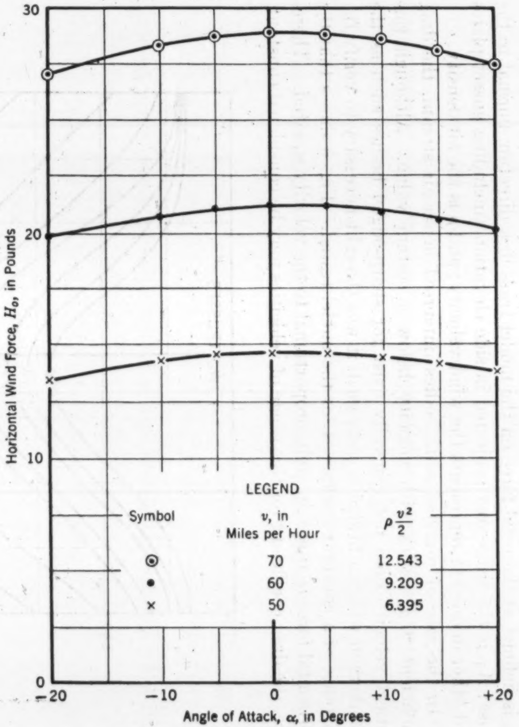

FIG. 6.—HORIZONTAL WIND ON A SINGLE TRUSS (A_T = 203.1 In.²)

H_o is defined as the total force on the model truss in a direction normal to the truss; A_T is the truss area projected in side elevation (including gusset plates and other details); v represents the wind velocity; and ρ is the air density.

In the case of rounded solid bodies immersed in an air stream, the drag coefficient, C_D, varies with velocity below a certain value. Although this critical velocity does not generally exist for sharp-edged bodies such as the members of which a bridge is composed, it was thought necessary to verify the existence of a constant coefficient for the model tested. Fig. 6 shows that the horizontal force is approximately proportional to the velocity squared. Therefore, the drag coefficient for this range of velocities may be considered constant.

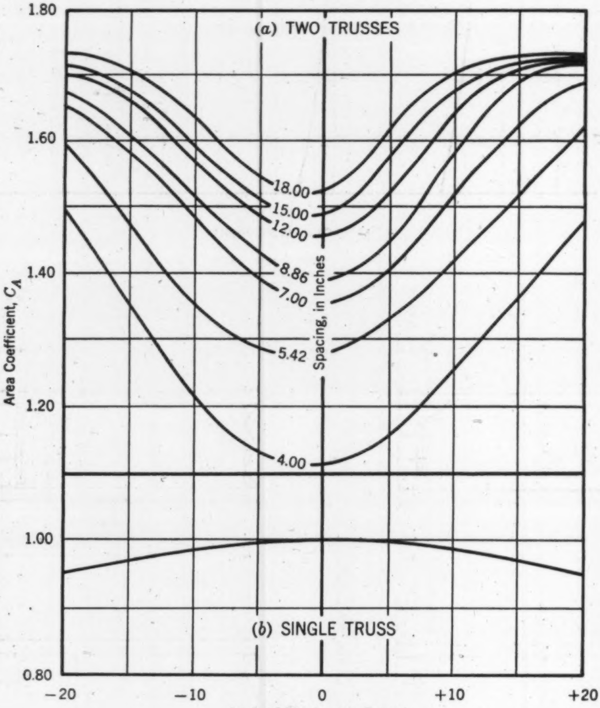

Fig. 7.—Area Coefficients

If the wind velocity is 70 miles per hr, the drag coefficient for a single truss at zero angle of attack is computed from Eq. 1 as $\dfrac{28.9 \times 144}{203.1 \times 12.543} = 1.63$.

The value of C_D is known to vary with "solidity"—defined as the ratio of the solid area of the members to the total area occupied by the truss in its vertical plane. The truss used in this experiment has a solidity of 0.25 which is fairly typical. Therefore, the drag coefficient given is applicable to most simple-span bridge trusses.

The two values of wind pressure usually used in bridge design are 30 lb per sq ft and 50 lb per sq ft. The tests on a single truss indicate that the wind velocities corresponding to these pressures are 84.9 miles per hr and 109.5 miles per hr, respectively.

In order to present the data in a manner consistent with design specifications, a new factor, C_A, was introduced into the basic equation—

$$H = C_A \, A_T \, C_D \, \rho \, \frac{v^2}{2} \ldots\ldots\ldots\ldots\ldots\ldots\ldots\ldots (2)$$

In this equation, $C_D = 1.63$, A_T is the elevation area of one truss, and C_A is the area coefficient. For any combination of the bridge components, or for any wind direction other than horizontal, C_A is the factor by which the area of one truss is multiplied to determine the effective area under the particular conditions. Thus, for a single truss subjected to an horizontal wind, C_A is unity. The factor C_A is a measure of the variation in total horizontal force on the model as the angle of attack is varied and other component parts are added to the single truss.

Fig. 7 shows how C_A varies with the angle of attack for the single truss. Positive angles indicate a wind component upward on the bridge. Fig. 7 also shows values of the area coefficient for various spacings of two parallel trusses. The extreme spacings tested correspond to 13.3 ft and 60 ft at full scale. The amount by which C_A exceeds unity represents the contribution of the leeward truss to the total horizontal force as well as the effect of variation in α. The total horizontal force and C_A increase directly with the truss spacing. If the trusses were very close together, the leeward members would be almost completely shielded by their windward mates. As the spacing is increased, the disturbance caused by the windward truss begins to disappear before the leeward truss is reached. At an infinitely wide spacing, the area coefficient would be 2.0. As the angle of attack increases from zero, the shielding effects are reduced, and the load on the leeward truss is increased.

As shown by Fig. 7, the load on the leeward truss varies widely as the truss spacing is changed; nevertheless, the effect of truss spacing is ignored in most specifications.

Meteorological data are scant from which the maximum angle of attack can be determined for design purposes. Although the maximum angle depends somewhat on the site of the structure, a reasonable range is ±15°. Within this range, the maximum area coefficient obtained for the 18-in. model truss spacing (equal to 60 ft at full scale) is 1.73. This value corresponds to a load on the leeward truss equal to 77% of that on the windward truss; it is considerably greater than the value of 50% contained in some specifications.

Fig. 8 shows values of C_A for all stages of completion of each of the four bridge types. When the floor system is added to the two trusses, the effect varies with the bridge type and the angle of attack. At most points the addition of the floor system decreases the total horizontal force which had acted on two trusses without floor system or bracing. Nowhere does the floor cause an appreciable increase in load. At the angle of attack corresponding to the maximum horizontal force on a complete bridge (−15° for the single-track railroad bridge and +15° for other types), the railroad floor systems cause the

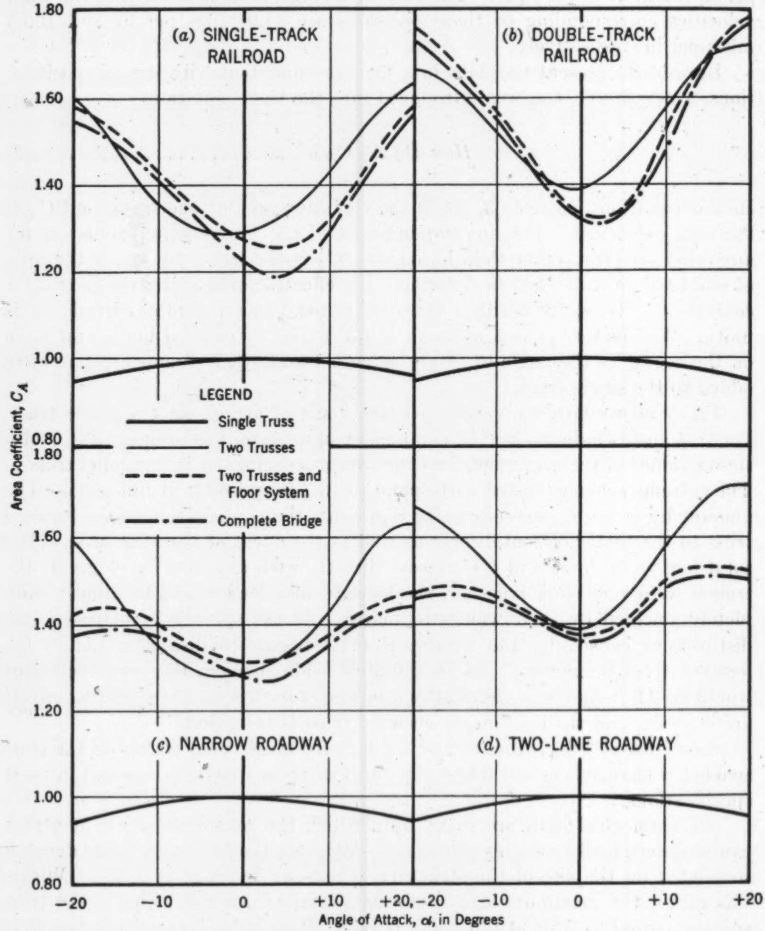

FIG. 8.—THE VARIATION IN AREA COEFFICIENT PRODUCED BY SUCCESSIVE ADDITION OF COMPONENTS, FOR FOUR FLOOR TYPES

wind load to increase slightly whereas the highway floors cause it to decrease considerably. This surprising lack of drag on the floor may be explained by the fact that the region shielded by the windward chord has a vertical dimension greater than the depth of the chord itself and may even contain the entire leading edge of the floor system. The only horizontal force on the floor is therefore the friction drag on its top and bottom surfaces. The floor system almost entirely shields the leeward chord and a reduction in drag results therefrom. If this reduction exceeds the friction drag on the floor, the net effect of adding the floor system is a decrease in the total horizontal wind force.

The situation described above varies with the angle of attack. As would be expected, the addition of the floor generally tends to increase the total horizontal load when the wind direction is down on the bridge (negative α) and to decrease the load when the wind has an upward component, as illustrated by Fig. 8. The relative position of the floor with respect to the chord is also important. As indicated by later tests, the wind load is greater if the floor position is above or below that in the prototype.

When the top lateral system is added to form the complete bridge, the total horizontal force is invariably decreased as indicated in Fig. 8. The decrease is very slight for the wide bridges, and somewhat larger for the narrow bridges.

Within the probable range of angle of attack (±15°) the maximum values of C_A for the four complete bridge types are as follows:

Bridge type	C_A
Double-track railroad	1.69
Single-track railroad	1.47
Two-lane highway	1.52
Narrow highway	1.42

EFFECT OF FLOOR POSITION

The next investigation involved the effect of the position of the floor system with respect to the trusses. In Fig. 9 the area coefficient of the wider bridge is plotted with four floor positions other than the "normal" position or that in

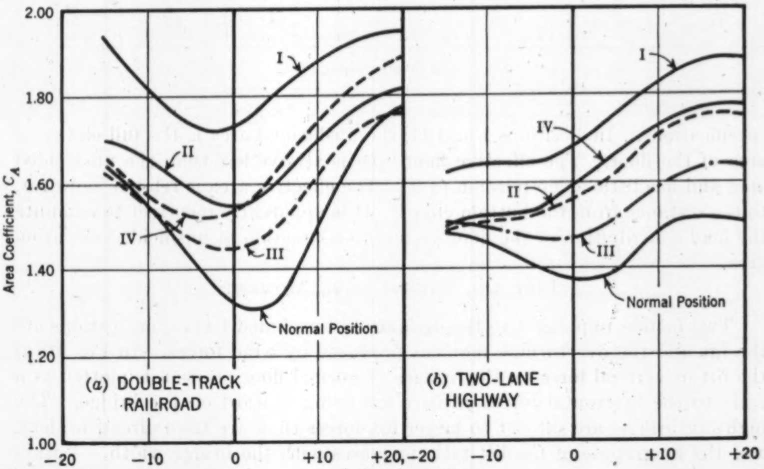

FIG. 9.—EFFECT OF FLOOR POSITION ON AREA COEFFICIENT

the prototype. In the normal position, the bottom of the floor beam was level with the bottom of the truss chord. Floor positions above and below the normal position were used and are indicated by Roman numerals according to the following key:

Position number	Vertical distance from normal, in inches
I	−3.5
II	−2.0
III	0.9
IV	2.5

Fig. 2 illustrates the normal position and Position IV.

In Table 1 are the changes in the area coefficients (ΔC_A) caused by the floor for each position tested, at an angle of attack corresponding to the maximum horizontal force. Also tabulated are the effective elevation areas of the floor ($\Delta C_A \times 203.1$ sq in.). These areas are compared with the unshielded area of the floor as seen in the side elevation, which is a factor considered in most specifications. In Positions I and II, the unshielded area is the full elevation area of the floor. The effective floor area is always less than the unshielded area and has little or no relation to it. The effective area is related, however, to the distance from the bottom chord. It is apparently incorrect to compute the load contribution of the floor system as a function of unshielded elevation area.

TABLE 1.—Comparison Between Effective and Unshielded Floor Area for $\alpha = 15°$

Floor position	Double-Track Railroad			Two-Lane Highway		
	ΔC_A, caused by the floor	Effective floor area[a]	Unshielded floor area[a]	ΔC_A, caused by the floor	Effective floor area[a]	Unshielded floor area[a]
I	0.25	51	82.5	0.19	39	91.6
II	0.09	18	82.5	0.07	14	91.6
Normal	0.01	2	30.8	−0.16	−33	38.7
III	0.04	8	71.8	−0.04	−8	79.7
IV	0.15	30	71.8	0.08	16	79.7

[a] In square inches.

Lift and Overturning Moment

Two factors important to the designer but excluded from specifications are the lift and the overturning moment produced by wind forces. In Fig. 10(*a*) the lift or vertical force on the bridges at normal floor position is plotted as a ratio to the horizontal force, positive lift being upward on the bridge. The highway bridges are subject to larger lift forces than are the railroad bridges, and the magnitude of the lift ratio increases with the bridge width. Within the probable range of α, the maximum vertical force on the two-lane highway bridge is six tenths of the horizontal force.

Plotted in Fig. 10(*b*) are curves of the effective overturning-moment arm expressed as a ratio of the truss depth. The moment is computed about the leeward bottom chord and the effective arm is defined as that moment divided by H. This moment arm is thus comparable to that normally used in design when lift is neglected. Except for that of the two-lane highway bridge, the moment arm is not far from the truss centroid. For the two-lane highway bridge, the maximum effective moment arm (at $\alpha = +15°$) is 0.72 of the truss depth. This value indicates that the maximum overturning moment is 50%

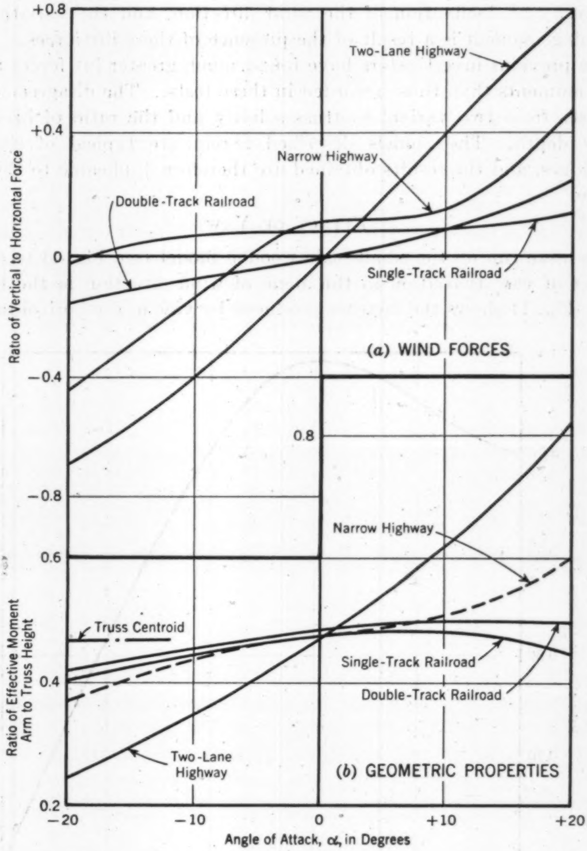

FIG. 10.—LIFT AND OVERTURNING-MOMENT ARM, AS RELATED TO α

greater than that normally used in design. Wider bridges would have greater values of lift and overturning moment.

When the wind is horizontal ($\alpha = 0$), the lift forces are not appreciable, and the overturning moment may be considered equal to that caused by the horizontal load applied at the truss centroid. The larger lift forces are caused primarily by an inclination of the wind direction, and the variation in the overturning moment is a result of the presence of these lift forces.

Some previous investigators have found much greater lift forces and overturning moments than those recorded in these tests. The disagreement probably arises from two variables—truss solidity and the ratio of bridge width to truss depth. The models described herein are typical of simple-span truss bridges, and the results obtained are therefore applicable to this type of structure.

Effect of Yaw

Tests were run on the small-scale wooden model (see Fig. 1) to determine the effect of yaw (variation in the angle of wind direction in the horizontal plane). Fig. 11 shows the increase produced by yaw in the horizontal force at zero angle of attack. The angle of yaw is expressed as ψ. The maximum increase is 9% and occurs at $\psi = 20°$. This increase is somewhat less for angles of attack other than zero.

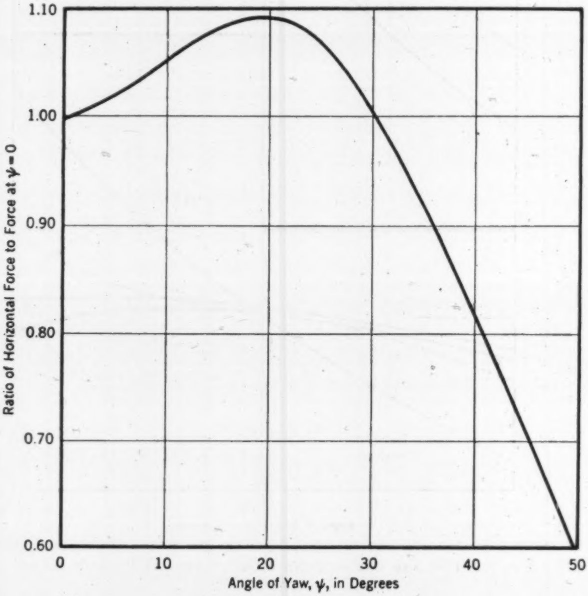

Fig. 11.—Effect of Yaw on the Ratio of the Horizontal Force to the Force at $\psi = 0$

FORCES ON A LOADED STRUCTURE

In order to determine the effect that a train produces on the horizontal force, scale-model box cars were placed on one track of the model. The resulting increase corresponded to a force of 238 lb per ft on the prototype at a wind velocity of 85 miles per hr, which corresponds to 30 lb per sq ft on a single truss. The design value usually specified is 300 lb per ft.

COMPARISON WITH SPECIFICATIONS

Based on the results described, the total horizontal force may be expressed as

$$H' = C_D \, C_\psi \, C_A \, A_T \, \rho \, \frac{v^2}{2} \ldots\ldots\ldots\ldots\ldots\ldots\ldots (3)$$

in which $C_D = 1.63$, $C_\psi =$ the yaw coefficient $= 1.05$, and $\rho \, \frac{v^2}{2} = 0.00256 \, v^2$ (v in miles per hr). Thus, $H' = 0.00438 \, C_A \, A_T \, v^2$ lb per sq ft.

This formula (with $v = 109.5$ miles per hr) is compared with present specifications at 50 lb per sq ft in Table 2. The loads computed are for the brass model. The wind velocity selected is that which produces 50 lb per sq ft on a single truss. Specifications do not indicate the wind velocity intended. The coefficient C_A is taken as the maximum value in the probable range of $\alpha(\pm 15°)$. The total horizontal load given by the specifications compares favorably with the experimental results and is always conservative. However, the method by which the loads are to be computed under these specifications is questionable.

TABLE 2.—COMPARISON OF HORIZONTAL WIND FORCES

Bridge type and floor position	EXPERIMENTALLY DETERMINED FORCE			FORCE INDICATED IN SPECIFICATIONS[a]		
	Trusses	Net effect of floor[b]	Total	Trusses	Net effect of floor	Total[b]
Normal floor position						
Double-track railroad...	125	1	126	141	−7	134
Single-track railroad...	107	3	110	141	−7	134
Two-lane highway......	125	−12	113	106	20	126
Narrow highway......	115	−9	106	106	20	126
Floor position IV:						
Double-track railroad...	125	11	136	141	21	162
Two-lane highway......	125	6	131	106	42	148

[a] Those of the American Association of State Highway Officials and of the American Railway Engineering Association. [b] In pounds.

The American Association of State Highway Officials (AASHO) specifies 50 lb per sq ft on 1.5 times the projected elevation area, including the trusses and floor system.[3] By this method, the load on the leeward truss is underestimated for customary truss spacings (see Fig. 7). In effect, the load on the floor is computed as the pressure multiplied by 1.5 times the unshielded floor area—a decidedly unrealistic procedure, as indicated in Table 1.

---

[3] "Standard Specifications for Highway Bridges," A.A.S.H.O., 1953.

The American Railway Engineering Association (AREA) specifies 50 lb per sq ft on the total projected elevation area plus the area of the leeward truss not shielded by the floor when seen in elevation.[3] With respect to the trusses, this procedure is conservative because the shielding of the leeward truss by its windward mate is entirely neglected. The effective area of the floor implied by this specification is the unshielded floor area minus the shielded part of the leeward truss. With this method, the effect of the floor agrees fairly closely with the experimental results.

The tests described in this paper include too few bridge types to warrant specific recommendations regarding design specifications for wind loads. It is nonetheless apparent that specifications could be improved by consideration of the effect of truss spacing. Further research is required to develop a more realistic approach to the determination of the contribution made by the floor system to the total wind resistance.

CONCLUSIONS

The following conclusions apply only to simple-span truss bridges with proportions similar to those of the model tested:

1. Wind pressures of 30 lb per sq ft and 50 lb per sq ft on a single truss completely separate from other parts of the structure correspond to wind velocities of approximately 85 miles per hr and 110 miles per hr, respectively.
2. The spacing of trusses has considerable effect on wind resistance. This fact is ignored by specifications (1953). As the spacing increases from 13.3 ft to 60 ft, the load on the leeward truss varies from 40% to 77% of that on the windward truss (see Fig. 7).
3. The effect of the floor system on the total horizontal load is generally small and bears little relation to the unshielded elevation area—a quantity considered by most specifications. The effect thus produced increases with the vertical distance from the floor to the truss chord.
4. Lift and the resulting overturning moment are small on railroad bridges but may be of considerable importance on wide highway spans. On the relatively narrow, two-lane bridge, the overturning moment is 50% greater than that normally used in design.
5. Accuracy in wind-tunnel tests does not require construction of large-scale bridge models showing minute details of fabrication.

ACKNOWLEDGMENTS

The tests described in this paper are a by-product of research done for the Corps of Engineers, United States Department of the Army, and were conducted in the Wright Brothers Wind Tunnel at the Massachusetts Institute of Technology, at Cambridge, under the supervision of John M. Cord and Warren B. Delano, Junior Members, ASCE, of the Department of Civil and Sanitary Engineering.

---

[3] "Specifications for Steel Railway Bridges," A.R.E.A., 1953.

DISCUSSION

F. B. Farquharson,[4] M. ASCE.—It is encouraging to learn of new data, such as the author's, regarding the wind forces to be expected on typical modern bridge sections. However, the writer urges further investigation of the effect of the Reynolds number on structures in which the shapes presented to the wind are of a blunt form.

The writer has searched the literature and finds meager test information (as of 1953) on the effect of the Reynolds number (**R**) on flat plates presented normal to the wind. Apparently, the only test data in this field of investigation are those published in 1925[5,6] by O. Flachsbart. He reported that the drag coefficient, C_D, was equal to 1.96 at **R** equal to 6,000 and remained constant at this value as **R** was decreased to 4,000. After **R** was decreased to below 3,000, C_D showed a marked decrease. At $\mathbf{R} = 1{,}600$, C_D reached a value of 1.67. By further reducing **R**, C_D was reported to have increased. These data are plotted in Fig. 12, in which $\mathbf{R} = V\,L$—the symbol V representing wind velocity (in feet per second) and L, the depth of the flat plate (in feet). The solid part of the curve for the flat plate represents the range of values studied by Mr. Flachsbart.

In investigating vortex frequencies in the wake of wings, M. Z. Krzywoblocki has stated that many investigators believe that, in the case of bodies having sharp edges, the vortex systems are geometrically similar throughout the entire range of the Reynolds number—excepting only the extremely low values.[7] This belief is equivalent to an assumption that the drag coefficient (C_D) for such sharp-edged bodies is constant relative to all Reynolds numbers above a low value. The investigations of Messrs. Flachsbart and Krzywoblocki are based on the classical theory of Theodor von Kármán,[8,9,10] Hon. M. ASCE, in which the mechanism of fluid resistance was explained through the study of the vortex pattern in the wake of the body. Subsequent tests[11] on circular cylinders revealed two critical regions on the curve relating the drag coefficient to the logarithm of the Reynolds number.

In Fig. 12, C_D for a circular cylinder is plotted against log **R**; a definite drop occurs in the curve in the vicinity of $\mathbf{R} \approx 1{,}800$, and the curve falls sharply where $\mathbf{R} \approx 200{,}000$.

A few years after these tests were made, it was demonstrated[12] that the Strouhal number, $S = f\,d/V$, is constant for a circular cylinder throughout a range of Reynolds numbers of approximately 1,000 to 50,000, but it increases sharply as C_D decreases at $\mathsf{R} \approx 100{,}000$. This information is also plotted in Fig. 12. In the Strouhal number, f represents the vortex frequency, and d, the diameter of the cylinder. Clearly, these critical values of the Reynolds number for a circular cylinder correspond to a drop in C_D, accompanied by a rise of the vortex frequency in the wake.

---

[4] Director, Eng. Experiment Station, Univ. of Washington, Seattle, Wash.

[5] *Zeitschrift für angewandte Mathematick und Mechanik*, Vol. 15, 1925, pp. 32–37.

[6] "Modern Developments in Fluid Mechanics," edited by S. Goldstein, Oxford University Press, Oxford, England, 1938, Vol. 2, p. 423.

[7] "Investigation of the Wing-Wake Frequency with Application of the Strouhal Number," by M. Z. Krzywoblocki, *Journal of the Aeronautical Sciences*, January, 1945, p. 31.

[8] *Göttingen Nachrichten*, 1911, p. 509.

[9] *Ibid.*, 1912, p. 547.

[10] "On the Mechanism of Fluid Resistance," by Theodor von Kármán and H. L. Rubach, *Physikalishe Zeitschrift*, Vol. 2, p. 49.

[11] *Reports and Memoranda (British) No. 102*, Aeronautic Research Committee, by E. F. Relf, 1914.

[12] *Reports and Memoranda (British) No. 917*, Aeronautic Research Committee, by E. F. Relf and L. F. Simmons, 1924.

E. F. Relf and other experimenters in this field have not revealed evidence regarding the excitation of regularly shed vortices for a circular cylinder beyond Reynolds numbers of approximately 100,000.

However, W. W. Pagon,[13] M. ASCE, while observing a smoke pattern around a pair of steel stacks (each 11 ft in diameter, in a wind of 53 miles per hr), found a distinct periodic vortex pattern at $\mathsf{R} = 5{,}500{,}000$, in which the vortex frequency had not increased as in Fig. 12 but corresponded to a Strouhal number of 0.188.

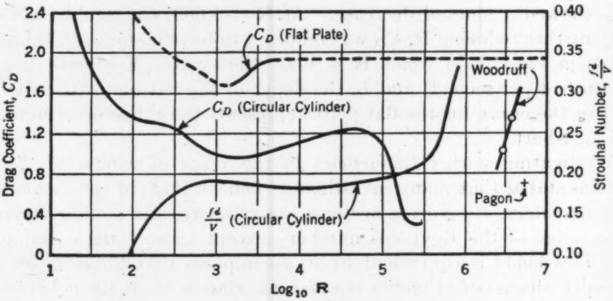

FIG. 12.—VARIATIONS IN C_D AND f WITH RESPECT TO THE REYNOLDS NUMBER

Glenn B. Woodruff,[14] M. ASCE, has recently observed a well-developed vortex pattern behind a stack of 11.4-ft diameter at two different wind velocities. At $V = 37$ ft per sec and $S = 0.225$, $\mathsf{R} = 2{,}670{,}000$; and at $V = 51$ ft per sec and $\mathsf{R} = 3{,}750{,}000$, $S = 0.267$. The data of Messrs. Pagon and Woodruff are plotted in Fig. 12 and are definitely outside the region reported by Mr. Relf and L. F. Simmons.

The reported information that produced the C_D-curve for a circular cylinder in Fig. 12 clearly indicates a critical region at a small Reynolds number and another, more distinct drop in C_D corresponding to a greater Reynolds number. The wind data contributed by Messrs. Pagon and Woodruff suggest that the maximum critical region may be higher than $\mathsf{R} = 2{,}500{,}000$. The meager data available for values of C_D for wind acting on a flat plate show a decrease at $\mathsf{R} \approx 1{,}800$, corresponding to the decrease in the C_D-curve for a circular cylinder. It is emphasized that the dashed projection of this curve to higher values of R is pure conjecture.

---

[13] "Aerodynamics and the Civil Engineer," by W. W. Pagon, *Engineering News-Record*, July 12, 1934.

[14] "Aerodynamic Stability of Suspension Bridges," by F. B. Farquharson, *Bulletin No. 116*, Pt. III, Eng. Experiment Station, Univ. of Washington, Seattle, Wash., June, 1952, p. 102.

Apparently the author's experiments were conducted at Reynolds numbers between 30,000 and 80,000, depending on wind velocities and the depth of the principal vortex producing surfaces normal to the wind. Thus, these tests are above the lower critical regions shown in Fig. 12 for a flat plate, but they are below the upper critical value of C_D for a circular cylinder. The definite similarity between the known part of the flat-plate curve and the corresponding part of the curve for the circular cylinder leaves the unexplored upper end of the flat-plate curve in an unsatisfactory state. More test data on the drag coefficients for flat surfaces at high Reynolds numbers—if the data substantiate the statement of Mr. Krzywoblocki concerning similarity of the vortex systems—would give one full confidence in the test data obtained at lower values of the Reynolds number.

In some regions of the earth it may be reasonable to design for wind velocities as high as 100 miles per hr (somewhat exceeding those considered in the author's tests), and one might anticipate some truss members having depths between 3 ft and 4 ft. In modern girder bridges, the depths might exceed 15 ft. For a wind having a velocity of 100 miles per hr, acting on a member 3 ft deep, $\mathsf{R} = 6{,}380 \times 146.5 \times 3 = 2{,}800{,}000$, and, if the velocity is 100 miles per hr and the depth 15 ft, $\mathsf{R} = 14{,}000{,}000$. Such values of R so far exceed any available test data or observation that it would seem desirable to obtain data on C_D for sharp-edged sections with R-values at least as great as 10,000,000.

Such a series of tests would have presented a formidable problem several years ago, but in the present era (1953) of large, high-speed wind tunnels, with balance systems designed for supersonic loads, the problem is comparatively simple. For example, a steel beam, 30 in. deep and weighing 121 lb per ft, tested at velocities between 50 miles per hr and 450 miles per hr, would yield the values of R shown in Table 3.

TABLE 3.—REYNOLDS NUMBER AND DRAG ON AN I-SECTION, 5 FT LONG AND 30 IN. DEEP, AT VARIOUS VELOCITIES[a]

v, in miles per hr	V, in ft per sec	R (dimensionless)	Drag,[b] in lb
50	73	1,164,000	126
100	147	2,340,000	512
200	293	4,670,000	2,034
300	440	7,020,000	4,570
400	587	9,360,000	8,150
450	660	10,500,000	10,320

[a] In this table $\mathsf{R} = 6{,}380\ V L$; $L = 2.5$ ft; thus, $\mathsf{R} = 15{,}950\ V$. [b] Drag, $H = C_D V^2 A \frac{\rho}{2}$, in which $C_D = 1.6$, and $\rho = 0.00237$ lb ft^{-4} sec^2.

The fourth column in Table 3 indicates the approximate load that the balance system would have to sustain for a beam 5 ft long in order to develop the Reynolds numbers listed in the third column. A test specimen as short as the one proposed here would require appropriate end plates to eliminate end losses.

The general question of the reliability of model tests was of great concern in the studies leading to the design of the new Tacoma Narrows Bridge (Tacoma, Wash.). A series of static tests were conducted using the largest model that could be mounted in the available wind tunnel. However, the capacity of the balance system limited the maximum velocity to 153 miles per hr, corresponding to a Reynolds number of 59,700 computed on the basis of the depth of the top chord of the truss.[15]

Before the collapse of the Tacoma Narrows Bridge, static wind-tunnel tests of a model of this bridge having an aspect ratio of 3.91 showed that the lift curve sloped negatively between attack angles of $-4°$ and $+3°$, but that the addition of end plates produced a positive slope. For a model having an aspect ratio of 9.27, the slope was positive. Further tests involving four different ratios of girder depth to width of bridge (d/b), and an aspect ratio of 4.91, showed that the slope of the lift curve changed from positive to negative at values of d/b slightly greater than 0.20 and remained so as d/b increased to 0.33, the limit of the tests.

These sections cannot be compared directly with truss-stiffened bridges; however, in Fig. 10(*a*), the curve for the narrow highway bridge shows a zero slope between α-values of 0° and 7°, and the curve for the wider highway bridge shows a 45° positive slope in this region. Possibly an increase in the small aspect ratio (2.8) might have had a great effect on the slope of both these curves.

JOHN M. BIGGS.[16]—Mr. Farquharson has raised a pertinent question regarding the validity of small-scale wind tunnel tests when applied to wind loads on actual structures.

The tests described in the paper were conducted at Reynolds numbers of between 18,000 and 70,000, using the average width of the truss members normal to the wind direction as the representative dimension. No variation of the drag coefficient within this range was detected. A wind velocity of 100 miles per hr on the prototype would correspond to a Reynolds number of 2,800,000. Of course, the results presented are applicable only if the drag coefficient is constant within the range of R which includes both model and prototype.

Theory indicates that sharp-edged elements such as flat plates or structural members have a constant C_D-value throughout this entire range of R. Mr. Farquharson states that test data which would verify this conclusion for flat plates are meager. This condition is true for rectangular plates; for sharp-edged circular disks, however, considerable information is available. These data verify the theoretical conclusion because the drag coefficient was found to be constant for values of R ranging from 5,000 to 4,440,000—the latter being the maximum test value attained.[17] This upper limit would include nearly all truss bridges.

The curve relating C_D and R for circular disks is almost identical in shape to that for a rectangular plate in the critical range of R-values less than approximately 5,000 (Fig. 12). It is more than probable that the two curves would be similar throughout and that the drag coefficient corresponding to **R**-values exceeding this critical range would be constant.

---

[15] "Aerodynamic Stability of Suspension Bridges," by F. B. Farquharson, *Bulletin No. 116*, Pt. IV, Eng. Experiment Station, Univ. of Washington, Seattle, Wash., April, 1954.

[16] Asst. Prof. of Structural Eng., Massachusetts Inst. of Technology, Cambridge, Mass.

[17] "Resistance of a Fifteen-Centimeter Disk," *Technical Note No. 252*, by James M. Shoemaker, National Advisory Committee for Aeronautics, Washington, D. C., 1926.

The major drag-producing components in a truss bridge are the truss members. It is logical to assume that the effect of the Reynolds number on these sharp-edged elements would be the same as that on flat plates rather than being similar to the effect on the circular cylinder cited by Mr. Farquharson. Therefore, it may be concluded that test data on model trusses may be applied to full-scale structures. Information from the suggested test program on actual structural elements would be desirable, however, as further verification of this conclusion.

In the paper, the writer concluded that it was apparently unnecessary to construct models that included minute details of fabrication. This conclusion was reaffirmed by a series of tests[18] conducted by Abraham Perera in the wind tunnel of the Massachusetts Institute of Technology.

Mr. Perera constructed and tested truss models cut from plywood of various thicknesses. These models represented only a single truss and were identical in elevation to the brass truss shown in Fig. 2. The elevation area on which the drag coefficient is based was the same for both the plywood and brass models, but the members of the plywood models were of solid, rectangular cross section and contained no structural details whatsoever. The results obtained were as follows:

Truss-model material	Member thicknesses, in inches	Drag coefficient, $\alpha = 0$
Brass	$\frac{5}{8}$	1.63
Plywood	$\frac{3}{8}$	1.65
Plywood	$\frac{1}{2}$	1.60
Plywood	$\frac{5}{8}$	1.63
Plywood	$\frac{3}{4}$	1.50
Plywood	1	1.45

These results indicate that accurate drag coefficients for a single truss can be obtained by using models which have no structural details and which simulate only the outlines of the truss members. The thickness of all the members of the brass truss was $\frac{5}{8}$ in., this dimension being consistent with the scale of the model. Plywood models of this thickness or less gave good results, but the use of larger thicknesses produced somewhat smaller coefficients. The conclusion implied is that the thickness of the model should be approximately to scale; the results, however, are not particularly sensitive to changes in this dimension.

The total load on the entire structure is given by the equation:

$$H = (C_A\, A_T)\, C_D\, \rho\, \frac{V^2}{2}.$$

---

[18] "Wind Tunnel Testing of Simplified Bridge Truss Models," by Abraham Perera, thesis presented, in January, 1954, to the Massachusetts Institute of Technology at Cambridge, Mass., in partial fulfilment of the requirements for the degree of Bachelor of Science.

The coefficient C_A for which curves have been given (Figs. 7, 8, and 9) is not appreciably affected by the type of truss. The nature of the truss as reflected in the coefficient C_D is the predominate influence on the total load. These tests on simple plywood models indicate that C_D for a particular truss type may be determined simply and inexpensively. By this procedure, the difficulties in the experimental determination of wind loads on a complete bridge may be greatly reduced.

AMERICAN SOCIETY OF CIVIL ENGINEERS
Founded November 5, 1852
TRANSACTIONS

Paper No. 2703

MASS-CONCRETE OPERATIONS IN THE ROCKY MOUNTAINS

BY GEORGE P. MCINDOE[1]

SYNOPSIS

Mass-concrete operations are conducted in a plant that is equipped with a primary crusher arrangement, an aggregate screening plant, a concrete batching plant, and a shuttle and cableway system. The particular plant under consideration is situated high in the Rocky Mountains adjacent to Boulder Creek Canyon at El. 7300, approximately 30 miles from Denver, Colo. The over-all arrangement was selected and designed with the primary objective being the establishment of an efficient and economical cableway operation. Considerable difficulties arose in locating the plant and its equipment and access roads because of the hazardous mountain slopes and high wind velocities that were encountered.

INTRODUCTION

On June 1, 1951, the contract was let to construct Reservoir Dam No. 22, a gravity-arch dam, located on South Boulder Creek in Colorado, for the Denver (Colo.) Municipal Water Department. The dam, when completed, will be 340 ft high, 1,000 ft long at its crest, and will contain 588,800 cu yd of mass concrete.

To state that the concrete-making operations at Reservior Dam No. 22 were "quite unusual" is a generous understatement. Following the completion of the design, various engineers and contractors described the location of the plant as "atop an ice-cream cone." The first question inevitably would be, "Why should these modern aggregate processing and batching facilities be situated on such a hazardous terrain?" The answer is that the location of the plant was based primarily on the location and operation of the cableway. The cableway was designed so that it required a minimum amount of excavation for its location. It also had to provide sufficient coverage of the dam. Once the position of the cableway was established from maps of the area, it

---

NOTE.—Published, essentially as printed here, in September, 1953, as *Proceedings-Separate No. 268*. Positions and titles given are those in effect when the paper was received for publication.

[1] Asst. Project Supt., Macco Corp., Paramount, Calif.

was decided that the remaining plant should be placed adjacent to the cableway traveling tail tower—a hazardous undertaking. Nevertheless, this location was the most practical, as is evident on consideration of the following operational points:

1. It proved economical to condense the primary crusher, aggregate screening plant, mixing plant, and cableway traveling tail tower into one area from the standpoint of operating labor and supervision.
2. Sufficient processed-aggregate storage piles could be placed in the area so that mass concrete could be poured continuously on a three-shift basis, taking into account a normal number of breakdowns in the screening plant.
3. Adequate raw-aggregate storage could be provided as a surge of supply for the screening plant, as slippery roads and difficult grades made hauling of raw aggregates an unreliable operation.
4. The site was best adapted for procuring raw aggregates from the various sources in the general area.

Raw Aggregate Materials

Investigations of many test-pit holes and quantity surveys along South Boulder Creek indicated that large amounts of natural river-run aggregates were available. Analyses of numerous pit samples indicated that the material was suitable for concrete aggregate. However, the results of these tests also showed that many problems would arise in processing aggregates that would meet the specifications required for this mass-concrete operation. Some test-pit holes showed that the material would probably fail to pass the Los Angeles (Calif.) Rattler Test Specification (10% at 100 revolutions). Test samples that showed traces of organic materials, mica particles, and clay pockets were found.

Screen analyses of the samples from the various test pits showed that there might be a deficiency in cobbles, minus 6 in. plus 3 in. (stone greater than 6 in. in diameter and less than 3 in. in diameter), and in certain sizes of sands. Inasmuch as it was most difficult to analyze the over-all gradation of the pit-run aggregates, it was decided to remedy the probable deficiencies by augmenting all natural aggregates with a suitable crushed-rock product. The specifications allowed for the substitution of crushed rock for concrete aggregate in any given amount.

Plant Capacity and Storage Requirements

As a result of the relatively short pouring season, the high altitude, the snow, the rain, and the imminent contract-completion date, it was decided that suitable aggregate storage should be provided to supply the concrete-batching operations with sufficient capacity to pour on a 6-day, 3-shift basis at a pouring rate of 1,800 cu yd of mass concrete per day. In order to maintain this schedule it was necessary to obtain an area in which 64,000 tons of processed material could be stored, of which 21,300 tons would be "live" storage. A raw storage of 18,000 tons was considered to be sufficient.

For this operation, a rate of 400 tons per hr (on an 8-hr day and 6-day week schedule) was considered adequate for the excavating, hauling, crushing, and screening plant.

Plant Site.—The exact location of the original plant site was determined by a study of the area with regard to the advisability of placing the plant adjacent to the right abutment (south side of the canyon), as shown in Fig. 1. It was immediately evident that the contractors would have to provide access roads to both sides of the canyon, primarily for the purpose of removing rock excavation from the right and left abutments of the dam. These access roads could also be used to locate and construct a suitable cableway. After many preliminary studies and surveys, it was found that these access roads could be constructed at a nominal cost. The more difficult problem, however, was the location of the plant site. Contour maps and other survey data were limited, the area was heavily timbered, and there were hazardous 300-ft precipices dropping sheerly to the river bottom. After making more extensive surveys, it was decided that the plant site should be situated adjacent to the right southern abutment (looking downstream). Because the traveling tail tower of the cableway was also to be located on this side of the canyon, and the space available for working area was greatly limited, the plant arrangement was necessarily compact; in several instances it was of unique design. Although large quantities of excavation were required to place all of the plant in such a

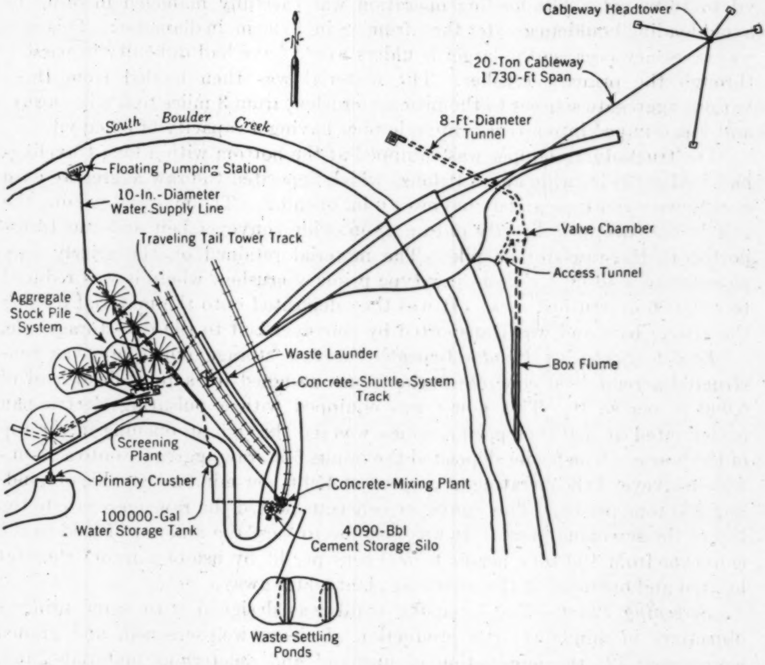
Cableway Headtower
20-Ton Cableway
1 730-Ft Span
8-Ft-Diameter
Tunnel
South Boulder Creek
Floating Pumping Station
10-In.-Diameter
Water Supply Line
Traveling Tail Tower Track
Valve Chamber
Access Tunnel
Aggregate
Stock Pile
System
Waste Launder
Box Flume
Concrete-Shuttle-System
Track
Screening
Plant
Primary Crusher
Concrete-Mixing Plant
100000-Gal
Water Storage Tank
4090-Bbl
Cement Storage Silo
Waste Settling
Ponds

FIG. 1.—PLOT PLAN OF RESERVOIR DAM NO. 22 ON SOUTH BOULDER CREEK IN COLORADO

mountainous and limited area (6 acres), the over-all design proved to be both practical and economical.

RAW MATERIALS OPERATION

Primary Crusher.—The pit-run materials were excavated from the river bottom by use of diesel-powered shovels equipped with 2½-cu-yd-capacity buckets and deposited into end-dump trucks having capacities of from 12 cu yd to 16 cu yd. The loading operation was carefully managed in order to avoid loading boulders greater than from 18 in. to 20 in. in diameter. This care was necessary because the larger boulders would have had difficulty in passing through the primary crusher. The material was then hauled from these various aggregate sources to the primary crusher, from 3 miles to 5 miles away, and was dumped into a truck-dump hopper having a capacity of 30 cu yd.

The truck-dump hopper was equipped at the bottom with a long traveling-pan feeder (36 in. wide and 8 ft long) which deposited the raw aggregate onto a stationary rail-type grizzly having a 6-in. opening. The material passing the grizzly bars dropped directly onto a 48-in.-wide conveyer belt and was transported to the raw-storage pile. The material retained on the grizzly bars passed into a 42-in. by 48-in. jaw-type primary crusher, where it was reduced to minus 6-in. crushed rock. It was then deposited onto the material passing the grizzly bars and was transported by conveyer belt to the raw-storage pile.

Feed to Screening Plant.—Beneath the raw storage pile there was constructed a reinforced concrete feeder house designed for a total dead load of 6,000 lb per sq ft. This house was equipped with a pulsating electric-pan feeder rated at 500 tons per hr, which was fed through an opening in the top of the house. The feeder deposited the minus 6-in. raw aggregate onto a 30-in.-wide conveyer belt operating at a speed of 450 ft per min and capable of handling 550 tons per hr. This conveyer belt transported the raw aggregate to the top of the screening plant. It was possible to vary the amount of feed to the conveyer from 100 tons per hr to 500 tons per hr by use of a feeder rheostat located and operated at the screening plant 200 ft away.

Screening Plant.—The screening plant was designed with three primary objectives in mind: (1) the production of clean, well-screened, and graded aggregates; (2) the elimination of unsound and deleterious materials; and, (3) the construction of a self-cleaning operating plant to minimize operating and clean-up labor.

The screening-plant building consisted of a structural-steel frame 24 ft wide, 60 ft long, and 60 ft high. The first major problem encountered in the design of the screening plant was that of supporting a solid trommel (18 ft long and 8 ft in diameter). The trommel was necessarily located on the fourth floor of the screening plant, approximately 50 ft above the ground. The trommel rotated at a rate of 14 rpm and passed from 400 tons per hr to 500 tons per hr of minus 6-in. aggregate.

The raw material entered the trommel from the 30-in.-wide conveyer belt. Approximately 300 gal of water per min were injected into the mouth of the trommel along with the aggregate. The twofold purpose of the trommel was to break up the unsound particles of aggregate and to clean and scrub the rock by its own abrasive action.

The aggregate leaving the trommel was then deposited onto a 5-ft by 10-ft, heavy-duty, two-deck, scalping and dewatering screen. At this point, four closed, aggregate circuits began:

a. Sand Processing.—The bottom deck of the scalping and dewatering screen was equipped with special wedge-type grizzly bars spaced at intervals of $\frac{3}{16}$ in. Through this 5-ft by 10-ft bottom deck passed all the minus No. 4 sand (sand that would not pass through a No. 4 screen) and the water, which flowed (by way of a launder) directly into a 14-ft-diameter hydroseparator. This hydroseparator was equipped with a slow-speed, four-blade, traveling rake rotating at approximately 5 rpm. The action of the rake kept the sand and water agitated, thus giving the sand ample time to drop from suspension. The hydroseparator was also equipped with a circular 14-in. by 14-in. overflow launder at the top, which carried away all the waste water, organic and floating matter, and particularly the bulk of the minus No. 100 material which remained in suspension in the water. The waste water leaving the top of the hydroseparator then flowed directly to the main waste flume.

The bottom of the hydroseparator was cone shaped and was equipped with an 8-in.-diameter rubber pinch valve, which regulated the passage of sand pulp at any desired water content. The adjustment of this pinch valve was one of the most critical operations of the sand circuit. The capacity of the hydroseparator under normal conditions was from 100 tons per hr to 125 tons per hr.

Because the sand passing through the pinch valve was clean and free from almost all organic and floating materials, it was then passed into a launder and transported onto a single-deck vibrating screen (4 ft by 10 ft); this screen was of the short-throw, pulsating type.

The single deck was equipped with a No. 16 wire-mesh screen cloth. Therefore, the sand was split into two definite gradations with the aid of high-pressure sprays acting directly on the screen. The sand which was retained on the top of the screen was a minus No. 4 plus No. 16 sand product, and under normal operation passed down a chute and onto an 18-in.-wide conveyer belt—thence directly to its respective storage pile. If, however, the natural pit-run sands were to consist of an excess amount of coarse sand, any or all of the material from the top deck of the previously mentioned screen could be by-passed to the sand-manufacturing circuit (rodmill). The sand passing this No. 16 wire cloth had a gradation of minus No. 16 plus No. 100, and flowed directly, by launders, into the sand wheel for final dewatering.

The operation of the sand-dewatering wheel was similar to the action of a slowly revolving wheel set in a settling tank. The wheel was 10 ft in diameter and 6 ft wide. Twelve buckets formed the outside diameter of the wheel. Each bucket was equipped with a set of overflow louvres, so that surface water could be removed by decanting; this first cycle was completed in 3 sec. The second cycle lasted from 15 sec to 20 sec, depending on the speed of the wheel. The water and sand were removed by a vacuum process through filtering brushes in the buckets. Air and water, but not sand, were filtered through full-length, round, and flat brushes at the bottom of the buckets. The backs of the buckets were completely enclosed and connected to an automatic valve which permitted air to be pulled through at the proper point in the cycle. The water drawn through the brushes was collected in a vacuum tank and returned to the main settling tank by a sand pump.

The vacuum was created by a turbine-type air compressor (2,500 cu ft per min to 3,500 cu ft per min) mounted over a vacuum tank. The sand thus was made dry enough at this stage of the vacuum cycle to crumble and fall forward down its chute to the sand-stacking conveyer.

The sand-dewatering wheel was operated at a speed of from ½ rpm to 1¼ rpm depending on the dryness and tonnage required. The speed could be varied immediately, as the unit was equipped with a variable-speed drive. The capacity of this wheel was 75 tons per hr at ¾ rpm for material containing no moisture. At 125 tons per hr the material had a moisture content of from 1½% to 2%. Extreme dryness was reached by processing 50 tons per hr at ½ rpm.

b. Sizing of Aggregates.—The material retained on the lower deck of the dewatering and scalping screen, a minus 6-in. plus No. 4 rock product, was transferred to a battery of four double-deck, vibrating, rock-sizing screens (4 ft by 14 ft). Two of these screens formed a parallel, identical top bank and two composed a parallel, identical lower bank. The material from the dewatering screen was deposited onto the upper bank of the sizing screens by use of a two-way, pants-leg-type chute, each leg being equipped with a control gate so that either or both of the screens of the upper bank could be fed with rock at any time.

Each of the upper two sizing screens was equipped with 3¼-in. opening wire cloth on the top deck and 1⅝-in. opening wire cloth on the bottom deck. The material retained on the top deck was, therefore, a minus 6-in. plus 3-in. rock product. The material passing the top deck, but retained on the bottom deck was a minus 3-in. plus 1½-in. rock product. These aggregates then fell into chutes and were deposited onto their respective stacking conveyers. The material passing the 1⅝-in. opening in the bottom decks of the upper sizing screens was deposited into a collection hopper and was then fed onto the lower bank of sizing screens. Each of the screens was equipped with ⅞-in. opening wire cloth on the top deck and $\frac{3}{16}$-in. opening wire cloth on the bottom deck, and therefore produced a minus 1½-in. plus ¾-in. rock and a minus ¾-in. plus No. 4 rock (pea gravel) on the top and bottom decks, respectively. In a similar manner, these aggregates fell into chutes and were deposited onto their respective stacking conveyers.

The material passing the bottom decks of the lower bank of sizing screens was a minus No. 4 sand and was small in amount. This sand passed into a collection hopper and onto a stationary grizzly where the coarser sand was retained and directed to the sand pump. The material passing the grizzly was fed into the main waste system.

All these screens were equipped with high-pressure jet sprays, which, on the sizing screens, gave the rock a third and final washing. The capacity of the sizing screens was chosen so that ample screening area would always be available. Also, in case of breakdown, the two screens on the left could operate independently of the two screens on the right and vice versa.

c. Crushed Rock Circuit.—The top deck of the dewatering and scalping screen was a plate-type screen. The upper half had 6½-in. openings and the lower half had 6-in. and 5½-in. openings. These openings were arranged to scalp off varying amounts of plus 5-in. rock. This retained material was deposited into a heavy-duty chute and thence into a surge box, from which it was transferred into either of two gyratory-type crushers.

The two gyratory crushers were of distinct types: One— a 4-ft, low-head type equipped with a fine grinding bowl, which produced a fine-graded product, particularly a rodmill-feed product; the other—a 4¼-ft, standard gyratory type, equipped with a course grinding bowl adapted for producing coarse crushed aggregates in large quantities. The product from these crushers was deposited onto a 24-in.-wide conveyer belt, which deposited the material onto a second conveyer belt. The second conveyer belt brought the crushed rock to the top of the screening plant and deposited it onto two 4-ft by 8-ft, double, flat-deck screens (by way of another pants-leg-type chute). The purpose of these screens was threefold:

First, the top deck was equipped with a ⅝-in. mesh wire cloth, and the material retained on this deck was approximately minus 1½-in. plus ¼-in. crushed rock. This material passed directly to the sizing screens and was screened again with the natural river-run aggregates.

Secondly, the material passing the ⅝-in. opening wire cloth and retained on the bottom deck (3/16-in. opening wire cloth) was a minus ½-in. plus ¼-in. product, suitable for a sand manufacturing process. This material was deposited into a two-way chute and could be diverted either to the sizing screens or onto an 18-in.-wide conveyer belt (for rodmill feed).

The third purpose of the flat-deck screens was to reclaim all sand manufactured by the crushers. This minus No. 4 product passed the lower deck of each screen, fell into a collection hopper, flowed into a launder (where water was added), and was deposited into the hydroseparator for washing and sizing (along with the natural sands).

d. Manufactured Sand.—The minus ½-in. plus ¼-in. rodmill-feed product from the 4-ft by 8-ft, flat-dock crushed-rock screens could be by-passed onto the 18-in.-wide conveyer. The rock placed on this conveyer traveled a distance of 25 ft and was then deposited into a 150-ton-capacity storage bin located just outside the screening plant. The material from this bin flowed (by gravity) through two openings at the bottom onto two reciprocating-type feeders equipped with variable-speed drives. These feeders deposited the material into each end of a 6-ft by 12-ft rodmill, where water was added. The amount of feed and water was calibrated so that any desired size of sand could be manufactured. The rodmill rotated at a rate of 15 rpm and was charged with 25 tons of high-carbon-steel grinding rods.

The manufactured sand product passed from the discharge located in the center at the bottom of the rodmill into a surge box, where a sand pump with a capacity of 60 tons per hr pumped the material 35 ft up to the hydroseparator through a 4-in.-diameter pipe line. Here the manufactured sand was blended with the natural sands and washed and sized.

Summary.—The screening-plant structure was 24 ft wide, 60 ft long, and 60 ft high. Through carefully engineered arrangements, design capacities, and equipment supports, it was possible to place in this structure a trommel, a dewatering and scalping screen, two crushed-rock screens, four sizing screens, a sand-scalping screen, a hydroseparator, a sand-dewatering wheel, and the tail sections of six outgoing stacking conveyers. In the same building the six aggregate products were screened.

Stock Piles

It was determined that approximately 21,300 tons of "live" processed-aggregate storage would be required to provide ample surge for the concrete-making operations. Because of the limited working area and the cone-shaped mountain on which the plant site was located, the only feasible solution was a T-shape arrangement of tunnels underneath the stock piles (Fig. 1). The top of the T was oriented toward the mixing plant, and was underneath the screened-aggregate stock piles of minus ¾ in. plus No. 4, minus 3 in. plus 1½ in., and minus 6 in. plus 3 in., respectively. The leg of the T was parallel to the screening plant and underneath the minus No. 16 plus No. 100 sand, the minus No. 4 plus No. 16 sand, and the minus 1½-in. plus ¾-in. screened-rock stock piles. This arrangement was economical for two reasons: First, the 24-in.-wide stacking conveyers (handling minus 6-in. plus 3-in., minus 3-in. plus 1½-in., and minus 1½-in. plus ¾-in. screened rock) were the three shortest conveyers, and the three 18-in.-wide stacking conveyers (handling the fine sand, coarse sand, and pea gravel) were the three longest conveyers. Secondly, locating the minus 6-in. plus 3-in. and minus 3-in. plus 1½-in. rock on the top of the T eliminated the necessity for transferring these large materials more than once, after they were in their respective stock piles. Approximately 600 lin ft of the 18-in.-wide conveyer and 380 ft of the 24-in.-wide conveyer were required to complete the stacking conveyer system; about 700 ft of corrugated multiplate pipe were required for the tunnel arrangement.

The three 18-in.-wide conveyers (handling the two sands and pea gravel) dumped directly onto their stock piles, each pile being 50 ft high. The three 24-in.-wide conveyers (handling the larger screened rock sizes) deposited their loads into shelf-type rock ladders approximately 55 ft high. Each rock ladder was supported on a reinforced concrete housing.

The corrugated multiplate pipe tunnels housed two 30-in.-wide conveyer belts. The conveyer in the leg of the T deposited its load onto the conveyer in the top of the T part of the tunnel. The latter conveyer ran 780 ft to the top of the mixing plant.

Underneath each stock pile were two hand operated gates. These gates acted as valves for the feeding of the rock onto the conveyer belt in the tunnel. Each rock size was conveyed to the mixing plant separately—that is, no blending of aggregates was made on the belts.

At the junction of the two tunnels a reinforced concrete structure 12 ft wide, 15 ft long, and 13 ft high was constructed. The dead load on the top of this junction house was assumed to be 5,000 lb per sq ft since this structure was necessarily located directly beneath the minus 6-in. plus 3-in. stock pile.

The stock pile system contained two piles of sand—one of fine sand (minus No. 16 plus No.100), and the other of coarse sand (minus No. 4 plus No. 16). The essential purpose of these two piles was to regulate the fineness modulus of the processed sand. It is quite probable that the natural pit-run sands contained either too much or too little of the minus No. 4 plus No. 16 size at different times (different excavation locations), but the over-all gradation of the natural sands was within the limits given in the specifications. Therefore, the minus No. 16 plus No. 4 stock pile acted as a surge when coarser sands were being excavated, and the minus No. 16 plus No. 100 stock pile acted similarly when finer sands were encountered.

It has previously been noted that no blending was made on the conveyer belt beneath the sand stock piles. Although this is a common practice in concrete making, it is also an inaccurate and unreliable process. Therefore, it was decided to transport separately the find sand and coarse sand to the mixing plant, where they could be weigh-batched, and consistent results could be obtained.

Cement Storage

Bulk cement was delivered at the Crescent (Colo.) railroad siding, approximately 3½ miles from the mixing-plant site. Here the Denver Water Board had installed a separate railroad siding for unloading bottom-dump cars. The cars were moved, after switching, with an electric car mover. Each car had a capacity of 400 bbl of bulk cement. The cement flowed by gravity from these cars into a screw-type feeder underneath the track. The screw feeder deposited the cement onto an enclosed 18-in.-wide by 60-ft-long conveyer belt, which in turn deposited the cement into a 1,750-bbl-capacity storage bin. All this equipment was designed with the knowledge that frequent high wind velocities would occur and that it would be necessary to provide for a moisture-proof system. The cement was then truck-hauled from the silo to a 4,090-bbl silo adjacent to the mixing plant. Here the cement was deposited into a truck-dump hopper, under which was located another screw feeder. This screw deposited the cement into a bucket elevator, which conveyed it upward and dumped it into a chute connected to the top of the silo. This screw feeder was oriented so that it could be used to convey cement from the bottom of the silo to the bucket elevator. The bucket elevator then dumped the cement into the chute. However, by use of a butterfly valve, the cement was directed to the mixing-plant storage bin, instead of to the silo.

Water Supply System

The water for the aggregate manufacturing, the concrete mixing, and the clean-up operations was supplied by four vertical turbine pumps mounted on a barge placed in a sump which had been blasted in South Boulder Creek Channel. Each pump was powered by a 150-hp, 440-volt motor; it supplied 1,000 gal per min, and operated under a total head of 500 ft. The pumps were automatically controlled by floatless liquid-level controls. Protection against surge was provided by the installation of an hydromatic check valve at each pump.

The four pumps were connected to a 25-ft section of 10-in.-diameter rubber hose by use of a pipe manifold. The hose was connected to a 10-in.-diameter steel pipe line leading to a 100,000-gal storage tank placed above the screening and mixing plant. From the pumps to the storage tank the total lift was 430 ft. The rubber hose provided a flexible connection between the steel pipe anchored on the mountain side and the floating pumping station and gave considerable latitude for variation in the water surface elevation of the river.

Mounting of the pumps on a barge was chosen as the most economical method since it was anticipated that the water storage in Reservoir Dam No. 22 would begin early in the 1953 construction season and that the water surface elevation would rise as the construction of the dam progressed.

In order to provide adequate working pressure for spray nozzles mounted over the vibrating screens, a booster pump was installed in the water service line at the screening plant. The design requirements called for the pump to supply 1,100 gal per min under a differential head of 150 ft.

Mixing Plant

The mixing plant for this project had a storage capacity for 500 cu yd of each of the six aggregate sizes and for 300 bbl of cement. The structure was 95 ft high with the storage bins located at the top. The six aggregate-storage bins surrounded the cement-storage bins located in the center. The aggregates were fed to these bins from the main 30-in.-wide conveyer by means of a swivel-type chute.

The aggregates were fed from their respective bins by gravity into the batching hopper. Each hopper was equipped with a separate scale and was operated automatically, with solenoid valves and air rams, from the main control panel. The materials from the weigh-batching hoppers were deposited into a mixing hopper where water was added. All the materials were then dumped into two 4-yd-capacity, revolving, tilting-type mixers. Each mixer had a capacity of 7 cu yd per hr, giving a total of 14 cu yd per hr for a mixing time of 2½ min.

Some of the salient features of this plant were the air-entrainment equipment, batching facilities, consistency-metering operation, and batch-by-batch recording of cement usage per cubic yard of concrete. All these features were fully automatic (controlled from a main panel by one operator).

When the concrete was satisfactorily mixed, it was dumped into an 8-cu-yd-capacity receiving hopper—first from one mixer and then from the other. The 8 cu yd of concrete were then deposited into an 8-cu-yd-capacity hopper on a flat car. The flat car was moved along a dinky track by a diesel-electric locomotive for a distance of from 200 ft to 700 ft to the cableway setting. Here the concrete was released by an automatic air-dumping device into an awaiting 8-cu-yd-capacity concrete bucket, which was placed on a deck 14 ft below the dinky track—soon to be picked up by the cableway hook.

Cableway

The cableway had a 109-ft-high stationary head tower located on the north, or left, side of the canyon. A movable tail tower 42 ft high was placed on the opposite side of the canyon. The head tower was supported on a concrete foundation and was guyed with two 3-in.-diameter back stay cables and two

2-in.-diameter front stay cables. Each back stay cable was jeweled into a socket which was bolted to two 4-in.-diameter, special steel anchor bolts imbedded in 115 cu yd of concrete. The front stay anchors were similarly connected to 60-cu-yd concrete anchors.

The movable tail tower traveled on 112-lb rail tracks on an arc approximately 550 ft long. The tower carried a concrete counterweight of 210 cu yd and was powered with a 100-hp, 2,200-volt induction motor which had a rated speed of 6 miles per hr.

The cableway span was 1,730 ft with the head tower main gut pin located at El. 7500.0 and the tail tower main gut pin located at El. 7387.0—a difference of 113 ft. All the cableway operations were controlled from the head-tower side.

Five different sizes of cables were required for the actual operation of the cableway: (1) The main gut was a 3-in.-diameter lock-coil-type cable. A 6% main-gut sag was used giving a low point at El. 7332 and a factor of safety greater than 3 for normal loads on the cable; a 40-ft-long carriage, from which the 8-cu-yd-capacity concrete bucket was lowered and elevated, traveled along the main gut. (2) A 1-in. diameter "endless line" 4,000 ft long moved the carriage back and forth. (3) A $\frac{7}{8}$-in.-diameter load line, also 4,000 ft long, lowered and elevated the concrete bucket. (4) A "button line" stretched from head tower to tail tower; this line kept the slack carriers, which received the slack of the load line, spaced. (5) A "messenger line" supported the floodlights for night operations.

The endless and load lines were operated from a two-drum hoist located at the foot of the head tower and powered by a 500-hp, 2,200-volt motor. Both drums had a rated speed of 2,900 ft per min. Using a four-part line, the hoisting speed for the concrete bucket was approximately 750 ft per min.

This cableway operation had a pouring rate of from 100 cu yd per hr to 120 cu yd per hr using a 8-cu-yd-capacity bucket.

CONCLUSION

At the time of completion, Reservoir Dam No. 22 was the highest concrete dam in Colorado. The contractor was faced with many problems in the planning and designing of the concrete-producing plant. The dam stands as evidence of the successful solution of these problems.

ACKNOWLEDGMENTS

The Macco-Puget Sound Construction Company, a joint venture between the Macco Corporation (Paramount, Calif.) and the Puget Sound Bridge and Dredge Company (Seattle, Wash.) were the builders of Reservoir Dam No. 22.

AMERICAN SOCIETY OF CIVIL ENGINEERS
Founded November 5, 1852
TRANSACTIONS

Paper No. 2704

AMPLIFICATION OF STRESS IN FLEXIBLE STEEL ARCHES

BY ROBERT S. ROWE,[1] A. M. ASCE

WITH DISCUSSION BY MESSRS. MILO S. KETCHUM, AND ROBERT S. ROWE

SYNOPSIS

A simplified method which is useful in solving problems pertaining to the amplification of stress in flexible steel arches has been devised. Only fundamental concepts are used; these are extended to include the displacement of the arch axis. The increase, or amplification, of the computed stress at the quarter point of the loaded part of the arch (when the displacements of the axis are included in the analysis) is developed and presented in graphic form.

The amplification chart is useful in showing the entire range of structural action for curved members subjected to axial compression and bending. The chart is divided into (1) the ordinary range, where the usual methods of structural mechanics apply with little error; (2) the flexible range, where the ordinary methods of analysis must be extended to include the effects of displacement; and (3) the dangerous range, where the amplification of stress is so large that there is a possibility of structural collapse.

The chart is valuable because it is a graphical presentation of the range of structural action for a given arch, the magnitude of the amplification when displacements of the axis are included in the analysis, and the modifications that may be made to reduce the amplification.

NOTATION

The letter symbols adopted for use in this paper are defined where they first appear, in the illustrations or in the text, and are arranged alphabetically, for convenience of reference, in Appendix I.

NOTE.—Published, essentially as printed here, in August, 1953, as *Proceedings-Separate No. 245.* Positions and titles given are those in effect when the paper or discussion was received for publication.

[1] Associate Prof. of Civ. Eng., Princeton Univ., Princeton, N. J.

INTRODUCTION

The arch is a structural form which has become increasingly important because of the need for long, unobstructed spans. A typical steel-arch bridge is shown in Fig. 1. This bridge is similar to the Rainbow Bridge at Niagara Falls, N. Y., and has the following properties:

Item	Symbol	Value
Span length	L	950 ft
Rise of arch	h	150 ft
Depth of arch rib	d	12 ft
Moment of inertia	I	12,300 in.^{2} ft^2
Section modulus	Z	24,600 in.^{3}
Area of cross section	A	554 in.^{2}
Radius of gyration	r	4.76 ft
Ratio of span length to rise of arch	L/h	6.3
Modulus of elasticity	E	30×10^6 lb per sq in.

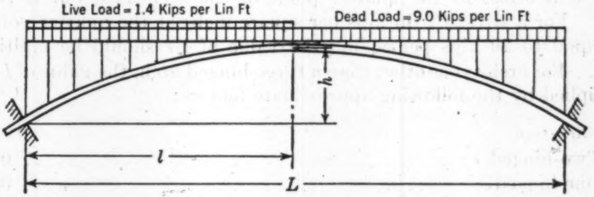
Live Load = 1.4 Kips per Lin Ft
Dead Load = 9.0 Kips per Lin Ft
h
l
L

FIG. 1.—A TYPICAL STEEL-ARCH BRIDGE

Considerable time is expended on the preliminary design and analysis of long-span steel arches because of the lack of a simplified method for performing these operations. It is not permissible to use the ordinary methods of structural mechanics for flexible arches, because the displacements (which are normally neglected) may increase or amplify the stresses which, in turn, further increase the displacements. It should be realized that any refinements which are introduced into an analysis are included for reasons of safety rather than economy.

In order to determine the stresses in an arch, it is first necessary to assume a preliminary design. In general, the effect of variations can only be determined by analyzing several designs. Because of the great amount of time and labor required in this process, elaborate analyses are seldom practical. A device useful in determining the preliminary design is termed an "amplification chart," whereby the structural action (as well as the effects of varying the proportions) can be visualized easily. This amplification chart can be modified for conditions other than those originally specified. Thus, one chart can serve for the various arch types, proportions, and loading, and for various computed stresses. The amplification chart is developed from simple structural concepts. The results obtained by use of the chart are extended, by successive correction, to include the displacement of the arch axis. These results agree closely with the results arrived at by using the formal methods of structural mechanics.

Much literature is available concerning those algebraic methods of analysis which include the effect of displacements of the arch axis (Bibliography, Appendix II). These methods of analysis are not of immediate concern. The details of design, the economics of design, the methods of proportioning arches, the methods of fabrication and erection, and the interaction of deck and rib will not be investigated.

AMPLIFICATION CHART

The amplification chart (Fig. 2) shows in graphic form the percentage of increase, or amplification, of the combined axial compression plus the transverse bending unit stress when the displacements of the axis are included in the analysis. Fig. 2 is based on a combined stress of 20 kips per sq in. at the quarter point of a three-hinged arch which supports a uniformly distributed live load on half of the span. This loading does not produce the maximum bending unit stress at the quarter point of the arch axis, but it is easy to analyze. For a stress f'_t (in kips per square inch) at the quarter point which is not equal to 20 kips per sq in., the value of l/r should be multiplied by $\sqrt{f'_t/20}$. For arch types other than a three-hinged arch, the value of l/r should be multiplied by the following approximate factors:

Arch type	Factor
Two-hinged	0.9
One-hinged	0.8
Hingeless	0.7

The pressure line for an unsymmetrically placed live load plus a symmetrically positioned dead load moves away from the arch axis. The displacements resulting from transverse bending are the moment arms for the dead load and the live load axial forces. Although the displacements are small, the additional bending moments may be large because the live-load plus the dead-load axial forces are large. In flexible members the bending stresses and displacements are increased, or amplified, by the additional bending moment resulting from the product of the large axial forces and the transverse bending displacements. The total combined axial compression and amplified bending stress f_t can be represented by

$$f_t = f_a + f_b \left[\frac{1}{1 - \frac{f_a}{n\,E} \left(\frac{L}{r} \right)^2} \right] \ldots\ldots\ldots\ldots\ldots\ldots (1)$$

in which f_a is the axial stress and f_b represents the bending stress, both before amplification and both resulting from the dead load and the live load. In Eq. 1 the term by which f_b is multiplied is the "amplification factor" which will be subsequently represented by Φ. In the amplification factor, n is a shape factor that depends on the loading and properties of the member. In

Fig. 2 the value of n is 1/10, and E is equal to 30 kips per sq in. The total stress (neglecting the effect of the displacements) can be represented by

$$f'_t = f_a + f_b \qquad (2)$$

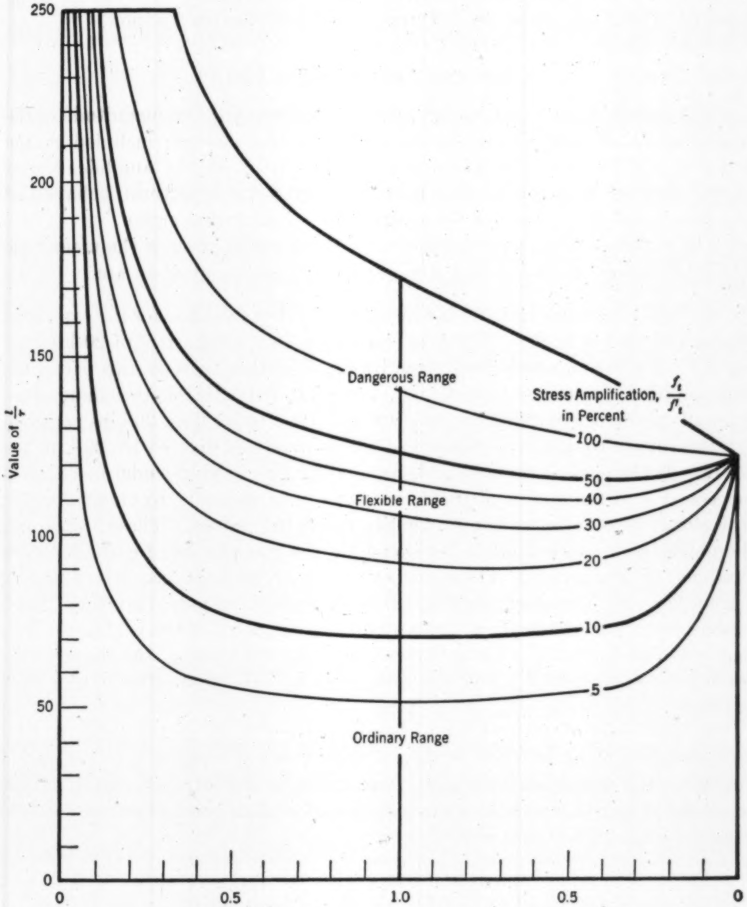

FIG. 2.—AMPLIFICATION CHART

Eq. 1 can be developed for a straight beam and then extended to include curved members and the various arch types. The magnitude of the errors resulting from the simplification in which displacements are considered will be investigated subsequently.

The amplification chart is based on Eq. 1. Fig. 2 shows the amplification of stress f_t/f'_t plotted against the slenderness ratio l/r and the ratio of axial stress and bending stress f_a/f_b or f_b/f_a. By use of both f_a/f_b and f_b/f_a, extremes can be shown conveniently on one chart. In addition to demonstrating the magnitude of the amplification of stress when displacements are included in the analysis, Fig. 2 also shows the arbitrary ranges of structural action.

USE OF THE AMPLIFICATION CHART

The amplification chart can be used (*a*) to determine the magnitude of the amplification of stress when displacements of the axis are included in the analysis, (*b*) to show the influence of modifications on the amplification of stress, and (*c*) to describe, in a general manner, the structural behavior of beam columns and arches for the entire range of structural action.

The ratios are computed as follows for the determination of the magnitude of amplification of the bending stress at the quarter point of an arch:

1. The slenderness ratio l/r is computed and then modified for the computed stress and type of arch. (Fig. 2 is based on a computed stress of 20 kips per sq in.) If the computed stress given by Eq. 2 is other than 20 kips per sq in., the modified slenderness ratio $(l/r)_{\text{mod}}$ needed to enter the chart is determined by multiplying the slenderness ratio for the stress other than 20 kips per sq in. by the square root of the quotient of the other stress divided by 20 kips per sq in. If the arch is three-hinged, no modification in the slenderness ratio is necessary. If the arch is of a different type, it is necessary to modify further the slenderness ratio by the previously tabulated values. These values can be determined approximately by sketching the pressure line for the loads on various types of arches. These coefficients are approximations, determined by "rounding off" computed values. It is important to note that these (l/r)-values pertain to the bending stress at the quarter point of the part of the arch subjected to live load. These values vary with the loading, the shape of the arch axis, the position along the arch axis, and the properties of the cross section.
2. The ratio of axial stress to bending stress, f_a/f_b, or the ratio, f_b/f_a, is computed—whichever is the smaller. These two ratios are all that are needed to enter the amplification chart. Variations in rise of arch, depth of rib, moment of inertia, and cross-sectional area are included when the ratio of axial and bending stress is determined.

Fig. 2 is entered from the abscissa with the ratios of either f_a/f_b or f_b/f_a (whichever is the smaller) and thence vertically up to the value of $(l/r)_{\text{mod}}$. The intersection represents the range of structural action and the magnitude of the amplification of the total stress at the quarter point when displacements of the axis are included in the analysis.

It is also possible to express the ratio of axial stress to bending stress in terms of the properties of the arch and the loading. Thus, a similar chart could be constructed in which the abscissas are expressed in terms of the ratio of the rise of arch to the depth of rib for a given cross section and the ratio of the dead load to live load at the quarter point of the arch for a given radius of gyration.

It may be of interest to note that the amplification of stress is little influenced for smaller values of l/r by variations in the ratio of f_a/f_b and f_b/f_a at either side of the point at which f_a is equal to f_b.

Example.—Consider a steel arch of proportions similar to those shown in Fig. 1. From the proportions of the arch rib and the loadings, the ratios needed to enter the chart are computed:

$$l = \frac{950 \text{ ft}}{2} = 475 \text{ ft} \ldots\ldots\ldots\ldots (3a)$$

and

$$r = \sqrt{\frac{I}{A}} = \sqrt{\frac{12{,}300 \text{ in.}^2 \text{ ft}^2}{554 \text{ in.}^2}} = 4.76 \text{ ft} \ldots\ldots\ldots\ldots (3b)$$

from which

$$\frac{l}{r} = \frac{475 \text{ ft}}{4.76 \text{ ft}} = 100 \ldots\ldots\ldots\ldots (3c)$$

Because Fig. 2 is based on a computed stress of 20 kips per sq in., it is necessary to modify the slenderness ratio for any other computed stress. The computed stress (from Eq. 2) is 19.1 kips per sq in.; therefore, the modified slenderness ratio would be

$$\left(\frac{l}{r}\right)_{\text{mod}} = \frac{l}{r}\sqrt{\frac{19.1}{20.0}} = 100\sqrt{\frac{19.1}{20.0}} = 97.5 \ldots\ldots\ldots\ldots (4)$$

The arch in Fig. 1 is hingeless; thus, the slenderness ratio is further modified by 0.70. The slenderness ratio needed to enter the chart is

$$97.5 \times 0.70 = 0.68 \ldots\ldots\ldots\ldots (5)$$

The ratio of the bending stress to the axial stress is then computed:

$$\frac{f_b}{f_a} = \frac{7.38}{11.72} = 0.63 \ldots\ldots\ldots\ldots (6)$$

The chart shown in Fig. 2 is entered with the ratio of f_b/f_a equal to 0.63—thence, vertically up to the value of l/r equal to 68. The intersection shows the range of structural action and the approximate value of the amplification of the stress when changes in the dimensions of the arch axis are included. The amplification of the stress at the quarter point, interpolated from the chart, is approximately 8%. It is of interest to note that the designers of the Rainbow Bridge computed a stress-amplification value of 7% (1).[2]

INFLUENCE OF MODIFICATIONS ON THE AMPLIFICATION OF STRESS

The amplification of stress in arches subjected to combined axial compression and bending is influenced by the slenderness ratio l/r, the type of arch, the ratio f_a/f_b, and the stress computed from Eq. 2. The amplification of stress can be reduced by decreasing the slenderness ratio. For a given length between inflection points, the amplification of stress decreases for increasing values of the radius of gyration.

---

[2] Numerals in parentheses, thus (1) refer to corresponding items in the Bibliography (Appendix II).

A higher allowable computed stress is permitted for certain types of steel and for wind load. The relative amplification of stress is influenced by variations in the allowable or computed stress (Eq. 2). An increase in the computed stress results in a disproportionate increase in amplification. The amplification chart is useful in showing the influence of changes in the computed stress. For example, consider an arch with a slenderness ratio of 100 and a computed stress, before amplification, of 20 kips per sq in. If the total stress is increased 50% (to 30 kips per sq in.), the slenderness ratio is modified by

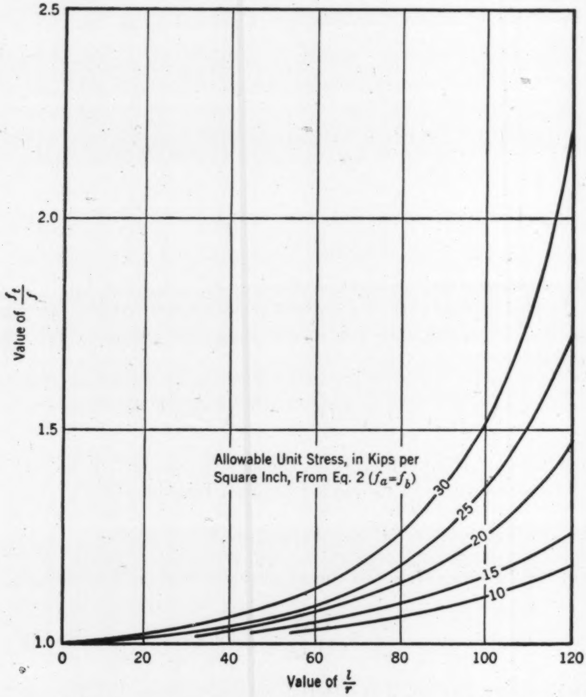

FIG. 3.—THE RELATIONSHIP BETWEEN STRESS AMPLIFICATION AND SLENDERNESS RATIO FOR VARIOUS VALUES OF ALLOWABLE UNIT STRESS

$$\sqrt{\frac{30}{20}} = \sqrt{1.5} = 1.23 \qquad (7)$$

The corresponding amplification is increased from 25% for l/r equal to 100, to 45% for l/r equal to 123—a net increase of 80%.

Fig. 3 shows the amplification of the total stress divided by the allowable stress f_t/f, plotted against the slenderness ratio, l/r, for various allowable unit stresses. This chart is based on the use of a flexible arch rib of silicon steel with a yield-point stress of 45 kips per sq in. For larger values of l/r, the amplification of the total stress becomes disproportionately larger than the corresponding increase in the allowable unit stress, f.

The amplification of stress is only slightly influenced by changes in f_a/f_b for values of l/r less than 80 when this ratio is approximately equal to unity. For a decrease in the relatively small values of f_a/f_b and f_b/f_a, the amplification of stress is decreased. This is true because there is little bending moment to be amplified in the range of all axial stress, and there are small axial forces to cause amplification in the range of all bending stress.

USE OF THE AMPLIFICATION CHART TO DESCRIBE STRUCTURAL ACTION

The amplification chart may be useful in describing the range of the structural action of arches. The chart has been divided into three arbitrary ranges: (a) The ordinary range, (b) the flexible range, and (c) the dangerous range.

The ordinary range shows that the analysis, by customary methods of structural mechanics, gives sufficiently accurate results. In the ordinary range, changes in the dimensions of the arch axis and changes in the displacement of the arch rib have little influence on the amplification of stress; therefore (to that degree) superposition of effects is applicable. In the ordinary range, for a given slenderness ratio of less than 70 and for values of f_a/f_b from 0.5 to 2.0, the amplification of stress remains sensibly constant, irrespective of the loading and proportions of the arch. For decreasing values of f_a/f_b and f_b/f_a less than 0.5, the amplification of stress decreases for constant values of l/r. Fig. 2 has been drawn for a total stress, before amplification, of 20 kips per sq in. If the computed stress is greater than 20 kips per sq in., it is necessary to consider the corresponding disproportionate increase in the amplification. In the ordinary range, elastic buckling is highly improbable except for relatively small values of f_b/f_a—at which values the amplification of displacements is relatively large.

In the flexible range, the ordinary methods of structural mechanics must be modified and extended to include the effects of displacements. Superposition of effects is not applicable, and it is not permissible to separate live load and dead load. The amplification of stress in this range has been arbitrarily limited from 10% to 50%. The area of constant amplification of stress for a given (l/r)-ratio is less pronounced in the flexible range than in the ordinary range. The amplification of stress increases for increasing values of f_a/f_b up to a certain value and then decreases. Variations in loading and in properties of the arch have more influence on the amplification of stress in the flexible range than in the ordinary range. Amplification of stress is more pronounced for small changes in the slenderness ratio. Attention is given to variations in the computed stress because increases in the computed stress result in disproportionate increases in the amplification. Elastic buckling may be possible at the relatively larger values of l/r and for values of f_a/f_b greater than unity.

In the dangerous range, the amplification of stress is greater than 50%. In this range the amplification of stress and displacement is so large that there is danger of elastic or plastic buckling. Small changes in the slenderness ratio are associated with disproportionate changes in the amplification. Variations in loading and in the properties of the arch are relatively more important in the dangerous range. For a constant value of l/r, increasing the ratio of f_a/f_b will result in elastic or plastic buckling. The line separating elastic and plastic buckling depends, to some extent, on the type of steel used. The higher allowable stresses associated with silicon and nickel steel result in disproportionate increases in amplification.

For an assumed arch, the amplification chart shows immediately if danger exists, and what modifications are indicated to avoid this danger without making elaborate computations.

AMPLIFICATION

The bending moment obtained from the pressure line for the live load only is not the actual moment in the structure. The bending resulting from vertical loads is increased (or amplified) by additional bending caused by the axial forces. Usually an arch is designed so that the pressure line for the loads fits the arch axis closely. The bending moment is computed by multiplying the thrust by the distance from the pressure line to the arch axis. If the displacements of the arch axis are neglected, the same bending moment will be determined for the live-load pressure line as for the dead-load pressure line plus the live-load pressure line. Thus, by the usual theory, it is permissible to separate the live load from the dead load and to add the partial effects to obtain the total effect.

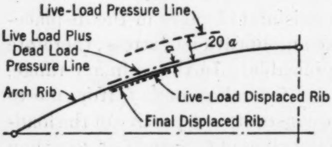

FIG. 4.—PRESSURE LINES

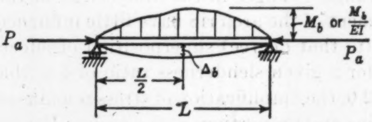

FIG. 5.—AXIAL AND TRANSVERSE LOADS ON A STRAIGHT BEAM

In flexible members the displacements of the arch axis, although small, may form a large part of the dead-load plus the live-load pressure line, as shown in Fig. 4. If the displacements of the arch axis are included, larger bending moments will be determined for the live-load plus the dead-load pressure line than for the live-load pressure line. The transverse displacements are moment arms for the combined live-load plus the dead-load axial forces. When the displacements of the axis are included, it is not permissible to separate the live load from the dead load. Not only are the bending moments and the displacements increased or amplified by the live-load plus dead-load axial forces, but the sums of the partial effects of the live load and the dead load are not equal to the total effect. However, it is often convenient to set an arbitrary allowable increase to the results obtained. This can be done by adding the effects of the displacements to the results obtained by assuming that the structure does not deform.

The stages of additional bending continue and may be represented by a mathematical series which may or may not converge. If the bending continues to increase (non-convergent series), the structure will collapse. In Fig. 5 there is shown a straight member subjected to both axial and transverse loads. Bending moment diagrams for beams subjected to various loading conditions are shown in Fig. 6. The equation for the displacement at the center of the beam is

$$\Delta = n \frac{M l^2}{E I} \qquad (8)$$

in which M is the ordinate of the bending moment diagram at the center of the beam.

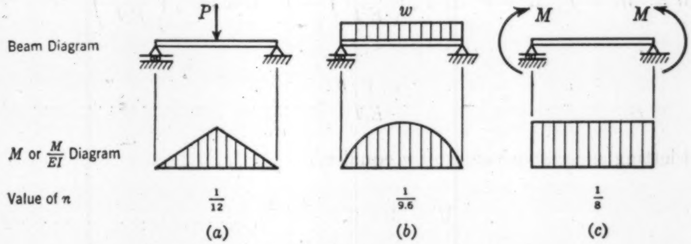

FIG. 6.—MOMENT DIAGRAMS FOR VARIOUS LOADINGS

The M-diagram—or the $(M/E I)$-diagram—is shown in Fig. 7. The value of n can be determined, by interpolation, for any other loading by superimposing the particular M-diagram (or the $(M/E I)$-diagram) on Fig. 7. In Fig. 7 the symbol M_{max} is the maximum bending moment (at the center of the span) and l_l is the distance from the left end of the span. The bending moment for the transverse loads is increased by additional bending caused by the axial forces. The shape factor for the transverse loads n_b is not the same as the shape factor for the axial loads n_a.

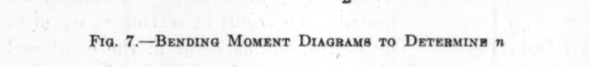

FIG. 7.—BENDING MOMENT DIAGRAMS TO DETERMINE n

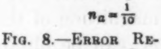

FIG. 8.—ERROR RESULTING FROM SETTING n_a EQUAL TO n_b

The additional bending moment (Fig. 5) is

$$M_{ad} = P_a \Delta_b \qquad (9a)$$

which causes a further displacement

$$\Delta_{ad} = \frac{n_a\, P_a\, \Delta_b\, l^2}{E\, I} \quad \text{(9b)}$$

and an increased bending moment

$$M'_{ad} = P_a \frac{n_a\, P_a\, \Delta_b\, l^2}{E\, I} \quad \text{(9c)}$$

This process is continued, and the total bending moment can be represented by

$$M = M_b + P_a\, \Delta_b + P_a\, \Delta_b\, n'_a \left(\frac{P_a\, l^2}{E\, I}\right) + P_a\, \Delta_b\, n'_a\, n''_a \left(\frac{P_a\, l^2}{E\, I}\right)^2 \cdot \cdot \cdot \quad \text{(10)}$$

If

$$\frac{n_a\, P_a\, l^2}{E\, I} < 1 \quad \text{(11a)}$$

and letting successive values of n equal n_a,

$$M = M_b + \frac{P_a\, \Delta_b}{1 - \dfrac{n_a\, P_a\, l^2}{E\, I}} \quad \text{(11b)}$$

Eq. 11*b* can also be written as

$$M = M_b \frac{1 - \dfrac{n_a\, P_a\, l^2}{E\, I} + \dfrac{n_b\, P_a\, l^2}{E\, I}}{1 - \dfrac{n_a\, P_a\, l^2}{E\, I}} \quad \text{(12)}$$

By setting n_a equal to n_b, an approximate expression is obtained—

$$M = \frac{M_b}{1 - \dfrac{n_a\, P_a\, l^2}{E\, I}} \quad \text{(13)}$$

Slight errors are caused by neglecting successive changes in n_a. A scale of the magnitude of the error in bending moment, as a result of setting n_a equal to n_b, can be obtained from Fig. 8. The corresponding error in the combined axial stress plus bending stress will be less than that shown in Fig. 8.

The quantity $\dfrac{1}{1 - \dfrac{n_a\, P_a\, l^2}{E\, I}}$ is the amplification factor Φ. Because

$$r^2 = \frac{I}{A} \quad \text{(14a)}$$

$$f_a = \frac{P_a}{A} \quad \text{(14b)}$$

and

$$f_x = \frac{E}{n_a \left(\frac{l}{r}\right)^2} \qquad \text{(14c)}$$

the amplification factor can also be written as

$$\Phi = \frac{1}{1 - \frac{f_a}{f_x}} \qquad \text{(14d)}$$

The total stress for a straight member subjected to both axial and transverse loads can be computed from

$$f_t = f_a + f_b \left(\frac{1}{1 - \frac{f_a}{f_x}} \right) \qquad \text{(15)}$$

The effects of temperature change, rib shortening, and movement of the abutment or hinge in a straight member are not included in Eq. 15.

This investigation and the amplification formula for an horizontal, straight member are applicable also to a curved member with supports on the same elevation. In Fig. 9(*a*) there is shown a curved member (circular for convenience) of rise *h* with a concentrated load at the center of the beam. If small changes in span length are neglected, the bending moment for the curved beam is the same as for the corresponding horizontal, straight beam. The displacement at the crown Δ_{ch} is slightly larger for a curved member than Δ_{bh} for a straight member. Consider a circular member with constant moment of inertia and various ratios of rise of arch to span length h/l. The ratio of the displacement at the center of a curved member (with concentrated load at the center) to a similarly supported and loaded straight beam is shown in Fig. 9(*b*). For arches of ordinary proportions, the increase in the displacement of a curved member over the displacements of a straight member is small and in most cases can be neglected. However, if it appears desirable to refine the computations to include the effect of curvature, the slenderness ratio can be increased by the small percentage shown in Fig. 9(*b*).

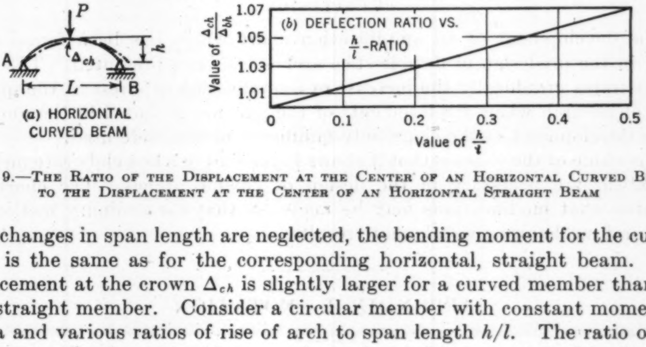

(*a*) HORIZONTAL CURVED BEAM

FIG. 9.—THE RATIO OF THE DISPLACEMENT AT THE CENTER OF AN HORIZONTAL CURVED BEAM TO THE DISPLACEMENT AT THE CENTER OF AN HORIZONTAL STRAIGHT BEAM

The displacement at the center of a beam is influenced by the difference in elevation of the end supports and by the shape of the beam. In Fig. 10 there are shown an horizontal inclined beam, an horizontal straight beam, and an inclined curved beam. The displacement at the center of a straight beam with supports on different elevations is greater than that occurring in the corresponding straight beam. The increase in displacement of the inclined beam over the horizontal beam is shown in Fig. 10(*d*). Values for an inclined curved beam are also shown. Thus, the amplification of stress in flexible-steel arch ribs may be determined approximately by Eq. 15 modified for additional bending.

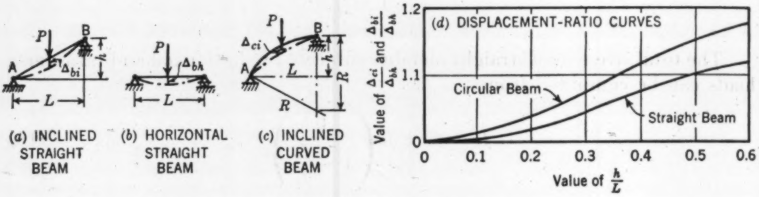

(*a*) INCLINED STRAIGHT BEAM (*b*) HORIZONTAL STRAIGHT BEAM (*c*) INCLINED CURVED BEAM (*d*) DISPLACEMENT-RATIO CURVES

FIG. 10.—THE DISPLACEMENT RATIO FOR STRAIGHT AND CURVED HORIZONAL AND INCLINED BEAMS

An estimate of the error introduced by neglecting the curvature of the axis and the relative difference in elevation between points of inflection can be determined from Fig. 10(*d*). For flexible-steel arch ribs of ordinary proportions, this error is usually small and can be neglected.

CONCLUSION

The development of an amplification chart which has been found to be useful in the predesign of flexible-steel arches has been presented. The chart demonstrates graphically the increase or amplification of stress at the quarter point of an arch when displacements of the axis are included in the analysis. In the development of the chart only familiar concepts were used.

The value of the chart is that it shows immediately when elaborate methods of analysis are necessary in the design of flexible arches. The chart also indicates what modifications may be made, so that the ordinary methods of structural mechanics give adequate results.

APPENDIX I. NOTATION

The following symbols, adopted for use in this paper and for the guidance of discussers, conform essentially with "American Standard Letter Symbols for Structural Analysis" (ASA Z10.8—1949) prepared by a committee of the American Standards Association with Society representation, and approved by the Association in 1949:

A = cross-sectional area;
d = depth of the arch rib;
E = modulus of elasticity;

f = allowable unit stress:

f_a = axial stress before amplification resulting from dead load and live load;

f_b = bending stress before amplification resulting from dead load and live load;

f_t = total combined axial compression and amplified bending stress;

f'_t = total stress before amplification;

f_x = critical stress;

h = rise of the arch;

I = moment of inertia;

L = span length;

l = one half span length;

l_l = distance from the left end of the span (Fig. 7);

M = bending moment;

M_{max} = maximum bending moment (Fig. 7);

n = shape factor:

n_a = shape factor for axial loads;

n_b = shape factor for transverse loads;

P = concentrated load;

R = radius of curvature of an arch;

r = radius of gyration;

Z = section modulus;

Δ_{bh} = deflection of horizontal straight beam;

Δ_{bi} = deflection of inclined straight beam;

Δ_{ch} = deflection of horizontal curved beam;

Δ_{ci} = deflection of inclined curved beam; and

Φ = amplification factor.

APPENDIX II. BIBLIOGRAPHY

(1) **"Rainbow Arch Bridge Over Niagara Gorge: A Symposium,"** *Transactions*, ASCE, Vol. 110, 1945, p. 33.

(2) **"Theory of Curved Beams,"** by C. G. Best, *Transactions*, ASME, Vol. 68, December 1946, pp. A 294–296.

(3) **"Récherches analytiques sur la flexion et la résistance des pièces courbes,"** by M. Bresse, Mallet-Bachelier, Paris, France, 1854.

(4) **"Die zentrische Knickung symetrisch belasteter gelenkloser Bogenträger mit veränderlichem Tragheitsmoment,"** by B. Busch, *Der Bauingenieur*, Vol. 18, 1937, pp. 812–820.

(5) **"Remarques sur l'application des formules de Bresse au calcul des arcs,"** by J. Courbon, *Annales des Ponts et Chaussées*, Vol. 115, 1945, pp. 427–437.

(6) **"The Relation of Structural Mechanics to Structural Engineering,"** by H. Cross, *Proceedings,* Fifth International Cong. of Applied Mechanics, 1939.

(7) **"Flexion et flamboyement des arcs minces,"** by P. A. Dauriac, *La Houille Blanche,* Vol. 2, 1947, pp. 233–248.

(8) **"Das Knicken von Bogenträgern bei unsymetrischer Belastung,"** by E. Deutsch, *Der Bauingenieur,* Vol. 21, 1940, pp. 353–360.

(9) **"Untersuchungen über die Knicksicherheit, die elastische Verformung und das Kriechen des Betons bei Bogenbrücken,"** by F. Dischinger, *ibid.,* Vol. 18, 1937, pp. 487-520, pp. 538–552, pp. 595–621.

(10) **"Elastische und plastische Verformungen der Eisentragwerke und insbesondere der Bogenbrücken,"** by F. Dischinger, *ibid.,* Vol. 20, 1939, pp. 53–63, pp. 286–294, pp. 426–437, pp. 563–572.

(11) **"Die Änderung des Spannungszustandes weitgespannter, flacher Eisenbetonbogen durch die plastische Dauerverformung des Betons,"** by A. Freudenthal, *Beton und Eisen,* Vol. 34, 1945, pp. 176–184.

(12) **"Deflection Theory for Arches,"** by A. Freudenthal, International Assn. for Bridge and Structural Eng., Swiss Federal Inst. of Technology, *Publications,* Zurich, Switzerland, Vol. 3, 1935, p. 100.

(13) **"Knickbelastung der Bogenträger,"** by J. Fritsche, *Bautechnik,* Vol. 3, 1925, p. 465.

(14) **"Theorie und Berechnung vollwandiger Bogenträger,"** by B. Fritz, Julius Springer, Inc., Berlin, Germany, 1934.

(15) **"Uber die Knicksicherheit vollwandinger Bögen,"** by E. Gaber, *Bautechnik,* Vol. 12, 1934, pp. 646–651.

(16) **"Verformungstheorie des eingespannten Bögen mit einer Stützlinienachse,"** by A. Hawranek, *Der Bauingenieur,* Vol. 18, 1937, pp. 719–727.

(17) **"Application des series trigonometriques a l'étude du flambement des arches,"** by M. Hupner, *Annales des Ponts et Chaussées,* Vol. 105, 1935, pp. 754–800.

(18) **"Beitrag zur Theorie weitgespannter Brückenbögen mit Kampfergelenken,"** by S. Kasarnowsky, *Der Stahlbau,* Vol. 6, 1931, p. 61.

(19) **"Die Methode der Grundkoordination,"** by G. Kruck, Gebrüder Leeman und Co., Zurich, Switzerland, 1937.

(20) **"Étude Génèrale du flambement des arches,"** by R. Levi, *Comptes Rendus,* Académie des Sciences, Vol. 220, 1945, pp. 436–438.

(21) **"Nôte sur le flambement et en particulier celui des arcs,"** by R. Levi, *Annales des Ponts et Chaussées,* Vol. 117, 1947, pp. 345–366.

(22) **"Formänderung und Festigkeit gekrummter Körper insbesondere der Ringe,"** by E. Linkler, *Der Civilingenieur,* Vol. 4, 1858, pp. 232–246.

(23) **"Der biegsame eingespannte Bögen,"** by J. Melan, *Der Bauingenieur,* Vol. 6, 1925, p. 143.

(24) **"Theorie und Berechnung der eisernen Bögenbrücken,"** by H. Müller-Breslau, *Baumgartner's Buchhandlung,* Leipzig-Berlin, Germany, 1880.

(25) **"Numerical Procedure for Computing Deflection, Moments, and Buckling Loads,"** by N. M. Newmark, *Transactions*, ASCE, Vol. 108, 1943, p. 1168.

(26) **"The Buckling of a Thin Circular Arch,"** by J. Ratzendorfer, *Engineering*, Vol. 150, 1940, pp. 284–285.

(27) **"Applications de la méthode des moindres carres du calcul des arcs,"** by W. Wierzbricke, *Publications*, Association International des Ponts and Charpentes, Vol. 5, 1937–1938, pp. 263–274, pp. 309–322, pp. 333–342, pp. 375–422, Vol. 6, 1938–1939, pp. 71–88, pp. 265–276.

(28) **"Steel Arch Analyzed and Designed by Semigraphical Methods,"** by Milo S. Ketchum, *Civil Engineering*, August, 1952, pp. 30–34.

DISCUSSION

Milo S. Ketchum,[4] A. M. ASCE.—A problem such as the one stated in the paper was described in connection with the design of the steel arches for the fieldhouse at the University of Wyoming in Laramie (28). In this description all stress values were given, and it will be of interest to compare the results by the two methods.

In the writer's analysis the amplification of stress is $(411 - 380)/380 = 8.2\%$. In the paper, the following constants are required:

$$L = 110.5 \text{ ft}, r \text{ (for 36WF150)} = 14.29$$

and

$$\frac{L}{r} = \frac{110.5 \times 12}{14.29} = 92.7.$$

The ratio of axial stress to bending stress is $3.62/9.80 = 0.370$. The reduced (L/r)-value, using the coefficient 0.90 for a two-hinged arch, is $92.7 \times 0.90 = 83.3$.

Using the foregoing values in Fig. 2 of the paper, the amplification ratio is approximately 10%. The writer considers this to agree closely with the more precise method.

This paper should be helpful to engineers making preliminary estimates of the amplification stresses or buckling stresses in steel arches—particularly for those arches used in buildings which by their nature do not permit long and elaborate studies.

Robert S. Rowe,[5] A.M. ASCE.—The discussion by Mr. Ketchum adds materially to the paper by presenting additional evidence to compare the results of the amplification of stress by a simplified and by a more precise method. The writer agrees with Mr. Ketchum that the use of the amplification chart should be helpful in making a preliminary estimate of the amplification of stress in steel arches, especially for problems where time-consuming studies may be indicated.

---

[4] Cons. Engr., Ketchum & Konkel, Cons. Engrs., Denver, Colo.

[5] Associate Prof. of Civ. Eng., Princeton Univ., Princeton, N. J.

AMERICAN SOCIETY OF CIVIL ENGINEERS
Founded November 5, 1852
TRANSACTIONS

Paper No. 2705

FREQUENCY OF EXCESSIVE RAINFALLS IN FLORIDA

By David B. Smith,[1] A. M. ASCE

Synopsis

A study of one aspect of the excessive rainfalls recorded at five locations in Florida is presented herein. This paper illustrates the empirical expressions which relate the intensity and frequency of occurrence of heavy rains of short duration. The method of analysis and the presentation of results follow those established in similar studies from other localities. A comparison is drawn with a study made in 1935. It is seen that only minor changes are necessary in applying the results of this previous work, even though the present study has lengthier records from which to draw.

Introduction

A proper balance between safety and economy in the construction and operation of many differing types of engineering structures depends on a working knowledge of the rainfall characteristics in the areas under consideration. Consequently, an analysis of the interrelations existing among the intensities, durations, and frequencies of excessive rainfalls is a necessary requirement for the engineering design of these structures.

The studies made by D. L. Yarnell, M. ASCE, supplied some of these data for the entire United States.[2] However, the unusual geography of Florida has created uncertainty as to the propriety of applying these data to local problems. Many additional basic data have been added to the rainfall records in the period from 1935 to 1954.

The purpose of this study is to analyze rainfall data in Florida in order to determine the frequency with which excessive rates of precipitation occur in various sections of the state. In this study attention is directed to high-intensity rainfall of durations from 5 min to 100 min.

Investigations of this type require long-time records such as those which are obtained from automatic recording rain gages. There were in 1950 seventy-

---

Note.—Published, essentially as printed here, in December, 1953, as *Proceedings-Separate No. 366*. Positions and titles given are those in effect when the paper was received for publication.

[1] Associate Prof. of Civ. Eng., Univ. of Florida, Gainesville, Fla.

[2] "Rainfall Intensity-Frequency Data," by D. L. Yarnell, *Miscellaneous Publications No. 204*, U.S.D.A., Washington, D. C., August, 1935.

seven recording rain gages in Florida, of which seventy-one were placed in operation subsequent to 1940. The six remaining stations were established at significantly earlier dates.

For statistical purposes data obtainable from the newer stations will yield results of a lesser order of precision than those data from the older stations. For this reason no station which had records of less than ten years was considered for inclusion in this study. This criterion eliminated all stations but six. Table 1 lists pertinent information relating to the five stations selected for this study. The records of the sixth station (Key West) were not readily available and were not included. The geographical location of the five stations is shown in Fig. 1.

TABLE 1.—RECORD DATA ON FLORIDA RAINFALL STATIONS SELECTED FOR STUDY

	First year of record	Last year included	Years of record	Number of storms analyzed
Pensacola	1902	1948	47.5	720
Apalachicola[a]	1922	1948	24.0	328
Tampa	1905	1948	44.6	751
Miami	1911	1948	38.3	712
Jacksonville	1896	1948	53.0	556

[a] Record discontinued from August, 1933, to January, 1937.

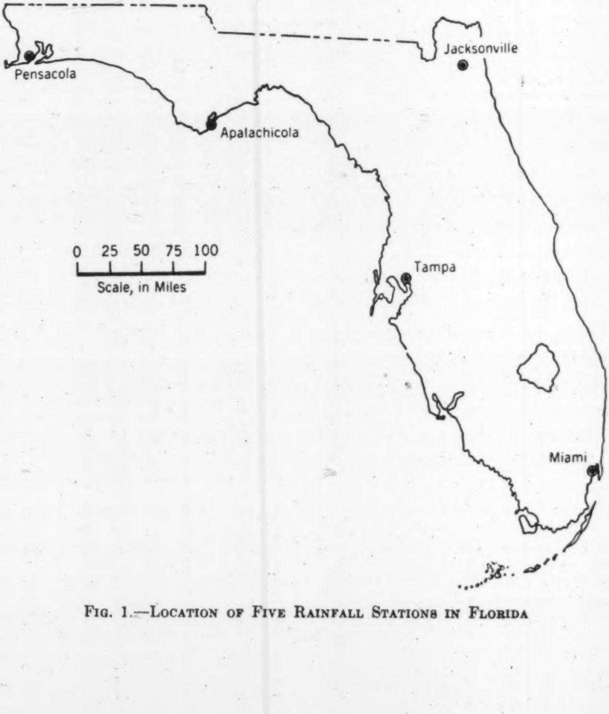

FIG. 1.—LOCATION OF FIVE RAINFALL STATIONS IN FLORIDA

RAINFALL RECORDS

The basic rainfall data were collected from the individual recording stations. This information included each entry of excessive precipitation in the daily record of the Weather Bureau, United States Department of Commerce (USWB), from the beginning of each record.

During the periods of record the USWB rule for defining—and the method of tabulating—excessive precipitation were changed. Prior to 1933, Florida storms attaining 1 in. or more in 1 hr or less were considered excessive. In 1933, however, the rate which differentiated excessive storms from others was changed to conform with

$$y_a = 2\,t_m + 30 \ldots\ldots\ldots\ldots\ldots\ldots\ldots\ldots (1)$$

in which y_a is the accumulated depth in hundredths of an inch, and t_m is the time in minutes.

In 1936 the method of tabulating excessive precipitation was also changed. The method previously used gave the accumulated depth of precipitation for each 5 min. during a storm. The tabulation began with the first 5-min. period in which at least 0.05 in. of rain were measured, after which the tabulation was continued for each succeeding 5-min period. The method established in 1936 furnishes a record of the maximum rainfall occurring during the storm for each time interval. The record shows the maximum amounts for 5 min, 10 min, 15 min, 20 min, 30 min, 45 min, 60 min, 80 min, 100 min, 120 min, 150 min, and 180 min.

Although this latter method tended to increase the amounts of rainfall measured during the various time increments, no distinction was made in the analysis of the two types of data. Also, the change made in the 1933 definition of excessive rainfalls tended to decrease the number of storms so recorded. This analysis, however, is not affected since the rates of rainfall which did not equal or exceed those indicated by Eq. 1 were discarded from the grouped data.

There are also certain inherent deficiencies in rainfall data of the type used. These factors have been investigated by A. J. Schafmayer, M. ASCE, and B. E. Grant,[3] and others.[4] However, most errors of this nature are minimized when long-time records such as those in this study are used.

ANALYSIS OF DATA

The method of analyzing the data followed conventional practice in the conversion of depths of rainfall into average rates.[5] These rates were grouped for each station to show the number of occasions when the average intensity of rainfall reached or exceeded an indicated intensity for an indicated duration. These compilations are given in Table 2. Interpolation into Table 2 yields the various durations of rainfall intensities which occurred once in 0.25 yr, 0.5 yr, 1 yr, 2 yr, 3 yr, 4 yr, and 6 yr at each station.

---

[3] "Rainfall Intensities and Frequencies," by A. J. Schafmayer and B. E. Grant, *Transactions*, ASCE, Vol. 103, 1938, p. 344.

[4] "Hydrology Handbook," ASCE *Manual of Engineering Practice No. 28*, 1949, p. 9.

[5] *Ibid.*, p. 16.

TABLE 2.—NUMBER OF OCCASIONS WHEN THE AVERAGE INTENSITY OF RAINFALL REACHED OR EXCEEDED THE INDICATED INTENSITY FOR THE INDICATED DURATION AT FIVE CITIES IN FLORIDA

Duration of Storm, in Minutes	AVERAGE INTENSITY, IN INCHES PER HOUR											
	1.5	2.0	2.5	3.0	3.5	4.0	4.5	5.0	5.5	6.0	6.5	7.0 and over
PENSACOLA												
5								94	59	43	22	16
10				324	201	116	76	44	22	14	7	4
15			342	205	109	63	35	20	11	5	3	2
20		381	247	136	69	40	26	14	8	3	3	3
30		216	123	57	32	17	8	2	2	1	1	1
45		103	52	21	11	6	1	1	1			
60	131	54	23	12	8	2	1					
80	72	30	15	10	4							
100	43	18	11	7								
APALACHICOLA												
5								42	28	20	7	3
10				138	86	49	27	18	9	3	2	2
15			144	87	45	22	10	5	3	1		
20		168	106	62	26	13	8	4	2			
30		96	49	24	9	4	1					
45		42	20	10	2							
60	61	25	10	1	1							
80	36	12	4	1								
100	17	4	1									
TAMPA												
5								87	59	36	22	13
10				324	191	130	80	47	30	14	3	2
15			344	226	131	71	39	23	12	4	2	1
20		383	252	155	83	42	23	15	7	2	1	
30		218	133	71	33	20	9	4	2			
45		101	41	22	13	7	3					
60	120	47	19	9	6	3						
80	59	20	10	6	4							
100	22	8	4	1								
MIAMI												
5								77	47	28	12	7
10				300	178	103	61	30	18	7	4	2
15			305	185	113	56	28	16	6	5	2	1
20		348	228	133	69	34	16	7	4	2	1	
30		193	112	62	34	11	5	3	2	2		
45		101	52	23	7	4	3	1				
60	111	60	27	9	5	2	1					
80	79	35	12	4	1	1						
100	46	21	8	1								
JACKSONVILLE												
5							171	114	70	44	24	13
10				299	201	127	79	45	28	13	5	3
15			333	209	132	79	42	25	10	7	1	
20		364	229	141	79	35	23	15	4	2		
30		193	105	55	28	18	6	4	1			
45		76	38	18	10	3						
60	73	34	14	7	1							
80	42	14	5									
100	24	8	2									

In empirical curve fitting, it was found that a two-parameter, reciprocal equation of the generalized form,

$$i = \frac{d}{j + t_a} \tag{2}$$

proved most adaptable for expressing the intensity-duration relationship found for each of the seven frequencies investigated. In Eq. 2, i is the average rainfall intensity in inches per hour, t_a denotes time in minutes over which the average intensity occurs, and d and j are constants for a given locality and frequency.

When Eq. 2 is converted to

$$\frac{1}{i} = Y + M\, t_a \tag{3}$$

it becomes a straight-line relation in which Y indicates the intercept value, and M is the value of the slope of the line. Fig. 2 shows the high degree of correlation obtained by the use of Eq. 3.

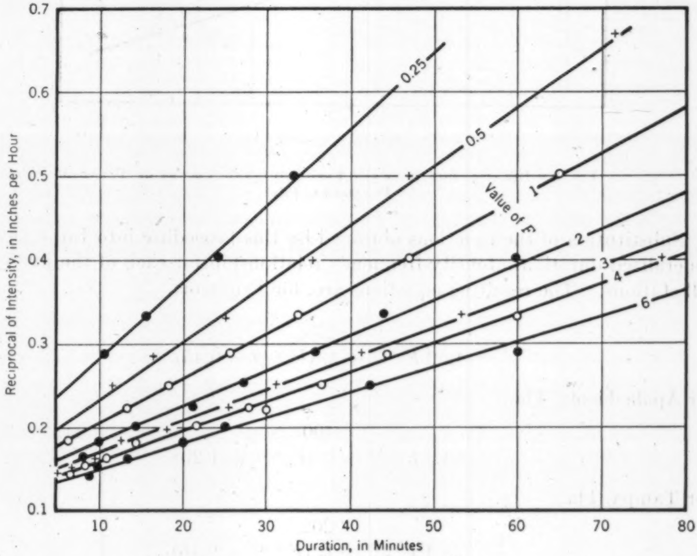

FIG. 2.—DURATION-INTENSITY RELATIONSHIPS FOR VARIOUS FREQUENCIES AT PENSACOLA, FLA.

An investigation of each set of data by the method of least squares produced the corresponding values of Y and M. In each of the thirty-five cases the coefficient of correlation was greater than 0.99.

Further examination revealed that the values of Y and M exhibit a logarithmic trend when compared with the average time intervals between occurrences.

Fig. 3 illustrates these relations at Pensacola, Fla. Application of the method of least squares produces the lines of best fit, the equations of which relate the values of Y and M to a unit of frequency, F, expressed as an average frequency of occurrence of once in the indicated number of years. In the Y-relationships the coefficient of correlation of the data was found to be less than -0.88 in each instance, and in the M-relationships the coefficient was less than -0.99.

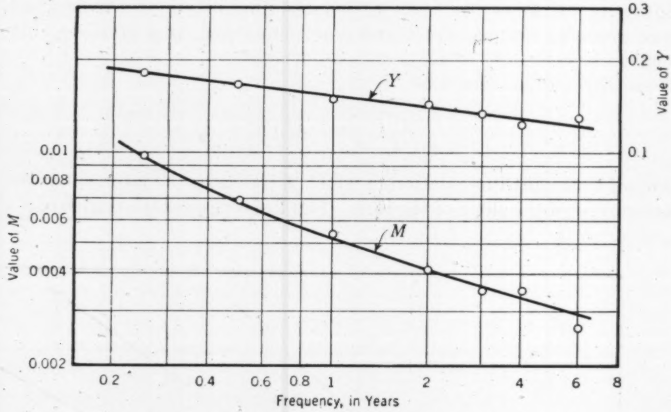

FIG. 3.—RELATIONSHIP BETWEEN FREQUENCY AND VALUES OF Y AND M AT PENSACOLA, FLA.

Substitution of the functions obtained by this procedure into Eq. 3 gave a generalized duration-intensity-frequency relationship for each of the five rainfall stations. The resulting equations are, for Pensacola,

$$i = \frac{278}{42.2\, F^{-0.12} + t_a\, (F^{-0.56} + 0.45)} \qquad (4a)$$

for Apalachicola, Fla.,

$$i = \frac{400}{63.2\, F^{-0.12} + t_a\, (F^{-0.77} + 1.20)} \qquad (4b)$$

for Tampa, Fla.,

$$i = \frac{202}{28.4\, F^{-0.10} + t_a\, (F^{-0.42} + 0.16)} \qquad (4c)$$

for Miami, Fla.,

$$i = \frac{370}{60.0\, F^{-0.11} + t_a\, (F^{-0.67} + 0.73)} \qquad (4d)$$

and for Jacksonville, Fla.,

$$i = \frac{231}{31.2\, F^{-0.08} + t_a\, (F^{-0.58} + 0.46)} \qquad (4e)$$

It can be seen that selection of a numerical value for *F* will reduce Eqs. 4 to a specific duration-intensity relationship of the form given by Eq. 2.

Comparison of Results

For rainfall durations of between 5 min and 100 min, Eqs. 4 furnish reliable information as to the average rainfall intensities which occur with an average frequency of once in 3 mo. to once in 6 yr. For less frequent occurrences, however, the precision with which an average rate of rainfall can be predicted also decreases. It was felt that a comparison of rarely observed rainfalls with the equivalent computed values would serve to demonstrate the range of reliability of the generalized equations. For this purpose a frequency of once in the period of years of record was selected at each station. The results are presented in Fig. 4 in which the dashed curve represents the computed data. The straight lines connect points of the maximum observed intensities on record.

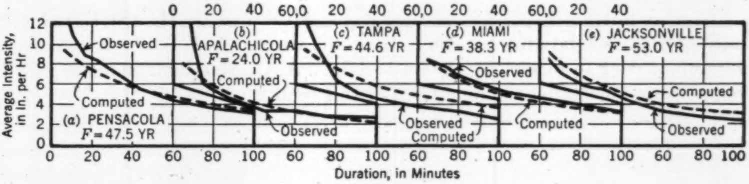

FIG. 4.—COMPARISON BETWEEN OBSERVED AND COMPUTED RAINFALLS FOR THE INDICATED FREQUENCIES FOR FIVE CITIES IN FLORIDA

It is noteworthy that (except at Tampa) the observed and computed values are in excellent agreement. The observed intensities of short duration tend to exceed the computed ones, but for longer durations these differences become relatively small. In general, then, it can be stated that the relations expressed for the various rainfall stations will permit extrapolation for frequencies less than those used in the derivations (less than once in 6 yr).

TABLE 3.—PERCENTAGE DEVIATION OF D. L. YARNELL'S RESULTS FROM PRESENT ANALYSIS FOR FIVE CITIES IN FLORIDA

Duration, in minutes	Pensacola	Apalachicola	Tampa	Miami	Jacksonville
5	4	11	1	11	1
15	−6	5	−4	2	−4
30	−12	3	−6	−2	−9
60	−18	−1	−11	−10	−11

A comparison of the results of this study with those of Mr. Yarnell[2] furnishes additional insight into the consistency of rainfall frequencies in Florida. Table 3 has been prepared for this purpose. Average intensities for durations of 5 min, 15 min, 30 min, and 60 min were obtained by interpolation of Mr. Yarnell's charts which showed the rainfalls to be expected on an average of once in 2 yr, 5 yr, 10 yr, and 25 yr. The corresponding intensities were computed by use of Eqs. 4. The values in Table 3 represent the deviation of Mr. Yarnell's results from those of this analysis. Each value is an average of the percentage variations found for the four frequencies listed.

At the five stations examined, a small but significant trend is in evidence. The records which have been added since the study made in 1935 show that for short durations the earlier study indicated intensities which were too large, but for longer durations the intensities appear to be somewhat less than this study demonstrates. No doubt these differences are caused by the change in the method of tabulation. The variations are not great, however, and it can be concluded that the rainfall characteristics at the five stations studied have not varied to any appreciable degree during the period of record.

ACKNOWLEDGMENTS

The work presented in this paper was performed under the sponsorship of the Division of Water Survey & Research, Florida State Board of Conservation, Tallahassee, Fla.

Charles Sutton, J. M. ASCE, and Rufus Musgrove, J. M. ASCE, reduced most of the basic data into usable form. The various USWB offices were most accommodating in furnishing the basic data. A. G. Matthews made excellent suggestions concerning the final form of this report.

AMERICAN SOCIETY OF CIVIL ENGINEERS
Founded November 5, 1852
TRANSACTIONS

Paper No. 2706

PLATES WITH BOUNDARY CONDITIONS OF ELASTIC SUPPORT

By S. J. Fuchs,[1] M. ASCE

With Discussion by Messrs. M. Z. v. Krzywoblocki, R. H. Wood, and S. J. Fuchs

Synopsis

A solution for the deflections, moments, and reactions in a rectangular plate under transverse load, supported at the corners, and with or without supporting beams at the panel boundaries, is presented in this paper. This solution can be classified as a unified one, since it is adaptable to most of the specific problems for which particular solutions have been developed. Provision is made for other classes of particular solutions for additional cases. The solutions for specific problems, expressed in a general form, differ only in the arbitrary constants appearing in the general form. These constants are evaluated by means of operational formulas, with dependence on parameters that are defined by the ratios of the flexural and torsional rigidities of the beams to the flexural rigidity of the plate, and by the proportions of the plate. To illustrate the procedure, the arbitrary constants are obtained for a rectangular plate under uniform load that is simply supported on beams of finite flexural rigidity on four sides. A particular value of the parameter of relative flexural rigidity for which the expressions for moment reduce to simple exact formulas also exists. Moment and reaction coefficients are evaluated at positions along the axes of symmetry and the boundaries of the simply supported plate for several values of the parameter of relative flexural rigidity. Experimental verification is obtained by use of introductory tests made on panels supported on beams of arbitrarily reduced flexural rigidity.

Notation

The letter symbols introduced in this paper are defined where they first appear, in the text or by illustration, and are assembled alphabetically in Appendix II for convenience of reference.

Note.—Published, essentially as printed here, in June, 1953, as *Proceedings-Separate No. 199*. Positions and titles given are those in effect when the paper or discussion was received for publication.

[1] Analyst, Loewy Construction Co., New York, N. Y.

INTRODUCTION

For the thin, elastic, rectangular laterally loaded plate that is supported at the corners, with or without tributary beams disposed at the panel boundaries, various important cases may be considered as corresponding to the limit values of the flexural and torsional rigidities of the beams. Thus, the clamped plate supported on rigid beams may be considered as corresponding to values of the flexural and torsional rigidities for the beams that approach infinity. Similarly, other combinations of limit values of these rigidities, which correspond to the solutions that are known for rectangular plates, are classified in Table 1, which applies to polygons in general. Therefore, a solution for the laterally loaded plate, involving formulas expressing a dependence on parameters corresponding to the torsional and flexural rigidities of the beams, may be considered a general solution as it would reduce to the known solutions for limit values of the parameters. The solution would also yield classes of solutions for intervening ranges of parametric values. The derivation and application of such a solution, with particular reference to the rectangular plate, will be investigated in this paper.

TABLE 1.—CLASSIFICATION DEFINED BY THE FLEXURAL AND TORSIONAL RIGIDITIES OF THE SUPPORTING BEAMS

		Flexural Rigidity, λ		
Line	Torsional Rigidity, H	$\lambda = 0$ (Plain support)	λ = finite (Flexural support)	$\lambda \to \infty$ (Nonflexural support)
1	$H = 0$ (Simple support)	plain, simple	flexural, simple	nonflexural, simple
2	H = finite (Torsional support)	plain, torsional	flexural, torsional	nonflexural, torsional
3	$H \to \infty$ (Clamped support)	plain, clamped	flexural, clamped	nonflexural, clamped

Historical Note.—The extensive and distinguished literature on the theory of plates can be acknowledged only inadequately by the brief list of references that are limited to a few distinct solutions (exclusive of difference-equation methods) which have been applied to a majority of the historic problems of thin, rectangular, transversely loaded plates.

The first of these solutions, for the deflection of panels on simple, nonflexural supports, was introduced by C. L. M. H. Navier[2] in 1820; it comprised a double infinite series of trigonometric terms. Other investigators have applied the same form of solution to the clamped plate, with or without nonflexural supports.

The next solution to appear, which was also important in the sense of initiating a new class of applications, was that of M. Lévy,[3] in 1899. The latter's primitive for the applicable differential equation may be expressed as $w = \sum_m Y_m \cos mx + \phi$, in which w is the deflection of the plate; m is an index of the summation; Y_m, in the complementary function, comprises hyperbolic functions in the variable y; x is the coordinate variable; and ϕ is a particular integral. Two applications of Lévy's result, by H. Hencky[4] and A. Nadai,[5] are also examples of a construction which often recurs in the literature. These applications involve the superposition of a pair of expressions (each of the same form) but with x and y, and a and b, mutually interchanged, in which a and b are the panel span lengths, measured parallel to the x-axis and y-axis, respectively. Mr. Hencky used a simple superposition of functions $f(x, y, a, b)$ and $f(y, x, b, a)$ in which f comprised Lévy's primitive for the problem of the clamped, nonflexurally supported panel. Mr. Nadai's method consisted in the construction of an orthonormalized set of functions w_k out of linear combinations of functions $w_n = u_n\ (x, y, a, b) + v_n\ (y, x, b, a)$, in which u_n and v_n essentially comprise the form of Lévy's solution.

---

[2] "Extrait des Recherches sur la Flexion des Plans élastiques," by C. L. M. H. Navier, *Bulletin des Sciences*, Société Philomathique de Paris, Vol. 10, 1823, pp. 94–102.

[3] "Sur l'Équilibre élastique d'une Plaque rectangulaire," by M. Lévy, *Comptes Rendus*, Vol. 129, 1889, pp. 535–539.

By a different mathematical method (that of the variational calculus) a third method was introduced by W. Ritz.[6] In this method, a series of functions was set up which satisfied the boundary conditions, and the coefficients of these functions were derived by minimum energy considerations. When, however (as in this investigation), the difficulty lies in the formulation of expressions that satisfy the boundary conditions, this method does not appear advantageous.

To satisfy the range of boundary conditions considered in this investigation, it is sufficient to use any convenient primitive of the differential equation which contains arbitrary constant coefficients. Of the known solutions, the primitive of Lévy is available for this purpose and may be conveniently used.

FORMULATION OF THE SOLUTION

In the formulation of the solution, the Kirchoff-Kelvin-Tait theory of boundary conditions is presupposed.[7] It has been shown[8] that, compared with more exact assumptions, the possible error by use of this theory is small for thin plates, and the error is confined to the narrow layers adjacent to the boundaries. By this theory two equations for each boundary edge are required in order to define the boundary conditions for a polygonal plate, or 2 n equations for a polygon of n sides. Furthermore, the plate is assumed to be thin, to have small deflections, and the middle surface is assumed to be inextensional, so that sides of elements that are normal before bending remain normal after bending. In agreement with these assumptions, the differential equation used is the fourth order bi-harmonic or plate equation:

$$N \left(\frac{\partial^2}{\partial x^2} + \frac{\partial^2}{\partial y^2} \right) \left(\frac{\partial^2 w}{\partial x^2} + \frac{\partial^2 w}{\partial y^2} \right) = p \ldots\ldots\ldots\ldots\ldots (1)$$

in which N is the flexural rigidity of the plate and p is the intensity of the distributed load. Since the complementary function or solution of the homogeneous part of this equation includes four constants of integration, $2\,n/4$ independent solutions in superposition are required to yield sufficient constants for application to the $2\,n$ equations—namely, $w_1 + w_2 + \cdots + w_{n/2}$. In the case of the parallelogram and, in particular, in that of the rectangle, $w = w_1 + w_2 + \phi$, in which w_1 and w_2 may be of the same form but with x, y, and a, b mutually interchanged; that is, $w_1 = f\,(x, y, a, b)$, and $w_2 = f\,(y, x, b, a)$.

---

[4] "Der Spannungszustand in rechteckigen Platten," by H. Hencky, Oldenbourg, Munich, Germany, 1913.

[5] "Die Elastischen Platten," by A. Nadai, Julius Springer, Berlin, Germany, 1925, pp. 180–184.

[6] "Über eine neue Methode zur Losung gewisser Variationsprobleme der mathematischen Physik," by W. Ritz, *Journal für reine und angewandte Mathematik*, Vol. 135, 1909, pp. 1–61.

[7] "Treatise on Natural Philosophy," by Lord Kelvin (W. Thomson) and P. G. Tait, Cambridge University Press, Cambridge, England, Part 11, 1883, pp. 188–192.

[8] "The Edge Effect in the Bending of Plates," by K. O. Friedrichs, in "Reissner Anniversary Volume: Contributions to Applied Mechanics," J. W. Edwards, Ann Arbor, Mich., 1949.

Therefore, both w_1 and w_2 are solutions of Eq. 1, but w_2 may be considered as resulting from a rotation of Cartesian axes from those of w_1. Since Eq. 1 is an invariant differential equation under rotation of axes, w_2 is of the same form as w_1, when referred to the new axes. More explicitly, denoting the new coordinates by primes, and with rotation through $-\pi/2$—

$$w_2 = f(x', y', a', b') = f(-y, x, -b, a) = f(y, x, b, a) \ldots\ldots (2)$$

—the negative signs being included in the arbitrary constants implicitly contained in Eq. 2.

For convenience, expressions similar to w_1 and w_2 which occur in the same form, but with x, y or a, b, or both, mutually interchanged, may be termed as being analogous to each other.

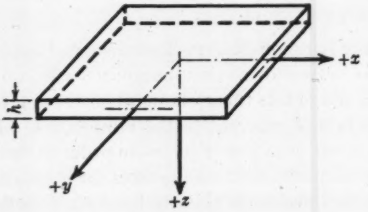

FIG. 1.—ORIENTATION OF THE PLATE AND THE COÖRDINATE AXES

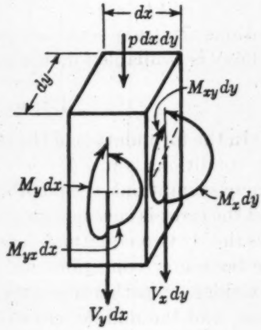

FIG. 2.—THE POSITIVE DIRECTIONS OF THE STRESS RESULTANTS

The process of superposition of component solutions referred to successively rotated Cartesian axes may be extended to the construction of a formal solution for the general polygon. However, the analysis contained in this paper is confined to symmetrical conditions of the rectangular plate. The boundaries and orientation of the plate are shown in Fig. 1, and the positive sense of the stress resultants is shown in Fig. 2. The flexural rigidity of the plate may be defined as $N = \frac{E\,h^3}{12}\,(1 - \mu^2)$, in which E represents the modulus of elasticity of the plate material; h is the thickness of the plate; and μ denotes Poisson's ratio for the plate material.

A complementary function of Eq. 1 utilized as a component solution to Eq. 2 is the primitive of Lévy:

$$w_1 = \frac{a^4}{N} \sum_{m}^{\infty} (A_{2m} \cosh \alpha y + B_{2m} \alpha y \sinh \alpha y) \cos \alpha x \ldots\ldots\ldots (3)$$

in which $\alpha = m \pi / a$, the index m being assumed to include all integers. Accordingly, application of Eq. 3 and its analogous expression in the expression for w yields, for symmetrical conditions of the rectangular plate under any symmetrical loading,

$$w = \frac{a^4}{N} \sum_{m}^{\infty} (A_{2m} \cosh \alpha y + B_{2m} \alpha y \sinh \alpha y) \cos \alpha x + \frac{b^4}{N} \sum_{m}^{\infty} (A_{1m} \cosh \beta x + B_{1m} \beta x \sinh \beta x) \cos \beta y + k_1 x^2 + k_2 y^2 + k_0 + \phi \ldots (4)$$

in which $\beta = m \pi / b$; the terms containing the arbitrary constants k_1, k_2, and k_0 are unaffected by the differential operator and are added for greater generality; and A_{1m}, A_{2m}, B_{1m}, and B_{2m} are arbitrary constant coefficients corresponding to each value of the index m of the series comprising the primitive of the plate differential equation.

Eq. 4, for each value of the index m, contains four arbitrary constants for application to the equations which define boundary conditions. As will be shown subsequently, all the classifications of Table 1 may be expressed by four equations, for either the symmetrical or antisymmetrical conditions of the rectangular plate. Accordingly, Eq. 4 is the solution embracing all the classifications of the boundary conditions listed in Table 1, subject to the determination of the corresponding four sets of constants, A_{2m}, A_{1m}, B_{2m}, and B_{1m}, consistent with the boundary conditions assigned.

It is evident that equations similar to Eq. 4 can be set up for the antisymmetrical and also for the general or nonsymmetrical plate conditions.

The set of four equations, which represents all the classifications of Table 1, expresses the equilibrium of the plate at its boundary edges. These equations may be written as[9]

$$[w_{yyy} + (2 - \mu) w_{xxy}]_{y=\pm b/2} = \lambda_2 (w_{xxxx})_{y=\pm b/2} \ldots\ldots\ldots\ldots (5)$$

$$[w_{xxx} + (2 - \mu) w_{yyx}]_{x=\pm a/2} = \lambda_1 (w_{yyyy})_{x=\pm a/2} \ldots\ldots\ldots\ldots (6)$$

$$[w_{yy} + \mu w_{xx}]_{y=\pm b/2} = \kappa_2 (w_{xxy})_{y=\pm b/2} \ldots\ldots\ldots\ldots (7)$$

$$[w_{xx} + \mu w_{yy}]_{x=\pm a/2} = \kappa_1 (w_{yyx})_{x=\pm a/2} \ldots\ldots\ldots\ldots (8)$$

Eqs. 5 and 6 are statements for the equilibrium of the transverse reaction between the plate and the beams at the edges $y = \pm b/2$ and $x = \pm a/2$, respectively. The parameters λ_2 and λ_1 denote the ratios of the flexural rigidities of the beams to the plate at the edges $y = \pm b/2$ and $x = \pm a/2$; that is, $\lambda_2 = E_2 I_2 / N$, $\lambda_1 = E_1 I_1 / N$, in which E_2 and E_1 denote the moduli of elasticity, and I_2 and I_1 the moments of inertia, of the corresponding beams. It is assumed that only forces transverse to the plane of the plate are transmitted between the plate and beams.

---

[9] "Theory of Plates and Shells," by S. Timoshenko, McGraw-Hill Book Co., Inc., New York., N. Y., 1940, p. 89.

Eqs. 7 and 8 are expressions for the equilibrium in the moment between the plate and the beams about the axes coinciding with the edges $y = \pm b/2$, $x = \pm a/2$, respectively. The parameters κ_2 and κ_1 denote the ratios of the torsional rigidities of the beams to the flexural rigidity of the plate at the edges $y = \pm b/2$, $x = \pm a/2$; that is, $\kappa_2 = H_2/N$ and $\kappa_1 = H_1/N$. It is assumed that longitudinal stresses caused by warping restraint may be neglected in the beams under torsion.

The various classifications in Table 1 correspond to setting at zero or allowing the values of λ_2 and λ_1, or κ_2 and κ_1, or both pairs of parameters to approach infinity. The central position in the table corresponds to all the finite values for all these parameters.

Eqs. 5 to 8 are the means for the determination of the constant coefficients for the solution of the problem. The process could be used in a straightforward manner as a means of obtaining a solution having general application to all the classifications of Table 1. However, to simplify the presentation, the method is applied to the simply, flexurally supported panel, corresponding to line 1 of Table 1.

SIMPLY, FLEXURALLY SUPPORTED RECTANGULAR PLATES UNDER UNIFORM LOAD

The formal solution for the simply, flexurally supported rectangular plates under uniform load is the inclusive solution given by Eq. 4. The particular integral utilized, corresponding to the uniform loading assigned, is

$$\phi = \frac{2\,p}{a\,N} \sum_{m=1,3,\cdots}^{\infty} s(m)\,\alpha^{-5}\cos\alpha\,x + \frac{2\,p}{b\,N} \sum_{m=1,3,\cdots}^{\infty} s(m)\,\beta^{-5}\cos\beta\,y \ldots (9)$$

in which $s(m)$ is a convenient method of representing the alternating sign; that is, $s(m) = (-1)^{(m-1)/2}$, with m equal to $1, 3, \cdots$ in succession. The problem reduces to one of determining the values of the arbitrary constants contained in the solution, consistent with Eqs. 5 to 8, by setting $\kappa_1 = \kappa_2 = 0$. Accordingly, Eq. 7 becomes, for simple support,

$$(w_{yy} + \mu\,w_{xx})_{y=\pm b/2} = 0 \ldots\ldots\ldots\ldots\ldots\ldots\ldots (10)$$

Substitution in Eq. 10, which is an equation for the derivatives of Eq. 4, yields

$$\begin{aligned} - s(m)\,\frac{2\,\mu\,p}{a\,N} \sum_{m=1,3,\cdots}^{\infty} \alpha^{-3}\cos\alpha\,x + 2\,k_2 + 2\,k_1\,\mu \\ + \frac{a^4}{N} \sum_{m=0,1,2,\cdots}^{\infty} \alpha^2 \left\{ \left[(1-\mu)\,A_{2m} + 2\,B_{2m} \right] \cosh\frac{b}{2}\,\alpha \right. \\ \left. + (1-\mu)\,B_{2m}\,\frac{b}{2}\,\alpha\,\sinh\frac{b}{2}\,\alpha \right\} \cos\alpha\,x = 0 \ldots (11) \end{aligned}$$

Eq. 11 can be regarded as a sum of an infinite set of equations, one equation for each value of m, and each equation containing, in all its terms, a factor comprising a trigonometric function of similar index. On elimination of this common factor, each equation is solved for the corresponding constant, A_{2m}, which results in

$$A_{2m} = \frac{s(m)\ 2\ \mu\ p\ \operatorname{sech} \frac{b}{2} \alpha}{a^5\ \alpha^5\ (1 - \mu)} - \left[\frac{2}{1 - \mu} + \frac{b}{2} \alpha \tanh \frac{b}{2} \alpha \right] B_{2m} \ldots\ldots (12a)$$

The evaluation of A_{2m} expressed by Eq. 12a and the trivial values $k_2 = k_1 = 0$ are sufficient to satisfy Eq. 11 for all values of x. Thus the monomial terms containing k_2 and k_1 are eliminated from the solution for problems of simple support.

Similarly, the equation analogous to Eq. 12a, obtained by application of Eq. 8 for the edge at $x = \pm\, a/2$, is

$$A_{1m} = \frac{s(m)\ 2\ \mu\ p\ \operatorname{sech} \frac{a}{2} \beta}{b^5\ \beta^5\ (1 - \mu)} - \left(\frac{2}{1 - \mu} + \frac{a}{2} \beta \tanh \frac{a}{2} \beta \right) B_{1m} \ldots\ldots (12b)$$

Eq. 5 becomes, on substitution of the appropriate derivatives of w,

$$\sum_{m=1,3,\ldots}^{\infty} \frac{2\ p}{b\ \beta^2} + \sum_{m=0,1,2,\ldots}^{\infty} a^4\ \alpha^3 \left\{ \left[(\mu - 1)\ A_{2m} + (1 + \mu)\ \beta_{2m} \right] \sinh \frac{b}{2} \alpha \right.$$
$$\left. + (\mu - 1)\ B_{2m} \frac{b}{2} \alpha \cosh \frac{b}{2} \alpha \right\} \cos \alpha\, x - \sum_{m=1,3,\ldots}^{\infty} \frac{s(m)\ 2\ p}{a\ \alpha} \lambda_2 \cos \alpha\, x$$
$$- \sum_{m=0,1,2,\ldots}^{\infty} \lambda_2\ a^4\ \alpha^4 \left[A_{2m} \cos \frac{b}{2} \alpha + B_{2m} \frac{b}{2} \alpha \sinh \frac{b}{2} \alpha \right] \cos \alpha\, x$$
$$+ \sum_{m=0,1,2,\ldots}^{\infty} s(m)\ b^4\ \beta^3 \left\{ \left[(\mu - 1)\ A_{1m} - 2\ (2 - \mu)\ B_{1m} \right] \cosh \beta\, x \right.$$
$$\left. + (\mu - 1)\ B_{1m}\ \beta\, x \sinh \beta\, x \right\} = 0 \ldots (13$$

The series of terms of Eq. 13, comprising mixed hyperbolic, trigonometric, and other functions, do not enable the solving for the unknown constants in a direct manner. However, by a process utilized by Hencky[4] (among others), the mixed terms are first expressed in equivalent trigonometric series, with a period of $2a$, which results in

$$\sum \cosh \beta\, x = \frac{2}{a} \sum \sum a_{1mn} \cos \alpha'\, x \ \ldots\ldots\ldots\ldots\ldots (14a)$$

$$\sum x \sinh \beta\, x = \frac{2}{a} \sum \sum b_{1mn} \cos \alpha'\, x \ldots\ldots\ldots\ldots\ldots (14b)$$

and

$$\frac{2\ p}{b} \sum_{m=1,3,\ldots}^{\infty} \frac{1}{\beta^2} = \frac{8\ p}{a\ b} \sum_{m=1,3,\ldots}^{\infty} \sum_{n=1,3,\ldots}^{\infty} \frac{s(n)}{\beta^2\ \alpha'} \cos \alpha'\, x \ldots\ldots\ldots (14c)$$

in which $s(n) = (-1)^{(n-1)/2}$, $\alpha' = n\, \pi/a$, and the indices are assumed to comprise all integers, except as otherwise indicated.

The order of summation of the double series shown in Eqs. 14 may be reversed by interchanging the indices m and n. On substitution in Eq. 13 of these series, with interchanged indices, and on elimination of the factor $\cos \alpha x$, the equation for each odd value of m is

$$\left[a^4 \alpha^3 (\mu - 1) \sinh \frac{b}{2} \alpha - \lambda_2 a^4 \alpha^4 \cosh \frac{b}{2} \alpha \right] A_{2m} + \left\{ a^4 \alpha^3 \left[(1 + \mu) \times \sinh \frac{b}{2} \alpha + (\mu - 1) \frac{b}{2} \alpha \cosh \frac{b}{2} \alpha \right] - \lambda_2 \frac{b}{2} a^4 \alpha^5 \sinh \frac{b}{2} \alpha \right\} B_{2m}$$
$$+ 2 \sum_{n=0,1,2,\cdots}^{\infty} \operatorname{sgn}' a^2 (\alpha')^3 \Big\{ b \left[(\mu - 1) A_{1n} - 2 (2 - \mu) B_{1n} \right] a_{1nm} + n (\mu - 1) B_{1n} b_{1nm} \Big\} = s(m) \frac{2 \lambda_2 p}{a \alpha} - \frac{s(m)\, 8 p}{a^2 \beta} \sum_{n=1,3,\cdots}^{\infty} \frac{1}{(\alpha')^2}$$
$$= s(m) \frac{2 \lambda_2 p}{a \alpha} - s(m) \frac{p}{\beta} \quad \ldots (15)$$

For each even value of the index m, the corresponding equation is homogeneous—that is, the right-hand side of Eq. 15 vanishes. Hence, it is sufficient to satisfy the equations for the boundary conditions by the trivial solutions for the constants of even index; that is,

$$A_{1m} = B_{1m} = A_{2m} = B_{2m} = 0, \quad m = 0, 2, 4, \cdots \quad \ldots (16)$$

Accordingly, the Fourier coefficients a_{1nm} and b_{1nm} of Eqs. 14, with interchanged indices, are evaluated only for odd values of m and n, corresponding to Eq. 15, by use of the expressions

$$a_{1nm} = \frac{s(m)\, 2 \alpha \cosh \frac{a}{2} \beta'}{(\alpha')^2 \left(\frac{m^2}{n^2} + \frac{a^2}{b^2} \right)} \quad \ldots (17a)$$

and

$$b_{1nm} = \frac{s(m)\, b \beta \sinh \frac{a}{2} \beta'}{(\alpha')^2 \left(\frac{m^2}{n^2} + \frac{a^2}{b^2} \right)} - \frac{s(m)\, 4 \beta \cosh \frac{a}{2} \beta'}{(\alpha')^3 \left(\frac{m^2}{n^2} + \frac{a^2}{b^2} \right)^2} \quad \ldots (17b)$$

These expressions for the Fourier coefficients and Eqs. 12 for A_{1m} and A_{2m} are simultaneously introduced into Eq. 15, and the terms resulting as coefficients of B_{2m} are simplified. On further simplification of the result by use of the summation,

$$\sum_{n=1,3,\cdots}^{\infty} \frac{1}{n^4 \pi^4 \left(\frac{a^2}{b^2} + \frac{m^2}{n^2} \right)} = - \frac{a}{4 m^3 \pi^3 b} \left(\tanh \frac{m \pi b}{2 a} - \frac{m \pi b}{2 a} \right) \quad \ldots (18)$$

and by the notation

$$B_{2m} = s(m)\, m^2 \pi^2 \cosh \frac{m \pi b}{2 a} B_{2m} \quad \text{. . . . . (19a)}$$

$$B_{1m} = s(m)\, m^2 \pi^2 \cosh \frac{m \pi a}{2 b} B_{1m} \quad \text{. . . . . (19b)}$$

$$\Gamma_{2m} = m \pi (3 + \mu) \tanh \frac{m \pi b}{2 a} + (\mu - 1) \frac{m^2 \pi^2 b}{2 a} \operatorname{sech}^2 \frac{m \pi b}{2 a} + \frac{2 m^2 \pi^2 \lambda_2}{(1 - \mu) a} \quad \text{. . (19c)}$$

and

$$\Gamma_{1m} = m \pi (3 + \mu) \tanh \frac{m \pi a}{2 b} + (\mu - 1) \frac{m^2 \pi^2 a}{2 b} \operatorname{sech}^2 \frac{m \pi a}{2 b} + \frac{2 m^2 \pi^2 \lambda_1}{(1 - \mu) b} \quad \text{. . (19d)}$$

the dimensionless form derived from Eq. 15 is

$$B_{2m} - \frac{8 (1 - \mu) b}{\Gamma_{2m} a} \sum_{m=1,3,\cdots}^{\infty} \frac{m^3}{n^3 \left(\dfrac{a^2}{b^2} + \dfrac{m^2}{n^2} \right)^2} B_{1n} = \frac{2 \lambda_2 2p}{m \pi (1 - \mu) a \Gamma_{2m}} - \frac{(1 - \mu) b p}{m \pi a \Gamma_{2m}}, \quad m = 1, 3, \cdots \text{. . (20a)}$$

An equation analogous to Eq. 20*a* can be derived from Eq. 6 and is of the form:

$$B_{1m} - \frac{8 (1 - \mu) a}{\Gamma_{1m} b} \sum_{n=1,3,\cdots}^{\infty} \frac{m^3}{n^3 \left(\dfrac{b^2}{a^2} + \dfrac{m^2}{n^2} \right)^2} B_{2n} = \frac{2 \lambda_1 2 p}{m \pi (1 - \mu) b \Gamma_{1m}} - \frac{(1 - \mu) p}{m \pi b \Gamma_{1m}}, \quad m = 1, 3, \cdots \text{. . (20b)}$$

The constants B_{1m}, B_{2m}, with m equal to $1, 3, \cdots$, which—with the related constants A_{1m} and A_{2m}—were required to satisfy the equations for the boundary conditions assigned, comprise the formal solution of the infinite sets of numerical equations represented by Eqs. 20.

In practice, the unknowns of Eqs. 20 are approximated by solving, in a conventional manner, partial sets of the numerical equations. An illustration of the procedure for the numerical application of Eqs. 20 is provided by the following example, which corresponds to an arbitrarily assigned value of the parameter λ.

Numerical Example.—To simplify the example, the plate is assumed to be square, and the sides are equal to a. The parametric value assigned to the plate is $\dfrac{\lambda}{a} = (1 - \mu) \dfrac{1}{4}$, in which $\mu = 0.15$. For the square plate, Eqs. 20

reduce to the same form, which for the numerical values assumed become

$$B_m - \frac{6.8\, m^3}{\Gamma_m} \sum_{n=1,3,\cdots}^{\infty} \frac{1}{n^3 \left(1 + \dfrac{m^2}{n^2}\right)^2} B_n = -\frac{0.35}{m\, \pi\, \Gamma_m}, \quad m = 1, 3, \cdots \ldots (21a)$$

A partial set of numerical equations is obtained from Eq. 21*a*, corresponding to the first six values of the index m; that is, $m = 1, 3, \cdots 11$. For a load of $p = 1$, these equations become

$$\begin{bmatrix} 0.8726 & -0.0153 & -0.0038 & -0.0014 & -0.0007 & -0.0004 \\ -0.0248 & 0.9771 & -0.0107 & -0.0052 & -0.0028 & -0.0016 \\ -0.0073 & -0.0128 & 0.9902 & -0.0063 & -0.0039 & -0.0025 \\ -0.0030 & -0.0067 & -0.0068 & 0.9945 & -0.0040 & -0.0029 \\ -0.0015 & -0.0038 & -0.0045 & -0.0042 & 0.9965 & -0.0027 \\ -0.0009 & -0.0023 & -0.0030 & -0.0031 & -0.0028 & 0.9976 \end{bmatrix} \begin{bmatrix} B_1 \\ B_3 \\ B_5 \\ B_7 \\ B_9 \\ B_{11} \end{bmatrix} \begin{matrix} = \\ = \\ = \\ = \\ = \\ = \end{matrix} \begin{bmatrix} -0.8350\times10^{-2} \\ -0.5015\times10^{-3} \\ -0.1289\times10^{-3} \\ -0.5115\times10^{-4} \\ -0.2533\times10^{-4} \\ -0.1435\times10^{-4} \end{bmatrix} \ldots(21b)$$

This set of numerical equations may be represented algebraically by the relationship $l\,c = r$, in which l is the matrix of the numerical coefficients on the left-hand side of Eqs. 21*b*; c is the column matrix comprising the unknowns B_m, with $m = 1, 3, \cdots$; and r is the column on the right-hand side of Eqs. 21*b*. The solution for c may be obtained by an iterative operational formula first reported by J. Morris,[10] and of the form:

$$c = l^{-1}\, r = (I + t + t^2 + \cdots)\, r \ldots\ldots\ldots\ldots\ldots (22a)$$

provided the matrix series indicated converges, in which t is the matrix l minus the unit diagonal; that is, $t = l - I$. Accordingly, substitution of the corresponding matrices into Eq. 22*a* yields, successively

$$\begin{array}{cccccc} r \; + & tr \; + & t(tr) \; + & t(t^2r) \; + & t(t^3r) \; = & c \; = B_m \\ -0.8350 & -0.1072 & -0.0140 & -0.0019 & -0.0002 & -0.9581\times10^{-2} \\ -0.5015 & -0.2202 & -0.0326 & -0.0043 & -0.0006 & -0.7591\times10^{-3} \\ -0.1289 & -0.0691 & -0.0116 & -0.0016 & -0.0002 & -0.2114\times10^{-3} \\ -0.5115 & -0.2971 & -0.0541 & -0.0077 & -0.0010 & -0.8715\times10^{-4} \\ -0.2533 & -0.1535 & -0.0296 & -0.0043 & -0.0006 & -0.4412\times10^{-4} \\ -0.1435 & -0.0931 & -0.0184 & -0.0027 & -0.0004 & -0.2580\times10^{-4} \end{array} \ldots(22b)$$

These values of the unknowns, on substitution into Eqs. 21*b*, agree to within one unit in the last significant digit of the respective right-hand side. The corresponding constants B_m and A_m, with $m = 1, 3, \cdots 11$, are computed by use of Eqs. 19 and 12 and converge rapidly, as follows:

$$(B_m) = (-0.3869\times10^{-3},\quad 0.1535\times10^{-6},\quad -0.6652\times10^{-9},\quad 0.6047\times10^{-11},$$
$$-0.8001\times10^{-13},\quad 0.1354\times10^{-14})$$

$$(A_m) = (0.1927\times10^{-2},\quad -0.1170\times10^{-5},\quad 0.7076\times10^{-8},\quad -0.8302\times10^{-10},$$
$$0.1348\times10^{-11},\quad -0.2702\times10^{-13})$$

These numerical values, multiplied by the applied load p, are inserted for the corresponding constants into Eq. 4. The result is the evaluation of w as a partial sum for the assigned values of the parameter λ.

---

[10] "On a Simple Method for Solving Simultaneous Linear Equations by a Successive Approximation Process," by J. Morris, *Journal*, Royal Aeronautical Soc., Vol. 39, 1935, p. 349.

Corroboration by Known Solutions.—It can be verified that, for $\lambda_1 \rightarrow \infty$ and $\lambda_2 \rightarrow \infty$, Eqs. 20 reduce to expressions that are known in literature for this limit case of nonflexural support.

Thus, for $\lambda_2 \rightarrow \infty$, from Eq. 20*a*,

$$B_{2m} = \frac{p}{m^3 \pi^3} \quad \text{(23a)}$$

$$B_{2m} = s(m) \frac{p}{m^5 \pi^5} \operatorname{sech} \frac{m \pi b}{2 a} \quad \text{(23b)}$$

and from Eq. 12*a*

$$A_{2m} = \frac{-\, s(m)\, p \left(2 + \dfrac{m \pi b}{2 a} \tanh \dfrac{m \pi b}{2 a}\right)}{m^5 \pi^5 \cosh \dfrac{m \pi b}{2 a}} \quad \text{(23c)}$$

Similarly, expressions analogous to Eqs. 23*b* and 23*c* for the constants B_{1m} and A_{1m} are derived by use of Eqs. 20*b* and 12*b*. These expressions for the values of B_{2m}, B_{1m}, A_{2m}, and A_{1m}, together with the formal expression for w in Eq. 4, complete the required solution. However, for the nonflexural case, Eq. 4 may be simplified since each solution for w_1 and w_2 separately satisfies the boundary conditions on all four sides. Since there can be only a unique solution, $w_1 = w_2 = w/2$, which is

$$\begin{aligned} 2\, p\, a^{-1} \sum_{m=1,3,\cdots}^{\infty} s(m)\, \alpha^{-5} \cos \alpha x + a^4 \sum_{m=1,3,\cdots}^{\infty} (A_{2m} \cosh \alpha y \\ + B_{2m}\, \alpha y \sinh \alpha y) \cos \alpha x = 2\, p\, b^{-1} \sum_{m=1,3,\cdots}^{\infty} s(m)\, \beta^{-5} \cos \beta y \\ + b^4 \sum_{m=1,3,\cdots}^{\infty} (A_{1m} \cosh \beta x + B_{1m}\, \beta x \sinh \beta x) \cos \beta y \quad \text{(24)} \end{aligned}$$

in which the constants A_{2m} and B_{2m} are evaluated by Eqs. 23*b* and 23*c*, and A_{1m} and B_{1m} by the analogous expressions. Thus, the left-hand side of Eq. 24, multiplied by two, agrees with a classical solution for this case of nonflexural support.[11]

It can be shown that, for the classification $\lambda_2 \rightarrow \infty$, and λ_1 finite, Eqs. 20 also reduce to corresponding expressions derived in the literature.

Other Assigned Loading.—For other load functions, particular integrals expressed as infinite trigonometric series may be introduced for ϕ in the formal solution, and equations similar to Eqs. 20 can be obtained by the same method of derivation. The left-hand sides of Eqs. 20 remain the same for all particular integrals expressed as infinite trigonometric series, evaluated for odd integer values of the index.

---

[11] "Theory of Plates and Shells," by S. Timoshenko, McGraw-Hill Book Co., Inc., New York, N. Y., 1940, p. 125.

NUMERICAL EVALUATIONS OF MOMENTS AND REACTIONS

Numerical evaluations were made by the writer of various moment and reaction coefficients for square plates over the full range of relative rigidities of the supporting beams. Rectangular plates, simply supported and uniformly loaded, were also investigated.

For square plates, values of the parameter λ were selected at intervals in the range from $\lambda = 0$ to $\lambda \rightarrow \infty$, and corresponding sets of computations of the constants B_m and A_m were computed as described previously. However, for greater accuracy, summations were carried for ten values of the index, and sets of ten numerical equations in each case were solved for the constants $\mathbf{B}_m$ with $m = 1, 3, \cdots, 19$, by the method of successive elimination as adapted for computing machines by P. D. Crout.[12]

Sets of moment and reaction coefficients were computed for ten distinct stations along the axes of symmetry, along the diagonals, and along the edges of the panel. The differential expressions used for the computation of the moments M_y comprise the left-hand side of Eq. 7. Similarly, M_x is expressed by the left-hand side of Eq. 8. The differential expressions used for the reaction at the edges $y = \pm\, b/2$ and $x = \pm\, a/2$ comprise, respectively, the left-hand sides of Eqs. 5 and 6. The evaluation for each station of the derivatives of w, appearing in the differential expressions, was effected by substitution of the constants A_m and B_m in the respective expressions for the derivatives of w, and by summation for values of $m = 1, 3, \cdots, 19$.

The results of these computations are shown in Table 2 and Figs. 3 to 7, in which $\mu = 0.15$.

TABLE 2.—MOMENT COEFFICIENTS AND DEFLECTIONS[a]

Quantity	RELATIVE STIFFNESS λ/a						
	0.0	0.10	0.25	0.36125	1.0	3.0	∞
C_{mxy}[b]	0.125	0.0635	0.0317	0.0187	−0.01082	−0.02834	−0.03941
$\frac{w_m}{p\, a^4/N}$	0.026340	0.020587	0.015981	0.013021	0.009044	0.006015	0.004062

[a] For square, simply supported plates under uniform load p. [b] $C_{mxy} = \frac{M_{xy}}{p\, a^2}$. Moment coefficients refer to twisting moments of the corners of the panel and the deflections are at the center of the panel.

A Particular Solution.—For panels corresponding to the parametric values,

$$\frac{\lambda_2}{a} = \frac{(1 - \mu)^2\, b}{2\, a} \qquad (25a)$$

and

$$\frac{\lambda_1}{b} = \frac{(1 - \mu)^2\, a}{2\, b} \qquad (25b)$$

it is found that the various expressions for moment and reaction reduce to simple exact formulas. Thus, in all cases which correspond to Eqs. 25, the right-hand

---

[12] "A Short Method for Evaluating Determinants and Solving Systems of Linear Equations with Real or Complex Coefficients," by P. D. Crout, *Transactions*, AIEE, Vol. 60, 1941, pp. 1235–1240.

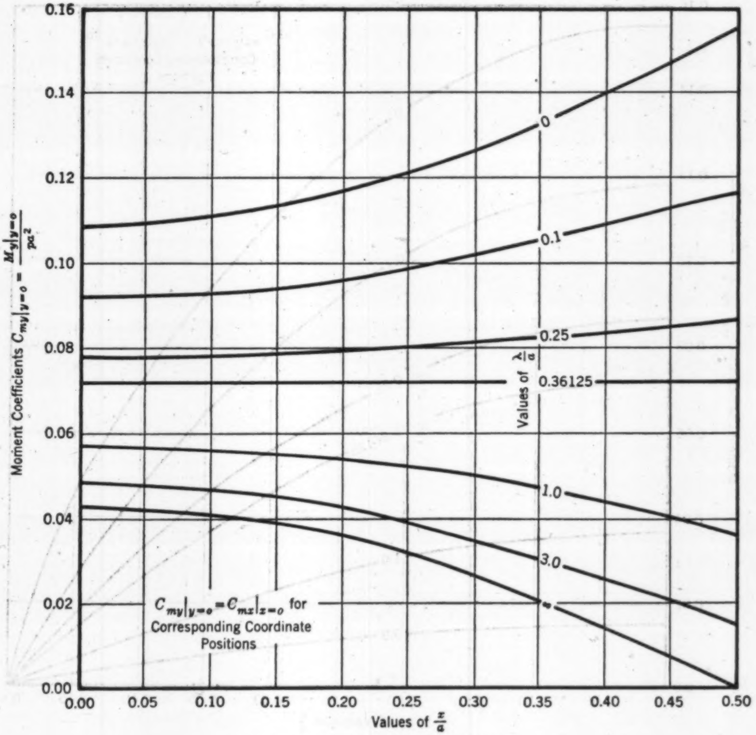

FIG. 3.—MOMENT COEFFICIENTS $C_{my}|_{y=0}$

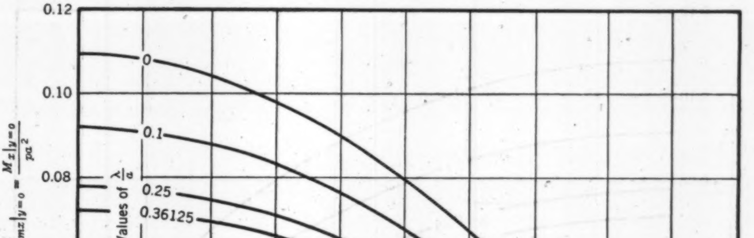

FIG. 4.—MOMENT COEFFICIENTS $C_{mx}|_{y=0}$

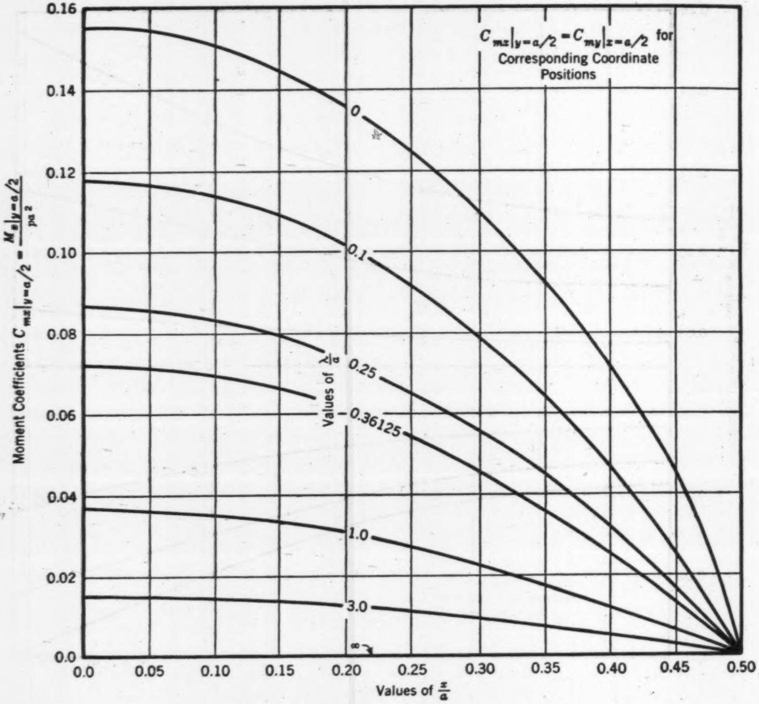

FIG. 5.—MOMENT COEFFICIENTS $C_{mx}|_{y=a/2}$

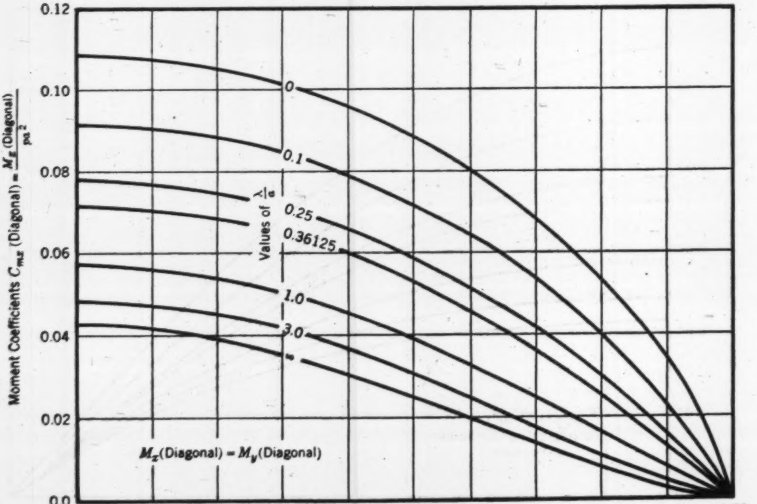

FIG. 6.—MOMENT COEFFICIENTS C_{mx} (DIAGONAL)

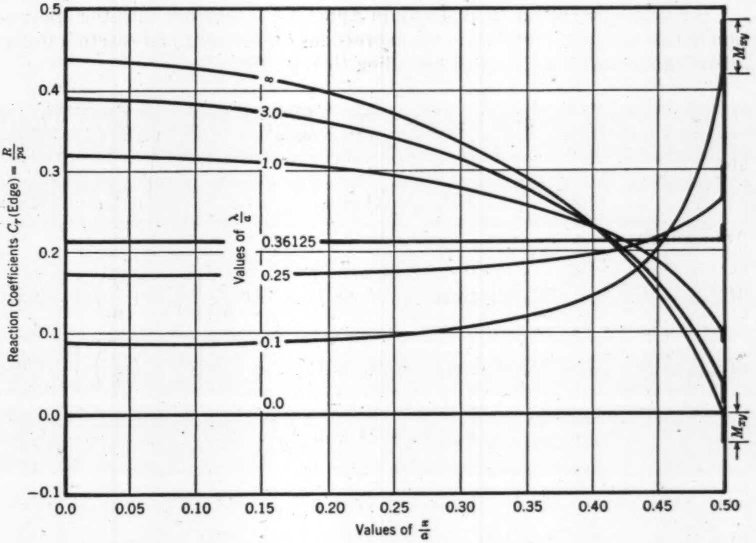

FIG. 7.—REACTION COEFFICIENTS C_r (EDGE)

sides of Eqs. 20 vanish; hence, in all these cases the trivial values $B_{2m} = B_{1m} = B_m = 0$ with $m = 1, 3, \cdots$, are sufficient to satisfy the equations for the boundary conditions. For all these cases, the corresponding constants obtained are

$$A_{2m} = \frac{s(m)\, 2\, \mu\, p \operatorname{sech} \dfrac{m\, \pi\, b}{2\, a}}{(1 - \mu)\, m^5\, \pi^5} \ldots\ldots\ldots\ldots\ldots\ldots (26a)$$

and

$$A_{1m} = \frac{s(m)\, 2\, \mu\, p \operatorname{sech} \dfrac{m\, \pi\, a}{2\, b}}{(1 - \mu)\, m^5\, \pi^5} \ldots\ldots\ldots\ldots\ldots\ldots (26b)$$

The terms containing A_m which appear in the various differential expressions for moment and reaction are further simplified for the values indicated by Eqs. 26, with the aid of the relationship

$$a^{-1} \sum_{m=1,3,\cdots}^{\infty} s(m)\, \alpha^{-3} \operatorname{sech} \alpha \frac{b}{2} \cosh \alpha\, y \cos \alpha\, x$$

$$= b^{-1} \sum_{m=1,3,\cdots}^{\infty} s(m)\, \beta^{-3} \operatorname{sech} \beta \frac{a}{2} \cosh \beta\, x \cos \beta\, y$$

$$+ a^{-1} \sum_{m=1,3,\cdots}^{\infty} s(m)\, \alpha^{-3} \cos \alpha\, x - b^{-1} \sum_{m=1,3,\cdots}^{\infty} s(m)\, \beta^{-3} \cos \beta\, y \ldots (27)$$

The derivation of Eq. 27 is shown in Appendix I, together with the application of this equation in reducing the expressions for moment and reaction to the following simple formulas (corresponding to Eqs. 25).

$$M_y|_{y=0} = 2\,(1+\mu)\,p\,b^2 \sum_{m=1,3,\dots}^{\infty} \frac{s(m)}{m^3\,\pi^3} = (1+\mu)\,\frac{p\,b^2}{16} \quad \dots\dots (28a)$$

and

$$M_x|_{x=0} = (1+\mu)\,\frac{p\,a^2}{16} \quad \dots\dots (28b)$$

Analogously,

$$M_x|_{y=0} = M_x|_{y=b/2} = M_x\,(\text{diagonal}) = M_x = (1+\mu)\,\frac{p\,a^2}{4}\left[\frac{1}{4} - \left(\frac{x}{a}\right)^2\right] \quad \dots (29a)$$

$$M_y|_{x=0} = M_y|_{x=a/2} = M_y\,(\text{diagonal}) = M_y = (1+\mu)\,\frac{p\,b^2}{4}\left[\frac{1}{4} - \left(\frac{y}{b}\right)^2\right] \quad \dots (29b)$$

$$V_y|_{y=b/2} = (1-\mu)\,\frac{p\,b}{4} \quad \dots\dots (30a)$$

$$V_x|_{x=a/2} = (1-\mu)\,\frac{p\,a}{4} \quad \dots\dots (30b)$$

and

$$M_{xy}|_{x=a/2,\ y=b/2} = M_{xy}|_{y=b/2,\ x=a/2} = -\tfrac{1}{8}\,\mu\,p\,a\,b \quad \dots\dots (31)$$

Eqs. 28 to 31 can be corroborated by the procedure previously described for sets of numerical evaluations, with numerical values determined from Eqs. 25 substituted for the constants A_m. A polynomial expression for w, conforming to Eqs. 25, and Eqs. 28 to 31, constructed independently of the general solution, is provided in Appendix I.

EXPERIMENTAL VERIFICATION

Experimental verification of the analysis previously presented was sought by two introductory tests of plates simply supported on beams of arbitrary flexural rigidity. Glass and gypsum plaster were selected as plate materials because of the ideal linearity of the stress-strain relationship to the point of rupture for both materials. It was thought that the test results could be simplified by the use of plaster that would allow for the casting of the model with the supporting beams embedded symmetrically within the slab thickness. Also, from preliminary tests with sample specimens, it was concluded that commercial resistance type strain gages are convenient to use with plaster models and yield consistent results.

Model Specifications and Test Procedure.—The test model dimensions and the details of support are shown in Fig. 8. The uniform loading was applied in each test by water contained in a rubberized fabric tank, placed in contact with the plate. The tank portions extending beyond the panel boundaries were supported independently of the panel in order to eliminate any vertical component of pull on the panel edges. Strains in the plate and beam surfaces were observed by means of SR-4 resistance strain gages, type A-5, bonded to the plates in the positions shown in the plan views.

Test 1.—The plate material consisted of commercial plate glass, nominally $\frac{1}{4}$ in. thick. The four supporting bars were of steel, with mitre cut at the ends and arranged in a frame, as shown in Fig. 8(*b*). The supports for the bars at each corner of the frame consisted of a small disc, which was laid flat on a rigid plane base. For this preliminary test, the gages were applied on one side of the glass plate and of the supporting bar. The glass was first placed with gages on the compression side. After taking initial readings, strain observations were recorded corresponding to three increments of water head. The water was then removed, the plate reversed, successive increments of load reapplied, and corresponding tensile strains recorded.

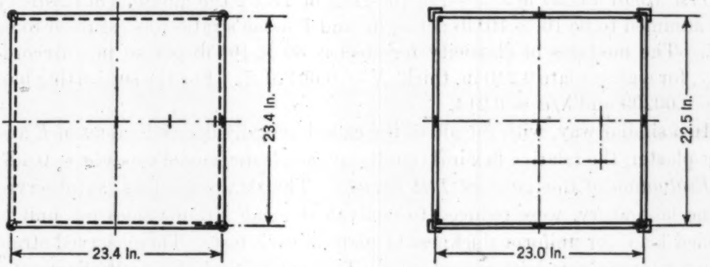
23.4 In.
23.4 In.
22.5 In.
23.0 In.

(*a*) PLAN VIEW, TEST PANEL 1

(*c*) PLAN VIEW, TEST PANEL 2

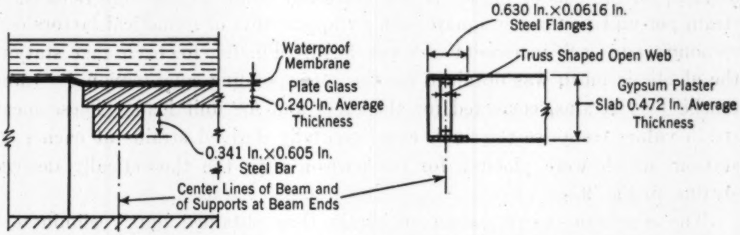
Waterproof Membrane
Plate Glass
0.240-In. Average Thickness
0.341 In.×0.605 In. Steel Bar
Center Lines of Beam and of Supports at Beam Ends
0.630 In.×0.0616 In. Steel Flanges
Truss Shaped Open Web
Gypsum Plaster Slab 0.472 In. Average Thickness

(*b*) SECTION, TEST PANEL 1

(*d*) SECTION, TEST PANEL 2

FIG. 8.—DETAILS OF TEST PANELS

Test 2.—The gypsum plaster used for the plate material was of a commercial variety with a water-plaster ratio of 70:100 by weight. The supporting beams, which were fabricated with open webs, were embedded in the cast slab along the edges and were connected at the panel corners to small blocks resting on jacks. Strain gages were applied on the top and bottom surfaces of the panel and supporting beams, usually in pairs at each gage station. Other gages, not indicated on the figure, were applied on the panel close to the beams, and on the beams close to the ends, to determine whether simple support was realized.

Successive increments of water head were applied and corresponding strain readings were recorded. Following each increment of head, the water was entirely removed to ascertain whether the strain readings reverted to the initial zero values with each release of the load.

The modulus of elasticity of the plaster was determined by specimens in the shape of small flat beams cast from the same batch as used for the test panel, and also by a specimen cut out from the test panel at the conclusion of the experiment. From tests of these specimens in flexure, a mean value was determined for the modulus of elasticity of the plaster of 1.22×10^6 lb per sq in. Poisson's ratio was determined experimentally to be 0.14.

Test Model Values of λ/a.—For the glass of Test 1 the modulus of elasticity was assumed to be 10×10^6 lb per sq in. and Poisson's ratio was assumed to be 0.21. The modulus of elasticity for steel is 30×10^6 lb per sq in. Accordingly, for a glass plate 0.240 in. thick, $N = 0.00120\,E$. For the supporting bar, $I_1 = 0.00200$ and $\lambda/a = 0.214$.

In a similar way, with the aid of the experimentally derived values of E and μ for plaster, the relative flexural rigidity of the plaster model was $\lambda/a = 0.407$.

Evaluation of Comparative Test Results.—The strain readings, as observed in the laboratory, were reduced to equivalent mean strain values per unit of applied load, for uniform thickness of plate in each test. The observed strain values were corrected for variation in actual thickness h_1 by multiplication of the original readings by the factor $0.24/h_1$, in the case of $\frac{1}{4}$-in. glass plate, and by $0.472/h_1$ for the plaster plate. These corrected strain values were reduced to strain per unit pound per square inch by application of numerical factors corresponding to each increment of water head. Finally, for each gage station, the algebraic mean was obtained for the corresponding compression $(-)$ and tensile $(+)$ strains, corrected for thickness and for unit load. These mean strain values comprise the final, experimentally derived strains at each gage station, which were plotted, for comparison with the theoretically derived strains, in Fig. 9.

The algebraic mean values of strain thus obtained partly eliminate a T-beam effect, whereby the strains on the top surface of the plate were consistently higher than the strains on the bottom surface, at the same gage stations. This effect was found during both tests and is attributed to the design of the panel supporting members. Accordingly, the test results shown in Fig. 9 include only algebraic mean values derived from gage readings where available in pairs—one reading for the top and one reading for the bottom surface, respectively, of plate or beam at each gage station.

For Test 2, the values plotted are the averages of these algebaric mean values for corresponding positions where available on two orthogonal axes, for various intensities of load. These average strain values further eliminate effects which are unsymmetrical with respect to the two axes.

Theoretically Derived Strain Values.—The value $\lambda/a = 0.214$, evaluated by means of the dimensions and elastic constants of model 1, agrees closely with $\lambda/a = 0.2125$, for which value of the parameter a numerical example was solved. Hence, corresponding to $\lambda/a = 0.2125$, theoretical strains $\epsilon_y|_{y=0}$, normal to an axis of the plate, were computed for points generally along the axis. These computations can be made with the aid of moment coefficients computed for corresponding positions, by means of the relationship

$$\epsilon_y = \frac{h}{2}\frac{\partial^2 w}{\partial y^2} = \frac{h}{2\,N}\frac{a^2}{(1-\mu^2)}\left(C_{my} - \mu\, C_{mx}\right) \ldots\ldots\ldots\ldots (32)$$

in which substitution is made for the dimensions h, a, and the ratio μ to conform to the test model. Theoretically derived strains thus computed for the conditions of Test 1 are plotted in Fig. 9 for comparison with test results.

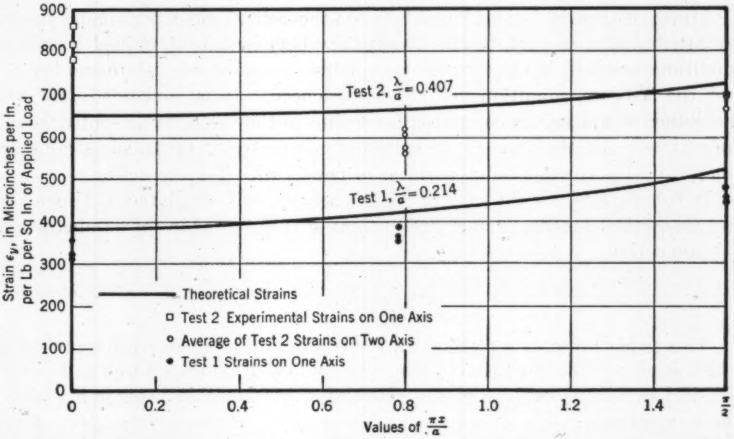

FIG. 9.—A COMPARISON OF TEST AND THEORETICAL STRAINS

Similarly, $\lambda/a = 0.407$, for model 2, is approximately equal to the parameter value 0.36125, for which the moment coefficients are expressed by exact formulas given by Eqs. 28 and 29. Hence, the moment coefficients for $\lambda/a = 0.407$ were obtained by use of Eqs. 28 and 29 and were corrected by interpolation in the sets of coefficients plotted in Figs. 2 to 5. The strains $\epsilon_y|_{y=0}$, for the conditions of Test 2, were then computed by means of Eq. 32 and plotted in Fig. 9.

Comparison Between Test and Theoretical Values.—For Test 1, the average deviation of the test strains plotted in Fig. 9, with respect to the corresponding theoretical values represented by the curve, is evaluated as 12.6%, based on the theoretical results.

For Test 2, the average deviation between respective theoretical and test values is 9.1%, where these test values represent averages derived from gage readings at corresponding positions on two orthogonal axes of the model. However, the average deviation thus computed does not include a considerable deviation (amounting to 23.6%) for a position on the test model where only uniaxial strains were available. At this position, the large deviation represents, in part, an apparent error due to the unsymmetrical strains experienced in model 2.

The curves of Fig. 9 refer only to points along the axes parallel to the panel edges. For the station on the diagonal axis, shown on the panel diagram at $(\pi x)/a = 0.8$ (approximately the quarter point), the theoretical and experimental values are, respectively, 476 and 466 microinches per in. per lb per sq in. of applied load, where, however, the experimental values are based only on uniaxial gage readings.

Test Conclusions.—The average deviations evaluated correspond to average test strain values which are 87% to 91% of the respective theoretical values. This numerical comparison, together with the graphical comparison of Fig. 9, leads to the conclusion of substantial corroboration of the analysis.

Moreover, the deviations found between theoretical and experimental strains are attributable, in part, to the discrepancy between the simplified boundary conditions assumed in the analysis (of vertical forces between plate and beams) and the T-beam condition actually experienced. It is concluded that the theoretical strain values computed according to the methods presented herein approximate the algebraic mean values of compressive and tensile strains developed on the corresponding surfaces of panels with T-beam action.

In future tests, for the sake of greater accuracy of correlation between test and theoretical results, further precautions should be taken for elimination of T-beam action.

CONCLUSIONS

This paper presents a method for the solution of boundary value problems, which is adapted to problems of transversely loaded plates, as well as to other physical problems, especially those involving harmonic or biharmonic differential equations.

The method is applied to the formulation of a solution for the problem of the rectangular plate, supported on beams along all the edges, for general values of parameters expressing the flexural and torsional rigidities of these beams. Most of the solutions in the literature on this subject apply to limit values of these parameters. As far as is known, the solution of this paper has not been obtained by other investigators.

The formal solution comprises an infinite series of terms with constant coefficients, dependent on the boundary conditions, as in most solutions of plate problems in literature. However, the determination of these constants involves the solution of sets of simultaneous linear equations. These constants, once obtained for the assigned values of the parameters and for the assigned plate proportions, serve thereafter for computation of stress and deflection coefficients for various positions in the corresponding panels. It is found that the convergence of the constants A_m and B_m with $m = 1,3, \cdots$ is very rapid. These constants, as used in expressions for shear and moment, occur in combinations of terms, the convergence of which, in extreme cases, is slow. In these extreme cases, however, the accuracy is still estimated as adequate for design or graphical purposes. Similar conclusions as to accuracy apply to the limit case, at which $\lambda \rightarrow \infty$, the solution for which is identical with the classic solution for nonflexural supports.

The detailed application of the formal solution, complete with numerical results, corresponds to the problem of simple, flexural support under uniform load. For this problem, a comparative numerical investigation was conducted of moment and reaction coefficients in relation to flexural rigidity of supporting beams. The graphs clearly show the considerable moments developed along the edges which comprise a characteristic feature of flexural support. Thus, in all square panels having a relative rigidity $\frac{\lambda}{a} < \frac{(1-\mu)^2}{2}$, the moments are maximum along the edges. The pattern of variation of reaction along the edges changes from concave downward to convex downward as the parameter lambda progresses from $\frac{\lambda}{a} > \frac{(1-\mu)^2}{2}$ to $\frac{\lambda}{a} < \frac{(1-\mu)^2}{2}$. As the parameter $\frac{\lambda}{a}$ decreases, equal increments in its value give rise to progressively larger changes in moment and shear.

For any rectangular panel, corresponding to the particular values $\frac{\lambda}{b} = \frac{(1-\mu)^2}{2}$ and $\frac{\lambda}{a} = \frac{(1-\mu)^2}{2}$, the derived expressions for moment reduce to simple exact formulas that represent parabolic cylinders superposed symmetrically with the axes of symmetry of the plate.

Maximum deflections, which are of general interest, are among the quantities that are easily obtained with extreme precision. From Table 2, these quantities are seen to vary from $0.026340 \frac{p\,a^4}{N}$ for $\lambda = 0$ to $0.004062 \frac{p\,a^4}{N}$ for $\lambda \to \infty$.

Introductory experimental results are found to be consistent with the theoretically computed corresponding data. The test results obtained also suggest improvements in the preparation and arrangement of panel specimens in future tests, so as to provide for increased accuracy of experimental corroboration of the theory.

Acknowledgment

This paper was based on a dissertation submitted in partial fulfillment of the requirements for the degree of Doctor of Applied Mechanics at the Polytechnic Institute of Brooklyn, at Brooklyn, New York, N. Y. Continued advice and constructive criticism and comments were received from H. J. Reissner, Professor of Aerodynamics and Aerostructures, and from M. S. Klamkin, Instructor of Mathematics, both of the faculty of the Polytechnic Institute of Brooklyn.

APPENDIX I. DERIVATION OF EQUATIONS

Since $w_1 = w_2$, application of the same differential operator to w_1 and w_2 yields

$$(w_1)_{xx} + (w_1)_{yy} = (w_2)_{xx} + (w_2)_{yy} \quad \text{(33)}$$

Substitution in Eq. 33, by termwise differentiation of Eq. 24, results in Eq. 27.

The following equations are obtained from Eq. 27 by termwise differentiation or integration—that is, by the differentiation of Eq. 27 with respect to y,

$$\sum_{m=1,3,\cdots}^{\infty} \frac{s(m)}{b\,\beta^2} \sin\beta\,y - \sum_{m=1,3,\cdots}^{\infty} \frac{s(m)}{b\,\beta^2} \operatorname{sech}\beta\,\frac{a}{2} \cosh\beta\,x \sin\beta\,y$$
$$= \sum_{m=1,3,\cdots}^{\infty} \frac{s(m)}{a\,\alpha^2} \operatorname{sech}\alpha\,\frac{b}{2} \sinh\alpha\,y \cos\alpha\,x \,. \,. \,(34a)$$

and by the integration of Eq. 27 with respect to y,

$$- \sum_{m=1,3,\cdots}^{\infty} \frac{s(m)}{b\,\beta^4} \sin\beta\,y + \sum_{m=1,3,\cdots}^{\infty} \frac{s(m)}{a\,\alpha^3}\, y \cos\alpha\,x$$
$$+ \sum_{m=1,3,\cdots}^{\infty} \frac{s(m)}{b\,\beta^4} \operatorname{sech}\beta\,\frac{a}{2} \cosh\beta\,x \sin\beta\,y$$
$$= \sum_{m=1,3,\cdots}^{\infty} \frac{s(m)}{a\,\alpha^4} \operatorname{sech}\frac{\alpha\,b}{2} \sinh\alpha\,y \cos\alpha\,x \,. \,. \,(34b)$$

and by the differentiation of Eq. 34*b* with respect to x,

$$- \sum_{m=1,3,\cdots}^{\infty} \frac{s(m)}{a\,\alpha^2}\, y \sin\alpha\,x + \sum_{m=1,3,\cdots}^{\infty} \frac{s(m)}{b\,\beta^3} \operatorname{sech}\beta\,\frac{a}{2} \sinh\beta\,x \sin\beta\,y$$
$$= - \sum_{m=1,3,\cdots}^{\infty} \frac{s(m)}{a\,\alpha^3} \operatorname{sech}\alpha\,\frac{b}{2} \sinh\alpha\,y \sin\alpha\,x \,. \,. \,(34c)$$

It may be noted that Eqs. 23 for the constants B_{1m} and B_{2m} are the equivalent, except for a constant factor, of Eqs. 26 for the constants A_{1m} and A_{2m}. Hence, on substitution into the differential expressions for moment,

$$M_y = - N\,(w_{yy} + \mu\,w_{xx}) \,\ldots\ldots\ldots\ldots\ldots\ldots\,(35a)$$

$$M_x = - N\,(w_{xx} + \mu\,w_{yy}) \,\ldots\ldots\ldots\ldots\ldots\ldots\,(35b)$$

of Eq. 4, Eqs. 26, and the trivial values $B_{1m} = B_{2m} = 0$ in which $m = 1,3,\cdots$, it is found, with the aid of Eq. 27, that all the terms containing A_{1m} and A_{2m} vanish from the resulting expressions, which readily reduce to Eqs. 28 and 29.

Similarly, Eq. 31, for twisting moment, is readily obtained with the aid of Eq. 34*c*, from the differential expression $M_{xy} = (1 - \mu)\,N\,w_{xy}$.

Also, Eqs. 30 are readily obtained with the aid of Eq. 34*a* from the differential expressions represented by the left-hand sides of Eqs. 5 and 6.

The polynomial expression for w is constructed to satisfy the boundary condition (Eq. 10) for simple support:

$$w = \frac{p}{32\,(1-\mu)\,N} \left[(a^2 - \mu\,b^2)\,x^2 - \tfrac{2}{3}\,x^4 \right.$$
$$\left. + (b^2 - \mu\,a^2)\,y^2 - \tfrac{2}{3}\,y^4 + 4\,\mu\,x^2\,y^2 - k_0 \right] \,. \,. \,(35c)$$

in which $k_0 = \dfrac{5}{24}\,(a^4 + b^4) - \mu\,\dfrac{a^2\,b^2}{4}$.

It is found that Eqs. 5 and 6 for equilibrium are also satisfied by Eq. 35*c*, provided that the values for λ_2 and λ_1 conform to Eqs. 25. Eqs. 28 to 31 follow from Eq. 35*c*.

APPENDIX II. NOTATION

The following letter symbols, adopted for use in the paper and for the guidance of discussers, conform essentially with "American Standard Letter Symbols for Structural Analysis" (ASA Z10.8—1949), prepared by a committee of the American Standards Association with ASCE participation, and approved by the Association in 1949.

$A_{1m}, A_{2m}, B_{1m}, B_{2m}$ = arbitrary constant coefficients corresponding to each value of the index m of the series comprising the primitive of the plate differential equation;

a = panel span length measured parallel to the x-axis;

b = panel span length measured parallel to the y-axis;

C_{mx} = moment coefficient for the moment M_x;

C_{my} = moment coefficient for the moment M_y;

C_r = reaction coefficient;

c = column matrix comprising the unknowns B_m with $m = 1,3,\cdots$;

E = modulus of elasticity of the plate material:

E_1 = modulus of elasticity of supporting beam material at edges $x = \pm \frac{a}{2}$;

E_2 = modulus of elasticity of supporting beam material at edges $y = \pm \frac{b}{2}$;

H_1 = torsional rigidity of the supporting beams at edge $x = \pm \frac{a}{2}$;

H_2 = torsional rigidity of the supporting beams at edge $y = \pm \frac{b}{2}$;

h = depth or thickness of the plate material;

I = unit diagonal in a matrix;

I_1 = moment of inertia of the cross-sectional areas of the supporting beams at edge $x = \pm \frac{a}{2}$;

I_2 = moment of inertia of the cross-sectional areas of the supporting beams at edge $y = \pm \frac{b}{2}$;

k_0, k_1, k_2 = constants used in the general equation;

l = matrix of the numerical coefficients on the left-hand side of Eq. 21*b*;

M_x = bending moment per unit length about axis parallel to the y-axis, considered to be positive when causing compression in the top fibers of the plate or beams;

M_y = bending moment per unit length about axis parallel to the x-axis, same sign convention as for M_x;

M_{xy} = twisting moment per unit length of section of plate normal to the x-axis;

M_{yx} = twisting moment per unit length of section of plate normal to the y-axis;
m = index of summation;
N = flexural rigidity of the plate material;
n = index of summation;
p = intensity of the distributed load, positive downward;
r = right-hand side of Eq. 21b;
$s(m) = (-1)^{(m-1)/2}$ with $m = 1,3,\cdots$;
$s(n) = (-1)^{(n-1)/2}$ with $n = 1,3,\cdots$;
t = matrix l minus the unit diagonal I;
w = deflection of the plate, positive downward;
x, y, z = Cartesian coördinates;
$\alpha = \dfrac{m\pi}{a}$;
$\alpha' = \dfrac{n\pi}{a}$;
$\beta = \dfrac{m\pi}{b}$;
$\beta' = \dfrac{n\pi}{b}$;
ϵ = strain in the plate;
κ_1 = ratio of the torsional rigidity H_1 to the flexural rigidity N at edge $x = \pm\dfrac{a}{2}$;
κ_2 = ratio of the torsional rigidity H_2 to the flexural rigidity N at edge $y = \pm\dfrac{b}{2}$;
$\lambda_1 = \dfrac{E_1 I_1}{N}$ at edge $x = \pm\dfrac{a}{2}$;
$\lambda_2 = \dfrac{E_2 I_2}{N}$ at edge $y = \pm\dfrac{b}{2}$;
μ = Poission's ratio; and
ϕ = a particular integral.

DISCUSSION

M. Z. v. Krzywoblocki[13].—An interesting approach has been presented by the author to the problem encountered in the investigation of elastically supported plates. It appears that Mr. Fuchs has underestimated the method offered by Mr. Ritz.[6] Although this method does not usually bear Mr. Ritz's name, it has furnished many successful solutions in the theory of plates.

In 1908 Mr. Ritz proposed an approximation method for solving the problems of a variational character.[14] He proved that under some conditions the minimizing sequence converges (but stated that the limit of convergence can be quite different from the sought for solution), and he applied his method to plate problems, vibrating-string problems, and the Dirichlet problem. Subsequent investigators have made use of Mr. Ritz's work but have failed to make the proper references to the initial investigation.[15,16,17] A comparison of Mr. Ritz's work with the subsequent investigations has been made by the writer.[18] It has been shown that the principle of least work (based on the method proposed by Mr. Ritz), depending on the choice of the minimizing sequence, may yield a rapid convergence (as shown in some of the examples of S. Timoshenko) or nonsensical results (as shown by the writer). It can be assumed that each particular type of boundary-value problem is characterized by its own most proper minimizing sequence.

Other approaches (developed by S. Bergman) to the problem under investigation are the integral-operator method[19] and the method of solving the boundary-value problem.[20] Mr. Fuchs did not mention this interesting method, proposed by Mr. Bergman in 1930 and applied by the writer in 1948.[21] Other methods which can be successfully applied are those that were developed by A. Weinstein[22,23,24,25] and R. V. Southwell.[26,27]

---

[13] Prof. of Gas Dynamics and Theoretical Aerodynamics, Univ. of Illinois, Urbana, Ill.

[14] "Variational Methods for the Solution of Problems of Equilibrium and Vibrations," by R. Courant, *Bulletin*, Am. Mathematical Soc., Vol. 49, 1943, pp. 1-23.

[15] "The Approximate Solution of Two-Dimensional Problems in Elasticity," by S. Timoshenko, *Philosophical Magazine*, Vol. 47, Series 6, 1924, pp. 1095-1104.

[16] "Strength of Materials," by S. Timoshenko, D. Van Nostrand Co., Inc., New York, N. Y., 1930, Vol. 1, p. 326, Paragraph 7.1.

[17] "Theory of Elasticity," by S. Timoshenko, McGraw-Hill Book Co., Inc., New York, N. Y., 1934, p. 150, Paragraph 43.

[18] "On the So-called Principle of Least Method," by M. Z. v. Krzywoblocki, *Proceedings*, First Midwestern Conference on Solid Mechanics, Univ. of Illinois, Urbana, Ill., April, 1953.

[19] "Über Schubknickung von isotropen und anisotropen Platten," by S. Bergman, *Proceedings*, Third International Cong. of Applied Mechanics, Stockholm, Sweden, 1930, pp. 82-87.

[20] "Neuere Probleme aus der Flugzeugstatik. Über die Knickung von rechteckigen Platten bei Schubbeanspruchung," by S. Bergman, *Prikladnaja Matematika i Mekhanika*, Vol. 2, 1935, pp. 207-224.

[21] "A General Approximation Method in the Theory of Plates of Small Deflection," by M. Z. v. Krzywoblocki, *Quarterly of Applied Mathematics*, April, 1948, pp. 31-52.

[22] "Étude des spectres des équations aux dérivées partielles de la théorie des plaques élastiques," by A. Weinstein, *Mémorial des sciences mathématiques*, No. 88, 1937.

[23] "On the Unified Theory of Eingenvalues of Plates and Membranes," by N. Arojszajn and A. Weinstein, *American Journal of Mathematics*, Vol. 64, 1942, pp. 623-643.

[24] "On the Bending of a Clamped Plate," by A. Weinstein and D. H. Rock, *Quarterly of Applied Mathematics*, Vol. 2, 1944, pp. 262-266.

[25] "On a Boundary Value Problem for a Clamped Plate," by A. Weinstein and J. A. Jenkins, *Transactions*, Royal Soc. of Canada, Section 3, 1946, pp. 59-67.

[26] "Relaxation Methods Applied to Engineering Problems," by L. Fox and R. V. Southwell, *Transactions*, Royal Soc. of London, Series A, Vol. 239, 1945, pp. 419-460.

[27] "Relaxation Methods Applied to Engineering Problems," by D. G. Christopherson, L. Fox, F. S. Shaw, and R. V. Southwell, *ibid.*, pp. 461-487.

R. H. Wood.[28]—An analytical solution which rarely has been attempted because of its complexity has been obtained by the author. The problem involved is the determination of the behavior of rectangular and square plates supported on elastic beams. It is not generally understood, however, what significance the solution has in relation to structural-engineering research.

A great deal of attention has been given to the design of multi-story building frames both in the elastic field[29] and by "plastic" methods to determine the point of collapse.[30] The next logical step would be to determine what additional effects—in terms of both the behavior at working conditions and the enhancement of the collapse load—can be produced by the presence of cladding. When there are reinforced concrete floors in a building, it has been found that the reduction of stress in the supporting beams can be so large that the resulting frame action is considerably modified. In Fig. 10 there is shown a floor being subjected to a distributed load of 12 tons. The maximum recorded stress was approximately $\frac{1}{4}$ ton per sq in. The corresponding stress computed for bare frame action would be many times this amount. Consequently, the Building Research Station at Garston, Watford, Hertfordshire, England, has commenced a systematic study of "composite action" by analysis, controlled tests in the laboratory, and field tests. It will be shown that the problem which Mr. Fuchs has investigated is one of considerable practical importance.

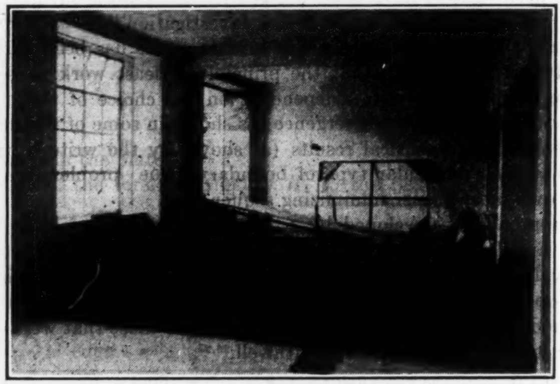

Fig. 10.—Floor Under Load

This particular floor-beam problem has been studied by the writer using the method of finite differences (for elastic behavior) and the "limit-analysis" method (for ultimate collapse); a general report on the relationship of the problem to the study of composite action in multi-story buildings is being prepared. In Fig. 11 there is shown the distribution of vertical reaction between floor and beam for a square slab with beams of equal stiffness. Fig. 11 has been drawn for the case in which Poisson's ratio is equal to zero. The British Code of Practice[31] allows the computations for elastic design to proceed on a basis of Poisson's ratio equal to zero, but as an alternative the beam loads, as shown by the dashed lines, can be used. It can be seen that Fig. 11 is of the same form as Fig. 7 after allowance has been made for the effect of Poisson's ratio. Similar agreement is found in the case of the bending moments across the center section (Fig. 12). The parameter relating beam stiffness ($E\,I$) to the flexural rigidity of the half slab $\left(N\,\frac{L}{2}\right)$ is

---

[28] Prin. Scientific Officer, Building Research Station, Garston, Watford, Hertfordshire, England.

[29] "An Economical Design of Rigid Steel Frames for Multi-Storey Buildings," by R. H. Wood, *Research Paper No. 10, National Building Studies*, Her Majesty's Stationery Office, London, England, 1951.

[30] "A Review of Recent Investigations into the Behavior of Steel Frames in the Plastic Range," by J. F. Baker, *Journal*, Inst. of C.E., London, England, January, 1949.

$$\gamma = \frac{E\,I}{N\,\frac{L}{2}} \qquad (36)$$

It is apparent that, when γ is equal to unity, a "twistless" case ensues (when μ is equal to zero)—each strip acting independently and resulting in a uniform reaction on each beam of $\frac{p\,L}{4}$ per unit length. It is interesting to note that the author has found (Fig. 7) that a uniform load on the beams can be produced in certain cases even when Poisson's ratio is not zero—that is, when the condition is not that of zero twist. Of even greater interest is the fact that the writer has discovered that a uniform beam reaction can ensue at the point of incipient plastic collapse when there is a considerable amount of twist present. This phenomenon might be termed "reaction-redistribution" and is of considerable importance in determining the behavior of composite systems near collapse.

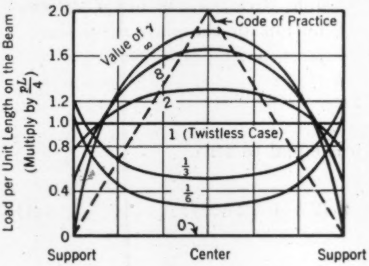

FIG. 11.—DISTRIBUTION OF LOAD INTENSITY ON THE SUPPORTING BEAMS ($\mu = 0$) FOR UNIFORM LOADING ON SQUARE SLAB

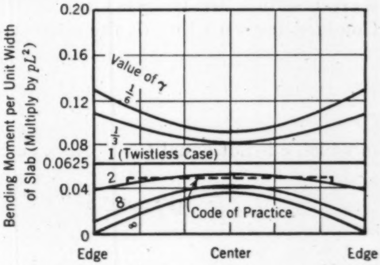

FIG. 12.—DISTRIBUTION OF BENDING MOMENT AT CENTER SECTION OF SLAB ($\mu = 0$) FOR UNIFORM LOADING ON SQUARE SLAB

There are some interesting features in the polynomial expression for the deflection of a plate. The writer has investigated the deflection of a composite slab-beam system and has found that the deflection can be expressed as

$$w = a + b\,x^2 + c\,x^4 + d\,y^2 + e\,y^4 \qquad (37)$$

---

[31] "The Structural Use of Normal Reinforced Concrete in Buildings," *British Standard Code of Practice C.P. 114*, British Standards Inst., London, England, 1948.

which is a twistless solution ($\mu = 0$), whereas Mr. Fuchs has found, for the more general case,

$$w = a + b\,x^2 + c\,x^4 + d\,y^2 + e\,y^4 + f\,x^2\,y^2 \quad \text{(38)}$$

In order that the support moments shall be zero, Eq. 38 leads to the restriction,

$$f = -\,6\,\mu\,e = -\,6\,\mu\,c \quad \text{(39a)}$$

and entails the necessary symmetry,

$$c = e \quad \text{(39b)}$$

which leads to the singular solution,

$$\gamma_x = \frac{E\,I_x}{N\,\dfrac{L_a}{2}} = \gamma_y = \frac{E\,I_y}{N\,\dfrac{L_b}{2}} = (1 - \mu)^2 \quad \text{(39c)}$$

for a rectangle of sides L_a and L_b.

It is interesting to note, however, that, if μ is small enough to be neglected, there results a greater generality in the possible variations in beam stiffness. Commencing with Eq. 37, the biharmonic equation for the plate results in

$$c + e = \frac{p}{24\,N} \quad \text{(40)}$$

in which c is not equal to e. Also, since μ is equal to zero,

$$M_x = -\,N\,\frac{\partial^2 w}{\partial x^2} = -\,N\,(2\,b + 12\,c\,x^2) \quad \text{(41)}$$

If M_x is equal to zero along the side $x = \pm L_a/2$,

$$b = -\,\frac{3}{2}\,c\,L^2_a \quad \text{(42a)}$$

and by symmetry

$$d = -\,\frac{3}{2}\,e\,L^2_b \quad \text{(42b)}$$

In the twistless case the beam-to-slab reaction is

$$V_x = Q_x - \frac{\partial M_{xy}}{\partial y} = -\,N\,\frac{\partial^3 w}{\partial x^3} = -\,24\,c\,x\,N \quad \text{(43a)}$$

Along $x = L_a/2$, Eq. 43a can be written as

$$V_x = -\,12\,L_a\,c\,N \quad \text{(43b)}$$

The load on the beam, however, is

$$E\,I_x \left(\frac{\partial^4 w}{\partial y^4}\right)_{x=L_a/2} = E\,I_x\,24\,e \dots\dots\dots\dots\dots\dots (44a)$$

so that

$$24\,e\,E\,I_x = -\,V_x = +\,12\,L_a\,c\,N \dots\dots\dots\dots\dots (44b)$$

which leads to

$$e = c\,\frac{N\,\frac{L_a}{2}}{E\,I_x} = \frac{c}{\gamma_x} \dots\dots\dots\dots\dots\dots\dots\dots (45a)$$

and

$$c = \frac{e}{\gamma_y} \dots\dots\dots\dots\dots\dots\dots\dots\dots (45b)$$

For Eqs. 45 to be applicable simultaneously, it is only necessary to have the less restrictive condition,

$$\gamma_x = \frac{1}{\gamma_y} \dots\dots\dots\dots\dots\dots\dots\dots\dots (46a)$$

or

$$\gamma_x\,\gamma_y = 1 \dots\dots\dots\dots\dots\dots\dots\dots\dots (46b)$$

It will be noticed from Eqs. 46 that there is now no restriction on the magnitudes of the beam stiffnesses. However, in this twistless case if one set of beams is strengthened, the other set must be weakened. The intensity of load on the beams is

$$\text{Along } x = \frac{L_a}{2}\,V_x = -\,\frac{p\,L_a}{2}\,\frac{1}{1+\frac{1}{\gamma_x}} \dots\dots\dots\dots\dots (47a)$$

$$\text{Along } y = \frac{L_b}{2}\,V_y = -\,\frac{p\,L_b}{2}\,\frac{1}{1+\frac{1}{\gamma_y}} \dots\dots\dots\dots\dots (47b)$$

Consequently, if Poisson's ratio is small, the reactions will be given approximately by Eqs. 47. However, because there is no restriction to the singular solution (Eq. 39*c*), it is easier to interpret the behavior of floor-beam systems.

This conception is enhanced when one attempts to determine if a twistless case can exist in continuous slab-beam systems, restricting the investigation to continuous rectangular panels supporting continuous uniform loading.

Assuming

$$N\,(1-\mu)\,\frac{\partial^2 w}{\partial x\,\partial y} = 0 \dots\dots\dots\dots\dots\dots\dots\dots (48)$$

at all points, then $\partial w/\partial y$ must be a function of y only. It follows that

$$\frac{\partial^4 w}{\partial y^4} = f'''\,(y) \dots\dots\dots\dots\dots\dots\dots\dots\dots (49)$$

Because this attempted solution represents, in effect, the behavior of independent strips, the load carried in the x-direction is not necessarily the same; therefore,

$$\frac{\partial^4 w}{\partial x^4} = \phi''' \, (x) \tag{50a}$$

from which

$$\nabla^4 w = \frac{\partial^4 w}{\partial x^4} + 2 \frac{\partial^4 w}{\partial x^2 \, \delta y^2} + \frac{\partial^4 w}{\partial y^4} = \phi''' \, (x) + 0 + f''' \, (y) = \frac{p}{N} \tag{50b}$$

If the load is shared in the proportion,

$$\phi''' \, (x) = \alpha \frac{p}{N} \tag{51a}$$

$$f''' \, (y) = (1 - \alpha) \frac{p}{N} \tag{51b}$$

then

$$\frac{\partial w}{\partial x} = \alpha \frac{p}{N} \frac{x^3}{6} + B \, x \tag{51c}$$

retaining only odd powers of x because of symmetry.

Since w is equal to zero at the corners,

$$w = \alpha \frac{p}{N} \left(\frac{x^4}{24} - \frac{L^2_a \, x^2}{48} + \frac{L^4_a}{384} \right) + (1 - \alpha) \frac{p}{N} \left(\frac{y^4}{24} - \frac{L^2_b \, y^2}{48} + \frac{L^4_b}{384} \right) \tag{52}$$

Along the edge, $y = L_b/2$, the combined reaction per unit length from the slabs on both sides is found to be $(1 - \alpha) \, p \, L_b$, and along the edge, $x = L_a/2$, the reaction is equal to $\alpha \, p \, L_a$ both of which are constant.

Because the beam is virtually built-in (because of continuity), the deflection of the long beams carrying this uniform load would be

$$w = \frac{1}{E \, I_y} (1 - \alpha) \, p \, L_b \left(\frac{x^4}{24} - \frac{L^2_a \, x^2}{48} + \frac{L^4_a}{384} \right) \tag{53}$$

but the slab deflection along $y = L_b/2$ is given by

$$w = \alpha \frac{p}{N} \left(\frac{x^4}{24} - \frac{L^2_a \, x^2}{48} + \frac{L^4_a}{384} \right) + \underbrace{(1 - \alpha) \frac{p}{N} \left(\frac{L^4_b}{384} - \frac{L^4_b}{192} + \frac{L^4_b}{384} \right)}_{\text{zero}} \tag{54}$$

Eqs. 53 and 54 are identical if

$$\frac{1}{E \, I_y} (1 - \alpha) \, p \, L_b = \alpha \frac{p}{N} \tag{55a}$$

or

$$\frac{E \, I_y}{N \, L_b} = \frac{1 - \alpha}{\alpha} = \gamma_{c,y} \tag{55b}$$

in which the subscript c denotes continuity, and each beam is now associated with a total width of slab of L_b.

Similarly,

$$\frac{E\,I_x}{N\,L} = \frac{\alpha}{1-\alpha} = \gamma_{c,x} \quad \text{(56a)}$$

from which

$$\gamma_{c,x}\,\gamma_{c,y} = 1 \quad \text{(56b)}$$

which is the condition relating slab and beam stiffnesses if the twistless case is to occur. This condition is valid for all values of Poisson's ratio, whereas the condition was only valid for μ equal to zero in the case of isolated panels. Of greater interest is the fact that Eq. 56*b* is exactly the same as the "less restricted" condition given by Eq. 46*b*. These twistless cases therefore serve as a landmark in a general study of the subject.

Fig. 13 shows the results obtained for the beam loads which appertain to continuous, square panels. Fig. 13 emphasizes the importance of studying the load distribution on the beams. The finite-difference results contain small errors which could be improved by using a finer mesh in the computations. The twistless case shows up prominently.

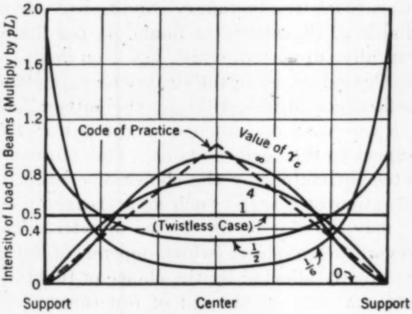

FIG. 13.—APPROXIMATE DISTRIBUTION OF LOAD INTENSITY ON THE BEAMS SUPPORTING CONTINUOUS SQUARE SLABS SUBJECTED TO CONTINUOUS UNIFORM LOADING

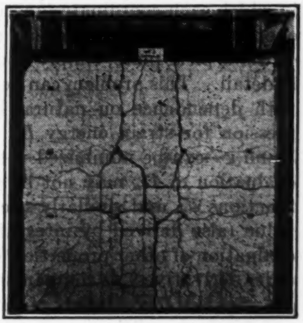

FIG. 14.—UNDERSIDE OF A COLLAPSED SLAB-BEAM SYSTEM

A brief introduction to the collapse of such slab-beam systems is of interest. Fig. 14 shows the collapse of a symmetrical square panel. The collapse mode is identified by the fracture lines (lines of full plastic moment) in the slab approximately along each center line and by the plastic hinges in the beams to form a mechanism. Above a certain critical ratio of beam-to-slab carrying capacity, theory indicates that the rectangular mode of collapse is abandoned in favor of a diagonal collapse of the slab. The supporting frame does not take part in this collapse. There is clearly a limiting load distribution collected by the beams, which is eventually insufficient to cause the beams to collapse. That is, this limiting load distribution is decided by the slab and beams working in unison. In general, it cannot be decided intuitively in advance and then coupled with a load factor.

Design on such a basis may, however, be intuitively correct in special cases. Consequently, Mr. Fuchs' analytical solution is a welcome and valuable addition to the information which is required in the study of composite structures in general.

S. J. Fuchs,[32] M. ASCE.—Interesting comments concerning developments in various aspects of the investigation of elastically supported plates have been offered by Messrs. Krzywoblocki and Wood.

Mr. Krzywoblocki's justifiable criticism is that the writer's brief comment relative to the method offered by Mr. Ritz appears to underestimate the method. Under the heading, "Introduction: Historical Note," it was stated that the usual application of the Rayleigh-Ritz method involves a minimizing sequence

$$w_n = c_1\psi_1 + c_2\psi_2 + \cdots + c_n\psi_n \qquad (57)$$

in which each coordinate function ψ_i satisfies the boundary conditions. However, functions are not readily available which satisfy the boundary conditions of the typical plate, simply and flexurally supported, which has been analyzed in detail. This problem can be investigated by use of the strain-energy method with dependence on natural boundary conditions; that is, the integral expression for strain energy D_n (w_n, λ, κ)—with dependence on the parameters λ and κ—can be minimized with respect to the coefficients c_i. This minimum evaluation of D_n may not be affected intimately by the choice of coordinate functions ψ_i, and similarly the evaluation of a scalar such as a characteristic value (also derived by integration) may likewise be unaffected directly. The evaluation of other properties, however, such as shear (which depends on third-order derivatives), is comparatively directly affected by the choice of functions ψ_i. By the formulation of the problem without the aid of functions which satisfy the conditions as imposed, the error involved in the evaluation of a property is probably increased. Furthermore, the strain-energy method as applied to the case of the typical, flexurally supported plate requires the solution of simultaneous linear equations—as is also necessary in the method offered by the writer.

In 1953 a strain-energy analysis of the clamped, flexurally supported plate was reported[33] by J. G. Sutherland, J. M. ASCE, L. E. Goodman, and N. M. Newmark, M. ASCE. Their problem admitted the use of coordinate functions, referred to previously, which facilitated the solution by satisfying the imposed boundary conditions. Certain functions, formed of combinations of Legendre polynomials, were utilized so as to satisfy explicitly the condition of zero normal slope around the boundary. For the sake of a comparison of results obtained by the alternative methods, some typical maximum moment coefficients derived by the strain-energy method[33] are listed in Table 3, together with corresponding coefficients obtained by the use of the writer's method. No shear coefficients were listed by Messrs. Sutherland, Goodman, and Newmark.[33] The complete analysis and numerical evaluation (by the writer's method) of the clamped, flexurally supported plate may be published subsequently.

---

[32] Chf. Stress Analyst, Loewy Construction Co., New York, N. Y.

[33] "Analysis of Plates Continuous over Flexible Beams," by J. G. Sutherland, L. E. Goodman, and N. M. Newmark, *Technical Report, Project NR-064-183*, Office of Naval Research, Washington, D. C., January, 1953.

The historical note was limited to a few standard solutions that have been applied to plate problems. A more extended survey would have required mention of the important methods developed by Mr. Bergman. The latter's integral-operator method, alluded to by Mr. Krzywoblocki, provides a solution for an assigned, linear, partial, differential equation as a transform of arbitrary functions. The method, however, appears to offer no particular facility in dealing with the boundary conditions typical of this subject. Futhermore, the method requires involved computations.[19,20] The writer's method is considered to be sufficiently general for many applications in engineering and was shown to reduce to standard solutions for particular cases.

TABLE 3.—MAXIMUM-MOMENT COEFFICIENTS FOR CLAMPED PLATES[a]

Coefficient	VALUE[b] OF λ_2/a AND λ/b				
	0.5	0.25	0.5	0.25	0.1
By Mr. Fuchs' method	VALUE OF b/a				
	1.0		0.75		
$-C_{mx}\|_{x=a/2,y=b/2}$	1/24	0.069043	0.035715	0.057866	0.097062
$-C_{my}\|_{x=a/2,y=b/2}$	1/24	0.069043	0.026785	0.046045	0.082592
By strain-energy method[c]	VALUE OF b/a				
	1.0		0.80		
$-C_{mx}\|_{x=a/2,y=b/2}$	1/24	0.06904	0.03704	0.06010	0.09951
$-C_{my}\|_{x=a/2\ y=b/2}$	1/24	0.06904	0.02963	0.05037	0.08775

[a] At the corners of flexurally supported clamped rectangular plates ($\mu = 0$) under uniform load, p. Thus, $M_x = C_{mx}\, p\, a^2$, and $M_y = C_{my}\, p\, a^2$. [b] Values of parameter λ refer to single panels, or one half of the total ridigity of the beam between adjacent panels. [c] As reported by Messrs. Sutherland, Goodman, and Newmark.

Mr. Wood's informative account of research on composite panel action conducted at the Building Research Station at Garston (England) indicates the alertness of investigators to the implications, in practice, of developments in the theory of transversely loaded panels. The coëfficients for moment and shear which Mr. Wood derived by another alternative method—that of difference equations—are of great value in providing the mutual corroboration required by the engineer.

The exact solution for the clamped plate classification can be derived conveniently by recognizing that the normal slope, hence the mixed derivatives

w_{xy}, vanish at each point on the boundary. Thus, it is sufficient to set f equal to zero in Eq. 38, and Eqs. 43 to 46 follow as shown.

It is agreed that elastic stress, computed (for example) by the coefficients from Table 3, are also of value in consideration of plastic stress. Thus, the residual stress caused by plastic action can be computed as the difference between plastic and elastic stress at a generic point provided that the residual effective shear does not exceed the yield strength in unloading. Thereafter, cycles of loading and unloading may be all-elastic; in these cases, elastic coefficients are necessary.

Flexurally supported panels are important in structural design. It has been usual to consider panels to be supported on beams of implied complete rigidity ($\lambda \rightarrow \infty$). The analyses and numerical data which have been made available for flexurally supported plates give the designer greater latitude and enable him to use supporting beams of arbitrary rigidity.

AMERICAN SOCIETY OF CIVIL ENGINEERS
Founded November 5, 1852
TRANSACTIONS

Paper No. 2707

AN INTERSTATE ROUTE AND ITS URBAN CONNECTIONS

By D. W. Ormsbee,[1] A. M. ASCE

Synopsis

The State of Colorado has within its borders 661 miles of federal-aid highways. This paper traces the development of the north-south highway through the state, the effect it will have on transportation within Colorado, and the cost of its construction. Special attention is given to the choice of the road's particular path and the deficiencies overcome by this highway.

The National System of Interstate Highways

A report on highway needs[2] states that:

> "The National System of Interstate Highways is the trunk line highway system of the United States. It connects all the largest cities and most of the larger ones. On its rural sections it serves 20% of the traffic carried by all rural roads. Its urban sections thus far designated, to which further designation will add an almost equal mileage, now serves more than 10% of the traffic moving over all city streets.
>
> This large measure of service is rendered by a network that includes only 1 percent of the country's total mileage of roads and streets. Without doubt, this system forms the most important connected network within the highway system for service of the economy of peace.
>
> The national military establishment has determined that this same system includes in its rural sections substantially the roads of greatest strategic importance for service of the highway necessities of war. The urban sections are rated with the same authority as of prime authority for war-time duty, and the additional urban designation desirable for service of wartime movements is identical in character with the additional needs of normal usage in peace."

This is the basis for the selection of a national system of interstate highways which several governmental groups determined as best serving both civil and military needs of the United States.

Note.—Published, essentially as printed here, in November, 1953, as *Proceedings-Separate No. 329*. Positions and titles given are those in effect when the paper was received for publication.

[1] Urban Engr., Urban Div., Dept. of Highways, Denver, Colo.

[2] "Highway Needs of the National Defense," by Thomas H. McDonald, *House Document No. 249*. 81st Cong., 1st Session, May 27, 1949, Chapters 1-2, p. 2.

The basic highway system was initiated by the Bureau of Public Roads (USBPR) in 1922. At that time the various state highway departments and the USBPR were engaged in selecting routes to comprise the federal-aid system. The United States War Department responded to a request from the USBPR for information as to the most strategic highways; the map provided by the War Department showed the important highways of the United States. It became known as the "Pershing map," and the highways represented on it were included in the federal-aid system. With revisions to May 15, 1941, this map was approved by the Secretary of War. The system of roads shown on it became known as the "strategic network," and was referred to as such in the Defense Highway Act of 1941.[3,4] The length of highways shown on the Pershing map was 78,800 miles.

On April 14, 1941, the President, Franklin D. Roosevelt, appointed a National Interregional Highway Committee to review data and suggestions presented by the USBPR. The USBPR had suggested that a more limited mileage of trunkline highways could be developed to serve national needs. Acting on the committee's report, the United States Congress directed that:[5]

> "There shall be designated within the continental United States a National System of Interstate Highways not exceeding 40,000 miles in total extent so located as to connect by routes, as direct as practicable, the principal metropolitan areas, cities, and industrial centers, to serve the national defense, and to connect at suitable border points with routes of continental importance in the Dominion of Canada and the Republic of Mexico. The routes of the National System of Interstate Highways shall be selected by joint action of the State highway departments of each State and the adjoining States, as provided by the Federal Highway Act of November 9, 1921, for the selection of the Federal-aid system. All highways or routes included in the National System of Interstate Highways as finally approved, if not already included in the federal-aid highway system, shall be added to said system without regard to any mileage limitation."

A system was accordingly selected by the several state highway departments and approved by the federal works administrator on August 2, 1947. The system approved was composed of 37,681 miles, leaving 2,319 miles of the 40,000-mile limitation for future selection. (It was expected that future selection would consist of circumferential or distributing routes within cities.) Some changes have been made, and Fig. 1 shows the 37,800-mile system.

The federal works administrator submitted to President Roosevelt a report, prepared in compliance with a directive from Congress, on the status of the improvements designated in accordance with the provisions of the act of 1944. The report supplemented all previous reports. The President transmitted this report to Congress, with recommendations for its consideration in relation to the continuance of federal aid for highway construction.[3]

The system in 1949 included 5,969 miles of streets in urban locales and 31,831 miles of rural roads located outside the limits of all towns and urban areas, representing 2% of all city streets and 1% of all rural roads. As of the

---

[3] "Highway Needs of the National Defense," by Thomas H. McDonald, *House Document No. 249*, 81st Cong., 1st Session, May 27, 1949.

[4] "Toll Roads and Free Roads," *House Document No. 272*, 76th Cong., 2d Session.

[5] Federal Highway Act: 1944, Sect. 7, Approved December 20, 1944.

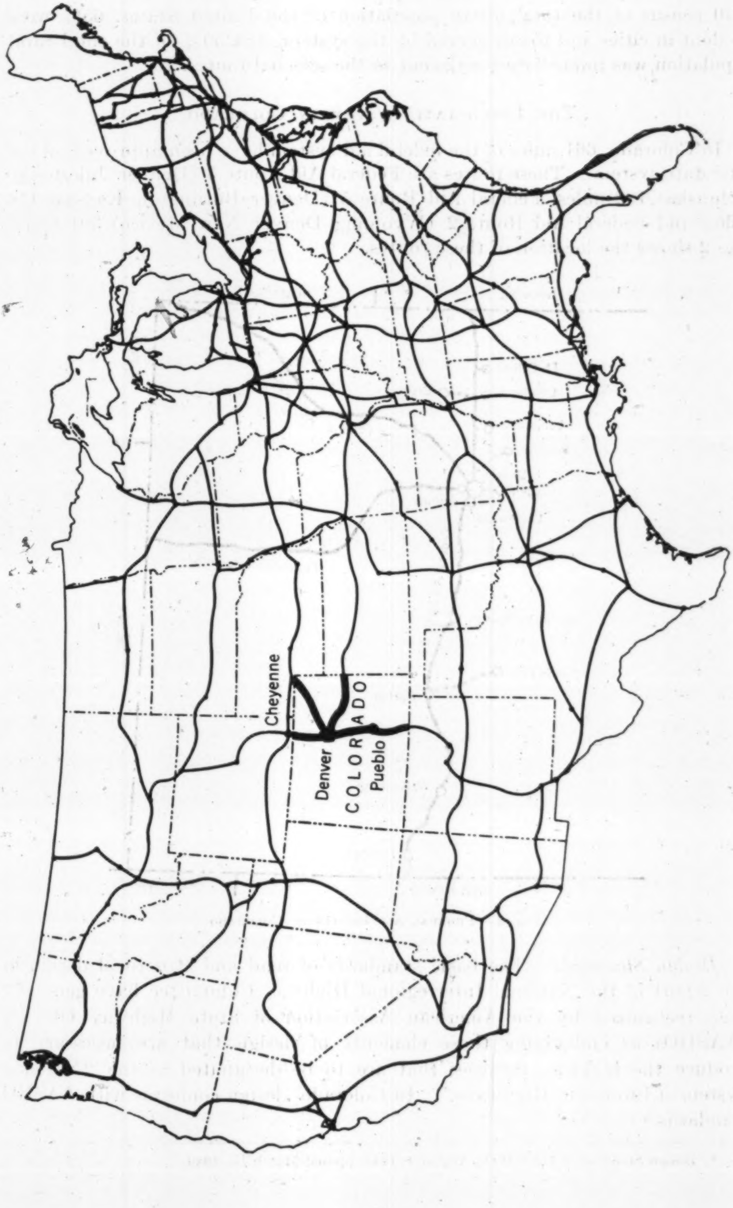
Cheyenne
Denver
COLORADO
Pueblo

FIG. 1.—NATIONAL SYSTEM OF INTERSTATE HIGHWAYS IN THE UNITED STATES

1940 census of the total urban population of the United States, 65% were resident in cities and towns served by the system, and 50% of the total rural population was immediately adjacent to the selected routes.

THE INTERSTATE SYSTEM IN COLORADO

In Colorado, 661 miles of the federal aid system have been approved on the interstate system. These routes are Federal Aid Route 3 (Denver–Julesburg–Nebraska) 182 miles, Federal Aid Route 5 (Denver–Burlington–Kansas) 178 miles, and Federal Aid Route 2 (Wyoming–Denver–New Mexico) 301 miles. Fig. 2 shows the location of these routes.

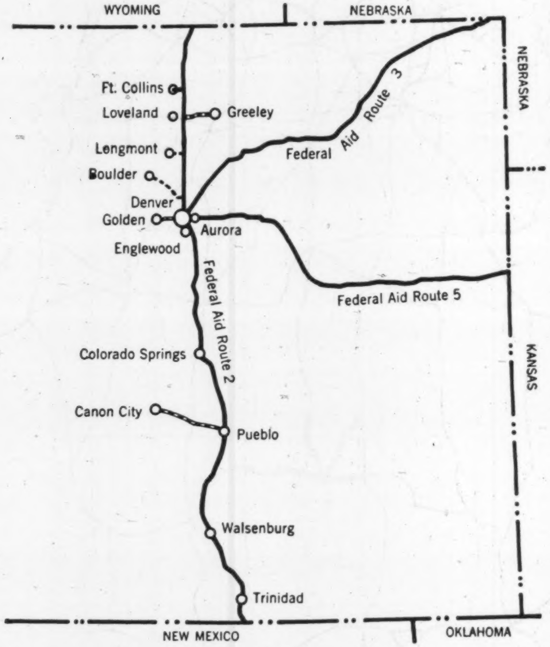
WYOMING
NEBRASKA
NEBRASKA
Ft. Collins
Loveland
Greeley
Longmont
Boulder
Denver
Golden
Aurora
Englewood
Federal Aid Route 3
Federal Aid Route 5
Federal Aid Route 2
Colorado Springs
KANSAS
Canon City
Pueblo
Walsenburg
Trinidad
NEW MEXICO
OKLAHOMA

FIG. 2.—FEDERAL AID ROUTES IN COLORADO

Design Standards.—The basic standards of road and structural design in the report of the National Interregional Highway Committee have generally been recognized by the American Association of State Highway Officials (AASHO) as embodying those elements of design that are necessary to produce the highway facilities that are to be designated as the "National System of Interstate Highways." In Colorado, design conforms with AASHO standards.[6]

---

[6] "Design Standard," A.A.S.H.O., August 1, 1945, revised March 15, 1949.

The standards proposed for the Colorado roads are intended for future traffic conditions. For the interim period, stage construction may be permitted—and for certain conditions may be necessary—to utilize values lower than the suggested minimum standards.

It was decided that the design should accommodate the thirtieth highest hourly traffic density of the year. The system provided safe and efficient facilities to serve the mixed traffic of passenger cars, motor buses, trucks, and truck combinations of a volume estimated to be that existing 20 years from the time of construction. Access to the roads was controlled by the purchase of access rights, or by the construction of frontage roads connecting the controlled-access points.

Separation of grades was required for all railroad crossings of two or more main-line tracks—regardless of traffic volume. Separation was justified (regardless of traffic volume) when six or more regular train movements were made on a single track. Protective devices were required at all railroad grade crossings. Vehicular cross traffic at grade was eliminated where design traffic density was 3,000 vehicles per hour or more. Traffic signal controls, channelized intersections, or stop controls were used where roads were not separated.

TABLE 1.—THE EFFECT OF LOCALE ON DESIGN SPEED

Location	Topography	DESIGN SPEED, IN MILES PER HOUR	
		Minimum	Desirable
Rural	Flat	60	70
Rural	Rolling	50	60
Rural	Mountainous	40	50
Urban		40	50

TABLE 2.—THE EFFECT OF DESIGN SPEED ON DEGREE OF CURVATURE

Design speed, in miles per hour	DEGREE OF CURVATURE[a]	
	Maximum	Desirable
70	4	3
60	6	5
50	9	7
40	14	11

[a] Based on the equation: Degree of curvature = 5,730/radius of curvature, in feet.

All curves with a curvature greater than 1° were superelevated. Curves sharper than 2° were designed with approach transition curves, and the maximum curvature was consistent with design speed. Sight distance requirements conformed to AASHO policy, with a preferred grade of 5% and an absolute maximum grade of 6%.

Design speeds were determined by use of Table 1, and the degree of curvature was selected by the use of Table 2.

Where the traffic density per lane was less than 200 vehicles per hour, 11-ft lanes were used. Where the density of traffic was 200 vehicles or more per hour, 12-ft lanes were constructed. In urban areas all surfacing or pavement lanes were 12 ft. Where a traffic density of 500 vehicles per hour existed (or was anticipated) the initial improvement was patterned to the ultimate development; in the case of a density of 800 vehicles per hour or more, a divided highway was constructed. Shoulders were built 10 ft wide, except in mountainous terrain, where a 4-ft width was maintained.

This paper is concerned with the status (as of 1953) and development of Federal Aid Route 2, termed the "north-south route," through Colorado between Wyoming and New Mexico. This route is a part of the interstate highway system, and it passes through the cities of Denver, Colorado Springs, Pueblo, Walsenburg, and Trinidad, and is close to Fort Collins, Loveland, Longmont, Greeley, Boulder, Golden, Aurora, Englewood, and Canon City. These fourteen of the twenty-one cities in Colorado with a population of 5,000 or more have a total population of 648,919—or 48.9% of the state's population of 1,325,089, and 78% of the population of all the cities. With the traffic on this road carrying the products of all phases of civilian and military enterprises, it is a vital part of the state and national economy.

The condition of this highway (as of 1951) is indicated in Fig. 3. The sufficiency rating was prepared by the planning and research division of the department of highways. With ratings based on structural adequacy, par 40; safety, par 30; and service, par 30; the condition of the route was as follows:

Sufficiency rating	Percent of route	Miles
80 to 100	46.4	140
70 to 79	32.0	96
Less than 70	14.0	42
Within cities	7.6	23

The appropriation for 1952 construction provided for approximately $3,670,000 for improvement of the route outside the cities. This was allocated to reconstruct the 42-mile roadway having a sufficiency rating of less than 70.

Fig. 3(*b*) is a graph showing the estimated practical capacity of the route, and the sections where surpluses or deficiencies in roadway capacity exist. Fig. 3(*c*) is a graph showing the capacity of a two-lane highway, fully developed as permitted by the terrain, with its deficiencies or surplus capacities for the traffic anticipated for 1972.

From Fig. 3 it can be seen that:

1. The sections on Federal Aid Route 2 indicated as overloaded correspond to sections rated under 80 on the sufficiency study, and the funds allocated for the 1952 construction program were properly assigned by the chief engineer and advisory board to correct the sections given lower rating.
2. The remainder of the route with a rating of less than 80 is in need of improvement.
3. The two-lane sections constructed to full standard will reach full practical capacity and hence require additional treatment.

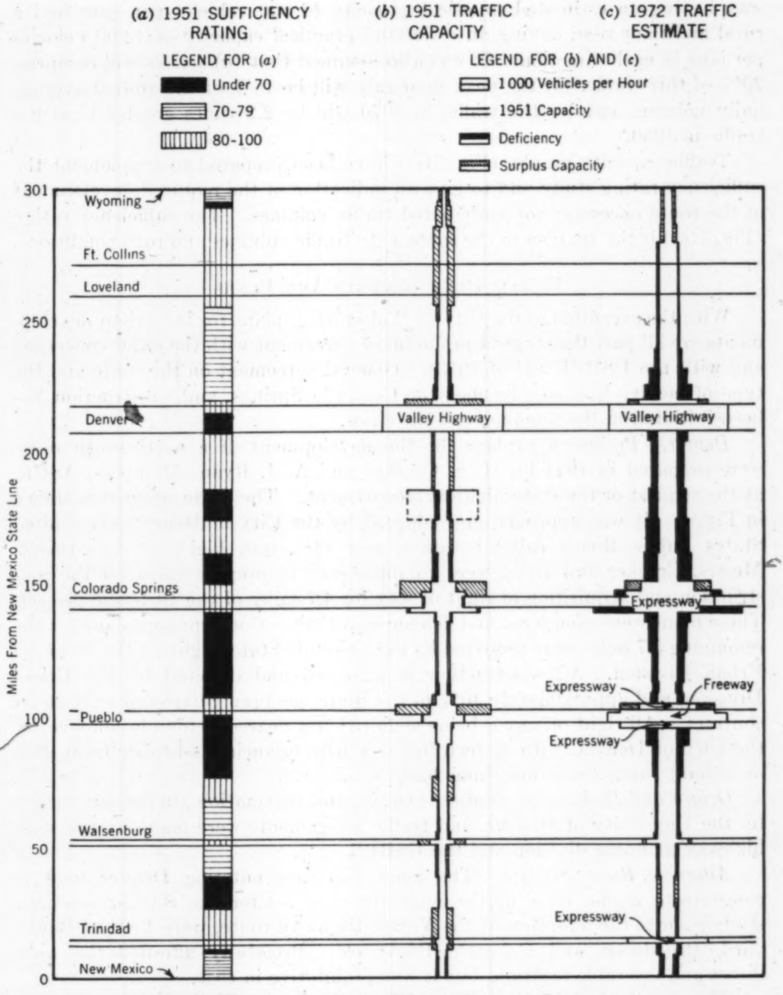

FIG. 3.—FEDERAL AID ROUTE 2 SUFFICIENCY AND CAPACITY

4. The route from Walsenburg to Fort Collins, assuming that traffic follows the estimated percentage of increase, must be improved beyond the capacity of a fully-developed two-lane road. Certain sections appear to require immediate attention.

The preparation of Fig. 3 was based on the data and methods outlined in a manual of the USBPR.[7] Fig. 3 is also based on a rural, two-way, two-lane highway having an estimated practical capacity of 900 vehicles per hour and a rural multilane road having an estimated practical capacity of 1,000 vehicles per lane in each direction. It was also assumed that (*a*) trucks will comprise 20% of this traffic, (*b*) the peak hour rate will be 16% of the annual average daily volume, and (*c*) the traffic in 1970 will be 2.2 times greater than the traffic in 1950.

---

[7] "Highway Capacity Manual," Bureau of Public Roads, U. S. Dept. of Commerce, Washington, D. C., 1950.

Traffic-capacity graphs (Fig. 3(*c*)) have been prepared to supplement the sufficiency rating study and to give an indication of the required development of the route necessary for anticipated traffic volumes. The sufficiency rating (Fig. 3(*a*)) is the analysis of the route as to traffic volumes and road conditions.

URBAN DEVELOPMENTS AND PLANS

With the exception of the City of Walsenburg, plans for the urban developments are all past the stage of preliminary agreement with the cities concerned and with the USBPR (as of 1953). General agreement on the route and the type of facility has been reached for Colorado Springs, and construction has been initiated in the remainder of the cities.

Denver.—Preliminary plans for the development of a north-south route were prepared in 1944 by H. S. Crocker and A. J. Ryan, Members, ASCE, at the request of the state highway department. The route selected is shown in Fig. 4. It was approved and adopted by the City of Denver, the United States Public Roads Administration, and the state highway department. Messrs. Crocker and Ryan were commissioned to prepare plans for the construction and acquisition of right of way for 4.7 miles of the 10.4-mile project. These plans were completed and delivered in 1946. Construction plans for the remaining 5.7 miles were prepared by the Colorado State Highway Department, Urban Division. All construction is managed and directed by the Urban Division, and approximately 40% of the route has been completed or is under contract. All right of way is being acquired and cleared to foundation level by the City of Denver, with its own funds or with financial assistance from state or federal funds on a matching basis.

Origin and Destination Studies.—Origin and destination studies were made by the University of Denver, and traffic assignments were made by the state highway planning division and the USBPR.

Alternate Route Studies.—The main highways entering Denver tend to concentrate traffic in a north-south direction. Alternate routes, receiving study prior to the adoption of the Valley Highway route, were Federal Boulevard, Broadway, and Colorado Boulevard. Broadway afforded the most direct and desirable location, but it was prohibitive in cost.

The location along the Platte River lowlands (Valley Highway) was selected as the most economical in construction and right of way. It was deemed superior to other routes also in respect to distribution and access to objective points of traffic. Not included in the Valley Highway plan itself, but developed by Messrs. Crocker and Ryan, was the Market Street plan. This route is complementary to the freeway plan, giving direct access to the principal industrial and commercial area of the city from Valley Highway. The construction of this route or a similar route was necessary to develop the full potential of Valley Highway.

Valley Highway, 10.4 miles long, extends from the northern city limit of Denver at West 52d Avenue to South Colorado Boulevard. On the north, there is a four-lane expressway for 2 miles, and funds were provided for an additional 6 miles on the interstate route, with a connection to the Boulder Turnpike. To the south, the interstate route is completed to Castle Rock, as a high-type, two-lane, concrete-pavement highway with four lanes provided on grades over 4%.

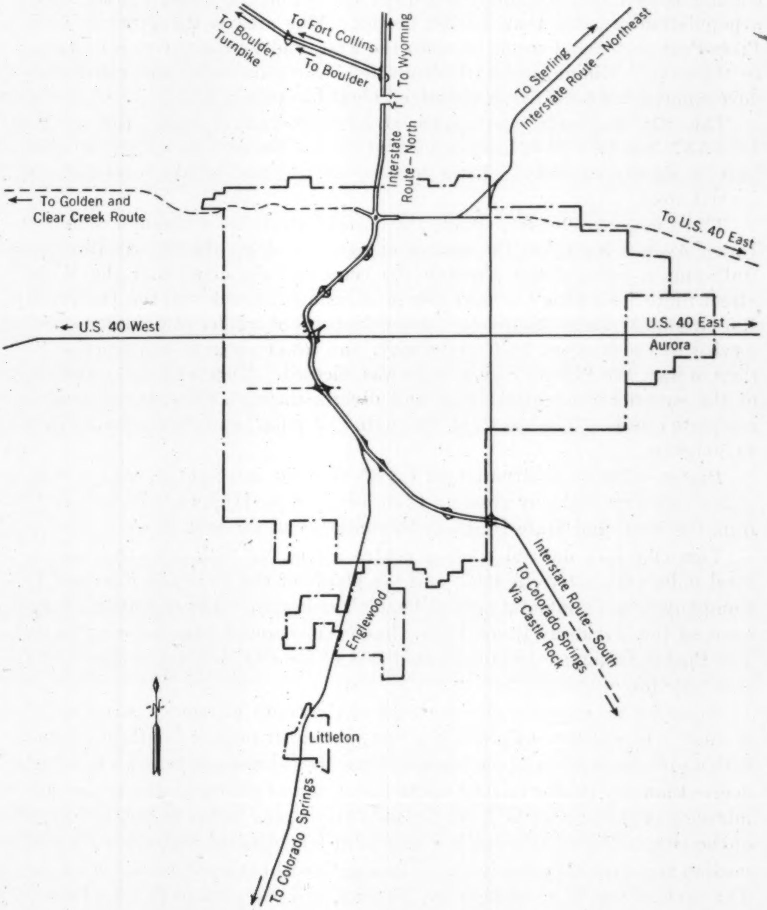
To Boulder Turnpike
To Fort Collins
To Boulder
To Wyoming
To Sterling
Interstate Route – Northeast
Interstate Route – North
To Golden and Clear Creek Route
To U.S. 40 East
U.S. 40 West
U.S. 40 East
Aurora
Interstate Route – South
To Colorado Springs Via Castle Rock
Englewood
Littleton
To Colorado Springs

FIG. 4.—VALLEY HIGHWAY IN DENVER, COLO.

The Valley Highway route within the city is a freeway. Access rights have not been secured, but sufficient width of right of way has been acquired to provide space for outer highway construction to protect the freeway. A typical section of the highway is shown in Fig. 5.

Colorado Springs.—Colorado Springs is situated on US 85-87 at its junction with US 24 and State Highway 94 on the east and US 24 on the west. Including Broadmoor, Manitou, and other developments, these highways serve a population of more than 75,000 people. This area is the gateway to the Pikes Peak region and scenic areas to the west, and tourist travel is important to the area. Mining and agriculture are basic industries, and considerable development has occurred in industrial plant location.

This city has wide north-south streets. Nevada Avenue, the route of US 85-87, has two 30-ft lanes separated by a wide median. Parallel streets have a similar capacity. These streets all traverse highly-developed residential areas.

Three major routes were made the basis of study for a through route—the Union Avenue route (on the eastern edge of the city), the Shooks Run route (following a railroad line through the center of the city), and the Walnut Street route (following the west side of Monument Creek and the Denver and Rio Grande Western Railroad). After analyses of traffic, community service, service to the western half of the city, and lower costs of construction and right of way, the Walnut Street route was selected. This route by-passes most of the superior residential areas and diverts through truck travel from inadequate routes. The length of the route is 4 miles, and its estimated cost is $4,500,000.

Pueblo.—Pueblo is situated on US 85-87 at its intersection with US 50, a prime east-west highway crossing Colorado. State Highways 76 and 96 enter from the west, and State Highway 96 continues to the east.

This city is a natural trading center served by four main-line railways. Steel mills were active in 1882, and the plants of the Colorado Fuel and Iron Company form an integral part of Pueblo's economy. The irrigation development of the Arkansas River Valley has been a sound basis for city growth. The Pueblo Ordnance Depot, located east of the city, is a major factor in the economic life of the city.

Plans for an expressway, with part of the route a freeway, were initiated in 1946. In addition to providing a rapid-transit facility for through traffic, with ample approaches to the business area, the expressway serves—to a higher degree than any similar facility which the state has planned—the movement of intracity peak-hour traffic from the industrial areas to the residential sections of the city. The expressway is a four 12-ft lane divided highway with a 30-ft median area and 10-ft shoulders. The length within the city limits is 5.4 miles. The over-all length of expressway, freeway, and connections is 8.3 miles.

The cost of the entire development was $7,500,000, of which $677,000 was expended prior to 1953.

Walsenburg.—Walsenburg is located at the junction of US 85-87 and State Highway 10 from the east, US 160 to the west, and State Highway 69 to the northwest. Through this city much of the traffic flows which originates in the San Luis Valley and the Durango areas of Colorado.

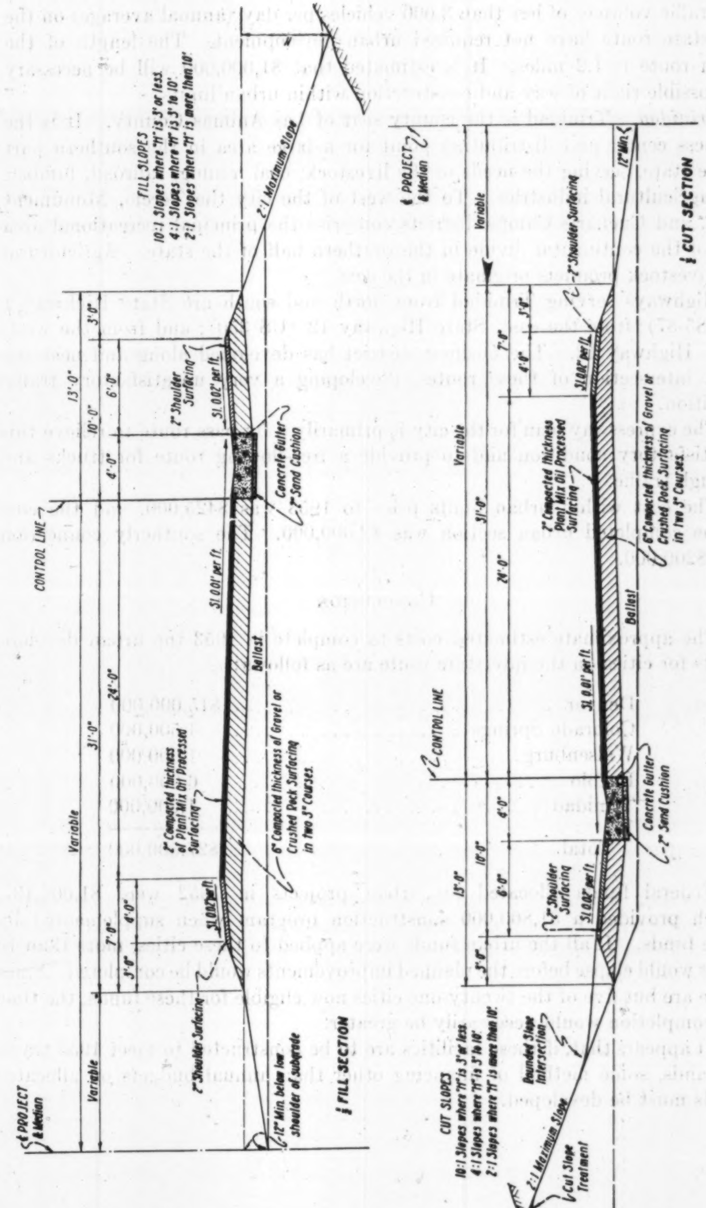

℄ PROJECT & Median
Variable
13'-0"
3'-0"
7'-0"
4'-0"
31'-0"
24'-0"
10'-0"
6'-0"
CONTROL LINE
Sl. 0.08' per ft.
Sl. 0.01' per ft.
Sl. 0.02' per ft.
2" Shoulder Surfacing
2" Compacted thickness of Plant Mix Oil Processed Surfacing
6" Compacted thickness of Gravel or Crushed Rock Surfacing in two 3" Courses.
Ballast
Concrete Gutter
2" Sand Cushion
12" Min. below low shoulder of subgrade
℄ FILL SECTION
FILL SLOPES
10:1 Slopes where "H" is 3' or less
4:1 Slopes where "H" is 3' to 10'
2:1 Slopes where "H" is more than 10'
2:1 Maximum Slope
H
CUT SLOPES
10:1 Slopes where "H" is 3' or less
4:1 Slopes where "H" is 3' to 10'
2:1 Slopes where "H" is more than 10'
Rounded Slope Intersection
Cut Slope Treatment
15'-0"
5'-0"
12" Min.
℄ CUT SECTION

FIG. 5.—TYPICAL SECTIONS OF THE VALLEY HIGHWAY

Traffic volumes of less than 3,000 vehicles per day (annual average) on the interstate route have not required urban development. The length of the urban route is 1.2 miles. It is estimated that $1,000,000 will be necessary for possible right of way and construction within urban limits.

Trinidad.—Trinidad is the county seat of Las Animas County. It is the business center and distributing point for a large area in the southern part of the state, serving the needs of the livestock, coal mining, railroad, lumber, and agricultural industries. To the west of the city the Tercio, Monument Lake, and Cucharis Camps districts comprise the principal recreational area east of the continental divide in the southern half of the state. Agricultural and livestock products originate in the east.

Highways serving Trinidad from north and south are State Highway 1 (US 85-87); from the east, State Highway 12 (US 350); and from the west, State Highway 12. The business district has developed along and near the main intersection of these routes, developing a very unsatisfactory traffic condition.

The expressway plan for the city is primarily a by-pass route to relieve this unsatisfactory condition and to provide a free-flowing route for trucks and through traffic.

The cost within urban limits prior to 1953 was $425,000, and the cost of the completed urban section was $2,000,000. The southerly connection cost $200,000.

CONCLUSION

The approximate estimated costs to complete in 1953 the urban developments for cities on the interstate route are as follows:

Denver	$15,000,000
Colorado Springs	4,500,000
Walsenburg	1,000,000
Pueblo	6,000,000
Trinidad	1,000,000
Total	$27,500,000

Federal funds allocated for urban projects in 1952 were $1,006,137, which provided a $1,800,000 construction program when supplemented by state funds. If all the urban funds were applied to these cities, more than 15 years would elapse before the planned improvements would be completed. Since these are but five of the twenty-one cities now eligible for these funds, the time for completion would necessarily be greater.

It appears that, if these facilities are to be constructed to meet 1953 traffic demands, some method of financing other than annual budgets on allocated funds must be developed.

AMERICAN SOCIETY OF CIVIL ENGINEERS
Founded November 5, 1852
TRANSACTIONS

Paper No. 2708

LIVE LOADING FOR LONG-SPAN HIGHWAY BRIDGES

By R. J. Ivy,[1] A. M. ASCE; T. Y. Lin,[2] A. M. ASCE; Stewart Mitchell,[3] M. ASCE; N. C. Raab,[4] M. ASCE; V. J. Richey,[5] A. M. ASCE; and C. F. Scheffey,[6] J. M. ASCE

With Discussion by Messrs. Louis Balog; Glenn B. Woodruff; William G. Byers; Kuang-Han Chu; and R. J. Ivy, T. Y. Lin, Stewart Mitchell, N. C. Raab, V. J. Richey, and C. F. Scheffey

Synopsis

The live loading used in designing highway bridges of short and medium spans is standardized by various codes, but the selection of a suitable live loading for long spans has been left to the discretion of the designing engineers. The writers have formulated herein a loading suitable for use as a design standard and a system of accompanying allowable unit stresses to provide for repetitions of stress and their effect upon highway bridges longer than 400 ft.

Introduction

The two standard codes now used for the design of bridges are that of the American Railway Engineering Association (11)[7] and that of the American Association of State Highway Officials (12) (AASHO). The former code applies to spans 400 ft and shorter, and the latter does not definitely state the limiting length for which the specifications govern; the AASHO does assert, however, that the live loading should be reduced for spans exceeding between 300 ft and 400 ft. The purpose of this paper is to furnish suggestions for such supplemental specifications concerning live loading and related subjects as are required for the design of long-span highway bridges.

Note.—The authors of this paper constitute a Joint Committee of the San Francisco, Calif., Section and Sacramento, Calif. Section, ASCE, as appointed November 15, 1950. Mr. Raab served as Joint Committee chairman. Published, essentially as printed here, in June, 1953, as *Proceedings-Separate No. 198*. Positions and titles given are those in effect when the paper was received for publication.

[1] Superv. Bridge Engr., State Div. of Highways, Sacramento, Calif.

[2] Associate Prof. of Civ. Eng., Univ. of California, Berkeley, Calif.

[3] Prin. Bridge Engr., Div. of Highways, Sacramento, Calif.

[4] Project Engr., San Francisco Bay Toll Crossings, Berkeley, Calif.

[5] Senior Bridge Engr., San Francisco Bay Toll Crossings, Berkeley, Calif.

[6] Dept. of Civ. Eng., Univ. of California, Berkeley, Calif.

[7] Numerals in parentheses, thus: (11), refer to corresponding items in the Bibliography (see Appendix).

The types of vehicles comprising the traffic on the various highways throughout the nation are quite varied, principally because of the nonuniformity of restrictions placed by the individual states on the size and weight of commercial carriers. The pattern of traffic including both automobiles and all the various types of trucks further complicates the problem of standardizing a live loading which could be used for long-span bridges.

The study for a design live loading for long-span highway bridges with related problems consisted of the following steps: (1) A review of the present status of live loading for highway bridges; (2) a review of loadometer station recordings; (3) a survey of long-span highway bridge traffic; (4) reduction of the data; (5) the formulation of design live loading; and (6) a study of related problems.

Various problems are interconnected with design live loading—such as reductions for multilane loadings, impact in long spans, fatigue of metals, economy, and safety. Most of these accompanying effects are being considered by other groups, and are therefore outside the scope of this paper.

REVIEW OF PRESENT STATUS

Various types of loads have been used to represent the maximum live load using the highways. Formerly the live loading used for highway bridges consisted of a load per square foot of roadway, the intensity decreasing with the loaded length of structure. As roadway stripping became prevalent, the H- and (H–S)-type of lane loading became standard for the shorter spans (12). For the longer loaded lengths, a uniform lane load with a concentration is now the most commonly-used method of evaluating the effects of live loading. A uniform load which is similar, but without concentration, is used by some engineers for the longer spans. On some projects, an empirical formula has been used, yielding a varying lane load, of which the intensity decreases in accordance with the loaded length.

The foregoing paragraph shows that there is no uniformity of practice regarding the design live loading for longer spans. Although some divergency might be unavoidable in order to meet the local conditions and special traffic requirements of a particular bridge, it is reasonable to assume that standardization of live loading for long spans is desirable.

LOADED LENGTH

The "loaded length" of a span is the length of loading required to produce the maximum live load stresses in individual members or maximum reactions in supports. Loaded lengths for simple, continuous, or other types of structures are those lengths—or summations of lengths—producing the maximum stresses or reactions of the same sign in any member. All reference in this paper to loaded span length will mean the loaded length that produces maximum stress.

BASIS FOR DESIGN LIVE LOADING

The basis of design for any long-span live loading will depend in general on the three fundamental variables listed below: (1) The weight and type of vehicles; (2) the vehicular pattern or arrangement of vehicles in a lane; and (3) the speed and spacing of vehicles.

Specific truck weights and truck types might not be representative of the vehicles traveling on all the various highways. The writers have endeavored, however, to select representative vehicle sizes, weights, and types recognized as legal in most states. An overweight truck would have a pronounced effect on the floor system of any structure or on any short-span structure; however, the longer spans are relatively insensitive to individual heavy concentrations.

The vehicular pattern, or arrangement of vehicles in a lane, varies momentarily because of the passing of the smaller and more maneuverable vehicles. The pattern also changes by the particular hour, day, month, and year. The vehicular pattern affects the longer spans more than it does the shorter spans. One or more design loads of known value can be placed on the shorter span to produce the maximum effect. On the longer spans, the accumulative effect of many of the heavier trucks produces the maximum results. Although the pattern of vehicles varies, some standard might be chosen to serve as a common basis for design.

Most highways carry traffic composed of automobiles, buses, and trucks. This mixed traffic produces a very light lane loading. Generally, the maximum proportion of automobiles to heavier vehicles is in the ratio of 4:1, and will produce, under ordinary conditions, a lane load of between 150 lb per lin ft and 250 lb per lin ft when operating at a very slow or zero speed with an allowance of about 8 ft between vehicles.

Even under mixed traffic conditions, it is conceivable that trucks alone could occupy traffic lanes for some distance, and some structures are built entirely for truck traffic. Also, there are times when civilian traffic is stopped in order to allow military convoys to pass. These conditions should be considered for any live loading for long spans.

The live loading used in the AASHO specifications (12) and the loadings referred to in this paper do not represent the heaviest truck-and-trailer combinations using the various highways in the United States. This loading is the result obtained from normal legal vehicles using the various highways.

TRAFFIC AND VEHICULAR SURVEYS

When considering the bases for design live loadings, the writers studied actual data derived from traffic studies of the lower deck of the San Francisco-Oakland Bay Bridge, in California, which is devoted entirely to heavy vehicular travel; records of the heavier vehicular traffic taken from rural loadometer stations; and studies of the weights and arrangement of vehicles in military convoys traveling the highways during maneuvers and under assignment.

To obtain a pattern of traffic on the lower deck of the San Francisco-Oakland Bay Bridge, a two-day count was taken during the peak hours. The lower deck of this bridge is composed of three 10.33-ft lanes carrying opposed traffic which uses the center lane for passing. Except for conditions peculiar to this particular bridge, these data are considered representative of segregated truck loadings which might exist on any long-span bridge. The information recorded was as follows: (1) The time of departure from tollgates; (2) classification of vehicles according to the number of axles; (3) the weight of the vehicle; and (4) the average speed of the vehicle during crossing.

Fig. 1 lists truck classifications mentioned in this paper, with diagrams of the typical vehicles for each type. The wheel-base measurement for each typical vehicle also is shown in Fig. 1.

A typical pattern of truck loadings obtained from the survey is shown in Table 1. From these data it is interesting to note that the heaviest trucks did not generally follow one another. A loading of the heaviest trucks in regular pattern would be a rare natural occurrence or a planned, regulated trip.

The actual maximum lane load obtained for the observed speed in the two-day recording of these data was only 145 lb per lin ft of lane, which is much less than the 640 lb per lin ft of lane specified by the AASHO.

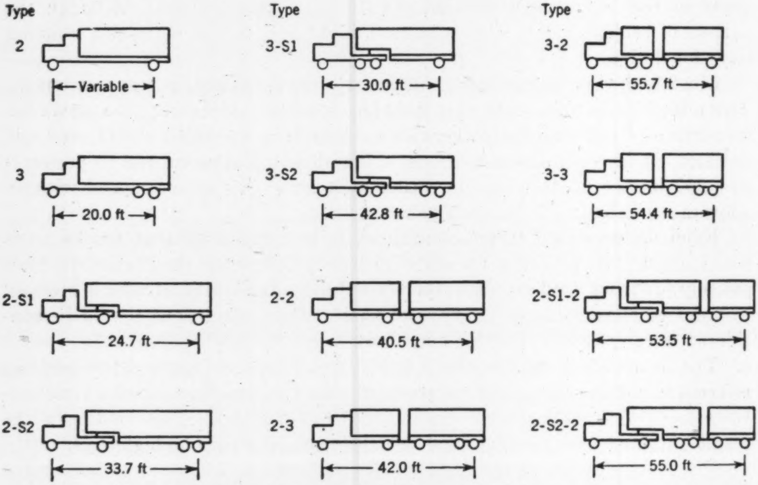

FIG. 1.—IDENTIFICATION OF TRUCK TYPES

The average weight of vehicles using the lower deck of the San Francisco-Oakland Bay Bridge is known to be less than the average weight of trucks using the highways. This is a result of the nature of the business the bridge handles and the restrictions placed on traffic using it. These factors may be summarized as follows: Short hauls, with 50% of the trucks either partly loaded or empty; prohibition of trucks carrying inflammable liquids; "peaking" of heavy bus and truck traffic at different hours; and buses which carry predominantely light loads after morning peak hours.

Records were obtained from various highway loadometer stations which showed samples of heavier vehicular loads than those found in the bridge study. Selected heavy trucks weighed at these stations averaged about 20% heavier than the vehicles using the lower deck of the San Francisco-Oakland Bay

Bridge. The actual loadometer-station pattern of the mixture of lighter trucks and heavier trucks was not obtained.

Weights and arrangement of military convoys were obtained from the manual (10) of the United States Department of the Army and from tables of organization and equipment for units such as an engineer combat battalion. This is one of the heaviest common units likely to use the highways. The average lane load with this type of unit spaced at 8 ft between vehicles is 620 lb per lin ft. The extremely heavy loads of the armored units, which would travel the highways only in an emergency, would follow normal military regulations of speeds and spacing in crossing bridges. Regulations specify 30 yd between vehicles; according to this restriction, the average lane load for a medium tank battalion is found to be 450 lb per lin ft.

TABLE 1.—TYPICAL TRUCK PATTERN (VEHICLE TYPES IDENTIFIED IN FIG. 1)

Typical axle types	DEPARTURE TIME			Truck weight, in pounds	Average speed, in miles per hour
	Hour	Minute	Second		
2	8	34	25	3,400	....
2-S1	8	34	25	28,500	25.0
2	8	34	30	26,900	30.5
2-S1	8	34	40	20,000	31.0
2	8	34	55	26,500	....
3-S2	8	35	00	56,000	26.1

REDUCTION OF TRAFFIC DATA

Before reducing the traffic data to a design live loading, speed and spacing of vehicles must be considered. In the case of the survey at the San Francisco-Oakland Bay Bridge, it was found that the average speed for all vehicles making the crossing was 34 miles per hr, although the posted speed limit for this deck is 35 miles per hr. The minimum average speed recorded was 18 miles per hr, and some stoppages occurred that resulted in zero speed.

To relate truck spacing to truck speed, the following equation was used:

$$D = K_1 v^2 + K_2 v + L + L' \qquad (1)$$

in which D is the safe following distance between centers of vehicles, in feet; K_1 is the vehicle braking constant, equal to 0.05; K_2 is the driver reaction constant, equal to 1.50; L is the length of the vehicle, in feet; L' is the minimum clear distance between vehicles, taken as 8 ft; and v is the velocity, in miles per hour.

The lane capacity, C, in vehicles per hour, may be obtained from the expression:

$$C = 5{,}280 \frac{v}{D} \qquad (2)$$

If the weight of a vehicle, in pounds, is denoted by the symbol W, the average lane load, in pounds per linear foot, is expressed as

$$w = \frac{W}{D} \qquad (3)$$

An average clear distance of 8 ft between two vehicles was measured in the field. This is the minimum space required for one vehicle to turn out and pass another when given the opportunity. Under no conditions were vehicles found stopped bumper to bumper.

TABLE 2.—AVERAGE WEIGHT AND LENGTH OF TRUCK

Truck type (see Fig. 1)	Average weight, in pounds	Over-all length, in feet	Number of trucks	Total weight, in kips	Total length, in feet
2	4,604	15.0	2,429	11,184	36,435
2	11,022	20.0	1,322	14,571	26,440
2	23,553	25.0	608	14,320	15,200
2-S1	24,568	29.7	367	9,017	10,900
2-S2	32,909	38.7	248	8,161	9,598
3-S2	44,088	47.8	209	9,214	9,990
3	17,547	25.0	177	3,106	4,425
2-S1-2	45,263	58.5	139	6,292	8,132
Others	48,264	57.8	130	6,274	7,514
Total			5,629	82,139	128,634
Average	14,592	22.9			

To determine the average length and weight of vehicles, the total truck traffic recorded during the period of the survey is shown in Table 2. A total of 5,629 trucks passed through the tollgates during these two 7-hr periods, yielding data from which was derived an average truck weight of 14.6 kips and an average length of 23 ft. Eq. 3 yields $W/D = 472$ lb per lin ft, in which D is the sum of the average over-all length plus L'.

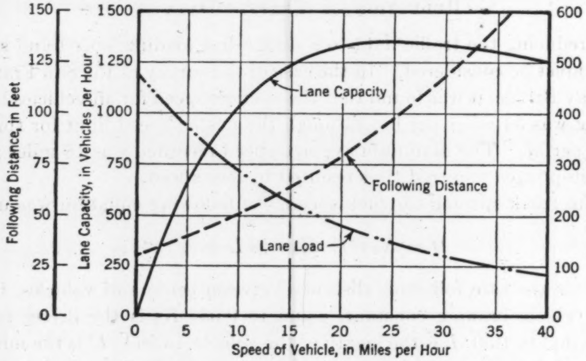

FIG. 2.—LANE LOADING CHARACTERISTICS

The average lane load for zero speed according to the information from one of the loadometer stations is 589 lb per lin ft. This loading is somewhat greater than the average loading of all trucks using the highways because only the larger and heavier loaded trucks are weighed at the loadometer stations; the loading recorded at these stations, therefore, would not be typical of the truck pattern to be discussed.

The lane capacity, following distance, and the lane load for various speeds are given in Table 3 and illustrated graphically in Fig. 2. The maximum lane capacities are obtained between speeds of 20 miles per hr to 30 miles per hr; the maximum lane load, however, is obtained at zero speed. The lane capacity for any structure depends on the physical characteristics of the particular lane—such as width, grades, alinement, shoulders, side obstructions, and other conditions. Lane capacities are also influenced by speed, safe following distances at various speeds, length, weight, and maneuverability of the vehicles.

The average truck listed in Table 2 is a composite vehicle representing all of the trucks recorded during the survey. The lane loads found on the basis of the composite truck (shown in Table 3) are of interest because they apply only to extremely long spans. These lane loads would be the lower limits for any live loading derived from the survey data. For shorter spans, the lane load would depend on the actual traffic patterns and would vary inversely with the loaded length. Actual patterns of the survey data were plotted, samples of which are shown in Fig. 3. In plotting these truck trains, the actual pattern at the tollgates was maintained. However, the spacing between the trucks has been shortened to a minimum of 8 ft. Any long-span bridge will have at least two lanes; simultaneous loading of two lanes with a pattern giving the maximum loading was considered improbable. Therefore, it was decided to use the maximum loading in one lane, averaged together with the loading for the same time period of the following day of the survey in the opposite lane. With these loading patterns established, uniform lane loads producing the same maximum moment and shear stresses, and producing maximum average lane loads, were determined for various loaded lengths. These equivalent loadings are shown in Fig. 4.

TABLE 3.—Lane Capacities and Loads

Speed, in miles per hour	Following distance, in feet	Lane capacity, in vehicles per hour	Lane loads, in pounds per foot
0	30.9	0	472
5	39.7	660	365
10	50.9	1,040	285
15	64.7	1,220	225
20	80.9	1,305	180
25	99.7	1,320	145
30	120.7	1,310	120
35	144.7	1,275	100
40	170.9	1,240	85

Design Live Loading

At first consideration of the establishment of a suitable live loading, it might appear that the pattern of mixed live loads found on the various highways and freeways in the United States should be the basis for any study of live loading.

However, the studies made in this paper indicate that a loading suitable for design purposes could not be obtained from a pattern composed of mixed traffic occurring on the various highways because of the high ratio of automobiles to trucks. This loading would be too light and would not account for the probability of the increased number, if not weight, of trucks in the future.

Spacing ft.	28.0	28.0	46.7	33.0	33.0	37.7	23.0	55.8	55.8	23.0	33.0	23.0	55.0	33.0	23.0	23.0	23.0	33.0	23.0	28.0	67.4	23.0	33.0	23.0	23.0	28.0
Truck Type	2	2	2-S2	2	2	2-S1	2	3-S2	3-S2	2	2	2	3-S2	2	2	2	2	2	2	2	3-3	2	3	2	2	2
Weight kips	7.5	9.5	17.0	21.0	26.9	30.0	3.6	25.0	66.5	2.9	27.8	2.9	29.5	26.9	10.0	3.6	3.4	26.9	3.4	14.0	71.0	3.2	37.0	7.1	3.6	12.0

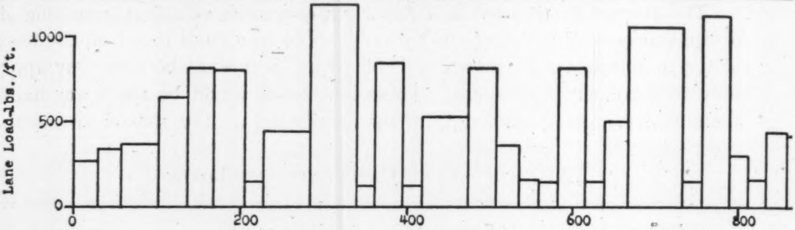

Jan. 24,

Spacing ft.	28.0	33.0	33.0	28.0	66.5	33.0	23.0	28.0	23.0	28.0	28.0	28.0	23.0	55.8	33.0	23.0	28.0	23.0	23.0	67.0	23.0	33.0	37.7	28.0	23.0	33.0	33.0
Truck Type	2	3	2	2	2-S1-2	2	2	2	2	2	2	2	2	3-S2	2	2	2	2	2	3-2	2	2	2-S1	2	2	2	2
Weight kips	9.2	11.0	21.0	10.5	53.0	26.4	3.0	16.0	2.9	9.5	13.7	8.5	3.8	21.0	18.4	3.4	17.0	4.0	3.6	65.0	2.8	24.8	25.0	9.0	3.2	19.5	24.8

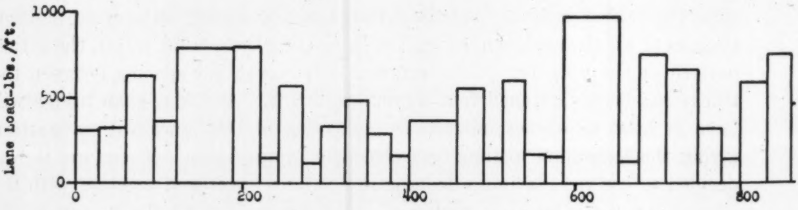

Jan. 25,

FIG. 3.—TYPICAL TRAFFIC PATTERN FOR THE LOWER DECK OF THE

The nearest approach to a maximum live loading, therefore, would seem to be the loading pattern of a military convoy occupying the entire length of a structure, or truck and bus traffic such as that running on the lower deck of the San Francisco-Oakland Bay Bridge. This latter loading, which excludes automobiles, has been found fairly representative of convoys that normally use the highways.

The variables involved make it evident that a single pattern for any one lane and for any one length should not be taken as a standard and applied to all lanes of a bridge. It is assumed that any modern bridge would have not

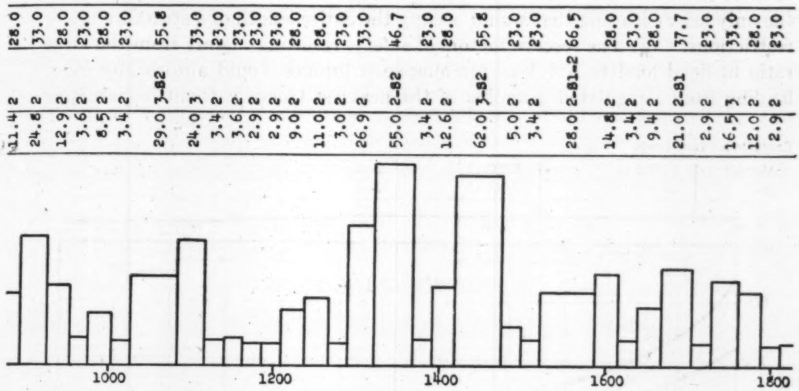

Loaded Length - ft.
1951 8:30:50 A.M. to 8:37:00 A.M., Incl.

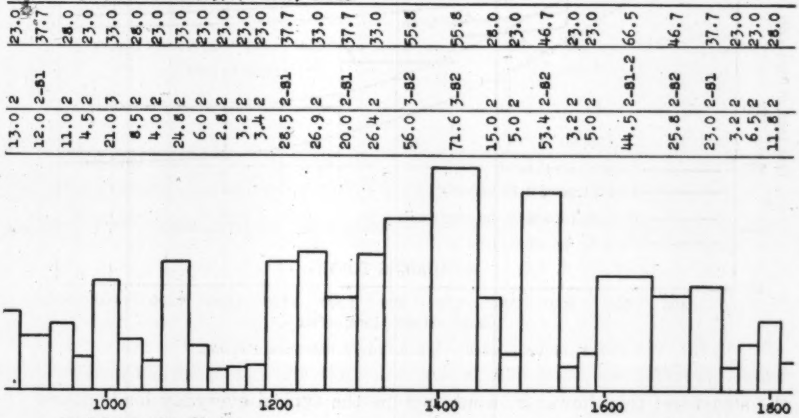

Loaded Length - ft.
1951 8:30:40 A.M. to 8:37:00 A.M., Incl.

SAN FRANCISCO–OAKLAND BAY BRIDGE—WESTBOUND TRAFFIC

less than two lanes, particularly a long-span structure on which the ratio of the width to the span would have to be maintained; consequently, the average of two typical lane patterns would be applied for any loaded length desired. The probability of having more than two lanes occupied by this average lane loading is provided for by the reduction factor in the AASHO design specifications (12).

A comparison of the data on heavy vehicles shows that the average truck on the highway is slightly heavier than the vehicles using the lower deck of the San Francisco-Oakland Bay Bridge. However, the total vehicular load on the highway is much less because the ratio of automobiles to trucks is between 4:1 and 5:1. It was decided to use the bridge pattern of loading because: (1) It more nearly fits the military convoy loading—which, it is believed, would be the only heavy loading that would occupy the entire length of a structure under restrictions. (2) The reserve factors of safety, resulting mainly from the large ratio of dead load to live load for long-span bridges, could absorb any overloading from a regulated grouping of the heaviest trucks without jeopardizing the structure; this, however, would not be the typical everyday loading and would probably never occur in the life of a structure. (3) The vehicular loading of a highway would in all cases carry mixed traffic which, in turn, would produce a lighter load than that assumed for the convoy load.

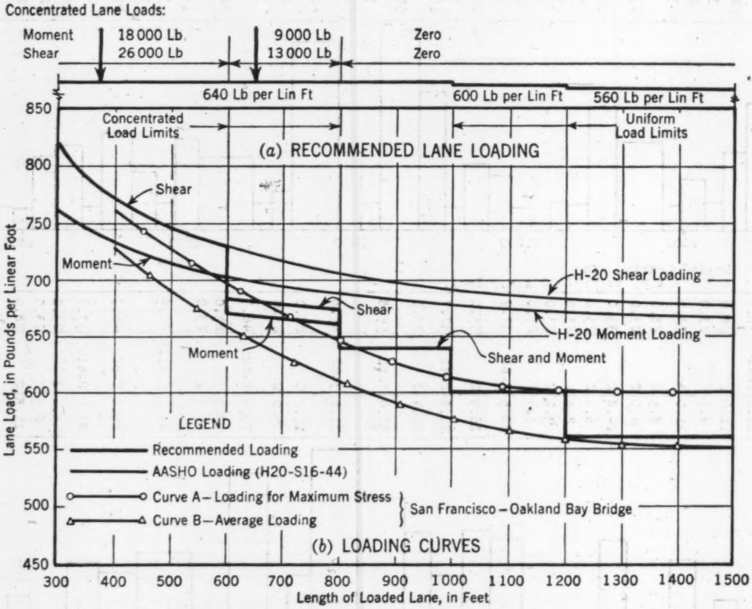

FIG. 4.—LIVE LOADING CURVES FOR LONG-SPAN BRIDGES

Several forms of loading were considered which would accurately, yet simply, represent the typical heavy vehicular pattern. It would appear, because of general usage of the AASHO live load, that some form of loading similar to this should be used for the longer spans. The recommended loading of Table 4, illustrated in Fig. 4, satisfies the vehicular pattern data and is in a form familiar to most designers.

Consideration was given to the types and limiting lengths of structures which would use this type of loading. Plate-girder bridges of one span or of more than one span, either simply supported or continuous, are usually limited by specifications to lengths not greater than 300 ft between supports. For continuous bridges, the concentrated loads should be placed so as to yield maximum reactions or stresses.

Simple-span truss bridges for highways have maximum lengths of between 500 ft and 600 ft. Here again, concentrated loads should be used to give the effect of local concentrations represented in the traffic patterns of Fig. 3.

Structures with clear spans of between 500 ft and 1,000 ft are generally cantilever bridges or continuous truss bridges. Members designed by the shorter loaded lengths will have the benefit of the concentrations. Main truss members, because of the longer loaded lengths, will be proportioned by the uniform load.

If spans are greater than 800 ft, the suspension-type bridge is nearly always considered, provided conditions at the site are favorable. Concentrated loads are difficult to apply in the analysis of a structure of this type, and the effect of concentrated loads on spans of 800 ft or greater is negligible.

TABLE 4.—RECOMMENDED MAXIMUM LIVE LOADING FOR LONG-SPAN BRIDGES

LOADED LENGTH, IN FEET		Uniform live load, in pounds per linear foot of lane	CONCENTRATED LIVE LOAD, IN POUNDS	
Minimum	Maximum		For moment	For shear
0	600	640	18,000	26,000
600	800	640	9,000	13,000
800	1,000	640	0	0
1,000	1,200	600	0	0
1,200	∞	560	0	0

This load provides a gradual reduction in intensity from the short bridges to the long-span bridges; however, sudden changes in live-load stresses will occur at the loaded lengths where the loadings change. These changes in both the web and chord stresses are less than 8% for the live load, and less than 2% when both live load and dead load are considered. The proportions of a member are ordinarily not changed for a variation of stress of this magnitude.

Fig. 4 shows graphically the variation of lane loads for different loaded lengths. The AASHO H20-S16-44 loading is included for comparison. Curve A represents the uniform lane load that will produce maximum flexural stresses and shear stresses; Curve B represents the maximum average lane load. Both curves are obtained from traffic patterns with two lanes loaded such as those shown in Fig. 3. Curves A and B envelop the curve representing the recommended live loading for long-span bridges.

RELATED SUBJECTS

The relationship between the live-load stresses and dead-load stresses in highway bridges does not remain constant with an increase of span; the live loading decreases somewhat, whereas the dead load increases more rapidly as the span increases.

Naturally, these ratios of live load to dead load will vary (even in spans of the same length) according to the width of the roadway, the type of loading, and other variables peculiar to a particular structure. Ratios of live load to dead load for various component parts of typical spans between 300 ft and 1,000 ft are listed in Table 5.

Attempts have been made to provide for the damaging effects of repeated stresses and for future increase in live loadings, by increasing the factor of safety for those parts which come into more direct contact with the live loading. The proportioning of these effects in the design of a structure has come to be known as "balanced design," and for large structures it is generally accomplished by either of the following two methods:

TABLE 5.—LOAD RATIOS, STRESSES, AND SAFETY FACTORS FOR VARIOUS BRIDGE COMPONENTS

Member	Ratio of Live Load to Dead Load		Unit Stress, in Pounds per Square Inch		Safety Factor	
	300-ft span	1,000-ft span	300-ft span	1,000-ft span	300-ft span	1,000-ft span
Slab	28.0:1	28.0:1	18,200	18,200	1.8	1.8
Stringers	4.0:1	3.0:1	19,200	19,500	1.7	1.7
Floorbeams	2.0:1	1.0:1	20,000	21,000	1.7	1.6
Verticals	1.1:1	0.7:1	20,800	21,500	1.6	1.5
Hangers	0.8:1	0.6:1	21,400	21,800	1.5	1.5
Web Members	0.6:1	0.2:1	21,800	23,000	1.5	1.4
Chords	0.3:1	0.2:1	22,600	23,000	1.5	1.4

1. Dual unit stresses are used, whereby the specified unit stress is applied to the live load, and a higher unit stress (usually one third greater) is applied to the dead load; or
2. The live loading is increased from that normally specified, and a higher unit stress is applied to both dead loads and live loads.

These two methods can be used with equal ease and success. If the first method is used, all dead-load stresses are reduced by one fourth and the unit stress applying to the live load is used. This method may be preferred because it is adaptable to any specification and no change is necessary in the unit stresses established, and because it does not imply that the established live loading should be increased.

Using the first method and applying unit stresses of 18,000 lb per sq in. for live load and 24,000 lb per sq in. for dead load, for members of carbon steel with an elastic limit of 33,000 lb per sq in., the combined unit stress and the factor of safety are listed in Table 5. The stresses listed are based on the corresponding ratios of dead load to live load. The lesser factors of safety are applied to the members carrying predominately dead load.

The dead load of a bridge can, in general, be divided into two parts: (1) The floor system, including the slab, stringers, and floorbeams; and (2) the trusses, including the longitudinal and transverse bracing. In very short spans, the weight of the floor system is generally greater than that of the trusses.

It can be visualized that, as the span length increases, the quantity of material used in the trusses exceeds that used in the floor system. The increase of truss material does not vary directly with, but as some power of, the span length. Also, as the span length increases, the distance on centers of trusses is increased to keep a satisfactory ratio of width to span. In turn, this change increases the length and weight of the bracing. The floor system, except for the floorbeams, increases directly with the bridge width. The floor system, even for the longer spans, will retain a somewhat constant factor of safety while the factor of safety for the trusses varies inversely with the span length.

The writers believe that an impact factor similar to that recommended by the AASHO should be retained even for the longer spans until better data are available. The intensity of impact varies inversely as the loaded length, and is in accord with the statements of the preceding paragraph.

CONCLUSION

The highway-bridge live loading presented in this paper for spans exceeding from 300 ft to 400 ft has been patterned after the present H20-S16-44 lane loading of the standard specifications of the AASHO (12). This type of loading is known universally and is commonly used in the United States. The live loading for long-span bridges, as described in this paper, accurately represents the survey data and the actual vehicular patterns indicated in these data.

Various methods to achieve balanced design for larger structures have been used. This has generally been accomplished by allowing greater dead-load unit stresses, so that the individual members of a structure can function more efficiently in their stress-carrying capacity.

The writers present this paper with the hope that it will stimulate widespread interest and further activity in the standardization of specifications for long-span highway bridges.

APPENDIX. BIBLIOGRAPHY ON LOADING FOR HIGHWAY BRIDGES

(1) **"The Weight Problem in Highway Transportation,"** *Bulletin No. 26*, Highway Research Board, National Research Council, Washington, D. C., July, 1950.

(2) **"Axle Load and Gross Load Trends,"** by T. B. Dimmick and John T. Lynch, *Public Roads*, February, 1950, p. 279.

(3) **"Distribution and Frequency of Heavy Freight Vehicles Based on H Loading Equivalents,"** by A. A. Jakkula and H. K. Stephenson, *Progress Report No. 5*, Texas Agri. and Mech. College, College Station, Tex., March 15, 1945.

(4) **"New Loading Advocated for Highway Bridges,"** by T. Y. Lin, *Civil Engineering*, April, 1949, p. 43.

(5) **"Determination of Permissible Vehicle Weights on Bridges of H Loading Design,"** by H. K. Stephenson, *Proceedings*, A.A.S.H.O., Washington, D. C., 1949.

(6) **"Sizes and Weights of Motor Vehicles Require Economic Study,"** by Herbert S. Fairbank, *Civil Engineering*, June, 1949, p. 40.

(7) **"A More Logical Highway Bridge Loading,"** by Stewart Mitchell, *ibid.*, May, 1945, p. 206.

(8) **"Truck Size and Weight Limits as They Affect Highway Design,"** *Engineering News-Record*, January 11, 1945, p. 96.

(9) **"Reflection on Standard Specifications for Structural Design,"** by Alfred M. Freudenthal, *Transactions*, ASCE, Vol. 113, 1948, p. 269.

(10) **"Construction and Routes of Communications,"** *Field Manual FM 5-10*, Corps of Engrs., Dept. of the Army, Washington, D. C.

(11) **"Specifications for Steel Railway Bridges for Fixed Spans Not Exceeding 400 Feet in Length,"** A.R.E.A., Chicago, Ill., 1947.

(12) "Standard Specifications for Highway Bridges," A.A.S.H.O., 5th Ed., Washington, D. C., 1949.

(13) **"Beitrag zur Frage der Durchbiegung von grossen Strassenbrücken im Zusammenhang mit Messungen an der Köln-Deutzer Rheinbrücke,"** by Franz Braun and Fritz Barth, *Der Bauingenieur*, Vol. 26, 1951, pp. 65–67.

(14) **"Die neue Strassenbrücke über den Rhein von Köln nach Deutz,"** by Fritz Leonhardt, *Die Bautechnik*, Vol. 26, 1949.

(15) **"Denkschrift zum Wiederaufbau der Rheinbrüke Düsseldorf-Neuss 1950–1951,"** J. Springer, Berlin, Germany, 1951.

(16) **"Grundzüge für ein Verfahren zur dynamischen Untersuchung von Brücken,"** by N. Streletzki, *Die Bautechnik*, Vol. 5, 1927, No. 41.

(17) **"Beitrag zur Brückenmesstechnik. Neuere Messungen dynamischer Brückenbeanspruchungen,"** by Rudolf Bernhard, *Der Stahlbau*, Vol. 1, 1928, No. 13.

(18) **"Stosswirkung bewegter Lasten auf Brücken,"** by N. Streletzki, *Bericht uber die II*, Internationale Tagung für Brückenbau und Hochbau, J. Springer, Vienna, Austria, 1929.

(19) **"Brücke und Fahrzeug, Betrachtungen über ihre dynamischen Zusammenhange,"** by Rudolf Bernhard, *Der Bauingenieur*, Vol. 11, 1930, No. 28.

(20) **"Dynamische Untersuchungen von Brücken und Hochbauten,"** by G. Reutlinger, *Publications*, IABSE, Leemann, Zurich, Switzerland, Vol. 1, 1932, pp. 387–410.

(21) **"Investigation of the Dead Load Stresses in the Mississippi River Veterans Memorial Bridge at East St. Louis, Illinois,"** by L. T. Wyly, R. W. Kluge, K. H. Lenzen, L. B. McGammon, M. B. Lágaard, and E. W. Larson, Jr., *Proceedings-Separate No. 219*, ASCE, July, 1953.

(22) **"Investigation of the Dead Load Stresses and Live Load Stresses in a 350 Ft Truss Span on the A.T. and S.F. System,"** *Committee 30 Bulletin 509*, A.R.E.A., Chicago, Ill., June–July, 1953.

DISCUSSION

Louis Balog.[8]—Specifications for the design live load of long-span highway bridges are incomplete without simultaneous reference to the permissible structural deformations. When the recommended live loads (listed in Table 4 and shown in Fig. 4) for computing deflections in accordance with the AASHO specifications (12) are used, bridges result that have an excessive vertical rigidity. The importance of the consideration of the actual deflection is indicated by the proportions and behavior of the bridges listed in Table 6. Schematic cross sections of these bridges are shown in Fig. 5.

The slender girder bridges built in Germany and listed in Table 6 could not have been built if their design live loads (which also included railway loadings) had been used in computing the permissible deflections in conformity with the AASHO specifications. It is always possible to satisfy the requirements pertaining to reasonably allowable stresses for the design live load if proper specifications permit deformations consistent with the safe use of the bridge.

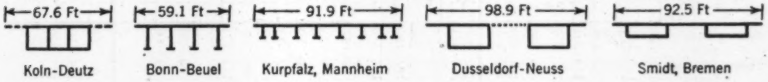

Fig. 5.—Schematic Cross Sections of the Bridges Listed in Table 6

Vertical Deflections.—The relation between the deflections caused by the design live load and the deflections caused by the actual live load is indicated by the results of the measurements made on the Köln-Deutz Bridge during the period from January, 1949, to March, 1949 (13). The movements of targets attached to the bridge at sections A and B were observed with a theodolite located as shown in Fig. 6(*a*). Figs. 6(*c*), 6(*d*), and 6(*e*) show the measured maximum vertical deflections (increased by vibrations) caused by peak traffic containing moving load concentrations (of weight and length shown) at recorded locations. The bridge was not noticed to have moved laterally. The smallness of the largest values of the measured deflections furnishes a scale for the improbability of the occurrence of design live-load deflections.

The measured maximum deflections at sections A and B were 1/2,790 and 1/4,360 of the span. In contrast, maximum deflections of 1/266 and 1/279 of these spans were computed for the design live load (14). The computed design live-load deflection of the Düsseldorf-Neuss Bridge is 1/230 of the center span (15) and those of the Kurpfalz Bridge are 1/359 and 1/488 of the center and side spans, respectively. The AASHO specifications (12) limit the deflection caused by the design live load plus impact to 1/800 of the span, and thus rule out the aforementioned bridges which are sufficiently rigid. These bridges are also eliminated by the requirements for the span-to-depth ratios of girders.

---

[8] Cons. Engr., Binghamton, N. Y.

The accuracy of evaluating the magnitude and location of the traffic loads on the Köln-Deutz Bridge received consideration. The deflections computed for the traffic loads (without knowledge of the measured values) were in satisfactory agreement with the measured values when a composite moment of inertia was used in the compressed lengths of the concrete flooring. When only the moment of inertia of the steel sections was used, the computed values increased 15% at Section A and 6.5% at Section B (13). Three significant facts have to be considered relative to the deflections of this structure: (*a*) The design live-load deflection is three times larger than that permitted by the AASHO specifications (12). (*b*) The actual maximum measured deflection was less than 10% of that caused by the design live load. (*c*) The bridge is so stiff torsionally that its tilting is negligible.

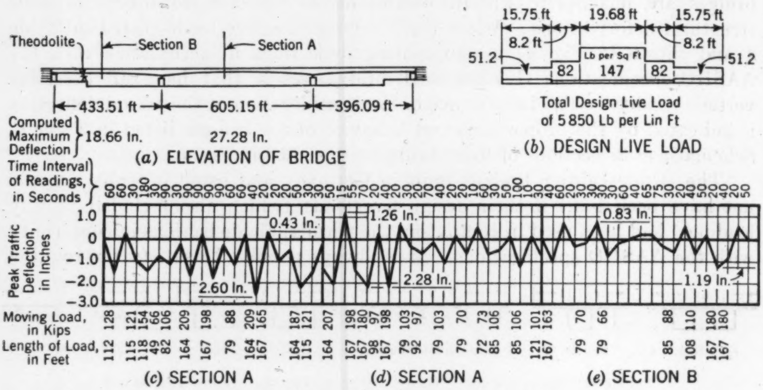

(*a*) ELEVATION OF BRIDGE

(*b*) DESIGN LIVE LOAD

(*c*) SECTION A

(*d*) SECTION A

(*e*) SECTION B

FIG. 6.—DESIGN LIVE LOAD, MEASURED PEAK LOADINGS, AND MAXIMUM DEFLECTIONS OF BRIDGE AT KÖLN-DEUTZ (GERMANY)

TABLE 6.—CONTINUOUS PLATE GIRDER BRIDGES WITH MONOLITHIC STEEL FLOORS

Bridge location (Germany)	Year completed	Length of girder, in feet[a]	LENGTH OF SPANS, IN FEET				SPAN-TO-DEPTH RATIO[b] FOR LONGEST SPAN	
			Span 1	Span 2	Span 3	Span 4	Midspan	Support
Köln-Deutz	1948	1434.75[c]	433.51	605.15	396.09		57.9	24.0
Bonn-Beuel	1949	1292.64[c]	324.80	643.04	324.80		65.0	24.0
Kurpfalz, Mannheim	1950	613.52[c]	184.05	245.40	184.05		54.8	23.7
Düsseldorf-Neuss....	1951	1351.70[d]	337.925	675.85	337.925		61.9	26.3
Smidt, Bremen.....	1952	724.40[d]	207.5	100.2	100.2	49.2	41.7	41.7

[a] Center to center of end bearings for the main river unit. [b] Average outside depth of steel. [c] Riveted construction. [d] Welded construction, riveted field connections.

Torsional Deflections.—The design live load located at the half width and full length of the center span produces 0.13% maximum transverse tilting of the Köln-Deutz Bridge. With a similar load at the center span and at the opposite half width of the side spans of the Düsseldorf-Neuss Bridge, the maximum tilting is 0.4% (15). Test loading with vehicles weighing 1,450 lb per lin ft placed along the curb in two thirds of the center span of the Kurpfalz Bridge produced a maximum tilting of 0.21%. The moment caused by this loading was slightly greater than 20% of the maximum torsional moment produced by the design live load.

Fig. 7 shows the loading producing the maximum computed transverse tilting of the Düsseldorf-Neuss Bridge and the corresponding moments (15).

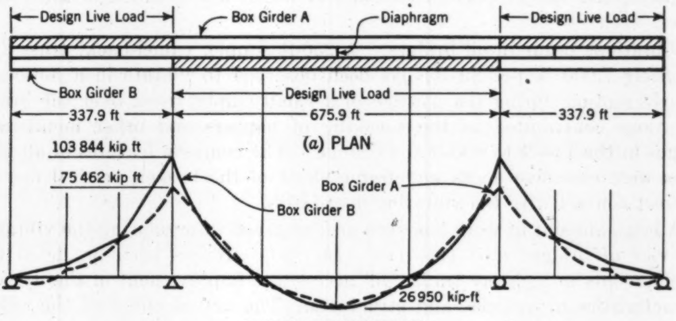

(a) PLAN

(b) MOMENT DIAGRAMS

Fig. 7.—Effect of Diaphragms in Equalizing Torsional Loading of Bridge at Düsseldorf (Germany)

It appears that diaphragms 20 ft long, two in the side spans and three in the center span, greatly equalize the moments between the two box girders. In the Smidt Bridge, cross frames, 23 ft long, spaced 68.9 ft and 78.7 ft in spans of 367.5 ft and 207.5 ft, respectively, assure that the four webs of the two box sections, about 23 ft wide and 8 ft deep, carry approximately equal shares of the torsional loadings of the bridge. The torsional deformations of these slender bridges are small.

Vibrations.—The vibrations of the spans of the Köln-Deutz Bridge resulting from rail traffic could be detected only by instruments. Occasionally, light trucks caused noticeable, slight vibrations of the longer side span. Vibrations of small amplitudes and frequencies of from 20 cycles per sec to 30 cycles per sec were observed at the handrails located at the ends of the 15-ft-long brackets. The computed natural frequency of the bridge is 0.4 cycle per sec and, with the design live load placed over the entire bridge, the fundamental frequency is 0.3 cycle per sec (14).

German highway-bridge specifications (1941) limited deflections to 1/500 of the span and permitted larger deflections for long spans without defining the limits of the deflections. Giving primary consideration to the fact that the slow vibrations of bridges were unnoticeable, Fritz Leonhardt made reference to the low natural frequency of the bridge and suggested that the permissible relative deflections of long-span bridges of low natural frequency be larger than for shorter spans of higher natural frequency (14). The behavior of the Köln-Deutz Bridge justified the basic characteristics of the design.

The experiences gained in the construction of the Köln-Deutz Bridge were utilized in the design of bridges built subsequently. The 4.72-in. concrete flooring (with exposed riding surface, anchored to steel-plate flanges having an area of 50,000 sq ft) was replaced by an asphalt flooring. Instead of rigid mortar connections between the precast elements, bitumen joints were used. The Köln-Deutz Bridge and the bridges built subsequently advanced girder design beyond the proportions the use of which was retarded in the United States.

Vibrations occur in all bridges. A 250-ft simple, camel-back, truss span (weighing 7,000 lb per lin ft) has been observed to vibrate in a noticeable no-node motion during the passage of a small empty truck over the bridge. Vibrations contributed to the breaking of hangers and other members of bridges in the 100-ft to 600-ft span range. The common features of all these spans were excessive depth and frame effect of the broken vertical member in direct contact with the vibrating floor beam.

A large amount of work has been accomplished in measuring the vibratory behavior of bridges (16) (17) (18) (19) (20). It has been predicted that developments in highway traffic will necessitate improvement of the dynamic characteristics of vehicles and structures. The actual effect of the vehicle on the structure is not expressed by the weight and the impact factor. The response of the bridge to these effects, however, depends on structural proportions and arrangements influencing dynamic behavior.

Conclusions.—The probability of the occurrence of the design live load decreases with increasing span and varies with bridge locations. Deflections and vibrations caused by the actual traffic govern the satisfactory behavior of long-span bridges not subject to objectionable wind vibrations.

Traffic-load observations and deflection and vibration measurements should be simultaneous in order to avoid the formulation of inconsistent specifications that arbitrarily limit the structural proportions and deflections.

The refinements in "balanced design" involve unattainable accuracy in making, shaping, fabricating, assembling, and erecting structural steel. These refinements are also unsuited for defining the factor of safety of various structural arrangements. Assuming standard quality materials, workmanship, and reasonable details, the magnitude of the stresses depends on the distribution of the actual loads, and the amplification of the stresses depends on the vibratory characteristics of the loads and of the structural arrangements. The specification of allowable-stress computations which only complicates the design should be avoided.

Specifications that do not agree with the actual behavior of structures hinder the use of existing knowledge. They present an obstacle to the use of available materials and to the development of efficient structural arrangements. The infrequent issuance of specifications and the rapid advances in structural techniques demand that any specification which is issued contain specific statements concerning its limited validity.

Glenn B. Woodruff,[9] M. ASCE.—The writer appreciates the immense amount of work performed by the authors and joins in the hope that there will result a standardization of specifications for long-span highway bridges. It is also hoped that further work may develop data that will lead to the improvement of specifications for bridges of shorter span. Although the chief purpose of the authors has been the proposal of a loading for long-span bridges, consideration has been given to related subjects.

Certain data and conclusions obtained by the authors can be summarized as follows:

1. The AASHO H20-S16-44 loading is accepted for spans of less than 600 ft. Assuming an increase of $\frac{1}{3}$ in this loading, an allowable base stress of 24 kips per sq in. for carbon steel is proposed.
2. The greatest loads (where more than one vehicle is involved) occur when traffic is stalled. Under this condition there are no dynamic forces.
3. On traffic lanes restricted entirely to commercial traffic, the percentage of the heavier vehicles is very small.

It can also be stated that:

a. It is the concensus of highway engineers that it is not economical to design pavements for loads exceeding legal limits. Unfortunately there will always be some cases of illegal loads exceeding such limits.

b. There exists little definite knowledge as to the magnitude of dynamic stresses in highway bridges. Such data as is available indicate that the AASHO specifications are conservative in this respect.

c. The history of both highway and railway bridges has been that of overdesigned trusses and girders in comparison with the design of the floor system.

The writer endorses the opinion of the authors that the design should be based on the largest combination of stresses that are probable during the life of the structure and the greatest unit stresses that are prudent. The authors mention various methods of achieving the result, but fail to mention the method which assumes the greatest probable live load and combines the stresses therefrom with those produced by other forces. Moreover, there appears little logic in restricting this proposal to "large structures." If a given unit stress is satisfactory in the chord of a long-span bridge, it should be even more conservative in the flanges of a plate girder or rolled beam.

The safety factors listed in Table 5 may be misleading because no provision is made for increase of live load. If the live load were increased by $\frac{1}{3}$, the factor would become 1.5 throughout. In addition to stresses produced by dead, live, and dynamic loadings, other stresses result from lateral and longitudinal forces and from changes in temperature. The stresses are not uniformly distributed across the member (21) (22).

The safety factors also may be misleading because the upper yield point, as determined by the mill "drop of beam" test, is above the true elastic limit.

---

[9] Cons. Engr., San Francisco, Calif.

It is wasteful to use a stress of 18 kips per sq in. for A-7 steel, but an increase of ⅓ is not recommended unless an allowance is included for the effects previously listed.

There are considerable data enabling the engineer to evaluate the heaviest probable single vehicle. From this point, the matter becomes one of selecting the most severe probable combination of these loads in a single lane, and then of combinations of these heavy loads in additional lanes. For a single lane, it appears logical to assume a vehicle (type S-2) loaded to the legal limit, and to add ⅓ to allow for illegal loading and other "unmeasurables." To this loading, it would be necessary to add an allowance for impact. For longer spans, an unusual (but possible) situation would be for any combination of three vehicles—one as previously described, the other two of the same type but loaded to legal limit—to "close up." In this case, no impact would be involved.

TABLE 7.—Comparison of Stresses Obtained by Use of the Authors' Loading and the Proposed Loading

Span, in feet	Number of lanes	Distance between curbs, in feet	Center-to-center distance for trusses, in feet	Live Load Plus Impact Stresses per Truss			
				Proposed Loading		Authors' Loading[a]	
				Maximum moment, in kip-feet	Reaction, in kips	Maximum moment, in kip-feet	Reaction, in kips
300	2	26	31	14,500	220	11,100	158
300	4	52	57	16,800	256	16,400	232
600	2	26	32	43,300	300	35,000	238
600	4	52	58	50,500	349	53,300	363
1,000	4	52	58	125,000	500	139,000	554
1,000	6	76	82	150,700	603	181,000	720
1,500	4	52	58	253,000	674	288,000	768
1,500	6	76	82	305,000	814	375,000	1,000

[a] Assuming reduction for multiple lanes in accordance with AASHO specifications. For four-lane bridges maximum stress occurs with three lanes loaded.

Assuming that the ultimate or maximum live loads are being considered, the H20-S16-44 loading—as well as those loadings recommended by the authors—appears to be inadequate. However, the probabilities of simultaneous loading in the other lanes are such as to justify a greater reduction than that permitted by the AASHO specifications. Accordingly, the writer proposes the following loadings:

1. *Single Lane.*—A vehicle (type 3-S2) with axle loads of 12 kips, 24 kips, 24 kips, 24 kips, and 24 kips, and axle spacing of 16 ft, 4 ft, 16 ft, to 30 ft, and 4 ft. To this loading, impact should be added according to the AASHO formula. This loading may be replaced by (1) a uniform load of 800 lb per lin ft for spans of less than 1,100 ft and 720 lb per lin ft for longer spans; (2) moment concentrations of 60 kips for spans of less than 600 ft, 300 kips for spans of between 600 to 1,000 ft, and zero kips for spans greater than 1,000 ft; and (3) shear concentrations of 80 kips for spans of less than 600 ft, 40 kips for spans of between 600 ft to 1,000 ft, and zero kips for spans greater than 1,000 ft. No impact should be added to these loads.

2. Additional Lanes.—One hundred percent of the load listed for a single lane is assumed in the lane nearest the truss being considered, 75% of the single-lane load in the lane farthest away from the truss being considered, and 25% of such load for a single lane in the other lanes.

A comparison of this proposal with that of the authors is shown in Table 7. The authors' proposal (for ultimate loads) appears to be low for two-lane bridges and excessive for bridges of four and six lanes.

A satisfactory live load is only part of a needed specification for the design of long-span highway bridges. The writer hopes the authors will continue their work in such a direction.

William G. Byers,[10] J.M. ASCE.—The value of the authors' paper is largely dependent on the value of the live loadings recommended in Table 4. These live loadings can best be evaluated by devising a standard of requirements for design loads in general and comparing the proposed loadings with the standard loadings.

It is suggested that the following requirements be used for the design loads: (*a*) The design load should produce stresses approximately equal to those caused by the maximum load that is likely to be carried by the structure. This maximum load should be estimated on the basis of the loads currently being carried by comparable structures with an allowance for probable future increases. (*b*) The design load should give only one value of live load for a given span length or loaded area. (*c*) The load pattern should be simple. (*d*) The design load should reflect actual conditions whereby the total live load never decreases with an increase in the span length.

The authors' proposed loading will satisfy the first three requirements if the larger of the two given values is specified for span lengths at which the load changes. The loading satisfies the fourth requirement except for span lengths near those at which the load changes. For example, the total load decreases 40,000 lb per lane as the span increases beyond 1,000 ft, and an additional in-increase of 66.7 ft is required to allow for the loss in total load. This condition could be remedied by using the following:

For spans of less than 500 ft, an H-20-S-16-44 loading should be used. This loading is represented by (1) w equal to 640 lb per ft, (2) the concentrated load for moment P_m equal to 18,000 lb, and (3) the concentrated load for shear P_v equal to 26,000 lb.

For spans of from 500 ft to 900 ft, w should equal 640 lb per ft; P_m should equal $18{,}000 - 45(L - 500) = 40{,}500 - 45\ L$; and P_v should be made equal to $26{,}000 - 65(L - 500) = 48{,}500 - 65\ L$.

For spans of from 900 ft to 1,300 ft, w should equal $640 - 0.2\ (L - 900) = 820 - 0.2\ L$, and P_m and P_v should both equal zero.

For spans that exceed 1,300 ft, w should equal 560 lb per ft, and P_m and P_v should both equal zero.

These recommendations are no more complex than the AASHO impact formula and could be combined with it, if desired, to give values of live load plus impact.

---

[10] Draftsman, Gulf, Colorado, and Santa Fe Ry. Co., Galveston, Tex.

Kuang-Han Chu,[11] A.M. ASCE.—There is no doubt that the loading specified in the existing (1953) AASHO specification is too high for long-span bridges, although there is some question as to the intensity that should be specified. The step loading suggested by the authors has some disadvantages. At the point where the loading changes from one step to another, the sudden changes in stress (although small in comparison to the total dead-load and live-load stress—but not small in comparison to the live-load stress) are nevertheless inconsistent. The percentage change of stress when the influence lines are similar to those shown in Figs. 8(*a*) and 8(*b*) (as in continuous bridges or arch bridges) may exceed those predicated by the authors (8% of live-load stress or 2% of total dead-load and live-load stress). Moreover, when the influence line is similar to that shown in Figs. 8(*a*) and 8(*b*), the higher intensity of loading for one step with shorter loaded length (L_1) may produce much greater stress than the loading in the next step with a loaded length between the zero points of the influence line (L_2). A loading which varies continuously with loaded length is preferable to step loading. In Table 8 are included suggested systems of loading which correspond closely with the authors' loading system and the data presented. In Table 8, ω is the uniform lane load in pounds per foot per lane.

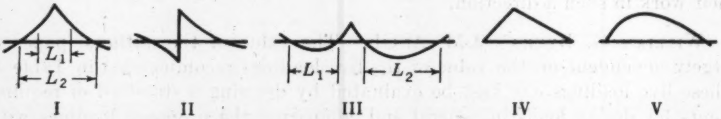

Fig. 8.—Types of Influence Lines

TABLE 8.—Loading Systems

Loaded Length l, in Feet	Loading Type	Equation for ω	Concentrated Lane Load, in Pounds	Remarks
400 to 800	A, for moment	$\omega = 400 + \frac{480{,}000}{l + 1{,}600}$	18,000	For negative moment of continuous spans (in Fig. 7(*c*) $l = L_1 + L_2$), two concentrations, each at a different span, shall be used.
	B, for shear	$\omega = 440 + \frac{200{,}000}{l + 600}$	26,000	...
Greater than 800[a]	C, for shear and moment	$\omega = 430 + \frac{330{,}000}{l + 700}$	...	For negative moment of continuous spans (in Fig. 7(*c*) $l = L_1 + L_2$), one concentration of 18,000 lb, placed so as to produce the maximum stress, shall be used.

[a] The loadings A and B (used for spans of from 400 ft to 800 ft) can also be used for spans that are greater than 800 ft, but loading C is simpler and therefore recommended.

The values given in Table 9 were obtained by using the loadings specified in Table 8 (based on a triangular-shaped influence line), the authors' loading, and the maximum and average loadings of the San Francisco-Oakland Bay Bridge in California.

---

[11] Structural Designer, D. B. Steinman, Cons. Engr., New York, N. Y.

Any concentration that is considerabley less than those concentrations specified by AASHO loses its significance in representing high concentration of axial load. Moving concentrations are useful in accounting for the effect of local load concentration in continuous bridges or arch bridges with influence lines similar to those shown in Figs. 8(*a*) and 8(*b*). The effect of the loads diminishes with increase in loaded length. With influence lines of the type shown in Fig. 8(*b*), loading B (with its high concentration) will produce approximately the same stress as loading A or loading C for *l* greater than 1,000 ft. However, with influence lines of triangular shape (Fig. 8(*d*)), loading B is slightly less than loading A or loading C for *l* in that range (Table 9). With influence lines of the types shown in Figs. 8(*d*) and 8(*e*), the uniform loads of loading C will always give stresses equal to or higher than those given by loading A or loading B (for *l* greater than 800 ft). From the comparison shown in Table 9, it appears that, if continuous-loading curves should be adopted in some set of specifications, some loading system similar to that suggested by the writer may merit consideration.

TABLE 9.—EQUIVALENT UNIFORM LOAD, IN POUNDS PER FOOT PER LANE

Loaded length, in feet	AUTHORS' LOADING		SAN FRANCISCO-OAKLAND BAY BRIDGE		LOADING TYPE		
	Moment	Shear	Maximum	Average	A	B	C
400	730	770	760	725	730[a]	770[a]	730
600	700 670	727 683	695	660	678[a]	694[a]	684
800	663 640	673 640	647	610	645[b]	648[b]	650[a]
1,000	640 600		610	575	620[b]	617[b]	624[a]
1,200	600 560		600	560	601[b]	594[b]	604[a]
1,500	560		600	550	579[b]	570[b]	580[a]
2,000	560		...	...	551[b]	543[b]	552[a]
3,000	560		...	...	516[b]	513[b]	519[a]
4,000	560		...	...	495[b]	497[b]	500[a]

[a] Recommended values. [b] Alternative values.

R. J. IVY,[12] A. M. ASCE, T. Y. LIN,[13] M. ASCE, STEWART MITCHELL,[14] M. ASCE, N. C. RAAB,[15] M. ASCE, V. J. RICHEY,[16] A. M. ASCE, AND C. F. SCHEFFEY,[17] J. M. ASCE.—The Joint Committee wishes to thank those who discussed the paper. The interest shown, and the variations in the proposed loadings, emphasize the need for a standardized live loading for highway bridges; the various opinions expressed in these discussions will be of great value to any group writing such a specification.

---

[12] Superv. Bridge Engr., State Div. of Highways, Sacramento, Calif.

[13] Associate Prof. of Civ. Eng., Univ. of California, Berkeley, Calif.

[14] Prin. Bridge Engr., State Div. of Highways, Sacramento, Calif.

[15] Project Engr., San Francisco Bay Toll Crossings, Berkeley, Calif.

[16] Senior Bridge Engr., San Francisco Bay Toll Crossings, Berkeley, Calif.

[17] Asst. Prof. of Civ. Eng., Univ. of California, Berkeley, Calif.

The writers restate their premise that the basis of a standardized live loading for long-span bridges should be the actual vehicles and traffic patterns found on the highways. It is believed that a "hand-picked" loading would be viewed with skepticism by the users of any such loads.

It is also recommended that the loading be presented in a form easy to use and familiar to most designers. Equations, curves, or tables should not be required in order to determine the proper load for each different loaded length. The writers are of the opinion that the steps in their proposed loading result in an ease of application that outweighs the hypothetical inaccuracy resulting therefrom.

Mr. Woodruff believes that the safety factors listed in the paper (Table 5) may be misleading. These factors were given as an example to illustrate the problem rather than as a definite conclusion.

Any increase in live loading during a period of several years affects all highway structures, and probably the only practical way of providing for a large increase in loading is either by strengthening the members of the structure or by decreasing the dead load. The latter procedure is probably the most practicable for long-span bridges and in most cases is accomplished in highway structures by the substitution of a lighter deck.

Messrs. Byers and Chu are concerned with the steps in the writers' proposed loading; both present alternate loadings in the form of equations which result in a lane loading that varies inversely with the loaded length. The writers considered such loadings and rejected them because of the complexity of application and loss of identity with the present AASHO standard live loads (12).

It should be noticed that the steps in the writers' loading curves occur in loaded lengths of more than 600 ft, on which the live loads, when used with other loading combinations, are a small percentage of the total design load used in the proportioning of structural members. This loading was recently applied to a large structure, now (1954) in the course of construction, with no recalculation of stresses and with ease of application.

The results in Table 9, based on live-load stresses, illustrate the close relationship of the loadings with those actually used and suggested. The writers remain convinced that not less than the 560-lb lane load should be used for spans exceeding 1,200 ft as most structures in this range (site conditions permitting) are suspension bridges, for which dead loads are not considered in the proportioning of the stiffening truss members.

As stated in the original paper, many related subjects must be considered before a comprehensive specification for long-span highway bridges can be formulated. As suggested by Mr. Balog, each subject, such as deflection, vibration, impact, and fatigue, merits a separate detailed study. The authors did not presume that their paper covered all phases of long-span bridge design. However, they believe that the adoption of a reasonable live loading for long-span bridges will lend impetus to the study of other conditions affecting structures.

AMERICAN SOCIETY OF CIVIL ENGINEERS
Founded November 5, 1852
TRANSACTIONS

Paper No. 2709

PEAK DISCHARGE FOR HIGHWAY DRAINAGE DESIGN

By Carl F. Izzard,[1] A. M. ASCE

With Discussion by Messrs. Max A. Kohler, Roy F. Warner,
N. E. Minshall, and Carl F. Izzard

Synopsis

The use of stream-flow records for determining the size of highway drainage structures is a logical procedure. This paper shows that, by developing regional flood curves, the peak rate of runoff on a stream can be estimated for a given frequency—whether or not stream gaging records are available for that particular stream. A graph is included that can be used for estimating peak rates of runoff on small watersheds to aid in culvert design.

Introduction

The present (1953) trend for determining the required waterways for bridges is to estimate the peak discharge and stage for some reasonable frequency of flood occurrence, and then to compute the waterway required to pass this flood with an amount of backwater tolerable for the conditions at the site. In cases where the flood flow is confined between the river banks, the bridge usually causes no appreciable contraction, and the primary concern is setting the superstructure high enough to clear the design flood. More commonly, however, a considerable proportion of the flood flow may be on the flood plain outside the banks of the main channel. In such cases the total length of the bridge is made less than the width of the flood plain, and may consist of a main channel crossing and one or more relief bridges.

Since a bridge usually costs more per foot than does embankment, the total cost of a valley crossing can be reduced by decreasing the length of the bridge. If the waterway is reduced excessively, however, the increased velocity through the opening may induce dangerous scouring action and the required

---

Note.—Published, essentially as printed here, in October, 1953, as *Proceedings-Separate No. 380*. Positions and titles given are those in effect when the paper was received for publication.

[1] Chf., Hydr. Branch, Div. of Research, Bureau of Public Roads, U. S. Dept of Commerce, Washington, D. C.

velocity head may cause excessive backwater. In order to estimate the velocity of flow through the contracted opening and backwater, the design discharge and its corresponding stage in the unobstructed channel must be known. Also the damage likely to be incurred if this flood is exceeded once in a given number of years must be compared with the increased cost of providing an opening large enough to eliminate or reduce the probable damage.

At the present rate of construction (1953) more than \$500,000,000 is spent annually for the construction of bridges and culverts. This amount is not sufficient to meet the demand generated by the obsolescence of existing structures caused by increased traffic volumes and increased traffic speeds. To make maximum use of limited funds, it is necessary to be certain that no bridge is built longer than is requisite. Unlike spillways on earth-fill dams, where loss of life as well as destruction of the dam may result if the spillway capacity is exceeded, bridges and roadways can usually be submerged without material damage. Determination of the tolerated frequency of the overflow of a roadway should include consideration of the character and volume of highway traffic and the length of time traffic is interrupted.

The magnitude and frequency of peak floods are therefore of primary concern to highway engineers. This paper seeks to focus attention on various methods of estimating floods—not only on streams for which discharge records are available, but also for ungaged streams.

FREQUENCY COMPUTATIONS

Tate Dalrymple, A.M. ASCE, has shown that, when mean annual floods on a group of watersheds having similar hydrologic characteristics are plotted against drainage area, the relationship can be approximated by a straight line on logarithmic graph paper.[2] Furthermore, a composite frequency curve can be drawn showing the ratio of the flood of a given frequency to the mean annual flood for any recurrence interval up to the period of record. This curve can also be extrapolated to a limited extent, if it is realized that the probable error increases as the recurrence interval exceeds the period of record. Thus, for ungaged watersheds within the same geographic region, the probable flood for any recurrence interval not greatly in excess of the period of record can be estimated with confidence. The procedure is to determine from a set of curves the mean annual flood corresponding to the drainage area, and then to multiply this by the ratio for the desired recurrence interval.

The Bureau of Public Roads, United States Department of Commerce (USBPR) applied this procedure with some modifications to particular regions with good results. The USBPR's procedure has been to prepare frequency curves for all stations having sufficient records, and then to plot the 25-yr flood against the drainage area. Watersheds having similar characteristics tend to "line up" on logarithmic graph paper, as will be shown subsequently.

A typical flood frequency curve for the Big Blue River at Randolph, Kans., is shown in Fig. 1. This figure has a ruling devised by Ralph W. Powell,[3] M. ASCE, for use with E. J. Gumbel's theory of extreme values.[4] Application of this theory requires the use of the peak flood for each year of record. The floods are tabulated in order of magnitude beginning with the greatest flood listed as Order No. 1. The plotting position is computed as $\frac{n+1}{m}$, in which n is the the number of years of record and m is the order number. In this case the maximum flood in 30 yr of record was 98,000 cu ft per sec. It is plotted at 31/1 = 31 yr. The next highest flood was 55,400 cu ft per sec and is plotted at 31/2 = 15.5 yr. Other floods are plotted in a similar manner. A straight line is then drawn to give the best fit to the plotted points. In Fig. 1 the maximum flood is out of line, and was ignored in drawing the frequency curve on the assumption that its recurrence interval should actually be much greater than the period of record. There is no reason why a 100-yr flood might not have occurred during this period.

---

[2] "Regional Flood Frequency," by Tate Dalrymple, *Research Report 11-B*, Highway Research Board, National Research Council, Washington, D. C., 1950.

[3] "A Simple Method of Estimating Flood Frequencies," by Ralph W. Powell, *Civil Engineering*, Vol. 13, February, 1943, pp. 105–6.

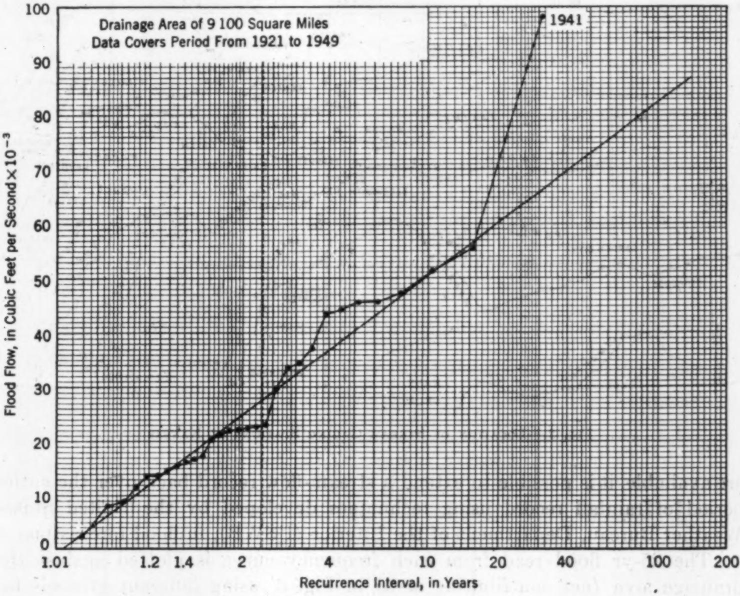

FIG. 1.—FREQUENCY CURVE FOR BIG BLUE RIVER AT RANDOLPH, KANS.

W. D. Potter has developed a simplified method of determining the position of the frequency curve. His method eliminates personal judgment,[5] and is recommended for use in statistical correlation studies of factors affecting peak rates of runoff.

---

[4] "Floods Estimated by the Probability Method," by E. J. Gumbel, *Engineering News-Record*, Vol. 134, June 14, 1945, pp. 833–837.

[5] "Simplification of the Gumbel Method for Computing Probability Curves," by W. D. Potter, *SCS-TP-78*, Soil Conservation Service, U.S.D.A., Washington, D. C., May, 1949.

Frequency curves have been prepared for all stations in Kansas for which there were records for at least 15 yr. The locations of these stations are shown in Fig. 2. A few of the shorter records were extended by establishing a correlation with nearby longer records as described by Mr. Dalrymple.[2] Another method for adjusting short records involves adjusting the peak rates according to a comparison of the rainfall experienced for the short period of runoff record with that for a much longer period. Where long rainfall records are available, it is possible to extend a stream-flow record back over the entire period of rainfall record using techniques developed by the United States Weather Bureau, Department of the Interior (USWB), in flood forecasting.

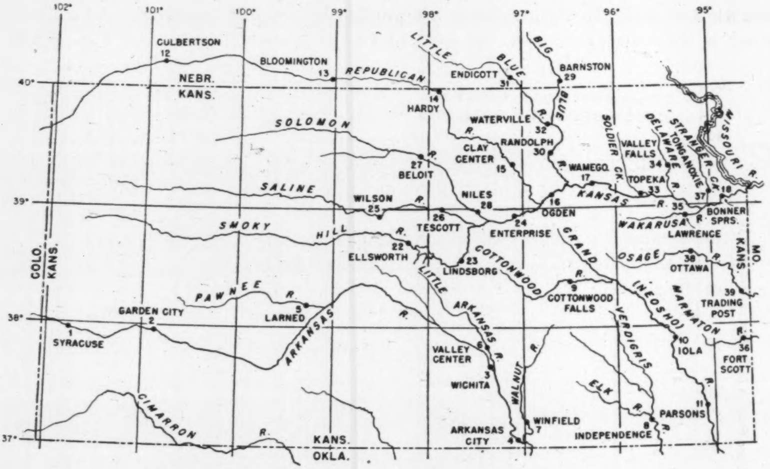
102°
101°
100°
99°
98°
97°
96°
95°
40°
39°
38°
37°
CULBERTSON 12
BLOOMINGTON 13
REPUBLICAN
LITTLE BLUE
BIG BLUE R.
ENDICOTT 31
BARNSTON 29
NEBR.
KANS.
14 HARDY
SOLOMON
WATERVILLE 32
RANDOLPH 30
CLAY CENTER 15
27 BELOIT
R.
SOLDIER CK.
DELAWARE R.
STRANGER CR.
TONGANOXIE
VALLEY FALLS 34
MISSOURI R.
WAMEGO 17
TOPEKA 33
37
18
KANSAS R.
SALINE
WILSON 25
R.
NILES 28
16 OGDEN
35
BONNER SPRS.
SMOKY HILL R.
26 TESCOTT
24 ENTERPRISE
WAKARUSA R.
LAWRENCE
22 ELLSWORTH
23 LINDSBORG
COTTONWOOD
GRAND
OSAGE
38 OTTAWA
R.
MO.
KANS.
COLO.
KANS.
PAWNEE R.
5 LARNED
GARDEN CITY 2
1 SYRACUSE
ARKANSAS
R.
LITTLE ARKANSAS R.
9 COTTONWOOD FALLS
R.
(NEOSHO)
MARMATON R.
VERDIGRIS
39 TRADING POST
10 IOLA
36 FORT SCOTT
6 VALLEY CENTER
3 WICHITA
WALNUT R.
ELK R.
11 PARSONS
CIMARRON R.
R.
KANS.
OKLA.
ARKANSAS CITY 4
WINFIELD 7
8 INDEPENDENCE
R.

FIG. 2.—LOCATION OF STREAM GAGING STATIONS IN KANSAS

The 25-yr flood read from each frequency curve is plotted against the drainage area (net contributing area) in Fig. 3, using different symbols for each of the several regions. The numbers shown with each point correspond to the gaging-station numbers shown in Fig. 2.

REGIONAL FLOOD CHARACTERISTICS

Regional Flood Curves.—Three lines have been drawn in Fig. 3 which are applicable, respectively, to various small rivers in eastern Kansas (east of 96.5° west long.), the Big Blue and Little Blue rivers, and the Kansas River tributaries west of Ogden. The dash line is an extension of a line that was found to fit 25-yr floods on small watersheds with mixed cover. This line was partly based on data from the Soil Conservation Service (SCS) United States Department of Agriculture Hydrologic Experiment Station at Hastings, Nebr., which is located at the headwaters of the Little Blue River.

Two of the peak runoff curves from the SCS report[6] have been plotted in Fig. 3. The upper curve applies to a watershed where the main channel has no meanders, and the lower curve applies to a watershed where the main channel is about 75% longer than the valley distance. It is of interest to note that the curve for the Big Blue and Little Blue rivers is almost directly in line with the latter curve. Stations 33, 35, and 37 in eastern Kansas plot below the line drawn for that region. A probable explanation is that these are all long, narrow watersheds. Another observation is that stations 5, 6, and 7 for the Arkansas River tributaries plot successively higher as they come closer to eastern Kansas. Station 5 has a magnitude comparable with the Kansas River tributaries immediately to the north.

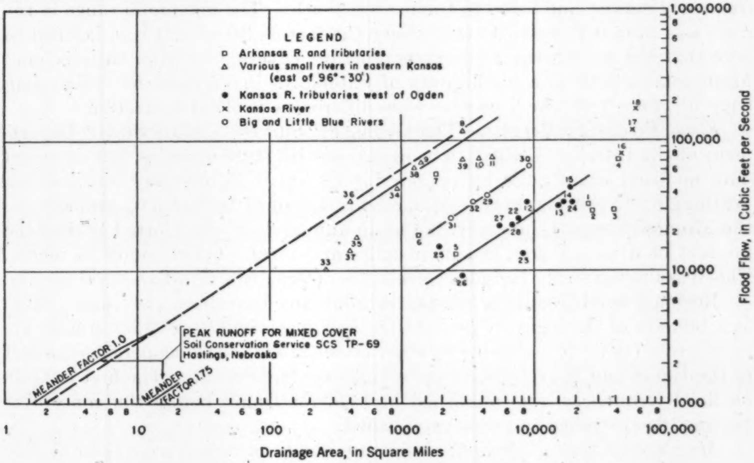

FIG. 3.—25-YR FLOODS IN KANSAS

As noted by R. W. Carter, A.M. ASCE, large rivers in Georgia that cross regional boundaries do not conform to curves established for the separate regions.[7] Station 16 on the Kansas River, not far downstream from the confluence with the Republican River, has a flood magnitude in line with the curve for the Kansas River tributaries. The flood peak increases markedly at station 17 after the Big Blue River joins the Kansas River and continues to rise as the mouth of the river is approached at station 18.

---

[6] "Rates of Runoff for the Design of Conservation Structures in the Central Great Plains of Nebraska and Kansas," by John A. Allis, *SCS-TP-69*, Soil Conservation Service, U.S.D.A., Washington, D. C., August, 1948.

[7] "Floods in Georgia—Frequency and Magnitude," by R. W. Carter, *Geological Survey Circular No. 100*, The Geological Survey, U. S. Dept. of the Interior, Washington, D. C., March, 1951.

Flood Frequency.—The curves in Fig. 3 can be used to estimate floods of other frequencies by multiplying the 25-yr flood by the following factors:

Frequency, in years	Factor
50	1.2
10	0.8
5	0.6

These factors are median values based on ratios obtained from the individual frequency curves, and listed to the nearest tenth. The maximum range in the ratio was from 0.07 below to 0.05 above the factors listed. It is of interest to note that the same range in frequency factors covers data from Georgia[7] and Minnesota[8] as well as a small group of watersheds in Virginia, for which data have not been published, despite wide differences in flood magnitude.

Flood Frequency Reports.—The Geological Survey, United States Department of the Interior (USGS), in cooperation with state agencies, has compiled data on flood frequencies by regions for Georgia,[7] Minnesota,[8] and western Washington,[9] following, in general, methods described by Mr. Dalrymple.[2] In the Minnesota report, however, the mean annual flood was plotted against the product of drainage area in square miles and mean annual runoff in inches. The Washington study includes correlation of peak runoff with several factors.

Regional flood frequency studies in Louisiana have been published (1952) as a bulletin of the highway department and the USGS.[10] Similar studies are in progress (1953) in a number of other states, usually as a cooperative project of the USGS and the respective state highway department. The first bulletin on flood frequencies was published in 1946 for Ohio[11] before the concept of regional flood studies had been established.

Maximum Floods of Record.—Maximum floods of record have been plotted against drainage area in Fig. 4 for the same Kansas stations that are shown in Figs. 2 and 3. The points scatter widely, as might be expected, because each point has a different frequency. No regional trends are evident except for stations 29, 30, 31, and 32 for the Big Blue and Little Blue rivers where the 1941 floods were uniformly about 1.5 times greater than a 25-yr flood. It is possible that a storm will occur on the Big Blue and Little Blue rivers similar to the 1935 storm that produced peaks illustrated by stations 12, 13, 14, and 15 on the Republican River. Maximum floods on the Big Blue and Little Blue rivers might then approach the magnitude of the Republican River floods or even exceed them. The 1951 flood, however, on the Neosho River (station 11) is so far above the magnitude of any other floods that a greater flood is a remote possibility. It is of interest to note that newly designed highway bridges, even though submerged, withstood the 1951 Neosho River flood with virtually no damage.

---

[8] "Magnitude and Frequency of Floods in Minnesota," by C. H. Prior, *Bulletin No. 1*, Div. of Waters, Minnesota Dept. of Conservation, St. Paul, Minn., November, 1949.

[9] "Floods in Western Washington," by G. L. Bodhaine and W. H. Robinson, *Geological Survey Circular No. 191*, The Geological Survey, U. S. Dept. of the Interior, Washington, D. C., 1952.

[10] "Floods in Louisiana—Magnitude and Frequency," by J. S. Cragwall, Jr., The Geological Survey, U. S. Dept. of the Interior, and the Louisiana Dept. of Highways, Baton Rouge, La., December, 1952.

[11] "Floods in Ohio—Magnitude and Frequency," by William P. Cross, *Bulletin No. 7*, Ohio Water Resources Board, Columbus, Ohio, October, 1946.

At the other extreme, frequency studies show that two of the maximum floods of record on the Verdigris River (station 8) and the Marmaton River (station 36) are approximately at the 25-yr flood frequency. Thus, highway bridges built to the maximum high water of record on these two streams would be applicable for only a 25-yr flood.

The regional flood-frequency curves in Fig. 3 are a better guide to economical bridge design than the maximum floods shown in Fig. 4, but maximum floods should be investigated. The highway bridge must be safe against destruction by such a flood, even though the approaches may be overtopped and partly destroyed.

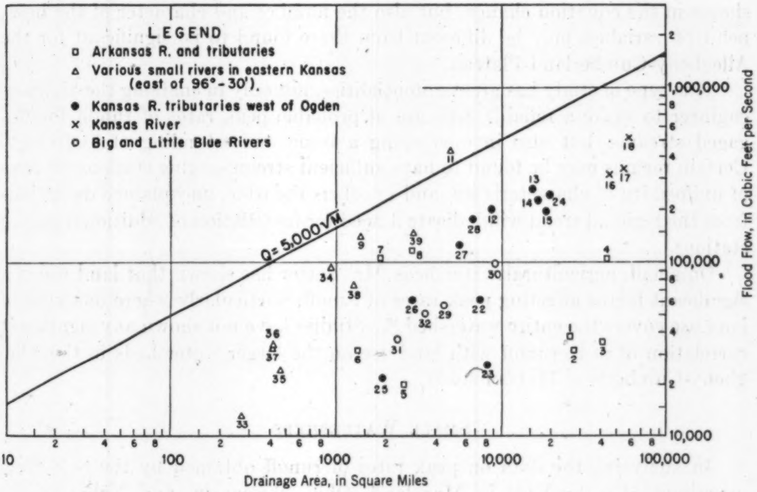

FIG. 4.—MAXIMUM FLOODS OF RECORD IN KANSAS

Analysis of Regional Flood Curves.—For ungaged watersheds within a given region for which a regional flood curve has been developed, the flood curve is a means of estimating the flood magnitudes for recurrence intervals not greatly in excess of the length of the records on which the curve is based. Such an estimate, based on a number of stations, is more reliable than an estimate based on a single record of an adjacent watershed with similar hydrologic characteristics.

Research is needed to discover the factors causing significant differences among watersheds in the same region. Why should points 10, 11, and 39 in Fig. 3 be below the peaks for other watersheds in eastern Kansas? Or why is point 25 relatively high, and point 23 relatively low in western Kansas?

Mr. Potter has demonstrated a solution to the problem in a study of peak rates of runoff from fifty-one watersheds in the Allegheny-Cumberland Plateau.[12] Six of these are experimental watersheds of the SCS, and the remainder are regular gaging stations of the USGS. Using multiple correlation, Mr.

---

[12] "Rainfall and Topographic Factors that Affect Runoff," by W. D. Potter, *Transactions*, Am. Geophysical Union, Vol. 34, No. 1, February, 1953.

Potter establishes correlation between peak rate of runoff per unit area for a 10-yr frequency and four independent factors. These factors are area of watershed, a topographic factor involving length and slope of the principal stream (which implicitly involves the shape of watershed), and two rainfall factors. The two rainfall factors involve the intensity of rainfall for a 1-hr duration, the annual amount of rainfall, and the number of excessive storms, as these vary geographically within the region. The relationships between these five variables are expressed in an equation. For forty-one of the fifty-one watersheds this equation gave peak rates of runoff which varied by not more than 25% with those derived directly from the runoff measurements. For other regions, further studies indicated that not only will the relationships shown in the equation change, but also the number and character of the independent variables may be different from those found to be significant for the Allegheny-Cumberland Plateau.

This type of study has great potentialities, not only in enabling the highway engineer to make a reliable estimate of probable peak rates of runoff for ungaged streams, but also in developing a basic understanding of hydrology. Certain regions may be found to have sufficient stream-gaging stations because of uniformity of characteristics, and in others the wide, unexplained deviations from the regional trend will indicate a need for installation of additional gaging stations.

On small, agricultural watersheds Mr. Potter has shown that land use is a significant factor affecting peak rates of runoff, particularly where one kind of land use covers the entire watershed.[13] Studies have not shown any significant correlation of peak runoff with land use on the larger watersheds in the Allegheny-Cumberland Plateau study.

SMALL WATERSHEDS

In analyzing the data on peak rates of runoff obtained by the SCS from experimental watersheds in Maryland, Ohio, Wisconsin, and Nebraska (as reported by Mr. Potter[13]), it was found that these peaks may be approximated by a single runoff curve to be adjusted by certain factors. This curve, shown in Fig. 5, gives the peak rate of runoff that may be expected to be equaled or exceeded on the average of once in 25 yr on mixed-cover watersheds in the humid section of the United States in localities where the rainfall factor is 1.0. The map in Fig. 6 shows values of the rainfall factor east of 101° west long. The factor is not given to the west of this meridian because of extreme local variations in rainfall intensity, and also because the application of the basic runoff curve to the western part of the United States has not been verified.

The factors for land use in the table of Fig. 5 are given for three classifications of land slope. Those for slopes greater than 2% are derived from the SCS data[13] and are reasonably reliable. The factors for flat and very flat land slopes are estimates based on the effect of slope in increasing surface detention and channel storage, and are therefore subject to correction when observed data become available. The frequency factors are based on the SCS report cited by Mr. Potter.[13] It should be noted that these factors are the same as those found applicable to rivers in Kansas. The term "mixed cover" deserves some explanation. The term is used to describe land use on a watershed with cultivated land, pasture, and woodland. This factor should be used wherever the watershed is not predominantly in one type of cover.

---

[13] "Surface Runoff from Agricultural Watersheds," by W. D. Potter, *Research Report No. 11-B*, Highway Research Board, National Research Council, Washington, D. C., 1950.

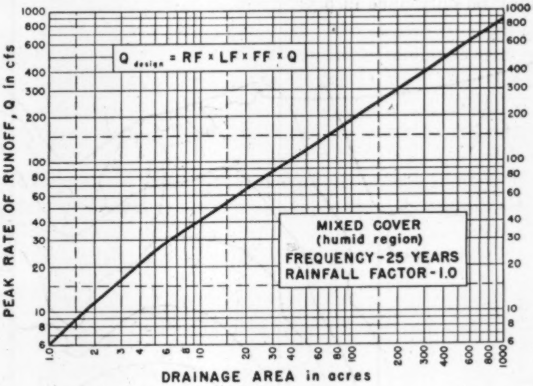

RAINFALL FACTOR (RF): See Figure 6

LAND USE AND SLOPE FACTORS (LF)

Land Slope	Steep over 2%	Flat 0.2%	Very flat, no ponds
100% Cultivated (row crops)	1.2	0.8	0.25
Mixed cover	1.0	0.6	0.2
Pasture	0.8	0.4	0.1
Woods, deep forest litter	0.3	0.2	0.05

FREQUENCY FACTORS (FF)

Frequency, years	5	10	25	50
Factor	0.6	0.8	1.0	1.2

FIG. 5.—PEAK RATES OF RUNOFF FOR WATERSHEDS OF LESS THAN 1,000 ACRES

The effect of soil type on peak rates of runoff has not been clearly established. For a longer frequency—such as 25 yr—the peak runoff probably occurs when the soil is nearly saturated by antecedent rainfall and, except for very pervious soils which can drain freely, the peak rate of runoff is assumed not to be affected by soil type. For more frequent floods it is likely that peak rates of runoff will be higher on the more impermeable soils.

Fig. 5 provides, for the humid portion of the United States, a simple method for estimating peak rates of runoff for use in the hydraulic design of culvert waterways for drainage areas of less than 1,000 acres. The close agreement of Fig. 5 with Fig. 3 suggests that the runoff curve can be extrapolated to larger drainage areas, although land-use factors will not apply. Unfortunately very few runoff data from which the curve might be extended are available on watersheds from 2 sq miles to 200 sq miles in area. If the curve is projected beyond 1,000 acres as a straight line, the land-use factors should converge on that for mixed cover. On larger watersheds the effect of channel storage does not cause differences in peak runoff caused by land use.

Mr. Potter has clearly demonstrated that the rational method of estimating peak rates of runoff is not applicable to agricultural watersheds because the runoff coefficient varies widely depending on the condition of the watershed when the storm occurs.[13] The maximum runoff corresponding to a given rainfall intensity may therefore have a frequency of once in 25 yr where the rainfall frequency may be only once in 5 yr.

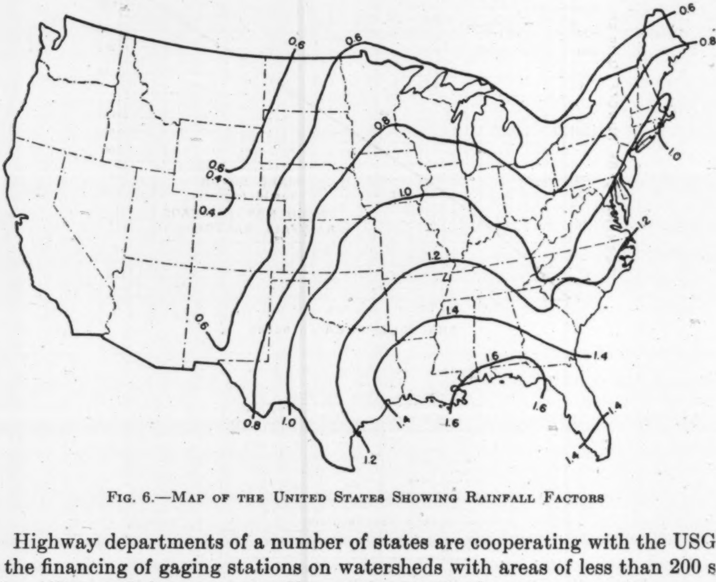

Fig. 6.—Map of the United States Showing Rainfall Factors

Highway departments of a number of states are cooperating with the USGS in the financing of gaging stations on watersheds with areas of less than 200 sq miles. Some of these are recording stations and others are crest stage gages. These stations must be maintained for at least 10 yr so that the length of record will constitute a sufficient sample for determination of regional flood frequency characteristics on watersheds in this size range.

Conclusions

Statistical analysis of peak runoff records for a period of years is a logical approach to estimating floods, because the runoff record has automatically integrated all the conditions effective on a given watershed. Many of these factors cannot be measured directly, and if they could it would still not be possible to anticipate the probability of any given combination of values of the variables. The regional flood-frequency curves demonstrate a close correlation between peak runoff for a given frequency and the size of the drainage area in a given region. Further studies will disclose the principal factors causing departure from the mean curve for a region, and may indicate reasons for differences between regional curves. Small agricultural watersheds with given land uses and areas have peak rates of runoff which correlate significantly with regional rainfall intensities. When peak runoff for mixed cover on small watersheds is expressed as a function of the drainage area size, the relationship is closely similar to that found for much larger watersheds in Kansas.

Maximum floods of record in Kansas show no well-defined relation to the size of the drainage area because the probable frequencies extend over a wide range. Consequently, the design of bridge waterways on the basis of maximum floods alone is a less satisfactory procedure than is the consideration of the probable frequency of a flood. The regional flood-frequency curves provide a method for ascertaining whether the maximum flood of record is an extreme event for which provision for maintenance of highway traffic cannot be justified on economic grounds, or is a flood which can be expected to occur frequently enough to justify provision of sufficient waterway to pass the entire flood without excessive backwater. High water elevations on the unobstructed stream, even if accurately established, are not adequate for the determination of bridge waterways, since the amount of backwater caused by the contracted opening depends on the flood discharge rate as well as on the stage.

DISCUSSION

Max A. Kohler,[14] A. M. ASCE.—The hydraulic design of highway structures is both an interesting and a timely subject. The importance of achieving an economical design is constantly increasing, and, as the time which can be justifiably devoted to the design of individual structures is limited, a generalized approach to the determination of the discharge to be used in the design is certainly useful and perhaps necessary.

Mr. Izzard has described methods for estimating the flood peaks having the specified recurrence interval from available discharge records. The work of Messrs. Dalrymple and Potter[2,5] on interpolation methods is cited by the author as well as the cooperative efforts of various state highway departments and the USGS in collecting stream-flow records from smaller watersheds. Mr. Izzard also makes mention of the feasibility of using USWB flood-forecasting techniques to extrapolate the stream-flow records.

The USWB has developed precipitation-runoff relations and related procedures for estimating flood peaks over much of the United States.[15,16] Although errors in the computed flood peaks can be appreciable, the effect of such errors on derived frequency curves is not great if the errors are essentially random. In fact, pilot studies (yet to be reported on) indicate that the reliability of a frequency curve based on a 10-yr record can be enhanced greatly if the record is extrapolated four-fold using a "forecasting" procedure.

Although the development of reliable precipitation-runoff relations requires a minimum of from 8 yr to 10 yr of stream-flow records, such relations are usually applicable to all basins larger than a few square miles that are located within large, fairly homogeneous areas. Unit hydrographs and other techniques for distributing the computed runoff volumes can be developed from the records for only a few storms. It is obvious, therefore, that stream-flow data collected from small drainage areas can be applied long before 10 yr have elapsed.

In using forecasting procedures for this purpose, there are two related facts which must be considered. First, precipitation data (the length of the record and the number of stations) are frequently insufficient to augment appreciably the observed stream-flow record. Second, the analysis requires considerable time and thus may not be economically justified except for the design of the more costly projects or the development of a generalized approach. Both deficiencies can be minimized, however, if it can be shown that the precipitation network utilized in the analysis need not be located in the basin under consideration, so long as the basin and the network are within an area of similar rainfall frequency regime. Most of the time required to estimate the maximum annual flood peaks for a period of years is spent in the processing of precipitation data. Thus, if the processed data can be used for numerous basins, the cost would become relatively small. It is believed that the area of applicability for a particular set of processed precipitation data could be determined by examination of intensity-duration-frequency maps. Because of the effect of topography on precipitation, it is obvious that rainfall data should not be transposed in mountainous terrain except with extreme caution.

---

[14] Chf. Research Hydrologist, Hydrologic Services Div., Weather Bureau, U. S. Dept. of Commerce, Washington, D. C.

[15] "Predicting the Runoff from Storm Rainfall," by M. A. Kohler and R. K. Linsley, *Research Paper No. 34*, Weather Bureau, U. S. Dept. of Commerce, Washington, D. C., September, 1951.

[16] "Applied Hydrology," by R. K. Linsley, M. A. Kohler, and J. L. H. Paulhus, McGraw-Hill Book Co. Inc., New York, N. Y., 1949, pp. 630–635.

It should be emphasized that this approach is a method of making full use of all available stream-flow data—and is not to be considered as a substitute for such data. Even so, the potentialities are believed to justify further investigation.

Roy F. Warner,[17] M. ASCE.—Present (1954) knowledge, experience, and highway drainage requirements have necessitated the new approach to the design of hydraulic structures which has been offered by Mr. Izzard. Much of the flood damage to highway structures has been the result of either a misapplication or an over-extrapolation of empirical formulas that were hardly more than "guessing rules" for a mode of transportation dependent on the unshod hoofs and wooden wheels of the nineteenth century.

The author has provided an excellent guide for the development of a detailed analysis of local-runoff characteristics for any region in the United States. Fortunately, stream-gaging observations have been kept for a sufficient period of time to provide a fairly reliable experience record for frequency analysis. The convenient manner in which runoff frequency is presented makes it easy for the engineer to determine a reasonable design runoff. Thus, waste is prevented by overdesigning for abnormally high floods, yet the structure can be consistent with anticipated maximum conditions of service.

It would be helpful if runoff-frequency studies were made on typical watersheds varying in size from 2 sq miles to 200 sq miles. Within this size range, numerous factors—meander, channel storage, ground cover, soil characteristics, distribution of precipitation, and water shed geometrics—exert an influence on the runoff. Representative regions within the major watersheds of each state should be studied to develop a basis for the adequate design of highway-drainage structures.

The cost of these studies would be minor compared to the half-billion dollars spent annually for the construction of highway bridges and culverts. A small fraction of 1% of the construction costs spent on frequency-runoff analysis of any state's major watersheds would result in enormous savings by avoiding overdesign of structures, by reducing reconstruction because of underdesign, and by avoiding or decreasing annual maintenance. The highway system in the United States is vast, but even so it is overtaxed by natural expansion and development. The system deserves to be constructed according to modern standards, with modern tools and by modern methods.

---

[17] Hydr. Engr.. Kansas City, Mo.

N. E. MINSHALL,[18] A. M. ASCE.—It is gratifying to note the progress that has been made in estimating peak rates of runoff for various frequencies on areas under measurement. The logical extension of these data to ungaged areas requires a thorough knowledge of the effect of many factors on rates of runoff. Mr. Izzard has drawn attention to various methods of estimating flood frequencies from gaged and ungaged areas. Two of the methods referred to by the author seem to be considerably at variance. Mr. Dalrymple plots the mean annual flood against the drainage areas as the basis for determining regional flood frequencies regardless of soil type, topography, shape of area, and vegetal cover.[2] Mr. Potter first outlines the general soil area and then attempts to determine the effect of various other factors within this area by multiple correlation.[12] It is regrettable that, as soil groupings are available for most of the United States, the data in all cases were not first grouped according to the major soil boundaries.

Relative to the effect of several of the principal topographic factors, Mr. Potter[12] states: "The index finally selected involves only the measurement of the length and slope of the principal waterway." This statement is essentially in agreement with that made[19] by Arnold B. Taylor and Harry E. Schwarz:

> "The study indicates that the most significant basin characteristics were drainage area, length of longest watercourse, length to center of area, and equivalent main stream slope."

In general, only the size of the drainage area has been considered in several of the flood-frequency reports cited by Mr. Izzard. Lack of adequate topographic maps was the cause of the failure to use other physiographic features in a multiple correlation.

It would seem more logical to group rainfall-runoff data by broad soil boundaries and then determine the cause for any unusual deviations from the mean line. For example, most of the stations shown in the claypan area of southeastern Kansas are near the upper line in Fig. 3. That points 33, 35, and 37 are below this line is probably because the soils in this area are more permeable than those in the extreme southeastern part of Kansas.

On small watersheds the approximate peak rates of runoff (modified by factors for variations in land use and rainfall) have been shown by the single curve in Fig. 5. Any such simplification which can be made reasonably should meet with the approval of all persons responsible for the design of small drainage structures. There is, however, the danger that such widespread application will lead to serious errors.

Fig. 5 and the table of land-use factors assume that (*a*) the soil type is not an important factor in determining the peak rates of runoff from small watersheds, (*b*) the cover is effective in flood reduction regardless of the soil, and (*c*) the slope of the land is the primary topographic influence, and little consideration need be given to the shape of the area or the slope of the main channel. The writer doubts that these exact limitations were intended by the author.

---

[18] Hydr. Engr., Soil and Water Conservation Branch, Agri. Research Service, U. S. Dept. of Agriculture, Madison, Wis.

[19] "Unit-Hydrograph Lag and Peak Flow Related to Basin Characteristics," by Arnold B. Taylor and Harry E. Schwarz, *Transactions*, Am. Geophysical Union, April, 1952.

It is stated (under the heading, "Small Watersheds") that "The effect of soil type on peak rates of runoff has not been clearly established." The more impermeable the soil, however, the more frequently will it be in a saturated condition; thus the chance of heavy runoff occurring during an excessive rainfall is increased. The two maximum rates of runoff on the watersheds at Fennimore, Wis., in 16 yr have both occurred as a result of very intense storms on dry soil. Tests made by the SCS, with the type F infiltrometer,[20] have shown that the minimum infiltration rates on a number of moderately permeable soils of Iowa, Illinois, and Wisconsin varied from 0.4 in. per hr for corn fields to more than 1 in. per hr for good hay fields or pasture.[21] In contrast with this, the minimum infiltration rates on the claypan areas of southern Illinois, Missouri, and southeastern Kansas are less than 0.1 in. per hr regardless of the type of vegetal cover. It is evident that the rainfall excesses are considerably higher on the impermeable soils.

The land-use factors given in the table in Fig. 5 for slopes greater than 2% might apply to the moderately permeable soils. It should be realized that the difference in infiltration rates between good and poor pasture may be as great as the difference between cultivated land and meadow land. Also, the engineer responsible for the design of small drainage structures has no assurance that a change in land ownership or other causes will not increase the severity of the cropping system. The engineer must provide for any such changes which might reasonably be expected to occur within the life of the structure.

Studies to determine rates and amounts of runoff from small agricultural watersheds were established by the SCS in 1938. Two groups of these watersheds located near Edwardsville, Ill., and Fennimore have been under the supervision of the writer since their inception. Reports—showing the general areas of application and estimated frequencies of peak rates of runoff—based on the first half of the period of record have been published.[22, 23]

Ralph W. Baird[24] has shown that the effect of conservation practices or crop cover on peak rates of runoff can be determined by comparing rates of rainfall minus runoff for the period of concentration for one watershed against another. Conservation practices on the base watershed must remain essentially unchanged for the entire period of record whereas the other watershed may have a few years of nonconservation practices followed by a period of conservation practices. This method of analysis was applied to the data obtained at Edwardsville and Fennimore, and the results are shown in Table 1.

The 27-acre area near Edwardsville was 96% cultivated during the years 1938, 1948, and 1949 and was 100% alfalfa continuously from 1940 to 1943, inclusive. The 50-acre area was approximately 100% pasture for the entire period of record, and the 290-acre area varied between 15% and 30% cultivated. Table 1 shows that peak rates of runoff on a 27-acre area of these claypan soils were reduced by approximately 10% for a complete change in cover from 100% cultivated to 100% alfalfa.

---

[20] "A Comparison of the Colorado and Type-F Artificial Rainfall Applicators, Hastings, Nebraska," by L. L. Kelly, Office of Research, Soil Conservation Service, U.S.D.A., Washington, D. C., August, 1940 (mimeographed).

[21] "The Sny Watershed," Illinois Interim Survey Report, U.S.D.A., Washington, D. C., June, 1950, Appendixes, Fig. 15.

[22] "Hydrologic Design of Farm Ponds and Rates of Runoff for Design of Conservation Structures in the Claypan Prairies," by D. B. Krimgold and N. E. Minshall, *Technical Publication No. 56*, Soil Conservation Service, U.S.D.A., Washington, D. C., May, 1945.

[23] "Rates of Runoff for the Design of Conservation Structures in the Upper Mississippi Valley Upland Loessial Areas," by N. E. Minshall, *Technical Publication No. 73*, Soil Conservation Service, U.S.D.A., Washington, D. C., January, 1949.

[24] "The Effect of Conservation Practices on Peak Rates of Runoff," by Ralph W. Baird, *Texas Engineer*, Vol. 16, November 8, 1946, pp. 8–15.

The 23-acre watershed at Fennimore was 60% cultivated during 1944 and 1945 and was less than 25% cultivated for all other years. The area had less than 10% cultivation during runoff-producing periods in 1938, 1942, and from 1947 through 1951. During these same periods, cover on the 171-acre area varied between 45% and 60% cultivated and, on the 330-acre watershed, varied between 35% and 50% cultivated. Table 1 indicates that peak rates of runoff on the 23-acre area of these moderately permeable soils were reduced by approximately one third when there was a reduction in percentage of area cultivated of from 60% to less than 10%. The percentage reductions in peak rates shown for these changes in vegetal cover are applicable only to the size of areas shown. The percentage reduction in rates of runoff, for a given change in percentage of cover, probably decreases as the size of the area increases.

TABLE 1.—PEAK RATES OF RUNOFF FOR VARIOUS FREQUENCIES[a]

Drainage area, in acres	Prevailing slopes, in percentages	Crop cover	PEAK RATE OF RUNOFF, IN CUBIC FEET PER SECOND, TO BE EXPECTED ONCE IN			
			5 yr	10 yr	25 yr	50 yr
		CLAYPAN PRAIRIES—EDWARDSVILLE, ILL.				
290	1 and 12	mixed[b]	480	625	800	930
50	1 and 12	pasture[c]	110	135	175	200
27	1	mixed	47	63	77	90
		cultivated[d]	51	67	81	95
		alfalfa[e]	43	59	73	86
Percentage reduction in runoff from 27-acre area by change from cultivated to alfalfa			15.7	11.9	9.9	9.5
		UPLAND LOESSIAL AREA—FENNIMORE, WIS.				
330	7	mixed[f]	315	425	595	660
171	6	mixed[g]	190	250	325	385
53	8	mixed	55	75	95	110
23	6	mixed	31	44	60	72
		60% cultivated[h]	37	50	67	80
		less than 10% cultivated[j]	20	31	44	54
Percentage reduction in runoff from 23-acre area by change from 60% cultivated to 10% cultivated			46	38	34	33

[a] On SCS watersheds. Based on period from 1938 to 1953. [b] Between 15% and 30% cultivated. [c] Approximately 100% for entire period of record. [d] 96% during 1938, 1948, and 1949. [e] 100% continuously from 1940 to 1943, inclusive. [f] Between 35% and 50% cultivated. [g] Between 45% and 60% cultivated. [h] During 1944 and 1945, less than 25% for all other years of record. [j] 1938, 1942, and 1947 through 1951.

Strict adherence to the curve in Fig. 5 may result in many inadequate designs, as is evidenced by the actual measured runoff rates and estimated frequencies shown in Table 2. The 25-yr frequency from the curve in Fig. 5

for the 50-acre pasture area near Edwardsville is approximately half that determined from the actual records. The runoff of 80 cu ft per sec for this area has been exceeded on the average of once every 2 yr. On the 290-acre area the estimated runoff of 420 cu ft per sec has been exceeded on the average of once every 3 yr. The 4-yr record for the Little Sioux watersheds in western Iowa is insufficient for use in a frequency analysis. The actual measured values for these areas do show that use of values from the curve in Fig. 5 can be dangerously low for this area. It is possible that the three floods shown on the 309-acre watershed all greatly exceeded the suggested 25-yr frequency.

TABLE 2,—COMPARISON OF THE 25-YR ESTIMATED PEAK RATES OF RUNOFF WITH ACTUAL MAXIMUM MEASURED DISCHARGES

Years of record	Drainage area, in acres	Type of cover	Type of soil	PEAK RATE OF RUNOFF IN CUBIC FEET PER SECOND FROM			
				Fig. 5	Watershed record	Actual measurement (maximum flood) during period of record	
				25-yr frequency		Date	Amount
				FENNIMORE, WIS.			
16	23 53 171 330	mixed mixed mixed mixed	mpsl[a]	63 112 235 370	60 95 325 595	June 28, 1945 June 28, 1945 Aug. 5, 1951 Aug. 5, 1951	62 87 304 565
				RALSTON CREEK, IOWA			
28	1,926	mixed and cultivated[b]	mpsl[a]	1,260	1,370	July 1, 1950	1,510
				EDWARDSVILLE, ILL.			
16	27 50 290	mixed pasture mixed	claypan	88 80 420	77 175 800	March 30, 1938 Aug. 14, 1946 Aug. 14, 1946	70 150 825
				McCREDIE, MO.			
11	155	pasture	claypan	165	300	Oct. 3-4, 1941	265
				LITTLE SIOUX, IOWA[c]			
4	63	mixed	mpsl[a]	125	...	June 15, 1950 July 2, 1951	315 315
4	151	mixed		250	...	June 15, 1950 July 2, 1951	680 400
4	309	mixed		360	...	June 15, 1950 June 17, 1950 July 2, 1951	1,750 620 950
3	49	cultivated		130	...	June 17, 1951	220
3	125	mixed		200	...	June 17, 1951	565

[a] The letters "mpsl" signify moderately permeable silt loam. [b] 35% cultivated. [c] Insufficient data for frequency analysis.

Crest-stage gages were established by the SCS in 1952 above twenty-two erosion-control structures in southwestern Wisconsin on drainage areas ranging in size from 250 acres to 2,500 acres. These gages show only the maximum peak rates between intervals of observation, but 10 yr, or more, of record will provide a reasonable approximation of flood frequencies. Because USGS topographic sheets are available for most of these areas, the data can also be of value in establishing the effect of various topographic features on the peak of runoff. Recording stations should be established on a number of areas to obtain the total seasonal and annual runoff for use as the basis for the design of small water-supply ponds and flood-retarding structures.

The writer doubts that reasonable accuracy in estimating peak rates of runoff from small ungaged drainage basins will be obtained until the results are grouped by soil types and an attempt is made to evaluate the effect of cover, land slope, shape of area, and slope of channel within each such area. Each soil group would have a curve similar to that shown in Fig. 5, but there would be additional factors if these curves showed a relationship for shape of area and slope of main channel. Sufficient data may not be available to establish such factors, but additional runoff-measuring installations should be made with this in mind.

CARL F. IZZARD,[25] A. M. ASCE.—The emphasis which Mr. Minshall places on the grouping of peak-discharge records according to soil type is fundamentally sound. This grouping should be the first step in attempting to discover the correlation of peak-runoff rate for a given frequency with other variables; otherwise a basic principle in statistical analysis—that samples be homogeneous—is violated. It is of interest to note that the USBPR has adopted the problem area map of the SCS as the criterion for geographic grouping of runoff data. This action stems from the highly significant correlations which have resulted from numerous applications of the criterion.

The Allegheny-Cumberland Plateau studied by Mr. Potter[12] is one problem area (designated B-15); the glaciated shale and sandstone area of New York, Pennsylvania, and Ohio (B-8) is another. Charts for estimating peak discharge in both of these areas have been published.[26]

The problem area map should have been used in grouping the watersheds in Kansas which are designated by various symbols in Fig. 3; watershed 7 would then have been classified with those for various small rivers in eastern Kansas because the Walnut River Basin lies entirely within the Central Basin physiographic area. (Subdivisions of broad physiographic areas are called problem areas.) The boundary line between the Central Basin and the Great Plains is actually about 1° west of the arbitrary boundary placed at 96°30′ to classify stations plotted in Fig. 3. Similarly, point 5 for the Pawnee River would have been grouped with the points shown by the solid-circle symbol, all of which are for watersheds wholly (or almost wholly) within the Great Plains area. The Blue River Basin straddles the boundary line between the Central Basin and the Great Plains areas and, quite reasonably, has a peak-discharge curve lying between the trend lines for those areas.

---

[25] Chf., Hydr. Branch, Div. of Research, Bureau of Public Roads, U. S. Dept. of Commerce, Washington, D. C.

[26] "Use of Indices in Estimating Peak Rates of Runoff," by William D. Potter, *Public Roads*, April, 1954, pp. 1–8.

The problem areas were determined, as the name suggests, primarily to assist the engineers of the SCS to formulate land-use programs aimed at solving conservation problems. Consequently, factors such as soils, geologic formation, topography, and degree of erosion were all considered. As these factors also influence the rate of runoff, it is not surprising to find that the problem area map is also an excellent guide to the homogeneous classification of runoff records.

When the paper was prepared (1951), the application of statistical-correlation techniques to the analysis of peak-runoff data had not been fully explored. However, enough work had been done to prove that peak runoff for a given frequency did correlate satisfactorily with the size of the watershed—provided the data were all for the same geographic area. Now (1954) it is possible not only to define boundaries but also to explore, as Mr. Minshall suggests, the reasons why individual watersheds show runoff peaks deviating from the mean curve for a problem area. Mr. Potter and the USBPR have found that the differences in peak runoff between problem areas may be as great as tenfold, whereas the meteorological and topographic indices seldom explain differences greater than twofold.

Mr. Minshall, therefore, rightfully challenges the application of Fig. 5 without regard to the problem area within which a watershed may lie. Fig. 5 was prepared (1950) to provide an approximate method of estimating the peak rate of runoff by considering only the factors which could be shown to be significant from analyses then available. A method is now being developed which will include a geographic index by problem areas as well as other indices. This method will apply to watersheds of less than 10,000 acres.

Whereas land use, as demonstrated by Mr. Minshall's records, is a significant factor (especially on small watersheds tending to one type of use), it is being ignored in the current studies for two reasons: (1) The available runoff data (USGS records) do not cover enough range in land use within each problem area so that significant correlations can be made. (2) The complex of land use in a given problem area (for watersheds larger than field size) tends to be similar because the soil type and the related characteristics are also similar. The exceptions in most cases will be evident from examination of an aerial photograph. The engineer is expected to use his judgment in raising or lowering the peak-runoff rate obtained for the average condition. He will also need to anticipate changes in land use, especially where forested or pasture lands may be subdivided for housing developments. Data on the effects of changes in land use, such as those being accumulated by Mr. Minshall and the SCS, will be an invaluable guide to the engineer.

Mr. Kohler mentions the possible use of rainfall-runoff relationships to extrapolate short runoff records from longer rainfall records. Where the rainfall-runoff relationship in a given problem area has already been established (for flood-forecasting purposes), this method is probably practical. Further tests of its practicality should be made; they might result in a re-examination of the rapidly expanding practice of installing crest-stage gages for obtaining records of peak runoff on small watersheds. Complete hydrographs are essential to the unit-hydrograph technique for estimating the peak discharge resulting from a given volume of excess rainfall. Synthetic unit hydrographs, as developed by Messrs. Taylor and Schwarz,[19] might have an application, but these also require complete hydrographs to establish the constants for a given problem area. However, if reliable results could be obtained with five years of record from continuous recording gages used in conjunction with a long period of rainfall record, the method suggested by Mr. Kohler might be more economical (and perhaps more reliable) than waiting ten or more years to get an adequate sample of annual floods from crest-stage gages.

Attention is directed to the fact that data relating rainfall intensity and duration for frequencies up to 10 yr are available for that part of the United States west of the 115th Meridian.[27] Such data can be used to establish rainfall indices for correlation with peak runoff in the part of the area not covered by Fig. 6. The other inadequacies of Fig. 6 are realized, and the USBPR is preparing, in cooperation with the USWB, rainfall index maps for the eastern half of the United States similar to those presented[26] by Mr. Potter.

Research on peak rates of runoff—directed toward the highway engineer's problem—is now (1954) involving the close cooperation of many government agencies at both state and federal levels. Also noteworthy is the effort being made in these research studies to make maximum use of the hydrologic data which have been accumulating in reports for many years. Analyses of the existing data are pointing out the deficiencies in the basic data and will be invaluable in the formulation of a stream-gaging program to fill the gaps.

---

[27] "Rainfall Intensities for Local Drainage Design in the United States—Part I West of the 115th Meridian," *Technical Paper No. 24*, Weather Bureau, U. S. Dept. of Commerce, Washington, D. C., August, 1953.

AMERICAN SOCIETY OF CIVIL ENGINEERS
Founded November 5, 1852
TRANSACTIONS

Paper No. 2710

DESIGN CHARTS FOR AIR CHAMBERS ON PUMP LINES

BY W. E. EVANS[1] AND C. C. CRAWFORD[2]

WITH DISCUSSION BY MESSRS. C. E. WITHERS; HENRY M. PAYNTER; AND W. E. EVANS AND C. C. CRAWFORD

SYNOPSIS

For controlling pressure surges following interruption of electric power to a pumping plant, the air chamber has certain advantages over other devices. If simplifying assumptions are made, surge conditions in a pump-discharge line having an air chamber can be expressed in terms of three other variables. The purpose of this paper is to present charts by which the required size of an air chamber for a particular pumping installation can be quickly determined for preliminary design purposes. The references, theories, and assumptions necessary for preparation of the charts are presented. An example is included that demonstrates the use of the charts.

NOTATION

The letter symbols introduced in this paper are defined where they first appear, in the text or by illustration, and are assembled alphabetically in Appendix II for convenience of reference.

INTRODUCTION

The transient pressures in pumping plants and their discharge lines after interruption of the flow of electric power to the pump motor may be objectionable. Corrective measures such as surge tanks, surge-suppressor valves, and air chambers are at the designer's disposal.

After it has been decided that certain types of pressure-control devices will meet design requirements, the final choice is usually based on a cost study of the various devices. The cost of an air chamber is determined primarily

---

NOTE.—Published, essentially as printed here, in September, 1953, as *Proceedings-Separate No. 273*. Positions and titles given are those in effect when the paper or discussion was received for publication.

[1] Engr., Design Div., Bureau of Reclamation, U. S. Dept. of the Interior, Denver, Colo.

[2] Engr., Design Div., Bureau of Reclamation, U. S. Dept. of the Interior, Denver, Colo.

by its size. This paper will present a set of data in chart form, from which the size of an air chamber can be determined quickly for preliminary design purposes.

For controlling pressure surges in pump-discharge lines, the air chamber has certain advantages over both the open-top surge tank and the valve-type surge suppresser. The air chamber can be built smaller than the surge tank, simplifying the foundation structure. Also, the air chamber can be a long cylinder having its axis parallel to the slope of the ground. This construction can, in some cases, drastically reduce foundation costs and may provide better resistance to earthquake and wind. The air chamber can be near the pump, whereas the surge tank cannot always be so located. The air chamber can be designed to reduce the downsurges in a pump-discharge line, thus preventing collapse of the line and water-column separation; ordinarily, surge-suppresser valves are not suitable for this important function. The principal disadvantage of the air chamber is that it must be provided with an air supply to replace the compressed air that is being lost by leakage or by going into solution. An idealized air-chamber installation is shown in Fig. 1.

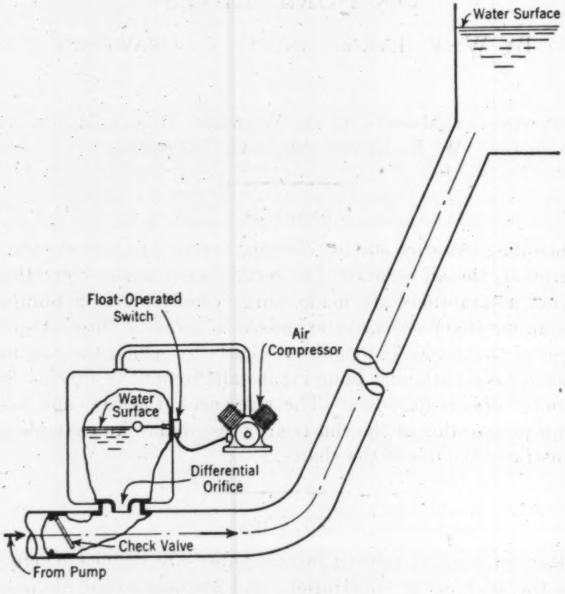

FIG. 1.—AN IDEALIZED AIR-CHAMBER INSTALLATION ON A PUMP-DISCHARGE LINE

THEORY

When an air chamber and check valve are in the line near the pump, power failure causes the head developed by the pump to drop rapidly, and a head differential is thus created across the air-chamber outlet. The air chamber begins to discharge into the pipe line to maintain the head and the flow. Soon, the head produced by the pump is less than that maintained by the air chamber, and the check valve closes; the pump coasts to a stop. Water will continue to be discharged from the pipe line at a diminishing rate, the air chamber supplying both the water and the energy. The water in the discharge line will reverse its direction and flow into the air chamber. While the water is flowing into the air chamber, the pressure in the discharge line will increase to exceed normal operating head and will produce the maximum head for the transient. Resurges in the pipe line will ensue with diminishing intensity.

R. W. Angus[3] has demonstrated a graphical method for computing transient hydraulic conditions in a pump-discharge line having an air chamber near the pump. The general method described by Mr. Angus has been adopted in making all water-hammer computations for the preparation of this paper.

Lorenzo Allievi[4] shows that the pressure surges in a pipe line equipped with an air chamber depend on the two parameters, ρ^* and σ^*, when friction is not considered. He then shows that, without frictional effects, chambers of normal size are ineffectual in controlling upsurges. Louis Bergeron,[5] in a discussion of Mr. Allievi's paper, describes a simple, effective, differential orifice for use in conjunction with an air chamber.

In his early work with water hammer, Mr. Allievi described the pipe-line characteristic, ρ, as

$$\rho = \frac{a V_o}{2 g H_o} \qquad (1)$$

in which a is the propagation velocity of water-hammer waves in the pipe line, in feet per second; H_o is the steady-state pressure head, in feet of water; and V_o is the steady-state velocity, in feet per second. By use of Eq. 1 all conduits in service can be classed in so far as water-hammer phenomena are concerned. The characteristic, ρ, is dimensionless and is a function of the ratio of the steady-state kinetic energy to the total potential energy in a unit length of the conduit. Since, in dealing with air chambers, the volume of the air is a function of the absolute pressure to which it is subjected, in order to facilitate computation the pipe-line characteristic was changed to

$$\rho^* = \frac{a V_o}{2 g H^*_o} \qquad (2)$$

in which H^*_o is the normal absolute pressure head in the pipe line at the entrance to the air chamber.

The parameter, developed by Mr. Allievi, that pertains to a pump-discharge line having an air chamber is

$$\sigma^* = \frac{2 g C_o H^*_o}{A L V^2_o} \qquad (3)$$

---

[3] "Air Chambers and Valves in Relation to Water-Hammer," by R. W. Angus, *Transactions*, ASME, Vol. 59, 1937, p. 661.

[4] "Air Chambers for Discharge Pipes," by Lorenzo Allievi, *ibid.*, p. 651.

[5] Discussion by Louis Bergeron of "Air Chambers for Discharge Pipes," by Lorenzo Allievi, *ibid.*, 1939, p. 441.

in which C_o is the volume of air in the air chamber at absolute pressure head H^*_o, in cubic feet; A is the cross-sectional area of the pipe line in square feet; and L is the length of the pipe line in feet. Eq. 3 expresses the ratio of steady-state potential energy of the air in the air chamber to the steady-state kinetic energy of the water in the discharge line.

Because σ^* varies directly with C_o (the initial volume of air in the chamber), the latter value must be maintained at its proper value in order that the air chamber can function as designed. The compressed air tends to dissolve. This dissolved air plus that lost through leakage must be continually replaced in order to keep the air chamber ready to function properly.

Because frictional resistance is essential to the efficient use of an air chamber in a pump-discharge line, a third variable (in addition to those shown by Mr. Allievi) will be used for this study. This variable, K, will be defined so that $K\,H^*_o$ is the total head loss for a flow of Q_o down the pipe line and into the air chamber where Q_o is the initial rate of flow in the pipe line, in cubic feet per second. A differential orifice similar to that described by Mr. Bergeron[5] will be used to create the head loss. Because of the differential orifice design, the head loss for flow from the air chamber will be less than that for flow into the chamber.

In order to use the graphical method of computation, and to express the results in terms of the proper parameters, it is required that an expression be developed to show the relationships among σ^*, ρ^*, the flow in the discharge line, and the volume of air in the air chamber. Such an expression can be obtained by algebraic manipulation of the basic relationships as follows: From Eqs. 2 and 3,

$$\sigma^* = \frac{C_o\,a}{A\,L\,V_o\,\rho^*} \qquad (4)$$

or

$$C_o = \sigma^*\,\rho^*\,Q_o\,\frac{L}{a} \qquad (5)$$

If the subscript n indicates the number of the time interval under study, one may let

$$c_n = \frac{C_n}{C_o} \qquad (6)$$

To fit the graphical solution, the interval of time used will be a fraction of the travel time of a wave, $f\,\frac{L}{a}$, in which f may take values of 2, 1, $\frac{1}{2}$, $\frac{1}{4}$, . . ., as the problem requires. Then

$$c_1 = \frac{\sigma^*\,\rho^*\,Q_o\,\frac{L}{a} + \frac{Q_1 + Q_o}{2}\,f\,\frac{L}{a}}{C_o} \qquad (7a)$$

and

$$c_1 = c_o + \frac{(Q_1 + Q_o)\,f\,\frac{L}{a}}{2\,\sigma^*\,\rho^*\,Q_o\,\frac{L}{a}} \qquad (7b)$$

If q_n is defined as being equal to Q_n/Q_o,

$$c_1 = c_o + \frac{(q_1 + q_o) f}{2 \sigma^* \rho^*} \qquad (8)$$

and for the time interval n,

$$c_n = c_{n-1} + \frac{(q_n + q_{n-1}) f}{2 \rho^* \sigma^*} \qquad (9)$$

which is the desired relationship. When $2 \rho^*$, σ^*, and K are fixed, Eq. 9 makes possible computation by the graphical method of the complete transient which follows power interruption. After σ^* and ρ^* are determined, Eq. 9 is independent of the value of L/a.

ASSUMPTIONS

For the purposes of making this study, it is assumed that (*a*) there is a check valve on the discharge side of the pump which closes immediately on power failure, and (*b*) the air chamber is situated near the pump. In addition, it is assumed that (*c*) the pressure-volume relationship for the air in the chamber may be expressed by

$$H^* C^{1.2} = \text{a constant}.$$

It is further assumed that (*d*) the ratio of the total head loss for the same flow into and from the air chamber is 2.5:1; (*e*) the air in the chamber is subjected to a head of H^*; (*f*) the head loss (surface friction and loss at the orifice) varies with the square of the velocity; and (*g*) during the transient condition following power failure, the condition of continuity of flow in the discharge line is maintained—that is, the water column remains intact throughout the length of the line.

These assumptions and simplifications are necessary because the variables involved are so numerous, and they permit a solution which yields usable results. By the use of assumption (*a*), the pump characteristics are eliminated as a consideration, but an abrupt wave is introduced that must be accounted for throughout the computations. Assumption (*c*) is a compromise between adiabatic and isothermal expansion. Normally, assumption (*d*) can be realized through proper orifice design. Theoretically, a higher ratio can be obtained, but the lower value is closer to that which will actually be obtained in ordinary practice. In assumption (*e*), the static head difference between the water surface in the air chamber and the center line of the pipe below the chamber is neglected. Normally, this difference in head is small compared to H^*, and the assumption is permissible. Assumption (*g*) limits the study to cases in which the water column remains intact. The study of conditions following breach of the water column is beyond the scope of this paper.

ORIFICE DESIGN

Restriction of flow into the air chamber (to control upsurges) results in some restriction on the flow from the chamber. Fig. 2 shows that the downsurge values at the pump are not increased as much by an increase in throttling

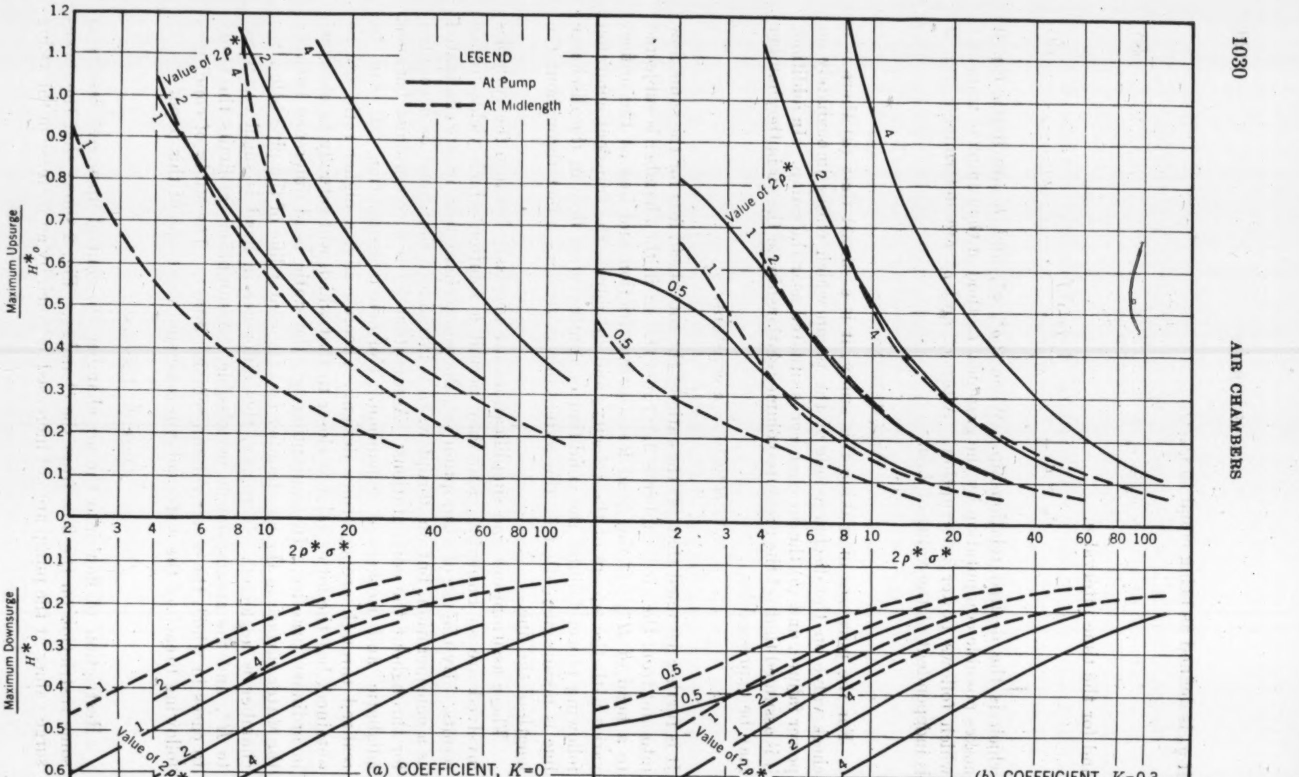

(a) COEFFICIENT, K=0

(b) COEFFICIENT, K=0.3

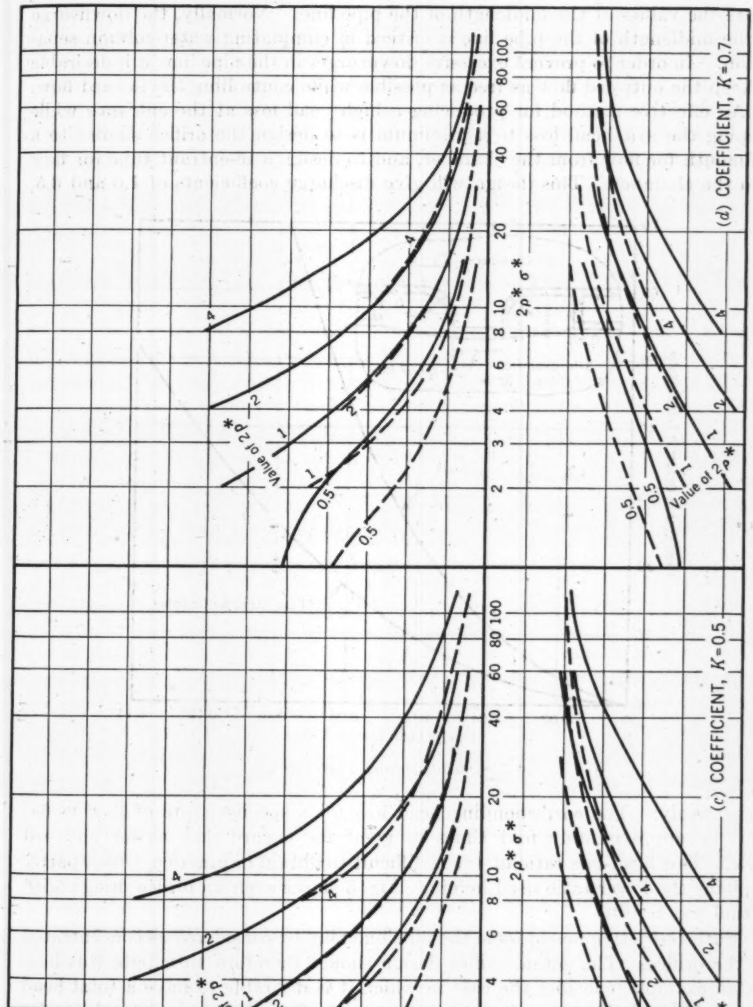

FIG. 2.—MAXIMUM SURGES FOR PUMP-DISCHARGE LINE EQUIPPED WITH THROTTLED AIR CHAMBER

as are the values at the midlength of the pipe line. Normally, the downsurge at the midlength of the pipe line is critical in eliminating water-column separation. In order to prevent excessive downsurges in the pipe line, it is desirable to keep the outward flow as free as possible while controlling the inward flow.

An effective method for producing a high head loss at the entrance while keeping the exit head loss to a minimum is to design the orifice similar to a bellmouth for flow from the chamber, and to design a re-entrant tube for flow into the chamber. This design will give discharge coefficients of 1.0 and 0.5, respectively. The corresponding head loss for a specified rate of flow would thus be approximately four times as great for inward flow as for outward flow. This head-loss ratio of 4:1 is difficult to obtain in practice, which partly explains the lower ratio used herein. Fig. 3 shows such an orifice design with actual test results.

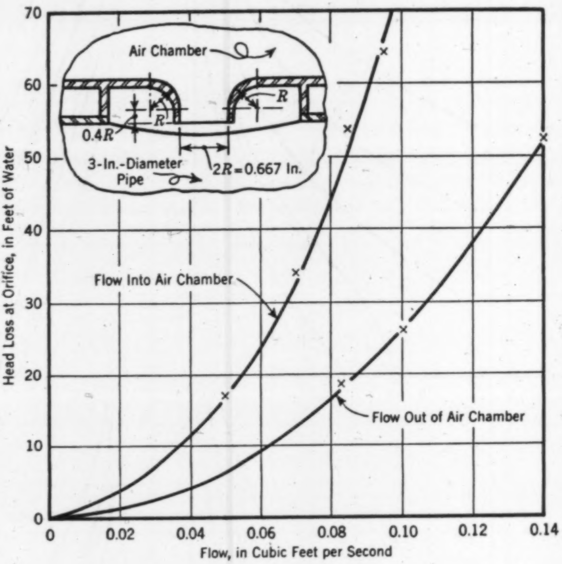

FIG 3.—ORIFICE-DESIGN TEST RESULTS

Surface-friction head loss in the pipe line may be considered as concentrated at the orifice. The actual orifice design should therefore anticipate this loss. As an example, consider the case in which it is desirable to have a total head loss of 50% of H^*_o for an inward flow equal to Q_o. The desired total loss for an outward flow of Q_o would then be 20% of H^*_o, or less. Assume that for a flow of Q_o the pipe-line, surface-friction loss is 5% of H^*_o. The orifice would then be designed for a head loss of 45% of H^*_o for an inward flow of Q_o, and a head loss of 15% of H^*_o for an outward flow of Q_o. Therefore, the actual orifice-design, head-loss ratio of inward flow to outward flow should be 3:1 which can be realized in practice by the suggested method.

THE CHARTS

For purposes of this study, certain simplifying assumptions have been made concerning the transient that follows power interruption. Under the conditions imposed by the assumptions, this entire transient is completely described by fixing the variables K, $2\rho^*$, and $2\rho^*\sigma^*$. In Fig. 2, the maximum upsurges and downsurges have been plotted in terms of these variables. Maximum upsurges and downsurges at the pump and at the midlength of the discharge line are plotted as percentages of H^*_o for various values of the descriptive variables.

Mr. Allievi[4] explains that the normal range of ρ^* is from 0.25 to 2.0 and that of σ^* is from 2 to 30. These ranges have been covered in Fig. 2. In order to include the effects of friction, the charts cover the range in values of K from 0.0 to 0.7. Values of K greater than 0.7 are considered unnecessary. Because of the great resistance to flow from the chamber, for $K = 0.7$, large air chambers are needed to control the downsurges whereas the upsurges are not greatly reduced. The downsurges can be controlled more efficiently by using smaller air chambers with less throttling.

Ordinarily, when an air chamber is being designed for a pump-discharge line, the values of L, a, V_o, Q_o, A, H^*_o, and g will be known. From these values, $2\rho^*$ can be computed. The allowable, maximum surge values may be dictated by specifications, operating conditions, or the profile of the discharge line. With the values of $2\rho^*$ and the maximum allowable surges known, values of K and $2\rho^*\sigma^*$ may be chosen from Fig. 2 such that the surge limitations are met. If the allowable surge conditions cannot be satisfied by data from the charts, probably some means other than an air chamber should be used to control the surges. When $2\rho^*\sigma^*$ has been determined, C_o can be computed from Eq. 5. The volume of the air chamber is then determined by considering that the chamber must contain adequate air above the upper emergency level (Fig. 4) to control the surges to desirable limits, and enough water below the lower emergency level to prevent unwatering. With allowances for the volume between the upper and lower emergency levels, the total required volume of the air chamber can be computed.

The minimum quantity of air that must be maintained in the air chamber—that is, the volume of the chamber above the upper emergency level—will be represented by C' which is numerically equal to the volume C_o necessary to control the pressure surges. By adding to this quantity the volume of the chamber between the upper and lower emergency levels (the factors affecting these levels will be discussed separately), one determines the initial volume of air in the chamber that will result in the lowest water-surface level following power failure. This new volume of air becomes C'' equal to C' plus the volume of air between the upper and lower emergency levels.

The downsurge at the pump with this initial volume of air can be determined from the curves by computing a new value of $2\rho^*\sigma^*$ based upon C'' instead of C'. Assuming that this expansion is isothermal, the total volume of the air chamber becomes $\frac{C'' H^*_o}{H^*_o - \text{downsurge at pump}}$.

The various control levels for the water surface in the air chamber insure that, whenever the pump is operating, the chamber contains sufficient quantities of air and water to protect the system in the event of power failure. If the water surface rises to the upper emergency level or drops to the lower emergency level, the automatic controls shut down the plant.

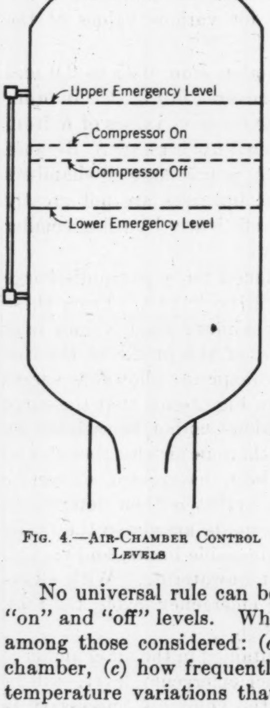
Upper Emergency Level
Compressor On
Compressor Off
Lower Emergency Level

FIG. 4.—AIR-CHAMBER CONTROL LEVELS

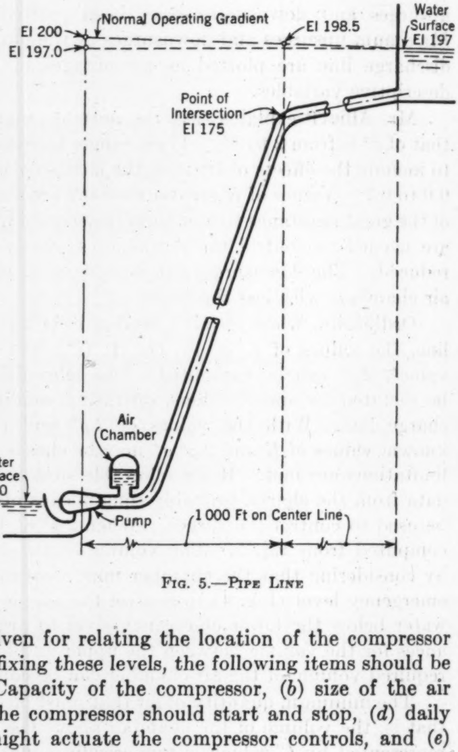
Normal Operating Gradient
El 200
El 197.0
El 198.5
Water Surface El 197
Point of Intersection El 175
Air Chamber
Water Surface El 0
Pump
1 000 Ft on Center Line

FIG. 5.—PIPE LINE

No universal rule can be given for relating the location of the compressor "on" and "off" levels. When fixing these levels, the following items should be among those considered: (*a*) Capacity of the compressor, (*b*) size of the air chamber, (*c*) how frequently the compressor should start and stop, (*d*) daily temperature variations that might actuate the compressor controls, and (*e*) how quickly the system is to be put back into operation after a prolonged shutdown.

The emergency levels can be at nominal distances above and below the compressor operating levels on those installations that have only one pump on a discharge line or that provide manual starting or stopping for individual pumps on the same line. However, if automatic starting and stopping of the individual pumps on the same line are required, the emergency levels should be sufficiently removed from the compressor operating levels to contain the surges produced by starting or stopping the largest of the pumps under the most critical initial conditions.

The data from Fig. 2 should be used primarily for purposes of estimation. In the final design of an installation having an air chamber, individual solutions similar to that shown by Mr. Angus[3] should be made to insure that the air chamber will fulfill design requirements.

ACKNOWLEDGMENTS

The writers gratefully acknowledge the helpful suggestions given by John Parmakian, M. ASCE, and the work done by J. R. Bruggeman and I. I. Pemberton, A.M. ASCE, who performed most of the individual solutions necessary to the preparation of the air-chamber charts. The writers are also indebted to R. H. Williams who prepared the drawings.

APPENDIX I. NUMERICAL EXAMPLE OF AIR-CHAMBER DESIGN

An example is included herein which demonstrates the use of Fig. 2. The pumping plant shown in Fig. 5 is to be fitted with an air chamber of a size such that the maximum head at the pump will be limited to 300 ft of water and the maximum negative head in the discharge line will be limited to 25 ft of water. In this example, Q_o is 100 cu ft per sec, A is 19.635 sq ft, V_o equals 5.093 ft per sec, and a equals 2,960 ft per sec. The absolute head is $H^*_o = 200$ ft + 34 ft = 234 ft. By Eq. 2, $2\,\rho^* = 2.00$. The allowable downsurge at midlength of the line is 198.5 ft − 175 ft + 25 ft $= 0.21\, H^*_o$. The allowable upsurge at the pump is 300 ft − 200 ft $= 0.43\, H^*_o$. From Fig. 2, the surge conditions can be met using the values,

$$K = 0.3,\ 2\,\rho^*\,\sigma^* = 21$$

and

$$K = 0.5,\ 2\,\rho^*\,\sigma^* = 44.$$

The volume of air in the chamber will vary directly as σ^*, so that the smaller value of $2\,\rho^*\,\sigma^* = 21$ will be used. For the values $2\,\rho^*\,\sigma^* = 21$, $2\,\rho^* = 2$, and $K = 0.3$:

The maximum upsurge at the pump $= 0.27\, H^*_o$.
The maximum downsurge at the pump $= 0.32\, H^*_o$.
The maximum downsurge at the midlength $= 0.21\, H^*_o$.

The surface-friction loss in the line for a flow of Q_o is 3 ft of water. The differential orifice should be designed to provide a head loss—for a flow of 100 cu ft per sec into the chamber—of (0.3) (234) − 3 = 67 ft. The minimum volume, C', equals C_o which, from Eq. 5, is 709 cu ft.

Assuming the volume between the upper and lower emergency levels to be 20% of C', $C'' = 1.20\, C'$; a corresponding value for $2\,\rho^*\,\sigma^*$ is 1.2 × 21, or 25.2. The maximum downsurge at the pump then becomes $0.30\, H^*_o$.

$$\text{The total air-chamber volume} = \frac{1.2 \times 709}{1 - 0.30} = 1{,}215 \text{ cu ft} \ldots\ldots (10)$$

APPENDIX II. NOTATION

The following letter symbols, adopted for use in the paper, and for the guidance of discussers, conform essentially with American Standard Letter Symbols for Hydraulics (ASA Z10.2—1942), prepared by a committee of the American Standards Association, with Society representation, and approved by the Association in 1942:

A = cross-sectional area of the pipe line, in square feet;
a = velocity of propagation of water-hammer waves in the pipe line, in feet per second;
C = volume of air in the air chamber at absolute pressure head H^*, in cubic feet:
  C' = volume in the air chamber above the upper emergency level, in cubic feet;
  C'' = volume in the air chamber above the lower emergency level, in cubic feet;
c_n = the term defined by Eq. 9;
f = a fraction, 2, 1, $\frac{1}{2}$, $\frac{1}{4}$, . . . ;
g = acceleration due to gravity, in feet per second per second;
H^* = absolute pressure head in the pipe line at the base of the air chamber, in feet of water;
K = a coefficient expressing the head loss at entrance to the air chamber such that $K\,H^*_o$ is the head loss for a flow of Q_o into the chamber;
L = length of pump-discharge pipe line, in feet;
n = the subscript used to indicate conditions at the nth time interval;
o = the subscript used to indicate steady-state conditions prior to power interruption;
Q = rate of flow in the pipe line, in cubic feet per second;
V = velocity of flow in the pipe line, in feet per second;
ρ^* = pipe line characteristic, dimensionless;
σ^* = air chamber characteristic, dimensionless; and
$*$ = the asterisk used in connection with ρ^*, σ^*, H^* to indicate that these quantities are based upon absolute, rather than gage, heads.

DISCUSSION

C. E. Withers.[6]—A check of several points on the charts (Fig. 2), using Mr. Angus' graphical solution for air chambers, will show that the charts are sufficiently accurate so that the graphical solution is necessary only for checking or for obtaining information about such transient hydraulic conditions in the system as are not indicated by the charts. Tests may have been conducted of a pump system with an air chamber, producing results substantiating the accuracy of the charts and proving the correctness of the entire conception of the transient hydraulic conditions in a pump system of this type. If so, the authors would increase the value of their charts by citing such results.

The authors explain that, for successful operation of an air chamber in a pump-discharge line, certain minimum requirements for the capacity of air and water in the tank must be maintained. This indicates the importance of being able to maintain the water level in the air chamber under all conditions of operation and the necessity for automatically shutting down the pumps if the proper water level cannot be maintained in the tank. Inasmuch as successful air-chamber operation is so dependent on successful water-level control, this fact deserves more attention. Fig. 6 is a schematic diagram of the water-level control for an air chamber. First, a check valve in the air line from the compressor eliminates the possibility of water backing up into the compressor due to malfunctioning of the air chamber. This valve should be guarded by a gate valve so that the check valve can be inspected or repaired without taking the air chamber out of operation.

As a second control, sight gages should cover the entire water-level range between the upper emergency water level and the lower emergency water level so that—if pumps are stopped by the water-level control system—the operator can see quickly whether the stoppage was caused by high water level or low water level in the tank. These gages are also required when the tank is first put in operation so that the operation of the water-level control system can be checked and altered, if necessary.

Third are water-level controls in the air chamber. These controls should be of the electric probe type to eliminate as many sources of malfunctioning as possible. The upper emergency water-level switch should stop all the pumps and should require manual restarting. This is necessary because, when the air chamber fills with water, the protection that it was designed to give to the system has been eliminated. The cause of the malfunctioning must be removed before the pumps are started again. Next is found the compressor-on water-level switch. Air leaks in the system and absorption of the air by the water will reduce the air pressure which must be renewed by the compressor. This water-level switch must be far enough below the upper emergency level so that, when the water level is slightly below the compressor-on level, a normal surge in the tank will not actuate the upper emergency water-level switch. The compressor-off water-level switch should be placed at some level slightly below the normal operating water level in the air chamber and far enough below the compressor-on level so that the compressor can operate for a reasonable time after it has been started. The lower emergency water-level switch will stop all the pumps and should require their manual restarting. This lower emergency water level must be far enough below the compressor-off water level to avoid its actuation by any normal surge in the tank. It must be high enough in the tank so that, when the water surface drops to this level and the pumps are stopped, the downsurge will not drain all the water out of the tank and allow air to enter the pump-discharge line. If after an air tank has been installed it is determined that every outage of power actuates the lower emergency water-level switch with such frequency that the air-chamber operation is objectionable, a time-delay switch can be installed so that the pumps can be started automatically; however, this delay must be short enough so that the pump-discharge lines will not have time to drain before the pumps are restarted.

---

[6] Mech. Engr., Denver, Colo.

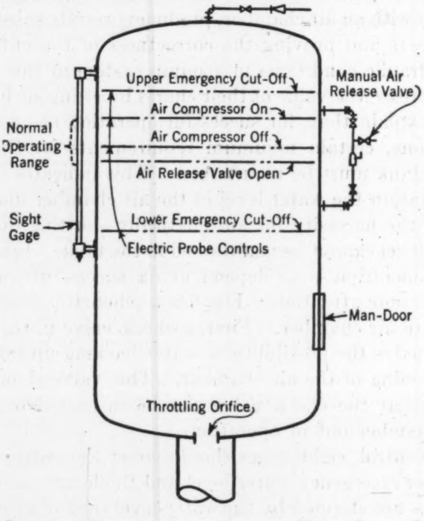
Upper Emergency Cut-Off
Manual Air Release Valve
Air Compressor On
Normal Operating Range
Air Compressor Off
Air Release Valve Open
Sight Gage
Lower Emergency Cut-Off
Electric Probe Controls
Man-Door
Throttling Orifice

FIG. 6.—SCHEMATIC DESIGN FOR AIR-CHAMBER WATER-LEVEL CONTROL

As a fourth control in some air chambers, particularly in installations designed for relatively low heads, it may be desirable to install a float-operated air-release valve slightly below the compressor-off water level. This valve will release air from the chamber whenever the water surface falls below this level and will prevent such factors as temperature change from resulting in an inadequate depth of water in the chamber. The size of this valve must be limited so that it will not release an excessive volume of air during a transient downsurge following a power interruption, thereby rendering the air chamber ineffective.

Lastly, a manual air-release valve should be installed between the compressor-off and the compressor-on water levels in order to provide some measure of manual control of the water in the tank during manual restarting of the pumps.

Any connections (manholes, for example) should be placed below the lower emergency water level so that any leaks can be readily detected.

HENRY M. PAYNTER,[7] J.M. ASCE.—Presentation of the authors' analytical results as charts directly applicable in design procedure is highly commendable.

The writer has been interested in the problem of air-chamber design and in related surge and water-hammer problems for several years.[8,9,10,11] He has determined to his satisfaction that the effects of the elasticity of the water column and pipe walls are negligible in the majority of pump-discharge lines—a conclusion which implies that the pressures in the tank and along the pipe are predominantly functions of the inertial parameter, σ^*, and that the elastic parameter, ρ^*, has only parasitic effects. This can be demonstrated by plotting the results as functions of σ^* instead of $2\,\rho^*\,\sigma^*$. The writer has replotted part of Fig. 2 ($K = 0$) as Fig. 7 in this manner. It is evident from Fig. 7 that the quantity, ρ^*, has only slight effects until it becomes very small (corresponding to extremely high static lifts). Also shown on the plot are the analytical curves A, B, C, and D for ρ^* infinite (a rigid water column). The equation for these curves is

$$\frac{1}{\sigma^*} = \sqrt[6]{1 + z}\left(5 + \frac{1}{1 + z}\right) - 6 \qquad (11)$$

in which $z = (\text{surge})/H^*_o$ and is defined by Fig. 7 as follows: Curve A shows z positive (upsurge); curve B shows z negative (downsurge); curve C shows z-values that are one half those of curve A; and curve D shows z-values that are one half those of curve B.

For the general case in which $K = 0$, the relation between extreme surges and chamber size may be written in terms of an arbitrary process exponent, n, as follows ($n \neq 1.0$ in Eq. 12 and $n = 1.0$ in Eq. 13):

$$\frac{1}{\sigma^*} = (n - 1)^{-1}\left[(1 + z)^{n-1/n} - 1\right] + (1 + z)^{-1/n} - 1 \qquad (12)$$

and

$$\frac{1}{\sigma^*} = \log_e (1 + z) + \frac{1}{1 + z} - 1 \qquad (13)$$

---

[7] Asst. Prof. of Hydr. Eng., Massachusetts Inst. of Technology, Cambridge, Mass.

[8] "Methods and Results from M.I.T. Studies in Unsteady Flow," by H. M. Paynter, *Journal*, Boston Soc. of Civ. Engrs., Vol. XXXIX, No. 2, April, 1952, p. 120.

[9] "Electrical Analogies and Electronic Computers: Surge and Water Hammer Problems," by H. M. Paynter, *Transactions*, ASCE, Vol. 118, 1953, p. 962.

[10] "The Stability of Surge Tanks," by H. M. Paynter, thesis presented to the Massachusetts Inst. of Technology, Cambridge, Mass., in 1949 in partial fulfilment of the requirement for the degree of Master of Science.

[11] "Transient Analysis of Certain Nonlinear Systems in Hydroelectric Plants," by H. M. Paynter, thesis presented to the Massachusetts Inst. of Technology, Cambridge, Mass., in 1951, in partial fulfilment of the requirement for the degree of Doctor of Science.

These results were first published in two pioneering papers of an Italian engineering scientist, Giuseppe Evangelisti of the University of Bologna.[12,13] Mr. Evangelisti also studied in exhaustive detail (by ingenious graphical analysis) the effects of the process exponent, *n*, the surge parameter, σ^*, the pipe friction loss, and the chamber throttling action.

Reproduced herewith are certain of the many design charts resulting from Mr. Evangelisti's studies. These curves, together with those of the authors, will aid in making the design of air chambers more straightforward.

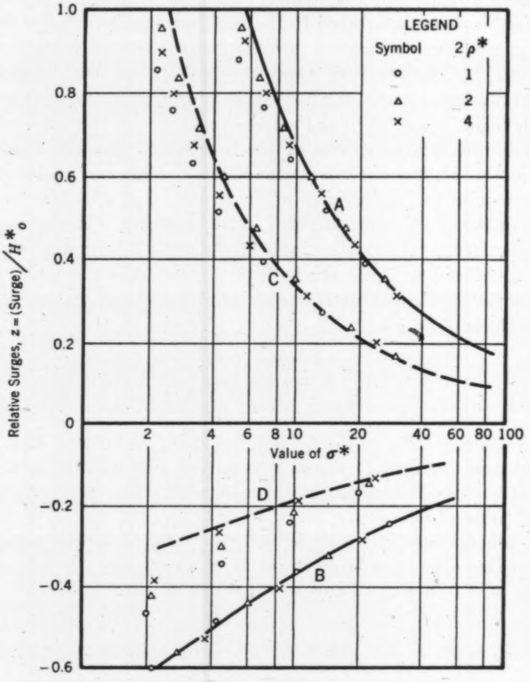

FIG. 7.—AIR-CHAMBER SURGES: $K = 0$; $n = 1.2$

Mr. Evangelisti's parameter, σ, has the form of the inverse of σ^* but is based on static values of head and volume instead of on the initial head and volume. For this reason, Fig. 8 and Table 1 are presented, indicating the slightly different notation of Mr. Evangelisti. It should be noted that the terms in the last two columns of Table 1 are not all equivalent, some being merely analogous.

---

[12] "L'impiego delle camere d'aria per attenuare i colpi d'ariete nelle condotte elevatorie," by G. Evangelisti, *L'Elettrotecnica*, Vol. XXII, April, 1935, No. 7.

[13] "Il colpo d'ariete nelle condotte elevatorie munite di camera d'aria," by G. Evangelisti, *L'Energia Elettrica*, Vol. XV, September, 1938.

Figs. 9, 10, 11, and 12 are adapted from Mr. Evangelisti's original charts.[13] They represent the upsurges and downsurges corresponding to the process and throttling conditions stipulated in each chart.

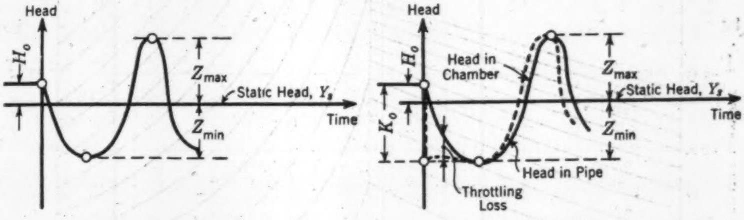

(*a*) CHAMBER WITHOUT THROTTLING

(*b*) CHAMBER WITH NORMAL THROTTLING

FIG. 8.—AIR-CHAMBER PERFORMANCE NOTATION, BASED ON VALUES OF STATIC HEAD AND VOLUME

The charts thus give the values of relative downsurge (at left) and upsurge (at right) corresponding to the values of the inertial parameter, σ, and the relative friction loss, $h_o = H_o/Y_s$, in which H_o is the initial friction loss and Y_s is the absolute static head. Figs. 11 and 12 indicate the reduction in surge resulting from the use of a symmetric throttling orifice (with the same loss factor for flow in either direction) proportioned to give a maximum initial drop equal to the final maximum downsurge as depicted in Fig. 8(*b*); this condition has been called "normal throttling." Greater or smaller throttling losses may be said to give overthrottling or underthrottling, respectively. All four of these charts are based on an assumed rigid water column and are therefore practically limited to values of ρ^* greater than unity. The effects for smaller values of ρ^* are as indicated in Fig. 2 and in Fig. 7 for K (or h_o) equal to zero.

TABLE 1.—COMPARATIVE TERMINOLOGY

Line	Term	Notation	
		Messrs. Evans and Crawford	Mr. Evangelisti
1	Air volume	C	U
2	Initial velocity	V_o	V_o
3	Initial absolute pressure head	H^*_o	$Y_s + H_o$
4	Minimum head at pump for maximum downsurge	H^*_o − downsurge	$Y_s - Z_{min}$
5	Maximum head at pump for maximum upsurge	H^*_o + upsurge	$Y_s + Z_{max}$
6	Initial pipe friction loss	....	H_o
7	Initial chamber throttling loss	....	K_o
8	Total head loss	$K\,H^*_o$	$H_o + K_o$
9	Chamber inertial parameter	$\sigma^* = \frac{2\,g\,H^*_o\,C_o}{V^2_o\,A\,L}$	$\sigma = \frac{V^2_o\,A\,L}{2\,g\,Y_s\,U_o}$

These graphs show that the greatest effect of elasticity is on the minimum pressure at the midlength, where the downsurge value approaches one half the value of the downsurge at the pump only if ρ^* is large; for lesser values of ρ^* the decelerating (minimum) design grade line along the pipe line is distinctly concave.

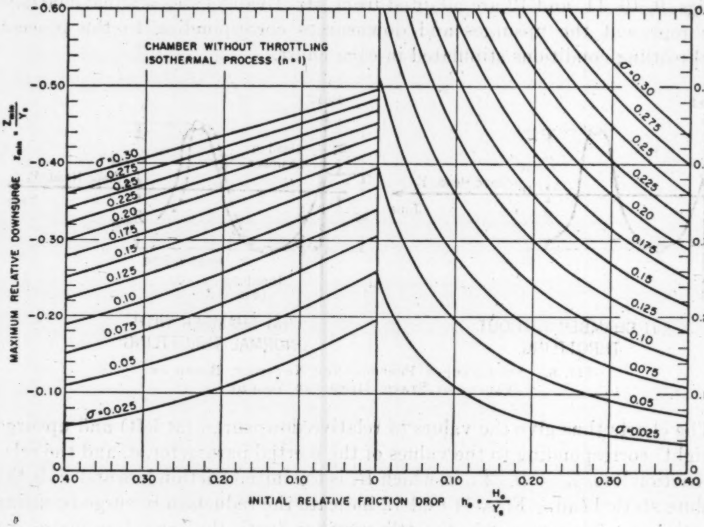
CHAMBER WITHOUT THROTTLING
ISOTHERMAL PROCESS (n=1)
MAXIMUM RELATIVE DOWNSURGE $z_{min} = \frac{Z_{min}}{Y_0}$
MAXIMUM RELATIVE UPSURGE $z_{max} = \frac{Z_{max}}{Y_0}$
INITIAL RELATIVE FRICTION DROP $h_0 = \frac{H_0}{Y_0}$
-0.60
-0.50
-0.40
-0.30
-0.20
-0.10
0
0.60
0.50
0.40
0.30
0.20
0.10
0
0.40
0.30
0.20
0.10
0
0.10
0.20
0.30
0.40
σ=0.30
0.275
0.25
0.225
0.20
0.175
0.15
0.125
0.10
0.075
0.05
σ=0.025

FIG. 9

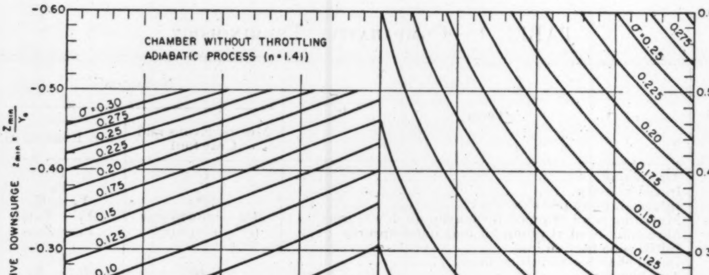
CHAMBER WITHOUT THROTTLING
ADIABATIC PROCESS (n=1.41)
MAXIMUM RELATIVE DOWNSURGE $z_{min} = \frac{Z_{min}}{Y_0}$
MAXIMUM RELATIVE UPSURGE $z_{max} = \frac{Z_{max}}{Y_0}$
INITIAL RELATIVE FRICTION DROP $h_0 = \frac{H_0}{Y_0}$
-0.60
-0.50
-0.40
-0.30
-0.20
-0.10
0
0.60
0.50
0.40
0.30
0.20
0.10
0.40
0.30
0.20
0.10
0
0.10
0.20
0.30
0.40
σ=0.30
0.275
0.25
0.225
0.20
0.175
0.15
0.125
0.10
0.075
0.05
σ=0.025
σ=0.25
0.275
0.225
0.20
0.175
0.150
0.125
0.10
0.075
0.05
σ=0.025

FIG. 10

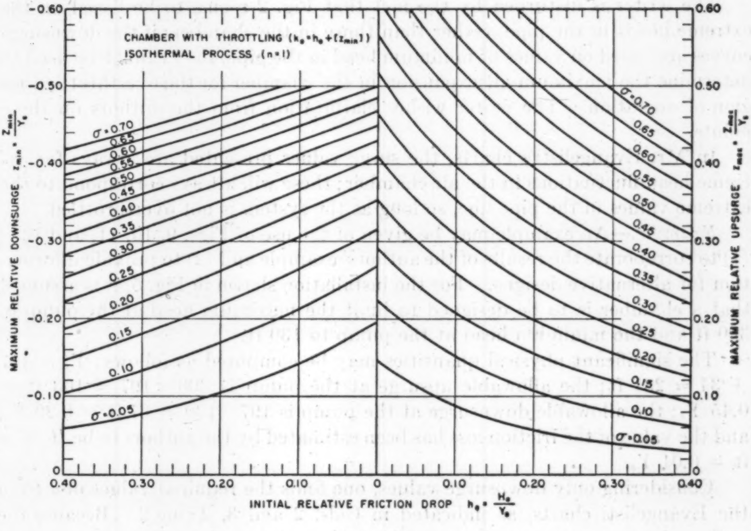
CHAMBER WITH THROTTLING ($k_a = h_a + [z_{min}]$)
ISOTHERMAL PROCESS (n=1)
-0.60
-0.50
-0.40
-0.30
-0.20
-0.10
0
0.60
0.50
0.40
0.30
0.20
0.10
0
σ=0.70
0.65
0.60
0.55
0.50
0.45
0.40
0.35
0.30
0.25
0.20
0.15
0.10
σ=0.05
σ=0.70
0.65
0.60
0.55
0.50
0.45
0.40
0.35
0.30
0.25
0.20
0.15
0.10
σ=0.05
0.40
0.30
0.20
0.10
0
0.10
0.20
0.30
0.40
MAXIMUM RELATIVE DOWNSURGE $z_{min} = \frac{Z_{min}}{Y_0}$
MAXIMUM RELATIVE UPSURGE $z_{max} = \frac{Z_{max}}{Y_0}$
INITIAL RELATIVE FRICTION DROP $h_0 = \frac{H_0}{Y_0}$

FIG. 11

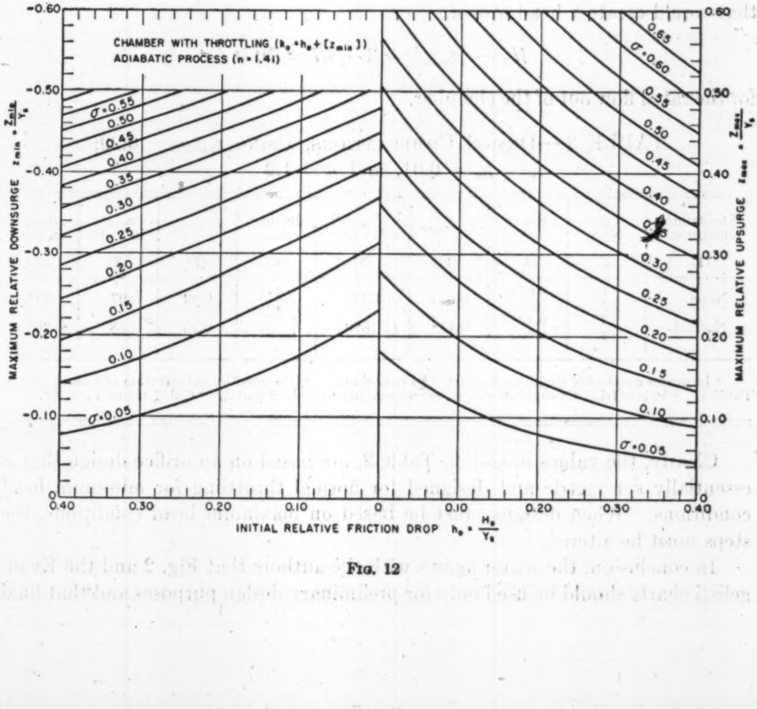
CHAMBER WITH THROTTLING ($k_a = h_a + [z_{min}]$)
ADIABATIC PROCESS (n = 1.41)
-0.60
-0.50
-0.40
-0.30
-0.20
-0.10
0
0.60
0.50
0.40
0.30
0.20
0.10
0
σ=0.55
0.50
0.45
0.40
0.35
0.30
0.25
0.20
0.15
0.10
σ=0.05
0.65
σ=0.60
0.55
0.50
0.45
0.40
0.35
0.30
0.25
0.20
0.15
0.10
σ=0.05
0.40
0.30
0.20
0.10
0
0.10
0.20
0.30
0.40
MAXIMUM RELATIVE DOWNSURGE $z_{min} = \frac{Z_{min}}{Y_0}$
MAXIMUM RELATIVE UPSURGE $z_{max} = \frac{Z_{max}}{Y_0}$
INITIAL RELATIVE FRICTION DROP $h_0 = \frac{H_0}{Y_0}$

FIG. 12

The writer is disturbed by the fact that Fig. 2 seems to be based on the extreme heads in the pipe, rather than those in the chamber; if the downsurge curves are based on values of minimum head in the pipe, they cannot be used to determine the maximum air expansion in the chamber for the overthrottled region of operation. The writer wishes clarification from the authors on these points.

In Mr. Evangelisti's charts, the surge values presented are always for extreme head fluctuations in the air chamber; these will always correspond to the extreme values in the pipe line, so long as the system is not overthrottled.

Example.—An example may be given of the use of Figs. 9, 10, 11, and 12—(1) to corroborate the results of the authors' example and (2) to provide information for alternative designs. For the installation shown in Fig. 5, it is assumed that a chamber is to be designed to limit the maximum head at the pump to 300 ft and the minimum head at the pump to 130 ft.

The significant physical quantities may be computed as follows: $Y_s = 197 + 34 = 231$ ft; the allowable upsurge at the pump is $300 - 197 = 103$ ft $= 0.45\ Y_s$; the allowable downsurge at the pump is $197 - 130 = 67$ ft $= 0.29\ Y_s$; and the value of the friction loss has been estimated by the authors to be $H_o = 3$ ft $= 0.01\ Y_s$.

Considering only downsurge values, one finds the required values of σ from the Evangelisti charts, as indicated in Cols. 2 and 3, Table 2. Because the authors have assumed a process exponent $n = 1.2$, the approximate required values of σ and z_{max} are the averages shown in Cols. 4 and 7.

To realize normal throttling it would be necessary to introduce an orifice that would create a head loss of

$$H_o + |z_{min}| = 3 + 67 = 70 \text{ ft}$$

for the rated flow out of the chamber.

TABLE 2.—DESIGN COMPUTATIONS, USING $z_{min} = -0.29$, $h_o = 0.01$, and $n = 1.2$

Throttling condition (1)	Fig. No.[a] (2)	Ratio σ[b] (3)	Average (4)	U_s, in cubic feet[c] (5)	Ratio,[d] z_{max} (6)	Average (7)	z_{max}, in feet[e] (8)	H_{max}, in feet (9)
None	1. 2.	0.07 0.04	0.055	1,240	0.44 0.40	0.42	97	294
Normal	3. 4.	0.13 0.09	0.11	620	0.25 0.25	0.25	58	255

[a] Indicates applicable Evangelisti chart. [b] From charts. [c] Obtained by substitution of values, line 9, Table 1. [d] Values from Evangelisti charts, corresponding to Cols. 2 and 3. [e] Col. 7 times Y_s.

Clearly, the values in Col. 9, Table 2, are based on an orifice design that is essentially symmetric and designed for normal throttling for minimum head conditions. When designs must be based on maximum head conditions, the steps must be altered.

In conclusion, the writer agrees with the authors that Fig. 2 and the Evangelisti charts should be used only for preliminary design purposes and that final detailed check computations should be made—graphically, numerically, or otherwise—using the basic dynamic equations for the system.

W. E. EVANS[14] AND C. C. CRAWFORD[15].—The writers are grateful to Messrs. Paynter and Withers for their constructive discussions. Mr. Paynter has provided a useful addition to the paper by his presentation of Mr. Evangelisti's design charts and by his comparisons between the two sets of data. The writers have recognized that most of the transient pressures in this type of system can be predicted with sufficient accuracy by using the rigid-water-column theory. However, the particularly important downsurge at the midlength of the discharge line cannot be so predicted; hence, the writers' use of the elastic-water-column theory.

The writers' downsurge charts are based on the minimum head in the pipe line. Mr. Paynter's argument that these values cannot be used rigorously to determine the maximum air expansion for the "overthrottled" region of operation is correct. However, the writers have chosen to use the minimum head from the charts for computing the maximum air expansion for two reasons:

1. In rare cases only will a system be overthrottled if the differential orifice is used as recommended by the writers; in these cases the tank will be estimated as slightly oversize.
2. This method is considered adequate for the stated "preliminary design purposes" for which the charts are intended.

No air chamber can perform as intended unless the controls function properly. Mr. Withers has ably discussed many of the control problems that confront the engineer responsible for the mechanical design of an air chamber.

---

[14] Engr., Design Div., Bureau of Reclamation, U. S. Dept. of the Interior, Denver, Colo.

[15] Engr., Design Div., Bureau of Reclamation, U. S. Dept. of the Interior, Denver, Colo.

AMERICAN SOCIETY OF CIVIL ENGINEERS
Founded November 5, 1852
TRANSACTIONS

Paper No. 2711

ELECTRICAL ANALOGS OF STATICALLY LOADED STRUCTURES

By Frederick L. Ryder[1]

Synopsis

The labor involved in the solution of indeterminate structures may be greatly reduced by the use of electrical analogs, especially in those cases where various choices of dimensions are to be investigated. There is a similarity between the structure and its analog which often permits the construction of the analog on a pictorial basis without regard to the governing equations.

In the electrical circuit, force and moment are simulated by current, and deflection and slope by voltage drop. The analogy is based on the fact that Castigliano's theorem and the principle of least work have their counterparts in certain electrical networks. The theory is developed for the two-dimensional truss and the three-dimensional truss, and for two-dimensional rigid frames and truss-frame combinations, including trusses with secondary stresses.

A working model of the necessary equipment, consisting of adjustable resistors and tapped transformers is described, and instructions are given for its use. Experimental results that are accurate to within 2.5% of the maximum values encountered have been obtained. A rapid numerical check is possible.

Notation

The letter symbols adopted for use in this paper are defined where they first appear, in the illustrations or in the text, and are arranged alphabetically, for convenience of reference, in the Appendix.

Introduction

Determinate trusses and rigid frames are relatively simple to analyze, as all forces and moments can be evaluated by considerations of equilibrium. The solution of indeterminate structures is contrastingly tedious because the forces and moments depend on the mutual compatibility of the deflections and

---

Note.—Presented at the Centennial Convocation, Chicago, Ill., September, 1952. Published, essentially as printed here, in December, 1953, as *Proceedings-Separate No. 376*. Positions and titles given are those in effect when the paper was received for publication.

[1] Senior Engr., Allen B. DuMont Labs., Passaic, N. J.

slopes, which are functions of the elastic parameters, as well as on equilibrium considerations.

An electrical instrument for the experimental solution of indeterminate framed structures has been devised by Vannevar Bush.[2] The instrument consists of adjustable resistors and tapped transformers which can be connected to simulate trusses and rigid frames of different configurations—the properties of the individual members being simulated by suitable setting of the resistors and selection of the transformer taps. Currents are introduced to simulate applied loads, and the internal forces and moments are simulated by certain other currents which are easily measured. This type of device has the advantage over purely mathematical instruments in that the governing equations need not be derived and is superior to mechanical models in regard to the speed and economy of changing the dimensions of the structure under investigation.

This paper continues Mr. Bush's work in the respect that the analysis of the analogous relationships existing between the structure and its corresponding electrical circuit are extended and generalized for trusses. For rigid frames, Mr. Bush introduced an analog for the two-dimensional case, in which the members were straight and disposed rectangularly. The analogy is based on the method of slope deflection, and requires the explicit simulation of the slopes and deflections as well as the moments and shears. This paper describes an analog which is applicable to all two-dimensional rigid frames, including those with curved members. Because this analog is based on the principle of least work, slope and deflection are not represented explicitly, the simulation being conducted in terms of forces, moments, and the elastic properties of the members. This analog can be extended to the three-dimensional rigid frame and to nonlinear rigid frames and trusses.

An approach quite different from Mr. Bush's has been followed by Gabriel Kron, who has described an electrical analog applicable to any framed structure in which the members are straight.[3] Mr. Kron's circuit elements consist of adjustable condensers and inductances, rather than the resistors and transformers used by Mr. Bush and the writer.

ANALOGOUS STRUCTURAL–ELECTRICAL ENERGY THEOREMS

The theorems on which the analogs are based are herewith summarized.[4]

Principle of Least Power.—In a circuit of resistors and ideal transformers that is supplied with given external alternating currents at a single frequency and phase angle, each internal current is a minimum, subject to the requirements of current-continuity. This is analogous to the principle of least work, which states that each internal force and moment in a structure is a minimum, subject to the requirements of equilibrium.

Castigliano's Theorem for Electrical Circuits.—In the circuit previously described, P denotes the power dissipated in the circuit; C is a supplied current, considered positive when leaving the circuit; and V denotes the voltage (measured below some arbitrary datum or ground) of the point at which C leaves the circuit.

---

[2] "Structural Analysis by Electric Circuit Analogies," by Vannevar Bush, *Journal*, The Franklin Institute, Vol. 217, March, 1934, p. 289.

[3] "Tensor Analysis and Equivalent Circuits of Elastic Structures," by Gabriel Kron, *ibid.*, Vol. 238, December, 1944, p. 399.

[4] "Network Analysis by Least Power Theorems," by F. L. Ryder, *ibid.*, Vol. 254, July, 1952, p. 47.

It can be shown that

$$V = \frac{1}{2}\frac{\partial P}{\partial C} \tag{1}$$

Eq. 1 is analogous to Castigliano's theorem for structures, which states that

$$\delta = \frac{\partial W_d}{\partial F} \tag{2}$$

and

$$\theta = \frac{\partial W_d}{\partial M} \tag{3}$$

in which W_d is the work of deformation; F and M are applied force and bending moment, respectively; and δ and θ are the deflection and slope, respectively, measured at the point of application of F or M. The absence of the factor $\frac{1}{2}$ in Eqs. 2 and 3 arises from the fact that electrical power equals the product of current and voltage, whereas the work of deformation is equal to one half the product of force and deflection, or of moment and slope. The following parameters may therefore be considered analogous:

Structure	Electrical circuit
Force	Current
Moment	Current
Deflection	Voltage
Slope	Voltage
Work	One half the power

The Ideal Transformer.—In constructing analogs based on the foregoing principles, ideal transformers are used. The behavior of such transformers is specified by the follow rules:

(1) The ratio of secondary voltage drop to primary voltage drop equals the turns ratio N.

(2) The ratio of secondary current to primary current is the negative reciprocal of the turns ratio N.

The voltage drop and the current must be measured in a selected direction for each winding. The number of turns is positive if positive current produces a flux in a specified direction in the transformer core; otherwise it is negative. These rules result in zero power loss in the transformer. The errors caused by the difference between practical and ideal transformers will be discussed subsequently.

Analog of the Pin-Connected Truss

Two-Dimensional Case.—A typical two-dimensional truss member, BH, is shown in Fig. 1 (*a*). Its analog consists of an x-branch and a y-branch, connected by an ideal transformer as shown in Fig. 1 (*b*). The arbitrarily oriented

Cartesian axes are indicated, as well as the angle of inclination, θ, the latter being measured from the x-axis to the direction of member BH. The reference direction for θ is that in which the y-axis is rotated 90° from the x-axis.

The force in branch BH is designated as F, and is considered positive if tensile. The alternating currents in the electrical branches are designated as F_x and F_y, respectively, and are at the same frequency and phase—the transformer-turns ratio being such that these currents are in the same ratio as the x-component and y-component of force F, measured in the branch direction chosen for the currents. To achieve this, the following must be satisfied:

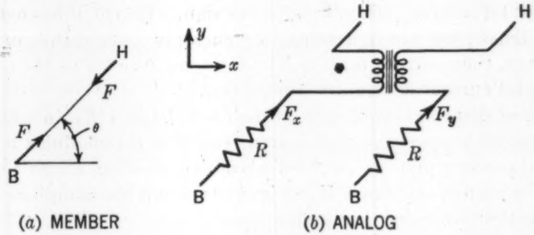

(a) MEMBER (b) ANALOG

FIG. 1.—TWO-DIMENSIONAL TRUSS MEMBER

$$\frac{N_x}{N_y} = -\tan\theta; \qquad (4)$$

in which N_x and N_y are the number of turns in the x-windings and y-windings of the transformer, respectively. The resultant current, whose rectangular components are F_x and F_y, is designated as F, as it is analogous to branch force. This resultant is not explicit in the analog.

The analog of the entire truss of which branch BH is a member consists of a separate x-network and y-network, each consisting of one branch for each truss member, the branches being connected in the same way as are the truss members. The separate networks are interconnected only magnetically—through the transformer cores. The x-components and y-components of the external forces, including both loads and reactions, are simulated by appropriately supplied x-currents and y-currents, at the same frequency and phase, the reference direction for these currents being considered as positive when leaving the network. According to the principles of least work and least power, the truss will be properly simulated if the equations of equilibrium are duplicated by the equations of current-continuity, and twice the work of deformation is duplicated by the power dissipation.

To compare the equations of equilibrium and current-continuity, the sum of the forces applied to joint B in the truss, and the currents leaving joint B in the analog are equated to zero. In the former case,

$$F'_x + F\cos\theta = 0 \qquad (5a)$$

and

$$F'_y + F\sin\theta = 0 \qquad (5b)$$

in which F'_x and F'_y are, respectively, the x-component and y-component of the resultant of all the forces applied to joint B by branches other than member BH and by the external forces, which include both loads and reactions. In the electrical case, Eq. 5 will be satisfied if F'_x is the total current, other than F_x, leaving joint B in the x-network, and can be composed of branch currents and supplied currents. A similar result is obtained for F'_y.

The force and current summations at joint H are similar to those at joint B, except that all terms are prefixed by a minus sign. Hence, if force components applied to a truss joint are represented by currents leaving the corresponding electrical joints, then current is analogous to force, in so far as the equations of equilibrium and current-continuity are concerned.

The work of deformation of each branch is $F^2L/(2\ A\ E)$, in which L is the length, A denotes the cross-sectional area, and E is the modulus of elasticity. The electrical power equals twice the work of deformation, a result that can be achieved if the branch resistance R in Fig. 1 (b) equals the compliance $L/(A\ E)$, in which case the power for the branch equals

$$P = (F^2_x + F^2_y)\ R = \frac{F^2\ L}{A\ E} \qquad (6)$$

the ideal transformer consuming no power. With this condition satisfied, and with the components of the loads and reactions duplicated by suitable currents, each resultant branch current F must simulate the corresponding branch force F. In reaching this conclusion it is unnecessary to write the structural and electrical equations which govern the values of the redundants, for these sets of equations must be identical, by the principles of least work and least power. The latter principle does not apply to the x-network and y-network separately, as stated by Mr. Bush and M. Hetenyi, but only to both networks combined.[5]

If it is imagined that the x-deflection and the y-deflection of the joints of a typical truss are computed by a conventional use of Castigliano's theorem—that is, by applying a load in the desired direction to each joint, writing the work of deformation in terms of the literal (nonnumerical) value of this load, and then applying Eq. 2, after which the load is given its actual value (which may be zero). The corresponding computation for the analog would be similar, but with applied x-current or y-current substituted for the load, and with deflection replaced by voltage. Hence, the x-component and y-component of deflection at any joint must be simulated by the corresponding voltages, measured below a datum corresponding to points of zero deflection, in the x-network and y-network.

This leads to two interesting conclusions. First, it is unnecessary to maintain at predetermined values the currents corresponding to reaction components, whether the reactions are redundant or not; if the electrical joints at which the corresponding deflection component is zero are grounded, the currents leaving these joints must correspond to the appropriate components of reaction force applied to the truss by its supports. Only the currents corresponding to load components, therefore, must be held at predetermined values.

---

[5] "Handbook of Experimental Stress Analysis," by M. Hetenyi, John Wiley & Sons, New York, N. Y., 1950, pp. 807–817.

Second, considering the interpretation of the voltage drops in Fig. 1(*b*); the drops across the resistors in the direction BH are $F_x L/(A\,E)$ and $F_y L/(A\,E)$, which correspond to the respective components of deflection associated with branch elongation. Because the total drops from joints B to H in each electrical branch must equal the corresponding components of total branch deflection, the transformer voltage drops must equal the approximate components of branch deflection caused by rotation. The rotational deflections are ordinarily of the same order of magnitude as the deflections caused by elongation.

In the special case in which a truss branch is parallel to the x-axis, the corresponding transformer and y-branch in the analog are omitted, the x-branch being shorted past its transformer terminals. This assures that the analog of the y-component of branch force is zero. A similar arrangement is used if the branch is parallel to the y-axis.

Considering the truss of Fig. 2(*a*), which is indeterminate to the second degree, F_{1-5} and F_{3-5} are suitable choices for the redundants. In the analog, Fig. 2(*b*), the horizontal branches appear only in the x-network, and the vertical branches only in the y-network. The inclined branches appear in both networks, the appropriate x-branch and y-branch being connected by transformers, the separate windings of which are represented symbolically by circles, and the mutual core by a dotted line, in a manner similar to that used by Mr. Bush. For branches 1–5 and 2–4 the value of N_x/N_y is -1, and for branches 2–6 and 3–5 it is $+1$, by use of Eq. 4. A resistance (represented by a rectangle) corresponding to branch compliance is placed in each electrical branch.

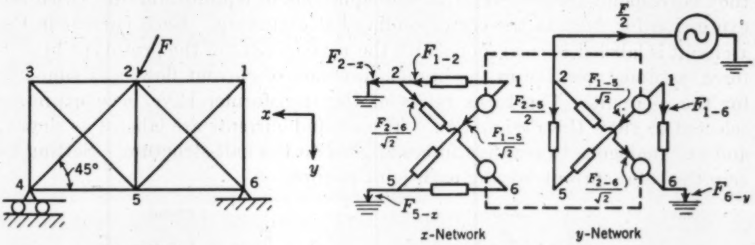

(*a*) TRUSS (*c*) ANALOG OF RIGHT HALF

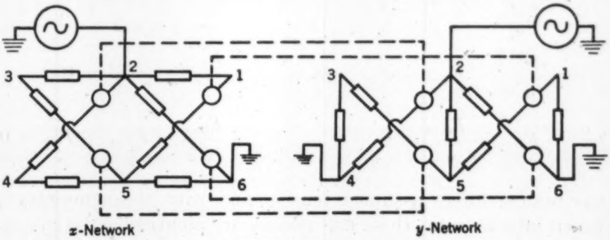

(*b*) ANALOG

FIG. 2.—TRUSS, INDETERMINATE TO THE SECOND DEGREE

To simulate the constraints imposed on the truss by its supports, joint 6 is grounded in the x-network and y-network, and joint 4 is grounded in the y-network. Appropriate alternating currents, at the same frequency and phase, are withdrawn from joint 2 to simulate the load components.

In the special case in which the load F is in the y-direction, the analog can be simplified by the considerations of symmetry. Joints 2 and 5 must have the same x-deflection, so that a vertical plane can be passed through the middle of the load and member 2–5. The datum for the measurement of the x-deflection is conveniently shifted to the plane of symmetry, while the datum for the y-deflection is at joint 6. Under these conditions the analog of only the right half of the truss need be considered, as shown in Fig. 2(c). The resistance in branch 2–5 must equal twice the associated compliance, while the current equals half the corresponding branch force, as the member was cut in half by the plane of symmetry.

The validity of the analog of Fig. 2(c) can be checked by writing the equations of current-continuity and the expression for power, and noting whether they correspond (respectively) to the equations of equilibrium and twice the expression for work in the corresponding half-structure. Each current in the x-circuit is labeled to correspond with the x-component of the prototype branch force, assumed positive in the branch direction of current flow, and similarly for the y-circuit. The turns ratios of the transformer have been expressly selected to allow this designation. The ground currents are labeled as shown, and are analogous to reaction forces applied to the half-structure. Setting to zero the total current leaving each joint in turn,

Joint	x-circuit	y-circuit
1......	$F_{1-2} + \frac{F_{1-5}}{\sqrt{2}} = 0$	$\frac{F_{1-5}}{\sqrt{2}} + F_{1-6} = 0$
2......	$- F_{1-2} - \frac{F_{2-6}}{\sqrt{2}} + F_{2x} = 0$	$\frac{F_{2-5}}{2} + \frac{F_{2-6}}{\sqrt{2}} + \frac{F}{2} = 0$
5......	$- \frac{F_{1-5}}{\sqrt{2}} - F_{5-6} + F_{5x} = 0$	$- \frac{F_{2-5}}{2} - \frac{F_{1-5}}{\sqrt{2}} = 0$
6......	$F_{5-6} + \frac{F_{2-6}}{\sqrt{2}} = 0$	$- \frac{F_{2-6}}{\sqrt{2}} - F_{1-6} + F_{6y} = 0$

With the branch forces assumed tensile, and with the symmetry of the structure taken into account, these expressions are identically the summations of x-components and y-components of force applied to each joint in the truss, so that the requirements of current-continuity and equilibrium are identical.

For the case in which all the truss branch compliances are equal, the power loss for Fig. 2(c) is

$$P = R \left(F^2_{1-2} + \frac{F^2_{2-5}}{2} + F^2_{5-6} + F^2_{1-6} + F^2_{1-5} + F^2_{2-6}\right) \ldots\ldots (7)$$

in which the branch resistance R (or $2R$, for branch 2–5) is set equal to the branch compliance $L/(A\,E)$. The work of deformation for the half-structure is half this quantity, so that the analogy is valid. Both the analog and the prototype can be solved analytically by substituting for the forces in Eq. 7 their values in terms of the redundant F_{1-5}, as obtained from the equations of current-continuity or equilibrium, and then setting to zero the partial derivative of the resulting expression with respect to F_{1-5}. The latter then has the value $F\sqrt{2/6}$, from which all other forces, deflection components, currents, and voltages can be determined. This necessitates the evaluation of the transformer voltage drops.

Scale Factor.—The scale factor is the ratio of any quantity in the prototype to its corresponding quantity in the analog. The scale factor relating force to current is S_F, and can be chosen arbitrarily. The scale factor S_C relates compliance (distance/force) to resistance, and also can be chosen arbitrarily. Relating deflection (which is dimensionally equal to force times compliance) to voltage (which is dimensionally equal to current times resistance) is the scale factor S_δ. Hence S_δ is the product of S_F and S_C.

Three-Dimensional Case.—The analog of a typical three-dimensional branch BH is shown in Fig. 3. The transformers relate F_x and F_z to F_y, keeping the currents in the same ratios as the respective x-component, y-component, and z-component of branch force. Alternatively, these transformers could be replaced by transformers relating F_y and F_z to F_x, or F_z and F_y to F_x. In any case, for transformers relating the x-current and y-current, the y-current and z-current, and the z-current and x-current, respectively, the transformer turns requirements are

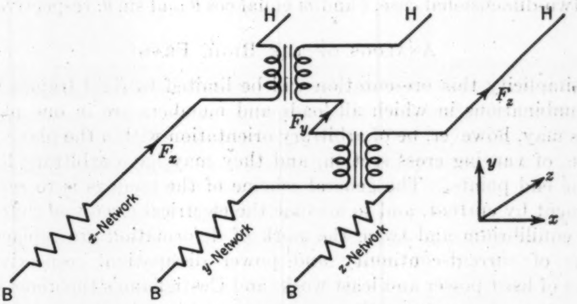

FIG. 3.—THREE-DIMENSIONAL TRUSS MEMBER

$$\frac{N_x}{N_y} = -\frac{m}{l}, \quad \frac{N_y}{N_z} = -\frac{n}{m}, \quad \frac{N_z}{N_x} = -\frac{l}{n} \quad \cdots\cdots\cdots\cdots\cdots \quad (8)$$

in which l, m, and n are the direction cosines of branch BH. In the special case in which a branch is perpendicular to one of the coordinate axes, the electrical branch corresponding to this axis is omitted, and only one transformer is needed for the purpose of relating the currents associated with the other two axes. If the branch is parallel to one of the coordinate axes, the electrical branches corresponding to the other axes are omitted, and no transformers are required.

The connection of the various electrical branches to form a complete analog, and the selection of grounds and the withdrawal of load currents, are governed by the same procedure as in the two-dimensional case. The resistances equal the compliances $L/(A\,E)$, the resistor and transformer voltage drops corresponding to appropriate components of deflection caused by branch elongation and rotation, respectively.

Unification of Branch Resistors.—In both the two-dimensional case and the three-dimensional case, the number of resistors can be reduced to one for each structural branch, by choosing a value of resistance which will leave the power dissipation unchanged. By the use of Castigliano's electrical theorem and the principle of least power, this reduction of the number of resistors will leave the analog unchanged with respect to branch currents and joint voltages; the transformer voltage drops will automatically adjust themselves to compensate for the changed resistor voltage drops. For the cases in which it is placed in the x-branch, y-branch, and z-branch, respectively, the value of the unified resistance is

$$\frac{R}{l^2}, \quad \frac{R}{m^2}, \quad \frac{R}{n^2} \qquad\qquad (9)$$

For the two-dimensional case, l and m equal $\cos\theta$ and $\sin\theta$, respectively.

ANALOGS OF THE RIGID FRAME

For simplicity this presentation will be limited to rigid frames and truss-frame combinations in which all loads and members are in one plane. The members may, however, be of arbitrary orientation within the plane, of irregular shape, of varying cross section, and they may have arbitrary loading between the end points. The general scheme of the analogs is to replace force and moment by current, and to arrange the electrical circuit so that the equations of equilibrium and twice the work of deformation are replaced by the equations of current-continuity and power dissipation, respectively. The principles of least power and least work, and Castigliano's theorems for electrical networks and structures then assure currents analogous to force and moment, and voltage drops analogous to deflection and slope.

Straight Member of Constant Cross Section, Loaded at End Points Only.—The typical member BH of length L is shown in Fig. 4(*a*), the parameters being F, the axial force applied to point B by member BH, and considered positive when tensile; S, the resultant shear applied to B by loads and by adjoining members, and considered positive when it tends to rotate BH in the direction of positive slope (which is the direction in which the y-coordinate is 90° removed from the x-coordinate); and M_{BH} and M_{HB}, the resultant moments applied to B and H, respectively, by loads and by adjoining members, and considered positive in the positive direction of slope. The forces at H are equal and opposite to those at B. Denoting by F'_x and the F'_y the components of the resultant force applied to B by the loads and by members other than BH, and noting that the resultant is also the resultant of S and $-F$,

$$F'_x = m\,S - l\,F \qquad\qquad (10a)$$

and

$$F'_y = -\,l\,S - m\,F \qquad\qquad (10b)$$

Moment summation yields

$$M_{BH} + M_{HB} + S\,L = 0 \quad\ldots\ldots\ldots\ldots (11)$$

The x-network and y-network of an electrical analog for the forces are shown in Fig. 4 (*b*), where the electrical quantities are denoted by the same symbols as the corresponding structural quantities. Current leaving a joint is analogous to a force component applied to the corresponding structural joint. Ideal transformers are used to fix the ratios of the currents, the required turns ratios being, for axial force, $\frac{N_x}{N_y} = -\frac{m}{l}$, and for shear force, $\frac{N_x}{N_y} = \frac{l}{m}$.

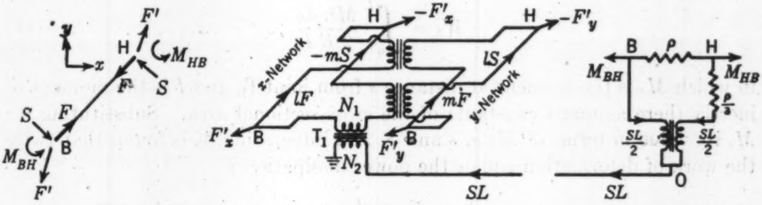

(*a*) MEMBER (*b*) FORCE ANALOG (*c*) MOMENT ANALOG

FIG. 4.—STRAIGHT MEMBER, LOADED AT END POINTS

The equations of current-continuity at joints B and H simulate Eqs. 10 of force summation. If the tensile and shear work is appreciable (unusual in the case of rigid frames), it can be simulated by inserting suitable resistors in the branches. By analogy with the tensile case, the shear resistance may be written as $\alpha L/(AG)$, in which G is the shear modulus, and α is the ratio of shear stress at the centroidal plane to S/A, the average shear stress.[6] It can be shown by Castigliano's theorems that the branch voltage drops simulate the corresponding components of total branch deflection. The resistor voltage drops in the tension and shear branches simulate deflection components caused by direct tension and direct shear, respectively.

In the special case in which the member is parallel to the x-axis, the currents analogous to x-shear and y-tension must be zero, so that the corresponding electrical branches are opened, no transformers then being required; and conversely for the case in which the member is parallel to the y-axis.

The moment relationships can be simulated in various ways, but a preferred form of the analog is indicated in Fig. 4 (*c*) with transformer-turns ratio equal to -1. The ($S\,L$)-current can be obtained by the indicated transformer tie-in with the x-shear branch, the turns ratio being

$$\frac{N_1}{N_2} = \frac{L}{m} \quad\ldots\ldots\ldots\ldots (12)$$

in which the units for L are arbitrary. Currents leaving joints B and H simulate moments applied to the corresponding structural joints. The equation of current-continuity is identical to Eq. 11 for moment equilibrium, whereas the power dissipation is

---

[6] "Strength of Materials, Part 1," by S. Timoshenko, D. Van Nostrand Co., Inc., New York, N. Y., 1940, p. 170.

$$P = \rho \left[M^2_{BH} + M_{BH}\, S\, L + \frac{(S\, L)^2}{3} \right] \ldots\ldots\ldots\ldots\ldots (13)$$

in which ρ is resistance analogous to bending compliance. The work of bending a straight beam is

$$W_b = \int_0^L \frac{M^2_s\, ds}{2\, E\, I} \ldots\ldots\ldots\ldots\ldots (14)$$

in which M_s is the moment at distance s from joint B, and I is the moment of inertia (here assumed constant) of the cross-sectional area. Substituting for M_s its value in terms of M_{BH}, s and S, and integrating, it is found that twice the work of deformation equals the power dissipation if

$$\rho = \frac{L}{E\, I} \ldots\ldots\ldots\ldots\ldots (15)$$

By Castigliano's theorems, it can be shown that the voltage drop from B to H in Fig. 4(*c*) represents the change of slope between B and H caused by bending. Also, the voltage drop from B to O represents $1/L$ times the bending deflection of H from the line tangential to the beam at B, in the direction of positive shear; and correspondingly for the voltage drop from H to O. The analog simulates conditions at the joints only, leaving the conditions along the structural branch to be computed separately.

To construct the analog for an entire rigid frame, points B and H for all branches are interconnected according to the configuration of the structure, a separate network being required for x-forces, y-forces, and moments. Electrical joints corresponding to points of zero x-deflection, y-deflection, or slope are grounded, and alternating currents of the same frequency and phase are withdrawn to simulate applied force components and moments. In many cases the force networks may be omitted, as will be shown.

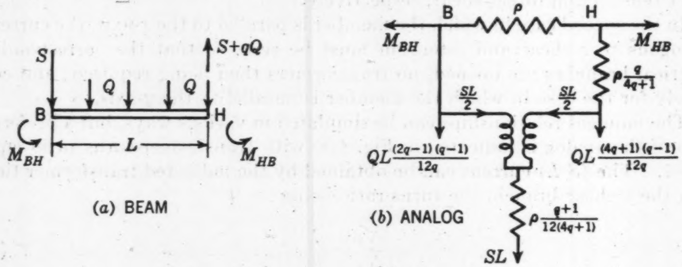

(*a*) BEAM

(*b*) ANALOG

FIG. 5.—BEAM UNDER CONCENTRATED LOADS

Some Special Members.—For simplicity, it will be assumed that in members other than the simple type previously described the work associated with direct shear and tension is negligible, so that only the moment analog need be considered. The general method of approach is to simulate the conditions of moment equilibrium and the bending work of deformation. By Castigliano's theorems, voltage drop between the joints which represent the ends of the member is analogous to change of slope.

Fig. 5 (*a*) shows a beam subjected to uniformly spaced loads Q. The analog is shown in Fig. 5 (*b*), in which q is the number of equal spaces between the loads. If the load Q exists at B, it may be added to S. The work associated with Q alone is not correctly simulated, but this work has a derivative only with respect to Q, and is therefore of no interest in the differentiations associated with Castigliano's theorem and the principle of least power. The analog may be reduced to the case of a uniformly distributed load Q', by letting the number of loads equal infinity.

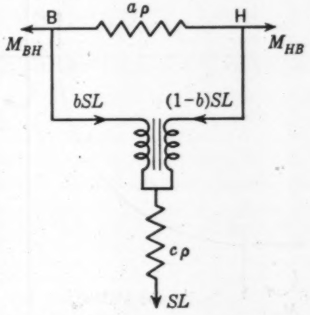

Fig. 6.—Analog of a Straight Member with Varying Moment of Inertia

Fig. 6 shows the analog of a beam loaded at the end points, and with a moment of inertia I varying linearly from I_B at B to I_H at H. The resistances are always positive, irrespective of the relative magnitudes of I_B and I_H. In Fig. 6

$$a = \log_e i \qquad (16a)$$

$$b = \frac{1}{\log_e i} - \frac{1}{i-1} \qquad (16b)$$

$$c = \tfrac{1}{2} + \frac{1}{i-1} - \frac{1}{\log_e i} \qquad (16c)$$

and

$$\rho = \frac{L}{E\,(I_H - I_B)} \qquad (16d)$$

in which $i = I_H/I_B$.

A quadrant member is shown in Fig. 7 (*a*), and its analog is shown in Fig. 7 (*b*), in which F_h and F_v are the unknown end forces exerted by adjacent members and $a = 0.3634$, $b = 0.6366$, and $c = 0.1880$. The sign of F_h must be reversed if the quadrant curves are positive in a clockwise direction from B to H. The simulation of twice the work of deformation is not perfect, the excess power, P_{ex}, being

$$P_{ex} = 0.0063\,\rho\,[(F_v\,r)^2 + (F_h\,r)^2] \qquad (17)$$

This excess power can usually be neglected, for it is of the order of magnitude of the direct shear and tension work, which is ordinarily ignored in rigid-frame problems.

Illustrative Examples.—Fig. 8 (*a*) represents a truss-frame combination in which the lower chord has an appreciable resistance to shear and bending, whereas the other members are slender, and thus act almost solely in tension and compression. The structure can also serve as a simple example of a rigidly connected truss in which some of the members are not slender, so that secondary stresses (associated with bending) are significant.

The analog is based only on the left half of the structure. The force networks, Fig. 8(*b*), are based on Fig. 4(*b*), the shear branches for member 1–2 and member 1–3 being omitted. The resistance in branch 1–3 must be doubled to account for the fact that this member is split in half. Joints 1 and 3 have the same x-deflection, by symmetry, and are chosen as the x-deflection datum, whereas the y-deflection datum is placed at joint 2. The applied current is $F/2$, by symmetry.

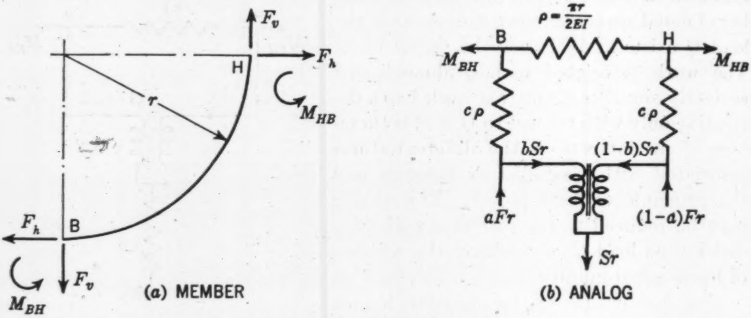
F_v
F_h
H
r
M_{HB}
F_h
B
F_v
M_{BH}
$\rho = \frac{\pi r}{2EI}$
B
H
M_{BH}
M_{HB}
$c\rho$
$c\rho$
bSr
$(1-b)Sr$
aFr
$(1-a)Fr$
Sr

(*a*) MEMBER (*b*) ANALOG

FIG. 7.—QUADRANT MEMBER

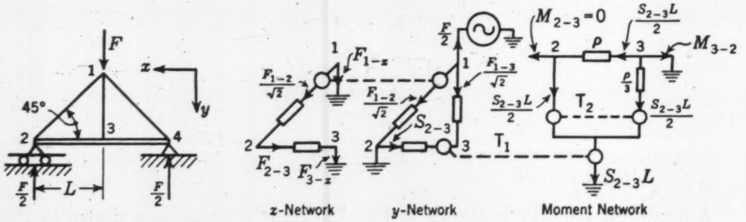
F
1
x
y
45°
2
3
4
$\frac{F}{2}$
L
$\frac{F}{2}$
1
F_{1-x}
$\frac{F_{1-2}}{\sqrt{2}}$
2
3
F_{2-3}
F_{3-x}
$\frac{F}{2}$
1
$\frac{F_{1-3}}{\sqrt{2}}$
$\frac{F_{1-2}}{\sqrt{2}}$
S_{2-3}
2
3
$M_{2-3} = 0$
$\frac{S_{2-3}L}{2}$
2
ρ
3
M_{3-2}
$\frac{\rho}{3}$
$\frac{S_{2-3}L}{2}$
T_2
$\frac{S_{2-3}L}{2}$
T_1
$S_{2-3}L$
x-Network
y-Network
Moment Network

(*a*) TRUSS-FRAME (*b*) ANALOG OF LEFT HALF

FIG. 8.—TRUSS-FRAME COMBINATION

The moment network is based on Fig. 4(*c*), and is open at joint 2 to indicate zero moment, and grounded at joint 3 to indicate the slope datum. The $(S_{2-3}\,L)$-current is obtained by transformer tie-in with the shear branch for member 2–3. The unit of length may be chosen arbitrarily so that the turns ratio of transformer T_1 has any convenient value.

The moment network can be simplified by the elimination of transformer T_2, as follows: The total power in the moment network is determined to be $\frac{\rho\,(S_{2-3}\,L)^2}{3}$. This is simulated by passing the $(S_{2-3}\,L)$-current through a resistance of value $\rho/3$. The disadvantage of this method is that there is no way of measuring the slope at joint 2, which in the moment network of Fig. 8(*b*) is simply the voltage of joint 2 below ground.

The validity of the analog of Fig. 8(*b*) is checked by comparing the equations of current-continuity and the expression for power with the equations of equilibrium and the expression for twice the work of deformation. All currents are labeled in accordance with Fig. 4, account being taken of the orientation of the coordinate axes in Fig. 8(*a*), and of the fact that M_{2-3} is zero. The ground currents are labeled as shown, and represent force and moment reactions acting on the half-structure. The summations of currents leaving the various joints are shown in Table 1.

TABLE 1.—CURRENTS LEAVING STRUCTURAL JOINTS

Joint	*x*-Network	*y*-Network	Moment-network
1	$\frac{F_{1-2}}{\sqrt{2}} + F_{1-x} = 0$	$\frac{F_{1-2}}{\sqrt{2}} + \frac{F_{1-3}}{2} + \frac{F}{2} = 0$	
2	$-\frac{F_{1-2}}{\sqrt{2}} - F_{2-3} = 0$	$-\frac{F_{1-2}}{\sqrt{2}} - S_{2-3} + F_{2y} = 0$	
3	$F_{2-3} + F_{3-x} = 0$	$-\frac{F_{1-3}}{2} + S_{2-3} = 0$	$\frac{2\,S_{2-3}\,L}{2} + M_{3-2} = 0$

With the sign conventions of Fig. 4(*a*), and with the symmetry of the structure considered, the equations of equilibrium are identical to the expressions of Table 1.

The power loss in Fig. 8(*b*) is

$$P = F^2_{1-2}\,R_{1-2} + \frac{F^2_{1-3}\,R_{1-3}}{2} + F^2_{2-3}\,R_{2-3} + S^2_{2-3}\,\frac{\alpha\,E\,R_{2-3}}{G} \ldots\ldots (18)$$

in which R is the branch resistance, except in the case of branches 1–3 and 2–3 in the *y*-network, in which the resistance is $2\,R_{1-3}$ and $\alpha\,E\,R_{2-3}/G$, respectively. If each R is set equal to the corresponding tensile compliance, then $\alpha\,E\,R_{2-3}/G$ is shear compliance, and Eq. 18 represents twice the tensile and shear work of the prototype half-structure.

The power dissipated in the moment network of Fig. 8(*b*) is

$$P = \frac{(S_{2-3}\,L)^2\,\rho}{3} \ldots\ldots\ldots\ldots\ldots\ldots\ldots\ldots (19)$$

Eq. 19 equals twice the bending work of the half-structure. All requirements for the validity of the analog are thus met.

Both the prototype and the analog can be solved by expressing the unknown forces and moments in terms of S_{2-3} (which is redundant) by means of the equations of current-continuity or equilibrium, and then setting to zero the partial derivative of the sum of tensile, shear, and bending work with respect to S_{2-3}. For the specific case in which $A_{1-2} = A_{1-4} = A_{1-3}\,\sqrt{2}$; A_{2-3} and A_{3-4} are large enough so that the work of direct shear and tension in these members is negligible; and $I_{2-3} = I_{3-4} = A_{1-3}\,L^2/12$, the value of S_{2-3} is found to equal $-F/8$.

With this value known, all other forces, moments, deflections, slopes, currents, and voltages can be evaluated.

Scale Factors.—In the force networks the scale factors S_F and S_C are arbitrary. The scale factor S_δ equals $S_F\, S_C$.

In the moment network, the scale factor S_M, relating moment to current, can be made the same as S_F, in which case it can be shown that S_B, the scale factor relating bending compliance $\left(\text{dimensions} = \dfrac{1}{\text{force} \times \text{distance}}\right)$ to resistance, is the same as S_C, and that S_θ, the scale factor relating slope (in radians) to voltage, equals S_δ. The power dissipation and the equations of current-continuity will be unchanged, however, if all currents are multiplied by any arbitrary factor f and the resistances by $1/f^2$, the voltages then being $1/f$ as large as before. The scale factors in the moment-network are then

$$S_M = \frac{S_F}{f} \qquad (20a)$$

$$S_B = S_C f^2 \qquad (20b)$$

and

$$S_\theta = S_\delta f \qquad (20c)$$

As a second example, Fig. 9(*a*) shows a rigid frame, loaded by a force F, in which the work of direct tension and shear is negligible, only the bending work being of interest. Because no force networks are used, S_{1-2} and S_{2-3} must be determined in terms of the load and the redundants, and the corresponding shear currents withdrawn from the bending network. By equilibrium considerations, it can be found that there is only one redundant, conveniently selected as the reaction F_1. In terms of F and F_1

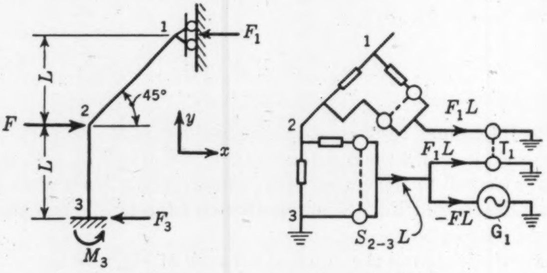

(*a*) FRAME (*b*) ANALOG

FIG. 9.—RIGID FRAME

$$S_{1-2} = \frac{F_1}{\sqrt{2}} \qquad (21a)$$

and

$$S_{2-3} = F_1 - F \qquad (21b)$$

The analog, shown in Fig. 9(*b*), can be developed as follows: The networks for member 1–2 and member 2–3 are first drawn according to Fig. 4(*c*), and are interconnected according to the configuration of the structure. Joint 3 is grounded to establish the slope datum, and joint 1 is opened to indicate zero moment. The shear currents must be interrelated according to Eqs. 21, without changing the number of redundants (in this case, one). This can be accomplished by selecting one shear current as redundant, then developing the other currents by the use of transformers and generators, as necessary. The selected redundant may be considered as $S_{2-3}L$. This redundant is separated into its component parts by use of generator G$_1$, the shear current for member 1–2 (F_1L) being established by the use of transformer T$_1$. For uniform cross section throughout the structure

$$F_1 = \frac{5\,F}{14 + 2\sqrt{2}} \qquad (22)$$

which can be used to check the validity of the entire analog.

Fig. 10(*a*) represents an irregular structure in which the work of direct tension and shear is considered insignificant. The joints are rigid except for joint 2, which is hinged. Member 1–2 and member 2–3 have the same constant moment of inertia *I*, whereas the moment of inertia for member 1–3 varies linearly from *I* at joint 1 to 2 *I* at joint 3. The reactions are determinate, and are as indicated in Fig. 10(*a*).

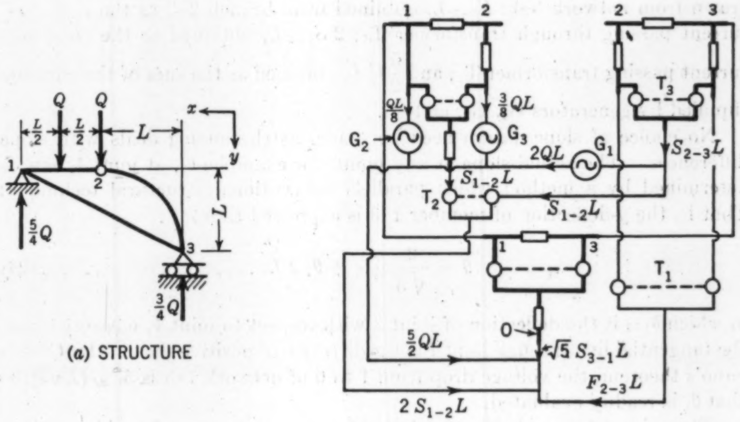

(*a*) STRUCTURE

(*b*) BENDING ANALOG

FIG. 10.—IRREGULAR STRUCTURE

To determine the bending network without using the force networks, it is necessary to find S_{1-2}, S_{3-1}, S_{2-3}, and F_{2-3} (the two latter terms being the shear and tension, respectively, in member 2–3 and joint 2) in terms of the loads and redundants. Applying the equations of force summation to each joint,

$$S_{2-3} = S_{1-2} + 2\,Q \qquad (23a)$$

and

$$S_{3-1} = -\frac{F_{2-3} + 2\,S_{1-2} + \frac{5}{2}\,Q}{\sqrt{5}} \ldots\ldots\ldots\ldots\ldots\ldots (23b)$$

in which S_{1-2} and F_{2-3} are selected as redundants. Applying moment summation to each member, it is found that there are no other redundants.

The bending analog, Fig. 10(*b*), may be developed as follows: The networks for the separate members are drawn according to Figs. 5, 6, and 7, and are interconnected according to the configuration of the structure, the connection between member 1–2 and member 2–3 being omitted to indicate zero moment at joint 2. Currents $S_{2-3}\,L$ and $F_{2-3}\,L$ are arbitrarily selected as the two redundants, it being necessary to develop the remaining shear currents, $S_{1-2}\,L$ and $\sqrt{5}\,S_{3-1}\,L$, by use of transformers and generators.

Current $S_{2-3}\,L$ is separated into its component parts by means of generator G_1. The part designated as $S_{1-2}\,L$ is then used to set up the shear current for member 1–2, with the aid of transformer T_2. To set up the shear current for member 3–1, the negative of the sum of the following three currents is withdrawn from network 3–1: $F_{2-3}\,L$, obtained from branch 2–3 as the combined current passing through transformer T_1; $2\,S_{1-2}\,L$, obtained as the combined current passing transformer T_2; and $\frac{5}{2}\,Q\,L$, obtained as the sum of the currents supplied by generators G_1, G_2, and G_3.

No choice of slope datum need be made, as the analog deals with slope differences. The actual slope at any point, for example, θ_1, at joint 1, can be determined by a method which parallels conventional structural technique: That is, the *y*-deflection of member 1–3 is expressed thus:

$$\theta = \frac{2}{\sqrt{5}}\,\delta_{1-3} + \theta_1\,2\,L \ldots\ldots\ldots\ldots\ldots\ldots (24)$$

in which δ_{1-3} is the deflection of joint 3 with respect to joint 1, measured from the tangential line through joint 1 in the direction of positive shear. By Castigliano's theorem, the voltage drop from 1 to 0 of network 1–3 is $\delta_{1-3}/(L\sqrt{5})$, so that θ_1 is readily evaluated.

The values of the redundants selected for the structure are found by analysis to be:

	F_{2-3}	S_{1-2}
Structure..........	$-1.511\,Q$	$-0.804\,Q$
Analog	$-1.489\,Q$	$-0.808\,Q$

The slight difference in the values is caused by the fact that the power dissipation in the analog is in excess, as explained for Fig. 7. With these values known, a complete check of the entire analog is facilitated.

EXPERIMENTAL EQUIPMENT, PROCEDURE, AND RESULTS

Fig. 11 shows a working model, the four essential parts of which are:

(1) Resistors. These are in the form of thirty calibrated rheostats, with the actuating knobs visible on the front panel. There are three types, with

maximum-resistance values of 100 ohms, 300 ohms, and 1,000 ohms, respectively. The resistances may be set to within 1% of the maximum value, and are used both in the analog and in conjunction with voltage sources, to be described subsequently, as a method of controlling load currents. Connections to the rheostats are made by use of the horizontally disposed screw-type terminal strips, each terminal being numbered to agree with the rheostat to which it is connected.

FIG. 11.—MEASURING INSTRUMENT

(2) Supply Transformers. These are of a conventional type, with 115-volt, 60-cycles-per-sec input, and with a plurality of independent 6-volt center-tapped secondaries, the latter being used as voltage sources or generators. Connection to the secondaries, of which there are six, is made by means of the last two vertically disposed terminal strips at the right of Fig. 11. The minimum resistance placed in series with each voltage source should be large enough to limit the current to a safe value in case of a short circuit in the analog.

(3) Computing Transformers. These are used in the analog, and have a nickel-iron core of about $\frac{1}{4}$ sq in. cross-sectional area, and two windings of five hundred turns of 24-gage wire. One of the windings is divided into five inde-

pendent parts having the following percentages of the total turns: 1%, 3%, 9%, 27%, and 60%. By connecting some or all of these in series, bucking or aiding, it is possible to vary the turns ratio (or its reciprocal) in steps of 1% from zero to 100%. There are twelve such transformers, each having its windings connected to one of the vertically disposed terminal strips, by means of which the turns ratio is selected and connection is made to the other elements of the analog.

(4) Measuring Circuit. This consists of the alternating current microammeter shown in Fig. 11, and an accurate rheostat with a dial arrangement which permits precise setting over the full range of ten turns. These elements can be used to measure voltage without drawing current from the analog, with the one necessity being to find the rheostat setting at which no current (in practice, minimum current) flows through the meter. For measuring negative voltage, the connections to the measured voltage are merely interchanged. Current is measured by noting the voltage drop across some known resistance.

Transformer Imperfections.—The accuracy of the instrument is limited chiefly by the departure of the computing transformers from ideality. At a frequency of 60 cycles per sec the important transformer imperfections are as follows:

(1) Equivalent Shunt Inductance. This arises from the fact that the transformer draws a small magnetizing current. Its effect can be practically eliminated by shunting a suitable fixed capacitance across the fixed winding. Such correction was not found necessary, however.

(2) Series Inductance. This is caused by leakage flux, and can be remedied by inserting a suitable fixed capacitor in series with the fixed winding, but this also was not considered necessary.

(3) Equivalent Shunt Resistance. This is associated with eddy current and hysteresis losses in the core, and can be dealt with as follows: As each transformer drop is measured, the resulting current drawn by the equivalent shunt resistance, about 7,500 ohms, is estimated. If this current is appreciable, in comparison to the analog currents, there is imposed on the transformer a compensating value of in-phase ampere turns of the correct magnitude and polarity just to sustain the core losses. This is preferably done by passing a suitable current through a special winding of few turns, so that the induced electromotive force will be small enough not to complicate the adjustment of the inserted current. The whole operation can be done very rapidly by the use of prepared charts relating transformer voltage drops to values of resistance which, when placed in series with a selected voltage source, will pass the required compensating current. This correction also was not used.

(4) Series Resistance. Series resistance is the resistance of each transformer winding (2 ohms for the fixed winding) and is compensated for by deducting it from a convenient analog resistance with which it is in series, the latter usually being much larger. For a given winding, the resistance to be deducted can also be referred to any analog resistance whose current is held in a fixed ratio with the winding current, by means of the following formula, which will leave the power unchanged:

$$R_r = R_w \frac{C^2_w}{C^2_r} \quad \text{..................} (25)$$

in which R_r and R_w are the referred and winding resistances, respectively, and C_r and C_w the referred and winding currents, respectively. This correction was used throughout the investigation.

Experimental Procedure.—The steps in setting a problem into the equipment are as follows:

1. The circuit diagram is drawn according to the various examples previously cited. Trusses and truss-frame combinations follow the explanations given in connection with Figs. 2 and 8. For rigid frames in which only the bending work is of interest, only the moment analog need be drawn. The forces which influence the bending work are determined separately in terms of the loads and redundants, the corresponding currents then being withdrawn from the analog, as in Figs. 9 and 10.

2. A scale factor is chosen between the structural compliances ($L/(A\,E)$, $L/(E\,I)$) and the corresponding electrical resistances. The latter is small in comparison with the equivalent shunt resistances of the transformers, and large compared to the winding resistances, the optimum compromise probably being reached with resistances of from 50 ohms to 300 ohms. The computing transformers are connected to yield the required turns ratios. After that, they are wired to the selected rheostats, which have been set to the proper values. The ground or datum points are then connected together.

3. Load currents are supplied by the voltage sources in series with resistances, the voltage drop across the resistances serving as an indication of current. The scale factor between force and moment and the corresponding currents is a matter of convenience.

4. The branch currents and joint voltages are measured. The former represent force or moment, which are readily converted to stress, and the latter represent slope or deflection. If the structure is seen to be of unsatisfactory design, the cross section of selected members can be altered by changing the setting of the associated rheostats. This change usually necessitates a readjustment of the load currents. Measurements are then made as before, and the whole process is repeated until the design is satisfactory.

5. A rapid numerical check can be made by noting whether the currents leaving each joint and the voltage drops around each current path sum to zero. This, however, does not reveal errors in the circuit diagram. A more thorough check can be conducted in purely structural terms, by noting whether the results satisfy the requirements of equilibrium, and whether the deflections and slopes are mutually compatible.

Experimental Results.—The structures of Figs. 2, 8, 9, and 10 were solved experimentally. The error is expressed as a percentage of the maximum values encountered. This manner of expressing error is considered more indicative of the overall accuracy than if the error is expressed as a percentage of each individual quantity. The latter can be much larger than the former, for members that are relatively lightly loaded. However, the error is of far less importance for these members than for the heavily loaded members.

The computing transformers were uncompensated, except that the winding resistances were subtracted from analog resistances where possible.

The units used were as follows: Resistance in ohms, voltage in divisions of the ten-turn rheostat, and current in divisions per ohm. In the experiments, one thousand divisions represented 6 volts.

Fig. 2(*c*). The branch resistance R was 100 ohms (200 ohms for branch 2–5), and F was 6.58. The joint voltages (from which the branch currents are computed) were measured, the greatest error compared to theoretical values being 2% of $F R$.

Fig. 8. The tensile compliance was represented by 100 ohms. For L equal to unity, the bending compliance resistor ρ would have been 1,200 ohms, which was considered too high compared to the transformer equivalent shunt resistance of 7,500 ohms. Hence L was set at 2, thus reducing ρ to 300 ohms, transformer T_1 then having a 2:1 turns ratio. The value of F was 7.94. The various currents were measured, the greatest error being 1.5% of F.

Fig. 9. The bending compliance resistor was 300 ohms for member 1–2 and $F L$ was 8.40. The currents were measured and were found to be accurate to within 1/2% of $F L$.

Fig. 10. The resistance simulating bending compliance was 300 ohms for member 3–1 and $Q L$ was 4.545. The voltages and currents were measured, the latter having the larger error—2.5% of $Q L$ as referred to the theoretical solution for the electrical analog. The small difference between the structure and its analog need not be charged against the latter, since it is caused by an excess of power comparable to the work caused by direct shear and tension, which is customarily ignored in rigid-frame computations. It was not possible to absorb the winding resistances of transformers T_1 and T_3 in any analog resistances, which may account for the somewhat larger error observed in this analog.

CONCLUSIONS

For two-dimensional trusses and three-dimensional trusses, the analog developed by Mr. Bush has been extended to include the simulation of indeterminate reactions and of deflections caused by branch rotation.

For two-dimensional rigid frames, there has been presented a new analog in which slope and deflection need not be simulated explicitly, as in Mr. Bush's analog, but are obtained automatically with a simulation based on force, moment, and elastic compliance. Furthermore, there is no limitation on the orientation or configuration of the members.

For trusses, the circuit diagram can be constructed on a purely pictorial basis. For rigid frames, the analog achieves its maximum economy when it is only partly pictorial, in which case it is necessary to solve the equations of equilibrium. It is unnecessary to derive the equations governing the mutual compatibility of the slopes and deflections, such as appear in explicit form in the method of slope deflection, in implicit form in the method of least work, and in iterative numerical form in the method of moment distribution. For irregular members, however, it is necessary to derive special analogs, as shown in Figs. 5, 6, and 7. Such analogs may be tabulated and used wherever applicable.

For the experimental solution of practical problems, an instrument such as that of Fig. 11, but large enough to accommodate structures of many members, may be necessary. This instrument would contain no component of unusual cost or difficulty of manufacture, or of limited life, such as vacuum tubes. The expected error would be of the order of 2% of the maximum values encountered in each problem. Should the error increase substantially for structures of many members, the computing transformers, which are the chief source of error, must be compensated.

With such an instrument in the hands of an experienced operator, it is estimated that the total experimental solution, including the construction of the circuit diagram, the making of the connections and setting of the values, and the measuring of the unknowns and converting them into structural quantities, will require a small fraction of the time required for analytical solution, for structures of at least moderate complexity and indeterminacy. The saving in time will be particularly great when an optimum design is sought, so that different choices of dimensions are to be explored. In such cases the successive solutions are obtained in a small fraction of the time required for the initial solution in contrast with conventional analytical methods, where much of the solving procedure must be repeated for each choice of dimensions.

ACKNOWLEDGMENT

This paper was based on a thesis which has been accepted by the faculty of the Graduate Division of the College of Engineering of New York University, in New York, N. Y., in partial fulfilment of the requirements for the degree of Doctor of Engineering Science.

APPENDIX. NOTATION

The following symbols, adopted for use in this paper and for the guidance of discussers, conform essentially with American Standard Letter Symbols for Structural Analysis (ASA Z10.8–1949), prepared by a committee of the American Standards Association, with Society representation, and approved by the Association in 1949:

A = cross-sectional area of a member;
B = end of a typical member;
C = supplied electrical current:
    C_r = referred currents;
    C_w = windings current;
E = modulus of elasticity;
F = axial force, current analogous to force:
    F_x, F_y = components of the axial force;
    F'_x, F'_y = components of the resultant of all forces on the end of a member;
    F_h, F_v = horizontal and vertical components of a force;
f = scale factor coefficient;
G = shear modulus;

$G_{1,2,\ldots}$ = generators in electrical network;
H = end of a typical member;
I = moment of inertia of a section;
L = length of a member;
l, m, and n = direction cosines of a member;
M = applied bending moment;
N = transformer-turns ratio;
O = point in an electrical network;
P = electric power dissipation:
  P_{ex} = excess power in an electrical network;
Q = concentrated loads;
Q' = uniformly distributed load;
q = number of spaces between concentrated loads;
R = branch resistance:
  R_r = referred resistance;
  R_w = windings resistance;
r = radius of curvature of curved member;
S = shear in member, current analogous to shear;
S_B = scale factor relating bending compliance to resistance;
S_C = scale factor relating compliance to resistance;
S_F = scale factor relating force to current;
S_M = scale factor relating moment to current;
S_δ = scale factor relating deflection to voltage;
S_θ = scale factor relating slope to voltage;
T_1, T_2 = transformers in electrical network;
V = voltage in electrical network;
W_b = work of bending;
W_d = work of deformation;
x, y, and z = rectangular coordinates;
α = ratio of maximum shear stress to average shear stress;
δ = elastic deflection;
θ = elastic slope of a beam; and
ρ = resistance analogous to bending compliance.

AMERICAN SOCIETY OF CIVIL ENGINEERS
Founded November 5, 1852
TRANSACTIONS

Paper No. 2712

RIVER-BED SCOUR DURING FLOODS

By E. W. Lane,[1] M. ASCE, and
W. M. Borland,[2] A.M. ASCE

With Discussions by Messrs. E. E. Dittbrenner; Emmett M. Laursen and Arthur Toch; and E. W. Lane and W. M. Borland

Synopsis

Scour in wide, steep rivers during floods is not general throughout the flooded reach since deposition occurs at wide sections. The measurements of river action are almost always made at narrow sections, causing a misconception that is not supported by studies of the transported sediment. In the design of a project for the protection and rehabilitation of the middle Rio Grande Valley in New Mexico, the question of the depth of scour of the river beds during floods assumed unusual importance. A study was made, therefore, to determine this depth. The study, its results, and revised theories based on it are explained in this paper.

Conditions in the Middle Rio Grande Valley

Before the intense agrarian use of the area by white settlers, the middle Rio Grande Valley had probably reached a sedimentation status approaching equilibrium, in which the sediment carried out of the valley nearly equaled the sediment brought into it by the Rio Grande and its tributaries. In recent years, however, a large portion of the upstream runoff has been used for irrigation, thus decreasing the flow downstream in the valley. In addition, overgrazing of the watershed has increased the sediment load brought into the main stream by tributaries. Evidence suggests that a secular change of climate may also be responsible. Thus, the load of sediment brought into the valley has increased, and the flow available to carry it out has decreased, with the result that the valley is filling at a rate that the latest measurements (1952) indicate to

---

Note.—Published, essentially as printed here, in August, 1953, as *Proceedings-Separate No. 254*. Positions and titles given are those in effect when the paper or discussion was received for publication.

[1] Cons. Hydr. Engr., Bureau of Reclamation, U. S. Dept. of the Interior, Denver, Colo.

[2] Head, Sedimentation Section, Hydrology Branch, Bureau of Reclamation, U. S. Dept. of the Interior, Denver, Colo.

be about ½ in. per year. The river bed at Albuquerque, N. Mex. (the principal city of the valley), had risen above the level of the streets by 1952.

This condition not only increases the danger of floods but also tends to raise the ground-water level on the agricultural land of the valley—threatening it with waterlogging. In addition, water-loving plants have grown up in the abandoned areas. This vegetation absorbs the available water to an extent that seriously decreases the water supply. The rise of the river bottom is thus threatening the future prosperity of the valley.

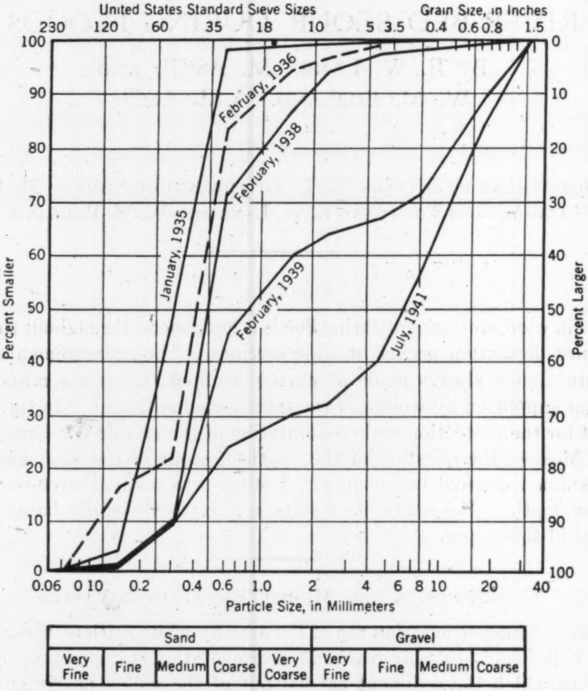

FIG. 1.—INCREASE IN COARSENESS OF BED MATERIAL BELOW LAKE MEAD, LOWER COLORADO RIVER

To remedy this condition, a plan of improvement, developed jointly by the Bureau of Reclamation, United States Department of the Interior (USBR), and the Corps of Engineers, United States Department of the Army, was approved by the 80th Congress in 1948.[3] The plan consists principally of the construction of (1) two dams for the storage of sediment and temporary retention of flood flows, and (2) control works whereby the channel scours out—and thus lowers—its bed. The storage of sediment in the basins and the release of the clarified water into the river channel is expected to make possible a lowering of the river bed through the picking up of the bed material by the clarified water. Considerable degradation of the stream below Lake Mead on the lower Colorado River has resulted from the release of clarified water. As will be shown, the rate of degradation in the Rio Grande Valley is related to the depth to which the river bed of this stream scours during floods. A study of the phenomenon was important for this reason.

---

[3] "Flood Control Act of 1948," *Public Law No. 858*, 80th Cong., U. S. Govt. Printing Office, Washington, D. C., 1948.

Observations made at Lake Mead indicate that, when the clarified water is released from the dams on the Rio Grande, the flow will carry away from the bed more fine particles than coarse particles. As a result, the average particle size of the bed material will gradually become larger. For example, Fig. 1 shows the increase in size of the bed material a short distance below Hoover Dam on the lower Colorado River. Since a specified flow cannot carry so large a volume of coarse as of fine material, this increase in bed coarseness will cause a slow decrease in scour volume. Thus, the rate of degradation will be reduced gradually, and the rate of lowering of the bed will become negligible. The rate at which the fine sand is removed and the length of time before the degradation rate becomes negligible depend on the depth to which the river bed is scoured during high flows, since the volume of fine material that can be removed by the river depends on the volume of this material that comes in contact with the flowing water. If the depth of scour is small, little fine material can be carried away before the bed becomes covered with coarse material; however, if the depth of scour is great, much fine material will be carried away before the average size becomes large. The removal of the small quantity with small depth of scour will lower the bed much less than the removal of the large amount if the depth of scour is great. It was necessary, therefore, to know the scour depth.

The middle Rio Grande is a steep stream having a slope of 4.5 ft per mile in the vicinity of Albuquerque, and it carries a heavy sediment load averaging at San Marcial (New Mexico) approximately 1.18% by weight. The river is generally wide, shallow, and relatively straight. The channel contains many islands that give it a "braided" pattern, similar to many others in the western United States.

THE COMMONLY ACCEPTED CONCEPT OF DEPTH OF SCOUR

Since the early 1900's, the discharges of the Rio Grande and other similar rivers in the western states have been measured thousands of times under widely varying flow conditions. In each of these observations, the cross section was determined by frequent soundings across the stream bed. As the flow of water in the stream increases, the increase in the average depth of the flowing water usually is found to exceed the rise in water-surface elevation. This indicates that the bottom of the stream has been scoured out. It is not uncommon for the bottom to recede as much as the water surface rises. When the flood crest is passed and the flow decreases, the bottom begins to fill, and when the flood has passed, the bottom has risen nearly to the level that existed before the flood. This is indicated by Fig. 2, which shows the changes in the river bed at the San Marcial gaging station on the Rio Grande during 1929.

Similar changes in the Rio Grande and other western rivers have been observed so frequently that it is the general impression of many experienced engineers that such action is normal for streams of this type. It is believed that, when a flood occurs, the bed of the stream (for the greater part of its length and width) scours materially and refills as the flood recedes. This opinion is widely held by men who have gaged the Rio Grande and is substantiated by observations of the effect that the floods exert on pilings driven for bank-protection work. These pilings are observed to rise suddenly in the water and float away, despite the fact that they are 40 ft long—with most of this length below the stream bottom. Bridges supported by 60-ft pilings have been washed out during such floods. If such deep scour occurs over the entire stream bottom during floods, the volume of river-bed material from which the finer particles can be drawn is great; a long time will elapse before the clear water from the proposed sediment-control reservoirs will stop the degradation of the stream bed by increasing the coarseness of the grain sizes.

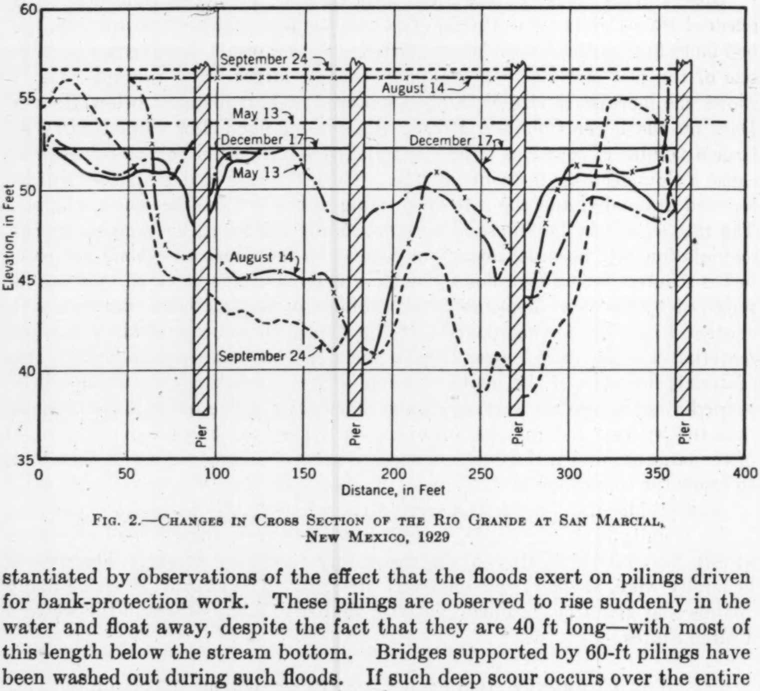

Fig. 2.—Changes in Cross Section of the Rio Grande at San Marcial, New Mexico, 1929

The Conflict Between Theoretical and Actual Sedimentation

The belief of many experienced observers—that the entire bed of the Rio Grande scours deeply during floods—seems to be based on quite conclusive evidence; but a quantitative examination proves even more conclusively that such deep general scour has not occurred during floods in recent years. If the Rio Grande scours downward several feet throughout its width and length, it must transport a large quantity of material down the river. Nearly all the material transported in the section of stream under study is deposited in the Elephant Butte Reservoir (New Mexico). The volume of sediment being deposited in this basin has been measured frequently, and the amount is known within a reasonable degree of accuracy. Comparison of this volume with that which would have to be moved into the reservoir with even so small an average depth of scour as 1.5 ft shows that the sediment actually deposited is decidedly less than would occur with this scour. Thus occurs the apparently conflicting evidence of the scour unquestionably observed by the stream gagers and the equally unquestionable lack of a corresponding volume of material deposited in the reservoir.

In quantitative terms, this difference may be shown by an example. The section of the Rio Grande from Cochiti (New Mexico) to San Marcial has a length of 160 miles and an average width of 1,170 ft, giving it a surface area of 22,700 acres. For each foot of average depth of scour below the elevation of the bed at the start of the flood, a volume of 22,700 acre-ft would, therefore, be carried into the lake. The average yearly volume of material carried into the lake is 18,276 acre-ft, of which only 1,800 acre-ft are composed of sand and larger sizes, such as would be scoured out of the stream bottom. Since floods sufficient to scour the river bed occur almost every year, it is evident that the average depth of scour during floods, even if all the deposited coarse material is assumed to be moved out of the bed, is of the order of magnitude of 0.08 ft.

Another proof of the nonexistence of large depths of scour over nearly the entire stream-bed area is that the measurements of sediment concentration made in the river do not show the presence of sufficiently large volumes of sand to account for a deep scouring of the channel bed. For a flood to scour an average of 5 ft of depth from the bed of the Rio Grande would require that it move 113,500 acre-ft of sediment, almost all sand, from the river bed. The concentrations in the Rio Grande below the mouth of the Rio Puerco sometimes become as great as 20% resulting mainly from flash floods from the Rio Puerco, which is probably the carrier of the highest sediment concentration of any stream in the United States (and possibly the world), 68% concentration by weight having been observed in it.[4] Above the mouth of the Rio Puerco, concentrations in the Rio Grande rarely reach above 5%. These high concentrations are of short duration and only a small part of them is composed of sand particles. Although the sand loads are great, no flows have been observed at the lower end of the river with sufficient volume of discharge and concentration of sand sizes to account for the 113,500 acre-ft of loss of material necessary to deepen the river bed an average of 5 ft.

Since the river bed refills as a flood recedes, an inflow of 113,500 acre-ft of sand would be required to provide this material, but no such flows have been observed. If this scouring action took place, there would be a high concentration of sand at the lower end of the valley during the first part of the flood, but a large flow with low concentration during the latter part of the flood. A high sediment concentration during the early part of the flood is commonly observed; the concentration differences between rising and falling floods, however, are insufficient to account for an extensive general scour.

---

[4] "Sedimentation Studies at Conchas Reservoir in New Mexico," by D. C. Bondurant, *Transactions*, ASCE, Vol. 116, 1951, p. 1283.

L. G. Straub, M. ASCE, has made extensive studies of the changes of river-bed level resulting from contractions, including both model studies and observations on the Missouri River.[5, 6] He reached the conclusion that the scour observed at contracted sections was not general throughout the length of the river.

A General Study of Scour

Since the data available on depth of scour in the Rio Grande were so conflicting that no satisfactory quantitative values could be obtained, the available literature bearing on this subject was studied with a view to obtaining more information on this subject. The principal information thus gleaned is summarized here.

Few measurements for the primary purpose of determining general bed scour have been made (1953). Most of the available data have been secured from measurements made primarily for other purposes, such as the determination of stream discharge or surveys to determine depths available for navigation. Observations of local scour (such as those made at bridge piers or abutments) are of no value in determining the general bed scour. The available data seem to deal with two general classes of rivers: (1) Large rivers of small or moderate slope, like the Mississippi and Missouri rivers, and (2) smaller rivers of steep slope, such as are often found in the western United States. The situation in these two types of streams differs somewhat. The larger rivers, if they flow in alluvial beds, generally consist of a series of bends between which are fairly straight reaches. In these straight reaches, the main channel of the river usually shifts from one side of the river to the other at places called "crossings." At ordinary stages the bends are usually deep and relatively narrow, and the crossings are wider and shallower.[7]

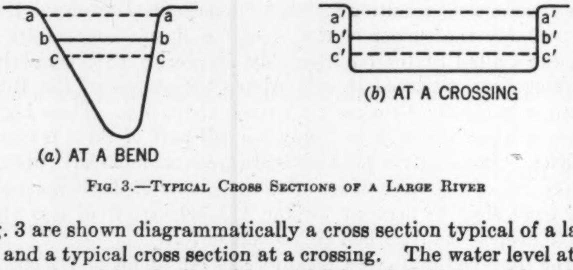

(a) AT A BEND

(b) AT A CROSSING

Fig. 3.—Typical Cross Sections of a Large River

In Fig. 3 are shown diagrammatically a cross section typical of a large river at a bend and a typical cross section at a crossing. The water level at medium stages is represented by the lines bb and b′b′, and at high and low discharges by aa and a′a′ and by cc and c′c′, respectively. At medium stages, the cross-sectional area of flow is almost the same in both cases; consequently the velocity of flow also is nearly the same. During floods, the water level rises to aa and a′a′—a rise of approximately the same height above bb and b′b′. Because the

---

[5] "Effect of Channel-Contraction Works upon Regimen of Movable Bed-Streams," by L. G. Straub. *Transactions*, Am. Geophysical Union, 1934, Pt. II, p. 454.

[6] *House Document No. 238*, by L. F. Straub, 73rd Congress, 2d Session, U. S. Govt. Printing Office, Washington, D. C., Appendix XV, p. 1150.

[7] "A Laboratory Study of the Meandering of Alluvial Rivers," by J. F. Friedkin, U. S. Waterways Experiment Station, Vicksburg, Miss., 1945, Plate V.

width at the crossing is considerably greater than that at the bend, the rise in water level increases the cross section at the crossing more than at the bend; therefore, the total cross-sectional area at the crossing becomes greater than that at the bend. This difference causes a lower velocity at the crossing than at the bend; hence the flow tends to produce less scour in the crossing than in the bend. At the low-water stage the opposite action occurs. The areas at the bends become larger than at the crossings, and more scour results at the crossings. At high-water stages, therefore, the pools usually scour out and deposition occurs at the crossings; whereas during low-water stages, the crossings scour out and the bends fill.

The Rio Grande is a relatively straight river and does not have the bends and crossings that characterize the large alluvial rivers, but it does have a series of alternately narrow and wide sections. If the river has approximately the same area in both types of sections at normal flows, during floods it should have larger areas at the wide sections and smaller areas at the narrow ones, producing deposit at the wide sections and scour at the narrow ones—the same action as that in large alluvial streams.

The fact that the bed of the Rio Grande is lowered during the period of floods (at least at certain places) is indicated by the cross sections shown in Fig. 2. These cross sections represent the bed of the river under the Santa Fe Railroad bridge at San Marcial in 1929. Some of the measurements were taken during the large flood of that year. At this place, the stream is contracted somewhat at high flows, and the presence of bridge piers doubtlessly increases the scour. The tendency of the bed to be deeper near the piers is evident at these sections. The piers are set at an angle with the direction of flow, which also increases the scouring effect.

Discharge measurements have been made in the Colorado River at Yuma, Ariz., since 1878. The great depths of stream-bed lowering that have been measured at this station during floods have received wide publicity and have been partly responsible for the belief that the bottoms of such streams are scoured deeply at flood stage. Some of the flow cross sections for the years 1912, 1916, and 1929 are shown in Fig. 4. The maximum increase in depth at the section is usually twice the rise in the water surface. These measurements were made from a cableway at a narrow section of the river where one or both banks are of scour-resistant material, and where the bed material is fine sand. Backwater curve studies made to determine levee grades below Yuma indicate that this degradation effect continues along a narrow reach of the river extending approximately 12 miles below Yuma.

In contrast with the deep stream-bed degradation at the Yuma station was the condition at the site of the Imperial Dam. A cable station was operated at this site for a short period before the dam was constructed. During this period the flow reached a maximum of 65,000 cu ft per sec. Although the bottom shifted considerably (being higher first on one side and then on the other), there was no appreciable change of the mean bottom level.

During the excavation for Hoover Dam, a sawed and planed 2-in. by 6-in. wooden plank was found in the river-bed material 50 ft below low-water surface and 40 ft below the bottom of the river channel. This discovery indi-

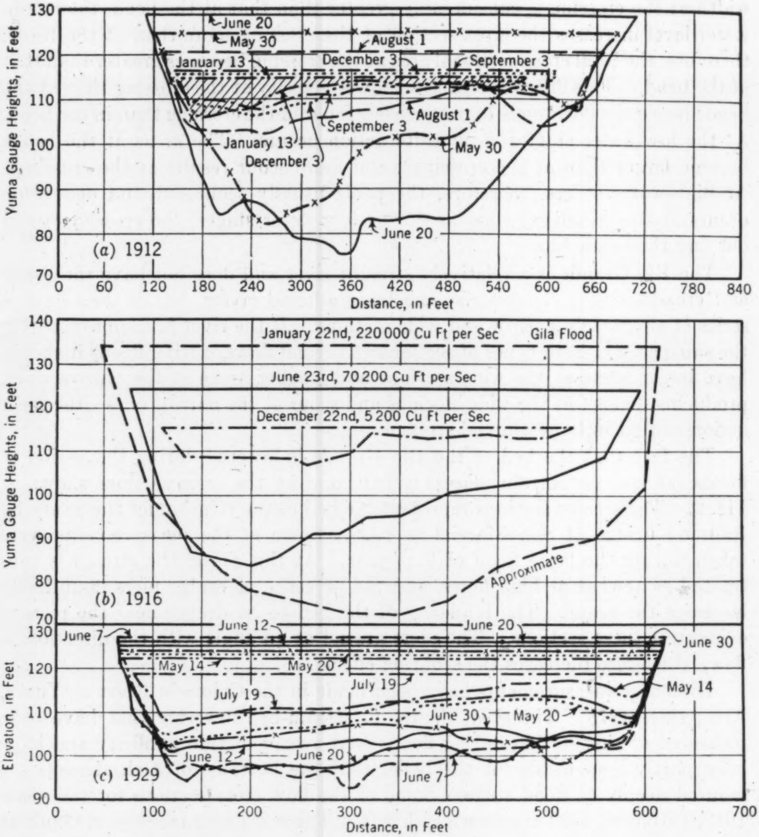

FIG. 4.—CHANGES OF A COLORADO RIVER CROSS SECTION AT YUMA, ARIZ.

cated that at some comparatively recent time, the river in this canyon had scoured out the bed to the depth of this plank.

Fig. 5 shows the cross sections at two stations on the Yellow River in China as described by J. R. Freeman.[8] These sections indicate the degradation of the bed of this stream during a flood. The cross sections were determined at gaging stations where the river was probably narrow. At one of them, rock was exposed nearby on one bank. For the shaded area in Fig. 5 (*b*), the gaging station is several hundred feet upstream from bedrock. At two other stations for which sections were not given, a similar degradation was observed. Mr. Freeman apparently believed that the degradation was continuous along the part of the river that he studied. Cross sections of the Verde River near

---

[8] "Flood Problems in China," by J. R. Freeman, *Transactions*, ASCE, Vol. 85, 1922, p. 1436.

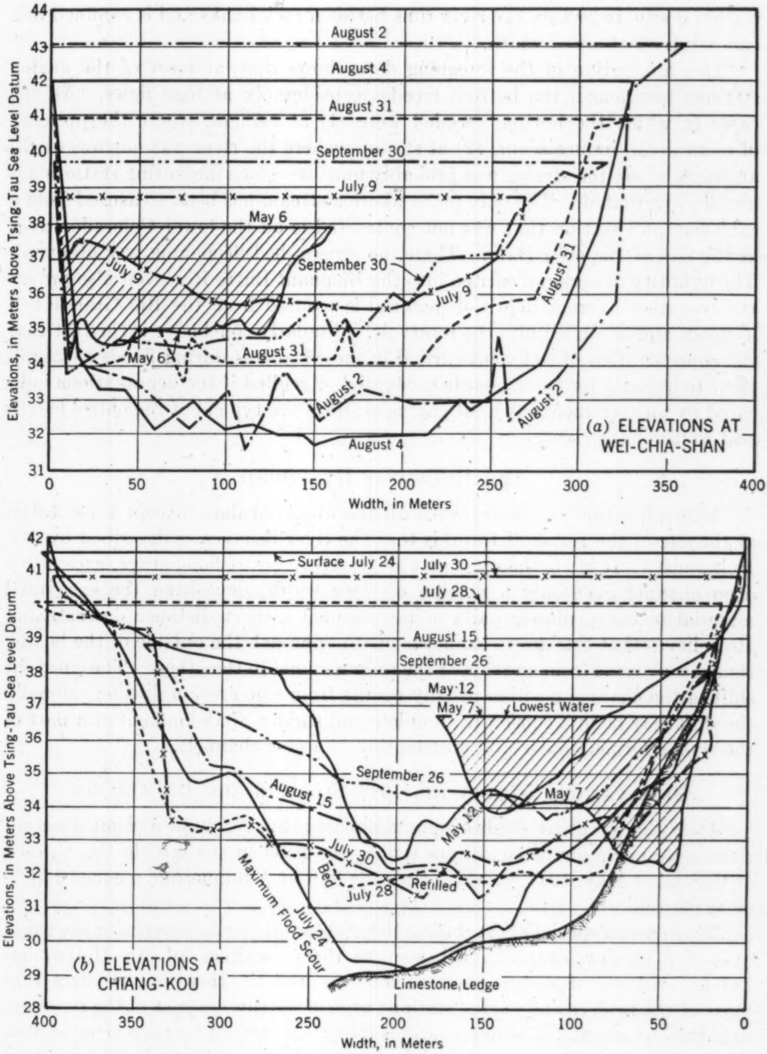

FIG. 5.—CHANGES OF YELLOW RIVER CROSS SECTIONS AT WEI-CHIA-SHAN AND CHIANG-KOU, CHINA, 1919
(1 METER = 3.28083 FT)

Fort McDowell, in Arizona, which indicate a considerable degradation of this stream at high flows, are provided by F. N. Holmquist.[9] This gaging station is situated where the river runs between rock banks and is confined to a comparatively limited width.

---

[9] "Behavior of Debris-Carrying Rivers in Flood," by F. N. Holmquist, *Engineering News-Record*, Vol. 94, 1925, pp. 362–365.

An examination of the foregoing data shows that, at most of the gaging stations mentioned, the bottom recedes considerably at high flows. All the cases in which the bottom receded were (1) at bridges, where the presence of piers would induce scour, (2) at stations where the river was narrow, or (3) at places where the stream was probably narrow—since measuring stations are usually so situated. The only place where a stream has been measured from a cableway at a section that was not contracted is on the lower Colorado River at the site of Imperial Dam. There, no stream-bed deepening was observed. The quantity of material carried into the Elephant Butte Reservoir also proves that no great average depth of material is scoured from the Rio Grande bed in floods and is carried into the reservoir. Similarly conclusive is the fact that the concentration of sediment carried in most streams during floods is insufficient to account for the amounts excavated or refilled if the degradations indicated by measurements at most gaging stations are typical of the entire length and width of the river.

The Holmquist Hypothesis

An explanation consistent with all the observed data, except those taken at the site of the Imperial Dam, is that the river behaves as described by Mr. Holmquist.[9] It is his theory that wide, steep rivers at flood stage, excavate a deep channel over only a portion of their width, depositing the excavated material in the shallower parts of the channel a short distance downstream. He believes that this deep channel tends to approach the outside of the bends; thus it may cross from one side of the river channel to the other. The constant shift of the channel position usually results from side erosion, but occasionally the shift may be by avulsion (a complete and sudden abandonment of a part of the river's former course and an adoption of a new channel).

Observations During the 1948 Flood in the Rio Grande

After the foregoing studies were completed, both ground and air observations were made of the conditions during the flood in the middle Rio Grande at the end of May, 1948, at which time the flow at Albuquerque reached 13,000 cu ft per sec.

There was a special effort during these observations to determine the existence of a narrow, deep channel, such as that described by Mr. Holmquist; but no evidence of such a phenomenon was found. However, the fact that most of the bridges and gaging stations were at narrow sections of the river was definitely observed. The observations that these narrow sections scour during floods agreed with the visual evidence, which also strongly indicated that the removed material was deposited at the next wide section downstream and not carried on down the river. These observations agree with all the other observed data on the middle Rio Grande, a fact which tends to confirm the accuracy of these observations.

This explanation also agrees with another observed condition—that the greatest danger to the levees along the middle Rio Grande is from the cutting of the banks, and that this cutting seems to be most active in the falling stages of a flood. It is believed that, during the height of the flood, deposits occur in the wide, shallow sections. Because of the shallow depth, a channel may be largely filled by a deposit of moderate depth, the volume of which is within the capacity of the stream to transport and lay down. Similarly, a bar may be formed to a height that equals a considerable percentage of the depth of the flow. When the flood recedes, the bottom topography may differ considerably from that which existed at the start of the flood because of these deposits; the former channel may be sufficiently blocked to force the stream to follow a new channel. If this channel impinges on the bank when the flow decreases, a new and unexpected scour occurs which under particularly unfavorable conditions may have serious consequences.

This is a different action from that which occurs on large alluvial rivers where the greatest bank cutting also accompanies a falling stage of the flood. In the case of the large river, this action is caused principally by (1) softening of the bank and the outward pressure at the bottom of the banks resulting from the return of the seepage water to the river, and (2) the sloughing of the high banks of saturated material exposed as the water recedes. This action is not important on the Rio Grande because the rise of the water during a flood is not large.

CONCLUSIONS

As a result of the studies described, it was concluded that during floods the bed of the Rio Grande (in general) scours at the narrow sections, and that most of the material thus removed is deposited in the next wide section downstream. This action causes the wide section to fill up somewhat and occasionally promotes channel changes in the wide sections which may cause the stream to attack the bank. It is believed that this action is typical of rivers in this category which includes most of the Great Plains rivers. It was also concluded that the common opinion that there is a general lowering of the bed of such streams during floods is unsound. The belief arises because the bottoms at gaging stations usually scour out; but such stations are in the great majority of cases situated at bridges or cableways where the rivers are narrow, and are not typical of the greater part of the length of the river. The unsoundness of the concept of a general lowering is proved by (1) the observation that the volume of deposit in the Elephant Butte Reservoir is less than that which would result from such scour, and (2) the lack of sufficient concentrations in the flowing water to carry such excavation during the rising flood or to deposit it as the flood recedes.

Although these general studies did not lead to a quantitative evaluation of the average depth of scour of the Rio Grande bed during flood, they proved that the scour was much less than it was generally believed to be by experienced hydrologists.

ACKNOWLEDGMENTS

The writers wish to acknowledge the helpfulness of the suggestions of Thomas Maddock, Jr., in the preparation of this paper.

DISCUSSION

E. E. Dittbrenner.[10]—The paper should be a considerable contribution toward the solution of the laws of stream behavior. Collection and analysis of specific data as presented by the authors are altogether too rare. The presentation highlights a characteristic problem, however, in that any attempt to isolate one of the characteristics of streams flowing in the channel built by them, sooner or later, leads to another facet, and so on ad infinitum.

This is well illustrated by the laboratory studies made during the 1940's at the United States Waterways Experiment Station, at Vicksburg, Miss., on the meandering of alluvial streams.[11] These are undoubtedly the most comprehensive studies ever made on these phenomena. Certainly some firm and hopeful data were developed. Beyond a doubt, most of the findings so well illustrated, will have their greatest value as knowledge progresses. The experimenters, however, were unable to put together an over-all solution of the laws governing stream characteristics. The model tests indicated among other things that, where erosion of the banks ceased, meandering ceased. On the other hand, if the banks were made erosion resistant, a deeper and narrower channel resulted under conditions otherwise the same. This illustrates rather graphically the difficulties students of stream behavior encounter.

The writer's attention was attracted by the authors' use of Fig. 3, depicting a section of a stable channel, between bends, as a rectangle. If his understanding of the authors' intent is correct—that is, a section between bends on a mature stable stream—this section will not be a rectangle. It will have a rounded ridge in midsection, dividing the channel into two sections—the top of this ridge being below the water surface, as shown in Fig. 6. This condition is a characteristic of what geologists call a mature or old river, and represents a channel at the "crossing" between two successive bends. Fig. 6 represents the section AA in Fig. 7.

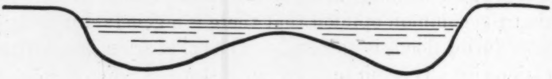

Fig. 6

There are many differences in streams; the authors have pointed out some of them. To classify them for study, an endless variety of categories or classifications is possible, but in the writer's opinion, the geologists have provided a simple classification based on their main interest in the earth's surface—erosion. They classify topography, streams, and valleys as youthful, mature, and old. In application, no exception need be made to these categories. They can occur together in any combination, and in most drainage areas they do.

Youthful valleys are V-shaped and generally straight. The stream that has made that valley is invariably a youthful stream, fairly straight, usually with a steep slope, ragged banks, eroding downward. A mature stream has reached—or nearly so—its base level with a gradient sufficient to carry its liquid and sediment discharge; it has attained the meandering stage and built a flood plain of a width determined by the stream's meander limits. The flood plain width has been established. As the stream gets older, these meanders continue to move downstream with respect to the channel. This movement brings alternate loops toward each other, eventually forming cutoffs and leaving oxbows. It is now an "old" stream. There is no degradation or aggradation in either the "mature" or old category, and there is no burden other than the sediment it moves from place to place in its channel, and receives from its tributaries.

---

[10] Div. Drainage Engr., Bureau of Public Roads, Dept. of Commerce, Albany, N. Y.

[11] "A Laboratory Study of the Meandering of Alluvial Rivers," by J. F. Friedkin, U. S. Waterways Experiment Station, Vicksburg, Miss., 1945.

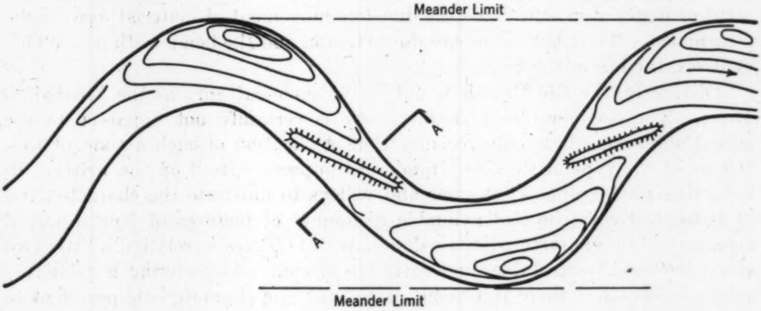

FIG. 7

The mature and old channels are stable; they shift relatively little, and then slowly. Generally, their slope is small—but for an alluvial valley, this is a relative matter, related to the quantity of flow. The same characteristics may be seen in large and small alluvial streams, but their slopes will be inverse to their discharges. The stream with a "steep" slope will usually be a "youthful" stream in a relatively narrow valley. (Precisely when a slope becomes steep may be an important element.) Its channel section is characteristically rectangular—but wider and shallower than in a mature or old stream handling the same drainage. The regularity of meanders is lacking. From what the writer has seen of the Rio Grande, this is the pattern of that stream—in fact, the pattern of most western streams. Mountain streams generally are of this pattern, regardless of the material in which they flow.

In the midwestern United States, parts of a large number of medium and large streams are alluvial streams, and in the mature or old category. Fig. 7 illustrates the former. Channel characteristics are a succession of pools in the bends, the pool having a triangular section, deepest at the outside bank. A diagonal bar crosses the channel between the two bends. The highest velocity in the stream will be found at the outside of the bend during high stages. At low stages, the highest velocity will be found over the bar, which tends to hold the pool elevation above it considerably higher than the pool below. At relatively low stages, flow across the bar is shallow and rapid. Col. Charles

R. Pettis,[12] M. ASCE, considered this "pool-and-rapid" an apt description of the normal stream found in at least the eastern Mississippi drainage basin.

In this type of stream, as the stage rises, the bottom of the pool is lowered by scour, and the bar below this pool is raised. On reversal of the stage, deposition occurs in the pool, and the bar erodes, but generally not as fast as the stage falls. On navigable streams, this bar must be dredged through before the stage gets too low, or else navigation ceases. This is an old story on such streams as the Mississippi River. The erosion of the bar resembles the movement of material in saltation—the dunelike movement of material seen on the stream bed. Thus, the bar moves downstream, and the bends with it. Which controls, the bar or the bends?

Obviously, the Rio Grande is not in the same category as the Mississippi River. The pool-and-rapid characteristic is certainly not apparent to the casual observer. It is only recently that application of such a concept to a stream of the type of the Rio Grande has impressed itself on the writer. In collecting photographs of streams and valleys to illustrate the characteristics of natural streams he had available a number of pictures of New England streams. Two characteristics predominate: (1) There is relatively little erosion—the banks are stable, and so is the stream. Meandering is relatively minor, even where there is a flood plain. (2) The characteristic pertinent to this discussion, however, is that the stream bed is a succession of steps. On the smaller streams this is immediately obvious. This is naturally not so evident on the larger streams.

In an investigation of scour around piers, an apparent inconsistency came to the writer's attention. A number of bridges in New England showed no such tendency, but rather the reverse—instead of scour, a deposit grew up around each pier. In a preliminary examination of a number of cases, one conclusion seemed to fit: Where the bridge was in a "rapid"—that is, on a bar—there was deposition around the piers. Where the bridge was in or across a pool, there was no deposition, and usually some scour around the piers. The predominant stream in New England, although lacking the well-developed, mature or old pool-and-rapid form of the mature stream, nevertheless has that characteristic in relatively straight channels. Very recently, the writer was furnished with photographs of the same phenomenon of deposition around the piers of a bridge over one of the larger midwestern rivers. Geometrically, the rivers on the high plains in the Rocky Mountain piedmont are similar to the New England streams, although their bed material certainly differs.

The authors cite a condition at the Imperial Dam station, at which scour during rise in stage failed to occur, as it did at all other stations noted. Obviously, this is a phenomenon of some significance. In the past generation many highway stream crossings have been built. Invariably, where these cross the channel of mature valleys, they do so at the edge of the valley over the pool, where scour will occur, both in the pool and around the pier. The writer has examined thousands of such crossings and at the moment can recall only one major crossing in midvalley. Therefore, it is expected that scour will always be found at a bridge pier. The crossing of a stream over the diagonal bar is seldom practicable, and one does not encounter any unexpected phenomena on that type of stream. On the youthful stream, the partly developed meanders and narrow valley do not limit the physical features of a stream crossing, and there is greater likelihood of crossing on a "bar." Apparently this is what has happened in New England. This could be the case at the Imperial Dam station.

---

[12] "A New Theory of River Flood Flow," by Charles R. Pettis, Ellisville, Miss., 1927 (privately published).

The "shingling" of a stream bed, which gives it erosion resistance, is doubtless more marked in the New England streams, which largely flow through a glacial detritus varying from fine clay to large boulders. The boulders form the "shingle." Bed movement is logically slow compared to western streams flowing in finer materials. During the lifetime of a New England resident, a bar would move downstream an unnoticeable amount. On western streams this bed movement logically would be faster; but there is more than one source of movement of bed material.

The authors refer to the evidence of bed movement on the Rio Grande to great depths during a flood rise. This is a common phenomenon in the western streams flowing through sand. It has also been noted in the straightened channels of midwestern streams—at least in fine bed material. Obviously, this is a phenomenon associated with only a large flow, and can be maintained only in that section of the stream and with the velocity of flow which brings that about. This would produce the movement of a large part of the bottom a certain distance during that flood—a wave of sand moving downstream. When the flow decreases, the wave will be dropped. Another rise in the same length may add to the previous wave. This may be what is occurring at Albuquerque now (1953). Some years ago, when discussing stage discharge relations on the Mississippi River with personnel at the Keokuk Dam, they called attention to a disturbing factor in this relationship which they could explain only by assuming that such a sand wave periodically moved down the river. The Mississippi River at this dam is geologically more advanced than the Rio Grande or the Kansas River, but it is more youthful than it is below the mouth of the Ohio River.

Of the recognized movements of bed material, three—saltation, the diagonal bar, and the deep bed movement of western streams—appear to be of a different character. The writer is beginning to question this apparent difference. At no stage of development is the stream free of bed movement, and this movement is in the form of a bar, a wave, or a pulse, whatever it may be called. Meandering appears to be affected, if not controlled, by sediment from bank erosion; yet nature seems to have imposed definite limits on the extent of the meanders, as many topographic maps will show. In the writer's experience, Colonel Pettis' formula[13] for the area of the flood prism in a mature valley is very accurate, and could be so only if meandering (and erosion) followed some law. However, no relationship between sediment load and meandering has been established. In the mature and old stream, the diagonal bar is classic. This stream has completed its downward erosion, and is merely passing on the sediment carried down from tributaries. Its slope is sufficient for this task.

---

[13] *The Military Engineer*, April–May, 1936.

It probably carries, relatively, the least sediment of any category—yet its meandering is the most pronounced. The youthful stream has a different task—to cut downward, and carry away, the material beneath it. When it has reached a balance of slope and channel size, it begins moving laterally to produce a flood plain as wide as the meander limits imposed by nature's laws. Under any conditions its activity results in a channel of a certain size and shape. In spite of ceaseless erosion of its banks, the channel size remains constant so long as the factors controlling its regime do not change. For instance, the Missouri River is one of those streams that are constantly gnawing their banks. As it does so, however, the other bank closes in behind it. Any sample of sediment includes this transfer. There is a certain amount of land in transition and out of cultivation for a certain period, but the total net area in the valley remains the same. For an individual who loses his farm, it is catastrophic. For the public at large, it has no physical significance.

There are many immediate problems pressing for a solution, but before great progress is made in advocating what today seems to be a panacea, it might be well to determine the laws governing the formation of channels by the streams occupying them. Perhaps this can be more easily done by working with the larger elements of stream similarity and differences, and by looking at the forest rather than the trees. If, for instance, one completely eliminates surface erosion, which many engineers advocate, what will the ultimate effect be on streams? It might be something highly objectionable. No one knows.

The authors' data appear to be consistent with what can be concluded from the foregoing—and bed movement contributes little to reservoir sedimentation. Any sample of sediment contains material in local transit; therefore it cannot be expected to be a reliable indicator of the amount of sediment carried to a reservoir or estuary. Certainly the final deposition must be less than any sediment sample would indicate.

At least, it is encouraging to find substantial evidence that major reservoirs are not doomed to an early end. The fact that there are a few small reservoirs that fill up quickly should provide valuable data for further comparative study of conditions which caused them to become full. Other reservoirs under superficially similar conditions do not fill up. It is the writer's belief that a determination of the laws controlling the formation of channels by the occupying streams will supply most, if not all, of the answers sought in sedimentation studies. Progress could very well be more satisfactory by studying the stream rather than its burden. Certainly, data of the kind presented by the authors are essential for that purpose, and many more are needed.

Emmett M. Laursen,[14] **A.M. ASCE, and Arthur Toch,**[15] **J.M. ASCE.**—The authors' stimulating exposition of sediment movement in alluvial streams recalls an approximate analysis made by the writers to indicate the order of magnitude of scour to be expected at a contraction. This analysis—originally conceived as a guide to the experimental studies of scour at bridge crossings conducted by the Iowa Institute of Hydraulic Research, State University of Iowa, at Iowa City—should have direct application to the authors' problem.

---

[14] Research Engr., Iowa Inst. of Hydr. Research, State Univ. of Iowa, Iowa City, Iowa.

[15] Instructor and Research Associate, Iowa Inst. of Hydr. Research, State Univ. of Iowa, Iowa City, Iowa.

A reach of a typical alluvial stream is represented schematically in Fig. 8. A part Q' of the flood discharge Q of such a stream flows over the flood plain. The vegetation on the flood plain will reduce the velocity of flow and inhibit sediment movement. Therefore, the overbank flow will carry a negligible amount of sediment as compared to the rate of transport in the main channel. At contracted sections the sediment-transport capacity will depend on the total discharge. Such conditions of discharge and transport can be described by the Manning equation of flow and the classical DuBoys equation of sediment-transport capacity. These relationships, involving an extension of those used by Mr. Straub[16] for simple contractions, take the form:

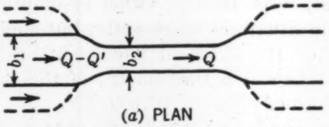

(a) PLAN

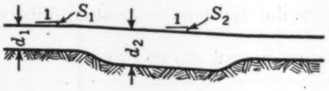

(b) PROFILE

FIG. 8.—TYPICAL REACH—ALLUVIAL STREAM

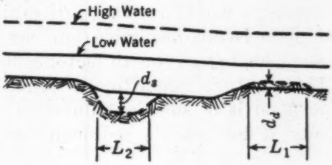

FIG. 9.—SCOUR AND DEPOSITION

$$Q - Q' = \frac{1.49}{n_1} b_1 \sqrt[3]{d^5_1} \sqrt{S_1} \qquad (1)$$

and

$$\left.\begin{aligned} Q_s &= C_s b_1 \tau_1 (\tau_1 - \tau_c) \\ \tau_1 &= \gamma d_1 S_1 \end{aligned}\right\} \qquad (2)$$

for the uncontracted section, and

$$Q = \frac{1.49}{n_2} b_2 \sqrt[3]{d^5_2} \sqrt{S_2} \qquad (3)$$

and

$$\left.\begin{aligned} Q_s &= C_s b_2 \tau_2 (\tau_2 - \tau_c) \\ \tau_2 &= \gamma d_2 S^2 \end{aligned}\right\} \qquad (4)$$

for the contracted section. In Eqs. 1 through 4, Q_s is the total sediment load, τ is the boundary shear, γ is the specific weight of water, n is the Manning roughness factor, and C_s is a coefficient of sediment discharge.

---

[16] "Approaches to the Study of Mechanics of Bed Movement," by L. G. Straub, *Proceedings*, Hydraulics Conference, State Univ. of Iowa, Iowa City, Iowa, 1940.

If the critical shear τ_c is neglected as being small in comparison to τ, a simultaneous solution of the equations for the depth ratio d_2/d_1 results in

$$\frac{d_2}{d_1} = \left(\frac{b_1}{b_2}\right)^{9/14} \left(\frac{Q}{Q - Q'}\right)^{12/14} \left(\frac{n_2}{n_1}\right)^{12/14} \ldots\ldots\ldots\ldots\ldots (5)$$

The first parenthesized factor on the right-hand side is the contraction effect determined by Mr. Straub, and the second and third factors embody the effects of overbank flow and of roughness, respectively. Other assumptions could be made which might describe some situations more aptly, but similar relationships would result. For example, if the sediment movement on the flood plain is not negligible but can be taken as a fraction Q'_s of the total sediment load Q_s, a fourth factor will be formed: $[(Q_s - Q'_s)/Q_s]^{3/14}$.

This analysis refers to the equilibrium conditions which will obtain only if the flood is of sufficient duration. According to the analysis, neither the velocity of flow nor the sediment size affects the depth of scour at equilibrium.

TABLE 1.—EXPECTED DEPTH OF SCOUR, d_s, IN FEET

Description	CONTRACTION EFFECT		OVERBANK EFFECT		COMBINED EFFECT	
	Low Water	High Water	Low Water	High Water	Low Water	High Water
b_1/b_2	2	2	1	1	2	2
$Q/(Q-Q')$	1	1	1	2	1	2
d_1	5	30	5	30	5	30
d_2	8	47	5	54	8	85
$L_1 = L_2$:						
d_s		9		12		35
d_d		5		12		17
$L_1 = 10\ L_2$:						
d_s		13		22		49
d_d		1		2		3

Laboratory experiments[17,18] on scour around bridge piers and abutments confirm that the equilibrium scour is independent of the absolute rate of transport. The length of time required to attain, or closely approach, equilibrium will depend on the absolute rate of transport and, therefore, on the velocity of flow and the sediment size. The rate of scour will be the difference between the rate at which sediment is supplied to the contracted section and the simultaneous excess capacity for transport prevailing at the section.

If, as the authors conclude, the material scoured from the contracted section does not go into suspension, deposition must occur in the next wider reach downstream as illustrated by Fig. 9. To show typical depths of scour that may be expected, Table 1 was prepared, based on the assumption that $d_d L_1 b_1 = d_s L_2 b_2$, and $n_1 = n_2$. Arbitrary values were selected for the ratios b_1/b_2 and $Q/(Q - Q')$, and for the low-water and high-water depths, d_1.

During the period of active scour and deposition, scour should begin at the upstream end of the contraction, where the capacity for sediment transport

---

[17] "Observations on the Nature of Scour," by E. M. Laursen, *Proceedings*, Fifth Hydraulics Conference, State Univ. of Iowa, Iowa City, Iowa, 1953.

[18] "A Generalized Model Study of Scour Around Bridge Piers and Abutments," by E. M. Laursen and A. Toch, *Proceedings*, Minnesota International Hydraulics Convention, Univ. of Minnesota, Minneapolis, Minn., 1953.

is greater than the supply of sediment, and deposition at the upstream end of the following wide reach, where the capacity is less than the supply. Such an intermediate stage is shown, to a shortened horizontal scale, in Fig. 9. Both effects normally progress downstream, approaching equilibrium, as the sections of excess and deficient capacity change position. A flash flood would not endure long enough to move the scoured material very far down the wide reach. If the length of the deposit equaled the length of the scoured area ($L_1 = L_2$ in Table 1), deep deposition would occur. A flood of longer duration would distribute the scoured material farther down the wide reach ($L_1 = 10\ L_2$ in Table 1), resulting in a shallower deposit and deeper scour.

As shown in Table 1, the depth of scour to be expected locally can be of the same order of magnitude as the rise in stage. Indeed, the combined contraction and overbank effects for the example chosen resulted in a scour depth that was almost double the height through which the surface rose. Thus the analysis gives an approximate quantitative solution that is in accord with the observed behavior of streams on alluvial plains as reported by the authors.

E. W. LANE,[19] M. ASCE, AND W. M. BORLAND,[20] A. M. ASCE.—Messrs. Laursen's and Toch's extension of Mr. Straub's development of the hydraulics of scour in a contraction in an open channel should be valuable in indicating the magnitude of scour that would occur in narrow sections of a river or at bridge openings, which greatly contracts the waterway of a stream.

Mr. Dittbrenner's discussion introduces many facts about rivers, collected over a long period of observation. He is right in pointing out the unorganized state of knowledge concerning the interaction of water and sediment in river formation. Because of the large number of variables involved and the constant fluctuation of many of them, this is inevitable. Considerable progress is being made in this science (1954), but for many years there will be wide gaps in the information pertaining thereto. Mr. Dittbrenner's statement that a stream determines the dimensions of the channel is true; recent publications[21] indicate that many engineers are reaching this conclusion.

Colonel Pettis' concept of a river as a series of pools and rapids which Mr. Dittbrenner mentions is a useful one, especially for mountain streams, but care must be taken not to use it where it does not apply.

Fig. 3 is admittedly a simplification, but it is believed that what it has left out does not detract appreciably from the soundness of the conclusions based on it.

Mr. Dittbrenner's contention that sediment travels in waves has some merit. Especially is this true in the wide reaches of sand-carrying streams. Field studies of the Niobrara River (Nebraska), the Loup River (Nebraska), and the middle Rio Grande all indicate that a larger percentage of their total loads moves by contact and saltation in the wider reaches rather than in the narrower reaches. The slower movement of these sand waves and dunes in the wide reaches of the stream accounts for considerable temporary storage of sediment in these places. However, the writers cannot conceive of a sand wave that would move as slowly as the rate indicated by Mr. Dittbrenner in discussing the Albuquerque situation.

---

[19] Cons. Engr., Bureau of Reclamation, U. S. Dept. of the Interior, Denver, Colo.

[20] Head, Sedimentation Section, Hydrology Branch, Bureau of Reclamation, U. S. Dept. of the Interior, Denver, Colo.

[21] "The Hydraulic Geometry of Stream Channels and Some Physiographic Implications," by Luna B. Leopold and Tom Maddock, Jr., *Professional Paper No. 252*, Geological Survey, U. S. Dept. of the Interior, Washington, D. C., 1953.

Stafford C. Happ, in a communication to the writers, has called attention to an error in their presentation, in that they have not considered the overbank deposits in estimating the average depth of scour along the Rio Grande during a flood. He cites studies indicating that two thirds as much by total volume (but twice as much sand) was deposited overbank as in the reservoir. He concludes, however, that this does not weaken the writers' principal contention—namely, that the whole bed of the river is not lowered during a flood.

Mr. Happ also supplies more data on the observation of the 68% sediment concentration observed in the Rio Puerco, which was mentioned by the writers. Since this is (so far as is known to the writers) a record concentration, it is important that its circumstances be firmly established. The following is quoted from his letter:

> "The record 68% concentration from the Rio Puerco is based on a sample collected by the writer [Mr. Happ] at an estimated discharge of 2,200 cu ft per sec to 3,200 cu ft per sec, 22 minutes after the beginning of a flash flow which attained a crest discharge of 3,000 cu ft per sec to 4,000 cu ft per sec some 15 to 20 minutes later. This was not a relatively large discharge for the Rio Puerco. The sample was taken from the upper foot of water in a pint bottle having a top opening of about 1½-in. diameter. Mechanical analysis, after drying and subsequent dispersion, showed 75% of the sediment to be sand (larger than 0.625 mm). Preceding and succeeding samples had 57% and 64% sediment concentrations, of which 66% and 71% were sand, respectively. A dozen other samples during the receding stages, over a period of about 12 hours, showed consistent, progressive decreases in sediment concentration and percentage of sand.
>
> "Progressive changes culminating in concentrations of the order of 30%–60% were measured during several other Rio Puerco flash flows, also with high but lesser proportions of sand. The proportion of sand generally increased with an increase in sediment concentration. The flows of high sediment concentration were notably smooth, oily and streaming in appearance, and had considerably fewer than usual surface waves, vortices and general appearances of turbulence."

The percentage is computed as the weight of the sediment divided by the sum of the weight of the sediment plus the weight of the water.

Since the paper was prepared, considerable information regarding the bed of the Rio Grande has been obtained by detailed surveys made by the USBR of a section of the river. No particularly high flows occurred during the period of observation. The results indicate that, at the discharges observed, channels deeper than average extend from the narrow, deep sections into the wider sections downstream, but these are not continuous and their positions are shifted occasionally. If an attempt is made to trace the narrow, deep channels downstream, it is found that they become shallow and disappear altogether; if the river is examined at the section where one of the channels vanishes, the beginning of another narrow, deep section is found within the wide reach of the river. The conclusion is that there are narrow, deep sections within the wide, shallow ones, but that they are discontinuous. No continuous, deep channel (such as that suggested by Mr. Holmquist) was observed.

An analysis by Ernest Pemberton, J. M. ASCE, was made of data collected by the Corps of Engineers, Albuquerque District, at the Bernalillo gaging station in the Rio Grande during the 1948 flood at a section 272 ft wide—which is somewhat narrower than the average width of the river. The section did not begin to deepen until a discharge of about 8,000 cu ft per sec was reached. At the peak discharge of about 13,000 cu ft per sec, the average scour was about 1.5 ft, and the maximum scour was about 5 ft. It was concluded that narrow, deep channels existed at periodic intervals throughout the length of the river. In the narrow reaches, these deep scour channels occur at the same location throughout a given flood, but in the wide reaches the deep channels are moved from one location to another. Continuous sounding at the cableway showed a cycle of scouring and filling occurring with little variation of discharge—a fact that suggests bed-load movement. It is believed that at such times the gradual and general changes in depth were caused by the passing of a large sand bar and that the local rapid lowering and raising of the bed level was caused by the movement of sand dunes.

In conclusion, it may be stated that the principal contention of the paper—that there is no general deepening of the entire length of the rivers of the Rio Grande type during floods—seems to have been accepted by the discussers. Although the preponderance of the evidence is against the existence of a continuous, narrow, deep channel in the Rio Grande, such as is suggested by Mr. Holmquist, the extent of the evidence is insufficient to preclude the possibility that it does not happen under certain conditions.

AMERICAN SOCIETY OF CIVIL ENGINEERS
Founded November 5, 1852
TRANSACTIONS

Paper No. 2713

HIGHWAY BRIDGES ON DEEP FOUNDATIONS

BY LOUIS DUCLOS,[1] M. ASCE

WITH DISCUSSION BY MR. ARTHUR V. WALKER

SYNOPSIS

Many bridges on deep foundations have been built in Louisiana, and these bridges have presented construction and design problems which have been overcome by basic engineering principles used in conjunction with sound construction methods. This paper outlines a few methods for determining the depths at which piers should be set, especially at bridge sites where rock cannot be reached. Although pier design is primarily the engineer's responsibility, it is concluded that the contractor should be allowed latitude in selecting the method of construction.

INTRODUCTION

The design and construction of deep foundations are among the most difficult operations involved in bridging a river. One of the most critical features of the design is the determination of the depth of the pier in locations where rock or other hard materials cannot be reached. It is necessary to determine the amount of penetration into the ground to assure that the base of the pier will be in material which can support the loads from the pier without excessive settlement. For channel piers, two factors of importance are the depth required to make the pier safe from undermining by scouring action and the amount of scouring which might occur.

SUBSURFACE CONDITIONS

Borings.—Borings should be made before the final design of the pier is attempted. If the length of the spans is determined by navigation requirements, as is usually the case for bridges over large streams or rivers, the piers should be located and the borings made at the exact location of the piers. Two borings should be made at each pier site, and additional borings should be

---

NOTE.—Published, essentially as printed here, in September, 1953, as *Proceedings-Separate No. 276.* Positions and titles given are those in effect when the paper or discussion was received for publication.

[1] Asst. Bridge Design Engr., Dept. of Highways, State of Louisiana, Baton Rouge, La.

made if the original borings indicate extensive variations in the subsurface material.

If the length of the spans is not fixed by navigation requirements, and there is some latitude in the choice of span length, sufficient preliminary borings should be made to establish a reasonably accurate soil profile. This procedure will permit making comparative layouts with the assurance that the preliminary pier designs for these layouts will not be too unlike the final pier designs. After the most economical or desirable layout is determined from the trial designs, the final borings are made at the selected pier locations.

The types of borings made are influenced by many factors. Wash borings, even for preliminary investigations, are generally considered unsatisfactory. Dry-sample borings furnish representative samples of the material, are considered satisfactory for preliminary investigations, and may furnish all the information necessary for the final design. However, in compressible cohesive soils undisturbed samples should be obtained in order that shear and consolidation laboratory tests can be made.

The depth of the borings is affected by many factors and cannot be predicted without some knowledge of the soil. In general, borings should be deep enough to assure that there are no soft compressible materials below the base of the piers which might cause undesirable settlements. To fulfil this condition, borings under the center of the pier must extend to a depth at which the additional pressure caused by the pier loads is not more than 10% greater than the average additional pressure immediately under the pier base. It is unlikely that this slight additional pressure would cause any appreciable settlement of the pier founded upon material at this depth. To determine this depth, it is necessary to make a trial design of the pier and to estimate the depth at which the additional pressure is only 10% greater than the average additional pressure immediately under the base as computed by use of the Boussinesq equation or the Westergaard equation.

Scouring Action.—After the borings have been made, the depth of the pier for stability and safety from scour must be determined. A preliminary estimate of the depth at which scouring might be expected to occur can be obtained from the log of the borings and an examination of the soil samples, but this estimate is mainly a question of judgment. The best guide as to the amount of scouring which can be expected is the examination of the history of neighboring bridges. After determining the minimum depth at which the pier would be safe from undermining, the base is located in material with the proper load-carrying capacity as determined by the nature of the material, the past experiences, and the laboratory tests. Consolidation tests indicate the permissible additional load for the allowable amount of settlement. The depth of the pier is usually determined by the anticipated depth of scour and not by the load-carrying capacity of the material.

CONSTRUCTION METHODS

Having established the depth of the pier and the allowable unit base pressure, the next step is to decide on the type and method of construction of the pier.

Bridges in Louisiana.—The first two highway bridges constructed on deep foundations in Louisiana by the Department of Highways were across Chef Menteur Pass and The Rigolets, the contracts for which were signed on July 19, 1927. Double-wall, cylindrical-steel caissons of the floating type were used on these two bridges, as well as on the bridges at Morgan City and Krotz Springs across the Atchafalaya River in Louisiana, the contracts for which were signed on September 30, 1931.

A double-wall, cylindrical-steel caisson to be sunk by open dredging consists of an outer and inner cylindrical-steel shell, the diameter of the inner shell being several feet less than the diameter of the outer shell. The inner and outer shells are braced together with horizontal frames, usually composed of angles, and are joined at the bottom with a conical plate to form a cutting edge that is heavily reinforced at the bottom edge where the conical plate joins the outside shell. The caisson material is usually shipped in sections and assembled at the bridge site. The caisson may be assembled on ways and launched like a ship, or it may be assembled on a barge—temporarily supported from a working dock by screws, or hoists, while the barge is flooded and floated out from under the caisson—after which the caisson is lowered into the water. After the caisson has been floated, it is towed into position and encircled by a ring of timber piles that hold the caisson in position. On occasion sheet-steel piling is driven inside the timber-pile ring to provide "quiet water" in order to permit easier handling and location of the caisson.

Caisson Design.—Concrete is deposited in the space between the inner and outer shells, after the caisson has been located, to cause the caisson to settle on the bottom of the stream. The shell is made of sufficient height to keep the top of the caisson above water. Additional sections of steel shell are added and more concrete is deposited; this process is continued until the concrete is brought above the water level, after which the shell is discontinued and the concrete above this height is deposited in removable forms. During this process material is excavated, with a clamshell bucket, in the dredging well (the area inside the inner steel shell) as is necessary to keep the caisson plumb and on line. After the concrete has been brought above the water level, the process of alternately pouring concrete and dredging and sinking is continued until the cutting edge reaches the required depth. If the material found at the proposed depth is unsatisfactory, the sinking is continued until the cutting edge is in satisfactory material, at which time the dredging well and cutting edge are cleaned out, and the concrete for the seal course is deposited under water.

Quite often the dredging well is unwatered to permit inspection of the pier and the seal course and to check more accurately the position of the cutting edge. Additional concrete is then poured into the well and the well is flooded.

The diameter of the caissons is influenced by several factors. The dimensions at the top of the pier are determined by the requirements of the superstructure, and these dimensions determine the minimum size of the caisson. The area of the base must be large enough so that the additional unit pressure under the base will not exceed the safe supporting capacity of the material upon which it rests. In determining the additional base pressure, it is customary to neglect the effect of skin friction, as it is not known how much of the material may be lost through scouring. Circular caissons are best adapted for bridges with relatively narrow roadways as in this case the minimum diameter required is not too large. For bridges with very wide roadways, where two caissons for each pier might be satisfactory, circular caissons may be utilized. Circular-steel shells are easily fabricated and assembled. The greatest advantage in the use of circular caissons is the ease of depositing the concrete for the seal course, since the tremie does not have to be moved from dredging well to dredging well as in the case of rectangular cellular open caissons. There is a division of opinion as to the relative difficulty of controlling circular and rectangular caissons during sinking operations.

The height of steel shell required is dependent on the depth of the water and the nature of the material to be penetrated. The caisson and concrete must be supported principally by skin friction, and the required height of the shell is determined by estimating the penetration which will be required to develop enough skin friction to support the caisson and the amount of concrete necessary to bring the top of the concrete above the water level. The height of the steel shell must be equal to the depth of the water, the penetration, and a sufficient freeboard height above the water level to provide for any expected rise of the water level. If the material in the river bottom is firm, the amount of shell required will not be much more than the depth of the water, but if the material is soft, the amount of shell required may be much greater. In addition, when the river bottom is soft and the water is deep, care must be taken that enough penetration is obtained before the concrete is brought up to a height at which the caisson will be unstable, thus reducing the danger of tipping.

CONSTRUCTION PROJECTS

At Chef Menteur Pass the bottom was of reasonably good material; the greatest amount of shell, 78 ft, was used at Pier 2 where the water was 54 ft deep at the beginning of construction. However, 110.5 ft of shell was required for Pier 3 on the bridge at Morgan City where the water was 53 ft deep at the beginning of construction.

The distance between the inner and outer shell of the caisson determines the weight of the caisson. Except for structural reasons, this dimension is varied in accordance with the type of material to be penetrated. If the material is soft it is desirable to keep the caisson light, whereas a heavier caisson is desirable in firm material to aid in overcoming skin friction during sinking. From the designer's viewpoint, the lighter pier is always desirable for economy of materials as well as for lighter loads on the soil. It is not economical to make the caisson excessively heavy to overcome any possible sinking condition which may occur. Additional effective weight for sinking can be obtained by removing water from the dredging well, thus reducing the effect of buoyancy. The caisson may also be temporarily loaded with pig iron, or compartments may be provided for loading with sand or water.

Fixed Jets.—To assist in the sinking operation, twenty-four fixed jets were built into the caissons for the bridges across Chef Menteur Pass and The Rigolets. These jets were located in quadrants in a circle immediately inside the extreme bottom of the cutting edge. Each quadrant had six jets and an independent feed pipe so that, if the pier should begin to lean, the jets on the high side could be used to aid in righting the pier. The object of these jets was to wash material from under the cutting edge into the dredging well.

In addition to these jets twenty-four additional fixed jets (also in four quadrants of six jets each, and each quadrant having an independent feed pipe) were provided on the caissons for the bridges across the Atchafalaya River at Morgan City and Krotz Springs. The outside jets were installed around the outer wall of the caissons, about 8 ft above the cutting edges, and were directed upward at a slope of about 3 horizontal on 12 vertical. The object of the outside jets was to reduce the friction between the caissons and the material being penetrated.

Fixed jets have a tendency to clog. On the four bridges mentioned previously, it was noted that, as the water pump connection was removed from the feed pipe, considerable back pressure developed. This resulted in a reverse flow through the jets, which helped to wash in material that eventually clogged the jets. Once the jets were clogged, it was impossible to clear more than one jet in each quadrant. In subsequent designs, the use of fixed jets was abandoned, and jetting wells 8 in. in diameter were cast in the walls of the caisson, half of these wells terminating just inside the extreme bottom of the cutting edge and the other half terminating higher up on the sloping face of the cutting edge. Movable jets operated in these jetting wells and along the outside of the caisson and were found to be more satisfactory than the fixed jets. These jetting wells provided an excellent means of making holes in hard material. Small charges of explosives placed in these holes aided in the sinking operation by shattering the hard material and forcing it into the dredging wells.

Great care should be taken to keep the caisson in a vertical position. When the caisson begins to lean, it may be difficult to correct this condition. Remedial measures include dredging on the outside of the high side of the caisson, loosening the ground on the outside by small charges of explosives, jetting on the inside and the outside of the high side, and rigging of lines to aid in pulling the pier over. In pneumatic caissons, blocks may be inserted under the cutting edge on the low side so as to increase the resistance to sinking on that side. If the cutting edge is out of position, the only way that the condition can be remedied is by leaning the pier and continuing the sinking. The type of construction used above the caisson may be any type that is preferred, but the dredging wells must be kept open until the sinking operation is completed.

Pier Sinking.—The contracts for the bridges at Morgan City and Krotz Springs provided that the initial sinking of the caissons be accomplished by the pneumatic process because it was feared that obstructions, such as submerged logs, might be encountered in the earlier stages of sinking. These obstructions could be more easily removed if the caisson were sunk by the pneumatic method than by any other method. It was further provided that the sinking under compressed air could be continued until the foundation material appeared free of obstructions or the limits of air pressure were reached. However, at Morgan City, because of the soft composition of the river bottom, it was thought best to sink the caissons some distance into this soft material before applying compressed air. Consequently, the caisson was designed with a removable circular steel diaphragm to form the roof of the working chamber. This roof could be lowered into the dredging well and bolted to a shelf by divers. The roof could be removed by the divers when the limits of pneumatic excavation were reached so that the sinking could be continued by open dredging. The construction of the caissons for the bridge at Krotz Springs was identical.

With 50 ft of concrete in the caisson of Pier 3 at Morgan City, the cutting edge reached a depth of 87.5 ft before the material in the dredging well could be removed to below the shelf provided for the roof of the working chamber (so that the roof could be installed and air applied). Sinking by the pneumatic process proceeded for 21 ft until the cutting edge was 109 ft below low water, at which time the roof was removed and sinking was continued by open dredging. The maximum pressure used was 46 lb per sq in. When completed, the cutting edge of the pier was 176.5 ft below low water, and was the world's deepest pier at the time of completion.

The caisson data for the four bridges previously mentioned are listed in Table 1.

TABLE 1.—CAISSON DATA FOR HIGHWAY BRIDGES IN LOUISIANA

Bridge location	Piers	Caisson diameter, in feet	Dredging-well depth, in feet	Depth below low water, in feet
Chef Menteur Pass.........	5	28	14	82 to 126.5
The Rigolets..............	5	28	14	92
Morgan City...............	4	44	20	112.9 to 176.5
Krotz Springs.............	4	44	20	140 to 150

Wax Lake Outlet.—The construction of the Wax Lake Outlet in St. Mary Parish, Louisiana, provided an additional outlet for the escape of the floodwaters from Six Mile Lake in the Lower Atchafalaya River Basin to the Gulf of Mexico, and necessitated the construction of a new highway bridge on U. S. Highway 90 (the Old Spanish Trail) near Calumet, La., the contract for which was signed on November 28, 1939. The Wax Lake Outlet was to be constructed with a bottom width of 300 ft at El. −45 (referred to Mean Gulf Level (MGL) at the bridge site).

Two deep channel piers were required by the adopted layout, as it was believed the channel might eventually scour under the action of floodwaters to approximately El. −90 MGL. The borings indicated that these piers should be at El −149 MGL to be safe from scouring and for the required stability, and the piers were constructed to within a foot of this depth.

The contract for the construction of this bridge included the excavation of the channel at the bridge site, which was not to be done until after the piers were completed. This rather unusual condition enabled the main channel piers to be constructed on dry land.

Open cylindrical concrete caissons, 38 ft in diameter and 40 ft high, with one dredging well 22 ft in diameter, and steel cutting edges 12 ft high, were used. All the concrete, except that in the cutting edges, was poured in removable forms which permitted examination of all the concrete before sinking. There are many advantages in being able to construct piers in this manner. The caissons can be constructed in exact position, and the difficulty of locating floating caissons in moving water is eliminated.

The design drawings provided for twenty-four 8-in.-diameter vertical jetting wells to be cast in the walls of the pier, twelve terminating near the cutting edge, and twelve terminating higher up on the sloping face of the cutting edge. In addition, the contractor decided to provide eighteen fixed horizontal jets on the outside of the caisson about 10 ft above the cutting edge, arranged in six segments of three jets, each segment having an independent feed pipe.

The determination of the height of the caisson for piers of this type is a matter of engineering judgment and experience. The caisson should be high enough to provide stability during construction and high enough to furnish a reasonable amount of weight to aid in the sinking operation. No particular difficulty was encountered in the sinking of the Wax Lake Outlet caissons. Concrete caissons 30 ft high have been used in a number of instances. Some engineers are of the opinion that caissons less than 30 ft high should be used with caution for deep-pier construction.

After the caissons had reached the proposed depth, it was found to be impossible to excavate closer than 7 ft from the cutting edges, and seal courses of tremie concrete 27 ft deep were poured under water. After this seal concrete hardened, the dredging wells were unwatered, the concrete was inspected, the laitance was removed from the top of the seal course, about 6 ft of concrete were deposited in the dry above the wet seal, and the dredging well was again filled with water.

Sand-Island Method

There are few opportunities to construct deep piers on dry land, but the "sand-island method" offers many of the same advantages. This method consists of erecting a large steel shell, penetrating some distance into the river bottom, and extending above the expected water level, which is then filled with sand. Concrete caissons can then be constructed on these sand islands completely above the water level. After completion of the pier, the shell is salvaged. Sand islands are vulnerable to erosion, however, as undermining of the steel shell will permit the fill material to escape. It is advisable to protect the bottom by mattresses.

On June 15, 1937, the contract was signed for the four channel piers for the Mississippi River bridge at Baton Rouge, La., and these piers were constructed by the sand-island method and were sunk by open dredging. Two of the sand islands were constructed with circular steel shells, and two were constructed with sheet-steel piling; the steel shells being used for Piers 3 and 4 were located in the deepest water. The depth of the water was 69 ft at Pier 3 and 40 ft at Pier 4 (below MGL).

Mattresses measuring 250 ft by 450 ft were constructed at the site of Piers 3 and 4, after which the timber piles for the construction docks were driven. Timber piles 108 ft long were driven at Pier 4, and piles 135 ft long were driven at Pier 3. The assembly of the shells, which were 111 ft in diameter at Pier 4 and 121 ft in diameter at Pier 3, was then begun. Several sections of shells, supported on the dock piles, were assembled. These sections were then lowered to a new connection with the dock piles by use of a number of hoist frames. Each frame was equipped with a hand hoist, located on the construction docks around the circumference of the shells, and the process was continued until the shells had penetrated 10 ft into the river bottom through the mattresses and extended 30 ft above low water. The shells were filled 15 ft above the water level with material obtained 2000 ft from the bridge. The fill material was loaded into barges by means of an hydraulic dredge, and the material was placed in the sand islands with clamshell buckets after the barges were towed to the pier site.

The depth of the water at Piers 2 and 5 was very much less than that at Piers 3 and 4, and the sand islands for these piers were constructed with sheet-steel piling. Rectangular, cellular concrete open caissons were constructed on the sand islands and were sunk to the required depths by open dredging, the deepest being Pier 2 which extended 183 ft below low water.

The sand-island method was used in the construction of three other bridges by the Department of Highways, State of Louisiana. On two of these bridges pneumatic concrete caissons were used, one across the Red River at Moncla, La. (the contract for which was signed in December, 1946), and one across the Red River near Miller's Bluff, La. (the contract for which was signed in March, 1951). Open concrete caissons were used on the third bridge across the Calcasieu River at Lake Charles, La., the contract for which was signed in February, 1948.

The Bridge at Lake Charles.—The bridge at Lake Charles has two 26-ft roadways, separated by a 4-ft median and two 3-ft sidewalks. One navigation channel, 200 ft wide, is provided with 135-ft vertical clearance. The two channel piers, Piers 4 and 5, were each constructed with two open cylindrical concrete caissons, 67.5 ft on centers.

The caissons for Piers 4 and 5 were originally designed as open double-wall steel cylindrical caissons, 36 ft high and 32 ft in diameter with 18-ft-diameter dredging wells. Concrete cylinders 31 ft in diameter with 18-ft dredging wells were provided above the caissons. These cylinders were 86 ft high at Pier 4 and 74 ft high at Pier 5, and were capped with 9 ft of concrete on which the pier shafts were constructed. An attempt was made to reduce the skin friction during sinking by decreasing the diameter of the pier from 32 ft to 31 ft at the top of the 36-ft-high caisson. The value of this offset is problematical in sand or in plastic soil, as the material probably flows in against the smaller diameter section.

After bids were received, in accordance with supplemental agreements with the contractor, the caissons were redesigned to eliminate the steel shells and to use concrete caissons of the same dimensions. Steel sheet pile sand islands were constructed, separate sand islands being used for each caisson. The depth of the water at low stage was 20 ft at each pier, and extreme high water was only 8 ft above low stage. The river bottom was firm and not subject to much scouring, all of which was very favorable to the sand-island method. The redesign of the piers resulted in a saving of approximately $50,000.00.

The caissons for Pier 4 extended 135 ft below low water, and those for Pier 5 were 122 ft deep. The material penetrated was predominately hard clay and sand; it was necessary to load the caissons to aid in the sinking operation, Cast iron pigs were used as weights. It would not have been economical to make the caisson heavy enough to avoid the use of temporary loading.

The Bridge at Moncla.—The bridge across the Red River at Moncla consists of one 360-ft vertical-lift span, flanked on each side by one 360-ft fixed high-level truss, requiring two channel piers and two bank piers, as the river was less than 1,000 ft wide at the selected bridging point. All four piers were constructed to the same depth, about 70 ft below extreme low water, as the banks of the Red River are generally subject to excessive caving. Some caving of the banks upstream from the bridge has occurred, and it is very likely that extensive bank protection works are necessary.

Pneumatic concrete caissons were used for all four piers, with the two channel piers being designed for use of the sand-island method. The caissons were very similar to those used at Miller's Bluff, described subsequently, the principal difference being that the caissons at Moncla had lenticular ends to lessen the scouring action of the water as much as possible, whereas those at Miller's Bluff had cylindrical ends. The cylindrical ends were used in an attempt to reduce the cost of the forms, as it was felt that the hydraulic qualities of the cylindrical ends were not greatly inferior to the lenticular ends.

The pneumatic process was selected for the construction of these piers because the borings indicated that the material might be too hard for open dredging. However, the contractor requested permission (which was granted) to start sinking the caissons by open dredging and to continue the open method until the nature of the material made it necessary to use the pneumatic method.

The Bridge at Miller's Bluff.—The bridge across the Red River at Miller's Bluff is a fixed high-level bridge providing 50-ft clearance above extreme high water (which is about 40 ft above low water) consisting of five 360-ft, high-level trusses flanked by I-beam spans. Although this crossing is approximately 250 miles upstream from Moncla, the Red River is wider at Miller's Bluff. This is because of the hard bluffs which form the east bank just upstream from the bridge location. These bluffs deflect the water against the west bank, causing caving. At the time the bridge survey was made (September, 1949) the west bank had been stable since 1938, which was the date of the earliest available accurate records. By July, 1950, 250 ft of the west bank had caved in, and the bridge layout was made on that basis. Pier 1 was set back approximately 450 ft from the west bank just inside the existing levee, and all six piers for the the five 360-ft trusses were designed as deep piers, extending about 65 ft below low water. The river bottom is composed of highly erodible materials, but the borings indicated that piers of this depth would be safe from undermining by scouring action. Bids were received for the construction of the substructure in January, 1951. By March, 1951, when the contract was signed, 250 ft more of the west bank had caved in. This was not unexpected, as the bridge had been planned so that 600 ft of caving would not endanger the structure. In the meantime, investigations were begun to determine what type of bank protection could be constructed to stop further loss of the bank, as it appeared to be more economical to force the river to remain under the bridge, rather than to extend the bridge over the river if the river were permitted to continue its westward movement.

Bids were received on August 8, 1951, for a system of trail and spur dikes extending about ½ mile upstream from the bridge. Dikes of this type have been constructed in numerous locations along the Red River by the Corps of Engineers, United States Department of the Army, and have proved to be very effective in preventing bank erosion. A contract for approximately $210,000.00 for bank protection works was signed on August 27, 1951. By September, 1951, an additional 300 ft of the west bank had caved in, which is about the limit for the bridge layout, and in the two years between September, 1949, and September, 1951, approximately 800 ft of bank, which had been stable for the previous 11 years, were lost.

All six piers are identical except for height, and consist of a concrete caisson 30 ft high and rectangular in shape with cylindrical ends, the extreme outside dimensions being 26 ft by 50 ft in plan; a lower shaft, also rectangular with cylindrical ends in plan, 60 ft high and extending above high water; and an upper shaft similar to the lower shaft except smaller in size, and differing in height for the various piers.

For maximum economy, the shafts were not tapered, and, except for the forms for the copings of the lower and upper shafts, only three outside forms were used by the contractor—one for the caissons (used 18 times), one for the lower shafts (used 36 times), and one for the upper shafts (used 18 times).

Sheet-steel pile sand islands were used for three of the piers, and the other three were constructed as dry-land piers. The caissons were sunk by a combination of open dredging and pneumatic excavation. Because the very hard material which makes pneumatic excavation necessary lies at some distance below the surface, the initial sinking of the caissons was accomplished by open dredging, and the pneumatic method was used when the material became too hard for open dredging. Two pay items were provided for excavation, one for open excavation, for which the contractor bid $3.70 per cu yd, and one for pneumatic excavation, for which the contractor bid $22.00 per cu yd.

Three dredging wells, each 8 ft in diameter, were provided in the caissons and lower shafts. Recesses were provided in these dredging wells, and when the open dredging was discontinued, concrete plugs 7 ft thick were poured into the wells above the water level and the man and material shafts fastened to flanges in the concrete plugs. The water was then forced out by compressed air, the men descended into the working chamber, and the sinking was continued. When the caisson was founded, the working chamber and wells in the caisson were filled with concrete, in the dry, under air pressure. The wells in the lower shaft were not filled.

The crossing at Miller's Bluff was the best location which could be found for this bridge, and it is rather typical of the Red River. Trouble has been experienced at practically all existing bridge locations, and bank protection works are vital.

CONCLUSIONS

It is desirable, in the preparation of plans and specifications, to permit the contractor considerable latitude in the method to be used in constructing piers. The most economical method may be determined by the type of equipment available to the contractors who are in a position to bid on the work. However, design of the piers is within the province of the engineer who should study both the construction methods and the construction costs.

DISCUSSION

Arthur V. Walker,[2] A. M. ASCE.—The state highway system in Louisiana has been developed principally since 1923. During that time a considerable number of large bridges have been constructed under the supervision of the Department of Highways, State of Louisiana. These bridges are particularly notable because of the nature of the soil in which their foundations were constructed, which in many instances required the sinking of piers to very great depths. Louisiana is traversed by many large navigable rivers. The soil, particularly in the southern half of Louisiana, is alluvial to great depths and is plastic and readily subject to lateral flow (or displacement) when subjected to load. It is regrettable that the considerable accomplishments, developments, and experiences of the bridge engineers of the Department of Highways were not published previously for the benefit of other engineers who might be concerned with similar problems. Mr. Duclos was engaged in the design of many of the bridges which are mentioned in the paper, and he is deserving of commendation for an excellent coverage of the subject.

All the bridges cited by Mr. Duclos were partly financed through the Federal Aid program administered by the Bureau of Public Roads, United States Department of Commerce. The writer became familiar with the problem of deep bridge foundations while associated with the design and construction of the second bridge across the Red River at Moncla, and the bridge across the Calcasieu River at Lake Charles. He became very familiar with the condition and service records of the other bridges cited by Mr. Duclos (with the exception of the bridge at Miller's Bluff) by means of annual maintenance inspections of these bridges.

The depth of scour which can be expected to occur at bridge piers after their construction is of major concern in choosing the depth to which the piers should be constructed. It is to be expected that local scour will take place at bridge piers as a result of the turbulence in the stream created by the presence of the piers. This local scour can be observed readily at many bridge piers during periods of low water. The local scour which is visible at low water is, however, often not a true indication of the actual extent of the scour during periods of high water and increased stream velocities because the scour holes become partly filled with silt as stream levels recede and velocities decrease. A sounding taken in the relatively quiet water inside the fender of the pivot pier of the original movable bridge at Moncla during the flood of April, 1945, indicated that the scour at this pier had extended to an elevation that was approximately 40 ft below the low-water ground level at this point. It is true that this particular observation was the result of an unusual set of circumstances —a levee break located 3 miles downstream which caused high velocities at the bridge and a deflection of the stream current from its usual direction of flow by serious bank caving immediately upstream from the bridge. However, bridge washouts are usually caused by unusual circumstances. In 1953 soundings were made around old railroad bridge piers on the delta of the Copper River in Alaska during both high-water stage and average-water stage, and it was found that at two of the piers the scour holes had become silted after the recession of high water to the extent of 7 ft at one pier and 4 ft at the other. This silting action occurred during a drop in the river level of only 5 ft.

---

[2] Div. Bridge Engr., Div. Ten, Bureau of Public Roads, U. S. Dept. of Commerce, Juneau, Alaska; formerly Dist. Bridge Engr., Bureau of Public Roads, U. S. Dept. of Commerce, Louisiana.

It is not always possible to anticipate the extent of erosion or bank caving which may take place at a bridge subsequent to its construction. However, if possible, the designer should locate the bridge piers so that they will not subsequently be subjected to large unbalanced lateral earth pressures because of erosion or bank caving which reasonably can be expected to occur. If bank caving is anticipated, the pier should be set well back from the river bank. In plastic soils, unbalanced lateral earth pressures can, over a period of years, result in a considerable leaning of bridge piers or abutments because of the increased footing pressures induced by these loads near the edges of the foundations. This movement of the bridge substructure often causes serious damage to the superstructure bearings and causes closure of, or damage to, deck expansion joints and adjacent parts of the bridge, particularly the concrete deck and curbs. Where substructure movement can be reasonably anticipated, it is well to provide generous openings at expansion joints to assure their continued functioning. During construction, the contractor should be required to distribute the material from the excavations in a manner so that avoidable unbalanced lateral earth pressures will not be induced against the substructure.

In the design of deep foundations, the designer should not be surprised to find that the usual relationships between foundation pressures (caused by dead load, live load, wind and longitudinal forces) in ordinary bridge substructures are much distorted. Where the piers are very deep and a considerable portion of their height is below any possible lower limit of scour, it is necessary to assume that horizontal loads of relatively short duration (such as wind loads and tractive loads) will be resisted by active horizontal earth reactions against the sides of the pier. To assume otherwise would require the bottom area of the pier footing to be so large as to be uneconomical and ridiculous. In checking the design of the bridge across the Calcasieu River at Lake Charles, it was found that the increased pressure on the foundations of the main river piers caused by the live load was only 4% of the total increased pressure resulting from both live load and dead load.

The interests of the bridge owner will best be served if the plans and specifications specially emphasize those results which are desired. Limitations and controls (other than those which are required by sound engineering principles) which place undue restrictions on the contractor's method of operation can only result in less than the maximum use of the contractor's knowledge, experience, and available equipment—with a consequent increase in the cost of the project. Contractors who engage in this type of construction usually have had a great deal of experience and have a better knowledge of the equipment available for the work and of the cost of performing the several detailed operations required in the construction than has the designer. Accordingly, maximum economy can be attained by allowing the contractor a wide choice of the methods of construction and specifying only the final results. Detailed plans for steel shells, fixed jets, and other details principally concerned with the method of operation could well be omitted from the plans and specifications and left to the choice of the contractor.

It would be of interest to examine plans for bridge piers of the type cited by the author. These would allow an engineer unfamiliar with this type of work to visualize the problem more clearly. Also of interest would be a tabulation of the unit friction values for the contact surface between the sides of the piers and the soil at various cutting-edge depths as actually experienced for the bridges cited. Information on the unit bearing values used under the pier footings for various types of soil would be informative as would a mention of the practice in Louisiana of expressing bearing values in terms of additional load over that load (caused by the weight of the superimposed earth) existing at the footing level before construction. The paper would be further enhanced by a more detailed presentation of the methods used and the sizes of charges employed in the use of dynamite inside the working chambers of the caissons when hard material was encountered.

AMERICAN SOCIETY OF CIVIL ENGINEERS
Founded November 5, 1852
TRANSACTIONS

Paper No. 2714

MECHANICS OF MANIFOLD FLOW

By John S. McNown,[1] M. ASCE

With Discussion by Messrs. Julio Escobar; M. R. Carstens and John Roberson; James J. Hartigan; Sadiq M. Niaz; James R. Barton; Ralph W. Powell; John K. Vennard and Darrhl I. Dentoni; and John S. McNown

Synopsis

Flow characteristics of branch points in manifolds involve complexities that the author has studied by combining results of experiment and of simplified analysis. The variation in head is studied for flow in a circular conduit with lateral inflow or outflow at right angles thereto. Theoretical results are shown to be insufficiently accurate for practical use except in a few instances. The systematized empirical results presented for the various types of flow should be helpful in the design of a variety of manifold systems.

Introduction

Changes in piezometric and total head at branch points are significant design criteria for various kinds of manifold systems. Dividing flows are present in sprinkler irrigation systems and in gas-burner manifolds, and both combining and dividing flows occur in lock manifolds and in complex water-supply systems. The complexity of the flow patterns at branch points precludes rigorous analysis, but a general understanding can be obtained by comparing the results of experiment and of simplified analysis. The geometry of the conduit and the junction is infinitely variable, but for an idealized form the significant characteristics of manifold flow can be determined.

From the designer's point of view, the analysis of flow in manifolds can be accomplished by predicting (*a*) the losses in regions of parallel flow, and (*b*) the changes in pressure and the losses at the junction. In some instances the branch points are so close that mutual interactions of successive junctions

---

Note.—Presented at the Centennial Convocation, Chicago, Ill., September, 1952. Published essentially as printed here, in August, 1953, as *Proceedings-Separate No. 258.* Positions and titles given are those in effect when the paper or discussion was received for publication.

[1] **Prof. of Mechanics and Associate Director, Iowa Inst. of Hydr. Research, State Univ. of Iowa, Iowa City, Iowa.**

affect these values; a useful simplification is nonetheless effected by considering a single branch point in a conduit in which the flow is otherwise uniform throughout a considerable distance upstream and downstream from the junction.

Because there is a marked difference between dividing and combining flows, the analyses and results for the two cases will be presented separately. In every instance considered, the diameter of the main pipe and the direction of flow therein are the same upstream and downstream from the junction, and the diameter of the lateral pipe is equal to, or less than, that of the main pipe. The axes of the lateral pipe and of the conduit are considered to intersect at right angles.

Since the early 1900's, studies of this topic have been made by investigators in several fields. In an excellent series of experiments at Munich, Germany,[2,3,4] D. Thoma's students conducted a systematic investigation of this phenomenon. These experiments will be referred to in this paper as the "Munich experiments." Publications, such as that by W. E. Howland,[5] A. M. ASCE, have been presented on the general problem of efflux from a perforated pipe. Manifold flow in irrigation systems was summarized by J. E. Christianson, A.M. ASCE, in 1942.[6] A comprehensive study of gas-burner manifolds was presented by J. D. Keller, Jr.[7]. Various aspects of the flow in lock manifolds have been described by E. Soucek, M. ASCE, and E. W. Zelnick,[8] A.M. ASCE, and G. R. Rich,[9] M. ASCE, among others. Although in most of these publications the conclusions reached were founded on experiment, useful analyses based on simplified versions of the momentum and energy principles have been presented by several of these writers and by H. Favre.[10] With E. Y. Hsu, A.M. ASCE, the writer presented an entirely different type of analysis using the free-streamline theory in determining the principal characteristics of the lateral efflux.[11] The various papers cited contain references to a number of others, among which is found diversified information that is, for the most part, either specialized or fragmentary.

THEORY

The energy equation can be written for both the main conduit flow and for that in the lateral, if a term is included to express energy loss. From a similarly simplified approach, one can write the momentum equation for the flow at the

---

[2] "Untersuchungen über der Verlust in rechtwinkligen Rohrverzweigungen," by G. Vogel, *Mit. des Hydr. Inst. der Tech. Hoch.*, Munich, Germany, Vol. I, 1926, pp. 75–90, and Vol. II, 1928, pp. 61–64. (Translation by Charles Voetsch, *Technical Memorandum No. 299*, USBR, 1932.)

[3] "Der Verlust in schiefwinkligen Rohrverzweigungen," by F. Petermann, *ibid.*, Vol. III, 1929, pp. 99–117. (Translation by H. N. Eaton and K. H. Beij, ASME, 1935.)

[4] "Beitrage zur Kenntnis der hydraulischen Verluste in Abzweigstücken," by E. Kinne, *ibid.*, Vol. IV, 1931, pp. 70–93. (Translated and abstracted by E. E. Halmos, *Engineering News-Record*, Vol. 108, 1932, p. 684.)

[5] "Gain in Head at Take-Offs," by W. E Howland, *Journal*, N.E.W.W.A., January, 1935, p. 14.

[6] "Hydraulics of Sprinkling Systems for Irrigation," by J. E. Christianson, *Transactions*, ASCE, Vol. 107, 1942, pp. 221–250.

[7] "The Manifold Problem," by J. D. Keller, Jr., *Journal of Applied Mechanics*, March, 1949, pp. 77–85.

[8] "Lock Manifold Experiments," by E. Soucek and E. W. Zelnick, *Transactions*, ASCE, Vol. 110, 1945, pp. 1357–1400.

[9] "Hydraulic Transients," by G. R. Rich, McGraw-Hill Book Co., Inc., New York, N. Y., 1951, pp. 206–213.

[10] "Sur les lois régissant le mouvement des fluides dans les conduites en charge avec adduction latérale," by H. Favre, *Revue Universelle des Mines*, Liége, Belgium, December, 1937, pp. 502–512.

[11] "Application of Conformal Mapping to Divided Flow," by J. S. McNown and E. Y. Hsu, *Proceedings*, Midwestern Conference on Fluid Dynamics, J. W. Edwards, Ann Arbor, Mich., 1951, pp. 143–155.

junction, provided that a term is included for (*a*) the indeterminate momentum of the flow in the lateral at the junction, or (*b*) the corresponding unbalanced force component acting on the wall at the lateral. In either equation, lack of knowledge of this one significant unknown makes direct application of the results impossible without recourse to experiment. The results obtained are nevertheless useful in assessing the observed characteristics of branching flow.

Dividing Flow.—Simplified forms of the energy and momentum equations can be written directly for describing dividing flow. The assumption is made that the mean velocity at each section in Fig. 1 (*a*) is representative of the flow at that section. Also, terms expressing the head losses are assumed to represent the difference between the total losses and the losses observed in normal conduit flow. For the flow that continues in the conduit, the change in piezometric head, Δh, is expressible in the following forms:

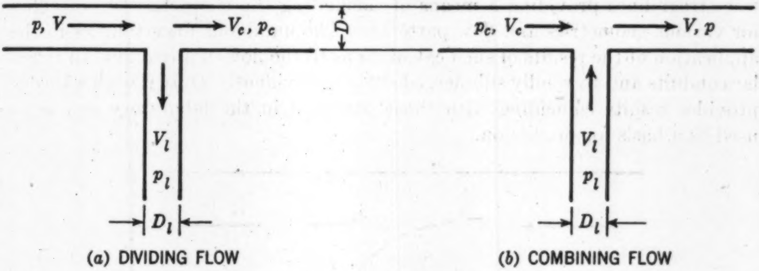

(*a*) DIVIDING FLOW (*b*) COMBINING FLOW

FIG. 1.—DEFINITION SKETCHES

$$\frac{\Delta h}{\frac{V^2}{2g}} = \frac{p_c - p}{\frac{\rho V^2}{2}} = 1 - \left(\frac{V_c}{V}\right)^2 - \frac{h_f}{\frac{V^2}{2g}} = \frac{Q_l}{Q}\left(2 - \frac{Q_l}{Q}\right) - \frac{h_f}{\frac{V^2}{2g}} \quad \ldots\ldots (1)$$

in which V is the average velocity, g the acceleration due to gravity, p the unit pressure, ρ the density, h_f the head lost through friction, and Q the discharge. The meanings of the subscripts c and l are indicated in Fig. 1. For the flow into the lateral a similar expression can be obtained, but for reasons presented in the following sections the various terms are related to the velocity head in the lateral:

$$\frac{\Delta h'}{\frac{V^2_l}{2g}} = \frac{p_l - p}{\frac{\rho\, V^2_l}{2}} = \left(\frac{V}{V_l}\right)^2 - 1 - \frac{h'_f}{\frac{V^2_l}{2g}} \quad \ldots\ldots\ldots\ldots (2)$$

in which the prime superscript refers to that portion of the flow which goes into the lateral.

In the momentum equation, inclusion of the resultant of the unbalanced pressures inside the lateral is required. As the direction of flow of the fluid into the lateral is inclined to the axis of the lateral, either the component of the resultant momentum in the direction of conduit flow or the force required to reduce it to zero must be included in a bulk momentum equation. If this force is represented by F, considered positive in the upstream direction, the momentum equation takes the following form:

$$\frac{\Delta h}{\frac{V^2}{2\,g}} = 2\left[1 - \left(\frac{V_c}{V}\right)^2 - \frac{F}{\rho\, Q\, V}\right] \ldots\ldots\ldots\ldots\ldots (3)$$

An exact solution was obtained in 1951[11] for the special case of irrotational two-dimensional branching flow, the classic Helmholtz-Kirchhoff theory of free streamlines providing a means of calculating the characteristics of efflux for various geometries and flow patterns. The numerous uncertainties in the application of the results of such calculations to the flow of a real fluid in circular conduits and to wholly submerged efflux are evident. Only if such a theory provides results coinciding with those observed in the laboratory can it be used as a basis for prediction.

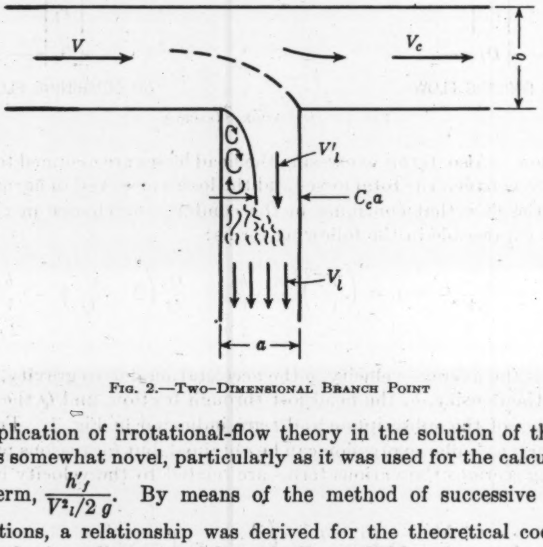

FIG. 2.—TWO-DIMENSIONAL BRANCH POINT

The application of irrotational-flow theory in the solution of this type of problem[11] is somewhat novel, particularly as it was used for the calculation of a head-loss term, $\frac{h'_f}{V^2_l/2\,g}$. By means of the method of successive conformal transformations, a relationship was derived for the theoretical coefficient of contraction for two-dimensional lateral efflux. With reference to Fig. 2 the relationship,

$$C_c = f\left(\frac{V_c}{V}, \frac{a}{b}\right) \ldots\ldots\ldots\ldots\ldots\ldots\ldots\ldots (4)$$

was defined in general but implicit form, and representative curves were presented.

The results represented by Eq. 4 were assumed to be applicable to the dividing flow of a real fluid in circular conduits with the provisions that (1) the ratio of the area of the lateral to the area of the main conduit was the same in each case, and (2) the energy loss was like that in an abrupt expansion downstream from a section at which the contraction of the jet could be assumed essentially complete. Thus, C_c was obtained for a value of a/b equal to $(D_l/D)^2$, and h'_f was computed from the known formula for head loss at a boundary enlargement,

$$h'_f = \frac{(V'_l - V_l)^2}{2\,g} \qquad (5)$$

in which V'_l is the velocity at the contracted section, $\frac{Q_l}{C_c\,A_l}$—A_l being the cross-sectional area of the lateral. It follows that the head loss for the flow in the lateral is

$$\frac{h'_f}{\frac{V^2_l}{2\,g}} = \left(\frac{1}{C_c} - 1\right)^2 \qquad (6)$$

One flaw in the analysis leading to Eq. 4 is that the stagnation point for the dividing streamline was forced to fall at the downstream edge of the opening regardless of the geometry and discharge ratio. As a consequence, a nonexistent partial barrier projecting into the flow was introduced in the analysis of the flow. For most significant values of Q_l/Q and a/b, the barrier was small and, on the basis of other computations, not particularly significant in its effect on the value of C_c. Additional calculations indicate the amount by which the downstream channel width should be altered to cause the stagnation point to fall at the proper place without artificial modification of the flow pattern.

Combining Flow.—Markedly different from dividing flow in physical characteristics, combining flow is nonetheless describable in general equation form by means of Eqs. 1 to 3 with minor modifications. The total flow, Q, occurs downstream from the junction in this case; the subscript, c, is used for the conduit flow upstream; and the direction of lateral flow is reversed (Fig. 1(*b*)). Because p_c is again greater than p, it is logical (if not conventional) to leave the equations in the forms given; only the sign of the last term in each equation must be changed. If γ denotes the specific weight, and if Δh is $(p_c - p)/\gamma$,

$$\frac{\Delta h}{\frac{V^2}{2\,g}} = 1 - \left(\frac{V_c}{V}\right)^2 + \frac{h_f}{\frac{V^2}{2\,g}} \qquad (7)$$

Similarly, if F is again considered positive in the upstream direction, the sign on the term $F/(\rho\,Q\,V)$ in Eq. 3 should be positive for combining flow:

$$\frac{\Delta h}{\frac{V^2}{2\,g}} = 2\left[1 - \left(\frac{V_c}{V}\right)^2 + \frac{F}{\rho\,Q\,V}\right] \qquad (8)$$

The irrotational-flow theory comparable to that presented for divided flow has not been found to produce useful results. The difference between the idealized flow pattern for plane motion and the real conduit flow seems to be considerably greater in this case. In the analysis it is assumed that the two jets coalesce, the entire downstream flow separating from the boundary as did the lateral flow in the preceding case. For this flow a coefficient of contraction and a head-loss value can also be computed. In an unpublished calculation, the losses thus computed were found to differ greatly from those measured by S. M. Niaz[12] for flow in circular conduits. It was concluded that the marked differences arose because the two jets did not coalesce as assumed. For laterals smaller in diameter than the main conduit, the lateral jet presumably pierced the main jet and left part of the conduit flow comparatively undisturbed—a state of flow for which the assumed flow pattern is inadequate.

The foregoing equations have been presented both to serve as a framework for the presentation and discussion of the experimental data, and to make possible the comparing and assessing of various simplified and therefore approximate analyses. M. L. Enger, M.ASCE, and M. I. Levy[13] proposed the neglect of the head-loss term in Eq. 1 and supported their idea by data from experiments for which D_l/D was small. Messrs. Soucek and Zelnick[8] and several discussers of that paper (including the writer) suggested and compared various assumptions for the indeterminate quantities of head loss and unbalanced force. Mr. Favre, in the study of combining flow, assumed the unbalanced force to be zero, and presented a detailed treatment of this kind of flow.[10] His assumption was found to produce results that corresponded well with those of the Munich experiments.[2,3,4] Actually, as is shown in the following sections, no simplified analysis is valid throughout a sufficient range of the significant variables to have general application beyond use as a reference for the comparison and evaluation of laboratory measurement.

LABORATORY INVESTIGATION

In the absence of a general analysis of manifold flow, laboratory studies must be conducted to augment the available knowledge of this subject. Because the geometry differs in each application, no exhaustive study of the various possible arrangements is feasible. General information can be obtained only by determining the characteristics of flow for a few manifolds of simple geometric form. The studies conducted at the Iowa Institute of Hydraulic Research, at Iowa City, Iowa, are comparable in this respect to those conducted at Munich under Mr. Thoma's supervision. A greater number of basic manifold shapes were investigated in the experiments in Germany, but the considerably more detailed results of the Iowa experiments make possible a more nearly complete interpretation of the phenomenon.

Throughout this study a brass pipe of 2-in. diameter (actual inside diameter, 2.06 in.) was used as the main conduit. A similar pipe and lengths of brass tubing 1 in. in diameter and ½ in. in diameter were used as laterals. All sections of pipe and tubing used were between 75 and 100 diameters long. The inside surfaces were smooth except for slight traces of chemical deposit. The three junctions were machined tees, the intersection being sharp-edged.

---

[12] "A Study of Converging Flow in Pipe Lines," by S. M. Niaz, thesis presented to the State Univ. of Iowa, Iowa City, Iowa, in 1947 in partial fulfilment of the requirement for the degree of Master of Science.

[13] "Pressures in Manifold Pipes," by M. L. Enger and M. I. Levy, *Proceedings*, A.W.W.A., May, 1929, p. 659.

For two special series of experiments, additional junctions were made. A second junction with a lateral of 1-in. diameter was constructed so that the effect of one lateral on another a short distance downstream could be studied. The second lateral and a short spacer were so constructed that the two could be placed 4, 8, or 14 conduit diameters apart. For the additional set of experiments, a junction was made in the form of a cross with two laterals of 1-in. diameter symmetrically connected on opposite sides of the conduit.

Water was supplied to the various pipe arrangements from a constant-level tank through a stilling tank (two stilling tanks in the case of combining flow). The flows were varied by changing valve settings either upstream from the stilling tanks or downstream from the conduit and lateral. Streamlined entrance sections were provided, and the two parts of the flow were measured either by direct weight or by a combination of direct weight and observations of a calibrated discharge meter at the inlet contraction. The equipment was arranged so that the total discharge could be measured independently and compared with the sum of the two component discharges as a check. Piezometer openings were provided at intervals of approximately 5 tube diameters for determination of the three pressure gradients. In observing the various piezometric heads, a pressure manifold and either a mercury-water differential gage or an air-water differential gage were used, readings being made to the nearest 0.001 ft.

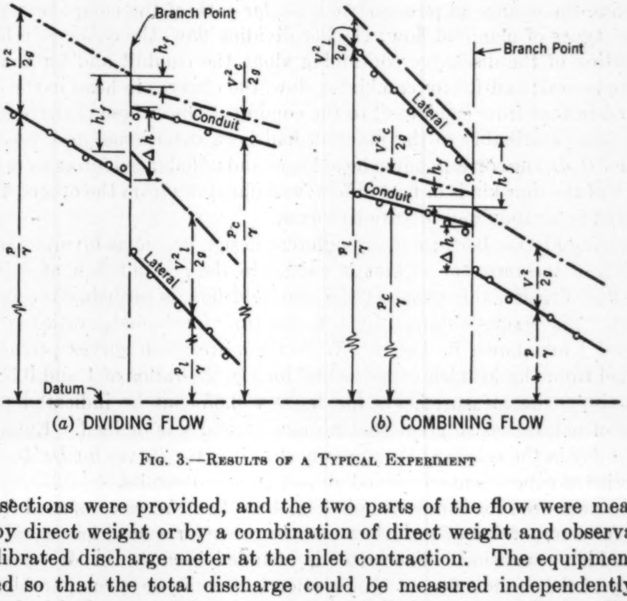
Branch Point
$\frac{V^2}{2g}$
h_f
h'_f
Δh
$\frac{V^2_c}{2g}$
Conduit
$\frac{p}{\gamma}$
$\frac{p_c}{\gamma}$
$\frac{V^2_l}{2g}$
Lateral
$\frac{p_l}{\gamma}$
Datum
Branch Point
$\frac{V^2_l}{2g}$
Lateral
$\frac{V^2_c}{2g}$
h_f
h'_f
Conduit
$\frac{p_l}{\gamma}$
Δh
$\frac{p_c}{\gamma}$
$\frac{V^2}{2g}$
$\frac{p}{\gamma}$

(*a*) DIVIDING FLOW (*b*) COMBINING FLOW

FIG. 3.—RESULTS OF A TYPICAL EXPERIMENT

Before measurements were made of the manifold flows, the head loss for uniform flow was determined for each of the various pipe sections. Plots were prepared relating the piezometric-head gradient to the discharge, so that the apparent gradient (as observed during individual runs) could be checked for each section of the pipe in every run. In this way large errors were eliminated, and the spread of the data was considerably reduced.

After each run the observed piezometric heads were plotted for the three sections of pipe, and straight lines of correct slope were then drawn through the sets of points in the region of undisturbed flow of each pipe. Runs for which the gradients were incorrect or poorly defined were disregarded. The lines were then extended to the branch point as indicated by the solid lines in Fig. 3. From these plots and from the observed discharge values the velocity heads, the total head (dash-dot lines), and the two head losses were computed as also indicated schematically in Fig. 3. Complete details of equipment and procedure are available elsewhere.[12,14,15,16]

OBSERVED RESULTS

From the tests described in the foregoing section, it was then possible to determine the change in piezometric head for each of the component parts of the two types of manifold flow: (1) For dividing flow, the changes in head for the portion of the discharge continuing along the conduit and for that going into the lateral; and (2) for combining flow, the changes in head in the conduit flow and in that from the lateral to the conduit. Once these changes in piezometric head ascribable to the junction had been determined as a function of Q_l/Q and D_l/D, the corresponding head losses and unbalanced forces were known. As each of the four kinds of flow differs fundamentally from the others, they are presented separately and in various forms.

Dividing Flow.—Because many different design problems involve the determination of the recovery of kinetic energy in the conduit flow at a junction where flow divides, this phase of the manifold flow is probably the most important. The results obtained by J. R. Barton[14] for diameter ratios (D_l/D) of 1, $\frac{1}{2}$, and $\frac{1}{4}$ are shown in Fig. 4. With them are mean curves presented by G. Vogel from the Munich experiments[2] for (D_l/D)-ratios of 1 and 0.58. Mr. Vogel also made measurements for $D_l/D = 0.35$, but he indicated that the scatter of points was so great that no mean trend was defined. Except for a discrepancy in the region of the uppermost part of the curves for $D_l/D = 1$, the two series of experiments achieved almost identical results.

Also presented for comparison in Fig. 4 are two curves computed from Eq. 1, one for a zero value of head loss and the other for a head loss equal to that in a sudden expansion. The latter is included because the decrease in the velocity of the conduit flow at the junction is in some ways comparable to that which occurs at an expansion. Evident from Fig. 4 are the facts that: (1) The gain in piezometric head is significantly large; (2) the head loss is never as much as one half that at an abrupt expansion; and (3) for small values of the ratio Q_l/Q, the head loss as computed is actually a sizable negative quantity.

The systematic occurrence of negative losses was also observed by Mr. Vogel,[2] Messrs. Soucek and Zelnick,[8] and J. A. Oakey,[17] M.ASCE, and cannot

---

[14] "A Study of Diverging Flow in Pipe Lines," by J. R. Barton, thesis presented to the State Univ. of Iowa, Iowa City, Iowa, in 1946 in partial fulfilment of the requirement for the degree of Master of Science.

[15] "Studies of Manifold Flow," by J. Escobar, thesis presented to the State Univ. of Iowa, Iowa City, Iowa, in 1948 in partial fulfilment of the requirement for the degree of Master of Science.

[16] "Studies of Multiple Laterals in Manifold Flow," by A. Yanes, thesis presented to the State Univ. of Iowa, Iowa City, Iowa, in 1951 in partial fulfilment of the requirement for the degree of Master of Science.

[17] "Hydraulic Losses in Short Tubes Determined by Experiments," by J. A. Oakey, *Engineering News-Record*, June 1, 1933, p. 717.

be ascribed to experimental error. A logical hypothesis is that the losses are negative because the square of the mean velocity was used in the energy equation without a correction factor to account for the effect of variation of velocity across the sections. Particularly for relatively small lateral discharges, the velocity of the water before flowing into the lateral is below average, both because the low velocities occur near the wall and because less force is required to divert the more slowly moving water. This hypothesis was tested in an approximate calculation, and resulting changes in the kinetic energy factor were found to be large enough to offset entirely the apparently negative losses. J. Escobar,[15] J.M.ASCE, performed confirming experiments in which the region in the conduit from which the lateral discharge came was delineated by means of observations of streams of dye injected into the water a short distance upstream from the junction. As expected, the lateral flow was found to come from a segment of the conduit in which the velocity was significantly below average. Additional verification of this hypothesis is available in the fact that, for a given

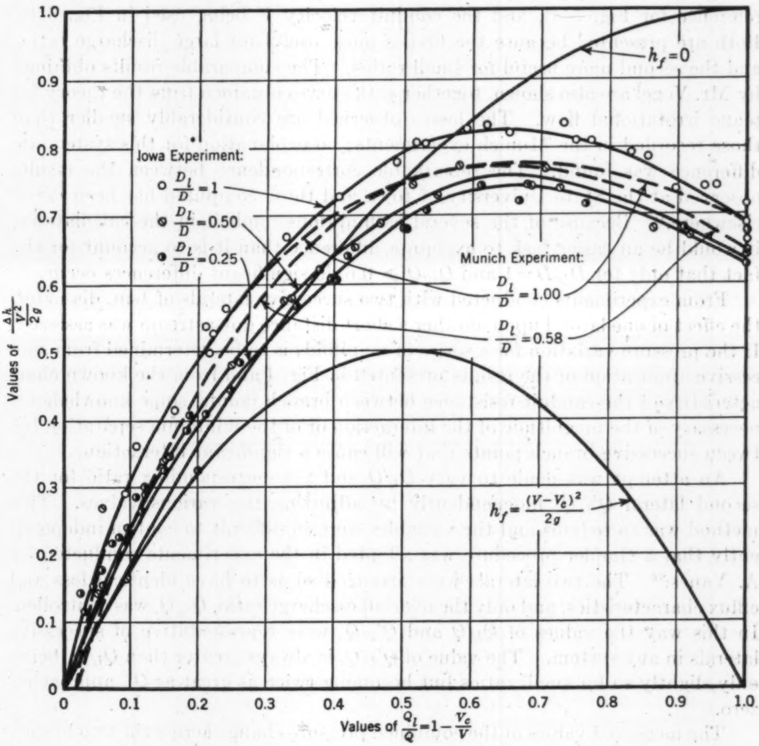

FIG. 4.—CHANGE IN PIEZOMETRIC HEAD IN THE CONDUIT FOR DIVIDING FLOW

discharge ratio, the larger the lateral the greater the segmental area from which the lateral could draw water with velocities below the average. Thus, as is indicated in Fig. 4, the apparent energy gain is greatest for the lateral having $D_l/D = 1$, and decreases with decreasing size of lateral.

The head loss for the flow that goes from the conduit to the lateral is shown in Fig. 5, the velocity head in the lateral based on $V_l = Q_l/A$ being used as a reference for Fig. 5(*a*), and the conduit velocity V being used in Fig. 5(*b*). Both are presented because the first is more useful for large discharge ratios and the second more useful for small ratios. The comparable results obtained by Mr. Vogel are also shown, together with curves obtained from the theory for plane irrotational flow. The losses observed are considerably smaller than those recorded in the Munich experiments; no explanation for this systematic difference was found. The remarkable correspondence between the results observed at the State University of Iowa and those computed has been noted elsewhere.[11] Because of the several assumptions implicit in the calculations, it would be an easier task to explain a difference than it is to account for the fact that only for $D_l/D=1$ and $Q_l/Q > 0.6$ do significant differences occur.

From experiments conducted with two successive laterals of 1-in. diameter, the effect of one lateral upon another a short distance downstream was assessed. If the pressure variation for a series of manifolds is to be determined from successive application of the results presented in Fig. 4 and from the known characteristics of the conduit resistance between branch points, some knowledge is necessary of the magnitude of the interaction or of the minimum separation between successive branch points that will cause a significant interaction.

An attempt was made to vary Q_l/Q and the corresponding ratio for the second lateral Q'_l/Q_c independently by adjusting the various valves. This method was so tedious and the variables were so difficult to control independently that a simpler procedure was adopted in the experiments conducted by A. Yanes.[16] The two laterals were arranged so as to have identical loss and efflux characteristics, and only the over-all discharge ratio, Q'_c/Q, was controlled. In this way the values of Q_l/Q and Q'_l/Q_c were representative of successive laterals in any system. The value of Q'_l/Q_c is always greater than Q_l/Q, being only slightly so for small ratios but becoming twice as great as Q'_c approaches zero.

The measured values of the combined pressure change across the two branch points were compared with those computed from Fig. 4 for the various lateral spacings (4, 8, and 14 conduit diameters). The results are not well defined because the quantity sought was a second-order difference, so that otherwise minor discrepancies caused sizable errors. From averages of the observed results, the measured recovery of piezometric head was found to be less than that indicated by Fig. 4, by about 15% for the 4-diameter spacing, by 10% for the 8-diameter spacing, and by less than 5% for the 14-diameter spacing. However, the values varied considerably with the discharge ratio. Probably no significant interaction would occur if the spacing were 20 conduit diameters or more.

In a study of a third secondary effect, the characteristics of a double lateral were determined. For the symmetrically placed 1-in.-diameter laterals, a

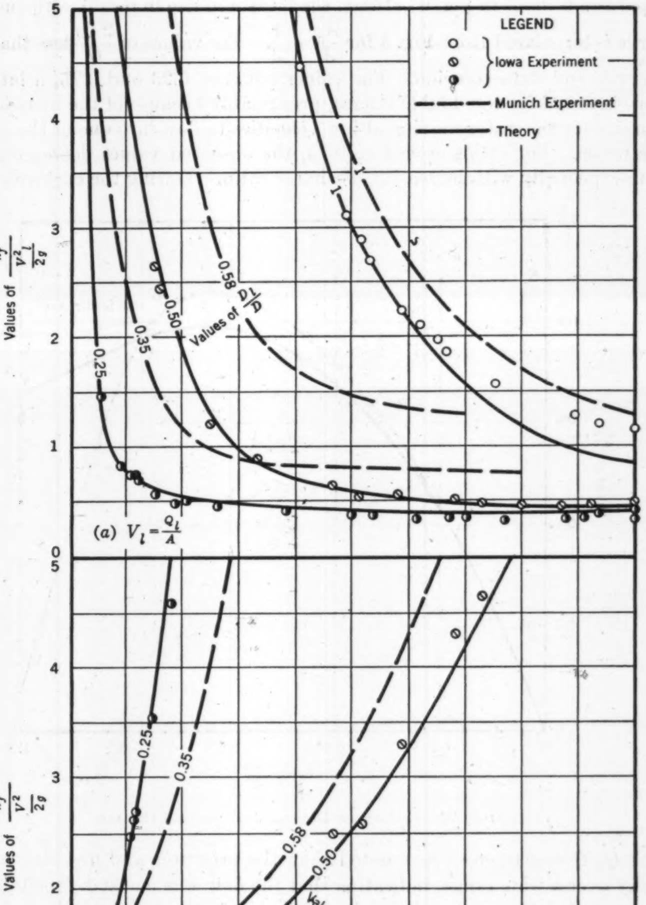

FIG. 5.—LOSS OF HEAD BETWEEN THE CONDUIT AND THE LATERAL FOR DIVIDING FLOW

comparison is made in Fig. 6 between the measured rise in piezometric head and a curve interpolated from Fig. 4 for $\frac{A_l}{A} = \frac{1}{2}$. For values of $\frac{2\,Q_l}{Q}$ less than 0.25, the curve and data coincide. For values between 0.25 and 0.75, a larger recovery is found for the double lateral, presumably because of the increased opportunity for the water moving at low velocities to flow into one or the other of the laterals. For ratios exceeding 0.75, the observed values decrease rapidly and unexpectedly with increasing discharge ratio. During the experiments for

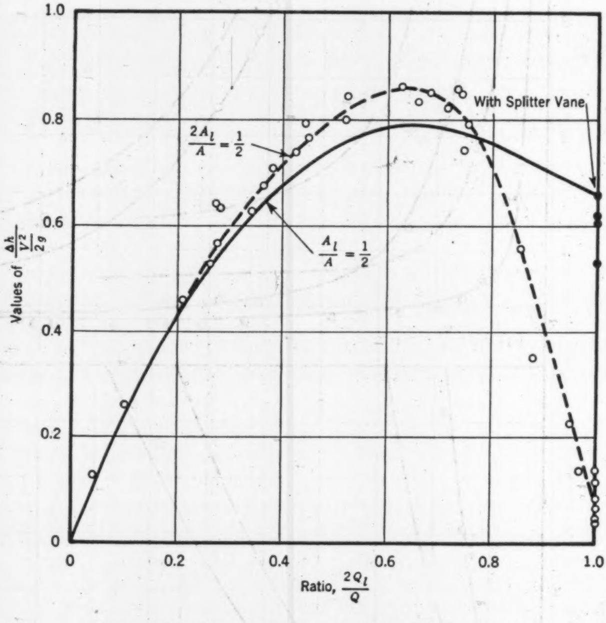

FIG. 6.—COMPARISON OF DOUBLE AND SINGLE LATERALS

which Q_l/Q was large, it was noted that the pressures and discharges varied rapidly over a wide range, indicating that the flow was markedly unstable. It was concluded that unequal division of flow into the two laterals took place, and that rapid and periodic changes in this division caused excessive losses. In obtaining the solid points in the figure the pipe was capped and a splitter vane was placed between the entrances to the laterals. With equal and stable division of the flow thus assured, the pressure rise became essentially that predicted from the single-lateral tests.

Combining Flow.—Experimental results for the drop in piezometric head in a conduit for combining flow were obtained by Mr. Niaz.[12] In Fig. 7, these are compared with Mr. Vogel's results, as revised by E. Kinne for $D_l/D = 1$. Similar trends were demonstrated by the two sets of experiments, although some differences are evident. Also included in Fig. 7 are two computed curves, one obtained from the Bernoulli equation and the other from the momentum equation. For the first of these, the head loss was set equal to zero, and for the second the unbalanced force was set equal to zero.

The pressure drop varied from 1.5 times to 2.5 times the change in kinetic energy. The unbalanced force, set equal to zero by Mr. Favre[10] for this type of flow, varied considerably with the diameter ratio. The force is sizable and in the downstream direction for $D_l/D = 1$ and almost equal in magnitude but in the upstream direction for $D_l/D = 1/4$. The marked difference results from the facts that the water coming from the large lateral must be accelerated and that that from the small lateral is considerably decelerated if Q_l/Q is nearly

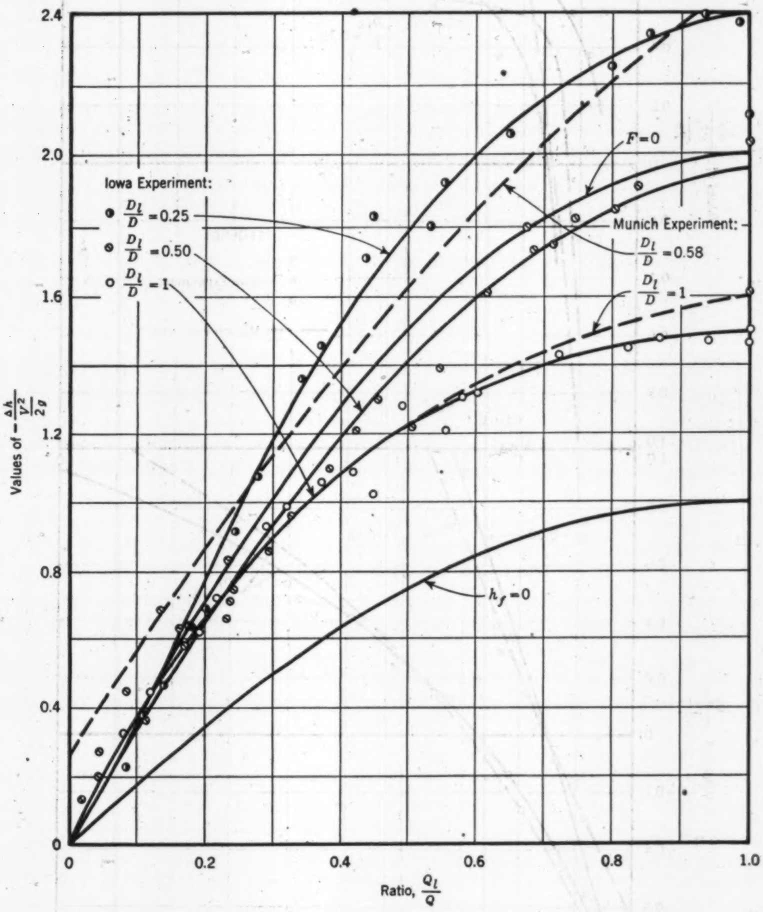

FIG. 7.—CHANGE IN PIEZOMETRIC HEAD IN THE CONDUIT FOR COMBINING FLOW

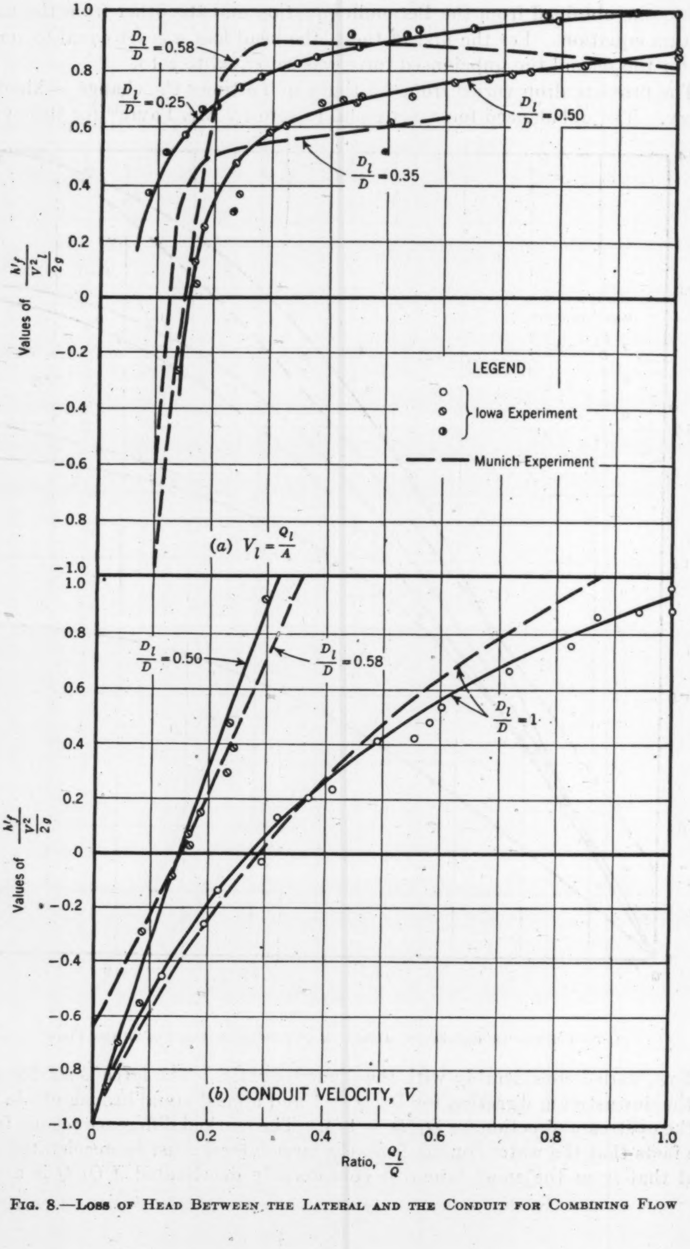

FIG. 8.—LOSS OF HEAD BETWEEN THE LATERAL AND THE CONDUIT FOR COMBINING FLOW

unity. In the comparison that Mr. Favre made with the Munich experiments, the apparent discrepancies were evidently assumed to be relatively unimportant.

To present the loss of head occurring in the lateral flow, it was also thought advantageous to use two plots. As shown in Fig. 8, the head loss is most conveniently represented in its ratio to the velocity head in the lateral if Q_l/Q is large. For small values of this ratio, particularly if $D_l/D = 1$, the velocity head downstream from the junction is a more significant reference. Negative losses again occur. These losses can be explained logically for the limiting case of $Q_l/Q = 0$, as pointed out by Mr. Vogel, since the pressure in the lateral is equal to that in the conduit at the junction, and the velocity is zero. Thus, for very small lateral discharges, a gain in energy takes place. However, this gain is also only apparent, as the water flowing from the lateral must go to a region in which the velocity is below average. Each of the curves approaches a value corresponding to $h'_f = - V^2/2\,g$ as $Q_l/Q \rightarrow 0$. In Fig. 8(*a*) this would correspond to large negative ratios as V_l is necessarily much less than V if Q_l/Q is sufficiently small.

Discussion of Results

The foregoing comparisons of observed and theoretical trends demonstrate that the characteristics of flow through manifolds must be predicted empirically, at least in part. Only for the one case of loss for the lateral efflux in dividing flow was close correspondence found between results predicted from a simplified theory and those observed in the laboratory. Even in this case the concurrence appears to be somewhat fortuitous.

In the several plots, the variations of the piezometric and total head are indicated for the circular smooth conduits tested both in the Iowa and in the Munich experiments. As these are for only one of a wide variety of possible geometrical arrangements, the results presented herein may well differ from those that would be obtained for other forms. Several modifications were tested in the Munich experiments, including modified lateral inlet sections and laterals making angles of 45° and 60° with the conduit. Also, in studies of typical lock manifolds and gas-burner manifolds, the characteristics of other geometrical forms have been determined. In most cases, the general trends noted in this study are the same as those for other manifold arrangements.

For estimation and sometimes for design, the results presented herein may prove to be satisfactory. In other projects, in which more accurate results are essential, a typical junction can be studied in the laboratory and the results can be used for the design of an entire manifold system. Messrs. Soucek and Zelnick followed this procedure and showed its effectiveness in studies of the Panama Canal locks. A difficulty in the direct application of the results for a single branch point is that trial computations, beginning with the outlet farthest downstream, must be made; and a final check is obtained only if the computed head at the upstream end corresponds to the design value. To avoid such trial solutions, M. R. Carstens,[18] J.M.ASCE, and Mr. Yanes[16] presented graphical methods that can be used directly. Mr. Carstens used the data presented in Fig. 4 in deriving a general design procedure for the distribution networks of sprinkler irrigation systems. Mr. Yanes devised a similarly general method of computing the flow in lock manifolds after the characteristics of a single port have been determined.

---

[18] "The Hydraulics of Sprinkler Irrigation Systems," by M. R. Carstens, *Bulletin No. 212*, Washington State Inst. of Technology, Pullman, Wash., May, 1951.

CONCLUSION

In a determination of the principal characteristics of the flow of fluids at a branch point in a conduit, the various effects are most logically treated separately. Changes in piezometric and total head have been determined for both combining and dividing flow, and for each case the two component parts of the flow have been analyzed separately. The various occurrences have been interpreted with reference to conventional equations of energy and momentum, so that indications were obtained of the magnitude of the head-loss term and of the resultant pressure on the wall of the lateral. The effect of lateral spacing was evaluated, and the characteristics of a symmetrical double lateral were found to coincide satisfactorily with those for a single lateral having the same effective area ratio.

The various results are presented as functions of the ratio of lateral discharge to total discharge and of the ratio of lateral diameter to conduit diameter. Although the results are also dependent on the shape of the conduit and the geometry of the lateral, those for circular conduits are thought to be representative of other manifold forms. During a period of nearly half a century various experimenters have published data for a variety of other forms, so that considerable information is available. In this paper the writer has presented new data and systematized the presentation and interpretation of the results. It is to be emphasized that tests on a single junction are usually sufficient in defining the characteristics of a complete manifold system. For many installations, the results presented herein should prove directly applicable.

ACKNOWLEDGMENTS

The experiments on which this paper is based were conducted under the writer's supervision by Messrs. Barton, Niaz, Escobar, and Yanes as a project of the Iowa Institute of Hydraulic Research. Funds for equipment used in this project in its early stages were provided by the American Society of Civil Engineers through the Engineering Foundation.

DISCUSSION

Julio Escobar,[19] **J. M. ASCE.**—Rather than having considered particular problems from the standpoint of their immediate or practical applications, the staff of the Iowa Institute of Hydraulic Research has been engaged in fundamental research into the mechanics of fluid motion. In evolving the different phases of the studies, newly learned basic principles are given coherent expression, and their experimental foundations are thoroughly evaluated.

Mr. McNown undertook such a basic investigation of the hydraulics of manifolds after the publication of the work of Messrs. Soucek and Zelnick[8] together with his discussion. After five years of research, Mr. McNown has published his findings—not as a series of graphs, tables, or charts applicable to the design of a particular type of manifold, lock, or water-supply system, but rather as an interpretation of the behavior of flow in the vicinity of laterals, together with a definition of the general principles governing the hydraulics of manifolds.

Among the many aspects of the problem, the explanation of the energy changes and the head losses that occur in the region of the lateral for dividing flow is particularly important. The writer was concerned with this phase of the investigation while at the University of Iowa and wishes to show how additional findings from his studies[15] are helpful in the understanding of certain phases of the phenomenon described by the author.

The apparent increase in the energy of flow past the lateral for small ratios of the lateral discharge to the total discharge is explained by the hypothesis that the lateral discharge comes from a region of low-velocity flow, in which kinetic energy relative to the remaining flow is less than average. Therefore, the equation of energy, from which Eq. 1 was established, should be modified[20] to include velocity correction coefficients,

$$\alpha_b \frac{V^2}{2\,g} = \alpha_c \frac{V^2_c}{2\,g} + \Delta h + h_f \ldots\ldots\ldots\ldots\ldots\ldots (9)$$

with reference to Fig. 9. If the velocity correction factors are redefined as

$$\text{and} \quad \left.\begin{aligned} \alpha_b &= 1 + \epsilon_b \\ \alpha_c &= 1 + \epsilon_c \end{aligned}\right\} \ldots\ldots\ldots\ldots\ldots\ldots (10)$$

and if Eq. 9 is rewritten in the form:

$$\Delta h + \epsilon_c \frac{V^2_c}{2\,g} - \epsilon_b \frac{V^2}{2\,g} = \frac{V^2}{2\,g} - \frac{V^2_c}{2\,g} - h_f \ldots\ldots\ldots\ldots (11a)$$

the pressure rise will be modified by two terms depending on the velocity heads and the velocity distributions upstream and downstream from the lateral. If Δh_c is the corrected pressure rise,

---

[19] Engr., Escobar y Venegas, Engrs., Bogotá, Colombia.

[20] "Elementary Mechanics of Fluids," by Hunter Rouse, John Wiley & Sons, Inc., New York, N. Y., 1946, p. 114.

$$\Delta h_c = \Delta h + \epsilon_c \frac{V_c^2}{2g} - \epsilon_b \frac{V^2}{2g} \qquad (11b)$$

and the final equation takes the form:

$$\frac{\Delta h_c}{\frac{V^2}{2g}} = 1 - \left(\frac{V_c}{V}\right)^2 - \frac{h_f}{\frac{V^2}{2g}} \qquad (11c)$$

The second member of Eq. 11*c* is the same as that of Eq. 1 plotted in Fig. 4. Therefore, the pressure rises may be computed and compared not only with the theoretical curves but with Mr. Barton's experimental curves, also plotted in Fig. 4

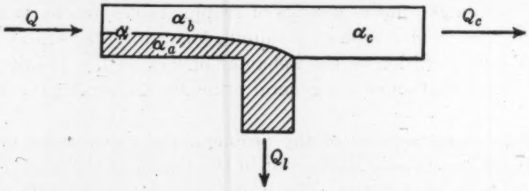

FIG. 9.—DIVISION OF FLOW

The remaining problem is the evaluation of the velocity correction factors, which are defined by the equation:

$$\alpha_e = \frac{1}{A}\int \left(\frac{v}{V}\right)^3 dA \qquad (12)$$

in which v is the velocity of a filament. Evaluation of α_e depends on the manner in which the main flow is divided in the region of the lateral. Once the cross-sectional area of the lateral discharge is known, the energy factors can be determined and applied to the general energy equation.

It was necessary to observe in the laboratory what part of the cross section of the main pipe contributed flow to the lateral. A Lucite tee of 2-in. conduit diameter and 1-in. lateral diameter was inserted in the experimental 2-in.-diameter pipe to enable the observation of the path followed by dyed droplets or by air bubbles injected at various points in a cross section a few inches upstream. The use of dye was somewhat troublesome because prolonged operation colored the recirculating supply and interfered with other experiments in the laboratory. Therefore, most of the exploratory measurements were made with air although later analysis showed that the dye solution was more accurate for the purpose.

Experiments showed that, for values of $Q_l/Q < 0.5$, the area for Q_l was bounded by slightly curved lines convex to the side of the lateral as shown in Fig. 10. For $Q_l/Q > 0.5$, the experiments did not show exactly the form of the

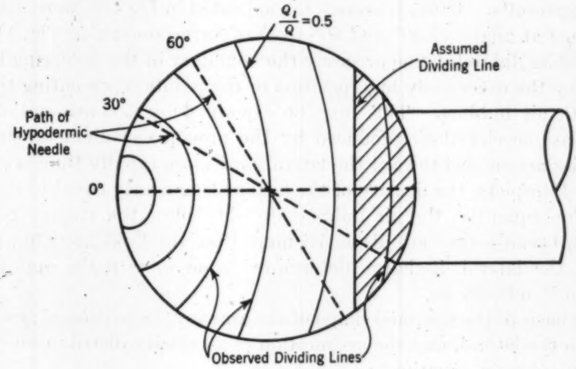

$\frac{Q_l}{Q}=0.5$
60°
Assumed Dividing Line
30°
Path of Hypodermic Needle
0°
Observed Dividing Lines

FIG. 10.—DEMARCATION BETWEEN LATERAL AND CONTINUING FLOW—FOR FLOW APPROACHING THE LATERAL

section, but the bounding curves seemed to be increased in curvature, so as to form almost closed boundaries as shown in Fig. 10.

In Fig. 11 are shown the results obtained from the tests with air and dye for a horizontal traverse of the hypodermic needle used for dye injection; the line shown was computed from the assumption (made for simplicity) that the area required for a given lateral discharge was limited by a vertical line as indicated in Fig. 11. This assumption was not exact but it was helpful in

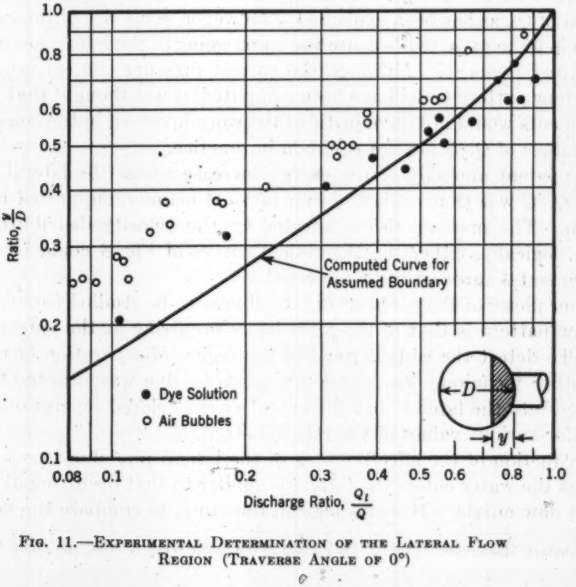

FIG. 11.—EXPERIMENTAL DETERMINATION OF THE LATERAL FLOW REGION (TRAVERSE ANGLE OF 0°)

interpreting results. Other traverses (as indicated in Fig. 10) were made along lines inclined at angles of 30° and 60° to that corresponding to Fig. 11.

Air bubbles did not define precisely the boundary of the diverging flow as is indicated by the excessively high position of the points representing the observation with air bubbles. This may be explained by a consideration of the relative mass accelerations produced by the pressure gradient at the outlet. The bubbles are carried toward the lateral pipe more rapidly than is the water or the dyed droplets, the density of the latter being nearly equal to that of the water. Consequently, the air bubbles do not follow the streamlines of the liquid and, because they are displaced more than the fluid particles, the cross section of the lateral discharge determined from their paths appears to be larger than it actually is.

On the basis of the assumed shape of the area for the portion of Q which was diverted to the lateral, and the assumption of a velocity distribution described by the von Kármán equation[21]:

$$\frac{v}{V} = \sqrt{f}\,\left(2.15 \log_{10} \frac{y}{r_o} + 1.43\right) + 1 \qquad (13)$$

(in which f is the coefficient of friction and r_o is the radius of the pipe), the energy factors were evaluated. From Eq. 11c it was possible to compute corrected values of the pressure rise across the lateral and to compare computed values with those of Mr. Barton's experiments.

For values of $Q_l/Q < 0.5$, all recomputed points showed that the energy gain previously found had been accounted for. For $Q_l/Q > 0.5$, all recomputed points were abnormally high, indicating a failure in the assumption of the form of the area of Q_l, as has been explained. However, some rise of the experimental points is to be expected because the water going to the lateral has more than average kinetic energy. Although the correct pressure rise corresponding to the exact flow pattern could have been computed, it was thought that the possible refinements would not have justified the work involved in the computations as large values of Q_l/Q are not common in practice.

The apparent anomaly of the energy increase across the lateral for small values of Q_l/Q was thus explained in a rational manner, supported by experimentation. The pressure rise is affected by the velocity distribution of the flow, and, logically, either the theoretical curves of Fig. 4 could be raised, or the experimental curves could be lowered.

Another phase of the problem of lateral flow to be studied from knowledge of the flow pattern is that of the form losses occurring at the entrance to the lateral. To detect the eddy formed in the region of separation of the lateral flow, another technique was developed whereby dye was injected through a hole drilled into the lateral, and the extent of the colored separation zone was recorded for various values of the ratio, Q_l/Q.

The reduction of the effective area of the lateral pipe due to separation of the flow as the water enters the lateral is similar to that occurring at an orifice plate or a flow nozzle. It seems logical, therefore, to compare the head losses in the lateral with those for such boundary transitions. Mr. McNown has shown the remarkable correspondence between the measured head losses and those based on theoretical considerations for plane irrotational flow. The writer also found good correspondence between his laboratory determination of the effective cross section of the lateral and that for either an abrupt enlargement (Eq. 5) or a nozzle. For the latter, the empirical equation recommended by H. S. Bean and S. R. Beitler[22]—

---

[21] "Elementary Mechanics of Fluids," by Hunter Rouse, John Wiley & Sons, Inc., New York, N. Y., 1948, p. 198.

$$h_f = \frac{(V'_l)^2 - V^2_l}{2\,g}\,(1 - C_c) \qquad \text{(14a)}$$

—was used. This equation takes the dimensionless form:

$$\frac{h_f}{\dfrac{V^2_l}{2\,g}} = \left(\frac{1}{C_c}\right)^2 - \frac{1}{C_c} + C_c - 1 \qquad \text{(14b)}$$

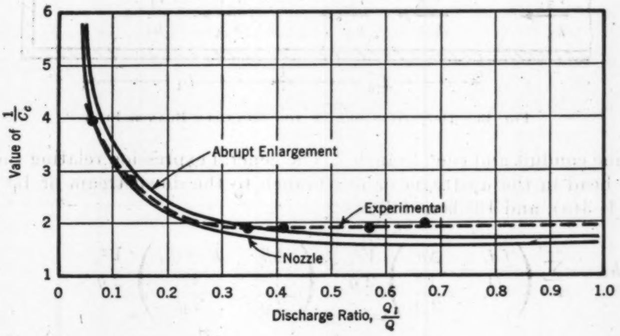

FIG. 12.—COMPARISON, OBSERVED AND COMPUTED EFFECTIVE CROSS SECTION OF THE LATERAL

Fig. 12 shows the computed and observed values of the effective cross section of the lateral for different values of the ratio, Q_l/Q. The contracted area decreases with values of Q_l/Q for small values of the latter, thus increasing the head losses because of the greater deceleration of the flow. For $Q_l/Q = 0.35$, the area ratio becomes essentially constant and approximately equal to 0.5. These empirical findings are comparable both to the computed and the experimental values presented in the paper.

M. R. CARSTENS,[23] A. M. ASCE, AND JOHN ROBERSON.[24]—The results presented in this paper demonstrate the value to the engineering profession of wisely directed graduate-student research programs. If the principal characteristics of the flow are defined for a single branch point in a conduit, it is possible to incorporate the results into the analysis of a multiple branching conduit system. The only additional restriction to such an analysis is that the branch points be separated by a sufficient length of straight conduit. The reported experiments indicate that a spacing of 20 diameters between branch points is sufficient. As mentioned by Mr. McNown, the multiple branch analysis must be begun at the farthest downstream branch and must be continued by successively accounting for the effects of each section of intervening main-line conduit and each branch. The general expression relating the piezometric head in the upstream or *n*th branch to the downstream or 1st branch (Figs. 1, 3(*a*), and 13) is as follows:

---

[22] "Research on Flow Nozzles," by H. S. Bean, and S. R. Beitler, *Transactions*, ASME, Vol. 60, April, 1938, p. 244.

[23] Associate Prof., School of Civ. Eng., Georgia Inst. of Technology, Atlanta, Ga.

[24] Asst. Hydr. Engr., Div. of Industrial Research, and Instructor in Civ. Eng., State College of Washington, Pullman, Wash.

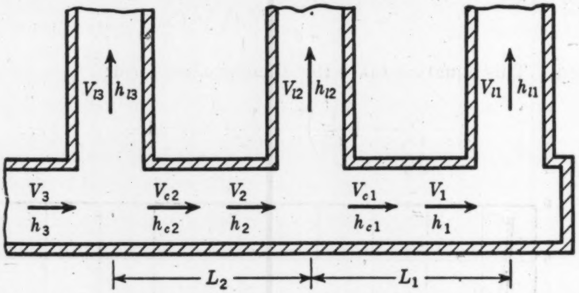

FIG. 13.—DEFINITION SKETCH FOR MULTIPLE BRANCH FLOW

$$h_{ln} - h_{l1} \doteq \sum_{i=1}^{n-1} \left(\frac{f\,L}{D} - \frac{\Delta h}{\frac{V^2}{2\,g}} \right)_i \frac{V^2{}_i}{2\,g} - \left(\frac{\Delta h}{\frac{V^2}{2\,g}} + \frac{h - h_l}{\frac{V^2}{2\,g}} \right)_n \frac{V^2{}_n}{2\,g} + \left(\frac{\Delta h}{\frac{V^2}{2\,g}} + \frac{h - h_l}{\frac{V^2}{2\,g}} \right)_1 \frac{V^2{}_1}{2\,g} \quad (15)$$

The parameter $f\,L/D$ is the loss coefficient for the straight pipe section between the branch points. The values of $\frac{\Delta h}{V^2/2\,g}$ can be determined directly from Fig. 4. The value of $\frac{h - h_l}{V^2/2\,g}$ can be determined from Fig. 5, as follows:

$$\frac{h - h_l}{\frac{V^2}{2\,g}} = \frac{h'_f}{\frac{V^2}{2\,g}} + \left(\frac{Q_l}{Q}\right)^2 \left(\frac{D}{D_l}\right)^4 - 1 \quad (16)$$

The computation procedure indicated by Eq. 15 is satisfactory for analysis of an installed system, but laborious trial computations are involved in the calculation for the design.

In many situations the multiple branch variables are limited, and the solution of Eq. 15 can be presented on a nomograph. Work was done by the

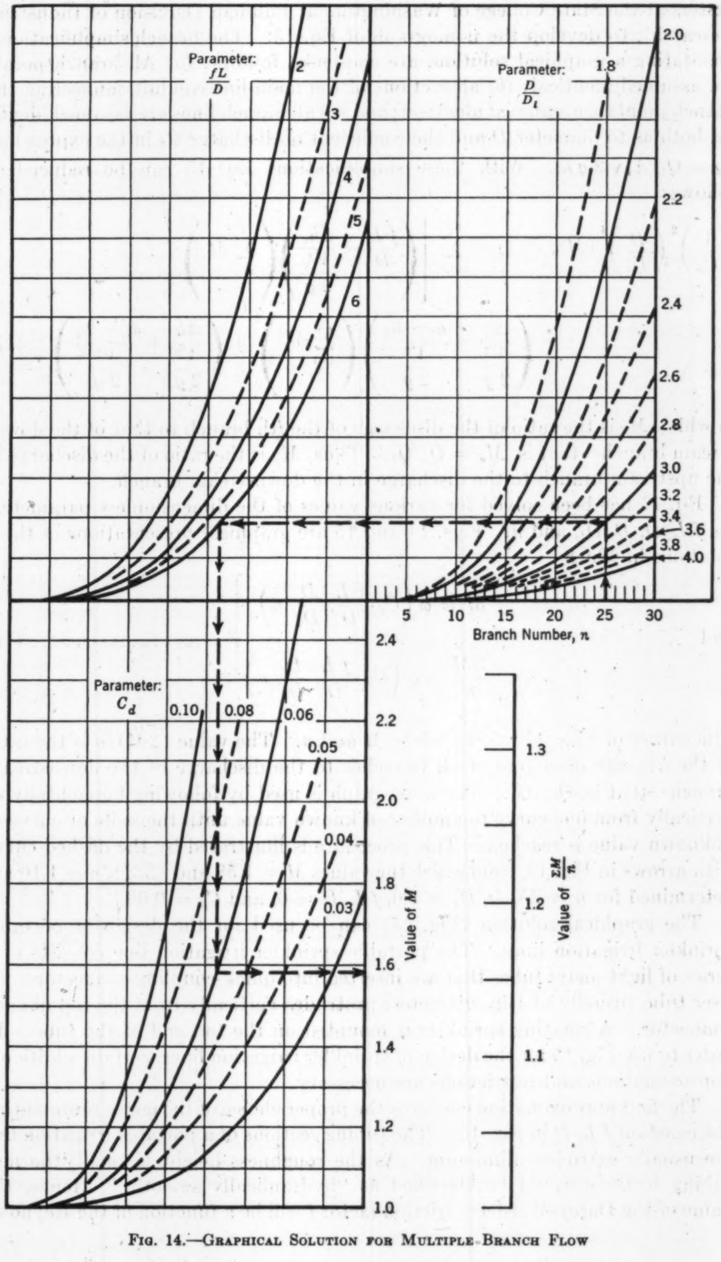

FIG. 14.—GRAPHICAL SOLUTION FOR MULTIPLE-BRANCH FLOW

writers at the State College of Washington, at Pullman (Division of Industrial Research), to develop the nomograph of Eq. 15. The branch simplifications, facilitating a graphical solution, are chosen as follows: (*a*) All branch points are assumed identical; (*b*) all sections of the main-line conduit connecting the branch points are assumed identical; and (*c*) all branch lines are assumed identical both as to diameter D and the coefficient of discharge C_d in the expression, $C_d = Q_l/A_l\sqrt{2\,g\,h_l}$. With these simplifications Eq. 15 can be reduced as follows:

$$\left(\frac{1}{C_d}\right)^2\left(\frac{D}{D_l}\right)^4(M^2_n - 1) = \sum_{i=1}^{n-i}\left[\left(\frac{f\,L}{D} - \frac{\Delta h_i}{\frac{V^2_i}{2\,g}}\right)\left(\sum_{i=1}^{i} M_i\right)^2\right] - \left(\frac{\Delta h}{\frac{V^2}{2\,g}} + \frac{h - h_l}{\frac{V^2}{2\,g}}\right)_n\left(\sum_{i=1}^{n} M\right)^2 + \left(\frac{\Delta h}{\frac{V^2}{2\,g}} + \frac{h - h_l}{\frac{V^2}{2\,g}}\right)_1 \quad \ldots(17)$$

in which M_i is the ratio of the discharge of the *i*th branch to that of the downstream branch—that is, $M_i = Q_i/Q_1$. Thus, M_n is the ratio of the discharge in the upstream branch to the discharge in the downstream branch.

Eq. 17 has been solved for various values of the dimensionless parameters C_d, $f\,L/D$, D/D_l, and n. Figs. 14 and 15 are graphical presentations of these solutions in which

$$\left.\begin{aligned} M &= \phi\left(C_d, \frac{f\,L}{D}, \frac{D}{D_l}, n\right) \\ \text{and} \qquad \frac{\Sigma M}{n} &= \phi\left(C_d, \frac{f\,L}{D}, \frac{D}{D_l}, n\right) \end{aligned}\right\} \quad \ldots\ldots\ldots\ldots\ldots\ldots(18)$$

The curves of Figs. 14 and 15 relate M and n. The value $(\Sigma M)/n$ is the ratio of the average discharge of all branches to the discharge of the downstream branch—that is, Q_{av}/Q_1. The nomograph is used by following horizontally or vertically from one curve to another of known value until the scale or curve of unknown value is reached. This procedure is illustrated by the dashed curve with arrows in Fig. 14, from which the values $M = 1.58$ and $(\Sigma M)/n = 1.16$ are determined for $n = 25$, $D/D_l = 3.0$, $f\,L/D = 6$, and $C_d = 0.06$.

The graphical solution (Fig. 15) can be used for the design of portable sprinkler irrigation lines. The portable sprinkler irrigation line consists of a series of light metal tubes that are inserted into quick-coupling connectors. A riser tube (usually of 1-in. diameter) protrudes vertically from the top of each connector. A rotating sprinkler is mounted on the top end of the tube. In order to use Fig. 15 for the design of sprinkler irrigation lines, certain additional approximations and restrictions are necessary.

The first approximation concerns the proper choice of the curve representing the constant $f\,L/D$ in Fig. 15. The tubing sections of a portable irrigation line are usually extruded aluminum. As the roughness height is small, the new tubing sections would be classified as "hydraulically smooth." Hence, the value of the Darcy-Weisbach friction factor f will be a function of the Reynolds number of each tubing section. The Reynolds number will be a minimum in the downstream section and will increase successively to a maximum in the upstream section. The best value of a constant f to replace the variable f can be determined by a summation of the terms $(f\,L/D)\,(V^2/2\,g)$. From this summation, the average velocity V_R to be used in computing the Reynolds number is found to be $V_R = V_1\sqrt{n(2\,n - 1)/6}$. Thus, one can determine the best value of the Reynolds number by using V_R. By referring to a standard curve relating f and the Reynolds number, the best value of f can be determined.

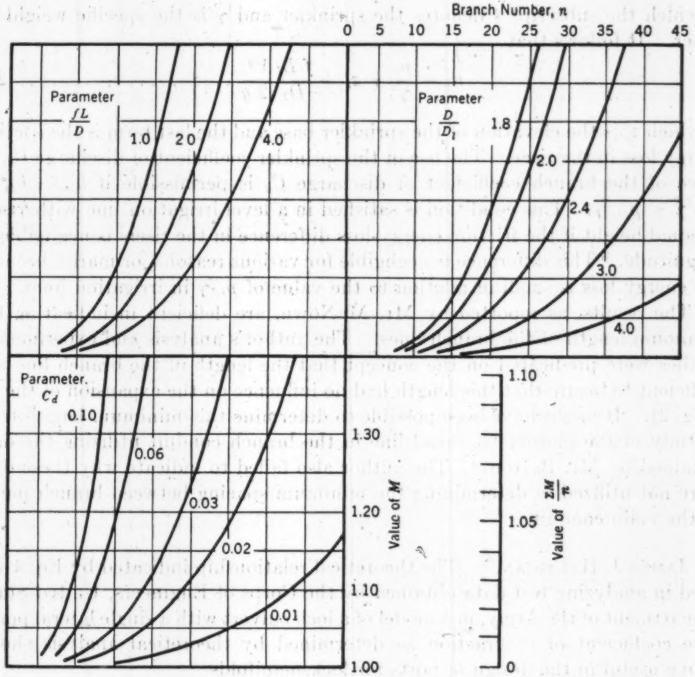

FIG. 15.—GRAPHICAL SOLUTION FOR MULTIPLE BRANCH FLOW

The parameter $f\,L/D$ is computed using this value of f together with the values of the properties of the repeating tubing sections, L and D.

In the design of sprinkler irrigation lines, using the sprinkler coefficient of discharge is much simpler than using the branch-line coefficient of discharge In Eq. 15, the difference $h_{ln} - h_{l1}$ was expressed in terms of the flow and the geometric properties. In Eq. 17 the values of h_{ln} and h_{l1} were eliminated, as previously explained, by the use of the branch discharge equation—that is,

$$h_l = \frac{V^2_l}{2\,g\,C^2_d} \qquad (19a)$$

Thus, the value,

$$h_{l_n} - h_{l_1} = \left(\frac{1}{C_d}\right)^2 \left(\frac{V^2{}_{l_n}}{2\,g} - \frac{V^2{}_{l_1}}{2\,g}\right) \ldots\ldots\ldots\ldots\ldots (19b)$$

was used in the derivation of Eq. 17. However, the discharge of a sprinkler is a function of the sprinkler geometry, and the pressure at the base of the sprinkler is

$$\frac{p_s}{\gamma} = \left(\frac{1}{C_{d_s}}\right)^2 \frac{V^2{}_l}{2\,g} \ldots\ldots\ldots\ldots\ldots\ldots\ldots\ldots (20)$$

in which the subscript *s* denotes the sprinkler and γ is the specific weight of water. It follows that

$$h_l = \frac{p_s}{\gamma} + z_s + \frac{f\,L_l}{D_l}\,\frac{V^2{}_l}{2\,g} \ldots\ldots\ldots\ldots\ldots\ldots (21)$$

in which z_s is the elevation of the sprinkler base and the last term is the friction energy loss in the riser. The use of the sprinkler coefficient of discharge C_{d_s} in place of the branch coefficient of discharge C_d is permissible if $h_{l_n} - h_{l_1} = p_{s_n}/\gamma - p_{s_1}/\gamma$. This condition is satisfied in a level irrigation line with risers of equal height if the friction energy-loss difference in the risers is negligible in magnitude. This difference is negligible for various reasons, primarily because the energy loss is small in relation to the value of p_s/γ in irrigation lines.

The results, as reported by Mr. McNown, are deficient in indicating the minimum length of the branch lines. The author's analysis and experimental studies were predicated on the concept that the length of the branch line was sufficient to insure that this length had no influence on the expansion of the jet (Fig. 2). It might have been possible to determine this minimum length from a study of the piezometric head line in the branch conduit utilizing the data obtained by Mr. Barton.[14] The author also failed to indicate why these data were not utilized in determining the minimum spacing between branch points in the main conduit.

JAMES J. HARTIGAN.[25]—The theoretical relationship indicated by Eq. 4 was used in analyzing test data obtained by the Corps of Engineers, United States Department of the Army, in a model of a lock culvert with a single lateral port.[26] The coefficient of contraction as determined by theoretical analysis should prove useful in the design of ports for lock manifolds.

Head losses between the conduit and port were determined from the sum of the piezometer head and the velocity head in the conduit on the upstream side of the port, and from the sum of the chamber water surface and the velocity head, $V^2{}_p/2\,g$, of the flow through the port computed on the basis of the outlet area exclusive of the rounded edges. References to port entrance and outlet are defined by direction in divided flow. Test data for combining flow are not included in this discussion. In a definition sketch such as Fig. 3(*a*), the chamber water surface would replace the upstream end of the piezometric pressure gradient in the lateral.

---

[25] Hydr. Engr., St. Paul Dist., Corps of Engrs., U. S. Dept. of the Army, St. Paul, Minn.

[26] *Hydraulic Laboratory Report No. 52*, St. Paul Dist., Corps. of Engrs., U. S. Dept. of the Army St. Paul, Minn., June, 1946.

In Fig. 16, head losses in terms of $V^2_p/2\,g$ are shown for four ports, three of which had rounded entrances and exits and the other, square edges. Dimensions of the ports are shown in Fig. 17, in which R denotes the radius. The long curved arrow in each plan view indicates direction of flow into the ports.

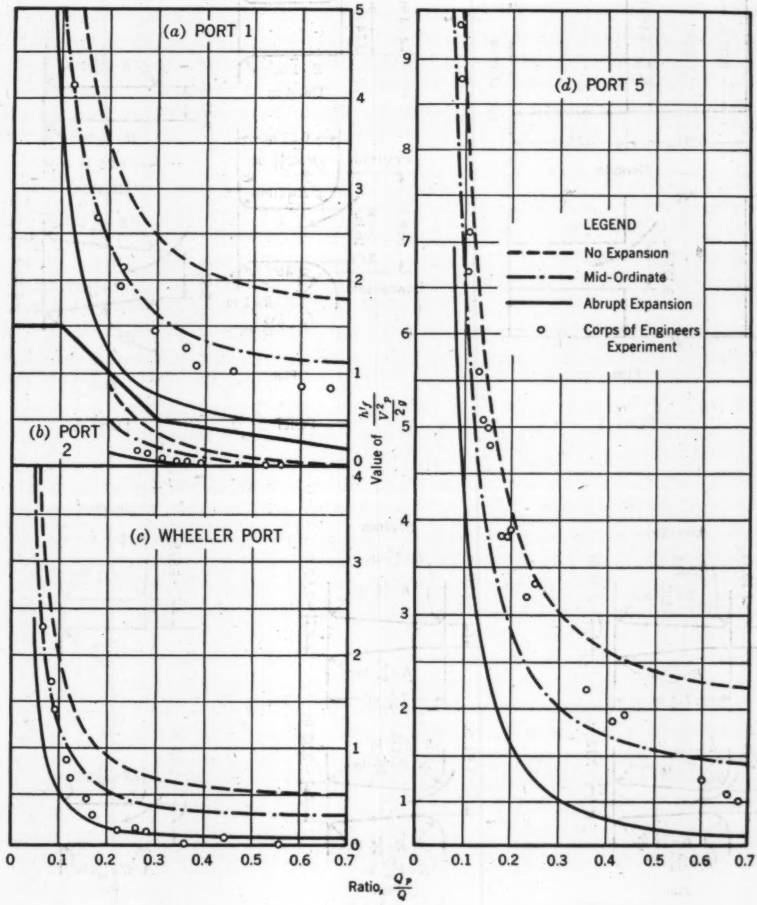

FIG. 16.—HEAD LOSS BETWEEN CONDUIT AND PORT IN DIVIDED FLOW

Although in each case the port was located at the bottom of the conduit, thus limiting contraction in the vertical direction to the top side, there seemed to be no reason for changing the areas to be used in determining the ratio of a/b in Eq. 4.

Evidently the ratio of port length to conduit width was large enough so that values of C_c computed for a barrier of infinite length were applicable. However, it was observed in the model that the ports were too short to allow complete expansion of the jet before reaching the outlet. Test data are therefore compared with the theoretical curve for head loss in an abrupt expansion and also for the condition of no expansion of the jet,

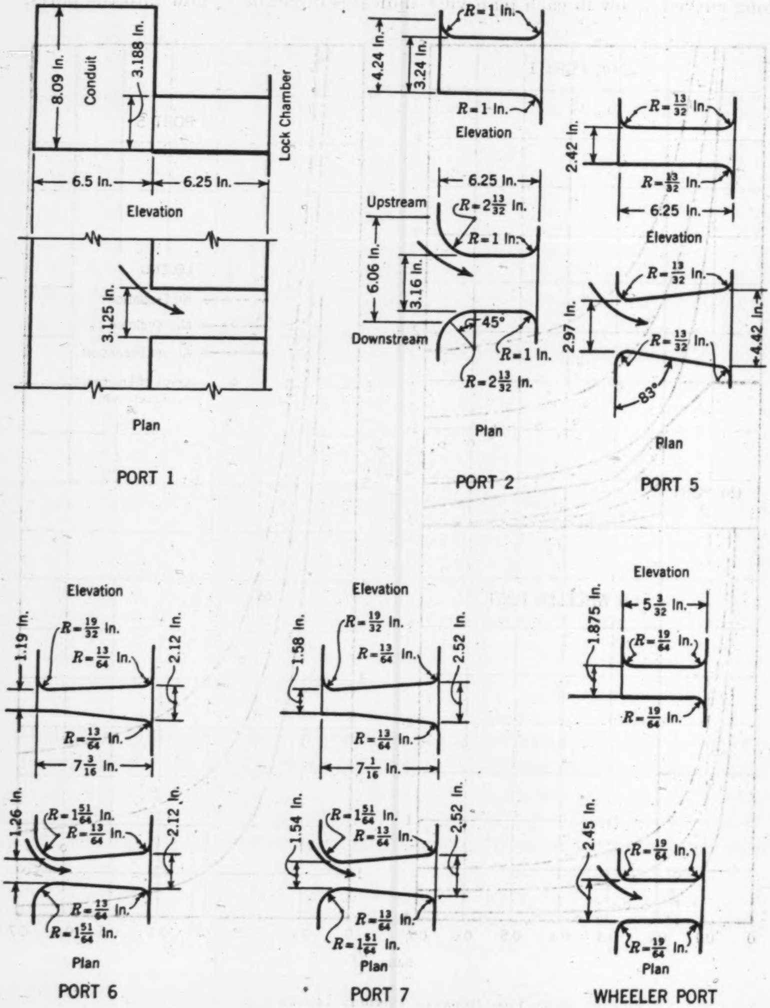
8.09 In.
Conduit
3.188 In.
Lock Chamber
6.5 In.
6.25 In.
Elevation
3.125 In.
Plan
PORT 1
R=1 In.
4.24 In.
3.24 In.
R=1 In.
Elevation
6.25 In.
Upstream
R=2 13/32 In.
R=1 In.
6.06 In.
3.16 In.
45°
Downstream
R=1 In.
R=2 13/32 In.
Plan
PORT 2
R=13/32 In.
2.42 In.
R=13/32 In.
6.25 In.
Elevation
R=13/32 In.
2.97 In.
R=13/32 In.
4.42 In.
83°
Plan
PORT 5
Elevation
1.19 In.
R=19/32 In.
R=13/64 In.
2.12 In.
R=13/64 In.
7 3/16 In.
1.26 In.
R=1 51/64 In.
R=13/64 In.
2.12 In.
R=13/64 In.
R=1 51/64 In.
Plan
PORT 6
Elevation
1.58 In.
R=19/32 In.
R=13/64 In.
2.52 In.
R=13/64 In.
7 1/16 In.
1.54 In.
R=1 51/64 In.
R=13/64 In.
2.52 In.
R=13/64 In.
R=1 51/64 In.
Plan
PORT 7
Elevation
1.875 In.
5 3/32 In.
R=19/64 In.
R=19/64 In.
2.45 In.
R=19/64 In.
R=19/64 In.
Plan
WHEELER PORT

FIG. 17.—PORT DESIGNS

$$h'_f = \left(\frac{V'_p}{2g}\right)^2 - \frac{V^2_p}{2g} \qquad (22)$$

in which V'_p is the velocity of the jet. A curve midway between the ordinates of the curves for abrupt expansion and no expansion is shown in Fig. 16 to help reference the test points.

The rounding of the entrance to the ports made indefinite the effective entrance area for determining the ratio a/b. Dimensions for Port 2 in Fig. 17 show the width and height used in determining the maximum effective entrance area. In addition to the upstream and top curvatures, the downstream curvature to the point where the radius subtends 45 degrees of arc is included.

Because in three-dimensional flow the contraction coefficient C_c is applicable to an area, values of $\sqrt{C_c}$ will apply to the width and height of the port. For Port 2 the jet would not be suppressed in the vertical until the value of C_c reached $\left(\frac{3.24}{4.24}\right)^2 = 0.584$. After determining the effective entrance area for the foregoing conditions, the value of $Q_p/Q = 0.7$ was obtained from a graph of Eq. 4. For greater values of Q_p/Q the port should flow full, and head loss computed on the basis of the contraction coefficient will be zero. For smaller values of Q_p/Q the jet would be contracted in elevation, but not in plan, until the maximum effective width could be used.

According to the theoretical analysis, the Wheeler Port will have a contracted jet smaller than the minimum port area throughout the range of values of Q_p/Q; thus, the theoretical curves remain greater than the value for $h'_f = 0$. Similar conditions exist for the square-edged Port 1. Unlike the author's theoretical curves in Fig. 5, which are fixed for a given ratio of D_l/D, the curves computed on the basis of a lateral having a larger entrance area than outlet area indicate lower values of head loss, and possibly zero head loss, as shown for Port 2 in Fig. 16.

Data for Port 5 are presented because the greatest range of the head-loss ratio was measured in tests on this port. However, Port 5 is probably the least practical of the four. It was assumed that the barrier in the plan view was of sufficient length to deflect the jet at an angle of 83°. Accordingly, a plot was made of Eq. 4 for the special case of the jet deflected 83°. However, for the range of available test data—that is, up to $Q_p/Q = 0.7$—it was found that values of C_c did not exceed by more than 1% the corresponding values for a jet having a 90° deflection angle. Values of C_c applicable to Port 5 would probably vary by less than 0.5% from those values for a jet having a 90° angle.

Fig. 16 shows that only for Port 5 are the head losses substantially above the midordinate line. For Ports 1 and 5, and for the Wheeler Port, there was some consistency in the relationship between the size of the jet and the outlet area of the port at the section where the head loss dropped below the midordinate curve.

Ports 6 and 7 were more efficient than Port 5. Flared 9° and 10.5°, respectively, these ports indicated head losses corresponding to values of Q_p/Q greater than 0.15, which did not exceed the loss that might be expected in gradual expansions twice as great.

In the operation of opposing side-wall manifolds having ports in one sidewall spaced midway between the ports in the opposite wall, the angle of efflux is important because any deviation from an angle of 90° will tend to interfere with the diffusion of jets. It is believed, therefore, that the possibility of determining the angle of efflux in divided flow by the author's theoretical analysis should also be useful in the design of port manifolds for navigation-lock hydraulic systems.

Sadiq M. Niaz.[27]—As a part of the study outlined by the author, the writer made detailed observations on certain phases of converging manifold flow. In particular, information was obtained concerning the terms for the head loss and the unbalanced force for this type of flow. These observations, together with alternative forms of plotting, are presented as an aid to interpreting the data.

From the application of a simplified energy relationship, the author obtained Eq. 7. Because the conduit velocity increases at the junction, the loss sustained by the conduit flow resembles that for flow through a boundary contraction. It can be expressed in terms of loss coefficients to be applied either to the velocity head of approach or to the difference between the upstream and downstream velocity heads; the two are simply related through the discharge ratio and the diameter ratio. Thus, from the latter alternative, the head loss can be expressed in the form:

$$h_f = j\left(\frac{V^2 - V^2_c}{2\,g}\right) = j\,\frac{V^2}{2\,g}\left(1 - \frac{V^2_c}{V^2}\right) \ldots\ldots\ldots\ldots (23)$$

in which j is a loss coefficient that varies with the aforementioned diameter and discharge ratios.

Eq. 7 can now be rewritten:

$$\frac{\Delta h}{\dfrac{V^2}{2\,g}} = \left[2\,\frac{Q_l}{Q} - \left(\frac{Q_l}{Q}\right)^2\right](1 + j) \ldots\ldots\ldots\ldots\ldots (24)$$

A family of curves for various constant values of j relates the dimensionless pressure change and the discharge ratio. In Fig. 18, curves representing Eq. 24 for various values of j are compared with the data obtained for convergent flow, this plot being an alternative to Fig. 7. The curve for $j = 0$ corresponds to the ideal condition of no head loss, and that for $j = 1$, to the condition of $F = 0$ assumed by Mr. Favre. The unbalanced force F is directed downstream for $j < 1$ and upstream for $j > 1$.

The experimental results indicate trends comparable to those for the curves corresponding to different values of constant j. For $D_l/D = \frac{1}{4}$ and $D_l/D = \frac{1}{2}$, the values of j are 1.38 and 0.95, respectively. The departure of the experimental curves from the theoretical curves for values of Q_l/Q less than 0.25 is due to the fact that for relatively small values of Q_l the type of mixing which occurs results in a smaller loss of head. For $D_l/D = 1.0$ the trend of the experimental curve is different from the direction of the theoretical curves because the water entering the conduit through the lateral always increases in velocity;

---

[27] Director Central Designs, Punjab Irrig. Dept., Lahore, Pakistan.

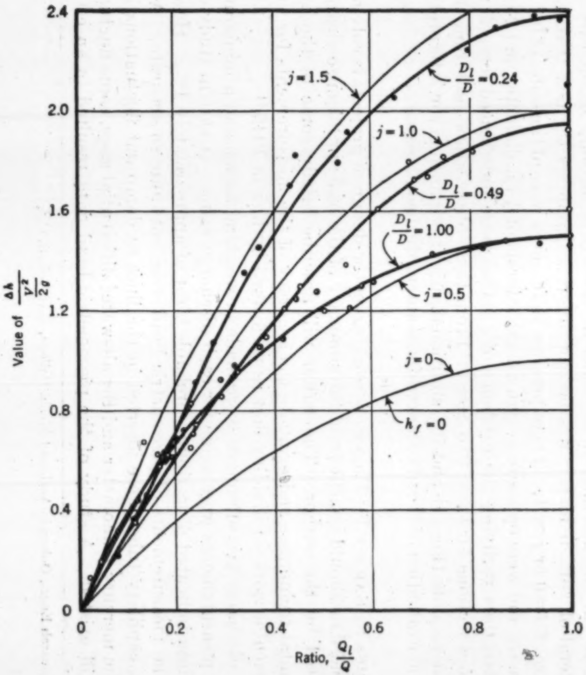

FIG. 18.—COMPARISON BETWEEN EQ. 24 AND FIG. 7

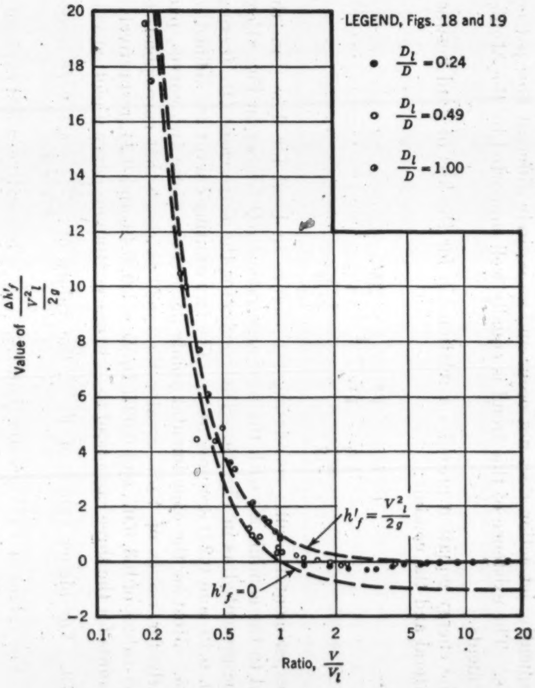

FIG. 19.—LOSS OF HEAD, FLOW FROM LATERAL TO CONDUIT

consequently, jet action does not occur and an entirely different flow pattern results. The existence of this trend is equally well supported by the Munich experiments.

The energy equation provides a relationship for the loss of head between the lateral and the conduit:

$$\frac{h'_f}{\frac{V^2_l}{2\,g}} = \frac{V^2}{V^2_l} - 1 + \frac{\Delta h'}{\frac{V^2_l}{2g}} \quad\quad (25)$$

The experimental results correlating the change in head for flow from the lateral to the conduit h'_f with the discharge ratio Q_l/Q (shown in Fig. 8) can also be presented as in Fig. 19. The results for the three cases (D_l/D equal to 1.0, 0.49, and 0.24) are presented. The two limiting curves are defined by Eq. 25. Most of the experimental points lie between these two curves, particularly for values of V_l/V greater than 0.30 (a range that corresponds to (Q_l/Q)-values of 0.3, 0.07, and 0.02 if $D_l/D = 1.0, 0.49$, and 0.24, respectively). The points for the three cases tend to form one continuous curve if plotted as in Fig. 19. For higher values of V_l/V, the values of $\frac{\Delta h'}{V^2_l/2\,g}$ are very nearly zero. For values of V_l/V greater than 1.0, $\frac{\Delta h'}{V^2_l/2\,g}$ is negative, a fact explained by the author.

The pressure measurements along the sides of the lateral closely adjacent to the junction showed that the pressure on one side differed from that on the other side only by amounts of the order of 0.005 ft of mercury in the case of the lateral of 1-in. diameter; this lack of difference confirms the fact that, for this case, $F \simeq 0$ or $j \simeq 1$. These pressure differences were of the order of 0.1 ft of mercury and were opposite in sign for the laterals of $\frac{1}{2}$-in. diameter and 2-in. diameter, thus verifying the existence of a rather large unbalanced force F in the two directions for these two cases. From these observations and from the alternative plots (Figs. 18 and 19), additional insight is gained in the interpretation and evaluation of the unbalanced force and of the head losses.

James R. Barton.[28]—Engineers working on the design of projects involving manifold flow should benefit from the summary of the basic problem so clearly presented by the author. The writer will describe briefly some of the experimental techniques and evaluate the accuracy of the measurements for the experimental work on dividing flow as performed by him in 1946.[14]

All discharge measurements were made in weighing tanks, and a minimum of two measurements were made for each discharge value. A careful study of these data indicated a maximum probable error of approximately 1%. However, the measurements of piezometric head were not quite so accurate. Although capillary tubes were inserted in the lines to damp out fluctuations in both the mercury manometer and the air-water differential gage, some fluctuation still existed. A study of the piezometric head data resulted in an estimated maximum probable error of about 2% with a possibility of a 3% error in the vicinity of the lateral where excessive disturbance occurred.

---

[28] Research Engr., Colorado Agri. and Mech. College, Fort Collins, Colo.

Determination of the proper hydraulic gradient for each pipe was a problem as the individual piezometric head measurements showed some scatter. In order to avoid repeatedly deciding what the exact slope should be on a particular run, each lateral and the main pipe were carefully calibrated by making a logarithmic plot of the Reynolds number against the hydraulic gradient. Each of these plots was based on a minimum of nine different slopes which in turn were based on a minimum of six point measurements of piezometric head. With these calibration plots, the correct slope could always be fitted to the piezometric head data for individual runs, even though the data exhibited some scatter. In the case of excessive scatter the run was discarded and repeated. A study of Fig. 3 will indicate that a change of slope of any of the hydraulic grade lines could have affected values of Δh and h'_f, especially when these terms were small. For this reason, the precaution of using the correct slope for each flow measurement is believed to have avoided some errors that might have resulted in a larger scatter of the data plotted in Figs. 4 and 5.

In order to illustrate the usefulness of the author's data as a guide in research or practice, the writer presents some findings of a project completed in 1949 by Grant Borg.[29] With the object of establishing a workable design for the underdrainage system of small rapid sand filters, Mr. Borg ran extensive tests on the discharge characteristics of a perforated-pipe underdrain. The research resulted in the establishment of certain relationships necessary for satisfactory distribution of wash water through the perforated-pipe system.

The equipment consisted of one 4-in.-diameter manifold with twelve 1-in.-diameter laterals attached to each side of the pipe so that all laterals were in a single plane. Orifices of various sizes were drilled in the bottom of the laterals. In this way, the 4-in.-diameter pipe acted as a manifold for the lateral pipes, and each lateral in turn was a manifold system for the orifices, which discharged into the atmosphere. Because the orifice discharge was not always at an angle of 90° to the center line of the lateral, Mr. Borg's data cannot be compared in the strictest sense with the author's data, but in some details an interesting qualitative comparison exists.

Of the comparisons that might be made, one will be included here to illustrate how the author's data would have been useful in the research in the Utah experiments. For small (D_l/D)-ratios, and varying (Q_l/Q)-ratios, the flow distribution through the orifices was nearly uniform, as Fig. 5 indicates it should be. For $D_l/D = \frac{1}{4}$, the value of $\frac{h'_f}{V^2_l/2\,g}$ remains essentially constant when the discharge ratio, Q_l/Q, is varied widely. However, as D_l/D increases, $\frac{h'_f}{V^2_l/2\,g}$ varies considerably relative to a wide range of (Q_l/Q)-values. The results of the Utah experiments clearly illustrated that, as the orifice was enlarged, the flow distribution became poorer because the ratio of $\frac{h'_f}{V^2_l/2\,g}$ varied considerably with variation in Q_l/Q, and the value of Q_l/Q at the first orifice on the lateral varied greatly from its value at the last orifice. The author's results could have been used as a guide for the Utah experiments, thereby reducing the total work required for a significant answer.

---

[29] "Design Data on Perforated-Pipe Underdrains for Small Rapid Sand Filters," by Grant Borg, thesis presented to the University of Utah, Salt Lake City, Utah, in 1949, in partial fulfilment of the requirement for the degree of Master of Science.

Ralph W. Powell,[30] M. ASCE.—Despite the many papers that have been written on manifold flow, the subject has remained in an unsatisfactory state. The author's treatment of the subject and the report on the results obtained at the Iowa Institute of Hydraulic Research are most welcome. However, the writer wishes to call attention to one important set of data on combining flow that apparently had not attracted the author's notice.

In 1931 Itaru Naramoto and Taijiro Kasai[31] reported a series of 651 test runs on combining flow in cylindrical pipes with intersection angles of 15°, 30°, 45°, 60°, 70°, 75°, 80°, 85°, and 90°, and (D_l/D)-ratios of 1.004, 0.815, 0.678, 0.666, 0.581, and 0.503. Unfortunately, only the total loss of energy was reported for most of these runs, without mention of the amount in the main pipe, and the amount in the lateral. However, for twenty-nine of the runs involving 90° intersections, the complete data are printed, and from these the writer has prepared Table 1.

TABLE 1.—Data from the Kyushu Experiments (Japan)

(a) $D_l/D = 1.004$					(b) $D_l/D = 0.503$				
Run	$\frac{Q_l}{Q}$	$\frac{2\,g\,\Delta h}{V^2}$	$\frac{2\,g\,h'_f}{V^2}$	$\frac{2\,g\,h'_f}{V^2_l}$	Run	$\frac{Q_l}{Q}$	$\frac{2\,g\,\Delta h}{V^2}$	$\frac{2\,g\,h'_f}{V^2}$	$\frac{2\,g\,h'_f}{V^2_l}$
1	0.135	0.450	−0.480	−26.7	1	0.135	0.396	−0.184	−0.642
2	0.233	0.627	−0.261	− 4.84	2	0.208	0.633	0.227	0.333
3	0.341	0.939	0.100	0.82	3	0.270	0.797	0.656	0.574
4	0.409	1.137	0.404	2.45	4	0.322	0.914	1.018	0.624
5	0.484	1.161	0.368	1.59	5	0.368	1.043	1.442	0.680
6	0.528	1.218	0.448	1.63	6	0.399	1.120	1.727	0.692
7	0.564	1.268	0.510	1.64	7	0.435	1.193	2.085	0.703
8	0.602	1.314	0.580	1.62	8	0.472	1.268	2.548	0.729
9	0.653	1.352	0.648	1.54	9	0.509	1.132	2.990	0.734
10	0.690	1.390	0.699	1.49	10	0.522	1.386	3.271	0.766
11	0.704	1.396	0.684	1.43	11	0.567	1.496	3.813	0.756
12	0.728	1.425	0.760	1.47	12	0.605	1.545	4.385	0.764
13	0.745	1.447	0.808	1.48	13	0.598	1.543	4.294	0.765
14	0.760	1.467	0.841	1.47					
15	0.767	1.453	0.846	1.43					
16	0.774	1.461	0.878	1.46					

In general, it shows close agreement with the data reported in the paper, most of the points lying between those lines in Figs. 7 and 8 that represent the Iowa and Munich experiments.

John K. Vennard,[32] A. M. ASCE, and **Darrhl I. Dentoni,**[33] J. M. ASCE. —The writers have done experimental work of a nature similar to that of the author and are thus in a position to appreciate the excellent and concise presentation of theories and facts in a field that seems to have all too many uncertainties.

---

[30] Prof. of Mechanics, The Ohio State Univ., Columbus, Ohio

[31] "On the Loss of Energy at Impact of Two Confined Streams of Water," by Itaru Naramoto and Taijiro Kasai, *Memoirs*, College of Eng., Kyushu Imperial Univ., Vol. VI, No. 3, Fukuoka, Japan, 1931.

[32] Prof. of Fluid Mechanics, Stanford Univ., Stanford, Calif.

[33] Junior Engr., Davis and Holman, Cons. Engrs., Stockton, Calif.

Since the completion of the thesis by Mr. Barton,[14] the senior writer has been interested in an apparently serious discrepancy between the results obtained in the Iowa experiments and those obtained in the Munich experiments for the case of dividing flow. This discrepancy is not evident in Fig. 4. In fact, the author asserts (under the heading, "Observed Results: Dividing Flow") that

> "Except for a discrepancy in the region of the uppermost part of the curves for $D_l/D = 1$, the two series of experiments [Iowa and Munich] achieved almost identical results."

From study of the Munich papers and comparison with Mr. McNown's interpretation of these in Fig. 4, the writers believe that the Munich curves have been mislabeled and that the results are not only not "identical" but exhibit a trend opposite to those obtained in the Iowa experiments. This apparent discrepancy led the junior writer to undertake an experimental program in an attempt to resolve the conflicting results obtained from these two carefully performed sets of experiments. Accordingly, tests were conducted in the Stanford Hydraulic Laboratory of Stanford University, Stanford, Calif., on five square-edged outlets having axes at 90° to a main conduit of 1.276-in. diameter. Lateral sizes were selected such that the diameter ratios, D_l/D, were 0.294, 0.392, 0.490, 0.642, and 0.830. The results were plotted in the manner suggested by the author in Figs. 4 and 5. Good agreement with the results of the Iowa and Munich experiments was obtained in the case of Fig. 5 and fair agreement in that of Fig. 4.

The Stanford tests were conducted in the same general manner as those at Iowa and Munich but differed in one detail—no piezometer connections were made in the laterals. The laterals consisted of smooth, straight sections of pipe between 27 and 30 diameters in length discharging freely to the atmosphere. The diameters were measured (volumetrically) with extreme care, and the hydraulic grade lines throughout the laterals were established from the Blasius friction factor and from the use of the generally accepted premise that the hydraulic grade line intersects the axis of the lateral in the plane of its outlet. The reliability of the Blasius friction factor, the correctness of the foregoing premise, and the adequacy of the previously mentioned length of lateral had been accurately confirmed by C-T. Chen[34] in a series of tests. Many piezometer connections were used to establish the hydraulic grade line throughout the main conduit, and the Blasius friction factor was again used as a guide in selecting the best line through the tops of the piezometer columns. Here again the reliability of the Blasius friction factor was demonstrated by close agreement between a line of predetermined slope and points obtained experimentally.

The Stanford results are presented in Fig. 20 and, because of Mr. McNown's explanation of Figs. 4 and 5, are presumably self-explanatory. However, the trend of the curves in Fig. 20(*a*) confirms the data obtained at Iowa rather than

---

[34] "Unestablished Flow Patterns Downstream from Square Edged Pipe Entrances," by C-T. Chen, thesis presented to Stanford Univ., Stanford, Calif., in 1952 in partial fulfilment of the requirement for the degree of Engineer.

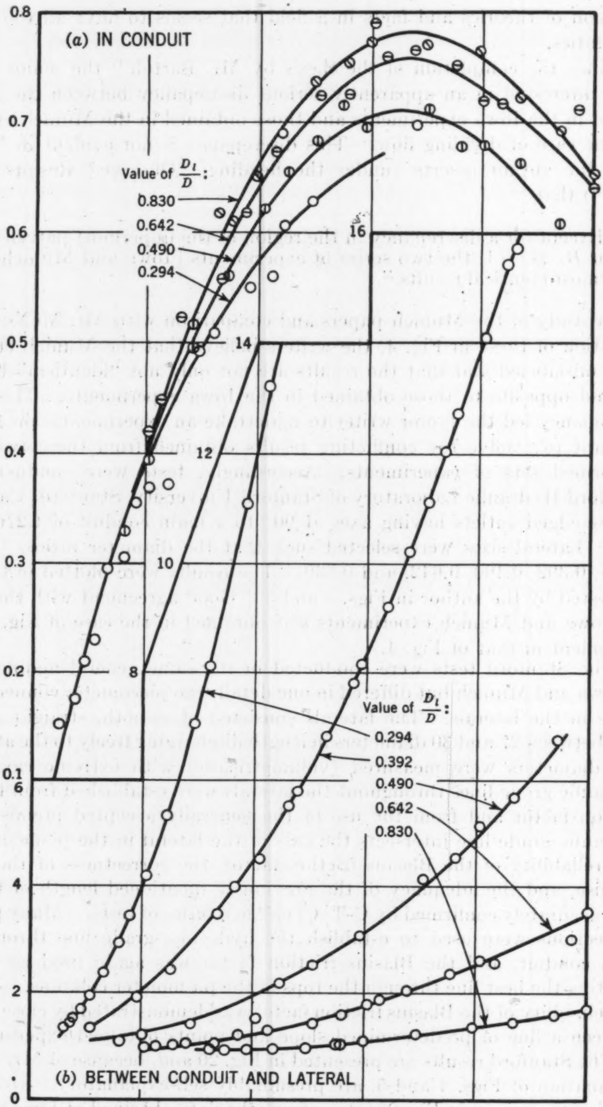

FIG. 20.—STANFORD EXPERIMENTAL RESULTS, DIVIDING FLOW

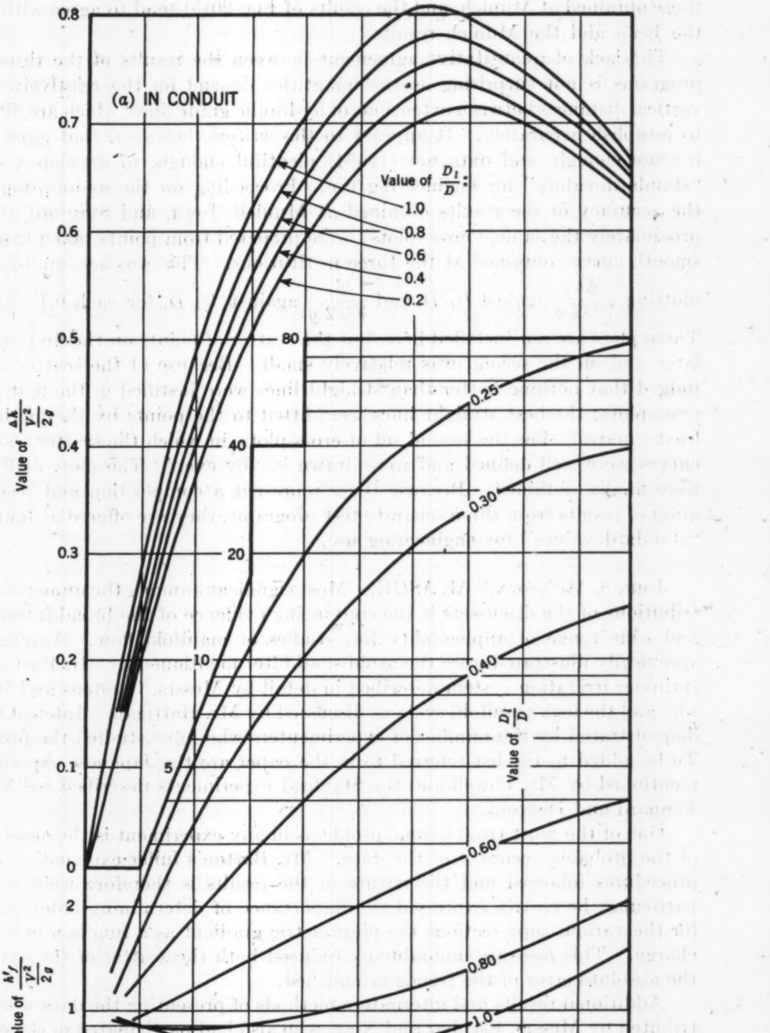

FIG. 21.—COMBINED RESULTS, DIVIDING FLOW

those obtained at Munich, and the results of Fig. 20(*b*) tend to agree with both the Iowa and the Munich results.

The lack of quantitative agreement between the results of the three test programs is not surprising as the quantities depend on the relatively small vertical distances between extensions of hydraulic grade lines, which are difficult to establish accurately. It appears to the writers, however, that agreement is close enough, and data now (1954) plentiful enough, to develop a set of "standard values" for engineering use. Proceeding on the assumption that the accuracy of the results obtained at Munich, Iowa, and Stanford are approximately the same, "cross-plots" were prepared from points taken from the smooth curves obtained at the three institutions. This was accomplished by plotting $\frac{\Delta h}{V^2/2\,g}$ against D_l/D, and $\frac{h'_f}{V^2/2\,g}$ against D_l/D, for each 0.1 of Q_l/Q. These plots are not included here, but the scatter of points on the first set was large and on the second was relatively small. Because of the scatter it was judged that nothing better than straight lines were justified in the first set of cross-plots; the best straight lines were fitted to the points by the method of least squares. For the second set of cross-plots, in which the scatter was less, curves were well defined and were drawn in "by eye." The plots of Fig. 21 were finally obtained. Because these represent a composition and reconciliation of results from three separate test programs, they are offered as tentative "standard values" for engineering use.

JOHN S. MCNOWN,[35] M. ASCE.—Most significant among the numerous contributions of the discussers is the convincing evidence of the broad interest in, and wide range of applicability for, studies of manifold flow. Applications specifically illustrated were the rapid sand filter mentioned by Mr. Barton, the sprinkler irrigation system described in detail by Messrs. Carstens and Roberson, and the lock manifold systems discussed by Mr. Hartigan. Interest is also demonstrated by the number of experimenters who have studied the problem. To be added to the list referred to in the paper are the Japanese experiments mentioned by Mr. Powell and the Stanford experiments described by Messrs. Vennard and Dentoni.

One of the most troublesome problems in any experiment is the assessment of the probable accuracy of the data. Mr. Barton's fuller explanation of the procedures followed and the nature of the results is therefore welcome. In particular, he clearly expressed the importance of determining independently for the various pipe sections the piezometric gradient as a function of the discharge. This measure undoubtedly reduced both the scatter of the data and the absolute error of the trends established.

Additional results and alternative methods of presenting the data were contributed by Messrs. Escobar and Niaz, who also had participated in the experiments on which the paper was based. Mr. Escobar demonstrated convincingly the way in which the transverse velocity distribution causes the apparently negative head losses in Fig. 4, and he observed the profile of the contracted jet in the lateral. In Fig. 12 he illustrated the close correspondence between experiment, empiricism, and theory relative to this particular problem. Mr. Niaz presented alternative plots, Figs. 18 and 19, for the combining flow. These show (1) the similarity of the loss to that in an abrupt contraction, and (2) the efficacy of plotting the head loss for the lateral flow against the ratio of the final velocity to the initial velocity for this flow. Although the latter plot introduces a degree of system to the results, the data in Fig. 19 appear on close inspection to be three curves, each involving a transition from the lower envelope curve to the upper one. The results for this type of flow are evidently difficult to depict in any completely satisfactory manner.

---

[35] Associate Director, Iowa Inst. of Hydr. Research, State Univ. of Iowa, Iowa City, Iowa.

The question of the minimum length of conduit or lateral necessary to establish the intended uniform flow was raised in two of the discussions. The velocity distribution approaches its ultimate form asymptotically with the distance downstream from the point of separation or major disturbance. Selection of the distance required for the effect of the branch point to vanish depends very much on the purpose for which the determination is to be made.

In reply to Mr. Hartigan's comment: In a distance of from 5 to 10 diameters, the primary characteristics of the separation and high-velocity jet disappear. The relevant questions asked by Messrs. Carstens and Roberson can be given only a provisional answer. A sprinkler unit also will show normal characteristics at a distance downstream of only a few diameters. Aside from the indication of the major flow conditions, the proposal to use the pressure taps as an indication of the degree to which the flow has been established is not reliable. The performance of a subsequent lateral, which was tested thoroughly by Mr. Yanes,[16] was surprisingly dependent on small changes in the velocity distribution. These changes cannot be detected accurately without many carefully made piezometers, and, even then, the significance of a small change in pressure would probably have been underestimated without the direct measurements of lateral performance.

Detection by Messrs. Vennard and Dentoni of the error both in labeling and in discussing the comparison of the Munich and Iowa experiments in Fig. 4 is greatly appreciated. Although most of the results correspond quite well, those for this case certainly do not. The differences are not large, but the trends are opposite. The comparable data from the Stanford experiments, generally confirming the Iowa test results, are thus particularly valuable; the summary plots presented by Messrs. Vennard and Dentoni should also be useful. However, the curves in Fig. 21 (*b*) should logically approach the limiting value of unity as Q_l/Q approaches zero. The curve for $D_l/D = 1.0$ is too high at the other end of the scale ($Q_l/Q = 1.0$). The suggested value of 1.5 is considerably greater than either the value of 1.3 from the Munich experiments or the value of 1.15 from the Iowa experiments. No data were given for $D_l/D = 1$ in the Stanford tests. If this curve had been lowered, the indicated trend of the curves would have been improved.

Also welcome is the corroboration provided by the additional data of the Japanese experiments[31] for combining flow. As Mr. Powell indicates, the correspondence among the several sets of data is close. For $D_l/D = 0.5$, data from the Iowa and Munich experiments differ somewhat (Figs. 7 and 8), and in these instances the data from the Japanese experiments are much closer to those from the Iowa experiments.

No matter how much care is given to the averaging of the various sets of data, the result will not be a final answer to all problems of manifold flow. In the paper it was emphasized that the data presented are for a single geometrical form of branch point or junction, and that the results obtained are representative rather than general. The variety of results presented by Mr. Hartigan for various lock ports well illustrates the variability with port geometry of one characteristic of the flow. For this reason, extreme refinement either in the processing of the data or in its application to any such design problem as the sprinkler system is unjustified.

By way of conclusion, the writer is gratified by the interest shown in the discussions, which are equivalent in length to nearly twice (in *Proceedings-Separates*) that of the paper itself, and by the fact that three of the investigators who participated in the Iowa tests contributed additional findings from their thesis investigations. The goals of the Society in fostering thorough discussion were met admirably by the discussers in that varied points of view were expressed, additional results were presented, and various findings were emphasized through repeated reference to them. The representative results obtained, reinforced in the discussions, should find application to a wide variety of practical problems.

AMERICAN SOCIETY OF CIVIL ENGINEERS
Founded November 5, 1852

TRANSACTIONS

Paper No. 2715

DESIGN OF FRAMES BY RELAXATION OF YIELD-HINGES

BY J. MORLEY ENGLISH,[1] A. M. ASCE

WITH DISCUSSION BY MESSRS. NOEL W. MURRAY, HERMAN TACHAU, AND J. MORLEY ENGLISH

SYNOPSIS

A method is herein developed for determining the loading condition that causes the collapse of a rigid frame structure. It is shown that the location of the "yield-hinges," when the structure is on the verge of collapse, is independent of the stiffness of the individual members. The method consists of (1) the arbitrary distribution of moment to the joints of the structure, and (2) the adjustment of this distribution by the trial-and-error method until the highest ratio of actual moment to limit moment—at any point in the structure—reaches a minimum. The locations of the yield-hinges are the points at which these minima occur.

The procedure is extended to account for the order in which the yield-hinges develop. This order is dependent on the stiffnesses of the members; therefore, the initial moment distribution must be consistent with the actual elastic properties of the structure. Similarly, the subsequent redistribution of moment—to minimize the highest values—is made in accordance with the elastic properties of the structure.

INTRODUCTION

If a system of loads acting on a rigid frame structure is increased slowly and proportionately, some point within the structure will reach its limiting elastic value of resisting moment. As the loading increases, the resisting moment at this point will increase at a diminishing rate, and the moment will increase slowly as the values of moment at other locations will tend to approach it. As other moments approach the end of the elastic range, corresponding

---

NOTE.—Published, essentially as printed here, in November, 1953, as *Proceedings-Separate No. 322*. Positions and titles given are those in effect when the paper or discussion was received for publication.

[1] Associate Prof. of Eng., Univ. of California Los Angeles, Calif.

points will in turn offer progressively less resistance to bending until a sufficient number of points attain their limiting moment values. When this occurs, the structure, as a part or as a whole, cannot effectively offer any further resistance to the loading and collapse becomes imminent. The magnitude of the loads at collapse, or at an arbitrarily defined deformation of the structure, should be considered as the true criterion for design rather than the surpassing of the elastic limit of the material at any point in the structure.

It is usually postulated that the relation between moment and angle change is as depicted in Fig. 1(*c*) rather than as shown in Fig. 1(*b*). Fig. 1(*b*) is derived from an assumption of the flat-topped stress-strain relationship shown in Fig. 1(*a*). The moment is considered to reach a maximum value M' without any angle change. After attaining this value, the moment is considered to remain constant for an unlimited angle change. Thus a point on a structure is a yield-hinge when the moment at that point is equal to M'.

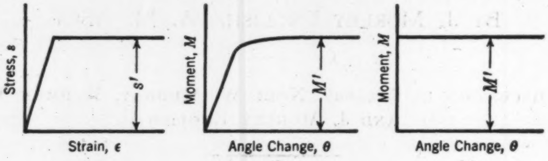

(*a*) (*b*) (*c*)

FIG. 1

Because the deformation in the elastic range and the elastic-plastic range is relatively insignificant in comparison to the subsequent unrestricted deformation, the usual postulate is unnecessarily restrictive. The loading path is unimportant if a constant maximum moment can be attained. The yield-hinge can develop as a result of any actual stress-strain relation or because of the instability of the flanges or web of a flanged section. However, the actual deflection of the structure will depend on the relationship between moment and angle change. Where it is required to determine this deflection, the assumption of a flat-topped relationship may not be correct.

CONDITIONS OF COLLAPSE

H. J. Greenberg and W. Prager, M. ASCE, have demonstrated a solution for the problem of the rigid frame structure wherein a number, λ, by which the actual loads must be multiplied to bring about collapse, is determined by guessing the collapse mode (that is, the location of the yield-hinges to produce collapse), and then verifying the validity of the guess by checking the statics and the yield conditions.[2] If the guess should prove to be incorrect, a yield condition will be found to be violated at some point. A revised guess is then made and the process is repeated until the correct solution is found. The principal disadvantage of this method is the inability of the analyst to guess the correct mode at the outset of the solution.

---

[2] "Limit Design of Beams and Frames," by H. J. Greenberg and W. Prager, *Transactions*, ASCE, Vol. 117, 1952, p. 447.

If it were known that the correct location of the yield-hinges is as shown in Fig. 2, the solution would be simple. In effect, the structure has been reduced to a mechanism by the introduction of the yield-hinges. The structure cannot support any further increase of load and so will collapse.

When the structure deflects a distance δ, measured horizontally at the point of application of the load, the external work is $\lambda P \delta$. The energy stored in the frame at any joint i will be $M'_i \theta_i$ (Fig. 1(*c*)). The assumption of no previous elastic deformation excludes consideration of elastic energy. Equating the internal work to the external work,

$$\sum \lambda P \delta = \sum M'_i \theta_i \ldots\ldots\ldots\ldots\ldots\ldots\ldots (1)$$

in which M'_i is the limit moment at joint i and θ_i is the angular deformation at joint i.

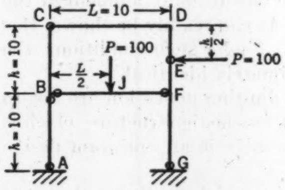

Fig. 2.—Rigid Frame Structure

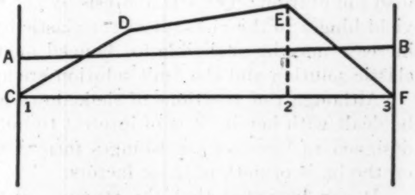

Fig. 3.—Moment Diagram

The angle change θ can always be related, by the geometry of the structure, to the deflection δ; thus,

$$\lambda = \frac{11\, M'}{3\, P\, h} \ldots\ldots\ldots\ldots\ldots\ldots\ldots (2)$$

Determination of Yield-Hinges.—The solution proposed by Messrs. Greenberg and Prager is easily obtained, provided the location of the yield-hinges can be predicted. The trial-and-error approach may be suitable for uncomplicated frames but becomes too complex for intricate structures. The method to be developed subsequently overcomes this difficulty by establishing the location of the yield-hinges as part of the solution. Another method which overcomes the difficulty inherent in the method presented by Messrs. Greenberg and Prager has been developed by P. S. Symonds and B. G. Neal.[8]

It is significant to note that nowhere in the development of Eq. 1 was it necessary to introduce the concept of member stiffness, whereas the elastic solution is dependent on the stiffness. The maximum value of M/M' in the elastic solution of the frame will determine the location of the first yield-hinge. The location of the maximum value of M/M' is dependent on the relative stiffnesses. Likewise, the order in which the other hinges develop is dependent on the member stiffnesses. The following principle may therefore be stated: The order in which yield-hinges develop, as all the loads on the structure are increased proportionally, will depend on the relative stiffnesses of the members of the structure. However, irrespective of the order in which the yield-hinges develop, the final locations of the yield-hinges will be unaltered.

---

[8] "Recent Progress in the Plastic Methods of Structural Analysis," by P. S. Symonds and B. G. Neal, *Journal*, The Franklin Institute, Pt. I, November, 1951, pp. 383–407; Pt. II, December, 1951, pp. 469–491.

This principle permits the arbitrary assignment of any value of member stiffness provided only that the final collapse condition is sought. Any arbitrary distribution of moment to the various joints of the frame—consistent with the requirements of statics—is tantamount to an arbitrary assignment of stiffnesses. Therefore, it is possible to obtain a moment distribution such that the maximum value of M/M' is the same at all points at which yield-hinges will develop. As the loads are increased, all such points will reach their limit moments simultaneously and all yield-hinges will form concurrently. Hence, the problem reduces to one of imagining an elastic structure designed to satisfy this requirement.

It is evident that in such a case the ultimate load will be greater than the load found from an elastic analysis by the ratio of the ultimate moment at the yield-hinges to the moment at the elastic limit. As can readily be shown, this increase may be negligible for flanged members. Under such conditions, the elastic solution and the limit solution are approximately identical.

Although the questions of shakedown and of limiting deflection are not to be dealt with herein, it is of interest to note that an elastic structure which is designed to have all yield-hinges form simultaneously is an optimum design on the basis of both of these factors.

It can be noted that the moment distribution which produces the same value for the maximum value of M/M' at all points that are to be yield-hinges will be that for which the maximum value of M/M' in the structure is minimized. This is implicit in Theorem I of Messrs. Greenberg and Prager,[2] and it can be readily seen with reference to a single-span restrained beam.

The moment diagram CDEF in Fig. 3 is a primary statics requirement for a simple-beam loading condition. The effect of end restraints superimposes the reference axis AB. Collapse will occur when the value of M/M' reaches unity at points 1, 2, and 3. Since it is required that the ratio M/M' for all three points reach unity simultaneously, the axis line AB is fixed such that

$$\frac{M_1}{M'_1} = \frac{M_2}{M'_2} = \frac{M_3}{M'_3} = \text{a minimum} \ldots\ldots\ldots\ldots\ldots (3)$$

F. Panlillio has applied this principle to a graphic solution of the problem of continuous beams.[4]

Since it would be difficult to determine analytically the moment distribution which would satisfy the requirements of Eqs. 3, any arbitrary distribution can be assumed. The point at which the maximum ratio of M_i/M'_i occurs will be a yield-hinge.

The loads can be considered to be large enough to cause the arbitrary elastic solution to have at least one moment in excess of the limit moment. Because a value of moment in excess of M' is a violation of the yield condition, the excess moment at the point must be redistributed (or relaxed) to locations that can accept the increased moment. The mechanics of this relaxation process are best illustrated by the following solutions of problems.

---

[4] "Theory of Limit Design Applied to Magnesium Alloy and Aluminum Alloy Structures," by F. Panlillio, *Journal*, Royal Aeronautical Soc., June, 1947.

Example 1.—The frame shown in Fig. 4 is loaded as indicated in Fig. 4(*a*). For simplicity, the limit moment is assumed to be the same for all points; that is, M' is equal to 100. The problem requires the determination of a multiplier λ by which the loads must be increased in order to cause collapse of the frame. Since M' is constant throughout, the moment values, rather than the ratios, are considered.

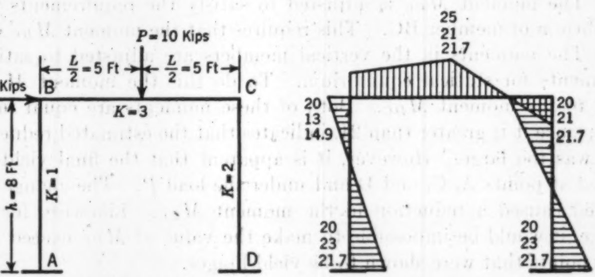

(*a*) LOADING CONDITION (*b*) MOMENT VALUES

FIG. 4.—SOLUTION OF EXAMPLE 1

Conditions of statics require that, regardless of the actual distribution of moments at the ends of the members, the member BC must support the simple beam moment of $(P\,L)/4$ and that the vertical members AB and CD must support the lateral moment $H\,h$. The distribution of moment may be guessed as $(H\,h)/4 = 20$, acting at each end of each vertical member. This would leave $(P\,L)/4 = 25$ to be resisted under load P. The moment values are recorded in Fig. 4(*b*). It can be seen that such a distribution of moment would correspond to an infinite stiffness of the member BC.

The maximum moment value of 25 at P indicates that this point will be a yield-hinge when P is increased by a factor λ. The value of 25 can be considered to have already exceeded the limit value and so must be reduced. That is, the yield-hinge at P must be relaxed by distributing the excess moment to some other point or points.

The distribution of moment which revealed that a yield-hinge will be formed at P was arbitrary. Any other distribution that would be statically correct could also have been assumed, although it probably would have revealed a different location for the first yield-hinge. For example, an assumption that the horizontal force was resisted entirely by equal moments at points A and D would indicate that these points would be yield-hinges. A series of such assumptions can thus reveal quickly the locations of most of the yield-hinges. This technique may also indicate the manner of blocking relaxations for the determination of the remaining yield-hinges. If the distribution first assumed is used, the procedure can be continued as follows:

1. A value by which the moment M_P under the load P can be reduced is estimated as 4 in this case. Then M_P will equal 21.

2. Because the object is to make a number of points reach the same final values, it is assumed that the change in M_P will produce a change in some other moment (or moments) to make it equal to a value of 21. Any moment can be used, but in this case the moment M_{CB} (at point C in member BC) is chosen. This nomenclature for representing moments will be used throughout the paper. That is, the moment will act at the end of the member corresponding to the first subscript, and the moment will occur in the member whose ends are denoted by the two subscripts.

3. The moment M_{BC} is adjusted to satisfy the requirements for statical equilibrium of member BC. This requires that the moment M_{BC} equal 13.

4. The moments in the vertical members are adjusted to satisfy the requirements for statical equilibrium. To do this the moment M_{AB} is made equal to the moment M_{DC}. Both of these moments are equal to 23. This value, since it is greater than 21, indicates that the estimated reduction of M_P by 4 was too large. However, it is apparent that the final yield-hinges are located at points A, C, and D and under the load P. The change which was effected caused a reduction in the moment M_{BC}. Likewise, for any other change, it would be impossible to make the value of M_{BC} exceed that of the other points that were shown to be yield-hinges.

5. The process is repeated by relaxing the excess values at points A and D or by revising the reduction of M_P by 4, until all four points have equal values. In this problem, this occurs at $M_{AB} = M_{CB} = M_{DC} = M_P = 21.7$.

6. The multiplier λ can be found by dividing M' by the final relaxed value of the maximum moment in the frame; thus $\lambda = \frac{100}{21.7} = 4.61$.

Example 2.—The frame of Fig. 2 is analyzed in Fig. 5. The sign convention adopted assumes that the moment at the end of a member is positive in the clockwise sense.

As in Example 1, it is not important what the initial distribution of moment is assumed to be. If the location of the yield-hinges were known, or could be guessed, the relaxation process might be completed more readily, as in Example 1. However, the solution is readily determinable, and it is not advantageous to spend time attempting to anticipate the location of the hinges.

In Example 2 the assumed distribution corresponds to infinite stiffness in the horizontal members and equal stiffnesses in the vertical members. The moment M_{FJ} is the largest—hence the first—yield-hinge. Relaxing the excess moment M_{FJ}, it is seen that the moment M_{BJ} next reaches a maximum. The moments M_{FJ} and M_{BJ} can be relaxed simultaneously until the moment M_{GF} appears as a yield-hinge. The process is continued, reducing by arbitrary increments all hinges that have been determined, until a minimum value, below which it is impossible to go without violating the requirement of statical equilibrium, is obtained. The final values are recognized by: (*a*) the fact that the same value is obtained at a sufficient number of points so that if these points were hinges, the structure would become a mechanism, and (*b*) any further attempted reduction of moment at one or more points will necessitate an increase of moment at some other point. The final maximum moment divided into the limit moment M' results in $\lambda = \frac{1{,}000}{273} = 3.67$.

General Solution.—In Examples 1 and 2, frames in which the limit moments were the same everywhere were investigated to simplify the problem. In an actual structure it is not likely that the limit moment will be the same for each point. The general problem, in which the limit moment can be any value, can be handled by recording the relative values of the limit moment on the frame after each relaxation, dividing the relaxed value by this relative limit moment.

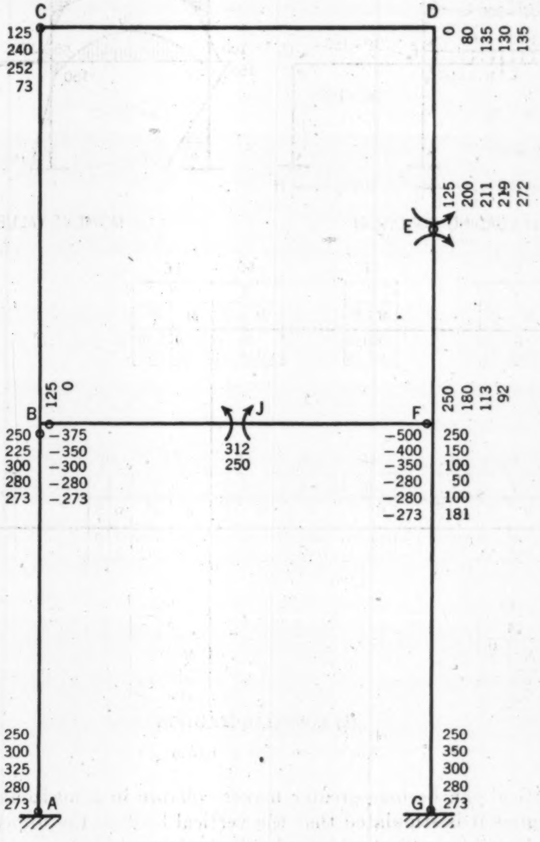
C
125
240
252
73
D
0
80
135
130
135
125
200
211
219
272
E
125
0
B
J
F
250
180
113
92
250
225
300
280
273
-375
-350
-300
-280
-273
312
250
-500
-400
-350
-280
-280
-273
250
150
100
50
100
181
250
300
325
280
273
A
250
350
300
280
G
273

FIG. 5.—SOLUTION OF EXAMPLE 2

The procedure may be performed as shown previously until the maximum ratio M/M' is minimized. The problem can be handled most readily by choosing a reference limit moment and relating this reference value to the limit moment at any point by a factor r. Then the moments after each distribution can be divided by the corresponding factor r. The r-values can be recorded on the frame as shown in Fig. 6 which is the solution for Example 3.

Example 3.—The complete solution for the frame shown in Fig. 6(*a*) is indicated in Fig. 6(*b*). In this solution local collapse is indicated by the development of hinges at points C, D, and E. However, hinges also are indicated at points A, B, G, H, J, and L. The fact that the moment M_{FJ} at one end of one vertical can become greater makes collapse in a horizontal mode impossible unless it is stipulated that the vertical load on the upper member of the frame be held constant while only the horizontal loads are increased. It should be noted that M_{FJ} is less than a limit moment because of the choice of distribution of moment. The moment could have been less than the limit moment at some other point or points. In fact, the location of the actual hinges in the lower structure is not revealed by the process.

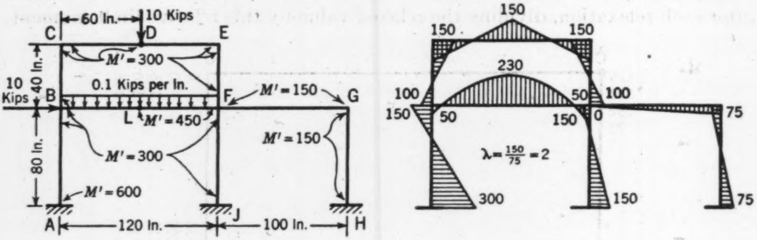

(*a*) LOADING CONDITION (*c*) MOMENT VALUES

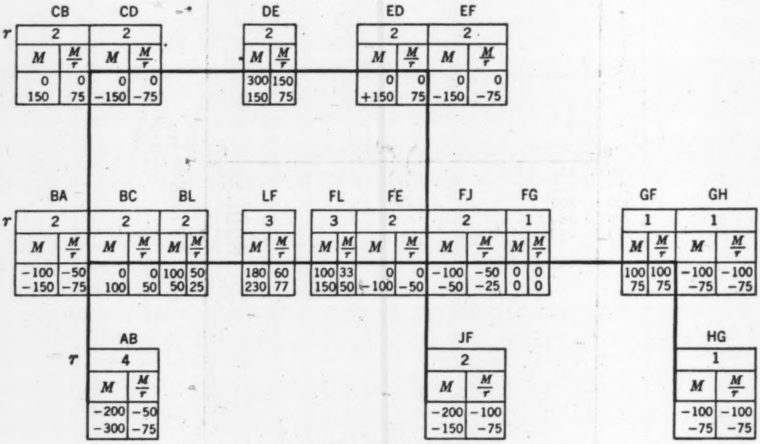

Member	r	M	$\frac{M}{r}$
CB	2	0 150	0 75
CD	2	0 −150	0 −75
DE	2	300 150	150 75
ED	2	0 +150	0 75
EF	2	0 −150	0 −75
BA	2	−100 −150	−50 −75
BC	2	0 100	0 50
BL	2	100 50	50 25
LF	3	180 230	60 77
FL	3	100 150	33 50
FE	2	0 −100	0 −50
FJ	2	−100 −50	−50 −25
FG	1	0 0	0 0
GF	1	100 75	100 75
GH	1	−100 −75	−100 −75
AB	4	−200 −300	−50 −75
JF	2	−200 −150	−100 −75
HG	1	−100 −75	−100 −75

(*b*) COMPLETE SOLUTION

Fig. 6.—Solution of Example 3

A further generalization is needed for the consideration of the case of a frame having unequal legs. In Example 3 the height of the vertical members in the frame were the same in any one story. This made it possible, during the distribution process, to maintain the total of the moments constant at the ends of the members. Actually, it is the shear which must be constant across any story section. Thus for member AB,

$$H = \frac{(M_{AB} + M_{BA})_i}{h_i} \quad \text{.......................} \quad (4)$$

Therefore, in the case of a frame having unequal legs it is necessary to recompute the total of the end moments after each distribution.

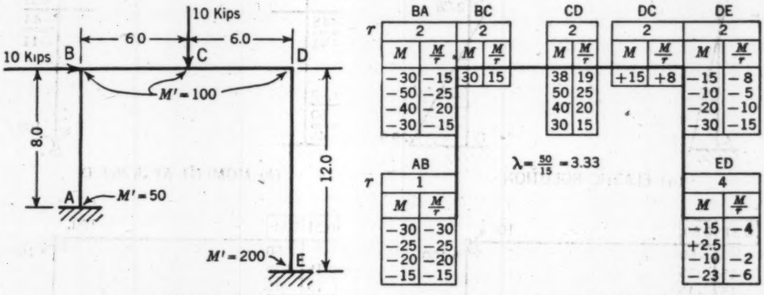
10 Kips
6.0
6.0
10 Kips
B
C
D
M′ = 100
8.0
12.0
A
M′ = 50
M′ = 200
E
BA
BC
CD
DC
DE
r
2
2
2
2
2
M
M/r
BA: −30, −50, −40, −30 | −15, −25, −20, −15
BC: 30 | 15
CD: 38, 50, 40, 30 | 19, 25, 20, 15
DC: +15 | +8
DE: −15, −10, −20, −30 | −8, −5, −10, −15
λ = 50/15 = 3.33
AB
r
1
AB: −30, −25, −20, −15 | −30, −25, −20, −15
ED
4
ED: −15, +2.5, −10, −23 | −4, −2, −6

(a) LOADING CONDITION (b) COMPLETE SOLUTION

FIG. 7.—SOLUTION OF EXAMPLE 4

Example 4.—The frame shown in Fig. 7(*a*) is solved in Fig. 7(*b*). The shear relation of Eq. 4 can be rearranged into a more convenient form to facilitate the solution of this example. Thus,

$$M_{AB} + M_{BA} = 80 - \tfrac{2}{3}\,(M_{CD} + M_{DC}) \quad \text{............} \quad (5a)$$

or

$$M_{CD} + M_{DC} = 120 - \tfrac{3}{2}\,(M_{AB} + M_{BA}) \quad \text{...........} \quad (5b)$$

ORDER OF THE DEVELOPMENT OF YIELD-HINGES

It has been shown previously that the individual member stiffnesses have no effect on the final location of the yield-hinges. Nevertheless, the stiffnesses do affect the order in which the yield-hinges form. Inasmuch as the design can be governed by considerations other than the condition for final collapse of the structure—for example, deflection—it often is desirable to know what yield-hinges have developed at intermediate stages. This can be accomplished by extending the application of the relaxation technique with proper regard to the actual stiffnesses of the members. In this case the excess moment at a point must be distributed by the elastic method developed by Hardy Cross, Hon. M. ASCE. However, the accuracy required is low because a relatively large percentage of error in the adjustment of the amount, which is itself only a fraction of the total moment, represents a correspondingly small error in the final answer.

The elastic solution for Example 1 is shown in Fig. 8(*a*). It is seen that the first yield-hinge will occur at joint D as a result of a maximum moment of 29.9. The excess moment at joint D can be eliminated by superimposing an opposite moment at that joint. The distribution of an arbitrarily applied moment of 100 at joint D is shown in Fig. 8(*b*), in which the factors for the distribution of moment at each joint are shown in boxes above the appropriate joint. In this case the sidesway unbalanced moment equals 139 and is balanced by moments of −50 at joint A, −45 at joint B, and −44 at joint C. The distributed moment values at the various points of the frame can be assumed to be influence coefficients for a moment change at joint D.

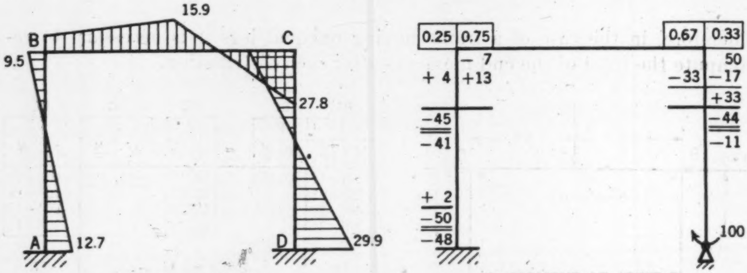
15.9
B
C
9.5
27.8
A
12.7
D
29.9
0.25
0.75
− 7
+ 4
+13
−45
−41
+ 2
−50
−48
0.67
0.33
50
−33
−17
+33
−44
−11
100

(*a*) ELASTIC SOLUTION (*b*) MOMENT AT JOINT D

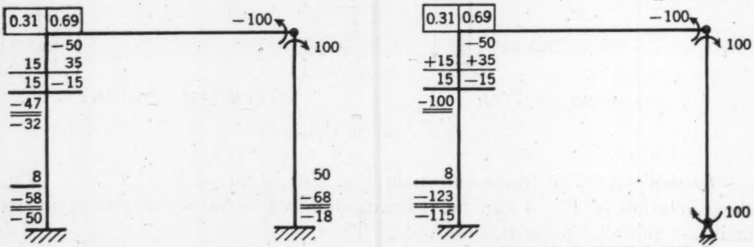
0.31
0.69
−50
15
35
15
−15
−47
−32
8
−58
−50
−100
100
50
−68
−18
0.31
0.69
−50
+15
+35
15
−15
−100
8
−123
−115
−100
100
100

(*c*) MOMENT AT JOINT C (*d*) MOMENT AT JOINT C AND D

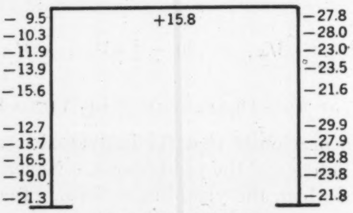
− 9.5
−10.3
−11.9
−13.9
−15.6
−12.7
−13.7
−16.5
−19.0
−21.3
+15.8
−27.8
−28.0
−23.0
−23.5
−21.6
−29.9
−27.9
−28.8
−23.8
−21.8

(*e*) FINAL DISTRIBUTION

FIG. 8.—ORDER OF DEVELOPMENT OF HINGES FOR EXAMPLE 1

By relaxing the moment at joint D an amount of 2 (Fig. 8(*e*)), joint C develops a maximum moment. Consequently a set of coefficients must be determined for joint C, as shown in Fig. 8(*c*). In this case the sidesway unbalanced moment equals 193 and is balanced by moments of −58 at joint A, −47 at joint B, and −68 at joint D.

The excess moment at joint C is reduced by 5 (Fig. 8(*e*)), but it is noted that the relaxation of the moment at joint C disturbs the value of the moment at joint D. Therefore, the moment at joint D must be reduced. Choosing a value of 5 for this reduction causes the moment at joints C and D to be approximately equal. The moment of 23.8 is greater than the moment of 21.7 that was completed in Example 1. This necessitates the relaxing of joints C and D simultaneously by adding the coefficients for joints C and D, as shown in Fig. 8(*d*). In Fig. 8(*d*) the sidesway unbalanced moment equals 223 and is balanced by moments of −123 at joint A and −100 at joint B. The distribution shown in Fig. 8(*d*) results in the final moments shown in Fig. 8(*e*).

CONCLUSION

The method that has been proposed for determining the final mode of collapse of a frame is simple and readily applicable for the solution of relatively complicated frames. The method does not require that the moment be constant with increasing angular distortion but only that the moment reach a maximum value from which it does not diminish.

The determination of the condition of final collapse is not the entire problem. In many cases the limit design of a rigid frame may be governed by (*a*) the limit of deformation, (*b*) the limit of stability, or (*c*) the need to guard against an inelastic stress reversal. Under these circumstances the ultimate loading will be less than the collapse value. Hence, a knowledge of the progress of collapse from yield-hinge to yield-hinge is required. The method determines this order of yield-hinge development in relation to the actual stiffnesses of the members.

DISCUSSION

Noel W. Murray.[5]—A method for determining the load factor of frameworks containing plastic hinges has been developed by the author. The method is simple in its application, and the physical steps involved are readily visualized.

There is, however, one way in which the arithmetical work can be simplified. The simplification can be attained by applying simple formulas to determine the carry-over moments which maintain equilibrium when the moment on one end is relaxed. Thus, if in Fig. 9(*a*) AB is a beam in a structure loaded by a concentrated load P at C (the center), the beam has moments M_A and M_B acting on its ends. These moments maintain equilibrium with the load P and the reactions R_A and R_B. Similarly, there is a moment M_C acting at C, as shown in Fig. 9(*b*). If the moment M_B is increased by ΔM_B, then M_A and M_C will have to be altered to maintain equilibrium of the beam. The increases ΔM_A and ΔM_C in M_A and M_C are found from the equations of equilibrium:

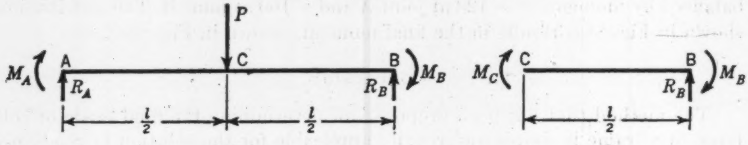

(*a*) (*b*)

Fig. 9.—Beam Subjected to a Concentrated Load at Its Center

$$M_A + M_B + \frac{P\,l}{2} - R_B\,l = 0 \qquad (6a)$$

and

$$M_C + M_B - \frac{R_B\,l}{2} = 0 \qquad (6b)$$

Eliminating R_B from Eqs. 6 results in

$$2\,M_C + M_B - M_A - \frac{P\,l}{2} = 0 \qquad (7)$$

On taking differentials, Eq. 7 leads to

$$2\,\Delta M_C + \Delta M_B - \Delta M_A = 0 \qquad (8)$$

Thus it can be seen that the moments can be varied at will without having to check the beam for equilibrium after each relaxation. For example, if joint A is held rigid and joint B is relaxed by 20 units of moment, $\Delta M_A = 0$ and $\Delta M_B = -20$, whence $\Delta M_C = +10$. This computation indicates that, in order to maintain equilibrium, the moment at C will have to be increased by 10.

---

[5] Asst. Lecturer, Eng. Dept., Univ. of Manchester, Manchester, England.

Eq. 8 is also applicable to a uniformly distributed load because member stiffness is not included. If P is placed at a distance $k\,l$ from A instead of being at the center, the equation corresponding to Eq. 8 is

$$\Delta M_C + k\,\Delta M_B - (1-k)\,\Delta M_A = 0 \qquad (9)$$

Herman Tachau,[6] A. M. ASCE.—The application of relaxation techniques to limit design is an important addition to structural analysis. Heretofore, using principles evolved[2] by Messrs. Greenberg and Prager, the location of yield-hinges had to be guessed. The method offered by Mr. English practically obviates all guesswork; the necessity for good judgment in selecting the locations of yield-hinges (or the initial distribution of moments) is reduced to a minimum. In addition, a useful procedure for tracing the order of the development of yield-hinges has been presented.

For continuous beams and simple rectangular frames, the mode of collapse and the correct locations of yield-hinges are predicted easily. The author's method of analysis will therefore be more useful when applied to complicated frameworks. The ultimate purpose of structural analysis is to benefit the designer. With this in mind, it has been pointed out[7] that (in practice) complicated frames are most likely to be subject to several different simultaneous loadings, the magnitudes of which vary independently of each other. For example, P and H in Fig. 4(*a*) may be increasing toward collapse at different rates. Cases of this sort can be investigated by plotting limiting values of P versus H to establish the "safe domain."[8, 9] The concept of the safe domain is similar to the graphical representation commonly used to define the various criteria of failure for stresses at a point in a body subjected to biaxial or triaxial loading.

Yield-hinges can occur between joints as well as at the joints. Therefore, in contrast to the moment-distribution method, it is important to record moment values at pertinent intermediate points. Such points would occur under concentrated loads and at other points where bending moments are high. In Example 2 (Fig. 5) only the first and final values of the positive moment at point J are shown. It would be preferable to record a value for each stage of the computations. Similarly, in Fig. 8(*e*), the positive moments under the load P should be written as: 15.8, 16.0, 19.2, 19.6, and 21.8. (The example illustrated by Fig. 8 would have been more realistic if M' had been varied in accord with the K-values.)

There exists a remote possibility—theoretically, at least—that the assumed initial distribution of moments may be so far from reality that the process might not converge. It may be of interest to investigate this possibility. Such an investigation has been performed for the method of moment distribution as applied to continuous beams.[10]

---

[6] Bridge Designer, New Mexico State Highway Dept., Santa Fe, N. M.

[7] "Limit Design of Beams and Frames," by H. J. Greenberg and W. Prager, *Transactions*, ASCE, Vol. 117, 1952, pp. 463–464.

[8] *Ibid.*, p. 482. Fig. 26.

[9] "Limit Analysis and Design," by W. Prager, *Journal*, A. C. I., Vol. 25, 1953, p. 300.

[10] "Convergence of Hardy Cross's Balancing Process," by Rufus Oldenburger, *Transactions*, ASME, Vol. 62, 1940, p. A-166.

The discussion of the paper by Messrs. Greenberg and Prager revealed many limitations and practical difficulties still to be overcome; most of that discussion applies here as well. Undoubtedly Mr. English has helped to pave the way toward a wider acceptance of limit design. His method will appeal to structural engineers because—as in the moment distribution—every step in the computations represents a physical action which can be readily visualized. This paper deserves careful study by all engineers interested in limit design.

J. Morley English,[11] A. M. ASCE.—An important simplification for checking the stability of each individual member of the frame has been recognized by Mr. Murray. The technique suggested is implicit in the method developed by the writer. A unique relationship exists between any change to the end moments and the moments throughout the member. This relationship can be explicitly determined in the form of Eq. 9. The use of such a relationship should facilitate the computational procedure, and Mr. Murray has made a valuable contribution in directing attention to this point.

Mr. Tachau has cited a practical limitation inherent in all ultimate-load methods of analysis for which the loads are assumed to increase proportionally to failure. All real structures are subjected to a combination of loads which can be applied in various orders. As a consequence, the most useful design approach will be to establish an envelope curve or domain of ultimate-loading combinations. Then, provided the actual loads (with a suitable safety factor) are within this domain, the structure may be presumed to be safe.

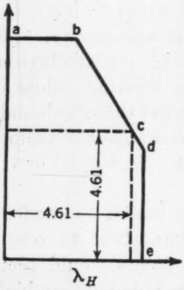

Fig. 10.—Envelope Curve for Horizonal and Vertical Loads

For example, one might consider the domain for P and H in Example 1 (under the heading, "Conditions of Collapse") the solution of which is illustrated in Fig. 4. If no load P were applied, the limit moments would develop at points A, B, C, and D in Fig. 4, and the value of λ_H would be equal to 5.0. If H is held constant at this ultimate-load value, a load P can still be applied until a further hinge develops under the point of load application. The value for λ_P is determined from the simple static solution of the beam BC because the moments at the ends cannot be changed without altering H. Thus, λ_P is equal to 4 (Fig. 10). It is evident that a further increase in P can only be accomplished by decreasing the value of H. This increase can proceed until local collapse of the beam is imminent. Thus, continuing this approach, the envelope curve can be completed. The solution of Example 1 was for a unique loading condition that determined one point on the envelope curve, point c in Fig. 10, where λ is the same for both the horizontal and vertical loads. It should be realized that the scope of the original investigation did not include the reverse-loading problem.

---

[11] Associate Prof. of Eng., Univ. of California, Los Angeles, Calif.

AMERICAN SOCIETY OF CIVIL ENGINEERS
Founded November 5, 1852
TRANSACTIONS

Paper No. 2716

LAMINAR TO TURBULENT FLOW IN A WIDE OPEN CHANNEL

BY W. M. OWEN[1]

WITH DISCUSSION BY MESSRS. YUICHI IWAGAKI; J. W. DELLEUR; RALPH W. POWELL AND CHESLEY J. POSEY; HENRY MAKSOUD; AND W. M. OWEN

SYNOPSIS

Theoretical equations are presented, involving the velocity and rate of laminar flow in rectangular channels and in channels of infinite width. Data taken at shallow depths on an open channel 1.5 ft wide and 20 ft long are plotted in a graph showing the relation between the friction factor and the Reynolds number. The point of departure of these data from the theoretical laminar flow line is taken to be the critical value of the Reynolds number at which the flow changes from laminar to turbulent. A thread of dye was also injected into the flow to determine whether the flow was laminar, turbulent, or transitional. The two methods of determining the critical velocity gave similar results.

1. INTRODUCTION

In spite of the extensive literature on the subject of open channel flow, little information is available on laminar flow and the transition from laminar to turbulent flow in open channels. The following quotation from a well-known textbook[2] on fluid mechanics is indicative of the present state of knowledge of this subject:

> "It might, in fact, be inferred from analogy with pipe flow that below some 'critical' velocity the resistance will be proportional to the first power of the velocity. The clear glassy non-distortive reflecting surface observed in any long straight reach of a deep and sluggish stream tends to strengthen this inference, while the behavior of small particles of suspended matter appears to show almost conclusively that at low speed motion takes place in stream lines."

NOTE.—Published, essentially as printed here, in April, 1953, as *Proceedings-Separate No. 188.* Positions and titles given are those in effect when the paper or discussion was received for publication.

[1] Development Engr., Airesearch Mfg. Co., Los Angeles, Calif.

[2] "Hydraulics and Its Applications," by A. H. Gibson, D. Van Nostrand Co., Inc., New York, N. Y., 1930, p. 295.

Observers engaged in the measurements of the discharge of natural streams testified that, from time to time, the method of measuring the discharge based on turbulent flow fails, and that the discharge appears to be varying approximately as the first power of the slope. In 1907, E. C. Thrupp[3] conducted experiments on the Thames and Kennet rivers in England and ascertained that, below an average velocity of 0.64 ft per sec, the velocities were approximately proportional to the slope, and above this velocity, the velocities were approximately proportional to the square root of the slope. Mr. Thrupp reached the conclusion that laminar flow existed below this critical value of the velocity, which would indicate that laminar flow existed at Reynolds numbers of several hundred thousand. If this conclusion is correct, the subject of laminar flow in open channels is not merely an academic one but is of vital interest to engineers engaged in open channel work. On the other hand, if the critical Reynolds number for open channel flow is the same, or somewhat lower, than that for closed conduits, as indicated by some writers, practically all open channel flow of interest to the hydraulic engineer would occur in the turbulent range, and the subject of laminar flow in open channels would be of little interest to the hydraulic engineer.

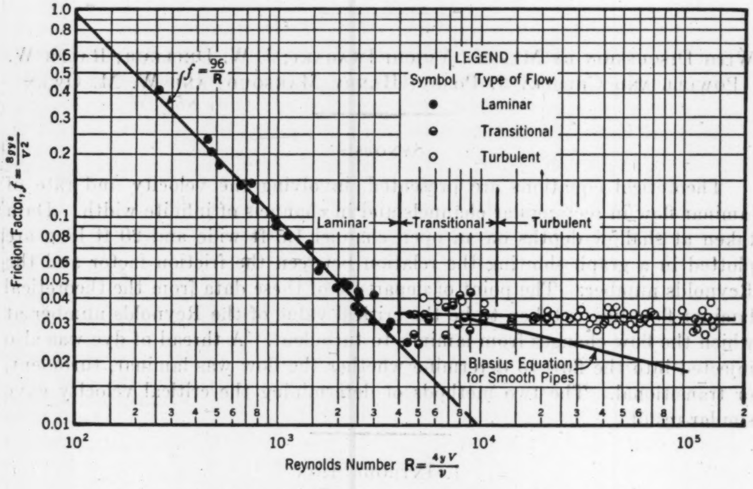

FIG. 1.—RELATION BETWEEN THE FRICTION FACTOR AND THE REYNOLDS NUMBER FOR A WIDE OPEN CHANNEL

The depth of water in the channel used in this investigation (1.5 ft wide) never exceeded 0.3 ft so that the flow conditions in the channel could be considered to approach the conditions of flow in a channel of infinite width. Determination of whether the flow was laminar or turbulent was made by noting both the variation of the resistance law (Fig. 1), and the behavior of a stream of colored water injected into the flow in the manner introduced by Osborne Reynolds.

---

[3] "Flowing Water Problems," by E. C. Thrupp, *Proceedings*, Inst. C. E., London, England, Vol. 171, 1907-1908, p. 346.

2. Apparatus and Procedure

Fig. 2 is a photograph of the glass-walled flume used in this investigation. The flume consists of a large reservoir containing a gravel baffle, an approach section, and a rectangular glass-walled channel 20 ft long and 1.5 ft wide. The bottom of the channel is made of polished brass plate. The support consists of a roller under the reservoir, about which the entire flume pivots, and threaded posts at the downstream end of the channel. The slope may be changed by turning nuts on the threaded posts by means of a suitable gear train. This channel was leveled carefully by means of a surveyor's instrument before the beginning of the tests. A counter mounted on the shaft of the slope-adjusting wheel was then set at zero, and the slopes for the various tests were determined from the reading of this counter. The bottom was found to be not perfectly flat, showing depressions and elevations in the order of magnitude of 0.01 in. These depressions and elevations may cause serious errors when small slopes and shallow depths are used. Preliminary tests were made to determine the smallest slopes at which consistent data could be taken, and no data appearing in this paper were taken for slopes below this value.

Fig. 2.—Laboratory Arrangement of the Glass-Walled Flume Used in the Investigation

The depth of water in the channel was controlled by a brass end gate. Two electric point gages, 10 ft apart, were used to measure the depth of water in the channel to the nearest 0.0005 ft. The rate of flow was determined by measuring the time necessary to collect a given weight of water in a tank mounted on a calibrated scale.

The nature of the flow in the channel was made visible by injecting colored water into the stream through a long glass tube (3 mm, outside diameter) parallel to the direction of the flow. The colored water was made by dissolving a few crystals of potassium permanganate in a beaker of water.

The test procedure was as follows: The channel was set at a given slope, and the tail gate was adjusted to give approximately the desired depth for the test. The supply-control valve was then adjusted until uniform flow was established. The rate of discharge, the depth, and the water temperature were then determined and recorded. Colored water was next introduced into the stream, and the nature of the flow was noted and recorded.

3. DERIVATION OF THE THEORETICAL EQUATIONS FOR THE VELOCITY DISTRIBUTION AND THE RATE OF FLOW FOR LAMINAR FLOW IN OPEN CHANNELS

General Equations for Laminar Flow in Channels of Rectangular Cross Section.—In deriving the following relationships, use will be made of the fact that the theoretical flow characteristics, such as velocity distribution and energy loss for an open channel of depth a and width $2\,b$ (Fig. 3), are exactly the same as those of one half of a closed conduit of depth $2\,a$ and width $2\,b$. The use of this fact simplifies the problem considerably, inasmuch as the boundary conditions are the same for all sides. The following equations are valid for all rectangular conduits and channels, subject to the restriction that depth a in the following equations must always be one half of the length of the shorter side.

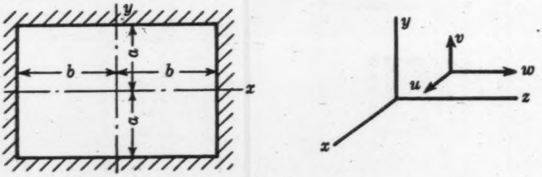

FIG. 3

The Navier-Stokes equations for this case reduce to

$$\nu\left(\frac{\partial^2 w}{\partial x^2}+\frac{\partial^2 w}{\partial y^2}\right)=-\,g\,\frac{\partial H}{\partial z}=-\,g\,S=\text{constant}\,\ldots\ldots\ldots\,(1)$$

or

$$\frac{\partial^2 w}{\partial x^2}+\frac{\partial^2 w}{\partial y^2}=-\,\frac{g\,S}{\nu}=-\,\mathrm{K}\,\ldots\ldots\ldots\ldots\ldots\ldots\,(2)$$

in which S is the slope of the channel, ν is the kinematic viscosity, and g is the acceleration of gravity. The boundary conditions are as follows: When

$$y=\pm\,a;\qquad w=0$$

and when

$$x=\pm\,b;\qquad w=0.$$

Eq. 2 is of the same form as the differential equation obtained in the problem of torsion of rectangular bars. The solution of this equation has been found, by S. Timoshenko,[4] to be

$$w = \frac{16\,K\,b^2}{\pi^3} \sum_{n=1,3,5}^{\infty} \frac{1}{n^3} (-1)^{(n-1)/2} \left(1 - \frac{\cosh \dfrac{n\,\pi\,y}{2\,b}}{\cosh \dfrac{n\,\pi\,a}{2\,b}}\right) \cos \frac{n\,\pi\,x}{2\,b} \quad \ldots\ldots(3)$$

Eq. 3 gives the velocity at any point of the cross section. The rate of flow, Q, in an open channel of depth a and width $2\,b$ may be determined from the following equation:

$$Q = \int_{-b}^{b} \int_{o}^{a} w\,dx\,dy \quad \ldots\ldots(4)$$

The solution of this equation has been found, by Mr. Timoshenko, to be

$$Q = \frac{2}{3}\,K\,b^3\,a \left(1 - \frac{192\,b}{\pi^5\,a} \sum_{n=1,3,5}^{\infty} \frac{1}{n^5} \tanh \frac{\pi\,n\,a}{2\,b}\right) \quad \ldots\ldots(5)$$

Derivation of the Theoretical Expression for the Friction Factor for Laminar Flow in a Channel of Infinite Width.—The following expressions for laminar flow in a channel of infinite width were given by Robert E. Horton, M. ASCE, H. R. Leach, A.M. ASCE, and R. Van Vliet,[5] M. ASCE. The velocity distribution ω is given by

$$\omega = \frac{g\,S}{2\,\nu} (a^2 - y^2) \quad \ldots\ldots(6)$$

the rate of flow per unit width by

$$q = \int_{-a}^{o} \omega\,dy = \frac{g\,S\,a^3}{3\,\nu} \quad \ldots\ldots(7)$$

and the average velocity, V, is equal to

$$V = \frac{q}{A} = \frac{g\,S\,a^2}{3\,\nu} \quad \ldots\ldots(8)$$

The Darcy equation for uniform flow in an open channel may be written as

$$S = \frac{f}{4\,R} \frac{V^2}{2\,g} \quad \ldots\ldots(9)$$

in which f is the friction factor and R is the hydraulic radius.

The characteristic dimension used is four times the hydraulic radius, so that the friction factors obtained will be comparable to those found for flow in pipes, using the diameter as the characteristic length. On substituting

---

[4] "Theory of Elasticity," by S. Timoshenko, McGraw-Hill Book Co., Inc., New York, N. Y., 1934.

[5] "Laminar Sheet Flow," by Robert E. Horton, H. R. Leach, and R. Van Vliet, *Transactions*, Am. Geophysical Union, 1933–1934, pp. 393–404.

Eq. 7 into Eq. 8 and simplifying,

$$f = \frac{24\,\nu}{q} \tag{10}$$

For two-dimensional flow $\overline{\mathsf{R}}$ (the Reynolds number) is equal to $4\,\frac{q}{\nu}$, and

$$f = \frac{96}{\overline{\mathsf{R}}} \tag{11}$$

A plot of this equation is shown along with the experimental data in Fig. 1.

General reading references in support of the theoretical parts of this paper are to be found in the works of A. H. Gibson[2]; Mr. Thrupp[3]; Mr. Timoshenko[4]; Messrs. Horton, Leach, and Van Vliet[5]; Lorenz G. Straub[6]; J. Allen[7]; R. J. Cornish[8]; L. Hopf[9]; H. Jefferys[10]; H. Levy[11]; and in "Some Experiments on Shallow Flows Over a Grassed Slope," presented[12] in 1939.

4. Experimental Results

The results of the experimental part of this investigation are summarized in Fig. 1, showing the relation between the friction factor and the Reynolds number plotted to logarithmic scales. The theoretical relationship for two-dimensional flow and Blasius' empirical relation for turbulent flow in smooth pipes is shown in addition to the experimental data. The data depicted by the solid circles are for test runs in which the thread of dyed water injected into the stream maintained a straight unbroken line for the entire length of the channel. The data designated by the half-solid circles are for test runs in which the dye thread was observed to oscillate but remained intact. The data shown by the open circles are for test runs in which the dye thread was observed to break up and to disclose the presence of vortices.

The critical Reynolds number is taken to be the value of the Reynolds number at which the average curve through the experimental data first departs from the theoretical curve for laminar flow. From the graph, the critical Reynolds number appears to be approximately 4,000.

The data near the critical Reynolds number were taken for both increasing (that is, laminar to turbulent) and decreasing (that is, turbulent to laminar) Reynolds numbers. No difference in the value of the critical Reynolds number was found for the two conditions. This result is believed to be caused by the fact that initial disturbance in the water was such that the upper and lower critical Reynolds numbers coincided.

---

[6] "Studies of the Transition Region Between Laminar and Turbulent Flow in Open Channels," by Lorenz G. Straub, *Transactions*, Am. Geophysical Union, 1939, pp. 649–653.

[7] "Streamline and Turbulent Flow in Open Channels," by J. Allen, *London, Edinburgh, and Dublin Philosophical Magazine and Journal of Science*, Vol. 17, No. 116, June, 1934, pp. 1081–1112.

[8] "Flow in a Pipe of Rectangular Cross-Section," by R. J. Cornish, *Proceedings*, Royal Soc. of London, Series A, Vol. 120, 1928, pp. 691–695.

[9] "Turbulenz bei einen Flusse," by L. Hopf, *Annalen der Physik*, Vol. 32, Sect. 4, April–July, 1910, pp. 777–808.

[10] "Flow of Water in an Inclined Channel of Rectangular Section," by H. Jefferys, *London, Edinburgh, and Dublin Philosophical Magazine and Journal of Science*, Vol. 49, No. 293, May, 1925, pp. 793–807.

[11] "On the Criterion for Stable Flow of a Fluid in a Uniform Channel," by H. Levy, *Proceedings*, Royal Soc. of Edinburgh, Vol. 41, Pt. 2, 1920–1921, pp. 136–147.

[12] "Some Experiments on Shallow Flows over a Grassed Slope," *Transactions*, Am. Geophysical Union, Pt. IV, 1939, pp. 653–656.

The "dip" in the curve and the scatter of data which characterize the transition region in the Stanton diagram for flow in pipes are also present in the data shown in Fig. 1.

The Blasius empirical relation is shown in Fig. 1, so that a comparison in the turbulent flow range of the friction factors for smooth pipes and the experimental data for the smooth channel used in this investigation might be made. The data from this investigation agree with the Blasius equation only for a small range of values in the transition region. The experimental data presented show an almost constant friction factor in the turbulent flow range, which is characteristic of the type of curve obtained for pipes of considerable roughness. The increasing degree of scatter, with increasing Reynolds numbers, may be explained by the fact that surface waves present at the higher values of Reynolds number made it difficult to determine depths in the channel.

5. CONCLUSION

From the results of this investigation, four general conclusions can be drawn concerning laminar flow and the transitions from laminar to turbulent flow, as applied to the flow of water in a wide open channel:

1. In the laminar range, the curve showing the relationship between the friction factor and the Reynolds number agrees well with the theoretical equation derived from the Navier-Stokes equations in Section 3 of this paper.
2. The value of the Reynolds number at which the flow first departs from the laminar state is approximately 4,000.
3. There is a transition from laminar to turbulent flow, which extends approximately from a Reynolds number of 4,000 to 11,000, in which the flow is neither truly laminar nor turbulent. There is considerable uncertainty as to the value of the friction factor in this range.
4. The data presented in this paper for the turbulent flow range are not in agreement with the smooth pipe curve of Blasius, but rather show an almost constant value of the friction factor.

Comment.—From the evidence presented herein, it would appear that it is unlikely that laminar flow would exist in large natural streams. The fact that the surface of the stream exhibits a smooth glassy surface, as noted by several writers, is no indication that the flow is laminar; possibly it indicates that only the surface velocity is lower than that necessary for capillary waves to form. Laminar open channel flow is known to exist in nature, however, with the flow of thin sheets of water over the surface of the ground.

The information contained in this paper may be of importance in the study of models of natural open channels. The rates of flow and the dimensions of the model are such that the Reynolds numbers frequently fall in the laminar or transitional range, as determined in this investigation. The fact that the flow in the prototype is turbulent, whereas that in the model may be either laminar or transitional, may be one cause of the difficulty in the verification of models.

ACKNOWLEDGMENT

This investigation was conducted in the Hydraulics Laboratory of the Department of Theoretical and Applied Mechanics, as a part of the work of the Engineering Experiment Station of the University of Illinois, at Urbana.

Acknowledgment is due H. L. Langhaar for his able assistance in the theoretical part of this paper, and to W. M. Lansford, M. ASCE, under whose direction a preliminary investigation was performed as a thesis project.

DISCUSSION

Yuichi Iwagaki.[13]—In the hydraulic laboratory of Kyoto University (Kyoto, Japan), the writer has performed an experiment[14] similar to that conducted by the author. In this experiment, a rectangular section, planed wood flume 40 cm (1.31 ft) wide, 19 cm (0.62 ft) deep, and approximately 18 m (59.1 ft) long (effective length of 10 m (32.8 ft)) was used; the experimental data were taken for slopes of 0.0021, 0.005, 0.01, 0.02, and 0.024, and the water depth varied from 0.16 cm (0.0053 ft) to 3.85 cm (0.126 ft).

Mr. Owen treated his experimental results as two-dimensional flow. Taking the maximum water depth as 0.3 ft, the ratio of water depth y to hydraulic radius R becomes

$$\frac{y}{R}=1+\frac{2\,y}{B}=1+\frac{0.6}{1.5}=1.4\ldots\ldots\ldots\ldots\ldots\ldots\ldots(12)$$

in which B is the width of the flume. The flow of water having such a depth cannot be regarded as two-dimensional flow. The relationship obtained by the writer between the friction factor f and the Reynolds number $\mathbf{R}$ is shown in Fig. 4. The solid line in Fig. 4 satisfies

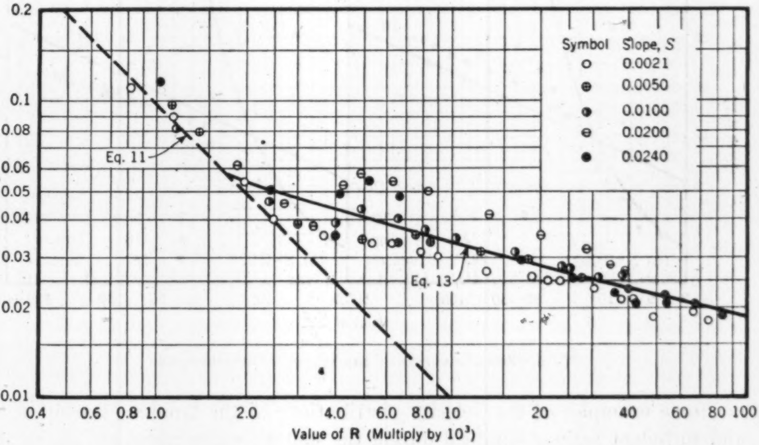

FIG. 4.—RELATION BETWEEN THE FRICTION FACTOR AND THE REYNOLDS NUMBER

$$\frac{1}{\sqrt{f}} = 2.033 \log\left(\mathbf{R}\sqrt{f}\right) - 1.081\ldots\ldots\ldots\ldots\ldots\ldots(13)$$

---

[13] Asst. Prof. of Hydraulics, Dept. of Civ. Eng., Kyoto Univ., Kyoto, Japan.

[14] "Studies on the Thin Sheet Flow (1st Report)," by Tojiro Ishihara, Yuichi Iwagaki, and Takeshi Goda, *Transactions*, Japan Soc. of Civ. Engrs., No. 6, 1951, pp. 31–38 (in Japanese).

Eq. 13 can also be obtained from the equation for the distribution of velocity in a smooth pipe

$$\frac{u}{V_f} = 5.5 + 5.75 \log \frac{V_f Z}{\nu} \qquad (14)$$

in which u is the velocity at the distance Z from the bottom and V_f the friction velocity. It is seen in Fig. 4 that the writer's experimental results tend to be plotted below the curve of Eq. 13 in the case of gentle slopes, and above the curve in the case of steep slopes. The reasons for these results have been explained by the writer.[15] The author's experimental data in the turbulent region (Fig. 1) show an almost constant value for the friction factor. This can be explained by the fact that the results obtained three dimensionally in Mr. Owen's experiment were expressed two dimensionally.

The values of the Reynolds number at the change from laminar to transitional flow and from transitional to turbulent flow are found in Fig. 4 to be 2,000 and 5,000, respectively. Both of these critical values are smaller than those found by the author, and this difference is caused by the amount of initial disturbance resulting from the shape of the entrance to the flume.

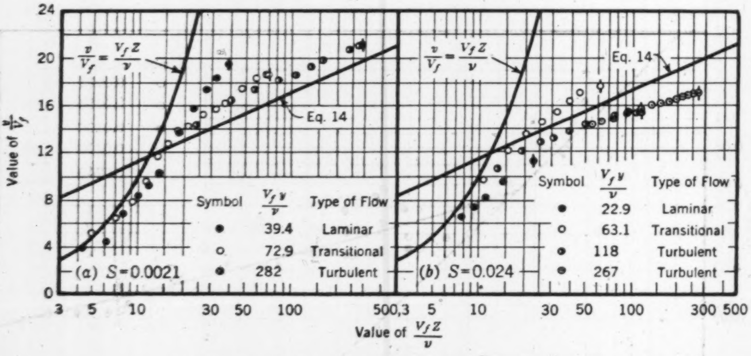

FIG. 5.—SOME EXAMPLES OF THE VELOCITY DISTRIBUTIONS

Some examples of the velocity distributions in the laminar, transitional, and turbulent regions obtained during the writer's experiments are shown in Fig. 5. The differences between the velocity distributions in each region are also shown in Fig. 5.

Investigations of flow with low Reynolds numbers are necessary for the examination of the problems of drainage and soil erosion. It is also important to develop the relationship between the type of flow, either laminar or turbulent, and sediment transportation.

---

[15] "On the Laws of Resistance to Turbulent Flow in Open Smooth Channels," by Yuichi Iwagaki, *Memoirs*, Faculty of Eng., Kyoto Univ., Vol. 15, No. 1, January, 1953, pp. 27–40.

J. W. DELLEUR,[16] J. M. ASCE.—The determination of the Reynolds number at which the transition from laminar flow to turbulent flow occurs in open-channel flow, and the relationship between the friction factor and the Reynolds number, fill a void in the knowledge of open-channel flow. The departure of the experimental data from the Blasius equation, shown in Fig. 1, is of special interest to those engineers investigating turbulent flow in open channels.

The applications of Mr. Owen's results are limited to smooth rectangular channels as his investigations were performed in a glass-walled flume with a smooth brass bottom. Determination of the effect of roughness, and preparation of a system of curves, similar to that shown in Fig. 1 (in which the relative roughness is a parameter), would seem to be the next steps to be undertaken.

The points which seem to need some clarification are whether the author's experiments actually led to a condition of uniform flow, and whether the flow was sufficiently two dimensional to justify the neglect of the side-wall effects.

First it seems questionable that a depth of 0.3 ft in a 1.5-ft-wide channel (that is, a ratio of width to depth of $\frac{1}{5}$) can be considered to approximate the flow conditions that exist in a channel of infinite width. The writer has studied phenomena in open-channel flow connected with the development of the turbulent boundary layer along the bottom of an open horizontal channel. The depth-to-width ratio which was used varied from $\frac{1}{6}$ to $\frac{1}{8}$, and it was found that the flow was not truly two dimensional. The results obtained show that the side-wall boundary layers have a substantial effect on the rate of growth of the bottom boundary layer.

The second point concerns the assumption of uniform flow made by the author in all his theoretical considerations and also his interpretation of the experimental data. The experimental flow was gaged to assure uniform depth. This gaging provided a constant mean velocity, but it did not necessarily assure a uniform velocity distribution throughout the test section. A uniform velocity distribution would be obtained if the boundary layer, which began at the entrance of the channel, were fully developed at the upstream end of the test section.

In Mr. Owen's experiments the boundary layer may not have been fully developed before the test section was reached. The formula for the development of the boundary layer along a flat plate leads to the conclusion that, for a Reynolds number of 3,000, under the test conditions indicated, a length of 9 ft (almost half the channel length) is required to obtain a full development of the boundary layer. Furthermore, A. E. Craya and the writer have found that the development of the boundary layer along the bottom of an horizontal channel is slower than that along a flat plate in an infinite fluid.[17] In unconfined flow, as along a flat plate in an infinite fluid, the displacement of the outer flow caused by the boundary layer disturbs the original flow around the body only slightly. However, in open-channel flow the boundary layer has a substantial influence on the frictionless flow outside the boundary layer. The effect of the side walls is to decrease further the rate of growth of the boundary layer along the bottom of the channel. It then appears that, in some of the author's experiments, the boundary layer may not have been completely developed before it reached the test section of the channel—that is, between the two electric point gages.

---

[16] Instructor in Civ. Eng., Columbia Univ., New York, N. Y.

[17] "An Analysis of Boundary Layer Growth in Open Conduits near Critical Regime," by A. E. Craya and J. W. Delleur, *CU-1-52-ONR-266 (10)-CE*, Dept. of Civ. Eng., Columbia Univ., New York, N. Y., 1952 (report to the Office of Naval Research).

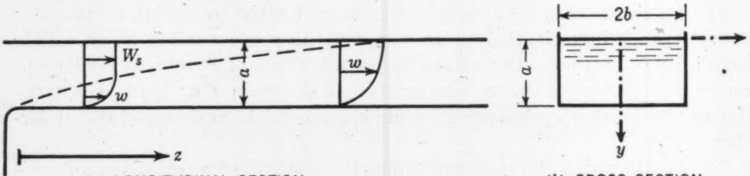

(*a*) LONGITUDINAL SECTION (*b*) CROSS SECTION

Fig. 6.—Sections of the Experimental Channel

To illustrate the boundary-layer growth, Fig. 6 shows the sections of the channel used by the writer to obtain the experimental data shown in Fig. 7.

Velocity-distribution measurements were taken for several flow conditions—ranging from laminar flow to turbulent flow—and for different values of the ratio, z/a. The channel used (Fig. 6) was 13.5 in. wide and 15 ft long. The velocity measurements were taken by using a pitot tube made of a hypodermic needle (outside diameter of 0.060 in. or 0.027 in.) mounted on a streamlined lucite stem. The vertical motion of the pitot tube was controlled to the nearest 0.0005 in. by a traverse gear. The velocity head was measured to the nearest 0.001 in. by a micromanometer which was described by R. C. Pankhurst[18] and by E. Ower.[19]

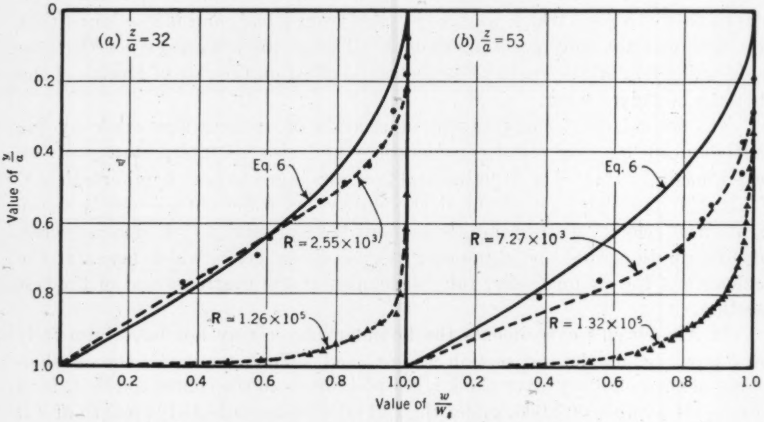

Fig. 7.—Velocity Profiles for Laminar and Turbulent Flows at the Same Relative Abscissa

---

[18] "Wind Tunnel Technique," by R. C. Pankhurst and D. W. Holder, Sir Isaac Pitman & Sons, Ltd., London, England, 1952.

[19] "The Measurement of Air Flow," by E. Ower, Chapman & Hall, London, England, 1933.

For the purpose of comparison, the theoretical velocity distribution given by Eq. 6 has been plotted in Fig. 7. It can be seen that the velocity distribution given by Eq. 3, at least for $x = 0$, converges rapidly to the values obtained from Eq. 6 when the ratio b/a in Eq. 3 increases beyond 10.

In Fig. 7(*a*), for $z/a = 32$, the curve for $\mathsf{R} = 2.55 \times 10^3$ shows that for this laminar flow the boundary layer is not fully developed and reaches only 75% of the depth of flow. However, there is good agreement between the experimental and the theoretical curves, and the values of the friction factor will not be greatly affected. In terms of a depth of 0.3 ft, the ratio z/a corresponds to an abscissa —$z = 9.6$ ft— almost at the center of the channel and within the test section. The curve (Fig. 7(*a*)) for turbulent flow at the same value of z/a but for $\mathsf{R} = 1.26 \times 10^5$ shows that the boundary layer is much less developed, and that it reaches approximately 40% of the depth of flow. This fact throws a greater doubt on the uniformity of flow for the turbulent range of Mr. Owen's experiments, and on the applicability of the friction factors computed therefrom to uniform flow.

In Fig. 7(*b*) are presented data similar to those shown in Fig. 7(*a*) for $z/a = 53$, and for a flow in the transitional zone with $\mathsf{R} = 7.27 \times 10^3$ as well as for a turbulent flow with $\mathsf{R} = 1.32 \times 10^5$. All curves for turbulent flow in Fig. 7 were taken essentially for the same flow conditions. The growth of the boundary layer was from 40% to 65% of the depth of flow (Fig. 7(*a*) to Fig. 7(*b*)).

The actual depths a and the surface velocities W_s used by the writer are given in Table 1.

TABLE 1.—DEPTHS AND SURFACE VELOCITIES CORRESPONDING TO FIG. 7

Relative abscissa z/a	Reynolds number R	Depth a, in feet	Surface velocity W_s, in feet per second
32	2.55×10^3	0.0410	0.150
32	1.26×10^5	0.1715	1.660
53	7.27×10^3	0.0965	0.182
53	1.32×10^5	0.1643	1.800

Regarding the velocity measurements in turbulent flow, it can be added that a roughness element was placed at the entrance of the channel so as to insure a turbulent boundary layer beginning at that point.

It would seem that Mr. Owen's experiments for laminar flow achieved a velocity distribution close to the theoretical distribution. However, in the case of turbulent flow, the experiments probably differed substantially from the assumed uniform flow. To assure uniform flow in the test section a longer entrance zone is probably necessary. For a closer analysis of data taken near the entrance, the boundary layer and side-wall effect should be considered.

Ralph W. Powell,[20] **and Chesley J. Posey,**[21] **Members, ASCE.**—The experimental results recorded by Mr. Owen are interesting and valuable. Eq. 3, however, is an equation which does not converge when $b > a$.

The difficulty is caused by the fact that Mr. Timoshenko measured a in the x-direction and b in the y-direction, and the author has interchanged them. Mr. Owen has tried to correct for this by interchanging a and b in Mr. Timoshenko's equation; but if b is to approach infinity, it must remain larger than a; thus, x and y should have been interchanged, and Eq. 3 should have been written as

$$w = \frac{16\,K\,a^2}{\pi^3} \sum_{n=1,3,5,\dots}^{\infty} \frac{1}{n^3}\,(-1)^{(n-1)/2} \left[1 - \frac{\cosh\dfrac{n\,\pi\,x}{2\,a}}{\cosh\dfrac{n\,\pi\,b}{2\,a}}\right] \cos\frac{n\,\pi\,y}{2\,a} \dots (15)$$

which reduces to

$$Q = \frac{2}{3}\,K\,a^3\,b\left(1 - \frac{192\,a}{\pi^5\,b} \sum_{n=1,3,5,\dots}^{\infty} \frac{1}{n^5} \tanh\frac{\pi\,n\,b}{2\,a}\right) \dots\dots\dots (16)$$

rather than Eq. 5. When $b = \infty$, Eq. 16 results in

$$q = \frac{Q}{2\,b} = \frac{K\,a^3}{3} = \frac{g\,S\,a^3}{3\,\nu} \dots\dots\dots\dots\dots\dots\dots (17)$$

which is the equation for an infinitely wide channel.

The maximum recorded depths in the 1.5-ft-wide channel were 0.3 ft. This causes some doubt as to whether the data should have been computed as though the width-to-depth ratio were infinite. On substituting $b/a = 5$ into Eq. 16, one finds that the laminar-flow discharge is theoretically reduced 12.6% by the effect of the side walls. The hydraulic radius in this case is 28.5% less than the depth. If the width-to-depth ratio of the various test runs had been similarly accounted for in Fig. 1, the points near the right side, where the discrepancy is the largest, would have moved downward and to the left, perhaps enough to give a more obvious downward trend to the curve in the turbulent range.

Although no theoretical solution is available for the turbulent case, the laminar solution (in which the actual width is taken into account) would seem to provide a sounder basis for the reduction of data than that in which the width-to-depth ratio is assumed to be infinite.

The statement in Sect. 3 that the

> "* * * velocity distribution and energy loss for an open channel of depth a and width $2\,b$ (Fig. 3) are exactly the same as those of one half of a closed conduit of depth $2\,a$ and width $2\,b$"

is open to question. The statement may be approximately true with regard to the energy loss when the flow is laminar (as shown by the author's experiments), but it is doubtful if it is true for velocity distribution, and the statement certainly is not true for either velocity distribution or energy loss when the flow is turbulent. If the statement were true, the maximum velocity would be at the middle of the free surface, whereas experiments show that the maximum velocity is generally depressed below the surface. Experiments have also shown that the discharge of a rectangular channel containing water flowing with uniform depth is not equal to half the discharge of a rectangular pipe twice as deep, flowing full, with the same hydraulic-gradient slope. Garbis H. Keulegan introduced the symbol $\bar{\epsilon}$ to measure the apparent "drag of the free surface" or, more accurately, the effect of the angle between the free surface and the side walls.[22] It appears that this effect is a three-dimensional effect, and that there is double-spiral flow when there is a free surface, which makes the resistance different from that in a full flowing pipe.

---

[20] Prof. of Mechanics, Ohio State Univ., Columbus, Ohio.

[21] Prof. and Head, Dept. of Civ. Eng., State Univ. of Iowa, Iowa City, Iowa.

It is not an established fact that velocity distributions for laminar flow in open channels correspond to half of the solutions of the Navier-Stokes equations for closed conduits. Measurements made by Ellis B. Pickett, in a triangular channel with one side vertical, showed a systematic deviation from the symmetry demanded by this type of theoretical solution.[23] No explanation seemed possible except in terms of an effect of the free surface.

There has been some difference of opinion as to the lower value of the critical Reynolds number for open-channel flow, and the author's value of approximately 4,000 is a significant contribution. The paper[6] by Mr. Straub, (based on data by Edward Silberman), reported a transition range of Reynolds numbers for a rectangular channel from 2,800 to 7,000. Other experimenters[24,25,26,27,28] have found somewhat different values and have conclusively shown that the precise value of the Reynolds number at which flow ceases to be laminar, and the value at which turbulent flow becomes established, depends on the shape of the cross section. This was made especially clear in the work reported by Peter Feng.[28]

The fact that model flow intended to simulate turbulent prototype flow may tend to be transitional or laminar by virtue of the decrease in Reynolds number (inherent in the scale change) has long been recognized as a cause of difficulty in the verification of open-channel models.[29]

There is another possible explanation for Mr. Owen's finding f to be practically constant in the turbulent range. Other investigations have found f to decrease with increasing Reynolds numbers when the channel is smooth.[30]

---

[22] "Laws of Turbulent Flow in Open Channels," by Garbis H. Keulegan, *Research Paper RP1151*, National Bureau of Standards, Washington, D. C., Vol. 21, December, 1938, p. 719, Eq. 48.

[23] "A Direct Optical Method for Measuring Fluid Velocities in Laminar Flow," by Ellis B. Pickett, thesis presented to the State Univ. of Iowa, Iowa City, Iowa, in 1950, in partial fulfilment of the requirement for the degree of Master of Science.

[24] "Experimental Studies of Viscous Flow in a Triangular Open Channel," by Sigurd W. Anderson, thesis presented to the Univ. of Minnesota, Minneapolis, Minn., in 1939, in partial fulfilment of the requirement for the degree of Master of Science.

[25] "Experimental Studies of Velocity Distribution at a Section in a 90° Triangular Channel," by Harry D. Purdy, thesis presented to the Univ. of Minnesota, Minneapolis, Minn., in 1947, in partial fulfilment of the requirement for the degree of Master of Science.

[26] "Flow in a Triangular Channel with Varied Boundary Roughness," by Joseph M. Forns, thesis presented to the Univ. of Minnesota, Minneapolis, Minn., in 1948, in partial fulfilment of the requirement for the degree of Master of Science.

[27] "A Study of Viscous Flow in an Open Channel Having a Circular Arc Cross-Section," by Daniel K. Donovan, thesis presented to the Univ. of Minnesota, Minneapolis, Minn., in 1949, in partial fulfilment of the requirement for the degree of Master of Science.

[28] "Experimental Studies of Viscous Flow in a Triangular Open Channel with Varied Central Vertex Angle," by Peter Chi-Te Feng, thesis presented to the Univ. of Minnesota, Minneapolis, Minn., in 1952, in partial fulfilment of the requirement for the degree of Master of Science.

[29] "Hydraulic Laboratory Practice," edited by John R. Freeman, ASME, New York, N. Y., 1929.

[30] "Resistance to Flow in Smooth Channels," by Ralph W. Powell, *Transactions*, Am. Geophysical Union, December, 1949.

Because the author states that the bottom of the channel had depressions and elevations of the order of 0.01 in., the question arises as to whether the channel was not acting as a rough channel. In Fig. 1 it can be seen that f has an average value, in the turbulent range, of approximately 0.034, which is equivalent to a Chezy coefficient whose value is 87. It has been found[31] that

$$C = 42 \log_{10} \frac{R}{\epsilon} \ldots\ldots\ldots\ldots\ldots\ldots\ldots\ldots (18)$$

in which C is Chezy's coefficient. A rough channel would give a value of C equal to 87 if $\frac{R}{\epsilon}$ were equal to 118. When R is equal to 0.15 ft, this would require ϵ to be 0.00127 ft or 0.0153 in.

Henry Maksoud.[32]—Useful experiments have been conducted by Mr. Owen with the purpose of studying laminar and turbulent flow in an open channel and the transition from one type of flow to the other. The conclusions reached are, however, open to question.

Although no complete and consistent study has been made, as of 1953, of the mechanics of laminar and turbulent flow in open channels, the quotation cited by the author in the Introduction as indicative of the present state of knowledge on the subject is misleading. In a later edition of the text,[33] the quoted paragraph has been omitted as obsolete.

In Sect. 4, Mr. Owen states that the upper and lower values of the critical Reynolds numbers appeared to be the same for his experiments and were approximately equal to 4,000. This statement does not follow the accepted definitions of upper and lower critical values of the Reynolds number.[34,35] The lower critical value of the Reynolds number defines a condition below which all turbulence entering the flow from any source will eventually be damped out by viscosity. The upper critical value of the Reynolds number defines a condition above which laminar flow can never exist, and, therefore, the flow is always turbulent.

It is the lower critical value which is of practical importance because a moving fluid is seldom so free from local disturbances that laminar flow will persist at higher values of the Reynolds number. Above this lower critical value the flow can be either unstable laminar, or turbulent. Unstable laminar flow is that which might change to turbulent depending on the magnitude and frequency of the disturbances that might occur. The flow with a Reynolds number of 4,000 in the author's experimental channel could have been classified as unstable laminar flow because it could have changed to turbulent flow if the flow had been sufficiently disturbed.

Since G. H. L. Hagen (in 1854) indicated the existence of two states of flow which are termed laminar and turbulent, the phenomenon of transition from one state to the other has been the subject of many studies, most of which concern flow in pipes. The results of much of the work differed regarding the true values for the lower and upper critical Reynolds numbers. The lower critical value for pipe flow is well defined. As to the upper critical value, attention is directed to the work of R. Comolet who experimented with flow in conduits of various shapes and reached values of the Reynolds number for circular tubes of 75,000 (50,000 was the highest value previously reached) for which the flow remained laminar.[36]

---

[31] "Resistance to Flow in Rough Channels," by Ralph W. Powell, *Transactions*, Am. Geophysical Union, August, 1950.

[32] Research Assistant, Iowa Inst. of Hydr. Research, State Univ. of Iowa, Iowa City, Iowa.

[33] "Hydraulics and Its Applications," by A. H. Gibson, Constable and Co., Ltd., London, England, 1952, p. 295.

[34] "Elementary Mechanics of Fluids," by H. Rouse, John Wiley & Sons, Inc., New York, N. Y., 1947, p. 174.

[35] "Elementary Fluid Mechanics," by J. K. Vennard, John Wiley & Sons, Inc., New York, N. Y., 1947.

The author considered the flow in the 1.5-ft-wide channel to approach that in an infinitely wide channel. Consequently, Mr. Owen selected the depth of flow rather than the hydraulic radius as the length term in the Reynolds number and for the computation of the friction coefficient. One of the consequences of this approximation is the constancy of the friction factor in the turbulent region as shown in Fig. 1. Had the hydraulic radius been used, the results would not have deviated markedly from the Blasius relationship for smooth pipes.

In the subsequent computations, the writer uses the scant amount of data given by the author to show that this deviation is largely the result of the use of the depth in place of the hydraulic radius. For illustration, one point has been taken from Fig. 1 which has approximately the following coordinates:

$$\mathsf{R} = \frac{4\,V\,y}{\nu} = 130{,}000 \ldots\ldots\ldots\ldots\ldots\ldots (19a)$$

and

$$f = \frac{8\,g\,y\,S}{V^2} = 0.0317 \ldots\ldots\ldots\ldots\ldots\ldots (19b)$$

A value of 0.3 ft is assumed by the writer for the depth y which according to the author is the maximum depth observed. The value of 1.2×10^{-5} for the kinematic viscosity is also assumed.

From Eqs. 19, the mean velocity was found to be equal to 1.3 ft per sec, and the slope was found to equal 0.000678. The hydraulic radius was computed from the known width and assumed depth, and with this hydraulic radius as the length parameter, the Reynolds number was found to be approximately 93,000. The friction factor was also recomputed and was found to be equal to 0.022. These values differ significantly from the values given in Eqs. 19. The new point, thus defined, if plotted in Fig. 1, would fall close to Blasius' relationship. This should be expected in the case of smooth channels having commonly used cross sections.

Had the author presented his data, a more complete analysis of the variation of the resistance coefficient with the Reynolds number could have been made. This analysis would be expected to indicate that, in the turbulent region, the Blasius and Kármán-Prandtl resistance equations for turbulent flow in smooth pipes serve as limits for the variation in resistance for open channels.

In the laminar region, the depths of flow are small, and the effect of using the depth of flow instead of the hydraulic radius is probably less marked. Nonetheless, in the laminar region, the ratio of depth to width (or other shape parameter) is, as shown by Mr. Powell,[37] the significant criterion for determining the resistance law. In contrast, there is considerable evidence from experimental studies in smooth, open channels[27] that the resistance law in the turbulent region is essentially independent of channel cross section.

---

[36] "Recherches sur la Genèse de la Turbulence dans les Conduites en Charge," by R. Comolet, *Publications Scientifiques et Techniques No. 246*, Ministère de l'Air, Paris, France, 1950.

W. M. Owen.[38]—It is not agreed that (as Messrs. Powell and Posey state) two errors are present in Eq. 3. The mathematical arguments which they have offered concerning the necessity for interchanging x and y can be shown to be incorrect. The assertion that the series in Eq. 3 diverges if $b > a$ is not substantiated by elementary convergence tests. As the absolute value of each term in the series is evidently less than $1/n^3$, the Weierstrass comparison test[39] shows that the series converges absolutely and uniformly throughout the rectangle and on its boundary, irrespective of the values of a and b. In fact, because the series $1 + 3^{-2} + 5^{-2} + \cdots$ can be used for comparison, the absolute value of the sum of the series in Eq. 3 is always less than $\pi^2/8$.

Obviously, the function defined by Eq. 3 satisfies the boundary condition, $w = 0$. Also, it can be seen by direct substitution that this function satisfies Eq. 1. Eq. 3 is therefore a solution of the boundary-value problem. Furthermore, it is the only solution as there is a theorem in potential theory which asserts that a problem of the Dirichlet type possesses only one regular solution.[40] How is this conclusion to be reconciled with the fact that the function proposed by Messrs. Powell and Posey (Eq. 15) is also a solution of the boundary-value problem? There is only one possible answer to this question. The two functions are identical; they merely have different representations. As the two expressions for w are equivalent, their integrals are equal. Consequently, Eqs. 5 and 16 are different representations of the same function, Q.

It is true that Eqs. 15 and 16 are better adapted for displaying the limits that are approached as b becomes infinite. An even simpler form of the equation for w is obtained if Eq. 15 is written as a sum of two series, and if the first series is evaluated by a Fourier series. Thus, there results

$$w = \tfrac{1}{2} K \left(a^2 - y^2\right) - \frac{16\, K\, a^2}{\pi^3} \sum_{n=1,3,\ldots}^{\infty} \frac{(-1)^{(n-1)/2} \cosh \dfrac{n \pi x}{2 a} \cos \dfrac{n \pi y}{2 a}}{n^3 \cosh \dfrac{n \pi b}{2 a}} \quad \ldots (20)$$

If b becomes infinite, the series in Eq. 20 approaches zero, and only the terms that represent the solution for the infinitely wide channels remain.

As noted by several of the discussers, the writer erred in the assumption that the flow was two-dimensional when the depths in the channel were approximately 0.3 ft. It should be noted, however, that the depth only approached this value at the higher values of the Reynolds number and that the depths for laminar flow were extremely shallow; therefore, the 12.6% error, as given by Messrs. Powell and Posey, is considerably greater than that which actually existed. As cited by Mr. Iwagaki, Messrs. Powell and Posey, and Mr. Maksoud, the data on the turbulent-flow region would actually plot downward and to the left in Fig. 1—thus, close to the Blasius curve for smooth pipes.

---

[37] "Resistance to Flow in Smooth Channels," by Ralph W. Powell, *Transactions*, Am. Geophysical Union, December, 1949, p. 878.

[38] Development Engr., Airesearch Mfg. Co., Los Angeles, Calif.

[39] "Theory and Application of Infinite Series," by K. Knopp, Stechert-Hafner, Inc., New York, N. Y., 1928.

[40] "Foundations of Potential Theory," by O. D. Kellogg, Dover Publications, New York, N. Y., 1953.

Messrs. Powell and Posey state that a sentence in Sect. 3 is open to question:

> "* * * velocity distribution and energy loss for an open channel of depth *a* and width 2 *b* (Fig. 3), are exactly the same as those of one half of a closed conduit of depth 2 *a* and width 2 *b*."

They also note that the statement is certainly not true for turbulent flow. This statement was made in a section entitled, "General Equations for Laminar Flow in Channels of Rectangular Cross Section;" it was not implied that it pertained to turbulent flow. Messrs. Powell and Posey cite the fact that the point of maximum velocity in turbulent flow is depressed below the surface, thus making this assumption invalid for turbulent flow. Both the writer's data and those presented by Mr. Delleur indicate that the assumption is at least approximately true for laminar flow.

The statement in Sect. 2 that the channel showed depressions and elevations in the order of 0.01 in. should be clarified. Both the brass bottom and the glass sides of the channel were exceptionally smooth; there were points, however, where the channel surface deviated from a plane by approximately 0.01 in. This deviation would probably cause an error in slope rather than in channel roughness.

Mr. Delleur is correct in stating that, in addition to the fact that at the higher Reynolds numbers or at greater depths the flow could not be considered two-dimensional, there exists some doubt as to whether the flow was uniform. However, no velocity traverses were made. With respect to Mr. Delleur's conclusions concerning the distance required for the development of the boundary layer in the tests, it should again be noted that the 0.3-ft depth applies only to the highest Reynolds numbers.

AMERICAN SOCIETY OF CIVIL ENGINEERS
Founded November 5, 1852
TRANSACTIONS

Paper No. 2717

ANALYSIS OF WATER HAMMER BY CHARACTERISTICS

BY C. A. M. GRAY,[1] A. M. ASCE

WITH DISCUSSION BY MESSRS. PIN-NAM LIN, HENRY M. PAYNTER, AND C. A. M. GRAY

SYNOPSIS

In the analysis of water-hammer problems the effects of friction, kinetic energy, and change in wave form may be negligible from the practical point of view. However, it is worthwhile to develop a general method of study that makes allowance for these factors, so that it can be seen what order of approximation is involved in neglecting them.

This paper presents a solution using the characteristics, or characteristic directions, of the equations that are involved in the water-hammer problem. The method evolved lends itself to a graphical treatment in some cases. The development of the method rather than the consideration of problems of practical significance is the concern of this paper.

NOTATION

The letter symbols introduced in this paper are defined where they first appear in the text, or by illustration, and are assembled alphabetically in Appendix II for convenience of reference.

INTRODUCTION

The analysis of water-hammer problems in hydraulic systems has been based primarily on the wave equation:

$$\frac{\partial^2 h}{\partial x^2} = \frac{1}{c^2}\frac{\partial^2 h}{\partial t^2} \qquad (1)$$

NOTE.—Published, essentially as printed here, in September, 1953, as *Proceedings-Separate No. 274*. Positions and titles given are those in effect when the paper or discussion was received for publication.

[1] Senior Lecturer, Univ. of Sydney, Sydney, Australia.

in which h is the head on the system, x is a length measured along the pipe, c equals the speed of surge, and t denotes time. Elegant solutions have been provided by Robert W. Angus[2,3,4] and G. R. Rich,[5] the former giving a graphical solution and the latter an analytical solution based on the Laplace-Mellin transformation. However, in neither case is it possible to incorporate the full effects of friction or kinetic energy, although an approximate correction for these effects has been given by Mr. Angus. Mr. Rich includes the effects of linear friction but neglects kinetic energy entirely, since his solution can deal only with linear quantities. In neither case can the effects of change in wave velocity be considered.

GENERAL THEORY FOR IDEAL CONDITIONS

The usual form of the equations of motion, neglecting viscosity, kinetic energy, and change in wave form, are

$$\frac{\partial u}{\partial x} = \frac{g}{c^2}\frac{\partial h}{\partial t} \quad \text{(2a)}$$

and

$$\frac{\partial u}{\partial t} = g\frac{\partial h}{\partial x} \quad \text{(2b)}$$

in which u is the velocity of the fluid and g denotes the acceleration due to gravity. For convenience, in Eqs. 2 the velocity u is measured in the opposite direction to that in which x is measured.

If Eq. 2a is multiplied by λ_1, Eq. 2b is multiplied by λ_2, and the two are added, there results

$$\lambda_1\frac{c^2}{g}\frac{\partial u}{\partial x} + \lambda_2\frac{\partial u}{\partial t} - \lambda_1\frac{\partial h}{\partial t} - \lambda_2 g\frac{\partial h}{\partial x} = 0 \quad \text{(3)}$$

If there is some curve in the xt-plane (Fig. 1), such that

$$\frac{dx}{dt} = \frac{\lambda_1}{\lambda_2}\frac{c^2}{g} = \frac{\lambda_2}{\lambda_1}g \quad \text{(4)}$$

then at any point on this curve $\frac{\lambda_1}{\lambda_2} = \pm\frac{g}{c}$. Thus through any point in the xt-plane there are two directions given by $\frac{dx}{dt} = \pm c$. If c is a constant, these directions define two straight lines, denoted by C_{pos} and C_{neg}, called the characteristics of Eqs. 2. For C_{pos} the equation of the line is

$$x + c\,t = \text{constant} \quad \text{(5a)}$$

---

[2] "Simple Graphical Solution for Pressure Rise in Pipes and Pump Discharge Lines," by Robert W. Angus, *The Engineering Journal*, Vol. 18, 1935, p. 72.

[3] "Water-Hammer Pressures in Compound and Branched Pipes," by Robert W. Angus, *Transactions*, ASCE, Vol. 104, 1939, p. 340.

[4] "Water Hammer in Pipes, Including Those Supplied by Centrifugal Pumps: Graphical Treatment," by Robert W. Angus, *Proceedings*, Inst. of Mech. Engrs., Vol. 136, 1937, p. 245.

[5] "Water-Hammer Analysis by the Laplace-Mellin Transformation," by G. R. Rich, *Transactions*, ASME, Vol. 67, 1945, p. 361.

and for C_{neg} the equation is

$$x - c\,t = \text{constant}. \qquad (5b)$$

Through every point in the xt-plane pass a C_{pos}-curve and a C_{neg}-curve. Consequently, each point in the xt-plane can be identified by the two curves passing through it.

Now, consider the changes in u and h along a C_{pos}-curve. From Eq. 3,

$$\frac{\lambda_1 c^2}{g}\left(\frac{\partial u}{\partial x} + \frac{\partial u}{\partial t}\frac{dt}{dx}\right) - \lambda_2 g\left(\frac{\partial h}{\partial x} + \frac{\partial h}{\partial t}\frac{dt}{dx}\right) = 0 \qquad (6a)$$

from which

$$\frac{c}{g}\frac{du}{dx} - \frac{dh}{dx} = 0 \qquad (6b)$$

in which $\frac{du}{dx}$ and $\frac{dh}{dx}$ are, respectively, the rate of change of u and h with regard to x along the C_{pos}-curve.

Alternatively,

$$\lambda_2\left(\frac{\partial u}{\partial x}\frac{dx}{dt} + \frac{\partial u}{\partial t}\right) - \lambda_1\left(\frac{\partial h}{\partial x}\frac{dx}{dt} + \frac{\partial h}{\partial t}\right) = 0 \qquad (7a)$$

from which

$$\frac{c}{g}\frac{du}{dt} - \frac{dh}{dt} = 0 \qquad (7b)$$

Therefore, from Eqs. 6b and Eq. 7b, the total change Δu in u and the total change Δh in h along the C_{pos}-curve are related by

$$\frac{c}{g}\Delta u = \Delta h, \qquad (8a)$$

and along the C_{neg}-curve, they are related by

$$\frac{c}{g}\Delta u = -\Delta h. \qquad (8b)$$

As an example, consider the sudden closure of the valve at the end of the pipe leading from the reservoir in Fig. 1(*a*).

The distance-time diagram is shown in Fig. 1(*c*); passing through each point there are two lines with slopes to the x-axis of ± $1/c$. The C_{pos}-curves are shown by solid lines and the dashed lines represent the C_{neg}-curves. Nothing occurs at any point along the pipe line AB until the first wave reaches that point. Thus, all the points on the line A_0B_0 in Fig. 1(*c*) have their initial u-value and h-value. This fact and the fact that the head at point B remains constant constitute the boundary data of the problem.

The velocity-head diagram is shown in Fig. 1(*d*). The points E_0, D_0, G_0, and B_0 are located by the use of the initial conditions of the problem. The points are coincident on the u-axis since all losses are neglected.

For the typical C_{neg}-characteristic, from Eq. 8*b*, since c is a constant, $\frac{dh}{du} = -\frac{c}{g}$. However, the velocity at A is zero for all times after the valve is closed. Hence, if a line is drawn through point E_0 in the *uh*-diagram, having a slope of $-\frac{c}{g}$, so as to intersect the *h*-axis, this intersection is A_1. All the points, A_1, A_2, A_3, and A_4, corresponding to times at the valve of $L/2c$, L/c, $3L/2c$, and $2L/c$, respectively, will coincide, since the lines E_0A_1, D_0A_2, and so on, in the *uh*-diagram have the same slopes and pass through a common point.

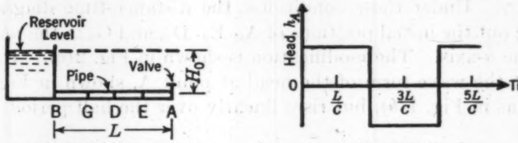
Reservoir Level
Pipe
Valve
H_0
B G D E A
L
Head, h_A
0
Time, t
$\frac{L}{c}$
$\frac{3L}{c}$
$\frac{5L}{c}$

(*a*) SCHEMATIC DIAGRAM (*b*) HEAD AT *A*

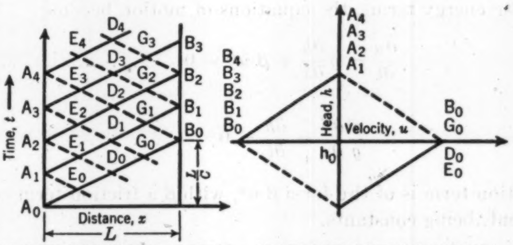
D4
E4
G3
B3
A4
E3
D3
G2
B2
D2
A3
E2
G1
B1
Time, t
D1
A2
E1
G0
B0
D0
A1
E0
$\frac{L}{c}$
A0
Distance, x
L
A4
A3
A2
A1
B4
B3
B2
B1
B0
Head, h
Velocity, u
B0
G0
D0
E0
h_0

(*c*) DISTANCE-TIME DIAGRAM (*d*) VELOCITY-HEAD DIAGRAM

FIG. 1.—SUDDEN CLOSURE, IDEAL CONDITIONS

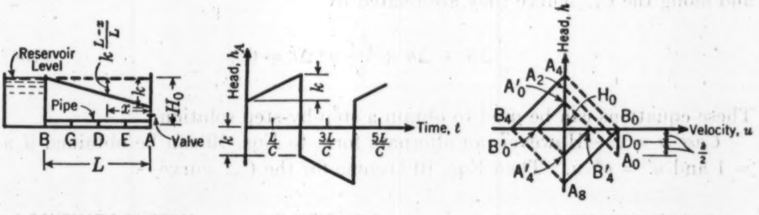
Reservoir Level
$k\frac{L-x}{L}$
k
H_0
Pipe
x
B G D E A
Valve
L
Head, h_A
k
k
Time, t
$\frac{L}{c}$
$\frac{3L}{c}$
$\frac{5L}{c}$
Head, h
A4
A2
A'0
H0
B4
B0
Velocity, u
B'0
D0
A0
$\frac{k}{2}$
A'4
B'4
A8

(*a*) SCHEMATIC DIAGRAM (*b*) HEAD AT *A* (*c*) VELOCITY-HEAD DIAGRAM

FIG. 2.—SUDDEN CLOSURE, NEGLECTING DISSIPATION AND KINETIC ENERGY

The B-points on the *uh*-diagram are obtained from the C_{pos}-curves drawn through the A-points. Since for the C_{pos}-characteristic $\frac{dh}{du} = \frac{c}{g}$, and at point B the head is always equal to H_0, the points B_1, B_2, B_3, and B_4 in the *uh*-plane are obtained by drawing lines through the corresponding A-points, having a slope of $\frac{c}{g}$ to the *u*-axis, and intercepting it at points B_1, B_2, B_3, and B_4. The remainder of the diagram is then completed as shown in Fig. 1 (*d*) in which the solid and dashed lines correspond to those of Fig. 1 (*c*).

However, the initial distribution of head along the pipe is not constant. In Fig. 2 the previous example is investigated assuming an initially linear distribution of head, as shown in Fig. 2 (*a*). In this case the head on the pipe is H_0, and the head decreases linearly throughout the length of the pipe, by an amount γ. Under these conditions, the distance-time diagram is similar to Fig. 1 (*c*), but the initial positions of A_0, E_0, D_0, and G_0 in the *uh*-plane are no longer on the *u*-axis. The modification is shown in Fig. 2 (*c*). It is of interest to note that the wave form of the head at point A, shown in Fig. 2 (*b*), is not flat-topped as in Fig. 1 (*b*), but rises linearly over the half period.

ANALYSIS WITH FRICTION INCLUDED

Neglecting the energy terms, the equations of motion become

$$\frac{\partial u}{\partial t} - g\frac{\partial h}{\partial x} + \beta\, u^n = 0 \qquad (9a)$$

and

$$\frac{c^2}{g}\frac{\partial u}{\partial x} - \frac{\partial h}{\partial t} = 0 \qquad (9b)$$

n which the friction term is of the form $\beta\, u^n$, with β a friction term coefficient and n an exponent, being constants.

As shown previously, the characteristics are given by the equations $\frac{dx}{dt} = \pm c$, and the total variations Δu and Δh of u and h along the C_{pos}-curve are related by

$$\frac{c}{g}\,\Delta u - \Delta h + \frac{\beta\, c}{g}\, u^n\, \Delta t = 0 \qquad (10a)$$

and along the C_{neg}-curve they are related by

$$\frac{c}{g}\,\Delta u + \Delta h + \frac{\beta\, c}{g}\, u^n\, \Delta t = 0 \qquad (10b)$$

These equations can be used to obtain a step-by-step solution.

Case n = 1.—However, an alternate form to Eqs. 10 can be obtained if $n = 1$ and $u' = e^{\beta t}\, u$. Then Eqs. 10 become for the C_{pos}-curve—

$$\frac{c}{g}\, e^{-\beta t}\, \Delta u' = \Delta h \qquad (11a)$$

and for the C_{neg}-curve—

$$\frac{c}{g}\, e^{-\beta t}\, \Delta u' = -\Delta h \qquad (11b)$$

For graphical solutions it is convenient to use dimensionless quantities. Therefore, let $u'_1 = \frac{u'}{u_0}$, $h_1 = \frac{g\, h}{c\, u_0}$, $\beta_1 = \frac{\beta\, L}{c}$, and $\tau = \frac{c\, t}{L}$, in which L is the length of pipe and u_0 is the initial velocity of the fluid. Then for the C_{pos}-curve, Eq. 11*a* becomes

$$e^{-\beta\tau}\,\Delta u'_1 = \Delta h_1 \tag{12a}$$

and for the C_{neg}-curve, Eq. 11*b* becomes

$$e^{-\beta\tau}\,\Delta u'_1 = -\,\Delta h_1 \tag{12b}$$

Since the friction term should be of the form $\beta\, u^2$, Eqs. 10 will be developed in a form suitable for graphical solution with $n = 2$.

Case $n = 2$.—As for the case of $n = 1$, a dimensionless form is most suitable. Therefore, let $u_1 = \dfrac{u}{u_0}$, $h_1 = \dfrac{g\,h}{c\,u_0}$, $\tau = \dfrac{c\,t}{L}$, and $\beta'_1 = \beta\, u_0 \dfrac{L}{c}$. Then for the C_{pos}-curve—

$$\Delta u_1 - \Delta h_1 + \beta'_1\, u^2_1\, \Delta\tau = 0 \tag{13a}$$

and for the C_{neg}-curve—

$$\Delta u_1 + \Delta h_1 + \beta'_1\, u^2_1\, \Delta\tau = 0 \tag{13b}$$

with the restriction that reversal of flow will change the sign of the friction term.

THE EFFECTS OF FRICTION

To illustrate the effects of friction, consider the case of $n = 1$, shown in Fig. 3, which represents a sudden closure of the valve at point A in the pipe line previously considered. Assuming initially a head loss of $0.125\,\dfrac{c\,u_0}{g}$ distributed linearly from reservoir to valve, and since $u_1 = e^{\beta t}\,\dfrac{u}{u_0}$, points A_0, E_0, D_0, G_0, and B_0 can be located in the *uh*-plane, shown in Fig. 3(*c*). From Eqs. 12, the slope $\dfrac{dh_1}{du_1}$ is known as a function of the time along the C_{pos} and C_{neg}-curves. If these curves are so flat that they can be approximated as a series of straight lines, then the slope of the curves $\dfrac{dh_1}{du_1} = \pm\, e^{-\beta\tau}$ in which τ is the

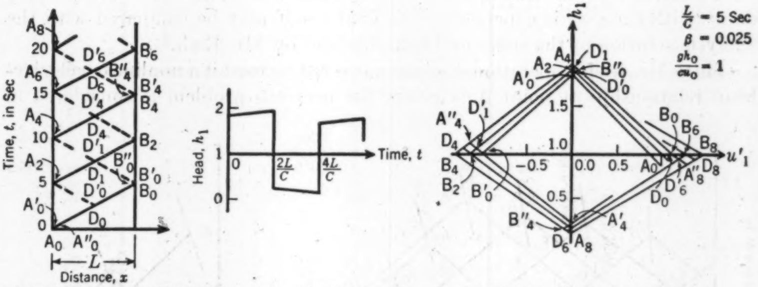
A8
20
A6
15
A4
10
A2
5
A'0
0
Time, t, in Sec
D'6
B''4
D6
D'4
D4
D'1
B''0
D1
D'0
D0
B6
B'4
B4
B2
B'0
B0
A0
A''0
L
Distance, x
2
1
0
Head, h1
0
2L/C
4L/C
Time, t
h1
L/C = 5 Sec
β = 0.025
gh0/cu0 = 1
A4
D1
A2
B''0
A'0
D'0
1.5
D'1
A''4
D4
B4
B2
B'0
1.0
−0.5
0.0
0.5
0.5
A0
B0
B6
B8
u'1
D8
A''8
D'6
D0
B''4
A'4
D6
A8

(*a*) DISTANCE-TIME DIAGRAM (*b*) HEAD AT *A* (*c*) VELOCITY-HEAD DIAGRAM

FIG. 3.—SUDDEN CLOSURE, LINEAR FRICTION

average time over the interval. For ease in graphical representation a comparatively large time interval of 2.5 sec is assumed.

Considering the point D_0 in Fig. 3(*a*)—D'_0 is located very close to point D_0, in time, along the C_{neg}-characteristic D_0A_2. Over this short period of time the head and velocity are very great. At D'_0, the first compression wave traveling up the pipe has passed a point $L/2$ from the valve. In order to use the previously mentioned approximation, it is necessary to find the points A'_0, D'_0, and so on.

Consider the point A''_0 along the C_{pos}-characteristic A_0B_0, very close to A_0. In Fig. 3(*c*) this is a point very close to A_0 and at the limit will coincide with A_0. To obtain A'_0, the C_{neg}-characteristic is drawn through A''_0 in the *xt*-diagram to intersect the *t*-axis. Since this time interval is so short, the slope in the $(u'_1\, h_1)$-diagram is $\dfrac{dh_1}{du_1} = -1$.

Therefore, through point A_0 a line is drawn, inclined towards the u'_1 axis at an angle of 135°, which intersects the h_1-axis at A'_0. To obtain D'_0 it is noted that it lies at the intersection of the C_{pos}-characteristic $A'_0B''_0$ and the C_{neg}-characteristic D_0A_2. Hence, in the $(u'_1\, h_1)$-plane, through A'_0 a line is drawn having a slope of $e^{-\beta\,(2.5+0)/2}$ and through D_0 a line is drawn having a slope of $-\,e^{-2.5\beta}$. The intersection of these lines locates the point D'_0. In a similar manner the head and velocity are obtained at all points along the characteristic B_0A_4. These can be used to extend the solution to the characteristic A_4B_4, and then, in turn, the information on A_4B_4 can be used to carry the solution as far as required, in exactly the same manner as the initial data were used along the characteristic A_0B_0.

The wave form for this case is shown in Fig. 3(*b*). The wave form shows a decay with time, as is expected. The final result may be compared with the analytic solution of the same problem obtained by Mr. Rich.[5]

Since Mr. Rich's operational solution can not be used if a nonlinear velocity-head relationship at point A is given, the previous problem is considered in

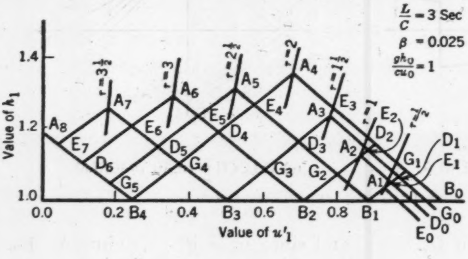

FIG. 4.—LINEAR CLOSURE, LINEAR FRICTION

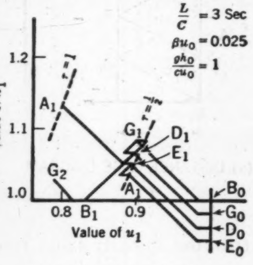

FIG. 5.—LINEAR CLOSURE, βu^2 FRICTION

Fig. 4 and Fig. 5, in which the velocity and head at point A are assumed to be related by an equation of the form $\dfrac{u_A}{u_0} = k\sqrt{\dfrac{h_A}{h_0}}$ for all time, in which u_A is the velocity at point A and h_A is the head at point A.

Fig. 4 shows the solution of the problem when the valve at point A closes in such a manner that k varies linearly from 1 to 0 in 12 sec, assuming a linear friction term. Fig. 5 considers the same problem but assumes a friction term of the form βu^2. The solution given in Fig. 4 follows the procedure for Fig. 3. However, some modification occurs in the solution presented in Fig. 5. Eqs. 13 apply to this case, and u_1 and h_1 are given along the C_{pos}-characteristic A_0B_0. Since the valve is closed continuously, no abrupt changes occur in u_1 and h_1 due to the passage of the surge. Thus the location of the points A'_0, E'_0, and so on, is obviated. This also applies to Fig. 4. In Fig. 5 the intervals of time taken are $t = L/4\,c$. It is assumed that over this period of time the term $\beta'_1\, u^2_1$ is sensibly constant and may be represented by its average value. If excessive variation occurs, as will be obvious in the solution, smaller increments of time must be taken.

In the velocity-head diagram, Fig. 5, the points E_0, D'_0, G_0, and B_0 are located by using the initial conditions. Then A_1 is located in the $(u_1\, h_1)$-plane. To obtain the average value of u_1 over the interval, a first approximation is made by assuming no friction, as in Fig. 6. From Fig. 6 $(u_1)_{aveg} = 0.96$ so that

$$0.075\ (u^2_1)_{aveg}\,\Delta\tau = 0.075 \times 0.96^2 \times \frac{1}{4} = 0.017.$$

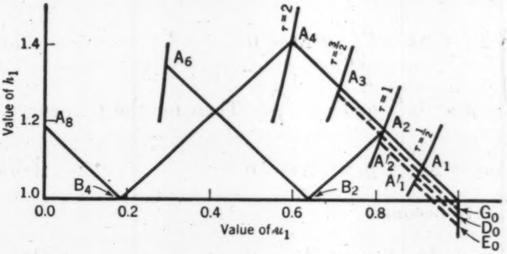

FIG. 6.—LINEAR CLOSURE

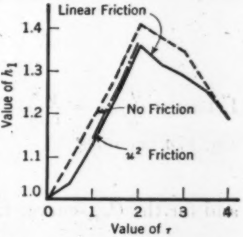

FIG. 7.—LINEAR CLOSURE, HEAD AT A

Since the increment Δu_1 is negative, $\Delta h_1 = |\,\Delta u_1\,| - 0.017$ in which Δh_1 is the increment of h_1 in going from E_0 to A_1 along the C_{neg}-characteristics E_0A_1. Therefore, from a point 0.017 horizontally to the left of E_0 in the $(u_1\, h_1)$-diagram a line is drawn at an angle of 135° to the horizontal. This line intersects the parabola $\tau = \frac{1}{2}$ at A_1. The same procedure is used for each element of the characteristic diagram.

Fig. 7 shows a comparison between the two forms of friction correction. The dimensionless head at the valve is plotted against time, using values of β in each case, to give the same head loss from reservoir to valve under the initial steady conditions. For the problem considered, it is seen that up to the maximum head there is a negligible difference. If no friction is assumed, the result obtained is only 4% in excess of the values obtained assuming friction.

Including the Effect of Kinetic Energy and Friction and Neglecting the Change in Wave Form.—The general equations of motion are

$$u \frac{\partial u}{\partial x} - \frac{\partial u}{\partial t} + g \frac{\partial h}{\partial x} + \beta u^n = 0 \dots\dots\dots\dots \tag{14}$$

and

$$\frac{c^2}{g} \frac{\partial u}{\partial x} - \frac{\partial h}{\partial t} + u \frac{\partial h}{\partial x} = 0 \dots\dots\dots\dots \tag{15}$$

in which u is measured in the direction opposite to that in which x is measured. As was done previously, Eq. 14 is multiplied by λ_1 and Eq. 15 is multiplied by λ_2, choosing λ_1/λ_2 so that $\lambda_1/\lambda_2 = \pm c/g$. The characteristics are given by

$$\frac{dx}{dt} = -\ (u \pm c) \dots\dots\dots\dots \tag{16}$$

and for the C_{pos}-characteristic—

$$\frac{c}{g} \Delta u - \Delta h + \frac{\beta\, c}{g} u^n \Delta t = 0 \dots\dots\dots\dots \tag{17a}$$

and for the C_{neg}-characteristic—

$$\frac{c}{g} \Delta u + \Delta h + \frac{\beta\, c}{g} u^n \Delta t = 0 \dots\dots\dots\dots \tag{17b}$$

Let $u_1 = \frac{u}{u_0}$, $h_1 = \frac{g\, h}{c\, u_0}$, $\beta_2 = \beta\, u^{n-1}{}_0 \frac{L}{c}$, and $\tau = \frac{c\, t}{L}$. Then for the C_{pos}-curve, Eq. 17*a* becomes

$$\Delta u_1 - \Delta h_1 + \beta_2\, u^n{}_1\, \Delta \tau = 0 \dots\dots\dots\dots \tag{18a}$$

and for the C_{neg}-curve, Eq. 17*b* becomes

$$\Delta u_1 + \Delta h_1 + \beta_2\, u^n{}_1\, \Delta \tau = 0 \dots\dots\dots\dots \tag{18b}$$

The characteristics given by Eqs. 17 are curved, and the solution will require these curves to be determined in the *xt*-plane, simultaneously with the *uh*-curve in the *uh*-plane. However no great difficulty is entailed, although a graphical solution is not possible.

Before indicating a solution, a few observations can be made. In dimensionless form Eq. 16 becomes,

$$\frac{dx_1}{d\tau} = -\left(u_1 \frac{u_0}{c} \pm 1\right) \dots\dots\dots\dots \tag{19}$$

in which $x_1 = \frac{x}{L}$, $\tau = \frac{c\, t}{L}$, and $u_1 = \frac{u}{u_0}$. For closure of the valve, u_1 is always less than 1, whereas generally u_0/c is of the order of 10^{-3}, so that the correction is of the order of 10^{-3}, and thus will be negligible. Therefore it appears that the kinetic energy can be safely neglected where conditions at the valve are not extremely sensitive to time since, considering only conditions at the valve, the curving of the characteristics can only affect time. This is shown in the following example.

Consider once again, the pipe discharging from a reservoir with a valve at the end, for which time of closure is 12 sec, $\frac{L}{c} = 3$ sec, $u_0 = 16$ ft per sec, and $c = 4{,}000$ ft per sec. A closure relation of the form $\frac{u_A}{u_0} = k\sqrt{h_A/h_0}$ is assumed in which k varies linearly with time.

Then for the C_{pos}-characteristics $\Delta x_1 = -(1 + 0.004\,u_1)\,\Delta\tau$ and for the C_{neg}-characteristics $\Delta x_1 = (1 - 0.004\,u_1)\,\Delta\tau$. Using values from Fig. 5 as a first approximation, $(u_1)_{aveg} = 0.96$ for the time interval E_0A_1. Hence, $\Delta\tau = \frac{1}{4}(1 - 0.00384) = 0.24904$ which gives the time corresponding to point A_1 in the $x_1\,\tau$-diagram. Thus in the $(u_1\,h_1)$-diagram, the parabola on which A_1 lies must be drawn for $\tau = 0.24904$. The next point located is E_1. Both time and heads are known at A_1 and D_0 and assuming the characteristics A_1E_1 and D_0E_1 are to be straight lines, two equations are obtained to compute τ and h at E_1. From Fig. 8, a general formula can be derived that is convenient when making these computations. From Fig. 8

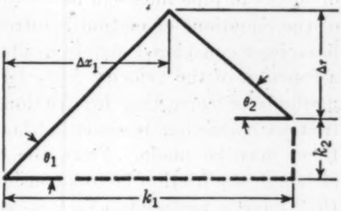

FIG. 8.—GENERAL CASE

$$\Delta\tau = \frac{k_1 - k_2\cot\theta_1}{\cot\theta_1 + \cot\theta_2} \quad \text{(20a)}$$

and

$$\Delta x_1 = (k_2 + \Delta\tau)\cot\theta_1 \quad \text{(20b)}$$

From Eqs. 20, E_1, $\cot\theta_1 = 0.9964$, and $\cot\theta_2 = 1.0036$, in which the estimated value of u_1 has been obtained from Fig. 5.

Hence, $\Delta\tau = 0.2495$, giving τ at E_1 equal to 0.7495. Consequently, for A_2, $\tau = \tau$ at $E_1 + \Delta\tau$ and $\Delta\tau = \frac{1}{4}(1 - 0.004 \times 0.85)$, which gives τ at A_2 equal to 0.9986. In a similar manner the coordinates of any point in the $x_1\,\tau$—diagram can be computed. The method of construction of the $(u_1\,h_1)$-diagram is unaltered.

VERIFICATION OF COMPUTATIONS

Since the use of the step-by-step method of solution will introduce cumulative errors, it is necessary to be able to check the error as the solution progresses. Referring to Eqs. 18, for the C_{pos}-curve—

$$(u_1)_G - (h_1)_G = (u_1)_F - (h_1)_F - \int_F^G \beta_1\, u^n{}_1\, d\tau \quad \text{(21a)}$$

and for the C_{neg}-curve—

$$(u_1)_G - (h_1)_G = (u_1)_F + (h_1)_F - \int_F^G \beta_1 \, u^n{}_1 \, d\tau; \ldots\ldots\ldots (21b)$$

in which F and G are two points on the characteristic. From the step-by-step solution, there is a value for u_1 at every point on a given characteristic. Thus the integrals in Eqs. 21 can be determined and, hence, values of h and u at G should agree with those obtained from the step-by-step solution.

CONCLUSION

From the illustrations it can be seen that a complete solution of the analysis of surges in pipe lines can be made when the conception of the characteristics of the equations of motion is introduced. In the paper two types of friction have been considered merely to illustrate the method—any form of friction as a function of the velocity could be used. However, notwithstanding existing methods of correcting for friction, it is clear that no steady-state form of friction correction is exact, although satisfactory approximations based on them may be made. From the examples considered, it can be seen that, although the friction factors considered on a steady-state basis are very great, they have a negligible effect on the maximum heads. This result may not apply to complex systems because of the retardation introduced. The kinetic energy correction, however, would seem to have been made incorrectly by previous investigators. As the paper shows, the correct basis for a kinetic energy correction is the ratio of the fluid velocity to the surge velocity. This is because only in exceptional cases will appreciable curving of the characteristics in the *xt*-plane occur. Thus, in general, velocity-head corrections are negligible.

No great difficulty should be found in applying the method to any case, no matter how complex. The procedure becomes apparent if the ideal case is taken as a guide, and for this the papers by Mr. Angus are available.[2,3,4]

APPENDIX I. ONE-DIMENSIONAL FLOW

Derivation of Equations.—If x is the direction of flow of a compressible fluid and u is measured in the same direction, then the Navier-Stokes equation for the flow of an ideal compressible fluid becomes

$$\frac{\partial u}{\partial t} + u \frac{\partial u}{\partial x} = - \frac{1}{\rho} \frac{\partial \rho}{\partial x} + \frac{g}{\rho} \frac{d}{dx} (\rho) \ldots\ldots\ldots\ldots\ldots\ldots (22)$$

in which p is the pressure on the fluid, and the z-axis is measured vertically downward and makes an angle α with the direction of flow.

If all the pressure changes are considered hydrostatic and $p' = p - \rho\, g\, z$, in which z is the distance from the z-axis, then Eq. 22 becomes

$$\frac{\partial u}{\partial t} + u\,\frac{\partial u}{\partial x} = -\,\frac{1}{\rho}\,\frac{\partial p'}{\partial x} \qquad (23)$$

By definition, if Δp is the change in pressure producing a change ΔV in volume of fluid V,

$$\Delta p = -\,K\,\frac{\Delta V}{V} \qquad (24)$$

in which K is the bulk modulus of the fluid.

However, since mass $= \rho\, V$, then $\frac{\Delta \rho}{\rho} = -\,\frac{\Delta V}{V}$, Eq. 24 becomes

$$\Delta p = K\,\frac{\Delta \rho}{\rho} \qquad (25)$$

in which ρ is the density of the fluid. From Eq. 25,

$$\frac{\partial p'}{\partial x} = \frac{K}{\rho}\,\frac{\partial \rho}{\partial x} \qquad (26a)$$

and

$$\frac{\partial p'}{\partial t} = \frac{K}{\rho}\,\frac{\partial \rho}{\partial t} \qquad (26b)$$

It is customary to express pressures in terms of the head of the flowing fluid, so by letting $p' = \rho\, g\, h$,

$$\frac{\partial p'}{\partial x} = g\left(\rho\,\frac{\partial h}{\partial x} + h\,\frac{\partial \rho}{\partial x}\right) = g\left(\rho\,\frac{\partial h}{\partial x} + \frac{\rho\, h}{K}\,\frac{\partial p'}{\partial x}\right) \qquad (27a)$$

from which

$$\frac{\partial p'}{\partial x} = \rho\,\frac{g\,\frac{\partial h}{\partial x}}{1 - \rho\,\frac{g\,h}{K}} \approx \rho\, g\,\frac{\partial h}{\partial x} \qquad (27b)$$

since $K \gg \rho\, g\, h$.

In a similar manner

$$\frac{\partial p'}{\partial t} = \rho\, g\,\frac{\partial h}{\partial t} \qquad (28)$$

Substituting Eq. 27b into Eq. 23,

$$\frac{\partial u}{\partial t} + u\,\frac{\partial u}{\partial x} = -\,g\,\frac{\partial h}{\partial x} \qquad (29)$$

The remaining equation required for the solution is given by the condition of continuity, which under the prescribed conditions takes the form:

$$\frac{\partial \rho}{\partial t} + \rho \frac{\partial u}{\partial x} + u \frac{\partial \rho}{\partial x} \quad \text{(30)}$$

By using Eqs. 26, 27*b*, and 28, Eq. 30 becomes

$$\frac{\partial u}{\partial x} = -\frac{\rho\, g}{K}\left(\frac{\partial h}{\partial t} + u \frac{\partial h}{\partial x}\right) \quad \text{(31)}$$

Eq. 29 and Eq. 31 are the equations governing the flow. As presented they are nonlinear. The usual procedure is to linearize them and to treat $C^2 = K/\rho$ as a constant. This is similar to neglecting the terms $u \frac{\partial u}{\partial x}$ and $u \frac{\partial h}{\partial x}$. Under these conditions, Eq. 29 and Eq. 31 become

$$\frac{\partial u}{\partial t} = -g \frac{\partial h}{\partial x} \quad \text{(32a)}$$

and

$$\frac{\partial u}{\partial x} = -\frac{g}{c^2} \frac{\partial h}{\partial t} \quad \text{(32b)}$$

With c as a constant, Eqs. 32 are further reduced to

$$\frac{\partial^2 h}{\partial x^2} = \frac{1}{c^2} \frac{\partial^2 h}{\partial t^2} \quad \text{(33a)}$$

$$\frac{\partial^2 u}{\partial t^2} = c^2 \frac{\partial^2 u}{\partial x^2} \quad \text{(33b)}$$

Effect of Friction.—If viscous effects are to be considered, an additional term $\nu \nabla^2 u$ must be added to the right side of Eq. 22. For steady one-dimensional viscous flow, $\nu \nabla^2 u$ is equal to $-\beta u$, in which β is a constant. Since $-\beta u$ is linear, it is the form usually adopted and added to the right side of Eq. 29.

It is often suggested that the allowance for friction should be made following the same form as the shock or eddy-loss developed for steady flow. In this case the term $\frac{f u^2}{2\, d} = \beta\, u^2$ is added to the right side of Eq. 29 (in which f is the friction factor and d is the diameter of the pipe), with the stipulation that under all conditions it will be effective in a direction opposing the velocity of flow.

APPENDIX II. LIST OF SYMBOLS

The following letter symbols, adopted for use in this paper and its discussion, conform essentially with American Standard Letter Symbols for Hydraulics (ASA Z10.2—1942), prepared by a committee of the American Standards Association, with Society participation and approved by the Association in 1942:

C_{pos} and C_{neg} = characteristics of the equations of motion;
c = speed of surge;
d = pipe diameter;
f = friction factor;
g = acceleration of gravity;
H_0 = head in the reservoir;
h = head of the system;
h_1 = dimensionless head $= \frac{g\,h}{c\,u_0}$;
K = bulk modulus;
k = effective coefficient of discharge at the valve;
L = length of pipe;
n = an exponent;
t = unit of time;
u = velocity of the fluid;
u_1 = dimensionless velocity $= \frac{u}{u_0}$;
x = distance measured along the pipe;
x_1 = dimensionless length $= \frac{x}{L}$;
z = distance from the z-axis;
β = a friction term coefficient;
γ = loss in head as a result of friction;
Δ = the total change in the quantity for the period under consideration;
λ = a number such that $\frac{\lambda_1}{\lambda_2} = \pm \frac{g}{c}$;
ρ = density of the fluid; and
τ = dimensionless time $= \frac{c\,t}{L}$.

(Subscripts 0, 1, 2, 3, . . . are used to indicate conditions along the pipe at successive time increments and the prime superscripts denote differential displacements of the points of study.)

DISCUSSION

Pin-Nam Lin.[6]—In 1947, J. Lamoen presented an application of the theory of characteristics to the analysis of water-hammer problems.[7] Mr. Lamoen's treatment was concerned with the following:

1. The case of negligible resistance and kinetic energy. Equations of characteristics were derived, and two equations were shown to be another form of the two equations forming the basis of the Schnyder-Bergeron graphical method.
2. The case of negligible kinetic-energy terms, but with the resistance term considered to be proportional to the mean velocity.
3. The case of negligible kinetic-energy terms, except that the resistance term was considered to be proportional to the square of the velocity. Numerical examples were given for the various cases, and the effect of the kinetic-energy term was elaborated upon.

The derivations given in Appendix I do not include the elasticity of the pipe wall. This inclusion is often desired in practical applications. When the elasticity is taken into account, the derivation of the equation of continuity is modified to the form:

$$\frac{\partial u}{\partial x} = -\frac{1 + \dfrac{K\,d}{E\,\delta}}{\dfrac{K}{\rho}}\left(\frac{\partial h}{\partial t} + u\,\frac{\partial h}{\partial x}\right) \quad \text{(34a)}$$

and

$$\frac{\partial u}{\partial x} = -\frac{g}{(c')^2}\left(\frac{\partial h}{\partial t} + u\,\frac{\partial h}{\partial x}\right) \quad \text{(34b)}$$

in which E is the modulus of elasticity of the pipe material and δ is the thickness of the pipe wall (assumed to be small in comparison with d).[8]

Eqs. 18 are of the same form as a pair of equations solved for the problem of unsteady flow in open channels. Both graphical[9,10] and semigraphical[11] methods of solution are available for this case. These methods could be adapted to the study of water-hammer problems.

---

[6] Asst. Prof., Dept. of Civ. Eng., Colorado Agri. and Mech. College, Fort Collins, Colo.

[7] "Le Coup de Bélier D'Allievi, Compte Tenu des Pertes de Charge Continues," by J. Lamoen, *Bulletin*, Centre d'Études, de Récherches et d'Essais scientifiques des Constructions du Genie Civil et d'Hydraulique fluviale, Tome II, Dosoer, Liège, Belgium, 1947, pp. 355–382.

[8] "Mathematical Engineering Analysis," by R. Oldenburger, Macmillan & Co., New York, N. Y., 1950, Chapter 13.

[9] "Calcul Graphique des Régimes Variables dans les Canaux," by A. Craya, *La Houille Blanche*, No. 1, November, 1945, p. 37.

[10] "Flood Routing," by B. R. Gilcrest, in "Engineering Hydraulics," edited by Hunter Rouse, John Wiley & Sons, Inc., New York, N. Y., 1950, Chapter X.

[11] "Numerical Analysis of Continuous Unsteady Flow in Open Channels," by Pin-Nam Lin, *Transactions*, Am. Geophysical Union, Vol. 33, 1952, pp. 226–234.

Henry M. Paynter,[12] J. M. ASCE.—The writer is impressed by Mr. Gray's excellent presentation of the principles of the method of characteristics as applied to elastic plane-wave problems. However, not enough credit has been given to earlier investigators such as: (1) Bernhard Riemann, who devised the mathematical techniques described for this very problem;[13] (2) Junius Massau, who innovated the graphical techniques for the solution of wave-propagation problems;[14,15] (3) O. Schnyder, who independently arrived at these constructions through the work of Lorenzo Allievi;[16] and (4) Louis Bergeron who extended these graphical techniques still further.[17,18]

The author commented on the incorrectness of the kinetic-energy assumptions of previous investigators but made no reference to the pertinent papers by D. Gaden and Mr. Schnyder[19,20] and Mr. Riemann.[13] These references are cited so that interested persons can avail themselves of some of the wealth of information contained in the prior studies of the problem.

As to the practical application of the graphical-characteristics techniques, it is believed that the conventional methods of combining pipe-friction losses at one or more points along the pipe have a sound rational basis. It is clear (from Mr. Gray's presentation) that, for all normal cases of water hammer in pipes and conduits, u is much smaller than c, and that, therefore, the characteristic equations are represented by Eqs. 10.

From Eqs. 10 it can be seen that the total variations in head can be written (by replacing $c\,dt$ by $\pm\,dx$) to give, along the C_{pos}-curve—

$$\frac{c}{g}\,du = dh + \frac{\beta\,u^n}{g}\,dx \ldots\ldots\ldots\ldots\ldots\ldots\ldots (35a)$$

and along the C_{neg}-curve—

$$-\,\frac{c}{g}\,du = dh + \frac{\beta\,u^n}{g}\,dx \ldots\ldots\ldots\ldots\ldots\ldots\ldots (35b)$$

If Eqs. 35 are integrated along the entire characteristic, the results can be written as

$$\frac{c}{g}\,\Delta u = \Delta h + h_{f\,\Delta x} \ldots\ldots\ldots\ldots\ldots\ldots\ldots (36a)$$

---

[12] Asst. Prof. of Hydr. Eng., Dept. of Civ. and San. Eng., Massachusetts Inst. of Technology, Cambridge, Mass.

[13] "Über die Fortpflanzung ebener Luftwellen von endlicher Schwingungsweite," by Bernhard Riemann, *Abhandlungen*, Gesellschaft der Wissenschaften Zu Göttingen, Mathematische—physikalische Klasse 8, Vol. 43, 1860.

[14] "L'intégration graphique," by Junius Massau, *Annales*, Association des Ingénieurs sortis des Écoles Spéciales de Gand, Vol. 12, 1889, p. 435.

[15] "Mémoire sur l'intégration graphique des équations aux dérivées partielles," by Junius Massau, *ibid.*, Vol. 23, 1900, p. 95.

[16] "Druckstösse in Pumpenleitungen," by O. Schnyder, *Schweizerische Bauzeitung*, Vol. 95, 1929, Nos. 22 and 23.

[17] "Méthode graphique génèrale de calcul des propagations d'ondes planes," by Louis Bergeron, *Mémoires*, Société des Ingénieurs Civils de France, 1937.

[18] "Du coup de bélier en hydraulique au coup de foudre en electricité." by Louis Bergeron, Dunod, Paris, France, 1940.

[19] "Des hypotheses admises pour l'établissement des équations du coup de bélier dans une conduite à caractéristique unique," by D. Gaden and G. Darrieus, *Rêvue Générale de l'Hydraulique*, May 12, 1939.

[20] "Coups de bélier des petites et des grandes amplitudes dans un milieu fluide animé d'une vitesse d'écoulement de valeur faible ou élevée," by D. Gaden and O. Schnyder, *Bulletin Technique de la Suisse Rumaude*, July 8, 1944.

and

$$-\frac{c}{g}\,\Delta u = \Delta h + h_{f\,\Delta x} \quad \ldots\ldots\ldots\ldots\ldots\ldots\ldots\ldots (36b)$$

respectively. In Eqs. 36

$$h_{f\,\Delta x} = \int_0^{\Delta x}\left(\frac{\beta\,u^n}{g}\right)dx = \int_0^{\Delta t} c\left(\frac{\beta\,u^n}{g}\right)dt \quad \ldots\ldots\ldots (37)$$

and $h_{f\,\Delta x}$ is the average value of the total head lost along the respective characteristic.

From Fig. 9 in which the pipe friction has been concentrated at a single point at the upstream end of the pipe, it can be seen (Fig. 9(*a*)) that the effect of the pipe-friction loss is determined quite closely by the illustrated process.

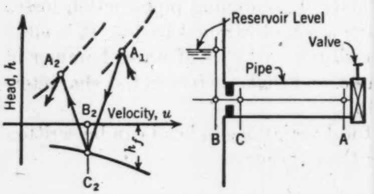

(*a*) VELOCITY-HEAD DIAGRAM (*b*) SCHEMATIC DIAGRAM

FIG. 9.—FRICTION LOSS CONCENTRATED AT ONE POINT

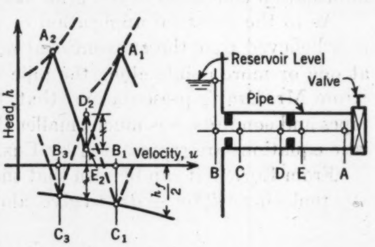

(*a*) VELOCITY-HEAD DIAGRAM (*b*) SCHEMATIC DIAGRAM

FIG. 10.—FRICTION LOSS CONCENTRATED AT SEVERAL POINTS

In this case, the measure of $h_{f\,\Delta x}$ is obtained by assuming that, for the round-trip time of the wave, the average value of $h_{f\,\Delta x}$ is approximated by the value of the head loss for the mean flow, or more specifically, the flow at the upstream end at the middle of a time increment of 2 L/c sec.

This is precisely the approach used by practitioners in this field. These engineers also group the losses at the downstream end or, more generally, at two or more points along the pipe to secure a better estimate of the frictional effects. A sample construction of this type is shown in Fig. 10.

It appears that, although the procedures described by Mr. Gray and those previously described have a common logical foundation, the latter constructions are more intuitively conceived and therefore more readily comprehended. Such constructions are less likely to cause error or confusion, although faster to apply.

Although the utility of the Schnyder-Bergeron-Angus graphical procedures is universally appreciated, prior to the appearance of Mr. Gray's paper the relationship of graphical approaches to the method of characteristics was not generally known, despite the applications of Mr. Massau's techniques to free surface flow and to the unsteady flow of gases. The author also deserves credit for drawing to the attention of English-speaking hydraulic engineers the fact that the effects of kinetic energy and distributed friction loss are simply accounted for within these methods. It should be equally clear from Mr. Gray's work (and from the cited references) that the effects of nonlinearities and nonuniformities on plane-wave propagation in all media can be studied with facility.

C. A. M. Gray,[21] A. M. ASCE.—The discussions offered by Messrs. Lin and Paynter have been primarily concerned with a bibliography on the analysis of the water-hammer problem by characteristics. It was believed that the treatment of hyperbolic partial differential equations by the method of characteristics or by Mr. Rieman's method required no further reference. However, further treatment (in English) of hyperbolic equations is available.[22,23] The application of the method of characteristics to open-channel flow has been investigated.[24]

It is not claimed that the treatment presented should replace the usual consideration of friction, but this method does allow intuitive derivation to be placed on a more exact basis and also allows some estimate of the approximation to be made. For example, in Fig. 9, the integral of Eq. 37 is only approximated by the velocity at the middle of the time interval $2\ L/c$ because the correction is small. This fact is shown readily by use of the *xt*-diagram which should be drawn in all cases as it identifies what is occurring in the *hv*-plane.

To derive a mathematically correct basis for the usual engineering approximation of friction joints, one must consider the two characteristics through some point (point 2) in the *xt*-plane; it must also be assumed that these characteristics pass through points 1 and 3 which lie on the C_{pos}-characteristic and C_{neg}-characteristic through point 2, respectively. It is further supposed that the values of u and h are known at these points.

Integrating along the C_{pos}-curve, there results from Eq. 10,

$$\begin{aligned}\frac{c}{g}u_2 - h_2 &= \frac{c}{g}u_1 - h_1 - \int_1^2 \frac{\beta\, c\, u^n}{g}\,dt\\ &= \frac{c\,u_1}{g} - h_1 - \frac{t_{21}}{2}\frac{\beta\, c}{g}\left(u^n{}_1 + u^n{}_2\right) \qquad \text{(38)}\end{aligned}$$

and along the C_{neg}-curve,

$$\begin{aligned}\frac{c}{g}u_2 + h_2 &= \frac{c}{g}u_3 + h_3 - \int_3^2 \frac{\beta\, c\, u^n}{g}\,dt\\ &= \frac{c\,u_3}{g} - h_3 - \frac{t_{23}}{2}\frac{\beta\, c}{g}\left(u^n{}_2 + u^n{}_3\right) \qquad \text{(39)}\end{aligned}$$

---

[21] Senior Lecturer, Univ. of Sydney, Sydney, Australia.

[22] "Partial Differential Equations of Mathematical Physics," by A. G. Webster, Hafner Publishing Co., Inc., New York, N.Y., 1950.

[23] "Supersonic Flow and Shock Waves," by R. Courant and K. O. Friedrichs, Interscience Publishing, Inc., New York, N. Y., 1948.

[24] "The Formation of Breakers and Bores," by J. J. Stoker, *Communications in Applied Mathematics*, New York Univ., New York, N. Y., Vol. 1, 1948.

in which the integrals have been evaluated by the trapezoidal rule and $t_{21} = t_2 - t_1$. Then, if

$$h''_2 = h_2 - \frac{t_{21}}{2} \frac{\beta\, c}{g} u^n{}_2 \qquad (40a)$$

$$h'_1 = h_1 + \frac{t_{12}}{2} \frac{\beta\, c}{g} u^n{}_1 \qquad (40b)$$

$$h'_2 = h_2 + \frac{t_{23}}{2} \frac{\beta\, c}{g} u^n{}_2 \qquad (40c)$$

and

$$h''_3 = h_3 - \frac{t_{23}}{2} \frac{\beta\, c}{g} u^n{}_3 \qquad (40d)$$

Eq. 38 becomes

$$\frac{c}{g} u_2 - h''_2 = \frac{c}{g} u_1 - h'_1 \qquad (41)$$

and Eq. 39 becomes

$$\frac{c}{g} u_2 + h'_2 = \frac{c}{g} u_3 + h''_3 \qquad (42)$$

Along the characteristics from point 1 to point 2 and from point 2 to point 3, friction can be neglected, provided it is concentrated at the joints at points 1, 2, and 3. At these points there will be a discontinuity in h which is given for point 2 by

$$h'_2 - h''_2 = \frac{t_{21} + t_{23}}{2} \frac{\beta\, c}{g} u^n{}_2 = \frac{L_{23} + L_{12}}{2} \frac{\beta\, u^n{}_2}{g} \qquad (43)$$

in which L_{23} and L_{12} denote $x_3 - x_2$ and $x_2 - x_1$, respectively. Thus, the analysis of friction can be performed to any degree of approximation by the use of friction-joints. It is to be noted from this analysis that there should always be joints at each end of the pipe. An alternative procedure based on the solution of Eqs. 38 and 39 by a method of successive approximation has been applied to some results.[25]

Concerning Mr. Lin's question regarding wall elasticity, the speed of the surge (an abrupt discontinuity) is the only quantity affected; Eqs. 22 and 30 are correct. However, the pressure-density relationship of the fluid must be modified, and Eq. 25 can be written as

$$\Delta p = K' \frac{\Delta \rho}{\rho} \qquad (44)$$

in which

$$K' = \frac{K}{1 + \dfrac{K\, d}{E\, \delta}} \qquad (45)$$

Thus, all results originally presented are correct, provided K' is substituted for K.

---

[25] "The Dissipation of Energy in Water Hammer," by C. A. M. Gray, *Australian Journal of Applied Science*, June, 1954, pp. 125–131.

AMERICAN SOCIETY OF CIVIL ENGINEERS
Founded November 5, 1852
TRANSACTIONS

Paper No. 2718

JOINT TRANSLATION BY CANTILEVER MOMENT DISTRIBUTION

By L. E. Grinter,[1] M. ASCE, and C. H. Tsao[2]

With Discussion by Messrs. T. C. Kavanagh; Ralph W. Stewart; W. Merchant; Jack R. Benjamin; Joseph G. Perri; Richard H. Hadley; Ming-Lung Pei; and L. E. Grinter and C. H. Tsao

Synopsis

The method of moment distribution of Hardy Cross, Hon. M. ASCE, has solved the problem of joint rotation in continuous structures in a simple manner. Joint translation (or sidelurch), however, has had to be dealt with in an indirect manner. The methods of correcting for sidesway include (1) an independent distribution of moments corresponding to each degree of freedom for translation, with interrelationships established by the solution of a number of simultaneous equations equal to the number of the degrees of freedom, (2) a sequence of partial sidesways, with joints restrained against rotation, which converge to the actual sidesway and form a series of corrections to the process of moment distribution, and (3) a reversed technique by which the computed or estimated movements of the joints that accompany sidelurch are used to determine the fixed-end moments for distribution. The method last mentioned has been effective in solving the problem of wind-stress analysis for tall buildings.

The concept of cantilever moment distribution is presented in this paper as a direct method of permitting joint translation to take place as an integral part of the process of moment distribution. Three techniques are suggested for application of the method: (*a*) In many structures involving identical columns or chords, complete freedom of sidelurch is permitted by cantilever moment distribution without any special correction. (*b*) For structures with unlike columns or chords an approximate solution by cantilever moment distribution that does not eliminate all restraining forces at the joints can be used. (*c*) Cantilever moment distribution can also be used to determine the moments and lateral deflections of a substitute structure having identical columns or chords.

Note.—Printed, essentially as printed here, in October, 1953, as *Proceedings-Separate No. 298.* Positions and titles given are those in effect when the paper or discussion was received for publication.

[1] Dean of the Graduate School, Univ. of Florida, Gainesville, Fla.

[2] Visiting Asst. Prof. of Civ. Eng., Univ. of Southern California, Los Angeles, Calif.

Following this analysis, the lateral joint movements of the substitute structure may be used in the previously cited reversed technique to determine a relatively accurate set of moments caused by sidesway in the structure with unlike columns or chords.

Moment Distribution

In the usual process of moment distribution, the relaxation or rotation of the joints, when joint translation is restricted, permits the reduction or loss of shear in members influenced by sidelurch. For example, the bent shown in Fig. 1(*a*) has fixed-end moments introduced into the columns as shown in Fig. 1(*b*), so that the sum of the column shears equals the applied load P. When the joints B and C, however, are permitted to rotate without translation, the process of moment distribution as developed by Hardy Cross, Hon. M. ASCE,[3] results in reduced column shears which no longer balance the load P. It is evident that a variation of this system of moment distribution would be useful for lessening or—preferably—preventing shear loss. In the Appendix an analysis of the method of moment distribution clarifies the fact that two factors defining the degree of fixity for each member, which are determinable from the actual or assumed conditions of end restraint, define a process of moment distribution. Of the infinite variety of distribution procedures possible, only one, termed "cantilever distribution," has the characteristic of allowing the member to undergo no change in shear as moment distribution occurs.

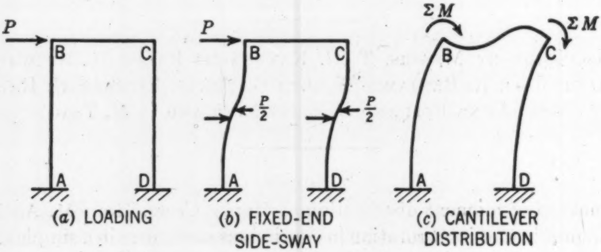

(*a*) LOADING (*b*) FIXED-END SIDE-SWAY (*c*) CANTILEVER DISTRIBUTION

Fig. 1.—A Simple Bent

Following the preparation of this paper, the writers became aware of other investigations of the subject of translation as a part of the process of moment distribution.[4, 5]

Cantilever Moment Distribution.—Fig. 1(*c*) shows the distortion of a symmetrical bent that moves freely under applied corner moments ΣM. Each column has a moment diagram which corresponds to a free cantilever, since identical columns have the same lateral deflections under equal applied moments. For such a cantilever the moment carry-over factor to the fixed end is -1.0, by use of the rotational sign convention introduced by one of the writers.[6] In Fig. 2 the slope θ, caused by a moment M, is $\frac{M\,L}{E\,I}$ as contrasted to $\frac{M\,L}{4\,E\,I}$ in Fig. 3. (L is the length of the column; I denotes the moment of inertia of the cross section of the column; and E is the modulus of elasticity of the column.) Hence, for cantilever moment distribution, the stiffness factor

---

[3] "Analysis of Continuous Frames by Distributing Fixed-End Moments," by Hardy Cross, *Transactions*, ASCE, Vol. 96, 1932, pp. 1–10.

[4] "'Degree of Fixity' Methods for Certain Sway Problems," by R. H. Wood and E. Goodwin, *The Structural Engineer*, July, 1952, pp. 153–162.

[5] "Analysis and Design of Columns in Frames Subject to Translation," by T. C. Kavanagh, *Column Research Council Report*, 1950.

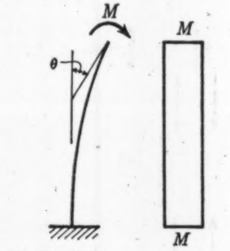

(a) COLUMN (b) BENDING MOMENT DIAGRAM

Fig. 2.—Cantilever Moments

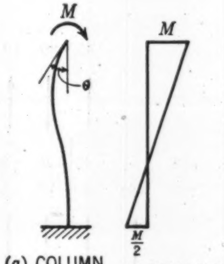

(a) COLUMN (b) BENDING MOMENT DIAGRAM

Fig. 3.—Rotation Without Translation

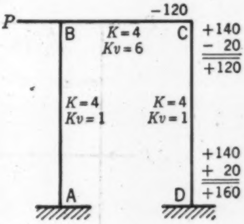

Fig. 4.—Analysis of a Simple Bent

is only 25% of the stiffness factor K that is used for a member in which joint translation is prevented. The stiffness factor and carry-over factor for cantilever moment distribution therefore equal $K/4$ and -1.0, respectively. These values can be compared with a stiffness factor of K and a carry-over factor of $+0.5$ for moment distribution without joint translation.

Cantilever Distribution for a Simple Bent.—Fig. 4 shows a simple bent with fixed-end columns and all members having the same K-values. The top member for antisymmetrical moments caused by sidesway has a stiffness, or resistance to equal end rotations, that is 1.5 times greater than its resistance to rotation at one end when the other end is fixed. Its corrected stiffness, or $K\,v$)-value is $1.5 \times 4 = 6$. The column as a cantilever has a ($K\,v$)-value equal to $0.25 \times 4 = 1$. The fixed-end column moments caused by the load P are $+140$ at each end of each column. When a moment distribution is performed at joint C of Fig. 4, the unbalanced moment of $+140$ causes a correction moment of $-(1/7) \times 140 = -20$ in member CD at end C, and a correction moment of $-(6/7) \times 140 = -120$ in member CB at end C. The carry-over factor for cantilever moment from joint C to support D is -1, which explains the correction moment of $+20$ at support D. Antisymmetry then results in the moments at support A and joint B. The final moments at points A and D are $+160$, and the corner moments at points B and C are $+120$. It can be seen that a single joint-moment distribution, using the cantilever concept for the columns, completed the analysis of this bent for sidesway.

---

[6] "Sign Conventions," by L. E. Grinter, *Engineering News-Record*, March 7, 1935, Vol. 114, p. 359.

Cantilever Distribution for a Multi-Story Bent.—In Fig. 5 a three-story bent is analyzed by cantilever distribution. There is antisymmetry of the moment diagrams for the girders; therefore, their stiffnesses are increased 50% and the moments are distributed at the joints of one column only. Fixed-end moments are proportional to the story shears for equal story heights and are +50, +100, and +150, respectively, from the third to the first story. The first joint to be balanced is B, at which the sum of the fixed-end moments is +250.

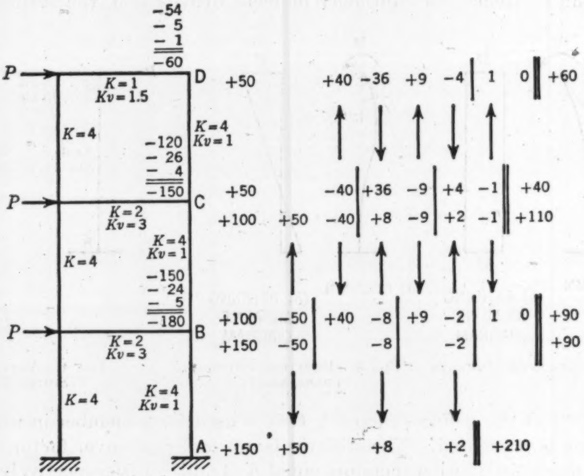

FIG. 5.—ANALYSIS OF A THREE-STORY BENT

Each column entering joint B is considered to act as a cantilever with its free end at joint B and its far ends, A and C, fixed against rotation. To maintain rotational continuity at joint B, the total fixed-end moment is distributed in proportion to the (*K v*)-values, and, to avoid a linear discontinuity at joint B, two of the three joints A, B, and C must provide freedom for lateral joint translation.

Considering the moment distribution at joint B, the division of moment according to the (*K v*)-values is −50 to each column and −150 to the girder. Then +50 is the carry-over moment to joint A and to joint C. At joint C the unbalanced moment is +200 and its distribution, according to (*K v*)-values, gives −40 to members CB and CD and −120 to the girder at joint C. The third joint to be balanced is D, after which the distribution sequence B-C-D is repeated twice to obtain the final convergence. When any joint is being balanced, the two columns entering the joint are dealt with as if they were cantilevers with fixed far ends that require freedom of sidesway at the joint being balanced and at the next joint above, to permit double cantilever deflection. All other joints beyond the next joint above the one being balanced translate the same distance as does the next joint above the one being balanced.

Parallel-Chord Vierendeel Truss, Upper and Lower Chords Having Equal Stiffnesses.—In Fig. 6 a parallel-chord Vierendeel truss is shown, with upper chord and lower chord of equal stiffnesses and loaded at the panel points only. Under the imposed loads, the joint A′ moves to a′, and joints B, C, D, and E deflect to b, c, d, and e, respectively. Neglecting direct-stress deformations, the deflected positions of the remainder of the joints are fixed by the geometry of the structure. If the entire truss is given a rigid-body rotation until member Aa′ is vertical, all web members will be vertical, and joints A and F will not be on the same level. Since the reactions at joints A and F are statically determinate, they are known and may be retained as forces acting on the ro-

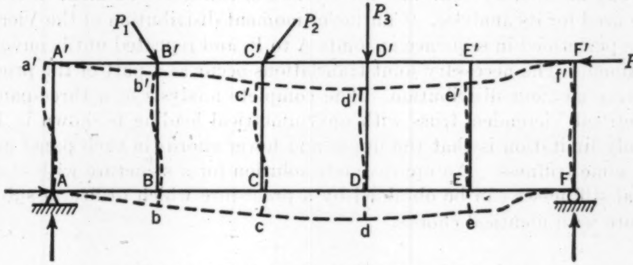
P1
P2
P3
A′
B′
C′
D′
E′
F′
P4
a′
b′
c′
d′
e′
f′
A
B
C
D
E
F
b
c
d
e

FIG. 6.—A PARALLEL-CHORD VIERENDEEL TRUSS

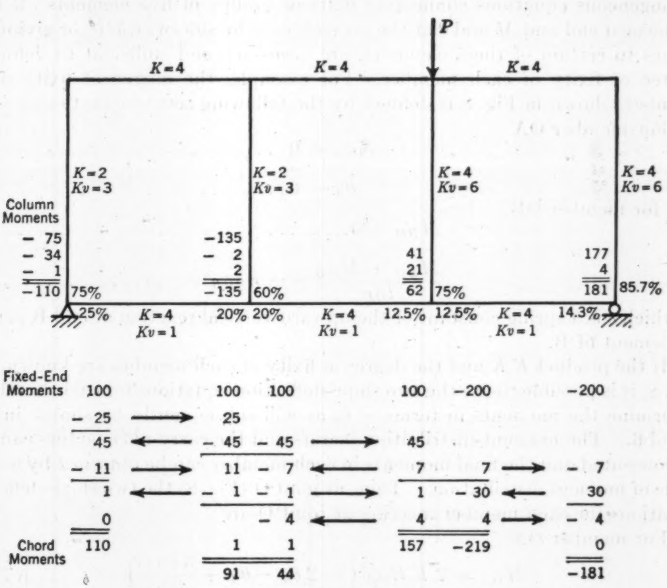
P
K=4
K=4
K=4
K=2
Kv=3
K=2
Kv=3
K=4
Kv=6
K=4
Kv=6
Column Moments
−75
−34
−1
−110
75%
−135
−2
2
−135
60%
41
21
62
75%
177
4
181
85.7%
25%
K=4
Kv=1
20%
20%
K=4
Kv=1
12.5%
12.5%
K=4
Kv=1
14.3%
Fixed-End Moments
100
100
100
100
−200
−200
−25
25
45
−45
−45
45
−11
11
−7
7
7
−7
1
−1
−1
1
−30
30
0
−4
4
4
−4
Chord Moments
110
1
1
157
−219
0
91
44
−181

FIG. 7.—AN UNSYMMETRICAL VIERENDEEL TRUSS

tated truss. The angle of rotation is so small that the directions of all forces can be considered to remain unchanged. The five degrees of freedom (four vertical joint movements and one horizontal movement) consist of the five free vertical deflections of joints B, C, D, E, and F. The parallel-chord Vierendeel truss with chords of equal stiffnesses is therefore structurally identical to the single-bay multi-story bent, and the method of cantilever moment distribution can be used for its analysis. Cantilever moment distribution of the Vierendeel truss is performed in sequence at joints A to F, and repeated until convergence is obtained. The necessary joint translations occur as a part of the process of cantilever moment distribution. The complete analysis of a three-panel unsymmetrical Vierendeel truss with unsymmetrical loading is shown in Fig. 7. The only limitation is that the upper and lower chords in each panel must be of the same stiffness. An approximate solution for a structure with chords of unequal stiffnesses can be obtained by a procedure which utilizes a substitute structure with identical chords.

APPENDIX. MOMENT DISTRIBUTION AND BOUNDARY CONDITIONS

The moment distributed to each member at a rigid joint depends entirely on (1) the product $E\,K$ of each member, and (2) the two properties of each member which together are called the "degree of fixity." Two linear, independent, homogeneous equations connecting pairs or groups of five elements (M and θ at the near end and M and θ at the far end, and the sidesway δ/l), or giving zero values to certain of these elements, are necessary and sufficient to define the degree of fixity of each member. For example, the degree of fixity of the members shown in Fig. 8 is defined by the following sets of equations:

For member OA

$$\delta_{OA} = 0 \qquad (1a)$$

and

$$\theta_A = 0 \qquad (1b)$$

and for member OB

$$M_{BO} = 0 \qquad (2a)$$

and

$$\frac{M_{BO} + M_{OB}}{l_{OB}} = - c\,\delta_{OB} \qquad (2b)$$

in which c is a spring constant or the upward vertical reaction at end B per unit settlement of B.

If the product $E\,K$ and the degree of fixity of each member are known, as in Fig. 8, it is possible to use the two slope-deflection equations for each member to determine the moments in terms of θ_0 as will subsequently be shown in Eqs. 5 and 6. The moment-distribution factors and the carry-over factors can then be computed and the final moments in each member can be obtained by a single cycle of moment distribution. Thus, at joint O (Fig. 8) the two slope-deflection equations for each member meeting at joint O are:

For member OA

$$M_{OA} = 2\,E\,K_{OA}\left(-\,2\,\theta_0 - \theta_A + \frac{3\,\delta_{OA}}{l_{OA}}\right) \qquad (3a)$$

and

$$M_{AO} = 2\,E\,K_{OA}\left(-\,2\,\theta_A - \theta_0 + \frac{3\,\delta_{OA}}{l_{OA}}\right)\ldots\ldots\ldots\ldots(3b)$$

and for member OB

$$M_{OB} = 2\,E\,K_{OB}\left(-\,2\,\theta_0 - \theta_B + \frac{3\,\delta_{OB}}{l_{OB}}\right)\ldots\ldots\ldots\ldots(4a)$$

and

$$M_{BO} = 2\,E\,K_{OB}\left(-\,2\,\theta_B - \theta_0 + \frac{3\,\delta_{OB}}{l_{OB}}\right)\ldots\ldots\ldots\ldots(4b)$$

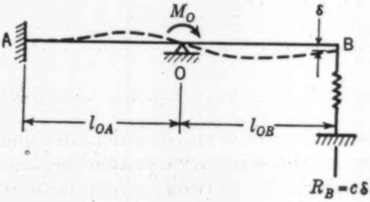

FIG. 8.—A CONTINUOUS GIRDER WITH ONE END ON AN ELASTIC SUPPORT

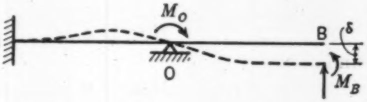

FIG. 9.—A CONTINUOUS GIRDER WITH ONE END DISPLACED VERTICALLY WITHOUT ROTATION

From Eqs. 1 and 3

$$M_{OA} = -\,4\,E\,K_{OA}\,\theta_0\ldots\ldots\ldots\ldots\ldots\ldots(5a)$$

and

$$M_{AO} = -\,2\,E\,K_{OA}\,\theta_0\ldots\ldots\ldots\ldots\ldots\ldots(5b)$$

from Eqs. 2 and 4

$$M_{OB} = \frac{-\,\theta_0}{\dfrac{1}{3\,E\,K_{OB}} + \dfrac{1}{c\,l^2}}\ldots\ldots\ldots\ldots\ldots\ldots(6a)$$

and

$$M_{BO} = 0\ldots\ldots\ldots\ldots\ldots\ldots\ldots\ldots(6b)$$

and from Eqs. 5 and 6 the moment-distribution factors and the carry-over factors are as follows:

$$M_{OA}\!:\!M_{OB} = 4\,E\,K_{OA}\!:\!\frac{1}{\dfrac{1}{3\,E\,K_{OB}} + \dfrac{1}{c\,l^2}}\ldots\ldots\ldots\ldots(7a)$$

$$M_{AO}\!:\!M_{OA} = 1\!:\!2\ldots\ldots\ldots\ldots\ldots\ldots\ldots\ldots(7b)$$

and

$$M_{BO}\!:\!M_{OB} = 0\ldots\ldots\ldots\ldots\ldots\ldots\ldots\ldots(7c)$$

The applied moment M_0 can be balanced by a single cycle of moment distribution:

$$M_{OA} = \frac{4\,E\,K_{OA}}{4\,E\,K_{OA} + \dfrac{1}{\dfrac{1}{3\,E\,K_{OB}} + \dfrac{1}{c\,l^2}}}\,M_0 \quad \text{(8a)}$$

$$M_{OB} = \frac{\dfrac{1}{\dfrac{1}{3\,E\,K_{OB}} + \dfrac{1}{c\,l^2}}}{4\,E\,K_{OA} + \dfrac{1}{\dfrac{1}{3\,E\,K_{OB}} + \dfrac{1}{c\,l^2}}}\,M_0 \quad \text{(8b)}$$

$$M_{AO} = \tfrac{1}{2}\,M_{OA} \quad \text{(8c)}$$

and

$$M_{BO} = 0 \quad \text{(8d)}$$

Principle Defining Moment Distribution.—The sets of two equations defining the degree of fixity of each member are called the boundary equations because they describe the end conditions of the member. These two equations must be independent of each other, independent of statics, and also independent of the two slope-deflection equations. From the previous example, the following principles are clear: Any two arbitrary, linear, independent, homogeneous boundary equations for ach member will define a system or process of moment distribution and vice versa. Any two linear, independent, homogeneous boundary equations will yield a formal process of moment distribution. However, many of these processes may not converge at all and many more will converge slowly. Evidently only those that converge reasonably rapidly can be used. In actual practice, the boundary equations are not chosen; they are often dictated by the geometry of the structure to be analyzed. To cite a few examples from among the infinite number of possible systems of moment distribution, Eqs. 2 are replaced by Eqs. 9 and 10. These equations are applicable to Fig. 9, in which the joint B is displaced vertically without rotation. For Fig. 9,

$$\theta_B = 0 \quad \text{(9)}$$

and

$$M_{BO} : M_{OB} = r \quad \text{(10)}$$

Eqs. 1, 9, and 10 define a process of moment distribution having the following characteristics:

$$M_{OA} : M_{OB} = K_{OA} : K_{OB}\,v_{OB} \quad \text{(11a)}$$

$$M_{AO} : M_{OA} = \tfrac{1}{2} \quad \text{(11b)}$$

and

$$M_{BO} : M_{OB} = r \quad \text{(11c)}$$

in which

$$v_{OB} = \frac{1}{2 - 2\,r} \quad \text{(12)}$$

Here θ_B is zero whereas δ_{OB} is not zero. Eq. 12 can be compared with $v = \frac{3}{4 - 2r}$ which applies to the case when $\delta_{OB} = 0$ whereas θ_B is not zero. It can be seen that v is a correction factor such that the product $K v$ represents the relative resistance to end rotation.

Cantilever Moment Distribution.—For the special case in which $r = -1$, Eq. 12 results in $v_{OB} = \frac{1}{4}$, and member OB takes no shear during moment distribution. Member OB acts similar to a cantilever fixed at B and loaded at O by the moment M_{OB}. For this reason this special process of moment distribution has been called "cantilever moment distribution." This method's unique property of producing no shear change during moment distribution makes it an excellent device for solving certain problems involving sidesway.

DISCUSSION

T. C. KAVANAGH,[7] M. ASCE.—The method of moment distribution described by the authors was developed in 1944 by Joseph G. Perri.[8] The method evolved as a result of an investigation of buckling problems for the Column Research Council of the Engineering Foundation.

The major part of Mr. Perri's research was concerned with all the aspects of wind problems. Also included in this investigation was the study of the "uniqueness principle" (stated by the authors in the Appendix) and of certain approximation methods. Additional research by the writer, under the sponsorship of the Column Research Council and the direction of the Council's Committee "D" (of which Mr. Grinter was a member), extended the method developed by Mr. Perri to (1) an embodiment of generalized translational and rotational stiffness factors and carry-over factors for both symmetrical and unsymmetrical frames and (2) a detailed application of the procedure to the buckling of columns in frameworks. This work[5] was the first research project completed by the Column Research Council and formed the starting point for an investigation currently (1953) being performed by the Council at the Pennsylvania State University at State College. This research project is concerned with the buckling of pony-truss chords or continuous columns on elastic supports.

The generalized moment-distribution procedure has been taught by the writer for a number of years in engineering schools in the eastern United States. The method has been introduced into a number of design offices with which Mr. Perri and the writer have been associated, and it has been used in many structural designs. The Perri method (the generalized moment-distribution procedure, or modified moment-distribution procedure using cantilever stiffnesses and carry-over factors, as the method has been variously named) has been particularly useful in design practice because of the frequent occurrence of symmetrical bents, in which case the procedure is quite simple.

This method has been expanded to include the effects of axial load and has also been adapted to the design of haunched members and frames with elastic joints (semirigid framing). A brief history of the development of the procedure is available.[5] The simplification resulting from symmetry was known to British engineers in 1950 and has been extended to include Vierendeel and similar trusses.[9]

The generalized moment-distribution procedure represents one of the most important single contributions to the development of the moment-distribution process that has been made since the original paper[3] of Mr. Cross. This method affords an opportunity for further developments by simplification and approximation.

---

[7] Prof. of Structural Eng. and Chairman of the Dept. of Civ. Eng., New York Univ., New York, N. Y.; partner, Praeger-Kavanagh, Engrs., New York, N. Y.

[8] "Modified Method of Moment Distribution for Analyzing Compression Members as Parts of Rigid Frames," by Joseph G. Perri, thesis presented to New York University, New York, N. Y., in June, 1948, in partial fulfilment of the requirement for the degree of Doctor of Science.

[9] "Sidesway in Symmetrical Building Frames," by N. Naylor, *The Structural Engineer*, April, 1950, p. 99.

Ralph W. Stewart,[10] M. ASCE.—The indirect solution shown by the authors in Fig. 4—in which is introduced the fictitious condition of cantilever flexure shown in Fig. 1—appears to be a roundabout procedure. A more direct approach would be to sketch the traverse of the final flexure as shown in Fig. 10. From Fig. 10, it can be seen that 3/7 of the sum of the column moments goes to the top of the columns and 4/7 of the sum goes to the bottoms, agreeing with the authors' result. In this solution the relative stiffnesses of the members are reduced to their lowest terms (unity). This is done rather than using a larger number which operates more conveniently with the special constants necessary for the cantilever-moment-distribution method.

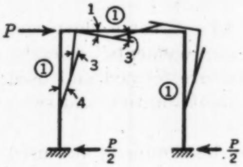

Fig. 10.—Traverse Analysis of a Simple Bent

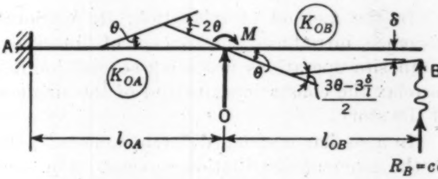

Fig. 11.—Traverse Analysis of a Continuous Girder with One End on an Elastic Support

The authors' moment-distribution equation (Eq. 8*a*) is derived from four standard slope-deflection equations. The same result can be obtained by a consideration of the basic properties of the flexed structure, and by the evaluation of the structure's flexure.

Fig. 11 shows the traverse of the elastic curves of this beam with the angles evaluated by a simple method. From the traverse principle (an end moment is equal to its appertenant flexure angle multiplied by the stiffness of the member) there results

$$M_{OA} = 4\,E\,K_{OA}\,\theta \quad \text{.......................} (13)$$

and

$$M_{OB} = \frac{3\theta - \frac{3\,\delta_{OB}}{l_{OB}}}{2}\,(2\,E\,K_{OB}) \quad \text{...............} (14)$$

However, it is also true that

$$M_{OB} = c\,\delta\,l \quad \text{...........................} (15)$$

From Eqs. 14 and 15,

$$\theta = \frac{c\,\delta\,l}{3\,E\,K_{OB}} - \frac{\delta}{l} \quad \text{.....................} (16)$$

Substituting Eq. 16 into Eq. 13 yields

$$M_{OA} = 4\,E\,K_{OA}\left(\frac{c\,\delta\,l}{2\,E\,K_{OB}}\right) - \frac{\delta}{l} \quad \text{.............} (17)$$

Dividing Eq. 17 by $c\,\delta\,l$ (the value of M_{OB}) results in Eq. 7*a*.

---

[10] Structural Engr., Los Angeles, Calif.

The traverse method can also be applied to the other problems presented by the authors. For the Vierendeel truss, however, the traverse method will probably show no advantage over the cantilever-moment-distribution method.

W. Merchant,[11] A. M. ASCE.—To the list of those papers which have investigated the subject of translation as a part of the process of moment distribution should be added a contribution by A. Bolton.[12] Mr. Bolton considered the effect of a joint rotation or the sway of a story to be a pattern of the moments and forces. A successive use of these elementary patterns to reduce the magnitude of restraints corresponds to the use of the ordinary process of moment distribution.

In the method of relaxation, R. V. Southwell,[13] to overcome slow convergence, introduced the concept of "block or group displacements" whereby composite operations involving several joints or stories are formed and used to relax the constraints, instead of the single steps of joint rotation and sway of the story.

In a similar manner, different moment patterns can be combined and used in the moment-distribution process. For example, if it is known (from the principle of symmetry) that two joints rotate an equal amount, a pattern can then be formed which satisfies this condition. Thus, moment patterns can be made to satisfy any known facts concerning the structure or the load.

The authors' method of cantilever moment distribution is an example of such a composite moment pattern. This method involves the equal rotation of the two ends of a member, combined with sufficient sway of the stories above and below the beam, so that the shear in these stories is unchanged. The identical device was used by Mr. Bolton[12] who termed it a "no shear operation."

It is of interest to note that moment patterns can be used in three ways to solve a problem: (1) In simple problems they can be synthesized almost by inspection. (2) In more difficult problems—such as a symmetrical, single-bay, multi-story frame—a successive correction can be made in exactly the same manner in which the method of moment distribution can be applied. (3) For multi-story, multi-bay frames; multi-bay, ridged, shed frames;[14] and similar structures successive approximation such as that involved in the relaxation method can be used.

Jack R. Benjamin,[15] A.M. ASCE.—Is cantilever moment distribution a general approach which is worthy of both study and application in the practice of structural engineering? All too many special procedures that give remarkably good solutions when applied to special academic problems have been evolved. Almost all of these are not satisfactory when applied to the routine problems of structural engineering.

---

[11] Reader in Applied Mechanics, College of Technology, Manchester, England.

[12] "A New Approach to the Elastic Analysis of Rigid Frames," by A. Bolton, *The Structural Engineer*, January, 1952, pp. 1-13.

[13] "Relaxation Methods in Engineering Science," by R. V. Southwell, Oxford University Press, Oxford, England, 1940.

[14] "The Analysis of Multi Bay Gabled Rigid Frames," by A. Bolton, *The Structural Engineer*, April, 1943, pp. 110-117.

[15] Associate Prof. of Structural Eng., Stanford Univ., Stanford, Calif.

The method of cantilever moment distribution appears to be practical for only very special problems. The basic weakness in this method is that transfer of shear from one column to another is impossible. Thus, the shear distribution must be found by some other procedure before the method can be applied. The only case in which this shear distribution can be made involves two legs and perfect symmetry such as those in the illustrative examples. Three or more legs or a lack of symmetry invalidate the approach.

The authors mention approximate procedures that are available to extend the method to more general problems. The use of a solution in which complete joint restraint is not removed is highly undesirable. The errors involved can be large, and the most obvious requirement—static equilibrium—is not satisfied. The method of cantilever moment distribution has been applied to several simple three-column and four-column bents, and the results were unacceptable. The use of substitute structures is undesirable because special techniques are required that not only obscure the process but also require an amount of study and mastery inconsistent with the usefulness of the procedure.

Messrs. Grinter and Tsao are to be complimented on the manner of presenting this method; too many technical papers are intelligible only to the writers.

JOSEPH G. PERRI.[16]—The method of cantilever moment distribution which has been presented by the authors is not original nor complete; it is merely one of the many possible solutions of the more general procedure developed by the writer in 1944.[8,5]

The writer has proved[8] that it is possible to select any values for the stiffness and carry-over factors of the columns and the beams provided that the initial moments are properly chosen. The writer has also proved that translational carry-over factors are not necessary whenever cantilever stiffnesses are used and proper initial moments are applied. The many examples offered by the writer,[8] and the practical application made in many engineering offices, cover the special case in which the column stiffness is equal to EI/L and its carry-over factor is -1. Both symmetrical and unsymmetrical configurations have been investigated.

RICHARD H. HADLEY,[17] J. M. ASCE.—In 1949 the writer presented a method[18] of determining sidesway stresses in rectangular rigid frames which is almost identical with that developed by the authors. Although the writer's approach to the problem was somewhat different from that of Messrs. Grinter and Tsao (the former being based on component moments, as suggested by Homer M. Hadley, M. ASCE), the final results appear to be similar, if not identical. This method has been taught at the University of Washington by A. L. Miller, M. ASCE, since 1949 and has been used subsequently by engineers in the northwestern part of the United States.

---

[16] Consultant, Structural Design Section, Eng. Div., Vitro Corp. of America, New York, N. Y.

[17] Partner, Hadley and Hadley, Cons. Engrs., Seattle, Wash.

[18] "Sidesway Analysis of Rectangular Rigid Frames by Component Moment Methods," by Richard H. Hadley, thesis presented to the University of Washington, Seattle, Wash., in 1949, in partial fulfilment of the requirement for the degree of Master of Science in Civil Engineering.

The writer's method is based on the fundamental concept that moments actually existing at the ends of a member can be considered to be the algebraic sum of two components—a shearing moment and a rotational moment. Shearing moments are of equal magnitude and act in the same direction; the rotational moments are of equal magnitude and act in opposite directions. Designating the end moments as M_1 and M_2, and having a proper regard for signs,

$$S = \frac{M_1 + M_2}{2} \qquad (18a)$$

and

$$R = \frac{M_1 - M_2}{2} \qquad (18b)$$

is which S is the shearing moment and R is the rotational moment.

A significant property of the shearing moments is that they transmit all the shear in a member while not producing any relative end rotation. The rotational moments transmit no shear and produce the entire change in the relative end rotation. For the solution of the equivalent bents mentioned by the authors, this concept of rotational and shearing moments develops into a method for the quick evaluation of those types of structures in which column stiffnesses are large in comparison to beam stiffnesses. In such a case, convergence is slow if one applies the method of cantilever moment distribution.

Methods presented by the writer have been used to analyze several irregular multi-story, multi-bay bents. Agreement with the results obtained by use of the slope-deflection theory was most satisfactory. Not only are the methods easy to apply, but any desired degree of accuracy can be readily obtained. In the case of irregular frames, shearing moments are altered by the necessary moment distribution to balance the joints. Precision can be easily re-established by reintroducing corrective shearing moments after each cycle of moment distribution. Because these methods permit both accuracy and ease of analysis, it is believed that they will become the standard method of approach for analyzing rectangular rigid frames subjected to loadings that cause sidesway.

MING-LUNG PEI,[19] J. M. ASCE.—A concise and direct method for solving rigid frames with sidesway has been presented by the authors. It should be noted, however, that the cantilever-moment-distribution method is valid only for symmetrical structures subjected to antisymmetrical loads. The method assumes that the ratios of the lateral displacements to the joint rotations for all columns in one story are the same. This is true only for symmetrical structures subjected to antisymmetrical loads.

When a symmetrical structure is subjected to unsymmetrical loadings, it is always possible to resolve the loadings into a symmetrical part and an antisymmetrical part. The symmetrical loading can be investigated by the regular moment-distribution method. The results of the antisymmetrical loading can be solved by the authors' cantilever-moment-distribution method. In Fig. 12(*a*) there is shown a simple symmetrical bent subjected to P, an unsymmetrical load. This load causes fixed-end beam moments of +56 and −28. In Fig. 12(*b*) the same bent is shown supporting two symmetrically placed loads $P/2$. These loads produce fixed-end beam moments of +42 and −42.

---

[19] Lecturer, The City College of New York, New York, N. Y.

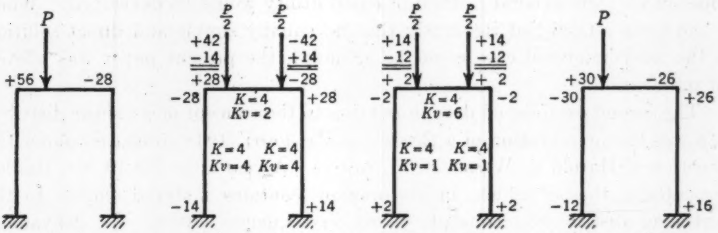

(*a*) LOAD AND FIXED-END BEAM MOMENTS

(*b*) SYMMETRICAL LOADS AND MOMENT DISTRIBUTION

(*c*) ANTI-SYMMETRICAL LOADS AND CANTILEVER MOMENT DISTRIBUTION

(*d*) LOAD AND MOMENTS OBTAINED BY SUPERPOSITION

FIG. 12.—APPLICATION OF THE PRINCIPLE OF SUPERPOSITION TO A SIMPLE BENT

By the moment-distribution method[3] the end moments in the bent are determined. There is shown in Fig. 12(*c*) the same symmetrical bent subjected to two antisymmetrical loads, $P/2$, which cause fixed-end beam moments of +14 and +14. By the cantilever-moment-distribution process the end moments are computed. Fig. 12(*d*) shows the symmetrical simple bent supporting the load P and the end moments which are determined by applying the principle of superposition to the results of Figs. 12(*b*) and 12(*c*).

L. E. GRINTER,[20] M. ASCE, AND C. H. TSAO.[21]—When any extraordinarily simple concept, such as cantilever moment distribution is published, it usually appears that the same or nearly the same concept has been developed in the minds of other investigators. Historical examples are too well known to enumerate. Because several of the discussers have been interested in establishing the priority of their work, it appears desirable to give the chronological development of the cantilever (or no-shear) distribution method as far as the evidence has been established.

The first recorded attempt to publish the cantilever distribution concept was made by the junior writer who presented a paper to the ASCE in January, 1948. This paper (entitled "Rigid Frame Analysis Through Iteration of Least Work Equations") contained the suggested use of a carry-over factor of −1 which is the basis of cantilever moment distribution. The paper was probably rejected for publication on the basis that the approach was overly mathematical. When the junior writer was enrolled as a graduate student at Illinois Institute of Technology (at Chicago) in 1948 and later presented this concept to the senior writer, the latter turned over to him some personal notes that also contained the cantilever distribution derived purely from physical considerations. The important concepts of the present paper, therefore, might have been published in 1948, except for the fact that the writers were interested in studying unsymmetrical structures which formed the basis for their joint studies during the following years. Publication was delayed in the hope that a more general method of equal utility would be developed. When it had been established rigorously that no equally simple and direct solution of the unsymmetrical case could be achieved, the present paper was offered for publication.

---

[20] Dean, Graduate School, and Director of Research, Univ. of Florida, Gainesville, Fla.

[21] Visiting Asst. Prof. of Civ. Eng., Univ. of Southern California, Los Angeles, Calif.

The second established date in relation to the concept of no-shear distribution was the presentation of a thesis[8] by Mr. Perri (1948) prepared under the direction of Harold E. Wessman, M. ASCE. A year later (1949) Mr. Hadley presented a thesis[18] which, in his opinion, contains material similar to the cantilever distribution concept. Next in sequence (1950), Mr. Kavanagh used the method developed by Mr. Perri in a report[5] of limited distribution.

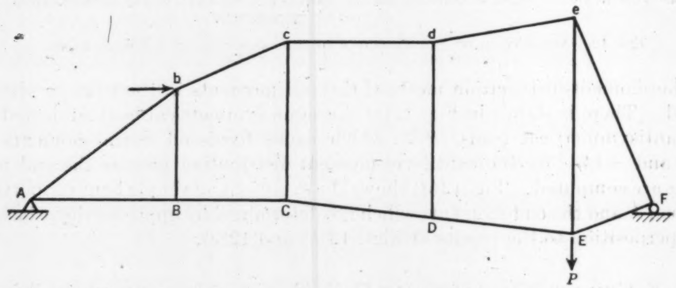

Fig. 13.—The Inclined-Chord Vierendeel Truss

Still in chronological order, the next established date was the presentation (1952) of a thesis[22] by the junior writer. Prepared under the guidance of the senior writer, this thesis contains the principle that: "Any two arbitrary, linear, independent, homogeneous boundary conditions for each member will define a method of moment distribution and vice versa." Applied to the analysis of the inclined-chord Vierendeel truss whose upper chord and lower chord have the same stiffness (Fig. 13), it was shown that joint translation will be automatically provided for if the following modified stiffness factors and carry-over factors are used:

Distribution ratio—

$$M_{CB} = M_{Cc} = M_{CD} = \frac{K_{BC}}{2\,(\alpha^2_{BC} + \alpha_{BC} + 1)} = K_{Cc} = \frac{\alpha^2_{CD}\,K_{CD}}{2\,(\alpha^2_{CD} + \alpha_{CD} + 1)} \quad (19)$$

---

[22] "The Analysis of the Vierendeel Truss and of the Wind Stresses in Tall Buildings," by C. H. Tsao, thesis presented to Illinois Inst. of Technology, at Chicago, Ill., in January, 1952, in partial fulfilment of the requirements for the degree of Doctor of Philosophy.

Carry-over factor to the left—

$$M_{BC} : M_{CB} = -\,\alpha_{BC} \qquad (20)$$

Carry-over fact to the right—

$$M_{DC} : M_{CD} = -\,\frac{1}{\alpha_{CD}} \qquad (21)$$

Carry-over factor for the web—

$$M_{cC} : M_{Cc} = 0 \qquad (22)$$

in which

$$\alpha_{BC} = \frac{\overline{Bb}}{\overline{Cc}} \qquad (23)$$

and

$$\alpha_{CD} = \frac{\overline{Cc}}{\overline{Dd}} \qquad (24)$$

Simple formulas are included[22] for the computation of fixed-end moments. These moments are balanced by the use of Eqs. 19 to 24 to obtain the final answer. It was also noted that, for the special case in which the value of α is unity, the inclined chords become parallel, and this method becomes the method of cantilever moment distribution.

The no-shear concept appears to have been first published[12] in England. This was followed by a paper[4] by R. H. Wood and E. Goodwin. It is perhaps superfluous to note that none of these publications or theses, except the thesis of the junior writer, was known to the writers until after the present paper had been accepted for publication by the ASCE.

In addition to the historical information, the writers appreciate the discussions by Messrs. Stewart, Merchant, Benjamin, and Pei; each of these discussions has added to the value of the paper. It is evident from these discussions that cantilever moment distribution is likely to be widely used as a supplement to ordinary moment distribution where a change in shear is to be avoided.

AMERICAN SOCIETY OF CIVIL ENGINEERS
Founded November 5, 1852
TRANSACTIONS

Paper No. 2719

TURBULENT BOUNDARY LAYER ON STEEP SLOPES

BY WILLIAM J. BAUER,[1] J. M. ASCE

WITH DISCUSSION BY MESSRS. G. HALBRONN, AND WILLIAM J. BAUER

SYNOPSIS

The development of the turbulent boundary layer in a fluid flowing down steep slopes controls not only the loss of head, but also the air entrainment. Prediction of the rate of growth of the layer is essential to proper spillway design. This paper describes a laboratory investigation of the variation in velocity distribution on smooth and rough channel beds for varying slopes and rates of discharge. The boundary-layer thickness, the coefficient of local resistance, and the parametric shape of the velocity profile are analyzed as functions of the Reynolds number and the relative roughness. Although these functions are shown to be in accordance with the general boundary-layer theory, they are essentially independent of both slope and discharge. A practical method is proposed for computing the limit of boundary-layer development on concrete spillways.

NOTATION

The letter symbols introduced in this paper are defined where they first appear, in the text, or by illustration, and are assembled alphabetically in the Appendix for convenience of reference.

INTRODUCTION

The boundary layer which develops on the steep slope of a spillway has important effects on the entire behavior of the fluid flow. The most important effect is the fact that the free surface of the flow may be made turbulent if the boundary layer attains a thickness approaching the thickness of the flow. Since a turbulent free surface is a prerequisite to air entrainment, and since the

---

NOTE.—Published, essentially as printed here, in September, 1953, as *Proceedings-Separate No. 281.* Positions and titles given are those in effect when the paper or discussion was received for publication.

[1] Senior Designer, Harza Eng. Co., Chicago, Ill.

boundary layer is the primary source of that turbulence, the significance of the layer's development on steep slopes lies in its connection with the air entrainment process and with the problems associated with the resulting bulking of flow.

The boundary layer influences the depth, the velocity, and the turbulence of the flow, and through its precipitation of the air entrainment process, also affects the density of the fluid. Without precise knowledge of these aspects of the flow and this property of the fluid, the design of structures associated with spillway floors becomes necessarily approximate, whereas an exact design would often be more economical.

BACKGROUND OF THE PROBLEM

Theory of the Boundary Layer Applied to Steep Slopes.—The assumption of a non-viscous fluid yields a solution to the well-known engineering problem of flow down steep slopes. Through application of the requirements of irrotationality and of the principles of conservation of energy and matter, together with the condition that the pressure be constant along the free surface, the velocity, the pressure, and the location of the free surface at any station along the slope can be determined. The curvilinear geometry of the boundary makes the analysis tedious, but offers no fundamental difficulty.

When viscosity is included in the problem, however, the expedient of separating the flow into two domains is used, as suggested by L. Prandtl in his original statement of the boundary layer concept.[2] Mr. Prandtl considered that, in many flow situations (particularly those involving fluids of low viscosity, of which water is a good example), the viscous effects are confined within a relatively narrow zone adjacent to the boundary; the greater part of the flow therefore behaves as if the fluid were non-viscous. Mr. Prandtl then proposed that these two domains be treated separately. The domain of large viscous effects is called the boundary layer; the domain of negligible viscous effects is termed the zone of near-potential flow, indicating the flow that is only slightly different from the potential flow of the non-viscous fluid. On a spillway, both domains exist contiguously—the near-potential flow being dominant at the upstream end of the spillway, and the boundary layer increasing in thickness in the direction of flow.

The flow in the near-potential domain remains essentially irrotational and free of shear forces. Flow in this domain is handled as if it were flow of a non-viscous fluid, except for its displacement in the direction away from the boundary. In a spillway problem, such displacement is never large enough to produce a significant difference between the magnitude of the actual velocity in the near-potential domain and that computed at the same station on the basis of irrotational flow. The displacement is significant in determining the location of the free surface, however.

The flow within the boundary layer is complicated by the presence of rotational flow and the internal shear, which reaches a maximum at the boundary. The nature of these two complications is understood only in the case of laminar flow, in which the viscous-shear relationship applies. The development of laminar boundary layers may be handled without resort to experimental measurement. Unfortunately, the transition from the laminar to the turbulent boundary layer usually occurs far upstream from the zone of interest, so that the laminar boundary layer constitutes no significant part of the spillway problem.

---

[2] "Über Flüssigkeiten bei sehr kleiner Reibung," by L. Prandtl, *Verhandlung*, Third International Mathematics Cong., Heidelberg, Germany, 1904.

The development of the turbulent boundary layer is governed by parameters which have customarily been determined by experiment. Similarly, the proposed solution depends on laboratory observations of the desired parameters. These parameters are then analyzed with respect to experience with turbulent flows. This empirical approach is the only one available in view of the lack of knowledge of the principles which govern turbulent flow.

In addition to locating both the point at which the free surface of the flow first becomes turbulent (because of the proximity of the turbulent boundary layer) and the free surface upstream from it, the aim of this study was to delineate the effect of continuous positive acceleration on the standard boundary-layer parameters. This latter goal culminates in a series of functional relationships presented graphically in a subsequent section. For better understanding of these relationships and their significance, a brief review of the analytical background of this study is necessary.

Definitions of Boundary-Layer Length Parameters.—In the case of turbulent boundary layers, the analysis is based on experimental evidence, which is interpreted according to a commonly accepted set of definitions. The nominal thickness of the boundary layer is designated by the symbol δ. This thickness is the normal distance from the boundary at which the magnitude of the velocity is approximately 99% of the value predicted by the theory of irrotational flow. A graphical presentation of this relationship is shown in Fig. 1.

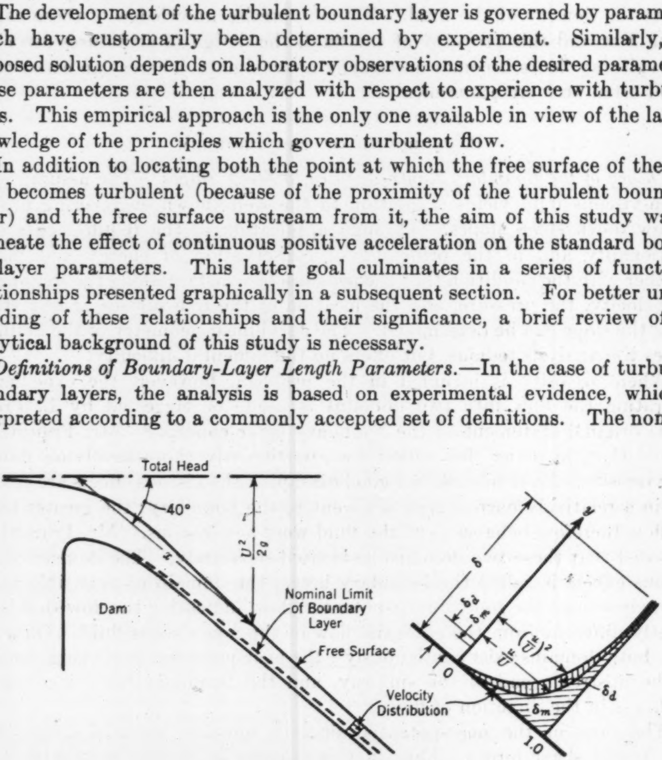

FIG. 1.—DEFINITION OF PARAMETERS

In addition to the nominal thickness, two parameters of other lengths are commonly used in the study of boundary layers. One of these is the displacement thickness, δ_d, which is the distance from the boundary that the potential flow has been displaced by the presence of the boundary layer. The other parameter is the momentum thickness, δ_m, which is a measure of the defect of momentum flux within the boundary layer. For two-dimensional flow, these two lengths are defined as

$$\delta_d = \int_0^\delta \left(1 - \frac{u}{U}\right) dy \ldots\ldots\ldots\ldots\ldots\ldots\ldots (1)$$

and

$$\delta_m = \int_0^\delta \left[\frac{u}{U} - \left(\frac{u}{U}\right)^2\right] dy \ldots\ldots\ldots\ldots\ldots\ldots (2)$$

in which u is the velocity at a point within the boundary layer, U denotes the velocity of the potential flow, and y is the normal distance from the boundary.

The von Kármán Momentum Equation.—Using the two length parameters δ_d and δ_m, T. von Kármán, Hon. M. ASCE, formulated the following expression[3] for the boundary shear in accelerating flows:

$$\frac{2\,\tau_0}{\rho\,U^2} = c_f = 2\,\frac{d\delta_m}{dx} + (\Lambda + 2)\,\frac{\delta_m}{U^2}\,\frac{dU^2}{dx} \ldots\ldots\ldots\ldots\ldots (3)$$

in which c_f is the local coefficient of boundary shear, τ_0 represents the intensity of boundary shear, ρ is the mass density of the fluid, x denotes the distance in the direction of flow, and Λ is a shape parameter of the velocity profile defined as δ_d/δ_m.

If the three functions that relate U, c_f, and Λ to x are known, then this expression can be numerically integrated to obtain δ_m as an explicit function of x. Of these three functions the first is given in the usual case, and the other two are often assumed according to the concepts of the boundary-layer behavior indicated by related experiments.

The von Kármán-Prandtl Velocity-Distribution Equations.—Many of the ideas concerning boundary layers find their basis in an abundance of experimental data concerning flow in pipes. Among them are the von Kármán-Prandtl velocity-distribution equations for turbulent flow near smooth and rough boundaries. The expressions given by Hunter Rouse, M. ASCE, are

$$\frac{u}{\sqrt{\frac{\tau_0}{\rho}}} = 5.75 \log_{10}\left(\frac{\sqrt{\frac{\tau_0}{\rho}}}{\nu}\,y\right) + 5.5 \ldots\ldots\ldots\ldots\ldots (4)$$

for smooth boundaries, and

$$\frac{u}{\sqrt{\frac{\tau_0}{\rho}}} = 5.75 \log_{10}\frac{y}{k} + 8.5 \ldots\ldots\ldots\ldots\ldots\ldots\ldots (5)$$

for rough boundaries.[4] These expressions were derived by Mr. von Kármán by applying the Prandtl mixing-length theory, assuming a constant shear stress throughout the region, and neglecting the laminar shear. The experimental data of J. Nikuradse[5] and others confirm the derivation.

---

[3] "Laminare und turbulente Reibung," by T. von Kármán, *Zeitschrift für angewandte Mathematik und Mechanik*, Vol. 1, 1921, p. 235.

[4] "Elementary Mechanics of Fluids," by Hunter Rouse, John Wiley and Sons, Inc., New York, N. Y., 1946.

Related Investigations.—Boundary-layer developments in uniform flow on flat plates have been both synthesized by a mathematical conversion of pipe-flow principles and measured in the laboratory. H. Schlichting presents an excellent review of the conversion techniques, as applied to both smooth and rough flat plates.[6] In both cases, the basic assumptions are that the thickness of the boundary layer corresponds to the radius of the pipe and that the shape of the velocity profile in the boundary layer is the same as that in a pipe. Although this last assumption is in error, the values of c_f obtained experimentally agree in the case of the smooth plate with those predicted through Mr. Schlichting's conversion techniques.

The development of the boundary layer in nonuniform flow was studied by E. Gruschwitz, who made measurements along the converging and diverging plane walls of a channel.[7] In developing this method of analysis, Mr. Gruschwitz presents the idea that the shape of the velocity profile may be characterized by a single parameter, which is different from Λ. With this as a background, Mr. Gruschwitz numerically integrates Eq. 3 and two empirical expressions. One of these expressions (for c_f) is obtained by conversion of pipe-flow principles according to the method previously indicated. The other expression is for the shape parameter, which is obtained by plotting the experimentally determined values of this quantity against the pressure gradient and the Reynolds number. Mr. Gruschwitz noted little dependence on the Reynolds number, and subsequently eliminated it from consideration in the relation for the shape parameter.

Another method for the computation of boundary-layer developments in flows with pressure gradients was presented by A. E. von Doenhoff and N. Tetervin.[8] Like Mr. Gruschwitz, Messrs. von Doenhoff and Tetervin consider the velocity profile susceptible to characterization by a single parameter. Unlike Mr. Gruschwitz, Messrs. von Doenhoff and Tetervin chose to use Λ as this parameter. In relating Λ to the pressure gradient, they noted a consistent variation with the Reynolds number not noted by Mr. Gruschwitz. This variation was eliminated by expressing Λ as a function of the quotient of the nondimensional pressure gradient and the coefficient of the boundary shear. For the determination of this latter quantity, Messrs. von Doenhoff and Tetervin used the Squire-Young formula, which was the result of experiments involving flows with both pressure increase and decrease. In this connection, Messrs. von Doenhoff and Tetervin noted that "* * * no systematic variation of the skin-friction coefficient with the shape parameter was indicated by the data."[8]

---

[5] "Strömunggesetze in rauhen Rohren," by J. Nikuradse, *Forschungsheft*, 361, Verein Deutscher Ingenieur, Berlin, Germany, 1933.

[6] "Boundary Layer Theory," by H. Schlichting, *Technical Memorandum Nos. 1217* and *1218*, National Advisory Committee for Aeronautics, Washington, D. C., 1949.

[7] "Die turbulente Reibungschicht in ebener Strömung bei Druckabfall und Druckanstieg," by E. Gruschwitz, *Ingenieur-Archiv*, Vol. II, 1931, p. 321.

[8] "Determination of General Relations for the Behavior of Turbulent Boundary Layers", by A. E. von Doenhoff and N. Tetervin, *Report No. 772*, National Advisory Committee for Aeronautics, Washington, D. C., 1943.

Another analysis was proposed by Mr. Tetervin and C. C. Lin for the determination of the turbulent boundary layers with pressure gradients.[9] The relationships obtained from laboratory observations were those between the pressure gradient and the boundary shear, as well as that between the integral of shearing stresses across the boundary layer and the pressure gradient. These relationships, together with a summary of analytical approaches to the determination of the turbulent boundary layer with pressure gradient, were obtained by P. S. Granville.[10]

In France, G. Halbronn[11] conducted an investigation similar to that undertaken by the writer, although Mr. Halbronn made no attempt to secure a controlled variation of the slope and roughness. Mr. Halbronn used Eq. 3, although in a somewhat different form, and assumed the velocity distribution and the shear relationship to be the same as that in a pipe. There resulted an expression which enabled Mr. Halbronn to determine the boundary-layer dimensions. Treating the flow outside the boundary layer as non-viscous flow, Mr. Halbronn was able to determine the loci of both the free surface and the upper limit of the boundary layer which was then projected to an intersection termed the critical point.

Mr. Halbronn compared the location of this critical point with observations made both in the laboratory and in the field. All Mr. Halbronn's laboratory measurements were made at values of $U\,x/\nu$ less than 4×10^6, whereas the investigations made by the writer were taken for the range from 1.4×10^6 to 3.7×10^7. Observations made by G. H. Hickox,[12] M. ASCE, of the flow on the spillway of Norris Dam at Norristown, Tenn., at values for the Reynolds numbers in the range from 1.5×10^8 to 1.5×10^9 were also compared to the analytical predictions. Further comparison was made with observations made of the flow on models of the spillway of Norris Dam and the spillway of Bort-les-Orgues Dam at Bort-les-Orgues, France. In all cases the agreement was good.

For a general treatment of boundary-layer characteristics the report by W. D. Baines,[13] J.M. ASCE, is more complete than that which has been presented.

EXPERIMENTAL ASPECTS

Equipment.—The approach to the problem of determining the turbulent boundary was made largely from an experimental standpoint. In order to achieve a systematic variation of the quantities involved, laboratory equipment designed especially for the project was constructed. This equipment provided for the introduction of nonturbulent flow to the crest of a steep flume of controlled slope and roughness. The dimensions were limited by the quantity of space and water available, but they were regarded as adequate for the determination of information for design purposes.

---

[9] "A General Integral Form of the Boundary-Layer Equation for Incompressible Flow with an Application to the Calculation of the Separation Point of Turbulent Boundary Layers," by N. Tetervin and C. C. Lin, *TN* 2158, National Advisory Committee for Aeronautics, Washington, D. C., August, 1950.

[10] "A Method for the Calculation of the Turbulent Boundary Layer in a Pressure Gradient," by P. S. Granville, *Report 752*, U. S. Dept. of the Navy, The David W. Taylor Model Basin, Washington, D. C., May, 1951.

[11] "Étude de la mise en régime des écoulements sur les ouvrages à forte pente," by G. Halbronn, thesis presented to the University of Grenoble, Grenoble, France, 1951.

[12] "Air Entrainment on Spillway Faces," by G. H. Hickox, *Civil Engineering*, ASCE, Vol. 15, 1945, p. 562.

[13] "A Literature Survey of Boundary-Layer Development on Smooth and Rough Surfaces at Zero Pressure Gradient," by W. D. Baines, *ONR Report*, Iowa Inst. of Hydraulic Research, Iowa City, Iowa, 1952.

The main feature of the equipment was a glass-lined flume, which was an open channel made in two sections—one 12 ft the other 4 ft long. Connecting the flume with the stilling tank were three spillway crests—one for each of the three slopes used. The function of the stilling tank was to deliver nonturbulent, potential-like flow to the spillway. This type of flow was obtained by using a large stilling tank equipped with a series of baffles, grids, and screens arranged in circular arcs. Two objectives were achieved by this arrangement: First, the presence of a pressure drop across each baffle, grid, and screen produced an effect which distributed the velocity in a potential-like pattern; second, the arrangement of coarse to fine gradation of the baffles, grids, and screen reduced the turbulence of the incoming flow to such a small scale that it was effectively dissipated before it reached the spillway crests. Thus, the only turbulence present within the flow on the slope was that engendered by the boundary itself.

Several sizes of stagnation tubes were used to make the stagnation-pressure surveys, but after experience with each, two were picked for general use. One was relatively small, with a diameter of 0.021 in., and one relatively large, being 0.084 in. in diameter. Results of the two were compared to discover at what distance from the boundary they began to agree. This point was reached when the center line of the large tube was approximately a diameter from the boundary. The fluctuations of the level of the mercury in the open manometer used with the large tube were evident as long as the tube was located within the boundary layer; they disappeared completely when the tube was moved to the nonturbulent zone outside the boundary layer. The line between the two domains was determinable with surprising precision on the basis of the presence and absence of the fluctuations, although the line was always outside the locus of $y = \delta$ by approximately a diameter of the tube. For most of the work, however, the small tube was used because the absence of fluctuations in the open manometer permitted more precise measurement of the stagnation pressure.

To determine the precise location of the tube with respect to the boundary, an Ames dial graduated to 0.001 in. was connected to the stagnation-tube support. The origin of the y-coordinate was determined in two ways. The first method was visual, the tube being viewed in a direction normal to its long axis with the observer's eye slightly above the plane of the glass floor, so that both the tube and its reflection were seen simultaneously. The second involved the use of a metal shim of known thickness placed between the glass and the tube; on initial contact an electrical circuit was completed. Since the visual method could be used under water, and since it agreed with the second method to within 0.001 in., it was used almost exclusively for all work done on the glass boundary. The value of the y-coordinate for all runs made with the rough boundary was measured from the midplane of the screen to the center line of the tube.

One series of runs was made with the glass boundary and a second series of runs with a boundary roughened by stretching a length of screen over the floor of the flume. The screen was 16-by-16 mesh, bronze wire of 0.010-in. diameter. This screen was chosen because it was uniform, easily reproducible, convenient to apply and remove, and low in cost. It was important to use a piece of screen completely free of folds, bulges, and kinks; only a perfect piece would lie flat on the glass without the use of an adhesive. In order to determine the effective roughness, a piece of screen from the same roll was applied to the floor of another laboratory flume. Uniform flow was established over the screen.

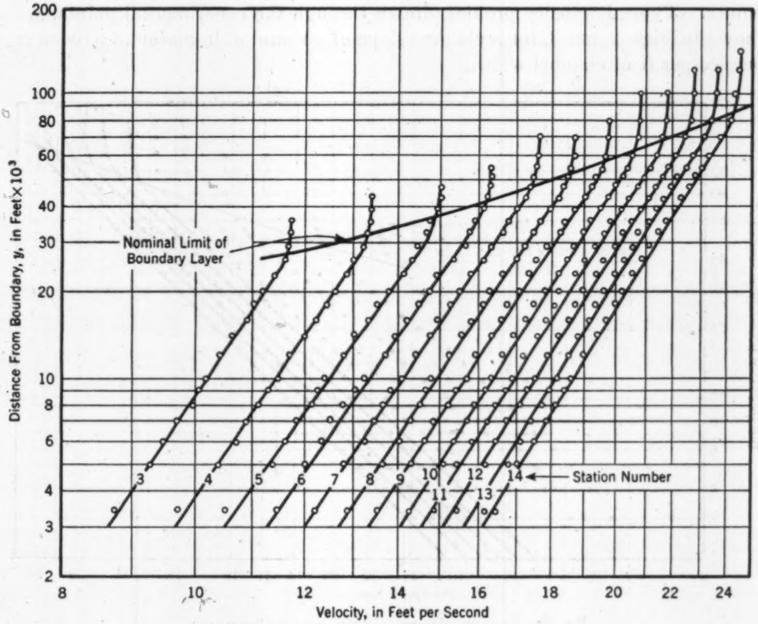

FIG. 2.—VELOCITY PROFILES WITH GLASS BOUNDARY

With knowledge of the discharge, the depth, and the slope, the values of f, k, and n could be computed. The equations used to determine f, the coefficient of friction, and n, the coefficient of roughness, were the Weisbach-Darcy and Manning expressions, respectively. The equations used to determine k, the equivalent Nikuradse roughness height, resulted from an application of the von Kármán-Prandtl velocity-distribution equations to the case of two-dimensional flow, as given by Mr. Rouse[4]—

$$\frac{1}{\sqrt{f}} = 2.03 \log_{10} \frac{y_0}{k} + 2.11 \quad \text{(6)}$$

—in which y_0 is the total thickness of the flow measured normal to the boundary. The resulting values of k and n indicated a roughness comparable to that of rough concrete. Thus, the development of the boundary layer over the 16-by-16 mesh is considered to be a good approximation to that occurring over rough concrete.

Data.—In making the stagnation-pressure surveys the measuring carriage was located at a fixed position on the flume and a normal traverse made. After making ten to thirty stagnation-pressure measurements at different normal distances from the boundary, the carriage was moved to the next station and the process repeated. The result was a characterization of the stagnation-pressure field by knowledge of its magnitude at many discrete points. Typical velocity profiles, drawn through the experimental points, are shown in Figs. 2 and 3, for a channel slope of 40° and a discharge of 3.68 cu ft per sec per ft of channel width.

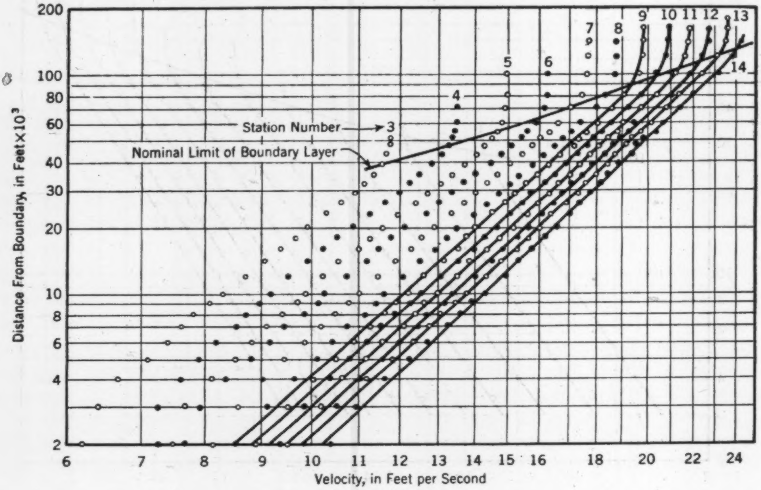

FIG. 3.—VELOCITY PROFILES WITH SCREEN BOUNDARY

In addition to the stagnation-pressure surveys, certain other observations were made by visual inspection of the appearance of the flow. The first thing to be noted was the effect of the walls of the flume in producing small waves which issued normal to the walls. Being superimposed on the general downstream motion of the water, the waves had a total velocity which was the vector sum of the celerity and the surface velocity of the fluid over which the wave was being propagated. Since the celerity of the waves was decreasing while the celerity of the fluid was increasing, the motion of the wave took place along a curve of such a shape that a region in the form of an inverted cusp in the central portion of the flow was largely unaffected by the presence of side boundaries.

Also to be observed was the fact that the free surface in the neighborhood of the critical point was characterized by a change within a relatively short distance from a smooth, glass-like, transparent appearance to one which was rough and nearly opaque. The apparent location of this transition was compared to the graphical location of the critical point. Comparison showed that slight disturbances of the surface occur upstream from the critical point because there is some turbulence outside the nominal boundary layer if the boundary-layer thickness is defined as occurring at $u/U = 0.99$. The effect intensifies rapidly from this point on, however, and reaches a well-developed stage at the critical point.

Careful measurement showed that energy loss in the domain outside the boundary layer is practically nonexistent. A flexible translucent tube completely filled with water was connected to the stagnation tube when the tube was located in the flow outside the boundary layer at the greatest possible distance from the stilling tank. The water level in this translucent tube rose to a distance above the water in the stilling tank almost exactly equal to the computed value of the velocity head at the point of comparison. If there was any energy loss, its magnitude was less than 0.001 ft in a region where the velocity head was about 10 ft.

ANALYSIS OF THE DATA

Dynamic Analysis.—Since the von Kármán momentum equation forms a major part of the dynamic analysis of the turbulent boundary layer, it is important to review its derivation. The net change in the momentum flux as the fluid passes through an elementary volume within the boundary layer, such as that shown in Fig. 4, is evaluated. The net change in the momentum flux in the x-direction is equated to the algebraic summation of all the forces

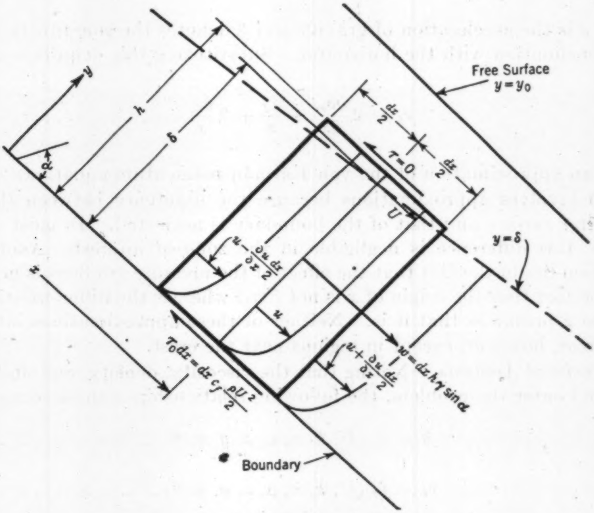

y
h
δ
α
x
Free Surface
$y = y_0$
$\frac{dx}{2}$
$\tau = 0$
$\frac{dx}{2}$
U
$y = \delta$
$u - \frac{\partial u}{\partial x}\frac{dx}{2}$
u
$u + \frac{\partial u}{\partial x}\frac{dx}{2}$
$w = dx\,h\,\gamma\,\sin\alpha$
$\tau_0\,dx = dx\,c_f\,\frac{\rho U^2}{2}$
Boundary

FIG. 4.—DEFINITION SKETCH

in that direction which act on this elementary volume of fluid. The integrals which arise from this application of the principle of conservation of momentum are simplified by using the definitions of δ_d and δ_m.

The forces acting on the elementary volume of fluid are the shear force at the boundary, the gravitational force, and the force due to the pressure gradient in the x-direction. The first of these forces can be expressed in terms of the coefficient of the local boundary shear. The combined effect of the last two forces is expressed in terms of the acceleration outside the boundary layer. This is done because this effect is not a function of distance from the boundary, and it is only the combination of the gravity and pressure gradient which produces acceleration of the fluid outside the boundary layer. On equating the net change in momentum flux to the summation of the forces acting on the elementary volume of fluid, there results

$$\rho\, U^2 \left[- \frac{\partial \delta_m}{\partial x} - \frac{1}{U} \frac{\partial U}{\partial x} (2\, \delta_m + \delta_d) + \frac{\delta}{U} \frac{\partial U}{\partial x} \right] dx = - c_f\, \rho\, \frac{U^2}{2}\, dx + \rho\, \delta\, U \frac{\partial U}{\partial x}\, dx \quad \text{. . (7)}$$

From Fig. 1,

$$x = \frac{U^2}{2\, g\, \mathbb{S}} \quad \text{. . . . . (8)}$$

in which g is the acceleration of gravity and $\mathbb{S}$ denotes the sine function of the angle of inclination with the horizontal. Substituting this definition into Eq. 7 yields

$$c_f = 2 \frac{\partial \delta_m}{\partial x} + \frac{\delta_d}{x} + 2 \frac{\delta_m}{x} \quad \text{. . . . . (9)}$$

which is an approximation of the von Kármán momentum equation.

Eq. 9 involves approximations because the difference between the slope of the water surface and that of the boundary is neglected. In most spillway problems, this difference is negligible in the zone of interest. Another approximation lies in the fact that the effect of the pressure gradient is neglected, and in the fact that the origin of x is not fixed whereas the differentiation with respect to x presumes that it is. Neither of these approximations introduces serious error, however, except in regions near the crest.

Dimensional Analysis.—Noting that the viscosity, density, and unit weight of the fluid enter the problem, the following relationships can be formed:

$$\delta = f_1\, (U, k, x, \mu, \rho, g, q, \mathbb{S}) \quad \text{. . . . . (10)}$$

$$c_f = f_2\, (U, k, x, \mu, \rho, g, q, \mathbb{S}) \quad \text{. . . . . (11)}$$

$$\Lambda = f_3\, (U, k, x, \mu, \rho, g, q, \mathbb{S}) \quad \text{. . . . . (12)}$$

in which μ is the dynamic viscosity of the fluid and q is the discharge per foot of width of spillway. Dimensionless combinations of these variables can be formed:

$$\frac{\delta}{x} = \phi_1\left(\frac{U\,x}{\nu}, \frac{k}{x}, \frac{U^2}{g\,x}, \frac{q}{U\,x}, \mathcal{S}\right)\dots\dots\dots\dots\dots\dots\dots(13)$$

$$c_f = \phi_2\left(\frac{U\,x}{\nu}, \frac{k}{x}, \frac{U^2}{g\,x}, \frac{q}{U\,x}, \mathcal{S}\right)\dots\dots\dots\dots\dots\dots\dots(14)$$

and

$$\Lambda = \phi_3\left(\frac{U\,x}{\nu}, \frac{k}{x}, \frac{U^2}{g\,x}, \frac{q}{U\,x}, \mathcal{S}\right)\dots\dots\dots\dots\dots\dots\dots(15)$$

From the definition of x, $\frac{U^2}{g\,x}$ is directly proportional to the slope of the boundary, so that in general the three dependent variables (Eqs. 13, 14, and 15) are functions of the Reynolds number, the relative roughness, the slope, and the ratio of the potential depth to x—the latter ratio being an interpretation of the dimensionless expression for the discharge. In the expressions for c_f and Λ, δ can be substituted for x without altering the validity of the procedure. The result is that the Reynolds number and the relative roughness are written in terms of the boundary-layer thickness. This immediately furnishes a basis for comparison with uniform flow in pipes or open channels. If x is retained, plots are obtained similar to those obtained from research on flat plates in uniform flow.

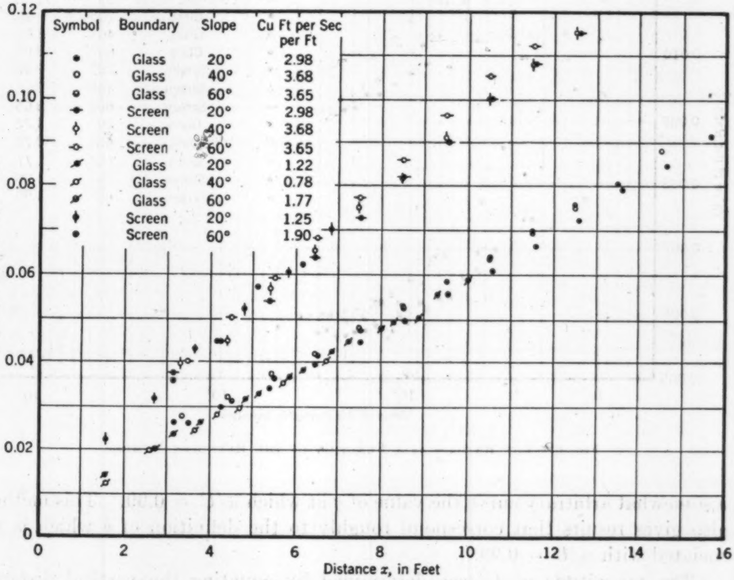

FIG. 5.—BOUNDARY-LAYER THICKNESS AS A FUNCTION OF THE DISTANCE IN THE DIRECTION OF FLOW

Analytical Techniques.—The values for δ_d and δ_m were obtained through numerical integration, in which the trapezoidal rule was used. An exception occurred in dealing with the region immediately adjacent to the boundary in which no stagnation-pressure measurements were possible. In this case an assumption was made which was roughly equivalent to the extrapolation of the velocity profile, according to a function of the form $u = J\, y^j$.

A graphical method was used to determine δ. The straight-line portion of a log-log plot of the velocity profile was extrapolated to its intersection with the line $u = U$. The value of y at this intersection was taken to be the value of δ. This method depends less on visual judgment than does reading from a somewhat arbitrary curve the value of y at which $u/U = 0.99$. This method also gives results that correspond roughly to the definition of δ which is associated with $u/U = 0.99$.

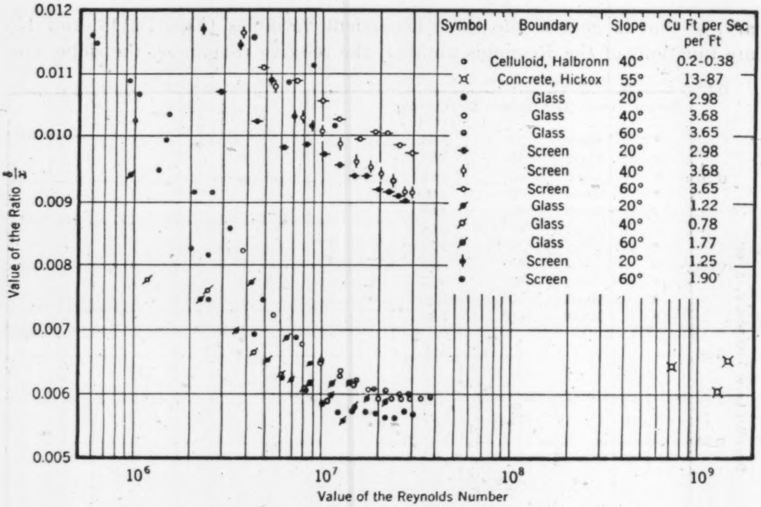

FIG. 6.—THE RATIO $\frac{\delta}{x}$ AS A FUNCTION OF THE REYNOLDS NUMBER

The magnitude of U was determined by equating the vertical distance between the water surface and the line of the total head to $U^2/(2\,g)$. The slight difference between the location of the actual surface and that of the potential flow is insignificant in this computation since the effect on U is a change in magnitude of about 0.05%.

Dimensional Plots.—The results of the analysis of the velocity profile are presented in dimensional form to afford a graphical view of the data. In Fig. 5, δ is plotted as a function of x, the points resulting from tests with both glass and screen boundaries, with all three slopes, and with various rates of discharge. All the points shown in Fig. 5 are presented in dimensionless form in Fig. 6.

Dimensionless Plots.—Fig. 6 shows δ/x as a function of the Reynolds number; the results obtained from different slopes, from different boundaries, and from different discharges are plotted on the same system of coordinates. In addition to the writer's observations, the values obtained by Mr. Halbronn and Mr. Hickox are also plotted. Neither of these experimenters presented data in the form plotted, so that it was necessary to deduce the points from the information which was presented. In Mr. Halbronn's work, the value of δ was obtained from the velocity profile by the same method applied to the data of this investigation. In the case of the observations made by Mr. Hickox on the spillway of Norris Dam, the thickness of the boundary layer was taken to be δ_d, plus the depth of the potential flow at the same discharge and at the same station on the slope.

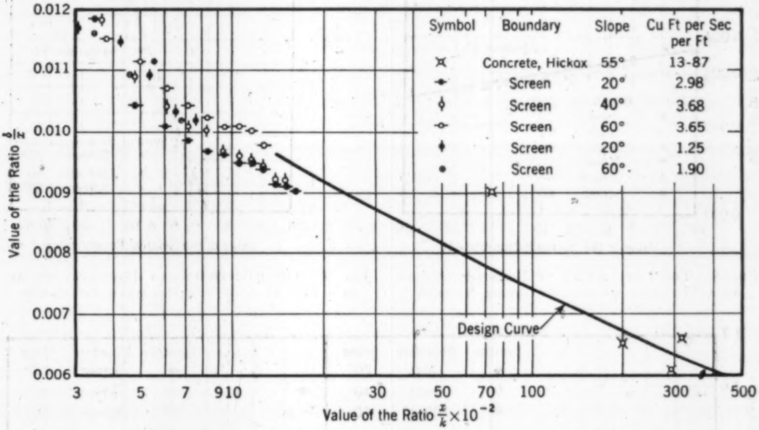

FIG. 7.—THE RATIO $\frac{\delta}{x}$ AS A FUNCTION OF THE RELATIVE ROUGHNESS

Fig. 7 shows δ/x as a function of the relative roughness, with results obtained from different slopes and different discharges being plotted on the same system of coordinates. The observations made by Mr. Hickox are plotted, with the assumption that the k of the concrete on the spillway of Norris Dam was 0.005 ft, corresponding to an average concrete surface texture. The value of k for the screen was taken as 0.009 ft, according to the results of the tests in uniform flow.

Fig. 8 shows c_f for both smooth and rough boundaries as a function of $\mathbf{R}$, the Reynolds number. The value of c_f was computed by applying Eq. 9 to the data obtained from the smooth curves drawn in plots of δ_d and δ_m as functions of x. The curve in Fig. 9 has the equation,

$$\frac{1}{\sqrt{c_f}} = 4.06 \log \sqrt{c_f}\, \mathbf{R}_\delta + 3.28 \quad \ldots\ldots\ldots\ldots\ldots\ldots (16)$$

in which $\mathbf{R}_\delta$ is the Reynolds number of the fluid in the boundary layer. Eq. 16

was obtained by substituting into Eq. 4 the point $y = \delta$, $u = U$, and expressing the boundary shear in terms of c_f.

Fig. 9 is the counterpart of Fig. 8, and shows c_f as a function of the relative roughness. A dashed line is drawn through the data and its equation is

$$\frac{1}{\sqrt{c_f}} = 4.06 \log \frac{\delta}{k} + 8.56 \qquad (17)$$

In Eq. 17, k for the screen was assumed to be 0.009 ft.

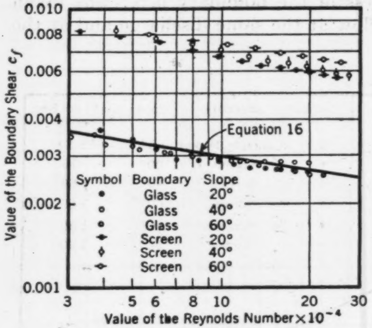

FIG. 8.—THE COEFFICIENT OF BOUNDARY SHEAR AS A FUNCTION OF THE REYNOLDS NUMBER

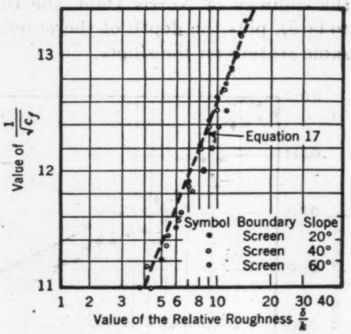

FIG. 9.—THE COEFFICIENT OF BOUNDARY SHEAR AS A FUNCTION OF THE RELATIVE ROUGHNESS

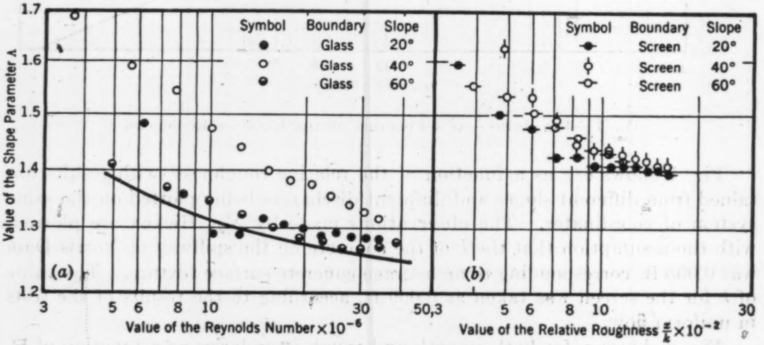

FIG. 10.—THE SHAPE PARAMETER AS A FUNCTION OF THE REYNOLDS NUMBER AND RELATIVE ROUGHNESS

Figs. 10(*a*) and 10(*b*) show the variation of the shape parameter Λ as a function of the Reynolds number and the relative roughness, respectively. The variation of Λ with the Reynolds number in flow over smooth flat plates has been approximated by Messrs. Tetervin and Lin[9] by the expression:

$$\log_{10} \Lambda = 0.5990 - 0.1980 \log_{10} \mathsf{R} + 0.0189 (\log_{10} \mathsf{R})^2 \qquad (18)$$

in which $\mathsf{R} = U\,\delta_m/\nu$ and ν is the kinematic viscosity of the fluid. A smooth curve representing Eq. 18 and the data obtained in this investigation are shown in Fig. 10(*a*).

DISCUSSION OF THE RESULTS

Role of the Discharge.—The discharge has an insignificant effect on the thickness of the boundary layer at a fixed value of x. This fact is illustrated in Fig. 5, and is shown in dimensionless form in Figs. 6 and 7. On inspection, it can be seen that points corresponding to the same slope and to the same boundary, but with much different rates of discharge, fall along the same line, within the limits of experimental variation. This does not mean the same thickness at the same station; it is only with reference to the parameter $x = \frac{U^2}{2\,g\,S}$ that the effect of the variable discharge becomes indeterminably small. This fact is basic to the solution of the full-scale problem. Therefore, only the parameter x need be used to define the position along the slope, and the development becomes identical to that occurring over the same boundary at any rate of discharge.

The discharge is significant in determining the depth of the flow, and hence the location of the critical point. The presence of a free surface limits the growth of the boundary layer, so that knowledge of the discharge is necessary to define that aspect of boundary-layer development.

Effect of the Slope.—As in the case of the discharge, slope has little effect on the thickness of the boundary layer at a fixed value of x. Although a slight difference between the developments occurring at the different slopes is apparent in some instances, it will be shown in the subsequent example that no important difference in the computed location of the critical point results from choosing slightly different values of δ/x. As in the case of the discharge, knowledge of the slope is essential in computing the depth of flow, and hence the location of the critical point.

The effect of the slope on c_f and on Λ is similar to its effect on δ/x, with consistent variation apparent in only a few instances. In the case of the rough boundary, both δ/x and c_f appear to have a positive correlation with slope. A less distinct trend in the same direction is indicated in the plot of Λ as a function of relative roughness (Fig. 10(*b*)). The effect in the case of the smooth boundary is indefinite, however.

Role of the Boundary Roughness.—Of all the variables encountered, the roughness of the boundary proved to be the most significant in determining the locus of the nominal thickness of the turbulent boundary layer. In Fig. 5, it is noted that all the points follow two distinct trends—one for the smooth boundary and one for the rough boundary. In Figs. 6 and 8, this grouping according to roughness is evident, although the delineation in Fig. 6 is not so distinct as that in Fig. 5.

The difference between the two trends evident in Fig. 6 is greatest in the middle range of Reynolds numbers, being small at very low and very high Reynolds numbers. This is to be expected on two accounts: First, at very low Reynolds numbers, the flow within the boundary layer is laminar, so that roughness of the boundary is of no consequence; and second, as the Reynolds number increases with increasing x, the thickness of the boundary layer is so large compared to the height of the roughness k that the boundary becomes effectively smooth. The latter fact is significant to the spillway problem because it makes possible, at high Reynolds numbers, a useful computation for the location of the critical point without a precise specification for the roughness of the boundary.

The roughness of the screen used in the laboratory investigation is probably greater than that encountered on most concrete spillways. The variation of the parameter δ/x on an actual concrete spillway should lie somewhere between that associated with the glass boundary and that associated with the screen boundary. Even if the concrete were as rough as the screen, however, the effect on the location of the critical point would not be great; hence, with the possible exception of the crest region, a very smooth spillway surface is not economically justified so far as its effect upon boundary-layer development is concerned.

The slope and the rate of discharge are unimportant, therefore, as far as the rate of growth of the boundary layer is concerned. The roughness of the boundary is significant near the crest—becoming less important with increasing distance along the slope.

Nominal Thickness of the Boundary Layer.—At high Reynolds numbers on both smooth and rough boundaries, δ is approximately a linear function of x. This is especially true with the smooth boundary. It is also true that the ratio δ/x continues to decrease as the Reynolds number increases; its rate of change is small enough, however, so that very little curvature of the locus $y = \delta$ results.

The variation of δ_m can be determined from the von Kármán momentum equation as follows:

$$\frac{d\delta_m}{dx} = \frac{1}{2}\left[c_f - (\Lambda + 2)\frac{\delta_m}{x}\right] \ldots\ldots\ldots\ldots\ldots\ldots (19)$$

The gradient of δ_m with respect to x is a function of the difference between two terms, both of which are decreasing in magnitude in the x-direction. In the usual case, c_f decreases more rapidly than does δ_m/x, so that the locus of δ_m is slightly concave downward. The nature of the equation is such, however, that little curvature is possible.

A significant effect is evident in the relationship among Λ, δ, and δ_m. Assuming that the velocity profile may be characterized by an expression of the form $u = M\,y^m$, applying the definition of δ_m, and solving for the ratio of δ/δ_m in terms of Λ, it is found that

$$\frac{\delta}{\delta_m} = \frac{\Lambda\,(\Lambda + 1)}{\Lambda - 1} \ldots\ldots\ldots\ldots\ldots\ldots\ldots\ldots (20)$$

The significance of this expression is that Λ is approaching unity in the region of interest. The denominator of the fraction on the right-hand side of Eq. 14 therefore decreases more rapidly than does the numerator. This means that δ is an increasing multiple of δ_m as the shape of the velocity profile progresses in the direction of a rectangular distribution. Thus, it is necessary that the locus of δ with respect to x be less concave in the direction toward the boundary than the locus of δ_m with respect to x. It is entirely possible, therefore, that the locus of δ with respect to x is actually linear at high Reynolds numbers, even if the locus of δ_m is not.

In the case of the rough boundary, the pronounced curvature of the locus of δ with respect to x is due primarily to the continuing decrease in the relative roughness, producing a more rapid change in the value of c_f as a function of x than is observed in the case of the smooth boundary. As the relative roughness approaches the limit at which it is effectively smooth, however, the variation in c_f will decrease, and at the same time the value of Λ will be near unity, so that again the locus of δ with respect to x is possibly linear.

Shape of the Velocity Profile.—The shape of the velocity profile associated with the development of the turbulent boundary layer on steep slopes is better approximated in most regions by an expression of the form $u = J\ y^j$ than one of the form $u = b \log y$. This is especially true at large values of the Reynolds number; it is not true at low values of the Reynolds number and within close proximity of the boundary. However, Eq. 18, obtained from consideration of boundary-layer developments over flat plates with zero pressure gradient, is an approximation to the values of Λ obtained experimentally. Fig. 10 indicates the degree of agreement. The effect of continuous acceleration over the experimental range has little bearing on the value of Λ expressed as a function of $U\ \delta_m/\nu$, as it is in Eq. 18. Hence, the value of Λ in boundary-layer development on steep slopes does not increase subsequently according to the predictions of Eq. 18, but continues to decrease at a diminishing rate. This is based on the consideration that large values of Λ are associated with imminent separation. It is impossible to imagine imminent separation in flow down steep slopes.

Coefficient of Boundary Shear for the Glass.—Application of Eq. 4 to the turbulent boundary layer on the glass steep slope yields an expression for c_f which is an excellent approximation to the results obtained experimentally. This is evident upon examination of the relative position of the smooth curve and the points plotted for the glass boundary in Fig. 8. Mr. Halbronn[11] made this assumption in his method of synthesis of the development. The presence of acceleration evidently has little influence on the ratio between the intensity of boundary shear and the dynamic pressure at the edge of the boundary layer. Therefore, despite the fact that the shape of the velocity profile within the boundary layer is different from that associated with flow in a pipe, the intensity of boundary shear is the same for the same maximum velocity, the same density, and the same Reynolds number.

Coefficient of Boundary Shear for the Screen.—In a similar manner, application of Eq. 5 to the turbulent boundary layer on the steep slope with the screen boundary yields an expression for c_f which is in excellent agreement with the experimental results, if the value of k for the screen is chosen to be a great deal less than the value indicated by a test of the screen in uniform flow in an open channel. The value of k which gives an expression equivalent to one derivable from Eq. 5 is 0.0021 ft; the value indicated by the test in uniform flow was 0.009 ft. The value of 0.0021 ft is nearly the thickness of the screen, two wire diameters being 0.0017 ft. However, both values of k indicate a roughness comparable to concrete with corresponding values of n equal to 0.012 and 0.015, respectively.

Any derivation for c_f as a function of the relative roughness which assumes the boundary shear to be composed entirely of form drag on elements of roughness, and which approximates the velocity profile by an expression of the form $u = b \log y$, will yield an expression of the form:

$$\frac{1}{\sqrt{c_f}} = M \log \frac{\delta}{k} + B \dots\dots\dots\dots\dots\dots (21)$$

in which the ratio $M/B = \log 30 = 1.477$. However, if it is assumed that the distribution of the velocity if of the form $u = J\, y^j$, there results

$$\log \frac{1}{\sqrt{c_f}} = j \log \frac{\delta}{k} + C_{v,r} \dots\dots\dots\dots\dots\dots (22)$$

in which $C_{v,r}$ is a constant dependent on the shape of the velocity profile and the height, shape, and density of the roughness.

The actual value of the roughness of the screen as expressed by a magnitude for k remains in doubt over a range of values which are associated with various concrete surface textures. The fact that the value lies within this range, however, renders the observations made in flow over the screen useful.

Application to the Design Problem

Outline of the Method of Approach.—A design problem requires the location of the critical point for a given discharge on a given spillway and the computation of the water-surface profile upstream from that point. The location of the critical point is determined by the graphical intersection of the projection of the locus of the nominal thickness of the turbulent boundary layer with the projection of the locus of the free surface. The locus of the nominal thickness of the boundary layer is determined with reference to either Fig. 6 or Fig. 7, depending on the roughness of the surface. The locus of the free surface is determined by adding to the depth of the potential flow the displacement thickness of the boundary layer, which is assumed to be from $\frac{1}{8}$ to $\frac{1}{10}$ of the thickness of the boundary layer, depending on the magnitude of the Reynolds number.

Illustrative Example.—A concrete spillway of indefinite length, with S equal to 0.80, and a roughness such that k is 0.005 ft, requires location of the critical point and the line of the free surface when the discharge is 360 cu ft per sec per ft of the spillway width.

With reference to the "Design Curve" of Fig. 7, computations can be made in the form shown in Table 1. The distance x is taken to be any reasonable distance along the slope at which the location of the water surface is desired. The value of x/k is the value of x divided by 0.005 ft. The value of δ/x is read from the design curve of Fig. 7. The value of δ is obtained by multiplication of the values of x and δ/x. The value of $U^2/(2\,g)$ is by definition the

TABLE 1.—Solution of the Illustrative Problem

x, in feet	$\frac{x}{k}$	$\frac{\delta}{x}$	δ, in feet	$\frac{U^2}{2g}$, in feet	$\frac{q}{U}$, in feet	y_0, in feet
50	1×10^4	0.0073	0.36	40	7.09	7.13
100	2×10^4	0.0066	0.66	80	5.00	5.07
200	4×10^4	0.0060	1.20	160	3.53	3.65
400	8×10^4	0.0055	2.20	320	2.50	2.72
600	1.2×10^5	0.0052	3.12	480	2.04	2.35

product of S and x—in this case $0.80\,x$. The value of U from the known magnitude of the velocity head having been determined, the discharge per foot is divided by U to obtain the potential thickness of flow, q/U. To this is added 10% of the thickness of the boundary layer in order to determine the actual thickness of the flow, y_0.

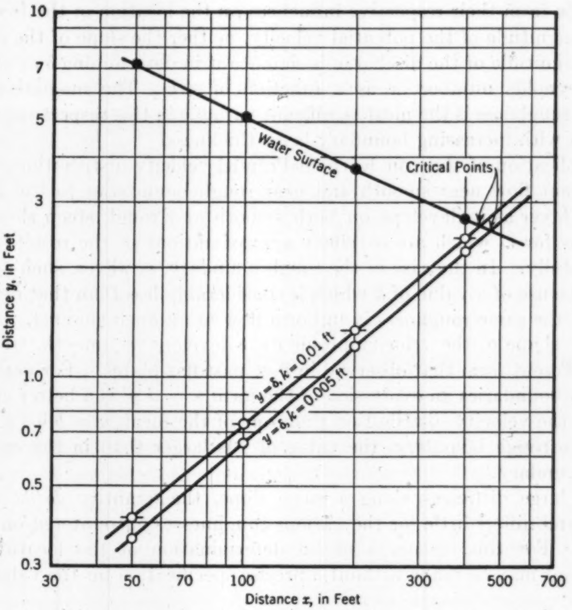

Fig. 11.—Graphical Solution of the Illustrative Problem

To locate the critical point, values of δ and y_0 obtained from Table 1, as functions of x, are plotted. This plot is shown in Fig. 11, which also shows the loci of the nominal thickness of the boundary layer and of the free surface. The desired value of x is found to be 470 ft.

To illustrate the effect of change in the roughness, the computation was repeated using the same situation, but with a roughness twice as large. The line "$y = \delta$, $k = 0.01$ ft" is the result of this computation. It can be seen that the difference between the values of x for the two cases is about 30 ft in 450 ft—a variation of less than 10%.

The order of magnitude of the changes in δ/x produced by a difference in slope is less than that involved in changing the roughness twofold. The design curve of Fig. 7 will thus suffice for all slopes.

After the value of x at the critical point has been determined, the corresponding station on the slope may be located by measuring the value of x in feet along the slope. The origin of coordinates is the intersection of the line of total head with a line drawn parallel to the slope through the water surface at the critical point. This procedure satisfies the definition of x.

CONCLUSIONS

The following conclusions seem justified on the basis of the foregoing results and discussion:

1. Aside from their respective influences on the location of the free surface and the magnitude of the potential velocity, neither the slope of the boundary nor the magnitude of the discharge is significant in determining δ as a function of the Reynolds number or as a function of x/k. The magnitude of the boundary roughness is the most significant variable in this respect, its influence decreasing with increasing boundary-layer thickness.
2. Application of the von Kármán-Prandtl velocity-distribution equations for turbulent flow near smooth and near rough boundaries to the turbulent boundary layer as it develops on both smooth and rough steep slopes yields expressions for c_f which are excellent approximations of the results obtained experimentally. In the case of the rough boundary, however, such agreement requires the use of a value of k which is considerably less than that determined by testing the same roughness in uniform flow in an open channel.
3. The shape of the velocity profile as it develops on smooth, steep slopes is little different from that observed in flow past flat plates. For both smooth and rough boundaries an expression of the form $u = J\, y^j$ is a better characterization of the velocity distribution than one of the form, $u = b \log y$. In the case of the rough boundary, the value of j is larger than in the case of the smooth boundary.
4. At large distances along a steep slope, the quantity $d\delta/dx$ is nearly constant and differs little for the various roughnesses encountered on concrete spillways. For this reason, a useful determination of the location of the critical point may be made without a precise specification for the value of k.

ACKNOWLEDGMENTS

The paper is based on a dissertation submitted in August, 1951, to the Graduate College of the State University of Iowa, at Iowa City, in partial fulfilment of the requirements for the degree of Doctor of Philosophy. The investigation was conducted in the laboratories of the Iowa Institute of Hydraulic Research (State University) under the direction of Mr. Rouse, and was sponsored by the Waterways Experiment Station of the Corps of Engineers, United States Department of the Army.

APPENDIX. NOTATION

The following letter symbols, adopted for use in this paper and its discussion, conform essentially with American Standard Letter Symbols for Hydraulics (ASA Z10.2-1942), prepared by a committee of the American Standards Association, with Society participation, and approved by the Association in 1942:

B = a constant, such that $M/B = \log 30$;

$C_{v,r}$ = a constant, dependent on velocity and roughness;

c_f = local coefficient of boundary shear;

f = Weisbach-Darcy coefficient of friction;

g = acceleration of gravity;

J, j = constants in the expression $u = J\, y^j$;

k = equivalent Nikuradse roughness height;

M = a constant, such that $M/B = \log 30$;

n = the Manning coefficient of roughness;

q = discharge per foot width of spillway;

R = Reynolds number of the fluid;

R_δ = Reynolds number of the fluid in the boundary layer;

S = the slope measured as the sine function of the angle of inclination with the horizontal;

U = velocity of the potential flow;

u = velocity at a point within the boundary layer;

W = weight of an elementary volume of the fluid;

x = distance in the direction of flow;

y = normal distance from the boundary;

y_0 = total thickness of the flow measured normal to the boundary;

γ = specific weight of the fluid;

δ = nominal thickness of the boundary layer;

δ_d = the distance that the potential flow has been displaced by the boundary layer;

δ_m = momentum thickness of the boundary layer;

Λ = shape parameter of the velocity profile;

μ = dynamic viscosity of the fluid;

ν = kinematic viscosity of the fluid;

ρ = mass density of the fluid; and

τ_0 = intensity of boundary shear.

DISCUSSION

G. Halbronn.[14]—A large number of experiments have been performed by Mr. Bauer which were concerned with boundary-layer development on spillways having various conditions of slope and roughness. This phenomenon was previously studied, both theoretically and experimentally.[15] It is of interest to compare the author's results with those obtained from a study of Eq. 3 when u is assumed to follow one of the relationships valid for the velocity distribution in the case of uniform flow within a pipe. The mathematical derivation can be evolved when:

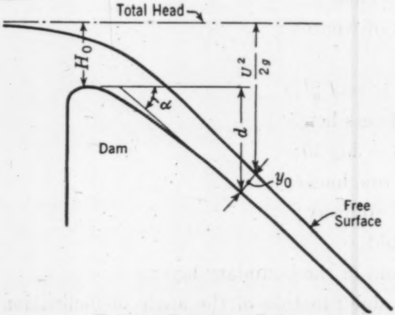

Fig. 12.—Definition Sketch

(a) The region under study is located away from the spillway crest. In this case

$$U=\sqrt{2\,g\,(d+H_0-y_0\cos\alpha)}\,.\qquad(23a)$$

can be expressed approximately as

$$U=\sqrt{2\,g\,(d+H_0)}\ldots(23b)$$

The terms in Eqs. 23 are defined in Fig. 12.

(b) The spillway, away from the crest, has a constant slope α. It can be seen that the boundary-layer thickness is independent of the flow near the crest and is dependent only on the local conditions. Therefore, the results are general.

When the spillway is smooth, Eq. 4 can be used if

$$\frac{k\sqrt{\frac{\tau_0}{\rho}}}{\nu}<5\ldots\ldots(24)$$

Letting

$$z=0.4\,\frac{U}{\sqrt{\frac{\tau_0}{\rho}}}=\frac{0.566}{\sqrt{c_f}}\ldots\ldots(25)$$

Eq. 4 can be written as

$$\frac{\delta}{x}=\frac{0.278}{\mathrm{R}_x}\,z\,e^z\ldots\ldots(26)$$

in which

$$\mathrm{R}_x=\frac{U\,x}{\nu}\ldots\ldots(27)$$

---

[14] Highway and Bridge Engr., 6th Elec. Dept., Grenoble, France.

[15] "Étude de la mise en régime des écoulements sur les ouvrages à forte pente. Application au problème de l'entrainement d'air," by G. Halbronn, *Houille Blanche*, 1952, No. 1, pp. 21–40; No. 3, pp. 347–371; No. 5, pp. 702–722.

Therefore, from Eq. 3,

$$\mathsf{R}_x = 4.35\, e^z (z^2 - 2.8\, z + 4.32) \ldots\ldots\ldots\ldots\ldots\ldots (28)$$

The variation of δ/x, as a function of R_x, is given in parametric form by Eqs. 26 and 28. This variation can be approximated by

$$\frac{\delta}{x} = 0.039\, \mathsf{R}^{-0.097}{}_x \ldots\ldots\ldots\ldots\ldots\ldots (29)$$

for $8.5 < z < 12.5$ $(0.00205 < c_f < 0.00443)$. If it is assumed[16] that

$$\frac{u}{\sqrt{\frac{\tau_0}{\rho}}} = 8.7 \left(\frac{y \sqrt{\frac{\tau_0}{\rho}}}{\nu} \right)^{1/7} \ldots\ldots\ldots\ldots\ldots\ldots (30)$$

then

$$\delta = 0.158\, \mathsf{R}^{-0.2}{}_x \ldots\ldots\ldots\ldots\ldots\ldots (31)$$

The curves corresponding to Eqs. 29 and 31 are shown in Fig. 13. For small values of the Reynolds number, the curves are in close agreement. This agreement indicates that the application of a logarithmic law to the experiments[15] is proper. In the range of Mr. Bauer's smooth-boundary experiments, Eq. 31 accounts for the observed increase of the thickness of the boundary layer. This agreement is expected as velocity profiles are better approximated

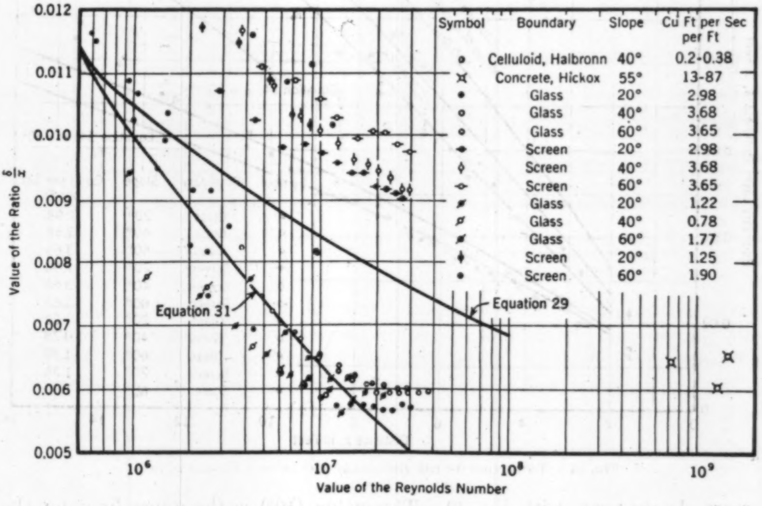

FIG. 13.—THE RATIO $\frac{\delta}{x}$ AS A FUNCTION OF R_x FOR SMOOTH BOUNDARIES

by an expression such as

---

[16] "Modern Developments in Fluid Dynamics," by S. Goldstein, Clarendon Press, Oxford, England, 1952, p. 339.

$$u = J\, y^j \quad \text{(32)}$$

than one in the form:

$$u = b \log_{10} y + c \quad \text{(33)}$$

although, in Fig. 2, j would be equal to 1/7.5. It was also observed that, for large values of the Reynolds number, the velocity profiles do not correspond to the logarithmic law. Because these larger Reynolds numbers occurred downstream from the critical point, it was assumed[15] that the poor agreement was caused by a physical change in the flow. The author's experiments show that this is not true.

It should be noted from Fig. 13 that, when the Reynolds number $\frac{2\, U\, \delta}{\nu}$ exceeds 10^5, the smooth-boundary experimental points depart from Eq. 31 and

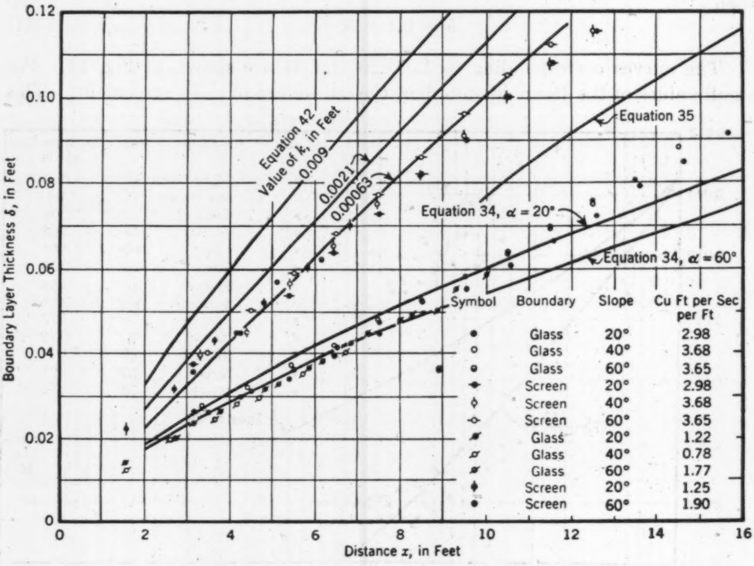

FIG. 14.—THICKNESS OF THE BOUNDARY LAYER AS A FUNCTION OF x

more closely agree with Eq. 29. This value (10^5) is the upper limit for the validity of Blasius' law.

Eq. 31 can also be written as

$$\delta \text{ (ft)} = \frac{0.0106}{S^{0.1}}\, x \text{ (ft)}^{0.7} \quad \text{(34)}$$

In Fig. 14 the curves corresponding to Eq. 34 for $\alpha = 20°$ and $\alpha = 60°$ are shown. As a result of the exponent 0.1 in Eq. 34, δ is approximately independent of S, but this fact has no special physical significance. Curves representing Eq. 29 in the form:

$$\delta\ (\text{ft}) = \frac{0.0104}{S^{0.0485}}\, x\ (\text{ft})^{0.8515} \quad \ldots\ldots (35)$$

are also shown in Fig. 14. These curves are in superposition.

In Fig. 15 there is shown the relationship between c_f and $\mathbf{R}_\delta$. This relationship is obtained by letting $u = U$ and $y = \delta$ in Eq. 30 to result in

$$c_f = 2\left(\frac{\sqrt{\frac{\tau_0}{\rho}}}{U}\right)^2 = 0.0463\ \mathbf{R}_\delta^{-\frac{1}{4}} \quad \ldots\ldots (36)$$

The smooth-boundary experimental points in Fig. 15 are farther from the curve of Eq. 36 than the same points are from the curve of Eq. 16 which corresponds to the logarithmic law. It is difficult to understand the reason for this deviation because the situation is reversed in Fig. 13, and both figures are only two different methods of representing the same result, obtained by substituting either Blasius' law or the logarithmic law in the von Kármán equation.

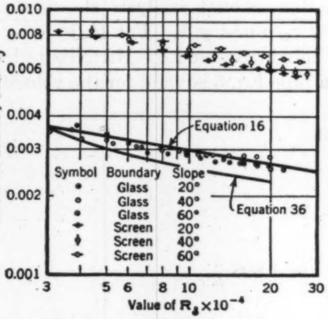

FIG. 15.—THE RELATIONSHIP BETWEEN c_f AND $\mathbf{R}_\delta$

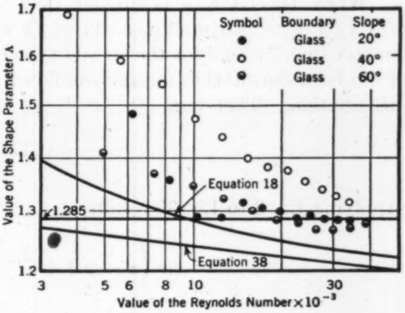

FIG. 16.—THE SHAPE PARAMETER AS A FUNCTION OF THE REYNOLDS NUMBER FOR SMOOTH BOUNDARIES

It is also of interest to study the values of the shape parameter Λ. The logarithmic law leads to

$$\delta_d = 1.765\,\sqrt{c_f}\,\delta \quad \ldots\ldots (37a)$$

and

$$\delta_m = 1.765\,\sqrt{c_f}\,\delta\,(1 - 3.54\,\sqrt{c_f}) \quad \ldots\ldots (37b)$$

Then, from Eq. 16,

$$\frac{\Lambda}{\Lambda - 1} = 1.15 \log_{10} \Lambda\mathbf{R} + 0.645 \quad \ldots\ldots (38)$$

Blasius' law leads to $\delta_d = \frac{\delta}{8}$, $\delta_m = \frac{7}{72}\,\delta$, and $\Lambda = \frac{9}{7}$. The corresponding curves are plotted in Fig. 16. The experimental points are somewhat scattered; nevertheless, the value $\Lambda = 1.285$ appears to be valid for large values of **R**. The curves for Eqs. 18 and 38 follow the general trend of the experimental points more accurately, although with a systematical displacement. It is worth while to note that the curve for Eq. 38 and the curve for the empirical law (Eq. 18) are in close agreement.

In Fig. 16 the experimental points shown by Mr. Bauer in Fig. 10(*a*) have been plotted exactly as shown in Fig. 10(*a*) with the value of the abscissa changed to "Value of the Reynolds Number $\times 10^{-3}$." Also, in Fig. 16 the curve for Eq. 18 is shown on the basis of the "new" abscissa. This value for the abscissa is correct, rather than Mr. Bauer's "Value of the Reynolds Number $\times 10^{-6}$," as can be seen by introducing into Eq. 18 the value of **R** equal to 10,000 so as to result in Λ equal to 1.287. It is true that introducing a value of **R** equal to 10,000,000 into Eq. 18 results in Λ equal to 1.380, but Messrs. Tetervin and Lin established Eq. 18 only for values of **R** between 1,500 and 40,000.

When $(k/\nu)\sqrt{\tau_0/\rho}$ is greater than 5, dimensional analysis shows that $u/\sqrt{\tau_0/\rho}$ depends simultaneously on $(y/\nu)\sqrt{\tau_0/\rho}$ and y/k. For $(k/\nu)\sqrt{\tau_0/\rho}$ greater than 71, and for the special type of roughness used by Mr. Nikuradse, it has been shown[4] that for uniform flow in a pipe Eq. 5 is valid for the velocity distribution. Therefore,

$$\frac{\delta}{x} = 0.0337\,\frac{k}{x}\,e^{z} \quad \text{(39)}$$

Applying Eq. 3 to Eq. 39 results in

$$e^{z}\left(z - 2.4 + \frac{2.24}{z}\right) = 1.898\,\frac{x}{k} \quad \text{(40)}$$

Eqs. 39 and 40 give the variation of δ/x as a function of x/k (shown in Fig. 17) which can be approximated by

$$\frac{\delta}{x} = 0.0447\left(\frac{x}{k}\right)^{-0.154} \quad \text{(41)}$$

for $6 < z < 9$ $(0.00395 < c_f < 0.0089)$ or, in a dimensional form:

$$\delta = 0.0447\,k^{0.154}\,x^{0.846} \quad \text{(42)}$$

The curves for Eq. 42 are shown in Fig. 14 for $k = 0.009$ ft, $k = 0.0021$ ft, and $k = 0.00053$ ft. This last value of k is seen to be in good agreement with the experimental data. The considerable variation of the values for k given in Fig. 14, in Fig. 9, or by the tests involving uniform flow (although, for a screen made with wire of an 0.0008-ft diameter, an equivalent sand roughness of 0.009 ft seems unexpected) leads one to believe that Eq. 5 does not agree with the observed velocity-profile distribution. In fact, if c_f is determined from the experimental points of Fig. 3 and from Eq. 3 and is then used to plot $u/\sqrt{\tau_0/\rho}$ as a function of y, a single curve does not result, as it would if Eq. 5 were applicable. It would be most interesting to investigate Mr. Bauer's data on rough bottoms by the method described by Boris A. Bakhmeteff.[17] By plotting $[(u/\sqrt{\tau_0/\rho}) - 5.75 \log_{10} (y/k)]$ as a function of $\log [(k/\nu) \sqrt{\tau_0/\rho}]$, it may be possible to determine the velocity distribution corresponding to the observations. Examination of Figs. 8 and 9 appears to show that $\sqrt{\tau_0/\rho}$ depends on both y/k and $(y/\nu) \sqrt{\tau_0/\rho}$.

Another manner of solving the problem might be by the use of prototype data obtained by the simple method followed by Mr. Hickox.[12] Such results (including a measured value for δ) have been published[18] by V. Michels, A.M. ASCE, and M. Lovely. These results, obtained at the Glennmaggie Dam in Australia, are as follows:

x, in feet	δ, in feet (measured)	δ, in feet (computed)
14	0.147	0.127
39	0.347	0.322
65	0.552	0.525

Plotted in Fig. 17 (with $k = 0.005$ ft for concrete) these points fall between the author's design curve and the curve of Eq. 41. The foregoing listing also shows the values of δ computed by the method used by Mr. Bauer in applying Mr. Hickox's data. However, it is noticeable that the measured values are larger than the computed ones. This is because the measured values account for the corrugation of the surface at the critical point.

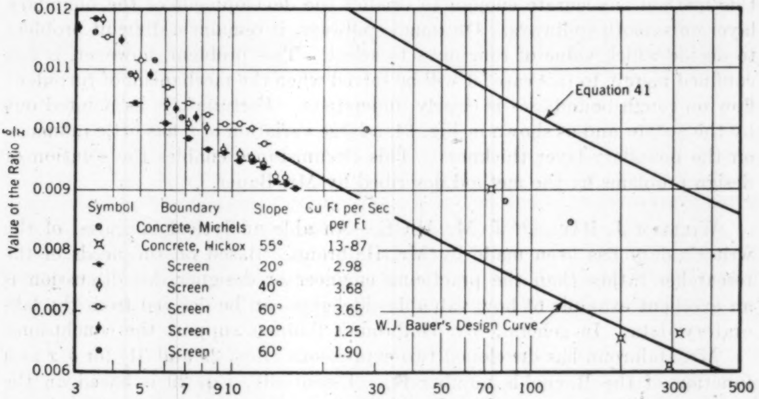

Fig. 17.—The Ratio $\frac{\delta}{x}$ as a Function of the Relative Roughness for Rough Boundaries

It is also true that the Manning coefficient for concrete can be expected to be between 0.013 and 0.016, corresponding approximately to 0.004 ft $< k <$ 0.016 ft. A change in the value of k which is used to plot the points in Fig. 17 results in a constant translation parallel to the abscissa. For these reasons, it can be concluded that, whereas the general trend of the design curve is known, its position is not accurately determined.

---

[17] "The Mechanics of Turbulent Flow," by Boris A. Bakhmeteff, Princeton University Press, Princeton, N. J., 1936, p. 90.

[18] "Some Prototype Observations of Air Entrained Flow," by V. Michels and M. Lovely, *Proceedings* Minnesota International Hydraulics Convention, Minneapolis, Minn., 1953, p. 403.

From Eq. 34 it can be seen that

$$\frac{d\delta}{dx} = \frac{0.0074}{\mathbb{S}^{0.1}} x^{-0.3} \ldots\ldots\ldots\ldots (43)$$

For x equal to 10 ft, $d\delta/dx$ equals 0.0037. The divergence of the boundary layer is then 0° 13′. In the same manner, from Eq. 42,

$$\frac{d\delta}{dx} = 0.0378 \left(\frac{k}{x}\right)^{0.154} \ldots\ldots\ldots\ldots (44)$$

For k/x equal to 0.0005, the divergence is 0° 40′. These low values for the divergence help one to understand why velocity distributions, valid in uniform flow, can also be applied to this case.

Mr. Bauer presents the experimental data on a physically sound basis. The data allow comparison with the results of a theoretical method of approach which was previously developed.[15] It is therefore possible to conclude that this method is accurate enough to predict the development of the boundary layer on smooth spillways. On rough spillways, it remains a difficult problem to decide which value of roughness to select. This problem, however, is not confined merely to this case; it will be solved when the mechanism of turbulent flow on rough boundaries is clearly understood. Fortunately, as pointed out by the author and as shown in Fig. 14, a large variation of k has little influence on the boundary-layer thickness. This circumstance enables the solution of design problems by the method described by Mr. Bauer.

WILLIAM J. BAUER,[19] J. M. ASCE.—An able analytical appraisal of the writer's data has been made by Mr. Halbronn. Based on the needs of the researcher rather than the practicing engineer or designer, his discussion is an excellent example of how valuable sidelights can be derived from the laboratory data. In general, Mr. Halbronn's findings support the conclusions.

Mr. Halbronn has developed two expressions (Eqs. 29 and 31) for δ/x as a function of the Reynolds number $\mathbf{R}_x$. Essentially, Eq. 29 is based on the assumption of velocity distribution of the form of Eq. 33, and Eq. 31 is based on one of the forms given in Eq. 32. Testing the hypotheses thus developed in the light of the data shown in Fig. 13, Mr. Halbronn concludes that an expression similar to Eq. 32 better approximates the shape of the velocity profile. It is felt, however, that the actual shape of the velocity profile within a turbulent boundary layer cannot be accurately approximated by simple mathematical expressions of the types considered (Eq. 32 and Eq. 33), except over specified limited ranges of the Reynolds number. It should be noted that in Figs. 2 and 3 there is a consistent deviation (however slight) of the experimental points from the straight line which represents an expression of the form of Eq. 32. The deviation increases with increased values of the Reynolds number, demonstrating the inadequacy (in this range of the Reynolds number) of the simple mathematical approximation.

---

[19] Senior Designer, Harza Eng. Co., Chicago, Ill.

Mr. Halbronn notes that in Fig. 2 the value of the exponent j of Eq. 32 would be 1/7.5. Actually, j in Fig. 2 decreases gradually as the Reynolds number increases, varying between 1/7.3 and 1/8. Similar trends were observed in the remainder of the data which were not published. Mr. Schlichting states[6] that beyond the range of validity of the Blasius law (the 1/7-power expression) "* * * a better approximation is obtained by the power 1/8, 1/9, or 1/10 instead of 1/7." The experimental data seem to confirm Mr. Schlichting's observation.

In analyzing the data for c_f, Mr. Halbronn has assumed a 1/7-power velocity distribution and has derived Eq. 36, an expression for c_f in terms of R_δ. On the basis of the previous comments, it is of interest to repeat the procedure for an 1/8-power velocity distribution. This procedure results in

$$c_f = 0.0427\ \mathsf{R}^{-2/9}{}_\delta \qquad (45)$$

The curve for Eq. 45 lies about as far above the data in Fig. 15 as Eq. 36 lies below, showing that the best fit would be associated with a value for j of between 1/7 and 1/8. This fit agrees with the previous indications as the observed values of j are between 1/7.3 and 1/8. It can be concluded, therefore, that the lack of agreement between Eq. 36 and the data is not caused by the inappropriateness of the form of the equation which has been used to approximate the velocity distribution, but rather to the use of an inappropriate value of j.

The excellent agreement between the data and Eq. 16 is surprising, as Mr. Halbronn has indicated, as this equation is based on the apparently inappropriate logarithmic velocity distribution. It is believed that this agreement is merely coincidental. The apparent agreement between the data and Eq. 31 in Fig. 13 is also somewhat coincidental as Eq. 31 is based on a slightly erroneous value of j, whereas the definition of δ in Fig. 13 does not agree exactly with the definition of δ used to derive Eq. 31. These two approximations have apparently tended to compensate for each other.

A misunderstanding has arisen concerning the significance of Fig. 10(a). Mr. Halbronn has suggested that the error lies in a mislabeling of the logarithmic abscissa scale. Actually, the proper abscissa scale for Fig. 10(a) ranges between 3×10^6 and 5×10^7 and is the value of $\mathsf{R}_x = U\,x/\nu$ and not $\mathsf{R}_{\delta m} = U\,\delta_m/\nu$. What the writer failed to explain was that Eq. 16 was first modified by a substitution of

$$\mathsf{R}_{\delta m} = f(\mathsf{R}_x) \qquad (46)$$

and then plotted in Fig. 10(a). Eq. 46 was determined from experimental data[20] (not published herewith).

In order to analyze the development on the rough bottom, Mr. Halbronn used the von Kármán-Prandtl velocity-distribution equations for uniform flow in pipe. Using Eq. 3 and Eq. 5 for the rough pipe (and making several necessary assumptions), he derived an expression for δ as a function of x and k, plotting it in Fig. 14 for three fixed values of k. Inasmuch as the assumed logarithmic velocity distribution is even further from the truth in the case of rough boundaries than in the case of smooth boundaries, the subsequent analytical results are of questionable value. In Fig. 3 are illustrated velocity profiles approximated by equations of the type of Eq. 32 wherein j ranges between 1/4.23 and 1/4.86. These values are far from the 1/7-exponent and 1/8-exponent which give better (yet inadequate) agreement with the logarithmic distribution.

---

[20] "The Development of the Turbulent Boundary Layer on Steep Slopes," by William J. Bauer, dissertation presented to the State Univ. of Iowa, at Iowa City, Iowa, in August, 1951, in partial fulfilment of the requirements for the degree of Doctor of Philosophy.

The writer is pleased with the insertion of additional prototype data into Fig. 17, as well as with the tabulated comparison between measured and computed values of δ on the Glennmaggie Dam. It is agreed that the position of the design curve in Fig. 17 is not accurately determined (k remains in doubt). It should be noted (as Mr. Halbronn noted) that the range of doubt is sufficiently small to permit solution of design problems by the method illustrated in Fig. 11. Conservatism would merely indicate the assumption of a reasonably large value for k.

AMERICAN SOCIETY OF CIVIL ENGINEERS
Founded November 5, 1852

TRANSACTIONS

Paper No. 2720

ANCHORED BULKHEADS

By Karl Terzaghi,[1] Hon. M. ASCE

With Discussion by Messrs. T. H. Wu; W. D. Bigler; J. Brinch Hansen; Gregory P. Tschebotarioff; Paul Baumann; Rudolf Briske; Norman D. Lea; S. Packshaw; J. Verdeyen and V. Roisin; and Karl Terzaghi

Synopsis

In Part I of this paper the fundamental assumptions made in existing methods of bulkhead design are compared with observational data published in the past few decades. The investigation shows that the discrepancies are too important to be ignored in the design.

Part II deals with the evaluation of the forces acting on anchored bulkheads and with the safety requirements. The importance of the errors involved in the estimates of the bending moments and the soil reactions depend, to a large extent, on the type of soils involved in the design problem, on the degree of complexity of the structure of the soil strata, on the degree of uniformity of the backfill material, and on the time and labor invested in the subsoil exploration. Therefore, it would be economically unjustified to select the allowable stresses and safety factors in the construction materials without taking into consideration the degree of reliability of the available data. The selection of these values requires experience and good judgment.

If the designer has only the results of a conventional subsoil exploration available, the problem must be solved on the basis of empirical values such as those contained in this paper. In connection with the design of bulkheads, involving unusual features not treated in this paper, the designer must improvise the procedure; and, in doing so, it will be found advantageous to consult the results of the experimental investigations summarized in Part I.

Notation

The letter symbols in this paper are defined where they first appear, in the text or by illustration, and are assembled alphabetically, for convenience of reference, in the Appendix.

---

[1] Prof. of the Practice of Civ. Eng., Harvard Univ., Cambridge, Mass.

Note.—Published, essentially as printed here, in September, 1953, as *Proceedings-Separate No. 262.* Positions and titles given are those in effect when the paper or discussion was received for publication.

I. THEORETICAL AND REAL PRESSURES OF ANCHORED BULKHEADS

TYPES OF BULKHEADS

Bulkheads are the retaining walls of the waterfront. Depending on the depth of penetration of the sheet piles, they are commonly divided into bulkheads with free earth support (Fig. 1 (*a*)) and bulkheads with fixed earth support (Fig. 1 (*b*)). The sheet piles of the second type are driven so deep into the ground that the bulkhead can fail only by bending or because of inadequate anchorage. If the sheet piles have been driven their full length (or almost full length) into natural ground, and the natural ground has then been removed by excavation, the bulkhead is referred to as a "dredge bulkhead." On the other hand, if the surface of the natural ground is approximately at the level of the dredge line, and the material between the natural ground surface and the level of the upper edge of the sheet piles was deposited after the sheet piles were driven, the bulkhead is called a "fill bulkhead."

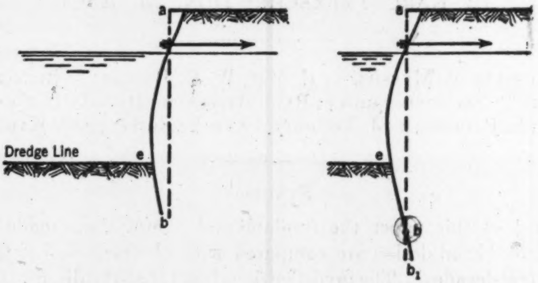

(*a*) FREE EARTH SUPPORT (*b*) FIXED EARTH SUPPORT

FIG. 1.—THE TWO EXTREME TYPES OF EARTH SUPPORT

CLASSICAL DESIGN ASSUMPTIONS

Although anchored bulkheads were probably in use in pre-Roman times, it appears that no attempt was made to design them on the basis of earth pressure computations until about 1910, when H. Krey, in Berlin, Germany, began to investigate the problem. Somewhat later he published an analytical procedure for bulkhead design. During the subsequent decades the Krey method was supplemented by various refinements including the "elastic line" and the "equivalent beam" method. In the United States, methods for the design of bulkheads on the basis of the classical earth pressure theories were developed and introduced into the practice of structural design by A. P. Pennoyer.[2] The fundamental assumptions on which all these procedures are based are illustrated in Fig. 2.

Fig. 2 (*a*) represents a bulkhead with free earth support. The inner face of the bulkhead is assumed to be acted upon by the active Coulomb pressure

---

[2] "Design of Sheet-Piling Bulkheads," by Raymond A. Pennoyer, *Civil Engineering*, November 1933, p. 615.

(pressure triangle, abc). The force that resists the outward movement of the buried part, eb, is represented by the shaded triangle, bef.

Fig. 2(*b*) shows a bulkhead with fixed earth support. The triangle, abc, represents the active earth pressure on the inner face. The assumed resistance against the outward movement of the buried part of the bulkhead is indicated by the pressure area, edb. Since the elastic line of the sheet piles forming an anchored bulkhead with fixed earth support is assumed to pass below a certain point b onto the right-hand, or inner, side of the original position of the bulkhead, it is also assumed that the earth pressure on the inner face changes at the elevation of point b from active to passive (line cc_1, Fig. 2(*b*)), whereas the pressure on the outer face changes at the same point from passive to active (line gg_1). The depth of penetration of the sheet piles (D) is computed in such a manner that the elastic line of the sheet piles satisfies the condition of fixed earth support. The computation is performed either by trial and error or on the basis of supplementary simplifying assumptions.

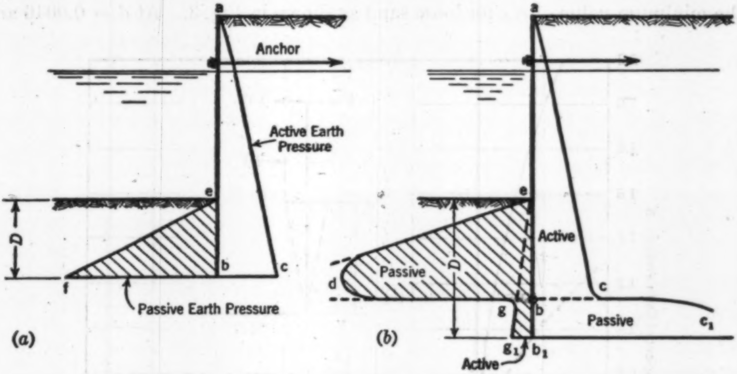

FIG. 2.—CLASSICAL CONCEPTIONS CONCERNING DISTRIBUTION OF EARTH PRESSURE ON BULKHEADS WITH (*a*) FREE AND (*b*) FIXED EARTH SUPPORT

At the time when the assumptions illustrated by Fig. 2 were originated, the physical conditions for the validity of these assumptions were still unknown. Since that time, many observational data have been accumulated which are incompatible with the original assumptions. Nevertheless, the methods of bulkhead design remained practically unchanged. The following sections of Part I contain a summary of those observational data which are at variance with the original assumptions. These data will then be used in Part II as a basis for a revision of the methods of design.

EFFECT OF WALL MOVEMENTS ON EARTH PRESSURE

The design methods illustrated in Fig. 2 involve the assumption that an infinitesimal yield of a lateral support is sufficient to reduce the intensity of the earth pressure to its minimum value and that a further yield has no influence on this pressure. This assumption is incompatible with the results of large-scale earth pressure tests[3] which furnished accurate information concerning relations among (1) the yield ratio $d = Y/H$ of a vertical wall (Fig. 3(*b*)) with height $H = 5$ ft, backfilled with coarse, clean sand in a loose or in a compacted state; (2) the coefficient of active earth pressure K_A; (3) the mobilized part ϕ' of the angle of internal friction ϕ; and (4) the angle of wall friction δ. The tests led to the following conclusions:

The assumed value K_A for the dense sand was its minimum value corresponding to $d = 0.0005$. This value was retained until the yield ratio became equal to 0.002. Further yield was associated with an increase of K_A toward the minimum value of K_A for loose sand as shown in Fig. 3. At $d = 0.0046$ an audible slip occurred in the backfill. Along the line of intersection between the surface of sliding and the surface of the backfill a low fault scarp appeared.

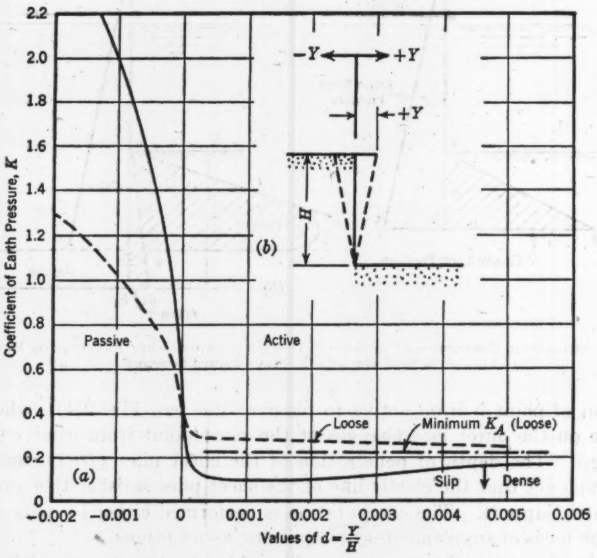

FIG. 3.—INFLUENCE OF RELATIVE DENSITY OF SAND AND EFFECTIVE YIELD Y ON COEFFICIENT OF EARTH PRESSURE

The value of K_A for loose sand decreased from 0.4 to 0.30 while the yield ratio d increased from zero to 0.0003. Further yield was associated with a less important decrease of K_A (Fig. 3(*a*)). At a yield ratio of $d = 0.007$, corresponding to the maximum distance through which the model retaining wall could be advanced, the value of K_A was still considerably greater than the minimum value for the dense sand (0.23), and no slip had yet occurred.

The angle of wall friction δ assumed its full value before the internal friction was completely active. On the other hand, when the wall was advanced toward the backfill over a distance of 0.002 H, the wall friction was still much smaller than its maximum value.

---

[3] "Large Retaining-Wall Tests. I. Pressure of Dry Sands," by Karl Terzaghi, *Engineering News-Record*, Vol. 112, 1934, pp. 136–140.

At any stage of the tests, as soon as the wall ceased to yield, both the angle of internal friction ϕ' and the angle of wall friction δ decreased slightly at a decreasing rate. Part of the decrease was probably caused by the fact that the backfill of the model retaining wall was subject to intermittent vibrations caused by passing trains.

The backfill of fill bulkheads is almost never compacted by artificial methods, and the average yield of the bulkhead hardly exceeds a fraction of 1% the height of the bulkhead. Therefore, it is unlikely that the lateral pressure of a sand backfill on an anchored bulkhead is as low as the active earth pressure of the fill material.

In the tests illustrated in Fig.3, the wall was not allowed to yield until the entire backfill had been placed. In practice, backfilling operations and yield take place simultaneously. In this case distinction must be made between total and effective yield. The term "effective yield" refers to that part of the total horizontal movement of a point on the back of a lateral support which occurs after the point has been buried. The value of the coefficient of earth pressure depends on the average effective yield of the support and not on the average total yield.

EFFECT OF WALL FRICTION ON PASSIVE EARTH PRESSURE

At the time when the analytical methods for bulkhead design came into existence, it was generally believed that the Coulomb method for computing passive earth pressure was as reliable as the Coulomb procedure for computing active earth pressure. Both are based on the assumption that the surface of sliding is plane. In Fig. 4(*a*) the surfaces of sliding are indicated by lines bc$_1$ (active wedge) and bd$_1$ (passive wedge).

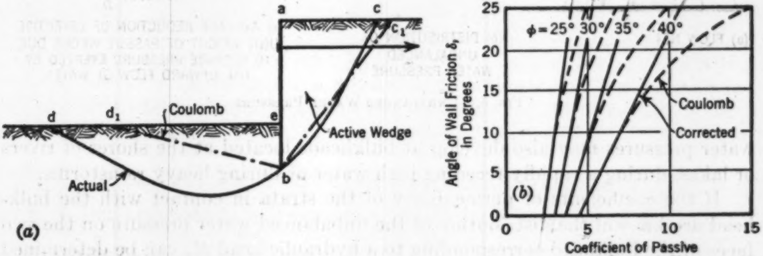

FIG. 4.—DIAGRAMS ILLUSTRATING ERRORS INVOLVED IN COULOMB'S ASSUMPTION THAT THE PASSIVE FAILURE TAKES PLACE ALONG A PLANE SURFACE OF SLIDING

If the Coulomb assumption represented by line bd$_1$ were justified, the coefficient of passive earth pressure K_P, of a sand with an angle of internal friction ϕ, would increase with increasing angle of wall friction δ, as shown in Fig. 4(*b*) by dashed lines. Subsequent theoretical investigations[4, 5] have shown

---

[4] "Theoretical Soil Mechanics," by Karl Terzaghi, John Wiley & Sons, Inc., New York, N. Y., 1943, pp. 42–63.

[5] *Ibid.*, pp. 100–105.

that the base of the active wedge (line bc, Fig. 4(*a*)) really is almost a plane. Therefore, the Coulomb minimum value for the active earth pressure is almost correct. However, in connection with the passive earth pressure, both the theory of plasticity and various experimental investigations led to the conclusion that the base of the passive wedge is not even approximately a plane. It consists of one curved section and one plane section, as indicated in Fig. 4(*a*) by line bd. On the basis of the knowledge of the actual shape of the surface of sliding, it was found by computation that the coefficient K_P of the passive earth pressure on a vertical lateral support (ratio between horizontal and vertical pressure at any depth below the surface) increases in accordance with the solid lines, and not the dashed lines, in Fig. 4(*b*).

UNBALANCED WATER PRESSURE

If an anchored bulkhead is located at the seashore, the earth pressure on the inner face of the sheet piles is a maximum at low tide. At the same time, the inner face is acted upon by an unbalanced water pressure because the water table behind the bulkhead lags behind the receding tide. Unbalanced water pressures may also develop at bulkheads located at the shores of rivers or lakes, during a rapidly receding high water or during heavy rainstorms.

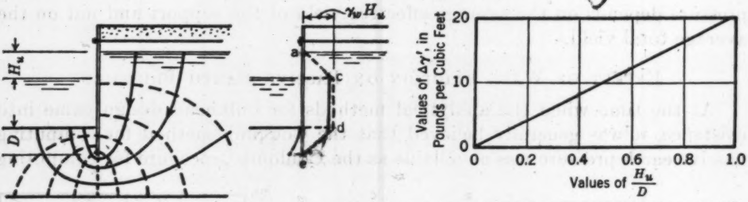

H_u
D
$\gamma_w H_u$
a
c
d
e
20
10
0
Values of $\Delta\gamma'$, in Pounds per Cubic Feet
0
0.2
0.4
0.6
0.8
1.0
Values of $\frac{H_u}{D}$

(*a*) FLOW NET

(*b*) DISTRIBUTION OF UNBALANCED WATER PRESSURE

(*c*) AVERAGE REDUCTION OF EFFECTIVE UNIT WEIGHT OF PASSIVE WEDGE DUE TO SEEPAGE PRESSURE EXERTED BY THE UPWARD FLOW OF WATER

FIG. 5.—UNBALANCED WATER PRESSURE

If the coefficients of permeability of the strata in contact with the bulkhead are known, the distribution of the unbalanced water pressure on the two faces of the bulkhead corresponding to a hydraulic head H_u can be determined by means of the flow net method, as shown in Fig. 5, for a dredge bulkhead with sheet piles driven into a homogeneous mass of fine, uniform sand.[6] Fig. 5(*a*) represents the flow net and Fig. 5(*b*), the corresponding distribution of the unbalanced part of the water pressure over the two faces of the bulkhead. Accurate flow nets for anchored bulkheads in contact with homogeneous sand have been published by J. McNamee.[7]

If the permeability of all the soil strata in contact with the bulkhead is practically the same, it can be assumed, without serious error, that the inner face of the bulkhead at any depth between the dredge line and the outside water level is acted upon by an unbalanced water pressure,

---

[6] "Theoretical Soil Mechanics," by Karl Terzaghi, John Wiley & Sons, Inc., New York, N. Y., 1943, p. 252.

[7] "Seepage into a Sheeted Excavation," by J. McNamee, *Geotechnique*, Vol. I, 1949, pp. 229–241.

$$P_u = \gamma_w H_u \quad \text{.........................} \quad (1)$$

in which γ_w is the unit weight of water. Below the dredge line, P_u decreases from $\gamma_w H_u$ to zero at the lower edge of the sheet piles, as indicated in Fig. 5(*b*) by the straight line, de.

If the permeability varies in vertical directions between wide limits, the determination of the distribution of the unbalanced water pressure may require the construction of a flow net.

When the water table in the backfill is above the free water level, the water percolates through the backfill in a downward direction, flows around the lower edge of the sheet piles, and rises beyond the outer face, as indicated in Fig. 5(*a*). The seepage pressure exerted by the rising ground water reduces the effective unit weight of the soil in contact with the outer face of the bulkhead and, as a consequence, it reduces the passive earth pressure. If i is the average hydraulic gradient in the soil adjoining the outer face, the corresponding reduction of the submerged unit weight γ' of the soil is[8]

$$\Delta\gamma' = i\,\gamma_w \quad \text{.........................} \quad (2)$$

Under the conditions illustrated in Fig. 5(*a*), the average value of i is somewhat smaller than $\frac{H_u}{3\,D}$. Hence, the effective unit weight of the soil in contact with the outer face of the bulkhead will be slightly greater than

$$\gamma' - \Delta\gamma' = \gamma' - \gamma_w \frac{H_u}{3\,D} \quad \text{.....................} \quad (3)$$

The relationship between $\Delta\gamma'$ and H_u/D is shown in Fig. 5(*c*). Within the backfill, the water percolates in a downward direction and it produces an increase of the effective unit weight of the fill by $\Delta\gamma''$. However $\Delta\gamma''$ is very much smaller than $\Delta\gamma'$ and does not require consideration.

LATERAL PRESSURE RESULTING FROM LINE LOADS

The first attempts to compute the lateral earth pressure p' per unit of length of a wall due to line loads, q', per unit of length, were made in the nineteenth century, before experimental data were available. Based on the Coulomb earth pressure theory, they led to the conclusion[9] that the intensity and the position of the center of the pressure caused by the line load depend on the angle of internal friction ϕ and the angle of wall friction δ. These conclusions are illustrated in Figs. 6(*a*) and 6(*b*). In Fig. 6(*b*) the abscissa of point s_1 represents the ratio m_1 between the width of the top surface of the "sliding wedge" (line ac, Fig. 4(*a*)) and the height H of a wall with a smooth back ($\delta = 0$) acted upon by the lateral pressure of very loose sand ($\phi = 30°$). The abscissa of point s_2 represents the corresponding m_1-value for a wall with a rough back ($\delta = 25°$), backfilled with dense sand ($\phi = 40°$). The ordinates of the dash-double-dot curves that pass through these points represent the ratio between the lateral pressure p' and the intensity q' of the line load computed by means of the Coulomb theory.

---

[8] "Soil Mechanics in Engineering Practice," by Karl Terzaghi and R. B. Peck, John Wiley & Sons, Inc., New York, N. Y., 1948, p. 54.

[9] *Ibid.*, p. 160.

At any given value of ϕ and δ the width $m_1 H$ of the top of the sliding wedge decreases slightly with increasing values of q'. If the line load is applied at a distance of less than $m_1 H$ from the crest of the wall, the value of p'/q' is independent of the position of the line load with reference to the crest of the wall. Therefore, on the left-hand side of points s_1 and s_2 the lines representing the (p'/q')-values are horizontal. If the line load moves to the right-hand side of points s_1 (loose sand) or s_2 (dense sand), the lateral pressure decreases rapidly and finally equals zero. The Coulomb theory also leads to the conclusion that the lateral pressure caused by a line load acts only on a narrow, horizontal strip. The elevation of this strip above the foot of the wall depends on the values ϕ and δ, and on the value m, which determines the position of the line load q' with reference to the crest of the wall (Fig. 6(*c*)). In Fig. 6(*a*) the position of the strips acted upon by the lateral force p' is indicated by horizontal arrows. To each arrow are added the values of ϕ and δ on which the computation of its position was based. In each of the four diagrams in Fig. 6(*a*) the two arrows indicate the extreme positions between which the theoretical center of the pressure caused by line loads on sand fills with different density may be located.

The conclusions based on the Coulomb theory concerning the lateral pressure resulting from line loads remained practically unchallenged until both the intensity and distribution of the lateral pressure were determined experimentally by E. Gerber[10] and M. G. Spangler,[11] M. ASCE. The backfill used by Mr. Gerber consisted of clean, uniform river sand with a grain size between 0.2 mm and 1.5 mm. The lateral support was practically rigid. It consisted of the concrete side wall of a rectangular pit, with a depth of 31 in. The lateral pressures caused by the line load were measured by means of pressure cells arranged in vertical rows. Mr. Spangler used as a backfill material pit run gravel with 13% particles passing the 200-mesh sieve. The lateral support consisted of a reinforced concrete cantilever wall, 84 in. high and 6 in. thick, which was free to tilt about the outer edge of the base of the base plate. In spite of the differences in the test conditions in these two sets of tests, there are no essential differences between the test results.

The solid curves in Fig. 6(*a*) represent the results of one of Mr. Gerber's series of tests performed on backfills with a height $H = 32$ in. (Fig. 6(*c*)). The surcharge, 0.4 ton per sq ft, covered a strip 6.3 in. wide and 25 in. long. The center line of the loaded strip was established, successively, at a distance $x =$ 3.1 in., 9.4 in., 15.5 in., and 22 in. from the upper edge of the wall, corresponding to values of m $(= x/H)$ of 0.1, 0.3, 0.5, and 0.7. The abscissas of the solid curves represent the values of the ratio $p \frac{H}{q'}$, p being the horizontal pressure per unit area on the back of the wall, and q' being the surcharge per unit of length of the loaded strip. In Fig. 6(*b*) the ordinates of the solid curve represent the ratio p'/q' between the measured lateral pressure p' per unit length of the wall and the line load q'.

---

[10] "Untersuchungen über die Druckverteilung im örtlich belasteten Sand," by E. Gerber, Zürich, Switzerland, 1929.

[11] "Horizontal Pressures on Retaining Walls Due to Concentrated Surface Loads," by M. G. Spangler, *Bulletin No. 140*, Iowa Eng. Experiment Station, Iowa City, Iowa.

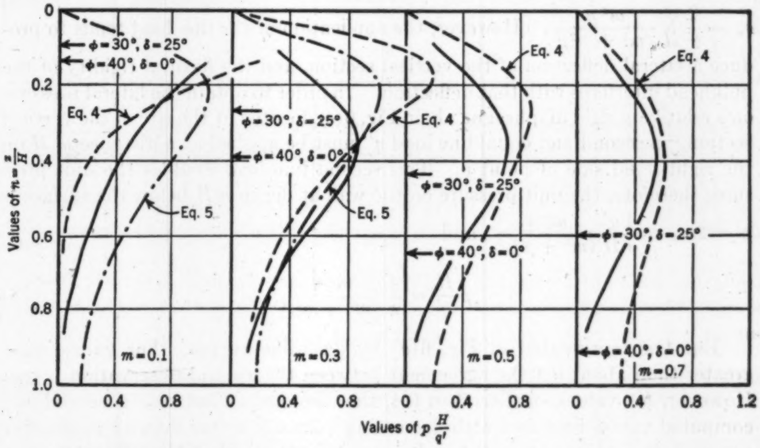

(*a*) DISTRIBUTION ALONG VERTICAL LINES

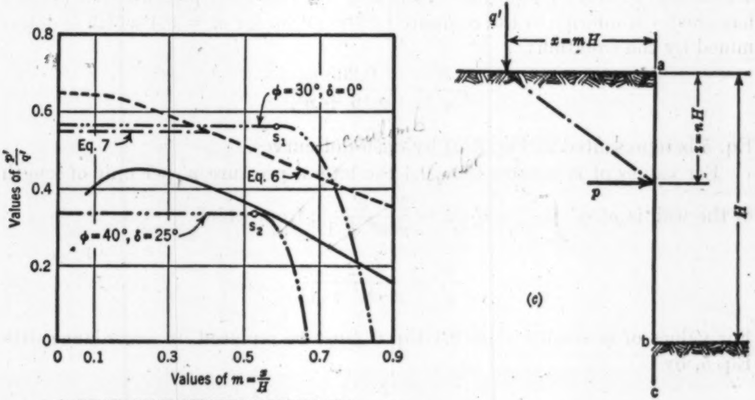

(*b*) RELATIONSHIP BETWEEN PRESSURE PER UNIT OF LENGTH OF BULKHEAD AND VALUES OF *m* FOR THE WALL SHOWN IN FIG. 6 (*c*)

FIG. 6.—MEASURED (PLAIN CURVES) AND COMPUTED (DASH AND DASH-DOT CURVES) LATERAL PRESSURE DUE TO LINE LOADS

According to the data shown in Fig. 6 the information furnished by the Coulomb theory concerning the intensity and distribution of the lateral pressure resulting from line loads is incompatible with the experimental data. More satisfactory is the agreement between the measured pressures and the

V 119 54 UMI

theory of Boussinesq.[12] According to this theory the horizontal unit pressure σ_x on a vertical section, ac, in Fig. 6(*c*) through a semi-infinite elastic medium, at a depth $n\,H$ below the surface, caused by a surface load q' per unit of length, acting on a line at a distance $m\,H$ from the vertical section is equal to $\sigma_x = \frac{2}{\pi}\frac{q'}{H}\frac{m^2\,n}{(m^2+n^2)^2}$. However, the application of the line load tends to produce a lateral deflection of the vertical section, and the flexural rigidity of the bulkhead interferes with that deflection. In order to obtain the lateral pressure on a relatively rigid diaphragm, ab, in Fig. 6(*c*), located at the site of the vertical section,[13] a second and equal line load q' must be applied at a distance $m\,H$ on the right-hand side of point a. This second line load doubles the unit pressure; therefore, the unit pressure on the wall at depth $n\,H$ below the surface is $p = 2\,\sigma_x = \frac{4}{\pi}\frac{q'}{H}\frac{m^2\,n}{(m^2+n^2)^2}$; and

$$p\,\frac{H}{q'} = \frac{4}{\pi}\,\frac{m^2\,n}{(m^2+n^2)^2}\ldots\ldots\ldots\ldots\ldots\ldots\ldots(4)$$

Eq. 4 is represented in Fig. 6(*a*) by dash-line curves. For values of m greater than about 0.4 the agreement between theory and observation is fair. However, for values smaller than 0.4, the discrepancy between observed and computed values increases with decreasing values of m (as shown by dash-line curves in Fig. 6(*a*) for $m = 0.1$ and $m = 0.3$). For such values of m (less than 0.4) it was found, by trial and error, that the observed pressure distribution has greater similarity to the computed distribution for $m = 0.4$ which is determined by the equation:

$$p\,\frac{H}{q'} = \frac{0.203\,n}{(0.16+n^2)^2}\ldots\ldots\ldots\ldots\ldots\ldots\ldots(5)$$

Eq. 5 is represented in Fig. 6(*a*) by dash-dot curves.

For values of m greater than 0.4 the lateral pressure p' per unit of length of the wall is $p' = \int_{n=0}^{n=1} p\,H\,dn = \frac{2}{\pi}\frac{q'}{m^2+1}$; from which

$$\frac{p'}{q'} = \frac{2}{\pi\,(m^2+1)}\ldots\ldots\ldots\ldots\ldots\ldots\ldots(6)$$

For values of m smaller than 0.4 Eq. 6 must be replaced, in accordance with Eq. 5, by

$$\frac{p'}{q'} = \frac{2}{\pi\,(0.16+1)} = 0.55\ldots\ldots\ldots\ldots\ldots\ldots\ldots(7)$$

In Fig. 6(*b*), Eq. 6 is represented by a dash line and Eq. 7 is represented by a dash-dot line.

The diagrams in Figs. 6(*a*) and 6(*b*) show that the values obtained by use of Eqs. 4 to 7 are consistently greater than the measured values. Part of the difference is due to the fact that the Gerber tests[10] were made with line loads having a length of not more than 0.8 H, whereas the computed values refer to line loads with infinite length. The remainder of the difference results from the fact that the Boussinesq theory is strictly applicable only to perfectly elastic materials. Since the computed values are too high, the differences partly compensate for the fact that the distribution of the (p'/q')-values under field conditions, may deviate to some extent from the observational curves which have been constructed on the basis of the test results reported by Mr. Gerber. The deviations are chiefly caused by the complex stress-strain relations for sands. Because of these relations the pressure distribution depends not only on the values of m and n contained in Eqs. 4 and 5, but also, to some extent, on the value of the ratio q'/H. Mr. Gerber's data were obtained only for one value of this ratio.

---

[12] "Theoretical Soil Mechanics," by Karl Terzaghi, John Wiley & Sons, Inc., New York, N. Y., 1943, p. 376.

[13] "Pressure Distribution on Retaining Walls," *Proceedings*, First International Conference on Soil Mechanics and Foundation Eng., Discussion by R. D. Mindlin, Cambridge, Mass., 1936, Vol. 3, pp. 155–156.

The observational data shown in Fig. 6 eliminated the Coulomb theory as a source of information concerning the lateral pressure produced by line loads, and they made it possible to establish empirical equations for estimating upper limiting values of the pressures produced by such loads.

They're high

LATERAL PRESSURE RESULTING FROM POINT LOADS

Intensity and distribution of the lateral pressure resulting from point loads were investigated by Messrs. Gerber[10] and Spangler.[11] The test results were practically identical. The point load in Mr. Gerber's tests consisted of a loaded circular slab with a diameter of 14 in. The slab rested upon the horizontal surface of a layer of clean, coarse sand with a depth of 32 in., at varying distances from the crest of the wall. Fig. 7 shows the distribution of the lateral pressure over the back of the wall. The pressure is greatest along the line of intersection, ab, between the wall and a vertical plane through the center of the load at right angles to the wall. Along this line, the unit pressure p_1 first increases with increasing depth, assumes a maximum value at a depth which is

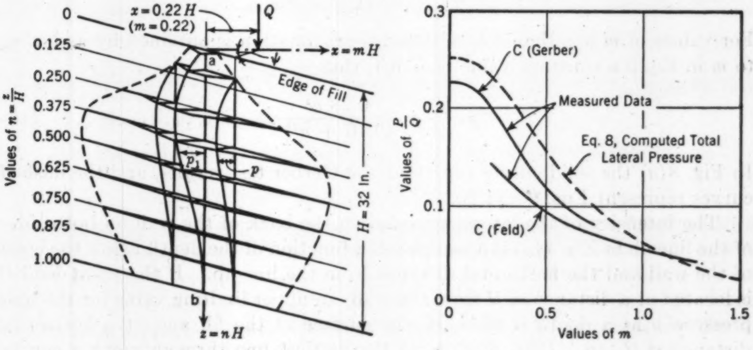

(a) OBSERVED PRESSURE DISTRIBUTION (E. GERBER)

(b)

FIG. 7.—LATERAL PRESSURE DUE TO POINT LOADS

V119 54 UMI

somewhat greater than the distance between load and wall, and then decreases again. At any depth the pressure decreases in horizontal directions with increasing distance from line ab.

Fig. 7 (*b*) shows the relationship between $m = x/H$ and the total intensity P of the lateral pressure caused by the point load Q. Curve C (Gerber) is based on test results[10] and curve C (Feld) on test data published by Jacob Feld,[14] M. ASCE. The lack of perfect agreement between observational curves obtained by different investigators is chiefly a result of the fact that the values of P/Q depend not only on m but also on various other factors such as the deflection ratio d for the lateral support and the ratio between Q and the ultimate bearing capacity of the backfill. Upper limiting values for P can be obtained by use of the empirical equation:

$$\frac{P}{Q} = \frac{0.25}{(1 + m^2)^2} \tag{8}$$

which is based on Mr. Gerber's test results. In Fig. 7 (*b*) Eq. 8 is represented by a dashed curve.

None of the existing theories (1953) account satisfactorily for the distribution over the inner face of a wall of the lateral pressure produced by a point load Q. For values of m greater than 0.4 the unit pressures p_1 along line ab (Fig. 7 (*a*)) can be estimated roughly by use of the empirical equation:

$$p_1 \frac{H^2}{Q} = 1.77 \frac{m^2\, n^2}{(m^2 + n^2)^3} \tag{9}$$

For values of m less than 0.4, a better approximation is obtained by assigning to m in Eq. 9 a constant value $m = 0.4$, thus—

$$p_1 \frac{H^2}{Q} = \frac{0.28\, n^2}{(0.16 + n^2)^3} \tag{10}$$

In Fig. 8 (*a*) the solid curves represent the Gerber test results, and the dashed curves represent Eqs. 9 and 10.

The intensity of the lateral pressure on the back of the wall on both sides of the line ab in Fig. 7 (*a*) is a complicated function of the depth below the crest of the wall and the horizontal distance from the line ab. If the point load Q is located at a distance $m\,H$ from the wall, an upper limiting value for the unit pressure p at a depth $n\,H$ below the surface of the fill and at a horizontal distance $m\,H \tan\psi$ (Fig. 8 (*b*)) from the vertical line through point a can be obtained by use of the empirical equation:

$$p = p_1 \cos^2 (1.1\,\psi) \tag{11}$$

In Eq. 11, p_1 is the unit pressure on the wall at depth $n\,H$ for $\psi = 0$. The value of p_1 is determined by Eq. 9 for m greater than 0.4 and by Eq. 10 for values of m smaller than 0.4. Eq. 11 is an empirical equation based on Mr. Gerber's test results.

---

[14] "Lateral Earth Pressure: The Accurate Experimental Determination of the Lateral Earth Pressure, Together with a Resume of Previous Experiments," by Jacob Feld, *Transactions*, ASCE, Vol. LXXXVI, 1923, pp. 1448–1505.

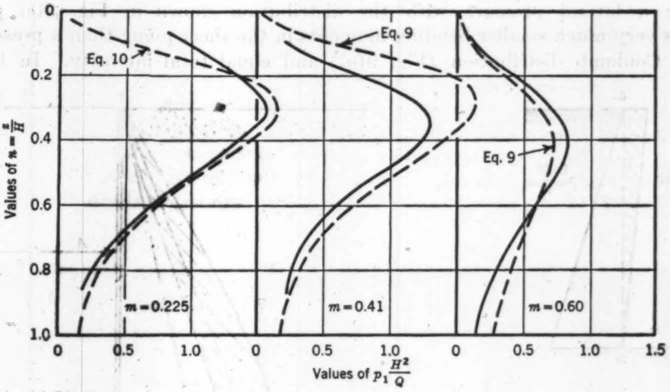

(*a*) PRESSURE PER UNIT OF AREA ALONG LINE a b IN FIG. 7 (*a*)

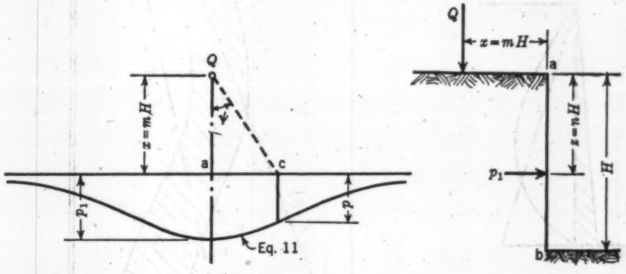

(*b*) PRESSURE ALONG HORIZONTAL LINES (*c*)

FIG. 8.—LATERAL PRESSURE PRODUCED BY POINT LOADS ON LATERAL SUPPORT

DISTRIBUTION OF EARTH PRESSURE

Theory and observation have shown that the distribution of the pressure on a lateral support is by no means necessarily in accordance with the Coulomb theory because it depends largely on the type of yield.[15] This fact is illustrated by Fig. 9 which represents the distribution of the lateral pressure on the back of a lateral support for three different types of yield. The effective yield at any depth below the surface is indicated by the width of the shaded area at that depth.

In connection with anchored bulkheads, the validity of the Coulomb theory was questioned for the first time in 1906 by Danish engineers on purely empirical grounds. It was argued that the lateral pressure on bulkheads is a minimum midway between the dredge line and the anchor line, as shown in Fig. 9(*c*). This conception received experimental support by tests performed by J.P.R.N. Stroyer[16] and received considerable attention because a lateral pressure with the distribution shown in Fig. 9(*c*) produces very much smaller bending moments in the sheet piling than a pressure with Coulomb distribution (Fig. 9(*a*)) and equal total intensity. In 1938

---

[15] "General Wedge Theory of Earth Pressure," by Karl Terzaghi, *Transactions*, ASCE, Vol. 106, 1941, pp. 68–80.

[16] "Earth Pressure on Flexible Walls," by J. P. R. N. Stroyer, *Journal*, Inst. of C. E., London, England, Vol. I, 1935, p. 94.

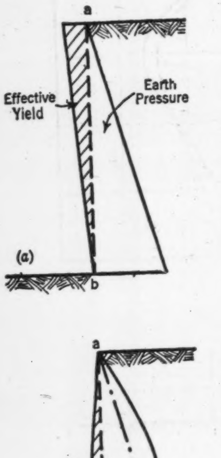
a
Effective Yield
Earth Pressure
(a)
b
a
(b)
b
a
(c)
b

Fig. 9.—Influence of Movement Type on Pressure Distribution

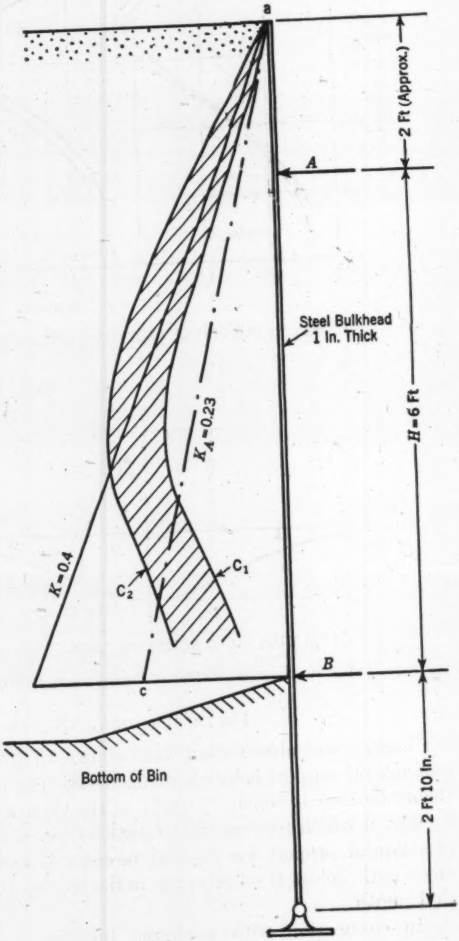
a
2 Ft (Approx.)
A
Steel Bulkhead 1 In. Thick
H=6 Ft
$K_A=0.23$
$K=0.4$
C_2
C_1
B
c
Bottom of Bin
2 Ft 10 In.

Fig. 10.—Intensity and Distribution of Active Earth Pressure on Inner Face of Relatively Stiff Model Bulkhead

J. Ohde computed the distribution of the earth pressure on flexible walls with fixed upper and lower edges and he also found that the pressure distribution should have the characteristics shown in Fig. 9(*c*). His theoretical conclusions were confirmed by large-scale tests performed by H. Press in 1948,[17] on a flexible wall 27 ft high. The inner face of the wall was paved with pressure cells.

---

[17] "Über die Druckverteilung im Boden hinter Wänden verschiedener Art," by H. Press, *Bautechnik Archiv*, W. Ernst and Son, Berlin, Germany, 1948, pp. 36–54.

Between the years 1944 and 1948 G. P. Tschebotarioff, M. ASCE, performed large-scale tests on bulkhead models.[18] He measured the lateral deflection and the extreme fiber stresses in the bulkheads at different elevations above their lower edge and he computed the pressure distribution on the basis of these data. He obtained the pressure distribution illustrated by Fig. 9(*c*) for bulkheads of the dredge type only. The distribution of the earth pressure on the inner face of the models of fill bulkheads was found to be similar to that shown in Figs. 10 and 11. The tests represented by Fig. 10 were made with a relatively stiff bulkhead with a maximum deflection equal to about 0.1% of the vertical distance *H* between the anchor line and the dredge line. The corresponding K_A-value was nearly 0.4, which is approximately equal to the coefficient of earth pressure at rest. The intensity and the distribution of the active earth pressure on more flexible bulkheads, having a deflection ratio of about 0.5%, is shown in Fig. 11. The corresponding K_A-value approximated

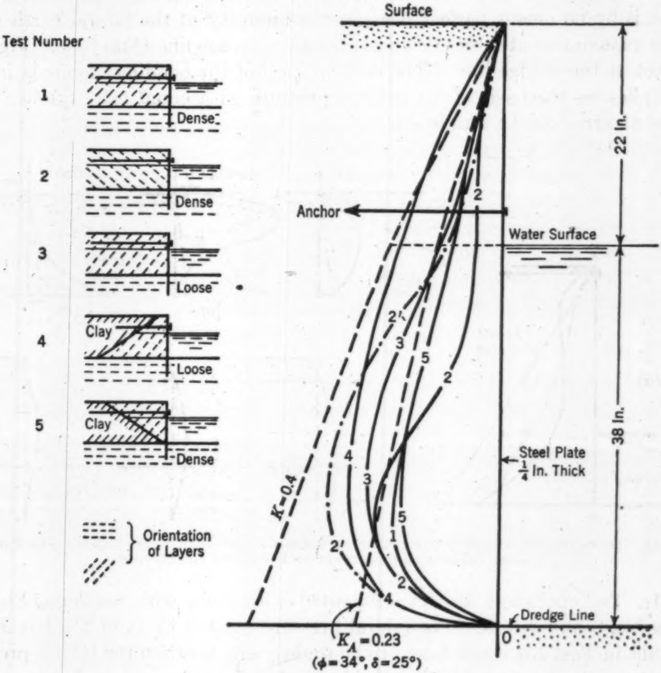

FIG. 11.—INTENSITY AND DISTRIBUTION OF ACTIVE EARTH PRESSURE ON THE INNER FACE OF RELATIVELY FLEXIBLE MODEL BULKHEADS

that of the active earth pressure. Curve 2′ represents Test No. 2 after compaction of the fill by vibration. The line marked $K_A = 0.23$ represents the Coulomb pressure computed on the assumption that $\phi = 34°$ and $\delta = 25°$. The line marked $K = 0.4$ represents the earth pressure at rest. All the test results showed that the lateral earth pressure was a maximum at some elevation above the dredge line. They also showed that the real pressure distribution depends on factors, such as the method of placing the fill, which do not receive any consideration in earth pressure theory. Hence, the agreement between the real pressure distribution and the Coulomb pressure distribution is by no means perfect because the intensity of the lateral earth pressure is a maximum at some elevation above the dredge line (Fig. 10 and Fig. 11) and not at the dredge line. The computation of the bending moments in the sheet piles on the basis of a Coulomb pressure with equal total intensity involves an error on the unsafe side.

---

[18] "Final Report. Large Scale Earth Pressure Tests with Model Flexible Bulkheads," by G. P. Tschebotarioff, Princeton Univ., Princeton, N. J., 1949.

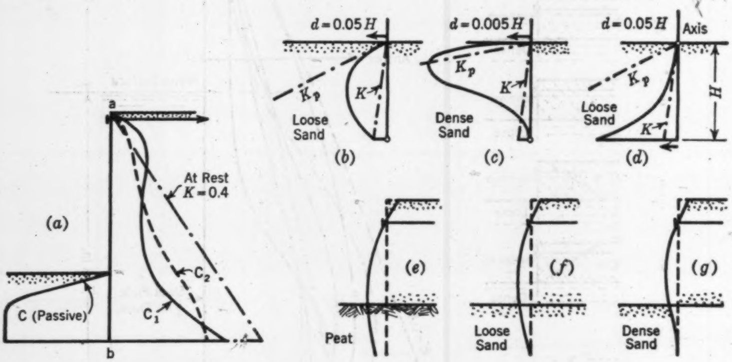

FIG. 12.—DIAGRAMS ILLUSTRATING THE EFFECT OF SUBSOIL CONDITIONS ON DISTRIBUTION OF PASSIVE EARTH PRESSURE AND ON TYPE OF BULKHEAD DEFLECTION

Mr. Tschebotarioff also experimented with composite backfills, Fig. 11, Tests No. 4 and No. 5. The lateral pressure exerted by sand fills backed by clay fills in Test No. 4 was found to be slightly greater than the lateral pressure of a continuous sand backfill with identical properties. The lateral pressure exerted by sand fills located between the bulkhead and a clay slope as in Test No. 5 was slightly smaller than that exerted by the fill in Test No. 4. P. W. Rowe determined the distribution of the earth pressure on a flexible wall directly by means of pressure cells in 1952.[19] In agreement with Mr. Tschebotarioff's findings, he obtained the pressure distribution for dredge bulkheads as shown in Fig. 9(*c*). However, he found that an anchor yield of 0.1% of the height of the bulkhead is sufficient to change the pressure distribution into one that agrees fairly closely with the Coulomb theory. The test results are illustrated in Fig. 12(*a*). In Fig. 12, curve C_1 represents the distribution of the earth pressure on the inner face of the model bulkhead prior to yielding of the anchorage and C_2 represents distribution after the bulkhead had yielded. The total intensity of the pressure remained almost unchanged.

---

[19] "Anchored Sheet-Pile Walls," by P. W. Rowe, *Proceedings*, Inst. of C. E., London, England, Vol. 1, Pt. 1, 1952, pp. 27–70.

The anchorage of Mr. Rowe's model bulkhead was allowed to yield after the sand in contact with the upper part of the outer face of the bulkhead had been removed by excavation, whereas in practice the anchorage yields gradually during the process of excavation. This difference may involve a considerable difference in the type of pressure distribution. However, the yield of the anchorage may exceed considerably the limiting value of 0.001 H, and the pounding of waves or traffic vibrations may contribute further to a modification of the pressure distribution. Hence, even in cases of dredge bulkheads it does not seem justified to depend on the benefits to be derived from a difference between the real pressure distribution and the distribution computed on the basis of the Coulomb theory.

Curve C(Passive), Fig. 12(*a*), shows the results of the measurement of the passive earth pressure that acted upon the buried part of the model bulkhead. In order to obtain supplementary information concerning the effect of the type of wall movement on the distribution of the passive earth pressure, Mr. Rowe experimented with a ⅜-in. steel plate that was buried to a depth of 2 ft in clean sand. The plate could be advanced toward the sand by rotation about a horizontal axis. The passive earth pressure on the wall was measured by use of seven pressure cells, spaced 3 in. on centers along the vertical axis of the area acted upon by the passive earth pressure. The test results are shown in Figs. 12(*b*), 12(*c*), and 12(*d*).

The pressure distribution represented by curve C(passive) in Fig. 12(*a*) is intermediate between those shown in Figs. 12(*c*) and 12(*d*), but none of them involves an increase of the passive earth pressure in simple proportion to the depth below the dredge line. With increasing flexibility of the buried part of the bulkhead, the movement of this part changes from a displacement almost parallel to the original position of the buried part into a movement by rotation about the lower edge of the bulkhead so that the distribution of the passive earth pressure becomes increasingly similar to that shown in Fig. 12(*b*), or Fig. 12(*c*).

INFLUENCE OF FLEXURAL RIGIDITY ON BENDING MOMENT

According to the theories of bulkhead analysis explained under the heading, "Classical Design Assumptions," and illustrated in Fig. 2, the conditions of end support and (as a consequence) the maximum bending moment in the sheet piles are independent of the flexural rigidity of the sheet piles. According to the same theories, the maximum bending moment decreases with increasing depth of sheet-pile penetration, whatever the flexural rigidity may be. These postulates are incompatible with what has been learned concerning the relation between horizontal displacement and horizontal soil reaction. The fallacies involved in the postulates have already been emphasized by Paul Baumann, M. ASCE, in connection with an analysis of the causes of the failure of Pier B in the Outer Harbor of the City of Long Beach, Calif.[20] In fact, if the sheet piles were perfectly rigid, the maximum bending moment would increase with increasing depth of pile penetration. However, no observational data were available concerning these important relationships until the results of Mr. Rowe's experimental investigations were published.[19]

---

[20] "Analysis of Sheet-Pile Bulkheads," by Paul Baumann, *Transactions*, ASCE, Vol. 100, 1935, pp. 707–797.

Mr. Rowe's model bulkheads consisted of metal plates of height H equal to from 20 in. to 36 in., and with different thicknesses. The dredge line (Fig. 13) was at a variable depth αH below the surface of the fill and the anchor line was at a depth βH. The vertical strains on the two surfaces of the metal plates were measured by strain gages spaced 2.5 in. vertically. The tests were performed using four different materials—coarse, clean sand; crushed rock (chips); pea gravel; and ashes. In one series of tests the materials were placed in a loose state and in a second series they were placed in a dense state. In each series of tests the extreme fiber stresses in the plate were measured by use of strain gages for different values of the free-height ratio α, anchor-level ratio β, surcharge ratio $\frac{q}{\gamma H}$, modulus of elasticity E of the wall, and the moment of inertia I of the cross section of the wall. The strain-gage readings furnished the data for computing the maximum bending moment in the plate for each set of test conditions.

According to the results of Mr. Rowe's analytical studies, which preceded the tests, the condition for similitude between the bulkhead model and the prototype is satisfied if the values α, β, $\frac{q}{\gamma H}$, and ρ are the same. The symbol ρ indicates the flexibility number of the sheet piles—

$$\rho = \frac{H^4}{E I} \quad \text{(12)}$$

in which I represents the rectangular moment of inertia of the piles. This conclusion is based on the tacit assumption that the modulus of elasticity of the sand increases in simple proportion to the depth below the dredge line. For loose sand, this assumption is at least approximately correct. For dense sand, the modulus of elasticity seems to increase more nearly with the square root of depth. Hence, if the sheet piles of a bulkhead are driven into dense sand, the conditions of end support will be less favorable than those of the model sheet piles embedded in sand with the same relative density.

The investigations led to the following conclusion, illustrated in Fig. 13. For very stiff bulkheads, the maximum bending moment M in the sheet piles is practically independent of the flexibility number and is equal to the value $M(\max)$ computed on the assumption of free earth support, Fig. 2(a). However, if ρ exceeds a certain value, the maximum bending moment M decreases with increasing values of ρ and finally approaches a value approximately equal to one third of $M(\max)$. The critical flexibility ρ_c at which the maximum bending moment starts to drop below the value of $M(\max)$ increases with decreasing relative density of the sand, as shown in Fig. 13. The value ρ_c is almost independent of the values of α, β, and $\frac{q}{\gamma H}$ in the range over which these quantities are likely to vary under actual conditions.

The fact illustrated by Fig. 13—that the bending moment in sheet piles decreases with increasing flexibility of the piles—is chiefly the result of the interdependence between the type of deflection of the buried part of the sheet piles and the corresponding distribution of the passive earth pressure. If the sheet piles, with a depth of penetration D, were perfectly rigid and the anchorage unyielding, the buried part of the sheet piles would rotate about the anchor line. The corresponding distribution of the earth pressure would be similar to that shown in Fig. 12(*d*), and the center of the pressure would be located at an elevation of less than $D/3$ above the lower edge of the piles.

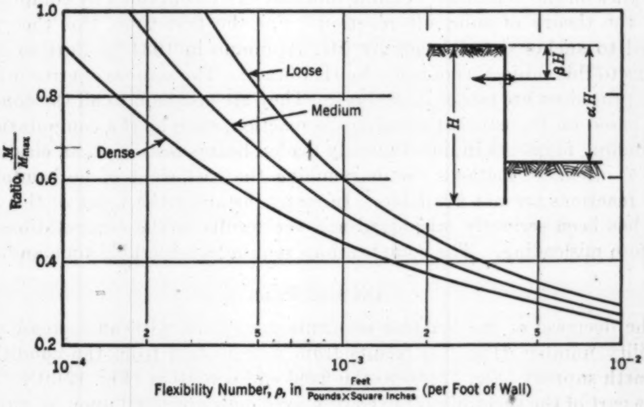

FIG. 13.—RELATION BETWEEN THE FLEXIBILITY NUMBER, ρ, OF SHEET PILES, AND BENDING-MOMENT RATIO, $\frac{M}{M\,(\text{max})}$ (LOGARITHMIC SCALE)

This condition corresponds to the ideal "free earth support." As the flexibility increases, the outward movement of the lower edge of the piles becomes smaller and smaller. The yield assumes the character of a yield by rotation about the lower edge, involving a pressure distribution as shown in Figs. 12(*b*) and 12(*c*). The elevation of the center of the passive pressure increases to more than $D/2$, whereby the "free span"—equal to the distance between anchor line and center of the passive pressure—decreases, and the maximum bending moment decreases with the third power of the span. Finally, if the piles are extremely flexible, the lowest part of the sheet piles will neither advance nor rotate. In other words, the lower ends of the sheet piles will be "fixed" as shown in Fig. 2(*b*).

The critical value ρ_c of the flexibility number increases with increasing compressibility of the soil because the resistance of the soil against tilt and outward movement of the buried part of the sheet piles decreases. This interdependence is illustrated in Figs. 12(*e*) to 12(*g*). If sheet piles are driven into peat (Fig. 12(*e*)), they receive "free earth support" even if they are made of a flexible material such as wood.

If sheet piles are driven into silt or clay, the initial end restraint may be important enough to produce "fixed earth support." However, as time goes on, the soil yields under the lateral pressure because of progressive consolidation. The final lateral displacement of the buried part of the sheet piles can be even greater than that of sheet piles driven into loose sand. The yield is associated with a transition from fixed earth support to free earth support, whereby the maximum bending moment in the sheet piles increases. A permanent fixed earth support for piles driven into a cohesive soil can hardly be expected, unless the soil has been heavily precompressed by overburden pressures that have subsequently been removed by natural processes such as erosion.

Approximate information concerning the influence of the flexibility of sheet piles on the maximum bending moment can be obtained by computation, using the theory of subgrade reaction. For the first time, this theory was applied to anchored bulkheads by Mr. Baumann in 1934.[20] Further contributions to this subject were made by H. Blum.[21] The sources of error involved in the procedure are rather important. They are common to all the computations based on the concept of subgrade reaction, such as the computations of the bending moments in nonuniformly loaded beams resting on an elastic subgrade.[22] Reliable methods for determining the coefficient of horizontal subgrade reactions are not available. In many instances the value of this coefficient has been seriously misjudged and the results of the computations were therefore misleading. The computations require considerable time and labor.

ANCHOR PULL

The decrease of the bending moments associated with an increase of the flexibility number (Fig. 13) results from a transition from the condition of free earth support (Fig. 12(*e*)) to the fixed end condition (Fig. 12(*g*)). If the lowest part of the sheet piles is fixed, the fixed ends are acted upon by moments that carry part of the lateral pressure on the inner face, and as a consequence the anchor pull is reduced.

Mr. Rowe's test results concerning the influence of the flexibility number on the anchor pull are shown in Fig. 14 for a value of $\beta = 0.2$. In Fig. 14, the ordinates represent the measured anchor pull in percentage of the pull corresponding to free earth support. According to the test results, the relieving effect of the fixed end condition depends not only on the relative density of the backfill, as does the bending moment (Fig. 13), but also on the values of the anchor-level ratio β and the free-height ratio α. The investigation also showed that the anchor pull decreases to some extent with increasing yield of the anchorage.

Since Mr. Rowe's data (illustrated in Fig. 13) have been published, there is no longer any justification for assuming fixed earth support without considering flexibility of the sheet piles.

THE SHEARING RESISTANCE OF SOILS AND THE ANGLE OF REPOSE

Whatever the design assumptions may be, the computation of the numerical values of the forces acting upon the bulkhead requires adequate knowledge of the shearing resistance of all the soils involved in the problem.

---

[21] "Beiträge zur Berechnung von Bohlwerken," by H. Blum, W. Ernst and Son, Berlin, Germany, 1951.

[22] "Theoretical Soil Mechanics," by Karl Terzaghi, John Wiley & Sons, Inc., New York, N. Y., 1943, pp. 345–346.

α

In the early days of bulkhead design, it was generally believed that the shearing resistance of a soil was equal to the normal pressure on the potential surface of sliding multiplied by the tangent of the slope angle at which the soil came to rest after it was dumped. This angle was called the angle of repose. For more than twenty years it has been known that there is no relationship between the shearing resistance and the tangent of the angle of repose except for clean, loose, and dust-dry sand. The angle of repose of any other material depends on both the characteristics of the material and the height of the slope. Therefore, it cannot be used as a basis for estimating the shearing resistance of the soil.

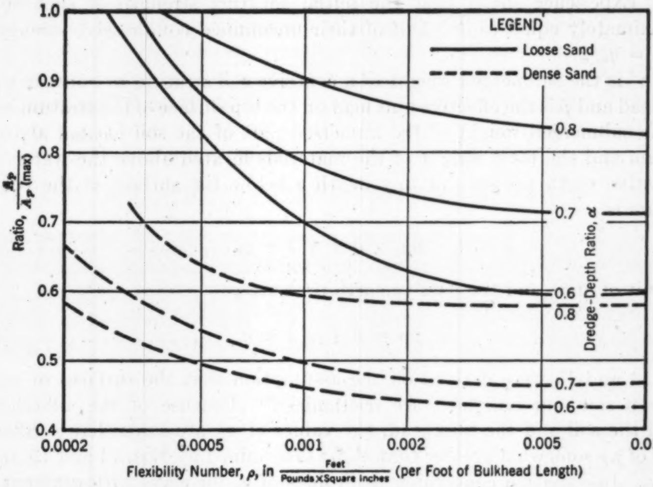

FIG. 14.—RELATION BETWEEN THE FLEXIBILITY NUMBER, ρ OF SHEET PILES, AND ANCHOR-PULL RATIO, $\frac{A_p}{A_p(\max)}$ FOR A β-VALUE OF 0.2

Whatever the characteristics of a soil may be, its shearing resistance can be divided into two components. One of them, commonly known as cohesion, is independent of the pressure, whereas the other one increases with increasing effective pressure $\bar{p}$ on the surface of sliding. The effective pressure $\bar{p}$ is equal to the difference between the total unit pressure p and the pore water pressure p_w. This fundamental relationship can be expressed approximately by the empirical equation:

$$s = c + (p - p_w) \tan \phi \qquad (13)$$

The limits of the validity of this equation are discussed in most references on soil mechanics.

For clean sand, $c = 0$ and $s = (p - p_w) \tan \phi$, in which s is the shearing resistance per unit of area. Cohesive soils, such as silt and clay, are commonly much more compressible than sand, and their permeability is very low. If the load on saturated, cohesive soil is increased—for example, by the deposition of a backfill—the application of the load, p, per unit of area, is associated with an equally important increase of the pore water pressure p_w because the excess water drains out of the loaded soil stratum very slowly. The corresponding increase of the second term on the right-hand side of Eq. 13 becomes equal to zero and, as a consequence, the loaded stratum performs during and immediately after the application of the load as if its angle of internal friction were zero. Experience shows that the initial shearing strength of such soils is approximately equal to one half of their unconfined compressive strength q_u, and $s = q_u/2$.

If γ' is the submerged weight of a cohesive soil stratum in contact with a bulkhead and $\bar{p}$ is the effective unit load on the top surface of the stratum caused by the submerged weight of the immersed part of the soil located above the stratum and the total weight of the materials located above the water table, the active earth pressure at any depth z below the surface of the cohesive stratum is

$$p_A = \bar{p} + \gamma' z - q_u \ldots\ldots\ldots\ldots\ldots\ldots\ldots (14)$$

per unit of area, and the passive earth pressure is

$$p_P = \bar{p} + \gamma' z + q_u \ldots\ldots\ldots\ldots\ldots\ldots\ldots (15)$$

Eqs. 14 and 15 were derived on the assumption that the surfaces of contact between soil and bulkhead are frictionless.[23] Because of the adhesion between the soil and the bulkhead, the values of p_A are somewhat smaller and those of p_P somewhat greater than those determined by Eqs. 14 and 15, respectively. Information concerning the values of q_u for clays with different consistencies is given in Table 1.

TABLE 1.—UNCONFINED COMPRESSIVE STRENGTH OF SILT AND CLAY

Consistency (the drillman's designation)	COMPRESSIVE STRENGTH, q_u, IN TONS PER SQUARE FOOT	
	Minimum	Maximum
Very soft	0	0.25
Soft	0.25	0.50
Medium	0.50	1.00
Stiff	1.00	2.00
Very stiff	2.00	4.00
Hard	4.00	∞

In the course of time, the shearing resistance of cohesive soils, such as silt or clay, increases because of progressive consolidation. Nevertheless, this process is harmful because the consolidation is associated with an increase of the maximum bending moment in the sheet piles, as previously explained under the heading, "Influence of Flexural Rigidity on Bending Moment."

If a cohesive soil, such as fine silt or clay, is deposited under water, consolidation hardly starts during construction. At any depth below the surface, the pore water pressure p_w almost equals the overburden pressure p at that depth, so that $(p - p_w)$ in Eq. 15 equals zero. Since the cohesion c of such backfills is also very small, the lateral earth pressure exerted by such a backfill and its resistance against lateral displacement are at any point equal to the vertical pressure in the fill at that point; hence,

---

[23] "Soil Mechanics in Engineering Practice," by Karl Terzaghi and R. B. Peck, John Wiley & Sons, Inc., New York, N. Y., 1948, pp. 147–150.

$$K_A = K_P = 1.00 \qquad (16)$$

Because of the absence of any definite relationship between the angle of repose and the shearing resistance of soils, reliable information concerning the active and passive earth pressure of the different soils in contact with an anchored bulkhead can be obtained only on the basis of: (1) The results of laboratory tests simulating the conditions under which the soils will be subject to shear in the field, or (2) empirical values derived from the results of tests such as those which will be proposed in Part II of this paper.

II. DESIGN OF ANCHORED BULKHEADS

Uncertainties Involved in the Design of Anchored Bulkheads

The experimental investigations described in Part I have made it possible to eliminate the most serious misconceptions associated with the customary methods of bulkhead design. On the basis of the findings, one can reliably estimate the forces exerted on anchored bulkheads by homogeneous layers of soil with known physical properties. Hence, the uncertainties involved in the design of bulkheads no longer result from inadequate knowledge of the fundamental principles involved. They are caused only by the fact that the structure of natural soil deposits is usually complex, whereas the theories of bulkhead design inevitably presuppose homogeneous materials. Not even the backfills composed of excavated and transported soils can be considered homogeneous. Because of local variations of the soil properties within the borrowpit area and segregation according to grain size during the process of underwater deposition, the characteristics of the backfill may change from place to place and its properties cannot be reliably determined by tests in advance of construction.

Because of these conditions, the most economical and expedient procedure consists in estimating the constants and coefficients—such as the unit weights and the coefficients of earth pressure—on the basis of the results of exploratory borings and of routine tests performed on representative samples, and compensating for the uncertainties involved in this procedure by an adequate margin of safety. More elaborate investigations are justified only in exceptional cases.

General Design Procedure

The design of anchored bulkheads requires several successive operations: (*a*) Evaluation of the forces that act on the inner face of the bulkhead, (*b*) determination of the depth of sheet-pile penetration, (*c*) computation of the maximum bending moments in the sheet piles, (*d*) evaluation of the anchor pull, and (*e*) selection of allowable stresses in the construction materials in accordance with the uncertainties involved in the evaluation of the acting forces.

Each operation is described herein under a separate subheading. The essential data required for performing the operations are obtained by exploratory borings at the site of the bulkhead and in the borrowpit area and by certain routine tests as specified subsequently.

At the site of the bulkhead, the borings must be supplemented by the standard penetration test[24] or an equivalent procedure to obtain information concerning the relative density of the strata of sand or of silty sand that will be in contact with the sheet piles. Drive-samples of the sand are secured, and a mechanical analysis is performed. The results define the general nature of the cohesionless strata. If layers of silt or clay are encountered, fairly undisturbed samples should be recovered and the natural water content, Atterberg limits, and the unconfined compressive strength q_u of these samples should be determined. If possible, the boring operations should be supplemented by field tests with the vane borer. This method of testing was developed in Sweden and it has been extensively used in the United States and in Canada.[25] The value of the natural water content is required for computing the full and the submerged unit weight, γ and γ', respectively, of the materials, and the value of the unconfined compressive stress q_u determines, according to Eqs. 14 and 15, the active and passive earth pressure of clay and silt.

The soils encountered at the bulkhead site and the backfill materials are classified on the basis of the following system: Clean sand (dense, medium,or loose); silty sand (dense, medium, or loose); and silt or clay (hard to very soft, as in Table 1). A sand should be classified as silty, if more than 5% passes the 200-mesh sieve.

Forces Acting on Inner Face of Bulkhead

Varieties of Forces.—Fig. 15 shows diagrammatic sections through bulkheads, ab. The sheet piles are driven into sand (Fig. 15(*a*)) and clay (Fig. 15(*b*)), respectively. Both bulkheads are backfilled with clean sand which has been sluiced into place.

The intensity of the forces acting on the inner face of each bulkhead is represented by the width of the pressure areas, numbered from I to IV on the left-hand side of ab. These forces include the following:

I. Active earth pressure produced by the weight of the backfill;
II. Active earth pressure produced by the uniformly distributed surcharge, q;
III. Unbalanced water pressure (see also Fig. 5); and
IV. Lateral pressure caused by line load q'.

The computation of the intensity of these forces must be preceded by an evaluation of the full and submerged unit weights of the various soils in contact with the inner face and of their coefficients of active earth pressure. In each figure the symbol $\overline{p}$ with subscripts indicates the effective vertical unit pressure on the different horizontal sections through the soil.

The active earth pressure exerted by the backfill depends on the coefficient of active earth pressure K_A of the fill material and on its effective unit weight.

---

[24] "Soil Mechanics in Engineering Practice," by Karl Terzaghi and R. B. Peck, John Wiley & Sons, Inc., 1948, p. 265.

[25] "The Vane Borer," by L. Cadling and S. Odenstad, *Proceedings*, Royal Swedish Geotechnical Inst., No. 2, 1950; Stockholm, Sweden.

It may be increased temporarily or permanently by a uniformly distributed surcharge, by line loads, or by mobile or stationary concentrated loads.

Unit Weights.—The effective unit weight depends on the position of the soil with reference to the water table. Above the water table, it is equal to the sum of the dry weight of the soil and the weight of the water contained in the voids (moist unit weight). Below the water table it is equal to the submerged weight of the soil particles. Limiting values for the moist and the submerged unit weights for cohesionless soils are given in Table 2. In the computation of the active earth pressure, the upper limiting values should be used unless the real unit weights have been estimated on the basis of test results. The unit weight of cohesive soils is determined by their natural water content *w*, and it can be computed by use of the equations given in Table 2.

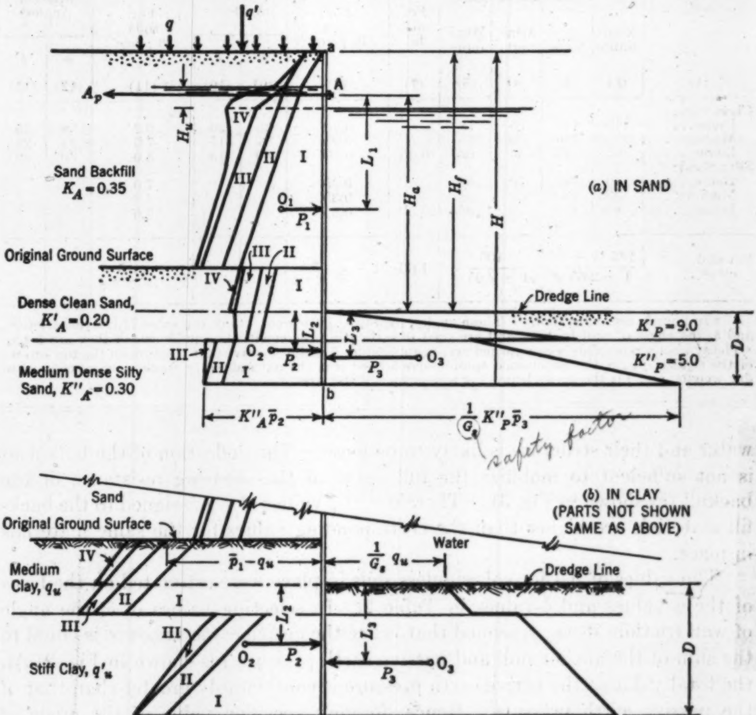
q'
q
a
A
A_p
H_u
IV
II
I
III
Sand Backfill
$K_A = 0.35$
L_1
H_a
H_f
H
(a) IN SAND
O_1
P_1
Original Ground Surface
III
II
IV
I
Dense Clean Sand,
$K'_A = 0.20$
Dredge Line
$K'_p = 9.0$
L_2
L_3
D
III
O_2
P_2
P_3
O_3
$K''_p = 5.0$
Medium Dense Silty Sand, $K''_A = 0.30$
II
I
b
$K''_A \bar{p}_2$
$\frac{1}{G_s} K''_p \bar{p}_3$
safety factor
Sand
(b) IN CLAY
(PARTS NOT SHOWN
SAME AS ABOVE)
Original Ground Surface
Water
$\bar{p}_1 - q_u$
$\frac{1}{G_s} q_u$
Medium Clay, q_u
Dredge Line
IV
II
I
III
L_2
L_3
D
III
O_2
P_2
O_3
P_3
Stiff Clay, q'_u
II
I
b
$\bar{p}_2 - q'_u$
$\bar{p}_3 + \frac{1}{G_s} q'_u$

FIG. 15.—FORCES ACTING ON BULKHEADS CONSISTING OF SHEET PILES DRIVEN INTO SAND AND INTO CLAY

Coefficients of Active Earth Pressure.—Design values for the coefficient of active earth pressure are in Table 2. The backfills are usually deposited under-

TABLE 2.—UNIT WEIGHTS OF SOILS, AND COEFFICIENTS OF EARTH PRESSURE

Type of soil	UNIT WEIGHT[a] OF MOIST SOIL, γ		UNIT WEIGHT[a] OF SUBMERGED SOIL, γ'		COEFFICIENT OF ACTIVE EARTH PRESSURE, K_A				COEFFICIENT OF PASSIVE EARTH PRESSURE, K_P		
	Minimum	Maximum	Minimum	Maximum	For backfill	For soils in place	Friction Angles[b]		For soils in place	Friction Angles[b]	
							ϕ	δ		ϕ	δ
(1)	(2)	(3)	(4)	(5)	(7)	(8)	(9)	(10)	(11)	(12)	(13)
Clean Sand:											
Dense......	110	140	65	78		0.20	38	20	9.0	38	25
Medium....	110	130	60	68		0.25	34	17	7.0	34	23
Loose......	90	125	56	63	0.35	0.30	30	15	5.0	30	20
Silty Sand:											
Dense......	110	150	70	88		0.25			7.0		
Medium....	95	130	60	68		0.30			5.0		
Loose......	80	125	50	63	0.50	0.35			3.0		
Silt and clay[c].......	$\frac{165\,(1+w)}{1+2.65\,w}$		$\frac{103}{1+2.65\,w}$		1.00	$1-\frac{q_u}{\overline{p}+\gamma\,\overline{z}}$			$1+\frac{q_u}{\overline{p}+\gamma\,\overline{z}}$		

[a] In pounds per cubic foot. These angles, expressed in degrees, are ϕ, the angle of internal friction, and δ, the angle of wall friction, and are used in estimating the coefficients under which they are listed. [c] The symbol γ represents γ or γ', whichever is applicable; $\overline{p}$ is the effective unit pressure on the top surface of the stratum; q_u is the unconfined compressive stress; w is the natural water content, in percentage of dry weight; and z is the depth below the top surface of the stratum.

water and their structure is likely to be loose. The deflection of the bulkhead is not sufficient to mobilize the full value of the shearing resistance of the backfill (as shown in Fig. 3). Therefore, the values of K_A assigned to the backfill materials are higher than the corresponding values for the same materials in place.

The values of K_A for cohesionless soils in place were estimated on the basis of the ϕ-values and δ-values in Table 2. In selecting values of δ, the angle of wall friction, it was reasoned that, since the active earth pressure is equal to the sum of the anchor pull and passive earth pressure (as shown in Fig. 2(*a*)), the total value of the active earth pressure is considerably greater than that of the passive earth pressure. Hence, for any specified value of the angle of wall friction, the resultant of the friction forces would tend to pull the sheet piles down. If the lower edge of the sheet piles were rigidly supported, the resultant would be carried by this rigid support. In reality, the resistance against a downward movement of the lower edge of the sheet piles is small. Therefore, the sheet piles will settle so that the total wall friction on the inner face will decrease until it becomes nearly equal to the friction force on the outer face. Because of this condition, the angle of wall friction for the active pressure was assigned smaller values than that for the passive earth pressure.

The K_A-value for dense sand can be much lower than the value of 0.2 given in Table 2, but this is only a possibility because the value of K_A depends, to a large extent, on the uniformity of the sand and the shape of the grains.[3] Therefore, the use of a lower value would be justified only if it has been computed on the basis of test results on representative samples.

Silty sand has been assigned greater K_A-values than clean sand with equal relative density because its angle of internal friction is likely to be smaller and its compressibility higher than that of clean sand with equal relative density. Furthermore, the evaluation of the relative density of silty sands by use of the standard penetration test appears to be much less reliable than that of clean sands. The K_A-values for silt and clay are represented in Table 2 by an equation that gives results which are on the safe side because the pressure reducing effect of the adhesion between soil and sheet piles has been disregarded.

Uniformly Distributed Surcharge.—The lateral unit pressure resulting from a uniformly distributed surcharge, q, per unit of area, is at any depth equal to q times the value of K_A for that depth (area II in Fig. 15).

Unbalanced Water Pressure.—The first step in studying the unbalanced water pressure is to estimate the greatest hydraulic head, H_w, in Fig. 5(*a*), which can be anticipated at the site of the bulkhead. This can be done on the basis of regional hydrographic data such as local tidal curves or flood records. If the coefficient of permeability of all the soils in contact with the bulkhead is of the same order of magnitude, the unbalanced water pressure associated with a head H_w can be estimated on the basis of the assumption represented by the broken line cde in Fig. 5(*b*). Area III in Fig. 15(*a*) has been plotted on this assumption. Otherwise, the effects of stratification on the distribution of the unbalanced water pressure must be considered. In any event, precautions must be taken to prevent the unbalanced water pressure from exceeding the estimated value even under exceptional conditions such as an outgoing spring tide combined with a heavy rainstorm. This may, for example, be accomplished by adequate surface drainage.

If the bulkhead is backfilled with a material—such as silt or soft clay—which does not begin to consolidate during construction, the initial water table in the backfill is located at the surface of the backfill. The coefficient of active earth pressure of such materials is equal to unity (Table 2). Therefore, the total lateral pressure of the backfill, earth and water pressure combined, is equal to the fluid pressure of a liquid the unit weight of which is equal to that of the saturated backfill material.

Line and Point Loads.—Line loads and point loads can be established only on the surface of backfills with adequate bearing capacity. Otherwise the loads must be carried by piles, and pile-supported loads have no influence on the lateral pressure.

Line loads are stationary, and the lateral pressure resulting from the loads is determined by Eqs. 4 and 5. Point loads are either stationary or mobile. The wheel loads of cranes that can be displaced on rails along the waterfront constitute mobile point loads. The unit pressures produced by a point load along the line of intersection ab (Fig. 7(*a*)) between the bulkhead and a vertical plane through the load at right angles to the bulkhead are determined by Eqs. 9 and 10. A mobile point load may occupy any position on the line along which it travels. Hence, every sheet pile may be acted upon by these pressures. However, if the point load is stationary, the unit pressures produced by the load decrease on both sides of the line ab, as shown in Fig. 7(*a*). Upper limiting values for these pressures are obtained by use of Eq. 11 (Fig. 8(*b*)).

V119 54 UMI

Figs. 6(*a*) and 8(*a*) show that the computed unit pressures on the lower part of the lateral supports are consistently greater than the real pressures. As a partial compensation for this difference, it should be assumed that the lateral pressure produced by line loads and point loads decreases, at the dredge line, to zero. Hence, in Eqs. 4, 5, 9, and 10, the value H should be made equal to the vertical distance H_f between the dredge line and the surface of the backfill. In Fig. 15 the lateral pressure caused by point loads or line loads is represented by area IV.

Depth of Sheet-Pile Penetration

Factors Determining Penetration Depth.—The investigations of Mr. Rowe have shown that no tangible benefits can be obtained by driving the sheet piles deeper than the depth required to assure an adequate margin of safety with respect to a failure resulting from an outward movement of the buried part of the sheet piles, and a sufficiently small horizontal displacement of the lower edge of the sheet piles.[19]

The resistance of a cohesionless soil against an outward movement of the buried part of the sheet pile depends on its effective unit weight and on the coefficient of passive earth pressure. The resistance of a cohesive soil such as silt or clay depends only on its unconfined compressive strength.

Unit Weights.—Because the passive earth pressure of a cohesionless soil decreases with decreasing unit weight, the computations should be made on the basis of the lower limiting values in Table 2, unless more accurate values have been obtained by tests on representative samples. Should the water table in the backfill be temporarily located above the free water level, as in Fig. 5(*a*), the reduction of the effective unit weight resulting from the seepage pressure associated with upward percolation through the soil in contact with the outer face of the bulkhead must be considered. If the coefficient of permeability of all the soils in contact with the bulkhead is of the same order of magnitude, the effective unit weight of the soil acted upon by the seepage pressure can be estimated by use of Eq. 3. Otherwise, an appropriate value for the hydraulic gradient i in equation Eq. 2 must be selected on the basis of the soil profile. In many instances the gradient i is too small to require any consideration.

Coefficients of Passive Earth Pressure.—Lower limiting values for the coefficients of passive earth pressure are in Col. 11, Table 2. The values of ϕ and δ used in the estimates of K_P-values for clean sand (Fig. 4) are in Cols. 12 and 13. The K_P-value for a well-graded dense sand or a mixture of sand and gravel can be almost twice as high as the tabulated value for dense sand. This, however, is only a possibility. Hence, higher values should be tolerated only if they are based on test results.

In the rare event that the buried part of an anchored bulkhead derives its lateral support from a sand fill, the sand can be assigned a K_P-value of 3.

Silty sand has been assigned smaller K_P-values than clean sand with equal relative density. This was done because of the conditions previously explained (under the heading, "Forces Acting on Inner Face of Bulkhead: Coefficients of Active Earth Pressure"). Very loose, silty sand cannot be expected to provide adequate lateral support for the buried part of sheet piles because of its high compressibility.

If the surface of the soil constituting the lateral support of the buried part of the bulkhead is not horizontal, the passive earth pressure must be determined by a graphical procedure on the basis of the ϕ-values and δ-values in Table 2. Since the assumption of a plane surface of sliding may involve important errors on the unsafe side (Fig. 4(*b*)), the logarithmic spiral method should be used.[26]

COMPUTATION OF DEPTH OF SHEET-PILE PENETRATION

The general principles in the computation of penetration depth are illustrated in Fig. 15. The area on the left-hand side of the bulkhead, ab, represents the active pressures on the inner face, and the area on the right-hand side represents the passive earth pressures, plotted on the assumption of free earth support.

The actual distribution of the passive earth pressure under conditions of free earth support (Fig. 12(*a*)) is approximately trapezoidal. However, the assumption of a trapezoidal distribution would complicate the computations considerably except in the rare event of a bulkhead with sheet piles driven into homogeneous ground. Therefore, the Coulomb concept is retained. In accordance with this concept, the passive earth pressure of homogeneous material increases in a manner similar to hydrostatic pressure (in simple proportion to the depth below the surface). The error resulting from this simplifying assumption is unimportant and on the safe side.

In order to provide for an adequate margin of safety with respect to a failure of the lateral earth support of the buried part of the sheet piles, the pressure areas on the right-hand side of line ab in Fig. 15(*a*) are constructed on the assumption that the coefficient of passive earth pressure is equal to the K_P-values in Table 2, divided by a safety factor G_s. If the sheet piles are driven into silt or clay, as in Fig. 15(*b*), the safety requirements are satisfied by assigning to the soil in contact with the outer face of the bulkhead a reduced unconfined compressive strength, $\frac{1}{G_s} q_u$. The conditions requiring consideration in the choice of G_s will be discussed, subsequently, under the heading, "Safety Requirements."

In Fig. 15, points O_1, O_2, and O_3 represent the centers of gravity of the pressure areas above the dredge line (O_1), and below the dredge line on the active side (O_2) and passive side (O_3) of the bulkhead. The total pressures represented by these areas are P_1, P_2, and P_3. The position of their lines of action are defined by the distances L_1, L_2, and L_3. The values of L_1 and P_1 are independent of the depth D of sheet-pile penetration. The depth D must satisfy the condition that the sum of all the moments about the anchor point A is equal to zero,

$$P_1 L_1 + P_2(H_a + L_2) = P_3(H_a + L_3) \qquad (17)$$

---

[26] "Theoretical Soil Mechanics," by Karl Terzaghi, John Wiley & Sons, Inc., New York, N. Y., 1943, pp. 100–113.

If the values of P_2, P_3, L_2, and L_3 are expressed in terms of the unknown quantity D, an equation of the third degree is obtained which can be solved for D.

Computation of Maximum Bending Moments

Free Earth Support.—If the profile of the soil into which the sheet piles will be driven is erratic or if no reliable data concerning the details of the soil profile are available, the maximum bending moment in the sheet piles should be computed on the assumption of free earth support. The acting forces are shown in Fig. 15(*a*) for bulkheads with lateral sand support and in Fig. 15(*b*) for bulkheads with clay support. The maximum bending moment can be determined by analytical or graphical methods in the usual manner.

Mr. Tschebotarioff has suggested computation of the maximum bending moment in the sheet piles on the assumption of fixed earth support irrespective of flexibility and of the relative density of the sand into which the sheet piles are driven.[18] Mr. Rowe showed that the errors involved in such a procedure can be very important and they are on the unsafe side.[19] Moment reduction caused by partly or completely fixed earth support can only be expected under the conditions to be described subsequently.

Moment Reduction Resulting from Flexibility Effects.—If the sheet piles are to be driven into a fairly homogeneous stratum of clean sand with known relative density, the maximum bending moment for free earth support can be reduced on the basis of the results of Mr. Rowe's investigations that are represented in Fig. 13. As an example, the reduction of the bending moments in sheet piles driven into sand with medium density will be considered.

The first step consists of computing the maximum bending moments for free earth support, M(max), and of the cross section of the piles required to withstand M(max). The conditions that must be considered in choosing the allowable fiber stresses f will be discussed subsequently (under the heading, "Safety Requirements"). The flexibility number ρ_1 of these piles is determined by Eq. 12.

At a specified value of M(max) the moment of inertia I and the corresponding flexibility number ρ_1 depend on the value assigned to the allowable fiber stresses and on the construction material. Hence, at a specified value of M(max), very different values of ρ_1 may be obtained, such as ρ_{1t} for timber piles, ρ_{1s} for steel piles, and ρ_{1c} for reinforced concrete piles.

The next step consists in plotting the moment-reduction curve, which is shown as the heavy curve in Fig. 16. This curve is obtained by multiplying the ordinates of the curve for sand with medium density in the Rowe diagram (Fig. 13) by M(max). The abscissa ρ_c of point C at which the curve starts to descend represents the critical flexibility number. If the flexibility number of the pile required by M(max) is smaller than ρ_c, the maximum bending moment in this pile is determined by the condition of free earth support and is equal to M(max).

In Fig. 16 the sheet piles with flexibility numbers ρ_1, such as ρ_{1t}, ρ_{1s}, and ρ_{1c}, are represented by points S. At a given value of M(max), the flexibility number of timber sheet piles with the required moment of inertia has the greatest value—designated as point S(timber)—and that of reinforced concrete piles the smallest value—designated as point S(concrete). Point S(steel), representing steel sheet piles, occupies an intermediate position.

If point S is located on the left-hand side of C, no moment reduction can be tolerated. A position of point S on the right-hand side of C indicates that the pile represented by the point is stronger than necessary because the maximum bending moment in the pile M_1 will be less than M(max). In order to select a more economical profile for the sheet piles, the allowable bending moments M', M'', $\cdots$ and the corresponding flexibility numbers ρ', ρ'', $\cdots$ for various weaker profiles are computed. In Fig. 16 these weaker sheet piles are represented by points such as S′(steel) with the ordinate M' and the abscissa log ρ'. All these points are located in proximity of a curve that intersects the moment-reduction curve at N, with abscissa log ρ_a and ordinate M_a. The corresponding moment reduction is $M(\max) - M_a$. However, because of the rudimentary state of present (1953) knowledge of the performance of bulkheads under field conditions, the computed bending moment M(max) should be reduced by not more than $\frac{1}{2}(M(\max) - M_a)$.

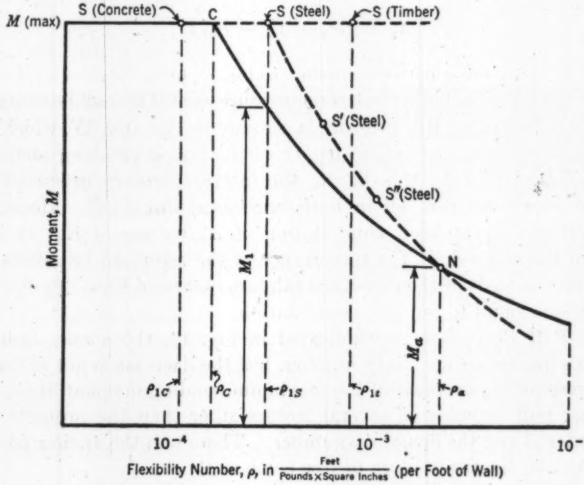

FIG. 16.—GRAPHIC PROCEDURE FOR DETERMINING TOLERABLE MOMENT REDUCTION

If the sheet piles are to be driven into a homogeneous stratum of dense or medium silty sand, Mr. Rowe's moment-reduction curves for medium and loose sand should be used instead of those for dense and medium sand. Sheet piles to be driven into loose, silty sand should be dimensioned for free earth support because the compressibility of such sands may be very high.

Sheet Piles Driven into Silt or Clay.—In Part I it was shown that the initial earth support for sheet piles driven into silt or clay is likely to be fixed. However, as time elapses, the end restraint decreases because of progressive consolidation of the soil resisting the lateral pressure of the buried part of the bulkhead. As the present (1953) state of knowledge concerning the effect of the progressive yield on the end restraint is limited, no moment reduction should be tolerated. The fundamental principles of the procedure have been explained in Part I.

ANCHOR PULL

Anchor Pull for Free Earth Support.—The anchor pull A_p for free earth support is determined by the condition that the sum of all the horizontal forces that act on the bulkhead (Fig. 15) is equal to zero:

$$A_p = (P_1 + P_2 - P_3)\, l \quad\dots\dots\dots\dots\dots\dots\dots (18)$$

in which l is the spacing between anchor rods.

The force P_1 also includes the lateral pressure caused by mobile or stationary point loads. In Fig. 15 this pressure is represented by area IV, which is equal to the lateral pressure per unit of length of the bulkhead along section ab in Fig. 7(*a*). According to this figure, the lateral pressure produced by the point load decreases from ab in both horizontal directions. Hence, if the backfill carries a point load, computation of A_p by use of Eq. 18 involves an error on the safe side. The importance of the error can be estimated and corrected on the basis of the experimental data shown in Figs. 7 and 8. Usually the error is too small to require consideration.

Anchor-Pull Reduction.—As indicated in Fig. 14, the anchor pull A_p decreases with increasing flexibility number, but the decrease is not as important as the corresponding decrease of the maximum bending moment M_1 in Fig. 13. The anchor pull depends on several factors other than the properties of the backfill material and the flexibility number. Therefore, the anchor pull should be computed on the assumption of free earth support.

SAFETY REQUIREMENTS

General Considerations.—The importance of the error involved in estimating the forces which act on the inner face of a bulkhead depends to a large extent on the degree of uniformity of the fill material, the complexity of the soil profile, and the amount of information which can be, or has been, secured concerning the significant soil properties. Therefore, it would be uneconomical to establish a rigid code concerning the safety factors and the allowable stresses. Designers who are not thoroughly familiar with the principles and techniques of soil mechanics are advised to consider only free earth support and to use large safety factors.

Passive Earth Pressure.—The safety factor G_s (Fig. 15(*a*)), with respect to a failure of the lateral earth support of piles driven into clean or silty sand, should be assigned a value between 2 and 3, depending on the accuracy with which the active earth pressure on the inner face of the bulkhead can be estimated.

If the earth support is derived from silt or clay, the limiting values for G_s (as shown in Fig. 15(*b*)) can be reduced to 1.5 and 2.0 because the K_P-value defined by Eq. 15 is on the safe side.

Whatever the subsoil conditions may be, the computed depth of sheet-pile penetration should always be increased by 20% as insurance against the effects of unintentional excess dredging, unanticipated local scour, and the presence of pockets of exceptionally weak material in the zone of passive earth pressure which have not been revealed in the borings. The corresponding increase of the cost of the bulkhead is small as compared to the increase of the margin of safety for all parts of the bulkhead associated with the excess penetration. The bending moments in the sheet piles and the anchor pull should be determined on the basis of the computed depth—and not of the increased depth—of sheet-pile penetration.

Allowable Fiber Stresses in Sheet Piles.—The maximum bending stresses f in the sheet piles of anchored steel bulkheads backfilled with clean sand can be made equal to at least two thirds of the yield point stress f_y. This recommendation also applies to dredge bulkheads supporting clean sand in place. If the backfill consists of hydraulically excavated, silty sand or a mixture of clean and silty sand, the real value of the coefficient of earth pressure can locally be considerably higher than the values given in Table 2 for silty sand because of the inevitable segregation of fine and coarse material during the process of deposition. Therefore, the fiber stress in the sheet piles of steel bulkheads backfilled with such materials should be assigned a value of not more than two thirds of the yield point. However, if a bulkhead is to be backfilled with hydraulically excavated clay or silt to which a coefficient of active earth pressure equal to unity is assigned, the sheet piles can safely be dimensioned on the basis of $f = f_y$ because the real lateral earth pressure cannot be greater than that which is computed.

The extreme fiber stresses in sheet piles having locks on the neutral axis depend largely on lock friction. Little information is available (1953) concerning the values that can safely be assigned to the lock friction in straight rows of sheet piles. Hence, it is advisable that such sheet piles be dimensioned on the assumption that the locks are lubricated. The flexibility number should be computed on the same basis. At a given value of M(max), the flexibility number for sheet piles dimensioned on the assumption of lubricated locks is considerably greater than the corresponding number for piles with "frozen locks." Therefore, a decrease of the friction in the interlocks can be associated with a decrease of the maximum bending moment in the sheet piles.

The allowable stresses for construction materials other than steel should be selected on the basis of the considerations that have been set forth for steel.

Allowable Stress in Anchor Rods.—Eq. 18, which is used for computing the anchor pull, involves the assumption that the distribution of the active earth pressure on the inner face is in accordance with the Coulomb theory. The real distribution may be somewhat different—as shown in Figs. 11 and 12—and the corresponding anchor pull may be greater than the computed anchor pull. Furthermore, if the uppermost part of the sheet piles is in contact with a soil having low compressibility and the lower part moves out (for example, because of progressive consolidation of the soil that provides the lateral earth support), the anchor pull increases. The anchor pull may also increase because of repeated application and removal of heavy surcharges. Finally, an unequal yield of adjacent anchorages produces an increase in the pull in some anchor rods, associated with a decrease in others. Because of these possibilities, the anchor rods should be dimensioned on the basis of more conservative allowable stresses than are applied to the design of sheet piles.

Supplementary Safety Provisions.—The first and foremost requirement for the success of a bulkhead project is avoiding, during construction, loading conditions which the designer has not anticipated. This vital aspect of the bulkhead problem has been investigated by J. R. Ayers, M.ASCE, and R. C. Stokes.[27] In addition to providing for an adequate margin of safety in the design and for protection of the construction materials against deterioration, it is also necessary to protect the bulkhead against the consequences of processes and events beyond the scope of theory.

If a bulkhead is at the seashore or at the bank of a swiftly flowing river, consideration should be given to the possibility that the scour along the foot of the exposed part of the outer face of the sheet piles may increase considerably the free height of the bulkhead, H_f (Fig. 15). The upper limiting value for the increase of H_f should be estimated on the basis of experience with local scouring action.

After the sheet piles for a fill bulkhead with submerged outer face are driven, a careful inspection should be made of the condition of the locks or joints. If gaps between adjacent sheet-piles are found, they should be plugged by divers. A case of important loss of soil caused by a flow of sand through gaps between sheet piles was reported by J. C. Gebhard.[28]

If the backfill material is very compressible or if the subsoil of the backfill contains layers of soft silt or clay, it is necessary to encase the anchor rods in large conduits with a circular or rectangular cross section that can follow the downward movement of the backfill without transmitting vertical forces onto the anchor rods. As an alternative, the rods could be supported at several points by piles, but then allowance must be made for the stresses in the tie rods caused by the earth load which acts on the rods between the points of support. On Pier C at Long Beach, it was found that the anchor rods embedded in the backfill carried a large part of the weight of the backfill lying above the level of the anchor line. This load increased considerably the tension in the rods.[29]

Bulkhead Failures.—All the bulkhead failures that have come to the writer's attention can be attributed to one of two causes. The designer has estimated earth pressure and earth resistance on the basis of the "angle-of-repose" concept, or else he has failed to notice a source of weakness in the ground below the level of the lower edge of the sheet piles.

It is known that there is no relationship between the angle of repose of a soil and its angle of internal friction except in the case of loose and dust-dry sand. Nevertheless, several bulkhead computations have been made in which soft clay was assigned an angle of internal friction of 11°, on the strength of the observation that the front part of a sheet of hydraulic-fill clay commonly has a slope approximating one on five. The bulkheads to which these computations referred have failed.

---

[27] "The Design of Flexible Bulkheads," by J. R. Ayers and R. C. Stokes, *Transactions*, ASCE, Vol. 119, 1954, p. 373.

[28] "Cave-Ins of Sandy Backfills," by J. C. Gebhard, *ibid.*, Vol. 114, 1949, pp. 490–498.

[29] "Field Study of a Sheet-Pile Bulkhead," by C. Martin Duke, *ibid.*, Vol. 118, 1953, p. 1131.

Some bulkheads with sheet piles driven into sand have failed because of an outward movement of both bulkhead and fill on a soft clay stratum beneath the sand. The design of the bulkheads and of the anchorage was satisfactory, but the designers failed to take heed of the subsoil of the stratum that provided the lateral support for the buried part of the sheet piles.

If the submerged natural earth in front of a bulkhead slopes downward in an offshore direction, the slope may fail along a surface of sliding located below the anchor and the lower edge of the sheet piles. Several bulkhead failures of this kind have occurred on the Whangpoo River at Shanghai, China. The subsoil consisted of river silt, the offshore slope was about one on two, and most of the failures occurred within two hours after low tide following spring tide.

At the present state of knowledge of the physical properties of soils (1953), all the aforementioned bulkhead failures could have been avoided by proper consideration of the results of exploratory borings and of a few identification tests on representative samples of the earth materials involved.

CONCLUSIONS

1. Since the time (1910 to 1930) when the current procedures (1953) for bulkhead computations originated, knowledge of the physical properties of earth materials and of the mechanics of earth pressure has increased vastly; yet the procedures remained practically unaltered. This paper contains suggestions for revisions on the basis of the experimental and observational data which have been secured during the last few decades.

2. Many bulkheads have been designed without adequate information concerning the relative density of the sand layers and the shearing strength of clay strata in contact with the bulkheads. Bulkheads designed in such a manner can be badly overdimensioned or they may be unsafe, depending on factors unknown to the designers. One of the most common causes of faulty design is the erroneous assumption that the shearing resistance of cohesive soils can be evaluated on the basis of an angle of repose.

3. The importance of the errors involved in the estimate of the soil constants appearing in the equations depends to a large extent on the complexity of the structure of the strata into which the sheet piles are driven, on the degree of uniformity of the material in the borrowpit area, and on the quality of the subsoil exploration. Therefore, it would be unwarranted to establish rigid rules for the factors of safety that should be used. One of the responsibilities of the designer is to evaluate the prevailing uncertainties and to choose the factors in accordance with his findings. Limiting values are proposed in this paper.

4. No bulkhead theory can possibly anticipate all the varieties of subsoil and hydraulic conditions that may be encountered in practice, and every case requires a certain amount of independent judgment. Hence, if the subsoil conditions do not conform to a standard pattern, designers who are not thoroughly familiar with the basic principles and techniques of soil mecahnics are advised to assume free earth support and to use conservative factors of safety. When solving unusual problems, the designer should consult the observational data (summarized in Part I) on which the design procedures are based.

ACKNOWLEDGMENTS

The writer expresses his thanks to A. E. Cummings, M. ASCE, S.D. Wilson, A.M. ASCE, and S. B. Avery, Jr., for valuable comments and suggestions. He is also indebted to Mr. Rowe who kindly placed at his disposal copies of the original records of various tests.

APPENDIX. NOTATION

The following letter symbols conform essentially with ASCE *Manual of Engineering Practice No. 22* ("Soil Mechanics Nomenclature") and American Standard Letter Symbols for Structural Analysis (ASA Z10.8—1949) prepared by a Committee of the American Standards Association, with ASCE participation, and approved by the Association in 1949:

A_p = anchor pull;
D = depth of sheet-pile penetration;
d = the ratio of deflection to the height of a wall;
E = the modulus of elasticity;
f = the allowable stress in bending of the piles;
f_y = the yield point;
G_s = the factor of safety;
H = the height of a lateral support, total length of sheet piles;
H_a = the vertical distance from the anchor to the dredge line;
H_f = the vertical distance between the dredge line and the surface of the backfill;
H_u = the vertical distance between the free water level and the water table in the backfill;
I = the moment of inertia of the cross section of a sheet pile;
i = the hydraulic gradient;
K_0 = the pressure coefficient for earth at rest;
K_A = the coefficient of active earth pressure (the ratio between the normal component of the earth pressure on the lateral support and the corresponding fluid pressure);
K_P = the coefficient of passive earth pressure;
L_1, L_2, and L_3 = the vertical distances from centers of pressure;
l = the anchor spacing;
M = the maximum bending moment in a sheet pile:
    M(max) = the maximum bending moment in a sheet pile computed on the assumption of free earth support;
    M' = the allowable bending moment for a sheet pile with a given flexibility number;
    M_a = the maximum bending moment in a sheet pile with flexibility number ρ_a;
    M_1 = the maximum bending moment in a sheet pile with a given flexibility number;

m = the ratio between the horizontal distance from the wall to the height of the wall;

n = the ratio between the depth below the surface of the backfill and the height of the wall;

P = the total normal pressure on a lateral support produced by a point load;

P_u = the unbalanced water pressure;

p = the unit pressure:

- p' = the horizontal pressure produced by a line load per unit of wall length;
- $\overline{p}$ = the effective unit pressure;
- p_A = intensity of active earth pressure;
- p_P = intensity of passive earth pressure;
- p_w = pore water pressure;
- p_1 = the horizontal unit pressure produced by a point load along the intersection between the inner face of a wall and a vertical section through the point load, perpendicular to the wall;

Q = a point load;

q = a uniformly distributed surcharge, per unit of area:

- q' = a unit line load;
- q_u = the unconfined compressive strength of cohesive soil;

s = the shearing resistance, per unit of area;

w = the natural water content, in percentage of the dry weight;

$x, y, z,$ = the variable distances in the directions X, Y, and Z;

α = the ratio between the depth of the dredge line below the surface of the backfill and the length of the sheet piles;

β = the ratio between the depth of the anchor line below the surface of the backfill and the length of the sheet piles;

γ = the unit weight of a soil including the weight of water contained in its voids:

- γ' = the submerged unit weight;
- $\overline{\gamma}$ = the effective unit weight of silt or clay (the saturated unit weight above the water table and the submerged unit weight below the water table);
- $\Delta\gamma'$ = the reduction in the submerged unit weight resulting from seepage pressure exerted by rising ground water;
- $\Delta\gamma''$ = the increase in the effective unit weight;
- γ_w = the unit weight of water;

δ = the angle of wall friction;

μ = the Poisson ratio;

ρ = the flexibility number;

ρ_a = the flexibility number corresponding to the point of intersection N in Fig. 16.

ρ_c = the critical flexibility number at which M becomes smaller than M(max);

σ = the normal stress;

σ_x = the horizontal unit pressure;

ϕ = the angle of internal friction;

ϕ' = the angle of partly mobilized internal friction; and

ψ = an angle defined by Fig. 8(*b*).

DISCUSSION

T. H. WU,[30] **J. M. ASCE.**—In his comprehensive treatment of the subject of bulkheads, Mr. Terzaghi has drawn extensively from the results of field measurements and large-scale model tests. The writer takes this opportunity to correlate the author's data with the results of some measurements made on the bracings of an open cut for a depressed trainway in El Paso, Tex. This bracing system was essentially an anchored bulkhead.

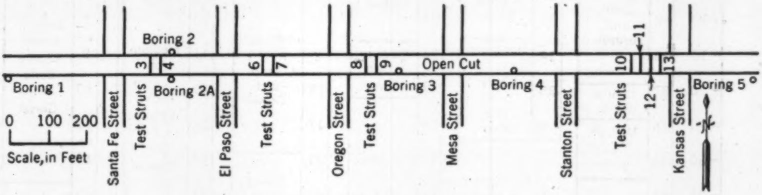
Boring 1
Boring 2
Boring 2A
Boring 3
Boring 4
Boring 5
Open Cut
3
4
6
7
8
9
10
11
12
13
Santa Fe Street
Test Struts
El Paso Street
Test Struts
Oregon Street
Test Struts
Mesa Street
Stanton Street
Test Struts
Kansas Street
0 100 200
Scale, in Feet
N

FIG. 17.—PLAN VIEW OF OPEN CUT

The open cut was 25 ft deep, and the bracing system consisted of a sheet-pile wall on each side of the cut supported at the top by continuous horizontal wales and cross struts. Fig. 17 shows the general layout of the open cut, and Fig. 18 shows the details of the bracing system.

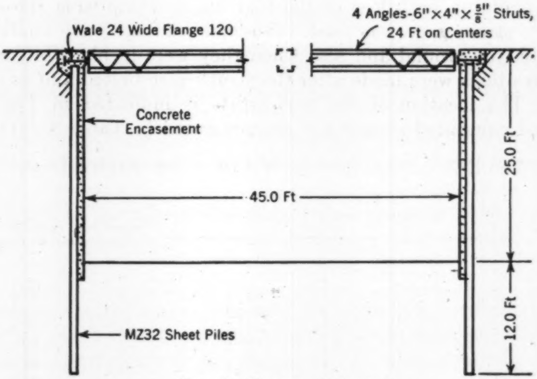
Wale 24 Wide Flange 120
4 Angles-6"×4"×5/8" Struts, 24 Ft on Centers
Concrete Encasement
45.0 Ft
25.0 Ft
12.0 Ft
MZ32 Sheet Piles

FIG. 18.—BRACING SYSTEM

The subsoil at the site was primarily sandy clay, coarse and medium sand, and gravel. The results of six borings are presented in Fig. 19. The values given in Fig. 19 in the columns under the letter "N" represent the number of blows per foot of penetration obtained by the standard penetration test.[24] In general the material west of Oregon St. was of medium density to a depth of

---

[30] Asst. Prof. of Civ. Eng., Michigan State College, East Lansing, Mich.

25 ft, and the standard penetration test resulted in 30 blows per ft. East of Oregon St. the material passed into the loose state, and the average number of blows was approximately 10. Below 25 ft the sand was dense; however, the average number of blows varied considerably.

The first step in the construction procedure was to drive the sheet piles and to excavate to a depth of 12 ft below ground level. The struts and wales were installed, and the cut was excavated to its final depth. Strain measurements were made on both legs of the four angles comprising the strut. An 8-in. portable strain gage was used. No-load readings were made when the struts were on the ground and also when they were in place but not bolted; subsequent readings were made after the struts were bolted and as excavation progressed. The location of the test struts is indicated in Fig. 17. The measured and computed strut loads are presented in Table 3. The average measured strut load represents the average of three strain measurements made after the excavation of the cut was completed. The maximum measured strut load shown in Table 3 is the largest load recorded in those measurements.

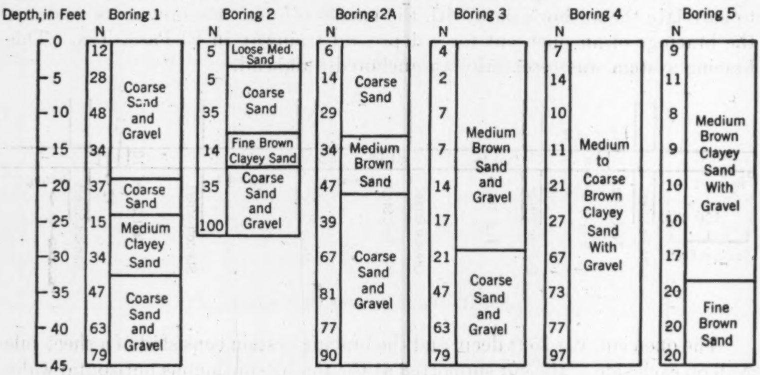

Depth, in Feet
0
5
10
15
20
25
30
35
40
45
Boring 1
N
12
28
48
34
37
15
34
47
63
79
Coarse Sand and Gravel
Coarse Sand
Medium Clayey Sand
Coarse Sand and Gravel
Boring 2
N
5
5
35
14
35
100
Loose Med. Sand
Coarse Sand
Fine Brown Clayey Sand
Coarse Sand and Gravel
Boring 2A
N
6
14
29
34
47
39
67
81
77
90
Coarse Sand
Medium Brown Sand
Coarse Sand and Gravel
Boring 3
N
4
2
7
7
14
17
21
47
63
79
Medium Brown Sand and Gravel
Coarse Sand and Gravel
Boring 4
N
7
14
10
11
21
27
67
73
77
97
Medium to Coarse Brown Clayey Sand With Gravel
Boring 5
N
9
11
8
9
10
10
17
20
20
20
Medium Brown Clayey Sand With Gravel
Fine Brown Sand

FIG. 19.—BORING LOGS

TABLE 3.—MEASURED AND COMPUTED STRUT LOADS

Strut No.	Measured Strut Load, in Kips		Strut load computed from fixed-earth-support theory, in kips
	Average	Maximum	
3	48.4	48.4	67.5
4	48.4	60.5	67.5
6	50.2	50.2	67.5
7	50.2	55.4	67.5
8	57.0	65.7	94.5
9	65.7	81.3	94.5
10	43.2	43.2	94.5
11	70.7	91.6	94.5
12	76.1	86.5	94.5
13	81.1	88.2	94.5

The earth pressures, required depth of sheet-pile penetration, and strut loads were computed in the following manner: Values of K_A and K_P equal to

0.25 and 7.0, respectively, were assigned to the sand of medium density (east of Oregon St.). The subsoil west of Oregon St. was considered to be loose silty sand with values of K_A and K_P equal to 0.35 and 3.0, respectively. These coefficients of active and passive earth pressures were obtained from Table 2. The required depth of sheet-pile penetration, as determined from Eq. 17, was approximately 7.5 ft for the loose silty sand. The penetration provided in this open cut was 12 ft. The loads on the struts, which correspond to the anchor pull described by the author, were computed for the fixed-earth-support condition as defined in Fig. 1 (*b*). The point of inflection of the sheet-pile wall was assumed to be 1.0 ft below the bottom of the cut. The computed strut loads are listed in Table 3, and the basis of the computations is shown in Fig. 20.

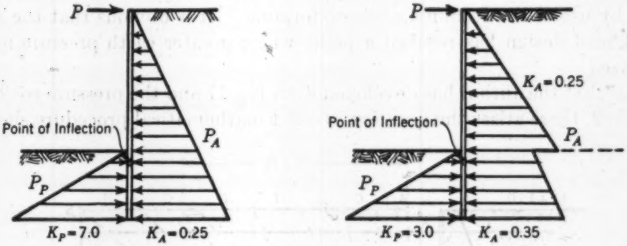

(*a*) STRUTS 3 TO 7 (*b*) STRUTS 8 TO 13

FIG. 20.—BASIS OF STRUT-LOAD COMPUTATION

Comparison of the measured and computed strut loads in Table 3 indicates that their agreement is satisfactory. The coefficients of active earth pressure, as deduced from the measurements, agree closely with those recommended by Mr. Terzaghi for loose silty sand and medium clean sand. It also appears that, when the sheet-pile penetration is increased to 1.5 times that required by Eq. 17, strut-load computations based on the fixed-earth-support condition would lead to better results than would Eq. 18 which is based on the free-earth-support condition.

Unfortunately, no reliable data on the movement of the sheet piles were obtained. The computed movement at the top of the sheet-pile wall for an excavation 12 ft deep (with no struts in place) was 0.008 ft. It was assumed in the computations that the sheet piles behaved as cantilevers resisting active earth pressure. After the struts were installed, no further movement was possible at the top. The computed movement was 0.0003 of the depth of the cut. This is approximately the movement that is required to develop the active earth pressure, according to the results shown in Fig. 3 (*b*).

Conclusion.—The results of the measurements on the open cut indicate that the coefficients of active earth pressure are close to those recommended by Mr. Terzaghi for loose silty sand and medium clean sand. The order of magnitude of the sheet-pile movement agrees with the amount of movement required to develop active earth pressure as determined by the author's tests. The depth of sheet-pile penetration in this cut was 1.5 times the required amount, and the measured strut loads show that the behavior of the sheet pile was close to the condition of fixed earth support. It is hoped that this information and correlation will be a contribution to the vast quantity of field data that are necessary to formulate design principles.

Acknowledgments.—De Leuw, Cather and Company of Chicago, Ill., designed the trainway and made the strut-load measurements with the assistance of C. P. Siess, M. ASCE, of the University of Illinois, at Urbana.

W. D. Bigler.[31]—Mr. Terzaghi's studies have answered some of the questions concerning lateral earth pressures acting upon tied bulkheads. There is ample evidence from strain-gage and pressure-gage measurements made on harbor structures in San Pedro Bay (California) that the final lateral force caused by backfill in confined areas is substantially greater than that determined by use of the Rankine pressure formula. It is obvious that the science of bulkhead design has reached a point where greater earth pressure must be recognized.

Now that the author has developed both Eq. 17 and the pressure coefficients of Table 2, there arises the question of what mathematical procedure should be used in computing the maximum bending moments and the required depth of penetration. Fig. 21 illustrates a suggested convenient procedure. Unit earth pressures have been selected from Table 2.

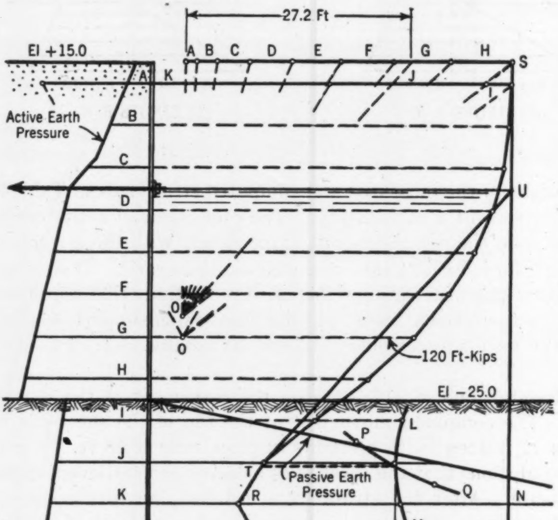

Fig. 21.—A Method for Determining the Maximum Bending Moment and the Required Depth of Penetration

In Fig. 21 the vertical line of the steel sheet-pile bulkhead is divided into spaces of convenient width (in this case a width of 5 ft). A force vector, A,

---

[31] Structural Engr., Long Beach, Calif.

B, . . . K, is computed for each space and placed at its midheight. Below the mud line, the vector is the algebraic sum of the active and passive pressures. The total available passive pressure is used to determine the bending moments.

The forces are drawn in the usual manner for graphically computing moments; the origin, 0, is placed directly below the left end of vector A; and the string polygon is drawn as shown. The abscissa at each point, such as line R–N, measures the cantilever moment caused by all earth forces above the point. This moment divided by the distance to the tie rod is equal to the tension required in the rod to maintain equilibrium. The tension is plotted with the vertical line S–N as a base to form the curve L–M.

Another curve, P–Q, is similarly drawn representing the shear above the reference point—that is, the active pressure minus the passive pressure. The intersection of the two curves determines the depth at which equilibrium is reached, and a line drawn horizontally to the string polygon at point T indicates the point of zero bending moment in the moment diagram. Line T–U is drawn, from which the maximum positive moment is scaled as 120 ft-kips, and the negative moment at the tie-rod as 45 ft-kips. This method of computing moments is applicable whether the length of embedment of the bulkhead is the minimum required or is sufficient to provide apparent fixity.

To find the required depth of penetration of the sheet piles, the earth-pressure forces below the mud line are recomputed on the basis of the passive pressure divided by a factor of safety; in this case G_s is assumed equal to 2. Likewise, the corresponding curves L–M and P–Q are reconstructed in a lower position. This final step, which is not shown in Fig. 21, indicates that the required penetration is 12.5 ft plus 20%, or 15 ft. Therefore, the value of H to be used in Eq. 12 is 52.5 ft.

Application of the moment-reduction curve of Fig. 16 indicates that a reduction of 27% is allowed. The final moment is therefore 0.73×120.0 ft-kips, or 87.6 ft-kips. If a steel-stress value of 22,000 lb per sq in. is used, the section modulus required is 47.8 in.^{3}, and a Z38 section ($S = 46.8$ in.^{3}) is required. The tie-rod tension is 27.2 kips per ft of bulkhead. Apparently the author's statement (under the heading, "Anchor Pull: Anchor-Pull Reduction") regarding reduction of anchor pull implies that reduction is not justified under usual conditions.

J. Brinch Hansen[32].—The errors involved in bulkhead design and the advances that have been made in this type of design have been clearly outlined by Mr. Terzaghi. The design procedure recommended by the author is a definite improvement on the methods which utilize only the classical earth-pressure distributions.

The decisive proof of the suitability of a design method, however, is its agreement with practical experience; in this connection the "Danish Rules" should be cited. This empirical method for the design of anchored bulkheads, which has been described[33,34] by Mr. Tschebotarioff, was developed by Danish engineers in 1926. Although numerous dredge and fill bulkheads designed from these rules have been constructed in water depths of up to 40 ft, no failures have been recorded except for a few cases of excessive anchor yield.

---

[32] Chf. Engr., Christiani and Nielsen, Copenhagen, Denmark.

[33] "Soil Mechanics, Foundations and Earth Structures," by G. P. Tschebotarioff, McGraw-Hill Book Co., Inc., New York, N. Y., 1951, p. 299.

[34] *Ibid.*, pp. 502–504.

Although certain details in the Danish Rules can be criticized, it is a fact that, by this method, a great number of sufficiently safe and economical bulkheads have been constructed. On the basis of this extensive practical evidence, it is maintained that any design method which consistently leads to greater dimensions than those required by the Danish Rules must be considered uneconomical.

If a comparison is made between the Danish Rules and Mr. Terzaghi's proposed method of design, the following will be found: In the Danish Rules the factor of safety for the passive earth pressure is nominally 2, but is actually approximately equal to 1.4 whereas Mr. Terzaghi recommends safety factors of from 2 to 3 and (in addition) a 20% increase of the computed driving depth. The moment reduction allowed in the Danish Rules is dependent on the flexibility of the wall and is usually about the same as that found by Mr. Rowe,[19] whereas Mr. Terzaghi proposes to account for only half of this reduction. The smaller driving depth specified by the Danish Rules means a further reduction of the moments.

In a certain typical case, it was found that Mr. Terzaghi's procedure (with a safety factor equal to 2 and an allowable stress equal to 2/3 of the yield stress) required a 75% greater driving depth (corresponding to 15% longer sheet piles) and a 60% greater section modulus of the wall than the Danish Rules.

A common feature of both Mr. Terzaghi's design method and the Danish Rules is that certain allowable stresses are specified which are independent of the flexibility of the wall. On the basis of Mr. Rowe's investigations,[19] however, it is evident that a comparatively rigid wall must possess a greater reserve of safety against failure than a more flexible wall which has almost exhausted its possibilities of redistributing the earth pressures. Therefore, it might be logical to vary the allowable stress with the flexibility of the wall.

The problem of the design of flexible anchored bulkheads is evidently one in which proportionality between total load and maximum stress does not exist, and in such a case the usual concept of allowable stresses is not suitable. In other fields of engineering such problems are investigated by considering the state of failure; the structure is then designed so as to possess a certain safety against failure. Similar design methods are also used for structures (such as slabs and shells) which might have been designed by the application of the theory of elasticity.

In the case of bulkheads and similar structures, a computation based on a state of failure (for example, one in which a yield hinge is supposed to develop in the wall) has until recently not been possible because methods have not been available for determining the earth pressures corresponding to arbitrary movements of the wall. However, following the development and application of such methods of investigation to anchored bulkheads and other earth-retaining structures,[35] nothing should now prevent the engineer from designing such structures on the basis of a state of failure.

---

[35] "Earth Pressure Calculation," by J. Brinch Hansen, The Danish Technical Press, Engineering House, Copenhagen, Denmark, 1953.

The only shortcoming of such a design method is that it does not provide information about the actual deformations of the structure under normal working conditions. This is less important for earth-retaining structures than for almost any other structure, however, because the former structures can (without detrimental effects) suffer deformations of a magnitude which would be unallowable for most other structures. Consequently, bulkheads would seem to be ideal objects for computational methods based on the state of failure.

Gregory P. Tschebotarioff,[36] M. ASCE.—The need for a revision of the wasteful conventional methods of anchored-bulkhead design has long been apparent. Mr. Terzaghi is to be complimented for emphasizing this need and for presenting an over-all review of developments in this field. Unfortunately, however, the paper contains several misstatements and omissions.

The writer's procedure for the design of anchored bulkheads driven into clean sand is discussed in Part II (under the heading, "Computation of Maximum Bending Moments: Free Earth Support"). The author states:

> "Mr. Tschebotarioff has suggested computation of the maximum bending moment in the sheet piles on the assumption of fixed earth support irrespective of flexibility and of the relative density of the sand into which the sheet piles are driven.[18] Mr. Rowe showed that the errors involved in such a procedure can be very important and they are on the unsafe side[19].'

This statement is not correct. It should be noted that Mr. Terzaghi refers only to Mr. Rowe's original paper[37] according to which the writer's method results in bending moments approximately 25% less than those obtained by the Danish Rules. It was shown subsequently that Mr. Rowe was incorrect and that the reverse is true—that is, the Danish Rules result in bending moments 25% less than those from the writer's method.[38] Mr. Rowe's original figure was corrected accordingly, and Mr. Rowe accepted the correction.[39] This point is of importance because a large number of bulkheads have been built in accordance with the Danish Rules and have performed satisfactorily. Subsequent remarks will demonstrate a fallacy in the reasoning on which Mr. Terzaghi based this comment relative to the writer's computation procedure.

The physical significance of the flexibility coefficient ρ as presented in the diagrams offered by Mr. Terzaghi and Mr. Rowe cannot be visualized easily. Therefore, Fig. 22(*a*) shows the relationship between the values of log ρ as given by the author (and by Mr. Rowe) and the values of the coefficient ρ expressed in more consistent units—square inches per pound per foot—and to the total length H for five typical steel sheet-pile sections. The coefficient ρ has dimensions that are the reciprocal of stress. The units "per ft" merely indicate that the moment of inertia I must be computed for a wall width of 1 ft. In Fig. 22(*b*) there are shown the structural curves for the same five sheet-pile sections, Mr. Rowe's bending-moment-reduction curves, and the line representing the writer's design proposal.

---

[36] Prof. of Civ. Eng., Princeton Univ., Princeton, N. J.

[37] "Anchored Sheet-Pile Walls," by P. W. Rowe, *Proceedings*, Inst. of C. E., London, England, Vol. 1, Pt. 1, 1952, p. 35, Fig. 8.

[38] Correspondence of G. P. Tschebotarioff of "Anchored Sheet-Pile Walls," by P. W. Rowe, *ibid.*, pp. 616–619.

[39] Correspondence of P. W. Rowe of "Anchored Sheet-Pile Walls," *ibid.*, p. 633.

This design-proposal line was obtained (to simplify comparisons) for the case in which α is equal to 0.7 and β equals 0.2, as used by Mr. Rowe.[37] It was further assumed that (1) the water level coincides with the anchor level; (2) the buoyant unit weight, γ^1, of the sand below the water level equals 0.6 times the weight, γ, of the sand above the water level; and (3) the surcharge is equal to zero. If H is taken in feet, the bending moment for free earth support, expressed in foot-pounds per foot, is

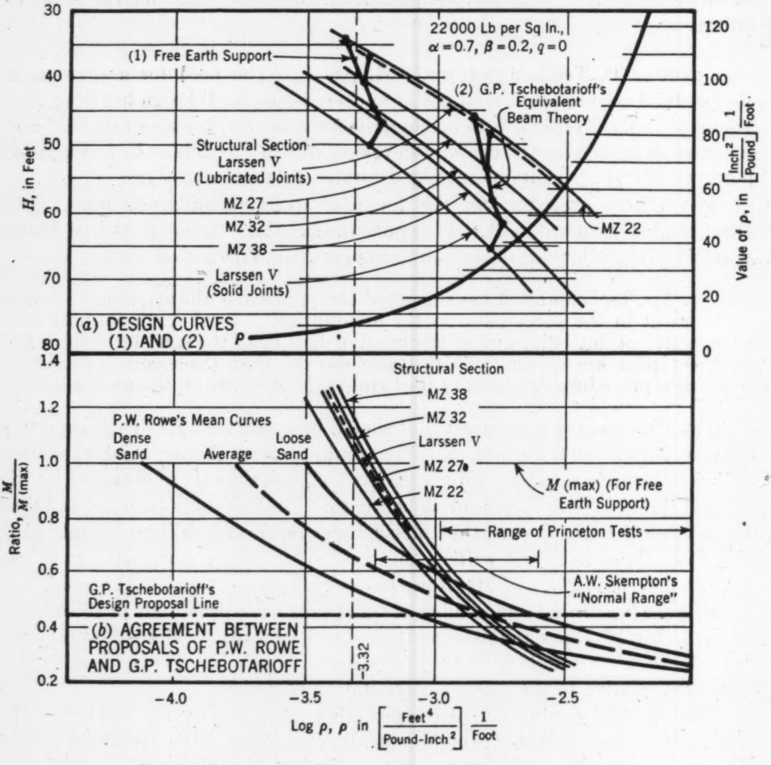

FIG. 22.—RELATIONSHIP BETWEEN H OR $M/M(\text{max})$ AND LOG ρ

$$M(\text{max}) = 0.0228\,\gamma\,K_A H^3 \ldots\ldots\ldots\ldots\ldots (19)$$

Similarly, the bending moment, M_T, used in the writer's design method which is illustrated in Fig. 23(*b*) is

$$M_T = 0.0102\,\gamma\,K_A H^3 \ldots\ldots\ldots\ldots\ldots\ldots (20)$$

The ratio of M_T from Eq. 20 and of $M(\text{max})$ from Eq. 19 equals 0.45, which value is plotted as a straight horizontal line in Fig. 22(*b*).

It should be noted that in Fig. 22(*b*) the average of the structural lines for the steel sheet piling, the design line proposed by the writer, and Mr. Rowe's mean curve for medium sand all intersect at approximately the same point. Thus, according to Mr. Rowe's data, the design proposal shown in Fig. 23(*b*) gives the strength required by a maximum tolerable flexibility of steel sheet piling. The structural curves for stiffer steel bulkheads (to the left of the intersection) will all be higher than Mr. Rowe's mean curve for medium sand and will therefore have a strength in excess of the increased strength required by their increased stiffness. Mr. Rowe selected a model bulkhead with the values of α equal to 0.7 and β equal to 0.2 to demonstrate the fact that a stiff bulkhead with log ρ equal to -3.32 was subjected (during his model tests with loose sand) to a bending moment approximately twice the value of the moment computed according to the writer's method (Fig. 23(*b*)). This fact is not questioned; however, it is a fallacy to believe that such a bulkhead would be unsafe.

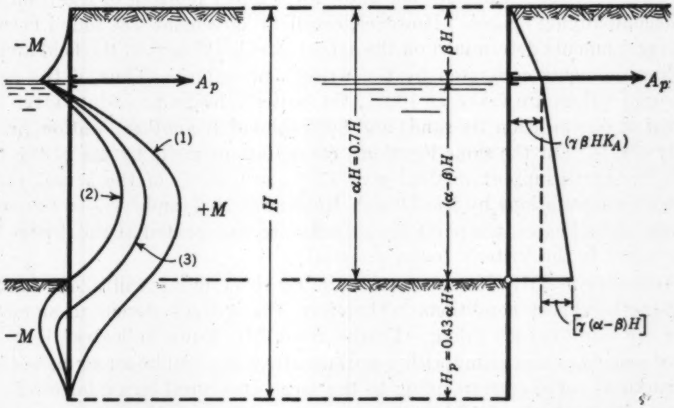

(*a*) INFLUENCE OF SHEET-PILE FIXATION ON THE BENDING-MOMENT CURVES

(*b*) FIXED-EARTH-SUPPORT METHOD FOR MAXIMUM FIXATION, IN CLEAN SAND

FIG. 23.—BENDING-MOMENT CURVES AND DESIGN METHOD

Example.—A wall made of MZ 38 steel sheet piling[40] that is 45 ft long (I equal to 281 in.^{4} per ft) has a flexibility coefficient ρ equal to 10.2 in.^{2} per lb per ft, and log ρ equal to -3.32. From Eq. 19—for K_A equal to 0.333 and γ equal to 105 lb per cu ft—M(max) is equal to 873,000 in.-lb per ft. According to Fig. 22(*b*) and Mr. Rowe's mean curve for loose sand, one should use 85% of M(max) or 742,000 in.-lb per ft. At a working stress of 22,000 lb per sq in. (that is, at $\frac{2}{3}$ of the yield stress, the minimum suggested by Mr. Terzaghi) an MZ 38 section (Z equal to 46.8 in.^{3} per ft) resists 1,030,000 in.-lb per ft, or 118% of M(max) (Fig. 22(*b*)). This is appreciably more than is needed according to Mr. Rowe's proposals. However, the use of the writer's design proposal for H equal to 45 ft, as shown in Fig. 22(*a*), would lead to the selection of the much more flexible and lighter MZ 22 section.

---

[40] "Carnegie-Illinois Steel Sheet Piling. Insert C, Z Piles," Carnegie-Illinois Steel Corp., Pittsburgh. Pa., February, 1936.

Thus, the writer's design proposal cannot be unsafe, and Mr. Terzaghi's use of Mr. Rowe's original paper[19] as a basis for his criticism is unjustified where steel sheet piles are concerned.

The design proposals shown in Fig. 23(*b*) have been substantiated by full-scale field measurements on steel sheet piling in the harbor of Bremen, Germany, by Dietrich Wiegmann.[41] The double anchorage—at two levels—of that steel sheet-pile wall does not allow for a direct plotting of the results on the accompanying figures. However, excellent agreement was found between bending moments determined on the actual steel bulkheads in the field and the bending moments computed by the writer's procedure. Thus, if the actual measured values are taken as 100%, the writer's design procedure gives 98% thereof at one location (in sand) and 96% thereof at another location (in stiff sandy clay). For the same locations, computations made by use of the Coulomb free-earth-support method give 170% and 133% of the actual values, whereas computations by the Danish Rules give 70% and 64% of the actual values. In all cases, the point of contraflexure was located at the dredge line, as assumed in the writer's design proposal.

According to Mr. Rowe's tests,[19] timber sheet piling will adapt itself to fixed-earth-support conditions. Therefore, the writer's design recommendations are safe for such piling. Furthermore, Mr. Rowe indicates[42] that reinforced concrete sheet piling with a working stress of 1,250 lb per sq in. will have a structural curve corresponding to the mean structural curve for steel sheet piling with a stress of 17,900 lb per sq in. (This working stress would be assigned in the United States to concrete having a 28-day strength of f'_c equal to 2,780 lb per sq in.) Hence the writer's findings, relative to steel sheet piles, are applicable to concrete of this quality which should normally be expected in present-day (1954) waterfront structures.

Fig. 16 shows that, for any concrete, tolerable moment reductions should be smaller than for steel. This is incorrect as Fig. 16 is applicable only to reinforced concrete sheet piles made of concrete having a very low strength (such as concrete having a 28-day strength of f'_c equal to 1,670 lb per sq in.) in which case only, according to Mr. Rowe,[42] any appreciable deviations from the writer's design proposals are to be expected. However, concrete of such poor quality should never be used in any properly designed waterfront structure. Such poor concrete may have been used in the first applications of reinforced concrete; yet early Danish bulkheads—although designed for bending moments at least 25% less than those which follow from the writer's design procedure[43, 44]—have performed satisfactorily. Thus, the writer's design proposal shown in Fig. 23(*b*) is entirely safe as evidenced by the field performance of reinforced concrete sheeting.

---

[41] "Der Erddruck auf Verankerte Stahlspundwände ermittelt auf Grund von Verformungsmessungen am Bauwerk," by Dietrich Wiegmann, dissertation approved by the Technische Hochschule (Technical University) of Hannover, Hannover, Germany, in 1953, for the award of the degree of Doktor-Ingenieur.

[42] "Anchored Sheet-Pile Walls," by P. W. Rowe, *Proceedings*, Inst. of C. E., London, England, Vol. 1, Pt. 1, 1952, p. 57, Fig. 21.

[43] "Soil Mechanics, Foundations and Earth Structures," by Gregory P. Tschebotarioff, McGraw-Hill Book Co., Inc., New York, N. Y., 1951, pp. 500–501.

[44] *Ibid.*, pp. 540–542.

The agreement (illustrated by Fig. 22(*b*)) among the structural curves for steel sheet piles, Mr. Rowe's mean curves, and the writer's design proposal is not accidental. The effects of the flexibility of sheet piles have been established and were taken into account by the writer's design proposal.[18] A contrary implication by Mr. Terzaghi is incorrect, as is the statement in Part I (under the heading, "Influence of Flexural Rigidity on Bending Moment") that "no observational data were available" concerning the effects of bulkhead flexibility "* * * until the results of Mr. Rowe's experimental investigations were published.[19]" Relevant observational data were obtained prior to Mr. Rowe's and were published by the writer.[18]

This is substantiated by Fig. 24, which reproduces data[45] from the report[18] quoted by Mr. Terzaghi. In Fig. 24 the test numbers in parentheses indicate the tests performed with originally loose sand. The same bulkhead thickness was used in all tests, but the vertical dimensions were varied according to three different scale factors. Thus (for α equal to 0.612), the scale factor equal to 1.00 corresponded to H equal to 73 in.; the scale factor equal to 1.17 corresponded to H equal to 83 in.; and the scale factor equal to 1.34 corresponded to H equal to 98 in. Most of the model bulkheads had an α-value of 0.612 $\left(\frac{H_p}{\alpha H}\text{ equal to }0.63\right)$. Tests 54 and (54A) had α equal to 0.700 $\left(\frac{H_p}{\alpha H}\right.$

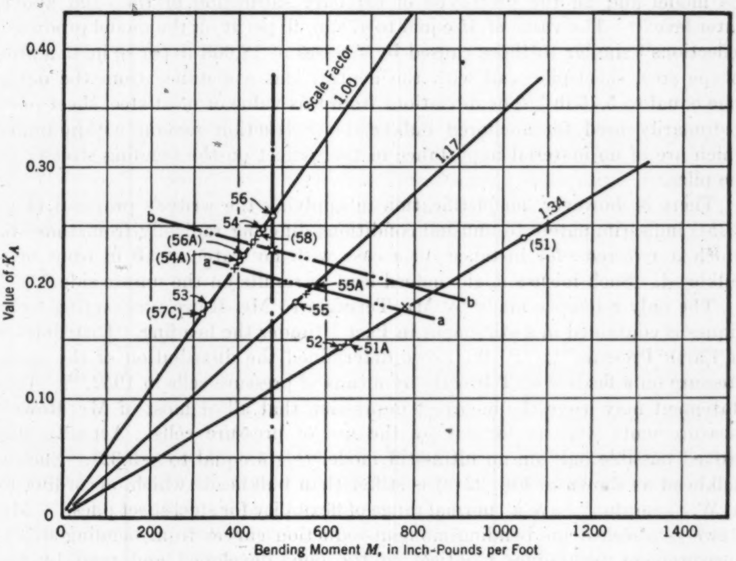

FIG. 24.—COMPARISON OF MEASURED BENDING MOMENTS AND DESIGN METHOD OF FIG. 22(*b*)

equal to 0.43) and H equal to 65 in. Tests 56 and (56A) had α equal to 0.786 $\left(\frac{H_p}{\alpha H}\right.$ equal to 0.27$\left.\right)$ and H equal to 57 in. The three inclined straight lines in Fig. 24 are the loci of bending moments for the bulkheads of the three flexibilities computed in accordance with the procedure shown in Fig. 23(*b*), as well as the K_A-values corresponding to the bending moments measured during the actual tests. The effect of increasing flexibility is shown by the fact that smaller values of K_A correspond to tests where the bulkhead had higher scale-factor values—hence, greater lengths and flexibilities. The line a–a corresponds to the average values of bulkhead tests with α equal to 0.612; the line b–b expresses the probable similar relationship for α equal to 0.700. The intersection between line b–b and a vertical line drawn through M equal to 478 in.-lb per ft results in a design value of K_A equal to 0.23 for model conditions. This value was then increased to compensate for a difference in the effects on the model and on the prototype of capillary saturation of the sand above water level.[18] The value of M equal to 478 in.-lb per ft on the model produced deflections[18] similar to those caused by stresses of 18,000 lb per sq in. in a prototype steel sheet-pile wall with the neutral axis a distance from the outer edge equal to 5.75 in. The deviations from this value of most steel sheet piles customarily used for anchored bulkhead construction remain within limits which are of no material importance in their effect on the bending stresses in the piles.

---

[45] "Final Report. Large Scale Earth Pressure Tests with Model Flexible Bulkheads," by G. P. Tschebotarioff, Princeton Univ., Princeton, N. J., 1949. Fig. 42.

There is, however, no justification in applying the writer's proposal (Fig. 23(*b*)) indiscriminately to unusual conditions differing radically from those to which it referred—for instance, to a case with no water at all in front of a bulkhead. Such misuse might indeed lead to results on the unsafe side.[42]

The only reference made by Mr. Terzaghi to Mr. Rowe's measuring techniques is contained in a statement in Part I (under the heading, "Distribution of Earth Pressure"); "P. W. Rowe determined the distribution of the earth pressure on a flexible wall directly by means of pressure cells in 1952.[19]" This statement may leave the incorrect impression that all or most of Mr. Rowe's measurements were performed by the use of pressure cells. Actually this proved possible only on an ultra-stiff model (log ρ equal to -3.32). Such a bulkhead as shown in Fig. 22(*a*) is stiffer than bulkheads which, according to A. W. Skempton[46] have a "normal range of flexibility for steel sheet piles." Mr. Rowe established his bending-moment-reduction curves from bending-strain-measurement techniques identical to the ones developed and used by the writer,[18] and not by pressure-cell measurements. The point is of importance for the understanding of this entire problem.[47]

Mr. Terzaghi and Mr. Rowe both overemphasize the effect of the original density of the sand and underemphasize the effect of variations in the depth of embedment of the piling. This is not justified.

Fig. 25(*a*) shows the alleged complete agreement between the writer's tests[18] and Mr. Rowe's mean curves as reported by Mr. Rowe.[19] Fig. 25(*b*) shows the actual relationship. Test 56 was omitted in Fig. 25(*a*), and the actual positions of tests 54 and (54A) are the reverse of the ones indicated by Mr. Rowe. This means that originally dense sands may lead to higher bending moments in the piling than originally loose sands. This seeming paradox is caused by the fact that the lateral resistance of a very loose submerged sand in front of the buried part of a bulkhead is not directly proportional to the initial density and to the static compression in a confined test of the sand, as Mr. Rowe suggested.[19] The lateral yield induces a simultaneous and appreciable vertical consolidation of a large mass of such sand under its own weight and under the action of the vertical shearing stresses, which are transmitted to it through wall friction by the bulkhead. This fact can be demonstrated in any seepage flume with transparent walls. The lateral bulkhead displacements y_D at the dredge line (Fig. 26) were only 75% larger during tests (54A) and (56A) with originally loose sands than the displacements y_D during tests 54 and 56 with originally dense sands.[18] The maximum displacements did not exceed $\frac{1}{4}$ in. on the model—approximately 2.5 in. on a prototype—a value which cannot be considered excessive. According to Mr. Rowe's confined tests, loose dry sand should compress 4.3 times as much as dense sand[19]—that is, 2.5 times more than the 75% higher value of lateral yield actually observed for submerged sand.

---

[46] "General Report Session 7: Earth Pressures," by A. W. Skempton, *Proceedings*, Third International Conference on Soil Mechanics and Foundation Eng., Zürich, Switzerland, Vol. II, 1953, p. 354.

[47] Discussion on Session 7 (Earth Pressures) by Gregory P. Tschebotarioff, *ibid.*, Vol. III, 1953.

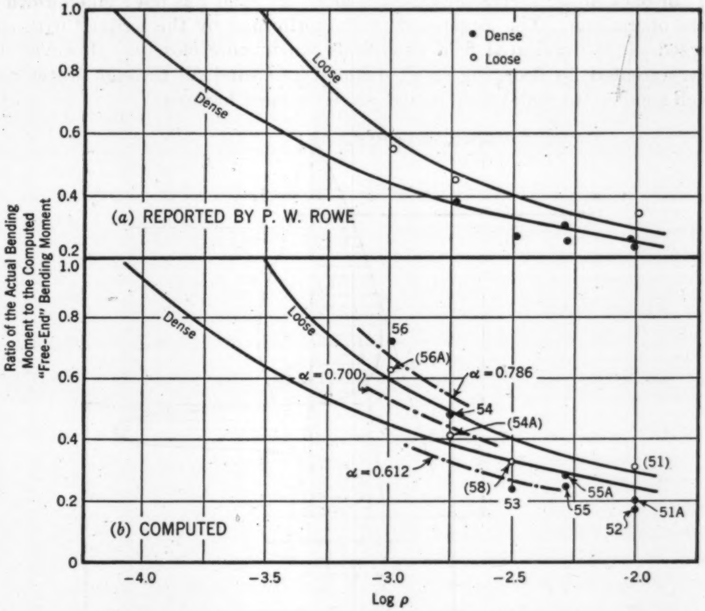

FIG. 25.—COMPARISON OF PRINCETON TEST RESULTS WITH P. W. ROWE'S MEAN CURVES

The actual effect of variations in the depth of embedment is indicated in Fig. 25(*b*). It is evident that with an increasing α-value—that is, with a decreasing depth of embedment—the moment reduction also decreases much more considerably than would follow from Mr. Rowe's mean curves shown in Fig. 13.

These discrepancies have the following explanation: Mr. Rowe performed his tests with dry sand only, and with a scale sufficiently small (H equal to 42 in.) to permit avoiding any shocks or vibrations during laboratory "dredging" or backfilling; therefore originally loose dry sand was not shaken down by these operations. The larger-scale tests performed by the writer[18] with submerged sands duplicated field conditions much more closely. However, the waves created by dropping small quantities of sand fill through water were much smaller (to scale) than actual waves in most harbors.

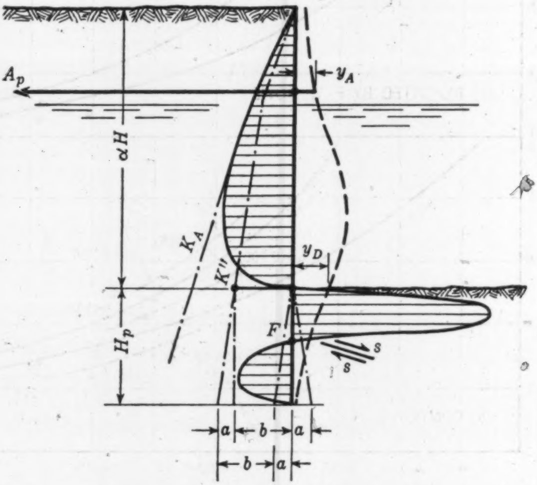

FIG. 26.—MAXIMUM EARTH PRESSURE VALUES, b, WHICH PROVIDED EFFECTIVE FIXATION OF TOE OF MODEL BULKHEAD

Except for the preceding reservations, the agreement between the results of Mr. Rowe's tests and the writer's is excellent. An examination of earlier summaries of the writer's findings[18, 48, 49] shows that the writer's tests established a number of points of fundamental importance for the analysis of bulkhead behavior; these points form the basis of Mr. Rowe's investigational procedures and findings. Some of these points are: (1) The breakdown of "arching" as a result of anchor yield; (2) the decrease of bending moments caused by the concentration of the passive pressures just below the dredge line, and by the decrease of active pressures just above the dredge line; and (3) the dependence of these pressure changes (at that boundary) on the bulkhead flexibility as it affects bulkhead displacements at the dredge line.[18, 48, 49] These limitations do not detract from the value of Mr. Rowe's achievements.

---

[48] "Soil Mechanics, Foundations and Earth Structures," by Gregory P. Tschebotarioff, McGraw-Hill Book Co., Inc., New York, N. Y., 1951, pp. 297–303, Figs. 10–41.

[49] *Ibid.*, pp. 505–516.

The writer has already welcomed[38, 47] Mr. Rowe's outstanding work both as a confirmation and as a development and extension of the writer's investigations. The writer recommends the use (with consistent units) of the coefficient ρ which Mr. Rowe introduced to define bulkhead flexibility. However, Mr. Terzaghi's suggestion that Mr. Rowe's bending-moment-reduction curves be used as a direct basis for field design ignores the fact that these curves reflect purely laboratory (stable) conditions and are not adapted to reflect field conditions.

The unwieldiness of the procedure is well illustrated by the fact that Mr. Terzaghi did not grasp its physical significance; hence he was led to the fallacy explained previously. The writer himself did not notice a similar fallacy at first and conceded too much.[38]

The advantages accruing from the routine use of Mr. Rowe's complex procedure are not apparent; especially if (as suggested by Mr. Terzaghi) one is arbitrarily to cut the moment reductions thereby obtained by one half.

Attention is drawn to the procedure illustrated in Fig. 23(*b*). The writer has shown[47] that this method can be easily adapted to reflect new field data concerning field imponderables, such as shocks resulting from wave action. These factors were not considered by either Mr. Rowe or Mr. Terzaghi. The type 2 bending-moment curves shown in Fig. 23(*a*) can be increased[47] to correspond to the type 3 curve (or type 1 curve), if so desired, for differing soil conditions or for stiffer bulkheads. This modified procedure is simpler and more flexible but fundamentally not different from the one suggested by Mr. Rowe, although the order of operations is reversed. Mr. Rowe used type 1 curves as a starting point and then reduced the maximum bending moments to correspond to curves of type 3 or type 2.

Mr. Terzaghi recommends no reduction of the free-earth-support moments for sheet piles driven into silt or clay on the basis that, in such soils, the end restraint decreases because of a progressive consolidation of the clay or silt resisting the lateral pressure on the back of the buried toe of the bulkhead. The accompanying reference to Part I of the paper (presumably to Fig. 1(*b*)) suggests that fixed-earth-support conditions occur only when the lower portion of the sheet pile has moved backward from its original position. This is a "classical" assumption which is tied to the belief that end restraint requires the mobilization of earth pressures of "passive" intensity. The writer's tests[18] have shown, however, that, in the case of sands, restraint of the toe of the bulkhead occurs even when it has moved out in the manner indicated in Fig. 1(*a*) and Fig. 26.

An analysis[50] has shown that the "classical" assumption that passive earth pressures have to be mobilized at the toe of a fixed-support bulkhead is incorrect. This was shown by the K''-values determined in accordance with Fig. 26. In all static tests with a depth of embedment corresponding to α equal to 0.612 and $\frac{H_p}{\alpha H}$ equal to 0.63, the K''-value varied between 0.07 and 0.23 with an average value for eight tests of K'' equal to 0.14. The effects of severe, deliberately produced vibration increased this value to $K'' = 0.23$. Thus, active pressures alone were sufficient to provide full end restraint for that particular depth of embedment. Recomputation[18] of the measured bending moments confirmed the validity of the pressure b from which these K''-values were computed. Even smaller K''-values will be obtained if they are referred to the $(a + b)$-pressures from a consideration of the shearing stresses S indicated in Fig. 26. These shearing stresses must decrease the active pressures a on the outer face of the buried portion of the bulkhead.

---

[50] "Einfluss der Gewölbebildung auf die Erddruckverteilung," by Gregory P. Tschebotarioff, Dissertation approved by the Rhine-Westfalian Technische Hochschule (Technical University) at Aachen, Germany, in 1952, for the award of the degree of Doktor-Ingenieur.

For tests 54 and (54A), with α equal to 0.7 and $\frac{H_p}{\alpha H}$ equal to 0.43, an average value (for the pressure b) for K'' of 0.45 was obtained. This value corresponds to earth pressures at rest. Only for the small depth of embedment (inadmissible in practice) of tests 56 and (56A) with α equal to 0.786 and $\frac{H_p}{\alpha H}$ equal to 0.27 was K'' equal to 0.85. This value is much smaller than the customarily assumed intensities of passive earth pressure.

Active and even neutral earth-pressure values can be relied on in clay and in silt soils. Thus, there is every reason to believe that appreciable end restraint will be permanently present in deep deposits of medium to stiff clay and silt, once a sufficient depth of bulkhead embedment is provided.

In discussing clay and silt soils, Mr. Terzaghi does not mention the use of a sand dike for the purpose of reducing fluid pressures of cohesive backfills. The writer's tests showed that such sand dikes are very effective when placed between a bulkhead and its fluid cohesive backfill.[18, 48, 49] The excavation of soft clay below the dredge line and its replacement by sand fill is also an effective measure[48, 49] since it provides a practical alternative for the use of the free-earth-support method which is frequently not feasible in such cases.

Paul Baumann,[51] M. ASCE.—An excellent treatise on anchored bulkheads has been presented by Mr. Terzaghi. The clarity with which the complexities inherent in bulkhead design are expounded is commendable. This paper should serve to dispel the idea, current among many engineers, that a bulkhead is just another retaining wall. The fact is that a bulkhead has little in common with the conventional retaining wall. A retaining wall is a simple, statically determinate structure, depending primarily on gravity for its stability. The anchored bulkhead, however, is a statically indeterminate structure, depending for stability primarily on its anchorage (that is, its restraint) at the lower end, its anchorage at or near the upper end, and the strength of the sheet piles.

The majority of bulkhead failures have resulted from faulty anchorage. Hence, the predomiant cause of failure has been in the foundation. The author stresses the need for exploratory borings to ascertain the possibility of critical changes in subsoil conditions. Unfortunately this practice is sometimes considered an unnecessary expense by engineers. Such borings should also serve to ascertain the density, the shearing strength, and the stress-strain relationship of the soil. This stress-strain relationship is termed (perhaps somewhat misleadingly) the "modulus of elasticity," so far as the linear part of this relation is concerned.

---

[51] Asst. Chf. Engr., County Flood Control Dist., Los Angeles, Calif.

It has been shown[52] that, by treating a sheet-pile bulkhead as a statically indeterminate structure and by evaluating the specific, passive resistance (e_f) as a function of both the depth and the stress-strain relationship—everything else being equal—relatively rigid sheet-piles require a greater depth of penetration (anchorage) than relatively flexible ones. Mr. Terzaghi, in Part II (under the heading, "Safety Requirements: Allowable Fiber Stresses in Sheet Piles"), suggests that the friction in the interlocks of steel sheet piles should be based on the assumption of lubricated conditions—that is, on the basis of a relatively great flexibility number. As H and E are constant for the identical wall, it follows that ρ varies inversely with I. Hence, if the friction in the interlock approached a "frozen" condition, the flexibility number would be much smaller and the rigidity of the sheet-pile wall would be much greater than that assumed. The depth of penetration might therefore be rendered unsafe. In consequence, it is considered better practice to design a sheet-pile bulkhead on the assumption of maximum, rather than minimum, rigidity. However, this procedure may actually result in higher bending stresses than those analyzed. The reason for this assumption of maximum rigidity is the lack of known bending failures in steel sheet-pile bulkheads whereas failures caused by insufficient penetration have been almost as frequent with this type of bulkhead as with any other type.

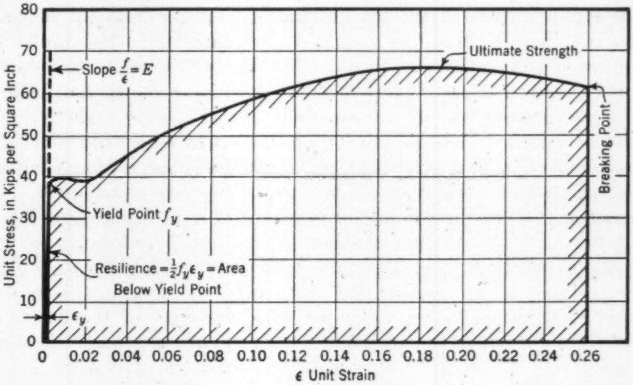

FIG. 27.—STRESS-STRAIN DIAGRAM FOR MEDIUM CARBON STEEL

When compared with other sheet-pile materials, steel has qualities which make it outstanding. The stress-strain relationship of medium carbon steel shown in Fig. 27 will serve to substantiate this statement. The yield point strength of this steel is approximately 40,000 lb per sq in., and the ultimate strength is approximately 68,000 lb per sq in. As Mr Terzaghi states, the allowable design stress should not exceed two thirds of the yield-point strength—that is, 26,700 lb per sq in. Hence, before the yield point is reached, the maximum bending moment would have to be 50% greater than analyzed, and the energy of deformation (the resilience) would then be 34 in.-lb per cu in. This value is quite small when compared with the 16,000 in.-lb per cu in. of energy required to reach the ultimate strength. Therefore, to cause structural failure, the energy required would be at least 700 times the energy associated with an allowable stress of 26,700 lb per sq in. The availability of such energy (cross-hatched area in Fig. 27) is, of course, unthinkable.

---

[52] "Analysis of Sheet-Pile Bulkheads," by Paul Baumann, *Transactions*, ASCE, Vol. 100, 1935, pp. 792-797.

The foregoing remarks should not be construed to suggest the under-designing of sheet-pile bulkheads. They are merely intended to show that anchorage failures are much more likely to occur than structural failures, so far as steel sheet-piles are concerned. In brief, it may be said that, in respect to structural qualities, there are steel sheet-piles and others.

RUDOLF BRISKE.[53]—In Part I (under the heading, "Distribution of Earth Pressure") Mr. Terzaghi, who is an advocate of the application of earth-pressure redistribution at flexible bulkheads, departs from his former considerations. In this paper the author makes use of the test results of Mr. Tschebotarioff and, especially, those of Mr. Rowe. These tests (which were concerned chiefly with the flexure of bulkheads) have shown that one cannot rely on a pressure redistribution to decrease moments indiscriminately. However, the tests did not show a basis for not using active-pressure redistribution.

Because of the plasticity of the backfill, the last deformation—and not the total deformation—of the structure causes the pressure distribution. Hence, a subsequent yield of the top of the bulkhead of approximately 0.001 *H* will cancel a prior pressure redistribution, as proved by Mr. Rowe's tests.[54] The author also states that, in practice, the anchorage yields gradually during the process of excavation. During the last stages of dredging, however, the deflection of the wall (when compared with the yield of the anchorage) is large, and (as a result of the anchorage) the yield of the top will be in a backward direction. Therefore, full pressure redistributions may occur at dredged bulkheads; also, at backfilled bulkheads, redistributions may be produced if the last critical deformation is an additional deflection of the bulkhead.[55] The total yield of the anchorage may be greater than the limiting value of 0.001 *H* if the last critical yield of the top of the bulkhead is smaller than this amount or is directed backward. By prestressing the anchorage, these conditions can be enforced.[55,56] Furthermore, a pressure redistribution will occur if the bulkhead yields plastically at a small factor of safety for the sheet piling.[35,56]

It is often stated that the pressure redistribution does not remain constant because the anchorage yields during the lifetime of a structure. However, a subsequent yield of the anchorage will cause an increase—or at least no decrease—of the anchor pull. In this manner, pressure redistribution is stabilized because anchor pull and bending moments are reciprocally dependent. That is, there will be a stable equilibrium between the increased anchor pull and the decreased bending moment.[55,56] Thus, a subsequent anchor yield will not cause a diminution of pressure redistribution if the anchor pull does not decrease.

---

[53] Engr., Berlin, Germany.

[54] Correspondence of "Anchored Sheet-Pile Walls," by P. W. Rowe, *Proceedings*, Inst. of C. E., London, England, Vol. 1, Pt. 1, 1952, pp. 616–647.

[55] "Erddruckverlagerung bei Spundwandbauwerken," by Rudolf Briske, Wilhelm Ernst and Sohn, Berlin, Germany, 1953.

[56] Discussion on Session 7 by Rudolf Briske, *Proceedings*, Third International Conference on Soil Mechanics and Foundation Eng., Vol. III, Zurich, Switzerland, 1954.

All bulkheads at which earth-pressure redistribution was accounted for have performed satisfactorily when the anchorage was safely constructed. Therefore, a German committee for quay walls has recommended reduction of the moments by one third, if the bulkheads are computed on the basis of a classical pressure distribution (that is, without redistribution of active pressures resulting from a bulkhead deflection).[57] The problem of flexure has been thoroughly investigated, but it is dangerous to neglect the problems of active-pressure redistribution. The cases in which redistribution can be accounted for may be as many as those in which flexure occurs. Which type of structure should be erected is a matter of economy.

Norman D. Lea,[58] **J. M. ASCE.**—The subject of anchored bulkheads has long been a disorganized one. Many engineers hold widely varying opinions and use widely different design procedures. Mr. Terzaghi's paper consolidates the gains in this field and should help in establishing design procedures and in planning research.

Irregular Surcharges.—It is common practice to use the area behind a bulkhead for the storage of bulk materials. The method of dealing with these irregular surcharges is not explicitly cited by Mr. Terzaghi. One is tempted to add the effects of a number of line loads approximating the irregular part of the surcharge to the effect of the uniform surcharge. The methods recommended for working with these two types of surcharge, however, are basically different. The procedure suggested by the author for line (or point) loads is independent of the type of soil. It is known, however, that the type of soil does have an influence; this effect is considered in the procedure recommended for uniform surcharges. Thus, one is led to question the recommended method for dealing with line loads. It certainly does not seem justified to extend this method for use with irregular surcharges.

The effect of the yield ratio is important. The tests performed[10, 11] by Messrs. Gerber and Spangler permitted little, if any, yield. Therefore, it is not surprising that the resulting pressures were approximately twice those determined by use of the Boussinesq theory[12] and that the influence of the type of material was small. With a greater yield, pressures reduce (in some instances) to much less than the Boussinesq value. There is some evidence, from the performance of structures, to indicate that bulkheads located in granular materials yield sufficiently to effect a permanent reduction of the pressure.

Thus, the writer suggests that, for irregular surcharges placed on granular materials, the Coulomb method should continue to be used, whereas twice the Boussinesq pressure should be used in cohesive materials.

---

[57] "Technischer Jahresbereicht über die Arbeiten des Ausschusses zur Vereinfachung und Vereinheitlichung der Berechnung und Gestaltung von Ufereinfassungen im Rahmen der Hafenbaztechnischen Gesellschaft und der Deutschen Gesellschaft fur Erd- und Grundbau," by E. Lackner, *Bautechnik*, Vol. 12, 1953, pp. 369–373.

[58] Assistant to the Vice-Pres., Foundation of Canada Eng. Corp., Ltd., Montreal, Que., Canada.

Lateral Earth Pressure in Cohesive Soils.—Mr. Terzaghi has been conservative in dealing with line loads; he has assumed practically no yield. In treating lateral earth pressures in cohesive soils, however, the reverse—unlimited yield—has been assumed; this may not be sufficiently conservative. The formula given in Table 2 for K_A in silt and clay assumes a full mobilization of the shear strength; this requires considerable yield. The writer has measured[59] such a yield of $\frac{1}{2}\%$, and it is conceivable that in some instances the yield necessary to mobilize the full shear strength may be at a rate of $\frac{1}{2}\%$ per year.

A further reason for being conservative in computing K_A for clays is that the formula in Table 2 will frequently result in a negative value. If, in such an instance, K_A is assumed to be zero, an unknown factor of safety is introduced. A further unknown factor of safety is introduced by neglecting the wall friction.

It is suggested that a factor of safety of 2 be introduced into the expressions given in Table 2: Thus,

$$K_A = 1 - \frac{q_u}{2(\bar{p} + \gamma\,\bar{z})} \qquad \text{(21a)}$$

and

$$K_P = 1 + \frac{q_u}{2(\bar{p} + \gamma\,\bar{z})} \qquad \text{(21b)}$$

Eqs. 21 should account conservatively for increased pressures caused by limited yield. Eq. 21*a* will also give a better approach to the problem in which K_A would have a negative value if the form shown in Table 2 were used.

Maximum Bending Moment.—In Part II (under the heading, "Computation of Maximum Bending Moments: Moment Reduction Resulting from Flexibility Effects") Mr. Terzaghi states "The first step consists of computing the maximum bending moments for free earth support * * *." It is presumed, although not stated by the author, that the passive resistance and pile length for this computation are determined for a factor of safety of unity. The writer suggests that for cohesive soils a factor of safety of 2 be introduced by using K_P from Eq. 21*b* in computing passive resistance and pile length.

Pile Length.—The author recommends that in determining pile length a factor of safety be introduced by using a fraction of the computed passive resistance. The length is then increased 20%—thus, a double factor of safety is introduced. When the problem involves clays and a factor of safety is used in the active pressure as well as in the passive pressure, then the extra 20% in length need not be considered.

Medium Clay.—The writer suggests that the term "medium" when applied to a clay be restricted to a description of the clay's plasticity. The term "firm" could be used to describe a clay having an unconfined compressive strength of 0.5 ton per sq ft to 1 ton per sq ft.

Increase of Shear Strength.—In Part I (under the heading, "The Shear Resistance of Soils and the Angle of Repose") it is stated that increased shear strength is harmful. This statement should be limited to the increased strength caused by passive pressure at the toe. This effect will normally be small, whereas the increased strength resulting from a surcharge can be large and beneficial.

---

[59] "Performance of Steel Sheet Piling Bulkhead," by Norman D. Lea, *Proceedings*, Third International Conference on Soil Mechanics and Foundation Eng., Zurich, Switzerland, Vol. II, 1953, p. 180.

Anchor Connections.—Particularly in clay soils, there is a great reduction in the load on the anchor rod when yielding is allowed. This yielding may not occur until the yield point of the metal is reached; it is thus important that all connections be stronger than the rods.

S. PACKSHAW,[60] M. ASCE.—A valuable service has been rendered by the review of the design of anchored bulkheads and by the summary of the research results in this field.

In Part I (under the heading, "Unbalanced Water Pressure") attention is drawn to the influence of seepage forces in reducing the passive pressure coefficient K_P. Hitherto this effect has been almost completely ignored, as if no reduction existed. However, this omission is qualified by the fact that the value of H_u in most bulkheads is small in comparison to the depth of penetration D. Thus, the corresponding reduction $\Delta\gamma'$ in the unit weight of the retained soil (Fig. 5(*c*)) may therefore amount to only a few pounds per cubic foot—an insignificant amount. If H_u exceeds approximately 3 ft, most designers attempt to relieve the hydrostatic head by providing weep holes in the bulkhead and, if necessary, filters.

The influence of seepage forces, however, is too important to be neglected when allowance must be made for higher values of H_u, particularly in cofferdams and sheeted excavations. Examination of Mr. McNamee's work[61,62] shows that the coefficient, 3, in Eq. 3 is actually (as stated by Mr. Terzaghi) somewhat greater—approximately 3.7 for a ϕ-circle wedge of failure. The difference, although not large, may be of some consequence in the design of a cofferdam.

The author has made extensive comments on Mr. Rowe's research[19] on the relationship between the flexibility of the wall and the bending moment that it has to withstand. In a joint contribution[63] with J. Owen Lake, A.M. ASCE, to the discussion of Mr. Rowe's paper, the writer compared the results of Mr. Rowe's method with the conventional fixed-earth-support procedure. In the latter procedure, G_s is assumed to be equal to unity, but there is, in fact, a substantial factor of safety against ground failure because the penetration is designed to be sufficiently great to assure fixity. A similar comparison to the author's method of design may be of value.

Fig. 28 shows three typical bulkheads with retained heights of 20 ft, 30 ft, and 40 ft. Fig. 29(*a*) and Fig. 29(*b*) show the relationship between the flexibility number and the bending moment (or stress) for these bulkheads when retaining loose sand and dense sand, respectively. In Fig. 29, notation such as 4B-228 is used to signify a 4B piling section[64] stressed to 22.8 kips per sq in. The corresponding penetrations and tie-rod loads are given in Table 4.

---

[60] Director, The British Steel Piling Co., Ltd., London, England.

[61] "Seepage into a Sheeted Excavation," by J. McNamee, *Geotechnique*, Vol. I, 1949, p. 235, Fig. 4.

[62] *Ibid.*, p. 235, Fig. 5.

[63] Correspondence of J. Owen Lake and S. Packshaw of "Anchored Sheet-Pile Walls," by P. W. Rowe, ***Proceedings***, Inst. of C. E., London, England, Vol. 1, Pt. 1, 1952, pp. 621–633.

[64] "Larssen Steel Sheet Piling," The British Steel Piling Co., Ltd., London.

In the conventional method of design, it is assumed that the wall will be fully fixed and that its deformation below the dredged level will be such that the passive pressures required for the formation of the necessary negative bending moment can be developed; there is no logical justification for this assumption. However, Mr. Rowe's research showed that full fixity (that is, a negative bending moment almost as great as the positive) always develops when the wall penetrates dense soil. On the other hand, only a small degree of fixity is obtained with walls that penetrate loose soil although there is some negative moment, however slight, in every case. Realizing that loose, noncohesive soils are rather uncommon in their natural state, it can be argued that most walls designed by the conventional method develop a major part of the required fixing moment. This statement will doubtless cause some satisfaction to those engineers who were compelled to use the conventional method prior to the publication of Mr. Rowe's research.

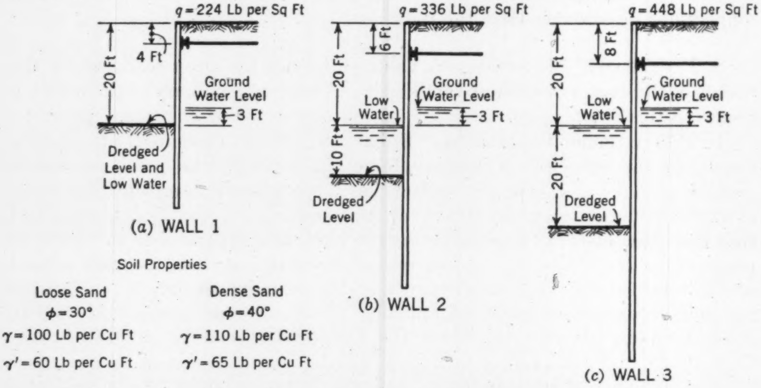
$q = 224$ Lb per Sq Ft
20 Ft
4 Ft
Ground Water Level
3 Ft
Dredged Level and Low Water
(a) WALL 1
$q = 336$ Lb per Sq Ft
6 Ft
20 Ft
Low Water
Ground Water Level
3 Ft
10 Ft
Dredged Level
(b) WALL 2
$q = 448$ Lb per Sq Ft
8 Ft
20 Ft
Low Water
Ground Water Level
3 Ft
20 Ft
Dredged Level
(c) WALL 3
Soil Properties
Loose Sand
$\phi = 30°$
$\gamma = 100$ Lb per Cu Ft
$\gamma' = 60$ Lb per Cu Ft
Dense Sand
$\phi = 40°$
$\gamma = 110$ Lb per Cu Ft
$\gamma' = 65$ Lb per Cu Ft

Fig. 28.—Retaining Walls Used for Comparing Design Methods

TABLE 4.—The Resulting Penetrations and Tie-Rod Loads for the

Wall	(a) Loose Sand, $\phi = 30°$							
	Penetration, in Feet				Tie-Rod Load, in Kips per Foot of Wall			
	Conventional	K. Terzaghi[a]	P. W. Rowe	K. Terzaghi, allowing full flexibility reduction[a]	Conventional	K. Terzaghi	P. W. Rowe[b]	K. Terzaghi, allowing full flexibility reduction
1	15.5	16.8	14.8	16.8	4.7	5.8	4.6	5.8
2	22.5	22.6	22.0	22.6	10.3	13.0	9.9	13.0
3	28.4	28.8	25.3	28.8	18.1	22.0	18.1	22.0

[a] Including the recommended addition of 20%. [b] Corresponding to a

The conventional method of designing anchored bulkheads (which was introduced[65] in 1931 and has been used for the design of thousands of retaining walls throughout the world) deserves another comment: There have been no known cases of failure or excessive deflection which could be attributed directly to the method of design and not to the causes referred to by the author in Part II (under the heading, "Safety Requirements: Bulkhead Failures"). This leads to the general conclusion that the conventional method, when applied with proper consideration of the site conditions, is not unsafe.

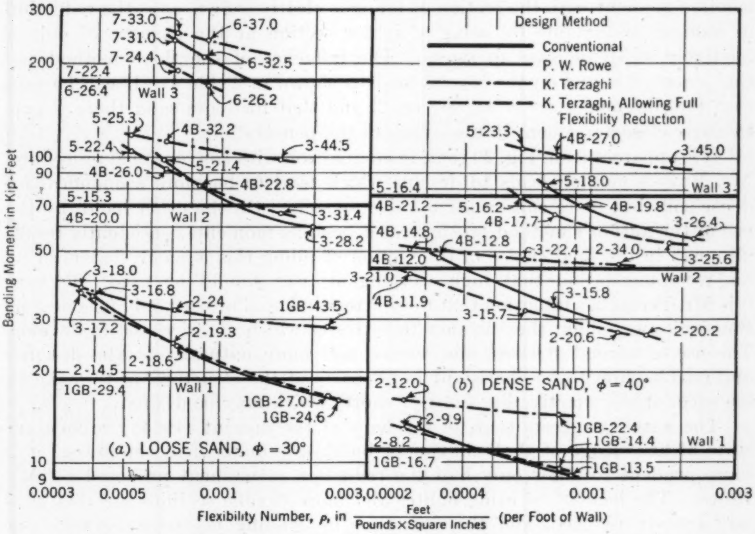

FIG. 29.—THE RELATIONSHIP BETWEEN BENDING MOMENT AND FLEXIBILITY NUMBER FOR THE RETAINING WALLS SHOWN IN FIG. 28

VARIOUS METHODS OF DESIGNING THE RETAINING WALLS SHOWN IN FIG. 28

(b) DENSE SAND, φ = 40°

PENETRATION, IN FEET				TIE-ROD LOAD, IN KIPS PER FOOT OF WALL				Wall
Conventional	K. Terzaghi[a]	P. W. Rowe	K. Terzaghi, allowing full flexibility reduction[a]	Conventional	K. Terzaghi	P. W. Rowe[b]	K. Terzaghi, allowing full flexibility reduction	
9.0	7.7	7.0	7.7	2.6	3.2	2.7	3.2	1
13.8	10.8	11.1	10.8	6.1	7.3	5.2	7.3	2
17.4	13.3	13.2	13.3	9.7	12.5	9.4	12.5	3

steel-pile section which will develop stresses within the perscribed limits.

---

[65] "Einspannungsverhältnisse bei Bohlwerken," by Hermann Blum, Wilhelm Ernst and Son, Berlin, Germany, 1931.

In Fig. 29(*a*) and Fig. 29(*b*) the results of the conventional method, which is unaffected by flexibility, are indicated by horizontal straight lines. The moments obtained by using Mr. Terzaghi's method were derived from one of the proprietary ranges of steel piling and are shown by the dash-dotted lines; those from Mr. Rowe's method are shown by solid lines. The variation in bending moment with the section of piling is clearly shown, as is the reduction in moment obtainable by using a lighter section at the expense of only a relatively small increase in stress. The influence of the three methods on the penetration and on the tie-rod loads is shown in Table 4. It can be seen that the differences are relatively small and that for loose sand there is particularly close agreement in the values of the penetration.

It is apparent from Fig. 29 that, in comparison with conventional procedure, Mr. Rowe's method leads to designs which tend to be more economical for dense soils but more conservative for loose soils. On the other hand, by the use of the author's method much greater bending moments consistently result, although in the final choice of the section of piling this is partly balanced by his recommendation that high working stresses should be used. Perhaps it is Mr. Terzaghi's intention that these stresses should be used only for selecting the section of piling; they are not the stresses which are expected to develop. The use of normal stresses, however, comes more naturally to the designer and enables him to be consistent in all parts of the structure, or to make allowance for the effective life (long or short) which may be desired.

The author suggests that, in the light of the present (1954) rudimentary state of knowledge of the behavior of bulkheads under field conditions, it is more prudent to allow only half the reduction in moment proposed by Mr. Rowe. The benefits of using lighter and more flexible sections are then proportionately reduced, and the difference in bending moments between one section and another often becomes so small that, within the limits of the range of available sections, it is not worth taking into account. To illustrate the effect of applying the full reduction proposed by Mr. Rowe to the author's method, curves shown by dashed lines have been included in Fig. 29. If these curves are used as a basis of design, it is suggested that more conservative stresses than those recommended by Mr. Terzaghi be used in the choice of a suitable section of piling.

Mr. Rowe has suggested[19] that design should be based on a factor of safety, G_s, of 1.5 in computing the passive pressure and that wall friction should be neglected. These recommendations actually result in G_s being at least 3. Mr. Rowe also introduces a horizontal shear force and a vertical end thrust at the bottom of the wall as secondary sources of moment reduction. One may doubt the existence of the end thrust or the importance of the shear force. In any case, these forces are small in comparison with the main cause of moment reduction—the flexibility of the wall—and may therefore be neglected without serious error. The reason for taking G_s equal to 1.5 and neglecting friction in determining the free-earth-support moment is that by doing so the computed moment can be made to agree with that which was actually measured in Mr. Rowe's tests on walls having less than the critical flexibility. A computation based directly on conventional earth-pressure theories, with an allowance made for wall friction and with no factor of safety, results in bending moments that are too large to agree with the test results. Probably, for similar reasons, Mr. Terzaghi recommends that the free-earth-support moment should be derived from the coefficients of Table 2, which allow for wall friction, divided by a factor of safety of not less than 2 (except in the case of silts or clays). The fact that the dashed curves in Fig. 29 (the author's design method allowing full flexibility reduction) are fairly close to the full lines (Mr. Rowe's method) is an indication that both procedures lead to similar results.

Mr. Terzaghi's advice that the penetration should always be designed with generous allowances for possible variations in the retained height and in the assessment of soil properties cannot be questioned. Indeed, one of the virtues of the conventional method is that it results in generous penetrations. However, the recommendation that, in determining the passive pressure, a substantial factor of safety should be used affects not only the penetration but also the bending moment. A figure[66] offered by Mr. Rowe gives the bending-moment curves for walls retaining loose sand and driven (*a*) into loose sand and (*b*) into sand which is dense below 0.6 H. The curves show that, in changing from dense sand to loose sand, the bending moment doubles (approximately). The application of a factor of safety of 2 to the value of K_P selected from Table 2 has a similar effect, and this effect becomes even more marked if the designer has to contend with material such as silty sand, for which the reduced value of K_P might be 2 or less.

It is inevitable that a change in the soil properties below the dredge line should influence the design of the piling above it. It appears, however, that an attempt should be made to separate the effect of the factor of safety on the penetration (and hence the over-all stability of the wall) from its effect on the bending moment and stress in the sheet piling. A simple method of performing this separation would be to use a factor of safety equal to unity and to allow for wall friction in determining the penetration for the free-earth-support condition. The penetration should then be increased by a factor of 2 (or more) so as to make it correspond approximately to the penetration for a fixed wall. Then the full flexibility reduction could be applied to the free-earth-support moment and a section selected which can withstand that moment without exceeding the normal stresses for the material. This procedure, however, has the disadvantage that the free-earth-support moment computed on this basis is substantially greater than the value of M(max) (Figs. 13 and 16) corresponding to that obtained by actual measurement in Mr. Rowe's tests. Whatever procedure is adopted, much must be left to the discretion of the designer and to his interpretation of the soil and site conditions. The amount of the reduction in the bending moment that may be made in mixed sand or silt and clay strata must also be decided by the individual designer.

Mr. Rowe found that, notwithstanding the care taken in installing the apparatus, there were substantial variations (up to 50%) in the tie-rod loads. However, these variations are likely to be much smaller in an actual bulkhead than in the model. The author suggests that no allowance should be made for the reduction in tie-rod load caused by the flexibility of the piling. Fig. 14 shows that for loose sand the reduction averages approximately 30% and that for dense sands it is greater than 50%. Although the tie rods and anchorages are only a minor part of the total cost of a bulkhead, the influence of flexibility seems too important to be neglected altogether. It is suggested, therefore, that (*a*) the tie-rod loads should be increased by 15% to 25% so as to allow for the differential yield of the tie rods and anchorages and (*b*) the full flexibility reduction should be permitted.

---

[66] "Anchored Sheet-Pile Walls," by P. W. Rowe, *Proceedings*, Inst. of C. E., London, England, Vol. 1, Pt. 1, 1952, p. 48, Fig. 16(a).

Mr. Terzaghi advises in Part II (under the heading, "General Design Procedure") that sand should be classified as silty if more than 5% passes the 200-mesh sieve. It would be instructive to have information concerning the line of demarcation between silty sand and silt, and the average values for K_A and K_P for (*a*) gravel or sand-and-gravel mixtures and (*b*) backfilling of broken rock.

In Eqs. 14 and 15 and in the corresponding pressure coefficients for silt and clay in Table 2, the author gives expressions which are applicable to smooth, frictionless walls. If adhesion is taken into account, the value of q_u can be multiplied by as much as 1.4 for the active pressure and 1.3 for the passive pressure[67] if the adhesion is equal to the shear strength of the clay. The effect of adhesion on the active pressure is relatively small, but it may be substantial on the passive pressure. This effect is in accordance with Mr. Terzaghi's recommendation in Part II (under the heading, "Safety Requirements: Passive Earth Pressure") of a somewhat lower value of G_s for silt and clay.

In Part II (under the heading, "Safety Requirements: Allowable Fiber Stresses in Sheet Piles") the author states that, if the piles have their locks on the neutral axis, the design should be based on the assumption that the locks are lubricated. Whether sections of piling of this type act as separate units, or whether the friction in the locks is sufficient to develop the full interlocked section modulus, has been discussed frequently and at length. It should also be realized that, although the piles behave as single sections when the locks are oiled, a sprinkling of dry sand will cause sufficient friction to develop approximately 75% of the interlocked modulus.[68] More friction, sufficient to develop almost the whole of the modulus, may be expected when the piles are driven into the ground. After the piles have been in position, even for a short time, the formation of rust inside the locks also causes them to act as solid joints.[69]

Mr. Terzaghi, in Part I (under the heading, "Influence of Flexural Rigidity on Bending Moment"), investigates the possibility of piles driven into clay behaving as "fixed" piles. The consolidation of the clay can be expected to cause a transition from a fixed-support condition to a free-support condition or to some intermediate stage. However, in the absence of any field observations it is impossible to state how long this process would take. It may be that even firm clay may be stiff enough to permit several decades to elapse before a substantial change in the condition of support occurs. Innumerable bulkheads have been designed by the conventional method to be fixed in clays of varying grades, but there is no evidence that any have developed the noticeable deflections which one would associate with the change to free support.

---

[67] "Earth Pressure and Earth Resistance," by S. Packshaw, *Journal*, Inst. of C. E., London, England, February, 1946.

[68] "Die Spannungen in der Larssenwand," by E. Lohmeyer, *Die Bautechnik*, 1937, No. 53.

[69] "Civil Engineering Code of Practice No. 4 (1954)—Foundations," Pt. 4, Inst. of C. E., London, England, 1954, Item 4.33072.

There is one other aspect of bulkhead design which deserves comment—namely, the necessity of providing an anchorage which is not only of sufficient size but is also able to withstand its loads with a minimum amount of movement or consolidation. On this basis, an anchorage consisting of backward and forward raking piles forming an A-frame seems to be of doubtful value unless capped with a platform which, together with the overlying soil, imposes a vertical load on the piles. The value of ordinary anchor blocks which develop their resistance from the passive pressure of the ground in front of them may be much reduced if the ground against which they are to bear is disturbed during excavation for the blocks and tie rods. Particular care should then be taken in selecting the quality of the material for the backfilling and in ramming it against the bearing faces of the blocks.

J. Verdeyen[70] and V. Roisin.[71]—Several of the concepts offered by Mr. Terzaghi are not agreed with by the writers. In the case of the forces acting on the inner face of a bulkhead, there is a linear distribution of active earth pressure (as shown in Fig. 15) when a bulkhead is loaded by soil placed behind the wall. The linear distribution also occurs in the case in which an excavation has been made along the face of a bulkhead which has an anchorage that yields so as to make the wall rotate about the foot. When the anchorage is nonyielding, however, the pressure distribution assumes that distribution shown in Fig. 30. The differences between Figs. 15 and 30 are quite important, as they result in theoretical loads on the anchorage that differ widely.

To illustrate the differences between the results obtained by use of the concepts offered in Figs. 15 and 30, the anchor pull A_p has been computed for Bulkheads A and B (shown in Fig. 31):

Bulkhead	A_p, in tons per linear yard	
	Fig. 15	Fig. 30
A	11	21
B	9.7	18

These differences appear to be quite large, and one might tend to discount the results obtained by the use of Fig. 30. Experimental investigation, however, has shown (Fig. 32(*a*)) that for Bulkhead A (with nonyielding supports) the value of A_p was even greater than 21 tons per lin yd.

Bulkheads A and B were used in 1953 on a project in Brussels, Belgium. The bulkhead wall and the props were made from DIN 22 and DIN 24 sections (Bulkhead B) and from DIN 32 sections (Bulkhead A). The properties of these sections are given in Table 5. The abscissa of Fig. 32 gives the time, in days, from the beginning of the project. At the end of the twenty-third day, the earth lying between Bulkhead A and the foot of the prop was removed until it was level with the lower face of the reinforced concrete floor on the left of Fig. 31(*a*). For Bulkhead B a period of 8 days was needed for a similar operation. Of the six type B bulkheads that were investigated, three (curves B9, B13, and B14 in Fig. 32(*b*)) had nonyielding supports, and three (curves B10, B11, and B12 in Fig. 31(*b*)) had supports that yielded $\frac{1}{5}$ in. The resulting mean curves show that the anchor pull on bulkheads with nonyielding supports is considerably greater than the anchor pull on bulkheads with yielding supports.

---

[70] Cons. Engr. and Prof. of Civ. Eng., Brussels Univ., Brussels, Belgium.

[71] Assistant in Civ. Eng., Brussels Univ., Brussels, Belgium.

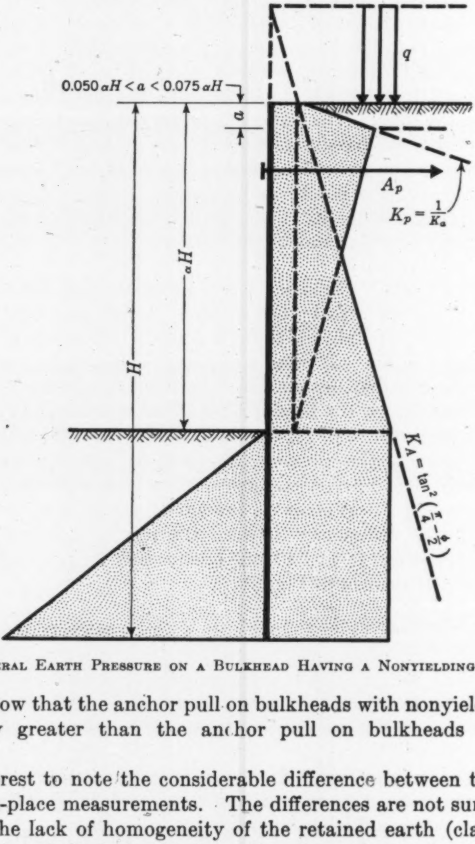
q
$0.050\,\alpha H < a < 0.075\,\alpha H$
a
A_p
$K_p = \frac{1}{K_a}$
αH
H
$K_A = \tan^2\left(\frac{\pi}{4} - \frac{\phi}{2}\right)$

FIG. 30.—LATERAL EARTH PRESSURE ON A BULKHEAD HAVING A NONYIELDING ANCHORAGE

It is of interest to note the considerable difference between the computed load and the in-place measurements. The differences are not surprising when one considers the lack of homogeneity of the retained earth (clay lentils and old foundations) and the lack of information about the mechanical properties of the soil. From an investigation of the neighboring soil, the following values were used in the theoretical determinations: $\phi = 35°$, $\delta = 0$, $c = 0$, $\gamma = 1.43$ tons per cu yd, and $\gamma' = 0.86$ tons per cu yd. Because of the lack of homogeneity, the computations may be considered to have an unsound basis. From the measurements, however, it can be seen that the deformability of the support greatly influences the anchor pull.

It is surprising that in Part II, under the heading, "Safety Requirements," Mr. Terzaghi makes no mention of the change in anchor pull with the passage of time. In the case of a backfilled bulkhead, it is believed prudent to use as the maximum load that load which corresponds to the restoration of the at-rest earth pressure. This load is characterized, according to Curt Kollbrunner,[72] by

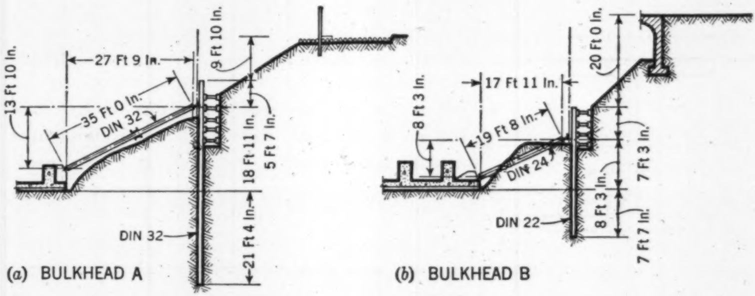

(a) BULKHEAD A (b) BULKHEAD B

FIG. 31.—CROSS SECTIONS OF EXPERIMENTAL BULKHEADS

$$K_0 = 1 + \tan^2 \phi \ldots\ldots\ldots\ldots\ldots\ldots\ldots (22)$$

Eq. 22 is applicable when the depth of embedment is less than a given depth, z_0, which is characteristic of the depth of the soil layers. Below this critical depth z_0, the pressure is assumed to be constant. Although Eq. 22 is applicable to loaded friction piles, it may be used for bulkheads because of the agreement between pressures computed from Eq. 22 and those pressures determined from an assumption of a linear distribution of pressure. In this manner, the safety of a sheet-pile anchored bulkhead decreases to a minimum value when the consolidation of the disturbed soil is complete. Therefore, different safety factors should be used for the time at which a bulkhead begins to act and for the time at which consolidation has occurred.

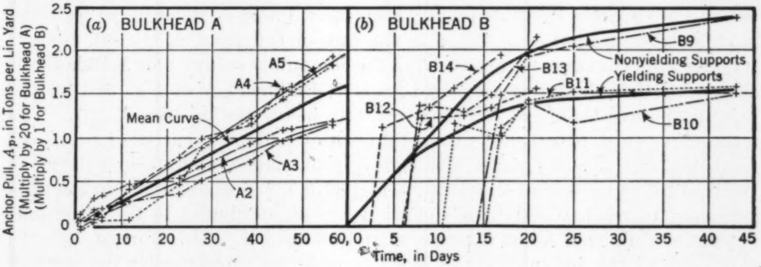

FIG. 32.—THE RELATIONSHIP BETWEEN ANCHOR PULL AND TIME FOR THE EXPERIMENTAL BULKHEADS

---

[72] "Fundation und Konsolidation," Vol. II, by Curt Kollbrunner, Schweizer Druck-und Verlagshaus, Zurich, Switzerland.

TABLE 5.—PROPERTIES OF BULKHEAD MEMBERS

Cross section	Section	Area, in square inches	h, in inches	b, in inches	a, in inches	e, in inches	I_x, in inches^4	I_y, in inches^4
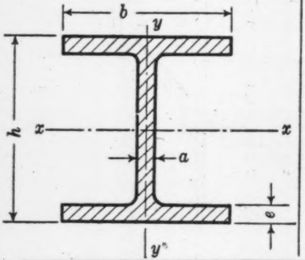	DIN 22	14.12	8.66	8.66	0.39	0.63	0.1934	0.0683
	DIN 24	17.25	9.45	9.45	0.43	0.71	0.2808	0.0996
	DIN 32	26.55	12.60	11.81	0.51	0.87	0.7748	0.2381

In the case of a bulkhead loaded as a result of an excavation along its face, the problem is similar—if the anchorage is deformable. If the support is nonyielding, however, the adoption of the modified pressure law proposed in Fig. 30 allows for a minimum safety against the restoration of the natural pressure.

In Part II, the author states (under the heading, "Safety Requirements: Allowable Stresses in Anchor Rods") "The anchor pull may also increase because of the repeated application and removal of heavy surcharges." This statement is acceptable; however, the effect of this phenomenon is minimized by Mr. Terzaghi. In fact, for Bulkhead A (Fig. 31(*a*)) measured A_p-values were approximately 1.5 times greater than the value of A_p determined from the modified pressure law (Fig. 30). In the case of Bulkhead A, the soil characteristics were the same as those used in the computation involving Bulkhead B. It appears that the larger measured loads at Bulkhead A were caused by the presence, above Bulkhead A, of a street with heavy traffic (Fig. 31(*a*)). The mean curve (Fig. 32(*a*)) shows that stabilization had not occurred at Bulkhead A at the end of sixty days, although approximate stabilization existed at Bulkhead B at the end of thirty days (Fig. 32(*b*)). This difference in the time necessary to reach a stabilized condition can be attributed to the vibrations present at Bulkhead A but not present at Bulkhead B. Therefore, it is necessary—during the design computations—to make an allowance for the increase of pressure caused by vibratory actions on the backfill, rather than introduce a correction to the safety factor at the conclusion of the computation.

Mr. Terzaghi has studied anchored bulkheads by performing a complete analysis of a bulkhead anchored at one level. The author implies that the method of investigation is also applicable to bulkheads anchored at several levels, but in this case a linear distribution of pressure does not exist. A more applicable and consistent representation of the pressure distribution is similar to that shown in Fig. 30.[73]

---

[73] "Nouvelle théorie du soutènement des excavations profondes," by J. Verdeyen and V. Roisin, *Annales*, L'Institut technique du Bâtiment et des Travaux Publics, Paris, France, June, 1952, No. 54, pp. 601–628.

Karl Terzaghi,[74] **Hon. M. ASCE.**—The well-documented case record offered by Mr. Wu is an instructive example of competent interpretation of the results of the subsoil exploration for the site of a dredged bulkhead.

The boring records indicated that the soil conditions west of Oregon St. were generally more favorable than were the conditions east of this street. Therefore, the designer decided to divide the bulkhead into two sections, meeting at Oregon St., and to design each section in accordance with the most unfavorable soil conditions encountered in this section. Table 3 illustrates the fact that this procedure was satisfactory and economical. In each section the scattering of the measured strut pressures from the average was considerable, but in both sections the maximum value was close to the value on which the design was based.

Mr. Bigler has proposed a convenient graphical procedure for solving Eq. 17.

A comparison between the writer's design procedure and the bulkhead design on the basis of the Danish Rules has been made by Mr. Hansen. The Danish Rules involve the assumption that the lateral pressure on the bulkhead increases from a minimum at about midheight of the bulkhead in an upward as well as in a downward direction. The experiments performed by Messrs. Tschebotarioff[18] and Rowe[19] indicate that such a pressure distribution develops only under special conditions. In practice, the existence of these conditions is rather uncommon; yet, according to Mr. Hansen, none of the bulkheads designed on the basis of the Danish Rules has failed. Hence, it can be concluded that the factor of safety for these bulkheads is considerably lower than the designers assumed—without being low enough to cause the bulkheads to fail. There is no doubt that the design of these bulkheads was economical; however, similar economies could be realized by reducing the factor of safety in design procedures which are based on more conservative assumptions concerning the distribution of the lateral pressure.

Also—according to Mr. Hansen—a comparatively rigid bulkhead (such as a bulkhead consisting of reinforced concrete sheet piles) has a greater reserve of strength than a flexible one because the flexible bulkhead has already exhausted the possibilities for a redistribution of the earth pressures, whereas the rigid one has scarcely begun its redistribution. Rigidity, however, is commonly associated with low deflection at failure, and a rigid bulkhead may fail before the deflection can produce a significant redistribution of the pressure. For the same reason, the struts in an open cut may fail by buckling before they have yielded sufficiently to induce a radical redistribution of pressure. Hence, the design of earth supports on the basis of the state of failure in the supported earth may lead in some, if not in many, cases to disappointing results.

Mr. Tschebotarioff's discussion is principally concerned with a comparison of his equivalent-beam method and Mr. Rowe's method of designing bulkheads composed of sheet piles driven into sand. Because this comparison is rather involved, one must begin with a brief review of the essentials of the subject (Fig. 22(*b*)).

---

[74] Prof. of the Practice of Civ. Eng., Harvard Univ., Cambridge, Mass.

In Fig. 22(*b*) the abscissa represents Mr. Rowe's flexibility number, ρ, which is a measure of the degree of flexibility of a sheet pile; the term ρ is defined in Eq. 12. The curves in Fig. 22(*b*) labeled "P. W. Rowe's Mean Curves" represent a digest of Mr. Rowe's test results. They show the relationship between flexibility number and moment reduction for dense, average, and loose sand.

From 1944 to 1948, Mr. Tschebotarioff performed tests[18] on bulkheads with various flexibility numbers. In Fig. 22(*b*) the range covered by these tests is labeled the "Range of Princeton Tests." It was found that the measured bending moments were approximately equal to those computed on the assumption that the upper part of the sheet piles is freely supported at the dredge line (Fig. 23(*b*)). This upper part was termed the "equivalent beam," and the procedure for computing the bending moments in the sheet piles is referred to in Fig. 22(*a*) as "G. P. Tschebotarioff's Equivalent Beam Theory." In Fig. 22(*b*) the moment reduction computed on the basis of this theory is represented by an horizontal line, labeled "G. P. Tschebotarioff's Design Proposal Line." The position of this line in Fig. 22(*b*) is independent of both the flexibility number and the density of the sand into which the piles were driven. Mr. Tschebotarioff qualified his recommendation by the following statement:

> "There is, however, no justification in applying the writer's proposal (Fig. 23(*b*)) indiscriminately to unusual conditions differing radically from those to which it referred * * *. Such misuse might indeed lead to results on the unsafe side.[42]"

However, before Mr. Rowe published his data[19] Mr. Tschebotarioff could not make any definite suggestions for the computation of the bending moments under "unusual conditions" because he had no observational data beyond the "Range of Princeton Tests" at his disposal. Furthermore, at that time he could not furnish any specific information concerning the limits for the validity of his theory because one of these limits was located in "unexplored territory," on the left side of the "Range of Princeton Tests" in Fig. 22(*b*).

Mr. Rowe supplemented Mr. Tschebotarioff's investigations by many more tests covering the entire range of conditions which can conceivably be encountered in designing bulkheads composed of sheet piles driven into sand. Furthermore, Mr. Rowe introduced into the investigations the concept of the flexibility number; he divided his test data into groups, according to flexibility number and relative density of the sand below the dredge line (all of which had not been done before). Mr. Rowe devised the graphical method of plotting his classified test results for which Fig. 22(*b*) is an example. The test results themselves are represented by the curves labeled "P. W. Rowe's Mean Curves." These curves illustrate the fact that the moment reduction depends on both the flexibility number and on the density of the sand, whereas Mr. Tschebotarioff's reduction factor is independent of these parameters.

At the present time (1954) "P. W. Rowe's Mean Curves" in Fig. 22(*b*) represent the only classified set of experimental data concerning the influence of flexibility and sand density on moment reduction. Therefore, these curves have been used by the writer as a basis for estimating the errors associated with Mr. Tschebotarioff's simplified procedure for computing the reduction factor.

The term "error on the unsafe side" indicates an excess of Mr. Rowe's reduction factor over Mr. Tschebotarioff's reduction factor, in percentage of the latter. Hence, if

$$r_T = \frac{M}{M\,(\text{max})} \qquad (23)$$

is the reduction factor computed by Mr. Tschebotarioff's theory for sheet piles with a given flexibility number ρ and if r_R is the reduction factor determined by the ordinate of Mr. Rowe's curve for loose sand—for sheet piles with the same flexibility number—the error is defined by

$$e_{RT} = 100\,\frac{r_R - r_T}{r_T} \qquad (24)$$

From Fig. 22(*b*) the following information can be obtained concerning the magnitude of these errors. Within the "Range of Princeton Tests" the error does not exceed 14%. Hence, within this range, Mr. Tschebotarioff's procedure represents an expedient and reliable method for computing the moment reduction. According to Fig. 22(*b*) the legitimate use of this procedure is limited to sheet piles with a flexibility number of more than approximately 18 in.^{2} per lb per ft—that is, within this range the designer can safely use the procedure of either Mr. Tschebotarioff or Mr. Rowe. However, at the left boundary of Mr. Skempton's "Normal Range," corresponding to a flexibility number of approximately 12 in.^{2} per ft and $\log \rho = 3.3$, the error on the unsafe side is 66%, which is excessive. Hence, if the flexibility number of the sheet piles is less than approximately 18 ($\log \rho = -3.0$), the moment reduction should be determined only by Mr. Rowe's curves.

Because Mr. Tschebotarioff's method of design is expedient, the following procedure is indicated: The sheet piles should be dimensioned by the equivalent-beam method. If the flexibility number is beyond the "Range of Princeton Tests," it is necessary to repeat the computation—this time by trial and error on the basis of Mr. Rowe's mean curves in Fig. 22(*b*), as described under the heading, "Computation of Maximum Bending Moments."

Mr. Rowe's procedure too cannot be considered perfect because tests conducted on a larger scale and under different conditions may furnish flexibility-moment reduction curves which are somewhat different from those he obtained. At the present time (1954), however, his data are the most reliable and accurate enough for all practical purposes.

It is agreed that, as Mr. Tschebotarioff recommends, the dimensions assigned by Mr. Rowe to the flexibility number should be replaced by square inches per pound per foot. The writer retained Mr. Rowe's dimensional equation for the purpose of facilitating comparison with Mr. Rowe's original data. The conversion can readily be performed by using the curve in Fig. 22(*a*).

In order to explain his procedure, Mr. Tschebotarioff described (under the heading, "Example") the design of a bulkhead 45 ft high, backfilled with sand. According to the equivalent-beam theory, the reduction factor r_T is 0.45, and the bending moments make necessary the use of an MZ-22 section, represented in Fig. 22(*b*) by the MZ-22 curve, with a value for $\log \rho$ of approximately $-$ 2.85.

If the sand into which the piles are driven were loose, Mr. Rowe's curve for loose sand would necessitate a reduction factor r_R of 0.54 for the same sheet piles. Hence, in accordance with Eq. 24, the error, e_{RT}, involved in using Mr. Tschebotarioff's procedure would be 20%, a tolerable error.

The bulkhead which Mr. Tschebotarioff used as an example was assumed to retain a backfill consisting of sand. If, however, the same bulkhead were backfilled with dredged silt or clay—which is not an unusual condition—curves 1 and 2 in Fig. 22(*a*) and the corresponding curves marked MZ 22 to MZ 38 in Fig. 22(*b*) would be displaced to the left, because much heavier sheet piles with a lower flexibility number would be required to support the backfill. As a consequence, r_R is much greater than 0.54, and the error becomes important.

According to Mr. Tschebotarioff, both Mr. Rowe and the writer overemphasize the influence of the relative density of the sand below the dredge line and underestimate the effect of the depth of sheet-pile penetration on the conditions of end support. To illustrate his argument concerning the influence of relative density on moment reduction, Fig. 25 was presented. The position of points 54, 54A, and 56 in Fig. 25(*b*) is abnormal indeed. However, in tests 54 and 54A the backfill carried a heavy surcharge, and in test 56 the depth of sheet-pile penetration had the abnormally small value of 0.27 H. These facts probably explain why Mr. Rowe did not show these points in his diagram from which Fig. 25(*a*) is derived.

In the writer's opinion the influence of relative density on the conditions of end support can hardly be overemphasized. This opinion is based chiefly on experiences in pile driving and on the results of loading tests. If a sand stratum is dense, piles meet refusal at a depth of a few feet below the surface, whereas, if the sand is loose, the piles can be driven without difficulty to a depth of several tens of feet. The differences in resistance to pile penetration are associated with equally important differences in compressibility, which determine the value of the "coefficient of horizontal subgrade reaction." This fact is shown by the differences in the settlement of bearing plates on dense and loose sand at equal load and loaded area.

The driving of a single row of sheet piles cannot be expected to convert a loose sand into a dense one. Therefore, it is maintained that the influence of the relative density of the sand below the dredge line on the conditions of end support is at least as important as the influence disclosed by Mr. Rowe's test results.[19] For the same reason, the writer considers it necessary to adapt the depth of sheet-pile penetration to the relative density of the sand, assigning a lower K_p-value to the loose sand than to the dense sand. The writer does not concur with Mr. Tschebotarioff's proposal to drive the sheet piles to a depth of 0.43 H irrespective of the density of the sand.

Mr. Tschebotarioff further discusses the criteria for active and passive earth-pressure conditions. In connection with retaining walls and arch abutments, the terms "active" and "passive" earth pressure have a well-defined meaning. At the lower end of the sheet piles of an anchored bulkhead the entire body of sand in contact with the sheet piles moves out, and the sheet piles move with reference to the sand. Under such conditions the terms "active" and "passive" become meaningless abstractions.

Mr. Tschebotarioff mentions methods of reducing the lateral pressure by the use of sand fills. This procedure was used successfully by the writer in 1941 with a cellular bulkhead.[75] Mr. Tschebotarioff's subsequent experimental investigations of this procedure (Fig. 11, tests 4 and 5) led to the same conclusions as did the preceding observations on a full-sized structure. The principle is simple: The lateral pressure on the bulkhead depends on the material in which the potential surface of sliding is located. Hence, by replacing an unstable material, such as soft silt, by a granular material having a high angle of internal friction, the pressure on the lateral support is reduced.

Mr. Baumann is correct in stating that stresses in a flexible bulkhead can be accurately computed only by treating the bulkhead as a statically indeterminate system. However, the basic equations contain the coefficient of horizontal subgrade reaction, and the observational data required for estimating this value are inadequate (as of 1954).

A comment is also made by Mr. Baumann concerning the allowable stresses in the steel. In this connection, distinction must be made between the bending stresses in the sheet piles and the tensile stresses in the anchor rods. In the sheet piles the yield point is reached only in those short sections where the bending moment is close to the maximum. Because of this fact the plastic deformation of the steel is localized, and the energy required to produce a large deflection of the sheet piles is relatively small. In the anchor rods, however, the yield point is reached almost simultaneously at every point between anchor and wale, and the rapid elongation which ensues when the steel is stressed beyond the yield point is inconsequential, provided the connections are stronger than the rod. In some cases it is even beneficial.

Both Mr. Baumann and Mr. Packshaw discuss the writer's recommendation that locks located in the neutral plane of a row of sheet piles should be considered frictionless. The friction which develops in the locks during the process of driving the sheet piles depends not only on the type of soil which is penetrated but also on the design of the locks. The locks of some types of sheet piles are fairly tight whereas others are loose. The importance of the influence of lock friction on the flexibility number and, as a consequence, on the allowable moment reduction is strikingly revealed by the two curves labeled "Larssen V (Lubricated Joints)" and "Larssen V (Solid Joints)" in Fig. 22(*a*). However, a reliable estimate of the lock friction is impracticable. Therefore, one should design on the basis of the more unfavorable assumption, which is to consider the locks to be frictionless.

It is contended by Mr. Packshaw that "* * * the conventional method, [of bulkhead design], when applied with proper consideration of the site conditions, is not unsafe." However, in some cases it may be somewhat uneconomical. If, for example, the sheet piles are to be driven into dense sand, the conventional method necessitates an excessive depth of sheet-pile penetration, as shown by the values in Table 4(*b*).

---

[75] "Shipways with Cellular Walls on a Marl Foundation," by M. M. FitzHugh, J. S. Miller, and Karl Terzaghi, *Transactions*, ASCE, Vol. 112, 1947, pp. 298–324.

With respect to Fig. 29, Mr. Packshaw states:

> "Perhaps it is Mr. Terzaghi's intention that these stresses should be used only for selecting the section of piling; they are not the stresses which are expected to develop."

This interpretation is perfectly correct. In order to explain his intention, the writer refers to the case record illustrated by Figs. 17, 18, and 19. The distance between the borings ranges between 300 ft and 500 ft. The soil conditions prevailing between the borings can only be approximated on the basis of the geological characteristics of the site; this procedure leaves a wide margin for error. The elevated position of the writer's curves in Fig. 29 with reference to the corresponding curves proposed by Mr. Rowe is intended to compensate for the inevitable errors involved in the interpretation of the boring records.

Mr. Packshaw also comments on the writer's proposal to tolerate not more than one half of the moment reduction determined by Mr. Rowe's curves. The writer himself was not quite satisfied with this proposal; therefore, it was decided to replace it by the following one, which appears to be more appropriate and, at the same time, is equivalent to the one suggested by Mr. Packshaw. If the boring records indicate that the sand is dense, the moment reduction should be computed by the use of Mr. Rowe's curve labeled "Medium" in Fig. 13, and, if they indicate a sand of medium density, the "Loose" curve should be used.

An attempt "to separate the effect of the factor of safety on the penetration (and hence the over-all stability of the wall) from its effect on the bending moment and stress in the sheet piling" is proposed by Mr. Packshaw. During the preparation of his paper the writer made several attempts of this kind; none of them led to a satisfactory result. Unless the subsoil conditions are very simple—and they seldom are—the designer is compelled to use his own judgment. No rules of general validity can be established.

Mr. Packshaw suggests that flexibility reduction be permitted not only for the bending moments in the sheet piles but also for the stresses in the anchor rods. The writer had originally intended to do this, but afterward he decided against it because of the uncertainties involved in the computation of the anchor pull.

The computation for the anchor pull is based on the assumption that the distribution of the active earth pressure on the bulkhead is in accordance with the classical earth-pressure theory. However, because of the rigidity of the anchorage (or of some other causes), arching may develop in vertical planes, whereupon the anchor pull is greatly increased. The performance of the bulkhead shown in Fig. 33 is an example of this phenomenon. The sheet piles were driven into dense sand, and the backfill consisted of clean sand compacted in layers. The pull on the anchor rods was computed without any flexibility reduction on the assumption that the angle of internal friction of the sand was 34°, which is a very conservative value for compacted sand. The tie rods were anchored to a reinforced concrete wall, forming one of the lateral boundaries of the backfill; therefore, the anchorage was very rigid. This condition is likely to increase the anchor pull considerably. Therefore, the allowable stress in the anchor rods was assigned the low value of 17 kips per sq in. Furthermore, it was specified that the anchor rods should be installed after the backfill was raised to the level of the rods and that the connections should be considerably stronger than the rods.

During construction, the elongation of the tie rods was measured at various stages of the backfilling operations by determining the change of the distance between the outer ends of the anchor rods and those of slender dummy rods ("stretch rods"), which were attached to the anchor rods without being subjected to tension. On the basis of the results of these measurements, the stress in the anchor rods was computed. After the filling operations were completed, the stresses in the anchor rods were 26 kips per sq in. Hence, the stresses exceeded the design stress by approximately 50%.

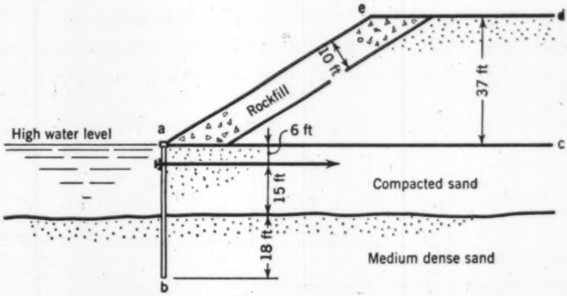

FIG. 33.—ANCHORED BULKHEAD IN DENSE SAND WITH SAND SURCHARGE AND BACKFILL

Mr. Packshaw inquires about the writer's conceptions concerning the line of demarcation between silty sand and silt. This most important question can only be answered by considering the angle of shearing resistance which has been assigned to these two materials. The increase Δs in the shearing resistance of a soil caused by an increase, Δp, of the pressure per unit of area on a potential surface of sliding is approximately equal to

$$\Delta s = (\Delta p - \Delta u) \tan \phi_s = \Delta p \tan \phi_a \ldots\ldots\ldots\ldots (25)$$

In Eq. 25 ϕ_s is the "true" angle of internal friction obtained by a consolidated-slow shear test or triaxial test; Δu is the excess hydrostatic pressure in the pore water of the soil associated with the total increase Δp of the unit pressure; and ϕ_a is the apparent angle of internal friction, also termed the angle of shearing resistance. The excess hydrostatic pressure Δu is caused by the time lag between the increase of the total pressure by Δp and the corresponding decrease of the water content of the soil.

For silty sand, the writer assumed that the excess water drains out of the soil almost as rapidly as the total pressure is increased. On this assumption $\Delta u = 0$,

$$\Delta s = \Delta p \tan \phi_s = \Delta p \tan \phi_a \ldots\ldots\ldots\ldots (26)$$

and

$$\phi_a = \phi_s = \phi \ldots\ldots\ldots\ldots (27)$$

The angle ϕ has been assigned values intermediate between 34° and 26°, depending on the relative density of the silty sand.

For silt it was assumed (as it was for clay) that the excess hydrostatic pressure is equal to the increase Δp of the total pressure ($\Delta u = \Delta p$) and that it retains its value until at least the end of the period of construction, when

$$\Delta s = (\Delta p - \Delta p) \tan \phi_s \ldots\ldots\ldots\ldots\ldots\ldots (28)$$

and

$$\phi_a = \phi = 0 \ldots\ldots\ldots\ldots\ldots\ldots\ldots\ldots (29)$$

There are many soils with properties intermediate between those of silty sand and silt, for which ϕ_a has a value intermediate between 26° and 0°.

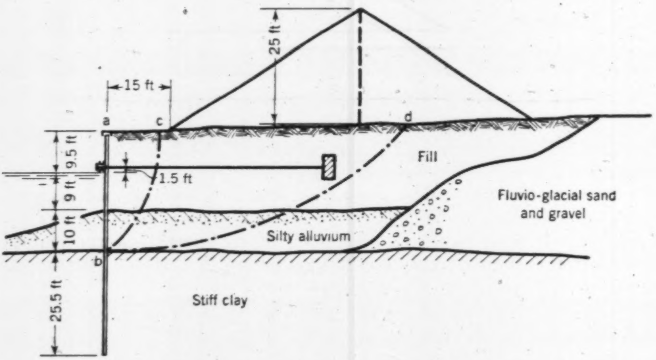

FIG. 34.—VERTICAL SECTION THROUGH AN ANCHORED BULKHEAD (BACKFILL OF SILTY SAND ON ALLUVIAL SILT)

According to the theory of consolidation, the value of ϕ_a for these soils depends on (*a*) the coefficient of consolidation of the soil, (*b*) the dimensions of the body of soil subject to an increase of pressure by Δp, and (*c*) the rate at which the pressure increases. The influence of the last two factors on the value of ϕ_a is illustrated in Fig. 34, representing a vertical section through an anchored bulkhead.

The sheet piles were driven through a layer of alluvial silt and fine silty sand to a depth of not less than 26 ft into stiff, glacial clay. The backfill consisted of silty sand. The deformations caused by the lateral pressure were imperceptible. Four years after the bulkhead was completed, a pile of sand with a diameter of 80 ft and a height of 25 ft was deposited within a few days on the surface of the backfill. According to Coulomb's theory the increase of the lateral pressure on the bulkhead caused by the weight of the sand should have amounted to less than 10% of the pressure exerted by the backfill. However, while the sand was being deposited, the upper edge of the bulkhead located next to the foot of the sand pile moved out 9 in., whereupon the surface of the backfill was no longer used as a storage space.

The excessive outward movement of the bulkhead was caused by the rapid application of the surcharge combined with the relatively low permeability of the alluvium. The rapid application of the surcharge produced an excess hydrostatic pressure in this material, whereupon the potential surface of sliding moved from position bc into position bd, and the shearing resistance along bd was inadequate.

If the thickness of the layer of silty alluvium at the base of the fill had been 2 ft rather than 10 ft, or if the pile of sand had gradually been built up in the course of several months rather than in a few days, the excess water would have drained out of the layer while the load was being increased. Consequently, the layer would have exhibited properties close to those of a silty sand and not to those of a silt, and the bulkhead would scarcely have moved. Under the conditions which actually prevailed, the alluvial layer performed in a manner similar to a typical silt, and the bulkhead almost failed.

On the basis of the facts previously outlined, no criterion of general validity can be established for discriminating between silty sand and silt. In order to learn under given conditions what value for ϕ could safely be assigned to a soil intermediate between sandy silt and silt, it would be necessary to perform consolidation and triaxial tests on representative samples of the soil in contact with the bulkhead. An estimate must then be made of the excess hydrostatic pressures which are likely to develop in the soil during the period of construction.

The instances in which such elaborate investigations would be justified economically are rather rare. Under normal conditions, the engineer has the choice of guessing as to what value of ϕ_a can be assigned safely to the soil (at the risk of overestimating this value) or proceeding on the pessimistic assumption that the "intermediate" material is a silt ($\phi_a = 0$).

Mr. Packshaw inquires concerning the values which should be assigned to gravel and to rock fill. For loose gravel the writer would use the values proposed for medium sand, and for dense gravel, those for dense sand—or even less conservative values. Rock fill is invariably deposited by dumping, and the resulting fill is relatively loose. For dumped rock fill the values assigned to medium sand appear to be appropriate.

The writer agrees with Mr. Packshaw that the possibility of the fixed earth support of sheet piles driven into firm clay or stiff silt gradually changing into a free earth support is rather remote. If the sheet piles are embedded in soft silt or soft clay, such transformation is irrelevant because in these cases the bulkheads have to be designed on the basis of the assumption of free earth support without moment reduction.

The writer shares Mr. Packshaw's aversion to anchorages consisting of piles forming an A-frame, unless the frames are capped with a platform carrying the weight of the superimposed fill. If a pile is acted upon by a force tending to pull it out of the ground, its resistance against pulling decreases rapidly with increasing upward displacement. Therefore, the tension piles of A-frames which do not carry any load may fail while the anchor rods are still intact. The writer has witnessed a failure of this type.

If the anchor pull is carried by anchor beams or anchor plates, the importance of thoroughly compacting the earth on the pressure side of the anchor cannot possibly be overemphasized. The writer appreciates that Mr. Packshaw has called attention to this fact.

The problem of computing the lateral pressure caused by irregular surcharges has been noted by Mr. Lea. He recommends that this pressure should be computed on the basis of Coulomb's theory. According to this theory, only that part of an irregular surcharge should produce an increase of the horizontal pressure on a lateral support which is located between the upper edge of the support and that of the potential surface of sliding.

In Fig. 35, ab represents an anchored bulkhead backfilled with sand; ac is the potential surface of sliding; and Q is a heavy, concentrated load located beyond ac. According to Coulomb's theory the influence of this load on the lateral pressure should be nil; yet there is no doubt that the application of this load is associated with an horizontal stretching of the underlying backfill, involving an outward movement of the entire wedge, acb, whereas the position of the anchor point A remains practically unaltered. As a consequence of this action, the lateral pressure on the bulkhead increases. Repeated removal and reapplication of the load would cause a further increase of this pressure.

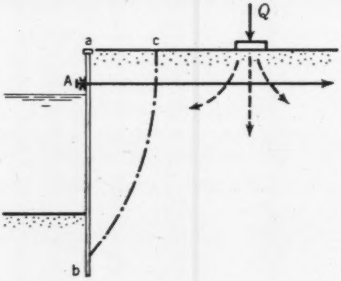

FIG. 35.—ANCHORED BULKHEAD WITH SAND BACKFILL SUPPORTING A LOAD, Q

In Fig. 33 the body of sand, acde, represents a surcharge. According to Coulomb's theory, the lateral pressure exerted by the backfill and the surcharge combined should have produced a stress in the anchor rods of approximately 17 kips per sq in. Because of the rigidity of the anchorage the actual stress was approximately 26 kips per sq in. The writer anticipated this condition, however, and the precautions previously cited were taken.

Considering these and various other facts, Mr. Lea's recommendation that the lateral pressure caused by irregular surcharges should be computed on the basis of Coulomb's theory does not appear to be a step in the right direction.

Coulomb's theory and the method proposed by the writer furnish the limits between which the real values may range. In some cases the designer may feel justified in determining the lateral pressure by Coulomb's theory, but this should not be established as a general rule. The description of bulkhead performance shown in Fig. 34 indicates the great variety of factors on which the lateral pressure caused by irregular surcharges depends.

Mr. Lea proposes that a factor of safety of 2 be introduced into the equations for K_A and K_P in Table 2, replacing these equations by Eqs. 21*a* and 21*b*. The value of q_u is usually determined by unconfined compression tests on seamless-tube samples, and these values are somewhat lower than the q_u-value of the undisturbed material. Furthermore, the adhesion between the soil and the sheet piles has been disregarded. It is believed, therefore, that the values defined by the equations in Table 2 are conservative, provided that they have been selected on the basis of the most unfavorable results of the soil tests and not on the basis of averages.

Mr. Lea implies that the writer determined "* * * the passive resistance and pile length * * * for a factor of safety of unity." In Part II (under the heading, "Computation of Depth of Sheet-Pile Penetration") the writer specified that the depth of sheet-pile penetration should be computed for a factor of safety G_s and under the subsequent heading, "Safety Requirements," values were assigned to G_s, ranging from 1.5 to 2. The additional 20% increase of the depth of sheet-pile penetration is not intended to increase the factor of safety. It is proposed for the purpose of compensating for the errors involved in the interpretation of the boring records. As the spacing between borings is commonly more than 100 ft, important errors are almost inevitable.

Mr. Lea also notes that the anchor connections should be stronger than the anchor rods. Departure from this rule constitutes faulty design.

Redistribution of the active earth pressure may occur on dredged bulkheads as well as on filled bulkheads, according to Mr. Briske. This statement is perfectly correct. At the same time it must be remembered that it is—and always will be—impracticable to determine, with certainty, in advance of construction, what type of earth-pressure distribution will ensue. Therefore, sound engineering practice requires that design be based on the more unfavorable possibility.

In order to establish a favorable redistribution of the lateral pressure, Mr. Briske recommends prestressing the anchor rods. Under no circumstances would the writer advocate such a procedure because under field conditions this procedure may increase both the stresses in the anchor rods and the bending moments in the sheet piles.

Messrs. Verdeyen and Roisin present the results of their observations on two recently constructed sheet-pile bulkheads (Fig. 31). These bulkheads, like the one shown in Fig. 34, support a surcharge consisting of a thick layer of sand with a steep slope descending to the upper edge of the sheet piles. The lateral pressure caused by such a surcharge is of the same order of magnitude as that resulting from a backfill. It may have any value between the Boussinesq value and the Coulomb value, depending on the yield of the anchorage. This fact alone eliminates the possibility of an accurate computation of the pressure. However, a slight yield of the anchor is sufficient to reduce the pressure to a value close to the minimum. This conclusion is corroborated by the observations on the bulkhead shown in Fig. 34. The Boussinesq pressure on this bulkhead exceeds the Coulomb pressure by several hundred percent and the yield of the anchor line was less than two tenths of one percent of the height of the bulkhead. However, the measured anchor pull exceeded the Coulomb value by not more than 50%.

A comparison between the measured and the Coulomb value of the earth pressure on bulkheads A and B in Fig. 31 cannot be made because no adequate data concerning the physical properties of the soils in contact with these bulkheads are available. These properties were unusual indeed because the lateral pressure on both bulkheads increased after completion by approximately 100%, whereas the pressure on the bulkhead in Fig. 33 became sensibly constant after the filling operations were completed.

In this connection, it was learned (by letter from Mr. Roisin) that the surcharge (the body of earth located above the level of the upper edge of the sheet piles) consists chiefly of coarse sand which was deposited at its present site in approximately 1880. The sand fill rests on fine, silty sand with layers of soft silt and clay ("sable ypresien") which is unstable in a saturated condition. The boundary between this material and the superimposed fill is located at the site of bulkhead A approximately at the elevation of the upper edge of the bulkhead and at bulkhead B approximately 15 ft below this edge. These conditions account for the extraordinary difference between the pressure per yard of length of the lateral supports (40 tons per yd at A and 2.5 tons per yd at B). However, judging from the design of the supports, such an important difference has not been anticipated.

It must also be considered that the water table was located approximately 10 ft above final grade of the excavation on the free side of the bulkheads. When the water table was reached, drainage wells were installed on the bottom of the braced trenches shown on the right side of the upper part of the sheet piles in Fig. 31, and the water table was lowered by pumping. The abnormal increase of the lateral pressure on the bulkhead after completed excavation operations can be accounted for by movements in the unstable ground, associated with the process of drainage by pumping and probably assisted by traffic vibrations.

Messrs. Verdeyen and Roisin ascribe the gradual increase of the lateral pressure exclusively to traffic vibrations and suggest that the coefficient of active earth pressure K_A of a backfill with an angle of internal friction ϕ may gradually assume a value

$$K'_A = K_0 = 1 + \tan^2\phi \qquad (30)$$

There are many old retaining walls, both in the United States and elsewhere, supporting the foot of railroad fills on lines subject to heavy traffic. None of them was designed with special allowance for the effects of traffic vibrations. If K'_A were one third of the value determined by Eq. 30, all these walls would have failed long since. The failures which have come to the writer's attention were a result of unfavorable foundation conditions, gradual or rapid softening of cohesive backfills, or formation of ice layers behind the back of the wall; none could be attributed to vibration effects.

It is noted by Messrs. Verdeyen and Roisin that the writer has not adequately considered the effects of repeated application and removal of surcharges on the lateral pressure. Every loading cycle produces a permanent increase of the lateral pressure. However, with an increasing number of cycles, the supplementary pressure produced by the cycle decreases and finally becomes zero. According to the writer's experience, the total increase is still well within the margin of safety, provided the lateral pressure caused by the surcharge has been computed by one of the procedures described in the paper.

Fig. 30 illustrates the proposals of Messrs. Verdeyen and Roisin concerning the assumptions which should be made about the distribution of the active earth pressure on the inner face of anchored bulkheads; this proposal appears to be over-conservative. The bulkhead shown in Fig. 18 is an example of the adequacy of the conventional assumption shown in Fig. 20. There are few anchored bulkheads with an anchorage as unyielding as the steel struts shown in Fig. 18; yet all the measured strut loads were smaller than those computed in the conventional manner.

The writer has reconsidered the recommendation in Part II (under the heading, "Computation of Maximum Bending Moments: Moment Reduction Resulting from Flexibility Effect"):

> "However, because of the rudimentary state of present (1953) knowledge of the performance of bulkheads under field conditions, the computed bending moment $M(\max)$ should be reduced by not more than $\frac{1}{2}(M(\max) - M_a)$."

This recommendation should be changed to read as follows:

> In order to compensate for the uncertainties involved in the assessment of the subsoil conditions between drill holes, the following procedure is recommended: If the test borings indicate that the sand below the dredge line is dense, the moments should be reduced in accordance with Mr. Rowe's "Average Curve." Otherwise, Mr. Rowe's curve for loose sand should be used.

The writer wishes to express his gratitude to the discussers for their valuable contributions. Their comments brought the controversial features of the topic clearly into prominence. Case records such as those illustrated by Figs. 18 and 31 demonstrate the practical value of careful observations on full-size bulkheads. Phenomena of the type described by Messrs. Verdeyen and Roisin are beyond the scope of theoretical forecast, and their existence can only be discovered by observations in the field.

In the last analysis, a paper dealing with anchored bulkheads does not serve its purpose unless it stimulates the thought and imagination of designers and makes them conscious of the consequences of the inevitable errors involved in the interpretation of the boring records and test results. Because of the great variety of subsoil conditions which may be encountered, the subject does, and always will, leave a wide margin for judgment—and also for misjudgment.

AMERICAN SOCIETY OF CIVIL ENGINEERS
Founded November 5, 1852
TRANSACTIONS

Paper No. 2721

THE ENGINEER AND WORLD POPULATION

ADDRESS AT THE SUMMER CONVENTION ATLANTIC CITY, N. J., JUNE 16, 1954

BY DANIEL V. TERRELL,[1] PRESIDENT, ASCE

During the past eight months it has been my duty as President of the American Society of Civil Engineers, and my privilege as an individual, to travel in all parts of the country and under all kinds of conditions. In doing this, I have met many people. Long periods in the air, on the train, or waiting for a flight which had been grounded, have given me time to reflect on these people and on the circumstances influencing their lives as well as mine. Such reflections lead to the obvious conclusion that collectively people create all the engineering problems which exist. By the same token, successful solutions to these problems are conducive to increases in population. These, in turn, produce greater demand for the skills of the engineer, and the two become thoroughly entwined.

Since the dawn of history, man has been in a constant struggle for his existence. Through a slowly but steadily developing power to outwit other creatures and devise machines to facilitate his work, man has gained considerable mastery over things in his surroundings. But progress in this direction throughout all the past centuries combined falls far short of the progress made in the first half of the present century, and still the pace is accelerating.

Obviously, population alone does not account for these circumstances, but population trends do reflect the upward climb. For example, in 1650 (which was but a short time after white settlements were started in North America), the population of the entire world was approximately 545 million. In 1900, this had increased to slightly more than 1.6 billion, and in 1950, it had reached the level of 2.5 billion. The world now has five times as many inhabitants as it had just 300 years ago, and almost twice as many as it had only 50 years ago.

The extent to which the multitudes depend on the engineer—and the engineer on the multitudes—is evident in several ways. In 1900, the United States, with a population of 76 million, had one engineer for each 400 workers. Today, with the population at 160 million, the ratio of engineers to workers is one to sixty. These disproportionate ratios and the trends in population growth for the same period of time emphasize the growing importance and the increasing stature of engineers in the economy of this country.

---

[1] Dean, College of Eng., and Director, Kentucky Eng. Experiment Station, Univ. of Kentucky, Lexington, Ky.

Near the turn of the century, 85% of our working population was needed to produce the necessary food. Now, no more than 15% of the working group is required for the production of food, and so far as our own needs are concerned we are constantly faced with the problem of consuming all the food we are able to produce. But the important point is that, through developments directly attributable to engineering skill, we have released large segments of our population from primitive toil on the farm to production of goods and services which were not even visualized a few years ago. In a large measure this transformation was brought about by the machines which the engineer develops so efficiently. However, no small part of it results from an ability to organize and to execute vast and complicated undertakings, regardless of their nature. This is rapidly becoming the field in which engineers are pre-eminent.

A large productive capacity is useless unless distribution, technical development, storage and preservation, advertising and communication to make the product known to the consumer, and a host of other elements keep pace with production. For all such lines of endeavor the engineer provides the foundation if not the guiding hand. This has become so well recognized in almost every field that the demand for graduates of engineering colleges has been greatly exceeding the supply. Through efforts to employ members of graduating classes from the various schools this year, many of you have become as familiar with the situation as I have.

Possibly most graduates regard this as a very fortunate situation, even though it presents them with a dilemma as to which of ten offers should be accepted. I too look upon it as a gratifying condition, and one providing great opportunity to each individual as well as to the profession which he is entering. But, at the same time, it is a severe handicap to our country and ultimately to the world at large. Within the past month the United States Department of Commerce has estimated that this year the number of students graduated from engineering colleges in Russia was twice as great as the number graduated from engineering colleges in this country. The dangers resulting from such a condition are easily recognized by all who hear the statement.

Despite the seriousness of this disparity for the present and for the foreseeable future, probably there are more serious consequences involved in our long-term economy. In an industrial system such as ours, nothing replaces knowledge and judgment, and we sacrifice progress when we restrict the production of those who can exercise knowledge and judgment. The problem has been recognized by many people and in many ways, but we have yet to take a very forward step toward solution of the problem.

Intense growth in population without commensurate technological development leads to conditions that are familiar to all of us. Because of the sensational treatment which the subject receives in textbooks of elementary schools, and in newspaper and magazine articles coming to the attention of adults, it is generally believed that a high density of population or a rapidly increasing birth rate inevitably leads to privation. But poverty, disease, and starvation in thickly-populated and backward areas are the results of ignorance and not the results of propagation. Real progress in human habitation and in human relations will be achieved when we can regard an increasing population in any part of the world as an increasing potential for the production and consumption of goods, rather than as an undesirable feature to be studied and combated in certain regions.

As recently as 1949, when I was traveling in some of the countries in Central America, I was deeply impressed by the tremendous waste of effort involved in the primitive agrarian economy of several sections. In field after field there were the familiar yoke of oxen, the crude plow, and from 8 to 10 workers following to assist in the cultivation and planting of a small plot of ground. This had been the method of their fathers and countless generations that preceded them. Not more than three generations ago it was the method of our ancestors. But under conditions where ignorance prevails, few realize the futility of the system. Even with years of experience on the part of those involved, the limited prospect for raising enough food to supply the simple needs of both the people and the oxen seems to go unnoticed. Who can measure the effort expended for small results, and who can measure the benefits that would be derived from one modern tractor and a person well enough informed to operate it?

One cannot avoid contrasting this condition with more pleasant circumstances that are now prominent in another of our western-hemisphere neighbor countries. The March, 1953, issue of *Civil Engineering*, and other publications as well, have given considerable recognition to private and public works programs in Venezuela. There, an economy founded largely on crude oil (with the recent addition of iron ore) is flourishing. Renovation of their capital city, extensive housing projects, and construction of the most expensive highway in the world are but a few of the many progressive steps that have been taken.

Granting the fact that mineral resources are abundant in this small country, it is still evident that not a foot of the splendid new highway would have been practical (even at the rate of 6 million dollars per mile) if engineers under the incentive of free enterprise had not developed in the United States rapid high-capacity, earth-moving equipment, modern efficient concrete plants, economical techniques for pipe-line construction, and the oil refinery as we know it today. Even with all these advantages, the economy of Venezuela is determined as much by world population as it is by the natural resources. During 1953, Venezuela produced 660 million barrels of crude oil—approximately one third the production in the United States. This would not have been feasible if Venezuela had been dependent on its own population of 5.5 million for the consumption of its chief product. Instead, it had access to a market created by thirty times as many people residing in this country alone, in addition to the other points of consumption throughout the world.

I have no doubt that for the present ox teams such as those tilling the soil of Central America in 1949 are also tilling the soil in Venezuela. But the death knell of the system has been sounded. An outmoded method of cultivation cannot long exist side by side with modern transportation, commerce, and education in Venezuela any more than it can in the United States.

The mere thought of dense population suggests India and its neighbors in Southeastern Asia. In the form to which it has been reduced since World War II, India still has 360 million people and a birth rate well in excess of 1,000 per hour. All but a few are born to be hungry throughout their lifetimes. The death rate is extremely high, life expectancy is very low, and approximately 85% of the population is illiterate. Engineers are almost too scarce to be mentioned, and the majority of people have no concept of the benefits provided through engineering endeavors. Even so, the engineering problems are there—existing in multitudes because the people are there. In reality, the potential for significant engineering contributions is greater in India than in the United States, but chances for utilizing more than a fraction of that potential during my lifetime are very remote. For the young members of our Society, the situation could be different.

Last year, upon his return from a three-month tour of Indonesia and Burma, a friend who is a sanitary engineer described for me some of the conditions which he had encountered in that part of the world. He had gone there with a United Nations team to study various public health factors. All excepting my friend were doctors from various member countries in the United Nations. One point in particular I remember very vividly: In the Indonesian capital city of Djakarta, which has a population of 2.8 million, there is no public water supply and no sewer system. The near-by river and a group of canals attendant to it serve both purposes. Hence, without benefit of treatment of any kind, the water consumed by the inhabitants is the same water used for all purposes of sanitation—if the term can be applied so loosely. If I remember correctly, there are only six engineers in the entire city, and probably doctors are almost equally scarce. Imagine, if you can, approximately half as many people as there are in the entire state of New Jersey crowded into the space of a few square miles. And imagine, too, the consequence of unsanitary conditions such as those described for Djakarta.

These disquieting facts are recounted, not to impress you with our superior standard of living, but to give you a vague estimate of some opportunities for engineering accomplishment that have gone practically untouched. These factors are important to us as engineers, and in the immediate prospect they are more important to us as individuals in a world where distances are rapidly shrinking. A high standard of living is not an unfailing defense against communist ideologies, but it does reduce the possibilities for Korean, Indochinese, and Guatemalan incidents.

Recently, in the magazine section of a well-known newspaper, I read an article posing the question, "How Many People Can The World Hold?" No one knows or dares to hazard a guess. In the same paper, however, I read other articles which led me to the conclusion that Americans in their usual spirit of cooperation are trying to find out. Statistics which were presented showed that in the period from 1940 to 1953 our population increased 21%, and that the increase was 19 million instead of the 8 million that had been predicted. The article went on to say that the production of baby food had increased from 270 million cans in 1940 to 1.5 billion cans in 1953, and that the toy industry had grown from an 84-million-dollar business to a 900-million-dollar business during the same period. In this particular instance, I can make no claims of exceptional contributions by the engineers, but I dare say that many of them are involved, one way or another, in taking care of the babies after they arrive.

Economists tell us that our current prosperity is not in danger of running out so long as current population trends continue. At the same time, sociologists and statisticians predict that the population of this country will reach 200 million by 1975, and as high as 375 million by 2050. Numbers alone give assurance that the demand for engineering services will remain great; but added to that is the restlessness that characterizes the times. Never before have we been so willing and eager to discard the old and seek something new which gives promise of greater comfort and convenience.

Tremendous housing projects, business centers, factories, and even entirely new cities, such as Levittown, Pa., spring up almost overnight in response to the demands. There is no hesitation whatever to dismantle or remove sound and usable structures when they stand in the way of progress. In every city, buildings representing valuable investments according to the tax books have been torn down to make way for parking lots. From any standpoint, the rate of change has been so great that the abilities of educational institutions, community planners, medical and public health agencies, and all other segments of government, business, and industry have been strained to keep pace.

In highways, for example, the boom is far greater than at any time in our history. Recently, Congress enacted a program of federal aid barely short of a billion dollars per year, which exceeds by 50% the largest appropriation made heretofore. Expenditures for toll roads and contributions by states, cities, and other political subdivisions will push the total highway program well beyond the 5-billion-dollar mark each year. Still, we find ourselves deeper in the "muddle," as it has been termed. Obviously we have better highways than we had before, but we expect more of them. According to one recent observation, everyone is some place where he does not care to be, and he is determined to go elsewhere.

It is interesting to note that in 1868 James Laurie, the first President of the American Society of Civil Engineers, prepared plans and advocated construction of an elevated railroad in New York City. The intent, of course, was to avoid the congestion of horse-drawn vehicles and provide what was then considered rapid transportation. It is also interesting yet irritating to note that the movement of motor traffic on the streets of New York today is hardly faster than the movement of horse-drawn traffic was 86 years ago. Despite our progress in means of transportation during the intervening years, increasing population and increasing use of the streets have recreated the same old problem in a slightly revised form. If the present trend continues, New Yorkers will soon be back on their feet—but in the best sense of the word. In contrast to the original solution to surface congestion, which carried the traffic above and on wheels, passenger "speedwalks" or pedestrian conveyors below ground seem to offer the best accommodations.

The engineering profession has reached a point of exceptional opportunity for its members, individually and collectively. This applies both to those who are well established and to those who are just entering the field. Some fields seem destined to continue in their traditional way—with vigor stemming from an expanding economy and an increasingly versatile service. In some industries, such as fuels, metals, and textiles, large segments are faced with the necessity of adapting themselves to the changing pattern of extinction. These changes present deep problems of technical development which engineers must face squarely and fully. Finally, as always, new industries are created every day. In our own times, new sources of energy and power are most prominent. With regard to these, it is well known that we have hardly pierced the surface. Likewise, we have hardly pierced the surface of distribution, which will carry the benefits of all types of industries to people throughout the world. The potential of world population is as enormous as atomic energy itself. Unfortunately, we have not found the key to unleashing this potential, as we have found the key to nuclear energy within the past few years.

From the standpoint of self-interest alone, we have much at stake in the conditions affecting people throughout the world; yet, from a professional standpoint, the stake is even greater. The reputation and the tenor of engineering have been built on knowledge, conscience, and determination to render service mainly to people in this country or to others with whom we have come into frequent contact. As the horizons of intercourse among nations are extended, our professional obligations go with them. Perhaps we cannot lead the way to higher levels, but we should be prepared to point the way. To do this we must first be aware of the people involved, for not only do the people benefit from our accomplishments—they create our problems.

MEMOIRS OF DECEASED MEMBERS

Abstracts

Honorary Members

Boris Alexander Bakhmeteff 1332
George Harrison Fenkell 1333
Sherman Melville Woodward 1335

Other Members

Henry James Alexander 1336
Verle Lorraine Austin 1337
Thomas Archibald Bedford 1337
Orris Bonney 1338
William Gerrie Brown 1339
Joseph L. Burkholder 1340
Frederick Julius Cellarius 1342
Louis Moses Chokla 1343
Albert Bernhardt Collins 1343
Arthur Coleman Comey 1344
George Davis Crow 1345
Joseph Herbert Davies 1346
Thomas Marsh Davis, Sr. 1347
Edward A. Dougherty 1348
Louis Warren Duffee 1350
Scotland G. Highland 1351
Arne Arthur Jakkula 1352
Lester Josef Newman Keliher 1353
Herbert Miller Knight 1354
John Crane McVea 1355
Fred William Morrill 1355
John Frederick Partridge 1356
John Cornelius Penn 1357
Harold Fred Percival 1358
St. George Tucker Richardson 1359
Robert Lawrence Rolfe 1361
Frank Charles Schroeder 1361
Walter Mickle Smith 1362
Edwin James Snow 1363
John Stearns 1365
Thomas Kennard Thomson 1366
Harvey Arthur Van Norman 1367
Fayette Samuel Warner 1369

BORIS ALEXANDER BAKHMETEFF, HON. M. ASCE[1]

DIED JULY 21, 1951

Boris Alexander Bakhmeteff, the son of Alexander P. and Julia (Novitsky) Bakhmeteff, was born on May 14, 1880, in Tiflis, Caucasus, Russia. He was educated at the Classical Gymnasium in Tiflis, the Institute of Engineers of Ways of Communication at St. Petersburg (Russia) from which he was graduated in 1903 with the degree of Civil Engineer, the Polytechnic Institute at Zurich (Switzerland), and the Polytechnic Institute Emperor Peter the Great at St. Petersburg. At the latter institution he received the degree of Doctor of Engineering in 1911.

Until the middle of World War I, Mr. Bakhmeteff served as professor of hydraulics and mechanics at the Polytechnic Institute Emperor Peter the Great, and as consulting engineer specializing in water power. During the war he was chief engineer of the great Dneiper hydraulic project, chief plenipotentiary of the Central War Industrial Committee to the United States, member of the Anglo-Russian Purchasing Commission, and vice-minister for Commerce and Industry. These successes led to his appointment in 1917 as head of the Extraordinary Commission and as the first Russian ambassador to the United States following the Czarist regime, a position he held nominally until 1922. He never returned to his native land but established practice as an hydraulic consultant in New York, N. Y. He became a United States citizen in 1935.

From 1931 he was professor of civil engineering at Columbia University, in New York, and after twenty years was made Honorary Professor, the fourth such recipient in the university's history. Professional services included membership on the Board of Consultants of the Panama Canal and chairmanship of the Society's Hydraulic Division and of its Committee on Research. He was the Society's representative to and chairman of the board of the Engineering Foundation; representative of the World Engineering Committee and of the Council of the American Association for the Advancement of Science; director of the Research Corporation; consultant to the United States Waterways Experiment Station, Vicksburg, Miss.; and chairman of a special Engineers Joint Council panel on legislation for a National Science Foundation. He was prominent in business and for years was chairman of the board of the Lion Match Company of New York. He also served as president and director of the No-Mercury Felt Corporation, and as director of the Potash Company of America.

Mr. Bakhmeteff was an innovator of advanced theories of fluid mechanics as well as an authority in the field of hydraulics. He published extensively, and, in America, his textbooks, "Hydraulics of Open Channels,"[2] and "Mechanics of

---

[1] Memoir prepared by Sydney Wilmot, M. ASCE.

[2] "Hydraulics of Open Channels," by Boris A. Bakhmeteff, McGraw-Hill Book Co., Inc., New York, N. Y., 1932.

Turbulent Flow,"[3] were outstanding. The latter, when translated and published in France, brought him the Grande Medàille de l'Association des Docteurs Ingénieurs de France. In recognition of his contributions to Society publications and technical discussions, he was awarded the James Laurie Prize (with Arthur E. Matzke, J.M. ASCE) in 1937; the J. C. Stevens Award (with Nicholas V. Feodoroff, A.M. ASCE) in 1944; and the Norman Medal (with William Allan, M. ASCE) in 1947. Mr. Bakhmeteff was an accomplished pianist and a conoisseur of painting. He was a quiet but generous philanthropist, and, as the director of Humanities Fund, Inc., and of the Russian Student Fund, he helped displaced persons to establish themselves in the United States. He contributed wholeheartedly to the Russian Orthodox Church in Manhattan, of which he was a member.

Mr. Bakhmeteff held membership in the American Society of Mechanical Engineers, the Institute of Aeronautical Sciences, the New York Academy of Sciences, the Foreign Policy Council, and the honorary societies of Sigma Xi and Tau Beta Pi. He was a fellow of the American Geographical Society.

Mr. Bakhmeteff was elected a Member of the American Society of Civil Engineers on March 13, 1917, and an Honorary Member on July 17, 1945. He became a Life Member in January, 1949.

GEORGE HARRISON FENKELL, HON. M. ASCE[1]

DIED NOVEMBER 8, 1949

George Harrison Fenkell, the son of Delaville L. and Sarah (Foote) Fenkell, was born in Chagrin Falls, Ohio, on February 4, 1873. He received his early education in the public schools of Chagrin Falls and entered the Engineering Department of the University of Michigan (Ann Arbor) in 1891. After completing one year's work in that institution, lack of finances necessitated his going to work in the spring of 1892, and he had no further formal education. In 1926 the University of Michigan recognized his high accomplishments as an engineer and awarded him the degree of Bachelor of Science in Engineering, *nunc pro tunc,* as of the class of 1895.

For a year prior to his entering college and from 1892 to 1896, Mr. Fenkell served as axman, rodman, chainman, instrumentman, and assistant engineer on railway location and construction. In the following six years he was associated with the Department of Water Supply of Detroit, Mich., as draftsman and chief draftsman and shared in the preparation of plans for a more adequate water supply for that city. Investigations of the causes of breaks in water mains and loss of head on curves led to the preparation of a paper[2] for which Mr. Fenkell and the co-authors were awarded the Norman Medal of the Society in 1902.

---

[3] "The Mechanics of Turbulent Flow," by Boris A. Bakhmeteff, Princeton University Press, Princeton, N. J., 1936.

[1] Memoir prepared by L. G. Lenhardt and Sydney Wilmot, Members, ASCE.

From 1902 until 1907, Mr. Fenkell was civil engineer for the City of Erie, Pa., in charge of design and construction of the Lake Erie Water Supply. In the following year he was called back to Detroit as civil engineer to the Board of Water Commissioners and held that position until 1913. Plans were made during this period for a new pumping station with a capacity of 216 million gallons daily. Mr. Fenkell's work as engineer of the water department was so outstanding that in 1913 he was drafted to be commissioner of public works of Detroit. During his administration a comprehensive plan for a sewer system for the city and its adjacent areas was completed, and the Department of Public Works was reorganized on an efficient basis. The total cost of the work of the department exceeded $20,000,000.

In 1918 Mr. Fenkell returned to the Department of Water Supply as general manager and held this position until he retired on August 1, 1938. The water department was completely mechanized under Mr. Fenkell's guidance. In 1923 the largest rapid sand filtration plant in the world was set in operation. In 1924 a large engineering force commenced work on a plan for a new water-supply system with investigations of filtration methods, construction methods, and materials. Springwells Station was put into operation in the spring of 1933. Mr. Fenkell's responsibility and accomplishment as general manager of the Detroit water department is best indicated by the fact that in 1918 he took over an inadequate plant valued at $18,425,000 and serving a population of 900,000, and at the end of his twenty years of service he left an adequate plant representing an investment of $118,000,000 and serving a population of 1,800,000.

He was active in Society affairs, serving as Director from 1923 to 1925. Mr. Fenkell served on the Recreation Commission of Detroit and was a member of the Engineering Board of Review of the Sanitary District of Chicago (Ill.). He held a commission as Lieutenant Colonel of Engineers in the Officers Reserve Corps from 1923 to 1926. He was an honorary member of the American Waterworks Association, a member of both the Michigan Engineering Society and the Detroit Engineering Society, and a representative of the Engineering Society of Detroit on the Engineering Council.

Mr. Fenkell was married to Jeanie Harris, at Rocky River, Ohio, on February 22, 1897. He is survived by his widow; a son, Neal H.; and a daughter, Margaret S. (Mrs. Winston Mather).

Mr. Fenkell was elected a Junior of the American Society of Civil Engineers on January 3, 1899; an Associate Member on October 1, 1902; a Member in July 1, 1909; and an Honorary Member on October 14, 1940.

---

[2] "Experiments at Detroit, Mich., on the Effect of Curvature upon the Flow of Water in Pipes," by Gardner S. Williams, Clarence W. Hubbell, and George H. Fenkell, *Transactions*, ASCE, XLVII, April, 1902, p. 1.

SHERMAN MELVILLE WOODWARD, HON. M. ASCE[1]

DIED SEPTEMBER 7, 1953

Sherman Melville Woodward, the son of Emerson Jewett and Amelia (Scaife) Woodward, was born on May 11, 1871, near Minneapolis, Minn. He went to grade school in Ridgefield, Minn., and received his high school education at the St. Louis (Mo.) Manual Training School. In 1888 Mr. Woodward entered Washington University at St. Louis and was graduated with high honors in engineering in 1893. In 1896 he received the degree of Master of Arts from Harvard University, at Cambridge, Mass.

Mr. Woodward's professional career began in 1893 when he was a science teacher in a high school in Youngstown, Ohio. From 1896 to 1904 he was professor of mechanics and physics at the University of Arizona at Tucson. In 1904 he became professor of steam engineering at the State University of Iowa, at Iowa City, and left one year later to become a drainage and irrigation engineer with the United States Department of Agriculture. Mr. Woodward returned to the University of Iowa in 1908 as professor of mechanics and hydraulics and served there until 1934, at which time he became chief water control planning engineer for the Tennessee Valley Authority (TVA) in the Knoxville (Tenn.) office. He held this position until his retirement in 1943. For the next nine years Mr. Woodward served as a consultant to the TVA.

Prior to his association with the TVA, he did a large amount of consulting engineering work including much of the hydraulic work of the Miami Conservancy District in Ohio. Among his consulting engagements, Mr. Woodward was on the board of consultants of the Chicago Sanitary District for a number of years. He was also a member of the Mississippi Valley Committee of the Public Works Administration during 1933 and 1934. Mr. Woodward was president of the Iowa City Savings Bank for six years and was the author of a number of articles and technical books.[2,3]

Mr. Woodward was a member of the American Society of Mechanical Engineers, the American Society for Engineering Education, and the American Association for the Advancement of Science. He belonged to Sigma Xi, Tau Beta Pi, the Rotary Club, the Irving Club, and the Knoxville Technical Society, and he participated fully in many kinds of civic work. He was a member of the Unitarian Church in Iowa City and was active in church affairs.

In 1897 Mr. Woodward was married to Gertrude B. Hughes in Tucson. The only child from this marriage was a daughter, Miriam (Mrs. Merlin Taylor). In 1916 Mr. Woodward was married to Christine M. Bachmiller in Dayton, Ohio. He is survived by his widow and three daughters, Amelia Jane (Mrs. M. Stanley Roberts, Jr.), Mary Elizabeth (Mrs. Charles Gillespie), and Sarah Melville (Mrs. Arthur Garrett, Jr.).

---

[1] Memoir prepared by Julian R. Fleming, A.M. ASCE.

[2] "Hydraulics of Steady Flow in Open Channels," by Sherman M. Woodward and Chesley J. Posey, John Wiley & Sons, Inc., New York, N. Y., 1941.

[3] "Hydraulics of the Miami Flood Control Project," by Sherman M. Woodward, Miami Conservancy District, Dayton, Ohio, 1920.

Mr. Woodward was elected a Member of the American Society of Civil Engineers on April 16, 1918, and an Honorary Member on October 12, 1942. He became a Life Member in January, 1943.

HENRY JAMES ALEXANDER, M. ASCE[1]

DIED MAY 8, 1953

Henry James Alexander, the son of Charles Henry and Sarah Abby (Marsh) Alexander, was born in Concord, N. H., on July 8, 1874. He attended Concord High School and entered the Lawrence Scientific School of Harvard University, at Cambridge, Mass., in September, 1896. He received the degree of Bachelor of Science in Civil Engineering in June, 1900.

After being graduated from high school, Mr. Alexander worked as a surveyor for the Boston and Maine Railroad on railroad surveys and construction in the White Mountain area. During summer vacations while in college and for a few months after graduation, he worked for the Massachusetts Highway Commission on surveys and construction of state highways. In the early part of 1901 he was employed by the Chicago, Burlington and Quincy Railroad on construction at Corning, Iowa. In June, 1901, he was appointed assistant engineer by the New York City Board of Rapid Transit Railroad Commissioners and was assigned to the construction of the Bronx section of the subway and the elevated approach to the first subway to be built in New York.

Mr. Alexander was engaged in subway construction for more than thirty years, during which time he was in charge of many difficult sections of the subway line, including the Broadway line from Herald Square to Times Square. He was also assigned to the construction of a reinforced concrete viaduct in the Borough of Queens, and he was engaged in the valuation of the various subway and elevated lines in New York City.

Mr. Alexander retired in March, 1934, and moved to Rockport, Mass., where he built a home and enjoyed his hobbies of gardening and color photography.

He was married to Lilly E. Robinson on June 2, 1906, in Concord. He is survived by two sisters, Grace J. and Maud M.

Mr. Alexander was elected an Associate Member of the American Society of Civil Engineers on March 7, 1906, and a Member on June 16, 1924. He became a Life Member in January, 1941.

---

[1] Memoir prepared by James P. Locke.

VERLE LORRAINE AUSTIN, M. ASCE[1]

DIED JULY 27, 1953

Verle Lorraine Austin, the son of Guy L. and Nina B. (Wilkinson) Austin, was born on July 29, 1896, in Nevinville, Iowa. He was educated at the University of Kansas, at Lawrence, and was graduated in 1921 with the degree of Bachelor of Science in Civil Engineering.

Mr. Austin served with the American Expeditionary Force in France during World War I. He taught school in Irving, Kans., during the fall of 1921. In January, 1922, he received an appointment as junior engineer with the United States Geological Survey (USGS) at Rolla, Mo., and he continued with this organization for his entire professional career. In March, 1930, he was transferred to the Texas District of the USGS as assistant engineer in the Water Resources Branch. Later, he was made office engineer in charge of computations for the Water Resources Branch, a position he held until his death.

He was a loyal member of the Methodist Church. He served as adjutant of the local post of the Veterans of Foreign Wars for many years and was responsible for its continued growth.

On June 11, 1924, Mr. Austin was married to Ethel Case. He is survived by his widow and two daughters.

Mr. Austin was elected an Associate Member of the American Society of Civil Engineers on October 29, 1934, and a Member on February 16, 1948.

THOMAS ARCHIBALD BEDFORD, M. ASCE[2]

DIED MARCH 14, 1953

Thomas Archibald Bedford, the son of Edward West and Huldah (Newton) Bedford, was born in Mansfield, Tex., on March 9, 1870. He was graduated from Southwestern University in Georgetown, Tex., in 1891.

After graduation, he was county engineer of Knox County, Texas, and was engaged in private practice for seven years. For the next five years he was division engineer of the Kansas City, Mexico & Orient Railway, in Texas and Mexico.

In 1908 he began his career in highway engineering. He took charge of the preliminary surveys of the system of county highways which San Diego County, California, had bonded itself to build. Later, he became principal assistant to A. B. Fletcher, chief engineer of the County Highway Commission.

---

[1] Memoir prepared by John A. Focht, M. ASCE.

[2] Memoir prepared by Fred J. Grumm, Thomas E. Stanton, and Thomas H. Dennis, Members, ASCE.

Mr. Bedford was appointed in 1911 division engineer in Division II of the newly organized California State Highway Department, which included Shasta, Siskiyou, Modoc, Lassen, Tehama, and Trinity counties. He located and supervised the construction of the Pacific Highway in the Sacramento River Canyon from Redding to Dunsmuir and built the first paved highways in this northern area. In 1923 he was transferred to Willits, Mendocino County, in Division I, which embraced the counties of Del Norte, Humboldt, Mendocino, and Lake.

During a year's leave of absence from the California State Highway Department, he was assistant general manager for the Kaiser Construction Company, building a system of paved highways in Cuba. On return to state service in 1929, he worked for the department of Surveys and Plans of the Division of Highways in Sacramento, Calif., until his retirement in 1939, locating many miles of the present state highway system in California.

On January 6, 1901, Mr. Bedford was married to Letitia Clay in Benjamin, Tex. He is survived by two sons, Thomas Archibald Bedford, Jr., and Clay H. Bedford; two daughters, Mrs. Frances Lindt and Mrs. Mary Sue Fitzgerald; seven grandchildren; and one great-grandchild.

Mr. Bedford was elected a Member of the American Society of Civil Engineers on September 6, 1910. He became a Life Member in January, 1941.

ORRIS BONNEY, M. ASCE[1]

DIED JULY 9, 1952

Orris Bonney, the son of Orris and Louise Wheelock (Corson) Bonney, was born in Grand Rapids, Mich., on September 19, 1895. He attended the public schools in Grand Rapids and studied engineering at the University of Michigan, at Ann Arbor, from which he was graduated in 1918 with the degree of Bachelor of Science in Civil Engineering.

He enlisted in the Sanitary Corps, United States Army, and served until his discharge after the Armistice. In 1919, Mr. Bonney entered the employ of the City Engineer's Office in Detroit, Mich., as a draftsman in the Sewer Department. He was promoted to senior assistant engineer in 1921 and was then assigned as principal assistant engineer in charge of the Public Sewer Department. In May, 1923, Mr. Bonney was employed as engineer in charge of sewerage investigation and study for the City of Columbus, Ohio. The remainder of his professional career was spent in Columbus, and his record shows continuing accomplishments and responsibility. In August, 1924, he was placed in charge of sewer design and construction, and from April, 1926, to January, 1928, he served as engineer in charge of sewerage relief. For the next thirteen years, Mr. Bonney was in charge of the design and construction of sewerage works aggregating approximately $12,000,000. He was appointed deputy chief engineer of the Columbus Division of Engineering and Construction in 1941 and in June, 1950, headed the newly established Division of Sewerage and Drainage, supervising all phases of planning, design, construction, maintenance, operation, and financing of the entire city system.

---

[1] **Memoir prepared by Carl W. Schoene, A.M. ASCE.**

Mr. Bonney was the author of two important papers for the Society.[2,3] In 1935 he and his co-authors received the Rudolph Hering Medal of the Society for the paper in *Transactions*. Mr. Bonney was a Registered Professional Engineer and Registered Surveyor in the State of Ohio and was a Registered Civil Engineer in the State of Michigan. He was active in Society affairs and served as President of the Central Ohio Section during 1930.

On August 20, 1921, Mr. Bonney was married to Alice Crosby Hallock in Detroit. In April, 1945, his wife died. In September, 1951, Mr. Bonney was married to Gertrude E. Ward in Columbus. He is survived by his widow and a daughter, Elizabeth K., from his previous marriage.

Mr. Bonney was elected a Junior of the American Society of Civil Engineers on February 25, 1924; an Associate Member on December 14, 1925; and a Member on May 12, 1930.

WILLIAM GERRIE BROWN, M. ASCE[1]

DIED NOVEMBER 19, 1951

William Gerrie Brown, the son of Robert Alexander and Isabella (Gerrie) Brown, was born in Lockport, Ill., on September 30, 1869. He attended primary schools at Lockport and Portland, Ore., and received his secondary school education in Portland.

From 1897 to 1903, Mr. Brown was engaged in construction work on the Columbia River. He was in charge of the operation of the Cascade Locks and worked on the South Jetty at the mouth of the river and on fortification construction at Fort Canby, Oregon. Later he worked on the organization and planning for the Multnomah Drainage Districts along the Columbia River. In 1906 Mr. Brown entered consulting engineering practice in Portland. He bought a part interest in Tenas Illihee Island on the lower Columbia River in Oregon in 1908 and developed the island by diking and drainage. He purchased a dredge for this work and also did other dredging in the area under contract. In 1911 Mr. Brown organized and planned work for the Blind Slough Drainage District (lower Columbia River) and constructed the works in 1914 and 1915.

---

[2] "Surveying Under Compressed Air," by Orris Bonney, *Civil Engineering*, January, 1933, p. 31.

[3] "Intercepting Sewers and Storm Stand-By Tanks at Columbus, Ohio," by John H. Gregory, R. H. Simpson, Orris Bonney, and Robert A. Allton, *Transactions*, ASCE, Vol. 99, 1934, p. 1295.

[1] Memoir prepared by Norman W. Haner, A.M. ASCE.

Mr. Brown became interested in the nut-growing business of the Willamette Valley and purchased a farm in 1919. He planned and constructed a nut-processing plant at Dundee, Ore., in 1937 and 1938, and he invented a multistage walnut dryer which is used extensively.

His construction engagements included the designing and building of the Oceanic Terminal in Portland in 1927 and 1928, which he rebuilt after a fire in 1934. In 1928 he assisted in the planning of the Ross Island Sand and Gravel Company plant in Portland.

Mr. Brown was the director of the Walnut Growers Cooperative at Dundee for many years and was honorary director of the North Pacific Nut Growers Cooperative during the later years of his life.

In 1896 Mr. Brown was married to Nina Elizabeth McClure. He is survived by a daughter, Doris.

Mr. Brown was elected a Member of the American Society of Civil Engineers on November 7, 1906. He became a Life Member in January, 1940.

JOSEPH L. BURKHOLDER, M. ASCE[1]

DIED APRIL 6, 1953

Joseph L. Burkholder, the son of Joseph and Susan Mary (Finney) Burkholder, was born in Roanoke, Ill., on October 11, 1884. He received his professional training at the University of Kansas, at Lawrence, as a member of the class of 1908. In April, 1948, the university awarded him the Distinguished Alumni Citation.

After beginning his career with the Santa Fe Railway Company, Mr. Burkholder entered the service of the Bureau of Reclamation, United States Department of the Interior, at Boise, Idaho, in 1910. He contributed materially in the early development of earth-moving equipment, including the type of dragline currently used, and he pioneered methods still used successfully in overcoming the problem of water-logged lands attending irrigation developments of the western United States. His accomplishments as assistant engineer in charge of drainage on the Boise project and later as drainage engineer for the Rio Grande project in El Paso, Tex., led to his appointment in 1919 as engineer in charge of all drainage and as inspector of earth-moving equipment for the Bureau. He held the latter position until 1922 when he accepted an assignment in Barahona, Dominican Republic, as assistant administrator in charge of engineering and construction of a $15,000,000 sugar development for the West Indies Sugar Corporation of New York, N. Y. Following the completion of this work, he accepted a position as resident engineer with C. E. Jacoby Engineering Company of Kansas City, Mo., in charge of investigations and planning for flood control projects for the North Wichita Drainage District of Kansas.

---

[1] Memoir prepared by J. F. Friedkin, M. ASCE, and Richard Stephens, A.M. ASCE.

In 1926, he was appointed chief engineer of the Middle Rio Grande Conservancy District in charge of the planning and construction of a $10,000,000 irrigation, drainage, and flood control project in central New Mexico. Few jobs have ever contained the many problems—financial and political, as well as engineering—that Mr. Burkholder encountered. Seldom have there been combined in one man the talents required for their successful solution. In 1933 the Metropolitan Water District of Southern California selected Mr. Burkholder to be assistant general manager in direct charge of the construction of the Colorado River Aqueduct which involved 92 miles of 16-ft-diameter tunnels, 58 miles of cut and cover conduit, 62 miles of lined canals, two dams, and incidental works. The aqueduct was completed at a saving of many millions of dollars under the original estimate. In 1938, Mr. Burkholder became senior engineer in charge of all investigation, design, and planning for the United States Section of the International Boundary Commission, United States and Mexico. He also served as technical consultant to the American Commissioner on the Agrarian Claims Commission, United States and Mexico.

With the entry of the United States into World War II, Mr. Burkholder's exceptional talents as an administrator led to his selection as operating manager for the Arundel Corporation and the Consolidated Engineering Company, Inc., both of Baltimore, Md., and the Hardaway Contracting Company of Columbus, Ga., in their joint-venture contract with the Bureau of Yards and Docks, United States Navy, for the construction in the Caribbean Islands of five naval bases and related facilities, costing about $145,000,000. In 1945, Mr. Burkholder became general manager and chief engineer of the San Diego County Water Authority of California, in which position he was prominent in the successful negotiations leading to the timely construction of the San Diego Aqueduct, averting an otherwise serious water shortage in the area. He was also one of the directors of the Metropolitan Water District of Southern California.

Outstanding as were Mr. Burkholder's material accomplishments in engineering and construction, he is best remembered by those who were privileged to have been associated with him as a builder of men.

Mr. Burkholder was a Past-President of the New Mexico Section of the Society. He was a registered civil engineer in California and held membership in Sigma Chi and Sigma Tau. He belonged to the Free and Accepted Masons and to the Rotary Club.

On May 27, 1911, Mr. Burkholder was married to Rebecca E. Moody in Lawrence. He is survived by his widow; four daughters, Jane (Mrs. W. D. Campbell), Elizabeth Sue (Mrs. E. V. Watts), Dorothy (Mrs. C. S. Williams), and Margaret (Mrs. G. H. Truran); one son, Joseph; and eleven grandchildren.

Mr. Burkholder was elected an Associate Member of the American Society of Civil Engineers on September 3, 1913, and a Member on August 28, 1922. He became a Life Member in January, 1948.

FREDERICK JULIUS CELLARIUS, M. ASCE[1]

DIED MARCH 28, 1953

Frederick Julius Cellarius, the son of Henry and Marie C. (Hessig) Cellarius, was born in Dayton, Ohio, on July 31, 1865. His mother was a native of Switzerland and his father emigrated to America from Germany. Mr. Cellarius was graduated from high school in Dayton in 1884. He then entered The Ohio State University at Columbus and was graduated in 1888 with the degree of Civil Engineer.

In 1894 Mr. Cellarius became assistant city engineer of Dayton and in 1908 was appointed city engineer. He held this position until 1912 when he went into private practice and devoted most of his time to municipal engineering. He was the consulting engineer on the installation of the sanitary sewer system of Miamisburg, Ohio, in 1919. Between 1920 and 1921, Mr. Cellarius supervised the moving of the village of Osborn to a new location, making way for the Huffman Dam, a part of the Miami Conservancy District Project. From 1912 to 1914 Mr. Cellarius served as a member of the Board of Park Commissioners of Dayton, and from 1936 to 1948 he was a member of the City Plan Board. For the first ten years of this period he served as president of the board. Mr. Cellarius published the first street maps of Dayton in 1891, and his firm, the Cellarius Engineering Company, published revisions in 1907, 1931, and 1948.

Mr. Cellarius was active in Society affairs, serving as President of the Dayton Section in 1927. He was one of the organizers of the Dayton Society of Professional Engineers and served as president of this society from 1934 to 1936. He was secretary-treasurer of the Ohio Society of Surveyors and Civil Engineers in 1900 and 1901, a member of the Board of Direction of the Ohio Society of Professional Engineers from 1936 to 1940, and a vice-president of this society in 1940. In 1942, Mr. Cellarius received a citation from the Ohio Society of Professional Engineers in recognition of his long record of engineering accomplishment in municipal planning and in the design of public works, and for his untiring leadership of engineering groups and the fine example he set for the profession. He was a member of the Free and Accepted Masons, the Scottish Rite, Commandery, Mystic Shrine, and the Dayton Engineers Club. He belonged to the Dayton Bicycle Club, the Rotary Club, Chi Phi, the Y.M.C.A., and the Dayton Art Institute.

Mr. Cellarius was married to Edith Garber. He is survived by his daughter, Catherine.

Mr. Cellarius was elected a Member of the American Society of Civil Engineers on April 2, 1912. He became a Life Member in January, 1937.

---

[1] Memoir prepared by John F. Hale, M. ASCE.

LOUIS MOSES CHOKLA, A.M. ASCE[1]

DIED JUNE 1, 1953

Louis Moses Chokla, the son of Moishe and Ranya Chokla, was born on January 21, 1881, at Falesti, Bessarabia, Russia. Before emigrating to the United States he attended the University of Odessa in Russia. After his arrival in this country, he attended The Cooper Union in New York, N. Y., in 1906 and 1907 and was graduated with the degree of Bachelor of Science in Civil Engineering at the University of Texas, at Austin, in 1913.

Following his graduation, Mr. Chokla worked on the construction of Elephant Butte Dam in New Mexico and spent the following few years in Texas on the staffs of the city engineers in San Antonio, Dallas, and Austin. From 1920 to 1922, he was in charge of the engineering work connected with the development of Highland Park West in Dallas. He was engaged in private engineering practice from 1936 to the end of his career. In 1940 Mr. Chokla founded the Department of Russian Language at Southern Methodist University at Dallas and taught there until his retirement because of ill health in 1951.

Mr. Chokla was a gifted linguist and was also the possessor of great technical knowledge. It was this combination of resources that enabled him to publish a number of translations from Russian geological research papers for Texas oil companies. He was proud of his ability to contribute something toward the development of private industry in the adopted country which had been so generous to him.

He was a member of the Modern Language Society, the American Association of University Professors, and the American Teachers Society of Eastern European Languages. He was a charter member of the Dallas Branch of the Texas Section of the Society.

In 1905 Mr. Chokla was married to Bassetta Shore in Falesti. He is survived by his only daughter, Sarah (Mrs. Gross).

Mr. Chokla was elected an Associate Member of the American Society of Civil Engineers on October 12, 1925. He became a Life Member in January, 1952.

ALBERT BERNHARDT COLLINS, A.M. ASCE[2]

DIED MARCH 13, 1953

Albert Bernhardt Collins, the son of Bernhardt and Henriette (Kautz) Collins, was born in New Brunswick, N. J., on June 9, 1893. His basic schooling was in Grand Rapids, Mich., and Philadelphia, Pa., and he attended the Grand

---

[1] Memoir prepared by Grayson Gill, M. ASCE.

[2] Memoir prepared by N. B. Hodgkinson, M. ASCE.

Rapids High School. Many years elapsed before Mr. Collins decided on an engineering career. He enrolled in the University of Southern California at Los Angeles in the civil engineering course, and in 1925 he obtained the degree of Bachelor of Science in Civil Engineering.

After being graduated from high school, Mr. Collins enlisted in the National Guard in 1916 and was called into uniform during the Pancho Villa skirmishes at the Mexican border. Shortly after the outbreak of World War I, he became a Sergeant in the 36th Division, United States Army, and was discharged in October, 1918. After a few years, Mr. Collins entered college and after graduation was employed by the Los Angeles County Flood Control District as an instrumentman. He soon became party chief and served in this capacity until 1932, with a one-year leave of absence (1929–1930) to obtain the degree of Master of Science from the University of Southern California. In 1932 Mr. Collins transferred to the Construction Division of the Flood Control District and worked as an inspector and foreman. In 1936 he was selected, because of his wide and varied field experience, to head the Permit Section of the Investigation Division, and in this position his reputation for integrity and great humanity spread through the country. In 1952 he was appointed to the position of assistant division engineer of the Investigation Division and, for the two months prior to his death, served in the District's Right of Way Engineering Division.

Mr. Collins devoted much of his time to boys' groups, such as the Boy Scouts, the Y.M.C.A., and the Mexican boys' group. He taught Sunday School classes, not only in his church but in others of his neighborhood, and he also gave freely of his time, interest, and engineering skill during the construction of the First Baptist Church in Huntington Park (California). He was a member of the Y.M.C.A. Board, the American Legion, the Huntington Park Planning and Zoning Commission, and the Rising Light Lodge of the Free and Accepted Masons in Huntington Park and was also active in Chi Epsilon. He was a registered professional civil engineer in the State of California.

In September, 1918, Mr. Collins was married to Marion Ida Davis. He is survived by his widow; one son, Marshall Davis; two granddaughters; and a sister.

Mr. Collins was elected an Associate Member of the American Society of Civil Engineers on October 24, 1932.

ARTHUR COLEMAN COMEY, M. ASCE[1]

DIED JANUARY 26, 1954

Arthur Coleman Comey, the son of Arthur M. and Kate (Coleman) Comey, was born at Somerville, Mass., on September 6, 1886. He was graduated, cum laude, from Harvard University at Cambridge, Mass., in 1907, with the degree of Bachelor of Arts and was later graduated from the Harvard School of Landscape Architecture.

---

[1] Memoir prepared by Carroll A. Farwell, M. ASCE.

Mr. Comey served as a lecturer and associate professor of city planning and landscape architecture at Harvard University. He taught at the Harvard School of Landscape Architecture, at the Harvard School of City Planning, and at its successor, the School of Regional Planning. In 1912, he entered private practice. During World War I he was a member of the Massachusetts Homestead Commission and served the United States Housing Corporation at Washington, D. C. He was associated with the State Planning Boards in Massachusetts and Maine and the New England Planning Commission, and he was a consultant in the selection of a site for the United Nations headquarters and also for the Tennessee Valley Authority. He wrote many books on planning subjects and served as associate editor of the *National Municipal Review.*

Mr. Comey became a member of the American Institute of Consulting Engineers in 1930 and was a fellow of the American Society of Landscape Architects. He also held membership in the American Civic Association, the National Conference on State Parks, the International Federation for Housing and Town Planning, the American Institute of National Defense, and the United States Housing Corporation. He was a member of the Harvard Faculty Club.

Mr. Comey was a devotee of the outdoor life. He was a member of the Harvard Mountaineering Club, the Chocorua Mountain Club (N. H.), the Appalachian Mountain Club, and the Appalachian Trail Conference. He served as secretary of the New England Trail Conference and as counselor of topography and exploration. In 1926 and 1928, Mr. Comey led a group of skiers to Mount Katahdin (Maine) to climb and descend the mountain on skis. These are believed to have been the first ski ascents of the mountain. He published many articles on matters of interest to the club.

In 1915 he was married to Eugenia Jackson, in 1930 to Janet Mowry, in 1950 to Elizabeth G. Pattee, and in 1954 he remarried his second wife. He is survived by his widow, two children by his first wife, and five grandchildren.

Mr. Comey was elected a Member of the American Society of Civil Engineers on December 14, 1925.

GEORGE DAVIS CROW, M. ASCE[1]

DIED DECEMBER 30, 1952

George Davis Crow, the son of William Jefferson and Sallie (Trammell) Crow, was born in Henderson, Tex., on April 4, 1888. He attended the public schools in Henderson and after graduation entered the University of Texas at Austin where he prepared for a civil engineer's career. Later he changed his course of study and was graduated in 1912 as an electrical engineer.

---

[1] Memoir prepared by John A. Focht, M. ASCE.

After graduation he worked as a mining engineer until World War I. He served as First Lieutenant in the 111th Engineers and participated in many of the important battles in France. After being separated from active duty, Mr. Crow went to Havana, Cuba, where he was an automobile dealer. He returned to Texas and in 1928 was employed by a road contractor, constructing many of the highways in the vicinity of Houston. During 1931 to 1938 he worked in the oil fields of east Texas and on irrigation projects in the Rio Grande Valley; in 1939 he opened a surveyor's office in Wharton, Tex. During 1941 he worked for a contracting firm, The Austin Company, building the Dow Chemical Plant at Freeport, Tex. He was associated with the Civil Aeronautics Administration in 1944 and 1945 on the construction of an airport at Conroe, Tex. For the next two years he was in Mexico staking out locations for radio range stations. Mr. Crow returned to airport construction in 1948 and continued until his retirement in 1952.

He was a civil engineer and a licensed land surveyor.

Mr. Crow is survived by a sister, Mrs. Emily Crow Downum, and four brothers, Madison K., Thomas Joel, Jefferson Brim, and Benge.

Mr. Crow was elected a Member of the American Society of Civil Engineers on December 5, 1949.

JOSEPH HERBERT DAVIES, M. ASCE[1]

DIED OCTOBER 7, 1953

Joseph Herbert Davies, the son of Joseph Edward and Daisy Florence (McAleer) Davies, was born in Columbus, Ohio, on August 12, 1902. After attending the public schools of Columbus, he enrolled in the Civil Engineering Department of The Ohio State University at Columbus. He was graduated in 1926 with the degree of Bachelor of Science in Civil Engineering.

After graduation he was supervisor of construction for the Highway Construction Company of Miami, Fla., in charge of road, pavement, and sewer work. In 1927 he moved to Long Beach, Calif., where he was employed as a structural engineer for the City of Long Beach. For one year he was in charge of the work on the Long Beach Municipal Auditorium, and, in 1933, after writing a detailed thesis concerning the auditorium, he received the degree of Civil Engineer from The Ohio State University.

After the severe Long Beach earthquake of March 10, 1933, Mr. Davies was in charge of all the emergency demolition work, inspection, and approval of buildings prior to re-occupancy. He also played a major part in the rewriting of California building codes which now require that the design of all construction be adequate to resist damage from seismic disturbances. In 1933 Mr. Davies left the employ of the city and opened a private engineering office. He was the structural engineer on more than thirty different elementary, high school, and college plants. During and after World War II, he was selected as the engineer for the design of major facilities for the Coast Guard, the Army, and the Navy. Mr. Davies made an extensive study of the subsidence phenomena which resulted in the gradual sinking of much of the Long Beach harbor area, and he was retained by the Ford Motor Company, Procter and Gamble Company, and other industrial concerns to design facilities for protection from this extensive subsidence. At the time of his death, his office was designing two large bridges soon to be erected in Long Beach. By official action of the Long Beach City Council, one of these bridges will be known as the J. H. Davies Memorial Bridge.

---

[1] Memoir prepared by James R. Bole, A.M. ASCE.

Mr. Davies was an active member of the American Association of Engineers, the Structural Engineers Association of California, the American Concrete Institute, the Consulting Engineers Association of California, and the American Society of Military Engineers. He was a registered civil and structural engineer in California. Much of his time was devoted to helping engineering students and young graduate engineers. He was a permanent sponsor of the Engineering Club of the Long Beach City College, and his friendly understanding and cooperation helped and inspired many young men. He was a member and director of the Chamber of Commerce and was a member of the County Planning Commission and the Board of Examiners and Appeals of the City Building Department. He belonged to the Free and Accepted Masons, the Scottish Rite of Long Beach, and the Al Malaikah Shrine Temple of Los Angeles. He was a member of Rotary International and, at the time of his death, was president of the Long Beach Rotary Club. He was an active worker in many youth organizations and was almost solely responsible for the low-cost construction of buildings for the Boys Clubs of Long Beach, the Long Beach Day Nurseries, and the Camp Fire Girls.

He is survived by his widow, Ann, and two daughters, Priscilla (Mrs. Gutknecht) and Nance (Mrs. Winston).

Mr. Davies was elected a Member of the American Society of Civil Engineers on November 12, 1940.

THOMAS MARSH DAVIS, SR., M. ASCE[1]

Died October 23, 1953

Thomas Marsh Davis, the son of John L. and Catherine (Marsh) Davis, was born in Centralia, Ill., on November 7, 1881. Mr. Davis attended grade school and high school in Centralia and studied civil engineering at the Armour Institute of Technology in Chicago, Ill., from 1901 to 1903.

The years from 1903 to 1905 were spent in homesteading in Klickitat County, Washington. At this time, Mr. Davis was also engaged in private engineering practice on land surveys. From 1905 to 1908 Mr. Davis was employed by the Centralia Coal Company in Centralia as paymaster, and he also conducted private classes in engineering. In 1908 he returned to Washington to spend five years in private engineering practice and served as chief deputy county engineer of Klickitat County, residing in Goldendale.

---

[1] Memoir prepared by Rene B. Wright, M. ASCE.

For the four-year period ending in 1917, Mr. Davis served as a resident engineer for the State Engineer's office on highway construction involving the first concrete pavement laid in the state of Oregon. In 1917 he was employed as senior highway engineer by the United States Bureau of Public Roads in Portland, Ore., and served with this agency until his retirement in February, 1951. For the last ten years of this period, Mr. Davis was district engineer in charge of all federal-aid highway construction in Oregon.

Mr. Davis was a member of Northwest Highway Engineers and served as president in 1933. He was active in Society affairs and served as Treasurer of the Oregon Section in 1946 and 1947.

Mr. Davis' two hobbies were gardening and color photography. He compiled an extensive file of 35-mm slides.

On June 11, 1905, Mr. Davis was married to Myrtle Denny in Corvallis, Ore. He is survived by two children, Catherine (Mrs. Frank W. Young) and Thomas M. Davis, Jr.

Mr. Davis was elected an Associate Member of the American Society of Civil Engineers on November 21, 1921, and a Member on April 9, 1951. He became a Life Member in January, 1952.

EDWARD A. DOUGHERTY, M. ASCE[1]

DIED FEBRUARY 27, 1952

Edward A. Dougherty, the son of Richard and Emma (Erwin) Dougherty, was born in New York, N. Y., on December 14, 1886. His father came from County Derry in Ireland, and his mother was born on a farm in Oakland County, Michigan. Mr. Dougherty was educated in the schools of New York. He attended DeWitt Clinton High School and the College of the City of New York and entered Columbia University in 1906, graduating with the degree of Civil Engineer in 1910. During the summer vacations he worked as a chainman for the New York Central Railroad.

After his graduation, Mr. Dougherty took a permanent position with the New York Central Railroad in the resident engineer's office at Yonkers, N. Y., and until 1916 he worked as rodman, inspector, instrumentman, transitman, and assistant engineer on major construction projects in New York State incident to the electrification of the railroad from Mott Haven to Croton-on-Hudson and to North White Plains, including such projects as three-tracking and four-tracking, elimination of grade crossing, and station improvements at Yonkers, Ossining, Mount Vernon, and White Plains, and the yard and engine terminal improvements at Harmon. During the next seven years Mr. Dougherty was assistant engineer in various departments of the railroad. From 1927 to 1935 he was designing engineer in the Engineering Department, Buffalo and East, in general charge of all trackwork and architectural and structural work, exclusive of bridge design or grade crossing eliminations. He had a leading part in developing many important projects in New York State, such as: The four-tracking of the Hudson Division of the railroad from Garrison to Beacon and from Chelsea to Poughkeepsie, the relocation of the Putnam Division tracks between Eastview and Briarcliff Manor, and the rearrangement of the Mott Haven yards and the Harmon yards. The plans for the relocation of the New York Central Railroad through Syracuse (N. Y.) on an elevated roadbed included the design of the passenger terminal, the station and subway, the express building and coach shop, several miles of retaining walls, and the coaling facilities at the DeWitt yards. Mr. Dougherty also participated in the designs for the St. John's Park freight terminal and the Cudahy Building in New York City (in connection with elevating the New York Central tracks) and the designs for the Central passenger terminal at Buffalo, N. Y.

---

[1] Memoir prepared by A. M. Westenhoff, M. ASCE.

From 1935 to 1938 Mr. Dougherty was assistant chief engineer of the New York Central Railroad, Buffalo and East, handling the construction of the West Side Highway between 79th Street and 181st Street in New York City. As the assistant to the vice-president of the New York Central Lines West in Chicago, Ill., Mr. Dougherty directed many grade separation projects, conducted negotiations with government agencies, and took an active part in legislative matters during the five years he served in this capacity. From 1943 to 1945, he was assistant general manager of the New York Central Lines West in Cleveland, Ohio. During that period an important project for constructing permanent bridges across Sandusky Bay in Lake Erie was completed, and extensive changes were made in the Collinwood engine terminal and yards at Cleveland. In 1945 Mr. Dougherty became chief engineer of the New York Central Lines West in Buffalo and directed many important engineering projects such as the construction of the Toledo passenger station, the reconstruction of the Cuyahoga River bridges at Cleveland, and the Diesel shop facilities at Stanley (Toledo), Collinwood, and Ashtabula, Ohio. Several coal roads in West Virginia and Illinois and grade crossing elimination projects were designed and constructed during this period.

Mr. Dougherty was active in Society affairs as a member of the executive committee of the Centennial Celebration Committee of the Society and a Director of the Centennial of Engineering, 1952. He was also a member of the American Railway Engineering Association and the Western Society of Engineers, and was chairman of Zone 5 Committee-Waterway Projects and the State of Michigan Railroads Engineers Committee, both committees of the Association of American Railroads.

Mr. Dougherty was married to Mary Kennedy in 1912. He is survived by his widow; one son, Richard Erwin; and two grandsons, Richard Edward and Steven John.

Mr. Dougherty was elected a Member of the American Society of Civil Engineers on April 22, 1946.

LOUIS WARREN DUFFEE, M. ASCE[1]

Died May 9, 1953

Louis Warren Duffee was born in Mobile, Ala., on November 28, 1884. He attended Barton Academy in Mobile and was graduated from Alabama Polytechnic Institute at Auburn in 1904 with the degree of Bachelor of Science in Civil Engineering. He returned to Alabama Polytechnic Institute in 1905 to prepare for the degree of Master of Science.

One of Mr. Duffee's first positions after graduation was as engineer in the construction of Ashland Place in Mobile—now one of the most beautiful residential sections of the city. His experience in this construction work was utilized in his master's thesis which dealt with the construction of Ashland Place. After receiving the degree of Master of Science, Mr. Duffee was employed by the Gulf Mobile and Northern Railroad (now the Gulf Mobile and Ohio Railroad) and served in various capacities, one of which was chief engineer. In 1917 Mr. Duffee was retained as chief engineer to build the Meridian and Bigbee Railroad.

He moved to Laurel, Miss., in 1919 and remained with the Gulf Mobile and Northern Railroad until 1922 when he entered private practice as architect and engineer. Later he worked with the Federal Works Agency in Jackson, Miss., and Atlanta, Ga., and with the Mississippi State Highway Department as project engineer. Mr. Duffee returned to Laurel in January, 1949, to continue his private practice. He was supervising architect for the Jones County Hospital in Laurel and for many buildings at Jones County Junior College and at the Ellisville State School.

Mr. Duffee was an Elder of the Presbyterian church. He was a member of the Free and Accepted Masons and the Rotary Club.

In 1913 he was married to Susie Sadler in New Albany, Miss. He is survived by his widow, and three children, Louis A. Duffee, Warren S. Duffee, and Mary Louise (Mrs. Frank A. Philips).

Mr. Duffee was elected an Associate Member of the American Society of Civil Engineers on February 4, 1913, and a Member on June 7, 1948.

---

[1] Memoir prepared by Roy C. Kuyrkendall, Jr., J. M. ASCE.

SCOTLAND G. HIGHLAND, A.M. ASCE[1]

Died October 25, 1953

Scotland G. Highland, the son of Capt. John Edgar and Lucinda Earle (Patton) Highland, was born near West Milford in Harrison County, West Virginia, on October 7, 1879. After his elementary education in the district schools, he attended West Virginia University at Morgantown, Iron City College at Pittsburgh, Pa., and G. W. Michael's School, in Logansport, Ind.

After working industriously during his youth in mercantile establishments, Mr. Highland became secretary and treasurer in 1906 of the Clarksburg (W. Va.) water plant. Following the completion of a modern filtration plant for the city in 1912, he was chosen as the general manager of this plant and of the Clarksburg Water Board and held this latter post until his retirement in April, 1953.

As general manager of the Clarksburg Water Board, Mr. Highland was distinguished by unusual ability. He provided an adequate supply of good water from a difficult source and at reasonable rates throughout his forty-seven years of service; at the same time, the capital value of the water system increased from $350,000 in 1909 to $3,636,243 on April 30, 1953, all of which increase was paid out of earnings of the Water Department. Mr. Highland was devoted to his job, was meticulous in his accounts, and worked continuously with the federal government and state authorities to secure a source of supply for the water system which would be of the highest quality. This intense interest in his duties—involving as they did the protection of the health of the city—and the esteem in which he was held by both his employees and employers made his sudden death a distinct and serious loss to the community.

Mr. Highland was an avid student throughout his life. He accumulated a large library, wrote of the geneology of the Highland family, and placed many other genealogical and historical items in the Library of Congress and other American libraries. It was in the realm of municipal water works, however, that Mr. Highland most diligently pursued his education, to the end that he prepared and read eight major papers at annual conventions of the American Water Works Association (AWWA), assisted in the preparation of the Manual of the American Water Works Practice for the AWWA, and, throughout his forty-seven years of service as general manager of the Clarksburg Water Board, contributed to the *Proceedings* of the AWWA.

He was a lifelong member of the Methodist Church. His devotion to the church was shown by his purchase of the Methodist Episcopal Church in West Milford (where his mother and father worshipped) which he restored and beautified. He belonged to Herman Lodge No. 6 of Clarksburg, Free and

---

[1] Memoir prepared by Frank D. McEnteer and George L. Coyle, Members, ASCE.

Accepted Masons, was a member of the AWWA, the New England Water Works Association, the West Virginia Conference on Water Purification, the American Geophysical Union, and the American Public Works Association, and was an associate member of the Engineering Societies of New England.

Mr. Highland was unmarried. He is survived by one brother, Cecil B. Highland, and one sister, Isophrene (Mrs. Emory E. Tetrick).

Mr. Highland was elected an Associate Member of the American Society of Civil Engineers on December 11, 1939.

ARNE ARTHUR JAKKULA, M. ASCE[1]

DIED MAY 30, 1953

Arne Arthur Jakkula, the son of August and Alma (Lyttinen) Jakkula, was born in Hancock, Mich., on March 19, 1904. He was graduated in 1926 from the University of Michigan at Ann Arbor with the degree of Bachelor of Science in Civil Engineering. He continued his studies there and was awarded the degrees of Master of Science and Doctor of Philosophy. He also obtained a professional degree in Civil Engineering from the University of Minnesota at Mineapolis.

Following graduation, Mr. Jakkula worked in various capacities for the Minnesota Highway Department, the United States Bureau of Public Roads, and the Westinghouse Electric Company. He joined the teaching staff of the Agricultural and Mechanical College of Texas at College Station in 1937 as a specialist in structural engineering. He served as a consultant on bridge design for the Texas Highway Department and conducted research on bridge problems for the Texas Engineering Experiment Station and the United States Bureau of Public Roads.

In recognition of his outstanding work in the field of suspension bridge design, Mr. Jakkula was named in 1942 a member of the advisory board of the Public Roads Administration to investigate suspension bridges after the failure of the Tacoma Narrows Bridge in the State of Washington. He was serving as chairman of the Committee on Interpretation and Analysis for this board at the time of his death. Mr. Jakkula was named the first executive director of the Agricultural and Mechanical Research Foundation, a non-profit corporation. Under his leadership, this organization established an enviable reputation, particularly in the field of oceanographic research in the Gulf of Mexico.

Mr. Jakkula was a member of Chi Epsilon, Tau Beta Pi, Sigma Xi, the Texas Academy of Science, the Texas Society of Professional Engineers, the National Society of Professional Engineers, and the American Society for Engineering Education. His works were published extensively during his lifetime.

---

[1] Memoir prepared by John A. Focht, M. ASCE.

In 1926 he was married to Myrta Danner in Minneapolis. He is survived by his widow; a daughter, Signe (Mrs. F. Moon); his mother; and two sisters, Florence, and Sigred (Mrs. L. J. Coffman).

Mr. Jakkula was elected a Junior of the American Society of Civil Engineers on January 16, 1928; an Associate Member on October 20, 1936; and a Member on November 9, 1942.

LESTER JOSEF NEWMAN KELIHER, A.M. ASCE[1]

DIED JANUARY 18, 1953

Lester Josef Newman Keliher, the son of Peter C. and Mary (Gardner) Keliher, was born in Saulte Sainte Marie, Mich., on March 6, 1891. He studied at the University of Michigan (at Ann Arbor) from which he received the degree of Bachelor of Science in Civil Engineering in 1914.

After serving in World War I, Mr. Keliher was employed by the Portland Cement Association, with headquarters in Chicago, Ill. He helped contractors promote the use of Portland Cement in the rapidly developing field of concrete construction throughout Minnesota, Illinois, Missouri, and Arkansas. Later, as head of the St. Louis (Mo.) Division, he made the major contribution to its educational and development work which resulted in the approval of the first bond issue in the State of Missouri for the construction of concrete roads.

While still a young man of twenty-nine, Mr. Keliher moved to Little Rock, Ark., where he organized the Keliher Construction Company, specializing in the construction of concrete highways. This activity shortly expanded to include concrete bridges, and it was in the bridge-construction field that he was best known. His company built bridges in Texas, Kansas, Arkansas, Oklahoma, Missouri, and Louisiana. The three-mile Bonet Carre Spillway Bridge and the Morganza Floodway Bridge in Louisiana are examples of his skill. In 1932 Mr. Keliher moved to Dallas, Tex., where he spent the remainder of his life. At the beginning of World War II he served as president of the Big Rock Stone and Material Company of Little Rock and contributed to the success of the construction of many Army projects in Arkansas.

During his later years, Mr. Keliher helped many young men get their start in the construction industry. These activities kept him in touch with the work he loved so well, and he derived much satisfaction from seeing his proteges advance in his chosen field. Mr. Keliher enjoyed his leisure—reading, hunting, and playing golf. He was a member of the Roman Catholic Church.

On July 3, 1916, Mr. Keliher was married to Hilda Filbert in Saginaw, Mich. He is survived by his widow; two daughters, Frances Louise (Mrs. W. J. Frank) and Hilda Jane (Mrs. L. L. Northup, Jr.); a son, Lester Josef Newman, Jr.; six sisters; and three brothers.

Mr. Keliher was elected an Associate Member of the American Society of Civil Engineers on August 28, 1922.

---

[1] Memoir prepared by Grayson Gill, M. ASCE.

HERBERT MILLER KNIGHT, M. ASCE[1]

Died August 18, 1948

Herbert Miller Knight, the son of Henry M. and Mary Boyd (Turner) Knight, was born on October 6, 1865, in Providence, R. I., and there spent his boyhood and young manhood. After attending the public schools of the city, he studied privately to further his professional life.

Following a few years at the engineering office of the City of Providence, where his most important assignment as resident engineer was the charge of the construction of the sewage-disposal plant near Fields Point, on Narragansett Bay, Mr. Knight became chief engineer for the Continental Compressed Air Company of Philadelphia, Pa. For this company, he was engaged in the construction of a unique hydro-pneumatic power plant in Norwich, Conn., a pioneering effort that left him always convinced of untold possibilities of the principles involved. From 1905 to 1910 he was design engineer and division engineer, respectively, for the City of Baltimore, Md., in charge of storm-water drains and the building of a sewage pumping station. For twelve years Mr. Knight was chief engineer on heavy construction work of canals, railroads, and bridges for the M. A. Talbot Company, in Rome, N. Y., and then with Grant Smith and Company, and Lacher, in New York, N. Y. Lock and dam construction for the New York State Barge Canal at Rome was one of his major projects.

Mr. Knight's major life's work began in 1922 when he became an engineer in the New York office of the Maryland Casualty Company and ended with his retirement in 1943 after a long span of active experience. He became an expert on engineering contracts and contract bonds, advising on claims and similar problems and displaying a deep understanding for both owner and contractor. He traveled extensively in the west and south. He also wrote widely on casualty and surety matters including a series in *Civil Engineering* in October, 1935, November, 1935, and January, 1936.

He belonged to the Engineers Club (New York), the Montclair (N. J.) Society of Engineers, and the Dunworkin Club of Montclair which he served as treasurer. Always he was a loyal churchman, for most of his life in the Baptist faith, and in his later years in the Central Presbyterian Church in Montclair.

Mr. Knight was a vivacious personality, keen of mind and memory and brilliant of expression. Two of his many inventions were a deep-sea floating dock or island and an automatic control for sewage, which was adopted in his Baltimore work. He spoke before technical meetings held by engineers of Yale University (New Haven, Conn.) and graduates of Brown University (Providence). He was an avid reader, enjoyed music, and wrote poetry.

On June 28, 1898, in Providence, he was married to Harriet E. Manning. He is survived by his widow.

Mr. Knight was elected a Member of the American Society of Civil Engineers on May 3, 1910. He became a Life Member in January, 1936.

---

[1] Memoir prepared by Sydney Wilmot, M. ASCE.

JOHN CRANE McVEA, M. ASCE[1]

DIED DECEMBER 16, 1952

John Crane McVea, the son of William and Jane (Crane) McVea, was born in Waelder, Tex., on April 3, 1876. He studied at the Moulton Institute at Moulton, Tex., and at the University of Texas, at Austin, from which he was graduated with the degree of Bachelor of Science in Civil Engineering in 1897.

After graduation Mr. McVea organized and designed a light plant for Flatonia, Tex. Five years later he sold the plant and joined the engineering staff of the Southern Pacific Railroad. He was transitman for this railroad on the Palacios Branch and on the Stockdale-Cuero Branch in Texas. Later he was resident engineer in charge of maintenance and structures on the Houston East and West Texas Railroad.

After twelve years of railroad work, he was employed bv the City of Houston as a draftsman. He was promoted, successively, to the positions of office engineer, assistant city engineer, and city engineer in 1919. He held the latter position until 1929. In this capacity he supervised civic improvements consisting of the installation of water mains, sanitary and storm sewers, and pavements. In 1941 Mr. McVea served as chief of surveys and maps in the City Utility Department, remaining until 1947 when he retired to private practice. During this last period of service with the city, he assisted greatly in the development of the San Jacinto Water project.

Mr. McVea was a senior deacon of the South Main Baptist Church. He was a charter member of the Houston Engineers Club, and before his death he was presented with a certificate for distinguished service by that group. He was a life member of the Salesmanship Club of Houston. He was a founder of the Sons of the Republic of Texas and a member of the Sons of the American Revolution. Mr. McVea was deeply versed in the history of the United States and particularly of Texas. He wrote the only history of the water department of Houston. Mr. McVea was an active member of the Texas Section of the Society, and he served as President in 1926.

He was married to Mary Faires in 1904. He is survived by his widow and a sister, Willie (Mrs. E. E. Smith).

Mr. McVea was elected an Associate Member of the American Society of Civil Engineers on November 28, 1916, and a Member on April 21, 1920. He became a Life Member in January, 1947.

FRED WILLIAM MORRILL, M. ASCE[2]

DIED MAY 25, 1953

Fred William Morrill, the son of William E. and Hattie (Davis) Morrill, was born in Haverhill, Mass., on July 26, 1885. He attended the Massachusetts

---

[1] Memoir prepared by John A. Focht, M. ASCE.

[2] Memoir prepared by a Committee of the Cincinnati Section consisting of H. D. Loring, *Chairman,* H. B. Luther, and H. W. Hanly, Members, ASCE.

Institute of Technology at Boston, Mass., where he was an outstanding student, and received the degree of Civil Engineer in 1907.

Shortly after graduation Mr. Morrill was appointed a professor at (the Imperial) Pei-Yong University in Tientsin, China, where he remained for three years. During his teaching career he acquired an understanding and affection for the Chinese people which were fully reciprocated by his Chinese associates. His study of the language and his vacation travels through the country contributed to his insight into Chinese society and culture, and his lifelong interest in the Orient. His brother, Arthur Morrill, succeeded him for a three-year term at Pei-Yong University, and their common knowledge of Chinese life and language was part of the background of a lifelong correspondence and sympathy.

In 1912 Mr. Morrill returned to Boston and spent several years as a structural designer with J. R. Worcester and with Fay, Spofford and Thorndike, consulting engineering firms of that city. He went to Cincinnati, Ohio, in 1915 and joined the engineering department of the Ferro Concrete Construction Company where he was senior structural engineer at the time of his death. Mr. Morrill's work covered a wide variety of structural designing projects for industrial, commercial, and public structures. He also acted as project engineer on some of the more important contracts executed by the company and was a director of the company. As the dean of the engineering staff, he was constantly sought for consultation by his colleagues who recognized his vast knowledge and his quality of a born teacher and clear thinker. In 1933 and 1934, on a leave of absence from the company, Mr. Morrill was acting professor of civil engineering at the University of Cincinnati.

Mr. Morrill was a registered engineer in Ohio and Indiana, a member of the Structural Provisions Sub-Committee of the Building Code Revision Committee of Cincinnati and was a past-president of the American Society of Philately, and of the Cincinnati Engineering Society. He was active in Society affairs and was a Past-President of the Cincinnati Section of the Society. Mr. Morrill was an elder, trustee, and clerk of the Session of the First United Church, Congregational-Presbyterian of Cincinnati.

He was married on September 19, 1914, to Beatrice Webster. He is survived by his widow and two daughters, Freda (Mrs. Irving Abrams) and Marjorie.

Mr. Morrill was elected an Associate Member of the American Society of Civil Engineers on July 6, 1920, and a Member on August 14, 1944.

JOHN FREDERICK PARTRIDGE, M. ASCE[1]

DIED OCTOBER 24, 1953

John Frederick Partridge, the son of John and Emily (Marriott) Partridge, was born in San Francisco, Calif., on April 7, 1891. He attended Leland Stanford University, at Stanford, Calif., and was graduated in 1912 with the degree of Civil Engineer.

---

[1] Memoir prepared by Julian R. Fleming, A.M. ASCE.

The long and varied career of Mr. Partridge began with land surveys, railroad and highway location, and highway construction from 1907 to 1911. In the next two years he was engaged in location, design, and construction of irrigation canals and structures for the South San Joaquin Irrigation District in California. Also during 1913 he was employed by the Hammon Engineering Company to make studies and surveys for river control. From 1914 to 1917 he was chief engineer in the pipe department of the Redwood Manufacturers Company in San Francisco. During World War I, Mr. Partridge was a Captain in the 23rd Engineers of the United States Army in France. After his return to the United States in 1919, he was engaged in an arch-dam construction project and an irrigation project in California. From 1921 to 1928 he was an hydraulic engineer for the California-Oregon Power Company. In 1929 Mr. Partridge went to Brazil as assistant engineer of the American and Foreign Power Company, doing investigation work on hydroelectric power plants. After his return to the United States he served during 1933 and 1934 as resident engineer on the Golden Gate Bridge project in California and on the San Francisco-Oakland Bay Bridge project. In 1934 he served with the National Park Service as park engineer in Yellowstone Park.

In 1934 Mr. Partridge was employed by the Tennessee Valley Authority (TVA). On the construction of Hiawassee Dam in North Carolina he served as civil engineer, office engineer, and assistant construction engineer. Later during the construction of Fort Loudoun Dam near Knoxville, Tenn., he was assistant construction engineer and later was construction engineer. In 1943 he received military leave from the TVA to become a Major in the United States Army. He served in Europe and later was promoted to Lieutenant Colonel. In 1947 he returned to the TVA as chief of the Construction Plant Branch, and he held this position until a few weeks before his death.

Mr. Partridge was a member of the American Legion, the Society of American Military Engineers, and the National Society of Professional Engineers. He belonged to Tau Beta Pi and Sigma Alpha Epsilon. He was a member of the Unitarian Church of Knoxville.

On February 11, 1915, Mr. Partridge was married to Vesta Reid in San Francisco. He is survived by his widow and two sons, John F., Jr., and Lawrence Reid.

Mr. Partridge was elected a Junior of the American Society of Civil Engineers on February 4, 1913; an Associate Member on January 19, 1920; and a Member on January 19, 1925.

JOHN CORNELIUS PENN, M. ASCE[1]

DIED JULY 20, 1952

John Cornelius Penn, the son of Jacob and Annigje (Stobbe) Penn, was born in Steenwyck, The Netherlands, on November 26, 1881, and emigrated to the United States in 1890. The Penn family settled in the Roseland District of Chicago, Ill., and Mr. Penn maintained a home in that section of the city throughout his life. After being graduated from Calumet High School in Chicago in 1901, Mr. Penn entered the Armour Institute of Technology (Chicago) and received the Bachelor of Science degree in June, 1905. The professional degree of Civil Engineer was awarded him by Armour Institute in May, 1910.

---

[1] Memoir prepared by F. W. Edwards, M. ASCE.

From 1905 to 1910, Mr. Penn served the City of Chicago as assistant engineer in the Bureau of Bridges. In 1910, he received an appointment as an instructor at Armour Institute of Technology and served that institution and its successor, Illinois Institute of Technology, until his retirement in 1949. A man of varied talents, Mr. Penn was, successively, instructor (1910 to 1914), assistant professor (1914 to 1918), associate professor of civil engineering (1918 to 1921), assistant registrar, registrar, assistant dean, dean (1928 to 1934), chairman of the administrative committee, head of the Civil Engineering Department, and professor of civil engineering (1937 to 1949). He was a lifelong student and teacher and left his mark on the lives of many students and associates.

The diversity of Mr. Penn's interests is partly indicated by the following organizations to which he belonged: Western Society of Engineers; American Society for Engineering Education; American Geographical Society; Chicago Astronomical Society; the Knickerbocker Society of Chicago; Theta Xi; Tau Beta Pi; and Chi Epsilon. Mr. Penn belonged to the Free and Accepted Masons. He was a member of the Dutch Reformed Church.

A particular interest in surveying persisted from his early work as a city engineer and a happy result was a book on surveying problems.[2] Many former students will best remember Mr. Penn as a result of the many years of close association at Camp Armour, the civil engineering summer camp in Vilas County, Wisconsin, where Mr. Penn served as the director. Many will also recall his interest in old maps and unusual clocks.

On June 6, 1922, Mr. Penn was married to Mae Van Wyngarden. He is survived by his widow; a daughter, Jane Ann (Mrs. W. C. De Young); three brothers, Hiram, Nicholas, and Henry; and two granddaughters, Linda Jean and Barbara Lee.

Mr. Penn was elected a Member of the American Society of Civil Engineers on February 10, 1936.

HAROLD FRED PERCIVAL, A.M. ASCE[1]

Died December 3, 1951

Harold Fred Percival, the son of Elijah C. and Anna Louise (Lloyd) Percival, was born in Petaluma, Sonoma County, California, on March 29, 1889. He obtained his grade school education in San Francisco, Calif., and attended Licks Technical High School where he studied civil engineering.

---

[2] "Elementary Surveying Problems for Field and Office," by John C. Penn, Chicago, Ill., 1942.

[1] Memoir prepared by Howard E. Blower, A.M. ASCE.

After graduation, Mr. Percival worked for the Western Pacific Railroad on the location of the route through rugged Feather River Canyon, above Oroville, Calif. He then attended the University of Nevada, at Reno, where he majored in civil engineering. In the field of sports at the university, he earned his letters in baseball and rugby, and as end in football.

Early in 1917, Mr. Percival enlisted in the United States Army (California Engineers) and was later transferred to the 42nd Rainbow Division, under Col. J. M. Johnson. In August, 1917, he was commissioned a Second Lieutenant and within a year was made Captain. During his eighteen months of service in France and Germany, he participated in the Champagne, Aisne-Marne, Saint Michel, and Meuse-Argonne offensives, and in the Defensive Sector. He was awarded the Purple Heart.

After his discharge from the Army, Mr. Percival worked on the Sutter Basin development in the Sacramento Valley (California). He organized the firm of Percival, Tibbals and Gans in Woodland, Calif. This firm did much of the early irrigation engineering in the Sacramento and San Joaquin valleys. The partnership was dissolved, and he was employed as a sales engineer for the California Corrugated Culvert Company in March, 1929.

Most of Mr. Percival's work with "Calco" was in the Sacramento Valley, where he sold drainage products to the farmer. He also sold to the irrigation and reclamation districts of the area and to many of the neighboring counties. Mr. Percival always engineered his installations well, and he had an almost endless list of customers who respected his decisions as an expert in the field of drainage and irrigation.

He was married to Marion Schumacher on November 17, 1920, in Berkeley, Calif. He is survived by his widow; a sister, Miss Ellita Percival; a daughter, Mrs. Robert Weeks; a son, John Percival; and a grandson, Alan Percival.

Mr. Percival was elected an Associate Member of the American Society of Civil Engineers on July 16, 1928.

ST. GEORGE TUCKER RICHARDSON, M. ASCE[1]

Died October 18, 1952

St. George Tucker Richardson, the son of Robert B. and Lucy Beverly (Tucker) Richardson, was born in Memphis, Tenn., on April 1, 1882. He was educated in public and private schools in Memphis and attended the University of Tennessee at Knoxville for two years as a student of engineering.

In 1901 Mr. Richardson left the university to become a surveyor for the Land Department of the Yazoo & Mississippi Valley Railroad, surveying its lands through the Yazoo Delta of the Mississippi River from Memphis to Vicksburg, Miss. Early in 1905 he left the railroad to enter private practice in Memphis. In the same year he was elected county surveyor of Shelby County,

---

[1] **Memoir prepared by Garner W. Miller and James R. Newman, Members, ASCE.**

Tennessee, and held that position from 1905 to 1927. During a large part of that period he also served as county engineer.

The list of Mr. Richardson's important surveying commissions must include the establishment of state and private boundary lines in the vicinity of the Centennial Cutoff in the Mississippi River in the lawsuit (originally styled "Stockley vs Cissna") which terminated in a suit between the States of Arkansas and Tennessee, tried before the United States Supreme Court. Mr. Richardson made his first survey in this vicinity in 1899, and he was active in the subsequent litigation until the matter was finally decided in March, 1918. From 1924 to 1928, Mr. Richardson was chief construction engineer for the Blair Construction Company of Detroit, Mich. He was in full charge of the field layouts, heavy machinery foundations, quantity estimates, and cost records on the Memphis Plant, the River Rouge Steel Mill (Michigan), and the Somerville (Massachusetts) plants of the Ford Motor Company. For nearly two years he represented the Blair Construction Company on a board of arbitration.

After another year of construction work in Michigan, Mr. Richardson returned to general practice in Memphis. During 1930 to 1947 his practice included drainage and sewer-system projects and surveys. The surveys on the Mississippi were primarily problems of accretion, reliction, reappearance, erosion, recession, and avulsion. Mr. Richardson became a nationally recognized authority in these matters, appearing as an expert witness, and doing research and offering testimony in important boundary disputes for the States of Arkansas and Tennessee, the U. S. Gypsum Company, and other large timber interests. Throughout his life, his work was characterized by ability, integrity, and untiring industry. One of his most important professional engagements was as land expert for the Anderson-Tully Lumber Company of Memphis and Vicksburg. He made numerous detailed surveys for this company involving several thousand acres of valuable timber land.

Mr. Richardson was an ardent hunter and fisherman throughout his life and was a member of the Horseshoe Lake Fishing Club of Crittenden County, Arkansas. He was a member of Grace St. Luke's Episcopal Church. He belonged to the Free and Accepted Masons (32nd degree), the Ancient Arabic Order of Nobles of the Mystic Shrine, the Engineers Club of Memphis, and the Tennessee Society of Professional Engineers. He was active in the affairs of the Mid-South Section of the Society and was Vice-President of the Memphis Branch.

He was married on June 11, 1906, to Ann Mussenden. He is survived by his widow; two brothers, Marquis D., and Gilmer; and a sister, Lena (Mrs. G. Gilmer).

Mr. Richardson was elected a Member of the American Society of Civil Engineers on September 8, 1947.

ROBERT LAWRENCE ROLFE, A.M. ASCE[1]

Died December 9, 1952

Robert Lawrence Rolfe, the son of Robert Mayo and Mattie (Kerr) Rolfe, was born in Memphis, Tenn., on December 6, 1887. He was educated at the University of Colorado at Boulder.

Mr. Rolfe's first position, which he held for eleven years, was with the United States Engineers Office, Mississippi River Commission, in Memphis. In 1919, he became associated with the firm of Gardner and Howe, Consulting Engineers, in Memphis. Later he became a partner and was in charge of the Dallas (Tex.) office. In 1932 he established his own firm in Dallas where he continued private practice until his death.

He was a member of the National Society of Professional Engineers, the Society of Military Engineers, and the Dallas Rotary Club. He was registered to practice as civil and structural engineer in Texas, New Mexico, Oklahoma, and Louisiana. Many imposing structures in the Southwestern United States stand as a monument to his skill as a structural engineer.

In 1915 Mr. Rolfe was married to Mary Price in Paris, Tex. He is survived by his widow and one son, Robert L., Jr.

Mr. Rolfe was elected a Junior of the American Society of Civil Engineers on September 5, 1911, and an Associate Member on March 14, 1916.

FRANK CHARLES SCHROEDER, M. ASCE[1]

Died February 2, 1953

Frank Charles Schroeder was born in Philadelphia, Pa., on February 17, 1883. He was awarded the degree of Bachelor of Science in Civil Engineering at the University of Wisconsin, at Madison, in 1907 and the degree of Civil Engineer in 1910.

At the age of eighteen Mr. Schroeder was an apprentice and draftsman at the Pencoyd Plant of the American Bridge Company at Philadelphia, Pa. During the eleven years following his graduation, he was engaged in the field of bridge design in Chicago, Ill., and in teaching at the University of Washington at Seattle, and at Columbia University in New York, N. Y. In 1918 he settled in Milwaukee, Wis., where he was engaged in engineering work until his retirement in 1949. Throughout his professional career he maintained a continuing interest in engineering students. To young men who were interested in an engineering career but were without sufficient means to secure an engineering education, Mr. Schroeder made substantial contributions of his time and resources.

---

[1] Memoir prepared by Grayson Gill, M. ASCE.

After his retirement he moved to Dallas, Tex., where he was active in the affairs of the Dallas Branch of the Society until his death. Mr. Schroeder was a member of the Free and Accepted Masons. He belonged to Tau Beta Pi and Delta Phi Zeta at the University of Wisconsin and was a member of the Wisconsin Alumni Club of Dallas. He was a registered professional engineer in Texas.

He is survived by his widow, Alma; a son, Frank C., Jr.; a sister; and a grandson.

Mr. Schroeder was elected an Associate Member of the American Society of Civil Engineers on September 3, 1912, and a Member on July 8, 1935. He became a Life Member in January, 1947.

WALTER MICKLE SMITH, M. ASCE[1]

DIED MARCH 12, 1953

Walter Mickle Smith, the son of George Davis and Mary Elizabeth (Davis) Smith, was born in Newberry, S. C., on October 26, 1867. He received his early education in the private schools of that city. In 1889, 1912, and 1933, respectively, the degrees of Bachelor of Science, Civil Engineer, and Doctor of Science were conferred upon him by the Citadel at Charleston, S. C. It was in this academy that he received preliminary instruction in the design of masonry arch bridges and dams under the tutelage of the late William Cain.

Mr. Smith was engaged in railroad construction at Chattanooga, Tenn., in 1890 and 1891. During the next ten years he was designer and consultant for the Corps of Engineers, United States Army, on jetty constructions and coast fortifications at Charleston and on fortification and government works at Portland, Me. In 1903, Mr. Smith was United States assistant engineer at Charleston. From 1905 through 1907 he acted as consultant on the preliminaries to construction of the Panama Canal and in the latter year was appointed division engineer and later designing engineer with the New York Board of Water Supply. With the successful designs of the great Kensico Dam, the Bronx and Rye earth dams (New York Board of Water Supply projects), and reinforced concrete highway bridges, Mr. Smith earned the prestige which placed him among the great contemporary engineers. One of these arch bridges had I-shaped ribs, a variation which established a precedent for his time.

In late 1914, Mr. Smith was called to Dayton, Ohio, to design the flood control structures for the Miami Conservancy District where his experience and application of engineering principles gained him admiration and cooperation. He was a strong advocate of the use of the theory of "least work," and by the use of this method designed three-hinged arch bridges, large diameter conduits under heavy transverse loads, and a canal lock wall containing a large diameter conduit. He resigned from the Miami Conservancy District and in 1919 initiated the plans for the Illinois Waterway which was completed in 1933. During the period of this work, he served as chief designing engineer, assistant chief engineer, chief engineer, and consultant. In addition to the Illinois Waterway project, the plans of the State Department of Public Works included flood control and drainage works for many of the waterways of the state. The plans for the Illinois Waterway called for canalization of the DesPlaines and Illinois rivers from Lockport, Ill., to the head of navigation at Starved Rock near Ottawa, Ill., and included head gates for the production of electric power at three dam sites, Brandon Road, Dresden Island, and Starved Rock. Mr. Smith continued with the state agency until his retirement in 1947. In addition to his work on the Illinois Waterway project, he acted as consultant in 1944 for the Greater Chicago Lake Water Company and Metropolitan Water Company, both of Chicago.

---

[1] Memoir prepared by Jay L. Southworth, A.M. ASCE, and Murray Blanchard, M. ASCE.

Mr. Smith spent the last six years of his life at his ancestral plantation at Glenn Springs, S. C. He will be remembered for his unusual ability to sell the idea of an engineering project under trying and difficult circumstances and for his desire to improve the technique of any design project, regardless of conventional use. Mr. Smith was a member of the National Geographic Society and of Pi Kappa Alpha. He belonged to the Presbyterian Church. Many lectures on engineering subjects, such as flood protection, were delivered by him, and he wrote numerous articles for engineering journals.

In 1889, Mr. Smith was married to Nettie Babcock McDonald. He is survived by a son, McDonald Davis, and a daughter, Patra Lee.

Mr. Smith was elected an Associate Member of the American Society of Civil Engineers on October 2, 1901, and a Member on April 3, 1906. He became a Life Member in January, 1936.

EDWIN JAMES SNOW, A.M. ASCE[1]

DIED FEBRUARY 16, 1952

Edwin James Snow, the son of Edwin P. and Jean (Todd) Snow, was born in Chicago, Ill., on May 6, 1907. He was a direct descendant of Stephen Hopkins of the *Mayflower*. Mr. Snow's formal education began in the public schools of Chicago. He was graduated from Austin High School and continued his studies at Crane Junior College (both in Chicago) and then at the University of Illinois at Urbana from which he was graduated with the degree of Bachelor of Science in Civil Engineering in 1931. Mr. Snow never ceased to study, doing graduate work at the University of Wisconsin at Madison in sanitary engineering, and later studying structural engineering at the State University of Iowa at Iowa City and geology at Augustana College at Rock Island, Ill.

---

[1] Memoir prepared by Mrs. Suzanne F. Snow and a Committee of the Tri-City Section consisting of Erwin E. Beaudry, Albert F. Burleigh, and Robert H. Hurlbutt, Associate Members, ASCE.

During "time-out" intervals, in which Mr. Snow earned funds to continue his studies, and in his vacation periods, he did sales work and general construction work. He also worked as rodman and inspector on paving and sewer projects, as transitman and rodman on property surveys, and was civil engineer on the design and inspection of new plants and layouts. He designed steel support towers for steam lines, a steel locomotive shed, and many small cranes and lifting devices. After his graduation Mr. Snow's first engineering job was with the Cook County Highway Department in Chicago as a junior engineer in the design division. In October, 1933, with his appointment as a junior civil engineer, Mr. Snow began a period of more than eighteen years of government service with the Rock Island District of the Corps of Engineers, United States Army. Among his earliest duties was the assignment in February, 1934 to inspect the construction of the Mississippi River Lock and Dam No. 21 at Quincy, Ill. His responsibility increased with the succeeding years as Mr. Snow became engaged in detailed design and project planning of flood-control reservoirs, in building construction for ordnance plants, and in airfield site investigations.

As the district's program returned to civil-works engineering after World War II, Mr. Snow was promoted to chief of the Flood Control Unit of the Design Branch, and in 1950 he became assistant chief of the Design Branch, Engineering Division. In the immediate post-war year, he directed his technical skill to the development of plans for flood-control projects—among them the protective works at Galena, Ill., the Coralville Reservoir on the Iowa River, and the Sny Basin in Adams, Pike, and Calhoun counties, Illinois. With the resumption of military construction at the onset of Korean hostilities, Mr. Snow designed an industrial building for the Rock Island Arsenal, and an extensive water-distribution system improvement for the Savanna Ordnance Depot at Savanna, Ill. He was one of the organizers of the engineering firm of Romine, Sindt, and Snow in Davenport, Iowa, in August, 1946, from which he withdrew in June, 1948.

Mr. Snow was particularly interested in the professional development of the younger engineers, aiding and guiding them whenever possible, and encouraging them to widen their horizons through affiliation with the Society. He was instrumental in the formation, in 1940, of the Tri-City Local Section to which he was constantly loyal, serving as President in 1945. Mr. Snow devoted much effort to the Quad-City Technical Council, an organization composed of the officers of the local sections of the founder societies and other professional engineering groups. He served as president of the Council in 1946.

A most important phase of Mr. Snow's life was his devotion to his church. He was a member of Christ Episcopal Church in Moline, Ill., which he served several terms as vestryman.

Mr. Snow was married on August 8, 1936, in the Episcopal Cathedral, at Quincy, to Suzanne Fawcett, daughter of the late Rt. Rev. Edward Fawcett, bishop of the Quincy diocese of the Episcopal Church. He is survived by his widow and two sons, Edwin Fawcett and James Todd.

Mr. Snow was elected a Junior of the American Society of Civil Engineers on October 26, 1931, and an Associate Member on July 10, 1940.

JOHN STEARNS, M. ASCE[1]

Died January 21, 1954

John Stearns, the son of John Lloyd and Ella (Powell) Stearns, was born on May 15, 1882, in Elizabeth, N. J. He was graduated from Cornell University, at Ithaca, N. Y., in 1906, with the degree of Civil Engineer.

Mr. Stearns was known nationally in engineering circles. He was with the Hughes Aircraft Company, in Culver City, Calif., from 1943 to 1954. During the first eight years of his employment, he was plant engineer and directed the design, engineering, and construction of new buildings for the company. He also supervised the construction of the dry dock and launching facilities at Long Beach (Calif.) for the famed Hughes Flying Boat, at Terminal Island (Calif.), as well as the launching of the boat at the time of its test run. In addition, all phases of maintenance for the company came under his direction. In 1951 he assumed the duties of executive assistant on the staff of the assistant general manager, which position he held until his death.

For six years, Mr. Stearns was with the Metropolitan Water District of Los Angeles, Calif. He was division engineer on the Colorado River Aqueduct (from 1932 to 1938); principal engineer in charge of construction at the Fleet Operating Base, Terminal Island (from 1940 to 1941); assistant project manager for W. A. Bechtel Company in the building of the Army Port of Embarkation at Oakland, Calif. (from 1941 to 1942); and assistant construction manager for the company, building the six-way shipyard at Sausalito, Calif. (from 1942 to 1943). He was a staff member of many private and governmental organizations including The Foundation Company of America, and the J. G. White Engineering Corporation, both of New York, N. Y.; vice-president of Frank Couzens, Incorporated; principal engineer for the Power Flood Control Survey, Federal Power Commission, Washington, D. C.; and assistant executive director of the Housing Authority, County of Los Angeles.

Mr. Stearns was a member of the National Society of Professional Engineers and Sigma Phi and was a registered civil engineer and mechanical engineer in the State of California.

He was married in 1911 to Melissa Daniel. He is survived by his widow; a daughter, Lee (Mrs. M. Coker); a grandson, John; three sisters, Harriet (Mrs. J. B. Stewart), Mary (Mrs. R. V. Barkalow), and Rosalie (Mrs. J. B. Johnson); and two brothers, Gen. Cuthbert Stearns and Dr. Robert L. Stearns.

Mr. Stearns was elected an Associate Member of the American Society of Civil Engineers on August 31, 1915, and a Member on September 26, 1933. He became a Life Member in January, 1950.

---

[1] Memoir prepared by Harold G. Tegart, A.M. ASCE.

THOMAS KENNARD THOMSON, M. ASCE[1]

DIED JULY 1, 1952

Thomas Kennard Thomson, the son of William Alexander and Lavinia Day (Newcomb) Thomson, was born in Buffalo, N. Y., on April 25, 1864. He earned the degree of Civil Engineer at the University of Toronto, in Toronto, Ont., Canada, in 1886, standing at the head of his class, and in 1913 received the first Doctor of Science degree awarded by that university, *honoris causa*. All his life Mr. Thomson combatted the handicap of deafness. His scholastic success he attributed largely to the understanding of his beloved professor, John Galbraith.

Before graduation and immediately following, Mr. Thomson spent a number of years in railroad and structural work. He was employed by the Canadian Pacific Railroad in the Canadian Rockies, by the Dominion Bridge Company in Lachine, Que., by the Pencoyd Bridge Company near Philadelphia, Pa., and by the Norfolk and Western Railroad on the Kenova Bridge over the Ohio River. His positions varied from field engineer to bridge designer. With this notable background of experience, he devoted most of the last sixty years of his life (from 1893 until his death) to consulting engineering, centering his activities in New York, N. Y., and specializing in deep foundations, a field in which he was an acknowledged authority. For nine years he was chief engineer for Arthur McMullen and Company in New York on heavy construction projects. He also served from 1911 to 1914 as a member of the official consulting board on the construction of the New York State Barge Canal, extending from Lake Erie to the Hudson River.

Mr. Thomson's boldness of conception resulted in a number of spectacular engineering projects which he sponsored for many years, such as his "Niagara Falls Junior," a proposal to utilize all the flow of the Niagara River with a 100-ft head created by a power dam across the gorge below the whirlpool. He advocated the extension of the southern part of Manhattan Island by hydraulic filling within coffer dams, large land extensions of New Jersey and Staten Island, and the filling of the East River after cutting a canal from Flushing Bay to Jamaica Bay. Mississippi floods according to his ambitious ideas could be conquered by building three huge supplementary rivers to the north and south, one in the east which would tap the Ohio River, and two through the western plains.

He proposed a twenty-mile timber belt from the Great Lakes to the Pacific Ocean, to be built along the northern border of the United States and to be used jointly as a national forest park by Canada and the United States. Some of his plans were appropriated and credited to others, such as the elevated belt-line highways and railroads for Manhattan. These unique conceptions, together with similar proposals for improving the harbors of Toronto, Buffalo, and San Francisco (Calif.), engaged his attention continually throughout his life.

---

[1] Memoir prepared by Sydney Wilmot, M. ASCE.

Mr. Thomson was a vigorous engineer—a valued friend to a host of professional leaders whom he met daily at the Engineers Club in New York City, and a constant inspiration to the younger generation. He was a member of the Engineering Society (which he founded in 1885) of the University of Toronto, the Canadian Club of New York (which he had served as president), and the Free and Accepted Masons.

There was no more loyal Society member than "T. K. T." From 1912 to 1914 he served on the Board of Direction. About that time, he originated the yearly Past and Present Officers' dinner in New York City, an event that he was always proud to attend. During his long membership, Mr. Thomson missed only two annual meetings. Likewise, he was intensely loyal to the Metropolitan Section. In addition to many oral comments and written discussions of *Proceedings* papers, he wrote chapters on foundations for the engineering textbook by Jacoby and Davis[2] and the engineering handbook edited by Hool and Johnson.[3]

On September 26, 1888, Mr. Thomson was married to Mary Julia Harvey in Toronto. He is survived by his widow; two daughters, Annis Eveleen and Mary Marjory; and three sons, Arthur Kennard, Walter Glencairn, and Harvey Stranraer.

Mr. Thomson was elected a Junior of the American Society of Civil Engineers on October 3, 1888; an Associate Member on June 3, 1891; and a Member on December 4, 1895. He became a Life Member in January, 1926.

HARVEY ARTHUR VAN NORMAN, M. ASCE[1]

DIED JANUARY 16, 1954

Harvey Arthur Van Norman, the son of Joseph Monroe and Martha (Halsel) Van Norman, was born in Victoria, Tex., on October 5, 1878, and was educated in the public schools of Los Angeles, Calif. His early ambition was to be an engineer, and through the advice and tutoring of engineering friends, correspondence courses, and intensive home study was laid the foundation for a brilliant and colorful career.

Mr. Van Norman's first employment was as a steam engineer at a pumping station near Yuma, Ariz. From 1899 to 1906 he was steam engineer for the Los Angeles Railway Company, steam engineer and superintendent of electrical construction for the Pacific Electric Railway, and superintendent of construction for the Los Angeles Gas and Electric Corporation. In February, 1907, Mr. Van Norman entered the service of the Water Department of the City of Los Angeles and soon thereafter was placed in charge of the construction of hydroelectric stations at Division Creek and Cottonwood Creek, in the Owens Valley, Ingo County, California. Power from these plants was used on the construction of the 240-mile-long Los Angeles Aqueduct project. Mr. Van Norman's association with this important project ultimately brought wide recognition of his ability as a builder. In 1909 he was in charge of the Owens Valley and Lone Pine sections of the aqueduct, and on January 1, 1912, he was placed in charge of the Mojave division of the aqueduct, where he was responsible for the difficult task of building the Jawbone, Antelope, Pine Tree, and Sand Canyon siphons. The Jawbone siphon was one of the most imposing items of construction on the aqueduct and, at the time of its completion, was considered the most outstanding pipe construction project in the United States.

---

[2] "Foundations of Bridges and Buildings," by H. S. Jacoby and R. P. Davis, McGraw-Hill Book Co., Inc., New York, N. Y., 1941, 3rd Ed., Chapter 10.

[3] "Handbook of Building Construction," Edited by G. A. Hool and N. C. Johnson, McGraw-Hill Book Co., Inc., New York, N. Y., 1929, pp. 350–369.

[1] Memoir prepared by a Committee of the Los Angeles Section consisting of Samuel B. Morris, Charles T. Leeds, and Burton S. Grant, Members, ASCE.

When the aqueduct was put into operation in 1913, Mr. Van Norman supervised its maintenance and operation. He continued in that position until 1923, when he was given a leave of absence to supervise the design and construction of the Los Angeles outfall sewer. He was retained by the Board of Public Works as city engineer from August, 1924, to October, 1925, when he was recalled by the Board of Water and Power Commissioners as assistant chief engineer of the water system. In November, 1929, Mr. Van Norman was appointed chief engineer and general manager of the Bureau of Water Works and Supply.

Mr. Van Norman assisted in making the original reconnaissance surveys and in planning the route of the Colorado River Aqueduct, which ultimately was constructed by the Metropolitan Water District of Southern California. Among his accomplishments as head of the water system were the construction of the Bouquet Reservoir and trunk line in 1934 and the Mono Basin extension of the Los Angeles aqueduct, which was completed in 1941. When the separate Water and Power Bureaus of Los Angeles were merged on November 1, 1943, Mr. Van Norman was appointed general manager and chief engineer of the entire Department of Water and Power and served until his retirement on September 30, 1944. He was retained thereafter by the department as an advisory engineer until his death.

Mr. Van Norman was a member of the National Association of Steam Engineers and a member and past-president of the California Section of the American Water Works Association, which he served as national director from 1939 to 1941. He served as Past-President of the Los Angeles Section of the Society and was affiliated with many business and civic organizations. He was a member of the Scottish Rite, Free and Accepted Masons (32nd degree), and was a member of the Elks.

On June 20, 1906, he was married to Bessie Christine Ross of Chicago, Ill. He is survived by two sisters, Lottie (Mrs. V. Scott) and Edna (Mrs. Albert Miller); two brothers, Claude H. and Dean M.; and nine nephews and nieces.

Mr. Van Norman was elected a Member of the American Society of Civil Engineers on May 8, 1922. He became a Life Member in January, 1949.

FAYETTE SAMUEL WARNER, A.M. ASCE[1]

DIED JANUARY 23, 1953

Fayette Samuel Warner, the son of A. Fayette and Mary (Gunn) Warner, was born on January 7, 1894, in Sunderland, Mass. He was graduated from Rensselaer Polytechnic Institute at Troy, N. Y., in 1921, with the degree of Civil Engineer and then attended the University of Pennsylvania, at Philadelphia, from which he was graduated with the degree of Master of Business Administration. In 1930 the same university awarded him the degree of Doctor of Philosophy.

Following graduation, Mr. Warner was a professor in the Wharton School of Finance and Commerce of the University of Pennsylvania. In 1926 he published an analysis of the reasons for the diversity in the cost of anthracite coal between the mine and the consumer. In Mr. Warner's paper[2] about the St. Lawrence Waterway, his well-documented forecast of water-born tonnage to and from the Great Lakes for the year 1950 has proved to be remarkably close to the Canadian estimates of today which are now used for justification of the St. Lawrence Seaway. Mr. Warner was appointed by the chairman of the Federal Power Commission (FPC) in 1933 to report on the Great Lakes-St. Lawrence Seaway and Power Project.[3] From 1934 until his death, Mr. Warner was on the staff of the FPC and acted as chief of the Research Division for the National Power Survey, and as director of the Chicago, Ill., regional office. He initiated and organized an analysis for a complete report on the power requirements and resources of the nation. In collaboration with the Forest Service he prepared a report on the water powers of Southeastern Alaska.[4]

In 1946 Mr. Warner collaborated in preparing a report on the hydroelectric power potential of the Drina River in Yugoslavia. The project, as conceived, would ultimately generate six billion kilowatt hours a year from several reservoirs in the Dinaric Alps. Mr. Warner took a great interest in the projects begun in 1941 by the FPC for the development of utility power from the wind. During twelve years of research in this field, he contributed greatly to the support of this work. Other research projects included a study in collaboration with the Department of the Interior for the use of Taconite, and a preliminary study for a comprehensive power development of the Yangtse Kiang River in China. At the time of his death, Mr. Warner was engaged in a long-range study of the hydro potentialities of the upper Columbia River and other important streams in the United States and Canada.

In 1923 he was married to Elsie (Leonard) in Lansing, Mich. He is survived by his children, Shirley Anne, Frank B., and Fayette Samuel, Jr.

Mr. Warner was elected an Associate Member of the American Society of Civil Engineers on December 23, 1932.

---

[1] Memoir prepared by Kenneth W. Ross, A.M. ASCE, Percy Thomas, and Philip Youtz.

[2] "The Future Movement of Iron and Coal in Relation to the St. Lawrence Waterway," by Fayette Samuel Warner, University of Pennsylvania Press, Philadelphia, Pa., 1930.

[3] "Great Lakes-St. Lawrence Seaway and Power Project," *Senate Document No. 116*, 73rd Cong., 2nd Session, U. S. Govt. Printing Office, Washington, D. C., March, 1934.

[4] "Water Powers of Southeastern Alaska," by Fayette Samuel Warner, Federal Power Comm. and Forest Service, U. S. Dept. of Agriculture, 1947.

TRANSACTIONS

OF THE

AMERICAN SOCIETY OF CIVIL ENGINEERS

INDEX

VOLUME 119

1954

Subject Index, Page 1373

Author Index, Page 1441

Titles of papers are in quotation marks when given with the author's name.

VOLUME 119

SUBJECT INDEX

ACCIDENTS
See HIGHWAYS AND ROADS—Safety; *see also* FAILURES . . .

ACCOUNTS AND ACCOUNTING
See COSTS . . . ; *also* Financing under relative subject

ADDRESSES
See AMERICAN SOCIETY OF CIVIL ENGINEERS—Addresses; *see also* under subject of address

AERIAL . . .
See also AIR . . .

AERIAL MAPS AND MAPPING
See MAPS AND MAPPING, AERIAL

AERIAL NAVIGATION
See AIR TRANSPORT

AERODYNAMICS
See AIR FLOW; *also* under relative subject

AERONAUTIC MAPS
See MAPS AND MAPPING, AERIAL

AGGREGATES AND AGGREGATION
"Mass-Concrete Operations in the Rocky Mountains," George P. McIndoe, 899.

AGREEMENTS
See CONTRACTS

AGRICULTURE
See FLOODS; IRRIGATION (cross references thereunder); LAND . . . ; RAINFALL; SOIL . . .

AIR . . .
See also AERIAL . . . ; AERO- . . . (cross references thereunder)

AIR CHAMBERS
See PIPE LINES

AIR COMPRESSORS AND COMPRESSION
"Design Charts for Air Chambers on Pump Lines," W. E. Evans and C. C. Crawford (with discussion), 1025.

AIRCRAFT
See also ELECTRONIC INSTRUMENTS
"Electronic Devices in Air Transport," F. B. Lee (with discussion), 60.
Landing study results relating to touchdown, turnoff and time on runway, 491.

AIR ENTRAINMENT
See WATER, FLOW OF . . .

AIRFIELDS
See AIRPORT . . .

AIR FLOW
"Wind Loads on Truss Bridges," John M. Biggs (with discussion), 879.

AIRPLANES
See AIRCRAFT; RADAR . . . (cross references thereunder); WHEEL LOADS

AIRPORT APPROACHES
"Zoning Maps for Airports," B. Everett Beavin, Sr., 277. *Discussion:* Harold M. Lewis, and B. Everett Beavin, Sr., 286.

AIRPORTS (structures and localities)
See also COSTS, AIRPORT; HANGARS (cross references thereunder); PAVEMENT AND PAVING; TRAFFIC, AIRPORT
"Aeronautical Charting and Mapping," Charles A. Schanck (with discussion), 151.
The categorization of airports and other United States Civil Aeronautics Administration regulations, 489.
Civil airport system requirements and needed improvements during and at the close of World War II, 583.
Forecasting capacity needs in planning the terminal building, 589, 590, 591, 592, 593.
Lighting improvements since 1946, 495, 498.
"Recent Airport Design and Development," Philip A. Hahn, 489. *Discussion:* Louis A. Nees, and Philip A. Hahn, 497.
"Special Procedures for Pavement Design," L. A. Palmer (with discussion), 542.
Terminal areas and buildings, 494.
Financing
"Revenue Bond Financing for Airport Improvements," James C. Buckley, 583.

AIR TANKS
See PIPE LINES

AIR TERMINALS
See AIRPORTS

AIR TRAFFIC
See TRAFFIC, AIR

AIR TRANSPORT
See also AIR TERMINALS (cross reference thereunder); TRANSPORTATION
"Aeronautical Charting and Mapping," Charles A. Schanck (with discussion), 151.
"Common system" as used in civil and military air transport in the United States, 61, 71.
Effect of jet transport on airport design standards, 493, 494, 498.
"Electronic Devices in Air Transport," F. B. Lee (with discussion), 60.

AIRWAYS

See AIR TRANSPORT

ALGAE

"Algae Responsible for Odor and Taste in Water Supplies," George J. Turre, 658.

ALGEBRA, MATRIX

See MATHEMATICS

ALLUVIATION

See BARS (alluvia); EROSION . . . ; SEDIMENT AND SEDIMENTATION; SILT AND SILTING; VALLEYS

AMERICAN SOCIETY OF CIVIL ENGINEERS

Addresses

1954—Address at the Summer Convention, Atlantic City, N. J., June 16, 1954, Daniel V. Terrell, 1325.

Committee Reports—Ice

"Ice Pressure against Dams": A Symposium, R. L. Hearn, R. F. Legget, D. A. Buzzell, D. McHenry, L. S. McLennan, E. N. Peterson, and G. R. Strandberg; Bertil Lofquist; A. D. Hogg, and G. E. Monfore (with discussion), 1.

Memoirs of Members. *See* name of member in Author Index

ANALOGS AND ANALOGIES

See under relative subject, e.g., STRUCTURES, THEORY OF

ANALYSIS, DESIGN

See under relative subject, e.g., STRUCTURES, THEORY OF

ANALYSIS OF DATA

See EQUATIONS; GRAPHICAL CHARTS; MATHEMATICS; STRUCTURES, THEORY OF; *see also* under relative subject

ANALYSIS, RADAR

See RAINFALL

ANALYSIS, STATISTICAL

See STATISTICAL ANALYSIS (cross references thereunder)

ANALYSIS, STRUCTURAL

See EQUATIONS; STRESS AND STRAIN; STRUCTURES, THEORY OF

ANCHORED BULKHEADS

See BULKHEADS

APPARATUS

See general types of apparatus, e.g., VIBRATION RECORDING APPARATUS; *also* under relative subject, e.g., ICE; METERS AND METERING, CURRENT; *also* INSTRUMENTS

APRONS

See DAMS

ARCHES

See also DAMS, MASONRY AND CONCRETE; STRESS AND STRAIN—Arches; STRUCTURES, THEORY OF . . .

Bibliography
Graphical method of analyzing the amplification of stress in flexible arches, 923.

ARCHITECTURE
See type of structure or structural part, e.g., BRIDGES

ASPHALT PAVEMENT AND PAVING
See PAVEMENT AND PAVING, BITUMINOUS

ASSOCIATIONS
See SOCIETIES, TECHNICAL (cross references thereunder)

ATOMIC BLAST
"Nonelastic Behavior of Bridges under Impulsive Loads," S. J. Fraenkel and L. E. Grinter, 309. *Discussion:* Robert J. Hansen and John S. Archer; and S. J. Fraenkel and L. E. Grinter, 329.

AUTOMOBILE . . .
See also MOTOR . . . ; TRAFFIC . . .

AUTOMOBILE PARKING
"The Engineer's Role in Metropolitan Traffic Planning," Lloyd Braff (with discussion), 713.

AUTOMOBILE TRUCKS
See MOTOR TRUCKS

AVIGATION
See AIRPORT APPROACHES

BACKWATER
"A Direct Step Method for Computing Water-Surface Profiles," Arthur A. Ezra (with discussion), 453.

BANKS AND BANK PROTECTION, RIVER
See RIVER BANKS AND BANK PROTECTION (cross references thereunder)

BARS (alluvia)
"River-Bed Scour during Floods," E. W. Lane and W. M. Borland (with discussion), 1069.

Bars (solid material)
See STRESS AND STRAIN—Bars (solid material)

BASINS (depression in earth's surface)
See RAINFALL; VALLEYS; *see also* RIVER BASINS (cross references thereunder)

BASINS, SETTLING (water supply)
See SETTLING BASINS (cross references thereunder)

BASINS, STILLING
See WATER, FLOW OF, OVER DAMS AND WEIRS

BEACHES
See EROSION, BEACH

BEAMS (General)

See also FLANGES (cross reference thereunder); STRESS AND STRAIN—Beams (General); STRUCTURES, THEORY OF—Beams and Girders (General); TORSION

"Deflection of Members of Variable Moment of Inertia," Anthony Hoadley, 499.

"Deflections of Laminated Beams," L. G. Clark, 721.

"The Equivalent Rectangle in Prestressed Concrete Design," John J. Peebles (with discussion), 292.

"Lateral Buckling of Channels and **Z**-Beams," H. N. Hill, 829.

"Rapid Computation of Flexural Constants," Thomas G. Morrison, 93. *Discussion:* Henry Malter, Paul Rogers, and Thomas G. Morrison, 103.

BEAMS, CONTINUOUS

See also STRESS AND STRAIN—Beams, Continuous; STRUCTURES, THEORY OF—Beams and Girders, Continuous

"Continuous Composite Steel and Concrete Beams," John Sherman, 810.

BEARING CAPACITY (foundations, rocks, soils)

For more general interpretation *see* cross references under LOAD

"Special Design Features of the Yorktown Bridge," Maurice N. Quade, 109.

"Special Procedures for Pavement Design," L. A. Palmer (with discussion), 542.

BED LOAD

See RIVERS; WATER, FLOW OF, IN OPEN CHANNELS

BED LOAD DISPOSAL

See SILT AND SILTING

BENDING

See BUCKLING; MOMENTS; STRESS AND STRAIN; *also* under relative structure, structural part or material, e.g., BEAMS

BENTS

See STRUCTURES, THEORY OF—Frames . . .

BIBLIOGRAPHY

See subheading Bibliography under relative subject. (Comprehensive bibliographical footnotes existing in individual papers in which books and other material are cited)

BIOGRAPHIES OF DECEASED MEMBERS

See cross reference under MEMOIRS OF DECEASED MEMBERS

BITUMEN

See PAVEMENT AND PAVING, BITUMINOUS

BLAST, ATOMIC

See ATOMIC BLAST

BORINGS

See also DRILLS AND DRILLING

"Anchored Bulkheads," Karl Terzaghi (with discussion), 1243.

Subsurface conditions and boring types and procedures for bridge piers, 1090.

BOUNDARY LAYER, THEORY OF (fluid flow)

See WATER, FLOW OF . . .

BRACING

See BUTTRESSES; TRUSSES

BREAKWATERS

See WATER PRESSURE

BRIDGE FLOORS AND FLOORING

See also STRESS AND STRAIN—Bridge Floors and Flooring

"Special Design Features of the Yorktown Bridge," Maurice N. Quade, 109.

BRIDGE PIERS

See also CONCRETE; COSTS, BRIDGE PIER; FOUNDATIONS

"Highway Bridges on Deep Foundations," Louis Duclos (with discussion), 1090.

Sand island method of constructing deep piers on dry land, 1096.

"Special Design Features of the Yorktown Bridge," Maurice N. Quade, 109.

BRIDGES (General)

See also BEAMS . . . ; CAISSONS; FOUNDATIONS, BRIDGE; IMPACT; STRESS AND STRAIN—Bridges; TRAFFIC, BRIDGE; TRUSS . . . ; WHEEL LOADS; WIND . . .

Bridge construction as related to highway flood flow location and frequency, 1005.

"Bridges on the West Virginia Turnpike," Elmer K. Timby, 737.

Design specifications for wind loadings on railroad and highway bridges, 879, 891, 892.

"Highway Bridges on Deep Foundations," Louis Duclos (with discussion), 1090.

"Live Loading for Long-Span Highway Bridges," R. J. Ivy, T. Y. Lin, Stewart Mitchell, N. C. Raab, V. J. Richey and C. F. Scheffey (with discussion), 981.

"Nonelastic Behavior of Bridges under Impulsive Loads," S. J. Fraenkel and L. E. Grinter (with discussion), 309.

Standard design codes existing and suggested supplemental specifications for live loads on long spans, 981.

Usage of design data drawings to convey all necessary information for any one bridge, 740.

Bibliography

Bibliography on loading for highway bridges, 993.

BRIDGES, ARCH

See ARCHES

BRIDGES, GIRDER

Continuous plate girder bridges in Germany with year of completion, girder and span lengths and behavior under stress, 996.

BRIDGES, MOVABLE (SWING)

"Special Design Features of the Yorktown Bridge," Maurice N. Quade, 109.

BRIDGES, SWING

See BRIDGES, MOVABLE (SWING)

BRIDGES, TRUSS

See also TRUSSES

"Wind Loads on Truss Bridges," John M. Biggs (with discussion), 879.

BRIDGE TRAFFIC

See TRAFFIC, BRIDGE

BUCKLING

Buckling of an ice sheet, 14.

"Lateral Buckling of Channels and Z-Beams," H. N. Hill, 829.

"Post-Buckling Strength of Redundant Trusses," E. F. Masur, 699.

"Stiffness Charts for Gusseted Members under Axial Load," John E. Goldberg (with discussion), 43.

BUILDING (process)

See CONSTRUCTION (cross references thereunder)

BUILDING MATERIALS

See MATERIALS OF CONSTRUCTION

BUILDINGS

See COSTS . . . ; EARTHQUAKES (cross references thereunder); FOUNDATIONS; MATERIALS OF CONSTRUCTION; ROOFS AND ROOFING; STRESS AND STRAIN; STRUCTURES . . . (cross references thereunder); STRUCTURES, THEORY OF; VIBRATION; *also* under type of building, e.g., AIR TERMINALS (cross reference thereunder)

BUILDING STONE

See STONE

BULKHEADS

See also COSTS, BULKHEAD; FAILURES, BULKHEAD; FOUNDATIONS, BULKHEAD; RETAINING WALLS; STRESS AND STRAIN—Bulkheads; WAVES

"Anchored Bulkheads," Karl Terzaghi, 1243. *Discussion:* T. H. Wu; W. D. Bigler; J. Brinch Hansen; Gregory P. Tschebotarioff; Paul Baumann; Rudolf Briske; Norman D. Lea; S. Packshaw; J. Verdeyen and V. Roisin; and Karl Terzaghi, 1281.

Danish Rules and Terzaghi design methods compared as related to factor of safety and moment reduction, 1285, 1286, 1287, 1300, 1310, 1311.

"Design Curves for Anchored Steel Sheet Piling," Walter C. Boyer and Henry M. Lummis, III (with discussion), 639.

"The Design of Flexible Bulkheads," James R. Ayers and R. C. Stokes, 373. *Discussion:* W. F. Heavey, Morgan S. Campbell, Walter C. Boyer, P. W. Rowe, Gregory P. Tschebotarioff, J. Owen Lake, Nai C. Yang, and David Hopkins, 384.

BUSES

See MOTOR BUSES

BUTTRESSES

"Dam Modifications Checked by Hydraulic Models," E. S. Harrison and Carl E. Kindsvater (with discussion), 73.

CABLES AND CABLEWAYS

"Mass-Concrete Operations in the Rocky Mountains," George P. McIndoe, 899.

CAISSONS

Design and usage of floating type double-wall, cylindrical steel caissons in highway bridge construction, 1092.

"Highway Bridges on Deep Foundations," Louis Duclos (with discussion), 1090.

"Special Design Features of the Yorktown Bridge," Maurice N. Quade, 109.

CANALS (General)

See also LOCKS; SILT AND SILTING, CHANNEL; WATER, FLOW OF, IN OPEN CHANNELS; WATER TRANSPORTATION; WAVES

CANALS (Geographical)

Commerce, in tons, through The Dalles–Celilo Canal section of the Columbia River, years 1870–2000, 142.

CAÑONS

See CANYONS

CANYONS

See also VALLEYS

"Mass-Concrete Operations in the Rocky Mountains," George P. McIndoe, 899.

CARRIERS

See AIRCRAFT; MOTOR . . . ; RAIL . . . ; SUBWAYS; TRANSPORTATION

CARS

See AUTOMOBILE . . . ; MOTOR . . . ; WHEEL LOADS; WHEELS

CARTOGRAPHY

See MAPS AND MAPPING . . .

CAR WHEELS

See WHEEL LOADS; WHEELS

CEMENT

See under structure

CHANNEL BANKS AND BANK PROTECTION

See WAVES

CHANNEL BEAMS

See BEAMS

CHANNEL RECTIFICATION

See BARS (alluvia); DIKES; WATER DIVERSION; WATER, FLOW OF, IN OPEN CHANNELS

CHANNELS (waterways)

See also EROSION, STREAM; RIVERS; SILT AND SILTING, CHANNEL; WATER DIVERSION; WATER, FLOW OF, IN OPEN CHANNELS; WATER POLLUTION (cross reference thereunder)

"A Direct Step Method for Computing Water-Surface Profiles," Arthur A. Ezra, 453. *Discussion:* I. H. Steinberg, C. A. M. Gray, Bob Buehler, Monir M. Kansoh, and Arthur A. Ezra, 463.

CHARTS

See GRAPHICAL CHARTS; HYDROGRAPHS; *see also* MAPS AND MAPPING . . . ; *also* under relative subject, e.g., AIR TRANSPORT; STIFFNESS

CHUTES, WATER FLOW THROUGH

See SPILLWAYS; WATER, FLOW OF, IN OPEN CHANNELS

CITIES

See also AIRPORTS; AUTOMOBILE PARKING; BUILDINGS (cross references thereunder); CITY PLANNING; COSTS . . . ; INDUSTRIAL . . . ; POPULATION; REGIONAL PLANNING; SEWAGE . . . ; STREETS; SUBWAYS; TRAFFIC, STREET; WATER FRONT (cross references thereunder); WATER SUPPLY (cross references thereunder); ZONING . . . ; *also* geographical subheadings under relative subject, e.g., HARBORS—New York, N. Y.; HIGHWAYS AND ROADS—Colorado

"Revenue Bond Financing for Airport Improvements," James C. Buckley, 583.

"Unified Mass-Transportation System for New York," William Reid (with discussion), 124.

CITY PLANNING (General)

See also REGIONAL PLANNING; STREETS; ZONING . . .

"City Planning Techniques," Russell H. Riley, 163.

"The Engineer's Role in Metropolitan Traffic Planning," Lloyd Braff (with discussion), 713.

CITY PLANNING (Geographical)

Dallas, Tex.

Revision of major thoroughfare plan as related to rapid population growth, 715.

New Orleans, La.

Comprehensive revision of original plan of New Orleans and problems encountered, 165.

CIVIL ENGINEERS AND ENGINEERING

See AMERICAN SOCIETY OF CIVIL ENGINEERS; ENGINEERS AND ENGINEERING (and cross references thereunder)

CLAY

See also SOILS

Unconfined compressive strength of silt and clay, 1264.

COAST

See SEACOAST (cross references thereunder)

COLUMNS

"Stiffness Charts for Gusseted Members under Axial Load," John E. Goldberg (with discussion), 43.

COMMERCE

See AIRPORTS; AIR TRANSPORT; CANALS; CHANNELS; CITIES; FREIGHT; HARBORS; LAKES; RIVERS; TRANSPORTATION; and other relative subject headings

COMMITTEE REPORTS

See AMERICAN SOCIETY OF CIVIL ENGINEERS—Committee Reports; *see also* under subject of report

COMPACTION

See BEARING CAPACITY; IMPACT; SOILS

COMPRESSION

See STRESS AND STRAIN

COMPRESSION, AIR

See AIR COMPRESSORS AND COMPRESSION

COMPRESSION MEMBERS

See COLUMNS

COMPRESSORS AND COMPRESSION

See under relative type, e.g., AIR COMPRESSORS AND COMPRESSION

COMPUTERS, ELECTRONIC

See ELECTRONIC INSTRUMENTS

CONCRETE (General)

See also AGGREGATES AND AGGREGATION; GRAVEL (cross references thereunder); PAVEMENT AND PAVING, CONCRETE; SAND; SLABS; STRESS AND STRAIN—Concrete . . . ; *also* under special structure or structural part, e.g., DAMS, MASONRY AND CONCRETE

"Mass-Concrete Operations in the Rocky Mountains," George P. McIndoe, 899.

Construction. *See* under special structure, e.g., INDUSTRIAL PLANTS

Effect of Natural Processes

Protection from freezing on the Granby Pumping Plant construction work, in Colorado, 538.

Placing

"The Granby Pumping Plant": A Symposium, W. R. Judd and W. H. Wolf; and R. J. Willson, 509.

Prestressing. *See* CONCRETE, PRESTRESSED

Slabs. *See* SLABS

CONCRETE DAMS

See DAMS, MASONRY AND CONCRETE

CONCRETE PAVEMENT AND PAVING

See PAVEMENT AND PAVING, CONCRETE

CONCRETE PLANTS

Conveyor types and transporting process for mass concrete operations in mountain areas, 902, 906, 907.

"Mass-Concrete Operations in the Rocky Mountains," George P. McIndoe, 899.

CONCRETE, PRESTRESSED

"Dam Modifications Checked by Hydraulic Models," E. S. Harrison and Carl E. Kindsvater (with discussion), 73.

"The Equivalent Rectangle in Prestressed Concrete Design," John J. Peebles, 292. *Discussion:* Fred E. Koebel, and John J. Peebles, 303.

CONCRETE, REINFORCED
See CONCRETE . . .

CONDUITS
See also CABLES AND CABLEWAYS; PIPE LINES; SUBWAYS
"The Granby Pumping Plant": A Symposium, W. R. Judd and W. H. Wolf; and R. J. Willson, 509.
"Mechanics of Manifold Flow," John S. McNown (with discussion), 1103.

CONNECTORS AND CONNECTIONS
See JOINTS . . .

CONSTRUCTION
See BUILDINGS (cross references thereunder); CONCRETE—Construction (cross reference thereunder); CONTRACTORS . . . ; CONTRACTS; COSTS . . . ; EXCAVATION; FAILURES . . . ; MATERIALS OF CONSTRUCTION; SOILS—Construction; SPECIFICATIONS (cross references thereunder); STRESS AND STRAIN . . . ; STRUCTURES, THEORY OF . . . ; *also* under type of construction, e.g., BULKHEADS; INDUSTRIAL PLANTS

CONSTRUCTION MATERIALS
See MATERIALS OF CONSTRUCTION

CONSTRUCTION PLANTS
See CONTRACTORS' PLANTS

CONSTRUCTION, UNDERWATER

CONTAMINATION, STREAM
See UNDERWATER CONSTRUCTION (cross references thereunder)
See WATER POLLUTION (cross reference thereunder)

CONTINUOUS BEAMS
See BEAMS, CONTINUOUS

CONTINUOUS FRAMES
See STRUCTURES, THEORY OF—Frames, Continuous

CONTINUOUS GIRDERS
See GIRDERS, CONTINUOUS (cross reference thereunder)

CONTINUOUS STRUCTURES
See STRUCTURES, THEORY OF

CONTRACTORS AND CONTRACTING
See also ENGINEERS AND ENGINEERING
Allowing contractor latitude in method used in constructing bridge piers, 1090.

CONTRACTORS' PLANTS
Equipment used in constructing Granby Pumping Plant, in Colorado, 526, 535.

CONTRACTS
See also SPECIFICATIONS (cross references thereunder)
"Bridges on the West Virginia Turnpike," Elmer K. Timby, 737.
Granby Pumping Plant construction contract, 525, 528, 533, 534, 538.

CONVENTIONS (AMERICAN SOCIETY OF CIVIL ENGINEERS)
See AMERICAN SOCIETY OF CIVIL ENGINEERS—Addresses

CONVEYORS AND CONVEYANCE
See under usage, e.g., CONCRETE PLANTS

COSTS (General)
See also subheading Financing under relative subject

COSTS (of work)
See COSTS . . .

COSTS, AIRPORT
Development and improvement cost estimates for major metropolitan centers in the United States, 584.

COSTS, BRIDGE PIER
Sand island method in relation to construction cost, 1097, 1101.

COSTS, BULKHEAD
Economy in usage of high tensile steel, 393.

COSTS, DIKE
Brush dike costs, 636, 638.

COSTS, DRILLING
Cost considerations in developing offshore operations in the Gulf of Mexico, 481, 482, 487, 488.

COSTS, HANGAR
Cost of hangar at Cleveland Hopkins Airport and other ports, 586, 591, 593.

COSTS, HIGHWAY AND ROAD
Colorado interstate route costs and estimates, 969.

COSTS, LANDSLIDE
1950 unit costs in estimating expenditures for landslide corrective measures, 685.

COSTS, PAVEMENT AND PAVING
Economical procedure for building airfield pavements to resist heavy wheel loads and thermal shock, 564.
Wave wash protection work costs, 636, 637.

COSTS, PILE AND PILE DRIVING
Driving and anchorage costs under utilization of certain methods of design, 640, 651.

COSTS, SEWAGE DISPOSAL
Actual costs of North Point Sewage Treatment Plant and Southeast Sewage Treatment Plant, and other treatment costs and estimates, at San Francisco, California, 786, 787, 790.

COSTS, TRAFFIC CONTROL (AIR TRAFFIC)
Cost of traffic control towers in relation to scheduled operations, 69.

COSTS, TRANSPORTATION
Allocation of costs in transportation facilities, 132.

COUNTY PLANNING
See REGIONAL PLANNING

CRACKING
See under relative subject, e.g., ICE

CREEP
See LANDSLIDES

CULVERTS
See DRAINAGE (cross references thereunder)

CURRENT METERS
See METERS AND METERING, CURRENT

CURRENTS
See RIVERS; TIDES; WATER . . .

CURVED STRUCTURES
See STRUCTURES, THEORY OF—Curved Structures

CURVES (backwater)
See BACKWATER

CURVES (design curves)
See relative subject of design, e.g., PILES AND PILE DRIVING

CURVES (graphic curves)
See GRAPHICAL CHARTS

CURVES, FREQUENCY
See under topic, e.g., RAINFALL

DAMPING
See STRESS AND STRAIN

DAMS (General)
See also GROUND WATER; MODELS, HYDRAULIC; RESERVOIRS; SPILLWAYS; WATER, FLOW OF, OVER DAMS AND WEIRS; WATER PRESSURE

Computation procedure for ice thrust calculations, 3, 6, 39.

"Dam Modifications Checked by Hydraulic Models," E. S. Harrison and Carl E. Kindsvater (with discussion), 73.

"Ice Pressure against Dams": A Symposium, R. L. Hearn, R. F. Legget, D. A. Buzzell, D. McHenry, L. S. McLennan, E. N. Peterson, and G. R. Strandberg; Bertil Lofquist; A. D. Hogg; and G. E. Monfore (with discussion), 1.

Profile of major dam projects on the Columbia River, 144, 145.

"Relief Well Systems for Dams and Levees," W. J. Turnbull and C. I. Mansur (with discussion), 842.

DAMS, GRAVITY
See DAMS, MASONRY AND CONCRETE

DAMS, MASONRY AND CONCRETE

Plan of Black Canyon Diversion Dam in Idaho, 414.

Plot plan and construction methods used in erecting Reservoir Dam No. 22, a gravity arch dam, on South Boulder Creek, in Colorado, 899, 901, 909.

DEBRIS CONTROL

"Wave-Wash Control on Mississippi River Levees," Rudolf Hertzberg, 628.

DEBRIS WAVES

See DEBRIS CONTROL

DEFINITIONS

See TERMINOLOGY

DEFLECTIONS

See DEFORMATION (cross references thereunder); MOMENTS; SIDESWAY (cross reference thereunder); SLOPE DEFLECTION; STRESS AND STRAIN; STRUCTURES, THEORY OF; VIBRATION; *also* under relative structure or structural part, e.g., BEAMS

DEFORMATION

See FAILURES . . . ; STRESS AND STRAIN; STRUCTURES, THEORY OF; *also* under specific type of stress, e.g., TORSION; *also* under type of structure, e.g., BRIDGES

DESIGN

See under relative subject, e.g., BRIDGES; CONCRETE, PRESTRESSED; *see also* DRAWINGS (cross reference thereunder); SPECIFICATIONS (cross references thereunder)

DESIGN ANALYSIS

See under relative subject, e.g., STRUCTURES, THEORY OF

DESIGN CURVES

See CURVES (design curves) (cross reference thereunder)

DIAGRAMS

See GRAPHICAL CHARTS; *see also* under relative subject, e.g., SEWAGE DISPOSAL

DIKES

See also COSTS, DIKE; LEVEES

Usage of low brush dikes to break waves prior to reaching levees, 631, 634, 637.

DISCHARGE

See METERS AND METERING, CURRENT; PUMPS AND PUMPING; WATER, FLOW OF . . .

DISCHARGE COEFFICIENTS

See under relative subject, e.g., SPILLWAYS; WATER, FLOW OF . . .

DISTORTION

See STRESS AND STRAIN; TORSION

DIVERSION

See WATER DIVERSION

DIVERSION DAMS

See DAMS

DOCKS AND WHARVES

See BULKHEADS; PILES AND PILE DRIVING

DOMES AND VAULTS

See ROOFS AND ROOFING; STRUCTURES, THEORY OF—Domes and Vaults

DRAINAGE

See RUNOFF; *also* under type of drainage, e.g., HIGHWAYS AND ROADS—Drainage

DRAWINGS

See under relative subject, e.g., BRIDGES; PIPE LINES

DREDGES AND DREDGING

Importance of dredging methods in bulkhead construction sequences, 381.

DRIFT CONTROL

See DEBRIS CONTROL

DRILLS AND DRILLING

See also BORINGS; COSTS, DRILLING

"Dam Modifications Checked by Hydraulic Models," E. S. Harrison and Carl E. Kindsvater (with discussion), 73.

"Offshore Petroleum Installations," Jack S. Toler, 480.

DROP STRUCTURES

See DAMS

DRUM GATES

See SPILLWAYS; WATER GATES, MOVABLE

DYNAMICS OF FLUIDS

See HYDRODYNAMICS

DYNAMICS OF GASES

See AERODYNAMICS (cross references thereunder)

DYNAMICS OF STRUCTURES

See STRUCTURAL DYNAMICS

DYNAMOMETERS

See INSTRUMENTS

EARTH . . .

See also GROUND . . . ; LAND . . . ; SOIL . . .

EARTH FAILURES

See FAILURES, EARTH

EARTH FLOW

See LANDSLIDES

EARTH MOVEMENTS

See EARTHQUAKES (cross references thereunder); LANDSLIDES

EARTH PRESSURE

"Anchored Bulkheads," Karl Terzaghi (with discussion), 1243.

"Design Curves for Anchored Steel Sheet Piling," Walter C. Boyer and Henry M. Lummis, III (with discussion), 639.

"The Design of Flexible Bulkheads," James R. Ayers and R. C. Stokes (with discussion), 373.

Examination of the Coulomb theory for lateral earth pressure, 1243.

"The Granby Pumping Plant": A Symposium, W. R. Judd and W. H. Wolf; and R. J. Willson, 509.

Soil pressure theories, 373, 391, 392, 394.

EARTHQUAKES

See STRUCTURES, THEORY OF—Earthquake Problems; VIBRATION

EARTHS

See SOILS

EARTHWORK

See also DRAINAGE (cross references thereunder); EMBANKMENTS (cross references thereunder); EXCAVATION; FOUNDATIONS . . . ; LEVEES; REVETMENT

"The Design of Flexible Bulkheads," James R. Ayers and R. C. Stokes (with discussion), 373.

Bibliography

Comprehensive bibliography on frozen ground, ice and snow, 619.

ECONOMICS

See also CONTRACTS; COSTS . . . ; *also* under subheading Financing under relative subject

"The Engineer and World Population": Address at the Summer Convention, Atlantic City, N. J., June 16, 1954, Daniel V. Terrell, 1325.

ELASTICITY

See also STRESS AND STRAIN

"Plates with Boundary Conditions of Elastic Support," S. J. Fuchs (with discussion), 935.

ELECTRIC ANALOGY

See STRUCTURES, THEORY OF

ELECTRIC ENGINEERS AND ENGINEERING

See under relative subject, e.g., LIGHTING (cross reference thereunder)

ELECTRIC RAILWAYS

See RAILROADS, ELECTRIC (cross reference thereunder)

ELECTRONIC COMPUTERS

See ELECTRONIC INSTRUMENTS

ELECTRONIC INSTRUMENTS

Course line and pictorial computer development, 63.

"Electronic Devices in Air Transport," F. B. Lee, 60. *Discussion:* P. C. Sandretto, and F. B. Lee, 70.

The omni-range system in air transport, 62.

Usage of radar, 64.

EMBANKMENTS

See DIKES; LEVEES; SOILS

EMPLOYEES AND EMPLOYMENT

Employing and training personnel in sewage treatment plants, 790, 796.

ENERGY

See AERODYNAMICS (cross references thereunder); HYDRODYNAMICS; KINETIC ENERGY (cross reference thereunder); STRUCTURAL DYNAMICS; STRUCTURES, THEORY OF; WATER, FLOW OF, IN OPEN CHANNELS

ENERGY, LOSS OF

See EVAPORATION; FRICTION; WATER, FLOW OF . . . ; WATER HAMMER

ENGINEERING

See ENGINEERS AND ENGINEERING

ENGINEERING AND WAR

See cross references under WAR AND ENGINEERING

ENGINEERING BIBLIOGRAPHY

See BIBLIOGRAPHY (cross references thereunder)

ENGINEERING GLOSSARIES

See TERMINOLOGY

ENGINEERING MECHANICS

See MECHANICS

ENGINEERING SOCIETIES

See AMERICAN SOCIETY OF CIVIL ENGINEERS

ENGINEERS AND ENGINEERING (General)

See also AMERICAN SOCIETY OF CIVIL ENGINEERS. (For memoirs of deceased members, *see* name of member in Author Index); CONTRACTORS . . . ; CONTRACTS; EMPLOYEES AND EMPLOYMENT; RESEARCH (cross references thereunder); TERMINOLOGY

"The Engineer and World Population": Address at the Summer Convention, Atlantic City, N. J., June 16, 1954, Daniel V. Terrell, 1325.

Government Relationships

"The Engineer's Role in Metropolitan Traffic Planning," Lloyd Braff (with discussion), 713.

ENTRAINMENT, AIR

See WATER, FLOW OF . . .

EQUATIONS

See also relative subject, e.g., WATER, FLOW OF (General)

Demonstration and use of Horner's method, 811.

EROSION, BEACH

"Wave-Wash Control on Mississippi River Levees," Rudolf Hertzberg, 628.

EROSION, STREAM

"Dam Modifications Checked by Hydraulic Models," E. S. Harrison and Carl E. Kindsvater (with discussion), 73.

"River-Bed Scour during Floods," E. W. Lane and W. M. Borland (with discussion), 1069.

ESTIMATES

See COSTS

ESTUARIES

See RIVERS

EVAPORATION

"Snow Hydrology for Multiple-Purpose Reservoirs," Herbert S. Riesbol (with discussion), 595.

EXCAVATION (General)

See also EARTH PRESSURE; EARTHWORK; FOUNDATIONS

"The Granby Pumping Plant": A Symposium, W. R. Judd and W. H. Wolf; and R. J. Willson, 509.

EXCAVATION, HYDRAULIC

See DREDGES AND DREDGING

EXPERIMENTS AND EXPERIMENTATION

See HYDRAULIC LABORATORIES; MODELS . . . ; TESTS AND TESTING (cross references thereunder); *also* under material, structure or structural part tested; *also* under relative subject

EXPLORATION

See BORINGS; EXCAVATION; FOUNDATIONS; PILES AND PILE DRIVING

EXPLOSION, ATOMIC

See ATOMIC BLAST

EXPRESSWAYS

See HIGHWAYS AND ROADS; TRAFFIC, STREET

FACT FINDING

See RESEARCH (cross references thereunder)

FACTOR OF SAFETY

See relative subject, e.g., BULKHEADS

FACTOR, ROUGHNESS

See cross reference under ROUGHNESS FACTOR

FAILURES (General)

See ACCIDENTS (cross references thereunder); BEARING CAPACITY; SAFETY (cross references thereunder); STRENGTH OF MATERIALS (cross references thereunder); STRESS AND STRAIN; STRUCTURES, THEORY OF

FAILURES, BULKHEAD

Causes and means of avoiding failures, 1276, 1296, 1298, 1303, 1311.

FAILURES, EARTH

"Analysis of Corrective Actions for Highway Landslides," R. F. Baker (with discussion), 665.

FILLING, HYDRAULIC

See HYDRAULIC FILLING

FILL, SETTLEMENT OF

See HYDRAULIC FILLING

FINANCE

See COSTS . . . ; ECONOMICS; *see also* subheading Financing under relative subject, e.g., AIRPORTS—Financing; HIGHWAYS AND ROADS—Financing

FLANGES

See STRESS AND STRAIN—Flanges

FLEXURE

See STRESS AND STRAIN; STRUCTURES, THEORY OF

FLOOD CONTROL

See FLOODS; RESERVOIRS, FLOOD CONTROL

FLOOD FORECASTING

See FLOODS

FLOODS (General)

See also DEBRIS CONTROL; LEVEES; RAINFALL; RESERVOIRS, FLOOD CONTROL; RUNOFF; SPILLWAYS

"A Direct Step Method for Computing Water-Surface Profiles," Arthur A. Ezra (with discussion), 453.

"Peak Discharge for Highway Drainage Design," Carl F. Izzard (with discussion), 1005.

"River-Bed Scour during Floods," E. W. Lane and W. M. Borland (with discussion), 1069.

FLOODS (Geographical)

Georgia

"Dam Modifications Checked by Hydraulic Models," E. S. Harrison and Carl E. Kindsvater (with discussion), 73.

Kansas

"Peak Discharge for Highway Drainage Design," Carl F. Izzard (with discussion), 1005.

Rio Grande River

Observations during 1948 flood in the Rio Grande River, 1078.

FLOORS AND FLOORING

See BRIDGE FLOORS AND FLOORING

FLOW

See AIR FLOW; EARTH FLOW (cross reference thereunder); FLOODS; GROUND WATER; MANIFOLD FLOW (cross reference thereunder); RUNOFF; SEEPAGE; SEWAGE . . . ; TURBULENCE; UNDERFLOW (cross references thereunder); WATER, FLOW OF . . .

FLOW, LAMINAR

See WATER, FLOW OF, IN OPEN CHANNELS

FLOW OF FLUIDS

See WATER, FLOW OF . . .

FLOW OF LIQUIDS

See WATER, FLOW OF . . .

FLOW OF OIL

See WELLS

FLOW OF SOLIDS

See EARTH FLOW (cross reference thereunder); SEDIMENT AND SEDIMENTATION; SILT AND SILTING . . . ; WATER, FLOW OF, IN OPEN CHANNELS

FLOW OF WATER

See WATER, FLOW OF . . .

FLUID FRICTION COEFFICIENTS

See FRICTION COEFFICIENTS, FLUID

FLUIDS, DYNAMICS OF

See HYDRODYNAMICS

FLUIDS, FLOW OF

See WATER, FLOW OF . . .

FORMULAS

See under relative subject, e.g., BEAMS; WATER, FLOW OF, IN PIPES

FOUNDATIONS (General)

See also BORINGS; CAISSONS; EARTH PRESSURE; EARTHQUAKES (cross references thereunder); EARTHWORK; EXCAVATION; FREEZING (cross references thereunder); PILES AND PILE DRIVING; WATER PRESSURE; *also* under special material, e.g., SAND; SOILS

"The Granby Pumping Plant": A Symposium, W. R. Judd and W. H. Wolf; and R. J. Willson, 509.

Bibliography

Comprehensive bibliography on frozen ground, snow and ice, 619.

FOUNDATIONS, BRIDGE

"Highway Bridges on Deep Foundations," Louis Duclos, 1090. *Discussion:* Arthur V. Walker, 1100.

FOUNDATIONS, BULKHEAD

"The Design of Flexible Bulkheads," James R. Ayers and R. C. Stokes (with discussion), 373.

FOUNDATIONS, PILE

See PILES AND PILE DRIVING

FOUNDATIONS, UNDERWATER

See also PILES AND PILE DRIVING

"Offshore Petroleum Installations," Jack S. Toler, 480.

"Relief Well Systems for Dams and Levees," W. J. Turnbull and C. I. Mansur (with discussion), 842.

FRAMES (General)

See STRESS AND STRAIN—Frames . . . ; STRUCTURES, THEORY OF —Frames . . . ; *see also* BEAMS; COLUMNS; GIRDERS . . . (cross references thereunder)

FRAMES, CONTINUOUS

See STRUCTURES, THEORY OF—Frames, Continuous

FRAMES, RIGID

See STRESS AND STRAIN—Frames, Rigid; STRUCTURES, THEORY OF —Frames, Rigid

FRAMEWORKS

See STRUCTURES, THEORY OF

FREEZING

See CONCRETE—Effect of Natural Processes; ICE

FREIGHT

See also MOTOR TRUCKS

"Unified Mass-Transportation System for New York," William Reid (with discussion), 124.

FREQUENCY CURVES

See under topic, e.g., RAINFALL

FRICTION

See also TURBULENCE

"Analysis of Water Hammer by Characteristics," C. A. M. Gray (with discussion), 1176.

"A Direct Step Method for Computing Water-Surface Profiles," Arthur A. Ezra (with discussion), 453.

FRICTION COEFFICIENTS, FLUID

"Friction Factors for Turbulent Flow in Pipes," Edward F. Wilsey, 331. *Discussion:* George A. Whetstone, 337.

"Laminar to Turbulent Flow in a Wide Open Channel," W. M. Owen (with discussion), 1157.

"Turbulent Boundary Layer on Steep Slopes," William J. Bauer (with discussion), 1212.

FUEL

See OIL . . .

GAGES (General)

See also METERS AND METERING . . . ; *also* cross references under INSTRUMENTS

GAGES, PRESSURE

Ice pressure gages, 9, 16, 21, 26, 28.

GAGES, RAIN

"Rainfall Studies Using Rain-Gage Networks and Radar," H. E. Hudson, Jr., G. E. Stout and F. A. Huff (with discussion), 248.

GAGES, STRAIN
"Stress meters" in ice pressure measuring, 24.

GAGING
See RIVERS

GASES, DYNAMICS OF
See AERODYNAMICS (cross references thereunder)

GATES
See under type of gate, e.g., WATER GATES, MOVABLE

GAUGES (measuring instruments)
See GAGES

GAUGING
See cross reference under GAGING

GEOGRAPHY
See relative technical subject, e.g., MAPS AND MAPPING . . .

GEOMETRY
See under relative subject, e.g., BEAMS

GIRDER BRIDGES
See BRIDGES, GIRDER

GIRDERS (General)
See BEAMS; CONNECTORS AND CONNECTIONS (cross reference thereunder); FLANGES (cross reference thereunder); STRUCTURES, THEORY OF—Beams and Girders; *also* under name of material

GIRDERS, CONTINUOUS
See STRUCTURES, THEORY OF—Beams and Girders, Continuous

GLOSSARIES
See TERMINOLOGY

GOVERNMENT
See ENGINEERS AND ENGINEERING—Government Relationships; PUBLIC . . . ; *also* LAW subject heading under related topic, e.g., ZONING LAW

GRADES, SUB-
See SUBGRADES (cross reference thereunder)

GRAPHICAL CHARTS
See also HYDROGRAPHS . . . ; *also* under relative subject, e.g., STRESS AND STRAIN—Arches
Development of method, similar to Williot-Mohr diagram, to determine deflections on curved beams having variable moment of inertia, 499, 506.
"A Direct Step Method for Computing Water-Surface Profiles," Arthur A. Ezra (with discussion), 453.

GRAPHIC CURVES
See cross reference under CURVES (graphic curves)

GRAVEL

See SAND; SEEPAGE; SOILS; STONE

GRAVITY DAMS

See DAMS, MASONRY AND CONCRETE

GROUND . . .

See also EARTH . . . ; LAND . . . ; SOIL . . .

GROUND MOVEMENTS

See EARTHQUAKES (cross references thereunder); LANDSLIDES

GROUND WATER

"Relief Well Systems for Dams and Levees," W. J. Turnbull and C. I. Mansur (with discussion), 842.

GROUNDWORK

See EARTHWORK; FOUNDATIONS

GROUTING

"Dam Modifications Checked by Hydraulic Models," E. S. Harrison and Carl E. Kindsvater (with discussion), 73.

GUSSET PLATES

See PLATES

HANGARS

See COSTS, HANGAR; *see also* AIRPORTS

HARBORS (General)

See also BULKHEADS; CHANNELS; FREIGHT; PILES AND PILE DRIVING

HARBORS (Geographical)

New York, N. Y.

Tidal action in New York Harbor as related to sewage distribution and detention, 435, 437, 449.

HEAD, LOSS OF

See FRICTION; WATER, FLOW OF . . .

HEALTH, PUBLIC

See PUBLIC HEALTH

HEAT MEASURING INSTRUMENTS

See TEMPERATURE MEASURING INSTRUMENTS

HIGHWAY BRIDGE FLOORS

See BRIDGE FLOORS AND FLOORING

HIGHWAY BRIDGES

See BRIDGES

HIGHWAYS AND ROADS (General)

See also BRIDGE FLOORS AND FLOORING; BRIDGES; COSTS, HIGHWAY AND ROAD; IMPACT; MOTOR . . . ; PAVEMENT AND PAVING; SNOW; STREETS; TRAFFIC, HIGHWAY AND ROAD; WHEEL LOADS

Costs. *See* COSTS, HIGHWAY AND ROAD

Drainage

"Peak Discharge for Highway Drainage Design," Carl F. Izzard, 1005. *Discussion:* Max A. Kohler, Roy F. Warner, N. E. Minshall and Carl F. Izzard, 1016.

Runoff from small experimental watersheds in Maryland, Ohio, Wisconsin and Nebraska, 1012, 1018, 1019.

Financing

"Bridges on the West Virginia Turnpike," Elmer K. Timby, 737.

Federal aid highway system (as initiated in 1922 by the United States Bureau of Public Roads), 970, 980.

Safety

"Analysis of Corrective Actions for Highway Landslides," R. F. Baker (with discussion), 665.

Traffic. *See* TRAFFIC, HIGHWAY AND ROAD

Transportation. *See* HIGHWAY TRANSPORTATION

HIGHWAYS AND ROADS (Geographical)

Colorado

"An Interstate Route and Its Urban Connections," D. W. Ormsbee, 969.

Urban developments and plans for interstate routes through cities of Denver, Colorado Springs, Pueblo, Walsenburg and Trinidad, 976.

West Virginia

"Bridges on the West Virginia Turnpike," Elmer K. Timby, 737.

West Virginia landslides in 1950–1951 and earlier, 665, 666, 667, 670, 672.

HIGHWAY TRAFFIC

See TRAFFIC, HIGHWAY AND ROAD

HIGHWAY TRANSPORTATION

See also TRANSPORTATION; VEHICLES (cross references thereunder)

"An Interstate Route and Its Urban Connections," D. W. Ormsbee, 969.

Network of the National System of Interstate Highways in the United States, in war and peace, with map, 969, 971.

"Unified Mass-Transportation System for New York," William Reid (with discussion), 124.

HINGES

See JOINTS

HOISTING MACHINERY

See under specific types of machines, e.g., DREDGES AND DREDGING

HOSE

See under relative technical subject, e.g., WATER, FLOW OF . . .

HOUSES (places of abode)

See also PLANTS (cross references thereunder)

Drainage. *See* PIPES AND PIPING (cross references thereunder)

HURRICANES

See WIND PRESSURE

HYDRAULIC EXCAVATION

See EXCAVATION, HYDRAULIC (cross reference thereunder)

HYDRAULIC FILLING

"Anchored Bulkheads," Karl Terzaghi (with discussion), 1243.

HYDRAULIC LABORATORIES

See also MODELS, HYDRAULIC

The St. Anthony Falls Hydraulic Laboratory equipment (at the University of Minnesota, in Minneapolis) suitable for studies of high velocity flow, 208.

HYDRAULIC MACHINERY

See under type of machinery, e.g., PUMPS AND PUMPING

HYDRAULIC MODELS

See MODELS, HYDRAULIC

HYDRAULICS

See also BREAKWATERS (cross reference thereunder); BULKHEADS; CANALS; CHANNEL . . . ; CONDUITS; COSTS . . . ; DAMS; DEBRIS CONTROL; DIKES; DRAINAGE (cross references thereunder); DREDGES AND DREDGING; EROSION . . . ; EVAPORATION; FAILURES . . . ; FLOOD . . . ; FLOW . . . (cross references thereunder); FLUID . . . (cross references thereunder); FOUNDATIONS . . . ; FRICTION . . . ; GAGES . . . ; GROUND WATER; GROUTING; HARBORS; HYDRAULIC . . . ; HYDRO– . . . ; IRRIGATION (cross references thereunder); LAKES; LEVEES; LOCKS; METERS AND METERING . . . ; MODELS, HYDRAULIC; PILES AND PILE DRIVING; PIPE LINES; PUMPS AND PUMPING; RAINFALL; RESERVOIRS . . . ; RETAINING WALLS; REVETMENT; RIVER . . . ; RUNOFF; SEA . . . ; SEDIMENT AND SEDIMENTATION; SEEPAGE; SEWAGE . . . ; SILT AND SILTING; SPILLWAY . . . ; SPRINKLERS AND SPRINKLING; STILLING BASINS (cross reference thereunder); STRESS AND STRAIN . . . ; TERMINOLOGY; TIDES; TURBULENCE; VALLEYS; WATER . . . ; WAVES; WELLS

"A Direct Step Method for Computing Water-Surface Profiles," Arthur A. Ezra (with discussion), 453.

"Friction Factors for Turbulent Flow in Pipes," Edward F. Wilsey (with discussion), 331.

"Mechanics of Manifold Flow," John S. McNown (with discussion), 1103.

"Turbulent Boundary Layer on Steep Slopes," William J. Bauer (with discussion), 1212.

HYDRAULIC STRUCTURES

See also under type of structure, e.g., DAMS; SPILLWAYS

Ice pressure against hydraulic structures, 1.

"Rating Curves for Flow over Drum Gates," Joseph N. Bradley (with discussion), 403.

HYDRODYNAMICS

"Analysis of Water Hammer by Characteristics," C. A. M. Gray (with discussion), 1176.

HYDROGRAPHS, RUNOFF

"Snow Hydrology for Multiple-Purpose Reservoirs," Herbert S. Riesbol (with discussion), 595.

HYDROLOGY

See also DRAINAGE (cross references thereunder); EVAPORATION; FLOODS; GROUND WATER; HYDROGRAPHS; LAKES; RAINFALL; RIVERS; RUNOFF; SEA WATER; SNOW; WATER . . .

"Frequency of Excessive Rainfalls in Florida," David B. Smith, 927.

"Rainfall Studies Using Rain-Gage Networks and Radar," H. E. Hudson, Jr., G. E. Stout and F. A. Huff (with discussion), 248.

HYDROMETRY

See WATER, FLOW OF . . .

HYDROSTATIC UPLIFT

See WATER PRESSURE

ICE

Computation procedure for ice thrust calculations, 3, 6, 39.

"Ice Pressure against Dams": A Symposium, R. L. Hearn, R. F. Legget, D. A. Buzzell, D. McHenry, L. S. McLennan, E. N. Peterson, G. R. Strandberg; Bertil Lofquist; A. D. Hogg; and G. E. Monfore, 1. *Discussion:* G. E. Monfore, Edwin Rose, and Bertil Lofquist, Edwin Rose, and G. E. Monfore, 17, 39.

Ice pressure problems and investigations in Switzerland, Norway, Sweden, Canada and the United States, 3, 4, 22, 26, 41.

Laboratory apparatus for measuring ice pressure, 8, 23, 24.

United States Bureau of Reclamation ice pressure testing procedure and apparatus, 32.

Bibliography

Comprehensive bibliography on ice, snow and frozen ground, 619.

Ice pressure against hydraulic structures, 4.

ICE PRESSURE

See ICE

ILLUMINATION

See LIGHTING (cross reference thereunder)

IMPACT

See also IMPULSE (cross references thereunder); VIBRATION; WHEEL LOADS

"Nonelastic Behavior of Bridges under Impulsive Loads," S. J. Fraenkel and L. E. Grinter (with discussion), 309.

"Radial Impact on an Elastically Supported Ring," Edward Wenk, Jr. (with discussion), 221.

IMPULSE

See STRUCTURAL DYNAMICS; *see also* IMPACT

INDUSTRIAL PLANTS

See also under specific type of plant, e.g., CONCRETE PLANTS

"The Granby Pumping Plant": A Symposium, W. R. Judd and W. H. Wolf; and R. J. Willson, 509.

INDUSTRY

See under relative technical classification, e.g., PUMPS AND PUMPING; *see also* EMPLOYEES AND EMPLOYMENT; LABOR; *also* under type of industry or industrial plant, e.g., CONCRETE PLANTS; CONTRACTORS' PLANTS

INFILTRATION

See FLOODS; GROUND WATER; LAND . . . ; RUNOFF; SEEPAGE

INFLUENCE LINES

See MOMENTS

INSTRUMENTS

See also GAGES; METERS AND METERING . . . ; *also* under general types of instruments, e.g., ELECTRONIC INSTRUMENTS; WATER INSTRUMENTS; *also* under specific type of instrument, e.g., DYNAMOMETERS (cross reference thereunder); *also* under usage; *see also* cross references under APPARATUS

Dynamometers to measure impact loads, 221, 235.

Electrical instrument for the experimental solution of indeterminate framed structures, 1047.

IRRIGATION (General)

See SPRINKLERS AND SPRINKLING; WATER SUPPLY (cross references thereunder)

JETTIES

See WAVES

JOINTS (General)

"Design of Frames by Relaxation of Yield-Hinges," J. Morley English (with discussion), 1143.

"Hipped Plate Analysis, Considering Joint Displacements," Ibrahim Gaafar (with discussion), 743.

"Joint Translation by Cantilever Moment Distribution," L. E. Grinter and C. H. Tsao (with discussion), 1195.

JOINTS, RIVETED

Theory which eliminates need for trial and error solution to find necessary number of rivets to limit the deflection of a laminated beam to a given amount, 721, 732, 734.

JOINTS, TRUSS

See TRUSSES

KINETIC ENERGY

See HYDRODYNAMICS

LABOR

See also cross references under INDUSTRY

Skilled and unskilled labor problems of contractors in construction of Granby Pumping Plant, in Colorado, 527.

LABORATORIES

See under relative subject; *also* under MODELS . . . ; TESTS AND TESTING (cross references thereunder) ; *also* under material, structure or structural part tested

LABORATORIES, HYDRAULIC

See HYDRAULIC LABORATORIES

LAKES (General)

See also WATER . . .

LAKES (Geographical)

Grand Lake, Colo.

"The Granby Pumping Plant": A Symposium, W. R. Judd and W. H. Wolf; and R. J. Willson, 509.

LAMINAR FLOW

See WATER, FLOW OF, IN OPEN CHANNELS

LAMINATED BEAMS

See BEAMS

LAND . . .

See also EARTH . . . ; GROUND . . . ; MAPS AND MAPPING, LAND; PUBLIC LANDS; SOIL . . .

LAND MAPS AND MAPPING

See MAPS AND MAPPING, LAND

LANDSLIDE LAW

Legal aspects of landslides, 697.

LANDSLIDES

See also COSTS, LANDSLIDE; FAILURES, EARTH

"Analysis of Corrective Actions for Highway Landslides," R. F. Baker, 665. *Discussion:* D. P. Krynine and Richard J. Woodward; and R. F. Baker, 690.

Detailed tabulation of corrective measures, specifying best applications of design principles involved, 677, 680.

Slip surface in landslides, 665.

Tabulated summary of data needed for design computations when using specified corrective measures, with estimated costs, 683, 685.

Bibliography

Comprehensive report and other publications cited, 666.

LATERAL PRESSURE

See EARTH PRESSURE; WATER PRESSURE

LAW

See LAW subject heading under related topic, e.g., ZONING LAW; *see also* CONTRACTS; GOVERNMENT (cross references thereunder)

LEAST WORK, PRINCIPLE OF

See STRUCTURES, THEORY OF

LEVEES

See also DIKES

"Relief Well Systems for Dams and Levees," W. J. Turnbull and C. I. Mansur (with discussion), 842.

"Wave-Wash Control on Mississippi River Levees," Rudolf Hertzberg, 628.

LIFTING MACHINERY

See HOISTING MACHINERY (cross reference thereunder)

LIGHTING

See AIRPORTS

LIMIT DESIGN, THEORY OF

"Design of Frames by Relaxation of Yield-Hinges," J. Morley English (with discussion), 1143.

LININGS

See under relative subject

LIQUIDS, FLOW OF . . .

See WATER, FLOW OF . . .

LOAD

See ATOMIC BLAST; BEARING CAPACITY; BUCKLING; EARTH PRESSURE; FAILURES . . . ; IMPACT; STRESS AND STRAIN; STRUCTURES, THEORY OF; VIBRATION; WATER PRESSURE; WHEEL LOADS; WIND PRESSURE; *also* under structure, structural member or part, e.g., BRIDGES; PLATES

LOAD, BED

See RIVERS; WATER, FLOW OF, IN OPEN CHANNELS

LOAD, SUSPENDED

See SEDIMENT AND SEDIMENTATION; SILT AND SILTING . . .

LOCKS

Effectiveness of manifold flow procedures as used in Munich and Iowa experiments when applied in studies of Panama Canal locks, 1117.

LOSS OF ENERGY

See EVAPORATION; FRICTION; WATER, FLOW OF . . . ; WATER HAMMER

LOSS OF HEAD

See FRICTION; WATER, FLOW OF . . .

MACHINERY

See under general types of machinery; *also* under specific type of machine, e.g., DREDGES AND DREDGING; *also* under usage, e.g., CONCRETE PLANTS

MANIFOLD FLOW

See WATER, FLOW OF, IN PIPES

MAPS AND MAPPING, AERIAL

"Aeronautical Charting and Mapping," Charles A. Schanck, 151. *Discussion:* E. S. Fabian, Phil M. Miles, and Charles A. Schanck, 158.

"Electronic Devices in Air Transport," F. B. Lee (with discussion), 60.

Factors to be considered in selecting a projection, 154.

MAPS AND MAPPING, LAND

"Zoning Maps for Airports," B. Everett Beavin, Sr. (with discussion), 277.

MARINE . . .

See SEA . . .

MASONRY

See CEMENT (cross reference thereunder); DAMS, MASONRY AND CONCRETE; STONE

MASONRY DAMS

See DAMS, MASONRY AND CONCRETE

MATERIALS, CONVEYANCE OF

See CONVEYORS AND CONVEYANCE (cross reference thereunder)

MATERIALS OF CONSTRUCTION

See also AGGREGATES AND AGGREGATION; CLAY; CONCRETE . . . ; EARTHWORK; EROSION . . . ; GRAVEL (cross references thereunder); PERMEABILITY OF MATERIALS (cross reference thereunder); SAND; SEEPAGE; SOILS; STEEL (cross references thereunder); STONE; STRENGTH OF MATERIALS (cross reference thereunder); STRESS AND STRAIN; STRUCTURES, THEORY OF . . . ; *also* under usage, e.g., PAVEMENT AND PAVING

Raw materials operation for mass concrete production in mountain regions, 902.

MATERIALS, STRENGTH OF

See STRENGTH OF MATERIALS (cross references thereunder)

MATERIALS, TESTING OF

See TESTS AND TESTING (cross references thereunder)

MATERIALS, WASTE

See cross references under WASTE DISPOSAL

MATHEMATICS

See also EQUATIONS; GRAPHICAL CHARTS; *also* under relative subject

Demonstration and use of Horner's method, 811.

"Group Loadings Applied to the Analysis of Frames," I. F. Morrison (with discussion), 338.

Method of group loadings used to orthogonalize simultaneous equations in analyzing structures, 340.

"Plates with Boundary Conditions of Elastic Support," S. J. Fuchs (with discussion), 935.

"Rapid Computation of Flexural Constants," Thomas G. Morrison (with discussion), 93.

Usage of matrix algebra in frame analysis, 353, 354.

MATRIX ALGEBRA

See MATHEMATICS

MEANDERS AND MEANDERING

See RIVERS

MEASURING INSTRUMENTS

See METERS AND METERING; TEMPERATURE MEASURING INSTRUMENTS

MECHANICAL ENGINEERS AND ENGINEERING

See MECHANICS; *see also* under relative subject, e.g., AUTOMOBILE . . . ; MACHINERY (cross references thereunder); MOTOR . . .

MECHANICS (General)

See also DYNAMICS (cross references thereunder); FLUIDS, FLOW OF (cross reference thereunder); HYDRAULICS; MATHEMATICS; STRENGTH OF MATERIALS (cross references thereunder); STRUCTURAL . . . ; STRUCTURES, THEORY OF; TESTS AND TESTING (cross references thereunder)

"Stresses in the Corners of Rigid Frames," Harvey C. Olander, 797.

MECHANICS, SOIL

See SOILS

MEMBERS (ASCE)

See AMERICAN SOCIETY OF CIVIL ENGINEERS. (For memoirs of deceased members, *see* name of member in Author Index)

MEMBERS, COMPRESSION

See COLUMNS

MEMBERS, STRUCTURAL

See BEAMS; COLUMNS; GIRDERS . . . (cross references thereunder); STRUCTURES, THEORY OF; *also* under structure, e.g., BRIDGES; *also* under name of material, e.g., CONCRETE

MEMOIRS OF DECEASED MEMBERS

See name of member in Author Index

METALLURGY

See under specific metal, e.g., STEEL (cross references thereunder)

METALS

See BARS (solid material) (cross reference thereunder); REINFORCED CONCRETE (cross reference thereunder); *also* under specific metal, e.g., STEEL (cross references thereunder)

METEOROLOGY

See EVAPORATION; RAINFALL

METERS AND METERING (General)

See also GAGES . . . ; INSTRUMENTS; WEIRS (cross references thereunder)

METERS AND METERING, CURRENT

"Rating Curves for Flow over Drum Gates," Joseph N. Bradley (with discussion), 403.

"Velocity Measurement of Air-Water Mixtures," Lorenz G. Straub, John M. Killen, and Owen P. Lamb, 207.

METERS AND METERING, WATER (stream velocity)

See METERS AND METERING, CURRENT

MILITARY ENGINEERS AND ENGINEERING

See under relative technical subject, e.g., AIRPORT . . . ; BRIDGES

MINERALOGY

See under relative technical subject, e.g., SOILS

MINERALS

See relative technical subject, e.g., CONCRETE; MATERIALS OF CONSTRUCTION

MODELS, HYDRAULIC

"Dam Modifications Checked by Hydraulic Models," E. S. Harrison and Carl E. Kindsvater, 73. *Discussion:* G. H. Hickox; and E. S. Harrison and Carl E. Kindsvater, 90.

"Relief Well Systems for Dams and Levees," W. J. Turnbull and C. I. Mansur (with discussion), 842.

Test results for relief well investigations, 859.

MODELS, STRUCTURAL

"Hipped Plate Analysis, Considering Joint Displacements," Ibrahim Gaafar (with discussion), 743.

"Plates with Boundary Conditions of Elastic Support," S. J. Fuchs (with discussion), 935.

"Wind Loads on Truss Bridges," John M. Biggs (with discussion), 879.

MOHR, WILLIOT-, DIAGRAM

See cross reference under WILLIOT-MOHR DIAGRAM

MOISTURE

See CONCRETE—Effect of Natural Processes; EVAPORATION; PAVEMENT AND PAVING . . . ; SEEPAGE; SOILS

MOMENT DISTRIBUTION

See MOMENTS; STRUCTURES, THEORY OF

MOMENTS

See also STRESS AND STRAIN; STRUCTURES, THEORY OF; *also* under specific type of stress, e.g., BUCKLING; TORSION

"Anchored Bulkheads," Karl Terzaghi (with discussion), 1243.

"Continuous Composite Steel and Concrete Beams," John Sherman, 810.

"Design of Frames by Relaxation of Yield-Hinges," J. Morley English (with discussion), 1143.

"Hipped Plate Analysis, Considering Joint Displacements," Ibrahim Gaafar (with discussion), 743.

"Numerical Analysis of Continuous Frames in Space," James Michalos, 565.

"Plates with Boundary Conditions of Elastic Support," S. J. Fuchs (with discussion), 935.

"Rapid Computation of Flexural Constants," Thomas G. Morrison (with discussion), 93.

"Stiffness Charts for Gusseted Members under Axial Load," John E. Goldberg (with discussion), 43.

"Stresses in the Corners of Rigid Frames," Harvey C. Olander, 797.

MOTOR BUSES

See also MOTOR VEHICLES; TRAFFIC . . .

"Unified Mass-Transportation System for New York," William Reid (with discussion), 124.

MOTOR CARS

See AUTOMOBILE . . . ; MOTOR VEHICLES; TRAFFIC . . .

MOTOR TRAFFIC

See TRAFFIC . . .

MOTOR TRANSPORTATION

See HIGHWAY TRANSPORTATION

MOTOR TRUCKING

See HIGHWAY TRANSPORTATION

MOTOR TRUCKS

See also MOTOR VEHICLES; TRAFFIC . . . ; WHEEL LOADS; WHEELS

Diagrams of trucks classified by type showing wheel base measurements, weight and speed, 984, 985, 986.

MOTOR VEHICLE ACCIDENTS

See HIGHWAYS AND ROADS—Safety

MOTOR VEHICLES

See also TRAFFIC . . . ; WHEEL LOADS

Number of registered vehicles in New York and New Jersey in 1925 and 1950, 127.

Variance in state standards and its influence on formulating a design live loading for long spans, 982, 987.

MOTORWAYS

See HIGHWAYS AND ROADS

MOUNTAINS

See CANYONS; WATER DIVERSION; *see also* VALLEYS

MOUNTAIN SLIDES

See LANDSLIDES

MOVABLE BRIDGES
See BRIDGES, MOVABLE

MOVABLE WATER GATES
See WATER GATES, MOVABLE

MULTI-PURPOSE RESERVOIRS
See RESERVOIRS, MULTI-PURPOSE

MUNICIPAL ENGINEERS AND ENGINEERING
See ENGINEERS AND ENGINEERING; *see also* AIRPORTS; BRIDGES; CITIES; CITY PLANNING; COSTS . . . ; HARBORS; PAVEMENT AND PAVING; SANITATION; SEWAGE . . . ; SNOW; STREETS; SUBWAYS; TRAFFIC, STREET; WATER . . . ; ZONING; and similar relative subjects

MUNICIPALITIES
See CITIES

NAVIGATION
See CANALS; CHANNELS; DAMS; ELECTRONIC INSTRUMENTS; FLOODS; HARBORS; LAKES; LOCKS; RIVERS; TIDES; WATER TRANSPORTATION

NAVIGATION, AIR
See AIR TRANSPORT

NETWORKS
See GAGES, RAIN; HIGHWAYS AND ROADS; HIGHWAY TRANSPORTATION; STRUCTURES, THEORY OF

NOMENCLATURE
See TERMINOLOGY

NUISANCES, ABATEMENT OF
See ODORS

OBITUARIES OF MEMBERS
See name of member in Author Index

OCEAN . . .
See also SEA . . . ; TIDES; WAVES

OCEAN BEACHES
See EROSION, BEACH

OCEAN CURRENTS
See EROSION, BEACH; TIDES; WAVES

OCEAN WAVES
See WAVES

ODORS
Odor causing algae, 658.

OIL, FLOW OF
See WELLS

OIL WELLS
See WELLS

OPEN CHANNELS
See CHANNELS; WATER, FLOW OF, IN OPEN CHANNELS

ORDNANCE
See METALS (cross references thereunder)

ORGANIZATIONS
See SOCIETIES, TECHNICAL (cross references thereunder)

ORIFICES
See WATER, FLOW OF, THROUGH ORIFICES

OSCILLATION
See VIBRATION; WAVES

PARKING REGULATIONS
See AUTOMOBILE PARKING

PAVEMENT AND PAVING (General)
See also COSTS, PAVEMENT AND PAVING; WHEEL LOADS
Recommended requirements for subbase materials for flexible and concrete pavements, 548.
Revisions of design standards for airport pavements with changing aircraft types, 493, 497, 498.
"Special Procedures for Pavement Design," L. A. Palmer, 542. *Discussion:* R. Horonjeff, and L. A. Palmer, 561.

PAVEMENT AND PAVING, ASPHALT
See PAVEMENT AND PAVING, BITUMINOUS

PAVEMENT AND PAVING, BITUMINOUS
"Wave-Wash Control on Mississippi River Levees," Rudolf Hertzberg, 628.

PAVEMENT AND PAVING, CONCRETE
"Wave-Wash Control on Mississippi River Levees," Rudolf Hertzberg, 628.

PERCOLATION
See GROUND WATER; SEEPAGE; SEWAGE DISPOSAL

PERMEABILITY OF MATERIALS
See SEEPAGE; STRENGTH OF MATERIALS (cross references thereunder)

PERSONNEL
See EMPLOYEES AND EMPLOYMENT

PETROLEUM
See OIL . . . (cross references thereunder)

PIERS (waterway structures)
See DOCKS AND WHARVES (cross references thereunder)

PIERS, BRIDGE
See BRIDGE PIERS

PILES AND PILE DRIVING

See also BEARING CAPACITY; COSTS, PILE AND PILE DRIVING; FOUNDATIONS, UNDERWATER

"Anchored Bulkheads," Karl Terzaghi (with discussion), 1243.

"Design Curves for Anchored Steel Sheet Piling," Walter C. Boyer and Henry M. Lummis, III, 639. *Discussion:* Gregory P. Tschebotarioff; and Walter C. Boyer and Henry M. Lummis, III, 651.

"The Design of Flexible Bulkheads," James R. Ayers and R. C. Stokes (with discussion), 373.

"Offshore Petroleum Installations," Jack S. Toler, 480.

PILLARS

See COLUMNS

PIN-CONNECTED TRUSSES

See TRUSSES, PIN-CONNECTED

PIPE LINES

See also PIPES AND PIPING (fluid conveyance); PUMPS AND PUMPING; SPRINKLERS AND SPRINKLING; WATER, FLOW OF, IN PIPES; WATER HAMMER

"Design Charts for Air Chambers on Pump Lines," W. E. Evans and C. C. Crawford, 1025. *Discussion:* C. E. Withers; Henry M. Paynter; and W. E. Evans and C. C. Crawford, 1037.

An idealized air chamber installation on a pump discharge line, 1026.

Schematic design for air chamber water level control, 1038.

PIPES AND PIPING (fluid conveyance)

See CONDUITS; PIPE LINES; WATER, FLOW OF, IN PIPES; WATER HAMMER

PITOT TUBES

See METERS AND METERING, CURRENT

PLANNING

See AIRPORTS; CITY PLANNING; REGIONAL PLANNING; STREETS —Planning and Design; ZONING . . .

PLANTS (industrial buildings and equipment)

See INDUSTRIAL PLANTS; *see also* under type of plant, e.g., CONCRETE PLANTS; CONTRACTORS' PLANTS

PLANTS, CONTRACTORS'

See CONTRACTORS' PLANTS

PLASTICITY

"Nonelastic Behavior of Bridges under Impulsive Loads," S. J. Fraenkel and L. E. Grinter (with discussion), 309.

PLATES

See also JOINTS; SLABS; STRESS AND STRAIN—Plates; STRUCTURES, THEORY OF—Plates

"Plates with Boundary Conditions of Elastic Support," S. J. Fuchs, 935. *Discussion:* M. Z. v. Krzywoblocki, R. H. Wood, and S. J. Fuchs, 959.

"Stiffness Charts for Gusseted Members under Axial Load," John E. Goldberg (with discussion), 43.

Bibliography

Plates with boundary conditions of elastic support, 959.

POLLUTION, STREAM

See WATER POLLUTION (cross reference thereunder)

POPULATION

Concentration of population in the United States and its influence on air transport, 67.

"The Engineer and World Population": Address at the Summer Convention, Atlantic City, N. J., June 16, 1954, Daniel V. Terrell, 1325.

PORE WATER PRESSURE

See WATER PRESSURE

POROSITY

See SEEPAGE

PORTS

See AIRPORTS; HARBORS

POWER (General)

See DAMS; DYNA- . . . (cross references thereunder); FUEL (cross reference thereunder); PUMPS AND PUMPING; WATER HAMMER

PRECIPITATION

See RAINFALL; SNOW

PRESIDENTIAL ADDRESSES (American Society of Civil Engineers)

See AMERICAN SOCIETY OF CIVIL ENGINEERS—Addresses; *see also* under subject of address

PRESSURE

See EARTH PRESSURE; HYDROSTATIC UPLIFT (cross reference thereunder); ICE; IMPACT; LATERAL PRESSURE (cross references thereunder); PUMPS AND PUMPING; STRESS AND STRAIN; WATER HAMMER; WATER PRESSURE; WAVES; WIND PRESSURE

PRESSURE GAGES

See GAGES, PRESSURE

PRESSURE TRANSMISSION THROUGH SOLIDS

See EARTH PRESSURE

PRESTRESSED CONCRETE

See CONCRETE, PRESTRESSED

PRIME MOVERS

See ENERGY (cross references thereunder); POWER (cross references thereunder)

PRINCIPLE OF LEAST WORK
See STRUCTURES, THEORY OF

PRINCIPLE OF SUPERPOSITION
See STRUCTURES, THEORY OF

PROPERTY (landed property)
See LAND . . . ; PUBLIC LANDS; STREETS—Planning and Design

PROTECTIVE WORKS
See under relative type; *see also* WAVES

PROTOTYPES AND MODELS
See MODELS

PUBLIC HEALTH
See also SANITATION (and cross references thereunder)
"Algae Responsible for Odor and Taste in Water Supplies," George J. Turre, 658.

PUBLIC LANDS
"Zoning Maps for Airports," B. Everett Beavin, Sr. (with discussion), 277.

PUBLIC SERVICES
See under type of service, e.g., SEWAGE DISPOSAL

PUBLIC UTILITIES
See SUBWAYS

PUBLIC WORKS
See COSTS . . . ; *see also* under type of structure or project

PUMPS AND PUMPING (General)
See also SEWAGE DISPOSAL
"Design Charts for Air Chambers on Pump Lines," W. E. Evans and C. C. Crawford (with discussion), 1025.
"The Granby Pumping Plant": A Symposium, W. R. Judd and W. H. Wolf; and R. J. Willson, 509.
Plan and profile of Granby Pumping Plant, in Colorado, 512, 518, 519.

RADAR
See AIR TRANSPORT; ELECTRONIC INSTRUMENTS

RADAR ANALYSIS
See RAINFALL

RAILROADS (General)
See BRIDGES . . . ; FREIGHT; SNOW; SUBWAYS
Design and Construction. *See* under relative subject, structure or structural part, e.g., BRIDGES

RAILROADS, ELECTRIC
See SUBWAYS

RAILROADS, UNDERGROUND
See SUBWAYS

RAILROAD TRACKS

See EARTHWORK; PAVEMENT AND PAVING; WHEEL LOADS

RAILROAD TRANSPORTATION

See RAIL TRANSPORTATION

RAIL TRANSPORTATION

See also FREIGHT

"Unified Mass-Transportation System for New York," William Reid (with discussion), 124.

RAILWAYS

See RAILROADS (cross references thereunder)

RAINFALL (General)

See also DRAINAGE (cross references thereunder); EVAPORATION; FLOODS; GAGES, RAIN; HYDROLOGY; RUNOFF; SEEPAGE; SNOW

Factors affecting area-depth relationships on individual basins, 253.

"Rainfall Studies Using Rain-Gage Networks and Radar," H. E. Hudson, Jr., G. E. Stout and F. A. Huff, 248. *Discussion:* Ven Te Chow; and H. E. Hudson, Jr., G. E. Stout, and F. A. Huff, 274.

RAINFALL (Geographical)

Florida

Excessive rainfall recording procedures changed by United States Weather Bureau, 929.

"Frequency of Excessive Rainfalls in Florida," David B. Smith, 927.

Muskingum Basin, Ohio

"Rainfall Studies Using Rain-Gage Networks and Radar," H. E. Hudson, Jr., G. E. Stout and F. A. Huff (with discussion), 248.

RAIN GAGES

See GAGES, RAIN

RAPID TRANSIT

See SUBWAYS

RECORDING APPARATUS

See under general types of apparatus, e.g., VIBRATION RECORDING APPARATUS; *see also* under relative subject

RECORDING INSTRUMENTS

See under relative subject

RECORD KEEPING

See GRAPHICAL CHARTS; HYDROGRAPHS . . . ; *see also* cross references under RECORDING . . . ; *see also* under relative subject, e.g., FLOODS; RAINFALL

RECREATIONAL FACILITIES

See CITY PLANNING

REDUNDANCE, STRUCTURAL

See STRUCTURES, THEORY OF

REFUSE DISPOSAL

See DEBRIS CONTROL; ODORS; SEWAGE DISPOSAL; SEWAGE SLUDGE

REGIONAL PLANNING

See also CITY PLANNING; ZONING . . .

"Zoning Maps for Airports," B. Everett Beavin, Sr. (with discussion), 277.

REINFORCED CONCRETE

See CONCRETE . . .

RELIEF WELLS

See WELLS

REPORTS OF COMMITTEES

See AMERICAN SOCIETY OF CIVIL ENGINEERS—Committee Reports; *see also* under subject of report

RESEARCH

See AMERICAN SOCIETY OF CIVIL ENGINEERS; HYDRAULIC LABORATORIES; LABORATORIES (cross references thereunder); MODELS . . . ; STRUCTURES, THEORY OF; SURVEYS (research data) (cross references thereunder); TESTS AND TESTING (cross references thereunder); *see also* under relative subject, e.g., RAINFALL; TRAFFIC, STREET

RESERVOIRS (General)

See also DAMS; EVAPORATION; LAKES; SPILLWAYS; WATER DIVERSION; WAVES

"A Direct Step Method for Computing Water-Surface Profiles," Arthur A. Ezra (with discussion), 453.

"The Granby Pumping Plant": A Symposium, W. R. Judd and W. H. Wolf; and R. J. Willson, 509.

"Ice Pressure against Dams": A Symposium, R. L. Hearn, R. F. Legget, D. A. Buzzell, D. McHenry, L. S. McLennan, E. N. Peterson, and G. R. Strandberg; Bertil Lofquist; A. D. Hogg; and G. E. Monfore (with discussion), 1.

RESERVOIRS, FLOOD CONTROL

"Snow Hydrology for Multiple-Purpose Reservoirs," Herbert S. Riesbol (with discussion), 595.

RESERVOIRS, MULTI-PURPOSE

"Snow Hydrology for Multiple-Purpose Reservoirs," Herbert S. Riesbol (with discussion), 595.

RESONANCE

See VIBRATION; WATER HAMMER; WAVES

RETAINING WALLS

See also BULKHEADS; EARTH PRESSURE; EARTHWORK; EMBANKMENTS (cross references thereunder); REVETMENT

"The Design of Flexible Bulkheads," James R. Ayers and R. C. Stokes (with discussion), 373.

REVETMENT

See also DIKES; LEVEES; RETAINING WALLS; WAVES

"Wave-Wash Control on Mississippi River Levees," Rudolf Hertzberg, 628.

RIGID FRAMES

See STRESS AND STRAIN—Frames, Rigid; STRUCTURES, THEORY OF —Frames, Rigid

RIVER BANKS AND BANK PROTECTION

See DIKES; EROSION, STREAM; FLOODS; LANDSLIDE . . . ; LEVEES; REVETMENT; SEDIMENT AND SEDIMENTATION

RIVER BANK STABILIZATION

See RIVER BANKS AND BANK PROTECTION (cross references thereunder)

RIVER BASINS

See DRAINAGE (cross references thereunder); RAINFALL; RESERVOIRS . . . ; VALLEYS

RIVER CHANNELS

See CHANNELS

RIVER MEANDERING

See RIVERS

RIVER RECTIFICATION

See RIVER REGULATION (cross references thereunder); *see also* other related RIVER . . . subject headings

RIVER REGULATION

See BARS (alluvia); DIKES; REVETMENT; RIVERS; WATER, FLOW OF, IN OPEN CHANNELS

RIVERS (General)

See also BARS (alluvia); BRIDGE . . . ; CHANNELS; DIKES; DREDGES AND DREDGING; EROSION, STREAM; FLOODS; HARBORS; HYDRAULIC LABORATORIES; HYDROLOGY; LEVEES; LOCKS; MODELS, HYDRAULIC; RAINFALL; RESERVOIRS; RETAINING WALLS; RUNOFF; SILT AND SILTING, CHANNEL; TIDES; VALLEYS; WATER . . . ; WAVES

Comprehensive studies on the meandering of alluvial streams, 1080.

"Sewage Disposal in Tidal Estuaries," Alexander N. Diachishin, Seth G. Hess and William T. Ingram (with discussion), 434.

RIVERS (Geographical)

Colorado River

"The Granby Pumping Plant": A Symposium, W. R. Judd and W. H. Wolf; and R. J. Willson, 509.

"River-Bed Scour during Floods," E. W. Lane and W. M. Borland (with discussion), 1069.

Columbia River

Commerce, in tons, through The Dalles–Celilo Canal section of the Columbia River, years 1870–2000, 142, 149, 150.

"Slackwater Improvement of the Columbia River," O. E. Walsh, 135.

East River

Tidal action in the East River in New York Harbor, 438, 449.

Hudson River

Tides and tidal currents in relation to physical characteristics of the river, 437, 449.

Kansas

Location of stream gaging stations in Kansas, 1008.

Mississippi River

"Relief Well Systems for Dams and Levees," W. J. Turnbull and C. I. Mansur (with discussion), 842.

"Wave-Wash Control on Mississippi River Levees," Rudolf Hertzberg, 628.

Rio Grande River

"River-Bed Scour during Floods," E. W. Lane and W. M. Borland (with discussion), 1069.

Western States

"Slackwater Improvement of the Columbia River," O. E. Walsh, 135.

RIVER TIDES

See TIDES

RIVER TRANSPORTATION

See WATER TRANSPORTATION

RIVER VALLEYS

See VALLEYS

RIVETED JOINTS

See JOINTS, RIVETED

ROADBEDS

See DRAINAGE (cross references thereunder); EARTHWORK; RAILROAD TRACKS (cross references thereunder)

ROADS

See HIGHWAYS AND ROADS

ROCK

See EARTH PRESSURE; STONE

RODS

See BARS (solid material) (cross reference thereunder)

RODS, TIE

See BULKHEADS

ROLLING STOCK

See WHEEL LOADS

ROOFS AND ROOFING

See also DOMES AND VAULTS (cross references thereunder); TRUSSES . . .

"Hipped Plate Analysis, Considering Joint Displacements," Ibrahim Gaafar (with discussion), 743.

ROUGHNESS FACTOR

See FRICTION COEFFICIENTS . . .

RUBBISH DISPOSAL

See REFUSE DISPOSAL (cross references thereunder)

RUNOFF (General)

See also FLOODS; HYDROGRAPHS, RUNOFF; RAINFALL; SNOW

"Peak Discharge for Highway Drainage Design," Carl F. Izzard (with discussion), 1005.

"Snow Hydrology for Multiple-Purpose Reservoirs," Herbert S. Riesbol (with discussion), 595.

RUNWAYS

See AIRPORT APPROACHES; AIRPORTS

SAFETY (General)

See EARTHQUAKES (cross references thereunder); HIGHWAYS AND ROADS—Safety

SAFETY FACTOR

See relative subject, e.g., BULKHEADS

SALINITY

See SEA WATER; WATER, FLOW OF, IN OPEN CHANNELS; WATER INSTRUMENTS

SALT WATER

See SEA WATER

SAND

See also GROUTING; PILES AND PILE DRIVING; SEDIMENT AND SEDIMENTATION; SEEPAGE; SILT AND SILTING; SOILS

"Anchored Bulkheads," Karl Terzaghi (with discussion), 1243.

Sand processing for mass concrete operations, 903, 905.

SAND BARS

See BARS (alluvia)

SANITARY ENGINEERS AND ENGINEERING

See SANITATION

SANITATION

See also DEBRIS CONTROL; DRAINAGE (cross references thereunder); HOUSES—Drainage (cross reference thereunder); ODORS; PIPES AND PIPING (cross references thereunder); PUBLIC HEALTH; REFUSE DISPOSAL (cross references thereunder); SEWAGE DISPOSAL; SEWAGE SLUDGE; WATER . . .

"Putting a Sewage Treatment Plant into Operation," Benjamin Benas, 785.

SCIENCE

See under specific science, e.g., HYDRAULICS; MATHEMATICS

SCIENTIFIC SOCIETIES

See AMERICAN SOCIETY OF CIVIL ENGINEERS; *see also* ENGINEERS AND ENGINEERING

SCOUR

See EROSION . . .

SEA . . .

See also OCEAN . . . (cross references thereunder)

SEACOAST

See HARBORS; OCEAN CURRENTS (cross references thereunder); TIDES; WAVES

SEA WATER

"Sewage Disposal in Tidal Estuaries," Alexander N. Diachishin, Seth G. Hess and William T. Ingram (with discussion), 434.

SEDIMENT AND SEDIMENTATION

See also SILT AND SILTING; TURBULENCE; WATER DIVERSION

"River-Bed Scour during Floods," E. W. Lane and W. M. Borland (with discussion), 1069.

SEEPAGE

"Relief Well Systems for Dams and Levees," W. J. Turnbull and C. I. Mansur (with discussion), 842.

SEISMOLOGY

See EARTHQUAKES (cross references thereunder)

SETTLEMENT OF FILL

See HYDRAULIC FILLING

SETTLEMENT OF STRUCTURES

See BEARING CAPACITY; EARTH PRESSURE; EMBANKMENTS (cross references thereunder); FOUNDATIONS . . . ; SOIL . . .

SETTLING BASINS (water supply)

See RESERVOIRS . . . ; SEDIMENT AND SEDIMENTATION

SEWAGE DISPOSAL (General)

See also COSTS, SEWAGE DISPOSAL; ODORS; PIPES AND PIPING (cross references thereunder); SEWAGE SLUDGE

Flow diagrams showing plant capacity and method of treatment, including sludge handling, 787, 789.

"Sewage Disposal in Tidal Estuaries," Alexander N. Diachishin, Seth G. Hess and William T. Ingram, 434. *Discussion:* Isadore Nusbaum; Alexander N. Diachishin, Seth G. Hess and William T. Ingram, 448.

SEWAGE DISPOSAL (Geographical)

San Francisco, Calif.

"Putting a Sewage Treatment Plant into Operation," Benjamin Benas, 785.

SEWAGE SLUDGE

See also SEWAGE DISPOSAL

SEWAGE SLUDGE

"Putting a Sewage Treatment Plant into Operation," Benjamin Benas, 785.

SEWAGE TREATMENT

See SEWAGE DISPOSAL

SEWAGE WORKS

See SEWAGE DISPOSAL

SEWERS

See DRAINAGE (cross references thereunder); PIPES AND PIPING (cross references thereunder); RAINALL; RUNOFF; WATER, FLOW OF, IN PIPES

SHEAR

"Analysis of Corrective Actions for Highway Landslides," R. F. Baker (with discussion), 665.

"Deflection of Laminated Beams," L. G. Clark, 721.

"Earthquake Stresses in Shear Buildings," Mario G. Salvadori (with discussion), 171.

"Special Procedures for Pavement Design," L. A. Palmer (with discussion), 542.

"Turbulent Boundary Layer on Steep Slopes," William J. Bauer (with discussion), 1212.

SHEARING STRESS

See SHEAR

SHEDS

See under relative type, e.g., WATERSHEDS (cross references thereunder)

SHEET PILING

See PILES AND PILE DRIVING

SHELL STRUCTURES

See DOMES AND VAULTS (cross references thereunder); PIPE LINES; PIPES AND PIPING (cross references thereunder); ROOFS AND ROOFING

SHIPS AND SHIPPING

See WATER TRANSPORTATION

SHOCK

See ATOMIC BLAST; EARTHQUAKES (cross references thereunder); IMPACT

SHORES AND SHORE PROTECTION

See BREAKWATERS (cross reference thereunder); EROSION, BEACH; RETAINING WALLS; WAVES; *see also* cross references under RIVER BANKS AND BANK PROTECTION

SIDESWAY

See STRUCTURES, THEORY OF—Frames . . .

SIDEWALKS (General)

See CONCRETE; PAVEMENT AND PAVING; STREETS

SILT AND SILTING (General)

Unconfined compressive strength of silt and clay, 1264.

SILT AND SILTING, CHANNEL

"River-Bed Scour during Floods," E. W. Lane and W. M. Borland, 1069. *Discussion:* E. E. Dittbrenner; Emmett M. Laursen and Arthur Toch; and E. W. Lane and W. M. Borland, 1080.

SLABS

See also PLATES; STRESS AND STRAIN—Slabs

"Continuous Composite Steel and Concrete Beams," John Sherman, 810.

SLIDES

See LANDSLIDES

SLIPS AND SLIPPAGE (movement of surfaces)

See LANDSLIDES

SLOPE DEFLECTION

"Stiffness Charts for Gusseted Members under Axial Load," John E. Goldberg (with discussion), 43.

Bibliography

Gusseted members under axial load, 44.

SLOPES, EARTH

See EARTHWORK

SLOPING CHANNELS

See CHANNELS

SLUDGE, SEWAGE

See SEWAGE SLUDGE

SNOW

"Snow Hydrology for Multiple-Purpose Reservoirs," Herbert S. Riesbol, 595. *Discussion:* Ray K. Linsley, R. W. Gerdel, Harold D. Hafterson, David M. Rockwood, and Herbert S. Riesbol, 614.

Bibliography

Comprehensive bibliography on snow, ice and frozen ground, 619.

SOCIAL PROBLEMS AND ENGINEERING

See ENGINEERS AND ENGINEERING

SOCIETIES, TECHNICAL

See AMERICAN SOCIETY OF CIVIL ENGINEERS; *see also* ENGINEERS AND ENGINEERING

SOIL . . .

See also EARTH . . . ; GROUND . . . ; LAND . . ,

SOIL MECHANICS

See SOILS

SOIL PRESSURE

See EARTH PRESSURE

SOILS (General)

See also BEARING CAPACITY; DRAINAGE (cross references thereunder); EARTH PRESSURE; EROSION . . . ; EVAPORATION; FOUNDATIONS . . . ; FRICTION . . . ; GRAVEL (cross references thereunder); GROUND . . . (cross references thereunder); LAND . . . (cross references thereunder); PAVEMENT AND PAVING; SAND; SEDIMENT AND SEDIMENTATION; SEEPAGE; SILT AND SILTING; *also* under name of soil structure, e.g., LEVEES

"Analysis of Corrective Actions for Highway Landslides," R. F. Baker (with discussion), 665.

"Relief Well Systems for Dams and Levees," W. J. Turnbull and C. I. Mansur (with discussion), 842.

Compaction. *See* BEARING CAPACITY

Construction

"Anchored Bulkheads," Karl Terzaghi (with discussion), 1243.

Tests and Testing

"The Granby Pumping Plant": A Symposium, W. R. Judd and W. H. Wolf; and R. J. Willson, 509.

SOIL TRANSPORTATION

See SILT AND SILTING

SOLIDS, FLOW OF

See EARTH FLOW (cross reference thereunder); SEDIMENT AND SEDIMENTATION; SILT AND SILTING . . . ; WATER, FLOW OF, IN OPEN CHANNELS

SOLIDS, PRESSURE TRANSMISSION THROUGH

See EARTH PRESSURE

SPACE STRUCTURES

See DOMES AND VAULTS (cross references thereunder); STRUCTURES, THEORY OF—Space Structures; WIND . . .

SPACE TRUSSES

See STRUCTURES, THEORY OF—Trusses and Trussed Structures; TRUSSES

SPECIFICATIONS

See under relative subject, e.g., BRIDGES; *see also* CONTRACTS

SPEED

See TRAFFIC . . .

SPILLWAY GATES

See SPILLWAYS

SPILLWAYS (General)

See also DAMS; STRESS AND STRAIN—Spillways; WATER, FLOW OF, OVER DAMS AND WEIRS

"Design of Side Walls in Chutes and Spillways," D. B. Gumensky, 355. *Discussion:* Leland S. Rhodes, G. S. Sarkaria, J. H. Douma, Edgar E. Foster, Thomas J. Rhone, and D. B. Gumensky, 362.

Examples of drum gate cross sections, 407.

"Rating Curves for Flow over Drum Gates," Joseph N. Bradley (with discussion), 403.

Snow evaporation and melt in its relation to spillway design, 603, 614, 620, 623, 624.

"Turbulent Boundary Layer on Steep Slopes," William J. Bauer (with discussion), 1212.

"Velocity Measurement of Air-Water Mixtures," Lorenz G. Straub, John M. Killen, and Owen P. Lamb, 207.

SPILLWAYS (Geographical)

Bartlett's Ferry Dam, Georgia

"Dam Modifications Checked by Hydraulic Models," E. S. Harrison and Carl E. Kindsvater (with discussion), 73.

Norris Dam

Flow observations (natural and model flow) compared to analytical predictions, 1217, 1225.

SPRINKLERS AND SPRINKLING (irrigation)

"Mechanics of Manifold Flow," John S. McNown (with discussion), 1103.

STABILITY

See AERODYNAMICS (cross reference thereunder); BUCKLING; HYDRODYNAMICS; MECHANICS; SOIL . . . ; STRUCTURES, THEORY OF

STATICALLY INDETERMINATE STRUCTURES

See INSTRUMENTS; STRUCTURES, CONTINUOUS (cross reference thereunder); STRUCTURES, THEORY OF; STRUCTURES, TRUSSED (cross reference thereunder)

STATIONS

See cross reference under TERMINALS

STATISTICAL ANALYSIS

See GRAPHICAL CHARTS; MATHEMATICS

STATISTICS

See relative subject

STEEL

See REINFORCED CONCRETE (cross reference thereunder); STRENGTH OF MATERIALS (cross references thereunder); *see also* under special structure or structural part, e.g., ARCHES; BEAMS . . . ; PILES AND PILE DRIVING

STIFFNESS

"Joint Translation by Cantilever Moment Distribution," L. E. Grinter and C. H. Tsao (with discussion), 1195.

"Lateral Buckling of Channels and **Z**-Beams," H. N. Hill, 829.

"Plates with Boundary Conditions of Elastic Support," S. J. Fuchs (with discussion), 935.
"Rapid Computation of Flexural Constants," Thomas G. Morrison (with discussion), 93.
"Stiffness Charts for Gusseted Members under Axial Load," John E. Goldberg (with discussion), 43.
Bibliography
Gusseted members under axial load, 44.

STILLING BASINS
See WATER, FLOW OF, OVER DAMS AND WEIRS

STONE
See also GRAVEL (cross references thereunder)
"The Granby Pumping Plant": A Symposium, W. R. Judd and W. H. Wolf; and R. J. Willson, 509.

STORAGE
See RESERVOIRS . . .

STORMS
See RAINFALL; SNOW; WAVES; WIND . . .

STORM WATER
See DRAINAGE (cross references thereunder); SEWAGE DISPOSAL; SEWERS (cross references thereunder)

STRAIN
See STRESS AND STRAIN

STRAIN GAGES
See GAGES, STRAIN

STREAM CONTAMINATION
See WATER POLLUTION (cross reference thereunder)

STREAM EROSION
See EROSION, STREAM

STREAM FLOW
See WATER, FLOW OF, IN OPEN CHANNELS

STREAMS
See RIVERS and cross references thereunder

STREET CLEANING
See REFUSE DISPOSAL (cross references thereunder)

STREETS
See also BRIDGES; CITIES; CITY PLANNING; CONDUITS; HIGHWAYS AND ROADS; IMPACT; MOTOR . . . ; PAVEMENT AND PAVING; PIPES AND PIPING (cross references thereunder); REFUSE DISPOSAL (cross references thereunder); SIDEWALKS (cross references thereunder); SUBWAYS; TRAFFIC, STREET; WHEEL LOADS; ZONING . . .

Planning and Design

"The Engineer's Role in Metropolitan Traffic Planning," Lloyd Braff (with discussion), 713.

STREET TRAFFIC

See TRAFFIC, STREET

STREET TRANSPORTATION

See HIGHWAY TRANSPORTATION; STREETS—Planning and Design; VEHICLES (cross references thereunder)

STRENGTH OF MATERIALS

See FAILURES . . . ; MECHANICS; STRESS AND STRAIN; *also* under specific material (*see* list of materials under MATERIALS OF CONSTRUCTION); *see also* under fabricated structure or structural part, e.g., BEAMS

STRESS AND STRAIN (General)

See also EARTH PRESSURE; EARTHQUAKES (cross references thereunder); ELASTICITY; FAILURES . . . ; GAGES, STRAIN; IMPACT; MOMENTS; STIFFNESS; STRENGTH OF MATERIALS (cross references thereunder); STRUCTURES, THEORY OF; TEMPERATURE; VIBRATION; WATER PRESSURE; WAVES; WHEEL LOADS; WIND PRESSURE; *also* under specific type of stress, e.g., BUCKLING; SHEAR; TORSION

"Deflection of Members of Variable Moment of Inertia," Anthony Hoadley, 499.

Arches

"Amplification of Stress in Flexible Steel Arches," Robert S. Rowe, 910. *Discussion:* Milo S. Ketchum, and Robert S. Rowe, 926.

Graphic chart presentation of amplification of computed stress at the quarter point of the loaded part of the arch, 910.

Bars (solid material)

Stiffness factors for a uniform bar, 53.

Beams (General). *See also* BUCKLING; SHEAR; STRESS AND STRAIN—Flanges; TORSION

"Rapid Computation of Flexural Constants," Thomas G. Morrison (with discussion), 93.

Beams, Continuous

"Continuous Composite Steel and Concrete Beams," John Sherman, 810.

Bridge Floors and Flooring

"Wind Loads on Truss Bridges," John M. Biggs (with discussion), 879.

Bridges (General). *See also* IMPACT; WIND . . .

"Live Loading for Long-Span Highway Bridges," R. J. Ivy, T. Y. Lin, Stewart Mitchell, N. C. Raab, V. J. Richey and C. F. Scheffey (with discussion), 981.

Buildings

"Earthquake Stresses in Shear Buildings," Mario G. Salvadori (with discussion), 171.

Influence of internal damping relating to earthquake stresses in shear buildings, 171, 177, 192, 204, 205.

Bulkheads

"Anchored Bulkheads," Karl Terzaghi (with discussion), 1243.

Concrete, Prestressed

"The Equivalent Rectangle in Prestressed Concrete Design," John J. Peebles (with discussion), 292.

Continuous Beams. *See* Beams, Continuous (hereunder)

Curved Structures. *See* STRUCTURES, THEORY OF—Curved Structures

Flanges

"Continuous Composite Steel and Concrete Beams," John Sherman, 810.

"Lateral Buckling of Channels and Z-Beams," H. N. Hill, 829.

Floors and Flooring. *See* Bridge Floors and Flooring (hereunder)

Frames, Rigid

"Design of Frames by Relaxation of Yield-Hinges," J. Morley English, 1143.

Discussion: Noel W. Murray, Herman Tachau, and J. Morley English, 1154.

"Stiffness Charts for Gusseted Members under Axial Load," John E. Goldberg (with discussion), 43.

Plates

"Hipped Plate Analysis, Considering Joint Displacements," Ibrahim Gaafar (with discussion), 743.

"Plates with Boundary Conditions of Elastic Support," S. J. Fuchs (with discussion), 935.

Slabs

"Plates with Boundary Conditions of Elastic Support," S. J. Fuchs (with discussion), 935.

Spillways

"Dam Modifications Checked by Hydraulic Models," E. S. Harrison and Carl E. Kindsvater (with discussion), 73.

Trusses and Trussed Structures

"Stiffness Charts for Gusseted Members under Axial Load," John E. Goldberg (with discussion), 43.

STRESSMETERS

See GAGES, STRAIN

STRESS, SHEARING

See SHEAR

STRINGERS

See BEAMS

STRUCTURAL ANALYSIS

See EQUATIONS; STRESS AND STRAIN; STRUCTURES, THEORY OF

STRUCTURAL DYNAMICS

See also AERODYNAMICS (cross references thereunder); EARTHQUAKES (cross references thereunder); VIBRATION

"Earthquake Stresses in Shear Buildings," Mario G. Salvadori (with discussion), 171.

"Nonelastic Behavior of Bridges under Impulsive Loads," S. J. Fraenkel and L. E. Grinter (with discussion), 309.

STRUCTURAL ENGINEERS AND ENGINEERING

See STRUCTURES . . . ; *also* under relative structure, e.g., BRIDGES

STRUCTURAL MATERIALS

See MATERIALS OF CONSTRUCTION

STRUCTURAL MEMBERS

See MEMBERS, STRUCTURAL (cross references thereunder)

STRUCTURAL MODELS

See MODELS, STRUCTURAL

STRUCTURAL REDUNDANCE

See STRUCTURES, THEORY OF

STRUCTURAL STEEL

See STEEL (cross references thereunder)

STRUCTURES (General)

See BUILDINGS (cross references thereunder); CONSTRUCTION (cross references thereunder); FOUNDATIONS . . . ; MATERIALS OF CONSTRUCTION; MODELS, STRUCTURAL; STRESS AND STRAIN . . . ; STRUCTURES, THEORY OF; VIBRATION; WIND . . . ; *also* under specific type of structure or related subject; *also* under general types of structures, e.g., HYDRAULIC STRUCTURES; SPACE STRUCTURES (cross references thereunder)

STRUCTURES, CONTINUOUS

See STRUCTURES, THEORY OF

STRUCTURES, CURVED

See CURVED STRUCTURES (cross reference thereunder)

STRUCTURES, DROP

See DAMS

STRUCTURES, HYDRAULIC

See HYDRAULIC STRUCTURES

STRUCTURES, SETTLEMENT OF

See BEARING CAPACITY; EARTH PRESSURE; EMBANKMENTS (cross references thereunder); FOUNDATIONS . . . ; SOIL . . .

STRUCTURES, SHELL

See SHELL STRUCTURES (cross references thereunder)

STRUCTURES, SPACE

See SPACE STRUCTURES (cross references thereunder)

STRUCTURES, STATICALLY INDETERMINATE

See STATICALLY INDETERMINATE STRUCTURES (cross references thereunder)

STRUCTURES, SUB-

See SUBSTRUCTURES (cross references thereunder)

STRUCTURES, THEORY OF (General)
See also STRESS AND STRAIN; *also* under type of structure or structural part
"Electrical Analogs of Statically Loaded Structures," Frederick L. Ryder, 1046.
"Nonelastic Behavior of Bridges under Impulsive Loads," S. J. Fraenkel and L. E. Grinter (with discussion), 309.
Bibliography
Gusseted members under axial load, 44.
Beams and Girders (General)
"Deflection of Laminated Beams," L. G. Clark, 721.
"Rapid Computation of Flexural Constants," Thomas G. Morrison (with discussion), 93.
Beams and Girders, Continuous
"Continuous Composite Steel and Concrete Beams," John Sherman, 810.
"Numerical Analysis of Continuous Frames in Space," James Michalos, 565.
Buildings
"Earthquake Stresses in Shear Buildings," Mario G. Salvadori (with discussion), 171.
Curved Structures
"Deflection of Members of Variable Moment of Inertia," Anthony Hoadley, 499.
Domes and Vaults
"Hipped Plate Analysis, Considering Joint Displacements," Ibrahim Gaafar (with discussion), 743.
Earthquake Problems
"Earthquake Stresses in Shear Buildings," Mario G. Salvadori (with discussion), 171.
Frames, Continuous
Application of the principle of superposition to a simple bent, 1209.
Chronological development of the cantilever (or no-shear) distribution method of correcting sidesway, 1209.
"Group Loadings Applied to the Analysis of Frames," I. F. Morrison, 338. *Discussion:* Bernard L. Weiner, and I. F. Morrison, 353.
"Joint Translation by Cantilever Moment Distribution," L. E. Grinter and C. H. Tsao, 1195. *Discussion:* T. C. Kavanagh; Ralph W. Stewart; W. Merchant; Jack R. Benjamin; Joseph G. Perri; Richard H. Hadley; Ming-Lung Pei; and L. E. Grinter and C. H. Tsao, 1204.
"Numerical Analysis of Continuous Frames in Space," James Michalos, 565.
"Stresses in the Corners of Rigid Frames," Harvey C. Olander, 797.
Frames, Rigid
Analogs of the rigid frame, 1054.
"Electrical Analogs of Statically Loaded Structures," Frederick L. Ryder, 1046.
"Group Loadings Applied to the Analysis of Frames," I. F. Morrison (with discussion), 338.
"Stiffness Charts for Gusseted Members under Axial Load," John E. Goldberg (with discussion), 43.
"Stresses in the Corners of Rigid Frames," Harvey C. Olander, 797.

Girders (General). *See* Beams and Girders (General) (hereunder)

Girders, Continuous. *See* Beams and Girders, Continuous (hereunder)

Plates

"Hipped Plate Analysis, Considering Joint Displacements," Ibrahim Gaafar, 743. *Discussion:* Herman Craemer; James M. Paulson and L. C. Maugh; R. Gartner; and Ibrahim Gaafar, 771.

"Plates with Boundary Conditions of Elastic Support," S. J. Fuchs (with discussion), 935.

Process of superposition as applied to plates with boundary conditions of elastic supports, 938.

Space Structures

"Numerical Analysis of Continuous Frames in Space," James Michalos, 565.

Trusses and Trussed Structures

"Electrical Analogs of Statically Loaded Structures," Frederick L. Ryder, 1046.

"Post-Buckling Strength of Redundant Trusses," E. F. Masur, 699.

"Stiffness Charts for Gusseted Members under Axial Load," John E. Goldberg, 43. *Discussion:* Leonard K. Stevens, 58.

STRUCTURES, TRUSSED

See STRUCTURES, THEORY OF—Trusses and Trussed Structures; TRUSSES

STRUCTURES, UNDERGROUND

See UNDERGROUND STRUCTURES (cross references thereunder)

STRUTS

See COLUMNS

SUB- . . .

See also UNDER- . . . (cross references thereunder)

SUBGRADES

See PAVEMENT AND PAVING

SUBSTRUCTURES

See CONCRETE; EARTHWORK; EXCAVATION; FOUNDATIONS; MASONRY (cross references thereunder); *also* under type of substructure, e.g., PIPE LINES; SUBWAYS

SUBURBS

See CITIES

SUBWAYS

See also RAILROAD TRACKS (cross references thereunder)

"Unified Mass-Transportation System for New York," William Reid (with discussion), 124.

SUPERPOSITION, PRINCIPLE OF

See STRUCTURES, THEORY OF

SURFACE PROFILES

See WATER SURFACE PROFILES (cross reference thereunder)

SURFACE RUNOFF

See RUNOFF

SURFACES, SLIPPAGE OF

See SLIPS AND SLIPPAGE (cross reference thereunder)

SURFACING

See AIRPORTS

SURGES (water surface)

See TANKS, AIR (cross reference thereunder); WAVES

SURVEYS (research data)

See under relative subject, e.g., RAINFALL; TRAFFIC . . . ; *see also* RESEARCH

SURVEYS AND SURVEYING (General)

See MAPS AND MAPPING; MATHEMATICS; PROPERTY (landed property) (cross references thereunder)

SUSPENDED LOAD

See SILT AND SILTING . . .

SWING BRIDGES

See BRIDGES, MOVABLE (SWING)

SYMBOLS

See under relative subject, e.g., HYDRAULICS; MATHEMATICS; STRUCTURES, THEORY OF

TANKS, AIR

See PIPE LINES

TASTES (in water)

Taste causing algae, 658.

TECHNICAL SOCIETIES

See AMERICAN SOCIETY OF CIVIL ENGINEERS; *see also* ENGINEERS AND ENGINEERING

TEMPERATURE

See also EVAPORATION; ICE

"Ice Pressure against Dams": A Symposium, R. L. Hearn, R. F. Legget, D. A. Buzzell, D. McHenry, L. S. McLennan, E. N. Peterson, and G. R. Strandberg; Bertil Lofquist; A. D. Hogg; and G. E. Monfore (with discussion), 1.

"Snow Hydrology for Multiple-Purpose Reservoirs," Herbert S. Riesbol (with discussion), 595.

TEMPERATURE MEASURING INSTRUMENTS

Development of salinity-temperature-depth (STD) indicator, 447.

TENSILE STRESS

See STRESS AND STRAIN

TENSION

See STRESS AND STRAIN

TERMINALS (structures and localities)

See AIR TERMINALS (cross reference thereunder)

TERMINOLOGY (Arranged hereunder by specific or comprehensive subject word when possible)

Airports. (Airport zoning, approach area, horizontal surface, conical surface, established elevation, airport reference point, turning bowl surface, and transitional surface defined), 277, 279, 280, 281.

Building and other structural rocking, 178.

Bulkheads. (Bulkhead types differentiated), 1244.

Cantilever moment distribution defined, 1203.

Clay. (Medium clay and firm clay suggested as terms), 1300.

Creep and landslide differentiated, 667.

Earth movements. (Landslides and similar terms as defined by specialists in the field), 667, 668, 669, 676, 690.

Estuaries. (Three types differentiated), 448.

Ground water. (Usage of "vadose" in upper subsurface water geological terminology), 694.

Hydrographs. (The hydrothermogram as a type of hydrograph), 611.

Loaded length on a bridge, 982.

Parameters. (Operation parameters in relation to mathematical definition), 619.

Paving materials. (Accuracy of nonfrost-susceptible materials as an expression), 564.

Radar echo contour maps defined, 268.

Sewage. (Mean age of sewage), 445.

Water flow through snow packs. (Channels known as "firn pipes" or "glands" which act as receivers of water in motion through snow packs), 618 623.

Watersheds. (Mixed cover as a land usage term), 1013.

Water supply. (Types of algae in potable water), 658.

TESTING MACHINES

See under use, material, structure or structural part tested

TESTS AND TESTING

See BUCKLING; ELASTICITY; FAILURES . . . ; IMPACT; LABORATORIES (cross references thereunder); MODELS . . . ; SHEAR; STRENGTH OF MATERIALS (cross references thereunder); STRESS AND STRAIN; STRUCTURES, THEORY OF; TORSION; WATER, FLOW OF . . . ; *see also* under material, structure or structural part tested, e.g., PLATES; SOILS—Tests and Testing

THEORIES

See cross references hereunder and under ANALYSIS OF DATA; *see also* under relative subject or its relative science, e.g., EARTH PRESSURE; TIDES

THEORY OF BOUNDARY LAYER (fluid flow)

See BOUNDARY LAYER, THEORY OF (cross reference thereunder)

THEORY OF LIMIT DESIGN

See LIMIT DESIGN, THEORY OF

THEORY OF STRUCTURES
See STRUCTURES, THEORY OF

THEORY OF SUPERPOSITION
See STRUCTURES, THEORY OF

THROTTLING
See WATER, FLOW OF, THROUGH ORIFICES

THRUST
See under relative structure, structural part or material, e.g., DAMS

TIDES
See also WAVES
General, classical and modified tide theories, 435, 443, 444, 451.

TIE RODS
See BULKHEADS

TORSION
"Lateral Buckling of Channels and **Z**-Beams," H. N. Hill, 829.
"Numerical Analysis of Continuous Frames in Space," James Michalos, 565.

TRACERS
See TIDES

TRACKS
See under type of track, e.g., RAILROAD TRACKS (cross references thereunder)

TRAFFIC (General)
See also FREIGHT; HIGHWAYS AND ROADS—Safety; TRANSPORTATION; WHEEL LOADS

TRAFFIC, AIR
See also COSTS, TRAFFIC CONTROL (AIR TRAFFIC)
"Electronic Devices in Air Transport," F. B. Lee (with discussion), 60.

TRAFFIC, AIRPORT
"Recent Airport Design and Development," Philip A. Hahn (with discussion), 489.

TRAFFIC, BRIDGE
"Bridges on the West Virginia Turnpike," Elmer K. Timby, 737.
"Live Loading for Long-Span Highway Bridges," R. J. Ivy, T. Y. Lin, Stewart Mitchell, N. C. Raab, V. J. Richey and C. F. Scheffey, 981. *Discussion:* Louis Balog; Glenn B. Woodruff; William G. Byers; Kuang-Han Chu; and R. J. Ivy, T. Y. Lin, Stewart Mitchell, N. C. Raab, V. J. Richey, and C. F. Scheffey, 995.
Procedure for traffic and vehicular surveys and reduction of traffic data, 983, 985.

TRAFFIC, BUS
See TRAFFIC, HIGHWAY AND ROAD; TRAFFIC, STREET

TRAFFIC, EXPRESSWAY
See TRAFFIC, STREET

TRAFFIC, HIGHWAY AND ROAD

"An Interstate Route and Its Urban Connections," D. W. Ormsbee, 969.

"Unified Mass-Transportation System for New York," William Reid (with discussion), 124.

TRAFFIC, STREET

See also AUTOMOBILE PARKING

"The Engineer's Role in Metropolitan Traffic Planning," Lloyd Braff, 713. *Discussion:* James L. Foley, Jr., 719.

Expressway planning to alleviate sudden traffic congestion conditions in Dallas, Texas, 716.

Use of origin-destination traffic survey in Dallas, Texas, in 1950, 716.

TRAFFIC, VEHICULAR

See TRAFFIC, HIGHWAY AND ROAD and other relative traffic headings hereunder

TRAIN . . .

See RAIL . . .

TRAINING WALLS

See SPILLWAYS

TRAIN LOADS

See WHEEL LOADS

TRANSIT, RAPID

See SUBWAYS

TRANSMISSION, PRESSURE, THROUGH SOLIDS

See EARTH PRESSURE

TRANSPORTATION

See also AIR TRANSPORT; CABLES AND CABLEWAYS; CANALS; CONVEYORS AND CONVEYANCE (cross reference thereunder); COSTS, TRANSPORTATION; FREIGHT; HIGHWAY TRANSPORTATION; RAILROADS (cross references thereunder); RAIL TRANSPORTATION; RIVERS; SOIL TRANSPORTATION (cross reference thereunder); STREET TRANSPORTATION (cross references thereunder); SUBWAYS; TERMINALS (cross reference thereunder); TRAFFIC; WATER TRANSPORTATION

"Unified Mass-Transportation System for New York," William Reid, 124. *Discussion:* John F. Kraus, 132.

TRUCKING

See HIGHWAY TRANSPORTATION

TRUCKS

See MOTOR TRUCKS

TRUSS BRIDGES

See BRIDGES, TRUSS

TRUSSED STRUCTURES

See STRUCTURES, THEORY OF—Trusses and Trussed Structures; TRUSSES

TRUSSES (General)

See also BRIDGES, TRUSS; STRESS AND STRAIN—Trusses and Trussed Structures; STRUCTURES, THEORY OF—Trusses and Trussed Structures

"Post-Buckling Strength of Redundant Trusses," E. F. Masur, 699.

Two theorems establishing upper and lower bounds to the ultimate load of a redundant truss, 707.

"Wind Loads on Truss Bridges," John M. Biggs (with discussion), 879.

TRUSSES, PIN-CONNECTED

Electrical analog of the pin-connected truss, 1048.

TRUSSES, VIERENDEEL

"Joint Translation by Cantilever Moment Distribution," L. E. Grinter and C. H. Tsao (with discussion), 1195.

TUBES

See CONDUITS; PIPE LINES; PIPES AND PIPING (cross references thereunder); PITOT TUBES (cross reference thereunder); SHELL STRUCTURES (cross references thereunder); SUBWAYS; WATER, FLOW OF, IN PIPES

TUNNELS, SUBWAY

See SUBWAYS

TUNNELS, WATER

See WATER DIVERSION

TURBULENCE (water agitation)

See also FRICTION . . . ; WATER, FLOW OF . . .

"Laminar to Turbulent Flow in a Wide Open Channel," W. M. Owen (with discussion), 1157.

"Turbulent Boundary Layer on Steep Slopes," William J. Bauer (with discussion), 1212.

TURBULENCE, WIND

See WIND . . .

TURNPIKES

See HIGHWAYS AND ROADS

TWISTING

See TORSION; *also* under relative material, structure or structural part, e.g., BEAMS

UNDER- . . .

See also SUB- . . .

UNDERFLOW

See SEEPAGE; WELLS

UNDERGROUND RAILWAYS

See SUBWAYS

UNDERGROUND STRUCTURES

See under type of structure, e.g., CONDUITS; SEWERS; *also* under related subject, e.g., SOILS

UNDERGROUND WATER

See GROUND WATER

UNDERWATER CONSTRUCTION

See under type of construction; *see also* EXCAVATION, HYDRAULIC (cross reference thereunder)

UNDERWATER FOUNDATIONS

See FOUNDATIONS, UNDERWATER

UNIT COSTS

See COSTS . . .

UNITED STATES WEATHER BUREAU

See under relative subject, e.g., RAINFALL

UNIT STRESSES

See STRESS AND STRAIN

UPLIFT, HYDROSTATIC

See WATER PRESSURE

URBAN . . .

See CITIES

UTILITIES

See PUBLIC UTILITIES (cross reference thereunder)

VALLEYS (General)

See also CANYONS

VALLEYS (Geographical)

Columbia River Basin

"Slackwater Improvement of the Columbia River," O. E. Walsh, 135.

Mississippi River Valley

"Relief Well Systems for Dams and Levees," W. J. Turnbull and C. I. Mansur (with discussion), 842.

Rio Grande Valley

"River-Bed Scour during Floods," E. W. Lane and W. M. Borland (with discussion), 1069.

VAULTS

See DOMES AND VAULTS (cross references thereunder)

VEHICLES

See under general types of vehicles, e.g., MOTOR VEHICLES; *also* under specific type of vehicle, e.g., AUTOMOBILE . . .

VEHICULAR TRAFFIC

See TRAFFIC . . .

VELOCITY

See HYDRODYNAMICS; WATER, FLOW OF . . .

VELOCITY DISTRIBUTION

See WATER, FLOW OF . . .

VELOCITY METERS

See WATER VELOCITY METERS (cross reference thereunder)

VESSELS

See cross reference under SHIPS AND SHIPPING

VIBRATION

See also EARTHQUAKES (cross references thereunder); IMPACT

"Earthquake Stresses in Shear Buildings," Mario G. Salvadori, 171. *Discussion:* John A. Blume; E. F. Masur; Edward Cohen, Edward Laing, and Leon S. Levy; and Mario G. Salvadori, 194.

"Radial Impact on an Elastically Supported Ring," Edward Wenk, Jr., 221. *Discussion:* John C. Burgess, and Edward Wenk, Jr., 246.

VIBRATION RECORDING APPARATUS

"Radial Impact on an Elastically Supported Ring," Edward Wenk, Jr. (with discussion), 221.

VIERENDEEL TRUSSES

See TRUSSES, VIERENDEEL

WALLS

See under relative structure or type of wall, e.g., BREAKWATERS (cross refence thereunder); BUILDINGS (cross references thereunder); BULKHEADS; JETTIES (cross reference thereunder); RETAINING WALLS; SPILLWAYS; *see also* BUTTRESSES; EARTHQUAKES (cross references thereunder)

WAR AND ENGINEERING

See WORLD WAR II (1941–1945) (cross reference thereunder); *also* cross references under MILITARY ENGINEERS AND ENGINEERING

WAREHOUSES

See BUILDINGS (cross references thereunder); FREIGHT

WASTE DISPOSAL

See DEBRIS CONTROL; ODORS; REFUSE DISPOSAL (cross references thereunder); SANITATION; SEWAGE DISPOSAL; SEWAGE SLUDGE; SEWERS (cross references thereunder); WATER POLLUTION (cross reference thereunder)

WASTE MATERIALS

See cross references under WASTE DISPOSAL

WASTE WATER

See SEWAGE DISPOSAL; SEWERS (cross references thereunder)

WATER . . .

See also BACKWATER; CONDUITS; COSTS . . . ; DAMS; DIKES; DRAINAGE (cross references thereunder); EROSION . . . ; EVAPORATION; FLOODS; FOUNDATIONS, UNDERWATER; GROUND WATER; HYDRAULIC . . . ; HYDRO- . . . ; ICE; IRRIGATION (cross references thereunder); METERS AND METERING; MODELS, HYDRAULIC; OCEAN . . . (cross references thereunder); PIPE LINES; PIPES AND PIPING (cross references thereunder); RAINFALL; RESERVOIRS; RUNOFF; SANITATION; SEA WATER; SEEPAGE; SETTLING BASINS (cross references thereunder); SEWAGE DISPOSAL; SEWERS (cross references thereunder); SPRINKLERS AND SPRINKLING; STORM WATER (cross references thereunder); TASTES (in water); TERMINOLOGY; TUNNELS, WATER (cross reference thereunder); TURBULENCE; WAVES; WELLS

WATER COLLECTION

See INFILTRATION (cross references thereunder); WELLS

WATER DISTRIBUTION

See CONDUITS; IRRIGATION (cross references thereunder); PIPES AND PIPING (cross references thereunder)

WATER DIVERSION

Diverting water across the Continental Divide (Rocky Mountains), 509, 526.

"The Granby Pumping Plant": A Symposium, W. R. Judd and W. H. Wolf; and R. J. Willson, 509.

WATER, FLOW OF (General)

See also FLOODS; FRICTION . . . ; GROUND WATER; HYDRAULICS; MODELS, HYDRAULIC; SPILLWAYS; TURBULENCE; WATER HAMMER; WELLS

The von Karman-Prandtl velocity distribution equations for turbulent flow near smooth and rough boundaries, 1215, 1219, 1232, 1235, 1241.

WATER, FLOW OF, FRESH WATER WITH SALT WATER

See WATER, FLOW OF, IN OPEN CHANNELS

WATER, FLOW OF, IN OPEN CHANNELS

See also BACKWATER; FLOODS; METERS AND METERING, CURRENT; RUNOFF; SILT AND SILTING, CHANNEL; WAVES

"Design of Side Walls in Chutes and Spillways," D. B. Gumensky (with discussion), 355.

"A Direct Step Method for Computing Water-Surface Profiles," Arthur A. Ezra (with discussion), 453.

Influence of salinity in tidal flow, 434.

Laboratory apparatus used to determine laminar to turbulent flow in a wide open channel, 1159.

"Laminar to Turbulent Flow in a Wide Open Channel," W. M. Owen, 1157. *Discussion:* Yuichi Iwagaki; J. W. Delleur; Ralph W. Powell and Chesley J. Posey; Henry Maksoud; and W. M. Owen, 1165.

"River-Bed Scour during Floods," E. W. Lane and W. M. Borland (with discussion), 1069.

"Sewage Disposal in Tidal Estuaries," Alexander N. Diachishin, Seth G. Hess and William T. Ingram (with discussion), 434.

"Snow Hydrology for Multiple-Purpose Reservoirs," Herbert S. Riesbol (with discussion), 595.

"Turbulent Boundary Layer on Steep Slopes," William J. Bauer, 1212. *Discussion:* G. Halbronn, and William J. Bauer, 1234.

"Velocity Measurement of Air-Water Mixtures," Lorenz G. Straub, John M. Killen, and Owen P. Lamb, 207.

WATER, FLOW OF, IN PIPES

See also PIPE LINES; PIPES AND PIPING (cross references thereunder); PUMPS AND PUMPING; SEWERS (cross references thereunder); SPRINKLERS AND SPRINKLING; WATER HAMMER; WATER PRESSURE

"Design Charts for Air Chambers on Pump Lines," W. E. Evans and C. C. Crawford (with discussion), 1025.

"Friction Factors for Turbulent Flow in Pipes," Edward F. Wilsey (with discussion), 331.

"Mechanics of Manifold Flow," John S. McNown, 1103. *Discussion:* Julio Escobar; M. R. Carstens and John Roberson; James J. Hartigan; Sadiq M. Niaz; James R. Barton; Ralph W. Powell; John K. Vennard and Darrhl I. Dentoni; and John S. McNown, 1119.

Variation in head in fluid flowing in a circular conduit with lateral inflow or outflow at right angles thereto, 1103.

WATER, FLOW OF, OVER DAMS AND WEIRS

"Dam Modification Checked by Hydraulic Models," E. S. Harrison and Carl E. Kindsvater (with discussion), 73.

"Design of Side Walls in Chutes and Spillways," D. B. Gumensky (with discussion), 355.

Effect of air entrainment in fast flowing water in chutes and spillways, 359.

"Rating Curves for Flow over Drum Gates," Joseph N. Bradley (with discussion), 403.

Side wall pressures at Grand Coulee Dam stilling basin on Columbia River, 368.

"Turbulent Boundary Layer on Steep Slopes," William J. Bauer (with discussion), 1212.

WATER, FLOW OF, THROUGH CHUTES

See SPILLWAYS; WATER, FLOW OF, IN OPEN CHANNELS

WATER, FLOW OF, THROUGH ORIFICES

Air chambers without throttling and with normal throttling indicating maximum relative downsurge and upsurge, 1041, 1045.

"Design Charts for Air Chambers on Pump Lines," W. E. Evans and C. C. Crawford (with discussion), 1025.

WATER FRONT

See BREAKWATERS (cross reference thereunder); BULKHEADS; HARBORS (cross references thereunder); JETTIES (cross reference thereunder); PILES AND PILE DRIVING; STREET TRANSPORTATION (cross references thereunder)

WATER GATES, MOVABLE

"Rating Curves for Flow over Drum Gates," Joseph N. Bradley, 403. *Discussion:* Guido Wyss; Sam Shulits; Bob Buehler; F. B. Campbell and A. A. McCool; and Joseph N. Bradley, 421.

WATER HAMMER

See also WATER PRESSURE

"Analysis of Water Hammer by Characteristics," C. A. M. Gray, 1176. *Discussion:* Pin-Nam Lin, Henry M. Paynter, and C. A. M. Gray, 1190.

"Design Charts for Air Chambers on Pump Lines," W. E. Evans and C. C. Crawford (with discussion), 1025.

Bibliography

Water hammer analysis by characteristics, 1177, 1190, 1191, 1193, 1194.

WATER INSTRUMENTS

See also under types of instruments, e.g., GAGES . . . ; METERS AND METERING, CURRENT

Development of salinity-temperature-depth (STD) indicator, 447.

St. Anthony Falls (SAF) velocity measuring instrument usage in traverses in air-water mixtures, 207.

"Velocity Measurement of Air-Water Mixtures," Lorenz G. Straub, John M. Killen, and Owen P. Lamb, 207.

WATER LEVEL CONTROL

See PIPE LINES

WATER MAINS

See PIPES AND PIPING (cross references thereunder); WATER SUPPLY (cross references thereunder)

WATER METERS AND METERING (stream velocity)

See METERS AND METERING, CURRENT

WATER PIPES AND PIPING

See PIPES AND PIPING (cross references thereunder)

WATER POLLUTION

See SEWAGE DISPOSAL

WATER POWER (General)

See DAMS; POWER (cross references thereunder)

WATER PRESSURE

See also GAGES, PRESSURE; PIPE LINES; WATER HAMMER; WAVES

"Anchored Bulkheads," Karl Terzaghi (with discussion), 1243.

"Dam Modifications Checked by Hydraulic Models," E. S. Harrison and Carl E. Kindsvater (with discussion), 73.

"Design of Side Walls in Chutes and Spillways," D. B. Gumensky (with discussion), 355.

Influence of pore pressure in correction of landslides, 692.

"Mechanics of Manifold Flow," John S. McNown (with discussion), 1103.

"Relief Well Systems for Dams and Levees," W. J. Turnbull and C. I. Mansur (with discussion), 842.

WATER, SEA

See SEA WATER

WATERSHEDS

See DRAINAGE (cross references thereunder); RAINFALL

WATER, STORM

See DRAINAGE (cross references thereunder); SEWAGE DISPOSAL: SEWERS (cross references thereunder)

WATER SUPPLY (General)

See ALGAE; DAMS; FLOODS; GAGES; GROUND WATER; IRRIGATION (cross references thereunder); METERS AND METERING; PIPE LINES; PIPES AND PIPING (cross references thereunder); PUMPS AND PUMPING; RAINFALL; RESERVOIRS; SETTLING BASINS (cross references thereunder); SILT AND SILTING; SPRINKLERS AND SPRINKLING; TASTES (in water); TUNNELS, WATER (cross reference thereunder); WATER . . . (related subject headings thereunder); WELLS

WATER SURFACE PROFILES

See BACKWATER

WATER SURFACE SURGES

See TANKS, AIR (cross reference thereunder); WAVES

WATER TRANSPORTATION

See also CANALS; CHANNELS; DOCKS AND WHARVES (cross references thereunder); FREIGHT; HARBORS; LOCKS; RIVERS; TRANSPORTATION; WATER FRONT (cross references thereunder)

"Slackwater Improvement of the Columbia River," O. E. Walsh, 135.

WATER TUNNELS

See TUNNELS, WATER (cross reference thereunder)

WATER, UNDERGROUND

See GROUND WATER

WATER VELOCITY METERS

See METERS AND METERING, CURRENT

WATER, WASTE

See SEWAGE DISPOSAL; SEWERS (cross references thereunder)

WATER WAVES

See WAVES

WATERWAYS (General)

See CANALS; CHANNELS; DOCKS AND WHARVES (cross references thereunder); HARBORS; OCEAN . . . (cross references thereunder); RIVERS; SEACOAST (cross references thereunder); WATER TRANSPORTATION

WATERWAY TRANSPORTATION

See WATER TRANSPORTATION

WATERWORKS (General)

See DAMS; PIPE LINES; PIPES AND PIPING (cross references thereunder); PUMPS AND PUMPING; RESERVOIRS; WATER SUPPLY (cross references thereunder)

WAVES

See also DEBRIS CONTROL; EROSION, BEACH; RETAINING WALLS; SHORES AND SHORE PROTECTION (cross references thereunder); TIDES; WATER PRESSURE

"Analysis of Water Hammer by Characteristics," C. A. M. Gray (with discussion), 1176.

"Offshore Petroleum Installations," Jack S. Toler, 480.

"Sewage Disposal in Tidal Estuaries," Alexander N. Diachishin, Seth G. Hess and William T. Ingram (with discussion), 434.

"Wave-Wash Control on Mississippi River Levees," Rudolf Hertzberg, 628.

WEATHER

See FLOODS; HYDROLOGY; METEOROLOGY (cross references thereunder); RAINFALL; SNOW; TEMPERATURE; WIND PRESSURE

WEATHER BUREAU, UNITED STATES

See under relative subject, e.g., RAINFALL

WEDGE-SHAPED MEMBERS, STRUCTURAL

See cross references under MEMBERS, STRUCTURAL

WEIRS

See DRUM GATES (cross references thereunder); WATER, FLOW OF, OVER DAMS AND WEIRS

WELLS

See also GROUND WATER

"Offshore Petroleum Installations," Jack S. Toler, 480.

"Relief Well Systems for Dams and Levees," W. J. Turnbull and C. I. Mansur, 842. *Discussion:* P. T. Bennett, John A. Focht, Jr.; W. H. Jervis; and W. J. Turnbull and C. I. Mansur, 862.

WHARVES

See DOCKS AND WHARVES (cross references thereunder)

WHEEL LOADS

Example of the graphical method of determining safe wheel loads for flexible pavements, 554, 555.

"Special Procedures for Pavement Design," L. A. Palmer (with discussion), 542.

WHEELS

Diagrams of trucks classified by type showing wheel base measurements, weight and speed, 984, 985, 986.

WILLIOT-MOHR DIAGRAM

See GRAPHICAL CHARTS

WIND PRESSURE

Gulf Coast hurricanes as related to offshore petroleum development construction design, 483.

Lift and overturning moment produced by wind forces on truss bridges, 888.

"Wind Loads on Truss Bridges," John M. Biggs, 879. *Discussion:* F. B. Farquharson, and John M. Biggs, 893.

WORK, COST OF

See COSTS

WORK, LEAST, PRINCIPLE OF

See STRUCTURES, THEORY OF

WORKS (industrial buildings and equipment)

See under general types of works, e.g., PUBLIC WORKS (cross references thereunder); *also* under specific type of works, e.g., SEWAGE WORKS (cross reference thereunder); WATERWORKS (cross references thereunder); *see also* cross references under HOUSES; PLANTS

WORLD WAR II (1941–1945)

See under relative technical subject, e.g., AIRPORTS

ZONING

See CITIES; CITY PLANNING; PROPERTY (cross references thereunder); REGIONAL PLANNING; STREETS—Planning and Design

ZONING LAW

Land use computation in zoning ordinances, 168.

"Zoning Maps for Airports," B. Everett Beavin, Sr. (with discussion), 277.

AUTHOR INDEX

(*including Memoirs of deceased members*)

ALEXANDER, HENRY JAMES
Memoir of, 1336.

ARCHER, JOHN S.
Impulsive loads, 329.

AUSTIN, VERLE LORRAINE
Memoir of, 1337.

AYERS, JAMES R.
"The Design of Flexible Bulkheads," 373.

BAKER, R. F.
"Analysis of Corrective Actions for Highway Landslides," 665.

BAKHMETEFF, BORIS ALEXANDER
Memoir of, 1332.

BALOG, LOUIS
Bridge loads, 995.

BARTON, JAMES R.
Manifold flow, 1134.

BAUER, WILLIAM J.
"Turbulent Boundary Layer on Steep Slopes," 1212.

BAUMANN, PAUL
Anchored bulkheads, 1296.

BEAVIN, B. EVERETT, SR.
"Zoning Maps for Airports," 277.

BEDFORD, THOMAS ARCHIBALD
Memoir of, 1337.

BENAS, BENJAMIN
"Putting a Sewage Treatment Plant into Operation," 785.

BENJAMIN, JACK R.
Joint translation, 1206.

BENNETT, P. T.
Relief wells, 862.

BIGGS, JOHN M.
"Wind Loads on Truss Bridges," 879.

BIGLER, W. D.
Anchored bulkheads, 1284.

BLUME, JOHN A.
Earthquake stresses, 194.

BONNEY, ORRIS
Memoir of, 1338.

BORLAND, W. M.
"River-Bed Scour during Floods," 1069.

BOYER, WALTER C.
"Design Curves for Anchored Steel Sheet Piling," 639.
Flexible bulkheads, 386.

BRADLEY, JOSEPH N.
"Rating Curves for Flow over Drum Gates," 403.

BRAFF, LLOYD
"The Engineer's Role in Metropolitan Traffic Planning," 713.

BRISKE, RUDOLF
Anchored bulkheads, 1298.

BROWN, WILLIAM GERRIE
Memoir of, 1339.

BUCKLEY, JAMES C.
"Revenue Bond Financing for Airport Improvements," 583.

BUEHLER, BOB
Drum gates, 421.
Water surface profiles, 470.

BURGESS, JOHN C.
Radial impact, 246.

BURKHOLDER, JOSEPH L.
Memoir of, 1340.

BUZZELL, D. A.
"Ice Pressure against Dams (symposium): Foreword," 1.

BYERS, WILLIAM G.
Bridge loads, 1001.

CAMPBELL, F. B.
Drum gates, 428.

CAMPBELL, MORGAN S.
Flexible bulkheads, 385.

CARSTENS, M. R.
Manifold flow, 1123.

CELLARIUS, FREDERICK JULIUS
Memoir of, 1342.

CHOKLA, LOUIS MOSES
Memoir of, 1343.

CHOW, VEN TE
Rainfall, 274.

CHU, KUANG-HAN
Bridge loads, 1002.

CLARK, L. G.
"Deflection of Laminated Beams," 721.

COHEN, EDWARD
Earthquake stresses, 203.

COLLINS, ALBERT BERNHARDT
Memoir of, 1343.

COMEY, ARTHUR COLEMAN
Memoir of, 1344.

CRAEMER, HERMAN
Hipped plates, 771.

CRAWFORD, C. C.
"Design Charts for Air Chambers on Pump Lines," 1025.

CROW, GEORGE DAVIS
Memoir of, 1345.

DAVIES, JOSEPH HERBERT
Memoir of, 1346.

DAVIS, THOMAS MARSH
Memoir of, 1347.

DELLEUR, J. W.
Laminar flow, 1167.

DENTONI, DARRHL I.
Manifold flow, 1136.

DIACHISHIN, ALEXANDER N.
"Sewage Disposal in Tidal Estuaries," 434.

DITTBRENNER, E. E.
River bed scour, 1080.

DOUGHERTY, EDWARD A.
Memoir of, 1348.

DOUMA, J. H.
Spillway side walls, 364.

DUCLOS, LOUIS
"Highway Bridges on Deep Foundations," 1090.

DUFFEE, LOUIS WARREN
Memoir of, 1350.

ENGLISH, J. MORLEY
"Design of Frames by Relaxation of Yield-Hinges," 1143.

ESCOBAR, JULIO
Manifold flow, 1119.

EVANS, W. E.
"Design Charts for Air Chambers on Pump Lines," 1025.

EZRA, ARTHUR A.
"A Direct Step Method for Computing Water-Surface Profiles," 453.

FABIAN, E. S.
Aeronautical mapping, 158.

FARQUHARSON, F. B.
Wind loads, 893.

FENKELL, GEORGE HARRISON
Memoir of, 1333.

FOCHT, JOHN A., JR.
Relief wells, 870.

FOLEY, JAMES L., JR.
Traffic planning, 719.

FOSTER, EDGAR E.
Spillway side walls, 368.

FRAENKEL, S. J.
"Nonelastic Behavior of Bridges under Impulsive Loads," 309

FUCHS, S. J.
"Plates with Boundary Conditions of Elastic Support," 935.

GAAFAR, IBRAHIM
"Hipped Plate Analysis, Considering Joint Displacements," 743.

GARTNER, R.
Hipped plates, 776.

GERDEL, R. W.
Snow hydrology, 615.

GOLDBERG, JOHN E.
"Stiffness Charts for Gusseted Members under Axial Load," 43.

GRAY, C. A. M.
"Analysis of Water Hammer by Characteristics," 1176.
Water surface profiles, 469.

GRINTER, L. E.
"Joint Translation by Cantilever Moment Distribution," 1195.
"Nonelastic Behavior of Bridges under Impulsive Loads," 309.

GUMENSKY, D. B.
"Design of Side Walls in Chutes and Spillways," 355.

HADLEY, RICHARD H.
Joint translation, 1207.

HAFTERSON, HAROLD D.
Snow hydrology, 619.

HAHN, PHILIP A.
"Recent Airport Design and Development," 489.

HALBRONN, G.
Turbulent layer, 1234.

HANSEN, J. BRINCH
Anchored bulkheads, 1285.

HANSEN, ROBERT J.
Impulsive loads, 329.

HARRISON, E. S.
"Dam Modifications Checked by Hydraulic Models," 73.

HARTIGAN, JAMES J.
Manifold flow, 1128.

HEARN, R. L.
"Ice Pressure against Dams (symposium): Foreword," 1.

HEAVEY, W. F.
Flexible bulkheads, 384.

HERTZBERG, RUDOLF
"Wave-Wash Control on Mississippi River Levees," 628.

HESS, SETH G.
"Sewage Disposal in Tidal Estuaries," 434.

HICKOX, G. H.
Hydraulic models, 90.

HIGHLAND, SCOTLAND G.
Memoir of, 1351.

HILL, H. N.
"Lateral Buckling of Channels and Z-Beams," 829.

HOADLEY, ANTHONY
"Deflection of Members of Variable Moment of Inertia," 499.

HOGG, A. D.
"Ice Pressure against Dams (symposium): Some Investigations in Canada," 22.

HOPKINS, DAVID
Flexible bulkheads, 396.

HORONJEFF, R.
Pavement design, 561.

HUDSON, H. E., JR.
"Rainfall Studies Using Rain-Gage Networks and Radar," 248.

HUFF, F. A.
"Rainfall Studies Using Rain-Gage Networks and Radar," 248.

INGRAM, WILLIAM T.
"Sewage Disposal in Tidal Estuaries," 434.

IVY, R. J.
"Live Loading for Long-Span Highway Bridges," 981.

IWAGAKI, YUICHI
Laminar flow, 1165.

IZZARD, CARL F.
"Peak Discharge for Highway Drainage Design," 1005.

JAKKULA, ARNE ARTHUR
Memoir of, 1352.

JERVIS, W. H.
Relief wells, 874.

JUDD, W. R.
"The Granby Pumping Plant (symposium): Foundations and Design," 510.

KANSOH, MONIR M.
Water surface profiles, 475.

KAVANAGH, T. C.
Joint translation, 1204.

KELIHER, LESTER JOSEF NEWMAN
Memoir of, 1353.

KETCHUM, MILO S.
Flexible arches, 926.

KILLEN, JOHN M.
"Velocity Measurement of Air-Water Mixtures," 207.

KINDSVATER, CARL E.
"Dam Modifications Checked by Hydraulic Models," 73.

KNIGHT, HERBERT MILLER
Memoir of, 1354.

KOEBEL, FRED E.
Prestressed concrete, 303.

KOHLER, MAX A.
Drainage design, 1016.

KRAUS, JOHN F.
Mass transportation, 132.

KRYNINE, D. P.
Landslides, 690.

KRZYWOBLOCKI, M. Z. v.
Elastic supports, 959.

LAING, EDWARD
Earthquake stresses, 203.

LAKE, J. OWEN
Flexible bulkheads, 392.

LAMB, OWEN P.
"Velocity Measurement of Air-Water Mixtures," 207.

LANE, E. W.
"River-Bed Scour during Floods," 1069.

LAURSEN, EMMETT M.
River bed scour, 1084.

LEA, NORMAN D.
Anchored bulkheads, 1299.

LEE, F. B.
"Electronic Devices in Air Transport," 60.

LEGGET, R. F.
"Ice Pressure against Dams (symposium) : Foreword," 1.

LEVY, LEON S.
Earthquake stresses, 203.

LEWIS, HAROLD M.
Zoning maps for airports, 286.

LIN, PIN-NAM
Water hammer, 1190.

LIN, T. Y.
"Live Loading for Long-Span Highway Bridges," 981.

LINSLEY, RAY K.
Snow hydrology, 614.

LOFQUIST, BERTIL
"Ice Pressure against Dams (symposium) : Studies of the Effects of Temperature Variations," 6.

LUMMIS, HENRY M., III
"Design Curves for Anchored Steel Sheet Piling," 639.

MAKSOUD, HENRY
Laminar flow, 1172.

MALTER, HENRY
Flexural constants, 103.

MANSUR, C. I.
"Relief Well Systems for Dams and Levees," 842.

MASUR, E. F.
Earthquake stresses, 201.
"Post-Buckling Strength of Redundant Trusses," 699.

MAUGH, L. C.
Hipped plates, 772.

McCOOL, A. A.
Drum gates, 428.

McHENRY, D.
"Ice Pressure against Dams (symposium): Foreword," 1.

McINDOE, GEORGE P.
"Mass-Concrete Operations in the Rocky Mountains," 899.

McLENNAN, L. S.
"Ice Pressure against Dams (symposium): Foreword," 1.

McNOWN, JOHN S.
"Mechanics of Manifold Flow," 1103.

McVEA, JOHN CRANE
Memoir of, 1355.

MERCHANT, W.
Joint translation, 1206.

MICHALOS, JAMES
"Numerical Analysis of Continuous Frames in Space," 565.

MILES, PHIL M.
Aeronautical mapping, 161.

MINSHALL, N. E.
Drainage design, 1018.

MITCHELL, STEWART
"Live Loading for Long-Span Highway Bridges," 981.

MONFORE, G. E.
Ice pressure, 17.
"Ice Pressure against Dams (symposium): Experimental Investigations by the Bureau of Reclamation," 26.

MORRILL, FRED WILLIAM
Memoir of, 1355.

MORRISON, I. F.
"Group Loadings Applied to the Analysis of Frames," 338.

MORRISON, THOMAS G.
"Rapid Computation of Flexural Constants," 93.

MURRAY, NOEL W.
Frame design, 1154.

NEES, LOUIS A.
Airport design, 497.

NIAZ, SADIQ M.
Manifold flow, 1132.

NUSBAUM, ISADORE
Tidal estuaries, 448.

OLANDER, HARVEY C.
"Stresses in the Corners of Rigid Frames," 797.

ORMSBEE, D. W.
"An Interstate Route and Its Urban Connections," 969.

OWEN, W. M.
"Laminar to Turbulent Flow in a Wide Open Channel," 1157.

PACKSHAW, S.
Anchored bulkheads, 1301.

PALMER, L. A.
"Special Procedures for Pavement Design," 542.

PARTRIDGE, JOHN FREDERICK
Memoir of, 1356.

PAULSON, JAMES M.
Hipped plates, 772.

PAYNTER, HENRY M.
Air chambers, 1039.
Water hammer, 1191.

PEEBLES, JOHN J.
"The Equivalent Rectangle in Prestressed Concrete Design," 292.

PEI, MING-LUNG
Joint translation, 1208.

PENN, JOHN CORNELIUS
Memoir of, 1357.

PERCIVAL, HAROLD FRED
Memoir of, 1358.

PERRI, JOSEPH G.
Joint translation, 1207.

PETERSON, E. N.
"Ice Pressure against Dams (symposium): Foreword," 1.

POSEY, CHESLEY J.
Laminar flow, 1170.

POWELL, RALPH W.
Laminar flow, 1170.
Manifold flow, 1136.

QUADE, MAURICE N.
"Special Design Features of the Yorktown Bridge," 109.

RAAB, N. C.
"Live Loading for Long-Span Highway Bridges," 981.

REID, WILLIAM
"Unified Mass-Transportation System for New York," 124.

RHODES, LELAND S.
Spillway side walls, 362.

RHONE, THOMAS J.
Spillway side walls, 368.

RICHARDSON, ST. GEORGE TUCKER
Memoir of, 1359.

RICHEY, V. J.
"Live Loading for Long-Span Highway Bridges," 981.

RIESBOL, HERBERT S.
"Snow Hydrology for Multiple-Purpose Reservoirs," 595.

RILEY, RUSSELL H.
"City Planning Techniques," 163.

ROBERSON, JOHN
Manifold flow, 1123.

ROCKWOOD, DAVID M.
Snow hydrology, 621.

ROGERS, PAUL
Flexural constants, 106.

ROISIN, V.
Anchored bulkheads, 1307.

ROLFE, ROBERT LAWRENCE
Memoir of, 1361.

ROSE, EDWIN
Ice pressure, 18, 39.

ROWE, P. W.
Flexible bulkheads, 388.

ROWE, ROBERT S.
"Amplification of Stress in Flexible Steel Arches," 910.

RYDER, FREDERICK L.
"Electrical Analogs of Statically Loaded Structures," 1046.

SALVADORI, MARIO G.
"Earthquake Stresses in Shear Buildings," 171.

SANDRETTO, P. C.
Electronic devices, 70.

SARKARIA, G. S.
Spillway side walls, 363.

SCHANCK, CHARLES A.
"Aeronautical Charting and Mapping," 151.

SCHEFFEY, C. F.
"Live Loading for Long-Span Highway Bridges," 981.

SCHROEDER, FRANK CHARLES
Memoir of, 1361.

SHERMAN, JOHN
"Continuous Composite Steel and Concrete Beams," 810.

SHULITS, SAM
Drum gates, 421.

SMITH, DAVID B.
"Frequency of Excessive Rainfalls in Florida," 927.

SMITH, WALTER MICKLE
Memoir of, 1362.

SNOW, EDWIN JAMES
Memoir of, 1363.

STEARNS, JOHN
Memoir of, 1365.

STEINBERG, I. H.
Water surface profiles, 463.

STEVENS, LEONARD K.
Gusseted members, 58.

STEWART, RALPH W.
Joint translation, 1205.

STOKES, R. C.
"The Design of Flexible Bulkheads," 373.

STOUT, G. E.
"Rainfall Studies Using Rain-Gage Networks and Radar," 248.

STRANDBERG, G. R.
"Ice Pressure against Dams (symposium): Foreword," 1.

STRAUB, LORENZ G.
"Velocity Measurement of Air-Water Mixtures," 207.

TACHAU, HERMAN
Frame design, 1155.

TERRELL, DANIEL V.
"The Engineer and World Population": Address at the Summer Convention, Atlantic City, N. J., June 16, 1954, 1325.

TERZAGHI, KARL
"Anchored Bulkheads," 1243.

THOMSON, THOMAS KENNARD
Memoir of, 1366.

TIMBY, ELMER K.
"Bridges on the West Virginia Turnpike," 737.

TOCH, ARTHUR
River bed scour, 1084.

TOLER, JACK S.
"Offshore Petroleum Installations," 480.

TSAO, C. H.
"Joint Translation by Cantilever Moment Distribution," 1195.

TSCHEBOTARIOFF, GREGORY P.
Anchored bulkheads, 1287.
Flexible bulkheads, 390.
Sheet piling, 651.

TURNBULL, W. J.
"Relief Well Systems for Dams and Levees," 842.

TURRE, GEORGE J.
"Algae Responsible for Odor and Taste in Water Supplies," 658.

VAN NORMAN, HARVEY ARTHUR
Memoir of, 1367.

VENNARD, JOHN K.
Manifold flow, 1136.

VERDEYEN, J.
Anchored bulkheads, 1307.

WALKER, ARTHUR V.
Deep foundations, 1100.

WALSH, O. E.
"Slackwater Improvement of the Columbia River," 135.

WARNER, FAYETTE SAMUEL
Memoir of, 1369.

WARNER, ROY F.
Drainage design, 1017.

WEINER, BERNARD L.
Group loadings, 353.

WENK, EDWARD, JR.
"Radial Impact on an Elastically Supported Ring," 221.

WHETSTONE, GEORGE A.
Friction factors, 337.

WILLSON, R. J.
"The Granby Pumping Plant (symposium): Construction," 525.

WILSEY, EDWARD F.
"Friction Factors for Turbulent Flow in Pipes," 331.

WITHERS, C. E.
Air chambers, 1037.

WOLF, W. H.
"The Granby Pumping Plant (symposium): Foundations and Design," 510.

WOOD, R. H.
Elastic supports, 960.

WOODRUFF, GLENN B.
Bridge loads, 999.

WOODWARD, RICHARD J.
Landslides, 690.

WOODWARD, SHERMAN MELVILLE
Memoir of, 1335.

WU, T. H.
Anchored bulkheads, 1281.

WYSS, GUIDO
Drum gates, 421.

YANG, NAI C.
Flexible bulkheads, 394.